Wiley Series on Polymer Engineering and Technology

*Richard F. Grossman and Domasius Nwabunma, Series Editors*

SECOND EDITION

# POLY(LACTIC ACID)

## Synthesis, Structures, Properties, Processing, Applications, and End of Life

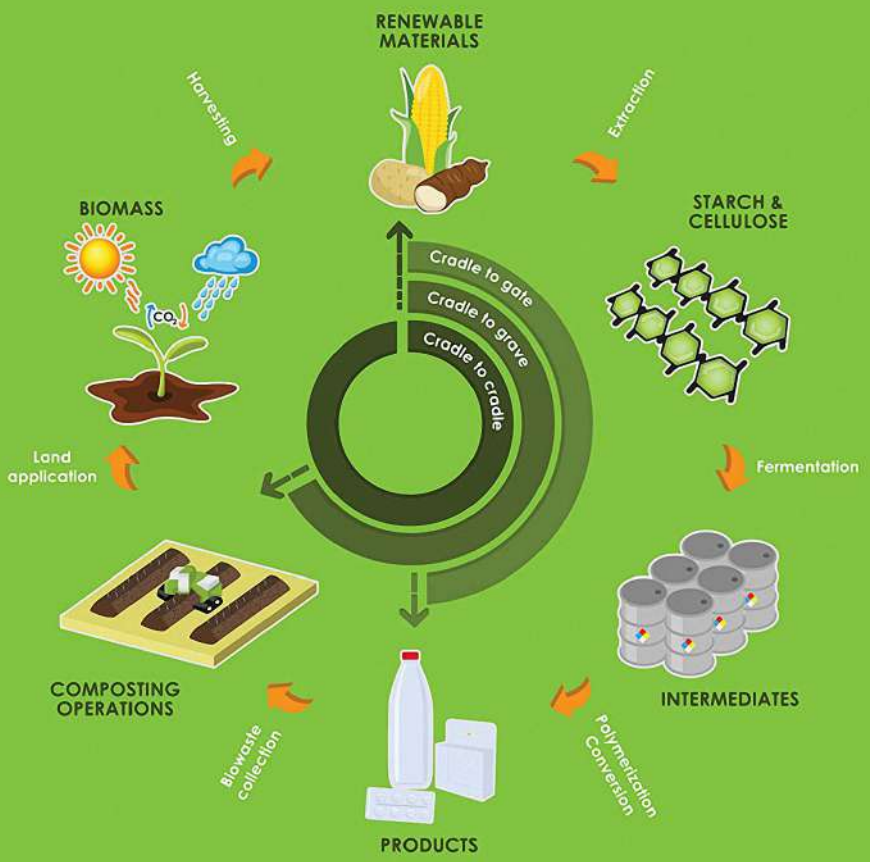


Edited by **RAFAEL A. AURAS, LOONG-TAK LIM, SUSAN E. M. SELKE, HIDETO TSUJI**

WILEY

**POLY(LACTIC ACID)**

**Wiley Series on Polymer Engineering and Technology**
**Richard F. Grossman and Domasius Nwabunma, Series Editors**

*Polyolefin Blends*
Edited by Domasius Nwabunma and Thein Kyu

*Polyolefin Composites*
Edited by Domasius Nwabunma and Thein Kyu

*Handbook of Vinyl Formulating, Second Edition*
Edited by Richard F. Grossman

*Total Quality Process Control for Injection Molding, Second Edition*
M. Joseph Gordon, Jr.

*Microcellular Injection Molding*
Jingyi Xu

*Poly(Lactic Acid): Synthesis, Structures, Properties, Processing, and Applications*
Edited by Rafael Auras, Loong-Tak Lim, Susan E.M. Selke, and Hideto Tsuji

*Hyperbranched Polymers: Synthesis, Properties, and Applications*
Edited by Deyue Yan, Chao Gao, and Holger Frey

*Advanced Thermoforming: Methods, Machines and Materials, Applications, and Automation*
Sven Engelmann

*Biopolymer Nanocomposites: Processing, Properties, and Applications*
Alain Dufresne, Sabu Thomas, Laly A. Pothan

*Polymers for PEM Fuel Cells*
Hongting Pu

*Polyurethanes: Science, Technology, Markets, and Trends*
Mark F. Sonnenschein

*Functional Polymer Coatings: Principles, Methods, and Applications*
Edited by Limin Wu and Jamil Baghdachi

*Polyurethanes: Science, Technology, Markets, and Trends, Second Edition*
Mark F. Sonnenschein

*Poly(lactic acid): Synthesis, Structures, Properties, Processing, Applications, and End of Life, Second Edition*
Edited by Rafael A. Auras, Loong-Tak Lim, Susan E.M. Selke, and Hideto Tsuji

# POLY(LACTIC ACID)

## Synthesis, Structures, Properties, Processing, Applications, and End of Life

### SECOND EDITION

Edited by

**RAFAEL A. AURAS**
**LOONG-TAK LIM**
**SUSAN E. M. SELKE**
**HIDETO TSUJI**

WILEY

This edition first published 2022


*Registered Office*
John Wiley & Sons, Inc., 111 River Street, Hoboken, NJ 07030, USA

*Editorial Office*
111 River Street, Hoboken, NJ 07030, USA

For details of our global editorial offices, customer services, and more information about Wiley products visit us at www.wiley.com.

Wiley also publishes its books in a variety of electronic formats and by print-on-demand.
Some content that appears in standard print versions of this book may not be available in other formats.



*Library of Congress Cataloging-in-Publication Data applied for*
Hardback ISBN: 9781119767442

Cover Design: Wiley
Cover Image: Courtesy of Rafael A. Auras

*To our students, mentors, and families.*

# CONTENTS

# LIST OF CONTRIBUTORS


**Hideki Abe**, Bioplastic Research Team, RIKEN Center for Sustainable Resource Science, Saitama, Japan

**Ashwini K. Agrawal**, Department of Textile Technology, Indian Institute of Technology, Hauz Khas, New Delhi, India

**Ann-Christine Albertsson**, Department of Fiber and Polymer Technology, KTH Royal Institute of Technology, Stockholm, Sweden

**Rafael Auras**, School of Packaging, Michigan State University, East Lansing, Michigan

**Sanchita Bandyopadhyay-Ghosh**, Engineered Biomedical Materials Research and Innovation Centre (EnBioMatRIC), Department of Mechanical Engineering, Manipal University Jaipur, Jaipur, India

**Anibal Bher**, School of Packaging, Michigan State University, East Lansing, Michigan; Materials Institute of Misiones (IMAM), CONICET-UNaM, Posadas, Misiones, Argentina

**Edgar Castro-Aguirre**, The Kraft Heinz Company, Glenview, Illinois

**Gian Domenico Cella,** Novamont SpA, Novara, Italy

**Kevin Cink**, Boston Scientific, Minneapolis, Minnesota

**Sukeewan Detyothin**, Department of Agro-Industry, Faculty of Agriculture Natural Resources and Environment, Naresuan University, Phitsanulok, Thailand

**John R. Dorgan**, Chemical Engineering and Materials Science, Michigan State University, East Lansing, Michigan

**Luca Fambri**, Department of Materials Engineering and Industrial Technologies and BIOtech Research Center, University of Trento, Trento, Italy

**Anna Finne-Wistrand**, Department of Fibre and Polymer Technology, KTH Royal Institute of Technology, Stockholm, Sweden

**Subrata Bandhu Ghosh**, Engineered Biomedical Materials Research and Innovation Centre (EnBioMatRIC), Department of Mechanical Engineering, Manipal University Jaipur, Jaipur, India

**Wim Groot**, Corbion, The Randstad, Netherlands

**Tanmay Gupta**, Engineered Biomedical Materials Research and Innovation Centre (EnBioMatRIC), Department of Mechanical Engineering, Manipal University Jaipur, Jaipur, India

**Akira Hiraishi**, Department of Environmental and Life Sciences, Toyohashi University of Technology, Toyohashi, Japan

**Shakira R. Hobbs**, Department of Civil Engineering, University of Kentucky, Lexington, Kentucky

**Yoshito Ikada**, Kyoto University, Kyoto, Japan; Department of Bioenvironmental Medicine, Nara Medical University, Kashihara, Nara, Japan

**Fabiola Iñiguez-Franco**, Niagara Bottling, LLC, Diamond Bar, California

**Saara Inkinen**, Laboratory of Polymer Technology, Åbo Akademi University, Turku, Finland; Nordic Catalyst, Vienna, Austria

**Tadahisa Iwata**, Graduate School of Agricultural and Life Sciences, Department of Biomaterial Sciences, The University of Tokyo, Tokyo, Japan

**Waree Jaruwattanayon**, Department of Agro-Industry, Faculty of Agriculture Natural Resources and Environment, Naresuan University, Phitsanulok, Thailand

**Ajay Kathuria**, Industrial Technology and Packaging, California Polytechnic State University, San Luis Obispo, California

**Vimal Katiyar**, Department of Chemical Engineering, Indian Institute of Technology Guwahati, Guwahati, India

**Yoshihiro Kikkawa**, National Institute of Advanced Industrial Science and Technology (AIST), Tsukuba, Japan

**Takeshi Kikutani**, School of Materials and Chemical Technology, Tokyo Institute of Technology, Yokohama, Japan

**Yoshiharu Kimura**, Center for Fiber and Textile Science, Kyoto Institute of Technology, Kyoto, Japan

**Kamlesh Kumar**, Council of Scientific and Industrial Research, Central Scientific Instruments Organization, Chandigarh, India

**Vijay Shankar Kumawat**, Engineered Biomedical Materials Research and Innovation Centre (EnBioMatRIC), Department of Mechanical Engineering, Manipal University Jaipur, Jaipur, India

**Amy E. Landis**, Department of Civil and Environmental Engineering, Colorado School of Mines, Golden, Colorado

**Loong-Tak Lim**, Department of Food Science, University of Guelph, Guelph, Ontario, Canada

**Carl T. Lira**, Department of Chemical Engineering and Materials Science, Michigan State University, East Lansing, Michigan

**Bimlesh Lochab**, Materials Research Laboratory, Department of Chemistry, School of Natural Sciences, Shiv Nadar University, Greater Noida, India

**Isabel M. Marrucho**, Centro de Quimica Estrutural and Departamento de Engenharia Quimica, Instituto Superior Tecnico, Universidade de Lisboa, Lisboa, Portugal

**Ken'ichiro Matsumoto**, Division of Applied Chemistry, Faculty of Engineering, Hokkaido University, Sapporo, Japan

**Laurent M. Matuana**, School of Packaging, Michigan State University, East Lansing, Michigan

**Claudio Migliaresi**, Department of Materials Engineering and Industrial Technologies and BIOtech Research Center, University of Trento, Trento, Italy

**Masatsugu Mochizuki**, Center for Fiber and Textile Science, Kyoto Institute of Technology, Kyoto, Japan

**Neha Mulchandani**, Department of Chemical Engineering, Indian Institute of Technology Guwahati, India

**Dennis Newby**, Department of Civil Engineering, University of Kentucky, Lexington, Kentucky

**Haruo Nishida**, Plas-N, Kitakyushu, Japan

**Mohammadreza Nofar**, Metallurgical & Materials Engineering Department, Istanbul Technical University, Maslak/Istanbul, Turkey

**Lars Peereboom**, Department of Chemical Engineering and Materials Science, Michigan State University, East Lansing, Michigan

**Elizabeth Peralta**, Centro de Investigación en Alimentación y Desarrollo, A.C. Hermosillo, Sonora, México

**Gabriele Perego**, Vanadis Srl, Colleretto Giacosa, Italy

**Talia Pincus**, Department of Civil Engineering, University of Kentucky, Lexington, Kentucky

**Jed Randall**, NatureWorks LLC, Minnetonka, Minnesota

**Suprakas Sinha Ray**, Centre for Nanostructures and Advanced Materials, DSI-CSIR Nanotechnology Innovation Centre, Council for Scientific and Industrial Research, Pretoria, Gauteng, Republic of South Africa; Department of Chemical Sciences, University of Johannesburg, Johannesburg, South Africa

**Nanjaporn Roungpaisan**, Rajamangala University of Technology Thanyaburi, Pathumthani, Thailand

**Sangeeta Sahu**, Materials Research Laboratory, Department of Chemistry, School of Natural Sciences, Shiv Nadar University, Tehsil Dadri, India

**Mohini Sain**, Department of Mechanical and Industrial Engineering, University of Toronto, Toronto, Ontario, Canada

**Wataru Sakai**, Faculty of Materials Science and Engineering Matsugasaki, Kyoto Institute of Technology, Sakyo-ku, Kyoto, Japan

**Hayati Samsudin**, Food Technology Division, School of Industrial Technology, Universiti Sains Malaysia, Penang, Malaysia

**Susan E. M. Selke**, School of Packaging, Michigan State University, East Lansing, Michigan

**Olav Sliekersl**, PURAC, Gorinchem, The Netherlands

**Anders Södergård**, Laboratory of Polymer Technology, Åbo Akademi University, Turku, Finland; Mirka Ltd, Jepua, Finland

**Uruchaya Sonchaeng**, School of Packaging, Michigan State University, East Lansing, Michigan; Department of Packaging and Materials Technology, Faculty of Agro-Industry, Kasetsart University, Bangkok, Thailand

**Herlinda Soto-Valdez**, Centro de Investigación en Alimentación y Desarrollo (CIAD), Hermosillo, Sonora, México

**Mikael Stolt**, Laboratory of Polymer Technology, Åbo Akademi University, Turku, Finland; Bayer Oy, Turku, Finland

**Shuko Suzuki**, The Queensland Eye Institute, South Brisbane, Queensland, Australia

**Wataru Takarada**, School of Materials and Chemical Technology, Tokyo Institute of Technology, Tokyo, Japan

**Midori Takasaki**, Faculty of Materials Science and Engineering, Kyoto Institute of Technology, Kyoto, Japan

**Kohji Tashiro**, Department of Future Industry-oriented Basic Science and Materials, Graduate School of Engineering, Toyota Technological Institute, Nagoya, Japan

**Hideto Tsuji**, Department of Applied Chemistry and Life Science, Graduate School of Engineering, Toyohashi University of Technology, Toyohashi, Japan

**Naoto Tsutsumi**, Faculty of Materials Science and Engineering, Kyoto Institute of Technology, Sakyo, Kyoto, Japan

**Jan Van Krieken**, Corbion, The Randstad, Netherlands

**Tim Vanyo**, NatureWorks LLC, Minnetonka, Minnesota

**Indra Kumari Varma**, Centre for Polymer Science and Engineering, Indian Institute of Technology, New Delhi, India

**Sicco de Vos**, Polymer Technology, AC Gorinchem, Gorinchem, The Netherlands

**Hai Wang**, Department of Polymer Science and Engineering, Faculty of Chemical, Environmental and Biological Science and Technology, Dalian University of Technology, Dalian, People's Republic of China

**Ja'Maya Wilson**, Department of Civil Engineering, University of Kentucky, Lexington, Kentucky

**Takeshi Yamada**, Department of Applied Chemistry and Life Science, Toyohashi University of Technology, Toyohashi, Japan

# PREFACE

The technological breakthrough at Cargill, Inc. in the early 1990s to produce high-molecular-weight PLA via commercially viable lactide ring-opening polymerization can be considered as the key milestone that paved the way to transform PLA from a specialty material to a commodity thermoplastic (Table P.1). Today, PLA has emerged as one of the mainstream biodegradable polymers that find many applications ranging from biomedical to single-use food packages.

More than 10 years have passed since the first edition of this volume was published in 2010. During this period, there have been considerable scientific advancements and technological developments of PLA. PLA continues to captivate the interests of technologists and researchers, as reflected by the sustained increase in the number of publications related to PLA (Figure P.1). The main goal for the second edition is to update the volume with new progress made on various topics of PLA. We made a minor change in the book title, adding "End of Life" to it given the expanded discussions related to this area.

Like the first edition, this volume is organized into five parts. In Part I, Chapters 1 and 2 cover various aspects of lactic acid/lactide monomers, including their physicochemical properties and production. Chapter 3 looks at different condensation reactions for the polymerization of PLA. To enhance the properties of PLA, modification involving copolymerization with lactic acid/lactide of different isomers is one of the strategies available today. These topics are presented in Chapter 4. This sets the stage for the discussions in Chapter 5 on fundamentals and technologies related to stereocomplex PLA produced by co-crystallization of PLLA/PDLA stereoisomers; topics discussed include stereoblock formation, copolymerization, and composite formation. Structures and phase transition behaviors of various crystals for PLA and PLLA/PDLA stereoisomer are reviewed in Chapter 6, along with comparison to related biodegradable polyesters.

Part II is dedicated to the techniques for material characterization for PLA. This part starts with Chapter 7 that focuses on spectroscopy techniques for PLA analysis, including UV–Vis, Fourier transform infrared, Raman, nuclear magnetic resonance spectroscopies. Chapters 8, 9, and 10 discuss the thermal, rheological, and mechanical properties of PLA, respectively, as affected by factors such as temperature, aging, annealing, molecular stereoregularity, copolymerization, and additive incorporation. Mass transport phenomena of gases and nonvolatile compounds in PLA have important implications on their end-use performance, especially in packaging applications. Chapters 11 and 12 discuss these topics in great depth.

Part III is made up of six chapters that are devoted to processing and conversion technologies for PLA. Chapter 13 summarizes the main conversion methodologies for PLA based on melt and solution processing (e.g., extrusion, injection molding, blow molding, thermoforming, fiber spinning). Other conversion techniques are presented in the subsequent chapters, including blending (Chapter 14), foaming (Chapter 15), composites and nanocomposites processing (Chapters 16 and 17). Chapter 18 looks at melt spinning process in greater depth, explicitly dealing with the mechanisms of fiber structure development.

Part IV covers the degradation and environmental issues of PLA. Bio- and physicochemical degradation phenomena of PLA are discussed in great length by various authors. Chapter 19 presents the mechanisms of photodegradation and radiolysis of PLA. Thermal degradation phenomena are highly relevant during the processing of PLA; Chapter 20 focuses on this topic wherein the authors address the apparent complexities of degradation kinetics through a multi-step complex reaction analysis method. Chapter 21 discusses the mechanisms of hydrolytic degradation, taking polymer (e.g., molecular structure/weight, highly ordered structures, blends) and medium (e.g., temperature, pH)

**TABLE P.1 Significant Events Related to PLA Production that Occurred Over the Past Few Decades**

| | |
|---|---|
| 2021 | NatureWorks production capacity reached 150,000 metric tons in Blair, NE, and a new plant of 75,000 metric tons in the Nakhon Sawan Province, Thailand was announced to be opened in 2024. Total Corbion produces 75,000 metric tons in Rayong, Thailand, and it announces a second plant in Grandpuits, France |
| 2015 | Enzyme-based technology by Carbios rendering biodegradation of PLA at mesophilic conditions |
| 2012 | Announcement of production of high-heat PLA by Total Corbion enabling durable applications |
| 2010 | Jung et al. employed recombinant *Escherichia coli* to produce PLA[a] |
| 2009 | PURAC, Sulzer, and Synbra announced production of PLA from solid lactide for foamed products |
| 2009 | Galactic and Total Petrochemicals from Belgium created a joint venture, Futerro, to begin PLA production |
| 2009 | Cargill, Inc. acquired full NatureWorks ownership from Teijin Ltd. |
| 2008 | Uhde Inventa Fischer and Pyramide Bioplastics announced large-scale production of PLA in Guben, Germany |
| 2008 | PURAC started to commercialize solid lactide monomers under PURALACT™ |
| 2007 | Teijin launched heat-resistant stereocomplex PLA under Biofront™ |
| 2007 | NatureWorks LLC and Teijin Limited formed 50–50 joint venture to market Ingeo™ biobased thermoplastic resins |
| 2005 | Cargill, Inc. acquired The Dow Chemical Company's share in Cargill-Dow LLC 50–50 joint venture |
| 2003 | Toyota produced and developed PLA for automotive applications |
| 1997 | Formation of Cargill-Dow LLC, a 50–50 joint venture of Cargill, Inc., and The Dow Chemical Company to commercialize PLA under the tradename NatureWorks™ |
| 1997 | Fiberweb (now BBA, France) introduced melt-blown and spunlaid PLA fabrics under Deposa™ brand name |
| 1996 | Mitsui Chemicals commercialize PLA produced by polycondensation route |
| 1994 | Kanebo Ltd. introduced Lactron® PLLA fiber and spun-laid nonwovens |
| 1990s | Cargill polymerized high-molecular-weight LA using commercially viable lactide ring-opening reaction |
| 1932 | Wallace Hume Carothers and coworkers polymerized lactide to produce PLA |
| 1845 | Théophile Jules Pelouze synthetized PLA by lactic acid condensation |

[a] Jung et al. [1].

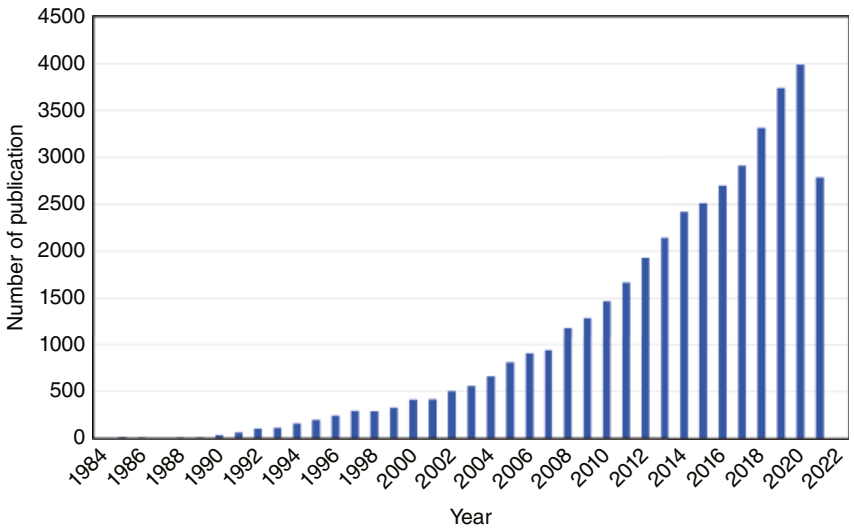


**FIGURE P.1** Number of publications since 1984 based on Web of Science search (accessed on 24 September 2021) using the keywords ("polylactide," "poly(lactic acid),", and "polylactic acid."

factors into considerations. Complementarily, Chapter 22 reviews the literature on enzymatic degradation, focusing on PLA derived from melt-crystallized, solvent-cast, and blend films. Recent advances in enzymes that degrade PLAs and their copolymers are also presented. The next two chapters deal with environmental issues, including topics such as life cycle assessment (Chapter 23) and end-of-life scenarios (Chapter 24). Finally, in Part V, various applications for PLA are discussed, including medical items (Chapter 25), packaging and consumer goods (Chapter 26), textiles (Chapter 27), and environmental applications (Chapter 28).

For completeness and better flow, we deliberately allowed some overlap between chapters so that they are relatively stand-alone. Chapter 1 is a reprint from the first edition. Chapter 9 is a reprint from Chapter 10 of the first edition. Since the theoretical framework of rheology for PLA remains

valid, we have decided to include this chapter in the present edition. In addition, a part of Chapter 20, "Spinning of poly(lactic acid) fibers," from the first edition is now incorporated in Chapter 13 of the present edition.

We are grateful to all authors who contributed their manuscripts and thankful to them for entrusting us to edit their contributions to meet the needs of this volume. It would not have been possible to complete this project without their participation and patience during the preparation of this book.

We hope that readers will find this updated edition of the book useful. We are looking forward to receiving comments and feedback regarding the content of this book.

September 2021
Rafael A. Auras
Loong-Tak Lim
Susan E. M. Selke
Hideto Tsuji

## REFERENCE

1. Y.K. Jung, T.Y. Kim, S.J. Park, S.Y. Lee, *Biotechnol. Bioeng.* 2010, *105*, 161–171

# AUTHOR BIOGRAPHIES

**Rafael A. Auras** is a professor at Michigan State University (MSU), School of Packaging, where he is a faculty member since 2004. He holds a PhD in Packaging from MSU, an MSc in materials science and technology from UNSAM, Buenos Aires, Argentina, and a BS in chemical engineering from FCEQyN, UNaM, Misiones, Argentina. He leads a research group working on the mass transfer in polymers, biodegradable polymers, life cycle assessment, and sustainable packaging systems. He has coauthored more than 200 publications, more than half of them related to poly(lactic acid) polymers.

**Loong-Tak Lim** holds a PhD (University of Guelph) and BSc (Acadia University) in food science. He is a professor in the Department of Food Science at the University of Guelph, where he is a faculty member since 2005. He works with graduate students on projects related to biopolymers, synthetic polymers, encapsulation, and controlled release technologies. He authored and coauthored more than 150 publications and several books. Before joining the University of Guelph, he was with Husky Injection Molding Systems Ltd. (Bolton, Canada), where he managed projects involving injection/stretch blow molding and package prototyping.

**Susan E. M. Selke** is a professor emeritus, Michigan State University, School of Packaging, where she was a faculty member for 36 years. She holds a BS in mathematics and MS and PhD in chemical engineering, all from MSU. In 2012, she was a recipient of the MSU Distinguished Faculty Award. She has authored or coauthored several books, as well as a number of book chapters, over 70 peer-reviewed journal articles, and many other publications. Her areas of expertise include packaging materials, especially plastics, degradability, and environmental impacts of packaging systems.

**Hideto Tsuji** is a professor in the Department of Applied Chemistry and Life Science, Graduate School of Technology at the Toyohashi University of Technology. He holds BS, MS, and PhD in polymer chemistry, from Kyoto University. His research areas include synthesis, structure, crystallization (including stereocomplexation), degradation, and properties of poly(lactic acid)-based materials. He has authored and coauthored more than 220 peer-reviewed journal articles, dozens of books, book chapters, review articles, and patents, which are cited more than 20,000 times.



# PART I

# CHEMISTRY AND PRODUCTION OF LACTIC ACID, LACTIDE, AND POLY(LACTIC ACID)

# 1

# PRODUCTION AND PURIFICATION OF LACTIC ACID AND LACTIDE

Wim Groot, Jan van Krieken, Olav Sliekersl, and Sicco de Vos

## 1.1 INTRODUCTION

Natural polymers, biopolymers, and synthetic polymers based on annually renewable resources are the basis for the twenty-first-century portfolio of sustainable, eco-efficient plastics [1]. These biosourced materials will gradually replace the currently existing family of oil-based polymers as they become cost- and performance-wise competitive. Polylactide or poly(lactic acid) (PLA) is the front runner in the emerging bioplastics market with the best availability and the most attractive cost structure. The production of the aliphatic polyester from lactic acid, a naturally occurring acid and bulk produced food additive, is relatively straightforward. PLA is a thermoplastic material with rigidity and clarity similar to polystyrene (PS) or poly(ethylene terephthalate) (PET). End uses of PLA are in rigid packaging, flexible film packaging, cold drink cups, cutlery, apparel and staple fiber, bottles, injection molded products, extrusion coating, and so on [2]. PLA is bio-based, resorbable, and biodegradable under industrial composting conditions [1, 3, 4].

PLA can be produced by condensation polymerization directly from its basic building block lactic acid, which is derived by fermentation of sugars from carbohydrate sources such as corn, sugarcane, or cassava, as will be discussed later in this chapter. Most commercial routes, however, utilize the more efficient conversion of lactide—the cyclic dimer of lactic acid—to PLA via ring-opening polymerization (ROP) catalyzed by a Sn(II)-based catalyst rather than polycondensation [2–6]. Both polymerization concepts rely on highly concentrated polymer-grade lactic acid of excellent quality for the production of high-molecular-weight polymers in high yield [2–4, 7].

Purification of lactic acid produced by industrial bacterial fermentation is therefore of decisive importance because crude lactic acid contains many impurities such as acids, alcohols, esters, metals, and traces of sugars and nutrients [4].

The lactide monomer for PLA is obtained from catalytic depolymerization of short PLA chains under reduced pressure [4]. This prepolymer is produced by dehydration and polycondensation of lactic acid under vacuum at high temperature. After purification, lactide is used for the production of PLA and lactide copolymers by ROP, which is conducted in bulk at temperatures above the melting point of the lactides and below temperatures that cause degradation of the formed PLA [4].

Processing, crystallization, and degradation behavior of PLA all depend on the structure and composition of the polymer chains, in particular the ratio of the L- to the D-isomer of lactic acid [2, 4, 6, 8, 9]. This stereochemical structure of PLA can be modified by copolymerization of mixtures of L-lactide and *meso*-, D-, or *rac*-lactide resulting in high-molecular-weight amorphous or semicrystalline polymers with a melting point in the range from 130 to 185°C [3, 4, 6–10].

Isotactic PLLA homopolymer—comprising L-lactide only—is a semicrystalline material with the highest melting point, while PLA copolymers with higher D-isomer content exhibit lower melting points and dramatically slower crystallization behavior, until they finally become amorphous at D-contents higher than 12–15% [8–10].

*Poly(Lactic Acid): Synthesis, Structures, Properties, Processing, Applications, and End of Life*, Second Edition.
Edited by Rafael A. Auras, Loong-Tak Lim, Susan E. M. Selke, and Hideto Tsuji.

For decades, ROP has been the preferred route to PLA for biomedical applications with small production volumes. PLLA and copolymers with *rac*-lactide, glycolide, and ε-caprolactone for resorbable biomedical applications have been produced by, for example, PURAC, previously known as CCA, since the 1970s [5]. Since the 1990s, the ROP concept is also used for high-volume production of PLA grades for other end uses.

Large-scale production of PLA, copolymers of L- and *meso*-lactide, was started in 2002 by a joint venture of Cargill and Dow under the name NatureWorks LLC. Nowadays, since July 1, 2009, NatureWorks LLC is again wholly owned by Cargill and has a production capacity of 140 ktpa for its Ingeo PLA grades in Blair, Nebraska [11].

The attractive price and commercial availability of lactic acid were important reasons why PLA became the first mass-produced bio-based polyester. The critical success factor for a final breakthrough of all green chemicals and plastics based on annually renewable materials is economic sustainability. Thus, the very basis of cost-competitive PLA is an industrial fermentative production process for lactic acid with efficient use of carbohydrates followed by excellent purification technology with minimum generation of by-products.

An important impulse for the expanding bioplastics market is the commercialization of lactide monomers for PLA by PURAC in 2008. Solid D- and L-lactides are now available in bulk quantities and can be polymerized into a whole range of tailor-made polylactides by continuous melt polymerization processes, like the technology based on static mixing reactors that was jointly developed by Sulzer and PURAC.

PLA offers an unprecedented market potential to lactic acid producers all over the world, but not all potential players can succeed, because PLA production poses stringent demands to lactic acid quality and price. The chemistry and physics of today's fermentative production and industrial-scale purification of lactic acid and lactide are the subject of this chapter.

## 1.2 LACTIC ACID

### 1.2.1 History of Lactic Acid

Lactic acid was discovered in 1780 by the experimental chemist Carl Wilhelm Scheele, who isolated "acid of milk" from sour whey [12, 13]. A further description of the history of lactic acid by Holten and Benninga shows that industrial production of lactic acid started in the United States in the 1880s [14, 15]. Avery patented and applied a process of fermentation of vegetable sugars [16]. The actual application was the use of a mixture of calcium lactate and lactic acid as baking powder. Unfortunately, this application was not a big success, but other applications in food and textile dyeing were developed.


(*S*)-Lactic acid
L-(+)-Lactic acid

(*R*)-Lactic acid
D-(−)-Lactic acid

**FIGURE 1.1** Two enantiomeric forms of lactic acid: (*S*)- and (*R*)-2-hydroxypropionic acid.

In 1950, the first commercial production of synthetic lactic acid started in Japan [15]. Lactonitrile was produced from acetaldehyde and hydrogen cyanide and hydrolyzed in the second stage to lactic acid. For some decades, synthetic lactic acid competed with lactic acid obtained by fermentation, but currently almost all lactic acid is produced by fermentation.

### 1.2.2 Physical Properties of Lactic Acid

Lactic acid (2-hydroxypropanoic acid) is the simplest 2-hydroxycarboxylic acid (or α-hydroxy acid) with a chiral carbon atom and exists in two enantiomeric forms (Figure 1.1).

The chirality of lactic acid often results in confusion regarding nomenclature. A number of different names are used in the literature. This confusion is the result of mixing the molecular structure and a physical property (optical rotation). (*S*)-Lactic acid (or L-lactic acid) has a slightly positive-specific optical rotation and is frequently named L-(+)-lactic acid [14]. However, a concentrated solution of (*S*)-lactic acid at equilibrium contains lactic acid oligomers, which results in an overall negative optical rotation. Therefore, it is advised to use the structural *R*/*S* notation or the older notation of L and D and avoid the + and − of the optical rotation (Table 1.1).

### 1.2.3 Chemistry of Lactic Acid

The lactic acid molecule has a hydroxyl and an acid functional group, which may result in intermolecular and intramolecular esterification reactions. The first step is the formation of a linear dimer (lactoyl lactic acid). This condensation reaction can proceed to higher oligomers and is promoted by removal of water. Also a cyclic dimer, lactide, is formed in small amounts. Lactide can be formed by intramolecular esterification of lactoyl lactic acid or by breakdown of higher oligomers. All reactions are equilibrium reactions (Figure 1.2).

Due to these reactions, a solution of lactic acid at equilibrium consists of monomeric lactic acid, dimeric lactic acid or lactoyl lactic acid, higher oligomers of lactic acid, and

**TABLE 1.1 Physical Properties of Lactic Acid [14]**

| Property | Value | Reference |
|---|---|---|
| CAS number | General: 50-21-5 | — |
| | (*S*)-Lactic acid: 79-33-4 | — |
| | (*R*)-Lactic acid: 10326-41-7 | — |
| Molecular weight (g/mol) | 90.08 | — |
| Formula | $C_3H_6O_3$ | — |
| Melting point (°C) | 18 (racemic) | [17] |
| | 53 (chiral pure) | [18] |
| Crystal structure | (*S*)-Lactic acid: orthorhombic, space group $P2_12_12_1$ | [19] |
| Solid density (g/mL) | 1.33 (solid, 20°C) | [20] |
| Solubility in water (wt%) | 86 (20°C, monomeric (*S*)-lactic acid) | [20] |
| Heat of fusion (kJ/mol) | (*S*)-Lactic acid: 16.8 | [21] |
| Boiling point (°C) | 122 (at 14 mmHg) | [22] |
| Liquid density (g/mL, 20°C) | 1.224 (100% undercooled liquid) | [22] |
| | 1.186 (80.8% solution in water) | [23] |
| Viscosity (mPa s) | 28.5 (85.3% solution in water, 25°C) | [23] |
| $pK_a$ | 3.86 | [24] |
| Specific heat (J/(g K) at 25°C) | Crystalline (*S*)-lactic acid: 1.41 | [25] |
| | Liquid lactic acid: 2.34 | [26] |

lactide. The ratios between all substances depend on the amount of water present; for example, a 90.1% lactic acid solution (total acidity) contains about 59.3% of monomeric lactic acid and 27.3% of lactoyl lactic acid and higher oligomers [14].

The condensation reactions are also the reason that it is quite difficult to obtain pure, solid, and enantiopure lactic acid. This can only be achieved by crystallization [27, 28]. The kinetics of the condensation reactions determine the stability of a solution of monomeric lactic acid and have a large influence on the stability of solid lactic acid.

### 1.2.4 Production of Lactic Acid by Fermentation

Almost all lactic acid available on the market is produced by fermentation. During fermentation, a suitable carbohydrate is converted to lactic acid by microorganisms. Although some of the microorganisms used, such as the mold *Rhizopus*, need oxygen for growth, the actual conversion of sugars to lactic acid is carried out without oxygen. As a matter of fact, the complete oxidation of a sugar to carbon dioxide and water is energetically much more favorable, so lactic acid is mainly formed under anaerobic conditions. Indeed, most lactic-acid-producing microorganisms are inactive when oxygen is continuously present in high amounts [29]. Upon entering the cell, the sugar is first converted to pyruvate by several enzymatic steps. This conversion yields chemical energy in the form of ATP (adenosine triphosphate) and reducing equivalents (NADH); see the reaction in Figure 1.3.

To recycle these reducing equivalents, microorganisms convert the pyruvate into the more reduced lactic acid; see the reaction in Figure 1.4.

In other words, lactic acid is mainly produced to keep the cellular processes going [30]. The chemical energy obtained is used by several processes elsewhere in the cell, for example cell growth, maintenance, and sometimes even motility.

The reaction in Figure 1.3 takes place in the so-called homofermentative lactic acid bacteria (LAB). Homofermentative bacteria have almost exclusively lactic acid as a

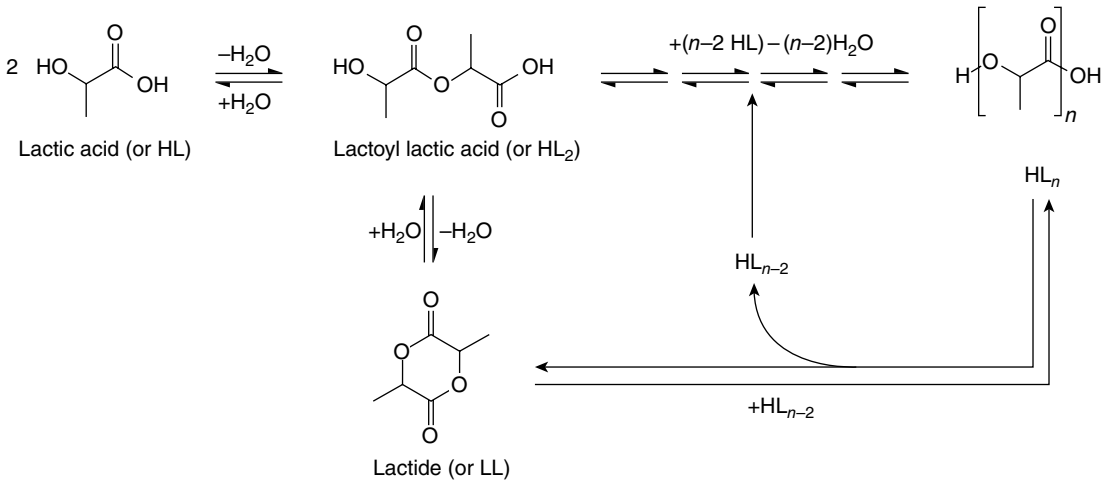


**FIGURE 1.2** Lactic acid condensation reactions: interchange between lactide, oligomers, and poly(lactic acid).

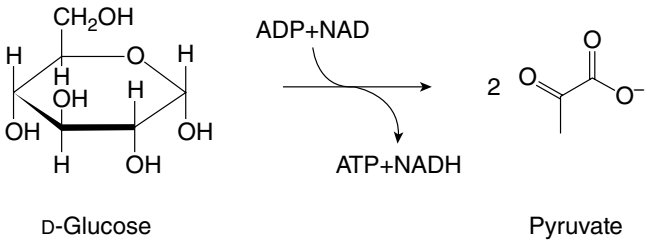


**FIGURE 1.3** During conversion of glucose to pyruvate, chemical energy (ATP) is generated, as well as reducing equivalents (NADH).

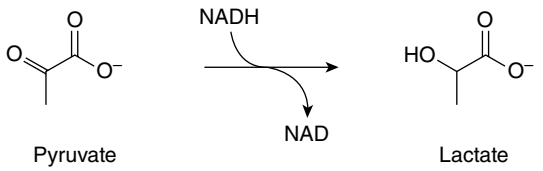


**FIGURE 1.4** Lactic acid formation from pyruvate: reoxidation of NADH and NAD takes place; NAD can be used again in the reaction of Figure 1.3.

fermentation product, in contrast to heterofermentative bacteria that produce a mixture of lactic acid, acetate, $CO_2$, and acetate or ethanol [31]. Heterofermentative bacteria were believed to use exclusively the so-called phosphoketolase pathway, and homofermentative bacteria were believed to use exclusively the glycolysis (Figure 1.3) that splits $C_6$ into two $C_3$ molecules [31].

The phosphoketolase pathway is a route where a $C_6$ is transformed to a $C_5$ sugar (and $CO_2$) and split into a $C_2$ and a $C_3$ molecule. The $C_3$ molecule is then converted to lactic acid, whereas the $C_2$ molecule is converted to acetate or ethanol. In the same traditional view, $C_5$ sugars were regarded as leading to this heterofermentative metabolism, which is less interesting from the point of view of industrial production as a lot of acetic acid or ethanol is produced simultaneously. Although some bacteria seem to fit well in this paradigm, more recent literature has shown that this view is oversimplified and somewhat obsolete for a number of reasons.

- Some heterofermentative bacteria are shown to have both pathways active at the same moment and produce mostly lactic acid under certain circumstances [32, 33].
- Pentoses can lead exclusively to lactic acid as a fermentation product [34].
- Lactic-acid-producing organisms that do not have a phosphoketolase pathway can still produce acetate or ethanol, formed by the usual mixed acid fermentation, via pyruvate. This is the case for, for example, *Lactococcus lactis* [35].

The reason why even heterofermentative bacteria prefer to produce mostly lactic acid is related to the fast generation of chemical energy and thus fast growth and acidification of the environment [32, 36, 37]. The fast growth and acidification gives lactic acid bacteria a competitive advantage and that is exactly why lactic acid bacteria are so troublesome in ethanol fermentations [38]. Lactic acid production is certainly not restricted to bacteria or fungi. Higher organisms, including humans, also use lactic acid formation for fast supply of energy in muscles when needed [39].

The uniformity in this biochemistry is in sharp contrast with the degrees of freedom one has in choosing the microbes, the acid-neutralizing agent, nutrients, and carbohydrates needed for industrial lactic acid fermentation. Only delicate weighing of the pros and cons of every possibility leads to an economically feasible fermentation.

***1.2.4.1 The Microbes*** There are several important features a microorganism used for the production of lactic acid must have in order to be industrially attractive:

- high productivity to reduce fermentation time,
- high conversion yield to reduce carbohydrate costs,
- ability to use cheap sources of nutrients to reduce nutrient costs,
- high-end concentration to reduce evaporation costs,
- low amount of by-products to increase purification yield, and, of course,
- the organisms must be robust with regard to contamination and infections.

Every microorganism has its own benefits and drawbacks, but lactobacilli (present in many food fermentations) and *Rhizopus* (a fungus) are the most reported [40]. Besides lactobacilli and *Rhizopus*, *Streptococcus*, *Pediococcus*, *Sporolactobacillus inulinus*, *Bacillus coagulans*, and several yeasts are mentioned in the excellent overview by Vaidya et al. [41].

Lactobacilli generally have high productivity, but special and often expensive nutrient requirements. *Rhizopus* needs much less nutrients, but has a lower yield, needs oxygen, and its morphology is sometimes difficult to handle. Of course, via genetic manipulation, researchers have tried to make an ideal lactic-acid-producing microorganism.

***1.2.4.2 Stereochemical Purity*** To make semicrystalline, high-melting PLA, stereochemically pure lactic acid is needed. Not all microorganisms yield such stereochemically pure lactic acid and some even produce a racemic mixture [29]. Therefore, a strain must be chosen that meets the quality demands. Finding such a strain that produces L-lactic acid in an economically feasible manner is relatively easy. Producing D-lactic acid by bacterial fermentation on an industrial scale is far more difficult.

Several natural D-lactic-acid-producing bacterial species exist; *Sporolactobacillus inulinus*, *Sporolactobacillus laevolacticus* (previously *Bacillus laevolacticus*), and *Lactobacillus delbrueckii* are among these bacteria [29, 42, 43]. Also, patents have been filed claiming the production of D-lactic acid by a genetically modified microorganism. Several different species such as *Kluyveromyces* and *Escherichia coli* have been claimed so far [44, 45].

***1.2.4.3 Nutrients*** The most well-known lactic-acid-producing organisms, such as *Lactobacillus* and *Lactococcus* species, are members of the taxonomic order of Lactobacillales, also commonly referred to as lactic acid bacteria. These lactic acid bacteria have their really complex nutrient need in common [29]. Vitamins and peptides need to be added to the medium to enable growth. This can be done by adding peptones, yeast extract, or corn steep liquor, but this is expensive. Nutrients for lactic acid production can also be derived from nutrient-rich waste streams such as rice bran, fish waste, or vinification lees [46–48].

***1.2.4.4 Neutralization*** Lactic acid fermentation inevitably leads to a drop in pH, and without neutralization the microorganism is quickly unable to continue the fermentation, as the environment becomes too acidic. Several bases can be used to neutralize the acidity during fermentation, and the choice of the base will determine the nature of the downstream processing (DSP). Most industrial lactic acid plants use $Ca(OH)_2$ or $CaCO_3$, which results in the production of a large amount of gypsum as a by-product.

A major challenge in lactic acid production is to find or construct an efficient microorganism that can produce at such a low pH that the fermentation does not require neutralization. Lactic acid bacteria are usually able to grow at low pH, but it is difficult to find an organism capable of producing lactic acid in reasonable amounts at pH close to the $pK_a$ of lactic acid [49]. Another solution is to construct a lactic-acid-producing yeast, but organisms like this still suffer from low productivities (amount of lactic acid produced per hour) and low final concentrations, leading to the requirement for large fermenter volumes and high amounts of water evaporation [50].

Some basic hurdles have to be overcome to improve the low-pH fermentation by yeasts. Although yeasts are very resistant to low pH, the export of lactate from the yeast cell to the outside medium costs them as much energy as they get from lactic acid production by fermentation. For this reason, lactic-acid-producing yeasts need reasonable amounts of oxygen to generate enough energy to survive [51]. In contrast, traditional lactic acid bacteria use another way to transport lactic acid across the membrane and even gain extra energy by exporting lactic acid to the medium [52].

***1.2.4.5 Carbohydrates for Lactic Acid Production*** In principle, any carbohydrate source containing pentoses ($C_5$ sugars) or hexoses ($C_6$ sugars) can be used for the production of lactic acid, although it is very rare that any particular microorganism is able to use all possible and available $C_5$ and $C_6$ sugars. Pure sucrose from sugarcane or sugar beets and glucose from starch are available in large amounts and readily fermentable. Polysaccharides such as cellulose or starch are more complex and need special pretreatment. When using less pure sources such as raw sugar beet juice, the impurities must be removed somewhere in the total lactic acid production process [53]. This can be done before, during, or after the fermentation. This often leads to special adaptations in the production plant. Last but not least, the local price and availability of the carbohydrate source determine the raw material of choice for industrial fermentation. Another usable disaccharide is lactose present in whey, as was used by Scheele when he discovered lactic acid in 1780 [12].

***1.2.4.6 Starch*** Starch occurs in discrete granules and is usually a mixture of two homopolymers of glucose, amylopectin, and amylose. Starch can be derived from corn, wheat, potato, or tapioca [54]. Although some microorganisms are able to degrade and ferment starch directly to lactic acid, most lactic-acid-producing microorganisms cannot hydrolyze starch themselves. A solution is to hydrolyze the starch to glucose prior to fermentation with the commercially available enzymes, α-amylase, and glucoamylase. This can be done in a separate process, so no incompatibilities are present between the optimal pH and temperatures of the enzymes on one hand and the optimal pH and temperature of the microbes on the other. However, if the right combination of enzymes, microorganisms, pH, and temperature is carefully chosen, the hydrolysis and fermentation can be carried out in one reactor. This process is generally called SSF (simultaneous saccharification and fermentation) [55]. Prior to SSF, the starch granules usually must be gelatinized at high temperature by cooking. However, even a cooker is optional nowadays as commercial enzymes are becoming available that are able to attack and hydrolyze the granules efficiently and fast enough at relatively low temperatures.

***1.2.4.7 Lignocellulose*** Sucrose and starch have in common that they are used for food and nowadays, with oil wells drying out and prices rising, also for biofuels. A decrease in the availability of fossil fuels is envisaged for the future, and with increasing population, more food is needed at reasonable prices. Therefore, the ideal raw material for biofuels and bioplastics is carbohydrates that are not edible. Such material is abundantly available around the globe as lignocellulose, like in corn stover or wheat straw. Lignocellulose consists of the glucose homopolymer cellulose, the heteropolymer hemicellulose, and lignin. Hemicellulose consists of hexoses and

pentoses. In all, lignocellulose contains roughly 80% fermentable sugars, but this largely depends on the source [54]. The remainder, lignin, is a phenolic polymer that is difficult to degrade and is not directly usable for lactic acid production. It may be used for energy production though, which can be returned to the lactic acid plant.

A purer source of cellulose without lignin is waste paper that can be used for lactic acid production at lab scale [56]. Thus, even this book can eventually be converted into PLA!

Complete utilization of cellulose and hemicellulose requires selection or genetic modification of an organism that is able to ferment pentoses. To obtain monosaccharides from the raw material, several pretreatments and/or separations are required. First, the lignocellulosic material is mechanically treated and then delignified (pulped) by strong alkali or acid treatment. The (hemi)cellulose part becomes more accessible for enzymes at the same time. Subsequent enzymatic treatment mainly yields glucose and xylose and some arabinose. The enzymatic treatment and subsequent fermentation can be done in separate reactors or in one fermenter, in an SSF concept similar to starch SSF [57].

***1.2.4.8 Batch versus Continuous Fermentation*** A process can be run in batch or continuous mode. In continuous mode, there is a constant flow of fermented sugar out of the reactor that is equal to a continuous flow of fermentation medium into the reactor. During batch fermentation, there can be an inflow of medium, but there is no outflow [58]. Batch fermentation needs to be inoculated with a starter culture every time, whereas this is not needed in a continuous fermentation setup. However, in case of problems, the continuous fermentation needs to be restarted, so an infrastructure for starter cultures is needed anyway. A high volumetric production rate can be achieved when combining continuous fermentation with biomass retention, leading to smaller fermenter size [59]. It must be stated that the lactic acid concentration is lower compared with batch culture [58]. The concentration of lactic acid influences the water balance in the production plant.

In all scenarios, microorganisms produce an aqueous lactic acid solution, comprising mainly lactate and counterions from the base, impurities from raw materials or fermentation by-products, residual sugars and polysaccharides, and the microorganism itself.

### 1.2.5 Downstream Processing/Purification of Lactic Acid

When Scheele discovered lactic acid, he recovered and purified the lactic acid from sour whey by saturation with lime, filtering off the crude calcium lactate, acidifying the crystal mass with "acid of sugar" (oxalic acid), filtering off the calcium oxalate, and evaporating to obtain a crude viscous lactic acid [12, 13]. Basically, this process with a calcium-based neutralized fermentation and sulfuric acid instead of oxalic acid is the same process used in industry today for the production of crude lactic acid. Drawbacks are the continuously rising costs of lime/chalk, sulfuric acid, and other chemicals and the disposal of large quantities of gypsum ($CaSO_4 \cdot 2H_2O$), as an unavoidable side product of this technology.

In such a process also the first downstream processing (DSP) step, biomass removal by filtration, can be accomplished relatively easily in a (mild) liming step, in essence quite similar to the traditional liming step to remove protein in sugar beet or sugarcane processing in sugar mills. A simplified block scheme of the traditional lactic acid production process including fermentation is shown in Figure 1.5.

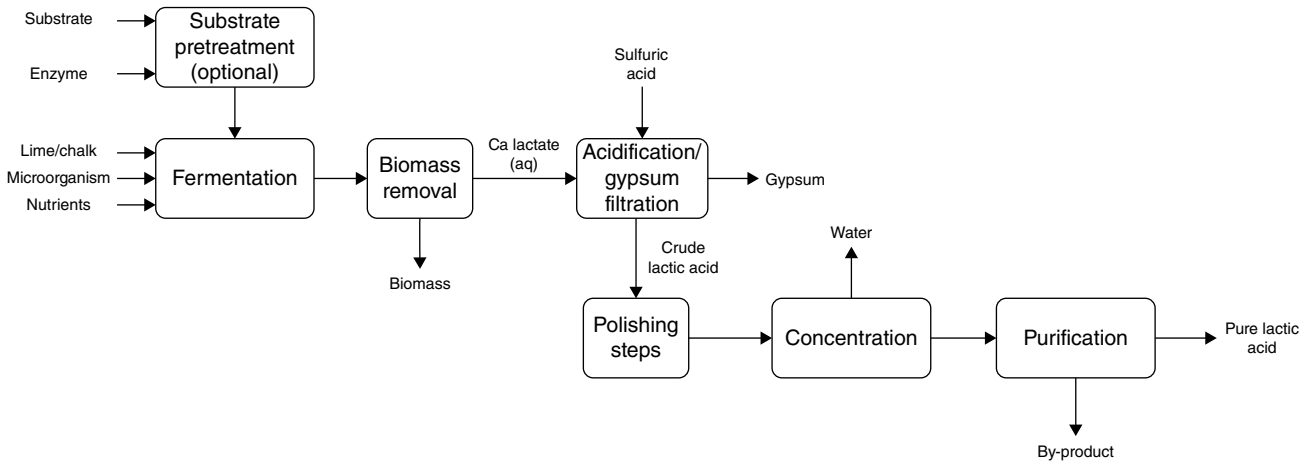


**FIGURE 1.5** Simplified block scheme of traditional lactic acid production process.

**TABLE 1.2 Summary of Lactic Acid Purification Methods**

| Lactic Acid Purification Method | Advantages | Disadvantages |
|---|---|---|
| Crystallization [27, 28] | Highly pure lactic acid product | Amount of mother liquor by-product, scalability |
| Esterification/distillation [52] | Highly pure acid, scale-up | Relatively high utility cost, amount of residue as by-product |
| Lactic acid distillation [27, 28, 53] | Good splitting for heavy compounds | Amount of residue as by-product |
| Extraction [54, 55] | Potentially high yield | Complex (e.g., for emulsion, entrainment issues), extractant cost |

***1.2.5.1 Purification Methods for Lactic Acid*** Crude lactic acid, which may be upgraded by simple active carbon treatment and/or ion exchange to remove impurities and salts, can be directly used in a large number of food applications. Traditionally, taste, smell, and heat stability for color formation have been used to express lactic acid quality. The presence of acids (e.g., acetic acid and pyruvic acid), alcohols (e.g., methanol and ethanol), and esters can directly influence taste and smell [4]. The presence of residual sugar and nitrogen compounds greatly influences heated color, that is, browning of the liquid upon heating. The formation of color upon heating prohibits the use of crude acid in foods that need to undergo pasteurization/sterilization. Over the decades, the demand for purer lactic acid with improved color stability upon heating has increased, as exemplified by the need for ultrapure lactic acid as a sodium lactate base in pharmaceutical infusion products. At present, a chemical engineer can choose from a number of mature industrial methods to purify lactic acid. Table 1.2 lists their relative advantages and disadvantages.

Choices in an overall process are governed by raw material costs, utility costs, and, last but not least, outlets for by-products.

The purification methods described above each involve considerable technological know-how:

- *Esterification/Saponification*. Esterification of lactic acid with methanol/ethanol yields systems with good separation characteristics to separate many impurities with different boiling points [60]. However, the energy demand of a full reaction/distillation route from crude acid to pure acid is high.
- *Crystallization*. Crystallization can yield an excellent lactic acid grade, but the yield is low.
- *Lactic Acid Distillation*. Industrial equipment is available to distill lactic acid at low vacuum. Higher-molecular-weight components such as sugar and protein will leave the system as a residue. Heat-stable lactic acid is obtained as the top product. In the stages of dewatering the crude lactic acid prior to distillation, the formation of oligomers will limit an overall high distillation yield.
- *Extraction*. An extraction/back-extraction process, for example, with the well-described tertiary amine systems, is a suitable way to purify lactic acid [61, 62]. The possible combination of extraction with low-pH fermentation yields an elegant concept to arrive at a gypsum-free process.

For future large-scale, low-cost lactide/PLA production, lactic acid DSP will need to meet new challenges:

- *Use of Low-Cost and Nonedible Substrates*. Whereas production of lactic acid from sucrose or glucose syrup is well established, crude sources (starches, sugars, or future lignocellulose hydrolysates) will form the next hurdle as they contain much more impurities and possible fermentation inhibitors.
- *Gypsum-Free Processing*. For large-scale, sustainable PLA production, a fermentation process that does not coproduce a mineral salt is a must.

***1.2.5.2 Gypsum-Free Lactic Acid Production*** Gypsum-free lactic acid production can be briefly categorized as follows:

- *Low-pH Fermentations Coupled to In Situ Product Removal*. As discussed in Section 1.2.4, fermentations can be carried out without neutralization at pH 2–3 with genetically modified yeast or at pH 4 with LAB with partial neutralization [50]. When a separation method to recover the undissociated acid is integrated with fermentation, a process route can be designed in which no gypsum is produced. In the literature, a number of separation methods are described with an emphasis on extraction [63]. Cost efficiency in the fermentation (e.g., nutrients, yield) and the practical processing of large dilute streams need breakthroughs for economical processing.
- *Electrochemical Splitting of a Neutral Lactate Salt*. Numerous articles have described the splitting of a lactate salt, notably sodium lactate, into lactic acid and the original base [64]. With this principle, a gypsum-free process can be designed, with electrodialysis

separate from or integrated with fermentation. The use of electrodialysis with new bipolar membranes is straightforward, but a large-scale commercial breakthrough as in the 1980s and 1990s with monopolar membranes for the chloro-alkali process is still pending. Electrodialysis involves relatively high electricity costs and a huge membrane area, but these costs may be managed in biorefinery concepts with integrated energy production.

- *Chemical Salt Splitting of a Lactate Salt*. Lactate salts can be split with the help of auxiliary chemicals and the regeneration of these chemicals. A patent by Baniel et al., for example, describes a method in which a sodium lactate solution is acidified with $CO_2$ under pressure, and simultaneously undissociated lactic acid is extracted and insoluble sodium bicarbonate ($NaHCO_3$) is formed [65].

Another patent describes the splitting of ammonium lactate by esterification with butanol while liberating ammonia [66]. In the distillation process, the butyl lactate can be hydrolyzed with water to liberate lactic acid. This is an interesting option, but the energy consumption and side reactions such as the formation of lactamide and racemization require attention.

Chemical salt splitting processes with the recycle of chemicals can be complex, but it is a challenge to develop a system with straightforward chemistry, high yield, low energy consumption, and good scalability.

***1.2.5.3 Modern Industrial Methods*** In overall process development, knowledge about dealing with impurities will be important. Residual sugar in the broth and sugar degradation products play a role throughout the process at the various levels of temperature and acidity. Color may be formed at any step from low- to high-boiling color precursors. Volatile acids such as acetic acid and formic acid will partition throughout DSP and their concentration in recycle streams must be prevented.

In the design of a modern lactic acid plant, mathematical models are indispensable. For example, the kinetic model of oligomerization of lactic acid and the right thermodynamic model for the gas/liquid equilibria are important in design for the concentration of lactic acid by evaporation, as well as for prepolymerization in the lactide route.

Lactic acid solutions and vapors are quite corrosive and knowledge of the material of construction is a must for a low-maintenance plant. Also, wastewater treatment is an integral part of a lactic acid plant. Aerobic systems are state of the art, but anaerobic systems are increasingly used to treat acid-containing wastewater streams. The biogas can then be profitably used for steam production. While a plant using sucrose has a net intake and net purge of water, future plants using crude, low-cost, water-rich substrates will need to pay more attention to the water balance and wastewater treatment.

Although the fermentation industry can be considered traditional, new technologies may quickly find uses. The rapid commercial application of filtration techniques such as in membrane bioreactors in wastewater treatment and the fast introduction of nanofiltration for making process water from river water are examples. The discovery of ionic liquids with high distribution coefficients for lactic acid in dilute solutions may lead to breakthroughs [67]. New steam boiler concepts that can handle residues can drastically change DSP layout in energy-efficient integrated biorefineries.

### 1.2.6 Quality/Specifications of Lactic Acid

The dehydration of lactic acid to make the prepolymer should start with an –OH to –COOH ratio of 1 : 1. All other components with –OH and –COOH functionality disrupt the stoichiometric balance and may be incorporated as comonomers during prepolymerization, which limits the final lactide production yield from lactic acid. Little public information is available on the technical and economic relationship between lactic acid quality and lactide synthesis. Only a few patents mention the effect of metal impurities on racemization [68, 69]. Stereochemical purity is one of the key parameters determining lactic acid purity.

Lactic acid purified by crystallization may be taken as the benchmark in lactide manufacture, but the expected unfavorable economics of making crystalline acid in relation to mother liquor processing may prevent its commercial use for lactide/PLA. The next level of quality with the right commercial relevance is heat-stable lactic acid. Heat stability puts constraints on the content of sugar, and thus on the DSP method used in the process. It is unlikely that suitable acid for making lactide will contain sugar because of the high temperatures involved (see the next section) and the well-known practical decomposition problems when sugars are cracked. In practice, this means that color, or actually heated color (color after heating of the acid), is an important indicator for the suitability of the acid for lactide/PLA production [6, 70]. The appeal for lactic acid with little or no sugar and the DSP methods mentioned in practice lead to demands for separation methods that are similar for sugar and other heavy components such as proteins, amino acids, and polysaccharides.

It is expected that the desired quality of lactic acid for making lactide/PLA will evolve, with overall process yields and economics as the criteria.

## 1.3 LACTIDE

### 1.3.1 Physical Properties of Lactide

The dehydrated, cyclic dimer of lactic acid is commonly called lactide (3,6-dimethyl-1,4-dioxane-2,5-dione). Due to the two asymmetric carbon atoms in the molecule, lactide exists in three different forms (Figure 1.6).

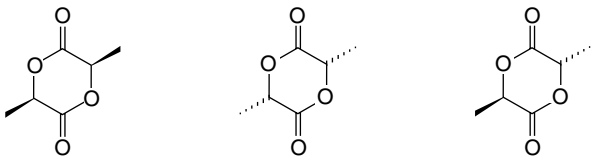


**FIGURE 1.6** The three diastereomeric structures of lactide (3,6-dimethyl-1,4-dioxane-2,5-dione).

In addition to the three diastereomeric structures mentioned above, also a racemate of D-lactide and L-lactide exists: *rac*-lactide or D,L-lactide (Table 1.3).

### 1.3.2 Production of Lactide

The synthesis of lactide was first described by Pelouze in 1845 [71]. He investigated the self-esterification of lactic acid by heating and driving off water and obtained a prepolymer that was no longer fully miscible with water. Upon continued heating of the prepolymer, he noticed that in a certain distillate fraction nice crystals were formed. He was able to deduce the chemical formula and gave the name "lactid" to the substance. An improved procedure was described in a patent by Gruter and Pohl in 1914 [72]. Lactic acid was self-esterified at 120–135°C, and air was drawn in to remove the water. Next, zinc oxide was added as a catalyst and lactide was distilled off under vacuum at 200°C. In practice, modern industry cannot dispense with this concept of thermal catalytic depolymerization for lactide production. A major step forward was the use of a tin catalyst, a frequently used coordinating catalyst in polymerizations, in the process. The general scheme of lactide manufacture including the purification is shown in Figure 1.7.

In the past two decades, several papers have appeared on lactide manufacture [73, 74]. A main underlying problem in understanding all information is that the reaction from oligomer to lactide is an equilibrium reaction. To pull the reaction toward the right, lactide must be withdrawn from the system. In reaction engineering terms, this means that the chemical kinetics of the reaction cannot be understood without consideration of the method and efficiency of lactide removal. In terms of know-how described in patents, this means that reported lactide production rates depend to a large extent on the geometry of the equipment in which lactide synthesis is performed and that provides for removal of lactide vapor from the reaction zone.

In modern chemical technology, one of the goals is to fully understand a given system, capture the knowledge in models to describe experimental work, and ultimately use these models to design, optimize, and debottleneck large-scale equipment. For the present system, this means that one must

**TABLE 1.3 Physical Properties of the Lactides**

| | Unit | D-Lactide | L-Lactide [6] | *meso*-Lactide | *rac*-Lactide |
|---|---|---|---|---|---|
| CAS number | | 13076-17-0 | 4511-42-6 | 13076-19-2 | 116559-43-4 |
| Molecular weight | g/mol | 144.12 | 144.12 | 144.12 | — |
| Melting point | °C | 96–97 | 96 | 53 [64] | 125 [6] |
| Boiling point | °C | — | — | — | 142 (20 mbar) [64] |
| Heat of fusion | J/g | — | 146 | 128 [64]; 118 [6] | 185 [6] |
| Heat of vaporization | kJ/mol | — | 63 | — | — |
| Solid density | g/mL | — | 1.32–1.38 | 1.32–1.38 [6] | — |
| Liquid viscosity | mPa s | — | 2.71 (110°C); 2.23 (120°C); 1.88 (130°C) | — | — |

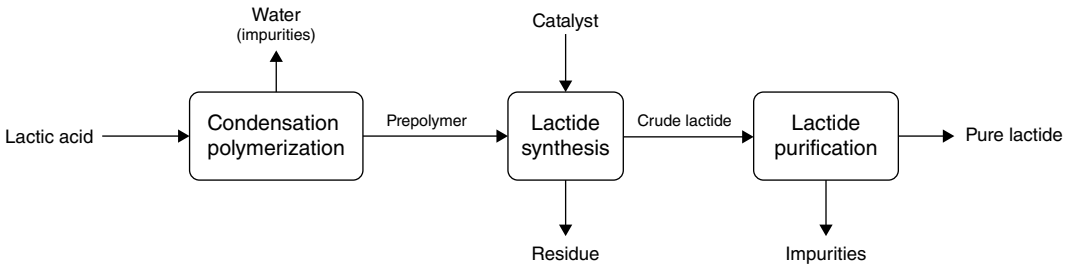


**FIGURE 1.7** Schematic illustration of lactide manufacture by thermal catalytic depolymerization of lactic acid oligomers.

develop process know-how on chemical kinetics and thermodynamics of lactide and HL oligomers, and on physical phenomena related to equipment design.

These aspects will be relevant for both the prepolymerization and the synthesis of lactide, as these chemical systems are highly similar. In practice, however, lactide synthesis is more complex as chemistry, recovery and type of equipment are intertwined, and the viscous nature of reaction mixtures requires special attention.

With these aspects in mind, the information on the lactide synthesis that can be found in the literature is summarized below.

***1.3.2.1 Prepolymerization*** A general procedure for batch prepolymerization is described in a patent by O'Brien et al. [75]. Typically, vacuum pressures of 70–250 mbar and temperatures up to 190°C are used to dewater lactic acid to a prepolymer with an average degree of polymerization (DP) of around 10 in a batch process time of 6 h. For lab-scale equipment, it was also found that thin film and rotating flask vacuum equipment showed faster reaction times than a stirred tank, indicating the importance of mass transfer of water in the already viscous prepolymer.

Continuous prepolymerization has also been described in a number of patents, for example, in stirred tanks in series or in evaporator-type equipment [68, 76, 77]. Usually patents describe prepolymers with a DP of 7–20 as feed to the lactide synthesis. Using modern HPLC methods, it has been shown that in oligomeric systems up to DP 10, an equilibrium is present with constant equilibrium constants between the oligomers [6, 72].

***1.3.2.2 Lactide Synthesis During Prepolymerization*** Because the composition of a mixture comprising lactic acid oligomers and lactide is governed by chemical equilibria, a prepolymerization exhibits relatively high concentrations of lactide ($HL_2$–$H_2O$–$L_2$ equilibrium) around DP 2. Sinclair et al. distilled these fractions to recover lactide, but the crude lactide was quite impure, which may prevent economical processing [73]. In hindsight, the patent describes trials to optimize Pelouze's original lactide synthesis without catalyst [71].

***1.3.2.3 Basic Research on Batch Lactide Synthesis and the Catalysts Used*** Noda and Okuyama reported on the batch synthesis of lactide from DP 15 prepolymer with various catalysts at 4–5 mbar and 190–245°C [74]. In a batch synthesis with 50 g of oligomer in a stirred flask, the evolution rate of crude lactide is rather constant and then starts to decline and the conversion levels off at 80–90%. The tin catalyst performed best compared with other catalysts and showed the lowest levels of racemization. Tin octoate (stannous 2-ethylhexanoate) is a liquid catalyst that can be handled easily, is food grade, and is widely available.

Thinking in terms of mechanisms, the equilibrium concentration of lactide in an oligomer mixture is 5% or less, and it will boil off at low vacuum [6, 68]. The catalyst increases the rate of lactide formation by facilitating lactide formation by backbiting from hydroxyl chain ends of oligomers [4, 74]. In a batch experiment, the rate is initially constant, but during synthesis esterification also occurs, and the DP of the polyester rises concomitantly. The melt viscosity of the reaction mixture increases accordingly and at the end of a batch process, mixing the highly viscous residue becomes very difficult, which limits the extent to which the residue can be depleted of lactide.

In engineering terms, this means that mass transfer of lactide from the liquid to the gas phase decreases as viscosity increases. The balance between lactide production and lactide removal plays a role in all experiments that one might want to investigate on lab scale. For example, catalyst concentrations of 0.05–0.2 wt% tin(II) octoate are mentioned in the literature, but traditional experiments to verify the order of the reaction for the catalyst are difficult because of the influence of mass transfer limitations.

***1.3.2.4 Continuous Synthesis*** In 1992, Gruber et al. [68] described a continuous lactide synthesis in which prepolymer is fed continuously to a reactor, crude lactide is evaporated under vacuum, and residue is removed. Typical operating conditions for the reactor were residence time around 1 h, vacuum pressure 4 mbar, temperature 213°C, and catalyst amount 0.05 wt% tin(II) octoate on feed. The conversion per pass was around 70%, and the overall yield was increased by recycling the residue to the lactic acid section of the process, where the oligomers are hydrolyzed again.

Especially in the patent literature, several different reactor types are described for continuous lactide synthesis:

- Stirred tank reactor with different stirrer types [76]. On a bench scale, the reactor is jacketed for heating.
- Stirred reactor with a distillation section on top of the reactor to fractionate the product [50].
- Thin film evaporator with a typical conversion of 80% on pilot scale [70].
- Horizontal wiped film evaporator. In a patent by Kamikawa et al. [77], the use of horizontal wiped film is described. In the horizontal mode, the residence time of the reaction mixture can be controlled and a conical form is used in which wipers transport the viscous residue.
- Distillation column. In a patent by O'Brien et al. [75], a distillation column with perforated plates and optional use of packing material and heating on the stage are described. In an experiment with a single tray, a DP 10 feed was fed to the top, and $N_2$ was used to strip the

lactide from the liquid. At different residence times, the conversion on the tray could be as high as 93% at 210–215°C. In other patents, the use of $N_2$ gas as a stripping agent is mentioned, but it is to be expected that in large-scale equipment the processing of large amounts of inert gases will be less economical compared with the use of vacuum systems.

Reviewing the literature provides a list of process aspects that need consideration in the design of a solventless synthesis operated with vacuum equipment.

- *Temperature*. Intrinsic reaction rates increase with temperature. At higher temperature also, the vapor pressure of lactide above the reaction mixtures increases. The reaction rate of racemization will also increase with temperature. In Witzke's Ph.D. study, information on activation energies can be found [6].
- *Pressure*. Pressures of 10 mbar or less are used. At higher pressures, the driving force for lactide evaporation will be lower, and the overall reaction rate will be lower. Low pressures will require detailed considerations of equipment size, vacuum systems, condensers, and so on.
- *Feed DP*. The feed DP has two effects. First, a low DP feed will contain more monomer lactic acid that boils at a lower temperature than lactide, and this will contaminate the crude lactide distilled off from the reactor. Also, monomer lactic acid can be released from DP 3 with the catalyst, leading to more acidity in the crude lactide. Second, it is to be expected that at a higher feed DP the residue in the reactor will have a higher DP and viscosity with consequences for equipment design. The influence of prepolymer DP on the *meso*-lactide level formed during lactide synthesis was discussed by Gruber et al. [69]. Increasing feed DP clearly resulted in a decrease in the lactic acid concentration in the crude lactide. A drawback is that the *meso*-lactide concentration also increased significantly.
- *Catalyst Concentration*. More catalyst will increase the overall reaction rate. In practice, this effect may not be linear, since next to kinetics mass transfer in the equipment will play a role.
- *Racemization*. In the production of stereochemically pure lactide, formation of the other lactic acid enantiomer and *meso*-lactide is unwanted. Higher temperatures, longer reaction times, and increased catalyst levels result in increased rates of racemization [4, 6, 69]. Since temperature and catalyst influence the rate of lactide formation as well, controlling the racemization rate can become quite complex.
- *Impurities*. Data in the literature on the role and fate of impurities from the feed in the synthesis are scarce. Some metal cations such as sodium and potassium in the feed increase racemization risk, while other metals (Al, Fe) are catalytically active in transesterification, resulting in competitive polylactide formation [68, 69]. Through corrosion, metals may be released in the residue and will build up there [6, 75]. Some patents discuss the presence of acid impurities in the process [6, 7, 67, 78]. Mono- and dicarboxylic fermentation acids are responsible for stoichiometric imbalance in the lactic acid polycondensation reaction. Consequently, the composition of the obtained lactic acid oligomer chains can differ from pure PLA, resulting in impeded and incomplete catalytic depolymerization of the oligomers into lactide. In PLA manufacture, degradation reactions play a role, mainly via *intramolecular chain scission*, and this may also affect lactide synthesis.

On the one hand, it can be concluded that the lactide synthesis is straightforward in the sense of making a prepolymer and releasing lactide by thermal catalytic depolymerization at low pressure. On the other hand, it can be concluded that the scale-up from a lab-scale process to an economical, large-scale process with high yield and no compromises on stereochemical purity is a complex multifaceted task.

### 1.3.3 Purification of Lactide

A lactide synthesis reactor invariably produces a crude lactide stream that contains lactic acid, lactic acid oligomers, water, *meso*-lactide, and further impurities. The specifications for lactide are stringent mainly for free acid content, water, and stereochemical purity. Basically, two main separation methods, distillation and crystallization, are currently employed for lactide purification:

- *Distillation*. Splitting the multicomponent mixture consisting of lactide, water, lactic acid, and its oligomers into pure fractions requires considerable know-how on kinetics and operation of vacuum equipment. Distillates and bottoms may be recycled, but the accumulation of impurities from the feed or the production of *meso*-lactide during the process requires careful fine-tuning of temperatures and residence times. Distillation is well described in the patent by Gruber et al. [68]. The crude lactide from the synthesis is distilled in the first column to remove the acids and water, and then *meso*-lactide is separated from lactide in the second column. As the boiling points of all compounds are in the range of 200–300°C, low pressures are used. Since the difference in boiling temperature of lactide and *meso*-lactide is quite small, this distillation requires a lot of theoretical stages (>30). The NatureWorks distillation uses a

series of distillation columns and is performed continuously [4]. Part of the distillation can also be integrated with the reaction [79].

- *Solvent Crystallization*. A commonly used laboratory method for lactide purification is recrystallization from mixtures of toluene and ethyl acetate [4]. Lactide of extremely high purity can be obtained by repeated crystallization with different toluene/ethyl acetate ratios. Several patents also mention the use of solvents for the crystallization of lactide, but for large scale, melt crystallization without the use of solvents is preferred.
- *Melt Crystallization*. Lactide crystallizes easily, and several patents describe how crystallization can yield lactide with required specifications regarding lactic acid content, oligomers, *meso*-lactide, and water. An early patent describes such a crystallization method and includes some information on the thermodynamic equilibria (eutectica) of the lactide/lactic and the lactide–*meso*-lactide system, which define the maximum yield as a function of these impurities in the feed [80]. In patents, the use of different types of equipment is mentioned: static equipment, falling film crystallizers, vertical column with scraper to remove crystal mass from the cooled wall, and scraped heat exchanger coupled to a wash column [70, 80, 81]. For large scale, it is a challenge to design and scale-up the crystallization equipment with respect to the needed heat transfer areas and hydrodynamics, and the possible increase of viscosity of mother liquor by oligomerization of lactide and residual acid.

The choice between distillation, crystallization, or novel separation methods such as absorption or membrane separation is determined by the desired stereochemical purity of the product. Crystallization yields highly pure lactide, suitable, for example, for high-melting PLLA homopolymer of high molecular weight. Affordable distillation equipment does not fully remove all *meso*-lactide, and consequently, a lactide monomer mixture for PLA copolymers with other thermal properties is obtained upon ring-opening polymerization.

The design of the separation system relies on detailed knowledge of the thermodynamic properties of the compounds and the kinetics of the reactive system. Obtaining such know-how requires sophisticated analytical methods for lactic acid and its oligomers, lactides, and residues. Impurities can also be formed in lactide synthesis, similar to PLA degradation reactions, and gas chromatography (GC) methods are needed to identify these compounds and determine their fate in the process.

### 1.3.4 Quality and Specifications of Polymer-Grade Lactide

The specifications and allowed impurity levels of lactide monomer for PLA are defined by the polymerization mechanism and the applied catalyst. PLA is commercially produced by ROP of lactides in bulk. The tin(II)-catalyzed process offers good control over molecular weight and reaction rate provided that it is performed in the absence of impurities such as water, metal ions, lactic acid, or other organic acids. Purification of crude lactides is therefore indispensable for the industrial manufacture of high-molecular-weight PLA ($M_w > 100$ kg/mol). In fact, lactide is the ultimate form of lactic acid, in its dehydrated and purest form.

***1.3.4.1 Role of the Catalyst and Initiator in Lactide Polymerization*** The theoretical description of the $Sn(Oct)_2$-catalyzed ROP of cyclic esters has been studied by many authors, but there does not appear to be a theory that consistently explains all experimental results of the coordination–insertion polymerization [3, 4, 82–84]. Different polymerization mechanisms may dominate, depending on polymerization conditions, catalyst and initiator concentration, and the presence of a solvent.

Here, it is assumed that lactide is polymerized in bulk with $Sn(Oct)_2$—a Lewis acid—and that the mechanism follows the model proposed by Kowalski et al. [84]. Since lactide is a cyclic ester, its ring can be opened by nucleophilic attack on the ester bond to start polymerization. Suitable initiators (nucleophiles) are water and alcohols, including the hydroxyl group of lactic acid. One ester linkage of a lactide ring is cleaved by reaction of the OH group of the initiator R—OH, creating a new R—O—C(O)— ester end group and an OH end group (Figure 1.8).

Every initiating molecule is covalently bonded as an end group to each polymer chain [84]. Via transesterification reactions, the 2-ethylhexanoate ligands of the $SnOct_2$ catalyst will also end up as octanoic ester groups in the polymer. In some papers, the Sn(II) catalyst is indicated as the initiator, presumably because lactide also polymerizes upon addition of that substance, and the effect of impurities is overlooked. An initiator—or *coinitiator*—is a substance that

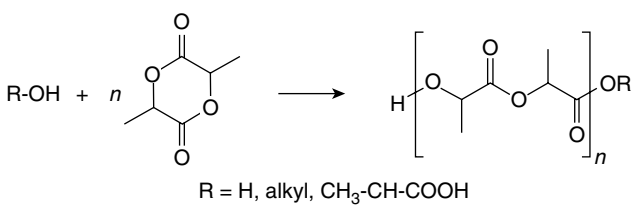


**FIGURE 1.8** Ring-opening polymerization of lactide to PLA initiated by an alcohol.

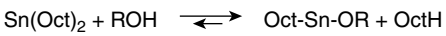


**FIGURE 1.9** Equilibrium reaction of tin octoate with alcohol initiator or impurities to form catalytically active tin alkoxide bonds Sn—O—R [76].

can start polymerization, in the case of lactide by opening the lactide ring, and thus offers control over molecular weight. This has to be a nucleophile and cannot be the Sn catalyst itself, as supported by the excellent work of Kowalski et al. who proved that $SnOct_2$ needs activation with R—OH (Figure 1.9) [84].

In a nutshell, the total hydroxyl content, including R—OH initiator and lactic acid impurities, determines the maximum attainable $M_n$ (number-average molecular weight) [4, 6]. The rate of polymerization is controlled by factors such as temperature and catalyst content, with the remark that a tin(II) octoate catalyst requires traces of the initiator to become active.

***1.3.4.2 Alcohols*** If water is the initiator, R equals H and hydrolysis of lactide produces lactoyl lactic acid ($HL_2$). Propagation with lactide in the presence of a polymerization catalyst produces PLA with a hydroxyl and one carboxylic acid end group, as if the PLA was obtained by polycondensation of lactic acid.

If the hydroxyl group of lactic acid acts as an initiator, PLA with one hydroxyl end group and a lactic acid end group (HOOC—$CH(CH_3)$—O—C(O)—) is obtained.

If the initiator itself is polymeric in nature, for example, polyethylene glycol (PEG), lactide can polymerize from the hydroxyl end group(s) of PEG resulting in PEG–PLLA diblock or triblock copolymers.

The molar ratio of monomer to initiator (M/I)—where initiator can also be read as total hydroxyl content—basically controls the final, average molecular weight ($M_n$) of the PLA. A high amount of initiator produces short polymer chains, and a low amount of initiator produces high-molecular-weight polymer. The lower the amount of potentially initiating hydroxyls in the lactide monomer, the higher the maximum attainable degree of polymerization [69]. Since water and lactic acid can both cause ring scission of the lactide and initiate polymerization, their amounts in the lactide must be low and should be specified.

***1.3.4.3 Carboxylic Acids*** Carboxylic acids are poor initiators, but they are believed to interfere with the commonly used Sn(II) polymerization catalyst. According to Kowalski, carboxylic acids may suppress the rate of polymerization by shifting the equilibrium between ROH and $Sn(Oct)_2$ to the inactive $Sn(Oct)_2$ side [83, 84]. Consequently, longer polymerization times are needed to achieve the desired molecular weight, accompanied by unavoidable degradation caused by the extra residence time at high temperature in the presence of a catalyst [84].

The effect of carboxylic acids on lactide polymerization rate was published in 1993 in patents by Ford and O'Brien [78, 85]. The results clearly show the dramatic rate-decreasing effect of organic acids: according to O'Brien, melt polymerization slows down by a factor of 2 upon increasing free acidity from less than 2 to between 2 and 4 meq/kg [85].

Witzke, however, states that the presence of lactic acid did not negatively influence polymerization rate [4, 6]. Lactic acid is therefore a practically used initiator that is already present in lactide as an impurity.

Lactic acid and its oligomers have a hydroxyl group and a carboxylic acid group. Consequently, a free acidity of 10 meq/kg—that is, 900 ppm expressed as lactic acid equivalents—in lactide corresponds to a hydroxyl concentration that limits $M_n$ to 100 kg/mol. Free acidity of 4 meq/kg sets a theoretical limit of 250 kg/mol to $M_n$.

Free acid and water content specifications are essential for any lactide grade; the lower the amount of hydroxyl impurities, the better the storage stability and product properties of the lactide.

***1.3.4.4 Metals*** Metal cations such as Sn, Zn, Fe, Al, and Ti not only accelerate polymerization, but can also affect hydrolysis, oxidation, racemization, or other degradation mechanisms of PLA and lactides [4, 6]. Consequently, the lactic acid used for lactide preparation should be very low (ppm) in metal cations in order to avoid considerable racemization during lactide synthesis.

O'Brien has shown that the formation of dark color of lactide was a direct function of the iron content of the material in which the lactide was in contact [86]. Other examples in the patent (Examples 7 and 8) demonstrate the desirability of having low alkali (e.g., sodium) content and minimizing the depolymerization temperature.

Cationic impurities such as sodium ions have no direct effect on lactide production rate, but the sodium content has a direct correlation with the *meso*-lactide content in the crude lactide [67, 87].

***1.3.4.5 Stereochemical Purity*** The higher the stereochemical purity of the lactide monomer, the higher the stereochemical purity of the obtained PLA, which controls material properties such as melting point, crystallinity and crystallization rate, and mechanical strength [8, 9, 88].

The strong dependence on D-isomer content presents an opportunity to control polymer properties. NatureWorks Ingeo PLA is easily processable and suitable as amorphous biopackaging material as a result of its relatively high *meso*-lactide content. The downside is the poor resistance to elevated temperatures (low heat distortion temperature, HDT) during transportation, storage, and use of articles produced from this bioplastic. *meso*-Lactide—which contains an L- and a D-isomer—is an unavoidable side product of lactide

production and must be separated from L- and D-lactides of high stereochemical purity.

Kolstad [9] investigated the crystallization behavior of copolymers of L-lactide and *meso*-lactide. He found that every 1% of *meso*-lactide comonomer—or D-isomer—causes a 3°C reduction in the melting point of the PLA copolymer. With 3% *meso*-lactide in PLA, crystallization is more than two times slower than PLLA under the same conditions. With 6% *meso*-lactide incorporation, the difference can be up to 10 times!

This underlines the need for a low *meso*-lactide content in the monomer mixture for semicrystalline PLA, because *meso*-lactide formation by racemization cannot be avoided during melt polymerization of lactides. According to Gruber and coworkers, racemization, which lowers the stereochemical purity of the PLA, is believed to be driven by factors such as temperature, pressure, time at a given temperature or pressure, the presence of catalysts or impurities, and relative concentrations of the two enantiomers at any given time during the polymerization process [88].

PLA grades for more demanding applications that require better heat resistance are achievable by stereocomplexation with PDLA [89]. This is only effective with PLA grades of high stereochemical purity. To prepare high-quality PLA, it is necessary to start with lactide monomers with the highest possible stereochemical purity, that is, the lowest *meso*-lactide content that is technically and economically achievable by purification.

D-Lactide can be obtained if one has the appropriate biochemistry to produce the D-enantiomer of lactic acid by fermentation of carbohydrates. Copolymerization of controlled mixtures of L- and D-lactides subsequently offers the advantage of precise control over PLA properties. Moreover, D-lactide is the monomer for the production of poly(D-lactide), which is able to form high-melting stereocomplex PLA via 1 : 1 racemic cocrystallization with P(L)LA, as will be discussed in Chapter 5 [89].

### 1.3.5 Concluding Remarks on Polymer-Grade Lactide

In conclusion, the most important quality specifications for lactide monomers are those of free acidity, water, metal ion content, and stereochemical purity.

- *Free acidity*, for example, lactic acid or lactoyl lactic acid, slows down the rate of polymerization and limits the achievable degree of polymerization. According to the patent literature, free acidity of polymer grade lactide should be <10 meq/kg, and preferably no more than 5 meq/kg.
- *Water* causes hydrolysis of lactide and also limits the attainable degree of polymerization of PLA.
- *Metal ions* need to be specified in low quantities, because Sn, Zn, Fe, and Al cations accelerate polymerization, but may also affect hydrolysis, oxidation, or other degradation mechanisms. Sodium in particular causes racemization even in ppm amounts.
- *Stereochemical purity* expresses the sum of *meso*-lactide and D-lactide in L-lactide and vice versa. The higher the stereochemical purity of the lactide monomer, the higher the stereochemical purity of the obtained PLA, which controls material properties such as melting point, crystallinity, and mechanical strength.

## REFERENCES


1. R. Narayan, Drivers & rationale for use of biobased materials based on life cycle assessment (LCA), GPC 2004 Paper Abstract #18, Michigan State University, 2004.
2. D. Garlotta, *J. Polym. Environ.* **2001**, *9*(2), 63–84.
3. A. P. Gupta, V. Kumar, *Eur. Polym. J.* **2007**, *43*, 4053–4074.
4. M. H. Hartmann, High molecular weight polylactic acid polymer, in: D. L. Kaplan (Ed.), *Biopolymers from Renewable Resources*, Springer, Berlin, 1998, Chapter 15, pp. 367–411.
5. J. Nieuwenhuis, *Clin. Mater.* **1992**, *10*, 59–67.
6. D. R. Witzke, Introduction to properties, engineering, and prospects of polylactide polymers, Ph.D. thesis, Department of Chemical Engineering, Michigan State University, East Lansing, MI, 1997.
7. D. E. Henton, P. Gruber, J. Lunt, J. Randall, Polylactic acid technology, in: A. K. Mohanty, M. Misra, L. T. Drzal (Eds.), *Natural Fibers, Biopolymers, and Biocomposites*, CRC Press, Boca Raton, FL, 2005, Chapter 16, pp. 527–577.
8. D. W. Grijpma, A. J. Pennings, *Macromol. Chem. Phys.* **1994**, *196*, 1649–1663.
9. J. J. Kolstad, *J. Appl. Polym. Sci.* **1996**, *62*, 1079–1091.
10. R. G. Sinclair, E. S. Lipinsky, U.S. Patent PATN 5,502,158, 1996 (to Ecopol LLC).
11. Cargill/NatureWorks LLC Press Release, July 1, 2009, available at http://www.natureworksllc.com (accessed date: July 24, 2009).
12. C. W. Scheele, *Kgl. Vetenskaps-Academiens nya Handlingar (Stockholm)* **1780**, *1*, 116–124.
13. L. Dobbin, *The Collected Papers of Carl Wilhelm Scheele*, G. Bell & Sons Ltd, London, 1931.
14. C. H. Holten, A. Müller, D. Rehbinder, *Lactic Acid*, Verlag Chemie, Weinheim, 1971.
15. H. Benninga, *A History of Lactic Acid Making*, Kluwer Academic Publishers, Dordrecht, 1990.
16. C. Avery, U.S. Patent 243,827, 1881 (to Avery Lactate Company).
17. F. Kraft, W. A. Dyes, *Ber. Dtsch. Chem. Ges.* **1895**, *28*, 2589–2597.
18. H. Borsook, H. M. Huffman, Y. P. Liu, *J. Biol. Chem.* **1993**, *102*, 449–460.


19. A. Schouten, J. A. Kanters, J. van Krieken, *J. Mol. Struct.* **1994**, *323*, 165–168.
20. PURAC internal data.
21. G. Saville, H. A. Gundry, *Trans. Faraday Soc.* **1959**, *55*, 2036–2038.
22. A. Šepitka, *Průmysl Potravin* **1961**, *13*, 661–665.
23. R. A. Troupe, W. L. Aspy, P. R. Schrodt, *Ind. Eng. Chem.* **1951**, *43*, 1143–1146.
24. W. Ostwald, *Z. Phys. Chem.* **1889**, *3*, 170–197, 241–288, 369–322.
25. H. M. Huffman, E. L. Ellis, H. Borsook, *J. Am. Chem. Soc.* **1940**, *62*, 297–299.
26. G. S. Parks, S. B. Thomas, D. W. Light, *J. Chem. Phys.* **1936**, *4*, 64–69.
27. J. van Breugel, J. van Krieken, A. Cerda Baro, J. M. Vidal Lancis, M. Camprubi Vila, WO 00/56693, 2000 (to PURAC).
28. J. van Krieken, WO 02/022546, 2002 (to PURAC).
29. W. P. Hammes, C. Hertel, The genera *Lactobaccilus* and *Carnobacterium*, in: M. Dworkin, S. Falkow, E. Rosenberg, K.-H. Schleifer, E. Stackebrandt (Eds.), *The Prokaryotes*, 3rd edition, Springer, New York, 2006, pp. IV/320 ff.
30. M. T. Madigan, J. M. Martinko, J. Parker, *Brock Biology of Microorganisms*, 9th edition, Prentice Hall, Englewood Cliffs, NJ, 2000, pp. 118–121.
31. O. Kandler, *Antonie van Leeuwenhoek* **1983**, *49*, 209–224.
32. C. Plumed-Ferrer, et al., *Appl. Environ. Microbiol.* **2008**, *74*, 5349–5358.
33. M. H. Saier, et al., *J. Bacteriol.* **1996**, *178*, 314–316.
34. A. M. Rodas, et al., *Int. J. Syst. Evol. Microbiol.* **2006**, *56*, 513–517.
35. M. Cocaign-Bousquet, C. Garrigues, P. Loubiere, N. D. Lindley, *Antonie van Leeuwenhoek* **1996**, *70*, 253–267.
36. A. P. Oliveira, J. Nielsen, J. Förster, *BMC Microbiol.* **2005**, *5*, 39.
37. B. Teusink, et al., *J. Biol. Chem.* **2006**, *281*, 40041–40048.
38. N. V. Narendranath, et al., *Appl. Environ. Microbiol.* **1997**, *63*, 4158–4163.
39. W. F. Kemper, et al., *Proc. Natl. Acad. Sci. USA* **2001**, *98*, 723–728.
40. Z. Ying Zhang, B. Jin, J. M. Kelly, *Biochem. Eng. J.* **2007**, *35*, 251–263.
41. A. Vaidya, et al., *Crit. Rev. Environ. Sci. Technol.* **2005**, *35*, 429–467.
42. O. Michio, K. Kimitoshi, Jpn. Patent 61293388, 1986 (to Daicel Chemical Industries).
43. J. P. de Boer, et al., *Appl. Environ. Microbiol.* **1993**, *59*, 2474–2478.
44. V. Rajgarhia, et al., WO 03/102201, 2003 (to Cargill Dow LCC).
45. M. Wada, et al., WO 05/033324, 2005 (to Mitsui Chemicals).
46. G. Bustos, A. B. Moldes, J. M. Cruz, J. M. Dominquez, *J. Agric. Food Chem.* **2004**, *52*, 801–808.
47. M.-T. Gao, et al., *Bioresour. Technol.* **2008**, *99*, 3659–3664.
48. M.-T. Gao, M. Hirata, E. Toorisaka, T. Hano, *Bioresour. Technol.* **2007**, *97*, 2414–2420.
49. T. J. Carlson, E. M. Peters, U.S. Patent 6,475,759, 2002 (to Cargill Inc.).
50. S. Saitoh, et al., *Appl. Environ. Microbiol.* **2005**, *71*, 2789–2792.
51. A. J. A. van Maris, et al., *Appl. Environ. Microbiol.* **2004**, *70*, 2898–2905.
52. W. N. Konings, et al., *Antonie van Leeuwenhoek Int. J. Gen. Mol. Microbiol.* **1997**, *71*(1–2), 117–128.
53. D. Visser, J. van Breugel, J. M. de Bruijn, P. A'Campo, WO 08/000699, 2008 (to PURAC Biochem BV).
54. R. L. Whistler, J. N. BeMiller, *Carbohydrate Chemistry for Food Scientists*, 1st edition, American Association of Cereal Chemist Inc., St. Paul, MN, 1997, 117 pp.
55. R. Anuradha, A. K. Suresh, K. V. Venkatesh, *Process Biochem.* **1999**, *35*, 367–375.
56. E. Y. Park, P. Ngoc Anh, N. Okuda, *Bioresour. Technol.* **2004**, *93*, 77–83.
57. S. I. Abe, M. Tagaki, *Biotechnol. Bioeng.* **1991**, *37*, 93–96.
58. S. Ding, T. Tan, *Process Biochem.* **2006**, *41*, 1451–1454.
59. E. Ohleyer, H. W. Blanch, C. R. Wilke, *Appl. Biochem. Biotechnol.* **1985**, *11*, 317–332.
60. A. A. Dietz, E. F. Degering, H. H. Shopmeyer, *Ind. Eng. Chem.* **1947**, *39*, 82–85.
61. B. I. Veldhuis-Stribos, et al., WO 0127064 A1, 2000 (to PURAC).
62. J. van Krieken, et al., WO 05123647A1, 2005 (to PURAC).
63. A. M. Eyal, et al., WO 9919290, 1999 (to Cargill Inc.)
64. M. Bailly, *Desalination* **2002**, *144*, 157–162.
65. A. M. Baniel, et al., U.S. Patent 5,510,526, 1994 (to Cargill Inc.).
66. A. Kumagai, et al., EP 0614983A3, 1996 (to Musashino).
67. J. Martak, S. Schlosser, *Sep. Purif. Technol.* **2007**, *57*, 483–494.
68. P. Gruber, et al., U.S. Patent 5,338,822, 1992 (to Cargill Inc.);U.S. Patent 5,258,488, 1993 (to Cargill Inc.).
69. P. Gruber, et al., U.S. Patent 6277951B1, 1999 (to Cargill Inc.).
70. P. Coszach, J. C. Bogaert, F. van Gansberghe, U.S. Patent 0014975A1, 2006 (to Galactic).
71. J. Pelouze, *J. Chem. Pharm.* **1845**, *53*, 112–124.
72. H. Pohl, U.S. Patent 1,095,205, 1914 (to Gruter).
73. R. G. Sinclair, R. A. Markle, R. K. Smith, U.S. Patent 9,205,167, 1992 (to Battelle).
74. M. Noda, H. Okuyama, *Chem. Pharm. Bull.* **1999**, *47*, 467–471.
75. W. O'Brien, L. A. Cariello, T. F. Wells, WO 9606092, 1995 (to Ecological Chemical Products Company).
76. T. Matsuo, et al., U.S. Patent 25222379A1, 2005 (to Hitachi/ Toyota).
77. M. Kamikawa, et al., EP 1873185A1, 2006 (to Hitachi).
78. Th. M. Ford, U.S. Patent 5,310,599, 1993 (to Du Pont de Nemours & Co.).
79. J. Meerdink, A. Södergard, WO 05056509A1, 2003 (to Hycail).

80. I. D. Fridman, J. Kwok, U.S. Patent 5,264,592, 1993 (to Camelot Industries).
81. R. U. Scholz, R. P. M. van der Steen, (2007), WO/2007/148975, Purification of Lactide Streams.
82. H. R. Kricheldorf, et al., *Macromolecules* **2000**, *33*, 702–709.
83. X. Zhang, et al., *J. Polym. Sci. Part A* **1994**, *32*, 2965–2970.
84. A. Kowalski, et al., *Macromolecules* **2000**, *33*, 7359–7370.
85. W. G. O'Brien, et al., DE 44044838A1, 1993 (to Du Pont de Nemours & Co.).
86. W. G. O'Brien, et al., U.S. Patent 5,521,278, 1994 (to Ecological Chemical Products).
87. P. Kruger, et al., U.S. Patent 6,005,067, 1998 (to Cargill Inc.).
88. P. Gruber, et al., WO 9509879A1, 1993 (to Cargill Inc.).
89. H. Tsuji, *Macromol. Biosci.* **2005**, *5*, 569–597.

# 2

# AQUEOUS SOLUTIONS OF LACTIC ACID

Carl T. Lira and Lars Peereboom

## 2.1 INTRODUCTION

Lactic acid is a three-carbon alpha hydroxy carboxylic acid. This chapter summarized some key properties of pure lactic acid and lactide, but primarily focuses on aqueous lactic acid solutions, that are of importance in purification. Lactic acid is typically marketed as aqueous solutions.

## 2.2 STRUCTURE OF LACTIC ACID

Lactic acid is a chiral molecule with two enantiomers, L-(+)-lactic acid (also known as *S*-lactic acid) and D-(−)-lactic acid (also known as (*R*)-lactic acid). L-lactic acid is dextrorotatory and D-lactic is levorotatory. The racemic mixture is termed *rac*-lactic acid. The L- and D-forms of lactic acid have melting points near 53°C, while *rac*-lactic acid has a melting point of 16.8°C (Table 2.1). The optically active forms will racemize slowly to *rac*-lactic acid when held at 200°C for 500 h [1].

Lactide is the dilactone of lactic acid. Having two stereocenters, lactide has three unique configurations: *SS* (L-lactide), *RR* (D-lactide), and *RS* (*meso*-lactide). Note that a blend of L-lactide and D-lactide is called *rac*- or DL-lactide and is not the same as *meso*-lactide. The lactides rotate polarized light in the opposite direction of the constituent lactic acids; *SS* (L-lactide) is levorotatory (−) and *RR* (D-lactide) is dextrorotatory. *Meso*-lactide is optically inactive. Melting points are indicated in Table 2.2.

The optical rotation for D- and L-forms of lactic acid in water is complicated by oligomer equilibration. Literature values for the optical rotation of L-lactic acid in water range from −13° to 3.9°. Bancroft and Davis [2] show that specific rotation ($[\alpha]_D$) for L-lactic acid as a function of apparent concentration changed linearly from 5.26° at 76 g/100 mL to 0.85° at 5 g/100 mL. Sodium lactate, on the other hand, exhibits nonlinear optical rotation with concentration and changes from −7.8° at 47 g/100 mL to −12.2° at 0.7 g/100 mL. They also showed that specific rotation of a freshly prepared lactic acid (76 g/100 mL) decreased from 5.2° to 1.37° over 17 days. The lactic acid was prepared by acidifying zinc lactate, filtering of zinc sulfate and removing the water under vacuum, keeping the temperature < 40°C. It should be noted that their structural interpretations were wrong. We recommend not to use optical rotation as a measure of the enantiomeric purity of lactic acid but instead rely on HPLC [3], GC [4], or NMR [5] methods.

## 2.3 VAPOR PRESSURE OF ANHYDROUS LACTIC ACID AND LACTIDE

Vapor pressure of anhydrous lactic acid has been measured by relatively few authors. Due to the challenges in purifying lactic acid, data are somewhat scattered. Table 2.3 summarizes data and the accepted data are plotted in Figure 2.1. Data are accepted based on consistency between values from multiple researchers by plotting with the expected approximate linear behavior on the coordinates of Figure 2.1. Many of the data are measurements provided by researchers using lactic acid for chemical synthesis. The accepted data are well represented by Equation 2.1 for vapor pressure $P^{sat}$ (in units

*Poly(Lactic Acid): Synthesis, Structures, Properties, Processing, Applications, and End of Life*, Second Edition.
Edited by Rafael A. Auras, Loong-Tak Lim, Susan E. M. Selke, and Hideto Tsuji.

**TABLE 2.1 Physical Properties of Lactic Acid**

| Property | Value | Isomer | Reference |
|---|---|---|---|
| Molar mass (g/mol) | 90.078 | D, L, rac | — |
| Melting point (°C) | 52.7 | D, L | [6] |
| | 16.8 | rac | [6] |
| Refractive index $[n]_D^{20}$ | 1.4265 | rac | [7] |
| p$K_a$ (22°C, $I$ = 0.1 M KCl) | 3.73 | rac | [8] |
| Octanol : water partition coefficients (log $K_{ow}$) | –0.93 | L | [9] |

**TABLE 2.2 Physical Properties of Lactide**

| Property | Value | Isomer | Reference |
|---|---|---|---|
| Molar mass (g/mol) | 144.13 | D, L, *meso*, *rac* | — |
| Melting point (°C) | 53–54 | *meso* | [10] |
| | 95–98 | L | [10] |
| | 95–98 | D | [10] |
| | 122–126 | rac | [10] |
| Specific rotation L-lactide | | | |
| $[\alpha]_D^{20}$ | –266 (c 1.00 dichloromethane) | — | [11] |
| $[\alpha]_D^{20}$ | –299 (c 1.00 toluene) | — | [11] |

**TABLE 2.3 Vapor Pressure of Anhydrous Lactic Acid**

| $T$ (K) | $P^{sat}$ (Pa) | Source | Accepted(A) or Rejected(R) |
|---|---|---|---|
| 351.15 | 13.332 | [13] | R |
| 352.65 | 39.997 | [14] | R |
| 355.15 | 66.66 | [15] | A |
| 358.15 | 133.32 | [15] | A |
| 369.15 | 133.32 | [16] | R |
| 377.15 | 599.95 | [17] | A |
| 392.15 | 1599.9 | [15] | A |
| 395.15 | 1866.5 | [15] | A |
| 395.15 | 1999.8 | [18] | A |
| 395.25 | 1599.9 | [19] | R |
| 400.65 | 2666.4 | [20] | A |
| 405.15 | 3333.1 | [21] | A |

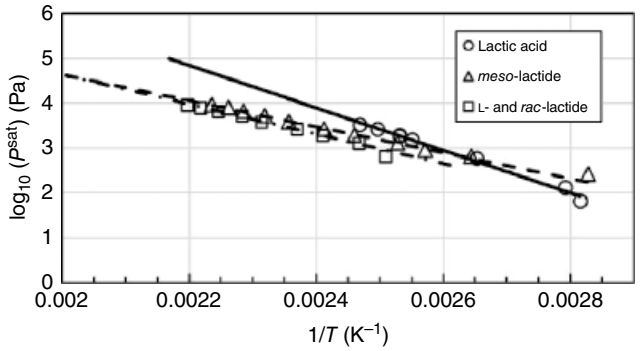


**FIGURE 2.1** Selected vapor pressures of anhydrous lactic acid selected from literature as summarized in Table 2.3.

of Pa) that is extrapolated in the figure for comparison with lactide vapor pressure data at higher temperatures. Care should be taken in using the extrapolation above 405 K because the vapor pressure may have a curvature on the log $P^{sat}$ vs. $1/T$ plot that is not captured by the extrapolation. Oligomerization and subsequent water evaporation are likely to occur during vapor pressure measurements, complicating the interpretation of the results.

$$\text{Lactic acid; } \log_{10} P^{sat}\left(\text{Pa}\right) = 15.217 - 4716.3/T\left(\text{K}\right) \quad (2.1)$$

Witzke [1] evaluated lactide vapor pressure data from a Boehringer Ingelheim patent [12], as well as data provided by Cargill. The Boehringer Ingelheim patent provides vapor pressure data and a distillation to separate *meso*-lactide from D- and *rac*-lactide. The Witzke thesis provides plots superimposing the Cargill data with the patent data but does not tabulate the Cargill data. The Boehringer Ingelheim vapor pressures are provided in the approximate range of 100 to 225°C and are represented by:

$$meso - \text{Lactide; } \log_{10} P^{sat}\left(\text{Pa}\right) = 10.4634 - 2909.8/T\left(\text{K}\right) \quad (2.2)$$

$$D - \text{and } rac - \text{Lactide; } \log_{10} P^{sat}\left(\text{Pa}\right) = 11.2451 - 3300.6/T\left(\text{K}\right) \quad (2.3)$$

The equations and the patent data are provided in Figure 2.1. Witzke was able to reproduce the patent distillation to separate *meso*-lactide from D- and *rac*-lactide using intermediate temperatures and a high reflux ratio.

## 2.4 OLIGOMERIZATION IN AQUEOUS SOLUTIONS

Lactic acid exits as primarily a monomer unit in dilute aqueous solutions, nominally <20 wt%. Aqueous solutions are acidic and thus undergo equilibrium esterification. At high acid concentrations, the equilibrium shifts to the longer esters and the solution viscosity increases. The oligomerization of the lactic acid is an equilibrium-limited reaction, dependent upon the acid and water concentrations. Two lactic acid molecules can esterify, yielding a dimer called lactoyllactic acid, $L_2$:

$$2L_1 \rightleftharpoons L_2 + H_2O \quad (2.4)$$

The $L_2$ can further react to form lactolyl–lactolyllactic acid, $L_3$

$$L_1 + L_2 \rightleftharpoons L_3 + H_2O \quad (2.5)$$

The structures of the species are shown in Figures 2.2 and 2.3. The step-wise condensation oligomerization

presents a significant challenge for performing separations and for modeling vapor–liquid equilibrium of aqueous solutions. The oligomerization can be represented by a succession of simultaneous equilibrium reactions with the same equilibrium constant.

$$L_1 + L_3 \rightleftharpoons L_4 + H_2O \tag{2.6}$$

$$L_1 + L_{j-1} = L_j + H_2O \tag{2.7}$$

where $L_4$ is the tetramer, and $Lj_{-1}$ and L$j$ are generic notation for oligomers of the lengths $j-1$ and $j$, respectively. While alternative combinations of reactions can be written, such as two $L_2$ molecules forming $L_4$, chemical equilibrium can be obtained with the most convenient combination of independent reactions. Other expressions of the equilibria can be obtained by combinations of the independent network. For generalization, addition of a monomer to a chain provides a series of reactions where each equilibrium constant is expected to be approximately the same numerical value.

The equilibrium constant can be expressed in terms of concentration or mole fraction equivalently because the reaction has no net change in moles. Assuming that the equilibrium constant $K_2$ for forming $L_2$, is the same for each condensation reaction $Kj$ for forming L$j$, as suggested by Flory [22]:

$$K_2 = K_j = \frac{x_{L_j} x_W}{x_{L_{(j-1)}} x_{L_1}} = \frac{n_{L_j} n_W}{n_{L_{(j-1)}} n_{L_1}} = \frac{[L_j][W]}{[L_{j-1}][L_1]} \qquad j \geq 2 \tag{2.8}$$

where $xi$ represents a mole fraction (e.g., $x_{L_j}$ represents the mole fraction of species L$j$), $ni$ represents a number of moles, and the square brackets indicate a concentration.

The equilibrium has been studied by Watson [23], Montgomery [24], and Ueda and Terajima [25] and Bezzi [26], but the basis of the concentrations is not always clear. The distribution was studied by Witzke [1] who suggested an equilibrium constant value of approximately 0.25. Vu et al. [27] performed calibrated HPLC analysis and titrations and found that a value of 0.2023 was suitable, which is used for the calculated equilibria below. The mole fractions, moles, or concentrations appearing in Equation 2.8 are those existing at equilibrium and not those used to prepare a solution.

The unreacted form of lactic acid ($L_1$) is called the monomer. The concentration resulting from the conversion of all lactic acid to monomer is called the apparent concentration or sometimes the superficial or formal concentration. In the work of Vu et al. [27], the percent equivalent monomer lactic acid, %EMLA$j$, denotes the percentage of apparent lactic acid represented by a particular oligomer. For example, the %EMLA$_2$ equals 10% when 10% of the apparent lactic acid molecules are dimers. The weight fraction is commonly referred to as the apparent (also known as superficial or formal) weight fraction. Using a superscript $i$ to indicate the initial moles, for a solution composed of $n_W^i$ moles of water (mass $m_W^i = 18.02 n_W^i$) and $n_L^i$ lactic acid (all $L_1$, mass $m_L^i = 90.08 n_L^i$), the apparent mole fraction of lactic acid is $n_L^i/(n_W^i + n_L^i)$ and the apparent weight fraction is $m_L^i/(m_W^i + m_L^i)$.

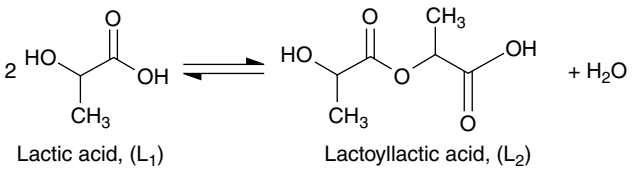


**FIGURE 2.2** Chemical structure of lactic acid and lactoyllactic acid.

## 2.5 EQUILIBRIUM DISTRIBUTION OF OLIGOMERS

The equilibrium and size distributions can be readily calculated using infinite series when the equilibrium constant is assumed to be independent of the oligomer length. Oligomer distribution is obtained by rearranging the material balances in terms of the equilibrium constant and subsequently empirically determining the equilibrium constant that represents the total titratable acid. The distribution is then verified against the smaller oligomers that are measurable. The equilibrium constant (Equation 2.8) can be rearranged as:

$$n_{L_j} = n_{L_{(j-1)}} \frac{n_{L_1} K}{n_W} = n_{L_{(j-1)}} p \qquad j \geq 2 \tag{2.9}$$

where $p$ is a lumped variable including the lactic acid monomer, free water, and equilibrium constant.

$$p = \frac{n_{L_1} K}{n_W} \tag{2.10}$$

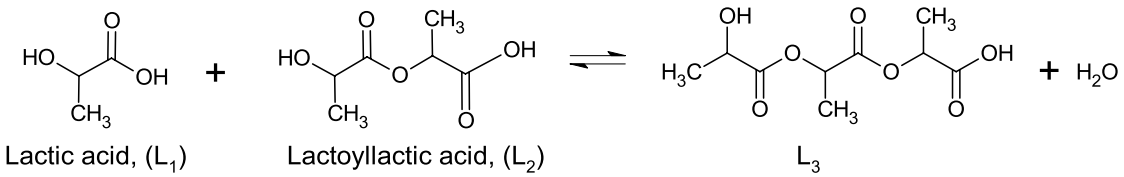


**FIGURE 2.3** Chemical reaction between lactic acid and lactoyllactic acid.

The variable $p$ represents the probability of bond formation. Although the value of $p$ depends on concentration, the quantity is the same for all oligomers at each concentration. Vu et al. [27] used the variable $r$, which is equivalent to the variable $p$ used here. Using recursion, we recognize that Equation 2.9 can be written as:

$$n_{L_3} = n_{L_2} p = n_{L_1} p^2; \qquad n_{L_4} = n_{L_3} p = n_{L_1} p^3 \tag{2.11}$$

$$n_{L_j} = n_{L_{(j-1)}} p = n_{L_1} p^{j-1} \qquad j \geq 2 \tag{2.12}$$

Each oligomer of length $j$ contains $j$ lactic acid molecules, so the apparent moles of lactic acid are given by the balance found by the closed form of the sum:

$$n_L^i = \sum j n_{L_j} = n_{L_1}\left(1 + 2p + 3p^2 + 4p^3 + \ldots\right) = n_{L_1} / (1-p)^2 \tag{2.13}$$

$$n_{L_1} = n_L^i (1-p)^2 \tag{2.14}$$

Equation 2.14 can be inserted into Equation 2.12 to give the Flory-Schulz distribution:

$$n_{L_j} = n_L^i p^{j-1} (1-p)^2 \qquad j \geq 2 \tag{2.15}$$

The water in an equilibrated solution is the sum of the apparent water plus the water from the condensation reaction. Each step during the condensation releases a water molecule, so an oligomer of length $j$ releases $(j-1)$ moles of water ($n_W$):

$$\begin{aligned} n_W &= n_W^i + \sum (j-1) n_{L_j} = n_W^i + n_{L_1} p\left(1 + 2p + 3p^2 + 4p^3 + \ldots\right) \\ &= n_W^i + n_{L_1} p / (1-p)^2 \end{aligned} \tag{2.16}$$

Recognizing Equation 2.13, we insert it into Equation 2.16 to obtain:

$$n_W = n_W^i + n_L^i p \tag{2.17}$$

Inserting Equations 2.14 and 2.17 into Equation 2.10, we develop a relation between the apparent number of moles and $K$ that can be solved to find $p$

$$K = \frac{p\left(n_W^i + n_L^i p\right)}{n_L^i (1-p)^2} \tag{2.18}$$

$$n_L^i (1-K) p^2 + \left(n_W^i + 2 n_L^i K\right) p - n_L^i K = 0 \tag{2.19}$$

$$p = \frac{2 n_L^i K}{\left(n_W^i + 2 n_L^i K\right) + \sqrt{\left(n_W^i\right)^2 + 4 n_L^i \left(n_L^i + n_W^i\right) K}} \tag{2.20}$$

For a given $K$ and apparent moles $n_L^i$ and $n_W^i$, Equation 2.20 provides a value of $p$. Then Equations 2.12 and 2.14 can be used to find the equilibrium moles of lactic oligomers and monomer, while Equation 2.17 provides the equilibrium moles of water. The titratable acidity is a measure of the true number of oligomers in solution because each oligomer has one free carboxylic acid group. The titratable acidity is

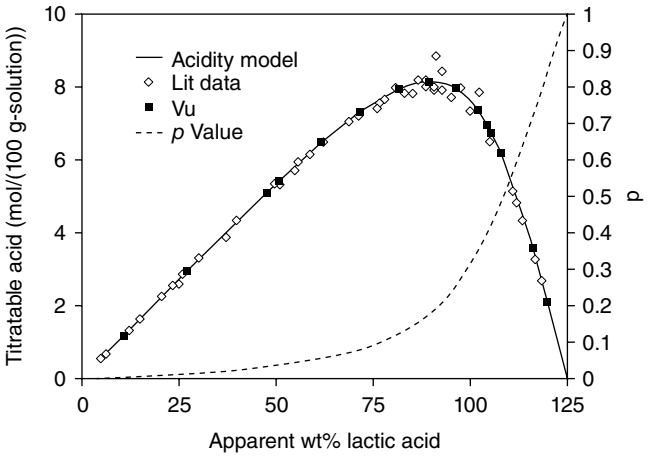


**FIGURE 2.4** Left axis—total titratable acidity tabulated by Holten [28] from various workers (◇) and measurements by Vu et al. [27] (■) compared to the model. Right axis—value of $p$ for the model as a function of apparent wt% using $K = 0.2023$.

$$\begin{aligned} \text{Titratable acidity} &= \sum n_{L_j} = n_{L_1}\left(1 + p + p^2 + p^3 + \ldots\right) \\ &= n_{L_1} / (1-p) = n_L^i (1-p) \end{aligned} \tag{2.21}$$

Because water is formed by polymerization and can be removed from the solution by evaporation, the material balance constraint for water is for equilibrium moles, $n_W \geq 0$, via Equation 2.17 and not the initial moles, $n_W^i \geq 0$. Thus, negative values of $n_W^i$ are feasible and the apparent weight fractions of water are negative at high degrees of oligomerization. Vu et al. [27] have regressed $K$ to fit titratable acidity and found a value of $K = 0.2023$. Using $K = 0.2023$, solutions of up to an apparent lactic acid concentration of 125 wt% lactic acid are theoretically feasible with an apparent water concentration of −25 wt%. The value of p and the titratable acidity are shown in Figure 2.4.

Several important relations can be developed. The distribution of oligomer lengths is given by the Flory-Schulz distribution [22]. The %EMLA$j$ for species $j$ is (note that a typographical error in equation 19 of Vu et al. [27] omits the 100):

$$\%\text{EMLA}_j = 100\, j p^{j-1} (1-p)^2 \tag{2.22}$$

Other useful results are:

$$\text{Number average oligomer length} = 1/(1-p) \tag{2.23}$$

$$\text{True wt\%water} = 100 + \left(\text{apparent wt\%LA}\right)\left(0.2p - 1\right) \tag{2.24}$$

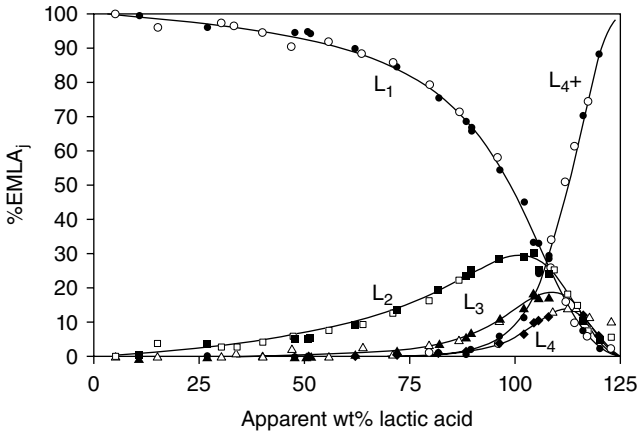


**FIGURE 2.5** The percent equivalent monomer lactic acid for $L_1$ through $L_4$. Open symbols are from Montgomery [24] and Ueda and Terajima [25]. Solid symbols are measured by Vu et al. [27].

$$\text{True wt\%L}_j = \left(0.8j + 0.2\right)\left(\text{apparent wt\%LA}\right) p^{j-1} \left(1-p\right)^2 \tag{2.25}$$

The %EMLA for the short oligomers are shown in Figure 2.5. The equilibrium constant is only weakly temperature dependent. Esterification reactions are commonly nearly thermoneutral. Recently, Feng et al. [29] performed potentiometric titration at temperatures between 8 and 100°C. They found that differences in the titratable acidity were only a couple percent mostly in the range of 60–80 apparent wt% lactic acid; minor differences were observed at other concentrations.

## 2.6 VAPOR–LIQUID EQUILIBRIUM

Vapor–liquid equilibria for aqueous solutions of lactic acid have been measured by Sanz et al. [30] and Vu [31]. Sanz et al. used gas chromatography to measure compositions of both phases. They reported only $L_2$ and $L_3$ oligomers of lactic acid. Both flame ionization and thermal conductivity detectors were used, which enabled quantification of the water. Details of the calculations using the peak areas were not provided. Due to the low volatility of oligomers, error in the overall lactic acid concentrations of the liquid phase is likely. Analysis of the data indicates that $p = x_{L_2}/x_{L_1}$ is nearly constant across the reported compositions, though $p$ should change as shown in Figure 2.6, indicating that the reported mole fractions are not representative of reaction equilibria.

Vu measured isobaric vapor–liquid equilibrium (VLE) data of lactic acid + water using a Fischer recirculating apparatus (model VLE 100D). Pure water, acetone, and ethanol were used to calibrate the pressure and temperature sensors. Heating was regulated to maintain a mean recirculation speed of 30 drops per minute. The mixtures were equilibrated for at least 12 h to ensure the equilibrium was reached, before each 0.5 mL sample was taken from condensed vapor and liquid for analyses. The equilibrium state was indicated by a constant pressure and temperature of the system. Vu further quantified the oligomers using a Hewlett-Packard 1090 Liquid Chromatograph, equipped with an ultraviolet detector (Hitachi L400H) at a wavelength of 210 nm. The mobile phase was acetonitrile (ACN) + water in a gradient mode (0% ACN ($t$ = 0) to 60% ACN ($t$ = 20 min) to 90% ACN ($t$ = 25 min) to 0% ACN ($t$ = 28 min) at 1.0 mL/min. The Novapak C18 column (3.9 × 150 mm) was used and both ACN and water were acidified by 2 mL of 85% (w/v) phosphoric acid per 1 L of solvent, equivalent to pH = 1.3. Further details are provided in [27].

VLE data of Vu are summarized in Tables 2.4 and 2.5. The rows in the two tables at the same temperature represent the coexisting phases. The true mole fractions represent the moles of a species divided by the total moles present in the equilibrated mixture. The subscripts denote the species as

**TABLE 2.4 Liquid Phase Mole Fractions of Lactic Acid + Water VLE at 101.33 kPa**

| $T$ (K) | True $x_{water}$ | True $x_{L_1}$ | True $x_{L_2}$ | True $x_{L_3}$ | True $x_{L_4}$ | Apparent $x_{LA}$ |
|---|---|---|---|---|---|---|
| 378.25 | 0.79 | 0.19 | 0.015 | 0.0012 | 0.0001 | 0.22 |
| 379.25 | 0.8 | 0.18 | 0.014 | 0.0011 | 0.000087 | 0.21 |
| 380.25 | 0.73 | 0.24 | 0.024 | 0.0023 | 0.00023 | 0.30 |
| 380.75 | 0.72 | 0.25 | 0.025 | 0.0025 | 0.00025 | 0.31 |
| 381.75 | 0.69 | 0.28 | 0.03 | 0.0033 | 0.00037 | 0.35 |
| 381.85 | 0.71 | 0.26 | 0.027 | 0.0027 | 0.0003 | 0.32 |
| 383.35 | 0.68 | 0.28 | 0.032 | 0.0035 | 0.0004 | 0.36 |
| 387.35 | 0.58 | 0.36 | 0.054 | 0.008 | 0.0012 | 0.50 |
| 391.65 | 0.53 | 0.39 | 0.066 | 0.011 | 0.0019 | 0.56 |
| 399.85 | 0.42 | 0.45 | 0.1 | 0.023 | 0.0051 | 0.74 |
| 402.25 | 0.46 | 0.43 | 0.087 | 0.018 | 0.0036 | 0.67 |
| 404.05 | 0.46 | 0.43 | 0.088 | 0.018 | 0.0036 | 0.67 |
| 409.15 | 0.42 | 0.45 | 0.1 | 0.023 | 0.0053 | 0.74 |

The coexisting vapor compositions are given in Table 2.5 for each temperature reported by Vu [31].

**TABLE 2.5 Vapor Phase Mole Fractions of Lactic Acid + Water VLE at 101.33 kPa.**

| $T$ (K) | True $y_{water}$ | True $y_{L_1}$ | True $y_{L_2}$ | True $y_{L_3}$ | True $y_{L_4}$ | Apparent $y_{LA}$ |
|---|---|---|---|---|---|---|
| 378.25 | 1 | 0.00051 | 2.9E−07 | 1.7E−10 | 9.6E−14 | 5.1E−04 |
| 379.25 | 1 | 0.00072 | 5.8E−07 | 4.7E−10 | 3.8E−13 | 7.2E−04 |
| 380.25 | 1 | 0.0011 | 1.5E−06 | 1.9E−09 | 2.4E−12 | 1.1E−03 |
| 380.75 | 1 | 0.00083 | 7.8E−07 | 7.4E−10 | 6.9E−13 | 8.3E−04 |
| 381.75 | 1 | 0.00097 | 0.000001 | 1.1E−09 | 1.2E−12 | 9.7E−04 |
| 381.85 | 1 | 0.0019 | 0.0001 | 0 | 0 | 2.1E−03 |
| 383.35 | 1 | 0.0024 | 0.0001 | 0 | 0 | 2.6E−03 |
| 387.35 | 1 | 0.003 | 0.0001 | 0 | 0 | 3.2E−03 |
| 391.65 | 0.99 | 0.012 | 0.0005 | 0 | 0 | 1.3E−02 |
| 399.85 | 0.98 | 0.021 | 0.0009 | 0 | 0 | 2.3E−02 |
| 402.25 | 0.98 | 0.022 | 0.0009 | 0 | 0 | 2.4E−02 |
| 404.05 | 0.98 | 0.015 | 0.0006 | 0 | 0 | 1.6E−02 |
| 409.15 | 0.97 | 0.03 | 0.0013 | 0.0001 | 0 | 3.3E−02 |

The coexisting liquid compositions are given in Table 2.4 for each temperature reported by Vu [31].

defined in Equations 2.4–2.6. The apparent mole fractions in the last column are calculated by taking a basis of one true mole, recognizing that the water in the analysis includes the water released by condensation of the oligomers, thus $n_W^i = n_W - \sum(j-1)n_{L_j}$, and the apparent moles of lactic acid are determined by $n_L^i = \sum j n_{L_j}$.

Comparison of the two data sets is informative, but the Sanz et al. data should be corrected for the missing oligomers. Only approximate analysis can be performed from the published data. The oligomerization model equations can be used to convert the Sanz et al. data for comparison. The relation $n_{L_j} = n_{L_{(j-1)}} p$ suggests a method to determine $p$, but the $p$ values found using the Sanz et al. data with the relation $p = x_{L_2}/x_{L_1}$ range from 0.23 to 0.29 when the $p$ values should be increasing with lactic acid concentration as in Figure 2.6. Values determined using the Sanz et al. data with the alternative relation $p = x_{L_1} K/x_W$ are reasonable and range from 0.007 to 0.64 when the value $K = 0.2023$ is used. Thus, for the Sanz et al. data, the apparent composition can be calculated from the reported $x_W$ and $x_{L_1}$ using Equation 2.10 with $K = 0.2023$ to determine $p$, and then using Equations 2.14 and 2.17 to find the apparent moles of lactic acid and water, from which the apparent mole fractions are calculated and plotted in Figure 2.7.

A similar analysis can be performed on the data of Vu. Using Equation 2.10, the $p$ values from the data range from 0.05 to 0.22. Analysis using $p = x_{L_2}/x_{L_1}$ and comparison with $p = x_{L_1} K/x_W$ shows a reasonable parity as shown in Figure 2.6, indicating that the data are much more consistent with equilibria. A comparison of the data of Vu with the manipulated data of Sanz et al. is shown in Figure 2.7. The Vu data at high concentrations are more scattered indicating some control issues with the recirculating apparatus. The data of Sanz et al. vary smoothly to higher concentrations indicating better circulation control. Though both data sets have some shortcomings, the agreement is remarkable

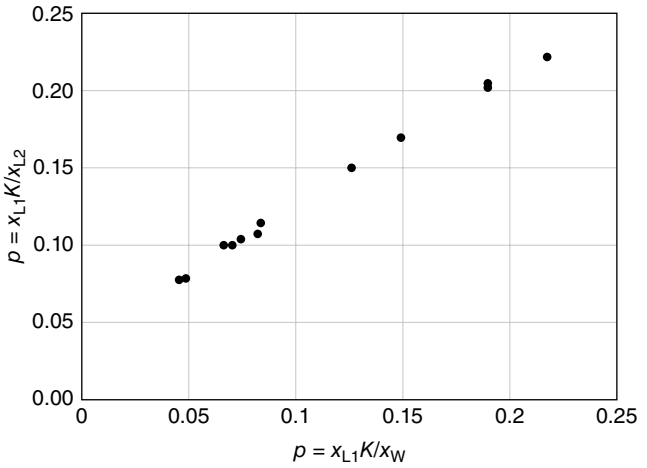


**FIGURE 2.6** Parity plot of $p$ values determined by two methods as explained in the text for data of Vu.

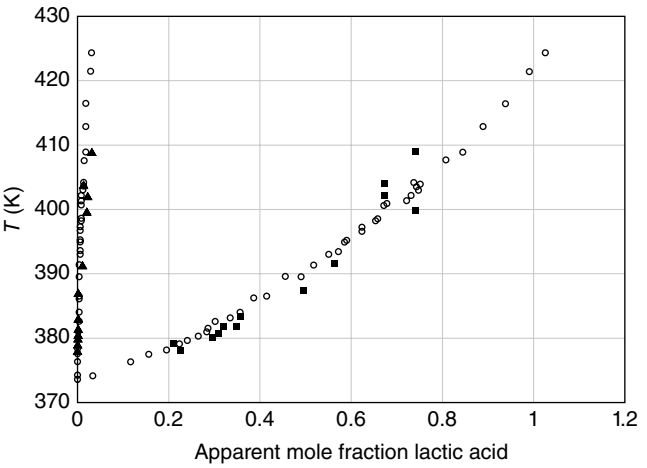


**FIGURE 2.7** VLE data for lactic acid + water at 101.33 kPa as reported by Vu compared to the manipulated data of Sanz et al. Data of Vu are filled symbols with triangles for the vapor phase and squares for the liquid phase.

for the complex experimental system. The data provide reasonable approximations for practitioners.

## 2.7 DENSITY OF AQUEOUS SOLUTIONS

Holten [28] fitted density data from Troupe et al. [32] using a third-order polynomial with each wt% fitted separately. The individual fits represent the experimental data within 0.2%. To provide practitioners a more rapid calculation, we have refitted the data of Troupe et al. using Equation 2.26 where coefficients $A$ and $B$ are linear functions of the apparent wt% lactic acid, $w$. The calculated densities, $\rho$, match experimental data within 0.3% as shown in Figure 2.8.

$$\rho\left(\text{g/mol}\right) = A \times T\left(^{\circ}\text{C}\right) + B \tag{2.26}$$

$$A\left(\text{g/mol}^{\circ}\text{C}\right) = -5.6822 \times 10^{-6} w + -4.4990 \times 10^{-4} \tag{2.27}$$

$$B\left(\text{g/mol}\right) = 2.4801 \times 10^{-3} w + 1.0091 \tag{2.28}$$

## 2.8 VISCOSITY OF AQUEOUS SOLUTIONS

Troupe et al. [32] observed that the viscosity increased over time as did the titratable acidity when a 75 apparent wt% lactic acid sample was freshly prepared from 85 wt%. At room temperature, it took more the 20 days to reach equilibrium. Equilibration of solutions is critical to obtain reliable viscosity data, and equilibration is slow at 20°C. Suggested equilibration times are provided by Vu et al. [27]. Troupe et al. fitted their viscosity data with Equation 2.29 where each wt% was fitted separately. The individual fits represent the experiments within 5%. For practitioners, we provide a rapid way to interpolate the viscosity. We have regressed the coefficients $A$ and $B$ for the common log of viscosity $\eta$,in cP, as a function of apparent wt% lactic acid as given in Equations 2.30 and 2.31. These correlations are compared with experimental data in Figures 2.9 and 2.10. The equations are within 10% except for the most concentrated measurement at 25°C where the error is 12%. For Equations 2.30 and 2.31, $w$ is apparent wt% lactic acid (Figures 2.9 and 2.10).

$$\log_{10} \eta\left(\text{cP}\right) = A + B \times \log_{10}\left(T\right)\left(\text{K}\right) \tag{2.29}$$

$$A = 2.7638 \times 10^{-3} w^2 - 4.2602 \times 10^{-2} w + 15.529 \tag{2.30}$$

$$B = -1.0507 \times 10^{-3} w^2 + 1.8037 \times 10^{-2} w - 6.2620 \tag{2.31}$$

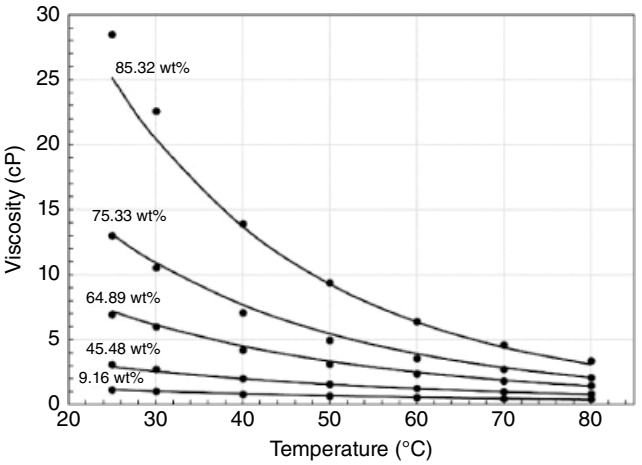


**FIGURE 2.9** Comparison of viscosity calculated using Equations 2.29–2.31 with experimental data of Troupe et al. as a function of temperature and apparent wt%.

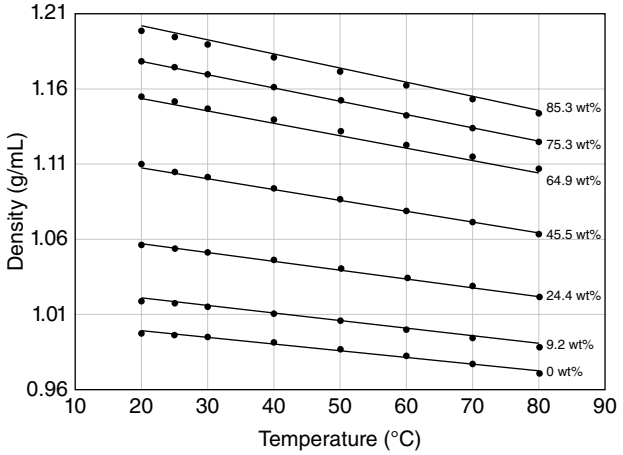


**FIGURE 2.8** Comparison of aqueous lactic acid density calculated using Equations 2.26–2.28 with experimental data of Troupe et al. as a function of apparent wt% and temperature.

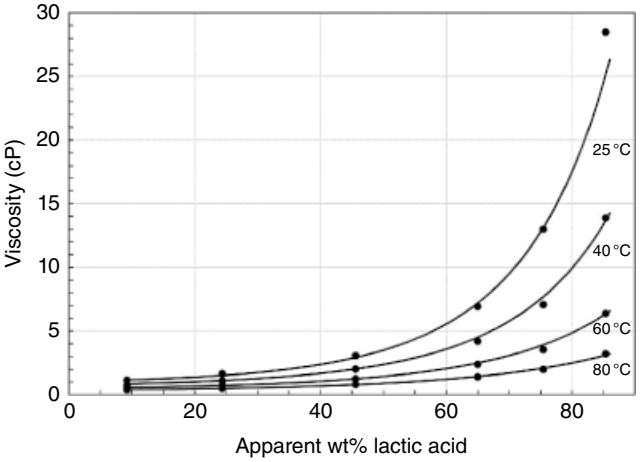


**FIGURE 2.10** Comparison of viscosity calculated using Equations 2.29–2.31 with experimental data of Troupe et al.

## 2.9 SUMMARY

Vapor pressure measurements of anhydrous lactic acid could potentially be affected by oligomerization which produces water. Many vapor pressure measurements are provided by investigators measuring vapor pressure during use of lactic acid in chemical synthesis. Oligomerization of aqueous lactic acid significantly influences optical rotation, bubble temperature, and viscosity. Property measurements of aqueous solutions require careful validation of oligomer equilibration. The titratable acidities of equilibrated aqueous solutions are well represented by the Flory-Schulz distribution which is a measure of the number of free acid groups in the equilibrated mixture.

## REFERENCES


1. D. R. Witzke, Introduction to properties, engineering, and prospects of polylactide polymers, *Ph.D. thesis*, Michigan State University, East Lansing, 1997.
2. W. D. Bancroft, H. L. Davis, The optical rotation of lactic acid, *J. Phys. Chem.* **1931**, *35*(9), 2508–2529.
3. H. Henry, N. Marmy Conus, P. Steenhout, Béguin A, Boulat O., Sensitive determination of D-lactic acid and L-lactic acid in urine by high-performance liquid chromatography-tandem mass spectrometry: D-lactic acid and L-lactic acid in urine, *Biomed. Chromatogr.* **2012**, *26*(4), 425–428.
4. X. Ding, S. Lin, H. Weng, J. Liang, Separation and determination of the enantiomers of lactic acid and 2-hydroxyglutaric acid by chiral derivatization combined with gas chromatography and mass spectrometry, *J. Sep. Sci.* **2018**, *41*(12), 2576–2584.
5. L. Zhang, A. F. Martins, P. Zhao, M. Tieu, D. Esteban-Gómez, G. T. McCandless, et al., Enantiomeric recognition of D- and L-lactate by CEST with the aid of a paramagnetic shift reagent, *J. Am. Chem. Soc.* **2017**, *139*(48), 17431–17437.
6. H. Borsook, H. M. Huffman, Y.-P. Liu, The preparation of crystalline lactic acid, *J. Biol. Chem.* **1933**, *102*(2), 449–460.
7. V. L. Novikov, O. P. Shestak, Reactions of hydrogen peroxide with acetylacetone and 2-acetylcyclopentanone, *Russ. Chem. Bull.* **2013**, *62*(10), 2171–2190.
8. J. Schott, J. Kretzschmar, S. Tsushima, B. Drobot, M. Acker, A. Barkleit, et al., The interaction of Eu(III) with organoborates—a further approach to understand the complexation in the An/Ln(III)–borate system, *Dalton Trans.* **2015**, *44*(24), 11095–11108.
9. C. T. Bowmer, R. N. Hooftman, A. O. Hanstveit, P. W. M. Venderbosch, N. van der Hoeven, The ecotoxicity and the biodegradability of lactic acid, alkyl lactate esters and lactate salts, *Chemosphere* **1998**, *37*(7), 1317–1333.
10. K. Masutani, Y. Kimura, Chapter 1. PLA synthesis. From the monomer to the polymer, in: A. Jiménez, M. Peltzer, R. Ruseckaite (Eds.), *Polymer Chemistry Series [Internet]*, Royal Society of Chemistry, Cambridge, 2014 [cited 31 March 2021], pp. 1–36. Available from: http://ebook.rsc.org/?DOI=10.1039/9781782624806-00001.
11. Feng L, X. Bian, Z. Chen, S. Xiang, Y. Liu, B. Sun, et al., Determination of D-lactide content in lactide stereoisomeric mixture using gas chromatography-polarimetry, *Talanta* **2017**, *164*, 268–274.
12. M. Muller, J. Hess, W.-G. Schnell, G. Entenmann, *Meso*-lactide, processes for preparing it and polymers and copolymers produced therefrom, US Patent 4,983,745, 1991.
13. H. Rinderknecht, C. Niemann, The esterification of acylated α-amino acids, *J. Am. Chem. Soc.* **1948**, *70*(7), 2605–2606.
14. B. Iselin, E. A. Zeller, 196. Über den enzymatischen Abbau von *l*-α-oxysäuren, *Helv. Chim. Acta.* **1946**, *29*(6), 1508–1520. https://dx.doi.org/10.1002/hlca.19460290618.
15. A. Šepitka, Physical-technical properties of lactic acid, *Prům. Potravin.* **1961**, *12*, 661–665.
16. E. Cherbuliez, H. Weniger, 255. Phosphorylations par les acides polyphosphoriques, *Helv. Chim. Acta.* **1946**, *29*(6), 2006–2017.
17. V. V. Perekalin, A. K. Petryaeva, M. M. Zobacheva, É. L. Metelkina, New method of synthesizing α-hydroxy and α-ketoacids, *Dokl. Chem.* **1966**, *166*, 217–219.
18. V. Ababi, A. Popa, Studiul echilibrului sistemului ternar: acid lactic—apă—solvent organic, *Analele Stiitifice Univ. Al Cuza Sect. I.* **1960**, *6*, 929–942.
19. G. Losse, G. Bachmann, Synthese von depsipeptiden, *Chem. Ber.* **1964**, *97*(9), 2671–2680.
20. D. Vorländer, R. Walter, Die mechanisch erzwungene Doppelbrechung der amorphen Flüssigkeiten im Zusammenhang mit der molekularen Gestalt, *Z. Für. Phys. Chem.* **1925**, *118U*(1), 1–30.
21. Y. Ogata, M. Inaishi, Preparation of DL-alanine by the reaction of (±)-2-chloropropionic acid with aqueous ammonia under pressure, *Bull. Chem. Soc. Jpn.* **1981**, *54*(11), 3605–3606.
22. P. J. Flory, Molecular size distribution in linear condensation polymers, *J. Am. Chem. Soc.* **1936**, *58*(10), 1877–1885.
23. P. D. Watson, Composition of lactic acid production of a highly concentrated acid, *Ind. Eng. Chem.* **1940**, *32*(3), 399–401.
24. R. Montgomery, Acidic constituents of lactic acid-water systems, *J. Am. Chem. Soc.* **1952**, *74*(6), 1466–1468.
25. R. Ueda, T. Terajima, The utilization of lactic acid obtained by fermentation, XII. Change in the polymers by dilution with water, *Hakko Kogaku Zasshi.* **1958**, *36*, 371–374.
26. S. Bezzi, L. Riccoboni, *Memorie della Classe di Scienze Fisiche, Matematiche e Naturali. Reale Accademia d'Italia* **1937**, *8*, 181–200.
27. D. T. Vu, A. K. Kolah, N. S. Asthana, L. Peereboom, C. T. Lira, D. J. Miller, Oligomer distribution in concentrated lactic acid solutions, *Fluid Phase Equilibria.* **2005**, *236*(1–2), 125–135.
28. C. H. Holten, A. Müller, D. Rehbinde, *Lactic Acid*, Verlag Chemie, International Research Association, Copenhagen, 1971.


29. S. Feng, S. Xiang, X. Bian, G. Li, Quantitative analysis of total acidity in aqueous lactic acid solutions by direct potentiometric titration, *Microchem. J.* **2020**, *157*, 105049.
30. M. T. Sanz, S. Beltran, B. Calvo, J. L. Cabezas, Vapor liquid equilibria of the mixtures involved in the esterfication of lactic acid with methanol, *J. Chem. Eng. Data.* **2003**, *48*(6), 1446–1452.
31. D. T. Vu, Properties and separations of plant-derived chemicals, Ph.D. thesis, Michigan State University, East Lansing 2007.
32. R. A. Troupe, W. L. Aspy, P. R. Schrodt, Viscosity and density of aqueous lactic acid solutions, *Ind. Eng. Chem.* **1951**, *43*(5), 1143–1146.

# 3

# INDUSTRIAL PRODUCTION OF HIGH-MOLECULAR-WEIGHT POLY(LACTIC ACID)

Anders Södergård, Mikael Stolt, and Saara Inkinen

## 3.1 INTRODUCTION

Polymers based on lactic acid (PLA) are the most promising category of polymers made from renewable resources. They are not only compostable and biocompatible but also processable with standard processing equipment. The properties of lactic-acid (LA)-based polymers vary to a large extent depending on the ratio between, and the distribution of, the two stereoisomers or other comonomers [1–3]. The polymers can be manufactured by different polymerization routes, which are schematically described below (Figure 3.1).

PLA of high molecular weight is most commonly made by ring-opening polymerization (ROP) of the ring-formed dimer, dilactide (lactide; 3,6-dimethyl-1,4-dioxane-2,5-dione), which is made by depolymerization of the polycondensed LA (2-hydroxypropanoic acid). This route is a two-step reaction that usually involves additional purification steps and is therefore costly. It is often stated in the art that the preparation of high-molecular-weight PLA by a direct dehydration condensation reaction is not feasible due to the equilibrium not favoring a high-molecular-weight polymer. PLA prepared from polycondensation has low molecular weight and poor mechanical properties and therefore is not suitable for many applications. The commercial interest for solving this problem has increased because of the need of cost-effective approaches in the manufacturing of LA-based polymers with a high molecular weight. Solvent-assisted polycondensation is one way to overcome this problem [4] and melt polycondensation followed by solid-state polycondensation is another one [5]. The third approach to achieve high-molecular-weight LA-based polymers is to utilize the terminal groups of the prepolymer in linking processes where a linking agent is employed [6]. Such prepolymers can be composed of solely one stereoisomer, combinations of D- and L-lactoyl units in various ratios, lactic acid in combination with other hydroxy acids, or di-/multifunctional comonomers. If the lactic acid is polycondensated in the presence of difunctional monomers (e.g., diols or diacids), the resulting prepolymer will have the same end groups in both chain ends; that is, the prepolymer is a telechelic macromer [6].

Since the first commercial products of lactic-acid-based polymers were introduced in the market by DuPont, Chronopol, and Cargill at the end of the 1980s and the beginning of the 1990s, PLA has been successfully commercialized by several companies and subsequently found use in several different end-product categories [7]. However, PLA was initially used mainly in medical applications [8], which continue to be an important field for some PLA producers [9]. Today, PLA is one of the most important bio-based and biodegradable polymers suitable for a wide variety of applications [10].

The unique position of PLA in the field of bio-based products is related to its processability, appearance, and properties such as mechanical strength and barrier. In addition to the medical sector, other uses of PLA include food and non-food packaging, food service ware, agricultural materials, durable goods, electronics, building, construction, and 3D-printing [11, 12]. Since 2005, the business of bio-based material production has grown significantly. In 2020, 18.7% (i.e., 395,000 metric tons) of the total annual production capacity of bioplastics was attributed to PLA [13].

The growth of industrial PLA production volumes was initially driven by (i) oil prices, as high crude oil price was

*Poly(Lactic Acid): Synthesis, Structures, Properties, Processing, Applications, and End of Life*, Second Edition.
Edited by Rafael A. Auras, Loong-Tak Lim, Susan E. M. Selke, and Hideto Tsuji.

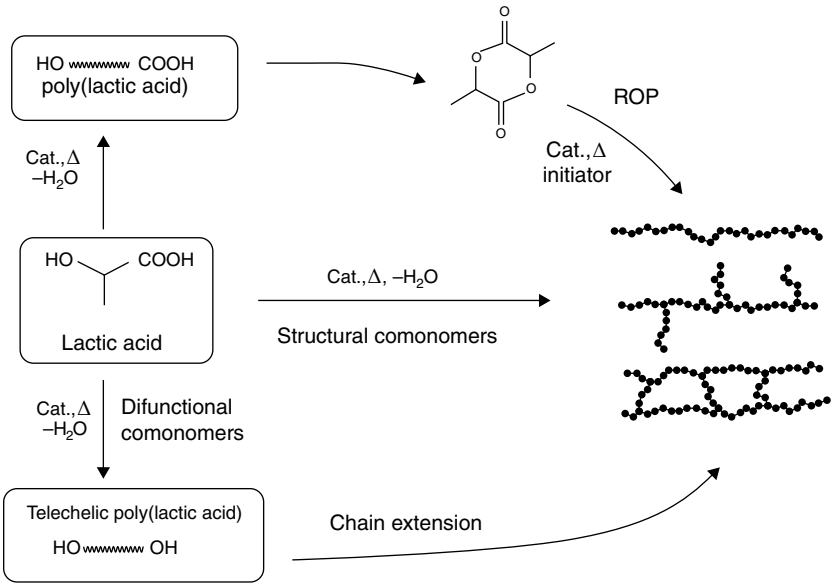


**FIGURE 3.1** Manufacturing routes for lactic-acid-based polymers.

reflected in the pricing of traditional polymers and in energy costs; (ii) factors related to legislation, as favorable legislation and government support made the use of bio-based materials an attractive option to traditional polymers; and (iii) image, as an increased awareness among brand owners and retailers made compostable and renewable products real alternatives with added value in terms of sustainability.

In the past decade, the commercial production of PLA has been boosted by the global shift in consumer awareness toward eco-friendly packaging, the technological developments and investments related to large-scale manufacturing, and the concurrent development of suitable applications and products. PLA is hence on its way to become a true commodity polymer.

At the moment, the American market leader, Natureworks, holds a leading position in terms of PLA production capacity (150,000 metric tons) [7], followed by Total Corbion PLA from the Netherlands with its 75,000 metric tons production site in Thailand [14]. Total Corbion PLA is additionally building a 100,000 metric tons PLA plant, which is to become operational in 2024, in France [15]. Also, Belgian Futerro [16] and Zhejiang Hisun Biodegradable Plastics Corporation [17] are significant PLA producers, with production capacities of 30,000 and 15,000 metric tons, respectively. The Austrian Weforyou Group and its subsidiary Jiangsu Supla Bioplastics should also be noted with their 10,000 metric tons production site in China [18]. Additionally, several other producers exist, and the market is expected to exhibit significant growth during the coming years due to new production sites in China, the United States, and Europe.

## 3.2 LACTIC-ACID-BASED POLYMERS BY POLYCONDENSATION

From a chemistry point of view, lactic acid can form PLA by means of the reaction of the hydroxyl and carboxylic acid groups of lactic acid. By removing the water formed during this condensation reaction, the reaction proceeds toward the product side, PLA:

$$\mathrm{HO-\left(CH\left(CH_3\right)COO\right)_n-H+HO-\left(CH\left(CH_3\right)COO\right)_m-H \longleftrightarrow HO-\left(CH\left(CH_3\right)COO\right)_{n+m}-H+H_2O}$$

where $n$ and $m \geq 1$.

The removal of water becomes more difficult and can be rate determining when producing a higher-molecular-weight PLA due to the increased viscosity of the reaction mixture. Through applying vacuum and high temperature, the water removal can be enhanced. However, during the polycondensation of lactic acid, other side reactions also occur, such as transesterification, resulting in the formation of ring structures of different sizes [19]. These side reactions have a negative influence on the properties of the polymer. The formation of ring structures, such as lactide, lowers the overall molecular weight and the removal of the lactide formed reduces the first-pass yield of the process. The formation of lactide cannot be excluded, but to suppress the lactide formation and increase the first-pass yield of the polycondensation reaction of lactic acid, the lactide can be returned back to the reaction mixture. A partial condenser (reflux condenser) or a rectification column placed on top of the polycondensation reaction can be used to recycle lactide back to the reaction

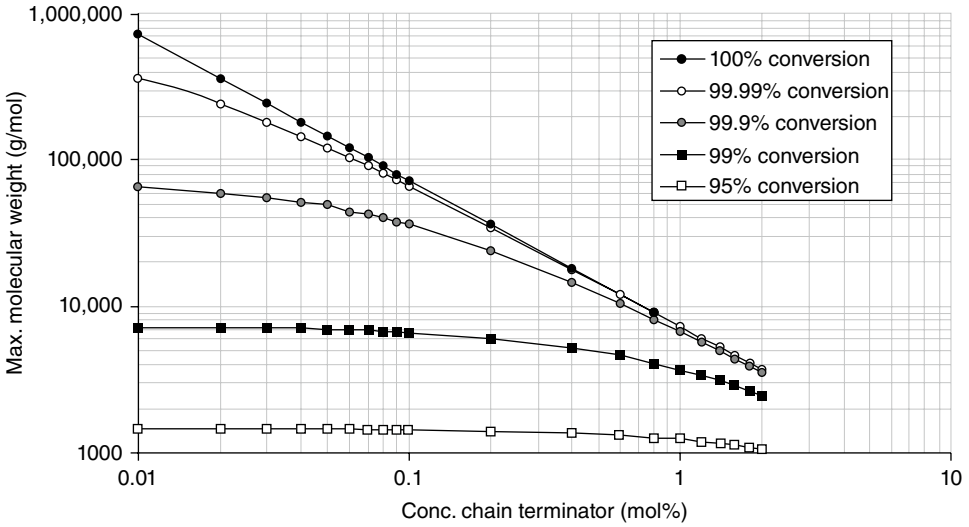


**FIGURE 3.2** Theoretical relation between concentration of chain terminator and number-average molecular weight ($M_n$) at different conversions of the functional groups.

mixture. The addition of stabilizers, such as antioxidants or phosphorous compounds, can reduce the coloration [20].

The lactide formation becomes substantial at high reaction temperatures (>200°C) [21]. To suppress the lactide formation, the polycondensation reaction should thus be carried out at temperatures below 200°C. Conducting the polycondensation at low temperatures again has a negative effect on the removal of water due to the relatively high viscosity of the reaction mixture in addition to a lowered reaction rate. Since polycondensation should be the main reaction, the removal of water should be as high as possible without allowing the reaction mixture to undergo hydrolysis and transesterification reactions.

Besides the removal of reaction water from the viscous reaction mixture, the quality of the monomer (lactic acid) with respect to chain terminators such as monocarboxylic acids (formic acid, acetic acid, propionic acid, etc.) or monohydroxy alcohols (methanol, ethanol, propanol, etc.) is important. To obtain a desired high molecular weight, the amount of end terminators must be limited. In Figure 3.2, the theoretical relationship between the concentration of chain terminator in mol% and the corresponding number-average molecular weight ($M_n$) at different conversions of the functional groups is shown. With a chain terminator content of 0.1 mol%, a maximum $M_n$ of 72,000 g/mol can be obtained at 100% conversion of the functional groups. This clearly demonstrates the importance of using high-purity lactic acid (often also called polymer-grade lactic acid) during the polycondensation reaction.

### 3.2.1 Direct Condensation

The preparation of PLA from lactic acid by direct condensation can be divided into three principal stages: (a) removal of the free water content; (b) oligomer polycondensation; and (c) melt polycondensation of high-molecular-weight PLA:

(a) Besides lactic acid, the feedstock also contains the so-called free water. Due to the equilibrium of lactic acid and water, some low amount of oligomers of lactic acid (linear dimer, linear trimer, etc.) can already be formed in this stage. To convert lactic acid to PLA, first the free water has to be removed. The evaporation of the free water requires a system having good heat transfer and can be carried out in commonly used evaporators, such as falling film evaporators. Flash evaporation can also be used to remove the free water in lactic acid feedstock.

(b) In the second stage, the lactic acid is converted into low-molecular-weight PLA or oligo(lactic acid). In this step, the removal of water is not critical because of the low viscosity of the reaction mixture. The rate-determining step in this stage is usually the chemical reaction, which is significantly affected by the catalyst used [22]. Traditional polycondensation catalysts are strong acids, and organometallic compounds are also commonly used catalysts. The low-molecular-weight PLA polycondensation can also be carried out in an evaporator or alternatively in a stirred reactor having an agitator that generates good radial and axial mixing. The loss of lactic acid due to entrainment can be overcome by using a reflux condenser, a demister package, or a rectification column. Preferably, this stage is carried out in a system having a narrow residence time distribution (plug-flow behavior) to obtain a prepolymer of lactic acid of narrow molecular weight distribution (small dispersion).

(c) The third stage is the melt-polycondensation in which the removal of water becomes critical. To enhance the polycondensation reaction, and not the transesterification reactions, the water formed in the reaction mixture should be removed efficiently. The rate-determining step in this phase is the mass transfer of water. To enhance both mass and heat transfer, the melt-polycondensation reaction should be applied in an apparatus having an efficient renewal of phase boundary layers. The apparatus should have intensive mixing and kneading in order to homogenize the reaction mixture. The removal of water from the viscous PLA mass can be further enhanced by carrying out the reaction under vacuum conditions in an inert atmosphere. A mathematical model for the polycondensation of lactic acid accounting for water removal by diffusion has been developed [23]. The increasing molecular weight of the PLA requires a system that can handle high-viscosity mass. Such an apparatus could be a rotating disk type of reactor, generating a good surface renewal to enhance the mass transfer of the water formed. Such an apparatus should also have very good heat transfer to have a homogeneous temperature profile in the reaction mixture. Especially the mechanical heat formed due to mixing and kneading of the highly viscous PLA should be controlled. In this stage also a plug-flow behavior is preferred to obtain a narrow molecular weight distribution.

Only a few studies have dealt with the influence of the catalyst when preparing PLA of high molecular weight through the direct bulk condensation reaction. In most studies with regard to catalysts, the polycondensations were carried out only to obtain low-molecular-weight polymers with an $M_w$ of a few thousands, before they were stopped. PLA having a molecular weight of as high as 130,000 g/mol (gel permeation chromatography (GPC) relative to polystyrene (PS) standards) was synthesized by direct bulk condensation polymerization at 180°C using titanium(IV) butoxide as catalyst [24]. In another study, several metal catalysts based on Ge, Sb, Zn, Fe, Al, Ti, and Sn were employed in the melt-polycondensation reaction [25]. The most efficient catalyst was SnO with regard to molecular weight of the PLA, but the yield was below 40% when using this catalyst at 180°C (20 h). However, when using *p*-toluenesulfonic acid as a co-catalyst with $SnCl_2$, the efficiency was drastically improved and molecular weights above 100,000 g/mol (GPC relative to PS standards in chloroform, 35°C) were achieved within 15 h of polycondensation. Sodium carbonate, calcium carbonate, and lanthanum oxide have also been used as catalysts when preparing PLA of high molecular weight [26]. Weight-average molecular weights ranging from 63,000 to 79,000 g/mol (GPC relative to PS standards in chloroform at 40°C) were obtained by melt-polycondensation but with poor yields (33–52%).

To achieve an increased molecular weight of the PLA, comonomers with functionality higher than two have been used. A process for making a star-shaped PLA was described, where the lactic acid is polycondensated in the presence of a polyhydroxyl compound having at least four hydroxyl groups [27]. The PLA obtained has a higher molecular weight than a polymer prepared without the use of comonomer, but the invention has a clear limit in obtainable molecular weight. If the polyhydroxyl compound is used in large amounts, the polymer will be hydroxyl terminated and the condensation reaction cannot continue, thus yielding a low-molecular-weight polymer. On the other hand, if the polyhydroxyl compound is used in small amounts, the effect of the polyhydroxyl compound will diminish and the polycondensation reaction will be a blend of star-shaped PLA and linear PLA. A hyperbranched PLA of high molecular weight was also manufactured by coupling a first prepolymer having at least three functional end groups with a second prepolymer having at least two functional end groups by a condensation reaction between the end groups in the prepolymers [28]. The improvement of the process was that the number of arms and/or molecular weight of the functionalized prepolymers could be accurately adjusted, thus affecting the properties of the resulting hyperbranched polymer in a desired way. Molecular weight in excess of 200,000 g/mol (GPC relative to PS standards in chloroform at 30°C) was obtained for the hyperbranched PLA.

Lactide has been used as a coreactant and yield enhancer in the polycondensation reaction of lactic acid [29]. $M_w$s in the range of 65,000–83,000 g/mol were obtained in 17–42 h (GPC, 40°C, chloroform), starting from 90 wt% lactic acid, when an inorganic solid acid catalyst (aluminum silicate) was used.

Copolymers with high enough molecular weight for practical use were prepared from succinic acid and 1,4-butanediol and minor amounts of lactic acid [30]. An increase in the reaction rate was reported when the aliphatic diol and the aliphatic dicarboxylic acid were polycondensated using a few mole percent of lactic acid and a germanium oxide catalyst.

### 3.2.2 Solid-State Polycondensation

The disadvantage of the PLA prepared by direct polycondensation is often a limited molecular weight in combination with a low yield. Some progress in increasing the molecular weight of the PLA has recently been achieved, though, by sequential melt/solid polycondensation [5, 31].

In sequential melt/solid-state polycondensation, the three first stages as described for direct polycondensation (i.e., removal of the free water content, oligomer polycondensation, and melt polycondensation) are utilized with an additional fourth stage. In the fourth stage, the melt-polycondensated PLA is cooled below its melting temperature, often followed by particle formation as it solidifies. The

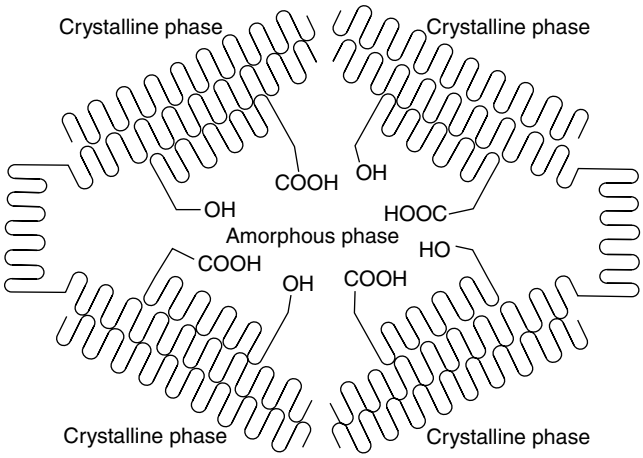


**FIGURE 3.3** Schematic description of the solid-state polycondensation.

solid particles are then subjected to a crystallization process, where two phases can be identified: a crystalline phase and an amorphous phase. It is believed that the reactive end groups, as well as the catalyst, are concentrated in the amorphous phase in between the crystals (Figure 3.3), thus yielding an apparent enhancement of the polycondensation rate although the polycondensation is performed in the solid state at a low temperature (i.e., below the melting temperature of the polymer). A metal catalyst can catalyze the solid-state polycondensation in the amorphous phase, as well as the melt-polycondensation. These catalysts can be different metals or metal salts, from metals such as Sn, Ti, and Zn.

The rate-determining step in solid-state polycondensation is the mass transport of the reaction water by molecular diffusion. The removal of water can be further enhanced by carrying out the reaction under vacuum conditions in an inert atmosphere.

A process for preparing PLA by sequential melt/solid-state polycondensation has been described [32]. The process comprises a liquid-phase polycondensation reaction step, followed by a solidification and particle formation step of the prepolymer formed, by crystallization of the prepolymer particles, and finally a solid-phase polymerization step. The weight-average molecular weight of linear PLA obtained by this process was above 100,000 g/mol, which in many cases was a 10-fold increase when compared with the prepolymer. The total process time to prepare the PLA was about 100 h, starting from 88% lactic acid. The weight-average molecular weight was determined by GPC at 40°C in chloroform compared with polystyrene standards. A similar process for making poly(hydroxycarboxylic acid) was described where a low-molecular-weight polycondensate was pelletized and crystallized, and a solid-phase polycondensation reaction step was performed by heating the pellets to a temperature not lower than the crystallization temperature [33]. According to the invention, pellets of poly(hydroxycarboxylic acid) of low molecular weight caused no blocking in the equipment, and it was possible to efficiently prepare poly(hydroxycarboxylic acid) of high molecular weight. The weight-average molecular weight obtained by this process was in the range of 128,000–152,000 g/mol (GPC, 40°C, chloroform) requiring a minimum solid-phase polycondensation reaction time of 40 h.

Stereoblock PLA was synthesized by solid-state polycondensation of a 1:1 mixture of PLLA and PDLA [34]. In the first step, PLLA and PDLA having a medium molecular weight were melt polycondensated. The PLLA and PDLA were then melt blended in a 1 : 1 weight ratio to allow the formation of their stereocomplex, and the blend was subjected to solid-state polycondensation. Some process optimization with regard to polymerization conditions was done and molecular weights exceeding 100,000 g/mol were obtained for the stereoblock PLA (GPC relative to poly(methyl methacrylate) (PMMA) standards with hexafluoroisopropanol (HFIP) as the eluent). In another study, it was found that the weight-average molecular weight of the resultant stereoblock PLA was strongly influenced by the lactide/oligomer content in the melt blend, which is determined by the melt-blending conditions because it is directly correlated with the crystallinity of the polycondensation products [35]. The effect of crystallization on the solid-state polycondensation of PLLA has also been investigated [36]. The results showed that the $M_w$ of the PLA reached a maximum value when a crystallization time of 30 min (105°C) and solid-state polycondensation of 35 h (135°C) were used.

### 3.2.3 Azeotropic Dehydration

In azeotropic dehydration, the same principle stages as in direct melt condensation of lactic acid are present, with the exception that the last high viscosity melt-polycondensation stage is eliminated because the polycondensation is performed in solution. The removal of the reaction water from the reaction medium thus becomes easier and a higher PLA molecular weight is achievable. The solvent, on the other hand, has to be dried from the water produced in the reaction using a drying agent (e.g., molecular sieve). Alternatively, fresh, dry organic solvent can be added during the reaction, which is undesirable from both an environmental and an economical point of view. Another disadvantage when using organic solvents in the dehydration reaction is that the prepared polymer has to be collected from the solvent, typically by using a nonsolvent for the polymer, and dried. These steps use extra labor, are time-consuming, and usually lower the yield of the raw material used. The boiling point of the solvent also sets a restriction on the polycondensation temperature that can be used. However, the optical purity of the PLA can be retained because of the lower temperature.

Several patent applications have been filed on the azeotropic dehydration of PLA. A process was claimed wherein the organic solvent was removed from the reaction mixture

and an additional solvent, that had a water content less than the water content of the solvent removed from the reaction mixture, was added to the reaction mixture [37]. The removed solvent was dried using, for example, molecular sieves, phosphorus pentaoxide, or metal hydrides and added back to the reaction mixture. In another similar application, the drying agent used was an ion exchange resin [38]. Examples of solvents that were claimed included anisole or diphenyl ether. Azeotropic dehydration of lactic-acid-containing impurities (e.g., chain terminators such as methanol, ethanol, acetic acid, and pyruvic acid) in a total amount of 0.3 mol% has also been reported [39]. When the lactic acid contained 0.16 mol% methanol, a molecular weight of 50,000 g/mol (viscometry, dichloromethane, 20°C) was obtained in diphenyl ether at 130°C using tin powder as a catalyst. A methanol content of 0.02 mol% yielded a PLA with $M_w$ of 320,000 g/mol using the same polycondensation procedure.

The effect of several different catalysts on the azeotropic dehydration of lactic acid in diphenyl ether has been studied [40]. The most effective catalysts were found to be Sn compounds (Sn powder, SnO, and $SnCl_2$), $Ni(OAc)_2$, and $CH_3$—Ph—$SO_3H$. Using these catalysts, weight-average molecular weights exceeding 100,000 g/mol according to GPC results relative to polystyrene standards (chloroform, 40°C) were obtained for the PLA. Haloiminium salts have also been utilized as polycondensation agents in azeotropic dehydration of hydroxycarboxylic acids, including lactic acid [41].

A process to further increase the $M_w$ of the hydroxycarboxylic acid copolymerization with polyfunctional compounds was described [42]. The polyfunctional compounds were those having three or more carboxylic end groups or hydroxyl groups. In addition to this, a second compound having two or more functional end groups was present in the reaction mix. A disadvantage of the invention is that all compounds are preferably added at the same time in the beginning of the reaction, thus giving an uncontrollable reaction and therefore also reproducibility problems.

## 3.3 LACTIC ACID-BASED POLYMERS BY CHAIN EXTENSION

### 3.3.1 Chain Extension with Diisocyanates

Chain extension with diisocyanates is undoubtedly the most commonly applied chain-extension approach for aliphatic polyesters (Figure 3.4). A large number of different diisocyanates have been used as linking molecules in the preparation of aliphatic poly(ester-urethane)s. Various isocyanates are listed in Table 3.1 together with the type of prepolymer used.

The most frequently used diisocyanate in the preparation of aliphatic poly(ester-urethane)s is 1,6-hexamethylene diisocyanate because of its low toxicity, and the use of this isocyanate will accordingly be discussed in detail. Numerous

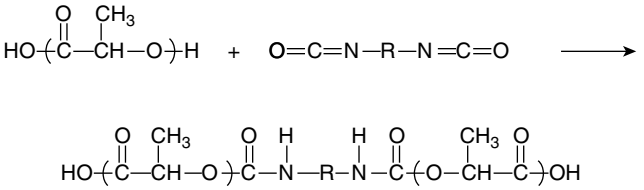

**FIGURE 3.4** Chain-extension reactions of LA-based prepolymers using diisocyanates.

**TABLE 3.1 Diisocyanates Used in the Preparation of Aliphatic Poly(ester-urethane)s**

| Name | Prepolymer Composition | Reference |
|---|---|---|
| 1,6-Hexamethylene diisocyanate | l-LA, 1,4-butanediol | [43] |
| 1,4-Butanediisocyanate | ε-caprolactone (CL), 1,4-butanediol | [44] |
| 1,6-Hexamethylene diisocyanate | 1,3-propanediol, succinic acid | [45] |
| 1,4-Butanediisocyanate | PLA, 1,4-butanediol | [46] |
| Methylenediphenyl diisocyanate | LA | [47] |
| 4,4′-Dicyclohexylmethane diisocyanate | l-LA, 1,4-butanediol | [48] |
| Isophorone diisocyanate | l-LA, 1,4-butanediol | [48] |
| Ethyl 2,6-diisocyanohexanoate | CL, glycolide, inositol | [49] |
| 1,6-Hexamethylene diisocyanate | l-LA, mandelic acid | [50] |
| 1,6-Hexamethylene diisocyanate | l-LA, malic acid | [50] |
| Methylene diphenyl isocyanate | l-LA, butyl glycidyl ether | [51] |

examples of the use of diisocyanate chain extension of aliphatic polyesters can be found in the scientific publications and in the patent literature [52–54].

***3.3.1.1 Chain-Extension Reaction Parameters*** The amount of diisocyanate determines to a large extent how the linking reaction proceeds. For a hydroxyl-terminated prepolymer and an equimolar amount of diisocyanate, the chain-extension reaction proceeds rapidly and the molecular weight reaches its maximum in a few minutes, after which the molecular weight starts to decrease due to thermal degradation [55]. Side reactions become more evident if the amount of diisocyanate is increased, which can be seen from an increase in weight-average molecular weight but not in the number-average molecular weight. This is caused by the formation of isocyanate-terminated prepolymers in excess of chain extender and the further reaction with urethane bonds yielding allophanates, branching, and eventually cross-linking. The terminal groups of the prepolymers are also important for the progress of the chain extension. Carboxylic acid end groups

can react with isocyanates and yield amides, carboxylic anhydrides, or ureas even if the reactivity with hydroxyl groups is significantly higher than with carboxylic acid groups. The presence of carboxylic acid end groups has furthermore been suggested to retard the reaction between hydroxyls and isocyanates [56]. The acid number of the prepolymers is consequently an important parameter and useful as a tool for controlling the chain-extension reaction [55, 57]. Molecular weight, molecular weight distribution, and long-chain branching can be varied by changing reaction conditions and acid number of the prepolymer. This gives a possibility for tailoring the viscoelastic properties of the polymer and tailoring LA-based polymers for specific processing equipment and conditions [57]. The third important parameter in the linking process is the catalyst, which will affect not only the reaction rate, but also the racemization. The racemization, that is, degree of lost tacticity, determines the ability of the poly(ester-urethane) to crystallize, which in turn will affect the mechanical and thermomechanical properties of the polymer. It can be concluded that the preparation of poly(ester-urethane) s can be best controlled by the following: (i) the presence of more than one type of end groups in the prepolymer being as low as possible; (ii) the semicrystalline nature being retained during both the prepolymer preparation and the linking steps; (iii) keeping the molecular weight of the prepolymer below a certain level to perform successful linking; and (d) using a catalyst that preferably is also nontoxic, with retained activity in both reaction steps [58].

***3.3.1.2 Properties of Poly(Ester-Urethane)s*** The thermal and mechanical properties of poly(ester-urethane)s are similar to those of polylactide prepared by ring-opening polymerization, but most of the poly(ester-urethane)s described in the literature are amorphous, with a few exceptions [58]. This means that some of the properties need to be improved to make useful end products. For many applications, the brittleness is an issue and for others the low heat resistance. Different approaches have been suggested for reducing the brittleness of PLA, for example, by copolymerization [59], blending [60], or adding plasticizing compounds [61].

The copolymerization approach has successfully been applied for poly(ester-urethane)s by equipping the prepolymers with elastomeric properties by copolymerization. CL–LA copolymers have been reported to result in a significant increase in the strain and the flexibility [62]. Table 3.2 shows the changes in the material properties that have been achieved by varying the prepolymer composition [50, 62].

The softening point of poly(ester-urethane)s based on CL–LA prepolymers can be varied to a large extent by changing the ε-caprolactone (CL) content. The properties of thermoplastic poly(L-lactic acid-*co*-ε-caprolactone-urethane)s changed according to the molar ratio of the monomers in the copolymer. Small amounts of CL increased the strain of the poly(ester-urethane)s, while at higher CL content the poly(ester-urethane)s exhibited lower strength but higher elongation [50, 62]. By utilizing well-defined four-armed CL–LA precursors that were cross-linked with diisocyanates, a variety of mechanical properties were attained [63].

The low heat deflection temperature of PLA limits its use for several application fields, such as in packaging materials and electronic components. The introduction of rigid building blocks [64] or cross-links [65] is known, for instance, to increase the glass transition temperature and/or heat resistance of LA-based polymers. The effect of different amounts of comonomers in the prepolymers on the $T_g$ and mechanical properties of poly(ester-urethane)s is demonstrated in Table 3.2. The heat resistance of poly(ester-urethane)s can be improved by the copolymerization of LA with D,L-mandelic acid. This broadening of the operating temperature range is of clear practical importance. The incorporation of other comonomers that impede rotation and make polymer chains less mobile also causes an increase in $T_g$, even if the same comonomers can depress the rate of polycondensation [50].

The hydrolysis behavior of amorphous LA-based poly(ester-urethane)s is similar to that of regular PLA, with a typical water absorption and a decrease in molecular weight followed by weight loss at a later stage [66]. The biodegradation of poly(ester-urethane)s has been evaluated in several studies [67]. It has been found that increasing the amount of diisocyanate used as a linking agent increases the biodegradation rate to some extent, which has been explained by an activating effect of a degradation product attributed to the linking agent. All the poly(ester-urethane)s in this study did biodegrade; that is, 90% of the theoretical $CO_2$ was

**TABLE 3.2 Thermal and Mechanical Properties of Poly(ester-urethane)s**

| Composition | Ratio | $T_g$ (°C) | Tensile Strength (MPa) | Strain (%) |
|---|---|---|---|---|
| LA : 1,4-butanediol | 98 : 2 | 53 | 47 ± 2 | 3.7/0.3 |
| LA : CL | 93 : 7 | 35 | 23 ± 3 | 420/20 |
| LA : CL | 63.7 : 36.3 | −5 | 1.6 ± 30.1 | 900/50 |
| LA : DL-mandelic acid : butanediol | 89.1 : 8.9 : 2 | 58 | 34 ± 38 | 1.8/0.4 |
| LA : DL-mandelic acid : butanediol | 78.9 : 19.1 : 2 | 60 | 49 ± 31 | 3.1/0.1 |

produced during six months, as stipulated by the European Committee for Standardization (CEN) for biodegradability of packaging materials [68]. In a further part of the study, the Flash test, which is based on the kinetic measurement of bioluminescence of *Vibrio fischeri*, was applied to evaluate the formation of potentially toxic metabolites in the compost matrix during the biodegradation. The poly(ester-urethane) based on 1,6-hexamethylene diisocyanate produced a toxic response in the test. The poly(ester-urethane) prepared by using 1,4-butane diisocyanate, on the other hand, did not show any toxic effects [67].

### 3.3.2 Chain Extension with Bis-2-Oxazoline

Bis-2-oxazolines were described in the 1960s as useful in the preparation of poly(ester-amide)s and manufacturing processes were later developed, for instance, for chain extension of aromatic polyesters [69, 70]. Bis-2-oxazolines have also been applied in the linking of LA-based prepolymers. Prepolymers with predominantly carboxylic acid termination were linked using 2,2′-bis(2-oxazoline) as chain extender [71]. 2-Oxazolines are inert toward aliphatic alcohols [72] and accordingly react selectively with the carboxyl end group of the prepolyester through ring-opening between positions 1 and 5 of the oxazoline, yielding compounds possessing both amide and ester bonds (Figure 3.5).

***3.3.2.1 Chain-Extension Reaction Parameters*** The molecular weight of the poly(ester-amide) strongly depends on the polymerization temperature and the molar ratio of oxazoline and carboxylic acid end groups [71]. High-molecular-weight polymers can be produced only within a narrow range of polymerization parameters. The amount of 2-oxazoline must be optimized because too high an excess of oxazoline results in a dominant blocking reaction and the hydroxyl end group concentration becomes too high, leading to faster degradation than polymerization. An optimal polymerization was achieved when a molar ratio of end groups of 1.2 : 1.0 (Ox/COOH) at 200°C was used. At lower temperature, the linking reaction is insufficient and at higher temperatures, significant thermal degradation takes place. At optimal conditions, the linking process can be completed in a few minutes [71].

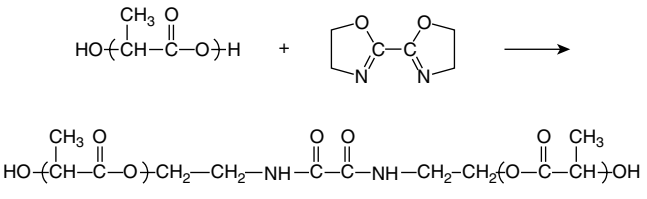

**FIGURE 3.5** Chain-extension reactions of LA-based prepolymers using bis-2-oxazolines.

***3.3.2.2 Properties of Poly(Ester-Amide)s*** Poly(ester-amide)s are, like poly(ester-urethane)s, amorphous polymers, but provide an interesting alternative to other biodegradable polyesters due to the incorporated oxamide linkage in the polyester backbone. This feature equips the polymer with different mechanical properties as well as stability when compared to poly(ester-urethane)s. A slightly higher mechanical strength and lower elongation have their origin in the rigid configuration of the linking agent. The presence of the oxamide linkage affects both the hydrolytic and the thermal stability. The blocking of the terminal groups reduces the melt degradation, and the increased hydrophilicity speeds up the hydrolytic degradation [55, 71, 73]. Poly(ester-amide)s undergo biodegradation well in the time framework stipulated in the norms. The ecotoxicity issue observed for the poly(ester-urethane)s prepared by 1,6-hexamethylenediisocyanate can also be avoided if 2,2′-bis(2-oxazoline) is used as the chain extender [67].

### 3.3.3 Dual Linking Processes

The selective reactivity of oxazolines provides a possibility of performing dual linking processes with both diisocyanates and oxazolines. It has been shown that the order of addition of the linking agent affects both the reaction and the structure of the polymers, for example, the degree of branching. Simultaneous addition of 2,2′-bis(2-oxazoline) and 1,6-hexamethylene diisocyanate results in a slower increase of the molecular weight than does sequential addition. This approach is of particular benefit in the linking of lactic acid prepolymers prepared by polycondensation of solely LA. Prepolymers with a higher molecular weight and lower acid number can be prepared without the addition of a diol. Linking with oxazoline will, in this way, both increase the molecular weight and further reduce the acid number, which will make the subsequent diisocyanate linking more successful and result in higher molecular weight, less thermal degradation, and shorter total reaction times [55]. The LA-based polymers prepared by dual linking with diisocyanates and 2-oxazolines exhibit properties of both poly(ester-urethane)s and poly(ester-amide)s. This, together with the fact that the dual linking process can be used for controlling the branching, opens a wider field of applications, for instance, in applications where the melt flow behavior or the hydrolytic degradation need to be tailored.

### 3.3.4 Chain Extension with Bis-Epoxies

Bis-epoxies have been reported to be useful for chain extending PLA. The epoxy groups can react both with hydroxyl groups and with carboxylic acid groups (Figure 3.6).

However, the latter reaction has been found to be the more rapid one. The opening of the epoxy ring yields a

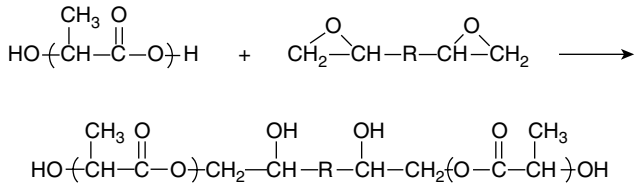

**FIGURE 3.6** Chain-extension reactions of LA-based prepolymers using bis-epoxies.

secondary hydroxyl, but this one does not readily react further with remaining epoxy groups [51].

## 3.4 LACTIC-ACID-BASED POLYMERS BY RING-OPENING POLYMERIZATION

The generally applied ROP process for polylactides involves three separate steps: polycondensation, lactide manufacturing, and ring-opening polymerization (Figure 3.1). All three chemical processes have basically been known for a long time. Carothers et al. [74] did the first observations on the reversible formation of the ring-formed dimer of α-hydroxy acids, and the self-condensation ability of LA was discovered even longer back in time [75]. The results of these pioneering works have later been utilized in further scientific studies, as well as in making and improving technically and economically feasible processes. The three different processes deal with a number of critical steps. Some of these issues are intrinsically present in all the steps of the manufacturing process due to the nature of the LA molecule, while other issues are generated in the separate process steps as a result of the processing conditions. The most crucial parameters are summarized below along with a summary of the harmful effects that can be seen in the PLA:

(a) *Racemization*. The racemization may have its origin in the optical purity of LA or be generated, which is pronounced in any of the process steps. An increased amount of the antipodal structure of the repeating unit will result in drastic changes in the crystallization behavior and eventually affect many other properties of the end products [76, 77].

(b) *Lactide Purity*. The lactide can contain impurities such as acids or oligomers formed during the depolymerization or purification step. The presence of impurities in the lactide and the amount thereof will affect polymerization rate, molecular weight, or both [78].

(c) *Residual Monomer Content*. The presence of residual lactide in the polymer and the amount thereof will have harmful effects on the performance of the polymer during processing and may also cause undesired property changes in the end products [79].

A few complete process descriptions going from LA to polylactide can be found in the literature, for instance, the Cargill process [80], the Inventa Fisher process [81], and the Boehringer process [82]. However, most references are found on newer scientific results and detailed process improvements, which will be discussed in the following sections.

### 3.4.1 Polycondensation Processes

Many technical processes involve esterification reactions, and these have traditionally been of main importance in the preparation of polyesters. Previous chapters have dealt with the preparation of mainly high-molecular-weight LA polymers involving polycondensation. This chapter focuses on processes where the polycondensation is a process step in the ROP polylactide manufacturing chain and the PLA prepared is generally of low molecular weight.

The lactide manufacturing is done by depolymerization of PLA that preferably is in the $M_w$ range of 400–2500 g/mol [83]. Both catalyzed and uncatalyzed polycondensation reactions of LA as such have been known as an industrial process since the 1940s and can be considered to be common knowledge [84]. This explains the fact that not more than a few relevant patents can be found for the polycondensation of LA into low-molecular-weight polymer. The patent literature found is mainly related to other inventions in connection with the polycondensation process, for instance, the use of different catalyst systems, such as solid inorganic catalysts containing alumina silicate [85] or alkali metal compounds [26]. The former reference also provides the conditions for the polycondensation processes in terms of temperature increase (from 105 to 150°C) along with pressure reduction (350–30 mmHg). Further references are related to technical solutions for the polycondensation process. One invention describes the production of an LA polycondensate with a degree of polymerization of 1.59–2.63 and immediately separation of the lactide contained in the polycondensate [86]. Another uses an adiabatic reactor at 120–180°C and has a recycling loop, and it eliminates the water vapor [87]. Two additional references for polycondensation processes focus on improving water removal [88, 89].

### 3.4.2 Lactide Manufacturing

It was earlier mentioned that the reversible lactide formation from polycondensated LA was initially explored by Carothers. He furthermore observed that temperature and pressure could be manipulated for pushing the equilibrium toward the lactide product. This was utilized later for the preparation of lactide, but the presence of other species (e.g., LA, water, lactoyllactic acid, lactoyllactoyllactic acid, and higher oligomers) necessitates further purification of the crude lactide to make it useful for polymerization purposes.

Various technologies for lactide manufacturing are found in the literature. Batch-wise or continuous manufacturing processes have been described, as well as the use of different catalysts [90, 91]. A typical manufacturing process on an industrial scale involves heating PLA to 130–230°C at reduced pressure in the presence of 0.05–1.0 wt% of tin dust, or an organic tin compound derived from a carboxylic acid having up to 20 carbon atoms, in such a way that the produced lactide is distilled off and the PLA is continually or batch-wise replenished [92]. In some processes, a fluid is used to make the separation of lactide more efficient. This can, for instance, be done by stripping off and recovering lactide from a gaseous nonreactive feed containing LA polycondensate [93]. It has been shown that keeping the crude lactide at elevated temperatures above the melting point prior to distillation for several hours will result in an increased LA oligomer content which enables a more efficient purification process [94]. The crude lactide will in most cases contain different impurities that will make the monomer mixture unsuitable for direct ring-opening polymerization as such. The optical purity, acid number, and yield of the lactide will accordingly affect the economy of the manufacturing to a large extent. There are mainly three purification approaches suggested in the literature: solvent-assisted purification, crystallization from the melt, and purification in the gas phase.

***3.4.2.1 Solvent-Assisted Purification*** Solvent-assisted purification has been described in both the scientific and the patent literature. The most commonly used method for purifying lactide is by crystallization from ethyl acetate or from toluene and subsequent drying of the lactide under vacuum [95, 96]. A few industrial processes for manufacturing and purifying lactide from solvents have been described in the patent literature. In one reference, lactide is purified by washing with $C_{4–12}$ ethers [97]. In another approach, lactide is recrystallized in a suitable solvent followed by azeotropic distillation of the solvent [98]. In the third approach, lactide is dissolved in an organic solvent that is immiscible with water, the solution is extracted with water, and the lactide is isolated from the organic solvent [99]. One method utilizes the difference in the hydrolytic degradation rate of *meso*- and L-lactide. The crude lactide is purified in water, whereby the *meso*-lactide is hydrolyzed into lactoyllactic acid and solubilized, whereas the pure L-lactide is crystallized and can be separated [100]. In a more recently described process, the crude lactide in vapor phase is cooled down, collected, and crystallized in a solvent (ethanol or propanol), and the crystals are filtrated. The crystallized lactide is dissolved and recrystallized in a subsequent process step [101].

***3.4.2.2 Melt Crystallization*** The differences in the melting points for D- or L-lactide and the *meso*-lactide can be used for separating the different lactides from each other and from other impurities. Crystallization of lactide from the melt has been described as a three-step industrial process including crystallization–sweating–melting [102]. The process can also be combined with other lactide manufacturing techniques to improve the lactide quality. Another process is described as an integrated process for the manufacture of purified lactide, where the final step requires that the concentrated lactide is subjected to melt crystallization to separate lactide fractions [103].

***3.4.2.3 Separation in the Gas Phase*** The differences in the boiling point of the different lactic acid species can be utilized in the purification of lactide. The most volatile compounds are water and LA; *meso*- and racemic pure lactides are less volatile, and lactic acid oligomers are often in the liquid phase. One purification method employs a gas stream for purification of an impure cyclic ester by passing a gaseous inert substance through the impure cyclic ester in a molten state and removing the gas stream, whereby the purified cyclic ester is recovered from the gas stream [104]. There are several references on lactide distillation processes applied on an industrial scale, and even if the processes are similar, they all have different detailed technical solutions. Some basic differences between the processes described are in many cases found in how the outlet for the purified lactide is arranged. In one method, the liquefied gaseous impurities are separated from the solidified lactide, after which the liquefied impurities are returned to the lactide synthesis step [105]. Another process involves producing pure lactide using a final step of purifying *meso*-lactide from L-lactide and/or D-lactide by distillation to give one *meso*-enriched purified lactide stream and one *meso*-depleted purified lactide stream [106]. A further and improved process uses a partial condensation of the rectified lactide, whereby the low boiling point gaseous fraction remains as a vapor and is discarded. The lactide fraction is condensed and passed in the liquid phase to a distillation column [107].

***3.4.2.4 Separation by Cooling*** In this method, a four-step process is applied. After polycondensation and depolymerization, the depolymerization product is led by a carrier gas, which preferably is nitrogen, through a cooling zone (–78–10°C) into a cold cyclone for separation of unreacted PLA from the mixture of lactide and depolymerization impurities. In the last step, the mixture of lactide and impurities are mixed with water (v/v ratio of 1/0.5–5) to separate lactide in a separation vessel to remove a liquid containing water and impurities formed at the top and to recover only lactide crystals from the bottom. The mixing may be performed at a temperature between 5 and 30°C. The unreacted LA separated can be recycled, and the process may be a continuous cyclic process. The method is advantageous in that the lactide can be obtained at a high yield by a simple method, compared to the above-mentioned conventional production methods [108].

### 3.4.3 Ring-Opening Polymerization

ROP of L-lactide is generally the most preferred route for preparing high-molecular-weight polylactide due to the possibility of an accurate control of the chemistry and thus varying the properties of the resulting polymers in a more controlled manner. This makes ROP well suited for a large-scale process. Polymerizations of lactide have successfully been carried out by using melt polymerization, bulk polymerization, solution polymerization, and suspension polymerization techniques. Each of these methods has its own advantages and disadvantages, but melt polymerization is generally considered the most simple and reproducible method and will be discussed later in detail [109].

***3.4.3.1 Reactor Design*** The simplest type of reactor system is a reaction vessel with an agitator. The number of vessels can vary depending on the desired polymerization conditions [110]. A combination of this type of reactor and a static mixer has also been developed for a continuous polymerization process for preparing polyesters from glycolide, lactide, or CL. The column type of plug-flow reactor is preferably equipped with agitation blades in order to ensure appropriate mixing [111]. A similar concept is described in another patent, but the static mixer here can optionally be linked to an extruder as the final process step [112]. A static mixer for continuous ROP of lactide is described in another US patent. The mixer is equipped with mixing elements designed to enable mixing in both axial and crosswise directions [113]. ROP can also be performed by reactive extrusion, provided that the residence time and catalyst efficiency match [114]. A more recent approach for ROP of lactide is described where the lactide is fed into a first polymerization step (e.g., a stirred vessel or loop-type bubble column) where pre-polymerization takes place. The pre-polymerized product is transferred to a second polymerization reactor where the polymerization step is conducted in a tubular reactor equipped with non-mixing baffles [115]. Another continuous ROP process for cyclic ester monomers has been developed to operate at temperatures between 100 and 240°C by continuously providing cyclic ester monomer and polymerization catalyst to a mixing reactor to form a pre-polymerized reaction mixture, which is transferred to a plug flow reactor where the reaction mixture is polymerized to a degree of polymerization of at least 90% whereafter the polymer is continuously removed from the plug flow reactor [116].

***3.4.3.2 Catalyst Systems*** A vast number of catalysts have been utilized in the ROP of lactide, of which the most studied are the carboxylates and alkoxides of Sn [117–126] and Al [127–133]. Of these, stannous 2-ethylhexanoate (tin octanoate) is the most intensively studied. The polymerization mechanism is believed to involve a preinitiation step, in which stannous 2-ethylhexanoate is converted to a stannous alkoxide by reaction with a hydroxyl-bearing compound. Then, the polymerization proceeds on the tin–oxygen bond of the alkoxide ligand, whereas the carboxylate itself is inactive in the polymerization [120]. Reviews with emphasis on Sn- and Al-catalyzed ring-opening polymerization have been published by Stridsberg et al. [134] and Slomkowski et al. [135]. Some kinetic studies were also included in the reviews. However, the highly active catalysts based on, for example, tin compounds are toxic [136], and efficient catalysts showing less toxicity based on Ca [137–143], Fe [95, 144–154], Mg [155–158], and Zn [158–165] have, therefore, been developed for lactide and lactone polymerization. Many of these, however, tend to cause racemization of PLA, especially when polymerizing at high temperatures. In addition to the aforementioned metals, Kricheldorf et al. [166] used other salts prepared from cations and anions belonging to the human metabolism in the ROP. Zinc lactate was found to be the most efficient of the tested catalysts with regard to reactivity and obtaining high-molecular-weight PLA. More recently, however, a potassium-based catalyst been reported to be more efficient in the ROP of polylactide to high molecular weight [167]. Other catalyst/initiator systems of low-toxicity metals for ROP have been discussed in a study by Okada [168].

Catalysts have been developed for the stereoselective ROP of lactides. In the early publications, semicrystalline PLAs were prepared from both *meso*-lactide (yielding syndiotactic PLA) and racemic lactide (yielding stereoblock isotactic PLA) using chiral aluminum catalysts containing bulky ligands [131, 132, 169]. After annealing, a $T_m$ of 152°C was obtained for the syndiotactic PLA and the racemic PLA was reported to have a $T_m$ of 191°C. The high $T_m$ for the latter PLA was believed to result from stereocomplex formation of synthesized stereoblock PLA. The work using aluminum catalysts in stereoselective polymerization has continued [133, 170–172], and other metal complexes have been utilized as well [158, 164, 173–175]. Many of the studies, though, were conducted only in solution; therefore, the selectivity of the catalyst in, for example, melt polymerization remains unclear. A review including discussion on the stereocontrolled ROP of *rac*- and *meso*-lactides has been published [176].

Metal-free catalysis of ROP was reviewed [177, 178]. Both organocatalytic (nucleophilic, cationic, and bifunctional) and enzymatic approaches were discussed.

***3.4.3.3 Post-Polymerization Treatments*** Post-polymerization treatments for PLA prepared by ROP are strongly related to the processing and processability of the polymer. The processing of PLA is more demanding than that of commodity plastics due to the hygroscopic nature and the limited melt stability that can lead to hydrolytic degradation. The post-polymerization treatments can mainly be divided into those performed in the melt as a finishing process or those

done as a subsequent and independent processing step. Excluded from this review are post-polymerization treatments involving simple polymer modification by the use of processing aids and other additives. The processes performed in the melt that are described in the literature are mainly focusing on improving the melt stability and the processability. Catalyst deactivation is one important feature that has been applied to PLA. Deactivators used include phosphorous-containing compounds [179–181], nitrogen-containing compounds [182], antioxidants [183], acrylic acid derivatives [184], and organic peroxides [185, 186]. The catalyst deactivation is generally performed in combination with a lactide removal process, which can be done by removing the low $M_w$ material at low pressures and at a temperature sufficiently high for distillation (devolatilization) [187, 188]. This process has been further developed by applying an inert gas flow in addition to the reduced pressure, which enables improved removal of the unreacted lactide [189]. The recovery of lactide has also been integrated in the polymerization process of new PLA as a means for improving the efficiency in the manufacturing chain [190]. Another way for reducing the lactide content of PLA is to apply solid-state polymerization of the residual lactide containing PLA below its $T_m$, which besides reducing the residual lactide content also increases the molecular weight of the polymer [191].

Separate post-polymerization treatments of PLA have also been described in the literature. Drying of the polymer is generally done before processing to minimize the thermohydrolysis and molecular weight reduction during the melt processing. Suggested drying conditions for crystallized PLA is in the temperature range of 65–90°C, using dehumidified air with a dew point of −40°C [192]. More recently, the end-of-life options of bio-based polymers have been brought into sustainability discussions. For PLA, this can be seen in the form of a number of suggested approaches on how to deal with waste materials from the polymerization process, the manufacturing process of end products, or the end product after its use. Converting of PLA into lower-molecular-weight polymers has been described, as well as the complete hydrolysis of the polymer into LA for use as new building blocks for either biosolvents or polymers [193–195].

## REFERENCES


1. H. Tsuji, Y. Ikada, *Macromol. Chem. Phys.* **1996**, *197*, 3483–3499.
2. J. Huang, M. S. Lisowski, J. Runt, E. S. Hall, R. T. Kean, N. Buehler, J. S. Lin, *Macromolecules* **1998**, *31*, 2593–2599.
3. A. Södergård, M. Stolt, *Prog. Polym. Sci.* **2002**, *27*, 1123–1163.
4. I. Ajioka, K. Enomoto, K. Suzuki, A. Yamaguchi, *J. Environ. Polym. Degrad.* **1995**, *3*, 225–234.
5. S.-I. Moon, C. W. Lee, I. Taniguchi, M. Miyamoto, Y. Kimura, *Polymer* **2001**, *42*, 5059–5062.
6. K. Hiltunen, M. Härkönen, J. V. Seppälä, T. Väänänen, *Macromolecules* **1996**, *29*, 8677–8682.
7. BCC Research LLC, Staff Report. PLS025G biodegradable polymers: global markets and technologies through 2022, BCC Research, Report Code PLS025G, June 2018, ISBN: 978-1-62296-759-9, 2018.
8. R. K. Kulkarni, K. C. Pani, C. Neuman, F. Leonard, *Arch. Surg.* **1966**, *93*, 839–843.
9. A broad range of standard, custom and specialized biodegradable polymers for medical applications. Available at https//healthcare.evonik.com/en/medical-devices/biodegradable-materials/resomer-portfolio (accessed date 18 April 2021).
10. We make Ingeo, a new material for plastics & fibers with unique properties that all begin with greenhouse gases. Available at https://www.natureworksllc.com (accessed date 5 May 2021).
11. Ingeo in use. Available at https://www.natureworksllc.com/Ingeo-in-Use (accessed date 18 April 2021).
12. Applications & solutions. Available at https://www.total-corbion.com/applications-solutions/ (accessed date 18 April 2021).
13. Bioplastics market data. Available at www.european-bioplastics.org/market/ (accessed date February 16, 2021).
14. About total Corbion PLA. Available at https://www.total-corbion.com/about-total-corbion-pla/ (accessed date 18 April 2021).
15. Total Corbion PLA announces the first world-scale PLA plant in Europe. Available at https://www.total-corbion.com/news/total-corbion-pla-announces-the-first-world-scale-pla-plant-in-europe/ (accessed date 18 April 2021).
16. *Bioplastics Magazine* **2020**, *15*(4), 24–25.
17. K. K. Jem, B. Tan, *Adv. Ind. Eng. Polym. Res.* **2020**, *3*, 60–70.
18. *Bioplastics Magazine* **2017**, *12*(04), 36–37.
19. S. Kéki, I. Bodnár, J. Borda, G. Deák, M. Zsuga, *J. Phys. Chem. B* **2001**, *105*, 2833–2836.
20. N. M. Qureshi, B. Woodfine, EP 0,937,743, 1999 (to Kobe Steel).
21. A. Duda, S. Penczek, *Macromolecules* **1990**, *23*, 1636–1639.
22. D. K. Yoo, D. Kim, D. S. Lee, *Macromol. Res.* **2005**, *13*, 68–72.
23. Y. M. Harshe, G. Storti, M. Morbidelli, S. Gelosa, D. Moscatelli, *Macromol. Symp.* **2007**, *259*, 116–123.
24. G. X. Chen, H. S. Kim, E. S. Kim, J. S. Yoon, *Eur. Polym. J.* **2006**, *42*, 468–472.
25. S.-I. Moon, C. W. Lee, M. Miyamoto, Y. Kimura, *J. Polym. Sci. Part A* **2000**, *38*, 1673–1679.
26. H. Maruyama, T. Murayama, N. Yanagisawa, N. Tsuzaki, EP 0,848,026, 1998 (to Kyowa Yuka).
27. Y. H. Kim, K. D. Ahn, Y. K. Han, S. H. Kim, J. B. Kim, U.S. Patent 5,434,241, 1995 (to Korea Institute of Science and Technology).

28. A. Södergård, M. Stolt, EP 1,525,249, 2005 (to Tate & Lyle Public Limited Co.).
29. N. Yanagisawa, T. Nezu, K. Hotta, T. Murayama, N. Tsuzaki, S. Kodama, H. Maruyama, Y. Yokomori, EP 0,823,448, 1998 (to Kyowa Hakko Kogyo).
30. K. Miyazaki, H. Noguchi, T. Ota, A. Kasai, H. Yamaoka, EP 0,792,901, 1997 (to Mitsubishi).
31. S.-I. Moon, I. Taniguchi, M. Miyamoto, Y. Kimura, C. W. Lee, *High Perform. Polym.* **2001**, *13*, 189–196.
32. Y. Terado, H. Suizu, M. Takagi, M. Ajioka, S. Hiraoka, M. Sakai, H. Suzuki, R. Shinagawa, S. Ogawa, Y. Kotaki, EP 0,953,589, 1999 (to Mitsui Chemicals).
33. S. Hiraoka, H. Tsuboi, M. Sakai, EP 1,114,840, 2001 (to Mitsui Chemicals).
34. K. Fukushima, Y. Furuhashi, K. Sogo, S. Miura, Y. Kimura, *Macromol. Biosci.* **2005**, *5*, 21–29.
35. K. Fukushima, Y. Kimura, *Macromol. Symp.* **2005**, *224*, 133–143.
36. H. Xu, M. Luo, M. Yu, C. Teng, S. J. Xie, *Macromol. Sci. Part B* **2006**, *45*, 681–687.
37. K. Enomoto, M. Ajioka, A. Yamaguchi, EP 0,572,675, 1993 (to Mitsui Chemicals).
38. K. Goto, Y. Mori, M. Miyamoto, EP 0,826,711, 1998 (to Mitsui Chemicals).
39. M. Ohta, S. Obuchi, Y. Yoshida, EP 0,603,889, 1994 (to Mitsui Chemicals).
40. M. Ajioka, K. Enomoto, K. Suzuki, A. Yamaguchi, *Bull. Chem. Soc. Jpn.* **1995**, *68*, 2125–2131.
41. S. Tamai, Y. Mori, K. Goto, K. Watanabe, O. Kohgo, K. Shimizu, T. Kataoka, T. Kuroki, W. Yamashita, H. Mizuta, T. Nagata, EP 0,769,512, 1997 (to Mitsui Chemicals).
42. Y. Terado, H. Suizu, C. Higuchi, M. Ajioka, EP 0,829,503, 1998 (to Mitsui Chemicals).
43. K. Hiltunen, J. V. Seppälä, M. Härkönen, *J. Appl. Polym. Sci.* **1997**, *63*, 1091–1100.
44. C. J. Spaans, J. H. de Groot, F. G. Dekens, A. J. Pennings, *Polym. Bull.* **1998**, *41*, 131–138.
45. Y. Liu, M. Söderqvist-Lindblad, E. Ranucci, A. C. Albertsson, *J. Polym. Sci. Part A* **2001**, *39*, 630–639.
46. Y. Di, S. Iannace, E. Di Maio, L. Nicolais, *Macromol. Mater. Eng.* **2005**, *290*, 1083–1090.
47. W. Zhong, J. Ge, Z. Gu, W. Li, X. Chen, Y. Zang, Y. Yang, *J. Appl. Polym. Sci.* **1999**, *74*, 2546–2551.
48. K. Hiltunen, J. V. Seppälä, M. Härkönen, *J. Appl. Polym. Sci.* **1997**, *64*, 865–873.
49. P. Bruin, G. J. Veenstra, A. J. Nijenhuis, A. J. Pennings, *Macromol. Chem. Rapid Commun.* **1988**, *9*, 589–594.
50. J. Kylmä, M. Härkönen, J. V. Seppälä, *J. Appl. Polym. Sci.* **1997**, *63*, 1865–1872.
51. P. Bonsignore, U.S. Patent 5,470,944, 1995 (to Arch Dev Corp.).
52. E. Ranucci, Y. Liu, M. Söderqvist-Lindblad, A. C. Albertsson, *Macromol. Rapid. Commun.* **2000**, *21*, 680–684.
53. C. J. Spaans, V. W. Belgraver, O. Rienstra, J. H. de Groot, R. P. H. Veth, A. J. Pennings, *Biomaterials* **2000**, *21*, 2453–2460.
54. J. V. Seppälä,M. Härkönen, K. Hiltunen, M. Malin, J. Kylmä, PCT/WO 9601863, 1996 (to Alko Group Ltd.; Neste Oy).
55. J. Kylmä, J. Tuominen, A. Helminen, J. V. Seppälä, *Polymer* **2001**, *42*, 3333–3343.
56. A. C. Draye, J. J. Tondeur, *J. Mol. Catal. A: Chem.* **1999**, *138*, 135–144.
57. A. Helminen, J. Kylmä, J. Tuominen, J. V. Seppälä, *Polym. Eng. Sci.* **2000**, *40*, 1655–1662.
58. M. Stolt, K. Hiltunen, A. Södergård, *Biomacromolecules* **2001**, *2*, 1243–1248.
59. D. W. Grijpma, G. J. Zondervan, A. J. Pennings, *Polym. Bull.* **1991**, *25*, 327–333.
60. M. E. Broz, D. L. var der Hart, N. L. Washburn, *Biomaterials* **2003**, *24*, 4181–4190.
61. N. Ljungberg, B. Wesslen, *J. Appl. Polym. Sci.* **2002**, *86*, 1227–1234.
62. J. Kylmä, J. V. Seppälä, *Macromolecules* **1997**, *30*, 2876–2882.
63. H. Tsuji, K. Tamura, Y. Arakawa, *RSC Adv.* **2019**, *9*, 7094–7106.
64. S. Inkinen, A. Södergård, M. Stolt, PCT/WO 2,008,056,136, 2008 (to Tate & Lyle Public Limited Co.).
65. D. W. Grijpma, E. Kroeze, A. J. Nijenhuis, A. J. Pennings, PCT/WO 9,313,154, 1993 (to DSM N.V.).
66. K. Hiltunen, J. Tuominen, J. V. Seppälä, *Polym. Int.* **1998**, *47*, 186–192.
67. J. Tuominen, J. Kylmä, A. Kapanen, O. Venelampi, M. Itävaara, J. V. Seppälä, *Biomacromolecules* **2002**, *3*, 445–455.
68. CEN 13432; European Standardization Committee, 2000. Packaging – Requirements for Packaging Recoverable Through Composting and Biodegradation – Test Scheme and Evaluation Criteria for the Final Accepance of Packaging.
69. K. Fukui, T. Kagiya, S. Narisawa, T. Maeda, GB 1,117,798, 1969 (to Sunimoto Chemical Co. Ltd.).
70. H. Inata, S. Matsumura, M. Ogasawara, EP 0,020,944, 1981 (to Teijin Ltd.).
71. J. Tuominen, J. V. Seppälä, *Macromolecules* **2000**, *33*, 3530–3535.
72. R. Po, L. Abis, L. Fiocca, R. Masani, *Macromolecules* **1995**, *28*, 5699–5705.
73. J. Tuominen, J. Kylmä, J. V. Seppälä, *Polymer* **2002**, *43*, 3–10.
74. W. H. Carothers, G. L. Dorough, F. J. van Natta, *J. Am. Chem. Soc.* **1932**, *54*, 761–772.
75. J. Pelouze, *Ann. Chemie* **1845**, *8*, 112–124.
76. D. W. Grijpma, A. J. Pennings, *Macromol. Chem. Phys.* **1994**, *195*, 1649–1663.
77. J. J. Kolstad, *J. Appl. Polym. Sci.* **1996**, *62*, 1079–1091.
78. X. Zhang, D. A. Macdonald, M. F. A. Goosen, K. B. Mcauley, *J. Polym. Sci. Part A* **1994**, *32*, 2965–2970.

79. S. Jacobsen, H. G. Fritz, P. Degée, P. Dubois, R. Jérôme, *Polymer* **2000**, *41*, 3395–3403.
80. J. J. Kolstad, D. R. Witzke, M. H. Hartmann, E. S. Hall, J. F. Nageroni, PCT/WO 9,950,345, 1999 (to Cargill Inc.).
81. L. Gerking, R. Hagen, K. Richter, F. Idler, W. Reimann, B. Hanzsch, PCT/WO 0,181,610, 2001 (to Inventa-Fisher GmbH).
82. D. Reichert, F.-D. Klingler, H. Schwall, A. Christmann, B. Buchholz, EP 0,372,221, 1990 (to Boehringer Ingelheim Pharma KG).
83. P. Gruber, E. Hall, J. Kolstad, M. Iwen, R. Benson, R. Borchardt, PCT/WO 9,509,879, 1995 (to Cargill Inc.).
84. P. D. Watson, *Ind. Eng. Chem.* **1948**, *40*, 1393–1397.
85. M. Tanaka, Y. Ogawa, T. Miyagawa, T. Watanabe, EP 0,172,636, 1986 (to Wako Pure Chem. Ind. Ltd.).
86. R. Sinclair, R. Markle, R. Smith, EP 0,552,226, 1993 (to Biopak Technology Ltd.).
87. R. Teissier, S. Tretjak, E. Burtin, PCT/WO 03,066,187, 2003 (to Atofina).
88. H. Maeda, K. Shimizu, Y. Kurishiru, E. Kawada, K. Fujisawa, EP 0,808,861, 1997 (to Kobe Steel Ltd.).
89. K. K. Bhatia, N. E. Drysdale, K. Lin, R. S. Nash, T. W. Stambaugh, PCT/WO 9,317,993, 1993 (to Du Pont).
90. M. Mueller, DE 3,632,103, 1988 (to Boehringer Ingelheim).
91. H. E. Bellis, K. K. Bhatia, WO 92/00292, 1992 (to Du Pont).
92. M. Mueller, DE 3,708,915, 1988 (to Boehringer Ingelheim).
93. K. K. Bhatia, EP 0,531,458, 1993 (to Du Pont).
94. J.J. De Vries, A.I. Cavaco Morao, A.B. De Haan, EP 3,288,930, 2018 (to Purac Biochem BV).
95. M. Stolt, A. Södergård, *Macromolecules* **1999**, *32*, 6412–6417.
96. J. W. Leenslag, A. J. Pennings, *Makromol. Chem.* **1987**, *188*, 1809–1814.
97. P. Hoessel, G. Hoffmann, F. Braun, D. Kratz, M. Brudermueller, T. Witzel, EP 0,588,222, **1994** (BASF AG).
98. P. Degee, P. Coszack, BE 1008099, 1996 (to Brussels Biotech SA).
99. K. S. de Vries, EP 0,275,581, 1988 (to Akzo NV).
100. K. Hiltunen, J. V. Seppälä, FI 105185, 1999 (to JVS Polymers Oy).
101. D.V. Wang, J. S. Chang, Y. K. Hwang, U. H. Lee, D. Y. Hong, S. K. Lee, K. H. Cho, P. P. Upare, US Patent 10,253,012, 2019 (to Korea Research Institute of Chemical Technology).
102. M. Stepanski, *First PLA World Congress*, Munich, 9–10 September 2008.
103. W. G. O'Brian, L. A. Cariello, T. F. Wells, EP 0,777,664, 1997 (to Ecological Chem. Prod.).
104. K. K. Bhatia, EP 0,531,462, 1993 (to Du Pont).
105. H. Ohara, M. Ogaito, DE 19,631,633, 1998 (to Shimadzu Corp.).
106. P. Gruber, E. Hall, J. Kolstad, M. Iwen, R. Benson, R. Borchardt, EP 1,247,808, 2002 (to Cargill Inc.).
107. M. Meerdink, A. Södergård, EP 1,694,626, 2005 (to Tate & Lyle Public Limited Co.).
108. D. S. Han, C. H. Hong, Hyundai Motor Co Ltd, S. H. Kim, J. Y. Seo, US Patent 2,012,302,724, 2012 (to Hyundai Motor Co).
109. A. J. Nieuwenhuis, *J. Clin. Mater.* **1992**, *10*, 59–67.
110. H. Ebato, S. Imamura, EP 0,661,325, 1995 (to Dainippon Ink and Chem.).
111. T. Iiyama, T. Sato, M. Yamada, EP 0,916,684, 1999 (to Daicel Chem.).
112. H. Ebato, S. Oya, Y. Kakizawa, H. Furuta, K. Arai, EP 0,618,250, 1994 (to Dainippon Ink and Chem.).
113. T. Morio, K. Yasutoshi, U.S. Patent 5,484,882, 1996 (to Dainippon Ink and Chem.).
114. S. Jacobsen, Darstellung von polylactiden mittels reaktiver extrusion, Ph.D. thesis, Universität Stuttgart, Germany, 2000.
115. R. Hagen, U. Muhlbauer, EP 2,188,047, 2012 (to Uhde Inventa Fischer GmbH).
116. R.E. Haan, P.P. Jansen, S.C. De Vos, J. Van Breugel, P.W. Kreis, S. Lanfranchi, EP 2,310,437, 2015 (to Purac Biochem BV, Sulzer Chemtech AG).
117. A. J. Nijenhuis, D. W. Grijpma, A. J. Pennings, *Macromolecules* **1992**, *25*, 6419–6424.
118. J. Dahlmann, G. Rafler, *Acta Polym.* **1993**, *44*, 103–107.
119. H. R. Kricheldorf, I. Kreiser-Saunders, C. Boettcher, *Polymer* **1995**, *36*, 1253–1259.
120. A. Kowalski, A. Duda, S. Penczek, *Macromolecules* **2000**, *33*, 7359–7370.
121. A. Kowalski, J. Libiszowski, A. Duda, S. Penczek, *Macromolecules* **2000**, *33*, 1964–1971.
122. H. R. Kricheldorf, I. Kreiser-Saunders, A. Stricker, *Macromolecules* **2000**, *33*, 702–709.
123. K. Stridsberg, M. Ryner, A. C. Albertsson, *Macromolecules* **2000**, *33*, 2862–2869.
124. M. Ryner, A. Finne, A. C. Albertsson, H. R. Kricheldorf, *Macromolecules* **2001**, *34*, 7281–7287.
125. K. B. Aubrecht, M. A. Hillmyer, W. B. Tolman, *Macromolecules* **2002**, *35*, 644–650.
126. H. R. Kricheldorf, B. Fechner, *Biomacromolecules* **2002**, *3*, 691–695.
127. P. Dubois, C. Jacobs, R. Jérôme, P. Teyssié, *Macromolecules* **1991**, *24*, 2266–2270.
128. A. Kowalski, A. Duda, S. Penczek, *Macromolecules* **1998**, *31*, 2114–2122.
129. P. Degée, P. Dubois, R. Jérôme, S. Jacobsen, H.-G. Fritz, *Macromol. Symp.* **1999**, *144*, 289–302.
130. J. L. Eguiburu, M. J. Fernandez-Berridi, J. San Roman, *Polymer* **2000**, *41*, 6439–6445.
131. T. M. Ovitt, G. W. Coates, *J. Polym. Sci. Part A* **2000**, *38*, 4686–4692.
132. C. P. Radano, G. L. Baker, M. R. Smith, *J. Am. Chem. Soc.* **2000**, *122*, 1552–1553.
133. Z. Zhong, P. J. Dijkstra, J. Feijen, *J. Am. Chem. Soc.* **2003**, *125*, 11291–11298.
134. K. M. Stridsberg, M. Ryner, A. C. Albertsson, *Adv. Polym. Sci.* **2002**, *157*, 41–65.

135. S. Slomkowski, S. Penczek, A. Duda, *Polym. Adv. Technol.* **2014**, *25*, 436–447.
136. M. C. Tanzi, P. Verderio, M. G. Lampugnani, M. Resnati, E. Dejana, E. Sturani, *J. Mater. Sci. Mater. Med.* **1994**, *5*, 393–396.
137. P. Dobrzynski, J. Kasperczyk, M. Bero, *Macromolecules* **1999**, *32*, 4735–4737.
138. Z. Zhong, M. J. K. Ankoné, P. J. Dijkstra, C. Birg, M. Westerhausen, J. Feijen, *Polym. Bull.* **2001**, *46*, 51–57.
139. Z. Zhong, P. J. Dijkstra, C. Birg, M. Westerhausen, J. Feijen, *Macromolecules* **2001**, *34*, 3863–3868.
140. Z. Zhong, S. Schneiderbauer, P. J. Dijkstra, M. Westerhausen, J. Feijen, *J. Polym. Environ.* **2001**, *9*, 31–38.
141. L. Piao, M. Deng, X. Chen, L. Jiang, X. Jing, *Polymer* **2003**, *44*, 2331–2336.
142. Z. Zhong, S. Schneiderbauer, P. J. Dijkstra, M. Westerhausen, J. Feijen, *Polym. Bull.* **2003**, *51*, 175–182.
143. D. J. Darensbourg, W. Choi, O. Karroonnirun, N. Bhuvanesh, *Macromolecules* **2008**, *41*, 3493–3502.
144. H. R. Kricheldorf, A. Serra, *Polym. Bull.* **1985**, *14*, 497–502.
145. H. R. Kricheldorf, C. Boettcher, *Macromol. Chem.* **1993**, *194*, 463–473.
146. A. Nakayama, N. Kawasaki, I. Arvanitoyannis, J. Iyoda, N. Yamamoto, *Polymer* **1995**, *36*, 1295–1301.
147. I. Arvanitoyannis, A. Nakayama, E. Psomiadou, N. Kawasaki, N. Yamamoto, *Polymer* **1996**, *37*, 651–660.
148. H. R. Kricheldorf, D. O. Damrau, *Macromol. Chem. Phys.* **1997**, *198*, 1767–1774.
149. A. Södergård, M. Stolt, *Macromol. Symp.* **1998**, *130*, 393–402.
150. A. Södergård, M. Stolt, EP 0,937,116, 1998 (to Fortum Oyj).
151. M. Stolt, K. Jalander, A. Södergård, *Polym. Prepr.* **1999**, *40*(2), 675–676.
152. B. J. O'Keefe, S. M. Monnier, M. A. Hillmyer, W. B. Tolman, *J. Am. Chem. Soc.* **2001**, *123*, 339–340.
153. P. Dobrzynski, J. Kasperczyk, H. Janeczek, M. Bero, *Polymer* **2002**, *43*, 2595–2601.
154. B. J. O'Keefe, L. E. Breyfogle, M. A. Hillmyer, W. B. Tolman, *J. Am. Chem. Soc.* **2002**, *124*, 4384–4393.
155. R. Dunsing, H. R. Kricheldorf, *Polym. Bull.* **1985**, *14*, 491–495.
156. H. R. Kricheldorf, S.-R. Lee, *Polymer* **1995**, *36*, 2995–3003.
157. J. Kasperczyk, M. Bero, *Polymer* **2000**, *41*, 391–395.
158. B. M. Chamberlain, M. Cheng, D. R. Moore, T. M. Ovitt, E. B. Lobkovsky, G. W. Coates, *J. Am. Chem. Soc.* **2001**, *123*, 3229–3238.
159. M. Bero, J. Kasperczyk, Z. J. Jedlinski, *Makromol. Chem.* **1990**, *191*, 2287–2296.
160. M. Bero, J. Kasperczyk, G. Adamus, *Makromol. Chem.* **1993**, *194*, 907–912.
161. G. Schwach, J. Coudane, R. Engel, M. Vert, *Polym. Bull.* **1994**, *32*, 617–623.
162. G. Schwach, J. Coudane, R. Engel, M. Vert, *Polym. Int.* **1998**, *46*, 177–182.
163. E. Bukhaltsev, L. Frish, Y. Cohen, A. Vigalok, *Org. Lett.* **2005**, *7*, 5123–5126.
164. T. R. Jensen, C. P. Schaller, M. A. Hillmyer, W. B. Tolman, *J. Organomet. Chem.* **2005**, *690*, 5881–5891.
165. H. Y. Chen, H. Y. Tang, C. C. Lin, *Macromolecules* **2006**, *39*, 3745–3752.
166. H. R. Kricheldorf, I. Kreiser-Saunders, D.-O. Damrau, *Macromol. Symp.* **1999**, *144*, 269–276.
167. Y. Lemmouchi, M. C. Perry, A. J. Amass, K. Chakraborty, E. Schacht, *J. Polym. Sci. Part A* **2008**, *46*, 5348–5362.
168. M. Okada, *Prog. Polym. Sci.* **2002**, *27*, 87–133.
169. T. M. Ovitt, G. W. Coates, *J. Am. Chem. Soc.* **1999**, *121*, 4072–4073.
170. K. Majerska, A. Duda, *J. Am. Chem. Soc.* **2004**, *126*, 1026–1027.
171. P. Hormnirun, E. L. Marshall, V. C. Gibson, A. J. P. White, D. J. Williams, *J. Am. Chem. Soc.* **2004**, *126*, 2688–2689.
172. Z. Tang, X. Chen, Y. Yang, X. Pang, J. Sun, X. Zhang, X. Jing, *J. Polym. Sci. Part A* **2004**, *42*, 5974–5982.
173. M. H. Chisholm, J. C. Gallucci, K. Phomphrai, *Inorg. Chem.* **2004**, *43*, 6717–6725.
174. M. H. Chisholm, J. C. Gallucci, K. Phomphrai, *Inorg. Chem.* **2005**, *44*, 8004–8010.
175. S. K. Russell, C. L. Gamble, K. J. Gibbins, K. C. S. Juhl, W. S. Mitchell III, A. J Tumas, G. E. Hofmeister, *Macromolecules* **2005**, *38*, 10336–10340.
176. S. Dutta, W.-C. Hung, B.-H. Huang, C.-C. Lin, *Adv. Polym. Sci.* **2012**, *245*, 219–284
177. D. Bourissou, S. Moebs-Sanchez, B. Martin-Vaca, *C. R. Chimie* **2007**, *10*, 775–794.
178. J. Pretula, S. Slomkowski, S. Penczek, *Adv. Drug Deliv. Rev.* **2016**, *107*, 3–16.
179. D. A. Rothrock and R. F. Conyne, GB 588834, 1947 (to Resinous Prod. & Chemical Co.).
180. N. A. Higgins, U.S. Patent 2,683,136, 1954 (to Du Pont).
181. T. Kusunoki, T. Unrinin, O. Morimoto, US Patent 8,642,717, 2014 (to Toyo Boseki).
182. G. Gobius du Sart, W. de Lang, WO 2020245063, 2020 (to Total Corbion PLA bv).
183. P. Gruber, J. J. Kolstad, E. S. Hall, R. S. E. Conn, EP 0,615,532, 2000 (to Cargill Inc.).
184. J. J. Kolstad, D. R. Witzke, M. H. Hartmann, E. S. Hall, J. F. Nageroni, EP 1,070,097, 2001 (to Cargill Inc.).
185. A. Södergård, J.-F. Selin, M. Niemi, C.-J. Johansson, K. Meinander, EP 0,737,219, 1999 (to Fortum Oyj).
186. S. C. de Vos, EP 2,271,696, 2012 (to Purac Biochem bv).
187. D. G. Lowrance, U.S. Patent 1,995,970, 1935 (to Du Pont).
188. P. Gruber, J. J. Kolstad, C. Ryan, EP 0,615,529, 1994 (to Cargill Inc.).
189. H. Ohara, S. Sawa, M. Ito, Y. Fujii, M. Oota, H. Yamaguchi, U.S. Patent 5,770,682, 1998 (to Shimadzu Corp.).
190. H. Ohara, T. Okamoto, U.S. Patent 5,728,847, 1998 (to Shimadzu Corp.).

191. H. Ohara, S. Sawa, T. Kawamoto, EP 0,664,309, 1995 (to Shimadzu Corp.).
192. Crystallizing and Drying of PLA, NatureWorks LLC, available at https://www.natureworksllc.com/~/media/Files/NatureWorks/Technical-Documents/Processing-Guides/ProcessingGuide_Crystallizing-and-Drying_pdf.pdf (accessed date 23 February 2021).
193. F. G. Hutchinson, EP 0,244,114, 1987 (to ICI PLC).
194. K. Yamamoto, T. Tani, T. Aoki, Y. Hata, EP 1,310,517, 2003 (to Wako Pure Chem. Ind. Ltd.; Tadeka Chem. Ind. Ltd.).
195. E. Feghali, L. Tauk, P. Ortiz, K. Vanbroekhoven, W. Eevers, *Polym. Degrad. Stab.* **2020**, *179*, 109241.

# 4

# DESIGN AND SYNTHESIS OF DIFFERENT TYPES OF POLY(LACTIC ACID)/POLYLACTIDE COPOLYMERS

Ann-Christine Albertsson, Indra Kumari Varma, Bimlesh Lochab, Anna Finne-Wistrand, Sangeeta Sahu, and Kamlesh Kumar

## 4.1 INTRODUCTION

High molar mass poly(lactic acid) (PLA) is obtained by either the polycondensation of lactic acid or ring-opening polymerization (ROP) of the cyclic dimer 2,6-dimethyl-1,4-dioxane-2,5-dione, commonly referred to as dilactide or lactide (LA). The stereochemistry of LA plays a crucial role in dictating the properties of the polymers which have already been described in earlier chapters (Chapters 1 and 3).

L-Lactide (LLA) is prepared with relatively high enantiopurity from corn starch fermentation, which polymerized to form poly(L-lactide) (PLLA). PLLA is a versatile, semicrystalline, degradable polymer with a relatively high melting ($T_m$) and glass transition temperature ($T_g$). PLLA has mechanical properties which makes it interesting for many applications such as degradable plastic for disposable consumer products [1–3]. It is also of interest in medical applications [4], due to its favorable interactions with the cells. PLLA is also explored as a degradable scaffold where the transplanted cells could remold their intrinsic tissue superstructural organization, and thereby led to the desirable three-dimensional structure and physiological functionality of a regenerated organ [5]. However, certain shortcomings of PLLA may need to be overcome to extend its applications. In particular, high crystallinity [6], brittle behavior with a very-low elongation at break value, and the hydrophobic nature of the polymer demands a long degradation time. The properties of PLLA are tailored by copolymerization (random, block, and graft), change in molecular architecture (hyperbranched polymers, star shaped, or dendrimers), introduction of polar groups such as carboxyl, amino, or thiol-based via end group or main-chain functionalization, or blending with other polymers. Physical properties, such as $T_g$, $T_m$, crystallinity, hydrophobicity, and mechanical properties are significantly affected by such modifications. Furthermore, functionalization of PLLA can provide specific bio-interactions with cells, which is specifically needed in tissue engineering. Several reviews have summarized how functionalization of lactide and copolymerization with other hydroxyl-acid-based monomers influence the properties and applications of the resultant copolymers [5, 7–15]. In this chapter, preparation of polymers and copolymers of LAs with different structures, using polycondensation and ROP, is described. The influence of macromolecular structure and composition on the properties of structurally modified polymers is also discussed. The stereocopolymers of LA prepared by the polymerization of various stereoisomers are discussed in a subsequent section in this book and will not be discussed here.

Typical comonomers and polymers which are used for lactic acid or LA copolymerization include glycolic acid or glycolide (GA) [16–22], poly(ethylene glycol) (PEG) or poly(ethylene oxide) (PEO) [17, 18, 21, 23–42], poly(propylene oxide) (PPO) [43, 44], β-butyrolactone (BL) [45–48], δ-valerolactone (VL) [49, 50], ε-caprolactone (CL) [22, 51–58], 1,5-dioxepan-2-one (DXO) [59–64], *p*-dioxanone [65–70], trimethylene carbonate (TMC) [58, 71], and *N*-isopropylacrylamide (NIPAAm) [41, 72–74]. The structures of some of these comonomers are given in Figure 4.1 [22, 42]. Monomer distribution (random or block)

*Poly(Lactic Acid): Synthesis, Structures, Properties, Processing, Applications, and End of Life*, Second Edition.
Edited by Rafael A. Auras, Loong-Tak Lim, Susan E. M. Selke, and Hideto Tsuji.

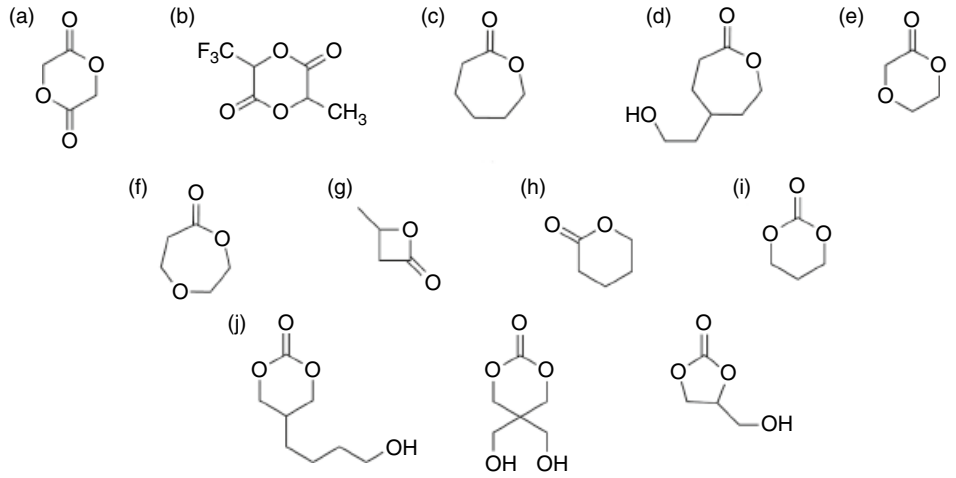


**FIGURE 4.1** Structures explored as comonomers with lactide monomer. (a) GA, (b) flourine substituted lactide monomer, (c) CL, (d) hydroxyl functionalized CL, (e) *p*-dioxanone, (f) DXO, (g) BL, (h) VL, (i) TMC, (j) hydroxyl functionalized cyclic carbonate derivatives.

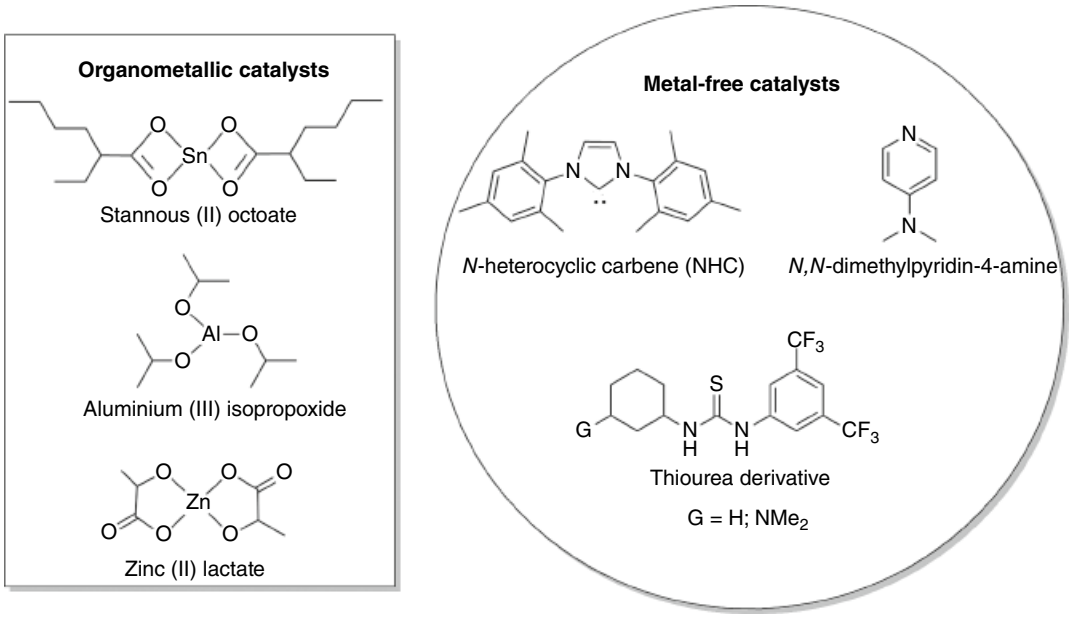


**FIGURE 4.2** Structures of catalysts used in lactide polymerization.

in the copolymers depends on the reactivity of monomer pairs, nature of the catalysts, and polymerization conditions.

Various catalysts and initiators used for ROP of LA monomers/comonomers are shown in Figure 4.2. Organometallic compounds such as stannous octoate $Sn(Oct)_2$, aluminum isopropoxide [75], and zinc salt [76] as oxides, carboxylates, and alkoxides are reported as effective catalysts/initiators for polymerization reaction. Among all catalysts, $Sn(Oct)_2$ is usually preferred as it mediates ROP reaction at a faster rate. However, resultant polymer showed a lower molar mass than when reaction was catalyzed by zinc metal or zinc lactate [13, 77]. $Sn(Oct)_2$ allows formation of atactic PLAs with well controlled architecture, linear and star shape, and that too with high efficiency. Despite the usage of high temperature (usually 140°C) and/or high pressure, $Sn(Oct)_2$ allows low percentage racemization [78]. Zn-catalyzed PLA exhibited higher hydrophilicity and degradation susceptibility than the Sn-mediated polymerization [19]. A partial esterification of alcohol chain ends in PLA by an octanoyl group is reported in $Sn(Oct)_2$ catalyzed polymerization reaction [79]. While in case of Zn, occurrence of an extra lactoyl group is likely observed [80].

Metallic salts can either be used alone or along with a co-initiator (water or alcohol) to affect polymerization of LA. Presence of co-initiators mainly alcohols allowed formation of different molecular architecture and controlled growth of

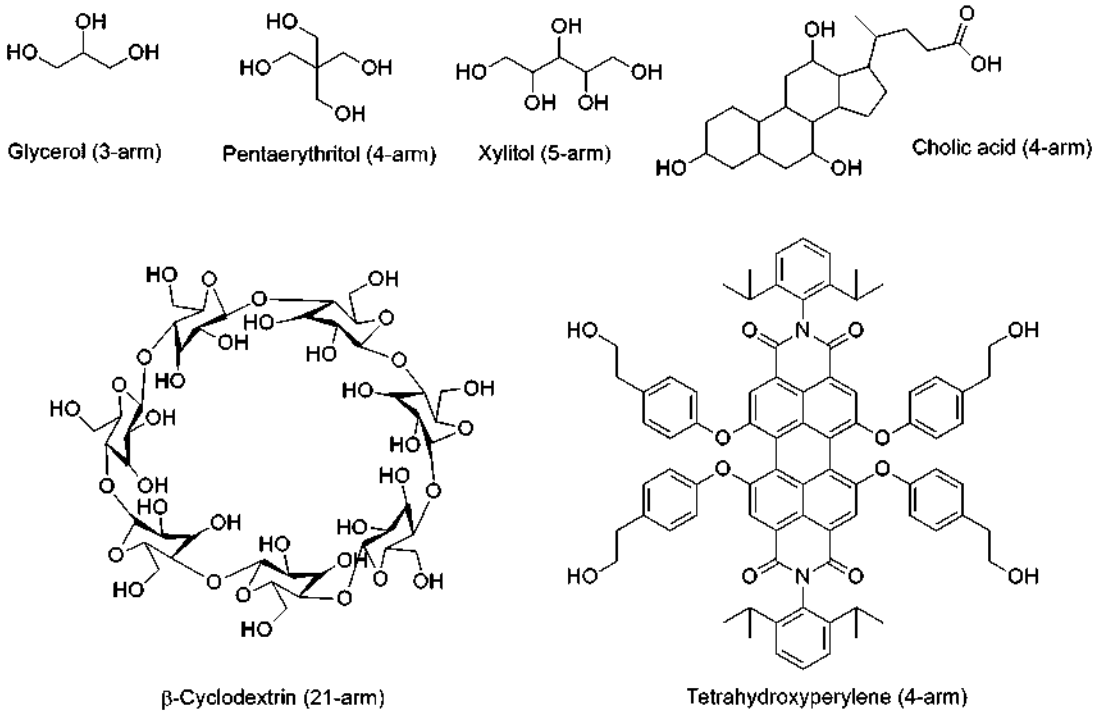


**FIGURE 4.3** Polyol cores used for synthesis of different architecture in lactide-based copolymers/polymers.

both the pristine and copolymers based on PLA. They form the cores, thus allows a different architectural growth of polymer in space. It is considered as an effective synthetic approach to tune the macromolecular structure of PLLA and thus the resultant polymer showed significantly different physical properties than that obtained otherwise. Linear to branched to star-shaped [81] polyol co-initiators utilized in LA polymerization are shown in Figure 4.3.

There are many examples of biocompatible and FDA-approved (Food and Drug Administration) medical devices, which contain polymers composed of LA with or without other comonomers. They may find utility in various commercial products ranging from surgical sutures, tissue engineering scaffolds to drug delivery systems [82]. Normally, $Sn(Oct)_2$ is used as catalyst during the polymerization, but utility of zinc lactate is also reported [13, 19, 77]. A Sn residue of 306 ppm is detected in PLA [77]. $Sn(Oct)_2$ itself has been found to be slightly cytotoxic, and it is reported that $Sn(Oct)_2$ is considered harmful at a dietary level of 0.1% [18, 83]. When polymerization reaction is pursued using high catalyst to monomer ratios, residues such as ethyl-2-hexanoic acid or hydroxy tin octanoate or tin oxide [79] are detected. However, such impurities can alternatively be removed by repeated dissolution and precipitation of polymer and/or in combination with other purification techniques. With the raising environmental and health concerns and knowing traces of metal-related toxicity in polymers, organo- or enzymatic-catalyzed polymerization reactions appeared as a safe and attractive alternative to metal-catalyzed systems. Organo- and enzymatic catalysis are comparatively nontoxic, mild, and eco-friendly in nature [84–86]. Unlike usual metallic catalysts (Sn, Zn, Ti, etc.), organocatalysts containing non-oxophilic moieties allow their easier removal, especially during the synthesis of oxygen-atom-rich polymers [87]. In general, organic catalysts being miscible within the monomer may allow a better control in polymerization conditions and thus provide avenues to modulate the copolymer composition. For example, combination of organocatalyst such as Brønsted acid (DPP, diphenylphosphate) and Brønsted base (DBU, 8-diazabicyclo[5.4.0]undec-7-ene) assist ROP of different type of monomers in one pot to form sequence controlled multiblock copolymers such as poly(VL-*b*-LA) and poly(VL-*b*-TMC-*b*-LA), which otherwise could not be realized in a single pot using either DPP or DBU as a catalyst [88].

## 4.2 COMONOMERS WITH LACTIC ACID/LACTIDE

### 4.2.1 Glycolic Acid/Glycolide

The polymerization of LA and GA can proceed by anionic, carbocationic, or coordination insertion mechanisms and is well described in the previous sections. Poly(lactic acid-*co*-glycolic acid) [poly(LA-*co*-GA) or PLGA] of varying molar masses and compositions are also available commercially.

Low molar mass PLGA, copolymers were prepared by the step-growth polycondensation of lactic acid and glycolic acid. Such copolymers are obtained by polycondensation reaction of the desired composition of monomers in the presence of heat. The reaction is favored in forward direction by removal of evolved water by distillation at atmospheric pressure or under vacuum conditions. The copolymers thus obtained are either brittle and glassy or waxy and sticky, depending on the feed composition and the resultant molar mass of the polymer. A copolymer with a weight-average molar mass of ≥15,000 g/mol was prepared by dehydration condensation of lactic acid and glycolic acid in diphenyl ether in the presence of tin powder [89].

On the other hand, high molar mass copolymers are prepared by ROP of LLA or DLA and 1,4-dioxane-2,5-dione or GA under inert atmosphere or in vacuum. The polymerization can be carried out in bulk, solution (tetrahydrofuran (THF), toluene, dioxane, etc.), or suspension or emulsion conditions. The temperature of bulk polymerization is generally in the range of 100–160°C, whereas in solution polymerization, low temperature (0–25°C) was used to minimize the side reactions (inter- and intra-molecular transesterifications). PLGA copolymers having lactoyl content of 70–90% were prepared by copolymerization at 160°C for 20 h using a desired ratio of monomers and $Sn(Oct)_2$ as a catalyst [21]. The weight-average molar mass of the copolymers ranged from 9.07 to $7.95 \times 10^4$ g/mol. Bulk polymerization of LLA and GA (75 : 25) using $Sn(Oct)_2$ at 60°C for 2 h (in vacuum to remove traces of water) and at 165°C for 4.5 h gave a polymer with weight-average molar mass of 50,000–70,000 g/mol [18].

Block copolymers of LA and GA have been synthesized by sequential addition of monomer onto the reactive chain end of polymer produced from another monomer and by using a hydroxyl-terminated homopolymer as a chain transfer agent [17]. Even small differences in the sequence of monomer units in PLGAs can be easily noticed and determined by ($^1$H and $^{13}$C) NMR. Especially, the diastereotopic methylene resonances for the glycolic units of the copolymers are well noticed in the $^1$H NMR. Thus, NMR technique is considered as sensitive and useful technique to provide a better structure–property correlation [90].

### 4.2.2 Poly(Alkylene Glycol)

The unique properties of PEG, such as solubility in water and polar organic solvents and its insolubility in nonpolar solvents such as ethyl ether and heptane, lack of toxicity, rapid clearance from the body [32], high mobility, and FDA approval of PEG based medical device or formulation for internal consumption, make it a suitable polymer for the preparation of block copolymers of LA or LA–GA. Copolymers of LLA with hydrophilic poly(ethylene oxide) and/or poly(propylene oxide) are vastly reported [25, 43, 44]. Several triblock copolymers of LLA, D,L-lactide (DLLA), and PEO, with PEO as the central block are reported in the literature [24]. These copolymers are more hydrophilic, flexible, and revealed a higher tendency to degrade than PLLA homopolymer [40]. The hydrophilic domains generated by the EO-based blocks act as surface modifier of hydrophobic LA-based domains of the microspheres and thus promote the stability of water-soluble molecules (e.g., λ-DNA) with efficient loading within these microspheres. The degradability and biocompatibility of these copolymers make them suitable candidates for controlled delivery of water-soluble molecules [39]. Diblock and triblock polymers were prepared by bulk or solution polymerization using stannous chloride [39], $Sn(Oct)_2$ [28, 35, 36], potassium *tert*-butoxide [91], sodium hydride [29], calcium hydride/Zn [34], or zinc metal [38] as catalysts. Block copolymers were also prepared in the absence of added catalyst [31].

High polymerization temperatures generally reduce the molar mass of the PLLA [35]. A wide range of copolymers were prepared by varying the molar mass of PEG (1000–30,000 g/mol) and LLA/PEG ratio in the initial feed. A representative structure of such triblock copolymers is depicted in Figure 4.4. The resultant triblock copolymers showed phase separation, due to the hydrophobic and hydrophilic nature of the segments in the polymer backbone, as shown by differential scanning calorimetry (DSC) and wide-angle X-ray scattering analysis (WAXS) studies.

Synthesis and applications of copolymers obtained by adding LA to PEG is widely reported in the literature [92–96]. Transesterification reaction of PLA ($M_w$ 5000–400,000 g/mol) with poly(alkylene ethers) ($M_w$ 500–50,000 g/mol) having ≥1 OH per polymer unit was carried out under melt conditions in the presence of $Ti(OBu)_4$ as a catalyst at 200°C to obtain a high molar mass PLA copolymer. The obtained copolymer showed better flexibility, transparency than that obtained by ROP of lactide in the absence of the above-mentioned polyalkylene glycol [97]. A synthetic strategy for the preparation of ABA

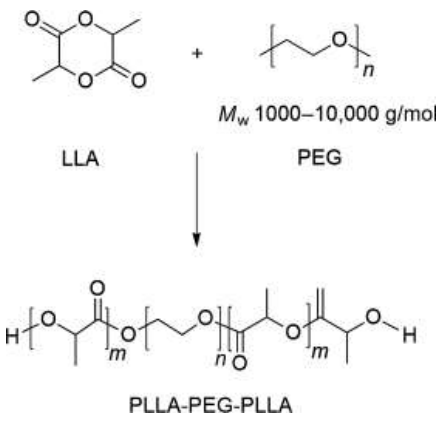


**FIGURE 4.4** Representative structure of triblock copolymer based on LLA and PEG [35].

triblock copolymers, consisting of poly(LLA-*co*-GA) and PEG synthesized under bulk conditions, is shown in Figure 4.5 [27].

LA has also been reacted to poly(propylene glycol)diglycidyl ether ($PPGDGE_{380}$) using $Sn(Oct)_2$ as catalyst. The resultant copolymers showed a range of properties, from weak elastomeric property to tougher thermoplastics, and it was tuned by the feed ratio of LLA and $PPGDGE_{380}$. The obtained copolymers were found to be more hydrophilic than neat PLA [98].

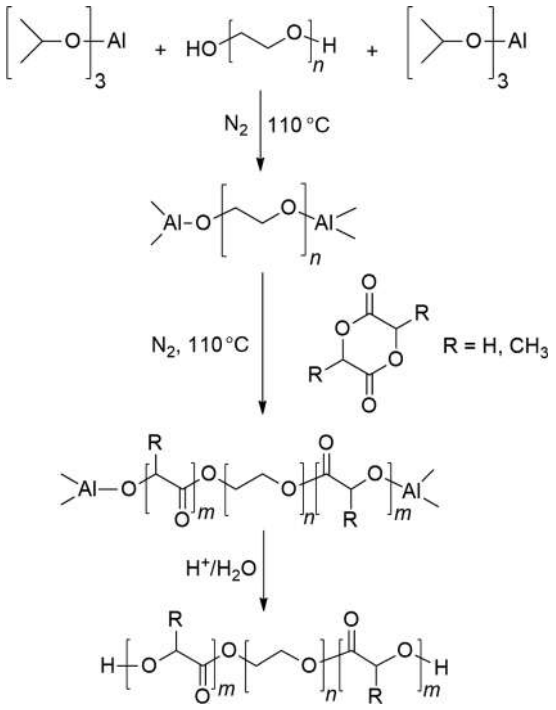


**FIGURE 4.5** Schematic diagram of the synthesis of ABA triblock copolymer using aluminum triisopropoxide as a catalyst [27].

Triblock comb-like copolymer containing fluorophilic, lipophilic, and hydrophilic units was obtained by first ROP of LA with polyethylene glycol methyl ether to form diblock copolymer, which was subsequently converted to macroinitiator to promote atom transfer radical polymerization (ATRP) of heptadecafluorodecyl methacrylate (FMA). Small-angle neutron scattering of poly(PEG-*b*-LA-*b*-FMA) bearing distinct numbers of perfluorinated pendant chains (5–20) confirmed existence of an outer shell of fluorinated polymer, which led to the formation of a nanocapsule morphology [99].

Cholesterol-tethered polymers found utility for attachment of cells. Cholesterol-linked PEG–PDLA copolymer was reported to promote osteoblast attachment and proliferation [37]. The existence of 5 and 15 ethylene glycol units in the copolymer promoted osteoblast attachment and growth, while incorporation of 30 ethylene glycol units prevented adhesion and proliferation. The strategy adopted for the synthesis of above copolymer is presented in Figure 4.6.

Stupp et al. [100] synthesized low molar mass oligomers of cholesterol-(L-lactide)$n$ with $n \leq 20$ in bulk conditions at 150°C. The cholesterol end group induced liquid crystalline properties and ensured self-assembly of the oligomers, which may be beneficial for interaction with the cells and provide opportunities to introduce additional bioactive substituents.

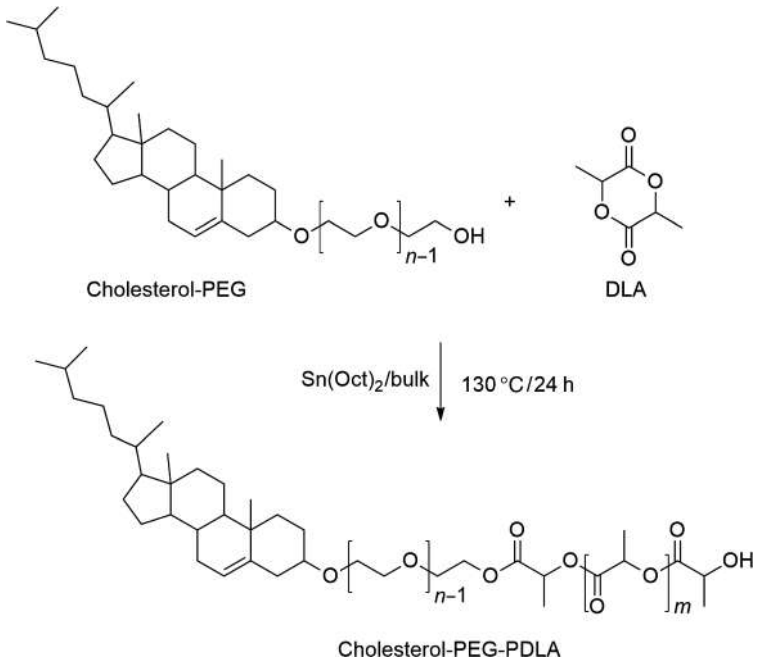


**FIGURE 4.6** Synthetic route for the preparation of cholesterol–PEG–PDLA [37].

In general, additional ring-substitution on lactide affects polymerization behavior detrimentally. For example, trimethyl GA requires a very higher temperature (180°C) and longer reaction time (24 h) than GA [101]. While tetramethyl GA due to high degree of substitution did not polymerize in the presence of $Sn(Oct)_2$ [102]. However, existence of different functional groups as a side chain in poly(α-hydroxy acid)s is interesting and provide avenues for further structural modification and exploration in various application. Certain groups such as alkene [103], allyl [104], alkyne [105, 106], carboxylic acid [107–110], hydroxyl [111], and amine [112, 113] is of profound interest as it allows further structural modifications. Mert et al. [114] reported a viable methodology for the formation of amine-functionalized PLA-PEG copolymers as shown in Figure 4.7.

PEG-grafted PLA is usually obtained by post-polymerization modification process via typical Huisgen cycloaddition reaction [105], initially D,L-lactide is polymerized in the presence of allyl glycidyl ether followed by subsequent PEG functionalization [115]. PEG-grafted PLA can be synthesized either based on the condensation of hydroxy acids with PEG side chains [116], or by typical ROP reaction of PEG-grafted lactide analogues [117].

Recently, ROP-induced crystallization-driven self-assembly (CDSA) of block copolymer, PLLA-*b*-PEG, prepared by ROP of LLA using a monofunctionalized PEG initiator in toluene, and triazabicyclodecene (TBD) as a catalyst is reported. The polymerization time observed was much shorter than the self-assembly relaxation time, which resulted in a nonequilibrium self-assembly process.

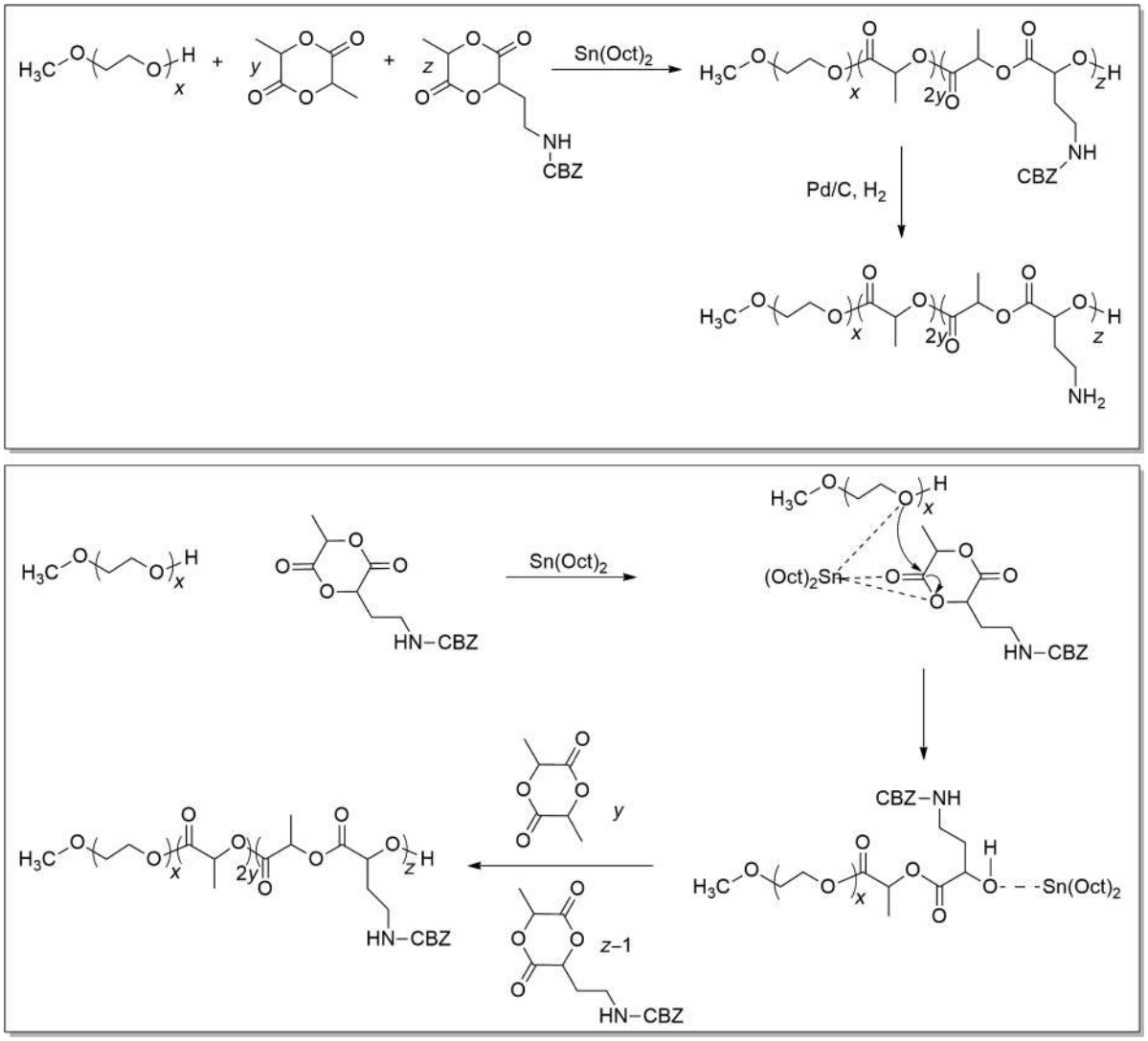


**FIGURE 4.7** Synthesis of protected and deprotected block copolymers. Polymerization mechanism of asymmetrical monomer with methylated PEG [114].

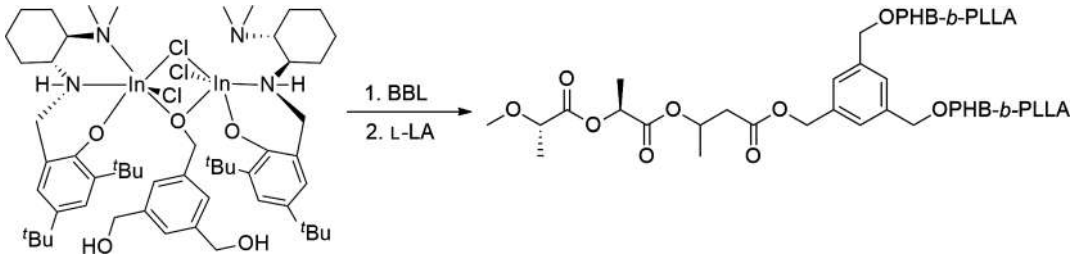


**FIGURE 4.8** Star-shaped copolymers of LA [119].

Traditionally, such self-assembly by CDSA typically occurred in dilute solutions (~1% solids w/w); however, above method allowed realization of such architectural growth at an extremely high solid (5–20% w/w) content [118].

### 4.2.3 δ-Valerolactone and β-Butyrolactone

There has not been much research considering copolymerization of LA with δ-valerolactone (VL) and β-butyrolactone (BL). Anionic block copolymerization of VL and LLA in the presence of potassium methoxide in THF at 20°C gave diblock copolymers with expected compositions and molar mass [49]. Slight racemization of LLA was observed during polymerization due to transesterification reactions.

Block copolymers of LA and BL have been prepared by first preparing a hydroxyl-terminated poly(β-butyrolactone) (PBL). The ROP of (*R*)-BL or (*RS*)-BL with distannoxanes as catalyst in the presence of 1,4-butanediol as initiator gave optically active poly[(*R*)-BL] or atactic poly[(*RS*)-BL] with secondary hydroxyl chain ends and oxytetramethylene units in the backbone. These polymers may be used to initiate the copolymerization of LA at the chain ends and form block copolymers. The optically active poly[(*R*)-BL] was found to be brittle, whereas atactic poly[(*RS*)-BL] showed elastomeric properties. Thus, ROP of [*RS*]-βBL with LLA could be used to prepare elastomeric copolymers, which may alleviate brittle behavior of pristine PLLA. However, utility of Sn(IV) compounds is known as active transesterification catalysts and may cause scrambling of monomer units when LLA is used as a comonomer. Therefore, a two-stage polymerization was carried out. In the first step, telechelic poly[(*RS*)-BL] in the molar mass range of 5000–12,000 g/mol was prepared at 100°C by maintaining the desired molar ratios of (*RS*)-BL and 1,4-butanediol and using Sn(IV) as catalyst. In the second stage, the desired ratio of hydroxyl-terminated poly[(*RS*)-BL] and LLA monomer was added and $Sn(Oct)_2$ was used as a catalyst and polymerization is carried out at 160°C [47]. Hori et al. [45] have also presented research about the synthesis of random copolymers using LLA and (*R*)-BL.

Various mono and bisbenzylalkoxy-bridged dinuclear indium complexes were explored as catalysts to form poly(hydroxybutyrate) (PHB) and star-shaped block copolymer, PHB-*b*-PLA, in the presence of branched alcohols suggests nature of catalyst governs the formation of macromolecular architecture (Figure 4.8) [119].

### 4.2.4 ε-Caprolactone

Copolymerization of LA and CL has been extensively established [51–58]. Random copolymers of DLLA ($r_1 = 10.8$) and CL ($r_2 = 0.37$) were prepared by using lanthanide halides as initiators [55]. High molar mass copolymers of LLA and CL using Al and Zn compounds (e.g., $Et_2AlOEt$, aluminum acetyl acetonate) as catalysts and a variation in microstructure from random to diblock copolymers are also reported [51]. In the case of aluminum acetyl acetonate, the reactivity ratio of LLA was 44 and CL was 0.25. The microstructure depended on the temperature and the kind of initiator used. Also, magnesium complex with 4-fluorophenol catalyst assisted as co-catalyst system for sequential polymerization of LLA and CL to form poly(CL-*b*-LA) [120]. In the ligand-assisted copolymerization, complexes with bulky substituents on the ligands yield a random arrangement, while less bulky substituents favor the formation of gradient copolymers, PLA-*gradual*-PCL. Alternating aluminum complexes bearing ligands containing electronegative atoms tends to favor CL polymerization rate selectively over LA [121, 122].

A series of copolymers of DLA and CL were synthesized by ROP using zinc lactate as a catalyst and carrying out the reaction at 145°C for 8 days. The formation of copolymers was confirmed by gel permeation chromatography (GPC), DSC and NMR. Interestingly, Kister et al. [53] used vibrational spectroscopy, particularly Raman spectroscopy, for determination of morphology, conformation, configuration, and composition of the copolymers. Raman spectroscopy thus appeared to be a suitable method for the identification of PDLA-*co*-PCL samples directly from solid samples without any special preparation.

Star-shaped polymers consist of many linear polymers fused at a central point with many chain end functionalities. Owing to this exclusive structure, star polymers exhibit some remarkable characteristics and properties, which are unattainable by simple linear polymers [123]. Adapting a dual reaction mode strategy, i.e., ROP with click reaction allowed formation of miktoarm star-shaped and inverse star-block copolymers of CL with LA to design novel structures [124]. Recently, synthesis of optically

active poly(lactic-*alt*-caproic acid) by cross-metathesis polymerization (CMP) followed by hydrogenation is adopted, which is seemingly an attractive synthetic approach for designing alternating aliphatic polyesters [125].

### 4.2.5 1,5-Dioxepan-2-One

Albertsson and coworkers [59, 60, 62–64] reported extensive studies on copolymers of LA and 1,5-dioxepan-2-one (DXO). Poly(1,5-dioxepan-2-one) (PDXO) is a completely amorphous and hydrophilic wax-like polymer with a $T_g$ of −39°C. When DXO is used as a comonomer with LA, it increases the hydrophilicity and rate of degradation of the copolymers as compared with PLA. The copolymers show characteristics of thermoplastic elastomers that are suitable for biomedical applications such as slowly degrading sutures, temporary implants, and drug vehicles. Although the synthesis of DXO was reported as early as 1972, Mathisen et al. [59] in 1989 described an improved reaction scheme with a high yield. The DXO block forms a soft amorphous block, while LLA block forms a hard-semicrystalline segment in the triblock copolymer of poly(LLA-*b*-DXO-*b*-LLA) [60, 62, 63]. Blocks of controlled lengths were synthesized using a tin oxide initiator. Degradable polyesters with strictly defined structure, unique mechanical properties, and tuned degradation profiles were prepared and characterized [64]. The morphology of spin-coated films of triblock copolymers poly(LLA-*b*-DXO-*b*-LLA) was characterized by AFM. These studies revealed the absence of nanoscale morphology in copolymer films [64].

### 4.2.6 Trimethylene Carbonate

Thermoplastic elastomers (TPEs) having unusual physical and chemical properties were prepared by copolymerization of LLA with TMC. Recently, a batch procedure for the preparation of degradable TPEs based on multiblock copolymers of LLA with TMC were reported [71] using a combination of ring-expansion polymerization and ROP. The initiator used was 2,2-dibutyl-2-stanna-1,3-oxepane. The block lengths were varied via the monomer/initiator and TMC/LLA ratio. These copolymers were transformed in situ into multiblock copolymers by ring-opening condensation with sebacoyl chloride (Figure 4.9). Li et al. [126] developed the synthesis of a PLA/PPC [poly(propylene carbonate)] multiblock copolymer based on a one-pot copolymerization of epoxides/carbon dioxide and LA using a ternary catalyst system that proceeds via an intermolecular chain transfer mechanism.

### 4.2.7 Poly(*N*-Isopropylacrylamide)

A block copolymer of *N*-isopropylacrylamide (NIPAAm) and LA may combine the thermosensitive property of poly(NIPAAm) and the degradation of PLA. Micelles from such copolymers can improve protein release properties. Temperature change can alter the hydrophilicity and conformation of PNIPAAm, which may affect the physicochemical properties of micelles of the polymer. Amphiphilic block copolymers of NIPAAm and LA were prepared by first synthesizing hydroxy-terminated PNIPAAm followed by ROP of LA in toluene using $Sn(Oct)_2$ as a catalyst (Figure 4.10) [73].

Similar copolymers have recently been synthesized by ROP of LA using the two hydroxyl groups of *S,S′*-bis(2-hydroxyethyl-2′-butyrate)trithiocarbonate (BHBT). The triblock copolymers PLA-*b*-PNIPAAm-*b*-PLA were synthesized by ROP of LA initiated by BHBT followed by reversible addition–fragmentation chain transfer (RAFT) polymerization of NIPAAm with a centered trithiocarbonate unit as a RAFT agent [74]. Self-organization of such

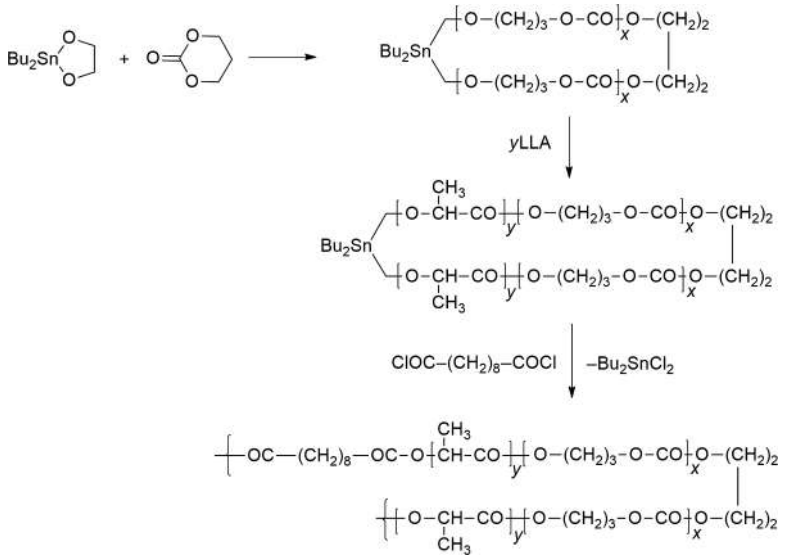


**FIGURE 4.9** Representative structure of multiblock copolymers based on LLA and TMC [71].

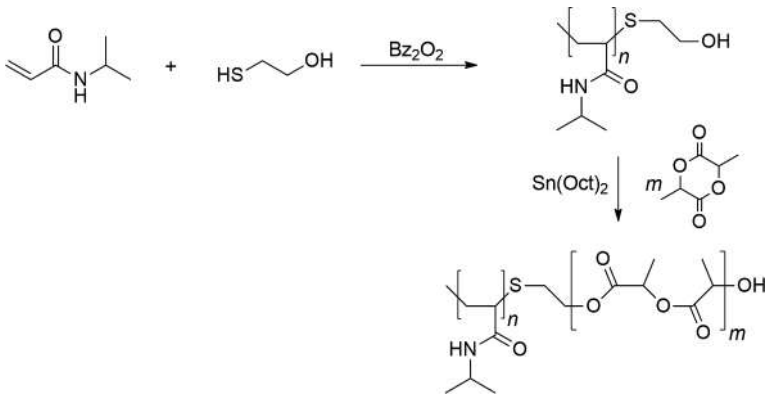


**FIGURE 4.10** Reaction sequence for preparation of PNIPAAm-*b*-PLA [72].

amphiphilic block copolymers in aqueous solutions indicated the formation of vesicles. Stabilization of vesicles was attained by cross-linking chain extension of the NIPAAm block using hexamethylene diacrylate [73]. Multifunctional micelles for cancer cell targeting, distribution, and anticancer drug delivery were prepared using poly(NIPAAm-*co*-methacrylic acid-*g*-DLA) and diblock copolymers [41].

### 4.2.8 Alkylthiophene (P3AT)

End-functionalized poly(3-alkylthiophene) (P3AT), where the alkyl side chain of thiophene moiety contains either 6 or 12 carbons in length, was used as a macroinitiator for ROP of LA, thereby yielding rod-coil block copolymers as shown in Figure 4.11 [127].

A semicrystalline block copolymer PLA-*b*-P3AT-*b*-PLA showed a tendency to phase segregate due to a self-assembly process. Alkaline etching of LA blocks from the polythiophene matrix led to the formation of nanoporous templates, which is useful to generate ordered nanostructures. Other block copolymers can be prepared by combining 3-(2′-ethyl) hexylthiophene (3EHT) and LA using a change-of-mechanism polymerization technique that utilizes two controlled polymerization techniques. A Grignard metathesis (GRIM) reaction is used to polymerize 3EHT to form bromine-terminated P3EHT, which is then end-functionalized with a hydroxyl group through a Suzuki coupling reaction to form the P3EHT–OH macroinitiator. Subsequent controlled ROP of D,L-LA using triethylaluminum results in the synthesis of P3EHT–PLA block copolymers [128]. It is unlikely to obtain complete functionalization of the P3EHT–$CH_2OH$ parent homopolymer with PLA, residual P3EHT in the reaction mixture was removed from P3EHT–PLA by selective precipitation in petroleum ether. Other block copolymers containing PEG and thiophene unit as 3-hexylthiophene (3HT), 3-dodecylthiophene (3DDT), and 3-(2′-ethyl)hexylthiophene (3EHT) blocks are also reported via azide-alkyne coupling reaction [129]. Thienyl-difluoroboron-PLA have been synthesized and used to explore oxygen-sensing capability based on phosphorescence [130].

### 4.2.9 Polypeptide

Hybrid copolymers constituted by short L-phenylalanine (Phe)*n* blocks (*n* ranging from 2 to 25) and LLA blocks of different length have been synthesized by ROP of LA using

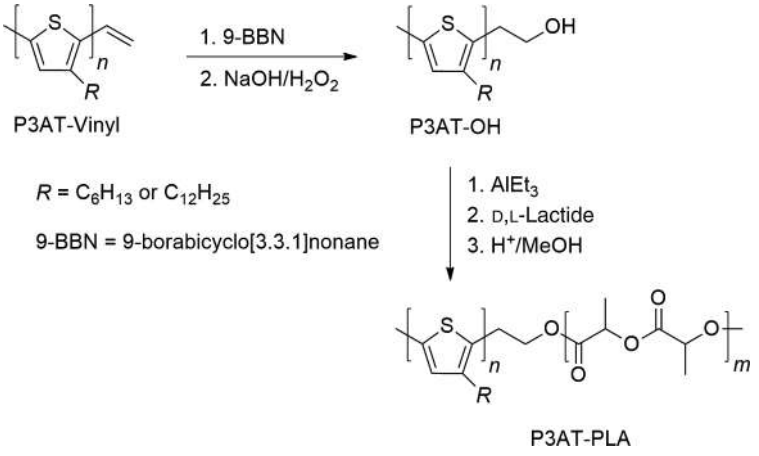


**FIGURE 4.11** Synthesis of 3-alkylthiophene and LLA-based block copolymer [127].

a Phe-oligopeptide as macroinitiator. A variable morphology from lozenge, flower-like, fibrillar structures, spheres, ringed spherulites, dendritic, microfibers, to braid-like microstructures was observed due to self-assembly of Phe-oligopeptides in the copolymer [131].

Recently amino-acid-based morpholine-2,5-diones (MD copolymerized with lactide using DBU : thiourea (TU) catalyst : co-catalyst system to form an interesting class of bio-based degradable polymers with low dispersity (8.1–25.2 kDa and $Đ = 1.13–1.18$) in short periods (5–10 min.) [132]. Ring-strain in monomer was found to affect the rate of homo- vs hetero-propagation of monomer units and dictated the nature and richness of units in the polymer backbone. As noticed, LLA exhibited a higher ring-strain compared with 3*S*,6*S*-dimethylmorpholine-2,5-dione (DMMD) monomer and thus LLA rapidly homopropagated at a higher rate, resulted in the formation of longer LLA block. This provided a platform for the selective incorporation of α-amino acids along a hydrolyzable polymer backbone, mimicking peptide that holds significant potential in biological applications. On the contrary, reverse behavior was observed in case of DMMD as it favored heteropropagation with LLA units [133]. In another work comparing "grafting to" versus "grafting from" strategies, the former appeared to be more successful at covalently linking the peptide to thiol functionalized PLA using thiol-ene click chemistry mediated by AIBN initiator [134]. Core-shell molecular bottlebrushes with a wormlike conformation related to the retention of the α-helical conformation of poly(L-glutamate) backbone obtained as side chains through the "grafting to" strategy on PLA-*b*-PEG copolymer was obtained using azide-alkyne cyclo-addition reaction [135]. Degradable poly[LA-*b*-(*N*-ε-carbobenzyloxy-L-lysine)] copolymers were obtained using LLA macroinitiators and led to controlled polymerizations with low dispersity [136]. Star-PLA bearing triethoxysilyl propyl groups and bifunctional silylated peptides found to react via sol-gel process to form cross-linked networks [117].

## 4.3 FUNCTIONALIZED PLA

PLAs having amino, carboxyl, or other functional (pendant or chain end) groups are well reported in the literature. These functional groups can be utilized for chemical modification or as binding sites for biomolecules to impart selective binding and adhesion. ROP of LLA or DLA using bis(hydroxymethyl) butyric acid (BHMBA) as an initiator and $Sn(Oct)_2$ as a catalyst at 130°C yielded PLA with pendant carboxyl groups. The chain extension of this polymer with diisocyanate yielded poly(ester–urethane) containing carboxyl groups as pendant functional groups [137].

Thiol-functionalized PEG-*b*-PLA was prepared by ROP of DLA using PEG disulfide as the macroinitiator. The disulfide bond was cleaved using tributylphosphine to generate a block copolymer having a thiol unit at the PEG end [138]. Finne-Wistrand and coworkers [139] utilized thiol chemistry to form redox responsive PLA-*b*-PEG nanoparticles. In addition, peptide-functionalized porous scaffolds were prepared by disulfide exchange reaction of pendant thiol groups in poly(LLA-*co*-CL) [140].

Functionalization of PLA by grafting of maleic anhydride (MAn) has been carried out in the presence of free radical initiators (*tert*-butyl peroxide and dicumyl peroxide) [141]. The presence of high succinic anhydride units in the grafts was confirmed by FTIR and NMR. Low percentage grafting was observed in PLA due to the presence of limited free radical sites [142].

Finne and Albertsson introduced a double bond in PLA by using 1,1-di-*n*-butyl-stanna-2,7-dixacyclo-4-heptene as initiator [143, 144]. The presence of a double bond in the LA macromonomer provided a variety of opportunities for further modification. For example, epoxidation was carried out with *m*-chloroperoxybenzoic acid (*m*CPBA) and a quantitative conversion of the double bond to epoxide was observed.

PLA-functionalized polyoxanorbornenes with one or two exo-PLA chains, as well as two endo-, exo-chains were prepared using $Sn(Oct)_2$ as a catalyst in the presence of mono- or di-alcohol derivatives of oxanorbornenes [145]. These macromonomers were then subjected to ring-opening metathesis polymerization (ROMP) to yield graft copolymers as shown in Figure 4.12.

A sequential ROP and ROMP reaction was carried out in the same pot to yield well-defined bottlebrush polymers. The process involved the synthesis of an LA-based macromonomer via ROP of DLA initiated by an alcohol-functionalized norbornene. This was followed by ROMP grafting-through process in the same pot to produce the bottlebrush polymer architecture [146]. Simple one-pot synthesis of block copolymers of norbornene and LA using a bifunctional initiator based on a ruthenium complex for the ROMP of norbornenes and an alcohol to initiate ROP of LLA using 1,5,7-triazabicyclo[4.4.0]dec-5-ene (TBD) as a catalyst is also reported [147]. Low molar mass oligoLAs end capped with fumarate groups were used for in situ cross-linkable scaffolds for tissue engineering [148]. Side-chain functionalized diastereomeric LAs were synthesized from commercially available amino acids and their subsequent polymerization or copolymerization [108]. This approach allows the incorporation of any protected amino acid for the preparation of functionalized cyclic monomers. The quantitative deprotection of amino acids lead to the formation of new functionalized LA-based polymers.

Protected functional LA copolymers can be synthesized by copolymerization of dibenzyloxy-substituted monomers with LA. Deprotection followed by modification with succinic anhydride with carboxyl side chains was

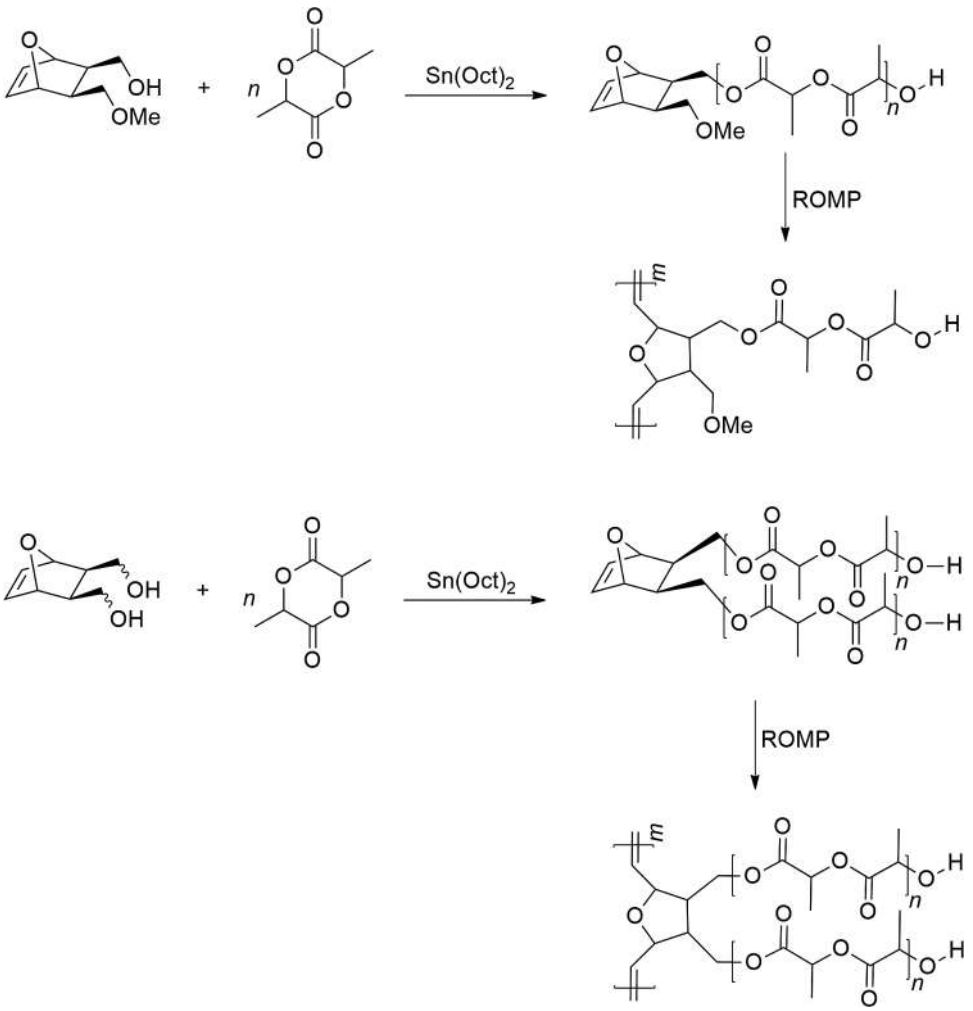


**FIGURE 4.12** Synthesis of oxanorbornenes and LA-based copolymers [145].

shown to be suitable for peptide coupling. Such a modification can control the attachment of cells in tissue engineering and other biomedical applications [109].

## 4.4 MACROMOLECULAR DESIGN OF LACTIDE-BASED COPOLYMERS

Studies on copolymers with LA having a core of LA (or another comonomer) and branches of another monomer (or LA comonomer) have been extensively reported in the literature. Graft copolymers having different architectures (linear branches, hyperbranched, star-like, brush-like, and comb-like) were synthesized to modify the properties of PLA. The hydrophilicity or crystallinity of these copolymers can be varied and controlled by preparing such architectures. A general reaction for the preparation of such copolymers is depicted in Figure 4.13.

Branched PLA is different from linear PLA in physical, thermal, and mechanical properties. Such polymers were prepared by using multifunctional alcohols, for example, inositol, pentaerythritol, glycerol, and so on [149–154]. Finne and Albertsson prepared four-arm star-shaped PLLA using novel spirocyclic tin initiators [149]. Kricheldorf et al. [150] polymerized LLA using bismuth triacetate and pentaerythritol as initiator and co-initiator, respectively. Kim et al. [151] and Arvanitoyannis et al. [152] used $Sn(Oct)_2$, tetraphenyl tin and pentaerythritol, respectively, as the initiator and co-initiator system for LLA polymerization. Similarly, Korhonen et al. [153] reported star-shaped polymers using co-initiators containing multiple hydroxyl groups.

As can be seen, many types of branched PLA are prepared by using organometallic catalysts and multifunctional alcohols. Figure 4.14 shows the synthesis of branched PLA using lipase PS (*Pseudomonas fluorescens*) catalyzed ROP of LA monomers (LLA, DLA, DLLA) [154].

Branched copolymers were also synthesized by the preparation of macromonomers. Various types of methacrylate-functionalized macromonomers are reported in the literature for the preparation of graft and star copolyesters. The reaction

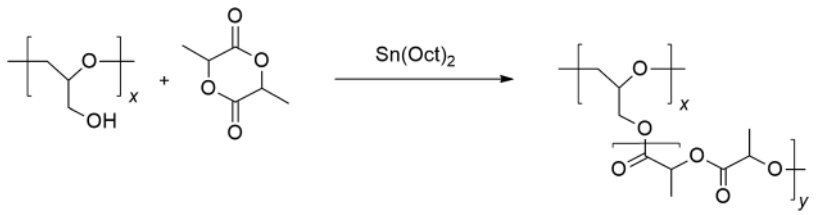


**FIGURE 4.13** Synthetic route for the preparation of branched PLLA.

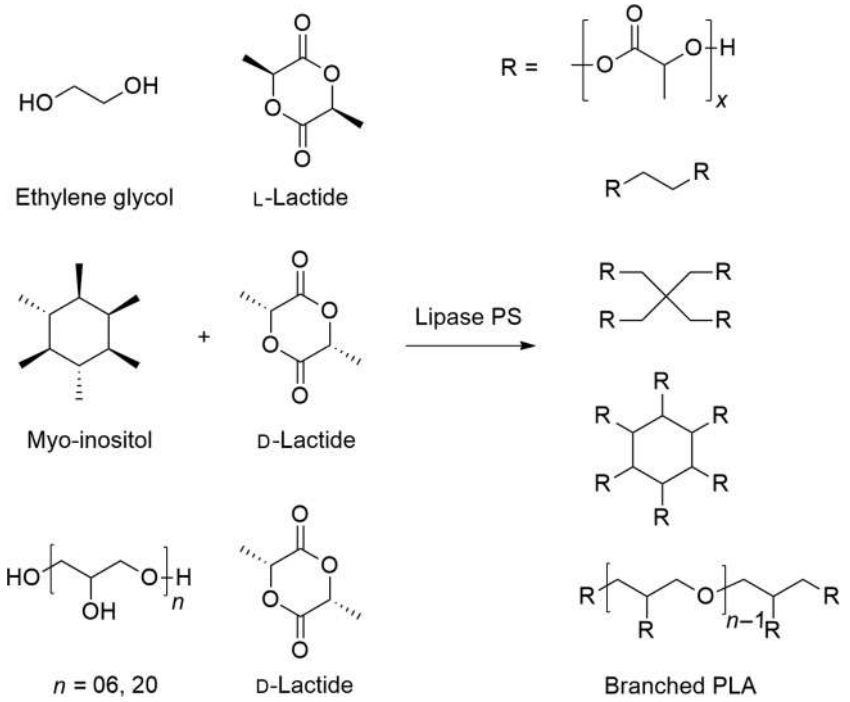


**FIGURE 4.14** Reaction scheme of enzymatic polymerization [154].

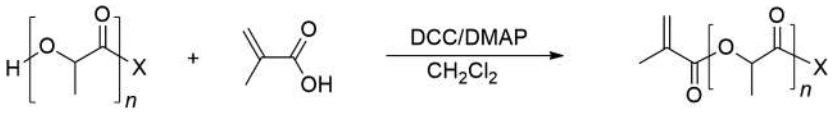


DCC = *N*, *N*′-dicyclohexylcarbodimide

DMAP = 4-dimethylaminopyridine

**FIGURE 4.15** Synthesis of macromonomers.

scheme used for the preparation of the macromonomers is depicted in Figure 4.15.

Segmented terpolymers of poly(alkylmethacrylate-*g*-DLA/dimethylsiloxane) were prepared by combination of a "grafting through" technique (macromonomer method) and controlled/living radical polymerization such as ATRP or RAFT. Different synthetic approaches for the ATRP synthesis of graft terpolymers can be adopted by either one-step copolymerization or two-step sequential approach. In a single-step approach, the low-molecular-weight methacrylate monomer [methyl methacrylate (MMA), butyl methacrylate (BuMA)] (Figure 4.16) was polymerized onto a LA or dimethylsiloxane (DMS) macromonomer. The second strategy was a two-step approach in which a graft copolymer containing one macromonomer is chain-extended with the copolymerization of the second macromonomer and the low-molecular-weight monomer, forming a second block–graft copolymer [155].

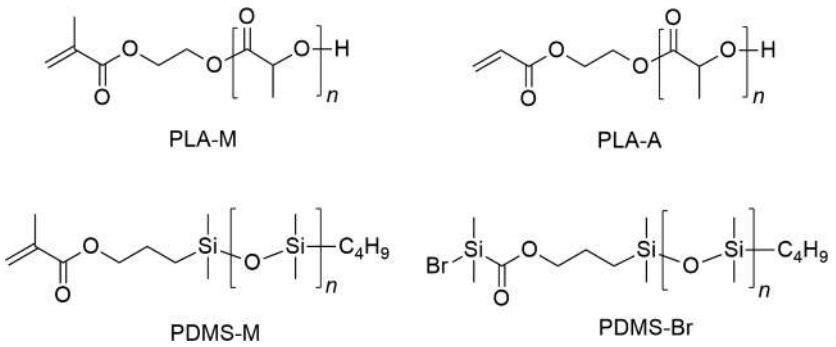


**FIGURE 4.16** Structure of LA- and DMS-based macromonomers and macroinitiators (M: methacrylate, A: acrylate) [155].

### 4.4.1 Graft Copolymers

As mentioned earlier, the macromolecular design of a polymer regulates its physico-chemical properties. Advanced structures such as combs, brushes, ladders, and so on were synthesized to meet the vast demands from different targeted applications of such polymers. Several graft copolymers based on LA are prepared to modify the properties such as degradability, transition temperatures ($T_g$ and $T_m$), morphology, mechanical properties, and solubility. Surface characteristics of PLA films were modified by grafting. Micelle structures, having a multifunctional core and hydrophobic shell, were developed with higher drug activity and lower material toxicity. Some of these modifications are described in the following text. The star-shaped highly branched polymers are discussed separately in Section 4.4.1.

To prepare degradable polymers, graft copolymers of LA acting as macromonomer and *t*-butylacrylate were prepared by free radical polymerization. An increase in LA units resulted in an increase in the degradation rate [156]. ATRP of MMA (96.5%) and (meth)acrylate-terminated LA-based macromonomer ($M_n$ 2800 g/mol, 3.5%) yielded a homogeneously branched poly(MMA-*g*-LA) of low dispersity ($Đ = 1.15$) [157]. The reactivity ratio of MMA for conventional radical polymerization is 1.09 while with ATRP is 0.57. This accounted for the lower dispersity of ATRP-synthesized poly(MMA-*g*-LA).

Degradable comb-like polymer can be prepared by free radical copolymerization of LA-based macromonomer with vinyl (*N*-vinylpyrrolidone) and acrylic [MMA, methacrylic acid (MA)] monomers [158]. ROP to form PLA is not limited to synthesis of polymer and then fabricate or apply for specific purpose. Even PLA growth can be initiated at the surface via surface-anchored poly(2-hydroxyethyl methacrylate) (HEMA), which can then initiate ROP of LA using $Sn(Oct)_2$ as a catalyst. An overall "bottle-brush" structure of the polymer was obtained due to the formation of surface-anchored poly(hydroxyethyl methacrylate-*g*-LA) [159].

PLA and its random copolymer with GA are grafted onto poly(vinyl alcohol) to increase hydrophilicity and manipulate the structure [160]. A novel comb-type PLA was prepared using a depsipeptide–lactide random copolymer having pendant hydroxyl groups as macroinitiator for graft polymerization of LA. The comb-type polymer had a lower $T_g$, $T_m$, and crystallinity than linear PLA [161].

A graft copolymer of poly(NIPAAm-*co*-methacrylic acid)-*g*-DLLA, [poly((NIPAAm-*co*-MAAc)-*g*-LA)], along with diblock copolymers of DLLA and EG and poly(2-ethyl-2-oxazoline) was used for the formation of mixed micelles with a multifunctional core and core/shell morphology. These micelles exhibited higher drug activity and lower material cytotoxicity than micelles based on formulation without the inclusion of diblock copolymers [162]. This formation of nanostructure allowed screening of the highly negative charges (due to the carboxylic groups) in the pristine graft copolymer.

New thermoresponsive, pH-responsive, and degradable nanoparticles comprising poly[DLA-*g*-(NIPAAm-*co*-methacrylic acid)] were prepared by grafting PDLA onto NIPAAm-*co*-methacrylic acid copolymer. A core–shell structure was formed with a hydrophilic outer shell and a hydrophobic inner core that exhibited a phase transition temperature above 37°C. The drug loading level of 5-fluorouracil (5-FU) as encapsulated nanoparticles from these copolymers could be as high as 20%. The release of 5-FU was controlled by the pH in the aqueous medium. These studies indicated that these nanoparticles can be used as a drug carrier for intracellular delivery of anticancer drugs [163].

In biological systems, an organism can create the proper organic matrix as a substrate for the nucleation and growth of inorganic crystals due to the interfacial interaction between inorganic and organic phases. In analogy, in vitro fabrication of novel inorganic/organic composites holds special relevance in several biomedical fields more specifically in implants/bone regeneration. Such applications demand appreciable interactions at the interface of the two; demanding appreciable biocompatibility and favourable bioactivity to induce growth of bone cells. To provide abovementioned benefits, ceramics (hydroxyapatite) along with PLA modified with other functionalities such as carboxyl groups found to mediate the process. This interaction assisted the nucleation sites of HA crystals and may be used as a template to

manipulate and control the growth and size of HA crystals necessary for bone growth. To affect the surface characteristics, photoinduced grafting appeared as a useful technique due to its usual advantages. Solvent cast PLA films were modified by grafting with vinyl acetate, acrylic acid, and acrylamide by a UV-induced photopolymerization process [164]. For the same purpose, PLA surfaces have also been modified by grafting poly(methacrylic acid) via photooxidation followed by UV-mediated polymerization. Thus, the introduced carboxyl groups due to MMA onto PLA surfaces acted as the nucleation sites of hydroxyapatite crystals. Nanohydroxyapatite/PLA composites with interfacial interaction between the two phases were prepared using these graft copolymers [165]. FTIR, XRD, and SEM studies supported that the modified PLA could act as a template to control the nucleation, growth, morphology, size, and distribution of hydroxyapatite crystals over the organic phase.

A thermoplastic polyolefin (TPO), more specifically TPO-*g*-PLA was prepared by grafting PLA onto maleic anhydride-functionalized TPO in the presence of 4-dimethyl aminopyridine (DMAP). A high reaction temperature and a high DMAP concentration resulted in the polymerization of LA. These copolymers were used as a compatibilizer for PLA/TPO blends. An increase in concentration of this copolymer from 0 to 2.5% resulted in an increase in elongation at break and tensile toughness of the blends [166].

Butanediamine (BDA)-*g*-PDLLA was synthesized by grafting maleic anhydride onto the side chains of PDLLA via melt-free radical polymerization using benzoyl peroxide as initiator. BDA was then grafted via an *N*-acylation reaction. The degradation behavior of these graft copolymers could be controlled by the content of BDA. Grafting of BDA onto PDLLA reduced or neutralized the acidity of PDLLA degradation products due to dangling amine component. Also a uniform degradation of these copolymers was observed in comparison with an acidity-induced autoaccelerating degradation featured by PDLLA [167].

New amphiphilic graft copolymers of hyaluronic acid (HA) were prepared by grafting both hydrophobic (PLA) and hydrophilic branches (PEG) on the PLA backbone. The copolymers (PLA-*g*-HA-*g*-PEG) were characterized by spectroscopic techniques. Branched PLA with various lengths of graft chains were synthesized by ROP of L- or D-lactide with polyglycidol as an initiator [168]. The branched PLLA revealed a lower $T_g$, $T_m$, crystallinity, and Young's modulus and higher strain at break than the corresponding linear PLLA or PDLA film.

The PLA surface was chemically modified by a single-step, nondestructive grafting technique using vinyl monomers such as acrylamide, maleic anhydride, and *N*-vinylpyrrolidone in the vapor phase. Benzophenone was used as a photo-initiator under solvent-free conditions. The modified surfaces exhibit higher wettability, and the grafting was verified by X-ray photoelectron spectroscopy, attenuated total reflection, FTIR, contact-angle measurements, and scanning electron microscopy. The graft chain pendant groups remain functional and can subsequently be modified so that a tailor-made surface with desired properties may be achieved [169].

Acrylic-acid-grafted PLA (PLA-*g*-AA) and multihydroxyl-functionalized multiwalled carbon nanotubes are melt blended to improve thermal stability and mechanical properties of the composite. The formation of a covalent bond (ester linkage) resulted in a significant improvement in compatibility [170]. Alternatively, carboxylic acid-functionalized multiwalled carbon nanotubes were grafted onto PLLA by a one-step in situ polycondensation reaction [171]. Acrylic-acid-grafted PLA, titanium tetraisopropylate, and starch blends were prepared by an in-situ sol–gel and melt blending processes. The carboxylic acid groups of acrylic acid act as a coordination site for the titania phase to form a Ti—O—C chemical bond. This resulted in a nanoscale dispersion of $TiO_2$ in the polymer matrix [172].

PLA-*g*-dextran having various lengths and number of grafted chains and sugar units were synthesized using the trimethylsilyl protection method. The surface of these films is believed to be covered with hydrophilic dextran segments, which led to the suppression of cell attachment and protein absorption onto the film [173–175]. In another study, PLA-*g*-dextran copolymers were synthesized by a three-step process: partial silylation of the dextran hydroxyl groups, ROP of DLA initiated by the remaining hydroxyl groups of dextran, followed by silyl ether deprotection under mild conditions. The emulsifying properties of these glycopolymers depend on the PLA/dextran ratio [176]. PLA-*g*-dextran and PLA-*g*-silylated dextran adopt a core–shell conformation in various solvents [177]. Studies on encapsulation and release behavior of bovine serum albumin from PLA-*g*-dextran revealed a higher loading than in PLLA microspheres [178].

Studies on gelatin-*g*-PLA were extensively reported in the literature. These degradable, in general, amphiphilic polymers are useful for parenteral drug delivery systems and tissue engineering. These copolymers were prepared by the ROP of LLA onto functionalized gelatin using bulk copolymerization at 140°C or solution copolymerization at 80°C with $Sn(Oct)_2$ as the catalyst. The number of grafting sites on the gelatin chain could be adjusted by partial trimethyl silylation of pendant hydroxyl, amino, and carboxylic acid groups [179].

Novel triblock copolymer PLGA-PEG-PLGA showed a pH-dependent hydrolytic degradation with itaconic acid (ITA), obtained from renewable resources, delivers a reactive double bond and carboxylic functional group to the end of PLGA-PEG-PLGA. The so obtained carboxylic groups containing copolymer (ITA/PLGA-PEG-PLGA was found to be more susceptible to hydrolytic degradation than the unmodified copolymer as reflected with nearly 45% decrease in $M_n$ value (in initial 10 days) when kept at pH 7.4 [180].

PLA lacks reactive functional groups and the presence of the polyester backbone limits further modification to alter its chemical and physical properties and advocate its applicability to vast domain. To overcome this limitation, PLA bearing functional side chains such as alkenes, alkynes, hydroxyl, amino, carboxylic acid, thiol, and azido groups have been prepared [105, 181–185]. Among these, azide or alkyne groups are valuable addition in its structure as it allows a facile coupling azide–alkyne [3+2] cycloaddition "click" chemistry under mild conditions. For example, pendant azide groups in PLA were reduced to amine to assist further modification to quaternary ammonium groups using copper-catalyzed [3+2] cycloaddition reaction. The resultant polymer showed an enhanced antimicrobial activity both in suspension and as a film [186]. Amphiphilic brush-grafted copolymers of PLA-*g*-POEGMA [POEGMA, poly[(oligoethylene glycol) methacrylate] revealed a molecular architecture upon assembly, which increase their potential as drug delivery carriers. The copolymer was prepared by ATRP of oligo(ethylene glycol) methacrylate (OEGMA) macromer using brominated PLA (Br-PLA) as a macroinitiator [187].

### 4.4.2 Star-Shaped Copolymers

A block copolyester formed by the condensation reaction of PLA with hydroxyl-terminated four-armed PCL macroinitiators are shown in Figure 4.17. This reaction was catalyzed by two different catalysts, $Sn(Oct)_2$ and $Fe(OAc)_2$. The so-formed block copolyester poly(ε-caprolactone-*b*-lactic acid) and its blend with poly(lactic acid) was explored for adhesive application [56]. Further crosslinking reaction of thus-obtained four-armed polymer with diisocyanate resulted in a biodegradable polymeric material composed of well-defined alternating hard and soft domains [188].

Precision synthesis of microstructures in star-shaped copolymers of CL, LLA, and DXO was accomplished using a spirocyclic tin initiator and $Sn(Oct)_2$ (cocatalyst) together with pentaerythritol ethoxylate (co-initiator) [189].

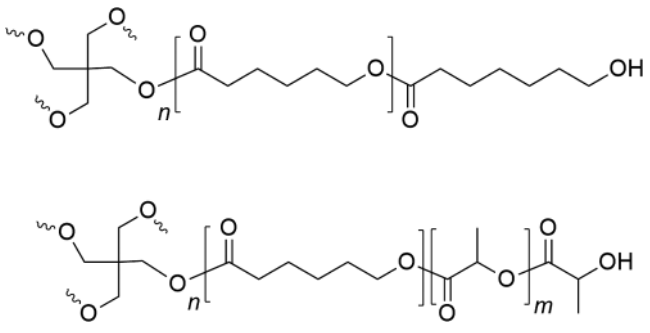


**FIGURE 4.17** Hydroxy end-functionalized star-shaped PCL macroinitiators [56].

Four-arm star-shaped DLLA oligomers of controlled molar mass and low dispersity were synthesized by using ethoxylated pentaerythritol initiator. The terminal hydroxyl group was converted to methacrylate (methacrylic anhydride) or 2-isocyanatoethyl methacrylate. Photo-crosslinking of these functional oligomers yielded networks with high gel contents. The $T_g$ of the copolymers depended on the prepolymer molar mass [190].

Star-shaped PEO–PLA showed a shorter degradation times in comparison to previously reported linear PLA and PLA-*b*-PEG copolymers, along with exceptional amphiphilic characteristics, which may be appealing for their utility as excellent candidates for drug release intracellular carriers [191]. The four-arm star-branched block copolymer of LA and EO was investigated for the release of anticancer drugs 5-FU and paclitaxel. The drug release of paclitaxel from the micellar nanoparticles could be better controlled, as compared with linear block copolymers. The cumulative drug release reaches 60 and 85% by 4th and 14th day, respectively [192]. A rapid and complete release of drug was due to the rapid degradation of micelles from the star-shaped copolymer, compared to the linear block copolymers. PEGylated copolymers with CL, VL, and LA were amphiphilic in nature and formed micelles with low critical micellar concentration (CMC) values in the range of ~$10^{-7}$–$10^{-8}$ M [193].

A copolymer having seven arms of poly(LA-*co*-2-ethyl-2-oxazoline) have been successfully prepared. Star-shaped copolymers were prepared by using tosylated β-cyclodextrin (β-CD) as a core while having LA and 2-ethyl-2-oxazoline copolymers as branches. The hydroxyl functional group of (Tosyl)7-β-CD was used as the initiator for ROP of LA. The hydroxyl chain end of PLA chain was later used for ROP of 2-ethyl-2-oxazoline [194].

A novel degradable chestnut-shaped polymer having a PLA shell and hyperbranched D-mannan (HBM) was synthesized by polymerization of LLA and HBM with DMAP as catalyst. The number of PLA chains on PLA–HBM could be controlled by the ratio of DMAP to sugar [195].

Hyperbranched vs linear polymer structures based on $Sn(Oct)_2$-mediated one-pot copolymerization of glycidol and LA can be achieved by controlling the reaction temperature. Usage of different temperature conditions allowed a controlled occurrence of epoxide ring opening that leads to hyperbranching. Epoxide ring opening was prevented in low-temperature solution polymerizations, resulted in essentially linear PLA functionalized with an epoxide end-groups [196].

LA has been polymerized in a star-shape to poly(amidoamine) dendrimer (PAMAM), the copolymer was synthesized by bulk polymerization of LA with PAMAM. Unlike the linear PLA with similar molar mass, PAMAM-*g*-PLA revealed a higher hydrophilicity and a faster degradation rate. The highly branched structure significantly accelerated the release of water-soluble bovine serum

albumin from these graft copolymers, whereas a time lag was observed in linear PLLA of similar molar mass [197].

### 4.4.3 Periodic Copolymers

Periodic lactide copolymers have garnered significant interest over a period of years and recently emerged as one of the upcoming strategy to affect polymer properties [90, 198–244]. Alternating copolymer is a subset of periodic copolymer. These copolymers hold special relevance as they offer good microstructure control by sequential arrangement of monomer with retention of their stereochemistry in polymer, as compared with random copolymers. Both step growth and chain growth polymerization have been used for the synthesis of periodic copolymers as shown in Figure 4.18.

Tsuji et al. [203] successfully synthesized s-PLA by adopting the procedure reported by Stayshich and Meyer [90, 204]. Usually s-rich PLA form amorphous polymers due to insufficient syndiotactity or crystallization, as determined by wide-angle X-ray diffractometry (WAXD). On the contrary, h-/i-rich (isotactic-rich) PLA showed existence of transient aggregate regions, stereocomplex (SC), which are believed to form due to enhanced interactions between L- and D-lactoyl unit sequences [205] in PLLA and PDLA. The occurrence of such domains is supported by crystalline infrared, terahertz (THz) vibrational spectroscopy, and crystal orbital density functional theory [206, 207]. SC formation of PLLA and PDLA as homopolymers and random copolymers is gaining significant attention. Interestingly, upon SC formation between PLLA and PDLA homopolymers and their copolymers, the resultant polymers showed an improved mechanical performance, resistance to hydrolytic degradation, and a higher thermal stability [208–215]. Thus, SC formation is advantageous feature as it presents opportunities for advancement in scope of polylactide chemistry [208–219]. For example, an increase in elastic modulus to 20 from 14 GPa of the PLLA/PDLA as SC vs homo-crystalline region, respectively, is achieved [220].

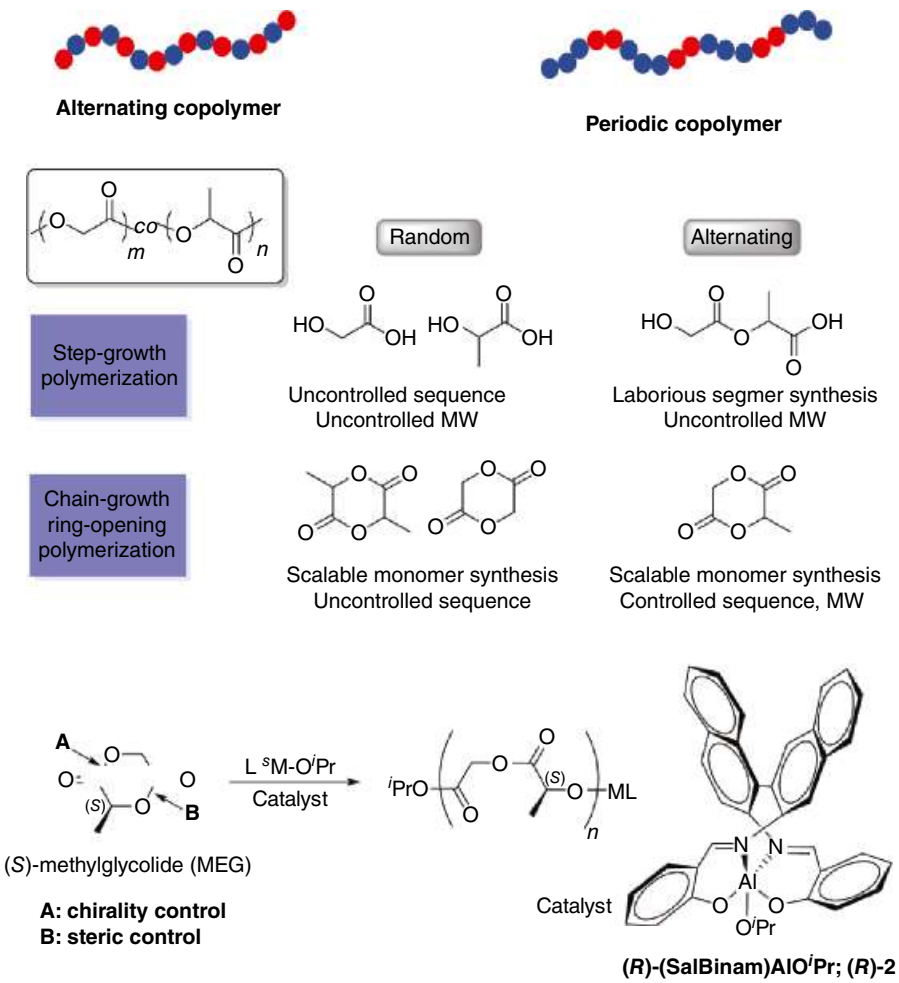


**FIGURE 4.18** Common routes to synthesize random and alternating PLGA and typical synthesis of stereo- and regio-selective ROP using (SalBinam)AlOR catalyst [199].

The origin of this substantial change is accounted to the strong interchain interactions between PLLA and PDLA. A high degree of SC formation is further noticed by incorporating additional structure motifs, which extends hydrogen bonding interactions between the polymer chains [221]. Even variation in catalyst assists in situ SC formation during monomer polymerization. For example, DL-lactide polymerization performed using achiral iron complexes as catalyst at ambient temperature resulted in SC formation [222]. Seemingly SC formation presents opportunities for advancement in scope of polylactide chemistry [208–219]. These favorable interactions offer a multitude in variation in resultant polymer properties, which are further guided by the variation in type, concentration, and sequence of monomer units in the polymer architecture [209, 210, 214, 223–228]. A retention of symmetry between PLLA and PDLA in the crystal lattice [206, 229], with a wide percentage variation in PLLA fractions (30–70%) is observed [207, 230].

Another approach for SC formation is observed by blending of enantiomeric PLLA and PDLA or upon synthesis of stereoblock copolymers with enantiomeric PLLA and PDLA blocks [208–215]. Besides homopolymers, binary and tertiary system containing PLLA and PDLA are also reported. Formation of such crystalline lattice formation in enantiomeric random, staggered random, and enantiomeric alternating copolymer blends of LLA or DLA with hydroxyalkanoic acids is supported by WAXD. Notably, in these repeating units, only one type of chiral center from lactic acid units existed. Recently, SC formation between enantiomeric alternating copolymers consisting of repeating units with two types of chiral centers, D,D-configured poly(DLA-*alt*-D-3-hydroxybutanoic acid) and L,D-configured poly(LLA-*alt*-D-3-hydroxybutanoic acid), is also reported [231]. A significant variation in the $T_m$ between the two polymers (233 vs 83°C) is observed. A very high value of the $T_m$ of SC crystal (~230°C) is observed, which is among the highest value reported in the aliphatic polyesters including poly(glycolate) [40].

Among other lactide copolymers, PLGA has garnered significant interest due to its nontoxic hydrolytic degradation pathway in vivo, with tunable degradation rates and $T_g$ value lies just above human body temperature for a random arrangement of units [232]. When PLGA is used for drug delivery application, the arrangement of GA and LA units are of paramount importance as they govern the degradation rates to affect a sustained drug release profile [233]. A slow but controlled polymer degradation property of copolymers renders them ideal candidates for the investigation to study the role of sequential arrangement of monomers. Alternating sequence copolymers of PLGA tend to degrade at slower but at a constant rate [234], thus allowing a sustained release of encapsulated guests, as compared to a random copolymer. Synthetic approaches adopted to affect arrangement of GA and LA units in polymer are shown in Figure 4.18. Usually, PLGA is synthesized by the ring-opening polymerization (ROP) of LA and GA, yielding a random copolymer [235]. In step-growth segmer assembly polymerization (SAP) produces PLGA with a repeating sequence that depends on the preformed oligomer used [90]. Repeating sequence copolymers (RSCs) with complex microarchitecture from lactic acid (LA) and glycolic acid (GA) such as poly(LA–GA), poly(GA–LA–GA), poly(LA–LA–GA), as syndiotactic, and isotactic were prepared by segmer assembly polymerization (SAP) approach [90]. End-groups of PLGA copolymers containing exact sequenced segmers, i.e., monodisperse units (2–8 monomer units) were further utilized for subsequent condensation polymerization by Li et al. [236]. The SAP approach is a laborious and multistep process. It is a direct polycondensation and produce alternating PLGA reliably but face challenges in controlling molecular weight and $Đ$ lies between 1.3 and 2. A 10 times higher rate of GA incorporation than LA is observed, which is attributed to the steric effect of the methyl substitution [237]. ROP of 3-methyl glycolide (MeG) has also been used to prepare alternating PLGA, with varying degrees of sequence [238, 239]. Alternating PLGA with a very high regioselectivity of 98% is achieved with (*S*)-MeG with a chirality-directed regioselective approach [240], for the sequence-controlled synthesis of PLGA as illustrated in Figure 4.18.

Meyer et al. [241] reported selectivity enhanced entropy-driven ring-opening metathesis polymerization (SEED-ROMP) for the preparation of copolymers with repeating sequences. In this strategy, a preformed sequence is embedded into a large cyclic macromonomer containing a reactive unit that can be systematically cleaved. Upon cleavage, the opened rings join with other units in a controlled manner to form long chains that incorporate sequenced units. Advantages offered by this methodology for formation of copolymers involves no dependence on the chemical behavior of the constituent monomers during polymerization reaction, easy scalability with a high degree of molecular weight control, and copolymers thus formed showed low dispersity. Selectivity-enhanced entropy-driven ring-opening metathesis polymerization (SEED-ROMP) of large, strain-free, ring-chain macromonomer with double bond as reactive unit form linear polymeric chains with specific sequence of monomer units. A *cis*- vs *trans*-double bond in macromonomer found to polymerize faster using a cis-selective Grubbs' catalyst in 10 min vs 2 h with similar conversion. Thus, current methodology offers a good synthetic control in designing well-defined controlled architecture for monomer arrangement in the polymers.

Abe and Tabata [242] demonstrated thermal properties and crystalline structures for a class of periodic aliphatic polyesters, with 3-hydroxybutyrate and lactate units, can be varied over a wide range of temperatures based on stereosequence manipulations. Similarly, a statistical variation in chain microstructure found to affect various hydrolytic

degradation rates in poly(lactide-*co*-ε-caprolactone) matrices [243].

Besides modification in synthetic strategy, a variation in catalyst design is also exploited. Organocatalysts such as phosphazene-based catalysts reported to form alternating PLGA with high regioselectivity and low dispersity [239]. Likewise, lactide-based polymers, the nature of SC formation differs significantly between pure enantiomeric alternating copolymers to enantiomeric alternating LA-based copolymers, poly(LLA-*alt*-GA)/poly(DLA-*alt*-GA) blends, as supported by WAXD and DSC [244].

## 4.5 PROPERTIES OF LACTIDE-BASED COPOLYMERS

The physical properties and degradability of PLA copolymers can be easily controlled by changes in the polymer architecture by altering the structure of monomers and feed ratio to affect the composition of the repeat units, flexibility of the chain, inclusion of labile linkages, molar mass, crystallinity, and orientation of the backbone chains. Tong summarized the $T_g$ and $T_m$ of various aliphatic polyesters depending upon the tacticity and functionality present in the polymer [245]. Properties of PLA depend on the stereoisomers used for their preparation. PLLA and PDLA are semicrystalline hard materials with modulus of 2.7 GPa, tensile strength of 50–70 MPa, elongation at break of 4%, flexural modulus of 5 GPa, and flexural strength of 100 MPa [246–249]. The $T_m$ is around 180°C and $T_g$ is 60–65°C. The molar mass of the polymer, as well as degree of crystallinity, showed a significant influence on the mechanical properties [250–254]. Polymerization of a racemic mixture of 1 : 1 D,D-LA and L,L-LA or *meso*-LA gave an amorphous polymer with a $T_g$ of 55–60°C and a tensile modulus of 1.9 GPa. The in vitro degradation of PLLA is much slower than PMLA (M = meso) due to its crystalline nature, and it takes two years for complete degradation of the former polymer. Surprisingly, a high crystallinity in the *rac*-PLA is observed when polymerization of a racemic monomer in the presence of a racemic catalyst, a chiral Schiff's base complex of aluminum was carried out [255]. This stereoselective mode of polymerization is accounted to the formation of stereocomplex as supported by powder X-ray diffraction and NMR studies. Ovitt and Coates reported the formation of isotactic stereoblock PLA where each enantiomerically pure block contained an average of 11 LA units. The polymer showed a $T_m$ of 179°C, which is higher than that of the enantiomerically pure polymer suggesting the cocrystallization of the enantiomeric blocks of the polymer [199, 256].

PLGA copolymers are less stiff than the homopolymer, but are biocompatible, and undergoes hydrolytic cleavage yielding harmless products. Copolymer compositions containing 25–79% GA are found to be amorphous in nature because of the disruption of regularity of the polymer chain by the other monomer and are therefore interesting for drug delivery devices. The degradability of the copolymers depends on the composition of the backbone. An increase in the GA content from 15 to 50% decreased the degradation time from 5–6 months to 1–2 months. The morphology of the polymeric matrix showed a pronounced effect on degradation rate because ester hydrolysis proceeds more rapidly in the amorphous state [257].

The transition temperatures of the copolymers, $T_g$ (68–58°C) and $T_m$ (160–141°C), decreased with a decrease in lactoyl content from 90 to 70%. Polymers having LA less than 85% did not show a $T_m$. The tensile stress at break of the PLGA copolymer films ($M_n$ value in the range of g/mol) decreased from 54 to 27 MPa with decreasing LA units from 90 to 70%. The elongation at break, however, increased with a decrease in LA content from 110 to 470% [18].

In biomedical applications, it is desirable to change the hydrophobic surface of PLGA to hydrophilic by surface treatments [258]. Some of these treatments include plasma discharge, corona discharge, and surface oxidation by chemical treatments [18, 258, 259]. Chemical treatment by 70% hydrochloric acid, 50% sulfuric acid, and 0.5 N NaOH resulted in a decrease in water contact angle of the surface from 73° to 60°, thereby showed an increase in hydrophilicity. The water contact angle for corona discharge and plasma discharge PLGA surfaces was in the range of 50–56° [20]. Such surface modifications resulted in an increase in adhesion, spreading, and cellular growth on the PLGA surface and may be helpful in improving the tissue compatibility of film and scaffold-type substrates. Three-dimensional PLGA porous scaffolds capable of controlled, sustained delivery using a foaming/particulate leaching method may be useful to regulate and enhance angiogenic factors (e.g., vascular endothelial growth factor) or gene transfer within a developing tissue [260, 261]. For example, amorphous PLGA copolymers having LA : GA ratios of 50 : 50, 75 : 25, and 85 : 15 foam to yield matrices with a porosity of up to 95%. PLGA 50 : 50 was found to be the most amenable to morphological changes during preparation of porous PLGA microparticles using a supercritical carbon dioxide pressure quench treatment of particles prepared using the conventional emulsion–solvent evaporation method [262].

In PLA-*b*-PEG copolymers, the LA blocks are hydrophobic while the EG blocks are soluble in water. As a consequence, such copolymers may form a micellar structure in water and are thus potential candidates for controlled drug delivery applications. The introduction of EG blocks in PLLA or PLGA copolymers increases flexibility and toughness. The $T_g$ of PLLA-*b*-PEG block copolymers showed a strong dependence on the composition and molar mass of the EG block [29]. A significant reduction in $T_g$ was observed by using high molar mass PEG or a high weight percent of PEG in the initial feed composition [263]. Microspheres

based on poly(DL-lactide) and triblock copolymers of PDLLA-*b*-PEG-*b*-PDLLA and loaded with λ-DNA were prepared by a conventional solvent evaporation method based on formation of multiple w1/o/w2 emulsion. The degradation profile of these microspheres was quite different because of more swelling in the triblock copolymer due to the presence of the EG block. This swelling helped in maintaining a more stable condition for DNA and minimized initial burst release [25].

The poly(LLA-*b*-VL) copolymers having the monomers in the ratio 57 : 43 showed two endothermic transitions in DSC, representing the $T_m$ of the VL and LLA block, around 52 and 156°C, respectively. However, only one $T_m$ was observed in the block copolymers having higher ratio of one comonomer (e.g., LLA : VL = 19 : 81 and 81 : 19) [49]. Thermoplastic elastomers based on block copolymers having semicrystalline LLA terminal blocks and an amorphous heterogeneous middle block were prepared from DXO and TMC using a cyclic five-membered tin oxide initiator. All the copolymers exhibited highly elastic behavior with a maximum stress at break of 35.6 MPa for a copolymer without DXO and maximum strain at break 1089% when the ratio DXO : TMC : LLA was 200 : 200 : 200 [264]. The mechanical properties of films of triblock copolymer based on LLA, DXO, and CL depend on the composition of the polymer backbone. Varying the composition of DXO, CL, and LLA in the copolymer varied the stress at break from 4 to 55 MPa and elongation at break from 25 to 1200% [265]. LLA/DLA block length ratio had a significant impact on the crystallization behavior of star-shaped PPO-*b*-PDLA-*b*-PLLA stereoblock copolymers. The overall crystallization rate decreased (half time of crystallization delayed from 2.85 to 5.31 min at 140°C) with the increase in LLA/DLA block length ratio from 7 : 7 to 28 : 7 [266].

ABA triblock copolymer architecture is particularly useful for designing pressure sensitive adhesives (PSAs). The A- and B-block usually comprised of glassy (minor, end component) and rubbery (major, central component), respectively. A-block provide physical crosslinks and mechanical strength, while B-block provide adhesion to the matrix. Commercial triblock copolymers adhesive properties could be improved by diluting entanglements in the central block. A-block based on LA [267–269], γ-methyl-α-methylene-γ-butyrolactone [270], and lactone acrylate [271] and B-blocks based on β-methyl-δ-valerolactone (βMδVL) [269] and ε-decalactone (PDL) [268] sound promising from sustainability and degradability perspective. Copolymers based on LA with PDL or menthide-based PSAs have also been reported because they can potentially degrade before or during the paper recycling process and simultaneously dilute entanglements and control viscosity, which are an essential criteria for their utility as PSAs [267]. An increase in the entanglement molar mass ($M_e$) value was controlled by increasing the length of alkyl substituents in poly(*n*-alkyl-δ-VL) without affecting the $T_g$ [272]. Recently, lactone sourced from cashewnut shell liquids (CNSLs)[273] seems to be promising sustainable approach being inexpensive, potentially degradable, and impart rubbery segment to affect rigidity of the block copolymer due to the presence of inherent long alkylene chain.

To impart surface hydrophilicity, porous scaffolds were successfully fabricated from copolymers of DXO, LLA, and ε-CL through a solvent casting and particulate leaching technique, in which methanol was used to wet and swell the composite before leaching, thereby leading to an interconnected porous network. In the DSC thermograms of these copolymers, only a single $T_g$ located between corresponding copolymers was observed, indicating thereby a continuous amorphous phase due to the randomness of the copolymers [274]. In another approach, better hydrophilicity is achieved by surface functionalization of the porous resorbable scaffolds by covalent grafting [275].

## 4.6 DEGRADATION OF LACTIDE HOMO- AND COPOLYMERS

PLA and its copolymers especially when used for biological applications, besides requirement of optimization of mechanical properties by engineering at the molecular level, also demands a fast degradation polymer rate (less than usual reported time of a couple of months or years). A careful designing of polymer structure is required to optimize both these properties. To achieve a controllable degradation time of polymer demands exploration to satisfy various other desired parameters that are guided by end-use application.

Hydrolysis of PLA under both alkaline and acidic conditions have been investigated. The presence of D-lactoyl units reduces the hydrolysis rate [276]. The hydrolysis of copolymers of poly(LA-*co*-GA) was investigated at 37 and 60°C for 80 days. A three-stage degradation was observed: during the first stage, the molar mass decreased rapidly with little mass loss; in the second stage, a severe mass loss was observed, and monomer formation was initiated; and in the third stage, via hydrolysis the oligomers were transformed to lactic acid and glycolic acid [277]. The GA units in the copolymers were hydrolyzed at a much faster rate than the LA units thus subsequently resulted in an increase in LA content in the remaining polymer.

Tacticity, nature, and length of sequencing in PLGAs found to affect the rate of degradation rate of PLGA. An alternating vs random PLGA exhibits a more gradual and constant degradation rate [90, 234, 236, 278]. Poly(LA-*co*-carbonate)s formed by polymerization of LA and 2-methyl-2-benzyloxycarbonyl-1,3-trimethylene carbonate (MBC) followed by catalytic hydrogenation led to debenzylation of poly(LA-*co*-MBC)s to form poly(LA-*co*-MCC)s containing carboxylic acid groups. The degradation rates were

significantly affected by their sequence distribution. The degradation rates significantly affected by LA–carbonate linkages in the main chains of copolymers with L–C/C–L linkages are more easily cleaved. The following descending trend of lactide–carbonate unit (L–C/C–L) > carbonate–carbonate unit (C–C) > lactide–lactide unit (L–L) of degradation is observed [279].

Hydrolysis of the triblock copolymer poly(LLA-*b*-DXO-*b*-LLA) of different compositions was studied in a buffered salt solution at 37°C and pH 7.4. The rate of degradation was influenced by the original molar mass of the sample, and the copolymer composition had no effect on the degradation [280]. During in vitro degradation carried out for 59 days for the elastic copolymers of DXO and LLA, both exhibited good retention of mechanical properties, with elongation at break 600–800% and elastic modulus 8–20 MPa.

The rate of degradation of PLA can be controlled by copolymerization with monomers such as CL, GA, DXO, α-malate, glycine, HEMA, and ethylene glycol. Blending of PLLA with other polymers was also attempted [62]. Recently, covalent grafting of PLA to tune the in vitro degradation rate was reported. Grafting was performed with acrylamide, *N*-vinylpyrrolidone, or acrylic acid. The in vitro rate of degradation was enhanced, and the grafted surface layer was found to be covalently attached to the surface [281].

Copolymers between LLA and TMC have been used to produce as multifilament fibers by high-speed melt-spinning process with an improved crystallinity [282]. The random copolymers of LLA and TMC (up to 18 mol%) enabled an overall longer service lifetime and a faster degradation kinetics than PLLA [283].

The rates of enzymatic hydrolysis (*proteinase K*) for branched PLLA (prepared from pentaerythritol with four branches and from polyglycerin with 22 branches) were found to be dependent on the average molar mass of the LLA block in the branched molecules, not on the overall molar mass of the samples [284].

The biodegradability of PLA has been extensively investigated in the literature [285–289]. PLLA and its copolymers degraded in the presence of different types of enzymes such as *pronase*, *bromelain*, *Rhizopus delemar lipase*, *lipase* from *Rhizopus arrhizus*, and *proteinase K* from *Tritirachium album* [285]. The enzymatic degradation by *proteinase K* was the subject of interest in several reports [276, 286–289]. Reeve et al. [286] carried out the degradation of a series of PLA stereocopolymers by *proteinase K* and observed that the enzyme preferentially attacks L-lactoyl units. The degradation of PLA stereocopolymers by *proteinase K* increased with a decrease in crystallinity and an increase in hydrophilicity of the polymers.

Recently, a method is devised to provide the real-time assessment of degradability of biomedical polymers at physiological conditions [290]. Screening of degradability extent of series of aliphatic polyesters was determined by time-dependent analysis of data obtained by polymer characterization and measuring the change in pH and released L-lactate molecules using electrochemical sensors. Such advancements in analysis are highly desired to provide a degradation metrics for pristine polylactides or as copolymers.

Even the nature of initiator used in LA polymerization affect degradation characteristics. For example, non-resorbable polyols such as xylitol and β-cyclodextrin can assist the synthesis of star-shaped polyester via ROP of natural xylitol with LLA. The mole fraction of xylitol used during the reaction was found to dictate the crystallinity of the polymer. Xylitol >6% resulted in amorphous polymer while less than 6% resulted in semicrystalline polymer. An increase in xylitol molar fraction concentration increased the rate of degradation of the polymer [291].

### 4.6.1 Drug Delivery from Lactide-Based Copolymers

The successful utilization of polymer materials within the living body is highly dependent on the structural architecture and monomer unit distribution in the polymer. Nanoparticles with a hydrophobic surface (e.g., PLA and PLGA) are rapidly taken up by the cells of the reticuloendothelial systems (RES) [292]. Polymer particles with a hydrophilic surface can avoid this uptake to a greater extent, thereby prolonging the lifetime in the blood circulation, which may help in efficient delivery of the therapeutic agent. Self-organizing block copolymers offers the possibility of entrapping a hydrophobic drug in the micelle core while the micelle's hydrophilic shell confers water solubility. Intelligent drug delivery vehicles can be designed by utilizing shell forming polymers that exhibit stimuli-responsive behavior. Block copolymers of DLA and NIPAAm are widely investigated as potentially useful carriers for targeted delivery [41, 72–74]. Particles prepared from an amphiphilic polymer usually possess tendency to self-organize besides providing functional sites where chemical modifications can be easily carried out. Such modifications may provide opportunities for altering specific surface characteristics such as charge, hydrophilicity, and targeting capabilities. Degradable graft copolymers with amino acids [lysine (Lys), aspartic acid (Asp), alanine (Ala), etc.] as polyester–polyamino acid hybrids have been prepared where the side chains can be at neutral pH poly(LA-*co*-Ala), positively charged poly(LA-*co*-Lys), or negatively charged (poly(LA-*co*-Asp). In such copolymers, the amine side chains tend to concentrate at the surface of the particles [293]. The capabilities of microparticles to serve as carriers in controlled drug release and delivery devices were demonstrated by encapsulation and release of rhodamine B, a low molar mass model.

The effect of morphology on the drug release in blends, as well as copolymers of LLA and DXO, was investigated

by Albertsson and coworkers. The microspheres obtained from blends were more compact and crystalline, while the copolymer microspheres had an amorphous structure that affected the hydrolysis under humid conditions. The storage stability of copolymers was studied for five months and was found to be less than that of blends due to their more crystalline and dense morphology [294]. Albertsson and coworkers [295] reported in another study a nondestructive preparation of resorbable polymer scaffolds with heparin and an osteo-inductive growth factor covalently bonded to the PLA surface. This was achieved by photochemical vapor-phase grafting of acrylamide and subsequent reduction of amide groups of polyacrylamide to amino groups for covalently linking heparin and immobilization of osteo-inductive growth factor, recombinant human bone morphogenetic protein-2, in the heparin layer.

A functionalized triblock copolymer PLA-PEG-PLA with polybasic carboxylic end groups revealed a high drug encapsulation efficiency due to favorable specific interactions between the polymer and loaded drug [296]. A redox-responsive behavior in copolymers of LLA and 3-m ethyl-6-(tritylthiomethyl)-1,4-dioxane-2,5-dione was achieved by postmodification of pendant thiol to disulfide group to assist glutathione-mediated release of hydrophobic molecules entrapped in polymer nanospheres [139]. The morphology and polymer architecture of polymers affects nanoscale vesicular structure, which shows a significant effect on release of entrapped species. The release rates of 5-FU and paclitaxel, widely used chemotherapeutics, were investigated in di-, tri-, and four-arm (star-branched) block copolymers of LA and EO. Micellar aggregates were prepared from these block copolymers and release rates were studied over three weeks. More complete drug release was observed in star-shaped polymers [192].

A nanoparticle carrier based on PLGA demonstrated both high biocompatibility and low toxicity and which was found to improve the efficacy of the drug with reduced side effects against lung cancer [297]. A copolymer of LA and CL alone or with renewable polymers such as chitosan as an electrospun membrane applications matrix shows application in tissue regeneration and drug delivery [298, 299]. The synergistic affect in properties is provided by utility of both synthetic and chitosan polymer. Penta-block copolymer, PLA-PCL-PEG-PCL-PLA, in the form of spherical micelles/nanovehicles are good for ocular drug permeability and drug delivery due to combination of hydrophobic/hydrophilic blocks with appreciable biocompatibility [300, 301].

A star-shaped cholic acid-core poly(CL-*ran*-LA)-*b*-PEG copolymer act as a promising drug-loaded biomaterial for liver cancer chemotherapy [302]. Further the protein fouling by enzymes was lowered by block copolymer nanoparticles through self-assembly of PEO-*b*-PLA [303]. Modified thiolated chitosan greatly increases its mucoadhesiveness and permeation properties, thus increasing the chances of nanoparticle uptake by the gastrointestinal mucosa and improving drug absorption for chemotherapy of lung cancer [304]. Linear and star-shaped amphiphilic PEG-*b*-PLA with or without β-cyclodextrin (β-CD) conjugation were synthesized. Oil-based formulations are formed by emulsion method in organic solvent with a defined core-shell structure and a particle size of ~150–300 nm. Such reverse micelles (RMs), consisting of a hydrophilic core surrounded by hydrophobic surface, were constructed using PEG-*b*-PLA-β-CD in nonpolar solvents and used to sequester hydrophilic guest molecules. They have attracted much attention as drug delivery cargos, as they can form a continuum with other lipid barriers in the body, such as skin lipids and cell membranes. This oil-based formulation fabricated from above-mentioned copolymer allowed a high percentage of protein loading, which is prudential for cellular delivery [305].

### 4.6.2 Radiation Effects

The effect of radiation (γ- and electron-beam) on the degradation of PLA and its copolymers received considerable attention in the past [274, 306, 307]. Irradiation of polymers generates free radicals that induce chemical changes such as chain scission and cross-linking. The atmosphere of the surroundings, irradiation dose, chemical composition, and morphology of the polymer influence the degradation mechanism. The type of end groups, pendant units, and copolymer structure (such as aromatic or aliphatic units) showed a significant effect on the stability of the polymers toward irradiation. In aliphatic polyesters, the ester linkage and the tertiary carbons in the branched polyesters are the preferred site for the degradation. Mechanical properties and molar mass are significantly affected by radiation. Therefore, the sterilization method should be carefully chosen. Ethylene oxide is mainly used when sterilizing degradable devices, by tuning the method can implants be sterilized without influencing the polymer. Electron beams and γ-rays are also used for the sterilization of implants [306]. Generally, a dose of 25 kGy is used for such purposes [308]. Albertsson and coworkers [309] reported that copolymerization of LLA with a small amount of CL or DXO increased the stability in comparison to PLLA. The most abundant low molar mass degradation product was identified as DXO.

## REFERENCES

1. K. J. Jem, B. Tan, *Adv. Ind. Eng. Polym. Res.* **2020**, *3*, 60.
2. E. C. Aguirre, F. I. Franco, H. Samsudin, et al., *Adv. Drug Deliv. Rev.* **2016**, *107*, 333.

3. How ingeo is made. https://www.natureworksllc.com/Products. (accessed 11 January 2021).
4. E. J. Bergsma, F. R. Rozema, R. R. Bos, et al., *J. Oral Maxillofac. Surg.* **1993**, *51*, 666.
5. G. J. Jagur, *Polym. Adv. Technol.* **2006**, *17*, 395.
6. J. W. Leenslag, A. J. Pennings, *Macromol. Chem. Phys.* **1987**, *188*, 1809.
7. S. Vainionpää, P. Rokkanen, P. Törmälä, *Prog. Polym. Sci.* **1989**, *14*, 679.
8. M. Spinu, C. Jackson, M. Keating, et al., *J. Macromol. Sci. Part A: Pure Appl. Chem.* **1996**, *33*, 1497.
9. W. Amass, A. Amass, B. Tighe, *Polym. Int.* **1998**, *47*, 89.
10. A. C. Albertsson, I. K. Varma, Aliphatic polyesters: synthesis, properties and applications, in: A. C. Albertsson (Eds.) *Degradable Aliphatic Polyesters*, Springer, Berlin, 2002, p. 1.
11. A. C. Albertsson, I. K. Varma, Aliphatic polyesters, in: Y. Doi, A. Steinbüchel (Eds.), *Biopolymers: Biology, Chemistry, Biotechnology, Applications, III*, Wiley-VCH, Verlag GmbH, Weinhiem, 2002, p. 1.
12. A. Södergärd, M. Stolt, *Prog. Polym. Sci.* **2002**, *27*, 1123.
13. A. C. Albertsson, I. K. Varma, *Biomacromolecules* **2003**, *4*, 1466.
14. T. Ouchi, Y. Ohya, *J. Polym. Sci. Part A: Polym. Chem.* **2004**, *42*, 453
15. I. K. Varma, A. C. Albertsson, R. Rajkhowa, et al., *Prog. Polym. Sci.* **2005**, *30*, 949.
16. M. C. Tanzi, P. Verderio, M. Lampugnani, et al., *J. Mater. Sci. Mater. Med.* **1994**, *5*, 393.
17. I. Barakat, P. Dubois, C. Grandfils, et al., *J. Polym. Sci. Part A: Polym. Chem.* **2001**, *39*, 294.
18. G. Khang, J. H. Choee, J. M. Rhee, et al., *J. Appl. Polym. Sci.* **2002**, *85*, 1253.
19. G. Schwach, J. Coudane, R. Engel, et al., *Biomaterials* **2002**, *23*, 993.
20. Y. Zhao, Z. Wang, J. Wang, et al., *J. Appl. Polym. Sci.* **2004**, *91*, 2143.
21. C. Min, W. Cui, J. Bei, et al., *Polym. Adv. Technol.* **2007**, *18*, 299.
22. M. Bednarek, *Prog. Polym. Sci.* **2016**, *58*, 27.
23. H. Younes, D. Cohn, *J. Biomed. Mater. Res.* **1987**, *21*, 1301.
24. D. Cohn, H. Younes, G. Marom, *Polymer* **1987**, *28*, 2018.
25. H. Younes, D. Cohn, *Eur. Polym. J.* **1988**, *24*, 765.
26. K. J. Zhu, L. Xiangzhou, Y. Shilin, *J. Appl. Polym. Sci.* **1990**, *39*, 1.
27. L. Youxin, T. Kissel, *J. Control. Release* **1993**, *27*, 247.
28. H. R. Kricheldorf, J. M. Haack, *Macromol. Chem. Phys.* **1993**, *194*, 715.
29. Z. Jedliński, P. Kurcok, W. Walach, et al., *Macromol. Chem. Phys.* **1993**, *194*, 1681.
30. H. R. Kricheldorf, C. Boettcher, *Macromol. Chem. Phys.* **1993**, *194*, 1653.
31. P. Cerrai, M. Tricoli, *Macromol. Rapid Commun.* **1993**, *14*, 529.
32. T. Yamaoka, Y. Tabata, Y. Ikada, *J. Pharm. Sci.* **1994**, *83*, 601.
33. X. Deng, C. D. Xiong, L. M. Cheng, et al., *J. Appl. Polym. Sci.* **1995**, *55*, 1193.
34. S. Li, S. Anjard, I. Rashkov, et al., *Polymer* **1998**, *39*, 5421.
35. J. M. Onyari, S. J. Huang, *Macromol. Symp.* **2003**, *193*, 143.
36. J. R. Mohammadi, S. Farnia, M. Sarbolouki, *J. Appl. Polym. Sci.* **1999**, *74*, 2004.
37. G. Yu, J. Ji, J. Shen, *J. Mater. Sci. Mater. Med.* **2006**, *17*, 899.
38. S. Li, M. Vert, *Macromolecules* **2003**, *36*, 8008.
39. X. Deng, Y. Liu, M. Yuan, et al., *J. Appl. Polym. Sci.* **2002**, *86*, 2557.
40. H. Tsuji, Polylactides, in: Y. Doi, A. Steinbüchel (Eds.), *Biopolymers: Biology, Chemistry, Biotechnology, Applications, III*, Wiley-VCH, Verlag GmbH, Weinhiem, 2002, p. 129.
41. C. K. Huang, C. L. Lo, H. H. Chen, et al., *Adv. Funct. Mater.* **2007**, *17*, 2291.
42. C. U. Lee, R. Khalifehzadeh, B. Ratner, et al., *Macromolecules* **2018**, *51*, 1280.
43. T. Yamaoka, Y. Takahashi, T. Ohta, et al., *J. Polym. Sci. Part A: Polym. Chem.* **1999**, *37*, 1513.
44. Y. Kimura, Y. Matsuzaki, H. Yamane, et al., *Polymer* **1989**, *30*, 1342.
45. Y. Hori, Y. Takahashi, A. Yamaguchi, et al., *Macromolecules* **1993**, *26*, 4388.
46. A. Nakayama, N. Kawasaki, I. Arvanitoyannis, et al., *J. Environ. Polym. Degrad.* **1996**, *4*, 205.
47. S. Hiki, M. Miyamoto, Y. Kimura, *Polymer* **2000**, *41*, 7369.
48. M. Bouyahyi, N. Ajellal, E. Kirillov, et al., *Chem. Eur. J.* **2011**, *17*, 1872.
49. P. Kurcok, J. Penczek, J. Franek, et al., *Macromolecules* **1992**, *25*, 2285.
50. A. Nakayama, N. Kawasaki, Y. Maeda, et al., *J. Appl. Poly. Sci.* **1997**, *66*, 741.
51. M. Bero, J. Kasperczyk, G. Adamus, *Macromol. Chem. Phys.* **1993**, *194*, 907.
52. Y. Shen, K. Zhu, Z. Shen, et al., *J. Polym. Sci. Part A: Polym. Chem.* **1996**, *34*, 1799.
53. G. Kister, G. Cassanas, M. Bergounhon, et al., *Polymer* **2000**, *41*, 925.
54. H. Tsuji, T. Yamada, *J. Appl. Polym. Sci.* **2003**, *87*, 412.
55. J. Broström, A. Boss, I. S. Chronakis, *Biomacromolecules* **2004**, *5*, 1124.
56. M. Stolt, M. Viljanmaa, A. Södergärd, et al., *J. Appl. Polym. Sci.* **2004**, *91*, 196.
57. H. Tsuji, Y. Tezuka, *Macromol. Biosci.* **2005**, *5*, 135.
58. H. Declercq, M. Cornelissen, T. Gorskiy, et al., *J. Mater. Sci. Mater. Med.* **2006**, *17*, 113.
59. T. Mathisen, K. Masus, A. C. Albertsson, *Macromolecules* **1989**, *22*, 3842.
60. A. C. Albertsson, A. Lófgren, *J. Macromol. Sci. Part A: Pure Appl. Chem.* **1995**, *32*, 41.
61. K. Stridsberg, A. C. Albertsson, *J. Polym. Sci. Part A: Polym. Chem.* **2000**, *38*, 1774.

62. M. Ryner A. C. Albertsson, *Biomacromolecules* **2002**, *3*, 601.
63. K. Stridsberg, M. Ryner, A. C. Albertsson, *Adv. Polym. Sci.* **2002**, *157*, 41.
64. A. Finne, N. Andronova, A. C. Albertsson, *Biomacromolecules* **2003**, *4*, 1451.
65. N. Bhattarai, S. R. Bhattarai, H. K. Yi, et al., *Pharm. Res.* **2003**, *20*, 2021.
66. N. Bhattarai, S. R. Bhattarai, M. S. Khil, et al., *Eur. Polym. J.* **2003**, *39*, 1603.
67. S. Bhattarai, S. Kim, K. Jang, et al., *Gene Ther.* **2007**, *14*, 476.
68. Y. Wang, M. Huang, Y. Luo, et al., *Polym. Degrad. Stab.* **2010**, *95*, 549.
69. R. Chen, J. Hao, C. Xiong, et al., *Adv. Eng. Mater.* **2010**, *12*, B504.
70. W. Ge, Y. Guo, H. Zhong, et al., *Cellulose* **2015**, *22*, 2365.
71. D. Pospiech, H. Komber, D. Jehnichen, et al., *Biomacromolecules* **2005**, *6*, 439.
72. F. Kohori, K. Sakai, T. Aoyagi, et al., *J. Control. Release* **1998**, *55*, 87.
73. M. Hales, C. K. Barner, T. P. Davis, et al., *Langmiur* **2004**, *20*, 10809.
74. Y. You, C. Hong, W. Wang, et al., *Macromolecules* **2004**, *37*, 9761.
75. P. Degée, P. Dubois, R. Jérôme, *Macromol. Chem. Phys.* **1997**, *198*, 1973.
76. H. R. Kricheldorf, D. O. Damrau, *Macromol. Chem. Phys.* **1998**, *199*, 1747.
77. G. Schwach, J. Coudane, R. Engel, et al., *Polym. Bull.* **1996**, *37*, 771.
78. D. J. Cameron, M. P. Shaver, *Chem. Soc. Rev.* **2011**, *40*, 1761.
79. H. R. Kricheldorf, I. K. Saunders, A. Stricker, *Macromolecules* **2000**, *33*, 702.
80. M. Vert, G. Schwach, R. Engel, et al., *J. Control. Release* **1998**, *53*, 5.
81. A. Michalski, M. Brzezinski, G. Lapienis, et al., *Prog. Polym. Sci.* **2019**, *89*, 159.
82. D. Pappalardo, T. Mathisen, A. F. Wistrand, *Biomacromolecules* **2019**, *20*, 1465.
83. V. J. Feron, A. P. de Groot, M. Spanjers, et al., *Food Cosmet. Toxicol.* **1973**, *II*(11), 85.
84. S. Matsumura, K. Mabuchi, K. Toshima, *Macromol. Rapid Commun.* **1997**, *18*, 477.
85. M. K. Kiesewetter, E. J. Shin, J. L. Hedrick, et al., *Macromolecules* **2010**, *43*, 2093.
86. H. Xia, S. Kan, Z. Li, et al., *J. Polym. Sci. Part A: Polym. Chem.* **2014**, *52*, 2306.
87. D. J. Coady, A. C. Engler, Y. Y. Yang, et al., *Polym. Chem.* **2011**, *2*, 2619.
88. X. Wang, J. Liu, S. Xu, et al., *Polym. Chem.* **2016**, *7*, 6297.
89. T. Kashima, T. Kameoka, C. Higuchi, et al., Aliphatic polyester and preparation process thereof. US Patent 5,428,126, 1995.
90. R. M. Stayshich, T. Y. Meyer, *J. Am. Chem. Soc.* **2010**, *132*, 10920.
91. H. R. Kricheldorf, C. Boettcher, *Macromol. Symp.* **1993**, *73*, 47.
92. R. Z. Xiao, Z. W. Zeng, G. L. Zhou, et al., *Int. J. Nanomed.* **2010**, *5*, 1057.
93. F. Coumes, C. Y. Huang, C. H. Huang, et al., *Biomacromolecules* **2015**, *16*, 3666.
94. Z. Jing, X. Shi, G. Zhang, et al., *Polym. Int.* **2015**, *64*, 1399.
95. J. Bao, G. Guo, W. Lu, et al., *Polymer* **2020**, *208*, 122965.
96. I. A. Pijpers, F. Meng, J. C. van Hest, et al., *Polym. Chem.* **2020**, *11*, 275.
97. T. Mihara, M. Takahashi, Poly(lactic acid)—syntheses, structures, properties, processing, and application, Jpn. Kokai Tokkyo Koho JP 2004231773, CAN 141:174937, 2004.
98. S. Castillejos, J. Cerna, F. Meléndez, et al., *Polymers* **2018**, *10*, 1184.
99. S. Houvenagel, L Moine, G. Picheth, et al., *Biomacromolecules* **2018**, *19*, 3244.
100. H. A. Klok, J. J. Hwang, S. N. Iyer, et al., *Macromolecules.* **2002**, *35*, 746.
101. G. L. Baker, M. R. Smith III, Process for the preparation of polymers of dimeric cyclic esters, US Patent 6,469,133, 2002.
102. H. Hall, Jr., A. Schneider, *J. Am. Chem. Soc.* **1958**, *80*, 6409.
103. J. Zou, C. C. Hew, E. Themistou, et al., *Adv. Mater.* **2011**, *23*, 4274.
104. M. Leemhuis, N. Akeroyd, J. A. Kruijtzer, et al., *Eur. Polym. J.* **2008**, *44*, 308.
105. X. Jiang, E. B. Vogel, M. R. Smith, et al., *Macromolecules* **2008**, *41*, 1937.
106. Q. Zhang, H. Ren, G. L. Baker, et al., *Polym. Chem.* **2015**, *6*, 1275.
107. Y. Kimura, K. Shirotani, H. Yamane, et al., *Macromolecules* **1988**, *21*, 3338.
108. W. W. Gerhardt, D. E. Noga, K. I. Hardcastle, et al., *Biomacromolecules* **2006**, *7*, 1735.
109. D. E. Noga, T. A. Petri, N. Wack, et al., *Polym. Prepr. (ACS Div. Polym. Chem.)* **2008**, *49*, 844
110. R. Ganugula, M. Arora, P. Saini, et al., *J. Am. Chem. Soc.* **2017**, *139*, 7203.
111. M. Leemhuis, C. V. Nostrum, J. Kruijtzer, et al., *Macromolecules* **2006**, *39*, 3500.
112. D. A. Barrera, E. Zylstra, P. T. Lansbury, et al., *Macromolecules* **1995**, *28*, 425.
113. Y. B. Lim, C. H. Kim, K. Kim, et al., *J. Am. Chem. Soc.* **2000**, *122* 6524.
114. M. O. Arıcan, S. Erdoğan, O. Mert, *Macromolecules* **2018**, *51*, 2817.
115. S. Sant, V. Nadeau, P. Hildgen, *J. Control. Release* **2005**, *107*, 203.
116. X. Jiang, M. R. Smith, G. L. Baker, *Macromolecules* **2008**, *41*, 318.
117. L. Arsenie, C. Pinese, A. Bethry, et al., *Eur. Polym. J.* **2020**, *139*, 109990.
118. P. J. Hurst, A. M. Rakowski, J. P. Patterson, *Nat. Commun.* **2020**, *11*, 1.

119. I. Yu, T. Ebrahimi, S. G. Hatzikiriakos, et al., *Dalton Trans.* **2015**, *44*, 14248.
120. R. M. Slattery, A. E. Stahl, K. R. Brereton, et al., *J. Polym Sci. Part A: Polym. Chem.* **2019**, *57*, 48.
121. T. Shi, W. Luo, S. Liu, et al., *J. Polym. Sci. Part A: Polym. Chem.* **2018**, *56*, 611.
122. C. J. Chang, C. F. Chiu, K. H. Wu, et al., *Polymer* **2020**, *202*, 122572.
123. M. Trollsås, J. L. Hedrick, *J. Am. Chem. Soc.* **1998**, *120*, 4644.
124. X. Yan, J. Li, T. Ren, *e-Polymers* **2018**, *18*, 559.
125. F. R. Zeng, J. M. Ma, L. H. Sun, et al., *Macromol. Chem. Phys.* **2018**, *219*, 1800031.
126. X. Li, C. Hu, X. Pang, et al., *Catal. Sci. Technol.* **2018**, *8*, 6452.
127. B. W. Boudouris, C. D. Frisbie, M. A. Hillmyer, *Macromolecules* **2008**, *41*, 67.
128. V. Ho, B. W. Boudouris, B. L. McCulloch, et al., *J. Am. Chem. Soc.* **2011**, *133*, 9270.
129. C. N. Kempf, K. A. Smith, S. L. Pesek, et al., *Polym. Chem.* **2013**, *4*, 2158.
130. C. A. DeRosa, M. Kolpaczynska, C. Kerr, et al., *ChemPlusChem* **2017**, *82*, 399.
131. E. Mayans, S. K. Murase, M. M. Pérez-Madrigal, et al., *Macromol. Chem. Phys.* **2018**, *219*, 1800168.
132. T. F. Burton, J. Pinaud, O. Giani, *Macromolecules* **2020**, *53*, 6598.
133. T. Kivijärvi, D. Pappalardo, P. Olsén, et al., *Eur. Polym. J.* **2020**, *131*, 109703.
134. J. Fagerland, D. Pappalardo, B. Schmidt, et al., *Biomacromolecules* **2017**, *18*, 4271.
135. H. Tang, Y. Li, S. H. Lahasky, et al., *Macromolecules* **2011**, *44*, 1491.
136. Y. L. Peng, Y. Huang, H. J. Chuang, et al., *Polymer* **2010**, *51*, 4329.
137. T. R. Cooper, R. F. Storey, *Macromolecules* **2008**, *41*, 655.
138. N. C. Kalarickal, S. Rimmer, P. Sarker, et al., *Macromolecules* **2007**, *40*, 1874.
139. T. Fuoco, D. Pappalardo, A. F. Wistrand, *Macromolecules* **2017**, *50*, 7052.
140. T. Fuoco, A. F. Wistrand, D. Pappalardo, *Biomacromolecules* **2016**, *17*, 1383.
141. V. H. Orozco, W. Brostow, W. Chonkaew, et al. (Eds.), *Macromol. Symp.* **2009**, *277*, 69.
142. R. Mani, M. Bhattacharya, J. Tang, *J. Polym Sci. Part A: Polym. Chem.* **1999**, *37*, 1693.
143. M. Ryner, A. Finne, A. C. Albertsson, et al., *Macromolecules* **2001**, *34*, 7281.
144. A. Finne, A. C. Albertsson, *J. Polym. Sci. Part A: Polym. Chem.* **2004**, *42*, 444.
145. I. Czelusniak, E. Khosravi, A. M. Kenwright, et al., *Macromolecules* **2007**, *40*, 1444.
146. S. C. Radzinski, J. C. Foster, J. B. Matson, *Macromol. Rapid Commun.* **2016**, *37*, 616.
147. H. Jung, N. T. Brummelhuis, S. K. Yang, et al., *Polym. Chem.* **2013**, *4*, 2837.
148. E. H. X. Jabari. *Polym. Prepr. (ACS Div. Polym. Chem)* **2006**, *47*, 353.
149. A. Finne, A. C. Albertsson, *Biomacromolecules* **2002**, *3*, 684.
150. H. R. Kricheldorf, H. H. Thiessen, G. Schwarz, *Biomacromolecules* **2004**, *5*, 492.
151. S. H. Kim, Y. K. Han, Y. H. Kim, et al., *Macromol. Chem. Phys.* **1992**, *193*, 1623.
152. I. Arvanitoyannis, A. Nakayama, N. Kawasaki, et al., *Polymer* **1995**, *36*, 2947.
153. H. Korhonen, A. Helminen, J. V. Seppälä, *Polymer* **2001**, *42*, 7541.
154. K. Numata, R. K. Srivastava, A. Finne-Wistrand, et al., *Biomacromolecules* **2007**, *8*, 3115.
155. J. F. Lutz, N. Jahed, K. Matyjaszewski, *J. Polym. Sci. Part A: Polym. Chem.* **2004**, *42*, 1939.
156. V. Langlois, K. Vallee-Rehel, J. J. Peron, et al., *Polym. Degrad. Stab.* **2002**, *76*, 411.
157. H. Shinoda, K. Matyjaszewski, *Macromolecules* **2001**, *34*, 6243.
158. J. Eguiburu, M. J. Fernandez-Berridi, J. San Román, *Polymer* **1996**, *37*, 3615.
159. J. B. Kim, W. Huang, C. Wang, et al., Bottle brush brushes: ring-opening polymerization of lactide from poly(hydroxyethyl methacrylate) surfaces, in: R. C. Advincula, W. J. Brittain, K. C. Caster, et al., *Polymer Brushes*, Wiley-VCH, New York, 2004, p. 105.
160. A. Breitenbach, D. Mohr, T. Kissel, *J. Control. Release* **2000**, *63*, 53.
161. F. Tasaka, Y. Ohya, T. Ouchi, *Macromolecules* **2001**, *34*, 5494.
162. C. L. Lo, K. M. Lin, C. K. Huang, et al., *Adv. Funct. Mater.* **2006**, *16*, 2309.
163. C. L. Lo, K. M. Lin, G. H. Hsiue, *J. Control. Release* **2005**, *104*, 477.
164. A. V. Janorkar, S. E. Proulx, A. T. Metters, et al., *J. Polym Sci. Part A: Polym. Chem.* **2006**, *44*, 6534.
165. Y. Xiao, D. Li, H. Fan, et al., *Mater. Lett.* **2007**, *61*, 59.
166. C. H. Ho, C. H. Wang, C. I. Lin, et al., *Polymer* **2008**, *49*, 3902.
167. Y. Luo, Y. Wang, X. Niu, et al., *Eur. Polym. J.* **2007**, *43*, 3856.
168. T. Ouchi, S. Ichimura, Y. Ohya, *Polymer* **2006**, *47*, 429.
169. U. Edlund, M. Källrot, A. C. Albertsson, *J. Am. Chem. Soc.* **2005**, *127*, 8865.
170. C. S. Wu, H. T. Liao, *Polymer* **2007**, *48*, 4449.
171. W. Song, Z. Zheng, W. Tang, et al., *Polymer* **2007**, *48*, 3658.
172. H. T. Liao, C. S. Wu, *J. Appl. Polym. Sci.* **2008**, *108*, 2280.
173. T. Ouchi, T. Kontani, Y. Ohya, *J. Polym. Sci. Part A: Polym. Chem.* **2003**, *41*, 2462.
174. T. Ouchi, T. Kontani, Y. Ohya, *Polymer* **2003**, *44*, 3927.
175. T. Ouchi, T. Kontani, T. Saito, et al., *J. Biomater. Sci. Polym. Ed.* **2005**, *16*, 1035.

176. J. Raynaud, B. Choquenet, E. Marie, et al., *Biomacromolecules* **2008**, *9*, 1014.
177. C. Nouvel, P. Dubois, E. Dellacherie, et al., *J. Polym. Sci. Part A: Polym. Chem.* **2004**, *42*, 2577.
178. T. Ouchi, T. Saito, T. Kontani, et al., *Macromol. Biosci.* **2004**, *4*, 458.
179. J. Ma, H. Cao, Y. Li, et al., *J. Biomater. Sci. Polym. Ed.* **2002**, *13*, 67.
180. J. Oborna, L. Mravcova, L. Michlovska, et al., *Express Polym. Lett.* **2016**, *10*, 361.
181. F. Jing, M. A. Hillmyer, *J. Am. Chem. Soc.* **2008**, *130*, 13826.
182. G. L. Fiore, F. Jing, Jr. V. G. Young, et al., *Polym. Chem.* **2010**, *1*, 870.
183. D. E. Borchmann, N. T. Brummelhuis, M. Weck, *Macromolecules* **2013**, *46*, 4426.
184. C. Wright, A. Banerjee, X. Yan, et al., *Macromolecules* **2016**, *49*, 2028.
185. P. P. Kalelkar, G. R. Alas, D. M.Collard, *Macromolecules* **2016**, *49*, 2609.
186. P. P. Kalelkar, Z. Geng, M. G. Finn, et al., *Biomacromolecules* **2019**, *20*, 3366.
187. P. P. Kalelkar, D. M. Collard, *Macromolecules* **2020**, *53*, 4274.
188. H. Tsuji, K.-i. Tamura, Y. Arakawa, *RSC Adv.* **2019**, *9*, 7094.
189. K. Odelius, A. C. Albertsson, *J. Polym. Sci. Part A: Polym. Chem.* **2008**, *46*, 1249.
190. A. S. Karikari, W. F. Edwards, J. B. Mecham, et al., *Biomacromolecules* **2005**, *6*, 2866.
191. L. E. Salaam, D. Dean, T. L. Bray, *Polymer* **2006**, *47*, 310.
192. P. Jie, S. S. Venkatraman, F. Min, et al., *J. Control. Release* **2005**, *110*, 20.
193. W. J. Lin, Y. C. Chen, C. C. Lin, et al., *J. Biomed. Mater. Res. Part B: Appl. Biomater.* **2006**, *77*, 188.
194. M. Adeli, Z. Zarnegar, R. Kabiri, *Eur. Polym. J.* **2008**, *44*, 1921.
195. T. Satoh, M. Tamaki, Y. Kitajyo, et al., *J. Polym. Sci. Part A: Polym. Chem.* **2006**, *44*, 406.
196. L. M. Pitet, S. B. Hait, T. J. Lanyk, et al., *Macromolecules* **2007**, *40*, 2327.
197. Q. Cai, Y. Zhao, J. Bei, et al., *Biomacromolecules* **2003**, *4*, 828.
198. T. M. Ovitt, G. W. Coates, *J. Am. Chem. Soc.* **1999**, *121*, 4072.
199. T. M. Ovitt, G. W. Coates, *J. Am. Chem. Soc.* **2002**, *124*, 1316.
200. A. Kapelski, J. Okuda, *J. Polym. Sci. Part A: Polym. Chem.* **2013**, *51*, 4983.
201. P. J. Dijkstra, H. Du, J. Feijen, *Polym Chem.* **2011**, *2*, 520.
202. J. C. Buffet, J. Okuda, *Polym. Chem.* **2011**, *2*, 2758.
203. H. Tsuji, Y. Arakawa, *Polym. Chem.* **2018**, *9*, 2446.
204. R. M. Stayshich, T. Y. Meyer, *J. Polym. Sci. Part A: Polym. Chem.* **2008**, *46*, 4704.
205. L. E. Chile, P. Mehrkhodavandi, S. G. Hatzikiriakos, *Macromolecules* **2016**, *49*, 909.
206. F. Zhang, H. W. Wang, K. Tominaga, et al., *J. Phy. Chem. Lett.* **2016**, *7*, 4671.
207. K. Tashiro, H. Wang, N. Kouno, et al., *Macromolecules* **2017**, *50*, 8066.
208. J. Slager, A. J. Domb, *Adv. Drug Deliv. Rev.* **2003**, *55*, 549.
209. H. Tsuji, *Macromol. Biosci.* **2005**, *5*, 569.
210. K. Fukushima, Y. Kimura, *Polym. Int.* **2006**, *55*, 626.
211. P. Pan, Y. Inoue, *Prog. Polym. Sci.* **2009**, *34*, 605.
212. M. Saravanan, A. J. Domb, *Eur. J. Nanomed.* **2013**, *5*, 81.
213. Y. Jing, C. Quan, B. Liu, et al., *Polym. Rev.* **2016**, *56*, 262.
214. H. Tsuji, *Adv. Drug Deliv. Rev.* **2016**, *107*, 97.
215. B. H. Tan, J. K. Muiruri, Z. Li, et al., *ACS Sustain. Chem. Eng.* **2016**, *4*, 5370.
216. Z. Li, B. H. Tan, T. Lin, et al., *Prog. Polym. Sci.* **2016**, *62*, 22.
217. H. Bai, S. Deng, D. Bai, et al., *Macromol. Rapid Commun.* **2017**, *38*, 1700454.
218. S. Thomas, E. B. Gowd, N. Kalarikkal (Eds.), *Crystallization in Multiphase Polymer Systems*, 1st edition, Elsevier, Amsterdam, 2017.
219. D. Bandelli, J. Alex, C. Weber, et al., *Macromol. Rapid Commun.* **2020**, *41*, 1900560.
220. S. Lee, M. Kimoto, M. Tanaka, et al., *Polymer* **2018**, *138*, 124.
221. J. Bao, X. Chang, G. Shan, et al., *Polym. Chem.* **2016**, *7*, 4891.
222. P. Marin, M. J.,L. Tschan, F. Isnard, et al., *Angew. Chem. Int. Ed.* **2019**, *58*, 12585.
223. N. Yui, P. J. Dijkstra, J. Feijen, *Macromol. Chem. Phys.* **1990**, *191*, 481.
224. K. Fukushima, Y. Furuhashi, K. Sogo, et al., *Macromol. Biosci.* **2005**, *5*, 21.
225. M. H. Rahaman, H. Tsuji, *Macromol. React. Eng.* **2012**, *6*, 446.
226. K. Masutani, C. W. Lee, Y. Kimura, *Polym J.* **2013**, *45*, 427.
227. L. Han, G. Shan, Y. Bao, et al., *J. Phy. Chem. B* **2015**, *119*, 14270.
228. L. Han, Q. Xie, J. Bao, et al., *Polym. Chem.* **2017**, *8*, 1006.
229. W. Zhou, K. Wang, S. Wang, et al., *ACS Macro Lett.* **2018**, *7*, 667.
230. K. Tashiro, N. Kouno, H. Wang, et al., *Macromolecules* **2017**, *50*, 8048.
231. H. Tsuji, K. Nakayama, Y. Arakawa, *RSC Adv.* **2020**, *10*, 39000.
232. F. Danhier, E. Ansorena, J. M. Silva, et al., *J. Control. Release* **2012**, *161*, 505.
233. J. A. Nowalk, J. H. Swisher, T. Y. Meyer, *Polym. Chem.* **2019**, *10*, 4930.
234. J. Li, S. N. Rothstein, S. R. Little, et al., *J. Am. Chem. Soc.* **2012**, *134*, 16352.
235. O. D. Cabaret, B. M. Vaca, D. Bourissou, *Chem Rev.* **2004**, *104*, 6147.
236. J. Li, R. M. Stayshich, T. Y. Meyer, *J. Am. Chem. Soc.* **2011**, *133*, 6910.
237. D. Gilding, A. Reed, *Polymer* **1979**, *20*, 1459.

238. C. M. Dong, K. Y. Qiu, Z. W. Gu, et al., *J. Polym. Sci. Part A: Polym. Chem.* **2000**, *38*, 4179.
239. K. Takojima, H. Makino, T. Saito, et al., *Polym. Chem.* **2020**, *11*, 6365.
240. Y. Lu, J. H. Swisher, T. Y. Meyer, et al., *J. Am. Chem. Soc.* **2021**, *143*, 4119.
241. A. L. Short, C. Fang, J. A. Nowalk, et al., *ACS Macro Lett.* **2018**, *7*, 858.
242. Y. Tabata, H. Abe, *Macromolecules* **2014**, *47*, 7354.
243. J. Fernández, E. Meaurio, A. Chaos, et al., *Polymer* **2013**, *54*, 2621.
244. H. Tsuji, M. Yamasaki, Y. Arakawa, *ACS App. Polym. Mater.* **2019**, *1*, 1476.
245. R. Tong, *Ind. Eng. Chem. Res.* **2017**, *56*, 4207.
246. D. Grijpma, A. Nijenhuis, P. Van Wijk, et al., *Polym. Bull.* **1992**, *29*, 571.
247. P. Törmälä, *Clin. Mater.* **1992**, *10*, 29.
248. L. Fambri, A. Pegoretti, R. Fenner, et al., *Polymer* **1997**, *38*, 79.
249. S. Jacobsen, H. G. Fritz, *Polym. Eng. Sci.* **1999**, *39*, 1303.
250. I. Engelberg, J. Kohn. *Biomaterials* **1991**, *12*, 292.
251. D. W. Grijpma, C. A. Joziasse, A. J. Pennings, *Macromol. Rapid Commun.* **1993**, *14*, 155.
252. D. W. Grijpma, A. J. Pennings, *Macromol. Chem. Phys.* **1994**, *195*, 1633.
253. G. Perego, G. D. Cella, C. Bastioli, *J. Appl. Polym. Sci.* **1996**, *59*, 37.
254. Y. Ikada, H. Tsuji, *Macromol. Rapid Commun.* **2000**, *21*,117.
255. C. P. Radano, G. L. Baker, M. R. Smith, *J. Am. Chem. Soc.* **2000**, *122*, 1552.
256. T. M. Ovitt, G. W. Coates, *J. Polym. Sci. Part A: Polym. Chem.* **2000**, *38*, 4686.
257. S. Mohapatra, S. Ranjan, N. Dasgupta, et al., *Nanoscience and Nanotechnology in Drug Delivery*, Elsevier, Amsterdam, 2018.
258. G. Khang, B. J. Jeong, H. B. Lee, et al., *Biomed. Mater. Eng.* **1995**, *5*, 259.
259. J. H. Lee, G. Khang, J. W. Lee, et al., *J. Colloid Interface Sci.* **1998**, *205*, 323.
260. M. Sheridan, L. Shea, M. Peters, et al., *J. Control. Release* **2000**, *64*, 91.
261. J. H. Jang, L. D. Shea, *J. Control. Release* **2003**, *86*, 157.
262. K. Koushik, U. B. Kompella, *Pharm. Res.* **2004**, *21*, 524.
263. R. Li, Y. Wu, Z. Bai, et al., *RSC Adv.* **2020**, *10*, 42120.
264. N. Andronova, A. C. Albertsson, *Biomacromolecules* **2006**, *7*, 1489.
265. M. Ryner, A. C. Albertsson, *Macromol. Symp.* **2001**, *175*, 11.
266. W. Li, Y. Ma, Z. Fan, *Polym. Eng. Sci.* **2015**, *55*, 2534.
267. J. Shin, M. T. Martello, M. Shrestha, et al., *Macromolecules* **2011**, *44*, 87.
268. S. Lee, K. Lee, Y. W. Kim, et al., *ACS Sustain. Chem. Eng.* **2015**, *3*, 2309.
269. T. R. Ewert, A. M. Mannion, M. L. Coughlin, et al., *J. Rheol.* **2018**, *62*, 161.
270. K. Ding, A. John, J. Shin, et al., *Biomacromolecules* **2015**, *16*, 2537.
271. H. Sajjad, W. B. Tolman, T. M. Reineke, *ACS Appl. Polym. Mater.* **2020**, *2*, 2719.
272. D. K. Schneiderman, M. A. Hillmyer, *Macromolecules* **2016**, *49*, 2419.
273. H. J. Kim, K. Jin, J. Shim, et al., *ACS Sustain. Chem. Eng.* **2020**, *8*, 12036.
274. K. Odelius, P. Plikk, A. C. Albertsson, *Biomacromolecules* **2005**, *6*, 2718.
275. M. Källrot, U. Edlund, A. C. Albertsson, *Macromol. Biosci.* **2008**, *8*, 645.
276. S. Li, A. Girard, H. Garreau, et al., *Polym. Degrad. Stab.* **2000**, *71*, 61.
277. M. Hakkarainen, A. C. Albertsson, S. Karlsson, *Polym. Degrad. Stab.* **1996**, *52*, 283.
278. Y. Wang, Z. Jia, J. Jiang, et al., *Macromolecules* **2019**, *52*, 7564.
279. X. Hua, X. Liu, D. Cui, *Macromolecules* **2020**, *53*, 5289.
280. K. Stridsberg, A. C. Albertsson, *Polymer* **2000**, *41*, 7321.
281. M. Källrot, U. Edlund, A. C. Albertsson, *Biomacromolecules* **2007**, *8*, 2492.
282. T. Fuoco, T. Mathisen, A. F. Wistrand, *Biomacromolecules* **2019**, *20*, 1346.
283. T. Fuoco, T. Mathisen, A. F. Wistrand, *Polym. Degrad. Stab.* **2019**, *163*, 43.
284. K. Numata, A. F. Wistrand, A. C. Albertsson, et al., *Biomacromolecules* **2008**, *9*, 2180.
285. H. Fukuzaki, M. Yoshida, M. Asano, *Eur. Polym. J.* **1989**, *25*, 1019.
286. M. S. Reeve, S. P. McCarthy, M. J. Downey, et al., *Macromolecules* **1994**, *27*, 825.
287. H. Cai, V. Dave, R. A. Gross, et al., *J. Polym. Sci. Part B: Polym. Phys.* **1996**, *34*, 2701.
288. S. Li, S. McCarthy, *Macromolecules* **1999**, *32*, 4454.
289. S. Li, M. Tenon, H. Garreau, et al., *Polym. Degrad. Stab.* **2000**, *67*, 85.
290. T. Fuoco, M. Cuartero, M. Parrilla, et al., *Biomacromolecules* **2021**, *22*, 949.
291. L. Teng, X. Xu, W. Nie, et al., *J. Polym. Res.* **2015**, *22*, 83.
292. R. Gref, Y. Minamitake, M. T. Peracchia, et al., *Science* **1994**, *263*, 1600.
293. G. Caponetti, J. S. Hrkach, B. Kriwet, et al., *J. Pharm. Sci.* **1999**, *88*, 136.
294. U. Edlund, A. C. Albertsson, *J. Polym. Sci. Part A: Polym. Chem.* **2000**, *38*, 786.
295. U. Edlund, S. Dånmark, A. C. Albertsson, *Biomacromolecules* **2008**, *9*, 901.
296. H. Zhang, L. Chang, B. Zhang, et al., *J. Biomater. Sci. Polym. Ed.* **2008**, *19*, 99.
297. J. Jiménez-López, M. M. El-Hammadi, R. Ortiz, et al., *Pharmacol. Res.* **2019**, *141*, 451.
298. R. Dorati, S. Pisani, G. Maffeis, et al., *Carbohydr. Polym.* **2018**, *199*, 150.

299. S. Pisani, R. Dorati, B. Conti, et al., *React. Funct. Polym.* **2018**, *124*, 77.
300. M. Alami-Milani, P. Zakeri-Milani, H. Valizadeh, et al., *Pharm. Dev. Technol.* **2020**, *25*, 704.
301. N. Jalilzadeh, N. Samadi, R. Salehi, et al., *Sci. Rep.* **2020**, *10*, 1.
302. W. Tao, X. Zeng, J. Zhang, et al., *Biomater. Sci.* **2014**, *2*, 1262.
303. C. E. de Castro, B. Mattei, K. A. Riske, et al., *Langmuir* **2014**, *30*, 9770.
304. L. Jiang, X. Li, L. Liu, et al., *Nanoscale Res. Lett.* **2013**, *8*, 1.
305. W. X. Gu, M. Zhu, N. Song, et al., *J. Mater. Chem. Part B: Polym. Phys.* **2015**, *3*, 316.
306. L. Montanari, M. Costantini, E. C. Signoretti, et al., *J. Control. Release* **1998**, *56*, 219.
307. S. C. J. Loo, C. P. Ooi, Y. C. F. Boey, *Polym. Degrad. Stab.* **2004**, *83*, 259.
308. J. S. C. Loo, C. Ooi, F. Boey, *Biomaterials* **2005**, *26*, 1359.
309. P. Plikk, K. Odelius, M. Hakkarainen, et al., *Biomaterials* **2006**, *27*, 5335.

# 5

# PREPARATION, STRUCTURE, AND PROPERTIES OF STEREOCOMPLEX-TYPE POLY(LACTIC ACID)

Neha Mulchandani, Yoshiharu Kimura, and Vimal Katiyar

## 5.1 INTRODUCTION

An intermolecular complex formed by macromolecules having identical chemical composition but different configuration of the repeating units is known as a stereocomplex (sc) [1]. The co-crystallization of the stereoisomers PLLA and PDLA results in the formation of a well-known crystal structure stereocomplex PLA (sc-PLA). The sc-PLA gained widespread recognition and acceptance ever since it was discovered by Ikada et al. [2] and patented by Murdoch and Loomis [3]. Stereocomplexation in PLA is attributed to the non-covalent interaction of the enantiomeric macromolecular chains. The sc-PLA crystals melt at a temperature ($T_m$) 50°C higher than the homochiral (hc) PLLA or PDLA crystals [4]. Apart from the improved heat resistance, sc-PLA has better mechanical performance and resistance to hydrolysis [5, 6] than PLLA and PDLA, allowing its exploration in pharmaceutical and biomedical applications. The homopolymers PLLA or PDLA have been utilized for short life applications such as agricultural mulch-films, disposable trays and bottles, and nonwovens. On the other hand, sc-PLA can be specifically adopted for high-performance applications such as structural and engineering plastics [7]. Several studies have also made use of sc-PLA for drug delivery application due to its improved barrier properties, which prevent the burst release and prolong the release of drugs [8]. The formation of sc crystals may therefore lead to the development of PLA-based materials with enhanced performance. The molecular weight, optical purity of the enantiomeric PLA, and tacticity are the governing parameters for the sc crystallization; lower optical purity or higher molecular weight likely hinders the sc crystallization [9, 10]. The formation of hc crystals is often more kinetically favorable than that of sc crystals during the crystallization of high-molecular-weight PLLA/PDLA blends. However, enhancing the interchain interactions between PLLA and PDLA by covalent or non-covalent means can improve the formation of sc crystallites [11]. Also, sc crystallizes much faster from the melt as compared with the α-form. Researchers have been studying the varied crystal morphologies of sc-PLA and the governing parameters for their formation. A preferential formation of sc can be attained by blending PLLA/PDLA in equimolar (1 : 1) ratio in solution. However, varying the ratios of PLLA/PDLA in the blend give rise to the formation of hc-PLA ($T_m$ ~ 180°C) along with sc-PLA ($T_m$ ~ 230°C). In order to improve the sc formation in non-equimolar blends of PLLA/PDLA, several methodologies have been adopted, some of which are highlighted in this chapter.

## 5.2 STEREOCOMPLEXATION IN POLY(LACTIC ACID)

Enantiomeric PLLA and PDLA are synthesized from L- and D-lactides ($T_m$ = 97.5°C) that are derived from L- and D- lactic acids, respectively. Both PLLA and PDLA are semicrystalline in nature and develop unique morphologies in their block copolymers due to the competition between crystallization and microphase separation, which expands their applications [12]. Intriguingly, mixing of a concentrated solution of PLLA with that of PDLA leads to the

*Poly(Lactic Acid): Synthesis, Structures, Properties, Processing, Applications, and End of Life*, Second Edition.
Edited by Rafael A. Auras, Loong-Tak Lim, Susan E. M. Selke, and Hideto Tsuji.

formation of an irreversible gel due to the formation of sc crystals as crosslinking points. The stereoselective interaction of the optically active PLLA and PDLA enantiomers results in the formation of optically inactive sc crystals consisting of PLLA and PDLA chains in an equimolar ratio [13, 14]. The formation of sc crystals was initially discovered from solution mixing and later from melt blending of both enantiomers. The sc crystals are characterized by the high melting temperature of ~230°C, which is ~50°C higher than that of homo-crystals of PLLA and PDLA [2]. The enantiomeric PLLA and PDLA chains are packed side by side in a sc crystal lattice, where hydrogen bond between the carbonyl and methyl groups of PDLA and PLLA is responsible for the complexation. The spherulites of sc-PLA do not have a ring-band structure at any crystallization temperature, unlike those of PLLA and PDLA homopolymers. Since the development of sc crystals is driven by the diffusion of the macromolecular chains of PLLA and PDLA in the crystallization process, the sc crystallizability is inversely proportional to their molecular weight. Accordingly, an equimolar blending of PLLA and PDLA (1 : 1) with high molecular weight (>100 kg/mol) often leads to the formation of homo-crystallites (larger extent) along with sc crystallites [15, 16]. Improved miscibility between the PLLA and PDLA chains can enhance the formation of sc in the PLLA/PDLA blend. The mesophase (an ordering of molecules which is intermediate between the crystalline and amorphous states) in sc-PLA can be observed by annealing the equimolar blends of PLLA/PDLA just above their $T_g$ due to the prevailing weak intermolecular interactions between high-molecular-weight (HMW) PLLA and PDLA chains [17]. The stereocomplex mesophase is more prevalent at a lower temperature due to the reduced molecular mobility, while at higher temperature, the formation of hc crystals is enhanced. Furthermore, blending of non-equimolar PDLA and PLLA results in various fractions of hc and sc crystallites. However, as reported by Woo et al., the non-equimolar blends of PDLA and 30–50% of low-molecular-weight PLLA lead to the formation of sc-PLA crystals. In such a case, a large amount of hc-PLA chains may be trapped and dispersed in the spherulites of sc-PLA crystals, thereby resulting in fluffy lamellae stacking of sc crystals [18].

Lately, attention has been paid to improving the melt crystallizability of sc-PLA to expand its applications, particularly in industries where melt processing of polymers is employed. The boundary viscosity average molecular weight ($\overline{M_v}$) for stereocomplexation from the melt is $6\times10^3$ g/mol, whereas that from the solution casting is $4\times10^4$ g/mol [19]. However, the ordinary melt crystallization leads to the formation of hc crystals together with sc crystals [20]. Therefore, efforts have been made to achieve exclusive formation of sc crystals from the melt [21, 22]. The use of polyethylene glycol (PEG) as a plasticizer has been reported to enhance the formation of sc crystallites in the HMW blends of PLLA and PDLA. The plasticizer facilitates the interaction between PLLA and PDLA chains by increasing the segmental mobility of the polymer chains, thereby leading to the formation of exclusive stereocomplexation during melt crystallization. The use of cellulose nanocrystals (CNCs) as a nucleating agent has also resulted in the improvement in stereocomplexation from melt. A higher loading of CNCs (~25 wt%) led to an accelerated growth of sc-PLA as reported by Jiang et al., which further expanded the industrial applications of sc-PLA [23]. Hence, the use of nucleating agents and plasticizers has become an alternate route to improve stereocomplexation in PLA. Additionally, an aryl amide derivative (TMB-5) has been adopted as a nucleating agent to promote sc crystallization in equimolar blends of PLLA/PDLA. Exclusive formation of sc crystals from the melt has been reported upon loading 0.5% TMB-5 in an equimolar PLLA/PDLA blend. However, the $T_m$ of sc-PLA is reduced from 230 to 200°C upon loading TMB-5 into the matrix of sc-PLA [24]. The formation of sc-PLA nanofibers by electrospinning has also been explored by several researchers [25–28]. The HMW blend of PLLA/PDLA has been subjected to electrospinning by Tsuji et al., where the sc crystallization is found to be enhanced with higher voltage. The nanofibers are prepared with dominant sc crystals and negligible amount of hc crystals. The formation and growth of sc crystals is attributed to the high voltage or electrically induced high shearing force used during the electrospinning process [29].

## 5.3 CRYSTAL STRUCTURE OF sc-PLA

sc-PLA often crystallizes in a triclinic or trigonal unit cell with both $3_1$ (or $3_1$ and $3_2$) PLLA and PDLA chains packed side by side [30] unlike the orthorhombic or pseudo-orthorhombic crystal forms of hc-PLA [31]. The crystal structure consisting of a triclinic unit cell (P1 symmetry with parallel chain orientation) was proposed in 1991 by Okihara et al., who reported a $3_1$ helical structure of PLLA and PDLA chains having a lamellar thickness of 0.87 nm, where the three enantiomeric chains penetrate one unit cell [32]. The unit cell parameters of a triclinic cell are given as $a = b = 9.16$ Å, $c = 8.7$ Å; $\alpha = \beta = 109.2°$, $\gamma = 109.8°$. The structure was different from that of the trigonal unit cell (R3c or R-3C group) described by Cartier et al., where the PLLA and PDLA chains have $3_2$ and $3_1$ conformations, respectively [33]. According to the modified trigonal structure, the triclinic cell was assumed to be a subcell of the larger trigonal cell where six helices penetrate one unit cell. The trigonal unit cell parameters may be given as $a = b = 14.98$ Å, $c = 8.7$ Å; $\alpha = \beta = 90°$, $\gamma = 120°$. The crystal was grown from non-equimolar blends of PLLA and PDLA,

which indicated that the co-crystallization of PLLA and PDLA chains could occur from their asymmetric ratio. However, the proposed model only took 1 : 1 PLLA and PDLA ratio into consideration. Stereocomplex structures with parallel and antiparallel orientation of the molecular chains were studied by molecular simulations by Brizzolara et al. who revealed that the parallel structure (P1) is more stable than the antiparallel structure (P/1). The structures were considered to be triclinic having cell parameters $a = 0.912$, $b = 0.913$, $c = 0.930$ nm, $\alpha = \beta = 110°$, $\gamma = 109°$ for the parallel structure (P1); and $a = 0.930$, $b = 0.940$, $c = 0.930$ nm, $\alpha = 111°$, $\beta = 112°$, $\gamma = 108°$ for the antiparallel structure (P/1). The growth mechanism of the triangular lamellar crystals in the sc formation was well supported by the molecular simulations [34]. Highly oriented stereocomplex samples were prepared in a study by Sawai et al. who adopted solvent casting technique to prepare the blend films followed by co-extrusion of the dried polymer blend (draw ratio = 14). The oriented samples showed 20 wide angle X-ray reflections that were reasonably indexed with a trigonal unit cell as proposed by Cartier et al. with a slight variation of the parameters, which were given as: $a = b = 1.50$, $c = 0.823$ nm, $\alpha = \beta = 90$ and $\gamma = 120°$ with R3c space group [35].

These structure models are proposed mainly for the PLLA/PDLA blend having a ratio of 50/50. However, stereocomplexation is also evident in PLLA/PDLA blends having the compositions of 30/70–70/30, for which a new structure model (space group P3) has been proposed by Tashiro et al. [36] on the basis of X-ray diffraction analysis. According to their model, the co-existence of PLLA and PDLA chains between the sc crystal lattice is profound for the PLLA/PDLA blend ratios in the range of 30/70–50/50–70/30. Beyond this range, the coexistence of PLLA and PDLA chains is not realizable due to their instability. A statistically disordered packing of PLLA and PDLA chains can be attributed to the P3 space group, unlike the symmetrical R3c model [36, 37]. The unit cell parameters reported by several researchers are tabulated in Table 5.1.

## 5.4 FORMATION OF STEREOBLOCK PLA

The stereoblock (sb) formation allows for the intermolecular and intramolecular mixing of the neighbouring L- and D-stereosequences, thereby leading to the preferential formation of sc crystallites. This is particularly important when synthesizing sc polymers of HMW. Block copolymerization has received enormous recognition in achieving the desired properties of the resulting materials. The composition of PLLA/PDLA, along with the number of blocks and chain length, can be varied to obtain a variety of diblock and multiblock copolymers with tailored properties. The molecular mixing of the enantiomeric PLLA and PDLA chains in the sb copolymers leads to the improved crystallinity [38–40).

### 5.4.1 Single-Step Process

The formation of sc-PLA usually occurs by blending PLLA/PDLA, which requires synthesis of the individual polymers by the ring-opening polymerization (ROP) of L- and D-lactides prior to blending the respective enantiomeric PLA chains. The sc-PLA thus formed exhibits improved thermal and mechanical properties; however, the process requires the formation of enantiopure polymers from the respective enantiopure monomers, which restricts its practical applications. In this regard, the single step preparation of sc-PLA has been explored from the readily available racemic lactide (*rac*-LA, or DL-lactide, 1 : 1 mixture of L- and D-lactides), which is inexpensive (Figure 5.1). The ROP of *rac*-LA usually yields amorphous polymers (atactic or heterotactic) having lower $T_g$ and $T_m$ than those of the isotactic PLA, i.e., PLLA and PDLA. The random arrangement of L- and D-lactide units in the backbone chain is usually observed upon polymerizing *rac*-LA with a limited scope of application. To extend the utilization of *rac*-LA precursor, significant efforts have been made in achieving the stereoselective polymerization of LA that causes the resulting stereochemistry in the product [41–43). The direct formation of sc-PLA from *rac*-LA has been achieved by Radano et al. using

**TABLE 5.1 Unit Cell Parameters Reported for the sc Crystals**

| | Okihara et al. [32] | Brizzolara et al. [34] | Cartier et al. [33] | Sawai et al. [35] | Tashiro et al. [36] |
|---|---|---|---|---|---|
| Crystal system | Triclinic | Triclinic | Trigonal | Trigonal | Trigonal |
| Chain conformation | $3_1$ | $3_1$ | $3_1$ and $3_2$ | $3_1$ and $3_2$ | $3_1$ |
| Unit cell parameter | | | | | |
| $a$ (nm) | 0.916 | 0.912 | 1.498 | 1.50 | 1.494 |
| $b$ (nm) | 0.916 | 0.913 | 1.498 | 1.50 | 1.494 |
| $c$ (nm) | 0.870 | 0.930 | 0.870 | 0.823 | 0.862 |
| $\alpha$ (°) | 109.2 | 110 | 90 | 90 | 90 |
| $\beta$ (°) | 109.2 | 110 | 90 | 90 | 90 |
| $\gamma$ (°) | 109.8 | 109 | 120 | 120 | 120 |
| $\rho_{calc}$ (g/cm$^3$) | 1.27 | 1.21 | 1.27 | 1.342 | — |

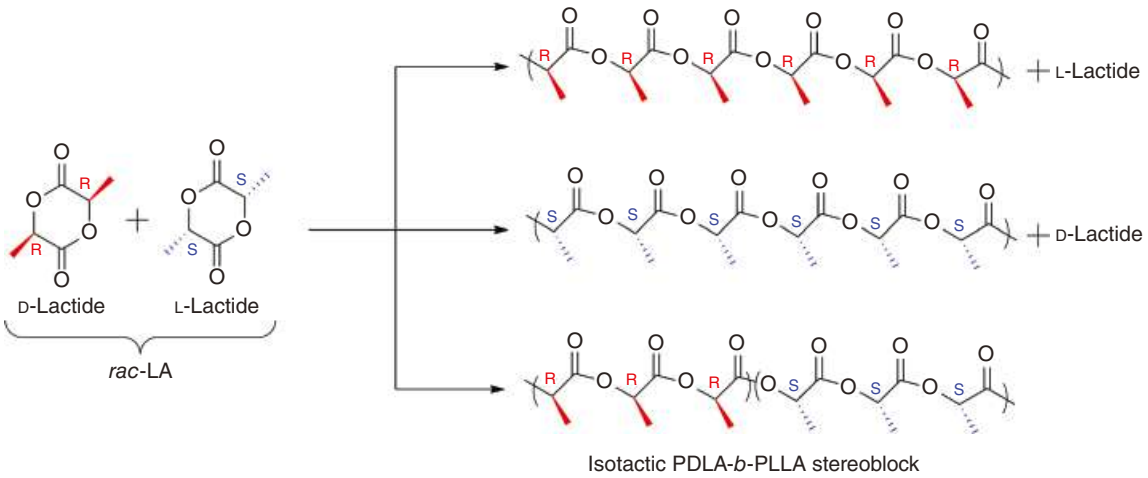


**FIGURE 5.1** Stereoblock PLA formation from rac-LA in a single step.

triethylaluminum-based catalysts [44]. The formation of sc-PLA is supported by XRD analysis; however, the lower degree of isotacticity reduces the $T_m$ of the resulting polymer to ~191°C as compared with ~230°C of the usual sc. The degree of crystallinity of sc-PLA is ~42% as determined from the enthalpy of fusion ($\Delta H_{fus}$). In another study, semi-crystalline stereoblock copolymers with HMW (~461 kg/mol) have been produced from *rac*-LA using chiral oxazolinyl aminophenolate magnesium complexes. The isoselective control of the magnesium complexes is affected by the chirality of the ligand, which may be modified to develop more efficient catalysts [45]. Furthermore, the ROP of *rac*-LA by a series of achiral iron complexes has been performed by Marin et al. to yield HMW stereoblock copolymers [46]. The stereoselective catalysts permit the formation of stereoblock copolymers under mild conditions. The catalyst complex also influences the tacticity of the resulting polymers and the stereochemistry. The thermal degradation temperature of the isotactic stereoblock PLA is increased up to ~350°C, which is reasonably dependent on its molecular weight [46]. The degradation temperature correlates more strongly with the molecular weight than with the stereoregularity. The developed stereoblock PLA having high molecular weight may be used for industrial applications.

### 5.4.2 Stepwise ROP

The well-known sequential polymerization has largely been employed to develop stereoblock PLA with high molecular weight and crystallinity [47]. The formation of diblock copolymers of PLLA and PDLA was first reported by Yui et al. by adopting the sequential ROP strategy using aluminum tris(2-propanolate) as a catalyst [48]. The interaction between the enantiomeric block sequences of di-stereoblock (di-sb) copolymers resulted in the formation of sc crystals with little homo-crystallization. The molecular weight of the diblock copolymers was reported to be ~20 kDa; however, it is often essential to obtain the polymers with HMW (more than 100 kDa) in order to render them processable and dimensionally stable for possible applications. The two-step ROP of L- and D-lactides has been conducted to form di-sb copolymers (PLLA–PDLA) where stannous octoate ($Sn(Oct)_2$) was employed as a catalyst (Figure 5.2). The prepolymer (PLLA or PDLA) having a molecular weight of <50 kDa was prepared in the first step and then purified to remove the residual lactide prior to synthesizing di-sb PLA having different block ratios of PLLA/PDLA in the second stage of ROP. The di-sb-PLA had a $M_w > 150$ kDa, which, when solution-cast into films, showed the formation of exclusive sc crystals. However, the heat deflection temperature of the di-sb PLA having a non-equivalent PLLA/PDLA ratio was somewhat lower, and the di-sb-PLAs having complementary PLLA/PDLA ratios were blended to adjust the whole PLLA/PDLA ratio to 50/50 and to increase the sc crystallinity [49]. In another study, tri-stereoblock (tri-sb) PLAs (ABA) having non-equivalent block compositions were prepared by a two-step ROP in the presence of 1,12-dodecanediol as an initiator. The bis-hydroxyl terminated PDLA was prepared in the first stage of ROP and purified to remove the residual D-lactide. In the second stage of ROP, L-lactide was used as a monomer to develop tri-sb copolymers (PLLA-PDLA-PLLA) with different compositions of PLLA and PDLA blocks (Figure 5.3). The molecular weight of tri-sb copolymers was higher than 100 kDa, and exclusive formation of sc crystals was found out without hc crystallization [50]. Another study applied a living polymerization system using magnesium-based catalysts for synthesizing sb copolymers by the sequential ROP of L- and D-lactides [51]. The first monomer L-lactide was consumed rapidly (in minutes) in the presence of a magnesium complex to yield PLLA with a narrow molecular weight distribution. This process was followed by the addition of D-lactide

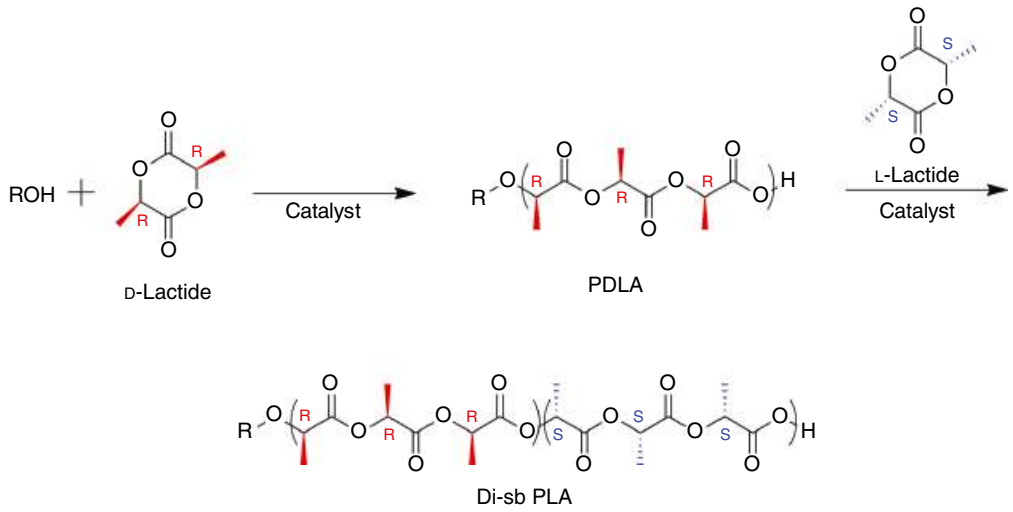


**FIGURE 5.2** Two-step ROP for the synthesis of di-sb-PLA.

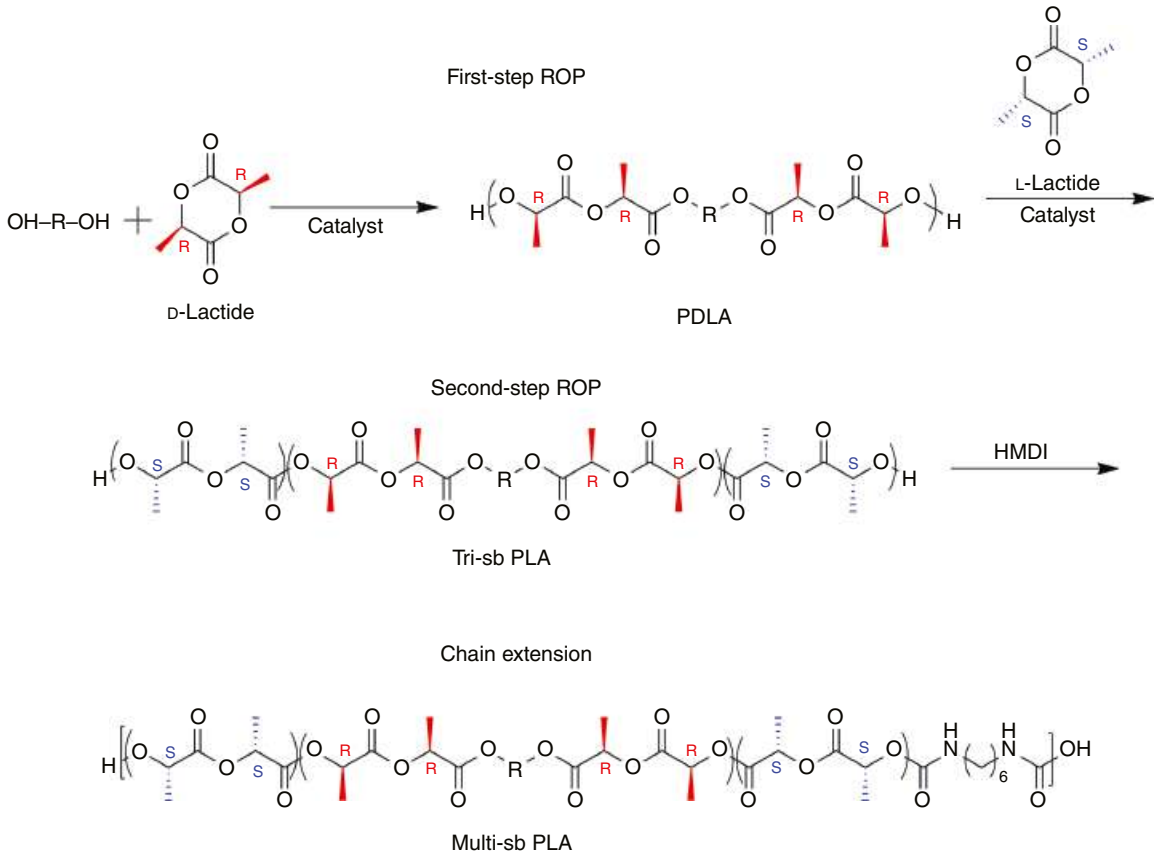


**FIGURE 5.3** Two-step ROP for the synthesis of tri-sb PLA followed by chain extension to form multi-sb-PLA.

monomer for formation of a PLLA-PDLA diblock copolymer with 500 repeating units within 30 min in a one-pot manner. The resultant diblock copolymer having a regulated molecular weight resulted in the exclusive formation of sc crystals.

### 5.4.3 Chain Coupling Method

***5.4.3.1 Chain Extension*** The formation of stereoblock copolymers by chain extension is another strategy well explored by researchers for tailoring the properties of PLA.

In a study reported by our group, the ROP of D- and L-lactides was performed to yield mono-maleimide-terminated PDLA (M-PDLA) and mono-anthracene-terminated PLLA (A-PLLA), respectively [52]. This was followed by the reaction of A-PLLA with hexamethylene diisocyanate (HMDI) to dimerize and form di-anthracene-terminated two-armed PLLA (A-PLLA-A). The stereo di- and tri-block copolymers were readily formed by the terminal Diels-Alder coupling reaction between A-PLLA/M-PDLA and A-PLLA-A/M-PDLA, respectively. This process resulted in the development of copolymers with improved thermomechanical and thermal properties due to the easy sc crystal formation. Extending the possibilities of applying Diels–Alder reactions to the sb-PLA formation, the isocyanate coupling of maleimide-terminated PLLA (M-PLLA) and furan-terminated PDLA (F-PDLA) was conducted to yield bis-maleimide-terminated PLLA (M-PLLA-M) and bis-furan-terminated PDLA (F-PDLA-F), which were mixed in 1 : 1 ratio in solution. The resulting solution was electrospun where the sc-PLA was formed by the terminal Diels–Alder coupling between the respective enantiomeric polymers [53]. The chain extension reaction was ascertained by the molecular weight of the electrospun fibers, which was found to increase from 10 to 45 kDa after the electrospinning and annealing. The fibers (as spun) were converted from the amorphous or semicrystalline state to the fully crystalline state by thermal annealing with the formation of sc crystals [53]. Chain extension by HMDI has also been used to develop multiblock copolymers with significantly improved mechanical properties. In line with this, tri-sb copolymers synthesized by two-step ROP have been subjected to chain extension by using HMDI to develop multiblock sb-PLA (multi-sb) copolymers. For example, tri-sb-PLA copolymers having equivalent composition of PLLA and PDLA enantiomers were reacted with HMDI to form multi-sb-PLA copolymers with controlled block sequences, which were reported to exclusively form sc crystallites by suppressing the hc crystallization [54]. The multi-sb copolymers having longer PLLA/PDLA blocks, upon annealing, showed improved thermo-mechanical properties along with higher sc crystallinity. It was remarked that the thermal properties of multi-sb copolymers can be tailored by controlling the block lengths of tri-sb-PLA [54]. The sc crystallization in multiblock copolymers by dynamic Monte Carlo simulations has been reported by Qiu et al. who identified the effect of block numbers and the crystallization temperature on the sc formation [55]. Several systems with alternating sequences of A and B were used, namely A/B blend, A–B diblock, tetrablock, octablock, and sixteen-block copolymers. In multiblock copolymers with low block numbers, sc formation was found to increase with increasing crystallization temperature. The effect of crystallization temperature was not detected for the multiblock copolymers with relatively high block numbers. The miscibility between the different blocks, the block length, and the size of the crystal thickness were reported to be the governing parameters for sc formation in the multiblock copolymers.

***5.4.3.2 Click Chemistry*** Click chemistry [56] has evolved as an efficient and simple approach to develop HMW sb-PLA with controlled block lengths and chain architecture. The combination of ROP and click chemistry has been shown by Han et al. to prepare HMW sb-PLA (PLLA–PDLA) with controlled composition and block length [57]. The sc-crystallinity was found to increase when the PLLA/PDLA block ratio approached 50/50, which also increased the storage modulus of HMW sb-PLA. In another study, Isono et al. applied the combination of sb and star polymer approaches and succeeded in synthesizing stereo-miktoarm star-shaped PLAs by a click coupling method [58]. This approach led to the preferential sc formation in the solution cast samples, without any homo-crystallite formation. The variation in the arm number also led to the variation in $T_m$ of the stereo-miktoarm star polymers, thereby providing a mechanism to tailor the physical properties of sc-type PLAs. Besides these approaches, the synthesis of cyclic stereoblock copolymers of PLLA and PDLA with head-to-head and head-to-tail configurations has been carried out by implementing the click chemistry and ring closing metathesis approaches [59]. The orientation of PLLA and PDLA segments in the cyclic structure may be controlled in a facile way by using this approach, along with modulated thermal properties.

***5.4.3.3 Polycondensation*** The melt polycondensation of low-molecular-weight PLLA/PDLA blends has been adopted to synthesize stereo multiblock PLAs having different block lengths. In contrast to the chain extension reaction, the stereo multiblock PLAs synthesized by melt-polycondensation have higher crystallizability due to the connecting ester groups [60]. Further, stereo multiblock copolymers were synthesized by melt-polycondensation as reported by Rahaman et al. with a wide range of block lengths [61], which led to the preferential formation of stereocomplex crystallites irrespective of the crystallization temperature and block length. In a study reported by our group, the PLLA and PDLA prepolymers were made by the melt-polycondensation technique and mixed to develop sb-PLA consisting of short sequences of D- and L-lactate units where the molecular weight was as high as 100 kDa at the reaction temperature of 180°C [62]. The molecular weight of the homopolymer PLLA or PDLA obtained by SSP was much higher than sc-PLA, even at a considerably lower reaction temperature. This fact was attributed to the partial chain racemization and difficulty of the elongated chains to crystallize out of the amorphous domain into the solid state. To enhance the crystallization of the elongated chains, it

was speculated that the presence of homo-crystallites may be essential. To further substantiate the hypothesis, non-equivalent mixtures of PLLA and PDLA were used for SSP [63]. The melt blending of PLLA and PDLA (medium molecular weight) obtained by melt-polycondensation of L- and D-lactic acids was performed to obtain sb-copolymers with different compositions and block sequences. The SSP reaction under mild conditions resulted in products with higher yield and larger molecular weight. The molecular weight and the composition of the block sequences were found to govern the thermal properties. The elongated chains of the homo-sequences were able to crystallize out from the reaction system to allow for the chain extension reaction. Thus, the necessity of the hc domain for developing sb-PLA with HMW by SSP was determined. Based on this evidence, a new design was proposed where the prepolymers PLLA and PDLA were mixed in the powder state (1 : 1) and subjected to heat treatment to form partial sc-crystallization at the boundaries, followed by conducting SSP without reaching the melt-blending state [64]. This method led the elongated hc chains to crystallize out from the reaction system along with an increase in the molecular weight. The block structure was formed by the hetero-coupling reaction in the minor sc-domain resulting in complete sc formation upon melt quenching. This method led to the formation of sc-PLA having HMW suitable for high temperature applications such as car parts and housings of electrical appliances. The SSP of PLA enantiomers using methanesulfonic acid (SO) has been conducted by Kanno et al. to form sb-PLA [65]. The sb copolymers were obtained with higher crystallinity when the chain length of the PLA was shorter. The structure and yield of the sb-PLA were affected by the catalyst system used [65]. The tin-based catalyst was found to induce side reactions during the SSP with a lower yield of sb-PLA and to reduce the glass transition temperature ($T_g$), whereas SO resulted in the inhibition of side reactions and formation of HMW sb-PLA with an efficient polymerization process. The molecular weight of the PLA starting materials and the catalyst used were found to be the governing parameters for synthesizing sb-PLA. Figure 5.4 shows a schematic representation of the methods used for developing sb-PLA.

## 5.5 STEREOCOMPLEXATION IN COPOLYMERS

The formation of sc-PLA has been studied with various copolymers of enantiomeric PLAs with other well-known bio-based/biodegradable polymers such as PCL, PEG, and so on due to the complementary properties of the counterparts, which may lead to materials with customized properties. The mechanical and thermal properties of representative bio-based/biodegradable polymers used for copolymerization are summarized in Table 5.2.

### 5.5.1 Stereocomplexation in Random and Alternating Lactic Acid or Lactide-Based Polymers

Stereocomplex crystallites can be formed only by the interaction of enantiomeric PLA chains (PLLA and PDLA), which can be controlled during melt processing. Further, sc-PLA has a limited ability to reform its crystallinity after

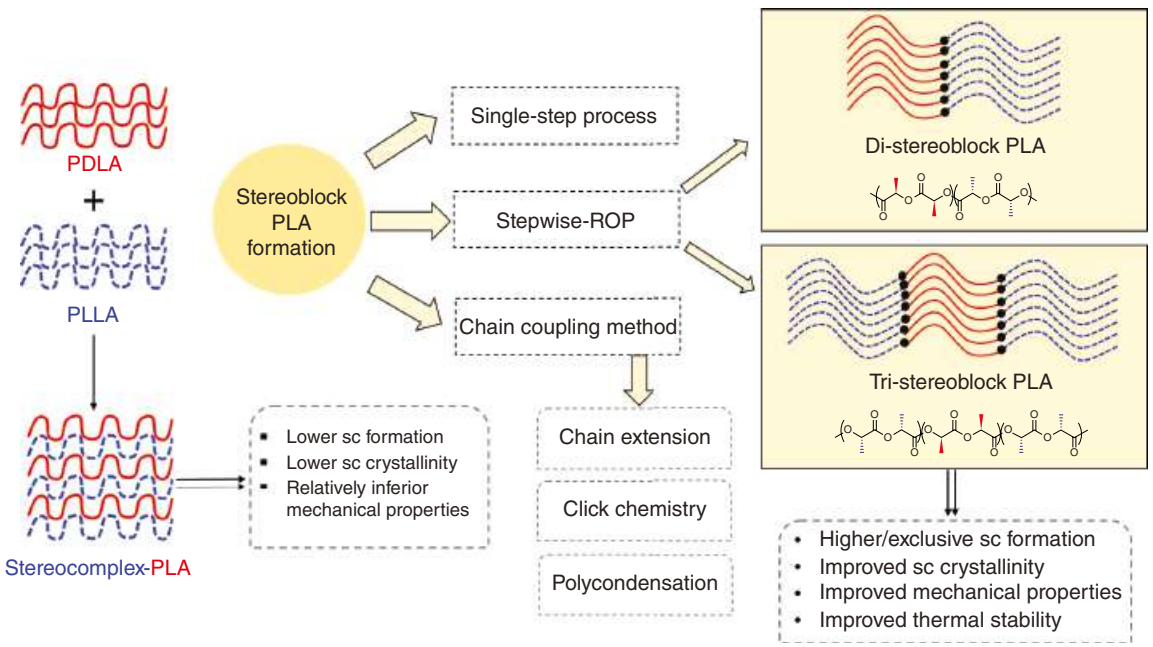


**FIGURE 5.4** Schematic representation of the methods adopted for developing sb-PLA.

**TABLE 5.2 Mechanical and Thermal Properties of the Representative Bio-Based/Bio-Degradable Polymers**

| | PLLA | sc-PLA | PGA | PHB | PCL |
|---|---|---|---|---|---|
| $T_m$ (°C) | 170–190 | 220–240 | 225–230 | 188–197 | 55–65 |
| $T_g$ (°C) | 50–65 | 65–72 | 40 | 5 | −60 |
| $\Delta H_m$ (J/g) | 93–203 | 142–155 | 180–207 | 146 | 136 |
| Density (g/cm$^3$) | 1.25–1.3 | 1.21–1.342 | 1.50–1.69 | 1.18–1.26 | 1.1–1.15 |
| Tensile strength (MPa) | 120–2260 | 880 | 80–980 | 180–200 | 8–16 |
| Young's modulus (GPa) | 6.9–9.8 | 8.6 | 3.9–1.4 | 4.9–5.9 | 0.1–0.4 |
| Elongation at break (%) | 12–16 | 30 | 30–40 | 50–70 | 100–2000 |

being melted (removal of thermal history). To improve the molecular interaction between PLLA and PDLA, Purnama et al. have studied stereocomplexation in the blend of PLLA and random copolymer (PDLCL) of D-lactide with small amount of caprolactone (CL) [66]. The small amount of CL units in PDLCL act as soft fraction (due to the presence of methylene linkage) in the polymeric system to provide relatively low glass transition and melting temperatures. Further, this soft fraction accelerates the PDLA chain movement to easily interact with PLLA chains, thereby resulting in improved melt stability of sc crystallites. They also reported that the system resulted in the maximum sc crystallinity when the amount of CL was 2.5 unit-mol%. It was however indicated that the excess use of CL may lead to overactive mobility of PDLA chains, ultimately affecting the stereocomplexation. In an another approach, Jikei et al. attempted to develop a segmented, random multiblock copolymer of PLLA and PCL and blended it with PDLA to improve the stereocomplexation [67]. The soft segment PCL aided in improving the elongation at break (over 400%) of PLLA, whereas preferential formation of stereocomplex crystallites in hard domain (containing PLLA and PDLA) contributed to enhancing the Young's modulus (over 400 MPa) and ultimately improved the overall toughness of the blend. In particular, the physical crosslinking in hard domain also contributed to enhance the thermal deformation stability of the blend.

Furthermore, stereocomplexation involving alternating copolymers comprising lactic acid (LA) units have been studied extensively. For example, blending of enantiomeric alternating copolymer of LA and glycolic acid (GA) having molecular weight of 5000 Da leads to preferential formation of stereocomplex crystallites as reported by Tsuji et al. [68]. They proposed that blending of alternating LA-based copolymers could be a versatile technique for the development of high-performance bio-based biodegradable materials with tunable physical properties and biodegradability. Yet another study reports the incorporation of alanine unit into LA units in random copoly(ester-amides) with ester and amide linkages leading to the preferential formation of sc crystallites [69]. However, the developed polymers contain low degree of polymerization, and to have them employed in the commercial scale utility, further development is needed.

### 5.5.2 sc-PLA–PCL Copolymers

Lately, there have been important advances in sc blends of PLA copolymers for biomedical implant applications. In a study reported by us [70], diblock copolymers of PCL-PLLA and PCL-PDLA were synthesized by two-step ROP followed by blending them in a 1 : 1 ratio to achieve sc blends of the enantiomeric diblock copolymers. Using this strategy, it was possible to obtain enantiomeric diblock copolymers having enhanced mechanical properties (28 MPa strength and ~80% elongation at break), which were also processed by the conventional injection moulding technique to develop cancellous bone screws (orthopedic implants). The study reported the thermomechanical stability of the cancellous bone screw at 121°C in comparison to commercial PLA (2003D, NatureWorks LLC). The stereococomplexed diblock copolymer was found to be stable at the sterilization temperature of biomedical devices, unlike the commercial PLA sample. The biocompatibility of the synthesized sc diblock copolymer blend was also ascertained by MTT (3-(4, 5-dimethylthiazol-2-yl)-2,5-diphenyl tetrazolium bromide) assay using MG-63 cells (human bone osteosarcoma). In another study reported by our group, the triblock copolymers of PLLA-PCL-PLLA and PDLA-PCL-PDLA were synthesized by sequential ROP, where the block length of the terminal as well the mid segment was tailored. The enantiomeric triblock copolymers were blended in equal ratios to achieve the sc blends of triblock copolymers. Such blends of triblock copolymers resulted in a significant improvement in the elongation at break (~400 - 700%) as well as Young's modulus (0.3 - 0.9 GPa), with a very low degree of sc crystallinity. The adhesion and growth of UMR-106 cells (rat bone osteosarcoma) on the surface of the developed sc triblock copolymer further indicated its non-toxic nature. [100].

### 5.5.3 sc-PLA–PEG Copolymers

Polyethylene glycol, being hydrophilic in nature, leads to the development of amphiphilic materials when used in combination with hydrophobic polymers [71, 72]. Amphiphilic copolymers based on PLA [73] have received attention in several applications including pharmaceutical, drug delivery [74, 75], hydrogels for tissue engineering [76], and so on. The aqueous self-assembly of amphiphilic PEG-sc-PLA copolymers has been reported by Noack et al. [77] where the block

**TABLE 5.3 Thermal and Mechanical Properties Reported for the sc-PLA-Based Copolymers and Composites**

| | Mulchandani et al. [70] | Mulchandani et al. [100] | Noack et al. [77] | Sun et al. [79] | Gupta et al. [80] | Gupta et al. [81] | Gupta et al. [82] |
|---|---|---|---|---|---|---|---|
| Copolymer/composite | sc-PLA/PCL | sc-PLA/PCL | sc-PLA/PEG | sc-PLA/GO | sc-PLA/chitosan | sc-PLA/CMC | sc-PLA/n-HAP |
| $T_{m,hc}$ (°C) | 171–177 | 167–173 | — | 150 | — | 152–180 | 152–178 |
| $T_{m,sc}$ (°C) | 210–235 | 218–222 | 140–200 | 210 | 192–208 | 211 | 210 |
| $\Delta H_{m,hc}$ (J/g) | 10–23 | 3.9–27.7 | — | — | — | — | 0–28 |
| $\Delta H_{m,sc}$ (J/g) | 30–42 | 22–45.3 | — | — | 20–40 | — | 17–55 |
| Crystallinity sc (%) | — | 1–9 | — | 40–70 | ~70 | 55 | 12–39 |
| Tensile strength (MPa) | 14–30 | 15–33 | — | — | 29–63 | 29–57 | 33–40 |
| Elongation at break (%) | 7–80 | 400–700 | — | — | — | 1.9–36 | 6.3–131 |
| Young's modulus (GPa) | 0.3–0.7 | 0.3 – 0.9 | — | — | 1.9–2.8 | — | — |

copolymers PEG–PLLA and PEG–PDLA were synthesized by ROP using polyethylene glycol monomethyl ether (PEG–OH) as a macroinitiator for the enantiomeric polymer blending. In these sc-block copolymers, the decreasing hydrophobic unit (lactide) content led to the increased formation of worm-like aggregates at ambient conditions. The preferential formation of spherical micelles was observed for the most related block copolymers (as revealed from the dynamic light scattering analysis), which became colloidally unstable upon increasing the crystalline PLA, leading to the formation of worm-like aggregates [77]. Bio-functional injectable hydrogels based on PEG-sc-PLA were reported by Wang et al. for cartilage tissue engineering [78]. The ROP of D- and L-lactides was performed using four-arm PEG as a macroinitiator to develop four-arm PEG-PDLA and PEG-PLLA copolymers, respectively. This was followed by synthesizing their cholesterol (Chol)-modified derivatives, namely four-arm PEG-PDLA-Chol and four-arm PEG-PLLA-Chol, by condensation reaction. The sc blends of the both enantiomers resulted in the stereocomplexes, scPLA (four-arm-PEG-PLA) and scPLA-Chol (four-arm PEG-PLA-Chol), which were employed as 3D scaffolds for cartilage tissue engineering. The cholesterol-modified sc-PLA-Chol had a higher critical gelation temperature, improved mechanical properties, better adhesion to chondrocytes, and slower degradation than the non-cholesterol-modified derivatives, which served as an appropriate material for cartilage regeneration. The thermal and mechanical properties of the sc-PLA-based copolymers and composites are reported in Table 5.3.

## 5.6 STEREOCOMPLEX PLA-BASED COMPOSITES

Stereocomplexation has been used by researchers to impart heat stability to composites. In principle, when the desired properties cannot be achieved by a single component, the incorporation of several fillers may lead to the tailored/desired properties. Stereocomplexed PLA is known for its enhanced thermal resistance, which has been incorporated and modified with fillers such as hydroxyapatite, chitosan, cellulose, graphene, and so on to obtain materials with customized properties. To this end, Total Corbion PLA, a European joint venture company, has already started the development of glass fiber-reinforced sc-PLA as an engineering plastic for automotive, aerospace, electronics, home appliance, marine, and construction industries [83]. Sun et al. have grafted graphene oxide (GO) to PDLA by ROP of D-lactide, where the OH groups on the GO acted as initiator [79]. The grafted PDLA was then blended with PLLA in solution for casting of sc nanocomposite films. The activation energy of crystallization was lowered along with an increased fraction of sc crystallites and improved crystallinity of the nanocomposites, as compared with the PLLA/PDLA blends without the GO filler. This effect may be attributed to the heterogeneous nucleation of GO. The cold crystallization, however, led to lower crystallinity, possibly due to the reduced chain mobility and hindered crystal growth resulting from the exfoliated GO sheets.

Furthermore, Gupta et al. have demonstrated the use of nano-amphiphilic chitosan to develop highly heat stable sc-PLA [80]. The grafting of chitosan to the oligomeric PLLA was done via in situ polycondensation of L-lactic acid to synthesize nano-amphiphilic chitosan. The PLLA-modified chitosan (0.5–1.5%) along with PLLA/PDLA (50/50) was melt blended using extrusion followed by injection moulding to form dumbbell sc nanocomposite specimens. Heat treatment (annealing above 160°C) led to the exclusive formation of sc crystals with ~40% crystallinity. Also, cooling the nanocomposite from the melt at 2°C/min increased the crystallinity to ~70% with an exclusive formation of sc crystals. The heat distortion temperature was elevated from 70(sc-PLA) to 145°C for the sc nanocomposite containing 1.5% filler. In another study, the use of nano-amphiphilic chitosan (1–3%) in the blends of PLLA/PDLA (50/50) has been demonstrated [20]. The filler was mixed with equal amounts of PLLA and PDLA and mixed by stirring followed by solvent casting into films. The solvent (chloroform) was allowed to evaporate at room temperature for 24 h followed by drying under vacuum at 50°C for 24 h and then annealing at 120°C for 2 h. The sc

crystallites were formed in the nanocomposites with a ~56% crystallinity, where the degree of stereocomplexation became higher upon melt cooling as compared with annealing the blend film of PLLA/PDLA (control). The nanocomposite films showed ~56% reduction in the oxygen permeability as compared with the blend film of PLLA/PDLA (control). The addition of the nanofiller also led to an increase in hydrophobicity of the nanocomposite, which was attributed to the increased surface roughness, as well as crystallinity. The viability of fibroblast cells (BHK-21) on the surface of the nanocomposites have been determined, manifesting the biocompatible behavior of the composite materials.

In another study, the biocomposites of sc-PLA were prepared by employing cellulose microcrystals (CMC) as a filler (1–10%). The ROP technique was used to develop PDLA-grafted CMC, which was mixed with PLLA at 50/50 ratio and melt extruded, followed by injection moulding to prepare the biocomposite specimens. The improved dispersion of CMC led to the formation of sc crystallites and suppressed the homo-crystallite formation. This CMC/sc-PLA biocomposites resulted in significant improvement of the tensile strength (~96%) as compared with sc-PLA along with a high storage modulus (~3500 Pa). The enhanced sc formation and the incorporation of CMC reduced the permeability of oxygen and water vapor, suggesting its potential for engineering and packaging applications [81].

The use of nano-hydroxyapatite (n-HAP) has drawn enormous attention in the biomedical field because hard biotissues such as human bones and teeth are composed of n-HAP. In order to exploit sc-PLA and n-HAP for biomedical applications, their biocomposites were prepared in a study by Gupta et al.; the n-HAP was grafted to PDLA via in situ ROP where the OH groups on n-HAP acted as initiating species. The grafting was confirmed by $^{13}C$ NMR and thermogravimetric analysis [82]. The grafted PDLA was blended with PLLA to develop sc biocomposites, which gave the exclusive formation of sc crystallites due to the improved dispersion of n-HAP and extended molecular surface area provided by the PDLA chains. The nanocomposites exhibited improved mechanical properties (~40 MPa in strength, ~132% elongation at break, and ~47% increase in storage modulus). The increase in crystallinity resulted in improved resistance to moisture, as well. The viability of BHK-21 cells on the nanocomposites revealed their applicability as a biomaterial.

These findings show that sc-PLA-based copolymers and composites are promising for addressing polymer processing and application concerns in the packaging and biomedical domains. The applications of sc-PLA-based copolymers and composites are shown in Figure 5.5.

## 5.7 Advances in Stereocomplex-PLA

Several processing techniques such as electrospinning [29, 84] and melt spinning [85] have gained enormous recognition for developing sc-PLA fibers with improved stereocomplexation [86–88]. Often, targeted biomedical applications require a controlled hierarchy, which may be possible by selectively modifying the surface of nanofibers [89]. One such method reported by Xie et al. is the combined use of electrospinning and a controlled polymerization technique for designing PLA nanofiber shish kebabs. The sc-PLA nanofibers produced by electrospinning are used as the shish where the secondary polymer (hc-PLA or sc-PLA) is decorated to form a kebab lamella. The soft epitaxy mechanism possibly leads to the formation of shish kebab structures where the sc-PLA nanofibers (shish) serve as the nucleating sites for kebab lamellae [25]. Such controlled mechanisms are of substantial importance when functionalizing the surface of nanofibers required for intended applications. Furthermore, the functionalization of sc-PLA using cyclodextrins has facilitated their use as pollutant absorbers

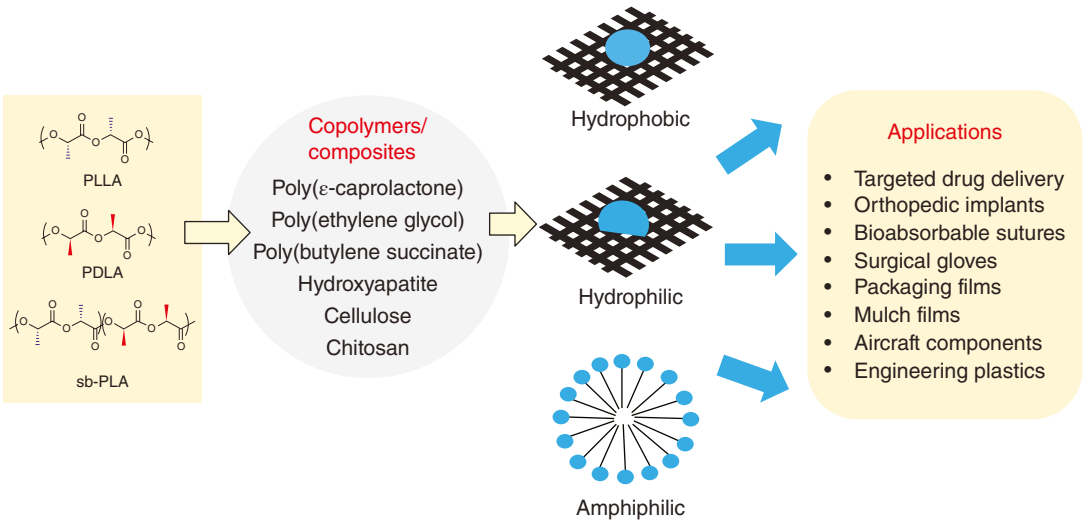


**FIGURE 5.5** Applications of the sc-PLA-based copolymers and composites.

and drug carriers [90]. The exclusive formation of sc-PLA has been achieved during electrospinning along with its functionalization, where the sub-micrometer dispersion of nanofillers, namely polyhedral oligomeric silsesquioxanes (POSS), has been established. The functionalized sc-PLA retains the capability of forming pure stereocomplex upon annealing [91]. Nevertheless, efforts have also been made to tune the hydrolytic degradation of sc-PLA by tailoring the backbone architecture. Stereocomplexation between PLLA and PDLA oligomers has been reported, where the polymer architecture and the end groups altered the hydrolytic degradation rate [92]. Namely, the linear sc architecture having alcoholic end groups exhibited an increased degree of stereocomplexation with higher hydrolytic stability. In contrast, for the polymer with carboxyl chain ends, the degradation was accelerated due to the lower degree of stereocomplexation. The use of sc-PLA has also been explored in textiles and membranes for oil–water separation. The modification of PLA nonwoven fabric by the formation of sc crystals has been reported by Zhu et al., where the sc crystal phase increased the surface roughness, as well as imparted oleophilicity to the fabric. The modification of the surface by sc-PLA increased the oil absorption capability by 30–40% [93], which can be repeatedly used for the same purpose. The sc-PLA, being brittle in nature, is limited to only specific applications. When exploring sc-PLA for tissue engineering applications, elasticity is often required for the scaffold materials to serve physiological functions [94, 95]. This may be made possible by using toughness modifiers [96, 97]. For example, poly(butylene adipate-*co*-terephthalate) (PBAT) may be regarded as a toughness modifier when loaded into the matrix of PLA to increase elongation and processability [98]. The sc-PLA/PBAT scaffolds with high porosity have been prepared by Kang et al. by non-solvent phase separation [99]. The sc-PLA-based scaffolds led to a uniform porous structure (as compared to PLLA- or PDLA-based scaffolds) having a wall thickness of ~1 μm, which may be due to the intermolecular forces between the enantiomeric PLA chains. The sc-PLA/PBAT scaffolds are capable of supporting the adhesion of fibroblast cells, which in turn accounts for its biocompatible nature.

## 5.8 CONCLUSIONS

Stereocomplexation in PLA has resulted in widespread acceptance accounting to its unique thermal, mechanical, and physical properties. The current chapter has underlined various techniques of achieving improved stereocomplexation in PLA, such as stereoblock formation, copolymerization, and composite formation. These techniques result in the formation of intended materials with customized properties, which have been manifested in the current chapter. Further, insights have been made into the melt-crystallizability of sc-PLA in view of improving its industrial applications. An emphasis has also been laid on improving the biocompatibility of sc-PLA-based materials for potential biomedical applications. It may be recognized that the bio-based polymers/copolymers/composites built on sc-PLA could replace the conventional polymers in multifaceted applications and reduce the human dependence on fossil resources, as well as the carbon dioxide loading on the global sphere.

## REFERENCES


1. M. Brzeziński, T. Biela, Stereocomplexed polylactides, in: S. Kobayashi, K. Müllen (Eds.), *Encyclopedia of Polymeric Nanomaterials*, Springer Berlin Heidelberg, Berlin, Heidelberg, 2014. p. 1–10.
2. Y. Ikada, K. Jamshidi, H. Tsuji, S. H. Hyon, Stereocomplex formation between enantiomeric poly(lactides), *Macromolecules* **1987**, *20*(4), 904–906.
3. J. R. Murdoch, G. L. Loomis, Polylactide compositions, US4719246A, 1988.
4. F. Luo, A. Fortenberry, J. Ren, Z. Qiang, Recent progress in enhancing poly(lactic acid) stereocomplex formation for material property improvement, *Front. Chem.* **2020**, *8*, 688.
5. D. Karst, Y. Yang, Molecular modeling study of the resistance of PLA to hydrolysis based on the blending of PLLA and PDLA, *Polymer* **2006**, *47*(13), 4845–4850.
6. H. Tsuji in vitro hydrolysis of blends from enantiomeric poly(lactide)s. Part 4: well-homo-crystallized blend and non-blended films, *Biomaterials* **2003**, *24*(4), 537–547.
7. M. Kakuta, M. Hirata, Y. Kimura, Stereoblock polylactides as high-performance bio-based polymers, *Polym. Rev.* **2009**, *49*(2), 107–140.
8. H. Tsuji, Poly(lactic acid) stereocomplexes: a decade of progress, *Adv. Drug Deliv. Rev.* **2016**, *107*, 97–135.
9. M. Saravanan, A. J. Domb, A contemporary review on—polymer stereocomplexes and its biomedical application, *Eur. J. Nanomed.* **2013**, *5*(2), 81–96.
10. P. Pan, Y. Inoue, Polymorphism and isomorphism in biodegradable polyesters, *Progr. Polym. Sci.* **2009**, *34*(7), 605–640.
11. L. Han, P. Pan, G. Shan, Y. Bao, Stereocomplex crystallization of high-molecular-weight poly(L-lactic acid)/poly(D-lactic acid) racemic blends promoted by a selective nucleator, *Polymer* **2015**, *63*, 144–153.
12. S. Nagarajan, D. Krishnan, V. P. Sivaprasad, E. Bhoje Gowd, Chapter 5—Crystallization behavior of crystalline–amorphous and crystalline–crystalline block copolymers containing poly(L-lactide), in: S. Thomas, P. M. Arif, E. B. Gowd, N. Kalarikkal (Eds.), *Crystallization in Multiphase Polymer Systems*, Elsevier, Amsterdam, 2018, pp. 93–122.
13. H. Tsuji, F. Horii, S. H. Hyon, Y. Ikada, Stereocomplex formation between enantiomeric poly(lactic acid)s. 2. Stereocomplex formation in concentrated solutions, *Macromolecules* **1991**, *24*(10), 2719–2724.
14. K. Scheuer, D. Bandelli, C. Helbing, C. Weber, J. Alex, J. B. Max, et al., Self-assembly of copolyesters into stereocomplex

crystallites tunes the properties of polyester nanoparticles, *Macromolecules* **2020**, *53*(19), 8340–8351.

15. B. Na, J. Zhu, R. Lv, Y. Ju, R. Tian, B. Chen, Stereocomplex formation in enantiomeric polylactides by melting recrystallization of homocrystals: crystallization kinetics and crystal morphology, *Macromolecules* **2014**, *47*(1), 347–352.
16. H. Tsuji, S. Yamamoto, Enhanced stereocomplex crystallization of biodegradable enantiomeric poly(lactic acid)s by repeated casting, *Macromol. Mater. Eng.* **2011**, *296*(7), 583–589.
17. R. Lv, N. Peng, T. Jin, B. Na, J. Wang, H. Liu, Stereocomplex mesophase and its phase transition in enantiomeric polylactides, *Polymer* **2017**, *116*, 324–330.
18. E. M. Woo, L. Chang, Crystallization and morphology of stereocomplexes in nonequimolar mixtures of poly(L-lactic acid) with excess poly(D-lactic acid), *Polymer* **2011**, *52*(26), 6080–6089.
19. L. Gardella, A. Basso, M. Prato, O. Monticelli, On stereocomplexed polylactide materials as support for PAMAM dendrimers: synthesis and properties, *RSC Adv.* **2015**, *5*(58), 46774–46784.
20. A. Gupta, N. Mulchandani, M. Shah, S. Kumar, V. Katiyar, Functionalized chitosan mediated stereocomplexation of poly(lactic acid): influence on crystallization, oxygen permeability, wettability and biocompatibility behavior, *Polymer* **2018**, *142*, 196–208.
21. L. Bouapao, H. Tsuji, Stereocomplex crystallization and spherulite growth of low molecular weight poly(L-lactide) and poly(D-lactide) from the melt, *Macromol. Chem. Phys.* **2009**, *210*(12), 993–1002.
22. T. Biela, A. Duda, S. Penczek, Enhanced melt stability of star-shaped stereocomplexes as compared with linear stereocomplexes, *Macromolecules* **2006**, *39*(11), 3710–3713.
23. L. Jiang, P. Lv, P. Ma, H. Bai, W. Dong, M. Chen, Stereocomplexation kinetics of enantiomeric poly(L-lactide)/poly(D-lactide) blends seeded by nanocrystalline cellulose, *RSC Adv.* **2015**, *5*(87), 71115–71119.
24. Z. Xiong, X. Zhang, R. Wang, S. de Vos, R. Wang, C. A. P. Joziasse, et al., Favorable formation of stereocomplex crystals in poly(L-lactide)/poly(D-lactide) blends by selective nucleation, *Polymer* **2015**, *76*, 98–104.
25. Q. Xie, X. Chang, Q. Qian, P. Pan, C. Y. Li, Structure and morphology of poly(lactic acid) stereocomplex nanofiber shish kebabs, *ACS Macro Lett.* **2020**, *9*(1), 103–107.
26. M. Septiyanti, A. A. Septevani, M. Ghozali, S. Fahmiati, E. Triwulandari, W. K. Restu, et al., Effect of solvent combination on electrospun stereocomplex polylactic acid nanofiber properties, *Macromol. Symp.* **2020**, *391*(1), 1900134.
27. N. Kurokawa, A. Hotta, Thermomechanical properties of highly transparent self-reinforced polylactide composites with electrospun stereocomplex polylactide nanofibers, *Polymer* **2018**, *153*, 214–222.
28. M. Spasova, N. Manolova, D. Paneva, R. Mincheva, P. Dubois, I. Rashkov, et al., Polylactide stereocomplex-based electrospun materials possessing surface with antibacterial and hemostatic properties, *Biomacromolecules* **2010**, *11*(1), 151–159.
29. H. Tsuji, M. Nakano, M. Hashimoto, K. Takashima, S. Katsura, A. Mizuno, Electrospinning of poly(lactic acid) stereocomplex nanofibers, *Biomacromolecules* **2006**, *7*(12), 3316–3320.
30. Y. Furuhashi, Y. Kimura, N. Yoshie, Self-assembly of stereocomplex-type poly(lactic acid), *Polym. J.* **2006**, *38*(10), 1061–1067.
31. L. Cartier, T. Okihara, Y. Ikada, H. Tsuji, J. Puiggali, B. Lotz, Epitaxial crystallization and crystalline polymorphism of polylactides, *Polymer* **2000**, *41*(25), 8909–8919.
32. T. Okihara, M. Tsuji, A. Kawaguchi, K.-I. Katayama, H. Tsuji, S.-H. Hyon, et al., Crystal structure of stereocomplex of poly(L-lactide) and poly(D-lactide), *J. Macromol. Sci. Part B* **1991**, *30*(1–2), 119–140.
33. L. Cartier, T. Okihara, B. Lotz, Triangular polymer single crystals: stereocomplexes, twins, and frustrated structures, *Macromolecules* **1997**, *30*(20), 6313–6322.
34. D. Brizzolara, H.-J. Cantow, K. Diederichs, E. Keller, A. J. Domb, Mechanism of the stereocomplex formation between enantiomeric poly(lactide)s, *Macromolecules* **1996**, *29*(1), 191–197.
35. D. Sawai, Y. Tsugane, M. Tamada, T. Kanamoto, M. Sungil, S.-H. Hyon, Crystal density and heat of fusion for a stereocomplex of poly(L-lactic acid) and poly(D-lactic acid), *J. Polym. Sci. Part B Polym. Phys.* **2007**, *45*(18), 2632–2639.
36. K. Tashiro, N. Kouno, H. Wang, H. Tsuji, Crystal structure of poly(lactic acid) stereocomplex: random packing model of PDLA and PLLA chains as studied by X-ray diffraction analysis, *Macromolecules* **2017**, *50*(20), 8048–8065.
37. K. Tashiro, H. Wang, N. Kouno, J. Koshobu, K. Watanabe, Confirmation of the X-ray-analyzed heterogeneous distribution of the PDLA and PLLA chain stems in the crystal lattice of poly(lactic acid) stereocomplex on the basis of the vibrational circular dichroism IR spectral measurement, *Macromolecules* **2017**, *50*(20), 8066–8071.
38. M. Spinu, C. Jackson, M. Y. Keating, K. H. Gardner, Material design in poly(lactic acid) systems: block copolymers, star homo- and copolymers, and stereocomplexes, *J. Macromol. Sci. Part A* **1996**, *33*(10), 1497–1530.
39. Z. Kan, W. Luo, T. Shi, C. Wei, B. Han, D. Zheng, et al., Facile preparation of stereoblock PLA from ring-opening polymerization of *rac*-lactide by a synergetic binary catalytic system containing ureas and alkoxides, *Front. Chem.* **2018**, *6*, 547.
40. M. Hirata, K. Masutani, Y. Kimura, Synthesis of ABCBA penta stereoblock polylactide copolymers by two-step ring-opening polymerization of L- and D-lactides with poly(3-methyl-1,5-pentylene succinate) as macroinitiator (C): development of flexible stereocomplexed polylactide materials, *Biomacromolecules* **2013**, *14*(7), 2154–2161.
41. R. H. Platel, L. M. Hodgson, C. K. Williams, Biocompatible initiators for lactide polymerization, *Polym. Rev.* **2008**, *48*(1), 11–63.
42. M. J. Stanford, A. P. Dove, Stereocontrolled ring-opening polymerisation of lactide, *Chem. Soc. Rev.* **2010**, *39*(2), 486–494.
43. C. M. Thomas, Stereocontrolled ring-opening polymerization of cyclic esters: synthesis of new polyester microstructures, *Chem. Soc. Rev.* **2010**, *39*(1), 165–173.
44. C. P. Radano, G. L. Baker, M. R. Smith, Stereoselective polymerization of a racemic monomer with a racemic catalyst: direct preparation of the polylactic acid stereocomplex from racemic lactide, *J. Am. Chem. Soc.* **2000**, *122*(7), 1552–1553.

45. J. Hu, C. Kan, H. Wang, H. Ma, Highly active chiral oxazolinyl aminophenolate magnesium initiators for isoselective ring-opening polymerization of *rac*-lactide: dinuclearity induced enantiomorphic site control, *Macromolecules* **2018**, *51*(14), 5304–5312.
46. P. Marin, M. J.-L. Tschan, F. Isnard, C. Robert, P. Haquette, X. Trivelli, et al., Polymerization of *rac*-lactide using achiral iron complexes: access to thermally stable stereocomplexes, *Angew. Chem. Int. Edn.* **2019**, *58*(36), 12585–12589.
47. H. Tsuji, T. Tajima, Relatively short poly(D-lactide) segments as intra-crystallization-accelerating moieties in stereo diblock poly(lactide)s, *Macromol. Mater. Eng.* **2014**, *299*(4), 430–435.
48. N. Yui, P. J. Dijkstra, J. Feijen, Stereo block copolymers of L- and D-lactides, *Makromol. Chem.* **1990**, *191*(3), 481–488.
49. M. Hirata, K. Kobayashi, Y. Kimura, Synthesis and properties of high-molecular-weight stereo di-block polylactides with nonequivalent D/L ratios, *J. Polym. Sci. Part A Polym. Chem.* **2010**, *48*(4), 794–801.
50. K. Masutani, C. W. Lee, Y. Kimura, Synthesis and thermomechanical properties of stereo triblock polylactides with non-equivalent block compositions, *Macromol. Chem. Phys.* **2012**, *213*(7), 695–704.
51. T. Rosen, I. Goldberg, V. Venditto, M. Kol, Tailor-made stereoblock copolymers of poly(lactic acid) by a truly living polymerization catalyst, *J. Am. Chem. Soc.* **2016**, *138*(37), 12041–12044.
52. K. Masutani, C. W. Lee, Y. Kimura, Synthesis and properties of stereo di- and tri-block polylactides of different block compositions by terminal Diels-Alder coupling of poly-L-lactide and poly-D-lactide prepolymers, *Polym. J.* **2013**, *45*(4), 427–435.
53. K. Masutani, C. W. Lee, R. Kanki, H. Yamane, Y. Kimura, Reactive electrospinning of stereoblock polylactides prepared via spontaneous Diels-Alder coupling of bis maleimide-terminated poly-L-lactide and bis furan-terminated poly-D-lactide, *Sen'i Gakkaishi* **2012**, *68*(3), 64–72.
54. K. Masutani, K. Kobayashi, Y. Kimura, C. W. Lee, Properties of stereo multi-block polylactides obtained by chain-extension of stereo tri-block polylactides consisting of poly(L-lactide) and poly(D-lactide), *J. Polym. Res.* **2018**, *25*(3), 74.
55. X. Qiu, R. Liu, Y. Nie, Y. Liu, Z. Liang, J. Yang, et al., Monte Carlo simulations of stereocomplex formation in multi-block copolymers, *Phys. Chem. Chem. Phys.* **2019**, *21*(24), 13296–13303.
56. N. Sugai, H. Heguri, K. Ohta, Q. Meng, T. Yamamoto, Y. Tezuka, Effective click construction of bridged- and spiro-multicyclic polymer topologies with tailored cyclic prepolymers (kyklo-Telechelics), *J. Am. Chem. Soc.* **2010**, *132*(42), 14790–14802.
57. L. Han, Q. Xie, J. Bao, G. Shan, Y. Bao, P. Pan, Click chemistry synthesis, stereocomplex formation, and enhanced thermal properties of well-defined poly(L-lactic acid)-*b*-poly(D-lactic acid) stereo diblock copolymers, *Polym. Chem.* **2017**, *8*(6), 1006–1016.
58. T. Isono, Y. Kondo, I. Otsuka, Y. Nishiyama, R. Borsali, T. Kakuchi, et al., Synthesis and stereocomplex formation of star-shaped stereoblock polylactides consisting of poly(L-lactide) and poly(D-lactide) arms, *Macromolecules* **2013**, *46*(21), 8509–8518.
59. N. Sugai, T. Yamamoto, Y. Tezuka, Synthesis of orientationally isomeric cyclic stereoblock polylactides with head-to-head and head-to-tail linkages of the enantiomeric segments, *ACS Macro Lett.* **2012**, *1*(7), 902–906.
60. M. H. Rahaman, H. Tsuji, Synthesis and characterization of stereo multiblock poly(lactic acid)s with different block lengths by melt polycondensation of poly(L-lactic acid)/poly(D-lactic acid) blends, *Macromol. React. Eng.* **2012**, *6*(11), 446–457.
61. M. H. Rahaman, H. Tsuji, Isothermal crystallization and spherulite growth behavior of stereo multiblock poly(lactic acid)s: effects of block length, *J. Appl. Polym. Sci.* **2013**, *129*(5), 2502–2517.
62. K. Fukushima, Y. Furuhashi, K. Sogo, S. Miura, Y. Kimura, Stereoblock poly(lactic acid): synthesis via solid-state polycondensation of a stereocomplexed mixture of poly(L-lactic acid) and poly(D-lactic acid), *Macromol. Biosci.* **2005**, *5*(1), 21–29.
63. K. Fukushima, M. Hirata, Y. Kimura, Synthesis and characterization of stereoblock poly(lactic acid)s with nonequivalent D/L sequence ratios, *Macromolecules* **2007**, *40*(9), 3049–3055.
64. K. Fukushima, Y. Kimura, An efficient solid-state polycondensation method for synthesizing stereocomplexed poly(lactic acid)s with high molecular weight, *J. Polym. Sci. Part A Polym. Chem.* **2008**, *46*(11), 3714–3722.
65. T. Kanno, H. T. Oyama, S. Usugi, Effects of molecular weight and catalyst on stereoblock formation via solid state polycondensation of poly(lactic acid), *Eur. Polym. J.* **2014**, *54*, 62–70.
66. P. Purnama, Y. Jung, S. H. Kim, Stereocomplexation of poly(L-lactide) and random copolymer poly(D-lactide-*co*-ε-caprolactone) to enhance melt stability, *Macromolecules* **2012**, *45*(9), 4012–4014.
67. M. Jikei, Y. Yamadoi, T. Suga, K. Matsumoto, Stereocomplex formation of poly(L-lactide)-poly(ε-caprolactone) multiblock copolymers with poly(D-lactide), *Polymer* **2017**, *123*, 73–80.
68. H. Tsuji, M. Yamasaki, Y. Arakawa, Stereocomplex formation between enantiomeric alternating lactic acid-based copolymers as a versatile method for the preparation of high performance biobased biodegradable materials, *ACS Appl. Polym. Mater.* **2019**, *1*(6), 1476–1484.
69. H. Tsuji, S. Sato, N. Masaki, Y. Arakawa, A. Kuzuya, Y. Ohya, Synthesis, stereocomplex crystallization and homo-crystallization of enantiomeric poly(lactic acid-*co*-alanine)s with ester and amide linkages, *Polym. Chem.* **2018**, *9*(5), 565–575.
70. N. Mulchandani, A. Gupta, K. Masutani, S. Kumar, S. Sakurai, Y. Kimura, et al., Effect of block length and stereocomplexation on the thermally processable poly(ε-caprolactone) and poly(lactic acid) block copolymers for biomedical applications, *ACS Appl. Polym. Mater.* **2019**, *1*(12), 3354–3365.
71. N. Mulchandani, A. Prasad, V. Katiyar, Chapter 4—Resorbable polymers in bone repair and regeneration, in: V. Grumezescu, A. M. Grumezescu (Eds.), *Materials for Biomedical Engineering*, Elsevier, Amsterdam, 2019, pp. 87–125.
72. C. Garofalo, G. Capuano, R. Sottile, R. Tallerico, R. Adami, E. Reverchon, et al., Different insight into amphiphilic PEG-PLA copolymers: influence of macromolecular architecture on the micelle formation and cellular uptake, *Biomacromolecules* **2014**, *15*(1), 403–415.

73. W. Zhang, D. Zhang, X. Fan, G. Bai, G. Yuming, Z. Hu, Stable stereocomplex micelles from Y-shaped amphiphilic copolymers MPEG–(scPLA)2: preparation and characteristics. *RSC Adv.* **2016**, *6*(25), 20761–20771.
74. C. Feng, M. Piao, D. Li, Stereocomplex-reinforced PEGylated polylactide micelle for optimized drug delivery, *Polym. (Basel)* **2016**, *8*(4), 165.
75. Y. Yu, J. Zou, L. Yu, W. Ji, Y. Li, W.-C. Law, et al., Functional polylactide-*g*-paclitaxel–poly(ethylene glycol) by azide–alkyne click chemistry, *Macromolecules* **2011**, *44*(12), 4793–4800.
76. N. Mulchandani, A. Gupta, V. Katiyar, Polylactic acid-based hydrogels and its renewable characters: tissue engineering applications, in: M. I. H. Mondal (Ed.), *Cellulose-Based Superabsorbent Hydrogels*, Springer International Publishing, Cham, 2019, pp. 1537–1559.
77. S. Noack, D. Schanzenbach, J. Koetz, H. Schlaad, Polylactide-based amphiphilic block copolymers: crystallization-induced self-assembly and stereocomplexation, *Macromol. Rapid Commun.* **2019**, *40*(1), 1800639.
78. C. Wang, N. Feng, F. Chang, J. Wang, B. Yuan, Y. Cheng, et al., Injectable cholesterol-enhanced stereocomplex polylactide thermogel loading chondrocytes for optimized cartilage regeneration, *Adv. Healthcare Mater.* **2019**, *8*(14), 1900312.
79. Y. Sun, C. He, Synthesis and stereocomplex crystallization of poly(lactide)–graphene oxide nanocomposites, *ACS Macro Lett.* **2012**, *1*(6), 709–713.
80. A. Gupta, A. K. Pal, E. M. Woo, V. Katiyar, Effects of amphiphilic chitosan on stereocomplexation and properties of poly(lactic acid) nano-biocomposite, *Sci. Rep.* **2018**, *8*(1), 4351.
81. A. Gupta, V. Katiyar, Cellulose functionalized high molecular weight stereocomplex polylactic acid biocomposite films with improved gas barrier, thermomechanical properties, *ACS Sustain. Chem. Eng.* **2017**, *5*(8), 6835–6844.
82. A. Gupta, A. Prasad, N. Mulchandani, M. Shah, M. Ravi Sankar, S. Kumar, et al., Multifunctional nanohydroxyapatite-promoted toughened high-molecular-weight stereocomplex poly(lactic acid)-based bionanocomposite for both 3D-printed orthopedic implants and high-temperature engineering applications, *ACS Omega* **2017**, *2*(7), 4039–4052.
83. Bioplastics MAGAZINE, "Total corbion PLA launches full stereocomplex PLA technology", Polymedia Publisher GmbH, Mönchengladbach, Germany, Issue 03, May 2018
84. A. Greiner, J. H. Wendorff, Electrospinning: a fascinating method for the preparation of ultrathin fibers, *Angew. Chem. Int. Edn.* **2007**, *46*(30), 5670–5703.
85. Y. Furuhashi, Y. Kimura, H. Yamane, Higher order structural analysis of stereocomplex-type poly(lactic acid) melt-spun fibers, *J. Polym. Sci. Part B-Polym. Phys.* **2007**, *45*, 218–228.
86. M. Takasaki, H. Ito, T. Kikutani, Development of stereocomplex crystal of polylactide in high-speed melt spinning and subsequent drawing and annealing processes, *J. Macromol. Sci. Part B* **2003**, *42*(3–4), 403–420.
87. M. Takasaki, H. Ito, T. Kikutani, Development of stereocomplex crystal of polylactide in high-speed melt spinning and subsequent drawing and annealing processes, *J. Macromol. Sci. Part B Phys.* **2007**, *42*(3 & 4), 403–420.
88. D. Masaki, Y. Fukui, K. Toyohara, M. Ikegame, B. Nagasaka, H. Yamane, Stereocomplex formation in the poly(L-lactic acid)/poly(D-lactic acid) melt blends and the melt spun fibers, *Sen'i Gakkaishi* **2008**, *64*(8), 212–219.
89. B. Wang, B. Li, J. Xiong, C. Y. Li, Hierarchically ordered polymer nanofibers via electrospinning and controlled polymer crystallization, *Macromolecules* **2008**, *41*(24), 9516–9521.
90. S. Boi, L. Pastorino, O. Monticelli, Multi applicable stereocomplex PLA particles decorated with cyclodextrins, *Mater. Lett.* **2019**, *250*, 135–138.
91. O. Monticelli, M. Putti, L. Gardella, D. Cavallo, A. Basso, M. Prato, et al., New stereocomplex PLA-based fibers: effect of POSS on polymer functionalization and properties, *Macromolecules* **2014**, *47*(14), 4718–4727.
92. S. Regnell Andersson, M. Hakkarainen, S. Inkinen, A. Södergård, A.-C. Albertsson, Customizing the hydrolytic degradation rate of stereocomplex PLA through different PDLA architectures, *Biomacromolecules* **2012**, *13*(4), 1212–1222.
93. C. Zhu, W. Jiang, J. Hu, P. Sun, A. Li, Q. Zhang, Polylactic acid nonwoven fabric surface modified with stereocomplex crystals for recyclable use in oil/water separation, *ACS Appl. Polym. Mater.* **2020**, *2*(7), 2509–2516.
94. N. J. Kaiser, K. L. K. Coulombe, Physiologically inspired cardiac scaffolds for tailored in vivo function and heart regeneration, *Biomed. Mater.* **2015**, *10*(3), 034003.
95. P. Mogha, A. Srivastava, S. Kumar, S. Das, S. Kureel, A. Dwivedi, et al., Hydrogel scaffold with substrate elasticity mimicking physiological-niche promotes proliferation of functional keratinocytes, *RSC Adv.* **2019**, *9*(18), 10174–10183.
96. X. Zhao, H. Hu, X. Wang, X. Yu, W. Zhou, S. Peng, Super tough poly(lactic acid) blends: a comprehensive review, *RSC Adv.* **2020**, *10*(22), 13316–13368.
97. H. Liu, J. Zhang, Research progress in toughening modification of poly(lactic acid), *J. Polym. Sci. Part B Polym. Phys.* **2011**, *49*(15), 1051–1083.
98. F. Wu, M. Misra, A. K. Mohanty, Super toughened poly(lactic acid)-based ternary blends via enhancing interfacial compatibility, *ACS Omega* **2019**, *4*(1), 1955–1968.
99. Y. Kang, P. Chen, X. Shi, G. Zhang, C. Wang, Preparation of open-porous stereocomplex PLA/PBAT scaffolds and correlation between their morphology, mechanical behavior, and cell compatibility, *RSC Adv.* **2018**, *8*(23), 12933–12943.
100. N. Mulchandani, K. Masutani, S. Kumar, H. Yamane, S. Sakurai, Y. Kimura, et al., Toughened PLA-b-PCL-b-PLA triblock copolymer based biomaterials: effect of self-assembled nanostructure and stereocomplexation on the mechanical properties, Polym. Chem. **2021**, *12*(26), 3806–3824.

# PART II

# PROPERTIES

# 6

# STRUCTURES AND PHASE TRANSITIONS OF PLA AND ITS RELATED POLYMERS

Hai Wang and Kohji Tashiro

## 6.1 INTRODUCTION

This chapter focuses on the structure and phase transition behavior of PLA and related polymers. The crystal modifications of PLA revealed so far are the mesophase [1–5], the δ (α′) phase [5–10], the α phase [11–16], the β phase [17–20], the γ phase [21, 22], the ε phase [23–26], and the stereocomplex (SC) between PLLA and PDLA [27–37]. The relationship between the chain conformation and aggregation state of chains in these crystalline modifications and the resulting intrinsic physical properties has to be understood for the improvement of the physicochemical property of PLA products. Besides, the unknowns about the crystal structure information make it difficult to fully understand the phase transition behaviors between the various crystal forms. In this way, the establishment of reliable and precise structures of PLA crystalline forms and the clarification of their phase transition behaviors are indispensable for the development of PLA.

The similar situation is seen also for the crystal structures of poly(3-hydroxybutyrate) (PHB). By adding one $CH_2$ unit to the basic chemical formula of PLA (─[─C*H($CH_3$)OCO─]$_n$─), PHB (─[─$CH_2$C*H($CH_3$)OCO─]$_n$─) is obtained. One skeletal C atom is optically asymmetric and so the PHB polymer chain may take also the L and D enantiomeric species similarly to those of PLLA and PDLA. This apparently slight difference of chemical structure between PLA and PHB, however, provides the remarkably different characters with respect to the helical chain conformation and the chain packing mode, as well as the crystallization behavior itself. Additionally, there are many kinds of aliphatic polyesters, which can show relatively high biodegradability comparable with that of PLA and PHB. For example, poly(ethylene adipate) (PEA) has the linear chemical formula without $CH_3$ side groups, ─[─$OCH_2CH_2OCO(CH_2)_4CO$─]$_n$─. In some cases, PEA is blended with PLA or PHB to control the biodegradability. To understand the crystallization behavior of PEA and PLA in these blends, it is indispensable to know the structure of PEA at the starting point.

In the present chapter, the crystal structures and phase transition behaviors of PLA are mainly discussed, but, at the same time, such related polyesters as PHB and PEA are also reviewed to extract the similarity and differences between these polyester compounds, from the structural points of view.

Although many review articles have been published about the structures, the phase transition behaviors and the relation between structure and property of these polymers [38–41], we need to realize the most reliable and accurate information, which were derived mainly from the quantitative analyses of the X-ray diffraction and vibrational spectroscopic data, are introduced in the present chapter.

## 6.2 STRUCTURAL STUDY OF PLA

### 6.2.1 Preparation of Crystal Modifications of PLA

To elucidate the detailed crystal structures and phase transition behaviors of PLLA, X-ray diffraction method of highly oriented and highly crystalline samples is most useful. Figure 6.1 shows that the various crystal modifications are obtained depending on the sample preparation conditions. When the sample in the molten state is quenched into ice water, predominantly amorphous-phase PLA is obtained [4, 5]. Casting

*Poly(Lactic Acid): Synthesis, Structures, Properties, Processing, Applications, and End of Life*, Second Edition.
Edited by Rafael A. Auras, Loong-Tak Lim, Susan E. M. Selke, and Hideto Tsuji.

PLA films using chloroform solution at room temperature also produces amorphous phase. The oriented PLLA sample of the mesophase is prepared by stretching the melt-quenched sample by four to five times the original length near the glass transition temperature ($T_g \sim 60°C$) [5]. The oriented δ form is obtained by annealing the as-drawn mesophase in the temperature range of 70–120°C. Annealing of the δ form at a higher temperature of 120–170°C induces a phase transition to the α form [5, 7, 9, 14]. The oriented β form cannot be obtained easily by the usual heat treatment of other such crystal modifications as the δ and α forms. To prepare the highly oriented pure β form, a high shear or tensile stress has to be applied to the oriented α form at a temperature higher than 120°C [17–20, 42–45]. The γ form is obtained as a single crystal by casting from hexamethylbenzene solution [21, 22]. A PLLA–$CO_2$ complex is prepared by treating the PLLA sample with supercritical fluid $CO_2$. The desorption of $CO_2$ under vacuum at room temperature gives the empty α″ form. PLLA forms a crystalline complex with organic solvents like cyclopentanone (CPO) and *N*,*N*-dimethylformamide (DMF), which is known as the ε form [25]. This complex is stable only at a low temperature; it transforms spontaneously to the α (or δ) form by leaving the sample at room temperature.

PLLA and PDLA are enantiomers with the same chemical formula but with the opposite configuration around the asymmetric carbon atoms or the opposite optical activity. The blend sample of PLLA and PDLA at 1 : 1 molar ratio was found to form the so-called stereocomplex (SC) [27]. However, the SC sample can be obtained in a wider range of PLLA/PDLA ratio of 7/3–3/7 [37, 46, 47].

Figure 6.2 shows the typical WAXD patterns of the uniaxially oriented PLA samples of the mesophase, δ, α, and β forms [5, 9, 14, 20], where an incident X-ray beam is a graphite-monochromatized Mo-Kα line (wavelength λ = 0.711 Å). Compared with the X-ray diffraction patterns observed for the general crystalline polymer samples, the α crystal form shows the *anomalously* beautiful X-ray diffraction pattern with many sharp spots, reflecting the well-developed

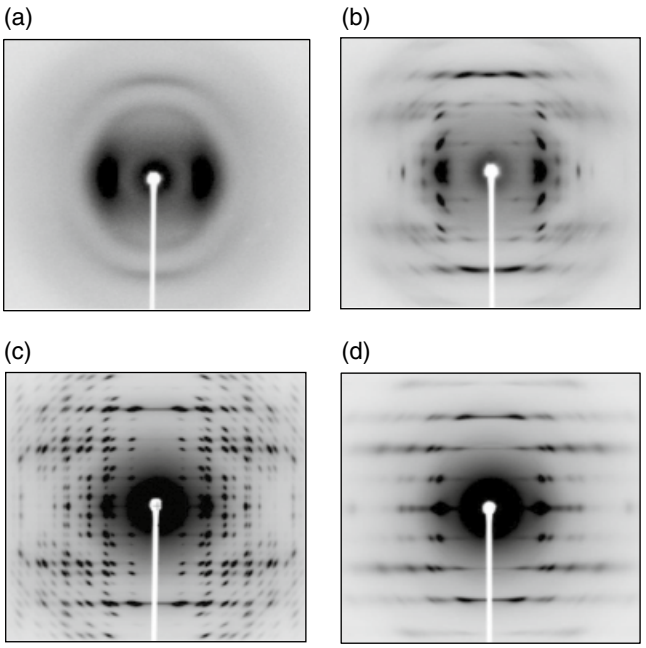


**FIGURE 6.2** 2D-WAXD patterns of PLLA (a) mesophase, (b) **δ** form, (c) **α** form, and (d) **β** form. Source: (a)–(c): Reproduced from Wasanasuk et al., *Macromolecules* 2011, 44, 9650–9660; (d): Wang et al., *Macromolecules* 2017, 50, 3285–3300.

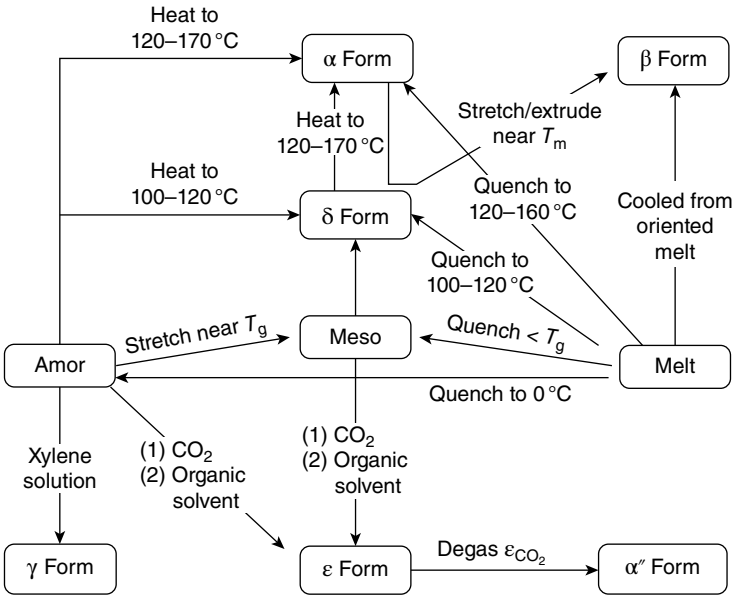


**FIGURE 6.1** Sample preparations and phase transitions of the various crystal modifications of PLLA.

crystal domains with highly regular chain packing mode. The diffraction pattern of the δ form is similar to that of the α form but diffuse as a whole, and the several characteristic diffraction peaks of the α form are lack, indicating that the δ form is not simply a disordered α form, but it is a crystalline form independent of the α form. The mesophase shows the further poor and diffuse diffraction pattern with the similar characteristic structural feature to those of the α and δ forms. The β form shows the remarkably different diffraction pattern from those of the abovementioned α and δ forms and meso phase. The streaks are more remarkable in the β form.

### 6.2.2 Crystal Structure of the α Form

The crystal structure of PLLA α form proposed at first was of the orthorhombic unit cell of $a = 10.7$ Å, $b = 6.45$ Å, $c$ (chain axis) = 27.8 Å [15], which contains the two chains of 10/3 helical conformation [13, 48], where 10/3 indicates that the 10 monomeric units are contained and the 3 turns in the repeating period. The internal rotation angles of the skeletal chain are approximately expressed as the repetition of *TTG* where *T* and *G* are trans and gauche bonds, respectively. The crystal structure was refined by Sasaki et al. by assuming the space group symmetry $P2_12_12_1$ [13]. However, several unsolved problems are still relevant in the abovementioned crystal structure analysis of the α form. For example, if the structure of the $P2_12_12_1$ space group is assumed correct, the molecular chain must be deformed more or less from the regular and uniform 10/3 helical conformation, since the unit cell possesses only the $2_1$ screw symmetries. If the $2_1$ screw axis passes through the center of the molecular chain along the *c* axis, the five monomeric units should form one crystallographically asymmetric unit. The total number of the atomic coordinates to be determined is remarkably large, making the structure analysis greatly difficult. A more serious problem is the usage of the space group $P2_12_12_1$ itself.

The observed X-ray diffraction pattern shows a series of 00*l* reflections containing the odd *l* values (003, 007 etc.) in addition to the even 00*l* peaks. This is not consistent with the extinction rule (00*l* with even *l* values) required for the space group $P2_12_12_1$.

In the X-ray structure analysis of the α form, the total number of the adjustable parameters of one asymmetric unit (i.e., the coordinates and thermal factors of the atoms in one asymmetric unit) is 101 for C and O atoms of isotropic thermal factors, and 306 for C, H, and O atoms of anisotropic thermal factors. So, for the determination of the accurate crystal structure of the α form, we need to collect the X-ray diffraction spots of about two to three times larger than the number of the parameters, i.e., 600–900 spots. The usage of an X-ray beam of a shorter wavelength is useful for this purpose. For example, the X-ray beam of 0.328 Å wavelength, generated from the synchrotron radiation facility, was incident to the ultra-drawn PLLA α form sample [14]. From the collected 2D-WAXD pattern, 700 independent diffraction spots were recognized, which are high enough when compared with the above-mentioned number of the adjustable parameters. The quantitative analysis was performed manually by reading the positions and integrated intensities of all the observed diffraction peaks. By taking the above-mentioned problems into consideration, the space group was reduced to the $P12_11$ of the monoclinic system, which is lower than the space group $P2_12_12_1$. The following unit cell parameters were obtained.

$$a = 10.683 \text{ Å}, b = 6.170 \text{ Å},$$
$$c\,(chainaxis) = 28.860 \text{ Å and } \gamma = 90°$$

The finally refined crystal structure, which can be assumed as the most accurate crystal structure of the α form, is shown in Figure 6.3. The two antiparallel L-helices are packed in the unit cell. The chain conformation is approximately a repetition of *TTG* sequences. But, the individual chain is not symmetric. The two chains are connected by the $2_1$ screw symmetry along the *b* axis to give the structure of the alternately upward and downward chains along the *c* axis. This model can reproduce the observed X-ray diffraction profiles along all the layer lines quite well as shown in Figures 6.4 and 6.5a.

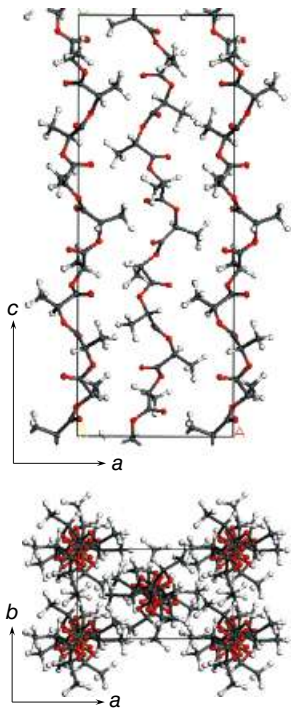


**FIGURE 6.3** Crystal structure of PLLA α form. The space group is $P12_11$. No symmetry is existent along the chain axis. The helical chains are packed upward and downward along the chain axis alternately. Source: Reproduced from Wasanusuk et al., *Macromolecules* 2011, 44, 6441–6452.

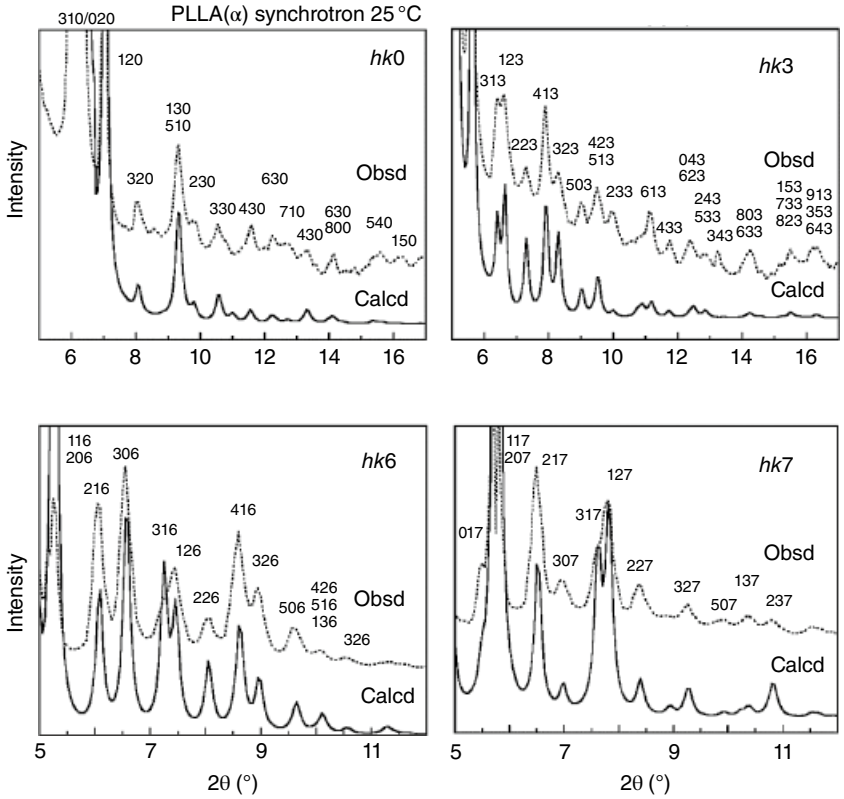


**FIGURE 6.4** Comparison between the observed (broken line) and calculated (solid line) X-ray diffraction profiles of PLLA **α** form for the several layer lines (25°C). Source: Reproduced from Wasanasuk et al., *Macromolecules* 2011, 44, 6441–6552.

The H atom positions, which are important for the theoretical calculation of the mechanical properties, can be determined from the quantitative analysis of the wide-angle neutron diffraction data, since the neutron beam is scattered almost equally by C, O, and H (and D) atomic species, which is quite in contrast to the X-ray scattering, in which the scattering amplitude is extremely small for H atoms compared with the C and O atoms [49].

As mentioned above, the finally-determined space group is $P2_1$. This symmetry reduction is needed to generate the 00*l* diffraction peaks of the odd *l* values (see Figure 6.5a). Strictly speaking, even this model could not reproduce the observed 00*l* profile perfectly, although most of the *hkl* diffraction peaks were reproduced satisfactorily enough (Figure 6.4). This situation requires introducing some structural disorder that was not considered in the structural analyses mentioned above. After many trials, the disordered domain model was found to reproduce the data quite well. Figure 6.5b shows that the domains of a specific size are gathered together with the relative height disorder. The relative-height shift between the domains is small (0.1–0.2 *c*), but it gives a good reproduction of the 00*l* diffraction profile as shown in Figure 6.5a. Since the domain size is large enough, the observed X-ray diffraction profiles of the general *hkl* peaks are not seriously affected [14].

### 6.2.3 Crystal Structure of the δ Form

The existence of the δ form (or the old name, α′ form) had been controversial for a long time. Historically, the suggestion of the δ form came from the measurement of the melt-isothermal crystallization rate, which showed an anomalous peak at around 110–118°C [1, 50]. The DSC thermogram showed double melting peaks in the cold-crystallization process [51]. Simultaneous DSC and WAXD measurement was performed as shown in Figure 6.6. The unoriented δ form sample was heated gradually, during which the 1D X-ray diffraction profile was measured stepwise. When the temperature increased to 148–165°C, the 203 and 116 diffraction peaks, which were originally single peaks, changed to double peaks and the relative intensity of these two peaks was exchanged, as indicated by the arrows. This indicates that these two phases are coexistent during the transition, implying a thermodynamically first-order transition. Besides, several peaks (210 and 213) started to appear, which were assigned to the diffraction peaks of the α form. In this way, the δ form is the crystal form thermodynamically independent of the α form.

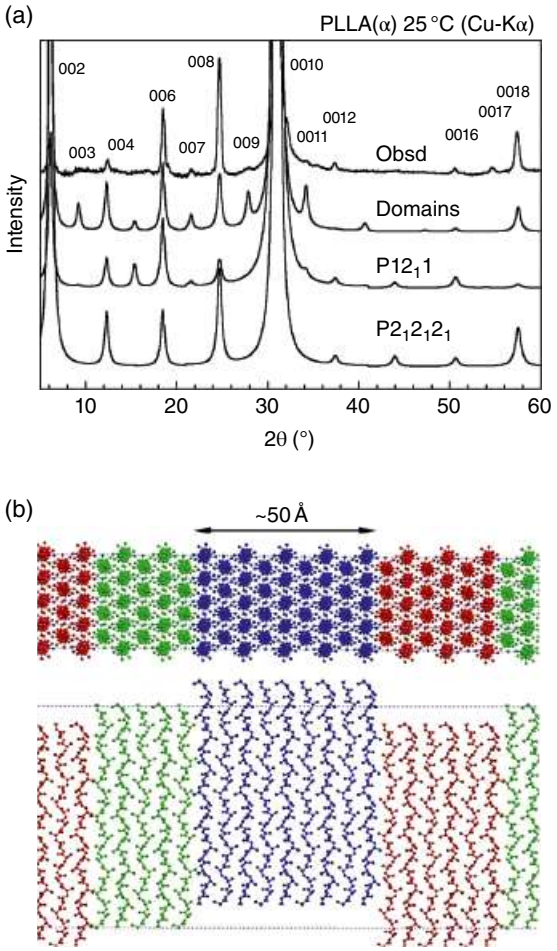


**FIGURE 6.5** (a) Comparison of the observed 00*l* reflection profile with the calculated curves for both of $P2_12_12_1$ and $P12_11$ models and for the disordered domain model. Source: Reproduced from Wasanusuk et al., *Macromolecules* 2011, 44, 6441–6452. (b) PLLA domain model (several tens Å size along the a axis).

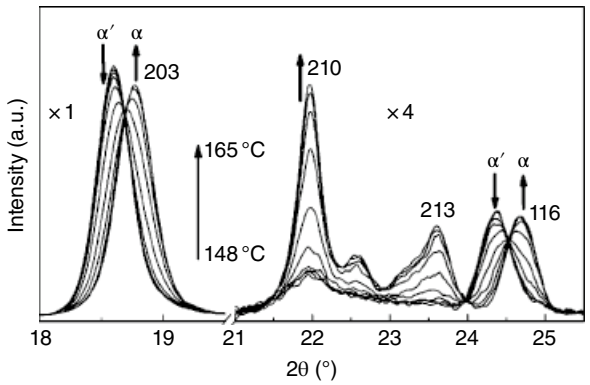


**FIGURE 6.6** Temperature dependence of the 1D WAXD profile measured in the phase transition from the **δ** (**α**') to **α** form of the unoriented PLLA sample (heating process). Source: Reproduced from Zhang et al., *Macromolecules* 2008, 41, 1352–1357.

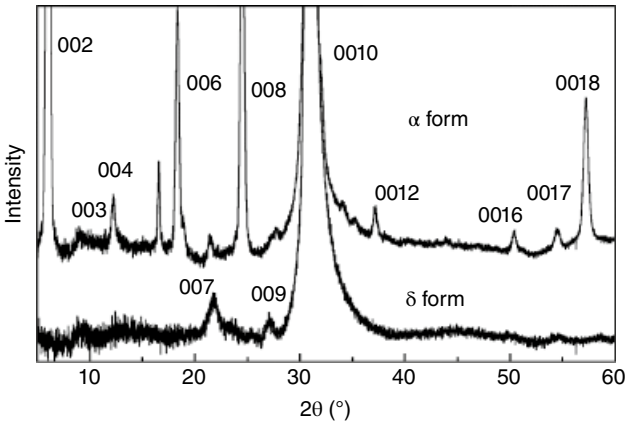


**FIGURE 6.7** Observed X-ray 00*l* reflection profiles of PLLA **α** and **δ** forms. Source: Reproduced from Wasanasuk and Tashiro, *Polymer* 2011, 52, 6097–6109.

The crystal structure of the δ form was proposed by analyzing the 2D X-ray diffraction pattern shown in Figure 6.2b, where the sample was prepared by stretching the melt-quenched sample followed by annealing at *ca*. 100°C. In contrast to the α form, the X-ray diffraction pattern is not very clear and consists of only the 41 broad diffraction spots. In addition, the diffuse streaks are detected relatively strongly along the layer lines, suggesting the existence of the remarkable disorder of the unit cell structure [9]. The orthogonal unit cell was proposed with the parameters $a$ = 10.80 Å, $b$ = 6.20 Å, and $c$ (chain axis) = 28.80 Å. As seen in the 00*l* profile (Figure 6.7), the 0010 peak is quite strong, but the others are appreciably broad and diffuse, which is different from the sharp 00*l* peaks observed for the α form. This indicates that the chains takes the 10/3 helical conformation, but they are deformed to more extent than the α form (Figure 6.3). The detailed analysis of the X-ray diffraction data revealed that not only the conformational disorder but also the chain packing disorder occurs in the crystal lattice of the δ form. In particular, the relative height between the neighboring chains is appreciably random compared with the α form, as seen from the more remarkable streaks along the layer lines of the 2D X-ray diffraction pattern [9]. Besides, the aggregation of the domains is also more highly disordered than the α form (see Figure 6.5b). The X-ray-coherent crystallite sizes, as evaluated from the half width of the various diffraction peaks using Scherrer's equation [52], are appreciably smaller than those of the α form (see Section 6.3.1).

### 6.2.4 Crystal Structure of the β Form

As for the structure of the β form, the two types of the crystal structure were previously proposed by the X-ray or electron diffraction data analysis: model (i) the orthorhombic type:

$a$ = 10.31 Å, $b$ = 18.21 Å, and $c$ (chain axis) = 9.00 Å, in which the six chains of 3/1 helical conformation are packed [17], and model (ii) the trigonal type with $a = b$ = 10.52 Å and $c$ (chain axis) = 8.80 Å, in which the three upward helices of 3/1 conformation are related by the space group symmetry $P3_2$ [18]. The present authors measured the 2D X-ray diffraction pattern using a Mo-Kα beam and analyzed it thoroughly (Figure 6.2d). The several diffraction peaks intrinsic to the β form could not be indexed reasonably by using the model (ii). Besides, the observed 000$l$ reflections along the chain axis do not satisfy the extinction rule requested for the $P3_2$ space group (the appearance of 000$l$ reflections with $l$ = 3, 6, 9, . . .) [20]. The 2D X-ray diffraction pattern was measured again using the incident X-ray beam of shorter wavelength (λ = 0.711 Å) than before, giving 40–50 observed diffraction spots in total [20]. The indexing of the observed peaks was made using the orthorhombic-type unit cell:

$$a = 10.41\ \text{Å},\ b = 18.02\ \text{Å, and}$$
$$c\,(chainaxis) = 9.00\ \text{Å at } 23°\text{C}.$$

The chain takes the 3/1 helical conformation [17, 18], and the six chains are packed in the unit cell, the same as the model (i). The 18 monomeric units are contained in the unit cell. According to the International Table for Crystallography [53], the orthorhombic unit cell must contain four or eight crystallographically asymmetric units. Therefore, if the orthorhombic system is assumed, the 18 monomeric units (or six chains) cannot be divided into the asymmetric units and are difficult to correlate with each other by the symmetric relation. So, the final space group symmetry selected is $P1$, which reproduced the observed X-ray diffraction data well. However, it was impossible to determine the packing structure of many such chains uniquely because the observed diffraction peaks are relatively small in number compared with the total number of the adjustable structure parameters. As the hints to construct the crystal structure model, two important phenomena were observed:

1. The α (or δ) form transforms to the β form by the application of tensile or shear force, wherein the alternate packing structure of the upward and downward chains must be kept between them.
2. The relationships of the unit cell size among the three crystalline forms are $a$ (α) ≈ $a$ (δ) ≈ $a$ (β), $b$ (α) ≈ $b$ (δ) ≈ $b$/3 (β), and $c$ (α) ≈ $c$ (δ) ≈ 3$c$ (β), suggesting that the positions of the chains in the cell might not change very much before and after the structural transition from the α to β form.

Then, the chain packing structure of the α form was used as an initial model of the β form, which was enlarged three times along the $b$-axis. The thus-constructed model consists of the alternate packing of the upward (U) chains and downward (D) 3/1 chains. The positions and relative orientations of these U and D chains were modified in various ways to obtain the best reproduction of the observed X-ray diffraction profiles. At present, the two possible models (model 2 and model 3) are considered as the best candidates for the β form (Figure 6.8). The U (and D) chains are surrounded by the U and D chains in a different environment depending on the local position, suggesting the frustrated structure as pointed out by Lotz et al. [18]. The comparison between the observed and calculated 1D-WAXD profiles is presented in Figure 6.9.

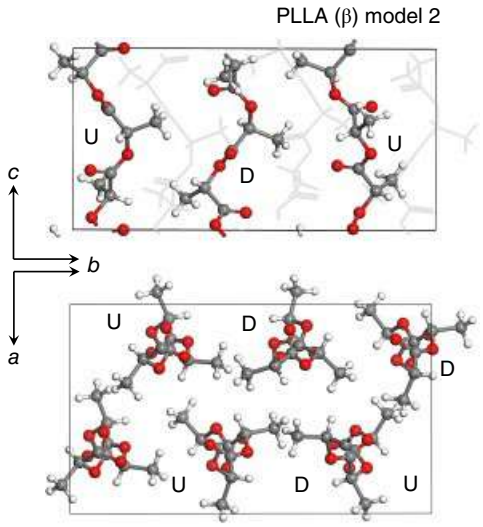


**FIGURE 6.8** Crystal structure of PLLA **β** form (model 2). Source: Reproduced from Wang et al., *Macromolecules* 2017, 50, 3285–3300

### 6.2.5 Structure of the Mesophase

The 2D X-ray diffraction pattern of the uniaxially oriented mesophase, prepared by stretching the amorphous sample around $T_g$, is shown in Figure 6.2a. The pattern is very broad and diffuse. The relative content of the mesophase increases with an increase of tensile drawing ratio of the original amorphous sample [54]. The X-ray data analysis revealed that the oriented mesophase contains the conformationally disordered 10/3 helical chains, which are gathered together to form the small domains of about 30 Å ($c$-axis) × 20 Å (lateral direction) size with low correlation between them [5]. By heating, the mesophase undergoes the stepwise disorder-to-order phase transformation to the δ and α forms [5] (refer to Section 6.3.1). These transitions were proposed to occur, not by the solid-to-solid process, but by the melt-recrystallization process, although not yet confirmed [55].

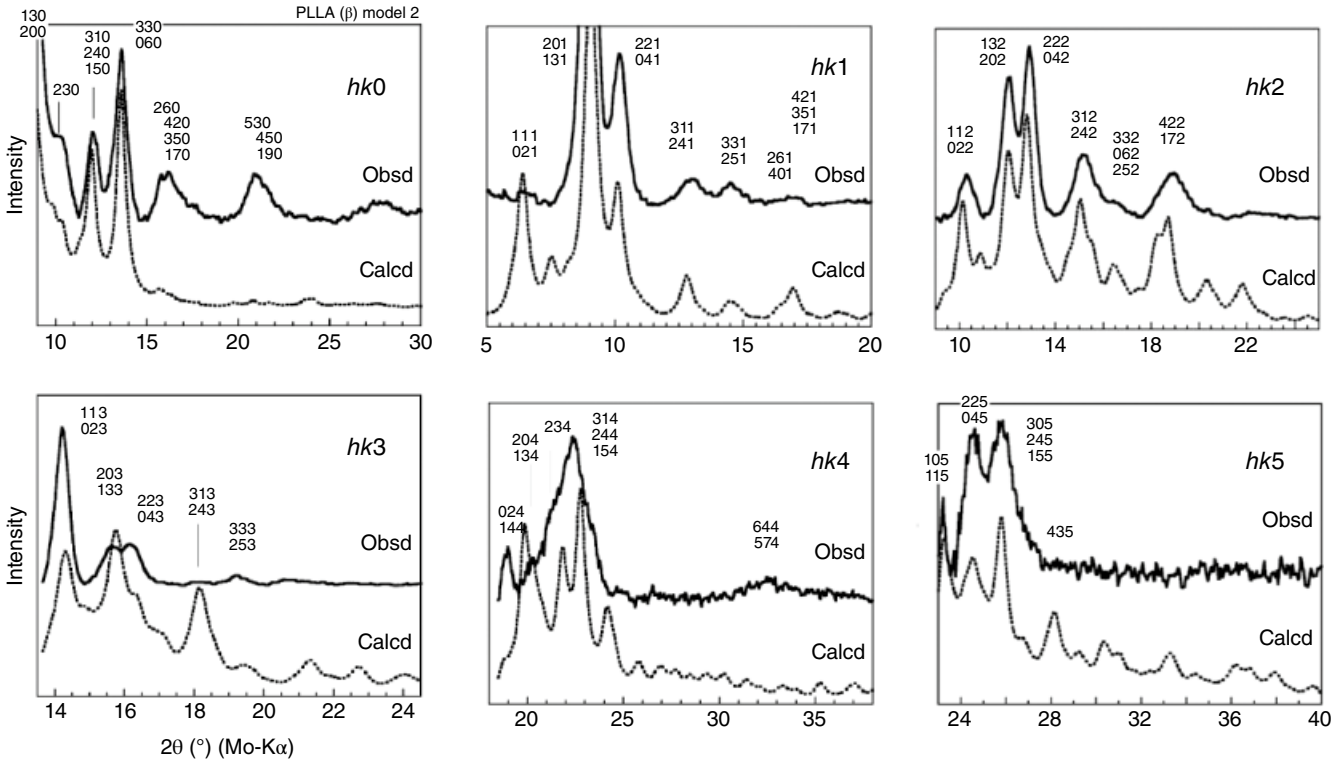


**FIGURE 6.9** Comparison of the observed X-ray diffraction profiles with those calculated for the structure model 2 of the **β** form. Source: Reproduced from Wang et al., *Macromolecules* 2017, 50, 3285–3300.

## 6.3 THERMALLY INDUCED PHASE TRANSITIONS

### 6.3.1 Phase Transition in Cold Crystallization

The crystallization phenomenon caused by heating the amorphous sample is known as cold-crystallization in contrast to the melt-crystallization that occurs during the cooling process from the molten state. The temperature-dependent 2D-WAXD patterns were measured for the uniaxially oriented mesophase sample in the cold-crystallization process, as shown in Figure 6.10 [5]. The mesophase started to transform to the δ form at around $T_g$. The δ form grew gradually during heating to 120°C. Once the sample was heated above 120°C, the δ form transformed to the α form. By further heating, the α form did not directly transform to the molten state, but it first changed to the mesophase once again and then to the melt. The growth of the crystallite size was estimated by analyzing the change of the half-width of the X-ray diffraction spots using Scherrer's equation [52]. Figure 6.11 shows the results obtained for the equatorial (200/110 peak) and meridional (0010 peak) directions. The starting mesophase has a quite small crystal size of *ca*. 30 Å (*c*-axis) × 20 Å (*ab*-plane). It changes gradually to the δ form with a larger size of *ca*. 75 Å (*c*-axis) × 100 Å (*ab*-plane). The α form developed from δ form has a larger crystal size of *ca*. 175 Å (*c*-axis) × 300 Å (*ab*-plane).

### 6.3.2 Phase Transition in the Melt Crystallization

As predicted from the phase diagram (Figure 6.1), quenching the melt gives various crystalline phases depending on the quenching temperature. The X-ray diffraction measurement revealed the details as shown elsewhere [5]. The mesophase was formed when the quenching temperature was near $T_g$. By quenching into 100–120°C, the δ crystal was formed. Cooling to the higher temperature caused crystallization to the α form.

Figure 6.12a and b show the time dependence of the infrared absorbance at 921 $cm^{-1}$ band, which is common to various crystal phases, measured in the temperature jump process from the amorphous phase or from the melt [5]. In these experiments, the temperature was changed quite sharply to a preset crystallization point by using a homemade temperature jump cell [56]. The crystallization rate *k* was estimated from the steepest slope of the intensity-vs-time curves at each temperature, as seen in Figure 6.12c. The crystallization rate started to increase above 70°C and showed a maximum at around 110°C, and then decreased with increasing temperature. These curves are similar to those of the spherulite growth rate measured with an optical microscope [50, 57]. The two important points are extracted from these experimental data. One is about the crystallization of the different crystal forms: in the low temperature region (70–110°C), the δ form is produced, while the α form is crystallized in the

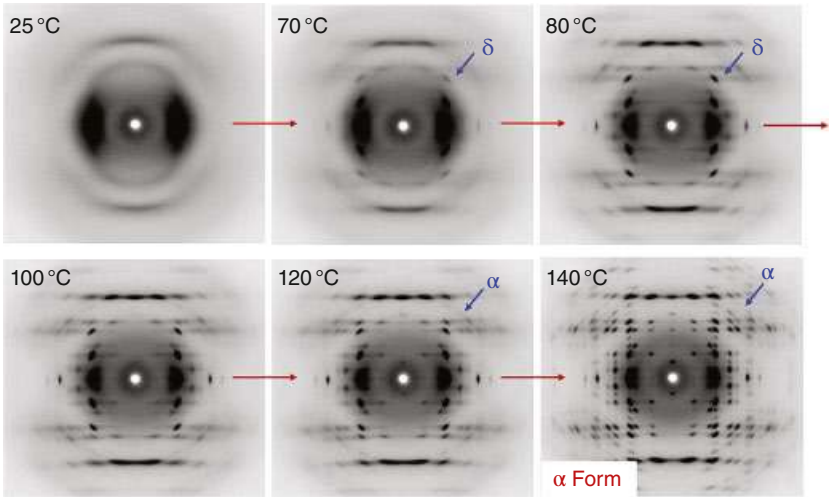


**FIGURE 6.10** Temperature dependence of 2D X-ray diffraction patterns of the oriented PLLA mesophase measured in the heating process. Source: Reproduced from Wasanasuk et al., *Macromolecules* 2011, 44, 9650–9660.

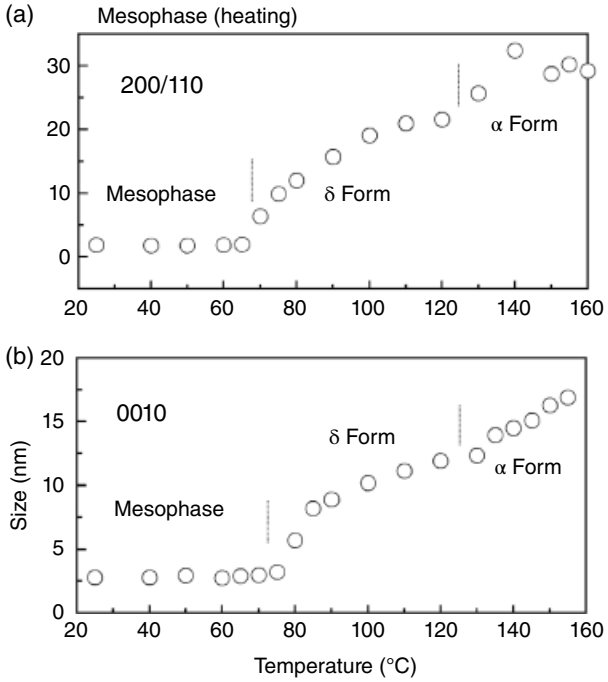


**FIGURE 6.11** The temperature dependence of the crystallite size estimated for the equatorial and meridional directions of the oriented PLLA sample during the cold crystallization process starting from the meso form. Source: Reproduced from Wasanasuk et al., *Macromolecules* 2011, 44, 9650–9660.

high temperature region (>110°C), as already mentioned above. Another point is about the crystallization rate. As seen in Figure 6.12c, the cold-crystallization gave the crystallization rate higher than the melt-crystallization when compared at the same crystallization temperature. The higher crystallization rate in the cold crystallization phenomenon was ascribed to the higher content of the crystalline nuclei produced in the cooling process from the amorphous phase compared with that from the molten state [58, 59].

### 6.3.3 Mechanically Induced Phase Transition

The study of the mechanically induced transition from the α to β form is important for the purpose of improving the mechanical properties of the bulk PLLA samples. As speculated from the sample preparation condition of the β form, the α-to-β transformation was considered to be induced primarily by shear applied along the helix axis of the α form [60]. Figure 6.13 shows the 2D X-ray diffraction

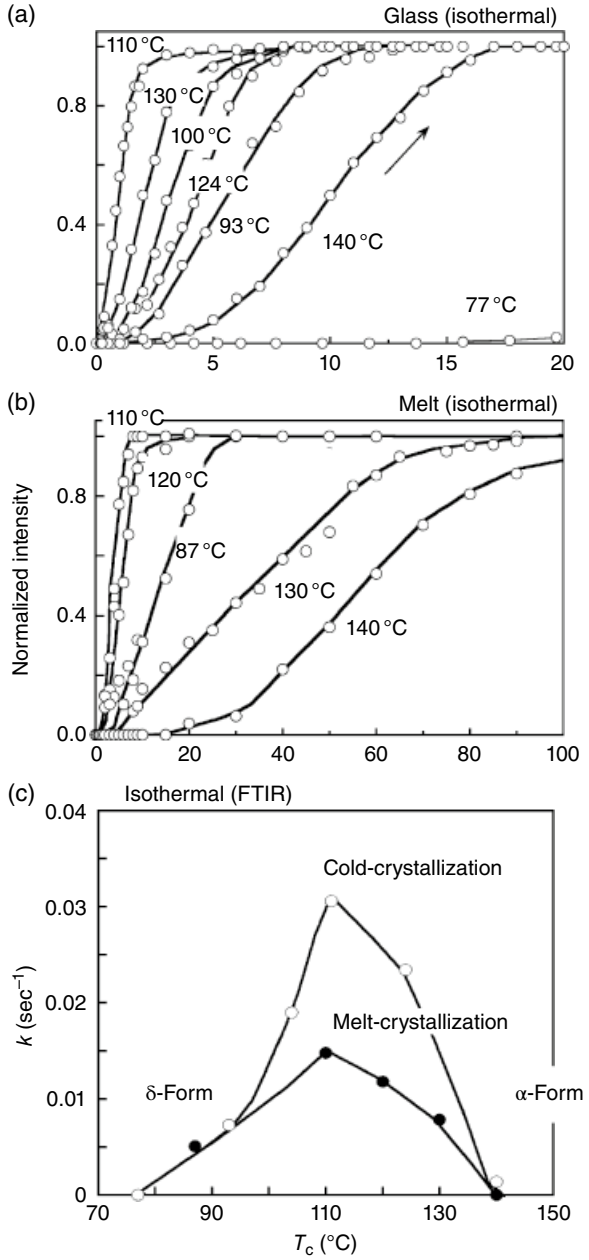


**FIGURE 6.12** (a) and (b) Time dependence of normalized intensity of the crystallization sensitive IR band at 921 $cm^{-1}$ measured in the isothermal crystallization processes at the various $T_c$. (c) Crystallization temperature dependence of the crystallization rate constant $k$ estimated from the data (a) and (b). Source: Reproduced from Wasanasuk et al., *Macromolecules* 2011, 44, 9650–9660.

patterns measured for the oriented α form samples stretched at 165°C at different drawing ratios. The drawing ratio (DR) of 6 gave almost pure and highly-oriented β form. The δ form was mainly obtained in the sample of DR 5. The stretching at DR 3 gave the X-ray diffraction pattern similar to that of the original α form, but the diffraction peaks are appreciably broad and diffuse. This state is named the disordered α form ($\alpha_d$) [20]. In this way, the stretching of the oriented α form at 165°C (below the melting point) induces the stepwise transformation of $\alpha \rightarrow \alpha_d \rightarrow \delta \rightarrow \beta$ in the solid state as the draw ratio increases.

Another experiment was performed by in situ measurement of the 2D WAXD pattern under a constant tensile stress in the continuous heating process beyond the melting point of the α form [20]. As shown in Figure 6.14, the starting sample was a highly oriented α form. A 1 MPa tensile stress was applied along the chain axis. At around 153°C, the X-ray diffraction pattern changed to that of the highly diffuse diffraction spots, i.e., the transformation to the $\alpha_d$ form. Further heating changed the X-ray pattern to that of the δ form (175°C), which finally disappeared at around 185°C. That is to say, the δ form was melted under tension at this temperature. However, the further increase of temperature by only 2°C caused the appearance of the X-ray diffraction pattern of the highly oriented β form with the characteristic diffuse pattern (in addition to a small amount of the $\alpha_d$ phase). The β form remained up to 207°C and finally disappeared at about 210°C. The process may be summarized as follows: the α form subjected to a tensile force $\rightarrow \alpha_d \rightarrow \delta \rightarrow$ melt $\rightarrow \beta \rightarrow$ melt. In this experiment, the phase transition temperature was high compared with those observed under normal conditions, which might be due to the overstressed state of the oriented sample subjected to a tensile force.

In this way, two different types of the formation process of the α to β form seem to exist. One is a solid-state transition via the $\alpha_d$ and δ forms at a relatively low temperature below the melting point (100–170°C; refer to Figure 6.13). Another one is observed near the melting point. The starting α form changes to the $\alpha_d$ form and to the δ form, then the melt of the δ form occurs in a highly superheated state, followed by the recrystallization to an extremely highly oriented β form (refer to Figure 6.14).

The more concrete image of the transformation process from the α to β form is discussed here by referring to the above-mentioned knowledge. As already seen in the previous section, PLLA β form takes a complicated and low-symmetric packing structure ($P1$) consisting of the six chains in the orthogonal unit cell. It must be noted that the chain packing mode is not random, but the upward and downward chains are packed in a systematic (but complicated) way. The geometrical relation of the crystal structure between the α (δ) and β forms is shown in Figure 6.15a. The unit cell size and chain positions in the *ab* plane are almost the same among these three crystalline forms. In the unit cells of the α and δ forms, the upward (U) and downward (D) chain stems are arrayed alternately at the corner and center positions of the unit cell along the *a* axis. In the crystal lattice of the β form, the U and D chain stems are arranged in a different way. How can we relate the chain packing structures between the α (δ) and β forms? One possible model is illustrated in Figure 6.15b. The

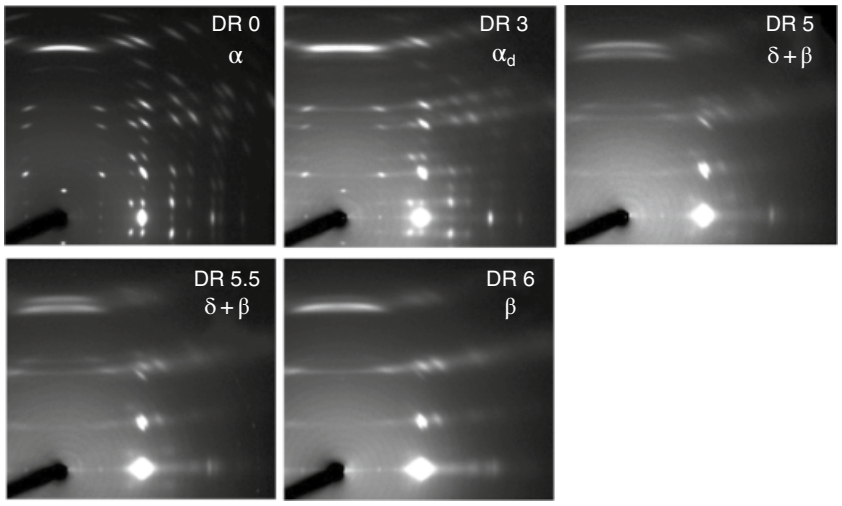


**FIGURE 6.13** The 2D WAXD patterns measured at 25°C for the uniaxially oriented PLLA samples prepared by drawing the oriented **α** form at 165°C. The drawing ratio DR = $(L - L_0)/L_0$ for the sample length L and $L_0$ (initial value). Source: Reproduced from Wang et al., Macromolecules 2017, 44, 3285–3300.

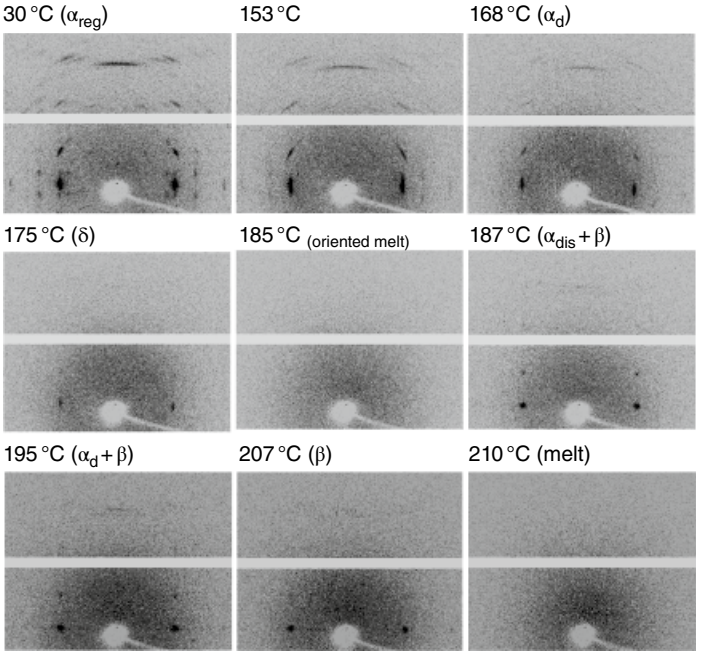


**FIGURE 6.14** Temperature dependence of 2D X-ray diffraction pattern of highly oriented α form under a constant tensile force (about 1 MPa). Source: Reproduced from Wang et al., *Macromolecules* 2017, 44, 3285–3300.

three diagonal arrays (A, B and A along the 110 planes) are focused now [see $(b-1)$]. By applying shear stress to the crystallite, the diagonal arrays of A are slipped in the positive direction along the 110 planes, while the B arrays in the opposite direction [$(b-2)$]. As a result, the new packing structure of U and D chain stems is created as shown in $(b-3)$. These chains are displaced furthermore along the *b* axis so that the total packing energy becomes lower, resulting in the β form [$(b-4)$]. During this process, the molecular chains change the conformation from 10/3 to 3/1 form. At the same time, the relative heights of the neighboring chains are disordered, and the domain size becomes smaller as known from the change of the X-ray diffraction width. The schematic illustration of the crystallite-size change is given in Figure 6.15c.

## 6.4 MICROSCOPICALLY-VIEWED STRUCTURE-MECHANICAL PROPERTIES OF PLA

The estimation of the mechanical property of an ideal crystalline state, or the ultimate mechanical property, is important as a guiding principle for the development of PLA

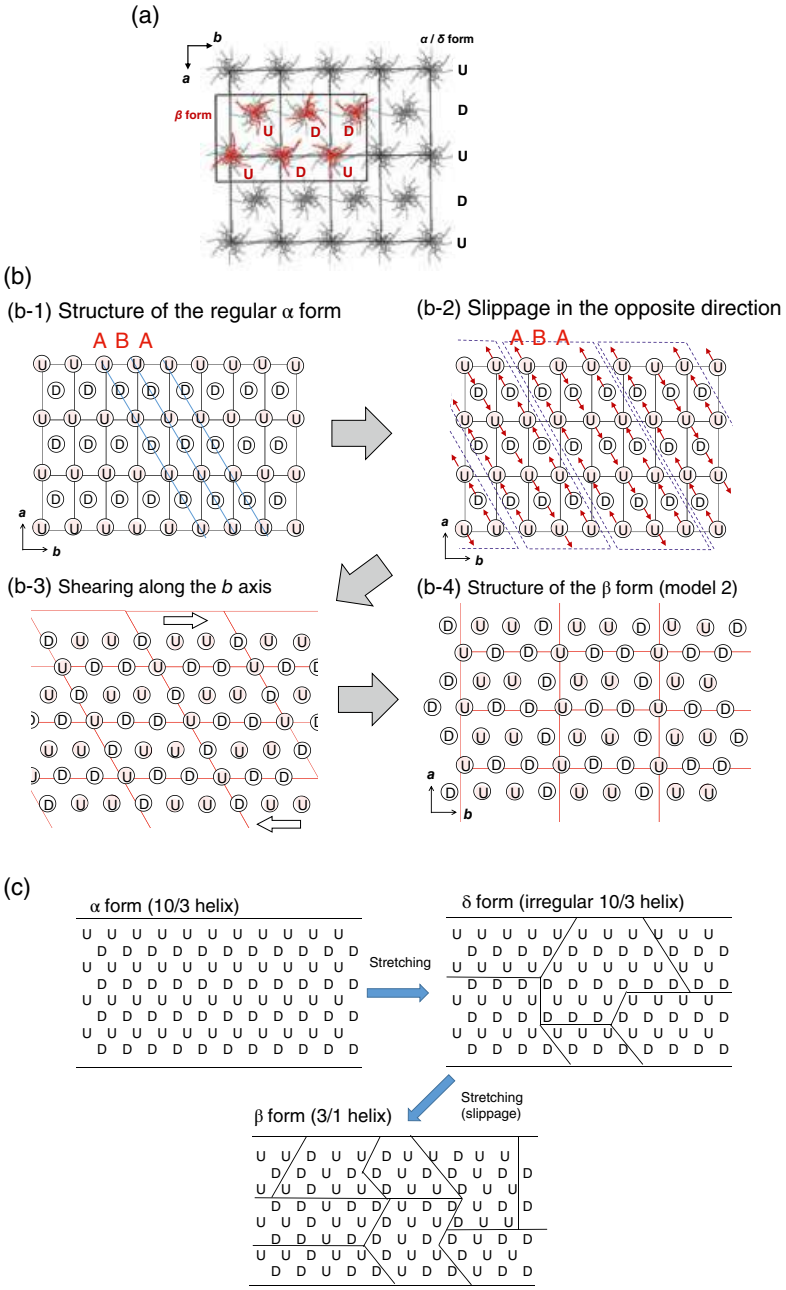


**FIGURE 6.15** (a) Comparison of the unit cell *ab*-plane structure between the α (δ) and β forms, where the model 2 is employed for the β form. The U and D indicate the upward and downward helical chains along the c axis, respectively. (b) A schematic illustration of the structural transformation model from the α (α′) form to the β form. The set of arrays A, B and A slip along the 110 planes. Source: Modified from the reference [20]. Reproduced from Wang et al., *Macromolecules* 2017, 44, 3285–3300. (c) The change of the X-ray coherent domain size in the transition process from the α to δ to β forms.

samples with excellent mechanical properties. The theoretical prediction of mechanical properties with high reliability can be made for the first time by using the accurate crystal structure information and the credible potential functional parameters, which can reproduce the various kinds of the experimentally obtained physical constants including the vibrational spectroscopic data [61–72]. The 3D elastic constant tensors of PLLA α [5], δ [9] and β forms [20] were calculated using the above-mentioned X-ray-analyzed crystalline structures:

PLLA α form

Elastic constants matrix,

$$\mathbf{c}(\mathrm{GPa}) = \begin{bmatrix} 2.50 & 6.48 & 7.15 & 0.00 & -1.45 & 0.00 \\ 6.48 & 12.38 & 9.07 & 0.00 & 2.28 & 0.00 \\ 7.15 & 9.07 & 17.87 & 0.00 & 3.98 & 0.00 \\ 0.00 & 0.00 & 0.00 & 15.03 & 0.00 & 3.18 \\ -1.45 & 2.28 & 3.98 & 0.00 & 0.21 & 0.00 \\ 0.00 & 0.00 & 0.00 & 3.18 & 0.00 & 3.90 \end{bmatrix}$$

Compliance tensors matrix,

$$\mathbf{s}\left(\mathrm{GPa}^{-1}\right)=\begin{bmatrix} 0.08 & -0.02 & 0.06 & 0.00 & -0.35 & 0.00 \\ -0.02 & 0.13 & -0.09 & 0.00 & 0.12 & 0.00 \\ 0.06 & -0.09 & 0.07 & 0.00 & 0.04 & 0.00 \\ 0.00 & 0.00 & 0.00 & 0.08 & 0.00 & -0.07 \\ -0.35 & 0.12 & 0.04 & 0.00 & 0.16 & 0.00 \\ 0.00 & 0.00 & 0.00 & -0.07 & 0.00 & 0.31 \end{bmatrix}$$

PLLA δ form

$$\mathbf{c}\ \left(\mathrm{GPa}\right)=\begin{bmatrix} 3.52 & 3.26 & 6.49 & 0.02 & -0.88 & -0.18 \\ 3.26 & 10.53 & 9.21 & -0.35 & -2.05 & 2.81 \\ 6.49 & 9.21 & 24.72 & 2.64 & 0.53 & -13.16 \\ 0.02 & -0.35 & 1.04 & -0.61 & 0.15 & 1.89 \\ -0.88 & -2.05 & 0.53 & 0.15 & 2.78 & -1.17 \\ -0.18 & 2.81 & -13.16 & 4.89 & -1.17 & 1.25 \end{bmatrix}$$

$$\mathbf{s}\left(\mathrm{GPa}^{-1}\right)=\begin{bmatrix} 0.63 & -0.05 & -0.13 & -0.26 & 0.20 & 0.00 \\ -0.05 & 0.16 & -0.04 & -0.17 & 0.12 & 0.00 \\ -0.13 & -0.04 & 0.08 & 0.21 & -0.10 & 0.00 \\ -0.26 & -0.17 & 0.21 & 0.55 & -0.19 & 0.20 \\ 0.20 & 0.12 & -0.10 & -0.19 & 0.54 & 0.00 \\ 0.00 & 0.00 & 0.00 & 0.20 & 0.00 & 0.02 \end{bmatrix}$$

PLLA β form

$$\mathbf{c}\left(\mathrm{GPa}\right)=\begin{bmatrix} 7.63 & 5.06 & 5.38 & 0.34 & 0.14 & -0.95 \\ 0.00 & 6.09 & 2.71 & 0.46 & -1.08 & 1.59 \\ 0.00 & 0.00 & 18.37 & 0.87 & -2.42 & 0.66 \\ 0.00 & 0.00 & 0.00 & 1.21 & -0.77 & 0.45 \\ 0.00 & 0.00 & 0.00 & 0.00 & 1.28 & 0.32 \\ 0.00 & 0.00 & 0.00 & 0.00 & 0.00 & 1.25 \end{bmatrix}$$

$$\mathbf{s}\left(\mathrm{GPa}^{--1}\right)=\begin{bmatrix} 0.081 & 0.015 & -0.004 & 0.175 & 0.167 & -0.249 \\ 0.00 & 0.089 & -0.043 & -0.231 & -0.208 & 0.24 \\ 0.00 & 0.00 & 0.065 & -0.045 & 0.034 & 0.100 \\ 0.00 & 0.00 & 0.00 & 0.919 & 0.188 & 0.578 \\ 0.00 & 0.00 & 0.00 & 0.00 & 0.621 & 0.578 \\ 0.00 & 0.00 & 0.00 & 0.20 & 0.00 & 0.019 \end{bmatrix}$$

The calculated Young's moduli along the *c*-axis ($E_c = 1/s_{33}$) are compared among the α, δ, and β forms, as shown below:

α form: $E_c$ = 14.7 GPa [66] (X-ray observed 13.76 GPa [66, 73])

δ form: $E_c$ = 12.5 GPa [66] (X-ray observed 12.58 GPa [66])

β form: $E_c$ = 15.4 GPa [20]

The experimental evaluation of the Young's modulus of the crystal lattice along the chain axis, which is often called the crystallite modulus, was performed using the X-ray diffraction method [67], where the crystalline strain along the chain axis was measured under constant tensile stresses by assuming the stress working on the crystalline region was equal to the stress of the bulk sample (the assumption of homogeneous stress distribution) [67, 72]. The agreement between the observed and calculated values is relatively good. The crystallite modulus changes depending on the conformational regularity of the PLLA chain: the mesophase (6.7 GPa) < the δ form (12.9 GPa) < the α form (14.7 GPa) < the β form (15.4 GPa). For reference, the X-ray-measured crystallite modulus of PLLA/PDLA stereocomplex is 20 GPa, in which the PLLA or PDLA chain takes a 3/1 helical conformation similar to that of the β form [73].

The crystallite modulus changes depending on the mechanical deformation mechanism of the molecular chain, i.e., the degree of change in the internal coordinates (bond lengths, bond angles, and torsional angles) induced by the external force [67–71]. For example, a planar-zigzag polyethylene chain is deformed by the stretching of C─C bonds and the deformation of C─C─C bond angles, resulting in a Young's modulus of 300 GPa [67, 69]. The deformation of a helical chain is induced mainly by the change of the torsional angles, giving 1–2 order lower modulus. The deformation of PLLA helical chains also occurs through the torsional angles around the skeletal C─C and C─O bonds. The disordered chain is more easily deformed due to the easier torsional angle changes. In addition, the methyl groups jutting from the main chain significantly increase the effective cross-sectional area of the chain. The synergetic effect of these two factors results in the above-mentioned order of the modulus among the meso, δ, α, and β forms. The crystallite modulus of PLLA chain (in the order of 15 GPa) is lower than those of *isotactic* polypropylene (34 GPa) and polyoxymethylene (70 GPa) [66, 70, 71], which can be understood from the difference of the chain conformation; the latter two polymers have a tighter and more rigid helical conformation than the PLA chain.

The anisotropic mechanical property is also important. The Young's modulus in the plane perpendicular to the chain axis is governed mainly by the H. . .H interatomic interactions between the neighboring chains [67]. The Young's modulus of PLLA in the lateral direction is in the same order as that of polyethylene, *isotactic* polypropylene, and so on [66, 67, 71].

## 6.5 STRUCTURE AND FORMATION OF PLLA/PDLA STEREOCOMPLEX

### 6.5.1 Reconsideration of the Crystal Structure

The stereocomplex of PLLA and PDLA was discovered in 1987 by Ikada et al., in which the blend samples of various L/D ratios were prepared from solution [27]. They reported

the formation of stereocomplex occurs apparently over a comparatively wide range of L/D ratio. But their conclusion was that the complexation occurs stoichiometrically at the 1 : 1 ratio only, and the excess amount of the component is crystallized into the α form or remains in the amorphous region.

The crystal structure of PLLA/PDLA stereocomplex was proposed by Okihara et al. by analyzing the WAXD and electron diffraction data [28, 33]. The unit cell dimensions were $a$ = 9.16Å, $b$ = 9.16Å, and $c$ (chain axis) = 8.70Å, $\alpha$ = 109.2°, $\beta$ = 109.2°, and $\gamma$ = 109.8°. As shown in Figure 6.16b, a pair of PLLA and PDLA chain stems of 3/1 helical conformation is packed in the triclinic unit cell of space group $P1$ with the statistically disordered mode: the upward and downward chains of the same handedness locate at 50% probability at a lattice site. On the basis of the X-ray powder diffraction data, the electron diffraction data of a single crystal and also the packing energy calculations, Brizzolara et al. suggested the importance of the van der Waals interactions between the PLLA and PDLA chains [74]. By analyzing the electron diffraction data of a stereocomplex single crystal, Cartier et al. proposed a model of the trigonal unit cell with $a = b$ = 14.98Å, $c$ (chain axis) = 8.70Å, $\alpha = \beta = 90°$ and $\gamma = 120°$ [75]. As shown in Figure 6.16a, the three couples of PLLA and PDLA pairs are packed in this large cell. They proposed the two candidates of the space group: $R3c$ and $R\bar{3}c$. In the former case, all the chains are directed toward the same direction concerning the upward and downward orientation along the chain axis. In the latter case, the upward and downward chains are positioned at 50% probability at one lattice site.

At this point, we have to remember one important experimental data, which was reported by the several researchers [27, 37, 46, 76]: the PLLA/PDLA stereocomplex is formed at an L/D mass ratio in the region of 7/3–4/6,

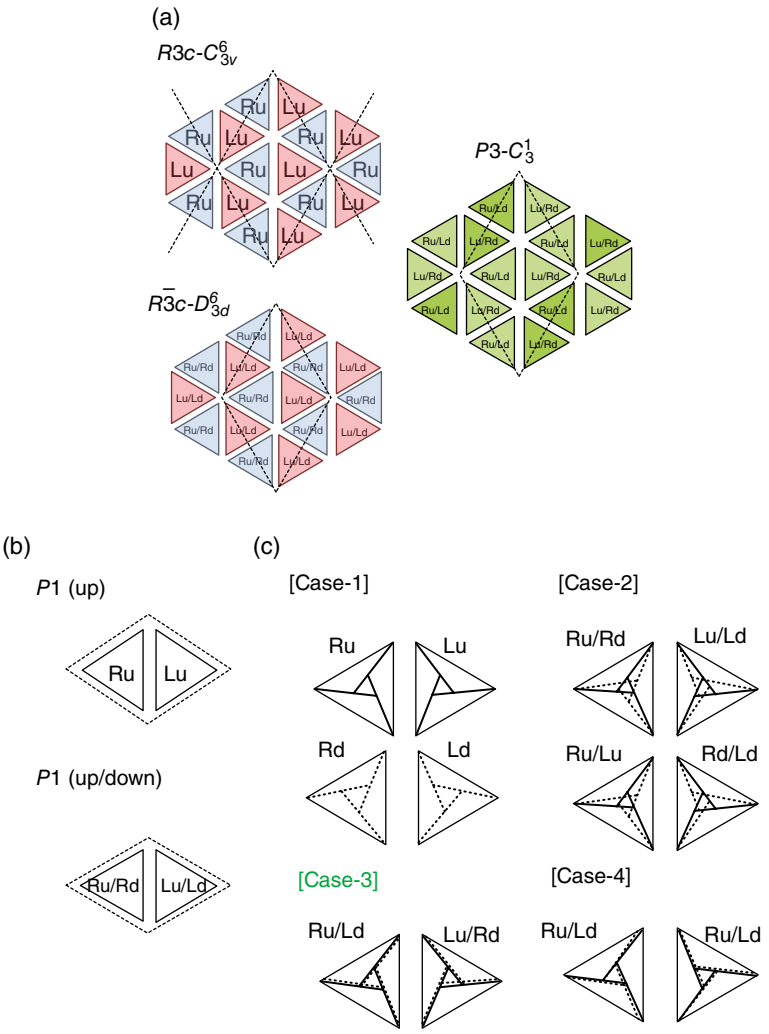


**FIGURE 6.16** (a) and (b) Various chain packing modes of PLA stereocomplex with L/D 50/50 ratio. (c) Illustrated structures of the R and L chain stems projected along the chain axis. Source: Reproduced from Tashiro et al., *Macromolecules* 2017, 50, 8048−8065.

not only at 5/5. The X-ray diffraction data are shown in Figure 6.17a and b. The sample films were blends of L/D 50/50 and 70/30 ratio, which were cast from the chloroform solution. The film was heated up continuously, during which the X-ray diffraction profile was measured stepwise. The starting samples showed the weak peaks of the α form in addition to the main amorphous halo. By heating, the α form peaks increased in intensity and disappeared at the melting point (~190°C). In parallel, the diffraction peaks of the stereocomplex started to appear and increased. These peaks disappeared at 230°C, the melting point of the stereocomplex. After being melted, the sample was cooled slowly toward the room temperature. During cooling, only the X-ray peaks of the stereocomplex appeared and increased in intensity. On the second heating, only these peaks were observed, and no trace of the α peaks was detected up to the melting. This finding was observed not only for the L/D = 50/50 sample but also for the L/D = 70/30 sample. Beyond the ratio 70/30, the blend sample showed a mixture of the X-ray diffraction peaks of the stereocomplex and the α form. The relative intensity for the stereocomplex and α form peaks is plotted against the L/D content as shown in Figure 6.17c. The pure stereocomplex was detected in the L/D ratio of 70/30–40/60. By combining the various experimental data, the most reasonable structure is the co-crystallization model of PLLA and PDLA chains at the various ratios.

Figure 6.18 shows the typical 2D-WAXD patterns of stereocomplex with different enantiomer ratios. The unit cell parameters are almost common to these stereocomplexes; $a = b = 14.94$ Å, $c$ (chain axis) = 8.624 Å, $\alpha = \beta = 90°$ and $\gamma = 120°$. Although the $R3c$ model is not necessarily reasonable in such a point that only R : L = 1 : 1 ratio is accepted, the X-ray equatorial line profile reproduces the observed data quite well, while the layer line profiles are not very well reproduced. In the case of the $R\bar{3}c$ model, the upward and downward chains of the same handedness are located at 50% at one lattice site. The oppositely-handed chains are positioned at the neighboring sites. As a result, this model gives the R : L = 1 : 1 ratio only. The $R\bar{3}c$ model did not reproduce the observed diffraction profiles very well, which can be deleted here from the preferential candidates. A new possible model of $P3$ space group was proposed by Tashiro et al., which can cover the stereocomplex produced in the range of L/D 7/3–4/6 [46, 47]. In the $P3$ model, the packing mode of the chains is similar to those of the above-mentioned two models. But, the two neighboring sites are symmetrically independent. This means that the pair of the neighboring sites (left and right sides) can be (R and R), (R and L) or (L and L) at an arbitrary ratio. However, the packing structure must be stereochemically reasonable. As mentioned above, the $R3c$ model can reproduce the X-ray equatorial line profile well, suggesting the projected structure of R and L chains should be the same as that predicted for the $R3c$ model (see Figure 6.16a). It is noticed that the right-handed upward (Ru)

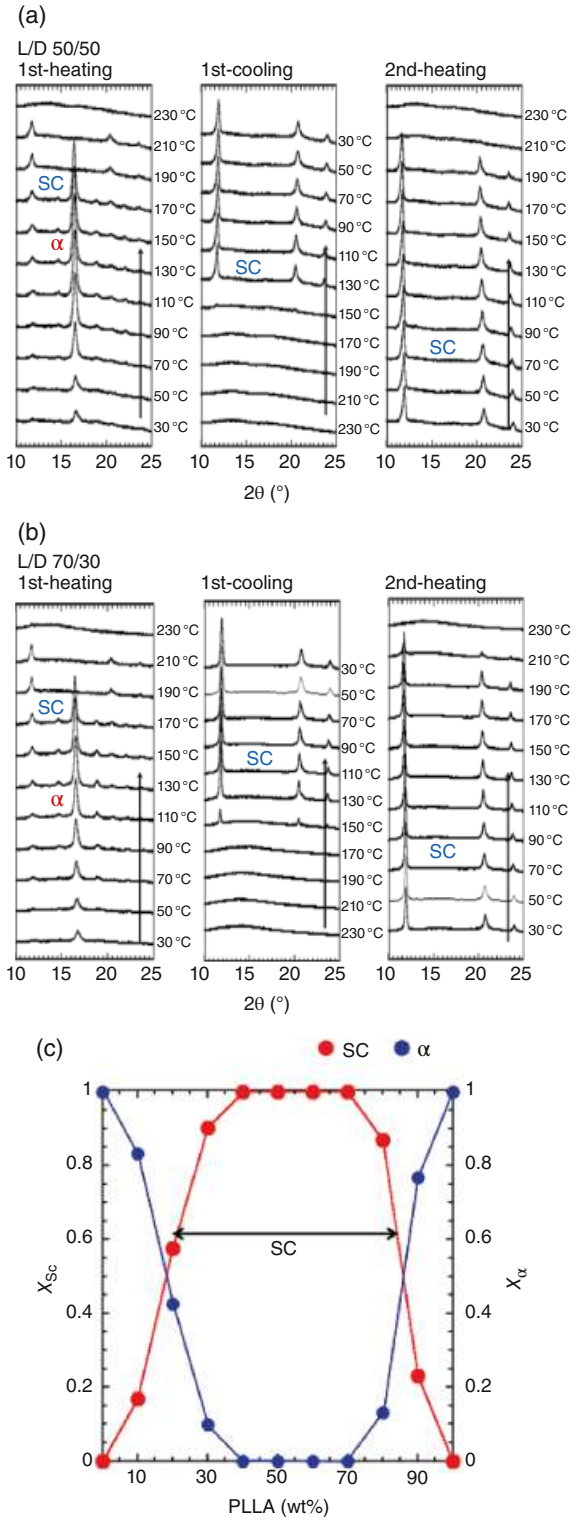


**FIGURE 6.17** Temperature dependence of X-ray diffraction profiles of the solution-cast films, (a) PLLA/PDLA 50/50 and (b) PLLA/PDLA 70/30 sample measured in the heating, cooling, and reheating processes. (c) The relative content of the **α** form and SC phase measured for the PLLA/PDLA blend samples with the various L/D contents on the basis of the X-ray diffraction data measured after cooling from the melt. Source: Reproduced from Tashiro et al., *Macromolecules* 2017, 50, 8048−8065.

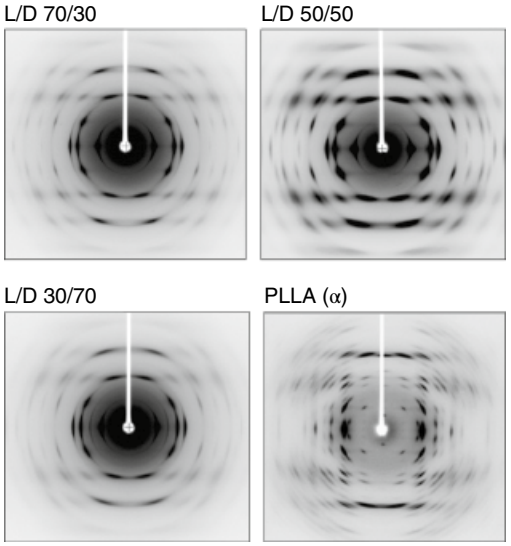


**FIGURE 6.18** 2-Dimensional X-ray diffraction diagrams of the uniaxially oriented SC phase of the PLLA/PDLA blend samples with the various L/D ratios. The diffraction diagram of the uniaxially oriented PLLA **α** form is shown here also for comparison. Source: Reproduced from Tashiro et al., *Macromolecules* 2017, 50, 8048–8065.

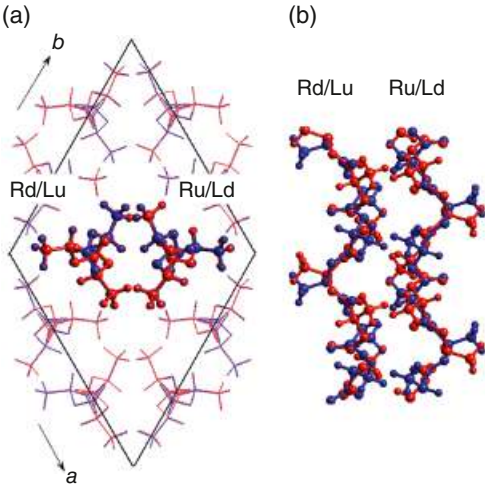


**FIGURE 6.19** Crystal structure of PLLA (L)/PDLA (R) stereocomplex. One lattice site is statistically occupied by a pair of Rd and Lu chains and the neighboring site by a pair of Ru and Ld chains: (a) along the c-axis and (b) along the 110 plane. Source: Reproduced from Tashiro et al., *Macromolecules* 2017, 50, 8048–8065.

chain and the left-handed downward (Ld) chain show the same projected structure perfectly (Figure 6.16c). The Lu and Rd chains are also in the same situation. Then, the plausible pair of the two neighboring sites is (Ru/Ld and Lu/Rd, case 3) or (Ru/Ld and Ru/Ld, case 4), as illustrated in Figure 6.16c. Finally, the model of case 3 was found as the best candidate to reproduce the observed X-ray diffraction data. The crystal structure is shown in Figure 6.19. Different from the case of the *R*3*c* model, the *P*3 model gives better agreement for all the layer-line profiles up to the higher angle regions as seen in Figure 6.20a. Besides, as already mentioned, the R and L chains can be located at one site with various ratios, satisfying well the experimental data shown in Figure 6.20.

### 6.5.2 Experimental Support of *P*3 Structure Model

The *P*3 structural model is consistent with the various experimental data. The details are discussed in the original paper [46, 47]. Several representative points are listed below:

1. According to the International Tables for Crystallography [53], the (000*l*) diffractions are expected to appear for $l = 6, 12, \ldots$ in the case of the *R*3*c* model. But no such extinction rule is predicted for the *P*3 model. As seen in the actually measured Weissenberg pattern shown in Figure 6.20b, the 0003 diffraction was clearly observed in addition to 0006, 00012 peaks. The *R*3*c* model cannot satisfy this result.
2. Once the stereocomplex is formed, it does not transform to the α form anymore even after many repetitions of melting and slow cooling (Figure 6.17). The L or D chains are supposed to be trapped into the stereocomplex region without a remarkable change of the spatial arrangements.
3. The experimental data including the formation of the spherulites and the single crystal of the stereocomplex and the SAXS data analysis [77, 78] are interpreted by assuming the existence of the stacked lamellar structure with the upward and downward chain stems (or the folded chain structure). The *R*3*c* model is difficult to apply for the interpretation of these experimental data.
4. Another important experimental evidence to show the reasonableness of the *P*3 model comes from the vibrational circular dichroism (VCD) data. The VCD is one powerful technique to distinguish the R and L chains in the crystal lattice. The right-handed and left-handed rotating IR beams (*r*- and *l*-circularly-polarized beams, respectively) are incident to the sample. The *l*-polarized IR beam is absorbed by the L chains and the *r*-polarized IR beam by the R chains. The absorbance difference, $\Delta Abs(\nu) = Abs^{L}(\nu) - Abs^{R}(\nu)$, is 0 if the L and D species are in the equal amounts in the sample, but it changes with other L/D blend ratios. Since the IR bands of the crystalline and amorphous phases can be distinguished easily, the measurement of $\Delta Abs$ for the crystalline bands can be used to study the *R*3*c* and *P*3 models. For the *R*3*c* model, the $\Delta Abs$ of the *crystalline bands* should be always 0 even when the L/D ratio is changed, while the $\Delta Abs$ may change depending on the R/L ratio for the *P*3 model.

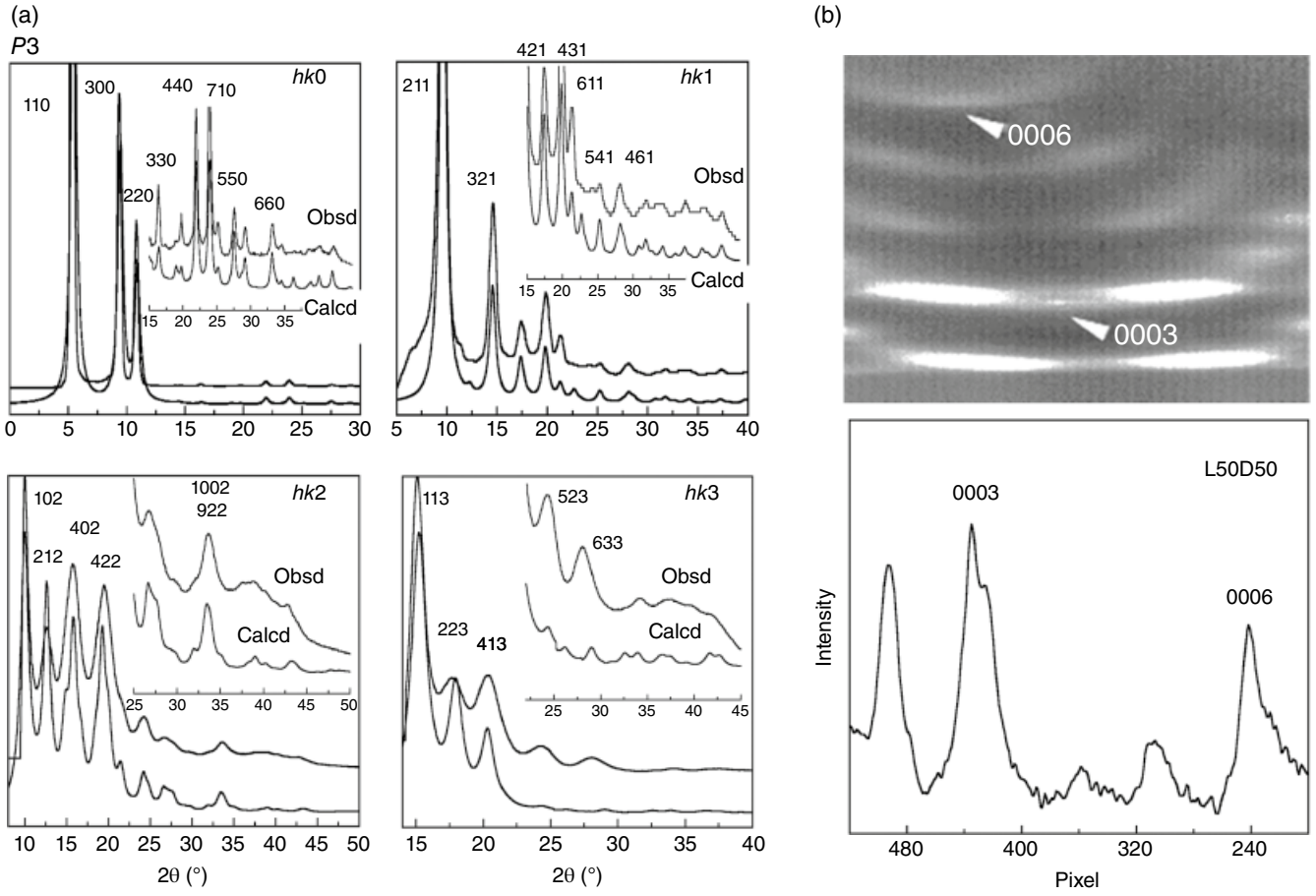


**FIGURE 6.20** (a) Comparison of the observed X-ray diffraction profiles along the various layer lines with those calculated for the L/D 50/50 stereocomplex model of the *P*3 space group symmetry. An incident X-ray is the Mo-K**α** line. (b) The Weissenberg 000*l* diffraction pattern measured for the L/D 50/50 stereocomplex. The diffraction profile was obtained by scanning the 2D pattern along the line of 000*l*. Source: Reproduced from Tashiro et al., *Macromolecules* 2017, 50, 8048−8065.

Figure 6.21a shows the experimental results collected for the PLLA (L)/PDLA (R) blend samples cast from chloroform solutions. The thus-prepared films are almost in the amorphous state. In the normal (not-circularly-polarized) IR spectra, the typical amorphous band is detected at about 1300 $cm^{-1}$, the absorbance of which does not change at all as long as the sample thickness is the same, because the L and R chains cannot be distinguished. But, the situation changes remarkably in the VCD spectra. Depending on the L/R content the $\Delta Abs$ changes between plus and minus values systematically. Figure 6.21a indicates that the L and R chains in the amorphous region are mixed homogeneously. Our attention should be drawn to the behavior of the crystallization-sensitive bands of the stereocomplex. In the normal IR spectra, the heat treatment caused a reduction of the amorphous band intensity (broken line) and a remarkable increase of the 1306 $cm^{-1}$ band, which is assigned to the crystalline stereocomplex phase (Figure 6.21b). In the VCD spectra, $\Delta Abs(\nu)$ of 1306 $cm^{-1}$ band changes systematically and quite clearly depending on the L/D ratio. This observation indicates that the L and R chains in the crystalline region of the stereocomplex changes their relative content systematically depending on the L/D blend ratio, being consistent with the X-ray observation. In this way, it is reasonable to conclude that the L and R chain stems co-crystallize in the same crystallite of the stereocomplex at various L/R contents in the region of $70/30 \leq L/R < 40/60$.

### 6.5.3 Formation Mechanism of Stereocomplex

The above-mentioned *P*3 model was built up by introducing the rigid 3/1 helical conformational chains. Because of no flexibility of the rigid chain form, some pairs of the H. . .H distances between the $CH_3$ units of the neighboring chains

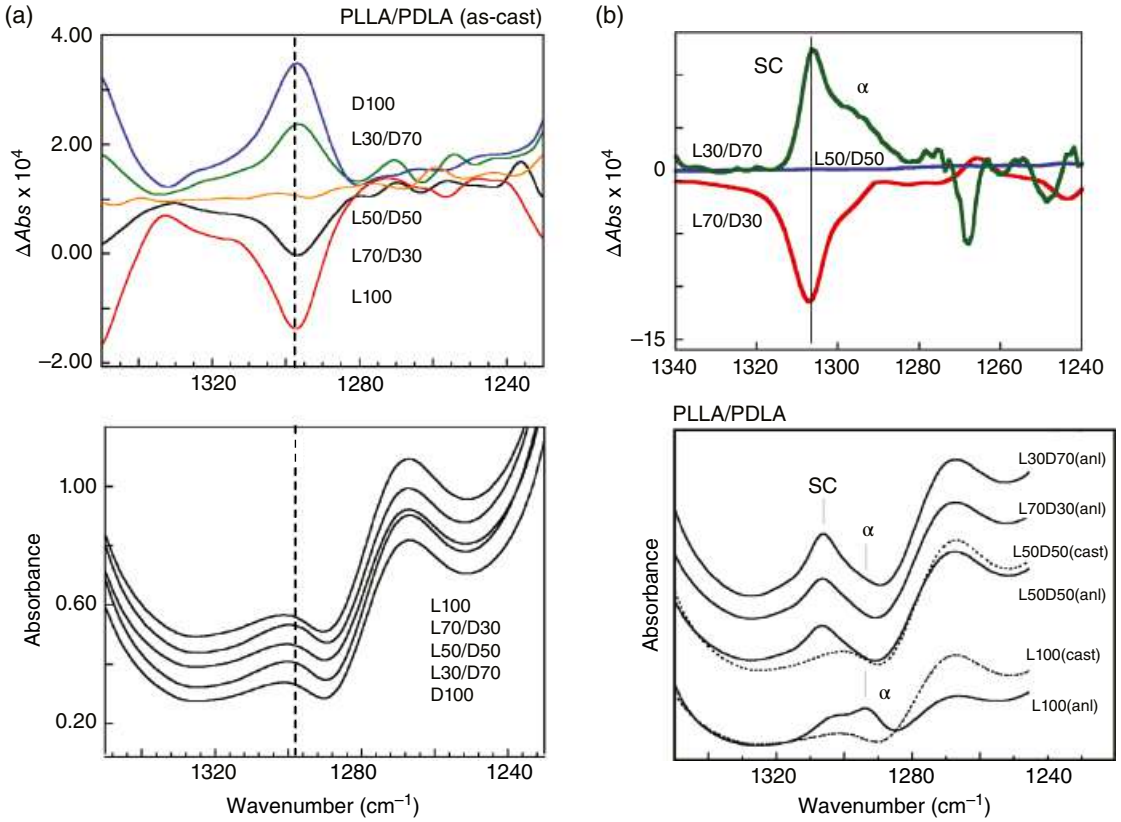


**FIGURE 6.21** (a) IR circular dichroism **Δ**Abs and IR spectra measured for a series of the solution-cast PLLA/PDLA blend samples with the various L/R ratios, and (b) a series of PLLA/PDLA blend samples before and after annealing. The crystalline band at 1306 $cm^{-1}$ shows a clear change of **Δ**Abs depending on the L/R ratio. Source: Reproduced from Tashiro et al., *Macromolecules* 2017, 50, 8066−8071.

are found to be too short compared with the sum of the van der Waals radius of the H atom. The energy calculation of the model clarified two key points about the chain packing mode. First, the packing of Rd–Ld pairs in the *R*3*c* unit cell is energetically stable with the H. . .H distance of about 2.6 Å. But the chain conformation is strictly constrained to possess the 3/1 helical symmetry required by the space group. Once the crystallographic $3_1$ helical symmetry is erased from the chains, as seen in the *P*3 model, the packing of such too rigid helical chains is energetically unacceptable and the chain conformation is spontaneously deformed so that the total energy becomes lower. Second, in the stereocomplex of the asymmetric R/L content, the population of the R/R (L/L) pairs increases statistically in addition to the R/L pairs. By modifying the chain conformation and the chain packing mode, an energetically stable structure can be attained for the crystal structure composed of only the Ru and Rd (or Ld and Lu) chain stems with the same unit cell parameters as mentioned above. These R/R (L/L) pairs are considered to exist as the locally stable structures in the stereocomplex. When the R/L ratio is beyond the critical value (refer to Figure 6.17c), the large domains of R (or L) chain stems transform to the packing structure of the α form with more stable energy.

Figure 6.22 illustrates the formation process of the stereocomplex crystal region in the amorphous film containing the random distribution of L and D (or R) chains. The domains of only L or D components and the region of randomly mixed L and D components are coexistent. These amorphous domains composed of only D or L components crystallize partially into the δ (or α) form, when the film is heated above the glass transition temperature. At a higher temperature, the α crystallites are melted. In the cooling process, these molten chains are aggregated to form the crystalline region of the stereocomplex. It is hard to imagine that they change drastically their spatial distribution to create the structure consisting of the *regularly- and alternately*-packed R and L chain components. It is more natural to consider that the heterogeneously distributed PDLA and PLLA chains co-crystallize together *without large change of their spatial arrangements*.

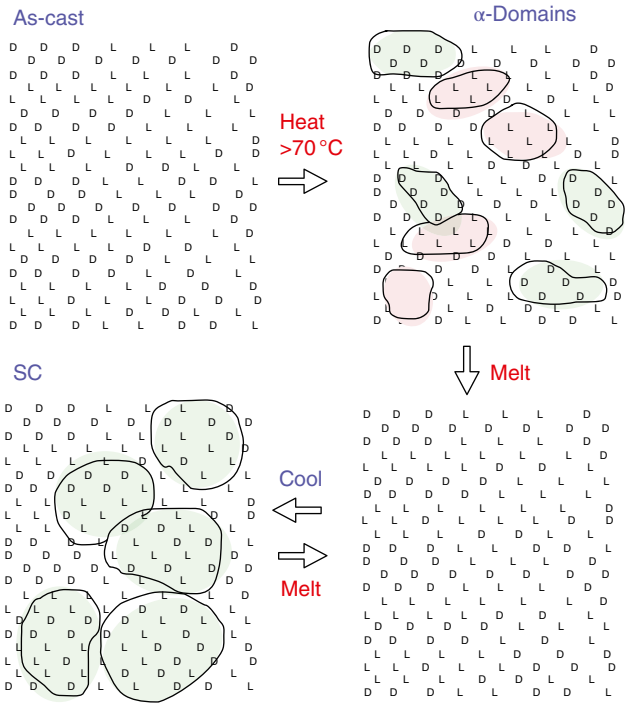


**FIGURE 6.22** A model of stereocomplex formation from the solution cast L/D blend sample. Here "D" is equivalent to "R." Source: Reproduced from Tashiro et al., *Macromolecules* 2017, 50, 8048–8065.

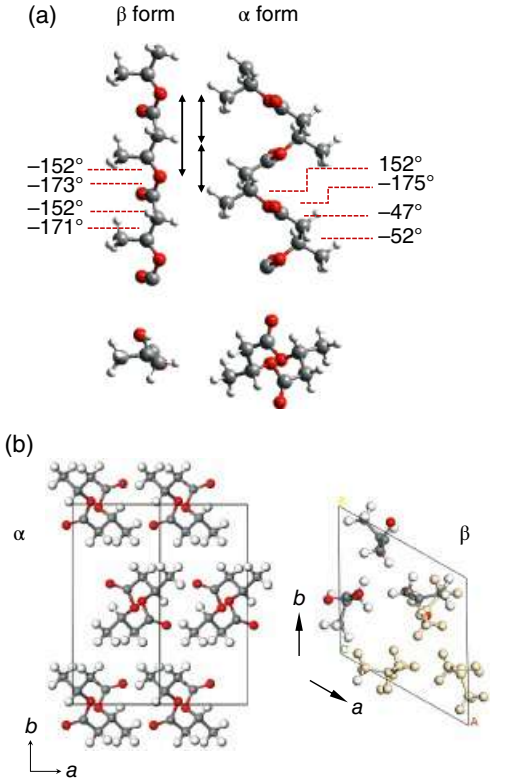


**FIGURE 6.23** (a) Chain conformation and (b) chain packing mode obtained for the PHB α and β forms. Source: Reproduced from Phongtamrug and Tashiro, *Macromolecules* 2019, 52, 2995–3009 and Wang and Tashiro, *Macromolecules* 2016, 49, 581–594.

## 6.6 PHB AND OTHER BIODEGRADABLE POLYESTERS

In addition to PLA, several aliphatic polyesters are becoming good targets for biodegradable and carbon-neutral multipurpose polymers, though they do not have necessarily the asymmetric carbon atoms on the skeletal chains. Because of the relatively high biodegradability, these various polyesters have become increasingly important in commodity field, including medical and pharmaceutical applications, food packaging, and even automobiles. To understand and improve their physical properties, it is needed to know how the combination between the ester parts and the aliphatic (and aromatic) segments affects the structure, phase transition, and crystallization behaviors in the different manner from those of the above-mentioned PLA case. In this section, several representative aliphatic polyesters are listed, and their structural characteristics are briefly described.

### 6.6.1 Poly(3-Hydroxybutyrate) (PHB)

***6.6.1.1 Crystal Structure of α Form*** PHB crystallizes usually as the α form. The orthorhombic unit cell parameters are $a$ = 5.76 Å, $b$ = 13.20 Å, and $c$ (chain axis) = 5.96 Å, in which the two 2/1 helical chains of *TTGG* conformation are packed with the $P2_12_12_1$ space group symmetry [79]. Figure 6.23 shows the crystal structure of the α form [80, 81]. In the IR spectra of the α form, the anti-symmetric CH stretching mode of $CH_3$ groups [$\nu_{as}$(CH)] was found to appear at appreciably high frequency side, 3009 $cm^{-1}$, which was interpreted as a result of the intermolecular $CH_3$. . .O(=C) interactions between the neighboring chains coming from the anomalously short H. . .O distance (2.62 Å) [80, 82].

***6.6.1.2 Crystal Structure of β Form*** The PHB β form is produced by strongly stretching an oriented α form sample [83]. It is actually impossible to obtain the pure β sample even when the sample is stretched up to the occurrence of fracture. Therefore, the observed X-ray diffraction pattern contains necessarily the two patterns of the α and β forms. Figure 6.24b shows the X-ray diffraction pattern of the pure β component, which was obtained by subtracting the diffraction pattern of the pure α form from the original pattern [81]. The equatorial line consists of the highly oriented spots, while the layer lines are quite diffuse. The unit cell parameters were determined as $a = b$ = 9.22 Å, $c$ (chain axis) = 4.66 Å and γ = 120°. The repeating period 4.66 Å corresponds to the almost extended chain conformation (see Figure 6.23a). After the many trial-and-error

processes, the structure model of the space group $P3_221$ was found to reproduce the observe diffraction profiles along all the layer lines reasonably. Figure 6.23b shows the thus-obtained crystal structure of the β form. The upward and downward chains are located at one lattice site at 50% probability. Figure 6.24c compares the observed diffraction profiles with those calculated for this model.

At this stage, we can compare the chain conformations of the various crystalline forms of PLA and PHB as follows. Roughly speaking, PLA takes the *TTG* chain conformation, though the *T* and *G* values vary slightly among the different crystal forms (α, δ, and β forms). On the other hand, the PHB α form takes the conformation of *TTGG* sequences, but the positions of these torsional angles are different from those of PLA chain although the local chemical structure is similar to each other. Besides, the strong stretching of the PHB chains causes the large change of the torsional angle from *G* to *T*. The rough comparison of the torsional angles is made as shown below, where $T \approx 160–180°$, $T' \approx 150–160°$, and $G \approx 50–80°$.

| | |
|---|---|
| PLA | . . .–$C(CH_3)$–C(O)–O–$C(CH_3)$–C(O)–O–$C(CH_3)$– |
| (α, δ, β) | $T'$ $T$ $G$ $T'$ $T$ $G$ |
| PHB | . . .–$CH_2$–C(O)–O–$C(CH_3)$–$CH_2$–C(O)–O–$C(CH_3)$–. . . |
| α | $G$ $G$ $T$ $T'$ $G$ $G$ $T$ $T'$ |
| β | $T$ $T'$ $T$ $T'$ $T$ $T'$ $T$ $T'$ |

It must be noted that the whole shapes of the chains are affected remarkably even when the changes of the torsional angles are not very large as seen well in the cases of PLA chains.

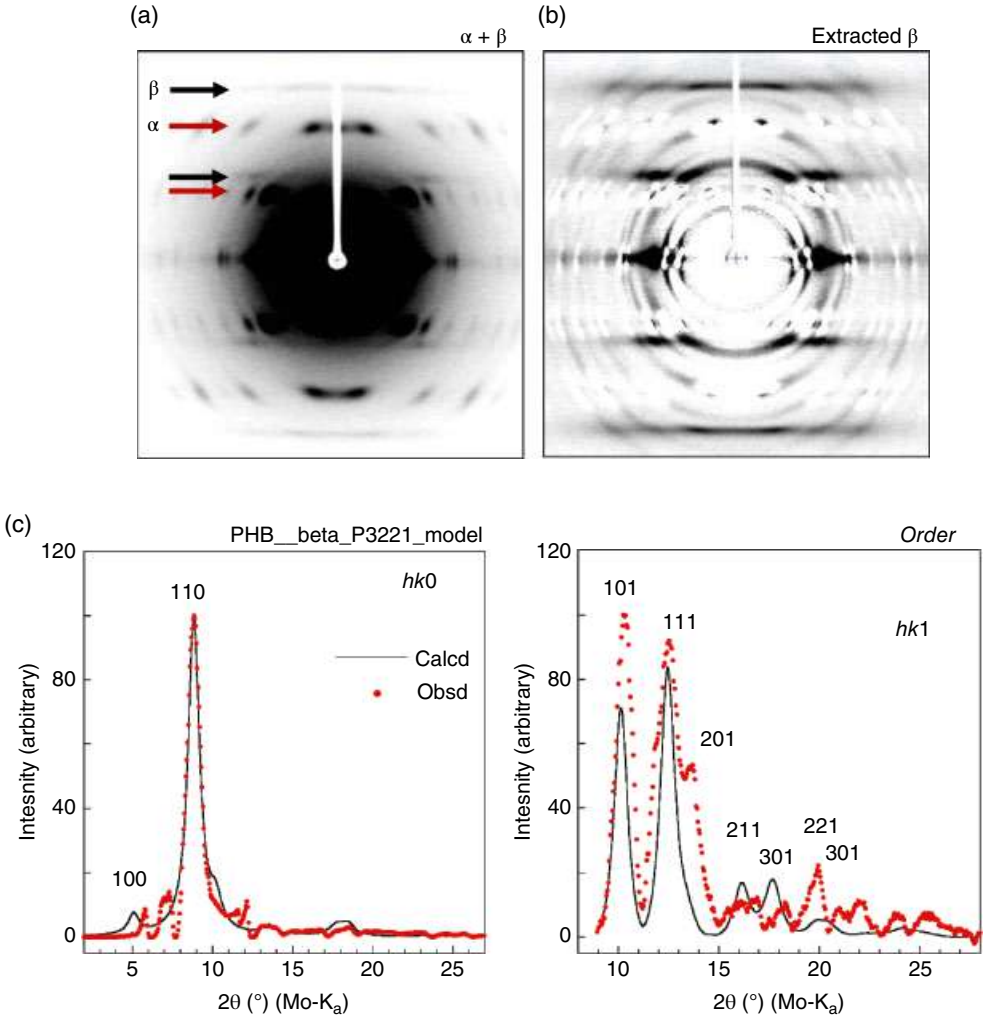


**FIGURE 6.24** The 2D X-ray diffraction patterns of PHB. (a) The mixture of the **α** and **β** forms, (b) the **β** form pattern obtained by the subtraction of the X-ray pattern of the pure α form from (a). (c) Comparison of the X-ray diffraction profiles along the various layer lines observed for PHB **β** form with those calculated for the model with the space group $P3_221$. Source: Reproduced from Phongtamrug and Tashiro, *Macromolecules* 2019, 52, 2995–3009.

***6.6.1.3 Transition Mechanism to the β Form*** As clarified by the IR spectral data analysis, the β form starts to appear above a constant stress point (critical stress σ*) and increases its content with stress [81]. Another important point is obtained from the SAXS data analysis. As shown in Figure 6.25a, the α form sample shows the meridional 2-point SAXS pattern. The long period of the stacked lamellae is about 200 Å. When the sample is stretched to 30–60% of the original length, the new long-period peak of about 400 Å period appeared. At the same time the diffuse scattering peak was detected along the equatorial line, the averaged period of which is about 90 Å. By taking all of the thus-collected experimental data into consideration, the transition mechanism of the β form crystal regions is described as illustrated in Figure 6.25b. Here the role of the tie chains is emphasized, which pass through the neighboring lamellae and the intervening amorphous region.

The original α crystallites form the regular lamellar stacking structure. As the sample is stretched, the short tie chain segments between the neighboring lamellae start to be tensioned strongly, and the high stress is locally generated in these tie chain parts (sometimes, the fraction of these rigid chains in the amorphous region are called RAF (rigid amorphous fraction) [84, 85]. When the local stress exceeds a critical value σ*, the transformation to the zigzag chain conformation of the β form starts to occur in the highly strained tie chain parts. The thus-created β crystalline bundles exist at the various positions with the averaged period 90 Å along the equatorial line. The α crystalline regions connected to the strained tie chains are also induced to transform to the β form. As a result, the repeating period of the β crystalline parts becomes quite long, compared with the part of the original α form. By increasing the stress furthermore, the highly tensioned tie chain segments cannot bear against the high local stress, and they are finally broken to generate the radicals. These radicals react with the neighboring chain segments and accelerate the breakage of the surrounding chain segments. As a result, micro-voids are generated. These micro-voids are fused into larger macro-voids, resulting finally in the rupture of the whole sample [72, 86].

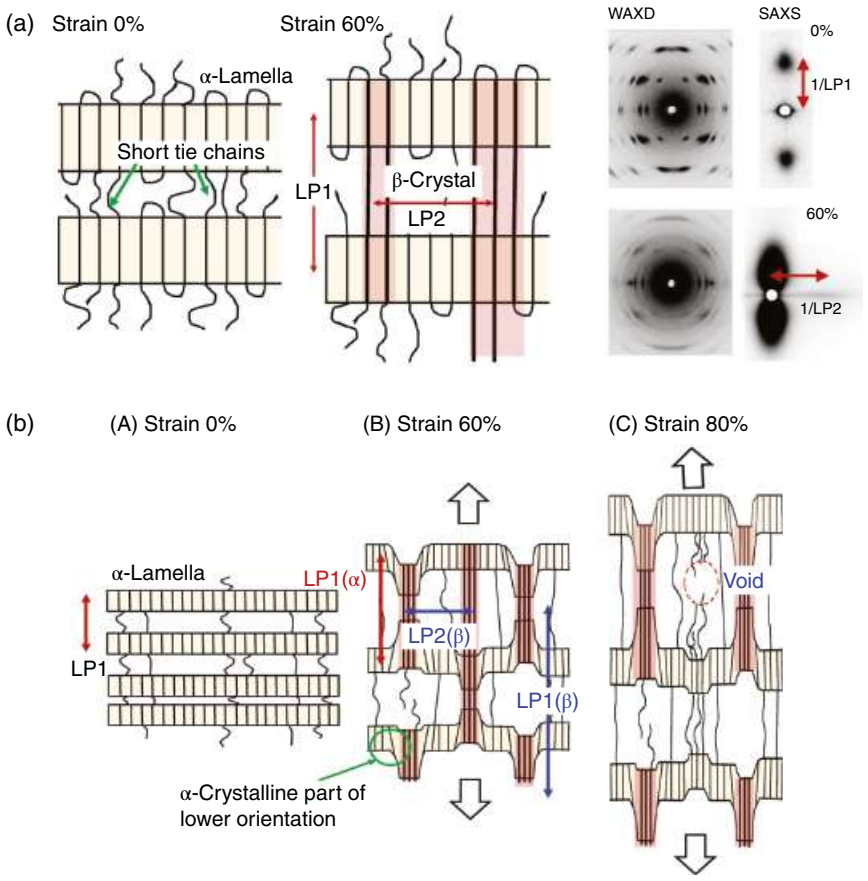


**FIGURE 6.25** (a) Images of the higher-order structure of the **α** and **β** forms of the oriented PHB sample. (b) The illustration of the higher-order structure change in the tensile deformation of the oriented PHB sample. Source: Reproduced from Phongtamrug and Tashiro, *Macromolecules* 2019, 528, 2995–3009.

### 6.6.2 Polyethylene Adipate (PEA)

PEA (—[—$OCH_2CH_2OCO(CH_2)_4CO$—]$_n$—) crystallizes to the α form with the unit cell parameters of $a = 5.47$ Å, $b = 7.23$ Å, $c$ (chain axis) = 11.72 Å and $\beta = 113.5°$ [87–89]. The two chains of almost zigzag type are packed in the unit cell with the $P2_1/a$ space group symmetry.

The spherulite of PEA α form gives a beautiful ring pattern as shown in Figure 6.26. The stepwise WAXD/SAXS measurements at 1 μm step using a synchrotron X-ray beam of 1 μm size revealed that the lamellae grow radially with the 180° twisting around the $a'$ axis at 7 μm pitch. On the other hand, the SEM observation of the fractured surface of the spherulite clarified that the spherulite consists of the discontinuous aggregation of the lamellar blocks in the radial direction [90]. These two observations, the lamellar twisting phenomenon and the discontinuous growth of lamellae, must be combined together consistently. In the growing spherulite of PEA α form, the molecular chains are attached on the front surface of the lamella, and the lamella grows with the small twisting of the plane sheet of the extended chain stems. Once when the 180° twisting is completed, a new lamella starts to generate *discontinuously* on the adjacent lamellar surface and grows with the twisting phenomenon. So far, as a general phenomenon of the ring-pattern spherulite, the twisted lamellae have been believed to grow *continuously* from the center. But the study of the PEA spherulite gave us a warning about such an unsound universal concept of the continuously growing process of the twisted lamellae.

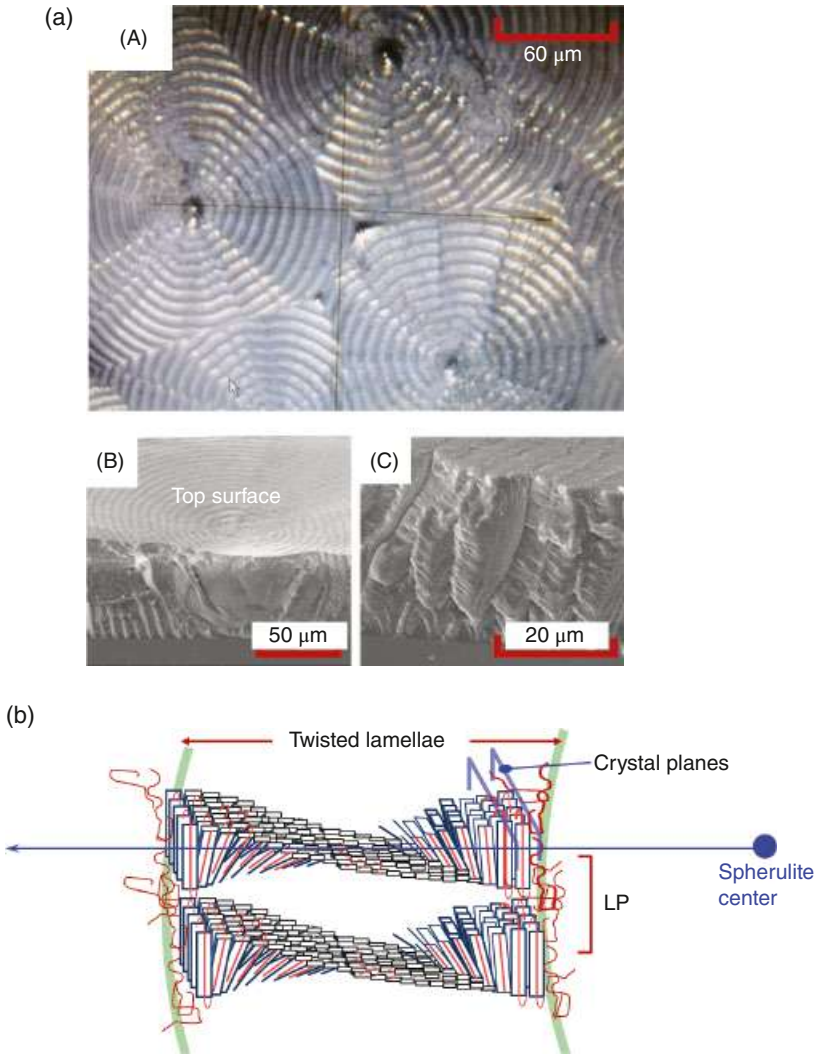


**FIGURE 6.26** (a) (A) polarized optical microscopic image and (B) and (C) SEM (scanning electron microscope) images measured for PEA spherulite. Source: Reproduced Woo et al., *Macromolecules* 2012, 45, 1375–1383.] (b) Illustration of the stacking structure of the twisted lamellae. Source: Reproduced from Tashiro et al., *Polymer Journal* 2019, 51, 131–141.

## 6.7 FUTURE PERSPECTIVES

Among many kinds of biodegradable polyesters, PLA is expected to be one of the most promising candidates. The present chapter described mainly the latest details of the crystal structure and phase transition of the various crystalline forms of this polymer. Some characteristics of such related polyesters as PHB and PEA are also compared briefly.

At this moment, there are many unsolved problems about these polymers. For example, we need to know the relation between the crystal structures and the morphology of the bulk PLLA sample. The complex hierarchical structure of the polymer makes it difficult to understand the structure–property relation from a wide range of structure. For example, the details of the structure evolution process in the isothermal crystallization from the melt are still ambiguous for these polyesters. Another important aspect of the biodegradable polyesters is related to the microscopically viewed investigation of their biodegradation process in the presence of bacteria. As described briefly about the phase transition of PHB, the role of taut tie chains passing through the stacked lamellae (or the rigid amorphous fraction, RAF) must be also revealed in association with the structure-property relation of the bulk samples [72].

In the long history of the biodegradable polyesters, many papers have reported their structural information. However, reliability of the crystal structure and chain conformation reported in the literature remain elusive. Different from the single crystals of low-molecular-weight compounds, the low accuracy of the analyzed structure might be fatal for the semicrystalline polymer substances because the poor X-ray diffraction data of small and broad diffraction spots are collected at best. It is important to always check whether the structure information is consistent with other experimental data, as exemplified from several case studies presented in this chapter.

## ACKNOWLEDGEMENTS

The author Kohji Tashiro, is grateful for many researchers who collaborated and encouraged him in the structure studies of PLA: Dr. Hideto Tsuji (Toyohashi University of Technology, Japan), Dr. Takashi Ohhara (Japan Atomic Energy Agency), Dr. Nobuo Niimura (Ibaraki University, Japan), Dr. Tomoji Ozeki (Tokyo Institute of Technology, (present) Nihon University, Japan), Dr. Kaewkan Wasanasuk (Toyota Technological Institute, (present) PTT Public Co., Thailand), Dr. Makoto Hanesaka (Toyota Technological Institute), Dr. Tetsuo Kanamoto (Tokyo University of Science,), Mr. Naoto Kouno (Toyota Technological Institute), Dr. Jun Koshobu and Mr. Keisuke Watanabe (Japan Spectroscopic Co. Ltd., Japan), Dr. Suwabun Chirachanchai (Chulalongkorn University, Thailand), Dr. Piyawanee Jariyasakoolroj (Chulalongkorn University, (present) Kasetsart University, Thailand), Dr. Wannee Chinsirikul (National Metal and Materials Technology Center, Thailand), and Dr. Hiroko Yamamoto (Toyota Technological Institute, (present) Aichi Synchrotron Radiation Center).

This work was supported by "the Strategic Project to Support the Formation of Research Base at Private University (2010–2014) and (2015–2019)" of MEXT, Japan, and also by the National Natural Science Foundation of China 22073015.

## REFERENCES

1. S. Iannace, L. Nicolais, Isothermal crystallization and chain mobility of poly(L-lactide), *J. Appl. Polym. Sci.* **1997**, *64*, 911–919.
2. G. Kokturk, E. Piskin, T. F. Serhatkulu, M. Cakmak, Evolution of phase behavior and orientation in uniaxially deformed polylactic acid films, *Polym. Eng. Sci.* **2002**, *42*, 1619–1628.
3. J. Hu, T. Zhang, M. Gu, X. Chen, J. Zhang, Spectroscopic analysis on cold drawing-induced PLLA mesophase, *Polymer* **2012**, *53*, 4922–4926.
4. J. Zhang, Y. Duan, A. J. Domb, Y. Ozaki, PLLA mesophase and its phase transition behavior in the PLLA–PEG–PLLA copolymer as revealed by infrared spectroscopy, *Macromolecules* **2010**, *43*, 4240–4246.
5. K. Wasanasuk, K. Tashiro, Structural regularization in the crystallization process from the glass or melt of poly(L-lactic acid) viewed from the temperature-dependent and time-resolved measurements of FTIR and wide-angle/small-angle X-ray scatterings, *Macromolecules* **2011**, *44*, 9650–9660.
6. J. Zhang, Y. Duan, H. Sato, H. Tsuji, I. Noda, S. Yan, Y. Ozaki, Crystal modifications and thermal behavior of poly(L-lactic acid) revealed by infrared spectroscopy, *Macromolecules* **2005**, *38*, 8012–8021.
7. J. Zhang, K. Tashiro, A. J. Domb, H. Tsuji, Confirmation of disorder α form of poly(L-lactic acid) by the X-ray fiber pattern and polarized IR/Raman spectra measured for uniaxially-oriented samples, *Macromol Symp* **2006**, *242*, 274–278.
8. J. Zhang, K. Tashiro, H. Tsuji, A. J. Domb, Disorder-to-order phase transition and multiple melting behavior of poly(L-lactide) investigated by simultaneous measurements of WAXD and DSC, *Macromolecules* **2008**, *41*, 1352–1357.
9. K. Wasanasuk, K. Tashiro, Crystal structure and disorder in poly(L-lactic acid) δ form (α′ form) and the phase transition mechanism to the ordered α form, *Polymer* **2011**, *52*, 6097–6109.
10. X. Chen, J. Kalish, S. L. Hsu, Structure evolution of α′-phase poly(lactic acid), *J. Polym. Sci. Part B Polym. Phys.* **2011**, *49*, 1446–1454.

11. J. Kobayashi, T. Asahi, M. Ichiki, H. Oikawa, H. Suzuki, T. Watanabe, E. Fukada, Y. Shikinami, Structural and optical properties of poly lactic acids, *J. Appl. Phys.* **1995**, *77*, 2957–2973.
12. C. Aleman, B. Lotz, J. Puiggali, Crystal structure of the α-form of poly (L-lactide), *Macromolecules* **2001**, *34*, 4795–4801.
13. S. Sasaki, T. Asakura, Helix distortion and crystal structure of the α-form of poly(L-lactide), *Macromolecules* **2003**, *36*, 8385–8390.
14. K. Wasanasuk, K. Tashiro, M. Hanesaka, T. Ohhara, K. Kurihara, R. Kuroki, et al., Crystal structure analysis of poly(L-lactic acid) α form on the basis of the 2-dimensional wide-angle synchrotron X-ray and neutron diffraction measurements, *Macromolecules* **2011**, *44*, 6441–6452.
15. P. De Santis, J. Kovacs, Molecular conformation of poly (*S*-lactic acid), *Biopolymers* **1968**, *6*, 299–306.
16. B. Eling, S. Gogolewski, A. J. Pennings. Biodegradable materials of poly(L-lactic acid): 1. Melt-spun and solution-spun fibres, *Polymer* **1982**, *23*, 1587–1593.
17. W. Hoogsteen, A. Postema, Crystal structure, conformation and morphology of solution-spun poly (L-lactide) fibers, *Macromolecules* **1990**, *23*, 634–642.
18. J. Puiggali, Y. Ikada, H. Tsuji, L. Cartier, T. Okihara, B. Lotz, The frustrated structure of poly (L-lactide), *Polymer* **2000**, *41*, 8921–8930.
19. K. Takahashi, D. Sawai, T. Yokoyama, T. Kanamoto, S. H. Hyon, Crystal transformation from the α- to the β-form upon tensile drawing of poly(L-lactic acid). *Polymer* **2004**, *45*, 4969–4976.
20. H. Wang, J. Zhang, K. Tashiro, Phase transition mechanism of poly(L-lactic acid) among the α, δ and β forms on the basis of the reinvestigated crystal structure of the β form, *Macromolecules* **2017**, *50*, 3285–3300.
21. L. Cartier, T. Okihara, Y. Ikada, H. Tsuji, J. Puiggali, B. Lotz, Epitaxial crystallization and crystalline polymorphism of polylactides, *Polymer* **2000**, *41*, 8909–8919.
22. B. Lotz, G. Li, X. Chen, J. Puiggali, Crystal polymorphism of polylactides and poly(pro-alt-CO): The metastable beta and gamma phases. Formation of homochiral PLLA phases in the PLLA/PDLA blends, *Polymer* **2017**, *115*, 204–210.
23. H. Marubayashi, S. Asai, M. Sumita, Guest-induced crystal-to-crystal transitions of poly(L-lactide) complexes, *J. Phys. Chem. B* **2013**, *117*, 385–397.
24. H. Marubayashi, S. Asai, M. Sumita, Crystal structures of poly(L-lactide)–$CO_2$ complex and its emptied form, *Polymer* **2012**, *53*, 4262–4271.
25. H. Marubayashi, S. Asai, M. Sumita, Complex crystal formation of poly(L-lactide) with solvent molecules, *Macromolecules* **2012**, *45*, 1384–1397.
26. H. Marubayashi, S. Akaishi, S. Akasaka, S. Asai, M. Sumita, Crystalline structure and morphology of poly(L-lactide) formed under high-pressure $CO_2$, *Macromolecules* **2008**, *41*, 9192–9203.
27. Y. Ikada, K. Jamshidi, H. Tsuji, S. H. Hyon, Stereocomplex formation between enantiomeric poly(lactides), *Macromolecules* **1987**, *20*, 904–906.
28. T. Okihara, Lattice disorders in the stereocomplex and of poly(L-lactide), *Bull. Inst. Chem. Res. Kyoto Univ.* **1988**, *66*, 271–282.
29. H. Tsuji, Y. Ikada, S. H. Hyon, Y. Kimura, T. Kitao, Stereocomplex formation between enantiomeric poly(lactic acid). VIII. Complex fibers spun from mixed solution of poly(D-lactic acid) and poly(L-lactic acid), *J. Appl. Polym. Sci.* **1994**, *51*, 337–344.
30. H. Tsuji, S. H. Hyon, Y. Ikada, Stereocomplex formation between enantiomeric poly (lactic acid)s. 4. Differential scanning calorimetric studies on precipitates from mixed solutions of poly (D-lactic acid) and poly (L-lactic acid), *Macromolecules* **1991**, *24*, 5657–5662.
31. H. Tsuji, F. Horii, S. H. Hyon, Y. Ikada, Stereocomplex formation between enantiomeric poly(lactic acid)s. 2. Stereocomplex formation in concentrated solutions, *Macromolecules* **1991**, *24*, 2719–2724.
32. H. Tsuji, S. H. Hyon, Y. Ikada, Stereocomplex formation between enantiomeric poly(lactic acid)s. 3. Calorimetric studies on blend films cast from dilute solution, *Macromolecules* **1991**, *24*, 5651–5656.
33. T. Okihara, M. Tsuji, A. Kawaguchi, I. Katayama, H. Tsuji, S. H. Hyon, Y. Ikada, Crystal structure of stereocomplex of poly(L-lactide) and poly(D-lactide), *J. Macromol. Sci. Part B Phys.* **1991**, *B30*, 119–140.
34. H. Tsuji, Y. Ikada, Stereocomplex formation between enantiomeric poly(lactid acid)s. 6. Binary blends from copolymers, *Macromolecules* **1992**, *25*, 5719–5723.
35. H. Fumitaka, Y. Ikada, Stereocomplex formation between enantiomeric poly(lactic acid)s. 7. Phase structure of the stereocomplex crystallized from a dilute acetonitrile solution as studied by high-resolution solid-state, *Macromolecules* **1992**, *25*, 4114–4118.
36. H. Tsuji, S. Hyon, Y. Ikada, Stereocomplex formation between enantiomeric poly(lactic acid)s. 5. Calorimetric and morphological studies on the stereocomplex formed in acetonitrile solution, *Macromolecues* **1992**, *25*, 2940–2946.
37. H. Tsuji, Y. Ikada, Stereocomplex formation between enantiomeric poly (lactic acids). 9. Stereocomplexation from the melt, *Macromolecules* **1993**, *26*, 6918–6926.
38. P. Pan, Y. Inoue, Polymorphism and isomorphism in biodegradable polyesters, *Prog. Polym. Sci.* **2009**, *34*, 605–640.
39. H. Tian, Z. Tang, X. Zhuang, X. Chen, X. Jing, Biodegradable synthetic polymers: preparation, functionalization and biomedical application, *Prog. Polym. Sci.* **2012**, *37*, 237–280.
40. H. Nakajima, P. Dijkstra, K. Loos, The recent developments in biobased polymers toward general and engineering applications: polymers that are upgraded from biodegradable polymers, analogous to petroleum-derived polymers, and newly developed, *Polymers* **2017**, *9*, 523.
41. B. Lotz, Crystal polymorphism and morphology of polylactides, in: M. DiLorenzo and R. Androsch *Synthesis, Structure and Properties of Poly(Lactic Acid)*, Springer, Cham, 2017. https://doi.org/10.1007/12_2016_15.
42. D. Sawai, K. Takahashi, T. Imamura, K. Nakamura, T. Kanamoto, S. H. Hyon, Preparation of oriented β-form poly(L-lacic acid) by solid state extrusion, *J. Polym. Sci. Part B Polym. Phys.* **2002**, *40*, 95–104.

43. D. Sawai, K. Takahashi, A. Sasashige, T. Kanamoto, Preparation of oriented β-form poly(L-lactic acid) by solid-state coextrusion: effect of extrusion variables, *Macromolecules* **2003**, *36*, 3601–3605.
44. D. Sawai, T. Yokoyama, T. Kanamoto, M. Sungil, S. H. Hyon, L. P. Myasnikova, Crystal transformation and development of tensile properties upon drawing of poly(L-lactic acid) by solid-state coextrusion: effects of molecular weight, *Macromol. Symp.* **2006**, *242*, 93–103.
45. J. F. Ru, S. G. Yang, D. Zhou, H. M. Yin, J. Lei, Z. M. Li, Dominant β-form of poly(L-lactic acid) obtained directly from melt under shear and pressure fields, *Macromolecules* **2016**, *49*, 3826–3837.
46. K. Tashiro, N. Kouno, H. Wang, H. Tsuji, Crystal structure of poly(lactic acid) stereocomplex: random packing model of PDLA and PLLA chains as studied by X-ray diffraction analysis, *Macromolecules* **2017**, *50*, 8048–8065.
47. K. Tashiro, H. Wang, N. Kouno, J. Koshobu, K. Watanabe, Confirmation of the X-ray-analyzed heterogeneous distribution of the PDLA and PLLA chain stems in the crystal lattice of poly(lactic acid) stereocomplex on the basis of the vibrational circular dichroism IR spectral measurement, *Macromolecules* **2017**, *50*, 8066–8071.
48. K. Aou, S. L. Hsu, Trichroic vibrational analysis on the α-form of poly (lactic acid) crystals using highly oriented fibers and spherulites, *Macromolecules* **2006**, *39*, 3337–3344.
49. R. J. Roe, *Methods of X-Ray and Neutron Scattering in Polymer Science*, Oxford University Press Inc., New York, 2000.
50. M. L. Di Lorenzo, Crystallization behavior of poly(L-lactic acid), *Eur. Polym. J.* **2005**, *41*, 569–575.
51. M. Yasuniwa, S. Tsubakihara, Y. Sugimoto, C. Nakafuku, Thermal analysis of the double-melting behavior of poly(L-lactic acid), *J. Polym. Sci. Part B Polym. Phys.* **2004**, *42*, 25–32.
52. A. L. Patterson, The scherrer formula for X-ray particle size determination, *Phys. Rev.* **1939**, *56*, 978–982.
53. T. Hahn (Ed.), *International Tables for Crystallography-Vol. A Space Group Symmetry*, 5th edition, Springer, Dordrecht, 2005.
54. G. Stoclet, R. Seguela, J. M. Lefebvre, S. Elkoun, C. Vanmansart, Strain-induced molecular ordering in polylactide upon uniaxial stretching, *Macromolecules* **2010**, *43*, 1488–1498.
55. G. Stoclet, R. Seguela, J. M. Lefebvre, C. Rochas, New insights on the strain-induced mesophase of poly(D,L-lactide): in situ WAXS and DSC study of the thermo-mechanical stability, *Macromolecules* **2010**, *43*, 7228–7237.
56. K. Tashiro, S. Sasaki, Structural changes in the ordering process of polymers as studied by an organized combination of the various measurement techniques, *Prog. Polym. Sci.* **2003**, *28*, 451–519.
57. M. L. Di Lorenzo, Determination of spherulite growth rates of poly(L-lactic acid) using combined isothermal and non-isothermal procedures, *Polymer* **2001**, *42*, 9441–9446.
58. H. Tsuji, Y. Ikada, Properties and morphologies of poly(L-lactide): 1. Annealing condition effects on properties and morphologies of poly(L-lactide), *Polymer* **1995**, *36*, 2709–2716.
59. H. Tsuji, Y. Tezuka, S. K. Saha, M. Suzuki, S. Itsuno, Spherulite growth of L-lactide copolymers: effects of tacticity and comonomers, *Polymer* **2005**, *46*, 4917–4927.
60. H. M. De Oca, I. M. Ward, Structure and mechanical properties of poly(L-lactic acid) crystals and fibers, *J. Polym. Sci. Part B Polym. Phys.*, **2007**, *45*, 892–902.
61. L. R. G. Treloar, Calculations of elastic moduli of polymer crystals: 1. Polyethlene and nylon 66, *Polymer* **1960**, *1*, 95–103.
62. T. Shimanouchi, M. Asahina, S. Enomoto, Elastic moduli of oriented polymers. I. The simple helix, polyethylene, polytetrafluoroethylene, and a general formula, *J. Polym. Sci.* **1962**, *59*, 93–100.
63. H. Sugeta, T. Miyazawa, A General method for calculating elastic moduli of helical polymer chains in crystals; application to poly(oxymethylene), *Polym. J.* **1970**, *1*, 226–231.
64. A. Odajima, T. Maeda, Calculation of the elastic constants and the lattice energy of the polyethylene crystal, *J. Polym. Sci. Part C Polym. Symp.* **2007**, *15*, 55–74.
65. D. N. Theodorou, U. W. Suter, Atomistic modeling of mechanical properties of polymeric glasses, *Macromolecules* **1986**, *19*, 139.
66. K. Wasanasuk, K. Tashiro, Theoretical and experimental evaluation of crystallite moduli of various crystalline forms of poly(L-lactic acid), *Macromolecules* **2012**, *45*, 7019–7026.
67. K. Tashiro, Molecular theory of mechanical properties of crystalline polymers, *Prog. Polym. Sci.* **1993**, *18*, 377.
68. K. Tashiro, M. Kobayashi, H. Tadokoro, Calculation of three-dimensional elastic constants of polymer crystals. 1. Method of calculation, *Macromolecules* **1978**, *11*, 908–913.
69. K. Tashiro, M. Kobayashi, H. Tadokoro, Three-dimensional elastic constants of polymer crystals. 2. Application to orthorhombic polyethylene and poly(vinyl alcohol), *Macromolecules* **1978**, 914–918.
70. K. Tashiro, M. Hanesaka, T. Ohhara, T. Ozeki, T. Kitano, T. Nishu, K. Kurihara, T. Tamada, R. Kuroki, S. Fujiwara, I. Tanaka, N. Niimura, Structural refinement and extraction of hydrogen atomic positions in polyoxymethylene crystal based on the first successful measurements of 2-dimensional high-energy synchrotron X-ray diffraction and wide-angle neutron diffraction patterns of hydrogenated, *Polym. J.* **2007**, *39*, 1253–1273.
71. K. Tashiro, M. Kobayashi, H. Tadokoro, Vibrational spectra and theoretical three-dimensional elastic constants of isotactic polypropylene crystal. An important role of anharmonic vibrations, *Polym J* **1992**, *24*, 899.
72. K. Tashiro, A role of taut tie chains in the heterogeneous stress distribution and mechanical deformation behavior of synthetic and natural fibers, *J. Fiber Sci. Technol.* **2021**, *77*, 88–117.
73. S. Lee, M. Kimoto, M. Tanaka, H. Tsuji, T. Nishino, Crystal modulus of poly (lactic acid)s, and their stereocomplex, *Polymer* **2018**, *138*, 124–131.
74. D. Brizzolara, H. J. Cantow, K. Diederichs, E. Keller, A. J. Domb, Mechanism of the stereocomplex formation between enantiomeric poly(lactide)s, *Macromolecules* **1996**, *29*, 191–197.

75. L. Cartier, T. Okihara, B. Lotz, Triangular polymer single crystals: stereocomplexes, twins, and frustrated structures, *Macromolecules* **1997**, *30*, 6313–6322.
76. X. Wang, R. Prud'homme, Dendritic crystallization of poly(L-lactide)/poly(D-lactide) stereocomplexes in ultrathin films, *Macromolecules* **2014**, *47*, 668–676.
77. H. Tsuji, Poly(lactide) stereocomplexes: formation, structure, properties, degradation, and applications, *Macromol. Biosci.* **2005**, *5*, 569–597.
78. H. Tsuji, Poly(lactic acid) stereocomplexes: a decade of progress, *Adv. Drug. Deliv. Rev.* **2016**, *107*, 97–135.
79. M. Yokouchi, Y. Chatani, H. Tadokoro, K. Teranishi, H. Tani, Structural studies of polyesters: 5. Molecular and crystal structures of optically active and racemic poly(β-hydroxybutyrate), *Polymer* **1973**, *14*, 267.
80. H. Wang, K. Tashiro, Reinvestigation of crystal Structure and intermolecular interactions of biodegradable poly(3-hydroxybutyrate) α-form and the prediction of its mechanical property, *Macromolecules* **2016**, *49*, 581–594.
81. S. Phongtamrug, K. Tashiro, X-ray crystal structure analysis of poly(3-hydroxybutyrate) β-form, *Macromolecules* **2019**, *52*, 2995–3009.
82. H. Sato, R. Murakami, A.Padermshoke, F. Hirose, K. Senda, I. Noda, Y. Ozaki, Infraredspectroscopy studies of CH···O hydrogen bondings and thermal behavior ofbiodegradable poly(hydroxyalkanoate), Macromolecules **2004**, *37*, 7203–7213.
83. T. Iwata, Y. Aoyagi, T. Tanaka, M. Fujita, A. Takeuchi, Y. Suzuki, K. Uesugi, Microbeam X-ray diffraction and enzymatic degradation of poly [(*R*)-3-hydroxybutyrate] fibers with two kinds of molecular conformations, *Macromolecules* **2006**, *39*, 5789–5795.
84. M. C. Righetti, Amorphous fractions of poly(lactic acid), in: M. L. Di Lorenzo, R. Androsch (Eds.), *Synthesis, Structure and Properties of Poly(Lactic Acid), Advances in Polymer Science*, vol. *279*, Springer, Berlin, 2017.
85. M. L. Di Lorenzo, M. C. Righetti, Crystallization-induced formation of rigid amorphous fraction, *Polym. Cryst.* **2018**, e10023.
86. S. N. Zhurkov, V. A. Zakrevskyi, V. E. Korsukov, Mechanism of submicrocrack generation in stressed polymers, *J. Polym. Sci. Part 2* **1972**, 10, 1509–1520.
87. C. S. Fuller, C. L. Erickson, An X-ray study of some linear polyesters, *J. Am. Chem. Soc.* **1937**, *59*, 344–351.
88. A. Turner-Jones, C. W. Bunn, The crystal structure of polyethylene adipate and polyethylene suberate, *Acta Crystallogr.* **1962**, *15*, 105–113.
89. S. Y. Hobbs, F. W. J. Billmeyer, Crystal unit-cell dimensions and densities of linear aliphatic polyesters, *J. Polym. Sci. Part A-2* **1969**, *7*, 1119–1121.
90. K. Tashiro, T. Yoshioka, H. Yamamoto, H. Wang, E. M. Woo, K. Funaki, H. Murase, Relationship between twisting phenomenon and structural discontinuity of stacked lamellae in the spherulite of poly(ethylene adipate) as studied by the synchrotron X-ray microbeam technique, *Polym. J.* **2018**, 9–12.

# 7

# OPTICAL AND SPECTROSCOPIC PROPERTIES

Isabel M. Marrucho

## 7.1 INTRODUCTION

Optical properties such as color, clarity, and refractive index are important in dyeing operations for textiles and in various packaging applications [1, 2]. Many of the physical properties of PLA are influenced by the ratio and distribution of the *R*- and *S*-lactic acid stereocenters in the polymer chain, which reflect its processing history including the stereochemistry *RR* (D-lactide), *SS* (L-lactide), *RS* (*meso*-lactide), or a racemic mixture (DL-lactide) of the feed composition, polymerization kinetics, and extent of transesterification and racemization (see Chapters 1–4). As this rich variety of structures leads to materials with different characteristics, ranging from fully amorphous to semicrystalline, a discussion of PLA optical properties across a broad range of stereooptical compositions is valuable.

Since most applications of PLA-based materials are in the solid state, detailed knowledge of the composition, bulk structure, and conformation of these materials is crucial. For example, it is well known that the most common crystalline structure of PLA is the α although other crystals, such as the β, δ, and γ have also been reported for some specific conditions [3]. As it will be shown below, spectroscopic techniques such as infrared and Raman spectroscopy are very useful analytical techniques in the elucidation of many aspects of the optical properties of solid-state PLA.

In this chapter, the main optical techniques used to characterize PLA-based polymers are discussed in four sections: (i) absorption and transmission of UV–Vis radiation; (ii) index of refraction; (iii) specific optical rotation; and (iv) Fourier transform infrared radiation (FTIR), Raman and nuclear magnetic resonance (NMR) spectroscopy.

## 7.2 ABSORPTION AND TRANSMISSION OF UV–VIS RADIATION

Since cheap nonbiodegradable petroleum-based materials play a dominant role in short-term use for food packaging, their replacement with PLA could provide a significant step towards a greener planet. In order to adequately preserve the quality of the food, the packaging materials have to provide efficient barriers against light, water vapor, atmospheric gases, and volatile organic compounds (VOCs) to prevent food degradation and oxidation and preserve aromas and flavors [4]. The absorption and transmission of light by polymers are especially important in the food packaging industry where the packaged goods are light sensitive. Also, γ irradiation is the common method used to sterilize packaging in pharmaceutical and food industry. However, the exposure of PLA to radiation can also accelerate its decomposition rate or change its properties [5].

Sensitive components of foods such as lipids, flavors, vitamins, and pigments may undergo degradation reactions when exposed to light. The spectrum and the intensity of the light source, the conditions of light exposure, and the light transmittance of the packaging material are factors that can dramatically affect the food quality. Thus, packaging plays a critical role in the prevention of photodegradation of food components during storage. For example, packaging can slow down oxidation of lipids, formation of unpleasant volatile compounds (methional, aldehydes, and methyl ketones), loss of vitamins (riboflavin, β-carotene, and vitamin C), production/degradation of free amino acids, increase of the peroxide value, discoloration of pigments, and so on by absorption of the incident light [6, 7].

*Poly(Lactic Acid): Synthesis, Structures, Properties, Processing, Applications, and End of Life*, Second Edition.
Edited by Rafael A. Auras, Loong-Tak Lim, Susan E. M. Selke, and Hideto Tsuji.

The design of the packaging for a specific food product involves not only the choice of the appropriate packaging material but also the addition of the right additives or stabilizers to the packaging in order to provide a more efficient UV–Vis light barrier, and thus a significant improvement in protected food quality during storage when compared to the nonprotected food to extend product shelf life.

The transmission of visible light (400–700 nm) and ultraviolet radiation (100–400 nm) is an important parameter in designing the right packaging to preserve and protect products until they reach the consumer. Although this is an extremely important subject in food packaging applications, to our knowledge, only Auras [8] measured visible and ultraviolet light barrier properties of PLA and compared them with the properties of commercial polymers traditionally used for food packaging. As can be seen in Figure 7.1 [9], at a wavelength of 225 nm, PLA shows a significant increase in UV light transmitted when compared with other standard polymers, reaching about 85% at 250 nm and 95% at 300 nm. Thus, most of the UV-B and UV-A radiation passes through the films. No UV radiation transmission was found in the lower UV wavelength range of 190–220 nm region. Within the group of conventional polymers, polystyrene (PS) and cellophane transmit less radiation in the UV range where most foods are more sensitive and polyethylene terephthalate (PET) does not transmit any light in this wavelength range. Low-density polyethylene (LDPE) shows the highest transmission of UV light followed by PLA [10].

When the subject of visible radiation is discussed, its relationship with colors cannot be forgotten. Each wavelength in the visible light band causes a particular sensation of color. The human eye is not equally sensitive to light emitted at all wavelengths. It is most sensitive to the light in the yellow and green areas of the visible spectrum. When visible light of many frequencies strikes a surface of an object, this object will selectively absorb, reflect, or transmit certain frequencies, thus changing the color perception by the human eye. This selectivity is due to the fact that different atoms and molecules have different natural frequencies of vibration, and they will selectively absorb different frequencies of visible light. Reflection and transmission of incident radiation occur because the frequencies of those light waves do not match the natural frequencies of vibration of the objects. When radiation in these frequencies strikes an object, the electrons in the atoms begin to vibrate. If the object is transparent, then the vibrations of the electrons are passed on to neighboring atoms through the bulk of the material and reemitted on the opposite side of the object. Light waves of such frequencies are said to be transmitted. If the object is opaque, then the vibrations of the electrons are not passed from atom to atom through the bulk of the material. Rather the electrons of atoms on the material's surface vibrate for short periods of time and then reemit the energy as a reflected light wave. Lights of such frequencies are said to be reflected. Transparent materials are materials that allow one or more frequencies of visible light to be transmitted through them. Several important parameters are currently used to characterize visible light transmission and color of plastics, such as transparency (ASTM D1746-03), haze (ASTM D1003), and degree of yellowness (ASTM D6290-05), which are based on the absorbance or transmission of UV–Vis light. The transparency, commonly known as "see through," is defined as the transmission of visible light in the 540–560 nm range [7]. The average transparency of food packaging films is around 95%. The degree of yellowness or the change in the degree of yellowness is a number calculated from spectrophotometric data that describes the change in color of a test sample from clear or white to yellow. PLA, PS, and LDPE have the same

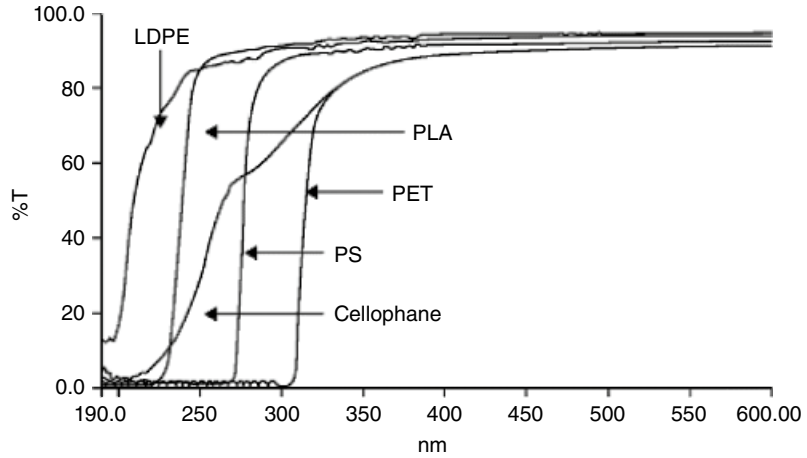


**FIGURE 7.1** Percent transmission versus wavelength for PLA (98% L-lactide), PS, LDPE, PET, and cellophane films. Source: Adapted from Ref. 8 with permission from Wiley-VCH Verlag GmbH & Co.

degree of yellowness, while cellophane and PET have higher values [9]. Since the light yellow color of PLA products could be a drawback in its applications in the packaging industry, creating a consumer perception that the package is old, additives are usually used.

The Commission Internationale de l'Eclairage (CIE) proposed the $L^*a^*b^*$ color space, where $L^*$ indicates lightness, $a^*$ is the red/green coordinate, and $b^*$ is the yellow/blue coordinate to measure color change in polymers. Auras et al. [7] reported for PLA $L^*$ value of $90.64 \pm 0.21$, $a^*$ value of $-0.99 \pm 0.01$, and $b^*$ value of $-0.50 \pm 0.04$ [8], but other values have been reported more recently such as 96.22, 0.24, 0.21 [11] or $92.1 \pm 0.1$, $-1.0 \pm 0.0$, $1.0 \pm 0.0$ [12], respectively, among others. The total color difference between the control film and the film with additives is given by

$$\Delta E = \sqrt{\left(\Delta L^*\right)^2 + \left(\Delta a^*\right)^2 + \left(\Delta b^*\right)^2} \tag{7.1}$$

where deltas for $L^*$ ($\Delta L^*$), $a^*$ ($\Delta a^*$) and $b^*$ ($\Delta b^*$) may be positive (+) or negative (−).

In particular, the development of color in PLLA when processed above its melting temperature is a quality issue in the production of PLLA-based products (implants, fabrics, textiles) by melt processing techniques, such as extrusion and injection molding. This problem adversely affects the properties and end use of the final product, making it suitable only for low-grade materials or where color is not an issue. As a matter of fact, discoloration has been considered as one of the most critical problems that arises during melt processing of aromatic polyesters, including PET [13, 14] and poly(trimethylene terephthalate) [15]. Wang et al. [16] successfully used UV–Vis spectroscopy for monitoring the process-induced degradation of PLLA during extrusion. UV–Vis spectroscopy provides a powerful and nondestructive tool for real-time detection of the thermal degradation of PLLA, which can be used to optimize the processing conditions since it is very sensitive to minute color changes in the PLLA melt. The analysis of the spectra allows the identification of a redshift of the absorption maximum of a polymer due to new chromophoric groups resulting from thermal degradation. It is known that the absorption maximum of a polymer is shifted to higher wavelengths when the number of conjugated double bonds increases [16, 17]. These authors concluded that pyrolytic elimination is the main degradation mechanism for dry PLLA and is responsible for the color formation and molecular weight reduction. On the other hand, hydrolysis in moist PLLA only reduces molar mass but does not contribute to a change in UV–Vis absorption. A similar study was carried out by Gupta and Deshmukh [18] using PLA in a benzene solution by following the n → p* transition characteristic of nondegraded PLA that occurs at 287 nm. Nevertheless, a blueshift of this absorption band occurs at 280 nm, suggesting that carbonyl carbon–oxygen bond cleavage is more efficient than other cleavages, which would result in the formation of –COOH groups on the polymer chain ends. Chugh and Lalla [19] dissolved PLA in chloroform and measured the maximum absorbance wavelength at 240 nm, which was attributed to the ester group present in the polymer.

Among the thermoplastic polymers used in 3D printing, PLA is the most often used in fused deposition modelling, as it is cheap, biodegradable, and does not release toxic fumes during the printing process. However, the final properties of the PLA filament are highly dependent on PLA grade and modifiers. Since PLA prints are quite vulnerable to high temperatures and direct sunlight, as the surface of the print can break up and deform [20], NatureWorks recently announced the introduction of a new PLA grade, Ingeo™ 3D700 for large format 3D printing from consumer to industrial applications [21]. The influence of selected parameters and modifications on the final properties of 3D printed PLA has also been investigated. For example, Mikolajczyk and Kuberski [20] studied five types of PLA filament with different dyes and the influence of UV radiation on the optical properties was studied. These authors concluded that although exposure to UV light caused only negligible changes in thermal properties of the prints, it significantly changed the optical properties of the PLA. Moreover, the UV light increased the transparency of the print. The absorbance changed over the exposure time; for some wavelengths the absorbance increased over time, but for the others the absorbance decreased or remained constant. The absorbance changes also differed between different colors of the filament.

Despite the attractive properties of PLA, the brittleness and low vapor and gas barrier properties of PLA are potential limitations, thus representing areas of current development. One avenue to address these limitations is the reinforcement of PLA [22]. Several reinforcement materials, from clay, to carbonaceous materials, cellulose, metal and metal oxides, and silicone, have been studied. Although the addition of small concentrations of reinforcement materials generally increases the transparency of the nanocomposite, an increase in opacity was observed for high concentrations, probably due to agregation, as shown by many authors. For example, Tabatabei and Ajji [23] showed that the haze of nanocomposite films decreased with clay concentration up to 5 wt%, but increased with further addition of the nanoclay. The orientation, mechanical, and optical properties of multilayer films of nanoclay filled PLA as the core layer and polyethylene (PE) as the skin layer obtained from the film blowing process were investigated.

Similarly, Orellana et al. [24] showed that the reinforcement of PLA varies as a function of the (CNC) cellulose

nanocrystal's morphology, functionality, polydispersity, and the processing conditions. PLA-CNC films showed significant optical transparency at low concentration (1–3%) of CNCs. More interestingly, polarized light microscopy images of the CNC nanocomposites revealed the formation of oriented CNC, which provided interesting colors (green, blue, and redish) to the composites at high CNC loadings. It was shown that a better dispersion of CNCs results in a better organization of the nanocomposites. However, the degree of alignment was found to be relatively low with CNC orientation pointing at multiple directions around the extrusion direction for the toughened composites, which has been attributed to the inherent spiral assembly of cellulose as reported in the literature. Kim et al. [25] studied PLA nanocomposite films fabricated with graphene oxide (GO) and single-walled carbon nanotubes (CNT) as a hybrid-co-filler with GOCNT fractions varying from 0.05 to 0.4% by weight and showed that UV–Vis radition transmission decreased up to 30% with increasing fraction of GOCNT and that the use of GOCNT blocked visible light more efficiently than the mono fillers of GO and CNT.

In a transparent and conductive film, optical transmittance and sheet resistance are two critical parameters to evaluate its quality and practical application in optoelectronic devices. For example, the addition of NiO in PLA clearly influences the surface color due to the black color of NiO [26]. UV penetration through the PLA/NiO films was prevented by the color of NiO nanoparticles, which can be properly used for UV protection. Opacity is the indication of the amount of light not permitted to travel through the packaging material, and high transparency indicates a low opacity value. The opacity for pure PLA was 45.8%; after the incorporation of 0.25 wt% of NiO, it increased to 77.88%. This was due to the presence of NiO blocking the penetration of light. After the addition of 0.25, 0.5, 0.75, and 1 wt% of NiO, the opacity value significantly increased to 77.88, 79.45, 81.26, and 85.64%. The opacity value was directly proportional to the amount of NiO added due to the strong scattering of light. The prevention of light transmission in the PLA polymer matrix was also because of the improper dispersion of NiO nanoparticles. It may be well understood that the well dispersed 1 nm thickness of nanomaterials in the polymer matrix does not obstruct the light passage because the nanomaterial size is smaller than the visible light wavelength. In another article, Wang et al. [27] presented the optical transmittances of Ag nanowire (NW) films with different AgNW area densities (36, 72, and 108 mg/m$^2$) deposited on glass or transferred by PLLA and PLLA/PDLA blend solution. For the same substrate, the optical transmittance of the film decreased with increasing AgNW area density due to the fact that more nanowires on the substrate can cause more light to be reflected and absorbed. Compared with the AgNW/Glass film, the optical transmittance of the AgNW/PLLA and AgNW/PLLA/PDLA film with the same AgNW area density dropped by about 2–4% and 10–20% due to the polymer crystallization.

## 7.3 REFRACTIVE INDEX

Refractive index is a fundamental physical property of a substance that is often used for its identification, to confirm its purity or to measure its concentration. By definition, the refractive index of a medium is a measure of how much the speed of light is reduced inside the medium. It is a fundamental optical property of polymers that is directly related to other optical, electrical, and magnetic properties. Knowledge about this property is valuable due to its application in the design of new optical polymeric materials. The addition of nanosized inorganic or organic dopants to polymers allows modification of the polymers' physical properties enabling the preparation of functionalized polymers with new application fields, such as, microoptics. For example, electron-rich organic dopants in polymers, can cause a pronounced increase in the refractive index.

Polymeric materials have refractive indices that depend on their structure. Lactic-acid-based polymers can contain enantiomers of both L- and D-lactic acid. The most common structures have above 90% L-lactic acid enantiomers and are semicrystalline. Below this percentage, PLA becomes fully amorphous. Hutchinson et al. [1] studied the change in the index of refraction for PLA by ellipsometric measurements. These authors did not find statistically significant differences in the refractive indices between samples of PLA with different enantiomeric compositions. Nevertheless, a decrease in the index of refraction (1.499–1.448) as the wavelength increased from 300 to 1300 nm was observed (Figure 7.2). This variation of index of refraction of PLA as a function of wavelength, λ (nm), can be described using the well-known Cauchy model, given by Equation 7.2.

$$n(\lambda) = (1.445 \pm 0.00075) + \frac{4892 \pm 143}{\lambda^2} \qquad (7.2)$$

Also, many semiempirical group contribution methods derived from the refractive indices of liquid organic compounds, as well as organic polymers, have been established and give reliable predictions. These group contribution calculations are based on the molecular weight and molecular volume of the monomer, the density of the polymer, and the chemical structure of the polymer. The molar refraction values corresponding to group contribution models such as Lorentz–Lorenz, Gladstone–Dale, Vogel, and Looyenga have been collected extensively by VanKrevelen [28]. Auras et al. [9] reported PLA refractive indices calculated by Lorentz–Lorenz ($n$ = 1.482), Gladstone–Dale ($n$ = 1.492), and Vogel methods ($n$ = 1.482).

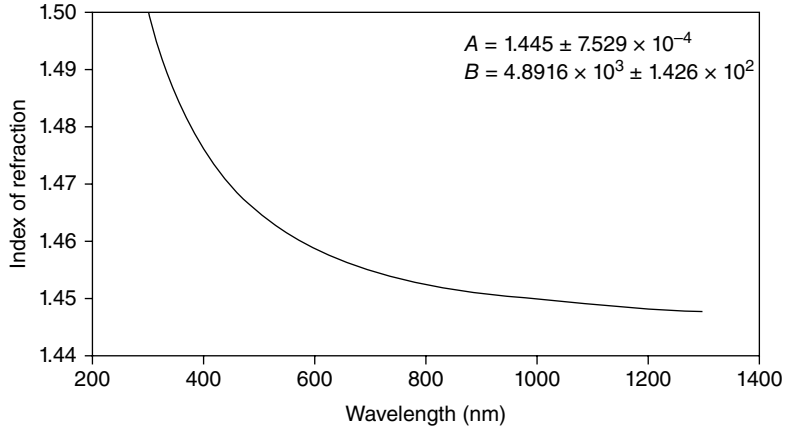


**FIGURE 7.2** Index of refraction for PLA as a function of wavelength from a global determination of the Cauchy parameters across all optical compositions. Source: Adapted from Ref. 1 with permission from American Chemical Society.

Malmgren et al. [29] determined the specific refractive index increment (d*n*/d*c*) for PLA with 16.4% of D-isomer, in chloroform. The resulting d*n* versus concentration curve was measured using a differential refractometer. Two similar values for the resulting slope, d*n*/d*c*, $0.0237 \pm 0.0034$ and $0.0240 \pm 0.0049$ mL/g, were reported due to the presence of air bubbles inside the sample. The obtained d*n*/d*c* values for PLA in chloroform are fairly small compared to those of other polymers such as polystyrene, which shows a d*n*/d*c* of 0.169 mL/g in chloroform. Olivier and Walkenhorst reported a d*n*/dc of PLA in tetrahydrofurane (THF) of 0.042 mL/g, which is 4.5 times smaller than a PS with the same molecular weight and concentration also in THF [30].

## 7.4 SPECIFIC OPTICAL ROTATION

The specific optical rotation of a pure material is an intrinsic property at a given wavelength and temperature when dissolved in a particular solvent. The specific optical rotation [α] of PLLA and PDLA polymers was measured in chloroform at a concentration of 1 g/dL at 25°C using a polarimeter and wavelength of 589 nm. The values of α for PDLA and PLA were approximately +150° and −150°, respectively [31–33]. The optical rotatory power along the *c*-axis of PLLA was found to be positive, while negative along the *a*-axis. This means that right-handed circularly polarized light propagates faster than left-handed circularly polarized light along the helix axis in PLLA. The reverse phenomenon takes place in PDLA. A gyration tensor component $g_{33}$ of PLLA crystal along the *c*-axis was found to be extremely large, a few orders of magnitude larger than in the usual optically active crystals. Thus, the helical molecular conformations in helical polymers such as PLLA and PDLA produce large optical activity. This phenomenon is important for the elucidation of gyro-optical properties of solids and is promising for new optical applications utilizing their large optical activity [34].

## 7.5 INFRARED AND RAMAN SPECTROSCOPY

Infrared spectroscopy is a nondestructive analytical technique used to identify mainly organic materials. In general terms, the state of order of a macromolecular system can be defined by its constitution, configuration, conformation, regularity, stereoregularity, conformational regularity, and crystallinity. Vibrational spectroscopy of a polymer can give information about the state of order by analyzing different types of bands caused by different phenomena such as stereoregularity and conformational regularity of the polymer chain and the crystallinity of the polymer. While the conformational regularity depends on the intramolecular interactions between neighboring chemical groups of the same chain, the crystallinity depends on the intermolecular forces between adjacent chains. It is well known that vibrational spectroscopy is sensitive to local molecular environments, so differences can be observed between these two types of interactions. On the other hand, while these two properties, conformational regularity and crystallinity, are strongly influenced by the pretreatment of the polymer sample and the experimental conditions, the stereoregularity is only affected by chemical reactions [35].

IR and Raman spectroscopies are very important tools for the characterization of the chemical and physical nature of polymers. Due to the high sensitivity of IR spectroscopy to changes in the dipole moment of a given vibrating group, this technique is extensively used to identify polar groups. In contrast, Raman spectroscopy is especially helpful in the characterization of the homonuclear polymer backbone due

to its sensitivity to changes in polarizability [35]. The characterization of polymers using vibrational spectroscopy is based on empirical interpretation of IR or Raman spectra, since the bands are assigned to the independent vibration of atomic groups in the macromolecule and give information about the structural features of the polymer such as chemical composition, configuration, conformation, and crystallinity. However, a complete theoretical treatment in terms of the vibrational behavior of the polymeric system can only be obtained when the spectra data are obtained from isotope-substituted polymer analogues and polarization measurements on the specimens.

### 7.5.1 Infrared Spectroscopy

Early studies on PLLA mainly focused on the identification of characteristic bands to investigate the polymer crystallinity. Since Fourier transform infrared (FTIR) spectroscopy is sensitive to the conformation and local molecular environment, this technique has also been used to elucidate the structure of the crystalline polymers. More recently, research on PLLA surface characterization using FTIR has been an object of interest. This section is divided into three parts: structural analysis, surface characterization, and crystallization studies.

*7.5.1.1 Structural Analysis: Band Assignment* The FTIR spectrum of a polymer in the fingerprint region ($\nu \leq 1500\,cm^{-1}$) is used to identify and characterize the material, since the observed peaks can be assigned to different vibration modes of chemical groups by comparison with cataloged FTIR spectra. Many authors [36–42] have used FTIR to characterize the structure of PLA-based materials (from new composite materials to polymer blends, to copolymers, to the effect of addition of plasticizers, just to mention a few) synthesized by different methods for different purposes and to evaluate differences between the obtained polymer and pristine PLA at different experimental conditions, confirming interactions between fillers and the polymer [43–46]. FTIR spectroscopy was used by several authors to measure the lactide concentration in a PLA matrix, using different signals to normalize the characteristic lactide absorbance [47–50]. FTIR has also been used to study the effect of the amorphous fraction on mechanical and optical properties of PLA below the glass transition temperature ($T_g$) and a three-phase model is proposed to explain how amorphous fraction changes with heat treatments and contributes to polymer modulus below $T_g$ [51].

Several important articles have been published concerning the infrared and Raman spectra of PLA-based polymers. For example, one reference work is the pioneering study of Kister et al. [50] on the morphology, conformation, and configuration of PDLA and poly(*meso*-lactide) stereocopolymers using vibrational spectroscopy. Figure 7.3 shows the IR of the PLA polymers. PLA*x* is the acronym used to represent homopolymers and stereocopolymers, where *x* is the percentage of

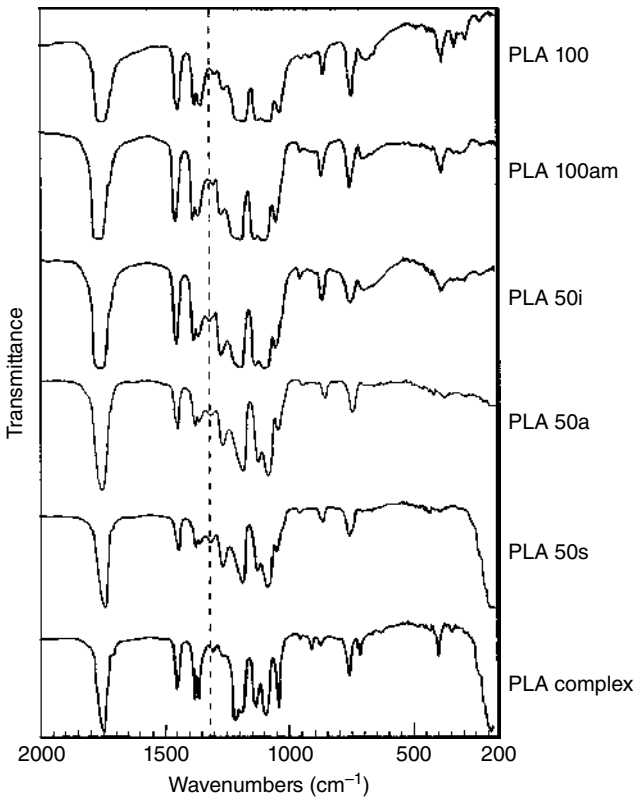


**FIGURE 7.3** Infrared spectra of poly(L-lactic acid)s: PLA 100 (semicrystalline), PLA 100am (amorphous), PLA 50i (isotactic), PLA 50a (atactic), PLA 50s (syndiotactic), and PLA complex (stereocomplex). (- - -) Band sensitive to the tacticity. Source: Adapted from Ref. 50 with permission from Elsevier.

L-lactyl units. The differences observed in the several bands in the position, shape, or splitting clearly indicate that FTIR is a powerful technique to study PLA-based polymers.

In Figures 7.4 and 7.5, the attenuated total reflection FTIR (ATR-FTIR) spectra of semicrystalline $PDLA_{2:98}$ and amorphous $PDLA_{20:80}$ films are presented [52].

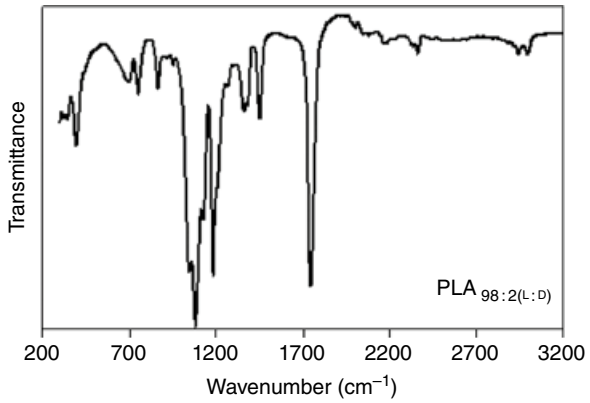


**FIGURE 7.4** Infrared spectra of semicrystalline 98 : 2 (L : D) poly(lactic acid) [52].

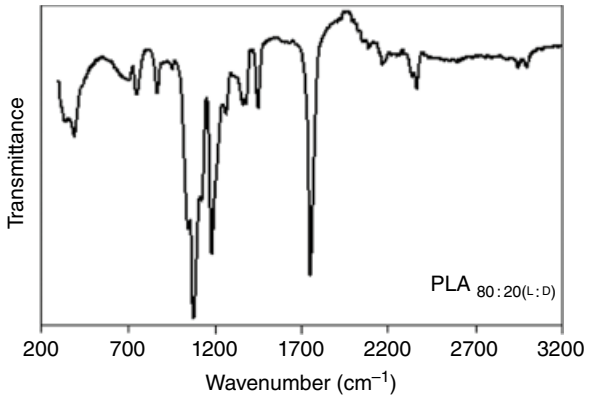


**FIGURE 7.5** Infrared spectra of amorphous 80 : 20 (L : D)poly (lactic acid) [47].

The general band assignments for PLA-based polymers are presented in Table 7.1. The strong IR bands at 2997, 2946, and 2877 $cm^{-1}$ are assigned to the CH stretching region (─$CH_{3(asym)}$, $CH_{3(sym)}$, and CH modes). The C═O stretching region appears in IR spectra at about 1759 $cm^{-1}$ as a broad asymmetric band mainly due to A and $E_1$ active modes. The $CH_3$ is responsible for the appearance of the band at 1456 $cm^{-1}$. The CH deformation and asymmetric bands appear at 1382 and 1365 $cm^{-1}$. Moreover, the CH bending modes result in the bands at 1315 and 1300 $cm^{-1}$.

The C═O stretching modes of the ester group appear at 1225 $cm^{-1}$ and the C─O─C asymmetric mode appears at 1090 $cm^{-1}$. At 956 and 921 $cm^{-1}$, the bands characteristic of the helical backbone vibrations with the $CH_3$ rocking modes can be observed. At 871 and 756 $cm^{-1}$ appear two bands that can be attributed to the amorphous and crystalline phases of PLA, respectively. The bands that appear below 300 $cm^{-1}$ are mainly due to the $CH_3$ torsion modes and the skeletal C–C torsions [9, 50–54].

***7.5.1.2 Surface Characterization*** Although transmission IR spectra contain information of both the bulk and the surface of the films, the majority of the signal arises from the bulk due to the much larger amount of polymer chains located there. However, a thorough knowledge of the surface structure of PLA is of great importance, since the surface constitutes a barrier to the surroundings and provides an adsorption site where chemical reactions can occur. A very suitable technique for surface studies of PLA is vibrational sum frequency generation (VSFG) spectroscopy. This is a nonlinear laser spectroscopy technique, which is inherently surface (and symmetry) sensitive under the electric dipole approximation for centrosymmetric systems.

A very interesting work on surface segregation and restructuring in PDLA and PLLA films of various thicknesses was presented by Paragkumar et al. [55] using ATR-FTIR. It was observed that PDLA surface segregation and the surface restructuring of methyl side groups are influenced by the polymer film thickness (e.g., poly(D, L-lactide). Films with thickness of 1 μm do not exhibit surface segregation of methyl side groups. On the other hand, thin and clear poly(L-lactide) film with 15 μm thickness undergo surface conformational changes upon solvent treatment with organic solvents such as toluene, acetone, tetrahydrofuran, and ethyl acetate. The solvent-treated surface of PLLA becomes hazy and milky white and its hydrophobicity increases compared with the untreated surfaces. FTIR spectroscopic analysis indicate that polymer chains at the surface undergo certain conformational changes upon solvent treatment. These changes are identified as the restricted motions of C─O─C segments and more intense and specific vibrations of methyl side groups. Another study [56] using VSFG methodology in the CH stretching region demonstrated that this technique can generate valuable information to track the changes on the surface and in the bulk structure of amorphous PLLA and PDLA films, and crystalline PLLA and PDLA/PLLA stereocomplex films. For crystalline PLA, strong surface and bulk signals caused by both the order and the symmetry of the space group were observed. Amorphous PLLA and racemically composed PDLA were found to consist of a relatively disordered bulk.

VSFG spectroscopy has been widely and successfully employed to probe vibrational modes in the high-frequency region (1500–4000 $cm^{-1}$) of the IR spectrum. However, these vibrations constitute highly localized modes. Therefore, such measurements mostly report on very local structural parts of the interfacial molecules (i.e., presence and orientation of ─$CH_3$, ─OH, and C─O groups). Recently, developments have been made to assess a wider variety of surface chemical groups, such as the amide group that allows for the identification of α-helices and β-sheets (in molecules where amide bonds are present). This type of structural information still depends on the presence of a single chemical group. In contrast to high-frequency localized modes, low-frequency (skeletal) modes are often composed of the movement of several chemical groups. Thanks to their delocalized nature, these modes are extremely sensitive to the 3D structure of molecules.

Very recently, Sugiharto et al. [57] showed that knowledge of the structure of the first few monolayers of the PLLA/air surface of a biodegradable polymer can be achieved by performing femtosecond VSFG spectroscopy. The crystalline structure of PLLA was determined to belong to the *P*212121 space group [58–60]. This particular combination of skeletal mode frequencies can be correlated to a helical structure in the polymer skeleton [60, 61].

The 3D surface structure of amorphous PLLA (L-A), crystalline PLLA (L-C), and racemic PDLLA (R) using femtosecond VSFG spectroscopy on delocalized modes in the fingerprint region for PLA was studied [62]. Figure 7.6 displays IR transmission spectra of the L-C, L-A, and R films. The IR spectra show some changes in the fingerprint region, which are characteristic of the three films.

**TABLE 7.1 Infrared Spectroscopy Data: Peak Band Assignments for Semicrystalline and Amorphous PLLA Infrared and Raman Spectra**

| IR υ ($cm^{-1}$) | | | | Raman υ ($cm^{-1}$) | | | | |
|---|---|---|---|---|---|---|---|---|
| Semicrystalline PLA | *I* | Amorphous PLA | *I* | Semicrystalline PLA | *I* | Amorphous PLA | *I* | Assignment |
| 3571 | w | | | | | | | νOH (free) |
| 2997 | M | 2997 | M | 2995 | S | 2997 | S | $\nu_{as}CH_3$ |
| | | | | 2970 | sh | | | $\nu_{as}CH_3$ |
| | | | | 2960 | sh | | | $\nu_{as}CH_3$ |
| 2947 | M | 2947 | M | 2943 | VS | 2942 | VS | $\nu_{s}CH_3$ |
| | | | | 2901 | w | | | νCH |
| 2882 | w | 2882 | w | 2877 | M | 2877 | M | νCH |
| 1760 | VS | 1760 | VS | 1773 | S | 1769 | S | ν(C–O) |
| | | | | 1763 | S | 1755 | sh | ν(C–O) |
| | | | | 1749 | S | | | ν(C–O) |
| 1452 | S | 1452 | S | 1452 | S | 1455 | S | $\delta_{as}CH_3$ |
| 1348, 1388 | S | 1385 | S | 1384, 1388 | M | 1386 | M | $\delta_{s}CH_3$ |
| 1368 | S | 1365 | sh | 1363, 1371 | M | 1365 | M | δ1CH + $\delta_{s}CH_3$ |
| 1360 | S | 1360 | S | 1356 | sh | 1355 | M | δ1CH + $\delta_{s}CH_3$ |
| 1300, 1313 | M | 1300, 1315 | M | 1293, 1302, 1315 | S | 1296, 1300 | S | δ2CH |
| 1270 | S | 1270 | S | | | 1264 | sh | δCH + νCOC |
| 1215 | VS | 1211 | VS | 1216 | M | 1216 | M | $\nu_{as}$COC |
| 1185 | VS | 1185 | VS | 1179 | M | 1183 | M | $\nu_{as}$COC |
| 1130 | S | 1130 | S | 1128 | S | 1128 | S | $r_{as}CH_3$ |
| 1090 | VS | 1090 | VS | 1092 | S | 1092 | S | $\nu_{s}$COC |
| 1045 | S | 1045 | S | 1042 | S | 1042 | S | νC–$CH_3$ |
| 960 | w | 960 | sh | 954 | Vw | 953 | sh | $rCH_3$ + νCC |
| 925 | w | | | 923 | M | | | $rCH_3$ + νCC |
| 875 | M | 873 | M | 873 | VS | 873 | VS | νC–COO |
| | | | | | | 790 | w | γC–O |
| 760 | S | 760 | S | 760 | sh | | | δC–O |
| 740 | sh | 740 | sh | 736 | M | 740 | M | δC–O |
| 715 | M | 710 | M | 711 | M | | | γC–O |
| | | | | | | 700 | Vw | γC–O |
| 695 | M | 690 | M | 675 | M | 682 | w | γC–O |
| | | | | 578 | w | 591 | w | $\delta_1$C–$CH_3$ + δCCO |
| 515 | w | | | 520 | M | | | $\delta_1$C–$CH_3$ + δCCO |
| 415 | sh | 415 | sh | 411 | S | 410 | sh | δCCO |
| 400 | M | 395 | M | 398 | S | 397 | S | δCCO |
| 350 | M | 345 | M | 347 | w | | | $\delta_2$C–$CH_3$ + δCOC |
| 300 | M | 300 | M | 308 | S | 316 | S | δσC–$CH_3$ + δCOC |
| 295 | sh | 295 | sh | 300 | w | 300 | S | COC deformation |
| | | | | 251 | M | 250 | M | τCC |
| 240 | M | 240 | M | 238 | M | 238 | w | τCC |
| | | | | 208 | M | 194 | w | τCC |
| | | | | 158 | S | 160 | S | Skeletal torsion |
| | | | | 117 | S | 116 | S | Skeletal torsion |
| | | | | 77 | S | 77 | S | Skeletal torsion |
| | | | | 60 | M | | | Skeletal torsion |

The intensity, *I*, of each band is classified as VS (very strong), S (strong), M (medium), w (weak), sh (shoulder), s (symmetrical), and as (asymmetric) [9, 50–54].

Figure 7.7 displays VSFG spectra taken in the vibrational fingerprint region of the same films. The spectra of these three chemically identical films show a large diversity, in contrast to the IR spectra in Figure 7.6, which reflects the secondary and tertiary structure of the biopolymer at the interface. Such dramatic changes are not observed in Figure 7.6 because in linear spectroscopy, all atomic groups in the film participate in generating the signal so that it is

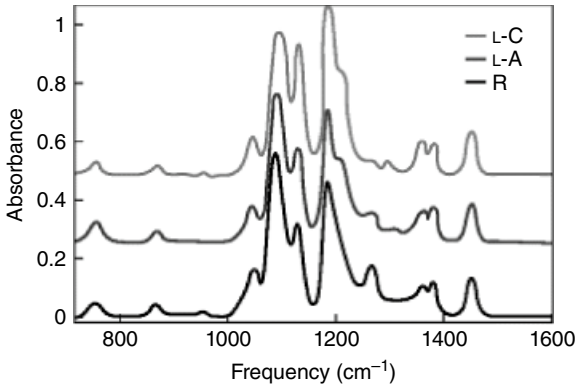


**FIGURE 7.6** Infrared spectra of L-crystalline (L-C), L-amorphous (L-A), and racemic (R) PLA films. Since the materials are chemically identical, only small differences displaying the average bulk structure are observed. Source: Adapted from Ref. 57 with permission from American Chemical Society.

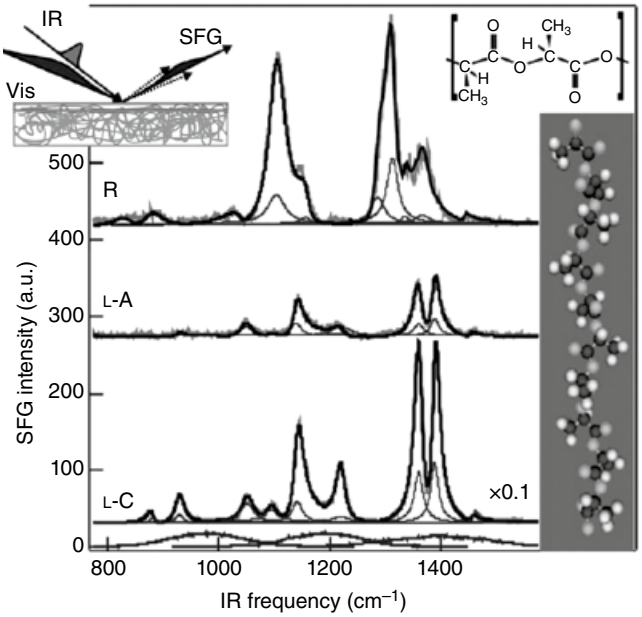


**FIGURE 7.7** VSFG spectra of the delocalized modes of L-crystalline (L-C), L-amorphous (L-A), and racemic (R) PLA films, taken with three different IR pulses, which are displayed in the bottom. The black lines are fits to the data in which all contributions to the reflected electrical sum frequency field are added. The gray Lorentzians display the most prominent vibrational modes. The chemical repeat unit of L-PLA is also shown, as well as a molecular model of a $10_3$ helix. In the top left panel, the VSFG experiment is illustrated. Source: Adapted from Ref. 57 with permission from American Chemical Society.

the average bulk structure that is compared and not the interfacial one. Direct comparison between the VSFG spectra and the data in Figure 7.6 is therefore not very meaningful when it comes to determining the interfacial structure. Thus, VSFG experiments in the fingerprint region are extremely sensitive to changes in the backbone structure of the outermost polymer monolayer at the polymer/air surface. This previously largely unexplored frequency region allows the determination of whether the interfacial biopolymers are ordered helices (L-C interface), disordered helices (L-A interface), or rather consist of heterogeneously composed chains (R interface).

***7.5.1.3 Crystallization Studies*** It is well known that IR is sensitive to the local molecular environment. Accordingly, it has been widely used to explore variations in the intra- and intermolecular interactions and structural changes in macromolecules during melting, crystallization, and phase transition behavior of polymers.

Pan et al. [63] carried out a temperature-variable FTIR to investigate the α and δ crystalline structure of polymorphic PLA and PDLA stereocomplex. The different crystal forms of PLA show distinct spectral features in line shapes and band/resonance splittings upon cooling to the cryogenic conditions. The well-resolved splittings in FTIR bands are absent in δ crystals, indicating the disordered conformation and loose molecular lateral packing within their crystal lattices. In α-form PLA, the tight lateral molecular packing results in extensive interchain interactions between the two antiparallel packed chain, predominantly due to dipolar interactions involving carbonyl, methyl, and methine groups. The significant FTIR frequency shifts of C═O, $CH_3$, CH vibration modes during stereocomplex crystallization of PLLA/PDLA blend and the appearance of spectral splittings at cryogenic conditions suggest the coexistence of weak C─H. . .O═C hydrogen bonds and dipolar interactions between PLLA and PDLA chains in the stereocomplex crystals of PLA. In conclusion, the lateral arrangement and packing of molecular chains in the crystalline phase, which are the origin of the interchain interactions, play an important role in the polymorphism of PLA. This might be an important factor influencing the physical proprieties (e.g., mechanical, barrier properties, and biodegradability) of PLA materials.

Generalized 2D correlation spectroscopy has been applied extensively to analyze IR spectra of polymers for three major reasons: first, it has powerful deconvolution ability for highly overlapped bands; second, it provides information about inter- and intramolecular interactions by correlating absorption band intensities of different functional groups; and third, the intensity changes of a specific sequence occurring during the measurement can be derived from the analysis of asynchronous spectra. In particular, the IR spectra of PLLA polymers are very sensitive to structural changes taking place during melt/crystallization.

Depending on the preparation conditions, three different crystalline modifications (α, δ, β, γ) can be attained for PLLA. Recently, the fine details of dynamic processes during the crystallization of PLLA have become a matter of keen interest. The orthorhombic structure of the β-form,

previously suggested from X-ray studies, was confirmed by trichroic vibrational analysis [60].

The structural evolution and crystallization dynamics of PLLA polymers during isothermal crystallization have been studied by IR spectroscopy. The 2D correlation analysis of time-dependent IR spectra collected during the melt crystallization process revealed details about the intermolecular interaction of the $CH_3$ and C–O groups and the conformational changes in the C–O–C backbone that are not easily detected by conventional one-dimensional spectra. It was found that the intermolecular interaction of the $CH_3$ group appears during both the induction period and the growth period of PLLA melt crystallization, while the intermolecular coupling of the C–O group can only be observed during the crystallization period. The order formation of the C–O–C backbone during the induction period of PLLA melt crystallization can also be clearly observed in the 2D synchronous spectra. These observations show that the weak interchain interactions play an important role in controlling the nucleation and growth of polymer crystallization [2].

Detailed analysis of the three crystallization-sensitive regions is presented below.

(a) The C═O stretching band region of 1860–1660 $cm^{-1}$. Despite extensive studies on the vibration spectra of PLLA α-crystal, the origin of spectral splitting is still not well interpreted, especially for the νC─O band. So far, it has been proposed that this splitting of the νC─O band can be attributed to intramolecular coupling [64] or correlation field splitting arising from interchain interactions, such as C─H**. . .**O hydrogen bonding [65, 66] or dipole-dipole [67]. Hydrogen bonding can be discarded from the analysis of the C─H stretching spectral region [60]. The intramolecular coupling is sensitive to the chain conformation and the distribution of conformers. The four components observed in the C─O stretching band of semicrystalline PLLA are attributed to the four possible conformers, gt, gg, tt, and tg, while in amorphous PLLA only bands corresponding to gt, gg, and tt conformers were found [64]. The correlation field splitting, also called factor group splitting or Davydov splitting, occurs due to the lateral interaction between the chains contained in the unit cell, splitting the absorption in a number of components. In the case of the orthorhombic unit cell of PLLA, the transition moments of the two adjacent PLLA chains can couple in phase or out of phase, leading to the splitting in the FTIR absorption [64].

(b) $CH_3$, CH bending, and the C─O─C stretching bands in the region of 1500–1000 $cm^{-1}$. Although in the range of 1500–1000 $cm^{-1}$, the bands are highly overlapped, the band splittings of the $CH_3$ asymmetric deformation mode and C─O stretching during melt crystallization mode can be clearly observed in time-dependent IR spectra. It was found that the 1458 $cm^{-1}$ band reflects the structural order of the $CH_3$ group, and the band at 1109 $cm^{-1}$ is related to the C─O─C *trans*-conformation in the crystalline phase of PLLA. From 2D correlation analysis, it can be concluded that $CH_3$ groups form a close interchain contact during the induction period, causing the distortion of the $10_3$ helix conformation of PLLA in α-crystals. On the other hand, the C─O groups of different PLLA chains do not come into close contact in the induction period [2].

The band at 1193 $cm^{-1}$ is sensitive not only to the structural adjustment of the C─O─C backbone but also to the structural order of the $CH_3$ group in the crystalline phase. From the analysis of the difference spectra and 2D correlation spectra in the 1500–1000 $cm^{-1}$ region, it is shown that the structural adjustment of the $CH_3$ group unambiguously precedes that of the ester group [67].

(c) The skeletal stretching and $CH_3$ rocking band region of 970–850 $cm^{-1}$. The absorption band at 921 $cm^{-1}$ is found to be characteristic of the α-crystals and the 871 $cm^{-1}$ band is sensitive to the $10_3$ helix conformation. The former corresponds to a shorter critical sequence length than the latter. The bands at 955 and 860 $cm^{-1}$ are proportional to the concentration of crystals in the α-form [2].

For polymorphic polymers, such as PLLA, the characteristic FTIR bands can be correlated to the different crystal modifications and typically stay distinguishable in a certain process. This makes it possible to illustrate the mechanism for a polymorphic transition process at the molecular level. It has been reported that when crystallized at 100–120°C, a mixture of δ- and α-crystals is formed. Since the PLLA δ- and α-crystals show different FTIR spectra [68, 69], the structural changes during the annealing process could be detected by using FTIR spectroscopy.

The disordered crystal (δ-form) of PLLA was found to transform into the α-form during the annealing process at elevated temperatures. The δ to α transition is very dependent on the annealing period ($t_a$: 0–1440 min) and annealing temperature ($T_a$: 120–160°C). For example, high annealing temperatures lead to a more rapid polymorphic transition compared with low annealing temperature. As shown in Figure 7.8, the changes in FTIR spectra upon annealing are mainly associated with the splitting of νC─O and νC─$CH_3$ indicating that the δ to α transition mainly involves the slight rearrangement of the chain conformation (especially related to the side groups) and packing manner in the unit cell to the more energy-favorable state, corresponding to the reduction of unit

cell dimensions. It was proposed that the δ to α transformation mainly proceeds by the direct solid–solid transition mechanism, since the direct solid–solid phase transition band (1500–1320 cm−1) was observed during the annealing process (Table 7.2). Moreover, it was found that $M_w$ affects the crystalline phase transition significantly. In low-molecular-weight PLLA samples, the δ to α transition is much faster and can proceed prominently even when annealed at relatively lower temperature [69, 70].

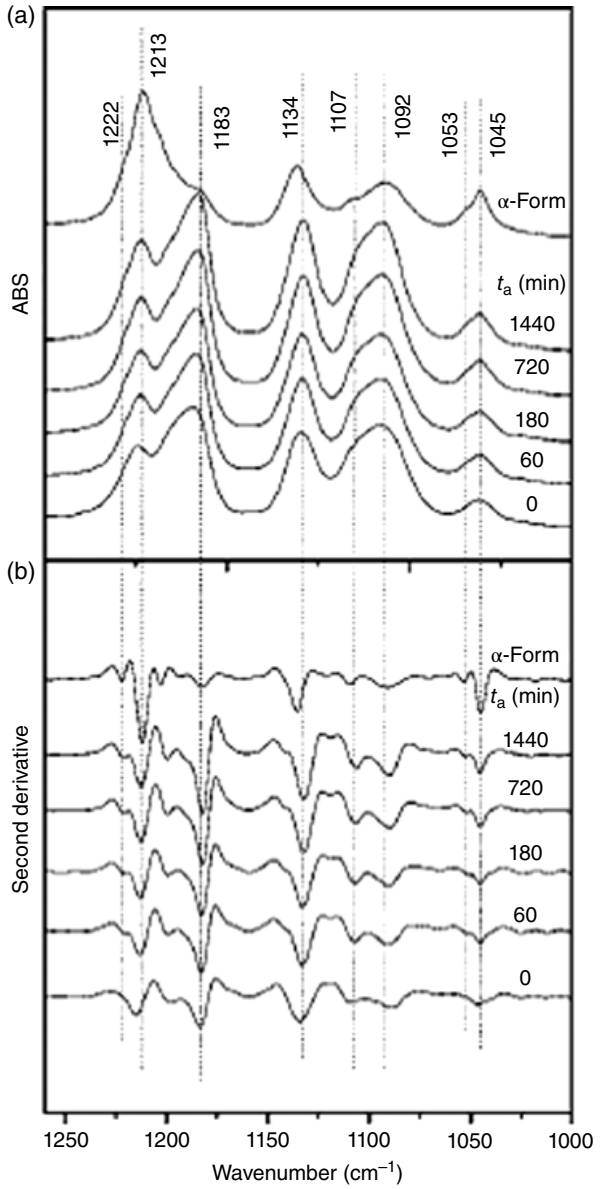


**FIGURE 7.8** FTIR spectra (a) and corresponding second derivatives (b) in the frequency region 1260–1000 cm−1 recorded for the normal PLLA118 α-crystal and annealed (at 150°C for various periods, $t_a$ (min)) PLLA118 δ crystals. Source: Adapted from Ref. 68 with permission from American Chemical Society.

**TABLE 7.2 Assignments for the FTIR Bands in the 1260–1000 cm−1 Region for PLLA δ- and α-Crystals [68]**

| IR Frequencies (cm−1) | | |
|---|---|---|
| δ | α | Assignments |
| 1213 | 1213 | |
| | 1222 | $\nu_{as}$(C–O–C) + $r_{as}$($CH_3$) |
| 1183 | 1183 | |
| 1134 | 1134 | $r_s$($CH_3$) |
| 1092 | 1092 | $\nu_s$(C–O–C) |
| 1107 | 1107 | |
| 1045 | 1045 | |
| 1053 | | $\nu$(C–$CH_3$) |

### 7.5.2 Raman Spectroscopy

The Raman spectra of PLA polymers are also characterized by a C—O stretching region. The C—O stretching mode in PLLA presents four active modes in the Raman region designated by A, B, $E_1$, and $E_2$, which could be observed at 1749, 1763, 1769, and 1773 cm−1, as mentioned in Table 7.1. The PDLA Raman spectrum is characterized by broad and asymmetric lines. Two bands at 1769 and 1749 cm−1 appear in both PDLA and PDLLA stereocopolymer spectra. As this region of the spectra is very sensitive to changes in helical chain structure, any perturbation due to the introduction of (D,D) or (D,L) units causes the appearance or disappearance of these bands. Stereocomplexes can be identified by a sharp peak at 1745 cm−1 and a broad diffusion band at 1760–1780 cm−1. This region proved to be very sensitive to the morphology and conformation. PLLA, PDLA, PLA complex, and poly(*meso*-lactic) stereocopolymers present $CH_3$ asymmetric deformation modes at about 1450 cm−1 in both IR and Raman spectra. Deconvolution analysis of the range between 1250 and 1400 cm−1 of the Raman spectra shows three groups of splitting bands at about 1390, 1360, and 1300 cm−1, which are assigned, respectively, to the A, B, E ($E_1$ and $E_2$) modes of the $CH_3$ and CH bending region [50]. Once again, it is possible to observe sharp and splitting peaks that characterize the semicrystalline PLAs, namely, PLLA and the PLA complex. As previously observed in the C—O stretching region, the amorphous state is characterized by asymmetric broad bands. For the (L,D)-PLA stereocopolymers, the bands at ∼1390 cm−1, due to $\delta_s CH_3$ symmetric deformation, and ∼1300 cm−1, due to δCH, are broad and with similar intensity and do not have significant shifts in the frequency. Next, we described the bands assigned to skeletal stretching and the $rCH_3$ rocking region, which appear between 1216 and 1179 cm−1. Unlike the IR bands, the symmetric and asymmetric C—O—C modes of the PLLA present low-intensity bands in the Raman spectrum. At 1128 and 1042 cm−1, two bands assigned to $r_{as}CH_3$ and

$\nu C{-}CH_3$ stretching, respectively, can be found. The $\nu C{-}COO$ stretching is responsible for the strong band at 873 cm$^{-1}$, which becomes broad and asymmetric for the (L,D)-PLA stereocopolymers and presents a shift to higher frequencies (880 cm$^{-1}$) for PLA complex. It is important to note the presence of a band at 920 cm$^{-1}$ for the PLLA and at 908 cm$^{-1}$ for the PLA complex (semicrystalline polymers), and the absence of any band near these frequencies in amorphous polymers (copolymers). The shifts in frequencies at which these bands appear for the semicrystalline polymers are mainly due to the different crystalline forms of each PLA. PLLA crystallizes preferably in left-handed helices while the crystalline PDLA (stereocomplex) adopts right-handed helices. Since the crystalline structure from the stereocomplex is racemic, the stereocomplex crystallizes in a triclinic unit cell to form a $3_1$ helical conformation known as the β-form. In contrast, the individual polyenantiomers crystallize in a pseudo-orthorhombic system with two $10_3$ helices, which is known as the α-form. The band at 920 cm$^{-1}$ is assigned to α-forms, while the other is due to β-forms [71]. Finally, in the low-frequency region, below 800 cm$^{-1}$, two bands, one of them in the range 736–760 cm$^{-1}$ and the other in the range 650–677–711 cm$^{-1}$, are observed for PLLA. The corresponding bands of the PLA complex are sharp and located at slightly higher frequencies and correspond to $\delta C{-}O$ and $\gamma C{-}O$. The bands of the δCCO mode appear between 398 and 411 cm$^{-1}$. For the PLA complex, the δCOC skeletal chain deformation band appears in the range of frequencies (291–309 cm$^{-1}$) as a split line, while bands characteristic of torsion modes are found at 239, 206, and 160 cm$^{-1}$. For PLLA, the associated bands are located at 230, 210, and 160 cm$^{-1}$. Raman spectra are more sensitive to modifications of chain morphology below 600 cm$^{-1}$ [50, 53] as we can see in Figure 7.9.

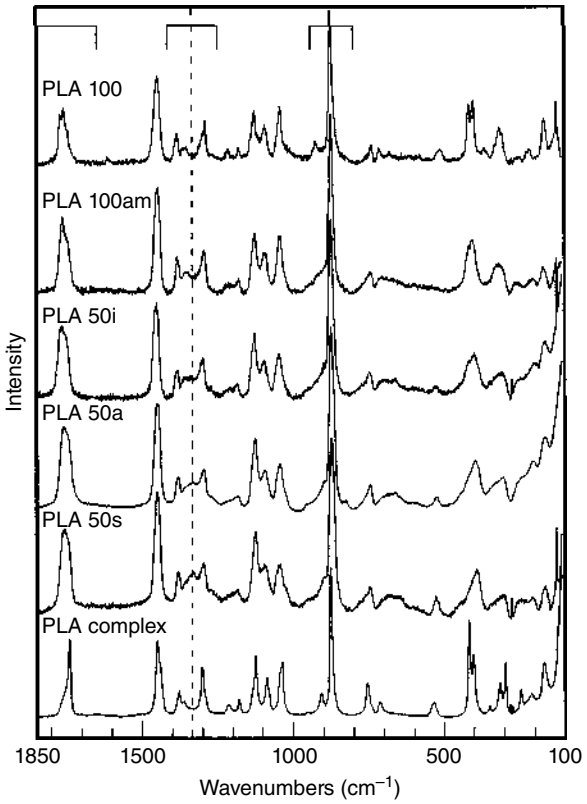


**FIGURE 7.9** Raman spectra of poly(L-lactic acid)s: PLA 100 (semicrystalline), PLA 100am (amorphous), PLA 50i (isotactic), PLA 50a (atactic), PLA 50s (syndiotactic), and PLA complex (stereocomplex). (- - -) Band sensitive to the tacticity. Source: Adapted from Ref. 50 with permission from Elsevier.

Polarized Raman spectroscopy is a powerful tool to quantify molecular orientation distributions, since it can be used for obtaining the fourth-order molecular orientation distribution coefficients, as well as the second order. This technique enables the molecular orientation distribution of the crystalline and the amorphous region to be determined independently. The PLLA Raman bands are assumed to be cylindrically symmetric owing to its helical molecular structure. A band at 926 cm$^{-1}$ was assigned to the crystalline regions only of PLLA, whereas another band at 875 cm$^{-1}$ was assigned to both crystalline and amorphous regions. The PLLA molecules were biaxially oriented in both amorphous and crystalline regions. The orientation distribution normal to the surface of the film was found to be broader in the amorphous regions than in the crystalline regions. Furthermore, a predominant unidirectional molecular orientation was observed in the crystalline region, whereas an isotropic molecular orientation distribution parallel to the surface was found for the amorphous phase [72].

Using Raman spectroscopy, Smith et al. [73] characterized the orientation of PLA films for food packaging. The study was carried out by monitoring the changes in bands assigned to the crystalline and amorphous phases, as well as its orientation. The uniaxial and biaxial oriented films were characterized by Raman depolarization and Raman band shifts, respectively. Figure 7.10 shows a Raman spectrum of an unoriented film. The bands between 415 and 398 cm$^{-1}$ are related to the $C{-}C{-}O$ bonds in the backbone. The band at 873 cm$^{-1}$ can be assigned to a stretch of the C–C bond. There are two bands at 397 and 410 cm$^{-1}$ with extreme sensitivity and selectivity to crystallization and orientation, which can be used to follow crystallization and to characterize orientation in the crystalline phase. The first band is assigned to the amorphous phase and the other is a crystalline band. When these films become oriented, these bands have marked shifts depending on the draw ratio, as can be seen in Figure 7.11 [73].

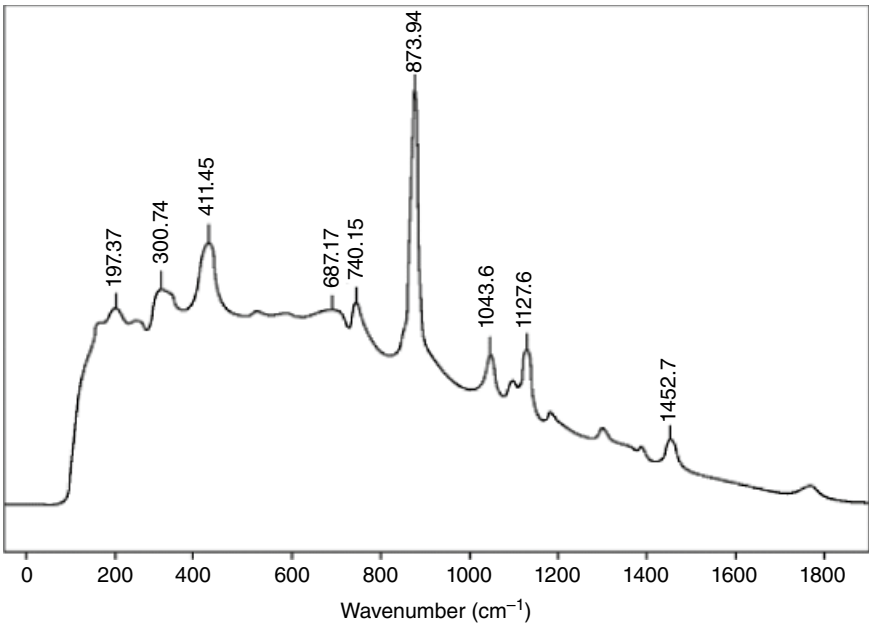


**FIGURE 7.10** Raman spectrum of a 4.1% D-PLA unoriented cast film. Source: Adapted from Ref. 73 with permission from John Wiley & Sons, Inc.

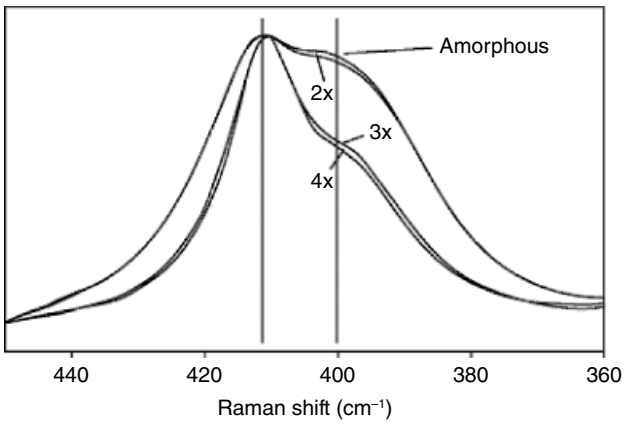


**FIGURE 7.11** Raman spectrum of a 4.1% D-PLA-oriented cast film. Source: Adapted from Ref. 73 with permission from John Wiley & Sons, Inc.

## 7.6 $^{1}$H AND $^{13}$C NMR SPECTROSCOPY

NMR spectroscopy has been used as a fundamental tool to understand the molecular structure of a wide variety of compounds. In polymer science, its applicability has proven to be extremely important for solid samples. The Zeeman interactions that happen between nuclei determine the average resonance frequency of a particular nuclear species, allowing the observation of specific elements without interferences of others present in the sample [72]. NMR is known to be one of the best techniques for the analysis of polymer stereochemistry and tacticity [74, 75]. Thus, there have been a large number of NMR tacticity studies of PLA at the tetrad level for CH protons and carbon, and partially at the hexad level for carbonyl carbon [76–86]. The assignments were assisted with quantum chemical calculations of chemical shifts [85, 86].

In the NMR spectra of PLA, the observed resonances can be assigned to stereosequence distribution in the polymer and reflect its history including the stereochemistry of the feed composition, polymerization kinetics, the catalyst used, and extent of transesterification and racemization [77–80]. The assignments are designated as various combinations of "*i*" isotactic pairwise relationship (*RR* and *SS*) and "*s*" syndiotactic pairwise relationship (*RS* and *SR*). In the NMR spectra, the combinations *RR* and *SS* are indistinguishable and have identical chemical shifts, as would *RS* and *SR* [77, 80]. Many of the physical properties of PLA are influenced by the amount and distribution of the *R* and *S* stereocenters in the polymer chain, which in turn is determined by the relative probability of a specific sequence of stereocenters occur in the polymer. It is well known that polymers with high stereo regularity are highly crystalline polymers. For example, isotactic PLA crystallizes at a faster rate and to a higher degree than the syndiotactic, and both racemic and *meso*-lactide form an amorphous polymer.

Zell et al. [81] assigned both the $^{1}$H and $^{13}$C NMR spectrum of the methine proton and carbon in PLA at the tetrad stereosequence level. They used a combination of 2D NMR experiments and selective $^{13}$C labeling and showed that the

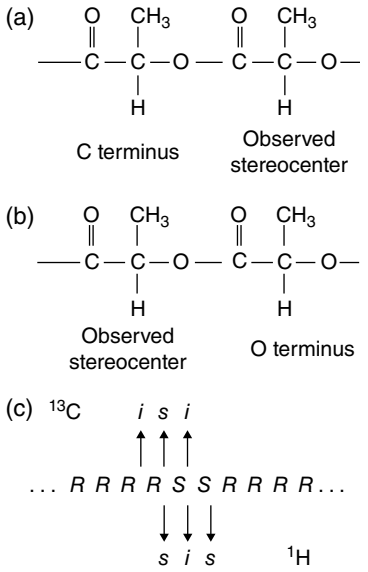


**FIGURE 7.12** Diagram illustrating the alternative interpretation of $^{1}H$ and $^{13}C$ stereosequences: (a) central pairwise relationship determined by lactic acid connected to C terminus, (b) central pairwise relationship determined by lactic acid connected to O terminus, (c) direction of central pairwise relationship of $^{1}H$ and $^{13}C$ resonances. Source: Adapted from Ref. 81 with permission from American Chemical Society.

central pairwise relationship in the $^{1}H$ NMR spectrum is determined by the stereocenter in the lactic acid unit attached to the O terminus. They also determined that in the $^{13}C$ NMR spectrum, the central pairwise relationship of the stereocenter in the lactic acid unit attached to the C terminus obtained consistent NMR and statistical data as can be seen in Figure 7.12. The chemical shifts of $^{13}C$ and $^{1}H$ nuclei in PLA are affected by the stereoconfiguration of two or three adjacent stereogenic centers on either side (hexad stereosensitivity) [82].

Kricheldorf et al. [79, 80] proposed assignments for the stereosequences of the known microstructures of PLA, which were more recently confirmed by Zell et al. [81]. Figure 7.13 presents the $^{1}H$ and $^{13}C$ spectra of PLA synthesized using 5% L-lactic and 95% D-lactic obtained by Zell et al. [81].

In the $^{1}H$ NMR spectrum, the *sis* resonance, which appears at 5.24 ppm, gives an integrated intensity of 2.64%. Integration of the resonance at 69.21 ppm (the *isi* resonance) in the $^{13}C$ NMR spectrum gives a value of 6.19% [81]. When the PLA is synthesized using primarily D-lactide and small amounts of L-lactide that was $^{13}C$ labeled in the carbonyl position, only two peaks can be observed in the carbonyl region due to the $^{13}C$ labels, which confirms that almost all the pairs of *S* stereocenters are surrounded on either side by several

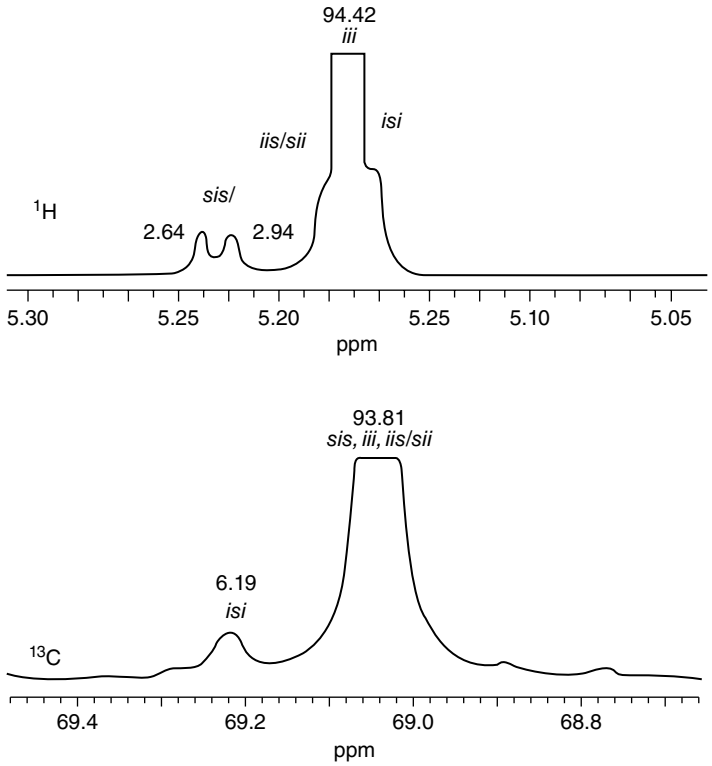


**FIGURE 7.13** $^{1}H$ and $^{13}C$ solution NMR spectra of PLA synthesized using 5% L-lactide and 95% D-lactide. Source: Adapted from Ref. 81 with permission from American Chemical Society.

*R* stereocenters [81]. The NMR spectra of PLA synthesized using (a) fully $^{13}$C labeled and (c) unlabeled 5% L-lactide and 95% *meso*-lactide are shown in Figure 7.14, along with (b) the NMR spectrum of poly(*meso*-lactide). The spectra in Figure 7.14b and c are almost identical since the stereosequence distributions for 5% L-lactide/95% *meso*-lactide and for 100% *meso*-lactide are almost identical. The NMR spectrum in Figure 7.14a is very different from the spectra in Figure 7.14b and c. The reason is that the signals from the fully $^{13}$C-labeled *S* stereocenters dominate the spectrum, which is similar to the situation observed in the one-dimensional $^{13}$C NMR spectrum. As a result of the splitting of the signals for the $^{13}$C-labeled *S* stereocenters into a doublet of doublets, the spectrum of the labeled polymer spans a larger chemical shift range (68.5–69.5 ppm) than the unlabeled polymer (69.0–69.4 ppm). The center of each set of doublet of doublets corresponds to the expected chemical shift value for an unlabeled carbon. The *sis* stereosequence is expected from both the unlabeled and labeled stereocenters. For the unlabeled *meso*-lactide component, an *isi* stereosequence is expected, while for the $^{13}$C-labeled stereocenters, an *isi* stereosequence is not expected. In the unlabeled *meso*-lactide region, the *sis* resonance appears at 69.0 ppm and is not split, while in the $^{13}$C-labeled L-lactide region, the *sis* resonance is centered at 69.0 ppm, but it is split into a doublet of doublets that extends ~0.4 ppm in both directions, spanning the region from 68.6 to 69.4 ppm. In addition, all of the other resonances expected due to the $^{13}$C-labeled L-lactide lie within 0.1 ppm of the *sis* resonance, making the total span of all resonances due to $^{13}$C-labeled L-lactide from 68.5 to 69.5 ppm (Figure 7.14). This experiment definitively proves that the peak at 69.0 ppm in the $^{13}$C NMR spectrum is due to *sis*. If the *isi* and *sis* stereosequence assignments were reversed, then the *sis* peak would be centered at 69.2 ppm and would span from 68.8 to 69.6 ppm. The solid line in Figure 7.14 shows where the *sis* peak would be centered, the short-dashed line shows where the *iss*/*ssi* peak would be centered, and the two long-dashed lines show where the *isi* peak would be centered and where the farthest peak in that doublet of doublets should be. Since there is no resonance at 69.6 ppm, the assignment of the peak at 69.0 ppm to *sis* and the peak at 69.2 ppm to *isi* must be correct. It is also possible to definitively assign the *iss/ssi* stereosequences to specific resonances in the $^{13}$C NMR spectrum. For a polymer that is synthesized with no isotopically labeled material, both the *iss* and *ssi* resonances will always have equal probability and therefore cannot be distinguished in the NMR spectrum. For PLA synthesized using 5% fully $^{13}$C-labeled L-lactide and 95% *meso*-lactide, both the *ssi* and *iss* stereosequences are expected from the large amount of *meso*-lactide, and these resonances will not be split in the NMR spectrum. When PLA is synthesized using 5% fully $^{13}$C-labeled L-lactide and 95% *meso*-lactide, only the *ssi* stereosequence will be split into a doublet of doublets because of $^{13}$C–$^{13}$C*J* coupling to the methyl and carbonyl carbons. No peak due to *iss* will be observed from the $^{13}$C-labeled stereocenters. If the *ssi* resonance is centered at 69.1 ppm, the doublet of doublets will overlap the doublet of doublets generated by the *iii*, *iis*, *sii*, and *sis* stereosequences, and the spectrum will span from about 68.7 to 69.5 ppm (Figure 7.6). If the *ssi* resonance occurs at 69.4 ppm, the doublet of doublets will span from 69 to 69.8 ppm. The $^{13}$C NMR spectrum in Figure 7.14a has no resonance above 69.5 ppm, indicating that the resonance at 69.1 ppm in Figure 7.14b is due to *ssi*, while the resonance at 69.4 ppm is due to *iss* [81].

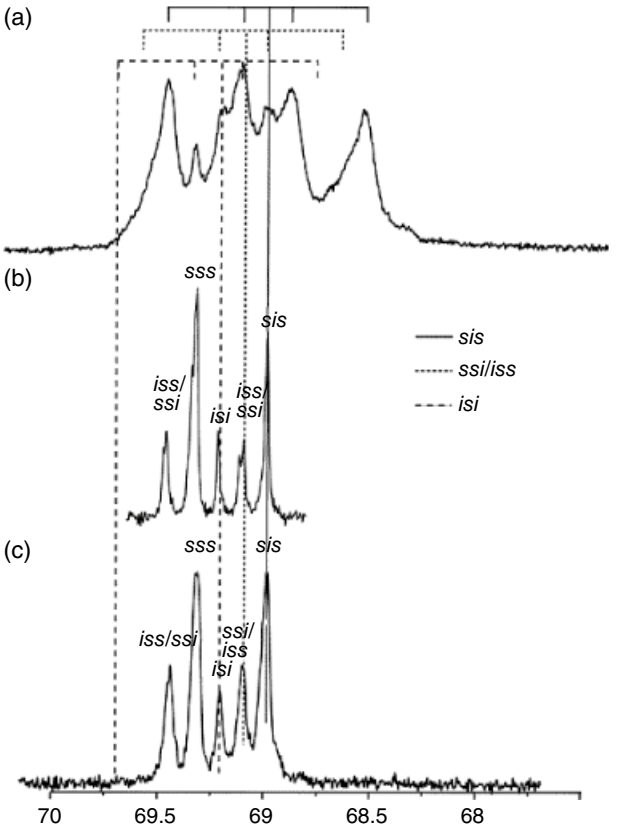


**FIGURE 7.14** $^{13}$C NMR spectra of PLA synthesized using (a) 5% fully $^{13}$C-labeled L-lactide and 95% *meso*-lactide, (b) *meso*-lactide, and (c) 5% L-lactide and 95% *meso*-lactide. Source: Adapted from Ref. 80 with permission from American Chemical Society.

Thakur et al. [82] studied PLA samples with various compositions of L-lactide, D-lactide, and *meso*-lactide: sample 1 had 3% of both L-lactide and D-lactide and 94% of *meso*-lactide; sample 2 had 51.5% of L-lactide, 1.5% of D-lactide, and 47% of *meso*-lactide; and sample 3 had 70.9% L-lactide, 0.9% D-lactide, and 28.2% *meso*-lactide. They found that the carbonyl resonance in $^{13}$C spectrum of PDLLA indicates a higher stereoselectivity than hexad and is most likely to be octad [82]. However, due to the high degree of overlap, the assignments of the peaks for octad stereosequences to carbonyl resonance and probably a hexad stereosensitivity to

methyl resonance are difficult. Based on hexad stereosequences, the authors [82] interpreted the $^{13}C$ methine resonances and the stereosequences *sss*, *isi*, *ssi*, and *iss* are well resolved and their assignments are consistent with previous studies made by Kricheldorf [80], Schindler and Harper [83], or Kasperczyk [78].

Although $^{1}H$ NMR allows good results regarding stereosequence probabilities, there are still some questions regarding the coupling between the methyl protons and the methine (—CH) protons at each of the stereogenic centers in PLA. As was observed from the analysis of $^{13}C$ spectra, also in $^{1}H$ spectra the peaks corresponding to hexad stereosequences can be observed (Figure 7.15). The intensity distribution of the various stereosequence resonances in the NMR spectra indicates a preference for syndiotactic addition during the polymerization process [82]. However, this preference decreases with increasing extent of polymerization. Steric hindrance at the polymer growing site is probably responsible for the syndiotactic stereospecificity, and the increasingly random lactide addition is due to interplay of kinetically and thermodynamically controlled reactions. Changes in viscosity during the melt polymerization additionally influence the stereochemistry. The effect of transesterification on the stereosequence distribution should be related to increasing time and hence increasingly randomize with increasing polymerization time until the stereosequence distribution in the polymer becomes random. The limiting invariant stereosequence intensity in PLA near equilibrium shows that transesterification and racemization are not frequent enough to influence the stereosequence distribution under typical polymerization conditions [82].

In another vein, Tsuji et al. [87] studied the phase structure of the stereocomplex obtained from the crystallization of racemic PLA in a dilute acetonitrile solution, using high-resolution solid-state $^{13}C$ NMR spectroscopy. The total spectrum reflecting quantitatively all the components has been resolved into four components by a line shape analysis, corresponding to the rigid and disordered racemic crystalline components, the noncrystalline region, where the segments of PDLA and PLLA are almost randomly mixed, and the crystalline component of homopolymers produced. The degree of crystallinity estimated as a sum of mass fractions of the rigid and disordered racemic crystalline components is in agreement with that determined by differential scanning calorimetry or X-ray diffractometry. Later, Tsuji et al. [88] also investigated the effects of crystallinity, water absorption, hydrolytic degradation, and tacticity on the solid structure

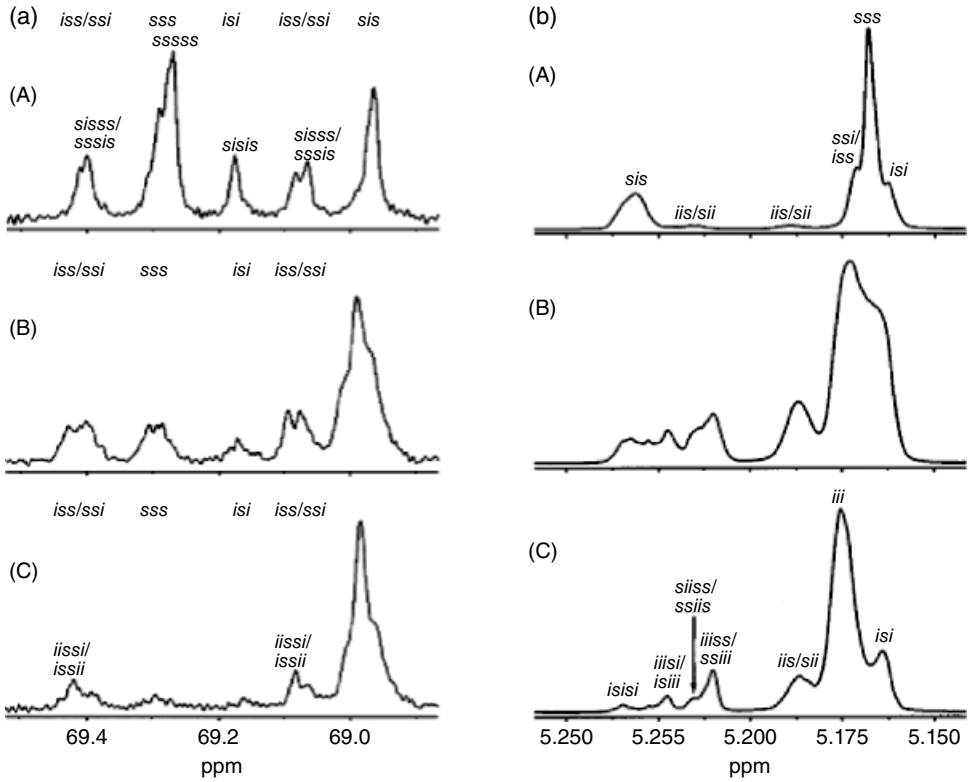


**FIGURE 7.15** (a) Methine resonances in the $^{13}C$ NMR spectra of poly(lactide) samples (A) 1, (B) 2, and (C) 3. The peak at about 68.95 ppm comprises resonances from *iii*, *iis*, *sii,* and *sis* core stereosequences. (b) Methine resonances in the homonuclear decoupled $^{1}H$ NMR spectra of poly(lactide) samples (A) 1, (B) 2, and (C) 3. Source: Adapted from Ref. 82 with permission from American Chemical Society.

and chain mobility of poly(lactide)s by using solid-state $^{13}C$ NMR spectroscopy. These authors showed that the crystallized PLLA in the dried, hydrated, and hydrolyzed states had two (rigid and soft) components which can be, respectively, assigned to the crystalline and non-crystalline components. Upon water absorption, the chain mobility in the non-crystalline component of crystallized PLLA remained unchanged, while in the crystalline component a high chain mobility was detected strongly suggesting that water molecules are incorporated in the crystalline lattice. Upon removal of the non-crystalline components by hydrolytic degradation of crystallized PLLA, the chain mobility was slightly higher in both crystalline and non-crystalline components by the lowered crystalline thickness and shortened non-crystalline chains. On the other hand, the non-crystalline specimens, PLLA quenched and PDLLA, also contain two (rigid and soft) components, with the similar conformation but different restricted states of chains, which cause high and low chain mobility.

The fine refinement of the crystal structure of the α-polymorph of L-polylactide was carried out by NMR crystallography, a complementary approach that combines NMR measurements, analysis of X-ray and neutron powder diffraction data, and advanced quantum mechanical calculations [63, 89]. Notably, GIPAW (gauge-including projector-augmented waves) method NMR parameters computed for fully optimized PLLA perfectly correlate with the experimental solid-state NMR spectra recorded at different spinning rates. This result means that the procedure in which GIPAW and NMR are combined can be used for the fine refinement of polymeric structure when only coarse X-ray data are available.

Statistical models (also known as reaction probability models) have been used extensively in polymer studies [90–92] since they provide fundamental understanding of polymerization processes and serve as a theoretical framework whereby NMR, molecular weight, fractionation, and polymerization kinetics data can be analyzed in a rational manner. In many cases, the models can assist in NMR spectral assignments and help to interpret the spectral intensities. For PLA, if the starting material is lactide (the cyclic dimer of lactic acid), the simplest model is the pair-addition Bernoullian model that takes into account the configuration of lactide. There are some variations on this model, depending on the details of the formulation used, which were applied to NMR data [78, 93, 94]. The fit was usually satisfactory when no transesterification or racemization was present. However, when transesterification and racemization occurred, a two-state (pair-addition Bernoullian and single-addition Bernoullian) model provides not only a better fit of the data but also allows to quantify the extent of transesterification and racemization, and potentially yields useful information on the polymerization mechanism [95].

## REFERENCES


1. M. H. Hutchinson, J. R. Dorgan, D. M. Knauss, S. B. Hait, *J. Polym. Environ.* **2006**, *14*, 119–124.
2. J. M. Zhang, H. Tsuji, I. Noda, Y. Ozaki, *J. Phys. Chem. B* **2004**, *108*, 11514–11520.
3. A. Jiménez, M. Peltzer, R. Ruseckaite (Eds.), *Poly(Lactic Acid) Science and Technology: Processing, Properties, Additives and Applications*, Royal Society of Chemistry, Cambridge, 2015, pp. 66–98.
4. N. S. Oliveira, J. Oliveira, T. Gomes, A. Ferreira, J. Dorgan, I. M. Marrucho, *Fluid Phase Equilibr.* **2004**, *222*, 317–324.
5. K. L. G. Ho, A. L. Pometto, *J. Environ. Polym. Degrad.* **1999**, *7*, 93–100.
6. K. N. Turhan, F. Sahbaz, *Polym. Int.* **2001**, *50*, 1138–1142.
7. M. Mathlouthi, *Food Packaging and Preservation*, Blackie, Glasgow, 1994, XVI + 275 pp.
8. R. Auras, B. Harte, S. Selke, *Macromol. Biosci.* **2004**, *4*, 835–864.
9. R. Auras, Ph.D. thesis, Michigan State University, East Lansing, MI, 2004, p. 268.
10. J. Lunt, D. W. Farrington, S. Davies, R. S. Blackburn, Poly(lactic acid) fibers, in: *Elsevier Science Biodegradable and Sustainable Fibres*, Woodhead Publishing Ltd., Cambridge, 2005, Chapter 6. ISBN 9781845690991.
11. S. W. Hwang, J. K. Shim, S. E.M. Selke, H. Soto-Valdez, L. Matuana, M. Rubino, R. Auras, *Polym. Int.* **2012**, *61*, 418–425.
12. A. Bher, I. U. Unalan, R. Auras, M. Rubino, C. E. Schvezov, *Polymers* **2018**, *10*, 95.
13. C. F. L. Ciolacu, N. R. Choudhury, N. K. Dutta, *Polym. Degrad. Stab.* **2006**, *91*, 875–885.
14. M. Edge, R. Wiles, N. S. Allen, W. A. McDonald, S. V. Mortlock, *Polym. Degrad. Stab.* **1996**, *53*, 141–151.
15. J. Ramiro, J. I. Eguiazabal, J. Nazabal, *J. Appl. Polym. Sci.* **2002**, *86*, 2775–2780.
16. Y. M. Wang, B. Steinhoff, C. Brinkmann, I. Alig, *Polymer* **2008**, *49*, 1257–1265.
17. F. Sondheimer, D. A. Benefraim, R. Wolovsky, *J. Am. Chem. Soc.* **1961**, *83*, 1675–1681.
18. M. C. Gupta, V. G. Deshmukh, *Colloid Polym. Sci.* **1982**, *260*, 514–517.
19. N. N. Chugh, J. K. Lalla, *Indian Drugs* **1990**, *27*, 516–522.
20. F. Mikołajczyk, S. Kuberski, *IOSR J. Polym. Text. Eng.* **2019**, *6*, 14–22.
21. NatureWorks (4 April 2021). https://www.natureworksllc.com/News-and-Events/Press-Releases/2021/2021-04-15-3D700-Release, accessed date 22 June 2021.
22. J. M. Raquez, Y. Habibi, M. Murariu, P. Dubois, *Prog. Polym. Sci.* **2013**, *38*,1504–1542.
23. S. H. Tabatabaei, A. Ajji, *Polym. Eng. Sci.* **2011**, *51*, 2151–2158.
24. J. L. Orellana, D. Wichhart, C. L. Kitchens, *J. Nanomater.* 2018, Article ID 7124260.

25. Y. Kim, J. S. Kim, S.-Y. Lee, R. L. Mahajan, Y.-T. Kim, *Int. J. Biol. Macromol.* **2020**, *144*, 135–142.
26. V. Ramji, M. Vishnuvarthanan, *Silicon* 2020 DOI: https://doi.org/10.1007/s12633-020-00839-x.
27. J. Wang, J. Yu, D. Bai, Z. Li, H. Liu, Y. Li, S. Chen, J. Cheng, L. Li, *Polymers* **2020**, *12*, 604.
28. D. W. VanKrevelen, *Properties of Polymers*, 3rd edition, Elsevier Science B.V., Amsterdam, The Netherlands, 1997.
29. T. Malmgren, J. Mays, M. Pyda, *J. Therm. Anal. Calorim.* **2006**, *83*, 35–40.
30. S. Olivier, R. Walkenhorst, *Materiaux*, **2002**, 1–5.
31. H. Tsuji, S. H. Hyon, Y. Ikada, *Macromolecules* **1991**, *24*, 5651–5656.
32. N. Yui, P. J. Dijkstra, J. Feijen, *Makromol. Chem.* **1990**, *191*, 481–488.
33. H. R. Kricheldorf, R. Dunsing, *Makromol. Chem.* **1986**, *187*, 1611–1625.
34. J. Kobayashi, T. Asahi, M. Ichiki, A. Oikawa, H. Suzuki, T. Watanabe, E. Fukada, Y. Shikinami, *J. Appl. Phys.* **1995**, *77*, 2957–2973.
35. H. W. Siesler, K. Holland-Moritz, *Infrared and Raman Spectroscopy of Polymers*, Marcel Dekker, New York, **1980**, VIII + 389 pp.
36. R. Mehta, V. Kumar, H. Bhunia, S. N. Upadhyay, *J. Macromol. Sci. Polym. Res.* **2005**, *C45*, 325–349.
37. M. Matsusaki, A. Kishida, N. Stainton, C. W. G. Ansell, M. Akashi, *J. Appl. Polym. Sci.* **2001**, *82*, 2357–2364.
38. M. H. Gutierrez-Villarreal, M. G. Ulloa-Hinojosa, J. G. Gaona-Lozano, *J. Appl. Polym. Sci.* **2008**, *110*, 163–169.
39. W. H. Song, Z. Zheng, W. L. Tang, X. L. Wang, *Polymer* **2007**, *48*, 3658–3663.
40. M. T. Khorasani, H. Mirzadeh, S. Irani, *Radiat. Phys. Chem.* **2008**, *77*, 280–287.
41. Y. S. Kim, E. S. Gil, T. L. Lowe, *Macromolecules* **2006**, *39*, 7805–7811.
42. Z. J. Ren, L. S. Dong, Y. M. Yang, *J. Appl. Polym. Sci.* **2006**, *101*, 1583–1590.
43. Y. Zhou, L. Lei, B. Yang, J. Li, J. Ren, *Polym. Test.* **2017**, *60*, 78e83.
44. H. Samsudin, H. Soto-Valdez, R. Auras, *Food Control* **2014**, *46*, 55–66.
45. L. Lopusiewicz, F. Jedra and M. Mizielinska, *Polymers* **2018**, *10*, 386–408.
46. C. Yang, H.Tang, Y. Wang, Y. Liu, J Wang, W. Shi, L. Li, *Food Packag. Shelf Life* **2019**, *22*, 100393.
47. B. Braun, J. R. Dorgan, S. F. Dec, *Macromolecules* **2006**, *39*, 9302–9310.
48. P. Degee, P. Dubois, S. Jacobsen, H. G. Fritz, R. Jerome, *J. Polym. Sci. Polym. Chem.* **1999**, *37*, 2413–2420.
49. M. Jalabert, C. Fraschini, R. E. Prud'Homme, *J. Polym. Sci. Polym. Chem.* **2007**, *45*, 1944–1955.
50. G. Kister, G. Cassanas, M. Vert, *Polymer* **1998**, *39*, 267–273.
51. T.-H. Yu, Y.-H. Su, H.-H. Huang, H.-J. Tsai, W.-K. Hsu, *Polym. Test.* **2020**, *91*, 106731.
52. C. M. B. Gonçalves, L. C. Tomé, J. A. P. Coutinho, I. M. Marrucho, *J. Appl. Polym. Sci.* **2011**, *119*, 2468–2475.
53. G. Kister, G. Cassanas, M. Vert, B. Pauvert, A. Terol, *J. Raman Spectrosc.* **1995**, *26*, 307–311.
54. D. Garlotta, *J. Polym. Environ.* **2001**, *9*, 63–84.
55. N. T. Paragkumar, E. Dellacherie, J. L. Six, *Appl. Surf. Sci.* **2006**, *253*, 2758–2764.
56. C. M. Johnson, A. B. Sugiharto, S. Roke, *Chem. Phys. Lett.* **2007**, *449*, 191–195.
57. A. B. Sugiharto, C. M. Johnson, H. B. De Aguiar, L. Alloatti, S. Roke, *Appl. Phys. Part B* **2008**, *91*, 315–318.
58. C. Aleman, B. Lotz, J. Puiggali, *Macromolecules* **2001**, *34*, 4795–4801.
59. S. Sasaki, T. Asakura, *Macromolecules* **2003**, *36*, 8385–8390.
60. K. Aou, S. L. Hsu, *Macromolecules* **2006**, *39*, 3337–3344.
61. S. H. Kang, S. L. Hsu, H. D. Stidham, P. B. Smith, M. A. Leugers, X. Z. Yang, *Macromolecules* **2001**, *34*, 4542–4548.
62. A. B. Sugiharto, C. M. Johnson, I. E. Dunlop, S. Roke, *J. Phys. Chem. C* **2008**, *112*, 7531–7534.
63. P. Pan, J. Yang, G. Shan, Y. Bao, Z. Weng, A. Cao, K. Yazawa, Y. Inoue, *Macromolecules* **2012**, *45*, 189–197.
64. E. Meaurio, E. Zuza, N. Lopez-Rodriguez, J. R. Sarasua, *J. Phys. Chem. B* **2006**, *110*, 5790–5800.
65. J. R. Sarasua, N. L. Rodriguez, A. L. Arraiza, E. Meaurio, *Macromolecules* **2005**, *38*, 8362–8371.
66. J. M. Zhang, H. Sato, H. Tsuji, I. Noda, Y. Ozaki, *Macromolecules* **2005**, *38*, 1822–1828.
67. J. M. Zhang, H. Tsuji, I. Noda, Y. Ozaki, *Macromolecules* **2004**, *37*, 6433–6439.
68. P. Pan, W. Kai, B. Zhu, T. Dong, Y. Inoue, *Macromolecules* **2007**, *40*, 6898–6905.
69. J. M. Zhang, Y. X. Duan, H. Sato, H. Tsuji, I. Noda, S. Yan, Y. Ozaki, *Macromolecules* **2005**, *38*, 8012–8021.
70. P. J. Pan, B. Zhu, W. H. Kai, T. Dong, Y. Inoue, *Macromolecules* **2008**, *41*, 4296–4304.
71. H. Bourque, I. Laurin, M. Pezolet, J. M. Klass, R. B. Lennox, G. R. Brown, *Langmuir* **2001**, *17*, 5842–5849.
72. M. Tanaka, R. J. Young, *Biomacromolecules* **2006**, *7*, 2575–2582.
73. P. B. Smith, A. Leugers, S. H. Kang, X. Z. Yang, S. L. Hsu, *Macromol. Symp.* **2001**, *175*, 81–94.
74. A.E. Tonelli, *NMR Spectroscopy and Polymer Microstructure: The Conformation Connection*, VCH Publishers, New York, 1989.
75. K. Matsuzaki, T. Uryu,T. Asakura, *NMR Spectroscopy and Stereoregularity of Polymers*, Japan Scientific Societies Press, Tokyo, Japan, 1996.
76. S. J. Spell (Ed.), *Characterization of Solid Polymers New Techniques and Developments*, Chapman & Hall, London, 1994, XII + 368 pp.

77. K. A. M. Thakur, R. T. Kean, E. S. Hall, M. A. Doscotch, E. J. Munson, *Anal. Chem.* **1997**, *69*, 4303–4309.
78. J. E. Kasperczyk, *Macromolecules* **1995**, *28*, 3937–3939.
79. H. R. Kricheldorf, C. Boettcher, K. U. Tonnes, *Polymer* **1992**, *33*, 2817–2824.
80. H. R. Kricheldorf, I. Kreisersaunders, C. Boettcher, *Polymer* **1995**, *36*, 1253–1259.
81. M. T. Zell, B. E. Padden, A. J. Paterick, K. A. M. Thakur, R. T. Kean, M. A. Hillmyer, E. J. Munson, *Macromolecules* **2002**, *35*, 7700–7707.
82. K. A. M. Thakur, R. T. Kean, E. S. Hall, J. J. Kolstad, T. A. Lindgren, M. A. Doscotch, J. I. Siepmann, E. J. Munson, *Macromolecules* **1997**, *30*, 2422–2428.
83. A. Schindler, D. Harper, *J. Polym. Sci. Part C* **1976**, *14*, 729–734.
84. K. A. M. Thakur, R. T. Kean, E. S. Hall, J. J. Kolstad, E. J. Munson, *Macromolecules* **1998**, *31*, 1487–1494.
85. K. Suganuma, K. Horiuchi, H. Matsuda, H.N. Cheng, A. Aoki, T. Asakura, *Macromolecules* **2011**, *44*, 9247–9253.
86. K. Suganuma, K. Horiuchi, H. Matsuda, H. N. Cheng, A. Aoki, T. Asakura, *Polym. J.* **2012**, *44*, 838–844.
87. H. Tsuji, F. Hori, M. Nakagawa, Y. Ikada, H. Odani, R. Kitamaru, *Macromolecules* **1992**, *25*, 4114–4118
88. H. Tsuji, S. Kamo, F. Horii, *Polymer*, **2010**, *51*, 2215–2220.
89. T. Pawlak, M. Jaworska, M. J. Potrzebowski, NMR crystallography of α-poly(L-lactide), *Phys. Chem. Chem. Phys.* **2013**, *15*, 3137–3145.
90. H. N. Cheng, Polymerization and statistical models, in: D. M. Grant, R. K. Harris (Eds.), *Encyclopedia of NMR*, Wiley, New York, 1996, pp. 3713–3721.
91. H. N. Cheng, Structural studies of polymers by solution NMR, *RAPRA Rev. Rep.* Rapra, Shrewsbury, **2001**, *11*(5), 19–22.
92. H. N. Cheng, M. Miri, Statistical models and NMR analysis of polymer microstructure. *ACS Symp. Ser.* **2011**, *1077*, 371–382.
93. B. M. Chamberlain, M. Cheng, R. Moore, T. M. Ovitt, E. B. Lobkovsky, G. W. Coates, *J. Am. Chem. Soc.* **2001**, *123*, 3229–3238.
94. J. Coudane, C. Ustariz-Peyret, G. Schwach, M. Vert, *J. Polym. Sci. Part A Polym. Chem.* **1997**, *35*, 1651–1658.
95. K. Suganuma, T. Asakura, M. Oshimura, T. Hirano, K. Ute, H. N. Cheng, *Polymer* **2019**, *11*, 725.

# 8

# CRYSTALLIZATION AND THERMAL PROPERTIES*

Luca Fambri and Claudio Migliaresi

## 8.1 INTRODUCTION

Poly(lactic acid) (PLA)-based products are largely being used for biomedical and environment-friendly applications [1–10]. Processing conditions and final properties of PLAs are strongly influenced by the crystalline or amorphous structure of the polymer [11–13]. Starting from the early work of Kulkarni et al. [14, 15] in 1966 and 1971, many papers addressed the evaluation of thermal properties and crystallinity of PLA or polylactide-based polymers.

The chiral nature of lactic acid results in distinct forms of polylactide, namely, poly(L-lactide) (PLLA), poly(D-lactide) (PDLA), and poly(D,L-lactide) (PDLLA), which are synthesized from the L-, D-, and D,L-lactic acid monomers, respectively, or from the corresponding L,L-lactide, D,D-lactide, and D,L-lactide, respectively [16]. Both L- and D-lactic acid stereoisomers are naturally occurring; however, most of the lactic acid in nature is L-type or sometimes racemic. The fact that lactic acid is produced in the human body in the L-enantiomeric form and the interest in the biomedical applications of this polymer have led research and production to concentrate on L-lactide or D,L-lactide polymers [17–19]. The D-isomer does not have many applications, except for use in particular medicinal chemicals, and for the synthesis of PDLA utilized for the preparation of stereocomplexed materials with PLLA.

Today petrochemical-based production gives a 50/50 mixture of the L- and D-forms, whereas mostly L-lactic acid is obtained from fermentation. In particular, high-purity L-lactic acid can be obtained starting from bacteria, fungi, algae, municipal wastes, or renewable vegetal sources [20]. The production of D-lactic acid is mainly based on fermentation, starting for instance from rice [21], orange peel waste [22], glucose, molasses, and corn steep liquor [23].

PLLA and PDLA are crystalline polymers due to the enantiomeric purity of the pristine monomers and the stereoregularity of the polymer chain. Conversely, the equimolar PDLLA, i.e., the equimolar relatively random copolymer of L- and D-lactic acid (or L- and D-lactide), is fully amorphous because of its irregular structure. The stereochemical configurations of PLLA (or PDLA) and PDLLA are analogous to those of isotactic polypropylene and atactic polypropylene. Syndiotactic PLA that can be polymerized from a stereoselective polymerization of *meso*-lactide [24], or synthesized by polycondensation of the dimer L-lactic acid-D-lactic acid [25], can be considered as an alternating D,L-lactic acid copolymer, analogous to syndiotactic polypropylene.

It is noteworthy that in the early work of Kulkarni et al. [15], the glass transition peak of PDLLA at about 60°C was misinterpreted and attributed to melting. Pure PLLA and PDLA have the same properties, that is, a glass transition temperature ($T_g$) between 50 and 70°C, a melting temperature ($T_m$) between 170 and 190°C, and a crystallinity of around 35% [1, 2, 7, 8, 26–33]. In the case of syndiotactic PLA, due to the different stereotactic configuration, lower $T_g$ and $T_m$ were found, equal to 34 and 155°C, respectively [24]. Crystallization, crystallinity degree, and thermal properties of PLLA depend on the polymer molecular weight, polymerization conditions, thermal history, purity, and so on. As reported by Ikada et al. [30], blending of PLLA and PDLA results in the formation of a stereocomplex with a crystalline structure different from that of each homopolymer and with a

* In memory of our colleague Amabile Penati, a mentor and a friend.

*Poly(Lactic Acid): Synthesis, Structures, Properties, Processing, Applications, and End of Life*, Second Edition.
Edited by Rafael A. Auras, Loong-Tak Lim, Susan E. M. Selke, and Hideto Tsuji.

$T_m$ reaching 230°C. Contradictory data are reported in the literature about the reference melting enthalpy of PLLA, $\Delta H_m^0$, ranging from 40 to 203 J/g. The most common values adopted for $\Delta H_m^0$ of PLLA are 93.6 J/g, as reported by Fisher et al. [26], or 140 J/g, as evaluated by Loomis et al. [34], or 106 J/g, as later determined by Sarasua et al. from the melt point depression [35].

## 8.2 CRYSTALLINITY AND CRYSTALLIZATION

Many authors have studied the crystalline structure of PLLA [36–82], either homopolymer, copolymers, or blends. PLLA crystals present several different structural conformations that can develop under different processing or treatment conditions. Various researches progressively reported and defined the α phase [51–55], the β phase [56–59], the γ phase [60, 61], the δ (α′) phase [59, 65–67]. Furthermore ordered conformations consisting in meso-structures [42, 62–64], co-crystallization with specific low molecular weight compounds (ε phase) [68, 69], and stereocomplex (SC) formation between PLLA and PDLA [70–72] have been reported.

In particular, melt or cold crystallization and solution spinning processes at low drawing temperatures and/or low hot draw ratios induce the formation of α-structures characterized by a left-handed $10_3$ helix that packs in an orthorhombic unit cell with parameters $a = 1.06$ nm, $b = 1.737$ nm, and $c = 2.88$ nm [51]. Stretching, solution spinning, or high hot draw ratios induce the formation of β-crystal structures, a unit cell with $a = 1.031$ nm, $b = 1.821$ nm, and $c = 0.900$ nm, and a chain conformation with left-handed $3_1$ helices [56]. The crystalline form named γ, which develops under epitaxial crystallization, is characterized by an orthorhombic unit cell with two antiparallel $3_1$ helices [60]. δ (α′) is a disordered crystalline form that develops in PLLA crystallized below 120°C and that typically converts into α-crystals upon heating [65, 73, 74]. The small exothermic peak in differential scanning calorimetry (DSC) just before melting has been interpreted as the crystallization of reduced mobility amorphous regions (rigid amorphous phase, RAF) [42], or transformation from δ(α′) to α-form [75], as supported by comparing XRD and DSC data [76].

Multiple melting or crystallization peaks have been reported [48] in calorimetric analysis after the isothermal crystallization of PLLA, with the melting of less perfect crystals (that form when crystallization is conducted at lower temperature), their reorganization in more perfect structures, and their final melting. Figure 8.1 shows a typical DSC analysis of thermal behavior of two amorphous PLAs, that is, a PDLLA ($M_w$ = 70 kDa) sample that is intrinsically amorphous and PLLA ($M_w$ = 200 kDa) that was quenched to the amorphous state by fast cooling at −100°C/min after melting. In both cases, the $T_g$ is evident and is located at about 65°C.

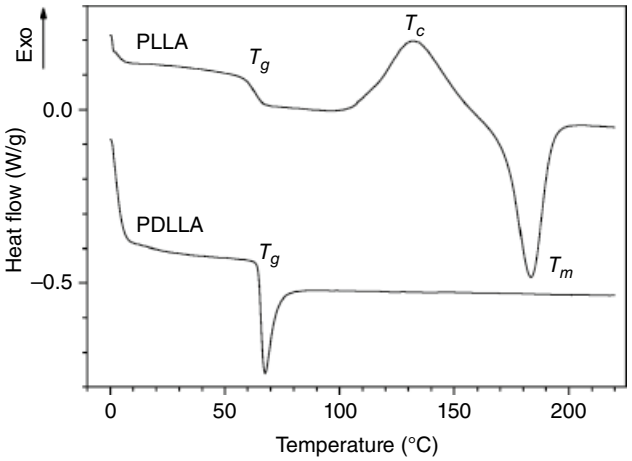


**FIGURE 8.1** Differential scanning calorimetry thermograms of amorphous PLLA and PDLLA (heating rate 10°C/min).

The crystallinity content ($X_c$) has been evaluated from the DSC data according to the following equation:

$$X_c = 100\left(\Delta H_m - \Delta H_c\right) / \left[\Delta H_m^0 \left(1 - f\right)\right] \qquad (8.1)$$

where $\Delta H_m$ and $\Delta H_c$ are the melting and the crystallization enthalpies, respectively, $\Delta H_m^0$ is the reference $\Delta H_m$ (93.6 J/g) for PLLA crystals having an infinite size [26], and $f$ is the weight fraction of the filler in the case of a composite.

Above $T_g$, PLLA exhibits an aging peak in the interval 65–90°C with an enthalpy of 8 J/g, which is typical of aged amorphous polymer. The longer the aging time and/or the closer the aging temperature to the $T_g$, the more intense is that peak. PLLA can reach an enthalpy value of about 10 J/g, as shown by Celli and Scandola [33]. On the other hand, the initial amorphous PLLA presents a broad crystallization peak in the range 100–160°C centered at about 132°C with $\Delta H_c$ = 38 J/g, followed by melting at 182°C with $\Delta H_m$ = 38 J/g. As determined by the equal values of the crystallization and melting enthalpies, the fast quenching produced a fully amorphous material. The variation of specific heat ($\Delta C_p$) at $T_g$ was 0.50 J/(g K).

Figure 8.2 shows the DSC thermograms of a commercial PLLA (L210 from Boehringer, Ingelheim, Germany) with a molecular weight of 200 kDa, subjected to the following three DSC runs at 10°C/min: (i) heating from 0 to 220°C; (ii) cooling from 220 to 0°C, and finally (iii) heating from 0 to 220°C. The initially crystalline polymer presented a $T_g$ at 73°C and $T_m$ at 192°C. During cooling, apparently no crystallization developed and the following thermal run on the initially amorphous materials showed glass transition ($T_g$ = 64°C), crystallization ($T_c$ = 127°C), and melting ($T_m$ = 181°C). Worth noting between the curves of Figures 8.1 and 8.2 is the difference in the crystallization temperature, which was lower for the slowly cooled

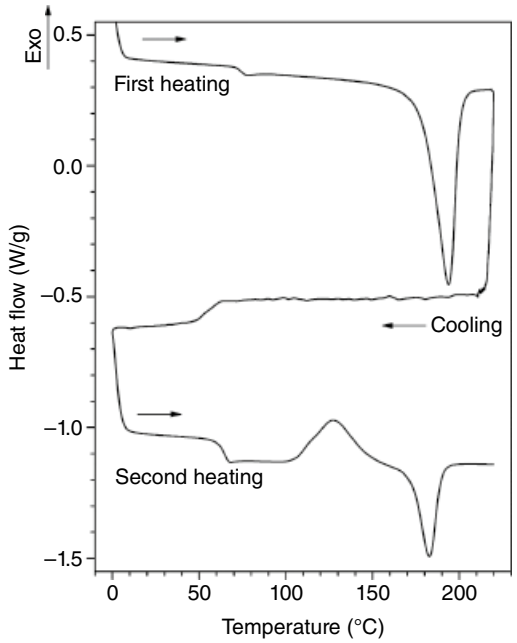


**FIGURE 8.2** DSC thermal cycles of PLLA 200 kDa (first heating, cooling, and second heating at ±10°C/min).

polymer, probably due to the formation of crystallization nuclei during cooling.

Table 8.1 lists $T_g$, $T_m$, $T_c$, $\Delta H_c$, and $\Delta H_m$ of various molecular weight PLLA samples, namely, 2, 30, and 200 kDa, respectively, subjected to the same DSC cycles presented in Figure 8.2.

Due to the favorable crystallization conditions during the polymerization process, all the products in the first scan display a high crystallinity between 51 and 73%, depending on their molecular weight, and a $T_m$ that is proportional to the molecular weight according to the classical Flory equation:

$$1/T_m = 1/T_m^* - 2RM_0/\Delta H_{mu}M_n \tag{8.2}$$

where $T_m^*$ is the $T_m$ at infinite molecular weight, $R$ is the gas constant, $\Delta H_{mu}$ is the heat of fusion per mole of the repeating unit, $M_0$ the molecular weight of the repeating unit, and $M_n$ is the number-average molecular weight.

The Flory–Fox equation

$$T_g = T_g^* - K/M_n \tag{8.3}$$

can also be used to predict the $T_g$ of polymers as a function of the molecular weight, $T_g^*$ being the $T_g$ at infinite $M_n$.

While in the first heating, $T_g$ values are higher than expected due to high crystallinity content (crystalline domains hinder the mobility of amorphous chains), as also confirmed from the low value of $\Delta C_p$ at $T_g$, the $T_g$ measured during cooling proportionally depends on molecular weight, in accordance with Equation 8.3. It is also interesting to note that during cooling PLLA (30 kDa) developed some crystallinity, whereas in the other cases crystallization was inhibited by the high content of terminal groups that acted as

**TABLE 8.1 Glass Transition Temperature ($T_g$), Change of Specific Heat at $T_g$ ($\Delta C_p$), Melting Peak Temperature ($T_m$) and Enthalpy ($\Delta H_m$), Crystallization Peak Temperature ($T_c$), and Enthalpy ($\Delta H_c$) for Different Molecular Weight of PLLA Samples. During a DSC Cycle of Heating–Cooling–Heating DSC Cycle of Between 0 and 220°C at ±10°C/min. Crystallinity ($X_c$) was Calculated According to Equation 8.1**

**(i) First Heating**

| $M_W$ (kDa) | $T_g$ (°C) | $\Delta C_p$ (J/(g K)) | $T_m$ (°C) | $\Delta H_m$ (J/g) | $X_c$ (%) |
|---|---|---|---|---|---|
| 2 | 58 | 0.17 | 147 | 48 | 51 |
| 30 | 79 | 0.06 | 171 | 68 | 73 |
| 200 | 73 | 0.22 | 192 | 67 | 72 |

**(ii) Cooling**

| $M_W$ (kDa) | $T_c$ (°C) | $\Delta H_c$ (J/g) | $T_g$ (°C) | $\Delta C_p$ (J/(g K)) |
|---|---|---|---|---|
| 2 | — | — | 39 | 0.56 |
| 30 | 96 | 21 | 50 | 0.32 |
| 200 | — | — | 55 | 0.50 |

**(iii) Second Heating**

| $M_W$ (kDa) | $T_g$ (°C) | $\Delta C_p$ (J/(g K)) | $T_c$ (°C) | $\Delta H_c$ (J/g) | $T_m$ (°C) | $\Delta H_m$ (J/g) | $X_c$ (%) |
|---|---|---|---|---|---|---|---|
| 2 | 43 | 0.54 | 107 | 9 | 142 | 9 | 0 |
| 30 | 55 | 0.32 | 97 | 21 | 174 | 50 | 31 |
| 200 | 64 | 0.51 | 127 | 25 | 181 | 26 | 1 |

defects in PLLA (2 kDa) and by the low mobility of the long PLLA (200 kDa) chains.

During the second heating, all the polymers showed glass transition, crystallization, and melting events. $T_g$ and $T_m$ directly depend on molecular weight. The different $T_g$ values measured during cooling and the following heating cycles of the amorphous PLLAs, that is, 39 versus 43°C for the 2 kDa PLLA and 55 versus 64°C for the 200 kDa PLLA, are due to a kinetic effect that depends on the molecular weight of the polymer. The lower $T_c$ of PLLA (30 kDa) is attributable to its crystallinity before the second heating cycle that acted as a nucleating agent and promoted further crystallization, up to 53%, as determined from the $\Delta H_m$. In the case of PLLA (2 kDa) and PLLA (200 kDa), the lower $\Delta H_m$ and the developed crystallinity of about 10 and 28%, respectively, once again are the effect of short and long polymer chains.

As a function of molecular weight, however, thermal treatments can produce different results, as shown by Migliaresi et al. [32, 38]. As presented in Figure 8.3, the crystallinity of the polymers increases with annealing time and with decreasing viscometric molecular weight ($M_v$). The lower the molecular weight, the higher the rate of crystallization. This increase, as discussed later in the chapter, could be attributed to kinetic effects and thermal degradation of $M_v$ during annealing. Often, this effect is not considered in the literature.

Migliaresi et al. [32] showed that low-molecular-weight PLLA ($M_v$ = 18 kDa) was able to crystallize and regain almost 65, 79, and 87% of its initial crystallinity, during cooling after full melting at −5, −1, and −0.5°C/min, attaining crystallinity contents of 38.5, 46.8, and 51.3%, respectively. Higher $M_v$ PLLA (156 and 425 kDa) developed only a little crystallinity when cooled at −5°C/min. As mentioned, mobility, and hence crystallization ability, is determined at any given molecular weight by the temperature of the system. Their data confirmed that same thermal histories lead to materials with substantially different crystallinity amounts as a function of the PLLA molecular weight. More importantly perhaps, Migliaresi et al. [32] evidenced that all treatments resulted in molecular weight degradation, as shown in Table 8.2. This also means that, at a given initial molecular weight, thermal cycles at different heating or cooling rates could result in polymers having actually different viscometric molecular weight $M_v$.

The effect of molar mass on PLLA $T_g$ and $T_m$ and on PDLLA $T_g$ is clearly shown in Figure 8.4. $T_g$ values of both PLLA and PDLLA show similar trend with molar mass, with a glass transition increase up to about 20 kDa molar mass and reached a threshold value thereinafter. At each $M_n$, PLLA displays higher $T_g$, attributable to the hindering effect exerted on the amorphous chain mobility by the crystalline regions. Worth noting is the similar trend for melting, with $T_m$ ranging from about 130 to about 180°C as a function of $M_n$.

The effect of the L- or D-content on the $T_g$ of PLA has been discussed by Lim et al. [13] and Dorgan et al. [83]. The $T_m$ of PLA is also a function of its optical purity. While the calculated theoretical $T_m$ values for pure PLLA are reported to be 215, 211–212, and 206°C by different authors, the maximum practical obtainable $T_m$ for pure PLLA is around 190°C [28, 41, 42].

**TABLE 8.2 Effect of Cooling Rate on the Residual Molar Mass of Different Viscometric Molecular Weight PLLAs, Previously Heated at 10°C/min to 220°C**

| Initial $M_v$ (kDa) | After Cooling at −100°C/min | After Cooling at −20°C/min | After Cooling at −5°C/min |
|---|---|---|---|
| 18 | 15 (−17%) | 14 (−22%) | 11 (−39%) |
| 31 | 26 (−16%) | 26 (−16%) | 25 (−19%) |
| 156 | 113 (−28%) | 111 (−29%) | 75 (−52%) |
| 425 | 364 (−15%) | 357 (−16%) | 225 (−49%) |

*Note*: Reprinted from Ref. 32. Copyright 1991, with permission from Elsevier.

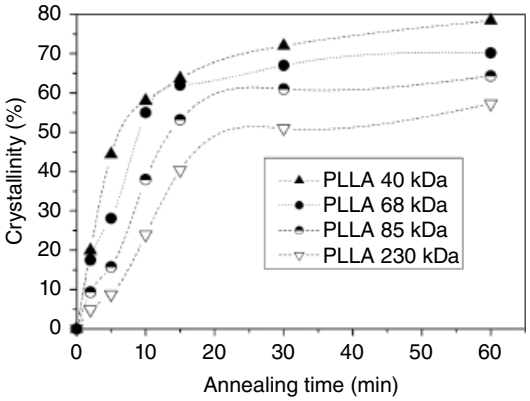


**FIGURE 8.3** Effect of annealing time on crystallinity of compression-molded PLLA at 160°C. *Source*: Adapted from Ref. 38.

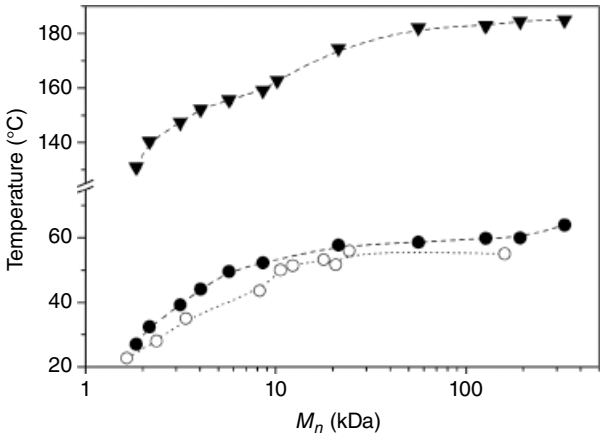


**FIGURE 8.4** $T_m$ of PLLA (▼) and $T_g$ of PLLA (•) and PDLLA (○) polymer as a function of molecular weight. *Source*: Adapted from Ref. 38 and authors' data.

The $T_g$ is better evidenced in dynamical mechanical thermal analysis (DMTA) as shown in Figures 8.5 and 8.6, where the storage modulus $E'$, loss modulus $E''$, and the damping or loss factor tan δ = $E''/E'$ are presented. In these plots, the temperatures corresponding to the tan δ or $E''$ peaks are taken as the $T_g$ values.

Both PDLLA (Figure 8.5) and PLLA (Figure 8.6) polymers exhibit a storage modulus in the glassy region of about 2 GPa with a slight difference due to the crystalline content of PLLA ($X$ = 55%). Crystallinity is, however, responsible for the much lower decrease of $E'$ and $E''$ of PLLA above $T_g$ while a progressive increase of damping occurs for PDLLA in the temperature range 100–120°C. Again, crystallinity accounts for the higher temperatures and width of the $E''$ peak of PLLA due to the constraints exerted by the PLLA crystalline domains on the amorphous region mobility. Crystallinity, however, can have an important effect on PLLA mechanical properties and can be affected by the molecular weight. As shown by Perego et al. [45], crystallinity of PLLA of different viscometric molecular weights and annealed at 105°C for 90 min increased from 3 to 13% to 42–65%, depending on the molecular weight. Although mechanical properties of low crystalline polymers, such as tensile strength or impact resistance, almost did not depend on $M_v$, crystallization induced significant differences in improving these properties markedly for higher $M_v$ polymers.

A secondary transition (beta-transition) attributed to the mobility of methyl group has been determined at −79°C for high crystallized PLLA polymerized by different catalysts [84].

Following the approach of Diez-Gutierrez et al. [85] that studied the effect of filler on the mechanical properties of talc/polypropylene composites, Fambri et al. [86] analyzed the effect of crystallinity on the storage modulus $E'$ of PLLA through a glass transition intensity factor defined as:

$$S = \left(E_g' - E_r'\right) / E_r' \tag{8.4}$$

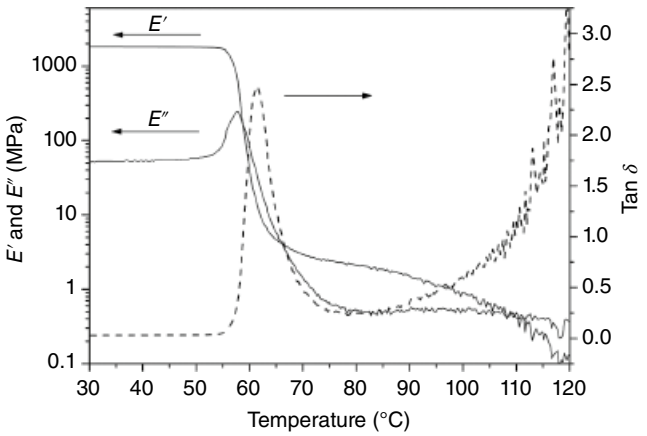


**FIGURE 8.5** Storage modulus E′, loss modulus E″, and damping tan δ of PDLLA. Heating rate 2°C/min and frequency 1 Hz.

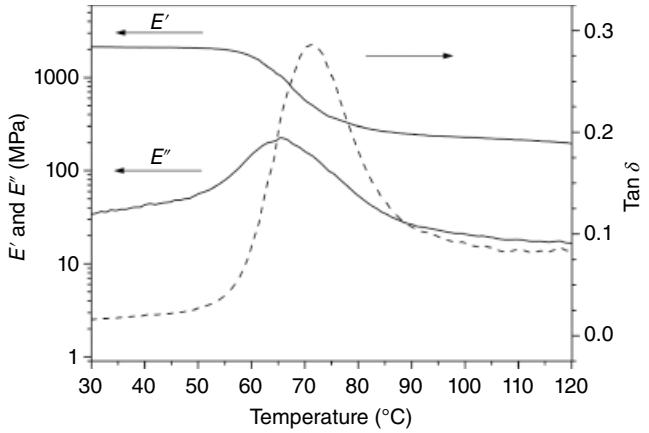


**FIGURE 8.6** Storage modulus E′, loss modulus E″, and damping tan δ of PLLA with a crystallinity of 55%. Heating rate 2°C/min and frequency 1 Hz.

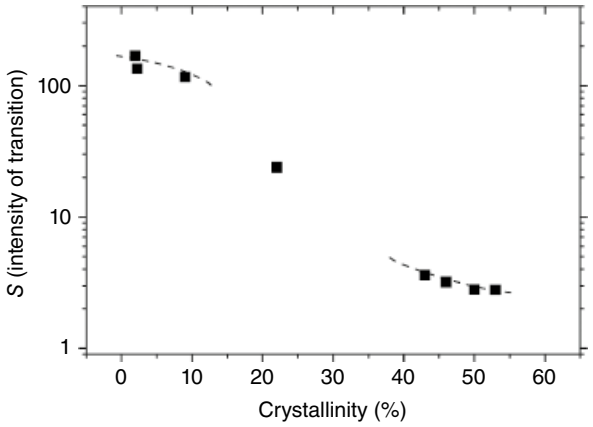


**FIGURE 8.7** Effect of crystallinity on the intensity of the transition S of compression molded samples. *Source*: Data from Ref. 38.

where $E_g'$ and $E_r'$ are the $E'$ values in the glassy and rubbery states taken at about 30°C below and above the $T_g$, that is, 30 and 90°C, respectively. Values of $S_{PDLLA}$ = 1173 and $S_{PLLA}$ = 7.5 can be calculated from data in Figures 8.5 and 8.6. A higher $S$ value indicates a superior mobility and/or a higher content of the amorphous phase. With increasing crystallinity, the intensity factor $S$ decreases, with an almost proportional dependence on crystallinity (Figure 8.7) for compression molded materials (data from Ref. 38).

Since the glass transition is a kinetic transition, the measured value depends on both heating rate and frequency. This is clearly evidenced by comparing DMTA curves of Figure 8.6 (at 2°C/min and 1 Hz) and the multifrequency DMTA analysis of Figure 8.8 (at 0.5°C/min and 3, 10, and 30 Hz). At increasing deformation frequencies, the storage moduli of the glassy and rubbery plateaus increase and the apparent $T_g$ is shifted to higher temperatures.

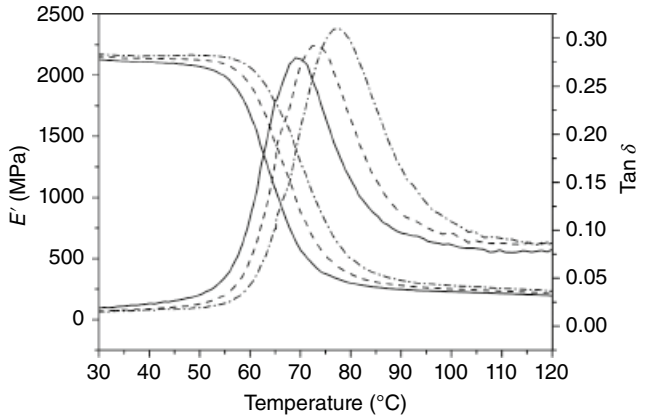


**FIGURE 8.8** Storage modulus $E'$ and damping factor tan $\delta$ of PLLA samples at various frequencies: 3 Hz (continuous line), 10 Hz (dashed line), and 30 Hz (dash-dotted line). Heating rate 0.5°C/min (from authors' data).

The apparent activation energy for the relaxation process can be calculated from the following equation:

$$\ln f = \ln f_0 - \left(E_a / RT\right) \tag{8.5}$$

where $f$ is the frequency in Hz, $T$ is the temperature of the maximum of the loss factor, $R$ is the ideal gas constant, and $E_a$ is the activation energy for the relaxation process. According to Equation 8.5, apparent $E_a$ of 553 and 620 kJ/mol were calculated for low- and high-molecular-weight PLLA, respectively [86].

In dynamic mechanical tests, the reduced chain mobility due to the crystalline domains is detected by a shift of the damping peak to higher temperatures, that is, the increase of $T_g$, as already stated in DSC analyses. In addition, as shown in Figure 8.9, the DMTA shows an increase of the elastic component of the viscoelastic behavior of the polymer as a significant reduction of the damping peak (data from Ref. 38). At the same time, the width of the tan $\delta$ peak increases as an effect of the larger distribution of amorphous chain mobility induced by the formation of a less-mobile distributed interphase [87, 88].

In practical injection molding conditions, there is little crystallization due to the high cooling rate. For this reason, methods to induce crystallization have been studied by using nucleating agents or plasticizers during polymer processing. By using 1% talc, the crystallization half time can be reduced to less than 1 min [89]. Other nucleating agents, such as montmorillonite, are less effective than talc [90]. Some organic compounds have also been studied, such as calcium lactate, *N*,*N*-ethylenebis(12-hydroxystearamide), benzoylhydrazide compounds, or sodium stearate [91–94]. The addition of 1% calcium lactate induced crystallization of a 90:10 L/D,L-PLA copolymer during the injection molding cycle [91].

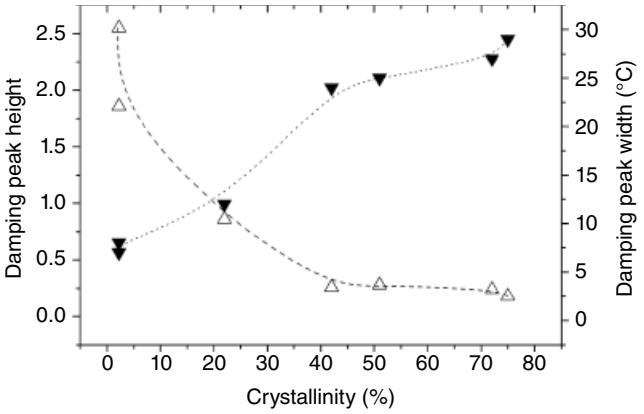


**FIGURE 8.9** Height (△) and width (▼) of damping peak of PLLA as a function of crystallinity. *Source*: Data from Ref. 38.

Kawamoto et al. [93] found that in the presence of a series of hydrazide compounds having different methylene chain numbers, the $T_c$, and $\Delta H_c$ of PLLA during cooling increased with the methylene chain number. In this study, decamethylene dicarboxylic dibenzoylhydrazide was the most effective in promoting crystal nucleation by increasing the PLA $T_c$ and $\Delta H_c$ to 131°C and 46 J/g, respectively. The addition of a plasticizer decreases the $T_g$. Common plasticizers used for PLA are poly(ethylene glycol) (PEG), triacetine, and citrate, laurate, and sebacate esters [31, 95–100]. The primary effect is the improvement of the polymer ductility and drawability, but also an increase in crystallization rate, as shown by Kulinski and Piorkowska [98] when PEG was added to PLLA.

## 8.3 CRYSTALLIZATION REGIME

Properties of PLA depend on purity and, for the racemic form, on the crystallinity. Crystal morphology and amount depend on the preparation (from melt or solution) and crystallization conditions (temperature and time) [101]. Moreover, crystallinity and crystalline structure affect mechanical properties of semicrystalline polymers, as well as the amount of the mobile amorphous fraction (MAF) and the rigid amorphous fraction (RAF) with properties that differ from those of the bulk. RAF is located at the interface with the crystalline domains and acts as the interphase in composites. Compositions of properly treated PLLA, the correspondent MAF/RAF content, their mechanical and other properties were investigated by Sarasua and coworkers [102, 103]. Mechanical properties of semicrystalline polymers have been modeled by using the approaches used for composite materials, with the crystals acting as the reinforcing phase in the amorphous matrix. For PLLA, the elastic moduli $E$ of crystalline, mobile amorphous and rigid amorphous fractions have been estimated [82] by using a modified Takayanagi mechanical model with $E_{MAF}$ being evaluated equal to 3.6 GPa

and $E_{MAF} < E_{RAF} < E_C$. In particular in Ref. 82, the tensile moduli for the δ(α')- and α-phases (11.2 and 14.8 GPa, respectively) were quantified, in agreement with other literature data, and the elastic moduli for the RAF linked to δ(α')-form and α-phase (5.4 and 6.1 GPa, respectively), the difference being due to the stronger constraints imposed by the more ordered α-crystals.

One of the first papers discussing the morphology and crystal growth of PLLA as a function of thermal treatment and molecular weight was published by Vasanthakumari and Pennings [36]. Following Hoffman and coworkers [104, 105], the growth rate ($G$) of a linear polymer crystal with chain folding can be expressed by

$$G = G_0 \exp\left[\frac{-u^*}{R\left(T_c - T_\infty\right)}\right] \exp\left[\frac{-K_g}{T_c \Delta T f}\right] \tag{8.6}$$

where $K_g$ is the nucleation constant, $u^*$ is the activation energy of chain mobility in the crystallization site, $\Delta T = \left(T_m^0 - T_c\right)$ is the difference between the equilibrium $T_m$ and the crystallization temperature, $f$ is a factor equal to $2T_c/\left(T_m^0 + T_c\right)$, $R$ is the gas constant, $T_\infty$ is the temperature at which all the motion associated with viscous flow ceases, and $G_0$ is the front factor. Equation 8.6 can be used to predict the crystallization rate of a number of polymers over a wide range of temperature.

As reported in Figure 8.10, the spherulite radius growth rate as a function of $T_c$ reached a maximum for all investigated molecular weights at temperatures ranging around 130°C and depending on the specific polymer molecular weight [36]. In particular, the higher the PLLA molecular weight, the lower the $G$, as generally observed for many polymers. Different cooling rates also induced variation in the crystal morphology, with the formation of regular geometry and defined spherulites at high $\Delta T$ and spherulites with irregular shape and a coarse-grained structure at lower $\Delta T$.

In the reported experiments [36], for all investigated molecular weights the spherulitic growth rate, $G$, reached a maximum at around 400 K. Slight different results have been later reported [43, 106] that indicated some dependence of the maximum spherulitic growth rate on the PLLA molecular weight and an unusual behavior for some intermediate molecular weight PLLAs with two maxima for $G$ related to different regimes of crystallization [46].

According to the Hoffman theory, polymers such as polyethylene present two different crystallization regimes characterized by the ratio of the corresponding nucleation constants $K_{gI}/K_{gII}$ = 2 [104, 105]. The presence of two crystallization regimes in PLLA was first confirmed by Vasanthakumari and Pennings [36] at 163°C for the highest of the PLLA molecular weights investigated, that is, for a polymer with viscometric molecular weight $M_v$ = 150 kDa, while lower molecular weight polymers presented only a regime II crystallization type.

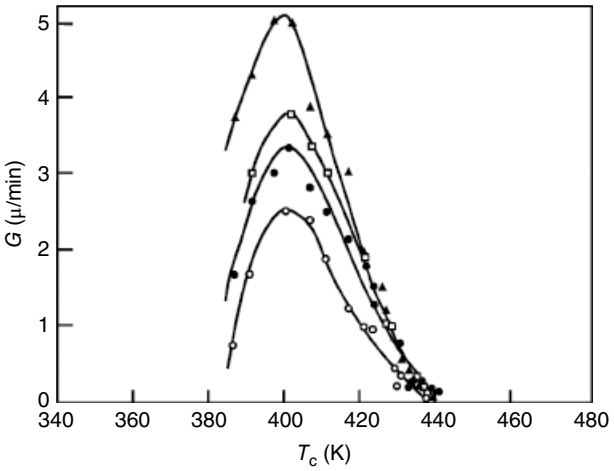


**FIGURE 8.10** Radius growth rate $G$ as function of crystallization temperature $T_c$ for different viscometric molecular weight samples of PLLA, that is, $M_v$ = 150 kDa (▲), 260 kDa (□), 350 kDa (•), and 690 kDa (○). *Source*: Reprinted from Ref. 36. Copyright 1983, with permission from Elsevier.

Tsuji and Ikada [41] studied the effect of different thermal treatments and annealing histories on solution cast PLLA films, which resulted in materials with different morphologies and physical properties. In particular, annealing was performed on films with three treatments: (a) as cast; (b) cast and molten; and (c) cast, molten, and quenched. Differences in crystallization were mainly attributed to the presence of preexisting spherulite nuclei before annealing, with the cast and molten film having the highest developed total crystallinity at any annealing temperature, resulting in the highest mechanical strength. An increase in crystallinity was observed in the annealing temperature range 100–160°C.

Mazzullo et al. [40] also found a regime III governed crystallization starting at 140°C, with $K_{gIII}/K_{gII}$ = 3.13. Several authors have then confirmed the presence of three distinct crystallization regimes, starting at different temperatures and with different constants [42, 46–48].

The crystallization mode of PLLA has also been analyzed by using the Avrami equation [107, 108]:

$$X_c = 1 - \exp\left(-kt^n\right) \tag{8.7}$$

By measuring the fraction of crystallized material, $X_c$, with time $t$, an $n$ value of 4 was evaluated by Miyata and Masuko [43], who observed in nonisothermal crystallization experiments from the melt, a remarkable increase in the polymer crystallization at low cooling rates and a maximum value of the isothermal crystallization rate at 105°C. A similar trend was observed by Iannace and Nicolais [42]. However, these results could be affected by the polymer thermal degradation induced at low cooling rates, as previously described by Migliaresi et al. [32].

Recently Fambri et al. [109] showed that the addition of 8%vol of fumed silica did not significantly affect the crystallization kinetics of commercial PLA, as determined by the comparison of *k* and *n* Avrami coefficients in the temperature range of 80–125°C. Other authors also reported slight or negligible increase of crystallinity depending on the hydrophilic or hydrophobic nature of the fillers [110, 111].

## 8.4 FIBERS

One of the first studies about the fabrication of PLA fibers were made by Kulkarni et al. [14, 15] and Kalb and Pennings [27]. PLA fibers can be produced by melt and solution spinning [28, 57, 112–120]. The two methods generate fibers with different mechanical properties and degradation rate, which can be explained in terms of the different developed crystal morphologies [56, 112, 115]. In both cases, the high shear rate induces orientation and chain alignment that in turn induces crystallization. Wide-angle X-ray scattering revealed the presence of two distinct crystal modifications in solution-spun fibers and in particular the origin of a so-called β-structure in hot drawn fibers. The β-structure seems to correspond with fibrillar morphology and bears most of the load applied to the fibers. It has been found that the redrawing of highly oriented PLLA film induces the transformation of the α-form crystallites into the β-form [57]. PLLA solution-spun fibers have better mechanical properties and also higher hydrolytic degradation stability [114].

Crystallinity developed in melt- and solution-spun fibers is reported in Figure 8.11 as a function of the applied draw ratio. In both cases, for draw ratios higher than 8–10, a maximum value of crystallinity equal to about 65 and 44% was reached for melt- and solution-spun fibers, respectively [115, 116]. Similar results were also found in the case of films where, after drawing, crystallinity significantly increased up to about 55% [117].

Melt spinning imparts intense thermal and mechanical stress on PLLA, resulting in a large reduction in molar mass that can reach 30–70% [30, 115]. Hence, when considering the crystallizability of polymer fibers, the effects of molecular weight and the thermal and mechanical drawing should be considered. Melt spinning of low-molecular-weight polymers, between 30 and 150 kDa, results in high crystallizability, especially during drawing. In a double-step process of fiber spinning followed by fiber drawing, crystallization from the melt should be properly controlled in order to preserve the ability for further orientation and crystallization. It was reported that depending on the fiber collecting rate, the crystallinity of as-spun fiber initially increased up to about 35%, and then decreased as the fiber collecting rate increased, due to the faster cooling rate of the higher surface area of the lower diameter fibers. Figure 8.12 shows the thermograms of PLLA melt-spun fibers collected at 1.8, 5, 10, and 20 m/min.

The different amorphous phase content is initially evidenced by the various $\Delta C_p$ at the $T_g$, 0.36, 0.19, 0.14, and 0.30 J/(g K). Moreover, it should be noted that the cold crystallization of these melt-spun fibers occurred during heating in the range of about 80–120°C, significantly lower than that of completely amorphous PLLA shown in Figure 8.1, with direct dependence on the preexistent nucleating crystalline domains and the oriented polymer structure. As already observed, at higher temperatures, a small exothermal peak of secondary crystallization at about 160°C precedes the melting. As shown in Figure 8.12, the DSC curves revealed two melting peaks, with the higher temperature one appearing as a shoulder in the highest rate collected fibers. The melting at about 188°C was due to crystallinity developed during the melt spinning process, whereas the peak at 180°C corresponded to the melting of crystals

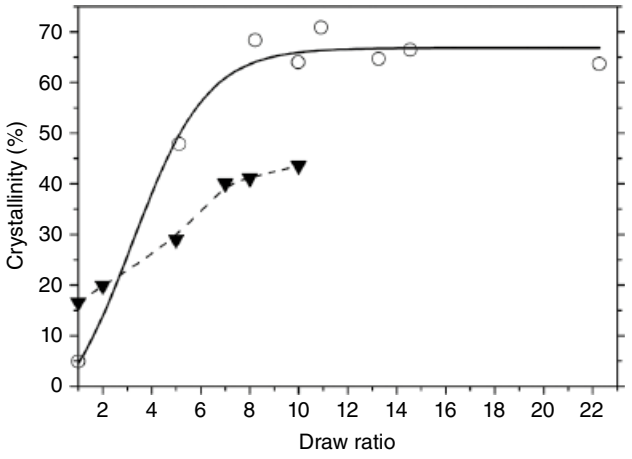


**FIGURE 8.11** Crystallinity of melt-spun PLLA fiber drawn at 160°C (○) and crystallinity of solution-spun PLLA fiber drawn at 190°C (▼) as a function of draw ratio.

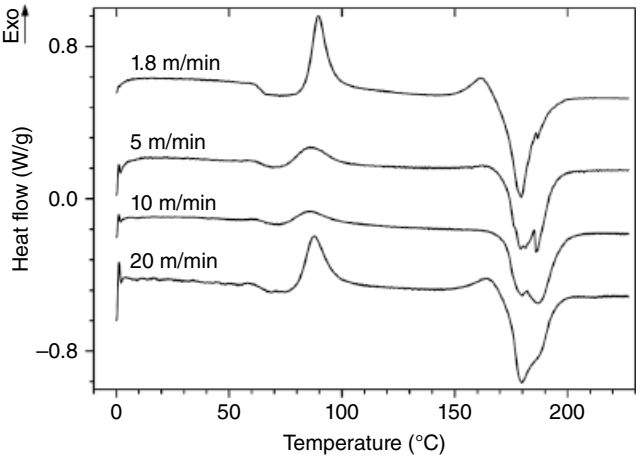


**FIGURE 8.12** DSC curves of melt-spun PLLA fibers collected at different rates, as indicated. *Source*: Reprinted from Ref. 115. Copyright 1997, with permission from Elsevier.

generated during the DSC analysis. The percentage crystallinity of the fiber can be evaluated as 5, 30, 37, and 10% for spinning process of 1.8, 5, 10, and 20 m/min, respectively. The drawing temperature is selected above the $T_g$ in order to modify the amorphous phase in the rubbery state; the initial crystallinity, the nucleation and growth rate according to the crystallization regimes I–III, the polymer chain mobility, and the polymer molecular weight are important factors for optimization of fiber orientation and crystallization. Typically, PLLA melt-spun fibers after drawing at 160°C reach a crystallinity of about 50–70% [29, 118]. Multiple melting peaks in as-spun fibers collected at high rate (range 1–6 km/min) were also described by Takasaki et al. and different phases, i.e., δ(α') and α, were obtained in dependence on the process. A partial melting peak of δ(α') crystals around 148.5°C and melting of α crystals above 169°C were reported [121].

In the case of solution spinning, the crystallinity of undrawn as-spun fiber was typically 30–40%, higher than that of melt-spun fibers (compare data of Figures 8.12 and 8.13), due to the lower spinning and cooling rate, and in general as a consequence of the more favorable conditions of solution crystallization. Solvent, in fact, acts as a plasticizer, resulting in a higher chain rearrangement capability.

On the other hand, high molecular weight (between 300 and 900 kDa) inhibits the development of high crystallinity due to the lower polymer chain mobility [116, 118, 119]. Figure 8.13 shows the first and second DSC scans of as-spun PLLA fibers produced from dry spinning. Low $T_g$ due to the residual solvent that acts as a plasticizer, and low $T_c$ and $T_m$ were observed in the first scan. In the second DSC scan after a mass loss of about 15% attributable to solvent removal, a $T_g$ of 65°C and crystallization and melting peaks at 140 and 180°C, respectively, with a crystallinity of about 25%, were observed.

These solution as-spun fibers can be drawn at a higher drawing temperature, above the expected $T_m$ (this is possible due to the high polymer molar mass and initial crystallinity). The DSC analysis revealed, after drawing at temperatures between 160 and 210°C, the formation of a double crystalline structure, with two melting peaks at about 160–170 and 190–200°C, as summarized in Table 8.3 and shown in thermograms of Figure 8.14.

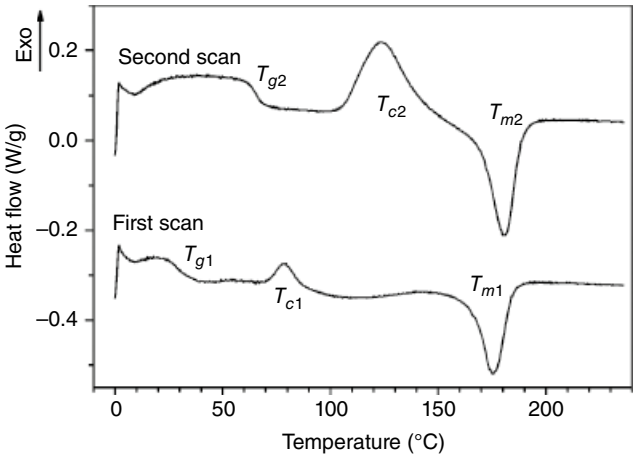


**FIGURE 8.13** First and second DSC scans of as-spun PLLA fibers produced by solution spinning (5% chloroform solution).

The higher the drawing temperature, the higher the total crystallinity and the enthalpy of the first melting peak at about 160–170°C, thus suggesting the formation of the β-phase, as previously indicated by Pennings and coworkers, in coexistence with the α-phase [52, 56, 113, 120]. At the same time, the $T_g$ was found to increase with the drawing temperature, reaching about 100°C, as a consequence of the high orientation of the crystallized fibers. Moreover, the progressive and remarkable reduction of $\Delta C_p$ from 0.1 to about 0.05 J/(g K) indicates both high packing and low mobility of the amorphous phase above $T_g$, once again due to the high orientation of the high-molecular-weight drawn PLLA fibers.

Stereocomplex crystals (SC) developed in fibers of PLLA and PDLA produced at high-speed spinning (up to10 km/min) have been deeply investigated. Multiple melting peaks were evidenced in fibers, and compared with WAXS spectra, in particular double peak at 170–180°C attributed to PLLA (and PDLA), and single melting peak of SC at 225°C [121–123]. More details are described and discussed in Chapter 18.

Copolymerization of L-lactide with other analogous cyclic lactones, such as D,L-lactide, D-lactide, glycolide, or ε-caprolactone, produces polymers with relatively

**TABLE 8.3 Glass Transition Temperature ($T_g$) and Change of Specific Heat at $T_g$ ($\Delta C_p$), Melting Peak Temperature ($T_m$) and Enthalpy ($\Delta H_m$), and Crystallinity ($X_c$) (from Equation 8.1) of Solution-Spun Fibers After Drawing at Various Temperatures**

| Drawing Temperature (°C) | | | First Melting Peak | | Second Melting Peak | | |
|---|---|---|---|---|---|---|---|
| | $T_g$ (°C) | $\Delta C_p$ (J/(g K)) | $T_m$ (°C) | $\Delta H_m$ (J/g) | $T_m$ (°C) | $\Delta H_m$ (J/g) | $X_c$ (%) |
| 160 | 83 | 0.13 | — | — | 190 | 29 | 31 |
| 170 | 81 | 0.12 | — | — | 189 | 29 | 32 |
| 180 | 87 | 0.11 | 155 | 5 | 199 | 27 | 34 |
| 190 | 98 | 0.09 | 169 | 16 | 203 | 17 | 35 |
| 200 | 92 | 0.09 | 167 | 17 | 201 | 21 | 41 |
| 210 | 97 | 0.04 | 172 | 26 | 195 | 18 | 47 |

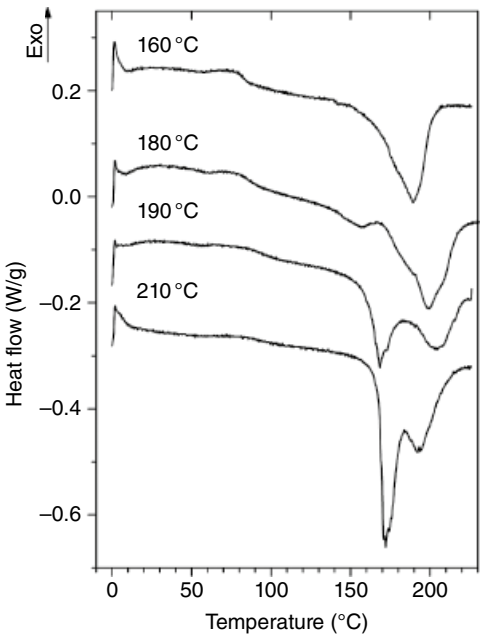


**FIGURE 8.14** DSC thermograms of solution-spun fibers after drawing at various temperatures (glass transition temperature and various melting peaks are evident) [116].

random distribution of comonomers. The $T_g$ of PLA copolymers decreases proportionally with the increasing glycolide or ε-caprolactone comonomer content, to some extent. Moreover, the presence of stereochemical defects in PLLA reduces $T_m$, rate of crystallization, and extent of crystallization of the resulting polymer. Gilding and Reed reported in 1979 that a sharp reduction of melting point to 120°C with the addition of 20% glycolide, with no crystallization occurring if glycolide content reached 25% [27]. Figure 8.15a and b summarizes some of their results. Similarly, the L/D,L-lactide copolymers present an almost linear $T_m$ depression, from 178°C for pure PLLA to 115°C for the 70/30 copolymer, and a $T_g$ decrease from 63 to about 55°C, as shown in Figure 8.16.

## 8.5 COMMERCIAL POLYMERS AND PRODUCTS

Several consumer applications have been progressively developed over the last few decades, and various commercial types of PLA are available in the market as a successful thermoplastic commodity for films [124], fibers [125], packaging containers, foamed products [126], cutlery, cups, bottles, and so on, produced with different processing technologies.

Commercial polymers are based on PLA composition with D,L copolymer content typically in the range of 0.5–15%. The role of D-comonomer is to modulate the enantiomeric purity and consequently to reduce both $T_m$ and the crystallinity content to favor a higher transparency for packaging applications. On the other hand, for textile applications and for some injection molding items, a certain level of regularity in polymer chains is required, and PLA polymers with $T_m$ in the range of about 170–180°C are typically used. Table 8.4 shows the results of DSC of selected PLA pellets, PLA products, and PLA composites. The corresponding thermograms are presented in Figure 8.17a–c, respectively. No crystallization of PLA pellets was observed in DSC at controlled cooling rate (−10°C/min).

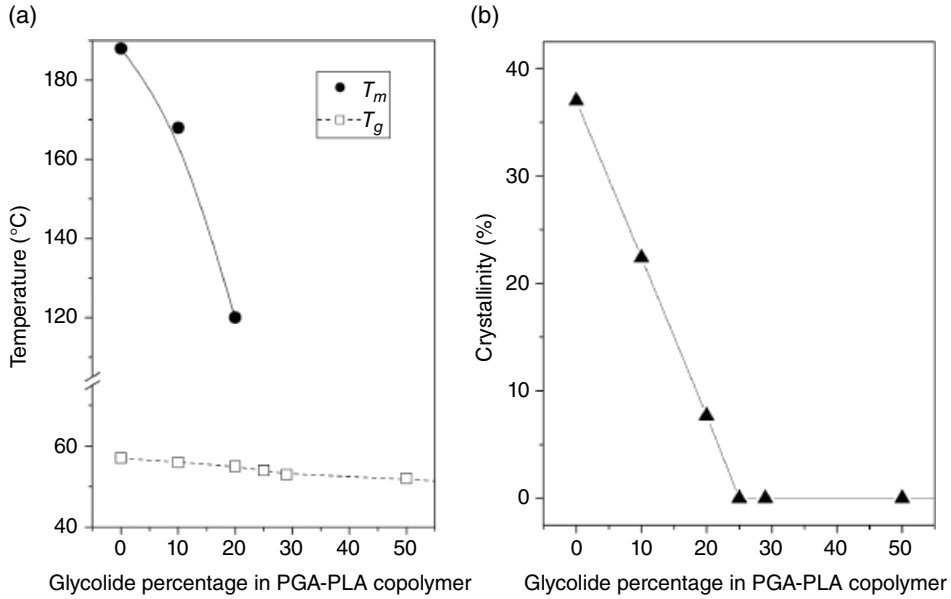


**FIGURE 8.15** Effect of composition on $T_g$, $T_m$ (a), and crystallinity (b) of L-lactide-*co*-glycolide copolymers as a function of glycolide content (adapted from literature). *Source*: Reprinted from Ref. 27. Copyright 1979, with permission from Elsevier.

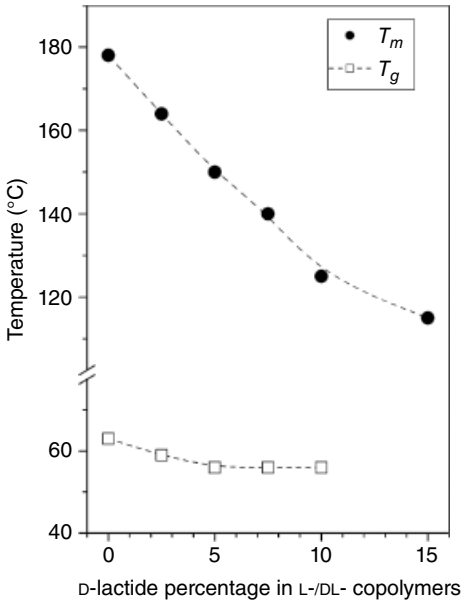


**FIGURE 8.16** $T_g$ and $T_m$ of poly-L-D,L-lactide as a function of D,L-lactide content. *Source*: Adapted from Ref. 37 and authors data.

It is worth noting that different levels of crystalline content of the pellets would require different drying treatment before processing. In particular almost amorphous polymers have to be dried below the $T_g$ (for instance 8 h at 40°C) in order to avoid adhesion in the rubbery state. On the other hand, typical drying conditions for crystallized pellets are 2 h at 90°C. Further discussion about drying PLA is provided in Chapter 13.

In terms of PLA filaments for additive manufacturing, in particular for fuse filament fabrication, specific compositions for PLA filaments for 3D printing have been formulated. A low crystallizability of PLA materials is required to improve the adhesion between the layers with typical processing conditions (nozzle temperature 180–220°C, bed temperature 40°C, deposition rate 40 mm/s). Both the characterized filaments (Figure 8.17b and Table 8.4) exhibited low crystallinity (1%), low crystallizability (up to 8%), and low melting peak (about 150°C), as result of a specifically selected copolymerization for maintaining a high content of amorphous phase.

PLA cups are usually produced from sheet casting and then thermoforming by selecting copolymers with $T_m$ of about 150°C, and low crystallizability (about 30%). Thermal data evidenced they are almost amorphous, resulting a relatively low crystallization enthalpy (6–19 J/g) at about 120°C and a low melting enthalpy (22–28 J/g). These thermal properties affect the maximum use temperature of PLA cups, that should not exceed 50°C (cups not suitable for hot liquids).

To overcome this limitation, blends of PLA with other polymers have been investigated thermally resistant up to 120°C [127], and PLLAs with improved mechanical properties and heat resistance have been developed with a procedure of cold crystallization from melt-stretched PLLA, to induce the formation of nanocrystals instead than large spherulites [128].

On the other hand, injection molded items (for instance, spoons for ice cream and sticks for fruit) are produced with PLA at high $T_m$ (170°C) and high crystallizability (40–48%). The two products, however, remained almost amorphous due to high rate in cooling after injection molding; and in DSC cooling at −10°C/min (thermograms not shown), no crystallization was observed, neither for PLA cups, nor for injection molded items.

The exothermal peak between 159–169°C was visible in Figure 8.17 for some thermograms of PLA material with the higher purity, and a certain content of crystallinity, as in the case of pellets of Ingeo® 2500 ($T_m$ 180°C and 45% crystallinity), PLA stick ($T_m$ 174°C) and PLA-GF30% ($T_m$ 176°C).

Moreover, PLA composites [129] and nanocomposites [130] have been also developed in order to improve thermal properties, mechanical behavior, barrier properties, electrical conductivity, and other specific properties. For instance, inorganic micro- and nanofillers, or natural fibers [131], micro- and nanocellulose [132] have been proposed for the preparation of PLA composites. Micrometric fillers such as talc [133], hydroxy apatite [88, 134–136] calcium carbonate [137, 138], and calcium sulfate [139–141], or nanoparticles as fumed silica [142] at concentrations between 5 and 40 wt% were added to various PLAs. In various cases, the fillers promoted crystallization, behaving as an heterogeneous nucleating agent. For instance, the nucleation role of talc in PLA composites was evidenced by a double melting peak attributable to different types of crystal domains [143]. Moreover, glass fiber can promote crystallization (Table 8.4). During the cooling step at −10°C/min, the crystallization peak of PLA-GF30 has been observed in the range 130–100°C (enthalpy 19.6 J/g) at higher temperature as compared with the unfilled PLA, showing the positive effect of nucleation on the glass surface.

In the case of PLA fibers containing 2% of fumed silica (FS), it is worth noting that the composite has a higher crystallinity content, due to the drawing process, but also an increase in $T_g$. In the second heating scan after cooling at −10°C/min (not reported for the sake of brevity), the $T_g$ at 61°C, crystallization peak at 108°C (30 J/g), and melting peak at 168°C (33 J/g) were detected. No significant variation of crystallinity was observed in the case of modified nanocellulose (LNC) and micro-crystalline-cellulose (MCC) composites with respect to the PLA matrix [144].

**TABLE 8.4 Thermal Data of Selected PLA Commercial Polymers (Pellets), Selected Common Products and Different Composites. Glass Transition Temperature ($T_g$), Crystallization and Melting Peak Temperatures ($T_c - T_m$), Enthalpy of Crystallization ($\Delta H_c$) and Melting ($\Delta H_m$), and Crystallinity Content ($X_c$) from Equation 8.1, Following DSC Analysis in the Range 0–200°C at ±10°C/min**

| Polymer | $T_g$ (°C) | Producer | $T_c$ (°C) | $T_m$ (°C) | $\Delta H_c$ (J/g) | $\Delta H_m$ (J/g) | $X_c$ (%) |
|---|---|---|---|---|---|---|---|
| PLE-005 pellet A | 59 | NaturePlast (F) | // | 138 | 0 | 3 | 3 |
| PLE-005 pellet C | 64 | NaturePlast (F) | // | 139 | 0 | 20 | 22 |
| 4032D pellet | 63 | NatureWorks LLC (US) | 104 | 172 | 30 | 33 | 3 |
| 2500 pellet | 69 | NatureWorks LLC (US) | 168 | 183 | 2 | 44 | 45 |
| **Product** | **$T_g$ (°C)** | **Processing** | **$T_c$ (°C)** | **$T_m$ (°C)** | **$\Delta H_c$ (J/g)** | **$\Delta H_m$ (J/g** | **$X_c$ (%)** |
| 3D filament-1 | 66 | Commercial (ϕ1.7 mm) extrusion | 128 | 150 | 1.1 | 1.8 | 1 |
| 3D filament-2 | 62 | Commercial (ϕ1.7 mm) extrusion | 129 | 151 | 7 | 8 | 1 |
| Cup-1 | 63 | Commercial 125 mL thermoforming | 121 | 150 | 6 | 22 | 17 |
| Cup-2 | 60 | Commercial 125 mL thermoforming | 117 | 150 | 19 | 28 | 9 |
| Ice-cream spoon | 60 | Injection molding | 99 | 171 | 38 | 40 | 2 |
| Stick | 60 | Injection molding | 93/158 | 174 | 42/3 | 48 | 5 |
| **PLA Composite** | **$T_g$ (°C)** | **Composition (processing)** | **$T_c$ (°C)** | **$T_m$ (°C)** | **$\Delta H_c$ (J/g)** | **$\Delta H_m$ (J/g)** | **$X_c$ (%)** |
| PLA-FS2 | 89 | Fumed silica 2% (fiber spinning and drawing) | // | 171 | 0 | 49 | 53 |
| PLA-LNC5* | 58 | Lauril nano cellulose 5% (film casting) | 135 | 166 | 10 | 12 | 2 |
| PLA-MCC10 | 59 | Micro crystalline cellulose 10% (filament extrusion) | 108 | 170 | 32 | 35 | 3 |
| PLA-T10 | 58 | Talc 10% (compression molding) | // | 160 | 0 | 35 | 42 |
| PLA-GF30 | 62 | Glass fiber 30% (compression molding) | 159 | 176 | 2 | 21 | 29 |

* From Ref. 144

## 8.6 DEGRADATION AND CRYSTALLINITY

The degradation kinetics of PLLA is largely affected by its crystallinity. As is known, degradation of PLA proceeds via hydrolysis, which is in turn controlled by the water diffusion in the free volume amorphous phase. In addition to crystallinity, other factors such as molecular weight, surface/volume ratio, purity, and chain orientation can greatly affect degradation kinetics [7].

Migliaresi et al. [145] compared the hydrolytic degradation of different molecular weight and crystallinity PLLAs, obtained by quenching or annealing treatments. As shown in Figure 8.18 for two different molecular weight PLLA polymers, as the degradation proceeds, crystallinity increases, reaching an almost equal value for the two polymers despite their largely different initial crystallinity levels (46% for 153 kDa and 6% for 103 kDa). This behavior was not attributable to the loss of amorphous degraded materials, because no appreciable mass loss was detected during the experiment.

A concomitant phenomenon associated with the molar mass reduction was the plasticizing effect of the water molecules diffusing into the amorphous regions, which provoked an increase in the chain segmental motions. Ultimately, the crystallinity increased when chain length became short enough to enable spatial rearrangement of the original amorphous regions into crystalline domains.

This was also found by Li et al. [146] who investigated the effect of morphology on the hydrolitic degradation of 130,000 $M_w$ poly(L-lactic acid) specimen processed by compression molding and quenched as amorphous or annealed as semicrystalline. In addition a surface-center differentiation of degradation was observed with the interior of the specimen degrading faster than the outer zone, due to the entrapment of degrading macromolecules. The occurrence of the phenomenon depends on the sample thickness.

The degradation-induced crystallization was also found by Tsuji et al. [147] who investigated the effects of crystallinity on the hydrolysis up to 36 months of high-molecular-weight

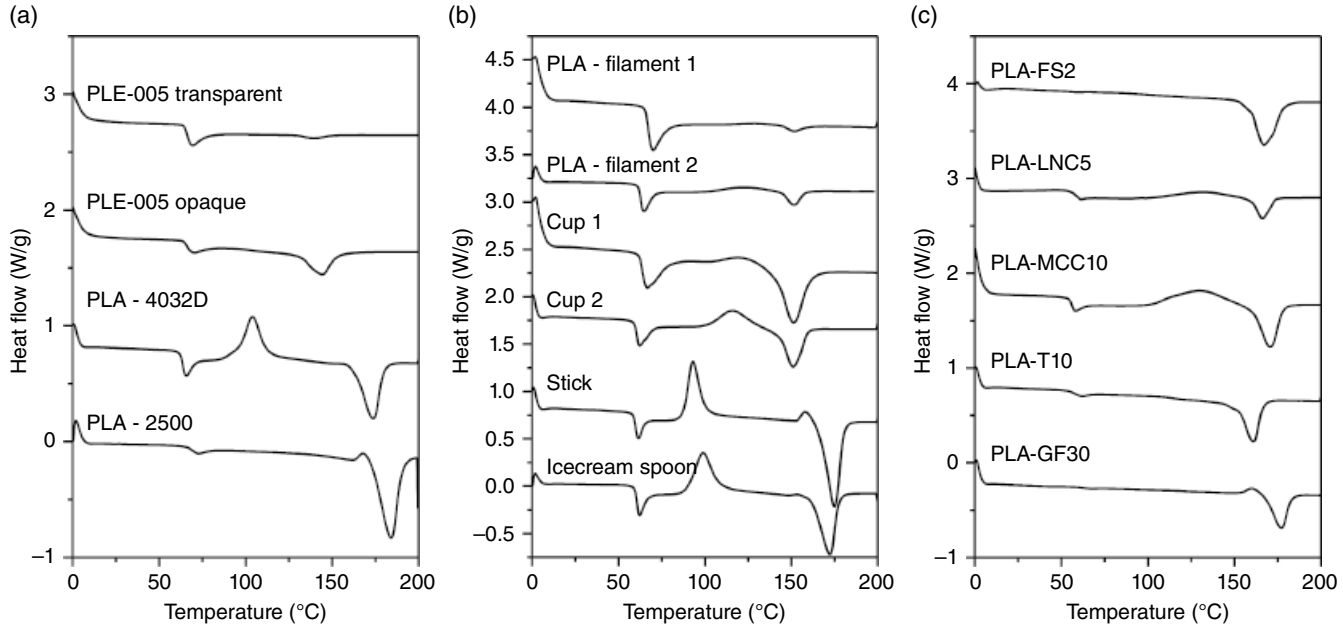


**FIGURE 8.17** DSC thermograms of selected commercial pellets (a), PLA products (b), and example of PLA composites (c).

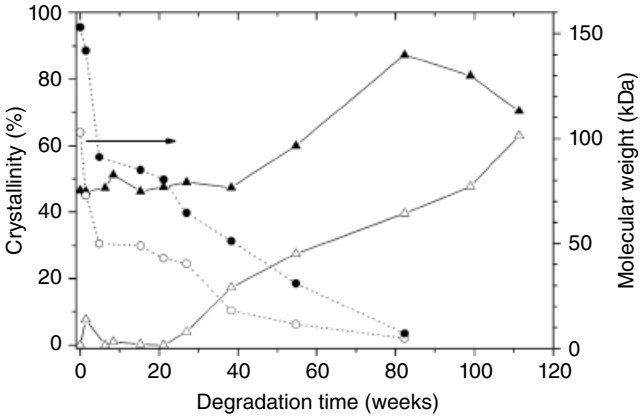


**FIGURE 8.18** Crystallinity percentage (△, ▲) and molecular weight (○, ●) as a function of degradation time in Ringer solution at 37°C for PLLA samples of initial low (open symbols) and high (filled symbols) crystallinity, respectively. *Source*: Adapted from Ref. 145.

PLLA films in a phosphate-buffered solution at 37°C. Worth noting and due to the degradation-induced crystallization are the increase of the induction period before mass starts to decrease with the decrease in the initial crystallinity of the PLLA films, and higher reduction of molecular weight as the initial crystallinity of the PLLA films increased when hydrolysis was carried out up to 24 months.

Chapter 21 deals in detail with the hydrolytic degradation and crystallinity.

The degradation-induced crystallization has a very important drawback for the biomedical use of PLLA as an implant material, which can last in the implant site for a very long time [145, 148]. Pistner et al. [148] observed in vivo an increase in crystallinity that reached 96% after 52 weeks of implantation in the dorsal muscle of rats. Even though they attributed such increase to the preferential degradation and cleavage of the amorphous regions, it is plausible that in this case the degradation induced partial rearrangement of the amorphous regions into a crystalline structure, as previously described [32]. The excessive longevity of PLLA in vivo, which is considered as a major drawback of the polymer for biomedical applications, can be in part related to the observed in vivo degradation-induced crystallization that slows down the hydrolytic attack on the compact stable crystalline regions. Also, residues of PLLA in vivo have been observed after seven years of implantation [149]. Also worth noting for biomedical uses of PLLA is the increase in crystallinity due to gamma ray irradiation with the formation of new thin crystal lamellae [150].

Commercial PLA with or without fillers shows a modification of thermal behavior during aging in hydrolytic or bacterial expositions, or in soil and compost. Fukushima et al. [151] reported the molecular weight reduction of PLA (Ingeo 4042D, NatureWorks LLC) after 4–17 weeks of compost and 10 days of presence of bacteria, the consequent modification of crystallizability with the reduction of crystallization peak from about 120 to 100°C, and the appearance of a secondary melting peak at around 135°C, near the main peak at 152°C. Accelerated hydrolysis at various temperatures (37°C, 58°C, 25–50°C) was also performed by various authors [152, 153].

Deroine et al. [154] showed that 4 mm thick specimens of commercial PLA (Ingeo 7001, NatureWorks LLC) easily

crystallized (36%) after 30 days at 50°C in water, whereas the process was slower at lower temperature (25–40°C) with a crystallinity content of about 2–10% after six months. The role of initial crystallinity was also compared by Pantani and Sorrentino [155] in injection-molded specimens 2 mm thick produced with PLA Ingeo 2002D (NatureWorks LLC), showing the progressive crystallization of polymer either in water or in compost. Luo [156] observed in a long-term hydrolytic degradation study of 0.5 mm thick sample of PLA 4032D (NatureWorks LLC) a progressive crystallization, and the effect of $TiO_2$ nanofiller in accelerating both degradation and crystallization kinetics.

## ACKNOWLEDGMENTS

The authors acknowledge N. Corradini, I. Dabrowska, C. Gavazza, D. Rigotti and M. Sebastiani for the preparation and DSC analysis of PLAs presented in Section 8.5.

## REFERENCES

1. T. H. Barrows, *Clin. Mater.* **1986**, *1*, 233–257.
2. I. Engelberg, J. Kohn, *Biomaterials* **1991**, *12*, 292–304.
3. M. Vert, G. Schwarch, J. Coudane, *J. Macromol. Sci. Pure Appl. Chem.* **1995**, *A32*, 787–792.
4. W. Amass, A. Amass, B. Tighe, *Polym. Int.* **1998**, *47*, 89–144.
5. Y. Ikada, H. Tsuji, *Macromol. Rapid Commun.* **2000**, *21*, 117–132.
6. D. A. Garlotta, *J. Polym. Environ.* **2001**, *9*, 63–84.
7. L. Fambri, C. Migliaresi, K. Kesenci, E. Piskin, Biodegradable polymers, in: R. Barbucci (Ed.), *Integrated Biomaterials Science*, Kluwer Plenum Publications, New York, 2002, Chapter 4, pp. 119–187.
8. H. Tsusj, Polylactide, in: Y. Doi, A. Steinbuchel (Eds.), *Biopolymers. Polyesters III. Applications and Commercial Products*, Wiley-VCH Verlag GmbH, Weinheim, 2002, Chapter 5, pp. 129–177.
9. N. Kumar, A. Ezra, T. Ehrenfroind, M. Y. Krasko, A. J. Domb, Biodegradable polymers, medical applications, in: H. F. Mark (Ed.), *Encyclopedia of Polymer Science & Technology*, 3rd edition, Wiley, Hoboken, NJ, 2003, Chapter 5, pp. 263–285.
10. S. Farah, D. G. Anderson, R. Langer, *Adv. Drug Deliv. Rev.* **2016**, *107*, 367–392.
11. R. von Oepen, W. Michaeli, *Clin. Mater.* **1992**, *10*, 21–28.
12. B. Gupta, N. Revagade, J. Hilborn, *Prog. Polym. Sci.* **2007**, *32*, 455–482.
13. L. T. Lim, R. Auras, M. Rubino, *Prog. Polym. Sci.* **2008**, *33*, 820–852.
14. R. K. Kulkarni, K. C. Pani, C. Neuman, F. Leonard, *Arch. Surg.* **1966**, *93*, 839–843.
15. R. K. Kulkarni, E. G. Moore, A. F. Hegyeli, F. Leonard, *J. Biomed. Mater. Res.* **1971**, *5*, 169–171.
16. A. P. Gupta, V. Kumar, *Eur. Polym. J.* **2007**, *43*, 4053–4074.
17. A. L. Lehninger, *Biochemistry*, 3rd edition, Worth Publishers Inc., New York, 1977.
18. J. Lunt, *Polym. Degrad. Stab.* **1998**, *59*, 145–152.
19. T. Maharana, B. Mohanty, Y. S. Negi, *Prog. Polym. Sci.* **2009**, *34*, 99–124.
20. Q. Jian, L. Xiang, Y. Chen, Y. Liu, Y. Pan, *Environ. Technol.* **2016**, *37*(19), 2457–2466.
21. C. W. Lee, *Fibers Polym.* **2007**, *8*, 571–578.
22. D. Bustamante, M. Tortajada, D. Ramón, A. Rojas. *Fermentation* **2020** *6*(1), 1–11.
23. S. Michelz Beitel, L. Fontes Coelho, J. Contiero, *Biomed Res. Inter.* **2020**, *3*, 1–13.
24. T. M. Ovitt, G. W. Coates, *J. Am. Chem. Soc.* **1999**, *121*, 4072–4073.
25. H. Tsuji, Y. Arakawa, *Polym. Chem.* **2018**, *9*, 2446–2457.
26. E. W. Fisher, H. J. Sterzel, G. Wegner, *Kolloid Z. Z. Polym.* **1973**, *251*, 980–990.
27. D. K. Gilding, A. M. Reed, *Polymer* **1979**, *20*, 1459–1464.
28. B. Kalb, A. J. Pennings, *Polymer* **1980**, *21*, 607–612.
29. S. H. Hyon, K. Jamshidi, Y. Ikada, Melt spinning of poly-L-lactide and hydrolysis of the fibre *in vitro*, in: S. W. Shalaby, A. S. Hoffmann, B. D. Ratner, T. A. Horbett (Eds.), *Polymers as Biomaterials*, Plenum Press, New York, 1984, pp. 51–65.
30. Y. Ikada, K. Jamshidi, H. Tsuji, S. H. Hyon, *Macromolecules* **1987**, *20*, 904–906.
31. H. Younes, D. Cohn, *Eur. Polym. J.* **1988**, *24*, 765–773.
32. C. Migliaresi, A. De Lollis, L. Fambri, D. Cohn, *Clin. Mater.* **1991**, *8*, 111–118.
33. A. Celli, M. Scandola, *Polymer* **1992**, *33*, 2699–2703.
34. G. L. Loomis, J. R. Murdoch, K. H. Gardner, *Polym. Prepr.* **1990**, *31*(2), 55.
35. J. R. Sarasua, R. E. Prud'homme, M. Wisniewski, A. Le Borgne, N. Spassky, *Macromolecules* **1998**, *31*, 3895–3905.
36. R. Vasanthakumari, A. J. Pennings, *Polymer* **1983**, *24*, 175–178.
37. K. Jamshidi, S. H. Hyon, Y. Ikada, *Polymer* **1988**, *29*, 2229–2234.
38. C. Migliaresi, D. Cohn, A. De Lollis, L. Fambri, *J. Appl. Polym. Sci.* **1991**, *43*, 83–95.
39. C. Marega, A. Marigo, V. Di Noto, R. Zannetti, A. Martorana, G. Paganetto, *Makromol. Chem.* **1992**, *193*, 1599–1606.
40. S. Mazzullo, G. Paganetto, A. Celli, *Progr. Colloid Polym. Sci.* **1992**, *87*, 32–34.
41. H. Tsuji, Y. Ikada, *Polymer* **1995**, *36*, 2709–2716.
42. S. Iannace, L. Nicolais, *J. Appl. Polym. Sci.* **1997**, *64*, 911–919.
43. T. Miyata, T. Masuko, *Polymer* **1998**, *39*, 5515–5521.
44. J. J. Kolstad, *J. Appl. Polym. Sci.* **1996**, *62*, 1079–1091.

45. G. Perego, G. D. Cella, C. Bastioli, *J. Appl. Polym. Sci.* **1996**, *59*, 37–43.
46. M. L. Di Lorenzo, *Polymer* **2001**, *42*, 9441–9446.
47. M. L. Di Lorenzo, *Eur. Polym. J.* **2005**, *41*, 569–575.
48. M. L. Di Lorenzo, *J. Appl. Polym. Sci.* **2006**, *100*, 3145–3151.
49. Y. Wang, J. F. Mano, *Eur. Polym. J.* **2005**, *41*, 2335–2342.
50. Y. Yuryev, P. Wood-Adams, M. C. Heuzey, C. Dubois, J. Brisson, *Polymer* **2008**, *49*, 2306–2320.
51. P. De Santis, A. Kovacs, *Biopolymers* **1968**, *6*, 299–306.
52. B. Eling, S. Gogolewski, A. J. Pennings, *Polymer* **1982**, *23*, 1587–1593.
53. C. Aleman, B. Lotz, J. Puiggali, *Macromolecules* **2001**, *34*, 4795–4801.
54. S. Sasaki, T. Asakura, *Macromolecules* **2003**, *36*, 8385–8390.
55. K. Wasanasuk, K. Tashiro, M. Hanesaka, T. Ohhara, K. Kurihara, R. Kuroki, T. Tamada, T. Ozeki, T. Kanamoto, *Macromolecules* **2011**, *44*, 6441–6452.
56. W. Hoogsteen, A. R. Postema, A. J. Pennings, G. Ten Brinke, P. Zugenmaier, *Macromolecules* **1990**, *23*, 634–642.
57. K. Takahashi, D. Sawai, T. Yokoyama, T. Kanamoto, S. H. Hyon, *Polymer* **2004**, *45*, 4969–4976.
58. H. Wang, J. Zhang, K. Tashiro, *Macromolecules* **2017**, *50*, 3285–3300.
59. J. Puiggali, Y. Ikada, H. Tsuji, L. Cartier, T. Okihara, B. Lotz, *Polymer* **2000**, *41*, 8921–8930.
60. L. Cartier, T. Okihara, Y. Ikada, H. Tsuji, J. Puiggali, B. Lotz, *Polymer* **2000**, *41*, 8909–8919.
61. B. Lotz, G. Li, X. Chen, J. Puiggali, *Polymer* **2017**, *115*, 204–210.
62. G. Kokturk, E. Piskin, T. F. Serhatkulu, M. Cakmak, *Polym. Eng. Sci.* **2002**, *42*, 1619–1628.
63. J. Hu, T. Zhang, M. Gu, X. Chen, J. Zhang, *Polymer* **2012**, *53*, 4922–4926.
64. K. Wasanasuk, K. Tashiro, *Macromolecules* **2011**, *44*, 9650–9660.
65. J. Zhang, K. Tashiro, H. Tsuji, A. J. Domb, *Macromolecules* **2008**, *41*, 1352–1357.
66. J. Zhang, Y. Duan, H. Sato, H. Tsuji, I. Noda, S. Yan, Y. Ozaki, *Macromolecules* **2005**, *38*, 8012–8021.
67. K. Wasanasuk, K. Tashiro, *Polymer* **2011**, *52*, 6097–6109.
68. H. Marubayashi, S. Akaishi, S. Akasaka, S. Asai, M. Sumita, *Macromolecules* **2008**, *41*, 9192–203.
69. H. Marubayashi, S. Asai, M. Sumita, *J. Phys. Chem. B* **2013**, *117*, 385–397.
70. T. Okihara, *Bull. Inst. Chem. Res. Kyoto Univ.* **1988**, *66*, 271–282.
71. H. Tsuji, Y. Ikada, *Macromolecules* **1993**, *26*, 6918–6926.
72. H. Tsuji, *Macromol. Biosci.* **2005**, *5*, 569–597.
73. P. Pan, W. Kai, B. Zhu, T. Dong, Y. Inoue, *Macromolecules* **2007**, *40*, 6898–6905.
74. P. Pan, B. Zhu, W. Kai, T. Dong, Y. Inoue, *Macromolecules* **2008**, *41*, 4296–4304.
75. R. Androsch, C. Schick, M. L. Di Lorenzo, *Macromol. Chem. Phys.* **2014**, *215*(11), 1134–1139
76. T. Kawai, N. Rahman, G. Matsuba, K. Nishida, T. Kanaya, M. Nakano, H. Okamoto, J. Kawada, A. Usuki, N. Honma, K. Nakajima, and M. Matsuda, *Macromolecules* **2007**, *40*, 9463–9469.
77. N. Delpouve, A. Saiter, E. Dargent, *Eur. Polym. J.* **2011**, *47*, 2414–2423.
78. Q. Ma, G. Georgiev, P. Cebe, *Polymer (Guildf)* **2011**, *52*, 4562–4570.
79. T. L. Nguyen, F. Bédoui, P.-E. Mazeran, M. Guigon, *Polym. Eng. Sci.* **2015**, *55*, 397–405.
80. M. L. Di Lorenzo, M. C. Righetti, *Polym. Cryst.* **2018**, *1*, 1–14.
81. A. Sangroniz, A. Chaos, M. Iriarte, J. del Río, J.-R. R. Sarasua, A. Etxeberria, *Macromolecules* **2018**, *51*, 3923–3931.
82. L. Aliotta, M. Gazzaro, A. Lazzeri, M. C. Righetti, *ACS Omega* **2020**, *5*(33): 20890–20902.
83. J. R. Dorgan, J. Janzen, M. P. Clayton, *J. Rheol.* **2005**, *49*, 607–619.
84. A. J. Ninjenhuis, D. W. Grijpma, A. J. Pennings, *Polym. Bull.* **1991**, *26*, 71–77.
85. S. Diez-Gutierrez, M. A. Rodriguez-Perez, J. A. Saja, J. I. Velasco, *Polymer* **1999**, *40*, 5345–5353.
86. L. Fambri, K. Kesenci, C. Migliaresi, *Polym. Compos.* **2003**, *24*(1), 100–108.
87. D. W. van Krevelen, *Properties of Polymers*, 3rd edition, Elsevier, Amsterdam, 1998, p. 402.
88. L. C. E. Struik, *Physical Aging of Amorphous Polymers and Other Materials*, Elsevier, Amsterdam, 1978.
89. T. Ke, X. Sun, *J. Appl. Polym. Sci.* **2003**, *89*, 1203–1210.
90. J. Y. Nam, S. S. Ray, M. Okamoto, *Macromolecules* **2003**, *36*, 7126–7131.
91. D. M. Bigg, *Conference Proceedings ANTEC: Annual Technical Conference*, Society of Plastics Engineers, Nashville, TN, 2003, pp. 2816–2822.
92. J. Y. Nam, M. Okamoto, H. Okamoto, M. Nakano, A. Usuki, M. Matsuda, *Polymer* **2006**, *47*, 1340–1347.
93. N. Kawamoto, A. Sakai, T. Horikoshi, T. Urushihara, E. Tobita, *J. Appl. Polym. Sci.* **2007**, *10*, 198–203.
94. H. Li, M. A. Huneault, *Polymer* **2007**, *48*, 6855–6866.
95. S. Jacobsen, H. G. Fritz, *Polym. Eng. Sci.* **1999**, *39*, 1303–1310.
96. O. Martin, L. Averous, *Polymer* **2001**, *42*, 6209–6219.
97. N. Ljungberg, B. Wesselen, *J. Appl. Polym. Sci.* **2002**, *86*, 1227–1234.
98. Z. Kulinski, E. Piorkowska, *Polymer* **2005**, *46*, 10290–10300.
99. Z. Ren, L. Dong, Y. Yang, *J. Appl. Polym. Sci.* **2006**, *101*, 1583–1590.
100. I. Pillin, N. Montrelay, Y. Grohens, *Polymer* **2006**, *47*, 4676–4682.

101. A. J. Müller, M. Ávila, G. Saenz, J. Salazar, Crystallization of PLA-based materials, in: A. Jiménez, M. Peltzer, R. Ruseckaite (Eds.), *Poly(Lactic Acid) Science and Technology: Processing, Properties, Additives and Applications*, Polymer science, series, Royal Society of Chemistry, Cambridge, 2014, pp. 66–98
102. J. del Río, A. Etxeberria, N. López-Rodríguez, E. Lizundia, J. R. Sarasua, *Macromolecules* **2010**, *43*(10), 4698–4707.
103. E. Lizundia, S. Petisco, J. R. Sarasua, *J. Mech. Behav. Biomed. Mater.* **2013**, *17*, 242–251.
104. J. I. Lauritzen, J. D. Hoffman, *J. Appl. Phys.* **1973**, *44*, 4340–4352.
105. J. D. Hoffman, G. T. Davis, J. I. Lauritzen, The rate of crystallization of linear polymers with chain folding, in: N. B. Hannay (Ed.), *Treatise on Solid State Chemistry*, Vol. *3*, Plenum Press, New York, 1976, Chapter 7.
106. R. V. Castillo, A. J. Muller, J. M. Raquez and P. Dubois, *Macromolecules* **2010**, *43*, 4149–4160.
107. M. J. Avrami, *J. Chem. Phys.* **1940**, *8*, 212–224.
108. M. J. Avrami, *J. Chem. Phys.* **1941**, *9*, 177–184.
109. L. Fambri, A. Dorigato and A. Pegoretti, *Appl. Sci.* **2020**, *10*, 6731.
110. D. Cao, L. Wu, *J. Appl. Polym. Sci.* **2009**, *111*(2), 1045–1050
111. R. H. Hakim, J. Cailloux, O. O. Santana, J. Bou, M. Sanchez-Soto, J. Odent, J. M. Raquez, P. Dubois, F. Carrasco, M. L. Maspoch, *J. Appl. Polym. Sci.* **2017**, *134*, 45367/1–45367/12.
112. J. A. Cicero, J. R. Dorgan, *J. Polym. Environ.* **2001**, *9*(1), 1–10.
113. S. Gogolewski, A. J. Pennings, *J. Appl. Polym. Sci.* **1983**, *28*, 1045–1061.
114. C. Migliaresi, L. Fambri, *Macromol. Symp.* **1997**, *123*, 155–161.
115. L. Fambri, A. Pegoretti, R. Fenner, S. D. Incardona, C. Migliaresi, *Polymer* **1997**, *38*, 79–85.
116. L. Fambri, A. Pegoretti, M. Mazzurana, C. Migliaresi, *J. Mater. Sci. Mater. Med.* **1994**, *5*, 679–684.
117. A. Fujimori, N. Ninomiya, T. Masuko, *Polym. Adv. Technol.* **2008**, *19*, 1735–1744.
118. A. Pegoretti, L. Fambri, C. Migliaresi, *J. Appl. Polym. Sci.* **1997**, *64*, 213–223.
119. I. Horacek, V. Kalisek, *J. Appl. Polym. Sci.* **1994**, *54*, 1751–1757.
120. J. W. Leenslag, A. J. Pennings, *Polymer* **1987**, *28*, 1695–1702.
121. M. Takasaki, N. Fukushi, M. Yoshizawa, S. Onosato, M. Hanada, W. Takarada, Y. Kawahara, T. Kikutani, H. Kobayashi, K. Tanaka, *J. Macromol. Sci. Part B Phys.* **2017**, *56*(3), 143–160.
122. N. Roungpaisan, W. Takarada, T. Kikutani, *J. Fiber Sci. Technol.* **2019**, *75*, 119–131.
123. T. Kikutani, Fiber formation through melt spinning of bio-polymers, in *Proceedings of International Conference on Technology and Social Science 2020 (ICTSS 2020)*, Kyriu, Japan, 2–4 December 2020.
124. R. J. Crawford, P. J. Martin, *Plastics Engineering*, 4th edition, Butterworth-Heinemann (Elsevier), Oxford, 2020, Chapter 1, pp. 36–44.
125. F. S. Fattahi, A. Khoddami, O. Avinc, Sustainable, renewable, and biodegradable poly(lactic acid) fibers and their latest developments in the last decade, in: S. Muthu, M. Gardetti (Eds.), *Sustainability in the Textile and Apparel Industries. Sustainable Textiles: Production, Processing, Manufacturing & Chemistry*, Springer, Cham, 2020.
126. T. Standau, C. Zhao, S. Murillo Castellón, C. Bonten and V. Altstädt, *Polymers* **2019**, *11*, 306/1–306/39.
127. M. Nofar, D. Sacligil, P. J. Carreau, M. R. Kamal, M.-C. Heuzey. *Int. J. Biol. Macromol.* **2019**, *125*, 307–360.
128. M. Razavi, S.-Q. Wang, *Macromolecules* **2019**, *52*(14), 5429–5441.
129. M. Murariu, P. Dubois, *Adv. Drug Deliv. Rev.* **2016**, *107*, 17–46
130. J. M. Raquez, Y. Habibi, M. Murariu, P. Dubois, *Prog. Polym. Sci.* **2013**, *38*, 1504–1542.
131. K. Oksman, M. Skrifvars, J. F. Selin, *Compos. Sci. Technol.* **2003**, *63*, 1317–1324.
132. C. Miao, W. Y. Hamad, *Cellulose* **2013**, *20*, 2221–2262.
133. S. Jain, M. M. Reddy, A. K. Mohanty, A. M. Misra, A. K. Ghosh, *Macromol. Mater. Eng.* **2010**, *295*, 750–762
134. Y. Shikinami, M. Okuno, *Biomaterials* **1999**, *20*(9), 859–877.
135. S. N. Nazhat, M. Kellomaki, P. Tormala, K. E. Tanner, W. Bonfield, *J. Biomed. Mater. Res.* **2001**, *58*, 335–343.
136. J. Russias, E. Saiz, R. K. Nalla, K. Gryn, R. O. Richtie, A. P. Tomsia, *Mater. Sci. Eng. C* **2006**, *26*, 1289–1295.
137. Y. Kasuga, H. Maeda, K. Kato, M. Nogami, K. Hata, M. Ueda, *Biomaterials* **2003**, *24*, 3247–3253.
138. H. Urayama, C. Ma, Y. Kimura, *Macromol. Mater. Eng.* **2003**, *288*, 562–568.
139. M. Murariu, A. D. Ferreira, P. Degee, M. Alexandre, P. Dubois, *Polymer* **2007**, *48*, 2613–2618.
140. M. Pluta, M. Murariu, A. D. Ferreira, M. Alexandre, A. Galeski, P. Dubois, *J. Polym. Sci. B Polym. Phys.* **2007**, *45*, 2770–2780.
141. K. Molnar, J. Moczo, M. Murariu, P. Dubois, B. Pukanszky, *Express Polym. Lett.* **2009**, *3*, 49–61.
142. A. Dorigato, M. Sebastiani, A. Pegoretti, L. Fambri, *J. Polym. Environ.* **2012**, *20*, 713–725.
143. D. Battegazzore, S. Bocchini, A. Frache, *Express Polym. Lett.* **2011**, *5*(10), 849–858.
144. D. Rigotti, R. Checchetto, S. Tarter, D. Caretti, M. Rizzuto, L. Fambri, A. Pegoretti, *Express Polym. Lett.* **2019**, *13*(10), 858–876.
145. C. Migliaresi, D. Cohn, L. Fambri, *J. Biomater. Sci. Polym. Ed.* **1994**, *5*(6), 591–606.
146. S. M. Li, H. Garreau, M. Vert, *J. Mater. Sci. Mater. Med.* **1990**, *1*, 198–206)
147. H. Tsuji, A. Mizuno, Y. Ikada, *J. Appl. Polym. Sci.* **2000**, *77*, 1452–1146.
148. H. Pistner, D. R. Bendix, J. Muhling, J. F. Reuther, *Biomaterials* **1993**, *14*, 291–298.
149. J. E. Bergsma, W. C. de Bruijn, F. R. Rozema, R. R. M. Bos, G. Boering, *Biomaterials* **1995**, *16*, 25–31.


150. D. Mililevic, S. Trifunovic, S. Galovic, E. Suljiovrujic, *Radiat. Phys. Chem.* **2007**, *76*, 1376–1380.
151. K. Fukushima, C. Abbate, D. Tabuani, M. Gennari, G. Camino, *Polym. Degrad. Stab.* **2009**, *94* 1646–1655.
152. K. Fukushima, D. Tabuani, C. Abbate, M. Arena, P. Rizzarelli, *Eur. Polym. J.* **2011**, *47*, 139–52.
153. K. Fukushima, D. Tabuani, M. Arena, M. Gennari, G. Camino, *React. Funct. Polym.* **2013**, *73*, 540–549.
154. M. Deroiné, A. Le Duigou, Y.-M. Corre, P.-Y. Le Gac, P. Davies, G. César, S. Bruzaud, *Polym. Degrad. Stab.* **2014**, *108*, 319–329.
155. R. Pantani, A. Sorrentino, *Polym. Degrad. Stab.* **2013**, *98*, 1089–1096.
156. Y.-B. Luo, X.-L. Wang, Y. Z. Wang, *Polym. Degrad. Stab.* **2012**, *97*, 721–728.

# 9

# RHEOLOGY OF POLY(LACTIC ACID)

John R. Dorgan

## 9.1 INTRODUCTION

The readers of this chapter are expected to come from a wide variety of backgrounds with varying degrees of expertise in polymer materials science. Accordingly, a detailed understanding of the rheological properties of polymers is, for many readers, an unknown subject. With these factors in mind, the first topic to be addressed is, *What is rheology and why is it important?*

Simply stated, rheology is the study of the flow and deformation of matter. Rheology is a subfield of continuum mechanics that combines elements of both solid and fluid mechanics. Polymer rheology is a highly advanced science that reveals very important features of polymeric materials like PLA. In particular, the *viscometry* of dilute polymer solutions is an effective means of determining fundamental properties of polymer molecules; these include the molecular weight and the characteristic ratio (subjects to be discussed in detail in this chapter). More important, the *melt rheology* of polymeric materials reflects the relationship between molecular structure and dynamic properties. Of these properties, the viscosity and elasticity of the molten polymer are of primary importance in processing of plastics into useful articles. For example, both the shear thinning viscosity and the strain hardening extensional behavior of PLA are of great importance in plastic processing operations such as extrusion and fiber spinning. With this very cursory discussion of the nature and importance of rheology in mind, the attentive reader will ask, *Is there anything particularly unique about the rheology of PLA?*

Indeed, the melt rheology of PLA is distinct from other commodity plastics in at least one important respect. Namely, the chemical stability of PLA can be adversely affected rather easily compared to most other polymeric molecules. At processing temperatures typically needed for semicrystalline PLA, namely, those above the melting temperature, both hydrolysis and pyrolysis can become important. Fortunately, commercially available PLAs are typically stabilized against thermal degradation. However, it is impossible to overstate *the importance of drying PLA sufficiently* prior to processing (or measuring its rheological properties!). Rheological measurements can provide direct evidence for the loss in molecular weight of improperly stabilized PLA in the molten state. Accordingly, in examining rheological data on PLAs, it is of particular importance to understand what, if any, chemical changes have taken place during the preparation and testing of the samples. In this regard, there is a clear link to dilute solution viscometry that can provide information about molecular weight in a simple test requiring only elementary equipment. As a final remark on the unique nature of PLA rheology, we can state that rheological measurements are particularly useful for assessing the effectiveness of both chemical stabilization against thermal degradation and of drying procedures meant to preclude hydrolytic degradation.

This chapter is organized to provide a short yet detailed understanding of the fundamental rheological properties of PLAs; extensive use of references is employed where appropriate. However, the chapter is meant to be self-contained, and so appropriate introductory material is also provided.

*Poly(Lactic Acid): Synthesis, Structures, Properties, Processing, Applications, and End of Life*, Second Edition.
Edited by Rafael A. Auras, Loong-Tak Lim, Susan E. M. Selke, and Hideto Tsuji.

Properties of the single chain are discussed and related to measurable quantities available from dilute solution viscometry. This is followed by a discussion of the single chain properties of PLA. Next, a brief discussion of the rheology of polymeric materials is provided. In this context, mathematical models are briefly discussed, including the empirical but useful Havriliak–Negami (HN) model that serves as the basis for the software provided with the text. Appropriate conclusions are drawn regarding the influence of PLA rheology on polymer processing operations. Finally, in an appendix to the chapter, a description of software enabling the prediction of melt rheological properties as a function of molecular weight, temperature, and shear rate is given.

## 9.2 FUNDAMENTAL CHAIN PROPERTIES FROM DILUTE SOLUTION VISCOMETRY

*Conformational analysis* is the study of how molecules can alter their overall geometry (their arrangement in space) through bond rotations. Such analysis is useful for understanding polymer properties, particularly solution properties. Molecular forces in polymeric materials dictate the conformation adopted and can be classified as either bonded or nonbonded. Bonded forces are strictly intramolecular and typically consist of strong covalent bonds. Nonbonded forces are weaker interactions and may be either intramolecular or intermolecular. Examples of nonbonded forces include hydrogen bonding, dipole and multipole interactions, and van der Waals forces (London dispersion forces). Flexibility of polymer chains should not be confused with individual bond flexibility. Polymers, which are considered flexible, are capable of assuming many different geometric conformations in space. Rigid polymers are those that are capable of assuming relatively few conformations due to the restricted bond rotations.

### 9.2.1 Unperturbed Chain Dimensions

The *freely jointed chain* is a model that treats the conformation of a polymer molecule as a mathematical random walk. This is a simple model for chain conformation in which

1. There are $n$ segments
2. Each skeletal bond is represented as a vector $l_i$
3. No restrictions are placed on the allowable bond angle between two adjoining segments (it is freely jointed)
4. All bond lengths are taken as the same and equal to $|l|$

The freely jointed chain can step back on itself; that is, it does not obey the physical reality of *excluded volume*. Excluded volume effects are caused by the fact that no two polymer segments may occupy the same position in space. The volume that one chain segment occupies is excluded from occupation by another segment. This effect serves to push segments away from one another and thus increase the overall dimensions of the chain.

The solvent in which a polymer is dissolved strongly affects its conformation. *Solvent quality* is a general terminology to describe how well a particular solvent can dissolve a particular polymer. In good solvents, a polymer chain adopts an open conformation and is expanded. In poor solvents, a polymer chain adopts a closed conformation and is collapsed. To be quantitative, a measure of the size of a polymer coil of a given molecular structure, molecular weight, and in a particular solvent environment is needed.

The *end-to-end vector*, $r$, connects the first and last segments of a polymer chain. For the freely jointed chain, its mean squared value may be calculated within the assumptions of the model from a consideration of a random walk of $n$ vectors, each of length $l$.

$$\left\langle r^2 \right\rangle_{\mathrm{o}} = nl^2 \tag{9.1}$$

Here, the brackets denote an ensemble average (the average over many chains) and the subscripted "o" denotes conditions referred to as *unperturbed*. A related measure of polymer size is the *radius of gyration*, $s$, which is defined as the average of the distance from a segment to the chain's center of mass; that is,

$$s^2 = \frac{1}{n+1}\sum_{i=1}^{n}\left(r_i - r_{\mathrm{c.o.m.}}\right)^2 \tag{9.2}$$

The radius of gyration can be considered as an average measure of the radius of a polymer coil.

*Theta conditions* are the actual conditions under which a real polymer chain assumes its unperturbed dimensions. The solvent is then called a *theta solvent* and the temperature at which the unperturbed dimensions are produced is called the *theta temperature*. The unperturbed dimensions are realized because of the balance of two competing processes, the first being excluded volume effects that favor open conformations and the second being unfavorable energetic contacts between the polymer and the solvent. Theta conditions mean that only short-range interactions dictate the polymer conformation because the inter- and intramolecular interactions are identical in enthalpic nature (i.e., the heat of mixing is zero).

### 9.2.2 Real Chains

The *characteristic ratio*, $C_\infty$, is a quantity that can be experimentally determined or calculated using advanced molecular simulation techniques. It is defined by

$$C_\infty = \lim_{n\to\infty} \frac{\left\langle r^2 \right\rangle_{\mathrm{o}}}{nl^2} \tag{9.3}$$

Equation 9.3 says that the characteristic ratio is a measure of how large the polymer coil is under unperturbed conditions relative to the freely jointed chain. That is, it is a measure of chain stiffness or how the chain conformation is extended compared to the freely jointed chain. Consider the compactness of the freely jointed chain—it can step back on and through itself; real chains all have characteristic ratios greater than unity (in fact, all real chains must be greater than two). For example, the characteristic ratio of poly(ethylene oxide) is 4.0, that of polyethylene is 6.7, and that of polystyrene is 10.0. Note that molecular structure influences the quantity as one would expect; the oxygen in poly(ethylene oxide) has no pendant groups and provides low energy bond rotations, whereas the bulky phenyl groups of polystyrene increase the value of $C_\infty$.

The expansion factor, $\alpha$, is used to characterize the size of polymer coils when they are not under unperturbed conditions—that is, to measure the effects of the polymer's environment on its overall dimensions. To do so, $\alpha$ is defined as the ratio of the root mean squared end-to-end vector relative to its value in the unperturbed state according to the following equation:

$$\alpha = \frac{\left\langle r^2 \right\rangle^{1/2}}{\left\langle r^2 \right\rangle_o^{1/2}} = \frac{\left\langle r^2 \right\rangle^{1/2}}{\left(C_\infty n l^2\right)^{1/2}} \tag{9.4}$$

The expansion factor is a function of the particular polymer, solvent, and conditions (primarily temperature) being considered.

Fundamental polymer chain characteristics such as the characteristic ratio and the molecular weight can be quantitatively related to the melt rheological response. Because of this fact, it is important to be able to characterize these quantities. Several techniques are available, with multiple angle laser light scattering (MALLS) playing an important role. However, viscometry is the simplest technique for characterizing polymer chains of known molecular architecture.

### 9.2.3 Solution Viscometry

The viscosity of a low-molecular-weight solvent can be dramatically increased by the addition of even a very small amount of high-molecular-weight polymer. The reason for this effect is that the large polymer coil disturbs the local flow, causing gradients in fluid velocity that dissipate energy, requiring additional work to cause flow, and therefore increasing viscosity. Because relative increases in viscosity can be measured using simple and inexpensive techniques, such measurements of dilute solution viscosities of polymer solutions have been widely practiced for a long time. A critical feature of such measurements is that they provide information on the fundamental chain properties discussed above; this information is available because the viscometry is a measure of the *hydrodynamic radius*, $R_h$, of the polymer coil in the solvent being used.

The hydrodynamic radius is defined based on a result from fluid mechanics developed by Stokes long ago, the so-called Stokes flow around a sphere. In Stokes flow, the proportionality constant between the force applied by the flowing fluid on the moving sphere and the velocity of the sphere is called the *friction coefficient* $\zeta$. For rigid bodies such as colloidal particles, the friction coefficient is given by

$$\zeta = 6\pi\eta_s R \tag{9.5}$$

where $\eta_s$ is the viscosity of the dispersing solvent and $R$ is the radius of the sphere. This result is generalized to provide a definition for the hydrodynamic radius of polymer coils in solution as

$$R_h = \frac{\zeta}{6\pi\eta_s} \tag{9.6}$$

That is, according to Equation 9.6, $R_h$ is the radius of a rigid spherical particle that has the same frictional coefficient as the dissolved polymer coil.

In dilute solution viscometry, the concentrations employed (measured in volume fraction, $\varphi$) are of the order $\varphi \approx 0.001$. That is, the concentration is below $c^*$, the so-called *overlap concentration*, at which polymer coils touch and interact. In dilute solution viscometry, the polymer coils are isolated in solution. In this dilute regime, the polymer molecules can be treated as spheres with diameters roughly equal to the root mean squared end-to-end distance, $D = \langle r^2 \rangle^{1/2}$.

If the molecules are considered to behave like hard spheres, which implies that the entrained solvent molecules move with the polymer coil, then the *Einstein–Batchelor equation* may be applied, which is as follows:

$$\eta = \eta_s \left[1 + 2.5\varphi + 7.6\varphi^2\right] \tag{9.7}$$

where $\eta$ is the viscosity of the solution (or suspension of spheres), $\eta_s$ is the viscosity of the pure solvent, and $\varphi$ is the *volume fraction of spheres*.

The volume fraction of spheres (polymer coils containing entrained solvent) can be found from

$$\varphi_s = \frac{\text{Volume of spheres}}{\text{Volume of solution}} = c_2 \frac{N_A\left(\pi D^3/6\right)}{M_2} \tag{9.8}$$

where $c_2$ is polymer concentration expressed in g/cm$^3$, $N_A$ is Avagadro's number, $M_2$ is the molecular weight of the polymer, and $D$ is the sphere diameter.

The nomenclature associated with viscosity measurements has changed and both new and old terminologies are encountered. Table 9.1 summarizes the nomenclature.

**TABLE 9.1 Nomenclature of Dilute Solution Viscometry**

| Symbol | New Name | New Units | Old Name | Old Units |
|---|---|---|---|---|
| $H$ | Solution viscosity | Pa s | Solution viscosity | Poise |
| $\eta_s$ | Solvent viscosity | Pa s | Solvent viscosity | Poise |
| $\eta_r = \eta/\eta_s$ | Viscosity ratio | — | Relative viscosity | — |
| $\eta_{sp} = \eta_r - 1$ | — | — | Specific viscosity | — |
| $\eta_{sp}/c_2$ | Viscosity number | mL/g | Reduced viscosity | dL/g |
| $(\ln \eta_r)/c_2$ | Logarithmic viscosity number | mL/g | Inherent viscosity | dL/g |
| $[\eta] = \lim_{c2\to 0}(\eta_{sp}/c_2)$ | Limiting viscosity number | mL/g | Intrinsic viscosity | dL/g |

For monodisperse polymer samples, a log–log plot of the limiting viscosity number against the polymer molecular weight ($M_2$) gives a straight line. This finding is the basis of the Mark–Houwink (MH) equation,

$$[\eta] = K_\Theta M_2^a \tag{9.9}$$

where $a$ and $K_\Theta$ are known as the Mark–Houwink parameters. These parameters depend on the specific polymer, solvent, and temperature under consideration. Values for these parameters are extremely important and so are tabulated in places like the *Polymer Handbook*.

Substitution of Equation 9.9 for the volume fraction of spheres into the Einstein–Batchelor equation along with the use of the root mean squared end-to-end distance for the sphere diameter gives rise to Equation 9.10.

$$[\eta] = \Phi\left(\frac{\langle r^2\rangle_o}{M_2}\right)^{3/2} \alpha^3 M_2^{1/2} \tag{9.10}$$

where $\Phi$ represents the *universal viscometric constant* (Flory constant) having a numerical value of $2.1\times10^{23}$ (cm$^3$/g) (g/[mol cm$^3$]) and $\alpha$ is the expansion factor discussed above.

The grouping in the parenthesis of Equation 9.10 can be related to the characteristic ratio and is nearly independent of the polymer molecular weight; the dependence of intrinsic viscosity on solvent quality is therefore proportional to the product $\alpha M_2$. In theta solvents, $\alpha$ is unity (the intrinsic viscosity scales with $M_2^{0.5}$) and in good solvents $\alpha$ is proportional to $M_2^{0.1}$ (the intrinsic viscosity scales with $M_2^{0.8}$). Comparison with Equation 9.1 suggests that the Mark–Houwink parameter should lie in the range $0.5 \le a \le 0.8$. Equation 9.10 may be used to find the expansion factor if theta conditions for the polymer solution are known,

$$\alpha = \left(\frac{[\eta]}{[\eta]_\theta}\right)^{1/3} \tag{9.11}$$

or may be used to find the molecular weight if the grouping in the parenthesis of Equation 9.10 and the expansion factor are known. This average molecular weight, $\bar{M}_v$, is known as the *viscosity average molecular weight*. On the basis of the expected range for the Mark–Houwink $a$ parameter, it can be seen that

$$\bar{M}_n < \bar{M}_v < \bar{M}_w \tag{9.12}$$

The viscosity average molecular weight always lies between the number-average and weight-average molecular weights; in good solvents, its value is close to the value of the weight-average molecular weight.

### 9.2.4 Viscometry of PLA

The molecular characterization of PLA depends on the accurate knowledge of its fundamental properties. These include such parameters as Mark–Houwink constants that relate intrinsic viscosity to molecular weights, theta-condition front factors ($K\Theta$) used to calculate single chain properties, and characteristic ratios ($C_\infty$) that give an indication of the bonding structure of polymers.

Unfortunately, literature reports on some fundamental properties of PLAs seriously disagree. For example, Table XVIII of a review on PLA [1] lists 15 different sets of MH constants [2], and agreement among the various sets is very poor. MH values tabulated in the above review can be evaluated and used to reconstruct data for a Stockmayer–Fixman plot. This analysis plots the intrinsic viscosity divided by the square root of the viscosity averaged molecular weight against the square root of the viscosity averaged molecular weight; it is used to determine the $K\Theta$ for the MH equation. Figure 9.1 shows the $K\Theta$ values so determined (vertical axis intercepts) to vary over a wide range, from lowest to highest, by a factor of 25! From this analysis [3], it was concluded that the state of the literature regarding Mark–Houwink parameters for PLA was inadequate.

The literature inconsistencies can be attributed to the following reasons:

1. Different definitions of the mean squared "monomer" step length
2. Different expansion factor models for correcting data obtained in good solvents to Q conditions, or neglecting of such correction altogether [4]

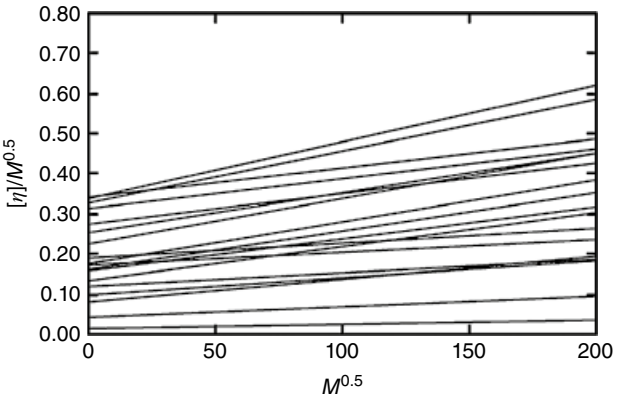


**FIGURE 9.1** Stockmayer–Fixman plots, reconstructed from published Mark–Houwink parameters, illustrating inconsistencies in the PLA literature. Rather than the wide range of values exhibited, the *y*-axis intercepts should be a common value equal to $K\Theta$.

3. Different assumed values for the viscosity function $F$ (or Flory constant) used to relate intrinsic viscosities to molecular dimensions in solution
4. Different methods of measuring molecular weights and subsequently relating them to dilute solution viscosities [4–10].

Because of the confused state of the literature, a careful study [3] was performed to determine appropriate physical constants for PLA under dilute solution conditions.

The results of this important study are summarized here with attention focused on the most important results useful for characterizing PLA. PLA homopolymers and optical copolymers spanning wide ranges of molecular weight and stereoisomer proportion were prepared by ring-opening polymerizations of L- and D-lactides using tin octanoate as the catalyst. The weight-average molecular weights produced spanned the range from below $10^4$ to over $10^6$ g/mol, and the range of enantiomer proportions was from 100 : 0 to 50 : 50.

As part of the careful characterization, both density and indices of refraction were determined and used to calculate the refractive index increment. The refractive index increment is an important physical property when light scattering measurements are conducted. The density of amorphous PLA was found using the data of Witzke [11] on densities above $T_g$, namely,

$$\rho(T) = \rho(T=0)\exp(\alpha T) = 1.2836\exp\left(-7.7\times10^{-4}T\right) \tag{9.13}$$

where density, $\rho$, is in g/cm$^3$ and temperature, $T$, is in °C. It is instructive to note that Equation 9.13 implies the density at room temperature for PLA is 1.258 g/cm$^3$. Refractive indexes were determined over the wavelength range 300–1300 nm for solid PLAs at room temperature using ellipsometry. The refractive indexes for all compositions can be represented to within experimental error by a two-term Cauchy expression:

$$n(\lambda) = (1.445 \pm 0.00075) + \frac{(4892 \pm 143)\,\text{nm}^2}{\lambda^2} \quad \text{for} \quad 300\,\text{nm} < \lambda < 1300\,\text{nm} \tag{9.14}$$

At the wavelength of the sodium D line, to which most tabulated solvent refractive indexes refer, evaluation of Equation 9.14 gives

$$n_{\text{PLA}}(589.2) = 1.459 \tag{9.15}$$

Densities ($\rho$) and refractive indexes ($n$) for various solvents were taken from standard tables [12–14], and the refractive indices of solvent mixtures were calculated according to classical [15] volume additivity of polarizabilities, namely,

$$\frac{n^2-1}{n^2+2} = \sum_i \varphi_i \frac{n_i^2-1}{n_i^2+2} \tag{9.16}$$

where the $\varphi_i$'s are volume fractions. The adoption of Equations 9.15 and 9.16 enables the calculation of refractive index increments (d$n$/d$c$) that are within experimental error of measured values. It is important to note that a molecular weight determined with an inaccurate d$n$/d$c$ value will be in error by a factor that is the square of the ratio of accurate and inaccurate d$n$/d$c$ values.

Samples were characterized by means of dilute solution viscometry in three different solvents: size exclusion chromatography (SEC), static multiangle light scattering, variable-angle spectroscopic ellipsometry, and melt rheology. More important, this study [3] also conclusively demonstrated consistency between solvents in determining the $K\Theta$ used to calculate single chain properties; Figure 9.2 shows the resulting Stockmayer–Fixman plot that should be compared with Figure 9.1. The resulting $K\Theta$ data provided by these experiments produce values of characteristic ratios ($C_\infty$) in the range $6.1 \pm 1.3$. These experimental values are in excellent agreement with molecular simulation [16].

As a result of the careful investigation by Dorgan and coworkers, the Schulz–Blaschke and Mark–Houwink constants for dilute PLA solutions in chloroform and in THF have been determined. For chloroform at 30°C, the correct values are $k_{SB}$ = 0.302, $K$ = 0.0131 mL/g, and $a$ = 0.759, while for THF at 30°C the correct values are $k_{SB}$ = 0.289, $K$ = 0.0174 mL/g, and $a$ = 0.736. The importance of having reliable and accurate values for the Mark–Houwink parameters is that they are needed in relating relative molecular weights determined by SEC to absolute molecular weights.

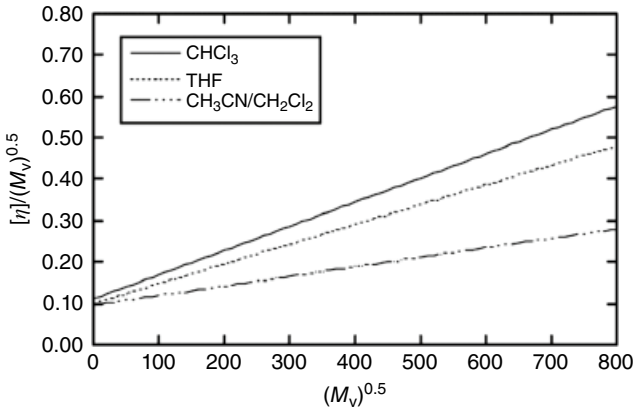


**FIGURE 9.2** Stockmayer–Fixman plots for three separate solvents from the study of Dorgan et al. showing consistency of the determined $K\Theta$ values (contrast with Figure 9.1).

Accordingly, without such information, it is very difficult to evaluate absolute molecular weight distributions for PLA, yet such information is critical in understanding a wide variety of phenomena.

In addition, there is a great utility of having reliable values for both Mark–Houwink and Schultz–Blaschke parameters in that the combination enables the measurement of an average molecular weight in a very simple viscometry experiment. Equation 9.17 gives an explicit formula for the intrinsic viscosity based only on the relative flow times for a single concentration experiment.

$$[\eta] = \frac{\eta/\eta_0 - 1}{c\left[1 + k_{SB}\left(\eta/\eta_0 - 1\right)\right]} = \frac{t^N/t_0^N - 1}{c\left[1 + k_{SB}\left(t^N/t_0^N - 1\right)\right]} \quad (9.17)$$

where $c$ is the concentration in g/mL and overtildes denote corrected flow times for the pure solvent and solution, $t_0$ and $t$, respectively. Accordingly, Equation 9.17 provides a direct method to obtain the intrinsic viscosity using a simple flow viscometer and a single concentration solution. With the value of intrinsic viscosity and the Mark–Houwink parameters, Equation 9.9 can be employed to find an absolute value for the viscometry averaged molecular weight. The application of Equation 9.17 is employed in the accompanying software program that enables the prediction of linear melt rheology based on the determination of molecular weight.

## 9.3 PROCESSING OF PLA: GENERAL CONSIDERATIONS

The bulk properties of PLA are greatly affected by the molecular weight of the polymer, the chain architecture (branched versus linear), and the degree of crystallinity [17, 18]. The relative proportions of L- and D-lactide in the polymer backbone determine the amount of crystallinity of a PLA sample. A diagram of representative backbones is provided in Figure 9.3; the mirror image stereochemistry of poly(L-lactide) with respect to poly(D-lactide) reflects the same relationship as the respective monomers. The lactide dimer obtained from the condensation of one L- and one D-lactic acid is called L,D-lactide (or *meso*-lactide)—a representative polymer structure obtained from this monomer is also shown in Figure 9.3.

The stereochemistry illustrated in Figure 9.3 profoundly affects crystallinity in PLA. Samples containing 87.5% L-lactide are completely amorphous, while samples with 92% L-lactide possess some crystallinity [19]. Polymers from 100% L-lactide can be nearly half-crystalline [20]. The melting point ($T_m$) range of crystalline PLA is 145–186°C [17], although a blend of 100% D-lactide and 100% L-lactide polymers in a "stereocomplex" forms a closely packed crystalline

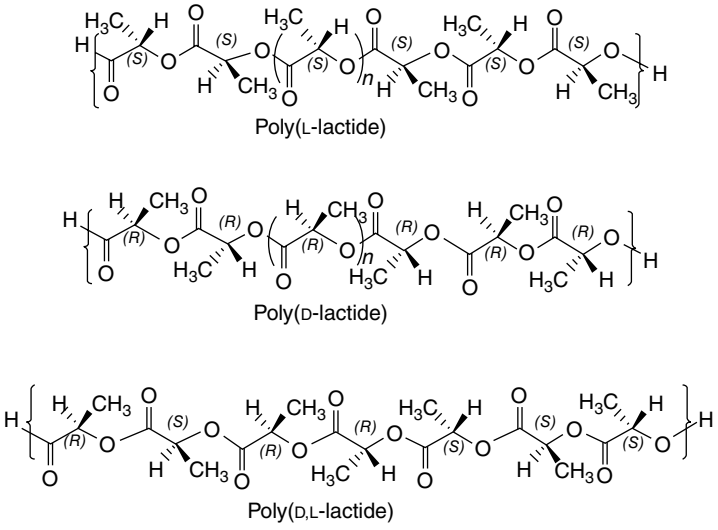


**FIGURE 9.3** Stereochemistry of L, D, and D,L-PLA backbones.

structure that increases the $T_m$ to 230°C [21]. The appearance of the PLA is also affected by the crystalline content. Amorphous PLA and low-crystalline PLA are clear materials with high gloss, while highly crystalline PLA is an opaque white material.

The molecular weight, structure, and crystallinity of PLA play important roles in its mechanical properties as well, including tensile strength, tensile modulus, and percent elongation to break [17, 18, 22]. Mechanical properties of solution-spun [23–27] and melt-spun [28–33] PLA fibers have been thoroughly investigated. It has been found that these properties are roughly equivalent to other polyesters, meaning that PLA can replace textiles based on nonrenewable resources. In addition, scanning electron microscopy (SEM) [23, 26, 29, 33] and wide-angle X-ray scattering (WAXS) [28, 34] have been useful in examining surface structure with respect to roughness and fracture surfaces. Understanding surface properties is important for dying and other textile finishing operations.

Cicero et al. have provided a complete characterization of the hierarchical fiber morphology from linear PLAs [35, 36], determining thermal, mechanical, and morphological properties of the fibers and showing that properties can be widely manipulated through a combination of processing temperature and draw ratio (the amount of stretching the fiber undergoes). Maximum tensile strength and modulus of 0.38 and 3.2 GPa, respectively, were obtainable. Again, such studies have been instrumental in establishing the suitability of PLA as a textile fiber. Atomic force microscopy showed that the fiber morphology was found to be highly fibrillar with microfibril diameters of ~40 nm. The same researchers have studied the effects of branching on fiber properties and morphology [37], and investigated the improvement of fiber properties specifically when thermally stabilized PLA is used [38]. These research studies provide several routes for optimizing the performance of PLA when used as a textile fiber.

## 9.4 MELT RHEOLOGY: AN OVERVIEW

Plastics are typically fabricated into useful articles in the molten state through melt flow, and therefore rheological properties of a polymer are considered to be of great importance. A polymer melt or solution can deform via shear, tensile (elongation), hydrostatic compression, or some combination of these. For introductory purposes, consider simple shear deformation as depicted in Figure 9.4. Here, a cubical volume element is undergoing a shear deformation due to an applied force, $F$, that acts parallel to one of the upper faces of the cube having a cross-sectional area of $A$. The shear stress, $\tau$, that results is defined according to Equation 9.18.

$$\tau = F / A \tag{9.18}$$

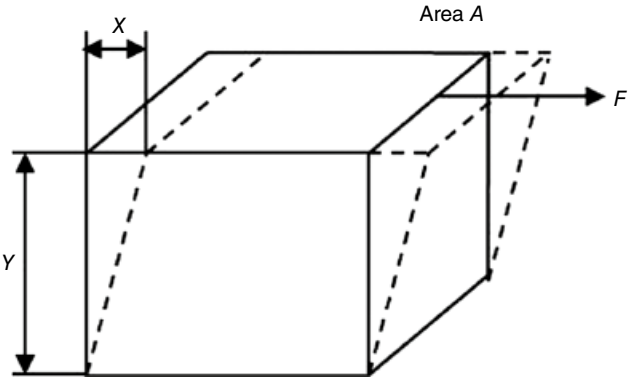


**FIGURE 9.4** Element undergoing shear deformation due to an applied force.

Provided the deformation is uniform, the shear strain, $\gamma$, is given by Equation 9.19

$$\gamma = X / Y \tag{9.19}$$

The velocity gradient, or shear rate, $\dot{\gamma}$, is also very important in describing the response of a polymer to deformation,

$$\dot{\gamma} = \frac{\mathrm{d}}{\mathrm{d}t}(\gamma) = \frac{\mathrm{d}}{\mathrm{d}t}\left(\frac{X}{Y}\right) = \frac{1}{Y}\frac{\mathrm{d}X}{\mathrm{d}t} = \frac{V}{Y} = \frac{\mathrm{d}V}{\mathrm{d}Y} \tag{9.20}$$

where $V$ denotes velocity of the fluid. The rate of deformation is characterized by the shear rate and rate dependence of properties is the hallmark of viscoelasticity that so dominates the behavior of polymer melts. Specifically, what is important is how fast is the rate of deformation relative to the rate at which molecular motions can occur. The relationship between these relative rates depends, of course, on the conditions of the flow, with temperature having a dominant effect.

The viscosity, $\eta$, is often described as the resistance of a material to flow; the greater the viscosity, the greater the force needed to deform the fluid. That is, viscosity relates the measurable shear stress to the imposed shear rate (or vice versa). For Newtonian fluids, the viscosity is independent of shear rate and the stress may be written as follows:

$$\tau = \eta\dot{\gamma} \tag{9.21}$$

From Equation 9.21, the dimensions of viscosity are stress multiplied by time, and in the SI system viscosity is measured in units of pascal-seconds (Pa s). For polymer melts and solutions, the fluid behavior is non-Newtonian, and Equation 9.21 must be modified to allow the viscosity to become a material function of the shear rate. Similarly, material elements may be deformed by pulling on opposite sides of the cube with an equal force; this constitutes an

extensional deformation that may be characterized by an extensional viscosity.

For solid materials, the relationship between stress, $\tau$, and strain, $\gamma$, is governed by the shear modulus, $G$,

$$\tau = G\gamma \tag{9.22}$$

For such elastic materials, there is no rate dependence. An elastic material subjected to an extensional deformation is characterized by a Young's modulus, $E$.

Consider the case of a time-varying shear deformation, specifically the case in which the strain is given by a sine wave of frequency $\omega$ and amplitude $A(\omega)$ according to Equation 9.23

$$\gamma(\omega) = A(\omega)\sin(\omega t) \tag{9.23}$$

The corresponding shear rate would be given by

$$\dot{\gamma}(\omega) = \omega A(\omega)\cos(\omega t) \tag{9.24}$$

For a viscous material, as defined by Equation 9.21, the stress would be

$$\tau(\omega) = \eta\dot{\gamma}(\omega) = \eta\omega A(\omega)\cos(\omega t) \tag{9.25}$$

whereas for an elastic material, as defined by Equation 9.22, the stress would be

$$\tau(\omega) = G\gamma(\omega) = GA(\omega)\sin(\omega t) \tag{9.26}$$

That is, for an elastic material, the stress would be in phase with the imposed strain; in contrast, Equation 9.25 shows that the stress would be 90° out of phase with the strain for a viscous material.

For viscoelastic materials such as polymer melts and solutions, the stress contains both in-phase and out-of-phase components. In the small deformation limit where the stress remains linear with respect to the amplitude of the applied strain, the response may be written as

$$\tau(\omega) = A(\omega)\left[G'(\omega)\sin(\omega t) + G''(\omega)\cos(\omega t)\right] \tag{9.27}$$

where the frequency (i.e., rate of deformation)-dependent moduli $G'(\omega)$ and $G''(\omega)$ are known as the storage and loss moduli, respectively. The storage modulus represents the elastic or in-phase response of the material and the loss modulus reflects the viscous or out-of-phase response. Due to their rate dependence, these are known as the dynamic moduli.

From the dynamic moduli, it is possible to construct a complex viscosity, the magnitude of which is given by Equation 9.28.

$$\left|\eta^*(\omega)\right| = \sqrt{\left(\frac{G'(\omega)}{\omega}\right)^2 + \left(\frac{G''(\omega)}{\omega}\right)^2} \tag{9.28}$$

The empirical Cox–Merz rule simply states that the magnitude of the dynamic viscosity as a function of the frequency is equal to the steady viscosity as a function of shear rate.

## 9.5 PROCESSING OF PLA: RHEOLOGICAL PROPERTIES

As discussed above, PLAs have physical properties useful in fibers, packaging, and other applications traditionally dominated by petroleum-based resins. Although the general literature on polylactides is extensive, only a few articles [39–43] have considered rheological properties. Measurements of dynamic, steady, and transient shear viscosities have been presented and the extensional data on PLA showed a strong strain hardening behavior [43].

The rheology of blends of linear and branched PLA architectures has also been comprehensively investigated [42, 44]. For linear architectures, the Cox–Merz rule relating complex viscosity to shear viscosity is valid for a large range of shear rates and frequencies. The branched architecture deviates from the Cox–Merz equality and blends show intermediate behavior. Both the zero shear viscosity and the elasticity (as measured by the recoverable shear compliance) increase with increasing branched content. For the linear chain, the compliance is independent of temperature, but this behavior is apparently lost for the branched and blended materials. These authors use the Carreau–Yasuda model, Equation 9.29, to describe the viscosity shear rate dependence of both linear and branched PLAs and their blends:

$$\eta = C_1\left[1 + \left(C_2\dot{\gamma}\right)^{C_3}\right]^{((C_4-1)/C_3)} \tag{9.29}$$

where $\eta$ is the viscosity, $\dot{\gamma}$ is the shear rate, and $C_1$–$C_4$ are material-dependent parameters. $C_1$ determines $\eta_0$ that decreases with increasing linear content. $C_2$ is the relaxation time corresponding approximately to the reciprocal of frequency for the onset of shear thinning. $C_3$ determines the shear thinning that increases with increasing branched PLA content; that is, branched PLA shear thins more strongly than the linear material. The increase of both $\eta_0$ and shear thinning with the addition of branching is also reported by other studies on PLA polymers with star polymer chain architectures.

Tensile and thermal properties of the linear-branched blends were also measured and found to be equal within the statistical error of the experiments. The results suggest that

excellent control over rheological behavior of PLA is possible through blending chain architectures without compromising mechanical properties.

The above studies do not, however, capture a systematic description of PLA rheology across a broad range of stereooptical compositions, as the materials studied possessed high (>90%) L-stereochemical center content. However, one study [3] does provide a comprehensive evaluation of the linear viscoelastic properties of PLA across a wide range of molecular weights and stereochemical compositions. The major points of this study are summarized here. This study also serves as the basis for the software included with this text for predicting viscoelastic properties of PLAs.

An important consideration in studying the melt rheology of PLA is melt stability; at high enough temperatures, PLA will degrade in molecular weight as time progresses. This makes melt stabilization crucial to good measurement science. The protocol put forth by Dorgan and coworkers consists of adding tris(nonylphenyl)phosphite (TNPP) as a stabilizer so that the measurement range could be extended to 200°C with negligible degradation. The TNPP concentration used is 0.35 wt%, and this was found to be suitable for the vicinity of 200°C by Lehermeier and Dorgan [42]. However, direct addition of neat additive to melts in an internal mixer [43] may be inadequate. Instead, weighed quantities of the polymers must be dissolved in and then recovered from fixed volumes of dichloromethane ($CH_2Cl_2$) solutions containing an appropriate concentration of TNPP by evaporation of the solvent in a vacuum oven at 40°C. This leaves appreciable $CH_2Cl_2$ dissolved in the solid polymer that must be removed by preheating the polymer to above the melting point (180°C) in a vacuum oven for 5 min. Subsequently, samples can be compression molded into disks suitable for rheological testing.

To facilitate data reduction, a model of the rheological response is desirable. The Havriliak and Negami (HN) model for complex viscosity is written as

$$\eta^*(\omega) = \eta_\infty + (\eta_0 - \eta_\infty)\left[1 + (i\tau_0\omega)^\alpha\right]^{(\nu-1)/\alpha} \tag{9.30}$$

This has five easily interpretable parameters, each corresponding to a readily discernible feature in a plot of log $|\eta^*|$ versus log $\omega$. The parameter $\eta_\infty$ is the often negligible or experimentally inaccessible high-frequency limiting value of $|\eta^*|$. In case $\eta_\infty$ is negligible, Equation 9.30 reduces to

$$\eta^*(\omega) = \eta_0\left[1 + (i\tau_0\omega)^\alpha\right]^{(\nu-1)/\alpha} \tag{9.31}$$

Taking the scalar magnitude of both sides of Equation 9.31 leads to

$$|\eta^*(\omega)| = \frac{\eta_0}{\left[1 + 2(\omega\tau_0)\cos(\alpha\pi/2) + (\omega\tau_0)^{2\alpha}\right]^{(1-\nu)/2\alpha}} \tag{9.32}$$

The effect of changing the model parameters of Equation 9.32 is presented in Figures 9.5–9.8.

Figure 9.5 shows the effect of changing $\eta_0$, the zero shear viscosity, while keeping all other parameters fixed. This figure demonstrates that $\eta_0$ is simply a vertical scaling factor that sets the low-frequency limiting value of $|\eta^*|$.

Figure 9.6 shows the effect of changing $\tau_0$, a characteristic viscous relaxation time. As discussed above, when the molecular motion is fast relative to the timescale for deformation, even a polymer melt will flow like a Newtonian liquid—the viscosity will be independent of the shear rate.

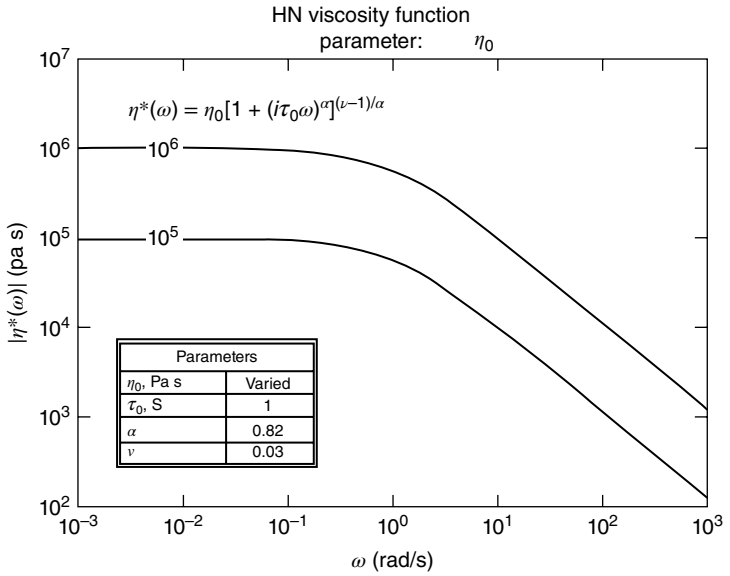


**FIGURE 9.5** Effect of changing the zero shear viscosity parameter in the HN model.

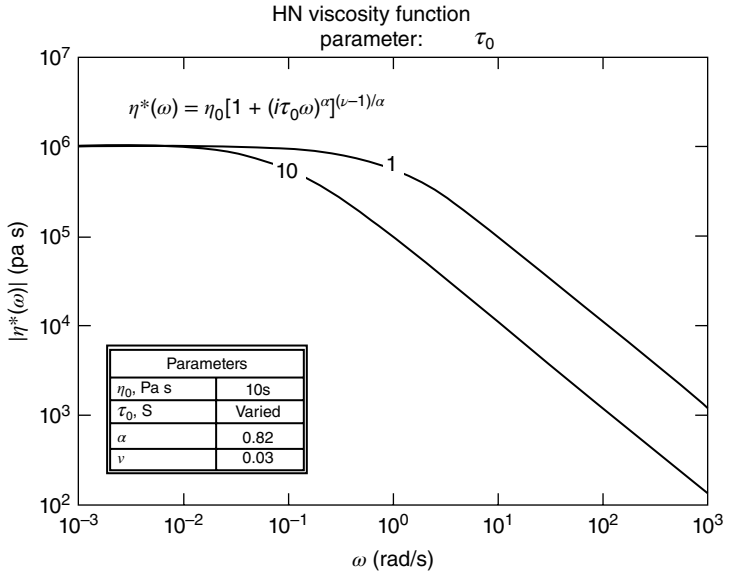


**FIGURE 9.6** Effect of changing the characteristic time parameter in the HN model.

However, when the deformation rate (the timescale of which is dictated by the inverse shear rate) exceeds the molecular relaxation rate, the polymers are deformed from their equilibrium conformations and shear thinning is observed. The value of $\tau_0$ in the model dictates when this transition takes place on the horizontal scale (frequency) as shown in Figure 9.6.

The parameter $\alpha$ is an inverse measure of the breadth of the relaxation spectrum, or a direct measure of the sharpness of the "knee" over which the transition from Newtonian flow to shear thinning takes place. The effect of changing this parameter is illustrated in Figure 9.7. This graph shows that a useful feature of Equation 9.32 is that the sharpness of the knee in the viscosity data may be easily adjusted independently of the high-frequency asymptotic slope through the parameter $\alpha$. However, values of $\alpha$ other than 1 cause an incorrect low-frequency scaling ($G'$ and $G''$ do not have appropriate slopes of 2 and 1, respectively, on a logarithmic scale), and accordingly the HN model should be considered only as a very useful empirical interpolating function.

Finally, as shown in Figure 9.8, $\nu - 1$ is the high-frequency limiting slope d[log $|\eta^*(\omega)|$]/d(log $\omega$) in the shear thinning regime. Examination of viscosities measured for model

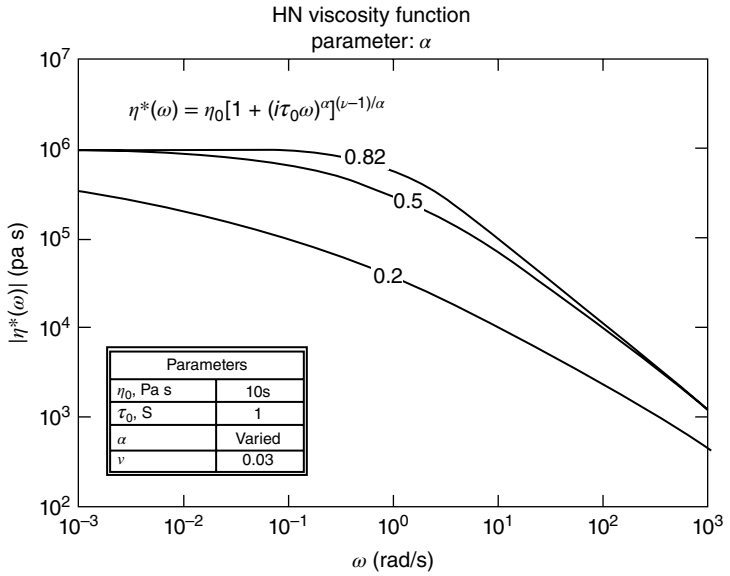


**FIGURE 9.7** Effect of changing α, the breadth parameter, in the HN model.

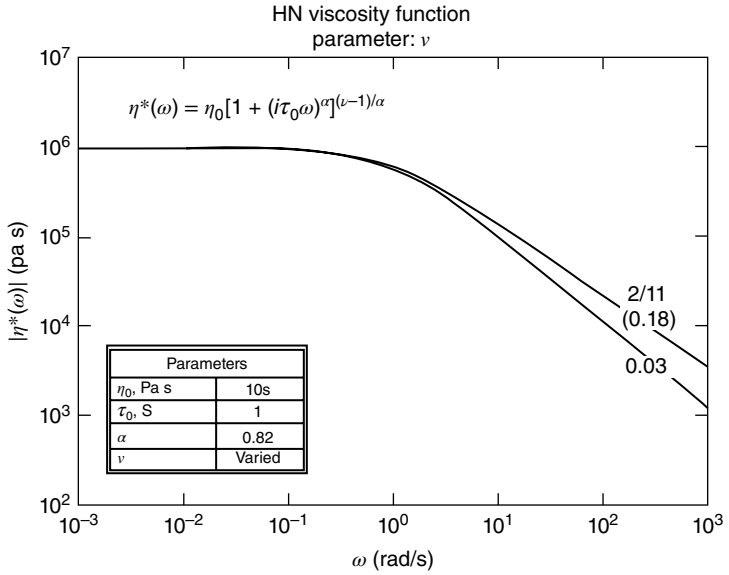


**FIGURE 9.8** Effect of changing the high-frequency $\nu$ parameter in the HN model.

linear flexible polymers of narrowly distributed high molecular weights and for the Curtis–Bird theoretical model [45] indicates a value of $\nu = 0.03 \pm 0.01$; therefore, $\nu$ is set equal to 0.03 in the model developed for linear PLAs.

Master curves based on the principle of time–temperature superposition can be constructed from measured values of $|\eta^*(\omega)|$ shifted vertically and horizontally as specified by Ferry [46]. Thus, horizontal shifting to a reference temperature $T_0$ and fitting provides the constants $c_1^0$ and $T_\infty$ (Vogel temperature) for the Williams–Landel–Ferry (WLF) shift factor $a_T$, where

$$-\log\left(a_T\right) = \frac{C_1\left(T - T_0\right)}{C_2 + \left(T - T_0\right)} = \frac{c_1^0\left(T - T_0\right)}{\left(T - T_\infty\right)} \qquad (9.33)$$

The average WLF parameters for PLA are $C_1 = 3.24\,\mathrm{K}^{-1}$ and $C_2 = 164.9\,\mathrm{K}$; the later correspond to a Vogel temperature of 288.25 K. Vertical shift factors given by $\rho_0 T_0/\rho T$ are first applied to the measured values of $G'$ and $G''$ using the known temperature dependence of density (Equation 9.13) before determining the shift factors [11]. This WLF temperature dependence is built into the accompanying software.

Figure 9.9 shows master curves ($G'$, $G''$, and $|\eta^*|$) for an amorphous PLA of high molecular weight. The symbols represent measurements shifted as described above. The continuous curves represent the best-fit two-mode HN model with frequency shifting factors for all temperatures calculated according to Equation 9.33 with a single pair of WLF constants. It is to be emphasized that the data is fit only to $|\eta^*|$ and the resulting values of $G'$ and $G''$ are calculated. Also,

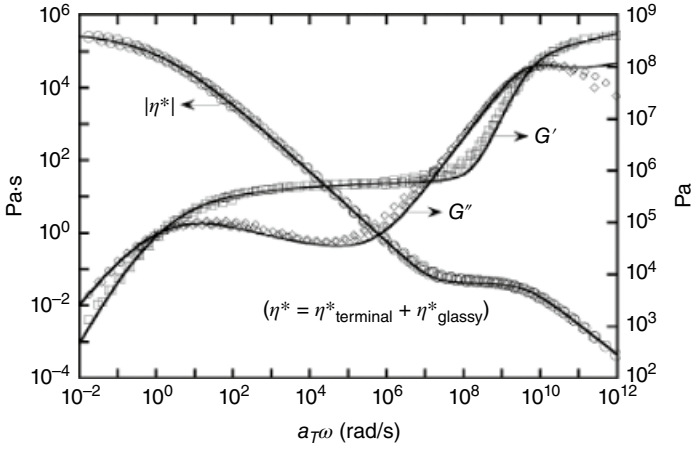


**FIGURE 9.9** Master curves for an amorphous PLA sample with a weight-average molecular weight $M_w$ = 570,000 g/mol over nearly 14 decades in frequency obtained via time–temperature superposition.

the $\eta_\infty$ parameter of the terminal mode serves as the $\eta_0$ for the glassy mode. The adopted phenomenological model is capable of describing the observed viscoelastic behavior over a large (nearly 14 decades) range of frequencies with a set of seven parameters.

Figure 9.10 presents measure of zero shear viscosities for a large collection of PLA samples. For the weight-average molecular weight range of $10^5$–$10^6$ g/mol and a reference temperature of 180°C, the zero shear viscosity is described well by the relationship regardless of the stereochemical composition. Likewise, average WLF parameters are $c_1 = 3.24\,\mathrm{K}^{-1}$ and $c_2 = 164.9\,\mathrm{K}$ across stereochemical composition. It is now clear that earlier reports [40, 41] of anomalously high scaling of the zero shear viscosity with molecular weight were artifacts of small data sets and thermal degradation. The present findings combined with an earlier study [43] in which samples have been stabilized against thermal degradation clearly demonstrate that the viscosity of PLA scales with molecular weight within the range is expected for linear flexible polymer chains. These findings [47] are built into the accompanying rheology software application.

Consistent values for plateau moduli, $G_N^0$, are obtained by integrations of either the relaxation spectra or the loss modulus [48] as described by Ferry [46]:

$$G_N^0 = \int_{\ln\tau_{min}}^{\ln\lambda} H(\tau)\,\mathrm{d}(\ln\tau) = \frac{2}{\pi}\int_{-\ln\lambda}^{-\ln\tau_{min}} G''(\omega)\,\mathrm{d}(\ln\omega) \tag{9.34}$$

where, in the limits of integration, $\ln\tau_{min}$ is the abscissa where the relaxation spectrum function $H$ has its minimum value in the transition zone and $\lambda$ is a longest relaxation time, beyond which $H(\tau) = 0$. The plateau modulus value determined using Equation 9.34 for the data of Figure 9.9 is 1.0 MPa; analysis across a wide set of PLA samples provides values for the plateau modulus of $1.0 \pm 0.2$ MPa.

Plateau modulus results can be used to infer characteristic ratios according to a chain packing model. A packing model for linear chains [49] gives the entanglement molecular weight (or molecular weight between entanglements) as

$$M_e = \rho RT / G_N^0 \tag{9.35}$$

and the same reference then gives the characteristic ratio in terms of $M_e$:

$$C_\infty = 10\rho^{-2/3}\left(M_e\right)^{-1/3} M_1/\bar{L}^2 \tag{9.36}$$

Additional characteristics of chains in the melt that are available from the packing scheme are the packing length [50],

$$p = \frac{M}{r_0^2 \rho N_A} \tag{9.37}$$

the tube diameter,

$$d_t = \left(\frac{M_e\left\langle r^2\right\rangle_0}{M}\right)^{1/2} \tag{9.38}$$

and the critical entanglement molecular weight [49]

$$M_c = 4.24\,p^{-0.65} M_e \tag{9.39}$$

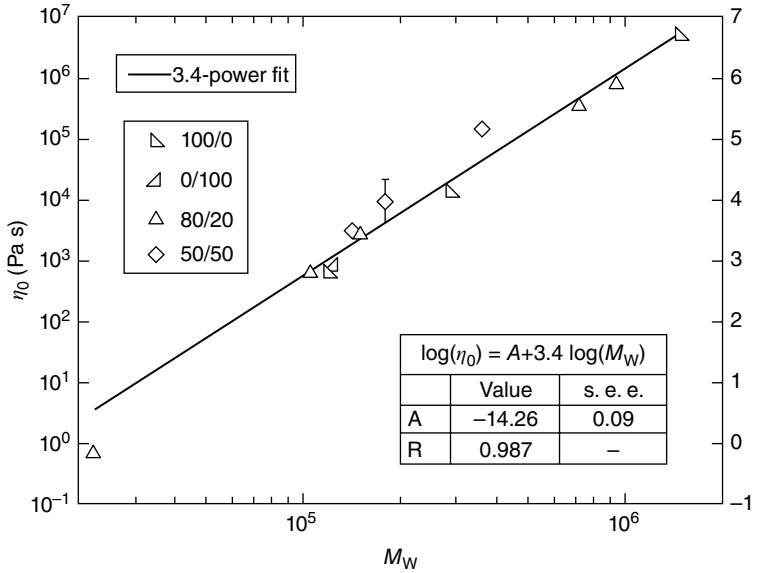


**FIGURE 9.10** Scaling of the zero shear viscosity against molecular weight for PLA samples of variable optical composition.

**TABLE 9.2 Flexible Linear Polymer Melt Chain Comparisons.**

| Polymer Characteristic | Value | | |
|---|---|---|---|
| | PLA (140°C) | PEO (140°C) | i-PP (190°C) |
| $M_l$ (relative molecular mass per backbone bond) | 24.02 | 14.68 | 21.04 |
| $\bar{L}^2$ (Å$^2$) | 2.05 | 2.11 | 2.37 |
| $\rho$ (g/cm$^3$) | 1.152 | 1.034 | 0.759 |
| $G_N^0$ (MPa) | 1.0 | 1.8 | 0.43 |
| $M_e$ (g/mol) | 3959 | 1973 | 6,797 |
| $M_e/M_l$ (backbone bonds) | 165 | 134 | 323 |
| $M_c$ (g/mol) | 9211 | 5330 | 13,635 |
| $M_c/M_l$ (backbone bonds) | 383 | 363 | 648 |
| $\langle r^2\rangle_o/M$ (Å$^2$) | 0.574 | 0.805 | 0.694 |
| $C_\infty$ | 6.7 | 5.6 | 6.2 |
| $p$ (packing length) (Å) | 2.51 | 1.99 | 3.15 |
| $d_t$ (tube diameter) (Å) | 47.7 | 39.9 | 68.7 |
| $d_t/p$ (Ronca–Lin ratio) | 19.0 | 20.0 | 21.8 |

$M_c$ represents the molecular weight that must be reached in order to have the zero shear viscosity follow the scaling of Figure 9.10. Rheological measurements combined with the packing model allow a comparison of various molecular parameters for PLA with other known polymer structures.

Table 9.2 collects various PLA properties obtained using Equations 9.35 and 9.36. For comparison, values for two other linear polymers are also tabulated: poly(ethylene oxide) (PEO) and isotactic polypropylene (i-PP). These polymers are selected because they share some common molecular features with PLA. It should be noted that a distinction should be made regarding the nature of the oxygen group in the PLA backbone as it is part of a rigid ester linkage. This distinction is evident in the data; the tube diameter and the number of backbone bonds between entanglements ($M_e/M_l$) in PLA is greater than in PEO as the latter molecule has greater rotational freedom about the oxygen linkage within its backbone. In this respect, the comparison with i-PP is suitable if the virtual bond model of Flory and Tonelli [5, 6] is adopted (i.e., a virtual bond between the two carbons is envisioned as a result of the rigidity of the ester group). An important result presented in Table 9.2 is the finding that the so-called Ronca–Lin ratio is approximately 20; if a higher value of $C_\infty$ were accepted, this ratio would change and linear PLA would be distinct from the hundreds of linear polymer chains to which the packing model has been applied [51].

Two other noteworthy physical properties result from the examination of the data. These are the critical molecular weight for entanglement and the molecular weight between entanglements. Table 9.2 shows that these values are about 9000 and 4000 g/mol, respectively. For linear polymer melts, a factor of about 2 is a usual finding in polymer physics.

## 9.6 CONCLUSIONS

Dilute solution viscometry and melt rheology are fundamental techniques for characterizing polymeric materials. Given PLA's growing importance, it is important to understand the fundamental chain properties that are reflected in the data obtained using these experimental methods.

When performed correctly on high-quality data, Stockmayer–Fixman fitting of intrinsic viscosity data for three different solvents yields a consistent Mark–Houwink scale factor for theta conditions of $K\Theta = 0.107 \pm 0.022$ mL/g. This corresponds to unperturbed chain dimensions described by a characteristic ratio $C_\infty = 6.5 \pm 0.9$. Equations 9.9 and 9.17 can be used to determine calibrated absolute values for the viscometry averaged molecular weight of typical commercial PLAs.

The melt rheological properties are consistent with the packing model propounded by Fetters and coworkers. Using the packing model and an experimentally measured plateau modulus = 1.0 MPa ± 20% leads to an implied $C_\infty$ in the range $6.7 \pm 0.7$. Simulation methods have also been used to estimate PLA characteristic ratios. The study of Blomqvist [16] may be summarized as indicating characteristic ratios in the range $6.1 \pm 1.3$, in excellent agreement with the experimental results. While Blomqvist's computational study does find a systematic trend with optical composition, the predicted magnitude of the effect is small and lies within the range of uncertainty of the experimental investigations. Appreciably, larger values of $C_\infty$ or a strong dependence of this ratio on optical composition is not confirmed either experimentally or via molecular simulation. The careful experimental work is consistent not only with recent simulation work but also with the pioneering work of Tonelli and Flory [5, 6], who reported a characteristic ratio of about 4.5 (based on real chemical bonds as opposed to the value of 2.0 for the virtual bond model) and a temperature dependence that leads to a value of about 6 at 180°C. Accordingly, values of $C_\infty$ determined by solution, melt rheology, and simulation now agree and imply that the polylactides are typical linear flexible polymers.

Rheological and thermal measurements on a comprehensive and well-characterized set of homopolymers and copolymers spanning wide ranges of molecular mass and stereoisomer proportions (L-content) have been reported in the literature [47]. Within the weight-average molecular weight range of $10^5$–$10^6$ g/mol and a reference temperature of 180°C, the zero shear viscosity is described well by $\log(\eta_0) = -14.26 + 3.4\log(M_w)$, the plateau modulus is $1.0 \pm 0.2$ MPa, and average WLF parameters are $c_1 = 3.24\ K^{-1}$ and $c_2 = 164.9$ K; the later correspond to a Vogel temperature of 288.25 K. The values of the glass transition temperatures at infinite molecular weight for 100, 80, and 50% L-content are 60.2, 56.4, and 54.6°C, respectively. Based upon a chain packing model, molecular parameters determined include a

packing length of 2.51 Å, a tube diameter of 47.7 Å, and a characteristic ratio of $6.5 \pm 0.9$, independent of stereoisomeric composition. The critical molecular weight for entanglement, $M_c$, is found to be near 9000 g/mol, while the molecular weight between entanglements, $M_e$, is about 4000 g/mol.

## APPENDIX 9.A DESCRIPTION OF THE SOFTWARE

The software consists of a Microsoft Excel workbook that can be downloaded from ftp://ftp.wiley.com/public/sci_tech_med/poly(lactic_acid). There are two tabs in the workbook: one is labeled "plot" and the other "worksheet." The plot tab presents a log–log plot of the magnitude of the dynamic viscosity and the moduli ($G'$ and $G''$) as a function of frequency (in rad/s).

The user can change values for independent variables in the worksheet and see the resulting predictions updated in the plot tab. In addition, tabular data are updated in the worksheet. Only three independent variables may be changed, and these are the relative viscosity, the concentration, and the temperature. These variables appear at the top of the worksheet labeled as "user input" and are in red.

The concentration corresponds to the concentration used in performing a 1-point experiment according to Equation 9.17 and is entered in units of g/dL. The relative viscosity is the ratio of corrected flow times for the solution of the entered concentration to that of the pure solvent. The temperature is entered in units of degree Celsius. The reference temperature is fixed at 180°C.

The program uses the input value of concentration and relative flow times to calculate a molecular weight according to Equations 9.17 and 9.9. This value is used to calculate a zero shear viscosity, and average values for the other parameters of the HN model discussed in the text are adopted to calculate the frequency dependence (i.e., to calculate the viscoelastic moduli as a function of shear rate). All the values adopted in the model are disclosed on the worksheet page.

## REFERENCES


1. D. Garlotta, A literature review of poly(lactic acid), *J. Polym. Environ.* **2001**, *9*, 63–84.
2. P. Kratochvil, U. W. Suter, Definitions of terms relating to individual macromolecules, their assemblies, and dilute polymer solutions (1988), *Pure Appl. Chem.* **1989**, *61*, 211–241.
3. J. R. Dorgan, J. Janzen, S. B. Hait, D. K. Knauss, Fundamental solution and single chain properties of polylactides, *J. Polym. Sci. Part B* **2005**, *43*, 3100–3111.
4. J. Ren, O. Urakawa, K. Adachi, Dielectric study on dynamics and conformation of poly(D,L-lactic acid) in dilute and semidilute solutions, *Polymer* **2003**, *44*, 847–855.
5. A. E. Tonelli, P. J. Flory, The configuration statistics of random poly(lactic acid) chains. I. Experimental results, *Macromolecules* **1969**, *2*, 225–227.
6. A. E. Tonelli, P. J. Flory, D. A. Brant, The configurational statistics of random poly(lactic acid) chains. II. Theory, *Macromolecules* **1969**, *2*, 227.
7. A. Schindler, D. Harper, Polylactide. II. Viscosity–molecular weight relationships and unperturbed chain dimensions, *J. Polym. Sci. Polym. Chem. Ed.* **1979**, *17*, 2593–2599.
8. S. H. Kim, Y. K. Han, Y. H. Kim, S. I. Hong, Multifunctional initiation of lactide polymerization by stannous octoate/pentaerythritol, *Makromol. Chem.* **1992**, *193*, 1623–1631.
9. C. A. P. Joziasse, H. Veenstra, D. W. Grijpma, A. J. Pennings, On the chain stiffness of poly(lactide)s, *Macromol. Chem. Phys.* **1996**, *197*, 2219–2229.
10. S. Kang, G. Zhang, K. Aou, et al., Raman and light scattering analysis of poly(lactic acid) flexibility. *Polym. Prepr.* **2002**, *43*, 896–897.
11. D. R. Witzke, Introduction to properties, engineering, and prospects of polylactide polymers, Ph.D. thesis. Michigan State University, East Lansing, MI, 1997, xxvi + 389 pp.
12. H. G. Elias, Isorefractive and isopycnic solvent pairs, in: J. Brandrup, E. H. Immergut (Eds.), *Polymer Handbook*, Wiley, New York, 1989, III/13–23 pp.
13. H. G. Elias, Refractive indices of common solvents, in: J. Brandrup, E. H. Immergut (Eds.), *Polymer Handbook*, Wiley, New York, 1989, III/25–28 pp.
14. D. Fleischer, Physical constants of the most common solvents, in: J. Brandrup, E. H. Immergut (Eds.), *Polymer Handbook*, Wiley, New York, 1989, p. III/29.
15. J. R. Partington, *An Advanced Treatise on Physical Chemistry*, Longmans/Green, London/New York, 1953.
16. J. Blomqvist, RIS Metropolis Monte Carlo studies of poly(L-lactic), poly(L,D-lactic) and polyglycolic acids, *Polymer* **2001**, *42*, 3515–3521.
17. L. Lu, A. G. Mikos, Poly(lactic acid), in: J. E. Mark (Ed.), *Polymer Data Handbook*, Oxford University Press, New York, 1999, pp. 627–633.
18. I. Engelberg, J. Kohn, Physico-mechanical properties of degradable polymers used in medical applications: a comparative study, *Biomaterials* **1991**, *12*, 292–304.
19. M. Vert, G. Schwarch, J. Coudane, Present and future of PLA polymers, *JMS. Pure Appl. Chem.* **1995**, *A32*, 787–796.
20. M. H. Hartman, High molecular weight polylactic acid polymers, in: D. H. Kaplan (Ed.), *Biopolymers from Renewable Resources*, Springer, Berlin, 1998, pp. 367–411.
21. Y. Ikada, K. Jamshidi, H. Tsuji, S. H. Hyon, Stereocomplex formation between enantiomeric poly(lactides), *Macromolecules* **1987**, *20*, 904–906.
22. M. H. Naitove, Push is on to commercialize biodegradable lactide polymers, *Plast. Technol.* **1995**, *March*, 15–17.

23. L. Fambri, A. Pegoretti, C. Migliaarsesi, Biodegradable fibres. Part I. Poly-L-lactic acid fibres produced by solution spinning, *J. Mater. Sci. Mater. Med.* **1994**, *5*, 679–683.
24. S. Gogolewski, P. Mainil-Varlet, The effect of thermal treatment on sterility, molecular and mechanical properties of various polylactide. I. Poly(L-lactide), *Biomaterials* **1996**, *17*, 523–528.
25. I. Horácek, V. Kalísek, Polylactide. I. Continuous dry spinning-hot drawing preparation of fibers, *J. Appl. Polym. Sci.* **1994**, *54*, 1751–1757.
26. J. W. Leenslag, S. Gogolewski, A. J. Pennings, Resorbable materials of poly(L-lactide). V. Influence of secondary structure on the mechanical properties and hydrolyzability of poly(L-lactide) fibers produced by a dry-spinning method, *J. Appl. Polym. Sci.* **1984**, *29*, 2829–2842.
27. J. W. Leenslag, A. J. Pennings, High-strength poly(L-lactide) fibres by a dry-spinning/hot-drawing process, *Polymer* **1987**, *28*, 1695–1702.
28. B. Eling, S. Gogolewski, A. J. Pennings, Biodegradable materials of poly(L-lactic acid): 1. Melt spun and solution-spun fibers, *Polymer* **1982**, *23*, 1587–1593.
29. L. Fambri, A. Pegoretti, R. Fenner, S. D. Incardona, C. Migliaresi, Biodegradable fibres of poly(L-lactic acid) produced by melt spinning, *Polymer* **1997**, *38*, 79–85.
30. S. D. Incardona, L. Fambri, C. Migliaresi, Poly-L-lactic acid braided fibres produced by melt spinning: characterization and in vitro degradation, *J. Mater. Sci. Mater. Med.* **1996**, *7*, 387–391.
31. K. Mezghani, J. E. Spruiell, High speed melt spinning of poly(L-lactic acid) filaments, *J. Polym. Sci. Part. B* **1998**, *36*, 1005–1012.
32. G. Schmack, B. Tändler, R. Vogel, R. Beyreuther, S. Jacobsen, H. G. Fritz, Biodegradable fibers of poly(L-lactide) produced by high-speed melt spinning and spin drawing, *J. Appl. Polym. Sci.* **1999**, *73*, 2785–2797.
33. X. Yuan, A. F. T. Mak, K. W. Kwok, et al., Characterization of poly(L-lactic acid) fibers produced by melt spinning, *J. Appl. Polym. Sci.* **2001**, *81*, 251–260.
34. W. Hoogsteen, A. R. Postema, A. J. Pennings, Crystal structure, conformation, and morphology of solution-spun poly(L-lactide) fibers, *Macromolecules* **1990**, *23*, 634–642.
35. J. A. Cicero, J. R. Dorgan, Physical properties and fiber morphology of poly(lactic acid) obtained from continuous two-step melt spinning, *J. Polym. Environ.* **2001**, *9*, 1–15.
36. J. A. Cicero, J. R. Dorgan, J. Janzen, et al., Supramolecular morphology of two-step melt-spun poly(lactic acid) fibers, *J. Appl. Polym. Sci.* **2002**, *86*, 2828–2838.
37. J. A. Cicero, J. R. Dorgan, J. Garrett, et al., Effects of molecular architecture on two-step melt-spun poly(lactic acid) fibers, *J. Appl. Polym. Sci.* **2002**, *86*, 2839–2846.
38. J. A. Cicero, J. R. Dorgan, S. F. Dec, D. M. Knauss, Phosphite stabilization effects on two-step melt-spun fibers of polylactide, *Polym. Degrad. Stab.* **2002**, *78*, 95–105.
39. G. Biresaw, C. J. Carriere, Interfacial tension of poly(lactic acid)/polystyrene blends, *J. Polym. Sci. Part B* **2002**, *40*, 2248–2258.
40. J. J. Cooper-White, M. E. Mackay, Rheological properties of poly(lactides). Effect of molecular weight and temperature on the viscoelasticity of poly(L-lactic acid), *J. Polym. Sci. Part B* **1999**, *37*, 1803–1814.
41. J. R. Dorgan, J. S. Williams, Melt rheology of poly(lactic acid): entanglement and chain architecture effects, *J. Rheol.* **1999**, *43*, 1141–1155.
42. H. J. Lehermeier, J. R. Dorgan, Melt rheology of poly(lactic acid): consequences of blending chain architectures, *Polym. Eng. Sci.* **2001**, *41*, 2172–2184.
43. L. I. Palade, H. J. Lehermeier, J. R. Dorgan, Melt rheology of high-L content poly(lactic acid), *Macromolecules* **2001**, *34*, 1384–1390.
44. H. J. Lehermeier, Poly(lactic acid): an environmentally benign polymer derived from corn: rheological and permeation properties, M.S. thesis, Colorado School of Mines, Golden, CO, 2000, xvii + 122 pp.
45. R. B. Bird, R. C. Armstrong, O. E. Hassager, *Dynamics of Polymeric Liquids*, Vol. *2*, 2nd edition, Wiley, New York, 1987.
46. J. D. Ferry, *Viscoelastic Properties of Polymers*, Wiley, New York, 1980.
47. J. R. Dorgan, J. Janzen, M. P. Clayton, et al., Melt rheology of variable L-content poly(lactic acid), *J. Rheol.* **2005**, *49*, 607–619.
48. J. M. Dealy, K. F. Wissbrun, *Melt Rheology and Its Role in Plastics Processing*, Van Nostrand Reinhold, New York, 1990.
49. L. J. Fetters, D. J. Lohse, W. W. Graessley, Chain dimensions and entanglement spacings in dense macromolecular systems, *J. Polym. Sci. Part B* **1999**, *37*, 1023–1033.
50. L. J. Fetters, D. J. Lohse, R. H. Colby, Chain dimensions and entanglement spacings, in: J. E. Mark (Ed.), *Physical Properties of Polymers Handbook*, AIP Press, New York, 1996, pp. 335–340.
51. L. J. Fetters, D. J. Lohse, S. T. Milner, W. W. Graessley, Packing length influence in linear polymer melts on the entanglement, critical, and reptation molecular weights, *Macromolecules* **1999**, *32*, 6847–6851.


# 10

# MECHANICAL PROPERTIES

Mohammadreza Nofar, Gabriele Perego, and Gian Domenico Cella

## 10.1 INTRODUCTION

Polylactide (PLA) is a glossy, high modulus (elastic modulus of about 3–4 GPa), and high strength (tensile strength of ~50–70 MPa) thermoplastic biopolymer with properties comparable to those of polystyrene (PS) and poly (ethylene terephthalate) (PET). The modulus and strength of PLA are higher than those of polypropylene (PP) and high-density polyethylene (HDPE). Aside from these high mechanical performances, its low elongation at break (i.e., low ductility), low toughness, and impact resistance limit PLA's usage. This is because PLA has a glass transition temperature ($T_g$) of about 55–65°C making it brittle at room temperature, fracturing through a crazing mechanism. Consequently, due to its comparable mechanical properties with those of the noted conventional petroleum-based polymers and upon enhancements in its ductility, toughness, and impact properties, PLA could be considered as a promising bioplastic in many commodity and engineering applications, such as plastic utensils, films and packaging, textiles and fibers, construction and automotive. Due to its biocompatibility and biodegradability, PLA is also widely used in biomedical applications, such as scaffolding, tissue engineering, and drug delivery [1–4]. In drug release applications, amorphous PLAs could sometime be preferred since the crystallinity could retard the degradation of PLA [5]. For applications where higher mechanical and thermomechanical properties are required, semicrystalline PLAs are often more favorable.

Homopolymers of PLA based on either L-lactic acid (i.e., PLLA) or D-lactic acid (i.e., PDLA) monomers are generally semicrystalline materials although their crystallization kinetics are slower than many other conventional semicrystalline thermoplastics. Homopolymer PLAs are, nowadays, still very expensive as their synthesis is not as cost-effective as that of copolymer PLAs. Therefore, their application is limited to mostly biomedical applications. In copolymer PLAs, the molecular backbone is generally based on L-lactic acid with a certain content of D-lactic acid monomers. The increase in D-lactic acid content suppresses the crystallizability of PLA [6]. In this context, the PLAs with D-content beyond 8 mol% are considered as fully amorphous systems, whereas those possessing D-content between 4 and 8 mol% are PLAs with very slow crystallization [1, 7, 8].

The properties and hence the application of various types of PLAs vary depending on their molecular weight, molecular structure (i.e., linear versus branched), and molecular configuration (i.e., D-lactic acid content). All these parameters significantly affect PLA's melt properties, crystallization kinetics, and hence its processability, as well as its final mechanical performance [8–10]. Although the molecular weight, structure, and configuration of PLA can substantially influence its crystallization and rheological properties, typically these parameters mainly influence the mechanical strength and modulus. In other words, its drawbacks, which are its brittleness and low toughness and impact strength, cannot be enhanced dramatically with such molecular modifications. It is worth mentioning that the mechanical properties of PLA are not significantly influenced by its synthesis methods [7, 11].

Due to the slow crystallization of PLA after various processing steps such as injection molding, annealing can be an approach to induce cold crystallization in crystallizable PLAs. Depending on the annealing temperature and time, various crystal structures can be induced depending on

*Poly(Lactic Acid): Synthesis, Structures, Properties, Processing, Applications, and End of Life*, Second Edition.
Edited by Rafael A. Auras, Loong-Tak Lim, Susan E. M. Selke, and Hideto Tsuji.

whether crystal nucleation or growth dominates. Although such induced cold crystallinity can enhance the modulus and strength of PLA and structures with a larger number of spherulites can positively affect the toughening of PLA, the control of crystallinity and the crystallization kinetics is not considered to be an effective approach to noticeably improve the ductility and impact properties of PLA [12].

Chain branching of PLA molecules has also been employed to enhance the low melt strength and slow crystallization kinetics of PLA, which can improve its poor processability, formability, and foamability [9, 13–21]. Such chain branching, however, does not generally greatly affect the final mechanical performance of PLA products.

The development of PLLA/PDLA blends, which introduces stereocomplex crystals, has been shown to be an effective route to enhance the melt rheological properties of PLA while enhancing its processability [22–28]. In the presence of such stereocomplex crystals, the final modulus and strength of PLA can be enhanced although the final ductility, toughness, and impact properties of PLA do not significantly improve. Moreover, PLLA and PDLA raw materials are expensive, and the development of PLLA/PDLA blends is still not fully cost-effective for commodity and engineering applications [27].

While the development of PLA composites and nanocomposites can improve the rheological properties, crystallization kinetics, and mechanical strength and stiffness of PLA, the use of fibers or micro-/nano-size reinforcements does not effectively enhance the ductility and impact resistance of PLA [29, 30].

Efforts to improve the major mechanical drawbacks of PLA (i.e., brittleness, low toughness, and impact strength) can, however, be tackled through copolymerization [31], plasticization [32, 33], blending with other polymers [27, 28], and development of microfibrillated composites (MFCs) of PLA [34, 35], which are the subject of other chapters. In this chapter, the mechanical properties of PLA materials are first introduced as a general framework. Along with that, the dependency of mechanical performance of PLA on temperature, relaxation and aging, annealing, orientation, stereoregularity of PLA molecules, and the use of reinforcements are explored. The effect of copolymerization, plasticization, and blending on the final mechanical properties of PLA are also discussed.

## 10.2 GENERAL MECHANICAL PROPERTIES AND MOLECULAR WEIGHT EFFECT

### 10.2.1 Tensile and Flexural Properties

Semicrystalline PLA has a tensile strength of approximately 50–70 MPa, tensile modulus of 3000–4000 MPa, elongation at break of 2–10%, flexural strength of 100 MPa, and flexural modulus of 4000–5000 MPa [2, 7, 11, 36–38]. PLA specimens obtained by a typical injection molding process are generally almost amorphous due to PLA's slow crystallization kinetics. In Tables 10.1 and 10.2, the results of physicochemical and mechanical characterization of, respectively, injection-molded crystallizable PLLA and amorphous

**TABLE 10.1 Mechanical Properties of PLLA Specimens with Different Molecular Weights [39]**

| Sample | PLLA I | | PLLA II | | PLLA III | |
|---|---|---|---|---|---|---|
| Annealing at 105°C | No | Yes | No | Yes | No | Yes |
| Molecular weight ($M_v$, Da) | 23,000 | 20,000 | 58,000 | 47,000 | 67,000 | 71,000 |
| $T_m$ (°C) | 178 | 178 | 179 | 180 | 181 | 178 |
| Crystallinity (%) | 9 | 70 | 9 | 52 | 3 | 45 |
| Tensile properties | | | | | | |
| Yield strength (MPa) | — | — | 68 | 68 | 70 | 70 |
| Tensile strength (MPa) | 59 | 47 | 58 | 59 | 59 | 66 |
| Yield elongation (%) | — | — | 2.3 | 2.2 | 2.2 | 2.0 |
| Elongation at break (%) | 1.5 | 1.3 | 5.0 | 3.5 | 7.0 | 4.0 |
| Elastic modulus (MPa) | 3550 | 4100 | 3750 | 4050 | 3750 | 4150 |
| Flexural properties | | | | | | |
| Flexural strength (MPa) | 64 | 51 | 100 | 113 | 106 | 119 |
| Maximum strain (%) | 2.0 | 1.6 | 4.1 | 4.8 | 4.7 | 4.6 |
| Elastic modulus (MPa) | 3650 | 4200 | 3600 | 4150 | 3650 | 4150 |
| Impact resistance | | | | | | |
| Izod, notched (kJ/m$^2$) | 1.9 | 3.2 | 2.5 | 7.0 | 2.6 | 6.6 |
| Izod, unnotched (kJ/m$^2$) | 13.5 | 18.0 | 18.5 | 34.0 | 19.5 | 35.0 |
| Heat resistance | | | | | | |
| HDT (°C) | 57 | 66 | — | — | 55 | 61 |
| Vicat penetration (°C) | 60 | 157 | 59 | 163 | 59 | 165 |
| Hardness | | | | | | |
| Rockwell hardness (scale H) | 85 | 84 | 83 | 84 | 88 | 88 |

**TABLE 10.2 Mechanical Properties of PDLLA Specimens with Different Molecular Weights [39]**

| Sample | PDLLA I | PDLLA II | PDLLA III |
|---|---|---|---|
| Molecular weight ($M_v$, Da) | 47,500 | 75,000 | 114,000 |
| Tensile properties | | | |
| Yield strength (MPa) | 49 | 53 | 53 |
| Tensile strength (MPa) | 40 | 44 | 44 |
| Yield elongation (%) | 1.7 | 1.4 | 1.5 |
| Elongation at break (%) | 7.5 | 4.8 | 5.4 |
| Elastic modulus (MPa) | 3650 | 4050 | 3900 |
| Flexural properties | | | |
| Flexural strength (MPa) | 84 | 86 | 88 |
| Maximum strain (%) | 4.8 | 4.1 | 4.2 |
| Elastic modulus (MPa) | 3500 | 3550 | 3600 |
| Impact resistance | | | |
| Izod, notched (kJ/m$^2$) | 1.8 | 1.7 | 1.8 |
| Izod, unnotched (kJ/m$^2$) | 13.5 | 14.0 | 15.0 |
| Heat resistance | | | |
| HDT (°C) | 51 | 50 | 50 |
| Vicat penetration (°C) | 52 | 53 | 52 |
| Hardness | | | |
| Rockwell hardness (scale H) | 78 | 72 | 76 |

poly(D,L-lactide) or *meso*-lactide (PDLLA) specimens with different molecular weights are presented [39].

From Tables 10.1 and 10.2, it is evident that in the selected range of molecular weights, the tensile and flexural properties of amorphous PDLLA and crystallizable PLLA are quite different. Tensile strength for PLLA typically ranges from about 50 to 70 MPa, while for PDLLA it ranges from 40 to 53 MPa. This difference is mainly related to the stereoregularity of the polymer chains, which are characterized, in the case of PLLA, by the presence of only *S*(−) chiral centers. It has been observed that after annealing at 105°C PLLA samples showed a crystallinity ranging from 45 to 70%, as revealed by DSC analysis (100% crystallinity = 93 J/g) [40]. Tensile strength of these PLLA samples ranged from 47 to 70 MPa in the same range of molecular weights. The effect of molecular weight on tensile and flexural properties is more evident in annealed PLLA than non-annealed PLLA and PDLLA specimens, with an increase of tensile strength from 47 to 66 MPa in the range of molecular weight between 20,000 and 70,000 g/mol (viscosity-average molecular weight, $M_v$). Above $M_v$ = 30,000–40,000 g/mol, the tensile and flexural properties of amorphous PLLA increase more gradually, while for annealed PLLA the same behavior is reached at higher molecular weight, near $M_v$ = 50,000–60,000 g/mol. In the case of PDLLA, the increase in tensile and flexural properties with molecular weight becomes less pronounced when the molecular weight is higher than 45,000–50,000 g/mol. A similar phenomenon is observed for non-annealed PLLA.

The dependence of PLA mechanical properties on its molecular weight has been investigated by many authors. According to the work of Engelberg and Kohn [38], the increase of molecular weight from 107,000 to 550,000 g/mol resulted in a 20% increase in tensile strength. In general, it seems that at high molecular weights, the variation of mechanical properties became less pronounced. Comparable values of tensile properties were observed by Grijpma et al. [41] who reported tensile strength of 47 MPa, elongation at break of 1.5%, and elastic modulus of 3650 MPa for unoriented PDLA with weight-average molecular weight of 241,000 g/mol. Slightly different tensile properties of commercial grade PLAs were also described by several authors [42, 43]. Extruded sheets of NatureWorks LLC amorphous PLA (grade 4060, with 12 mol% D-lactic acid content, and melt flow rate, MFR, of 7–10 g/10 min at 210°C) showed tensile strength of 44 MPa, elongation at break of 7%, and elastic modulus of 2500 MPa. Semicrystalline PLA from NatureWorks LLC (grade 4032, with 1.5 mol% D-lactic acid content, and MFR of 7 g/10 min at 210°C) was characterized by tensile strength of 54 MPa, elongation at break of 9%, and elastic modulus of 2600 MPa. The differences among the values reported in the literature are quite small; however, it is useful to highlight that the commercial PLA is manufactured by copolymerizing L-lactide with small amounts of *meso*-lactide to reduce material crystallinity and decrease brittleness. Another study reported tensile properties for commercial PLLA with $M_w$ = 84,000 g/mol manufactured by Mitsui Fine Chemicals (grade Lacea H.100-E, with 1 mol% D-lactic acid content, and MFR of 8 g/10 min at 190°C), which showed tensile strength of 66 MPa, elongation at break of 1.8%, and elastic modulus of 3300 MPa [44]. A lower value of elastic modulus was reported for PLLA with $M_w$ = 350,000 g/mol manufactured by Purac of 1151 MPa, with a yield stress of 62 MPa and strain at break of 14.5% [45]. It has been suggested that different methods used for specimen preparation and testing can contribute to different mechanical properties. Nevertheless, data reported in the literature are rather consistent in reporting PLA as having high elastic modulus, high tensile strength, and low deformability.

### 10.2.2 Impact Resistance

The impact resistance of PLA is significantly affected by notching. The values of Izod impact resistance of PLLA fall in the range of 2.0–3.0 kJ/m$^2$ for low-crystallinity (3–9%) samples. The values obtained with more crystalline PLLA (45–70%) are in the range of 3.0–7.0 kJ/m$^2$ [39]. PDLLA is characterized by lower values, with notched Izod impact resistance ranging from 1.5 to 2.0 kJ/m$^2$. In the case of

unnotched impact strength, the difference between PLLA samples of different crystallinity is even higher; samples of PLLA with low crystallinity (3–9%) show values ranging between 13 and 20 kJ/m$^2$, while samples with higher crystallinity (32–75%) are characterized by unnotched impact strength of 18–35 kJ/m$^2$. Other literature data shows values of notched impact strength of PLLA in the range of 2.0–2.6 kJ/m$^2$ [46] and unnotched impact strength of 12 kJ/m$^2$ [41]. A dependence of notched impact strength on notch radius was observed by Grijpma et al. [41], who reported that the strength values decreased from 2.2 to 1.2 kJ/m$^2$ when the radius decreased from 1.00 to 0.10 mm.

It is interesting to note that material processing has considerable effect on the impact resistance of PLA. Very-high molecular-weight PLLA ($M_v$ = 780,000 g/mol) shows impact strength values that decrease significantly from 47 kJ/m$^2$ for as-polymerized polymer to 12 kJ/m$^2$ for compression molded samples of the same material [47]. This behavior is clearly due to the loss of crystallinity associated with the fast cooling during the compression molding process.

PLA impact resistance also depends on molecular weight. Charpy impact strength values of 8 and 15 kJ/m$^2$ have been reported for PDLLA having molecular weight of 78,000 and 108,000 g/mol, respectively [41, 47]. More generally, Charpy impact strength values obtained with PDLLA range from 3.5 to 22 kJ/m$^2$, related to different molecular weights, while PLLA is characterized by values ranging from 10 to 35 kJ/m$^2$ [37, 48].

Therefore, since PLA is a material that is characterized by relatively low values of impact resistance, the effect of crystallinity and molecular weight must be taken into consideration in practical applications.

### 10.2.3 Hardness

Rockwell hardness of PLA generally ranges between 70 and 90 according to scale H [11, 39] and around 120 according to scale L [11]. The Rockwell hardness of PLLA is affected very little by crystallinity, as evidenced by the values reported in the literature that range from 83 to 88 H for amorphous PLLA and from 82 to 88 H for semicrystalline PLLA. Also, the dependence of Rockwell hardness on molecular weight appears quite small (Tables 10.1 and 10.2). However, the effect of $T_g$ is more evident. PDLLA, in fact, is characterized by lower hardness values, ranging from 72 to 78 H. The lower hardness values for PDLLA as compared with PLLA can be explained in terms of the lower $T_g$ of PDLLA [39].

Among biodegradable polymers, PLA is characterized by high elastic modulus and high hardness. These characteristics, which influence the applications of this material, are strictly related to its chemical composition. The presence of vicinal and regularly distributed polar ester groups, in fact, affects physicochemical interactions between polymer chains, thereby reducing the possibility of chain shear during physical deformation. Polar interchain interactions and the consequent high $T_g$, therefore, are the origin of the high hardness of PLA.

## 10.3 TEMPERATURE EFFECT

Enantiomerically pure PLLA is a semicrystalline polymer with a $T_g$ of 60–70°C and a melting point of about 180°C. Dynamic mechanical analysis (DMA) of PLLA reveals the α-relaxation associated with $T_g$ of the amorphous phase, as a maximum of tan δ peak and by loss modulus ($E''$) curves. The values reported in the literature for the maximum of the tan δ peak range from 65 to 72°C, measured at 1 Hz [48–50]. As expected, the a-relaxation temperature ($T\alpha$) values associated with glass transition of PLLA differ from the data obtained by DSC measurements. Lower $T_g$ values of PLLA are obtained by loss modulus, $E''$ curves, ranging from 52 to 60°C [50–54].

The $E''$ peak temperature is 58°C for amorphous PLA and 60°C for semicrystalline PLLA, while the tan δ peak is at 65°C for both materials [50]. The storage modulus of PLLA shows a rapid decrease at the temperature corresponding to α-relaxation; however, it is interesting to note that before this decrease there is a slight storage modulus ($E'$) increase. This behavior can be interpreted as the rearrangement of macromolecules, relieving the stress generated during processing. This cold crystallization process takes place at a temperature beyond the PLA's $T_g$ [52]. Therefore, DMA can be easily used to characterize the nonequilibrium crystallization of PLLA.

As shown in Tables 10.1 and 10.2, the heat deflection temperature (HDT) for PLA do not change much with molecular weight. Amorphous and semicrystalline PLLA show HDT values of 55–57°C and 60–66°C, respectively; therefore, PLA HDT seems to be minimally influenced by its crystallinity, with the crystalline PLA having slightly higher heat resistance than the amorphous PLA. This is due to the main effect of $T_g$ on HDT—an effect that is very similar in both cases. HDT value for PDLLA is around 50°C, and this difference is easily understandable if we take into consideration the physicochemical properties of this material; in fact, PDLLA exhibits the lowest $T_g$, around 50°C, approximately corresponding to its HDT value.

Vicat penetration is more influenced by the PLA's crystallinity. In the case of PDLLA and amorphous PLLA, Vicat penetration values of 52–53°C and 59–60°C, respectively, were reported. Also, these values are very near to the $T_g$ of the polymers. On the other hand, semicrystalline PLLA presents very different behavior, with Vicat penetration values of 157–165°C. This marked difference in Vicat penetration measurements is related to the contribution of crystallinity to thermomechanical properties of this material at a microscopic level [11, 39].

**TABLE 10.3 Influence of Temperature on PLA Flexural Properties [39]**

| Sample | PDLLA | PLLA Quenched | PLLA Annealed |
|---|---|---|---|
| Molecular weight ($M_v$, Da) | 75,000 | 58,000 | 47,000 |
| $T_g$ (°C) | 50 | 58 | 59 |
| Crystallinity (%) | 0 | 9 | 52 |
| **Properties at 23°C** | | | |
| Flexural strength (MPa) | 86 | 100 | 113 |
| Maximum strain (%) | 4.1 | 4.1 | 4.8 |
| Elastic modulus (MPa) | 3550 | 3600 | 4150 |
| **Properties at 36°C** | | | |
| Flexural strength (MPa) | 60 | 77 | 83 |
| Maximum strain (%) | 3.3 | 3.9 | 4.3 |
| Elastic modulus (MPa) | 2800 | 3400 | 3600 |
| **Properties at 56°C** | | | |
| Flexural strength (MPa) | 0.2 | 0.4 | 28 |
| Maximum strain (%) | n.d. | 8 | 7.5 |
| Elastic modulus (MPa) | 25 | 50 | 950 |

The available literature on PLA mechanical properties at different temperatures is reported in Table 10.3 [39]. As shown, the flexural properties of PDLLA, amorphous PLLA, and semicrystalline PLLA at 23, 36, and 56°C are different. At 36°C, the flexural modulus decreased by 30, 23, and 26% as compared with the 23°C data for PDLLA, PLLA quenched, and PLLA annealed, respectively. However, increasing the temperature to 56°C resulted in a marked drop of the flexural strength of PDLLA to 0.2 MPa. This result is expected due to glass transition at 50°C together with the lack of crystallinity for the PDLLA polymer. Similarly, the quenched amorphous PLLA shows a substantial reduction of flexural strength to 0.4 MPa at 56°C. Only annealed semicrystalline PLLA maintains useful mechanical properties of 28 MPa flexural strength. Evidently, a small amount of crystallinity (9%) for the quenched PLLA is not sufficient to provide thermomechanical properties that are useful in practice. Therefore, only PLLA that has been subjected to proper crystallization, by means of annealing, orientation, or nucleation, can offer useful properties for end-use applications where the temperature is greater than 50°C.

## 10.4 RELAXATION AND AGING

When PLLA is quenched from the melt and vitrified, a nonequilibrium glassy state is reached. Even in the glass, short-range mobility produces molecular rearrangements that drive the thermodynamic variables closer to their equilibrium values. The mobility of the polymer chains, that is, the ability to eliminate excess free volume, is directly related to temperature.

Figure 10.1 shows the dynamic mechanical spectrum reported by Celli and Scandola [55] for PLLA after heating at 200°C to erase the thermal history. The solid line refers to a

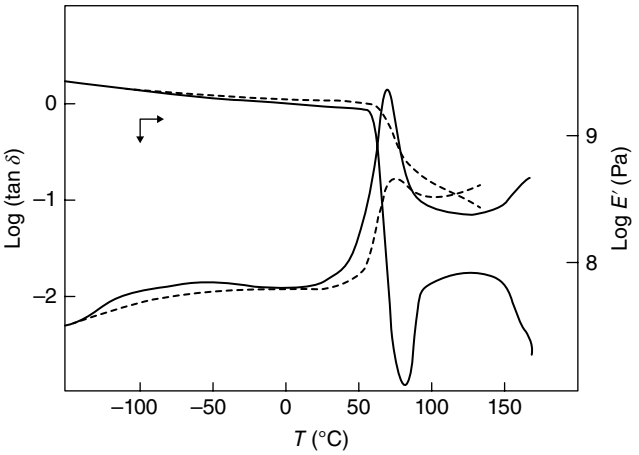


**FIGURE 10.1** Dynamic mechanical spectrum of poly(L-lactic acid) Resomer L 214, $M_v$ = 690,000, (—) first run, (- - -) second run [55].

sample quenched in a water–ice mixture after extrusion, while the broken line depicts an immediate rerun on the same sample, after cooling from 160°C. Below room temperature, no relaxation process is apparent in either curve, that is, the dynamic mechanical loss tangent is as low as $10^{-2}$ over the range of −150 to 20°C [55]. The absence of any loss phenomena below $T_g$ capable of mechanical energy dissipation is likely the reason for the observed brittleness of glassy PLLA of lower molecular weight. In the first run on the quenched PLLA, the loss tangent curve shows an intense relaxation peak in the range 50–80°C (peak value 70°C), which is associated with a steep drop in modulus. This relaxation phenomenon corresponds to the glass/rubber transition of PLLA, and its intensity indicates that a large fraction of the sample has been frozen in the glassy amorphous state after extrusion. The abrupt increase in $E'$ above 80°C reflects a sudden increase in rigidity of the material and indicates that, above $T_g$, the polymer chains have acquired enough mobility to crystallize during the DMA run.

The occurrence of crystallization is clearly demonstrated by the spectrum obtained in an immediate rerun (broken line in Figure 10.1), where the $T_g$ of PLLA appears as a tan δ peak of moderate intensity associated with a small decrease in the storage modulus. In this instance, only a small fraction of the sample undergoes the glass transition, owing to the presence of a significant crystalline phase. The crystallites cause the observed broadening of the tan δ peak [55].

Figure 10.2 shows how the glass transition region of the viscoelastic spectrum of PLLA is affected by aging. Here, the broken curves refer to a sample aged for nine days at 48°C, while the solid lines are for a sample without aging, which was obtained after an immediate rerun of the same sample cooled from 100°C. The aging effect is exemplified as decreasing the loss factor and increasing the storage modulus over the whole temperature range tested. As a result of aging, the mechanical characteristics of PLLA change due to

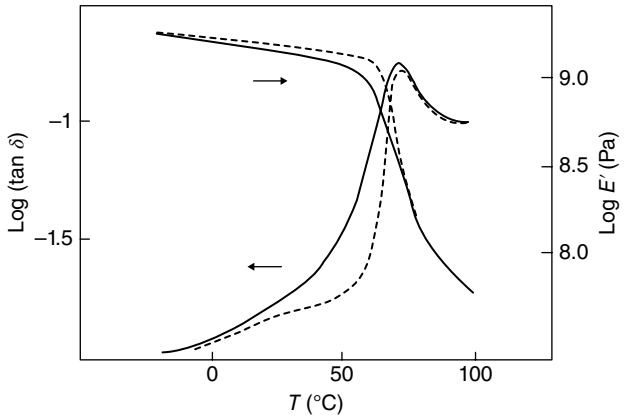


**FIGURE 10.2** Influence of aging on the dynamic mechanical spectrum of PLLA. Aging time: (—) zero, (- - -) nine days at 48°C [55].

the reduced ability for the material to dissipate energy through a reduction of molecular motion. The increased rigidity also results in a more brittle material [55].

Hot recoverable strain is also an important parameter directly related to the thermomechanical conditions applied during processing. PLA hot recoverable strain increases steadily with increasing shear stress due to increased molecular orientation. The tests performed on injection-molded PLA specimens show longitudinal shrinkage ranging from 5.7 to 10.6%, depending on the shear rate used during the injection molding process. This relationship is, however, quite moderate and it tends to diminish as the shear rate increases [56].

## 10.5 ANNEALING

As already stated, injection-molded PLA parts are generally amorphous, because of the slow crystallization kinetics of PLA. In general, the process of crystallization in semicrystalline polymers results in embrittlement of the material and hence results in a decrease of fracture toughness. The effect of annealing on the fracture toughness of PLLA has been investigated in material samples quenched and annealed in the work of Park et al. [57]. PLLA samples prepared by a quenching procedure show $T_g$ of 64°C, $T_m$ of 168°C, and crystallinity ($X_c$) of 2.7%, while those of the annealed samples are characterized by 66°C, 169°C, and 48%, respectively [57]. As evidenced by these data, $T_g$ and $T_m$ slightly increased due to the annealing treatment, which results in crystallization. Generally, the annealed material has higher $X_c$ ranging from 45 to 70%, as determined by DSC analysis, depending on its molecular weight.

In impact tests, different types of crack growth behavior were observed by polarized optical microscopy of annealed PLLA specimens, as illustrated in Figure 10.3 from the work of Park et al. [57].

The quenched sample that has been subjected to quasistatic deformation (Figure 10.3a) exhibits multiple crazes in the vicinity of the crack tip typical for amorphous polymers. Under the impact effect, the number of crazes is significantly reduced, as evidenced by Figure 10.3b. The annealed samples show cracks that propagate through spherulites and along spherulite boundaries with few or no crazes formed around the main crack. Also, in the annealed samples it is possible to observe that crack branching occurs at the quasistatic deformation rate, whereas only single cracks are observed at the impact rate [57]. The toughness of PLLA under impact loading is therefore increased by annealing.

The crystallization temperature peak of PLLA has been estimated to be about 123°C, and therefore a proper temperature for annealing is around 100°C. At this thermal condition, crystal growth is faster than at lower temperature. This is illustrated in Figure 10.4, where the microstructures of PLLA specimens annealed at 70 and 100°C at different treatment times are shown with polarized optical microphotography. The size of spherulites increases with annealing time and temperature, whereas the spherulite density increases with decreasing temperature [58].

From a quantitative point of view, the $X_c$ of quenched PLLA is generally around 3%, while PLLA annealed at 70 and 100°C can reach $X_c$ of 23 and 56%, respectively [58]. The storage modulus, $E'$, of PLLA, both quenched and annealed at 70°C, shows a sudden decrease around 60°C that is close to the $T_g$ of 64°C. This is evidenced by an $E'$ value that ranges between 5 and 10 MPa at 80°C. PLLA specimens annealed at 100°C maintain a higher value of storage modulus above 60°C, with $E'$ around 1000 Pa at 80°C, due to the $X_c$ contribution to the mechanical properties [58].

Samples of PLLA that have been annealed at 100–110°C are characterized by higher elastic modulus and lower strain at break in comparison to amorphous material (Table 10.1). These data agree well with those reported in the literature [7, 45]. In general, annealing of PLLA is accompanied by increases in tensile and flexural strengths, as well as impact resistance and thermomechanical properties. This increase of mechanical properties seems to reach a maximum around an $X_c$ of 65%. Above this value, material embrittlement becomes predominant [7]. By increasing the annealing temperature from 110 to 160°C, it is possible to increase the elastic modulus while decreasing the strain at break and tensile strength. Samples annealed at 120°C exhibit ductile failure while those annealed at 150°C have transitioned to brittle failure [45]. Even though PLLA deformability is slightly reduced by annealing, its thermomechanical properties are markedly improved by increasing the material $X_c$.

In another study, it was also revealed that the annealing of the injection molded crystallizable PLAs at different annealing temperatures and for different annealing times could differently enhance the crystallinity of PLA through different

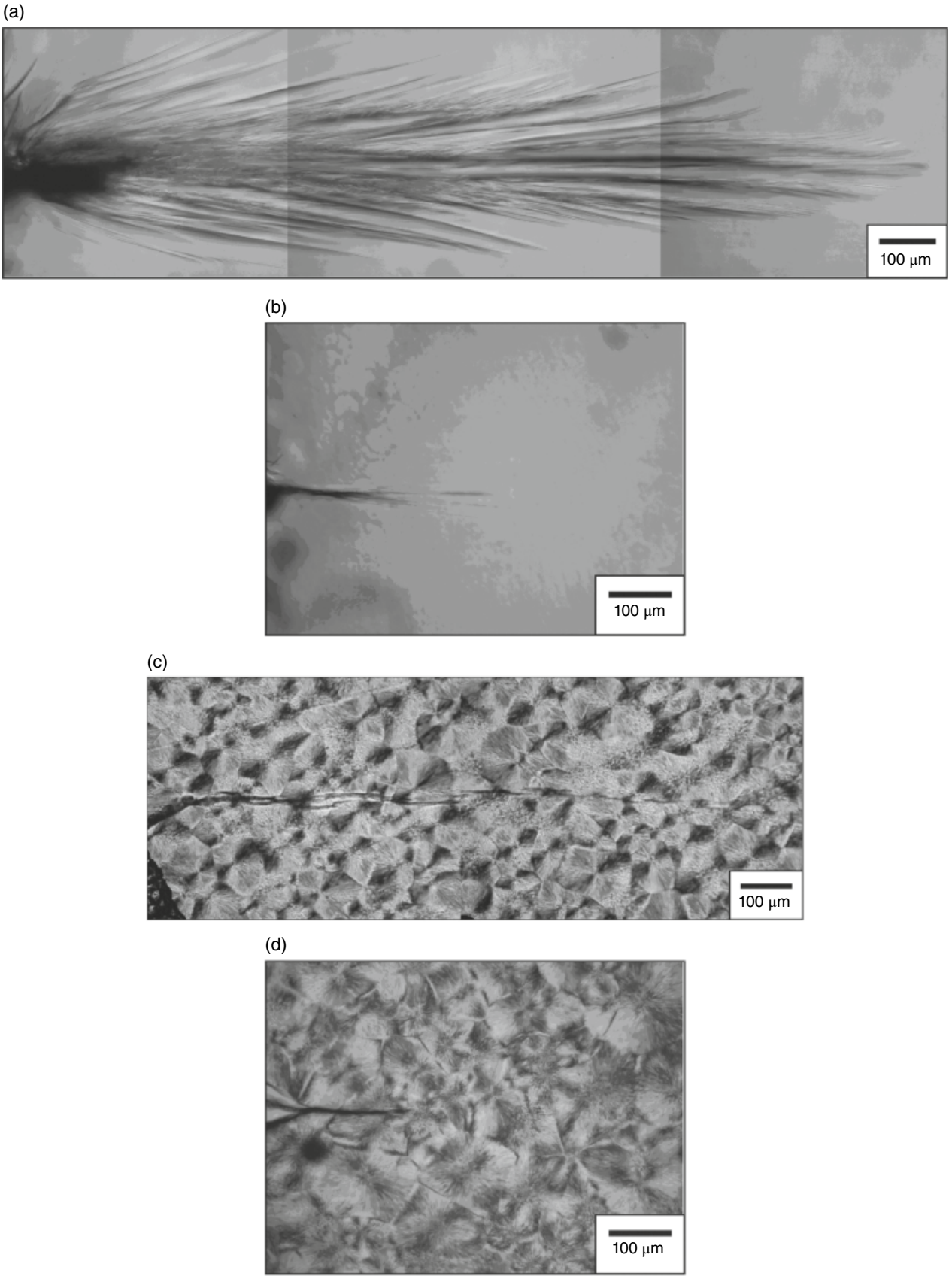


**FIGURE 10.3** Polarizing micrographs of crack behavior of PLA: (a) quenched static, (b) quenched impact, (c) annealed static, (d) annealed impact [57].

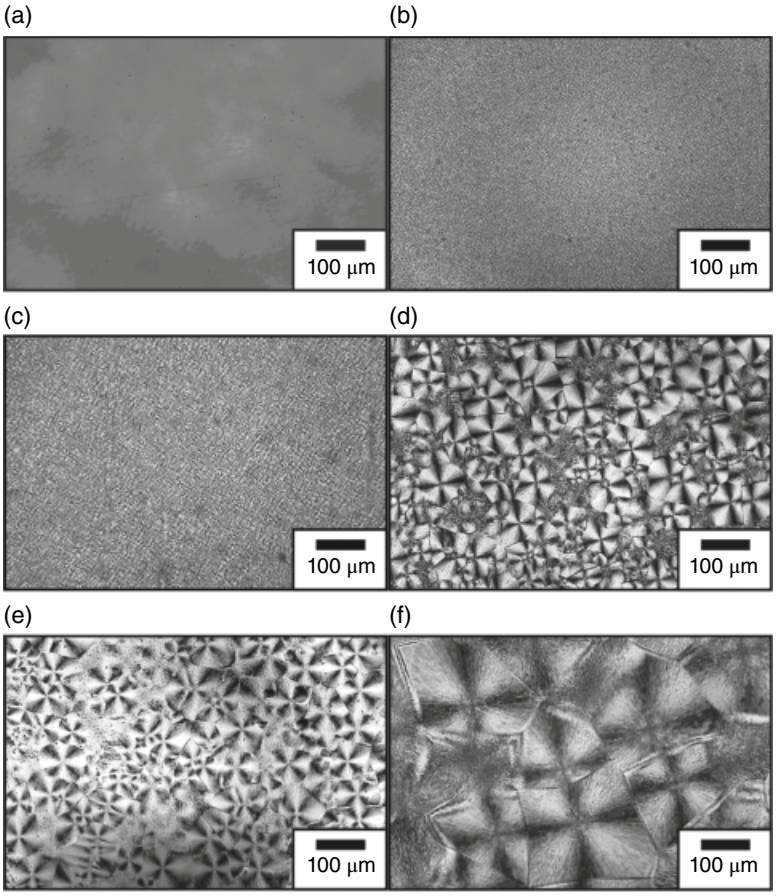


**FIGURE 10.4** Polarized micrographs of PLLA annealed microstructures: (a) 70°C/3 h, (b) 70°C/8 h, (c) 70°C/24 h, (d) 100°C/3 h, (e) 100°C/8 h, (f) 100°C/24 h [58].

crystallization mechanisms [12]. Such annealing turns the PLA opaque due to the induced crystallinity. It was illustrated that when the annealing temperature decreases from 80 to 65°C, the full crystallization in PLA samples could be obtained during a longer annealing time as the molecular mobility reduces with decreasing temperature. While full crystallization occurs over 30 h at 65°C, it takes around 30 min at 80°C to achieve a similar degree of crystallinity. At lower annealing temperatures, due to the lower molecular mobility, the crystal nucleation mechanism dominates the crystallization kinetics of PLA. Such larger number of crystal nuclei in samples annealed at a lower temperature could further reduce the molecular mobility and the crystal growth mechanism, and hence a longer time to reach full crystallization. On the other hand, at higher annealing temperature, the higher molecular mobility could facilitate the crystal growth mechanism of smaller number of nucleated crystals and thereby the full crystallization could occur in a shorter period. Although in annealed samples at both temperatures (until full crystallization) the final degrees of crystallinity are comparable, the difference in crystallization mechanism can influence the final mechanical performance of the annealed samples. Figure 10.5 illustrates how the tensile properties of PLA are affected after annealing at 65 and 80 C. As shown, the tensile strength and modulus of PLA were more noticeably enhanced in PLAs annealed at 65°C while the ductility was not influenced. In annealed samples at 65°C, the toughness was more noticeably enhanced than that of the annealed PLA at 80°C. This is because of the presence of a larger number of spherulites in samples annealed at 65°C, which influenced the strength and modulus of PLA, thereby revealing its toughening effect on the final performance of PLA samples. As seen, although the crystallization affects the final mechanical performance of PLA, it did not improve the ductility of PLA [12].

## 10.6 ORIENTATION

Mechanical orientation is another method for improving the mechanical properties of PLA due to its morphological change from α-crystallites into β-crystallites upon drawing. This process converts the otherwise fragile polymer into a versatile and useful material for practical tools, packaging, and biomedical applications, although the major mechanical

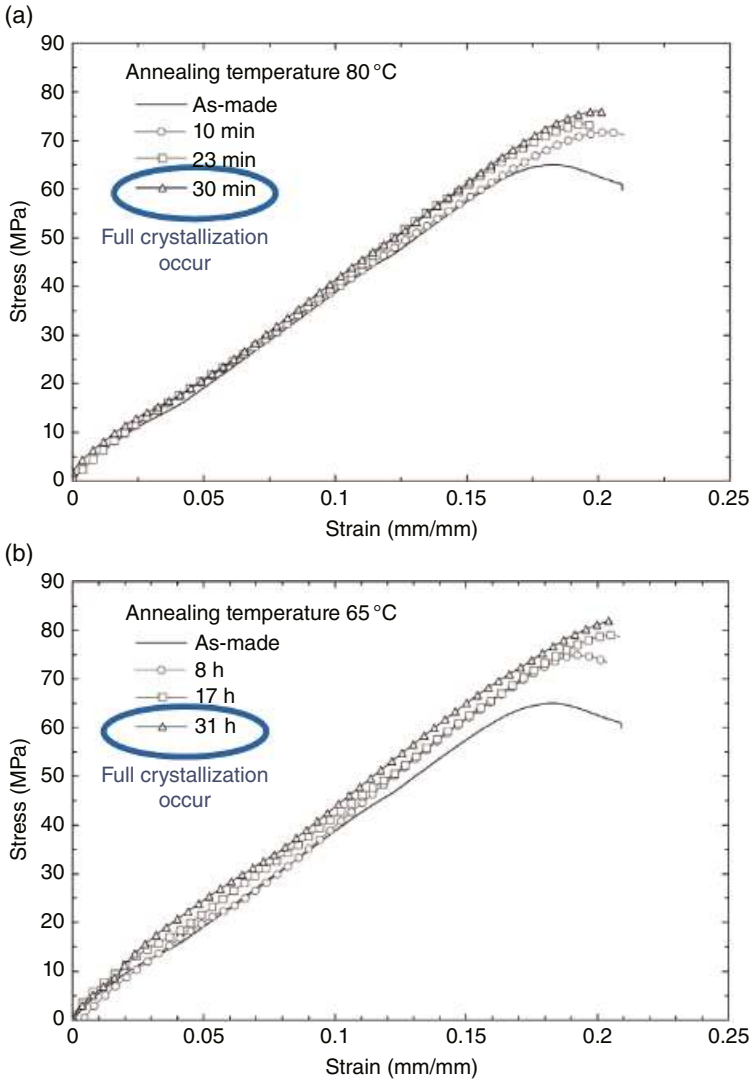


**FIGURE 10.5** Tensile stress-stain behavior of neat PLA compared with that of annealed samples at (a) 80°C and (b) 65°C [12].

performance drawbacks (i.e., brittleness and low toughness and impact strength) are still not resolved.

At room temperature, PLA is a brittle polymer, which fractures through a crazing mechanism. Research conducted using simultaneous small-angle X-ray scattering (SAXS) and tensile testing showed that the craze features increase in size with the extent of deformation [45]. The submicron cracks increase in height while decreasing in diameter, showing that the cracks elongate in the loading direction. This is consistent with visual observation during deformation, in which samples are observed to thin out and elongate in the loading direction. In dry amorphous PLLA, although new crazes are constantly formed during deformation, the dominating factor during deformation may be the changing dimensions of crazes that are generated soon after yield. Simultaneous SAXS and tensile testing of annealed PLLA results in a characteristic pattern that has been observed and discussed by several authors and interpreted as combined cavitation and fibrillated shear. This deformation mechanism is not uncommon in polymeric lamellar systems [45].

Crazing involves the extension of polymeric chains forming fibrils that span the craze [41]. The brittle fracture behavior in tensile and impact testing is due to the crazing mechanism through which the polymer fails. Due to the very localized nature of this process, the craze fails, and wide crack growth occurs. The crazing behavior of PLA is shown in Figure 10.6, illustrating the slight deformation of a specimen, followed by cracking.

It should be noted that when PDLLA is tested in the compression mode, crazing is suppressed, and its behavior is quite ductile. Here, the sample yields at a compressive strain of more than 30% and a compressive stress more than 100 MPa [41].

Another significant route to improve PLA mechanical properties is drawing and orientation. As reported by

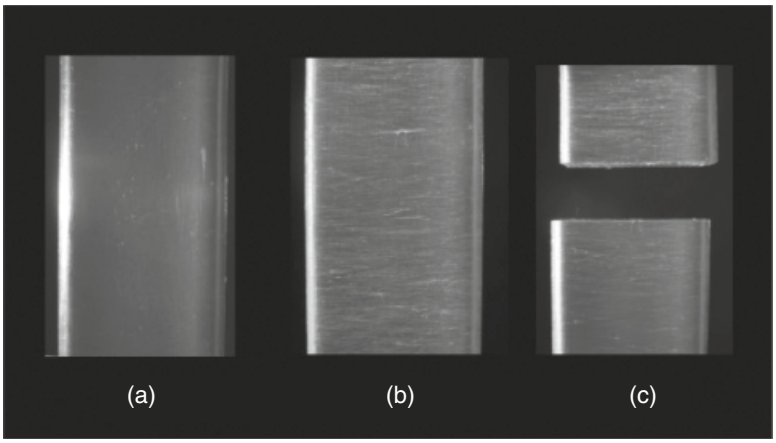


**FIGURE 10.6** Brittle fracture of amorphous PLA: (a) specimen before deformation, (b) crazes at a strain of 3.5%, (c) break at 5.5% strain. Source: Photos were kindly provided by Novamont SpA.

Grijpma et al. [41], PLA orientation at a stretch ratio of $\lambda = 2.5$ increases tensile strength from 47 (unoriented polymer) to 73 MPa (oriented polymer), elongation at break from 1.5 to 48%, Young's elastic modulus ($E$) from 3650 to 4490 MPa, and impact strength (Izod, 0.25 mm notch) from 1.6 to 5.9 kJ/m$^2$. However, perpendicular to the direction of orientation, the mechanical properties are usually poorer. It is therefore important to have biaxial molecular orientation to minimize anisotropy and obtain strong PLA films with improved mechanical properties.

There are two kinds of crystalline structures in PLA, depending on the formation conditions: the α-form (orthorhombic), which is obtained by crystallization from melt or solution, and the β-form (orthorhombic or trigonal). When an amorphous PLLA film is drawn by tensile force above the $T_g$, an oriented film with α-crystallites is obtained. When a PLLA semicrystalline film with α-crystallites is drawn, some of the α-crystallites are transformed into the oriented β-crystallites, depending on the draw conditions. The β-crystallites are generated upon tensile drawing at a high temperature and higher draw ratio, whereas drawing at a lower temperature and/or a lower draw ratio leads to α-crystallites. Thus, the drawn products of PLLA commonly consist of α-crystallites or a mixture of α- and β-crystallites [59, 60].

Biaxial orientation of PLLA film is effective in increasing the tensile strength, elongation at break, and elastic modulus. Stretching conditions may be selected within the range of 1.5–6 times in both the longitudinal and lateral directions. However, in view of film strength and evenness of thickness, stretching is preferably two times or more in both directions. The stretching is typically carried out at a temperature between the $T_g$ and $T_m$ of the material, between 70 and 90°C, depending on the stretching method [61].

The tensile strength of a semicrystalline PLLA film can be increased from 50 to 60 MPa (unoriented film) to 100–200 MPa (biaxially oriented film), while elongation at break can change from 10 to 50–150% and the elastic modulus increase from 2500 MPa to around 3300 MPa, in the machine direction [42, 61]. These data are also confirmed by mechanical testing of commercial grade PLA 4042D (~8 mol% D-lactic acid content) from NatureWorks LLC. Biaxial orientation of the extrusion cast film results in machine direction (MD) elongation at break of 160% and cross direction (CD) elongation at break of 100% [62]. The same material, when extruded without biaxial orientation, has much lower elongation at break values of only around 10%. Elmendorf tear strength values for these materials after orientation, however, are 6 and 5 N/mm in MD and CD, respectively. For unoriented samples, the Elmendorf tear strengths in MD and CD are 4 and 8 N/mm, respectively [62]. The contribution of biaxial orientation in improving the mechanical properties of PLA films is therefore quite evident, and this route represents an important tool for manufacturing biodegradable PLA films with good characteristics for several practical applications.

The development of different microstructures because of the thermomechanical conditions during injection molding depends upon the operative parameters involving melt processing temperature, the injection flow rate, and holding pressure. The shear stress predominantly controls the hot recoverable strain applied during processing and the degree of crystallinity, and both parameters increase with increasing PLA shear stress. The work of Ghosh et al. [26, 63] with optically pure PLLA shows that a low melt processing temperature facilitates the attainment of a high level of molecular orientation and higher degree of crystallinity. The elongation at break increases with increasing molecular orientation and decreases with increasing crystallinity. Both the level of molecular orientation and crystallinity contribute to the maximum tensile strength of injection molded specimens.

The development of crystal-induced self-reinforced PLA materials has also been reported by Zengwen et al. [64] and

Xie et al. [65]. A semicrystalline PLA with a certain degree of crystallinity was melt processed through an extruder at processing temperatures around the melting temperature of the PLA where not all crystals were molten. Zengwen et al. showed that the presence of unmelted micro-crystals during film blowing could significantly enhance the strain at break and tensile strength of the blown films. Xie et al. also revealed that the stretching of the extrudates could generate a nanofibrillar PLA structure throughout its unmelted crystallites, which could enhance the strain at break, tensile strength, and toughness of the final PLA product. Along these efforts, recently Nofar et al. [66] illustrated that through the generation of fiber-like crystal structure of a semicrystalline PLA in an amorphous PLA matrix could significantly enhance the melt rheological properties of the amorphous PLA. In this approach, and through the incorporation of other ductile polymers, the mechanical performance of the developed system is expected to be enhanced although this idea is still in its early research stage.

## 10.7 STEREOREGULARITY

As already described, PLA can be manufactured to give a wide range of properties because of the chiral nature of lactide. The mechanical characteristics of PLA are known to depend on the choice and distribution of stereoisomers within the polymer chains. High-purity L- and D-lactide form stereoregular isotactic PLLA and PDLA, respectively, with equivalent physicochemical and mechanical properties. These are semicrystalline polymers with a high $T_m$ around 175–180°C and a $T_g$ in the 60–70°C range. The racemic D,L-lactide and *meso*-lactide, on the other hand, form atactic PDLLA and *meso*-PLA, which are amorphous materials [67–69].

It is quite interesting to compare the behavior of commercial grade PLA 4030D, which was prepared with nominal 98% L-lactide, with the characteristics of PLA 4040D, prepared with nominal 94% L-lactide. While tensile strength and elastic modulus are comparable for both materials and only slightly higher for PLA 4040D, the elongation at break appears quite different. PLA 4030D shows elongation at break values of 11% MD and 5% CD, while for PLA 4040D values are 78% MD and 97% CD. These data show that, besides biaxial orientation, film-grade PLLA may benefit from a small amount of amorphous PLA, possibly because of lower crystallite dimensions [43].

It has been observed that a 1 : 1 mixture of pure PLLA with pure PDLA yields a stereocomplex of the two polymers during crystallization or polymerization. The PLA stereocomplex consists of racemic crystalline structures in which PLLA and PDLA chains are packed side by side, with a 1 : 1 ratio of L : D monomer units [2, 69, 70]. While the melting temperature of α- and β-crystalline forms of PLA falls in the range 170–180°C, the $T_m$ of PLA stereocomplex is between 220 and 230°C [70]. The high $T_m$ of PLLA/PDLA stereocomplex makes it a difficult material for processing; however, it is interesting to note that the comparison between PLLA/PDLA equimolar blends and the starting materials shows mechanical properties that are markedly improved.

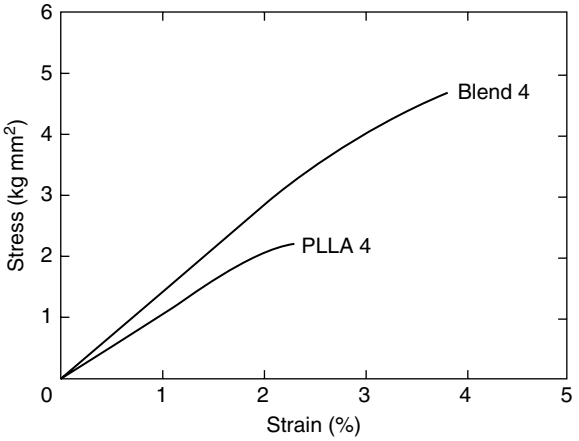


**FIGURE 10.7** Stress–strain curves for blend film and non-blended PLLA film. The blend was a 1 : 1 mixture of PLLA with $M_w$ = 150,000 g/mol and PDLA with $M_w$ = 150,000 g/mol [71].

Figure 10.7 shows the stress–strain curve for a film obtained from a 1 : 1 blend of PLLA:PDLA, both having a molecular weight $M_w$ = 150,000 g/mol, compared to the behavior of the film made with the PLLA component. Tensile strength and elongation at break of this blended PLA are 46 MPa and 3.8%, respectively. These values are higher than the values for PLLA alone, which are 22 MPa and 2.3%, respectively [71]. The difference in mechanical properties between PLLA/PDLA blend film and PLLA is due to the different morphology of these polymers, as evidenced by Figure 10.8. As can be seen, the PLLA films are composed of normal spherulites, whereas for the blend films, microcrystallites are observed [71]. When the orientation of PLA film is performed on equimolar blends of PLLA and PDLA, in which a mixture of stereocomplex crystallites and α-crystallites are formed [68, 71], it exhibits relevant mechanical effects.

Sawai et al. studied the mechanical properties of a stereocomplex PLA film prepared by casting from a solution of an equimolar blend of PLLA and PDLA [72]. The film was uniaxially drawn by solid-state coextrusion and characterized by DMA. The optimum draw temperature that resulted in the highest draw and mechanical properties was 200°C. The maximum tensile modulus and strength, for the samples with an extrusion draw ratio of 16 and prepared by solid-state coextrusion of a highly crystalline stereocomplex film, were 9500 and 410 MPa, respectively. Furthermore, the PLA stereocomplex films with an extrusion draw ratio of 16 exhibited excellent thermomechanical

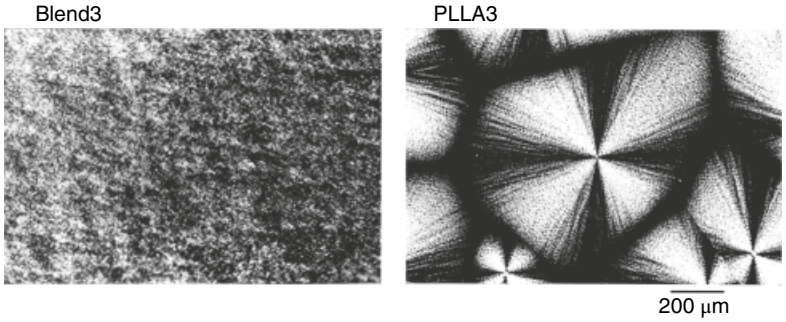


**FIGURE 10.8** Representative polarizing microscopic photographs of 1 : 1 PLLA:PDLA blend and PLLA films. The molecular weight of PLLA and PDLA are 120,000 and 100,000 g/mol, respectively [71].

stability as evaluated by the $E'$ measured as a function of temperature. The reported $E'$ values at room temperature, 100, and 200°C, were 9500, 7000, and 3000 MPa, respectively [72]. Equimolar amounts of PLLA and PDLA stereocomplex are therefore characterized, upon orientation, by the most relevant mechanical and thermomechanical properties in PLA family.

## 10.8 SELF-REINFORCED PLA COMPOSITES

Self-reinforced composites of PLA have also been introduced as a method to develop new composites with enhanced modulus and strength. In such self-reinforced composites, PLA fibers are simply embedded within PLA films as the matrix, mostly through using compression molding. The fibers could be produced through melt and electrospinning or melt drawing [73–77]. Somord et al. [78] revealed that reinforcing PLA films with electrospun PLA nanofibers could, to some degree, improve the ductility and toughness of the PLA matrix. Slight improvements of the final ductility and toughness in self-reinforced PLA composites have also been reported. Such self-reinforcement of PLA systems may, however, be limited due to the restrictions in producing PLA fibers, while the manufacturing of the corresponding composites is also mainly limited to lamina stacking and compression molding [66].

## 10.9 PLA NANOCOMPOSITES

The development of composites improves the strength and stiffness of PLA. The need of using high fibers content or particulate reinforcements with high density have motivated industries and scientists to move toward using nanofillers. The use of low nanofiller content can significantly improve those properties of PLA that could be achieved in their composite counterparts with higher filler contents. Upon achieving a good dispersion within the matrix, these nanofillers or nanoparticles, depending on the aspect ratio, can significantly improve the strength and stiffness of PLA. Meanwhile, nanoparticles can dramatically enhance the rheological and crystallization behavior of PLA and hence its processability. Table 10.4 shows how the incorporation of nanofillers in PLA can enhance different PLA properties. This should be noted that still such nanofillers could not significantly enhance ductility, toughness, and impact properties of PLA [29].

The nanoparticles, depending on their shape and functionality, can also induce some functional features in their nanocomposite counterparts. For instance, while nanoclay platelets can improve the barrier properties, the use of

**TABLE 10.4 Overview of Main End-Use Characteristics of PLA Nanocomposites [29]**

| Nanofiller Type | Main Enhancements in Mechanical Performance |
|---|---|
| PLA clay-based nanocomposites | |
| Layered silicates | Stiffness, high tensile and flexural strength, high heat distortion temperature |
| Sepiolite | Thermo-mechanical improvements |
| Halloysite | High tensile strength and tensile/storage modulus, good impact properties |
| PLA nanocellulose-based nanocomposites | |
| Cellulose nanocrystals (CNC), cellulose nanofiber (CNF), bacterial cellulose (BC) | Improved tensile strength, tensile/storage modulus |
| PLA carbonaceous-based nanocomposites | |
| Carbon nanotube (CNT) | Improved tensile strength and modulus |
| Graphene derivatives | Thermal stability, better lubrication, and abrasion resistance |
| PLA silicon-based nanocomposites | |
| Silica | Thermal stability, enhancement in tensile strength, and ductility |
| Polyhedral oligomeric silsesquioxane (POSS) | Enhanced storage and tensile modulus |

conductive nanoparticles such as carbon nanotubes (CNTs) can induce electrical conductivity. Hybrid nanocomposites can also be developed to induce multifunctionalities. The incorporation of nanoclay and CNTs, for instance, can result in PLA nanocomposites with both sorption-ability from nanoclay and electrical conductivity from CNTs. Further details are provided in Chapter 17.

## 10.10 COPOLYMERIZATION

One of the methods, although expensive, that was initiated more than two decades ago is to develop copolymers of PLA with other tough, ductile, and/or elastomeric monomers [31, 79]. Rubber modification through copolymerization is very effective in increasing the toughness of PLA; however, this is accompanied by significant reduction of elastic modulus and tensile strength. In early studies, copolymers of L-lactide and ε-caprolactone as biodegradable elastomeric implant materials were developed with high toughness and ductility [80]. Supertough PLA products were also introduced by developing poly(lactide-*co*-glycolide) copolymers modified with ε-caprolactone [81]. Furthermore, ductility and toughness were highly improved when trimethylene carbonate and caprolactone were copolymerized with lactide and then blended with PLA [82]. Due to the biocompatibility and hydrophilicity of ethylene glycol, it is considered as another common copolymer with PLA [31]. Recently, Fan et al. [83, 84] revealed how the use of flexible copolymers of PLA can effectively be incorporated in drug delivery and oxygen carriers in biomedical treatments. Detail information of these copolymers are provided in Chapters 4 and 14.

## 10.11 PLASTICIZATION

PLA is characterized by good mechanical properties and clarity in addition to satisfactory processability; however, its brittleness is its major drawback for many applications [33]. For PLA, Elmendorf tear test values range from 5 to 15 N/mm, which is quite low compared to conventional film grade polyolefins. As PLLA is like polystyrene, it is also a comparatively brittle and stiff polymer with low deformation at break. Moreover, extrusion casting of PLA film for packaging and many other applications is relatively difficult compared to other polymers. In fact, there is no tolerance for PLA film tearing or cracking when subjected to forces during package manufacturing [52]. It is therefore important to modify these properties in such a way that PLA can compete with other more flexible commodity polymers such as PE, PP, PET, or PVC.

There are several means of improving the flexibility of PLLA by modifying its physical properties, such as through copolymerization. An example of a suitable comonomer is ε-caprolactone, which can result in soft copolymers [80, 85]. Also blending with biomaterials, such as thermoplastic starch [48], is a feasible method to prepare PLA-based materials that can be successfully used for film manufacturing. However, an interesting and practical route to modify the mechanical properties of PLLA consists of introducing biodegradable plasticizers in this material composition [32]. In general, plasticizers improve the ductile characteristics of PLA. It is also well known that lactide monomer itself is an effective plasticizing agent for PLLA, but it has the disadvantage of rapid migration due to its low molecular weight. The plasticization of PLLA with lactide therefore results, besides accelerated aging, in a stiff polymer with a sludgy surface [11, 37].

The introduction of plasticizers in the formulation of semicrystalline polymers such as PLA can in principle reduce not only the $T_g$ of the amorphous phase but also the $T_m$ of the crystalline domains. Even though the $T_m$ of PLLA can be in part reduced without significantly affecting its thermomechanical properties, from a practical point of view it is quite important to also avoid depressing the melting point excessively. Therefore, the choice of a suitable plasticizer for PLA must take this aspect into consideration, with the aim of plasticizing the polymer without affecting its heat resistance and without modifying its compostability. A second aspect to be considered is the drop of tensile strength, which should be minimized as much as possible.

Labrecque et al. demonstrated good miscibility of PLA with different citrate esters at up to 20–30% by weight of plasticizer concentration, depending on the type of citrate employed [33]. Tensile strength and elongation at break of PLA plasticized with citrate esters are reported in Table 10.5 and show a marked effect of plasticizer at concentrations between 10 and 30%.

As expected, all the plasticizers decrease the tensile strength of PLA significantly (by about 50%) even at 10% concentration, and the deterioration is larger at higher concentrations. On the other hand, elongation at break does not show significant change at the lower concentrations but significantly increases at higher concentrations in all cases [33].

Similar data have been published by Ljungberg et al. showing that stress at break of PLA is lowered from 62 MPa for neat material to 30 MPa in the presence of 15% triacetine and to 35 MPa with 15% tributyl citrate, after one day of storage. Elongation at break changes from 6% for the selected PLA to 355% and to 350%, respectively, with 15% triacetine and with 15% tributyl citrate [86, 87]. They also reported data about DMA characteristics of plasticized PLA. Figure 10.9 shows the evolution of viscoelastic storage and loss moduli as a function of temperature for pressed films of neat PLA and blends containing 15 wt% plasticizer. TbC, TbC-3, and TbC-7 are, respectively, tributyl citrate and oligomeric tributyl citrate obtained by transesterification with diethylene

**TABLE 10.5 Thermal and Mechanical Properties of PLA Plasticized with Different Citrate Esters [33]**

| | $T_g$ (°C) | $T_m$ (°C) | $\Delta H$ (J/g) | Tensile Strength (MPa, Yield) | Elongation at Break (%) |
|---|---|---|---|---|---|
| PLA | 59.1 | 145.2 | 0.79 | 51.7 | 7 |
| Triethyl citrate (wt%) | | | | | |
| 10 | 42.1 | 134.1 | 0.31 | 28.1 | 21.3 |
| 20 | 32.6 | 130.9 | 2.86 | 12.6 | 382 |
| 30 | 22.0 | 126.8 | 7.57 | 7.2 | 610 |
| Tributyl citrate (wt%) | | | | | |
| 10 | 40.4 | 143.1 | 0.06 | 22.4 | 6.2 |
| 20 | 17.6 | 139.0 | 19.1 | 7.1 | 350 |
| Acetyl triethyl citrate (wt%) | | | | | |
| 10 | 50.8 | 141.7 | 0.91 | 34.5 | 10 |
| 20 | 30.0 | 138.1 | 0.91 | 9.6 | 320 |
| 30 | 14.2 | 131.6 | 18.34 | 7.6 | 228 |
| Acetyl tributyl citrate (wt%) | | | | | |
| 10 | 25.4 | 139.2 | 1.4 | 17.7 | 2.3 |
| 20 | 17.0 | 138.9 | 3.9 | 9.2 | 420 |

glycol, having 3 and 7 repeating units. The thermograms show the α-relaxation (between 30 and 60°C) of the materials and the effects of cold crystallization (between 80 and 100°C). It is clearly shown in Figure 10.9a that the drop in storage modulus following the α-relaxation is found at a lower temperature for the plasticized materials as compared with neat PLA. The same trend can be observed in Figure 10.9b, where $T\alpha$ is significantly decreased for all the plasticized materials, with the plasticizer having the lowest molecular weight, that is, TbC, being the most effective [54].

Malonate esters, such as diethyl bishydroxymethyl malonate (DBM), have also been tested as plasticizers for PLA. These compounds lowered $T_g$ of PLLA from an initial value of 54 to 30°C with 15 wt% and to a $T_g$ of 5°C with plasticizer at 25 wt%. However, at a concentration of 20–25 wt%, phase separation occurs because of saturation of the amorphous phase of PLA. Aging a blend containing 15 wt% DBM for four months at ambient temperature also leads to phase separation and to the migration of the plasticizer to the film surface. Malonate oligomers, prepared by reacting DBM with acid chlorides, lead to more stable materials in aging tests [51, 53]. It is also worth mentioning here the need to select PLA plasticizers that are stable during material aging to avoid unfavorable property changes during the intended material life.

Poly(ethylene glycol) (PEG) is another compound that has been tested as a plasticizer for PLA [44]. According to Martin and Avérous [48], PEG with a molecular weight of 400 g/mol reduces the $E$ of a pure PLLA from an initial value of 2050 to 1488 MPa at a concentration of 10% and to 976 MPa at 20%, while the elongation at break increases from the initial level of 9 to 26 and 160%, respectively [48]. However, PEG tends to migrate from the PLA matrix if not copolymerize.

In general, the storage modulus drop associated with the $T_g$ of plasticized PLA decreases almost linearly with increasing plasticizer concentration, from 67°C for pure PLA to 54 and 46°C for a PEG concentration of 10 and 20%. The work of Martin and Avérous shows that plasticization of the same PLLA with oligomeric lactic acid (OLA) reduces the elastic modulus from 2050 to 1256 MPa at 10% plasticizer and to 744 MPa at 20% plasticizer, while elongation at break increases to 32 and 200%, respectively [48]. In general, the $T_g$ values of plasticized PLA can be predicted with Fox's law [32]. Plasticization of PLA affects significantly the mechanical properties of this material; however, the choice of a plasticizer and its concentration requires great attention to avoid losing physicochemical characteristics such as heat of fusion and, consequently, thermomechanical properties.

## 10.12 PLA BLENDS

The brittleness and low toughness and impact strength of PLA have motivated scientists and industries to develop its blends with other thermoplastics, preferably biopolymers, that possess high impact strength and ductility [27, 28]. Blending, which is more practical and cost-effective compared to copolymerization, can offer a variety of properties depending on the developed morphologies and the phase compatibility [88, 89]. Hence, PLA blends with a wide range of properties can be developed for various applications from commodity and engineering to biomedical [28]. A number of studies have explored the processing and properties of various types of PLA blends [27]. Among biopolymers, the mostly explored polymers for blending with PLA are polycaprolactone (PCL) [90, 91], thermoplastic starch (TPS) [92, 93], polyhydroxyalkanoates (PHAs) [94–96], poly(butylene adipate-*co*-terephthalate) (PBAT) [97–101], poly(butylene succinate-*co*-adipate) (PBSA) [102–105], and

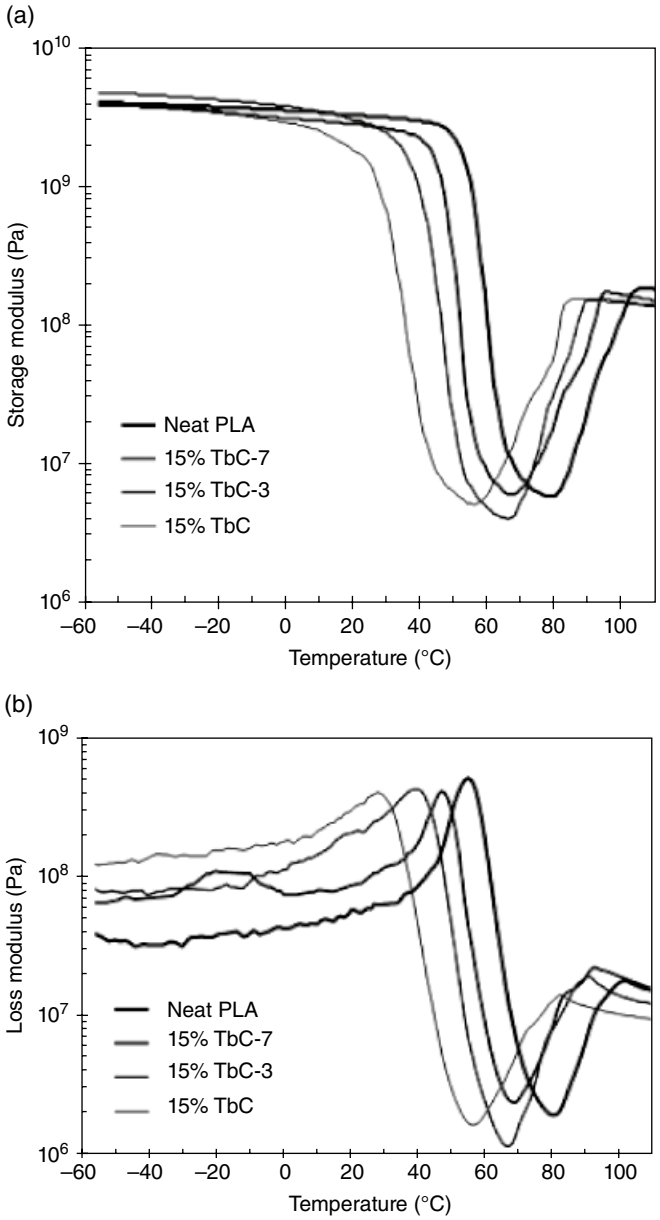


**FIGURE 10.9** (a) Storage modulus curves as a function of temperature from DMA runs comparing blends containing 15 wt% TbC, TbC-3, and TbC-7 with neat PLA. (b) Loss modulus curves as a function of temperature from DMA runs comparing blends containing 15 wt% TbC, TbC-3, and TbC-7 with neat PLA. TbC, TbC-3, and TbC-7 are, respectively, tributyl citrate and oligomeric tributyl citrate obtained by transesterification with diethylene glycol, having 3 and 7 repeating units [54].

poly(butylene succinate) (PBS) [106–108]. Among synthetic non-compostable thermoplastics, rubber [109–111] and thermoplastic polyurethane (TPU) [112–115] have been widely considered for blending with PLA due to their high flexibility.

While blends of PLA/PCL are more preferred for biomedical applications where enhancements of mechanical performance may not be crucial, blends of PLA with PHAs have also been investigated for mostly packaging applications. Among PHAs, since poly(3-hydroxybutyrate) (PHB) exhibits high stiffness and crystallinity, it is often copolymerized with 3-hydroxyvalerate to form poly(3-hydroxybutyrate-*co*-3-hydroxyvalerate) (PHBV) with improved flexibility and processability. Increasing hydroxyvalerate content in PHB increases the ductility, reduces the stiffness, melting temperature, and crystallinity of PHB. Poly(3-hydroxybutyrate butyrate-*co*-3-hydroxyhexanoate) (PHBHHx or PHBH) is another copolymer of PHB with reduced crystallinity, broader processing window, higher flexibility, and lower tensile strength and modulus compared with PHB [116].

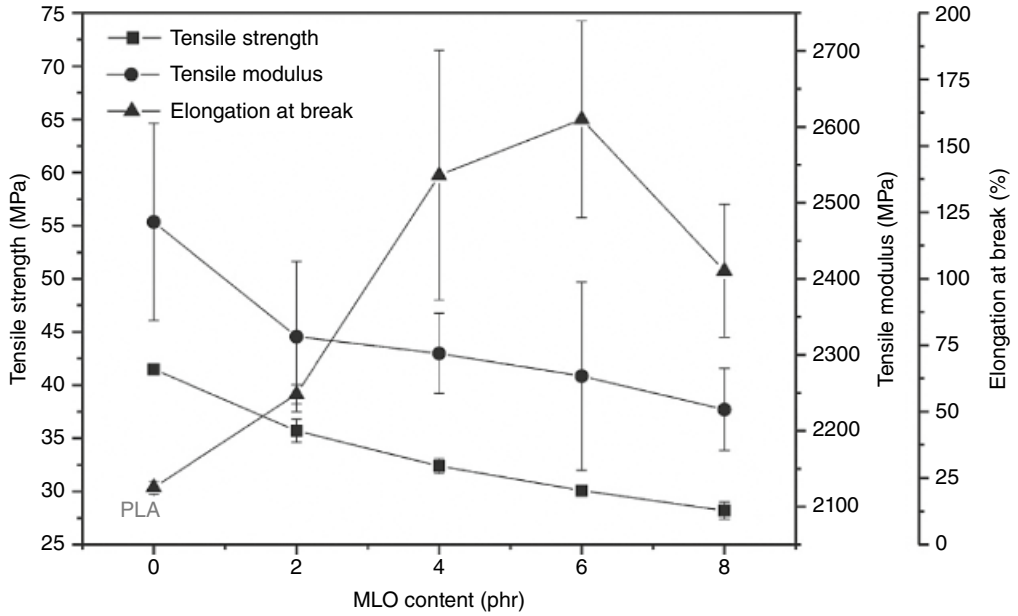


**FIGURE 10.10** Tensile mechanical properties of TPS/PLA (70w/30w) blends with varying MLO content [28, 118].

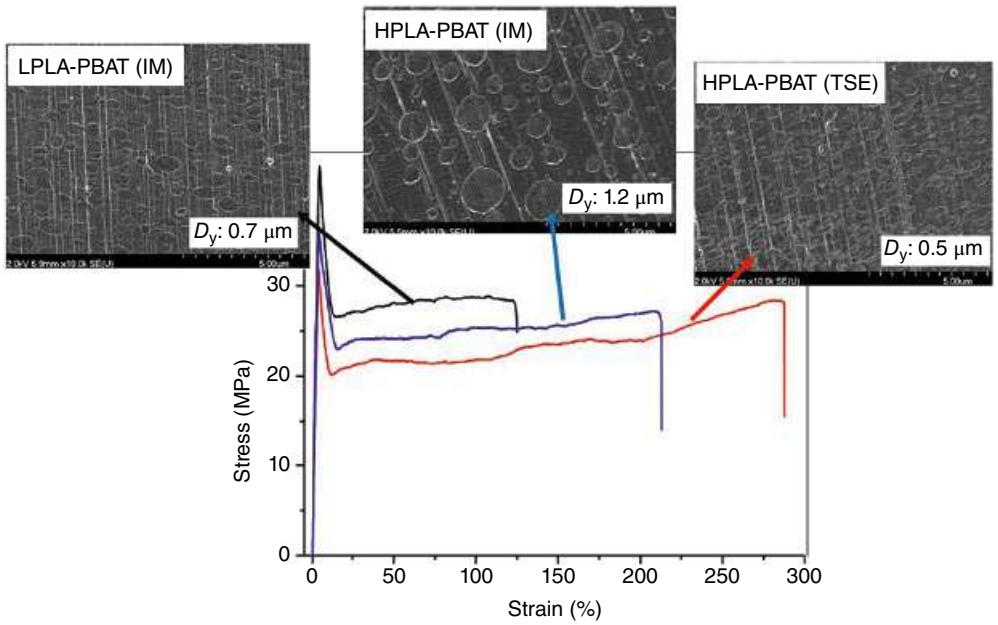


**FIGURE 10.11** The processing-morphology-tensile properties relationship of PLA/PBAT (75w/25w) blends. The scale bar is 5 µm and the average droplet diameter size is provided [28, 103].

In PLA/TPS systems, plasticizers such as citric acid have been mostly incorporated. Citric acid could lower the viscosity of PLA/TPS blends, lowers interfacial tension, and results in a finer dispersion of TPS minor phase [117]. Maleinized linseed oil (MLO) was also used at different ratios to gelatinize starch [118]. Figure 10.10 shows how the tensile strength, modulus, and elongation at break of PLA/TPU (70w/30w) blends could vary with the addition of MLO when using melt extrusion process. As seen, the elongation at break of PLA/TPU blends increased over 160% with the addition of only 6 phr MLO [118].

Blends of PLA/PBAT, PLA/PBSA, and PLA/PBS have also been of a great interest over the last decade mostly for packaging applications. It has been demonstrated that processing and the viscoelastic features of the blend components could significantly influence the final mechanical performance of the blends. Figure 10.11 shows the morphology and tensile properties relationship of the PLA/PBAT

(75w/25w) blends with various PBAT droplet sizes. This was while low- and high-molecular-weight PLAs were incorporated as the matrix (i.e., LPLA and HPLA). The blends were processed at 160°C and 100 rpm in an internal mixer (IM) or in a twin-screw extruder (TSE). As seen, the droplet size reduction of PBAT could improve the strain at break and toughness of PLA more efficiently. This is because the applied load could be transferred from the matrix through a larger available surface area to the PBAT droplets. When comparing LPLA–PBAT (IM) with HPLA–PBAT (IM), the ductility is increased from around 150 to 200%. Although the larger droplet morphology in HPLA-PBAT (IM) is expected to suppress the ductility and toughness, the presence of a PLA matrix with a higher molecular weight and hence higher molecular entanglement seems to have a more dominant effect on ductility improvements. In comparison of HPLA–PBAT (IM) with HPLA–PBAT (TSE), the later revealed a higher ductility of around 265%. The higher interfacial area in the PLA–PBAT blend with finer morphology favors the stress transfer from one phase to another, and hence, the PBAT dispersed phase could further contribute to improving the ductility and toughness of the PLA matrix [28, 103].

In PLA blends with synthetic non-compostable thermoplastics, various studies reported that the efficiency of rubber as the minor phase on toughening and improving the ductility of PLA is limited up to a certain rubber content. Such efficiency has been reported up to around 10–20 wt% of rubber content and the further addition of various rubber types lead to the suppression of the final properties of the blend. In PLA/TPU blends, the ductility and impact strength improved with increasing TPU content, although the tensile strength and modulus decreased accordingly. Figure 10.12 summarizes the mechanical properties of PLA/TPU blends with data adapted from different studies (Figure taken from [27, 28]). As depicted, the property variation trends are quite similar in most of studies where no compatibilizers have been utilized [27]. Detailed discussion of PLA blends is presented in Chapter 14.

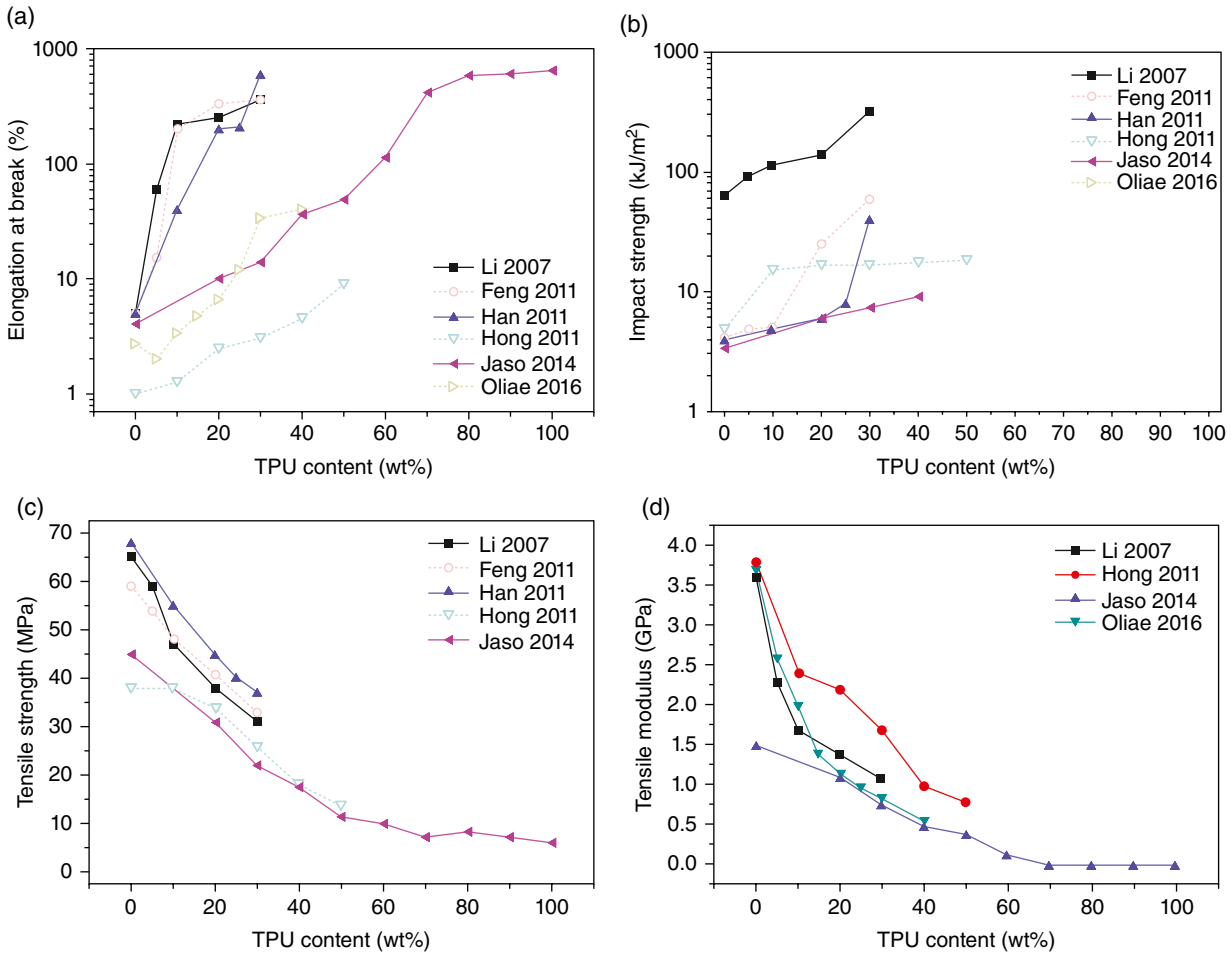


**FIGURE 10.12** (a) Elongation at break, (b) impact strength, (c) tensile strength, and (d) tensile modulus of the PLA/TPU blends. Source: Data adapted from different studies. The corresponding references on the graphs are separately available in [27, 28].

## 10.13 CONCLUSIONS

PLA has attracted the attention of industry for packaging and biomedical applications because of its biodegradability characteristics, in addition to its good mechanical and physicochemical properties. From a general point of view, PLA is a rigid, semicrystalline material, with tensile strength ranging from 50 to 70 MPa, modulus of elasticity of 3000–4000 MPa, and elongation at break of 2–5%. However, the toughness of PLA polymers can be successfully modified to meet specific applications by changing the formulation and manufacturing process. Thus, PLA is a versatile polymer that can be converted into several materials having useful properties for many different applications. The copolymerization of L-lactide with minor amounts of *meso*-lactide or D,L-lactide offers materials with lower brittleness and better film properties.

In general, annealing improves the thermomechanical properties. Therefore, extrusion or injection molding of PLA must be optimized. Proper crystallization of PLLA significantly improves the thermomechanical behavior, and this is an important requisite for applications at temperatures of 40–50°C or higher. Biaxial orientation of PLLA film is an important method to increase tensile strength, elongation at break, and modulus of elasticity. Here, the stereocomplex formed by equimolar amounts of PLLA and PDLA, particularly when subjected to biaxial orientation, exhibits very interesting thermomechanical properties and is therefore a promising material for new applications. The use of chain extenders or the development of PLA-based composites or nanocomposites can also enhance the processability of PLA through enhancing its crystallization and melt rheological properties. However, these approaches are more effective in enhancing the strength and stiffness of the final PLA product. The major drawbacks of PLA are its brittleness, low toughness, and low impact strength. Efforts to improve these major mechanical drawbacks of PLA have, so far, been tackled through copolymerization, plasticization, and blending with other polymers. Among these approaches, while copolymerization is not cost-effective, blending is a more practical and cheaper approach for achieving a compatible blend system. Blending PLA with appropriate thermoplastics or plasticization of PLA can improve the elongation at break of PLA to about 300% while the toughness and impact strength values can also be noticeably enhanced.

## REFERENCES


1. R. Auras, B. Harte, S. Selke, An overview of polylactides as packaging materials, *Macromol. Biosci.* **2014**, *4*,835–864. https://doi.org/10.1002/mabi.200400043.
2. D. Garlotta, A literature review of poly (lactic acid), *J. Polym. Environ.* **2001**, *9*(2), 63–84. https://doi.org/10.1023/A:1020200822435.
3. R. E. Drumright, P. R. Gruber, D. E. Henton, Polylactic acid technology, *Adv. Mater.* **2000**, *12*, 1841–1846. https://doi.org/10.1002/1521-4095(200012)12:23<1841::AID-ADMA1841>3.0.CO;2-E.
4. B. Gupta, N. Revagade, J. Hilborn, Poly (lactic acid) fiber: an overview, *Prog. Polym. Sci.* **2007**, *32*, 455–482. https://doi.org/10.1016/j.progpolymsci.2007.01.005.
5. S. E. Atalay, B. Bezci, B. Özdemir, Y. A. Göksu, A. Ghanbari, A. Jalali, M. Nofar, Thermal and environmentally induced degradation behaviors of amorphous and semicrystalline PLAs through rheological analysis, *J. Polym. Environ.* **2021**, *29*(10), 3412–3426. https://doi.org/10.1007/s10924-021-02128-z.
6. M. Nofar, A. Ameli, and C. B. Park, The thermal behavior of polylactide with different D-lactide content in the presence of dissolved $CO_2$, *Macromol. Mater. Eng.* **2014**, *299*(10), 1232–1239. https://doi.org/10.1002/mame.201300474.
7. A. Södergård, M. Stolt, Properties of lactic acid based polymers and their correlation with composition, *Prog. Polym. Sci.* **2002**, *27*(6), 1123–1163. https://doi.org/10.1016/S0079-6700(02)00012-6.
8. S. Saeidlou, M. A. Huneault, H. Li, C. B. Park, Poly (lactic acid) crystallization, *Prog. Polym. Sci.* **2012**, *37*, 1657–1677. https://doi.org/10.1016/j.progpolymsci.2012.07.005.
9. M. Nofar, R. Salehiyan, S. Sinha Ray, Rheology of poly (lactic acid)-based systems, *Polym. Rev.* **2019**, *59*(3), 465–509. https://doi.org/10.1080/15583724.2019.1572185.
10. L. T. Lim, R. Auras, M. Rubino, Processing technologies for poly (lactic acid), *Prog. Polym. Sci.* **2008**, *33*, 820–852. https://doi.org/10.1016/j.progpolymsci.2008.05.004.
11. M. Ajioka, K. Enomoto, K. Suzuki, A. Yamaguchi, Basic properties of polylactic acid produced by the direct condensation polymerization of lactic acid, *J. Polym. Environ.* **1995**, *3*, 225–234. https://doi.org/10.1246/bcsj.68.2125.
12. Y. Srithep, P. Nealey, L. S. Turng, Effects of annealing time and temperature on the crystallinity and heat resistance behavior of injection-molded poly (lactic acid), *Polym. Eng. Sci.* **2013**, *53*(3), 580–588. https://doi.org/10.1002/pen.23304.
13. A. Jalali, M. A. Huneault, M. Nofar, P. C. Lee, C. B. Park, Effect of branching on flow-induced crystallization of poly (lactic acid), *Eur. Polym. J.* **2019**, *119*, 410–420. https://doi.org/10.1016/j.eurpolymj.2019.07.045.
14. M. Nofar, W. Zhu, C. B. Park, J. Randall, Crystallization kinetics of linear and long-chain-branched polylactide, *Ind. Eng. Chem. Res.* **2011**, *50*, 13789–13798. https://doi.org/10.1021/ie2011966.
15. M. Nofar, W. Zhu & C. B. Park, Effect of dissolved $CO_2$ on the crystallization behavior of linear and branched PLA, *Polymer* **2012**, *53*, 3341–3353. https://doi.org/10.1016/j.polymer.2012.04.054.
16. N. Najafi, M. C. Heuzey, P. J. Carreau, D. Therriault, C. B. Park, Mechanical and morphological properties of injection molded linear and branched-polylactide (PLA) nanocomposite foams, *Eur. Polym. J.* **2015**, *73*, 455–465. https://doi.org/10.1016/j.eurpolymj.2015.11.003.


17. N. Najafi, M. C. Heuzey, P. J. Carreau, D. Therriault, C. B. Park, Rheological and foaming behavior of linear and branched polylactides, *Rheol. Acta.* **2014**, *53*, 779–790. https://doi.org/10.1007/s00397-014-0801-3.
18. N. Najafi, M. C. Heuzey, P. Carreau, D. Therriault, Quiescent and shear-induced crystallization of linear and branched polylactides, *Rheol. Acta.* **2015**, *54*, 831–845. https://doi.org/10.1007/s00397-015-0874-7.
19. T. Standau, M. Nofar, D. Dörr, H. Ruckdäschel, V. Altstädt, A review on multifunctional epoxy-based Joncryl® ADR chain extended thermoplastics, *Polym. Rev.* **2021**, 1–55. https://doi.org/10.1080/15583724.2021.1918710
20. M. Nofar, C. B. Park, *Polylactide Foams: Fundamentals, Manufacturing, and Applications*, Elsevier, William Andrew, Cambridge, MA. 2017.ISBN: 9780128139912.
21. M. Nofar, C. B. Park, Poly (lactic acid) foaming, *Prog. Polym. Sci.* **2014**, *39*(10), 1721–1741. https://doi.org/10.1016/j.progpolymsci.2014.04.001.
22. L. Wang, R. E. Lee, G. Wang, R. K.M. Chu, J. Zhao, and C. B. Park, Use of stereocomplex crystallites for fully-biobased microcellular low-density poly(lactic acid) foams for green packaging, *Chem. Eng. J.* **2017**, *327*, 1151–1162. https://doi.org/10.1016/j.cej.2017.07.024.
23. S. Saeidlou, M. A. Huneault, H. Li, and C. B. Park, Poly(lactic acid) stereocomplex formation: application to PLA rheological property modification, *J. Appl. Polym. Sci.* **2014**, *131*, 40173. https://doi.org/10.1002/app.41073.
24. S. Saeidlou, M. A. Huneault, H. Li, P. Sammut, and C. B. Park, Evidence of a dual network/spherulitic crystalline morphology in PLA stereocomplexes, *Polymer* **2012**, *53*, 5816–5824. https://doi.org/10.1016/j.polymer.2012.10.030.
25. Y. Srithep, D. Pholharn, L. S. Turng, and O. Veang-In, Injection molding and characterization of polylactide stereocomplex, *Polym. Degrad. Stab.* **2015**, *120*, 290–299. https://doi.org/10.1016/j.polymdegradstab. 2015.07.017.
26. H. Tsuji, Poly (lactic acid) stereocomplexes: a decade of progress, *Adv. Drug Deliv. Rev.* **2016**, *107*, 97–135. https://doi.org/10.1016/j.addr.2016.04.017.
27. M. Nofar, D. Sacligil, P. J. Carreau, M. R. Kamal, M. C. Heuzey, Poly (lactic acid) blends: processing, properties and applications, *Int. J. Biol. Macromol.* **2019**, *125*, 307–360. https://doi.org/10.1016/j.ijbiomac.2018.12.002.
28. M. Nofar, *Multiphase Polylactide Blends: Towards Sustainable and Green Environment*, Elsevier, Amsterdam, 2021. ISBN: 9780128241509.
29. J.-M. Raquez, Y. Habibi, M. Murariu, P. Dubois, Polylactide (PLA)-based nanocomposites, *Prog. Polym. Sci.* **2013**, *38*, 1504–1542. https://doi.org/10.1016/j.progpolymsci.2013.05.014.
30. E. Vatansever, D. Arslan, and M. Nofar, Polylactide cellulose-based nanocomposites, *Int. J. Biol. Macromol.* **2019**, *137*, 912–938. https://doi.org/10.1016/j.ijbiomac.2019.06.205.
31. R. M. Rasal, A. V. Janorkar, D. E. Hirt, Poly (lactic acid) modifications, *Prog. Polym. Sci.* **2010**, *35*, 338–356. https://doi.org/10.1016/j.progpolymsci.2009.12.003.
32. I. Pillin, N. Montrelay, Y. Grohens, Thermo-mechanical characterization of plasticized PLA: is the miscibility the only significant factor?, *Polymer* **2006**, *47*, 4676–4682. https://doi.org/10.1016/j.polymer.2006.04.013.
33. L. V. Labrecque, R. A. Kumar, V. Davé, R. A. Gross, S. P. McCarthy, Citrate esters as plasticizers for poly(lactic acid), *J. Appl. Polym. Sci.* **1997**, *66*, 1507–1513. https://doi.org/10.1002/(SICI)1097-4628(19971121)66:8<1507::AID-APP11>3.0.CO;2-0.
34. A. R. Kakroodi, Y. Kazemi, M. Nofar, C. B. Park, Tailoring poly (lactic acid) for packaging applications via the production of fully bio-based in situ microfibrillar composite films, *Chem. Eng. J.* **2017**, *308*, 772–782. https://doi.org/10.1016/j.cej.2016.09.130.
35. A. Jalali, J. H. Kim, A. M. Zolali, I. Soltani, M. Nofar, E. Behzadfar, C. B. Park, Peculiar crystallization and viscoelastic properties of polylactide/polytetrafluoroethylene composites induced by in-situ formed 3D nanofiber network, *Compos. B. Eng.* **2020**, *200*, 108361. https://doi.org/10.1016/j.compositesb.2020.108361.
36. H. Urayama, T. Kanamori, Y. Kimura, Microstructure and thermomechanical properties of glassy polylactides with different optical purity of the lactate units, *Macromol. Mater. Eng.* **2001**, *286*, 705–713. https://doi.org/10.1002/1439-2054(20011101)286:11<705::AID-MAME705>3.0.CO;2-Q.
37. S. Jacobsen, H. G. Fritz, Plasticizing polylactide—the effect of different plasticizers on the mechanical properties, *Polym. Eng. Sci.* **1999**, *39*, 1303–1310. https://doi.org/10.1002/pen.11517.
38. I. Engelberg, J. Kohn, Physico-mechanical properties of degradable polymers used in medical applications: a comparative study, *Biomaterials* **1991**, *12*, 292–304. https://doi.org/10.1016/0142-9612(91)90037-B.
39. G. Perego, G. D. Cella, C. Bastioli, Effect of molecular weight and crystallinity on poly(lactic acid) mechanical properties, *J. Appl. Polym. Sci.* **1996**, *59*, 37–43. https://doi.org/10.1002/(SICI)1097-4628(19960103)59:1<37::AID-APP6>3.0.CO;2-N.
40. E. W. Fischer, H. J. Sterzel, G. Wegner, Investigation of the structure of solution grown crystals of lactide copolymers by means of chemical reactions, *Kolloid Z. Z. Polym.* **1973**, *251*, 980–990. https://doi.org/10.1007/BF01498927.
41. D. W. Grijpma, H. Altpeter, M. J. Bevis, J. Feijen, Improvement of the mechanical properties of poly(D,L-lactide) by orientation, *Polym. Int.* **2002**, *51*, 845–851. https://doi.org/10.1002/pi.988.
42. L. Yu, H. Liu, F. Xie, L. Chen, X. Li, Effect of annealing and orientation on microstructures and mechanical properties of polylactic acid, *Polym. Eng. Sci.* **2008**, *48*, 634–641. https://doi.org/10.1002/pen.20970.
43. R. A. Auras, B. Harte, S. Selke, R. J. Hernandez, Mechanical, physical, and barrier properties of poly(lactide) films, *J. Plast. Film Sheet.* **2003**, *19*, 123–135. https://doi.org/10.1177/8756087903039702.
44. M. Baiardo, G. Frisoni, M. Scandola, M. Rimelen, D. Lips, K. Ruffieux, E. Wintermantel, Thermal and mechanical properties

of plasticized poly(L-lactic acid), *J. Appl. Polym. Sci.* **2003**, *90*, 1731–1738. https://doi.org/10.1002/app.12549.

45. A. C. Renouf-Glauser, J. Rose, D. F. Farrar, R. E. Cameron, The effect of crystallinity on the deformation mechanism and bulk mechanical properties of PLLA, *Biomaterials* **2005**, *26*, 5771–5782. https://doi.org/10.1016/j.biomaterials.2005.03.002.
46. K. S. Anderson, K. M. Schreck, M. A. Hillmyer, Toughening polylactide, *Polym. Rev.* **2008**, *48*, 85–108. https://doi.org/10.1080/15583720701834216.
47. D. W. Grijpma, A. J. Nijenhuis, P. G. T. van Wijk, A. J. Pennings, High impact strength as-polymerized PLLA, *Polym. Bull.* **1992**, *29*, 571–578. https://doi.org/10.1007/BF00296720.
48. O. Martin, L. Avérous, Poly(lactic acid): plasticization and properties of biodegradable multiphase systems, *Polymer* **2001**, *42*, 6209–6219. https://doi.org/10.1016/S0032-3861(01)00086-6.
49. Z. Ren, L. Dong, Y. Yang, Dynamic mechanical and thermal properties of plasticized poly(lactic acid), *J. Appl. Polym. Sci.* **2006**, *101*, 1583–1590. https://doi.org/10.1002/app.23549.
50. Z. Kulinski, E. Piorkowska, Crystallization, structure and properties of plasticized poly(L-lactide), *Polymer* **2005**, *46*, 10290–10300. https://doi.org/10.1016/j.polymer.2005.07.101.
51. N. Ljungberg, D. Colombini, B. Wesslén, Plasticization of poly(lactic acid) with oligomeric malonate esteramides: dynamic mechanical and thermal film properties, *J. Appl. Polym. Sci.* **2005**, *96*, 992–1002. https://doi.org/10.1002/app.21163.
52. N. Ljungberg, B. Wesslén, Preparation and properties of plasticized poly(lactic acid) films, *Biomacromolecules* **2005**, *6*, 1789–1796. https://doi.org/10.1021/bm050098f.
53. N. Ljungberg, B. Wesslén, Thermomechanical film properties and aging of blends of poly(lactic acid) and malonate oligomers, *J. Appl. Polym. Sci.* **2004**, *94*, 2140–2149. https://doi.org/10.1002/app.21100.
54. N. Ljungberg, B. Wesslén, Tributyl citrate oligomers as plasticizers for poly (lactic acid): thermo-mechanical film properties and aging, *Polymer* **2003**, *44*, 7679–7688. https://doi.org/10.1016/j.polymer.2003.09.055.
55. A. Celli, M. Scandola, Thermal properties and physical ageing of poly (L-lactic acid), *Polymer* **1992**, *33*, 2699–2703. https://doi.org/10.1016/0032-3861(92)90440-8.
56. S. Ghosh, J. C. Viana, R. L. Reis, J. F. Mano, Effect of processing conditions on morphology and mechanical properties of injection-molded poly(L-lactic acid), *Polym. Eng. Sci.* **2007**, *47*, 1141–1147. https://doi.org/10.1002/pen.20799.
57. S. D. Park, M. Todo, K. Arakawa, Effect of annealing on the fracture toughness of poly(lactic acid), *J. Mater. Sci.* **2004**, *39*, 1113–1116. https://doi.org/10.4028/www.scientific.net/KEM.261-263.105
58. S. D. Park, M. Todo, K. Arakawa, M. Koganemaru, Effect of crystallinity and loading-rate on mode I fracture behavior of poly(lactic acid), *Polymer* **2006**, *47*, 1357–1363. https://doi.org/10.1016/j.polymer.2005.12.046.
59. D. Sawai, K. Takahashi, A. Sasashige, T. Kanamoto, Preparation of oriented β-form poly(L-lactic acid) by solid-state coextrusion: effect of extrusion variables, *Macromolecules* **2003**, *36*, 3601–3605. https://doi.org/10.1021/ma030050z.
60. K. Takahashi, D. Sawai, T. Yokoyama, T. Kanamoto, S. H. Hyon, Crystal transformation from the α-to the β-form upon tensile drawing of poly (L-lactic acid), *Polymer* **2004**, *45*, 4969–4976. https://doi.org/10.1016/j.polymer.2004.03.108.
61. S. Kumar, S. Akhtar, V. Kumar, Biaxially oriented biodegradable film based on polylactic acid: a brief review, *Popular Plast. Packag.* **2005**, *50*, 85–89.
62. NatureWorks technical data sheet, available from: http://www.natureworksllc.com/product-and-applications/natureworks-biopolymer/technical-resources/~/media/Product%20and%20Applications/NatureWorks%20Biopolymer/Technical%20Resources/Technical%20Data%20Sheets/TechnicalDataSheet_4042D_pdf.ashx (accessed December 2009).
63. S. Ghosh, J. C. Viana, R. L. Reis, J. F. Mano, Oriented morphology and enhanced mechanical properties of poly(L-lactic acid) from shear controlled orientation in injection molding, *Mater. Sci. Eng. A* **2008**, *490*, 81–89. https://doi.org/10.1016/j.msea.2008.01.003.
64. C. Zengwen, H. Pan, J. Bian, L. Han, H. Zhang, L. Dong, Y. Yang, Transform poly (lactic acid) packaging film from brittleness to toughness using traditional industrial equipments, *Polymer* **2019**, *180*, 121728. https://doi.org/10.1016/j.polymer.2019.121728.
65. L. Xie, X. Sun, Y. Tian, F. Dong, M. He, Y. Xiong. Self-nanofibrillation strategy to an unusual combination of strength and toughness for poly(lactic acid), *RSC Adv.* **2017**, *7*, 11373–11380. https://doi.org/10.1039/C6RA27643A.
66. M. Nofar, M. Mohammadi, P. J. Carreau, Super enhancement of rheological properties of amorphous PLA through generation of a fiberlike oriented crystal network, *J. Rheol.* **2021**, *65*(4), 493–505. https://doi.org/10.1122/8.0000234.
67. R. Mehta, V. Kumar, H. Bhunia, S. N. Upadhyay, Synthesis of poly(lactic acid): a review, *Polym. Rev.* **2005**, *45*, 325–349. https://doi.org/10.1080/15321790500304148.
68. C. C. Chen, J. Y. Chueh, H. Tseng, H. M. Huang, S. Y. Lee, Preparation and characterization of biodegradable PLA polymeric blends, *Biomaterials* **2003**, *24*, 1167–1173. https://doi.org/10.1016/S0142-9612(02)00466-0.
69. J. R. Dorgan, H. Lehermeier, M. Mang, Thermal and rheological properties of commercial-grade poly(lactic acid)s *J. Polym. Environ.* **2000**, *8*, 1–9. https://doi.org/10.1023/A:1010185910301.
70. M. Spinu, C. Jackson, M. Y. Keating, K. H. Gardner, Material design in poly(lactic acid) systems: block copolymers, star homo- and copolymers, and stereocomplexes, *J. Macromol. Sci. A* **1996**, *33*, 1497–1530. https://doi.org/10.1080/10601329608014922.
71. H. Tsuji, Y. Ikada, Stereocomplex formation between enantiomeric poly(lactic acid)s. XI. Mechanical properties and morphology of solution-cast films, *Polymer* **1999**, *40*, 6699–6708. https://doi.org/10.1016/S0032-3861(99)00004-X.
72. D. Sawai, M. Tamada, T. Kanamoto, Development of oriented morphology and mechanical properties upon drawing of stereo-complex of poly(L-lactic acid) and poly(D-lactic acid) by solid-state coextrusion, *Polym. J.* **2007**, *39* 953–960. https://doi.org/10.1295/polymj.PJ2007038.

73. O. Gil-Castell, J. D. Badia, S. Ingles-Mascaros, R. Teruel-Juanes, A. Serra, A. Ribes-Greus, Polylactide-based self-reinforced composites biodegradation: individual and combined influence of temperature, water and compost, *Polym. Degrad. Stab.* **2018**, *158*, 40–51. https://doi.org/10.1016/j.polymdegradstab. 2018.10.017.
74. W. Jia, R. H. Gong, and P. J. Hogg, Poly (lactic acid) fiber reinforced biodegradable composites, *Compos. Part B. Eng.* **2014**, *62*, 104–112. https://doi.org/10.1016/j.compositesb. 2014.02.024
75. R. Li, D. Yao, Preparation of single poly(lactic acid) composites, *J. Appl. Polym. Sci.* **2008**, *107*, 2909–2916. https://doi.org/10.1002/app.27406.
76. K. P. Matabola, A. R. De Vries, F. S. Moolman, A. S. Luyt, Single polymer composites: a review, *J. Mater. Sci.* **2009**, *44*, 6213–6222. https://doi.org/10.1007/s10853-009-3792-1.
77. C. Gao, L. Yu, H. Liu, L. Chen, Development of self-reinforced polymer composites, *Prog. Polym. Sci.* **2012**, *37*(6), 767–780. https://doi.org/10.1016/j.progpolymsci.2011.09.005.
78. K. Somord, O. Suwantong, N. Tawichai, T. Peijs, N. Soykeabkaew, Self-reinforced poly(lactic acid) nanocomposites of high toughness, *Polymer* **2016**, *103*, 347–352. https://doi.org/10.1016/j.polymer.2016.09.080.
79. G. Theryo, F. Jing, L. M. Pitet, M. A. Hillmyer, Tough polylactide graft copolymers, *Macromolecules* **2010**, *43*, 7394–7397. https://doi.org/10.1021/ma101155p.
80. D. W. Grijpma, G. J. Zondervan, A. J. Pennings,High molecular weight copolymers of L-lactide and ε-caprolactone as biodegradable elastomeric implant materials, *Polym. Bull.* **1991**, *25*, 327–333. https://doi.org/10.1007/BF00316902.
81. C. A. P. Joziasse, M. D. C. Topp, H. Veenstra, D. W. Grijpma, A. J. Pennings, Supertough poly(lactide)s, *Polym. Bull.* **1994**, *33*, 599–605. https://doi.org/10.1007/BF00296170.
82. D. W. Grijpma, R. D.A. Van Hofslot, H. Supèr, A. J. Nijenhuis, A. J. Pennings, Rubber toughening of poly(lactide) by blending and block copolymerization, *Polym. Eng. Sci.* **1994**, *34*, 1674–1684. https://doi.org/10.1002/pen.760342205.
83. Z. Fan, Z. Xu, H. Niu, N. Gao, Y. Guan, C. Li, et al., An injectable oxygen release system to augment cell survival and promote cardiac repair following myocardial infarction, *Sci. Rep.* **2018**, *8*, 1371–1398. https://doi.org/10.1038/s41598-018-19906-w.
84. Z. Z. Fan, M. Fu, Z. Xu, B. Zhang, Z. Li, H. Li, et al., Sustained release of a peptide-based matrix metalloproteinase-2 inhibitor to attenuate adverse cardiac remodeling and improve cardiac function following myocardial infarction, *Biomacromolecules* **2017**, *18*, 2820–2829. https://doi.org/10.1021/acs.biomac.7b00760.
85. G. Perego, T. Vercellio, G. Balbontin, Copolymers of L- and D,L-lactide with 6-caprolactone: synthesis and characterization, *Macromol. Chem.* **1993**, *194*, 2463–2469. https://doi.org/10.1002/macp.1993.021940905.
86. N. Ljungberg, T. Andersson, B. Wesslén, Film extrusion and film weldability of poly(lactic acid) plasticized with triacetine and tributyl citrate, *J. Appl. Polym. Sci.* **2003**, *88*, 3239–3247. https://doi.org/10.1002/app.12106.
87. N. Ljungberg, B. Wesslén, The effects of plasticizers on the dynamic mechanical and thermal properties of poly(lactic acid), *J. Appl. Polym. Sci.* **2002**, *86*, 1227–1234. https://doi.org/10.1002/app.11077.
88. C. W. Macosko, Morphology development and control in immiscible polymer blends, *Macromol. Symp.* **2000**, *149*, 171–184. https://doi.org/10.1002/1521-3900(200001)149:1<171::AID-MASY171>3.0.CO;2-8.
89. B. D. Favis, Polymer alloys and blends: recent advances, *Can. J. Chem. Eng.* **1991**, *69*, 619–625. https://doi.org/10.1002/cjce.5450690303.
90. H. Tsuji, Y. Ikada, Blends of aliphatic polyesters. I. Physical properties and morphologies of solution-cast blends from poly(DL-lactide) and poly(E-caprolactone), *J. Appl. Polym. Sci.* **1996**, *60*, 2367–2375. https://doi.org/10.1002/(SICI)1097-4628(19960627)60:13<2367::AID-APP8>3.0.CO;2-C.
91. H. Tsuji, Y. Ikada, Blends of aliphatic polyesters. II. Hydrolysis of solution-cast blends from poly(L-lactide) and poly (E-caprolactone) in phosphate-buffered solution, *J. Appl. Polym. Sci.* **1998**, *67*, 405–415. https://doi.org/10.1002/(SICI)1097-4628(19980118)67:3<405::AID-APP3>3.0.CO;2-Q
92. N. Chapleau, M. A. Huneault, H. Li, Biaxial orientation of polylactide/thermoplastic starch blends, *Int. Polym. Process.* **2007**, *22*, 412–418. https://doi.org/10.3139/217.2185.
93. M. A. Huneault, H. Li, Morphology and properties of compatibilized polylactide/thermoplastic starch blends, *Polymer* **2007**, *48*, 270–280. https://doi.org/10.1016/j.polymer.2006.11.023.
94. S. Iannace, L. Ambrosio, S. J. Huang, L. Nicolais, Poly(3-hydroxybutyrate)-*co*-(3-hydroxyvalerate)/poly-L-lactide blends: thermal and mechanical properties, *J. Appl. Polym. Sci.* **1994**, *54*, 1525–1535. https://doi.org/10.1002/app.1994.070541017.
95. Y. Kikkawa, T. Suzuki, T. Tsuge, M. Kanesato, Y. Doi, H. Abe, Effect of phase structure on enzymatic degradation in poly(L-lactide)/atactic poly(3-hydroxybutyrate) blends with different miscibility, *Biomacromolecules* **2009**, *10*, 1013–1018. https://doi.org/10.1021/bm900117J.
96. Z. Bartczak, A. Galeski, M. Kowalczuk, M. Sobota, R. Malinowski, Tough blends of poly(lactide) and amorphous poly([*R*,*S*]-3-hydroxy butyrate)–morphology and properties, *Eur. Polym. J.* **2013**, *49*, 3630–3641. https://doi.org/10.1016/j.eurpolymj.2013.07.033.
97. M. Nofar, M. C. Heuzey, P. J. Carreau, M. R. Kamal, Effects of nanoclay and its localization on the morphology stabilization of PLA/PBAT blends under shear flow, *Polymer* **2016**, *98*, 353–364. https://doi.org/10.1016/j.polymer.2016.06.044.
98. M. Nofar, M. C. Heuzey, P. J. Carreau, M. R. Kamal, J. Randall, Coalescence in PLA-PBAT blends under shear flow: effects of blend preparation and PLA molecular weight, *J. Rheol.* **2016**, *60*(4), 637–648. https://doi.org/10.1122/1.4953446.
99. R. Salehiyan, M. Nofar, K. Malkappa, S. S. Ray, Effect of nanofillers characteristics and their selective localization on morphology development and rheological properties of melt-processed polylactide/poly(butylene adipate-*co*-terephthalate) blend composites, *Polym. Eng. Sci.* **2020**, *60*(11), 2749–2760. https://doi.org/10.1002/pen.25505.

100. M. Nofar, M. C. Heuzey, P. J. Carreau, M. R. Kamal, Nanoparticle interactions and molecular relaxation in PLA/PBAT/nanoclay blends, *Exp. Res.* **2020**, *1*, E47. https://doi.org/10.1017/exp.2020.54.
101. D. S. Sarul, D. Arslan, E. Vatansever, Y. Kahraman, A. Durmus, R. Salehiyan, M. Nofar, Preparation and characterization of PLA/PBAT/CNC blend nanocomposites, *Colloid Polym. Sci.* **2021**, *299*(6), 987–998. https://doi.org/10.1007/s00396-021-04822-9.
102. M. Nofar, A. Maani, H. Sojoudi, M. C. Heuzey, P. J. Carreau, Interfacial and rheological properties of PLA/PBAT and PLA/PBSA blends and their morphological stability under shear flow, *J. Rheol.* **2015**, *59*(2), 317–333. https://doi.org/10.1122/1.4905714.
103. M. Nofar, A. Tabatabaei, H. Sojoudiasli, C. B. Park, P. J. Carreau, M. C. Heuzey, M. R. Kamal, Mechanical and bead foaming behavior of PLA-PBAT and PLA-PBSA blends with different morphologies, *Eur. Polym. J.* **2017**, *90*, 231–244. https://doi.org/10.1016/j.eurpolymj.2017.03.031.
104. M. Nofar, R. Salehiyan, U. Ciftci, A. Jalali, A. Durmus, Ductility improvements of PLA-based binary and ternary blends with controlled morphology using PBAT, PBSA, and nanoclay, *Compos. B. Eng.* **2020**, *182*, 107661. https://doi.org/10.1016/j.compositesb.2019.107661.
105. M. Nofar, H. Oguz, D. Ovalı, Effects of the matrix crystallinity, dispersed phase, and processing type on the morphological, thermal, and mechanical properties of polylactide-based binary blends with poly[(butylene adipate)-*co*-terephthalate] and poly[(butylene succinate)-co-adipate], *J. Appl. Polym. Sci.* **2019**, *136*(23), 47636–47647. https://doi.org/10.1002/app.47636.
106. D. Ji, Z. Liu, X. Lan, F. Wu, B. Xie, M. Yang, Morphology, rheology, crystallization behavior, and mechanical properties of poly(lactic acid)/poly(butylene succinate)/dicumyl peroxide reactive blends, *J. Appl. Polym. Sci.* **2013**, *131*. https://doi.org/10.1002/app.39580.
107. M. Harada, T. Ohya, K. Iida, H. Hayashi, K. Hirano, H. Fukuda, Increased impact strength of biodegradable poly(lactic acid)/poly(butylene succinate) blend composites by using isocyanate as a reactive processing agent, *J. Appl. Polym. Sci.* **2007**, *106*, 1813–1820. https://doi.org/10.1002/app.26717.
108. Y. Deng, N. Thomas, Blending poly(butylene succinate) with poly(lactic acid): ductility and phase inversion effects, *Eur. Polym. J.* **2015**, *71*, 534–546. https://doi.org/10.1016/j.eurpolymj.2015.08.029.
109. S. Ishida, R. Nagasaki, K. Chino, T. Dong, Y. Inoue, Toughening of poly(L-lactide) by melt blending with rubbers, *J. Appl. Polym. Sci.* **2009**, *113*, 558–566. https://doi.org/10.1002/app.30134.
110. M. Kowalczyk, E. Piorkowska, Mechanisms of plastic deformation in biodegradable polylactide/poly(1,4-cis-isoprene) blends, *J. Appl. Polym. Sci.* **2011**, *124*, 4579–4589. https://doi.org/10.1002/app.35489.
111. R. Jaratrotkamjorn, C. Khaokong, V. Tanrattanakul, Toughness enhancement of poly(lactic acid) by melt blending with natural rubber, *J. Appl. Polym. Sci.* **2011**, *124*, 5027–5036. https://doi.org/10.1002/app.35617.
112. F. Feng, L. Ye, Morphologies and mechanical properties of polylactide/thermoplastic polyurethane elastomer blends, *J. Appl. Polym. Sci.* **2010**, *119*, 2778–2783. https://doi.org/10.1002/app.32863.
113. E. Oliaei, B. Kaffashi, S. Davoodi, Investigation of structure and mechanical properties of toughened poly(L-lactide)/thermoplastic poly(ester urethane) blends, *J. Appl. Polym. Sci.* **2015**, *133*, 43104–43117. https://doi.org/10.1002/app.43104.
114. Y. Kahraman, B. Özdemir, V. Kılıç, Y. Alkan Goksu, M. Nofar, Super toughened and highly ductile PLA/TPU blend systems by in situ reactive interfacial compatibilization using multifunctional epoxy-based chain extender, *J. Appl. Polym. Sci.* **2021**, *138*(20), 50457. https://doi.org/10.1002/app.50457.
115. M. Nofar, M. Mohammadi, P. J. Carreau, Effect of TPU hard segment content on the rheological and mechanical properties of PLA/TPU blends, *J. Appl. Polym. Sci.* **2020**, *137*(45), 49387. https://doi.org/10.1002/app.49387.
116. E. Bugnicourt, P. Cinelli, A. Lazzeri, V. Alvarez, Polyhydroxyalkanoate (PHA): review of synthesis, characteristics, processing and potential applications in packaging, *Express Polym. Lett.* **2014**, *8*, 791–808. https://doi.org/10.3144//expresspolymlett.2014.82.
117. N. Wang, J. Yu, P. R. Chang, X. Ma, Influence of citric acid on the properties of glycerol-plasticized dry starch (DTPS) and DTPS/poly (lactic acid) blends, *Starch-Starke* **2007**, *59*, 409–417. https://doi.org/10.1002/star.200700617.
118. J. M. Ferri, D. Garcia-Garcia, L. Sánchez-Nacher, O. Fenollar, R. Balart, The effect of maleinized linseed oil (MLO) on mechanical performance of poly (lactic acid)-thermoplastic starch (PLA-TPS) blends, *Carbohydr. Polym.* **2016**, *147*, 60–68. https://doi.org/10.1016/j.carbpol.2016.03.082.

# 11

# MASS TRANSFER

Uruchaya Sonchaeng and Rafael Auras

## 11.1 INTRODUCTION

Poly(lactic acid) (PLA), like other polymers, is permeable to gases, vapors, and volatile organic compounds. Mass transfer parameters such as permeability (*P*), diffusion (*D*), and solubility (*S*) coefficients have been reported for PLA. Compared to the number of publications on other PLA properties, the literature related to PLA mass transfer is limited. Moreover, the measuring conditions and reported units of the mass transfer parameters are inconsistent. In the first edition of the book, several of the mass transfer values of PLA were summarized [1]. In this edition, we updated the latest published information regarding mass transfer of PLA. We converted the mass transfer parameters (*P*, *D*, and *S*) of PLA to standard units before comparing these parameters to offer the readers a broader understanding of the mass transfer of PLA. Some useful mass transfer data with units that could not be converted to standard units due to the lack of thickness or partial pressure information are discussed separately.

In general, PLA is considered a moderate barrier polymer in the context of mass transfer. Thus, a polymer described as a "good barrier" or "high barrier" means it has low mass transfer, which usually refers to low *P*. Similarly, a polymer with "poor barrier" has high mass transfer and refers to high *P*. PLA may be referred to as poly(L-lactic acid) (PLLA), poly(D-lactic acid) (PDLA), or poly(DL-lactic acid) (PDLLA) depending on the isomerism of the monomer(s). In this chapter, we will use the generic abbreviation PLA and specify the material with its stereoisomer composition; for example, 94% L is a PLA sample with 94% L-lactide or L-lactic acid in its final form. The readers may refer to the original references for the material details. When discussing mass transfer, the gas or vapor of interest will be subscripted to the parameter; for example, $P_{O_2}$ is *P* for oxygen gas. The term "gas" in this chapter refers to non-condensable gases such as $O_2$ and the term "vapor" refers to condensable gases such as water and organic vapors. The molecules discussed in this chapter are gases and vapors, unless stated otherwise.

When compared with common commercial films (Figure 11.1), $P_{O_2}$, $P_{CO_2}$, and $P_{N_2}$ of PLA are higher than those of poly(ethylene terephthalate) (PET) but mostly lower than those of polyethylene (PE), polystyrene (PS), and polypropylene (PP). As for water vapor, PLA has higher $P_{H_2O}$ than those of PET, PE, PS, and PP. PLA by itself is not suitable when high barrier against gases and water vapor is necessary. Modifications of PLA such as varying stereoisomerism of PLA monomers in the manufacturing process, coextruding or blending PLA with a high barrier polymer, or utilizing nanocomposites or radiation technology can help improve barrier properties of PLA. The effects of these modifications on PLA mass transfer parameters are discussed in this chapter.

Most of the reported mass transfer parameters of PLA have been compared and interpreted based on an assumption that PLA has only two phases, namely, a crystalline fraction (CF) and an amorphous fraction. The relatively new concept that the amorphous fraction in semicrystalline polymers can be separated into a rigid amorphous fraction (RAF) and a mobile amorphous fraction (MAF) has been proven to be applicable to semicrystalline PLA, as well as other semicrystalline polymers like PET [2–6]. We will use this new concept (known as a three-phase model) to explain some inconsistent mass transfer values in PLA as reported in the literature.

*Poly(Lactic Acid): Synthesis, Structures, Properties, Processing, Applications, and End of Life*, Second Edition.
Edited by Rafael A. Auras, Loong-Tak Lim, Susan E. M. Selke, and Hideto Tsuji.

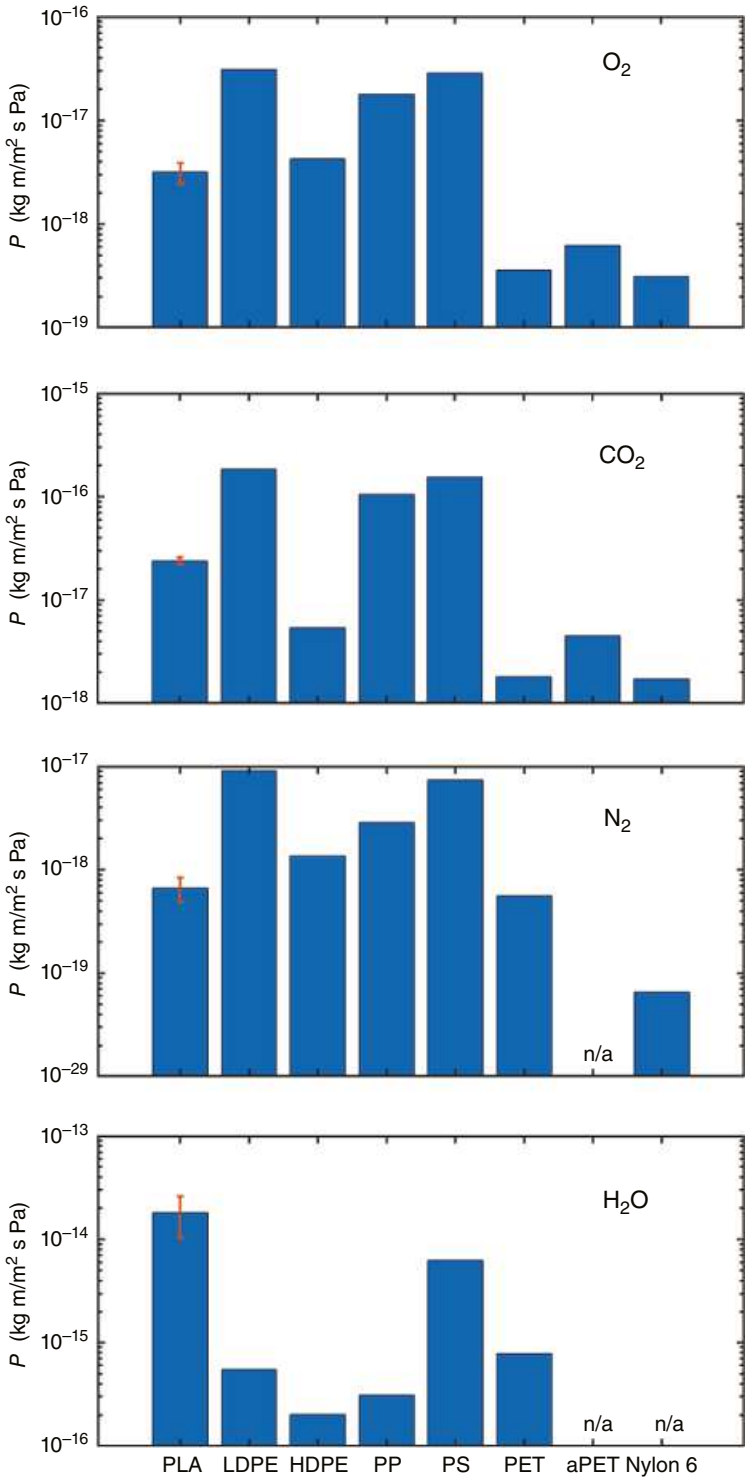


**FIGURE 11.1** Comparisons of permeability coefficients ($P$) of $O_2$, $CO_2$, and $N_2$ gases and water vapor at 25°C in poly(lactic acid) (PLA), low-density polyethylene (LDPE), high-density polyethylene (HDPE), polypropylene (PP), polystyrene (PS), poly(ethylene terephthalate) (PET), and amorphous PET (aPET). Values for PLA are averages of reported experimental data and are shown with error bars. *Source:* Data from [7–11].

## 11.2 BACKGROUND ON MASS TRANSFER IN POLYMERS

A mathematical approach to evaluate mass transfer, followed by a review of common experimental methods to quantify mass transfer in polymers and a brief discussion of factors affecting mass transfer, are provided in this section. Figure 11.2 illustrates the mass transfer processes in a homogeneous polymeric film. The mass transfer starts with permeant sorption on a side of the film where the permeant has high chemical potential, followed by permeant diffusion through the polymer matrix toward the low chemical potential side, and then permeant desorption from the surface where the permeant has low chemical potential. These three processes are called the permeation process. To maintain thermodynamic equilibrium, the permeant molecules permeate through a polymer from high to low chemical potential. A compound has a higher chemical potential on the higher concentration side of the film, and vice versa [12].

Diffusion process in a film can be described by Fick's first law of diffusion:

$$F = -D\frac{dc}{dx} \tag{11.1}$$

where $F$ is the diffusion flux, $D$ is the diffusion coefficient or diffusivity, $c$ is the permeant concentration, $x$ is the direction of movement of the permeant (across the film thickness), and $dc/dx$ is the concentration gradient in the direction of the flow. Equation 11.1 can be used at steady state when the permeant concentration is independent of time. There are cases where the permeant interacts with the polymer, causing a deviation from a straight line during the diffusion process (illustrated as curve dashed lines in Figure 11.2). The diffusion process in these cases does not follow Fickian behavior and is usually referred to as non-Fickian diffusion [13–15]. Assuming no interaction between the permeant and the polymer, Henry's law can be used to express the relationship between the permeant concentration and its solubility coefficient ($S$) and partial pressure ($p$) at steady state.

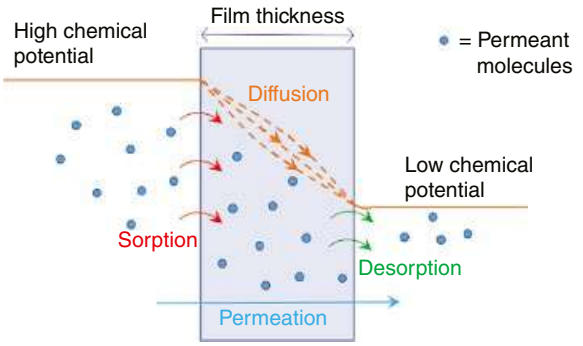


**FIGURE 11.2** Permeation of permeant molecules from a higher to a lower chemical potential membrane.

$$c = Sp \tag{11.2}$$

At steady state, the flux, $F$, in Equation 11.1 is the amount of permeant ($Q$) passing through a surface of unit area ($A$) per unit time ($t$) and can be written as:

$$F = \frac{Q}{At} \tag{11.3}$$

Combining Equations 11.1 through 11.3, the permeability coefficient ($P$) can be described as:

$$P = DS = \frac{QL}{At\Delta p} \tag{11.4}$$

where $L$ is the film thickness and $\Delta p$ is the partial pressure gradient of the permeant. Sometimes the term transmission rate ($TR$) is reported instead of $P$:

$$TR = \frac{Q}{At} \tag{11.5}$$

$TR$ values are commonly reported for water vapor and oxygen gas, namely, water vapor transmission rate ($WVTR$) and oxygen transmission rate ($OTR$). From Equations 11.4 and 11.5, $TR$ can be converted to $P$ when the values of $L$ and $\Delta p$ are known.

While Equation 11.4 applies to the permeation process at steady state, Fick's second law describes the process during the unsteady state [16]:

$$\frac{dc}{dt} = \frac{d}{dx}\left(D\frac{dc}{dx}\right) \tag{11.6}$$

where $dc/dt$ is the rate of change of the permeant concentration as a function of time. Assuming $D$ is independent of time, position, and concentration, Equation 11.6 can be written as:

$$\frac{dc}{dt} = D\frac{d^2c}{dx^2} \tag{11.7}$$

Equation 11.7 can be solved numerically if the unsteady state and steady state portions of the mass transfer are included and Henry's law applies:

$$\frac{F_t}{F_\infty} = \left(\frac{4}{\sqrt{\pi}}\right)\left(\sqrt{\frac{L^2}{4Dt}}\right)\sum_{n=1,3,5,\ldots}^{\infty}\exp\left(\frac{-n^2L^2}{4Dt}\right) \tag{11.8}$$

where $F_t$ is the permeant flux through the film at time $t$ during the unsteady state portion and $F_\infty$ is the permeant flux at steady state [17]. Based on the mass transfer profile (i.e., both unsteady and steady state portions) from Equation 11.8,

$D$ can be estimated from:

$$D = \frac{L^2}{7.199 t_{0.5}} \tag{11.9}$$

where $t_{0.5}$ is the time when $F_t/F_\infty = 0.5$. $P$ can be calculated when the value of $F_\infty$ is known:

$$P = \frac{F_\infty L}{\Delta p} \tag{11.10}$$

These equations, including the relationships in Equation 11.4, must be used with care. While they apply to mass transfer of a permeant in a polymeric film, some permeation phenomena cannot be simplified, especially for glassy polymers, because of their restricted chain mobility.

Various methods can be used to determine mass transfer parameters in polymeric films. Isostatic and quasi-isostatic methods are often used for measuring permeability of gases and vapors [18, 19]. In these methods, one side of the film is exposed to a known concentration of a test gas or vapor, and the concentration of the gas or vapor permeated to the other side of the film is measured. $P$ can be determined from the steady state flux based on Equation 11.4 or Equation 11.10, $D$ from Equation 11.9 if the unsteady state data are available, and $S$ can then be estimated from the $P = DS$ relationship in Equation 11.4. For sorption measurements, which are common for vapors and volatile organic compounds [20], the film is exposed to a constant concentration or vapor pressure of the permeant and the change in weight of the film is monitored. Absorption-based instruments such as quartz crystal microbalance (QCM) and quartz spring microbalance (QSM) can measure $D$ and $S$, from which $P$ can be estimated from Equation 11.4. How the mass transfer data are obtained (i.e., through a direct measurement or from an estimation through other parameters) should be clearly specified as it may influence data accuracy.

As temperature increases, the diffusion of gases and vapors is enhanced which affects permeation. The Arrhenius equations [21] describe the temperature dependence of these mass transfer parameters:

$$P = P_0 \exp\left(-\frac{E_P}{RT}\right) \tag{11.11}$$

$$D = D_0 \exp\left(-\frac{E_D}{RT}\right) \tag{11.12}$$

$$S = S_0 \exp\left(-\frac{\Delta H_S}{RT}\right) \tag{11.13}$$

where $P_0$, $D_0$ and $S_0$ are the pre-exponential factors for $P$, $D$, and $S$, respectively, and can be derived from mass transfer experimental data. $E_P$ is the activation energy of permeation, $R$ is the universal gas constant, $T$ is temperature in Kelvin, $E_D$ is the activation energy of diffusion, and $\Delta H_S$ is the heat of sorption. Equations 11.14 and 11.15 further describe the relationship of $E_P$, $E_D$, and $\Delta H_S$:

$$E_P = E_D + \Delta H_S \tag{11.14}$$

$$\Delta H_S = \Delta H_C + \Delta H_M \tag{11.15}$$

where $\Delta H_C$ is the heat of condensation and $\Delta H_M$ is the heat of mixing.

## 11.3 MASS TRANSFER PROPERTIES OF NEAT PLA FILMS

This section focuses on key findings in mass transfer properties of neat PLA films, which depend on the grades of PLA, film processing, and/or thermal history. The mass transfer parameters measured by different instruments from different groups of researchers also contribute to variations in the results. We recommend readers check the original source of the data for details of the materials and methods. Mass transfer properties of modified PLA films are discussed later in Section 11.4.

### 11.3.1 Mass Transfer of Gases

The mass transfer parameters of gases are important in determining PLA applications. Pure $O_2$ is a strong oxidizing agent and, thus, mass transfer of $O_2$ is a crucial factor for packaged oxidation-sensitive food products [22]. Similarly, the level of $O_2$ affects microbial growth and fresh produce respiration rate, which can be seen in various applications of modified atmosphere packaging (MAP) [23–27]. Gases such as $CO_2$, $N_2$, nitrous oxide ($N_2O$), and ethylene ($C_2H_4$) are also used in MAP. Chlorine dioxide ($ClO_2$) is an oxidizing agent, which has been used for food packaging disinfection [28]. While the above are gases that have been associated with the shelf life of the packaged food product, other gases are commonly used in mass transfer experiments. For example, $H_2$ is used because it is the smallest chemical molecule, He because it is the smallest noble gas, and methane ($CH_4$) because it is the simplest saturated hydrocarbon. In the following sections, the mass transfer parameters ($P$, $D$, and $S$) of these gases in neat PLA films are compiled and discussed. Interestingly, the reports for mass transfer parameters of $O_2$ in the literature are more extensive compared with other gases. This could be attributed to the abundance of $O_2$ in air and its oxidizing nature. Therefore, a dedicated section on mass transfer of $O_2$ is provided in Section 11.3.2. When discussing mass transfer parameters of gases in neat PLA in this chapter, an arbitrary glass transition temperature ($T_g$) of 58°C is used to separate ranges below and above $T_g$, and the values of $P$, $D$, and $S$ are converted into and compared in S.I. units, i.e., kg m/m$^2$ s Pa

for $P$, $m^2/s$ for $D$, and $kg/m^3$ Pa for $S$. Reported data with units that could not be converted into S.I. units are discussed separately or excluded.

***11.3.1.1 Gas Permeability*** Arrhenius plots of $P$ of gases in neat PLA films at 0% relative humidity (RH) are shown in Figure 11.3. Even with new data from recent works [11, 24, 29–31] added, the overall $P$ for $O_2$, $CO_2$, $N_2$, $N_2O$, $H_2$, He, and $CH_4$ gases are not much different from what was previously reported [7]; the overall $P$ of these gases are lower than $8\times10^{-17}$ kg m/m$^2$ s Pa below $T_g$, and lower than $3\times10^{-16}$ kg m/m$^2$ s Pa above $T_g$. The magnitude of $P$ of pure gases at 0% RH follows this trend: $P_{CO_2} > P_{He} > P_{N_2O} > P_{H_2} > P_{O_2} > P_{N_2} > P_{CH_4}$ below $T_g$, with the trend of $P_{CO_2} > P_{O_2} > P_{H_2} > P_{N_2}$ above $T_g$, similar to the trends reported by other authors [11, 32–34]. However, information for $P_{N_2O}$ and $P_{CH_4}$ is still lacking, and more data are needed to confirm the trend. The regression lines for the Arrhenius equation show strong linear relationship with $P$ increasing as temperature increases, with a discontinuity at $T_g$. The steeper slope of the regression line above $T_g$ indicates a greater effect of change in temperature on $P$ in the temperature range above $T_g$ than below $T_g$. The reported $P_{ClO_2}$ values [35] were in the range of $5.4\times10^{-17}$ kg m/m$^2$ s Pa at 23°C to $9.4\times10^{-16}$ kg m/m$^2$ s Pa at 40°C. However, since $P_{ClO_2}$ values were measured at 50% RH, they were not plotted in Figure 11.3. Some data were excluded as the researchers claimed that the reported data were out-of-range due to material defects [36].

For $CO_2$, $O_2$, $N_2$, and $CH_4$, their $P$ values (measured at 20–35°C and 0% RH) linearly increased as their molar mass (i.e., molecular weight, $M_w$) increased, and linearly decreased as their kinetic diameter increased [7]. However, for small and light gases such as He and $H_2$, their $P$ values did not fall on the same linear trend. These two gases are small and light, which may result in high $D$ [87, 88] and very low $S$ [89], leading to different mass transfer behaviors than those of other gases. Nevertheless, data on $D$ and $S$ of He and $H_2$ are not available to confirm this assumption.

*11.3.1.1.1 Factors Affecting Gas Permeability* In the following sub-sections, the main factors that affect $P$ of gases are discussed. As mentioned earlier, due to the massive data available for $O_2$, this gas is discussed separately in Section 11.3.2.

*Temperature:* An Arrhenius relationship is observed for $P_{CO_2}$ [33, 59, 80, 83], $P_{N_2}$ [33, 85], $P_{H_2}$ [32, 33], as well as $P_{N_2O}$ [24] as shown in Figure 11.3 with a discontinuity of the slope at $T_g$. Different researchers reported different $E_P$ values for gases [7, 24, 31], which could be due to different PLA sources, processing methods, or thermal treatment. Table 11.1 summarizes $E_P$, $E_D$, and $\Delta H_S$ values for gases in PLA. All the reported $E_P$ and $E_D$ values are positive, indicating an increase in $P$ and $D$ as temperature increases within the range of the test temperatures. $\Delta H_S$ values are mostly negative or low.

*Relative humidity*: RH can affect barrier properties of PLA, such as by inducing crystallization or plasticizing the polymer matrix, resulting in non-Fickian mass transfer phenomena [14, 93] as described by the solution of the general Equation 11.6. There were no reports of $P$ for

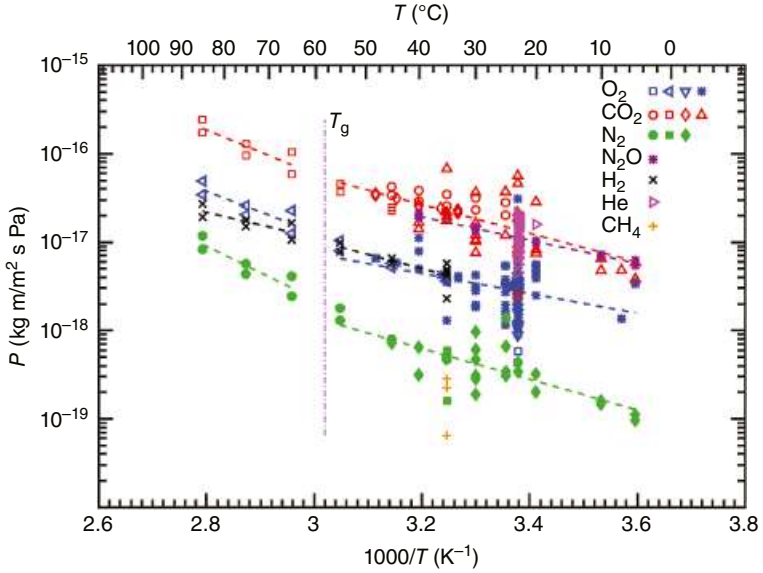


**FIGURE 11.3** Arrhenius plot of permeability coefficients ($P$) of $O_2$, $CO_2$, $N_2$, $N_2O$, $H_2$, He, and $CH_4$ at 0% RH. Data references: $O_2$ □ [37], ◁ [33], ∇ [38], * [11, 30–32, 39–82]. $CO_2$ ○ [83], □ [33], ◊ [59], Δ [11, 24, 32, 42, 50, 60, 63, 64, 73–75, 80, 84]. $N_2$ ● [33], ■ [32], ♦ [11, 24, 42, 54, 66, 80, 85]. $N_2O$ * [24]. $H_2$ × [32, 33]. He ▷ [38, 41, 47, 52, 86]. $CH_4$ + [32]. The vertical dash-dotted line is an arbitrary $T_g$ set at 58°C, and the dashed lines are from linear regressions of reported experimental data below and above $T_g$.

**TABLE 11.1 $E_P$, $E_D$, and $\Delta H_S$ for Selected Gases at 0% RH, Except for $ClO_2$ at 50% RH**

| Gas | $T$ (°C) | PLA Type | $E_P$ (kJ/mol) | $E_D$ (kJ/mol) | $\Delta H_S$ (kJ/mol) | Ref. |
|---|---|---|---|---|---|---|
| $CO_2$ | 5–40 | 30 μm thick[a] | 26.7 | 31.0 | −9.9 | [24] |
| | 5–40 | 40 μm thick[a] | 22.2 | 21.2 | 0.8 | [24] |
| | 23–45 | 98.7% L | 18.1 | 36.3 | −18.4 | [80] |
| | 23–45 | 80% L | 17.8 | 32.2 | −13.9 | [80] |
| | 23–45 | 50% L | 14.3 | 34.8 | −25.4 | [80] |
| | 35–85 | 96% L | 48.9 | n/a | n/a | [33] |
| | 35–85 | 96 : 88% L blends | 41.5 | n/a | n/a | [33] |
| | 33–48 | Biophan[b] | 27.9 | n/a | n/a | [59] |
| | 33–48 | Biophan[b] after high-pressure | 21.0 | n/a | n/a | [59] |
| | 25–45 | 98% L (4030D[c]) | 15.6 | n/a | n/a | [83] |
| | 25–45 | 94% L (4040D[c]) | 19.4 | n/a | n/a | [83] |
| | 20–40 | 80% L | n/a | n/a | −21.88 | [90] |
| | 10–40 | 98% L | n/a | n/a | −23.14 | [91] |
| | 30–50 | 80% L | n/a | n/a | −22.22 | [92] |
| | 30–50 | 98% L | n/a | n/a | −21.58 | [92] |
| | 5–58 | Various PLAs from literature | 21.6 | 4.6 | −22.4 | [7] |
| | 59–90 | Various PLAs from literature | 47.9 | n/a | n/a | [7] |
| $N_2$ | 5–40 | 30 μm thick[a] | 12.9 | 5.1 | 8.0 | [24] |
| | 5–40 | 40 μm thick[a] | 27.0 | 40.4 | −14.3 | [24] |
| | 35–85 | 96% L | 59.0 | n/a | n/a | [33] |
| | 35–85 | 96 : 88% L blends | 52.8 | n/a | n/a | [33] |
| | 25–45 | 98% L (4032D[c]) | 28.4 | n/a | n/a | [85] |
| | 23–45 | 98.7% L | 34.6 | 59.3 | −25.0 | [80] |
| | 23–45 | 80% L | 40.9 | n/a | n/a | [80] |
| | 23–45 | 50% L | 35.0 | n/a | n/a | [80] |
| | 5–58 | Various PLAs from literature | 31.5 | n/a | n/a | [7] |
| | 59–90 | Various PLAs from literature | 57.0 | n/a | n/a | [7] |
| $H_2$ | 35–85 | 96% L | 33.5 | n/a | n/a | [33] |
| | 35–85 | 96 : 88% L blends | 27.0 | n/a | n/a | [33] |
| | 5–58 | Various PLAs from literature | 30.7 | n/a | n/a | [7] |
| | 59–90 | Various PLAs from literature | 27.3 | n/a | n/a | [7] |
| $CH_4$ | 0–50 | 96% L | 13.0 | n/a | n/a | [36] |
| $C_2H_4$ | 5–40 | 30 μm thick[a] | 31.6 | n/a | n/a | [24] |
| | 5–40 | 40 μm thick[a] | 24.5 | n/a | n/a | [24] |
| $N_2O$ | 5–40 | 30 μm thick[a] | 25.2 | 19.9 | 5.2 | [24] |
| | 5–40 | 40 μm thick[a] | 25.7 | 41.2 | −24.8 | [24] |
| $ClO_2$ | 23–40 | EVLON[d] | 129.0 | n/a | n/a | [35] |

$T$: temperature, n/a: information not available.
[a]% L unknown.
[b]PLA from NatureWorks LLC.
[c]PLA from Treofan.
[d]PLA from BI-AX International Inc.

pure gases as a function of RH, except for $P_{O_2}$, which will be discussed in Section 11.3.2. Samuel et al. [94] reported $P_{N_2}$ for neat PLA at 50% RH and 22°C of $7.23 \times 10^{-24}$ kg m/m$^2$ s Pa. The value is lower than $P_{N_2}$ of neat PLA tested by other authors [54, 85] at 0% RH and similar temperature (25°C). This could be attributed to different instruments or measurement methods and sample preparation, as it is unlikely that PLA is a stronger barrier to $N_2$ at 50% RH. However, more studies for $P_{N_2}$ at different RH conditions are needed to verify the result.

Crystallinity and L : D ratio: The data on how the degree of crystallinity ($X_c$) of PLA films affects $P$ of pure gases vary. Some authors have reported an increase in $P$ of gases as $X_c$ increases, while others reported an opposite trend. Yet others reported no change, and some reported an increase and then a decrease, as shown in Table 11.2. It is known that the L : D ratio of PLA affects $X_c$ of neat PLA film. A L-lactide ratio of more than 92% yields a semicrystalline PLA and normally, $X_c$ increases as L-lactide increases. Furthermore, $X_c$ of PLA film may vary from different processing

**TABLE 11.2 Changes in Mass Transfer Parameters of Gases in PLA Film as Degree of Crystallinity ($X_c$) Increases or L : D Ratio of PLA Film Changes**

| PLA | Gas(es) | $T$ (°C) | RH (%) | Change | Ref. |
|---|---|---|---|---|---|
| 96% L | $H_2$, $CO_2$, $O_2$, $N_2$, $CH_4$ | 35 | 0 | $P$ increased ($X_c$ 0–9%) then decreased ($X_c$ 9–40%) | [32] |
| n/a | $CO_2$ | 23 | 0 | $P$ decreased ($X_c$ 2–10%) | [75] |
| 96% L | $CO_2$ | 35–55 | 0 | No change in $P$ ($X_c$ 7–25%) | [33] |
| 96% L | $CO_2$ | 65–85 | 0 | $P$ increased ($X_c$ 7–25%) | [33] |
| 98% L | $CO_2$, $O_2$ | 30 | 0 | $P$ decreased ($X_c$ 4–37%) | [96] |
| 50 : 50 blends[a] | $CO_2$, $O_2$ | 30 | 0 | $P$ decreased ($X_c$ 10–60%) | [96] |
| n/a | He | 23 | 0 | No change in $P$ ($X_c$ 2–39%) | [41] |
| 98% L | He | 23 | 0 | $P$ decreased ($X_c$ 2–40%) | [47] |
| 99% L | He | 23 | 0 | $P$ increased ($X_c$ 2–40%) then decreased ($X_c$ 40–60%) | [47] |
| 92% L | He | 23 | 40–60 | $P$ decreased ($X_c$ 3–43%) | [55] |
| 96% L | He | 23 | 0 | No change in $P$ ($X_c$ 1–20%) then $P$ decreased ($X_c$ 30–44%) | [38] |
| 99% L | He | 23 | 0 | No change in $P$ ($X_c$ 2–40%) then $P$ decreased ($X_c$ 50–63%) | [38] |
| 50–98% L | $CO_2$ | 30 | 0 | $D$ decreased (50–80% L) then increased (80–98% L) | [80] |
| 96% L | $CO_2$ | 35 | 0 | $D$ increased ($X_c$ 0–20%) then decreased ($X_c$ 20–40%) | [32] |
| 96% L blends | $CO_2$ | 35 | 0 | $D$ increased ($X_c$ 7–25%) | [97] |
| 98% L | $CO_2$ | 30 | n/a | No change in $D$ ($X_c$ 4–37%) | [96] |
| 50 : 50 blends[a] | $CO_2$ | 30 | 0 | No change in $D$ ($X_c$ 10–60%) | [96] |
| 50–98% L | $CO_2$ | 30 | 0 | $S$ decreased (50–80% L) then increased (80–98% L) | [80] |
| 98% L | $CO_2$ | 30 | n/a | $S$ decreased ($X_c$ 4–37%) | [96] |
| 50 : 50 blends[a] | $CO_2$ | 30 | 0 | $S$ decreased ($X_c$ 10–60%) | [96] |

n/a: information not available.
[a]50 : 50 blends of 98 and 2% L.

techniques and thermal histories, such as annealing or quenching time and temperature. $P$ is expected to decrease as $X_c$ increases because the impermeable crystalline domain in the polymer matrix should increase the tortuous path for the diffusion of the permeant in the film. However, some authors reported decreasing $P_{CO_2}$ as %L-lactide increases (i.e., $X_c$ increases) [80, 83], which may be explained using the three-phase model. Details about the three-phase model can be found in Chapter 6. In short, the existence of large free volume (FV) of the RAF when the RAF vitrifies during the crystallization process (de-densification of the RAF) can lead to an increase in mass transfer of permeants such as gas molecules. Kanehashi et al. [95] conducted data analysis on different crystalline polymers. Their findings that for PLA at low $X_c$, $P$ and $D$ of $CO_2$, $O_2$ and $N_2$ slightly increased as $X_c$ increased or were not affected by $X_c$ support the three-phase model. These authors reported that at high $X_c$, $P$ and $D$ decreased as $X_c$ increased.

***11.3.1.2 Gas Diffusion*** Figure 11.4 shows Arrhenius plots of $D$ for $O_2$, $CO_2$, $CH_4$, and $N_2$ in PLA films at 0% RH. Overall, $D$ values of $O_2$, $CO_2$, $CH_4$, and $N_2$ at 0% RH are less than $1\times10^{-11}$ m²/s below $T_g$. A trend of $D_{O_2} > D_{N_2} > D_{CO_2}$ is observed, which agrees well with other reported data [24]. Data for $D$ of gases are only available for the temperature range above PLA's $T_g$. Sonchaeng et al. [7] evaluated a relationship between average $D$ values of gases measured within the temperature range of 20–35°C and 0% RH and the critical volumes ($V_c$) of $O_2$, $CO_2$, $CH_4$, and $N_2$ and reported that gases with lower $V_c$ had higher $D$, which is in good agreement with other reported data [24, 32]. $D_{ClO_2}$ measured at 23°C and 50% RH is lower than $D_{CO_2}$, $D_{CH_4}$, and $D_{N_2}$ but higher than $D_{O_2}$. However, as mentioned before, $D$ values of the other gases are measured at 0% RH, so the results may not be comparable.

*11.3.1.2.1 Factors Affecting Gas Diffusion Temperature*: $D_{CO_2}$ at each temperature were reported by different researchers [24, 32, 80, 97] using different sources of PLA films, which resulted in large variability in the estimated $E_D$ values shown in Table 11.1. Siracusa et al. [24] contributed data for $E_D$ of different gases such as $CO_2$, $N_2$, and $N_2O$ in the temperature range of 5–40°C and 0% RH. The reported $E_D$ values for their neat PLA films of 30 and 40 μm thickness are different. There is no further information regarding the film sources.

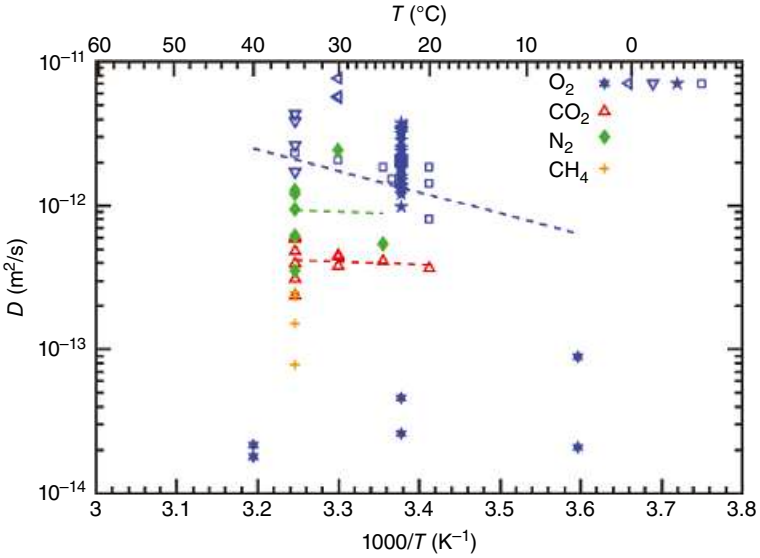


**FIGURE 11.4** Arrhenius plots of diffusion coefficients ($D$) for $O_2$, $CO_2$, $N_2$, and $CH_4$. Data references: $O_2$ ✶ [69], ◁ [80], ∇ [32], ★ [38], □ [11, 49, 52, 53, 55, 56, 63, 68, 97]. $CO_2$ Δ [11, 32, 63, 80, 97]. $N_2$ ◆ [11, 32, 80, 97]. $CH_4$ + [32]. The dashed line represents a least squares linear regression of each gas from the reported experimental data.

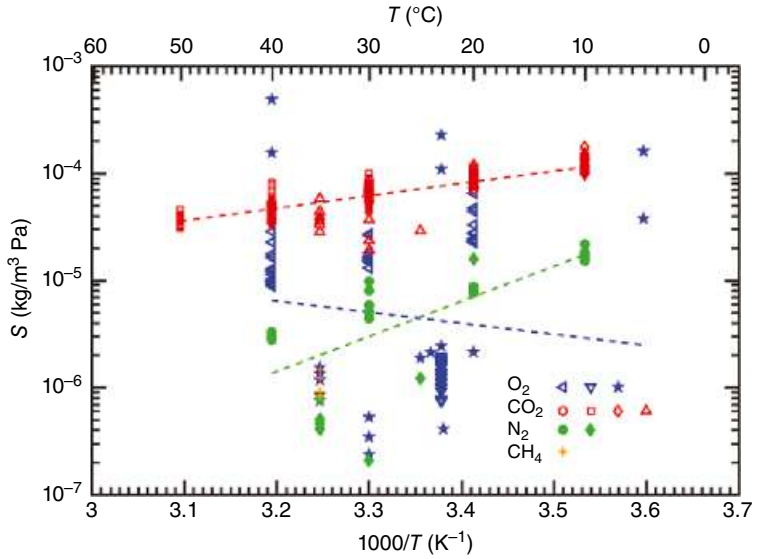


**FIGURE 11.5** Arrhenius plots of solubility coefficients ($S$) for $O_2$, $CO_2$, $N_2$, and $CH_4$. Data references: $O_2$ ◁ [90], ∇ [38], ★ [11, 32, 53, 55, 63, 69, 80, 97]. $CO_2$ ○ [90], □ [98], ◊ [91], **Δ** [11, 32, 63, 80, 97]. $N_2$ ● [90], ◆ [11, 32, 80, 97, 99]. $CH_4$ + [32]. The dashed line represents a least squares linear regression of each gas from the reported experimental data.

*Relative humidity*: Experimental data for $D$ of gases in PLA film at different RH are important to assess the effect of RH on $D$; they are missing in the reviewed literature.

*Crystallinity and* L : D *ratio:* Varying effects of $X_c$ and L : D ratio on $D$ of gases are shown in Table 11.2. An explanation of the initial increase and then decrease in $D$ could be the RAF de-densification, as discussed earlier in Section 11.3.1.1.1. Sangroniz et al. [96] reported that PLA 98% L with different annealing times (i.e., different $X_c$) showed no significant change in $D_{CO_2}$. The authors suggested that $D$ was reduced by an increase in $X_c$ and, at the same time, increased by an increase in FV. Therefore, the resulting $D_{CO_2}$ was the counterbalance of both effects and remained unchanged.

***11.3.1.3 Gas Solubility*** Figure 11.5 shows the Arrhenius plots of $S$ for $O_2$, $CO_2$, $N_2$, and $CH_4$ in PLA films at 0% RH. Overall, $S$ of these gases is lower than $4.9\times10^{-4}$ kg/m³ Pa below $T_g$. A trend of $S_{CO_2} > S_{N_2}$ is observed, which agrees well with other reported data [24]. However, due to the variation in $S_{O_2}$ values, the trend for $S_{O_2}$ compared to $S$ of other

gases cannot be assessed. Data for $S$ of gases are only available for the temperature range above PLA's $T_g$.

Siracusa et al. [24] reported $S$ values of $CO_2$, $N_2$, and $N_2O$ in the temperature range of 5–40°C and 0% RH. The results showed that $S_{N_2O} > S_{CO_2} > S_{O_2} > S_{N_2}$. However, because of the unit inconsistency, the values were not plotted in Figure 11.5. $S_{ClO_2}$ measured at 23°C and 50% RH is higher than $S$ of other gases reported in Figure 11.5.

*11.3.1.3.1 Factors Affecting Gas Solubility Temperature:* $\Delta H_S$ values of gases are shown in Table 11.1. Siracusa et al. [24] reported data for $\Delta H_S$ of different gases such as $CO_2$, $N_2$, and $N_2O$ in the temperature range of 5–40°C and 0% RH. The authors found that $\Delta H_S$ varied for neat PLA with different thicknesses (30 and 40 µm). However, no information about the type or source of their PLA film was provided. Except for $\Delta H_S$ for 40-µm thick PLA reported by Siracusa et al. [24] as positive values, $\Delta H_S$ values for other films are negative.

*Relative humidity:* To date, there is no literature available on the effect of RH on $S$ of gases.

*Crystallinity and* L : D *ratio*: Data from selected authors [80, 90, 92, 96, 98] suggest that $S$ increases as % L-lactide increases, but decreases as $X_c$ increases. While the result is contradictory since generally $X_c$ increases as L-lactide increases, this can be attributed to different processing techniques and the three-phase model in PLA. Data analyzed by Kanehashi et al. [95] showed decreasing $S$ values of $CO_2$, $O_2$, and $N_2$ as $X_c$ increased. Sangroniz et al. [96] reported decreasing $S_{CO_2}$ values of PLA 98% L as $X_c$ increased, mostly due to the reduction of FV in the amorphous region.

***11.3.1.4 Remarks for Gases*** Overall, $P$ values of gases increase as temperature increases, with different trends below and above $T_g$, i.e., $P_{CO_2} > P_{He} > P_{N_2O} > P_{H_2} > P_{O_2} > P_{CH_4}$ below $T_g$, and $P_{CO_2} > P_{O_2} > P_{H_2} > P_{N_2}$ above $T_g$. While there are clear trends for $P$, trends for $D$ and $S$ of gases below $T_g$ are not clear due to a large variation in the data. There is no information regarding $D$ and $S$ of gases above $T_g$. Furthermore, the effects of RH on mass transfer parameters have not been established due to lack of data. In addition to mass transfer data for pure gases, data for mass transfer of mixed gases such as air and mixtures of $N_2O/O_2$ intended for MAP applications are available [24]. Recently, the three-phase model has been confirmed to exist in semicrystalline PLA and the FV in the RAF has successfully accounted for some unusual mass transfer behaviors as shown in this section. A large amount of data for mass transfer of $O_2$ presented in Section 11.3.2 will contribute to more understanding of mass transfer of gases in PLA.

### 11.3.2 Mass Transfer of Oxygen

As mentioned earlier, mass transfer of $O_2$ is an important factor in determining PLA's end uses. Hence, mass transfer measurements, especially $P_{O_2}$, are commonly performed to characterize PLA. As a result, abundant mass transfer data of $O_2$ in PLA films are available in the literature. These data have been compiled and are discussed in this section.

Figure 11.3 shows $P_{O_2}$ as compared to $P$ of other gases at 0% RH. As discussed earlier, overall $P$ values increase as temperature increases, with a change in the slope of the regression line across $T_g$. In addition to $P_{O_2}$ at 0% RH, there are reported data for $P_{O_2}$ measured at different temperature and RH conditions. Therefore, Figure 11.6 presents $P_{O_2}$

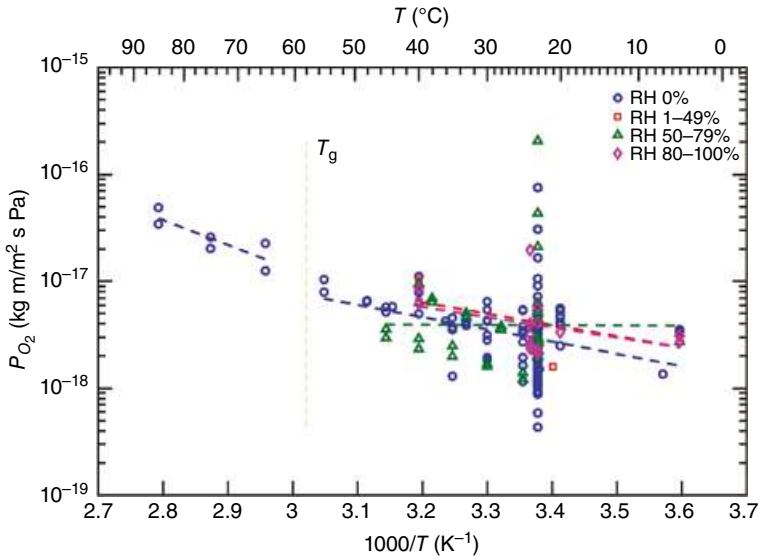


**FIGURE 11.6** Permeability coefficients of oxygen ($P_{O_2}$) in PLA films between 5 and 90°C and 0 and 100% RH. The vertical dashed line is an arbitrary $T_g$ of 58°C. Data references: ○ [11, 30–33, 37–54, 56–82, 96, 100, 101], □ [62, 69, 102, 103], Δ [44, 62, 69, 77, 83, 104–115], ◊ [39, 53, 69, 116–121].

values grouped by ranges of RH in an Arrhenius plot. Above $T_g$, $P_{O_2}$ values are between $1.2\times10^{-17}$ and $4.8\times10^{-17}$ kg m/m$^2$ s Pa. Below $T_g$, most $P_{O_2}$ values fall in the range of $1\times10^{-18}$–$2\times10^{-17}$ kg m/m$^2$ s Pa. The values of $D_{O_2}$ and $S_{O_2}$ are available only below $T_g$ and they vary greatly (data not shown). The overall range of $D_{O_2}$ measured at different temperature and RH conditions [7] is between $1.8\times10^{-14}$ and $8.4\times10^{-12}$ m$^2$/s, while the overall range of $S_{O_2}$ [7, 11] is between $2.4\times10^{-7}$ and $4.9\times10^{-4}$ kg/m$^3$ Pa. The effects of temperature or RH on $D_{O_2}$ and $S_{O_2}$ are inconsistent, which will be discussed in the following section. Wide variation around ambient temperature suggests that the PLA films might have been obtained from different sources.

***11.3.2.1 Factors Affecting Mass Transfer of Oxygen*** *Temperature:* Overall, $P_{O_2}$ values increase as temperature increases, as seen from the Arrhenius plot in Figure 11.6. Experimental conditions and the values of $E_P$, $E_D$, and $\Delta H_S$ for $O_2$ in PLA at different RH are summarized in Table 11.3. In contrast to the discontinuity in the regression lines below and above $T_g$ shown in Figure 11.6, Komatsuka and Nagai [33] reported a linear trend for $P_{O_2}$ values between 45 and 85°C. Besides data from these authors, we have not found other reported $P_{O_2}$ values above $T_g$. The reason could be the change in mechanical properties of PLA at temperature range above its $T_g$, which complicates the mass transfer experiment. Based on the positive $E_D$ values reported in Table 11.3, $D_{O_2}$ values seem to increase as temperature increases. However, the data have high variability. Similarly, the $\Delta H_S$ values also vary.

*Relative humidity*: Table 11.4 summarizes changes in mass transfer parameters for $O_2$ in PLA as RH increases. Most of the data show that $P_{O_2}$ values are not affected by RH at low or ambient temperature, implying that the test conditions and the time range of the experiments did not induce hydrolysis in PLA. Auras et al. [69] reported that at 40°C, as RH increased, $E_P$ and $\Delta H_S$ of $O_2$ decreased, while $E_D$ of $O_2$ increased. More data for mass transfer parameters of $O_2$ at different RH conditions are needed to verify the effect of RH.

*Crystallinity and* L : D *ratio*: Table 11.5 summarizes how $X_c$ and L : D ratio of neat PLA films affect mass transfer parameters of $O_2$ in PLA. With plenty of data for mass transfer of $O_2$, many authors have confirmed the three-phase model in semicrystalline PLA [7, 38, 55, 96, 122, 123]. Nassar et al. [123] reported that the occurrence of the RAF increased FV and resulted in an accelerated pathway for diffusion of small molecules such as $O_2$. An increase in FV due to the RAF corresponds with the research on the evolution of FV in crystallized PLA by Del Río et al. [124]. Experimental results from Guinault et al. [38.] agree with collective data from Sonchaeng et al. [7], which show an increase in $P_{O_2}$ as

**TABLE 11.3 $E_P$, $E_D$, and $\Delta H_S$ of $O_2$ in PLA**

| $T$ (°C) | RH (%) | PLA Type | $E_P$ (kJ/mol) | $E_D$ (kJ/mol) | $\Delta H_S$ (kJ/mol) | Ref. |
|---|---|---|---|---|---|---|
| 5–40 | 0 | 30 μm thick[a] | 21.8 | 19.1 | 0.9 | [24] |
| 5–40 | 0 | 40 μm thick[a] | 20.5 | 32.2 | −11.8 | [24] |
| 5–40 | 0–90 | 98% L | 23.4 | 1.0–5.0 | 17.0–22.7 | [69] |
| 5–40 | 0–90 | 94% L | 20.5 | 5.1–28.0 | n/a | [69] |
| 17–50 | 0 | 94% L | 21.0 | n/a | n/a | [31] |
| 23–38 | 50 | n/a | 45.1 | 45.2 | −0.1 | [111] |
| 23–45 | 0 | 98.7% L | 24.0 | 42.7 | −19.2 | [80] |
| 23–45 | 0 | 80% L | 24.9 | 40.8 | −15.9 | [80] |
| 23–45 | 0 | 50% L | 26.6 | 68.8 | −42.0 | [80] |
| 25–45 | 70 | 98% L | 41.4 | n/a | n/a | [83] |
| 25–45 | 70 | 94% L | 28.4 | n/a | n/a | [83] |
| 35–85 | 0 | 96% L | 47.9 | n/a | n/a | [33] |
| 35–85 | 0 | 96 : 88% L blends | 41.4 | n/a | n/a | [33] |
| 5–58 | 0 | Various PLAs from literature | 21.8 | 28.2 | 26.7 | [7] |
| 5–58 | 1–49 | Various PLAs from literature | 19.6 | 7.8 | 12.4 | [7] |
| 5–58 | 50–79 | Various PLAs from literature | 18.9 | 58.0 | −40.3 | [7] |
| 5–58 | 80–100 | Various PLAs from literature | 18.8 | 14.8 | −4.9 | [7] |
| 59–90 | 0 | Various PLAs from literature | 44.5 | n/a | n/a | [7] |

*T*: temperature, n/a: information not available.
[a]% L unknown.

**TABLE 11.4 A Summary of Changes in Mass Transfer Parameters of $O_2$ in PLA at Different RH**

| PLA Type | $T$ (°C) | RH (%) | Change as RH Increases | Ref. |
|---|---|---|---|---|
| 94% L | 5, 23, 40 | 0–90 | No change in $P_{O_2}$ at 5 and 23°C but $P_{O_2}$ decreased at 40°C | [69] |
| 98% L | 5, 23, 40 | 0–90 | No change in $P_{O_2}$ at 5 and 23°C but $P_{O_2}$ decreased at 40°C | [69] |
| 94% L | 23 | 0–50 | No change in $P_{O_2}$ | [44] |
| n/a | 23 | 0–75 | No change in $P_{O_2}$ | [62] |
| 96% L | 23 | 0–50 | No change in $P_{O_2}$ | [77] |
| 94% L | 5, 23, 40 | 0–90 | $D_{O_2}$ increased (at 5, 23, and 40°C) | [69] |
| 98% L | 5, 23, 40 | 0–90 | $D_{O_2}$ increased (at 5, 23, and 40°C) | [69] |
| n/a | 24 | 0 and 80 | $D_{O_2}$ slightly increased | [53] |
| 94% L | 5, 23, 40 | 0–90 | $S_{O_2}$ decreased (at 5, 23, and 40°C) | [69] |
| 98% L | 5, 23, 40 | 0–90 | $S_{O_2}$ decreased (at 5, 23, and 40°C) | [69] |

n/a: information not available.

$X_c$ increases up to around 40% and a decrease in $P_{O_2}$ above this $X_c$ level as shown in Figure 11.7.

***11.3.2.2 Remarks for Oxygen*** Despite being the most researched gas on mass transfer parameters of PLA, there still are not enough data at different temperature and RH with different $X_c$ to better understand how well PLA films perform as an oxygen barrier. The three-phase model should be considered when designing experiments; for example, $X_c$ of semicrystalline PLA film should be determined.

### 11.3.3 Mass Transfer of Water Vapor

Water causes food to deteriorate, including changes in texture, microbial growth, freezer burn, non-enzymatic browning, and weight change [126]. The permeability of a polymeric film to water vapor can play a key role in affecting these changes in a packaged food product [127]. The values of mass transfer parameters of water vapor in PLA film vary at different temperature and RH conditions, as well as with different compositions or treatments of PLA. While PLA is known to undergo hydrolysis, which leads to PLA degradation, the topics on mass transfer of liquid water and hydrolytic degradation of PLA are beyond the scope of this chapter. The readers may refer to Chapter 21 for such information.

To summarize the trends for $P_{H_2O}$ in neat PLA, data from the literature were separated into different test conditions, mainly temperature and RH, and plotted in Figure 11.8. The majority of $P_{H_2O}$ data from the literature were measured at 38°C and 90% RH, which are the recommended test conditions for the gravimetric method measurement [128]. Measurements at ambient temperatures (23–25°C) and different RH ranges are also abundant. The values of $P_{H_2O}$ shown in Figure 11.8 fall between $1.1\times10^{-19}$ and $1.6\times10^{-13}$ kg m/m$^2$ s Pa with a majority of the values within the range of $10^{-16}$–$10^{-13}$ kg m/m$^2$ s Pa. The wide variation in the data may be due to different types of films used, as well as different film processing and measurement methods applied. The values of

**TABLE 11.5 Changes in Mass Transfer Parameters of $O_2$ in PLA Films as Degree of Crystallinity ($X_c$) Increases or L : D Ratio of PLA Film Changes**

| PLA | $T$ (°C) | RH (%) | Change | Ref. |
|---|---|---|---|---|
| 98% L | 23 | 0 | $P_{O_2}$ decreased ($X_c$ ~2–40%) | [47] |
| 99% L | 23 | 0 | $P_{O_2}$ increased ($X_c$ 2–40%) then decreased ($X_c$ 40–63%) | [47] |
| 99% L | 23 | 50 | $P_{O_2}$ decreased ($X_c$ 14–46%) | [125] |
| 96% L blends | 35 | 0 | $P_{O_2}$ increased ($X_c$ 7–25%) | [97] |
| 50–99% L | 30 | 0 | $P_{O_2}$ increased (50–99% L) | [80] |
| 92% L | 23 | 0 | $P_{O_2}$ slightly increased ($X_c$ 3–43%) | [55] |
| 94 and 98% L | 5 | 0 | $D_{O_2}$ increased ($X_c$ 25–40%), $D_{O_2}$ decreased (94–98% L) | [69] |
| 94 and 98% L | 40 | 0 | $D_{O_2}$ slightly decreased ($X_c$ 25–40%), $D_{O_2}$ slightly increased (94–98% L) | [69] |
| 50–99% L | 30 | 0 | $D_{O_2}$ decreased (50–80% L) | [80] |
| 50–99% L | 30 | 0 | No change in $D_{O_2}$ (80–99% L) | [80] |
| 92% L | 23 | 0 | No change in $D_{O_2}$ ($X_c$ 3–43%) | [55] |
| 96% L | 35 | 0 | $D_{O_2}$ increased ($X_c$ 0–20%) then decreased ($X_c$ 20–40%) | [32] |
| 96% L | 20 | 0 | $D_{O_2}$ decreased ($X_c$ 0–46%) | [52] |
| 96 and 99% L | 23 | 0 | $D_{O_2}$ increased ($X_c$ 2–40%) | [38] |
| 96 and 99% L | 23 | 0 | $D_{O_2}$ decreased ($X_c$ 40–63%) | [38] |
| 96% L blends | 35 | 0 | $D_{O_2}$ decreased ($X_c$ 7–25%) | [33] |
| 94 and 98% L | 5–40 | 0–90 | $S_{O_2}$ decreased ($X_c$ 25–40%), $S_{O_2}$ slightly increased (94–98% L) | [69] |
| 96% L | 35 | 0 | $S_{O_2}$ slightly decreased ($X_c$ 0–40%) | [32] |
| 96% L blends | 35 | 0 | $S_{O_2}$ decreased ($X_c$ 7–25%) | [97] |
| 92% L | 23 | 0 | $S_{O_2}$ decreased ($X_c$ 3–43%) | [55] |

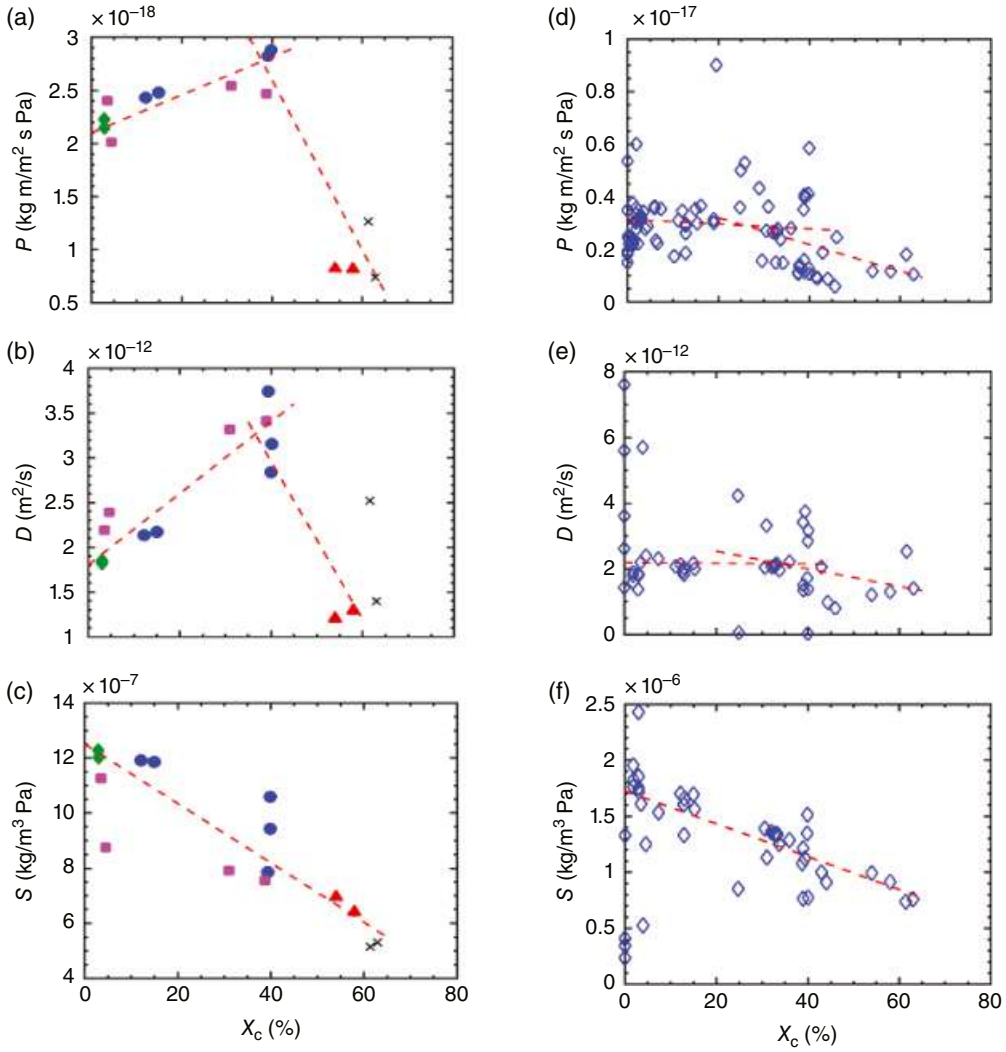


**FIGURE 11.7** (a–c) $P_{O_2}$, $D_{O_2}$, and $S_{O_2}$ measured at 23°C and 0% RH shown in original units as presented by Guinault et al. [38] with symbols indicating temperature conditions of the crystallization treatment for PLA: ♦ extruded sample, ● 85°C, ■ 90°C, ▲ 120°C, × 140°C. (d–f) $P_{O_2}$, $D_{O_2}$, and $S_{O_2}$ (shown with ◊ symbol) at 20–35°C and 0% RH [7].

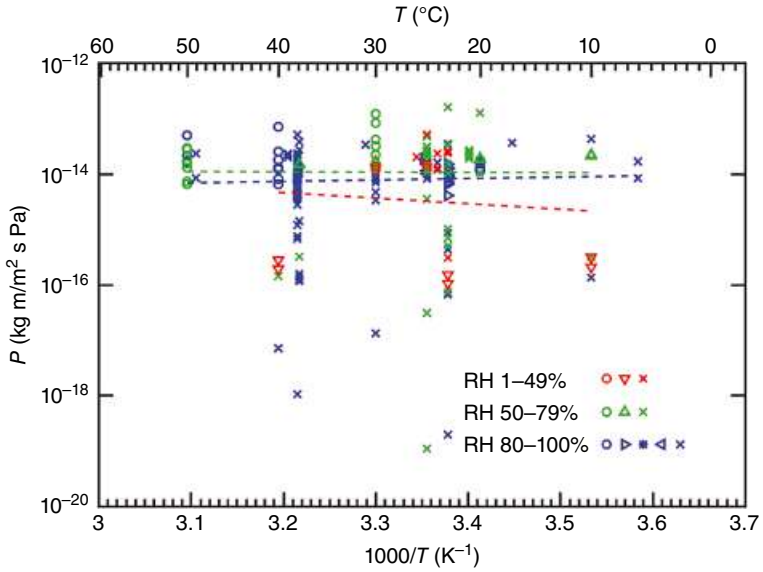


**FIGURE 11.8** Arrhenius plots of water vapor permeability coefficients ($P_{H_2O}$) in PLA films between 6 and 50°C grouped by different relative humidity (RH) ranges. Each dashed line is from linear regression of the data in each RH range group. References: ○ [59], ∇ [131], × [39, 53, 62, 63, 134–137], ○ [129], ▲ [83], × [10, 29, 31, 49, 59, 61, 71, 72, 74, 101, 103, 108, 109, 115, 131, 138–149], ○ [129], ▷ [37],* [150], ◁ [151], × [10, 29, 31, 71, 72, 74, 103, 108, 109, 143–149].

$P_{H_2O}$, $D_{H_2O}$, and $S_{H_2O}$ are only available below $T_g$. The overall range of $D_{H_2O}$ measured at different temperature and RH [14, 111, 129–133] is between $2\times10^{-15}$ and $1\times10^{-10}$ m²/s, while the overall range of $S_{H_2O}$ [111, 129, 131] is between $5\times10^{-4}$ and $1\times10^{-1}$ kg/m³ Pa. Several authors [14, 15] reported that diffusion of water vapor in PLA was concentration-dependent, i.e., water vapor diffusion did not follow Fick's laws. Davis et al. [14] suggested that the diffusion process could be separated into two stages. The first stage is the water uptake due to the concentration gradient and the second stage is controlled by stress relaxation or swelling of PLA.

#### *11.3.3.1 Factors Affecting Mass Transfer of Water Vapor*

*Temperature*: In an Arrhenius plot shown in Figure 11.8, data for $P_{H_2O}$ values scatter and the underlying trends for the effects of temperature are not clearly distinguished. Experimental conditions and the values of $E_P$, $E_D$, and $\Delta H_S$ for water vapor in PLA films at different RH are summarized in Table 11.6. The $E_P$ data vary greatly; some values are positive while other values are negative. Data for $E_D$ and $\Delta H_S$ for water vapor in PLA films are scarce. The negative $E_P$ indicates a decrease in $P_{H_2O}$ as temperature increases, which may be explained by the three-phase model, where the RAF de-densification has less effect as temperature increases.

*Relative humidity*: As shown in Figure 11.8, there are not enough data to draw a conclusion about the effect of RH on $P_{H_2O}$. Other authors [31, 62, 83, 129] reported no change in $P_{H_2O}$ at different RH ranges.

*Crystallinity and* L : D *ratio*: The effects of $X_c$ on mass transfer of water vapor in PLA films vary greatly. Table 11.7 presents how $X_c$ and L : D ratio of neat PLA films affect the mass transfer parameters of water vapor in PLA films. As discussed earlier, the crystalline region is impermeable and that should imply a decrease in $P_{H_2O}$ as $X_c$ increases, which was reported in some cases. The reported increase in $P_{H_2O}$ and $D_{H_2O}$ as $X_c$ increases may be attributed to the three-phase model, i.e., the de-densification of the RAF. The data on the effects of $X_c$ on $S_{H_2O}$ are scarce; in general, $S_{H_2O}$ decreases when $X_c$ increases.

#### *11.3.3.2 Remarks for Water Vapor*

Data on mass transfer of water vapor are abundant compared to data for other gases or vapors. However, these data are scattered due to the many factors that affect the mass transfer parameters of water in PLA films including the test conditions, the film processing, and treatments. Non-Fickian behavior of water diffusion [14, 15], film swelling and solvent-induced crystallization [158], and water cluster formation [159–161] make interpretation and prediction of the experimental results more complicated. Recently, researchers [96, 157] have been taking the three-phase model into account, which contributed to increased understanding of PLA mass transfer behaviors. However, comprehensive research is still needed to examine the mass transfer of water vapor in PLA film. Mostly, the main issue is the lack of full characterization of the films.

### 11.3.4 Mass Transfer of Organic Vapors

Mass transfer of organic vapors in PLA is important for food packaging, especially for food products that are susceptible to odor or flavor changes, as well as for some packaging technologies involving organic vapors such as MAP, antimicrobial packaging, and intelligent packaging [162]. So, knowledge about mass transfer properties of organic vapors in polymeric films is crucial to develop optimal packaging for specific food products. However, such data for PLA are not readily available. Figure 11.9 shows a plot of $P$ of different organic vapors in PLA films from the literature [24, 45, 73, 85, 163–165] against $M_w$ of the vapor permeants. In general, $P$ decreases as $M_w$ increases. The highest $P$ value in Figure 11.9 is $1.5\times10^{-13}$ kg m/m² s Pa from acetaldehyde measured at 10°C [73] and the lowest is $7.3\times10^{-23}$ kg m/m² s Pa from eucalyptol measured at 15°C [165]. The same group of authors [165–167] reported $P$ values of eucalyptol and estragole at 25°C that differed by several orders of magnitude, which could be due to different methods and models used for estimation of $P$. The reported $P$ value for *trans*-2-hexanal [73] measured at 23°C and 50% RH is $2.9\times10^{-13}$ kg m/m² s Pa, which is slightly higher than the highest value for $P$ for other

**TABLE 11.6 $E_P$, $E_D$, and $\Delta H_S$ of Water Vapor in PLA Films**

| $T$ (°C) | RH (%) | PLA Type | $E_P$ (kJ/mol) | $E_D$ (kJ/mol) | $\Delta H_S$ (kJ/mol) | Ref. |
|---|---|---|---|---|---|---|
| 10–38 | 50 | 98% L, 40% $X_c$ | −9.8 | n/a | n/a | [83] |
| 10–38 | 50 | 94% L, 25% $X_c$ | −10.1 | n/a | n/a | [83] |
| 20–50 | 90 | Different L : D ratios | n/a | 24–53 | −19–−41 | [129] |
| 6–49 | 100 | Crystalline | −0.1 | n/a | n/a | [152] |
| 6–49 | 100 | Amorphous | 5 | n/a | n/a | [152] |
| 25–45 | 10–90 | 88% L[a] | 31.4 | n/a | n/a | [14] |
| 25–45 | 10–90 | 88% L[b] | 39.2 | n/a | n/a | [14] |
| 10–31 | 50–85 | 94% L | −7.5 | n/a | n/a | [31] |

$T$: temperature, n/a: information not available.
[a]Measured by time-resolved FTIR-ATR spectroscopy.
[b]Measured by quartz spring microbalance.

**TABLE 11.7 Changes in Mass Transfer Parameters of Water Vapor in PLA Films as Degree of Crystallinity ($X_c$) Increases or L : D Ratio of PLA Film Changes**

| PLA Type | $T$ (°C) | RH (%) | Change | Ref. |
|---|---|---|---|---|
| 94 and 98% L | 10, 20 | 50 | $P_{H_2O}$ increased ($X_c$ 25–40%, 94–98% L) | [83] |
| 94 and 98% L | 30, 38 | 50 | $P_{H_2O}$ decreased ($X_c$ 25–40%, 94–98% L) | [83] |
| Semicrystalline | 20–50 | 90 | $P_{H_2O}$ decreased ($X_c$ 11–46%) | [129] |
| Amorphous | 20–50 | 90 | No change in $P_{H_2O}$ (50–100% L) | [129] |
| n/a | 6–49 | 100 | $P_{H_2O}$ decreased ($X_c$ 0–66%) | [152] |
| 88, 94 and 98% L | 38 | 90 | $P_{H_2O}$ decreased ($X_c$ 0–50%) | [150] |
| n/a | 25 | 90 | $P_{H_2O}$ increased ($X_c$ 0–30%), then no change ($X_c$ > 30%) | [151, 153] |
| 99% L | 38 | 90 | No change in $P_{H_2O}$ ($X_c$ 0–39%), then a rapid decrease ($X_c$ > 39%) | [154] |
| 94% L biaxially drawn | 25 | n/a | No change in $P_{H_2O}$ ($X_c$ 0–31%)* | [155] |
| Untreated and pasteurized films | 25 | 30 | $P_{H_2O}$ decreased (with similar $X_c$, $P_{H_2O}$ decreased due to structure changes in pasteurized films) | [59] |
| 88 and 98% L | 38 | 90 | $P_{H_2O}$ decreased | [156] |
| 96% L | 23 | 100 | $D_{H_2O}$ increased (amorphous to semicrystalline) | [37] |
| 96% L | 23 | 20–70 | $S_{H_2O}$ decreased ($X_c$ 0–35%) | [157] |

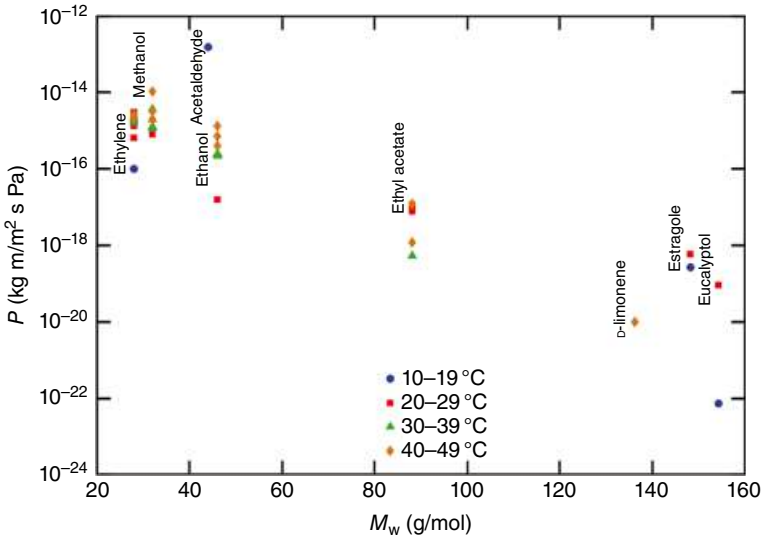


**FIGURE 11.9** $P$ of different volatile organic compounds in PLA films grouped by similar test temperatures versus molecular weight ($M_w$) at 0% RH. References: ethylene [24], methanol [85], acetaldehyde [73], ethanol [85], ethyl acetate [45, 163], D-limonene [164], estragole [165], eucalyptol [165].

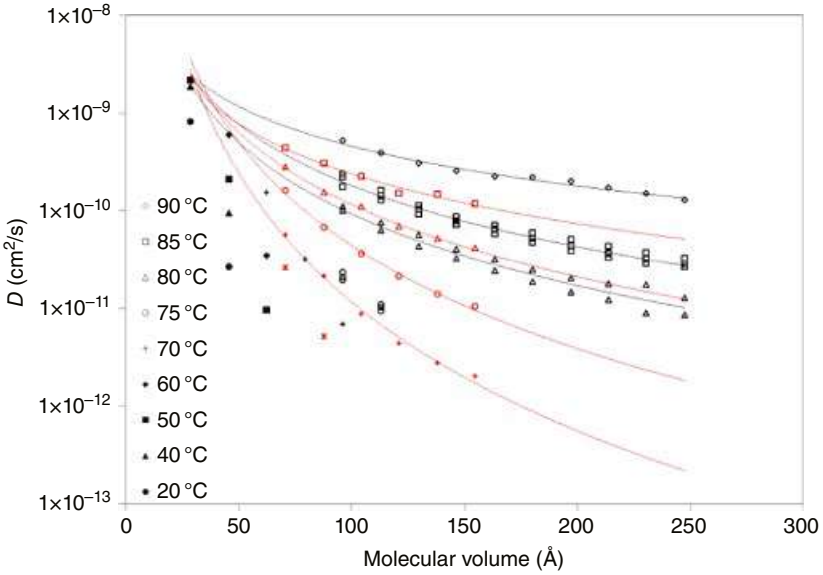


**FIGURE 11.10** Correlation between the molecular volume of the permeants and their diffusion coefficients ($D$) in PLA films (30 μm) at various temperatures. Black dots: *n*-alkanes, red dots: 1-alcohols, solid lines: predicted correlation based on [171]; figure reproduced from [170].

volatile organic compounds at 0% RH as shown in the figure. Due to different functional groups of these compounds and variation in the measurement methods, test conditions, and film samples, it is difficult to correlate $P$ with $M_w$ or predict $P$ for other molecules or compounds from the available data.

A plot of $D$ values of organic vapors from literature [45, 46, 163–165, 168] versus their molecular volume (figure not shown) suggested that $D$ decreased as the molecular volume increased [7]. Moreover, the Arrhenius relationship at 0% RH of $S$ of organic vapors from the literature [45, 55, 91, 163–166, 168, 169] did not show any increasing or decreasing trend in $S$ as the temperature increased. The highest $D$ for organic vapors is $7.0\times10^{-13}$ m²/s from ethyl acetate measured at 25°C [55] and the lowest at $1.2\times10^{-17}$ m²/s from estragole measured at 15°C [165]; the highest $S$ is 6.8 kg/m³ Pa from estragole measured at 25°C [166] and the lowest is $4.7\times10^{-7}$ kg/m³ Pa from ethyl acetate measured at 25°C [55]. Welle et al. [170] conducted experiments on diffusion of organic molecules such as homologous series of straight-chain alkanes (methane to tetradecane) and straight-chain alcohols (propanol to octanol) in two commercial PLA films at various temperature ranges. They reported strong correlations between molecular volume of the permeants and their $D$ values for a 30 μm PLA film, as shown in Figure 11.10.

***11.3.4.1 Factors Affecting Mass Transfer of Organic Vapors*** Factors affecting mass transfer of organic vapors in PLA films are presented in Table 11.8. Besides the effects of temperature, RH, $X_c$, and L : D ratio, which are reported in the following sub-section, Welle et al. [170] reported strong correlations of molecular volumes of permeants with $D$ and $E_D$ for straight-chain alkanes and straight-chain alcohols.

*Temperature*: In general, as seen from the data reported in Table 11.8, $P$ and $D$ increase as temperature increases. On the contrary, $S$ slightly decreases as temperature increases.

*Relative humidity*: Data on how RH affects mass transfer of organic vapors in PLA are not available, which could be due to the complication of the measurement methods and instrumentation.

*Crystallinity and* L : D *ratio*: Not many data are available on how $X_c$ or L : D ratio affect mass transfer of organic vapors in PLA films. In most cases, reported in Table 11.8 $P$ and $D$ decrease as $X_c$ increases. It is also crucial to be aware that organic vapors can induce crystallization in PLA, especially under long exposure time, as noted in Table 11.8.

***11.3.4.2 Remarks for Organic Vapors*** The change in $X_c$ from vapor-induced phenomena can complicate the mass transfer process, which may violate the basic mathematics explained in Section 11.2. This complication must be taken into consideration for PLA applications involving these vapors. Moreover, consideration of the effect of multi-compound permeation is essential for developing relevant applications.

## 11.4 MASS TRANSFER PROPERTIES OF MODIFIED PLA

With technology and knowledge such as polymer blends, composites, nanotechnology, stereocomplexity, and radiation, various properties of PLA can be enhanced. This section covers modifications of PLA that affect PLA's barrier properties. Section 11.4.4 provides information on mass transfer of PLA in other forms, rather than film.

**TABLE 11.8 Factors Affecting Mass Transfer Properties of Organic Vapors in PLA**

| Vapor | $T$ (°C) | RH (%) | PLA Type | Finding | Remark | Ref. |
|---|---|---|---|---|---|---|
| Ethylene | 5–40 | 0 | n/a, 30 µm | $P$ increased as $T$ increased | $E_P$ = 12.9 kJ/mol | [24] |
| Ethylene | 5–40 | 0 | n/a, 40 µm | $P$ increased as $T$ increased | $E_P$ = 27.0 kJ/mol | [24] |
| Eucalyptol | 15–25 | 0 | n/a, 30 µm | $P$ increased 2.2 times as $T$ increased | | [165] |
| Estragole | 15–25 | 0 | n/a, 30 µm | $P$ increased 1258 times as $T$ increased | | [165] |
| Ethyl acetate | 30–45 | 0 | 98% L | $P$ increased as $T$ increased | | [164] |
| Methanol | 25 | 0 | 96% L | No change in $P$ as exposure time increased | Permeant induced crystallization | [85] |
| Methanol | 35, 45 | 0 | 96% L | $P$ decreased as exposure time increased | Permeant induced crystallization | [85] |
| Ethanol | 25–35 | 0 | 96% L | No change in $P$ as exposure time increased | Permeant induced crystallization | [85] |
| Ethanol | 45 | 0 | 96% L | $P$ decreased as exposure time increased | Permeant induced crystallization | [85] |
| Eucalyptol | 15–25 | 0 | n/a, 30 µm | $D$ increased ~four times as $T$ increased | | [165] |
| Estragole | 15–25 | 0 | n/a, 30 µm | $D$ increased ~14 times as $T$ increased | | [165] |
| Ethyl acetate | 30–45 | 0 | 98% L | $D$ increased as $T$ increased | | [164] |
| Ethyl acetate | 25 | 0 | n/a | $D$ decreased as $X_c$ increased | Permeant induced crystallization | [55] |
| $n$-alkanes and 1-alcohols | 70–90 | 0 | Biaxially-oriented[a] | $D$ correlated well with molecular volume of permeant and $E_P$ | $E_P$ ~ 50–150 | [170] |
| Ethyl acetate | 30–45 | 0 | 98% L | $S$ slightly decreased as $T$ increased | | [164] |
| Ethylene | 10–40 | 0 | 98% L | $S$ slightly decreased 43% as $T$ increased | | [91] |
| Ethylene | 10–40 | 0 | 98% L annealed | $S$ slightly decreased 50% as $T$ increased | | [91] |
| Ethylene | 30 | 0 | 98% L annealed | $S$ decreased as $X_c$ increased (10–20% $X_c$) | | [91] |

$T$: temperature, n/a: information not available.
[a]A commercial PLA film.

### 11.4.1 PLA Stereocomplex and PLA Blends

While data for stereocomplex PLA (sc-PLA) and blends of PLA of different L : D ratio are included in a discussion for neat PLA because the base material is still PLA, it is worth mentioning sc-PLA and blends of PLA separately in this section as their mass transfer properties can be much different from those of neat PLA. More detail about sc-PLA can be found in Chapter 5.

The equimolar mixture of homochiral PLAs, i.e., poly(L-lactide) and poly(D-lactide), can form sc-PLA [172, 173]. In general, sc-PLA has higher $X_c$ than neat PLA. Sangroniz et al. [96] reported that blends of 50 : 50 poly(L-lactide), PLLA, and poly(D-lactide), PDLA, showed a stereocomplex structure and behaved differently from neat PLA. $D_{CO_2}$ and $S_{CO_2}$ values decreased due to crystallite formation, which the FV in RAF could not counterbalance. $P_{O_2}$ also decreased because the stereocomplex formation resulted in RAF reduction. Tsuji and Tsuruno [151] reported a reduction in $P_{H_2O}$ at 25°C of sc-PLA film when compared with $P_{H_2O}$ of pure PLLA and PDLA films in $X_c$ range 0–30%. Varol [173] also reported lower $P_{O_2}$, $P_{N_2}$, and $P_{CO_2}$ for sc-PLA than homopolymer PLA films at 25°C. Similar to sc-PLA, Bai et al. [174] used a nucleating agent to induce parallel-aligned shish-kebab-like crystals with interlocked boundaries in PLA with 98% L. The structure formed a dense wall and prevented gas permeation, which resulted in lower $P_{O_2}$.

Blends of PLA with other polymers affect its mass transfer properties. Chapter 14 provides an extensive discussion of PLA blends. When PLA is blended with a better barrier polymer, the blends tend to have better barrier than the neat PLA. This trend is demonstrated in recent works such as $P_{CO_2}$

of PLA blends with poly(3-hydroxybutyrate) (PHB) [34], $P_{He}$ of PLA blends with poly(3-hydroxybutyrate-*co*-3-hydroxyvalerate (PHBV) [86], and $P_{O_2}$ and $P_{H_2O}$ of PLA blend with poly[(butylene succinate)-*co*-adipate] (PBSA) [103]. Vice versa, PLA blends with poorer barrier polymer such as chitosan yielded blends with poorer barrier to water vapor than that of the neat PLA [175].

### 11.4.2 PLA Nanocomposites

Modifications of PLA using clays such as montmorillonite (MMT) and organo-montmorillonites (OMMT) are covered in Chapter 17. Some examples of these modifications that affect PLA mass transfer parameters are as follows. Koh et al. [42] studied the properties of PLA/layered silicate nanocomposite membranes where OMMT, namely, Cloisite® 15A, Cloisite 20A, and Cloisite 30B (C30B), were used as layered silicates. The authors found that $P_{CO_2}$, $P_{N_2}$, and $P_{O_2}$ measured at 30°C decreased as organoclay content increased. PLA/C30B showed an increased barrier performance to gases compared with PLA composites with other clays. The authors attributed the enhanced barrier to tortuosity for the permeation in the nanocomposite membrane. The authors also showed that with the same type of organoclay, gas molecules with smaller kinetic diameter have higher gas permeability values, i.e., $P_{CO_2} > P_{O_2} > P_{N_2}$. This is illustrated in Figure 11.11, which also shows a greater impact of C30B at higher content on reducing $P$ of gases.

Darie et al. [176] reported that PLA with 3 wt% Cloisite 93A reduced $P_{O_2}$ and $P_{CO_2}$ (measured at 23°C and 0% RH) by half compared with those of neat PLA. A highly hydrophilic Dellite® clay reduced $P_{O_2}$ and $P_{CO_2}$ even more when tested at the same conditions. In addition to the tortuosity from the clay, the authors attributed the reduction in $P_{O_2}$ and $P_{CO_2}$ to higher crystallinity of the PLA/clays. Şengül et al. [177] reported $P_{O_2}$ at 30°C and 0% RH of PLA/nanoclay films from four commercially modified MMT clays with different surface modifiers. The presence of nanoclays lowered $P_{O_2}$ in a manner with the higher wt% of clay, the lower the $P_{O_2}$. This finding that $P_{O_2}$ decreases as the amount of nanoclay increases has been reported elsewhere [178]. The authors also reported a decrease in $P_{H_2O}$ at 38°C and 90% RH of the PLA/nanoclay films compared with that of neat PLA. Some authors reported increasing $P_{O_2}$ after a certain amount of nanoclay was added. For example, Li et al. [179] studied PLA/OMMT nanocomposites and found that $P_{O_2}$ (measured at 23°C and 30% RH) decreased as wt% OMMT increased up to 6%. Adding greater than 6 wt% OMMT resulted in increasing $P_{O_2}$, which the authors attributed to poor dispersion of the clay. There are a number of research works on improving barrier properties of PLA using nanoclays [84, 180, 181]; however, at this juncture, PLA nanocomposites with high barrier properties are still not commercialized.

Several researchers have used cellulose nanocrystals (CNC) [15, 31, 140, 182, 183] and cellulose nanofibers (CNF) [118, 184] to create tortuosity for the permeation process and improve PLA barrier properties to permeants such as $O_2$ and water vapor. Most of these works reported improvement of the gases and water barrier properties of the compounded PLA films.

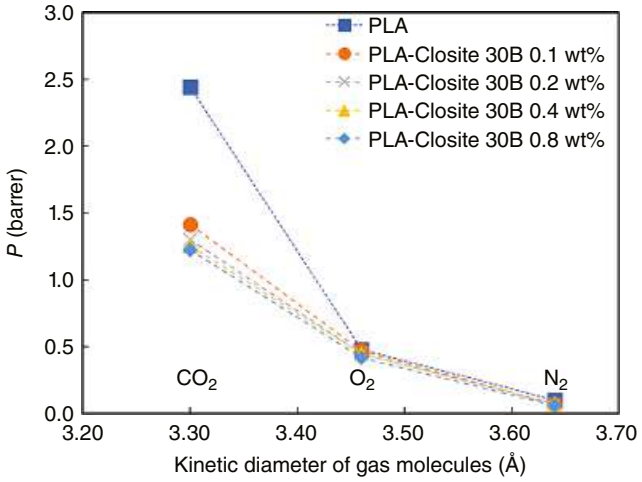


**FIGURE 11.11** Gas permeabilities of PLA and PLA/organoclay (Cloisite 30B) with different wt% of organoclay as a function of the kinetic diameters of gas molecules; figure adapted from [42].

### 11.4.3 Other PLA Modifications

Malinowski et al. [185] examined the effect of electron radiation on the properties of PLA film with 96.5% L. When 3 wt% triallyl isocyanurate (TAIC) was used as a crosslinking agent, non-irradiated film, and the film irradiated at a low dose (10 kGy) had greater $P_{H_2O}$ at 38°C and 90% RH than that of neat PLA. This was attributed to the plasticizing effect of TAIC. However, the film irradiated at doses above 10 kGy showed gradual decreases in $P_{H_2O}$ as the radiation doses increased, which was attributed to the growing crosslinking of PLA. There is little information on the effects of radiation on mass transfer of gases and vapors in PLA film although some food products are commercially irradiated after packaging.

Surface modification and coating have also been implemented in PLA to improve barrier properties. For example, Siracusa et al. [60] reported the surface treatments of PLA using silicon oxide, anti-UV, and varnish resulted in lower $P_{O_2}$ and $P_{CO_2}$ compared with unmodified PLA. Kim et al. [65] coated PLA films with ink formulations that contained C30B nanoclay and reported lower $P_{O_2}$ and $P_{H_2O}$ as the amount of the clay increased.

### 11.4.4 PLA in Other Forms

While the focus of this chapter is PLA and modified PLA films, there are mass transfer parameters reported for PLA as a coating layer and as rigid and flexible packaging. This section

briefly includes the information for references that could contribute to the understanding of PLA mass transfer properties.

Rhim et al. [186] measured $P_{H_2O}$ of PLA-coated paperboard intended for a single-use paper cup and found $P_{H_2O}$ decreased exponentially as the concentration of the PLA coating solution increased. A similar experiment on paperboard used for corrugated box liners [187] yielded similar results, with reduction in $P_{H_2O}$ values when the concentration of PLA in the coating increased up to 3 w/v%. At 4 and 5 w/v% PLA, the $P_{H_2O}$ values reached a plateau. The authors also noted that $P_{H_2O}$ values of solvent-cast PLA films [101, 138, 188] were two orders of magnitude lower than those of the base paperboard.

In some early works by Haugaard et al. [189, 190], PLA was evaluated as a rigid package for unpasteurized orange juice, which included measurements of $P_{O_2}$, $P_{CO_2}$, and $P_{H_2O}$ of PLA cups. Joo et al. [191] studied mass transfer properties, including $P_{O_2}$, $P_{CO_2}$, and $P_{H_2O}$, of an oriented PLA snap-fit package for blackberry fruit. Holm et al. [22] measured *OTR* and *WVTR* of a PLA thermoformed tray for semi-hard cheese. For flexible packaging, PLA bags were assessed as packaging for fresh-cut produce in two studies [26, 27], in which $P_{O_2}$, $P_{CO_2}$, $P_{H_2O}$, as well as *P* of ethanol vapor were reported.

## 11.5 FINAL REMARKS

Over the past decade, advances in knowledge about mass transfer properties of PLA have been centered on better understanding the effect of the three-phase structure, i.e., the CF, RAF, and MAF, in semicrystalline PLA. New experimental designs and interpretation of mass transfer results have been much more in-depth. More research has been done to understand better the mass transfer parameters and the factors affecting these parameters. Even so, there is still a lack of information regarding the factors affecting mass transfer properties of PLA, such as the RH and PLA morphology. Data for mass transfer parameters at some temperature ranges, especially above PLA's $T_g$, are needed. We now have different approaches in making stereocomplex PLAs, which shows better barrier performance than neat PLA, albeit still at a higher cost. Additional barrier improvements can be obtained by creating composites, nanocomposites, and using surface treatments such as coating and surface modification. With such advancement in the research on PLA barrier properties, PLA applications should have excellent market expansion.

## ACKNOWLEDGMENTS

The authors acknowledge the constructive review and suggestions from Dr. Eva Almenar at the School of Packaging, Michigan State University.

## REFERENCES

1. E. Almenar, R. Auras, Chapter 12. Permeation, sorption, and diffusion in poly(lactic acid), in: R.A. Auras, L.T. Lim, S.E.M. Selke and H. Tsuji, (Eds.) *Poly(Lactic Acid), Synthesis, Structures, Properties, Processing, and Applications*, 2010, pp. 155–179.
2. S. F. Nassar, S. Domenek, A. Guinault, G. Stoclet, N. Delpouve, C. Sollogoub, Structural and dynamic heterogeneity in the amorphous phase of poly(L,L-lactide) confined at the nanoscale by the coextrusion process, *Macromolecules* **2018**, *51*, 128–136. https://doi.org/10.1021/acs.macromol.7b02188.
3. M. C. Righetti, M. Gazzano, N. Delpouve, A. Saiter, Contribution of the rigid amorphous fraction to physical ageing of semi-crystalline PLLA, *Polymer (Guildf)* **2017**, *125*, 241–253. https://doi.org/10.1016/j.polymer.2017.07.089.
4. N. Delpouve, M. Arnoult, A. Saiter, E. Dargent, J.-M. Saiter, Evidence of two mobile amorphous phases in semicrystalline polylactide observed from calorimetric investigations, *Polym. Eng. Sci.* **2014**, *54*, 1144–1150. https://doi.org/10.1002/pen.23657.
5. A. Magoń, M. Pyda, Study of crystalline and amorphous phases of biodegradable poly(lactic acid) by advanced thermal analysis, *Polymer (Guildf)* **2009**, *50*, 3967–3973. https://doi.org/10.1016/j.polymer.2009.06.052.
6. S. F. Nassar, N. Delpouve, C. Sollogoub, A. Guinault, G. Stoclet, G. Régnier, et al., Impact of nanoconfinement on polylactide crystallization and gas barrier properties, *ACS Appl. Mater. Interfaces* **2020**, *12*, 9953–9965. https://doi.org/10.1021/acsami.9b21391.
7. U. Sonchaeng, F. Iñiguez-Franco, R. Auras, S. Selke, M. Rubino, L. T. Lim, Poly(lactic acid) mass transfer properties, *Prog. Polym. Sci.* **2018**, *86*, 85–121. https://doi.org/10.1016/j.progpolymsci.2018.06.008.
8. S. E. M. Selke, J. D. Culter, *Mass Transfer in Polymeric Packaging Systems: Sorption, Diffusion, Permeation, and Shelf Life. Plastics Packaging*, Carl Hanser Verlag GmbH & Co. KG, München, Germany, 2016, pp. 353–393. https://doi.org/10.3139/9783446437197.014.
9. G. Li, W. Luo, M. Xiao, S. Wang, Y. Meng, Biodegradable poly(propylene carbonate)/layered double hydroxide composite films with enhanced gas barrier and mechanical properties, *Chin. J. Polym. Sci.* **2016**, *34*, 13–22. https://doi.org/10.1007/s10118-016-1720-9.
10. S. Roy, J. W. Rhim, Preparation of bioactive functional poly(lactic acid)/curcumin composite film for food packaging application, *Int. J. Biol. Macromol.* **2020**, *162*, 1780–1789. https://doi.org/10.1016/j.ijbiomac.2020.08.094.
11. T. Messin, S. Marais, N. Follain, A. Guinault, V. Gaucher, N. Delpouve, et al., Biodegradable PLA/PBS multinanolayer membrane with enhanced barrier performances, *J. Membr. Sci.* **2020**, *598*, 117777. https://doi.org/10.1016/j.memsci.2019.117777.
12. A. H.-D. Cheng, *Poroelasticity, Theory and Applications of Transport in Porous Media*, Springer International Publishing, Switzerland, 2016. https://doi.org/10.1007/978-3-319-25202-5_1.

13. A. R. Berens, H. B. Hopfenberg, Diffusion and relaxation in glassy polymer powders: 2. Separation of diffusion and relaxation parameters, *Polymer (Guildf)* **1978**, *19*, 489–496. https://doi.org/10.1016/0032-3861(78)90269-0.
14. E. M. Davis, M. Minelli, M. Giacinti Baschetti, Y. A. Elabd, Non-Fickian diffusion of water in polylactide, *Ind. Eng. Chem. Res.* **2013**, *52*, 8664–8673. https://doi.org/10.1021/ie302342m.
15. E. Espino-Pérez, J. Bras, G. Almeida, C. Plessis, N. Belgacem, P. Perré, et al., Designed cellulose nanocrystal surface properties for improving barrier properties in polylactide nanocomposites, *Carbohydr. Polym.* **2018**, *183*, 267–277. https://doi.org/10.1016/j.carbpol.2017.12.005.
16. P. Meares, Transient permeation of organic vapors through polymer membranes, *J. Appl. Polym. Sci.* **1965**, *9*, 917–932. https://doi.org/10.1002/app.1965.070090310.
17. R. A. Pasternak, J. F. Schimscheimer, J. Heller, A dynamic approach to diffusion and permeation measurements. *J. Polym. Sci. Part A-2 Polym. Phys.* **1970**, *8*, 467–479. https://doi.org/10.1002/pol.1970.160080312.
18. D. S. Lee, L. Piergiovanni, K. L. Yam, *Food Packaging Science and Technology*, Taylor & Francis, Boca Raton, FL, 2008.
19. S. E. M. Selke, J. D. Culter, *Plastics Packaging: Properties, Processing, Applications, and Regulations*, 3rd edition, Hanser Publications, Cincinnati, OH, 2016.
20. J. Crank, G. S. Park, *Diffusion in Polymers*. Academic Press, New York, 1968.
21. D. W. Van Krevelen, K. Te Nijenhuis, Properties determining mass transfer in polymeric systems, in: D. W. Van Krevelen, K. Te Nijenhuis (Eds.), *Properties of Polymers: Their Correlation with Chemical Structure; Their Numerical Estimation and Prediction from Additive Group Contributions*, 4th edtion, Elsevier, Amsterdam, The Netherlands, 2009, pp. 655–702. https://doi.org/10.1016/B978-0-08-054819-7.00018-2.
22. V. Holm, G. Mortensen, J. Risbo, Quality changes in semi-hard cheese packaged in a poly(lactic acid) material, *Food Chem.* **2006**, *97*, 401–410. https://doi.org/10.1016/j.foodchem.2005.05.016.
23. A. Mistriotis, D. Briassoulis, A. Giannoulis, S. D'Aquino, Design of biodegradable bio-based equilibrium modified atmosphere packaging (EMAP) for fresh fruits and vegetables by using micro-perforated poly-lactic acid (PLA) films, *Postharvest Biol. Technol.* **2016**, *111*, 380–389. https://doi.org/10.1016/j.postharvbio.2015.09.022.
24. V. Siracusa, M. Dalla Rosa, A. Iordanskii, Performance of poly(lactic acid) surface modified films for food packaging application, *Materials (Basel)* **2017**, *10*, 850. https://doi.org/10.3390/ma10080850.
25. M. La Zazzera, M. L. Amodio, G. Colelli, Designing a modified atmosphere packaging (MAP) for fresh-cut artichokes, *Adv. Hortic Sci.* **2015**, *29*, 24–29. https://doi.org/10.13128/ahs-21301.
26. N. Page, J. González-Buesa, E. T. Ryser, J. Harte, E. Almenar, Interactions between sanitizers and packaging gas compositions and their effects on the safety and quality of fresh-cut onions (*Allium cepa* L.). *Int. J. Food Microbiol.* **2016**, *218*, 105–113. https://doi.org/10.1016/j.ijfoodmicro.2015.11.017.
27. J. González-Buesa, N. Page, C. Kaminski, E. T. Ryser, R. Beaudry, E. Almenar, Effect of non-conventional atmospheres and bio-based packaging on the quality and safety of *Listeria monocytogenes*-inoculated fresh-cut celery (*Apium graveolens* L.) during storage, *Postharvest Biol. Technol.* **2014**, *93*, 29–37. https://doi.org/10.1016/j.postharvbio.2014.02.005.
28. S. Singh, P. K. Maji, Y. S. Lee, K. K. Gaikwad, Applications of gaseous chlorine dioxide for antimicrobial food packaging: a review, *Environ. Chem. Lett.* **2021**, *19*, 253–270. https://doi.org/10.1007/s10311-020-01085-8.
29. N. Ploypetchara, P. Suppakul, D. Atong, C. Pechyen, Blend of polypropylene/poly(lactic acid) for medical packaging application: physicochemical, thermal, mechanical, and barrier properties, *Energy Procedia* **2014**, *56*, 201–210. https://doi.org/10.1016/j.egypro.2014.07.150.
30. E. Lizundia, M. C. Penayo, A. Guinault, J. L. Vilas, S. Domenek, Impact of ZnO nanoparticle morphology on relaxation and transport properties of PLA nanocomposites, *Polym. Test* **2019**, *75*, 175–184. https://doi.org/10.1016/j.polymertesting.2019.02.009.
31. S. S. Karkhanis, N. M. Stark, R. C. Sabo, L. M. Matuana, Water vapor and oxygen barrier properties of extrusion-blown poly(lactic acid)/cellulose nanocrystals nanocomposite films, *Compos. Part A Appl. Sci. Manuf.* **2018**, *114*, 204–211. https://doi.org/10.1016/j.compositesa.2018.08.025.
32. H. Sawada, Y. Takahashi, S. Miyata, S. Kanehashi, S. Sato, K. Nagai, Gas transport properties and crystalline structures of poly(lactic acid) membranes, *Trans. Mater. Res. Soc. Jpn.* **2010**, *35*, 241–246. https://doi.org/10.14723/tmrsj.35.241.
33. T. Komatsuka, K. Nagai, Temperature dependence on gas permeability and permselectivity of poly(lactic acid) blend membranes, *Polym. J.* **2009**, *41*, 455–458. https://doi.org/10.1295/polymj.PJ2008266.
34. V. Siracusa, S. Karpova, A. Olkhov, A. Zhulkina, R. Kosenko, A. Iordanskii, Gas transport phenomena and polymer dynamics in PHB/PLA blend films as potential packaging materials, *Polymers (Basel)* **2020**, *12*, 1–19. https://doi.org/10.3390/polym12030647.
35. S. Netramai, M. Rubino, R. Auras, B. A. Annous, Mass transfer study of chlorine doxide gas through polymeric packaging materials, *J. Appl. Polym. Sci.* **2009**, *114*, 2929–2936. https://doi.org/10.1002/app.30869.
36. H. J. Lehermeier, J. R. Dorgan, J. D. Way, Gas permeation properties of poly(lactic acid), *J. Membr. Sci.* **2001**, *190*, 243–251. https://doi.org/10.1016/S0376-7388(01)00446-X.
37. M. Drieskens, R. Peeters, J. Mullens, D. Franco, P. J. Iemstra, D. G. Hristova-Bogaerds, Structure versus properties relationship of poly(lactic acid). I. Effect of crystallinity on barrier properties, *J. Polym. Sci. Part B Polym. Phys.* **2009**, *47*, 2247–2258. https://doi.org/10.1002/polb.21822.
38. A. Guinault, C. Sollogoub, V. Ducruet, S. Domenek, Impact of crystallinity of poly(lactide) on helium and oxygen barrier properties, *Eur. Polym. J.* **2012**, *48*, 779–788. https://doi.org/10.1016/j.eurpolymj.2012.01.014.
39. M. D. Sanchez-Garcia, E. Gimenez, J. M. Lagaron, Novel PET nanocomposites of interest in food packaging applications and

comparative barrier performance with biopolyester nanocomposites, *J. Plast. Film Sheeting* **2007**, *23*, 133–148. https://doi.org/10.1177/8756087907083590.

40. S. R. Chowdhury, Some important aspects in designing high molecular weight poly(L-lactic acid)-clay nanocomposites with desired properties, *Polym. Int.* **2008**, *57*, 1326–1332. https://doi.org/10.1002/pi.2464.
41. G. Colomines, S. Domenek, V. Ducruet, A. Guinault, Influences of the crystallisation rate on thermal and barrier properties of polylactide acid (PLA) food packaging films, *Int. J. Mater. Form.* **2008**, *1*, 607–610. https://doi.org/10.1007/s12289-008-0329-0.
42. H. C. Koh, J. S. Park, M. A. Jeong, H. Y. Hwang, Y. T. Hong, S. Y. Ha, et al., Preparation and gas permeation properties of biodegradable polymer/layered silicate nanocomposite membranes, *Desalination* **2008**, *233*, 201–209. https://doi.org/10.1016/j.desal.2007.09.043.
43. A. Bhatia, R. K. Gupta, S. N. Bhattacharya, H. J. Choi, Effect of clay on thermal, mechanical and gas barrier properties of biodegradable poly(lactic acid)/poly(butylene succinate) (PLA/PBS) nanocomposites, *Int. Polym. Process.* **2010**, *25*, 5–14. https://doi.org/10.3139/217.2214.
44. S.-W. Cho, M. Gällstedt, M. S. Hedenqvist, Properties of wheat gluten/poly(lactic acid) laminates, *J. Agric. Food Chem.* **2010**, *58*, 7344–7350. https://doi.org/10.1021/jf1003144.
45. G. Colomines, V. Ducruet, Ć. Courgneau, A. Guinault, S. Domenek, Barrier properties of poly(lactic acid) and its morphological changes induced by aroma compound sorption, *Polym. Int.* **2010**, *59*, 818–826. https://doi.org/10.1002/pi.2793.
46. V. Ducruet, S. Domenek, A. Guinault, C. Courgneau, M. Bernasconi, C. Plessis, Barrier properties of PLA towards oxygen and aroma compounds, *Ital. J. Food Sci.* **2010**, *23*, 59–62.
47. A. Guinault, C. Sollogoub, S. Domenek, A. Grandmontagne, V. Ducruet, Influence of crystallinity on gas barrier and mechanical properties of PLA food packaging films, *Int. J. Mater. Form.* **2010**, *3*, 603–606. https://doi.org/10.1007/s12289-010-0842-9.
48. J. F. Martucci, R. A. Ruseckaite, Three-layer sheets based on gelatin and poly(lactic acid), part 1, Preparation and properties, *J. Appl. Polym. Sci.* **2010**, *118*, 3102–3110. https://doi.org/10.1002/app.32751.
49. C. Courgneau, S. Domenek, A. Guinault, L. Avérous, V. Ducruet, Analysis of the structure-properties relationships of different multiphase systems based on plasticized poly(lactic acid), *J. Polym. Environ.* **2011**, *19*, 362–371. https://doi.org/10.1007/s10924-011-0285-5.
50. D. Elangovan, U. Nidoni, I. E. Yuzay, S. E. M. Selke, R. Auras, Poly (L-lactic acid) metal organic framework composites. Mass transport properties, *Ind. Eng. Chem. Res.* **2011**, *50*, 11136–11142. https://doi.org/10.1021/ie201378u.
51. A. Guinault, G. H. Menary, C. Courgneau, D. Griffith, V. Ducruet, V. Miri, et al., The effect of the stretching of PLA extruded films on their crystallinity and gas barrier properties, *AIP Conf. Proc.* **2011**, *1353*, 826–831. https://doi.org/10.1063/1.3589618.
52. E. Picard, E. Espuche, R. Fulchiron, Effect of an organomodified montmorillonite on PLA crystallization and gas barrier properties, *Appl. Clay Sci.* **2011**, *53*, 58–65. https://doi.org/10.1016/j.clay.2011.04.023.
53. M. D. Sanchez-Garcia, D. Nordqvist, M. Hedenqvist, J. M. Lagaron, Incorporating amylopectin in poly(lactic acid) by melt blending using poly(ethylene-*co*-vinyl alcohol) as a thermoplastic carrier. II. Physical properties, *J. Appl. Polym. Sci.* **2011**, *119*, 3708–3716. https://doi.org/10.1002/app.32891.
54. X. Wen, K. Zhang, Y. Wang, L. Han, C. Han, H. Zhang, et al., Study of the thermal stabilization mechanism of biodegradable poly(L-lactide)/silica nanocomposites, *Polym. Int.* **2011**, *60*, 202–210. https://doi.org/10.1002/pi.2927.
55. C. Courgneau, S. Domenek, R. Lebossé, A. Guinault, L. Avérous, V. Ducruet, Effect of crystallization on barrier properties of formulated polylactide, *Polym. Int.* **2012**, *61*, 180–189. https://doi.org/10.1002/pi.3167.
56. S. Domenek, Ć. Courgneau, A. Guinault, V. Ducruet, Effect of crystallization of poly(lactide) on barrier properties, *Fifth International Symposium on Food Packaging*, Berlin, Germany, 2012.
57. K. Fukushima, A. Fina, F. Geobaldo, A. Venturello, G. Camino, Properties of poly(lactic acid) nanocomposites based on montmorillonite, sepiolite and zirconium phosphonate, *Express Polym. Lett.* **2012**, *6*, 914–926. https://doi.org/10.3144/expresspolymlett.2012.97.
58. M. Jamshidian, E. Arab Tehrany, F. Cleymand, S. Leconte, T. Falher, S. Desobry, Effects of synthetic phenolic antioxidants on physical, structural, mechanical and barrier properties of poly lactic acid film, *Carbohydr. Polym.* **2012**, *87*, 1763–1773. https://doi.org/10.1016/j.carbpol.2011.09.089.
59. L. Sansone, A. Aldi, P. Musto, E. Di Maio, E. Amendola, G. Mensitieri, Assessing the suitability of polylactic acid flexible films for high pressure pasteurization and sterilization of packaged foodstuff, *J. Food Eng.* **2012**, *111*, 34–45. https://doi.org/10.1016/j.jfoodeng.2012.01.034.
60. V. Siracusa, I. Blanco, S. Romani, U. Tylewicz, P. Rocculi, M. D. Rosa, Poly(lactic acid)-modified films for food packaging application: physical, mechanical, and barrier behavior, *J. Appl. Polym. Sci.* **2012**, *125*, E390–E401. https://doi.org/10.1002/app.36829.
61. E. Espino-Pérez, J. Bras, V. Ducruet, A. Guinault, A. Dufresne, S. Domenek, Influence of chemical surface modification of cellulose nanowhiskers on thermal, mechanical, and barrier properties of poly(lactide) based bionanocomposites, *Eur. Polym. J.* **2013**, *49*, 3144–3154. https://doi.org/10.1016/j.eurpolymj.2013.07.017.
62. H. Fukuzumi, T. Saito, A. Isogai, Influence of TEMPO-oxidized cellulose nanofibril length on film properties, *Carbohydr. Polym.* **2013**, *93*, 172–177. https://doi.org/10.1016/j.carbpol.2012.04.069.
63. C. M. B. Gonçalves, L. C. Tomé, H. Garcia, L. Brandão, A. M. Mendes, I. M. Marrucho, Effect of natural and synthetic antioxidants incorporation on the gas permeation properties of poly(lactic acid) films, *J. Food Eng.* **2013**, *116*, 562–571. https://doi.org/10.1016/j.jfoodeng.2012.12.034.

64. A. Kathuria, M. G. Abiad, R. Auras, Deterioration of metal-organic framework crystal structure during fabrication of poly(L-lactic acid)mixed-matrix membranes, *Polym. Int.* **2013**, *62*, 1144–1151. https://doi.org/10.1002/pi.4478.
65. H. K. Kim, S. J. Kim, H. S. Lee, J. H. Choi, C. M. Jeong, M. H. Sung, et al., Mechanical and barrier properties of poly(lactic acid) films coated by nanoclay-ink composition, *J. Appl. Polym. Sci.* **2013**, *127*, 3823–3829. https://doi.org/10.1002/app.37663.
66. A. M. Pinto, J. Cabral, D. A. P. Tanaka, A. M. Mendes, F. D. Magalhães, Effect of incorporation of graphene oxide and graphene nanoplatelets on mechanical and gas permeability properties of poly(lactic acid) films, *Polym. Int.* **2013**, *62*, 33–40. https://doi.org/10.1002/pi.4290.
67. N. A. Ali, F. Tariq, M. Noori, Gas barrier properties of biodegradable polymer nanocomposites films, *Chem. Mater. Res.* **2014**, *6*, 44–51.
68. L. Di Maio, P. Scarfato, M. R. Milana, R. Feliciani, M. Denaro, G. Padula, et al., Bionanocomposite polylactic acid/organoclay films: functional properties and measurement of total and lactic acid specific migration, *Packag. Technol. Sci.* **2014**, *27*, 535–547. https://doi.org/10.1002/pts.2054.
69. R. Auras, B. Harte, S. Selke, Effect of water on the oxygen barrier properties of poly(ethylene terephthalate) and polylactide films, *J. Appl. Polym. Sci.* **2004**, *92*, 1790–1803. https://doi.org/10.1002/app.20148.
70. T. Phupoksakul, M. Leuangsukrerk, P. Numpiboonmarn, A. Somwangthanaroj, T. Janjarasskul, Properties of poly(lactide)-whey protein isolate laminated films, *J. Sci. Food Agric.* **2014**, *95*, 715–721. https://doi.org/10.1002/jsfa.6775.
71. R. Avolio, R. Castaldo, G. Gentile, V. Ambrogi, S. Fiori, M. Avella, et al., Plasticization of poly(lactic acid) through blending with oligomers of lactic acid: effect of the physical aging on properties, *Eur. Polym. J.* **2015**, *66*, 533–542. https://doi.org/10.1016/j.eurpolymj.2015.02.040.
72. Y. Byun, K. Rodriguez, J. H. Han, Y. T. Kim, Improved thermal stability of polylactic acid (PLA) composite film via PLA–β-cyclodextrin-inclusion complex systems, *Int. J. Biol. Macromol.* **2015**, *81*, 591–598. https://doi.org/10.1016/j.ijbiomac.2015.08.036.
73. A. Kathuria, S. Al-Ghamdi, M. G. Abiad, R. Auras, The influence of $Cu_3(BTC)_2$ metal organic framework on the permeability and perm-selectivity of PLLA-MOF mixed matrix membranes, *J. Appl. Polym. Sci.* **2015**, *132*, 42764/1–42764/10. https://doi.org/10.1002/app.42764.
74. N. Moazeni, Z. Mohamad, N. Dehbari, Study of silane treatment on poly-lactic acid(PLA)/sepiolite nanocomposite thin films, *J. Appl. Polym. Sci.* **2015**, *132*, 41428/1–41428/8. https://doi.org/10.1002/app.41428.
75. M. A. Ortenzi, L. Basilissi, H. Farina, G. Di Silvestro, L. Piergiovanni, E. Mascheroni, Evaluation of crystallinity and gas barrier properties of films obtained from PLA nanocomposites synthesized via "in situ" polymerization of L-lactide with silane-modified nanosilica and montmorillonite, *Eur. Polym. J.* **2015**, *66*, 478–491. https://doi.org/10.1016/j.eurpolymj.2015.03.006.
76. F. Morel, E. Espuche, V. Eronique Bounor-Legar, O. Persynn, M. Lacroix, Impact of coated calcium carbonate nanofillers and annealing treatments on the microstructure and gas barrier properties of poly(lactide) based nanocomposite films, *J. Polym. Sci. Part B Polym. Phys.* **2016**, *54*, 649–658. https://doi.org/10.1002/polb.23957.
77. X. Yang, H. Xu, K. Odelius, M. Hakkarainen, Poly(lactide)-*g*-poly(butylene succinate-*co*-adipate) with high crystallization capacity and migration resistance, *Materials (Basel)* **2016**, *9*, 313/1–313/15. https://doi.org/10.3390/ma9050313.
78. R. A. Auras, S. P. Singh, J. J. Singh, Evaluation of oriented poly(lactide) polymers vs. existing PET and oriented PS for fresh food service containers, *Packag. Technol. Sci.* **2005**, *18*, 207–216. https://doi.org/10.1002/pts.692.
79. C. Thellen, C. Orroth, D. Froio, D. Ziegler, J. Lucciarini, R. Farrell, et al., Influence of montmorillonite layered silicate on plasticized poly(L-lactide) blown films, *Polymer (Guildf)* **2005**, *46*, 11716–11727. https://doi.org/10.1016/j.polymer.2005.09.057.
80. L. Bao, J. R. Dorgan, D. Knauss, S. Hait, N. S. Oliveira, I. M. Maruccho, Gas permeation properties of poly(lactic acid) revisited, *J. Membr. Sci.* **2006**, *285*, 166–172. https://doi.org/10.1016/j.memsci.2006.08.021.
81. L. Cabedo, J. Luis Feijoo, M. Pilar Villanueva, J. M. Lagarón, E. Giménez, Optimization of biodegradable nanocomposites based on aPLA/PCL blends for food packaging applications, *Macromol. Symp.* **2006**, *233*, 191–197. https://doi.org/10.1002/masy.200690017.
82. V. K. Holm, S. Ndoni, J. Risbo, The stability of poly(lactic acid) packaging films as influenced by humidity and temperature, *J. Food. Sci.* **2006**, *71*, E40–E44. https://doi.org/10.1111/j.1365-2621.2006.tb08895.x.
83. R. A. Auras, B. Harte, S. Selke, R. Hernandez, Mechanical, physical, and barrier properties of poly(lactide) films, *J. Plast. Film Sheeting* **2003**, *19*, 123–135. https://doi.org/10.1177/8756087903039702.
84. Y. Li, P.-G. Ren, Q. Zhang, T.-T. Shen, J.-H. Ci, C.-Q. Fang, Properties of poly(lactic acid)/organo-montmorillonite nanocomposites prepared by solution intercalation, *J. Macromol. Sci. Part B* **2013**, *52*, 1041–1055. https://doi.org/10.1080/00222348.2013.781937.
85. S. Sato, T. Wada, R. Ido, Y. Murakoshi, S. Kanehashi, K. Nagai, Dependence of alcohol vapor-induced crystallization on gas and vapor permeabilities of poly(lactic acid) films, *J. Appl. Polym. Sci.* **2014**, *131*, 40140/1–40140/9. https://doi.org/10.1002/app.40140.
86. M. Boufarguine, A. Guinault, G. Miquelard-Garnier, C. Sollogoub, PLA/PHBV films with improved mechanical and gas barrier properties, *Macromol. Mater. Eng.* **2013**, *298*, 1065–1073. https://doi.org/10.1002/mame.201200285.
87. A. R. Berens, G. S. Huvard, Particle size distribution of polymer powders by analysis of sorption kinetics, *J. Dispers. Sci. Technol.* **1981**, *2*, 359–378. https://doi.org/10.1080/01932698108943918.
88. A. R. Berens, H. B. Hopfenberg, Diffusion of organic vapors at low concentrations in glassy PVC, polystyrene, and PMMA, *J. Membr. Sci.* **1982**, *10*, 283–303. https://doi.org/10.1016/S0376-7388(00)81415-5.

89. P. Tremblay, M. Savard, J. Vermette, R. Paquin, Gas permeability, diffusivity and solubility of nitrogen, helium, methane, carbon dioxide and formaldehyde in dense polymeric membranes using a new on-line permeation apparatus, *J. Membr. Sci.* **2006**, *282*, 245–256. https://doi.org/10.1016/j.memsci.2006.05.030.
90. N. S. Oliveira, J. Oliveira, T. Gomes, A. Ferreira, J. Dorgan, I. M. Marrucho, Gas sorption in poly(lactic acid) and packaging materials, *Fluid Phase Equilib.* **2004**, *222–223*, 317–324. https://doi.org/10.1016/j.fluid.2004.06.032.
91. N. S. Oliveira, C. M. Gonçalves, J. A. P. Coutinho, A. Ferreira, J. Dorgan, I. M. Marrucho, Carbon dioxide, ethylene and water vapor sorption in poly(lactic acid), *Fluid Phase Equilib.* **2006**, *250*, 116–124. https://doi.org/10.1016/j.fluid.2006.10.009.
92. N. S. Oliveira, J. Dorgan, J. A. P. Coutinho, A. Ferreira, J. L. Daridon, I. M. Marrucho, Gas solubility of carbon dioxide in poly(lactic acid) at high pressures: thermal treatment effect, *J. Polym. Sci. Part B Polym. Phys.* **2007**, *45*, 616–625. https://doi.org/10.1002/polb.20969.
93. F. Iñiguez-Franco, R. Auras, G. Burgess, D. Holmes, X. Fang, M. Rubino, et al., Concurrent solvent induced crystallization and hydrolytic degradation of PLA by water-ethanol solutions, *Polymer (Guildf)* **2016**, *99*, 315–323. https://doi.org/10.1016/j.polymer.2016.07.018.
94. C. Samuel, J.-M. Raquez, P. Dubois, PLLA/PMMA blends: a shear-induced miscibility with tunable morphologies and properties? *Polymer (Guildf)* **2013**, *54*, 3931–3939. https://doi.org/10.1016/j.polymer.2013.05.021.
95. S. Kanehashi, A. Kusakabe, S. Sato, K. Nagai, Analysis of permeability; solubility and diffusivity of carbon dioxide; oxygen; and nitrogen in crystalline and liquid crystalline polymers, *J. Membr. Sci.* **2010**, *365*, 40–51. https://doi.org/10.1016/j.memsci.2010.08.035.
96. A. Sangroniz, A. Chaos, M. Iriarte, J. del Río, J.-R. Sarasua, A. Etxeberria, Influence of the rigid amorphous fraction and crystallinity on polylactide transport properties, *Macromolecules* **2018**, *51*, 3923–3931. https://doi.org/10.1021/acs.macromol.8b00833.
97. T. Komatsuka, A. Kusakabe, K. Nagai, Characterization and gas transport properties of poly(lactic acid) blend membranes, *Desalination* **2008**, *234*, 212–220. https://doi.org/10.1016/j.desal.2007.09.088.
98. N. S. Oliveira, J. Dorgan, J. A. P. Coutinho, A. Ferreira, J. L. Daridon, I. M. Marrucho, Gas solubility of carbon dioxide in poly(lactic acid) at high pressures. *J. Polym. Sci. Part B Polym. Phys.* **2006**, *44*, 1010–1019. https://doi.org/10.1002/polb.20746.
99. R. A. Auras, Solubility of gases and vapors in polylactide polymers, in: T. M. Letcher (Ed.), *Thermodynamics, Solubility and Environmental Issues*, Elsevier, London, 2007, pp. 343–368. https://doi.org/10.1016/B978-044452707-3/50021-5.
100. A. Marra, C. Silvestre, D. Duraccio, S. Cimmino, Polylactic acid/zinc oxide biocomposite films for food packaging application, *Int. J. Biol. Macromol.* **2016**, *88*, 254–262. https://doi.org/10.1016/j.ijbiomac.2016.03.039.
101. J.-W. Rhim, A. K. Mohanty, S. P. Singh, P. K. W. Ng, Effect of the processing methods on the performance of polylactide films: Thermocompression versus solvent casting, *J. Appl. Polym. Sci.* **2006**, *101*, 3736–3742. https://doi.org/10.1002/app.23403.
102. J. M. Lagaron, L. Cabedo, D. Cava, J. L. Feijoo, R. Gavara, E. Gimenez, Improving packaged food quality and safety. Part 2, nanocomposites, *Food Addit. Contam.* **2005**, *22*, 994–998. https://doi.org/10.1080/02652030500239656.
103. V. Ojijo, S. Sinha Ray, R. Sadiku, Concurrent enhancement of multiple properties in reactively processed nanocomposites of polylactide/poly[(butylene succinate)-*co*-adipate] blend and organoclay, *Macromol. Mater. Eng.* **2014**, *299*, 596–608. https://doi.org/10.1002/mame.201300306.
104. V. Katiyar, N. Gerds, C. B. Koch, J. Risbo, H. C. B. Hansen, D. Plackett, Melt processing of poly(L-lactic acid) in the presence of organomodified anionic or cationic clays, *J. Appl. Polym. Sci.* **2011**, *122*, 112–125. https://doi.org/10.1002/app.33984.
105. D. Battegazzore, J. Alongi, A. Frache, Poly(lactic acid)-based composites containing natural fillers: thermal, mechanical and barrier properties. *J. Polym. Environ.* **2014**, *22*, 88–98. https://doi.org/10.1007/s10924-013-0616-9.
106. D. Battegazzore, S. Bocchini, J. Alongi, A. Frache, F. Marino, Cellulose extracted from rice husk as filler for poly(lactic acid): preparation and characterization, *Cellulose* **2014**, *21*, 1813–1821. https://doi.org/10.1007/s10570-014-0207-5.
107. R. B. Valapa, G. Pugazhenthi, V. Katiyar, Fabrication and characterization of sucrose palmitate reinforced poly(lactic acid) bionanocomposite films, *J. Appl. Polym. Sci.* **2015**, *132*, 41320/1–41320/10. https://doi.org/10.1002/app.41320.
108. B. Palai, S. Mohanty, S. K. Nayak, Synergistic effect of polylactic acid(PLA) and poly(butylene succinate-*co*-adipate) (PBSA) based sustainable, reactive, super toughened eco-composite blown films for flexible packaging applications, *Polym. Test.* **2020**, *83*, 106130. https://doi.org/10.1016/j.polymertesting.2019.106130.
109. N. P. Risyon, S. H. Othman, R. K. Basha, R. A. Talib, Characterization of polylactic acid/halloysite nanotubes bionanocomposite films for food packaging, *Food Packag. Shelf Life* **2020**, *23*, 100450. https://doi.org/10.1016/j.fpsl.2019.100450.
110. C. Swaroop, M. Shukla, Development of blown polylactic acid-MgO nanocomposite films for food packaging, *Compos. Part A Appl. Sci. Manuf.* **2019**, *124*, 105482. https://doi.org/10.1016/j.compositesa.2019.105482.
111. G. Flodberg, I. Helland, L. Thomsson, S. Bodil Fredriksen, Barrier properties of polypropylene carbonate and poly(lactic acid) cast films, *Eur. Polym. J.* **2015**, *63*, 217–226. https://doi.org/10.1016/j.eurpolymj.2014.12.020.
112. C. Aulin, E. Karabulut, A. Tran, L. Wågberg, T. Lindström, Correction to transparent nanocellulosic multilayer thin films on polylactic acid with tunable gas barrier properties, *ACS Appl. Mater. Interfaces* **2013**, *5*, 10395–10396. https://doi.org/10.1021/am404037r.
113. H. D. Huang, P.G. Ren, J. Z. Xu, L. Xu, G. J. Zhong, B. S. Hsiao, et al., Improved barrier properties of poly(lactic acid) with randomly dispersed graphene oxide nanosheets,

*J. Membr. Sci.* **2014**, *464*, 110–118. https://doi.org/10.1016/j.memsci.2014.04.009.

114. L. Xie, H. Xu, J.-B. Chen, Z.-J. Zhang, B. S. Hsiao, G.-J. Zhong, et al., From nanofibrillar to nanolaminar poly(butylene succinate): paving the way to robust barrier and mechanical properties for full-biodegradable poly(lactic acid) films, *Appl. Mater. Interfaces* **2015**, *7*, 8023–8032. https://doi.org/10.1021/acsami.5b00294.
115. Y. Zhu, G. G. Buonocore, M. Lavorgna, L. Ambrosio, Poly(lactic acid)/titanium dioxide nanocomposite films: influence of processing procedure on dispersion of titanium dioxide and photocatalytic activity, *Polym. Compos.* **2011**, *32*, 519–528. https://doi.org/10.1002/pc.21068.
116. H. Ortiz-Vazquez, J. Shin, H. Soto-Valdez, R. Auras, Release of butylated hydroxytoluene (BHT) from poly(lactic acid) films, *Polym. Test.* **2011**, *30*, 463–471. https://doi.org/10.1016/j.polymertesting.2011.03.006.
117. J. Ambrosio-Martín, A. López-Rubio, M. José Fabra, M. Angel López-Manchado, A. Sorrentino, G. Gorrasi, et al., Synergistic effect of lactic acid oligomers and laminar graphene sheets on the barrier properties of polylactide nanocomposites obtained by the in situ polymerization pre-incorporation method, *J. Appl. Polym. Sci.* **2016**, *133*, 42661/1–42661/11. https://doi.org/10.1002/app.42661.
118. M. D. Sanchez-Garcia, J. M. Lagaron, On the use of plant cellulose nanowhiskers to enhance the barrier properties of polylactic acid, *Cellulose* **2010**, *17*, 987–1004. https://doi.org/10.1007/s10570-010-9430-x.
119. M. D. Sanchez-Garcia, J. M. Lagaron, Novel clay-based nanobiocomposites of biopolyesters with synergistic barrier to UV light, gas, and vapour, *J. Appl. Polym. Sci.* **2010**, *118*, 188–199. https://doi.org/10.1002/app.31986.
120. S. Sinha Ray, M. Okamoto, Biodegradable polylactide and its nanocomposites: opening a new dimension for plastics and composites, *Macromol. Rapid Commun.* **2003**, *24*, 815–840. https://doi.org/10.1002/marc.200300008.
121. J. Ambrosio-Martín, M. J. Fabra, A. Lopez-Rubio, J. M. Lagaron, Melt polycondensation to improve the dispersion of bacterial cellulose into polylactide via melt compounding: enhanced barrier and mechanical properties, *Cellulose* **2015**, *22*, 1201–1226. https://doi.org/10.1007/s10570-014-0523-9.
122. S. Sato, T. Nyuui, G. Matsuba, K. Nagai, Correlation between interlamellar amorphous structure and gas permeability in poly(lactic acid) films, *J. Appl. Polym. Sci.* **2014**, *131*, 40626/1–40626/6. https://doi.org/10.1002/app.40626.
123. S. F. Nassar, A. Guinault, N. Delpouve, V. Divry, V. Ducruet, C. Sollogoub, et al., Multi-scale analysis of the impact of polylactide morphology on gas barrier properties, *Polymer (Guildf)* **2017**, *108*, 163–172. https://doi.org/10.1016/j.polymer.2016.11.047.
124. J. Del Río, A. Etxeberria, N. López-Rodríguez, E. Lizundia, J. R. Sarasua, A PALS contribution to the supramolecular structure of poly(L-lactide), *Macromolecules* **2010**, *43*, 4698–4707. https://doi.org/10.1021/ma902247y.
125. Y. Byun, S. Whiteside, R. Thomas, M. Dharman, J. Hughes, Y. T. Kim, The effect of solvent mixture on the properties of solvent cast polylactic acid (PLA) film, *J. Appl. Polym. Sci.* **2012**, *124*, 3577–3582. https://doi.org/10.1002/app.34071.
126. E. Almenar, Chapter 9. Food shelf life, in: M. B. Omary (Ed.), *Introduction to Food Packaging*, Wiley-Blackwell Publishing Limited, Oxford, 2020, p. 400.
127. E. Almenar, Innovations in packaging technologies for produce, in: M. I. Gil and R. M. Beaudry (Eds.), *Controlled and Modified Atmospheres for Fresh and Fresh-Cut Produce*, Elsevier, Philadelphia, PA, 2020, pp. 211–264. https://doi.org/10.1016/B978-0-12-804599-2.00012-0.
128. ASTM E96/E96M-16, *Standard Test Methods for Water Vapor Transmission of Materials*, ASTM International, West Conshohocken, PA, 2016. https://doi.org/10.1520/E0096_E0096M-16.
129. G. L. Siparsky, K. J. Voorhees, J. R. Dorgan, K. Schilling, Water transport in polylactic acid (PLA), PLA/polycaprolactone copolymers, and PLA/polyethylene glycol blends, *J. Environ. Polym. Degrad.* **1997**, *5*, 125–136. https://doi.org/10.1007/BF02763656.
130. D. Cava, E. Gimenez, R. Gavara, J. M. Lagaron, Comparative performance and barrier properties of biodegradable thermoplastics and nanobiocomposites versus PET for food packaging applications, *J. Plast. Film Sheeting* **2006**, *22*, 265–274. https://doi.org/10.1177/8756087906071354.
131. N. Gulati, Use of QCM technology for measuring barrier properties of biodegradable packaging material, MS thesis, Michigan State University, East Lansing, MI, 2008.
132. J. Yoon, H. Jung, M. Kim, E. Park, Diffusion coefficient and equilibrium solubility of water molecules in biodegradable polymers, *J. Appl. Polym. Sci.* **2000**, *77*, 1716–1722. https://doi.org/10.1002/1097-4628(20000822)77:8<1716::AID-APP8>3.0.CO;2-F.
133. F. De Santis, G. Gorrasi, R. Pantani, A spectroscopic approach to assess transport properties of water vapor in PLA, *Polym. Test.* **2015**, *44*, 15–22. https://doi.org/10.1016/j.polymertesting.2015.03.015.
134. M. D. Sanchez-Garcia, E. Gimenez, J. M. Lagaron, Morphology and barrier properties of solvent cast composites of thermoplastic biopolymers and purified cellulose fibers, *Carbohydr. Polym.* **2008**, *71*, 235–244. https://doi.org/10.1016/j.carbpol.2007.05.041.
135. A. Du, G. A. Gelves, D. Koo, U. Sundararaj, R. Cairncross, Water transport in polylactide and polylactide/montmorillonite composites, *J. Polym. Environ.* **2013**, *21*, 8–15. https://doi.org/10.1007/s10924-012-0540-4.
136. B. S. Bouakaz, I. Pillin, A. Habi, Y. Grohens, Synergy between fillers in organomontmorillonite/graphene-PLA nanocomposites, *Appl. Clay Sci.* **2015**, *116–117*, 69–77. https://doi.org/10.1016/j.clay.2015.08.017.
137. K. Taleb, I. Pillin, Y. Grohens, S. Saidi-Besbes, Polylactic acid/Gemini surfactant modified clay bio-nanocomposites: morphological, thermal, mechanical and barrier properties, *Int. J. Biol. Macromol.* **2021**, *177*, 505–516. https://doi.org/10.1016/j.ijbiomac.2021.02.135.
138. J. W. Rhim, J. H. Lee, P. K. W. Ng, Mechanical and barrier properties of biodegradable soy protein isolate-based films

coated with polylactic acid, *LWT—Food Sci. Technol.* **2007**, *40*, 232–238. https://doi.org/10.1016/j.lwt.2005.10.002.

139. J.-W. Rhim, S.-I. Hong, C.-S. Ha, Tensile, water vapor barrier and antimicrobial properties of PLA/nanoclay composite films, *LWT—Food Sci. Technol.* **2009**, *42*, 612–617. https://doi.org/10.1016/j.lwt.2008.02.015.
140. E. Fortunati, M. Peltzer, I. Armentano, L. Torre, A. Jiménez, J. M. Kenny, Effects of modified cellulose nanocrystals on the barrier and migration properties of PLA nano-biocomposites, *Carbohydr. Polym.* **2012**, *90*, 948–956. https://doi.org/10.1016/j.carbpol.2012.06.025.
141. L. F. Boesel, M. De Geus, L. Thöny-Meyer, Effect of PLA crystallization on the structure of biomimetic composites of PLA and clay, *J. Appl. Polym. Sci.* **2013**, *129*, 1109–1116. https://doi.org/10.1002/app.38698.
142. E. Fortunati, F. Luzi, D. Puglia, F. Dominici, C. Santulli, J. M. Kenny, et al., Investigation of thermo-mechanical, chemical and degradative properties of PLA-limonene films reinforced with cellulose nanocrystals extracted from *Phormium tenax* leaves, *Eur. Polym. J.* **2014**, *56*, 77–91. https://doi.org/10.1016/j.eurpolymj.2014.03.030.
143. E. Fortunati, S. Rinaldi, M. Peltzer, N. Bloise, L. Visai, I. Armentano, et al., Nano-biocomposite films with modified cellulose nanocrystals and synthesized silver nanoparticles, *Carbohydr. Polym.* **2014**, *101*, 1122–1133. https://doi.org/10.1016/j.carbpol.2013.10.055.
144. J. Shojaeiarani, D. S. Bajwa, N. M. Stark, T. M. Bergholz, A. L. Kraft, Spin coating method improved the performance characteristics of films obtained from poly(lactic acid) and cellulose nanocrystals, *Sustain. Mater. Technol.* **2020**, *26*, e00212. https://doi.org/10.1016/j.susmat.2020.e00212.
145. Y. Wang, Y. Qin, Y. Zhang, M. Yuan, H. Li, M. Yuan, Effects of *N*-octyl lactate as plasticizer on the thermal and functional properties of extruded PLA-based films, *Int. J. Biol. Macromol.* **2014**, *67*, 58–63. https://doi.org/10.1016/j.ijbiomac.2014.02.048.
146. A. Abdulkhani, J. Hosseinzadeh, S. Dadashi, M. Mousavi, A study of morphological, thermal, mechanical and barrier properties of PLA based biocomposites prepared with micro and nano sized cellulosic fibers, *Cellul. Chem. Technol.* **2015**, *49*, 597–605.
147. J. H. Lim, J. A. Kim, J. A. Ko, H. J. Park, Preparation and characterization of composites based on polylactic acid and beeswax with improved water vapor barrier properties, *J. Food Sci.* **2015**, *80*, 2471–2477. https://doi.org/10.1111/1750-3841.13081.
148. Y. Qin, Y. Wang, W. Yan, Y. Zhang, L. Hongli, M. Yuan, Effect of hexadecyl lactate as plasticizer on the properties of poly(L-lactide) films for food packaging applications, *J. Polym. Environ.* **2015**, *23*, 374–382. https://doi.org/10.1007/s10924-014-0702-7.
149. H. Y. Yu, X. Y. Yang, F. F. Lu, G. Y. Chen, J. M. Yao, Fabrication of multifunctional cellulose nanocrystals/poly(lactic acid) nanocomposites with silver nanoparticles by spraying method, *Carbohydr. Polym.* **2016**, *140*, 209–219. https://doi.org/10.1016/j.carbpol.2015.12.030.
150. Z. Duan, N. L. Thomas, Water vapour permeability of poly(lactic acid): crystallinity and the tortuous path model, *J. Appl. Phys.* **2014**, *115*, 64903–64909. https://doi.org/10.1063/1.4865168.
151. H. Tsuji, T. Tsuruno, Water vapor permeability of poly(L-lactide)/poly(D-lactide) stereocomplexes, *Macromol. Mater. Eng.* **2010**, *295*, 709–715. https://doi.org/10.1002/mame.201000071.
152. R. Shogren, Water vapor permeability of biodegradable polymers, *J. Environ. Polym. Degrad.* **1997**, *5*, 91–95. https://doi.org/10.1007/bf02763592.
153. H. Tsuji, R. Okino, H. Daimon, K. Fujie, Water vapor permeability of poly(lactide)s: Effects of molecular characteristics and crystallinity, *J. Appl. Polym. Sci.* **2006**, *99*, 2245–2252. https://doi.org/10.1002/app.22698.
154. M. Cocca, M. L. Di Lorenzo, M. Malinconico, V. Frezza, Influence of crystal polymorphism on mechanical and barrier properties of poly(L-lactic acid), *Eur. Polym. J.* **2011**, *47*, 1073–1080.https://doi.org/10.1016/j.eurpolymj.2011.02.009.
155. N. Delpouve, G. Stoclet, A. Saiter, E. Dargent, S. Marais, Water barrier properties in biaxially drawn poly(lactic acid) films, *J. Phys. Chem. B* **2012**, *116*, 4615–4625. https://doi.org/10.1021/jp211670g.
156. Z. Duan, N. L. Thomas, W. Huang, Water vapour permeability of poly(lactic acid) nanocomposites, *J. Membr. Sci.* **2013**, *445*, 112–118. https://doi.org/10.1016/j.memsci.2013.06.008.
157. J. Trifol, D. Plackett, P. Szabo, A. E. Daugaard, M. Giacinti Baschetti, Effect of crystallinity on water vapor sorption, diffusion, and permeation of PLA-based nanocomposites, *ACS Omega* **2020**, *5*, 15362–15369. https://doi.org/10.1021/acsomega.0c01468.
158. S. Sato, D. Gondo, T. Wada, S. Kanehashi, K. Nagai, Effects of various liquid organic solvents on solvent-induced crystallization of amorphous poly(lactic acid) film, *J. Appl. Polym. Sci.* **2013**, *129*, 1607–1617. https://doi.org/10.1002/app.38833.
159. R. A. Cairncross, J. G. Becker, S. Ramaswamy, R. O'connor, Moisture sorption, transport, and hydrolytic degradation in polylactide, *Appl. Biochem. Biotechnol.* **2006**, *131*, 774–785. https://doi.org/10.1385/ABAB:131:1:774.
160. A. Du, D. Koo, G. Theryo, M. A. Hillmyer, R. A. Cairncross, Water transport and clustering behavior in homopolymer and graft copolymer polylactide, *J. Membr. Sci.* **2012**, *396*, 50–56. https://doi.org/10.1016/j.memsci.2011.12.030.
161. H. Ebadi-Dehaghani, M. Barikani, H. A. Khonakdar, S. H. Jafari, U. Wagenknecht, G. Heinrich, On $O_2$ gas permeability of PP/PLA/clay nanocomposites: a molecular dynamic simulation approach, *Polym. Test.* **2015**, *45*, 139–151. https://doi.org/10.1016/j.polymertesting.2015.05.010.
162. T. Janjarasskul, P. Suppakul, Active and intelligent packaging: the indication of quality and safety, *Crit. Rev. Food Sci. Nutr.* **2018**, *58*, 808–831. https://doi.org/10.1080/10408398.2016.1225278.
163. R. A. Auras, Investigation of polylactide as packaging material, Ph.D. thesis, Michigan State University, East Lansing, MI, 2004.
164. R. Auras, B. Harte, S. Selke, Sorption of ethyl acetate and d-limonene in poly(lactide) polymers, *J. Sci. Food Agric.* **2006**, *86*, 648–656. https://doi.org/10.1002/jsfa.2391.

165. P. Leelaphiwat, R. A. Auras, J. B. Harte, P. K. C. Ong, V. Chonhenchob, Barrier properties of polymeric packaging materials to major aroma volatiles in herbs, *MATEC Web Conf.* **2016**,*67*,06100.https://doi.org/10.1051/matecconf/20166706100.
166. P. Leelaphiwat, R. A. Auras, G. J. Burgess, J. B. Harte, V. Chonhenchob, Preliminary quantification of the permeability, solubility and diffusion coefficients of major aroma compounds present in herbs through various plastic packaging materials, *J. Sci. Food Agric.* **2018**, *98*, 1545–1553. https://doi.org/10.1002/jsfa.8626.
167. P. Leelaphiwat, V. Chonhenchob, S. P. Singh, J. Kruenate, U. Wichai, P. K. C. Ong, Transport coefficients of eucalyptol through various polymeric films, *Packag. Technol. Sci.* **2012**, *25*, 161–172. https://doi.org/10.1002/pts.967.
168. S. Domenek, M. Pronnier, A. Guinault, C. Plessis, V. Ducruet, The sorption of aroma compounds influences the thermomechanical properties of PLA, *Biopol2007*, Alicante, Spain, 2007.
169. R. Salazar, S. Domenek, V. Ducruet, Aroma sorption in polylactide, *Fifth International Symposium on Food Packaging*, Berlin, Germany, 2012.
170. F. Welle, J. Ewender, R. Auras, U. Sonchaeng, Diffusion of organic molecules in poly(lactic acid) films, *29th IAPRI Symposium on Packaging*, Twente, The Netherlands, 2019.
171. J. Ewender, F. Welle, Determination of the activation energies of diffusion of organic molecules in poly(ethylene terephthalate), *J. Appl. Polym. Sci.* **2013**, *128*, 3885–3892. https://doi.org/10.1002/app.38623.
172. H. Tsuji, Poly(lactic acid) stereocomplexes: a decade of progress, *Adv. Drug. Deliv. Rev.* **2016**, *107*, 97–135. https://doi.org/10.1016/j.addr.2016.04.017.
173. N. Varol, Advanced thermal analysis and transport properties of stereocomplex polylactide, Ph.D. thesis, Normandie Université, Caen, France, 2019.
174. H. Bai, C. Huang, H. Xiu, Q. Zhang, H. Deng, K. Wang, et al., Significantly improving oxygen barrier properties of polylactide via constructing parallel-aligned shish-kebab-like crystals with well-interlocked boundaries, *Biomacromolecules* **2014**, *15*, 1507–1514. https://doi.org/10.1021/bm500167u.
175. P. Shan Teo, W. Shyang Chow, Water vapour permeability of poly(lactic acid)/chitosan binary and ternary blends, *KMUTNB Int. J. Appl. Sci. Technol.* **2014**, *7*, 23–27. https://doi.org/10.14416/j.ijast.2014.01.001.
176. R. N. Darie, E. Pâslaru, A. Sdrobis, G. M. Pricope, G. E. Hitruc, A. Poiată, et al., Effect of nanoclay hydrophilicity on the poly(lactic acid)/clay nanocomposites properties, *Ind. Eng. Chem. Res.* **2014**, *53*, 7877–7890. https://doi.org/10.1021/ie500577m.
177. B. Şengül, R. M. A. El-abassy, A. Materny, N. Dilsiz, Poly(lactic acid)/organo-montmorillonite nanocomposites: synthesis, structures, permeation properties and applications, *Polym. Sci. Ser. A* **2017**, *59*, 891–901. https://doi.org/10.1134/S0965545X17060098.
178. A. H. Mohsen, N. A. Ali, Mechanical, color and barrier, properties of biodegradable nanocomposites polylactic acid/nanoclay, *J. Bioremediat. Biodegrad.* **2018**, *09*. https://doi.org/10.4172/2155-6199.1000455.
179. F. Li, C. Zhang, Y. Weng, Improvement of the gas barrier properties of PLA/OMMT films by regulating the interlayer spacing of OMMT and the crystallinity of PLA, *ACS Omega* **2020**, *5*, 18675–18684. https://doi.org/10.1021/acsomega.0c01405.
180. M. A. Busolo, P. Fernandez, M. J. Ocio, J. M. Lagaron, Novel silver-based nanoclay as an antimicrobial in polylactic acid food packaging coatings, *Food Addit. Contam. Part A* **2010**, *27*, 1617–1626. https://doi.org/10.1080/19440049.2010.506601.
181. S. Girdthep, P. Worajittiphon, R. Molloy, T. Leejarkpai, W. Punyodom, Formulation and characterization of compatibilized poly(lactic acid)-based blends and their nanocomposites with silver-loaded kaolinite, *Polym. Int.* **2015**, *64*, 203–211. https://doi.org/10.1002/pi.4775.
182. L. M. Matuana, S. S. Karkhanis, N. M. Stark, R. C. Sabo, Cellulose nanocrystals as barrier performance enhancer of extrusion-blown PLA films for food applications, *Adv. Mater. TechConnect Briefs 2016* **2016**, *3*, 1–4.
183. E. Fortunati, M. Peltzer, I. Armentano, A. Jiménez, J. M. Kenny, Combined effects of cellulose nanocrystals and silver nanoparticles on the barrier and migration properties of PLA nano-biocomposites, *J. Food Eng.* **2013**, *118*, 117–124. https://doi.org/10.1016/j.jfoodeng.2013.03.025.
184. S. S. Nair, H. Chen, Y. Peng, Y. Huang, N. Yan, Polylactic acid biocomposites reinforced with nanocellulose fibrils with high lignin content for improved mechanical, thermal, and barrier properties, *ACS Sustain. Chem. Eng.* **2018**, *6*, 10058–10068. https://doi.org/10.1021/acssuschemeng.8b01405.
185. R. Malinowski, P. Rytlewski, M. Żenkiewicz, Effects of electron radiation on properties of PLA, *Arch. Mater. Sci. Eng.* **2011**, *49*, 25–32.
186. J.-W. Rhim, J.-H. Kim, Properties of poly(lactide)-coated paperboard for the use of 1-way paper cup, *J. Food Sci.* **2009**, *74*, E105–E111. https://doi.org/10.1111/j.1750-3841.2009.01073.x.
187. J.-W. Rhim, J.-H. Lee, S.-I. Hong, Increase in water resistance of paperboard by coating with poly(lactide), *Packag. Technol. Sci.* **2007**, *20*, 393–402. https://doi.org/10.1002/pts.767.
188. J. W. Rhim, K.A. Mohanty, S. P. Singh, P. K. W. Ng, Preparation and properties of biodegradable multilayer films based on soy protein isolate and poly(lactide), *Ind. Eng. Chem. Res.* **2006**, *45*, 3059–3066. https://doi.org/10.1021/ie051207+.
189. V. K. Haugaard, B. Danielsen, G. Bertelsen, Impact of polylactate and poly(hydroxybutyrate) on food quality, *Eur. Food. Res. Technol.* **2003**, *216*, 233–240. https://doi.org/10.1007/s00217-002-0651-6.
190. V. Haugaard, C. Weber, B. Danielsen, G. Bertelsen, Quality changes in orange juice packed in materials based on polylactate, *Eur. Food Res. Technol.* **2002**, *214*, 423–428. https://doi.org/10.1007/s00217-001-0474-x.
191. M. Joo, N. Lewandowski, R. Auras, J. Harte, E. Almenar, Comparative shelf life study of blackberry fruit in bio-based and petroleum-based containers under retail storage conditions, *Food Chem.* **2011**, *126*, 1734–1740. https://doi.org/10.1016/j.foodchem.2010.12.071.


# 12

# MIGRATION AND INTERACTION WITH CONTACT MATERIALS

Herlinda Soto-Valdez and Elizabeth Peralta

## 12.1 INTRODUCTION

The term migration is generally used to describe the transfer of substances from packaging (e.g., polymerization residuals, additives, and decomposition products) to food. The word migration is used to describe the movement of contaminants from a package into food after the explosive growth of plastics during the second half of the twentieth century. The increasing use of biodegradable materials in packaging, such as PLA, and the possibility of degradation during the contact with the food, can bring an additional issue, that is, the migration of decomposition products such as monomers, oligomers, and other products of degradation. Additionally, in the last 10 years, there has been a significant increase in the number of publications related to active packaging in which additives such as antioxidant and antimicrobial agents have been used as components of PLA formulations. In many cases, these additives are to be released to the food in contact with the PLA by migration processes.

## 12.2 MIGRATION PRINCIPLES

Migration is the result of diffusion and equilibrium processes involving the transfer of low molecular mass compounds from a plastic package into a food or food simulant. The migrants diffuse through the amorphous portion of the polymer matrix toward the interface where they are partitioned between the two media until their chemical potential values in both the polymer and the food reach equilibrium. Migration can be mathematically described by Fick's second law (Equation 12.1):

$$\frac{\partial C}{\partial t} = D\left(\frac{\partial^2 C}{\partial x^2}\right) \tag{12.1}$$

where $C$ is the concentration of the migrant at position $x$ and time $t$ and $D$ is the diffusion coefficient (also known as diffusivity) of the migrant [1]. Since this equation is not easy to apply directly to practical cases, solutions have been developed, taking pertinent considerations to make it applicable to different cases. The theoretical background of the migration process and the development of different solutions are described by Crank [1], Limm and Hollifield [2], Chatwin [3], Hamdani et al. [4], Garde et al. [5], Sonchaeng et al. [6]. One of the most used models to describe and predict migration is expressed in Equation 12.2:

$$\frac{M_t}{M_\infty} = 1 - \sum_{n=1}^{\infty} \frac{2\alpha\left(1+\alpha\right)}{1+\alpha+\alpha^2 q_n^2} \exp\left(-\frac{Dq_n^2 t}{l^2}\right) \tag{12.2}$$

where $M_t/M_\infty$ represents the mass of the migrant diffused to the food at time $t$ and divided by the mass diffused at equilibrium. The thickness of the film or sheet is represented by $l$, $t$ is the contact time, and $D$ is again the Fickian diffusion coefficient of the migrant in that system [1, 3, 5–7]. $D$ is a kinetic parameter that represents the magnitude of the diffusion of a migrant diffused across a unit area per unit time ($cm^2/s$). $D$ is constant and independent of time when there is

*Poly(Lactic Acid): Synthesis, Structures, Properties, Processing, Applications, and End of Life*, Second Edition.
Edited by Rafael A. Auras, Loong-Tak Lim, Susan E. M. Selke, and Hideto Tsuji.

no interaction among the components of the system. The $q_n$ values are the nonzero positive roots of tan $q_n = \alpha q_n$ and $\alpha$ is:

$$\alpha = \frac{V_s}{K_{p,s} V_p} \tag{12.3}$$

where $V_s$ and $V_p$ are the molar volume of the food simulant and the plastic, respectively, $K_{p,s}$ is the partition coefficient of the migrant between the plastic and the food simulant, which at lower concentration can be assumed constant and calculated from the ratio of the concentration of the migrant in the plastic ($C_{p,\infty}$) and the food simulant ($C_{s,\infty}$) at equilibrium:

$$K_{p,s} = \frac{C_{p,\infty}}{C_{s,\infty}} \tag{12.4}$$

Considering a system composed of migrant/packaging material/food, the migration process has been divided into three classes: (i) class 1 or nonmigrating systems, where $D$ is close to zero (less than $10^{-12}$ cm$^2$/s); (ii) class 2 or independent migration that is not controlled by food but its presence may accelerate migration (larger than $10^{-9}$ cm$^2$/s); and (iii) class 3 or leaching, where migration is controlled by the presence of food (less than $10^{-12}$ cm$^2$/s in the absence of food but $10^{-9}$ cm$^2$/s or more in its presence) [8]. As an example, $D$ values for lactic acid from PLA to water, 50% ethanol, and 95% ethanol have been estimated as $8\times10^{-16}$, $1.5\times10^{-15}$, and $2.3\times10^{-15}$ cm$^2$/s, respectively (40°C) [9]. These low values may be considered to belong to class 1 or nonmigrating systems. Similar $D$ values for lactide (LA) from PLA to aqueous systems have been reported as $1.4\times10^{-16}$ and $3.8\times10^{-15}$ cm$^2$/s (23°C) [10]. These values also belong to class 1 and increased to $1.5–2.8\times10^{-13}$ cm$^2$/s at 43°C and will be expected to keep increasing at higher temperatures as discussed in this chapter. Eventually, the migration process will be affected by degradation of the polymer, hydrolysis of the LA dimer to lactic acid, and consequently, $T_g$.

## 12.3 LEGISLATION

One of the functions of packaging is to protect food from external contamination. Therefore, the fact that packaging itself can be a source of contamination brought some concerns to consumers, governments, and industries. The use of plastics in contact with food has increased dramatically during the last 50 years [11]. As a result, nowadays there is detailed legislation in different countries. It has not been possible to harmonize them into one global legislation, in spite of many attempts. Although there are similarities in the legislation, it may vary from region to region [12].

In general, legislation related to migration states the rules to assure the safety of the materials used in contact with food with the purpose to decrease the consumer's risk. They may include lists of polymers, monomers, and additives permitted to be used in packaging materials, global and specific migration limits, composition limits, and procedures to calculate the estimated daily intake (EDI) for certain migrants. They also lay down the conditions and procedures to perform migration studies (food simulants, temperature, time, analytical procedures, etc.).

In the United States of America (USA), the Food and Drug Administration (FDA) considers migrants transferred from food contact materials to food as "indirect food additives," and they are regulated in separate sections of title 21 of the Code of Federal Regulations parts 174–178 (21CFR174–21CFR178) [13]. In 1995, PLA was tested and identified to be Generally Recognized as Safe (GRAS) to be used in contact with food [10]. Regarding legislation applicable to potential migrants from PLA, according to CFR 184.1061 [14], lactic acid is affirmed as a food ingredient GRAS for individuals beyond infancy. This substance can be used as an antimicrobial, curing, or pickling agent. Also, it functions as a flavor enhancer, flavoring agent, adjuvant, pH control agent, solvent, and vehicle. The only restriction in the regulation is that lactic acid should not be added to infant foods and infant formulas, at levels higher than those recommended by the current good manufacturing practice. This restriction is based on the possibility that the limited ability of infants to metabolize the D-isomer of lactic acid may lead to an organic acidosis [10]. No comments related to LA or PLA oligomers are included.

The European Union (EU) published the Framework Regulation No. 1935/2004 for materials and articles intended to come into contact with food [15]. In addition, Commission Regulation No. 2023/2006 defines the requirements of good manufacturing practices [16], and Commission Regulation EU No. 10/2011 is a specific regulation for plastic packaging materials and substances intended to come into contact with food [17]. Lactic acid is included in Annex 1 of this regulation (Union list of authorized monomers, other starting substances, macromolecules obtained from microbial fermentation, additives, and polymer production aids) as a substance that is allowed to be used as a monomer or other starting substances and as an additive or polymer production aid. There is no specific migration limit applicable to lactic acid; therefore, the global migration limit is applicable (60 mg/kg). LA or PLA oligomers are not included. The most recent (at the time of this writing) amendment of regulation No. 10/2011 was published in September 2020 (1245) [18], which included the approval of montmorillonite clay modified with hexadecyltrimethylammonium bromide in the list of authorized substances, as an additive up to 4% w/w, in PLA intended for storage of water at ambient temperature or below. The rationale for this approval was based on the fact that once dispersed in the PLA plastic, the montmorillonite particles

can form platelets with one or two dimensions in the nanoparticle range. The nanoparticles are not expected to migrate as they are oriented parallel to the plastic surface and fully embedded within the polymer.

In South America, food contact materials are regulated by the Common Market Group (Grupo Mercado Común, GMC) of South America (MERCOSUR, Mercado Común del Sur). The General Provisions of GMC Resolution 56/92 presents a positive list of monomers, other starting substances and polymers authorized for the manufacture of food contact plastics and equipment in contact with food (GMC/RES 02/12) [19]. Lactic acid is included in the list of monomers without restriction or specification of use. A positive list of additives used for the manufacture of plastics and coatings intended to be in contact with food is in GMC/RES 39/19 [20]. LA or PLA oligomers are not included in any of the lists.

In 2016, China published two general standards related to food contact materials that are compulsory (abbreviated as GB): GB 4806.1-2016 National Food Safety Standard—General safety requirements for food contact materials and articles and GB 9685-2016 National Food Safety Standard—Standard for the use of additives for food contact materials and articles. English translations of the standards are available from several websites [21, 22]. PLA is listed as a plastic permitted for use in contact with food at temperatures not higher than 100°C. Regarding migration test methods, there are several GB standards that have been published since 2015 [12]. GB 31604.1-2015 National Food Safety Standard—General rules for migration test of food contact materials and articles [23], is the regulation equivalent to some annexes of the Commission Regulation EU No. 10/2011 [17]. Zhou et al. in 2020 compared this legislation to those of the EU and USA in a publication not yet translated to English [24].

In Japan, the Food Sanitation Act authorizes the Ministry of Health, Labor and Welfare (MHLW) to establish the specifications and standards for food, food additives, food contact materials, etc. In 2020, MHLW published a revised version of the positive lists, consisting of two notifications on synthetic resins in food contact materials and articles [25, 26]. Notification no. 195 establishes a migration limit of 0.01 mg/kg of food for polymers and additives not listed in the positive lists. Notification no. 196 includes specifications for base polymer resins, base polymer additives, monomers, and additives. This notification presents two tables in which there are restrictions for the use of PLA and lactic acid. Table 1 refers to *Base polymers for plastics* and the restriction "not more than 6% in the base polymer components" applies only to the stereoisomer D-lactic acid which is poorly metabolized by mammalians (explained in Section 12.4.1). Table 2 refers to *Base polymers for coatings* with restrictions applicable to any lactic acid (L- D- and the DL- mixture). Table 12.1 summarizes the testing conditions recommended by legislation in the United States of America [13, 34], the European Commission [15, 17], MERCOSUR [28], China [23], and Japan [25–27].

## 12.4 MIGRATION AND TOXICOLOGICAL DATA OF LACTIC ACID, LACTIDE, DIMERS, AND OLIGOMERS

Migrants from PLA may include lactic acid, the linear dimer of lactic acid (lactoyl-lactic acid), other oligomers of PLA ($n$ = 3–13), and the cyclic dimer of lactic acid (LA). Their chemical structures are shown in Figure 12.1.

### 12.4.1 Lactic Acid

Lactic acid (2-hydroxypropanoic acid) is considered the main migrant from PLA, since the other species are expected to hydrolyze to lactic acid either in the aqueous or the acidic media commonly found in food systems or in the human digestive tract [10]. Lactic acid is widely used in food and is considered safe when used both as an intentional food ingredient and when naturally occurring in food. Its L-isomer, D-isomer, and DL-mixture are considered as food ingredients with no limitations other than current good manufacturing practice, except when used in infant foods and infant formulas [14]. Lactic acid is a chiral acid. The two stereoisomers are metabolized in different manners in mammals. L-Lactic acid is a common compound of intermediary metabolism in mammals that is formed by the utilization of glycogen for energy in muscle. L-Lactic acid is then oxidized to pyruvic acid in the liver by L-lactic acid dehydrogenase. The other stereoisomer, D-lactic acid, is also absorbed from the intestinal tract, but it is poorly metabolized by mammalians because they do not have D-lactic acid dehydrogenase. Thus, this isomer is not utilized as a source of energy, and it can accumulate in cells to produce an organic acidosis. It can penetrate tissues such as the brain and interfere with normal metabolic processes [10].

Lactic acid has shown an oral LD50 value of 3.543 g/kg in rats [29], 4.88 g/kg in mice, and 1.81 g/kg in guinea pigs [10]. The LD50 value can be defined as the dose of an agent (lactic acid in this case) that is sufficient to kill 50% of a population of animals within a certain time. Lactic acid has also shown skin irritation in rabbits at 500 mg/24 h and severe irritation of the eye in rabbits at 750 µg/kg [29].

The first study of migration of lactic acid from PLA to food simulants was reported in 1995 by Conn et al. [10], who performed a safety assessment of PLA for use as a food contact polymer by following FDA regulations. However, they used 8% alcohol as a food simulant and higher temperatures (26 and 43°C) than those recommended by FDA (Table 12.1). This study included the migration of dimers

**TABLE 12.1 General Conditions to Determine Migration from Materials Intended to be in Contact with Food, According to Different Legislations**

| Food | Simulant | Temperature (°C) | Time |
|---|---|---|---|
| **United States of America (USA)** | | | |
| Aqueous and acidic | 10% Ethanol | 20 or 40, 121, 100 (at reflux) | 10 days, 2 h followed by 10 days at 40°C |
| Low- and high-alcoholic | 10–50% Ethanol | 20 or 40 | 10 days |
| Fatty | Food oil (corn oil), HB 307, Miglyol 812, 95% or absolute ethanol, 50% ethanol or isooctane | 20 or 40, 121 | 10 days or 2 h followed by 10 days at 40°C |
| **European Union (EU)** | | | |
| Aqueous | 10% Ethanol | 5, 20, 40, 50, 60, 70, or 100 or at reflux | 5 min, 0.5, 1, 2, 6, 24 h, 3 or 10 days |
| Acidic (pH ≤ 4.5) | 3% Acetic acid | Same as above | Same as above |
| Low- and high-alcoholic | 20–50% Ethanol | Same as above | Same as above |
| Fatty | Vegetable oil | 5, 20, 40, 50, 60, 70, 100, 121, 130, 150, or 175 | Same as above |
| Dry solid food | Poly(2,6-diphenyl-*p*-phenylene oxide) | Same as above | Same as above |
| Dairy products | 50% Ethanol. Fermented milks and sour cream: 3% Acetic acid | 5, 20, 40, 50, 60, 70, or 100 or at reflux | Same as above |
| **Mercado Común del Sur (MERCOSUR)** | | | |
| Aqueous | Distilled water | 5, 20, 40, 70, or 100 or at reflux | 0.5, 1, 2, 4, 24 h or 10 days |
| Acidic (pH ≤ 4.5) | 3% Acetic acid | Same as above | Same as above |
| Alcoholic (5–10%) | 10% Ethanol | Same as above | Same as above |
| Alcoholic (>10%) | For foods with alcohol content greater than 10%: ethanol solution in the same concentration as that of the food | Same as above | Same as above |
| Fatty | 95% Ethanol, rectified olive oil, sunflower oil, corn oil or a synthetic triglyceride mixture | 5, 20, 40, 60, 70, 100, 121, 130, 150, or 175 | Same as above |
| Dairy products | 50% Ethanol. Fermented milks and sour cream: 3% acetic acid | 5, 20, 40, 70, or 100 or at reflux | Same as above |
| **China** | | | |
| Aqueous, non acidic foods | 10% Ethanol or water | 5, 20, 40, 50, 60, 70, or 100 or at reflux | 0.5, 1, 2, 6, 24 h, 3 or 10 days |
| Acidic (pH < 5) | 4% Acetic acid | Same as above | Same as above |
| Low- and high-alcoholic | 20 and 50% Ethanol | Same as above | Same as above |
| Fatty | Vegetable oil | 5, 20, 40, 50, 60, 70, 100, 121, 130, 150, or 175 | Same as above |
| Dairy products | 50% Ethanol. Fermented milks and sour cream: 3% acetic acid | 5, 20, 40, 50, 60, 70, or 100 or at reflux | Same as above |
| **Japan** | | | |
| Normal (pH > 5) | Water | 60 or 95 (at reflux) | 30 min |
| Acidic (pH ≤ 5) | 4% Acetic acid | 60 or 95 (at reflux) | 30 min |
| Alcoholic | 20% Ethanol | 60 | 30 min |
| Fatty | Heptane | 25 | 60 min |

For specific applications, see European Commission [15, 17], USA [13, 34], MERCOSUR [28], China [23], and Japan [25–27].

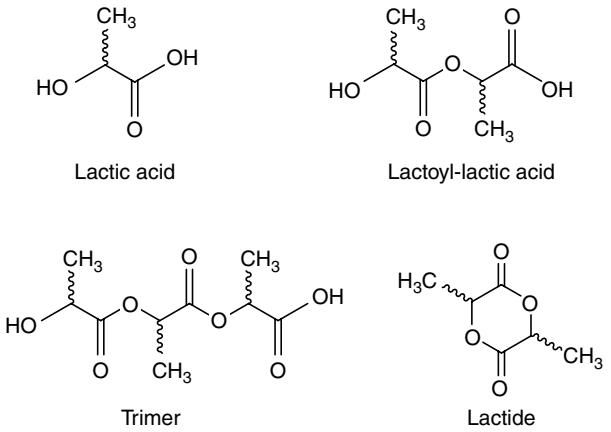


**FIGURE 12.1** Chemical structures of lactic acid, linear dimer of lactic acid (lactoyl-lactic acid), PLA trimer, and the cyclic dimer of lactic acid.

and trimers. The objective of this study was to determine whether PLA could be considered as GRAS when used in articles to hold or to package food (disposable cutlery, cups, plates, straws, stirrers, lids and cups, including containers for foods dispensed at delicatessens and fast-food shops). PLA films (0.51–0.64 mm thickness) were manufactured for that study with residual LA monomer from 0.3 to 2.5%. Samples of the polymer were exposed to food-simulating solvents (aqueous, acidic, and fatty) under conditions that reproduced the most severe temperature/time circumstances to which food would be exposed while in contact with PLA. Four categories of scenarios were tested. Category 1 represented most uses of PLA, including applications with food service-ware and other single-use disposable articles. These short-term experiments were performed for 0.5–24 h at 26°C. Category 2 simulated circumstances where PLA articles are used repeatedly as house-ware articles and in applications where foods are dispensed at delicatessens and fast-food establishments and then taken home and stored before consumption. These experiments were performed for one day at 26 and 43°C. Category 3 included special applications such as containers for hot foods. This experiment was performed for one day at 60°C. Category 4 included those applications where PLA is used as a food-packaging material. These experiments were performed for 1–15 days at 23 and 43°C. The study was reported in 1995, when use of PLA for packaging applications was still very limited.

The second important study that contributed to the knowledge of lactic acid migration from PLA was reported in 2008 by Mutsuga et al. [30] from the National Institute of Health Sciences in Japan. They also studied the migration of LA and oligomers (*n* up to 13) from PLA, strictly according to the Japanese legislation. The objective of this study was to identify and quantify migrants from four commercial PLA films (0.5–0.7 mm thickness and containing 0.025, 0.108, 0.120, and 0.160% of residual LA monomer) to food simulants recommended by the Japanese legislation (Table 12.1). Liquid chromatography coupled to mass spectrometry was used for the identification and quantification of the migrants.

Both studies by Conn et al. [10] and Mutsuga et al. [30] included hydrolysis experiments in order to quantify all the migrants as lactic acid in food simulants. The stability of lactic acid and oligomers and the effect of temperature and time on migration were also determined. In both the studies, the migration solutions were saponified with sodium hydroxide before quantification by liquid chromatography.

In 2013, Dopico-García et al. [31] reported the decomposition products of PLA that remained in the material due to the contact effect with food simulants. These authors determined the trapped degradation products of PLA (lactic acid and oligomers) in the matrices of two materials: PLA 7000D (Ingeo®, Naturework LLD) and a polymer blend based on PLA consisting of a co-polyester and additives (Bio-FlexW® 6510, FKuR Kunststoff GmbH). The second material was 70% biobased and the specific formulation was not reported. Bars of 4 × 10 × 80 mm were produced by injection molding and immersed in pure water at 40°C for six months to simulate the service life. Bar samples were taken at 0.0, 1.0, 2.2, 4.5, and 6.5 months. Lactic acid and oligomers were microwave extracted with water. Lactic acid was directly determined by liquid chromatography, and the sample was subjected to alkali hydrolysis to indirectly determine oligomers as lactic acid. The difference between both determinations was considered as hydrolyzed oligomers. At the beginning of the experiment (storage time: zero months), the level of both decomposition products was 185 and 215 µg/g in the bars made of PLA and the polymer blend, respectively. At one month of contact, the level decreased to 148 and 137 µg/g, respectively. The reduction was because at time zero the materials did not experience any contact with water, with no release of the original decomposition products that were in the materials. From 1 to 6.5 months of contact, the decomposition products (sum of lactic acid and hydrolyzed oligomers) increased up to 303 µg/g in the PLA material, from which >60% corresponded to oligomers. Regarding the polymer blend, at 6.5 months the sum reached 1077 µg/g with proportions of oligomers ≤40%. This behavior showed that the polymer blend may have contained a higher proportion of shorter chain oligomers than the PLA material. Although the release of the lactic acid and oligomers in water was not measured, these PLA decomposition products are potential migrants that could diffuse to aqueous food products at long periods of time at room temperature. A test carried out with a previous heating at 70°C did not show important differences when compared with the samples not heated, leading to the conclusion that the PLA chains suffered scissions during the aging test at 40°C. These results were complemented with determinations of $M_w$ and $M_n$, showing a considerable decrease. At the end, the authors

concluded that PLA may need addition of stabilizers to maintain the properties of the food package used in contact with aqueous food products.

Di Maio et al. [32], in 2014, reported the migration of lactic acid from monolayer PLA films added with 0, 3, and 6% of a nanofiller based on the organo-modified montmorillonite, Cloisite®30B. They used PLA 4032D (1.5% of D-isomer). The films were produced by the cast extrusion process, and the migration tests were performed by immersion in the food simulants 3% acetic acid and 50% ethanol for 10 days at 40°C [17]. The dimers, trimers, and oligomers that migrated to the simulants were hydrolyzed to lactic acid before quantification by liquid chromatography. The levels of lactic acid migration in the acidic simulant were undetectable or close to the limit of quantification, being the highest of 0.25 mg/dm$^2$ in the films with 3% of the nanofiller. Although these levels were always measurable in 50% ethanol, with the highest value of 2.4 mg/dm$^2$ in the films with 6% of the nanofiller. All the results of lactic acid migration for the three films were well below the applicable generic migration limit of 10 mg/dm$^2$ or 60 mg/kg [17]. In another study, the same authors [33] produced three-layer blown films with addition of 4% of the same nanofiller (Cloisite30B) in the middle layer. The outer and middle layers were made of PLA 4032D (semi-crystalline with 1.4% of D-isomer) and the inner layer (to be in contact with food) of PLA 4060D (amorphous with 12% of D-isomer). The authors [33] tested the migration of lactic acid in 50% ethanol at 40°C (1–10 days) using a glass migration cell for single-side contact [17]. The levels of lactic acid migration (by liquid chromatography) were from around 2 to nearly 2.5 mg/dm$^2$ for the film without nanofiller and to nearly 5 mg/dm$^2$ for the films with the nanofiller. In all cases, the migration did not reach the applicable limit 10 mg/dm$^2$ equivalent to 60 mg/kg. The authors reported that during the contact, ethanol penetrated the PLA, swelling the inner layer of the films and promoting the migration phenomena. This behavior was explained by an amorphous-to-crystalline transition phenomena that was observed with a change from transparent to white color, and presence of cavities after the samples were removed from the migration cells. Iñiguez-Franco et al. [9], in 2016, reported that the swelling in PLA films when in contact with 50% ethanol produced higher levels of hydrolysis than with 95% ethanol and pure water. This hydrolysis was related to the amount of water molecules available for chain scission that contributed to a decrease in molecular weight, thereby increasing the migration of lactic acid. Therefore, the presence of similar proportions of water and ethanol are needed to produce the swelling and hydrolysis of the PLA chains. These authors performed alkali hydrolysis to the material released during 120 days of contact at 40°C to quantify the total lactic acid as 700 mg/L in 50% ethanol, while the release was <50 and <20 mg/L in water and 95% ethanol, respectively. Scarfato et al. [33] reported that the addition of the nanofiller increased the level of migration of lactic acid due to a decrease of PLA molecular weight (13%) during the film production process. It is important to highlight that in 2020 the EU commission approved the substance montmorillonite clay modified with hexadecyltrimethylammonium bromide in the list of authorized substances, as an additive up to 4% w/w, in PLA intended for storage exclusively of water, at ambient temperature or below [18]. According to Di Maio et al. [32] and Scarfato et al. [33], the addition of the nanofiller improved the mechanical and barrier properties of the films in spite of the hydrolysis of the polymer during the manufacturing process. With respect to the effect on the migration of lactic acid, there was an increase during the time in 50% ethanol, but the levels remained within the allowable limits. No increase of migration was detected in the acidic simulant.

***12.4.1.1 Migration to Aqueous Simulants*** Conn et al. [10] found that for short-time and single-use applications, the migration of lactic acid from PLA (1.8% residual LA monomer) to the aqueous simulant reached 2.5 and 10.7 µg/in.$^2$ (0.039 and 0.166 mg/dm$^2$) at 26 and 43°C, respectively, when the contact time was 0.5 h. Migration at 26°C increased to 6.1 and 11.2 µg/in.$^2$ (0.095 and 0.174 mg/dm$^2$) at 24 h and 10 days, respectively. By this time, the experiment had reached equilibrium. However, at 43°C lactic acid increased to 29.2 µg/in.$^2$ (0.453 mg/dm$^2$) at 24 h and showed a linear increasing trend. The authors did not report long-term migration at 43°C, but they reported an experiment using PLA sheet with a residual LA monomer of 0.8% showing levels of migration up to 55.1 µg/in.$^2$ (0.854 mg/dm$^2$) at 10 days. However, the above values derived from aqueous simulants may not reflect the quantity of lactic acid diffused to a food product or drink under similar circumstances. To estimate the actual diffusion in foods, the following FDA guideline is often used by the industry [34]: ". . . if 1 µg of a substance is extracted from one square inch of packaging material into 10 g of food or food simulant, the estimated concentration in food is 0.1 mg/kg . . ." As the volume of the simulants used in the report was 10 mL, a maximum level of migration of lactic acid of 5.51 mg/kg in an aqueous food is expected in 10 days. Further, the FDA recommends the use of accelerated testing for 10 days at 40°C to simulate room temperature storage. However, for polymers that are used with food at temperatures below their $T_g$, such as PLA, FDA considers that accelerated testing for 10 days at 40°C might underestimate the migration that would occur during the entire food-contact scenario. Therefore, FDA [34] recommends that ". . . migration data obtained over 10 days at 40°C should be extrapolated to 30 days in order to better approximate migration levels expected after extended periods of time at ambient conditions." Even though Conn et al. [10] performed the

experiment at 43°C instead of 40°C, we can estimate a maximum level of migration of lactic acid of 16.53 mg/kg of an aqueous food at room temperature. The same authors reported that the natural content of lactic acid in buttermilk and yogurt is 10 g/kg; therefore, the migration value estimated is about a thousandth of that, which is too low to be considered a risk.

Mutsuga et al. [30] reported long-term migration of lactic acid into water at 40°C for one, three, and six months. At the end of the experiment, lactic acid reached levels of 0.84 and 2.65 µg/in.$^2$ (0.013 and 0.041 mg/dm$^2$) for PLA containing 0.025 and 0.108% of residual LA monomer, respectively. However, it reached levels of 25.03 and 15.55 µg/in.$^2$ (0.388 and 0.241 mg/dm$^2$) for PLA containing 0.120 and 0.160% of residual LA monomer, respectively. These values are lower than 55.1 µg/in.$^2$ (0.854 mg/dm$^2$) reported by Conn et al. [10] at 10 days at 43°C. This was due to the lower residual LA monomer and the composition of the simulant since Conn et al. [10] used 8% ethanol instead of water. It is also important to recall that Mutsuga et al. [30] used commercial PLA with 0.025–0.160% of residual lactide monomer and Conn et al. [10] used PLA with 0.3–1.8% of residual lactide monomer. Mutsuga et al. [30] also found a small decrease in the PLA molecular weight in their experiments. Besides lactic acid and LA, oligomers (up to $n = 13$) were identified by liquid chromatography coupled to mass spectrometry. From these results, they speculated that the decomposition of the polymer occurred by the removal of some LA units from the end of the chains. LA and oligomers generated from PLA decomposed to lactic acid during the test periods.

In another experiment, Conn et al. [10] estimated the migration when aqueous hot food is dispensed into PLA containers and consumed while cooling. They immersed PLA sheets (residual LA monomer of 0.8%) in 8% ethanol at 60°C, immediately allowed it to cool to room temperature, and analyzed the samples after 24 h giving a migration level of lactic acid of 24.3 µg/in.$^2$ (2.43 mg/kg of aqueous food). This value is 2.5 times higher than that reported after 24 h at 26°C (0.96 mg/kg) and slightly lower than that reported after 24 h at 43°C (2.77 mg/kg). Therefore, the use of aqueous hot food in PLA containers may more than double the migration of lactic acid compared to the case when the container is used for food at room temperature. It is important to point out that the $T_g$ of PLA can range from 27–57 [35] to 66.1–71.4°C [36], depending on the molecular weight and crystallinity. Consequently, the polymer could have been in a rubbery state at the beginning of the contact. However, it was not enough to increase the migration of lactic acid to more than that obtained for 10 days at 43°C.

Mutsuga et al. [30] reported lactic acid migration from four types of PLA sheets to water at 60°C for 30 min. The levels of migration ranged from 0.77 to 1.48 µg/in.$^2$ (0.012 to 0.023 mg/dm$^2$), which were much lower than the levels reported by Conn et al. [10], because the residual monomer in the PLA samples used in Mutsuga's studies was about one tenth of that used by Conn et al. [10]. Also, the aqueous simulant in Mutsuga's experiment was water, whereas Conn et al. [10] used 8% ethanol. Moreover, Conn immersed the PLA sheets in the simulant at 60°C and allowed them to cool at room temperature for 24 h. Mutsuga et al. [30] also extended the migration experiment to 1, 5, and 10 days at 60°C to simulate the case where PLA lunch boxes are kept warm in a hot vendor. At the end of the experiment, lactic acid reached levels of 3.87 and 17.10 µg/in.$^2$ (0.060 and 0.265 mg/dm$^2$) for PLA containing 0.025 and 0.108% of residual LA monomer, respectively. The PLA samples containing 0.120% of residual LA monomer reached levels of 56.65 µg/in.$^2$ (0.878 mg/dm$^2$). Interestingly, in spite of the differences in the experimental conditions (residual LA monomer concentration, test temperature, and the composition of the simulant), this value is very similar to the 55.1 µg/in.$^2$ (0.854 mg/dm$^2$) reported by Conn et al. [10] after 10 days at 43°C. Regarding the PLA samples containing 0.160% of residual LA monomer, the level of lactic acid at 10 days reached the unexpected quantity of 2709.6 µg/in.$^2$ (42.01 mg/dm$^2$). The decrease in molecular weight of PLA at 60°C was more noticeable than at 40°C. Moreover, the sample containing 0.160% of residual LA monomer had broken down completely, and the dried test sample had lost its elasticity and collapsed easily into powder. Additional information that could be related to that susceptibility to decompose was that this sample in particular had a high percentage of D-lactic acid (11.3%). An additional experiment was carried out by Mutsuga et al. [30] to simulate the use of lunch boxes in a microwave oven at over 100°C. They performed the experiment with water at 95°C. After 120 min of contact, lactic acid reached levels of 2.84, 10.84, 15.35, and 63.74 µg/in.$^2$ (0.044, 0.168, 0.238, and 0.988 mg/dm$^2$) for PLA containing 0.025, 0.108, 0.120, and 0.160% of residual LA monomer, respectively. These values are lower than those reported for 10 days at 60°C, especially the sample with 0.120% of residual LA monomer. They did not report the effect of the experimental conditions on the molecular weight. But, the short contact time did not allow the level of hydrolysis products recorded at 60°C for PLA sheets with 0.120 and 0.160% of residual LA monomer.

Mutsuga et al. [30] also determined the effect of different temperatures (20–95°C) on the migration of lactic acid from a PLA sheet containing 0.12% of residual LA monomer. The contact time with water was 30 min. The migration levels of lactic acid did not show considerable changes from 20 to 80°C (1.55 to 1.29 µg/in.$^2$, respectively, equivalent to 0.024 and 0.020 mg/dm$^2$) but increased when temperature increased to 95°C (2.32 µg/in$^2$ or 0.036 mg/dm$^2$). According to the authors, this increase could be related to the migration of LA and decomposition to lactic acid under this condition.

***12.4.1.2 Migration to Acidic Simulants*** Conn et al. [10] found that migration of lactic acid from PLA sheets with 0.3 and 0.8% of residual LA monomer in an acidic simulant (3% acetic acid) was <16.6 µg/in.$^2$ (0.257 mg/dm$^2$, limit of detection) and 18.6 µg/in.$^2$ (0.288 mg/dm$^2$) at 43°C, respectively. The contact time was 24 h. The experiment with PLA sheets with 0.3% of residual LA monomer was extended to 15 days with no detection of migrants. According to the FDA interpretation [34], the maximum level of migration of lactic acid is 1.86 mg/kg in acidic food in 24 h at room temperature, which is slightly lower than the 2.92 mg/kg found for the aqueous simulant at the same temperature and time, but with higher residual LA monomer (1.8%).

In another experiment, Conn et al. [10] observed haze formation at 102 and 69 h in PLA sheets with 0.8 and 1.8% of residual LA monomer in contact with 3% acetic acid at 43°C. Similar behavior was observed in the same samples in contact with 8% ethanol. No hazing was reported in PLA sheets with 0.3% of residual LA monomer during 15 days of contact with the acidic simulant. The authors concluded that hazing was a function of the residual monomer content, but not a function of the solvent. Crystallization could have contributed to the hazing effect. Similar behavior was reported by Manzanarez-López et al. [37] for PLA films in contact with ethanolic solutions and was related to an increase of crystallinity due to hydrolysis of the amorphous regions. In this work, the level of hazing increased with temperature (23–43°C). This behavior has not been reported for PLA in contact with 3% acetic acid. Tsuji and Nakahara [38] studied films of PLLA in contact with different acidic solutions finding that crystallization of PLLA chains occurs during the hydrolysis of the polymer.

The studies conducted by Mutsuga et al. [30] included an experiment of short-term (60°C, 30 min) migration of lactic acid from the four PLA sheets mentioned above in 4% acetic acid as an acid food simulant. Lactic acid reached levels of 0.52, 2.19, 2.26, and 2.58 µg/in.$^2$ (0.008, 0.034, 0.035, and 0.040 mg/dm$^2$) for PLA containing 0.025, 0.108, 0.120, and 0.160% of residual LA monomer, respectively. In general, these values are slightly higher than those found in water at the same conditions showing that during the short-time contact, there was no effect of the acidity on lactic acid migration from PLA. The authors also reported that lactic acid is stable under these experimental conditions.

Di Maio et al. [32] reported migration to 3% acetic acid as described in Section 12.4.1. The levels of migration (10 days at 40°C) from PLA films (with 1.5% of D-isomer) added with 0, 3 and 6% of the nanofiller Cloisite30B were from non-detectable to 0.25 mg/dm$^2$ (equivalent to 16.2 µg/in.$^2$). This value was close to that reported by Conn et al. [10] for migration from PLA sheets with 0.3% of residual LA monomer in the same acidic simulant. The value was also close to the limit of detection of the method [10].

***12.4.1.3 Migration to Fatty Food Simulants*** Conn et al. [10] measured migration of lactic acid using PLA sheet with low molecular weight ($M_w$ = 112,000 Da) and high residual LA monomer (2.5%). Fractionated C8–C10 coconut oil triglycerides (Miglyol) were used as a fatty food simulant and the experiment was performed at 43°C for 10 days. They reported migration levels of lactic acid from 23.1 µg/in.$^2$ (0.358 mg/dm$^2$ at one day of contact) to 27.9 µg/in.$^2$ (0.433 mg/dm$^2$ at 10 days of contact). These values are about one fifth the migration of lactic acid in 8% ethanol from the same PLA samples. According to the FDA interpretation [34] and being aware that 10 mL of oil weighs less than 10 g, a maximum level of migration of lactic acid of 2.79 mg/kg of a fatty food is expected in 10 days at room temperature. This value is about one sixth of the maximum level estimated for aqueous food. Therefore, if PLA is already used for water bottles, it could be used as packaging material for vegetable oil with less risk of lactic acid migration.

Mutsuga et al. [30] reported an experiment on short-term (25°C, 1 h) migration of lactic acid from the four PLA sheets mentioned above to heptane as fatty food simulant. No migrants were detected in any of the samples.

***12.4.1.4 Migration to Liquor Simulants*** Mutsuga et al. [30] also reported short-term experiments (60°C, 30 min) using 20% ethanol as a simulant for liquor. They found migration of lactic acid from the four PLA sheets mentioned above ranging from 0.84 to 1.54 µg/in.$^2$ (0.013 to 0.024 mg/dm$^2$). These values were very similar to those reported for water under the same conditions. Lactic acid was shown to be stable under these experimental conditions.

### 12.4.2 Lactide

Lactide (3,6-dimethyl-1,4-dioxane-2,5-dione)—LA is a cyclized dimer of lactic acid (anhydrous lactic acid) and is used in the manufacture of PLA resin (see Chapters 1–4) for the plastic industry. The compound exists as a translucent white powder or clear flakes, is odorless at room temperature but emits an acrid plastic odor when heated. LA decomposes when exposed to moisture to form the linearized lactic acid dimer followed by hydrolysis to lactic acid monomer [39].

The primary toxic effect of LA exposure is eye and skin irritation, which increases in severity in the presence of moisture. LA has an estimated oral LD50 value of greater than 5 g/kg in rats and an estimated dermal LD50 value greater than 2 g/kg for rabbits [40]. In dose-response evaluations, NOAEL (no observed adverse effect level) is the highest tested dose of a substance at which no adverse effect is found. LOAEL (lowest observed adverse effect level) is the lowest tested dose of a substance at which an adverse effect is observed. These are basic levels in risk assessment studies [41]. In a study [39] conducted to determine the

toxicity of LA when the compound was administrated orally in gelatin capsules to beagle dogs, the researchers reported clinical signs of irritation of the alimentary tract after two weeks of daily oral doses of 1000 and 2500 mg/kg body weight per day. At the same doses, dogs showed reduction in body weight gain, and erosion and ulceration of the stomach and esophagus. All dogs survived at the end of the study. No clinical signs of toxicity were reported for daily oral doses of 100 mg/kg body weight per day and lower after 13 weeks. Therefore, the NOAEL after subchronic oral dosing in dogs was considered to be 100 mg/kg [39]. Based on these data, the Food Safety Commission of Japan settled on an acceptable daily intake (ADI) of LA of 0.1 mg/kg per day [30].

Mutsuga et al. [30] quantified migration of LA among other oligomers from the four commercial PLA sheets mentioned above, using liquid chromatography coupled to mass spectrometry. In a short-term (60°C, 30 min) migration experiment, LA reached 6.26 μg/in.$^2$ (0.097 mg/dm$^2$) in water, 7.87 μg/in.$^2$ (0.122 mg/dm$^2$) in 4% acetic acid, and 15.55 μg/in.$^2$ (0.241 mg/dm$^2$) in 20% ethanol from PLA containing 0.160% of residual LA monomer. The values for the films containing 0.025, 0.108, and 0.120% of residual LA monomer were from nondetectable to 5.42 μg/in.$^2$ (0.084 mg/dm$^2$).

In a long-term migration experiment [30] in water (60°C, 10 days), LA levels reached 2567.7 μg/in.$^2$ (39.81 mg/dm$^2$) with the sample containing 0.160% of residual LA monomer and a ratio of D-lactic acid of 11.3%. Meanwhile, levels less than 7.74 μg/in.$^2$ (0.120 mg/dm$^2$) were recorded for the PLA samples containing 0.025, 0.108, and 0.120% of residual LA monomer. In another experiment on migration in water at 95°C (120 min) and 40°C (six months), the same material showed 193.2 and 15.54 μg/in.$^2$ (2.99 and 0.241 mg/dm$^2$) of LA migration, respectively. Lower migration was seen when compared to the experiment at 60°C (10 days). Therefore, temperatures higher than the $T_g$ increase migration of LA to water, and this is critical at long contact times.

Regarding the stability of the cyclic dimer, Conn et al. [10] reported a half-life of 3 h for LA in an aqueous medium (8% ethanol) at room temperature. Meanwhile, Mutsuga et al. [30] reported that solutions of LA of 1 μg/mL in 20% ethanol, 4% acetic acid, and water were stable at 60°C for 30 min (103.3, 98.7, and 99.4%, respectively). However, only 73.0 and 21.0% of LA were recovered from the solution in water after 1 and 10 days at 60°C, respectively.

Ubeda et al. [42] reported the identification of cyclic and linear oligomers in PLA by dissolution of the material in dichloromethane and precipitation with ethanol. The components in the soluble residue were separated, identified, and quantified by ultraperformance liquid chromatography-mass spectrometry quadrupole time-of-flight (UPLC-QTOF-MS). Several oligomers were identified as described in the Section 12.4.3, but LA monomer was not detected due to its difficult ionization in the mass spectrometer, compared to the oligomers.

### 12.4.3 Oligomers

Mutsuga et al. [30] reported that in a short-time migration experiment (60°C, 30 min), only PLA containing 0.160% residual LA monomer released 7.48 μg/in.$^2$ (0.116 mg/dm$^2$) of oligomers up to $n$ = 13, particularly to 20% ethanol simulant. Regarding the migration experiments to water, levels of 61.93 (40°C, six months), 8761.30 (60°C, 10 days), and 12.00 μg/in.$^2$ of oligomers (95°C, 120 min) were reported for the same PLA sheet (these levels are equivalent to 0.960, 135.834, and 0.186 mg/dm$^2$, respectively). This behavior was similar to the migration of LA. The PLA sheets containing 0.025, 0.108, and 0.120% of residual LA monomer gave levels of oligomers from nondetectable to 66.71 μg/in.$^2$ (1.034 mg/dm$^2$).

In 2012, Bor et al. [43] reported the migration of cyclic oligomers from three films produced by casting from commercial PLA (Hycail HM1011, NatureWorks 5200 D and a stereocomplex Hycail PLLA/PDLA). The films were tested by immersion in water, 3% acetic acid, 10% ethanol, 96% ethanol and isooctane, at 25°C for 7 and 50 days. The authors considered that the matter lost from the films corresponded to cyclic oligomers of PLA and they were identified by electrospray ionization—mass spectrometry. The most dominant oligomers identified were $n$ = 6–17, higher than the $n$ = 13 reported by Mutsuga et al. [30]. At seven days of contact, the mass lost was in the range of 3–5% in water, 3% acetic acid, 10% ethanol and isooctane (overall migration of 5–11 mg/dm$^2$) and at 50 days increased to 8–12% (overall migration of 7–19 mg/dm$^2$). Meanwhile, the mass losses in 96% ethanol were 9–14% at seven days of contact with no increase after 50 days (overall migration of 19–24 mg/dm$^2$). Some of the films exceeded the limit of overall migration established as 10 mg/dm$^2$ [17]. The authors concluded that the cyclic oligomers were present in the original unaged materials. Then, the higher levels of migration in 96% ethanol were influenced by their higher solubility in ethanol compared to that in water-based simulants and isooctane. The increased mass losses at 50 days of storage were due to hydrolysis of PLA and cyclic oligomers. They also mentioned that the use of ethanol as a fatty food simulant for PLA materials could overestimate the overall migration values. Regarding the mass lost from the stereocomplex PLLA/PDLA film, it was always lower than that lost from the other regular PLA films tested (Hycail HM1011 and NatureWorks 5200 D), which were mainly composed by PLLA. In 2014, the same authors [44] reported the effect of stereocomplexation on the migration of oligomers from the PLLA/PDLA film compared to the regular PLLA films mentioned above. The films were tested for migration in water

and 10% ethanol under microwave heating at 40, 60, 80, and 95°C for 10, 30, 60, and 120 min. The samples were also conventionally heated for 60 min at 60°C. The increasing time and temperature showed an increase in migration of linear oligomers. After 120 min at 95°C, oligomers ($n$ = 5–15) migrated from both regular PLLA (mass loss = 16%) and stereocomplex PLLA/PDLA (mass loss = 8%). The 50% of reduction in mass lost from the stereocomplex films was consistent in water and 10% ethanol at most of the tested conditions. With respect to the effect of microwave and conventional heating, the microwave heating caused higher mass loss as compared with the conventional heating. The authors concluded that stereocomplexation increased the migration resistance of PLA during microwave and conventional heating. Thus, this material could have potential in single-use microwave applications.

In 2013, Dopico-García [31] quantified the oligomers trapped in the polymer matrix of PLA bars (PLA and a polymer blend described in Section 12.4.1) during immersion in pure water at 40°C for six months to simulate their service life. As explained in that section, oligomers were hydrolyzed to be quantified as lactic acid by liquid chromatography. In this case, the release of oligomers in water was not measured; instead, they analyzed the decomposition products that were accumulating in the plastic bars. During the time of contact with water, there was a reduction in $M_n$ and $M_w$ of almost 60% in PLA and 20% in the polymer blend, compared with the unaged materials. This behavior showed that a high proportion of the molecular chains had suffered scissions and agreed with the increase of the concentration of oligomers determined at the end of the experiment. Also, an increase of the linear oligomers compared to the cyclic ones was observed as a consequence of the hydrolytic degradation due to the aging in water.

The identification, quantification, and migration of PLA oligomers in a material made of a blend of PLA and a biodegradable fossil-based polyester (not identified) was reported by Ubeda et al. [42]. The authors developed a methodology based on a total dissolution/precipitation procedure with dichloromethane and ethanol as solvent and antisolvent systems, respectively. Instead of hydrolyzing PLA oligomers to lactic acid for indirect quantification, the molecules were separated, identified, and quantified by an UPLC-QTOF-MS system. The analyses were performed in the PLA blend pellets and films, and also in the migration food simulants (95% ethanol, 10% ethanol and 3% acetic acid) after testing at 60°C for 10 days. It is important to notice that such temperature is near the $T_g$ of the PLA, and this condition is recommended in the EU legislation for simulation of food storage above six months at room temperature and below, including heating up to 70°C for up to 2 h, or heating up to 100°C for up to 15 min [17]. Thirty-nine PLA oligomers made of repeated monomer units of [lactic acid] ($C_3H_4O_2$) and with different structures were identified. Among them, 24 were identified in total dissolution of pellets and film samples, 12 were cyclic, and 12 linear. The value of $n$ ranged from 5 to 16, similar to that reported in [30, 43]. Ten out of the twenty-four were found in the migration simulants, as well as fifteen new molecules formed in the reaction between PLA oligomers and food simulants (OH─[lactic acid]$_n$─H and $CH_3$─$CH_2$─O─ [lactic acid]$_n$─H). The value of $n$ ranged from 3 to 15 for the oligomers with hydroxyl group and from 2 to 15 for those with ethoxy groups. The cyclic monomer LA was not found in the plastic or migration simulants because this molecule is difficult to ionize in the mass spectrometer; however, it is not discarded as a potential migrant in the PLA blend. Regarding the effect of the high temperatures applied to process the films, there were no changes in the identity and concentration of the oligomers in the pellets and films. In these materials, only cyclic oligomers ($n$ = 5–11) and linear oligomers with a hydroxyl group ($n$ = 5–8) were detected with no detection of those with ethoxy groups. With respect to concentration, the cyclic oligomers were 5–20 times higher than the linear ones in the plastic. As for the oligomers migrated to the food simulants, only linear molecules were found, with no presence of cyclic oligomers detected in the pellets and films. Ubeda et al. [42] performed additional experiments to test that cyclic oligomers did not migrate to the food simulants and the linear ones came from the PLA polymer that, during the contact, released these oligomers due to hydrolysis processes. The levels of migration in the three simulants were very low (≤0.6 mg/kg of simulant).

Aznar et al. [45] also worked with pellets and films made of the blend of PLA used in [42]. Among the potential migrants, three PLA cyclic oligomers ($n$ = 6, 7, and 9) were identified and other two ($n$ = 5 and 8) at very low concentrations. None of them were found to migrate to 95% ethanol, 10% ethanol, and 3% acetic acid when tested at 60°C for 10 days. The authors explained that the oligomers could have migrated and reacted with the simulants inducing a cycle opening and formation of new compounds. In fact, they found the same structures reported in [42], six linear PLA oligomers (OH─[lactic acid]$_n$─H, $n$ = 3–8), which were at higher levels in the 3% acetic acid compared with those in 10% and 95% ethanol. Also, in the ethanolic simulants, they detected seven different linear PLA oligomers ($CH_3$─$CH_2$─O─[lactic acid]$_n$─H), at higher level in 95% ethanol compared with that of 10% ethanol.

## 12.5 EDI OF LACTIC ACID

Conn et al. [10] presented a detailed discussion of the average daily intake of lactic acid from food sources that was estimated as 924 mg/day for those two years of age and older. In addition, 377 mg/day for calcium lactate was estimated for the same group. Regarding infants' consumption of lactic acid, breast milk contains 60 mg/L of L-lactic acid with an estimated daily intake as high as 10 mg/kg. From a different perspective, a breast-fed infant weighing 4 kg

would consume about 36 mg of L-lactic acid/day from both human and formula milk.

To estimate the consumer exposure to substances migrated from food packaging, the FDA has published a list of consumption factors (CF) [34] needed, among other data, to compute the dietary concentration of a specific migrant. A CF describes the fraction of the daily diet expected to contact specific packaging materials. It represents the ratio of the weight of all food contacting a specific packaging material to the weight of all food packaged. To calculate the dietary concentration of lactic acid (L- and D-lactic acid) originated from PLA, Conn et al. [10] followed the recommendations published in the FDA guidelines for industry [34]. They [10] considered a CF of 5% for PLA, which corresponds to the minimum CF permitted by the FDA. This value, however, may be modified as the use of PLA in food packaging increases. They also considered the data from the migration studies of PLA performed in different food simulants and reported in the same paper [10]. From these, a dietary concentration of 0.018 mg/kg of lactic acid was computed. This value translates to an EDI of no more than 0.054 mg/day/person of L- and D-lactic acid from food in contact with PLA. This value is very small when compared with the average daily intake of lactic acid from general food sources, 924 mg/day/person (two years of age and older).

Regarding consumer exposure to D-lactic acid, in 1995 Conn et al. [10] took the dietary concentration of 0.018 mg/kg of lactic acid as an indirect food additive from all-purpose uses of PLA and considering that PLA would never have more than 50% of D-lactic acid (usually 0–10% at that time), a maximum dietary concentration of 0.009 mg/kg value was estimated for this isomer for which intake is controlled for infants. From these estimations, Conn et al. [10] confirmed that PLA was safe and GRAS for use in fabricating articles intended to be in contact with food. A commercial racemic PLA (50 : 50 L-lactic acid : D-lactic acid) is used for high-temperature applications [46], which was already considered by Conn et al.'s [10] estimations in 1995, as the worst-case scenario. At present, in order to update the dietary exposure to lactic acid, a new CF that considers the actual level of use of PLA as material in contact with food is needed.

## 12.6 OTHER POTENTIAL MIGRANTS FROM PLA

The plastics industry has been introducing new formulations of PLA with additives intended to improve the properties of the final article. Plasticizers, stabilizers, and other substances are now integrated in the articles that will be in contact with food.

One of the drawbacks of PLA is its brittleness that can be reduced by combining with starch [47], mineral and polymeric additives [47], degradable polyesters [47], poly(ethylene glycol) [48], poly(propylene glycol) [49], aliphatic–aromatic copolyesters [47], and so on. Most of these compounds have relatively high $M_w$ that avoids their diffusion through the PLA polymer matrix. However, other additives, such as glycerol [47], sorbitol [50], tributyl citrate [51], glycerol triacetate [51], acetyl tributyl citrate (ATBC) [52], and so on, may also be used as plasticizers in PLA. These compounds have low $M_w$ with a potential to diffuse through the polymeric matrix when used in packaging or articles in contact with food. In spite of that, a limited number of works related to the migration of plasticizers from PLA have been published, among them those added with ATBC. Höglund et al. [52] reported the migration of the hydrophobic plasticizer ATBC from PLA to water at 37 and 60°C for one year. Although the additive was insoluble in water, it was released immediately after the first contact. Once in water, ATBC was degraded, and its products increased with the time of contact. Aliotta et al. [53] studied the migration of ATBC from films made of a PLA/poly(butylene succinate) blend added with ATBC (20%) and other additives like micro and nanometric calcium carbonate. The films were stored at 60°C and between two paper sheets for absorption of the ATBC released from the films. The weight loss of the films was periodically measured for two months. They found that micrometric calcium carbonate at 7% was more effective in hindering the ATBC migration, compared with the nanometric salt.

Other additives used in PLA formulations are slip additives (natural waxes) [47], impact modifiers (sodium alkyl sulfonate) [47], melt strength modifiers (epoxy-functional styrene/acrylic oligomer) [54], inorganic fillers [55] and so on. He et al. [55] reported the migration of metal elements from a dinner plate made of PLA added with talc (nucleating agent) and calcium carbonate. The food simulant was in 3% acetic acid and the migration conditions as follows: at 40°C (10 days), 60°C (6 days), and 70°C (6 days). The results showed that the migration increased with time and at short times the release of metals was from the surface of the plate. Meanwhile, at longer times the release of metals was from the surface and the interior of the plate. The authors found that the migration of aluminum, barium, iron, and zinc was within the allowable specific migration limit. The EDI values of calcium and magnesium were also within the tolerable upper intake levels.

Although the companies that produce these resins, additives, or masterbatches claim to have been approved for materials in contact with food, there are no reports of migration to food or food simulants to show that they comply with the legislation when used in PLA. New additives for PLA and their impurities should be tested for migration into food or food simulants in order to confirm their safety before they are used for food packaging.

## 12.7 CONCLUSIONS

Lactic acid is considered the main migrant from PLA, since dimers, trimers, and oligomers hydrolyze to lactic acid either in the aqueous or the acidic media commonly found in food systems or in the human digestive tract. The EDI of lactic

acid as indirect additive in food in contact with PLA is <0.054 mg/day/person, which is very small when compared with the EDI of lactic acid from food sources (924 mg/day/person). Therefore, the use of PLA in contact with food is safe with no health risk for consumers when used at temperatures lower than the $T_g$ of the polymer.

LA and PLA oligomers are not currently included in any legislation. They could be considered as non-intentionally added substances (NIAS). Cyclic oligomers are produced during processing of PLA and have low potential to migrate to food or food simulants. Linear oligomers are produced during the contact of PLA with aqueous, acidic, and ethanolic food simulants and have high potential to migrate.

The use of aqueous hot food in PLA containers may more than double the migration of lactic acid compared with the case when the container is used for food at room temperature. This is critical in PLA with higher percentage of residual LA monomer. With respect to migration of lactic acid to fatty food simulants, it is very low.

Regarding the application of PLA in contact with alcoholic solutions (liquors, antibacterial gel, etc.), films in contact with 50% ethanol presented swelling and higher levels of hydrolysis than with 95% ethanol and pure water. This phenomenon contributes to a decrease in the molecular weight and an increase in the migration of lactic acid to solutions with similar proportions of water and ethanol.

PLA is relatively stable at 40°C over six months in aqueous systems. But, at 60°C or above the $T_g$, the polymer decomposes and the level of lactic acid increases. This tendency is more critical in PLA containing high D-lactic acid levels. However, migration of oligomers from a PLLA/PDLA stereocomplex was half of that obtained from regular PLA during microwave and conventional heating.

The levels of migration of additives, like plasticizers, from PLA formulations is considerable and other additives are incorporated to decrease it. The new formulations of PLA with new additives should be tested for migration into food or food simulants in order to confirm their compliance with relevant legislation.

## REFERENCES


1. J. Crank, *The Mathematics of Diffusion*, 2nd edition, Oxford Science Publications, Oxford, 1975, p. 414.
2. W. Limm, H. C. Hollifield, Effects of temperature and mixing on polymer adjuvant migration to corn oil and water, *Food Addit. Contam.* **1995**, *12*(4), 609–624.
3. P. C. Chatwin, Mathematical modeling, in: L. L. Katan (Ed.) *Migration from Food Contact Materials*, Blackie Academic & Professional, London, 1996, pp. 26–50.
4. M. Hamdani, A. Feigenbaum, J. M. Vergnaud, Prediction of worst case migration from packaging to food using mathematical models, *Food Addit. Contam.* **1997**, *14*(5), 499–506.
5. J. A. Garde, R. Catalá, R. Gavara, Cinética de la migración, in: R. Catalá, R. Gavara (Eds.) *Migración de antioxidantes en polipropileno. Migración de Componentes y Residuos de Envases en Contacto con Alimentos*,Instituto de Agroquímica y Tecnología de Alimentos, Valencia, 2002, pp. 219–232.
6. U. Sonchaeng, F. Iñiguez-Franco, R. Auras, S. Selke, M. Rubino, L. T. Lim, Poly(lactic acid) mass transfer properties, *Prog. Polym. Sci.* **2018**, *86*, 85–121 [cited 14 July 2020]. Available from: https://doi.org/10.1016/j.progpolymsci.2018.06.008
7. I. Siró, É. Fenyvezi, L. Szente, B. De Meulenaer, F. Devlieghere, J. Orgoványi, et al., Release of alpha-tocopherol from antioxidative low-density polyethylene film into fatty food simulant: influence of complexation in beta-cyclodextrin, *Food Addit. Contam.* **2006**, *23*(8), 845–853.
8. G. L. Robertson. Safety and legislative aspects of packaging, in: *Food Packaging: Principles and Practice*, Marcel Dekker, Inc., New York, 1993, pp. 622–662.
9. F. Iñiguez-Franco, R. Auras, G. Burgess, D. Holmes, X. Fang, M. Rubino, et al., Concurrent solvent induced crystallization and hydrolytic degradation of PLA by water-ethanol solutions, *Polymer*, **2016** *99*, 315–323 [cited 9 March 2021]. Available from: http://dx.doi.org/10.1016/j.polymer.2016.07.018
10. R. E. Conn, J. J. Kolstad, J. F. Borzelleca, D. S. Dixler, L. J. Filer Jr., B. N. LaDu Jr., et al., Safety assessment of polylactide (PLA) for use as a food-contact polymer, *Food Chem. Toxicol.* **1995**, *33*(4), 273–283.
11. R. Geyer, Production, use, and fate of synthetic polymers, in: T. M. Letcher (Ed.), *Plastic Waste and Recycling*, Academic Press London, 2020, pp. 13–32.
12. N. Thomis, S. S. Peter, A. Danek, C. Wang, Global food contact compliance, *Intertek*, 2017 [cited 28 February 2021]. Available from: https://www.intertek.com/knowledge-education/global-food-contact-compliance-wp/.
13. Code of Federal Regulations (US), 21CFR174-178, *Indirect Food Additives*, 2021 [cited 31 March 2021]. Available from: https://www.ecfr.gov/cgi-bin/text-idx?SID=e5cc124de298eb0eb9eced0d1956d7ed&mc=true&tpl=/ecfrbrowse/Title21/21cfrv3_02.tpl#0.
14. Code of Federal Regulations (US), 21CFR184.1061 Direct food substances affirmed as generally recognized as safe, *Lactic acid*, 2021 [cited 31 March 2021]. Available from: https://www.ecfr.gov/cgi-bin/text-idx?SID=f22de9f5e8b2e346aa143535a1a540d3&mc=true&node=se21.3.184_11061&rgn=div8.
15. European Commission (EC), Regulation (EC) No. 1935/2004 of the European Parliament and of the Council of 27 October 2004 on materials and articles intended to come into contact with food, *OJEU* **2004**, *L338*, 4–17 [cited 6 March 2021]. Available from: https://eur-lex.europa.eu/legal-content/EN/TXT/PDF/?uri=CELEX:32004R1935&from=EN.
16. European Commission (EC), Commission Regulation (EC) No 2023/2006 of 22 December 2006 on good manufacturing practice for materials and articles to come into contact with food. *OJEU* **2006**, *L384*, 75–78 [cited 6 March 2021]. Available from: https://eur-lex.europa.eu/legal-content/EN/TXT/PDF/?uri=CELEX:32006R2023&from=EN.

17. European Commission (EC), Commission Regulation (EU) No 10/2011 of 14 January 2011 on plastic materials and articles intended to come into contact with food, *OJEU* **2011**, *L12*, 1–89 [cited 6 March 2021]. Available from: https://eur-lex.europa.eu/legal-content/EN/TXT/PDF/?uri=CELEX:32011R0010&from=ES.
18. European Commission (EC), Commission Regulation (EU) 2020/1245 of 2 September 2020 amending and correcting Regulation (EU) no 10/2011 on plastic materials and articles intended to come into contact with food, *OJEU* **2020**, *L288*, 1–17 [cited 6 March 2021]. Available from: https://eur-lex.europa.eu/legal-content/EN/TXT/PDF/?uri=CELEX:32020R1245&from=EN.
19. GMC/RES 02/12, Reglamento técnico MERCOSUR sobre lista positiva de monómeros, otras sustancias de partida y polímeros autorizados para la elaboración de envases y equipamientos plásticos en contacto con alimentos, 2012 [cited 19 January 2021]. Available from: http://extwprlegs1.fao.org/docs/pdf/mrc112771.pdf.
20. GMC/RES 39/19, Reglamento técnico MERCOSUR sobre lista positiva de aditivos para la elaboración de materiales plásticos y revestimientos poliméricos destinados a entrar en contacto con alimentos (derogación de la resolución GMC N° 32/07), 2019 [cited 19 January 2021]. Available from: https://normas.mercosur.int/simfiles/normativas/73869_RES_039-2019_ES_RTM%20Lista%20Positiva%20Aditivos%20Pl%C3%A1sticos.pdf.
21. ChemSafetyPRO, GB 4806.1-2016 National Food Safety Standard: General Safety Requirements on Food Contact Materials and Articles, 2017 [cited 23 May 2021]. Available from: https://www.chemsafetypro.com/Topics/Food_Contact/GB_4806.1-2016_General_Safety_Requirements_on_Food_Contact_Materials_and_Articles.html#:~:text=07%20Views%3A%209219-,GB%204806.1%2D2016%20National%20Food%20Safety%20Standard%3A%20General%20Safety%20Requirements,materials%20and%20articles%20(FCMs).
22. ChineseStandard.net, GB 4806.1-2016 National Food Safety Standard—General Safety Requirements on Food Contact Materials and Articles, 2021 [cited 23 May 2021]. Available from: https://www.chinesestandard.net/PDF/English.aspx/GB4806.1-2016.
23. Boarding Card, GB 31604.1-2015 National Food Safety Standard—General Rules for Migration Test of Food Contact Materials and Articles, 2017 [cited 28 March 2021]. Available from: http://food.bjboardingcard.com/english/uploadfile/2017/0619/20170619035010173.pdf.
24. Y. Zhou, Y. Weng, Z. Huang, L. Wang, X. Diao, X. Song, Analysis of regulations and standards for food packaging materials in domestic and foreign countries. *China Plastics* **2020**, *34*(12), 70–76 [cited 2021 Mar 13]. Available from: https://doi.org/10.19491/j.issn.1001-9278.2020.12.012.
25. United States Department of Agriculture (USDA), Japan translates positive list of food packaging and container substances, 2020 [cited 8 March 2021]. Available from: https://www.fas.usda.gov/data/japan-japan-translates-positive-list-food-packaging-and-container-substances.
26. Food Packaging Forum, Japan releases revised positive list for FCMs, 2020 [cited 3 December 2020]. Available from: https://www.foodpackagingforum.org/news/japan-releases-revised-positive-list-for-fcms.
27. T. Nakanishi, Y. Kawamura, K. Joichi, Y. Watanabe, T. Sugimoto, Y. Abe, et al., Establishment of test methods for overall migration test into vegetable oil applied to food contact materials intended for contact with oils and fatty foods, *J. Food Hyg. Soc. Jpn.* **2018**, *59*(5), 193–199.
28. GMC/RES 32/10, Reglamento técnico MERCOSUR sobre migración en materiales, envases y equipamientos plásticos destinados a estar en contacto con alimentos (derogación de las resoluciones N° 30/92, 36/92, 10/95, 11/95, 15/97, 32/97, 33/97, 38/98 y 56/02), 2010 [cited 24 November 2020]. Available from: https://normas.mercosur.int/simfiles/normativas/25302_RES_032-2010_ES_Migracion.pdf.
29. J. T. Baker, *Material Safety Data Sheet (MSDS) for Lactic Acid*, Mallinckrodt Chemicals, Phillipsburg, NJ, 2008 [cited 21 February 2021]. Available from: https://us.vwr.com/assetsvc/asset/en_US/id/8266925/contents.
30. M. Mutsuga, Y. Kawamura, K. Tanamoto, Migration of lactic acid, lactide and oligomers from polylactide food-contact materials, *Food Addit. Contam. Part A* **2008**, *25*(10), 1283–1290.
31. S. Dopico-García, A. Ares-Pernas, J. Otero-Canabal, M. Castro-López, J. M. López-Vilariño, V. González-Rodríguez, M. J. Abad-López, Insight into industrial PLA aging process by complementary use of rheology, HPLC, and MALDI, *Polym. Adv. Technol.* **2013**, *24*(8), 723–731 [cited 14 July 2020]. Available from: https://doi.org/10.1002/pat.3136.
32. L. Di Maio, P. Scarfato, M. R. Milana, R. Feliciani, M. Denaro, G. Padula, et al., Bionanocomposite polylactic acid/organoclay films: functional properties and measurement of total and lactic acid specific migration, *Packag. Technol. Sci.* **2014**, *27*(7), 535–547 [cited 15 February 2021]. Available from: https://doi.org/10.1002/pts.2054.
33. P. Scarfato, L. Di Maio, M. R. Milana, S. Giamberardini, M. Denaro, L. Incarnato, Performance properties, lactic acid specific migration and swelling by simulant of biodegradable poly(lactic acid)/nanoclay multilayer films for food packaging, *Food Addit. Contam. Part A [Internet]* **2017**, *34*(10), 1730–1742 [cited 15 February 2021]. Available from: https://doi.org/10.1080/19440049.2017.1321786.
34. Food and Drug Administration (US), Guidelines for industry: preparation of premarket submissions for food-contact substances (chemistry recommendations), 2007 [cited 9 March 2021]. Available from: https://www.fda.gov/regulatory-information/search-fda-guidance-documents/guidance-industry-preparation-premarket-submissions-food-contact-substances-chemistry.
35. M. O. Omelczuk, J. W. McGinity, The influence of polymer glass transition temperature and molecular weight on drug release from tablets containing poly(DL-lactic acid), *Pharm Res.* **1992**, *9*(1), 26–32.
36. R. A. Auras, B. Harte, S. Selke, R. Hernandez, Mechanical, physical, and barrier properties of poly(lactide) films, *J. Plast. Film Sheet.* **2003**, *19*(2), 123–135.

37. F. Manzanarez-López, H. Soto-Valdez, R. Auras, E. Peralta, Release of α-tocopherol from poly(lactic acid) films, and its effect on the oxidative stability of soybean oil, *J. Food. Eng.* **2011**, *104*, 508–517 [cited 15 May 2021]. Available from: https://doi.org/10.1016/j.jfoodeng.2010.12.029.
38. H. Tsuji, K. Nakahara, Poly (L-lactide). IX. Hydrolysis in acid media, *J. Appl. Polym. Sci.* **2002**, *86*(1), 186–194.
39. C. D. Hébert, H. D. Giles, J. E. Heath, D. B. Hogan, J. P. Modderman, R. E. Conn, Toxicity of lactide in dogs after 2 and 13 weeks of daily oral dosing, *Food Chem. Toxicol.* **1999**, *37*(4), 335–342.
40. Material Safety Data Sheet (MSDS) for DL-Lactide, Sigma-Aldrich, Saint Louis MO, 2018 [cited 21 February 2021]. Available from: https://www.chemblink.com/MSDS/MSDSFiles/95-96-5_Sigma-Aldrich.pdf.
41. Environmental Protection Agency (US). Reference Dose (RfD): Description and Use in Health Risk Assessments [Internet], 1993 [cited 11 March 2021]. Available from: https://www.epa.gov/iris/reference-dose-rfd-description-and-use-health-risk-assessments.
42. S. Ubeda, M. Aznar, P. Alfaro, C. Nerín, Migration of oligomers from a food contact biopolymer based on polylactic acid (PLA) and polyester, *Anal. Bioanal. Chem. [Internet]* 2019, *411*, 3521–3532 [cited 27 February 2021]. Available from: https://doi.org/10.1007/s00216-019-01831-0.
43. Y. Bor, J. Alin, M. Hakkarainen, Electrospray ionization-mass spectrometry analysis reveals migration of cyclic lactide oligomers from polylactide packaging in contact with ethanolic food simulant, *Packag. Technol. Sci. [Internet]* **2012**, *25*(7), 427–433 [cited 27 February 2021]. Available from: DOI: https://doi.org/10.1002/pts.990.
44. Y. Bor, J. Alin, M. Hakkarainem. Polylactide stereocomplexation leads to reduced migration during microwave heating in contact with food simulants, *J. Food Eng.* **2014**, *134*, 1–4 [cited 11 May 2021]. Available form: https://doi.org/10.1016/j.jfoodeng.2014.02.017.
45. M. Aznar, S. Ubeda, N. Dreolin, C. Nerín, Determination of non-volatile components of a biodegradable food packaging material based on polyester and polylactic acid (PLA) and its migration to food simulants, *J. Chromatogr. A* **2019**, *1583*, 1–8 [cited 27 February 2021]. Available from: https://doi.org/10.1016/j.chroma.2018.10.055.
46. *Improving heat-resistance of PLA using poly(D-lactide), Bioplastics Magazine*, 2008, 02 [cited 11 August 2009]. Available from: https://www.bioplasticsmagazine.com/en/magazine/online-archive/
47. J. Markarian, Biopolymers present new market opportunities for additives in packaging,. *Plastic Addit. Comp.* **2008**, *10*(3), 22–25.
48. S. Jacobsen, H. G. Fritz. Plasticizing polylactide—the effect of different plasticizers on the mechanical properties, *Polym. Eng. Sci.* **1999**, *39*(7), 1303–1310.
49. Z. Kulinski, E. Piorkowska, K. Gadzinowska, M. Stasiak, Plasticization of poly(l-lactide) with poly(propylene glycol), *Biomacromolecules* **2006**, *7*, 2128–2135.
50. X. Zhang, B. Yang, B. Fan, H. Sun, H. Zhang, Enhanced nonisothermal crystallization and heat resistance of poly (L-lactic acid) by D-sorbitol as a homogeneous nucleating agent, *ACS Macro Lett.* **2021**, *10*(1), 154–160 [cited 30 March 2021]. Available from: https://dx.doi.org/10.1021/acsmacrolett.0c00830.
51. N. Ljungberg, T. Andersson, B. Wesslén, Film extrusion and film weldability of poly(lactic acid) plasticized with triacetine and tributyl citrate, *J. Appl. Polym. Sci.* **2003**, *88*(14):3239–3247.
52. A. Höglund, M. Hakkarainen, A. C. Albertsson, Migration and hydrolysis of hydrophobic polylactide plasticizer, *Biomacromolecules* **2010**, *11*(1), 277–283 [cited 30 March 2021]. Available from: https://doi.org/10.1021/bm901157h.
53. L. Aliotta, A. Vannozzi, L. Panariello, V. Gigante, M. B. Coltelli, A. Lazzeri, Sustainable micro and nano additives for controlling the migration of a biobased plasticizer from PLA-based flexible films, *Polymers* **2020**, *12*(6), 1366 [cited 30 March 2021]. Available from: doi:https://doi.org/10.3390/polym12061366.
54. L. M. Sherman, Plastic technology, 2008 [cited 30 March 2021]. Available from: http://www.ptonline.com/articles/200807fa1.html.
55. J. F. He, X. G. Lv, Q. B. Lin, Z. Li, J. Liao, C. Y. Xu, et al., Migration of metal elements from polylactic acid dinner plate into acidic food simulant and its safety evaluation, *FPSL* **2019**, *22*, 100381 [cited 9 March 2021]. Available from: https://doi.org/10.1016/j.fpsl.2019.100381.

# PART III

# PROCESSING AND CONVERSION

# 13

# PROCESSING OF POLY(LACTIC ACID)

Loong-Tak Lim, Tim Vanyo, Jed Randall, Kevin Cink, and Ashwini K. Agrawal

## 13.1 INTRODUCTION

The use of poly(lactic acid) (PLA) in packaging and other consumer products has increased considerably over the past decade. This trend is driven by its sustainable production feedstock, end-of-life options to support circular economy initiatives (e.g., composting and recycling), similar processing characteristics as common thermoplastics (i.e., can be processed using existing production equipment with minimal modification), and property features suitable in a wide variety of applications. The development of large-scale polymerization methods that allows economical production of high-molecular-weight PLA polymer is another driver that had broadened its industrial appeal for packaging, food service ware, fibers, 3D printing, electronics, automotive, and other consumer products [1–7].

Melt processing is the most widely used method for converting PLA resins into end products. This process is characterized by heating the polymer above its melting point ($T_m$), shaping the molten polymer into the desired configuration, followed by cooling to stabilize its dimensions. Further crystallization of PLA can be achieved by orientation and/or annealing. Examples of melt-processed PLA include injection-molded disposable cutlery, thermoformed containers and cups, injection-stretch-blown bottles, extruded cast and oriented films, extrusion coatings on paper substrates, and melt-spun fibers for nonwovens, textiles, carpets, and staple fibers [2, 5, 8]. Another processing technique is based on dissolving the polymer in a suitable solvent to form a solution, which is then spun into filaments or cast into films. This chapter provides an overview of the main process technologies for PLA and presents the material properties needed for selected processing technologies. In this chapter, foaming, blending, and composite forming are not considered since these topics are discussed elsewhere in this book.

## 13.2 PROPERTIES OF PLA RELEVANT TO PROCESSING

Commercial PLA resins are copolymers of L-lactic acid and D-lactic acid. Whether polymerized by condensation polymerization of lactic acid or ring-opening polymerization of lactide, all polymers in this family are considered as PLA. The main commercial route to producing PLA is via ring-opening polymerization of lactide, which is available as L-lactide, D-lactide, M-lactide, and D,L-lactide or *rac*-lactide. The L-lactide is made up of two L-lactic acid molecules, while D-lactide two D-lactic acid molecules. The M-lactide, or *meso*-lactide, is made from one L-lactic acid and one D-lactic acid molecule. On the other hand, D,L-lactide is a 1 : 1 molar mixture of D-lactide and L-lactide that forms a unique crystalline structure. Poly(L-lactide) is produced from L-lactide and has the same polymer structure as the condensation reaction polymer of L-lactic acid, poly(L-lactic acid), and both structures are referred to as PLLA. It is common for poly(L-lactide) to be described as poly(L-lactic acid). The same is true for the opposite stereo structure made from D-lactide or D-lactic acid, PDLA. A broad range of stereo structures can be made by using combinations of lactide isomers [9]. In some cases, ring-opening polymerization of lactides can result in very different stereo sequences as

*Poly(Lactic Acid): Synthesis, Structures, Properties, Processing, Applications, and End of Life*, Second Edition.
Edited by Rafael A. Auras, Loong-Tak Lim, Susan E. M. Selke, and Hideto Tsuji.

compared to those observed in polymers prepared from lactic acid condensation, as two lactyl units from a given lactide can add to the polymer chain together to preserve the lactide stereochemistry. Poly(M-lactide) is a good example of a polymer with properties unique to the lactide polymerization process, where no more than two L-lactyl or two D-lactyl units can exist in a single sequence along the polymer chain.

PLA of different structural, thermal, and mechanical properties can be produced by varying the proportion of the monomeric isomers. PLA polymers with L-isomer content greater than 90% tend to be more crystalline than those with lower optical purity. Moreover, $T_m$, glass transition temperature ($T_g$), and crystallinity decrease with decreasing L-isomer content [10–12]. Typically, PLA articles that require heat-resistant properties can be thermoformed or injection-molded using PLA resins of less than 2% D-isomer and heterogeneous nucleating agents to increase crystallinity. In most fiber applications, PLA polymers with high optical purity are used to develop high levels of crystallinity with enhanced thermal stability. Molecular orientation greatly increases in the rate of crystallization during processing. In contrast, when higher heat resistance is not required, PLA resins of higher D-isomer contents (4–8%) are more suitable for thermoforming and two-stage stretch-blow-molding products because they are less prone to crystallization during the reheating step [13]. Thus, it is important to select the appropriate resin grade to match with the target applications.

PLA is often a semi-crystalline polymer. It has a relatively high $T_g$ but a low $T_m$ relative to $T_g$ when compared with other thermoplastics (Figure 13.1). The $T_g$ of PLA ranges from 35 to 60°C depending on molecular weight, physical aging, polymer architecture, and degree of crystallinity [14]. The addition of lasticizers can further reduce the $T_g$. Above $T_g$, PLA is a rubbery material, while below $T_g$ it becomes glassy, but it can still creep until it is cooled to its β transition temperature at approximately −45°C, below which it behaves like a brittle polymer [15]. In applications where mechanical properties are important, such as packaging materials, fibers, and surgical fixtures, crystalline PLA polymers with $T_g$ of 50–60°C are commonly used. The thermal transition temperatures not only dictate dimensional stability performance but also affect the processing window and thermodynamics of crystallization. The thermal transition temperatures of PLA are also dependent on the optical purity of the polymer. Decreasing the optical purity of PLA reduces both $T_g$ and $T_m$ (Table 13.1). Quenching the polymer from the melt at a high cooling rate (e.g., >500°C/min, such as during injection molding) usually results in highly amorphous "quenched" polymer. PLA polymers with low crystallinity tend to undergo rapid aging in several days under ambient conditions [18, 19]. This phenomenon is an important contributor to the embrittlement of PLA. With amorphous PLA, the $T_g$ dictates the upper use temperature for some applications, as the condition before dimensional deformation occurs. For semicrystalline polymers, the maximum practical obtainable peak melting point, $T_m$, for stereochemically pure PLA (either L or D) is around 180°C with a melting enthalpy of 40–70 J/g (35–65%). PLA of such high crystallinity can bear load above $T_g$ and has a useful dimensional stability up to the onset of melting. The presence of opposite isomers in the PLA structure can depress the $T_m$ by as much as 50°C, which in some processes, can result in wider processing windows,

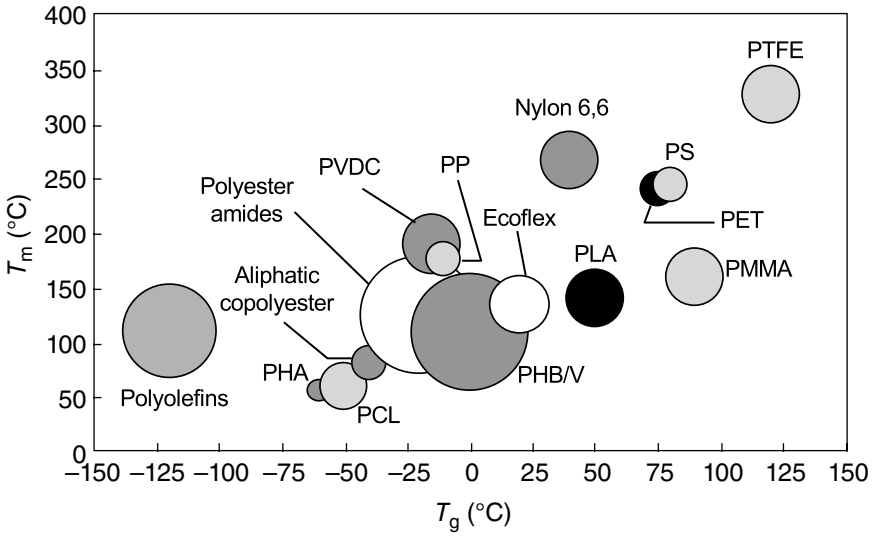


**FIGURE 13.1** Comparison of glass transition and melting temperatures of PLA with other thermoplastics. Source: Reproduced from Ref. 16 with permission from Elsevier.

**TABLE 13.1 Primary Transition Temperatures of Selected PLA Copolymers [17]**

| Copolymer Ratio | $T_g$ (°C) | $T_m$ (°C) |
|---|---|---|
| 100/0 (L/D,L)-PLA | 63 | 178 |
| 95/5 (L/D,L)-PLA | 59 | 164 |
| 90/10 (L/D,L)-PLA | 56 | 150 |
| 85/15 (L/D,L)-PLA | 56 | 140 |
| 80/20 (L/D,L)-PLA | 56 | 125 |

higher stretch ratios, more forgiving heating cycles, lower sealing temperatures, or faster production speeds than polymers with elevated $T_m$. Lower $T_m$ also allows for lower extrusion melt temperatures, thereby reducing thermal and hydrolytic degradations, as well as decreasing residual monomer fuming during processing.

During extrusion, the process temperature must be greater than $T_m$ to form a homogeneous melt, but low enough to minimize polymer degradation. Generally, the process temperature is set to 30–50°C above $T_m$ to ensure the crystalline phase is completely melted and to obtain optimal viscosity. Most often, the upper processing temperature for PLA in extrusion is recommended to be kept below 240°C, but some processes may require a processing temperature of as high as 260°C. During the cooling phase of molding, sufficient solidification cooling time must be provided to cool the part below $T_g$ to stabilize its dimensions. When molding high crystallinity PLA articles, hot molds are used with cycle times optimal for resin formulated with nucleating agents to crystallize the part while holding its dimensions on the mold or within the mold cavity. In many converting processes, the operating temperatures are set above $T_g$ but well below $T_m$ to bring the polymer to a rubbery state, so it is pliable enough for shaping and stretching. This will induce polymer chain orientation and stress-induced crystallization to enhance physical properties (e.g., biaxial orientation of film, stretch blow molding of bottles, drawn fibers, thermoforming).

Residual lactide polymerization catalysts present in the resin are also known to catalyze depolymerization, hydrolysis, and other side reactions [20, 21]. This may explain the large variation of molecular weight drop for melt-processed PLA reported in the literature. For instance, Witzke [21], Perego et al. [22], and Gogolewski et al. [23] reported molecular weight losses for injection-molded PLA parts of 5–52, 50–88, and 14–40%, respectively. Injection-molded PLA made from properly dried PLA resins and optimal processes should exhibit molecular weight loss of less than 10% [24]. To stabilize the polymer during melt processing, the removal or deactivation of the residual catalyst(s) is important to minimize process variability, molecular weight loss, and property changes. Strategies to improve the melt stability of PLA can be found in many patents [20, 25, 26]. Due to the different polymerization processes and technologies used, it is possible that the melt stability of PLA may be different from supplier to supplier.

## 13.3 MODIFICATION OF PLA PROPERTIES BY PROCESS AIDS AND OTHER ADDITIVES

Additives are formulated into PLA during processing to enhance its material properties and/or to facilitate processing. These additives, in either solid or liquid form, can be incorporated into PLA during melt extrusion. In a solid masterbatch system, concentrated additives are blended with PLA resin, compounded in an extruder, cooled, and cut into granules/pellets. During a later product fabrication step, these concentrated solid particles are added accurately to the extruder hopper by using a dosing unit at the target let-down ratio, together with PLA resins. In a liquid additive system, the additive is pre-dispersed in a liquid carrier by the supplier. The liquid additive is pumped into a mixer unit where PLA resins are mixed and coated with the additive before entering the feed section of the extruder. During the injection molding of PLA with a liquid additive system, it is important to ensure that the liquid carrier does not cause screw slippage, which can result in inconsistent screw recovery (i.e., fluctuating recovery time), poor melt mixing, and excessive cycle time variation.

PLA is relatively brittle with low elongation (<10%) and low impact strength (~2.1 kJ/m$^2$ or 0.4 ft lb/in. notched Izod impact), which can present end-use performance, handling, and processing challenges. The brittleness of PLA is related to its molecular structure; the carbonyl group presents a coplanar rigid structure with the adjacent oxygen atoms on the backbone. Moreover, the carbonyl group is in proximity to the carbon atom. The molecular structure gives rise to relatively rigid chain segments with a low degree of chain entanglement as compared with other polymers. For example, the critical entanglement molecular weight for PLA is considerably higher than polycarbonate (8300 and 1780 g/mol, respectively) [27]. Increasing shear yielding and craze density by blending with polymeric or non-polymeric additives is a key strategy to enhance the toughness of PLA polymers. The additives are often traditional impact modifiers, alloys with non-traditional polymers, or composites made with reinforcing agents. Typically, dried PLA resins are melt-blended with these impact modifiers in a compounder or twin-screw extruder, by adapting mixing elements to avoid excessive shear and elevated temperature that can cause substantial PLA degradation. A split feed extruder hopper is needed if the PLA resins are to be dried online. Commercially available impact modifiers for PLA include core-shell impact modifiers and soft thermoplastics for blends. Core-shell impact modifiers are available from several companies and may vary in composition and particle

size. Commonly, the core is made from butadiene, styrene-butadiene, silicone-acrylate, or butyl acrylate. The shell is often made from polymers of methyl methacrylate or methyl methacrylate-styrene. A common core-shell combination is butyl acrylate core-PMMA shell (e.g., KaneAce®, Biostrength®). Polymeric impact modifiers tend to have a lower melting point than PLA. Traditional soft thermoplastic additives include ethylene copolymer (e.g., Biomax®), ethylene-vinyl acetate (EVA; e.g., Escorene®), ethylene acrylic elastomer (EAE; e.g., Vamac®), polyether block amide elastomer (e.g., Pebax Rnew®), and so on. Nontraditional soft thermoplastic additives include polycaprolactone (PCL, e.g., Capa®), polybutylene succinate (PBS, e.g., BioPBS®), low crystallinity poly(hydroxyl alkanoates), and aliphatic-aromatic copolyester (PBAT, e.g., Ecoflex®). Commercial nucleating agents, designed to reduce PLA crystal spherulite size, can enhance the ability to absorb energy and arrest crack propagation. Examples are aromatic sulfonate derivatives (e.g., Lak-301®), magnesium oxysulfate (e.g., HPR-803i®), high aspect ratio calcium carbonate minerals (e.g., EMforce® Bio), and so on [28, 29].

While these additives enhanced the toughness, flexibility, and impact strength of PLA, they can increase optical opacity and whiteness of the products, depending on the level of modifier added (1–30%) [28]. In addition, the compostability and biodegradation properties of the PLA could be impacted, especially at high loading levels, unless the additive is also compostable or biodegradable when exposed to the desired conditions. For example, blends of PLA and Ecoflex, trade named as ecovio®, have improved toughness while maintaining compostability certifications. Here, a fossil-based modifier polymer, poly(butylene adipate-*co*-butylene terephthalate) (PBAT; derived from 1,4-butanediol, adipic acid, and terephthalic acid monomers), is itself biodegradable [30].

Other additives are incorporated into PLA to increase the melt strength to reduce melt sagging and necking phenomena for improved processing, such as during blown film extrusion, film and sheet extrusion, and foaming operations. Blends with high-molecular-weight acrylic-based additives (e.g., Paraloid™ BPMS, Biostrength® 700) enhance the melt strength of PLA during thermal processing. Typically, added at 2–5% concentration, the additive enhances the melt strength of PLA through the entanglement of high-molecular-weight acrylic with PLA polymer chains, thereby creating a physical network that resists melt breakage during extension [30, 31]. With a reactive approach, a chain extender acts differently by grafting or coupling PLA chains to maintain the molecular weight and/or creating a branched network to improve melt strength properties. The reviews by Zhao et al. [27] and Rasal et al. [31] provide a comprehensive overview of various reactive modifications of PLA. Lower-molecular-weight polymers with multifunctional epoxy side groups are commonly used for branching PLA via reaction with the PLA carboxylic acid end group (e.g., Joncryl® ADR-4468) [32]. Branching of PLA can also be driven through free radical reactions at the PLA α carbon after hydrogen abstraction, initiated using organic peroxides. Multifunctional allyl coagents are used to optimize branching versus degradation reactions [33].

PLA articles are inherently grippy or sticky due to their high surface coefficient of friction (COF), which may cause process and downstream processing difficulties such as sticking of films to themselves (i.e., blocking) or to rollers, difficulties in stacking of sheets, sticking of parts to the mold after injection molding or thermoforming, nesting of thermoformed packages, and so on. To overcome these processing difficulties, anti-block or slip agents are often used. For example, fatty acid amides are commonly used slip additives. Because they are not thermodynamically compatible with the polymer, they migrate to the surface of the PLA product, forming a crystalline structure that reduces the COF. Nonmigratory inorganic anti-block, slip agents provide immediate COF reduction by roughening the film surface at the microscopic level. Some commercial slip agents are Avient's OnCap™ Bio Additives and its Cesa®-bloc antiblock masterbatch, and Sukano's Sukano® PLA dcS511 [34]. These additives may affect the degradation and biodegradation behaviors of PLA.

Reheat additives are often added during the injection molding of PLA preforms for two-stage bottle manufacturing processes (Section 13.8). Because PLA is relatively more transparent to infrared radiation than PET, reheat additives are added to enhance the infrared energy absorbance in the oven so that PLA preforms can be effectively reheated in stretch-blow-molding machines designed for PET bottle production. Color pigments and toners are sometimes added during extrusion of PLA to provide color and visual options for certain food packaging and consumer applications.

Although additives are useful to facilitate processing and to enhance the end-use performance of PLA, they may affect the biodegradability and other properties of the resulting PLA products. As an example, adding $CaCO_3$ as a reinforcing agent to PLA not only raises modulus and ductility, but significantly affects thermal degradation during processing and reduces the rate of biodegradation [35, 36]. Fukuda and Tsuji reported that the enzymatic hydrolysis of PLLA was accelerated by the addition of anatase-type $TiO_2$, but the presence of rutile-type $TiO_2$ inhibited the hydrolytic degradation [37]. The potential impact of additives on compostability must be considered, especially if the product needs to comply with ASTM and ISO compostability certification requirements. For food contact applications, the additives used may require food compliance and regulatory approval based on geography, additive amounts, and conditions of use.

## 13.4 DRYING AND CRYSTALLIZING

PLA is a hygroscopic polymer that readily absorbs moisture from the air. Moisture present in PLA resin can induce hydrolytic degradation at elevated temperature during melt extrusion, resulting in a decrease in molecular weight and weakening of physical properties. Therefore, PLA resins must be dried before melt processing to less than 250 ppm (0.025%) moisture content to maximize the retention of molecular weight (<0.1 relative viscosity loss) [37]. Taubner and Shishoo reported that processing of wet PLLA resin (equilibrated at 20°C, 65% RH to give 0.3% moisture content) with an initial $M_n$ of 40,000 g/mol in a twin-screw extruder at 210°C resulted in considerable decreases of $M_n$ to 18,400 and 12,000 g/mol, respectively, at 20 and 120 rpm screw rotation speeds, respectively [38]. Lower decrease in $M_n$ was observed with the dried PLLA at 33,600 and 30,200 g/mol, respectively. By using dynamic sweep rheology, Speranza et al. reported similar decreases in the complex viscosity values of polymer melts for the undried PLLA resin (Ingeo™ 4032D; $M_n$ = 130,000 g/mol, dispersity $M_w/M_n$ = 1.9) over a temperature range of 180 to 220°C. Their mathematical models showed that both hydrolysis and thermal degradation contributed to the reduction of melt viscosity [39]. These observations highlight the importance of proper drying before PLA extrusion.

During the production of plant fiber-reinforced PLA composites, considering the moisture-sensitivity of PLA at elevated temperature, one would expect the drying of the natural fibers to be important. These natural fibers are hygroscopic and contain 6–10% of moisture at 50–70% relative humidity conditions. Interestingly, van den Oever et al. showed that undried plant fiber (ramie, flax, and cotton; 6–9% moisture content), when incorporated at 30% fiber level to commercial-grade PLA, did not induce substantial degradation after 13 min of compounding, as determined from intrinsic viscosity and melt flow index analyses. They concluded that not all moisture present in the biomasses is available in causing PLA polymer cleavage [40].

During the processing of PLA polymers, the drying of crystallized resins typically takes place in the range of 65–90°C, using dry air with a dew point of –40°C or lower. The required drying time depends on the drying temperature and volumetric air flow rate. The half-time values at different drying temperatures for amorphous and crystalline resin pellets, using –40°C dew point air at 0.016 $m^3$/min per kg resin, are summarized in Table 13.2. To calculate the drying time, consider a polymer with an initial moisture content of 1600 ppm, which is to be dried to 200 ppm at 80°C. With a half-time of 1.3 h, a total drying time of 3.9 h is needed [37]. Moisture analyzers can be used to determine the moisture content in the polymer. Coulometric Karl-Fischer titration works well for very low water measurement levels (e.g., 100 ppm).

**TABLE 13.2 Drying Half-Times for PLA Pellets Under –40°C Dew Point and Airflow Rate of 0.016 $m^3$/min/kg [37]**

| Drying Temperature (°C) | Drying Half-Time (h) |
|---|---|
| Amorphous pellets | |
| 40 | 4.0 |
| Crystalline pellets | |
| 40 | 4.3 |
| 50 | 3.9 |
| 60 | 3.3 |
| 70 | 2.1 |
| 80 | 1.3 |
| 100 | 0.6 |

Amorphous pellets must be dried below $T_g$, typically around 43–50°C, to prevent the resin pellets from sticking together, causing bridging and plugging of the dryer. Most commercial-grade PLA resin pellets are crystallized and can be dried at higher temperatures to shorten the drying time. By visual comparison, virgin crystalline pellets are opaque in appearance, whereas virgin amorphous pellets are clear.

Drying of PLA is commonly achieved using a closed-loop dual-bed regenerative desiccant-type dryer. Here, resin pellets in a hopper are purged with dry air generated by the desiccant bed. During the operation, one desiccant bed is in the process air stream and removes moisture from the resin, while the other standby bed is being regenerated (Figure 13.2). The hot air from the process stream removes the moisture from the resin and circulates back to the dryer where it is cooled. The moisture in the returned air is picked up by the desiccant. The air is then reheated before it is channeled back to the hopper. When the dew point of the process air is greater than the set point, the desiccant goes into the regeneration cycle where the desiccant is heated to strip the moisture from the desiccant and vent it to the atmosphere. Meanwhile, the process air is directed to the standby desiccant that was previously dried. Cooling units are typically installed between the drying hopper and the desiccant bed to prevent the air temperature from spiking in the supply air, which could cause pellet blocking when drying amorphous PLA.

Amorphous, optically pure PLA stereoisomer compositions (e.g., >95% PLLA) can be quiescently crystallized using properly designed crystallizing equipment available in the plastics industry. Reclaimed materials such as post-industrial scrap or recycled material may or may not be crystalline. For example, trim scraps from thermoforming or cast sheet are amorphous, while scrap materials from high-orientation processes (e.g., fibers, biaxially orientated films) are crystalline. Crystallizing prevents the amorphous materials from sticking together at temperatures greater than the

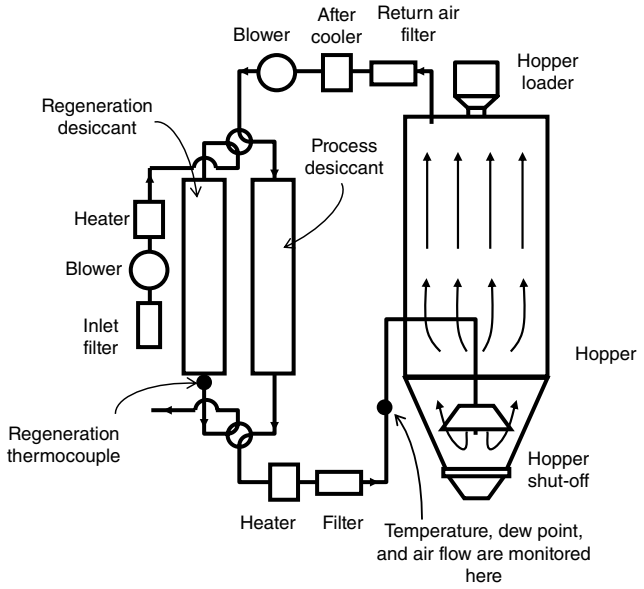


**FIGURE 13.2** Typical closed-loop dual-bed regenerative desiccant-type dryer for drying PLA before extrusion.

$T_g$ (>55–60°C). Once crystallized, the material can be dried at higher temperatures without blocking and fed into the melt extrusion process without screw sticking/slip issues. Reclaim and trim scrap may vary in shape, size, and bulk density, so material handling will need to be optimized [41].

There are numerous crystallizer machines available in the market. Typically, PLA is best processed using designs that have some type of mixing to prevent material agglomeration. Uniform heating of the material bed is important during mixing. Some designs may require start-up using pre-crystallized material before introducing the amorphous material. The optimal temperature to crystallize PLA will depend on its optical purity. Crystallization temperatures of 100–110°C are typically suitable for optically pure PLLA grades (>98% PLLA), whereas lower optically pure materials (94–98% PLLA) should be crystallized using lower temperatures (85–100°C) to prevent premature material bed sticking and clumping [41]. Crystallization times and extent of crystallinity level depend on several factors, such as material grade, temperature, and heat transfer. Low-optical-purity PLA grades that are essentially amorphous should not be loaded into crystallizers as they will not crystallize, or crystallize too slowly, and cause blocking issues. Depending on the operation, even material that has been processed through a crystallizer may need to be dried further to reduce the moisture content to acceptable levels before melt extrusion.

During storage, PLA resins are susceptible to hydrolytic degradation if exposed to elevated temperature and humidity conditions. The effects of storage temperature and humidity on the molecular weight of PLA were elucidated by Henton et al. (Figure 13.3) [15]. These results highlight the importance of protecting the resins from hot and humid environments during storage. Commercial PLA resins are shipped in differently sized containers, ranging from small sample bags to large gaylord boxes to rail cars. Unused resins should be in sealed containers to prevent uptake of moisture from the air and prevent foreign contamination.

Dryerless extrusion systems are an alternative option for extrusion processing of PLA without pre-drying. It also eliminates the need for a crystallizer to process the regrind

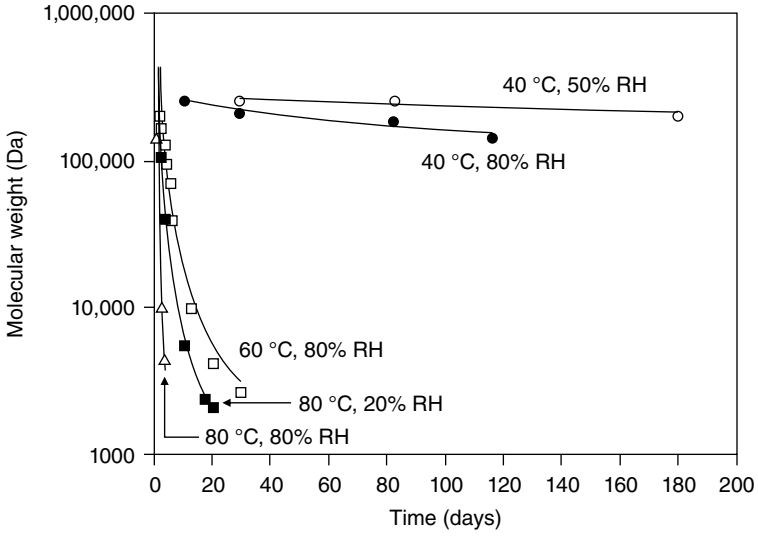


**FIGURE 13.3** Plots of molecular weight loss of PLA versus time under different environment conditions. Plots are recreated based on the original data published by Henton et al. [15].

before drying. Such machines use a vacuum venting system to remove moisture during melt extrusion before the moisture has a chance to significantly hydrolyze the PLA. This can be a significant advantage on production lines that swing between different polymers as it eliminates the need of cleaning the dryer and crystallizer hoppers. It also has the advantage of less overall energy use. However, good raw material and processing practices are required to keep the load on the vacuum system manageable, as residual lactide monomer in PLA resin and the tendency for PLA to reform lactide during processing can be problematic. In addition, the vapor removal system should be designed to efficiently condense and remove lactide without plugging the vent lines. Finally, an optimal designed system to capture the lactide stream and prevent it from reaching the vacuum system is necessary. The entire system should be manufactured from materials that resist chemical attack from lactic acid and can be emptied/cleaned in an efficient manner (e.g., heating venting lines to prevent early condensation, regular cleaning of filters/traps). Proper selection of vacuum levels at the vent site is important to create conditions for the desired level of lactide removal without unnecessary load on the vacuum pumps. Optimal conditions will increase the run time between cleaning cycles of the condensable materials in the collection system.

## 13.5 EXTRUSION

Extrusion is the key unit operation for converting solid PLA into a homogeneous melt for fabrication in many manufacturing processes, such as sheet extrusion, injection molding, single-stage stretch-blow molding, film blowing, and melt spinning. PLA can be processed using general purpose screws consisting of three sections (Figure 13.5a): (i) Feed section—acts as an auger that receives the polymer pellets and conveys the polymer into the screw; (ii) Transition section—also known as the compression or melting section, is characterized by decreasing flight depth to compress the pellets, drives energy into the pellets through friction, and enhances their contact with the barrel. Heat from friction and shear mixing converts the solid pellets into molten liquid; (iii) Metering section—this section has a constant and shallow flight depth, which acts as a pump to meter accurately the required quantity of molten polymer. The screw length-to-diameter (L/D) ratio, defined as the ratio of the flighted length of the screw to its outer diameter, is a characteristic that contributes to the total shear and the residence time of the melt. Screws with large L/D ratio provide greater shear heating, higher mixing, and longer melt residence time in the extruder.

Commercial-grade PLA resins typically can be processed using a conventional extruder equipped with a general-purpose screw with L/D ratio of 24–30. Extruder screws for processing PET, which typically have low shear for gentle mixing to minimize resin degradation and acetaldehyde generation, are suitable for processing PLA resin [5]. While PLA may be processed in extruders designed for polyolefins, such systems are usually not optimal. PLA has a solids density of about 1.24 g/mL, which is higher than that of polyolefins (0.91–0.96 g/mL). If the extruder is already operating at close to maximum power of the screw drive, the extruder may not have enough power to process PLA at equivalent mass flow output due to its substantially higher density [42]. Processing of polypropylene (PP) typically requires higher shear rates and a longer L/D screw than PLA. Therefore, PP screw is usually not optimal for processing PLA as it tends to result in melt temperatures higher than required and can cause a loss in molecular weight. Another important screw parameter is the compression ratio, which is frequently estimated from the ratio of the flight depth in the feed section to the flight depth in the metering section. The greater the compression ratio a screw has, the greater the shear heating it provides. The recommended compression ratio for PLA processing is in the range of 2–3, depending on the polymer grades [43].

During the plasticating process, PLA resin pellets are fed to the extruder from a hopper at the upstream end of a barrel. The screw, driven by an electric or hydraulic motor, rotates and transports the material downstream, toward the opposite end of the barrel. The heat required to raise the temperature above $T_m$ is provided by the heaters wrapped around the barrel and the frictional heat generated by the shear mixing from the rotating screw. To ensure that all the crystalline phases are melted and to achieve an optimal melt viscosity for processing, the screw is designed to input the correct amount of frictional energy, and the heater set point is usually 200–210°C, which is about 30–50°C above $T_m$. Melt rheological properties of PLA have a profound effect on how the polymer flows during extrusion. Since the PLA rheological properties are highly dependent on temperature, molecular weight, and shear rate, they must be taken into consideration during tooling design, process optimization, and process modeling/simulation. Across a large range of extrusion processes, shear melt viscosities of high-molecular-weight PLA are on the order of 100–2000 Pa s at shear rates of 10–50 $s^{-1}$ at their desired process temperature. PLA grades for injection molding have been reported to have $M_w$ of 100,000 Da, while those for cast film extrusion have an $M_w$ of as high as 300,000 Da [44]. Commercially available $M_w$ for high-molecular-weight PLA generally ranges from about 100,000 to 210,000 Da, relative to linear polystyrene standards.

Melt processing of PLA in an extruder will result in molecular degradation, the extent of which depends on the

temperature and shear applied. Mysiukiewicz et al. investigated the extrusion processing parameters and thermomechanical degradation of four grades of unmodified commercial Ingeo™ Biopolymers (4043D, 2500HP, 3100HP, and 3260HP, with $M_w$ of 202,000, 193,250, 148,250, and 107,500 Da, respectively) in a co-rotating twin-screw extruder with D = 16 mm and L/D = 40, equipped with a capillary die of diameter of D = 8 mm with die temperature ranging from 120° to 260°C [45]. They reported the effect of screw rotation speed and extrusion temperature on the weight average molecular weight values, as predicted from the zero-shear viscosity ($\eta_0$) calculated from the Carreau-Yasuda equation (Figure 13.4). Overall, the polymers exhibited minimal degradation up to 200°C. With low-melt-flow-index (MFI) polymer grades (4032D and 2500HP), substantial decreases in $\eta_0$ were observed above 220°C. With the high-MFI polymers (3100HP and 3260HP), increased screw rotation speed reduced polymer degradation. Although higher screw rpm increased shear mixing, the combined material shear-thinning and reduced residence time reduced the extent of overall polymer degradation.

The degradation of PLA during melt processing can be attributed to: (i) hydrolysis induced by trace amounts of water; (ii) zipper-like chain end depolymerization; (iii) oxidative, random main-chain scission; (iv) intermolecular transesterification to monomer and oligomeric esters; and (v) intramolecular transesterification resulting in the formation of monomer and oligomeric esters of low $M_w$ [46]. Kopinke et al. [47] reported that above 200°C, PLA can degrade through intra- and intermolecular ester exchange, *cis*-elimination, and radical and concerted nonradical reactions, resulting in the formation of small molecules, including CO, $CO_2$, acetaldehyde, and methylketene. In contrast, McNeill and Leiper [48] proposed that the thermal degradation of PLA is primarily driven by nonradical, "backbiting" ester interchange reactions involving the ─OH chain ends. Depending on the point in the backbone at which the reaction occurs, the by-product can be cyclic oligomers, lactide, or acetaldehyde plus carbon monoxide. Similar degradation mechanisms were reported by Kopinke et al. [47]. The formation of these small molecules during melt extrusion of PLA, such as acetaldehyde, must be minimized, especially for food packaging applications. The migration of acetaldehyde can result in off-flavor that may impact the organoleptic properties and consumer acceptance of the product [49, 50].

The formation of low-molecular-weight species due to thermal process degradation is generally undesirable. Efforts have been made to detect the degradation products and to elucidate the degradation reactions [47, 51–54]. Oligomers were reported to form at temperatures higher than 230°C [51]. The formation of lactide due to depolymerization has primary and secondary consequences. Besides reducing PLA melt viscosity and melt elasticity, the volatile lactide can cause fuming and/or fouling of processing equipment such as chill rolls, molds, and tooling surfaces [55]. Fouling is characterized by the gradual build-up of lactide condensing and crystallizing on the equipment surfaces, commonly known as plate out. To overcome this problem, fume exhaust

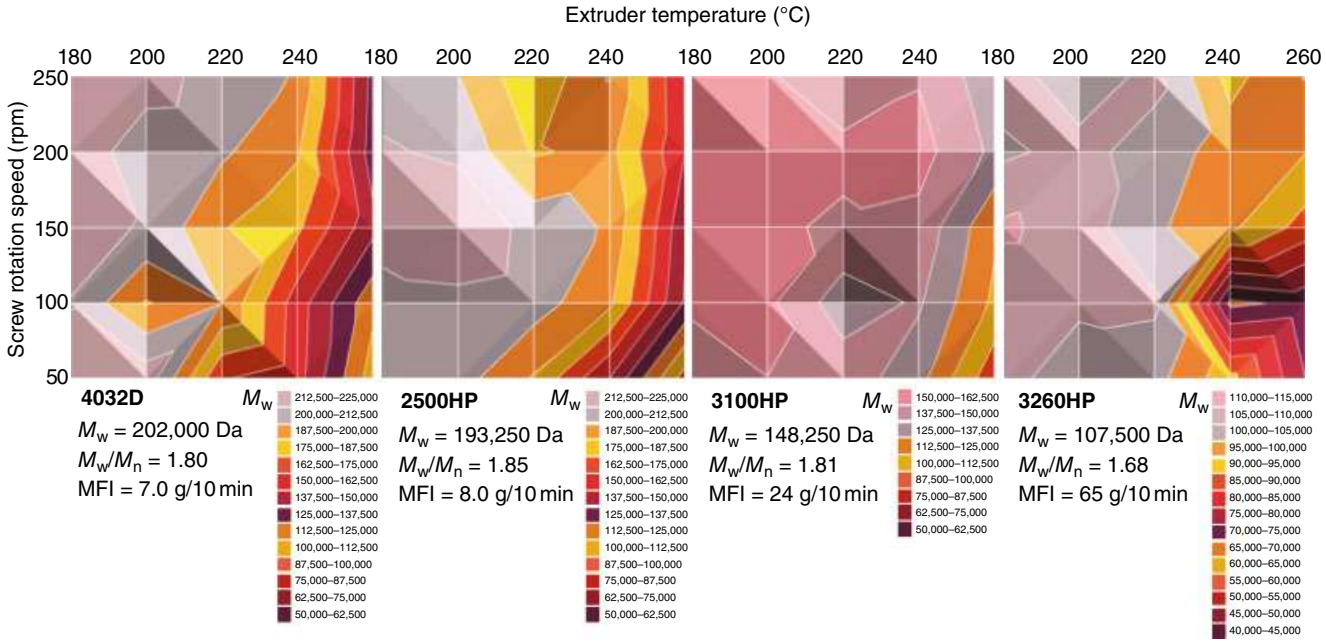


**FIGURE 13.4** Effects of twin-screw extruder temperature and screw rotation speed on the predicted molecular weight of different Ingeo™ biopolymers. Adapted from Mysiukiewicz et al. [45] under the Creative Commons Attribution (CC BY 4.0).

engineering is employed near die faces and melt extrusion areas. During material quenching and fabrication, such as cooling of cast sheet on chill rolls or solidifying in injection molds, the temperature of the equipment is optimized to reduce the tendency of lactide plate out. Lactide monomer was found to undergo racemization to form *meso*-lactide during intentional exhaustive depolymerization at high temperatures [51]. Recovered monomer stereo purity could impact the material properties of PLA polymerized from pyrolyzed lactide. Some control of stereo purity when depolymerizing lactide has been studied for chemical recovery via pyrolysis using catalysts that allowed for lower pyrolysis temperatures [52].

## 13.6 INJECTION MOLDING

Injection molding is a highly efficient process for forming parts that are complex in shape and require high-dimensional precision. All injection molding machines have an extruder for plasticating the polymer melt. Unlike a standard extruder, the extruder unit for the injection molding machine is designed such that the screw can reciprocate within the barrel to allow for the buildup of polymer melt in front of the screw during screw recovery. When the target volume of melt is accumulated, the screw can slide forward to inject the melt into the mold cavities (Figure 13.5b). Most injection molding machines for PLA are based on the reciprocating

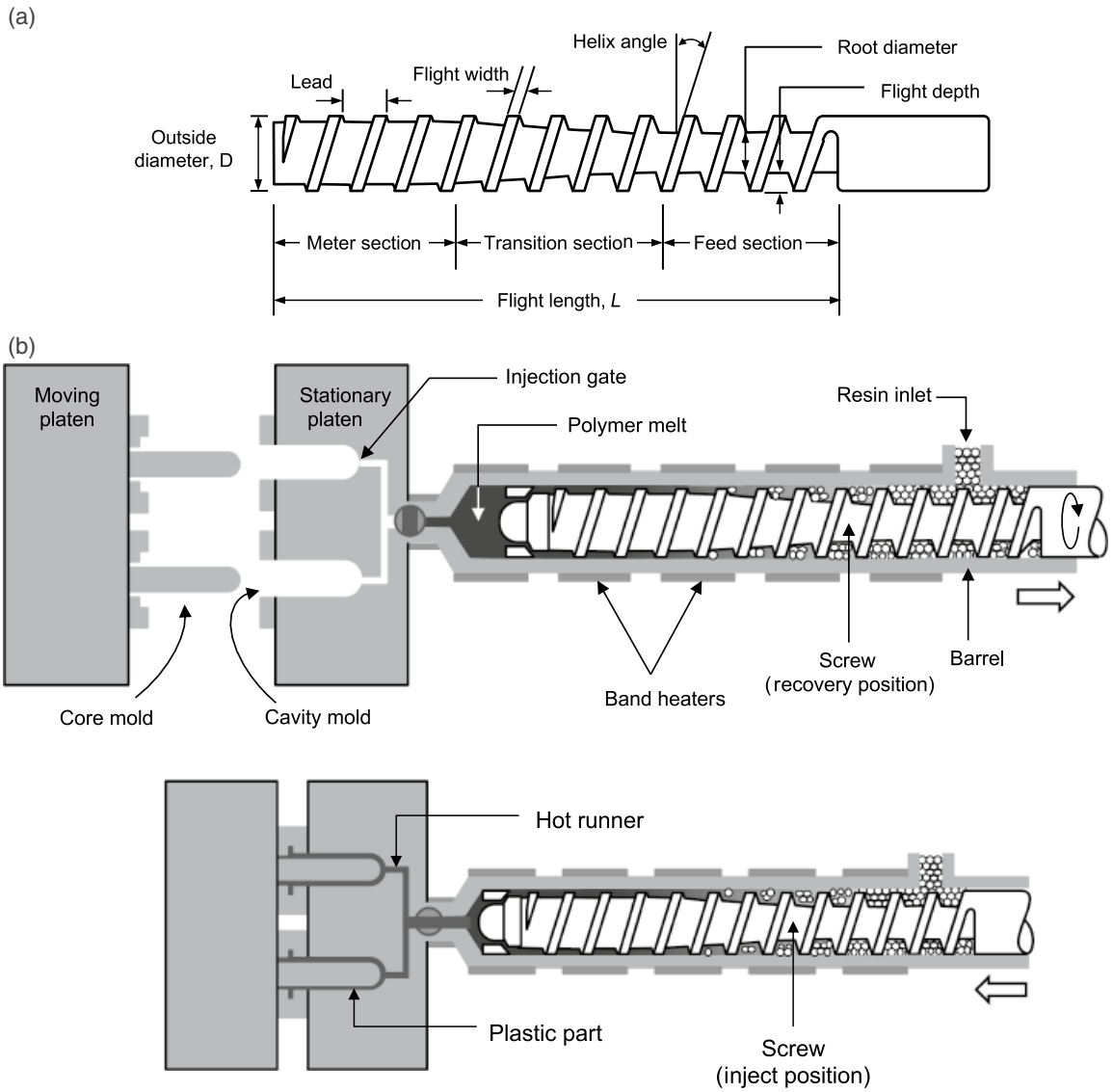


**FIGURE 13.5** (a) Typical geometries of a screw for single-screw extruder; (b) major components of an injection molding machine showing the extruder (reciprocal screw) unit and injection molds. Top: the screw rotates and slides backward to allow polymer melt to accumulate in front of the screw. Bottom: the mold clamps up followed by moving the screw forward to inject polymer melt into the hot runner and fill the mold cavities.

screw extruder, although in some systems a shooting pot and extruder may be integrated within a single machine. Here, the extruder plasticates and transfers the melt into the shooting pot under relatively low injection pressure. The melt is then injected into a mold, manifold, or hot runner under high pressure by a plunger in the shooting pot. While the reciprocating machine must stop the screw rotation during the injection and packing phases, the screw for this type of injection molding machine can plasticate and recover during much of the molding cycle, thereby presenting several advantages over its reciprocating counterpart, including shorter cycle time, smaller screw motor drive, more consistent melt quality, and more consistent shot size [56].

During a typical injection process, the beginning of mold close is usually taken as the start of an injection molding cycle (Figure 13.6). Immediately after the mold clamps up, the nozzle opens, and the screw moves forward to inject the polymer melt into the mold cavity. To compensate for the material shrinkage during cooling in the mold, the screw is maintained in the forward position with a prescribed holding pressure. At the end of the holding phase, the nozzle is shut off and the screw begins to recover, while the part continues to be cooled and solidify in the mold. During the recovery phase, the screw rotates and conveys the polymer forward along the screw. Concurrently, the screw slides backward within the barrel against a controlled back pressure exerted on the screw by a hydraulic cylinder. To ensure that the part is dimensionally stable enough to withstand the opening stroke of the molds, sufficient cooling time must be provided. In the molding cycle, heat removal takes place predominantly during the fill, hold, and cool phases, although the mold opening phase also contributes to partial cooling since one side of the part (the core-contacting side) is still being cooled on the mold surface prior to ejection.

Cycle time is an important process parameter that is often optimized to maximize the production throughput. As shown in Figure 13.6, minimizing the duration for non-process events (i.e., mold opening/closing, mold clamp-up/unclamp, part ejection) will reduce the cycle time. Lowering the mold temperature can also increase the heat extraction rate from the polymer. However, to reduce the propensity of lactide condensation on the cold tooling surfaces, which can affect the surface finish and weight of the molded articles, the mold temperature should be optimized based on the tooling design, material, additives used, and the molding process conditions. Typically, the minimal mold temperatures range from 25 to 30°C. The use of molds with polished surfaces, in conjunction with an increased injection speed during fill, can also reduce the deposition of the lactide layers. To further shorten the injection molding cycle time, it is common to transfer the partially cooled molded article to a post-mold cooling device (e.g., direct contact on a chilled surface and/or convective cooling by forced air). This frees up the mold for receiving the next shot while the molded parts are being cooled outside the molds, thereby increasing the production throughput.

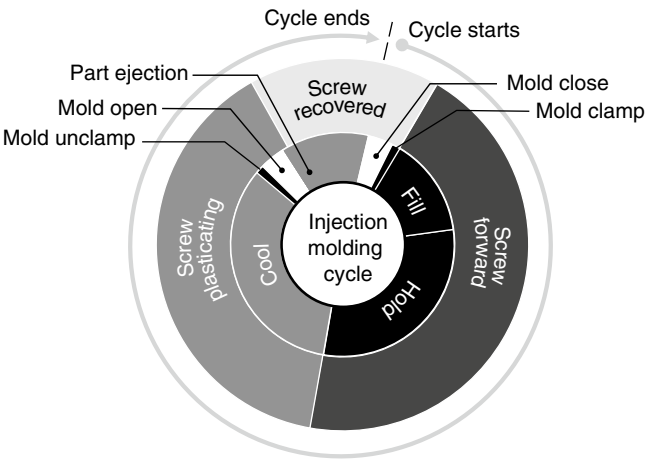


**FIGURE 13.6** Typical cycle events for an injection molding process.

The fill, hold, and cool events have an important implication for the shrinkage behaviors of injection-molded PLA articles. The shrinkage effect can be elucidated using a pressure–volume–temperature (PVT) diagram (Figure 13.7) [57]. During injection molding, the polymer is first subjected to isothermal injection of the polymer melt into the mold cavity, during which the pressure increases as the polymer is being injected and packed to the holding pressure (trace a–b in Figure 13.7). The polymer then undergoes isobaric cooling in the holding phase (trace b–c), followed by isochoric cooling. When the polymer cools below the freezing point, the gate freezes and the pressure in the mold cavities decreases to one atmospheric pressure (trace c–d). Finally, in the cooling phase, the article continues to cool isobarically to room temperature (trace d–e). The change in specific volume during the final isobaric cooling (trace d–e) dictates the extent of part shrinkage ($\Delta V$). The hold pressure and temperature play an important role in determining article shrinkage. In Figure 13.7, another process with higher holding pressure is presented (trace a–b′–c′–d′–e). Here, by holding the part at higher pressure, the total part shrinkage is reduced to $\Delta V'$. Although increasing pressure can reduce part shrinkage, the maximum hold pressure is limited by the machine clamp force. The use of elevated hold pressure can lead to the formation of "flash" caused by the excessive flow of melt into the mold parting line.

The PVT relationship can be modeled mathematically using the modified two-domain Tait model [58–60]:

$$v(T,p) = V_0(T)\left[1 - C\ln\left(1 + \frac{p}{B(T)}\right)\right] + V_t(T,p) \quad (13.1)$$

where $v(T, p)$ is specific volume at temperature $T$ and pressure $P$, $V_0$ is specific volume at zero-gauge pressure, and

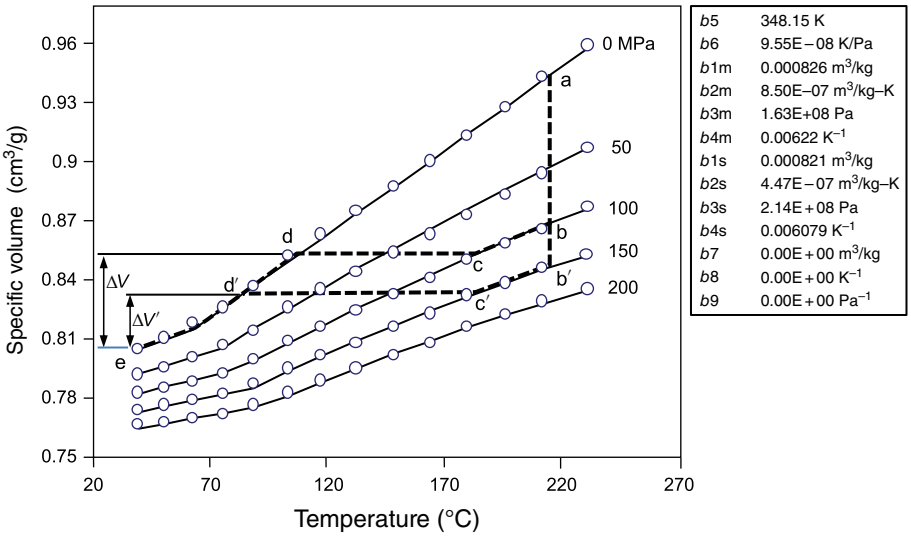


**FIGURE 13.7** PVT plots for PLA polymers (NatureWorks LLC, 4.25% D-isomer) [57]. The continuous lines represent the fitted results based on the two-domain-modified Tait model (Equation 13.1).

$C$ is a dimensionless constant, 0.0894. When the temperature of the material is greater than the transition temperature, $V_0(T)$ and $B(T)$ are determined by $b_{1m}$, $b_{2m}$, $b_{3m}$, $b_{4m}$, and $b_5$ as follows:

$$V_0(T) = b_{1m} + b_{2m}(T - b_5) \tag{13.2}$$

$$B(T) = b_{3m} \exp\left[-b_{4m}(T - b_5)\right] \tag{13.3}$$

When the material temperature is lower than the transition temperature, $V_0(T)$ and $B(T)$ are determined by $b_{1s}$, $b_{2s}$, $b_{3s}$, $b_{4s}$, and $b_5$ as follows:

$$V_0 = b_{1s} + b_{2s}(T - b_5) \tag{13.4}$$

$$B(T) = b_{3s} \exp\left[-b_{4s}(T - b_5)\right] \tag{13.5}$$

The constants have some physical meanings. Constants $b_{1m}$ and $b_{2m}$ are related to the intercept and slope of melt-state $V$–$T$ line, respectively, when $P = 0$. On the other hand, $b_{1s}$ and $b_{2s}$ are related to the intercept and slope for the solid-state $V$–$T$ lines when $P = 0$. Constants $b_{3m}$, $b_{4m}$, $b_{3s}$, and $b_{4s}$ affect the shape of the $V$–$T$ plots when $P \neq 0$. Constant $b_5$ is the transition temperature at zero pressure. Because the transition temperature, $T_{trans}(P)$, is often pressure dependent, it is often correlated with pressure and the transition temperature at zero-gauge pressure ($b_5$) as follows:

$$T_{trans}(P) = b_5 + b_6 p \tag{13.6}$$

Here, $b_6$ is related to the magnitude of change of transition temperature with pressure. For non-amorphous materials, an additional transition function may be required:

$$V_t(T, p) = b_7 \exp\left[b_8(T - b_5) - b_9 p\right] \tag{13.7}$$

The estimated parameter values for the modified two-domain Tait model are shown in the inserts in Figure 13.7. This model is often used for numerical simulation of injection molding processes involving finite element analysis for predicting the shrinkage behavior of injection-molded articles.

The crystallinity of the injection-molded PLA articles is dependent on the cooling rate, cooling time, and crystallizability of the PLA being processed. Quenching crystallizable polymer from the melt at a high cooling rate may result in a predominantly amorphous part, which will show an exothermic crystallization peak upon subsequent reheat by DSC, while slow cooling tends to produce a polymer with higher crystallinity and lower enthalpy of crystallization upon reheat. The optical purity of PLA also affects the crystallinity of PLA during cooling. In general, the crystallization half-time of PLA increases about 40% for every 1% of *meso*-lactide in the polymerization mixture [61].

Heated molds, in the range of 100–130°C, can be used to crystallize highly crystallizable PLA formulations prior to ejection, with cycle times dictated by the polymer crystallization rate and setup time. Crystallization of PLA can be enhanced by incorporating a heterogeneous nucleating agent in the polymer during extrusion. This lowers the surface free energy barrier for nucleation and enables crystallization to take place at higher temperature when cooling. Kolstad [61] showed that talc can be added to PLLA to effectively modify the crystallization rate of the polymer. With 6% talc added to PLLA, the crystallization half-time of the polymer at 110°C was reduced from 3 min to approximately 25 s. At the same percent of talc, for 3% *meso*-lactide

copolymerized with the L-lactide, the half-time was reduced from about 7 to about 1 min [61]. Similarly, Li and Huneault [62] reported that the lowest crystallization induction period and maximum crystallization speeds were observed around 100°C in their study comparing the crystallization kinetics of talc and montmorillonite (MMT, Closite $Na^+$) for 4.5% D-isomer PLA. By adding 1% of talc, the crystallization half-time of PLA was decreased from a few hours to 8 min. In contrast, the MMT tested was less effective as a nucleating agent; the lowest half-time achieved was 30 min. Randall showed that the crystallization half-time, when cooled from the melt, for PLA could be reduced below 15 s with the addition of a commercial heterogeneous nucleating agent (LAK-301) from Takemoto Oil & Fat [63]. Other researchers have also shown that PLLA/PDLA stereocomplex crystallites can act as nucleator for PLLA to accelerate its crystallization rate [64].

Injection-molded PLA articles quenched to cold temperatures tend to exhibit larger extension at break compared to those aged at room temperature due to changes in the glass transition enthalpy of relaxation. The development of brittleness during physical aging can be attributed to the reduction of free volume caused by the rapid relaxation toward the equilibrium amorphous state [12, 18, 21]. Cai et al. [19] showed that the endothermic enthalpy relaxation ($\Delta H_{rel}$) for PLA (96% L-lactide) increased with increasing aging time (Figure 13.8). They also showed that as the aging temperature increased toward the $T_g$, the rate of physical aging also became faster. However, when the aging temperature went above the $T_g$ (60°C), the excess enthalpy relaxation was reduced, indicating that physical aging was no longer taking place [19]. Celli and Scandola [18] observed a similar aging trend for PLLA using DSC and DMA. They observed that the extent of aging increased with decreasing molecular weight, which was attributed to the increased chain terminals that possess higher freedom of motion than the internal chain segments [18]. Since aging below $T_g$ is mainly related to the amorphous phase of the polymer, increasing the crystallinity of the polymer (e.g., by reducing the D-isomer composition or using nucleating agents) will reduce the aging effect. Furthermore, the crystallites formed also act like physical cross-links to restrict the polymer chain mobility.

Annealing of injection-molded PLA articles after molding at temperatures higher than $T_g$ and below $T_m$ can induce crystallization to improve their thermal stability. Perego et al. [22] showed that crystallization of injection-molded PLLA parts by annealing at 105°C for 90 min increased tensional and flexural elasticity, Izod impact strength, and heat resistance. After annealing PLLA and PLA copolymers, two melting peaks appeared in a DSC scan, as observed by Yasuniwa et al. [65]. They reported that the low temperature $T_m$ peak height increased with increasing heating rate, whereas the high temperature $T_m$ decreased. The double-melting peak behavior was explained based on a melt recrystallization model, in which small and imperfect crystals changed successively into more stable crystals through melting and recrystallization. Perez-Fonseca et al. studied the effect of thermal annealing on the mechanical and thermal properties of biocomposites by injection molding of commercial-grade PLA (Ingeo™ 3251D) compounded with

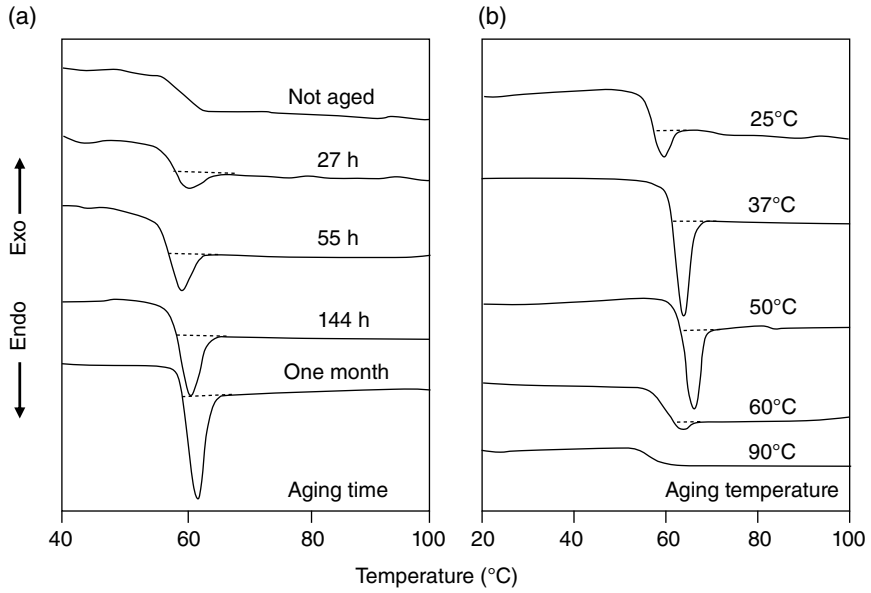


**FIGURE 13.8** Effects of temperature and time on the aging of injection-molded 4% D-lactide PDLA specimens. (a) DSC curves of PLA aged at room temperature for various aging times. (b) DSC curves of PLA annealed for 24 h at different temperatures. Source: Adapted from Ref. 19 with permission from John Wiley and Sons.

agave, coir, and pine, up to 30% fiber content, using twin-screw extrusion [66]. Annealing of the injection-molded biocomposites at 105°C for 1 h increased their impact strength and flexural modulus while decreasing flexural strength. Thermal stability of the composites was enhanced. Although the SEM micrographs showed good interfacial contact between PLA and the fillers (agave, coir, or pine) without the use of any coupling agent, the reduced tensile and flexural strengths with increasing fiber contents suggest limited fiber–matrix adhesion. The DSC analysis showed that PLA crystallinity of the biocomposite was decreased, as compared with the neat polymer, when fibers were added. However, thermal annealing increased the crystallinity of the biocomposites, up to 10% level for PLA–pine biocomposites, and increased the impact strength and flexural modulus of both neat PLA and all the biocomposites. They reported that longer fibers, such as those from coir and agave, produced biocomposites with higher impact strength compared with neat PLA. But pine fibers containing higher wax contents resulted in lower tensile and flexural strength [66].

During microinjection molding of small parts with micrometer dimensions, filling is often challenging due to premature freezing of the polymer in the mold cavity. The use of high temperature and increased injection speed can impact the crystallization process and result in substantial polymer degradation. De Meo et al. reported using dynamic in-mold local temperature control for micro-injection molding of thin PLA articles (200 µm thick) to control the solidification of the polymer melt [67]. In their study, they developed a mold with inserts and heating elements based on a thin/flexible resistance layer of high-power density, capable of increasing mold temperature by tens of °C/s, which was separated from the mold using a thin insulation layer. Due to the small thermal mass involved during microinjection molding, this setup allowed rapid heating when the polymer melt reached the mold cavity and rapid cooling after the heating element was switched off. They reported that at 25°C, the solidification of melt prevented the molding of the thin article. However, increasing the mold surface temperature above 120°C increased flow length considerably. Moreover, after filling the mold, reducing and holding the temperature at which the maximal crystallization rate occurred for the polymer (~105°C) could enhance the crystallinity of the molded part [67]. Using a similar setup, Liparoti et al. evaluated the replication of micro- and nanofeatures for microinjection molding of two commercial PLA polymers (Ingeo™ 3251D: 90 kDa, 1% D-enantiomer; 4032D: 210 kDa, 2% D-enantiomer) [68]. They reported that mold heating time that was longer than the filling time increased the surface microfeatures of the mold article, as revealed by atomic force microscopy. Melt viscosity significantly affected the replication of microfeatures, i.e., 3251D had higher replication accuracy than 4032D. However, viscosity had a negligible effect on the replication of nanofeatures [68].

## 13.7 FILM AND SHEET CASTING

PLA polymers of various optical purities have been successfully extruded using conventional extruders. In cast film extrusion, the molten PLA is extruded through a lip die and quenched on highly polished chrome rollers that are cooled with circulating water. Figure 13.9 shows the main components for a typical extrusion cast line for producing biaxially oriented PLA film. The casting of PLA film and sheet is practically identical; the main difference between them is their stiffness/flexibility owing to the difference in their thicknesses. Typically, films are ≤0.076 mm (0.003″ or 3 mils) in thickness, while sheets are typically ≥0.25 mm (0.01″ or 10 mils). Usually, the die gap is set to 10% or 25–50 µm (1–2 mils) greater than the target sheet thickness [37]. Due to the thermal sensitivity of PLA, the use of external deckles on the die to adjust the film width should be avoided since the degraded resin behind the deckles can lead to edge instability.

Sheet and film forming can be achieved on a three-roll stack. Because of the low melt strength of PLA, a horizontal roll stack configuration is preferred. To avoid the condensation of lactide monomers and slippage of web on the rollers, relatively high roller temperatures (25–50°C) are usually used. Lactide monomer buildup around the die can be further prevented by using an exhaust system. Good contact between the web and rolls is also important to minimize lactide buildup. To reduce the chance of trapping air and to reduce film or sheet defects, it is recommended that the die be positioned as close as possible to the entrance nip and slightly higher than the nip to accommodate the slight drooping of the molten PLA web [37] with vertical rolls. To cast PLA film, Ljungberg et al. used a 200 mm fishtail die with a 300–400 µm split gap and a casting air gap of 15 mm [69]. Generally, hydraulic roll stands, capable of producing pressure around 800–900 lb/linear in. (143–161 kg/cm) of die, are required to prevent floating of the rolls that would result in uneven PLA surfaces, edge instability, and neck-in [37]. Casting of PLA film usually requires edge pinning (electrostatic or low-pressure air) to eliminate streaking, reduce neck-in, and improve edge stability [70]. Slitting and web handling of PLA is similar to PS. Edge trimming of PLA should be carried out with rotary shear knives since razor knives may yield rough edges and web breaks. Winding of the PLA web should be done with good tension control to obtain a consistent gauge.

While the elastic modulus and tensile strength of PLA are comparable to PET, the elongation at break for quenched PLA is considerably lower, only a few percent. Thus, quenched neat PLA is not suitable for applications where toughness, high impact strength, and high elongation are required. However, mechanical orientation can improve the toughness of PLA films. As shown in Table 13.3, oriented PLA film has higher tensile strength, modulus, and in

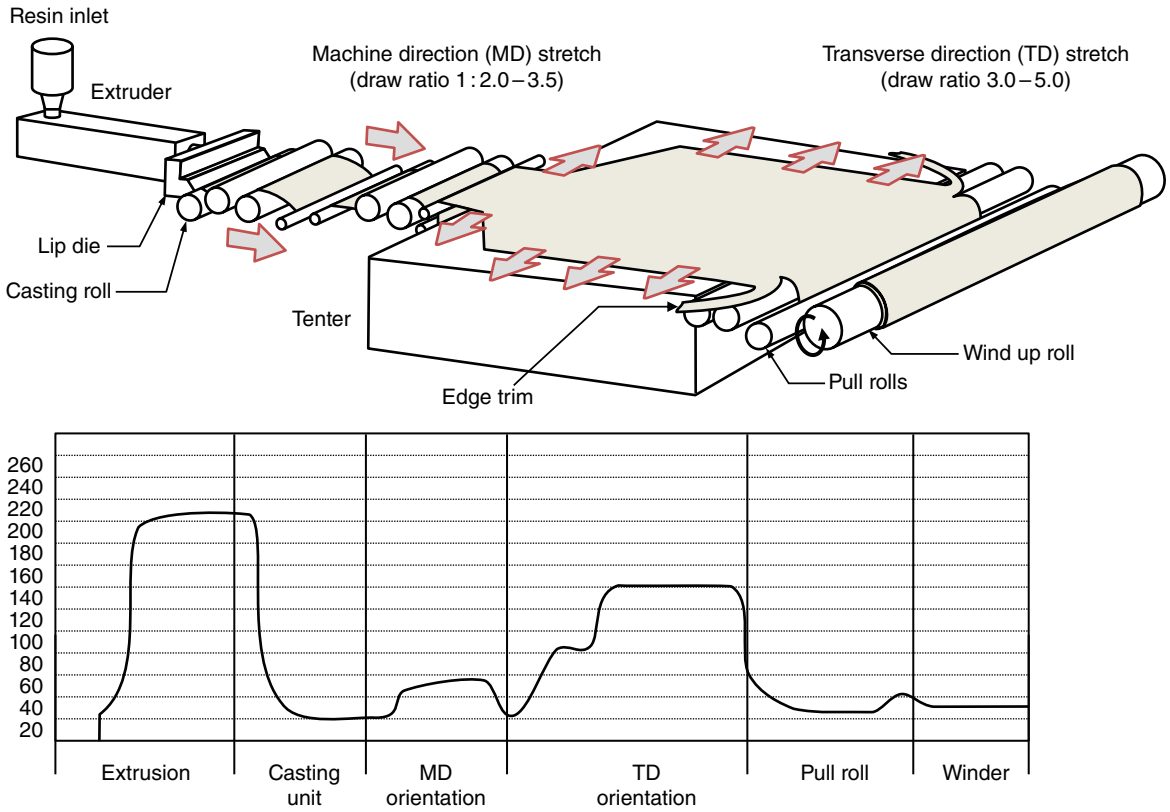


**FIGURE 13.9** Biaxially oriented extrusion cast film machine and typical temperature conditions used during biaxial orientation film casting. Source: Adapted from Refs 18 and 63.

**TABLE 13.3 Mechanical Properties of 90/10 (L/D,L) PLA ($M_w$ 145,000 Da) Under Different Processing Conditions [17]**

| Processing Conditions | Tensile Strength (MPa) | Modulus (GPa) | Elongation (%) |
|---|---|---|---|
| Injection molded | 53.4 | 1.03 | 4.6 |
| Injection molded followed by annealing at 130°C for 5 min | 58.6 | 1.29 | 5.1 |
| Extruded and biaxially oriented | 80.9 | 3.41 | 41.2 |
| Extruded, biaxially oriented, followed by heat set at 100°C for 10 min | 70.1 | 2.76 | 20.7 |

Biaxial orientation 3×3 was conducted at 85°C on 1.5 mm thick specimens.

**TABLE 13.4 Recommended Drawing Conditions in the Machine and Transverse Direction for PLA [70]**

| Section | Temperature (°C) |
|---|---|
| Machine direction | |
| Preheat | 45–65 |
| Slow draw | 55–70 |
| Fast draw | 70–75 |
| Annealing | 45–55 |
| Transverse direction | |
| Preheat | 65–70 |
| Draw | 70–85 |
| Annealing | 125–140 |

elongation at break than the quenched PLA from an injection molding process [17].

Uniaxial orientation of PLA can be achieved during film casting in conventional machine-direction orientation rolls. Typical drawing temperatures for PLA films in the machine direction (MD) and transverse direction (TD) are presented in Table 13.4. MD stretch ratios of 1:2.0–3.5 and TD stretch ratios of 1:2.0–5.0 are commonly used [70, 71]. As expected, the proportion of D- and L-isomers influences the strain-induced crystallinity. Moreover, the crystallinity decreases substantially as the stereo purity of the polymer decreases [13]. The amount of crystallinity attained through orientation depends on the mode of stretching (sequential versus simultaneous), strain rate, temperature, and annealing conditions [13, 72, 73]. High strain rate, low temperature, and high stretch ratio favor strain-induced crystallization during orientation. Taking the competitive crystallization and relaxation effects into consideration, Lee et al. [73] concluded that the optimal drawing temperature to obtain highly

oriented PLLA films ($M_W$ of 190,000 g/mol) is about 80°C. In contrast, Gruber et al. [20] used somewhat lower temperatures in their process for biaxial orientation of PLA with $M_n$ of 100,000–150,000 g/mol and with 10–20% *meso*-lactide content (65–72°C and 20°C for preheat and cooling rolls, respectively, for MD stretching; 63–70°C and circulated ambient air cooling for TD drawing).

Since the $T_g$ of biaxially oriented films is relatively low (~56°C), they tend to shrink when heated above this temperature. One strategy to induce thermal stability is by heat-setting, during which the oriented film is restrained at elevated temperature to relieve the residual stress. Bigg [17] heat-set biaxially oriented PLA films of 90/10 (L/D,L) copolymer ratio at 110°C for 10 min. A moderate reduction in tensile strength and modulus occurred, but the heat-set materials could be thermoformed at 75°C to produce dimensions that were stable at temperatures up to 100°C. Ou and Cakmak [72] prepared biaxially oriented PLA films by stretching cast PLA in both MD and TD to different ratios, followed by annealing these films at 110°C for 8 min to induce crystallinity and dimensional stability. Their wide-angle X-ray (WAXS) results showed that simultaneous biaxial stretching of PLA film did not impart significant crystalline order in the as-stretched films. However, annealing the films while they were held between in the grips resulted in dramatic development of crystalline order. In sequential stretching, the crystalline order built up during the first stretching was destroyed during the second stretching. This study highlighted that the properties of PLA films are dependent on the stretching sequence used during the orientation process [72]. Simultaneous biaxial orientation allowed higher planar stretch ratios (4.5 MD × 5.2 TD) than the sequential mode (2.2 MD × 6.0 TD), resulting in films with stronger mechanical properties (Figure 13.10) [71]. At slow deformation rates (<1 $s^{-1}$), the strain rate has a minimal effect on the stress–strain behaviors of PLLA. However, at higher strain rates typically encountered during extrusion casting, the nonlinear viscoelastic behavior is strongly dependent on the temperature and strain rate; in particular, the strain hardening phenomenon becomes more prominent, especially at lower stretching temperatures (Figure 13.11). Moreover, the stress–strain behavior is strongly dependent on the mode of deformation (e.g., simultaneous, sequential, versus width constraint) [74].

Recently, Xu et al. reported an interesting phenomenon in the ductile behavior of PLA films (2003D Ingeo™; $M_w$ 223,000 Da) prepared by melt-stretching. The melt-drawn films were prepared by uniaxially stretching PLA melt existing from the slit die (200°C) at melt draw ratios (MDR = chill roll speed/extrudate speed) ranging from 40 to 120, by adjusting the chill roll speed and extrudate velocity at the die exit [75]. The stretched melts were cast on a chiller roll at 50°C, forming cast films ranging from 30 to 12 μm in thickness. The melt-drawn films exhibited unusual ductility during tensile deformation. For example, at 40 MDR, the melt-drawn PLA exhibited elongation at break as high as 270% at room temperature (Figure 13.12b). The DSC thermograms showed that the melt-stretched samples were largely amorphous, although increasing MDR from 40 to 120 resulted in ~15°C decrease in the cold crystallization temperature during the first DSC heating scan (Figure 13.12a). Their wide- and small-angle X-ray scattering results suggested that the ductile deformation was related to the rigid amorphous fraction (RAF) transformation to mesophase and mobile amorphous fraction (MAF) chain extension. They proposed that the molecular orientation that took place during melt stretching formed the RAF weakly connected to the MAF, which served as the initial crystalline nuclei for cold crystallization (Figure 13.12c). Uniaxial stretching of melt drawn film in the yield region resulted in RAF chain slippage with an increase in MAF and mesophase. In the plateau region, MAF is being deformed in

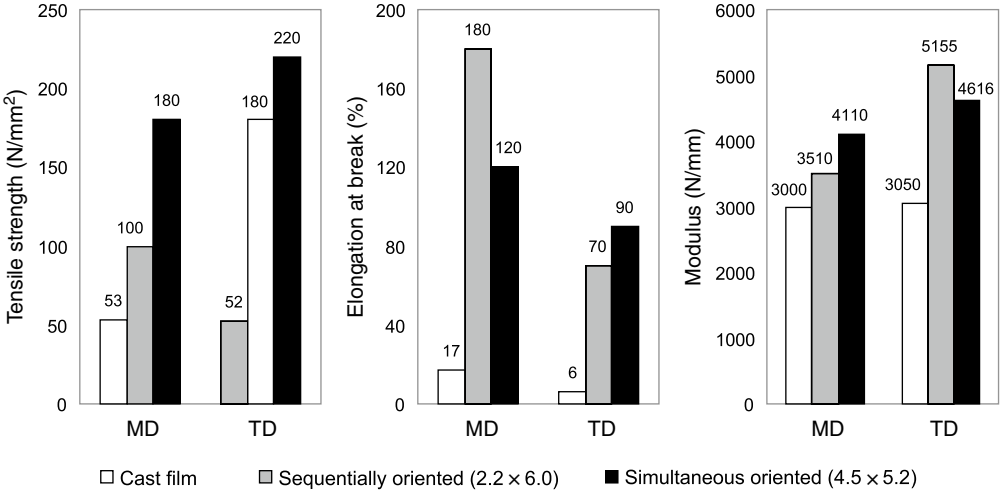


**FIGURE 13.10** Comparison of PLA films' mechanical properties. Source: Graphs are created based on the data from Ref. 71.

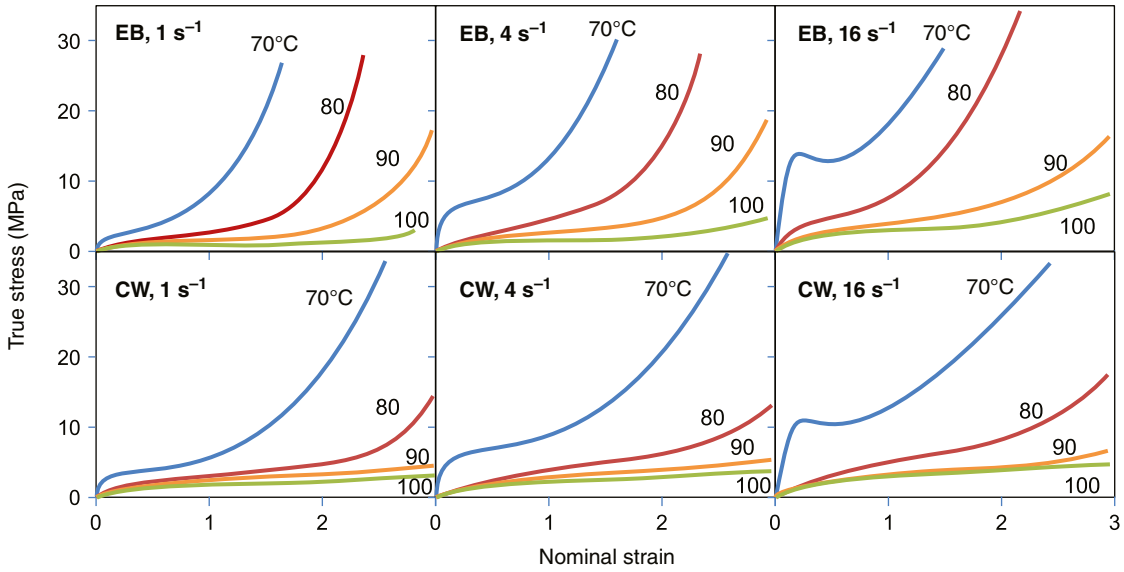


**FIGURE 13.11** Effects of strain rate, temperature, and mode of biaxial orientation on the stress–strain behaviors of PLLA sheeting (Purapol LX175; 96% L-isomer; 231 kDa molecular weight). EB: equal biaxial stretching; CW: constant width stretching. Source: Figures are recreated based on the data from Ref. 74 under the Creative Commons CC BY license.

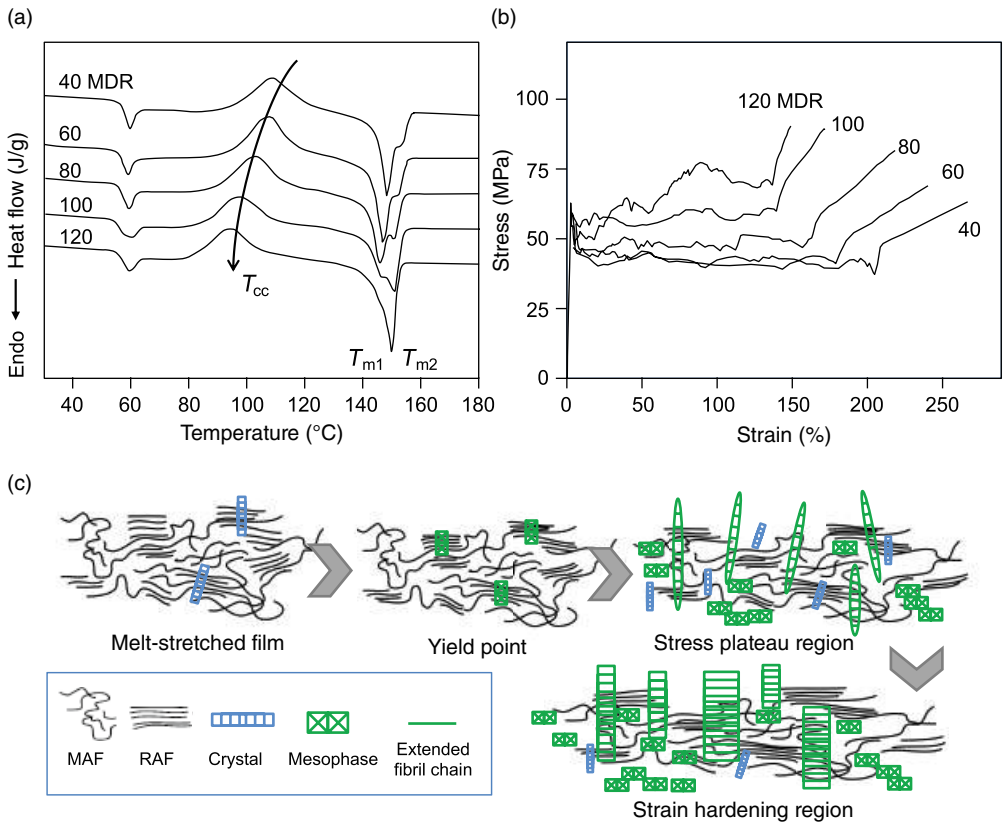


**FIGURE 13.12** (a) DSC thermograms of PLA films prepared at different melt-draw ratio (MDR). (b) Tensile properties at room temperature of PLA films as affected by MDR. (c) Conceptual representations of changes in structural elements contents of PLA during tensile deformation. MAF: mobile amorphous fraction; RAF: rigid amorphous fraction. Source: Adapted from Xu et al. Ref. 75 with permission from John Wiley and Sons.

the stretch direction with concomitant strain-induced crystallization. In the strain-hardening region, small crystals are broken and transformed into mesophase. Hence, while there is an increase in chain orientation and chain packing, it did not increase the perfection of the crystals [75].

Commercial PLA grades that are processed into biaxially oriented films include Ingeo 4043D (4.3% D) and Ingeo 4032D (1.5% D). Properties for 25.4 μm film (1.0 mil) after stretching 3.5× in MD and 5× in TD listed in the NatureWorks technical data sheets show elongation-at-break values in the MD direction of 160–180% for these films, with TD elongation-at-break of 100% [76]. The films can be heat set after TD stretching, resulting in enhanced resistance to boiling water shrinkage. These materials are routinely processed into rigid, ductile, clear films at industrial scale.

PLA is often coextruded with other polymers to form multilayer structures to enhance its performance properties. One patent disclosed a method to produce a multilayer biaxially oriented PLA film to enhance moisture barrier properties through sputter coating the PLA film with a thin layer of a metal primer (e.g., copper, titanium, nickel) [77]. The metal priming process was achieved using electrical corona-discharge treatment in a controlled $N_2/CO_2$ atmosphere excluding $O_2$, at 500–1000 ng/cm$^2$ coverage. The treated surface was then subjected to vacuum vapor deposition with aluminum. The metal primer layer improved the metal adhesion of the subsequent metal layer (30–60 nm thickness), resulting in enhanced gas barrier as compared with aluminum metalized PLA film without this pre-treatment. Reportedly, the metalized film had a water vapor transmission rate of lower than 0.5 g/m$^2$ day at 38°C and 90% RH. Because of the thin metalized coating applied, the multilayer PLA film still met compostable standards.

Noda et al. [78] disclosed a method of coextruding multilayer laminate film consisting of polyhydroxyalkanoate (PHA) copolymer (copolymer of 3-hydroxybutyrate with 3-hydroxyhexanoate) and PLA to impart softness to the PLA, and at the same time reduce the tackiness of the PHA. By preventing the web from sticking to itself or the processing equipment, the speed of production and product quality can be improved. Lee et al. co-extruded PLA with a biodegradable aliphatic-aromatic copolymer, poly(butylene adipate-co-terephthalate) (PBAT), to form alternating multilayer sheeting structures of up to 95 layers at about 245 μm total thickness. The sheeting samples were then pre-heated and stretched into 20 μm films [79]. At the same PLA : PBAT 70 : 30 blend ratio, the direct blend composite was substantially hazier and lower in light transmittance than the multilayer structures. The direct blend resulted in lower PLA crystallization temperature (94°C) than the neat PLA (118°C), while the extent of crystallization temperature depression was lower for those of the multilayer structures (122, 108, 108°C for 5-, 43-, and 95-layer structures, respectively). Moreover, the $\Delta H_m$ decreased with increasing number of layers as the interfaces probably due to two-dimensional spatial constraints on crystal lamellae growth [79].

## 13.8 STRETCH BLOW MOLDING

PLA bottles formed by the injection-stretch-blow molding (ISBM) process are subjected to biaxial orientation in the axial and hoop directions to impart mechanical and barrier properties. The crystallites produced during the strain-induced crystallization also reduce the aging effect since they can act as physical cross-links to stabilize the amorphous phase, thereby reducing its brittleness and the effect of aging [21].

The first step of ISBM involves the injection molding of the preform followed by inflating it in a blow molding machine. In a two-stage process, preforms are heated by a series of infrared lamps to 80–110°C (Figure 13.13a). Different power settings are usually applied to the infrared lamps to achieve a preform temperature profile optimal for stretching the preform into a bottle of uniform wall thickness distribution. The preform is then transferred to the blow molding station, where it is stretched by a stretch rod in the axial direction (Figure 13.13b) at a speed of 1–1.5 m/s (Figure 13.13c–e). During the pre-blow phase (Figure 13.13d and e), compressed air of 0.5–2.0 MPa is admitted to the preform through the blow nozzle to partially inflate the preform to prevent it from touching the stretch rod during the axial stretching. After the stretch rod pins the preform to the mold base, air pressure is ramped up to 3.8–4.0 MPa to fully inflate the preform to take the shape of the blow mold and to imprint the surface details of the bottles (Figure 13.13f and g). The high blow pressure is maintained for several seconds to allow the bottle to cool down before allowing the compressed air to exhaust (Figure 13.13h). The blow mold temperature for PLA is typically set at around 35°C. The mold halves are opened and the bottle (Figure 13.13i) is finally ejected. In a single-stage process, similar operations are used except that the injection-molded preforms are partially cooled down to 100–120°C and immediately transferred to the blow molding station for blowing without going through the reheat phase.

PLA exhibits strain hardening when it is stretched beyond its natural stretch ratio. This phenomenon can be leveraged to minimize wall thickness variation of the stretch blown PLA bottle, by developing a preform that matches the target bottle size and shape, such that optimal stretch ratios are achieved during blow molding. Preforms that are understretched will result in bottles with excessive wall thickness variation, heavy bases, weak mechanical properties, and poor aesthetic appeal (e.g., lens defect below the support ledge region). On the contrary, overstretched bottles can also result in stress whitening due to the formation of

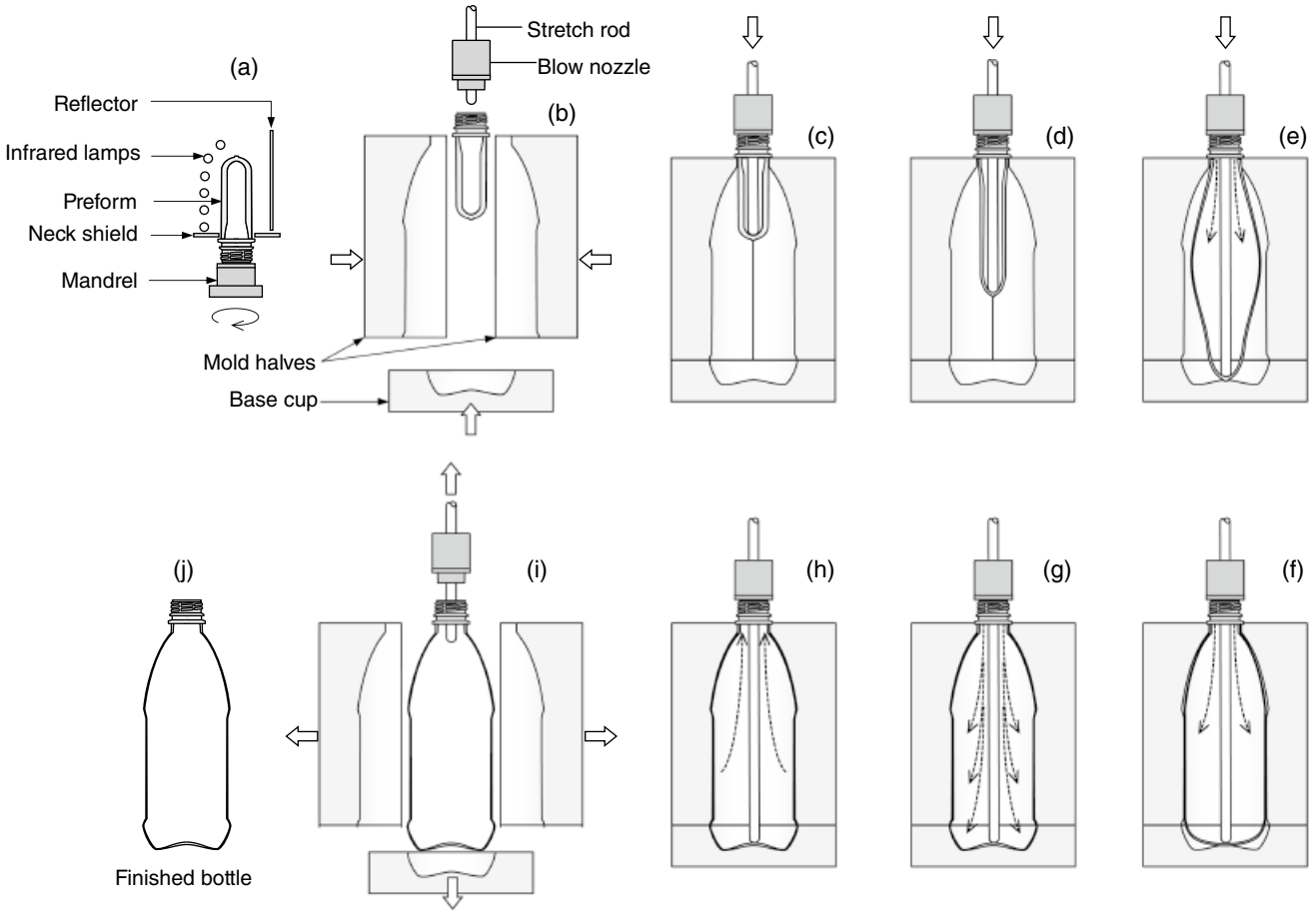


**FIGURE 13.13** Injection-stretch-blow molding cycle of PLA bottle: (a) preform reheat; (b) transfer preform into blow mold; (c)–(e) axial stretching by stretch rod; (e, f) hoop stretching with low pressure air; (g) final blow with high pressure air; (h) air exhaust; (i) withdraw stretch rod and open blow mold; and (j) eject bottle.

microcracks on the bottle surfaces that scatter light. Typical commercial grade PLA resins for bottle applications require preform axial stretch ratios of 2–3 and hoop stretch ratios of 3–4, with the desirable planar stretch ratio of 8–11 [80]. Considering that the ultimate crystallinity after stretching tends to decrease with decreasing stereoisomeric purity of the polymer [13], the optimal stretch ratios are expected to vary depending on the grade of PLA used. Depending on the shape of the stretch-blown articles, critical subtle features (e.g., standard versus reversed taper, step changes, transition points on the core/cavity) may be incorporated into the preform design to achieve optimal bottle side wall thickness distribution.

PLLA is biocompatible and bioabsorbable and hence ideal for biomedical implant applications (see details in Chapter 25). One of the emerging biomedical applications of PLLA is to be used as a bioresorbable vascular scaffold (BVS) for the surgical treatment of coronary heart diseases. Such BVSs are produced by stretch-blow molding like the production of bottles but without involving a stretch rod. Here, a section of an extruded PLLA preform tubing (~1.5 mm outer diameter) is enclosed within a mold and heated above $T_g$ and inflated with air pressure, forming an expanded tube of about 3.5 mm outer diameter and wall thickness of 150 μm. While the inflation induces circumferential molecular orientation, simultaneous or sequential stretching along the axial direction results in the orientation of molecular chains. The expanded tube is laser-cut to create axial struts and azimuthal rings. It was then crimped over a delivery balloon, reducing its OD to about 1.7 mm in the crimped state [74, 81]. Ailianou et al. [81] applied X-ray microdiffraction and reported the presence of multiple, micron-scale morphologies in the crimped BVS, which are important to confer ductility to PLLA and resist fracture upon deployment [81]. On the other hand, Wang et al. applied Raman spectroscopy and finite element analysis to look at the spatial degradation of PLLA BVS and concluded that the stresses generated from crimping and inflation can cause a loss of structural integrity and result in asymmetric degradation due to the introduction of irregularities in the microstructure during the fabrication and implantation process [82].

## 13.9 EXTRUSION BLOWN FILM

Blown film extrusion is an efficient process with low scrap rates. Depending on the material and process conditions, the process can produce some level of biaxial orientation, which provides different film properties versus completely unoriented films. However, orientation is typically lower in blown film samples versus films made using a higher orientation process, such as biaxially oriented films. In the extrusion blown film process, molten PLA is extruded to form a tube using an annular die. By blowing air through the die head, the tube is inflated into a thin tubular bubble and cooled. The size of the bubble is maintained by a certain internal pressure. The tube is then shaped in a collapsing frame, flattened in the nip rolls and taken up by the winder (Figure 13.14). The ratio of bubble diameter ($D_f$) to the die diameter ($D_0$) is called the blow-up ratio (BUR). BUR ratios of 2–4 with a die temperature of 190–200°C have been used for extrusion blowing of PLA films [84, 85]. At a given take-up speed ($V_f$), increasing the BUR will form a larger bubble, thereby increasing film width, enhancing orientation in the hoop direction, reducing blown film thickness ($h_f$), and promoting quicker cooling. On the other hand, increasing the winder take-up speed increases the orientation in the machine direction and film length, but decreases film thickness. The ratio of the $V_f$ to the extrudate speed ($V_0$) is termed the draw ratio (DR), which is also equal to the ratio of the die gap ($h_0$) to the film thickness, divided by the BUR. Typically, DR values range from 10 to 14. By varying the BUR, screw speed, air pressure, and winder speed, films of different thicknesses (10–150 μm) and degree of orientation can be achieved. Below the $T_g$, PLA is a stiff, glassy polymer, and care must be taken with the design and operation of the extrusion blown system to ensure that the film is at appropriate temperatures during collapsing and nip operations to prevent unwanted wrinkles.

The extrusion blown film process requires the use of polymer with relatively high melt strength. Compared to polyolefins, PLA has lower melt strength and is more prone to processing issues such as draw resonance, helical instability, frost-line oscillation, "breathing," "dancing," and bubble sag [86]. Although blown film extrusion of PLA can be achieved without the incorporation of a melt strength enhancer, precise control of processing temperature,

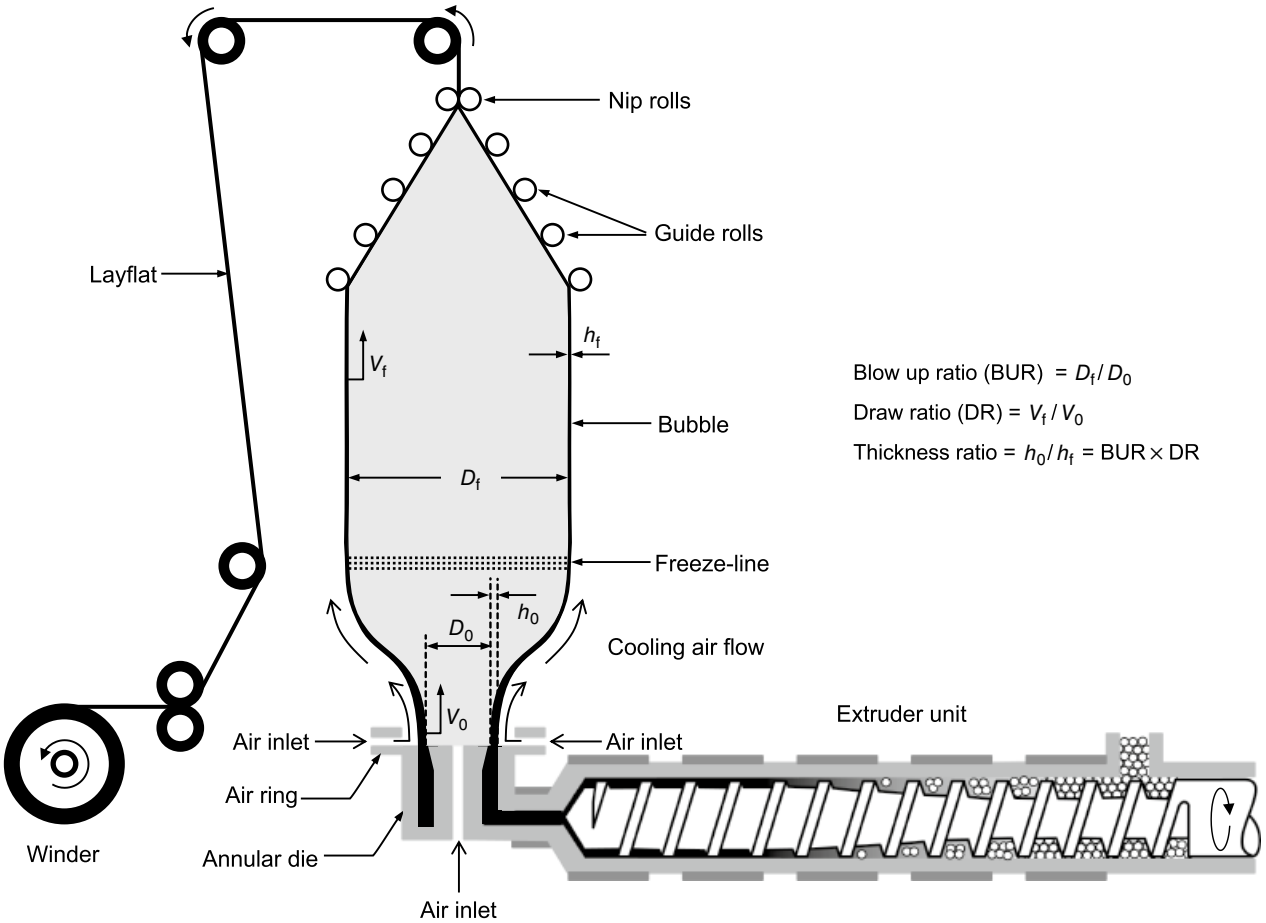


**FIGURE 13.14** Blow film extruder and key process parameters. $V_f$: take-up speed, $V_0$: velocity of material at the exit of die, $h_f$: thickness of film, $h_0$: thickness of tube, $D_f$: diameter of tubular film, $D_0$: diameter of tube. Source: Adapted from Ref. 83.

processing speed ratio (i.e., ratio of the speed of take-up rollers to the rotational screw speed of the extruder) and internal air pressure must be achieved [87]. Heat management in the bubble collapse is also an important variable to consider during take-up and winding to prevent blocking and fusing of the film. To expand the extrusion blown processing window, viscosity enhancers are often added to increase the melt strength of the polymer. These additives protect the polymer from degradation and/or couple polymer chains to attenuate the overall loss of molecular weight and viscosity of the polymer melt. Karkhanis and Matuana evaluated a multifunctional epoxy (Joncryl® ADR 4468) approved by the U.S. Food and Drug Administration for food-grade applications, for modifying PLA (Ingeo 4044D) by chain extension and introducing branching in the polymer. Their extrusion blown film was processed with a BUR of 5 into thicknesses of about 27 µm. They reported a maximal loading of the chain extender of 0.5%, beyond which a substantial increase in viscosity hampered the extrusion blown processing. The incorporation of the additive reportedly resulted in a substantial reduction in crystallinity and improved the ductility of the PLA films [88]. Similarly, Mallet et al. incorporated 0.5% Joncryl ADR 4368 epoxy chain extender to PLA (Ingeo 4032D) along with a ternary formulation (1% *N*,*N*′-ethylene bis(stearamide) as slip additive; 1% talc as nucleating agent; and 10% poly(ethylene glycol) as plasticizer) [86]. The addition of these additives significantly enhanced the process stability with an increase of the BUR from 7 to 12 at high DR, thereby expanding the processing window considerably. Other coupling agents reported in the literature include copolymers of styrene, methyl methacrylate, glycidyl methacrylate, and peroxy compounds (e.g., *tert*-butylperoxybenzoate, dibenzoylperoxide, *tert*-butylperoxyacetate) [84, 85].

Since PLA films are quite stiff and have high surface COF, collapsing the bubble in the nip rolls tends to produce permanent wrinkles. This problem can be overcome by incorporating anti-adhesion agents during extrusion, such as talc, $TiO_2$, and $CaCO_3$. Slip additives (e.g., oleamide, stearamide, *N*,*N*′-ethylenebis(stearamide), oleyl palmitamide) have also been added to reduce the COF [85]. Typically, a slip additive concentration of less than 0.5–1.0% by polymer weight is used, as excessive amounts will compromise the ability of print inks and labels to adhere to the film surface. Blending PLA with other biopolymers such as PBAT is a common strategy for the production of blown films with mechanical properties suitable for applications such as carrier bags, agricultural mulch films, and organic waste bags [89].

## 13.10 THERMOFORMING

Thermoforming is a common manufacturing method for food serviceware and packaging containers without complicated features (e.g., undercuts, detail imprints, small radius features). Low-to-mid-gauge (<1 mm) PLA sheets have been successfully thermoformed into disposable cups, single-use food trays, lids, yogurt cups, and blister packages. Figure 13.15 shows the typical steps for thermoforming of

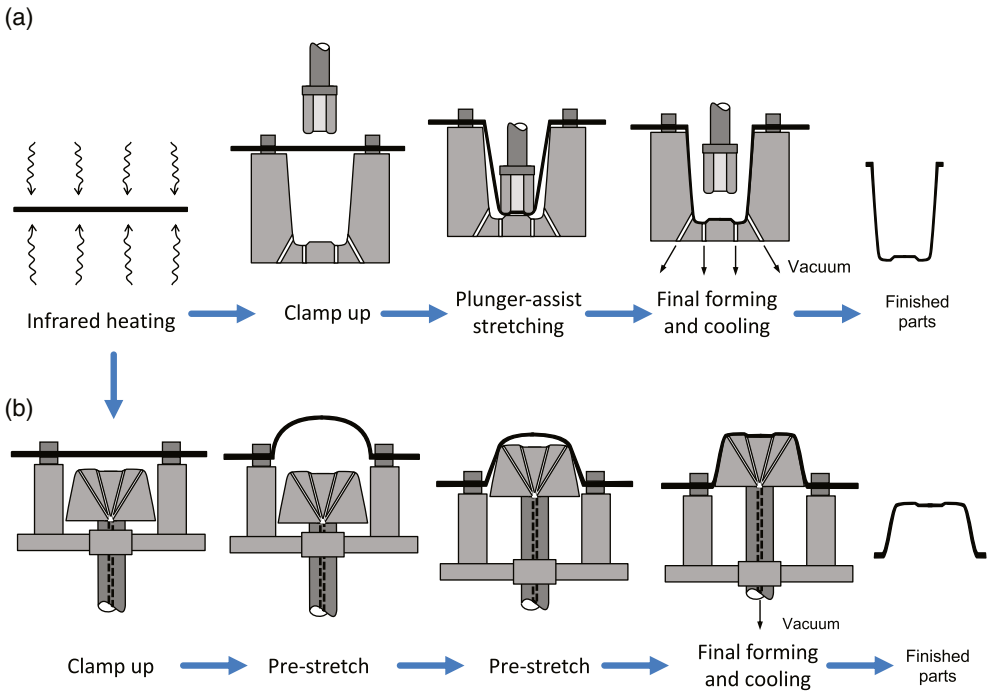


**FIGURE 13.15** Thermoforming of heated PLA sheet over a negative mold using plug-assist drawing (a) and a positive mold using reverse drawing processes (b).

PLA containers. In this process, PLA sheet is clamped on the mold frame and heated to a forming temperature above $T_g$ for optimal material stretching, while avoiding over-heating to prevent sheet drooping, poor thickness distribution, and heat-induced crystallization. In the plug-assist thermoforming process, a plug or plunger pushes the heated PLA sheet into the mold cavity. The air trapped in the mold cavity is evacuated by a vacuum pump, forcing the PLA sheeting to conform to the shape of the mold. Shaping may be assisted by compressed air or positive pressure on the opposite side of the sheet to push the sheet on to the mold surface. In a reverse draw process, the mold pushes toward the heated sheet, followed by vacuum suction to draw the sheet toward the mold surface. The stretched article cools on the mold until it is rigid enough for demolding. The thermoformed part is then trimmed to form the final product. Depending on the part design, plug-assist stretching, or prestretching may be used to achieve uniform part thickness.

Heating of PLA sheet for thermoforming is generally achieved by infrared (IR) radiation absorption from heater elements, although convection and conductive heating may also be used. To prevent excessive thinning of areas such as corners and deep-drawn regions of thermoformed articles, the temperature distribution of the PLA sheet can be controlled by zone-heating with separate controllers in different oven positions. Because each polymer has an optimum IR absorbance frequency, the heater element should be set at the temperature at which most energy is absorbed by the polymer. Typically, PLA is thermoformed in the range of 80–110°C [90], although crystallized PLA sheet may be thermoformed at higher temperatures [91, 92]. In the case of thermoforming during form-fill-seal operations, equipment will often not have an oven, but will use actuated platens and contact heating over multiple cycles to warm the sheet in specific positions. Usually, aluminum molds are used for thermoforming PLA containers. Molds, trim tools, and ovens designed for thermoforming of PET, high impact polystyrene (HIPS), and oriented polystyrene (OPS) can be used for forming PLA containers. However, molds for thermoforming of PP may not be used interchangeably for PLA because PP shrinks considerably more than PLA during cooling. For a given part thickness, cooling times required for PLA containers in the mold tend to be higher than for PET and PS containers due to the lower $T_g$ and thermal conductivity of PLA polymers [90].

Orientation of polymer chains during thermoforming increases toughness of PLA containers. Regions of PLA articles that are highly drawn are less brittle as compared with flanges and lips that received minimal orientation. Molecular weight of PLA may affect the thermoforming behaviors; high-molecular-weight polymer may not produce satisfactory mold surface definitions while low-molecular-weight polymer may result in thinning around corners of molded articles and areas where deep draws occurred. As expected, thermoforming behaviors are dependent on the D- and L-isomer contents due to changes in strain-induced crystallization and self-leveling behavior. Poloskei et al. investigated the thermoforming behaviors of PLA sheets derived from Ingeo biopolymers of various D-lactide contents (4032D, 1.4% D; 2003D, 4.3% D; 4060D, 12% D). The PLA sheets were thermoformed using a rig for burst test and involved pushing the specimens using a ball fixture (deformation rate 50–500 mm/s; test temperatures 25–75°C) that approximated the biaxial deformation during thermoforming [93]. With a slow crystallization rate, they reported that 4060D resulted in thermoformed samples of low crystallinity and tensile strength independent of both temperature and deformation rate. However, with lower D-contents, 2003D and 4032D exhibited strain-rate-dependent crystallinity; their tensile strength increased linearly with deformation rate at 65°C, but not at 25°C [93].

Aritake [94] disclosed a composition comprised of a mixture of amorphous (L- or D-isomer of less than 92% purity) and crystalline (L- or D-isomer of greater than 94% purity) PLA polymers that showed good thermoforming ability with improved impact and heat resistance compared with the amorphous extruded sheet. The thermoforming process was carried out by preheating the oriented sheet to 145°C and using a mold temperature of 60°C. To prevent excessive sheet sagging during heating, the extruded sheet was heat set by stretching 2.8 times in the transverse direction at 75°C, followed by heat fixing at 135°C for 30 s while applying tension. Reportedly, the treatment resulted in sheet that shrunk by less than 5% in the longitudinal and transverse directions when placed in a 90°C oven for 30 min [94].

To accelerate the crystallization during thermoforming, heterogeneous nucleating agents are incorporated into PLA. One patent disclosed a method to induce crystallinity corresponding to melting enthalpy of about 15 J/g by heating the PLA sheet prior to thermoforming. Nucleating agents, such as talc of less than 1 μm particle size, were added at about 5–10% to enhance crystallization during preheating [91], and further crystallization during forming and cooling, which led to heat stable parts even with chilled molds. Similarly, Deetuam et al. investigated the isothermal cold crystallization kinetics and properties of thermoformed PLA composites, as affected by the addition of talc (3 μm), calcium carbonate (5 μm), and cassava starch (12 μm), loaded at 1–10% filler levels [92]. At isothermal temperature of 100°C, they reported that the highest crystallization rate constant and the shortest crystallization half-time for the PLA/talc composites, implying that talc was the most effective among the nucleating agents tested. Furthermore, surface-functionalized talc by silanization with 3-aminopropyltriethoxysilane further accelerated the cold crystallization rate and enhanced the composite material properties due to improved interfacial interaction between the talc particles and the thermoformed PLA matrix [92]. Ethylenebis(stearamide) has also been used as an effective

PLA crystal nucleating agent during heating and is often an ingredient for crystalline thermoforming applications.

While amorphous and low-crystallinity PLA polymers are commercially fit-for-use for room temperature and chilled uses, the low $T_g$ of PLA polymer prevents amorphous PLA from being used in food serviceware and packaging applications where high thermal stability is needed (e.g., hot filled parts, cups for hot beverages, microwave-able package). Nucleated and crystallized PLA parts are useful for elevated temperature applications, which can be processed in thermoforming using two-stage equipment. The first stage shapes the part on a heated mold, set at temperatures that facilitate crystallization, and the second stage is a chilled mold to remove heat before trimming and collecting. PET is often processed this way for dual ovenable trays and has the common nomenclature CPET for crystalline PET. The abbreviation for such parts made from PLA is CPLA. Production speeds of CPLA products are dependent on the material and equipment and are a function of crystallization and stiffening time. To increase the thermal stability of thermoformed PLA bowls, Lee et al. laminated PLA foam sheet (Ingeo 8052D, 4.7 mol% D-isomer) with a high heat deflection temperature (HDT) solid PLA skin layer (Ingeo 2500HP, 0.4 mol% D-isomer content). With a high HDT skin layer of thickness of 100 μm or greater, the thermoformed bowl could withstand 99°C water for more than 13 min with minimal deformation [95].

Extruded sheets for thermoforming made from neat PLA are relatively brittle at room temperature, and therefore material handling may require some additional considerations. During thermoforming, to ensure smooth feeding and to prevent web breakage, a tight radius should be avoided in the unwind stations and skeleton rewind stations. A minimum rewind radius of 25 cm is recommended [40]. If the PLA sheet needs to be trimmed before thermoforming, it should be heated to temperatures near 90°C to prevent cracking. In a roll-fed machine, the PLA sheet is usually fed by two parallel motorized spike chains. The spikes pierce the edge of the sheet and convey it through the thermoforming line. Since extruded PLA sheet is quite brittle, edge-strip heating (contact or radiant) is recommended to prevent cracking or punching out of small particles. Incorporating impact modifier additives can dramatically improve the ductility of PLA for thermoforming processing and can reduce or eliminate many of the brittleness concerns.

Storage conditions for the PLA sheet stock should be controlled. As a guide, PLA should not be stored at temperatures above 40°C as the sheet may block and resist unwinding due to its low $T_g$. PLA waste from the trimming process can be ground and added to the extruder to recycle the material. Typically, PLA regrind of less than 40–50% is used to prevent significant change in the performance of thermoformed PLA containers. Since the regrind may be amorphous trim scrap, proper material handling, drying, crystallizing, and/or melt extrusion conditions may need to be optimized to prevent blocking in dryers, hoppers, extrusion feed throats, or sticking to extrusion screws.

## 13.11 MELT SPINNING

Many commercial grades of PLA polymers are available for melt spinning of fibers. PLLAs with a range of viscosity-average molecular weight ($M_v$) of around $0.5–3.5 \times 10^5$ Da have been processed via melt extrusion and then hot drawing [96–98]. PLA fiber extrusion is carried out above the $T_m$, in the temperature range of 185–240°C, through a spinneret. Lower extrusion temperatures may be used for polymers with low optical purity. Low moisture content (<50–100 ppm) is necessary to minimize hydrolytic degradation when higher melt process temperatures are used for fiber spinning. Before fiber melt extrusion, the polymer is commonly dried to moisture content of about 50 ppm. A typical melt spinning setup consists of (i) extruder; (ii) manifold distribution arrangement for the melt; (iii) metering pump to regulate polymer flow rate; (iv) spin pack to filter and extrude the polymer melt or spin dope through fine holes; (v) quench duct for cooling the extruded polymer filaments and solidifying them; and (vi) winder to pull and wind the solidified filament. This arrangement is shown schematically in Figure 13.16. The entire line from extruder output to the spin pack is maintained at a constant spinning temperature.

A general-purpose single-screw extruder of 24 : 1 to 32 : 1 L/D with feed throat cooling is common for processing PLA [100]. A mixing tip is generally recommended along with static mixers in the product stream to ensure temperature uniformity, as well as optimum additive dispersion and melt polymer homogeneity. Table 13.5 shows a typical melt temperature profile for PLA. The extruder melts the polymer and then compresses the fluid to remove any trapped gasses including air/nitrogen that is drawn along with the fed polymer chips. It also acts as a polymer fluid pump and provides the necessary pressure that is required for the polymer to flow from the extruder to the metering pump.

For monofilament spinning, a spinneret plate with one hole spins a single filament, which is then wound on a bobbin. Typical spinneret plates for monofilaments have a single spinneret hole with a diameter of about 0.5–1 mm. The denier (weight in grams of 9000 m long filament) of such filaments are in excess of 20. To produce multifilament yarn, the spinneret plate has numerous holes arranged in a particular pattern, and all the extruded filaments from this spin pack are wound together on one bobbin. Holes are arranged in a staggered configuration to allow enough separation between holes to prevent filaments from sticking to

each other due to extrudate swelling and to ensure cooling air is available to all the filaments in the quenching zone. Uniform and consistent melt temperature control is necessary for optimal PLA melt spinning. For example, vapor heat transfer medium systems have been employed to achieve melt spinning temperatures at the desired PLA melt temperature. Good melt filtration is also important, especially for melt spinning of fine fibers, to prevent fiber breaks in spinning and drawing due to contamination. Recommended capillary dimensions for a PLA fiber with a solid, round cross-section range from 0.2 to 0.35 mm diameter, typically with a L/D ratio of 2–4. Larger capillaries may be necessary for fibers greater than 6 denier per filament (dpf). Capillaries for different shaped cross-sections should be designed to provide for the desired shape, pressure drop, fiber fineness, and drawing to ensure optimal processing and final properties. After exiting from the spinneret die, the extruded filament is stretched as it passes through an air quench zone (or chamber) shielded from the outside air by a quench shield. This has a mild flow of cooling air at about 15–30°C with low-to-moderate relative humidity. When the spinning filaments are exposed to the cooling air, heat is removed, which facilitates solidification through crystallization. As soon as the temperature of the spun filament reaches the $T_g$, the spinning process is complete. Typical quenching conditions for PLA are shown in Table 13.6, but quenching conditions need to be optimized for a product depending upon the output rate, denier, the number of filaments, die design, and the cross-sectional shape of the spinning filament. A monomer exhaust system is preferred to prevent the buildup of residual lactide around the spinneret face and the quench screen.

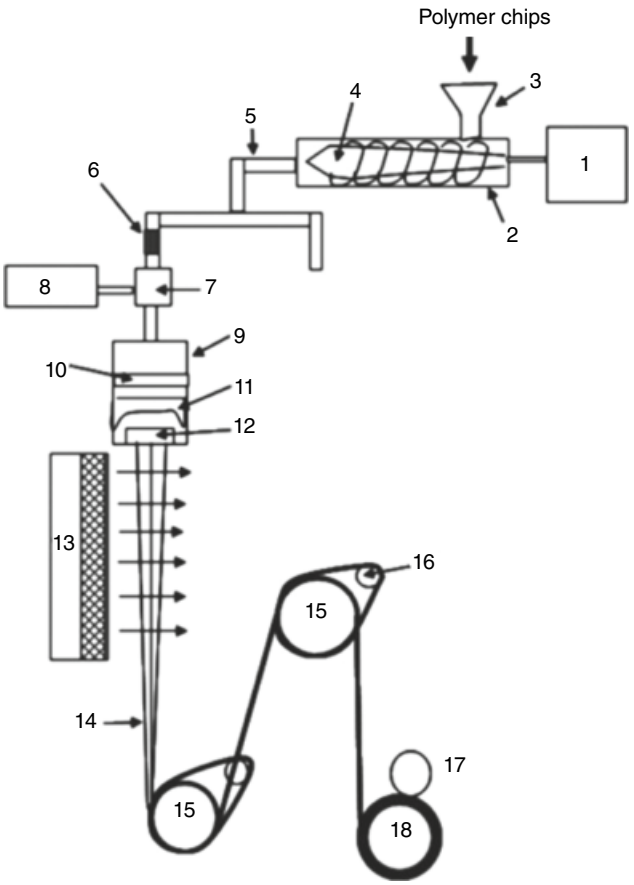


**FIGURE 13.16** Schematic representation of melt spinning setup: (1) extruder drive, (2) extruder, (3) hopper, (4) screw, (5) manifold, (6) static mixer, (7) metering pump, (8) metering pump drive, (9) spin pack, (10) mesh filters, (11) distributor, (12) spinneret, (13) crossflow quench chamber, (14) freshly spun yarn, (15) godet, (16) idler roller, (17) friction-driven winder, (18) yarn bobbin. Source: Reproduced with from Ref. 99 with permission from John Wiley and Sons.

**TABLE 13.5 Typical Melt Temperature Profile for PLA**

| Extrusion Area | Melt Temperature Setting (°C) |
|---|---|
| Feed throat | 25 |
| Zone 1 | 200 |
| Zone 2 | 220 |
| Zone 3 | 230 |
| Melt pump | 235 |
| Spin head | 235 |

*Notes*: (1) Temperatures are only starting points and may need to be altered. Target PLA melt temperatures (after melt pump) should be in the range of 235 ± 5°C. (2) PLA resins should not be processed at temperatures above 250°C due to excessive thermal degradation.

The filaments are given a spin finish at the end of the spinning line (just after the glass transition is reached) by one of the many techniques, such as kiss-roll or nozzle spray. The finish is normally sprayed onto the filaments in high-speed spinning machines. Readers may refer to the literature for information on spin finish functions and their formulation [101].

The next important device is the take-up winder. Usually, the yarn is not wound directly on the winder but is passed through a take-up godet, or a set of godet rollers (Figure 13.16). This breaks the vertical path of the spinning and allows the winder to be adjusted easily in the available space. Also, in an integrated system, the spun filaments may be subsequently drawn between the two godets before winding (also known as in-line spin-draw frames). The spinning speed is determined by the speed of the first

**TABLE 13.6 Typical Quenching Conditions for PLA**

| Quench Parameter | Typical Target |
|---|---|
| Quench air velocity (m/s) | 0.26–1.5 |
| Quench air temperature (°C) | 10–20 |
| Monomer exhaust velocity (m/s) | 0.26–2.0 |
| Spacer or shroud length (mm) | 50–100 |

rotating surface that the filament contacts after coming out of the quench chamber. This can be the first take-up godet or the take-up winder if the spun filaments are directly wound onto the winder without breaking their vertical path.

The winders may be friction-driven, where the bobbin is driven by a friction roller so that the surface speed of the winder remains constant throughout the formation of the yarn package. However, friction rollers are not optimal for high-speed spinning machines because, when the spinning yarn encounters such surfaces, it can get abraded. Therefore, bobbin winders that are directly driven by a motor are more commonly used. To compensate for the increasing speed as the diameter of the bobbin package increases, a feedback mechanism is installed, where the speed of the winder is regulated to maintain constant tension in the spinning line. PLA can be spun over a wide range of take-up speeds, but typically runs between 1100 and 1850 m/min for as-spun or staple fiber processing.

PLLA filaments can be spun at high speed, with take-up velocities of up to 5000 m/min [98, 102]. The crystallinity, birefringence, tensile strength, Young's modulus, and yield strength all exhibit maxima at take-up velocities between 3000 and 4000 m/min. The boiling water shrinkage exhibits a minimum in this range. This implies that a stable morphology is developed through strain-induced crystallization at this speed. The maximum tensile strength of the as-spun filaments has been reported to be 385 MPa and the maximum modulus to be 6 GPa. As the spinning speed is increased, the effect of air drag and inertial forces on the total stress value of the spinline increases substantially. Many studies have modeled the high-speed spinning process of various polymers to explain the spinline dynamics [103–106].

Partially oriented yarn (POY), highly oriented yarn (HOY), and spunbond melt spinning are products produced using relatively high filament velocities to achieve improved mechanical properties with dimensional stability. Nonwoven melt spun processes such as spunbond use air aspiration and a venturi system to draw the fibers and to make a random web on a forming belt for collection and bonding. Instead of drawing filaments from the die, melt-blown processes use hot air to push filaments away from the die and onto a collection belt or drum for subsequent fabric bonding and winding. The high velocity hot air enables the fiber melt stream to draw and thin significantly, creating very fine fibers. This allows for unique nonwoven structures to be produced, which capitalize on the large fiber surface area for applications such as air and liquid filtration. Melt-blown PLA fibers are typically produced with low orientation, low crystallinity, and low shrinkage [63]. Bonding is used to alter the properties of nonwovens, such as tensile properties and softness. Various methodologies can be used such as thermal calendering using different engraving patterns, through-air oven, hydroentangling by water jets, and the use of chemical binding agents.

PLA fibers produced by melt spinning may result in a reduction of molecular weight if processing conditions such as melt temperature, residence time, and resin drying are not properly optimized and managed. The literature has many examples of high molecular weight loss during spinning. In one study, the molecular weight was reduced from 330,000 to about 120,000 and 105,000 Da for as-spun and drawn fibers, respectively [97]. The degradation percentage is higher when higher shear rates are applied, as in the case of higher molecular weight PLA. The molecular weight degradation is attributed to ester group cleavage due to rapid hydrolysis reactions with residual water in the polymer at high melt-spinning temperatures. Modification of PLLA by end capping through acetylation of terminal carboxylic acid groups did not improve thermal stability during fiber melt spinning at 200°C in comparison with the untreated polymer [107]. The molecular weight degradation in melt spinning has been found to be much higher than the slight $M_w$ drop (about 6%) observed in fibers produced by a dry solution spinning process. The decrease of $M_n$ during melt spinning also leads to lower orientation and crystallinity in PLA fibers. As a result, the longer the period of applied thermal history, the lower are the tensile strength and modulus of the fibers [108]. Melt stability of PLA may vary substantially, depending on how it was produced and processed [109].

After spinning, fiber is subjected to drawing in a two-stage system. In the case where a thick filament tow (tow band) is being converted into staple fibers, the use of a predraw bath is recommended [100]. Initially, the tow temperature is raised to 25–50°C using sufficiently long predraw baths. These baths also enable saturation of the tow with moisture and finish. During predraw, the tow should not be heated above the $T_g$ of PLA (~58°C), otherwise the tow could begin to draw, which leads to many problems. Nip rolls are also recommended for the predraw rolls to minimize tension on the fiber tow band before drawing. During the first draw stage, the tow temperature is increased and maintained between 45 and 70°C. The draw roll is cooled on the post draw stand to prevent the tow band from sticking to the rolls. The recommended tow temperature for the second draw stage is between 70 and 90°C. Failure to reach recommended temperatures in the stage 2 draw zone may result in fiber with an excessive amount of shrinkage once the fiber is heat-set under relaxed conditions.

PLA can be drawn over a wide range of draw ratios. The optimal draw ratio is dependent upon the type of polymer used, the as-spun orientation level, and the desired tensile properties for the product. PLA staple fiber is typically drawn in the 3–4× range [100]. The percentage of the total draw ratio is typically split into 70 and 30 between the first and second stages, respectively, and often requires further optimization at the process and manufacturing lines. Drawing improves the mechanical properties of PLA

filaments. Higher birefringence is observed for fibers drawn at higher drawing temperatures. Birefringence increases with increasing draw ratio of up to 5 and subsequently levels off. Overdrawing of the fibers is possible if draw temperatures are too low and/or draw ratios are too high. Overdrawing may induce micro-crazing within the fiber interior or on the fiber surface, causing light to diffract making the fibers look opaque. If overdrawing occurs, the mechanical properties of the fibers may be comprised.

Heat-setting is carried out to improve dimensional stability of the spun fibers at elevated temperatures. During heat-setting, fiber tow is heated to the temperature of PLA crystallization so that polymer chains both relax and reorganize to form new crystalline regions. This helps to relieve the internal stresses that were developed during the drawing process. The development of new crystalline regions adds to the total crystal network and helps to lock in the drawn structure of the fiber. The crystal network helps the fiber-resist thermal shrinkage during subsequent operations or use. For staple fiber processing, roll heat-setting may be used, where the fiber tow band is annealed under tension using various heated godet roll configurations. Across PLA types, annealing conditions will depend on several factors, such as the optical purity and polymer molecular weight, the degree of melt orientation, the degree of drawn orientation, line set-up, tow band size and total denier, and roll heat transfer efficiency. Roll heat-set temperatures from 100 to 125°C have been used on high optical purity PLLA resins. For cotton-type staple fiber properties, the drying oven heat-set temperature conditions should not exceed the roll heat-set temperature. Otherwise, excessive fiber shrinkage may occur. Low optical purity PLA fiber grades may not be heat-set at such high temperature, as fiber fusing, fiber sticking, and melting may occur on the hot rolls. Water bath drawing and annealing of PLA has been employed for low optical purity PLA fibers to help minimize fiber sticking and shrinkage. For PLA, roll heat-setting under tension has less of an effect on changing the tensile properties (e.g., increase in fiber tenacity and modulus and decrease in fiber elongation) versus PET staple fibers.

Continuous hot air dryers are recommended for final drying and heat-setting of the staple fiber tow band. The dryers should have multiple zones with a cooling zone at the dryer exit. Temperature control is critical, as the objective is to efficiently dry the fiber, which may mean exposing the fiber to temperatures as close to the melting point as possible without melting the fiber. Recommended drying temperatures for crystalline and higher-melting-point PLA fibers range from 120 to 140°C. Heat-setting can also be carried out in dry air at 80–140°C, depending on PLA type, orientation level, roll heat-set conditions, fiber fineness, and oven residence time. Drying and heat setting fibers made from lower optical purity amorphous PLA grades may cause melting, fusing, and excessive shrinkage at too high temperatures (typically $>T_g$ of the amorphous PLA resin grade). Low drying temperatures may be required. The fiber tow band is typically introduced into the drying oven in a zig-zag fashion onto the oven conveyor belt, so it is not in contact with itself to allow the fiber to free shrink and anneal but not fuse together when cooling and exiting the dryer. Greater free shrinkage may occur with fiber tow that has not been roll heat-set under tension.

PLA conjugate staple fibers, filaments, or nonwovens using similar approaches during melt-spun fabrication techniques with heat bonding properties can be prepared by using two types of PLA polymers with different optical purity. The core is formed from a PLA polymer with higher optical purity and the sheath from a PLA polymer with lower optical purity. The lower $T_m$ of the PLA of lower optical purity provides a safe temperature range for melt bonding of conjugate fibers. In one of the studies [110], PLLA with optical purity 99% and melt flow rate (MFR) of 25 g/10 min as the core and another with optical purity 90% and MFR of 15 g/10 min as the sheath were together melt spun at a 1 : 1 weight ratio, cooled, lubricated, and wound. Subsequently, these were formed into a tow, drawn to a total draw ratio of 2.2, crimped in a stuffing box, lubricated, dried, and cut to give staple fibers with tenacity (measure of break stress equal to load divided by specific weight of the fiber) of 3.5 g/denier. The conjugate fibers develop fiber-to-fiber bonding on heat treating for 5 min at the air temperature of 130°C.

The mechanical properties of melt-spun fibers are dependent on the extrusion conditions. In a lab-scale melt-spinning operation at low speeds [97], the tensile modulus increases steeply at first from 2.8 to 4.1 GPa, reaching almost constant values for higher spinning speeds (20 m/min). Whereas yield stress and strength increase linearly with spinning speed to values of 128 and 209 MPa, respectively, strain at break decreases rapidly at first from 580% (1.8 m/min) to 94% (at 5 m/min), and then slowly to 60% (at 10 m/min) and 23% (at 20 m/min). At industrial spinning speeds, the highest values of tensile strength and modulus of as-spun fibers are obtained at around 3000–4000 m/min [98]. Elongation at break shows a similar trend as described above with values decreasing sharply from 160% at 1000 m/min to about 50% at 3000 m/min, followed by a slower decrease to 30–40% at 5000 m/min. Stress–strain curves for as-spun samples produced from a copolymer of L-lactide (92%) and *meso*-lactide (8%) at different spinning speeds are given in Figure 13.17. With increasing spinning velocity, the cold crystallization shifts toward lower temperatures and the crystallinity increases.

Hot drawing and annealing of the melt-spun filaments is performed to improve their mechanical properties. The higher the draw ratio, the better are the mechanical properties (modulus and strength), as is normally the case for thermoplastic fibers. Also, the drawing temperature has a

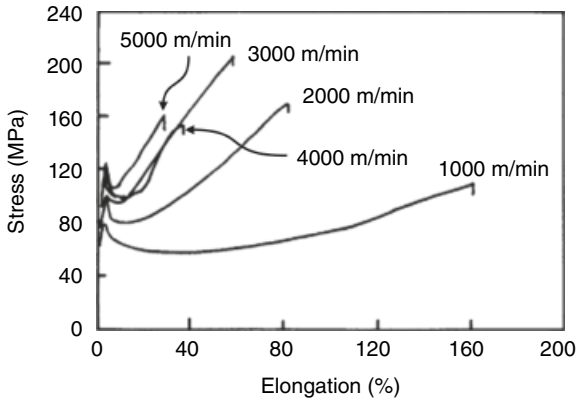


**FIGURE 13.17** Stress–strain plots of the high-speed-spun PLA fibers. Source: Plots are recreated based on the data from Ref. 98 with permission from John Wiley and Sons.

significant effect on mechanical properties. Fibers from PLA copolymer spun at 200 m/min can be drawn to a draw ratio of up to 6, resulting in a tensile strength of about 460 MPa and elongation-at-break of about 20% [98]. The maximum possible draw ratio is dependent upon the spinning speeds and tends to have lower values ranging from 160 to 30% for samples spun at higher speeds, that is, 1000 and 5000 m/min, respectively. Crystallinity of the as-spun samples is typically in the range of 35–40%, which upon drawing and annealing can increase to approximately 65%.

## 13.12 SOLUTION SPINNING

PLA can be solution-spun when specialty high-performance fibers or filaments are required. In solution spinning, the polymer is dissolved in a solvent to form a viscous spin dope solution. The solvent is removed from the extruded polymer solution by either coagulation or evaporation to allow solidification of the fiber filaments.

There are two main solution spinning methods, wet and dry spinning. When the spin dope solution is extruded inside a coagulation bath containing a nonsolvent, the process is known as wet spinning (Figure 13.18a). One variant of wet spinning is known as the dry-jet wet spinning, wherein the polymer solution is extruded in the air followed by regenerating the fiber in a coagulation bath (Figure 13.18b). When the extrudate is injected into a heated chamber of air, the process is known as dry spinning (Figure 13.18c). The spinneret plate is typically made of stainless steel or platinum with spinneret hole diameter ranging from 0.025 to 0.05 mm and L/D ratio of 1. Both the diameter and length of the spinneret are much smaller than those used for melt spinning, since the viscosity of the polymer solution is significantly lower (3000–7000 cP) than that of the polymer melt. The holes are also placed very close to each other because the elasticity of the polymer solution is considerably lower than that in melt spinning with minimal extrudate swell.

Wet spinning of PLLA has been carried out by extruding the spin dope solutions, prepared in chloroform solvent, into

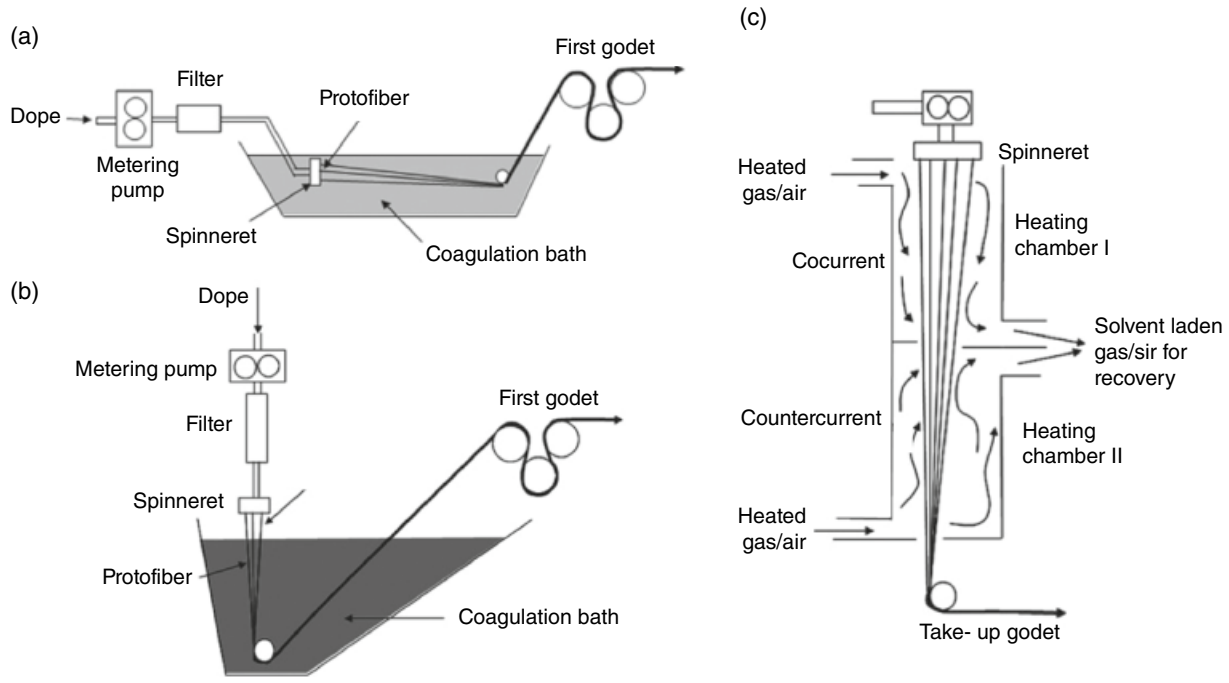


**FIGURE 13.18** Schematic representations of immersion-jet wet spinning (a); dry-jet wet spinning (b); and dry spinning (c) methods. Source: Reproduced from Ref. 99 with permission from John Wiley and Sons.

a coagulation bath containing toluene at 110°C [96]. The coagulation fluid is allowed to flow along the filaments (cocurrent) to facilitate the exchange of solvent and nonsolvent with the coagulating filament without creating excessive fluid drag force. The PLLA concentrations used are in the range of 6–12% depending on the molecular weight (in the range of $3–5 \times 10^5$ Da) of the polymer used. Molecular weights lower than $3 \times 10^5$ Da are unsuitable for wet spinning due to low solution viscosity at the extrusion temperature. The fiber from the coagulation bath is washed several times, dried, stretched, crimped, and/or heat set before winding it as a filament or cutting it into staple fibers. Low spinning speeds of about 25–35 cm/min at the laboratory scale are reported to give fibers with no orientation. Dry-jet wet spinning is believed to modify the outer layer of the extruded fibers. This in turn reduces rates of diffusion of both solvent and nonsolvent across the boundary of the precipitating fiber. However, the ratio of the rates of solvent to nonsolvent diffusion increases substantially. This results in collapsing of the coagulating fiber into a compact defect-free structure. In one study [111, 112], chloroform/methanol was used as the solvent/nonsolvent system. The study involved varying the draw ratio, take-up speed, drawing temperature, and heat setting temperature. The draw ratio had a significant influence on the crystallinity and tensile strength of the spun fiber. Tenacity values of 5.3 g/d (0.60 GPa) and modulus of 72 g/d (8.2 GPa) were achieved at a draw ratio of 8.

In dry spinning of PLLA, heated solution of polymer in chloroform is extruded through a multi-hole spinneret into a chamber of heated air, where the solvent evaporates to produce solidified and partially crystallized PLLA filaments. The solvent and the gas are separated and recycled back into the spinning system. The solidified filaments are collected on bobbins or guided through a set of godets to washing baths containing nonsolvent to remove traces of the solvent present inside the spun filaments. The filaments are subsequently drawn, dried, crimped, heat-set, and cut to staple fibers as required.

Studies have indicated that the use of binary solvents, such as a mixture of chloroform (good solvent) and toluene (poor solvent) [113], may lead to filaments with improved tensile properties. Scanning electron micrographs reveal that, compared with pure chloroform spun PLLA fibers, those spun from a chloroform/toluene mixture have more porous fiber morphologies due to rapid phase separation in the presence of toluene. Such PLLA fibers have high initial crystallinity and good drawability. PLLA is usually dry spun from a dope solution maintained at 70°C into an environment maintained at 60°C. On the other hand, spinning the dope at room temperature gave rise to extrudate distortion (solution fracture). The researchers adopted two approaches for making the dope solution in mixed solvent: first, by the direct dissolution of PLLA in the solvent mixture; or second, by first dissolving PLLA in chloroform followed by addition of toluene. With the first approach, the as-spun filaments obtained had lower tenacity (1.35 GPa) and limited drawability (maximum draw ratio achievable, $\lambda_{max} = 8$) [113]. Apparently, the dissolution of PLLA in the solvent mixture did not take place readily in the first case. Also, prolonged heating of the spinning solution can result in the degradation of the polymer. In the second approach, highly crystalline PLLA was readily dissolved in the good solvent, that is, chloroform at room temperature leading to highly expanded coil configurations at moderate polymer concentrations. The addition of the poor solvent (i.e., toluene) resulted in shrinkage of these molecular chain coils and was eventually followed by crystallization. Therefore, the second approach is more desirable. The composition of the binary solvent system used for making dope solution has been shown to have a great influence on the structure and properties of the fiber. The values of maximum draw ratio and tenacity are found to be influenced by the quality of solvent used for dry spinning. Figure 13.19 depicts the tenacity of PLLA fibers ($M_v = 9 \times 10^5$ Da) spun from 4% (w/v) polymer solutions in various chloroform/toluene mixtures at 60°C and subsequently hot drawn to different draw ratios ($\lambda$) at 204°C gas temperature. The ultimate tenacity of the fibers prepared shows a pronounced maximum of 2.1 GPa at a toluene volume fraction of 0.6. The drawability and tenacity decrease on either side of the binary solvent composition [113]. Moreover, the PLLA concentration of the spinning solutions influences the spinnability and ultimate fiber tenacity; the

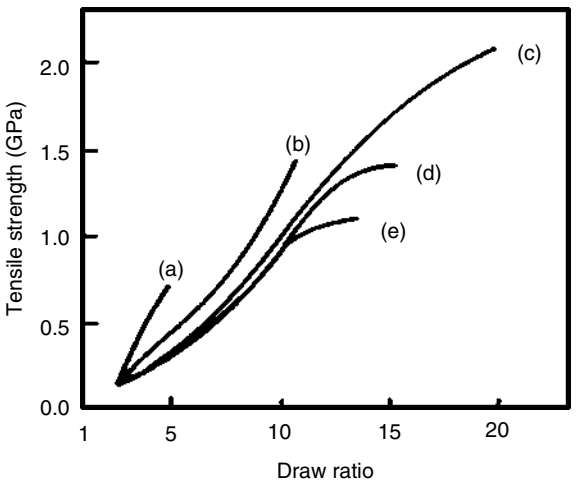


**FIGURE 13.19** Effect of chloroform/toluene ratio in the PLLA (viscosity-average molecular weight $9 \times 10^5$ Da) spinning solution (4% (w/v), 60°C) on the fiber drawability at 204°C and subsequent tensile strength of the filaments. (a) 0 (chloroform); (b) 0.5; (c) 0.6; (d) 0.7; and (e) 1 (toluene). Source: Adapted from Ref. 113 with permission from Elsevier.

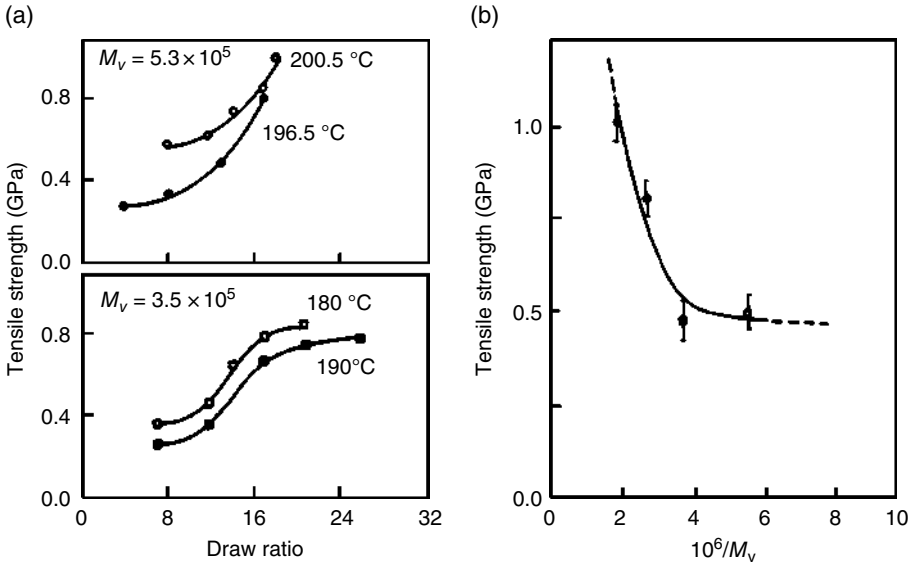


**FIGURE 13.20** (a) Dependence of the tensile strength on the draw ratio for two samples of PLLA with different $M_v$ drawn at indicated temperatures. (b) Effect of the reciprocal viscosity-average molecular weight on the maximum tensile strength of wet spun PLLA fibers. Fibers were drawn at optimum temperatures to maximum draw ratio. Source: Adapted from Ref. 96 with permission from Elsevier.

tenacity first increases and then decreases with increasing concentration of polymer. The concentration at which maximum tenacity is obtained also depends upon the molecular weight of the polymer.

The draw ratio has a direct impact on the mechanical properties of the fibers. The higher a fiber can be drawn (higher draw ratio), the higher is the tensile strength achieved. The maximum achievable draw ratio is dependent upon the preparation of the dope and the composition of the dope. Figure 13.20a illustrates the dependence of the tensile strength on the draw ratio for wet-spun PLLA fibers obtained from polymers with $M_v$ of $3.5 \times 10^5$ and $5.3 \times 10^5$ Da [96]. For the samples with lower molecular weight, the ultimate mechanical properties are obtained at draw ratios between 18 and 25. On the other hand, the highest achievable draw ratio was about 18 for the high-molecular-weight PLLA polymer. However, no plateau was observed for the higher molecular weight samples, indicating that the drawing limits and optimal drawing conditions that would lead to the maximum tensile strength have not yet been attained [96].

Solution-spun PLLA fibers can be continuously hot-drawn in a tube heated at 160–220°C. At this range, the actual temperature of the fiber is expected to be lower than the $T_m$ of the crystallites present in it. Wide-angle X-ray experiments showed that a crystal transition in PLLA fibers takes place at 190–204°C [113]. Fibers hot drawn up to 190°C revealed a usual α-modification. At higher temperatures (up to 204°C), the α-form was found to be gradually replaced by the β-form. PLLA fibers hot drawn at the optimum drawing temperature (204°C) consisted of the β-form only. This β-form probably is the load bearing structure in PLLA fibers. The sudden lowering of tensile properties due to drawing in the temperature range of 190–204°C is ascribed to the presence of both crystal types in these fibers [113].

Figure 13.20b shows the dependence of the maximum tensile strength on the reciprocal of viscosity-average molecular weight of PLLA fibers wet solution spun in toluene at 110°C and drawn at the optimum temperature [96]. The tensile strength of the PLLA fibers was not influenced by $M_v$ in the range of $1.0 \times 10^4$ to $3.0 \times 10^5$ Da. Similar behavior was observed for melt-spun fibers with low $M_v$ in the range $2 \times 10^4$ to $1.8 \times 10^5$ Da. For fibers solution-spun from higher molecular weight PLLAs, the tensile strength increases strongly with the molecular weight, reaching values of more than 1.0 GPa. Tensile strength of more than 2 GPa at optimum draw ratio has been reported for fibers dry spun from polymer of $9 \times 10^5$ Da $M_v$ using an optimum binary solvent of 40 : 60 chloroform : toluene (v/v) [113].

Stereocomplex PLA fibers have been produced by wet and dry spinning methods in chloroform by first preparing PDLA and PLLA solutions separately at 5–10 g/dL, followed by mixing the two solutions in an equimolar ratio. The conditions for both dry and wet spinning are given in Table 13.7 [114]. Solution spinning of the PDLA and PLLA mixture of $M_v$ below $4 \times 10^4$ Da tends to be difficult, because the stereocomplexation yields a macrogel too quickly. On the other hand, spinning of the complex fiber is possible at molecular weights as high as $10^5$ Da. At high molecular weight, complexation between PDLA and PLLA proceeds at a very slow rate even though the dope has a high concentration. The extruded dope of stereocomplex polymer tends to break

**TABLE 13.7 Typical Conditions for Dry and Wet Spinning of Stereocomplex [114]**

| | Wet Spinning | Dry Spinning |
|---|---|---|
| *Dope (in $CHCl_3$)* | | |
| PDLA : PLLA | 1 : 1 | 1 : 1 |
| Concentration (g/dL) | 5–8 | 9–10 |
| *First Coagulation Bath* | | |
| Composition | EtOH/$CHCl_3$ = 10/3 (v/v) | — |
| Temperature (°C) | 40 | — |
| *Second Coagulation Bath* | | |
| Composition | EtOH/$CHCl_3$ = 10/1 (v/v) | — |
| Temperature (°C) | 20 | — |
| *Drying Column* | | |
| Temperature (°C) | — | 60 |
| Length (cm) | — | 50 |

easily before solvent extraction or evaporation takes place. Therefore, lowering of the applied tensile force on the dope is essential during spinning to obtain the complex fiber. Further, rapid coagulation tends to produce fiber with many voids. Lowering the coagulation rate produces translucent fibers in wet spinning. In contrast, dry spinning produces transparent complex fibers, suggesting a lower number of voids compared with the wet-spun fibers [114]. Drawing of complex fibers is difficult at temperatures above 180°C, probably because of melting of the crystallites of the homopolymers. When the fibers are drawn at 160°C to a draw ratio of 13, the maximum attainable tensile strength and Young's modulus for dry-spun stereocomplex fibers have been observed to be about 0.92 and 8.6 GPa, respectively [114]. These values are comparable to those obtained for PLLA fibers. Interestingly, elongation at break of the dry-spun stereocomplex fibers is practically independent of the drawing temperature but decreases with increasing draw ratio.

## 13.13 ELECTROSPINNING

One variation of PLA solution spinning (Section 13.12) is known as electrospinning. Unlike conventional solution spinning which relies on extrusion and mechanical drawing to form fiber, the electrospinning process uses electrostatic forces to a spin polymer solution into ultrafine fiber. Moreover, electrospun PLA fibers are substantially smaller in diameter (typically submicron) than typical solution spun fibers. The electrospinning process produces continuous fibers randomly laid down as nonwovens with extremely large surface areas ideal for applications such as filtration, textiles, tissue engineering, drug delivery, and encapsulation. The low-temperature process is beneficial for the encapsulation of drugs, nutraceuticals, and bioactive agents that are thermally labile [115–117].

When a pendant droplet of a polymer solution is electrically charged with a positive or negative electrode (Figure 13.21a), the resulting electrostatic repulsion on the droplet surface causes it to elongate, forming a characteristic feature known as a "Taylor cone," named after Geoffrey Taylor, who conducted detailed investigations of electrostatic phenomenon in fluids in the 1960s [118, 119]. At a certain critical level of applied voltage (e.g., 10–20 kV when the spinneret tip and collector are separated at 10–20 cm), the electrostatic repulsion overcomes the surface tension of the solution, thereby forming a continuous jet that ejects toward an electrically grounded collector. As the polymer jet takes flight in the air, the solvent vaporizes rapidly, producing a fibrous nonwoven laid on the collector. The bending instability that occurs as the polymer jet approaches the collector is the main contributor to the formation of the ultrafine fiber.

A typical electrospinner is made up of four main components: (i) DC power supply capable of supplying greater than 10 kV, (ii) spinneret or surface where the fiber jet is formed, (iii) mechanism to deliver spin dope solution to the spinneret/surface, and (iv) electrically grounded stationary or moving collector where the fiber is laid down as a nonwoven. The setup for the single-spinneret approach is straightforward (Figure 13.21a) and hence widely adopted by researchers in the laboratory setting, although the production throughput is low, on the order of several milliliters per hour of polymer solution. To increase the production rate, multiple-spinneret and free-surface techniques have been developed, in conjunction with a conveyor belt to achieve a continuous process [120–122]. In one free-surface approach, the spin dope solution is deposited uniformly on a wire that serves as the spinning electrode (30–50 kV), by using a carriage that moves back and forth along the wire. The charged spin dope solution erupts as numerous jets toward a collector substrate (e.g., paper, spunbond nonwoven) positioned between the spinning electrode and a ground electrode (Figure 13.21b).

Electrospinning is governed mainly by Coulombic, electric field, viscoelastic, and surface tension forces. The interaction between these forces dictates the electrospinning process behavior and morphology of the resulting materials [123, 124]. By modifying the solution properties (e.g., concentration, viscosity, surface tension, electrical conductivity) and electrohydrodynamic processing conditions (stationary versus dynamic collector, electric field strength, temperature, spinning electrode design, etc.) fibers of diameters in the hundreds of nanometers and different morphologies are achievable. For example, an increase in spin dope solution viscosity (e.g., increase concentration or increase molecular weight) tends to stabilize the polymer jet, forming uniform fiber of increased diameter while preventing the formation of beads. On the other hand, an increase in surface tension tends to produce droplets and/or produce fibers embedded with beads. Electrospinning of highly conductive

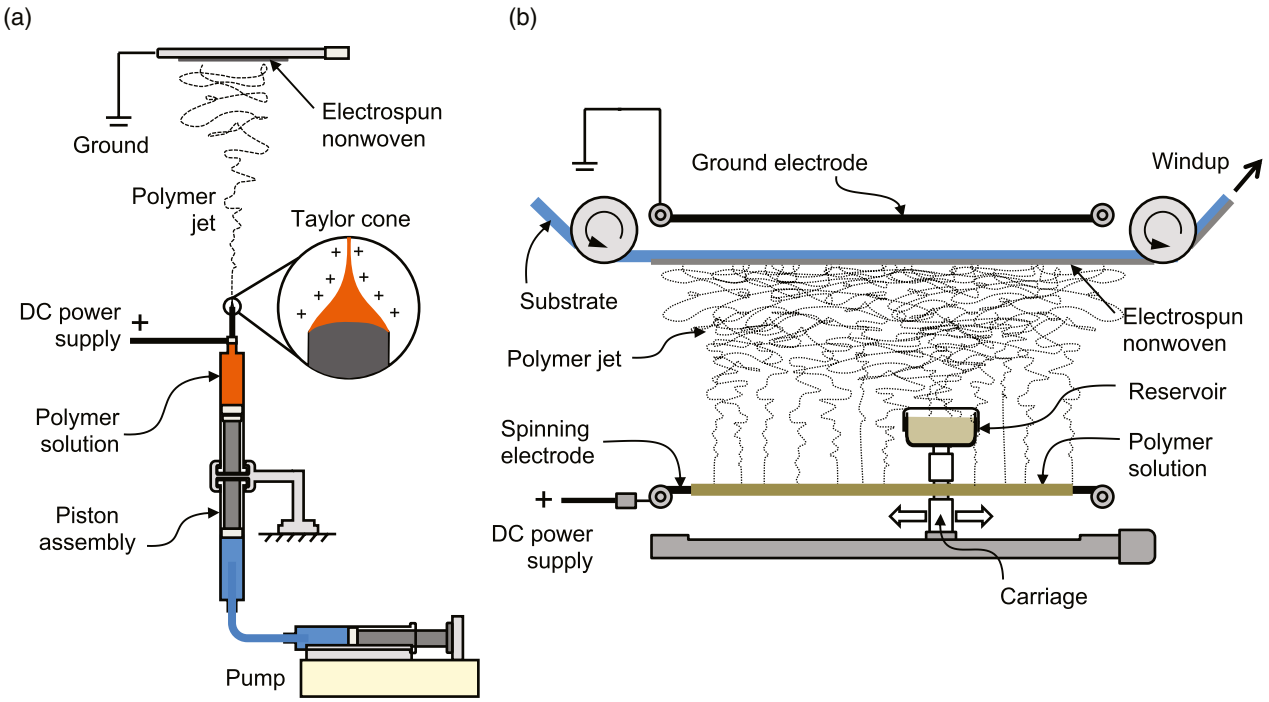


**FIGURE 13.21** Schematic representations of typical single-spinneret (a) and free-surface wire (b) setups for electrospinning of PLA nonwovens.

solutions can be challenging due to electric charge leakage that weakens the electric field force at the Taylor cone and reduces the Coulombic repulsion on the fiber surface essential to induce stretching [123, 124].

Judicious solvent selection (polar protic, polar-aprotic, nonpolar) is important to ensure its thermodynamic compatibility with the polymer, as well as to provide an optimal evaporation rate essential for preventing premature drying of spin dope solution at the spinneret or forming wet nonwoven. Typical solvents used for PLA and process conditions used for electrospinning are summarized in Table 13.8. In general, PLA solutions with lower polymer concentrations favor the formation of smaller diameter fibers but had less consistent morphology and tended to contain beads as compared with PLA fibers electrospun from polymer solutions at higher concentrations (Figure 13.22 a and b). These defects can be overcome by incorporating an organic or inorganic salt, such as pyridinium formate (PF), $KH_2PO_4$, $NaH_2PO_4$, or NaCl, in the fiber-forming solution to enhance its electrical conductivity (Figure 13.22 c and d) [131, 140]. The type of solvent used will also affect the surface morphology of the fiber. PLA fibers electrospun from chloroform, 2,2,-trifluoroethanol, and 1,1,1,3,3,3-hexafluoro-2-pro panol have smooth surface morphologies [129, 134]. In contrast, PLLA solution of 5% prepared using dichloromethane as solvent produced fibers with pore structures [141].

For spin dope prepared in volatile solvent, premature solidification of the solution at the spinneret will result in inconsistent fiber morphology and disruption of the electrospinning process. To overcome this problem, a second solvent is often added to depress the vapor pressure of the primary solvent. For instance, a binary solvent of 9 : 1 (w/w) $CHCl_3$ : dimethylformamide (DMF) can be used for preparing PLA spin dope solution to prevent the premature drying at the spinneret that tends to cause stringing and/or flow blockage. Here, DMF is added to depress the vapor pressure of $CHCl_3$ [129, 137]. Electrospun PLA fibers prepared using this binary solvent exhibited porous skin morphologies (Figure 13.22e). This porous morphology can be attributed to the large difference in volatility between the two compatible solvents and different compatibility of PLA in pure $CHCl_3$ (soluble) and DMF (limited solubility) [137]. During the electrospinning process, $CHCl_3$ evaporates rapidly from the surface, leaving DMF-rich (PLA-depleted) domains that formed pore imprints on the fiber surface after the remaining solvent was evaporated. On the other hand, the addition of a nonvolatile 1,3-dibenzylethane-2-pentyl imidazolidine (a precursor of hexanal) to the PLA solution (0.9 : 1 PLA : imidazolidine, w/w) resulted in fibers with smooth surface morphology (Figure 13.22f) due to the compatible nature of the imidazolidine with both solvents [137].

To modify the material properties and impart functionality to the electrospun PLA fibers, polymer blends and additives are often used in the spin dope solution formulation. Dai and Lim functionalized PLA nonwovens by uniformly

entrapping mustard seed meal particulates within the electrospun fibers [129]. Poly(ethylene oxide) (PEO) was added to PLA solution prepared in 9 : 1 (w/w) $CHCl_3$ : DMF to increase hydrophilicity of the electrospun fiber for moisture-triggered release applications. The incorporation of PEO into the PLA resulted in significantly thicker fibers (Figure 13.22h) than the pristine PLA (Figure 13.22g) and PEO fibers, implying that there was a dilation of free volume in the blended polymer fiber due to reduced chain-chain packing. The addition of allyl isothiocyanate (AITC) to the $CHCl_3$ : DMF solvent, at 5% (w/w) level, resulted in smooth fibers (Figure 13.22i) [138]. However, at an elevated AITC level (20% w/w), a drastic change in the electrohydrodynamics occurred, resulting in the formation of uniform spheres of diameter ~3 μm and fiber of ~100 nm in diameter (Figure 13.22j). The competitive dissolution of AITC in chloroform might have reduced the solvent quality for the PLA polymer, causing rapid phase separation of the solvent (AITC and DMF) from the polymer as chloroform evaporated.

Using the Hansen solubility parameters concept, Jash et al. formulated an alternate solvent for PLA that is less toxic (Class 3 ICH list) based on a blend of 9 : 1 (w/w) ethyl formate : dimethyl sulfoxide (EF : DMSO) [127]. The resulting fibers prepared from a 10% PLA spin dope solution had a smooth ribbon morphology (Figure 13.22k), as opposed to the porous surface morphologies as observed in fibers prepared from chloroform-based solvent (Figure 13.22e). The incorporation of 1,3-dibenzylethane-2-phenyl imidazolidine (a benzaldehyde precursor) into the spin dope solution suppressed the vapor pressure of the binary EF:DMSO solvent, delaying the solidification of polymer jet and thereby stretching it into thinner fibers (Figure 13.22l). The rod shape entities, as indicated with arrows in Figure 13.22l are likely the benzoic acid crystals formed due to the hydrolysis of the imidazolidine precursor.

To prepare composite PLA fibers comprise of two incompatible phases, surfactants have been used to prepared spin dope emulsions followed by electrospinning. For instance, Zhou and Lim immobilized glucose oxidase in polylactide (PLA) fibers [128]. The glucose oxidase-containing PLA fibers were electrospun from emulsions prepared by dispersing aqueous glucose oxidase in PLA dissolved in chloroform : DMF 9 : 1 (w/w) blend, using sorbitan monopalmitate as an emulsifier. The remnant inclusions of the dispersed phase, which formed after coalescence and drying of the aqueous droplets after spinning, can be seen in Figure 13.22n. In comparison, the pristine PLA fibers had more consistent morphologies and had larger diameters than the glucose oxidase composite fibers (Figure 13.22m). The smaller fiber diameter observed for the composite fibers may be related to the increased electrical conductivity of the spin dope emulsion that exerted a greater Columbic charge repulsion and imposed a greater stretching on the fiber jet than the neat PLA spin dope solution.

Besides spinning from organic solvents, PLA can be electrospun into fiber from the melt phase. While this approach is desirable to eliminate the use of organic solvents that are often toxic, melt phase electrospinning is prone to thermal degradation due to the elevated temperature involved, which is needed to reduce the melt viscosity to a point conducive for jetting and promoting the bending instability phenomenon needed to stretch the fiber. Moreover, the melt electrospun fiber tends to be larger in diameter than those prepared from spin dope solution, by one to two orders of magnitude. Zhou et al. [142] deployed an electrospinning setup where the polymer was held in a heated reservoir at 200°C, spinneret at 255°C, and electrospinning chamber at 80°C, producing fibers of average diameter of 0.13 mm. They reported a significant $M_v$ decrease from 186,000 to 40,000 Da in the first hour of electrospinning due to thermal degradation [142]. To reduce the extent of thermal degradation, several strategies may be employed, such as using polymers of high MFI. Koenig et al. were able to electrospin PLA polymers with MFI values (15–30, 65, and 70–85 g/10 min at 210°C for Ingeo Biopolymer 6201D, 6260D, and 6252D, respectively), at nozzle temperatures ranging from 220 to 230°C, using pilot scale equipment [139]. The nozzle and collector were separated at 11 cm with a positive voltage applied to the collector of 60 kV while grounding the spinneret comprised of 600 nozzles. Smooth fibers were obtained with the standard fiber-spinning grade 6201D resulting in the thickest fibers (Figure 13.22o), while the melt-blown grade 6252D had the smallest fiber diameter, averaging at 0.81 μm (Figure 13.22p).

To avoid prolonged heating of PLA in the melt, Ogata et al. electrospun PLA in the melt phase using a $CO_2$ laser [143]. This technique relies on using a laser beam to melt the PLA polymer locally, thus minimizing the thermal degradation due to prolonged heat exposure, which has been observed previously for melt electrospinning. This setup produced fibers with diameter smaller than 1 μm. These solvent-free approaches to produce submicron PLA fibers are more environmentally benign than the typical solution electrospinning processes and have the potential to increase the production of electrospun PLA fibers.

PLA has been successfully electrospun into nonwoven scaffolds for the regeneration of cardiac, neural, bone, and blood vessel tissues [125, 126, 130, 132]. PLA has been electrospun into different forms of ultrafine fiber and used as a carrier for bioactive agents, including antibiotics [133], anticancer drugs [135, 144], antibacterial silver nanoparticles [145], and enzymes [128]. Other composite PLA fibers containing nanocomponents such as nanoclay (montmorillonite) and $TiO_2$ nanoparticles have also been successfully produced using the electrospinning technique [144, 146].

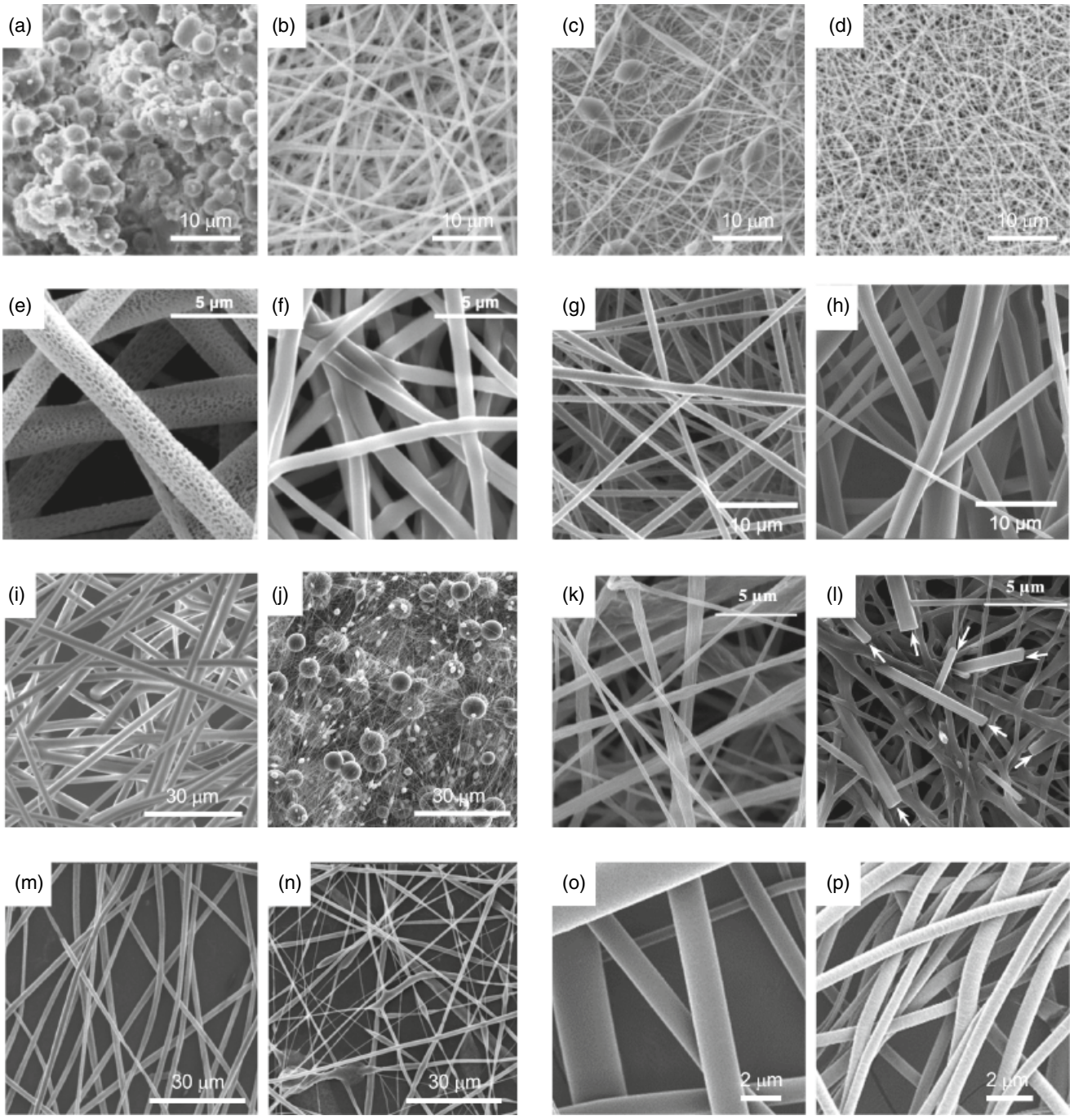


**FIGURE 13.22** SEM micrographs of electrospun PLA fibers. Spin dope solutions prepared in dimethyl formamide solvent: (a) 20% (w/w) PLA; (b) 35 wt% PLA; (c) 25% (w/w) PLA + 1% wt% $KH_2PO_4$; (d) 30% (w/w) PLA + 1% wt% NaCl. Source: Adapted from Ref. 131 with permission from Elsevier. Spin dope solutions prepared in chloroform : DMF (9 : 1, w/w): (e) 10% (w/w) PLA; and (f) 10% PLA (w/w) + 11% (w/w) 1,3-dibenzylethane-2-pentyl-imidazolidine. Source: Adapted from Ref. 137 with permission from Springer Nature. Spin dope solutions prepared in chloroform : DMF (9 : 1, w/w) binary solvent: (g) 9% (w/w) PLA; and (h) 9% (w/w) PLA + 1% (w/w) 300 kDa PEO. Source: Adapted from Ref. 129 with permission from Elsevier. Spin dope solutions prepared in chloroform : DMF (9 : 1, w/w) binary solvent: (i) 10% (w/w) PLA + 5% (w/w) AITC; and (j) 10% (w/w) PLA + 20% (w/w) AITC. Source: Adapted from Ref. 138 with permission from Elsevier. Spin dope solutions prepared in 9 : 1 (w/w) EF : DMSO solvent: (k) 10% (w/w) PLA; and (l) 9% (w/w) PLA + 10% (w/w) 1,3-dibenzylethane-2-phenyl imidazolidine. Source: Adapted from Ref. 127 under the Creative Commons CC BY license. Spin dope solutions prepared in chloroform : DMF 9 : 1 (w/w): (m) 10% (w/w) PLA; and (n) 10% (w/w) PLA continuous phase dispersed with glucose oxidase aqueous phase using sorbitan monopalmitate as an emulsifier. Source: Adapted from Ref. 128 with permission from John Wiley and Sons. PLA fibers electrospun from melt phase at 230°C nozzle temperature: (o) Ingeo Biopolymer 6201D (MFI 15–30 g/10 min at 210C); and (p) Ingeo Biopolymer 6252D (MFI 70–85 g/10 min at 210°C). Source: Adapted from Ref. 139 under the Creative Commons CC BY license.

**TABLE 13.8 Electrospinning Process Conditions for PLA Polymers**

| Ref. | Grade | Spin-dope | Dia. (mm)[a] | Dist. (cm)[b] | Volt. (kV)[c] | Feed Rate (mL/h)[d] | Collector Type | Fiber Dia. (μm) |
|---|---|---|---|---|---|---|---|---|
| [125] | PLA | 20% (w/v) in $CHCl_3$ | — | 15 | 25 | 0.1 | Rotating mandrel | 1.0–2.0 |
| [126] | PLA | 14% (w/v) in 15 : 3 $CHCl_3$ : DMF | — | 20 | 13 | 1.5 | Rotating mandrel | 0.8–3.0 |
| [127] | 1.4% D-lactide | 10% (w/w) in 9 : 1 EF : DMSO | 0.6 | 20 | 18 | 5.0 | Stationary plate | 0.7–1.1 |
| [128] | 1.4% D-lactide | 10% (w/w) in 9 : 1 $CHCl_3$ : DMF | 0.6 | 16 | 10 | 1.0 | Stationary plate covered with LDPE film | 0.6–2.0 |
| [129] | 1.4% D-lactide | 9% (w/w) in 9 : 1 $CHCl_3$ : DMF | 0.6 | 15 | 11 | 3.0 | Stationary plate covered with aluminum foil | 0.8–1.1 |
| [130] | 5% D-lactide | 10% (w/w) in HFP | — | 15 | 30 | 6.0 | Stationary plate | 0.9–1.0 |
| [131] | 5% D-lactide | 20–35% (w/w) in 1.5 : 1 (w/w) DCM : DMF | 0.7 | 15 | 20–30 | 1.2 | Rotating drum | 0.2–1.0 |
| [132] | PLLA | 1–5% (w/w) in 70 : 30 DCM : DMF | 0.7–1.2 | 10 | 12 | 1.0 | Stationary aluminum plate and rotating disk | 0.1–3.0 |
| [133] | PLLA | 14% (w/v) in $CHCl_3$ | — | 30 | 15 | 18–21 | Stainless steel sheet on rotating drum | 3.0–6.0 |
| [134] | PLA | 12% (w/v) in HFP or 11% (w/v) TFE | 0.50 | 20 | 11 | 0.3 | Stainless steel drum at 600 rpm | 0.1–2.2 |
| [135] | PLLA | 5.5–6% (w/w) in $CHCl_3$ | 0.4 | 18 | 45–50.4 | 3.0–4.2 | Stationary | 0.3–1.0 |
| [136] | PLLA/PDLA | 4 g/dL $CHCl_3$ | 0.5 | 10 | −12 or −25 | 6 | Rotating drum covered with aluminum foil | 0.4–2.7 |

DMF: dimethylformamide; HFP: 1,1,1,3,3,3-hexafluoro-2-propanol; TFE: 2,2-trifluoroethanol; DCM: dichloromethane; EF: ethyl formate; DMSO: dimethyl sulfoxide.

[a] Spinneret diameter.

[b] Spinneret–target distance.

[c] Applied voltage.

[d] Spin dope solution feed rate.

## 13.14 FILAMENT EXTRUSION AND 3D-PRINTING

3D-printing, also known as additive manufacturing, is defined by American Society for Testing and Materials as the "process of joining materials to make objects from three-dimensional (3D) model data, usually layer by layer, as opposed to subtractive manufacturing methodologies" [147]. 3D-printing has become an attractive fabrication process for certain applications since custom designs and complex geometries can be created without the need for expensive upfront costs for tooling and molds. This has allowed for the prototyping and manufacturing of articles to be more efficient, leading to faster design iterations, and shorter product development cycles. Compared to other traditional extrusion processes, additive manufacturing is ideal for small- to medium-volume production scales. New developments in 3D-printing equipment design, processing, and material formulations continue to enable further market adoption and novel end-use applications.

Profile extrusion is used in the fabrication of many plastic consumer products, such as tubing, piping, trim molding, and cable coating. Profile-extruded monofilament has become a popular choice for the fused filament fabrication 3D-printing process. With fused filament fabrication, a plastic monofilament is melted and extruded through a small capillary die and then continuously layered and cooled in a specifically designed three-dimensional fashion onto a substrate for part build and collection (Figure 13.23). Besides monofilament, 3D-printing may also employ direct-to-print from resin in a machine that includes melt extrusion to process the resin through the capillary die for 3D-part building. Fused filament fabrication is just one type of additive manufacturing process. Other approaches include stereolithography, selective laser sintering, jetting, and metal printing [149].

PLA has many attributes that are well suited for the 3D-printing process and its application. For example, printed part characteristics such as high resolution and dimensional accuracy, good adhesion to build plates (e.g., no heating needed), strong interlayer adhesion resulting in less warping or curling, and low odor (no strong, greasy, or oily smell while printing) are attractive performance features [150]. PLA grades can easily be modified to meet end-use requirements. Formulations have been developed to provide functionality such as impact strength, stiffness, thermal resistance, low part warpage, modification to layer adhesion for support structure and design, and filled materials such as carbon fibers, metal powders, glass, or colorants. These features make PLA and formulated grades well suited for many different types of 3D-printers and for a broad range of applications. For example, 3D-printing of PLA using the fused fabrication process is used for such applications as mold tool prototyping, medical devices

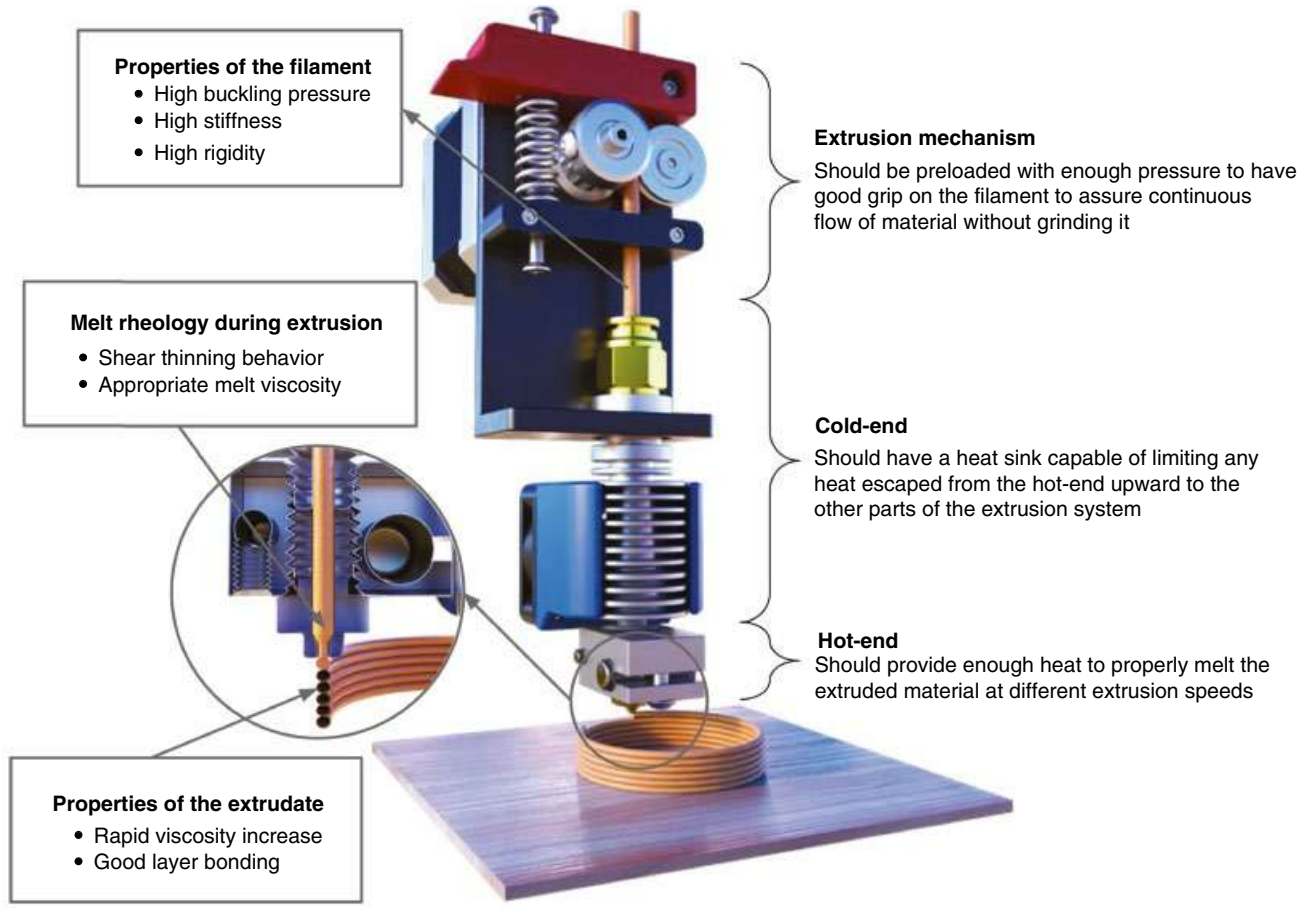


**FIGURE 13.23** Typical printing extruder head configuration for the fused filament fabrication 3D-printing process. Source: Reproduced from Ref. 148 with permission from Springer Nature.

requiring custom shapes and designs, metal casting, print models for pre-surgical planning, and tooling for big volume mold applications [151].

Conventional profile extrusion equipment can be used to produce PLA monofilament for 3D-printing. General purpose single-screw extruders with l/d ratios in the range of 24:1 to 36:1 are acceptable. To ensure profile diameter consistency, it is critical to minimize extruder surging through process optimization of resin drying, pellet feed, temperature, and pressure control. Melt pumps may also be required in some cases. Molten extrudate out of the die is typically quenched using a series of water baths, with some systems using air. Good temperature control for cooling is critical. After cooling, the filament is collected and wound onto spools. Spool sizes can vary, depending on the application and supply chain requirements. In some cases, filament is wound on larger rolls to be back-wound off-line into smaller package sizes. When winding PLA filament onto spools, good tension control is critical and should be monitored to ensure the filament is not damaged due to high winding tension. This is especially important during back-winding from a larger to smaller spool.

Since 3D-printers operate volumetrically, on-line gauge measurement during filament production is critical to ensure process and product uniformity. Typically, multi-axis laser gauges and scanning devices are used to measure filament diameter and ovality during production. Required filament diameters depend on the 3D-printing machine and die head configuration, but the most common are 1.75 mm and 2.85 mm in diameter. If the filament is not within diameter and ovality tolerances required by the 3D-printing machine, then printer jambs may occur, or the part build volume may change during printing. In some cases, print builds may take hours to create and complete. So significant time is lost if the filament fails after a significant portion of the print was in progress, but not yet complete.

## 13.15 CONCLUSION: PROSPECTS OF PLA POLYMERS

PLA is a highly versatile polymer and, via hydrolysis followed by biodegradation, an inherently biodegradable polymer that can be tailor-made into different resin grades for

processing into a wide range of products. The increasing acceptance of PLA can be partly attributed to its unique properties, as well as processing characteristics being similar to other well-established thermoplastics, which allows converters to process the polymer using conventional production equipment with minimal or no modification. PLA has attractive natural properties such as high stiffness-to-weight ratio, tunable crystallization, oil and grease resistance, good organoleptics, low carbon footprint, and industrial compostability. PLA polymers offer competitive advantages over existing petroleum-based polymers in several applications, such as containers/packages for short shelf-life food products, replacement of petroleum-based plastics in single-use consumer products such as paper coated cups, fibers and nonwovens for breathable garments, nonwovens for liquid and air filtration, profile extruded parts, monofilament and 3D-printed articles, flexible and rigid films, coatings, and bioabsorbable implants. Recent technological advances have enhanced the performance characteristics for PLA, through resin formulation, blends with other polymers, inclusion of impact modifiers, formation of micro- and nanocomposites, coating with high-barrier materials, polymer modification, and so on. The hydrolysis rate of PLA has also been shown to be a tunable parameter that scientists and engineers can modify to a significant degree for both rapid degradation and durable product needs. As the production of PLA products continues to increase, various end-of-life processes for PLA such as composting, mechanical recycling, and chemical recycling may be leveraged to embrace new circular economy initiatives. Recent technical and commercial developments have broadened the performance and value of PLA materials and have allowed for expansion into a wide variety of industries.

## REFERENCES


1. R. Datta, M. Henry, *J. Chem. Technol. Biotechnol.* **2006**, *81*, 1119–1129.
2. C. J. Weber, V. Haugaard, R. Festersen, G. Bertelsen, *Food Addit. Contam.* **2002**, *19*, 172–177.
3. K. Kimura, Y. Horikoshi, *Fujitsu Sci. Technol. J.* **2005**, *41*, 173–180.
4. S. Serizawa, K. Inoue, M. Iji, *J. Appl. Polym. Sci.* **2006**, *100*, 618–624.
5. Anonymous, *Bioplast. Mag.* **2008**, *3*(03/08), 24–26.
6. Anonymous, *Bioplast. Mag.* **2006**, *1*(02/06), 18–19.
7. Anonymous, *Bioplast. Mag.* **2007**, *2*(01/07), 14–18.
8. V. Siebott, *Bioplast. Mag.* **2007**, *2*(01/07), 28–29.
9. R. Auras, B. Harte, S. Selke, *Macromol. Biosci.* **2004**, *4*, 835–864.
10. H. Urayama, S. I. Moon, Y. Kimura, *Macromol. Mater. Eng.* **2003**, *288*, 137–143.
11. H. Tsuji, Y. Ikada, *Macromol. Chem. Phys.* **1996**, *197*, 3483–3499.
12. J. R. Dorgan, J. Jansen, M. P. Clayton, *J. Rheol.* **2005**, *49*, 607–619.
13. R. E. Drumright, P. R. Gruber, D. E. Henton, *Adv. Mater.* **2000**, *12*, 1841–1846.
14. G. L. Baker, E. B. Vogel, M. R. Smith III, *Polym. Rev.* **2008**, *48*, 64–84.
15. D. E. Henton, P. Gruber, J. Lunt, J. Randall, Polylactic acid technology, in: A. K. Mohanty, M. Misra, L. T. Drzal (Eds.), *Natural Fibers, Biopolymers, and Biocomposites*, Taylor & Francis, Boca Raton, FL, 2005, pp. 527–577.
16. L. T. Lim, R. Auras, M. Rubino, *Prog. Polym. Sci.* **2008**, *33*, 820–852.
17. D. M. Bigg, Effect of copolymer ratio on the crystallinity and properties of polylactic acid copolymers, *SPE ANTEC Technical Papers*, 1996, pp. 2028–2039.
18. A. Celli, A. Scandola, *Polymer* **1992**, *33*, 2699–2703.
19. H. Cai, V. Dave, R. A. Gross, P. McCarthy, *J. Polym. Sci.* **1996**, *B34*, 2701–2708.
20. P. R. Gruber, J. J. Kolstad, C. M. Ryan, E. S. Hall, R. S. E. Conn, U.S. Patent 5,484,881, 1996.
21. D. R. Witzke, Introduction to properties, engineering, and prospects of polylactide polymers, Ph.D. thesis, Michigan State University, East Lansing, MI, 1997.
22. G. Perego, G. D. Cella, C. Bastioli, *Polymer* **1996**, *59*, 37–43.
23. S. Gogolewski, M. Jovanovic, S. M. Perren, *Polym. Degrad. Stabil.* **1993**, *40*, 313–322.
24. NatureWorks LLC, Minnetonka, MN, 2007, Personal communication.
25. P. R. Gruber, S. P. Jeffrey, J. J. Kolstad, R. S. E. Conn, C. M. Ryan, U.S. Patent 5,446,123, 1995.
26. H. Suizu, M. Takagi, M. Ajioka, A. Yamaguchi, U.S. Patent 5,496,923, 1996.
27. X. Zhao, H. Hu, X. Wang, X. Yu, W. Zhou, S. Peng, *RSC Adv.* **2020**, *10*, 13316.
28. N. Likittanaprasong, M. Seadan, S. Suttiruengwong, *Mater. Sci. Eng.* **2015**, *87*, 012069.
29. V. Nagarajan, K. Zhang, M. Misra, A. K. Mohanty, *ACS Appl. Mater. Interfaces* **2015**, *7*, 11203–11214.
30. K. O. Siegenthaler, A. Kunkel, G. Skupin, and M. Yamamoto, *Adv. Polym. Sci.* **2012**, *245*, 91–136.
31. R. M. Rasal, A. V. Janorkar, D. E. Hirt, *Prog. Polym. Sci.* **2010**, *35*, 338–356.
32. J. R. Randall, K. Cink, J. C. Smith, U.S. Patent Application US2008/0050603A1, 2008.
33. J. R. Randell, A. Kulshrestha, N. Hossieny, *PCT application WO2019152264*, 2019.
34. Anonymous, *Plast. Addit. Compd.* **2007**, *11/12*, 32–35.
35. R. Renstad, S. Karlsson, A. Sandgren, A. C. Albertsson, *J. Environ. Polym. Degrad.* **1998**, *6*, 201–221.
36. P. C. Wernett, D. Prendes, J. Doll, J. Miller, The reinforcement of polylactic acid by a newly engineered mineral designed to provide ductility and greatly enhance impact resistance of PLA-mineral composites, *Innovation Takes Root Conference*, Las Vegas, NV, 17–18 September 2008.


37. N. Fukuda, H. Tsuji, *J. Appl. Polym. Sci.* **2005**, *96*, 190–199.
38. V. Taubner, R. Shishoo, *J. Appl. Polym. Sci.* **2001**, *79*, 2128–2135.
39. V. Speranza, A. D. Meo, R. Pantani, *Polym. Degrad. Stabil.* **2014**, *100*, 37–41.
40. M. J. A. van den Oever, B. B. J. Mussig, *Compos. Part A* **2010**, *41*, 1628–1635.
41. Anonymous, Crystallizing and drying Ingeo biopolymer, NatureWorks LLC, Minnetonka, MN. https://www.natureworksllc.com. Accessed on 21 December 2021
42. Anonymous, Production of NatureWorks polylactide films on blown film equipment designed for producing low density polyethylene film, NatureWorks LLC, Minnetonka, MN. https://www.natureworksllc.com. Accessed on 21 December 2021.
43. Anonymous, Ingeo™ biopolymer 4060D technical data sheet for heat seal layer in coextruded oriented film, NatureWorks LLC, Minnetonka, MN. https://www.natureworksllc.com. Accessed on 21 December 2021.
44. D. Garlotta, *J. Polym. Environ.* **2001**, *9*, 63–84.
45. O. Mysiukiewicz, M. Barczewski, K. Skórczewska, D. Matykiewicz, *Polymers* **2020**, *12*, 1333.
46. A. Sodergard, M. Stold, *Prog. Mater. Sci.* **2002**, *27*, 1123–1163.
47. F. D. Kopinke, M. Remmler, K. Mackenzie, M. Moder, O. Wachsen, *Polym. Degrad. Stabil.* **1996**, *53*, 329–342.
48. I. C. McNeill, H. A. Leiper, *Polym. Degrad. Stabil.* **1985**, *11*, 309–326.
49. A. Bashir, A. A. Al-Uraini, M. Jamjoom, A. Al-Khalid, M. Al-Hafez, S. Ali, *J. Macromol. Sci.* **2002**, *A39*, 1407–1433.
50. N. Sugaya, T. Nakagawa, K. Sajurai, M. Morita, S. Onodera, *J. Health Sci.* **2001**, *47*, 21–27.
51. T. Tsukegi, T. Motoyama, Y. Shirai, *Polym. Degrad. Stabil.* **2007**, *92*, 552–559.
52. Y. Fan, H. Nishida, Y. Shirai, T. Endo, *Green Chem.* **2003**, *5*, 575–579.
53. F. Khabbaz, S. Karlsson, A. C. Albertsson, *J. Appl. Polym. Sci.* **2000**, *78*, 2369–2378.
54. C. Westphal, C. Perrot, S. Karlsson, *Polym. Degrad. Stabil.* **2001**, *73*, 281–287.
55. J. J. Kolstad, D. R. Witzke, M. H. Hartmann, E. S. Hall, J. Nangeroni, U.S. Patent 6353086B1, 2002.
56. H. Rees, *Understanding Injection Molding Technology*, Hanser Gardner Publications, Inc., Cincinnati, OH, 1995.
57. Moldflow Material Testing Report, MAT2238 NatureWorks PLA, NatureWorks LLC, Minnetonka, MN, 2004.
58. X. Chen, Mathematical modeling of the in-mold coating process for injection molded thermoplastic parts, Ph.D. thesis, Ohio State University, Columbus, OH, 2003.
59. L. Capt, The pressure-volume-temperature behavior and the effect of pressure on crystallization kinetics of polyethylene resins, M.Sc. thesis, McGill University, Montreal, Quebec, Canada, 1999.
60. R. Y. Chang, C. H. Chen, K. S. Su, *Polym. Eng. Sci.* **1996**, *36*, 1789–1795.
61. J. J. Kolstad, *J. Appl. Polym. Sci.* **1996**, *62*, 1079–1091.
62. H. Li, M. A. Huneault, *SPE ANTEC Papers*, 2007, pp. 2615–2618.
63. J. R. Randall, Today's Ingeo™ products for the fiber industry, *Innovation Takes Root Conference*, Orlando, FL, 17–19 February 2014.
64. H. Tsuji, H. Takai, S. K. Saha, *Polymer* **2006**, *47*, 3826–3837.
65. M. Yasuniwa, S. Tsubakihara, Y. Sugimoto, C. Nakafuku, *J. Polym. Sci. Part B* **2004**, *42*, 25–32.
66. A. A. Perez-Fonseca, J. R. Robledo-Ortız, R. Gonzalez-Nunez, D. Rodrigue, *J. Appl. Polym. Sci.* **2016**, *133*, 43750.
67. A. De Meo, F. De Santis, R. Pantani, *Polym. Eng. Sci.* **2018**, *58*, 586–591.
68. S. Liparoti, V. Speranza, R. Pantani. *Materials* **2018**, *11*, 1442.
69. N. Ljungberg, T. Andersson, B. Wesslen, *J. Appl. Polym. Sci.* **2003**, *88*, 3239–3247.
70. NatureWorks, PLA processing guide for biaxially oriented film, NatureWorks LLC, Minnetonka, MN. https://www.natureworksllc.com. Accessed on 21 December 2021.
71. C. Aigner, *Bioplast. Mag.* **2007**, *2*(07/04), 25–27.
72. X. Ou, M. Cakmak, *SPE ANTEC Papers*, 2003, pp. 1701–1705.
73. J. K. Lee, K. H. Lee, B. S. Jin, *Eur. Polym. J.* **2001**, *37*, 907–914.
74. H. Wei, S. Yan, S. Goel, G. Menary, *Int. J. Mater. Forming* **2020**, *13*, 43–57.
75. R.-J. Xu, Z.-Q. Tian, J.-Y. Xie, C.-H. Lei, *Polym. Crystal.* **2019**, *2*, e10072
76. Anonymous, Ingeo™ biopolymer 4043D/4032D technical data sheet, NatureWorks LLC, Minnetonka, MN. https://www.natureworksllc.com. Accessed on 21 December 2021.
77. J. R. Cloutier, T. Mizumura, K.P. Chang, U.S. Patent 9314999B2, 2016.
78. I. Noda, E. B. Bond, D. H. Melik, U.S. Patent 6,808,795, 2004.
79. D.-Y. Lee, S. H. Lee, M. S. Cho, J. D. Nam, Y. Lee, *Polym. Int.* **2014**, *64*, 581–585.
80. Anonymous, NatureWorks PLA ISBM bottle guide, NatureWorks LLC, Minnetonka, MN, 2005.
81. A. Ailianou, K. Ramachandran, M. B. Kossuth, J. P. Oberhauser, J. A. Kornfield, *PNAS* **2016**, *113*, 11670–11675
82. P.-J. Wang, N. Ferralis, C. Conway, J. C. Grossman, E. R. Edelman. *PNAS* **2018**, *115*, 2640–2645
83. T. A. Osswald, *Polymer Processing Fundamentals*, Hanser Gardner Publications, Inc., Cincinnati, OH, 1998.
84. A. Sodergard, J. F. Selin, M. Niemi, C. J. Johansson, K. Meinander, U.S. Patent 6559244B1, 2003.
85. E. C. Tweed, H. M. Stephens, T. E. Riegert, U.S. Patent Application 2006/0045940A1, 2006.
86. B. Mallet, H. Lamnawar, A. Maazouz, *Polym. Eng. Sci.* **2014**, *54*, 840–857.
87. S. S. Karkhanis, N. M. Stark, R. C. Sabo, L. M. Matuana, *J. Appl. Polym. Sci.* **2017**, *134*, 45212

88. S. S. Karkhanis, L. M. Matuana, *Polym. Eng. Sci.* **2019**, *59*, 2211–2219.
89. https://plastics-rubber.basf.com/global/en/performance_polymers/products/ecovio.html; https://plastics-rubber.basf.com/global/en/performance_polymers/products/ecoflex.html. Accessed on 12 September 2021.
90. Anonymous, Processing guide for thermoforming articles, NatureWorks LLC, Minnetonka, MN, 2005.
91. R. C. Bopp, J. Whelan, U.S. Patent 2008/0258357A1, 2008.
92. L. Deetuam, C. Samthong, S. Choksriwichit, A. Somwangthanoroj, *Iran. Polym. J.* **2020**, *29*, 103–116.
93. K. Poloskei, G. Csezi, S. Hajba, T. Tabi, *Polym. Eng. Sci.* **2020**, *60*, 1266–1277.
94. T. Aritake, European Patent Application EP 1577356A1, 2005.
95. R. E. Lee, Y. Guo, H. Tamber, M. Planeta, S. N. S. Leung, *Ind. Eng. Chem. Res.* **2016**, *55*, 560–567.
96. B. Eling, S. Gogolewski, A. J. Pennings, *Polymer* **1982**, *23*, 1587–1593.
97. L. Fambri, A. Pegoretti, R. Fenner, S. D. Incardona, C. Migliaresi, *Polymer* **1997**, *38*, 79–85.
98. G. Schmack, B. Tandler, R. Vogel, R. Beyreuther, S. Jacobsen, H. G. Fritz, *J. Appl. Polym. Sci.* **1999**, *73*, 2785–2797.
99. A. K. Agrawal. Spinning of poly(lactic acid) fibers, in: R. Auras, L.-T. Lim, S. E. M. Selke, H. Tsuji (Eds.), *Poly(Lactic Acid): Synthesis, Structures, Properties, Processing, and Applications*, John Wiley & Sons, Inc., Hoboken, NJ, 2010, pp. 323–342.
100. NatureWorks Polymer Processing Guides—Crystallizing and Drying of PLA, NatureWorks LLC, Minnetonka, MN, 2007.
101. (a) P. Bajaj, Spin finishes for manufactured fibres, in: V. B. Gupta, V. K. Kothari (Eds.), *Manufactured Fibre Technology*, Chapman & Hall, London, 1997, pp. 139–169. (b) V. B. Gupta, Melt spinning processes, in: V. B. Gupta, V. K. Kothari (Eds.), *Manufactured Fibre Technology*, Chapman & Hall, London, 1997, pp. 67–97.
102. K. Mezghani, I. E. Spruiell, *J. Polym. Sci. Part B* **1998**, *36*, 1005–1012.
103. A. K. Doufas, A. J. McHugh, C. Miller, J. Non-Newton. *Fluid Mech.* **2000**, *92*, 27–66.
104. J. S. Kim, S. Y. Kim, *J. Appl. Polym. Sci.* **2000**, *76*, 446–456.
105. A. J. McHugh, A. K. Doufas, *Compos. Part A Appl. Sci. Manuf.* **2001**, *32*, 1059–1066.
106. A. K. Doufas, A. J. McHugh, C. Miller, A. Immaneni, *J. Non-Newton. Fluid Mech.* **2000**, *92*, 81–103.
107. S. H. Hyon, K. Jamshidi, Y. Ikada, Melt spinning of poly-L-lactide and hydrolysis of the fiber in vitro, in: S. W. Shalaby, A. Hoffman, B. Ratner, T. Horbett (Eds.), *Polymers as Biomaterial*, Plenum Press, New York, 1984, p. 65.
108. S. W. Chun, S. H. Kim, Y. H. Kim, H. J. Kang, *Polymer (Korea)* **2000**, *24*, 656–663.
109. P. R. Gruber, J. J. Kolstad, E. S. Hall, R. S. E. Conn, C. M. Ryan, US Patent 5,338,822, 1994.
110. F. Matsuoka, K. Hashimoto, Poly(lactic acid)-type conjugate staple fibers with good biodegradability and heat-bonding properties consisting of two types of lactic acid polymers with different optical purity and nonwoven fabrics therefrom and manufacture thereof, JP 2001049533, CAN 134:179858, 2001.
111. B. Gupta, N. Revagade, N. Anjum, B. Atthoff, J. Hilborn, *J. Appl. Polym. Sci.*, **2006**, *101*(6), 3774–3780.
112. B. Gupta, N. Revagade, N. Anjum, B. Atthoff, J. Hilborn, *J. Appl. Polym. Sci.*, **2006**, *100*, 1239.
113. J. W. Leenslag, A. J. Pennings, *Polymer* **1987**, *28*, 1695–1702.
114. H. Tsuji, Y. Ikada, S. H. Hyon, Y. Kimura, T. Kitao, *J. Appl. Polym. Sci.* **1994**, *51*, 337–344.
115. L.-T. Lim, Chapter 7—Electrospinning and electrospraying technologies for food and packaging applications, in: Y. Dong, A. Baji, S. Ramakrishna (Eds.), *Electrospun Polymers and Composites: Ultrafine Materials, High Performance Fibres and Wearables*, Elsevier Ltd., Duxford, United Kingdom, 2020, pp. 217–259.
116. D. I. Braghirolli, D. Steffens, P. Pranke, *Drug Discov. Today*, **2014**, *19*, 743–753.
117. W. E. Teo, S. Ramakrishna, *Nanotechnology* **2006**, *17*, R89–R106.
118. G. Taylor, *Proc. R. Soc. A Math. Phys. Eng. Sci.* **1966**, *291*, 145–158.
119. G. Taylor, *Proc. R. Soc. A Math. Phys. Eng. Sci.* **1969**, *313*, 453–475.
120. B. Chu, B. S. Hsiao, D. Fang, U.S. Patent 6,713,011, 2004.
121. M. A. Gogins, T. M. Weik, U.S. Patent 6,716,274, 2004.
122. W. S. Lee, S. M. Jo, S. G. Go, S. W. Chun, U.S. Patent 6,616,435, 2003.
123. L.-T. Lim, A. C. Mendes, I. S. Chronakis, *Adv. Food Nutr. Res.* **2019**, *88*, 167–234.
124. S. Ramakrishna, K. Fujihara, W. E. Teo, T. C. Lim, Z. Ma, *An Introduction to Electrospinning and Nanofibers*, World Scientific, Singapore, 2005.
125. H. W. Kim, H. H. Lee, J. C. Knowles, *J. Biomed. Mater. Res.* **2006**, *79A*, 643–649.
126. C. M. Vaz, C. van Tuijl, C. V. C. Bouten, F. P. T. Baaijens, *Acta Biomater.* **2005**, *1*, 575–582.
127. A. Jash, G. Paliyath, L.-T. Lim, *RSC Adv.* **2018**, *8*, 19930.
128. Y. Zhou, L.-T. Lim, *J. Food Sci.* **2009**, *74*, C170–C176.
129. R. Dai, L.-T. Lim, *Food Res. Int.* **2015**, *77*, 467–475.
130. X. Zong, H. Bien, C. Y. Chung, L. Yin, D. Fang, B. S. Hsiao, B. Chu, E. Entcheva, *Biomaterials* **2005**, *26*, 5330–5338.
131. X. Zong, K. Kim, D. Fang, S. Ran, B. S. Hsiao, B. Chu, *Polymer* **2002**, *43*, 4403–4412.
132. F. Yang, R. Murugan, S. Wang, S. Ramakrishna, *Biomaterials* **2005**, *26*, 2603–2610.
133. E. R. Kenawy, G. L. Bowlin, K. Mansfield, J. Layman, D. G. Simpson, E. H. Sanders, G. E. Wnek, *J. Control. Release* **2002**, *81*, 57–64.

134. E. S. Medeiros, L. H. C. Mattoso, R. D. Offeman, D. F. Wood, W. J. Orts, *Can. J. Chem.* **2008**, *86*, 590–599.
135. X. Xu, L. Yang, X. Xu, X. Wang, X. Chen, Q. Liang, J. Zeng, X. Jing, *J. Control. Release* **2005**, *108*, 33–42.
136. H. Tsuji, M. Nakano, M. Hashimoto, K. Takashima, S. Katsura, A. Mizuno, *Biomacromolecules* **2006**, *7*, 3316–3320.
137. A. Jash, L.-T. Lim, *J. Mater. Sci.* **2018**, *53*, 2221–2235.
138. A.-C. Vega-Lugo, L.-T. Lim, *Food Res. Int.* **2009**, *42*, 933–940.
139. K. Koenig, F. Langensiepen, G. Seide, *e-Polymers* **2020**, *20*, 233–241.
140. Z. Jun, H. Hou, A. Schaper, J. H. Wendorff, A. Greiner, *e-Polymers* **2003**, *9*, 1–9.
141. M. Bognitzki, W. Czado, T. Frese, A. Schaper, M. Hellwig, M. Steinhart, A. Greiner, J. H. Wendorff, *Adv. Mater.* **2001**, *13*, 70–72.
142. H. Zhou, T. B. Green, Y. L. Joo, *Polymer* **2006**, *47*, 7497–7505.
143. N. Ogata, S. Yamaguchi, N. Shimada, G. Lu, T. Iwata, K. Nakane, T. Ogihara, *J. Appl. Polym. Sci.* **2007**, *104*, 1640–1645.
144. M. Song, C. Pan, J. Li, X. Wang, Z. Gu, *Electroanalysis* **2006**, *18*, 1995–2000.
145. X. Xu, Q. Yang, Y. Wang, H. Yu, X. Chen, X. Jing, *Eur. Polym. J.* **2006**, *42*, 2081–2087.
146. Y. H. Lee, J. H. Lee, I. G. An, C. Kim, D. S. Lee, Y. K. Lee, J. D. Nam, *Biomaterials* **2005**, *26*, 3165–3172.
147. Y. Huang, M. C. Leu, J. Mazumder, A. Donmez, *J. Manuf. Sci. Eng.* **2015**, *137*, 014001
148. B. Shaqour, M. Abuabiah, S. Abdel-Fattah, A. Juaidi, R. Abdallah, W. Abuzaina, M. Qarout, B. Verleije, P. Cos, *Int. J. Adv. Manuf. Technol.* **2021**, *114*, 1279–1291.
149. M. V. den Eynde, P. V. Puyvelde, *Adv. Polym. Sci.* **2018**, *282*, 139–158.
150. https://www.natureworksllc.com/Products/3D-series-for-3D-printing. Accessed on 13 September 2021.
151. http://www.mdc.umn.edu/medworx/3Dprinting.html; https://www.lulzbot.com/learn/tutorials/3d-print-patterns-investment-casting; https://all3dp.com/2/lost-pla-casting-guide/; https://composites.umaine.edu/am-projects/. Accessed on 13 September 2021.

# 14

# BLENDS

Ajay Kathuria, Sukeewan Detyothin, Waree Jaruwattanayon, Susan E. M. Selke, and Rafael Auras

## 14.1 INTRODUCTION

Poly(lactic acid) (PLA) has increasingly gained momentum as a mass polymer across industrial sectors including packaging, textiles, agriculture, transport, and electronics due to its biodegradability, compostability, biocompatibility, and bio-based origin. The production of PLA reached 400,000 t in 2020 [1]. PLA has various inherent limitations such as its brittle nature, lack of toughness, poor gas barrier performance, and low heat deflection temperature (HDT) [2]. As discussed in the previous chapters, the stereochemical composition (i.e., L- and D-lactic acid, L-LA, and D-LA) of PLA can be used to manipulate molecular architecture, morphology, and crystallinity by introducing irregularity in the poly(L-lactic acid) (PLLA) molecular arrangement [3, 4]. In addition to molecular design control, molecular orientation, and processing conditions such as cooling rate and drawing parameters have been used to control the crystallinity in order to obtain the desired mechanical performance necessary for extending PLA's applications [5]. However, mechanical orientation of macro-molecules is not feasible for all PLA applications (e.g., injection molded articles). Furthermore, PLA functional properties may not be adequate for some designed applications. To improve strength, toughness, overcome the inherent brittle nature of PLA, and improve biodegradability, blending it with other polymers is a pragmatic commercially viable strategy. Another reason for adding PLA into fossil-derived polymers is to increase the bio-based carbon content of those polymeric matrices and reduce the environmental footprint of the final polymeric structure.

Various polymers have been blended with PLA for improving its properties, including nonbiodegradable polymers such as polyolefins [6–8], vinyl polymers [9, 10], elastomers [11], rubbers [12, 13], and biodegradable polymers such as thermoplastic starch [14, 15], polyanhydrides [16], aliphatic polyesters [17, 18], and aliphatic-aromatic co-polyesters [18–20]. PLA has also been blended with low-molecular-weight modifiers and plasticizers [20–22]. Simple melt blends of PLA have been commonly reported as thermodynamically unfavorable and immiscible. Poor compatibility, low interfacial adhesion, and immiscibility are widely seen as challenges due to the low entropy of mixing and large molecular structure [2, 23, 24]. Depending on the polymer structure, miscible, immiscible, or multiphase structures present in the polymer can be identified from studying the morphology, rheology, and glass transition temperature ($T_g$) [24–26]. Miscible polymers are characterized by a single thermal transition, single amorphous phase, or co-crystallization of blended polymer domains in the crystal lattice. Immiscibility creates several phases, which generates complex flow behavior and rheological properties. Furthermore, immiscible polymers have low interfacial adhesion leading to debonding at low stress and poor mechanical performance. However, immiscible blends have been reported as a growing sub-section of polymeric materials with the technological advances in compatibilization methodologies leading to stable microstructures. Nanostructured addition compatibilization, reactive compatibilization techniques, catalyst presence at the interphase, addition of chemicals or free radicals, ternary blends, and racemic polylactide blend formation have been widely researched to achieve various thermal and mechanical parameters, such as enhanced toughness, desired flexibility, chain mobility, requisite melt strength, and processing stability. Figure 14.1 shows a schematic representation of droplet, laminar, fiber, co-continuous,

*Poly(Lactic Acid): Synthesis, Structures, Properties, Processing, Applications, and End of Life*, Second Edition.
Edited by Rafael A. Auras, Loong-Tak Lim, Susan E. M. Selke, and Hideto Tsuji.

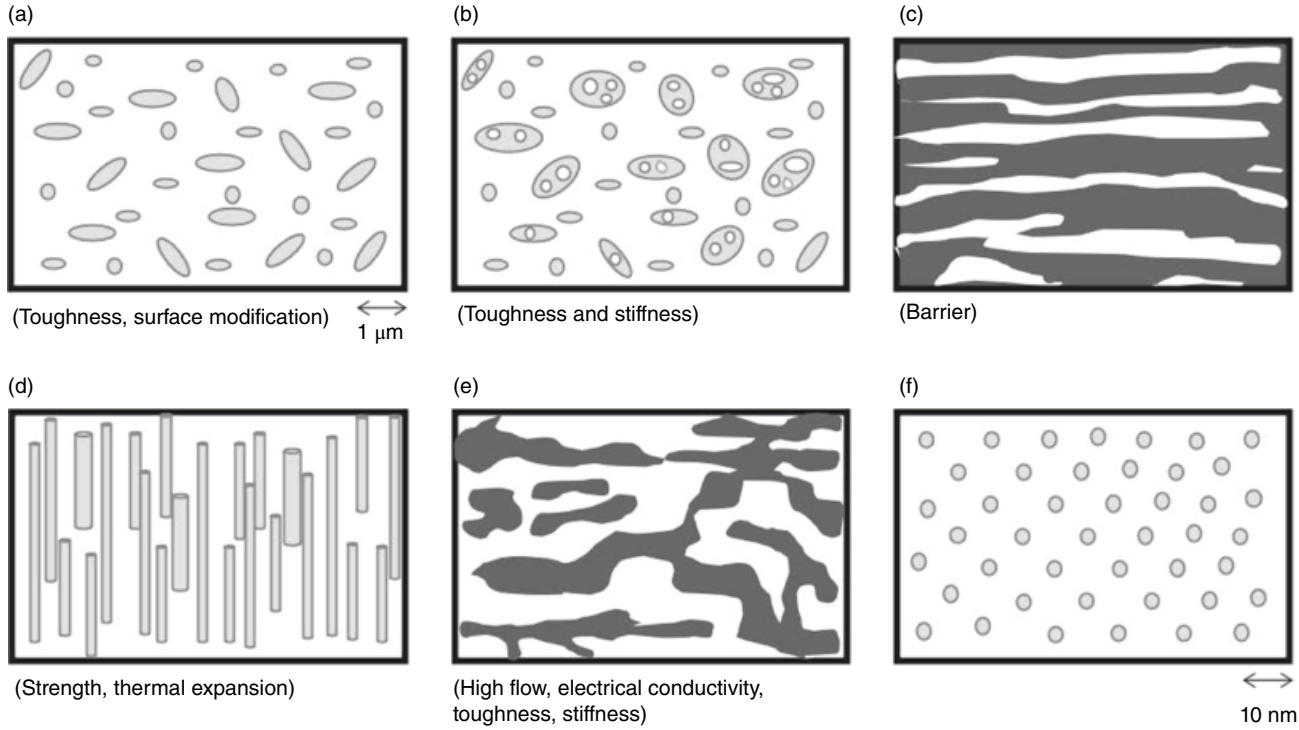


**FIGURE 14.1** Representation of different morphologies developed during melt blending: (a) drops, (b) double emulsion, (c) laminar, (d) fibers, (e) co-continuous, and (f) ordered microphases. *Source:* Adapted from Ref. 26.

and ordered microphase structures generally observed in polymer blends. In droplet microstructure, generally drops <1 μm can improve elastic performance and toughness; laminar-like microstructures can be useful for improving the barrier performance; fiber structures suit high-strength material needs; co-continuous morphologies occur due to coalescence when the melt viscosity difference between two polymers is large and can be deployed for conductive polymer needs; ordered microphases are currently produced by advancing blending techniques such as selective dissolution or 3D printing.

Various theoretical methods such as Hildebrand, Hansen Solubility Parameters, cohesive energy density (CED), and Flory-Huggins interaction parameters have been used to predict and model the interfacial strength and desired functional performance, which are influenced by morphological structure, coupling agents, and compatibilizers [27–30]. Monte Carlo and molecular dynamics simulations have also been utilized to predict structural properties and miscibility of blends by studying glass transition temperature, chain mobility, and interchain pair correlations, which directly affect the obtained morphology and functional performance [31, 32].

In this chapter, the morphological structures and mechanical and physical properties of these PLA blends are briefly discussed and reviewed. This review is divided into three main subsections: (i) PLA-non-biodegradable polymer blends; (ii) PLA-biodegradable polymer blends; and (iii) plasticization of PLA.

## 14.2 PLA NONBIODEGRADABLE POLYMER BLENDS

PLA has been blended with nonbiodegradable polymers to improve HDT, brittleness, and barrier performance and to increase the bio-based content of fossil-derived polymers. A second objective has been to develop morphologies suitable for medical applications. Among the main polymer families that have been blended with PLA, polyolefins, vinyl and vinylidene polymers and copolymers, elastomers, and rubbers have been widely studied.

### 14.2.1 Polyolefins

High toughness, good impact strength, and low cost make polyolefins such as polyethylene (PE) and polypropylene (PP) promising candidates to toughen PLA for commercial applications including packaging. Blending PLA with polyolefins improves thermal stability and reduces hydrolytic degradation. However, the immiscibility of polyolefin/PLA blends due to the differences in their chemical structure generally results in weak interfacial adhesion (indicated by poor dispersion, a very broad size distribution, and distinct particle interfaces) and poor mechanical properties. Table 14.1 shows a summary of the properties of PLA nonbiodegradable polymer blends.

**TABLE 14.1 Summary of the Mechanical Properties of Nonbiodegradable Polymer and PLA Blends**

| Polymer | Composition Ratio | Compatibilizer | Ratio | Blending Method | Young's Modulus (MPa) | Tensile Strength (MPa) | Elongation at Break (%) | Tensile Toughness ($MJ/m^3$) | Impact Resistance/ Strength (J/m) | Reference |
|---|---|---|---|---|---|---|---|---|---|---|
| PLA | — | — | — | — | — | — | — | — | 12 ± 4 | [6] |
| PLA/LLDPE | 80/20 | — | — | MB | — | — | — | — | 34 ± 1 | [6] |
| PLA/LLDPE | 80/20 | PLLA-PE block (5–30) | 5 | MB | — | — | — | — | 36 ± 5 | [6] |
| PLA/LLDPE | 80/20 | PLLA-PE block (30–30) | 5 | MB | — | — | — | — | 460 ± 60 | [6] |
| PLLA | | — | — | — | — | — | — | — | 20 ± 2 | [6] |
| PLLA/LLDPE | 80/20 | — | — | MB | — | — | — | — | 350 ± 230 | [6] |
| PLLA/LLDPE | 80/20 | PLLA-PE block (5–30) | 5 | MB | — | — | — | — | 510 ± 60 | [6] |
| PLLA/LLDPE | 80/20 | PLLA-PE block (30–30) | 5 | MB | — | — | — | — | 660 ± 50 | [6] |
| PLLA | — | — | — | — | 2400 ± 60 | 62.1 ± 1.0 | 4 ± 1 | 1.5 ± 0.1 | 20 ± 2 | [35] |
| LLDPE1 | — | — | — | — | 8.0 ± 0.5 | 10.8 ± 0.4 | 960 ± 40 | 56 ± 3 | — | [35] |
| PLLA/LLDPE1 | 80/20 | — | — | MB | 1680 ± 140 | 21.9 ± 6.4 | 23 ± 6 | 6.7 ± 1.6 | 490 ± 200 | [35] |
| PLLA/LLDPE1 | 80/20 | PLLA-PE block | 5 | MB | 1320 ± 110 | 24.3 ± 1.1 | 31 ± 18 | 7.7 ± 4.8 | 760 ± 50 | [35] |
| PLLA/LLDPE1 | 80/20 | PLA-PE block | 5 | MB | 1200 ± 40 | 23.0 ± 1.3 | 26 ± 16 | 6.3 ± 4.0 | 730 ± 40 | [35] |
| PLLA/LLDPE1 | 80/20 | PLLA-PEP block | 5 | MB | 1190 ± 20 | 23.0 ± 1.8 | 19 ± 7 | 4.3 ± 1.5 | 710 ± 40 | [35] |
| PLLA/LLDPE1 | 80/20 | PLA-PEP block | 5 | MB | 1200 ± 40 | 22.6 ± 0.7 | 27 ± 17 | 5.9 ± 3.9 | 660 ± 40 | [35] |
| LLDPE2 | — | — | — | — | 120 ± 5 | 21.7 ± 2.7 | 740 ± 140 | 96 ± 32 | — | [35] |
| PLLA/LLDPE2 | 80/20 | — | — | MB | 1570 ± 70 | 29.5 ± 1.9 | 16 ± 7 | 4.7 ± 2.2 | 50 ± 8 | [35] |
| PLLA/LLDPE2 | 80/20 | PLLA-PE block | 5 | MB | 1330 ± 60 | 26.7 ± 3.4 | 33 ± 27 | 8.5 ± 7.0 | 230 ± 30 | [35] |
| PLLA/LLDPE2 | 80/20 | PLA-PE block | 5 | MB | 1270 ± 90 | 23.8 ± 1.7 | 62 ± 46 | 16 ± 12 | 420 ± 30 | [35] |
| PLLA/LLDPE2 | 80/20 | PLLA-PEP block | 5 | MB | 1310 ± 60 | 25.2 ± 0.9 | 15 ± 6 | 3.8 ± 1.4 | 220 ± 30 | [35] |
| PLLA/LLDPE2 | 80/20 | PLA-PEP block | 5 | MB | 1290 ± 70 | 23.4 ± 1.0 | 26 ± 9 | 6.1 ± 2.1 | 150 ± 30 | [35] |
| HDPE | — | — | — | — | 440 ± 60 | 10.4 ± 3.7 | 150 ± 40 | 19.4 ± 6.8 | — | [35] |
| PLLA/HDPE | 80/20 | — | — | MB | 1710 ± 60 | 41.8 ± 2.1 | 2.9 ± 0.2 | 0.7 ± 0.1 | 12 ± 6 | [35] |
| PLLA/HDPE | 80/20 | PLLA-PE block | 5 | MB | 1590 ± 60 | 44.5 ± 1.9 | 3.7 ± 0.5 | 1.0 ± 0.2 | 24 ± 9 | [35] |
| PLLA/HDPE | 80/20 | PLA-PE block | 5 | MB | 1540 ± 90 | 42.3 ± 2.5 | 4.2 ± 0.8 | 1.2 ± 0.3 | 32 ± 7 | [35] |
| PLLA/HDPE | 80/20 | PLLA-PEP block | 5 | MB | 1440 ± 90 | 27.7 ± 1.1 | 14 ± 8 | 3.7 ± 2.4 | 42 ± 7 | [35] |
| PLLA/HDPE | 80/20 | PLA-PEP block | 5 | MB | 1390 ± 90 | 25.0 ± 1.1 | 13 ± 4 | 3.3 ± 0.0 | 64 ± 20 | [35] |
| PLLA | — | — | — | — | 2560 ± 170 | 69.7 ± 4.2 | 4.1 ± 1.5 | 1.8 ± 0.3 | 22 ± 4 | [34] |
| LLDPE | — | — | — | — | 11 ± 2 | 22.6 ± 1.8 | 840 ± 59.8 | 920 ± 140 | No break | [34] |
| PLLA/LLDPE | 80/20 | PE-*b*-PLLA | — | SB | 1520 ± 62 | 33.5 ± 3.3 | 10.4 ± 1.2 | 3.0 ± 0.5 | 22 ± 3 | [34] |
| PLLA/LLDPE | 80/20 | PE-*b*-PLLA | 2 | SB | 1510 ± 81 | 33.2 ± 1.4 | 19.5 ± 0.1 | 5.5 ± 1.7 | 77 ± 5 | [34] |
| PLLA/LLDPE | 80/20 | PE-*b*-PLLA | 5 | SB | 1490 ± 90 | 33.0 ± 1.7 | 27.4 ± 8 | 8.3 ± 2.2 | 185 ± 28 | [34] |
| PLLA/LLDPE | 80/20 | PE-*b*-PLLA | 10 | SB | 1460 ± 30 | 31.4 ± 2.6 | 35.3 ± 16.7 | 10.1 ± 2.6 | 283 ± 65 | [34] |
| PLA/LDPE | 80/20 | — | — | MB | — | 7.8 | 6.6 | — | — | [7] |
| PLA/LDPE | 80/20 | PE-GMA8 | 5 | MB | — | 9.2 | 77.9 | — | — | [7] |
| PLA/LDPE | 20/80 | — | — | MB | — | 7.1 | 16.4 | — | — | [7] |
| PLA/LDPE | 20/80 | PE-GMA8 | 5 | MB | — | 11.5 | 50.5 | — | — | [7] |
| PLA/LDPE | 80/20 | PE-GMA25 | 5 | MB | — | 32.0 | 4.0 | — | — | [7] |

(*Continued*)

**TABLE 14.1 (Continued)**

| Polymer | Composition Ratio | Compatibilizer | Ratio | Blending Method | Young's Modulus (MPa) | Tensile Strength (MPa) | Elongation at Break (%) | Tensile Toughness ($MJ/m^3$) | Impact Resistance/ Strength (J/m) | Reference |
|---|---|---|---|---|---|---|---|---|---|---|
| PLA/LDPE | 20/80 | PE-GMA25 | 5 | MB | — | 7.4 | 29.5 | — | — | [7] |
| PLA | — | — | — | — | 1316 ± 29 | 68.8 ± 0.6 | 7.2 ± 0.1 | — | — | [49] |
| PLA/PS | 75/25 | — | — | MB | 1310 ± 52 | 49 ± 2.0 | 5.3 ± 0.5 | — | — | [49] |
| PLLA | — | — | — | — | 2147.6 | 55.9 | 4.5 | — | — | [79] |
| PEVAc85 | — | — | — | — | 608.0 | 13.7 | 244.9 | — | — | [79] |
| PLLA/PEVAc85 | 90/10 | — | — | SB[a] | 1804.4 | 45.1 | 4.7 | — | — | [79] |
| PLLA/PEVAc85 | 70/20 | — | — | SB[a] | 1314.1 | 32.4 | 6.9 | — | — | [79] |
| PLLA/PEVAc85 | 50/50 | — | — | SB[a] | 1274.9 | 16.7 | 10.2 | — | — | [79] |
| PLLA/PEVAc85 | 30/70 | — | — | SB[a] | 1284.7 | 16.7 | 9.0 | — | — | [79] |
| PLLA/PEVAc85 | 10/90 | — | — | SB[a] | 627.6 | 13.7 | 208.9 | — | — | [79] |
| EVOH | — | — | — | — | 1067 ± 453.2 | 1.98 ± 0.62 | 16.5 ± 4.62 | — | — | [86] |
| PLLA/EVOH | 40/60 | — | — | SB | 860 ± 643.1 | 1.73 ± 0.77 | 2.70 ± 1.28 | — | — | [86] |
| PLLA/EVOH | 80/20 | TNBT | 0.3 | RSB | 1303 ± 493.3 | 0.55 ± 0.35 | 1.77 ± 0.55 | — | — | [86] |
| PLLA/EVOH | 60/40 | TNBT | 0.3 | RSB | 1711 ± 385.0 | 1.78 ± 0.58 | 9.34 ± 18.9 | — | — | [86] |
| PLLA/EVOH | 50/50 | TNBT | 0.3 | RSB | 1661 ± 412.9 | 1.59 ± 0.72 | 12.2 ± 8.12 | — | — | [86] |
| PLLA/EVOH | 40/60 | TNBT | 0.3 | RSB | 1198 ± 392.3 | 1.16 ± 0.15 | 21.6 ± 5.51 | — | — | [86] |
| PLLA/EVOH | 20/80 | TNBT | 0.3 | RSB | 1447 ± 355.9 | 1.43 ± 0.65 | 9.44 ± 2.97 | — | — | [86] |
| PLA | — | — | — | — | 2220 ± 500 | 54.2 ± 2.5 | 6.0 ± 0.1 | 2.3 ± 0.5 | 73 ± 17 | [98] |
| TPO | — | — | — | — | — | 7.3 | 1000 | — | — | [98] |
| PLA/TPO | 80/20 | — | — | MB | 1460 ± 30 | 34.7 ± 0.7 | 15.4 ± 1.4 | 4.6 ± 1.0 | 137 ± 21 | [98] |
| PLA/TPO | 80/20 | TP06PL08 | 1.0 | MB | 1210 ± 20 | 35.6 ± 0.4 | 99.1 ± 22.4 | 25.7 ± 6.3 | No break | [98] |
| PLA/TPO | 80/20 | TP06PL08 | 2.5 | MB | 1200 ± 10 | 33.1 ± 0.5 | 128.4 ± 18.2 | 29.9 ± 4.8 | No break | [98] |
| PLA/TPO | 80/20 | TP06PL08 | 5.0 | MB | 1100 ± 10 | 34.6 ± 0.7 | 107.2 ± 35.4 | 27.4 ± 0.8 | No break | [98] |
| PLA/TPO | 80/20 | TP06PL04 | 2.5 | MB | 1100 ± 30 | 30.1 ± 1.3 | 181.9 ± 10.1 | 38.5 ± 2.1 | No break | [98] |
| PLA/TPO | 80/20 | TP06PL16 | 2.5 | MB | 1100 ± 20 | 33.5 ± 0.8 | 101.7 ± 16.5 | 24.7 ± 3.8 | No break | [98] |
| PLA/TPO | 80/20 | TP13PL04 | 2.5 | MB | 1160 ± 20 | 31.0 ± 0.3 | 162.8 ± 30.2 | 37.1 ± 7.6 | No break | [98] |
| PLA/TPO | 80/20 | TP13PL08 | 2.5 | MB | 1180 ± 10 | 32.7 ± 0.7 | 140.8 ± 17.9 | 33.1 ± 4.4 | No break | [98] |
| PLA/TPO | 80/20 | TP13PL16 | 2.5 | MB | 1210 ± 80 | 33.3 ± 0.4 | 99.3 ± 19.3 | 22.9 ± 6.3 | No break | [98] |
| PLA/TPO | 80/20 | TPMA06 | 5.0 | MB | 1060 ± 20 | 32.4 ± 0.4 | 52.2 ± 12.6 | 13.1 ± 3.3 | No break | [98] |
| PLLA | — | — | — | — | 2024 | 65.5 | 4.0 | — | 69.7 | [89] |
| ABS | — | — | — | — | 807 | 32.9 | 122 | — | 425 | [89] |
| PLLA/ABS | 50/50 | — | — | MB | 1294 | 38.8 | 3.5 | — | 48.3 | [89] |
| PLLA/ABS | 50/50 | SAN-GMA | 5 | MB | 1327 | 42.9 | 18 | — | 119.7 | [89] |
| PLLA/ABS | 50/50 | SAN-GMA/ETPB | 5/0.02[b] | RMB | 1358 | 43.6 | 23.5 | — | 162.8 | [89] |

| Polymer | Composition Ratio | Compatibilizer | Ratio | Blending Method | Young's Modulus (MPa) | Tensile Strength (MPa) | Elongation at Break (%) | Tensile Toughness ($MJ/m^3$) | Impact Resistance/ Strength (J/m) | Reference |
|---|---|---|---|---|---|---|---|---|---|---|
| PLLA/ABS | 70/30 | — | — | MB | 1554 | 46.7 | 3.1 | — | 63.8 | [89] |
| PLLA/ABS | 70/30 | SAN-GMA | 5 | MB | 1405 | 43.6 | 20.5 | — | 81.1 | [89] |
| PLLA/ABS | 70/30 | SAN-GMA/ETPB | 5/0.02[b] | RMB | 1352 | 44.6 | 23.8 | — | 123.9 | [89] |
| PLLA | — | — | — | — | 1582.5 | 18.1 | 10.2 | — | — | [97] |
| PLLA/PIP | 80/20 | — | — | SB | 982.2 | 6.3 | 2.5 | — | — | [97] |
| PLLA/PIP-*g*-PVAc | 80/20 | — | — | SB | 1065.0 | 14.6 | 14.3 | — | — | [97] |
| PLA | — | — | — | — | ~1800 | ~61.0 | ~6.5 | — | ~2200[c] | [95] |
| PLA/EXL2330 | 99/1 | — | — | MB | ~1740 | ~58.7 | ~7.0 | — | ~2300[c] | [95] |
| PLA/EXL2330 | 95/5 | — | — | MB | ~1655 | ~56.5 | ~7.5 | — | ~2700[c] | [95] |
| PLA/EXL2330 | 90/10 | — | — | MB | ~1515 | ~52.5 | ~8.2 | — | ~4000[c] | [95] |
| PLA/EXL2314 | 99/1 | — | — | MB | ~1715 | ~56.5 | ~7.4 | — | ~2100[c] | [95] |
| PLA/EXL2314 | 95/5 | — | — | MB | ~1670 | ~57.0 | ~8.3 | — | ~2150[c] | [95] |
| PLA/EXL2314 | 90/10 | — | — | MB | ~1530 | ~53.2 | ~10.8 | — | ~2200[c] | [95] |

MB: melt blending; SB: solution blending; RMB: reactive melt blending; and RSB: reactive solution blending.

[a] Miscible blend.

[b] per hundred parts of resin (phr).

[c] Unit of impact strength is $J/m^2$.

***14.2.1.1 PLA-PE Blends*** Due to the significant difference in surface energy, polarity, chemical structure, and low entropy, PLA-PE blends have been widely reported as immiscible [6–8, 31–35]. To improve compatibility, researchers have investigated block copolymers as compatibilizers; among these investigations, PLA-PE block copolymers have been widely researched [6, 7, 31]. Wang et al. [34] studied 80 : 20 PLLA-LLDPE blends compatibilized with PE-PLLA block copolymer (PE-*b*-PLLA) in 2, 5, and 10 wt% ratio. In the uncompatibilized binary blends, large dispersed LLDPE spherical particles with an average size of 25.7 μm were observed in the PLLA matrix using scanning electronic microscopy (SEM) (Figure 14.2), which decreased to 3.5, 2.5, and 1.7 μm for 2, 5, and 10 wt% ratio of compatibilized blends, respectively. The decrease in the LLDPE droplet size and interfacial surface adhesion as a function of copolymer compatibilizer was accredited to the reduced surface tension and enhanced compatibility. Similar trends were observed in mechanical properties, such as Izod impact strength (283 J/m) and toughness (10.1 MJ/m$^3$) for 10% compatibilizer added to PLA/LDPE 80 : 20 blend. In addition to the dispersed phase droplet size, toughening of the matrix depends on the dispersed phase distribution impacting the matrix ligament thickness and distance between two dispersed particles. If a critical matrix ligament thickness (MLT) is achieved during blending, it helps in the yielding of a polymer with improved toughness. Such a toughening mechanism has been reported with rubber particles and hybrid fillers [35–37]. The critical MLT depends on the matrix-filler system, which can be calculated using Equation 14.1:

$$T = d\left[\left(\frac{\pi}{6\varphi}\right)^{1/3} \exp\left(1.5\ln^2\sigma\right) - \exp\left(0.5\ln^2\sigma\right)\right] \quad (14.1)$$

where $T$ is the matrix ligament thickness, $d$ is the average particle diameter, ϕ is volume fraction of the filler, σ is the particle size distribution parameter defined by Equation 14.2:

$$\ln\sigma = \sqrt{\frac{\sum_{i=1}^{N}\left(\ln d_i - \ln d\right)}{\sum_{i=1}^{N} n_i}} \quad (14.2)$$

In another study, Anderson et al. [35] reported the theoretically calculated critical MLT values for 80–20 PLA-LLDPE and PLA-HDPE matrices compatibilized with four types of PLA-*b*-PE copolymers; the final ternary blends

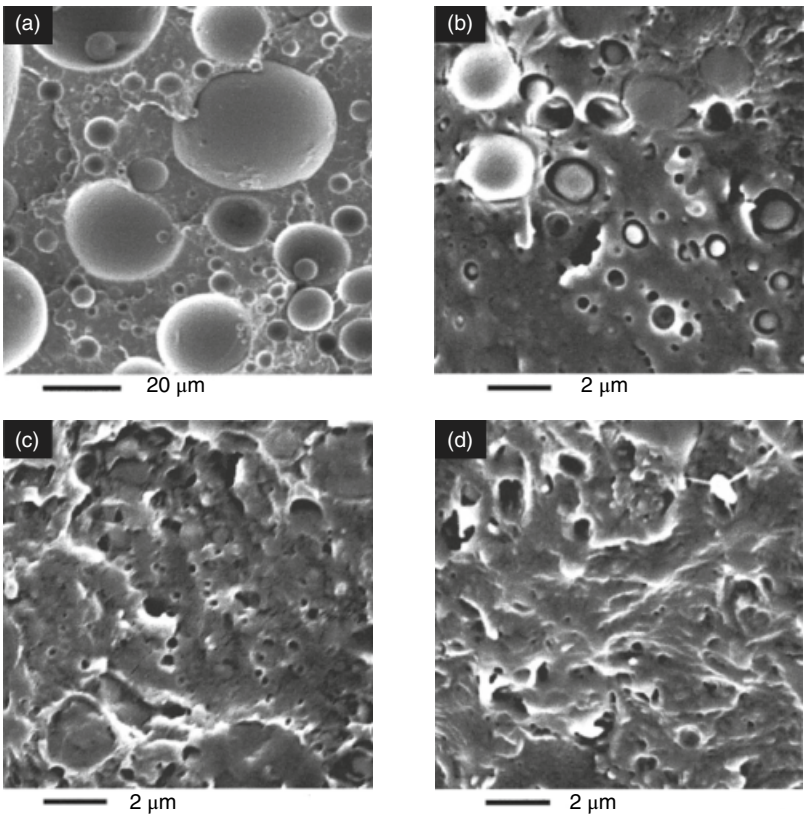


**FIGURE 14.2** Scanning electron micrographs of cryofractured surfaces of (a) 80 : 20 : 0; (b) 80 : 20 : 2; (c) 80 : 20 : 5; and (d) 80 : 20 : 10 PLLA/LDPE/PE-*b*-PLLA blends. *Source:* Reprinted from Ref. 34. Copyright 2001, with permission from John Wiley & Sons, Inc.

contained 5% compatibilizer. Depending on the combination of matrix and compatibilizer used, investigators reported critical MLT values ranging between 0.3 and 1.5 μm. Interfacial adhesion was studied using the dual cantilever method and 180°C peel test. PLA-PE block copolymers were reported with improved interfacial adhesion. PLA-LLDPE compatibilized ternary systems with good adhesion demonstrated improved impact strength to 730–760 J/m and tensile toughness ranging from 6.3 to 7.7 MJ/m$^3$. Furthermore, improved adhesion was linked to the entanglement and the co-crystallization ability of the block copolymer. SEM images of impact bar fracture surfaces of PLA-LLDPE ternary blends are shown in Figure 14.3.

The addition of reactive compatibilizers such as a copolymer of ethylene and acrylic acid (EAA) with 9.54% acrylic acid (AA) and PE containing polar units of glycidyl methacrylate (PE-GMA) to improve the compatibility of LDPE and PLA blends was investigated (PLA LACTY9031 was provided by Shimadzu, Japan) [7]. EAA did not improve the compatibility with PLA, but PE-GMA did. Increasing the GMA content to 25 wt% in PE-GMA(PE-GMA25) enhanced the compatibility with PLA but decreased its compatibility with LDPE [7]. PE-GMA8 (8 wt% GMA)

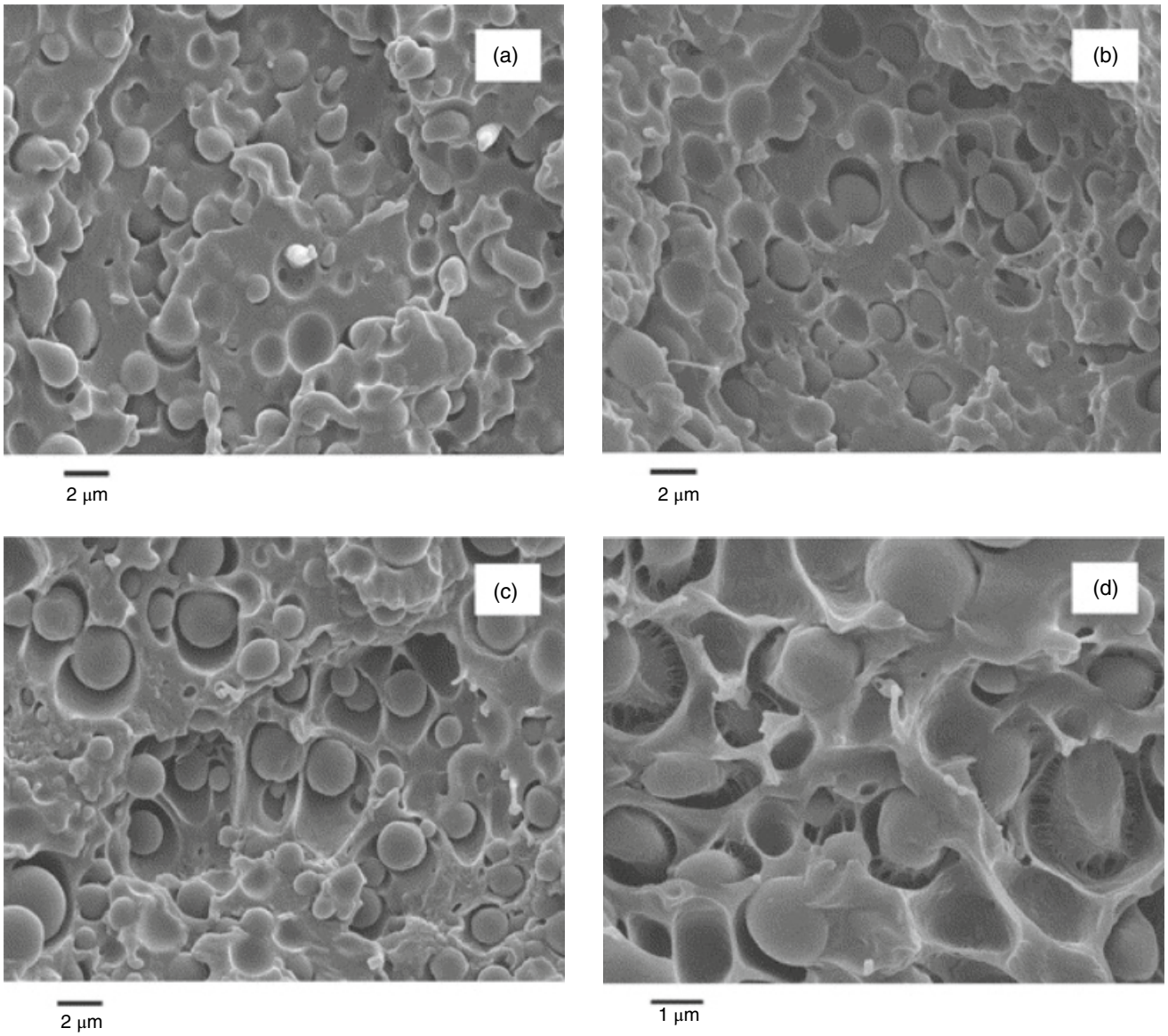


**FIGURE 14.3** SEM images of 80/20 wt% PLLA/LLDPE2 impact bar fracture surfaces. Images were taken behind notch area: (a) with 5 wt% D,L-lactide PLA-PE block copolymer; (b) with 5 wt% D,L-lactide PLA-poly(ethylene-alt-propylene) (PLA-PEP) block copolymer; (c) with 5 wt% PLLA-poly(ethylene-alt-propylene) (PLLA-PEP) block copolymer; and (d) with 5 wt% PLLA-PE block copolymer (higher magnification). *Source:* Reprinted from Ref. 35. Copyright 2004, with permission from Elsevier.

did not affect the thermal properties of the blends, but improvement in the mechanical properties of LDPE/PLA (20/80) with 5% PEGMA8 compared to blends without GMA (maximum stress of 0.8 kgf/mm$^2$ and strain at break of 6.6%) was observed. Adding PE-GMA8 at 5 wt% to the blend provided a maximum stress of 0.94 kgf/mm$^2$ and strain at break of 77.9% compared to 3.26 kgf/mm$^2$ and 4.0% for the blend with 5 wt% PE-GMA25 [7]. Reactive blends of HDPE/PLA/PE grafted with maleic anhydride (MA) (PE--*g*-MA) at the ratio of 60/30/10 exhibited poorer flexibility and higher strength and stiffness compared to HDPE [38]. Adding PE-*g*-MA did not improve interfacial adhesion between HDPE and PLA. However, an increase of surface energy of the blend promoted the adhesion of *Pseudomonas fluorescens* on the compatibilized HDPE/PLA surface [38].

Su et al. [39] predicted the morphologies of in situ compatibilized LLDPE/PLA/GMA-grafted poly(ethylene-octene) copolymer (mPOE) by using spreading coefficients and interfacial tensions calculated from the harmonic mean. They predicted that in 90 wt% PLA, mPOE would spread on LLDPE. Therefore, they encapsulated LLDPE, dispersed it in a PLA matrix, and correlated the results obtained from differential scanning calorimetry (DSC), SEM, and wide-angle X-ray diffraction (WAXD) for the blends. Fourier transform infrared (FTIR) spectroscopy analysis revealed the interaction between the end carboxyl and/or hydroxyl groups of PLA with the epoxy groups of mPOE [39]. The compatibilized LLDPE/PLA blends showed smaller domain sizes from 1.6–3.2 to <0.5 μm, lower crystallization temperature ($T_c$) (from ca. 103 to 96°C), and less crystallinity (from 34.2 to 24.1%) compared with the physical blends [39].

Zolali et al. [32] investigated the morphology of PLA/PE-based ternary blends of PLA, PE, and three different compatibilizing components, i.e., poly(ε-caprolactone) (PCL), poly(ethylene-methyl acrylate) (EMA), and ethylene-methyl acrylate-glycidyl methacrylate (EMA-GMA). For equal ratios of PLA-PE blends (50/50) and with 10% compatibilizer, a continuous phase morphology was observed with a layer of compatibilizer localized at the interface completely wetted by the compatibilizer. Compatibilizer layer thicknesses of 1.9, 0.6, and 0.5 μm were observed for PCL, EMA, and EMA-GMA indicating reduced interfacial interaction for EMA and EMA-GMA compared with PCL. The average phase sizes of PLA in the ternary blends dropped to 5.8 and 4.6 μm for PLA/EMA/LLDPE 45/10/45 and PLA/EMA-GMA/LLDPE 45/10/45, respectively, compared with PLA/LLDPE 50/50 blends. No significant change in the PLA phase size was observed for PLA/PCL/LLDPE 45/10/45, supporting the reduced interfacial tension ($\Gamma$) and better compatibility. They measured PE-PLA interfacial tension ($\Gamma_{PE\text{-}PLA}$) of 6.4 mN/m (180°C). However, $\Gamma_{PE\text{-}PLA}$ discrepancies have been noticed; some other researchers reported 5 and 11 mN/m [40, 41]. To investigate the discrepancies, Gu et al. [42] measured PLA/PE interfacial tension using immiscible PE/PS/PLA ternary blends. They estimated $\Gamma_{PE\text{-}PLA} \sim 10.5 \pm 1.4$ mN/m.

Thurber et al. [8] studied reactive compatibilization of PE-PLA-hydroxyl functionalized PE ternary blends using stannous octoate ($SnOct_2$) catalyst. Localization of $SnOct_2$ catalyst at the interface of the PLA-PE blend generated PLA-PE copolymer, which improved the compatibility between PE and PLA by decreasing the blended polymer droplet size in the matrix, improving dispersion and adhesion. Localization and enhanced compatibility of $SnOct_2$ resulted in favorable solubility parameters estimated around 20.0 MPa$^{1/2}$, which falls between the solubility parameters of the two polymers. On the other hand, $SnCl_2$ performed poorly because of its significantly higher solubility parameter, $\delta = 42.3$ MPa$^{1/2}$.

***14.2.1.2 PLA-PP Blends*** PP is a popular plastic due to low prices, high hydrophobicity, reasonable stiffness and high HDT. In general, physical blending of a PLA matrix with PP increased HDT, strain at break, decreased crystallinity and decreased elongation. PP has a higher complex viscosity compared to PLA; therefore, the complex viscosity of PLA/PP blends increases with increasing PP content. However, the mechanical performance depends on the compatibilizer used for blending PLA with PP, dispersed phase particle size, and its homogenous distribution which may be impacted by the compatibilizer. Various researchers [43–45] utilized polar compatibilizers containing polar carbonyl groups for improved compatibility of nonpolar PP with polar PLA. Lee et al. [45] studied the effect of hybrid compatibilizer composed of polypropylene-maleic anhydride (PP-*g*-MAH) and polyethylene-glycidyl methacrylate (PE-*g*-GMA) on the mechanical, rheological, and morphological properties. PP/PLA/compatibilizer were blended at a 60/30/10 ratio with varying PP-*g*-MAH to PE-*g*-GMA ratio. The degree of compatibility of PP, PLA, and hybrid modifier blends was analyzed by the Palierne emulation model using weighted relaxation spectra and the degree of compatibility correlated with relaxation time obtained from experimental data. Hybrid compatibilizers performed better compared to single compatibilizers by reducing the dispersed-phase particle size.

Ebadi-Dehaghani et al. [46] studied the effect of a terpolymer compatibilizer of ethylene, butylacrylate, and glycidylmethacrylate (EBAGMA) on the morphology and rheology of PP-PLA blends. For the purpose of this study, a PP-rich phase (75/25) and PLA-rich phase (25/75) were compatibilized with 2.5, 5, and 7.5 wt% compatibilizer. The addition of EBAGMA increased storage modulus, loss modulus, and complex viscosity. Peak storage and loss moduli were observed using 2.5 wt% EBAGMA for both PP-rich phase and PLA-rich phase. Therefore, 2.5 wt% was determined as the optimum value. A higher viscosity of PP ($\eta_{PP}/\eta_{PLA} > 1$) led to a smaller PLA droplet size (0.54 μm) in the PP-rich phase due to the ease of deformation, which further decreased to 0.28 μm with the addition of 5% EBAGMA.

### 14.2.2 Vinyl and Vinylidene Polymers and Copolymers

***14.2.2.1 Polystyrene/PLA Blends*** Blends of atactic polystyrene (PS) and PLA exhibited interfacial tensions of 5.4 ± 1.3 (at 170–200°C) and 6.1 ± 1.4 (at 200°C) mN/m, determined by embedded fiber retraction (EFR) and a modified deformed drop retraction, respectively [47, 48]. Therefore, blending of the PS/PLA pair is expected to produce an immiscible, incompatible blend. The mechanical, rheological, and thermal properties, including IR spectra and morphologies of physical PS/PLA blends produced by melt mixing, were reported elsewhere [47–51]. Overall, the addition of PS, which has a greater viscosity and thermal stability than PLLA, resulted in increases of melting temperature ($T_m$) (PLA component) and zero-shear viscosity, while heat capacity and tensile properties decreased with an increase of PS [49–51]. The production and characterization of spun-cast PS/PLA films were reported in the studies of Lim et al. [52] and Leung et al. [53, 54]. Topologies, PLA surface enrichment, and water contact angles of blend films at various composition ratios were explored to determine their effects on osteoblast adhesion of blend films [52]. The osteoblast adhesion of blend films was enhanced by increasing the PLLA weight fraction from 0.7 to 0.9 [52]. Leung et al. [53] characterized the phase morphology and quantified the chemical composition of spun-cast PS/PLA films by atomic force microscopy (AFM) and synchrotron-based X-ray photoemission electron microscopy (X-PEEM). They reported that a phase inversion of spun-cast PS/PLA films with a weight ratio of 40/60 (0.7 wt% dichloromethane solution) occurred with annealing above the $T_g$ of PLA (70°C for 1 h), and the use of these films for adsorption of human serum albumin was investigated [53, 54].

PS/PLA blends with a co-continuous structure are one of the most attractive blends for generating biodegradable controlled-release devices and tissue engineering scaffolds, since after selective removal of the PS phase from the blends, highly structured and completely interconnected porous PLA structures are obtained [48, 55–57]. The pore size, pore distribution, and void volume of the co-continuous structures can be tailored by controlling the influencing factors or adding compatibilizers [48, 53, 55–57]. Sarazin and Favis [58] reported that co-continuous PS/PLLA blends, produced by melt mixing at 200°C with a blade mixing speed of 50 rpm and mixing time of 7 min, had dual-phase continuity between 40 and 75% PS. The volume average pore diameter ($d_v$) after extraction of the PS phase increased from around 1.3 to 3.2 μm with an increase of PS volume from 40 to 70%, while the interfacial area per unit volume was constant (1 $\mu m^{-1}$) over the range of PS volume examined (40–70%). Annealing the blends at 200°C for 90 min induced coalescence in the microstructure and the number average pore diameter ($d_n$) and $d_v$ increased from 1.3 to 9.2 and 1.9 to 72.2 μm, respectively, with 50/50 PS/PLLA blends. Adding a diblock PS-*b*-PLLA (24,000-*b*-28,000) effectively improved the compatibility of the PS/PLLA blend when PS was present at a high-volume fraction. With 12 wt% of PS-*b*-PLLA based on the PS phase, the compatibilized PS/PLLA blends possessed dual-phase continuity with 40–60% PS, a small $d_v$ (from 0.8 to 1.1 μm), and a larger interfacial area per unit volume (from 1.7 to 4 $\mu m^{-1}$). In addition, the PS-*b*-PLLA blend was very effective in preventing coalescence during annealing [48]. The effects of quiescent annealing on coarsening co-continuous structures of PS/PLLA blends were further investigated by Yuan and Favis [55]. They showed that higher annealing temperature (from 190 to 220°C) and longer annealing time (from 0 to 90 min) enhanced the coarsening mechanism, resulting in an increase of $d_v$ (from 1 to 140 μm) in a co-continuous structure. However, time and temperature of annealing had only a minor effect on coarsening the co-continuous structures of compatibilized PS/PLLA blends ($d_v$ increased from 1 to <5 μm). It was also proposed that the degradation of PLLA during annealing could increase the rate of coarsening of PS/PLLA blends [55]. The *in vitro* degradation of highly structured, interconnected porous PLLA after extraction of the PS phase was investigated at accelerated temperature (70°C for 16 weeks) [58]. Porous and nonporous PLLAs exhibited a similar reduction of intrinsic viscosity and $T_m$, while the decrease in crystallinity of porous PLLA was faster compared with nonporous PLLA [58].

Fabrication of co-continuous PS/PLA blends with a gradient porous structure (GPS) for selective applications (e.g., graded membranes for enhanced filtration and graded porous beams for structural applications) was studied by Yao et al. [56]. They melt-blended PLA (4032D, $M_n$ = 330 kDa) and PS ($M_n$ = 590 kDa) at 200°C with a mixing speed of 60 rpm. The viscosity ratio of PLA over PS (0.7) at this blending condition produced a co-continuous PS/PLA blend at a weight ratio of 50/50. GPS of co-continuous PS/PLA blends can be created during annealing under a temperature gradient (200–25°C) and different types of thermal boundaries since the zero-shear viscosity of PS and PLA strongly depends on the temperature, and the rate of coarsening is a function of temperature (Figure 14.4) [56].

The application of highly structured, interconnected porous PLA, made from a co-continuous PS/PLA blend at a volume ratio of 50/50 with the PS phase removed by using cyclohexane, for the controlled release of bovine serum albumin (BSA) was also investigated [59, 60]. Due to the differences in chemical nature (BSA is hydrophilic, and PLA is hydrophobic), BSA was quickly released (89% after 2 h) from the highly structured, interconnected porous PLA ($d_n$ = 1.56 μm according to the BET nitrogen adsorption method) [57]. The release profiles of BSA can be designed by modifying the surface of the porous PLA through a layer-by-layer (LbL) deposition of polyelectrolytes to improve adhesion between the BSA and the PLA surface. This results in a slower release of BSA compared with the unmodified surfaces [57, 60]. Another technique to extend delivery times and reduce the burst release effect of BSA is immersing the highly structured,

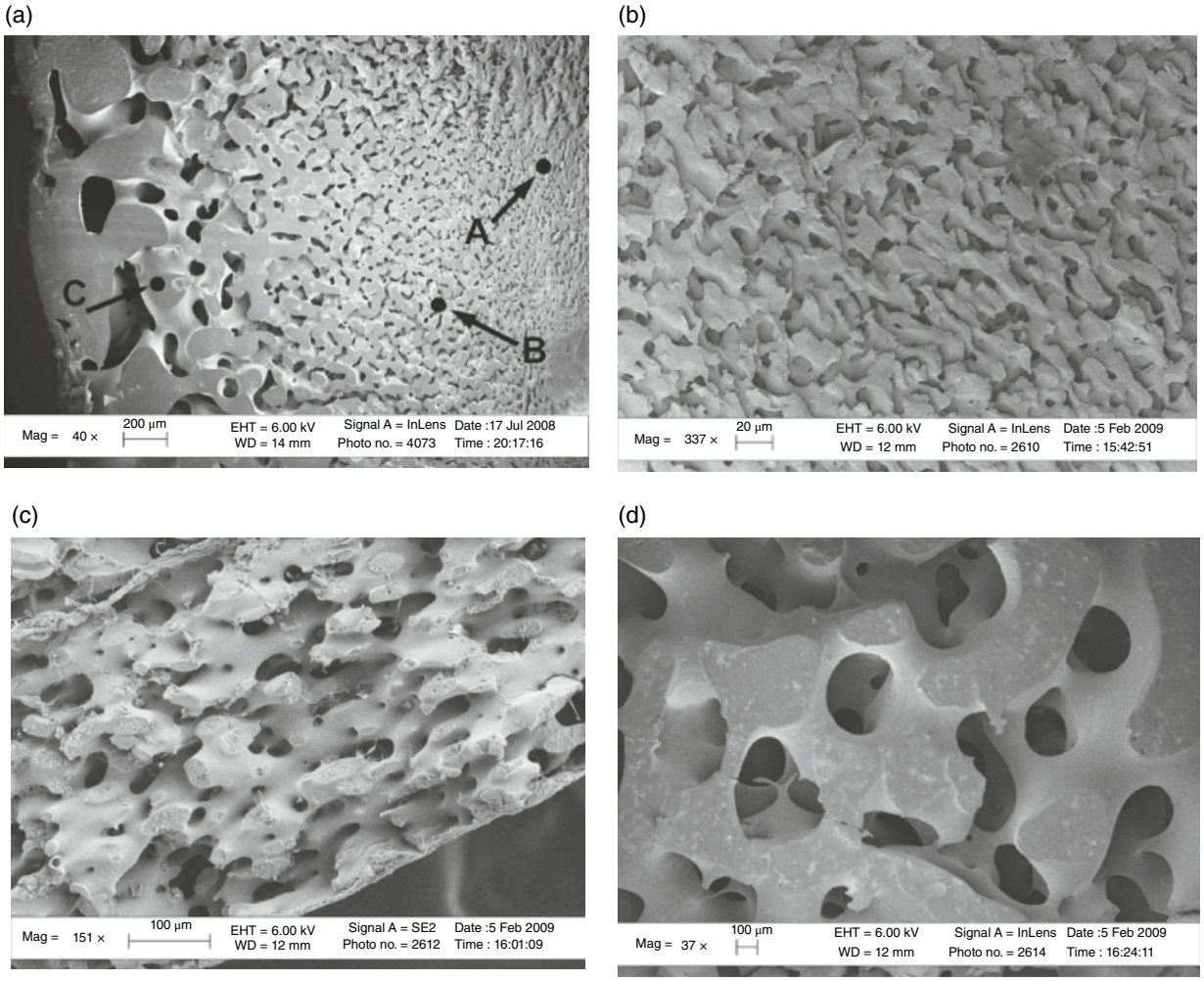


**FIGURE 14.4** Gradient porous structure from 1-D thermal gradient: (a) overall structure, (b) cross-sectional structure at location A, (c) cross-sectional structure at location B, and (d) cross-sectional structure at location C. *Source:* Reprinted from Ref. 56. Copyright 2009, with permission from the American Chemical Society.

interconnected porous PLA (open-cell), loaded with BSA, in solvent (e.g., chloroform) to build closed-cell porous blends [57, 58]. Partially closed-cell systems were prepared by cutting the end or edge of closed cell porous blends [60]. The compressive mechanical properties of highly structured, interconnected porous PLA (open-cell, closed-cell, open-cell with hollow center tube, and nonporous) were examined by Sarazin et al. [58]. The effects of interconnected pores of PLA (open-cell and partially closed-cell) and LbL polyelectrolytes on the release of BSA were also discussed by Xiang et al. [60].

Kaseem et al. [61] studied the effect of blending PLA/PS on the melt flow behavior. PLA/PS 30/70, 50/50 and 70/30 ratio were evaluated for the study. Viscosity of blends increased with increasing PS ratio due to its higher viscosity than PLA. Shear thinning behavior observed in all the blend compositions increased with increasing shear rate, with the highest shear rate sensitivity observed in 70/30 blends. PLA/PS 70/30 blends also exhibited the lowest viscous activation energy (109 kJ/mol), indicating viscosity stability over a wider temperature window.

Guo et al. [62] prepared blends of PLA, PS (or high impact polystyrene) 7 : 3 blends with 0–10% random styrene methyl methacrylate copolymer (SMMA) as a compatibilizer. They reported PS/SMMA and PLA/SMMA work of adhesion ($W_a$) values of 64.13 and 64.28 mN/m respectively, which are higher than $W_a$ of PLA-PS blend systems, supporting the compatibilization effect of SMMA. Impact toughness of PLA/PS and PLA/HIPS improved by 58% to 23.78 J/m and 56% to 36.34 J/m with the addition of 1.2 and 1.5% SMMA respectively, when compared with the respective binary uncompatibilized blends. A higher concentration of compatibilizer reduced the impact strength.

***14.2.2.2 Poly(Vinyl Phenol)/PLA Blends*** Poly(vinyl phenol), poly(4-vinyl phenol), poly(*p*-vinyl phenol), or poly(*p*-hydroxystyrene) (PVPh), a synthetic amorphous

polymer containing a hydroxyl group attached as a pendent phenyl ring, is a strong proton donor [63–66]. The interactions of the hydroxyl group of PVPh with proton-accepting functional groups such as ester, carbonyl, ether, and pyridine groups originate intermolecular hydrogen bonding [63, 64, 67]. Combined with a small difference in solubility parameters of PVPh ($10.6\,cal^{0.5}/cm^{1.5}$) and PLLA ($10.1\,cal^{0.5}/cm^{1.5}$), the result is that polymer blends of PVPh and PLLA can be miscible [63, 64, 67, 68]. Earlier studies of solution blends from tetrahydrofuran (THF) comprised of PVPh ($M_w$ = 30 kDa) and PLLA ($M_w$ = 105 kDa) at ratios of 10/90, 20/80, 30/70, 40/60, 60/40, and 80/20 indicated partially miscible blends, determined by DSC and FTIR analyses [68]. The blends containing PVPh of 10–60 wt% had one $T_g$ that was very close to the $T_g$ of PLLA (65°C) and slightly increased with increasing PVPh content. With a PVPh content of 80 wt%, two $T_g$s at 78°C (close to PLLA) and 143°C (close to PVPh, 159°C) were observed, with no detectable $T_m$. The addition of PVPh also reduced the kinetic crystallizability, enthalpy of cold crystallization, and crystallization of PLLA, which were attributed to the partial miscibility of the PVPh/PLLA blends. The weak hydrogen bonding interaction of PVPh and PLLA was determined by the shifts of the hydrogen-bonded hydroxyl band of PVPh (from 3323 to 3385 $cm^{-1}$) and the carbonyl stretching band of PLLA (from 1759 to 1751 $cm^{-1}$) with a rise of new hydrogen-bonded carbonyl groups of PLLA at 1700 $cm^{-1}$ [68].

In later studies, miscible blends of PVPh ($M_w$ = 25 kDa)/PLLA ($M_w$ = 153 kDa), as reflected by $T_g$, $T_m$, and FTIR spectra, were observed with solution in *N*,*N*-dimethylformamide (DMF) and with solution/precipitation blends of PVPh ($M_v$ = 30 kDa)/PLLA ($M_v$ = 320 kDa) using dioxane/hexane [69, 70]. An interlamellar (IL) morphology was observed when the solution blend was obtained from DMF. The PVPh was expelled into the IL regions during the crystallization of PLLA [54]. For the solution blends obtained from dioxane/hexane, a negative Flory-Huggins polymer-polymer interaction parameter value of $\chi_{12} = -0.42$ was observed, indicating the formation of a thermodynamically miscible PVPh/PLLA blend. Moreover, a large negative value of the $q$ parameter ($q = -78$; defined as the fitting constant related to the strength of the interaction) in Kwei's equation (Equation 14.3) indicated that the miscibility of PVPh/PLLA was due to a weak interaction [70]. In the cases where the systems have symmetric deviations from linearity, Kwei's equation can be expressed as follows:

$$T_g = w_1 T_{g1} + w_2 T_{g2} + q w_1 w_2 \qquad (14.3)$$

where $w_1$ and $w_2$ are the weight fractions of components 1 and 2, respectively; $T_{g1}$ and $T_{g2}$ are the $T_g$ of the neat components, i.e., PVPh and PLLA, respectively.

In contrast, solution blends of PVPh ($M_v$ = 30 kDa)/PLLA ($M_v$ = 320 kDa) produced from dioxane exhibited a phase separation (two $T_g$s of PVPh and PLLA) with a high PVPh content (>60 wt%) due to the $\Delta\chi$ effect, a phase separation effect induced by the solvent [70]. Solution blends of amorphous/amorphous polymers, PVPh/ poly(DL-lactide) (PDLLA), from methyl ethyl ketone (MEK) were immiscible, whereas solution blends from THF exhibited phase separation with PVPh content greater than 60 wt% [71, 72]. The spinodal phase diagrams (phase separation) of PVPh/PDLLA blends from THF can be simulated using an association model with small values of the inter-association constant ($k_A < 5$) [71]. Solution prepared blends prepared with THF/hexane were miscible with $q$ value of −87 obtained from Kwei equation. FTIR data suggested hydrogen bonding interactions between ─OH group of PVPh and ─C═O group of PDLLA [72, 73]. The phase behavior, interactions, and crystallinity of ternary blends of PVPh ($M_w$ = 22 kDa), PLLA ($M_w$ = 152 kDa), and poly(D-lactic acid) (PDLA) ($M_w$ = 124 kDa) at weight ratios of 2/49/49, 5/47.5/47.5, 10/45/45, and 20/40/40, prepared by solution casting from dioxane, were investigated [74]. The ternary blends exhibited one $T_m$ around 220°C (due to a PLLA/PDLA stereocomplex), a single composition-dependent $T_g$ (close to PLA), and a single composition-dependent $T_c$ (due to a PLLA/PDLA stereocomplex) that increased with increasing PVPh content. On the other hand, the equilibrium $T_m$ and cold crystallization of the ternary blends decreased with an increase of PVPh content. The Hoffman-Weeks plots and Flory-Huggins theory showed an $\chi_{12} = -0.88$ indicating that the ternary blends were thermodynamically miscible. The addition of a small amount of PVPh (up to 10 wt%) also enhanced the crystallization rate and reduced the spherulite size of PLLA/PDLA stereocomplex. However, the addition of a high amount of PVPh may lead to phase separation in the PVPh/PLLA/PDLA blends [74].

Performance of the polymer blends can be significantly impacted by the crystal structure and morphology. Nurkhamidah et al. [75] investigated morphology and crystal growth of low-molecular-weight PLLA/PVPh (70/30) using polarized optimal microscopy (POM), birefringence, and AFM. In the crystalline area, the polymer blend crystallized at 120°C demonstrated three types of crystalline morphologies differing in shape and optical properties. Type 1 showed hexagonal crystals with weak birefringence and a positive sign of the spherulites. Type 2 spherulites packed with dendritic crystals having strong birefringence with a negative sign of the spherulites. Type-3 demonstrated a mix of Type-1 and Type-2 spherulites.

#### *14.2.2.3 Poly(Ethylene-co-Vinyl Acetate)/PLA Blends*

Poly(ethylene-*co*-vinyl acetate) or ethylene/vinyl acetate copolymer (PEVAc) is a synthetic random copolymer of hydrophobic ethylene and hydrophilic vinyl acetate (VA)

monomers. PEVAc has a $T_g$ below room temperature and low viscosity (300 Pa s at 180°C) compared to PLLA (5340 Pa s at 180°C) [76]. The properties of PEVAc depend on the VA content and molecular weight. An increase in VA content results in lower crystallinity, better clarity and flexibility, and higher adhesion strength of PEVAc [77]. The miscibility of PEVAc and PLLA is expected to increase with increasing VA content, as visible in Figure 14.5 [78]. Solution blends of star-shaped PLLA ($M_w$ = 41.9 kDa) with PEVAc70 ($M_w$ = 285 kDa with 70 wt% of VA) were reported as immiscible, but with PEVAc85 ($M_w$ = 646 kDa with 85 wt % of VA), the solution blends were reported as miscible without microheterogeneity, as determined by a single composition-dependent $T_g$ following the Fox equation (Equation 14.4), $\chi_{12}$ of −0.043, and a depression of $T_m$ of PLLA with increasing PEVAc content [79].

$$\frac{1}{T_g} = \frac{W_{PLLA}}{T_{gPLLA}} + \frac{W_{PEVAc85}}{T_{gPEVAc85}} \tag{14.4}$$

where $W$ is the weight fraction of each polymer. Adding PEVAc85 reduced crystallinity, crystallization rate, and spherulitic growth rate of the blend. The tensile modulus and strength at break of PEVAc85/star-shaped PLLA blends decreased with an increase of PEVAc85 content, but elongation at break dramatically increased in blends containing 90 wt% PEVAc85 (Table 14.1) [79]. Solution/precipitation or melt blends of PEVAc and PLA ($M_w$ = 120 kDa) were reported to be immiscible; a co-continuous (bicontinuous) phase morphology was observed with blends containing 50–70 wt% PEVAc [80]. The incorporation of PLA in the blend increases Young's modulus, which improves the suitability of blends for semiconductive applications [76]. Katada et al. [76] reported that immiscible blends of PEVAc (containing 42 wt% VA) with PLLA ($M_w$ = 557 kDa) filled with a conductive filler, carbon black (CB), had higher electrical conductivity than single PEVAc filled with CB. However, the dispersion state, surface area, and electrical volume resistance of the CB in the blends were similar to those in PEVAc.

To date, most studies of PEVAc/PLA blends have been focused on controlled drug release systems. Its hydrolytic erodible character makes PLA unsuitable to serve as a long-term controlled release device [80, 81]. The loss of mechanical integrity due to bulk erosion can occur within three to four months; hence, the addition of nondegradable PEVAc helps prolong the induction period for PLA hydrolysis and reduces the weight loss rate [80]. Dollinger and Sawan [81] observed that rod-shaped devices prepared from solution/precipitation/melt extrusion of PEVAc/PLA possessed a longer induction period for PLA hydrolysis and a more constant rate of weight loss of PLA than blends prepared from extrusion melt blending, due to better homogeneity of the solution blends. PLA ($M_w$ = 15–25 kDa) also prevented coalescence or clumping of PEVAc (containing 60% VA) during the preparation of PEVAc/PLA

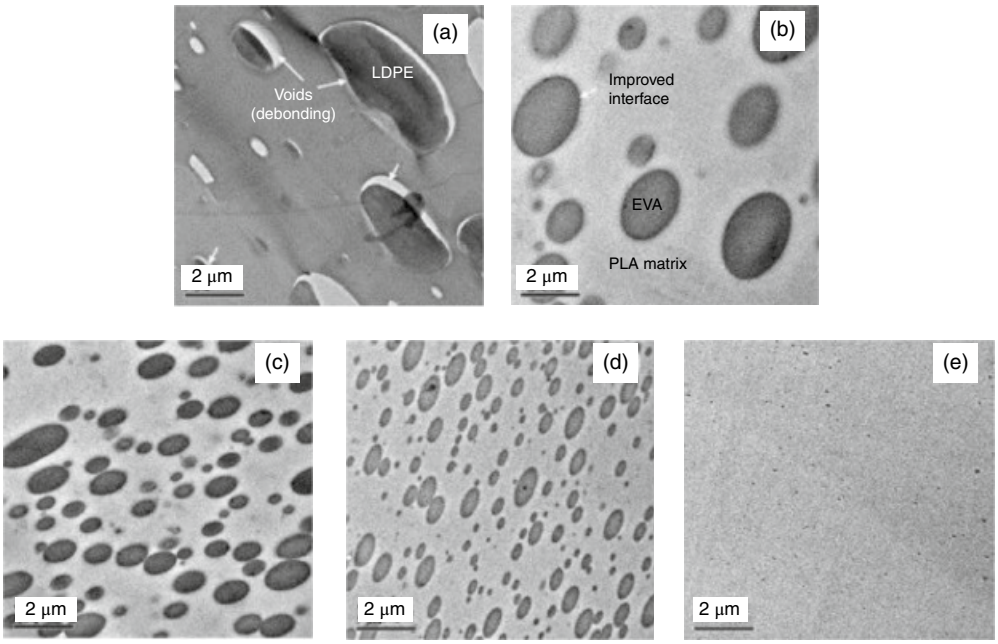


**FIGURE 14.5** TEM images (scale bar = 2 μm) of the PLA/EVA (80/20) blends with VA content in EVA copolymers: (a) 0 wt%; (b) 40 wt%; (c) 50 wt%; (d) 70 wt%; and (e) 90 wt%. The dark domains are dispersed EVA particles, while the bright matrix is PLA. The slight orientation of the EVA particles in these images was most probably formed in section-preparation (70 nm in thickness). *Source:* Reprinted from Ref. 78. Copyright 2012, with permission from Elsevier.

microspheres to encapsulate a low water-soluble taxol [82]. The 50/50 blend microsphere had encapsulation efficiencies between 95 and 100% taxol [82]. This blend microsphere was effective in the inhibition of angiogenesis, which was determined by using the chick chorioallantoic membrane (CAM) model. Kenawy et al. [83] studied the controlled release of tetracycline (using solution-cast film and electrospun fibers) by making 50/50 blends of PEVAc ($M_w$ = 60.4 kDa with 40 wt% VA) and PLA ($M_w$ = 205 kDa). The release of tetracycline from the blend film was similar to that from PLA cast film. For PEVAc cast film and PLA electrospun fiber, the release rate of tetracycline remained constant after the induction period, whereas the rate of tetracycline release from the blend electrospun fiber and from the PEVAc electrospun fiber kept increasing. After 120 h, the release of tetracycline from PLA film, PLA fiber, PEVAc film, PEVAc fiber, blend film, and blend fiber were approximately 5, 32, 8, 63, 23, and 39%, respectively [83]. The higher release of drug from the fiber devices is likely due to their greater surface area as compared with the film devices [83].

The effects of uncoated or coated polymeric microspheres made from blends of PEVAc/PLA (50/50) on the activation of neutrophils causing some localized inflammation compared to three types of pristine polymers (PLA, PCL, and polymethyl methacrylate [PMMA]) were investigated by Jackson et al. [84]. The neutrophil activation induced by polymers and polymer blends was very low. Among the plasma-coated microspheres, the PEVAc/PLA blend exhibited the lowest activation, whereas among the immunoglobulin-coated microspheres, the blend had the highest activation [84].

Zhang et al. [85] vulcanized and compatibilized various PLA/EVA blend compositions using 0.15–1% 2,5-dimethyl-2,5-di(*tert*-butylperoxy)hexane (AD); peroxide produced by AD decomposition crosslinked EVA and PLA, which generated a three-dimensional networked gel. The effect of EVA content and AD content on the properties of the blends was evaluated for PLA/EVA 70/30 blends. PLA/EVA 70/30 blends with varying 0–1% AD maintained tensile strength ~32 MPa while improving elongation at break for all the blend compositions with AD, with the highest strain and notched izod impact strength of 109.3% and 88.7 kJ/m$^{-2}$ observed for 70/30/0.3 ratios of PLA/EVA/AD. Improved mechanical properties were ascribed to the uniform morphology. Stress whitening was observed during deformation, indicating cavities and craze formation in the blends.

***14.2.2.4 Poly(Ethylene-co-Vinyl Alcohol)/PLA Blends*** Poly(ethylene-*co*-vinyl alcohol) or ethylene vinyl alcohol (EVOH), a semicrystalline random copolymer, is synthesized by a controlled hydrolysis of poly(vinyl acetate) (PVAc) [77]. Most of the EVOH properties are related to the amount of vinyl alcohol (which provides intermolecular forces) and ethylene content (which provides molecular flexibility) [77]. To induce grafting between the hydroxyl groups of EVOH and the terminal carboxylic group of PLLA, an esterification catalyst, tetrabutoxy titanate (TNBT), was added in solution blends of EVOH/PLLA ($M_w$ = 25 kDa) [24]. Compared to EVOH, the grafted copolymer blends had small decreases in the EVOH $T_m$ and $T_c$, as well as a significant decrease in the heat of fusion. At PLLA content higher than 60 wt%, PLLA showed a $T_m$ different from that of EVOH [86]. The grafted blends of PLLA/EVOH had lower tensile strength (0.55–1.78 MPa), lower elongation at break (1.77–21.6%), and higher tensile modulus (1.2–1.7 GPa) than EVOH (1.98 MPa, 16.5%, and 1.1 GPa, respectively) (Table 14.1). The grafted EVOH/PLLA blend at 60/40 exhibited higher compatibility (as determined from SEM micrographs) and better tensile properties (tensile strength of 1.16 MPa, elongation at break of 21.6%, and tensile modulus of 1.2 GPa) than the physical blend at a similar ratio (1.73 MPa, 2.7%, and 0.9 GPa, respectively) [86].

Gui et al. [87] observed that melt blending PLA with EVOH promoted PLA degradation due to a transesterification reaction, which resulted in decrease in the mechanical properties and viscosity. Distinct PLA and EVOH phases were visible in SEM analysis, indicating materials immiscibility. Oxygen and water vapor permeability values of blends decreased with increasing EVOH ratio due to its better barrier performance compared with PLA. Warangkhana et al. [88] fabricated PLA-EVOH (80/20) blends with 5–20 per hundred parts of resin (phr) poly(ethylene-*co*-glycidyl methacrylate) (EGMA) compatibilizer. The compatibilization improved mechanical performance, including elongation and impact strength, with optimum performance observed at 10 phr EGMA.

***14.2.2.5 Acrylonitrile–Butadiene–Styrene Copolymer/PLA Blends*** Acrylonitrile–butadiene–styrene copolymer (ABS), an amorphous graft copolymer comprised of a rigid linear styrene–acrylonitrile copolymer (SAN) grafted to rubbery butadiene, has been used to toughen engineering plastics [77, 89]. To improve compatibility of the immiscible ABS/PLLA blends and improve their mechanical properties, reactive melt blending of ABS and PLLA ($M_w$ = 170 kDa) was performed using 5% of a styrene–acrylonitrile–glycidyl methacrylate copolymer (SAN-GMA) as a reactive compatibilizer with and without 0.02 phr of ethyltriphenyl phosphonium bromide (ETPB) as a catalyst [89]. SAN-GMA epoxy ring was considered to react with ─OH or COOH end groups of PLLA producing grafted copolymer, which improves compatibility. The highest compatibility of immiscible ABS/PLLA, as determined from SEM micrographs, was obtained from reactive blending with ETPB (Figure 14.6).

The reactive blends of PLLA and SAN-GMA with ETPB exhibited two separate $T_g$s suggesting immiscibility and improved impact strength (123.9–162.8 kJ/m$^2$). PLLA/ABS

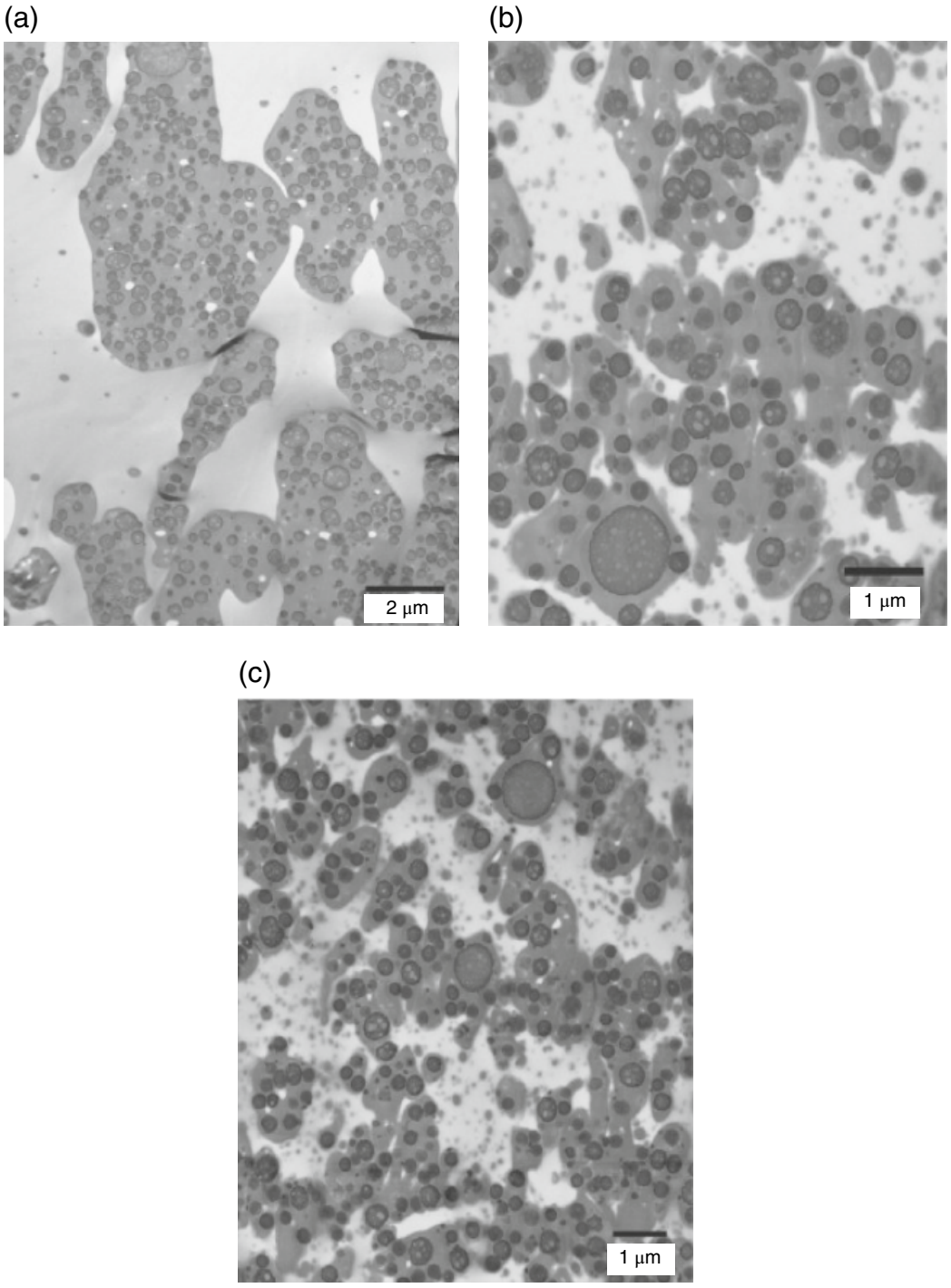


**FIGURE 14.6** TEM image of (a) uncompatibilized PLLA/ABS = 50/50 blend, (b) PLLA/ABS = 50/50 blend with 5 wt% SAN-GMA, and (c) PLLA/ABS = 50/50 blend with 5 wt% SAN-GMA and 0.02 phr ETPB. *Source:* Reprinted from Ref. 89. Copyright 2008, with permission from Elsevier.

50/50 blend 5 wt% SAN-GMA and 0.02 phr ETPB reactive blend demonstrated higher tensile properties (tensile modulus of 1.4 GPa, tensile strength of 43.6 MPa, and elongation at break of 23.5%) compared with physical blends and blends without ETPB [89]. Increasing ABS content significantly improved the impact strength of the reactive blends. The increase in compatibility and enhanced mechanical properties of ABS/PLLA was attributed to interactions of epoxy rings in SAN-GMA (induced by ETPB) with carboxyl or hydroxyl end groups of PLLA, generating PLLA-*g*-SAN

copolymers that act as compatibilizers for the ABS/PLLA blends [89].

Abt et al. [90] produced PLA/ABS blends by reactive extrusion. PLA was first modified using multifunctional styrene-acrylic multifunctional chain extender to improve its rheological properties, referred to as $PLA_{Rex}$. Then, $PLA_{Rex}$, ABS, and ABS-grafted maleic-anhydride (ABS-*g*-Ma) compatibilizer were melt blended. Unmodified PLA/ABS 70/30 blends without compatibilizer exhibited large ABS nonhomogeneous domains due to immiscibility. Introduction of compatibilizer reduced dispersed phase size to <1 μm, indicating a decrease in interfacial tension. Carrasco et al. [91] also reported improved thermal stability with the addition of ABS-*g*-Ma compatibilizer.

### 14.2.3 Rubbers and Elastomers

***14.2.3.1 Core-Shell Rubber PLA Blends*** Cavitation of core-shell rubber particles consisting of copolymers with rigid cores and flexible shells have been widely reported for various polymer matrices including PLA [35–37, 92]. Such core-shell copolymers impart high toughness without reducing the modulus of the polymer matrix compared to traditional blends. Toughness depends on various factors including core-shell particle size, rubber-shell thickness, and particle morphology. The toughening effect can be divided into three stages: (i) stress concentration and dilatation; (ii) void and shear band formation; and (iii) shear yielding. For toughening to occur, particles should be uniformly dispersed and the ligament thickness, the distance between two nearby dispersed particles, should be below a critical value. Once the critical cavitation condition is met, cavitation in the particle or at the interface follows plastic deformation and shear yielding of the matrix, leading to energy absorption. Core-shell particles can be designed so that under mechanical stress the debonding process occurs at the interface, causing fibrillation in the continuous polymer domain. The rigid shell may consist of polymeric material such as PMMA, which can act as a compatibilizer and improve the adhesion between the rubbery core and the host matrix. Lee et al. [93] studied the toughening mechanism of 10–30 phr acrylic core-shell rubber particles, consisting of poly(butyl acrylate) core and PMMA shell, in the PLA matrix. For 30 phr core-shell rubber particles, elongation at break of blends improved from 15 to 235%, due to debonding at the interface of PLA and the rigid PMMA shell. The shear viscosity and storage modulus of blends increased with increasing core-shell rubber particle phase ratio.

Core-shell particle consisting of soft rubbery cores with surface functionalized thermoplastic hard shells such as grafting of PMMA with epoxy functional groups have been researched [94, 95]. PMMA grafted with epoxy functional groups (Paraloid EXL2314) and ungrafted PMMA (Paraloid EXL2330) exhibited similar reduction in tensile strength and modulus of the blends with increasing rubber content (1–10 wt%). The impact strength of PLA blends improved with Paraloid EXL2330 (from 2.2 to 4 $kJ/m^2$), while a higher strain at break was obtained with the addition of Paraloid EXL2314 (Table 14.1) [95]. EXL2330/PLA blend composites with 5 wt% organic-modified montmorillonite (MMT)-Cloisite 30B-had a greater tensile modulus and lower strain at break than neat PLA but had a smaller decrease in impact and tensile strengths compared with the EXL2330/PLA blend alone [95].

In another study [96], core-shell nanoparticles were synthesized using a stiff esterified starch core and elastic poly(ethyl acrylate) (PEA) shell, as the esterification process improves emulsifying performance of starch. The melt blending of these nanoparticles improved the flexibility, impact strength, and toughness of PLA. PLA-starch-PEA nanoparticles 80/20 blends demonstrated improved elongation (412%) and impact strength (31.4 $kJ/m^{-2}$) with the addition of 20% nanoparticles.

***14.2.3.2 Poly(cis-1,4-Isoprene)/PLA Blends*** Poly(*cis*-1,4-isoprene) (PIP), a major component of natural rubber (NR), and isoprene rubber (IR) are synthesized by polymerization of isoprene. Besides being a ductile material that could be used to toughen PLA, PIP also has strain crystallization ability [97]. However, solution blends of PIP with a copolymer of LLA and bipentaerythritol-starshaped PLLA were immiscible. The PIP/star-shaped PLLA at a ratio of 20/80 wt% showed lower tensile strength, modulus, elongation at break, and toughness than the star-shaped PLLA [97]. To improve compatibility, PIP was modified by grafting with PVAc to obtain a graft copolymer (PIP-*g*-PVAc) [97]. The mechanical properties of PIP-*g*-PVAc/star-shaped PLLA (20/80) increased. In particular, its elongation at break (14.3%) was greater than that of star-shaped PLLA with an elongation at break of 10.2%. PIP-*g*-PVAc/star-shaped PLLA blends containing 60 and 80 wt% of PIP-*g*-PVAc exhibited two $T_g$s, as shown in Table 14.2 [97].

**TABLE 14.2 Thermal Properties of PLLA/PIP-*g*-PVAc Blend [97]**

| | $T_g$ (°C) | $T_m$ (°C) |
|---|---|---|
| PIP-*g*-PVAc | −57.0/27.6 | N.O.[a] |
| PLA/PIP-*g*-PVAc 20/80 | −58.0/28.0 | N.O.[a] |
| PLA/PIP-*g*-PVAc 40/60 | −60.3/31.0 | 146.1 |
| PLA/PIP-*g*-PVAc 60/40 | 35.3 | 147.9 |
| PLA/PIP-*g*-PVAc 80/20 | 41.1 | 148.7 |
| PLLA | 50.3 | 149.7 |
| PVAc | 20.0 | N.O.[a] |
| PIP | −60.0 | N.O.[a] |

*Source*: Adapted from Ref. 97. Copyright 2000, with permission from Elsevier.
[a]Not observed.

#### *14.2.3.3 Poly(Ethylene Octene) Copolymer/PLA Blends*

Poly(ethylene-octene) copolymer, a thermoplastic polyolefin elastomer (TPO), was melt blended with PLA at a ratio of 20/80 wt% [98]. The difference in polarities of the two polymers led to thermodynamic immiscibility and phase separation of the final blends as determined by the Molau test. Therefore, a copolymer of TPO-*g*-PLA (TPO-PLA) synthesized via functionalization of TPO and MA with benzoyl peroxide (BPO), followed by esterification of the MA-functionalized TPO (TPO-MAH) with PLA using 4-dimethylaminopyridine (DMAP) as a catalyst, was introduced to improve the compatibility of the TPO/PLA blends. The use of 5 wt% TPO-PLA in the binary blend of PLA and TPO resulted in an emulsion solution when dissolved in ethyl acetate (Molau test), lasting at least for 24 h, indicating that TPO-PLA should be effective in stabilizing a TPO dispersed phase in a PLA continuous phase [98]. TPO-PLA was effective in reducing the TPO dispersed phase domain size (from 6.2 to 4.5–2.1 μm, Figure 14.7), increasing elongation at break (from 15.4 to 99.1–181.9%), and increasing the Izod impact strength (from 137 J/m to nonbreak) without large decreases of tensile strength (from 34.7 to 30.1–35.6 MPa) or tensile modulus (from 1.46 to 1.10–1.21 GPa) compared with the neat blend (Table 14.1) [98]. The properties of the compatibilized TPO/PLA blends were related to the TPO-PLA architecture that depended on the reactant formulation (i.e., amounts of BPO, MAH, and DMAP) and the ratio of TPO-PLA in the blend [98]. DMAP content had a greater effect on flexibility and toughness of compatibilized blends than did BPO and MAH (percentage of functionalization via grafting). The smaller the amount of DMAP used, the longer was the PLA segment in the TPO-PLA, leading to greater flexibility and toughness, as well as smaller TPO particle size in the blend. Comparing the two compatibilizers, TPO-PLA promoted compatibility of TPO/PLA blends better than TPO-MAH [98].

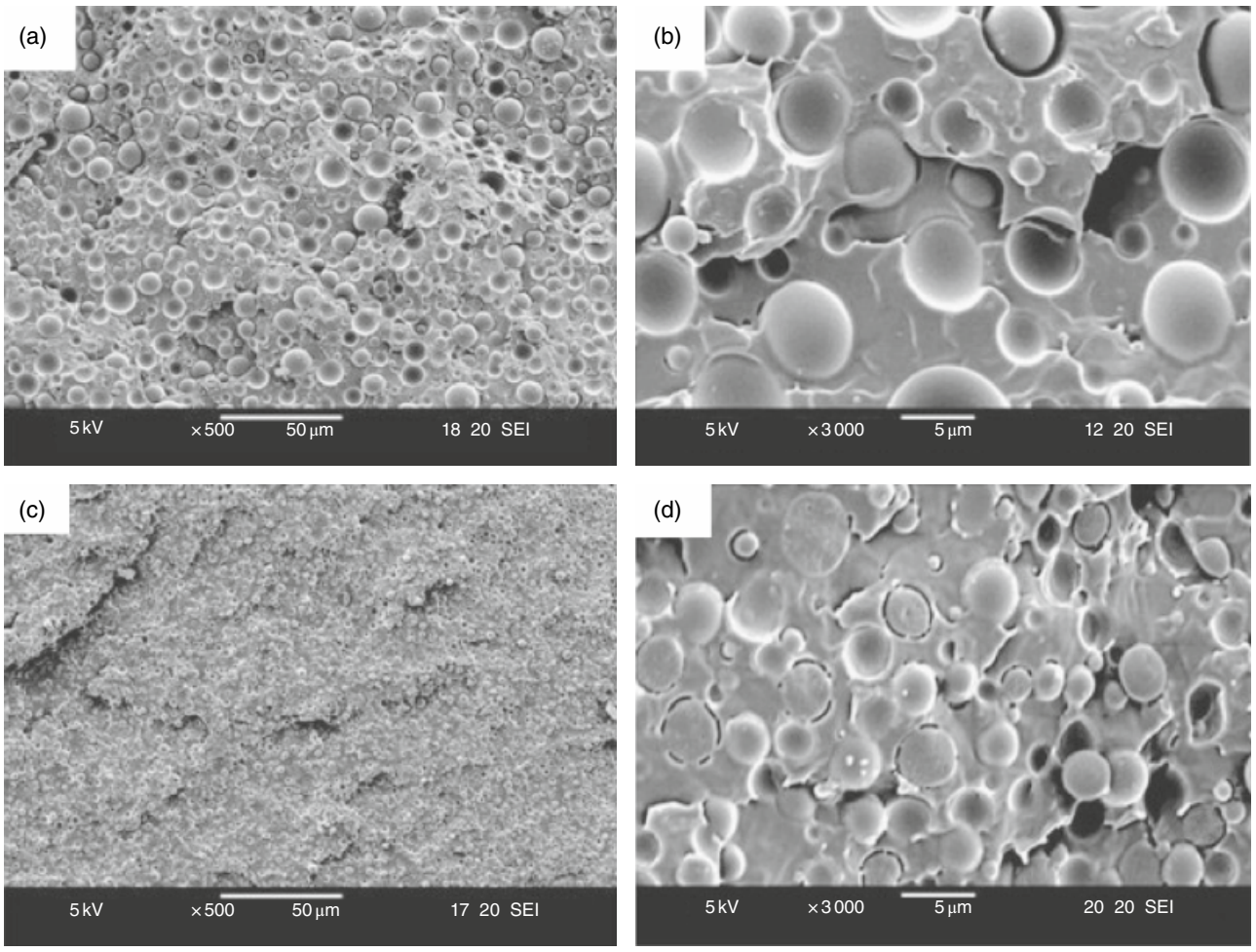


**FIGURE 14.7** Cryofractured surface morphology of PLA/TPO (80/20) blend: (a) without TPO-PLA, 500×; (b) without TPO-PLA, 3000×; (c) with 5 wt% TPO-PLA copolymer, 500×; (d) with 5 wt% TPO-PLA copolymer, 3000×. *Source:* Reprinted from Ref. 98. Copyright 2008, with permission from Elsevier.

### 14.2.4 PLA/PMMA Blends

Due to their biocompatibility and inert nature, PLA-PMMA blends have been studied. Recently, various researchers reported that PLA-PMMA forms miscible blends due to the amphiphilic nature of PMMA [99–102]. However, the miscibility is dependent on various factors including the blend fabrication methodology, processing conditions, molecular weight composition, and chirality. Zuo et al. [103] blended PLA with styrene–acrylonitrile (SAN) or acrylonitrile butadiene styrene (ABS) using 1–10% PMMA. Tensile strength, impact strength, and elongation improved for all PMMA compatibilized blends; however, optimum performance was reported below 5% PMMA content. Samuel et al. [102] fabricated PLA-PMMA blends using solvent casting and melt-blending techniques. Immiscible blends with phase-separated morphology were obtained by solvent casting using chloroform, whereas twin screw extrusion blending at 210°C provided miscible PLLA-PMMA morphological phases for all composition ranges due to high shear. The authors further investigated the reversibility of miscible blends by mixing the melt processed blends in chloroform and solvent casting. A phase separated immiscible state was retrieved by the blends with two $T_g$ at 61.2 and 109.5°C corresponding to PLLA and PMMA constituent polymeric domains, respectively. For the melt-extruded miscible blends, the $O_2$, $CO_2$, and $N_2$ permeability coefficients dropped as a function of PMMA concentration in the blends. For 40% PMMA content, a 60–80% drop in $O_2$, $CO_2$, and $N_2$ permeability coefficient was observed. Also, transparency, high-storage modulus (3 GPa) at room temperature, and Izod impact strength (2.4–2.6 kJ/m$^2$) were retained, suggesting a miscible morphology of the PLLA-PMMA blends.

Canetti et al. [99] studied the miscibility of PLA-PMMA blends using interaction parameters and nucleation constant. Single $T_g$ measured values for all the blend ratios coincided with theoretical calculations as predicted by the Fox law and Gordon Taylor equations, indicating miscibility in the amorphous phase. Higher elastic modulus and tensile strength values were observed in 60/40 and 50/50 blends compared with those of the neat PLLA or PMMA matrices. At lower PMMA concentrations (up to 20%), an increase in the PMMA concentration resulted in a decrease in the bulk crystallization. To further understand the morphology, crystallization kinetics behavior, and kinetics, the authors investigated 70/30 blends using a polarized optical microscope before and after isothermal crystallization at 130 and 145°C. Co-existence of PLA-PMMA domains was observed in the Maltese-cross spherulites configuration at both the temperatures as can be seen in optical microscope images shown in Figure 14.8a–d; the larger spherulite size at 145°C was ascribed to fewer nuclei at higher temperature. The single $T_g$ and absence of unseparated domains are indicative of miscible morphology.

Because of the miscibility of PLA-PMMA blends, it has been used as a compatibilizer. Guo et al. [100] reported a single $T_g$ between 63 and 98°C for various PLA-PMMA compositions, processed at 180°C for 10 min. As observed using DSC, the $T_g$ progressively increased with an increase in the weight fraction of PMMA in the blend. The tan($\delta$) peak obtained from dynamic mechanical analyzer (DMA), a representative of $T_g$, coincided with the DSC data. The compatibility was further supported with SEM. Due to PMMA's compatibility, it was introduced as a compatibilizer into PLA and PBAT blends [99, 100]. The developed ternary blend had mechanical performance comparable with that of the conventional polymers due to good miscibility of PMMA with PLA and PBAT. PMMA concentrations below 10% showed improved performance by localizing at the PLA-PBAT interface, thereby improving interfacial adhesion and the compatibility of ternary blends. PLA-PMMA-PBAT (62 : 8 : 30%) demonstrated enhanced impact strength of 168 J/m, around 73% improvement as compared with PMMA-PBAT (70 : 30) binary blends.

Zhang et al. [104] studied blends of PMMA/PDLLA at various concentrations. The blends prepared by solution precipitation were characterized by DSC. All the PMMA/PLA blend compositions demonstrated a single $T_g$ (Figure 14.9a). The authors fitted the Gordon–Taylor equation (Equation 14.5) to understand the interaction between the two polymers (Figure 14.9b):

$$T_g = T_{g1} - \left[ k w_2 T_{g2} \right] + \left[ T_{g1} / w_1 \right] - k w_2 \qquad (14.5)$$

where $w_1$ and $w_2$ are the weight content of each polymer phase, and $T_{g1}$ and $T_{g2}$ are their $T_g$, respectively. The calculated value of the adjustable parameter ($k$) supported weak interaction between the two polymers. Separate $T_g$s were observed for the PMMA phase and the PLA phase for the films prepared by solution casting, which indicates the immiscible nature of the blends.

Lu et al. [105] added wood fibers (WFs), ranging from 105 to 900 μm, into PLA-PMMA using melt compounding to reduce cost and to improve hydrophilicity for accelerating hydrolytic degradation. All composites showed improved mechanical performance compared to PLA. Composites containing PLA/PMMA-WFs—80/20 (WF-PMMA ratio 8 : 2) with particle size 150–180 μm demonstrated better performance compared with other tested compositions with improvement in tensile, flexural bending strength and Young's modulus by around 10, 37, 4, and 32% approximately, compared with the PLA matrix. Large wood fibers act as stress concentrators. To understand hydrolytic degradation, tests were conducted on PLA and PLA/WF/PMMA (WF particle size 150–180 μm) at 50°C in alkali liquor, known to promote wood fiber degradation, at pH 12.5. Faster degradation was observed in PLA/WF/PMMA, as compared

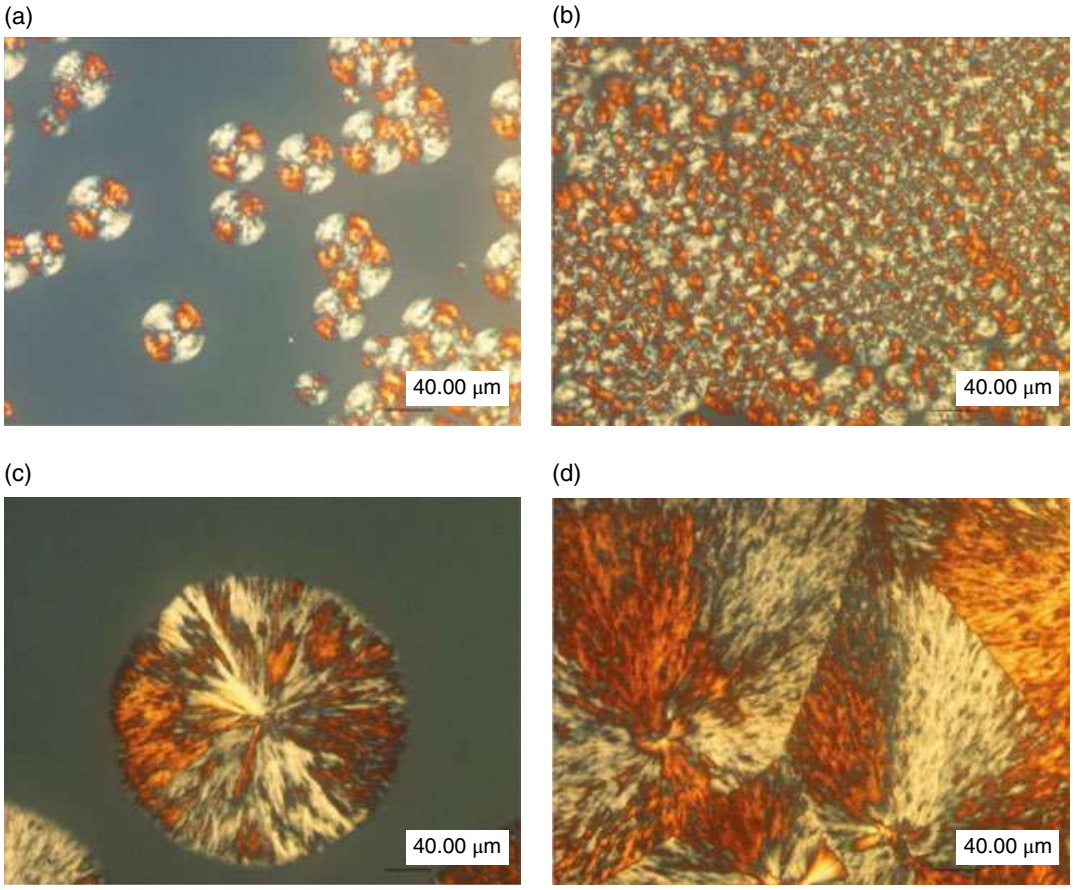


**FIGURE 14.8** Optical micrographs of PLA/PMMA 70/30 blend: during (a) and at the end (b) of the isothermal crystallization at 130°C, during (c) and at the end (d) of the isothermal crystallization at 145°C. *Source:* Reprinted from Ref. 99. Copyright 2014, with permission from John Wiley & Sons, Inc.

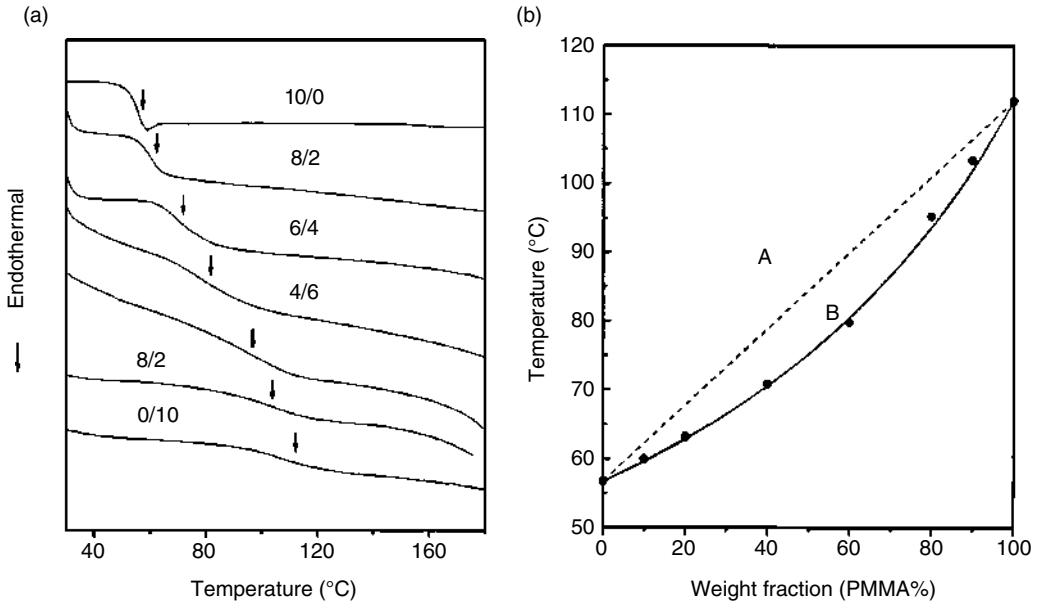


**FIGURE 14.9** (a) DSC thermogram in the second heating runs for solution/precipitation PDLLA/PMMA blends with compositions from 100 : 0 to 0 : 100, (b) $T_g$ versus composition in solution/precipitation PDLLA/PMMA blends. (•) Experimental results. Line A corresponds to the weight average, and line B is drawn according to Equation 14.5 with $k = 0.5$. *Source:* Reprinted from Reference 104 Copyright 2003, with permission from John Wiley and Sons, Inc.

with PLA, degrading most of the matrix in 10 days with a residual mass of 10%.

Yao et al. [106] investigated PLA/PMMA blend foams at 75/25, 50/50, and 25/75 wt% compositions for medical applications such as cell growth. Factors such as solubility and carbon dioxide diffusivity played an important role in these applications. Gas solubility was studied using a microelectronic balance. The Henry's law constant for $CO_2$ in the blends increased with increasing PLA content. Foam morphologies of the blends and neat polymers were investigated with respect to the effects of pressure and temperature. PLA/PMMA blends improved the foam morphologies compared to the neat polymers. More detail about these blends can be found in Chapter 15.

## 14.3 PLA/BIODEGRADABLE POLYMER BLENDS

Blends of PLA with other biodegradable polymers are mostly sought to maintain its biodegradability and sometimes compostability. Different biodegradable polymers are now commercially available and the market for these polymer blends is increasing. Table 14.3 summarizes their mechanical properties and the subsections below describe most of their properties.

### 14.3.1 Polyanhydrides

Polyanhydrides, having organic and hydrophobic backbones with anhydride linkages, are gaining interest as biodegradable materials for drug delivery systems because they are biocompatible, nonmutagenic, noncytotoxic, and noninflammatory [107]. In addition, the high hydrolytic sensitivity of the anhydride bonds on the surface results in rapid degradation, while the hydrophobic backbone prevents the penetration of water into the polymer matrix [107, 108]. Therefore, the hydrolytic degradation of polyanhydrides mainly occurs via a surface erosion mechanism. The main shortcomings of these polymers are poor mechanical strength, high reactivity with amine and nucleophilic groups, and high susceptibility to organic solutions, especially at elevated temperature, which limit their use in other applications besides drug release devices [107–109]. Hence, the focus has been on the potential use of polyanhydrides/PLA blends as implants for controlled delivery of drugs.

***14.3.1.1 Poly(Sebacic Anhydride)/PLA Blends and Poly(Anhydride-co-Amide)/PLA Blends*** Poly(sebacic anhydride) (PSA), a semicrystalline aliphatic anhydride, and PLA its blends were observed as "a uniform mixture" when PSA of $M_w$ = 54.9 kDa was solution or melt-blended with low-molecular-weight PDLLA ($M_w$ = 2 kDa) [110]. Davies et al. [111] characterized the surface of spun-cast films, prepared from solution blends of PSA ($M_w$ = 25 kDa), with low-molecular-weight PDLLA, $M_w$ = 2 kDa) at various ratios (25/75, 50/50, and 75/25). By using static secondary ion mass spectrometry (SSIMS) and X-ray photoelectron spectroscopy (XPS), surface enrichment with PLA was observed in all the miscible PSA/PLA blends. The surface topologies, recorded by AFM, revealed a particulate surface structure [111]. Immiscible blends of this polymer pair were observed when PSA was blended with high-molecular-weight PLA. Phase separation and/or surface enrichment of PLA were found at any ratio of the blends [16, 110–113]. PSA microdomains in the PLA matrix were observed with an increase in PLA content (≥40%) [13]. In general, PLA decreased the crystallinity of the PSA component in PSA/PLA blends and lengthened the degradation times of PSA/PLA and poly (anhydride-*co*-amide)/PLA blends [16, 111–114]. Shakesheff et al. [113] investigated the erosion kinetics of PLA ($M_w$ = 50 kDa) and PSA ($M_w$ = 25 kDa) blends at various ratios (70/30, 50/50, 30/70), compared with PLA and PSA, by using simultaneous in situ AFM and surface plasmon resonance (SPR) analysis. In a pH 11 buffer solution, the maximum rate of SPR shift of spin-cast PSA films was 100 times greater than that of spun-cast PLA films. The erosion of blend films goes through three distinct stages, in which the erosion kinetics at the initial and final stages are similar to the erosion kinetics of PSA and PLA films, respectively. The intermediate stage showed an intermediate rate of erosion, and the transition stage was extended with an increase of PLA [113]. In addition, it was proposed that the surface enrichment with PLA in PSA/PLA blends should retard the initial surface erosion kinetics of these polymer blends [16]. The effects of PSA/PLA blends on drug release were also investigated [110, 115]. In physiological conditions, PSA and PLA were metabolized and completely expelled from the body within 2–4 and 12–16 weeks, respectively [111]. Hence, the drug release and degradation periods can be designed by varying ratios of the polymer pair. Domb [110] reported that the *in vitro* release of bupivacaine-HCl followed first-order kinetics with an increase of PSA content. At 17 days, the release of bupivacaine-HCl was 15, 22, 30, 80, and 100 wt% from the polymer blends containing a PSA component of 10, 20, 30, 50, and 100 wt%, respectively. Chen et al. [115] studied the possibility of using PSA ($M_w$ = 3.5 kDa)/PDLLA ($M_w$ = 110 kDa) blends as carriers for *in vitro* and *in vivo* controlled release of ofloxacin for the treatment of chronic osteomyelitis and in the prophylaxis of bone infection. PLA/PSA 90/10 blends containing blend/ofloxacin ratio 8 : 1 exhibited *in vivo* average drug concentration 20.1 ± 10.3 μg/g, in the bones of rabbits during the eight weeks of study, indicating potential of PLA/PSA blends for drug delivery.

### 14.3.2 Vinyl and Vinylidene Polymers and Copolymers

***14.3.2.1 Poly(Vinyl Alcohol)/PLA Blends*** Poly(vinyl alcohol) (PVOH) is a synthetic, water-soluble, biodegradable, and biocompatible polymer [116–118]. Shuai et al. [118]

**TABLE 14.3 Summary of the Mechanical Properties of Biodegradable Polymer and PLA Blends**

| Polymer | Composition Ratio | Compatibilizer | Ratio | Blending Method | Young's Modulus (MPa) | Tensile Strength (MPa) | Elongation at Break (%) | Tensile Toughness ($MJ/m^3$) | Impact Resistance/ Strength (J/m) | Reference |
|---|---|---|---|---|---|---|---|---|---|---|
| PLLA | — | — | — | — | 970.8 | 32.4 | 3.9 | — | — | [123] |
| PLLA/PVOH | 80/20 | — | — | SB | 1127.8 | 37.3 | 5.3 | — | — | [123] |
| PLLA/PVOH | 60/40 | — | — | SB | 1461.2 | 54.9 | 7.4 | — | — | [123] |
| PHB | — | — | — | SB | 3589.2 | 85.3 | 3.7 | — | — | [156] |
| PLA/PHB | 40/60 | — | — | SB | 2687.0 | 63.7 | 27.7 | — | — | [156] |
| PLLA | — | — | — | — | 2214.7 | 64.6 | 6.9 | — | — | [367] |
| PBS | — | — | — | — | 326.3 | 32.1 | 320.6 | — | — | [367] |
| PLLA/PBS | 75/25 | — | — | MB | 1075.2 | 44.7 | 71.8 | — | — | [367] |
| PLLA/PBS | 75/25 | TFC | 2 | MB | 1407.9 | 45.2 | 75.5 | — | — | [367] |
| PLLA/PBS | 75/25 | TFC | 5 | MB | 1624.6 | 45.8 | 100.6 | — | — | [367] |
| PLLA/PBS | 75/25 | TFC | 10 | MB | 1990.3 | 46.7 | 118.1 | — | — | [367] |
| PLLA | — | — | — | — | — | 69.3 ± 0.9 | 4 ± 0.4 | — | 2500 ± 500[a] | [180] |
| PLLA/PBS | 80/20 | — | — | MB | — | 56.4 ± 1.0 | 250 ± 40 | — | 3700 ± 300[a] | [180] |
| PLLA/PBS | 80/20 | DCP | 0.05 | RMB | — | 50.0 ± 0.6 | 277 ± 45 | — | 12,100 ± 1300[a] | [180] |
| PLLA/PBS | 80/20 | DCP | 0.10 | RMB | — | 49.3 ± 0.9 | 249 ± 40 | — | 30,000 ± 2700[a] | [180] |
| PLLA/PBS | 80/20 | DCP | 0.15 | RMB | — | 45.1 ± 0.5 | 254 ± 57 | — | 18,700 ± 1000[a] | [180] |
| PLLA/PBS | 80/20 | DCP | 0.20 | RMB | — | 44.7 ± 0.2 | 252 ± 42 | — | 14,600 ± 2500[a] | [180] |
| PLLA | — | — | — | MB | — | 69.3 ± 0.9 | 4 ± 1 | — | 28 ± 2 | [368] |
| PLLA/PBSA | 70/30 | — | — | MB | — | 43.3 ± 0.6 | 343 ± 14 | — | 56 ± 5 | [368] |
| PBAT | — | — | — | MB | 61 ± 2 | 19 ± 3 | 831 ± 186 | — | — | [369] |
| PLA/PBAT | 70/30 | — | — | MB | 965 ± 98 | 38 ± 1 | 8.7 ± 1.4 | — | — | [369] |
| PLA1 | — | — | — | — | 2996 ± 52 | 33 ± 7 | 13 ± 3 | — | — | [232] |
| PLA2 | — | — | — | — | 2893 ± 235 | 48 ± 5 | 8 ± 4 | — | — | [232] |
| PBAT | — | — | — | — | 66 ± 12 | 15 ± 7 | 670 ± 84 | — | — | [232] |
| PLA1/PBAT | 90/10 | — | — | MB | 2882 ± 124 | 36 ± 8 | 17 ± 8 | — | — | [232] |
| PLA1/PBAT | 75/25 | — | — | MB | 2425 ± 136 | 30 ± 12 | 97 ± 23 | — | — | [232] |
| PLA1/PBAT | 65/35 | — | — | MB | 2182 ± 241 | 27 ± 9 | 91 ± 31 | — | — | [232] |
| PLA2/PBAT | 75/25 | — | — | MB | 1935 ± 110 | 38 ± 2 | 47 ± 25 | — | — | [232] |
| PLA2/PBAT/atbc | 75/25/10 | — | — | MB | 1778 ± 111 | 18 ± 2 | 87 ± 32 | — | — | [232] |
| PLA2/PBAT/atbc | 75/25/20 | — | — | MB | 870 ± 70 | 18 ± 4 | 150 ± 38 | — | — | [232] |
| PLA2/PBAT/atbc | 75/25/30 | — | — | MB | 62 ± 29 | 18 ± 5 | 250 ± 60 | — | — | [232] |
| PLA/PBAT | 90/10 | — | — | MB | — | ~28 | ~60 | — | ~6000[a] | [234] |
| PLA/PBAT | 90/10 | T-GMA | 2 | RMB | — | ~27 | ~120 | — | ~14,000[a] | [234] |
| PLA/PBAT | 90/10 | T-GMA | 5 | RMB | — | ~30 | ~190 | — | ~16,000[a] | [234] |
| PLA/PBAT | 90/10 | T-GMA | 10 | RMB | — | ~27 | ~140 | — | — | [234] |
| PLLA | — | — | — | SB | — | 28.1 | 19.33 | — | — | [237] |
| PTAT | — | — | — | SB | — | 13.7 | 1513.3 | — | — | [237] |
| PLLA/PTAT | 75/25 | — | — | SB | — | 24.6 | 97.0 | — | — | [237] |
| PLLA/PTAT | 50/50 | — | — | SB | — | 7.1 | 34.0 | — | — | [237] |
| PLLA/PTAT | 25/75 | — | — | SB | — | 1.1 | 285.3 | — | — | [237] |
| PLA | — | — | — | — | 1814 | 46.8 | 5.1 | — | — | [243] |

| Polymer | Composition Ratio | Compatibilizer | Ratio | Blending Method | Young's Modulus (MPa) | Tensile Strength (MPa) | Elongation at Break (%) | Tensile Toughness ($MJ/m^3$) | Impact Resistance/ Strength (J/m) | Reference |
|---|---|---|---|---|---|---|---|---|---|---|
| PLA/PAE | 95/5 | — | — | MB | 1517 | 48.1 | 161.5 | — | — | [243] |
| PLA/PAE | 90/10 | — | — | MB | 1633 | 40.9 | 194.6 | — | — | [243] |
| PLA/PAE | 80/20 | — | — | MB | 1240 | 23.7 | 184.6 | — | — | [243] |
| PLA/PAE | 70/30 | — | — | MB | 1050 | 24.6 | 367.2 | — | — | [243] |
| PLA | — | — | — | — | 3540 | 65 | 4.0 | — | 64[a] | [247] |
| PLA/PU | 95/5 | — | — | MB | 2414 | 59.2 | 58.5 | — | 91.5[a] | [247] |
| PLA/PU | 90/10 | — | — | MB | 1810 | 47 | 220 | — | 112.8[a] | [247] |
| PLA/PU | 80/20 | — | — | MB | 1489 | 38.1 | 250 | — | 138[a] | [247] |
| PLA/PU | 70/30 | — | — | MB | 1203 | 31.5 | 363 | — | 315[a] | [247] |
| PLA | — | — | — | — | 2500±200 | 68±2 | 3±0.5 | — | — | [256] |
| PLA/PEG | 90/10 | — | — | SB | 900±50 | 26±1 | 180±10 | — | — | [256] |
| PLA/PEG | 80/20 | — | — | SB | 150±20 | 4±0.5 | 260±20 | — | — | [256] |
| PLA/PEG | 70/30 | — | — | SB | 20±2 | — | 300±30 | — | — | [256] |
| PLA | — | — | — | — | 3430±90 | 63.1±1.6 | 3.8±0.4 | — | — | [292] |
| PLA/SPI | 30/70 | — | — | MB | 3960±220 | 12.4±2.0 | 1.3±0.1 | — | — | [292] |
| PLA/SPI | 30/70 | PEOX | 1 | MB | 3820±290 | 18.1±2.0 | 1.8±0.3 | — | — | [292] |
| PLA/SPI | 30/70 | PEOX | 3 | MB | 3730±250 | 19.4±1.5 | 1.9±0.1 | — | — | [292] |
| PLA/SPI | 30/70 | PEOX | 5 | MB | 3750±180 | 20.1±1.7 | 1.9±0.1 | — | — | [292] |
| PLA/SPC | 30/70 | PEOX | — | MB | 4430±280 | 19.3±0.6 | 1.7±0.1 | — | — | [292] |
| PLA/SPC | 30/70 | PEOX | 1 | MB | 4520±260 | 20.3±1.0 | 1.8±0.1 | — | — | [292] |
| PLA/SPC | 30/70 | PEOX | 3 | MB | 4380±160 | 22.0±1.2 | 1.9±0.1 | — | — | [292] |
| PLA/SPC | 30/70 | PEOX | 5 | MB | 4250±100 | 22.5±1.2 | 2.1±0.2 | — | — | [292] |
| PLA | — | — | — | — | 4461±106 | 40.7±3.8 | 2.1±0.3 | — | — | [297] |
| SF | — | — | — | — | 2876±89 | 23.2±2.1 | 2.0±0.7 | — | — | [297] |
| PLA/SF | 2/98 | — | — | SB | 3057±91 | 28.0±2.5 | 6.5±1.8 | — | — | [297] |
| PLA/SF | 5/95 | — | — | SB | 3227±82 | 30.4±1.8 | 5.5±1.1 | — | — | [297] |
| PLA/SF | 7/93 | — | — | SB | 3420±78 | 33.3±1.7 | 3.0±1.0 | — | — | [297] |
| PLA/SF | 10/90 | — | — | SB | 3480±62 | 28.5±2.3 | 2.2±0.2 | — | — | [297] |
| PLA | — | — | — | — | — | ~57 | ~14 | — | ~12,000[a] | [299] |
| TKGM | — | — | — | — | — | ~5 | ~380 | — | ~22,000[a] | [299] |
| PLA/TKGM | 80/20 | — | — | MB | — | ~45 | ~50 | — | ~13,000[a] | [299] |
| PLA/TKGM | 60/40 | — | — | MB | — | ~37 | ~230 | — | ~14,000[a] | [299] |
| PLA/TKGM | 50/50 | — | — | MB | — | ~22 | ~400 | — | ~16,000[a] | [299] |
| PLA/TKGM | 40/60 | — | — | MB | — | ~14 | ~410 | — | ~17,000[a] | [299] |
| PLA/TKGM | 20/80 | — | — | MB | — | ~10 | ~520 | — | ~27,000[a] | [299] |
| PLA | — | — | — | — | 384±35 | 52.5±5.9 | 3.6±0.5 | — | — | [306] |
| Chitosan | — | — | — | — | 534±44 | 82.4±8.5 | 5.2±0.9 | — | — | [306] |
| PLA/chitosan | 30/70 | — | — | SB | 406±51 | 54.5±2.9 | 4.1±0.5 | — | — | [306] |
| PLA/chitosan | 20/80 | — | — | SB | 433±35 | 64.4±5.1 | 4.2±0.9 | — | — | [306] |
| PLA/chitosan | 10/90 | — | — | SB | 470±20 | 72.7±1.8 | 4.9±0.5 | — | — | [306] |
| PDLLA | — | — | — | — | 89.3±4.92 | 3.09±0.21 | 5.1±1.33 | — | — | [308] |

(*Continued*)

**TABLE 14.3 (Continued)**

| Polymer | Composition Ratio | Compatibilizer | Ratio | Blending Method | Young's Modulus (MPa) | Tensile Strength (MPa) | Elongation at Break (%) | Tensile Toughness ($MJ/m^3$) | Impact Resistance/ Strength (J/m) | Reference |
|---|---|---|---|---|---|---|---|---|---|---|
| Chitosan | — | — | — | — | 37.6±2.23 | 2.1±0.16 | 13.5±2.36 | — | — | [308] |
| PDLLA/chitosan | 80/20 | — | — | SB | 75.8±3.44 | 2.63±0.17 | 6.4±1.01 | — | — | [308] |
| PDLLA/chitosan | 60/40 | — | — | SB | 63.5±2.91 | 2.24±0.13 | 7.5±1.45 | — | — | [308] |
| PDLLA/chitosan | 40/20 | — | — | SB | 54.7±3.35 | 1.72±0.24 | 8.3±1.62 | — | — | [308] |
| PDLLA/chitosan | 20/80 | — | — | SB | 45.2±3.58 | 1.35±0.19 | 9.7±1.87 | — | — | [308] |
| PLLA | — | — | — | | 106.4±5.15 | 3.21±0.31 | 4.7±1.09 | — | — | [308] |
| PLLA/chitosan | 80/20 | — | — | SB | 83.7±4.29 | 2.76±0.27 | 5.9±1.32 | — | — | [308] |
| PLLA/chitosan | 60/40 | — | — | SB | 69.1±3.17 | 2.35±0.13 | 6.8±1.87 | — | — | [308] |
| PLLA/chitosan | 40/20 | — | — | SB | 58.8±3.72 | 1.86±0.11 | 7.7±1.69 | — | — | [308] |
| PLLA/chitosan | 20/80 | — | — | SB | 48.9±2.64 | 1.49±0.24 | 8.6±1.43 | — | — | [308] |
| PLA | — | — | — | — | 1390 | 33.3 | 10 | — | — | [314] |
| H-chitosan | — | — | — | — | 240 | 1.8 | 890 | — | — | [314] |
| PLA/H-chitosan | 80/20 | — | — | SB | ~950 | ~17 | ~14 | — | — | [314] |
| PLA/H-chitosan | 60/40 | — | — | SB | ~620 | ~11 | ~10 | — | — | [314] |
| PLA/H-chitosan | 50/50 | — | — | SB | ~570 | ~4.5 | ~6 | — | — | [314] |
| PLA/H-chitosan | 40/60 | — | — | SB | ~560 | ~4 | ~10 | — | — | [314] |
| PLA/H-chitosan | 20/80 | — | — | SB | ~300 | ~2.5 | ~41 | — | — | [314] |
| PLLA | — | — | — | MB | ~3000 | ~63 | ~10 | — | — | [178] |
| PBSL | — | — | — | MB | ~700 | ~35 | ~15 | — | — | [178] |
| PLLA/PBSL | 99/1 | — | — | MB | ~2900 | ~62 | ~10 | — | — | [178] |
| PLLA/PBSL | 99/5 | — | — | MB | ~2800 | ~62 | ~60 | — | — | [178] |
| PLLA/PBSL | 90/10 | — | — | MB | ~2550 | ~57 | ~170 | — | — | [178] |
| PLLA/PBSL | 80/20 | — | — | MB | ~2500 | ~53 | ~130 | — | — | [178] |
| PLLA/PBSL | 60/40 | — | — | MB | ~2200 | ~47 | ~160 | — | — | [178] |
| PLLA/PBSL | 40/60 | — | — | MB | ~1700 | ~36 | ~205 | — | — | [178] |
| PLLA/PBSL | 20/80 | — | — | MB | ~1200 | ~37 | ~270 | — | — | [178] |
| PLA | — | — | — | — | ~1350 | ~56 | ~6 | ~3 | — | [187] |
| Bionolle#3000 | 90/10 | — | — | — | ~1320 | ~53 | ~8 | ~163 | — | [187] |
| PLA/Bionolle#3000 | 80/20 | — | — | MB | ~1060 | ~43 | ~200 | ~4 | — | [187] |
| PLA/Bionolle#3000 | 70/30 | — | — | MB | ~950 | ~46 | ~300 | ~70 | — | [187] |
| PLA/Bionolle#3000 | 50/50 | — | — | MB | ~800 | ~50 | ~400 | ~112 | — | [187] |
| PLA/Bionolle#3000 | 70/30 | — | — | MB | ~380 | ~51 | ~500 | ~130 | — | [187] |
| PLA/Bionolle#3000 | 100 | — | — | MB | ~200 | ~49.5 | ~600 | ~148 | — | [187] |
| PLLA/PEO | 60/40 | — | — | SB | — | ~28 | ~70 | — | — | [265] |
| PLLA/PEO | 60/40 | PVAc | 2 | SB | — | ~28.5 | ~110 | — | — | [265] |
| PLLA/PEO | 60/40 | PVAc | 5 | SB | — | ~27 | ~115 | — | — | [265] |
| PLLA/PEO | 60/40 | PVAc | 7 | SB | — | ~24.5 | ~115 | — | — | [265] |
| PLLA/PEO | 60/40 | PVAc | 10 | SB | — | ~22.5 | ~125 | — | — | [265] |
| PLLA/PCL | 80/20 | — | — | SB | 590±200 | 22±4 | 11±3 | — | — | [364] |
| PLLA/PCL | 80/20 | Cop1 | 5 | SB | 600±100 | 21±1 | 24±6 | — | — | [364] |

| Polymer | Composition Ratio | Compatibilizer | Ratio | Blending Method | Young's Modulus (MPa) | Tensile Strength (MPa) | Elongation at Break (%) | Tensile Toughness ($MJ/m^3$) | Impact Resistance/ Strength (J/m) | Reference |
|---|---|---|---|---|---|---|---|---|---|---|
| PLLA/PCL | 80/20 | Cop1 | 10 | SB | 1040±80 | 19±2 | 31±8 | — | — | [364] |
| PLLA/PCL | 80/20 | Cop1 | 15 | SB | 840±240 | 17±2 | 14±7 | — | — | [364] |
| PLLA/PCL | 80/20 | Cop2 | 5 | SB | 820±210 | 21±2 | 19±4 | — | — | [364] |
| PLLA/PCL | 80/20 | Cop2 | 10 | SB | 690±220 | 16±1 | 7±1 | — | — | [364] |
| PLLA/PCL | 50/50 | — | — | SB | 800±190 | 13±1 | 4±1 | — | — | [364] |
| PLLA/PCL | 50/50 | Cop1 | 5 | SB | 780±30 | 9±1 | 4±1 | — | — | [364] |
| PLLA/PCL | 50/50 | Cop1 | 10 | SB | 690±50 | 6±1 | 3±1 | — | — | [364] |
| PLLA/PCL | 50/50 | Cop2 | 5 | SB | 750±120 | 9±1 | 4±1 | — | — | [364] |
| PLLA/PCL | 50/50 | Cop2 | 10 | SB | 760±60 | 9±1 | 4±1 | — | — | [364] |
| PDLLA/PCL | 80/20 | — | — | SB | 810±40 | 18±1 | 5±1 | — | — | [364] |
| PDLLA/PCL | 80/20 | Cop1 | 5 | SB | 690±190 | 13±1 | 7±3 | — | — | [364] |
| PDLLA/PCL | 80/20 | Cop1 | 10 | SB | 650±50 | 11±1 | 46±13 | — | — | [364] |
| PDLLA/PCL | 30/70 | — | — | SB | 520±60 | 9±1 | 5±1 | — | — | [364] |
| PDLLA/PCL | 30/70 | Cop1 | 5 | SB | 530±30 | 10±1 | 5±1 | — | — | [364] |
| PDLLA/PCL | 30/70 | Cop1 | 10 | SB | 390±30 | 7±1 | 5±1 | — | — | [364] |
| PLLA | — | — | — | SB | 19.8±3.0 | 34.1±2.5 | 56.3±1.9 | — | — | [365] |
| PLLA/PCL | 80/20 | — | — | SB | 20.7±1.4 | 41.2±1.5 | 129.5±32.9 | — | — | [365] |
| PLLA/PCL | 60/40 | — | — | SB | 10.7±2.2 | 19.3±1.9 | 152.1±11.8 | — | — | [365] |
| PLLA/PCL | 50/50 | — | — | SB | 8.1±2.8 | 16.9±13 | 139.6±17.4 | — | — | [365] |
| PLLA | — | PEO-b-PPO | 2 | SB | 10.5±1.0 | 25.4±3.0 | 84.7±2.2 | — | — | [365] |
| PLLA/PCL | 80/20 | PEO-b-PPO | 2 | SB | 9.5±1.2 | 20.1±1.4 | 129±4.8 | — | — | [365] |
| PLLA/PCL | 60/40 | PEO-b-PPO | 2 | SB | 4.7±0.7 | 12.9±0.8 | 130±14.2 | — | — | [365] |
| PLLA/PCL | 50/50 | PEO-b-PPO | 2 | SB | 6.6±0.7 | 10.4±0.5 | 123.7±13.3 | — | — | [365] |
| PLA | — | — | — | — | 2275.3 | 48.3 | 3 | — | — | [366] |
| PCL | — | — | — | — | 175.8 | 18.6 | 600 | — | — | [366] |
| PLA/PCL | 80/20 | — | — | MB | 584.7 | 44.2 | 28 | — | — | [366] |
| PLA/PCL | 60/40 | — | — | MB | 751.5 | 19.4 | 5 | — | — | [366] |
| PLA/PCL | 40/60 | — | — | MB | 164.1 | 18.6 | 23 | — | — | [366] |
| PLA/PCL | 20/80 | — | — | MB | 111.7 | 20.1 | 440 | — | — | [366] |
| PLA/PCL | 80/20 | TPP | 2 | RMB | 1013.5 | 33.1 | 127 | — | — | [366] |
| PLA/PCL | 60/40 | TPP | 2 | RMB | 710.2 | 23.6 | 7 | — | — | [366] |
| PLA/PCL | 40/60 | TPP | 2 | RMB | 344.0 | 11.4 | 3 | — | — | [366] |
| PLA/PCL | 20/80 | TPP | 2 | RMB | 197.9 | 17.2 | 560 | — | — | [366] |
| PLLA | — | — | — | — | 5200±300 | 56.8±2.0 | 0.5±0.04 | — | — | [370] |
| PCL | — | — | — | — | 400±100 | 17.4±0.4 | 400±19.0 | — | — | [370] |
| PLLA/PCL | 80/20 | — | — | MB | 3000±700 | 20.7±1.7 | 1.3±0.1 | — | — | [370] |
| PLLA/PCL | 60/40 | — | — | MB | 1500±100 | 17.3±2.8 | 4.3±0.8 | — | — | [370] |
| PLLA/PCL | 40/60 | — | — | MB | 1000±10 | 15.2±0.2 | 19.5±2.4 | — | — | [370] |
| PLLA/PCL | 20/80 | — | — | MB | 600±100 | 12.5±1.9 | 52.5±2.1 | — | — | [370] |

MB: melt blending; SB: solution blending; and RMB: reactive melt blending.
[a]Unit of impact strength is $J/m^2$.

studied miscibility of solvent cast blends of PLA with amorphous PVOH (a-PVOH) and syndiotactic PVOH (s-PVOH) using thermal, infrared, and X-ray diffraction spectroscopy. Partially miscible, more flexible (compared to PLA) blends with two $T_g$s were reported. Partial compatibility, existed in the amorphous areas, was attributed to hydrogen bonding between the polar carbonyl groups in PLA and hydroxyl groups in PVOH, as revealed by FTIR [118]. Separate immiscible crystalline PLA and PVOH phases existed in the blends. Yeh et al. [119] reported that a PLA/PVOH 80/20 (wt%) blend composition had increased molecular interactions as observed in the carbonyl peak shift from 1758 to 1752 $cm^{-1}$ in FTIR spectroscopy. During the polarized light microscopy studies, PLA spherulite radial growth rate was the fastest in the 80/20 blends, as compared to neat PLA or other blend compositions. In another study [120], partial immiscibility and phase separation between PLA and PVOH was attributed to the difference in the solubility parameters of PLLA (22.7 $J^{0.5}/cm^{1.5}$ calculated; 19–20.5 $J^{0.5}/cm^{1.5}$ experimental) and PVOH (21.6 $J^{0.5}/cm^{1.5}$ calculated; 25.8–29.1 $J^{0.5}/cm^{1.5}$ experimental). These studies indicated that the solution blends of PVOH/PLLA were partly miscible at best, with PLLA- and PVOH-rich continuous domains [118, 120]. Molecular modeling and molecular dynamics simulations by the mesoscopic dynamic theory and thermodynamic approaches were used to predict the compatibility of PVOH/PLLA blends and validate the experimental results [121]. The modeling results showed slight miscibility in the blend at a ratio of 90/10 (PVOH/PLLA), as indicated by $\chi_{AB} = 0.134$ compared to $\chi_{AB,critical} = 0.143$ [125]. Increasing the PLLA content (25, 50, 75, and 90%) resulted in higher $\chi_{AB}$ (0.270, 0.363, 0.654, and 0.540) than $\chi_{AB,critical}$; hence, these polymer blends were predicted to be immiscible [121, 122].

The addition of PVOH, with high-melt viscosity and lower initial thermal degradation compared with PLA, led to an increase of melt viscosity and a decrease of initial degradation temperature of the blends [119]. A small decrease of PVOH crystallinity in solution blends of a-PVOH/PLLA containing 10–50 wt% a-PVOH was observed, whereas the enthalpy of fusion of s-PVOH in solution blends of s-PVOH/PLLA blends at similar ratios increased [118, 120]. In addition, PLLA crystallinity decreased in solution blends of a-PVOH or s-PVOH with PLLA except at the ratio of 10/90 (PVOH/PLLA) [118]. Shuai et al. [118] reported that the blends of a-PVOH or s-PVOH with PLLA containing 10–90% PVOH had lower tensile strength than neat PVOH or PLLA. The lowest tensile strength was found with the 50/50 blend. The blends had lower elongation at break than PLLA except for the blend comprised of 10 wt% PLLA. Tsuji and Muramatsu [120] reported that the tensile strength/modulus and elongation at break of blend films decreased with increasing PLLA content (50–90 wt%), but owing to swelling of PVOH, a wet state blend film (film immersed in distilled water for 24 h) had a slight increase of elongation at break and a dramatic decrease of tensile strength/modulus compared to a dry-state blend film. However, tensile strength/modulus of the wet-state blend films increased with increasing PLLA content, and the blend film comprised of 90 wt% PLLA had the highest tensile strength and modulus values than the wet PLLA and wet PVOH [120]. The addition of 20–40 wt% PVOH promoted enzymatic and nonenzymatic autocatalytic hydrolysis of PLLA [123]. After nonenzymatic autocatalytic hydrolysis in phosphate-buffered solution (pH 7.4) containing sodium azide for 2–12 months, the $T_g$, $T_c$, and $T_m$ of PLLA in the blends decreased, but the degree of crystallinity of PLLA in blend films increased with increasing PVOH content [123]. The tensile strength and Young's modulus of PVOH/PLLA blend films also decreased. More information about hydrolysis of these blends can be found in Chapter 21.

Li et al. [9] plasticized PLA-EVOH blends with a novel lacti-glyceride plasticizer, prepared by transesterification of glycerol and L-lactic acid using stannous octoate catalyst, $Sn(Oct)_2$. The transesterification reaction reduced hydrophobicity while maintaining good compatibility as observed during contact angle studies. PVOH was first plasticized with lacti-glyceride in 7 : 3 ratio. The plasticized PVOH was melt-blended with PLA. The tensile strength of EVOH-PLA: 90 : 10 blends improved from 35.4 to 39.6 MPa, while elongation improved from 248 to 305%. The plasticization effect was supported with minor drop in $T_g$. In addition to the plasticization effect, the authors concluded that the synthesized molecules served as a compatibilizer for the designed ternary blend system.

***14.3.2.2 Poly(Vinyl Acetate)/PLA Blends*** Melt blends of PLA-PVAc have been reported miscible by various researchers [122, 124] due to the interaction between proton acceptors, carboxyl groups of PLA, and the proton-donating α-hydrogens of PVAc [124]. A single $T_g$ was observed from all the blend compositions. However, favorable tensile strength and % elongation of PLA-PVAc blends were observed from 5 to 30% PVAc, which could be related to good dispersion of PVAc in the PLA matrix at low concentrations, although the SEM images provided in the article were lacking clarity. After fixed annealing between Teflon-coated aluminum plates at 70°C for 15 min, the tensile strength at yield of the film decreased from around 58.6 to 41.7 MPa with a dramatic increase of elongation at break from around 20 to 225% compared to extruded blend film [124]. However, it was observed that in the extruded films, the aging process induced relaxation of polymer chains, leading to decreased segmental mobility and flexibility. The fabricated blends also demonstrated slower enzymatic degradation rates than PLA.

It was observed that PVAc resided in the interlamellar regions of the PLA spherulites and roughened their texture (Figure 14.10) [122]. The addition of a small amount of

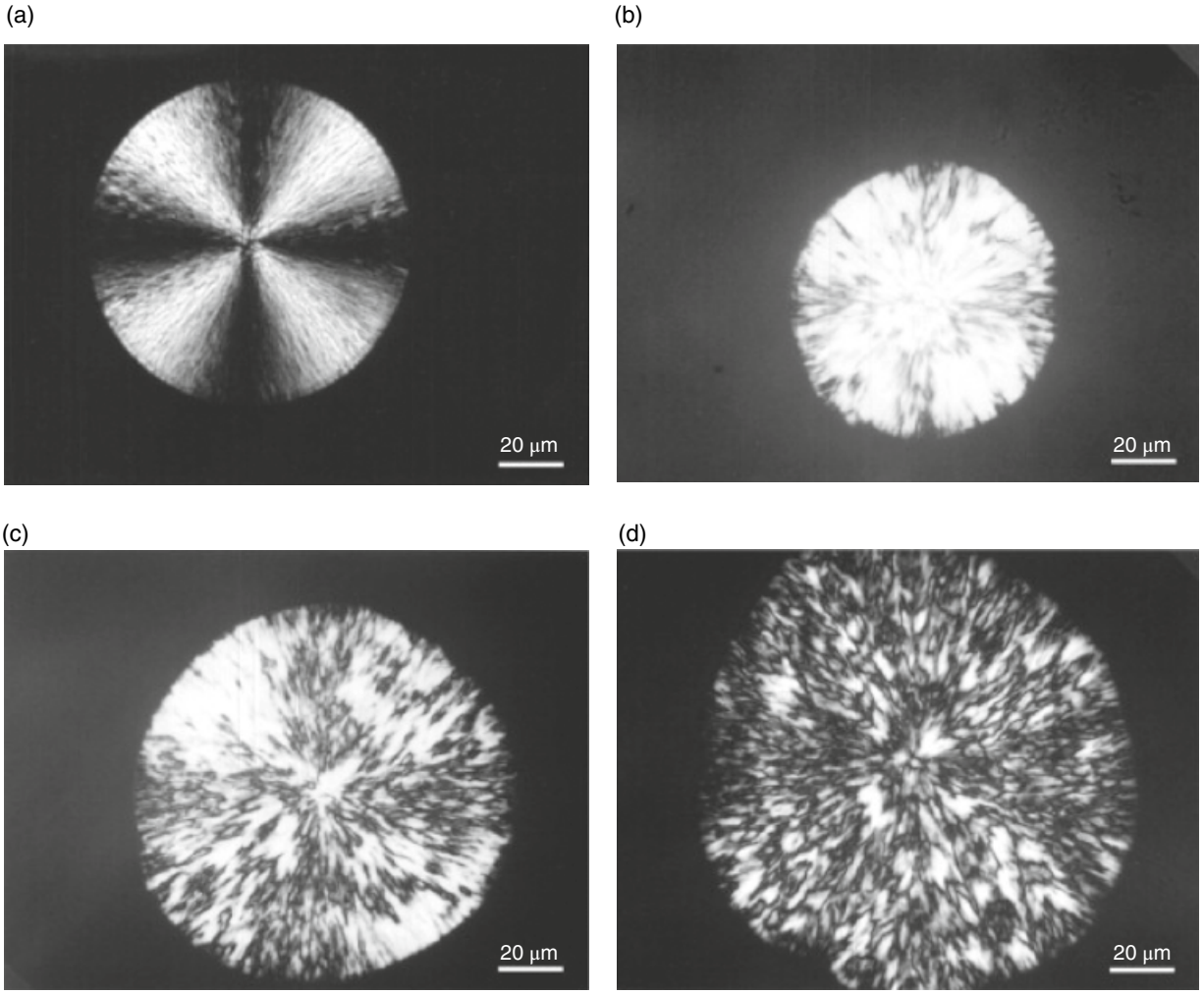


**FIGURE 14.10** Polarized optical micrographs of PLA/PVAc blends, isothermally crystallized at 130°C for various periods of time: (a) neat PLA for 30 min; (b) 70/30 for 50 min; (c) 50/50 for 70 min; and (d) 30/70 for 90 min. *Source:* Reprinted from Ref. 122. Copyright 2003, with permission from Elsevier.

PVAc (5 wt%) increased tensile strength at yield (from ca. 48 to 58 MPa) and elongation at break (from ca. 10 to 20%) of the extruded blend films compared to neat PLA film [124].

The incorporation of the more hydrophobic polymer PVAc, which has a surface tension of 24.85 dyn/cm$^2$, lowered the hydrophilicity of PLA (surface tension of 43.5 dyn/cm$^2$). Hence, PVAc-PLA blends containing 5–30 wt% PVAc exhibited surface energies of 21.75–16.2 dyn/cm$^2$. In turn, the adhesion properties of the blends, such as enzymatic adhesion on film surfaces was lower than that of pristine PLA [124]. Therefore, the enzymatic degradation of PVAc/PLA blends with proteinase K was considerably slower than the neat PLA [124, 125].

***14.3.2.3 Poly(Vinyl Acetate-co-Vinyl Alcohol)/PLA Blends*** PLA-PVAc blends have been reported as miscible in 5–30% PVAc content but it slows the enzymatic degradation. Therefore, to enhance miscibility and to accelerate degradation, various researchers blended PLA with poly(vinyl acetate-co-vinyl alcohol) (PVAc-*co*-VA) to introduce the hydrophilic hydroxyl groups. Park et al. [122] fabricated blends of PLA with (PVAc-*co*-VA), synthesized by controlled hydrolysis of PVAc. Blends with 10% hydrolyzed PVAc (PVAc-*co*-VA 10) were miscible when PLA and PVAc-*co*-VA 10 were blended in 90/10% ratio. A further increase in the degree of hydrolysis of PVAc to 20% or more, as well as increase in the PLA-PVAc-*co*-VA 10 content, rendered blends immiscible, which was evident with two separate $T_g$ and observed in the microscopy studies.

***14.3.2.4 Poly(Vinyl Pyrrolidone)/PLA Blends*** Poly(*N*-vinylpyrrolidone), also known as poly(*N*-vinyl-2-pyrrolidone) and poly(vinyl pyrrolidone) (PVP), is an amorphous, nonionic water-soluble, and biocompatible

synthetic polymer used in biomedical (e.g., retarding agent in drugs, plasma expander, drug delivery system), biochemical (e.g., hair sprays, skin care products), food (e.g., fruit juices), and textile [126–129] industries. PVP degrades hydrolytically quickly, but high $M_w$ (>20 kDa) PVP cannot be expelled from the body, causing undesirable side effects [128–130]. Due to its pyrrolidone rings containing a proton accepting carbonyl moiety, PVP is a good proton acceptor [131, 132]. Solution-blended films of PVP ($M_w$ = 30 kDa) with PDLLA ($M_w$ = 150 kDa) or PLLA ($M_w$ = 55 kDa) prepared by using chloroform were reported to be immiscible [126]. The cold crystallization process of PLLA in the blends was retarded (increased $T_c$) with increasing PVP content. No interaction between PVP and PLLA was observed by FTIR, but the blends of PVP/PDLLA exhibited a shift of the C═O stretching vibration of PVP peak at 1672 $cm^{-1}$ to a higher wavenumber, 1684 $cm^{-1}$, with PVP content of 40 wt% [126]. The use of solution blends of PVP ($M_w$ = 40 kDa)/PLA ($M_w$ = 5 kDa) as a controlled drug release system was studied by Morita et al. [133]. They reported good agreement between *in vitro* and *in vivo* results showing that an increase in PVP content increased both the release rate of fluorometholone (FLM) from rod-shaped ocular implants and the weight loss of implants. With PVP content of 0, 30, and 50 wt%, the amounts of FLM released in 10 days obtained in vivo were around 25, 45, and 90 wt%, respectively, and the weight losses of implants comprised of PVP/PLA/FLM observed for one day was about 13, 43, and 55 wt%, respectively. According to SEM observations, the enhancement of controlled release and weight loss of PVP/PLA blends were attributed to rapid degradation and leaching of PVP [133].

Nanoscale fibers with specific surface topologies can be prepared from solution blends of PVP/PLA in dichloromethane ($CH_2Cl_2$) using electrospinning [134]. The characteristics of phase behavior and phase boundaries of PVP ($M_w$ = 360 kDa)/PDLLA ($M_w$ = 54 kDa)/$CH_2Cl_2$ and PVP ($M_w$ = 360 kDa)/PLLA ($M_w$ = 148 kDa)/$CH_2Cl_2$ are shown in Figure 14.11 [134]. In both cases, phase separation (dispersed–matrix phase morphology with a major component of PVP or PLA and co-continuous phase morphology with equal polymer components) induced by rapid solvent evaporation occurred at earlier stages of fiber formation [134]. To create specific surface topologies, the selective removal of the PVP or PLA phase was performed by ultrasonic agitation in water or by annealing fibers at high temperature (above $T_g$s of components and/or $T_m$ of PLLA) (i.e., 200°C for 3 h). For example, with fibers comprised of PVP as a major component, the selective removal of the PVP phase resulted in fibers with a porous structure, whereas the removal of PLA led to a core (PLA)-shell (PVP) morphology [134].

Bonan et al. [135] fabricated PLA/PVP fibrous membranes containing 20% copaiba oil using solution blow spinning. Copaiba oil imparted antimicrobial barrier properties. The addition of PVP accelerated the degradation of fibers due to higher hydrophilicity, opening opportunities for medical applications including wound dressing.

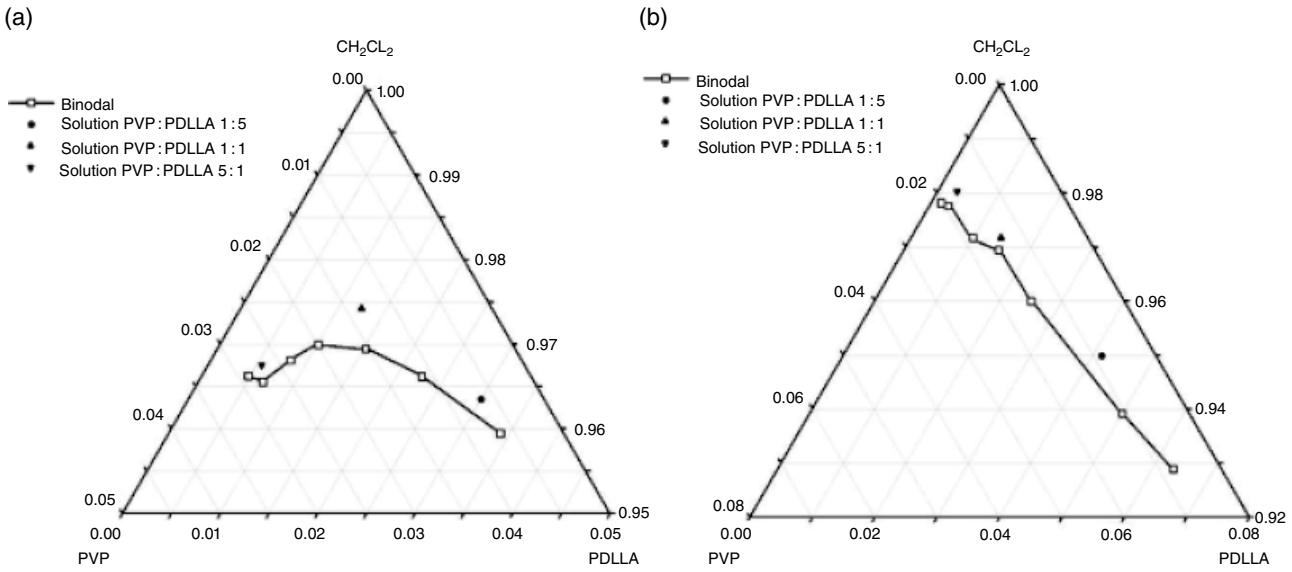


**FIGURE 14.11** Ternary phase diagrams obtained by turbidity measurements at room temperature: (a) PVP/PDLLA/$CH_2Cl_2$ and (b) PVP/PLLA/$CH_2Cl_2$. The solid symbols show the compositions of the solutions used for electrospinning, and the hollow squares mark the phase boundary. The concentrations are given in wt%. *Source:* Reprinted from Ref. 134. Copyright 2001, with permission from John Wiley & Sons, Inc.

### 14.3.3 Aliphatic Polyesters and Copolyesters

***14.3.3.1 Poly(ε-Caprolactone)/PLA Blends*** PCL is a water-insoluble nontoxic, biodegradable, biocompatible petroleum-based aliphatic polyester synthesized by ring-opening polymerization of ε-caprolactone (ε-CL) [136, 137]. It is a soft and flexible polymer with low $T_g$ (−60°C) and $T_m$ (55–70°C) [136, 137]. It is FDA approved for medical implants and controlled drug delivery applications [138] due to the ability of ester linkages to degrade under physiological conditions (pH 7.4) and bioreabsorption. However, its high degree of crystallinity (45–60%) and its high hydrophobicity are responsible for its slow degradation [137]. PLA can be blended with PCL to improve its toughness and impact strength while maintaining its rigidity. Also, PCL's low melting point, low thermal stability, and slow biodegradability limit its commercial application, which can be overcome by blending with PLA.

Various studies have reported immiscibility and phase separation in PLA-PCL blends [137, 139, 140]. Optimized PLA-PCL melt-blended morphologies with suitable micromechanical performance can be obtained. Ostafinska et al. [141] reported a synergistic effect of viscosity (PLA/PCL viscosity ratio ~ 1), composition, and processing parameters producing a droplet-particle-type morphology up to 20–25 wt% of PCL (~0.6 μm diameter). A blend with 30% PCL led to broader particle size due to coalescence, while further increase in the PCL content generated a co-continuous morphology. PLA/PCL 80/20 blends produced PCL droplets in a PLA matrix, which increased the impact strength by 16 times compared with a PLA matrix. The improved impact strength and toughness can be explained by a cavitation mechanism [142]; for such a mechanism to occur, a minimal suitable filler size is needed.

In other research, Bai et al. [143] studied the interaction of PCL droplet diameter and crystallinity on the impact strength of PLA/PCL (80/20) blends. Crystallinity was controlled by the extruder screw speed, mold temperature, and nucleating agent added to the blends. Crystallinity of the PLA matrix impacted the average diameter ($d_w$) range ideal for maximum impact performance. PLA blends with relatively low crystallinity (6.5–9.5%) demonstrated good impact strength at particle sizes of 0.7–1.1 μm. On the other hand, matrices with high crystallinity (46–48%) exhibited superior impact strength for particle sizes of 0.2–0.4 μm, which was in agreement with research reported elsewhere [144]. Blends with a higher crystallinity matrix roughly demonstrated two times better impact strength than amorphous blends. The notched Izod impact strength for amorphous and crystalline matrices as a function of particle size are represented in Figure 14.12 [143].

Tsuji et al. [145] found that the addition of PCL at contents below 10 wt% accelerated the crystallization of PLLA, mainly due to a nucleation-assisting effect of PCL. Tsuji et al. [146] also blended PLLA ($M_n$ = 500 kDa) and PCL ($M_n$ = 120 kDa), without or mixed with 10 wt% poly(L-lactide-*co*-ε-CL) P(LLA-*co*-CL) ($M_n$ = 170 kDa), by solution casting. The addition of P(LLA-*co*-CL) decreased the number density of spherulites in PLLA and PCL films. The $T_m$ of PLLA and PCL did not change due to the addition of P(LLA-*co*-CL). The addition of P(LLA-*co*-CL) also increased the tensile strength and the Young's modulus of the blend films. Tsuji and Yamada [147] studied the enzymatic hydrolysis of these blended films (PLLA and PCL added with 10 wt% P(LLA-*co*-CL) in the presence of proteinase K and *Rhizopus arrhizus* lipase by weighing the films. The addition of P(LLA-*co*-CL) decreased the hydrolyzabilities of the PLLA and PLLA/PCL (50/50) films by proteinase K and the hydrolyzabilities of PCL and PLLA/PCL (50/50) films by *R. arrhizus* lipase solutions. The reduction in hydrolyzability was attributed to the miscibility of P(LLA-*co*-CL) with PLLA

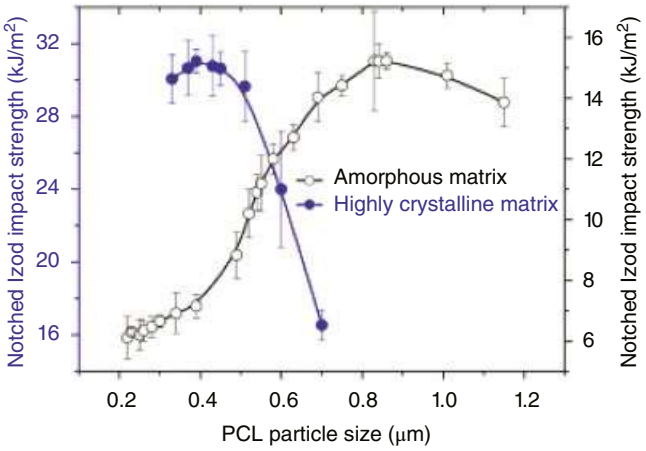


**FIGURE 14.12** Comparison of the difference in optimum particle size for toughening PLLA/20PCL blend with an amorphous PLLA matrix and for that with a highly crystalline PLLA matrix. *Source:* Reprinted from Ref. 143. Copyright 2013, with permission from Elsevier.

and PCL that may disturb the adsorption of the two enzymes.

Przybysz-Romatowska et al. [148] prepared PCL-*g*-PLA copolymer using dicumyl peroxide (DCP) or di-(2-*tert*-butyl-peroxyisopropyl) (BIB) peroxide initiator by chemically reacting PCL/PLA (3/1) using 1% initiator in xylene at 140°C and in situ compatibilizing by direct melt-blending PCL/PLA (3/1) with 1 or 5 wt% initiator in a Brabender® mixer at 170°C. Uncompatibilized blends (75% PCL/25% PLA) displayed a sea-island morphology with a spherical PLA dispersed phase. Compatibilization with PCL-*g*-PLA improved compatibility and phase adhesion between the two phases while preventing coalescence. The storage modulus of all compatibilized compositions was reported to improve from 10 to 40% due to reactive compatibilization as compared with PCL/PLA 75/25 uncompatibilized blend. In situ melt blending and BIB peroxide displayed higher reactive blending as observed in thermo-mechanical and morphological analysis.

***14.3.3.2 Polyhydroxyalkanoate/PLA Blends*** Poly[(*R*)-3-hydroxyalkanoate]s are biologically produced by microorganisms. Some of the polymers in this family are commercially available but have intrinsic performance and processing limitations, such as poor melt strength, poor thermal stability, low elongation, high tackiness, high crystallization, and large spherulite size [149]. Poly[(*R*)-3-hydroxybutyrate] (PHB), a linear highly crystalline stereoregular polymer, is a popular polymer from the PHA family. To tailor its properties, PHB has been copolymerized with other monomers such as 3-hydroxyvalerate, 3-hydroxyhexanoate to produce (PHBV) and poly[(*R*)-3-hydroxybutyrate-*co*-(*R*)-3-hydroxyhexanoate] (PHBHHx). Copolymerization with 3-hydroxyvalerate or 3-hydroxyhexanoate imparts side chain branches in the polymer which hinder crystallization, provide flexibility, increase toughness, and reduce melting temperature. The extent of change in these properties is strongly dependent on the type of comonomer, its branch size, and its content in the final polymer configuration [149]. PHAs are available under the trade names Biopol™, Nodax™, and Mirel™. PLA/PHB and PLA/PHBV have been reported to be immiscible when high molecular weights, required for mass application, are blended [150–153], due to low entropy. However, theoretical [31] and experimental studies [154] have confirmed miscibility when either of the two, or both, polymers are blended at low molecular weight (<20 kDa) [31, 153, 155] due to higher entropy. Also, as observed in some of the other blends, the PLA/PHA extrusion melt-compounding process produced better miscibility or dispersion due to higher shear force and shear thinning, compared with solvent cast material that has generally been reported to be immiscible [155, 156]. Gerard et al. [157] studied PLA/PHBV miscibility over a wide range of compositions using DSC and microscopic studies. Two melting peaks were observed at 150 and 170°C, indicating immiscibility. Poor interfacial adhesion was observed in SEM images except for PLA/PHBV 90/10 composition. Zhang et al. [156] reported that PHB/PDLLA blends prepared by solvent casting were completely immiscible with clear separate glass transition temperatures. Microscopic studies also revealed two distinct phases. However, greater polymer chain interactions were observed between PLA and PHB in melt-blended compositions as observed in DSC studies. Samples exposed to higher temperature (200°C) exhibited more miscibility, which can possibly be due to small-scale in situ transesterification copolymerization. The presence of PHB in the PLA matrix has also been reported to increase the HDT and accelerate the degradation kinetics of the PLA [158, 159].

Various studies have focused on understanding the mechanical performance of PLA/PHA blends. In general, blending PLA with PHB, PHBV, or PHBHHx decreased the elastic modulus of PLA [155, 160]. Iannace et al. [155] reported a decrease in yield stress and interference in the stress-induced crystallization during tensile testing in PLA-PHBV blends. PHBHHx/PDLLA blends have been reported immiscible by various researchers [161, 162]. The PHBHHx chain retained a helical structure in the blends. However, a reduction in the percentage crystallinity was observed during DSC studies [154]. Blending PLA with PHBHHx reduced the elastic modulus and increased toughness and ductility of the blends [149, 160].

Richards et al. [161] compounded PLA and PHBV (12% valerate content) in 25/75, 50/50, and 75/25 wt% composition. Foams were prepared with $CO_2$ as a blowing agent at 65, 75, and 95°C. Enthalpy of fusion of the blends increased with increasing PHBV content, ascribed to the higher crystallization of PHBV compared to PLA. PHBHHx in the PLA matrix improved the toughness and imparted ductility to the blends [149]. PHBHHx particles were dispersed in the amorphous phase of the PLA matrix below 20 wt% concentration. Good dispersion was associated with low interfacial energy between PLA and PHA. Furukawa et al. [153] reported that PHB and PHBHHx were immiscible in PLLA. The $T_g$ of PLA and PHBHHx did not change significantly. The $T_c$ of PLLA in the PHB/PLLA and PHBHHx/PLLA blends shifted, respectively, to lower and higher temperatures with an increase in the PHB or PHBHHx component. IR spectra of the blends were analyzed and weak amorphous bands of PLLA were observed in the spectra of the 80/20 PHBHHx/PLLA blend. Amorphous bands of PHBHHx were not observed in the spectra of the 20/80 PHBHHx/PLLA blend.

A new medium-molecular-weight PHA consisting of six comonomers, 3-hydroxyhexanoate, 3-hydroxyoctanoate, 3-hydroxydecanoate, 3-hydroxydodecanoate, *cis*-3-hydroxydodec-5-enoate and *cis*-3-hydroxydodec-6-enoate, was produced using glycerol by *Pseudomonas mediterranea*,

a gram-negative bacterium, which can be potentially used as a softener and lubricant for higher $M_w$ biopolymers including PLA-PHA blends [162]. Botta et al. [163] prepared PLA/PHA melt blends at 95 : 5, 90 : 10 and 85 : 10 ratios. Blended compositions were melt-processable due to a decrease in melt viscosity as PHA molecules acted as lubricants; with 15% addition of PHA, the viscosity of PLA dropped by 40%. Due to poor miscibility, spherical PHA droplets ranging from 1–2 to 2–8 μm in the PLA matrix were observed in SEM studies; the droplet size increased as a function of PHA content. The tensile tests of compression-molded sheets demonstrated ductile behavior and increased toughness. Elongation at break for PLA/PHA 90/10 and 85/15 blends were reported to be 43 and 48% respectively, compared to 5.2% for the PLA matrix, with 16 and 24% increase in the impact strength. A slight decrease in $T_g$, measured from tan $\delta$ peaks, as a function of PHA content, was observed. The $T_g$ of PLA dropped by 5°C with the addition of 15% PHA.

#### *14.3.3.3 Poly(Butylene Succinate)/PLA Blends*

Poly(butylene succinate) (PBS), a linear aliphatic polyester, is commercialized under various trade names such as Bionolle™ (grade 1000 series), Enpol (G4560 M, G4560J), BioPBS™ by various companies [164, 165]. It is produced via a polycondensation reaction of glycol (1,4-butanediol) and aliphatic dicarboxylic acid (succinic acid), both of which can be bio-derived. The properties and processing behavior of PBS are very similar to polyethylene, with a $T_g$ of −32°C, $T_m$ of 114–115°C, crystallinity of 35–45%, and HDT of 97°C at 0.45 MPa [164–167]. Due to its flexibility, toughness, and biodegradability, PBS has been blended with PLA to improve mechanical performance of PLA without compromising biodegradability of the polymer blends [168, 169]. PLA and PBS are thermodynamically immiscible [166, 167, 170] with high interfacial tension ∼1.13 mN/m, obtained using a thread retraction method [167]. However, some researchers reported reasonably strong interactions and partial miscibility for PBS content ≤10% [171–173]. To produce miscible blends, Srithep et al. [174] blended PLA with 2–10% low-molecular-weight PLA-PBS block copolymer ($M_w$ = 7700 Da), using a solvent casting technique. A miscible blend with increased chain mobility and increased MFI was obtained. Yield stress decreased along with increased strain, suggesting chain mobility and a plasticization effect. At 8% PLA-PBS copolymer concentration, elongation increased from 10 to 60% compared with PLA. Deng et al. [175] reported PLA-PBS partial miscibility for PBS content <20%; for 10–40% PBS and PLA, co-continuous phases were observed; above 40% PBS became the only continuous phase with a dispersed PLA phase.

The addition of PBS (>50 wt%) increased the viscosity of PBS/PLA blends, and a strong shear thinning behavior at low frequencies was found with the 50/50 wt% blend [171]. Two distinct $T_m$s of PBS and PLA were observed in the physical melt blends, indicating a dual lamellar stack model (each polymer crystallizes separately, and each polymer's lamellae are formed at different locations) [171, 174]. The shift of the $T_c$ and $T_m$ of PLA to lower temperatures and the increased bulk crystallinity in the blends with increasing PBS content, indicating that the PBS has enhanced the crystallization of PLA in the blends [168, 171, 176, 177]. Bhatia et al. [171] observed miscibility of PBS/PLA blends comprised of PBS content not greater than 20 wt%, while Yokohara and Yamaguchi [168] observed immiscibility of PBS ($M_w$ = 150 kDa) and PLA ($M_w$ = 350 kDa) in the molten state, and blends comprised of 5–20 wt% PBS exhibited a PBS dispersed phase in a PLA matrix. The interfacial tension of PBS and PLA (3.5 mN/m), estimated from a rheological emulsion model, also indicates immiscibility of this polymer pair [168].

Ostrowska et al. [170] found PLA/PBS blends with immiscible phases, but interaction between two polymers was observed, affecting structural arrangement and crystallization phases, as observed by carbonyl peak shift in FTIR spectra and decrease in $T_g$ of the PLA phase in the blends. In general, the authors reported the elongation of PLA increased and tensile strength decreased with the addition of PBS. The dispersion of the polymer and phase morphology had significant impacts on the mechanical performance. Higher elongation (>300%) in blends with PBS content above 50% was observed, which could be due to a co-continuous PBS phase in the composition. For PLA-PBS 10/90 composition, >600% elongation was observed, which was higher than that for neat PBS and neat PLA polymers. Also, PLA-PBS 90/10 blends had a higher tensile strength than PLA-PBS 60/40, 50/50, 40/60, 30/70, 20/80 blends, which was ascribed to the good dispersion of PBS in the PLA. Similar mechanical performance trends were observed by other researchers [171, 178].

Researchers have reported that the biodegradability of polymer blends was enhanced with the addition of PBS in the PLA matrix [169]. Higher biodegradation, which increased with increase in PBS content, was accredited to submicron gaps due to immiscibility of the two polymers increasing the moisture exposure, hydrophilicity, and accelerating hydrolytic degradation. Some researcher studied the effect of $O_2$ or Ar plasma treatment to improve the compatibility of the blends [179]. The plasma treatment enhanced the phase dispersion; however, no enhancement in biodegradation was observed, which can be explained by the increased compatibility and reduction in sub-micron voids and moisture exposure.

In PLA/PBS blends, several researchers reported PBS behaves as a nucleating agent at temperatures lower than its melting point, enhancing the crystallization rate of PLA [168, 177, 180]. Spherulite sizes of crystals were observed by POM [177] and increase in the cold crystallization peak

during thermal studies [168]. PLA/PBS blend configurations up to 30 wt% PBS showed a large extent of smaller spherulites due to the limited volume of PBS in those droplet structures [177]. Higher PBS concentrations led to clear phase separation due to crystallization.

#### *14.3.3.4 Poly(Butylene Succinate-co-Adipate)/PLA Blends*

Poly (butylene succinate-*co*-adipate) (PBSA) is a random aliphatic copolyester comprised of 1,4-butanediol, succinic acid, and adipic acid. PBSA has lower thermal properties ($T_g$ of −45°C, $T_c$ of 50–53°C, $T_m$ of 93–95°C, crystallinity of 20–35%, and HDT of 69°C at 0.45 MPa, more flexibility (tensile strength of 34–47 MPa, tensile elongation of 400–900%, and flexural modulus of 323–340 MPa), compared with PBS [181–183]. Due to its branched structure, it has lower crystallinity compared with PBS. As a result of reduced crystallinity, PBSA exhibits higher impact strength, higher biodegradation rate, higher flexibility, higher elongation, lower tensile strength, and melting point [183]. PBSA is relatively more expensive than other biopolymers, so to decrease its price and to improve PLA's toughness and processability, PBSA and PLA have been blended.

PLA/PBSA blends have been reported to be immiscible [184–187]. Adding PBSA reduced the stiffness and improved toughness, strain hardening, and flexibility of the blends (Table 14.3), as well as maintained flexibility during aging [186, 187]. PBSA/PLA blends exhibited lower thermal stability and greater decomposition activation energy compared with the individual polymer components [186].

Aliotta et al. [184] investigated PLA/PBSA blends up to 40% PBSA content using a twin-screw extruder followed by injection molding. The elongation at break increased as a function of PBSA content in the blends. They reported that PLA-PBSA 80/20 and 60/40 blends had 86.7 and 192.8% elongation, respectively, with the stress at break also showing an inverse relationship with PBSA content. However, only a minor increase in the stress at break for 40% PBSA content was observed as compared with the 80/20 blend, which was ascribed to the change from droplet to co-continuous morphology. A similar morphological change was reported by other researchers for 40% PBSA content. To compatibilize the blends, 2% Joncryl® ADR 4468 epoxy oligomer (EO) was added to the 80/20 and 60/40 blends, resulting in reduced interfacial tension and increased adhesion. The compatibilizer reduced the melt flow rate (MFR) and increased torque values recorded during extrusion processing due to reactive extrusion, which increased branching, molecular weight, and entanglement density. Figure 14.13 a and b show the MFR and torque, respectively, as a function of PBSA content with or without EO.

Other researchers [188, 189] have also reported compatibilized super tough PLA PBSA blends prepared by in situ reactive extrusion using active epoxy oligomers, for extending chains and introducing branches, increasing the melt strength

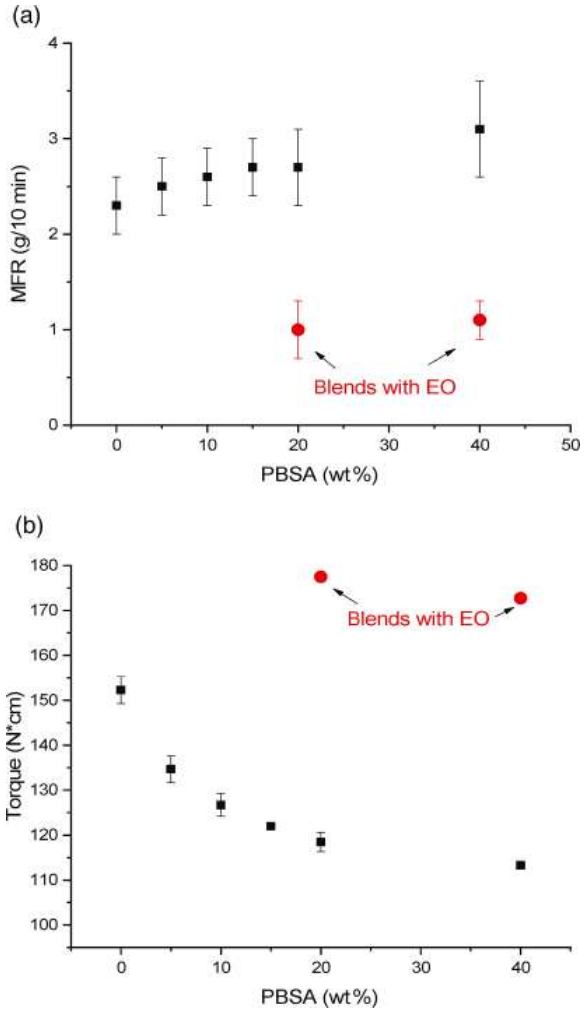


**FIGURE 14.13** (a) Trend of MFR as a function of PBSA content; (b) trend of torque as a function of PBSA content [184]. Reproduced under the Creative Common CC BY 4.0.

and thermal stability. Ojijo et al. [188] reported that with addition of 0.6 wt% multifunctional epoxy-based Joncryl ADR 4368 chain extender in a PLA/PBSA 60:40 blend, the droplet size of the PBSA decreased from 2.69 to 0.7 µm, indicating improved compatibilization, and impact strength increased (38.4 kJ/m$^2$) along with greater flexibility (elongation ~179%).

Suwanamornlert et al. [190] prepared PLA/PBSA 70/30 blends with 3 and 6% thymol for retarding fungal growth in packaged food. The films containing 6% thymol demonstrated effectiveness against growth of *Aspergillus* spp. and *Penicillium* spp. for the tested 24-day period. The addition of PBSA and thymol decreased the $T_g$, $T_m$, oxygen, and gas barrier properties of PLA due to increased chain mobility and the plasticization effect of thymol.

#### *14.3.3.5 Poly(Butylene Succinate-co-L-Lactate)/PLA Blends*

Poly(butylene succinate-*co*-L-lactate) (PBSL), an aliphatic copolymer composed of 1,4-butanediol and succinic and

L-lactic acid, with 3% lactate content, has been produced under the trade name of GS PLA by Mitsubishi Chemical Co., Ltd., Japan [178, 191, 192]. PBSL has a $T_g$ of −20°C and $T_m$ of 110°C. Tensile strength, Young's modulus, and elongation at break of PBSL engineering thermoplastics are 3 MPa, 1.8 GPa, and 5%, respectively, and the corresponding properties of PBSL film are 55 MPa (tensile strength at yield), 0.55 GPa, and 450%, respectively [191]. The improved performance of film could be ascribed to orientation of polymeric chain. PBSL/PLA blends are immiscible and a morphology of PBSL domains dispersed in a PLA matrix was observed with a high amount of PLLA (60%) [178, 192–195]. As expected, increasing the amount of ductile PBSL reduced strength and stiffness (strength and tensile and flexural modulus) and promoted flexibility (elongation at break) and toughness of PBSL/PLLA blends compared to PLLA [178, 193, 194]. Chou et al. [195] blended PLLA with 25 and 75% PBSL using melt blending. Partially immiscible blends with two $T_g$s with reduced brittleness and improved toughness were reported. Annealing the blends improved the flexural modulus of PLLA/PBSL blends. The thermal stability and MFI (melt flow index) of these blends gradually increased with PBSL content; with 30 wt% PBSL, the blend had thermal stability higher than that of neat PLLA over the whole tested temperature range [194]. An increase of PBSL content also enhanced cold crystallization and both isothermal and non-isothermal crystallization of PLLA [178]. In addition, PBSL behaved as an effective nucleator below 120°C [193]. Shibata et al. [178] and Vilay et al. [194] compared the properties and characteristics of PBSL/PLLA blends with PBS/PLLA and PCL/PLLA blends. They reported that PBSL was more effective in promoting the crystallization of PLLA and increasing the elongation at break than PBS. Furthermore, PBSL/PLLA blends exhibited slightly higher mechanical and thermal properties than PCL/PLLA blends [178, 194]. The use of 2 wt% lysine triisocyanate (LTI) promoted compatibility of the PBSL/PLLA blend (20/80), as observed in the electron microscopy images, by an unclear interface between the two phases, as well as improvement in the impact absorption performance [196].

Nishida et al. [192] studied the effect of 0–6% multifunctional epoxy-based chain extender on the molecular structure, mechanical properties, miscibility, compatibility, and morphology of PLLA/PBSL 70/30 blends. Uncompatibilized PLLA/PBSL blends revealed a sea-island morphology; with the addition of 2% PBSL, the domain size dropped with improved tensile strain, suggesting better miscibility, which was ascribed to grafting. Broader melting peaks indicated an amorphous nature of PLA observed in the compatibilized blend due to chain extension hindering crystallinity. SEM images, shown below in Figure 14.14, revealed 1–5 μm PBSL droplets in the uncompatibilized blends, which decreased to 0.5 μm for blends with 2% chain extender and further disappeared for blends with 6% chain extender, suggesting miscible blends.

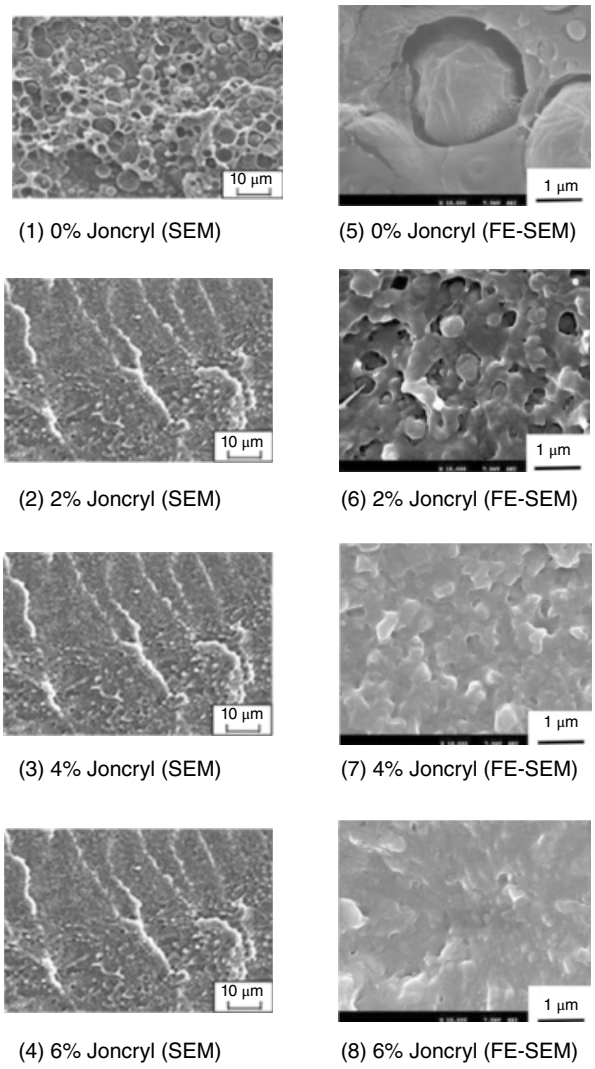


**FIGURE 14.14** SEM and FE-SEM images of the cryo-surfaces of the PLLA/PBSL blends at high magnification. *Source:* Reprinted from Ref. 192. Copyright 2021, Reproduced with permission from Elsevier.

***14.3.3.6 Poly(Butylene Succinate-co-Butylene Carbonate)/PLA Blends*** Poly(butylene succinate-*co*-butylene carbonate) (PBS-*co*-BC) or PBSC or polyester carbonate (PEC) is an aliphatic random copolymer composed of butylene succinate units and butylene carbonate units. It has a $T_g$ of −26°C, $T_m$ of 106°C, and similar properties to PP and PE, which can be tailored by controlling the ratio of carbonate content. It has been synthesized by Mitsubishi Gas Chemical Company [197, 198]. Miscible PLLA/PEC blends with interpenetrated spherulites (IPS), with PEC spherulites inserted into the interfibrillar regions of edge-on lamellae in the PLLA spherulites, were reported [197]. Various

researchers have credited IPS formation to simultaneous crystal growth. Various investigators have suggested that in general the polymer with higher $T_m$ generally crystallizes first, significantly impacting the crystallization behavior of the second polymer in the blend [199]. It can spatially restrict the second polymer. Polymers with similar melting points are more likely to crystallize simultaneously, exhibiting an IPS structure [197]. Another study reported miscibility of solvent cast semicrystalline PEC and semicrystalline PLLA blends, with a single $T_g$, which fit the Fox equation [200]. The growth rate of PEC spherulites was faster than that of PLLA spherulites [200].

***14.3.3.7 Poly(Glycolic Acid)/PLA Blends*** Poly(glycolic acid) or poly(glycolide) (PGA) is a biodegradable linear aliphatic polyester that can be obtained from fossil or bio-derived resources [201]. It is synthesized by polycondensation of glycolic acid or ring-opening polymerization of glycolide [202]. PGA has a $T_g$ and $T_m$ of 35–40 and 220–230°C, respectively. It has high HDT and a tensile modulus of 7.0 GPa. Due to its stereoregularity, it has high crystallinity, around 45–55%, which makes it a high barrier material insoluble in various organic solvents [202–204].

Its high water sensitivity makes it relatively low hydrolytic stable, which results in fast molecular and mechanical performance degradation making it suitable for medical applications including sutures, implants, and drug delivery [203]. However, its water sensitivity and fast degradation can be controlled by blending with PLA. These characteristics make it suitable for use in the biomedical area for tissue regeneration, surgical applications, and drug delivery. However, due to the limiting factors of fast degradation of PGA and a high $T_m$, blending of PGA and PLA is a choice for slowing down its degradation since PLA has a longer degradation period, and the blend may have a lower $T_m$ [204].

You et al. [205] prepared PGA-PLA electro-spun fibers composed of various ratios (90/10, 70/30, 50/50, and 30/70) solution blended in 1,1,1,3,3,3-hexafluoro-2-propanol (HFIP) solvent. Phase-separated immiscible blend fibers were obtained due to the crystalline structure of the components. A co-continuous phase morphology, with a circular and homogeneous pore size distribution, was observed during SEM studies after chloroform extraction of PLA.

Pandey et al. [206] claimed that microwave radiation was a clean, fast, and effective way of blending. Blends were produced with PGA/PLLA ratios of 33/67, 50/ 50, and 67/33 in chloroform and then subjected to radiation. The chloroform helped maintain the temperature of the process and was quickly evaporated. The resulting blends were compatible, especially the 50/50 blend, as determined by FTIR, $^1$H NMR, and DSC. The blends had linkages between the carboxylic acids of PGA and PLLA (according to FTIR). In addition, the blends mostly had one $T_m$. The linkages of the two polymers, which were determined by the $CH_2$ peak absorption, showed that the blends were actually copolymers.

In another work, You et al. [207] investigated the degradation behavior of PLA and PGA blends. The in vitro degradation of 90/10 and 70/30 ratios of PGA to PLA after eight days resulted in the production of short fragments due to the fast degradation and low molecular weight of PGA, while the degradation of ratios of 50/50 and 30/70 PGA/PLA did not significantly change. Furthermore, after 35 days, the 90/10 PGA/PLA ratio had a weight loss of approximately 60%, whereas less than 20% was lost in the 30/70 ratio PGA/PLA.

***14.3.3.8 Poly(Lactic-*co*-Glycolic Acid)/PLA Blends*** Poly(lactic-*co*-glycolic acid) (PLGA) is a biodegradable linear aliphatic copolymer of lactic acid units and glycolic acid units. PLGA is obtained by random ring-opening copolymerization of those units with catalysts such as $Sn(Oct)_2$. Mechanical, functional, and physicochemical properties depend upon lactic acid content (varies from 50 to 95%); the structures appear to be amorphous rather than crystalline with $T_g$ of 40–65°C [208]. PLGA, widely studied for drug delivery applications, is susceptible to hydrolytic degradation as observed with other aliphatic polyesters [209]. Although enzyme-catalyzed degradation mechanisms have been proposed, they have not been supported by any strong evidence [210]. The hydrolytic degradation results in the formation of the constituent monomeric units of the polymer. As both monomers are byproducts of metabolic pathways in organic bodies and have no adverse health impacts, it is suitable for biomedical applications. The hydrolytic degradation rate is dependent upon various factors including crystallinity, molecular weight, microsphere diameter or surface area, water diffusivity or hydrophilicity, chemical composition, including glycolic acid content, among others [210]. It is expected that higher glycolic acid content leads to faster degradation. However, the 50:50M ratio of lactic acid glycolic acid demonstrated the fastest degradation, potentially due to low crystallinity. Thus, by controlling the molar ratio of two monomeric units, the degradation rate and the drug release rate can be controlled for various therapeutic applications [211].

Carmagnola et al. [212] reported solvent cast PLLA-PLGA immiscible binary blends with a two-phase morphology and two $T_g$s. in vivo tests were performed to understand the inflammatory response, which was affected by degradation rate. Molecular weight changes were measured every two weeks up to eight weeks; a faster degradation rate was observed for 75/25 PLLA/PLGA blends compared with PLLA, particularly after fourth week. In blends, faster PLGA phase degradation created a porous surface on the samples.

PLLA-PLGA microspheres have been studied for drug delivery applications. However, microspheres have a high initial release rate of encapsulated active pharmaceutical

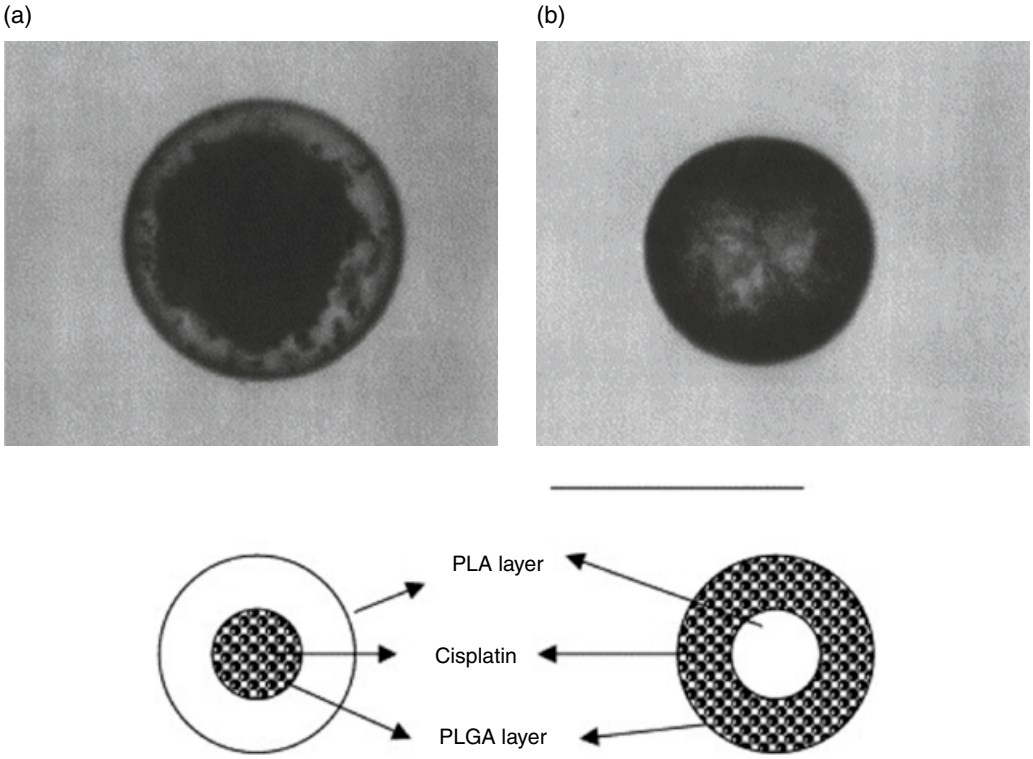


**FIGURE 14.15** Optical microphotograph of the typical multi-reservoir-type microsphere: (a) Type A, localization of drug powder in internal layer; (b) type B, localization of the drug powder in external layer. The length of a bar indicates 50 μm. *Source:* Reprinted from Ref. 213. Copyright 2005, Reproduced with permission from Elsevier.

ingredients (APIs), which can cause side effects. Matsumoto et al. [213] reported two-phase PLGA/PLA blends. The API were included in the PLGA phase and the release kinetics of API depended on the phase morphology. With higher PLGA content, the PLA became the dispersed phase and the model drug Cisplatin was located in the outer wall, whereas as with greater PLA content, the drug was in the inner PLGA part of microsphere, as shown in Figure 14.15. The dark area is Cisplatin localized in the PLGA phase. The microsphere on the left side of the figure, which has PLGA and the model drug inside, had a lower release rate than the one on the right. Blanco-Prieto et al. [214] reported similar results.

For biomedical applications, a microsphere of a 50/50 PLGA/PLA blend was used to deliver timolol maleate, which is an active drug ingredient for minimizing elevated intraocular pressure (IOP) causing glaucoma. The material was able to continuously deliver the drug for 107 days [215]. The control release property of these systems is strongly affected by many factors such as copolymer composition, molecular weight, and nature of the chain end groups. The chain end groups in PLA and PGA are hydroxyl and carboxyl groups, which are called uncapped polymer types, or if the carboxyl groups are esterified, these polymers are called capped. Blanco-Prieto et al. [214] found that a microsphere with 50/50 PLGA/capped PLA had a lower release rate and lower initial burst than the same ratio blend with uncapped PLA due to the lower hydrophilicity of the capped PLA. This, in turn, lowered the degradation rate.

### 14.3.4 Aliphatic–Aromatic Copolyesters

***14.3.4.1 Poly(Butylene Adipate-co-Terephthalate)/PLA Blends*** Poly(butylene adipate-*co*-terephthalate) (PBAT), a mostly fossil-derived linear random co-polyester, is obtained by modification of poly(butylene terephthalate) (PBT), an aromatic polyester, with an aliphatic BA unit (1,4-butanediol and adipic acid monomers) [216, 217]. The aliphatic fraction provides biodegradability, while the aromatic fraction offers useful performance properties; thus, the desired mix of those properties can be achieved with 35–55 mol% of terephthalic acid (aromatic dicarboxylic acid) [218–220]. PBAT has a moderate $T_m$ (110–125°C) and low $T_g$ (−35 to −25°C). The high toughness and high flexibility (ultimate elongation at break 700%), along with biodegradation, makes PBAT a good candidate for toughening PLA for various industrial applications including packaging [217, 218, 220–222]. The large difference in solubility parameters between PBAT (22.95 $cal^{0.5}/cm^{1.5}$) and PLLA (10.1 $cal^{0.5}/cm^{1.5}$) indicates immiscibility of this polymer pair [223, 224].

Gigante et al. [225] blended PLA with PBAT and observed a droplet morphology with droplet size ranging from 0.1 to 1 μm for PBAT content ranging from 10 to 25%. The small PBAT droplet size along with good interfacial adhesion improved the elongation of PLA to around 300 and 350% for 20 and 25% PBAT content; similar elongation numbers have been reported by other researchers along with improved notched Izod impact toughness [226]. Above 30% the particle size significantly increases due to coalescence, leading to weaker structures and co-continuous structure was reported for 50 : 50 PLA/PBAT blends [227]. As expected, a drop in the tensile modulus and tensile strength was observed as a function of PBAT ratio [226, 228]. The onset of cold crystallization, % crystallinity, $T_g$, and $T_m$ decreased as PBAT content increased [228]. The toughening mechanism of PLA/PBAT blends could be explained by a cavitation process initiated due to debonding at the interface of the two polymers, observed by SEM, as elaborated in some of the other sections of this book chapter [229]. PLA and PBAT exhibit non-Newtonian fluid behavior (shear thinning), while PBAT has a higher steady shear viscosity and higher melt elasticity at low frequencies [229, 230]. Thus, the incorporation of PBAT resulted in increasing melt elasticity of PBAT/PLA blends [230]. The addition of PBAT led to reduction of the Newtonian region, flow index ($n < 1$, indicating stronger shear-thinning behavior), and flow activation energy of the polymer pair [230]. MFR of PLA increased with an increase in the PBAT content [225]. PBAT/PLA blends exhibited a lower shear viscosity at higher shear rates than PLA. The flexible PBAT molecular chains also broadened the processing temperature range and helped improve processability of PLA in extrusion [229, 230].

The oxygen and water vapor permeability coefficients of PLA/PBAT blends, critical for various food packaging applications, increased with the addition of PBAT [231]. The increase in the permeability was associated with the addition of flexible PBAT to glassy PLA, which increased the chain mobility and free volume. The oxygen and water vapor permeability coefficients of plastic film composed of various blend ratios are presented in Table 14.4.

Compatibilizers or plasticizers have been used to improve the miscibility of these immiscible binary blends. Plasticization of PBAT/PLA blends (comprised of 10–25 wt % PBAT) with acetyl tributyl citrate (ATBC) (from 5 to 30 wt %) decreased $T_g$, $T_c$, and $T_m$ and increased the degree of crystallization (up to 6%), gas and water vapor permeabilities of the blends, and the diameter of the PBAT dispersed phase [232]. Compared with the PBAT/PLA blend (25/75) alone, adding ATBC significantly decreased tensile modulus (from 1.94 to 0.06 GPa) and tensile strength (from 38 to 18 MPa), but highly increased elongation at break (from 47 to 250%) [232]. Compatibilization of PLA/PBAT 70/30 blends by transesterification using tetrabutyl titanate (TBT) during reactive melt-extrusion processing was reported by Lin and others [233]. Elongation at break and impact strength of PLA/PBAT 70/30 blend increased from ~65 to 298% and 5 to 9 kJ/m$^2$, respectively, with addition of 0.5% TBT. SEM images of impact fractured surface indicated a decrease in the dispersed phase size (PBAT) to 0.5 μm with addition of 0.5% TBT [233].

**TABLE 14.4 Oxygen and water vapor permeability coefficients of the films [231]**

| | P $O_2$ ([cm$^3$.mm. m$^{-2}$.d$^{-1}$.bar$^{-1}$)] | P $H_2O$ ([g.mm.d$^{-1}$. m$^{-2}$)]* |
|---|---|---|
| PLA | 33.4 | 1.3 |
| PLA PBAT 80 20 | 40.9 | 1.4 |
| PLA PBAT 60 40 | 50.3 | 2.8 |
| PLA PBAT 40 60 | 61.9 | 2.9 |
| PLA PBAT 20 80 | 71.8 | 3.0 |
| PBAT | 84.0 | 3.1 |

*Note: Oxygen barrier properties were measured at 23 °C. Water barrier properties were measured at 23 °C and 50% of relative humidity.

To improve compatibility of PBAT and PLA (comprised of 10–40 wt% PBAT), 1–10 wt% of a reactive agent—a random terpolymer of ethylene, acrylic ester, and glycidyl methacrylate (T-GMA, $M_w$ = 240,000 g/mol, GMA content = 8%, LOTADER, ARKEMA Corp.) was incorporated during extrusion melt blending [234]. T-GMA increased the complex viscosity, impact strength, elongation at break, and toughness without a severe reduction of tensile strength. A finer phase structure, decrease in shear-thinning tendency, and only slight effects on thermal properties (increased $T_c$, decreased $T_m$ and degree of crystallinity) of PBAT/PLA blends were also observed with the incorporation of T-GMA [234].

Ma et al. [235] in situ compatibilized PLA-PBAT blends using 0.1–1% dicumyl peroxide (DCP) to initiate reaction between PLA and PBAT molecules, producing PLA-*g*-PBAT copolymers. The compatibilized interface reduced PBAT domain size and improved interfacial adhesion. Copolymerization reactions generated a branched network structure, which increased complex viscosity and storage modulus ($G_0$) as a function of DCP content. Consequently, the compatibility of the two components improved, which was reflected in reduced PBAT domain size, as shown in Figure 14.16, and enhanced interfacial adhesion leading to improved notched Izod impact toughness from 60 to 110 J/m. Toughness increased up to 0.6% DCP content due to cavitation of the matrix at the interface and an ideal dispersed phase domain size.

Al-Itry et al. [19] studied in situ compatibilization of PLA-PBAT blends using 0.25 and 0.5% Joncryl ADR EO. In binary uncompatibilized PLA-PBAT 80/20 blends, the elongation at break increased to 50% compared to brittle PLA (~14%). With the addition of 0.25 and 0.5% compatibilizer, the elongation at break further improved to 116 and 135%, respectively. The reduced brittleness was ascribed to ester linkages developed between PLA and PBAT due to EO. Detailed rheological analysis supported the formation of PLA-EO-PBAT at the interface.

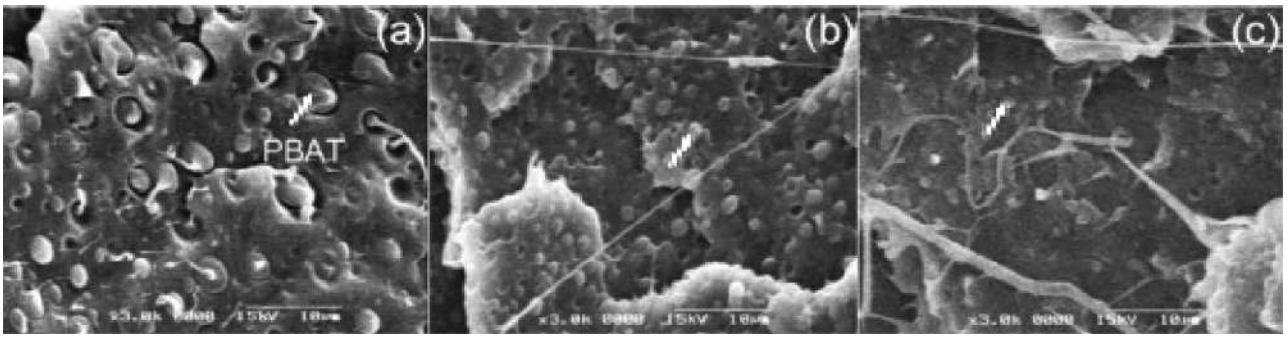


**FIGURE 14.16** SEM images (scale bar = 10 μm) of cryo-fracture surfaces of the PLA/PBAT (80/20) blends with DCP content of (a) 0 wt%, (b) 0.1 wt%, and (c) 0.5 wt%. The PBAT domains are indicated by arrows in the images. The number average diameters of the PBAT domains in the (a), (b), and (c) samples are 1.05, 0.63, and 0.52 μm, respectively. *Source:* Reprinted from Ref. 235. Copyright 2014, Reproduced with permission from Elsevier.

***14.3.4.2 Poly(Tetramethylene Adipate-co-Terephthalate)/PLA Blends*** Poly(tetramethylene adipate-*co*-terephthalate) (PTAT or PTMAT) is a petrochemical-based, aliphatic–aromatic co-polyester-modified from PBAT [236]. It is produced by reaction of tetramethylene glycol and adipic and terephthalic acids [236]. PLLA was solution blended with PTAT to improve its hydrophilicity and processability to levels comparable with PLGA [237]. This polymer pair was predicted to be miscible since PLLA and PTAT have similar solubility parameters of 19.70 and 19.83 $J^{0.5}/cm^{1.5}$, respectively. DMA testing revealed the characteristic two $T_g$s of each polymer in solution-cast films of PTAT/PLLA blends (25/75, 50/50, and 75/25), and an increase of PTAT was found to decrease $T_m$ and crystallinity of the blend films, as determined by DSC. The height mode roughness of the solution blend films determined by AFM was in the order of PTAT/PLLA 50/50 > PTAT/PLLA 25/75 > PTAT/PLLA 75/25 (37.39, 27.66, and 25.71 nm, respectively). The mechanical properties of PTAT/PLLA blends are shown in Table 14.3 [237].

### 14.3.5 Elastomers and Rubbers

***14.3.5.1 Natural Rubber and Epoxidized Natural Rubber PLA Blends*** Natural rubber (NR), a renewable bioresource, has been studied to improve the elasticity and compatibility of PLA due to its unique combination of toughness, biodegradability, biocompatibility, and low cost. However, as evident from the difference in their solubility parameters PLA (10.1 $cal.cm^{-31/2}$) and NR (7.75 $[cal.cm^{-31/2}]$), they are incompatible [238]. At low NR concentration, dispersed rubber droplet morphology has been observed since the NR concentration increases droplet coalescence. Bitnis et al. [239] reported that PLA blended with 10% NR provided optimal toughening performance compared with other PLA-NR compositions. Compatibilized and epoxidized rubber (ENR) have been widely used to increase surface adhesion, reduce droplet coalescence, and decrease the droplet size of dispersed rubber phase for enhanced toughness [240].

Epoxidized natural rubber (ENR), having higher reactivity and better mechanical properties than NR, could be a good candidate to toughen PLLA since compatibility between the polymer pairs could be generated via interaction of the epoxy group from the ENR and the ester group from PLLA [241]. However, the naturally occurring proteins of ENR may prohibit formation of ester linkages between epoxy and ester groups. Therefore, NR (high ammonia NR latex) was modified by deproteinization, epoxidization with peracetic acid, and depolymerization to produce liquid deproteinized natural rubber with epoxy groups (LEDPNR) [241]. For comparison, liquid natural rubber having epoxy groups (LENR) was prepared following the LEDPNR modification method except for the deproteinization. LEDPNR or LENR, containing around 43 mol% epoxy, was solution-blended with PLLA at a ratio of 40/60. The slight changes in $T_g$s of the blends (an increase in LEDPNR or LENR's $T_g$ and a decrease of PLLA's $T_g$) and a small reduction in the PLLA's $T_m$ were more obvious with LEDPNR/PLLA blends than with LENR/blends. $^{13}C$ nuclear magnetic resonance (NMR) spectra revealed the existence of an ester linkage peak only when the LEDPNR/PLLA blend underwent a heat treatment of 200°C for 20 min after mixing [241].

Nematollahi et al. [240] studied PLA-NR and PLA-NR-ENR. Elongation of PLA improved from 4.89 to 72.01% with the addition of 10% NR. The elongation at break further improved to 223% for PLA/NR/ENR (90 : 7 : 3) ternary blends. The improvement in flexibility and toughness of blends was achieved with 20–25% sacrifice in both tensile strength and modulus of the blends. The increased flexibility was supported by the compatibilization effect of ENR, due to polar groups and $\pi$–$\pi$ interactions produced by the unsaturated groups, resulting in decreased rubber droplet size, with average particle size of 0.92 μm, and uniform

distribution, as observed in the SEM images. Increased plastic deformation was also ascribed to the cavitation mechanism due to debonding of the rubber particles at the interface of the PLA and rubber particles.

Bijarimi et al. [242] evaluated PLA/ENR blends with varying composition of NR and Liquid NR (LNR) and lower $M_w$ NR prepared by photooxidation to evaluate their effect on morphology and compatibility. In all the blends, the PLA ratio was maintained at 40% with 5–15% NR or LNR with the balance of ENR. For PLA/ENR/NR 40/55/5 blends, tensile strength and elongation improved by 47 and 300%, respectively, compared with PLA/ENR 40/60 blends, which was ascribed to improved dispersion and compatibility. On the other hand, the addition of NR decreased the tensile strength of the blends.

***14.3.5.2 Polyamide Elastomer/PLA Blends*** Polyamide elastomer (PAE), a thermoplastic elastomer, is a biodegradable polyether block amide comprised of polyamide-12 (PA) (22 wt%) and poly(tetramethylene oxide) (78 wt%) as the hard and soft segments, respectively [243]. It was expected that the polyether segment would be compatible with PLA, and PA can form hydrogen bonds with PLA, enhancing the compatibility between PAE and PLA. The incorporation of PAE (5–30 wt%) resulted in a significant increase of elongation at break (from 5.1 to 367.2%) and decrease of tensile strength (from 46.8 to 24.6 MPa) compared to pristine PLA. An increase of PAE content reduced the $T_g$s of PLA and PAE and $T_c$ of the blends. Interestingly, PAE/PLA blends exhibited a shape memory ability after high deformation, which was also reported in chitosan/PLLA blends [244]. According to Zhang et al. [243], the inherent brittleness of PLA limits its shape memory ability. By blending with 10 wt% PAE, the deformed specimens after stretching to 100% strain can reform to the original shape within 3–8 s after heating at 80–90°C, with retention of 92% of the original mechanical properties.

Gug et al. [245] studied PLA/PA-11 50/50 blend catalyzed using 0.5% *p*-toluenesulfonic acid (TsOH) for improving compatibility due to an ester-amide exchange reaction; however, the catalyst leads to degradation. To stabilize the molecular weight, 2–6% tris (nonylphenyl) phosphite (TNPP) as a coupling agent was added during processing. The effect of catalyst, stabilizer, and processing parameters (screw speed: 250–2000 rpm) on the morphology, mechanical performance, and degradation behavior of the blend was observed. All compositions contained PA11 droplets dispersed in the PLA matrix, TNPP stabilized uniform droplet size and prevented coalescence at 250 rpm. However, at 2000 rpm degradation was reported in both polymers. The blend with 4% TNPP and 0.5% TsOH demonstrated >10% improvement in both tensile strength and Young's modulus as compared with the unmodified PLA/PA11 50/50 binary blend.

***14.3.5.3 Poly(Ether)Urethane Elastomer/PLA Blends*** Poly(ether)urethane (PU) elastomer is a biodegradable thermoplastic elastomer where the soft segment is a polyether, which generally possesses good low-temperature properties [246]. Blends of PLA and PU elastomer (5–30 wt%) exhibited changes in thermal and mechanical properties that were similar to PAE/PLA blends [247]. In addition, PU elastomer reduced the crystallinity of PLA. Compared with PLA, PU elastomer/PLA blends had lower tensile strength (from 65 to 31.5 MPa) and greater elongation at break (from 4 to 363%) and impact strength (from 64 to 315 J/m$^2$) (Table 14.3) [247].

Zhang et al. [248] compatibilized a PLA/ thermoplastic polyurethane (TPU) blend with 0–4% polyurethane elastomer prepolymer (PUEP) via melt-blending reactive extrusion. In all blend compositions, the PLA fraction was maintained at 70 wt%. With an increase in the PUEP content, impact strength and elongation at break increased without any statistically significant change in the tensile strength. For the PLA/TPU/PUEP 70/26/4 blend, impact strength and elongation increased by ~80 kJ/m$^2$ and ~90%, respectively, compared with ~10 kJ/m$^2$ and 15% reported for the PLA/TPU 70/30 blend, which was accredited to a decrease in the TPU particle size from 2 to 1 μm with the addition of PUEP compatibilizer. No significant change in thermal properties including $T_{cc}$ and % crystallinity were observed, which indicates improved mechanical performance is primarily linked to morphological changes leading to shear yielding, crazing, and cavitation.

***14.3.5.4 Poly(ε-CL/L-Lac)/PLA Blends, Polytrimethylene Carbonate/PLA Blends, and Poly(TMC/ε-CL)/PLA Blends*** Hydrolytically degradable rubbers (i.e., poly(ε-CL/L-lactide (L-lac), polytrimethylene carbonate (PTMC), and poly (trimethylene carbonate (TMC/ε-CL)) were synthesized and solution blended with PLA [249]. Due to differences in the Fedors solubility parameters-PLA 22.75 J$^{0.5}$/cm$^{1.5}$, PTMC 21.47 J$^{0.5}$/cm$^{1.5}$, poly(TMC/ε-CL) rubber 21.09 J$^{0.5}$/cm$^{1.5}$, and poly(ε-CL/L-lac) rubber 21.49 J$^{0.5}$/cm$^{1.5}$, PLA/rubber blends should form immiscible blends, confirmed by the presence of two $T_g$s in the blends. To investigate the effects of matrix crystallinity on impact and tensile strengths, PLAs composed of different LLA/DLA ratios (PLLA, PDLLA (95/5), and PDLLA (50/50)) were blended with poly(ε-CL/L-lac) rubbers (0–30 wt%). Poly(ε-CL/L-lac) rubber had a $T_g$ around −28°C, and the relatively long sequence of LLA segments was capable of crystallization. Incorporation of poly(ε-CL/L-lac) rubber dramatically increased the Dynstat unnotched impact strength and significantly decreased the tensile strength of the blends, with the order PLLA > PDLLA (95/5) > PDLLA (50/50). Annealing of poly(ε-CL/L-lac)/PDLLA (95/5) blends at 90°C for 30 min slightly increased tensile and impact strengths and heat of fusion, indicating strong phase separation [249]. To enhance the toughness of

amorphous PDLLA (85/15), poly(TMC/ε-CL) rubber, an amorphous high-molecular-weight copolymer with a very low $T_g$ (−43°C), and PTMC, a semicrystalline, low-molecular-weight polymer with $T_m$ of 36°C and $T_g$ of 20°C, were introduced into PDLLA (85/15) [249]. The addition of 20 wt% rubber resulted in nonbreakable materials (determined by the Dynstat unnotched impact test), Izod impact strengths of 52–63 (with PTMC) and 293–520 J/m (with poly(TMC/ε-CL)), tensile strengths of 39.2 (with PTMC) and 36 MPa (with poly(TMC/ε-CL)), and elongation at break of 40 (with PTMC) and 130% (with poly(TMC/ε-CL)). Another approach to improve the interfacial adhesion in the blend and reduce the particle size of the dispersed phase is segmented block copolymerization. The blend of PDLLA (85/15) with 20 wt% triblock copolymer (composed of D,L-Lactide (DLLA) (85/15)/ TMC/DLLA (85/15)) exhibited tensile and Dynstat impact strengths similar to that of the poly(TMC/ε-CL)/PDLLA blend but had greater elongation at break (280%). The mechanical properties of those blends are comparable to acrylonitrile–butadiene–styrene copolymer (ABS) nonbreakable by the Dynstat unnotched impact test, 258 J/m Izod notched impact strength, and 33 MPa tensile strength [249].

### 14.3.6 Poly(Ester Amide)/PLA Blends

Polymers containing both ester and amide groups in the repeating unit are categorized as poly(ester amide)s (PEA). Ester groups are hydrophobic, while amides are hydrophilic. The presence of both groups in a single chain can help in utilizing PEA in a variety of applications. They are generally popular in biomedical applications because of their biodegradable and nontoxic nature. They can be metabolized by living tissues. PEA can be categorized as saturated PEA, unsaturated PEA, and hyperbranched PEA (HBP). Unsaturated PEAs can cross-link with other molecules, especially vinyl polymers. Unsaturated PEAs are relatively more hydrophobic than saturated PEA [250].

HBP has recently received lot of attention because of its ability to significantly modify the rheology of polymers. The high reactivity of these three-dimensional dendritic molecules can be related to the presence of many peripheral terminal functional groups. HBP has high solubility, low melt viscosity, and is biodegradable [250]. Its use can help to improve the stiffness and toughness of polymers through melt blending or reactive extrusion. PLA modified with HBP is reported to have lower $T_g$ than the neat polymer [251]. Lin et al. [251] blended PLA with HBP and observed that adding a small amount of HBP (2.5%) resulted in a significant decrease in the complex viscosity of PLA. This has been ascribed to a decrease in the entanglement and increase in the free volume of the blends. Crystallization of the blends increased compared with neat PLA. PLA, HBP/PLA (2.5/97.5), and HBP/PLA (10/90) had 20, 31, and 34.9% crystallinity, respectively. The blends demonstrated significant improvement in elongation at break compared with neat PLA. Zhang et al. [252] melt-blended PLA with HBP up to 20% HBP in the PLA matrix. FTIR results support intermolecular hydrogen bonds between PLA and HBP, which restricts the mobility of PLA. The miscibility of HBP in PLA decreased with an increase in the concentration of the HBP. DSC thermograms showed two $T_g$s for compositions containing 10% or more HBP in the PLA matrix. Good miscibility was found below 10% concentration. The blends showed significant improvement in stiffness and toughness compared with neat PLA. The dispersed HBP in the PLA improved the mechanical properties. However, at 15 and 20% HBP concentrations, the mechanical properties sharply dropped, which was attributed to cavities of a wide distribution of size and shape that were present in the HBP phase.

### 14.3.7 Polyethers and Copolymers

***14.3.7.1 Poly(Ethylene Glycol)/PLA Blends*** Poly(ethylene glycol) (PEG) is a biodegradable hydrophilic thermoplastic with no reported toxic effects [253]. PEG is prepared by oxidation of ethylene with air or oxygen to obtain ethylene oxide, followed by an exothermic polymerization. Depending on its molecular weight, which ranges from 1 to 20 kDa, PEG is a liquid or a wax. In addition, the crystalline polymer, with a $T_g$ of −60 to −75°C, is water soluble across the above-mentioned range of molecular weights. The higher the molecular weight, the lower is the solubility. PEG can be dissolved in acetone, alcohol, benzene, chloroform, and dichloromethane but not in diethyl ether. Currently, PEG is used as a binder, lubricant, carrier, and coating in the food, pharmaceutical, and textile industries [254, 255].

PEG in PEG/PLA blends is used to enhance the hydrophilicity of PLA and to increase its degradation rate and the rate of drug release [253]. Moreover, PEG/PLA blends showed greater strength with lower deformation than PLA. In these blends, PEG acts as a plasticizer for PLA (see also Section 14.4) [256, 257]. PEG/PLA blends can be fabricated by either solution or melt blending [254]. Younes and Cohn [258] reported that solution blends containing more than 20 wt% of either compound can crystallize, and the resulting blends are semi-miscible. Jiang and Schwendeman [259] reported shifts of $T_g$ and $T_m$ in the blends indicating that they were semi-miscible. For melt blending, it was found that adding PEG below 30 wt% to PLA decreased the $T_g$ of PLA from 57 (neat PLA) to 37°C (PEG/PLA of 30/70) [254]. However, when the amount of PEG was higher than 30 wt%, no $T_g$ was found by DSC. Hu et al. [256, 260] reported similar results. Thermographs have shown that PEG is miscible with a single $T_g$, however blends are not stable and phase separation is observed with aging. Baiardo et al. [255] stated that the $T_g$ of the blend decreased

(at the same weight fraction) when the molecular weight of PEG decreased. As PEG content increased from 0 to 30%, a decrease in storage modulus ($E'$) occurred. Inversely, the modulus of the blend increased at PEG contents greater than 30% due to an increase in the PEG crystallinity (PLA100/PEG0, $E'$ = 2.51 GPa; PLA90/PEG10, $E'$ = 2.42 GPa; PLA70/PEG30, $E'$ = 1.75 GPa; PLA50/PEG50, $E'$ = 1.80 GPa; PLA30/PEG70, $E'$ = 1.96 GPa). Similarly, tensile strength and modulus decreased when PEG content increased, while elongation at break increased, especially at lower molecular weights of PEG [254, 255, 257].

Takhulee et al. [261] utilized molecular dynamic and dissipative particle dynamics simulations to predict miscibility using the Flory-Huggins interaction parameter ($\chi$) and radial distribution. Simulations ($\chi$ parameter) indicated miscibility of 10–30 wt% PEG. Experimental results supported miscibility up to 30% PEG in the binary blends. A single $T_g$ was observed for PLA–PEG 90/10, 80/20 and 70/30 blends; phase separation was observed for PEG content >30 wt%, as also reported elsewhere [254, 256, 260].

The degradation of PLA/PEG blends was reported to be higher than that of neat PLA [262]. When PEG content was equal or lower than 30 wt%, the weight loss occurred mainly due to the enzymatic degradation of PLA. Above 30 wt% of PEG, the weight loss mainly occurred due to the dissolution of PEG [254]. Correspondingly, Cai et al. [253] stated that PEG content decreased from the blends because of hydrolysis (buffer solution at pH 7.4, 37°C).

#### *14.3.7.2 Poly(Ethylene Oxide)/PLA Blends*

Poly(ethylene oxide) (PEO) can be described as PEG with a molecular weight greater than 20 kDa. Blends of PEO/PLA can be obtained by solution and melt-blending methods. The resulting blends were immiscible between 35 and 60 wt% of PEO as indicated by the presence of two transition temperatures ($T_g$ and $T_m$), with a lower $T_g$ corresponding to PEO and a higher $T_g$ corresponding to PLA [263, 264]. At lower PEO values (lower than 35 wt%), a single $T_g$ between 33 and 17°C was observed; however, at higher PEO values (higher than 60 wt%), a single $T_g$ between −63 and −78°C was observed. At PEO content of 70, 90, and 100 wt%, crystallinity was observed [263, 265]. Kim et al. [266] added two types of compatibilizers to improve the compatibility of the blends: block copolymers of PEG/PLLA and PVAc. PLLA/PEO blend of 60/40 without the block copolymer compatibilizer was immiscible. When added with the compatibilizer, the blends showed two $T_m$s, one of PLLA and another of PEO. The $T_m$ of PLLA was nearly constant at around 141°C. The $T_m$ of PEO in the PEO/star-shaped PLLA blend shifted to lower temperatures. The addition of PVAc at below 5 wt% levels did not significantly affect the melting temperatures and elongation at break. At the same PVAc content, the tensile strength of the solution blends was higher than that of the melt blends [266]. Ghosh et al. [265] reported the fabrication of porous lamellar PLLA scaffolds using "conventional injection molding of a 50/50 wt% blend of PLLA (69 kDa) and PEO (100 kDa) followed by swelling and Selective Porogen leaching." The 50/50 blend of PEO/PLLA had a biphasic structure, containing a homogeneous PLLA/PEO phase and a PEO-rich phase. The blends were designed to have alternating layers of homogeneous PEO/PLLA phase and PEO-rich phase. The lamellae were continuous in the injection molding flow direction with a thickness of less than 1 μm. Final porosities of the blends were 57–74%, with pore sizes of around 50–100 μm, and tensile elastic moduli were between 580 and 800 MPa. Processing temperature affected the size of the lamellae, the swelling of the pores, the porosity, and the yield strain of the blends. The lower the $T_m$, the thicker were the lamellae, and the lower the swelling, porosity, and yield strain. The viscosity of both neat polymers influenced the morphology of the blend. Defects in the lamellae decreased both the modulus and the tensile strength of the blends [265]. Tsuji et al. [267] produced porous PLLA films by water extraction of PEO from solution-cast PLLA and PEO blend films. Changing the blend ratio and the $M_w$ of PEO controlled the pore size and porosity of the PLLA films. The pore size of the PLLA films increased as the $M_w$ of PEO was augmented.

Li et al. [268] studied the effect of annealing on the morphology of PLA/PEO 80/20 and 50/50 blends using POM and SEM. Samples were annealed at 90, 110, and 125°C. In the control PLA samples, spherulite size increased with increasing temperature. Impact toughness of PLA/PEO 50/50 increased by 300% to 27.6 kJ/m$^2$ after annealing at 125°C, which was accredited to PEO-rich interspherulite sections promoting plastic deformation. Impact strength increased with increase in annealing temperature due to increase in the spherulite size and interspherulite plasticity.

An in vitro degradation study of 50/50 PEO/PLLA found that the blend degraded over a period of 14 days in $KH_2PO_4$—NaOH buffer solution due to diffusion of water and dissolution of PEO, while neat PLLA did not exhibit degradation under these conditions [269]. The phase separation of the blend was more obvious when the blends were in buffer solution than when they were not immersed in the buffer solution. An in vivo study conducted in rats showed that the blend could be used for bone formation [269].

#### *14.3.7.3 Poly(Ethylene Oxide)-b-Poly(Propylene Oxide)-b-Poly(Ethylene Oxide) Triblock Copolymer/PLA Blends*

Pluronic™ is a trade name for poloxamers, which are nonionic triblock copolymers of PEO chains on the two ends of the molecules with a poly(propylene) oxide (PPO) chain in the middle. The PEO chain is hydrophilic, while the PPO chain is hydrophobic. The polymer properties can be tailored

depending on the content ratio of the constituents. Due to the combined hydrophobic and hydrophilic properties in the structure (amphiphilic), it can be used as a stabilizer and a surfactant. It also can enhance miscibility and water absorption of polymers, and it has low toxicity itself. Pluronic has been used in drug delivery devices for controlled release purposes [270].

Blends of Pluronic/PLA are used in controlled release drug systems for reducing the initial burst of drugs, prolonging drug release, and modifying PLA degradation behavior through adjusting the ratio and types of Pluronic in the blend. Blending of the polymers can be achieved by solution blending. Park et al. [271] reported that blends of Pluronic/PLA produced via solution in methylene chloride had gel formation, especially in the Pluronic blend with higher PEO than PPO content. The degree of porosity can be manipulated by varying the Pluronic content. Dissolution of Pluronic from the blend resulted in a distribution of pores in the structure. The Pluronic/PLA blends were compatible and had a lower $T_g$ than neat PLA, demonstrating the plasticizing effect of Pluronic. Lee et al. [272] and Mahoney et al. [273] found greater segregation of the blend on the surface than in the bulk for spun-cast material. The PPO segments appeared predominantly on the surfaces of the material, while the PEO segments were predominantly within the bulk phase [272–274]. This segregation appeared in the blend in all blend compositions, and its degree increased with increasing Pluronic content [273]. Kiss et al. [275, 276] reported that a decrease in contact angle indicated improved wettability for the blends than for neat PLA. They also reported that the concentration of Pluronic on the surface was higher than in the bulk and that the amount of Pluronic on the surface varied with the type and content of Pluronic in the blend [275].

Park et al. [271] found that weight loss of the blends was evident after one week in phosphate-buffered saline (PBS) at pH 7.4 and 37°C. The 70/30 PLA/Pluronic F-108 ($M_w$ = 14.6 kDa and 80 wt% ethylene oxide, soluble in water) blends had weight loss greater than 20%, while 80/20 PLA/Pluronic P-104 ($M_w$ = 5.9 kDa and 40 wt% ethylene oxide, moderate solubility in water) had weight loss of 7.5%. The presence of PEO embedded in the amorphous PLA structure increased the interaction with water. However, the presence of the hydrophobic structure (PPO) and semicrystalline nature of the blend prevented rapid degradation.

In a study of controlled release, BSA, a protein, was used as a model drug. The absorption of BSA in the blend decreased compared with that in neat PLA [275]. With the presence of longer PEO chains in Pluronic, a considerable decrease in BSA absorption was obtained [276]. For controlled release, the incorporation of a greater proportion of hydrophobic component (PPO) than the hydrophilic component (PEO) in the blend enabled the reduction in the initial burst of BSA, a model drug, due to lower water absorption. This led to slower release of the BSA [271].

### 14.3.8 Annually Renewable Biodegradable Materials

***14.3.8.1 Lipid/PLA Blends*** Soybean oil is one of the most important plant triglycerides, comprised of glycerol esterified with around 84% major unsaturated fatty acids (i.e., linoleic, oleic, and linolenic acids) and 16% saturated fatty acids (i.e., palmitic and stearic acids) [277]. The cloud point measurement of binary mixtures of soybean oil ($M_n$ = 880 Da) and PLLA exhibited an upper critical solution temperature (UCST)—all the blends above the critical temperature are miscible in all proportions [278]. The blend of soybean oil and PLLA ($M_n$ = 740 Da) had $\chi_{12}$ of 0.35, indicating thermodynamic immiscibility. Addition of 5 wt% compatibilizer, poly(isoprene-*b*-lactide) block copolymer (ILLA), into melt blends of soybean oil and PLLA increased the amount of incorporated soybean oil in the blends (from 6 to 20 wt%) and induced phase inversion, in which high amounts of PLLA (75–90 wt%) were dispersed in a soybean oil matrix (20–5 wt%). The droplet sizes of dispersed soybean oil decreased, and their size uniformity increased with increasing isoprene volume fraction in the ILLA. In contrast to melt blends, phase-inverted blends induced by ILLA were not observed with solution blends of soybean oil and PLLA [278].

Robertson et al. [279] blended cross-linking polymerized soybean oil and PLLA to increase the toughness of PLLA. Poly(isoprene-*b*-L-lactide), PI-PLLA, block copolymers were used as compatibilizers. Blends of polymerized soybean oil and PLLA of 85 : 15 ratio and 5 wt% PI-PLLA showed tensile toughness as high as four times greater than that of unmodified PLLA.

Epoxidized soybean oil (ESO) is produced via the conversion of the double bonds of soybean oil with peracids or peroxides, resulting in more reactive oxirane or epoxide moieties, promoting chemical reactions [280–282]. ESO is normally used to plasticize and/or stabilize poly(vinyl chloride) (PVC), chlorinated rubber, and PVOH emulsions [245, 246]. The effects of ESO as a PLA plasticizer were reported elsewhere [280–282]. In summary, ESO lowered $T_g$, cold crystallization temperature ($T_{cc}$), $T_m$, enthalpy of cold crystallization ($\Delta H_{cc}$), $\Delta H_m$, tensile strength, and tensile modulus of PLA [259, 264]. The highest elongation at break (38%) was found in a plasticized PLA with 20 wt% ESO [281]. The complex viscosity of the plasticized PLA decreased, whereas the melt strength of the plasticized PLA increased with incorporation of ESO [280, 283, 284].

Lecithin (an amphiphilic phospholipid) was solution-blended with PLLA to improve hydrophilicity and cytocompatibility of PLLA [285]. With 5 wt% lecithin, the solution cast blend film possessed an optimum hydrophilic surface, providing the highest adhesion and proliferation of

mesenchymal stem cells (MSCs) with a very low toxicity toward MSCs [285].

***14.3.8.2 Protein/PLA Blends*** Wheat gluten consists of proteins: gliadin, glutenin, globulin, and albumin [286]. Once plasticized, wheat gluten exhibits good cohesive, adhesive, viscoelastic, and film-forming properties, as well as high gas barrier [287, 288]. The incorporation of wheat gluten reduced the heat resistance and recrystallization of PLA [289]. Compared with PLA melt blended with wheat gluten cross-linked via inter- or intramolecular ε (γ-glutamyl) lysine isopeptidic bonds by using the transglutaminase enzyme (XL gluten), wheat gluten/PLA blends had lower activation energies ($E_a$) measured using DSC, indicating a weaker interference of wheat gluten with the PLA structure as compared with PLA/XL gluten [290]. Furthermore, since a single composition-dependent $T_g$ of XL gluten/PLA blends fitted well with the Kwei equation, these blends were predicted to be miscible [290]. Further research is needed to better understand these blends.

Soy protein concentrate (SPC) is comprised of more than 65% protein and 18–20% carbohydrate, whereas soy protein isolate (SPI) contains more than 90% protein and about 1% carbohydrate [291, 292]. The higher the protein content (mostly globulin) of soy protein materials, the higher is their melt viscosity and hydrophilicity [291, 292]. Thus, preformulated SPI (containing sodium sulfite and sodium tripolyphosphate to improve moisture resistance, lubricant, and plasticizers)/PLA blends had higher viscosity and lower water resistance than preformulated SPC/PLA blends and neat PLA [292]. Compared with the preformulated SPI/PLA blends, the preformulated SPC/PLA blends had a finer co-continuous phase morphology with a low degree of orientation and higher tensile properties. The cold crystallization and crystallinity of PLA in the blends including their Young's modulus was enhanced by an increase of (preformulated) soy protein, but the tensile strength and elongation at break of the blends decreased with an increase in soy protein content [292, 293]. The addition of a compatibilizer, poly(2-ethyl-2-oxazoline) (PEOX), was more effective in promoting tensile strength, elongation at break (Table 14.3), and water resistance of the preformulated SPI/PLA blends than those of the preformulated SPC/PLA blends [292]. The enhancement of tensile properties and water resistance was also observed when sodium bisulfate and methylene diphenyl diisocyanate (MDI) were used to compatibilize the immiscible SPI/PLA blends [293]. However, those compatibilized blends mostly exhibited lower tensile strength and elongation at break with greater Young's modulus than neat PLA [292, 293]. Furthermore, the compatibilized blends had an ultimate water absorption similar to the physical blends [293].

Silk fibroin (SF) is one of the strongest natural fibers and is obtained from the silkworm *Bombyx mori* [294]. It is crystalline, has high molecular weight, and consists of block copolymer-like proteins. It is used in biomedical applications due to its biocompatibility and biodegradability with minimum inflammation (especially when sericin—a glue-like protein—was removed; this process is called degumming) [294, 295]. PLA-SF homogeneous stable macro-phase binary blends were observed in thermal studies with network morphology for PLA/SF 50/50 blends [296].

However, regenerated SF films (degummed SF, which involves a conformational transition from random coil/α-helix to β-sheet during solution casting) in a dry state have poor mechanical properties [297]. Cast solution films of SF/PLA (100 kDa) containing 2–10 wt% PLA, in which PLA is dispersed in an SF matrix, exhibited higher thermal stability compared with SF films because the interactions of SF and PLA induced a conformational transition of SF from silk I (α-helix conformation) to silk II (β-pleated sheet). The hydrophobicity, tensile strength (28–33 MPa), and elastic modulus (3.1–3.5 GPa) of the blends increased and their swelling capacity decreased with an increase in PLA content. Furthermore, the blends had higher elongation at break (6.5–2.2%) than neat polymers. Compared to cast solution PLA film, the biocompatibility (determined by plasma protein absorption) and the growth of L929 mouse fibroblast cells of the blends were improved [297]. Hu et al. [298] reported that a microsphere SF/PLLA blend (50/50) as a porous scaffold to deliver human hepatocellular carcinoma HepG2 cells was more successful than a neat PLA scaffold. They reported that "the hepatocellular compatibility and lower level of inflammatory response make the PLLA/fibroin scaffold a promising candidate for hepatic tissue engineering."

***14.3.8.3 Carbohydrate/PLA Blends*** Thermoplastic konjac glucomannan (TKGM) is a graft copolymer synthesized from konjac glucomannan (KGM) (a high-molecular-weight polysaccharide composed of β-(1–4)-linked D-mannose and D-glucose with a low amount of acetyl groups) grafted with vinyl acetate (VAc) and methyl acrylate (MA) (KGM/VAc/MA: 1/1.6/2.4), using ammonium persulfate as an initiator [299]. Hence, TKGM contains a polyether and a mannose as soft and hard polymer segments, respectively. Melt blends of TKGM and PLA ($M_n$ = 100 kDa) are thermodynamically miscible as evidenced by a single composition-dependent $T_g$ (decreased with increased TKGM), one-phase morphology, and interactions between TKGM and PLA of the blends. The incorporation of TKGM improved the melt strength of PLA, while the melt processing properties of TKGM were improved with addition of PLA. The addition of TKGM between 20 and 80 wt% also decreased $T_m$ of the PLLA in the blends (from ca. 152 to 148°C) and $\Delta H_m$ (from 6.9 to 0.2 J/g) of PLA, lowered tensile strength (from ca. 57 to 10 MPa), and improved impact strength (from 11.9 to 26.9 kJ/m$^2$) and elongation at break (from ca. 14 to 520%) compared with neat PLA. Interestingly, the blends with 80%

TKGM had higher impact strength and the blends containing at least 50% TKGM had higher elongation at break than pristine polymers (Table 14.3) [299].

Chitin or poly(β-[1–4]-*N*-acetyl-D-glucosamine) or poly (β-(1–4)-2-acetamido-2-deoxy-D-glucose), the second most abundant biopolymer after cellulose, is found in insect exoskeletons, shells of crustaceans, cell walls of fungi, microfauna, and plankton [300–302]. It has antimicrobial and film-forming properties [300]. The addition of a small amount of chitin ($M_w$ = 400 kDa) (0–6.0 mmol) increased viscosity of chitin/PDLLA ($M_w$ = 200 kDa) blend solutions and improved processability of PDLLA for nanofibrous electrospinning, as well as thinning and improving the uniformity of nanofiber diameters [300].

Chitosan is formed by alkaline deacetylation of chitin [303, 304]. It is hydrophilic with a weak basic property and more soluble with higher antimicrobial activity than chitin [301, 303]. Considering its biocompatibility, biodegradability, nontoxicity, bioadhesion, chelating and film-forming properties, and its affinity for nerve cells, chitosan is a promising material for biomedical, (active/edible) food packaging, food, and water treatment applications [301, 303, 305, 306]. The cast blend films of the blend solutions (i.e., chitosan (80–85% degree of deacetylation (DDA) dissolved in acetic acid and PLA ($M_w$ = 49 kDa) dissolved in chloroform and then blended) containing 10–30% PLA were immiscible (determined from $T_g$s, FTIR spectra, and tensile moduli) [306]. The addition of PLA enhanced water vapor barrier but decreased tensile properties of the blends. Due to the immiscibility of the blends, their tensile moduli obtained experimentally were much lower than the tensile moduli of miscible blends calculated from the parallel, series, and the Davies models.

Sebastien et al. [307] reported that solution blended films of chitosan (98% DDA)/PLA ($M_w$ = 49 kDa) composed of 10–30% PLA with 16.6% PEG (PEG 400) as a plasticizer had reduced water solubility (35–30%) and moisture absorption and an unexpected increase in water vapor transmission rate (from $1.88 \times 10^{-11}$ kg/m$^2$ s Pa at 10 wt% PLA to 2.52 kg/m$^2$ s Pa at 30 wt% PLA,) with increased PLA content to 30 wt%. The plasticized blend films exhibited antifungal activity against *Fusarium moniliforme, Fusarium proliferatum, and Aspergillus ochraceus* [307]. The use of a two-step solution/extraction method for preparing chitosan ($M_v$ = 1710 kDa and 86.3% DDA)/PDLLA ($M_v$ = 1130 kDa) or PLLA ($M_v$ = 152 kDa) blend membranes resulted in partially miscible blends when the blends were prepared under optimized processing conditions, such as the composition ratio of mixed solvents, as well as the concentrations of component solutions and extraction solvents [308]. The swelling index (SI) increased with the amount of chitosan. A lower thermal degradation temperature was observed with blends containing 50 wt% chitosan.

Meng et al. [244] blended PLLA with chitosan (85% DDA). They also prepared the films similar to Suyatma et al. [306] by first dissolving separately chitosan in acetic acid (1 wt%) and PLLA in chloroform (1 wt%). After the chitosan and PLLA were completely dissolved, the two solutions were mechanically blended by stirring so that a homogeneous solution was prepared. Chitosan/PLLA films were cast onto polytetrafluoroethylene-coated plates. The films were characterized by DSC and DMA. They investigated shape memory effects through field observations. Chitosan was reported to have no obvious influence on the shape fixity ratio but increasing chitosan content decreased the shape recovery ratio markedly, especially at high chitosan content.

Suyatma et al. [306] and Li et al. [309] prepared melt blends of chitosan/PLA at a temperature of 160–180°C. Water sorption and biocompatibility (due to an increase of hydrophilicity) of chitosan/PLA blends increased with increasing chitosan content [305, 309, 310]. Injection-molded specimens prepared from melt-blended 50/50 chitosan (85% DDA)/PLA had lower $T_g$ and $T_c$ than PLA, and lower tensile strength and elongation at break but higher tensile modulus [305]. Currently, the main application of chitosan/PLA blends is in the biomedical area. Different techniques have been used to fabricate scaffolds. For example, melt blending and sodium chloride were used to design the degree and the size of scaffold porosity [309]. The porous membrane scaffolds were prepared by a combination of solvent extraction, liquid–solid separation, and freeze-drying [303, 311]. Nerve conduits for peripheral nerve regeneration were fabricated with a mold casting/infrared dehydration technique, whereas micro/nanofibers from electrospinning were used in a native extracellular matrix for tissue engineering [312]. In summary, the addition of PLA helped provide a finer morphology, reduced beading, and increased the average fiber diameter of chitosan/PLA spun fibers. On the other hand, increasing chitosan reduced the tensile strength, Young's modulus, compressive stress, and compressive modulus but enhanced elongation at break of chitosan/PLA porous membranes [303, 311]. After immersion in PBS solution (0.2 M, pH 7.4) for 2 h, the hydrated chitosan/PLA porous membrane had lower mechanical properties except for significantly higher elongation at break compared with the dry membranes [303]. The basicity of chitosan also restrained the self-catalysis of PLA (the acceleration of PLA degradation due to its low molecular weight acidic products); thus, the blend scaffolds had slower degradation in vitro than pristine PLA [309, 311]. Finally, PLA promoted the tensile intensity of chitosan/PLA nerve conduits; meanwhile biocompatibility of the blends was enhanced with chitosan [313]. The blend nerve conduits had a relative generative rate (RGR) of 83.67 following ISO 10993-5 (RGR ≥ 75%), indicating good biocompatibility, and exhibited the potential to serve as a nerve conduit.

To improve blend solubility in organic solvents and modify its hydrophobic nature, chitosan can be chemically modified by acylation (e.g., hexanoyl chitosan (H-chitosan

and *O*-lauroyl chitosan OCS)) [314, 315]. Three solvents (i.e., chloroform, dichloromethane, and THF) were used to investigate the effects of solvents on properties of H-chitosan/PLA ($M_v$ = 70 kDa) blends prepared by solution casting [316]. On the basis of Hildebrand solubility parameters ($\delta$), 9.2 (chloroform), 9.6 (dichloromethane), 9.1 (THF), 9.3 (H-chitosan), and 9.4 (PLA) $cal^{0.5}/cm^{1.5}$, the authors proposed that solution blends in chloroform or dichloromethane should be more miscible than solution blends in THF. Overall, regardless of solvents, the composition dependence of $T_g$ and $T_m$ of the PLA/H-chitosan containing 20–40 wt% H-chitosan suggested partial miscibility. However, the blends exhibited phase-separated morphologies. H-chitosan also decreased the apparent degree of crystallinity of PLA in the blends. The blends prepared from dichloromethane exhibited the highest crystallinity [316]. Tensile strength and Young's modulus of the blends (20–80 wt% H-chitosan) prepared from THF decreased significantly with an increase of H-chitosan [314]. The elongation at break of the blends prepared from THF (ca. 12–42%) was not enhanced with an increase in ductile H-chitosan (elongation at break of 890%). The organic solvents also affected the spinnability of H-chitosan/PLA blend solutions for electrospinning [317]. The blend solutions had apparent shear viscosity lower than the neat PLA and neat H-chitosan. The viscosities of blends in chloroform (156–770 cp) were higher than those in dichloromethane (34.5–121 cp). The electrospun blend fibers prepared from chloroform solution had a rough surface without beads when the blends contained up to 50 wt% H-chitosan. In contrast, the electrospun fibers prepared from dichloromethane exhibited beading. The average diameters of electrospun blend fibers increased with increasing PLA content. Electrospun blend fibers containing 20–40 wt% H-chitosan prepared from chloroform possessed one-stage thermal degradation, which was very close to the thermal degradation of PLA, and the heat of fusion of PLA in the blends decreased with increased H-chitosan [317].

Solution blend membranes of OCS/PLLA composed of 20–80% OCS were determined to be compatible based on FTIR and WAXD results [315]. Furthermore, there was no phase separation in the blend membrane containing 50 wt% OCS. Addition of OCS decreased $T_m$ and the crystalline band of PLLA, with emergence of a broad exothermic peak at about 80–90°C in the blend membranes determined by DSC.

***14.3.8.4 Starch/PLA Blends*** PLA-starch blends have been extensively investigated due to price, commercial availability, natural abundance, biodegradability, and mechanical properties. So, a separate summary of the properties are shown in Table 14.5. Gelatinization or plasticization of starch granules, a semicrystalline material, by mixing with low amount of plasticizer under high pressure and shear force at moderate temperature weakens the strong intra- and intermolecular bonding of starch molecules and facilitates the formation of hydrogen bonding between starch and plasticizer. Plasticized starch or thermoplastic starch (TPS) is an amorphous material with lower $T_g$, which improves its processability.

However, the interfacial adhesion between PLA and starch phases of the blend is poor due to the difference in their surface energies and high interfacial tension. Surface energies of thermoplastic cassava starch and PLA are about 66 and 50 $mJ/m^2$, respectively. The interfacial tension of about 7.9 $mJ/m^2$ is classified as high with a spreading coefficient of about −8.4 $mJ/m^2$ [318–321]. Physical blends of thermoplastic starch and PLA are thermodynamically immiscible. Therefore, many approaches to improve the compatibility between two phases have been explored [318, 322–324]. This section focuses on thermoplastic starch PLA blends compatibilized using low-molecular-weight coupling agents, modified vegetable oils, nanofillers, and functionalized polymers. Among these, compatibilizers containing isocyanate groups, aromatic diisocyanates, such as toluene diisocyanates, phenylene diisocyanates, methylene diphenyl diisocyanates and aliphatic diisocyantes such as lysine diisocyanates, hexamethylene diisocyanates are attractive. The urethane linkages are formed via crosslinking between isocyanate group of diisocyantes (DI) with the hydroxyl group of starch, carboxyl, or hydroxy terminal group of PLA. Thus, the urethane crosslinks between starch and PLA, and within PLA and within starch are represented in Figure 14.17. As isocyanate groups are highly reactive, the unreacted methylene diphenyl diisocyanates (MDI) residues in the blend are not expected to be present [318, 324, 325]. The use of DI, especially MDI, as compatibilizers of PLA/starch blends have been reviewed elsewhere [318, 322, 324].

The elongation at break of PLA and starch (20–60%) or TPS blends (10–40%) with MDI (0.05–1.5%) are up to 6.1 and 3.2%, respectively [322]. Modified TPS with 3, 5, 7 wt% of MDI and 0.05 wt% dibutyltindilaurate and then blended with PLA at the ratio of 20–80 was investigated [326]. Among the blends with and without MDI modification, the blend with 5 wt% of MDI (PLA/$M_5$-$TPS_1$) had better impact and tensile properties. The average impact strength, tensile strength, tensile modulus, and elongation at break of PLA/$M_5$-$TPS_1$ were 27 J/m, 33 MPa, 2441 MPa, and 1.7%, respectively, as compared with those properties of PLA/$TPS_1$ (16 J/m, 35 MPa, 1847 MPa, 1.57%, respectively). The compatibilized blend also demonstrated lower $T_g$, $T_{cc}$, water absorption, and water permeability than those of the physical blend [326].

Grafting of 5 wt% hexamethylenediisocyanate (HDI) onto native corn starch with ditin butyl dilaurate (DBTDL) as a catalyst and then with PLA at the ratio of 30/70 was examined [327]. Impact strength and tensile strength decreased with the addition of grafted starch. The addition of 5 wt% castor oil (CO) in the HDI-grafted starch (HGST)/PLA

**TABLE 14.5 Summary of the Mechanical Properties of Some PLA and Starch Blends With and Without Compatibilizer**

| Polymer | | TPS Component | Compatibilizing Additive | | Blending Method | Young's Modulus | Tensile Strength | Elongation at Break | Tensile Toughness | Impact Strength | Ref. |
|---|---|---|---|---|---|---|---|---|---|---|---|
| | Ratio (wt%) | | | Ratio (wt%) | | (MPa) (GPa)* | (MPa) | (%) | (MJ/m$^3$) | (J/m) (kJ/m$^2$)** | |
| PLA | 100 | | | — | Corotating hot | 1.41* | 62.1 | 5.69 | — | — | [287] |
| PLA/wheat St | 55/45 | | | — | mixer | 1.73* | 36.0 | 2.58 | — | — | |
| | | | MDI | 0.25 | | 1.89* | 62.3 | 4.37 | — | — | |
| | | | | 0.5 | | 1.94* | 66.7 | 4.40 | — | — | |
| | | | | 1.0 | | 1.94* | 64.9 | 4.77 | — | — | |
| | | | | 2.0 | | 1.92* | 65.3 | 4.50 | — | — | |
| PLA | 100 | | | | Batch mixer of | 1958 ± 20 | 56 ± 3 | 2.3 ± 0.1 | — | 25 ± 2 | [288] |
| PLA/TPS$_1$ | 80/20 | Tapioca starch/ | | — | TPS | 1847 ± 70 | 35 ± 1 | 1.57 ± 0.1 | — | 16 ± 2 | |
| PLA/TPS$_2$ | 75/25 | water/ | | — | modification | 1754 ± 53 | 32 ± 8 | 2 ± 0.15 | — | 14 ± 1 | |
| PLA/TPS$_3$ | 65/35 | glycerol: | | — | and polymer | 1740 ± 1 | 24 ± 4 | 1.2 ± 0 | — | 14.3 ± 1 | |
| PLA/TPS$_4$ | 55/45 | 70/5/25 | | — | blending | 1740 ± 1 | 28 ± 5 | 1.6 ± 0 | — | 14 ± 0.5 | |
| PLA/M$_3$-TPS$_1$ | 80/20 | | MDI w/ | 3 | | 1935 ± 141,935 ± 14 | 32 ± 0.5 | 1.4 ± 0.2 | — | 20 ± 1.2 | |
| PLA/M$_3$-TPS$_1$ | 80/20 | | DBTDL | 5 | | 2441 ± 24 | 33 ± 0 | 1.7 ± 0 | — | 27 ± 1 | |
| PLA/M$_3$—TPS$_1$ | 80/20 | | catalyst | 7 | | | 30 ± 2 | 1.5 ± 0.1 | — | 24 ± 1.6 | |
| | | | | | | 2366 ± 16 | | | | | |
| PLA/E$_1$—TPS$_1$ | 80/20 | | ESO w/ | 1 | | 2543 ± 40 | 31 ± 1 | 2.1 ± 0.15 | — | 25 ± 0.5 | |
| PLA/E$_3$-TPS$_1$ | 80/20 | | TEA | 3 | | 2500 ± 33 | 34 ± 10 | 4.5 ± 0.1 | — | 30 ± 2 | |
| PLA/ E$_5$—TPS$_1$ | 80/20 | | catalyst | 5 | | | 32 ± 3 | 4.0 ± 0 | — | 28 ± 2.3 | |
| PLA | 100 | | | | Twin-screw | 3000 ± 20 | 65 ± 3 | 5.0 ± 1 | — | 18 ± 2** | [289] |
| PLA/corn St | 70/30 | | | — | extrusion | 2700 ± 30 | 50 ± 1 | 6.0 ± 1 | — | 10 ± 1** | |
| PLA/corn St/CO | 65/30/5 | | | — | | 2850 ± 80 | 40 ± 1 | 7.0 ± 1 | — | 11 ± 1** | |
| PLA/HGST$_1$ | | | | | | | | | | | |
| PLG/HGST$_1$/CO | 70/30 | | HDI w/ | 5 | | 2900 ± 50 | 42 ± 1 | 2.5 ± 1 | — | 13 ± 1** | |
| PLG/HGST$_2$/CO | 65/30/5 | | DBTDL | 5 | | 2530 ± 60 | 28 ± 1 | 45 ± 5 | — | 25 ± 2** | |
| PLG/HGST$_3$/CO | 65/30/5 | | catalyst | 8 | | 2450 ± 50 | 31 ± 2 | 50 ± 5 | — | 32 ± 1** | |
| | 65/30/5 | | | 11 | | 2500 ± 70 | 33 ± 1 | 68 ± 5 | — | 41 ± 2** | |

(*Continued*)

**TABLE 14.5 (Continued)**

| Polymer | | TPS Component | Compatibilizing Additive | | Blending Method | Young's Modulus | Tensile Strength | Elongation at Break | Tensile Toughness | Impact Strength | Ref. |
|---|---|---|---|---|---|---|---|---|---|---|---|
| | Ratio (wt%) | | | Ratio (wt%) | | (MPa) (GPa)* | (MPa) | (%) | (MJ/m$^3$) | (J/m) (kJ/m$^2$)** | |
| PLA | 100 | Cassava starch/ | — | — | Mixer-compression molding | 2680±44 | 51.2±5.2 | 2.4±0.3 | — | — | [334] |
| TPCS | 100 | Glycerol: | — | — | | 9.9±0.6 | 1.1±0.0 | 56.9±6.4 | — | — | |
| PLA/TPS/PLA-*g*-MA-L101 | 56/30/14 | 70/30 | MA/L101 | 2/0.65 | | 1620±408 | 24.5±6.1 | 2.6±0.7 | — | — | |
| PLA/TPS/PLA-*g*-MA-DCP | 56/30/14 | | MA/DCP | 2/0.65 | | 1760±54 | 28.4±1.3 | 2.6±0.3 | — | — | |
| PLA | 100 | | | | | | | | | | |
| PLA/TPS | 70/30 | | | | | | | | | | |
| PLA/TPS/PLA-g-MA-L101 | 56/30/14 | | — | — | Twin-screw extrusion-compression molding | 1930±323 | 44.6±2.9 | 2.0±0.1 | — | — | |
| PLA/TPS/PLA-*g*-MA-DCP | 56/30/14 | | — | — | | 741±142 | 11.5±2.4 | 1.2±0.2 | — | — | |
| | | | MA/L101 | 2/0.65 | | 980±130 | 12.3±5.5 | 1.1±0.5 | — | — | |
| PLA | 100 | | MA/DCP | 2/0.65 | | 700±367 | 16.1±3.5 | 1.4±0.2 | — | — | |
| PLA/TPS | 70/30 | | | | | | | | | | |
| PLA/TPS/PLA-*g*-MA-L101 | 56/30/14 | | | | | | | | | | |
| PLA/TPS/PLA-*g*-MA-DCP | 56/30/14 | | | | | | | | | | |
| | | | — | — | Twin-screw extrusion-cast film extrusion | 1180±83 | 22.5±2.6 | 6.0±1.1 | — | — | |
| | | | — | — | | 172.0±37.9 | 1.57±0.3 | 11.6±1.2 | — | — | |
| | | | MA/L101 | 2/0.65 | | 780±130 | 11.9±2.0 | 23.4±2.1 | — | — | |
| | | | MA/DCP | 2/0.65 | | 920±130 | 10.5±5.8 | 48.7±2.1 | — | — | |
| PLA | 100 | Cassava starch/ | GRH | | Twin-screw extrusion | 1.2±0.1* | 24.7±0.7 | 8.9±5.1 | 1.3±0.7 | — | [335] |
| PLA-GRH | 100 | Glycerol: | MA/L101 | 0.1 | | 2.2±0.3* | 43.2±1.5 | 21.2±5.7 | 5.3±1.1 | — | |
| PLA-*g*-MA/TPS | 70/30 | 70/30 | MA/L101 | 2/0.65 | | 0.7±0.1* | 11.0±1.5 | 23.9±2.1 | 2.3±0.5 | — | |
| | 70/30 | | MA/L101 W/ GRH | 2/0.65 W/0.1 | | 0.8±0.1* | 13.7±1.1 | 103.4±2.7 | 13.0±1.4 | — | |
| PLA-*g*-MA/TPS-GRH | | | | | | | | | | | |
| P-PLA | 100 | PLA/ATBC: 87.5/12.5 | — | — | Twin-screw extrusion | 814.4±26.8 | 26.6±1.9 | 43.2±3.2 | — | — | [336] |
| TPS | 100 | Wheat starch/ | — | — | | 1.9±0.2 | 1.4±0.2 | 91.5±7.5 | — | — | |
| P-PLA/TPS | 70/30 | glycerol/ | — | — | | 331.2±17.2 | 10.2±0.9 | 7.2±0.8 | — | — | |
| P-PLA/TPS/PLA-*g*-MA-2 | 70/30/2 phr | distilled water: | MA/L101 | 5/0.6 | | 624.3±21.3 | 15.6±1.2 | 16.5±1.1 | — | — | |
| P-PLA/TPS/PLA-*g*-MA-4 | 70/30/4 phr | 66.5/28.5/5 | | | | | | | | | |
| P-PLA/TPS/PLA-*g*-MA-6 | 70/30/6 phr | | | | | 469.0±18.8 | 16.1±0.6 | 19.9±0.9 | — | — | |
| P-PLA/TPS/PLA-*g*-MA-8 | 70/30/8 phr | | | | | | | | | | |
| | | | | | | 539.6±23.7 | 13.9±1.1 | 10.7±1.3 | — | — | |
| | | | | | | 390.5±19.4 | 8.0±0.9b | 4.5±0.8 | — | — | |

| Polymer | | TPS Component | Compatibilizing Additive | | Blending Method | Young's Modulus | Tensile Strength | Elongation at Break | Tensile Toughness | Impact Strength | Ref. |
|---|---|---|---|---|---|---|---|---|---|---|---|
| | Ratio (wt%) | | | Ratio (wt%) | | (MPa) (GPa)* | (MPa) | (%) | ($MJ/m^3$) | (J/m) ($kJ/m^2$)** | |
| PLA | 100 | | | | Extrusion | 1276 ± 84 | 48 ± 3 | 4.5 ± 0.3 | — | — | [338] |
| TPS | 100 | Yam starch/ | | | | 95 ± 12 | 8.1 ± 1.1 | 35 ± 5 | — | — | |
| PLA/TPS | 50/50 | Glycerol: | | | | 242 ± 5 | 7.2 ± 0.8 | 6.8 ± 0.8 | — | — | |
| PLA/TPS/ESO | 50/50 | 1/0.25 | ESO*** | 1.5 | | 485 ± 9 | 15.2 ± 0.9 | 12.1 ± 0.5 | — | — | |
| PLA/TPS/ESO | 50/50 | | | 3.0 | | 501 ± 7 | 14.1 ± 1.1 | 11.8 ± 1.1 | — | — | |
| PLA | 100 | Potato starch/ | | — | Melt mixing | 542 ± 16.3 | 16.4 ± 0.56 | 2.12 ± 0.68 | — | — | [341] |
| TPS | 100 | glycerol: 70/30 | | — | | 146 ± 6.2 | 1.82 ± 0.23 | 3.61 ± 0.84 | — | — | |
| PLA/TPS | 40/60 | w/ NaMMT dispersion | | — | | 305 ± 14.6 | 5.63 ± 0.32 | 4.32 ± 0.87 | — | — | |
| PLA/TPS/$NaMMT_{0.5}$ | 40/60 | | NaMMT | 0.5 | | 325 ± 17.2 | 7.29 ± 0.48 | 6.68 ± 0.98 | — | — | |
| PLA/TPS/$NaMMT_{1.0}$ | 40/60 | | | 1.0 | | 329 ± 13.8 | 7.95 ± 0.33 | 6.05 ± 1.24 | — | — | |
| PLA | 100 | | | | Miniature | 3018 ± 50 | 69 ± 1 | 5 ± 1 | — | 18 ± 1.0 | [340] |
| PLA/ESO | 90/10 | | | | twin-screw | 2727 ± 15 | 62 ± 2 | 6 ± 2 | — | 19 ± 0.5 | |
| PLA/corn starch | 90/10 | | | | extrusion | 2855 ± 20 | 57 ± 2 | 6 ± 1 | — | 14 ± 1.0 | |
| PLA/starch/ESO | 80/10/10 | | | | | 2406 ± 10 | 38 ± 2 | 64 ± 5 | — | 30 ± 1.0 | |
| | 80/10/10 | | | | | | | | | | |
| PLA/MGST1/ESO | 80/10/10 | | MGST1: | | | 2264 ± 13 | 36 ± 1 | 78 ± 5 | — | 34 ± 0.5 | |
| | 80/10/10 | | Starch/MA | 60/2.6 | | | | | | | |
| PLA/MGST2/ESO | 70/20/10 | | MGST2: | | | 2412 ± 30 | 41 ± 1 | 112 ± 10 | — | 38 ± 0.7 | |
| | 60/30/10 | | Starch/MA | 60/5.4 | | | | | | | |
| PLA/MGST3/ESO | 65/30/5 | | MGST3: | | | 2510 ± 20 | 43 ± 2 | 140 ± 10 | — | 42 ± 1.0 | |
| | 58/30/12 | | Starch/MA | 60/8.0 | | | | | | | |
| PLA/MGST3/ESO | 55/30/15 | | | | | 2318 ± 18 | 35 ± 1 | 96 ± 6 | — | 36 ± 1.2 | |
| PLA/MGST3/ESO | | | | | | 1769 ± 20 | 25 ± 2 | 63 ± 5 | — | 31 ± 1.0 | |
| PLA/MGST3/ESO | | | | | | 2063 ± 15 | 32 ± 1 | 56 ± 5 | — | 28 ± 1.0 | |
| PLA/MGST3/ESO | | | | | | 1366 ± 10 | 19 ± 1 | 68 ± 3 | — | 36 ± 0.8 | |
| PLA/MGST3/ESO | | | | | | 1057 ± 25 | 16 ± 2 | 32 ± 5 | — | 23 ± 1.0 | |

(*Continued*)

**TABLE 14.5 (Continued)**

| Polymer | Ratio (wt%) | TPS Component | Compatibilizing Additive | Ratio (wt%) | Blending Method | Young's Modulus (MPa) (GPa)* | Tensile Strength (MPa) | Elongation at Break (%) | Tensile Toughness ($MJ/m^3$) | Impact Strength (J/m) ($kJ/m^2$)** | Ref. |
|---|---|---|---|---|---|---|---|---|---|---|---|
| PLA | 100 | Corn starch/ | | | Extrusion | 3930±64 | 67±1.5 | 6.1±0.3 | — | — | [342] |
| TPS | 100 | Glycerol: | | | | 1550±60 | 19±0.7 | 2.7±0.6 | — | — | |
| PLA/MPLA/TPS | 60/10/30 | 70/30 | MPLA: | 10 | | 3264±64 | 33±1.5 | 4±0.3 | — | — | |
| | 60/10/30/3 | | PLA/MA/ | | | | | | | | |
| PLA/MPLA/TPS/P | 60/10/30/3/1 | P = silicone rubber | DCP | | | 3450±60 | 41±0.7 | 22±0.6 | — | — | |
| PLA/MPLA/TPS/P/1 $SiO_2$ | 60/10/30/3/3 | plasticizer | | | | | | | | | |
| PLA/MPLA/TPS/P/3 $SiO_2$ | 60/10/30/3/5 | | $SiO_2$ | 1 | | 2660±29 | 36±0.6 | 60±1.8 | — | — | |
| PLA/MPLA/TPS/P/5 $SiO_2$ | 60/10/30/3/1 | | | | | | | | | | |
| PLA/MPLA/TPS/P/1 A-$SiO_2$ | 60/10/30/3/3 | | | 3 | | 3060±51 | 33±0.4 | 63±7.3 | — | — | |
| PLA/MPLA/TPS/P/3 A-$SiO_2$ | 60/10/30/3/5 | | | | | | | | | | |
| PLA/MPLA/TPS/P/5 A-$SiO_2$ | | | | 5 | | 3210±33 | 34±0.4 | 88±5.9 | — | — | |
| | | | A-$SiO_2$ | 1 | | 2990±44 | 34±1.4 | 91±0.2 | — | — | |
| | | | | 3 | | 3110±35 | 33±1.0 | 72±2.0 | — | — | |
| | | | | 5 | | 3130±28 | 30±0.7 | 45±0.2 | — | — | |

*Note*: * Values are reported in GPA; ** Values are reported in $kJ/m^2$. St: starch; MDI: methylenediphenyl diisocyanate; DBTDL: dibutyltindilaurate; ESO: epoxidized soybean oil; TEA: triethylamine; CO: castor oil; HDI: hexamethylenediisocyanate; MA: maleic anhydride; L101: 2,5-bis(*tert*-butylperoxy)-2,5-dimethylhexane; DCP: dicumyl peroxide; GRH: graphene nanoplatelets; ATBC: acetyl tributyl citrate; ESO***: epoxidized sesame oil; NaMMT: sodium montmorillonite; MPLA: maleated polylactide; $SiO_2$: neat silica; A-$SiO_2$: modified (having amine functional groups) spherical silica.

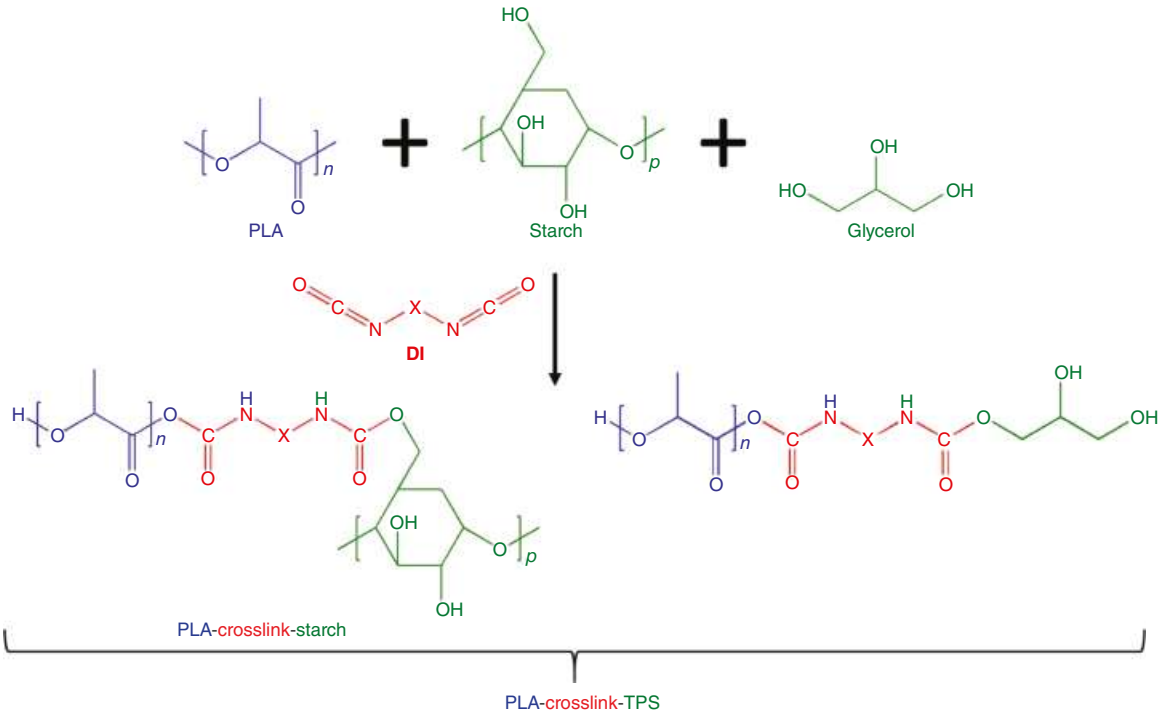


**FIGURE 14.17** Chemical reactions of the PLA-starch (TPS) crosslinking process using DI as the coupling agent. *Source:* Reprinted from Ref. 324. Copyright 2018, Reproduced with permission from Elsevier.

(30/65) improved the mechanical properties and degree of crystallinity. These properties further improved with increase in HGST 5, 8, and 11 wt%, nomenclature HGST1, HGST2, and HGST3, respectively. The average impact strength, tensile strength, elongation at break and degree of crystallinity of the PLA/HGST1-3 (5–11% HDI)/CO (65/30/5) blends were 25–41 kJ/m$^2$, 28–33 MPa, 45–68% and 10.3–13.1%, respectively, when compared with the PLA/HGST1-1 (5% HDI)/CO (65/30/5). The properties of PLA/starch blend were 10 kJ/m$^2$, 50 MPa, 6% and 0%, respectively, and the properties of PLA/starch/CO blend were 11 kJ/m$^2$, 40 MPa, 7% and 3%, respectively. The shear viscosity of the blends ranked in descending order were PLA > PLA/HGST, PLA/starch > PLA/HGST3/CO > PLA/HGST2/CO > PLA/HGST1/CO > PLA/starch/CO [327]. However, the carcinogenic potential of isocyanates limits their use in food contact materials such as food packaging [322, 328].

Another compatibilization technique that has been widely used for PLA/starch blends is functionalization by grafting to generate the reactive polymers (compatibilizers). The polymer is functionalized by mixing with small-molecular-weight functional groups (e.g., anhydride, hydroxyl, isocyanate, and epoxide) and suitable initiators (e.g., peroxide), then reactive blending with nonreactive polymer. The reactive polymer forms in situ graft copolymers, reducing interfacial tension and increasing interfacial adhesion, which reduce dispersed phase particle size and result in a uniform morphology with improved mechanical properties as discussed in previous sections [320, 321, 329]. Acrylic acid, glycidyl metracrylate (GMA), and maleic anhydride (MA) are normally used for reactive blending of PLA/starch. The hydroxyl groups of starch are crosslinked with carboxylic acid groups of AA, epoxide groups of GMA, and anhydride groups of MA [324]. Among these compatibilizers, MA, a polar monomer, is extensively used because of its low toxicity, high reactivity, no tendency for homopolymerization under grafting conditions, and ease of handling [324].

The studies of reactive compatibilized blends of PLA/starch with MA and peroxide initiators (e.g., dicumyl peroxide (DCP), 2,5-bis(*tert*-butylperoxy)-2,5-dimethylhexane (Luperox™ 101 or L101)) producing PLA-*g*-MA are reviewed elsewhere [318, 321, 323]. The reactive extrusion blending can be performed either in one-step or two-step processes. Jang et al. [330] investigated thermal properties, morphology, and biodegradability of the compatibilized one-step PLA/TPS blend with MA as compatibilizer (PSMA), the compatibilized two-step PLA/MTPS blends (PSMATPS), and PLA/starch blends (PS). As per obtained morphology, they reported that MA was a better compatibilizer than MATPS. PSMA exhibited higher biodegradability and degree of crystallinity. The degree of crystallinity of PSMA, PSMATPS, and PS (at 70/30 of PLA and starch) were reported as 36, 14–24, and 9%, respectively. The smaller TPS droplets and more uniform dispersion were observed from the reactive blend with a one-step process, whereas the reactive blends with a two-step process showed the greater improvement in elongation at

**TABLE 14.6 Sample Composition and Screw Speed for Production of PLA-*g*-MA [333]**

| Sample | Nominal MA (wt%) | L101 | TSE[a] Screw Speed (rpm) |
|---|---|---|---|
| PLA-*g*-MA A | 4.5 | 0.047 | 18 |
| PLA-*g*-MA B | 2 | 0.2 | 10 |
| PLA-*g*-MA C | 4.5 | 0.425 | 18 |
| PLA-*g*-MA D | 2 | 0.65 | 10 |
| PLA-*g*-MA E | 2 | 0.65 | 25 |
| PLA-*g*-MA F | 7 | 0.65 | 10 |

[a]Twin screw extruder.

break [331]. For the two-step modification, the reactive compatibilized blends with TPS ratios of 27 and 60% elongation increased to 200 and 180%, respectively.

The effects of grafted MA level and PLA molecular weight of PLA-*g*-MA on the properties and morphology of reactive binary blends (PLA-*g*-MA/TPS) and ternary blends (PLA/PLA-*g*-MA/TPS) were examined. PLA functionalized with MA and L101 using a twin-screw extruder to generate PLA-*g*-MA having different amounts of grafted MA (presented in Table 14.6) and/or $M_n$, and their properties were characterized [332, 333]. The thermoplastic cassava starch (TPCS) blends produced with PLA-*g*-MA A, B, C, and D were nomenclature as 7rPT A, B, C, and D, respectively. Figure 14.18 shows the SEM micrographs of the physical or reactive binary blends at 30 wt% TPS prepared with functionalized PLA, after removing TPS domains by acid etching [333]. Greater dispersion and uniformity of TPS domains in the PLA-*g*-MA continuous phase were observed when PLA-*g*-MA with a small amount of grafted MA (0.05 wt%) and high $M_n$ of 70 kDa (7rPT A) was used. The binary reactive blends containing higher amounts of grafted MAs (0.26–0.47 wt%) had smaller TPS domain sizes, but the variation of TPS domain sizes increased. Furthermore, larger TPS domains (≥4 μm) were found in the PLA-*g*-MA matrix having high-grafted MA (≥0.4 wt%) and lower $M_n$ (≤50 kDa), which are 7rPT C and 7r PT D.

Interfacial tension of the blends reduced with an increase of grafted MA, facilitating the finer domain. But the increase of grafted MA and decrease of $M_n$ of PLA-*g*-MA decrease the matrix viscosity, enhance chain scission and dynamic coalescence, resulting in large domains. The properties of reactive ternary blends (PLA/PLA-*g*-MA/TPS) were also studied using PLA-*g*-MA having 0.52% grafted MA and $M_n$ of 45 kDa as a compatibilizer. The blends with different amounts of grafted MA (approximately 0.05, 0.10, 0.25, 0.40% based on PLA-*g*-MA and PLA weights) and 30 wt% of TPS were prepared. The blend at the ratio of PLA/PLA-*g*-MA/TPCS 56/14/30, which had grafted MA around 0.1 wt% showed the highest value of average elongation at break (145%), compared with that of PLA and 70/30 of PLA/TPS (2.8 and 81%, respectively). PLA had average Young's modulus and tensile strength at break of 2.8 GPa and 65.9 MPa, whereas the physical and compatibilized blends had Young's Modulus of 2.2 and 2.4 GPa, respectively, and similar tensile strength of 38.9 MPa [333].

Types of peroxide initiator, techniques of reactive blending of PLA/PLA-*g*-MA/TPS, and film production were examined [334]. PLA-*g*-MA was functionalized with 2 wt% MA and 0.65 wt% L101 or DCP. PLA/PLA-*g*-MA/TPS were blended at the ratio of 56/14/30 by wt. Compared to L101, DCP performed as a better initiator. Extruded cast film, made from compatibilized polymer (PLA/PLA-*g*-MA-DCP/TPS) which was blended using a twin-screw extruder, had the longest elongation at break (48.7% with tensile strength of 10.5 MPa), the lowest reduction of PLA molecular weight, and the lowest transmittance of UV-Visible light (<20%). SEM images after the removal of the starch phase exhibited a better distribution of TPS domains in the compatibilized blend of PLA/PLA-*g*-MA-DCP/TPS (PLA-*g*-TPCS-DCP) (Figure 14.19).

The researchers also investigated the effect of graphene (GRH) nanoplatelets on the properties of PLA-*g*-TPCS [335]. PLA was functionalized with 2 wt% MA and 0.65% L101 and then blended with TPCS at the ratio of 70–30 wt% (PLA-*g*-TPCS) and finally mixed with 0.1 wt% GRH (PLA-*g*-TPCS-GRH) in a twin-screw extruder. Films were made by using cast film extrusion. The elongation at break and toughness of PLA-*g*-TPCS-GRH film (103.4% and 13.0 MJ/m$^3$, respectively) highly increased compared with PLA (8.9% and 1.3 MJ/m$^3$, respectively) and PLA-*g*-TPCS (23.9% and 2.3 MJ/m$^3$, respectively). The oxygen and water vapor permeability coefficients of PLA-*g*-TPCS-GRH film ($0.9\times10^{17}$ kg m/m$^2$ s Pa and $6.1\times10^{14}$ kg m/m$^2$ s Pa, respectively) were lower than those of PLA ($2.2\times10^{17}$ kg m/m$^2$ s Pa and $6.6\times10^{14}$ kg m/m$^2$ s Pa, respectively) and PLA-*g*-TPCS ($2.0\times10^{17}$ kg m/m$^2$ s Pa and $6.6\times10^{14}$ kg m/m$^2$ s Pa, respectively). The authors mentioned that GRH nanoplatelets in the PLA-*g*-TPCS-GRH agglomerated at the interface and the crack bridging mechanism enhanced film toughening.

Another group of researchers studied the effect of PLA--*g*-MA on compatibilized blends of PLA plasticized with 12.5 wt% acetyl tributyl citrate (P-PLA) and then blended with TPS. The polymer pair was compatibilized with PLA--*g*-MA, containing 5 wt% MA and 0.6 wt% of L101, at various PLA-*g*-MA contents (0–8 phr) and the sheets were made using hot-pressing [336]. The results showed that the optimum incorporation of PLA-*g*-MA at 4 phr in P-PLA/TPS (70/30 by wt) had better morphological and rheological properties. Interestingly, this blend had average tensile strength of 16.1 MPa and elongation at break of 19.9% compared to those properties of P-PLA, TPS, and the physical blend, which were 26.6 MPa and 43.2%, 1.4 MPa and 91.5%, and 10.2 and 7.2%, respectively.

The effect of maleinized vegetable oil on toughening of PLA/TPS was investigated. It was expected that the highly

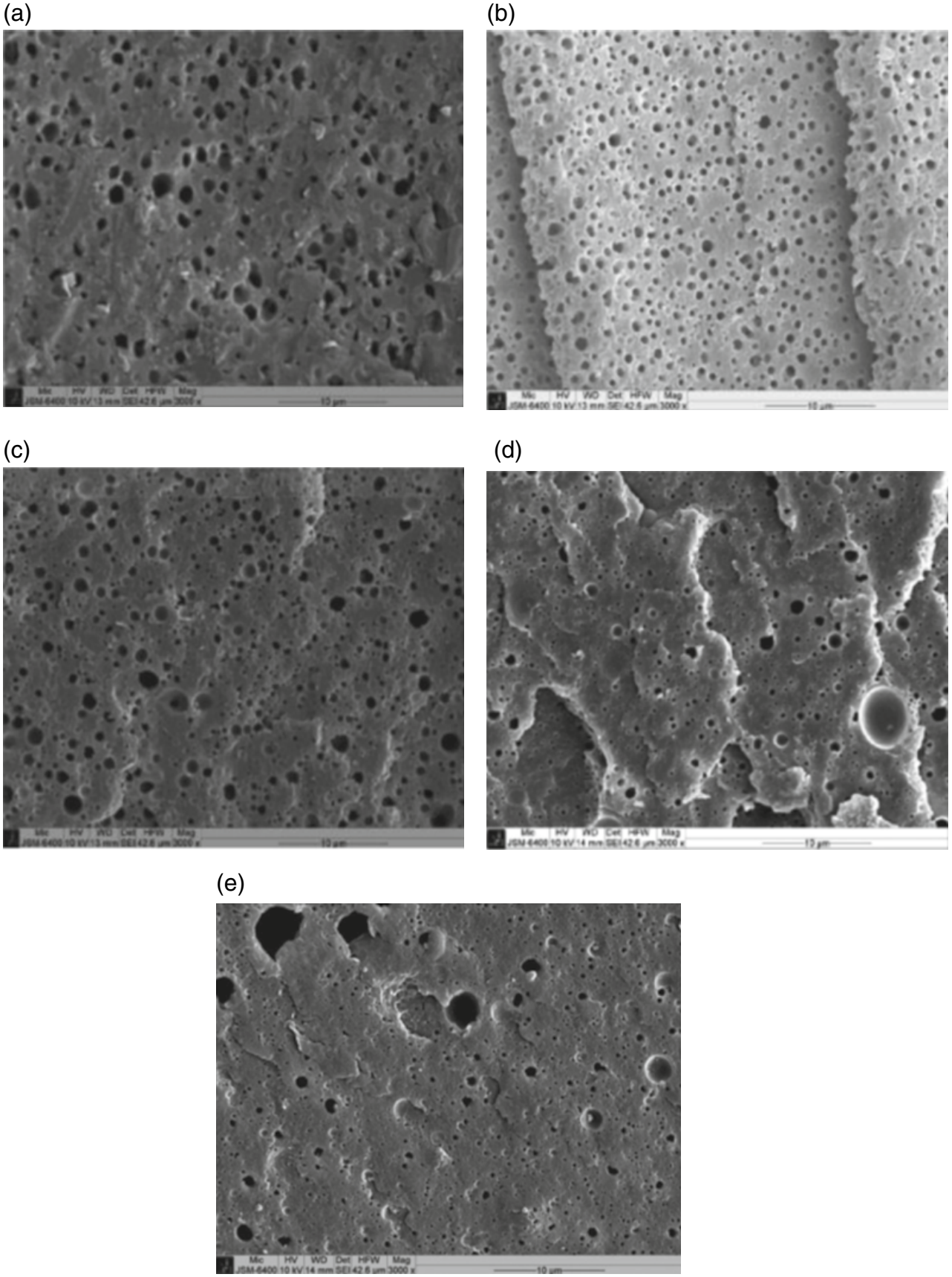


**FIGURE 14.18** SEM micrographs after removing TPCS domains by acid etching of physical and reactive blends (a) 7PT, (b) 7rPT A, (c) 7rPT B, (d) 7rPT C, and (e) 7rPT D. *Source:* Reprinted from Ref. 333. Copyright 2018, Reproduced with permission from John Wiley & Sons, Inc.

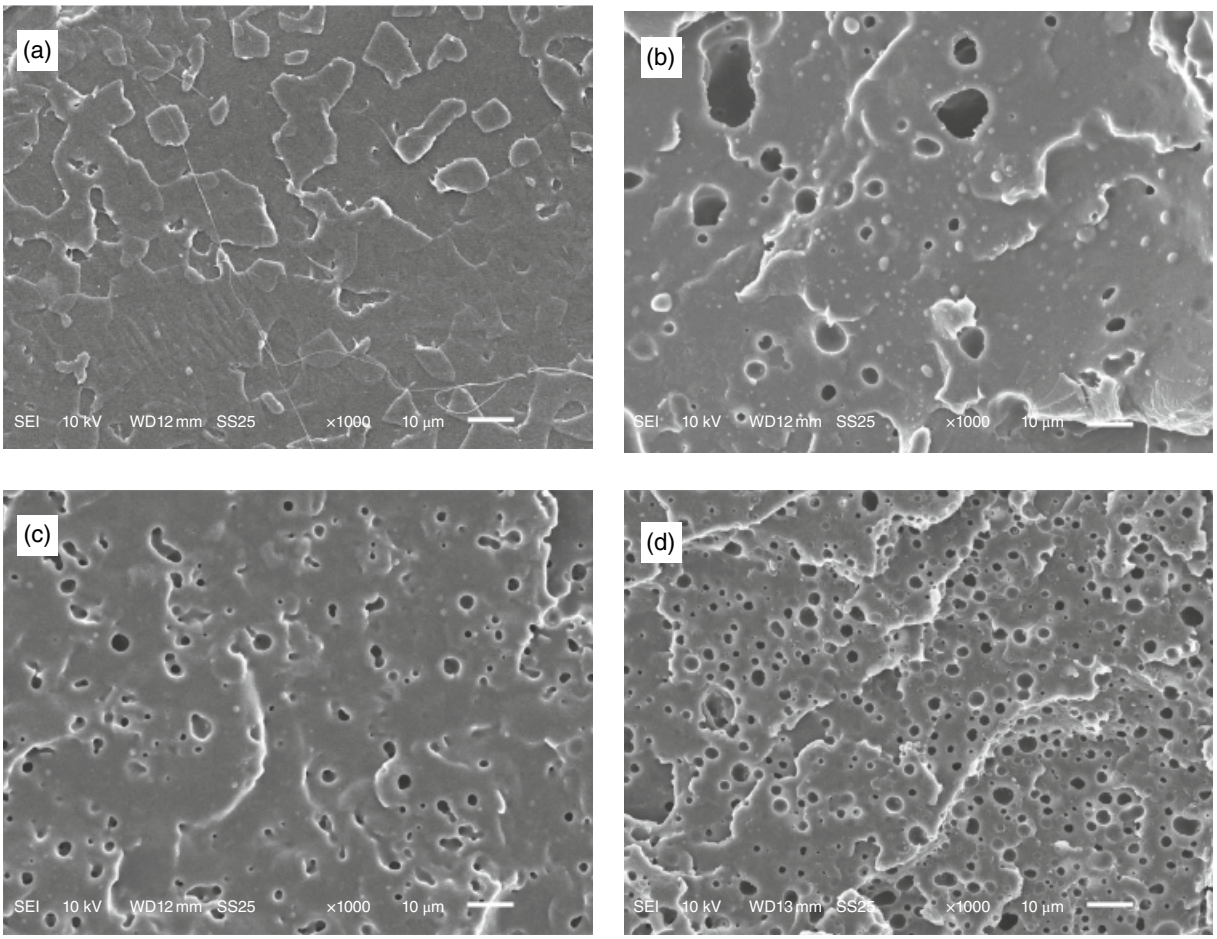


**FIGURE 14.19** SEM images of PLA, physical, and reactive blends: (a) PLA, (b) PLA-TPCS, (c) PLA-*g*-TPCS-L101, (d) PLA-*g*-TPCS-DCP. *Source:* Reprinted from Reference [334]. Copyright 2018, Reproduced with permission from John Wiley & Sons, Inc.

reactive acid/anhydride groups in maleinized vegetable oils can possibly have plasticizing and a compatibilizing/chain extension effects on the blends [337]. The interactions of MA groups in maleinized vegetable oil with some hydroxyl groups in PLA end chains and partially hydrolyzed PLA chains can induce a chain extension effect and with hydroxyl groups in TPS provide a compatibilization effect. In this work, PLA/commercial TPS/maleinized linseed oil (MLO) at the ratio of 70/30 wt./0–8 phr were blended in a twin-screw extruder. The specimens were made by injection molding. The highest elongation at break of the blends (160%) was found in the PLA/TPS blended with 6 phr MLO, having tensile strength of about 30 MPa, compared to those of PLA (7% and 64 MPa, respectively) and the blend without MLO (21.5% and 41.5 MPa, respectively). The blend with 6 phr MLO had an average Charpy impact energy value of 9.5 kJ/m$^2$, Shore D hardness of 64.8, Vicat softening temperature of 47.4°C, and HDT of 44.4°C, whereas the blend without MLO had values of 5.3 kJ/m$^2$, 68.2, 50.6°C and 49.4°C, respectively. MLO had a plasticizing-compatibilizing effect, which was observed from the decrease of $T_g$ using DSC and DMA and increase in compatibility by using field emission scanning electron microscopy.

Epoxidized vegetable oil is another interesting option as a coupling agent to improve the chemical affinity of PLA and starch blends. The principle is that the epoxidized groups of the modified oil can form hydrogen bonds with the terminal hydroxyls of PLA and starch. Accordingly, epoxidized sesame oil (ESO), having a 58.4% degree of substitution, was mixed in a mixture of 50TPS and 50PLA at the mass fraction of 0.013 and 0.026 ($ESO_{1.5}$ and $ESO_3$, respectively) and then pelletized [338]. The films were made by compression molding. ESO had plasticizing and coupling effects on the blends as evidenced by optical and SEM micrographs. The blend films with ESO showed more compact, smoother, and soft surfaces, fewer cracks and were more homogeneous than film without ESO. The blend films with $ESO_{1.5}$ and $ESO_3$ had lower water vapor permeability (2.63–2.17 g mm/kPa h m$^2$), higher tensile strength (15.2–14.1 MPa), and elongation at break (12.1–11.8%), compared to the properties of the blend film without ESO (3.68 g mm/kPa h m$^2$, 7.2 MPa and 6.8%, respectively).

Modified vegetable oils such as tung oil anhydride (TOA) and epoxidized soybean oil have been used as plasticizers or coupling agents in the blend of PLA/starch granules and PLA/MA-grafted starch (MGST), respectively [339, 340]. The industrial grade TOA in the PLA-starch blend was expected to develop interactions between anhydride groups of TOA and hydroxyl groups of the starch particles, developing a flexible layer on the surface of the starch granules in the PLA matrix, which was confirmed by FTIR and SEM [339]. The addition of 5–12 wt% TOA in the PLA and starch with a fixed amount of 30 wt% starch highly improved the impact strength and enhanced the elongation at break from ~7% (70/30 PLA/starch) to ~32% (63/30/7 PLA/starch/TOA). According to SEM images, TOA existed at the interface of PLA/starch for 5% TOA content. For blends containing >7 wt% TOA, small independent TOA droplet existing in the PLA matrix indicats immiscibility between PLA and TOA [339]. Comparing blends with native starch granules and functionalized starch granules (MA-*g*-starch, MGST), MGST having degree of substitution of 0.12 blended with PLA and epoxidized soybean oil at the ratio of 10/80/10 by wt showed the highest impact strength and elongation at break. This blend had impact strength of 42 kJ/m$^2$, tensile strength of 43 MPa, and elongation at break of 140%, whereas the blend with native starch at a similar ratio of components (native starch/PLA/epoxidized soybean oil of 10/80/10) had 30 kJ/m$^2$, 38 MPa and 64%, respectively. It was concluded that the better compatibility of the blends resulted from the reaction between the epoxy groups on the epoxidized soybean oil, the MA groups on MGST, and the end carboxylic acid groups of PLA [340].

Other approaches such as the use of nanofillers to improve the properties, as well as compatibility of the immiscible blends, have also been investigated. For example, 0.5 and 1 phr of unmodified nanoclay sodium montmorillonite (NaMMT) were mixed in TPS solution during gelatinization, cast, and dried, then finally melt mixed with PLA at the ratio of 60/40 (NaMMT–TPS/PLA), using a Brabender mixer [341]. A glucose-reduced graphene oxide (rGO) was dispersed in acetyl *tert*-butyl citrate (ATBC), mixed with glycerol-plasticized corn starch/PLA and extruded using a corotating twin-screw extruder [342]. Improvement in compatibility of the blends was reported in both experiments. The highest elongation at break (6.68%) was found in (0.5–60/40) NaMMT-TPS/PLA with tensile strength and water absorption of 7.29 MPa and 44.49%, respectively, whereas the blend without NaMMT had those properties of 4.32%, 5.63 MPa and 48.63%, respectively [341]. Addition of 5 mass% of rGO in TPS/PLA blend (70/30) improved notched Izod impact strength (36 J/m) and elongation at break (15.1%) with tensile strength of 5 MPa. The blend without rGO showed those properties of 16 J/m, 4.7% and 7.3 MPa, respectively [342].

Various amounts of nanosilica ($SiO_2$) and modified spherical silica (A-$SiO_2$) nanoparticles, having amine functional groups, were used in blends of PLA, TPS, and compatibilizer (maleated PLA (MPLA) containing 0.68 wt% of grafted maleic anhydride at a ratio of 60/30/10 with and without plasticizer, polydimetylsiloxanol (Plastosil M-2000) [305]. The tensile strength and elongation at break of PLA/MPLA/TPS increased by using plasticizer from 33 to 41 MPa and 4 to 22%, respectively. Increasing amounts of $SiO_2$ at the level of 1, 3, 5 wt% in the plasticized PLA/MPLA/TPS blends resulted in tensile strength of 36, 33, 34 MPa, respectively, and elongation at break of 60, 63, and 88%. The highest elongation at break (91% with tensile strength of 34 MPa) was found in the plasticized PLA/MPLA/TPS mixed with 1 wt% of A-$SiO_2$. This could be a consequence of the intensive interfacial interactions among the hydrogen bonds of the anhydride groups of the MPLA, the hydroxyl groups of the starch, and amine groups of the silica [343]. However, increasing amounts of A-$SiO_2$ to 3 and 5 wt% resulted in a slightly decrease of tensile strength (33 and 30 MPa) and decreased elongation at break (72 and 45%).

Different approaches to improving the compatibility of PLA/TPS blends were examined [344]. TPS/PLA at the ratios of 90/10, 75/25, and 60/40 were blended with different compatibilizers: 2 wt% peroxide (BP), 2 wt% MDI, and 1 wt% PLA grafted amylose (A-*g*-PLA) with number average molecular weight of 1200 g/mol and PLA weight fraction of 0.34. Decreasing the TPS content reduced the elongation at break. At the ratio of 90/10 (PS/PLA), the compatibilized blend with BP had the highest elongation at break of about 31% with tensile strength of 3.1 MPa > the compatibilizer blend with A-*g*-PLA (about 19% and 4.5 MPa, respectively) > the compatibilized blend with MDI (about 15% and 2.7 MPa, respectively), where the physical blend showed that properties of about 21% and 3.3 MPa. Increasing BP content to 4 wt% decreased the tensile properties and addition of 4 wt% of MDI did not significantly improve the tensile properties. It was concluded that A-*g*-PLA provided the best compatibilization effect since the tensile properties of the compatibilized blend increased without a decrease in elongation at break [344].

The effects of PLA-*g*-maleated TPS (PLA-*g*-MTPS) on the compatibility and properties of plasticized PLA and TPS blends were investigated [345]. To obtain the copolymers, PLA resins were blended with the prepared MTPS in the presence of Luperox®101 (0.25 and 1.0 pph, indicating as PLA-*g*-MTPS No.1 and PLA-*g*-MTPS No.2, respectively). The acid numbers of PLA-*g*-MTPS No. 1 and No. 2 were 359 and 364 mg NaOH/g, respectively. Plasticized PLA was prepared by compounding PLA with 50 pph of glycerol triacetate and 0.75 pph of Luperox231 (1,1-di-(*tert*-butylperoxy)3, 5,5-trimethyl cyclohexane) to induce branching of the PLA molecules and improve the melt strength of the molten PLA.

Lastly, 5 wt% of each PLA-*g*-MTPS copolymer was blended with plasticized PLA and TPS (80/20, 30/70 and 60/40 by wt). The properties of the compatibilized blends with copolymers were compared to the physical blends (no compatibilizer) and the compatibilized blends with PLA-*g*-MA [345]. The tensile strength, elongation at break, and toughness of the compatibilized and non-compatibilized blends greatly decreased with increasing TPS content from 20 to 40 wt%. However, the compatibilized blends with PLA-*g*-MTPS No. 1 exhibited the highest mechanical properties at every blend ratio. The best mechanical properties were obtained from the compatibilized blend at the ratio of 80/20 with PLA-*g*-MPTS No. 1. This compatibilized blend had tensile strength of ~4 MPa, elongation at break of ~540%, and toughness of ~6.1 J, whereas the physical blend had properties of ~3.5 MPa, ~ 510%, and toughness of ~5.1 J. Significant differences in the mechanical properties between the compatibilized blend with PLA-*g*-MTPS No. 1 and the non-compatibilized blend were observed in the blend at the ratio of 30/70; the morphologies of each at blend are shown in Figure 14.20 [345].

The compatibility of the PLA/TPS blend at the ratio of 50/50 wt% increased with addition of oligo(lactic acid)-grafted starch (OLA-*g*-starch), evidenced by SEM micrographs (Figure 14.21) [346]. Increasing amounts of OLA-*g*-starch (1, 2, 3, and 5 wt%) in the blends tended to increase elongation at break, and decrease water vapor and oxygen permeabilities, respectively. The highest elongation at break (~37% with tensile strength of ~20 MPa) and lowest WVP (~5500 g mil/m$^2$ day atm) and OP (~770 cc mil/m$^2$ day atm) were observed in the PLA/TPS with 5 wt% of OLA-*g*-starch. The physical blend had elongation at break of 9% with tensile strength of 21 MPa, WVP of 6596 g mil/m$^2$ day atm and OP of 1014 cc mil/m$^2$ day atm [346].

## 14.4 PLASTICIZATION OF PLA

Various studies have been conducted on imparting flexibility to PLA by plasticization using adipate [347], citrate [348–351], PEG [21, 260, 352, 353], glycerol and oligomeric lactic acid, partial fatty acid esters, and poly(propylene glycol) [354, 355]. The selection of plasticizer for PLA is constrained by factors such as biodegradability, miscibility, nonvolatility, and nontoxic nature of the plasticizer. PLA exhibits ductile

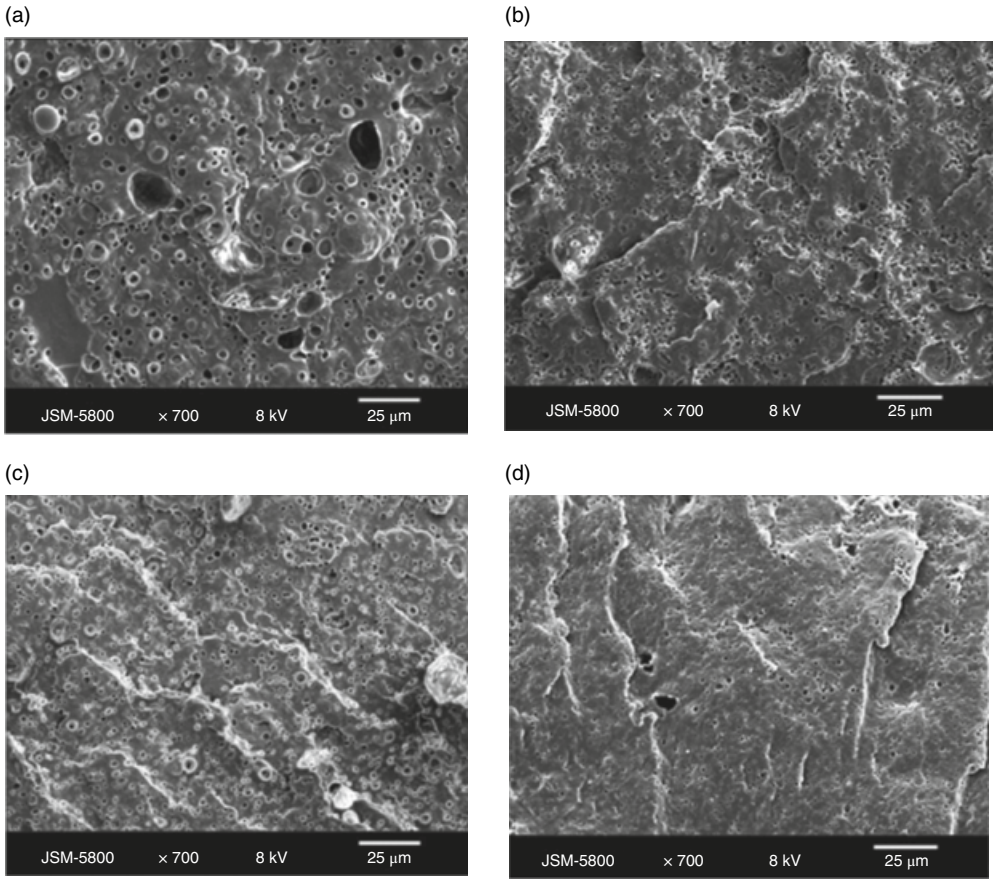


**FIGURE 14.20** SEM micrographs of various PLA/TPS blends (70/30 by wt) after acid etching of TPS; the blend without a compatibilizer (a), the blend with PLA-*g*-MA (b), the blend with PLA-*g*-MTPS No. 1 (c), the blend with PLA-*g*-MTPS No. 2 (d). *Source:* Reprinted from Ref. 345. Copyright 2012, Reproduced with permission from John Wiley & Sons, Inc.

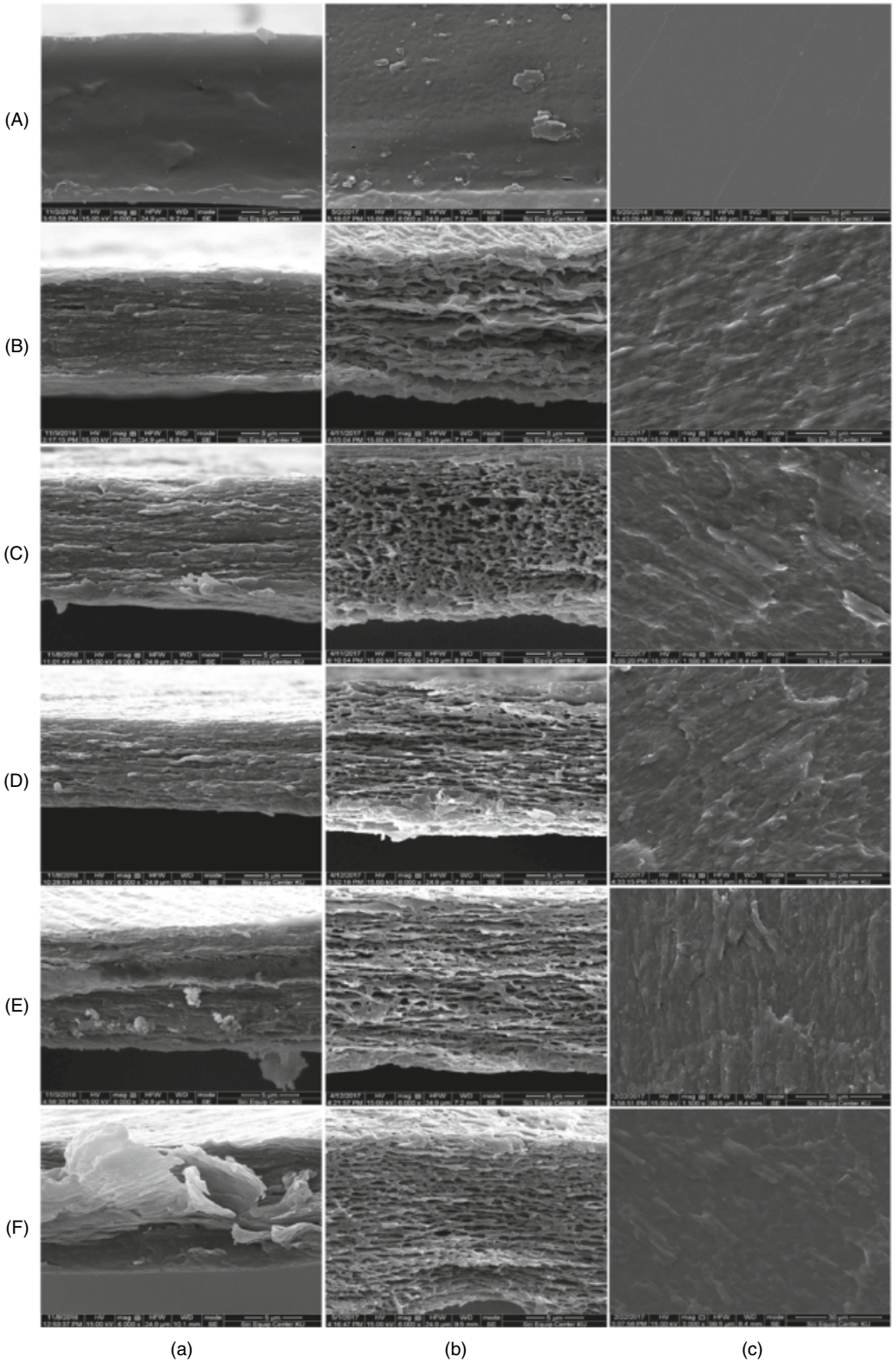


**FIGURE 14.21** (a) SEM micrographs of tensile fractured surfaces (in MD), (b) SEM micrographs of cryogenically fractured surfaces after immersion in 6 N of HCl solution at ambient temperature for 3 h, and (c) SEM micrographs of film surfaces of different film samples: (A) PLA, (B) PLA/TPS blend, and (C–F) PLA/TPS/OLA-*g*-starch blends containing different concentrations of OLA-g-starch: (C) 1 wt%, (D) 2 wt%, (E) 3 wt%, and (F) 5 wt%. *Source:* Reprinted from Ref. 346. Copyright 2020, Reproduced with permission from Elsevier.

behavior when the $T_g$ of PLA drops below 35°C [260]. Ductility of PLA increased with the increase in the plasticizer content (Figure 14.22) [355]. Low-molecular-weight molecules such as tributyl citrate (TBC), triethyl citrate (TEC), lactide molecules, diethyl bis(hydroxymethyl), and triacetin are effective plasticizers for PLA below 25% concentration of plasticizer [349, 356, 357]. An increase in the molecular weight decreases the efficiency of the plasticizer [355] and can lead to phase separation. Plasticizer tends to migrate upon aging, which leads to increase in the crystallinity. High-molecular-weight plasticizers tend to show phase separation from the PLA matrix. The higher the plasticizer content, the higher is the chain mobility of PLA, which leads to faster cold crystallization.

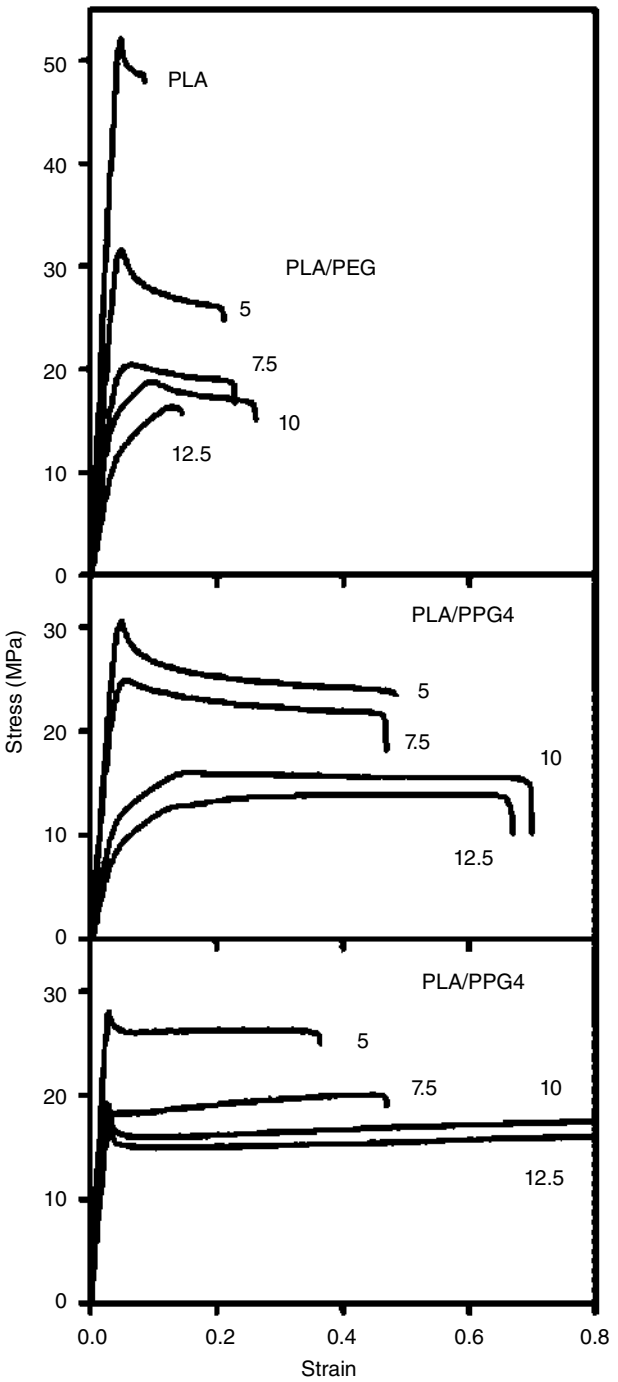


**FIGURE 14.22** Stress–strain plots for neat PLA, PLA/PPG4 ($M_w$ = 425 g/mol), PLA/PPG1 ($M_w$ = 1000 g/mol), and PLA/PEG blends. PPG: poly(propylene glycol); PEG: poly(ethylene glycol). Plasticizer content indicated in the figure, using numbers 5, 7.5, 10, and 12.5. *Source:* Reprinted from Ref. 355. Copyright 2006, Reproduced with permission from Elsevier.

PEG ($M_w$ < 20 kDa) acts as an efficient plasticizer for PLA [260, 353]. The decrease in the $T_g$ of PLA is directly related to the amount of plasticizer. Details about the effect of PEG in PLA blends are explained in Section 14.3.7.1. Li et al. [358] plasticized PLA with 10% PEG, with $M_w$ varying from 400 to 4000 g/mol, using a twin-screw extruder. A significant decrease in $T_g$ along with increase in strain was reported in all the compositions, supporting the plasticization effect. A larger drop in the $T_g$ was observed with lower $M_w$ PEG plasticizers. PLA-10% PEG 400 ($M_w$ = 400 g/mol) had a $T_g$ of 39°C, whereas PLA-10% PEG 4000 ($M_w$ = 4000 g/mol) had a $T_g$ of 44°C. PEG crystallizes with aging, leading to phase separation. Aging increases the modulus and crystallinity of the PEG/PLA system. After 500 h of aging at 23°C and 50% RH, elongation at break of PLA/PEG 30% blends dropped from 500 to 250% [260]. A further increase in the aging to 1800 h did not significantly affect the tensile properties. The increase in the crystallinity can be correlated to enhanced mobility of the polymer chain with the addition of the plasticizer [260]. It was also observed that aging leads to the development of spherulites in the PLA. Figure 14.23 shows polarized light microscopy of PEG/PLA. The PEG/PLA blend had spherulites 70 μm in diameter. Aging significantly increased the spherulite density of the PEG/PLA [260].

Citrate plasticizers are nontoxic and approved for various food packaging and medical applications. Due to favorable solubility parameters and low molecular weight, PLA is miscible with TBC and TEC (Table 14.7) [359]. The good solubility of PLLA with TEC and TBC can also be attributed to the polar interaction between the ester groups in PLA and the citrate plasticizers. However, the boiling point of these plasticizers is close to the processing temperature of PLLA, leading to probable partial evaporation of the plasticizer during extrusion. The $T_g$ of PLLA decreases linearly with an increase in the TBC content [349]. Ljungberg and Wesslen [350] investigated the plasticization of PLA with TBC oligomers. They showed that at lower molecular weights of TBC, the migration from the bulk of PLLA to the film surface is higher. To overcome this migration issue, they increased the molecular weight of TBC. TBC trimers and heptamers prepared by transesterification were added at 10, 15, and 20 wt% to the PLA matrix. Low-molecular-weight molecules were more effective as plasticizers. Phase

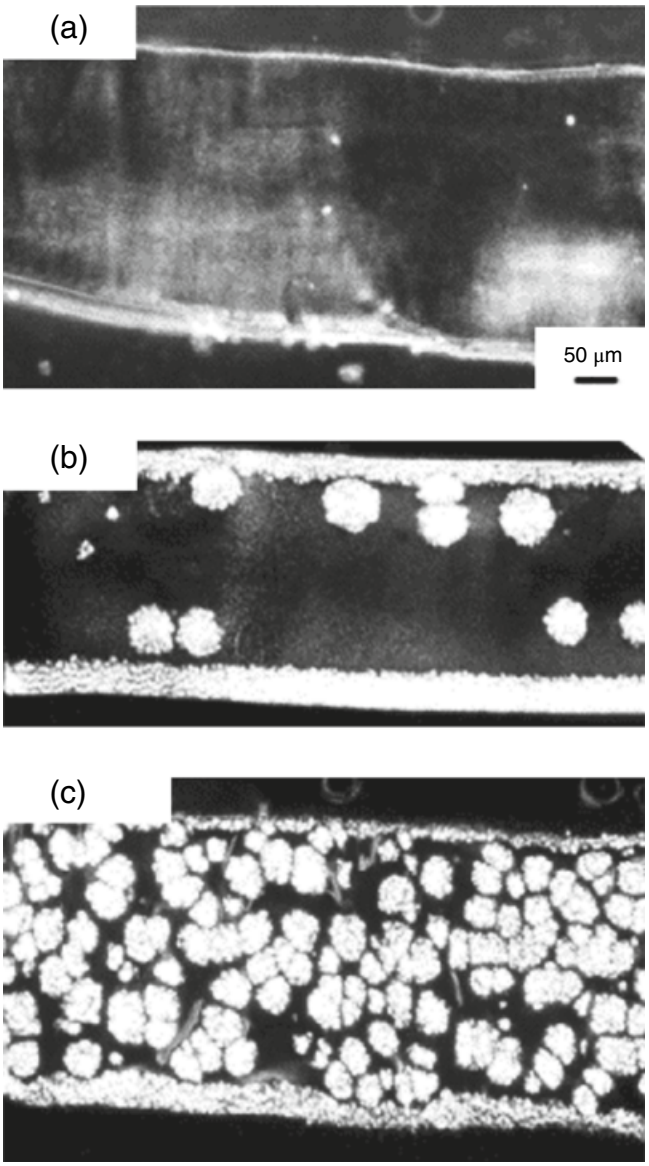


**FIGURE 14.23** Cross sections of the PLA/PEG 70/30 blend as viewed in the polarizing light microscope after aging at ambient conditions for different periods of time: (a) 0.2 h, (b) 75 h, and (c) 1800 h. *Source:* Reprinted from Ref. 260. Copyright 2003, Reproduced with permission from Elsevier.

separation occurred in TBC trimer at 10 and 15 wt%. For 20 wt% TBC trimer in the PLA matrix, migration was observed. High-molecular-weight plasticizer molecules reached saturation at a lower weight percentage.

Yang et al. [360] produced PLA cross-linked with 0.5 wt% triallyl isocyanurate (TAIC) and 0.5 wt% DCP, plasticized with dioctyl phthalate (DOP) plasticizer. Cross-linking helped in improving the thermal stability of PLA, and plasticization helped in dispersing the cross-linking agents. The addition of 15% DOP completely separated the agglomerated cross-linked particles, and 10% DOP decreased the $T_g$ of cross-linked PLA to 41 from 58°C and increased the elongation at break to 147%. The $T_m$ of PLA also dropped from 179 to 161°C. Nonhomogeneous blends and phase separation were observed for 12.5 and 15% DOP in PLA. SEM micrographs obtained from fractured surfaces revealed DOP droplets in the PLA matrix at 15% DOP concentration (Figure 14.24) [360].

**TABLE 14.7 Hansen Solubility Parameters of PLA and Popular Plasticizers [359]**

| | $\delta_D$ | $\delta_P$ | $\delta_H$ | Molar Volume | Distance |
|---|---|---|---|---|---|
| Poly(lactic acid) | 18.88 | 4.61 | 7.61 | 72.4 | — |
| Lactide monomers | 17 | 8.3 | 28.4 | 73.8 | 21.4 |
| Diethylene glycol | 16.6 | 12 | 20.7 | 94.9 | 15.7 |
| Diethyl malonate | 16.1 | 7.7 | 8.3 | 152.5 | 6.4 |
| Triacetine | 16.5 | 4.5 | 9.1 | 188.2 | 5.0 |
| Acetyl triethyl citrate | 16.6 | 3.5 | 8.6 | 279.9 | 4.8 |
| Tri-n-butyl citrate (TBC) | 16.6 | 3.8 | 10.1 | 345.5 | 5.3 |
| Triethyl citrate | 16.5 | 4.9 | 12 | 243 | 6.5 |
| Glycerol | 17.4 | 12 | 29.3 | 73.3 | 23.1 |

*Note*: PLA values were determined according to the Hansen solubility parameters method with 18 solvents and $R$ value = 5.6. The distance for the plasticizer was calculated according to distance = $[4(\delta_{Ds}-\delta_{Dp})^2+(\delta_{Ps}-\delta_{Pp})^2+(\delta_{Hs}-\delta_{Hp})^2]^{1/2}$; more explanation about this methodology can be obtained in Chapter 7 of the first edition. Unit for $\delta_D$, $\delta_P$, and $\delta_H$ is $MPa^{1/2}$ and for the molar volume is g/mol.

Hoglund et al. [361] evaluated the migration and hydrolysis of PLA, PLA plasticized with ATBC, and ATBC plasticized PLA surface grafted with acrylic acid at 37 and 60°C. The migration studies were conducted in deionized water for up to 364 days. ATBC plasticizer migrated from PLA to the water solution and hydrolyzed. The rate of degradation in the PLA plasticized with ATBC decreased compared with unplasticized PLA. It was observed that acrylic-acid-grafted oligomers migrated easily to the surface.

Burgos et al. [362] plasticized PLA with 15–25 wt% oligomeric lactic acid (OLA), due to the similar chemical structure and solubility parameter values of PLA ($19.5\,J^{1/2}\,cm^{3/2}$) and OLA ($17.7\,J^{1/2}\,cm^{3/2}$). Increase in the chain mobility as a function of plasticizer content was evident in the drop in the $T_g$, onset of cold crystallization and binodal melting peaks accredited to α and α′ crystals (generally reported when $T_{cc}$ of PLA < 100°C). As expected, the oxygen permeability increased, and tensile modulus ($E$) dropped as a function of the plasticizer content. To understand the effect of physical aging, samples stored at 23°C and 50% RH were tested using a tensile tester after 3, 10, 30, 60, and 90 days. Elongation at break of PLA (15%), which increased to ~175%, dropped to the value of the control (around 4%). However, PLA-20% OLA and PLA-25% OLA maintained their ductile-flexible behavior up to 90 days.

In summary, as for other polymers, small molecules are more efficient plasticizers than large molecules for PLA, and miscibility of PLA with a plasticizer from the same chemical

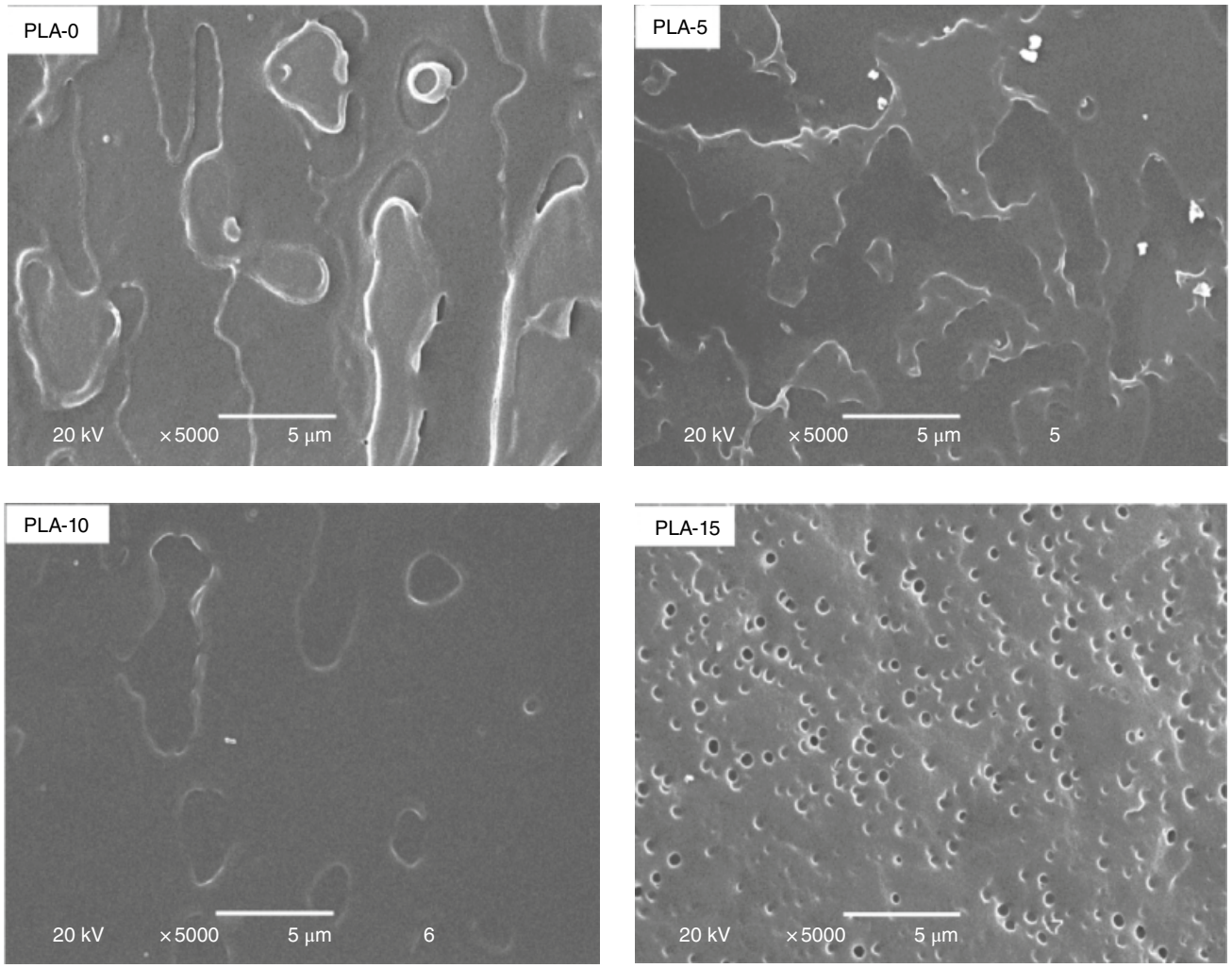


**FIGURE 14.24** SEM micrographs of the fracture surfaces of the samples: cross-linked PLA and the blends of cross-linked PLA with 5, 10, and 15 wt% of DOP. *Source:* Reprinted from Ref. 360, Copyright 2009, Reproduced with permission from John Wiley & Sons, Inc.

family decreases with an increase in the molecular weight of the plasticizer [363]. This can be ascribed to the fact that low-molecular-weight plasticizers have higher entropy of mixing compared to high-molecular-weight plasticizers. Aging leads to an increase in crystallization and phase separation.

## 14.5 CONCLUSIONS

PLA blends with nonbiodegradable polymers, biodegradable polymers, and plasticized PLA compositions were summarized in this chapter. Most of the PLA blends are immiscible or partly miscible at best due to unfavorable thermodynamics. However, at times, excellent mechanical performance such as improved toughness can be obtained by blending partly miscible polymers at certain determined blending proportions. The performance is contingent on the constituent polymers, their phase morphology, and interfacial characteristics, which are dependent on viscoelastic behavior and processing history. The dispersed phase morphology has significant impact on the properties and mechanical performance of the final structure. Smaller particle size distribution is indicative of relatively better surface interaction and low surface tension. Comparable viscosities of blending polymers along with shear during processing may also contribute to better mixing and smaller drop size. Higher interfacial tension may lead to coalescence, which in turn would generate bigger droplet size of the dispersed phase. Some polymers such as PMMA and poly(vinyl acetate-*co*-vinyl alcohol) have been found to be miscible with PLA. Existence of co-crystallized domains in PLLA-PMMA support good miscibility. In most cases, various polymer modification or compatibilization

strategies such as the use of ternary and block copolymers helped reduce interfacial tension and produce blends with desired properties. It was also observed by various researchers that melt extrusion processing allowed better dispersion and morphology compared to solvent casting. This could be explained by the fact that melt blending is done at higher temperature leading to chemical reactions such as transesterification in the case of polyesters, in addition to other favorable rheological effects such as shear thinning.

## REFERENCES


1. Nova Institute, European bioplastics. Bioplastics market data, Available from: https://www.european-bioplastics.org/market/. Accessed on 24 January 2021.
2. X. Zhao, H. Hu, X. Wang, X. Yu, W. Zhou, S. Peng, Super tough poly(lactic acid) blends: a comprehensive review, *RSC Adv.* **2020**, *10*, 13316–13368.
3. L. T. Lim, R. Auras, M. Rubino, Processing technologies for poly(lactic acid), *Prog. Polym. Sci.* **2008**, *33*, 820–852.
4. R. Auras, B. Harte, S. Selke, An overview of polylactides as packaging materials, *Macromol. Biosci.* **2004**, *4*, 835–8640.
5. E. Castro-Aguirre, F. Iniguez- Franco, H. Samsudin, X. Fang, R. Auras, Poly(lactic acid)-mass production, processing, industrial, and end of life, *Adv. Drug Deliv. Rev.* **2016**, *107*, 333–366.
6. K. S. Anderson, S. H. Lim, M. A. Hillmyer, Toughening of polylactide by melt blending with linear low-density polyethylene, *J. Appl. Polym. Sci.* **2003**, *89*, 3757–3768.
7. Y. F. Kim, C. N. Choi, Y. D. Kim, K. Y. Lee, M. S. Lee, Compatibilization of immiscible poly (L-lactide) and low-density polyethylene blends, *Fibers Polym.* **2004**, *5*, 270–274.
8. C. M. Thurber, Y. Xu, J. C. Myers, T. P. Lodge, C. W. Macosko, Accelerating reactive compatibilization of PE/PLA blends by an interfacially localized catalyst, *ACS Macro Lett.* **2015**, *4*(1), 30–33.
9. H.-Z. Li, S.-C. Chen, Y.-Z. Wang, Thermoplastic PVA/PLA blends with improved processability and hydrophobicity, *Ind. Eng. Chem. Res.* **2014**, *53*(44), 17355–17361.
10. X. Liao, H. Zhang, Y. Wang, L. Wu, G. Li, Unique interfacial and confined porous morphology of PLA/PS blends in supercritical carbon dioxide, *RSC Adv.* **2014**, *4*, 45109–45117.
11. R. Nehra, S. N. Maiti, J. Jacob, Analytical interpretations of static and dynamic mechanical properties of thermoplastic elastomer toughened PLA blends, *J. Appl. Polym. Sci.* **2018**, *135*, 45644.
12. K. Pongtanayut, C. Thongpin, O. Santawitee, The effect of rubber on morphology, thermal properties and mechanical properties of PLA/NR and PLA/ENR blends, *Energy Procedia* **2013**, *34*, 888–897.
13. S. Ishida, R. Nagasaki, K. China, T. Dong, Y. Inoue, Toughening of poly(L-lactide) by melt blending with rubbers, *J. Appl. Polym. Sci.* **2009**, *113*, 558–566.
14. P. Muller, J. Bere, E. Fekete, J. Moczo, B. Nagy, M. Kallay, B. Gyarmati, B. Pukanszky, Interactions, structure and properties in PLA/plasticized starch blends, *Polymer* **2016**, *103*, 9–18.
15. R. Nasseri, R. Ngunjiri, C. Moresoli, A. Yu, Z. Yuan, C. Xu, Poly(lactic acid)/acetylated starch blends: effect of starch acetylation on the material properties, *Carbohydr. Polym.* **2020**, *229*, 115453.
16. X. Chen, S. L. McGurk, M. C. Davis, C. J. Roberts, K. M. Shakesheff, S. J. B. Tendler, P. M. Williams, J. Davies, A. C. Dwakes, A. Domb, Chemical and morphological analysis of surface enrichment in a biodegradable polymer blend by phase-detection imaging atomic force microscopy, *Macromolecules* **1998**, *31*, 2278–2283.
17. I. Burzic, C. Pretschuh, D. Kaineder, G. Eder, J. Smilek, J. Masilko, W. Kateryna, Impact modification of PLA using bio-based biodegradable PHA biopolymers, *Eur. Polym. J.* **2019**, *114*, 32–38.
18. M. Nofar, A. Tabatabaei, H. Sojoudiasli, C. B. Park, P. J. Carreau, M. C. Heuzey, M. R. Kamal, Mechanical and bead foaming behavior of PLA-PBAT and PLA-PBSA blends with different morphologies, *Eur. Polym. J.* **2017**, *90*, 231–244.
19. R. Al-Itry, K. Lammnawar, A. Maazouz, Rheological, morphological, and interfacial properties of compatibilized PLA/PBAT blends, *Rheol. Acta* **2014**, *53*, 501–517.
20. E. Quero, A. J. Muller, F. Signori, M.-B. Coltelli, S. Bron, Isothermal cold-crystallization of PLA/PBAT blends with and without the addition of acetyl tributyl citrate, *Macromol. Chem. Phys.* **2012**, *213*, 36–48.
21. Z. Kulinski, E. Piorkowska, Crystallization, structure and properties of plasticized poly(L-lactide), *Polymer* **2005**, *46*, 10290–10300.
22. R. N. Darie-Nita, C. Vasile, A. Irimia, R. Lipsa, M. Rapa, Evaluation of some eco-friendly plasticizers for PLA films processing, *J. Appl. Polym. Sci.* **2016**, *133*, 43223.
23. J.-B. Zeng, K.-A. Li, A.-K. Du, Compatibilization strategies in poly(lactic acid)-based blends, *RSC Adv.* **2015**, *41*(5), 32546–32565.
24. S. Mishra, R. Sahoo, L. Unnikrishnan, A. Ramadoss, S. Mohanty, S. K. Nayak, Enhanced structural and dielectric behaviour of PVDF-PLA binary polymeric blend system, *Mater. Today Commun.* **2021**, *26*, 101958.
25. C. R. Lopez-Barron Rheological and morphological study of cocontinuous polymer blends during coarsening, *J. Rheol.* **2012**, *56*, 1315.
26. S. Biswas, S. S. Panja, S. Bose, Tailored distribution of nanoparticles in bi-phasic polymeric blends as emerging materials for suppressing electromagnetic radiation: challenges and prospects, *J. Mater. Chem. C* **2018**, *6*, 3120–3142.
27. S. Kasmi, A. Gallos, J. Beaugrand, G. Païs, F. Allais, Ferulic acid derivatives used as biobased powders for a convenient plasticization of polylactic acid in continuous hot-melt process, *Eur. Polym. J.* **2019**, *110*, 293–230.
28. K. Adamska, A. Voelkel, A. Berlinska, The solubility parameter for biomedical polymers—application of inverse gas chromatography, *J. Pharm. Biomed. Anal.* **2016**, *127*, 202–206.


29. J. Y. Park, S. Y. Hwang, W. J. Yoon, E. S. Yoo, S. S. Im, Compatibility and physical properties of poly(lactic acid)/poly(ethylene terephthalate glycol) blends, *Macromol. Res.* **2012**, *20*, 1300–1306.
30. R. P. White, J. E. G. Lipson. Free volume, cohesive energy density, and internal pressure as predictors of polymer miscibility, *Macromolecules* **2014**, *47*, 3959–3968.
31. A. D. Glova, S. G. Falkovich, D. I. Dmitrienko, A. V. Lyulin, S. V. Larin, S. V. Nazarychev, M. Karttunen, S. V. Lyulin, Scale-dependent miscibility of polylactide and polyhydroxybutyrate: molecular dynamics simulations, *Macromolecules* **2018**, *51*(2), 552–56.
32. A. M. Zolali, B. D. Favis, Toughening of cocontinuous polylactide/polyethylene blends via an interfacially percolated intermediate phase, *Macromolecules* **2018**, *51*(10), 3572–3581.
33. Y. Xu, J. Loi, P. Delgado, V. Topolkaraev, R. J. McEneany, C. W. Macosko, M. A. Hillmyer, Reactive compatibilization of polylactide/polypropylene blends, *Ind. Eng. Chem. Res.* **2015**, *23*, 6108–6114.
34. Y. Wang, M. A. Hillmyer, Polyethylene-poly(L-lactide) diblock copolymers: synthesis and compatibilization of poly(L-lactide)/polyethylene blends, *J. Polym. Sci. A Polym. Chem.* **2001**, *39*, 2755–2766.
35. K. S. Anderson, M. A. Hillmyer, The influence of block copolymer microstructure on the toughness of compatibilized polylactide/polyethylene blends, *Polymer* **2004**, *45*(26), 8809–8823.
36. S. Wu, A generalized criterion for rubber toughening, *J. Appl. Polym. Sci.* **1998**, *35*, 549–561.
37. A. Kathuria, M. G. Abiad, R. Auras. Toughening of poly(L-lactic acid) with $Cu_3BTC_2$ metal organic framework crystals, *Polymer* **2013**, *54*, 6967–6986.
38. A. V. Machado, I. Moura, F. M. Duarte, G. Botelho, R. Nogueira, A. G. Brito, Evaluation of properties and biodeterioration potential of polyethylene and aliphatic polyesters blends, *Int. Polym. Process.* **2007**, *22*, 512–518.
39. Z. Su, Q. Li, Y. Liu, H. Xu, W. Guo, C. Wu, Phase structure of compatibilized poly(lactic acid)/linear low-density polyethylene blends, *J. Macromol. Sci. Part B* **2009**, *48*, 823–833.
40. J. Wang, B. H. Lessard, M. Maric, B. D. Favis, Hierarchically porous polymeric materials from ternary polymer blends, *Polymer* **2014**, *55*, 3461–3467.
41. A. T. Hedegaard, L. Gu, C. W. Macosko, Effect of extensional viscosity on cocontinuity of immiscible polymer blends, *J. Rheol.* **2015**, *59*, 1397.
42. L. Gu, C. W. Macosko, Evaluating PE/PLA interfacial tension using ternary immiscible polymer blends, *J. Appl. Polym. Sci.* **2021**, *138*: e50623 (1–5).
43. Z. Bai, Q. Dou, Rheology, morphology, crystallization behaviors, mechanical and thermal properties of poly(lactic acid)/polypropylene/maleic anhydride-grafted polypropylene blends, *J. Polym. Environ.* **2018**, *26*, 959–969.
44. T. W. Yoo, H. G. Yoon, S. J. Choi, M. S. Kim, Y. H. Kim, W. N. Kim, Effects of compatibilizers on the mechanical properties and interfacial tension of polypropylene and poly(lactic acid) blends, *Macromol. Res.* **2010**, *18*, 583–588.
45. H. S. Lee, J. D. Kim, Effect of a hybrid compatibilizer on the mechanical properties and interfacial tension of a ternary blend with polypropylene, poly(lactic acid), and a toughening modifier, *Polym. Compos.* **2012**, *33*, 1154–1161.
46. H.. Ebadi-Dehaghani, H. A. Khonakdar, M. Barikani, S. H. Jafari, U. Wagenknech, An investigation on compatibilization threshold in the interface of polypropylene/polylactic acid blends using rheological studies, *J. Vinyl Addit. Technol.* **2016**, *22*, 19–28.
47. G. Biresaw, C. J. Carriere, Interfacial tension of poly(lactic acid)/polystyrene blends, *J. Polym. Sci. B* **2002**, *40*, 2248–2258.
48. P. Sarazin, B. D. Favis, Morphology control in co-continuous poly(L-lactide)/polystyrene blends: a route towards highly structured and interconnected porosity in poly(L-lactide) materials, *Biomacromolecules* **2003**, *4*, 1669–1679.
49. G. Biresaw, C. Carriere, Compatibility and mechanical properties of blends of polystyrene with biodegradable polyesters, *Compos. A: Appl. Sci. Manuf.* **2004**, *35*, 313–320.
50. A. Mohamed, S. H. Gordon, G. Biresaw, Poly(lactic acid)/polystyrene bioblends characterized by thermogravimetric analysis, differential scanning calorimetry, and photoacoustic infrared spectroscopy, *J. Appl. Polym. Sci.* **2007**, *106*, 1689–1696.
51. F. C. Felker, G. Biresaw. Rheology and morphology of extruded blends of polystyrene with biodegradable polyesters, *J. Biobaased Mater. Bioenergy* **2007**, *1*, 401–408.
52. J. Y. Lim, J. C. Hansen, C. A. Siedlecki, R. W. Hengstebeck, J. Cheng, C. N. Winograd, H. J. Donahue, Osteoblast adhesion on poly(L-lactic acid)/polystyrene demixed thin film blends: effect of nanotopography, surface chemistry, and wettability, *Biomacromolecules* **2005**, *6*, 3319–3327.
53. B. O. Leung, A. P. Hitchcock, J. L. Brash, A. Scholl, A. Doran, Phase segregation in polystyrene-polylactide blends, *Macromolecules* **2009**, *42*, 1679–1684.
54. B. O. Leung, A. P. Hitchcock, R. Cornelius, J. L. Brash, A. Scholl, A. Doran, X-ray spectromicroscopy study of protein adsorption to a polystyrene-polylactide blend, *Biomacromolecules* **2009**, *10*, 1838–1845.
55. Z. Yuan, B. D. Favis, Macroporous poly(L-lactide) of controlled pore size derived from the annealing of co-continuous polystyrene/poly(L-lactide) blends, *Biomaterials* **2004**, *25*, 2161–2170.
56. D. Yao, W. Zhang, J. G. Zhou, Controllable growth of gradient porous structures, *Biomacromolecules* **2009**, *10*, 1282–1286.
57. P. Salehi, P. Sarazin, B. D. Favis, Porous devices derived from co-continuous polymer blends as a route for controlled drug release, *Biomacromolecules* **2008**, *9*, 1131–1138.
58. P. Sarazin, N. Virgilio, B. D. Favis, Influence of the porous morphology on the in vitro degradation and mechanical properties of poly(L-lactide) disks, *J. Appl. Polym. Sci.* **2006**, *100*, 1039–1047.
59. L. Jiang, B. Liu, J. Zhang, Properties of poly(lactic acid)/poly(butylene adipate-*co*-terephthalate)/nanoparticle ternary composites, *Ind. Eng. Chem. Res.* **2009**, *48*, 7594–7602.
60. Z. Xiang, P. Sarazin, B. D. Favis, Controlling burst and final drug release times from porous polylactide devices derived

from co-continuous polymer blends, *Biomacromolecules* **2009**, *10*, 2053–2066.

61. M. Kaseem, Y. G. Ko, Melt flow behavior and processability of polylactic acid/polystyrene (PLA/PS) polymer blends, *J. Polym. Environ.* **2017**, *25*, 994–998.
62. X. Zuo, Y. Xue, L. Wang, Y. Zhou, Y. Yin, Y.-C. Chuang, C.-C. Chang, R. Yin, M. H. Rafailovich, Y. Guo. Engineering styrenic blends with poly(lactic acid), *Macromolecules* **2019**, *52*, 20, 7547–7556.
63. M. R. Landry, D. J. Massa, C. J. T. Landry, D. M. Teegarden, R. H. Colby, T. E. Long, P. M. Henrichs, A survey of polyvinylphenol blend miscibility, *J. Appl. Polym. Sci.* **1994**, *54*, 991–1011.
64. D. J. T. Hill, A. K. Whittaker, K. W. Wong. Miscibility and specific interactions in blends of poly(4-vinylphenol) and poly(2-ethoxyethyl methacrylate), *Macromolecules* **1999**, *32*, 5285–5291.
65. L. T. Lee, E. M. Woo, Miscible blends of poly(4-vinyl phenol)/poly (trimethylene terephthalate), *Polym. Int.* **2004**, *53*, 1813–1820.
66. J. Wang, M. K. Cheung, Y. L. Mi, Miscibility and morphology in crystalline/amorphous blends of poly(caprolactone)/poly(4-vinylphenol) as studied by DSC, FTIR, and $^{13}C$ solid state NMR, *Polymer* **2002**, *43*, 1357–1364.
67. S. W. Kuo, F. C. Chang. Effect of inert diluent segment on the miscibility behavior of poly(vinylphenol) with poly(acetoxystyrene) blends, *J. Polym. Sci. B* **2002**, *40*, 1661–1672.
68. L. L. Zhang, S. H. Goh, S. Y. Lee, Miscibility and crystallization behavior of poly(L-lactide)/poly(*p*-vinylphenol) blends. *Polymer* **1998**, *39*, 4841–4847.
69. H. L. Chen, H. H. Liu, J. S. Lin, Microstructure of semicrystalline poly(L-lactide)/poly(4-vinylphenol) blends evaluated from SAXS absolute intensity measurement, *Macromolecules* **2000**, *33*, 4856–4860.
70. E. Meaurio, E. Zuza, J. R. Sarasua, Miscibility and specific interactions in blends of poly(L-lactide) with poly(vinylphenol), *Macromolecules* **2005**, *38*, 1207–1215.
71. L. L. Zhang, S. H. Goh, S. Y. Lee. Miscibility and phase behavior of poly(D,L-lactide)/poly(*p*-vinylphenol) blends, *J. Appl. Polym. Sci.* **1998**, *70*, 811–816.
72. E. Meaurio, E. Zuza, J. R. Sarasua, Direct measurement of the enthalpy of mixing in miscible blends of poly(DL-lactide) with poly(vinylphenol), *Macromolecules* **2005**, *38*, 9221–9228.
73. E. Zuza, E. Meaurio, A. Etxeberria, J. R. Sarasua, Exothermal process in miscible polylactide/poly(vinyl phenol) blends: mixing enthalpy or chemical reaction? *Macromol. Rapid Commun.* **2006**, *27*, 2026–2031.
74. S. H. Li, E. M. Woo, Kinetic analysis on effect of poly(4-vinyl phenol) on complex-forming blends of poly(L-lactide) and poly(D-lactide), *Polym. J.* **2009**, *41*, 374–382.
75. S. Nurkhamidah, E. M. Woo, Mechanisms of multiple types of lamellae and spherulites in poly(L-lactic acid) interacting with poly(4-vinyl phenol), *Macromol. Chem. Phys.* **2013**, *214*, 2345–2354.
76. A. Katada, Y. F. Buys, Y. Tominaga, S. Asai, M. Sumita, Relationship between electrical resistivity and particle dispersion state for carbon black filled poly(ethylene-*co*-vinyl acetate)/poly(L-lactic acid) blend, *Colloid Polym. Sci.* **2005**, *284*, 134–141.
77. S. E. M. Selke, J. D. Culter, R. J. Hernandez, *Plastics Packaging: Properties, Processing, Applications, and Regulations*, Hanser Gardner Publications, Cincinnati, OH, 2004.
78. P. Ma, D. G. Hristova-Bogaerds, J. G. P. Goossens, A. B. Spoelstra, Y. Zhang, P. J. Lemstra, Toughening of poly(lactic acid) by ethylene-*co*-vinyl acetate copolymer with different vinyl acetate contents, *Eur. Polym. J.* **2012**, *48*, 146–154.
79. J.-S. Yoon, S.-H. Oh, M.-N. Kim, I.-J. Chin, Y.-H. Kim, Thermal and mechanical properties of poly(L-lactic acid) poly(ethylene-*co*-vinyl acetate) blends, *Polymer* **1999**, *40*, 2303–2312.
80. H. M. Dollinger, S. P. Sawan, *Polym. Prepr.* **1990**, *31*, 442–443.
81. H. M. Dollinger, S. P. Sawan. *ACS Symp. Ser.* **1991**, *469*, 181–193.
82. H. M. Burt, J. K. Jackson, S. K. Bains, R. T. Liggins, A. M. Oktaba, A. L. Arsenault, W. L. Hunter, Controlled delivery of taxol from microspheres composed of a blend of ethylene-vinyl acetate copolymer and poly (D,L-lactic acid), *Cancer Lett.* **1995**, *88*, 73–79.
83. E. R. Kenawy, G. L. Bowlin, K. Mansfield, J. Layman, D. G. Simpson, E. H. Sanders, G. E. Wnek, Release of tetracycline hydrochloride from electrospun poly(ethylene-*co*-vinylacetate), poly(lactic acid), and a blend, *J. Control. Release* **2002**, *81*, 57–64.
84. J. K. Jackson, C. M. K. Springate, W. L. Hunter, H. M. Burt, Neutrophil activation by plasma opsonized polymeric microspheres: inhibitory effect of Pluronic F127, *Biomaterials* **2000**, *21*, 1483–1491.
85. N. Zhang, X. Lu, Morphology and properties of super-toughened bio-based poly(lactic acid)/poly(ethylene-*co*-vinyl acetate) blends by peroxide-induced dynamic vulcanization and interfacial compatibilization, *Polym. Test.* **2016**, *56*, 354–363.
86. C. M. Lee, E. S. Kim, J. S. Yoon, Reactive blending of poly(L-lactic acid) with poly(ethylene-*co*-vinyl alcohol), *J. Appl. Polym. Sci.* **2005**, *98*, 886–890.
87. Z. Gui, W. Zhang, C. Lu, S. Cheng, Improving the barrier properties of poly(lactic acid) by blending with poly(ethylene-*co*-vinyl alcohol), *J. Marcomol. Sci. Part B* **2013**, *52*, 685–700.
88. P. Warangkhana, J. C. Sadhan, M. Rathanawan, Preparation and characterization of reactive blends of poly(lactic acid), poly(ethylene-*co*-vinyl alcohol), and poly(ethylene-*co*-glycidyl methacrylate), *AIP Conf. Proc.* **2015**, *1664*, 030007.
89. Y. Li, H. Shimizu, Improvement in toughness of poly(L-lactide) (PLLA) through reactive blending with acrylonitrile–butadiene–styrene copolymer (ABS): morphology and properties, *Eur. Polym. J.* **2009**, *45*, 738–746.
90. T. Abt, M. R. Kamrani, J. Cailloux, O. Santana, M. Sanchez-Soto, Modification of poly(lactic) acid by reactive extrusion and its melt blending with acrylonitrile-butadiene-styrene, *Polym. Int.* **2020**, *69*, 794–803.

91. F. Carrasco, O. O. Santana, J. Cailloux, M. Sanchez-Soto, M. L. Maspoch, Poly(lactic acid) and acrylonitrile-butadiene-styrene blends: influence of adding ABS-*g*-MAH compatibilizer on the kinetics of the thermal degradation, *Polym. Test.* **2018**, *67*, 468–476.
92. G. M. Kim, G. H. Michler, Micromechanical deformation processes in toughened and particle filled semicrystalline polymers. Part 2: Model representation for micro mechanical deformation processes, *Polymer* **1998**, *39*, 5699–5703.
93. J. Y. Lee, S. H. Kwon, I. J. Chin, H. J. Choi, Toughness and rheological characteristics of poly(lactic acid)/acrylic core-shell rubber blends, *Polym. Bull.* **2019**, *76*, 5483–5497.
94. S. Sohn, S. Kim, S. I. Hong, Synthesis and application of poly(butadiene-*g*-acrylonitrile–styrene) core–shell rubber particles for use in epoxy resin toughening. I. Synthesis of poly(butadiene-*g*-acrylonitrile–styrene). *J. Appl. Polym. Sci.* **1996**, *61*, 1259–1264.
95. T. N. Li, L. S. Turng, S. Q. Gong, K. Erlacher, Polylactide, nanoclay, and core-shell rubber composites, *Polym. Eng. Sci.* **2006**, *46*, 1419–1427.
96. Y. Wang, Q. Hu, T. Li, P. Ma, S. Zhang, M. Du, M. Chen, H. Zhang, W. Dong, Core–shell starch nanoparticles and their toughening of polylactide, *Ind. Eng. Chem. Res.* **2018**, *57*(39): 13048–13054.
97. H.-J. Jin, I.-J. Chin, M.-N. Kim, S.-H. Kim, J.-S. Yoon, Blending of poly(L-lactic acid) with poly(*cis*-1,4-isoprene), *Eur. Polym. J.* **2000**, *36*, 165–169.
98. C. H. Ho, C. H. Wang, C. I. Lin, Y. D. Lee, Synthesis and characterization of TPO–PLA copolymer and its behavior as compatibilizer for PLA/TPO blends, *Polymer* **2008**, *49*, 3902–3910.
99. M. Canetti, A. Cacciamani, F. Bertin, Miscible blends of polylactide and poly(methyl methacrylate): morphology, structure, and thermal behavior, *J. Polym. Sci. B Polym. Phys.* **2014**, *52*, 1168–1177.
100. Y. Guo, X. Zuo, Y. Xue, Y. Zhou, Z. Yang, Y. Chuang, C. Chang, G. Yuan, S. K. Satija, D. Gersappe, M. H. Rafailovich, Enhancing impact resistance of polymer blends via self-assembled nanoscale interfacial structures, *Macromolecules* **2018**, *51*, 3897–3910.
101. J. L. Eguiburu, J. J. Iruin, M. J. Fernandez-Berridi, J. San Roman, Blends of amorphous and crystalline polylactides with poly(methyl methacrylate) and poly(methyl acrylate): a miscibility study, *Polymer* **1998**, *39*, 6891–6897.
102. C. Samuel, J.-M. Raquez, P. Dubois, PLLA/PMMA blends: a shear-induced miscibility with tunable morphologies and properties, *Polymer* **2013**, *54*, 3931–3939.
103. X. Zuo, Y. Xue, Y. Zhou, Y. Yin, T.-D. Li, L. Wang, Y.-C. Chuang, M. H. Rafailovich, C. C. Chang, Y. Guo, The use of low cost, abundant, homopolymers for engineering degradable polymer blends: compatibilization of poly(lactic acid)/styrenics using poly(methyl methacrylate), *Polymer* **2020**, *186*, 122010.
104. G. Zhang, J. Zhang, S. Wang, D. Shen, Miscibility and phase structure of binary blends of polylactide and poly(methyl methacrylate), *J. Polym. Sci. B* **2003**, *41*, 23–30.
105. W. Lu, Z. Shuai, Z. Yanhua, Parallel advances in improving mechanical properties and accelerating degradation to polylactic acid, *Int. J. Biol. Macromol.* **2019**, *125*, 1093–1102.
106. B. S. Yao, A. V. Nawaby, X. Liao, R. Burk, *J. Cell. Plast.* **2007**, *43*, 385–398.
107. N. Kumar, R. S. Langer, A. J. Domb, Polyanhydrides: an overview, *Adv. Drug Deliv. Rev.* **2002**, *54*, 889–910.
108. L. S. Nair, C. T. Laurencin, Biodegradable polymers as biomaterials, *Prog. Polym. Sci.* **2007**, *32*, 762–798.
109. L. J. Suggs, S. A. Moore, A. G. Mikos, in: J. E. Mark (Ed.), *Physical Properties of Polymers Handbook*, Springer, New York, 2007.
110. A. J. Domb, Degradable polymer blends. I. Screening of miscible polymers, *J. Polym. Sci. A Polym. Chem.* **1993**, *31*, 1973–1981.
111. M. C. Davies, K. M. Shakesheff, A. G. Shard, A. Domb, C. J. Roberts, S. J. B. Tendler, P. M. Williams, Surface analysis of biodegradable polymer blends of poly(sebacic anhydride) and poly(DL-lactic acid), *Macromolecules* **1996**, *29*, 2205–2212.
112. K. M. Shakesheff, M. C. Davies, C. J. Roberts, S. J. B. Tendler, A. G. Shard, A. Domb, In situ atomic force microscopy imaging of polymer degradation in an aqueous environment, *Langmuir* **1994**, *10*, 4417–4419.
113. K. M. Shakesheff, X. Y. Chen, M. C. Davies, A. Domb, C. J. Roberts, S. J. B. Tendler, P. M. Williams, Relating the phase morphology of a biodegradable polymer blend to erosion kinetics using simultaneous in situ atomic force microscopy and surface plasmon resonance analysis, *Langmuir* **1995**, *11*, 3921–3927.
114. Z. Q. Zhang, X. M. Su, H. P. He, F. Q. Qu, Synthesis, characterization, and degradation of poly(anhydride-*co*-amide)s and their blends with polylactide, *J. Polym. Sci. A Polym. Chem.* **2004**, *42*, 4311–4317.
115. L. Chen, H. Wang, J. Wang, M. Chen, L. Shang, Ofloxacin-delivery system of a polyanhydride and polylactide blend used in the treatment of bone infection, *J. Biomed. Mater. Res. Part B Appl. Biomater.* **2007**, *83*, 589–595.
116. V. H. Sangeetha, R. B. Valapa, S. K. Nayak, T. O. Varghese. Super toughened renewable poly(lactic acid) based ternary blends system: effect of degree of hydrolysis of ethylene vinyl acetate on impact and thermal properties, *RSC Adv.* **2016**, *6*, 72681–72691.
117. J. H. Wu, C.-P. Wu, M. C. Kuo, Y. Tsui, Characterization and properties of reactive poly(lactic acid)/ethylene-vinyl alcohol copolymer blends with chain-extender, *J. Polym. Environ.* **2016**, *24*, 129–138.
118. X. Shuai, Y. He, N. Asakawa, Y. Inoue, Miscibility and phase structure of binary blends of poly(L-lactide) and poly(vinyl alcohol). *J. Appl. Polym. Sci.* **2001**, *81*, 762–772.
119. J.-T. Yeh, M.-C. Yang, C.-J. Wu, X. Wu, C.-S. Wu, Study on the crystallization kinetic and characterization of poly(lactic acid) and poly(vinyl alcohol) blends, *Polym. Plast. Technol. Eng.* **2008**, *47*, 1289–1296.
120. H. Tsuji, H. Muramatsu, Blends of aliphatic polyesters. IV. Morphology, swelling behavior, and surface and bulk

properties of blends from hydrophobic poly(L-lactide) and hydrophilic poly(vinyl alcohol), *J. Appl. Polym. Sci.* **2001**, *81*, 2151–2160.

121. S. S. Jawalkar, T. M. Aminabhavi, Molecular modeling simulations and thermodynamic approachesto investigate compatibility/incompatibility of poly(L-lactide)and poly(vinyl alcohol) blends, *Polymer* **2006**, *47*, 8061–8071.
122. J. W. Park, S. S. Im, Miscibility and morphology in blends of poly(L-lactic acid) and poly(vinyl acetate-*co*-vinyl alcohol), *Polymer* **2003**, *44*, 4341–4354.
123. H. Tsuji, H. Muramatsu, Blends of aliphatic polyesters: V non-enzymatic and enzymatic hydrolysis of blends from hydrophobic poly(L-lactide) and hydrophilic poly(vinyl alcohol), *Polym. Degrad. Stab.* **2001**, *71*, 403–413.
124. A. M. Gajria, V. Dave, R. A. Gross, S. P. McCarthy, Miscibility and biodegradability of blends of poly(lactic acid) and poly(vinyl acetate), *Polymer* **1996**, *37*, 437–444.
125. J. P. Mahalik, G. Madras Enzymatic degradation of poly(D, L-lactide) and its blends with poly(vinyl acetate), *J. Appl. Polym. Sci.* **2006**, *101*, 675–680.
126. G. Zhang, J. Zhang, X. Zhou, D. Shen, Miscibility and phase structure of binary blends of polylactide and poly (vinylpyrrolidone), *J. Appl. Polym. Sci.* **2003**, *88*, 973–979.
127. M. Teodorescu, M. Bercea, Poly(vinylpyrrolidone)—a versatile polymer for biomedical and beyond medical applications, *Polym. Plast. Technol. Eng.* **2015**, *54*, 923–943.
128. C.-C. Chi, S.-H. Wang, T.-T. Kuo, Localized cutaneous polyvinylpyrrolidone storage disease mimicking cheilitis granulomatosa, *J. Cutan. Pathol.* **2006**, *33*, 454–457.
129. A. K. Andrianov, A. Marin, P. Peterson, Water-soluble biodegradable polyphosphazenes containing *N*-ethylpyrrolidone groups, *Macromolecules* **2005**, *38*, 7972–7976.
130. Z. Xing, T. Xie, G. Yang, Novel biodegradable amphiphilic poly(*e*-caprolactone)/poly(*N*-vinylpyrrolidone) blends via successive in situ polymerizations, *J. Appl. Polym. Sci.* **2009**, *111*, 1676–1683.
131. M. M. Feldstein, G. A. Shandryuk, S. A. Kuptsov, N. A. Plate, Coherence of thermal transitions in poly(*N*-vinyl pyrrolidone)–poly(ethylene glycol) compatible blends 1. Interrelations among the temperatures of melting, maximum cold crystallization rate and glass transition, *Polymer* **2000**, *41*, 5327–5338.
132. S. N. Cassu, M. I. Felisberti, Poly(vinyl alcohol) and poly(vinyl pyrrolidone) blends: miscibility, microheterogeneity and free volume change, *Polymer* **1997**, *38*, 3907–3911.
133. Y. Morita, H. Saino, K. Tojo, Polymer blend implant for ocular delivery of fluorometholone, *Biol. Pharm. Bull.* **1998**, *21*, 72–75.
134. M. Bognitzki, T. Frese, M. Steinhart, A. Greiner, J. H. Wendorff, A. Schaper, M. Hellwig, Preparation of fibers with nanoscaled morphologies: Electrospinning of polymer blends, *Polym. Eng. Sci.* **2001**, *41*, 982–989.
135. R. F. Bonan, P. R. F. Bonan, A. U. D. Batista, Poly(lactic acid)/poly(vinyl pyrrolidone) membranes produced by solution blow spinning: structure, thermal, spectroscopic, and microbial barrier properties, *J. Appl. Polym. Sci.* **2017**, *134*, 44802.
136. I. Fortelny, A. Ujcic, L. Fambi, and M. Slouf, Phase structure, compatibility, and toughness of PLA/PCL blends: a review, *Front. Mater.* **2019**, *6*, 206.
137. J. S. Lyu, J.-S. Lee, J. Han, Development of a biodegradable polycaprolactone film incorporated with an antimicrobial agent via an extrusion process, *Sci. Rep.* **2019**, *9*, 20236.
138. O. S. Manoukian, M. R. Arul, N. Sardashti, T. Stedman, R. James, S. Rudraiah, S. G. Kumbar, Biodegradable polymeric injectable implants for long-term delivery of contraceptive drugs, *J. Appl. Polym. Sci.* **2018**, *134*(14), 46068.
139. S. Wachirahuttapong, C. Thongpin, N. Sombatsompop, Effect of PCL and compatibility contents on the morphology, crystallization and mechanical properties of PLA/PCL blends, *Energy Procedia* **2016**, *89*, 198–206.
140. B. Imre, B. Pukanszky, Compatibilization in bio-based and biodegradable polymer blends, *Eur. Polym. J.* **2013**, *49*, 1215–1233.
141. A. Ostafinska, I. Fortelny, M. Nevoralova, J. Hodan, J. Kredatusova, M. Slouf, Synergistic effects in mechanical properties of PLA/PCL blends with optimized composition, processing, and morphology, *RSC Adv.* **2013**, *5*, 98971–98982.
142. C. B. Bucknall, D. R. Paul, Notched impact behavior of polymer blends: part 2: dependence of critical particle size on rubber particle volume fraction, *Polymer* **2013**, *54*, 320–329.
143. H. Bai, C. Huang, H. Xiu, Y. Gao, Q. Zhang, Q. Fu, Toughening of poly(L-lactide) with poly(ε-caprolactone): combined effects of matrix crystallization and impact modifier particle size, *Polymer* **2013**, *54*, 5257–5266.
144. H. Bai, H. Xiu, J. Gao, H. Deng, Q. Zhang, M. Yang, and Q. Fu, Tailoring impact toughness of poly(L-lactide)/poly(ε-caprolactone) (PLLA/PCL) blends by controlling crystallization of PLLA matrix, *ACS Appl. Mater. Interfaces* **2012**, *4*, 897–905.
145. H. Tsuji, M. Swada, L. Bouapao, Biodegradable polyesters as crystallization-accelerating agents of poly(L-lactide), *ACS Appl. Mater. Interfaces* **2009**, *1*, 1719–1730.
146. H. Tsuji, T. Yamada, M. Suzuki, S. Itusno, Effects of poly(L-lactide-*co*-ϵ-caprolactone) on morphology, structure, crystallization, and physical properties of blends of poly(L-lactide) and poly(ϵ-caprolactone), *Polym. Int.* **2003**, *52*, 269–275.
147. H. Tsuji, T. Yamada, Blends of aliphatic polyesters. VIII. Effects of poly(L-lactide-*co*-ε-caprolactone) on enzymatic hydrolysis of poly(L-lactide), poly(ε-caprolactone), and their blend films, *J. Appl. Polym. Sci.* **2003**, *87*, 412–419.
148. M. Przybysz-Romatowska, J. Haponiuk, K. Formela, Poly(ε-caprolactone)/poly(lactic acid) blends compatibilized by peroxide initiators: comparison of two strategies, *Polymers* **2020**, *12*, 228.
149. I. Noda, M. M. Satkowski, A. E. Dowrey, C. Marcott, Polymer alloys of nodax copolymers and poly(lactic acid), *Macromol. Biosci.* **2004**, *4*, 269–275.

150. T. Furukawa, H. Sato, R. Murakami, J. Zhang, Y.-X. Duan, I. Noda, S. Ochiai, Y. Ozaki, Structure, dispersibility, and crystallinity of poly(hydroxybutyrate)/poly(L-lactic acid) blends studied by FT-IR microspectroscopy and differential scanning calorimetry, *Macromolecules* **2005**, *38*(15): 6445–6454.

151. M. Zhang, N. L. Thomas, Blending polylactic acid with polyhydroxybutyrate: the effect on thermal, mechanical, and biodegradation properties, *Adv. Polym. Technol.* **2011**, *30*, 67–79.

152. Liu Q., Wu C., Zhang H., Deng B. Blends of polylactide and poly(3-hydroxybutyrate-*co*-3-hydroxyvalerate) with low content of hydroxyvalerate unit: morphology, structure, and property, *J. Appl. Polym. Sci.* **2015**, *132*, 42689.

153. T. Furukawa, H. Sato, R. Murakami, J. Zhang, I. Noda, S. Ochiai, Y. Ozaki, Comparison of miscibility and structure of poly(3-hydroxybutyrate-*co*-3-hydroxyhexanoate)/poly(L-lactic acid) blends with those of poly(3-hydroxybutyrate)/poly(L-lactic acid) blends studied by wide angle X-ray diffraction, differential scanning calorimetry, and FTIR microspectroscopy, *Polymer* **2007**, *48*, 1749–1755.

154. S.-M. Lai, Y.-H. Liu, C.-T. Huang, T.-M. Don, Miscibility and toughness improvement of poly(lactic acid)/poly(3-hydroxybutyrate) blends using a melt-induced degradation approach, *J. Polym. Res.* **2017**, *24*, 102.

155. S. Iannace, L. Ambrosio, S. J. Huang, L. Nicolais, Poly(3-hydroxybutyrate)-*co*-(3-hydroxyvalerate)/poly-L-lactide blends: thermal and mechanical properties, *J. Appl. Polym. Sci.* **1994**, *54*, 1525–1536.

156. L. L. Zhang, C. D. Xiaong, X. M. Deng, Miscibility, crystallization and morphology of poly(hydroxybutyrate)/poly(D/L-lactide blends), *Polymer* **1996**, *37*, 235–241.

157. T. Gerard, T. Budtova, Morphology and molten-state rheology of polylactide and polyhydroxyalkanoate blends, *Eur. Polym. J.* **2012**, *48*, 1110–1117.

158. M. Nofar, D. Sacligil, P. J. Carreau, M. R. Kamal, M.-C. Heuzey, Poly(lactic acid) blends: processing, properties and applications, *Int. J. Biol. Macromol.* **2019**, *125*, 307–360.

159. N. Loureiro, J. Esteves, J. Viana, S. Ghosh, Mechanical characterization of polyhydroxyalkanoate and poly(lactic acid) blends, *J. Thermoplast. Compos. Mater.* **2015**, *28*(2):195–213.

160. Y. Gao, L. Kong, L. Zhang, Y. Gong, G. Chen, N. Zhao, X. Zhang, Improvement of mechanical properties of poly(DL-Lactide) films by blending of poly(3-hydroxybutyrate-*co*-3-hydroxyhexanoate), *Eur. Polym. J.* **2006**, *42*, 764–775.

161. E. Richards, R. Rizvi, A. Chow, H. Naguib, Biodegradable composite foams of PLA and PHBV using subcritical $CO_2$, *J. Polym. Environ.* **2008**, *16*, 258–266.

162. F. Pappalardo, M. Fragalá, P. G. Mineo, A. Damigella, A. F. Catara, R. Palmeri, A. Rescifina, Production of filmable medium-chain-length polyhydroxyalkanoates produced from glycerol by *Pseudomonas mediterranea*, *Int. J. Biol. Macromol.* **2014**, *65*:89–96.

163. L. Botta, M. C. Mistretat, S. Palermo, M. Fragala, F. Pappalardo, Characterization and processability of blends of polylactide acid with a new biodegradable medium-chain-length polyhydroxyalkanoate, *J. Polym. Environ.* **2015**, *23*, 478–486.

164. Y. Ichikawa, T. Mizukoshi, Bionolle (polybutylenesuccinate), in: B. Rieger, A. Künkel, G. Coates, R. Reichardt, E. Dinjus, T. Zevaco (Eds.), *Synthetic Biodegradable Polymers. Advances in Polymer Science*, vol. *245*, Springer, Berlin, Heidelberg, 2011.

165. L. Sisti, G. Totaro, P. Marchese, PBS makes its entrance into the family of biobased plastics, in S. Kalia, L. Avérous (Eds.), *Biodegradable and Biobased Polymers for Environmental and Biomedical Applications*, Wiley, Hoboken, NJ, 2016, 225–285.

166. S. Su, R. Kopitzky, S. Tolga, S. Kabasci, Polylactide (PLA) and its blends with poly(butylene succinate) (PBS): a brief review, *Polymers* **2019**, *11*, 1193.

167. D. Wu, L. Yuan, E. Laredo, M. Zhang, W. Zhou, Interfacial properties, viscoelasticity, and thermal behaviors of poly(butylene succinate)/polylactide blend, *Ind. Eng. Chem. Res.* **2012**, *51*, 2290–2298.

168. T. Yokohara, M. Yamaguchi, Structure and properties for biomass-based polyester blends of PLA and PBS, *Eur. Polym. J.* **2008**, *44*, 677–685.

169. Y.-P. Wang, Y.-J. Xiao, J. Duan, J.-H. Yang, C.-L. Zhang, Accelerated hydrolytic degradation of poly(lactic acid) achieved by adding poly(butylene succinate), *Polym. Bull.* **2016**, *73*, 1067–1083.

170. J. Ostrowska, W. Sadurski, M. Paluch, P. Tynski, J. Bogusz, The effect of poly(butylene succinate) content on the structure and thermal and mechanical properties of its blends with polylactide, *Polym. Int.* **2019**, *68*, 1271–1279.

171. A. Bhatia, R. K. Gupta, S. N. Bhattacharya, H. J. Choi, Compatibility of biodegradable poly(lactic acid) (PLA) and poly(butylene succinate) (PBS) blends for packaging application, *Korea-Austr. Rheol. J.* **2007**, *19*, 125–131.

172. E. Hassan, Y. Wei, H. Jiao, Y. Muhuo, Dynamic mechanical properties and thermal stability of poly(lactic acid) and poly(butylene succinate) blends composites, *J. Fiber Bioeng. Inform.* **2013**, *6*, 85–94.

173. L. Jompang, S. Thumsorn, J. W. On, P. Surin, C. Apawet, T. Chaichalermwong, Poly(lactic acid) and poly(butylene succinate) blend fibers prepared by melt spinning technique, *Energy Procedia* **2013**, *34*, 493–499.

174. Y. Srithep, O. Veang-in, D. Pholharn, L. Turng, J. Morris, Improving polylactide toughness by plasticizing with low molecular weight polylactide-poly(butylene succinate) copolymer, *J. Renew. Mater.* **2021**, *9*(7), 1267–1281.

175. Y. Deng, N. L. Thomas, Blending poly(butylene succinate) with poly(lactic acid): ductility and phase inversion effects, *Eur. Polym. J.* **2015**, *71*, 534–546.

176. J. W. Park, S. S. Im, Morphological changes during heating in poly(L-lactic acid)/poly(butylene succinate) blend systems as studied by synchrotron X-ray scattering, *J. Polym. Sci. B Polym. Phys.* **2002**, *40*, 1931–1939.

177. J. W. Park, S. S. Im, Phase behavior and morphology in blends of poly(L-lactic acid) and poly(butylene succinate), *J. Appl. Polym. Sci.* **2002**, *86*, 647–655.

178. M. Shibata, Y. Inoue, M. Miyoshi, Mechanical properties, morphology, and crystallization behavior of blends of poly(L-lactide) with poly(butylene succinate-*co*-L-lactate) and poly(butylene succinate), *Polymer* **2006**, *47*, 3557–3564.

179. T. Hirotsu, K. Nakayama, C. Tagaki, T. Watanabe, Plasma surface treatments of melt-extruded uniaxial blend sheets of PLLA/PBS, *J. Photopolym. Sci. Technol.* **2004**, *17*, 179–184.

180. R. Wang, S. Wang, Y. Zhang, C. Wan, P. Ma, Toughening modification of PLLA/PBS blends via in situ compatibilization, *Polym. Eng. Sci.* **2009**, *49*, 26–33.

181. M. Seggiani, R. Altieri, P. Cinelli, A. Esposito, A. Lazzeri, Thermoplastic blends based on poly(butylene succinate-*co*-adipate) and different collagen hydrolysates from tanning industry: I-processing and thermo-mechanical properties, *J. Polym. Environ.* **2021**, *29*, 392–403.

182. T. Fujimaki, Processability and properties of aliphatic polyesters, 'BIONOLLE', synthesized by polycondensation reaction, *Polym. Degrad. Stab.* **1998**, *59*, 209–214.

183. R. Muthuraj, M. Misra, A. K. Mohanty, Studies on mechanical, thermal, and morphological characteristics of biocomposites from biodegradable polymer blends and natural fibers, biocomposites-design and mechanical performance, in: M. Mishra, J. K. Pandey, A. K. Mohanty (Eds.), *Bicomposites*, *Woodhead Publishing Series in Composites Science and Engineering*, Woodhead Publishing 2015, pp. 931–140.

184. Aliotta, L., Vannozzi A., Canesi I.,Cinelli P., Coltelli M.-B., Lazzeri A., Poly(lactic acid) (PLA)/poly(butylene succinate-co-adipate) (PBSA) compatibilized binary biobased blends: melt fluidity, morphological, *Thermo-Mech. Micromech. Anal. Polym.* **2021**, *13*, 218.

185. Y. Ding, W. Feng, D. Huang, B. Lu, P. Wang, G. Wang, J. Ji, Compatibilization of immiscible PLA-based biodegradable polymer blends using amphiphilic di-block copolymers, *Eur. Polym. J.* **2019**,*118*, 45–52.

186. S. Lee, J. W. Lee, Characterization and processing of biodegradable polymer blends of poly(lactic acid) with poly(butylene succinate adipate), *Korea-Austr. Rheol. J.* **2005**, *17*, 71–77.

187. S. P. McCarthy, R. A. Gross, W. Ma, U.S. Patent 5,883,199, 1999.

188. V. Ojijo, S. S. Ray, Super toughened biodegradable polylactide blends with non-linear copolymer interfacial architecture obtained via facile in situ reactive compatibilization, *Polymer* **2015**, *80*, 1–17.

189. V. Ojijo, S. S. Ray, R. Sadiku, Toughening of biodegradable polylactide/poly(butylene succinate co adipate)blends via in situ reactive compatibilization, *ACS Appl. Mater. Interfaces* **2013**, *5*(10), 4266–4276.

190. P. Suwanamornlert, N. Kerddonfag, A. Sane, W. Chinsirikul, W. Zhou, V. Chonhenchob, Poly(lactic acid)/poly(butylene-succinate-*co*-adipate) (PLA/PBSA) blend films containing thymol as alternative to synthetic preservatives for active packaging of bread, *Food Packag. Shelf Life* **2020**, *25*, 100515.

191. L. Shen, J. Haufe, M. K. Patel, Product overview and market projection of emerging bio-based plastics: PRO-BIP 2009: Final report, Group Science, Technology and Society (STS), Copernicus Institute for Sustainable Development and Innovation, Utrecht University, Utrecht, The Netherlands, 2009.

192. M. Nishida, X. Liu, S. Furuya, M. Nishida, T. Takayama, M. Todo, Effect of chain extender on morphology and tensile properties of poly(L-lactic acid)/poly(butylene succinate-*co*-L-lactate) blends. *Mater. Today Commun.* **2021**, *26*, 101852.

193. M. Shibata, N. Teramoto, Y. Inoue, Mechanical properties, morphologies, and crystallization behavior of plasticized poly(L-lactide)/poly(butylene succinate-*co*-L-lactate) blends, *Polymer* **2007**, *48*, 2768–2777.

194. V. Vilay, M. Mariatti, Z. Ahmad, K. Pasomsouk, M. Todo, Characterization of the mechanical and thermal properties and morphological behavior of biodegradable poly(L-lactide)/poly(ε-caprolactone) and poly(L-lactide)/poly(butylene succinate-*co*-L-lactate) polymeric blends, *J. Appl. Polym. Sci.* **2009**, *114*, 1784–1792.

195. P.M. Chou, M. Mariatti, A. Zulkifli, M. Todo, Changes in the crystallinity and mechanical properties of poly(L-lactic acid)/poly(butylene succinate-*co*-L-lactate) blend with annealing process, *Polym. Bull.* **2011**, *67*, 815–830.

196. V. Vannaladsaysy, M. Todo, T. Takayama, M. Jaafar, Z. Ahmad, K. Pasomsouk, Effects of lysine triisocyanate on the mode I fracture behavior of polymer blend of poly(L-lactic acid) and poly(butylene succinate-*co*-L-lactate), *J. Mater. Sci.* **2009**, *44*, 3006–3009.

197. T. Ikehara, Y. Nishikawa, T. Nishi, Evidence for the formation of interpenetrated spherulites in poly(butylene succinate-*co*-butylene carbonate)/poly(L-lactic acid) blends investigated by atomic force microscopy, *Polymer* **2003**, *44*, 6657–6661.

198. M. Weng, Z. Qiu, Miscibility and crystallization behavior of biodegradable poly(butylene succinate-*co*-butylene carbonate) and tannic acid blends, *Thermochim. Acta* **2014**, *575*, 262–268.

199. Z. Qiu, Chapter 8—Crystallization behavior of miscible semicrystalline polymer blends, in: T. Sabu, A. P. Mohammed, E. G. Bhoje, K. Nandakumar, *Crystallization in Multiphase Polymer Systems*, Elsevier, Amsterdam, The Netherlands, 2018, ISBN 9780128094532.

200. S. Hirano, Y. Nishikawa, Y. Terada, T. Ikehara, T. Nishi, Miscibility and crystallization behavior of crystalline/crystalline polymer blends. Poly(ester carbonate)/poly(L-lactic acid), *Polym. J.* **2002**, *34*, 85–88.

201. P. Saini, M. Arora, M.N.V. Ravi Kumar. Poly(lactic acid) blends in biomedical applications. *Adv. Drug Deliv. Rev.* **2016**, *107*, 47–59.

202. P. K. Samantaray, A. Little, D. M. Haddleton, T. McNally, B. Tan, Z. Sun, W. Huang, Y. Ji, C. Wan, Poly(glycolic acid) (PGA): a versatile building block expanding high performance and sustainable bioplastic applications, *Green Chem.* **2020**, *22*, 4055–4081.

203. L. N. Woodard, M. A. Grunlan, Hydrolytic degradation and erosion of polyester biomaterials, *ACS Macro Lett.* **2018**, *7*(8), 976–982.

204. K. J. Jem, B. Tan, The development and challenges of poly(lactic acid) and poly(glycolic acid), *Adv. Ind. Eng. Polym. Res.* **2020**, *3*, 60–70.

205. Y. You, J. H. Youk, S. W. Lee, B. M. Min, S. J. Lee, W. H. Park, Preparation of porous ultrafine PGA fibers via selective dissolution of electrospun PGA/PLA blend fibers, *Mater. Lett.* **2006**, *60*, 757–760.

206. A. Pandey, G. C. Pandey, P. B. Aswath, Synthesis of polylactic acid-polyglycolic acid blends using microwave radiation. *J. Mech. Behav. Biomed. Mater.* **2008**, *1*, 227–233.

207. Y. You, S. W. Lee, J. H. Youk, B. M. Min, S. J. Lee, W. H. Park, in vitro degradation behavior of non-porous ultra-fine poly(glycolic acid)/poly(L-lactic acid) fibers and porous ultra-fine poly(glycolic acid) fibers, *Polym. Degrad. Stab.* **2005**, *90*, 441–448.

208. M. A. Valderrama, R.-J. V. Putten, G.-J. M. Gruter, PLGA barrier materials from $CO_2$. The influence of lactide comonomer on glycolic acid polyesters, *ACS Appl. Polym. Mater.* **2020**, *2*, 2706–2718.

209. P. Blasi, Poly(lactic acid)/poly(lactic-*co*-glycolic acid)-based microparticles: an overview. *J. Pharm. Investig.* **2019**, *49*, 337–346.

210. J. M. Anderson, M. S. Shive, Biodegradation and biocompatibility of PLA and PLGA microspheres, *Adv. Drug Deliv. Rev.* **2012**, *64*, 72–82.

211. R. A. Jain, The manufacturing techniques of various drug loaded biodegradable poly(lactide-*co*-glycolide) (PLGA) devices, *Biomaterials* **2000**, *21*, 2475–2490.

212. I. Carmagnola, T. Nardo, P. Gentile, C. Tonda-Turo, C. Mattu, S. Cabodi, P. Defilippi, V. Chiono, Poly(lactic acid)-based blends with tailored physicochemical properties for tissue engineering applications: a case study, *Int. J. Polym. Mater. Polym. Biomater.* **2015**, *64*, 90–98.

213. A. Matsumoto, Y. Matsukawa, T. Suzuki, H. Yoshino, Drug release characteristics of multi-reservoir type microspheres with poly(DL-lactide-*co*-glycolide) and poly(DL-lactide), *J. Control. Release* **2005**, *106*, 172–180.

214. M. J. Blanco-Prieto, M. A. Campanero, K. Besseghir, F. Heimgatner, B. Gander, Importance of single or blended polymer types for controlled in vitro release and plasma levels of a somatostatin analogue entrapped in PLA/PLGA microspheres, *J. Control. Release* **2004**, *96*, 437–448.

215. J. P. Bertram, S. S. Saluja, J. McKain, E. B. J. Lavik, Sustained delivery of timolol maleate from poly(lactic-*co*-glycolic acid)/poly(lactic acid) microspheres for over 3 months, *Microencapsulation* **2009**, *26*, 18–26.

216. J. Jian, Z. Xiangbin, H. Xianbo, An overview on synthesis, properties and applications of poly(butylene-adipate-*co*-terephthalate)-PBAT, *Adv. Ind. Eng. Polym. Res.* **2020**, *3*, 19–26.

217. F. V. Ferreira, L. S. Cividanes, R. F. Gouveia, L. M. F. Lona, An overview on properties and applications of poly(butylene adipate-*co*-terephthalate)-PBAT based composites, *Polym. Eng. Sci.* **2019**, *59*: E7–E15.

218. T. Kijchavengkul, R. Auras, M. Rubino, S. Selke, M. Ngouajio, R. T. Fernandez, Biodegradation and hydrolysis rate of aliphatic aromatic polyester,. *Polym. Degrad. Stab.* **2010**, *95*, 2641–2647.

219. C. Y. Han, J. Bian, H. Liu, L. Dong, Effect of γ-radiation on the thermal and mechanical properties of a commercial poly(butylene adipate-*co*-terephthalate), *Polym. Int.* **2009**, *58*, 691–696.

220. T. Kijchavengkul, R. Auras, M. Rubino, M. Ngouajio, R. T. Fernandez, Assessment of aliphatic-aromatic copolyester biodegradable mulch films. Part I: field study, *Chemosphere* **2008**, *71*, 942–953.

221. H. Moustafa, C. Guizani, C. Dupont, V. Martin, M. Jeguirim, A. Dufresne, Utilization of torrefied coffee grounds as reinforcing agent to produce high-quality biodegradable PBAT composites for food packaging applications, *ACS Sustain. Chem. Eng.* **2017**, *5*(2), 1906–1916.

222. G. Zehetmeyer, S. M. M. Meira, J. M. Scheibel, R. V. B. Oliveira, R. M. D. Soares, Influence of melt processing on biodegradable nisin-PBAT films intended for active food packaging applications, *J. Appl. Polym. Sci.* **2016**, *133*, 43212.

223. E. Meaurio, E. Zuza, J. R. Sarasua, Miscibility and specific interactions in blends of poly(L-Lactide) with poly(vinyl phenol), *Macromolecules* **2005**, *38*, 1207–1215.

224. P. H. S. Kumara, N. Nagasawa, T. Yagi, M. Tamada, Radiation-induced crosslinking and mechanical properties of blends of poly(lactic acid) and poly(butylene terephthalate--*co*-adipate), *J. Appl. Polym. Sci.* **2008**, *109*, 3321–3328.

225. V. Gigante, I. Canesi, P. Cinelli, M. B. Coltelli, A. Lazzeri, Rubber toughening of polylactic acid (PLA) with poly(butylene adipate-*co*-terephthalate) (PBAT): mechanical properties, fracture mechanics and analysis of ductile-to-brittle behavior while varying temperature and test speed, *Eur. Polym. J.* **2019**, *115*, 125–137.

226. X. Wang, S. Peng, H. Chen, X. Yu, X. Zhao, Mechanical properties, rheological behaviors, and phase morphologies of high-toughness PLA/PBAT blends by in-situ reactive compatibilization, *Compos. Part B* **2019**, *173*, 107028.

227. E. J. Dil, P. J. Carreau, B. D. Favis, Morphology, miscibility and continuity development in poly(lactic acid)/poly(butylene adipate-*co*-terephthalate) blends, *Polymer* **2015**, *68*, 202–212.

228. J.-T. Yeh, C.-H. Tsou, C.-Y. Huang, K.-N. Chen, C.-S. Wu, W.-L. Chai, Compatible and crystallization properties of poly(lactic acid)/poly(butylene adipate-*co*-terephthalate) blends, *J. Appl. Polym. Sci.* **2010**, *116*, 680–687.

229. L. Jiang, M. P. Wolcott, J. Zhang, Study of biodegradable polylactide/poly(butylene adipate-*co*-terephthalate) Blends. *Biomacromolecules* **2006**, *7*, 199–207.

230. S. Y. Gu, K. Zhang, J. Ren, H. Zhan, Melt rheology of polylactide/poly(butylene adipate-*co*-terephthalate) blends, *Carbohydr. Polym.* **2008**, *74*, 79–85.

231. A. Pietrosanto, P. Scarfato, L. D. Maio, M. R. Nobile, L. Incarnato, Evaluation of the suitability of poly(lactide)/poly(butylene-adipate-*co*-terephthalate) blown films for chilled and frozen food packaging applications, *Polymers* **2020**, *12*, 804.
232. Coltelli M. B., I. D. Maggiore, M. Bertold, F. Signori, S. Bronco, F. Ciardelli, Poly(lactic acid) properties as a consequence of poly(butylene adipate-co-terephthalate) blending and acetyl tributyl citrate plasticization. *J. Appl. Polym. Sci.* **2008**, *110*, 1250–1262.
233. S. Lin, W. Guo, C. Chen, J. Ma, B. Wang, Mechanical properties and morphology of biodegradable poly(lactic acid)/poly(butylene adipate-*co*-terephthalate) blends compatibilized by transesterification, *Mater. Des.* **2012**, *36*, 604–608.
234. N. W. Zhang, Q. F. Wang, J. Ren, L. Wang, Preparation and properties of biodegradable poly(lactic acid)/poly(butylene adipate-*co*-terephthalate) blend with glycidyl methacrylate as reactive processing agent, *J. Mater. Sci.* **2009**, *44*, 250–256.
235. P. Ma, X. Cai, Y. Zhang, S. Wang, W. Dong, M. Chen, P. J. Lemstra, In-situ compatibilization of poly(lactic acid) and poly(butylene adipate-*co*-terephthalate) blends by using dicumyl peroxide as a free-radical initiator, *Polym. Degrad. Stab.* **2014**, *102*, 145–151
236. A. M. Clarinval, J. Halleux, in: R. Smith (Ed.), *Biodegradable Polymers for Industrial Applications*, CRC Press, Boca Raton, FL, 2005.
237. T. Y. Liu, W. C. Lin, M. C. Yang, S. Y. Chen, Miscibility, thermal characterization and crystallization of poly(L-lactide) and poly(tetramethylene adipate-*co*-terephthalate) blend membranes, *Polymer* **2005**, *46*, 12586–12594.
238. H. Moustafa, N. E. Kissi, A. I. Abou-Kandil, M. S. Abdel-Aziz, A. Dufresne, PLA/PBAT bionanocomposites with antimicrobial natural rosin for green packaging, *ACS Appl. Mater. Interfaces* **2017**, *9*(23), 20132–20141
239. N. Bitnis, R. Verdejo, P. Cassagnau, M. A. Lopez-Manchado, Structure and properties of polylactide/natural rubber blends, *Mater. Chem. Phys.* **2011**, *129*, 823–831.
240. M. Nematollahi, A. Jalali-Arani, H. Modarress, High-performance bio-based poly(lactic acid)/natural rubber/epoxidized natural rubber blends: effect of epoxidized natural rubber on microstructure, toughness and static and dynamic mechanical properties, *Polym. Int.* **2019**, *68*, 439–446.
241. P. T. Nghia, N. Siripitakchai, W. Klinklai, T. Saito, Y. Yamamoto, S. Kawahara, Compatibility of liquid deproteinized natural rubber having epoxy group (LEDPNR)/poly(L-lactide) blend, *J. Appl. Polym. Sci.* **2008**, *108*, 393–399.
242. M. Bijarimi, S. Ahmad, R. Rasid, Mechanical, thermal and morphological properties of poly(lactic acid)/epoxidized natural rubber blends, *J. Elastomers Plast.* **2014**, *46*(4), 338.
243. W. Zhang, L. Chen, Y. Zhang, Surprising shape-memory effect of polylactide resulted from toughening by polyamide elastomer, *Polymer* **2009**, *50*, 1311–1315.
244. Q. Meng, J. Hu, K. C. Ho, F. Ji, S. Chen, The shape memory properties of biodegradable chitosan/poly(L-lactide) composites, *J. Polym. Environ.* **2009**, *17*, 212–224.
245. J. Gug, J. Soule, B. Tan, M. J. Sobkowicz, Effects of chain-extending stabilizer on bioplastic poly(lactic acid)/polyamide blends compatibilized by reactive extrusion, *Polym. Degrad. Stab.* **2018**, *153*, 118–129.
246. J. M. Margolis, in: C. A. Harper (Ed.), *Modern Plastics Handbook*, McGraw-Hill, New York, 2000.
247. Y. Li, H. Shimizu, Toughening of polylactide by melt blending with a biodegradable poly(ether)urethane elastomer, *Macromol. Biosci.* **2007**, *7*, 921–928.
248. H.-C. Zhang, B.-H. Kang, L.-C. Chen, X. Lu, Enhancing toughness of poly(lactic acid)/thermoplastic polyurethane blends via increasing interface compatibility by polyurethane elastomer prepolymer and its toughening mechanism, *Polym. Test.* **2020**, *87*, 106521.
249. D. W. Grijpma, R. D. A. Vanhofslot, H. Super, A. J. Nijenhuis, A. J. Pennings, Rubber toughening of poly(lactide) by blending and block copolymerization, *Polym. Eng. Sci.* **1994**, *34*, 1674–1684.
250. X. Li, Y. Su, Q. Chen, Y. Lin, Y. Tong, Y. Li, Synthesis and characterization of biodegradable hyperbranched poly(ester-amide)s based on natural material, *Biomacromolecules* **2005**, *6*, 3181–3188.
251. Y. Lin, K.-Y. Zhang, Z.-M. Dong, L.-S. Dong, Y.-S. Li, Study of hydrogen-bonded blend of polylactide with biodegradable hyperbranched poly(ester amide), *Macromolecules* **2007**, *40*, 6257–6267.
252. W. Zhang, Y. Zhang, Y. Chen, Modified brittle poly(lactic acid) by biodegradable hyper branched poly(ester amide), *Iran. Polym. J.* **2008**, *17*, 891–898.
253. Q. Cai, J. Bei, S. Wang, in vitro study on the drug release behavior from polylactide-based blend matrices, *Polym. Adv. Technol.* **2002**, *13*, 534–540.
254. M. Sheth, R. A. Kumar, V. Dave, R. A. Gross, S. P. McCarthy, Biodegradable polymer blends of poly(lactic acid) and poly(ethylene glycol), *J. Appl. Polym. Sci.* **1997**, *66*, 1495–1505.
255. M. Baiardo, G. Frisoni, M. Scandola, M. Rimelen, D. Lips, K. Ruffieux, E. Wintermantel, Thermal and mechanical properties of plasticized poly(L-lactic acid), *J. Appl. Polym. Sci.* **2003**, *90*, 1731–1738.
256. Y. Hu, Y. S. Hu, V. Topolkaraev, A. Hiltner, E. Baer. Aging of poly(lactide)/poly(ethylene glycol) blends. Part 2. Poly(lactide) with high stereoregularity, *Polymer* **2003**, *44*, 5711–5720.
257. K. Sungsanit, N. Kao, S. Bhattacharya, Properties of linear poly(lactic acid)/polyethylene glycol blends, *Polym. Eng. Sci.* **2012**, *52*, 108–116.
258. H. Younes, D. Cohn, Phase separation in poly(ethylene glycol)/poly(lactic acid) blends, *Eur. Polym. J.* **1988**, *24*, 765–773.
259. W. Jiang, S. P. Schwendeman, Stabilization and controlled release of bovine serum albumin encapsulated in poly(D,L-lactide) and poly(ethylene glycol) microsphere blends, *Pharm. Res.* **2001**, *18*, 878–885.
260. Y. Hu, M. Rogunova, V. Topolkaraev, A. Hiltner, E. Baer, Aging of poly(lactide)/poly(ethylene glycol) blends. Part 1.

Poly(lactide) with low stereoregularity, *Polymer* **2003**, *44*, 5701–5710.

261. A. Takhulee, Y. Takahashi, Vao-soongnern V., Molecular simulation and experimental studies of the miscibility of polylactic acid/polyethylene glycol blends, *J. Polym. Res.* **2017**, *24*, 8.
262. M. Bijarimi, S. Ahmad, R. Rasid, M. A. Khushairi, M. Zakir, Poly(lactic acid)/poly(ethylene glycol) blends: mechanical, thermal and morphological properties, *AIP Conf. Proc.* **2016**, *1727*, 020002.
263. A. N. Gaikwad, E. R. Wood, T. Ngai, T. P. Lodge. Two calorimetric glass transitions in miscible blends containing poly(ethylene oxide), *Macromolecules* **2008**, *41*, 2502–2508.
264. K. S. Kim, I. J. Chin, J. S. Yoon, D. S. Kim, S. H. Kim, Effect of PLA-PEO block copolymers on the compatibility of PLA/PEO blends, *Polymer (Korea)* **1996**, *20*, 497–505.
265. S. Ghosh, J. C. Vianac, R. L. Reis, J. F. Mano, Development of porous lamellar poly(L-lactic acid) scaffolds by conventional injection molding process, *Acta Biomater.* **2008**, *4*, 887–896.
266. K. S. Kim, I. J. Chin, J. S. Yoon, H. J. Choi, D. C. Lee, K. H. Lee, Crystallization behavior and mechanical properties of poly(ethylene oxide)/poly(L-lactide)/poly(vinyl acetate) blends, *J. Appl. Polym. Sci.* **2001**, *82*, 3618–3626.
267. H. Tsuji, R. Smith, W. Bonfield, Y. Ikada, Porous biodegradable polyesters. I. Preparation of porous poly(L-lactide) films by extraction of poly(ethylene oxide) from their blends, *J. Appl. Polym. Sci.* **2000**, *75*, 629–637.
268. J.-Z. Li, J. M. Schultz, C. M. Chan, The relationship between morphology and impact toughness of poly(L-lactic acid)/poly(ethylene oxide) blends, *Polymer* **2015**, *63*, 179–188.
269. D. C. Coraca, E. A. R. Duek, C. A. Padovani, J. A. Camilli, Osteointegration of poly(L-lactic acid)PLLA and poly(L-lactic acid) PLLA/poly(ethylene oxide) PEO implants in rat tibiae, *J. Mater. Sci. Mater. Med.* **2008**, *19*, 2699–2704.
270. R. Satchi-Fainaro, R. Duncan, *Polymer Therapeutics II: Polymers as Drugs, Conjugates and Gene Delivery Systems*, Springer, Berlin, 2006.
271. T. G. Park, S. Cohen, R. Langer, Poly(L-lactic acid)/pluronic blends: characterization of phase separation behavior, degradation, and morphology and use as protein-releasing matrixes, *Macromolecules* **1992**, *25*, 116–122.
272. J. W. Lee, E. D. Jeong, E. J. Cho, J. A. Gardella, W. Hicks, R. Hard, F. V. Bright, Surface-phase separation of PEO-containing biodegradable PLLA blends and block copolymers, *Appl. Surf. Sci.* **2008**, *255*, 2360–2364.
273. C. M. Mahoney, J. Yu, A. Fahey, J. A. Gardella, SIMS depth profiling of polymer blends with protein based drugs, *Appl. Surf. Sci.* **2006**, *252*, 6609–6614.
274. C. M. Mahoney, J. Yu, J. A. Gardella, Depth profiling of poly(L-lactic acid)/triblock copolymer blends with time-of-flight secondary ion mass spectrometry, *Anal. Chem.* **2005**, *77*, 3570–3578.
275. E. Kiss, M. G. Takacs, I. Bertoti, E. I. Vargha-Butler, Surface properties of poly(lactic/glycolic acid)–pluronic® blend films, *Polym. Adv. Technol.* **2003**, *14*, 839–846.
276. E. Kiss, K. Dravetzky, K. Hill, E. Kutnyanszky, A. Varga, Protein interaction with a pluronic-modified poly(lactic acid) Langmuir monolayer, *J. Colloid Interface Sci.* **2008**, *325*, 337–345.
277. F. S. Guner, Y. Yagci, A. T. Erciyes, Polymers from triglyceride oils, *Prog. Polym. Sci.* **2006**, *31*, 633–670.
278. K. H. Chang, M. L. Robertson, M. A. Hillmyer, Phase inversion in polylactide/soybean oil blends compatibilized by poly(isoprene-*b*-lactide) block copolymers, *ACS Appl. Mater. Interfaces* **2009**, *1*, 2390–2399.
279. M. L. Robertson, K. Chang, W. Gramlich, M. A. Hillmyer, Toughening of polylactide with polymerized soybean oil, *Macromolecules* **2010**, *43*, 1807–1814.
280. Y.-Q. Xu, J.-P. Qu, Mechanical and rheological properties of epoxidized soybean oil plasticized poly(lactic acid), *J. Appl. Polym. Sci.* **2009**, *112*, 3185–3191.
281. G. Biresaw, Z. S. Liu, S. Z. Erhan, Investigation of the surface properties of polymeric soaps obtained by ring-opening polymerization of epoxidized soybean oil, *J. Appl. Polym. Sci.* **2008**, *108*, 1976–1985.
282. L. Quiles-Carrillo, S. Duart, N. Montanes, S. Torres-Giner, R. Balart, Enhancement of the mechanical and thermal properties of injection-molded polylactide parts by the addition of acrylated epoxidized soybean oil, *Mater. Des.* **2018**, *140*, 54–63.
283. F. Ali, Y. W. Chang, S. C. Kang, J. Y. Yoon, Thermal, mechanical and rheological properties of poly (lactic acid)/epoxidized soybean oil blends, *Polym. Bull.* **2009**, *62*, 91–98.
284. Y. Xu, M. You, J. Qu, Melt rheology of poly (lactic acid) plasticized by epoxidized soybean oil, *Wuhan Univ. J. Nat. Sci.* **2009**, *14*, 349–354.
285. Z. H. Xu, Q. Y. Wu, Effect of lecithin content blend with poly (L-lactic acid) on viability and proliferation of mesenchymal stem cells, *Mater. Sci. Eng. C* **2009**, *29*:1593–1598.
286. J. John, J. A. Tang, M. Bhattacharya, Processing of biodegradable blends of wheat gluten and modified polycaprolactone, *Polymer* **1998**, *39*, 2883–2895.
287. I. Olabarrieta, M. Gallstedt, I. Ispizua, J. R. Sarasua, M. S. Hedenqvist, Properties of aged montmorillonite–wheat gluten composite films, *J. Agric. Food Chem.* **2006**, *54*, 1283–1288.
288. M. Mastromatteo, S. Chillo, G. G. Buonocore, A. Massaro, A. Conte, M. A. D. Nobile, Effects of spelt and wheat bran on the performances of wheat gluten films, *J. Food Eng.* **2008**, *88*, 202–212.
289. A. A. Mohamed, S. H. Gordon, C. J. Carriere, S. J. Kim, Thermal characteristics of polylactic acid/wheat gluten blends, *J. Food Qual.* **2006**, *29*, 266–281.
290. A. A. Mohamed, J. Y. Xu, Thermal and kinetic properties of poly(lactic acid) and transglutaminase-crosslinked wheat gluten blends, *J. Appl. Polym. Sci.* **2007**, *106*, 214–219.
291. S. N. Swain, S. M. Biswal, P. K. Nanda, P. L. Nayak, Biodegradable soy-based plastics: opportunities and challenges, *J. Polym. Environ.* **2004**, *12*, 35–42.
292. J. Zhang, L. Jiang, L. Zhu, J. Jane, P. Mungara, Morphology and properties of soy protein and polylactide blends, *Biomacromolecules* **2006**, *7*, 1551–1561.

293. K. Fang, B. Wang, K. Sheng, X. S. Sun, Properties and morphology of poly(lactic acid)/soy protein isolate blends, *J. Appl. Polym. Sci.* **2009**, *114*, 754–759.

294. A. R. Murphy, D. L. Kaplan, Biomedical applications of chemically-modified silk fibroin, *J. Mater. Chem.* **2009**, *19*, 6443–6450.

295. G. L. Jones, A. Motta, M. J. Marshall, A. J. E. Haj, S. H. Cartmell, Osteoblast: osteoclast co-cultures on silk fibroin, chitosan and PLLA films, *Biomaterials* **2009**, *30*, 5376–5384.

296. F. Wang, H. Wu, V. Venkataraman, X. Hu, Silk fibroin-poly(lactic acid) biocomposites: effect of protein-synthetic polymer interactions and miscibility on material properties and biological responses, *Mater. Sci. Eng. C* **2019**, *104*, 109890.

297. H. Zhu, X. Feng, H. Zhang, Y. Guo, J. Zhang, J. Chen. Structural characteristics and properties of silk fibroin/poly(lactic acid) blend films, *J. Biomater. Sci. Polym. Ed.* **2009**, *20*, 1259–1274.

298. K. Hu, Q. Lv, F. Z. Cui, L. Xu, Y. P. Jiao, Y. Wang, Q. L. Feng, H. L. Wang, L. Y. Huang, A novel poly(L-lactide) (PLLA)/fibroin hybrid scaffold to promote hepatocyte viability and decrease macrophage responses, *J. Bioact. Compat. Polym.* **2007**, *22*, 395–410.

299. C. Xu, X. Luo, X. Lin, X. Zhuo, L. Liang, Preparation and characterization of polylactide/thermoplastic konjac glucomannan blends, *Polymer* **2009**, *50*, 3698–3705.

300. H. S. Kim, J. T. Kim, Y. J. Jung, D. Y. Hwang, H. J. Son, J. B. Lee, S. C. Ryu, S. H. Shin, Preparation and characterization of nanofibrous membranes of poly(D,L-lactic acid)/chitin blend for guided tissue regenerative barrier, *Macromol. Res.* **2009**, *17*, 682–687.

301. K. V. H. Prashanth, R. N. Tharanathan, Chitin/chitosan: modifications and their unlimited application potential—an overview, *Trends Food Sci. Technol.* **2007**, *18*, 117–131.

302. J. L. Shamshina, P. Berton, R. D. Rogers, Advances in functional chitin materials: a review, *ACS Sustain. Chem. Eng.* **2019**, *7*(7), 6444–6457.

303. Y. Wan, Q. Wu, S. Wang, S. Zhang, Z. Hu, Mechanical properties of porous polylactide/chitosan blend membranes, *Macromol. Mater. Eng.* **2007**, *292*, 598–607.

304. R. Grande, A. J. F. Carvalho, Compatible ternary blends of chitosan/poly(vinyl alcohol)/poly(lactic acid) produced by oil oil-in-water emulsion processing, *Biomacromolecules* **2011**, *12*, 907–914.

305. V. M. Correlo, L. F. Boesel, M. Bhattacharya, J. F. Mano, N. M. Neves, R. L. Reis, Properties of melt processed chitosan and aliphatic polyester blends, *Mater. Sci. Eng. A* **2005**, *403*, 57–68.

306. N. E. Suyatma, A. Copinet, L. Tighzert, V. Coma, Mechanical and barrier properties of biodegradable films made from chitosan and poly (lactic acid) blends, *J. Polym. Environ.* **2004**, *12*, 1–6.

307. F. Sebastien, G. Stephane, A. Copinet, V. Coma, Novel biodegradable films made from chitosan and poly(lactic acid) with antifungal properties against mycotoxinogen strains, *Carbohydr. Polym.* **2006**, *65*, 185–193.

308. Y. Wan, H. Wu, A. X. Yu, D. J. Wen, Biodegradable polylactide/chitosan blend membranes, *Biomacromolecules* **2006**, *7*, 1362–1372.

309. L. Li, S. Ding, C. Zhou, Preparation and degradation of PLA/chitosan composite materials, *J. Appl. Polym. Sci.* **2004**, *91*, 274–277.

310. V. M. Correlo, E. D. Pinho, I. Pashkuleva, M. Bhattacharya, N. M. Neves, R. L. Reis, Water absorption and degradation characteristics of chitosan-based polyesters and hydroxyapatite composites, *Macromol. Biosci.* **2007**, *7*, 354–363.

311. Y. Wan, Y. Fang, H. Wu, X. Y. Cao, Porous polylactide/chitosan scaffolds for tissue engineering, *J. Biomed. Mater. Res. A* **2007**, *80A*, 776–789.

312. J. Xu, J. H. Zhang, W. Q. Gao, H. W. Liang, H. Y. Wang, J. F. Li, Preparation of chitosan/PLA blend micro/nanofibers by electrospinning, *Mater. Lett.* **2009**, *63*, 658–660.

313. F. Xie, Q. F. Li, B. Gu, K. Liu, G. X. Shen, in vitro and in vivo evaluation of a biodegradable chitosan–PLA composite peripheral nerve guide conduit material, *Microsurgery* **2008**, *28*, 471–479.

314. M. Peesan, P. Supaphol, R. Rujiravanit, Preparation and characterization of hexanoyl chitosan/polylactide blend films, *Carbohydr. Polym.* **2005**, *60*, 343–350.

315. Y. Z. Liao, M. H. Xin, M. C. Li, S. Su, Preparation and characterization of *O*-lauroyl chitosan/ polylactide blend membranes by solution-casting approach, *Chin. Chem. Lett.* **2007**, *18*, 213–216.

316. M. Peesan, P. Supaphol, R. Rujiravanit. Effect of casting solvent on characteristics of hexanoyl chitosan/polylactide blend films. *J. Appl. Polym. Sci.* **2007**, *105*, 1844–1852.

317. M. Peesan, R. Rujiravanit, P. Supaphol, Electrospinning of hexanoyl chitosan/polylactide blends, *J. Biomater. Sci. Polym. Ed.* **2006**, *17*, 547–565.

318. L. Long Yu, E. Petinakis, K. Dean, H. Liu, Poly(lactic acid)/starch blends, in: R Auras, L. T. Lim, S. Selke, H. Tsuji (Eds.), *Poly(Lactic Acid): Structures, Production, Synthesis, and Application*, John Wiley & Sons, New York, 2010.

319. Detyothin, S., Production and characterization of thermoplastic cassava starch, functionalized poly(lactic acid), and their reactive compatibilized blends, Ph.D. thesis, School of Packaging, Michigan State University, East Lansing, MI, 2012, p. 257.

320. W. Baker, C. Scott, G. H. Hu, *Reactive Polymer Blending*, Hanser Publishers, Munich, 2001, 289 p.

321. D. R. Paul, C. B. Bucknall, *Polymer Blends Volume1: Formulation*, John Wiley and Sons, Inc., New York, 2000, 600 p.

322. J. Muller, C. Gonzalez-Martinez, A. Chiralt, Combination of poly(lactic) acid and starch for biodegradable food packaging, *Materials* **2017**, *10*, 952.

323. K. Hamad, M. Kaseem, M. Ayyoob, J. Joo, F. Deri, Polylactic acid blends: the future of green, light and tough, *Prog. Polym. Sci.* **2018**, *85*, 83–127.

324. J. J. Koh, X. Zhang, C. He, Fully biodegradable poly(lactic acid)/starch blends: a review of toughening strategies, *Int. J. Biol. Macromol.* **2018**, *109*, 99–113.
325. H. Wang, X. Sun, P. Seib, Strengthening blends of poly(lactic acid) and starch with methylenediphenyl diisocyanate, *J. Appl. Polym. Sci.* **2001**, *82*, 1761–1767.
326. K. Sukhila, S. Mohanty, S. K. Nayak, Renewable resource based blends of polylactic acid (PLA) and thermoplastic starch (TPS) using novel reactive compatibilization, *J. Polym. Mater.* **2017**, *34*, 525–538.
327. Z. Xiong, L. Zhang, S. Ma, Y. Yang, C. Zhang, Z. Tang, J. Zhu, Effect of castor oil enrichment layer produced by reaction on the properties of PLA/HDI-*g*-starch blends, *Carbohydr. Polym.* **2013**, *94*, 235–243.
328. N. Noivoil, R. Yoksan, Compatibility improvement of poly(lactic acid)/thermoplastic starch blown films using acetylated starch, *J. Appl. Polym. Sci.* **2020**, *138*, 49675.
329. L M. Robeson, *Polymer Blends: A Comprehensive Review*, Hanser Publishers, Munich, 2007, 459 p.
330. W. Y. Jang, B. Y. Shin, T. J. Lee, R. Narayan, Thermal properties and morphology of biodegradable PLA/starch compatibilized blends, *J. Ind. Eng. Chem.* **2007**, *13*, 457–464.
331. M. A. Huneault, H. Li, Morphology and properties of compatibilized polylactide/thermoplastic starch blends, *Polymer* **2007**, *48*, 270–280.
332. S. Detyothin, S. E. M. Selke, R. Narayan, M. Rubino, R. Auras, Reactive functionalization of poly(lactic acid), PLA: effects of the reactive modifier, initiator and processing conditions on the final grafted maleic anhydride content and molecular weight of PLA, *Polym. Degrad. Stab.* **2013**, *98*, 2697–2708.
333. S. Detyothin, S. E. M. Selke, R. Narayan, M. Rubino, R. Auras, Effects of molecular weight and grafted maleic anhydride of functionalized polylactic acid used in reactive compatibilized binary and ternary blends of polylactic acid and thermoplastic cassava starch, *J. Appl. Polym. Sci.* **2015**, *132*, 42230.
334. A. Bher, R. Auras, C. E. Schvezov, Improving the toughening in poly(lactic acid)-thermoplastic cassava starch reactive blends, *J. Appl. Polym. Sci.* **2018**, *135*, 46140.
335. A. Bher, I. U. Unalan, R. Auras, M. Rubino, C. E. Schvezov, Toughening of poly(lactic acid) and thermoplastic cassava starch reactive blends using graphene nanoplatelets, *Polymers* **2018**, *10*, 95 (1–18).
336. M. R. A. Moghaddam, S. M. A. Razavi, Y. Jahani, Effects of compatibilizer and thermoplastic starch (TPS) concentration on morphological, rheological, tensile, thermal and moisture sorption properties of plasticized polylactic acid/TPS blends, *J. Polym. Environ.* **2018**, *26*, 3202–3215.
337. J. M. Ferri, D. Garcia-Garcia, L. Sánchez-Nacher, O. Fenollar, R. Balart, The effect of maleinized linseed oil (MLO) on mechanical performance of poly(lactic acid)-thermoplastic starch (PLA-TPS) blends, *Carbohydr. Polym.* **2016**, *147*, 60–68.
338. M. Bohórquez-Ayala, D. Rojano-Quiroz, R. González-Cuello, L. García-Zapateiro, R. Ortega-Toro, Application of modified vegetable oil for improvement of biodegradable materials based on thermoplastic starch (PLA-TPS) blends, *Rev. Mex. Ing. Quim.* **2021**, *20*, 423–433.
339. Z. Xiong, L. Chao, S. Ma, J. Feng, Y. Yang, R. Zhang, J. Zhu, The properties of poly(lactic acid)/starch blends with a functionalized plant oil: tung oil anhydride, *Carbohydr. Polym.* **2013**, *95*, 77–84.
340. Z. Xiong, Y. Yang, J. Feng, X. Zhang, C. Zhang, Z. Tang, J. Zhu, Preparation and characterization of poly(lactic acid)/starch composites toughened with epoxidized soybean oil, *Carbohydr. Polym.* **2013**, *92*, 810–816.
341. B. Ayana, S. Supratim, B. B. Khatua, Highly exfoliated eco-friendly thermoplastic starch (TPS)/poly (lactic acid)(PLA)/clay nanocomposites using unmodified nanoclay, *Carbohydr. Polym.* **2014**, *110*, 430–439.
342. W. H. Ferreira, K. Dahmouche, C. T. Andrade, Tuning the mechanical and electrical conductivity properties of graphene-based thermoplastic starch/poly(lactic acid) hybrids, *Polym. Compos.* **2019**, *40*, E1131–E1142.
343. R. Jeziorska, A. Szadkowska, E. Spasowka, A. Lukomska, M. Chmielarek, Characteristics of biodegradable polylactide/thermoplastic starch/nanosilica composites: effects of plasticizer and nanosilica functionality, *Adv. Mater. Sci. Eng.* **2018**, 4571368, 1–15.
344. E. Schwach, J.-C. Six, L. Averous, Biodegradable blends based on starch and poly(lactic acid): comparison of different strategies and estimate of compatibilization, *J. Polym. Environ.* **2008**, *16*, 286–297.
345. J. Wootthikanokkhan, P. Kasemwananimit, N. Sombatsompop, A. Kositchaiyong, S. Isarankurana Ayutthaya, N. Kaabbuathong, Preparation of modified starch-grafted poly(lactic acid) and a study on compatibilizing efficacy of the copolymers in poly(lactic acid)/thermoplastic starch blends, *J. Appl. Polym. Sci.* **2012**, *126*, E389–E396.
346. N. Noivoil, R. Yoksan, Oligo(lactic acid)-grafted starch: a compatibilizer for poly(lactic acid)/thermoplastic starch blend, *Int. J. Biol. Macromol.* **2020**, *160*, 506–517.
347. V. P. Martino, A. Jimenez, R. A. Ruseckaite, Processing and characterization of poly(lactic acid) films plasticized with commercial adipates, *J. Appl. Polym. Sci.* **2009**, *112*, 2010–2018.
348. L. V. Labrecque, R. A. Kumar, V. Dave, R. A. Gross, McCarthy S. P., Citrate esters as plasticizers for poly(lactic acid), *J. Appl. Polym. Sci.* **1997**, *66*, 1507–1513.
349. N. Ljungberg, B. Wesslen, The effects of plasticizers on the dynamic mechanical and thermal properties of poly(lactic acid), *J. Appl. Polym. Sci.* **2002**, *86*, 1227–1234.
350. N. Ljungberg, B. Wesslen, Tributyl citrate oligomers as plasticizers for poly (lactic acid): thermo-mechanical film properties and aging, *Polymer* **2003**, *44*, 7679–7688.
351. Y. Lemmouchi, M. Murariu, A. M. D. Santos, A. J. Amass, E. Schacht, P. Dubois, Plasticization of poly(lactide) with blends of tributyl citrate and low molecular weight poly(D,L-lactide)-*b*-poly(ethylene glycol) copolymers, *Eur. Polym. J.* **2009**, *45*, 2839–2848.

352. O. Martin, L. Averous, Poly(lactic acid): plasticization and properties of biodegradable multiphase systems, *Polymer* **2001**, *42*, 6209–6219.

353. Y. Hu, Y. S. Hu, V. Topolkaraev, A. Hiltner, E. Baer, Crystallization and phase separation in blends of high stereoregular poly(lactide) with poly(ethylene glycol), *Polymer* **2003**, *44*, 5681–5689.

354. Z. Kulinski, E. Piorkowska, K. Gadzinowska, M. Stasiak, Plasticization of poly(L-lactide) with poly(propylene glycol), *Biomacromolecules* **2006**, *7*, 2128–2135.

355. E. Piorkowska, Z. Kulinski, A. Galeski, R. Masirek, Plasticization of semicrystalline poly(L-lactide) with poly(propylene glycol), *Polymer* **2006**, *47*, 7178–7188.

356. N. Ljungberg, B. Wesslen, Preparation and properties of plasticized poly(lactic acid) films, *Biomacromolecules* **2005**, *6*, 1789–1796.

357. I. Pillin, N. Montrelay, Y. Grohens, Thermo-mechanical characterization of plasticized PLA: is the miscibility the only significant factor?, *Polymer* **2006**, *47*, 4676–4682.

358. D. Li, Y. Jiang, S. Lv, X. Liu, J. Gu, Q. Chen, Y. Zhang, Preparation of plasticized poly (lactic acid) and its influence on the properties of composite materials, *PLoS One* **2018**, *13*(3), e0193520.

359. C. M. Hansen, *Hansen Solubility Parameters*, CRC Press, Boca Raton, FL, 2007.

360. S.-L. Yang, Z.-H. Wu, B. Meng, W. Yang, The effects of dioctyl phthalate plasticization on the morphology and thermal, mechanical, and rheological properties of chemical crosslinked polylactide, *J. Polym. Sci. B* **2009**, *47*, 1136–1145.

361. A. Hoglund, M. Hakkarainen, A. C. Albertsson, Migration and hydrolysis of hydrophobic polylactide plasticizer, *Biomacromolecules* **2010**, *11*, 277–283.

362. N. Burgos, V. P. Martino, A. Jimenez, Characterization and ageing study of poly(lactic acid) films plasticized with oligomeric lactic acid, *Polym. Degrad. Stab.* **2013**, *98*, 651–658.

363. H. W. Xiao, W. Lu, J. T. Yeh, Effect of plasticizer on the crystallization behavior of poly(lactic acid), *J. Appl. Polym. Sci.* **2009**, *113*, 112–121.

364. Y. H. Na, Y. He, S. Shuai, Y. Kikkawa, Y. Doi, Y. Inoue, Compatibilization effect of poly(ε-caprolactone)-*b*-poly(ethylene glycol) block copolymers and phase morphology analysis in immiscible poly(lactide)/poly(ε-caprolactone) blends, *Biomacromolecules* **2002**, *3*, 1179–1186.

365. C. C. Chen, J. Y. Chueh, H. Tseng, H. M. Huang, S. Y. Lee, Preparation and characterization of biodegradable PLA polymeric blends, *Biomaterials* **2003**, *24*, 1167–1173.

366. L. Wang, W. Ma, R. A. Gross, S. P. McCarthy, Reactive compatibilization of biodegradable blends of poly(lactic acid) and poly(ε-caprolactone), *Polym. Degrad. Stab.* **1998**, *59*, 161–168.

367. G. X. Chen, H. S. Kim, E. S. Kim, J. S. Yoon, Compatibilization-like effect of reactive organoclay on the poly(L-lactide)/poly(butylene succinate) blends, *Polymer* **2005**, *46*, 11829–11836.

368. Y. Wang, J. F. Mano, Biodegradable poly(L-lactic acid)/poly(butylene succinate-*co*-adipate) blends: miscibility, morphology, and thermal behavior, *J. Appl. Polym. Sci.* **2007**, *105*, 3204–3210.

369. C. N. Ludvik, G. M. Glenn, A. P. Klamczynski, D. F. Wood, Cellulose fiber/bentonite clay/biodegradable thermoplastic composites, *J. Polym. Environ.* **2007**, *15*, 251–257.

370. N. Lopez-Rodriguez, A. Lopez-Arraiza, E. Meaurio, J. R. Sarasua, Crystallization, morphology, and mechanical behavior of polylactide/poly(ε-caprolactone) blends, *Polym. Eng. Sci.* **2006**, *46*, 1299–1308.

# 15

# FOAMING

Laurent M. Matuana

## 15.1 INTRODUCTION

A continuous increase in oil prices and environmental concerns about the use of petroleum-based plastics have led to a growing interest in bio-based plastics. Poly(lactic acid) (PLA), a plastic derived from fermented plant starch, is fast becoming one of the popular alternatives to traditional petroleum-based plastics. Even though PLA has been known for more than a century, it has only been used commercially in recent years in a number of biocompatible/bioabsorbable biomedical devices, packaging applications, and so on. Factors that contributed to the success of PLA in these applications include its physical properties, as well as favorable compostable and degradation characteristics [1].

Despite these attractive properties, PLA has considerable drawbacks. It is more expensive, more brittle, and has lower impact resistance than many petroleum-derived commodity plastics [2–6], in addition to having a narrow processing window due to its sensitivity to hydrolytic and thermal degradation [7]. All these factors may greatly limit its applicability in packaging applications where materials require flexible polymer film, because industrial production lines cannot tolerate film cracking or tearing when folded or subjected to force during manufacturing.

To broaden its applications, PLA is often blended with various additives such as lubricants, plasticizers, or a second polymer [3–6, 8–10]. Unfortunately, this approach can increase the manufacturing cost owing to the cost associated with the additives [2]. Previous efforts to reduce the cost of PLA included blending it with fillers such as cellulosic fibers or starch [5, 6, 11]. However, the lowered cost due to filler addition is usually achieved at the expense of other properties such as the ductility (lower elongation at break) and lower impact resistance, because the incorporated brittle cellulosic fibers alter the ductile mode of failure of the matrix, making the composites more brittle than neat polymer [12–14]. Efforts are continuously being made to further reduce the cost of PLA while enhancing its flexibility and toughness.

Foaming technology, such as microcellular foaming, is a well-known process to enhance the ductility and impact resistance of a polymer matrix in addition to providing a significant expansion ratio and weight reduction in plastic parts. The high expansion ratio induced by foaming generally reduces the material cost and consumption in mass-produced plastic parts without a major compromise in the required properties [15, 16].

This chapter is focused on the foaming agents/processes used in foam production, factors affecting the creation, growth, and stabilization of cells, as well as the properties of PLA foams.

## 15.2 PLASTIC FOAMS

A plastic foam can be defined as a plastic material with a cellular structure. Generally, it consists of a minimum of two phases: a gas phase dispersed in a solid plastic matrix phase. The gaseous phase contained in voids or cells is often referred to as the blowing or foaming agent. The solid plastic component can be based on neat resins, polymer blends, or alloys, which may contain fillers of fibrous or other morphologies [17–19].

*Poly(Lactic Acid): Synthesis, Structures, Properties, Processing, Applications, and End of Life*, Second Edition.
Edited by Rafael A. Auras, Loong-Tak Lim, Susan E. M. Selke, and Hideto Tsuji.

Foam properties are greatly affected by density and the cell geometry, size, and shape. Generally, cellular plastics are classified as open cell or closed cell. In closed-cell foams, each cell is completely enclosed by a thin wall or membrane of plastic in such a manner that the gas phase for each cell is independent of the other cells, whereas in open-cell foams, the individual cells are interconnected in such a manner that fluid can pass from one cell to another.

Cell geometry (i.e., open versus closed cells, size, and shape), which depends on the process used for the production of the foamed plastic, determines certain properties, thereby influencing its suitable types of applications. In open-cell foams, the gas phase is inevitably air and thus offers little resistance to the permeation of liquids and gases, making them only most suitable for acoustical insulation and in cushioning applications. In contrast, in closed-cell foam, the cell walls act as a barrier to gases and liquids. Therefore, closed-cell foams have lower permeability than open-cell foams. If the gas phase in closed-cell foams has low thermal conductivity, then these foams will provide better thermal insulation properties than the open-cell foams that are air filled.

Foam properties depend strongly on the chemical and physical nature of the matrix. Nevertheless, the composition of the gaseous phase from the blowing agent also has an important effect on certain properties such as thermal resistance, acoustical insulation, and so on.

## 15.3 FOAMING AGENTS

The foaming agents used to produce the cellular structure during the foaming operation fall into two classes: physical foaming agents (PFAs) and chemical foaming agents (CFAs).

### 15.3.1 Physical Foaming Agents

Physical foaming agents undergo only a physical change during foaming [18, 20]. The change may involve volatilization (boiling) of a liquid, or the release of a compressed gas to atmospheric pressure after diffusion into a solid or molten polymer while under pressure. The most common physical foaming agents are those based on low boiling point organic liquids such as hydrocarbons and halogenated hydrocarbons, which develop cells within the plastic material by changing from liquid to gas during foaming under the influence of heat. Nitrogen ($N_2$), carbon dioxide ($CO_2$), and argon (Ar) constitute another group of substances belonging to this class that are introduced into the foaming process as compressed gases. When physical blowing agents are used in foaming, the gas phase of the foam is chemically identical with the blowing agent.

Hydrocarbons (e.g., *n*-pentane, *n*-butane) and halogenated hydrocarbons (e.g., chlorofluorocarbons or CFCs) used to be the most common foaming agents owing to their high solubility in polymer melts. They produce low-density foam at a relatively low pressure. However, the use of CFCs was phased out in the 1990s because of their contribution to the depletion of the earth's ozone layer. Hydrocarbon foaming agents such as *n*-butane are also not preferable due to their high flammability. Inert gases are growing in use as alternative foaming agents [17, 18].

### 15.3.2 Chemical Foaming Agents

Chemical foaming agents are materials that are stable at normal storage temperature. However, under well-defined temperature (or reaction conditions), they provide a gas (or gases) by undergoing a chemical reaction, which results in the dissolution (or decomposition) of the original molecule, yielding one or more gases for polymer expansion, while forming one or more solid residues that remain in the foamed polymer [18–21]. Usually, the decomposition of CFAs is thermally induced, although there are a few examples where decomposition is chemically initiated. Since the residues are almost always more stable than the original foaming agent and do not form part of the gas produced, the gas phase of the resulting foam is different from the blowing agent when CFAs are used in foaming. CFAs as a class may also be subdivided into two major categories: endothermic and exothermic. The types and characteristics of some commercially available CFAs are listed in Table 15.1.

***15.3.2.1 Endothermic CFAs*** Endothermic CFAs continuously absorb heat during decomposition. Generally, they have a broad decomposition temperature, although materials

**TABLE 15.1 Characteristics of Some Commercially Available CFAs [20]**

| Names | Types | Decomposition Temperature (°C) | Gas Evolution ($cm^3/g$) | Main Gas Evolved | Additional Gases |
|---|---|---|---|---|---|
| Sodium bicarbonate | *endo* | 160–210 | 120 | $CO_2$ | |
| Azodicarbonamide | *exo* | 205 | 210–220 | $N_2$ | $NH_3$, CO, $CO_2$ |
| *p*,*p*′-Oxybis(benzene) sulfonyl hydrazide (OBSH) | *exo* | 160 | 125 | $N_2$ | $H_2O$ |
| *p*-Toluenesulfonyl semicarbazide (TSSC) | *exo* | 232 | 140 | $N_2$ | $NH_3$, CO, $CO_2$ |
| 5-Phenyltetrazole (5PT) | *exo* | 240–250 | 200 | $N_2$ | |

with narrow decomposition temperature ranges are now available [18, 20]. Formulations of endothermic foaming agents are based on a variety of chemistries, such as sodium bicarbonate/citric acid derivatives [21]. Carbon dioxide is the major gas evolved during chemical decomposition reactions of these agents. The endothermic characteristic of these products has been reported to have a cooling, stabilizing effect on the polymer melt, and to help reduce cooling cycle times. Since the components of these blends are essentially food additives, they are generally regarded as safe from a toxicity standpoint [20]. Endothermic CFAs, which absorb process heat during reaction, have a more controlled reaction and produce a smaller cell structure than exothermic agents. Smaller cells improve the elongation at break, although larger bubbles improve impact strength. Smaller cells generally result in a smoother surface appearance [21].

***15.3.2.2 Exothermic CFAs*** Exothermic CFAs generate heat as they decompose. They have more narrow decomposition temperature ranges and have a higher gas yield per gram of CFA compared with endothermic types (Table 15.1) [18, 20, 21]. A popular blowing agent of this class is azodicarbonamide (ADC). The gas evolved by exothermic CFAs is mainly nitrogen. Other gases such as CO, $CO_2$, and $NH_3$ may also be given off in lesser amounts. $N_2$ has a slow rate of diffusion through polymers and is useful for obtaining maximum density reduction, that is, it is a very efficient expanding gas for most polymers. Most of the exothermic CFAs listed in Table 15.1 have FDA sanction for use in foams coming into contact with food [20].

About 88% of global CFA volume is ADC, with 5% in endothermic foaming agents and 7% of the volume in various other types [21]. However, endothermic CFAs are expected to grow slightly faster than the exothermic CFAs due to both technical and regulatory concerns about exothermic CFA use. Processors' preference for fine cell structure and the prohibition by the European Food Safety Authority of the use of ADC in food contact materials due to its decomposition into toxic by-products are the driving forces for the future increased use of endothermic CFAs in many applications [21].

Therefore, the selection of any CFA should be based on the characteristics of the resin and processing conditions, since both classes of chemical foaming agents have their advantages and drawbacks. It has been reported that for most molding and extrusion applications, the general rule of thumb is to select a CFA that has a decomposition, or gas release, temperature closely matching the processing temperature to be used for the polymer [20].

Over the past years, blends of exothermic and endothermic CFAs are increasingly used to exploit the exothermic CFA's high gas yield and expansion ability, as well as the small cell structure induced by the endothermic agents.

## 15.4 FORMATION OF CELLULAR PLASTICS

The fundamentals of foam formation have been reviewed in detail by a number of authors [17–19]. Therefore, only the main concepts will be reviewed in this chapter. Cellular plastics are produced through several methods, irrespective of cell structure (open or closed). However, the most commonly used methods for cellular PLA are the following:

1. Thermal decomposition of foaming agent generating $N_2$ or $CO_2$, or both, within the polymer mass by the application of external heat.
2. Expansion of a gas dissolved in a molten or solid resin mix by reducing the pressure in the system.

Regardless of the blowing agent used, the formation of plastic foam involves three specific and critical steps:

1. Dissolution of a blowing agent in the polymer.
2. Bubble formation or nucleation of cells.
3. Growth and stabilization of cells.

### 15.4.1 Dissolution of Blowing Agent in Polymer

The dissolution of gas into the polymer depends on the type of foaming agent used. For CFA, the blowing agent is introduced into the polymer melt by applying heat, inducing its thermal decomposition, and thus generating $N_2$ or $CO_2$, or both. In contrast, in the case of physical foaming agents, the blowing agent is directly injected into the polymer melt (or solid) by using a special delivery system that provides high pressure and accurately meters the mass flow of gas to the processing equipment.

In both cases, the key requirement for a uniform and controlled cell structure is a homogeneous polymer–gas solution. This is controlled by two factors: the solubility of the blowing agent gas in the polymer and the sorption kinetics. The achievement of equilibrium solubility is determined by the sorption kinetics, and this is therefore a time-dependent process. This process can be accelerated by raising the melt temperature and using screw designs that promote good mixing of the polymer melt and injected gas [15, 16, 22–24].

### 15.4.2 Bubble Formation

When the dissolved gas reaches a saturation limit in the polymer, it becomes supersaturated and finally diffuses out of the polymer system to form voids or bubbles [17–19]. The formation of bubbles represents a nucleation process in which voids are formed either without nucleating agent (self-nucleation process) or with solid nucleating agents at the liquid–solid interface (heterogeneous process). An increase in the free energy of the system ($\Delta F$) is required for

the formation of bubbles in a liquid or molten plastic system, as given by the following equation:

$$\Delta F = \gamma A \tag{15.1}$$

where $\gamma$ is the surface tension of the liquid and $A$ is the total interfacial area.

It appears from Equation 15.1 that the formation of a bubble becomes easier by lowering the surface tension at the location of bubble formation.

While it is apparently difficult to produce desirable foams by a self-nucleation process [25, 26], it has been reported that the most successful foam systems contain nucleating agents [17–19]. The addition of external nucleating agents (e.g., solid particles such as talc, nanoclay) is important because they provide sites for nucleation of cells. Indeed, nucleating agents may be effective surface tension depressants that eliminate the need for the foaming gas to separate the liquid from itself to form bubbles. Rather, the foaming gas diffuses from the polymer system into the microvoids, causing them to grow, instead of nucleating new bubbles [17–19].

### 15.4.3 Bubble Growth and Stabilization

Once the cells are generated, they continue to grow as long as they encounter little resistance. Cell growth occurs due to the diffusion of the gas from the polymer into the nucleated cell and by expansion owing to the elevated temperature or external pressure drop [17, 19]. At equilibrium, the gas pressure in a bubble is usually larger than the pressure in the surrounding melt, as given by Equation 15.2:

$$\Delta p = \frac{2\gamma}{r} \tag{15.2}$$

where $r$ is the radius of the bubble.

Several authors have pointed out that when there are two adjacent bubbles of different sizes, the gas pressure in the small cell is greater than that in the larger one. The difference in pressure between the two bubbles ($\Delta p_1^2$) having radii of $r_1$ and $r_2$ is given by [17, 19]

$$\Delta p_1^2 = 2\gamma\left(\frac{1}{r_1} - \frac{1}{r_2}\right) \tag{15.3}$$

One can notice from Equation 15.3 that the gas will tend to diffuse from the smaller bubble into the larger one because of the pressure difference in the cells. Then the two cells will become one larger cell (cell coarsening) [24].

Stabilization of bubbles is accomplished by cooling the foamed molten plastic to provide the necessary increase in viscosity. In this stage, the temperature of the melt is one of the most important process parameters because it affects the stability of the foam. An increase in the temperature of the melt during processing implies a decrease in melt viscosity and melt strength, as well as the surface tension, making the thinning of the cell walls easier, which potentially leads to their rupture. An increase in the temperature of the melt tends to expand the foam first, after which grown cells may collapse due to lack of stabilization of the structure. Conversely, when the temperature of the melt is too low, foaming is limited because the material solidifies before the bubbles have the possibility to expand fully [14].

The final cell population density of the foam decreases due to cell coalescence and cell coarsening. These two outcomes of the bubble growth mechanism should be reduced because fine-celled foams have better mechanical, thermal, and acoustical properties. Therefore, stabilization is critical to prevent cell wall rupture caused by excessive thinning.

It should also be pointed out that cell wall rupture may be important for the formation of open-cell foams while cell wall thinning and rupture must be avoided for the production of closed-cell foams. In either case, there is an optimum processing temperature window and viscoelastic properties of the polymer for foaming.

## 15.5 PLASTIC FOAMS EXPANDED WITH PHYSICAL FOAMING AGENTS

Although various types of physical foaming agents are used in the production of polymeric foams, supercritical fluids such as $CO_2$ and $N_2$ are the commonly used foaming agents for PLA for several reasons. Supercritical fluids of $CO_2$ especially possess many advantageous properties including inertness, low cost, nonflammability, environmentally friendly, and so on. Its critical point is relatively low (31.1°C and 7.38 MPa) and easily attained. $CO_2$ reduces the viscosity and interfacial surface energy of polymer melts, which have a significant influence on the foaming process. It is also possible to quickly dissolve sufficient $CO_2$ in a polymer melt due to its high diffusivity.

### 15.5.1 Microcellular Foamed Polymers

A microcellular polymer is a foamed plastic characterized by a cell population density (or the number of cells nucleated per unit volume of the original unfoamed polymer) in the range of $10^9$–$10^{15}$ cells/cm$^3$ with fully grown cells being smaller than 10 μm in average size. These unique features differentiate microcellular foam (MCF) from conventional cellular foam (produced with CFAs), where the cell size ranges from 100 to 10,000 μm, and there is a very nonuniform cell size distribution (cell population density in the range of $10^4$–$10^6$ cells/cm$^3$). In general, foams with very fine cells (microcellular foams) exhibit stronger mechanical

properties than foams with larger cells (conventional foams). MCF technology foams plastics using a physical blowing agent in its supercritical state to create a swarm of bubbles in the polymer matrix.

The concept of microcellular thermoplastic foam was developed in the 1980s by researchers at the Massachusetts Institute of Technology and was based on the idea that the creation of a very large number of microbubbles, smaller than the preexisting natural flaws in a polymer, can reduce the material cost and consumption in mass produced plastic parts without compromising mechanical properties [15, 16].

Since then, interest in the production of MCF materials has grown for several reasons. In particular, they offer the benefits of reduced material usage and lowered weight while enhancing the impact strength (up to fivefold increase over unfoamed plastic) [27, 28], toughness (up to fivefold increase over unfoamed plastic) [28], fatigue life (up to 14-fold increase over unfoamed plastic) [29], and thermal stability [30]. These improvements are due to the presence of a very high cell population density of minute bubble cells. These small bubbles inhibit crack propagation by blunting the crack tip and increasing the amount of energy needed to propagate the crack [15]. The presence of these cells can also reduce the specific density of the polymer by 75% or more [31, 32]. With such unique properties, microcellular plastics can be used in a large number of innovative industrial applications, including lightweight and high-strength parts for the automotive and aerospace industries. Other applications include packaging materials, furniture, sports equipment, filtration membranes, and thermal/electrical insulators [33].

Microcellular foams can be produced by noncontinuous processes such as a batch process [2, 12, 15, 16, 31, 32, 34, 35], continuous processes such as extrusion and injection molding [24, 33, 36, 37], or by a semicontinuous process [38]. Since the semicontinuous process is not extensively used in the scientific community or in the industry, it will not be described in this chapter. Readers are encouraged to refer to Ref. 38 for detailed information on this process. To date, microcellular foams have been produced in amorphous polymers [12, 31, 32, 34], semicrystalline polymers [35], and elastomers [16]. Recently, MCF structures have also been produced in plastics filled with inorganic nanoparticles (montmorillonite) [39–43], as well as organic cellulosic fiber-filled plastic composites [12, 31, 32, 34, 37].

### 15.5.2 Solid-State Batch Microcellular Foaming Process

Martini and coworkers developed the two-stage batch microcellular foaming process using three different steps: (i) formation of a gas/polymer solution, (ii) cell nucleation, and (iii) cell growth and stabilization [16].

***15.5.2.1 Formation of Gas/Polymer Solution*** The formation of gas/polymer solution is achieved by saturating the polymer with a nonreactive gas such as $N_2$ or $CO_2$ in a high-pressure vessel with moderate pressure (<850 MPa) at room temperature (Figure 15.1a). Mixtures of $N_2$ and $CO_2$ gases can also be used. Saturation with high pressure (30 MPa) can also be achieved by heating up the pressure chamber (or using an autoclave) [39–43]. At equilibrium, the polymer has absorbed gas to form a uniform polymer/gas solution.

The formation of a gas/polymer solution depends on gas absorption and diffusion into the polymer matrix, which can be affected by the nature of the polymer matrix (amorphous versus semicrystalline), gas type, saturation pressure, and temperature [44, 45]. The sorption behaviors of gas in polymers can be explained by Henry's law (gas solubility), as shown in the following equations [46]:

$$C = k_D P \tag{15.4}$$

$$D = D_0 \exp\left(\frac{-\Delta E_D}{RT}\right) \tag{15.5}$$

where $C$ is the volumetric concentration of gas at standard temperature and pressure per volume of polymer, $k_D$ is the Henry's law constant, $P$ is the applied saturation gas pressure, $D$ is the diffusion coefficient, $D_0$ is the diffusion coefficient constant, $\Delta E_D$ is the activation energy for diffusion of the gas in the polymer, $R$ is the gas constant, and $T$ is the absolute temperature.

Equation 15.4 shows that the concentration of gas in the polymer is directly proportional to the gas pressure. Increasing the pressure can increase the gas absorption and diffusion to facilitate the formation of a gas/polymer single-phase solution. Increasing the saturation temperature increases the gas diffusion rate into the polymer. However, this decreases the gas concentration at a specific pressure.

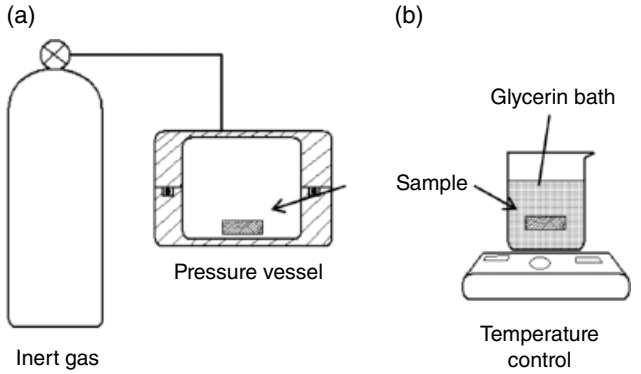


**FIGURE 15.1** Schematic of a batch microcellular foaming process (a) gas saturation and (b) foaming [34].

Detailed investigations on the fundamental interaction of various gases with PLA in different temperature and pressure ranges with subsequent gas-induced morphological changes in the polymer can be found in Refs 44, 45, and, 47–51 and in Chapter 11.

***15.5.2.2 Cell Nucleation*** After the gas/polymer single-phase solution is formed, the gas-saturated specimen is foamed under a variety of processing conditions. To produce microcellular foamed structures, the gas-saturated samples are subjected to a rapid pressure drop and a rapid temperature increase (Figure 15.1b) that result in nucleation and growth of billions of gas nuclei [52, 53]. The sudden drop of gas concentration creates a thermodynamic instability in the gas/polymer solution, which is the main driving force for nucleation of microcells.

The nucleation process is important because it determines the cell population densities, cell morphology, and the mechanical properties of the microcellular foams. The nucleation of cells in the polymer can be homogeneous, heterogeneous, or a mixed mode nucleation (both).

In homogeneous nucleation, nucleation sites are formed right through the mass of the polymers at a molecular level. This homogeneous nucleation is driven by thermodynamic instabilities and a certain amount of work is required in order to homogeneously create a nucleus [54–56]. This amount of work or the activation energy for homogeneous nucleation ($\Delta G_{hom}$) is defined as:

$$\Delta G_{hom} = \frac{16\pi\gamma_{bp}^3}{3\Delta P^2} \tag{15.6}$$

where $\gamma_{bp}$ is the surface energy of the polymer–bubble interface and $\Delta P$ is the saturation gas pressure.

According to the theory proposed by Colton and Suh [54–56], the rate that bubbles nucleate homogeneously ($N_{hom}$) is given by

$$N_{hom} = C_0 f_0 \exp\left(\frac{-\Delta G_{hom}}{kT}\right) \tag{15.7}$$

where $C_0$ is the concentration of gas molecules, $k$ is the Boltzmann's constant, and $f_0$ is the frequency factor for gas molecules joining the nucleus, which is related to the interfacial tension ($\gamma_{bp}$) and the mass of the gas molecules ($m$) by the following equation:

$$f_0 = \left(\frac{2\gamma_{bp}}{\pi m}\right)^{0.5} \tag{15.8}$$

Note from Equation 15.6 that a higher gas saturation pressure lowers the activation energy for homogeneous nucleation, and accordingly results in a higher nucleation rate (Equation 15.7).

As previously mentioned, heterogeneous nucleation occurs at the interface between the polymer and another phase. Generally, the addition of external nucleating agents provides sites for heterogeneous nucleation of cells due to their reduction of surface energy at the polymer–bubble interface. The heterogeneous nucleation rate ($N_{het}$) is given by an equation similar to the one describing homogeneous nucleation [54–56]:

$$N_{het} = C_1 f_1 \exp\left(\frac{-\Delta G_{het}}{kT}\right) \tag{15.9}$$

where $C_1$ is the concentration of heterogeneous nucleation sites, which is directly related to the particle concentration and gas molecules, and $f_1$ is the frequency factor for gas molecules joining the nucleus.

Gibbs free energy (activation energy barrier) for heterogeneous nucleation ($\Delta G_{het}$) can be expressed as follows:

$$\Delta G_{het} = \frac{16\pi}{3\Delta P^3}\gamma_{bp}^3 f(\theta) \tag{15.10}$$

where $f(\theta) = (1/4)(2+\cos\theta)(1-\cos\theta)^2$, $\theta$ is the contact angle at the polymer–additive interface.

***15.5.2.3 Cell Growth and Stabilization*** Once the cells have nucleated, they will continue growing provided that little resistance is encountered. In general, the cell growth process is controlled by the gas diffusion rate and the viscoelastic properties of the gas/polymer solution. Variations in foaming time and temperature (e.g., longer foaming time and higher temperature) can enhance the cell growth process, because of reduced polymer matrix stiffness and increased gas diffusion rate. After foaming, the specimen is immediately dipped into a water bath to freeze the foam structure and minimize the deterioration of cells through cell coalescence during bubble growth [2, 12]. Figure 15.2 shows the cell morphology (closed cells) of semicrystalline PLA foamed through a batch microcellular process using $CO_2$ as a blowing agent.

***15.5.2.4 Effects of the Nature of Polymer Matrix and Processing Conditions on the Morphology of Microcellular PLA Foams*** The nature of the polymer and the processing conditions can have a strong influence on the foaming ability of the polymer matrix. Indeed, some parameters such as solubility of gas in the polymer matrix, the rate of gas diffusion in and out of the nucleated cells, the surface energy at the polymer–bubble interface, the crystallinity of the polymer, the viscoelastic properties of the polymer/gas solution, and the amount of gas loss during foaming process have an effect not only on the porous morphologies generated in the matrix

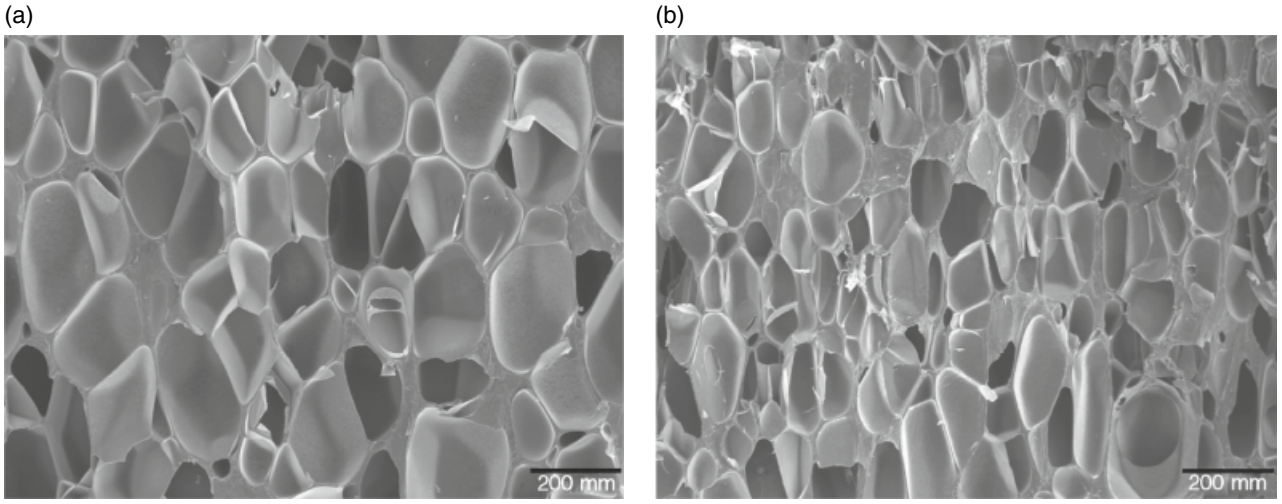


**FIGURE 15.2** SEM micrographs of amorphous PLA (8302D, NatureWorks, 10% D-lactic acid content) foamed at 150°C for 5 s in a batch process. Specimens were saturated with $CO_2$ at room temperature for 48 h at (a) 400 psi and (b) 600 psi (unpublished images from Matuana).

but also on the mechanical properties of the foamed plastic [12, 32, 34, 52, 53].

*15.5.2.4.1 Crystallinity* Changes induced by the gas are an important factor to be considered when designing cellular structures for specific applications because changes in the physical properties of a polymer can affect the morphology developed in foamed sample [57, 58]. Since the sorption of gas is known to induce crystallization in polymers from the plasticizing effect of gas at high concentrations, the solubility and diffusion coefficients of $CO_2$ in a copolymer of poly(L-lactic acid) (PLLA) and poly(DL-lactic acid) (PDLLA) were measured at room temperature and pressures up to 5.8 MPa. An X-ray diffraction analysis of the resulting products showed that conditioning PLA with $CO_2$ induces crystallinity in the polymer as expected and the degree of crystallinity increases with increasing saturation pressure (Table 15.2) [57, 58].

The greatest increases in crystallinity under room temperature conditions were observed at pressures between 2.1 and 2.8 MPa, and this induced crystallinity significantly affected the PLA foamability. In fact, lower saturation pressure (up to 2.8 MPa) led to more uniform microcellular structures with cell diameters on the order of 30–40 μm and a cell density of $7.93 \times 10^7$ cells/cm$^3$. In contrast, foam structures became inhomogeneous and cell size decreased with an increase in saturation pressure, owing to the rapid diffusion of $CO_2$ out of the polymer. As a result, the density of the foamed sample was almost similar to that of unfoamed material. SEM micrographs shown in Figure 15.2 also depict the $CO_2$-induced crystallinity in PLA since the cell size decreased with an increase in saturation pressure.

It is recognized that the solubility and diffusivity of gas in semicrystalline polymers are a function of the degree of crystallinity because gas does not dissolve in the crystallites [34, 59–61]. Increasing the mass fraction of crystallite in the polymer leads to the reduction of the amorphous matrix mass fraction. As a result, the solubility and diffusivity of gas are reduced since the gas does not dissolve in the crystallites, and the crystallites tend to obstruct the movement of gas molecules in the polymer [34]. Since the crystal domains in semicrystalline PLA do not absorb gas, the induced crystallinity in PLA by $CO_2$ must have reduced the amount of gas available in the amorphous region due to the lower amorphous volume fraction, thus affecting the morphology developed in the foamed polymer.

In foam processes, improving the crystallization kinetics of PLA can enhance its low melt strength and thus improve its foamability significantly [62–65]. The crystallization behavior of linear and branched PLA was investigated in the presence of dissolved $CO_2$ using high-pressure and regular

**TABLE 15.2 Pressure Dependence of $CO_2$-Induced Crystallization in PLLA at 25°C for 24 h and Cell Morphology of PLLA Foams [57, 58]**

| | | Properties of PLLA Foamed at 100°C for 5 s[a] | |
|---|---|---|---|
| Saturation Pressure (MPa) | Crystallinity (%) | Cell Size (μm) | Foam Density (g/cm$^3$) |
| 0 | | | ~1.25 |
| 2.1 | 13.1 | | |
| 2.8 | 16.0 | 30–40 | 0.35 |
| 3.4 | 20.8–24 | <10 | 1.10 |
| 4.1 | 23.4 | | |
| 5.8 | 23.6 | | |

[a] PLLA used was copolymer of poly-L-lactic acid and poly-DL-lactic acid with a D-lactide content of 1.1–1.7% (Unitika Ltd., Japan).

differential scanning calorimeter but without foaming the samples [64, 65]. Both isothermal and non-isothermal melt crystallization results showed that increasing the $CO_2$ pressure decreased the crystallization half-time. A very high (maximum) crystallinity was observed at a low $CO_2$ pressure of 15 bar attributed to the formation of more close-packed and larger perfect crystals. The crystallinity decreased at elevated pressures (45 bar) because a larger number of less close packed crystals were formed, i.e., the formation of smaller and more imperfect crystals.

A methodology for the preparation of microcellular PLA foams with high-volume expansion ratio by crystallization induction modification was proposed recently [66]. Phenylphosphonic acid zinc salt (PPZn) was used as an effective crystallization nucleating agent since its addition improved the crystallinity and crystallization temperature of unfoamed PLA. Neat PLA and PLA/PPZn batch-foamed by saturating the samples in an autoclave for 120 min at a saturation pressure of 10 MPa and saturation temperature of 144°C showed no foam structure was observed in neat PLA. In contrast, cellular morphology was fully developed in PLA/PPZn. The cell population density of PLA/PPZn foam was about $1.0 \times 10^{11}$ cells/cm$^3$ and the average cell size of 1.9 μm. This was attributed to the poor melt elasticity of linear PLA and the addition of PPZn increased its melt elasticity by increasing the number of high melting temperature crystals [66].

*15.5.2.4.2 Micron-/Nano-Sized Fillers and Nanofoams* Using a batch foaming process in an autoclave, Okamoto and his colleagues reported for the first time the preparation and characterization of neat PLA and PLA/nanocomposite foams having structures from microcellular to nanocellular [39, 41]. The nanocomposites contained 5 wt% of two different types of layered silicates organically modified with two different types of alkylammonium cations, octadecylammonium (ODA) and octadecyltrimethylammonium (SBE). A morphological correlation was established between the dispersed silicate particles with nanometer dimensions in the bulk and the formed closed-cell structure after foaming (Table 15.3).

The nanocomposite foams showed smaller cell size and higher cell population density compared with neat PLA foam. This behavior was attributed to the dispersed silicate particles that acted as nucleating sites for cell nucleation. Characterization of the interfacial tension between bubble and matrix revealed that the incorporation of nanoclay-induced heterogeneous nucleation because of a lower activation energy barrier compared with homogeneous nucleation [41]. In addition, SEM micrographs of nanocomposites (not shown here) showed that the grown cells having diameter of ~200 nm were localized along the dispersed nanoclay particles in the cell wall. The dispersed nanoclay particles acted as nucleating sites for cell formation and the cell growth occurred on the surfaces of the clays.

It should be pointed out that the role of crystallization in cell nucleation was not addressed, although $CO_2$ gas molecules can induce crystallization of the PLA matrix [57, 58], making the interpretation of the data presented in Table 15.3 difficult since one cannot separate the heterogeneous nucleating effect of nanoclay from the effect of $CO_2$-induced crystallinity on cell nucleation and growth.

Comparison between the two nanocomposites revealed that the number of the stacked individual silicate layers ($D/d_{001}$) for PLA/SBE nanocomposites was much lower than for PLA/ODA nanocomposites, suggesting that intercalated silicate layers were more homogeneously and finely dispersed in PLA/SBE than in PLA/ODA (Table 15.3). The nature of the dispersion also plays a vital role in controlling the size of the cell during foaming since PLA/SBE5 nanocomposites had "nanocellular" structure as opposed to the microcellular structure of the PLA/ODA5 nanocomposites.

The concentration of organically modified layered silicates also has a strong effect on the cell size and cell density of PLA and PLA nanocomposites [42, 43]. Compared with neat PLA, the nanocomposites foamed at 110°C using a 20 : 80 $CO_2$ : $N_2$ mixture as the blowing agent in a batch foaming process exhibited reduced cell size and increased cell density, even at very low organoclay content (Figure 15.3).

This behavior can be ascribed to increased cell nucleation due to the presence of the heterogeneous bubble nucleation

**TABLE 15.3 Morphological Properties of Unfoamed and Foamed PLA/Nanocomposites [39, 41]**

| | Properties of Foams | | | XRD Results | | |
|---|---|---|---|---|---|---|
| Specimens[a] | ρ (g/cm$^3$) | $d$ (μm) | $N_0$ (×10$^{-11}$ cells/cm$^3$) | $d_{001}$ (nm) | $D \approx d_{clay}$ (nm) | $D/d_{001}$ |
| Neat PLA | ~1.2 | ~230 | (<10$^5$) | | | |
| PLA/ODA nanocomposite[b] | 0.5 | 2.6 | 3.56 | 3.03 | 38.0 | 12.5 |
| PLA/SBE nanocomposite[b] | 0.6 | 0.4 | 1172 | 2.85 | 12.4 | 4.4 |

[a] PLA had a D-lactic acid content of 1.1–1.7% (Unitika Co. Ltd., Japan).

[b] The nanocomposites contained 5 wt% of organically modified layered silicates. All specimens were saturated with $CO_2$ in autoclave at elevated temperature (140–165°C) and pressure (~10 MPa) for 2 h.

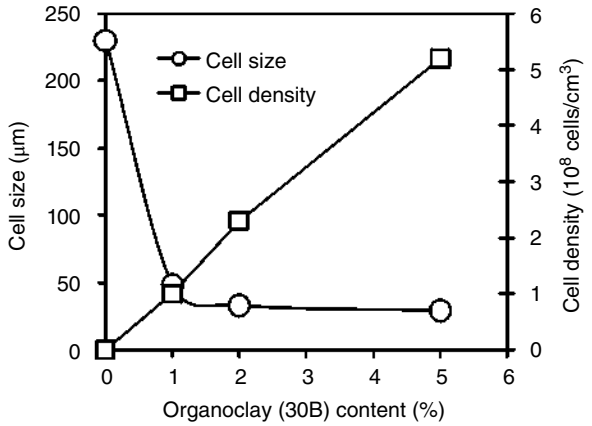


**FIGURE 15.3** Dependence of cell size and cell density of PLA (NatureWorks 3000D, Cargill Dow) and PLA nanocomposites on the concentration of organically modified layered silicates (organoclay Cloisites 30B, Southern Clay Products, Inc., Texas) [42]. Cloisite 30B is the montmorillonite modified with methyl, tallow (~65% C18, ~30% C16, ~5% C14), and bis-2-hydroxy ethyl quaternary ammonium salt.

sites. With the increase of organoclay content, the cell size decreased and both cell and foam densities were increased. Nanocomposites with higher organoclay content (10%) were poorly foamed due to the intrinsically high viscosity and elasticity caused by organoclay exfoliation and chain extension/branching, which reduced the cell growth.

Other micron-sized and nano-sized materials like talc, nanoclay, cellulose nanocrystals (CNCs), cellulose nanofibers (CNFs), wood flour, wood fibers, and so on have also been utilized to increase the nucleation rate in PLA even at low addition levels [37, 67–74]. Additionally, the incorporation of these materials in PLA improves its low melt strength and viscosity, thus enhancing its foaming.

A study has shown that the addition of pine wood flour into PLA matrix acts as a heterogeneous nucleating agent and rheology modifier [37]. A one order of magnitude increase in the extensional viscosity was achieved in PLA melt after the addition of 20% wood flour. However, there was no significant change on the void fraction of $CO_2$-extrusion microcellular PLA foam after the addition of wood flour [37].

PLA/cellulosic fiber composites based on fibers from northern bleached softwood kraft (NBSK) and black spruce medium density fiberboard (MDF) with poly(ethylene glycol) (PEG) as a lubricant were microcellular injection molded [67]. The incorporation of 25 phr NBSK and MDF fibers led to foamed composites with higher cell population density, smaller average cell size, and narrower cell size distribution (more uniform cell structure) compared with the neat PLA counterpart. This improved foam morphology was attributed to the cell nucleating effects of fibers and the increase in the melt strength of the PLA matrix by the addition of NBSK and MDF fibers [67].

The nucleating and rheological effects of cellulose nanofibers (CNFs) [68–70] and cellulose nanocrystals (CNCs) [69–71] in the $CO_2$ supercritical batch foaming process of PLA have been investigated. The introduction of various amounts of CNFs significantly improved the morphology of PLA foams by reducing the average cell size and increasing the cell population density. Interestingly, the addition of CNFs offered the potential to generate nanoporous structures in PLA foams [68].

Similar results were obtained with PLA/CNC nanocomposites containing two types of CNC particles, including pristine CNC (pCNC) and acetylated CNC (aCNC) [69]. PLA foam had uniform microcellular morphology with an average cell size of 35.6 μm and expansion ratio of 3.8 times. The addition of 3 wt.% pCNC and aCNC nanoparticles increased the expansion ratios of PLA foams to 4.9 and 6.7 times, respectively, while decreasing their average cell sizes to 25.1 and 21.7 μm, respectively. As a result, the cell population density of PLA foams increased from $3.91 \times 10^{10}$ to $1.2 \times 10^{11}$ and $2.0 \times 10^{11}$ cells/cm$^3$ by adding pNCN and aCNC, respectively. These morphological changes of PLA foams in the presence of CNC particles are attributed to the synergistic effects caused by nucleation and increased melt strength [69]. Like CNFs, the presence of CNC also provides the possibility of producing nanocellular structures in PLA. Nanocomposite foams containing aCNC had finer cell size and higher cell population density than their counterparts with pristine CNC (pCNC) due to better aCNC dispersion into PLA matrix, which favored crystal nucleation. Since the nucleating efficiency of the nanoparticles is generally compromised by their aggregation in the polymer matrix, better dispersion of nanoparticles can provide higher amounts of nucleating sites [68, 71].

Microcellular foamed PLA was also successfully produced in a batch process using up to 10 wt% talc [72]. An approximately 45% decrease in cell size from 15.4 to 8.5 μm, as well as a 298% increase in cell population density were reported with 3 wt% talc loading, owing to the heterogeneous nucleation caused by talc, which significantly increased the crystallinity of the PLA matrix [72].

The addition of nanoclay Cloisite® 30B into a PLA matrix has been reported to significantly improve the cell morphology of foamed samples produced through a low-pressure foam injection molding (LPFIM) and high-pressure FIM (HPFIM) equipped with mold opening and gas counter pressure [73]. Nanocomposite foams with average cell size of less than 50 μm and void fraction of as high as 55% were achieved in PLA by adding nanoclay [73]. Similarly, another type of clay, organophilic montmorillonite (OMMT), was also employed to enhance the foaming performance of PLA/poly(butylene succinate) (PBS) blends [74]. The PLA/PBS blends with 3 wt% OMMT showed a sixfold increase in the cell population density and 45% decrease in average cell size from 475.6 to 261.4 μm [74].

The manufacture of nanocellular polymer foams, which are characterized by average cell size less than 1 μm and cell density greater than $10^{12}$ cells/cm$^3$, has attracted wide attention in academic and industrial fields in recent years [75–82]. A facile batch foaming method using constant foaming temperature slightly lower than the melting temperature of PLA has been recently employed to fabricate nanocellular PLA foams in the presence of supercritical $CO_2$ [75]. Linear PLA (Grade 2003D) was modified with 1 wt% multifunctional epoxy-based chain extender (CE) and 0.01 wt% hydroxyl-functionalized graphene (HG) through a melt blending method to improve its crystallization behavior, rheological properties, and foaming behavior. A nanocellular structure was successfully produced in a PLA/CE/HG sample foamed at 130°C. The nanofoam had average cell size, cell population density, and volume expansion ratio of 350 nm, $1.76 \times 10^{13}$ cells/cm$^3$, and 3.7 times, respectively. This was attributed to the heterogeneous nucleating effect of HG for the cell nucleation and the crystallization nucleation, as well as the improvement of the rheological properties of PLA by the addition of HG and CE [75]. Additionally, processing at low foaming temperature (below PLA's melting temperature) increases PLA's viscosity, which is helpful for restricting cell growth, resulting in fine cells, high cell population density, but low volume expansion ratio.

Transition from microcellular to nanocellular PLA foams has also been reported by other investigators by controlling viscosity, branching, and crystallization [82]. PLA modified with crosslinking agents and foamed using supercritical nitrogen close to the crystallization temperature (~140°C) yielded sub-micron size cells, and the foam had a high cell population density on the order of $10^{11}$ cells/cm$^3$ [82].

Recently, bead foam technology was introduced as another innovative new way to produce nanocellular foam products in a batch process [79]. In this technology, expanded PLA bead foams were developed with a double crystal melting peak using long chain branched PLA (LCB-PLA) (Ingeo™ 8051D NatureWorks® LLC) with high crystallization kinetics. The gas saturation foaming conditions must be carefully controlled to achieve nanocellular foam, and details are given in Refs 64 and 65. The $CO_2$ pressure influences the kinetics of the high melting temperature crystals, which enhances cell nucleation and foam expansion. Using this approach, nanocellular PLA bead foams with a threefold expansion ratio and average cell sizes of 350 nm were developed using low saturation temperatures. This development was attributed to the large number of perfect crystals generated during $CO_2$ saturation, which promoted heterogeneous cell nucleation while delaying cell growth [64, 65].

*15.5.2.4.3 Foaming Conditions* The foaming time and/or the foaming temperature are important process variables for controlling the density and porous morphology of PLA foams owing to their effects on the viscoelastic properties of the polymer (Figure 15.4) [2]. The foamability of PLA is also influenced by the gas concentration [66, 83].

A density lower than 1.04 g/cm$^3$ could not be achieved in PLA foamed at 90°C, regardless of the foaming time, implying that higher foaming temperature is required to produce foamed PLA samples with high expansion ratios. The appropriate foaming temperature for PLA seems to be around 150°C, which is close to its melting temperature. Shorter foaming times appeared to be preferable because the lowest density was achieved when the samples were foamed at 150°C for 5 s. Longer foaming time tended to increase the density, probably due to the accelerated gas loss and cell collapse phenomena, which led to the subsequent smaller volume expansion [2, 12]. Significant reduction in density (up to 39%) or equivalently an increase in expansion ratio (more than twofold expansion) could be achieved by creating microcellular foamed structures in PLA samples.

The dependence of the foam density ($\rho$) on the foaming temperature ($T_f$) under different $CO_2$ pressures (14–30 MPa) was also investigated. Using $T_g$ depressions (corresponding to $\Delta T_g$), master plots of ρ versus $T_f + \Delta T_g$ were constructed using data for both neat PLA and PLA-based nanocomposites [41]. Two distinct behaviors were observed (Figure 15.5).

Foam density remained constant (~1.0 g/cm$^3$) at $T_f + \Delta T_g < 140$°C. This region was termed the nanocellular region since the cell size was nanometer in size and larger cell density ($10^{14}$ cells/cm$^3$) was achieved in foamed samples. The density of foamed samples abruptly decreased beyond $T_f$, and then attained a minimum constant value of approximately 0.3 g/cm$^3$ as the reduced temperature ($T_f + \Delta T_g$) increased above 150°C (a microcellular region). In this region, the cell size increased (~100 μm) while a significant reduction was noticed in the cell density ($10^8$ cells/cm$^3$). This trend is due to the competition between

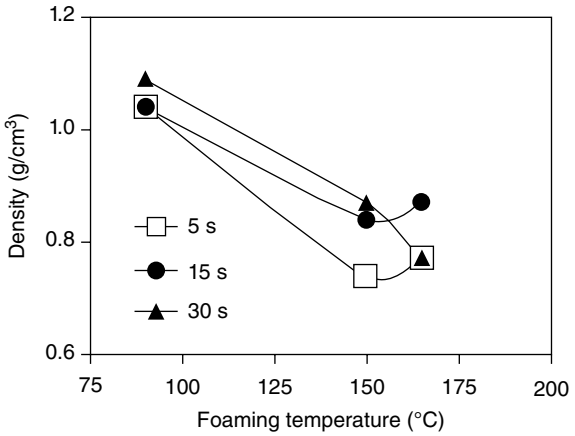


**FIGURE 15.4** Effects of foaming time and foaming temperature on the density of PLLA foams (Biomer L9000 supplied by Biomer Krailling, Germany). The melting temperature and density of PLLA were 180°C and 1.21 g/cm$^3$, respectively. Specimens were saturated with $CO_2$ at room temperature at 850 psi for 24 h [2].

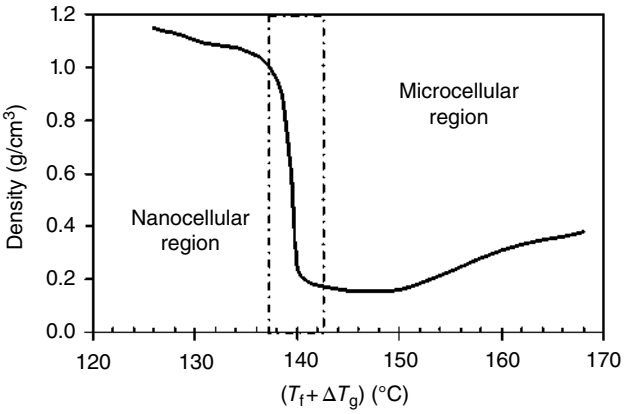


**FIGURE 15.5** Master plot of density versus $T_f + \Delta T_g$ (reduced foaming temperature) using data of both neat PLA and PLA-based nanocomposites foamed under various $CO_2$ pressures (14–30 MPa) [41]. Nanocomposite specimens and PLA type are described in Table 15.3.

cell nucleation and cell growth. Cell nucleation dominates at the low $T_f$ range (up to 140°C), owing to a large supply of $CO_2$ molecules in the system coupled with the high viscosity of the matrix, which suppresses cell growth. In contrast, cell growth and coalescence occurred at higher $T_f$ (>150°C) due to the low viscosity of the system. The critical temperature was around 140°C, where the morphology of foamed samples changed from nanocellular to a microcellular structure.

The morphology of PLA modified with 0.5 phr of PPZn, a crystallization nucleating agent, and 5 phr of multifunctional epoxy-based chain extender (CE), a styrene-acrylic oligomer with a number average molecular weight less than 3000 g/mol and an average functionality more than four, is also affected by the saturation temperature [66]. The cell morphology of PLA/CE/PPZn batch-foamed by saturating the samples in an autoclave for 120 min at a saturation pressure of 10 MPa showed a decrease in both volume expansion ratio from 45.9 to 10.2 times and average cell size from 431.0 to 4.3 μm; but a significant increase in cell population density from $7.0 \times 10^5$ to $8.5 \times 10^{10}$ cells/cm$^3$ as the saturation temperature decreased from 152 to 144°C.

The property of foams also depends on other processing parameters like saturation pressure and time [83]. Study of the influence of $CO_2$ saturation pressure and time on the $CO_2$ solubility and expansion ratio of batch-microcellular foamed PLA indicates that low saturation pressure is preferable to produce foamed PLA specimens with homogeneous morphology and high volume expansion. The results suggest the need for a critical gas concentration of approximately 9.4% for significant foam expansion to occur in PLA (10-fold expansion over unfoamed PLA). Increasing the concentration of $CO_2$ beyond this critical value has a deleterious effect on the volume expansion, i.e., foam expansion decreases significantly. The foaming conditions associated with such an elevated expansion ratio involved a lower gas saturation pressure up to 2.76 MPa (400 psi), which corresponds to a critical gas concentration of approximately 9.4%. At this condition, a saturation time of four days was required for $CO_2$ diffusion in 1.5–2.0 mm thick PLA samples [35, 83].

*15.5.2.4.4 Melt Rheology* Rheological characteristics of the melt are critical during the growth of the newly formed nuclei and the subsequent stabilization of the foamed cellular structure. During cell growth, the viscosity of the expanding melt should be low enough to allow the elongational deformation of the melt while, during the stabilization of the cellular structure, the strain-induced hardening behavior of polymer should be sufficient to withstand the stretching force at the latter stage of the bubble growth, avoiding the collapse of the newly foamed structure [43, 84, 85].

One of the limitations for using PLA is its processing instability due to its thermal, oxidative, and hydrolytic degradation during processing [7]. Such degradation leads to the cleavage of polymer chains (i.e., decrease in molecular weight), resulting in deterioration of the rheological properties of the melted polymer. Such deterioration should be avoided for processing requiring high levels of extensional viscosity and elasticity. Another shortcoming of PLA is its very low melt viscosity, which may also affect the growth and stabilization of cells during the foaming process. Attempts have been made to enhance the foamability of PLA by controlling the melt rheology of PLA through increasing the molecular weight to compensate for the molecular weight decrease caused by processing degradation and to increase the melt viscosity [35, 66, 84–92].

PLA is a linear polymer and thus has low melt strength due to a lack of chain entanglement. This can be mitigated by inducing branching in the polymer chain. Usually, branching is introduced in PLA through melt blending with chain extenders, which cause chain extension and branching in the polymer. Examples of these additives include diisocyanates, epoxides, anhydrides, carbodiimide, and so on. Branched and chain-extended PLA generally shows improved melt strength and extensional viscosity and is better suited for foaming [35].

PLA with L-lactide >92 wt% was reactively modified in the melt by sequentially adding 1,4-butanediol and 1,4-butane diisocyanate (BDI) as low-molecular-weight chain extenders. Modified PLA contained different ratios of OH of PLA to BDI (samples M1 and M2 in Table 15.4).

The molecular weights (both $M_w$ and $M_n$) for modified samples (M1 and M2) increased significantly compared to unmodified PLA because of chain extension. The effect of excess BDI was evidenced by the higher $M_w$ and $M_n$ for modified PLA sample M2 compared to M1, caused by more linking reactions. In addition, modified PLA samples showed

**TABLE 15.4 Molecular Weight and $T_g$ of Unfoamed PLA (L-lactide >92 wt%, NatureWorks) and Properties of PLA Foams [43, 85]**

| | Properties of Solids | | | Properties of Foams | | |
|---|---|---|---|---|---|---|
| Samples | $M_n$ ($\times 10^3$ g/mol) | $M_w$ ($\times 10^3$ g/mol) | $T_g$ (°C) | $\rho$ (g/cm$^3$) | $d$ (μm) | $N_0$ ($10^8$ cells/cm$^3$) |
| Neat PLA | 57 | 124 | 61.8 | 0.125 | 227 | 0.008 |
| Modified PLA (M1)[a] | 84 | 225 | 63.2 | 0.067 | 37 | 1.886 |
| Modified PLA (M2)[b] | 107 | 308 | 63.7 | 0.092 | 24 | 6.682 |

[a] The ratio of OH of PLA to BDI was 1 : 1 (OH/BDI = 2 : 1).
[b] The OH/BDI = 1 : 1, that is, the amount of BDI was excessive compared to M1 sample.

slightly higher $T_g$ than the unmodified resin, due to the higher molecular weight and chain cross-linking. Cross-linking increased the $T_g$ of the polymer by introducing restrictions in chain mobility [86]. Modified PLA samples with increased molecular weights showed enhanced melt viscosity and elasticity [84, 85]. The higher viscosity and elasticity for the chain extended/cross-linked PLA resins allowed the production of PLA foams with smaller cell size, higher cell density, and lower foam density compared to the unmodified PLA foam (Table 15.4).

Recently, long-chain branched (LCB) polylactide (LCB-PLA) was prepared by UV-induced reaction extrusion with trimethylolpropane triacrylate (TMPTA). The effect of the long-chain branching structure on the cell morphologies of PLA foamed in a batch process with supercritical $CO_2$ was analyzed [87]. Nanocells were formed in PLA and LCB-PLA branched with 0.5 wt% TMPTA when foamed with supercritical $CO_2$ at 142°C. Additionally, LCB-PLA foams showed better cell morphology (less coalescence, no collapse, and uniform cell distribution) than linear PLA under higher pressure due to increased matrix strength and higher nucleation potential [87].

LCB of PLA was also successfully prepared by a two-step functional group reaction of the end hydroxyl groups of PLA with pyromellitic dianhydride (PMDA) and then the triglycidyl isocyanurate (TGIC) through reactive processing [88]. The tree-like LCB chain structure generated from the functional group reactions contributed remarkably to the improvement of strain hardening of linear PLA (Grade 2002D) under elongational flow, which improved considerably the foaming ability during batch processing with $CO_2$. No clear foam structures were observed in neat PLA because of its low melt strength. In contrast, a well-developed and uniform foam morphology was achieved in the branched PLA/PMDA/TGIC sample due to its improved melt strength caused by the tree-like LCB chain structure [88].

Star-shaped LCB-PLA has also been prepared by melt transesterification with trimethylolpropane triacrylate (TMPTA) in the presence of zinc oxide nanoparticles (nano-ZnO) as a transesterification accelerant [89]. LCB-PLA showed a higher melt strength compared with neat PLA (2003D). Extrusion foamed samples using azodicarbonamide (ADC) as the foaming agent indicated that LCB-PLA had smaller average cell size (52 μm for LCB-PLA vs. 140 μm for neat PLA), higher cell density, and less occurrence of cell collapse, and slower crystallization speed than neat PLA, which benefited from the improvement of melt strength and strain hardening owing to the introduction of LCB structures in PLA.

Improvements in PLA foam characteristics have also been reported with other chain extenders such as multifunctional aziridine [90], polystyrene/poly(glycidyl methacrylate) random copolymer [91], or by the free radical branching/linking of PLA with dicumyl peroxide (DCP) [92].

Excellent foam morphology has been recently obtained in PLA modified with 5 phr multi-functional epoxy-based CE, a styrene-acrylic oligomer with a number average molecular weight less than 3000 g/mol and average functionality of more than four [66]. The volume expansion of microcellular batch-foamed PLA at a saturation pressure of 10 MPa and temperature of 145°C increased from 1.6 to 10.6 times due to the increase of melt elasticity of PLA. PLA/CE foam had cell population density and average cell size of $9.5 \times 10^{10}$ cells/cm$^3$ and 4.3 μm, respectively. The properties were not characterized for neat PLA foam due to the lack of developed cell structures [66].

Other investigators have also branched PLA with polystyrene/poly(glycidyl methacrylate) random copolymer CE through melt compounding and reported an increase in complex viscosity and elongational viscosity after branching [91]. The addition of CE increased the cold crystallization temperature but decreased the degree of crystallinity of PLA. Owing to the improved visco-elastic properties, branched PLA foamed in a batch process with supercritical $CO_2$ (12 MPa and 140°C for 2 h) exhibited smaller cell size and higher density than neat PLA foam. The reported average cell size and cell population density of PLA branched with 1 wt% CE were 27.6 μm and $4.2 \times 10^7$ cell/cm$^3$, respectively, compared with 36.9 μm and $1.5 \times 10^7$ cell/cm$^3$ for neat PLA foam.

Despite promising results, most of the CEs used to ease the foamability of PLA are not approved for food contact because of toxicity issues. For instance, trimethylolpropane triacrylate has been reported to cause rare types of cancer in

**TABLE 15.5 Effect of Epoxy-functionalized and Food-Grade-Approved Chain Extender (Joncryl® ADR4468 from BASF Corporation) on the Rheological and Foam Properties of PLA (4044D) [35, 96]**

| CE Contents | Physical Properties | | | | | Foam Morphology[e] | | | |
|---|---|---|---|---|---|---|---|---|---|
| in PLA (wt%)[a] | End Torque (N m)[b] | $M_w$ (g/mol)[c] | $\chi$ (%)[c] | $\eta_a$ (Pa s)[d] | $\eta_e$ (Pa s)[d] | $\phi$ (μm)[f] | $V_f$ (%)[f] | $\varphi$ | $N_0$ ($10^9$ cells/cm$^3$)[f] |
| 0 | 2.8 | 212,139 | 3.8 | 371.8 | 6607.1 | 11 | 56.6 | 2.6 | 0.7 |
| 0.25 | 3.4 | 339,817 | 3.1 | — | — | 8 | 74.2 | 4.0 | 4.3 |
| 0.5 | 5.6 | 474,904 | 2.3 | — | — | 16 | 83.1 | 6.0 | 0.7 |
| 1.0 | 8.1 | 582,952 | 0.9 | 742.2 | 18,247.3 | 19 | 86.4 | 7.6 | 0.2 |

[a] Joncryl ADR4468, an epoxy-functionalized and food-grade-approved chain extender (CE) provided by BASF Corporation.
[b] Recorded from melt blending in a three-piece internal mixer/measuring head at 200°C for 5 min with the rotor speed set at 35 rpm.
[c] $M_w$ and $\chi$ are the weight-average molecular weight and percent crystallinity (first heat) of PLA.
[d] $\eta_a$ and $\eta_e$ are the apparent shear viscosity and apparent extensional viscosity of the melt, respectively, measured at constant apparent shear rate of 386 s$^{-1}$ and strain rate of 73.5 s$^{-1}$.
[e] Samples were saturated with $CO_2$ at 400 psi pressures (2.76 MPa) at room temperature for at least four days and foamed at 150 C for 15 s.
[f] Average cell size ($\phi$), density reduction or void fraction ($V_f$), the volume expansion ratio ($\varphi$), cell-population density ($N_0$).

mice [93], whereas isocyanates are also known for their toxicity [94]. Other chain extenders are styrene-based additives, and styrene is a known carcinogen [95].

Recently, novel food-grade multifunctional epoxies with varying reactivities that are approved for food contact by the Food and Drug Administration in the United States have been developed [96]. These novel food grade multifunctional epoxies (CEs) are effective and efficient in branching PLA (4044D) [35, 96] and improving its foamability since the addition of 0.25 wt% increased end mixing torque, shear, elongational viscosity, and molecular weight but decreased crystallinity of PLA, due to chain entanglements (Table 15.5). Unlike neat PLA foams that showed a low expansion and poor cell morphology owing to its low elongational viscosity, chain-extended PLA foams had a homogeneous structure and fine cells (Figure 15.6), as well as a high void fraction (up to ~85%) and high volume expansion ratio (an eightfold expansion over unfoamed PLA). These improvements are attributed to the high elongational viscosity, suggesting that melt properties of branched PLA were appropriate for optimum cell growth and stabilization during foaming [35].

Suitable macromolecular architecture modification has a great influence on the viscoelastic properties of the PLA matrix, resulting in enhanced PLA foamability, allowing a finer control of the final foam cellular structure and, at the same time, reducing the final foam density [43].

### 15.5.3 Microcellular Foaming in a Continuous Process

A continuous microcellular process was developed to overcome some disadvantages of the batch process, such as the long time required for the gas saturation of the solid polymer and the poor cost-effectiveness of the batch process [23, 24, 97–100]. This technology was also developed in the 1990s by researchers at the Massachusetts Institute of Technology, and it is commercialized under the trade name of MuCell. The MuCell microcellular foam technology for injection molding and extrusion equipment is commercialized by Trexel, Inc. (Woburn, MA).

The continuous microcellular process is also based on the concept of thermodynamic instability and a much shorter time is needed for saturation of polymer with

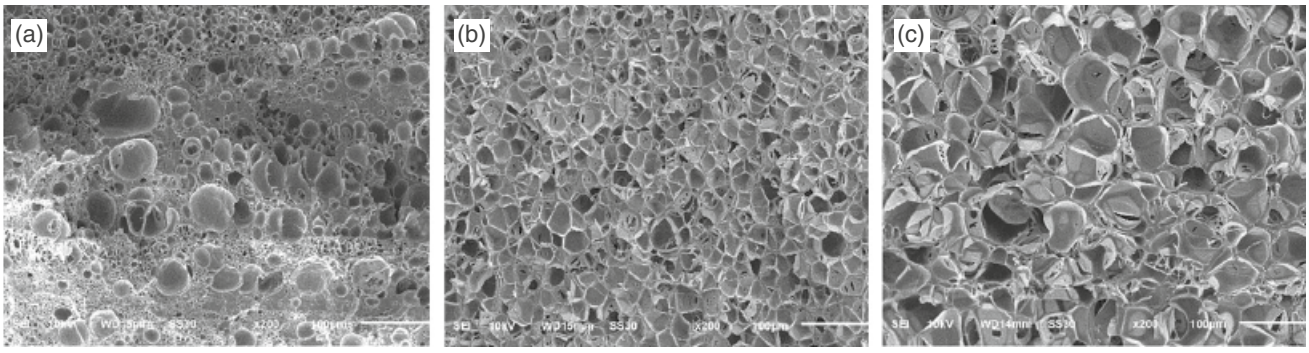


**FIGURE 15.6** SEM micrographs (×200) of neat PLA (a) and PLA branched with 0.5% (b) and 1% (c) epoxy-functionalized and food-grade-approved chain extender (Joncryl ADR4468 from BASF Corporation). Specimens were saturated with $CO_2$ at room temperature at 400 psi (2.76 MPa) for at least four days and foamed at 150°C for 15 s (Unpublished images from Matuana, L.).

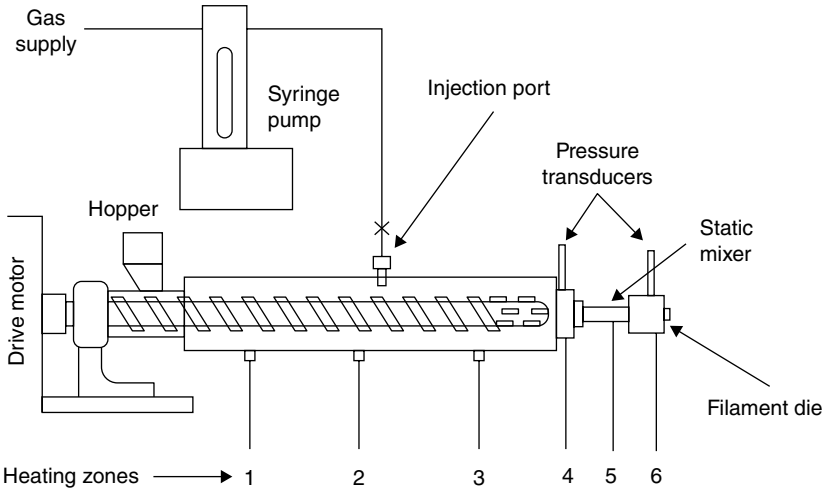


**FIGURE 15.7** Schematic of the extrusion foaming system.

gas [99]. As described by Park, when the polymer is melted in the extrusion barrel, a metered amount of gas is delivered to the polymer melt [99]. The injected gas diffuses into the polymer matrix at a much high rate because of convective diffusion induced in the extrusion barrel at an elevated temperature [97]. As with a batch process, there are three specific steps in a continuous microcellular extrusion process: (i) formation of polymer/gas solution, (ii) cell nucleation, and (iii) shaping and cell growth [23, 24, 99–103]. A typical schematic of the overall continuous microcellular experimental equipment is illustrated in Figure 15.7.

A uniform solution is achieved by the injection of gas to its solubility limit and ensuring complete dissolution of the gas using a diffusion-enhancing device such as a static mixer [97, 98]. This requires modification of the existing equipment by adding a supercritical fluid (SCF) delivery system that provides high pressure and accurately metered mass flow of SCF to the processing equipment [22]. Modification to the barrel, screw, and die is also needed to achieve a single-phase solution [22]. The formation of a uniform solution of polymer and gas is essential since undissolved gas pockets can generate undesirable large voids [99]. Finally, microcell nucleation occurs in a rapid pressure drop nucleation nozzle [23, 98]. The nucleated bubbles continue to grow to the desired final size during shaping at the die exit. The final foam structure is determined by the conditions under which the three steps of the process are performed [23].

The pressure drop rate is correlated to the thermodynamic instability necessary to generate the nuclei and, mainly, affects foam morphology. The gas concentration is directly correlated to the availability of gas necessary for cell growth, influencing the final density of the foamed plastic [104]. The pressure drop rate in the die ($-\mathrm{d}p/\mathrm{d}t$) is expressed as follows [24]:

$$\frac{-\mathrm{d}p}{\mathrm{d}t} \approx \frac{-\Delta p}{\Delta t} \approx \frac{-\Delta p q}{\pi r_0^2 L} \tag{15.11}$$

where $\Delta t$ is the average residence time of the flowing polymer/gas solution in the nozzle, $L$ is the length of the nozzle, $q$ is the volumetric flow rate, and $r_0$ is the radius of the nozzle.

Cell nucleation is significantly increased by increasing the rate of pressure drop at the die, irrespective of the blowing agent content or external nucleating agents. A higher pressure drop rate will be achieved when the nozzle radius is smaller, according to Equation 15.11. Detailed information on the calculation of the pressure drop rate for polymers can be obtained from Refs 23 and 24.

Compared with the batch foaming process, relatively few publications feature continuous microcellular foaming of PLA in extrusion or injection molding equipment [3, 5, 37, 63, 105–111], but the number of publications has considerably increased during the past 10 years.

#### *15.5.3.1 Microcellular Extrusion of PLA Foams*

*15.5.3.1.1 Effects of Nucleating Agent and Crystallinity* A thorough investigation of the continuous extrusion foaming of amorphous PLA using $CO_2$ as a blowing agent has been reported by Reignier et al. [105, 106]. The density and porous morphology characteristics of foams produced under various injection pressures (2.5–9 MPa), $CO_2$ contents (1.8–9.3 wt%), processing temperatures (90–100°C), and also by adding 0.5 wt% talc into the resin are summarized in Table 15.6.

Different behaviors can be seen with the data listed in Table 15.6. The concentration of gas had a limited impact on the density reduction of neat PLA at lower $CO_2$ content. Below 5 wt% $CO_2$, a smaller number of cells were nucleated and both the density and the cell population density remained

**TABLE 15.6 Effect of $CO_2$ Content on the Physical Characteristics of Neat PLA and PLA/Talc Foamed in a Continuous Extrusion Process [105, 106]**

| Injection Pressure (MPa) | $CO_2$ Content (wt%) | Density (g/cm³) | | Cell Population Density (cells/cm³) | | Cell Size (μm) | |
|---|---|---|---|---|---|---|---|
| | | Neat[a] | Talc[b] | Neat | Talc | Neat | Talc |
| 2.5 | 1.8 | 0.51 | 0.88 | $10^4$ | $10^6$ | 420 | 60 |
| 4.2 | 3.2 | 0.60 | ~0.90 | $10^4$ | $10^6$ | 380 | 60 |
| 5.3 | 4.3 | 0.84 | 0.55 | $10^4$ | $10^7$ | 220 | 60 |
| 6.4 | 6.4 | 0.22 | | | | >160 | |
| 7.4 | 7.3 | 0.024 | 0.03 | $10^7$ | $10^7$ | >120 | 60 |
| 9 | 8.2 | 0.021 | | $10^8$ | | ~80 | |
| 10 | 9.3 | 0.021 | | $10^8$ | | | |

[a] PLA (NatureWorks 8302D with D-lactic acid content of 9.85%).
[b] Samples contained 0.5 wt% talc.

almost constant. However, above 7 wt% $CO_2$, lower density foams with a large number of nucleated cells were produced. The density remained constant while the cell population density slightly increased with $CO_2$ content. Since higher gas concentration favors the nucleation of large number of cells, the results imply that a critical gas concentration of ~7 wt% is required to achieve low-density foams. The highly expanded foams had a high open-cell content.

Interestingly, the narrow processing window associated with this critical threshold, that is, low-density foams and high nucleation rate ($10^7$–$10^8$ cells/cm³), involved an injection pressure (or an equivalent gas concentration) that corresponds to the critical pressure of $CO_2$ (7.38 MPa). Consequently, extrusion foaming of PLA with $CO_2$ requires high processing injection pressures to prevent premature foaming, despite the high solubility of $CO_2$ in PLA. High $CO_2$ injection pressure would favor the generation of small $CO_2$ clusters due to the presence of local density inhomogeneities of the physical foaming agent when injected near its supercritical state. As a result, $CO_2$ clusters would act as gas nuclei that favor heterogeneous nucleation.

Talc affected the cell morphology of PLA foams at lower $CO_2$ content since its addition into the matrix led to foams with much finer cells and higher cell population density compared to neat PLA foams, a clear indication that talc particles act as heterogeneous nucleating sites for cell nucleation (Table 15.6). Nevertheless, the effect of talc on the cell morphology disappeared at higher $CO_2$ contents since the samples processed with or without talc had similar porous morphologies. This indicates that the rate of cell nucleation was not a limiting factor as expected from the high concentration of gas used during foaming process.

Microcellular extrusion of amorphous PLA resin intended for fiber melt spinning (6300D from NatureWorks, unknown D-lactic acid content) has also been produced with $CO_2$ to study the expansion dependency on the amount of blowing agent (2–9 wt%) and cell population density [107]. Both the foam density and cell population density decreased to a minimum, then increased with increase in the foaming agent content, suggesting two competing mechanisms exist during foaming. Densities in the 20–700 kg/m³ range were produced with cell sizes of around 100 μm and cell population density of $10^5$ cells/cm³.

The crystallinity development in PLA during the foam extrusion process significantly affects the cell morphology of PLA foam by enhancing its expansion and cellular structure. Mihai et al. foamed three different PLA grades with different D-lactic acid contents using various $CO_2$ concentrations to develop the crystallinity in PLA foams and understand the role of the achieved crystallinity on cell morphology of PLA foams (Table 15.7) [63, 109].

The crystallinity of PLA foams decreases with the D-lactic content but increases with $CO_2$ content for semicrystalline PLA. Conversely, crystallinity does not develop in PLA foams with D-lactic content of 10%, confirming its amorphous behavior (Table 15.6). Low density achieved in semicrystalline PLA foamed at lower $CO_2$ contents, particularly at conditions that lead to significant crystallinity development (i.e., 7 and 9%), results because the formation and growth of PLA crystal nuclei induced by $CO_2$ in the extrusion die increases the foam nucleation density. In contrast, lower density foam requires high $CO_2$ content for amorphous PLA. The paper neglected to include the number of cells nucleated in PLA [63, 109].

While these previous studies offered valuable insights, demonstrating the continuous extrusion process of PLA foamed with supercritical $CO_2$, the morphology achieved in foamed PLA of some studies failed to satisfy the definition of microcellular foam due to lower cell population density (less than $10^9$ cells/cm³) with cells being larger than 60 μm in average size. Distinctions between these features and microcellular foam persist, where the cell population density

**TABLE 15.7 Effect of D-Lactic Acid Content on the Crystallinity Developed in PLA Foams and PLA Foam Density [63, 109]**

| D-Lactic Acid Content in PLA (%)[a] | Crystallinity in PLA Foams (%) | | | Density of PLA Foams (kg/m³) | | |
|---|---|---|---|---|---|---|
| | 5% $CO_2$ | 7% $CO_2$ | 9% $CO_2$ | 5% $CO_2$ | 7% $CO_2$ | 9% $CO_2$ |
| 2% (PLA 4032D) semicrystalline | 5 | 25 | 45 | 400 | 32 | 35 |
| 4% (PLA 2002D) semicrystalline | 0 | ~8 | 18 | — | 44 | 41 |
| 10% (PLA 8302D) amorphous | 0 | 0 | 0 | 1000 | 315 | 40 |

[a] All PLA are from NatureWorks™.

ranges from $10^9$ cells/cm$^3$ and up, with fully grown cells being smaller than 10 μm in average size. Continuous extrusion of microcellular PLA with fine cell size (<10 μm) and high cell density ($10^9$ cells/cm$^3$ and up) will enable not only the production of foamed materials with superior mechanical properties compared to their solid counterparts but also the production of foamed structures in thin film.

*15.5.3.1.2 Effect of Melt Rheology* The classical nucleation theory (Equations 15.7 and 15.9) predicts that minimizing the free energy barrier for nucleation ($\Delta G$) will promote high cell nucleation rates. Although many relevant factors can affect the cell nucleation rate (Equations 15.7 and 15.9), a higher pressure drop of the gas/polymer solution lowers the free energy barrier to initiate nucleation (Equations 15.6 and 15.10), resulting in a higher nucleation rate. Park demonstrated that the pressure drop rate in the die ($-\mathrm{d}p/\mathrm{d}t$) given by Equation 15.11 correlates with the thermodynamic instability necessary to nucleate a high number of cells, that is, the higher the pressure drop rates, the higher the cell population densities [24, 99].

Since the pressure drop rate depends on the nozzle geometry ($r_0$ and $L$) and polymer flow properties ($\Delta p$ and $q$) (Equation 15.11), these process and material variables may be effective for controlling the cell nucleation during continuous microcellular processing [111].

Controlling the melt rheology through processing temperatures as a strategy to alter the rate of pressure drop during foaming is an appropriate approach to produce microcellular PLA with cell population densities on the order of $10^9$ cells/cm$^3$ and cell sizes of around 10 μm [111]. Processing temperature greatly influences the density and porous morphology of foams owing to its effects on the melt viscosity as described by the Arrhenius relation [112]

$$\eta = A_0 \exp\left(\frac{E_a}{RT}\right) \tag{15.12}$$

with $\eta$ as the melt viscosity, $A_0$ a constant, $R$ the universal gas constant, $T$ the absolute temperature, and $E_a$ the activation energy of melt flow.

Generally, as the processing temperature varies, the melt viscosity changes inversely, that is, the higher the processing temperature, the lower the melt viscosity, and vice versa, subsequently leading to a change in the pressure generated during extrusion process. Melt viscosity, an important parameter in foaming, affects the pressure built in the system, thus affecting the cell nucleation rate. Additionally, melt viscosity plays an important role during the growth and stabilization of nucleated cells [111].

Matuana and Diaz [111] examined the effect of processing temperature on the pressure drop rate, cell population density, and average cell size to understand the nucleation mechanisms in PLA foamed in a continuous extrusion process (Figure 15.8 and Table 15.8).

Not only does the temperature affect the melt viscosity, but also the cell nucleation rate owing to its effect on the pressure that develops in the system during the extrusion of microcellular PLA (Table 15.8). When processing at high temperature, PLA nucleates fewer bubbles (Figure 15.8). Processing at high temperature lowers the melt viscosity of the resin, thus preventing sufficient pressure from building in the system, consequently resulting in lower pressure drop rate (Table 15.8). The increase in gas diffusivity, which promotes gas loss to the environment, may also account for a smaller amount of injected $CO_2$ available for cell nucleation. Conversely, processing at a lower temperature significantly increases the cell nucleation rate owing to the fact that high melt viscosity induced high pressure drop rate. The number of nucleated bubbles, with the order of $10^9$ cells/cm$^3$ and the average cell size less than 10 μm (Table 15.8), satisfy the definition of microcellular plastics [111].

As mentioned, the rheology of the polymer melt is an important parameter in foaming. The low melt strength and the high diffusivity of the blowing (e.g., $CO_2$, water) agents through PLA create difficulty in the production of PLA foams with high expansion ratio and microcellular

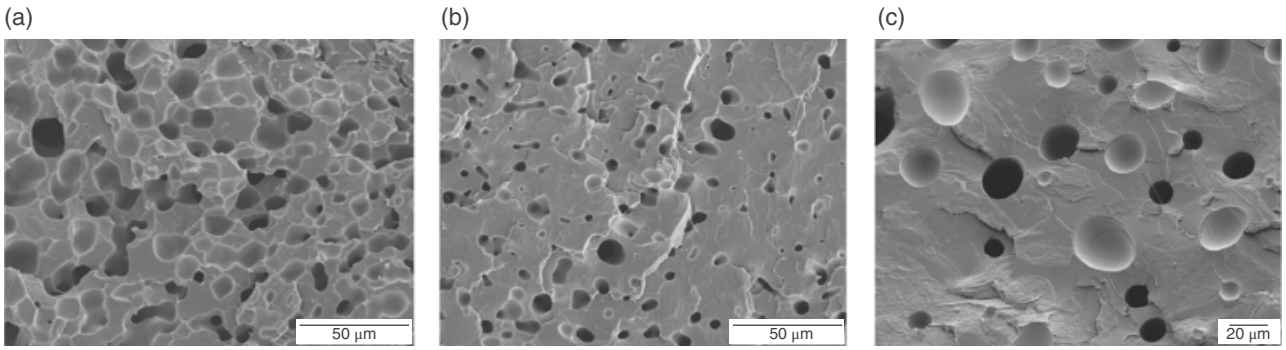


**FIGURE 15.8** Effect of processing temperature profile levels on the cell morphology of PLA foamed at (a) low, (b) intermediate, and (c) high temperatures. All pictures were taken at the same magnification (750×) (unpublished images from Matuana).

**TABLE 15.8 Effect of Processing Temperature Profile on the Pressure Drop Rate, Cell Population Density, and Average Cell Size of Foamed PLA Samples [111]**

| Temperature Profile Levels | Pressure Drop Rate (GPa/s) | Cell Population Density ($10^9$ cells/cm$^3$) | Average Cell Size (μm) |
|---|---|---|---|
| High[a] | 32.8 | 0.01 | 25.9 |
| Intermediate[b] | 38.3 | 0.2 | 9.3 |
| Low[c] | 45.5 | 1.0 | 8.8 |

[a] Temperature varied from 180 to 160°C from the hopper to the die.
[b] Temperature varied from 170 to 150°C from the hopper to the die.
[c] Temperature varied from 160 to 140°C from the hopper to the die.

closed-cell structures in the foam extrusion process. Despite the production of cell population densities exceeding $10^9$ cells/cm$^3$ in both linear and branched PLA foamed on a tandem extrusion system using $CO_2$ as the physical blowing agent, typically, a fully branched PLA has a higher melt strength and produces foams with higher expansion ratio and closed-cell content compared to a linear PLA with a similar molecular weight distribution (Table 15.9) [110]. Nonetheless, the very low crystallinity developed in PLA foams (<2%), in contrast with the results reported by other investigators (Table 15.7) [109], suggests that the $CO_2$ does not always induce the formation of crystal nuclei during the foam extrusion process. Crystallization dynamics depend on the residence time of the gas/polymer solution in the extrusion die [110].

Extensive work has been carried out over the past years to enhance the foamability of PLA through the use of chain extenders as described in Section 15.5.2.4.4 [35, 66, 84–92]. Chain extenders are also used to produce foams in a continuous extrusion process.

The effect of chain branching of amorphous PLA (aPLA) and semicrystalline (cPLA) matrices with multifunctional styrene-acrylic epoxy copolymer on their foamability in a one-step extrusion process with up to 9% $CO_2$ has been investigated [113]. The melt shear and elongational viscosities of both aPLA and cPLA increased with the CE content.

**TABLE 15.9 Morphological Characteristics of Linear PLA (PLA 2002D) and Branched (Proprietary Formulation, NatureWorks) Foamed on a Tandem Extrusion System Using 9% Carbon Dioxide as the Physical Blowing Agent [110]**

| Die Temperature(°C) | Expansion Ratio[a] | | Cell Population Density ($10^9$ cells/cm$^3$)[a] | |
|---|---|---|---|---|
| | Linear | Branched | Linear | Branched |
| 115 | — | 41 | — | 0.4 |
| 120 | 18 | 30 | 1.5 | 0.3 |
| 130 | 4 | 5 | 0.8 | 0.6 |

[a] Data extrapolated from figures in Ref. 109.

Unfortunately, increased melt elasticity of PLA did not correlate with the foaming ability of the amorphous grade since the foam structure and expansion of aPLA were not improved by the branching, regardless of the CE addition level. This was caused by the lower foaming temperatures achieved during aPLA foaming that restricted the reactivity of the chain extender. The cPLA foam structure and expansion were affected by the increase of the chain extender content only at 5% $CO_2$, where chain extended-cPLA foams exhibited lower densities and larger cell sizes than the neat cPLA counterpart.

The use of DCP modified PLA in foam extrusion with supercritical $CO_2$ was recently proposed for the first time as another effective approach to improving the foamability of PLA [92]. The characteristics of PLA-DCP foams were compared with those obtained with neat PLA and PLA branched with multifunctional epoxide (MFE). DCP is a free radical initiator and encourages random branching in PLA. Both modifications lead to an increase in melt strength, but the highest increase was shown for the PLA modified with DCP that also showed strain hardening. Neat PLA had foam density (45 kg/m$^3$) similar to that of MFE-modified PLA, while there was a 28.9% decrease in the density of PLA treated with DCP (32 kg/m$^3$). PLA treated with DCP also had finer cells (130 μm) than neat PLA foams (358 μm) [92].

#### *15.5.3.2 Microcellular Injection Molding of PLA Foams*

Foam injection molding (FIM) is semi-continuous foam processes employed to manufacture shaped foam parts. Supercritical nitrogen gas is usually used in this process due to its stronger nucleation ability [70, 76, 78, 114]. FIM is a process similar to conventional injection molding, except that it also requires a special supercritical fluid (SCF) delivery system that provides high pressure and accurately metered mass flow of SCF to the processing equipment [22], like in the case of the microcellular continuous extrusion process. Modification to the barrel, screw, and die is also needed to achieve a single-phase solution [22]. The FIM process is divided into two groups: low-pressure foam injection molding (LPFIM) and high-pressure FIM (HPFIM). Foams with nonuniform cell structure are obtained by the LPFIM process with cell population density generally between 10 and $10^3$ cells/cm$^3$, whereas foams with more uniform cell structures and cell population density in the range of $10^4$–$10^8$ cells/cm$^3$ are achieved with the HPFIM process [70, 114], which are lower compared with those achieved with $CO_2$-batch and extrusion foam processing.

Remarkably, research on foam injection molding (FIM) process has received substantial attention during the past decade as witnessed by a significant increase in the number of publications on the FIM process [67, 70, 73, 76, 78, 108, 114–117].

Neat PLA, PLA/cellulose fiber composites (10–30 wt%) and PLA/carbon nanotube nanocomposites were

successfully foamed in a microcellular injection molding process using $N_2$ gas [108, 117]. All foamed samples exhibited a sandwich-type structure, with solid walls encapsulating a foamed core. This morphology was attributed to several factors such as (i) rapid cooling at the polymer–mold interface that hampered cell nucleation and (ii) gas loss from the polymer to the environment that escaped through the mold vents, among others (Table 15.10).

Neat PLA foam exhibited nonuniform and larger cells owing to its lower viscosity. The average cell size decreased with the addition of fibers into the matrix, as expected. The increased melt viscosity of the matrix induced by the incorporation of fiber may have affected the growth of cells during foaming [31, 32, 34, 118–122]. The cell population density of the composites was nearly two orders of magnitude higher than that achieved in neat PLA foam, indicating that cellulose fibers provide numerous nucleation sites.

The addition of nanoclay Cloisite 30B into a PLA matrix (3001D) has been reported to significantly improve the cell morphology of foamed samples produced through a low-pressure foam injection molding (LPFIM) and high-pressure FIM (HPFIM) equipped with mold opening and gas counter pressure [73]. Nanocomposite foams with average cell size less than 50 μm and void fraction as high as 55% were achieved in PLA by adding nanoclay [73]. Similar results were reported by other investigators who also produced PLA (3001D) foams using the conventional injection molding process and activated azodicarbonamide as a chemical blowing agent [115]. The average cell size of PLA decreased from 68 to 35 μm, whereas the cell population density increased from $3.2 \times 10^6$ to $17.2 \times 10^6$ cells/cm$^3$ using 0.5 wt% nanoclay (Cloisite 30B). The effect of talc addition levels on the foaming behavior PLA samples foamed using LPFIM process was also investigated. The addition of 5 wt% talc significantly improved the foaming properties such as cell density, cell size, and structural uniformity [116]. Microcellular foamed structures have also been developed in PLA/cellulosic fiber composites through the FIM process [67]. The incorporation of 25 phr cellulosic fibers led to foamed composites with higher cell population density, smaller average cell size, and narrower cell size distribution (more uniform cell structure) compared with neat PLA (4032D) counterpart. This improved foam morphology was attributed to the cell nucleating effects of fibers and the increase in the melt strength of PLA matrix by the addition of cellulosic fibers [67].

**TABLE 15.10 Cell Morphology of Microcellular Injection Molded Neat PLA and PLA/Cellulosic Fiber Composites [117]**

| Samples[a] | Density (kg/m$^3$) | Cell Size (μm) | Cell Density (cells/cm$^3$) |
|---|---|---|---|
| Neat PLA | 1070 | 16.5 | $35 \times 10^7$ |
| PLA–10% fiber | 1120 | 5.0 | $60 \times 10^8$ |
| PLA–30% fiber | 1140 | 3.0 | $20 \times 10^9$ |

[a] PLA (NatureWorks PLA 3001D, 1.5% D-lactic acid, density = 1240 kg/m$^3$).

## 15.6 PLA FOAMED WITH CHEMICAL FOAMING AGENTS

CFAs influence the viscoelastic properties of the matrix and the cell morphology of foamed plastics in different manners, because of the differences in their thermal decomposition behaviors [118]. Endothermicity has been reported to be a desirable property because the foaming agent absorbs heat during its decomposition, which cools the polymer, increases the viscosity of the melt, stabilizes the cellular structure, and reduces cell coalescence [20, 21]. Smaller cells improve tensile strength and elongation at break, although larger bubbles improve impact strength [21]. In contrast, exothermic CFAs generate a lot of heat upon their decomposition. This heat may soften the polymer matrix and favor the occurrence of cell coalescence during the foaming process, resulting in a poor cellular structure with large bubbles [118]. Although there have been many studies on foaming of plastics using CFAs [118–122], little has been published on foaming of neat PLA using CFAs [107], although the number of publications has increased in the past years [123–128].

### 15.6.1 Effects of CFA Content and Type

Investigation has shown that a homogeneous and finer cell morphology could be successfully achieved in PLA foamed in an extrusion process with a proper combination of polymer melt-flow index, CFA content, and processing speed (Figure 15.9) [123]. The melt-flow index must lie within the range that provides a melt viscosity low enough to allow cell formation and growth but high enough to prevent cell coalescence.

The density of PLA foams is affected by the concentration of endothermic CFA. It decreases with an initial increase in CFA content, reaches a minimum value, and then increases as CFA content continues to increase (Figure 15.10) [123].

The U-shape in Figure 15.10 is expected because the number of nucleated cells and their growth, which controls the density reduction during the foaming process, are strongly dependent on the amount of gas molecules dissolved in the molten polymer matrix [12, 52, 53, 120, 122]. With the increase in CFA content, the amount of gas dissolved in the matrix for cell nucleation and growth increases. This favors the growth of cells resulting in reduced density. However, the opposite trend could be attributed to the cell growth mechanism, which depends also on the amount of gas dissolved in the polymer matrix during the foaming process. Once the cells are nucleated, they continue to grow as long as there is enough gas to diffuse into the nucleated cells,

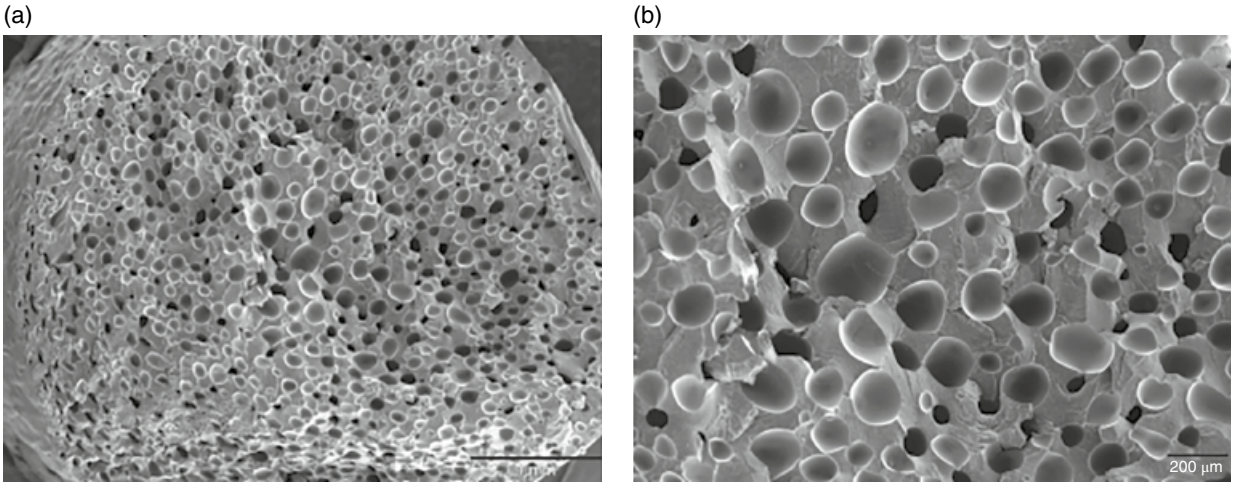


**FIGURE 15.9** SEM of amorphous PLA 8302D (NatureWorks, 10% D-lactic acid content) foamed with 0.5% endothermic CFA (BIH40 from Boehringer Ingelheim Chemicals, which is sodium salt of polycarbonic acid + carbonate compounds) at 40 rpm: (a) 30× and (b) 70× magnifications [123].

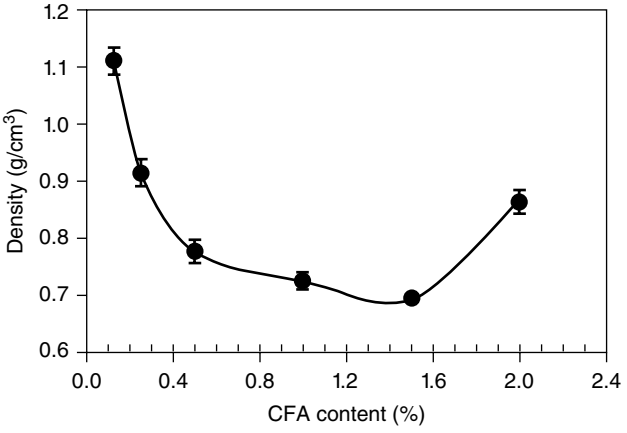


**FIGURE 15.10** Effect of endothermic CFA (BIH40) content on the density of amorphous PLA 8302D foamed at 40 rpm. The extrusion processing temperatures were set at 180–180–175–170°C from the hopper to the die [123].

and the polymer can be expanded [12, 118, 120, 122]. The density of the foamed sample will decrease as the CFA content increases because of the cell growth. However, once the nucleated cells are fully grown, cell coalescence and/or collapse may take place with a further increase in the CFA content. In particular, if cell coalescence occurs, the average cell size will increase and the density of the resulting foamed samples will increase [12]. This phenomenon is known as the gas containment limit [121].

A gas containment limit was also reported for amorphous PLA (6300D, NatureWorks) foamed with various concentrations (0.2–3.2 wt%) of exothermic foaming agent (azo) [107]. However, a bubble growth model with surface vaporization was inadequate in describing the foam density increase at increasing foaming agent content. Instead, analysis of the foamed rod diameter suggested premature gas separation from the polymeric melt before foaming occurred at higher gas content, which adversely affected foaming efficiency [107].

The influence of different CFA types and their applicability to produce PLA foams by extrusion have been evaluated using a wide range of commercially available conventional exothermic (azodicarbonamide) and endothermic (citric acid/baking soda) CFAs [124]. The properties of extrusion foamed PLA with 2 wt% of these CFAs are listed in Table 15.11. For exothermic CFA (ADCA), PLA 8052D produced a higher number of both nucleated cells per unit volume and expansion of cells, which resulted in lower density compared to PLA 2003D. Opposite results were obtained with the endothermic CFA (BS) because its decomposition products include water, which probably hydrolyzed the PLA, thus decreasing its melt pressure, viscosity, and melt strength during the foaming process. Since the weight average molecular weight of 2003D (180,477 Da) is greater that of PLA 8052D, it resisted degradation by hydrolysis and produced better cell morphology than the 8052D counterpart. The compression strength values of foams produced with exothermic CFA (ADCA) were similar for the two types of PLA. Overall, the results suggest the exothermic azodicarbonamide CFA added to PLA 8052D in 2 wt% is a favorable foaming agent to produce PLA foam at 190°C.

The cellular structure of PLA obtained using an extrusion process with various chemical foaming agents has also been reported in the literature [125–128].

### 15.6.2 Effect of Processing Conditions

Processing temperature is one of the most important variables in the extrusion foaming process because it affects

**TABLE 15.11 Cell Morphology and Compressive Strength of PLA Foamed with 2 wt% of Exothermic and Endothermic CFAs at 190°C**

| | Cell Population Density (cells/cm$^3$)[a] | | Volume Expansion Ratio (times)[a] | | Density (g/cm$^3$)[a] | | Foam Strength (MPa)[a,d] | |
|---|---|---|---|---|---|---|---|---|
| CFA Type | 8052D[b] | 2003D[c] | 8052D[b] | 2003D[c] | 8052D[b] | 2003D[c] | 8052D[b] | 2003D[c] |
| Azodicarbonamide (ADCA) | 4.82 | 4.17 | 2.38 | 2.18 | 0.53 | 0.57 | 22.4 ± 0.7 | 22.8 ± 0.6 |
| citric acid/baking soda (BS) | 0.56 | 1.91 | 1.24 | 1.53 | 1.00 | 0.81 | – | – |

Source: Adapted from Ref. 124.

[a] All PLA have a density of 1.24 g/cm$^3$ and are from Ingeo Biopolymer, NatureWorks© LLC, Minnetonka, MN, USA.

[b] PLA 8052D (4.5 mol% D-lactide content), $T_m$ = 153.3°C, MFI = 7/10 g/min; MW = 153,235 Da.

[c] PLA 2003D (4.3 mol% D-lactide content), $T_m$ = 150.9°C, MFI = 2/10 g/min; MW = 180,477 Da.

[d] Foam strength tests were performed on specimens considered acceptable (void fraction >40%) and the compression strength was measured at 10% deformation.

both the melt viscosity and the amount of gas given off upon the thermal decomposition of CFA [118–120]. However, high processing temperatures should be avoided due to the thermal instability of PLA. Similarly, a lower melt temperature should not be used to prevent only partial decomposition of the CFA. The extruder barrel temperature profile should be set up based on the melting temperature of the polymer and the decomposition temperature of CFA [123].

The extruder's rotational screw speed also affects the density of PLA foams. The density of foamed samples decreases with the processing speed up to a certain speed and then increases as the processing speed increases further (Figure 15.11) [123].

As mentioned, density reduction depends strongly on the concentration of gas dissolved in the molten polymer matrix [118–122]. Since the residence time for the molten polymer matrix was too long in the extruder's barrel at slower speed (20 rpm), most of the gas generated was either lost to the environment or cell coalescence occurred in foamed samples, thereby increasing the density of foamed samples. The gas generated during processing at moderate speed (e.g., 40 rpm) was effectively used for bubble nucleation and growth, leading to low-density foam. Faster processing speeds (above 40 rpm) lead to an incomplete decomposition of the CFA. As a result, a lesser amount of gas will be available for bubble growth, which leads to increased density of the part [123].

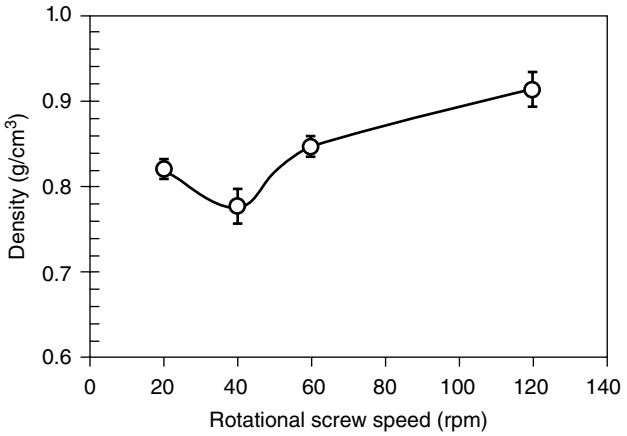


**FIGURE 15.11** Effect of rotational screw speed on the density of amorphous PLA 8302D foamed with 0.5% CFA (BIH40). The extrusion processing temperatures were set at 180–180–175–170°C from the hopper to the die [123].

## 15.7 MECHANICAL PROPERTIES OF PLA FOAMS

Currently, most studies on microcellular PLA are centered on understanding the mechanisms of bubble nucleation, growth, and stabilization. The relationships between morphological and mechanical properties of PLA foams are not well established because their mechanical properties have not been extensively characterized.

### 15.7.1 Batch Microcellular Foamed PLA

A significant improvement in the impact strength can be achieved in PLA by introducing a microcellular structure in the matrix. The notched Izod impact strengths of foamed PLA samples are, in general, three to four times larger than those of the unfoamed counterparts depending on the density of the samples (Table 15.12) [2].

The fourfold increase in notched Izod impact strength of foamed PLA over unfoamed could be attributed to the presence of small bubbles that inhibit crack propagation by blunting the crack tip and increasing the amount of energy needed to propagate the crack [15]. It is also believed that the struts and cell walls of the foam structure absorb the energy during deformation, and thereby increase the impact strength [32].

Foaming reduced both the ultimate strength and tensile modulus of the samples. In contrast, the specific strength and modulus were improved, implying that both the tensile strength at break to weight and modulus to weight ratios are not compromised by microcellular foaming (Table 15.13) [2].

**TABLE 15.12 Influence of Density on the Impact Strength of Unfoamed and Microcellular Foamed PLA [2]**

| Foaming Conditions[a] | Density ($g/cm^3$) | Notched Izod Impact Strength (J/m) |
|---|---|---|
| Unfoamed | 1.21 | 21 ± 4 |
| Foamed at 150°C for 5 s | 0.74 | 85 ± 23 |
| Foamed at 150°C for 15 s | 0.84 | 76 ± 31 |

[a] PLA specimens (Biomer L9000, Krailling, Germany) were saturated with $CO_2$ at room temperature at 850 psi for 24 h.

**TABLE 15.13 Tensile Properties of Unfoamed and Batch Microcellular Foamed PLA [2]**

| Samples[a] | Specific Stress at Break ($MPa/g/cm^3$)[b] | Specific Modulus ($GPa/g/cm^3$)[b] | Strain at Break (%) | Energy at Break (J) |
|---|---|---|---|---|
| Unfoamed PLA | 30 | 2.3 | 1.5 | 0.4 |
| Foamed PLA | 37 | 2.1 | 2.9 | 1.5 |

[a] PLA (Biomer L9000 supplied by Biomer (Krailling, Germany) were saturated with $CO_2$ at 23°C, 850 psi, and foamed at 150°C for 5 s.
[b] The densities of unfoamed and foamed PLA were 1.21 and 0.74 $g/cm^3$, respectively.

Due to the presence of foamed microcells, significant improvements were achieved in both the strain at break (up to a twofold increase over unfoamed PLA) and the toughness or energy at break (up to a fourfold increase over unfoamed PLA). The results imply that foaming enhances the ductility of PLA and are in agreement with the impact resistance data listed in Table 15.12.

The effect of uniaxially stretching on the stiffness of neat PLA foamed films and counterparts reinforced with microcrystalline cellulose (MCC) has been investigated [129, 130]. The stiffness of neat PLA-foamed films through a $CO_2$ batch process increased by approximately four times when they are mechanically stretched above the glass transition temperature [129]. This large increase in stiffness is attributed to an increase in crystallinity and alignment of the foam cell walls. These results corroborated other studies that reported increases in the crystallinity of PLA by up to 35% due to expansion from foaming [131] and that the crystallinity of solid PLA films reached a maximum at a stretch ratio of 4 [132]. Stretching of PLA reinforced with 10 wt% MCC gave an approximately 3.5 times improvement in the normalized tensile elastic modulus over unreinforced foams. This increase in stiffness with stretching was attributed mainly to cell wall alignment in the machine direction since the degree of crystallinity remained unchanged [130].

LCB of PLA with PMDA and then TGIC is suitable approach for improving the mechanical properties of PLA foamed in a batch process [88]. The tensile strength of LCB PLA (~63 MPa) increased slightly compared with the original linear PLA (~58 MPa). Conversely, the notched Izod impact strength improved significantly by introducing LCB (~36 J/m) compared to the neat PLA counterpart (~24 J/m). The increased impact strength was related to the change in crystallization by the presence of LCB.

The tensile properties of $CO_2$-batch foamed neat PLA and PLA filled with 3 wt% of aCNC were evaluated [69]. Neat PLA foam had an average cell size of 35.6 μm and population density of $3.91 \times 10^{10}$ cells/$cm^3$ compared to 21.9 μm and $1.93 \times 10^{11}$ cells/$cm^3$, respectively, for the nanocomposites with aCNC. The nanocomposite foam showed higher strength (10.7 MPa) as compared with neat PLA (9.5 MPa), with almost an identical modulus (~202–204 MPa). However, the nanocomposites had lower elongation at break (39.6%) than the neat PLA foam (53.7%) [69].

### 15.7.2 Extrusion of PLA

The compression properties of amorphous PLA foamed in a continuous extrusion process using $CO_2$ as a blowing agent are summarized in Table 15.14. Correlations were found by plotting the compressive modulus ($E$) and stress at yield ($\sigma$) as a function of $CO_2$ content. The decreased modulus and strength with increasing $CO_2$ content is due to the high level of plasticization induced by the residual $CO_2$ for specimens foamed at higher $CO_2$ content [105, 106].

Compression strengths of $CO_2$-extrusion-foamed neat PLA and PLA modified with DCP were evaluated [92]. Neat PLA (7001D) showed a foam density of (45 $kg/m^3$) and average cell size of 358 μm compared with 32 $kg/m^3$ and 130 μm, respectively, for PLA treated with DCP. Higher foam strength and stiffness were achieved with the foams from modified PLA. At 10% deformation, the compression stresses were 73 ± 1 Pa for neat PLA and 151 ± 4 Pa for PLA-DCP despite having a much lower density. The compression modulus also increased from 1.13 MPa (neat PLA) up to 2.93 MPa for PLA-DCP. This outstanding performance of PLA-DCP foams was attributed to their smaller cells.

The mechanical properties of neat PLA and reinforced PLA foamed with chemical foaming agents were also studied. As listed in Table 15.11, the compression strength values of foams produced with exothermic azodicarbonamide were similar for two different types of PLA [124]. The effect

**TABLE 15.14 Physicomechanical Properties of Low-Density PLA Foams [105, 106]**

| | Physical Properties[a] | | Compression Properties | |
|---|---|---|---|---|
| $CO_2$ Content (wt%) | Density ($g/cm^3$) | Cell Size (μm) | Strength (MPa) | Modulus (MPa) |
| 7.3 | 0.024 | 125 | 0.081 | 4.1 |
| 8.6 | 0.022 | 100 | 0.074 | 2.8 |
| 9.3 | 0.021 | 70 | 0.070 | 2.1 |

[a] PLA (NatureWorks 8302D with D-lactic acid content of 9.85%).

of wood flour content (15 and 30 wt%) on the dynamic mechanical properties of PLA and PLA/wood flour composites foams generated through an extrusion process with CFA was also assessed [125]. The mechanical properties of PLA foams were improved by the addition of wood flour into the matrix. Both the storage modulus ($E'$) and loss modulus ($E''$) of composites increased with wood flour content [125].

### 15.7.3 Microcellular Injection Molding of PLA

Static and dynamic properties of solid and microcellular injection-molded neat PLA and PLA/cellulose fiber composites are listed in Table 15.15. The addition of fibers increased the specific tensile modulus and storage modulus for both solid and microcellular specimens, while the specific tensile strength was not affected. Conversely, the presence of fibers led to a significant decrease in both strain at break and toughness of PLA foams, clearly suggesting that the ductility of PLA/cellulose fiber composites was not enhanced by creating a cellular structure through a microcellular injection molding process [117].

## 15.8 FOAMING OF PLA/STARCH AND OTHER BLENDS

There has been a growing interest in the development of starch-based products in recent years. Starch-based foams have been seen as a potential alternative to expandable polystyrene. PLA/starch (native and acetylated) composites can be foamed with both physical and chemical foaming agents in conventional processing equipment [5, 133–137]. PLA has some significant drawbacks such as low melt strength, slow crystallization rate, poor processability, brittleness, low service temperature, which limit its applications. These limitations are overcome by blending PLA with other polymers. Foamed PLA blends are used in various applications [133–142].

Biodegradable foams derived from PLA ($M_w$ = 120 kDa and 36% crystallinity, Shimadzu, Japan) and corn starch (75% amylopectin and 25% amylose) were prepared by extrusion using water (0–40 wt%) as a blowing agent and talc as a nucleating agent. The extrusion processing conditions (i.e., temperature profiles, die diameter, and screw speed) and material compositions (i.e., water content, PLA/starch ratio, nucleation agent content) were the critical variables affecting the average cell size and their distribution. Foams consisting of both open and closed cells with a relatively fine cellular size and uniform cell distribution were obtained by controlling these variables [134]. The presence of PLA significantly improved the water resistance of the foam and its recovery capacity, especially in high moisture conditions. However, the compression modulus of the foams was negatively related to the foam bulk density [135].

Low-density open-cell foams (25 kg/m$^3$) were obtained by microcellular extrusion of semicrystalline PLA (2002D, 4% D-lactic acid content, NatureWorks) and starch (75% amylopectin and 25% amylose) blends using a $CO_2$ concentration of 8 wt% [10]. Interfacial modification of PLA/starch blends using maleated PLA was necessary to obtain a fine cell structure and low-density foam. The use of 0.5 wt% talc did not modify the foam structure, clearly indicating that the rate of cell nucleation was not a limiting factor as expected from the high concentration of gas used during the foaming process [105, 106].

Blends of 75 wt% amorphous PLA with 25 wt% poly[(butylene adipate)-*co*-terephthalate] (PBAT) and poly[(butylene succinate)-*co*-adipate] (PBSA) were also prepared and foamed using supercritical $CO_2$ in a lab-scale autoclave foaming chamber. Microcellular bead foams of different cellular structures ranging from low-density open cell to high-density closed cell were manufactured by using blends [138, 139].

Similarly, microcellular foams of PLLA/poly(butylene adipate-*co*-terephthalate) (PBAT) blends with or without poly(D-lactide) (PDLA) were prepared via a batch foaming process with supercritical $CO_2$ [140]. PLLA/PBAT foams exhibited an open-cell structure due to the soft immiscible PBAT phase as separated domains. The average cell size decreased, while the cell population density increased with further addition of PDLA in the PLLA/PBAT blends.

**TABLE 15.15 Static Tensile and Dynamic Properties of Solid (S) and Microcellular (M) Injection-Molded Neat PLA and PLA/Cellulose Fiber Composites (PLA–30% CF) [117]**

| | Density (kg/m$^3$) | | Specific Strength (MPa/kg/m) | | Specific Modulus (MPa/kg/m) | | Strain (%) | | Specific Toughness (MPa/kg/m) | | Storage Modulus at 40°C (MPa) | |
|---|---|---|---|---|---|---|---|---|---|---|---|---|
| Samples[a] | S | M | S | M | S | M | S | M | S | M | S | M |
| Neat | 1220 | 1070 | 0.054 | 0.045 | 1.6 | 1.6 | 5.5 | 5.7 | 0.0020 | 0.0019 | 2050 | 2500 |
| PLA–30% CF | 1240 | 1140 | 0.060 | 0.048 | 2.2 | 2.3 | 5.1 | 3.5 | 0.0022 | 0.0010 | 3200 | 3700 |

[a] PLA (NatureWorks PLA 3001D, 1.5% D-lactic acid, density = 1240 kg/m$^3$).

Recently, the foaming behavior of PLA/PBS/cellulose fiber (CF) composites for hot cups and lids packaging applications has been studied [141]. The PLA/PBS and PLA/PBS/CF composites with various amounts of CF (5, 10, and 15 phr) were foamed in injection molding using 2.5 phr of sodium bicarbonate ($NaHCO_3$) as the blowing agent. As expected, the number of closed cells increased, and the cell distribution was more uniform, when the amount of CF in PLA/PBS blend was increased because the addition of CF in PLA/PBS blend decreased its viscosity. The morphology of composite foams after immersion in hot water at 75°C for 30 min indicated that the number of cells in the foam increased. The flexural strength and modulus of composite biofoams before and after immersion in hot water increased with increasing CF content. The PLA/PBS composite with 15 phr of CF was identified as suitable for hot cup or lid packaging applications [141].

Foams of biopolymer blends made by thermoplastic starch (TPS) addition to PLA (PLA and TPS) were successfully manufactured by hot-melt extrusion with supercritical $CO_2$ as a blowing agent at various extruder die temperatures and $CO_2$ contents [142]. Irrespective of the experimental conditions, a 50/50 (in wt%) PLA/TPS blend was poorly foamed due to the strong incompatibility between both biopolymers. The best structures were obtained for the blend consisting of 80/20 (in wt%). The nucleation was also greater in the 80/20 blend, and the average cell size decreased with die temperature reduction. However, the cell distribution remained inhomogeneous due to poor affinity between both polymers since no coupling agent for better interfacial adhesion was used in the blend. This blend behaved like pure PLA foam with high porosity levels of up to 96%. Interestingly, a threshold die temperature separating a closed cell porosity (at lowest temperatures) and an open cell structure (above the threshold) was clearly observed at 95°C, which is significantly lower than the 109°C obtained with pure PLA foam, attributable to the addition of TPS in PLA, which changed its melt strength [142].

## REFERENCES


1. D. Garlotta, *J. Polym. Environ.* **2001**, *9*, 63–84.
2. L. M. Matuana, *Bioresour. Technol.* **2008**, *99*, 3643–3650.
3. C. Xing, L. M. Matuana, *J. Appl. Polym. Sci.* **2016**, *133*, 43201.
4. S. Vijayarajan, S. E. M. Selke, L. M. Matuana, *Macromol. Mater. Eng.* **2014**, *299*, 622–630.
5. K. A. Afrifah, L. M. Matuana, *Macromol. Mater. Eng.* **2012**, *297*, 167–175.
6. K. A. Afrifah, L. M. Matuana, *Polym. Int.* **2013**, *62*, 1053–1058.
7. S. S. Karkhanis, N. M. Stark, R. C. Sabo, L. M. Matuana, *Polym. Eng. Sci.* **2018**, *58*, 1965–1974.
8. K. A. Afrifah, L. M. Matuana, *Macromol. Mater. Eng.* **2010**, *295*, 802–811.
9. B. W. Chieng, N. A. Ibrahim, Y. Y. Then, Y. Y. Loo, *Molecules* **2014**, *19*, 16024–16038.
10. M. Mihai, M. A. Huneault, B. D. Favis, H. Li, *Macromol. Biosci.* **2007**, *7*, 907–920.
11. S. Pilla, S. Gong, E. O'Neil, R. M. Rowell, A. M. Krzysik, *Polym. Eng. Sci.* **2008**, *48*, 578–587.
12. L. M. Matuana, C. B. Park, J. J. Balatinecz, *Polym. Eng. Sci.* **1997**, *37*, 1137–1147.
13. L. M. Matuana, C. B. Park, J. J. Balatinecz, *J. Vinyl Addit. Technol.* **1997**, *3*, 265–273.
14. L. M. Matuana, R. T. Woodhams, J. J. Balatinecz, C. B. Park, *Polym. Compos.* **1998**, *19*, 446–455.
15. F. A. Waldman, The processing of microcellular foam, S.M. thesis, Department of Mechanical Engineering, Massachusetts Institute of Technology, Cambridge, MA, 1982.
16. J. E. Martini, N. P. Suh, F. A. Waldman, Microcellular closed cell foams and their method of manufacture, U.S. Patent 4,473,665, 1984.
17. D. Klempner, V. Sendijarevic, *Handbook of Polymeric Foams and Foam Technology*, 2nd edition, Hanser Gardener Publications, Inc., Cincinnati, OH, 2004, p. 584.
18. S. T. Lee, *Foam Extrusion*, 2nd edition, CRC Press, Boca Raton, FL, 2014.
19. S. T. Lee, *Polymer Foams Innovations in Processes, Technologies, and Products*, CRC Press, Boca Raton, FL, 2017.
20. R. L. Heck, III, *J. Vinyl Addit. Technol.* **1998**, *4*, 113–116.
21. J. Markanian, *Plast. Addit. Compd.* **2006**, *9*, 22–25.
22. J. Vanvuchelen, C. Perugini, M. Deweerdt, L. Chen, T. Burnham, *J. Cell. Plast.* **2000**, *36*, 148–157.
23. C. B. Park, D. F. Baldwin, N. P. Suh, *Polym. Eng. Sci.* **1995**, *35*, 432–440.
24. C. B. Park, Continuous production of high-density and low-density microcellular plastics in extrusion, in S. T. Lee (Ed.), *Foam Extrusion: Principles and Practice*, Technomic Publishing Co., Inc., Lancaster, PA, 2000, pp. 263–305.
25. R. Cole, *Adv. Heat Transfer* **1974**, *10*, 86–166.
26. M. Blander, J. L. Katz, *AIChE J.* **1975**, *21*, 833–848.
27. D. I. Collias, D. G. Baird, *Polym. Eng. Sci.* **1995**, *35*, 1178–1183.
28. D. I. Collias, D. G. Baird, *Polym. Eng. Sci.* **1995**, *35*, 1167–1177.
29. K. A. Seeler, V. Kumar, *J. Reinf. Plast. Comp.* **1993**, *12*, 359–376.
30. M. Shimbo, D. F. Baldwin, N. P. Suh, The viscoelastic behavior of microcellular plastics with varying cell size, *Polym. Eng. Sci.* **1995**, *35*, 1387–1393.
31. L. M. Matuana, C. B. Park, J. J. Balatinecz, *Cell. Polym.* **1998**, *17*, 1–16.
32. L. M. Matuana, C. B. Park, J. J. Balatinecz, *Polym. Eng. Sci.* **1998**, *38*, 1862–1872.
33. C. B. Park, A. H. Behravesh, R. D. Venter, *Polym. Eng. Sci.* **1998**, *38*, 1812–1823.

34. L. Matuana-Malanda, C. B. Park, J. J. Balatinecz, *J. Cell. Plast.* **1996**, *32*, 449–467.
35. K. B. Venkatesan, S. S. Karkhanis, L. M. Matuana, *J. Appl. Polym. Sci.* **2021**, *138*, e50686.
36. X. Han, K. W. Koelling, D. L. Tomasko, L. J. Lee, *Polym. Eng. Sci.* **2003**, *43*, 1206–1220.
37. L. M. Matuana, C. A. Diaz, *Ind. Eng. Chem. Res.* **2013**, *52*, 12032–12040.
38. V. Kumar, H. G. Schimer, A semi-continuous process to produce microcellular foams, U.S. Patent 5,684,055, 1997.
39. Y. Fujimoto, S. Sinha Ray, M. Okamoto, A. Ogani, K. Yamada, K. Ueda, *Macromol. Rapid Commun.* **2003**, *24*, 457–461.
40. S. S. Ray, M. Okamoto, *Macromol. Mater. Eng.* **2003**, *288*, 936–944.
41. Y. Ema, M. Ikeya, M. Okamoto, *Polymer* **2006**, *47*, 5350–5359.
42. Y. Di, S. Iannace, E. Di Maio, L. Nicolais, *J. Polym. Sci. Part B* **2005**, *43*, 689–698.
43. C. Marrazzo, E. Di Maio, S. Iannace, *J. Cell. Plast.* **2007**, *43*, 123–133.
44. Y. Sato, M. Yamane, A. Sorakubo, S. Takishima, H. Masuoka, H. Yamamoto, *Takasugi Jpn. Symp. Thermophys. Prop.* **2000**, *21*, 196–198.
45. M. Takada, S. Hasegawa, M. Ohshima, *Polym. Eng. Sci.* **2004**, *44*, 186–196.
46. J. Crank, *The Mathematics of Diffusion*, 2nd edition, Oxford University Press, New York, 1975, p. 414.
47. N. S. Oliveira, J. Dorgan, J. A. P. Coutinho, A. Ferreira, J. L. Daridon, I. M. Marrucho, *J. Polym. Sci. Part B* **2006**, *44*, 1010–1019.
48. N. S. Oliveira, J. Dorgan, J. A. P. Coutinho, A. Ferreira, J. L. Daridon, I. M. Marrucho, *J. Polym. Sci. Part B* **2007**, *45*, 616–625.
49. N. S. Oliveira, J. Oliveira, T. Gomes, A. Ferreira, J. Dorgan, I. M. Marrucho, *Fluid Phase Equilib.* **2004**, *222–223*, 317–324.
50. N. S. Oliveira, C. M. Goncalves, J. A. P. Coutinho, A. Ferreira, J. Dorgan, I. M. Marrucho, *Fluid Phase Equilib.* **2006**, *250*, 116–124.
51. L. Bao, J. R. Dorgan, D. Knauss, S. Hait, N. S. Oliveira, I. M. Marucho, *J. Membr. Sci.* **2006**, *285*, 166–172.
52. D. F. Baldwin, C. B. Park, N. P. Suh, *Polym. Eng. Sci.* **1996**, *36*, 1437–1445.
53. D. F. Baldwin, C. B. Park, N. P. Suh, *Polym. Eng. Sci.* **1996**, *36*, 1446–1453.
54. J. S. Colton, N. P. Suh, *Polym. Eng. Sci.* **1987**, *27*, 485–492.
55. J. S. Colton, N. P. Suh, *Polym. Eng. Sci.* **1987**, *27*, 493–499.
56. J. S. Colton, N. P. Suh, *Polym. Eng. Sci.* **1987**, *27*, 500–503.
57. X. Hu, A. V. Nawaby, H. E. Naguib, M. Day, K. Ueada, X. Liao, ANTEC Technical Papers, 2005, pp. 2670–2673.
58. X. Liao, A. V. Nawaby, P. Whitfield, M. Day, M. Champagne, J. Denault, *Biomacromolecules* **2006**, *7*, 2937–2941.
59. A. S. Michaels, H. J. Bixler, *J. Polym. Sci.* **1961**, *50*, 393–412.
60. A. S. Michaels, H. J. Bixler, *J. Polym. Sci.* **1961**, *50*, 413–439.
61. D. W. Van Krevelen, *Properties of Polymers*, 3rd edition, Elsevier Science Publishers, New York, 1990, p. 875.
62. J. Wang, W. Zhu, H. Zhang, C. B. Park, *Chem. Eng. Sci.* **2012**, *75*, 390–399.
63. M. Mihai, M. A. Huneault, B. D. Favis, *J. Appl. Polym. Sci.* **2009**, *113*, 2920–2932.
64. M. Nofar, A.Tabatabaei, A. Ameli, C. B. Park, *Polymer* **2013**, *54*, 6471–6478.
65. M. Nofar, W. Zhu, C. B. Park, *Polymer* **2012**, *53*, 3341–3353.
66. P. Chen, W. Wang, Y. Wang, K. Yu, H. Zhou, X. Wang, J. Mi, *Polym. Degrad. Stab.* **2017**, *144*, 231–240.
67. W. Ding, D. Jahani, E. Chang, A. Alemdar, C. B. Park, M. Sain, *Compos. A: Appl. Sci. Manuf.* **2016**, *83*, 130–139.
68. J. Dlouhá, L. Suryanegara, H. Yano, *Soft Matter* **2012**, *8*, 8704–8713.
69. Y. Qiu, Q. Lv, D. Wu, W. Xie, S. Peng, R. Lan, H. Xie, *Cellulose* **2018**, *25*, 1795–1807.
70. M. P. Motloung, V. Ojijo, J. Bandyopadhyay, S. S. Ray, *Polymers* **2019**, *11*, 1270.
71. C. J. Xu, D. F. Wu, Q. L. Lv, L. Yan, *J. Phys. Chem. C.* **2017**, *121*,18615–18624.
72. A. Huang, P. Yu, X. Jing, H. Y. Mi, L. H. Geng, B. Y. Chen, X. F. Peng, *J. Macromol. Sci. Part B* **2016**, *55*, 908–924.
73. A. Ameli, D. Jahani, M. Nofar, P. U. Jung, C. B. Park, *Compos. Sci. Technol.* **2014**, *90*, 88–95.
74. J. Zhou, Z. Yao, C. Zhou, D. Wei, S. Li, *J. Appl. Polym. Sci.* **2014**, *131*, 40773.
75. X. Wang, J. Mi, H. Zhou, X. Wang, *J. Mater. Sci.* **2019**, *54*, 3863–3877.
76. C. Okolieocha, D. Raps, K. Subramaniam, V. Altstadt, *Eur. Polym. J.* **2015**, *73*, 500–519.
77. P. Muanchan, H. Ito, *Microsyst. Technol.* **2018**, *24*, 655–662.
78. M. Nofar, C. B. Park, *Prog. Polym. Sci.* **2014**, *39*, 1721–1741.
79. M. Nofar, A. Ameli, C. B. Park, *Polymer* **2015**, *69*, 83–94.
80. S. K. Yeh, Y. R. Chen, T. W. Kang, T. J. Tseng, S. P. Peng, C. C. Chu, S. P. Rwei, W. J. Guo, *J. Polym. Res.* **2018**, *25*, 30.
81. M. D. Leon, V. Bernardo, M. A. Rodriguez-Perez, *Macromol. Mater. Eng.* **2017**, *302*, 1700343.
82. P. Tiwary, C. B. Park, M. Kontopoulou, *Eur. Polym. J.* **2017**, *91*, 283–296.
83. L. M. Matuana, O. Faruk, *eXPRESS Polym. Lett.* **2010**, *4*, 621–631.
84. M. Xanthos, U. Yilmazer, S. K. Dey, J. Quintans, *Polym. Eng. Sci.* **2000**, *40*, 554–566.
85. Y. Di, S. Iannace, E. Di Maio, L. Nicolais, *Macromol. Mater. Eng.* **2005**, *290*, 1083–1090.
86. J. Tuominen, J. Kylma, J. Seppala, *Polymer* **2002**, *43*, 3–10.
87. S. Li, G. He, X. Liao, C. B. Park, Q. Yang, G. Li, *RSC Adv.* **2017**, *7*, 6266–6277.
88. J. Liu, L. Lou, W. Yu, R. Liao, R. Li, C. Zhou, *Polymer* **2010**, *51*, 5186–5197.


89. L. Yang, Z. Yang, F. Zhang, L. Xie, Z. Luo, Q. Zheng, *Polymers* **2018**, *10*, 796.
90. L. Gu, Y. Xu, G. W. Fahnhorst, C. W. Macosko, *J. Rheol.* **2017**, *61*, 785–796.
91. M. Zhou, P. Zhou, P. Xiong, X. Qian, H. Zheng, *Macromol. Res.* **2015**, *23*, 231–236.
92. T. Standau, S. M. Castellón, A. Delavoie, C. Bonten, V. Altstädt, *E-Polymers* **2019**, *19*, 297–304.
93. National Toxicology Program, *Natl. Toxicol. Program Tech. Rep. Ser.* **2012**, *576*, 1.
94. J. Pauluhn, *Toxicol. Sci.* **2000**, *58*, 173–181.
95. K. C. Leibman, *Environ. Health Perspect.* **1975**, *11*, 115–119.
96. S. S. Karkhanis, L. M. Matuana, *Polym. Eng. Sci.* **2019**, *59*, 2211–2219.
97. C. B. Park, N. P. Suh, *J. Manuf. Sci. Eng. Trans. ASME* **1996**, *118*, 639–645.
98. C. B. Park, N. P. Suh, *Polym. Eng. Sci.* **1996**, *36*, 34–48.
99. C. B. Park, The role of polymer/gas solutions in continuous processing of microcellular polymers, Ph.D. thesis, Department of Mechanical Engineering, Massachusetts Institute of Technology, Cambridge, MA, 1993.
100. D. F. Baldwin, C. B. Park, N. P. Suh, *Polym. Eng. Sci.* **1996**, *36*, 1425–1435.
101. C. B. Park, L. K. Cheung, *Polym. Eng. Sci.* **1997**, *37*, 1–10.
102. C. B. Park, L. K. Cheung, *Cell. Polym.* **1998**, *17*, 221–251.
103. A. H. Behravesh, C. B. Park, M. Pan, R. D. Venter, *Polym. Prepr.*, **1996**, *37*, 767–768.
104. H. E. Naguib, C. B. Park, N. Reichelt, *J. Appl. Polym. Sci.* **2004**, *91*, 2661–2668.
105. J. Reignier, R. Gendron, M. F. Champagne, *Cell. Polym.* **2007**, *26*, 83–115.
106. J. Reignier, R. Gendron, M. F. Champagne, SPE ANTEC Technical Papers, 2006, pp. 2710–2714.
107. S. T. Lee, L. Kareko, J. Jun, *J. Cell. Plast.* **2008**, *44*, 293–305.
108. S. Pilla, A. Kramschuster, S. Gong, A. Chandra, L. Turng, *Int. Polym. Process.* **2007**, *12*, 418–428.
109. M. Mihai, M. A. Huneault, B. D. Favis, SPE ANTEC Technical Papers, 2009, pp. 31–35.
110. J. Wang, W. Zhu, C. B. Park, J. Randall, SPE ANTEC Technical Papers, 2009, pp. 36–40.
111. L. M. Matuana, C. A. Diaz, *Ind. Eng. Chem. Res.* **2009**, *49*, 2186–2193.
112. A. Wong, S. N. Leung, G. Y. G. Li, C. B. Park, *Ind. Eng. Chem. Res.* **2007**, *46*, 7107.
113. M. Mihai, M. A. Huneault, B. D. Favis, *Polym. Eng. Sci.* **2010**, *50*, 629–642.
114. G. Llewelyn, A. Rees, C. A. Griffiths, *J. Cell. Plast.* **2020**, *56*, 647–675.
115. N. Najafi, M. C. Heuzey, P. J. Carreau, D. Therriault, C. B. Park, *Eur. Polym. J.* **2015**, *73*, 455–465.
116. A. Ameli, D. Jahani, M. Nofar, P. U. Jung, C. B. Park, *J. Cell. Plast.* **2013**, *49*, 351–374.
117. A. Kramschuster, S. Pilla, S. Gong, A. Chandra, L. Turng, *Int. Polym. Process.* **2007**, *12*, 436–445.
118. Q. Li, L. M. Matuana, *J. Appl. Polym. Sci.* **2003**, *88*, 3139–3150.
119. L. M. Matuana, Q. Li, *Cell. Polym.* **2001**, *20*(2), 115–130.
120. L. M. Matuana, Q. Li, *J. Thermoplast. Compos. Mater.* **2004**, *17*, 185–199.
121. L. M. Matuana, F. Mengeloglu, *J. Vinyl Addit. Technol.* **2002**, *8*(4), 264–270.
122. F. Mengeloglu, L. M. Matuana, *J. Vinyl Addit. Technol.* **2001**, *7*, 142–148.
123. L. M. Matuana, O. Faruk, C. A. Diaz, *Bioresour. Technol.*, **2009**, *100*, 5947–5954.
124. Á. Kmetty, K Litauszki, D. Réti, *Appl. Sci.* **2018**, *8*, 1960.
125. J. Ludwiczak, M. Kozlowski, *J. Biobased Mater. Bioenergy* **2015**, *9*, 227–230.
126. J. Ludwiczak, M. Kozlowski, *J. Polym. Environ.* **2014**, *23*, 137.
127. J. M. Julien, J. C. Bénézet, E. Lafranche, J. C. Quantin, A. Bergeret, M. F. Lacrampe, P. Krawczak, *Polymer* **2012**, *53*, 5885–5895.
128. J. M. Julien, J. C. Quantin, J. C. Bénézet, A. Bergeret, M. F. Lacrampe, P. Krawczak, *Eur. Polym. J.* **2015**, *67*, 40–49.
129. S. Hussain, A. R. Dickson, *Express Polym. Lett.* **2019**, *13*, 18–26.
130. S. Hussain, K. Parker, J. P. Garancher, *J. Cell. Plast.* **2017**, *53*, 513–523
131. J. P. Garancher, A. Fernyhough, *Polym. Degrad. Stab.* **2014**, *100*, 21–28.
132. R. E. Drumright, P. R. Gruber, D. E. Henton, *Adv. Mater.* **2000**, *12*, 1841–1846.
133. A. Hao, Y. Geng, Q. Xu, Z. Lu, L. Yu, *J. Appl. Polym. Sci.* **2008**, *109*, 2679–2686.
134. J. F. Zhang, X. Sun, *J. Appl. Polym. Sci.* **2007**, *106*, 857–862.
135. J. F. Zhang, X. Sun, *J. Appl. Polym. Sci.* **2007**, *106*, 3058–3062.
136. Q. Fang, M. A. Hanna, *Trans. ASABE* **2000**, *43*, 1715–1723.
137. J. Guan, M. A. Hanna, *Ind. Eng. Chem. Res.* **2005**, *44*, 3106–3115.
138. M. Nofar, A. Tabatabaei, H. Sojoudiasli, C. B. Park, P. J. Carreau, M. C. Heuzey, M. R. Kamal, *Eur. Polym. J.* **2017**, *90*, 231–244.
139. M. Nofar, D. Sacligil, P. J. Carreau, M. R. Kamal, M. C. Heuzey, *Int. J. Biol. Macromol.* **2019**, *125*, 307–360.
140. X. Shi, J. Qin, L. Wang, L. Ren, F. Rong, D. Li, R. Wang, G. Zhang, *RSC Adv.* **2018**, *8*, 11850–11861.
141. S. Vorawongsagul, P. Pratumpong, C. Pechyen, *Food Packag. Shelf Life* **2021**, *27*, 100608. https://doi.org/10.1016/j.fpsl.2020.100608.
142. M. Chauvet, M. Sauceau, F. Baillon, J. Fages, *J. Appl. Polym. Sci.* **2021**, *138*, 50150.

# 16

# COMPOSITES

Tanmay Gupta, Vijay Shankar Kumawat, Subrata Bandhu Ghosh, Sanchita Bandyopadhyay-Ghosh, and Mohini Sain

## 16.1 INTRODUCTION

A composite is defined as a material that combines two or more distinct constituents or phases, where one or more of the discontinuous phases (reinforcements) are dispersed in another continuous phase (matrix) in order to obtain tailor-made characteristics and properties. The reinforcing agent can be particulate, fibrous or structural in nature. While a particulate reinforcement has almost equal dimensions in all directions, a fiber has a much greater length than its width. Structural reinforcements on the other hand are three dimensional in nature. In fiber-reinforced polymer composites, fibers are used to carry the load while the polymeric matrices act as mediums for stress transfer as well as to bind the fibers together, while preserving their position and orientation. The matrices also protect the fibers from abrasion and environmental damage upon exposure to elevated temperature and humidity. Because of the distinct advantages that they have over traditional materials, polymer composites are being used in an increasing number of engineering applications.

Although, a number of conventional thermoset and thermoplastic polymer matrices are used in composite production, the depletion of petroleum resources, disposal problems after use, and the introduction of new stringent legislation have created a surge of interest in bio-derived polymer matrix materials. Poly(lactic acid) (PLA) is one such biopolymer, which apart from being used in the packaging industries, has gained a lot of attention as a matrix in composites [1–5]. It is one of the most promising biodegradable polymers owing to its mechanical property profile, thermoplastic processability, and biological properties, such as biocompatibility and biodegradability. PLA can be produced from renewable bio-based resources such as starch and sugars. Physical properties of PLA can be tailored by material modifications. In addition, PLA is a high-strength and high-modulus polymer, with excellent flavor and aroma barrier properties [6]. It can be easily processed by conventional processing techniques used for thermoplastics like injection molding, blow molding, thermoforming, and extrusion.

However, widespread application of PLA is limited because of high cost compared with commodity thermoplastics such as polyethylene (PE) and polypropylene (PP), brittleness, and low thermal stability [7–10]. One approach to increase the usability of PLA is to add fibrous reinforcements in order to produce materials at a comparable or lower cost while maintaining or improving the material properties. The reinforcement of polymers with filler is also common in composite production. Recently, interest has grown in the use of nanoscale fillers because of their distinctive advantages, such as dramatic improvement in mechanical properties with low filler content, to produce new value-added products.

## 16.2 PLA MATRIX

This section gives a brief overview of PLA matrix. For further reading, readers should refer to Chapters 1, 4, and 5. As with other commodity polymers, PLA actually refers to a large family of compounds that includes copolymers with other monomers. The monomer, that is, lactic acid (2-hydroxypropanoic acid), is the simplest hydroxy acid

*Poly(Lactic Acid): Synthesis, Structures, Properties, Processing, Applications, and End of Life*, Second Edition.
Edited by Rafael A. Auras, Loong-Tak Lim, Susan E. M. Selke, and Hideto Tsuji.

with an asymmetric carbon atom and exists in two optically active configurations (D and L). Generally, two major routes are followed for the synthesis of PLA, such as polycondensation polymerization of D- or L-lactic acid and ring-opening polymerization of the corresponding lactide [6, 11].

Properties of PLA are highly related to the number of chiral repeating units and correspondingly the stereoregularity of the polymer. For example, poly(92% L-lactide) is slightly crystalline, whereas poly(87.5% L-lactide) is a completely amorphous biodegradable polymer. In general, poly(L-lactide) (PLLA) exhibits higher mechanical strength than poly(D-lactide) (PDLA) and poly(D/L-lactide) (PDLLA, a blend of D, L enantiomers) [12]. The mechanical properties of PLA can also be varied to a large extent ranging from soft, elastic plastic to stiff and high-strength plastic by varying crystallinity, polymer structure, molecular weight, material formulation (plasticizers, blend, coupling agents, etc.), and processing. Plasticization increases the chain mobility and favors PLA organization and crystallization. PLA presents a moderate permeability to water and oxygen [13]. Also, the biodegradability of the polymers depends considerably on the type of enantiomer. For instance, PDLA exhibits a faster degradation rate than the PLLA form [14]. Moreover, the PDLLA form exhibits a higher permeability to oxygen and water, rendering it even more susceptible to degradation. In fact it was reported that the half-life of PLLA-based gastric-retentive screws is around 24 months, as opposed to 12 months for PDLLA-based screws [15]. Furthermore, the solubility of PLA is highly dependent on the molar mass, degree of crystallinity, and other co-monomers present in the polymer. Both PLLA and PDLA can be dissolved in chlorinated or fluorinated organic solvents, with excellent solubility observed in dioxane and 1,1,1,3,3,3-hexafluoro-2-propanol [16]. Chloroform and dichloromethane (DCM) are also used to prepare PLA solutions [17]. PLA has a glass transition temperature ($T_g$) in the range of 55–70°C and melts at 170–180°C [18]. PLA can be plasticized using oligomeric lactic acid (OLA), citrate ester, or low-molecular-weight poly(ethylene glycol) (PEG), which is a feature of great interest for adjusting mechanical characteristics [19].

## 16.3 REINFORCEMENTS

The primary engineering properties of a composite are derived predominantly from the mechanical and physical properties of the discontinuous phase. The PLA-matrix (continuous phase) acts as an adhesive binder, having considerably lower tensile strength and a greater amount of elasticity. To optimize the overall properties of composite materials (viz. interfacial interactions, stabilization, degradation etc.), appropriate selection of reinforcements (such as fibers, micro- and nanofillers) and processing techniques are critically important [20–22]. This section summarizes the most relevant information about types of micro/macro reinforcements in PLA-based composites.

In a fiber-reinforced PLA (FR-PLA) composite, the amount of fiber loading significantly governs its overall properties such as stiffness, strength, maximum elongation, heat resistance [23]. Additional factors such as desired dynamic behavior, environmental impact, price, and processing costs inform the selection criteria for the fibers, their loading, composite processing, and so on.

In response to increasing demands for PLA-based composite, a variety of new fillers and whiskers are being incorporated in the PLA-matrix. In fact, fillers, such as talc, graphene, and nanocellulose may act as nucleation sites for PLA chains, thereby resulting in improved crystallinity, faster cycle times, improved heat resistance, etc. [24]

An important factor that must be considered to maximize benefits from fibers and fillers is their uniform dispersion within the PLA-matrix. This is usually obtained by controlled addition of fibers/fillers during melt compounding, visual or microscopic inspection of the mix, optimizing process parameters such as throughput rate, temperature, rpm, and so on. Moreover, optimization of filler particle size is also important as finer particles lead to higher toughness and better appearance; however, the processing cost may increase [25]. Meanwhile, challenges related to fiber/filler addition may include increased viscosity, degradation (loss of molecular weight and color, appearance), poor interfacial compatibility, shear heating, and reduced biodegradability.

### 16.3.1 Natural Fiber Reinforcement

Natural FR-PLA composites are attractive because both the reinforcement (natural fiber) and matrix (PLA) are obtained from renewable resources. From an environmental and economic perspective, natural fibers are also considered as an eco-friendly, low cost, renewable, locally available alternative to synthetic fibers (glass, carbon, aramid fiber, etc.) [26]. Furthermore, research has shown the opportunity of achieving enhanced mechanical and thermal properties, such as high specific stiffness, superior toughness, tunable degradability, and recyclability through natural FR-PLA [27–31]. Such reinforcements can be subdivided into three categories: plants (viz. flax, jute, cotton, hemp), animals (viz. silk, wool), and mineral fibers (viz. inorganic whiskers, asbestos). Generally, plant fibers, owing to their easy availability, are more popularly used as natural fiber reinforcements.

***16.3.1.1 Plant Fiber Reinforcements*** Plant fibers are hydrophilic in nature as they contain strongly polarized hydroxyl groups. Most plant fibers are derived from lignocellulosic biomass, which is the most abundant renewable biomaterial, distributed in the form of plants, trees, and crops [32]. The main components of these plant fibers are

cellulose (α-cellulose), hemicellulose, lignin, pectin, waxes, and some water-soluble compounds. Among these, the quantity of cellulose governs the amount of hydrogen bonds and other linkages, which are principally responsible for their strength and stiffness [32, 33]. Similarly, hemicellulose acts as a linkage between the fibrous cellulose and lignin. Lignin is a phenolic compound that acts as a stiffening agent to hold the cellulose molecules within the cell walls.

The challenges pertaining to plant FR-PLA composites are:

- Interfacial adhesion between hydrophilic fiber and hydrophobic PLA. Weak interfacial adhesion may result in poor mixing, thereby affecting the mechanical properties of the composite [34].
- Processing temperature of lignocellulosic plant fibers. This is restricted to be less than 250°C in air, beyond which fiber degradation may occur [35].
- High moisture absorption of natural fibers. This results in swelling and void formation at the interfaces, adversely affecting the mechanical properties and dimensional stability of composites.
- Low microbial resistance and susceptibility to degradation. This restricts the successful exploitation of plant fibers for durable composite applications, posing serious problems during shipping, storage, and composite processing.
- Nonuniformity in dimensions and mechanical properties. This may be true even for individual plants within the same cultivation.

Table 16.1 shows the chemical composition and mechanical properties of different plant fiber reinforcements traditionally used to produce PLA-based composites.

Fibers from natural resources such as kenaf [36], rayon [37], hemp [38], and bamboo [39] have been incorporated in the PLA matrix to realize superior mechanical performance including improved heat resistance, tensile, and impact strength. For example, the incorporation of bamboo fibers (extracted either by steam explosion or alkali treatment of raw bamboo) in PLA improved its overall performance [39]. Higher bending strength of composite was obtained when steam-exploded filaments were used. The impact strength also improved with increasing fiber length. In other studies, hemp [40] or jute [31] micro-braided yarns were used to fabricate continuous fiber-reinforced composites having superior toughness. Wood FR-PLA composites have also demonstrated improvement in both flexural strength and flexural modulus. With 40% fiber volume fraction, a flexural strength of 115 MPa and 200% increase in flexural modulus was obtained [34]. Similarly, wood FR-PLA composites fabricated using the fused deposition modelling (FDM)-based 3D printing exhibited 15 and 24% increase in compressive strength and internal bond strength, respectively. The group also reported that the extrusion temperature during 3D printing had a substantial impact on the surface color, density, and mechanical properties of the resulting composites [41].

***16.3.1.2 Animal Fiber Reinforcements*** Although plant fiber-based reinforcements have been frequently utilized and studied, little effort has been invested toward studying animal FR-PLA composites [43]. Nevertheless, chicken feathers, silk, and wool are some examples of source materials from which high-quality animal-based fibers may be obtained [44, 45]. Keratin fibers obtained from chicken feathers (CFF) have been used to reinforce the PLA matrix to achieve fully biodegradable composites [44, 46]. CFF have several distinctive features such as high aspect ratio, surface toughness, flexibility, hydrophobicity, and a highly organized morphology characterized by a complex hierarchical structure. Incorporation of CFF in PLA at various loadings has resulted in improvement of both mechanical performance (viz. compressive strength, Young's modulus, flexural modulus, and hardness) and thermal stability of the composites in comparison to neat PLA [43, 47, 48]. Ayutthaya et al. prepared keratin nanofibers from CFF. These were used to prepare keratin/PLA composites having high surface activity toward fabrication of efficient biosensors and filtration devices [49].

**TABLE 16.1 Chemical Composition and Mechanical Properties of Different Plant Fiber Reinforcements [23, 42]**

| | Chemical Composition (wt%) | | | | | Mechanical Properties | | | |
|---|---|---|---|---|---|---|---|---|---|
| Fiber Type | α-Cellulose | Hemi-cellulose | Lignin | Pectin | Waxes | Density (g/cm$^3$) | Young's Modulus (GPa) | Tensile Strength (MPa) | Elongation at Break (%) |
| Flax | 71 | 18–21 | 2.2 | 2.3 | 1.7 | 1.54 | 27.5–85 | 345–2000 | 1–4 |
| Jute | 60–72 | 14–20 | 12–13 | – | 0.5 | 1.44 | 10–30 | 393–773 | 1.5–1.8 |
| Hemp | 68 | 15 | 10 | 1 | 0.8 | 1.47 | 17–70 | 368–800 | 1.6 |
| Sisal | 65 | 12 | 10 | 10 | 2 | 1.4–1.5 | 9–22 | 350–700 | 2–7 |
| Ramie | 68–77 | 13–16 | ~0.7 | 1.9 | ~0.4 | 1.5–1.6 | 27–128 | 400–1000 | 1.2–3.8 |
| Kenaf | 45–57 | 21.5 | 8–13 | 3–5 | – | 1.2 | 14–53 | 240–930 | 1.6 |
| Cotton | ~83 | ~6 | – | – | – | 1.5–1.6 | 5.5–12.6 | 287–597 | 7–8 |

Silk fibers are among the most extensible continuous fibers, with their tensile strength being among the highest for natural fibers [50]. Furthermore, favorable bonding of silk fibers with the polymer matrix makes it a promising candidate for reinforcing PLA scaffolds for tissue engineering applications. Cheung et al. [51] studied thermal as well as mechanical behavior of silk FR-PLA composite scaffolds. The group concluded that optimized fiber length and weight fraction (5 mm and 5% w/w, respectively) were crucial toward improving the mechanical properties of composites like micro-hardness, elasticity, and ductility. Ho et al. [52] demonstrated a reduction in crystallization temperature and crystallization enthalpy, along with an enhancement in storage modulus upon the incorporation of silk in PLA. In another application, silk fibroin/gelatin/PLA-based porous composite scaffolds were developed for cartilage tissue engineering. These composite cartilages exhibit good biocompatibility and long-term in vivo stability, crucial for effective rehabilitation of damaged tissue [53].

### 16.3.2 Synthetic Fiber Reinforcement

Synthetic fibers are frequently used as reinforcements in polymer matrices to produce high-performance composites. Because of their tunability and superior mechanical/thermal performance, synthetic fibers are often preferred to natural fibers in a PLA matrix [54, 55]. Synthetic fibers such as glass fiber (GF), carbon fiber (CF), aramid fiber, and basalt fiber have been explored with PLA matrix. GF-reinforced composites, for example, have the favorable characteristics of high strength to weight ratio; relatively low cost; ease of fabrication; good electrical insulation; good dimensional stability in addition to good resistance to moisture, heat, and corrosion. Silica glass fibers are among the most popular synthetic fiber reinforcements that are used in PLA composites [56]. However, machining glass FR-PLA composites is relatively challenging and results in reduced tool-life when fabricating using conventional machining processes [57]. In a study by Akindoyo et al. [58] incorporation of 10% (w/w) GF in PLA resulted in the improvement of mechanical strength and modulus of the composite, but reduced the degree of crystallinity of PLA. In a subsequent study, however, Wang et al. [59] reported enhanced tensile strength, flexural modulus, and impact strength (by 162.5, 266.4 and 232.5% respectively) at 20% (w/w) filler loading. Additionally, the optimized processing enhanced crystallinity of the PLA composite, thereby improving the heat deflection temperature (HDT) from 50.6 to 148.8°C.

GF based on borate and phosphate are also popular reinforcements for PLA owing to their outstanding mechanical properties; good heat resistance; low cost; superior bioactivity; and biodegradability, thereby making them suitable for use in biomedical and green packaging applications [60–62]. Felfel et al. [63] investigated iron-doped phosphate GF reinforcement in PLA matrix. At 18% (w/w) loading, these composites demonstrated superior flexural strength and modulus values (115 MPa and 9 GPa, respectively). Another study on phosphate-based GF reported that the incorporation of $B_2O_3$ (5–10%) in glass composition resulted in the improvement of the fiber's mechanical properties. The incorporation of these fillers in a PLA matrix not only improved degradation characteristics in vitro but also enhanced cellular viability [64].

To further improve the performance of the PLA matrix, CF reinforced PLA (CFR-PLA) composites have been studied for potential applications in the automotive and biomedical industries [65, 66]. For example, PLA-based composites reinforced with randomly oriented, chopped CF having superior mechanical properties were used to produce partially degradable bone plates [67]. These composites, however, were not sufficient for use in high-load situations. Long CF angle-ply composite laminates were therefore investigated. Composite micromechanical analysis was used in determining the optimum fiber layup for the long CFR-PLA composite plates. Although improved mechanical performance was achieved with a 0/45° laminate layup, hydrolytic degradation properties were found to be insufficient to prevent delamination in aqueous environments [66]. Alternatively, incorporation of a small amount of soft poly(ether)-urethane into the matrix proved effective in toughening the CFR-PLA composite [54]. Their results confirmed significantly improved impact strength, accompanied by an increase in yield strength and Young's modulus (46% and 235%, respectively). A relatively new technique involves fabricating complex shapes via 3D printing (3DP) of short CFR-PLA filaments [68]. Computed tomography (CT) of these composites revealed a high degree of fiber alignment in the print direction. Hu et al. [69] investigated 3DP of continuous CFR-PLA composites using a coaxial extrusion mold. The group concluded that low layer thickness and low printing speed resulted in maximum flexural strength and modulus values (610 MPa and 40 GPa, respectively).

### 16.3.3 Organic Filler Reinforcement

Organic fillers have the benefit of being inherently biodegradable. Among the naturally occurring organic fillers that have been used with a PLA matrix, the most important ones are cellulose [70], wood flour [71, 72], starch [73], rice hulls [74], sugar beet pulp (SBP) [75, 76], and oilseed crops [77].

***16.3.3.1 Wood-Based Filler*** Wood fiber (WF)-based reinforcement aids in the reduction of material costs in addition to providing specific properties, such as high biodegradability, high specific stiffness, and low density [78]. While wood-dust-filled PLA composites have traditionally been prepared by melt compounding and injection molding [71], recently they have also been prepared using

3DP techniques [41]. It has been reported that PLA composites reinforced with maple hardwood fiber produced by a combination of melt blending and injection molding exhibited improved tensile and flexural modulus of 2.5 GPa and 8.22 GPa, respectively (at 50% w/w loading) [79]. Elsewhere, Madyan et al. reported that sieved wood FR-PLA composite exhibited five times higher tensile and flexural strength (~15 MPa and ~13 MPa, respectively), compared with unsieved wood FR-PLA samples [80]. The reinforcement effect of raw WF on PLA-matrix, however, is limited owing to its hydrophilicity [81]. This issue may be addressed by the use of fiber surface modifications such as silanization to improve the interfacial adhesion between the matrix and filler [71].

Several recent studies investigated the mechanical behavior of 3DP wood FR-PLA composites [82]. For example, Le Duigou et al. reported that filament extrusion aids in aligning the fibers in the axial direction of the extrudate, positively affecting both the water intake capacity and tensile properties of the composite [83]. In fact, commercial WF-filled PLA filaments for 3DP are widely available, targeting products for both aesthetic and functional use [84].

Microcrystalline cellulose (MCC) (particle size 10–15 μm) is crystalline cellulose that is derived from acid hydrolysis of wood pulp. MCC has been used as a whisker reinforcement in a PLA matrix [85, 86]. These composites, however, possess poor or no adhesion with the PLA-matrix. As such, it was hypothesized that the full potential of MCC can be achieved after separation of the fillers into nanowhiskers [86]. PLA-based composites based on these nanowhiskers are described in Section 16.4.

***16.3.3.2 Starch*** Starch is an abundant biodegradable polymer that has been incorporated in PLA to prepare composites primarily targeting single-use, short-term applications [2, 5, 19]. Apart from reducing costs, starch can act as a nucleating agent for PLA. Starch, however, being hydrophilic in nature lacks compatibility with PLA. Moreover starch-based PLA composite are susceptible to water damage [73]. Techniques such as use of a maleic anhydride grafting system, or addition of compatible polymers (viz. polyvinyl alcohol (PVA), and polycapralactone (PCL)) have been adopted to compatibilize starch with PLA. Moreover, blending PLA with PCL and/or PVA also improves the water endurance of starch-PLA composites [87–89].

Previous work on starch-PLA composites showed that starch can be effectively used to augment the biodegradability of the PLA-based composite [90, 91]. Móczó et al. [92] investigated the reinforcing effect of starch in a PLA matrix using a compression molding method by incorporating glycerol as a plasticizer. Their results showed enhanced stiffness and strength of the composite. In the presence of a plasticizer, starch granules are swollen and gelatinized, which ensures some degree of compatibility between PLA and the starch polymer [19]. Olaiya et al. [93] studied the combined effect of starch and chitin particles on PLA. The PLA–chitin–starch composite revealed significant improvement in filler dispersion and mechanical properties in comparison to binary blends of PLA–chitin and PLA–starch. However, the effect of chitin addition on the dynamic mechanical properties of the composite was more pronounced than that of starch.

***16.3.3.3 Agricultural Waste-Based Filler*** Toward utilization of agricultural waste, research interest has been on the rise to develop composites based on such materials. One key candidate among these is cellulosic rice straw (RS) owing to its abundant availability [94]. The carbohydrate components of RS are similar to other reinforcing natural fibers, primarily consisting of lignin, cellulose, and hemicellulose. The presence of high silica content (up to 20% w/w) and resistance to bacterial decomposition endow RS with considerable potential as a reinforcing filler [95]. Zhu et al. [96] investigated the reinforcing effect of attapulgite (ATP) nanorod-modified RS (MRS) on PLA. MRS/PLA composites with 2 wt% ATP concentration exhibited tensile strength improvement of 18.6% compared with RS/PLA composites. In another study, rice husk powder (RHP) treated with maleic anhydride polypropylene (MAPP) and maleic anhydride polyethylene (MAPE) coupling agents was used as a reinforcing filler in a PLA-matrix. Their results established that MAPP-treated RHP/PLA composite demonstrated the highest tensile and flexural strength at all filler loadings [97].

Chrysanthemum filler-based PLA composites have also been explored by Chun et al. [98] to produce biodegradable PLA composites exhibiting improved elongation at break and tensile strength in comparison to pristine PLA. Agricultural waste from the oil industry can also be utilized for fabrication of environmentally friendly composites. The use of ground oil-cake (postproduction waste from oil industries) is mainly limited to the preparation of animal feed. As such, oilseed crops like cuphea, lesquerella, and milkweed have been used as natural source of fillers for PLA resin [77]. Barczewsk et al. [99] investigated the plasticization effect of a low-cost linseed cake (LC) filler on the PLA matrix. Their results showed improved rheological properties of PLA–LC composites, which in turn had potential applicability in the production of extruded or injection molded parts.

### 16.3.4 Inorganic Filler Reinforcement

Similar to organic fillers, PLA composites of inorganic fillers such as talc, calcium phosphate, hydroxyapatite (HA), and metal hydroxides have attracted considerable research interest. Yu et al. [100] found that talc ($Mg_3Si_4O_{10}(OH)_2$) can considerably enhance the crystallinity of PLA. Similarly, Shakoor et al. [101] developed talc-PLA composite with enhanced Young's modulus, tensile strength, and crystallinity,

due to the nucleating effect of talc. Carbonaceous fillers, viz. graphene, carbon nanotubes (CNT), and carbon black (CB), have also been used as conductive inorganic fillers for the preparation of biodegradable PLA nanocomposites [102–104]. Furthermore, Li et al. [102] reported that appropriate dispersion techniques and aspect ratio of the graphene content played a significant role in improving mechanical performance.

Another category of inorganic fillers is bio-ceramics. They possess good bioactive properties and can induce strong bonding between the defective bone sites and the implanted composite material, along with improved mechanical performance and biodegradation profiles [105, 106]. Due to their bio-resorbability, PLA/HA composites have attracted considerable attention for tissue engineering [107]. Such composites could be tailored for use in load-bearing biomedical applications as well [108]. However, interfacial adhesion between the PLA matrix and HA particles is a key challenge in such composites. According to Senatov et al. [109], the lack of interfacial adhesion between PLA and pristine HA deteriorates the crack resistance properties of the composite during cyclic loading. Additionally, high loading of HA filler in bone composite scaffolds is critical for enhancing bioactivity and osteointegration [105]. Corcione et al. [110] developed porous HA/PLA composite scaffolds with up to 50% (w/w) HA loading for bone tissue engineering (BTE), using low-cost FDM-based 3DP to biomimic the microstructure of native bone. Figure 16.1 shows a typical 3DP PLA/HA bone scaffold. It has been demonstrated in numerous studies that the lattice shape of such scaffolds greatly affects the overall scaffold performance. As such, 3DP scaffolds require optimization of not only material parameters, but the scaffold design as well [111]. Typical inorganic fillers for PLA composites in biomedical applications include mineral salts such as calcium carbonate, calcium phosphate, calcium sulfate, and so on [112, 113].

Other types of inorganic fillers for PLA include metal hydroxides, clay, mica, etc., which can be used for tuning its mechanical behavior, biodegradability, thermal behavior including flame retardancy [114–116], etc., targeting a plethora of applications.

### 16.3.5 Laminated/Structural Composites

Over the years, a majority of PLA bonded laminated composites have primarily included bamboo fabric, kenaf, wooden laminate plies, gelatin, PVA films, etc. [36, 117–121] for synthesizing fully biodegradable products. Some laminated composites, however, have also included carbon-fiber-based reinforcements to achieve higher performance [122, 123]. Further improvement in performance may be realized by improving the compatibility of fibers with the matrix through surface treatment of fibers with coupling agents such as 3-aminopropyltriethoxysilane [36]. A variety of other techniques for surface modification of reinforcements and PLA composites will be discussed in subsequent sections.

PLA-based biodegradable laminated composites have been applied in various applications. For example, PLA-bonded composites (comprised of 0° and ±45° laminae layups), reinforced either with physiologically inert carbon fiber or with in vivo degradable calcium phosphate glass fibers, were used to prepare bone fixation plates [123]. Elsewhere, structural products such as laminated panels reinforced with wood veneer (pine, spruce, or birch) [117] were developed by hot-pressing amorphous PLA at 140°C.

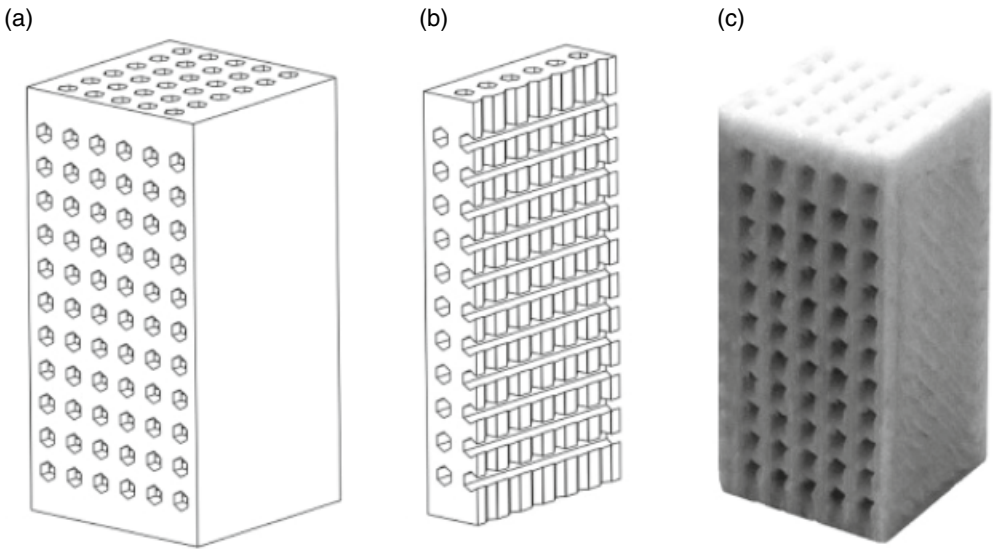


**FIGURE 16.1** (a) Computer model, (b) cut-section of computer model, and (c) 3D-printed PLA/HA scaffold [109].

These composites exhibited a tensile strength of 8.7 MPa along with appreciable bond line strength and could adequately withstand water immersion. Similarly, bamboo reinforcement in PLA either as woven fabrics [118] or as strips [119] has been reported for engineering structural applications. Morales et al. demonstrated that cost-effective composite panels could be developed using PLA-bonded bamboo laminates [119]. In fact, these laminates had overall mechanical behavior similar to that of E-glass/epoxy laminates.

Laminated PLA-based films have also been developed for food packaging applications. For example, Cho et al. reported laminated films of glycerol-plasticized wheat gluten supported by PLA to improve oxygen and moisture barrier properties [121]. Elsewhere, PVA-bonded PLA films were compatibilized by incorporating hydrophobized cellulose fibrils in the PVA phase [120], resulting in improved tensile strength, 20% reduction in moisture absorption and diffusion rate, and up to 40% improvement in peel strength compared to unfilled samples. Moreover, PLA-based laminated composites are now commercially available as disposable, biodegradable food containers, and packaging films [124–126]. Such products are often comprised of molded pulp laminated with PLA as a waterproofing layer. These products aim to reduce the $CO_2$ footprint through reduced processing temperature as compared with traditional plastics and through the prospect of $CO_2$ sequestration following PLA's degradation and absorption in the soil. In other research, low-density PLA foam sheets were laminated with PLA sheets having high HDT as an effective alternative to polystyrene (PS) foams in hot fill packaging applications [127].

A few studies have also been reported on the use of PLA-based laminated composites as functional materials. Liu et al. reported CNT- and PLA-based braided, angle-ply laminated composites having thermal shape memory for use as smart actuators. These composites exhibited high recovery force and a critical temperature (for shape recovery) around 60°C [128]. In yet another interesting report, the piezoelectric behavior of PLLA has been harvested for use as nanogenerator in wearable electronics [129]. Herein, meso-PLA electret-based triboelectric nanogenerator having triangular waveform was sandwiched between double-layered (PLA and PLLA) piezoelectric nanogenerators (as shown in Figure 16.2), resulting in a remarkable 0.31 mW power output at 70 V and 25 μA current at the resonance frequency of 19.7 Hz from the developed cantilever shape.

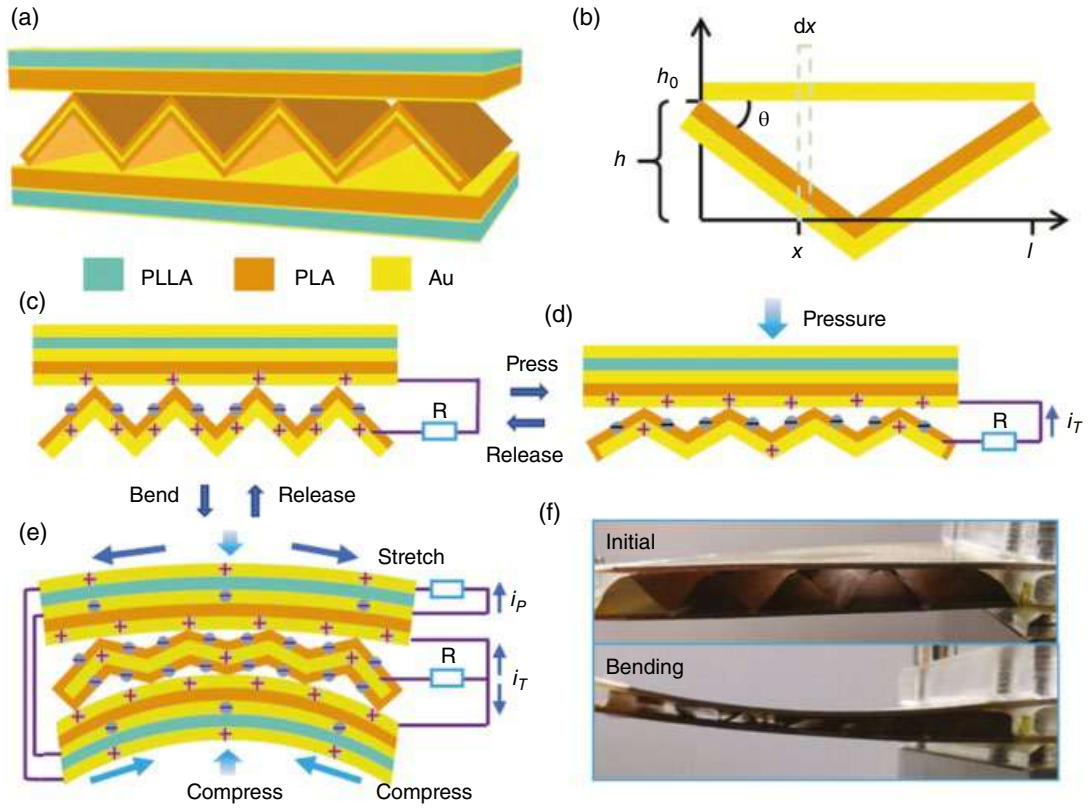


**FIGURE 16.2** Schematic diagram of hybrid nanogenerator (NG): (a) Schematic of hybrid NG. (b) Enlarged schematic of triboelectric NG device having triangle waveform. (c) Schematic diagram representing charge distribution in hybrid NG at initial state, (d) compression mode, and (e) bending mode. (f) Photographs of the initial and bending state of the hybrid NG [129].

## 16.4 NANOCOMPOSITES

Over the years, polymer nanocomposites have attracted increased attention, where nanotechnology is applied to produce materials with remarkable improvements in properties and performance. The most popular approach to produce this new family of composite materials is to introduce nanoscale particles into a polymer matrix to produce polymer/nanoparticle composites. Nanocomposites are often classified based on the type of nanofillers such as carbonaceous nanoparticles (viz. graphene, carbon nanotubes etc.), organic nanofillers (including bio-based fillers derived from cellulose, chitin, etc.), inorganic nanomaterials (including layered silicates, titanates, ceramic nanoparticles, etc.), and finally as metallic nanoparticles of gold, silver, platinum, etc. [115, 130, 131] Recently, a variety of PLA nanocomposites comprising of hybrid nanofillers [132, 133] with greater tunability in material properties have also been reported. Owing to the superior properties of nanomaterials and their immense potential for use as nanofillers, PLA-based nanocomposites have garnered considerable research attention during the last two decades. Figure 16.3 shows a summary of research articles published on PLA-based nanocomposites, demonstrating a clear increase in research interest in this domain. The current section aims to introduce the methods by which PLA-based nanocomposites are being developed for various applications. A more detailed discussion of the specific applications may be found in subsequent sections of the chapter. Moreover, Chapter 17 deals extensively with the production and properties of PLA nanocomposites.

Among organic fillers, bio-based nanofillers, viz. nanocellulose and its derivatives [134, 135], nano-chitin [136], nano-lignin [137], are often incorporated in a PLA matrix toward the development of "green-nanocomposites." Such bio-nanocomposites are not only being developed for biomedical applications [133], but also as high-performance products for a variety of industrial applications such as electronic sensors, displays, automotive products, and textiles [138–141]. Among these nano-reinforcements, cellulosic nanofibers or cellulose nano-whiskers (CNWs) are promising for enhancing the mechanical performance of the PLA matrix [142]. As such, CNWs have generated considerable research interest in recent years.

Although, lower loading of CNW resulted in marginal improvement in mechanical behavior [143, 144], studies incorporating 5% (w/w) CNW in PLA have reported 5- and 22-fold increase in tensile strength and Young's modulus, respectively [145]. Moreover, the addition of hydrophilic CNWs improved the degree of crystallinity from 6% (for pristine PLA nanofibers) to 14.1% and 21.6% for PLA/5CNWs and PLA/10CNWs composite nanofibers, respectively, indicating its potential in tissue engineering and membrane filtration applications [142]. Furthermore, many studies investigated metallic nanoparticles, such as Ag, Pt, Au, Sr, and Zn, for their effect in enhancing the conductive, catalytic, antimicrobial, and bioactive behavior of PLA-matrix [146–151].

Nanosilicates are one of the most commonly used inorganic nanoparticle reinforcements for polymer nanocomposites. Different types of modified montmorillonite clays, such as Cloisite® 20A, Cloisite 30B, and Cloisite $Na^+$,

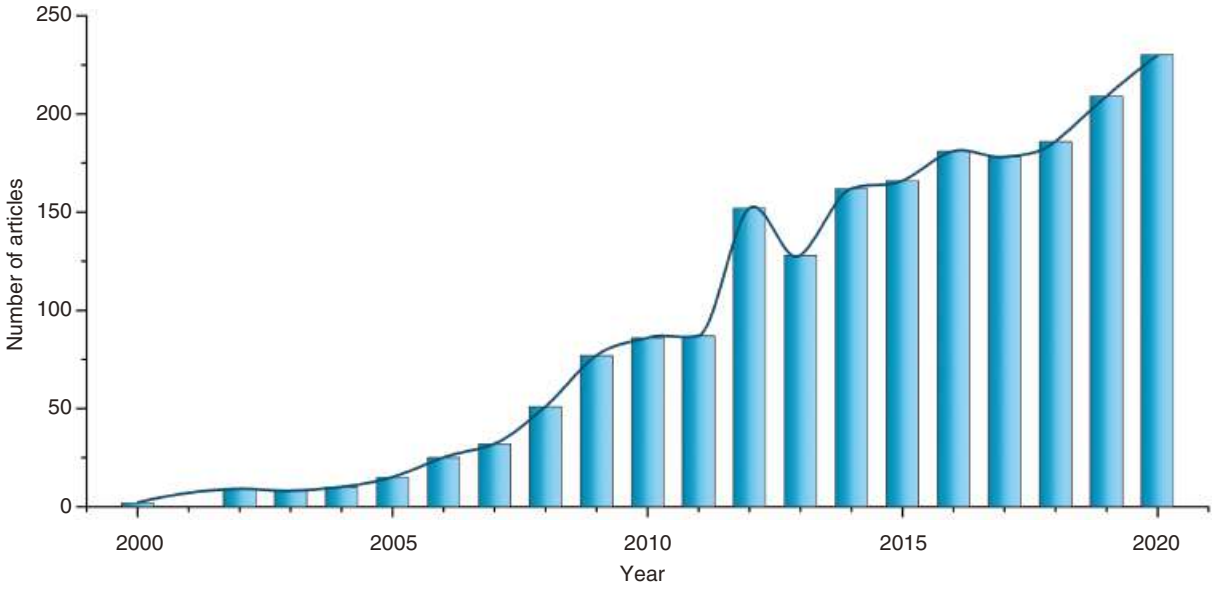


**FIGURE 16.3** Number of research articles published on PLA-based nanocomposites, as obtained from Scopus database with the following keywords: "poly lactic acid nanocomposite," "PLA nanocomposite," "poly lactic acid nano-composite," or "PLA nano-composite" from 2000 to 2020.

have been used for PLA-based composite films [114, 115]. The crystallization behavior of PLA/clay nanocomposites indicated that the nanoparticles can act as nucleating agents for PLA crystallization. The degree of clay miscibility with the matrix and the clay dispersion state in the PLA matrix both significantly influence the crystallization behavior and final morphology of the nanocomposites. Various approaches have been successfully developed to fabricate PLA/clay nanocomposites, namely, in situ polymerization intercalation, melt intercalation, solution intercalation, solution casting techniques, etc. [115] The inclusion of well-dispersed nanosilicates in polymers has led to substantial modification in properties, including increased storage modulus, HDT, gas barrier, tensile and flexural properties, along with reduced flammability. X-ray diffraction studies have revealed that good affinity between the organo-modified clay and the PLA matrix exists in an intercalated nanocomposite. The rate of biodegradation of neat PLA can also increase significantly after nanocomposite preparation [152]. Owing to the potential for significant property improvement, many studies have been directed toward the development of PLA nanocomposites exploiting the benefits of biodegradable PLA and nanolayered silicates [153–162]. Alternatively, various metallic oxide nanoparticles have been explored for modifying the flame retardancy, thermal, electronic properties, etc., of the base material [14, 133, 163]. Yet another key application of such inorganic materials is in the biomedical industry [164]. Herein, bioactive nanoparticles such as hydroxyapatite (HA) [165, 166], tricalcium phosphate (TCP) [167], and bio-glass [168], have been demonstrated to be efficient in improving tissue regeneration capability of PLA-based scaffolds.

Additionally, carbon-based nanoparticles (such as graphene, CNT, and their functionalized derivatives), owing to their facile synthesis, extreme strength, thermal stability, and electrical conductivity, have been a popular choice for inclusion in PLA matrix [104, 130, 169–176]. CNTs exhibit unique physical and mechanical properties, which has led to a significant amount of research in effectively utilizing them as reinforcements in polymer composites. For example, multiwalled carbon nanotubes (MWCNTs) have an outside diameter of 10–20 nm, and length of 10–30 mm, resulting in a specific surface area greater than 200 $m^2$/g, with tensile strength exceeding 60 GPa [177]. Both surface compatibilization and dispersion of MWCNTs are crucial for translating these properties in the nanocomposites. PLA nanocomposites containing various functionalized MWCNTs have been prepared by solution casting, melt compounding [172], or extrusion through a twin-screw extruder [173–175] (with a high shear rate configuration) followed by injection molding.

While efficient nanofiller dispersion has been a key concern for most nanocomposites, a modern trend has been toward designing the micro/nanostructure of composites in an attempt to tailor their overall mechanical behavior. Recently, a hierarchical structure called "hybrid sheesh kebab" was developed by employing customized ZnO whiskers and intensive shear flow. It is comprised of a central nano-whisker, flow-induced row-nuclei closely wrapping the whisker, a thin layer of periodically arranged primary kebabs, and a thicker transcrystalline layer of secondary kebabs. The result is a nearly 2.5-fold improvement in impact toughness (11.5 kJ/$m^2$), and doubling of the tensile strength (119.4 MPa), along with substantially enhanced HDT, and almost perfect UV light shielding efficiency [178].

In other studies, PLA-based nanocomposites were designed to bio-mimic the "staggered" arrangement seen in natural composites, such as nacre. These materials are comprised of a compliant polymeric phase and a stiff inorganic phase, arranged in a "staggered" manner similar to that of brick and mortar, thereby endowing the composite with superior fracture toughness through its efficient crack deflection, and fracture energy dissipation mechanisms. Narducci et al. reported PLA-based tough composites comprised of carbon fiber micropatterned in a staggered manner [180]. Elsewhere, a similar arrangement was realized using amorphous lamellae of alumina as the hard, and PLA as the soft phase (as seen in Figure 16.4) to prepare optically transparent nanocomposites having an extraordinary toughness of 103 MJ/$m^3$ and elongation at break of 500% [179].

## 16.5 SURFACE MODIFICATION

The fiber/matrix interfacial compatibilization during the production of reinforced composites can significantly influence the composite properties. Enhancement of mechanical performance in multicomponent systems is often ascribed to strong interfacial adhesion between the different phases. Therefore, a proper strategy to achieve improved interfacial adhesion is necessary to obtain satisfactory performance of the composites. In other instances, surface modification of the composites, such as chemical coating, and selective etching may also be done toward tuning their properties, such as surface activity, electrochemical response, and bioactivity.

### 16.5.1 Filler Surface Modification

Several studies optimized the properties of natural FR-PLA composites through enhancing fiber–matrix adhesion. Pretreatment of fibers, such as chemical modification, is a promising approach to form covalent bonds between the fiber and the matrix. One of the most common and efficient methods is alkali treatment (e.g., 2% NaOH aqueous solution) of fibers with successful results [9, 36, 38, 181]. Other pretreatment techniques such as surface esterification and cyanoethylation [182] have also been used for improving interfacial adhesion in natural fiber PLA composites by introducing functional groups on the fibers. For example,

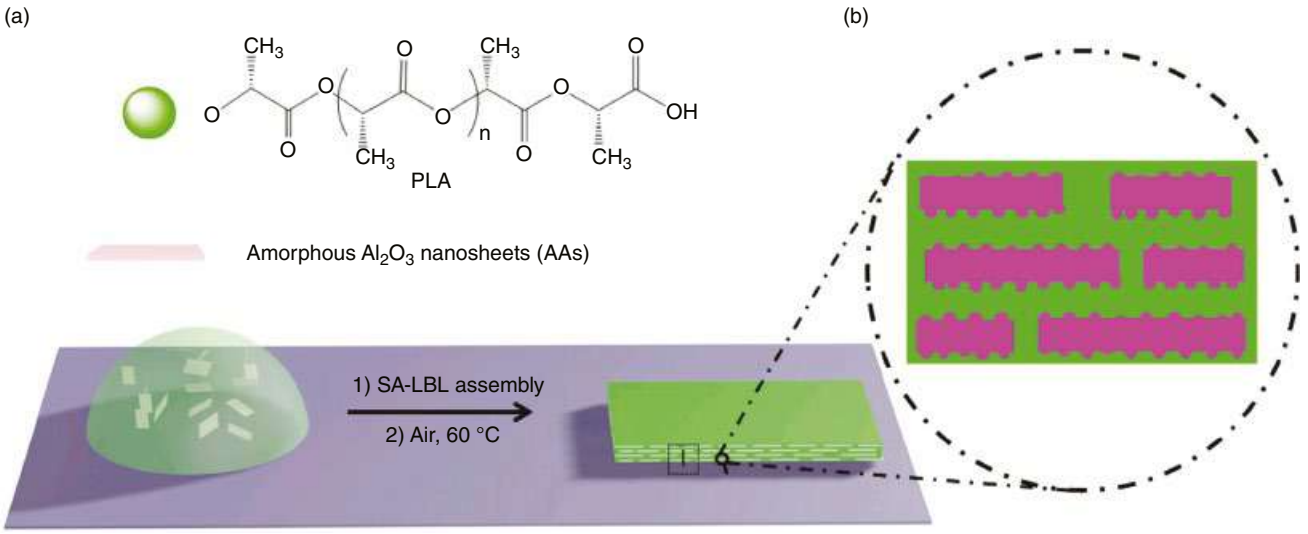


**FIGURE 16.4** (a) Schematic illustration of the fabrication of nacre inspired nanocomposite through controlled assembly of amorphous alumina nanosheets and PLA. (b) Magnified view of bricks-and-mortar layered structure unit [179].

improvement in flexural modulus has been possible when alkali-treated abaca fibers were used as reinforcement with PLA resin [182]. A further improvement in flexural modulus was possible when the same fibers were esterified [182].

In other instances of filler surface modification, amine functionalization of microcrystalline cellulose (MCC) was done to modify its rheological behavior. Furthermore, incorporation of surface modified MCC in the PLA matrix resulted in improved hydrophilicity and tensile strength of the composite [183]. In another study, nanofillers such as graphene oxides (GOs) were used as templates for the growth of highly crystalline hydroxyapatite (HA) nanorods [166]. HA surface modification improved exfoliation of GO sheets along with imparting bioactivity to the HA-GO/PLA composite, resulting in improved cell viability and an eightfold increase in mechanical toughness. As discussed in the previous section [120], interfacial interaction between PLA and PVA laminates was improved by incorporating hydrophobized cellulose fibrils.

### 16.5.2 Compatibilizing Agent

Another way to ensure appropriate adhesion between the reinforcements and PLA matrix is the use of coupling agents. Coupling agents are often used with glass fibers or coated fillers to enhance their interfacial adhesion with the matrix polymer [184]. Maleated compounds and silanes are generally used as coupling agents. In most cases, coupling agents improve the degree of cross-linking in the interface region and offer a suitable bonding result. Interactions between the anhydride groups of maleated coupling agents and the hydroxyl groups of natural fibers can overcome incompatibility problems between the fiber and the matrix. Silane coupling agents such as 3-aminopropyltriethoxysilane (APS) undergo hydrolysis in a solvent (viz. water) to produce silanol, which then reacts with the ─OH group of the natural fibers, forming stable covalent bonds with the fiber surface [185]. The amine groups from APS-modified fibers can in-turn bond with COO─ sites on the hydrolyzed PLA backbone. Sometimes, a combination of both alkali and silane treatments is used to obtain the desired performance. For example, silane- and alkali-treated kenaf fibers were used to reinforce PLA. These composites were fabricated using a film stacking method, which resulted in enhanced mechanical properties of treated composite specimens compared to untreated specimens [36]. Another study reported treatment of pineapple leaf fiber with maleated anhydride polyethylene (MAPE) as a compatibilizing agent. The study concluded that although the tensile strength was reduced with MAPE treatment, the composites exhibited an overall improvement in flexural and impact behavior [186]. In another study, ramie fiber was treated with maleic anhydride (MA) using benzoyl peroxide (as an initiator for MA and PLA) in the fabrication of ramie fiber-reinforced PLA composite. The microstructural results indicated that addition of PLA-*g*-MA (3% w/w) provided better adhesion between the ramie fiber and PLA matrix, thereby resulting in improved tensile, flexural, and impact strength (64.30 MPa, 112.4 MPa and 7.1 kJ/m$^2$ respectively) [187]. In a separate study, it was reported that incorporation of compatibilized micro/nanofiller within the PLA-matrix can be highly effective in toughening the composites owing to efficient transfer and dissipation of fracture energy [141]. Accordingly, He et al. reported tough PLA/poly(butylene succinate) blends reinforced with epoxy-functionalized

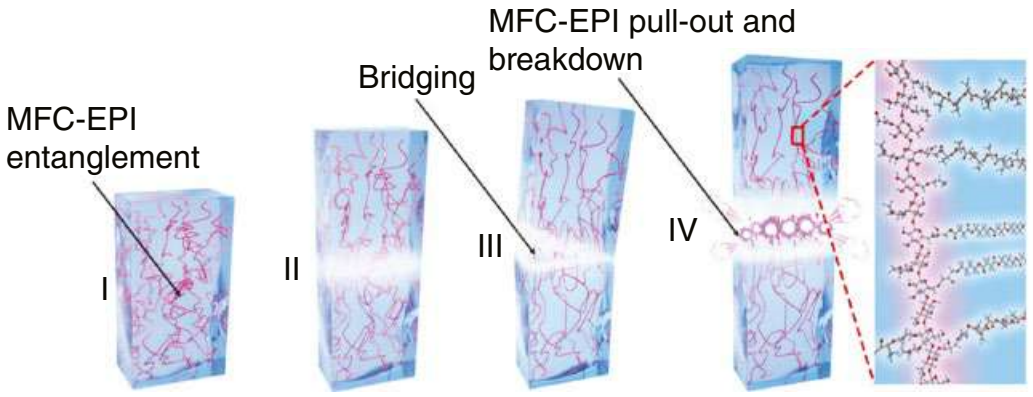


**FIGURE 16.5** Schematic illustration representing mechanism for fracture toughening in PLA matrix reinforced with functionalized cellulose microfibrils (10 wt%) [140].

cellulose microfibrils (as seen in Figure 16.5) [140]. These reinforcements formed microbridges during mode I fracture deformation, thereby impeding the rate of crack growth. Owing to high interfacial interaction between the filler and the matrix, these composites exhibited tensile strength of up to 71.4 MPa and 273% elongation at failure, accompanied by fivefold improvement in impact toughness. Occasionally, an adhesion promoter may also be used to increase the interfacial interactions between the fiber and the matrix. For example, lignin was used as an adhesion promoter in cotton FR-PLA composites, resulting in improved modulus and tensile strength (approximately 25 and 10% improvement, respectively) but decreased impact properties [188].

### 16.5.3 Composite Surface Modification

As opposed to filler surface modification, the key motivation for modifying the surface of a composite is (i) modification of the surface's chemical nature, or (ii) increasing the surface energy (by altering porosity, surface roughness, etc.). Modern biomedical scaffolds are often surface-treated with a biomolecule to improve their behavior under physiological conditions. For example, surface modification of PLA-based composites with arginine-glycine-aspartic acid peptides (RGD) through plasma treatment or physical absorption was done [189, 190], resulting in improved cellular adhesion and proliferation. Other surface modifiers, such as nano-HA and hydrophilic biopolymers, have also been explored for improving bioactivity of the composite [191–196]. Such composites are summarized in Table 16.2. Moreover, surface activation becomes crucial for conductive composites in sensing applications to reduce the kinetic barrier through a variety of pretreatments such as chemical etching [197], laser etching [198], or ionic plasma treatment [149, 199]; such treatments are discussed in more detail in Section 16.8.4.

## 16.6 PROCESSING

Several laboratory processing techniques have been developed by researchers for processing of PLA composites. The studies have revealed two important considerations for a suitable processing technique: (i) the impact of processing on the reinforcement and (ii) the impact of processing on polymer degradation. With natural fiber composites, additional challenges during processing include: variation in raw material quality, poor compatibility of fiber and matrix, and the poor thermal stability of fibers. Additionally, differences in bulk density in natural fibers can lead to feeding problems and poor dispersion of fibers within the matrix.

### 16.6.1 Conventional Processing

With almost all traditional processing techniques, a compounded pelletized feed stock is produced that can then be further processed with various techniques, such as injection molding, extrusion, compression molding, film casting, foaming, and thermoforming. These processing techniques have successfully been used in producing PLA composites and the product qualities have been compared. Pultrusion is another manufacturing process wherein continuous lengths of reinforced polymer structural shapes can be produced with constant cross sections. The process involves pulling the raw materials (rather than pushing, as is the case in extrusion) through a heated steel forming die using a continuous pulling device. Long jute fiber-reinforced PLA composites have been prepared by a pultrusion process followed by injection molding that resulted in good impregnation of resin into the jute fiber bundles [203]. From the results of the long and short hemp fiber/PLA composites produced using different processing conditions, it was found that long fiber/PLA composite produced by film stacking produced the best results in terms of mechanical performance [38]. Table 16.3 describes some of the different techniques used in developing PLA composites.

**TABLE 16.2 Surface Modification of PLA-Based Composites**

| Coating | Physical Property Change | Results | Advantage |
|---|---|---|---|
| Calcium-phosphate-filled chitosan or gelatin hydrogel [194] | Significant contact angle increase | Chitosan aids in certain anti-infection property, gelatin is attractive for bone ingrowth | Simplicity, adaptability, and versatility |
| Polydopamine, nano-HA, ponericin G1, and gelatin [191] | Completely hydrophilic and stronger affinity for serum | Early increase in cell proliferation, improved calcium deposition, and antibacterial behavior | Exhibits long-term antibacterial activity |
| Collagen [192] | — | Excellent cellular adhesion 3D-printed PLA grafts | Improved cell adhesion can improve overall tissue ingrowth |
| Stromal-derived factor (SDF-1) and collagen [193] | — | Good biocompatibility and cellular growth, proliferation of endothelial cells, osteoblasts etc. | Supports osteogenesis and neo-vascularization |
| Nanofibrous forsterite-gelatin [195] | Increase in elastic modulus | Appreciable apatite layer formation upon immersion in SBF solution | Has hierarchical structure |
| Antibiotics loaded Poly(lactic-co-glycolic acid) [196] | — | Efficient regeneration of rabbit femur tissue | Effective treatment of critical-sized bone defect |
| Arginine-glycine-aspartic acid peptides [189, 190, 201, 202] | Increase in surface wettability | Increase in cellular proliferation and adhesion | General method for improving bone tissue regeneration capability of scaffold |

*Source*: Adapted from [200].

**TABLE 16.3 Processing Techniques Employed for Fabrication of PLA Composites**

| Composite | Composite Fabrication Technique | References |
|---|---|---|
| Flax fiber–PLA | Injection molding, film stacking | [204] |
| Hemp fiber–PLA | Compression molding, extrusion + injection molding, extrusion + compression molding | [38, 205] |
| Lyocell fabric–PLA | Compression molding | [205] |
| Rayon–PLA | Extrusion + injection molding | [37, 206] |
| Hemp fiber/lyocell fiber–PLA | Carding + compression molding | [205] |
| Nonwoven random glass mat–PLA | Film stacking | [207] |
| Glass fiber/PLA | Filament blending + supercritical gas foaming | [208] |
| Wood fiber–PLA | Kinetic mixing + injection molding | [209] |
| Abaca–PLA | Twin rotary mixing + injection molding | [182, 210] |
| MCC–PLA | Twin-screw extrusion + injection molding | [85] |
| Kenaf fiber–PLA | Compression molding | [36, 211, 212] |
| Cotton fiber–PLA | Carding + compression molding | [188] |
| Bioactive glass fiber–PLA | Injection molding | [213] |
| MWCNT–PLA | Film casting, twin-screw extrusion + injection molding, twin-screw extrusion + compression molding, melt compounding + compression molding | [172–175] |
| Nanoclay filler–PLA | Solvent casting + compression molding | [114, 115] |
| $CaCO_3$ filler–PLA | Twin-screw extrusion | [112] |
| $CaSO_4$ filler–PLA | Continuous kneading + compression molding | [204] |
| Oilseed filler–PLA | Twin-screw extrusion + injection molding | [77] |
| Carbonated hydroxyapatite-PLA | Emulsion/solvent evaporation (for microsphere preparation) + selective laser sintering (SLS) | [214] |
| Hydroxyapatite or nanoclay-PLA | Direct mixing of nanofiller and PLA + SLS | [215, 216] |
| GO-PLA + TPU | Solvent casting + Filament extrusion + FDM | [217] |
| GO-PLA + TPU | In situ active filament mixing + FDM | [218] |
| TPU nanofiber-PLA | Melt extrusion via eccentric rotor extruder | [219] |

### 16.6.2 3D Printing

Over the years, PLA-based bioplastics have been fabricated into desired products for various applications via traditional routes available to thermoplastic polymers discussed above. Adaptation of PLA and its composites to additive manufacturing or 3D printing (3DP) techniques has further invigorated this effort and enabled the fabrication of products for even more diverse applications [14]. It may be said that

while preparation of composites aids in tailoring the material properties of pure PLA, 3DP facilitates rapid customization of its geometrical features. In addition, 3DP enables fast prototyping along with freedom of design, through its ability to manufacture customizable and complex shapes while minimizing wastage.

Extrusion-based 3DP processes such as fused deposition modelling (FDM) are the most widely employed 3DP technologies for PLA, owing to its suitability for such processes. Moreover, PLA-based prints have reduced warpage owing to lower printing temperature than ABS [220, 221]. The 3DP of PLA composites has readily been adopted in the biomedical industry towards tissue engineering scaffolds, surgical models, patient-specific instruments, etc. [200, 222, 223] Varga et al. reported PLA-based 3D-printed wrist splints (Figure 16.6) reinforced with different loadings of $CaCO_3$ for added rigidity [224]. These splints were customized for individual patients, thereby allowing a better fit and hence were better in immobilizing the injured limb, besides being more comfortable than traditional ones. PLA-based 3DP scaffolds allow fabrication of shapes precisely customized for each patient, in addition to control over their microarchitecture. Recently, PLA-based bone tissue scaffolds filled with metallic particles, CNT, GNP, $Fe_2O_3$, etc.; having controlled microarchitecture along with appreciable bioactivity and controllable in vivo degradability were reported [225, 226]. Also, Chen et al. reported tough, deformable 3DP scaffolds comprised of a thermoplastic polyurethane (TPU) and PLA blend filled with GO [217], prepared through solvent casting followed by filament extrusion. Addition of TPU aided in the reduction of rigidity and brittleness of the scaffold, while GO acted as a conductive reinforcement. The scaffolds exhibited favorable cellular proliferation at 0.5% GO loading, establishing their potential in tissue regeneration. Moreover, Kennedy et al. reported in situ blending of TPU- and CNT-filled PLA as a means of simplifying the production process and allowing greater controllability of the blending parameters [218]. Another key application of 3DP of PLA composites has been in the development of electrochemical sensors for detection of a wide range of analytes, such as, heavy metals [199], explosive chemicals [227], biomolecules like glucose, uric acid, and serotonin [147, 223, 228, 229].

Apart from FDM, selective laser sintering (SLS) is another 3DP technique that has been employed for fabrication of PLA-based products. SLS, however, is relatively less favored owing to difficulty in synthesis of PLA powder with enough flowability and sphericity [223]. Not only are PLA-based sintered products difficult to fabricate, they also exhibit inferior mechanical properties (as opposed to traditional fabrication routes) arising from poor coalescence of the sintered PLA particles [215]. Nevertheless, SLS allows better resolution than FDM. Additionally, sintering of PLA can be tailored to maintain adequate surface roughness and porosity. As such, a few studies involving hydroxyapatite (HA)-filled PLA composites have been reported to exhibit promising potential for SLS-based scaffolds in bone tissue engineering applications [214, 216].

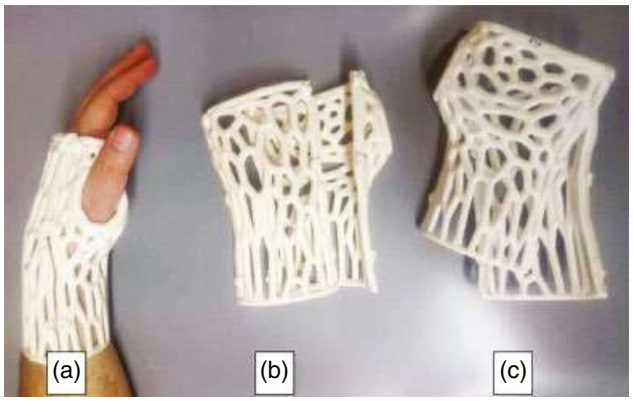


**FIGURE 16.6** 3D scanned and printed models of wrist splints of (a) gypsum PLA, i.e., high $CaCO_3$ loading, (b) Modell PLA, i.e., medium $CaCO_3$ loading, and (c) pristine PLA compositions [224].

## 16.7 PROPERTIES

### 16.7.1 Mechanical Properties

Mechanical performances of PLA-based composites are expressed by several factors such as nature and characteristics of reinforcements (including types, extraction method, volume fraction ratio, aspect ratio, surface treatment, fiber orientation etc.), filler loading, wettability, interfacial compatibility and bond strength, thermal stability, composite manufacturing process, filler dispersion and orientation, and crystallinity of the matrix.

#### *16.7.1.1 Static Mechanical Properties*

Natural fiber-reinforced PLA composites generally possess good stiffness and tensile characteristics. In general, tensile and flexural modulus results are improved by increasing the content of cellulose or cellulose-based reinforcements in PLA-based composites. In contrast, tensile and flexural strength remain practically unchanged or are worsened. This stems from the fact that tensile or flexural modulus is only measured at very small strain when simple physical contact of components is sufficient to transfer the stress, whereas tensile and flexural strength are very sensitive to the fiber/matrix interfacial adhesion and the interface plays a crucial role in transferring the stress from the matrix to the fibrous phase. Surface modification of fibers or compatibilizers are often used to ensure improved mechanical strengths of the composites. With hemp fiber composites, for example, 40% volume fraction of alkali-treated fibers showed the best mechanical properties considering tensile strength, Young's

modulus, and flexural strength, whereas the elongation and stress at break decreased with an increasing amount of fibers for all examined systems [38, 182]. Similarly, stiffness and tensile strength of PLA–rayon fiber composites (having 25% fiber weight fraction) manufactured by injection molding approximately doubled compared with the pure matrix [206]. For PLA–abaca fiber composites, although flexural modulus increased, flexural strength did not increase regardless of the fiber treatment [210]. Even the effect of the surface treatment of the abaca fiber on the flexural modulus of the composite was not very significant. The impact properties of PLA natural fiber composites are often worse than those of the pure matrix. For widespread application of natural fiber-reinforced composites, this fact is often the limiting factor. For example, with injection-molded flax fiber-reinforced PLA composite with a fiber mass content of 40%, although the stiffness was doubled, the impact strength was halved compared to pure PLA [37, 230]. Poor impact properties of bast fiber-reinforced PLA composites can be improved by admixing cellulose fibers with higher elongation at break values compared to bast fibers alone. Accordingly, tensile strength and impact strength could both be increased compared to hemp–PLA composites by using a mixture of hemp and lyocell fibers (25% improvement of tensile strength, 160% increase in Charpy impact strength) [205]. The Young's modulus was also slightly higher (4%) than that of the lyocell–PLA composite. Multilayered PLA–lyocell laminate composites showed considerably higher Izod impact strength than neat PLA. Impact strength could actually be more than tripled compared with the pure PLA matrix. However, compared to the pure PLA matrix, no improvement in impact strength was achieved by using kenaf fibers [231]. In some cases, kenaf–PLA composites had only about half the impact strength of the pure matrix [188]. When lignin powder was used as an adhesion promoter in cotton–PLA composites, tensile strength and Young's modulus were increased by 9 and 19%, respectively. However, the impact strength was decreased by 17% after addition of lignin powder, although it was still higher than that of the pure matrix. Presumably, the presence of lignin caused embrittlement of the composites, and it was concluded that impact strength was reduced by the embrittlement of the composites [188]. However, when recycled wood fiber (RWF) was used as a reinforcement for PLA matrix, the toughness of PLA decreased significantly [232]. This could be attributed to the facts that (i) RWF may act as stress concentrators in the composites; and (ii) RWF is rigid and brittle. Similar to the observed trend with toughness, the elongation at break also decreased with the addition of RWF, owing to the decreased deformability of PLA because of the restriction imparted by the rigid filler. However, the modulus of the PLA–RWF composites increased significantly when compared with pure PLA. The increase in modulus could be almost three- and fourfold with the addition of 10 and 20% RWF, respectively. This can be partially attributed to the much higher modulus exhibited by the RWFs compared with the PLA matrix. Glass fiber-reinforced PLA composites show both increased flexural strength and flexural modulus with increasing fiber content [207, 208]. Flexural strength reached 220 MPa, and flexural modulus was 14.3 GPa with bioactive glass–PLA composite [207].

The evaluation of the mechanical properties of PLA–MCC composites demonstrated that the tensile modulus was improved with increased MCC content, but tensile strength and elongation at break decreased [85]. Scanning electron microscopy (SEM) showed that the MCC remained as aggregates of crystalline cellulose fibrils, which explains the poor mechanical properties [85]. Furthermore, the fracture surfaces of MCC composites were indicative of poor adhesion between MCC and the PLA matrix.

Adding MWCNT to PLA enhanced the tensile strength of the nanocomposites. The composites after water cross-linking treatment exhibited better mechanical properties than the un-crosslinked composite because of strong chemical intramolecular bonding. The water cross-linking method involves a reaction with free radical initiators followed by condensation of water, leading to the cross-linking of the polymer matrix. Mechanical property tests showed that adding 1 phr (part per hundred) MWCNT improved the tensile strength of the nanocomposite by 13%. MWCNT dispersion in PLA was enhanced by covalent or hydrogen bonding between MWCNT and PLA. The flexural strengths of pristine PLA and 4 phr-modified MWCNT–PLA composites were 102.3 and 120.2 MPa, respectively (representing a difference of 17.5%) [173, 174]. Small- and wide-angle x-ray scattering measurements on solvent cast PLA–organoclay nanocomposite found that the silicate layers could not be individually well dispersed in the PLA–clay blend [114]. Although the tensile strength of PLA films decreased slightly after compounding with nanoclays, those of the composite films were still comparable to those of widely used plastic films such as high-density polyethylene (HDPE), polypropylene, and polystyrene (PS).

Surface-grafted HA–PLA composites show good mechanical properties, as modified HA particles are well dispersed in the PLA matrix, and the adhesion between modified HA particle and PLA matrix is improved after modification of HA particles. The tensile strength of *g*-HA/ composites increased with *g*-HA content and showed a maximum at 5–10 wt% *g*-HA addition [233, 234]. Thereafter, the tensile strength of *g*-HA/composites decreased as *g*-HA content increased further due to the strong tendency of HA to aggregate. Incorporation of nanosized $CaCO_3$ has also been shown to improve the mechanical properties of the composites. For example, the tensile modulus of the PLA composites filled with 5, 10, 20, and 30 wt% $CaCO_3$

**TABLE 16.4 Mechanical Properties of PLA Composites**

| Composite | Process Route | Tensile Strength (MPa) | Young's Modulus (GPa) | Elongation at Break (%) | Impact Strength (kJ/m$^2$) | References |
|---|---|---|---|---|---|---|
| PLA–hemp (40%) | Compression molding | 57.5 | 8.1 | 1.2 | 9.5 | [38, 182] |
| PLA–lyocell (40%) | Compression molding | 82 | 6.8 | 4.1 | 39.7 | [205] |
| PLA-hemp (20%) / lyocell (20%) | Compression molding | 71.5 | 7 | 1.7 | 24.7 | [205] |
| PLA–kenaf (40%) | Film stacking | 52.8 | 7.1 | 1.05 | 8.9 | [9, 36] |
| PLA–flax (40%) | Injection molding | 46.4 | 7.9 | — | 11 | [204] |
| PLA–flax (40%) | Compression molding | 99 | 6 | — | — | [204] |
| PLA–cotton (40%) | Carding + compression molding | 41.2 | 4.2 | 2.9 | 28.7 | [188] |
| PLA–RWF (20%)/ silane (0.5%) | Injection molding | 56.1 | 2.7 | — | — | [232] |
| PLA–cuphea (30%) | Injection molding | 37.9 | 1.5 | 7.9 | — | [77] |
| PLA–$CaCO_3$ (5%) | Extrusion | 55.3 | 2.3 | 2.7 | — | [112] |
| PLA–SBP (10%) | Mixing + vacuum drying | 37.5 | 1.04 | 6.7 | — | [75, 76] |
| PLA–MCC (10%) | Extrusion + injection molding | 38.2 | 4.1 | 1.8 | NS | [85, 86] |

nanofiller was found to be higher than that of the neat PLA [112]. The addition of talc (10 wt%) to PLA–wood flour composites improved the tensile modulus. Treatment with 1 and 3 wt% silane led to a higher tensile modulus for the composites, compared with neat PLA and PLA/wood flour composites without silane treatment, owing to increased fiber–matrix interfacial adhesion [71]. Table 16.4 shows static mechanical properties of some PLA composites prepared using different processing techniques.

#### *16.7.1.2 Dynamic Mechanical Properties*

Dynamic mechanical analysis (DMA) provides information about the response of a given material to an oscillatory deformation as a function of the temperature. DMA results are expressed in terms of three main parameters: (i) the storage modulus ($E'$), corresponding to the elastic response to the deformation; (ii) the loss modulus ($E''$), corresponding to the plastic response to the deformation; and (iii) the loss factor ($\tan\delta = E''/E'$), which is the ratio of the loss modulus to the storage modulus, useful for determining the occurrence of molecular mobility transitions, such as the glass transition temperature ($T_g$). In the transition region, tan δ indicates the imperfections in the elasticity of a polymer [235].

Ferreira et al. [236] reported reduction in crystallinity upon incorporation of RGO within PLA matrix using melt-extrusion, thereby resulting in the reduction of tan δ peak and increased chain mobility. This behavior of composite led to the increase in maximum strain ($\varepsilon_m$), which was further observed through thermally induced shape memory tests. Murphy and Collins [237] developed a novel, fully biodegradable 3DP microcrystalline cellulose (MCC)-reinforced PLA composite with 1, 3, and 5% loading. The DMA results indicated that 3 wt% MCC loading had the highest $E'$ below $T_g$, while $E'$ of 5 wt% loading was the greatest above $T_g$. In other studies, DMA of PLA–MCC, PLA–WF, and PLA–WP (wood pulp) composites indicated that the composites exhibited improved thermal stability when compared to pristine PLA [85, 238]. It was observed that the tan δ peak (α-transition) increased from 67°C for pure PLA to 70°C for WF and 69.1°C for WP and MCC reinforcements. A slight shift to higher temperature was observed with increasing filler content. Talib et al. [239] investigated the dynamic mechanical properties of 0–60% (w/w) randomly oriented kenaf FR-PLA at 1 Hz. The group reported a decrease in tan δ peak when the filler loading exceeded 50% (w/w). Elsewhere, the improvement in dynamic mechanical properties such as increased crystallinity and reduced $E''$ around $T_g$ in sisal FR-PLA bio-composites was ascribed to the nucleating effect of sisal fibers [240]. For CB/PLA composites $E'$ did not change much below $T_g$, but above $T_g$ the $E'$ value decreased rapidly with increasing temperature [241]. In a study involving layered silicate-filled PLA nanocomposites, higher $E'$ was recorded for nanocomposites; moreover, this change was more prominent at temperatures above $T_g$ [242]. This has been attributed to the mechanical reinforcement effect of silicate particles along with extensive intercalation of the polymer within silicate layers. For example, with organically modified layered silicate-reinforced PLA nanocomposite (PLA/qC2 18-MMT4), the increase in $E'$ was 52% in the temperature range of −20 to 0°C, while in the temperature range of 80–90°C, the increase was 96%. Due to the softening of the PLA matrix above $T_g$, the effect of interactions between silicate particles and the polymeric chains become more prominent, thereby resulting in greater increase in $E'$.

### 16.7.2 Thermal Properties

Thermal properties of pristine PLA such as thermal degradation temperature and heat deflection temperature (HDT) are not sufficient for most engineering applications. HDT suggests the upper service temperature limit for a polymer matrix. The HDT of kenaf FR-PLA laminated composites was found to be considerably higher (170°C) than that of neat PLA (64.5°C) [36, 211, 212]. Composites with silane- and alkali-treated kenaf fibers exhibited even higher HDT (175°C). The enhancement is primarily derived from the improved adhesion between the matrix and fiber. The improved heat resistance may also be attributed to the increase in modulus upon incorporation of kenaf fiber in the PLA matrix. Composites with silane-treated reinforcements generally exhibit a higher HDT, indicating that the interfacial bond strength and wettability of the fiber significantly influence the heat resistance properties of the composite.

With hemp FR-PLA composites, it was observed that $T_g$ of the PLA–hemp composites decreased slightly with increasing hemp content. Furthermore, with increasing fiber content, the ability of PLA matrix to recrystallize improved on heating above $T_g$. For example, the temperature of the cold crystallization peak ($T_{cc}$) decreased from 120°C for pure PLA to 114.5°C for the 70/30 PLA–hemp sample (the corresponding onset temperature being reduced from about 110 to 105°C) [38]. The enthalpy of cold crystallization ($\Delta H_c$) and enthalpy of melting ($\Delta H_m$) of the PLA matrix in the composites also increased with the increase in the hemp content, indicating an improvement in the degree of crystallinity. These findings suggest the occurrence of a nucleating effect of the fibers on the crystallization of PLA. Furthermore, thermogravimetric analysis (TGA) of the composites, carried out in both nitrogen and air, showed that the degradation of the fiber-filled systems started earlier than that of pristine PLA, independently of the presence of the plasticizer. The degradation temperature in a nitrogen atmosphere was in the range of 320–330°C for PLA–hemp samples, in comparison with 375°C for neat PLA [38]. Similarly, the addition of RWF enhances the crystallinity of PLA because RWFs can act as nucleating agents during the crystallization process. The $T_{CC}$ of PLA shifted to lower temperatures with the addition of RWFs. With oilseed fillers (cuphea, lesquerella, milkweed), the type of filler affected the thermal behavior of the resulting PLA composite. While addition of cuphea and lesquerella resulted in the reduction of $T_g$, $T_m$, degradation onset temperatures, and heat capacity; the incorporation of milkweed in PLA induced no significant change in $T_g$ or $T_m$.

Moreover, high HDT can be achieved in nanocomposites even at a low nanofiller loading. For example, the HDT of 1 phr MWCNT/PLA nanocomposite after 7 h water cross-linking reaction was 106°C, while that of virgin PLLA was 62°C [174]. This finding is useful in making biodegradable containers. Similar improvement in HDT has been reported upon incorporation of a variety of nanofillers such as RGO, nanosilica, organically modified nanoclay, or even their hybrids [243–247]. In particular, a low loading of MWCNT-silica hybrid nanoparticles (0.5%) in PLA matrix could result not only in an increase in the tensile strength by two-folds (95 MPa) but also in a 50°C increase in HDT [244].

### 16.7.3 Flame Retardancy

Over the years, consumption of PLA-based materials owing to their biodegradability has increased considerably. PLA, however, is a slow-burning material, with unfavorable flammability and dripping combustion, which has hindered its use near electric fields, in the automotive industry or as textiles in upholstery, the apparel industry, etc. [248] Such bioplastics are often required to possess a certain degree of flame retardancy [415]. Accordingly, a considerable amount of effort has been invested in improving the flame retardancy of PLA-based products. Flame retardancy in PLA may be developed through (i) use of nonreactive systems (such as inorganic fillers) [163, 248, 249]; (ii) use of reactive systems such as intumescent fire retardants [250, 251]; or (iii) by developing inherently flame-retardant polymers such as chain extension/functionalization of PLA chain with appropriate flame retardants [252].

Although, traditional flame retardant additives are based on metal salts such as those from aluminum, and magnesium [116], these have limited compatibility with organic polymer chains. Therefore, a new class of materials called metal–organic frameworks (MOFs) have been recently adopted as flame retardant additive owing to their improved affinity to PLA, arising from the presence of organic ligands [253]. MOF incorporation improves the thermal properties in addition to the overall physio-mechanical properties of PLA. For example, Shi et al. developed nano-MOF-filled PLA composites with improved dielectric and flame retardant behavior making it suitable for disposable electronic/electrical applications [254]. Alternatively, commercially available surface-modified montmorillonite nanoclays (such as Cloisite 30B and Bentone® 104-B104) have been incorporated for synthesis of PLA-based textiles having high thermal stability and reduced heat release rate (up to 46%) at low nanofiller loading [114, 255].

Carbon-based nanofillers such as MWCNT have also been reported to improve the heat stability of the PLA matrix and improve its flame retardant properties [256]. These improvements, however, are usually limited in nature and need to be augmented through other means. To this end, Gu et al. reported 9,10-dihydro-9-oxa-10-phosphaphanthrene-10-oxide (DOPO) functionalized MWCNTs incorporated in PLA along with a conventional metallic flame retardant (aluminum hypophosphite) [257]. DOPO has been sought after recently as a promising halogen-free flame retardant [252]. The synergistic incorporation of these flame

retardant additives allowed the realization of a UL 94 V-0 flame retardancy rating and a high limiting oxygen index (LOI), accompanied by 18% improvement in tensile strength.

Furthermore, to prepare halogen-free flame retardant (HFFR), intumescent fire retardation (IFR) is being touted as a promising candidate [258]. Conventionally, IFRs are comprised of (i) an acid source; (ii) a carbon source; and (iii) a blowing agent. A recent focus has been toward the preparation of bio-based green composites, with a significant amount of effort towards replacement of the petroleum-based carbon sources with the likes of lignin, starch, etc. [250, 251, 259] All these composites have been reported to achieve UL 94 V-0 flame retardancy rating, and a LOI up to 34.5. These were ascribed to the creation of free volume in the PLA matrix, and the agglomeration of lignin and/or starch particles, which impedes the heat transfer.

### 16.7.4 Degradation

According to ISO and CEN definitions, biodegradation is degradation caused by biological activity, especially by enzymatic action, leading to a significant change in the chemical structure of the exposed material and resulting in the production of carbon dioxide, water, mineral salts (mineralization), and new microbial cellular constituents (biomass) [260]. Many methods have been proposed to evaluate the biodegradability of a material, and some are standardized either for a liquid medium or for soil and/or compost medium (a complex biological environment with an active microbiological community) [261, 262]. Biodegradation of PLA proceeds through two steps: initial abiotic hydrolysis of the ester linkages, followed by enzymatic breakdown of lower molecular weight fragments [263, 264]. The hydrolytic degradation rate is primarily dependent on moisture and temperature. No microorganisms are involved in the primary phase, which is useful for product storage, and in food packaging applications. When the molecular weight is sufficiently decreased due to hydrolytic degradation, microorganisms then break down the lower molecular weight oligomers into carbon dioxide and water. The overall degradation rate is found to increase in a compost environment due to the presence of an active microbial community. It has been observed that biodegradation of pure PLA is slow in soil [265–267].

Biodegradation of PLA can be modified by blending with suitable polymers or reinforcements. Biodegradation studies performed on composites produced from PLA, thermoplastic starch (TPS), and short natural fiber (coir) showed a higher level of biodegradation (higher amounts of evolved $CO_2$) than PLA, probably due to the TPS domains being preferentially attacked by microorganisms [262]. Fibers seemed to play a secondary role in the process. Composites made with SBP and PLA, when buried in soil for four weeks at 40°C, revealed erosion of the PLA matrix [76]. The loss of SBP particles, either through erosion or mechanical loss, created a new surface for water penetration. This, in turn, was responsible for degradation of the continuous PLA phase. Furthermore, the organic acids generated by SBP digestion by microbes reduced the pH value in the microenvironments, which accelerated PLA hydrolysis. Surface modification of fiber reinforcements has also been found to influence the overall biodegradation rate. When the biodegradability of acetic anhydride-treated abaca fiber-reinforced PLA composite was evaluated by the soil burial test, no weight loss was observed after six months [210]. Penetration of water or microorganisms through the fiber/matrix interface was restrained owing to higher interfacial adhesion resulting from the surface modification of the fiber. Higher water penetration increases the degradation rate as seen in nanofilled $TiO_2$/PLA composites. It was also reported that these nanocomposites exhibit heterogeneous degradation, which is substantially influenced by filler loading and dispersion [268]. In another study, cellulose nanocrystal (CNC) and/or lignin-filled PLA composite films for food packaging application were prepared [137]. Not only did the ternary composite exhibit improved mechanical and antibacterial properties, it also possessed superior degradability in comparison to both pristine PLA and binary CNC or lignin filled PLA. In fact, the films consisting of 3% lignin degraded by up to 90% in 15 days under composting conditions (Figure 16.7) [129], which the authors attributed primarily to the lower crystallization ability of lignin. Moreover, controlled biodegradability of PLA composites is vital for biomedical applications [269], such as those for neural or bone tissue regeneration [270, 271]. This is because the in vivo degradation of the bioresorbable scaffold guides the overall regeneration process of the damaged tissue.

### 16.7.5 Shape Memory Properties

Smart materials, in particular shape memory polymers (SMP), are a class of materials that exhibit time-dependent responses to external stimuli, such as temperature, electricity, light, and magnetic field. SMPs may allow for the creation of products that automatically react to their environment without the need for heavy, expensive, and complex electronic actuation systems, and have recently been applied to a variety of industries, such as textile, aerospace, biomedical, and soft robotics [272–277]. The shape memory effect arises from the structural changes related to the so-called net-points and switching phases [278] within the material, occurring in response to the external stimuli. PLA-based smart materials were first reported in 2000 [279]. These, however, were limited in application, owing to their failure when programming strain exceeded 10% [280], and therefore have been modified using polymer blends, reinforcing fillers, etc., aimed toward improving their elastic modulus, strength, and deformability.

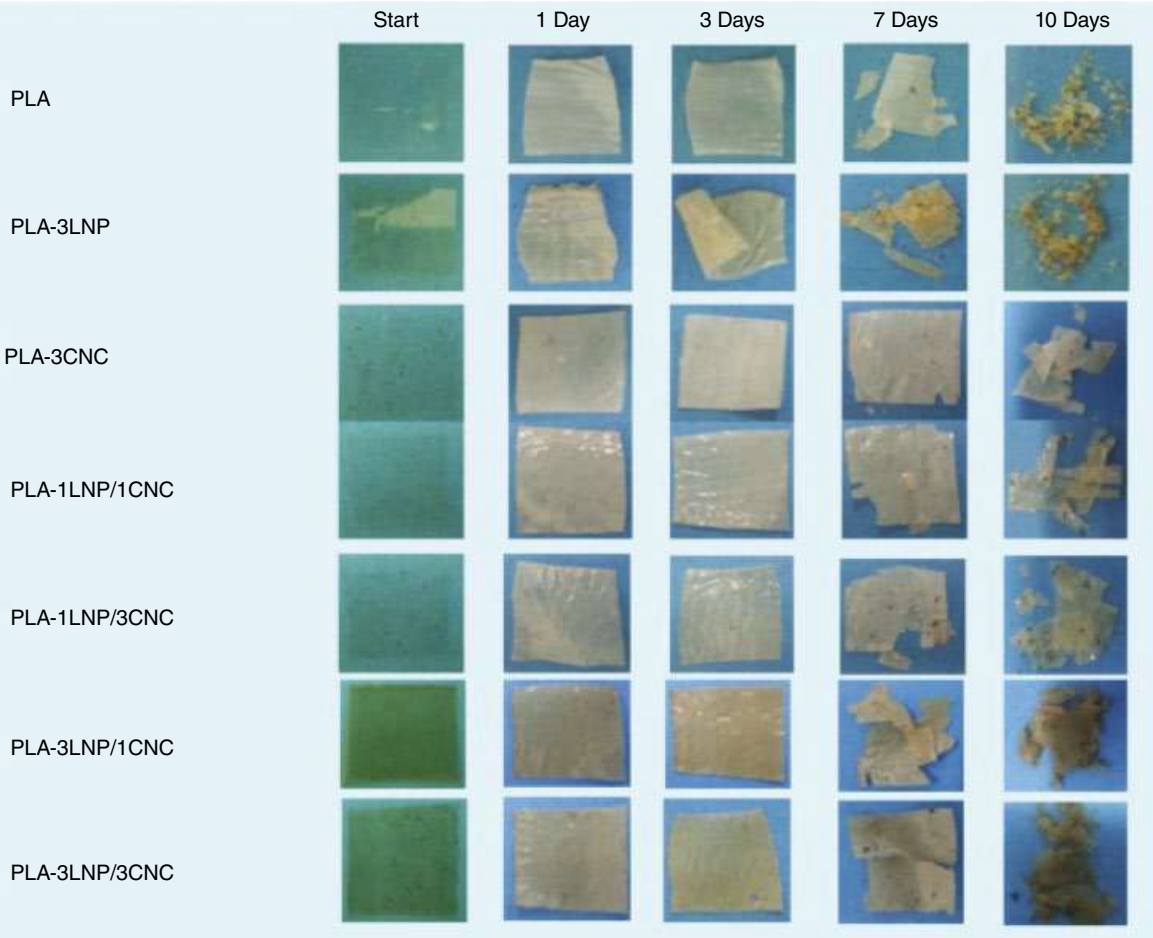


**FIGURE 16.7** Visual observation of pristine PLA and PLA-based nanocomposites at initial stage and after different stages of disintegration upon composting at 58°C [137].

The shape memory effect in PLA-based materials is primarily based on thermal activation; these may also be triggered by stimuli such as chemical, electric potential change [280, 281]. Xiu et al. reported incorporation of carbon black (CB) in a blend of PLA and TPU toward improving the recovery performance, as well as to widen the viable range of polymer compositions [103]. These were realized through preferential localization of CB in the TPU phase and formation of a co-continuous structure, as opposed to the sea-island-like structure of the pristine PLA-TPU blend. This work was further extended toward developing CB-PLA-TPU composites having electroactive shape-memory [281]. In a similar work, PLA-TPU reinforced cellulose nanofiber (CNF) bio-nanocomposites were studied for shape memory behaviors. At optimal filler loading, the nanocomposite exhibited up to 55% improvement in recovery force accompanied by appreciable strain recovery [282]. In another study, multiple SMP with high recovery stress was reported upon efficient incorporation of functionalized graphene in PLA-PCL blend [283]. The material exhibited temporary shapes at two temperatures, 0° and 65°C, which showed recovery at 65 and 165°C. Similar thermal shape memory was also observed in 3D-printed laminated composites using oriented fibers (45°/−45°) of PLA and PCL [284]. Interestingly, these were used to 3D print flower-like shapes (as shown in Figure 16.8), which shriveled upon rapid cooling, and blossomed again upon heat treatment at the transition temperature.

## 16.8 APPLICATIONS

PLA and its copolymers have several end-use applications. The key applications include short shelf-life products such as plastic bags for carrying household waste, overwrap and lamination films, barriers for sanitary products and diapers, planting, disposable cups and plates, and so on [230]. Hydrolytic degradability of PLA has generated a lot of interest for biomedical applications such as drug delivery systems [285–289], protein encapsulation and delivery [290–292], development of microspheres [293–297], hydrogels [298], bone screws [299], sutures [300, 301],

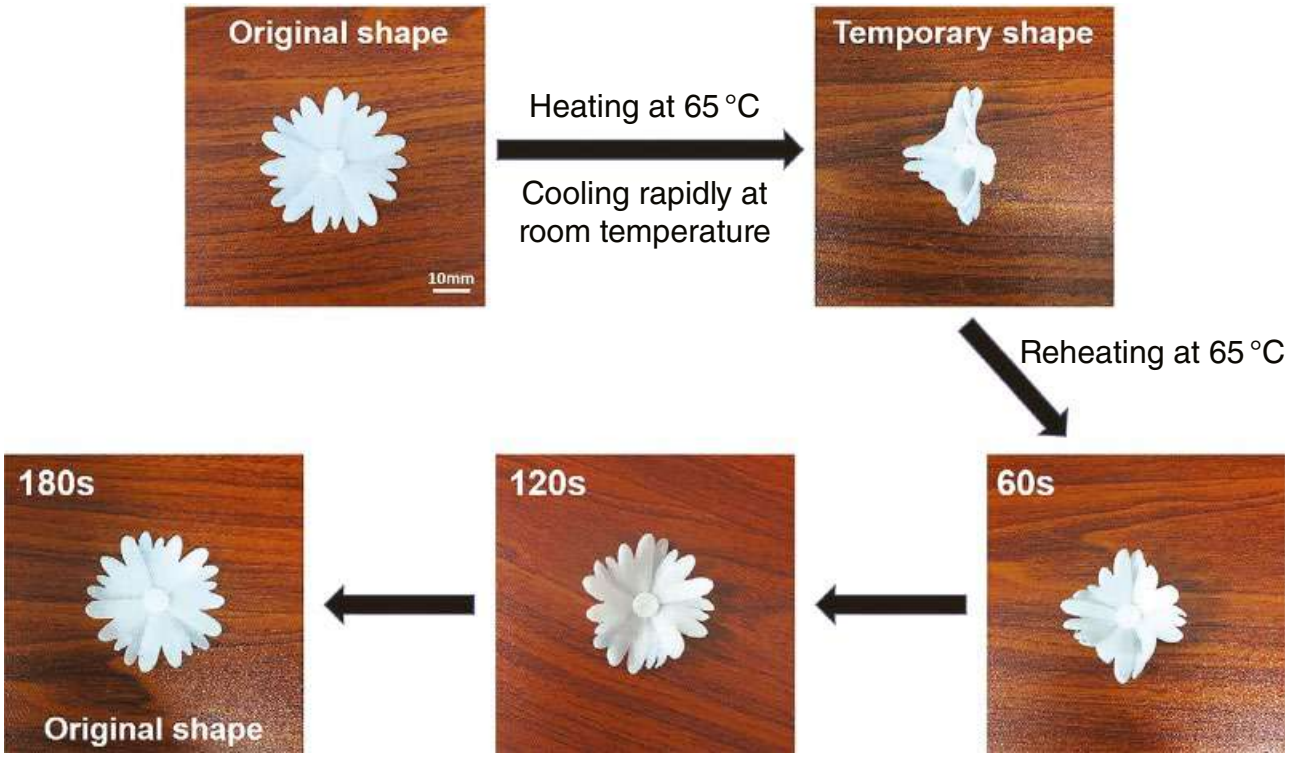


**FIGURE 16.8** Photographs displaying the thermo-responsive shape memory effect of the 3D-printed flower [284].

scaffolds [302], and so on. However, as also mentioned previously, pristine PLA has limited applicability. The use of suitable reinforcement, however, brings enormous opportunities to tailor the product properties. As such, a considerable amount of research has been dedicated toward expanding the potential uses of PLA as composites for applications ranging from biomedical industry to conventional thermoplastics. A few industry specific applications of such PLA-based composites are discussed in the following sections.

### 16.8.1 Biomedical Applications

Development of PLA-based biocomposite scaffolds is one of the emerging research areas in biomedical applications due to their bioactivity, biocompatibility, biodegradability, controlled drug release ability, and drug encapsulation. In recent years, PLA-based bio-nanocomposites have gained much attention due to their ability to meet diverse clinical requirements [303]. One way to produce high-performance PLA bio-nanocomposites is to reinforce PLA with metallic nanofillers (silver, gold, platinum etc.), bioactive ceramic filler (TCP, HA), CNCs, and graphene-based nanoparticles (GNP) to achieve the high mechanical properties, thermal conductivity, and optimized degradation. Moreover, improvement in surface roughness through these nanofillers further helps in enhancing cellular proliferation, migration, and adhesion.

Zhang et al. [304, 305] fabricated 3D-printed PLA/HA composite scaffolds and investigated their bone tissue regeneration capabilities and inflammation behavior in vivo. Their results indicated promising osteo-conductivity and biocompatibility of the printed scaffolds, along with minimal inflammation response, making them a potential candidate for rehabilitation of critical size bone defect. Recently, a surface-engineering approach was used to develop functionalized micro-porous 3D-printed PLA/HA scaffolds [306]. The group reported that the modified surfaces of composite scaffolds resulted in enhanced osteogenic activity through improved cellular proliferation and adhesion.

PLA nanocomposites incorporating functionalized GNP have now become popular in the biomedical field due to their outstanding properties, such as enhanced mechanical behavior, electrical conductivity, biodegradability, and biocompatibility. Wu et al. [307] showed that graphene nanosheets can be effectively used to both increase or decrease the degree of crystallinity of the nanocomposite by altering the loading and synthesis method of the nanofiller. This behavior can be of significant consequence, since degree of crystallinity directly impacts the in vivo degradation rate of PLA [308]. Marques et al. [309] fabricated PLLA/HA/GO composites to study their potential for application in biomedical scaffolds. Chen et al. [217] developed 3D-printed hybrid nanocomposites of thermoplastic polyurethane (TPU)/PLA/GO (Figure 16.9a and b) using a combination of solvent mixing and FDM. Their results demonstrated that TPU aided in improving the toughness of the composite, while the presence of GO resulted in improved

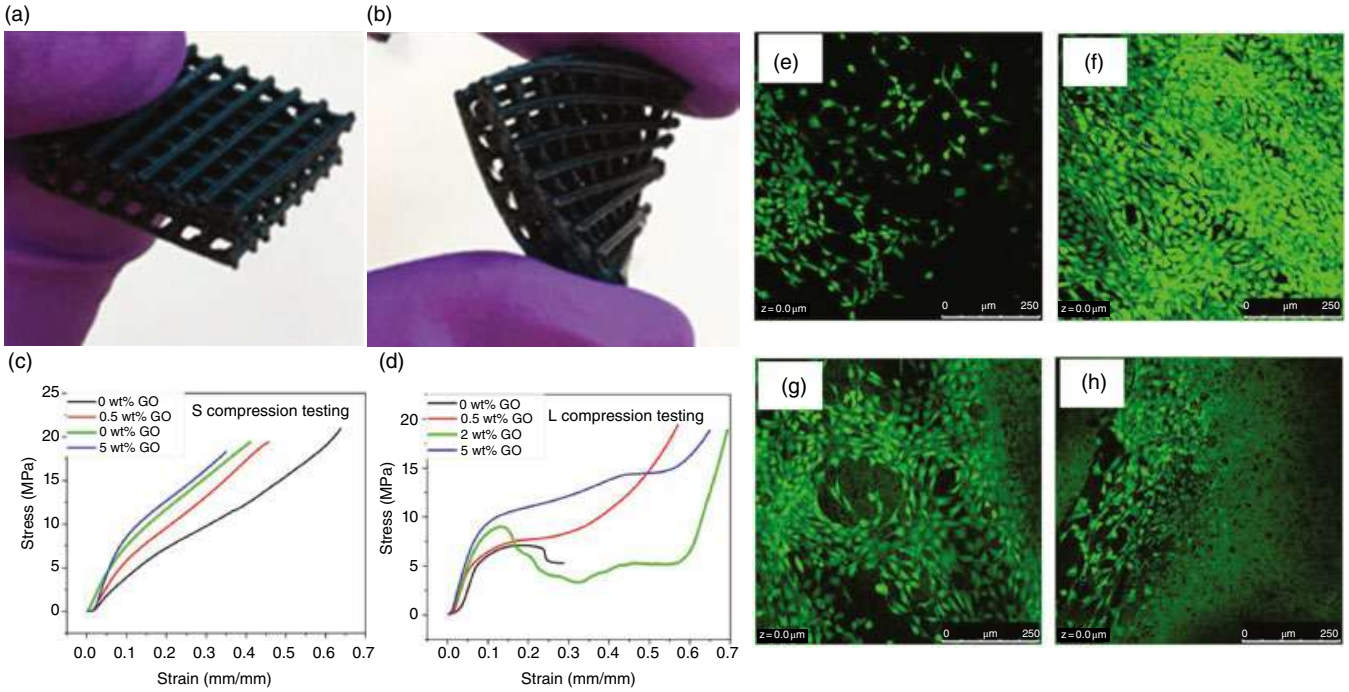


**FIGURE 16.9** (a) 3D-printed TPU/PLA/GO nanocomposites, (b) deformability of the micro-lattice, (c) S-compression curves, (d) L-compression curves with different GO loadings. Cell viability as seen through green stains at varying GO loading (e) 0 wt%, (f) 0.5 wt%, (g) 2 wt%, and (h) 5 wt%. *Source:* [217]. Copyright (2017) American Chemical Society.

mechanical performance, in addition to excellent cellular adhesion, viability, and proliferation responses.

PLA composites have also been employed to prepare fixation devices, such as screws [310], bone plates [123, 311], and bone clips [312], toward repair of traumatic bone and ligament injury. For example, Mg nanoparticle and α-tocopherol-filled PLA was used to 3D print degradable and bioactive bone fixation screws [313]. In another study, Yeon et al. [314] developed customized 3D-printed PLA/HA and PLA/HA/silk composite bone clips. These bone clips exhibited good mechanical stability and biocompatibility during in vitro testing. Furthermore, reduced invasiveness of the operative procedures used for implanting these bone clips suggested their potential as effective internal fixation devices. However, long degradation time and lower osteointegration have prompted modification of PLA chains with hydrophilic groups such as poly(lactic-*co*-glycolic acid) (PLGA), which exhibits better tunability of in vivo degradation and enhanced bioactivity [315, 316]. Recently, polymer blends of PLA and poly(L-lactide-*co*-ε-caprolactone) (PLCL) were used as self-fastening screws [317]. These polymers exhibited thermal shape memory near human body temperature. Consequently, these screws could be fastened without application of intense mechanical force, thereby eliminating debris. Incidentally, the current challenges of these bone fixation screws, such as limited mechanical properties and bioactivity, can be overcome by use of bioactive reinforcements like Bioglass®, HA, and Mg nanoparticles.

Non-orthopedic applications of PLA include surgical devices, viz., forceps, retractors, surgical planners [14, 318, 319]. In a recent report by Tzounis et al. [320], Ag nanoparticles were immobilized on 3D-printed PLA toward development of advanced, low cost surgical equipment having built-in antimicrobicidal properties. PLA composites, in addition, have shown considerable promise in drug delivery systems owing to long retention time and sustained drug release, thereby ensuring longer bio-availability of the drug molecules [164, 318, 321–323]. Drug-loaded micro/nano PLA particles have been particularly effective in anticancer treatment owing to their high specificity, reduced side effects, relapse inhibition, etc. [324–328] Moreover, stimuli-responsive drug delivery systems can be used to deliver drugs with a high degree of spatial and temporal control. For instance, near-infrared (NIR) sensitive hollow Au nanoshells were loaded with requisite drug and incorporated in sub-micron PLA particles [329]. NIR irradiation of these particles at the targeted sites led to rapid heating of the polymeric composites, releasing the Au nanoshells within. These nanoparticles exhibited a controlled drug elusion profile. In another work, an antitumor drug (metformin) along with nano-HA was incorporated in a PLA scaffold [330]. As a result, the developed degradable scaffold exhibited dual functionality, i.e., simultaneous enhancement of bone tissue regeneration (through HA particles), along with inhibition of bone tumor (via controlled release of metformin).

PLA has also been used in cardiovascular devices, such as stents [331–333], vascular grafts [334, 335], and heart

valves [336, 337]. Additionally, PLA composites with potential application in cardiovascular tissue engineering are also being developed [338, 339]. Such materials primarily comprise of nano/microfibrillar PLA scaffolds, which allow enhanced mass transport and cellular proliferation. Moreover, they incorporate additives, such as polyaniline (PANI), CNT, synthetic and natural biopolymers, adhesive peptides and other biomolecules, toward tuning the bioactivity of the composites (through enhanced conductivity, cellular adhesion, contractility, reduced hemolytic activity and coagulation etc.) [340–345].

### 16.8.2 Packaging Applications

PLA is attractive as a packaging material owing to its tensile strength, which is comparable to that of petroleum-derived thermoplastics. Additionally, PLA can degrade under commercial composting conditions and may be sealed at relatively low temperatures. However, certain drawbacks such as brittleness, limited thermal stability and gas barrier properties, and poor resistance to solvents of the neat PLA limit its use for food packaging applications [346]. Research efforts are being made to overcome some of these impediments through development of PLA-based composites. For example, cellular composites based on PLA and fibers are of interest in packaging sectors where light weight and limited lifetimes are desired [208]. Moreover, considering the benefits obtained with nanoscale distribution of nanofillers within a polymer matrix (viz., enhanced gas and solvent barrier properties, improved mechanical, and optical properties even at low filler loading), PLA-based nanocomposites have been exploited for food, as well as non-food packaging applications [114, 115, 415]. PLA nanocomposites prepared with organically modified montmorillonite clays, such as Cloisite 30B and 20A, demonstrated enhanced barrier against water vapor transmission. The improvement was ascribed to the tortuous path required for water vapor diffusion and a correspondingly higher diffusion path length arising from the impermeable clay layers dispersed within the polymer matrix [347]. Elsewhere, PLA reinforced with Bentonite® (a layered silicate) and MCC exhibited promising results in terms of reduction in transmission of UV and visual light radiation, which can be advantageous in packaging applications, considering that UV and visible light can have a negative effect on the quality of packed food. At 530 nm, transmissivity was 29% for bentonite nanocomposite and only 5% for MCC nanocomposite as compared with 86% light transmission through pure PLA [348].

In a similar work, synergistic incorporation of dual nanofillers CNT and GO in PLA films was reported to have resulted in the reduction of 30% in UV transmissivity and 67% in oxygen permeability, along with 75% increase in tensile strength of the film [349]. In another work, halloysite nanotubes (HNT) and chitosan (Ch)-filled PLA films were plasticized with triethyl citrate (TEC) and glycerol triacetate (GTA), allowing for extraordinary extensibility accompanied by improved UV and gas barrier properties [350]. Moreover, a variety of inorganic nanomaterials such as MgO, $TiO_2$, ZnO, and $SiO_2$ have been explored as fillers in PLA, as an effective means for improving UV and gas barrier properties of the packaging films, along with refinement of crystallization behavior of PLA [351–354]. Additionally, a few of these reinforcements (such as ZnO) have been useful in improving the antimicrobial behavior of the nanocomposite [355, 356].

Antimicrobial packaging has been an emerging area of study. Typically, these involve incorporation of an antimicrobial agent toward potential applications as packaging materials for a variety of foods including meat, fish, poultry, bread, cheese, fruits, vegetables [308, 357, 358]. The antimicrobial action of the film could help control the growth of pathogenic and spoilage microorganisms on the food. In one such example, pectin particles were incorporated into a PLA matrix, wherein the composite could absorb and store hydrophilic antimicrobial compounds such as nisin [359]. The incorporation of pectin created a rough and craggy surface, which was hydrophilic and facilitated the access and absorption of nisin by a diffusion–absorption technique. Similarly, PEG and glycerol were added to PLA for increasing its hydrophilicity [146]. These films were further reinforced with Ch, plasma etched, and sputtered with Ag nanoparticles; this imparted the films with superior microbicidal properties, with antimicrobial activity exceeding 99.99%. A more recent interest in such antimicrobial PLA films is the use of bio-based additives, resulting in greener products. Accordingly, bio-based dual nanofillers cellulose nanocrystal (CNC) and nano-Lignin (nLig) were incorporated in PLA films [137]. While nLig was used a natural antioxidant and antimicrobial agent in the film, CNC was included to improve its physio-mechanical properties, viz., gas barrier, tensile strength. Surprisingly, however, the nanocomposite material exhibited up to 90% degradation in 15 days under composting conditions.

### 16.8.3 Automotive Applications

Owing to increasingly stringent environmental regulations, research on developing biodegradable composites for automotive applications has gained a lot of momentum. Some of these composites have already been incorporated for car interior and exterior uses. There are potential benefits of using PLA-based composites in a car, as the concept of a "green car" is appealing from both consumer and manufacturer's points of view. Automotive manufacturers are exploring various applications of PLA composites. Compression-molded PLA has been developed by Toyota for potential application in spare tire covers [360]. Moreover, research carried out at Ford has shown that by optimizing the injection molding process and by incorporating suitable filler into the PLA matrix, the composite can be tailored for automotive applications [361].

In their model U concept car, Ford has used PLA for the canvas roof and carpet mats [362]. Toyota began using PLA resin in some cars in 2003, including the Raum and Prius models [362]. In spite of satisfying the environmental regulations, technical products based on pristine PLA fail to fully satisfy all the mechanical and thermal performance requirements for automotive applications [363, 364]. Accordingly, micro and/or nanofillers, impact-modifiers, plasticizers, thermal stabilizers, etc., have been explored toward tailoring the properties of the base material [14, 365]. Moreover, in the modern context, synthesis of "green products" entails not only the use of an ecofriendly PLA matrix but also the use of similarly green additives [366].

High-impact toughness and strength are key requirements for a vehicle's exterior parts; as such PLA blends comprising of TPU, natural rubber (NR), PCL, etc., as impact modifiers have frequently been explored [367–369]. For example, PLA-TPU blend with polyurethane elastomer prepolymer as compatibilizer was reported to have an impact strength of 81.3 kJ/m$^2$ [370]. In another study, TPU nanofibers were incorporated in PLA matrix using an innovative "eccentric roller extruder," resulting in an impact toughness of 73.5 kJ/m$^2$ along with a 12-fold increment in elongation at break [219]. Toward simultaneous improvement of toughness and strength of the polymer, incorporation of nanofillers such as functionalized silica nanoparticles in the TPU-PLA blends has also been reported [371].

As for the interior parts, adequate mechanical properties, thermal stability, moisture resistance, aesthetic appearance for application in door trims, spare tyre covers, car floor mats, seat covers, air filter housing have been reported [372, 373]. Often, these products include short natural fibers such as jute, flax, hemp, and kenaf in the PLA matrix. Replacement of petroleum-based polystyrene foams is another area where PLA-based products are being sought after [374] in automotive interior applications. In few studies, PLA-based foams reinforced with cellulosic microfibers, prepared using supercritical $CO_2$, have been reported to exhibit adequate compression strength and thermal insulation properties [375, 376]. Moreover, heat resistance and in certain instances flame retardation in automotive products like timing belt covers, upholstery, etc., have become important requirements.

However, issues such as cost affordability, scalability, and raw material availability are key concerns, which have limited the wider adoption of PLA composite products in the automotive industry.

### 16.8.4 Sensing and Other Electronic Applications

Owing to its biodegradability and renewability, a considerable effort has been directed toward the development of PLA-based composites for electronic applications, as well [361]. PLA-based materials in electronic applications are being employed in two primary ways: (i) as housing for electronic components or (ii) as conductive electroactive materials toward use in electrodes, sensors, electromagnetic interference (EMI) shielding, etc. [377–379]

In 2006, Japan's NEC Corp. developed PLA–kenaf composites for use as casings of cellular phones [380]. Addition of kenaf fiber greatly increased the heat resistance, toughness, and modulus of PLA, making it suitable for electronic applications. Moreover, the inclusion of the fiber improved its crystallization rate and ease of molding. In 2005, Fujitsu used flame-retardant PLA composite in personal computer housings [381]. A highly flame-retardant PLA composite is also being developed by NEC by adding metal hydroxide to PLA for use in electronic products such as PCs [382]. In a subsequent report, nonedible plant-based fillers were incorporated in PLA matrix for use in electronic packaging [383]. These biocomposites exhibited improved performance in terms of heat resistance, durability, water absorption, and moldability. In a separate investigation, it was shown that cross-linked carbon fiber reinforcement in a PLA-matrix can be employed to achieve high heat conductivity. With 10% w/w carbon fiber, the heat diffusion ability of PLA–carbon fiber reinforcement was comparable to stainless steel, while at 30% w/w carbon fiber reinforcement, the heat diffusion ability was twice that of stainless steel. This is useful in improving heat release issues caused by the latest and future small- and thin-sized electronic products (mobile phones, laptops, etc.), as conventional heat release devices such as fans and sheets are difficult to incorporate in products that are becoming smaller and slimmer [361].

Toward improving electrical conductivity of otherwise poorly conducting polymer like PLA, formation of a continuous network of the electrically conducting additive is crucial [384, 385]. As such, incorporation of conductive polymers and/or conductive nanofillers, owing to their high specific surface area and correspondingly low percolation threshold, becomes a viable option [386–388]. Recently, a high-strength hybrid PLA nanocomposite filled with cellulose nanocrystal (CNC) and PANI was reported to exhibit conductivity up to 2.16 S/m [139]. This was attributed to the grain structure refinement effect of CNC on PLA, resulting in efficient dispersal of PANI. Similarly high conductivity was observed in CNT-filled blend of ethylene-vinyl acetate (EVA) and PLA, owing to the formation of a co-continuous network within the polymers accompanied by preferential deposition of CNT in the EVA phase of the nanocomposite [389].

As opposed to metal-based products, polymeric EMI shields are easier to process, resistant to corrosion, and are lightweight [390]. A variety of conductive polymers and/or nanofillers have been used toward improving the shielding efficiency (SE) of the polymers, with PLA-based biodegradable composites being of particular interest. In general, a majority of fillers act by increasing the electromagnetic reflectivity of the composite, such as those based on metallic nanoparticles [391, 392]. Recently, MXene (a class of two-dimensional inorganic compounds)-based composites, owing

to their minimal thickness, and high conductivity, have been reported to exhibit an SE of 39.6 dB using 1.9 mm thick composite films [393]. Moreover, carbon-based filers (such as CB, CNT, and graphene) owing to their superior conductivity, high thermal stability, mechanical strength, and low percolation threshold have garnered considerable interest for EMI shielding applications [394–396]. Accordingly, graphene-reinforced PLA has been widely explored in a wide range of frequencies in the X band, K band, Ka band, and even in terahertz frequency ranges with appreciable SE [393, 397–400]. In fact, multiphasic PLA composites with biochar and graphite have been suggested to exhibit an SE of 30 dB in the K band range using films having a meager 0.25 mm thickness [397].

Another key application of PLA-based composites is in sensing applications, a vast majority of which are based on electrochemical behavior of the sensor [14]. Nevertheless, a few reports exploring the resistive changes in MWCNT-filled PLA fibers upon exposure to a variety of solvents such as water, *n*-hexane, ethanol, and methanol have been reported as means for detecting leakage [401]. Sensing capabilities of RGO- and CNT-filled PLA nanocomposites have also been studied [402]. Notably, percolation thresholds for RGO and CNT were 0.11 and 0.80%, respectively, with CNT-based sensors exhibiting noteworthy stability in conductance response to applied cyclic strain.

Disposable, biodegradable PLA-based electrodes can be prepared with relative ease and can be effectively used for electrochemical detection of a variety of analytes. Moreover, easy adaptability of these materials to FDM-based 3D printing further adds to the diversity of such applications. For instance, 3D-printed conductive PLA-based electrodes may be used for the detection of metallic ions like Cu in bioethanol [403], or for heavy metals like Hg, Cd, Pb with limit of detection (LOD) of 6.1 nM for Hg and 20 nM for Cd, Pb. These were prepared using GNP-PLA electrodes activated through incorporation of Bi microparticles on the surface [199]. In general, surface activation may be required to improve performance of sensors by improving their surface conductivity and thereby reducing the kinetic barrier, through use of appropriate techniques, such as electrochemical pretreatment [229], conductive ion sputtering, and surface etching. For example, selective, controlled etching of GNP-PLA electrodes using femtosecond laser pulses was demonstrated by Paula et al. as an effective surface activation strategy [198]. Elsewhere, selective digestion of PLA in GNP-PLA electrodes using proteinase-κ was used as an effective environmentally benign strategy toward activating GNP [197].

Furthermore, the biocompatibility of PLA in addition to its biodegradability has inspired the development of a variety of PLA-based biosensors [404]. Recently, Silva et al. reported highly efficient 3D-printed RGO-filled PLA-based biosensors for detecting serotonin levels in urine samples using differential-pulse voltammetry with a LOD as low as 0.032 μM [228]. A majority of the conventional biosensors are amperometric in nature, with glucose oxidase (GOx) enzyme-based glucose sensors being the most extensively studied [405–408]. Similarly, 3D-printed GNP-PLA was used for blood plasma glucose detection with LOD 15 μM with high precision and overnight recovery greater than 90% [227]. Moreover, this work was extended for detecting nitrite levels in saliva and uric acid in urine samples with an impressive LOD of 0.03 and 0.02 μM, respectively. Blood-plasma-based glucose detection, however, is inherently inconvenient, requiring invasive procedures such as finger-pricking, thereby, driving the research for minimally invasive or noninvasive techniques in glucose detection [409]. Accordingly, microneedle (MN)-based biosensors have been developed to access a variety of biomolecules (as shown in Figure 16.10) without causing discomfort to the patient [410]. Zhang et al. reported PLA-based MN biosensors, capable of

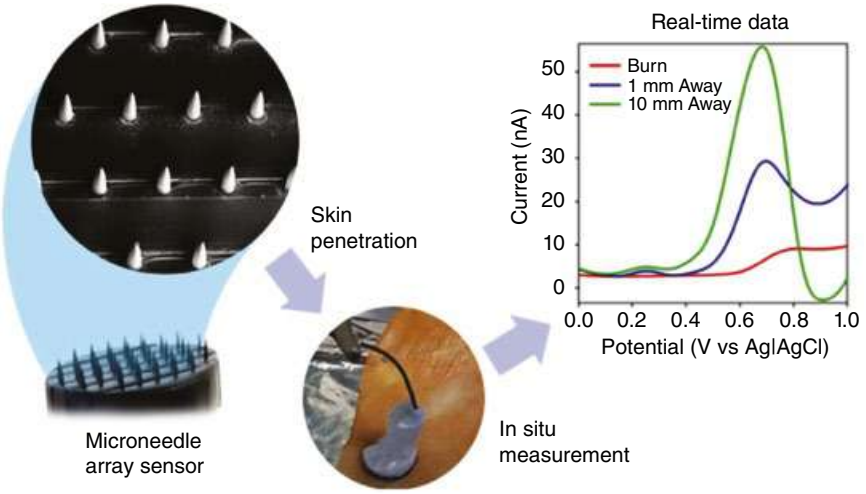


**FIGURE 16.10** MWCNT/PLA microneedle-based sensor for dermal biosensing, (from left to right) conductive microneedle sensor array, minimally invasive sensing of target skin tissue, and electrochemical signal generated by biosensor at varying distances from burn site [410].

selective detection of glucose levels with a LOD of 40 μM and a sensitivity of 8.09 μA/mM [148]. As an added advantage, MN arrays can further be used in sensitive detection of other biomarkers such as ascorbic acid [410], or even transdermal administration of therapeutics, such as drugs, vaccines. [411–413]. However, enzyme-based sensors are susceptible to degradation over time, owing to depletion of enzyme activity [414]. As such, Pt-catalyzed, PLA-based, enzyme-free electrochemical glucose sensors have been reported [149]. These Pt-PLA nanocomposite biosensors are capable of noninvasive glucose detection through sweat with a LOD as low as 0.19 nM.

## 16.9 FUTURE DEVELOPMENTS AND CONCLUDING REMARKS

Growing concerns over greenhouse gas emissions, depletion of fossil fuels, and fluctuation of oil prices have revived interest in the use of biodegradable materials. Waste disposal is another major driving force in stimulating the growth of biodegradable materials, as it is now being realized that continued expansion of landfills is not a solution. All these have been significant contributing factors in leading to research into PLA-based composite materials. PLAs have been recognized for their biodegradability and their susceptibility to hydrolytic degradation. They are produced from renewable resources and have high mechanical performance, comparable with those of commercial polymers. Although the higher price of PLA limits its general application, it is anticipated that better manufacturing practices, advancement in technologies, and multicomponent systems will not only bring down the cost, but a range of property benefits can also be realized. In this respect, there is a great potential to use PLA composites in a number of unexplored applications by replacing conventional polymers.

The use of natural fibers as reinforcements with PLA is of significant interest, since it can lead to the development of a new range of low-cost biodegradable composites with tailored properties. However, the environmental stability of natural fiber composites is a key issue of concern. Poor compatibility between hydrophobic PLA and hydrophilic natural fibers, high sensitivity of natural fibers toward moisture, and relatively poor thermal stability are some of the challenges that need to be overcome in extending the use of PLA-based natural fiber composites. The development of processing technologies, and use of proper fiber treatments, compatibilizers and/or coupling agents will lead to the production of composites with optimum properties to meet end-use requirements. Increasing commercial interest in these biodegradable composites, as well as demands for environmentally friendly material, leads to the responsibility and obligation of researchers to develop PLA composites with comparable or better properties at reasonable cost. Introducing nanoscale reinforcements into a PLA matrix to produce nanocomposites is one of the most effective approaches to enhance the properties of neat PLA, since the enhancements can be achieved using low filler loadings. PLA-based nanocomposites, in fact, has been an area of key research focus in the last decade. Such technologies, however, require a synergistic combination of bio-based materials and nanotechnology to produce a new generation of sustainable materials, which in turn has led to the emergence of the so-called green-nanocomposites. These nanocomposite alternatives could provide a considerable competitive advantage for manufacturers while being environmentally benign. Yet another emerging trend, especially in the last decade, has been the adoption of 3D printing technologies. These technologies allow greater control of the product geometry, opening up new avenues for enhanced control over product microarchitecture at a fraction of the cost.

While there are enormous opportunities for PLA composites to expand their horizons by entering into new markets, the future growth and sustainability of PLA composites is reliant on continued research, which will help in producing technically viable and economically feasible PLA composites of the future.

## REFERENCES


1. R. A. Gross, B. Kalra, Biodegradable polymers for the environment, *Science*[Internet] **2002**, *297*(5582), 803–807 [cited 9 March 2021]. Available from: https://science.sciencemag.org/content/297/5582/803.
2. C. Bastioli, Global status of the production of biobased packaging materials, *Starch/Staerke* **2001**, *53*(8), 351–355 [cited 9 March 2021]. Available from: https://onlinelibrary.wiley.com/doi/10.1002/1521-379X(200108]53:8%3C351::AID-STAR351%3E3.0.CO;2-R.
3. S. Pilla, S. Gong, E. O'Neill, R. M. Rowell, A. M. Krzysik, Polylactide-pine wood flour composites, *Polym. Eng. Sci.*. **2008**, *48*(3):578–587 [cited 9 March 2021]. Available from: http://doi.wiley.com/10.1002/pen.20971.
4. J. R. Dorgan, H. Lehermeier, M. Mang, Thermal and rheological properties of commercial-grade poly(lactic acids)s, *J. Polym. Environ.* **2000**, *8*(1), 1–9 [cited 9 March 2021]. Available from: https://link.springer.com/article/10.1023/A:1010185910301.
5. J. F. Zhang, X. Sun, Mechanical properties of poly(lactic acid)/starch composites compatibilized by maleic anhydride, *Biomacromolecules* **2004**, *5*(4), 1446–1451 [cited 9 March 2021]. Available from: https://pubmed.ncbi.nlm.nih.gov/15244463/.
6. Q. Fang, M. A. Hanna, Rheological properties of amorphous and semicrystalline polylactic acid polymers, *Ind. Crops Prod.* **1999**, *10*(1), 47–53.
7. K. S. Anderson, S. H. Lim, M. A. Hillmyer, Toughening of polylactide by melt blending with linear low-density polyethylene, *J. Appl. Polym. Sci.* **2003**, *89*(14), 3757–3768

[cited 9 March 2021]. Available from: http://doi.wiley.com/10.1002/app.12462.

8. M. S. Huda, L. T. Drzal, A. K. Mohanty, M. Misra, Effect of chemical modifications of the pineapple leaf fiber surfaces on the interfacial and mechanical properties of laminated biocomposites, *Compos. Interfaces* **2008**, *15*(2–3), 169–191 [cited 9 March 2021]. Available from: https://www.tandfonline.com/doi/abs/10.1163/156855408783810920.
9. M. S. Huda, L. T. Drzal, M. Misra, A. K. Mohanty, K. Williams, D. F. Mielewski, A study on biocomposites from recycled newspaper fiber and poly(lactic acid), *Ind. Eng. Chem. Res.* **2005**, *44*(15), 5593–5601 [cited 9 March 2021]. Available from: https://pubs.acs.org/doi/abs/10.1021/ie0488849.
10. M. A. Huneault, H. Li, Morphology and properties of compatibilized polylactide/thermoplastic starch blends, *Polymer (Guildf)* **2007**, *48*(1), 270–280 [cited 9 March 2021]. Available from: https://linkinghub.elsevier.com/retrieve/pii/S0032386106012651.
11. D. Garlotta, A literature review of poly(lactic acid), *J. Polym. Environ.* **2001**, *9*(2), 63–84 [cited 9 March 2021]. Available from: https://link.springer.com/article/10.1023/A:1020200822435.
12. R. Datta, M. Henry, Lactic acid: recent advances in products, processes and technologies—a review, *J. Chem. Technol. Biotechnol.* **2006**, *81*(7), 1119–1129 [cited 9 March 2021]. Available from: https://onlinelibrary.wiley.com/doi/10.1002/jctb.1486.
13. C. J. Weber, Biobased packaging materials for the food industry: status and perspectives: a european concerted action, 2000 [cited 9 March 2021]. Available from: https://books.google.com.co/books?id=W9OQAAAACAAJ.
14. M. L. Di Lorenzo, R. Androsch (Eds.), *Industrial Applications of Poly (Lactic Acid)*, 1st edition, Springer International Publishing, Cham, Switzerland, 2018, pp. 1–33 (Advances in Polymer Science; vol. 282]. Available from: https://link.springer.com/book/10.1007%2F978-3-319-75459-8.
15. S. Zhang, A. M. Bellinger, D. L. Glettig, R. Barman, Y. A. L. Lee, J. Zhu, et al., A pH-responsive supramolecular polymer gel as an enteric elastomer for use in gastric devices, *Nat. Mater.* **2015**, *14*(10), 1065–1071. Available from: http://www.nature.com/articles/nmat4355.
16. H. Tsuji, K. Sumida, Poly(L-lactide): V. Effects of storage in swelling solvents on physical properties and structure of poly(L-lactide), *J. Appl. Polym. Sci.* **2001**, *79*(9), 1582–1589. Available from: https://onlinelibrary.wiley.com/doi/10.1002/1097-4628(20010228]79:9%3C1582::AID-APP60%3E3.0.CO;2-7.
17. M. Rissanen, A. Puolakka, P. Nousiainen, M. Kellomäki, V. Ellä, Solubility and phase separation of poly(L,D-lactide) copolymers, *J. Appl. Polym. Sci.* **2008**, *110*(4), 2399–2404 [cited 9 March 2021]. Available from: http://doi.wiley.com/10.1002/app.28769.
18. A. Södergård, M. Stolt, Properties of lactic acid based polymers and their correlation with composition, *Prog. Polym. Sci.* **2002**, *27*(6), 1123–1163 [cited 9 March 2021]. Available from: https://linkinghub.elsevier.com/retrieve/pii/S0079670002000126.
19. O. Martin, L. Avérous, Poly(lactic acid): plasticization and properties of biodegradable multiphase systems, *Polymer (Guildf)* **2001**, *42*(14), 6209–6219 [cited 9 March 2021]. Available from: https://linkinghub.elsevier.com/retrieve/pii/S0032386101000866.
20. S. B. Ghosh, Bandyopadhyay-S. Ghosh, M. Sain, Composites, in: R. Auras, L.-T. Lim, S. E. M. Selke, H. Tsuji (Eds.), *Poly(Lactic Acid)*, 1st edition, John Wiley & Sons, Inc., Hoboken, NJ, 2010, pp. 293–310.
21. M. Murariu, P. Dubois, PLA composites: from production to properties, *Adv. Drug Deliv. Rev.* **2016**, *107*, 17–46. Available from: https://linkinghub.elsevier.com/retrieve/pii/S0169409X16301028.
22. D. K. Rajak, D. D. Pagar, R. Kumar, C. I. Pruncu, Recent progress of reinforcement materials: a comprehensive overview of composite materials, *J. Mater. Res. Technol.* **2019**, *8*(6), 6354–6374. Available from: https://linkinghub.elsevier.com/retrieve/pii/S2238785419312086.
23. O. J. Shesan, A. C. Stephen, A. G. Chioma, R. Neerish, E. S. Rotimi, Fiber-matrix relationship for composites preparation, in: A. Pereira, F. Fernandes (Eds.), *Renewable and Sustainable Composites*, IntechOpen, London, 2019. Available from: https://www.intechopen.com/books/renewable-and-sustainable-composites/fiber-matrix-relationship-for-composites-preparation.
24. G. Wypych (Ed.), Application of nucleating agents in specific polymers, in: *Handbook of Nucleating Agents*, 1st edition, Elsevier, Toronto, 2016, pp. 127–181. Available from: https://linkinghub.elsevier.com/retrieve/pii/B9781895198935500125.
25. C. DeArmitt, R. Rothon, Particulate fillers, selection, and use in polymer composites, in: R. Rothon (Ed.), *Fillers for Polymer Applications*, Springer International Publishing, Cham, Switzerland, 2017, pp. 3–27. Available from: http://link.springer.com/10.1007/978-3-319-28117-9_1.
26. M. Li, Y. Pu, V. M. Thomas, C. G. Yoo, S. Ozcan, Y. Deng, et al., Recent advancements of plant-based natural fiber–reinforced composites and their applications, *Compos. Part B Eng.* **2020**, *200*, 108254. Available from: https://linkinghub.elsevier.com/retrieve/pii/S1359836820333047.
27. K. Phogat, S. Kanwar, D. Nayak, N. Mathur, S. B. Ghosh, S. Bandyopadhyay-Ghosh, Nano-enabled poly(vinyl alcohol) based injectable bio-nanocomposite hydrogel scaffolds, *J. Appl. Polym. Sci.* **2020**, *137*(23), 1–9.
28. U. Kulshrestha, T. Gupta, P. Kumawat, H. Jaiswal, S. B. Ghosh, N. N. Sharma, Cellulose nanofibre enabled natural rubber composites: microstructure, curing behaviour and dynamic mechanical properties, *Polym. Test.* **2020**, *90*(January), 106676.
29. Z. Yang, X. Feng, M. Xu, D. Rodrigue, Properties of poplar fiber/PLA composites: comparison on the effect of maleic anhydride and KH550 modification of poplar fiber, *Polymers (Basel)* **2020**, *12*(3), 729. Available from: https://www.mdpi.com/2073-4360/12/3/729.
30. L. Mohammed, M. N. M. Ansari, G. Pua, M. Jawaid, M. S. Islam, A review on natural fiber reinforced polymer composite and its applications, *Int. J. Polym. Sci.* **2015**, *2015*, 1–15. Available from: http://www.hindawi.com/journals/ijps/2015/243947/.

31. R. Siakeng, M. Jawaid, H. Ariffin, S. M. Sapuan, M. Asim, N. Saba, Natural fiber reinforced polylactic acid composites: a review, *Polym. Compos.* **2019**, *40*(2), 446–463. Available from: https://onlinelibrary.wiley.com/doi/abs/10.1002/pc.24747.
32. L. C. Hao, S. M. Sapuan, M. R. Hassan, R. M. Sheltami, Natural fiber reinforced vinyl polymer composites, in: S. M. Sapuan, H. Ismail, E. S. Zainudin (Eds.), *Natural Fibre Reinforced Vinyl Ester and Vinyl Polymer Composites* 1st edition, Elsevier, Cambridge, 2018. p. 27–70. Available from: https://linkinghub.elsevier.com/retrieve/pii/B9780081021606000020.
33. V. K. Thakur, A. S. Singha, Natural fibres-based polymers: Part I—mechanical analysis of Pine needles reinforced bio-composites, *Bull. Mater. Sci.* **2010**, *33*(3), 257–264. Available from: http://link.springer.com/10.1007/s12034-010-0040-x.
34. Y. Zhou, M. Fan, L. Chen, Interface and bonding mechanisms of plant fibre composites: an overview, *Compos. Part B Eng.* **2016**, *101*, 31–45. Available from: https://linkinghub.elsevier.com/retrieve/pii/S1359836816303274.
35. A. Hart, J. Summerscales, Effect of time at temperature for natural fibres, *Procedia Eng.* **2017**, *200*, 269–275. Available from: https://linkinghub.elsevier.com/retrieve/pii/S1877705817328710.
36. M. S. Huda, L. T. Drzal, A. K. Mohanty, M. Misra. Effect of fiber surface-treatments on the properties of laminated bio-composites from poly(lactic acid) (PLA) and kenaf fibers, *Compos. Sci. Technol.* **2008**, *68*(2), 424–432 [cited 9 March 2021]. Available from: https://linkinghub.elsevier.com/retrieve/pii/S0266353807002643
37. B. Bax, J. Müssig, Impact and tensile properties of PLA/Cordenka and PLA/flax composites, *Compos. Sci. Technol.* **2008**, *68*(7–8), 1601–1607 [cited 9 March 2021]. Available from: https://linkinghub.elsevier.com/retrieve/pii/S026635380800016X.
38. R. Hu, J. K. Lim, Fabrication and mechanical properties of completely biodegradable hemp fiber reinforced polylactic acid composites, *J. Compos. Mater.* **2007**, *41*(13), 1655–1669 [cited 9 March 2021]. Available from: http://journals.sagepub.com/doi/10.1177/0021998306069878.
39. R. Tokoro, D. M. Vu, K. Okubo, T. Tanaka, T. Fujii, T. Fujiura, How to improve mechanical properties of polylactic acid with bamboo fibers, *J. Mater. Sci.* **2008**, *43*(2), 775–787. Available from: http://link.springer.com/10.1007/s10853-007-1994-y.
40. S. Kobayashi, K. Takada, Processing of unidirectional hemp fiber reinforced composites with micro-braiding technique, *Compos. Part A Appl. Sci. Manuf.* **2013**, *46*(1), 173–179. Available from: https://linkinghub.elsevier.com/retrieve/pii/S1359835X12003466.
41. T. C. Yang, Effect of extrusion temperature on the physico-mechanical properties of unidirectional wood fiber-reinforced polylactic acid composite (WFRPC) components using fused depositionmodeling, *Polymers (Basel)* **2018**, *10*(9), 976. Available from: http://www.mdpi.com/2073-4360/10/9/976.
42. A. Célino, S. Fréour, F. Jacquemin, P. Casari, The hygroscopic behavior of plant fibers: a review, *Front. Chem.* **2014**, *1*(JAN), 1–12. Available from: http://journal.frontiersin.org/article/10.3389/fchem.2013.00043/abstract.
43. B. O. Baba, U. Özmen, Preparation and mechanical characterization of chicken feather/PLA composites, *Polym. Compos.* **2017**, *38*(5), 837–845. Available from: http://doi.wiley.com/10.1002/pc.23644.
44. Y. Q. Zhao, K. T. Lau, T. Liu, S. Cheng, P. M. Lam, H. L. Li, Production of a green composite: mixture of poly (latic acid) and keratin fibers from chicken feathers, *Adv. Mater. Res.* **2008**, *47–50*, 1225–1228. Available from: https://www.scientific.net/AMR.47-50.1225.
45. A. L. Martínez-Hernández, C. Velasco-Santos, M. Icaza De, V. M. Castaño, Mechanical properties evaluation of new composites with protein biofibers reinforcing poly(methyl methacrylate), *Polymer (Guildf)* **2005**, *46*(19 SPEC. ISS.), 8233–8238 [cited 9 March 2021]. Available from: https://linkinghub.elsevier.com/retrieve/pii/S0032386105009092.
46. N. Reddy, Y. Yang, Structure and properties of chicken feather barbs as natural protein fibers, *J. Polym. Environ.* **2007**, *15*(2), 81–87. Available from: http://link.springer.com/10.1007/s10924-007-0054-7.
47. U. Özmen, B. O. Baba, Thermal characterization of chicken feather/PLA biocomposites, *J. Therm. Anal. Calorim.* **2017**, *129*(1), 347–355. Available from: http://link.springer.com/10.1007/s10973-017-6188-5.
48. S. Cheng, K.-t. Lau, T. Liu, Y. Zhao, P. M. Lam, Y. Yin, Mechanical and thermal properties of chicken feather fiber/PLA green composites, *Compos. Part B Eng.* **2009**, *40*(7), 650–654. Available from: https://linkinghub.elsevier.com/retrieve/pii/S1359836809000729.
49. S. Isarankura Na Ayutthaya, S. Tanpichai, W. Sangkhun, J. Wootthikanokkhan, Effect of clay content on morphology and processability of electrospun keratin/poly(lactic acid) nano-fiber, *Int. J. Biol. Macromol.* **2016**, *85*, 585–595. Available from: https://linkinghub.elsevier.com/retrieve/pii/S0141813016300423.
50. M. Ramesh, C. Deepa. Processing of green composites, in: P. K. Rakesh, I. Singh (Eds.), Springer Singapore, Singapore, 2019, pp. 47–72. (Materials Horizons: From Nature to Nanomaterials). Available from: http://link.springer.com/10.1007/978-981-13-6019-0.
51. H. Y. Cheung, K. T. Lau, X. M. Tao, D. Hui, A potential material for tissue engineering: silkworm silk/PLA biocomposite, *Compos. Part B Eng.* **2008**, *39*(6), 1026–1033. Available from: https://linkinghub.elsevier.com/retrieve/pii/S1359836808000048.
52. M. P. Ho, K. T. Lau, H. Wang, D. Bhattacharyya, Characteristics of a silk fibre reinforced biodegradable plastic, *Compos. Part B Eng.* **2011**, *42*(2), 117–122. Available from: https://linkinghub.elsevier.com/retrieve/pii/S1359836810001733.
53. T. Li, B. Liu, Y. Jiang, Y. Lou, K. Chen, D. Zhang, L-Polylactic acid porous microspheres enhance the mechanical properties and in vivo stability of degummed silk/silk fibroin/gelatin scaffold, *Biomed. Mater.* **2021**, *16*(1), 015025. Available from: https://iopscience.iop.org/article/10.1088/1748-605X/abca11.
54. H. Xiu, X. Qi, Z. Liu, Y. Zhou, H. Bai, Q. Zhang, et al., Simultaneously reinforcing and toughening of polylactide/

carbon fiber composites via adding small amount of soft poly(ether)urethane, *Compos. Sci. Technol.* **2016**, *127*, 54–61. Available from: https://linkinghub.elsevier.com/retrieve/pii/S0266353816300677.

55. S. D. Varsavas, C. Kaynak, Weathering degradation performance of PLA and its glass fiber reinforced composite, *Mater. Today Commun.* **2018**, *15*, 344–353. Available from: https://linkinghub.elsevier.com/retrieve/pii/S2352492817302453.
56. G. Mittal, K. Y. Rhee, Mišković-V. Stanković, D. Hui, Reinforcements in multi-scale polymer composites: processing, properties, and applications, *Compos. Part B Eng.* 2018, *138*(November 2017), 122–139. Available from: https://linkinghub.elsevier.com/retrieve/pii/S1359836817335813.
57. S. Prakash, Experimental investigation of surface defects in low-power $CO_2$ laser engraving of glass fiber-reinforced polymer composite, *Polym. Compos.* **2019**, *40*(12), 4704–4715. Available from: https://onlinelibrary.wiley.com/doi/abs/10.1002/pc.25339.
58. J. O. Akindoyo, M. D. H. Beg, S. Ghazali, H. P. Heim, M. Feldmann, M. Mariatti, Simultaneous impact modified and chain extended glass fiber reinforced poly(lactic acid) composites: mechanical, thermal, crystallization, and dynamic mechanical performance, *J. Appl. Polym. Sci.* **2021**, *138*(5), 49752. Available from: https://onlinelibrary.wiley.com/doi/10.1002/app.49752.
59. G. Wang, D. Zhang, B. Li, G. Wan, G. Zhao, A. Zhang, Strong and thermal-resistance glass fiber-reinforced polylactic acid (PLA) composites enabled by heat treatment, *Int. J. Biol. Macromol.* **2019**, *129*, 448–459. Available from: https://linkinghub.elsevier.com/retrieve/pii/S014181301930443X.
60. C. Zhu, I. Ahmed, A. Parsons, Y. Wang, C. Tan, J. Liu, et al., Novel bioresorbable phosphate glass fiber textile composites for medical applications, *Polym. Compos.* **2018**, *39*, E140–E151. Available from: http://doi.wiley.com/10.1002/pc.24499.
61. B. Yu, C. Geng, M. Zhou, H. Bai, Q. Fu, B. He, Impact toughness of polypropylene/glass fiber composites: interplay between intrinsic toughening and extrinsic toughening, *Compos. Part B Eng.* **2016**, *92*, 413–419. Available from: https://linkinghub.elsevier.com/retrieve/pii/S1359836816001542.
62. D. S. Cousins, Y. Suzuki, R. E. Murray, J. R. Samaniuk, A. P. Stebner, Recycling glass fiber thermoplastic composites from wind turbine blades, *J. Clean Prod.* **2019**, *209*, 1252–1263. Available from: https://linkinghub.elsevier.com/retrieve/pii/S0959652618333195.
63. R. M. Felfel, I. Ahmed, A. J. Parsons, P. Haque, G. S. Walker, C. D. Rudd, Investigation of crystallinity, molecular weight change, and mechanical properties of PLA/PBG bioresorbable composites as bone fracture fixation plates, *J. Biomater. Appl.* **2012**, *26*(7), 765–789. Available from: http://journals.sagepub.com/doi/10.1177/0885328210384532.
64. N. Sharmin, M. S. Hasan, A. J. Parsons, C. D. Rudd, I. Ahmed, Cytocompatibility, mechanical and dissolution properties of high strength boron and iron oxide phosphate glass fibre reinforced bioresorbable composites, *J. Mech. Behav. Biomed. Mater.* **2016**, *59*, 41–56. Available from: https://linkinghub.elsevier.com/retrieve/pii/S1751616115004853.
65. A. Ionita, Y. J. Weitsman, On the mechanical response of randomly reinforced chopped-fibers composites: data and model, *Compos. Sci. Technol.* **2006**, *66*(14), 2566–2579. Available from: https://linkinghub.elsevier.com/retrieve/pii/S0266353806000376.
66. Y. Z. Wan, Y. L. Wang, X. H. Xu, Q. Y. Li, in vitro degradation behavior of carbon fiber-reinforced PLA composites and influence of interfacial adhesion strength, *J. Appl. Polym. Sci.* **2001**, *82*(1), 150–158. Available from: http://doi.wiley.com/10.1002/app.1834.
67. M. Zimmerman, J. R. Parsons, H. Alexander, The design and analysis of a laminated partially degradable composite bone plate for fracture fixation, *J. Biomed. Mater. Res.* **1987**, *21*(3 SUPPL. 3), 345–361. Available from: https://pubmed.ncbi.nlm.nih.gov/3429470/.
68. T. Hofstätter, I. W. Gutmann, T. Koch, D. B. Pedersen, G. Tosello, G. Heinz, et al., Distribution and orientation of carbon fibers in polylactic acid parts produced by fused deposition modeling, in: *Proceedings—ASPE/Euspen 2016 Summer Topical Meeting: Dimensional Accuracy and Surface Finish in Additive Manufacturing*, Raleigh, 2016, pp. 44–49. Available from: http://aspe.net/technical-meetings/2016-additive-manufacturing/.
69. Q. Hu, Y. Duan, H. Zhang, D. Liu, B. Yan, F. Peng, Manufacturing and 3D printing of continuous carbon fiber prepreg filament, *J. Mater. Sci.* **2018**, *53*(3), 1887–1898. Available from: http://link.springer.com/10.1007/s10853-017-1624-2.
70. N. F. Zaaba, M. Jaafar, H. Ismail, Tensile and morphological properties of nanocrystalline cellulose and nanofibrillated cellulose reinforced PLA bionanocomposites: a review, *Polym. Eng. Sci.* **2021**, *61*(1), 22–38. Available from: https://onlinelibrary.wiley.com/doi/10.1002/pen.25560.
71. S. Y. Lee, I. A. Kang, G. H. Doh, H. G. Yoon, B. D. Park, Q. Wu, Thermal and mechanical properties of wood flour/talc-filled polylactic acid composites: effect of filler content and coupling treatment, *J. Thermoplast. Compos. Mater.* **2008**, *21*(3), 209–223 [cited 9 March 2021]. Available from: http://journals.sagepub.com/doi/10.1177/0892705708089473.
72. B. L. Shah, S. E. Selke, M. B. Walters, P. A. Heiden, Effects of wood flour and chitosan on mechanical, chemical, and thermal properties of polylactide, *Polym. Compos.* **2008**, *29*(6), 655–663. Available from: http://doi.wiley.com/10.1002/pc.20415.
73. F. J. Rodriguez-Gonzalez, B. A. Ramsay, B. D. Favis, High performance LDPE/thermoplastic starch blends: a sustainable alternative to pure polyethylene, *Polymer (Guildf)* **2003**, *44*(5), 1517–1526. Available from: https://linkinghub.elsevier.com/retrieve/pii/S0032386102009072.
74. B. Dimzoski, Bogoeva-G. Gaceva, G. Gentile, M. Avella, M. E. Errico, V. Srebrenkoska, Preparation and characterization of poly(lactic acid)/rice hulls based biodegradable composites, *J. Polym. Eng.* **2008**, *28*(6–7), 369–384. Available from: http://eprints.ugd.edu.mk/1724/.
75. V. L. Finkenstadt, C. K. Liu, P. H. Cooke, L. S. Liu, J. L. Willett, Mechanical property characterization of plasticized sugar beet pulp and poly(lactic acid) green composites using acoustic emission and confocal microscopy, *J. Polym. Environ.* **2008**, *16*(1), 19–26 [cited 9 March 2021]. Available from: https://link.springer.com/article/10.1007/s10924-008-0085-8.

76. L. S. Liu, M. L. Fishman, K. B. Hicks, C. K. Liu, Biodegradable composites from sugar beet pulp and poly(lactic acid), *J. Agric. Food Chem.* **2005**, *53*(23), 9017–9022 [cited 9 March 2021]. Available from: https://pubs.acs.org/doi/abs/10.1021/jf058083w.
77. V. L. Finkenstadt, C. K. Liu, R. Evangelista, L. S. Liu, S. C. Cermak, Hojilla-M. Evangelista, et al., Poly(lactic acid) green composites using oilseed coproducts as fillers, *Ind. Crops Prod.* **2007**, *26*(1), 36–43 [cited 9 March 2021]. Available from: https://linkinghub.elsevier.com/retrieve/pii/S0926669007000052.
78. C. Clemons, Wood-plastic composites in the United States: the interfacing of two industries, *For. Prod. J.* **2002**, *52*(6), 10–18. Available from: https://www.fs.usda.gov/treesearch/pubs/8778.
79. C. Way, D. Y. Wu, D. Cram, K. Dean, E. Palombo, Processing stability and biodegradation of polylactic acid (PLA) composites reinforced with cotton linters or maple hardwood fibres, *J. Polym. Environ.* **2013**, *21*(1), 54–70. Available from: http://link.springer.com/10.1007/s10924-012-0462-1.
80. O. A. Madyan, Y. Wang, J. Corker, Y. Zhou, G. Du, M. Fan, Classification of wood fibre geometry and its behaviour in wood poly(lactic acid) composites, *Compos. Part A Appl. Sci. Manuf.* **2020**, *133*, 105871. Available from: https://linkinghub.elsevier.com/retrieve/pii/S1359835X20301093.
81. Y. Du, T. Wu, N. Yan, M. T. Kortschot, R. Farnood, Fabrication and characterization of fully biodegradable natural fiber-reinforced poly(lactic acid) composites, *Compos. Part B Eng.* **2014**, *56*, 717–723. Available from: https://linkinghub.elsevier.com/retrieve/pii/S1359836813005258.
82. Y. Tao, H. Wang, Z. Li, P. Li, S. Q. Shi, Development and application ofwood flour-filled polylactic acid composite filament for 3D printing, *Materials (Basel)* **2017**, *10*(4), 339. Available from: http://www.mdpi.com/1996-1944/10/4/339.
83. A. Le Duigou, M. Castro, R. Bevan, N. Martin, 3D printing of wood fibre biocomposites: from mechanical to actuation functionality, *Mater. Des.* **2016**, *96*, 106–114. Available from: https://linkinghub.elsevier.com/retrieve/pii/S0264127516301654.
84. L. Gregurić, Wood filament: the basics & best brands for wood PLA | All3DP. All3DP.com. [cited 9 April 2021]. Available from: https://all3dp.com/2/wood-filament-for-a-3d-printer-explained-compared/.
85. A. P. Mathew, K. Oksman, M. Sain, Mechanical properties of biodegradable composites from poly lactic acid (PLA) and microcrystalline cellulose (MCC), *J. Appl. Polym. Sci.* **2005**, *97*(5), 2014–2025 [cited 11 March 2021]. Available from: http://doi.wiley.com/10.1002/app.21779.
86. K. Oksman, A. P. Mathew, D. Bondeson, I. Kvien, Manufacturing process of cellulose whiskers/polylactic acid nanocomposites, *Compos. Sci. Technol.* **2006**, *66*(15), 2776–2784. Available from: https://linkinghub.elsevier.com/retrieve/pii/S026635380600100X.
87. L. Averous, N. Fauconnier, L. Moro, C. Fringant, Blends of thermoplastic starch and polyesteramide: processing and properties, *J. Appl. Polym. Sci.* **2000**, *76*(7), 1117–1128. Available from: https://onlinelibrary.wiley.com/doi/10.1002/(SICI)1097-4628(20000516)76:7%3C1117::AID-APP16%3E3.0.CO;2-W.
88. L. Avérous, Biodegradable multiphase systems based on plasticized starch: a review, *J. Macromol. Sci. Polym. Rev.* **2004**, *44*(3), 231–274. Available from: http://www.tandfonline.com/doi/abs/10.1081/MC-200029326.
89. J. J. Koh, X. Zhang, C. He, Fully biodegradable poly(lactic acid)/starch blends: a review of toughening strategies, *Int. J. Biol. Macromol.* **2018**, *109*, 99–113. Available from: https://linkinghub.elsevier.com/retrieve/pii/S0141813017343027.
90. O. Wilfred, Z. Fan, W. Wang, H. Tai, R. Marriott, Q. Liu, et al., Biodegradation of polylactic acid and starch composites in compost and soil, *Int. J. Nano Res.* **2018**, *1*(2), 1–11. Available from: https://innovationinfo.org/articles/IJNR/IJNR-1-107.pdf.
91. T. M. Ogunrinola, U. Akpan, Production of cassava starch bioplastic film reinforced with poly-lactic acid (PLA), *Int. J. Eng. Res. Adv. Technol.* **2018**, *4*(8), 56–61. Available from: https://ijerat.com/index.php/ijerat/article/view/408.
92. J. Móczó, D. Kun, E. Fekete, Desiccant effect of starch in polylactic acid composites, *Express Polym. Lett.* **2018**, *12*(11), 1014–1024. Available from: http://www.expresspolymlett.com/letolt.php?file=EPL-0009205&mi=c.
93. N. G. Olaiya, I. Surya, P. K. Oke, S. Rizal, E. R. Sadiku, S. S. Ray, et al., Properties and characterization of a PLA-chitin-starch biodegradable polymer composite, *Polymers (Basel)* **2019**, *11*(10), 1656. Available from: https://www.mdpi.com/2073-4360/11/10/1656.
94. D. Jiang, M. Pan, X. Cai, Y. Zhao, Flame retardancy of rice straw-polyethylene composites affected by in situ polymerization of ammonium polyphosphate/silica, *Compos. Part A Appl. Sci. Manuf.* **2018**, *109*, 1–9. Available from: https://linkinghub.elsevier.com/retrieve/pii/S1359835X18300642.
95. M. Avella, A. Buzarovska, M. E. Errico, G. Gentile, A. Grozdanov, Eco-challenges of bio-based polymer composites, *Materials (Basel)* **2009**, *2*(3), 911–925. Available from: http://www.mdpi.com/1996-1944/2/3/911.
96. L. Zhu, J. Qiu, W. Liu, E. Sakai, Mechanical and thermal properties of rice straw/PLA modified by nano attapulgite/PLA interfacial layer, *Compos. Commun.* **2019**, *13*, 18–21. Available from: https://linkinghub.elsevier.com/retrieve/pii/S2452213918301311.
97. M. H. M. Hamdan, J. P. Siregar, M. R. M. Rejab, D. Bachtiar, J. Jamiluddin, C. Tezara, Effect of maleated anhydride on mechanical properties of rice husk filler reinforced PLA matrix polymer composite, *Int. J. Precis. Eng. Manuf. Green Technol.* **2019**, *6*(1), 113–124. Available from: http://link.springer.com/10.1007/s40684-019-00017-4.
98. K. S. Chun, C. M. Yeng, C. P. May, T. K. Yeow, O. T. Kiat, C. K. How, Effect of coupling agent content on properties of composites made from polylactic acid and chrysanthemum waste, *J. Vinyl Addit. Technol.* **2020**, *26*(1), 10–16. Available from: https://onlinelibrary.wiley.com/doi/abs/10.1002/vnl.21710.
99. M. Barczewski, O. Mysiukiewicz, J. Szulc, A. Kloziński, Poly(lactic acid) green composites filled with linseed cake as an agricultural waste filler. Influence of oil content within the filler on the rheological behavior, *J. Appl. Polym. Sci.* **2019**, *136*(24), 47651. Available from: https://onlinelibrary.wiley.com/doi/abs/10.1002/app.47651.

100. L. Yu, H. Liu, F. Xie, L. Chen, X. Li, Effect of annealing and orientation on microstructures and mechanical properties of polylactic acid, *Polym. Eng. Sci.* **2008**, *48*(4), 634–641. Available from: http://doi.wiley.com/10.1002/pen.20970.

101. A. Shakoor, N. L. Thomas, Talc as a nucleating agent and reinforcing filler in poly(lactic acid) composites, *Polym. Eng. Sci.* **2014**, *54*(1), 64–70. Available from: http://doi.wiley.com/10.1002/pen.23543.

102. S. Li, J. Liu, D. Wang, Y. Chen, H. Wei, Z. Qin, et al., Research progress on preparation and performance of bio-degradation PLA/graphene nanocomposites, in: *DEStech Transactions on Materials Science and Engineering*, AMST, 2017. Available from: http://dpi-proceedings.com/index.php/dtmse/article/view/11320.

103. H. Xiu, Y. Zhou, J. Dai, C. Huang, H. Bai, Q. Zhang, et al., Formation of new electric double percolation via carbon black induced co-continuous like morphology, *RSC Adv.* **2014**, *4*(70), 37193–37196. Available from: http://dx.doi.org/10.1039/C4RA06836J.

104. H. Tsuji, Y. Kawashima, H. Takikawa, S. Tanaka, Poly(L-lactide)/nano-structured carbon composites: conductivity, thermal properties, crystallization, and biodegradation, *Polymer (Guildf)* **2007**, *48*(14), 4213–4225 [cited 9 March 2021]. Available from: https://linkinghub.elsevier.com/retrieve/pii/S0032386107004922.

105. S. V. Dorozhkin, Calcium orthophosphate deposits: preparation, properties and biomedical applications, *Mater. Sci. Eng. C* **2015**, *55*, 272–326. Available from: https://linkinghub.elsevier.com/retrieve/pii/S0928493115300837.

106. A. El-Ghannam, Bone reconstruction: from bioceramics to tissue engineering, *Expert Rev. Med. Devices* **2005**, *2*(1), 87–101. Available from: http://www.tandfonline.com/doi/full/10.1586/17434440.2.1.87.

107. J. M. Ferri, J. Jordá, N. Montanes, O. Fenollar, R. Balart, Manufacturing and characterization of poly(lactic acid) composites with hydroxyapatite, *J. Thermoplast. Compos. Mater.* **2018**, *31*(7), 865–881. Available from: http://journals.sagepub.com/doi/10.1177/0892705717729014.

108. K. V. Niaza, F. S. Senatov, S. D. Kaloshkin, A. V. Maksimkin, D. I. Chukov, 3D-printed scaffolds based on PLA/HA nanocomposites for trabecular bone reconstruction, *J. Phys. Conf. Ser.* **2016**, *741*(1), 012068. Available from: https://iopscience.iop.org/article/10.1088/1742-6596/741/1/012068.

109. F. S. Senatov, K. V. Niaza., A. A. Stepashkin, S. D. Kaloshkin, Low-cycle fatigue behavior of 3D-printed PLA-based porous scaffolds, *Compos. Part B Eng.* **2016**, *97*, 193–200. Available from: https://linkinghub.elsevier.com/retrieve/pii/S1359836816305194.

110. S. M. Espinoza, H. I. Patil, E. San Martin Martinez, R. Casañas Pimentel, P. P. Ige, Poly-ε-caprolactone (PCL), a promising polymer for pharmaceutical and biomedical applications: focus on nanomedicine in cancer, *Int. J. Polym. Mater. Polym. Biomater.* **2020**, *69*(2), 85–126. Available from: https://www.tandfonline.com/doi/full/10.1080/00914037.2018.1539990.

111. S. Mondal, T. P. Nguyen, V. H. Pham, G. Hoang, P. Manivasagan, M. H. Kim, et al., Hydroxyapatite nano bioceramics optimized 3D printed poly lactic acid scaffold for bone tissue engineering application, *Ceram Int.* **2020**, *46*(3), 3443–3455. Available from: https://linkinghub.elsevier.com/retrieve/pii/S0272884219329062.

112. H. S. Kim, B. H. Park, J. H. Choi, J. S. Yoon, Mechanical properties and thermal stability of poly(L-lactide)/calcium carbonate composites, *J. Appl. Polym. Sci.* **2008**, *109*(5), 3087–3092 [cited 11 March 2021]. Available from: http://doi.wiley.com/10.1002/app.28229.

113. L. C. Lin, S. J. Chang, S. M. Kuo, G. C. C. Niu, H. K. Keng, P. H. Tsai, Preparation and evaluation of β-TCP/polylactide microspheres as osteogenesis materials, *J. Appl. Polym. Sci.* **2008**, *108*(5), 3210–3217. Available from: http://doi.wiley.com/10.1002/app.27309.

114. S. Solarski, F. Mahjoubi, M. Ferreira, E. Devaux, P. Bachelet, S. Bourbigot, et al., (Plasticized) polylactide/clay nanocomposite textile: thermal, mechanical, shrinkage and fire properties, *J. Mater. Sci.* **2007**, *42*(13), 5105–5117 [cited 9 March 2021]. Available from: http://link.springer.com/10.1007/s10853-006-0911-0.

115. J. W. Rhim, S. I. Hong, C. S. Ha, Tensile, water vapor barrier and antimicrobial properties of PLA/nanoclay composite films, *LWT—Food Sci. Technol.* **2009**, *42*(2), 612–617. Available from: https://linkinghub.elsevier.com/retrieve/pii/S0023643808000613.

116. M. Norouzi, Y. Zare, P. Kiany, Nanoparticles as effective flame retardants for natural and synthetic textile polymers: application, mechanism, and optimization, *Polym. Rev.* **2015**, *55*(3), 531–560. Available from: http://www.tandfonline.com/doi/full/10.1080/15583724.2014.980427.

117. W. J. Grigsby, A. Puri, M. Gaugler, J. Lüedtke, A. Krause, Bonding wood veneer with biobased poly(lactic acid) thermoplastic polyesters: potential applications for consolidated wood veneer and overlay products, *Fibers* **2020**, *8*(8), 50. Available from: https://www.mdpi.com/2079-6439/8/8/50.

118. A. Porras, A. Maranon, Development and characterization of a laminate composite material from polylactic acid (PLA) and woven bamboo fabric, *Compos. Part B Eng.* **2012**, *43*(7), 2782–2788.

119. A. P. Morales, A. Güemes, A. Fernandez-Lopez, V. C. Valero, L. S. de La Rosalano, Bamboo-polylactic acid (PLA) composite material for structural applications, *Materials (Basel)* **2017**, *10*(11), 1286 [cited 13 March 2021]. Available from: http://www.mdpi.com/1996-1944/10/11/1286.

120. T. Kittikorn, W. Chaiwong, E. Stromberg, R. M. Torro, M. Ek, S. Karlsson, Enhancement of interfacial adhesion and engineering properties of polyvinyl alcohol/polylactic acid laminate films filled with modified microfibrillated cellulose, *J. Plast. Film Sheeting* **2020**, *36*(4), 368–390 [cited 23 March 2021]. Available from: http://journals.sagepub.com/doi/10.1177/8756087920915745.

121. S. W. Cho, M. Gällstedt, M. S. Hedenqvist, Properties of wheat gluten/poly(lactic acid) laminates, *J. Agric. Food Chem.* **2010**, *58*(12), 7344–7350 [cited 23 March 2021]. Available from: https://pubs.acs.org/doi/abs/10.1021/jf1003144.

122. A. N. Dickson, K. A. Ross, D. P. Dowling, Additive manufacturing of woven carbon fibre polymer composites, *Compos. Struct.* **2018**, *206*, 637–643.


123. M. C. Zimmerman, H. Alexander, J. R. Parsons, P. K. Bajpai, The design and analysis of laminated degradable composite bone plates for fracture fixation, in: T. L. Vigo, A. F. Turbak (Eds.), *High-Tech Fibrous Materials*, 1st edition, ACS Symposium Series 457, 1991 [cited 23 March 2021], pp. 132–148. Available from: https://europepmc.org/article/med/3429470.

124. Food and beverage pulp packaging—molded pulp engineering, 2018 [cited 23 March 2021]. Available from: https://www.moldedpulpengineering.com/category/food-and-beverage-pulp-packaging/.

125. Polylactic acid laminating manufacturing/biodegradable products knowledge/biodegradable product manufacturer & supply by Happiness Moon, [cited 23 March 2021]. Available from: https://www.paperpulp-tableware.com/polylactic-acid-Laminating-Manufacturing.html.

126. E. Bryant, You can't recycle foam food containers. Here's why, 2017 [cited 23 March 2021]. Available from: https://www.democratandchronicle.com/story/news/local/columnists/bryant/2017/04/28/polystyrene-foam-containers-recycling-styrofoam/100976548/.

127. R. E. Lee, Y. Guo, H. Tamber, M. Planeta, S. N. S. Leung, Thermoforming of polylactic acid foam sheets: crystallization behaviors and thermal stability, *Ind. Eng. Chem. Res.* **2016**, *55*(3), 560–567 [cited 23 March 2021]. Available from: https://pubs.acs.org/doi/abs/10.1021/acs.iecr.5b03473.

128. Y. Liu, W. Zhang, F. Zhang, J. Leng, S. Pei, L. Wang, et al., Microstructural design for enhanced shape memory behavior of 4D printed composites based on carbon nanotube/polylactic acid filament, *Compos. Sci. Technol.* **2019**, *181*, 107692 [cited 23 March 2021]. Available from: https://linkinghub.elsevier.com/retrieve/pii/S026635381930171X.

129. S. Gong, B. Zhang, J. Zhang, Z. L. Wang, K. Ren, Biocompatible poly(lactic acid)-based hybrid piezoelectric and electret nanogenerator for electronic skin applications, *Adv. Funct. Mater.* **2020**, *30*(14), 1908724. Available from: https://onlinelibrary.wiley.com/doi/abs/10.1002/adfm.201908724.

130. J. M. Raquez, Y. Habibi, M. Murariu, P. Dubois, Polylactide (PLA)-based nanocomposites, *Prog. Polym. Sci.* **2013**, *38* (10–11), 1504–1542. Available from: http://dx.doi.org/10.1016/j.progpolymsci.2013.05.014.

131. A. Sharif, S. Mondal, M. E. Hoque, Polylactic acid (PLA)-based nanocomposites: Processing and properties, in: *Bio-based Polymers and Nanocomposites: Preparation, Processing, Properties & Performance*, Springer International Publishing, Cham, Switzerland, 2019, pp. 233–254 [cited 9 March 2021]. Available from: https://link.springer.com/chapter/10.1007/978-3-030-05825-8_11.

132. K. Piekarska, P. Sowinski, E. Piorkowska, M. M. U. Haque, M. Pracella, Structure and properties of hybrid PLA nanocomposites with inorganic nanofillers and cellulose fibers, *Compos. Part A Appl. Sci. Manuf.* **2016**, *82*, 34–41 [cited 9 March 2021]. Available from: https://linkinghub.elsevier.com/retrieve/pii/S1359835X15004297.

133. A. Basu, M. Nazarkovsky, R. Ghadi, W. Khan, A. J. Domb, Poly(lactic acid)-based nanocomposites, *Polym. Adv. Technol.* **2017**, *28*(8), 919–930. Available from: http://doi.wiley.com/10.1002/pat.3985

134. K. Jin, Y. Tang, X. Zhu, Y. Zhou, Polylactic acid based biocomposite films reinforced with silanized nanocrystalline cellulose, *Int. J. Biol. Macromol.* **2020**, *162*, 1109–1117 [cited 9 March 2021]. Available from: https://linkinghub.elsevier.com/retrieve/pii/S0141813020336436.

135. L. K. Kian, N. Saba, M. Jawaid, M. T. H. Sultan, A review on processing techniques of bast fibers nanocellulose and its polylactic acid (PLA) nanocomposites, *Int. J. Biol. Macromol.* **2019**, *121*, 1314–1328 [cited 9 March 2021]. Available from: https://linkinghub.elsevier.com/retrieve/pii/S0141813018331519.

136. M. B. Coltelli, P. Cinelli, V. Gigante, L. Aliotta, P. Morganti, L. Panariello, et al., Chitin nanofibrils in poly(lactic acid) (PLA) nanocomposites: dispersion and thermo-mechanical properties, *Int. J. Mol. Sci.* **2019**, *20*(3), 504. Available from: http://www.mdpi.com/1422-0067/20/3/504.

137. W. Yang, E. Fortunati, F. Dominici, G. Giovanale, A. Mazzaglia, G. M. Balestra, et al., Effect of cellulose and lignin on disintegration, antimicrobial and antioxidant properties of PLA active films, *Int. J. Biol. Macromol.* **2016**, *89*, 360–368. Available from: http://dx.doi.org/10.1016/j.ijbiomac.2016.04.068.

138. A. A. Singh, M. E. Genovese, G. Mancini, L. Marini, A. Athanassiou, Green processing route for polylactic acid-cellulose fiber biocomposites, *ACS Sustain. Chem. Eng.* **2020**, *8*(10), 4128–4136. Available from: https://dx.doi.org/10.1021/acssuschemeng.9b06760.

139. X. Wang, Y. Tang, X. Zhu, Y. Zhou, X. Hong, Preparation and characterization of polylactic acid/polyaniline/nanocrystalline cellulose nanocomposite films, *Int. J. Biol. Macromol.* **2020**, *146*, 1069–1075. Available from: https://doi.org/10.1016/j.ijbiomac.2019.09.233.

140. L. He, F. Song, D. F. Li, X. Zhao, X. L. Wang, Y. Z. Wang, Strong and tough polylactic acid based composites enabled by simultaneous reinforcement and interfacial compatibilization of microfibrillated cellulose, *ACS Sustain. Chem. Eng.* **2020**, *8*(3), 1573–1582.

141. J. K. Muiruri, S. Liu, W. S. Teo, J. Kong, C. He, Highly biodegradable and tough polylactic acid-cellulose nanocrystal composite, *ACS Sustain. Chem. Eng.* **2017**, *5*(5), 3929–3937. Available from: https://pubs.acs.org/doi/10.1021/acssuschemeng.6b03123.

142. W. Liu, Y. Dong, D. Liu, Y. Bai, X. Lu, Polylactic acid (PLA)/cellulose nanowhiskers (CNWs) composite nanofibers: microstructural and properties analysis, *J. Compos. Sci.* **2018**, *2*(1), 4. Available from: http://www.mdpi.com/2504-477X/2/1/4.

143. S. H. Sung, Y. Chang, J. Han, Development of polylactic acid nanocomposite films reinforced with cellulose nanocrystals derived from coffee silverskin, *Carbohydr. Polym.* **2017**, *169*, 495–503. Available from: https://linkinghub.elsevier.com/retrieve/pii/S0144861717304265.

144. S. Montes, I. Azcune, G. Cabañero, H. J. Grande, I. Odriozola, J. Labidi, Functionalization of cellulose nanocrystals in choline lactate ionic liquid, *Materials (Basel)* **2016**, *9*(7), 499. Available from: http://www.mdpi.com/1996-1944/9/7/499.

145. Q. Shi, C. Zhou, Y. Yue, W. Guo, Y. Wu, Q. Wu, Mechanical properties and in vitro degradation of electrospun bio-nanocomposite mats from PLA and cellulose nanocrystals, *Carbohydr. Polym.* **2012**, *90*(1), 301–308. Available from: https://linkinghub.elsevier.com/retrieve/pii/S014486171200464X.

146. M. Turalija, S. Bischof, A. Budimir, S. Gaan, Antimicrobial PLA films from environment friendly additives, *Compos. Part B Eng.* **2016**, *102*, 94–99. Available from: http://dx.doi.org/10.1016/j.compositesb.2016.07.017.

147. A. M. López Marzo, C. C. Mayorga-Martinez, M. Pumera, 3D-printed graphene direct electron transfer enzyme biosensors, *Biosens. Bioelectron.* **2020**, *151*(October 2019), 111980. Available from: https://linkinghub.elsevier.com/retrieve/pii/S0956566319310577.

148. B. L. Zhang, Y. Yang, Z. Q. Zhao, X. D. Guo, A gold nanoparticles deposited polymer microneedle enzymatic biosensor for glucose sensing, *Electrochim. Acta* **2020**, *358*, 136917. Available from: https://linkinghub.elsevier.com/retrieve/pii/S0013468620313104.

149. J. Y. Han, M. Li, H. Li, C. Li, J. Ye, B. Yang, Pt-poly(L-lactic acid) microelectrode-based microsensor for in situ glucose detection in sweat. *Biosens Bioelectron* **2020**, *170*(August), 112675. Available from: https://doi.org/10.1016/j.bios.2020.112675.

150. T. Wu, B. Li, W. Wang, L. Chen, Z. Li, M. Wang, et al., Strontium-substituted hydroxyapatite grown on graphene oxide nanosheet-reinforced chitosan scaffold to promote bone regeneration, *Biomater. Sci.* **2020**, *8*(16), 4603–4615 [cited 9 March 2021]. Available from: https://pubs.rsc.org/en/content/articlehtml/2020/bm/d0bm00523a.

151. Y. Li, Y. Yang, Z. Fang, X. Chen, Y. Wang, J. Kang, et al., Osteoinductivity and antibacterial properties of strontium ranelate-loaded poly(lactic-*co*-glycolic acid) microspheres with assembled silver and hydroxyapatite nanoparticles, *Front. Pharmacol.* **2018**, *9*(APR), 368 [cited 9 March 2021]. Available from: http://journal.frontiersin.org/article/10.3389/fphar.2018.00368/full.

152. Sinha S. Ray, K. Yamada, M. Okamoto, K. Ueda, Control of biodegradability of polylactide via nanocomposite technology, *Macromol. Mater. Eng.* **2003**, *288*(3), 203–208 [cited 9 March 2021]. Available from: http://doi.wiley.com/10.1002/mame.200390013.

153. S. S. Ray, K. Yamada, M. Okamoto, A. Ogami, K. Ueda, New polylactide/layered silicate nanocomposites, 4. Structure, properties and biodegradability, *Compos. Interfaces* **2003**, *10*(4–5), 435–450. Available from: https://www.tandfonline.com/doi/full/10.1163/156855403771953687.

154. R. Hiroi, S. S. Ray, M. Okamoto, T. Shiroi, Organically modified layered titanate: A new nanofiller to improve the performance of biodegradable polylactide, *Macromol. Rapid. Commun.* **2004**, *25*(15), 1359–1364 [cited 9 March 2021]. Available from: http://doi.wiley.com/10.1002/marc.200400173.

155. J. H. Chang, Y. U. An, G. S. Sur, Poly(lactic acid) nanocomposites with various organoclays. I. Thermomechanical properties, morphology, and gas permeability, *J. Polym. Sci. Part B Polym. Phys.* **2002**, *41*(1), 94–103 [cited 9 March 2021]. Available from: http://doi.wiley.com/10.1002/polb.10349.

156. N. Ogata, G. Jimenez, H. Kawai, T. Ogihara, Structure and thermal/mechanical properties of poly(L-lactide)-clay blend, *J. Polym. Sci. Part B Polym. Phys.* **1997**, *35*(2), 389–396 [cited 9 March 2021]. Available from: https://onlinelibrary.wiley.com/doi/10.1002/(SICI)1099-0488(19970130]35:2%3C389::AID-POLB14%3E3.0.CO;2-E.

157. M. A. Paul, C. Delcourt, M. Alexandre, P. Degée, F. Monteverde, A. Rulmont, et al., (Plasticized) polylactide/(organo-)clay nanocomposites by in situ intercalative polymerization, *Macromol. Chem. Phys.* **2005**, *206*(4), 484–498 [cited 9 March 2021]. Available from: http://doi.wiley.com/10.1002/macp.200400324.

158. J. Y. Nam, S. S. Ray, M. Okamoto, Crystallization behavior and morphology of biodegradable polylactide/layered silicate nanocomposite, *Macromolecules* **2003**, *36*(19), 7126–7131 [cited 9 March 2021]. Available from: https://pubs.acs.org/doi/abs/10.1021/ma034623j.

159. S. S. Ray, M. Okamoto, New polylactide/layered silicate nanocomposites, 6a melt rheology and foam processing, *Macromol. Mater. Eng.* **2003**, *288*(12), 936–944 [cited 9 March 2021]. Available from: http://doi.wiley.com/10.1002/mame.200300156.

160. S. S. Ray, P. Maiti, M. Okamoto, K. Yamada, K. Ueda, New polylactide/layered silicate nanocomposites. 1. Preparation, characterization, and properties, *Macromolecules* **2002**, *35*(8), 3104–3110 [cited 9 March 2021]. Available from: https://pubs.acs.org/doi/abs/10.1021/ma011613e.

161. S. S. Ray, K. Okamoto, K. Yamada, M. Okamoto, Novel porous ceramic material via burning of polylactide/layered silicate nanocomposite, *Nano Lett.* **2002**, *2*(4), 423–425 [cited 9 March 2021]. Available from: https://pubs.acs.org/doi/abs/10.1021/nl020284g.

162. S. S. Ray, M. Bousmina, Biodegradable polymers and their layered silicate nanocomposites: in greening the 21st century materials world, *Prog. Mater. Sci.* **2005**, *50*(8), 962–1079 [cited 9 March 2021]. Available from: https://linkinghub.elsevier.com/retrieve/pii/S0079642505000320.

163. S. Bourbigot, G. Fontaine, Flame retardancy of polylactide: an overview, *Polym. Chem.* **2010**, *1*(9), 1413–1422. Available from: http://xlink.rsc.org/?DOI=c0py00106f.

164. S. Liu, S. Qin, M. He, D. Zhou, Q. Qin, H. Wang, Current applications of poly(lactic acid) composites in tissue engineering and drug delivery, *Compos. Part B Eng.* **2020**, *199*, 108238 [cited 9 March 2021]. Available from: https://linkinghub.elsevier.com/retrieve/pii/S1359836820332881.

165. R. Zhang, H. Hu, Y. Liu, J. Tan, W. Chen, C. Ying, et al., Homogeneously dispersed composites of hydroxyapatite nanorods and poly(lactic acid) and their mechanical properties and crystallization behavior, *Compos. Part A Appl. Sci. Manuf.* **2020**, *132*(November 2019), 105841. Available from: https://doi.org/10.1016/j.compositesa.2020.105841.

166. C. Chen, X. Sun, W. Pan, Y. Hou, R. Liu, X. Jiang, et al., Graphene oxide-templated synthesis of hydroxyapatite nanowhiskers to improve the mechanical and osteoblastic

performance of poly(lactic acid) for bone tissue regeneration, *ACS Sustain. Chem. Eng.* **2018**, *6*(3), 3862–3869. Available from:https://pubs.acs.org/doi/10.1021/acssuschemeng.7b04192.

167. L. Cao, Q. Chen, L. B. Jiang, X. F. Yin, C. Bian, H. R. Wang, et al., Bioabsorbable self-retaining PLA/nano-sized β-TCP cervical spine interbody fusion cage in goat models: an in vivo study, *Int. J. Nanomed.* **2017**, *12*, 7197–7205. Availablefrom:https://www.dovepress.com/bioabsorbable-self-retaining-planano-sized-beta-tcp-cervical-spine-int-peer-reviewed-article-IJN.
168. D. Canales, M. Saavedra, M. T. Flores, J. Bejarano, J. A. Ortiz, P. Orihuela, et al., Effect of bioglass nanoparticles on the properties and bioactivity of poly(lactic acid) films, *J. Biomed. Mater. Res. Part A* **2020**, *108*(10), 2032–2043. Available from: https://onlinelibrary.wiley.com/doi/abs/10.1002/jbm.a.36963.
169. Y. T. Shieh, G. L. Liu, Effects of carbon nanotubes on crystallization and melting behavior of poly(L-lactide) via DSC and TMDSC studies, *J. Polym. Sci. Part B Polym. Phys.* **2007**, *45*(14), 1870–1881 [cited 9 March 2021]. Available from: http://doi.wiley.com/10.1002/polb.21184.
170. G. X. Chen, H. S. Kim, B. H. Park, J. S. Yoon, Synthesis of poly(L-lactide)-functionalized multiwalled carbon nanotubes by ring-opening polymerization, *Macromol. Chem. Phys.* **2007**, *208*(4), 389–398 [cited 9 March 2021]. Available from: http://doi.wiley.com/10.1002/macp.200600411
171. G. X. Chen, H. Shimizu, Multiwalled carbon nanotubes grafted with polyhedral oligomeric silsesquioxane and its dispersion in poly(L-lactide) matrix, *Polymer (Guildf)* **2008**, *49*(4), 943–951 [cited 9 March 2021]. Available from: https://linkinghub.elsevier.com/retrieve/pii/S0032386108000499.
172. D. Wu, L. Wu, M. Zhang, Y. Zhao, Viscoelasticity and thermal stability of polylactide composites with various functionalized carbon nanotubes, *Polym. Degrad. Stab.* **2008**, *93*(8), 1577–1584. Available from: https://linkinghub.elsevier.com/retrieve/pii/S0141391008001328.
173. C. F. Kuan, H. C. Kuan, C. C. M. Ma, C. H. Chen, Mechanical and electrical properties of multi-wall carbon nanotube/poly(lactic acid) composites, *J. Phys. Chem. Solids* **2008**, *69*(5–6), 1395–1398 [cited 9 March 2021]. Available from: https://linkinghub.elsevier.com/retrieve/pii/S0022369707006245.
174. C. F. Kuan, C. H. Chen, H. C. Kuan, K. C. Lin, C. L. Chiang, H. C. Peng, Multi-walled carbon nanotube reinforced poly (L-lactic acid) nanocomposites enhanced by water-crosslinking reaction, *J. Phys. Chem. Solids* **2008**, *69*(5–6), 1399–1402 [cited 9 March 2021]. Available from: https://linkinghub.elsevier.com/retrieve/pii/S0022369707006208.
175. K. Kobashi, T. Villmow, T. Andres, P. Pötschke, Liquid sensing of melt-processed poly(lactic acid)/multi-walled carbon nanotube composite films, *Sens. Actuators B Chem.* **2008**, *134*(2), 787–795 [cited 9 March 2021]. Available from: https://linkinghub.elsevier.com/retrieve/pii/S0925400508004346.
176. Z. Terzopoulou, P. A. Klonos, A. Kyritsis, A. Tziolas, A. Avgeropoulos, G. Z. Papageorgiou, et al., Interfacial interactions, crystallization and molecular mobility in nanocomposites of poly(lactic acid) filled with new hybrid inclusions based on graphene oxide and silica nanoparticles, *Polymer (Guildf)* **2019**, *166*(January), 1–12. Available from: https://doi.org/10.1016/j.polymer.2019.01.041.
177. H. I. Kim, M. Wang, S. K. Lee, J. Kang, N.am J. Do, L. Ci, et al., Tensile properties of millimeter-long multi-walled carbon nanotubes, *Sci. Rep.* **2017**, *7*(1), 9512. Available from: http://www.nature.com/articles/s41598-017-10279-0.
178. H. Xu, L. Xie, J.-B. Chen, X. Jiang, B. S. Hsiao, G. J. Zhong, et al., Strong and tough micro/nanostructured poly(lactic acid) by mimicking the multifunctional hierarchy of shell, *Mater. Horizons* **2014**, *1*(5), 546–552. Available from: http://dx.doi.org/10.1039/C4MH00085D.
179. K. Chen, J. Ding, L. Li, G. Shang, Y. Yue, L. Guo, Amorphous alumina nanosheets/polylactic acid artificial nacre, *Matter* **2019**, *1*(5), 1385–1398. Available from: https://doi.org/10.1016/j.matt.2019.09.012.
180. F. Narducci, K. Y. Lee, S. T. Pinho, Realising damage-tolerant nacre-inspired CFRP, *J. Mech. Phys. Solids* **2018**, *116*, 391–402. Available from: https://doi.org/10.1016/j.jmps.2018.04.004.
181. R. Gunti, A. V. Ratna Prasad, A. V. S. S. K. S. Gupta. Preparation and properties of successive alkali treated completely biodegradable short jute fiber reinforced PLA composites, *Polym. Compos.* **2016**, *37*(7), 2160–2170. Available from: http://doi.wiley.com/10.1002/pc.23395.
182. N. Teramoto, K. Urata, K. Ozawa, M. Shibata, Biodegradation of aliphatic polyester composites reinforced by abaca fiber, *Polym. Degrad. Stab.* **2004**, *86*(3), 401–409 [cited 9 March 2021]. Available from: https://linkinghub.elsevier.com/retrieve/pii/S0141391004001545.
183. X. Yin, Y. Li, P. Weng, Q. Yu, L. Han, J. Xu, et al., Simultaneous enhancement of toughness, strength and superhydrophilicity of solvent-free microcrystalline cellulose fluids/poly(lactic acid) fibers fabricated via electrospinning approach, *Compos. Sci. Technol.* **2018**, *167*, 190–198. Available from: https://linkinghub.elsevier.com/retrieve/pii/S0266353818312247.
184. F. Suzuki, T. Mochizuki, Resin molded article. United States Patent Application, US20040180990A1, 2003 [cited 12 March 2021]. Available from: https://patents.google.com/patent/US20040180990A1/en?oq=20040180990.
185. A. K. Bledzki, S. Reihmane, J. Gassan, Properties and modification methods for vegetable fibers for natural fiber composites, *J. Appl. Polym. Sci.* **1996**, *59*(8), 1329–1336 [cited 12 March 2021]. Available from: https://onlinelibrary.wiley.com/doi/10.1002/(SICI)1097-4628(19960222]59:8%3C1329::AID-APP17%3E3.0.CO;2-0.
186. J. P. Siregar, J. Jaafar, T. Cionita, C. C. Jie, D. Bachtiar, M. R. M. Rejab, et al., The effect of maleic anhydride polyethylene on mechanical properties of pineapple leaf fibre reinforced polylactic acid composites, *Int. J. Precis. Eng. Manuf. Green Technol.* **2019**, *6*(1), 101–112. Available from: http://link.springer.com/10.1007/s40684-019-00018-3.
187. T. Yu, N. Jiang, Y. Li, Study on short ramie fiber/poly(lactic acid) composites compatibilized by maleic anhydride, *Compos. Part A Appl. Sci. Manuf.* **2014**, *64*, 139–146. Available from: https://linkinghub.elsevier.com/retrieve/pii/S1359835X14001432.

188. N. Graupner, Application of lignin as natural adhesion promoter in cotton fibre-reinforced poly(lactic acid) (PLA) composites, *J. Mater. Sci.* **2008**, *43*(15), 5222–5229 [cited 21 March 2021]. Available from: https://link.springer.com/article/10.1007/s10853-008-2762-3.

189. M. Gutiérrez-Sánchez, V. A. Escobar-Barrios, A. Pozos-Guillén, D. M. Escobar-García, RGD-functionalization of PLA/starch scaffolds obtained by electrospinning and evaluated in vitro for potential bone regeneration, *Mater. Sci. Eng. C* **2019**, *96*, 798–806. Available from: https://linkinghub.elsevier.com/retrieve/pii/S0928493118311767.

190. B. Bhushan, R. Kumar, Plasma treated and untreated thermoplastic biopolymers/biocomposites in tissue engineering and biodegradable implants, in: *Materials for Biomedical Engineering*, Elsevier, Amsterdam, The Netherlands, 2019, pp. 339–369. Available from: https://linkinghub.elsevier.com/retrieve/pii/B9780128169018000110.

191. X. Li, Y. Wang, M. Guo, Z. Wang, N. Shao, P. Zhang, et al., Degradable three dimensional-printed polylactic acid scaffold with long-term antibacterial activity, *ACS Sustain. Chem. Eng.* **2018**, *6*(2), 2047–2054 [cited 31 March 2021]. Available from: https://pubs.acs.org/doi/abs/10.1021/acssuschemeng.7b03464.

192. M. Cavo, S. Scaglione, Scaffold microstructure effects on functional and mechanical performance: integration of theoretical and experimental approaches for bone tissue engineering applications, *Mater. Sci. C. Eng.* **2016**, *68*, 872–879.

193. U. Ritz, R. Gerke, H. Götz, S. Stein, P. M. Rommens. A new bone substitute developed from 3D-prints of polylactide (PLA) loaded with collagen i: an in vitro study, *Int. J. Mol. Sci.* **2017**, *18*(12), 2569 [cited 31 March 2021]. Available from: http://www.mdpi.com/1422-0067/18/12/2569.

194. M. Schneider, C. Günter, A. Taubert, Co-deposition of a hydrogel/calcium phosphate hybrid layer on 3D printed poly(lactic acid) scaffolds via dip coating: towards automated biomaterials fabrication, *Polymers (Basel)* **2018**, *10*(3), 275 [cited 31 March 2021]. Available from: http://www.mdpi.com/2073-4360/10/3/275.

195. S. Naghieh, E. Foroozmehr, M. Badrossamay, M. Kharaziha, Combinational processing of 3D printing and electrospinning of hierarchical poly(lactic acid)/gelatin-forsterite scaffolds as a biocomposite: mechanical and biological assessment, *Mater. Des.* **2017**, *133*, 128–135.

196. Y. C. Chou, D. Lee, T. M. Chang, Y. H. Hsu, Y. H. Yu, E. C. Chan, et al., Combination of a biodegradable three-dimensional (3D)—printed cage for mechanical support and nanofibrous membranes for sustainable release of antimicrobial agents for treating the femoral metaphyseal comminuted fracture, *J. Mech. Behav. Biomed. Mater.* **2017**, *72*, 209–218.

197. C. L. Manzanares-Palenzuela, S. Hermanova, Z. Sofer, M. Pumera, Proteinase-sculptured 3D-printed graphene/polylactic acid electrodes as potential biosensing platforms: towards enzymatic modeling of 3D-printed structures, *Nanoscale* **2019**, *11*(25), 12124–12131. Available from: http://xlink.rsc.org/?DOI=C9NR02754H.

198. K. T. Paula, G. Gaál, G. F. B. Almeida, M. B. Andrade, M. H. M. Facure, D. S. Correa, et al., Femtosecond laser micromachining of polylactic acid/graphene composites for designing interdigitated microelectrodes for sensor applications, *Opt. Laser Technol.* **2018**, *101*, 74–79. Available from: https://doi.org/10.1016/j.optlastec.2017.11.006.

199. J. G. Walters, S. Ahmed, I. M. Terrero Rodríguez, G. D. O'Neil, Trace analysis of heavy metals (Cd, Pb, Hg) using native and modified 3D printed graphene/poly(lactic acid) composite electrodes, *Electroanalysis* **2020**, *32*(4), 859–866. Available from: https://onlinelibrary.wiley.com/doi/abs/10.1002/elan.201900658.

200. X. Chen, G. Chen, G. Wang, P. Zhu, C. Gao, Recent progress on 3D-printed polylactic acid and its applications in bone repair, *Adv. Eng. Mater.* **2020**, *22*(4), 1901065. Available from: https://onlinelibrary.wiley.com/doi/10.1002/adem.201901065.

201. A. L. Coolen, C. Lacroix, P. Mercier-Gouy, E. Delaune, C. Monge, J. Y. Exposito, et al., Poly(lactic acid) nanoparticles and cell-penetrating peptide potentiate mRNA-based vaccine expression in dendritic cells triggering their activation, *Biomaterials* **2019**, *195*, 23–37. Available from: https://linkinghub.elsevier.com/retrieve/pii/S0142961218308536.

202. C. Guo, Y. Niu, Cellular automaton simulation for degradation of poly lactic acid with acceleratable reaction-diffusion model, *ACS Biomater. Sci. Eng.* **2019**, *5*(4), 1771–1783. Available from: https://pubs.acs.org/doi/10.1021/acsbiomaterials.9b00015.

203. T. Fujiura, K. Sakamoto, T. Tanaka, Y. Imaida, A study on preparation and mechanical properties of long jute fiber reinforced polylactic acid by the injection molding process, *WIT Trans. Built Environ.* **2008**, *97*, 231–240 [cited 12 March 2021]. Available from: www.witpress.com.

204. A. Le Duigou, P. Davies, C. Baley, Seawater ageing of flax/poly(lactic acid) biocomposites, *Polym. Degrad. Stab.* **2009**, *94*(7), 1151–1162 [cited 9 March 2021]. Available from: https://linkinghub.elsevier.com/retrieve/pii/S0141391009000792

205. N. Graupner, Improvement of the mechanical properties of biodegradable hemp fiber reinforced poly(lactic acid) (PLA) composites by the admixture of man-made cellulose fibers, *J. Compos. Mater.* **2009**, *43*(6), 689–702 [cited 12 March 2021]. Available from: http://journals.sagepub.com/doi/10.1177/0021998308100688.

206. J. Ganster, H. P. Fink, Novel cellulose fibre reinforced thermoplastic materials, *Cellulose* **2006**, *13*(3), 271–280. Available from: https://link.springer.com/article/10.1007/s10570-005-9045-9.

207. I. Ahmed, P. S. Cronin, E. A. Neel, A. J. Parsons, J. C. Knowles, C. D. Rudd, Retention of mechanical properties and cytocompatibility of a phosphate-based glass fiber/polylactic acid composite, *J. Biomed. Mater. Res. Part B Appl. Biomater.* **2009**, *89*(1), 18–27 [cited 9 March 2021]. Available from: http://doi.wiley.com/10.1002/jbm.b.31182.

208. M. Bühler, P. E. Bourban, J. A. E. Månson, Cellular composites based on continuous fibres and bioresorbable polymers, *Compos. Part A Appl. Sci. Manuf.* **2008**, *39*(12):1779–1786. Available from: https://linkinghub.elsevier.com/retrieve/pii/S1359835X08001437.

209. M. S. Huda, L. T. Drzal, M. Misra, A. K. Mohanty, Wood-fiber-reinforced poly(lactic acid) composites: evaluation of the physicomechanical and morphological properties, *J. Appl. Polym.*

*Sci.* **2006**, *102*(5), 4856–4869 [cited 9 March 2021]. Available from: http://doi.wiley.com/10.1002/app.24829.

210. M. Shibata, K. I. Takachiyo, K. Ozawa, R. Yosomiya, H. Takeishi Biodegradable polyester composites reinforced with short abaca fiber, *J. Appl. Polym. Sci.* **2002**, *85*(1), 129–138. Available from: http://doi.wiley.com/10.1002/app.10665.
211. M. Avella, Bogoeva-G. Gaceva, Bužarovska A., M. E. Errico, G. Gentile, A. Grozdanov, Poly(lactic acid)-based biocomposites reinforced with kenaf fibers, *J. Appl. Polym. Sci.* **2008**, *108*(6), 3542–3551 [cited 9 March 2021]. Available from: http://doi.wiley.com/10.1002/app.28004.
212. T. Nishino, K. Hirao, M. Kotera, K. Nakamae, H. Inagaki, Kenaf reinforced biodegradable composite, *Compos. Sci. Technol.* **2003**, *63*(9), 1281–1286 [cited 9 March 2021]. Available from: https://linkinghub.elsevier.com/retrieve/pii/S026635380300099X.
213. E. Pirhonen, G. Grandi, P. Törmälä, Bioactive glass fiber/polylactide composite, *Key Eng. Mater.* **2001**, *192–195*, 725–728. Available from: https://www.scientific.net/KEM.192-195.725.
214. W. Y. Zhou, S. H. Lee, M. Wang, W. L. Cheung, W. Y. Ip, Selective laser sintering of porous tissue engineering scaffolds from poly(L-lactide)/carbonated hydroxyapatite nanocomposite microspheres, *J. Mater. Sci. Mater. Med.* **2008**, *19*(7), 2535–2540 [cited 27 March 2021]. Available from: https://link.springer.com/article/10.1007/s10856-007-3089-3.
215. J. Bai, R. D. Goodridge, R. J. M. Hague, M. Okamoto, Processing and characterization of a polylactic acid/nanoclay composite for laser sintering, *Polym. Compos.* **2017**, *38*(11), 2570–2576 [cited 27 March 2021]. Available from: http://doi.wiley.com/10.1002/pc.23848.
216. X. Huang, S. Lin, Y. Hu, Y. Liao, W. Wang, Z. Zhang, et al., Preparation and characterization of digital coral hydroxyapatite artificial bone scaffolds based on 3D printing, *J. Biomater. Tissue Eng.* **2018**, *8*(7), 1038–1045 [cited 27 March 2021]. Available from: http://www.ingentaconnect.com/content/10.1166/jbt.2018.1831.
217. Q. Chen, J. D. Mangadlao, J. Wallat, A. De Leon, J. K. Pokorski, R. C. Advincula, 3D printing biocompatible polyurethane/poly(lactic acid)/graphene oxide nanocomposites: anisotropic properties, *ACS Appl. Mater. Interfaces* **2017**, *9*(4), 4015–4023. Available from: https://pubs.acs.org/doi/10.1021/acsami.6b11793.
218. Z. C. Kennedy, J. F. Christ, Printing polymer blends through in situ active mixing during fused filament fabrication, *Addit. Manuf.* **2020**, *36*(May), 101233. Available from: https://doi.org/10.1016/j.addma.2020.101233.
219. Y. He, Z.-t. Yang, J.-p. Qu, Super-toughed poly(lactic acid)/thermoplastic poly(ether)urethane nanofiber composites with in-situ formation of aligned nanofibers prepared by an innovative eccentric rotor extruder, *Compos. Sci. Technol.* **2019**, *169*(May 2018), 135–141. Available from: https://doi.org/10.1016/j.compscitech.2018.11.002.
220. M. N. Hafsa, M. Ibrahim, M. S. Wahab, M. S. Zahid, Evaluation of FDM pattern with ABS and PLA material, *Appl. Mech. Mater.* **2014**, 55–59 [cited 27 March 2021]. Available from: https://www.scientific.net/AMM.465-466.55.
221. A. Rodríguez-Panes, J. Claver, A. M. Camacho, The influence of manufacturing parameters on the mechanical behaviour of PLA and ABS pieces manufactured by FDM: a comparative analysis, *Materials (Basel)* **2018**, *11*(8), 1333 [cited 27 March 2021]. Available from: http://www.mdpi.com/1996-1944/11/8/1333.
222. M. Maniruzzaman (Ed.), *3D and 4D Printing in Biomedical Applications*, Wiley-VCH Verlag GmbH & Co. KGaA, Weinheim, Germany, 2019 [cited 27 March 2021]. Available from: http://doi.wiley.com/10.1002/9783527813704.
223. M. Van den Eynde, P. Van Puyvelde, 3D printing of poly(lactic acid), in: M. L. Di Lorenzo, R. Androsch (Eds.), *Industrial Applications of Poly(Lactic Acid)*, 1st edition, Springer, Cham, 2018 [cited 27 March 2021], pp. 139–158. Available from: https://link.springer.com/chapter/10.1007/12_2017_28.
224. P. Varga, D. Lorinczy, L. Toth, A. Pentek, M. Nyitrai, P. Maroti, Novel pla-caco3 composites in additive manufacturing of upper limb casts and orthotics-a feasibility study, *Mater. Res. Express* **2019**, *6*(4), 045317. Available from: https://iopscience.iop.org/article/10.1088/2053-1591/aafdbc.
225. F. Alam, V. R. Shukla, K. M. Varadarajan, S. Kumar, Microarchitected 3D printed polylactic acid (PLA) nanocomposite scaffolds for biomedical applications, *J. Mech. Behav. Biomed. Mater.* **2020**, *103*, 103576. Available from: https://doi.org/10.1016/j.jmbbm.2019.103576.
226. F. Alam, K. M. Varadarajan, S. Kumar, 3D printed polylactic acid nanocomposite scaffolds for tissue engineering applications, *Polym. Test.* **2020**, *81*, 106203. Available from: https://doi.org/10.1016/j.polymertesting.2019.106203.
227. R. M. Cardoso, D. P. Rocha, R. G. Rocha, J. S. Stefano, R. A. B. Silva, E. M. Richter, et al., 3D-printing pen versus desktop 3D-printers: fabrication of carbon black/polylactic acid electrodes for single-drop detection of 2,4,6-trinitrotoluene, *Anal. Chim. Acta.* **2020**, *1132*, 10–19. Available from: https://linkinghub.elsevier.com/retrieve/pii/S0003267020307662.
228. V. A. O. P. Silva, Fernandes-W. S. Junior, D. P. Rocha, J. S. Stefano, R. A. A. Munoz, J. A. Bonacin, et al., 3D-printed reduced graphene oxide/polylactic acid electrodes: a new prototyped platform for sensing and biosensing applications, *Biosens. Bioelectron.* **2020**, *170*, 112684. Available from: https://linkinghub.elsevier.com/retrieve/pii/S0956566320306734.
229. E. Vaněčková, M. Bouša, Š. Nováková Lachmanová, J. Rathouský, M. Gál, T. Sebechlebská, et al., 3D printed polylactic acid/carbon black electrodes with nearly ideal electrochemical behavior, *J. Electroanal. Chem.* **2020**, *857*, 113745. Available from: https://doi.org/10.1016/j.jelechem.2019.113745.
230. K. Oksman, M. Skrifvars, J. F. Selin, Natural fibres as reinforcement in polylactic acid (PLA) composites, *Compos. Sci. Technol.* **2003**, *63*(9), 1317–1324 [cited 12 March 2021]. Available from: https://linkinghub.elsevier.com/retrieve/pii/S0266353803001039.
231. S. Ochi, Mechanical properties of kenaf fibers and kenaf/PLA composites, *Mech. Mater.* **2008**, *40*(4–5), 446–452 [cited 12 March 2021]. Available from: https://linkinghub.elsevier.com/retrieve/pii/S0167663607001573.

232. S. Pilla, S. Gong, O'E. Neill, L. Yang, R. M. Rowell, Polylactide-recycled wood fiber composites, *J. Appl. Polym. Sci.* **2009**, *111*(1), 37–47. Available from: http://doi.wiley.com/10.1002/app.28860.

233. S. W. Kuo, C. F. Huang, Y. C. Tung, F. C. Chang, Effect of bisphenol A on the miscibility, phase morphology, and specific interaction in immiscible biodegradable poly(ε-caprolactone)/poly(L-lactide) blends, *J. Appl. Polym. Sci.* **2006**, *100*(2), 1146–1161 [cited 11 March 2021]. Available from: http://doi.wiley.com/10.1002/app.23227.

234. J. Li, X. L. Lu, Y. F. Zheng, Effect of surface modified hydroxyapatite on the tensile property improvement of HA/PLA composite, *Appl. Surf. Sci.* **2008**, *255*(2), 494–497 [cited 11 March 2021]. Available from: https://linkinghub.elsevier.com/retrieve/pii/S0169433208015067.

235. N. Saba, M. Jawaid, O. Y. Alothman, M. T. Paridah, A review on dynamic mechanical properties of natural fibre reinforced polymer composites, *Constr. Build. Mater.* **2016**, *106*, 149–159. Available from: https://linkinghub.elsevier.com/retrieve/pii/S0950061815307479.

236. W. H. Ferreira, C. T. Andrade, The role of graphene on thermally induced shape memory properties of poly(lactic acid) extruded composites, *J. Therm. Anal. Calorim.* **2021**, *143*(4), 3107–3115. Available from: http://link.springer.com/10.1007/s10973-020-09402-7.

237. C. A. Murphy, M. N. Collins, Microcrystalline cellulose reinforced polylactic acid biocomposite filaments for 3D printing, *Polym. Compos.* **2018**, *39*(4), 1311–1320. Available from: http://doi.wiley.com/10.1002/pc.24069.

238. I. Turku, T. Kärki, Research progress in wood-plastic nanocomposites: a review, *J. Thermoplast. Compos. Mater.* **2014**, *27*(2), 180–204. Available from: http://journals.sagepub.com/doi/10.1177/0892705713486131.

239. R. A. Talib, I. S. M. A. Tawakkal, K. Abdan, The influence of mercerised kenaf fibres reinforced polylactic acid composites on dynamic mechanical analysis, *Key Eng. Mater.* **2011**, *471–472*, 815–820. Available from: https://www.scientific.net/KEM.471-472.815.

240. Z. Samouh, K. Molnar, F. Boussu, O. Cherkaoui, R. El Moznine, Mechanical and thermal characterization of sisal fiber reinforced polylactic acid composites, *Polym. Adv. Technol.* **2019**, *30*(3), 529–537. Available from: http://doi.wiley.com/10.1002/pat.4488.

241. W. Ning, Z. Xingxiang, Y. Jiugao, F. Jianming, Partially miscible poly(lactic acid)-blend-poly(propylene carbonate) filled with carbon black as conductive polymer composite, *Polym. Int.* **2008**, *57*(9), 1027–1035 [cited 11 March 2021]. Available from: http://doi.wiley.com/10.1002/pi.2442.

242. S. S. Ray, M. Okamoto Biodegradable polylactide and its nanocomposites: opening a new dimension for plastics and composites, *Macromol. Rapid Commun.* **2003**, *24*(14), 815–840 [cited 9 March 2021]. Available from: http://doi.wiley.com/10.1002/marc.200300008.

243. P. J. Jandas, S. Mohanty, S. K. Nayak, Thermal properties and cold crystallization kinetics of surface-treated banana fiber (BF)-reinforced poly(lactic acid) (PLA) nanocomposites, *J. Therm. Anal. Calorim.* **2013**, *114*(3), 1265–1278 [cited 9 March 2021]. Available from: http://link.springer.com/10.1007/s10973-013-3102-7.

244. Y. W. Hsu, C. C. Wu, S. M. Wu, C. C. Su, Synthesis and properties of carbon nanotube-grafted silica nanoarchitecture-reinforced poly(lactic acid), *Materials (Basel)* **2017**, *10*(7), 829 [cited 9 March 2021]. Available from: http://www.mdpi.com/1996-1944/10/7/829.

245. A. Nuzzo, S. Coiai, S. C. Carroccio, N. T. Dintcheva, C. Gambarotti, G. Filippone, Heat-resistant fully bio-based nanocomposite blends based on poly(lactic acid), *Macromol. Mater. Eng.* **2014**, *299*(1), 31–40 [cited 9 March 2021]. Available from: http://doi.wiley.com/10.1002/mame.201300051.

246. F. L. Jin, R. R. Hu, S. J. Park, Improvement of thermal behaviors of biodegradable poly(lactic acid) polymer: a review, *Compos. Part B Eng.* **2019**, *164*, 287–296 [cited 9 March 2021]. Available from: https://linkinghub.elsevier.com/retrieve/pii/S1359836818325435.

247. P. Chen, Y. Wang, T. Wei, Z. Meng, X. Jia, K. Xi, Greatly enhanced mechanical properties and heat distortion resistance of poly(L-lactic acid) upon compositing with functionalized reduced graphene oxide, *J. Mater. Chem. A* **2013**, *1*(32), 9028–9032 [cited 9 March 2021]. Available from: http://xlink.rsc.org/?DOI=c3ta12060k.

248. X. W. Cheng, J. P. Guan, R. C. Tang, K. Q. Liu, Improvement of flame retardancy of poly(lactic acid) nonwoven fabric with a phosphorus- containing flame retardant, *J. Ind. Text.* **2016**, *46*(3), 914–928. Available from: http://journals.sagepub.com/doi/10.1177/1528083715606105.

249. O. Avinc, R. Day, C. Carr, M. Wilding, Effect of combined flame retardant, liquid repellent and softener finishes on poly(lactic acid) (PLA) fabric performance, *Text. Res. J.*. **2012**, *82*(10), 975–984. Available from: http://journals.sagepub.com/doi/10.1177/0040517511418557.

250. A. Cayla, F. Rault, S. Giraud, F. Salaün, V. Fierro, A. Celzard, PLA with intumescent system containing lignin and ammonium polyphosphate for flame retardant textile, *Polymers (Basel)* **2016**, *8*(9), 331. Available from: http://www.mdpi.com/2073-4360/8/9/331.

251. R. Zhang, X. Xiao, Q. Tai, H. Huang, J. Yang, Y. Hu, Preparation of lignin-silica hybrids and its application in intumescent flame-retardant poly(lactic acid) system, *High Perform. Polym.* **2012**, *24*(8), 738–746. Available from: http://journals.sagepub.com/doi/10.1177/0954008312451476.

252. S. Yu, H. Xiang, J. Zhou, M. Zhu, Enhanced flame-retardant performance of poly (lactic acid) (PLA) composite by using intrinsically phosphorus-containing PLA, *Prog. Nat. Sci. Mater. Int.* **2018**, *28*(5), 590–597. Available from: https://doi.org/10.1016/j.pnsc.2018.09.002.

253. D. Elangovan, I. E. Yuzay, S. E. M. Selke, R. Auras, Poly(L-lactic acid) metal organic framework composites: optical, thermal and mechanical properties, *Polym. Int.* **2012**, *61*(1), 30–37. Available from: http://doi.wiley.com/10.1002/pi.3186.

254. X. Shi, X. Dai, Y. Cao, J. Li, C. Huo, X. Wang, Degradable poly(lactic acid)/metal-organic framework nanocomposites exhibiting good mechanical, flame retardant, and dielectric

properties for the fabrication of disposable electronics, *Ind. Eng. Chem. Res.* **2017**, *56*(14), 3887–3894. Available from: https://pubs.acs.org/doi/10.1021/acs.iecr.6b04204.

255. S. Solarski, M. Ferreira, E. Devaux, G. Fontaine, P. Bachelet, S. Bourbigot, et al., Designing polylactide/clay nanocomposites for textile applications: effect of processing conditions, spinning, and characterization, *J. Appl. Polym. Sci.* **2008**, *109*(2), 841–851. Available from: http://doi.wiley.com/10.1002/app.28138.
256. S. Bourbigot, G. Fontaine, A. Gallos, S. Bellayer, Reactive extrusion of PLA and of PLA/carbon nanotubes nanocomposite: processing, characterization and flame retardancy, *Polym. Adv. Technol.* **2011**, *22*(1), 30–37. Available from: http://doi.wiley.com/10.1002/pat.1715.
257. L. Gu, J. Qiu, Y. Yao, E. Sakai, L. Yang, Functionalized MWCNTs modified flame retardant PLA nanocomposites and cold rolling process for improving mechanical properties, *Compos. Sci. Technol.* **2018**, *161*, 39–49. Available from: https://doi.org/10.1016/j.compscitech.2018.03.033.
258. C. Réti, M. Casetta, S. Duquesne, S. Bourbigot, R. Delobel, Flammability properties of intumescent PLA starch and lignin, *Polym. Adv. Technol.* **2008**, *19*(6), 628–635. Available from: http://doi.wiley.com/10.1002/pat.1130.
259. R. Zhang, X. Xiao, Q. Tai, H. Huang, Y. Hu, Modification of lignin and its application as char agent in intumescent flame-retardant poly(lactic acid), *Polym. Eng. Sci.* **2012**, *52*(12), 2620–2626. Available from: http://doi.wiley.com/10.1002/pen.23214.
260. U. Pagga, Biodegradability and compostability of polymers-test methods and criteria for evaluation, *J. Environ. Polym. Degrad.* **1996**, *4*(3), 173–178 [cited 12 March 2021]. Available from: https://link.springer.com/article/10.1007/BF02067451.
261. M. Itävaara, S. Karjomaa, J. F. Selin, Biodegradation of polylactide in aerobic and anaerobic thermophilic conditions, *Chemosphere* **2002**, *46*(6), 879–885 [cited 12 March 2021]. Available from: https://pubmed.ncbi.nlm.nih.gov/11922068/0.
262. R. Iovino, R. Zullo, M. A. Rao, L. Cassar, L. Gianfreda, Biodegradation of poly(lactic acid)/starch/coir biocomposites under controlled composting conditions, *Polym. Degrad. Stab.* **2008**, *93*(1), 147–157 [cited 12 March 2021]. Available from: https://linkinghub.elsevier.com/retrieve/pii/S014139100700300X.
263. Y. Tokiwa, A. Jarerat, Biodegradation of poly(L-lactide), *Biotechnol. Lett.* **2004**, *26*, 771–777 [cited 12 March 2021]. Available from: https://link.springer.com/article/10.1023/B:BILE.0000025927.31028.e3.
264. Y. Tokiwa, B. P. Calabia, Biodegradability and biodegradation of poly(lactide), *Appl. Microbiol. Biotechnol.* **2006**, *72*, 244–251 [cited 12 March 2021]. Available from: https://link.springer.com/article/10.1007/s00253-006-0488-1.
265. B. A. Ramsay, V. Langlade, P. J. Carreau, J. A. Ramsay, Biodegradability and mechanical properties of poly-(β-hydroxybutyrate- co-β-hydroxyvalerate)-starch blends, *Appl. Environ. Microbiol.* **1993**, *59*(4), 1242–1246 [cited 12 March 2021]. Available from: https://aem.asm.org/content/59/4/1242.
266. T. Iwata, Y. Doi, Morphology and enzymatic degradation of poly(L-lactic acid) single crystals, *Macromolecules* **1998**, *31*(8), 2461–2467 [cited 12 March 2021]. Available from: https://pubs.acs.org/doi/abs/10.1021/ma980008h.
267. R. T. MacDonald, S. P. McCarthy, R. A. Gross, Enzymatic degradability of poly(lactide): effects of chain stereochemistry and material crystallinity, *Macromolecules*. **1996**, *29*(23), 7356–7361 [cited 12 March 2021]. Available from: https://pubs.acs.org/doi/abs/10.1021/ma960513j.
268. Y. Luo, Z. Lin, G. Guo, Biodegradation assessment of poly (lactic acid) filled with functionalized titania nanoparticles ($PLA/TiO_2$) under compost conditions, *Nanoscale Res. Lett.* **2019**, *14*(1), 56. Available from: https://nanoscalereslett.springeropen.com/articles/10.1186/s11671-019-2891-4.
269. M. A. Elsawy, K. H. Kim, J. W. Park, A. Deep, Hydrolytic degradation of polylactic acid (PLA) and its composites, *Renew. Sustain. Energy Rev.* **2017**, *79*, 1346–1352. Available from: https://linkinghub.elsevier.com/retrieve/pii/S1364032117307876.
270. Z. Wang, Y. Wang, Y. Ito, P. Zhang, X. Chen, A comparative study on the in vivo degradation of poly(L-lactide) based composite implants for bone fracture fixation, *Sci. Rep.* **2016**, *6*(1), 20770. Available from: http://www.nature.com/articles/srep20770.
271. F. Xie, F. L. Qing, B. Gu, K. Liu, X. S. Guo, in vitro and in vivo evaluation of a biodegradable chitosan-PLA composite peripheral nerve guide conduit material, *Microsurgery* **2008**, *28*(6), 471–479. Available from: http://doi.wiley.com/10.1002/micr.20514.
272. Y. Liu, H. Lv, X. Lan, J. Leng, S. Du, Review of electroactive shape-memory polymer composite, *Compos. Sci. Technol.* **2009**, *69*(13), 2064–2068. Available from: https://linkinghub.elsevier.com/retrieve/pii/S0266353808002923.
273. J. Leng, X. Lan, Y. Liu, S. Du, Shape-memory polymers and their composites: stimulus methods and applications, *Prog. Mater. Sci.* **2011**, *56*(7), 1077–1135. Available from: https://linkinghub.elsevier.com/retrieve/pii/S0079642511000429.
274. Q. Zhao, H. J. Qi, T. Xie, Recent progress in shape memory polymer: new behavior, enabling materials, and mechanistic understanding, *Prog. Polym. Sci.* **2015**, *49–50*, 79–120. Available from: https://linkinghub.elsevier.com/retrieve/pii/S0079670015000477.
275. J. Hu, Y. Zhu, H. Huang, J. Lu, Recent advances in shape-memory polymers: structure, mechanism, functionality, modeling and applications, *Prog. Polym. Sci.* **2012**, *37*(12), 1720–1763. Available from: https://linkinghub.elsevier.com/retrieve/pii/S0079670012000706.
276. Y. Chen, C. Chen, H. U. Rehman, X. Zheng, H. Li, H. Liu, et al., Shape-memory polymeric artificial muscles: mechanisms, applications and challenges, *Molecules* **2020**, *25*(18), 4246. Available from: https://www.mdpi.com/1420-3049/25/18/4246.
277. G. Scalet, Two-way and multiple-way shape memory polymers for soft robotics: an overview, *Actuators* **2020**, *9*(1), 10.
278. M. Behl, A. Lendlein, Shape-memory polymers, *Mater. Today* **2007**, *10*(4), 20–28. Available from: https://linkinghub.elsevier.com/retrieve/pii/S1369702107700470.

279. R. S. Langer, A. Lendlein, A. Schmidt, H. Grablowitz, Biodegradable shape memory polymers, *Smart Mater. Bull.* **2001**, *2001*, 14. Available from: https://patents.google.com/patent/US6160084A/en.

280. J. Xu, J. Song, Polylactic acid (PLA)-based shape-memory materials for biomedical applications, in: L. Yahia (Ed.) *Shape Memory Polymers for Biomedical Applications*, 1st edition, Elsevier, Cambridge, 2015, pp. 197–217. Available from: https://linkinghub.elsevier.com/retrieve/pii/B9780857096982000106.

281. X. Qi, H. Xiu, Y. Wei, Y. Zhou, Y. Guo, R. Huang, et al., Enhanced shape memory property of polylactide/thermoplastic poly(ether)urethane composites via carbon black self-networking induced co-continuous structure, *Compos. Sci. Technol.* **2017**, *139*, 8–16. Available from: http://dx.doi.org/10.1016/j.compscitech.2016.12.007.

282. M. Barmouz, A. H. Behravesh, Shape memory behaviors in cylindrical shell PLA/TPU-cellulose nanofiber bio-nanocomposites: analytical and experimental assessment, *Compos. Part A Appl. Sci. Manuf.* **2017**, *101*, 160–172. Available from: http://dx.doi.org/10.1016/j.compositesa.2017.06.014.

283. F. Khademeh Molavi, I. Ghasemi, M. Messori, M. Esfandeh, Nanocomposites based on poly(L-lactide)/poly(ε-caprolactone) blends with triple-shape memory behavior: effect of the incorporation of graphene nanoplatelets (GNps), *Compos. Sci. Technol.* **2017**, *151*, 219–227. Available from: http://dx.doi.org/10.1016/j.compscitech.2017.08.021.

284. H. Liu, H. He, B. Huang, Favorable thermoresponsive shape memory effects of 3D printed poly(lactic acid)/poly(ε-caprolactone) blends fabricated by fused deposition modeling, *Macromol. Mater. Eng.* **2020**, *305*(11), 2000295. Available from: https://onlinelibrary.wiley.com/doi/10.1002/mame.202000295.

285. Y. Hu, X. Jiang, Y. Ding, L. Zhang, C. Yang, J. Zhang, et al., Preparation and drug release behaviors of nimodipine-loaded poly(caprolactone)-poly(ethylene oxide)-polylactide amphiphilic copolymer nanoparticles, *Biomaterials* **2003**, *24*(13), 2395–2404 [cited 12 March 2021]. Available from: https://linkinghub.elsevier.com/retrieve/pii/S0142961203000218.

286. M. Singh, B. Shirley, K. Bajwa, E. Samara, M. Hora, D. O'Hagan, Controlled release of recombinant insulin-like growth factor from a novel formulation of polylactide-co-glycolide microparticles, *J. Control. Release* **2001**, *70*(1–2), 21–28 [cited 12 March 2021]. Available from: https://linkinghub.elsevier.com/retrieve/pii/S0168365900003138.

287. T. Ouchi, T. Saito, T. Kontani, Y. Ohya, Encapsulation and/or release behavior of bovine serum albumin within and from polylactide-grafted dextran microspheres, *Macromol. Biosci.* **2004**, *4*(4), 458–463 [cited 12 March 2021]. Available from: http://doi.wiley.com/10.1002/mabi.200300106.

288. J. C. Olivier, Drug transport to brain with targeted nanoparticles, *NeuroRx* **2005**, *2*(1), 108–119 [cited 12 March 2021]. Available from: https://link.springer.com/article/10.1602/neurorx.2.1.108.

289. J. L. Bourges, S. E. Gautier, F. Delie, R. A. Bejjani, J. C. Jeanny, R. Gurny, et al., Ocular drug delivery targeting the retina and retinal pigment epithelium using polylactide nanoparticles, *Investig. Ophthalmol. Vis. Sci.* **2003**, *44*(8), 3562–3569 [cited 12 March 2021]. Available from: http://iovs.arvojournals.org/article.aspx?doi=10.1167/iovs.02-1068.

290. T. Chandy, G. S. Das, R. F. Wilson, G. H. R. Rao, Development of polylactide microspheres for protein encapsulation and delivery, *J. Appl. Polym. Sci.* **2002**, *86*(5), 1285–1295. Available from: http://doi.wiley.com/10.1002/app.11139.

291. T. G. Park, M. J. Alonso, R. Langer, Controlled release of proteins from poly(L-lactic acid) coated polyisobutylcyanoacrylate microcapsules, *J. Appl. Polym. Sci.* **1994**, *52*(12), 1797–1807. Available from: http://doi.wiley.com/10.1002/app.1994.070521214.

292. P. Caliceti, S. Salmaso, N. Elvassore, A. Bertucco, Effective protein release from PEG/PLA nano-particles produced by compressed gas anti-solvent precipitation techniques, *J. Control. Release* **2004**, *94*(1), 195–205. Available from: https://linkinghub.elsevier.com/retrieve/pii/S0168365903004851.

293. S. Y. Kim, I. G. Shin, Y. M. Lee, Preparation and characterization of biodegradable nanospheres composed of methoxy poly(ethylene glycol) and DL-lactide block copolymer as novel drug carriers, *J. Control. Release* **1998**, *56*(1–3), 197–208 [cited 12 March 2021]. Available from: https://linkinghub.elsevier.com/retrieve/pii/S0168365998000832.

294. H. Murakami, M. Kobayashi, H. Takeuchi, Y. Kawashima, Further application of a modified spontaneous emulsification solvent diffusion method to various types of PLGA and PLA polymers for preparation of nanoparticles, *Powder Technol.* **2000**, *107*(1–2), 137–143 [cited 12 March 2021]. Available from: https://linkinghub.elsevier.com/retrieve/pii/S0032591099001825.

295. H. Arimura, Y. Ohya, T. Ouchi, H. Yamada, Preparation of polylactide microspheres having positively or negatively charged surfaces, *Macromol. Biosci.* **2003**, *3*(1), 18–25 [cited 12 March 2021]. Available from: http://doi.wiley.com/10.1002/mabi.200390001.

296. X. Deng, Y. Liu, M. Yuan, X. Li, L. Liu, W. X. Jia, Preparation and characterization of poly-DL-lactide-poly(ethylene glycol) microspheres containing λDNA, *J. Appl. Polym. Sci.* **2002**, *86*(10), 2557–2566 [cited 12 March 2021]. Available from: http://doi.wiley.com/10.1002/app.11178.

297. M. Pluta, A. Galeski, M. Alexandre, M. A. Paul, P. Dubois, Polylactide/montmorillonite nanocomposites and microcomposites prepared by melt blending: structure and some physical properties, *J. Appl. Polym. Sci.* **2002**, *86*(6), 1497–1506 [cited 12 March 2021]. Available from: http://doi.wiley.com/10.1002/app.11309.

298. S. Li, Bioresorbable hydrogels prepared through stereocomplexation between poly(L-lactide) and poly(D-lactide) blocks attached to poly(ethylene glycol), *Macromol. Biosci.* **2003**, *3*(11), 657–661 [cited 12 March 2021]. Available from: http://doi.wiley.com/10.1002/mabi.200350032.

299. I. Kallela, T. Iizuka, A. Salo, C. Lindqvist, Lag-screw fixation of anterior mandibular fractures using biodegradable polylactide screws: a preliminary report, *J. Oral Maxillofac. Surg.* **1999**, *57*(2), 113–118 [cited 12 March 2021]. Available from: https://linkinghub.elsevier.com/retrieve/pii/S0278239199902203.

300. A. Viinikainen, H. Göransson, K. Huovinen, M. Kellomäki, P. Törmälä, P. Rokkanen, Material and knot properties of braided polyester (Ticron®) and bioabsorbable poly-L/D-lactide (PLDLA) 96/4 sutures, *J. Mater. Sci. Mater. Med.* **2006**, *17*(2), 169–177 [cited 12 March 2021]. Available from: https://link.springer.com/article/10.1007/s10856-006-6821-5

301. Y. Baimark, R. Molloy, N. Molloy, J. Siripitayananon, W. Punyodom, M. Sriyai, Synthesis, characterization and melt spinning of a block copolymer of L-lactide and ε-caprolactone for potential use as an absorbable monofilament surgical suture, *J. Mater. Sci. Mater. Med.* **2005**, *16*(8), 699–707 [cited 12 March 2021]. Available from: https://link.springer.com/article/10.1007/s10856-005-2605-6.

302. R. Zhang, P. X. Ma, Biomimetic polymer/apatite composite scaffolds for mineralized tissue engineering, *Macromol. Biosci.* **2004**, *4*(2), 100–111 [cited 12 March 2021]. Available from: http://doi.wiley.com/10.1002/mabi.200300017.

303. A. Buzarovska, S. Dinescu, L. Chitoiu, M. Costache, Porous poly(L-lactic acid) nanocomposite scaffolds with functionalized $TiO_2$ nanoparticles: properties, cytocompatibility and drug release capability, *J. Mater. Sci.* **2018**, *53*(16), 11151–11166. Available from: http://link.springer.com/10.1007/s10853-018-2415-0.

304. H. Zhang, X. Mao, Z. Du, W. Jiang, X. Han, D. Zhao, et al., Three dimensional printed macroporous polylactic acid/hydroxyapatite composite scaffolds for promoting bone formation in a critical-size rat calvarial defect model, *Sci. Technol. Adv. Mater.* **2016**, *17*(1), 136–148. Available from: https://www.tandfonline.com/doi/full/10.1080/14686996.2016.1145532.

305. H. Zhang, X. Mao, D. Zhao, W. Jiang, Z. Du, Q. Li, et al., Three dimensional printed polylactic acid-hydroxyapatite composite scaffolds for prefabricating vascularized tissue engineered bone: an in vivo bioreactor model, *Sci. Rep.* **2017**, *7*(1), 15255. Available from: http://www.nature.com/articles/s41598-017-14923-7.

306. L. R. Jaidev, K. Chatterjee, Surface functionalization of 3D printed polymer scaffolds to augment stem cell response, *Mater. Des.* **2019**, *161*, 44–54. Available from: https://linkinghub.elsevier.com/retrieve/pii/S0264127518308244.

307. D. Wu, Y. Cheng, S. Feng, Z. Yao, M. Zhang, Crystallization behavior of polylactide/graphene composites, *Ind. Eng. Chem. Res.* **2013**, *52*(20), 6731–6739. Available from: https://pubs.acs.org/doi/10.1021/ie4004199.

308. S. C. Agwuncha, E. R. Sadiku, I. D. Ibrahim, B. A. Aderibigbe, S. J. Owonubi, O. Agboola, et al., Poly(lactic acid) biopolymer composites and nanocomposites for biomedicals and biopackaging applications, in: V. K. Thakur, M. K. Thakur, M. R. Kessler (Eds.), *Handbook of Composites from Renewable Materials*, 1st edition, John Wiley & Sons, Inc., Hoboken, NJ 2017, pp. 135–169. Available from: http://doi.wiley.com/10.1002/9781119441632.ch153.

309. P. A. A. P. Marques, G. Gonçalves, M. K. Singh, J. Grácio, Graphene oxide and hydroxyapatite as fillers of polylactic acid nanocomposites: preparation and characterization, *J. Nanosci. Nanotechnol.* **2012**, *12*(8), 6686–6692. Available from: http://www.ingentaconnect.com/content/10.1166/jnn.2012.4565.

310. G. Narayanan, V. N. Vernekar, E. L. Kuyinu, C. T. Laurencin, Poly (lactic acid)-based biomaterials for orthopaedic regenerative engineering, *Adv. Drug Deliv. Rev.* **2016**, *107*, 247–276. Available from: https://linkinghub.elsevier.com/retrieve/pii/S0169409X16301259.

311. A. Mehboob, S. H. A. Rizvi, S. H. Chang, H. Mehboob, Comparative study of healing fractured tibia assembled with various composite bone plates, *Compos. Sci. Technol.* **2020**, *197*(March), 108248. Available from: https://doi.org/10.1016/j.compscitech.2020.108248.

312. Y. K. Yeon, H. S. Park, J. M. Lee, J. S. Lee, Y. J. Lee, M. T. Sultan, et al., New concept of 3D printed bone clip (polylactic acid/hydroxyapatite/silk composite) for internal fixation of bone fractures, *J. Biomater. Sci. Polym. Ed.* **2018**, *29*(7–9), 894–906. Available from: https://www.tandfonline.com/doi/full/10.1080/09205063.2017.1384199.

313. I. Antoniac, D. Popescu, A. Zapciu, A. Antoniac, F. Miculescu, H. Moldovan, Magnesium filled polylactic acid (PLA) material for filament based 3D printing, *Materials* **2019**, *12*(5), 1–13.

314. Y. K. Yeon, H. S. Park, J. M. Lee, J. S. Lee, Y. J. Lee, M. T. Sultan, et al., New concept of 3D printed bone clip (polylactic acid/hydroxyapatite/silk composite) for internal fixation of bone fractures, *J. Biomater. Sci. Polym. Ed.* **2018**, *29*(7–9), 894–906. Available from: https://www.tandfonline.com/doi/full/10.1080/09205063.2017.1384199.

315. W. Dong, X. Huang, Y. Sun, S. Zhao, J. Yin, L. Chen, Mechanical characteristics and in vitro degradation kinetics analysis of polylactic glycolic acid/β-tricalcium phosphate (PLGA/β-TCP) biocomposite interference screw, *Polym. Degrad. Stab.* **2021**, *186*, 109421. Available from: https://doi.org/10.1016/j.polymdegradstab. 2020.109421.

316. T. M. B. K. dos Santos, C. Merlini, Á. Aragones, M. C. Fredel, Manufacturing and characterization of plates for fracture fixation of bone with biocomposites of poly (lactic acid-*co*-glycolic acid) (PLGA) with calcium phosphates bioceramics, *Mater. Sci. Eng. C* **2019**, *103*(October 2018), 109728. Available from: https://doi.org/10.1016/j.msec.2019.05.013.

317. Y. Liu, H. Cao, L. Ye, P. Coates, F. Caton-Rose, X. Zhao, Long-chain branched poly(lactic acid)-*b*-poly(lactide-*co*-caprolactone): structure, viscoelastic behavior, and triple-shape memory effect as smart bone fixation material, *Ind. Eng. Chem. Res.* **2020**, *59*(10), 4524–4532.

318. V. DeStefano, S. Khan, A. Tabada, Applications of PLA in modern medicine, *Eng. Regen.* **2020**, *1*(April), 76–87. Available from: https://doi.org/10.1016/j.engreg.2020.08.002.

319. R. P. Pawar, S. U. Tekale, S. U. Shisodia, J. T. Totre, A. J. Domb, Send orders for reprints to reprints@benthamscience.net biomedical applications of poly(lactic acid), *Rec. Pat. Regen. Med.* **2014**, *4*, 40–51. Available from: https://www.ingentaconnect.com/contentone/ben/rpgm/2014/00000004/00000001/art00004?crawler=true.

320. L. Tzounis, P. I. Bangeas, A. Exadaktylos, M. Petousis, N. Vidakis, Three-dimensional printed polylactic acid (PLA) surgical retractors with sonochemically immobilized silver nanoparticles: the next generation of low-cost antimicrobial surgery equipment, *Nanomaterials* **2020**, *10*(5), 985.

321. J. Li, J. Ding, T. Liu, J. F. Liu, L. Yan, X. Chen, Poly(lactic acid) controlled drug delivery, in: M. L. Di Lorenzo, R. Androsch (Eds.), *Industrial Applications of Poly(Lactic Acid)*. 1st edition, Springer, Cham, 2017, pp. 109–138. Available from: http://link.springer.com/10.1007/12_2017_11.

322. D. da Silva, M. Kaduri, M. Poley, O. Adir, N. Krinsky, J. Shainsky-Roitman, et al., Biocompatibility, biodegradation and excretion of polylactic acid (PLA) in medical implants and theranostic systems, *Chem. Eng. J.* **2018**, *340*, 9–14. Available from: https://doi.org/10.1016/j.cej.2018.01.010.

323. J. He, X. Hu, J. Cao, Y. Zhang, J. Xiao, li J. Peng, et al., Chitosan-coated hydroxyapatite and drug-loaded polytrimethylene carbonate/polylactic acid scaffold for enhancing bone regeneration, *Carbohydr. Polym.* **2021**, *253*, 117198. Available from: https://linkinghub.elsevier.com/retrieve/pii/S0144861720313710.

324. G. Lv, F. He, X. Wang, F. Gao, G. Zhang, T. Wang, et al., Novel nanocomposite of nano $Fe_3O_4$ and polylactide nanofibers for application in drug uptake and induction of cell death of leukemia cancer cells, *Langmuir* **2008**, *24*(5), 2151–2156. Available from: https://pubs.acs.org/doi/10.1021/la702845s.

325. Z. Yuan, X. Zhao, J. Zhao, G. Pan, W. Qiu, X. Wang, et al., Synergistic mediation of tumor signaling pathways in hepatocellular carcinoma therapy via dual-drug-loaded pH-responsive electrospun fibrous scaffolds, *J. Mater. Chem. B* **2015**, *3*(17), 3436–3446. Available from: http://xlink.rsc.org/?DOI=C5TB00206K.

326. X. Zhao, Z. Yuan, L. Yildirimer, J. Zhao, Z. Y. Lin, Z. Cao, et al., Tumor-triggered controlled drug release from electrospun fibers using inorganic caps for inhibiting cancer relapse, *Small* **2015**, *11*(34), 4284–4291. Available from: https://onlinelibrary.wiley.com/doi/10.1002/smll.201500985.

327. D. D. Nguyen, L. J. Luo, J. Y. Lai, Effects of shell thickness of hollow poly(lactic acid) nanoparticles on sustained drug delivery for pharmacological treatment of glaucoma, *Acta Biomater.* **2020**, *111*, 302–315. Available from: https://linkinghub.elsevier.com/retrieve/pii/S1742706120302610.

328. P. Makvandi, U. Josic, M. Delfi, F. Pinelli, V. Jahed, E. Kaya, et al., Drug delivery (nano)platforms for oral and dental applications: tissue regeneration, infection control, and cancer management, *Adv. Sci.* **2021**, *8*(8), 2004014. Available from: https://onlinelibrary.wiley.com/doi/10.1002/advs.202004014.

329. R. Campardelli, Della G. Porta, L. Gomez, S. Irusta, E. Reverchon, J. Santamaria, Au-PLA nanocomposites for photothermally controlled drug delivery, *J. Mater. Chem. B* **2014**, *2*(4), 409–417. Available from: http://xlink.rsc.org/?DOI=C3TB21099E.

330. W. Tan, C. Gao, P. Feng, Q. Liu, C. Liu, Z. Wang, et al., Dual-functional scaffolds of poly(L-lactic acid)/nanohydroxyapatite encapsulated with metformin: simultaneous enhancement of bone repair and bone tumor inhibition, *Mater. Sci. Eng. C* **2021**, *120*, 111592. Available from: https://linkinghub.elsevier.com/retrieve/pii/S0928493120335104.

331. W. Hadasha, D. Bezuidenhout, Poly(lactic acid) as biomaterial for cardiovascular devices and tissue engineering applications, in: M. L. Di Lorenzo, R. Androsch (Eds.), *Industrial Applications of Poly(Lactic Acid)*, 1st edition, Springer, Cham, 2017, pp. 51–77. Available from: http://link.springer.com/10.1007/12_2017_27.

332. M. S. Singhvi, S. S. Zinjarde, D. V. Gokhale, Polylactic acid: synthesis and biomedical applications, *J. Appl. Microbiol.* **2019**, *127*(6), 1612–1626.

333. A. J. Guerra, P. Cano, M. Rabionet, T. Puig, J. Ciurana, 3D-printed PCL/PLA composite stents: towards a new solution to cardiovascular problems, *Materials* **2018**, *11*(9), 1679. Available from: http://www.mdpi.com/1996-1944/11/9/1679.

334. N. Mokhtari, A. Zargar Kharazi, Blood compatibility and cell response improvement of poly glycerol sebacate/poly lactic acid scaffold for vascular graft applications, *J. Biomed. Mater. Res. Part A* **2021**, *109*(12), 2673–2684. Available from: https://onlinelibrary.wiley.com/doi/10.1002/jbm.a.37259.

335. C. Li, F. Wang, G. Douglas, Z. Zhang, R. Guidoin, L. Wang, Comprehensive mechanical characterization of PLA fabric combined with PCL to form a composite structure vascular graft, *J. Mech. Behav. Biomed. Mater.* **2017**, *69*, 39–49. Available from: https://linkinghub.elsevier.com/retrieve/pii/S1751616116303836.

336. F. Oveissi, S. Naficy, A. Lee, D. S. Winlaw, F. Dehghani, Materials and manufacturing perspectives in engineering heart valves: a review, *Mater. Today Bio.* **2020**, *5*, 100038. Available from: https://linkinghub.elsevier.com/retrieve/pii/S259000641930064X.

337. L.-y. Long, C. Wu, X.-f. Hu, Y.-b. Wang, Biodegradable synthetic polymeric composite scaffold-based tissue engineered heart valve with minimally invasive transcatheter implantation, *Polym. Adv. Technol.* **2020**, *31*(11), 2422–2432. Available from: https://onlinelibrary.wiley.com/doi/10.1002/pat.5012.

338. D. A. Stout, B. Basu, T. J. Webster, Poly(lactic-*co*-glycolic acid): carbon nanofiber composites for myocardial tissue engineering applications, *Acta Biomater.* **2011**, *7*(8), 3101–3112. Available from: https://linkinghub.elsevier.com/retrieve/pii/S1742706111001930.

339. F. Flaig, H. Ragot, A. Simon, G. Revet, M. Kitsara, L. Kitasato, et al., Design of functional electrospun scaffolds based on poly(glycerol sebacate) elastomer and poly(lactic acid) for cardiac tissue engineering, *ACS Biomater. Sci. Eng.* **2020**, *6*(4), 2388–2400. Available from: https://pubs.acs.org/doi/10.1021/acsbiomaterials.0c00243.

340. W. E. E. Nabofa, O. O. Alashe, O. T. Oyeyemi, A. F. Attah, A. A. Oyagbemi, T. O. Omobowale, et al., Cardioprotective effects of curcumin-nisin based poly lactic acid nanoparticle on myocardial infarction in guinea pigs, *Sci. Rep.* **2018**, *8*(1), 16649. Available from: http://www.nature.com/articles/s41598-018-35145-5.

341. M. Santoro, S. R. Shah, J. L. Walker, A. G. Mikos, Poly(lactic acid) nanofibrous scaffolds for tissue engineering, *Adv. Drug Deliv. Rev.* **2016**, *107*, 206–212. Available from: https://linkinghub.elsevier.com/retrieve/pii/S0169409X16301296.

342. Y. Niu, F. J. Stadler, J. Fang, M. Galluzzi, Hyaluronic acid-functionalized poly-lactic acid (PLA) microfibers regulate vascular endothelial cell proliferation and phenotypic shape expression, *Coll. Surf. B Biointerf.* **2021**, *206*, 111970. Available from: https://linkinghub.elsevier.com/retrieve/pii/S0927776521004148.

343. Y. Liu, S. Wang, R. Zhang, Composite poly(lactic acid)/chitosan nanofibrous scaffolds for cardiac tissue engineering, *Int. J. Biol. Macromol.* **2017**, *103*, 1130–1137. Available from: https://linkinghub.elsevier.com/retrieve/pii/S014181301730911X.

344. T. Dvir, B. P. Timko, M. D. Brigham, S. R. Naik, S. S. Karajanagi, O. Levy, et al., Nanowired three-dimensional cardiac patches, *Nat. Nanotechnol.* **2011**, *6*(11), 720–725. Available from: http://www.nature.com/articles/nnano.2011.160.

345. B. Sun, S. Liu, R. Hao, X. Dong, L. Fu, B. Han, Rgd-peg-pla delivers mir-133 to infarct lesions of acute myocardial infarction model rats for cardiac protection, *Pharmaceutics* **2020**, *12*(6), 1–28. Available from: https://www.mdpi.com/1999-4923/12/6/575.

346. L. Cabedo, J. L. Feijoo, M. P. Villanueva, J. M. Lagarón, E. Giménez, Optimization of biodegradable nanocomposites based on aPLA/PCL blends for food packaging applications, *Macromol. Symp.* **2006**, *233*(1), 191–197. Available from: http://doi.wiley.com/10.1002/masy.200690017.

347. E. L. Cussler, S. E. Hughes, W. J. Ward, R. Aris, Barrier membranes, *J. Memb. Sci.* **1988**, *38*(2), 161–174. Available from: https://linkinghub.elsevier.com/retrieve/pii/S0376738800808777.

348. L. Petersson, K. Oksman, Biopolymer based nanocomposites: comparing layered silicates and microcrystalline cellulose as nanoreinforcement, *Compos. Sci. Technol.* **2006**, *66*(13), 2187–2196. Available from: https://linkinghub.elsevier.com/retrieve/pii/S0266353805004872.

349. Y. Kim, J. S. Kim, S. Y. Lee, R. L. Mahajan, Y. T. Kim, Exploration of hybrid nanocarbon composite with polylactic acid for packaging applications, *Int. J. Biol. Macromol.* **2020**, *144*, 135–142. Available from: https://doi.org/10.1016/j.ijbiomac.2019.11.239.

350. A. A. Singh, S. Sharma, M. Srivastava, A. Majumdar, Modulating the properties of polylactic acid for packaging applications using biobased plasticizers and naturally obtained fillers, *Int. J. Biol. Macromol.* **2020**, *153*, 1165–1175. Available from: https://doi.org/10.1016/j.ijbiomac.2019.10.246.

351. C. Swaroop, M. Shukla, Development of blown polylactic acid-MgO nanocomposite films for food packaging, *Compos. Part A Appl. Sci. Manuf.* **2019**, *124*(June), 105482. Available from: https://doi.org/10.1016/j.compositesa.2019.105482.

352. S. D. F. Mihindukulasuriya, L. T. Lim, Nanotechnology development in food packaging: a review, *Trends Food Sci. Technol.* **2014**, *40*(2), 149–167. Available from: https://linkinghub.elsevier.com/retrieve/pii/S0924224414002131.

353. A. Marra, C. Silvestre, D. Duraccio, S. Cimmino, Polylactic acid/zinc oxide biocomposite films for food packaging application, *Int. J. Biol. Macromol.* **2016**, *88*, 254–262. Available from: https://linkinghub.elsevier.com/retrieve/pii/S014181301630263X.

354. C. V. Garcia, G. H. Shin, J. T. Kim, Metal oxide-based nanocomposites in food packaging: Applications, migration, and regulations, *Trends Food Sci. Technol.* **2018**, *82*, 21–31. Available from: https://linkinghub.elsevier.com/retrieve/pii/S092422441830092X.

355. H. Zhang, M. Hortal, M. Jordá-Beneyto, E. Rosa, M. Lara-Lledo, I. Lorente, ZnO-PLA nanocomposite coated paper for antimicrobial packaging application, *LWT—Food Sci. Technol.* **2017**, *78*, 250–257. Available from: http://dx.doi.org/10.1016/j.lwt.2016.12.024.

356. R. T. De Silva, P. Pasbakhsh, S. M. Lee, A. Y. Kit, ZnO deposited/encapsulated halloysite-poly (lactic acid) (PLA) nanocomposites for high performance packaging films with improved mechanical and antimicrobial properties, *Appl. Clay Sci.* **2015**, *111*, 10–20. Available from: http://dx.doi.org/10.1016/j.clay.2015.03.024.

357. D. S. Cha, M. S. Chinnan, Biopolymer-based antimicrobial packaging: a review, *Crit. Rev. Food Sci. Nutr.* **2004**, *44*(4), 223–237. Available from: http://www.tandfonline.com/doi/abs/10.1080/10408690490464276.

358. J. H. Han, Antimicrobial food packaging, in: R. Ahvenainen (Ed.), *Food Technology*, 1st edition Woodhead Publishing, Cambridge, 2000, pp. 56–65. Available from: https://linkinghub.elsevier.com/retrieve/pii/B9781855736757500080.

359. L. S. Liu, V. L. Finkenstadt, C. K. Liu, T. Jin, M. L. Fishman, K. B. Hicks, Preparation of poly(lactic acid) and pectin composite films intended for applications in antimicrobial packaging, *J. Appl. Polym. Sci.* **2007**, *106*(2), 801–810. Available from: http://doi.wiley.com/10.1002/app.26590

360. T. Sekito, Y. Miyake, M. Matsuda, Performance improvement of eco plastics/poly lactic acid, SAE Technical Papers 2006. Available from: https://www.sae.org/content/2006-01-0335/.

361. S. Serizawa, K. Inoue, M. Iji, Kenaf-fiber-reinforced poly(lactic acid) used for electronic products, *J. Appl. Polym. Sci.* **2006**, *100*(1), 618–624. Available from: http://doi.wiley.com/10.1002/app.23377.

362. O. Skepticism, S. Technology, 科学技術 (Science and technology) と科学・技術 (Science and technology) について 戸田工業株式会社 創造本部京藤倫久, in: F. T. Wallenberger, N. E. Weston (Eds.), *October*, 1st edition, Springer US, Boston, MA, 2017, pp. 401–405. Available from: http://link.springer.com/10.1007/978-1-4419-9050-1_1.

363. E. F. H. Pennekamp, *Plastics in the Automotive Industry*, Woodhead Publishing Limited, 1970. Available from: http://www.sciencedirect.com/science/book/9781855730397.

364. A. Bouzouita, Notta-D. Cuvier, J. M. Raquez, F. Lauro, P. Dubois, Poly(lactic acid)-based materials for automotive applications, in: M. L. Di Lorenzo, R. Androsch (Eds.), *Advances in Polymer Science*, 1st edition, Springer, Cham, 2018, pp. 177–219. Available from: http://link.springer.com/10.1007/12_2017_10.

365. D. Notta-Cuvier, J. Odent, R. Delille, M. Murariu, F. Lauro, J. M. Raquez, et al., Tailoring polylactide (PLA) properties for automotive applications: effect of addition of designed additives on main mechanical properties, *Polym. Test.* **2014**, *36*, 1–9. Available from: https://linkinghub.elsevier.com/retrieve/pii/S0142941814000658.

366. R. Arjmandi, A. Hassan, Z. Zakaria, Polylactic acid green nanocomposites for automotive applications, in: M. Jawaid, M. S. Salit, O. Y. Alothman (Eds.), *Green Energy and Technology*, 1st edition, Springer, Cham, 2017, pp. 193–208. Available from: http://link.springer.com/10.1007/978-3-319-49382-4_9.

367. V. H. Sangeetha, H. Deka, T. O. Varghese, S. K. Nayak, State of the art and future prospectives of poly(lactic acid) based blends and composites, *Polym. Compos.* **2018**, *39*(1), 81–101. Available from: http://doi.wiley.com/10.1002/pc.23906.

368. K. Hamad, M. Kaseem, M. Ayyoob, J. Joo, F. Deri, Polylactic acid blends: the future of green, light and tough, *Prog. Polym. Sci.* **2018**, *85*, 83–127. Available from: https://linkinghub.elsevier.com/retrieve/pii/S0079670018300212.

369. C. Zhang, T. Zhai, L. S. Turng, Y. Dan, Morphological, mechanical, and crystallization behavior of polylactide/polycaprolactone blends compatibilized by L-lactide/caprolactone copolymer, *Ind. Eng. Chem. Res.* **2015**, *54*(38), 9505–9511. Available from: https://pubs.acs.org/doi/10.1021/acs.iecr.5b02134.

370. H. C. Zhang, B.-h. Kang, L. S. Chen, X. Lu, Enhancing toughness of poly (lactic acid)/thermoplastic polyurethane blends via increasing interface compatibility by polyurethane elastomer prepolymer and its toughening mechanism, *Polym. Test.* **2020**, *87*(April), 106521. Available from: https://doi.org/10.1016/j.polymertesting.2020.106521.

371. F. Yu, H. X. Huang, Simultaneously toughening and reinforcing poly(lactic acid)/thermoplastic polyurethane blend via enhancing interfacial adhesion by hydrophobic silica nanoparticles, *Polym. Test.* **2015**, *45*, 107–113. Available from: http://dx.doi.org/10.1016/j.polymertesting.2015.06.001.

372. Corbion, Total Corbion PLA [cited 8 March 2021]. https://www.total-corbion.com/news/total-corbion-p. Available from: https://www.corbion.com/bioplastics/total-corbion-pla.

373. Green Car Congress, Mitsubishi motors develops green plastic: bamboo-fiber reinforced plant-based resin, Mitsubishi Motors Develops Green Plastic: Bamboo-Fiber Reinforced Plant-Based Resin, 2006 [cited 8 March 2021]. Available from: https://www.greencarcongress.com/2006/02/mitsubishi_moto.html.

374. D. de Guzman, ZealaFoam—a biodegradable alternative to polystyrene, *Green Chemicals* Blog, 2015 [cited 8 March 2021]. Available from: http://www.biopolymernetwork.com/content/Zealafoam/90.aspx%0A%0Ahttps://greenchemicalsblog.com/2015/08/17/video-zealafoam-a-biodegradable-alternative-to-polystyrene/.

375. K. Bocz, T. Tábi, D. Vadas, M. Sauceau, J. Fages, G. Marosi, Characterisation of natural fibre reinforced PLA foams prepared by supercritical $CO_2$ assisted extrusion, *Express Polym. Lett.* **2016**, *10*(9), 771–779. Available from: http://www.expresspolymlett.com/letolt.php?file=EPL-0007064&mi=c.

376. K. Oluwabunmi, D'N. A. Souza, W. Zhao, T. Y. Choi, T. Theyson, Compostable, fully biobased foams using PLA and micro cellulose for zero energy buildings, *Sci. Rep.* **2020**, *10*(1), 17771. Available from: http://www.nature.com/articles/s41598-020-74478-y.

377. X. Wang, H. Bai, Z. Yao, A. Liu, G. Shi, Electrically conductive and mechanically strong biomimetic chitosan/reduced graphene oxide composite films, *J. Mater. Chem.* **2010**, *20*(41), 9032–9036. Available from: http://xlink.rsc.org/?DOI=c0jm01852j.

378. T. J. Rivers, T. W. Hudson, C. E. Schmidt, Synthesis of a novel, biodegradable electrically conducting polymer for biomedical applications, *Adv. Funct. Mater.* **2002**, *12*(1), 33–37. Available from: https://onlinelibrary.wiley.com/doi/10.1002/1616-3028(20020101]12:1%3C33::AID-ADFM33%3E3.0.CO;2-E

379. A. Giri, R. Bhowmick, C. Prodhan, D. Majumder, S. K. Bhattacharya, M. Ali, Synthesis and characterization of biopolymer based hybrid hydrogel nanocomposite and study of their electrochemical efficacy, *Int. J. Biol. Macromol.* **2019**, *123*, 228–238. Available from: https://linkinghub.elsevier.com/retrieve/pii/S0141813018327119.

380. Developed kenaf-added bioplastic for mobile phones, NEC Corporation press release, 2005 [cited 25 March 2021]. Available from: http://www.nec.co.jp/press/ja/0506/1402.html.

381. K. Kimura, Y. Horikoshi, Bio-based polymers, *FUJITSU Sci Tech J.* **2005**, *41*(2), 173–180. Available from: https://www.fujitsu.com/global/documents/about/resources/publications/fstj/archives/vol41-2/paper07.pdf

382. Launched a business PC equipped with a function to reduce power consumption by up to 30% and visualize power consumption, NEC Corporation press release, 2010 [cited 25 February 2021]. Available from: http://www.nec.co.jp/press/ja/1001/1201.html.

383. NEC reduces production energy for cellulose-based bioplastic_ press releases _ NEC, NEC Corporation press release, 2014 [cited 25 March 2021]. Available from: https://www.nec.com/en/press/201405/global_20140508_02.html.

384. T. Gupta, A. Pradhan, Bandyopadhyay-S. Ghosh, S. B. Ghosh, Thermally exfoliated graphene oxide reinforced stress responsive conductive nanocomposite hydrogel, *Polym. Adv. Technol.* **2019**, *30*(9), 2392–2401. Available from: https://onlinelibrary.wiley.com/doi/abs/10.1002/pat.4685.

385. V. Garg, T. Gupta, S. Rani, Bandyopadhyay-ghosh S., B. Ghosh, L. Qiao, et al., A hierarchically designed nanocomposite hydrogel with multisensory capabilities towards wearable devices for human-body motion and glucose concentration detection, *Compos. Sci. Technol.* **2021**, *213*(May), 108894. Available from: https://doi.org/10.1016/j.compscitech.2021.1088940.

386. S. S. Ashraf, M. Frounchi, S. Dadbin, Gamma irradiated electro-conductive polylactic acid/polyaniline nanofibers, *Synth. Met.* **2020**, *259*, 116204. Available from: https://linkinghub.elsevier.com/retrieve/pii/S0379677919305235.

387. S. Peng, P. Zhu, Y. Wu, S. G. Mhaisalkar, S. Ramakrishna, Electrospun conductive polyaniline-polylactic acid composite nanofibers as counter electrodes for rigid and flexible dye-sensitized solar cells, *RSC Adv.* **2012**, *2*(2), 652–657. Available from: https://pubs.rsc.org/en/content/articlehtml/2012/ra/c1ra00618e.

388. J. Li, W. J. Peng, Z. J. Fu, X. H. Tang, H. Wu, S. Guo, et al., Achieving high electrical conductivity and excellent electromagnetic interference shielding in poly(lactic acid)/silver nanocomposites by constructing large-area silver nanoplates in polymer matrix, *Compos. Part B Eng.* **2019**, *171*, 204–213. Available from: https://linkinghub.elsevier.com/retrieve/pii/S1359836819300782.

389. Y. Y. Shi, J. H. Yang, T. Huang, N. Zhang, C. Chen, Y. Wang, Selective localization of carbon nanotubes at the interface of poly(L-lactide)/ethylene-*co*-vinyl Acetate resulting in

lowered electrical resistivity, *Compos. Part B Eng.* **2013**, *55*, 463–469. Available from: http://dx.doi.org/10.1016/j.compositesb.2013.07.012.

390. Kruželák J., A. Kvasničáková, Hložeková K., I. Hudec, Progress in polymers and polymer composites used as efficient materials for EMI shielding, *Nanoscale Adv.* **2021**, *3*(1), 123–172. Available from: http://xlink.rsc.org/?DOI=D0NA00760A.
391. R. Singh, S. G. Kulkarni, Nanocomposites based on transition metal oxides in polyvinyl alcohol for EMI shielding application, *Polym. Bull.* **2014**, *71*(2), 497–513. Available from: http://link.springer.com/10.1007/s00289-013-1073-2.
392. Y. J. Yim, Y. M. Baek, S. J. Park, Influence of nickel layer on electromagnetic interference shielding effectiveness of CuS-polyacrylonitrile fibers, *Bull. Korean Chem. Soc.* **2018**, *39*(12), 1406–1411. Available from: https://onlinelibrary.wiley.com/doi/abs/10.1002/bkcs.11615.
393. Y. Wang, L. Liang, Z. Du, Y. Wang, C. Liu, C. Shen, Biodegradable PLA/CNTs/Ti3C2Tx MXene nanocomposites for efficient electromagnetic interference shielding, *J. Mater. Sci. Mater. Electron.* **2021**, *32*(21), 25952–25962. Available from: http://link.springer.com/10.1007/s10854-021-05377-9.
394. A. F. Ahmad, Ab S. Aziz, Z. Abbas, S. J. Obaiys, K. A. Matori, M. H. M. Zaid, et al., Chemically reduced graphene oxide-reinforced poly(lactic acid)/poly(ethylene glycol) nanocomposites: preparation, characterization, and applications in electromagnetic interference shielding, *Polymers (Basel)*[Internet] **2019**, *11*(4), 661. Available from: https://www.mdpi.com/2073-4360/11/4/661.
395. S. Frackowiak, J. Ludwiczak, K. Leluk, K. Orzechowski, M. Kozlowski, Foamed poly(lactic acid) composites with carbonaceous fillers for electromagnetic shielding, *Mater. Des.* **2015**, *65*, 749–756. Available from: https://linkinghub.elsevier.com/retrieve/pii/S0261306914007961.
396. E. G. Barathi Dassan, A. Anjang Ab Rahman, M. S. Z. Abidin, H. M. Akil, Carbon nanotube-reinforced polymer composite for electromagnetic interference application: a review, *Nanotechnol. Rev.* **2020**, *9*(1), 768–788. Available from: https://www.degruyter.com/document/doi/10.1515/ntrev-2020-0064/html.
397. J. Tolvanen, J. Hannu, M. Hietala, K. Kordas, H. Jantunen, Biodegradable multiphase poly(lactic acid)/biochar/graphite composites for electromagnetic interference shielding, *Compos. Sci. Technol.* **2019**, *181*(May), 107704. Available from: https://linkinghub.elsevier.com/retrieve/pii/S0266353819303446.
398. D. Bychanok, P. Angelova, A. Paddubskaya, D. Meisak, L. Shashkova, M. Demidenko, et al., Terahertz absorption in graphite nanoplatelets/polylactic acid composites, *J. Phys. D Appl. Phys.* **2018**, *51*(14), 145307. Available from: https://iopscience.iop.org/article/10.1088/1361-6463/aab1a5.
399. S. Kashi, R. K. Gupta, S. N. Bhattacharya, R. J. Varley, Experimental and simulation study of effect of thickness on performance of (butylene adipate-*co*-terephthalate) and poly lactide nanocomposites incorporated with graphene as stand-alone electromagnetic interference shielding and metal-backed microwave abso. *Compos. Sci. Technol.* **2020**, *195*(February), 108186. Available from: https://doi.org/10.1016/j.compscitech.2020.108186.
400. Q. Zeng, Z. Du, C. Qin, Y. Wang, C. Liu, C. Shen, Enhanced thermal, mechanical and electromagnetic interference shielding properties of graphene nanoplatelets-reinforced poly(lactic acid)/poly(ethylene oxide) nanocomposites, *Mater. Today Commun.* **2020**, *25*(June), 101632. Available from: https://doi.org/10.1016/j.mtcomm.2020.101632.
401. P. Pötschke, T. Andres, T. Villmow, S. Pegel, H. Brünig, K. Kobashi, et al., Liquid sensing properties of fibres prepared by melt spinning from poly(lactic acid) containing multi-walled carbon nanotubes, *Compos. Sci. Technol.* **2010**, *70*(2), 343–349. Available from: http://dx.doi.org/10.1016/j.compscitech.2009.11.005.
402. C. Hu, Z. Li, Y. Wang, J. Gao, K. Dai, G. Zheng, et al., Comparative assessment of the strain-sensing behaviors of polylactic acid nanocomposites: reduced graphene oxide or carbon nanotubes, *J. Mater. Chem. C* **2017**, *5*(9), 2318–2328. Available from: http://dx.doi.org/10.1039/c6tc05261d.
403. A. F. João, A. L. Squissato, E. M. Richter, R. A. A. Muñoz, Additive-manufactured sensors for biofuel analysis: copper determination in bioethanol using a 3D-printed carbon black/polylactic electrode, *Anal. Bioanal. Chem.* **2020**, *412*(12), 2755–2762.
404. C. L. Manzanares Palenzuela, F. Novotný, P. Krupička, Z. Sofer, M. Pumera, 3D-printed graphene/polylactic acid electrodes promise high sensitivity in electroanalysis, *Anal. Chem.* **2018**, *90*, 5753–7.
405. J. E. Oliveira, L. H. C. Mattoso, E. S. Medeiros, V. Zucolotto, Poly(lactic acid)/carbon nanotube fibers as novel platforms for glucose biosensors, *Biosensors* **2012**, *2*(1), 70–82. Available from: http://www.mdpi.com/2079-6374/2/1/70.
406. G. Chakraborty, P. Dhar, V. Katiyar, G. Pugazhenthi, Applicability of Fe-CNC/GR/PLA composite as potential sensor for biomolecules, *J. Mater. Sci. Mater. Electron*. **2020**, *31*(8), 5984–5999. Available from: http://link.springer.com/10.1007/s10854-020-03036-z.
407. C. Chen, X. L. Zhao, Z. H. Li, Z. G. Zhu, S. H. Qian, A. J. Flewitt, Current and emerging technology for continuous glucose monitoring, *Sensors (Switzerland)* **2017**, *17*(1), 182. Available from: http://www.mdpi.com/1424-8220/17/1/182.
408. A. Abdalla, B. A. Patel, 3D-printed electrochemical sensors: a new horizon for measurement of biomolecules, *Curr. Opin. Electrochem.* **2020**, *20*, 78–81. Available from: https://linkinghub.elsevier.com/retrieve/pii/S2451910320300909.
409. W. V. Gonzales, A. T. Mobashsher, A. Abbosh, The progress of glucose monitoring—a review of invasive to minimally and non-invasive techniques, devices and sensors, *Sensors (Switzerland)* **2019**, *19*(4), 800. Available from: https://www.mdpi.com/1424-8220/19/4/800.
410. E. Skaria, B. A. Patel, M. S. Flint, K. W. Ng. Poly(lactic acid)/carbon nanotube composite microneedle arrays for dermal biosensing, *Anal. Chem.* **2019**, *91*(7), 4436–4443. Available from: https://pubs.acs.org/doi/10.1021/acs.analchem.8b04980

411. J. W. Lee, J. H. Park, M. R. Prausnitz, Dissolving microneedles for transdermal drug delivery, *Biomaterials* **2008**, *29*(13), 2113–2124. Available from: https://linkinghub.elsevier.com/retrieve/pii/S0142961207010605.

412. Y. C. Kim, J. H. Park, M. R. Prausnitz, Microneedles for drug and vaccine delivery, *Adv. Drug Deliv. Rev.* **2012**, *64*(14), 1547–1568. Available from: https://linkinghub.elsevier.com/retrieve/pii/S0169409X12001251.

413. M. R. Prausnitz, Microneedles for transdermal drug delivery, *Adv. Drug Deliv. Rev.* **2004**, *56*(5), 581–587. Available from: https://linkinghub.elsevier.com/retrieve/pii/S0169409X03002394.

414. S. Y. Oh, S. Y. Hong, Y. R. Jeong, J. Yun, H. Park, S. W. Jin, et al., Skin-attachable, stretchable electrochemical sweat sensor for glucose and pH detection, *ACS Appl. Mater. Interfaces* **2018**, *10*(16), 13729–13740. Available from: https://pubs.acs.org/doi/10.1021/acsami.8b03342.

415. Malik N, Kumar P, Ghosh SB, Shrivastava S. Organically Modified Nanoclay and Aluminum Hydroxide Incorporated Bionanocomposites towards Enhancement of Physico-mechanical and Thermal Properties of Lignocellulosic Structural Reinforcement. *J. Polym. Environ*. **2018**, *26*(8), 3243–9. Available from: http://link.springer.com/10.1007/s10924-018-1184-9

# 17

# NANOCOMPOSITES: PROCESSING AND MECHANICAL PROPERTIES

Suprakas Sinha Ray

## 17.1 INTRODUCTION

Over the last few years, biodegradable polymers from renewable resources have attracted great research attention [1]. Biodegradable polymers are defined as those that undergo microbially induced chain scission, leading to mineralization [2]. Specific conditions in terms of pH, humidity, oxygenation, and the presence of some metals are required to ensure the biodegradation of such polymers. Renewable sources of polymeric materials offer an alternative to sustainable development of economically and ecologically attractive technology. The innovations in the development of biodegradable feedstock, the preservation of fossil-based raw materials, complete biodegradation, the reduction in the volume of garbage and compostability in the natural cycle, protection of the climate through the reduction of carbon dioxide released, as well as the application of agriculture resources for the production of green materials, are some of the reasons why such materials have attracted academic and industrial interest.

One of the most promising polymers in this direction is polylactide (PLA) because it is made 100% from agricultural products and is industrially compostable [3]. PLA has balanced mechanical properties, thermal plasticity, and biodegradability. It is commercially available as a promising polymer for various end-use applications [4, 5]. Increasing the realization of the various intrinsic properties of PLA, coupled with the knowledge of how such properties can be improved to achieve compatibility with thermoplastics processing, manufacturing, and end-use requirements, has fuelled technological and commercial interests in PLA.

Over the last decade, a wealth of investigation has been performed to enhance the mechanical properties and the impact resistance of PLA. Most studies focus on biodegradable and nonbiodegradable fillers, plasticizers, or blending of PLA with other polymers [6–13]. As a result, PLA can now compete with other low-cost biodegradable/biocompatible and commodity polymers.

In recent years, the excitement surrounding nanoscience and technology has resulted in the creation of revolutionary material combinations. These new materials circumvent classical material performance trade-offs through new properties and exploiting unique synergisms between constituents when the length scale of the morphology and the critical length associated with the fundamental physics of a given property coincide. Nanostructured materials or nanocomposites based on polymers have been an area of intense industrial and academic research over the last one and a half decades [14–19]. In principle, nanocomposites are an extreme case of composite materials in which interfacial interactions between two phases are maximized. In the literature, the term nanocomposite is generally used for polymers with submicrometer dispersions. In polymer-based nanocomposites, nanometer-sized inorganic or organic particles are homogeneously dispersed as separate particles in a polymer matrix. Nanoparticles can be classified based on their nanoscale dimensions and shape that includes (i) one-dimensional needle- or tube-like structures (e.g., inorganic nanotubes, carbon nanotubes, sepiolites); (ii) two-dimensional platelet structures (e.g., layered silicates); and (iii) sphere-like three-dimensional structures (e.g., silica, zinc oxide).

*Poly(Lactic Acid): Synthesis, Structures, Properties, Processing, Applications, and End of Life*, Second Edition.
Edited by Rafael A. Auras, Loong-Tak Lim, Susan E. M. Selke, and Hideto Tsuji.

This chapter provides an overview of recent developments in PLA-based nanocomposites. First, processing and characterization of nanocomposites are presented, including those that are key to achieving significant enhancement of properties through optimal dispersion and homogeneous distribution of the nanofiller. Various morphological and rheological characterization techniques are discussed to provide insight into the quality of dispersion and distribution, which is imperative for quality control. Thus, processing of nanocomposites and their characterization are crucial steps in the development of nanocomposites of superior properties. Second, the effect of nanofillers on mechanical properties is discussed in the context of the selection of a suitable nanofiller critical to developing nanocomposites of desired mechanical properties for various applications. The mechanical properties of the nanocomposites, as influenced by the morphological characteristics and other properties of the nanofiller, are discussed.

## 17.2 NANOCLAY-CONTAINING PLA NANOCOMPOSITES

Over the last two decades, polymer nanocomposites based on nanoclay minerals have attracted great interest from researchers in industry and in academia. These materials often exhibit concurrent improvements in several properties as compared to the neat polymer, including increased moduli/strength, enhanced heat resistance, decreased gas permeability/flammability, and increased degradability of biodegradable polymers [2, 7, 12]. These materials have also been proven to be unique model systems to study the structure and dynamics of polymers in confined environments [20, 21].

Ogata et al. [22] first reported the preparation of PLA-organoclay blends by dissolving the PLA in hot chloroform in the presence of dimethyldistearylammonium-modified montmorillonite (MMT) (2C18MMT). In the case of PLA/MMT composites, wide-angle X-ray diffraction (WXRD) and small-angle X-ray scattering (SAXS) showed that the nanoclay particles could not be intercalated in the PLA/MMT blends when prepared by the solvent-cast method. In other words, the nanoclay existed in the form of tactoids, consisting of several stacked silicate monolayers. These tactoids are responsible for the formation of particular geometrical structures in the blends, which lead to the formation of superstructures in the thickness of the blended film. This kind of structural feature increases the Young's modulus of the hybrid.

Then, Bandyopadhyay et al. [23] reported the preparation of intercalated PLA-organoclay nanocomposites with much improved mechanical and thermal properties. Two different kinds of clay, fluorohectorite (FH) and MMT, both modified with dioctadecyltrimethyl ammonium cation, were used for the preparation of nanocomposites with PLA.

Ray et al. [24, 25] used the same melt intercalation technique for the preparation of intercalated PLA-organoclay nanocomposites. WXRD patterns and transmission electron microscope (TEM) observations clearly established that the silicate layers were intercalated and randomly distributed in the PLA matrix. The incorporation of a very small amount (0.2–0.5 wt%) of poly(ε-caprolactone) oligomer(*o*-PCL) as a compatibilizer in the nanocomposites led to a better parallel stacking of the silicate layers and also to much stronger flocculation when compared with the nanocomposites without *o*-PCL. This observation is due to the hydroxylated edge–edge interaction of the silicate layers. Owing to the interaction between clay platelets and the PLA matrix in the presence of a very small amount of *o*-PCL, the strength of the disk–disk interaction plays an important role in determining the stability of the clay particles and hence the enhancement of mechanical properties of such nanocomposites.

In subsequent research, Ray et al. [26, 27] prepared PLA nanocomposites with organically modified synthetic fluorine mica (OMSFM). For the characterization of structure and morphology of prepared nanocomposites, they first used WXRD and conventional TEM (CTEM), and high-resolution TEM (HRTEM), to examine the final structure of the PLA/clay nanocomposites (PLACNs). In their further study [28–31], Ray et al. prepared a series of PLA-based nanostructured materials with various types of organoclays (4 wt% loading) to investigate the effect of organic modification on the morphology, properties, and degradability of the final nanocomposites. Table 17.1 summarizes the characteristics and abbreviation of four different types of organoclays. The structural and morphological characterization using WXRD and TEM indicates the formation of four different types of nanocomposites formation. When ODA was used as an organoclay, an intercalated and flocculated nanocomposite was formed. In the case of SBE, an intercalated nanocomposites was formed; whereas disordered intercalated or near to exfoliated nanocomposite was formed in case of SAP organoclay. Finally, MEE organoclay leads to the formation of a mixture of intercalated and exfoliated PLA/MEE nanocomposite.

Maiti and his co-workers [32] prepared a series of PLA-based nanostructured materials with three different types of pristine clays, i.e., saponite (SAP), MMT, and synthetic mica (SM). These clays were modified with alkylphosphonium salts having different chain lengths. In their work, they first tried to determine the effect of varying the chain length of the alkylphosphonium modifier on the properties of the organoclay and how the various oganoclays behaved differently with the same organic modifier. They also studied the effects of dispersion, intercalation, and the aspect ratio of the clay on the properties of PLA. The WXRD and TEM results show that, with a modified of the same chain length, the degree of dispersion of silicate particles was higher in the

**TABLE 17.1 Characteristics of Four Different Organoclays**

| Organoclay Abbreviation | Pristine Clay | Particle Length (nm) | Cation Exchange Capacity (meq/100 g) | Surfactant Used for Modification | Supplier | Nanocomposite Code Containing 4 wt% Organoclay |
|---|---|---|---|---|---|---|
| ODA | Montmorillonite | 150–200 | 110 | Octadecylammonium cation | Nanocor Inc., USA | PLA/ODA |
| SBE | Montmorillonite | 100–130 | 90 | Octadecyltrimethyl ammonium cation | Hojun Yoko Co., Japan | PLA/SBE |
| SAP | Saponite | 50–60 | 86.6 | Hexadecyltributyl phosphonium cation | CO-OP Chemicals, Japan | PLA/SAP |
| MEE | Synthetic fluorine mica | 200–300 | 120 | Dipolyoxyethylene alkyl (coco) metylammonium cation | CO-OP Chemicals, Japan | PLA/MEE |

case of SM-containing PLA nanocomposite; whereas SAP-containing nanocomposite showed lowest degree of dispersion of silicate particles in PLA matrix. According to the authors, this observation is linked with the higher exchange capacity of SM clay.

Paul et al. [33] used an in situ intercalative method for the preparation of exfoliated PLA-clay nanocomposites. They used two different kinds of organoclays (C30B and C25A, Southern Clay Products) for the preparation of nanocomposites with PLA. In their typical synthetic procedure, the clay was first dried overnight (20 h) at 70°C in a ventilated oven, and then under reduced pressure at the same temperature, directly in the flame-dried polymerization vial for 3.5 h. A 0.025 molar solution of L-lactide in dried tetrahydrofuran (THF) was then transferred under nitrogen to the polymerization vial, and the solvent was eliminated under reduced pressure. The polymerization was conducted in bulk at 120°C for 48 h, after 1 h of clay swelling in the monomer melt. When C30B was used, the polymerization was co-initiated by a molar equivalent of triethylaluminium ($AlEt_3$), with respect to the hydroxyl groups borne by the ammonium cations of the filler, in order to form aluminium alkoxide active species and was added before the L,L-lactide. The catalyst, Sn $(Oct)_2$ (monomer/Sn$(Oct)_2$ = 300), was used to catalyze the polymerization of L,L-lactide in the presence of C25A. The same research group also reported the preparation of plasticized PLA/MMT nanocomposites by a melt intercalation technique [34]. The organoclay used was MMT modified with bis-(2-hydroxyethyl) methyl (hydrogenated tallow alkyl) ammonium cations. X-ray diffraction (XRD) analyses confirmed the formation of intercalated nanocomposites, which significantly improved Young's modulus (59%) when compared with neat PLA. Chang et al. [35, 36] reported the preparation of PLA-based nanocomposites with three different organoclays ($C_{16}$–MMT, DTA–MMT Cloisite® 25A, C25A) via a solution intercalation method. They used *N*,*N*′-dimethylacetamide (DMA) for the preparation of the nanocomposites. The XRD patterns indicated the formation of intercalated nanocomposites for all the three organoclays tested. TEM images proved that most of the clay layers were dispersed homogeneously in the PLA matrices, although some clusters or agglomerated particles were also detected. To understand the structure–property relationship in various nanocomposites, the thermomechanical properties and the gas permeability of neat PLA and various nanocomposites were measured. The results showed that the final properties of the nanocomposites depended on the nature of organoclay used for the preparation of nanocomposites and the organoclay content in the polymer matrix. When thermal stability (at 2% weight loss) of PLA/$C_{16}$–MMT and PLA/C25A nanocomposites was compared with neat PLA, the thermal stability was linearly decreased with an increase in both $C_{16}$–MMT and C25A organoclays; whereas thermal stability of PLA/DTA-MMT nanocomposite was unaffected with DTA-MMT loadings.

Krikorian et al. [37] explored the effect of compatibility of different organic modifiers on the extent of dispersion of layered silicate layers in a PLA matrix. Three commercially (Southern Clay Product, Inc.) available organoclays, such as Cloisite C30B, C30B; C25A; and Cloisite 15A (C15A) were used as a reinforcement phase. To have a rough understanding of degree of compatibility of the neat PLLA with different organoclays, the authors used the group contribution methods of Fedors, Van Krevelen, Hoy, Small, and Hoftyzer–Van Krevelen [37] to calculate the solubility parameters ($\delta$) for each of the organic modifiers used in the organoclays and neat PLLA. Nanocomposites were prepared by using the solution-intercalation film-casting technique. The WXRD patterns of various nanocomposites showed that the increased compatibility between the organoclay and PLA matrix increases the tendency of the silicate particles to exfoliate and randomly distribute in the PLLA matrix. The highest degree of dispersion was achieved in the case of

PLA/C30B nanocomposite. The TEM observation supported the conclusion made from WXRD results. All nanocomposites showed a significant improvement in mechanical properties when compared with neat polymer, and it was consistent with the degree of dispersion of silicate layers in the nanocmposites.

Lee et al. [38] prepared PLA/MMT nanocomposite for the purpose of tailoring mechanical stiffness of porous PLA scaffold systems. They used a salt leaching/gas foaming method for the preparation of nanocomposite scaffolds. A viscous PLA solution with a concentration of 0.1 g/mL was prepared by dissolving the PLA polymer in chloroform. $NH_4HCO_3$/NaCl salt particles sieved in the range of 150–300 μm and dimethyl dehydrogenated tallow ammonium-modified MMT (2M2HT-MMT) clays were added to the PLA solution and thoroughly mixed. The amount of the 2M2HT-MMT clay was 2.24, 3.58, and 5.79 vol% to PLA. The paste mixture of polymer/salts/solvent was then cast on a glass slide. A cast film was obtained after being air-dried under atmospheric pressure for 2 h. When the film became semi-solid, a two-step salt leaching was performed. The film was first immersed in a 90°C hot water bath to leach out the $NH_4HCO_3$ particles, concomitantly generating gaseous ammonium and carbon dioxide in the polymer matrix. When no gas bubbles were generated, the film was subsequently immersed into another beaker containing hot water (~60°C) for 30 min to leach out the remaining NaCl particles. Finally, the samples were freeze-dried for two days. From the XRD patterns, it was seen that the pure 2M2HT-MMT demonstrated a sharp peak at $2\theta = 3.76°$, and this peak was not observed in the case of nanocomposites, indicating the formation of exfoliated PLA/2M2HT-MMT nanocomposite with improved tensile and flexural properties, but they did not report any TEM observation.

Recently, various authors reported the preparation of PLA/clay nanocomposites using different processing routes [39–43]. Pillai et al. [44] prepared PLA/palygorsite (Paly) nanocomposites by solvent casting in chloroform. Both pristine and organically modified palygorskite (Org-Paly), prepared by cation exchange reaction between Paly with a quaternary ammonium salt [di(hydrogenated tallow) dimethyl ammonium chloride], were used for nanocomposite preparation. Field-emission scanning electron microscope (FESEM) was used to study the morphological characteristics of the nanocomposites. As observed in both TEM and SEM images, PLA containing 2 wt% Paly exhibited a reasonably good extent of dispersion. A higher extent of nanoparticle aggregation, along with interfacial debonding, was observed in nanocomposites containing Org-Paly as compared to those containing the same loading of Paly. The higher tendency of Org-Paly to aggregate in the PLA matrix was ascribed to the fact that Org-Paly particles had less-stable surfactant molecules adsorbed on their surfaces. Recently, an improvement in the quality of clay dispersion has also been achieved by the modification of the processing equipment used in melt mixing [45, 46]. Wu et al. [45] used an eccentric rotor extruder (Figure 17.1a) to achieve continuous elongational flow in the fabrication of PLLA/OMMT nanocomposites. Their XRD (Figure 17.1b) and TEM (Figure 17.1c) results revealed a uniform dispersion of the nanoclay particles, which were found to exist mostly as intercalated structures.

The low-frequency values of storage modulus ($G'$) and loss modulus ($G''$) of the nanocomposites, in melt rheology studies, were found to increase montonically with increase in clay concentration. Moreover, the frequency dependence of the viscoelastic response of the nanocomposites were lower than that of neat PLLA. When the clay concentration was higher than 3 wt%, $G'$ became independent of frequency in the low-frequency region, exceeding $G''$ over the entire frequency range, indicating pseudo-solid-like behavior. The nanocomposites exhibited higher storage modulus ($E'$) than neat PLLA in temperature sweep studies of dynamic mechanical analyzer (DMA). However, the presence of intercalated structures did not result in a significant broadening of the loss modulus ($E''$) and tan $\delta$ curves from DMA studies. This observation was attributed to the unrestricted segmental movement at the organic–inorganic interface regions of the nanocomposites. The researchers proposed a mechanism for the dispersion of OMMT in the presence of an elongation flow field. They suggested that the double-side exfoliation might have occurred during elongational flow that was more effective in achieving a superior quality of dispersion than the layer-by-layer peeling mechanism that was exhibited during shear flow.

It can be concluded that melt processing can be successfully employed to produce PLA nanoclay composites exhibiting superior dispersion of silicate layers. Surface modification of the nanoclay, proper choice of processing conditions, and the use of compatibilizers help in achieving nanocomposites of superior morphology and hence properties.

## 17.3 CARBON-NANOTUBES-CONTAINING PLA NANOCOMPOSITES

In the last decade, carbon nanotubes (CNTs) have garnered more and more interest from both scientists and engineers because of their extraordinary high strength/modulus (the strongest material known today), excellent electrical conductivity, high thermal conductivity, stability, and low density, which can be associated with their high aspect ratio and one-dimensional tubular structure. These properties offer tremendous potential in applications such as nano-engineering and bionanotechnology.

Compared to PLA/clay nanocomposites, there is less literature on the production of PLA/CNT nanocomposites. In most cases, PLA/CNT nanocomposites have been synthesized by

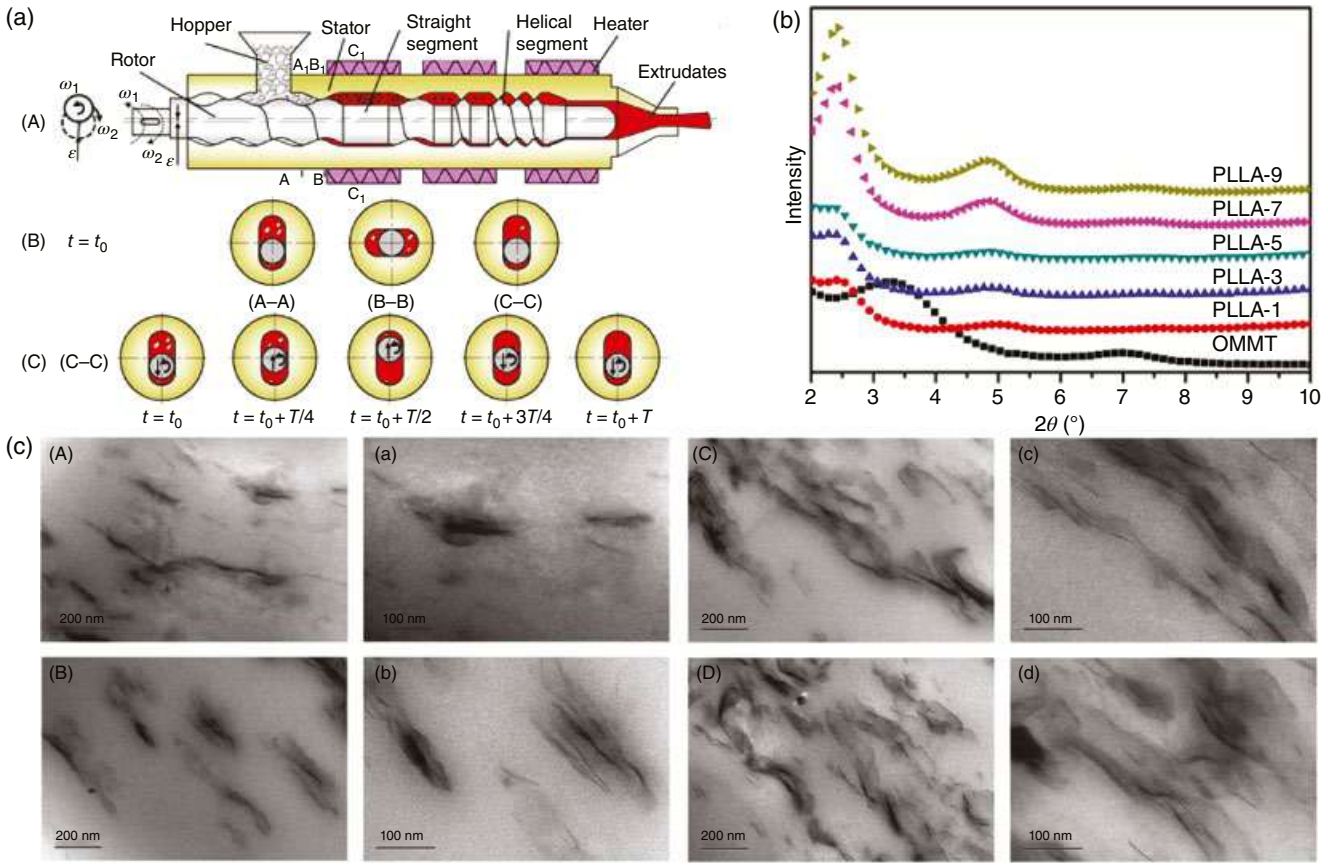


**FIGURE 17.1** (a) The schematic diagram of eccentric rotor extrusion system: (A) the overall extruder setup; (B) different cross section view; and (C) position of stator and rotor at different times of one cycle for section C–C. (b) X-ray diffractometer curves of neat organo-modified montmorillonite (OMMT) and poly(L-lactide) (PLLA)/OMMT nanocomposites. (c) Transmission electron microscope morphology of poly(L-lactide) (PLLA)/organo-modified montmorillonite (OMMT) nanocomposites in different OMMT concentration. (A) and (a) PLLA-1; (B) and (b) PLLA-3; (C) and (c) PLLA-5; (D) and (d) PLLA-7. Numbers 1, 3, 5, and 7 indicate the loadings of OMMT in PLA/OMMT nanocomposites. *Source*: Reproduced with permission. Ref. [45]. Copyright 2017, John Wiley & Sons, Ltd.

solvent casting or by melt mixing. Usually, the key challenge in the production of PLA/CNT nanocomposites is to achieve the desired degree of dispersion and distribution of the CNTs, without adversely affecting their structural integrity, so as to achieve a combination of low percolation threshold and superior mechanical properties. High shear and a prolonged mixing time during melt mixing are expected to facilitate the dispersion of CNTs in the PLA matrix. But this may simultaneously result in breakage of the CNTs, thus altering their structural integrity. Thus, optimization of process parameters must be carried out to attain the desired objectives.

Moon et al. [47] prepared PLA/multiwalled CNTs (MWCNTs) nanocomposites by solvent casting. For the synthesis of nanocomposites, they used two methods. In the first method, a 10 wt% solution of PLA in chloroform was prepared, which was then combined with previously dispersed MWCNTs in chloroform, and the whole mixture was sonicated for 6 h. Subsequently, the mixture was poured into Teflon dishes and dried at room temperature for one week. The resulting sample was vacuum-dried at 80°C for 8 h. In the second method, the as-cast composite films from the first method were folded and broken into pieces of 0.5–1.0 $cm^2$ and stacked between two metal plates. This stack was then hot pressed at 200°C and 150 $kgf/cm^2$ for 15 min to form 100–200 μm thick films. TEM analysis showed uniform dispersion of MWCNTs in the PLA matrix. This uniform dispersion of MWCNTs in PLA matrix resulted in significant increases in the electrical conductivity of the obtained PLA/MWCNTs composite. In comparison to neat PLA (1 GPa), the PLA/MWCNTs composite (2.5 GPa) showed improved Young's modulus.

Chen et al. [48] synthesized PLA/CNT nanocomposites using a "grafting to" technique. To understand the effect of molecular weight on the properties of the final nanocomposites, they used PLA of three different molecular weights. For the preparation of nanocomposites, carboxylic-acid-functionalized MWCNT (MWCNT-COOH) was first reacted with excess thionel chloride ($SOCl_2$) for 24 h under reflux

and then the residual $SOCl_2$ was removed by reduced pressure distillation to yield the acyl-chloride-functionalized MWCNT (MWCNT-COCl). The MWCNT-COCl was added to chloroform, and then the reactor was immersed in an oil bath at 70°C with methanol stirring for 1 h to remove the solvent. The reaction was allowed to proceed for 24 h at 180°C and 1 atm. The resulting reaction medium was dissolved in excess chloroform and vacuum filtered three times through 0.22 μm polycarbonate membrane to yield the MWCNT-*g*-PLLA hybrid by filtering the chloroform soluble substances such as the unbound PLLA. The MWCNT-*g*-PLLA hybrids were prepared using PLLAs of four molecular weights, 1000, 3000, 11,000, and 15,000 Da, which are abbreviated as MWCNT-*g*-PLLA1, MWCNT-*g*-PLLA2, MWCNT-*g*-PLLA3, and MWCNT-*g*-PLLA4, respectively. The composition of the resulting MWCNT-*g*-PLLA nanocomposites was confirmed by Fourier transform infrared (FTIR) spectroscopy. Results showed retention of PLLA even after extensive washing with a good solvent for the PLLA. The Raman analysis revealed the D- and G-bands of the MWCNT at 1287 and 1598 $cm^{-1}$ for both MWCNT-COOH and MWCNT-*g*-PLLA2, which were attributed to the defects and disorder-induced peaks and tangential-mode peaks. The peak intensity of the MWCNT-*g*-PLLA2 was weaker than that of the MWCNT-COOH, which means that the characteristic absorption peaks were strongly attenuated due to the grafted PLLA. The thermogravimetric analysis (TGA) and TEM observations indicated that the amount of grafted PLLA and its morphology depended strongly on the molecular weight of the PLLA. As the molecular weight of the PLLA increased from 1000 to 3000, the PLLA coating on the MWCNT became thicker and more uniform. When the molecular weight of the PLLA was increased further to 11,000 and 15,000, the surface of the MWCNT was not covered wholly but was sparsely stained with the PLLA. The grafted PLLA formed folds exhibiting a squid leg-like morphology. The MWCNT-*g*-PLLA prepared using PLLA with molecular weight of 3000 was more readily dispersed in inorganic solvents such as chloroform and dimethylformamide (DMF) than that obtained using other PLLAs. This was attributed to the higher PLLA content and the smaller area of the MWCNT surface. The MWCNT-*g*-PLLA composite with high-molecular-weight PLLA showed improved thermal stability and Young's modulus when compared with PLLA synthesized without MWCNTs. Recently, Song et al. [49] reported a one-step synthesis of PLA-*g*-MWCNT nanocomposite.

Li et al. [50] have reported an effective method of coupling PLA and CNTs without the use of any chemical treatment. The researchers achieved the same by tailoring the crystalline microstructure through the production of hybrid crystalline fibrils (shish), in which the CNTs were coated with extended PLA chains. Shish structures in PLA/CNT nanocomposite (containing 0.3 wt% CNT) were achieved by means of multistage stretching extrusion, in which fishtail channels were connected in series to create an intense extensional flow. Their processing equipment consisted of a conventional extruder equipped with a series of eight-layer multiplying elements (LMEs) (Figure 17.2a). The PLA/CNT melt in each LME was segmented into two left and right parts by means of a divider. Each melt section was passed through two up and down fishtail channels, respectively. The melt streams were vertically recombined before they entered the next LME. As shown in Figure 17.2b, connecting eight LMEs in series led to an extremely high-melt volume deformation ratio, which brought about the extension of PLA chains, leading to the formation of homogeneous and hybrid shish structures, as depicted in Figure 17.2c. For comparison, neat PLA was also extruded, both without and with LMEs, and designated as PLA-0 and PLA-8, respectively. The formation of shish structures endow a PLA/CNT composite with superior elongation at break (34.9%), strength (94.7 MPa), and modulus (2877 MPa), outperforming the conventional CNT/PLA nanocomposite with increase on elongation at break (502%), strength (31%), and modulus (53%).

## 17.4 GRAPHENE-CONTAINING PLA NANOCOMPOSITES

Graphene, an atomically thin 2-D honeycomb material composed of $sp^2$-hybridized carbon atoms, has gained significant importance since its rediscovery in 2004 [51]. Because of its unique structural and electronic features [52]. PLA/graphene nanocomposites have been regarded as promising materials in many applications.

Li et al. [53] produced PLA/graphene nanocomposites by solution-blending of PLA with liquid-phase exfoliated graphene. PLA solution in chloroform was stirred with graphene dispersion at 40°C for 4 h to obtain a homogeneous PLA/graphene solution, which was then poured into a polytetrafluoroethylene mould after being sonicated for 10 min. The solvent was evaporated at room temperature to obtain PLA/graphene nanocomposite film, which was dried under vacuum to remove traces of the solvent. TEM and XRD studies of the nanocomposite films indicated that no re-aggregation of GSs occurred after being blended with PLA. Tensile strength of the nanocomposites was significantly higher than that of the neat polymer, indicating a reinforcing effect of the nanofiller. Recently, Kim and Jeong [54] prepared exfoliated graphene (EG) by acid treatment of micron-sized natural graphite (NG). PLA/EG nanocomposites were produced by melt compounding. The graphite nanoplatelets of PLA/EG nanocomposites were found to be dispersed uniformly and no aggregates were observed, unlike PLA/NG composites. Similarly, Chakraborty et al. [55] enhanced the dispersion of graphene by coating PLA pellets with a masterbatch prior to melt mixing.

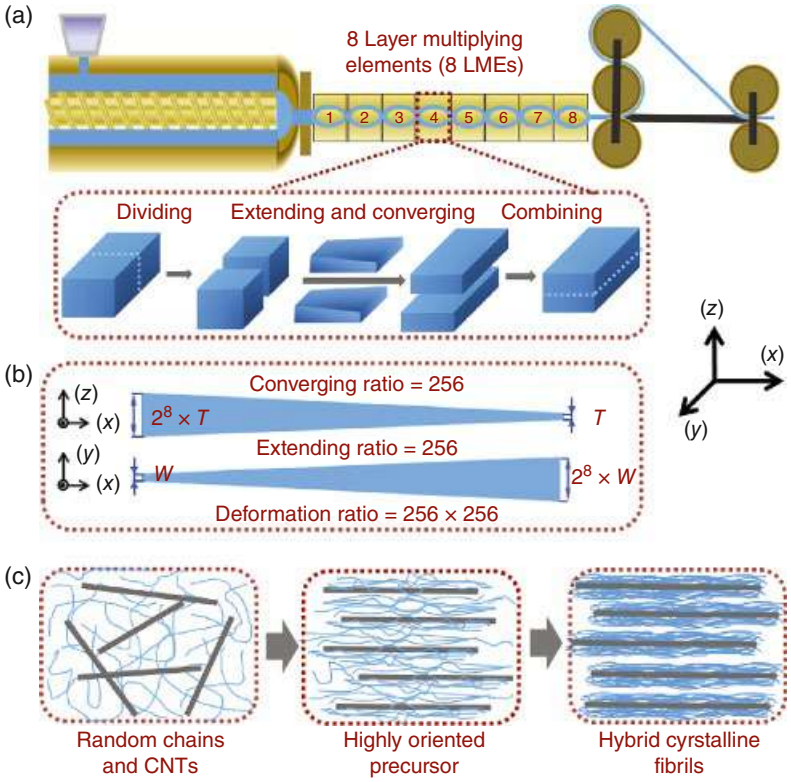


**FIGURE 17.2** (a) Schematic of multistage stretching extrusion system; (b) the converging ($x$, $z$ plane), extending ($x$, $y$ plane) and volume deformation ratio of CNT/PLA melt after flow through eight LMEs; and (c) structure evolution for the hybrid crystalline fibrils (shish). *Source*: Reproduced with permission. Ref. [50]. Copyright 2018, Elsevier.

Cao et al. [56] prepared solvent-free graphene nanosheets (GNSs) by means of freeze drying. Compared to those produced by vacuum filtration process, the lyophilized GNS powders were light, loosely packed, and suitable for redispersion, by means of sonication in solvents like DMF. The ability of the lyophilized GNS powders to be redispersed in organic solvents facilitated their incorporation into PLA through a solution-based processing method. In this method, PLA was added to a dispersion of lyophilized GNSs in DMF. The mixture was coagulated with methanol, filtered, and the floculant (PLA/graphene nanocomposite) was vacuum dried. Nanocomposite containing 0.2 wt%, prepared in this way, was found to possess uniformly dispersed GNSs and exhibited better mechanical properties than neat PLA. Findings of key literature related to dispersion/structure achieved in the processing of PLA/CNT nanocomposites using various techniques are presented in Table 17.2.

## 17.5 NANOCELLULOSE-CONTAINING PLA NANOCOMPOSITES

Investigations have been conducted on the preparation of PLA/cellulose nanocrystal (CNC) nanocomposites by melt mixing. It has been observed that the applied shear and extensional forces in melt mixing are not sufficient to overcome the strong bonds between the hydrophilic CNC particles. Furthermore, high processing temperatures along with shear forces may lead to thermal degradation of the CNCs [63, 64]. Various strategies have been implemented to enhance the dispersion of CNCs in PLA without causing thermal degradation. These include the use of different methods of preparation of CNCs, [65, 66] CNC surface modification [66–70], and the use of surfactants/compatibilizers [71–76]. PLA/CNC nanocomposites have also been prepared using various hybrid methods, involving wet (e.g., solution casting, liquid feeding, spin-coating) and dry (e.g., melt mixing) processes used in combination. Among these methods, liquid-assisted feeding of CNC into extruder has proven to be ineffective in achieving a superior quality of dispersion along with improvement in properties [77, 78]. However, the preparation of a masterbatch of CNC in a polymer by means of solution casting [79], spin-coating [80] or in situ polymerization [68], and diluting the masterbatch with PLA through melt mixing has been found to be effective in enhancing the quality of CNC dispersion.

The methods, which are used for enhancement of dispersion of CNC during melt processing with PLA, are also used for solvent casting. Sanchez-Garcia and Lagaron [81] compared the properties of solvent cast PLA/CNC nanocomposites, using CNC prepared by different methods. A better dispersion was

**TABLE 17.2 Processing Techniques and Structures of PLA/CNT, PLA/Graphene Nanocomposites**

| Fillers | Functionalization | Processing | Structure | Ref. |
|---|---|---|---|---|
| **CNTs** | None | Solvent casting in chloroform | Uniform dispersion at a micron scale | [47] |
| | None | Melt processing in a torque rheometer | Polymer-polymer network, polymer-CNTs network and CNTs-CNTs network | [53] |
| | Surface modification with hexadecyl amine | Melt processing in twin-screw extruder | Homogeneous dispersion of CNTs with some microscale dispersion of CNT bundles | [57] |
| | Surface modification with dodecylamine | Solution blending in chloroform | Uniform distribution of individual nanoscale particles and larger aggregates | [58] |
| | Acyl-chloride functionalization using $SOCl_2$, followed by grafting with PLLA | Solvent casting in chloroform | Uniform dispersion with CNT-*g*-PLLA wrapped with PLLA | [59] |
| | Carboxylic-acid functionalization using sulfuric acid and nitric acid in 1 : 3 molar ratio, followed by grafting with PLLA | Solution blending in chloroform | Uniform dispersion without aggregation | [60] |
| | None | Melt processing in TSE with masterbatch dilution | Uniform dispersion | [52] |
| | None | Melt processing using multistage stretching extrusion | Superior dispersion comprising shish structures | [50] |
| **Graphene** | None | Melt processing in Brabender kneader | Exfoliation with the presence of some aggregates | [61] |
| | None | Solution blending in chloroform | Highly exfoliated | [62] |
| | None | Melt blending in micro-compounder with masterbatch dilution | Superior dispersion and uniform distribution | [55] |
| | None | Melt processing in TSE | Uniform dispersion without aggregation | [54] |

achieved with CNC particles produced by freeze-drying as compared to those produced by solvent exchange, as evident in TEM studies and also in the transparency of the nanocomposite samples. In studies on PLA/CNC nanocomposites produced by solvent casting, improvement of dispersion by surface modification of CNC has mainly been achieved by surface silylation [82, 83] or surface acetylation [84, 85]. Xu et al. [84] used surface acetylation of CNC to achieve homogeneous and nanoscale dispersion of CNC in solvent cast PLA/CNC nanocomposites, as confirmed by morphological studies, as well as by the transparency of the films produced (Figure 17.3). Fortunati et al. [86] and Petersson et al. [87] have employed the surfactant Beycostat A B09 (acid phosphate ester of ethoxylated nonylphenol) for achieving improved dispersion of CNC in PLA/CNC nanocomposites prepared by solvent casting.

## 17.6 OTHER NANOPARTICLE-CONTAINING PLA NANOCOMPOSITES

Hiroi et al. [9] prepared PLA/organically modified layered titanate (OHTO) nanocomposites by a melt-extrusion method. The OHTO (dried at 120°C for 8 h) and PLA were first dry-mixed by shaking them in a bag. The mixture was then melt-extruded using a twin-screw extruder (KZW15-30TGN, Technovel Corp.) operated at 195°C (screw speed 300 rpm, feed rate 22 g/min) to yield nanocomposite strands. XRD patterns and TEM observations showed the formation of intercalated structures. Recently, Nishida et al. [88] reported the preparation of $Al(OH)_3$-based nanocomposites of PLA to achieve the chemical recycling of flame-resistant PLA. For the preparation of PLLA/$Al(OH)_3$ hybrids, PLLA was first synthesized by the ring opening polymerization of L-lactide catalyzed by Sn(2-ethylhexanoate)$_2$. The obtained PLLA was purified in a three-stage process by first extracting the catalyst and residues from the PLLA/chloroform solution with a 1 M HCl aqueous solution, and then washing with distilled water until the aqueous phase became pH neutral. Finally, the polymer was precipitated by methanol addition before vacuum drying. The purified PLLA was then mixed with $Al(OH)_3$ in a prescribed weight ratio in a chloroform solution and vigorously stirred for 1 h to disperse the inorganic particles uniformly. The mixture was then cast on glass Petri dishes. The resulting nanocomposite showed an improved thermal stability and flame resistance

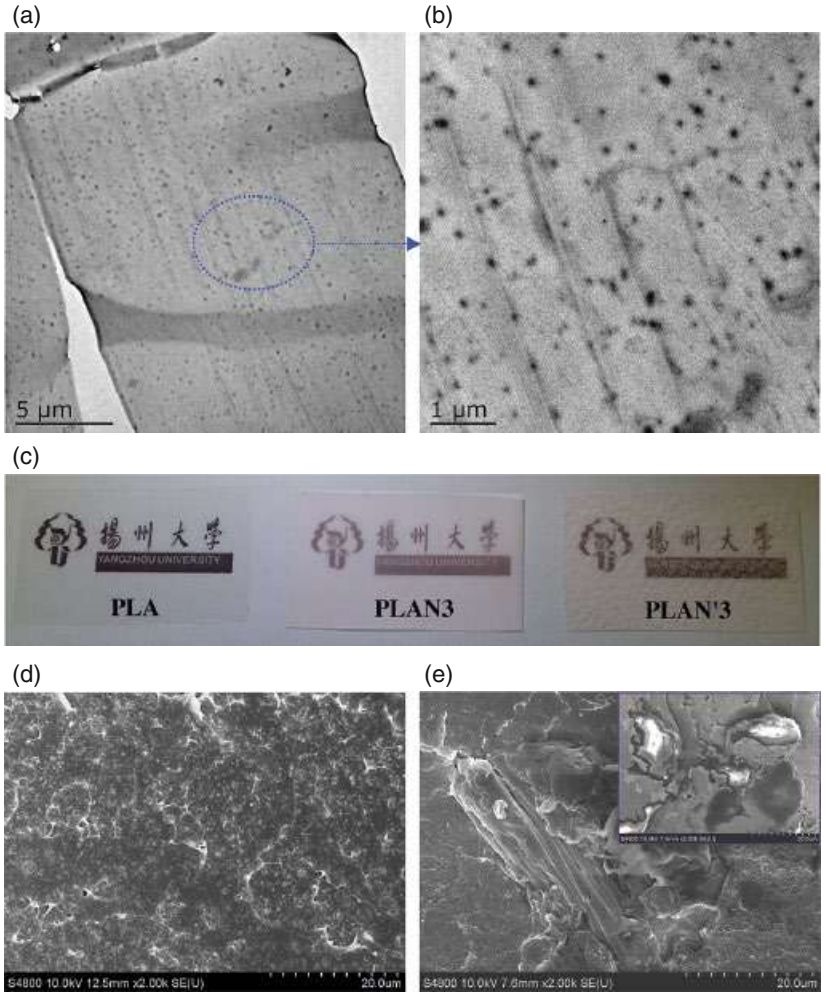


**FIGURE 17.3** (a, b) Transmission electron microscope images of PLAN3 (3 wt% acetylated-CNC), (c) optical images of neat PLA, PLA/3modified-CNC, and PLA/3CNC (3 wt% unmodified-CNC), and (d, e) Scanning electron microscope images of PLAN3 and PLAN'3 samples. *Source*: Reproduced with permission. Ref. [84]. Copyright 2016, Elsevier.

properties when compared with neat PLA and PLA/$Al(OH)_3$ composite prepared using a solvent casting technique.

## 17.7 MECHANICAL PROPERTIES OF PLA-BASED NANOCOMPOSITES

Nanocomposites consisting of PLA and nanofillers frequently exhibit significant improvement in mechanical properties when compared to those of pure polymers, through: (i) the nanoparticle itself can provide added stiffness and strength due to its own mechanical properties; (ii) the nanoparticle can prevent failure by impeding crack propagation; and (iii) changes in the structure of polymer chains close to the nanoparticle surface can modify the mechanical properties [2, 89, 90]. The extent of improvement in mechanical properties has been found to depend on the aspect ratio of nanoparticles [2] and the extent of dispersion, the latter being dependent on the nanoparticle loading and the mixing conditions during melt processing [91]. Table 17.3 reports typical improvements in the mechanical properties of PLA achieved by the incorporation of various nanofillers.

In addition to the mechanical properties, certain nanofillers such as CNTs and graphene impart properties specific to special applications. Due to their inherent electrical properties, CNTs and graphene have been used for fabricating conductive polymer composites (CPCs). In polymer/CNT nanocomposites, formation of 3D network of CNT occurs above a certain concentration called the percolation threshold. Conductivity is not observed in a polymer/CNT nanocomposite until the volume fraction of the CNTs reaches the percolation threshold. Many factors determine the electrical conductivity of PLA/CNT nanocomposites. These include the volume fraction, dimensions (aspect ratio), the degree of dispersion of the CNTs, conductivity and orientation of the CNTs, the interfacial energy between the PLA matrix and the CNTs, as well as the interphase zone

**TABLE 17.3 Improvement (with Respect to Neat PLA) in Mechanical Properties of PLA Nanocomposites Achieved with Various Nanofillers**

| Nanofiller | Filler Loading (wt.%) | Method of nanocomposite preparation | Improvement in Tensile Modulus (%) | Improvement in Tensile Strength (%) | Improvement in Flexural Modulus (%) | Improvement in Flexural Strength (%) | Ref. |
|---|---|---|---|---|---|---|---|
| MMT modified with octadecyl ammonium cation | 4 | Melt mixing | — | — | 17 | 53 | [2] |
| C30B | 4 | Melt mixing | 40 | 81 | — | — | [91] |
| Sepiolite treated with silane | 1.5 | Solvent casting | 100 | 24 | — | — | [92] |
| Sepiolite functionalized with aminosilane groups | 10 | Melt mixing | — | — | 20 | 9 | [78] |
| Halloysite nanotubes modified with benzoalkonium chloride | 4 | Melt mixing | 19 | 21 | 18 | 26 | [77] |
| CNC with surface grafted PLA chains | 2 | Solvent casting | 40 | 35 | — | — | [93] |
| CNC | 5 | Preparation of pickering emusion followed by drying and compression moulding | — | — | 36 | 19 | [94] |
| Acetylated carbon nanofiber | 5 | Solvent casting | 81 | 100 | — | — | [95] |
| Carboxylic functionalized MWNT | 5 | Melt processing | 15 | 20 | 25 | 20 | [96] |
| Graphene | 0.4 | Solvent casting | 156 | 40 | — | — | [97] |
| Graphene | 0.25 | Melt blending of freeze-dried graphene/poly(ethylene glycol) masterbatch with PLA | 126 | 51 | 35 | 46 | [98] |

**TABLE 17.4 Improvement in Properties Achieved in PLA/Nanocomposites**

| Nanofiller | Improvement in Properties Achieved | Refs. |
|---|---|---|
| **Layered Silicates** | Gas barrier property | [2, 7, 105] |
| | Biodegradability | [2, 7, 105] |
| | Fire retardant properties | [2, 7, 105] |
| **HNT** | Gas barrier property | [106, 107] |
| | Biodegradability | [108] |
| | FR properties | [109] |
| **Sepiolite** | Gas barrier property | [104, 110] |
| | Thermal stability | [111] |
| | FR properties | [112] |
| **CNC** | Gas barrier property | [113, 114] |
| | Biodegradability | [115] |
| | Thermal stability | [115] |
| | FR properties | [115] |
| **CNF** | Gas barrier property | [116, 117] |
| **CNT** | Biodegradability | [118] |
| | Thermal stability | [119] |
| | FR properties | [112] |
| | Electrical conductivity | [120, 121] |
| **Graphene** | Gas barrier property | [102, 103] |
| | Thermal stability | [120] |
| | FR properties | [61] |
| | Electrical conductivity | [122, 123] |
| Hydroxyapatite | Cytocompatibility | [124, 125] |
| **ZnO** | UV absorption, antibacterial and self-cleaning properties | [126, 127] |
| **Silver** | Antibacterial properties | [128, 129] |
| **$Fe_3O_4$** | Superparamagnetic properties | [130, 131] |

between the PLA matrix and the CNTs [26, 99, 100]. A low electrical percolation threshold of CNTs helps in maintaining the mechanical, physical, rheological, and electrical properties of nanocomposites at a lower product cost [101]. One way of achieving a low percolation threshold is to use well-dispersed CNTs of high aspect ratio and high conductivity [102, 103]. Another method is based on the concept of "double percolation." In this method, the CNTs are added into an immiscible polymer blend, which has a co-continuous morphology. The CNTs are selectively located in one phase of the blend, which leads to a significant reduction in percolation threshold [104]. Table 17.4 summarizes key literature related to improvement in properties, other than mechanical properties, achieved in PLA nanocomposites.

## 17.8 POSSIBLE APPLICATIONS AND FUTURE PROSPECTS

New environmental policies, societal concerns, and growing environmental awareness have triggered the search for products and processing alternatives that are more environmentally benign. PLA is considering as an alternative to the existing petroleum-based plastic materials. However, the intrinsic properties of the unmodified PLA, such as its low crystallinity (ca. 40%) and rigidity, and slow degradation, put limits on its wide range of applications [132, 133]. PLA-based nanostructured materials offer unique combinations of properties including biodegradability and thermoplastic processibility that may be exploited in applications, such as in packaging of agricultural products, and disposable materials. The versatility of the nanofillers to transform into various shapes and morphologies along with good mechanical properties has led to a wide range of applications. The thermoplastic character of PLA is very useful in allowing the transformation of the polymer materials into various shapes. The apparel sector is particularly promising. For example, the University of Tennessee (USA) has been active in work on spunlaid and melt-blown nonwovens based on PLA. Kanebo Ltd (Japan) has produced a PLA fiber under the brand name LACTRONTM, which was exhibited in garments during the Nagano Olympics under the umbrella of "Fashion for the Earth" [134]. The low modulus of the fiber has been exploited for better drape and feel of fabrics. A market for PLA and PLA-based nanostructured materials has also been developed in sportswear, especially as an inner wicking layer.

Because of the excellent oxygen barrier and water vapor barrier properties, as well as superior mechanical properties, transparency along with biodegradability, PLA nanocomposites are excellent food packaging materials, which would provide enhanced shelf life to food items. CPCs based on PLA/CNT and PLA/graphene nanocomposites find application in sensors and electromagnetic interference shielding. Because of their biodegradability and cytocompatibility, PLA/graphene, PLA/HA, and PLA/CNT nanocomposites are used in a variety of biomedical applications like scaffolds and drug delivery.

Although a significant amount of research has been conducted on PLA nanocomposites, much work is still required to better understand the structure–property–processing relationship of nanocomposites, to achieve a superior state of dispersion and distribution of nanoparticles with little or no use of surfactants/compatibilizers. Although extensive studies have been conducted on PLA/clay nanocomposites, more work needs to be done on clays of different morphologies, such as sepiolite and palygorskite. There is limited understanding of nanocomposites containing a mixture of different nanofillers. Development of such nanocomposites will help in achieving the synergistic benefits of various nanofillers, thus broadening the spectrum of applications. There is scope for developing a greater understanding of the sustainability of products based on various PLA nanocomposites, through life cycle assessment.

## ACKNOWLEDGMENT

The author thanks the Department of Science and Innovation and Council for Scientific and Industrial Research for financial support.

## REFERENCES

1. Y. Ikada, H. Tsuji, *Macromol. Rapid Commun.* **2000**, *21*, 117.
2. S. S. Ray, M. Bousmina, *Prog. Mater. Sci.* **2005**, *50*, 982.
3. P. Gruber, M. O'Brien, Polylactides NatureWorksTM PLA, in: Y. Doi, A. Steinbuchel (Eds.), *Biopolymers in 10 Volumes, Volume 4, Polyesters III Applications and Commercial Products*, Wiley-VCH, Weinheim, 2002, p. 235.
4. Q. Fang, M. A. Hanna, *Ind. Crops Prod.* **1999**, *10*, 47.
5. J. D. Gu, M. Gada, G. Kharas, D. Eberiel, S. P. McCarthy, R. A. Gross, *Polym. Mater. Sci. Eng.* **1992**, *67*, 351.
6. O. Martin, L. Averous, *Polymer* **2001**, *42*, 6209.
7. A. K. Mohanty, L. T. Drzal, M. Misra, *Polym. Mater. Sci. Eng.* **2003**, *88*, 60.
8. A. K. Mohanty, M. Misra, G. Hinrichsen, *Macromol. Mater. Eng.* **2000**, *276*, 1.
9. R. Hiroi, S. S. Ray, M. Okamoto, T. Shiroi, *Macromol. Rapid Commun.* **2004**, *25*, 1359.
10. J. E. Mark, *Acc. Chem. Res.* **2006**, *39*, 881.
11. S. S. Ray, A. O. C. Iroegbu, *ACS Omega* **2021**, *6*, 4511.
12. H. W. Kim, H. H. Lee, J. C. Knowles, *J. Biomed. Mater. Res.* **2006**, *79A*, 643.
13. S. N. Nazhat, M. Kellomaki, P. Tormala, K. E. Tanner, W. Bonfield, *J. Biomed. Mater. Res.* **2001**, *58*, 335.
14. S. S. Ray, M. Okamoto, *Prog. Polym. Sci.* **2003**, *28*, 1539.
15. M. Zanetti, S. Lomakin, G. Camino, *Macromol. Mater. Eng.* **2000**, *279*, 1.
16. M. Biswas, S. S. Ray, *Adv. Polym. Sci.* **2001**, *155*, 167.
17. M. Alexander, P. Doubis, *Mater. Sci. Eng.* **2000**, *R28*, 1.
18. P. C. LeBaron, Z. Wang, T. J. Pinnavaia, *J. Appl. Clay. Sci.* **1999**, *15*, 11.
19. S. Sinha Ray, in H. S. Nalwa (Ed.), *Polymeric Nanostructures and Their Applications*, Volume *1–2*, American Scientific Publishers, Los Angeles, 2007.
20. S. S. Ray, *J. Ind. Eng. Chem.* **2006**, *12*, 811.
21. S. W. Brindly, G. Brown, *Crystal Structure of Clay Minerals and their X-ray Diffraction*, The Mineralogical Society, London, 1980.
22. N. Ogata, G. Jimenez, H. Kawai, T. Ogihara, *J. Polym. Sci. Part B Polym. Phys.* **1997**, *35*, 389.
23. S. Bandyopadhyay, R. Chen, E. P. Giannelis, *Polym. Mater. Sci. Eng.* **1999**, *81*, 159.
24. S. S. Ray, P. Maiti, M. Okamoto, K. Yamada, K. Ueda, *Macromolecules* **2002**, *35*, 3104.
25. S. S. Ray, K. Yamada, M. Okamoto, K. Ueda, *Nano. Lett.* **2002**, *2*, 423.
26. S. S. Ray, K. Yamada, A. Ogami, M. Okamoto, K. Ueda, *Macromol. Rapid Commun.* **2002**, *23*, 943.
27. S. S. Ray, K. Yamada, M. Okamoto, A. Ogami, K. Ueda, *Chem. Mater.* **2003**, *15*, 1456.
28. S. S. Ray, K. Yamada, M. Okamoto, Y. Fujimoto, A. Ogami, K. Ueda, *Polymer* **2003**, *44*, 6633.
29. S. S. Ray, K. Yamada, M. Okamoto, K. Ueda, *Polymer* **2003**, *44*, 857.
30. S. S. Ray, K. Yamada, M. Okamoto, K. Ueda, *J. Nanosci. Nanotechnol.* **2003**, *3*, 503.
31. S. S. Ray, K. Yamada, M. Okamoto, A. Ogami, K. Ueda, *Compos. Interfaces* **2003**, *10*, 435.
32. P. Maiti, K. Yamada, M. Okamoto, K. Ueda, K. Okamoto, *Chem. Mater.* **2002**, *14*, 4654.
33. M. A. Paul, M. Alexandre, P. Degee, C. Calberg, R. Jerome, P. Dubois, *Macromol. Rapid Commun.* **2003**, *24*, 561.
34. M.-A. Paul, M. Alexandre, P. Degee, C. Henrist, A. Rulmont, P. Dubois, *Polymer* **2003**, *44*, 443.
35. J.-H. Chang, Y. U. An, G. S. Sur, *J. Polym. Sci. Part B Polym. Phys.* **2003**, *41*, 94.
36. J. H. Chang, Y. U. An, D. Cho, E. P. Giannelis, *Polymer* **2003**, *44*, 3715.
37. V. Krikorian, D. J. Pochan, *Chem. Mater.* **2003**, *15*, 4317.
38. J. H. Lee, T. G. Park, H. S. Park, D. S. Lee, Y. K. Lee, S. C. Yoon, J. D. Nam, *Biomaterials* **2003**, *24*, 2773.
39. A. Kramschuster, S. Gong, L. S. Turng, T. Li, T. Li, *J. Biobased Mater. Bioenergy* **2007**, *1*, 37.
40. P. H. Nam, A. Fujimori, T. Masuko, *e-Polymers* **2004**, article no. 005.
41. P. H. Nam, A. Fujimori, T. Masuko, *J. Appl. Polym. Sci.* **2004**, *93*, 2711.
42. N. Ninomiya, P. H. Nam, A. Fujimori, T. Masuko, *e-Polymers* **2004**, article no. 41.
43. P. H. Nam, M. Kaneko, N. Ninomiya, A. Fujimori, T. Masuko, *Polymer* **2004**, *46*, 7403.
44. S. K. Pillai, V. Ojijo, S. S. Ray, *J. Appl. Polym. Sci.* **2014**, *131*, 40414.
45. T. Wu, Y. Tong, F. Qiu, D. Yuan, G. Zhang, J. Qu, *Polym. Adv. Technol.* **2018**, *29*, 41.
46. Y. Luo, H. Y. Liu, G. Z. Zhang, J. P. Qu, *IOP Conference Series: Materials Science and Engineering*, Institute of Physics Publishing, 2017, vol. *213*, p. 012018.
47. S. Moon, F. Jin, C. J. Lee, S. Tsutsumi, S. H. Hyon, *Macromol. Symp.* **2005**, *224*, 287.
48. G. X. Chen, H. S. Kim, B. H. Park, J. S. Yoon, *J. Phys. Chem. B* **2005**, *109*, 22237.
49. W. Song, Z. Zheng, W. Tang, X. Wang, *Polymer* **2007**, *48*, 3658.
50. C. Li, J. Guo, T. Jiang, X. Zhang, L. Xia, H. Wu, S. Guo, X. Zhang, *Carbon* **2018**, *129*, 720.
51. C. S. Wu, H. T. Liao, *Polymer* **2007**, *48*, 4449.
52. T. Villmow, P. Pötschke, S. Pegel, L. Häussler and B. Kretzschmar, *Polymer* **2008**, *49*, 3500.

53. Y. Li, D. Yin, W. Liu, H. Zhou, Y. Zhang, X. Wang, *Int. J. Biol. Macromol.* **2020**, *163*, 1175.
54. I. H. Kim, Y. G. Jeong, *J. Polym. Sci. Part B Polym. Phys.* **2010**, *48*, 850.
55. G. Chakraborty, A. Gupta, G. Pugazhenthi, V. Katiyar, *J. Appl. Polym. Sci.* **2018**, *135*, 46476.
56. Y. Cao, J. Feng, P. Wu, *Carbon* **2010**, *48*, 3834.
57. J. Ramontja, S. S. Ray, S. K. Pillai, A. S. Luyt, *Macromol. Mater. Eng.* **2009**, *294*, 839.
58. M. J. Sobkowicz, R. Sosa, J. R. Dorgan, *J. Appl. Polym. Sci.* **2011**, *121*, 2029.
59. Y. T. Shieh, G. L. Liu, *J. Polym. Sci. Part B Polym. Phys.* **2007**, 45, 1870.
60. J. T. Yoon, S. C. Lee, Y. G. Jeong, *Compos. Sci. Technol.* **2010**, *70*, 776.
61. M. Murariu, A. L. Dechief, L. Bonnaud, Y. Paint, A. Gallos, G. Fontaine, S. Bourbigot, P. Dubois, *Polym. Degrad. Stab.* **2010**, *95*, 889.
62. X. Li, Y. Xiao, A. Bergeret, M. Longerey, J. Che, *Polym. Compos.* **2014**, *35*, 396.
63. C. Miao, W. Y. Hamad, *Cellulose* **2013**, *20*, 2221.
64. H. M. Ng, L. T. Sin, S. T. Bee, T. T. Tee, A. R. Rahmat, *Polym. Plast. Technol. Eng.* **2017**, *56*, 687.
65. M. R. Kamal, V. Khoshkava, *Carbohydr. Polym.* **2015**, *123*, 105.
66. S. Spinella, G. Lo Re, B. Liu, J. Dorgan, Y. Habibi, P. Leclère, J. M. Raquez, P. Dubois, R. A. Gross, *Polymer* **2015**, *65*, 9.
67. V. Khoshkava, M. R. Kamal, *Biomacromolecules* **2013**, *14*, 3155.
68. A. L. Goffin, J. M. Raquez, E. Duquesne, G. Siqueira, Y. Habibi, A. Dufresne, P. Dubois, *Biomacromolecules* **2011**, *12*, 2456.
69. E. Lizundia, E. Fortunati, F. Dominici, J. L. Vilas, L. M. León, I. Armentano, L. Torre, J. M. Kenny, *Carbohydr. Polym.* **2016**, *142*, 105.
70. Y. Habibi, S. Aouadi, J. M. Raquez, P. Dubois, *Cellulose* **2013**, *20*, 2877.
71. D. Bondeson, K. Oksman, *Compos. Interfaces* **2007**, *14*, 617.
72. E. Fortunati, I. Armentano, Q. Zhou, A. Iannoni, E. Saino, L. Visai, L. A. Berglund, J. M. Kenny, *Carbohydr. Polym.* **2012**, *87*, 1596.
73. M. P. Arrieta, E. Fortunati, F. Dominici, E. Rayón, J. López, J. M. Kenny, *Polym. Degrad. Stab.* **2014**, *107*, 139.
74. A. Gupta, W. Simmons, G. T. Schueneman, D. Hylton, E. A. Mintz, *ACS Sustain. Chem. Eng.* **2017**, *5*, 1711.
75. J. Chen, H. He, P. Yu, Y. Jia, S. Meng, J. Wang, *Polym. Compos.* **2018**, *39*, 3092.
76. W. Yang, F. Dominici, E. Fortunati, J. M. Kenny, D. Puglia, *RSC Adv.* **2015**, *5*, 32350.
77. A. P. Mathew, A. Chakraborty, K. Oksman, M. Sain, *ACS Symposium Series*, American Chemical Society, 2006, vol. *938*, pp. 114.
78. E. M. Sullivan, R. J. Moon, K. Kalaitzidou, *Materials* **2015**, *8*, 8106.
79. D. Bagheriasl, F. Safdari, P. J. Carreau, C. Dubois, B. Riedl, *Polym. Compos.* **2019**, *40*, E342.
80. J. Shojaeiarani, D. S. Bajwa, N. M. Stark, *Carbohydr. Polym.* **2018**, *190*, 139.
81. M. D. Sanchez-Garcia, J. M. Lagaron, *Cellulose* **2010**, *17*, 987.
82. A. Pei, Q. Zhou, L. A. Berglund, *Compos. Sci. Technol.* **2010**, *70*, 815.
83. S. Qian, K. Sheng, K. Yu, L. Xu, C. A. Fontanillo Lopez, *J. Mater. Sci.* **2018**, *53*, 10920.
84. C. Xu, J. Chen, D. Wu, Y. Chen, Q. Lv, M. Wang, *Carbohydr. Polym.* **2016**, *146*, 58.
85. T. Mukherjee, M. J. Tobin, L. Puskar, M. A. Sani, N. Kao, R. K. Gupta, M. Pannirselvam, N. Quazi, S. Bhattacharya, *Cellulose* **2017**, *24*, 1717.
86. E. Fortunati, F. Luzi, D. Puglia, R. Petrucci, J. M. Kenny, L. Torre, *Ind. Crops Prod.* **2015**, *67*, 439.
87. L. Petersson, I. Kvien, K. Oksman, *Compos. Sci. Technol.* **2007**, *67*, 2535.
88. H. Nishida, Y. Fan, T. Mori, N. Oyagi, Y. Shirai, T. Endo, *Ind. Eng. Chem. Res.* **2005**, *44*, 1433.
89. S. Laske, W. Ziegler, M. Kainer, J. Wuerfel, C. Holzer, *Polym. Eng. Sci.* **2015**, *55*, 2849.
90. M. P. Motloung, T. G. Mofokeng, V. Ojijo, S. S. Ray, *Polym. Eng. Sci.* **2022**, doi: https://doi.org/10.1002/pen.25798.
91. J. H. Lee, S. H. Park, S. H. Kim, *Polymers* **2020**, *12*, 178.
92. A. N. Frone, S. Berlioz, J. F. Chailan, D. M. Panaitescu, *Carbohydr. Polym.* **2013**, *91*, 377.
93. H. Almasi, B. Ghanbarzadeh, J. Dehghannya, A. A. Entezami, A. K. Asl, *Food Packag. Shelf Life* **2015**, *5*, 21.
94. A. Kiziltas, B. Nazari, E. Erbas Kiziltas, D. J. Gardner, Y. Han, T. S. Rushing, *Carbohydr. Polym.* **2016**, *140*, 393.
95. J. M. Raquez, Y. Murena, A. L. Goffin, Y. Habibi, B. Ruelle, F. DeBuyl, P. Dubois, *Compos. Sci. Technol.* **2012**, *72*, 544.
96. M. Martínez-Sanz, A. Lopez-Rubio, J. M. Lagaron, *Biomacromolecules* **2012**, *13*, 3887.
97. J. Ambrosio-Martín, M. J. Fabra, A. Lopez-Rubio, J. M. Lagaron, *Cellulose* **2015**, *22*, 1201.
98. L. C. Tomé, R. J. B. Pinto, E. Trovatti, C. S. R. Freire, A. J. D. Silvestre, C. P. Neto, A. Gandini, *Green Chem.* **2011**, *13*, 419.
99. A. A. Gusev, H. R. Lusti, *Adv. Mater.* **2001**, *13*, 1641.
100. M. A. Ortenzi, L. Basilissi, H. Farina, G. Di Silvestro, L. Piergiovanni, E. Mascheroni, *Eur. Polym. J.* **2015**, *66*, 478.
101. N. Devi, S. S. Ray, *Polym. Eng. Sci.* 2022, doi: https://doi.org/10.1002/pen.25876.
102. B. S. Bouakaz, I. Pillin, A. Habi, Y. Grohens, *Appl. Clay Sci.* **2015**, *116–117*, 69.
103. R. B. Valapa, G. Pugazhenthi, V. Katiyar, *RSC Adv.* **2015**, *5*, 28410.
104. P. Russo, S. Cammarano, E. Bilotti, T. Peijs, P. Cerruti, D. Acierno, *J. Appl. Polym. Sci.* **2014**, *131*, 39798.
105. R. Banerjee, S. S. Ray, *Polym. Eng. Sci.* **2021**, *61*, 617.

106. W. L. Tham, B. T. Poh, Z. A. Mohd Ishak, W. S. Chow, *J. Therm. Anal. Calorim.* **2016**, *126*, 1331.
107. N. Najafi, M. C. Heuzey, P. J. Carreau, *Polym. Eng. Sci.* **2013**, *53*, 1053.
108. P. Krishnaiah, C. T. Ratnam, S. Manickam, *Appl. Clay Sci.* **2017**, *135*, 583.
109. G. Stoclet, M. Sclavons, B. Lecouvet, J. Devaux, P. Van Velthem, A. Boborodea, S. Bourbigot, N. Sallem-Idrissi, *RSC Adv.* **2014**, *4*, 57553.
110. N. Moazeni, Z. Mohamad, N. Dehbari, *J. Appl. Polym. Sci.* **2015**, *132*, 41428.
111. M. Liu, M. Pu, H. Ma, *Compos. Sci. Technol.* **2012**, *72*, 1508.
112. T. D. Hapuarachchi, T. Peijs, *Compos. Part A Appl. Sci. Manuf.* **2010**, *41*, 954.
113. D. Arslan, E. Vatansever, D. S. Sarul, Y. Kahraman, G. Gunes, A. Durmus, M. Nofar, *Polym. Compos.* **2020**, *41*, 4170.
114. P. Dhar, D. Tarafder, A. Kumar, V. Katiyar, *RSC Adv.* **2015**, *5*, 60426.
115. Q. Shi, C. Zhou, Y. Yue, W. Guo, Y. Wu, Q. Wu, *Carbohydr. Polym.* **2012**, *90*, 301.
116. J. Trifol, D. Plackett, C. Sillard, P. Szabo, J. Bras, A. E. Daugaard, *Polym. Int.* **2016**, *65*, 988.
117. H. Y. Yu, H. Zhang, M. L. Song, Y. Zhou, J. Yao, Q. Q. Ni, *ACS Appl. Mater. Interfaces* **2017**, *9*, 43920.
118. H. Norazlina, A. A. Hadi, A. U. Qurni, M. Amri, S. Mashelmie, Y. Kamal, *Polym. Bull.* **2019**, *76*, 1453.
119. Y. Zhou, L. Lei, B. Yang, J. Li, J. Ren, *Polym. Test.* **2018**, *68*, 34.
120. J. Huang, C. Mao, Y. Zhu, W. Jiang, X. Yang, *Carbon* **2014**, *73*, 267.
121. K. Zhang, H. O. Yu, Y. D. Shi, Y. F. Chen, J. B. Zeng, J. Guo, B. Wang, Z. Guo, M. Wang, *J. Mater. Chem. C* **2017**, *5*, 2807.
122. Y. Gao, O. T. Picot, E. Bilotti, T. Peijs, *Eur. Polym. J.* **2017**, *86*, 117.
123. Y. Fu, L. Liu, J. Zhang, *ACS Appl. Mater. Interfaces* **2014**, *6*, 14069.
124. A. Kramschuster, L. S. Turng, W. J. Li, Y. Peng, J. Peng, *Proceedings of the ASME First Global Congress on NanoEngineering for Medicine and Biology 2010, NEMB2010*, American Society of Mechanical Engineers Digital Collection, 2010, pp. 175.
125. S. Morelli, S. Salerno, J. Holopainen, M. Ritala, L. De Bartolo, *J. Biotechnol.* **2015**, *204*, 53.
126. M. Murariu, Y. Paint, O. Murariu, J.-M. Raquez, L. Bonnaud, P. Dubois, *J. Appl. Polym. Sci.* **2015**, *132*, 42480.
127. M. Murariu, A. Doumbia, L. Bonnaud, A. L. Dechief, Y. Paint, M. Ferreira, C. Campagne, E. Devaux, P. Dubois, *Biomacromolecules* **2011**, *12*, 1762.
128. K. Shameli, M. Bin Ahmad, W. Md Zin Wan Yunus, N. A. Ibrahim, R. A. Rahman, M. Jokar, M. Darroudi, *Int. J. Nanomed.* **2010**, *5*, 573.
129. X. Xu, Q. Yang, Y. Wang, H. Yu, X. Chen, X. Jing, *Eur. Polym. J.* **2006**, *42*, 2081.
130. X. Zheng, S. Zhou, Y. Xiao, X. Yu, X. Li, P. Wu, *Colloids Surf. B Biointerfaces* **2009**, *71*, 67.
131. S. Taccola, A. Desii, V. Pensabene, T. Fujie, A. Saito, S. Takeoka, P. Dario, A. Menciassi, V. Mattoli, *Langmuir* **2011**, *27*, 5589.
132. B. Gupta, N. Revagade, J. Hilborn, *Prog. Polym. Sci.* **2007**, *32*, 455.
133. R. Leaversuch, Plastic technology, On-line article, 2002, www.plastictechnology.com/articles/200209fa3.html (accessed September).
134. J. Lunt, A. L. Shafer, *J. Ind. Text.* **2000**, *29*, 191.

# 18

# MECHANISM OF FIBER STRUCTURE DEVELOPMENT IN MELT SPINNING OF PLA

Nanjaporn Roungpaisan, Midori Takasaki, Wataru Takarada, and Takeshi Kikutani

## 18.1 INTRODUCTION-FUNDAMENTALS OF STRUCTURE DEVELOPMENT IN POLYMER PROCESSING

Characteristics of polymer products vary significantly depending on the processing conditions; however, the relation between "processing" and "properties" is not straightforward. The missing link between these two factors is the "structure." For better understanding of polymer processing, both the relation between processing conditions and resultant high-order structure, as well as the relation between high-order structure and properties of resultant products need to be clarified. Melt spinning is ideal for investigating the structure development behavior of polymers because it can be regarded as a simple steady-state and unidirectional process. It is also important to note that the ultimate characteristics of polymers can be realized only through the formation of fibers in which molecular chains are highly oriented along the fiber axis.

For melt processing, crystalline polymers can be categorized into two groups [1]. The first group includes polymers with a glass transition temperature ($T_g$) lower than room temperature. The crystallization rate of these polymers needs to be high enough so that the polymer can crystallize in the cooling process during the melt processing. Polyethylene (PE), polypropylene (PP), and so on are categorized into this group. The second group involves polymers with $T_g$ higher than room temperature. Most of the so-called engineering plastics such as poly(ethylene terephthalate) (PET) and polyamide (PA) are categorized into this group. These polymers normally have relatively low crystallization rates. Accordingly, in the cooling process, these polymers are cooled to room temperature without crystallization. The resultant products are in an amorphous state and require an additional annealing process to induce crystallization for enhancing the thermal stability.

One of the important categories of bio-based and/or biodegradable polymers is aliphatic polyester. Except for poly(glycolic acid) (PGA) [2, 3] and poly(lactic acid) (PLA) with $T_g$ of 40 and 60°C, respectively, other aliphatic polyesters normally have lower $T_g$ and low crystallization rate. These characteristics result in melt processing difficulty. For example, it was reported that in the melt spinning process of bio-based aliphatic polyesters, such as poly(3-hydroxybutyrate-*co*-3-hydroxyhexanoate) (PHBH), fibers extruded from the spinneret reach the take-up bobbin without crystallization and tend to stick together [4]. This is because the crystallization rate of PHBH is relatively low with its $T_g$ (0°C) much lower than room temperature, i.e., the fibers are in a rubbery state at room temperature. From this viewpoint, PLA is advantageous for producing products through melt processing in comparison with most other aliphatic polyesters because PLA has $T_g$ higher than room temperature.

In the first edition of this book, *Poly(lactic acid)*, Agrawal contributed a chapter on melt spinning from the engineering aspect [5]. The equipment and processing aspects of melt spinning are now covered in Chapter 13 of this volume. In this chapter, the melt spinning process will be discussed mainly from the viewpoint of fiber structure development.

*Poly(Lactic Acid): Synthesis, Structures, Properties, Processing, Applications, and End of Life*, Second Edition.
Edited by Rafael A. Auras, Loong-Tak Lim, Susan E. M. Selke, and Hideto Tsuji.

## 18.2 HIGH-SPEED MELT SPINNING OF PLLAs WITH DIFFERENT D-LACTIC ACID CONTENT

Structure development in fiber processing of PLA varies considerably depending on its optical purity and molecular weight. Among the papers on structure development of PLA through melt spinning [6–9], Schmack et al. investigated the effect of optical purity of L-lactic acid-rich PLA (PLLA) on fiber structure development in a high-speed melt-spinning process [8, 9]. They used PLLAs with optical purity of 1–8% and a take-up velocity range of up to 5 km/min.

High-speed melt spinning of PLLA pellets with low, middle, and high D-lactic acid content (PLA-L, PLA-M, PLA-H) supplied by Cargill Dow Polymers LLC (currently Nature Works LLC) was carried out in another study [10]. The polymers were mainly composed of L-lactic acid, and the D-lactic acid contents of the three polymers were 1.5, 8.1, and 16.4%, respectively. The polymers were extruded from a spinneret with a single hole of 0.5 mm diameter at a throughput rate of 5.0 g/min. The extrusion temperatures were 230, 220, and 220°C for PLA-L, PLA-M, and PLA-H, respectively. The high-speed winding system was placed 3.3 m below the spinning head. The highest take-up velocities attained for the three polymers were 10, 9, and 8 km/min.

The thinning behavior of filaments in a high-speed melt-spinning process was investigated by using a noncontact back-illumination-type diameter monitor. The variations of filament diameter along the spin-line for the three polymers are shown in Figure 18.1. Smooth diameter attenuation was observed at 1 km/min for all the polymers. Increasing the take-up velocity resulted in increased downstream deformation, while diameter profiles in the upper stream did not show significant change. In PLA-L, abrupt diameter attenuation, which usually is referred to as neck-like deformation [11–13], started to occur at 5 km/min. With an increase in the take-up velocity, the neck-like deformation became more distinct and its position shifted closer to the spinneret. It is well known that neck-like deformation occurring in the high-speed melt-spinning process is normally accompanied by orientation-induced crystallization [14, 15], i.e., the crystallization caused by the stress-induced acceleration of the crystallization rate.

### 18.2.1 Wide-angle X-ray Diffraction

Wide-angle X-ray diffraction (WAXD) patterns of selected high-speed spun fibers are shown in Figure 18.2. An isotropic amorphous halo was observed at low take-up velocities for all fiber samples. Concentration of scattering intensity to the equator proceeded with an increase in the take-up velocity.

In PLA-L, a pair of sharp reflections appeared on the equator at 4 km/min, and distinct crystalline reflections of α-form were observed above 5 km/min. In PLA-M, a pair of sharp reflections on the equator appeared at 5 km/min, and crystalline reflections were observed above 6 km/min. In comparison with the PLA-L fibers, the intensity of the crystalline reflections for PLA-M fibers was weaker, indicating lower crystallinity of these fibers. In PLA-H, a pair of

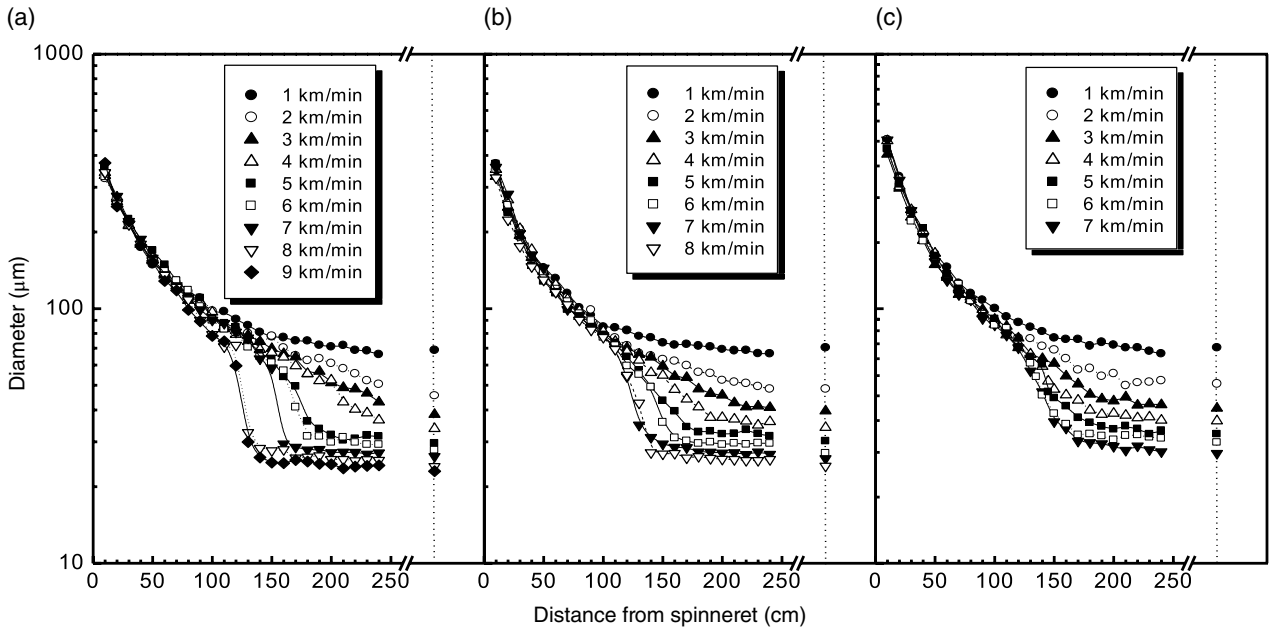


**FIGURE 18.1** Diameter profiles of the spin-lines of (a) PLA-L, (b) PLA-M, and (c) PLA-H measured at various take-up velocities. Data on dotted line denotes the diameter of as-spun fibers. Source: Reproduced from Ref. 10 with permission from Taylor & Francis Group.

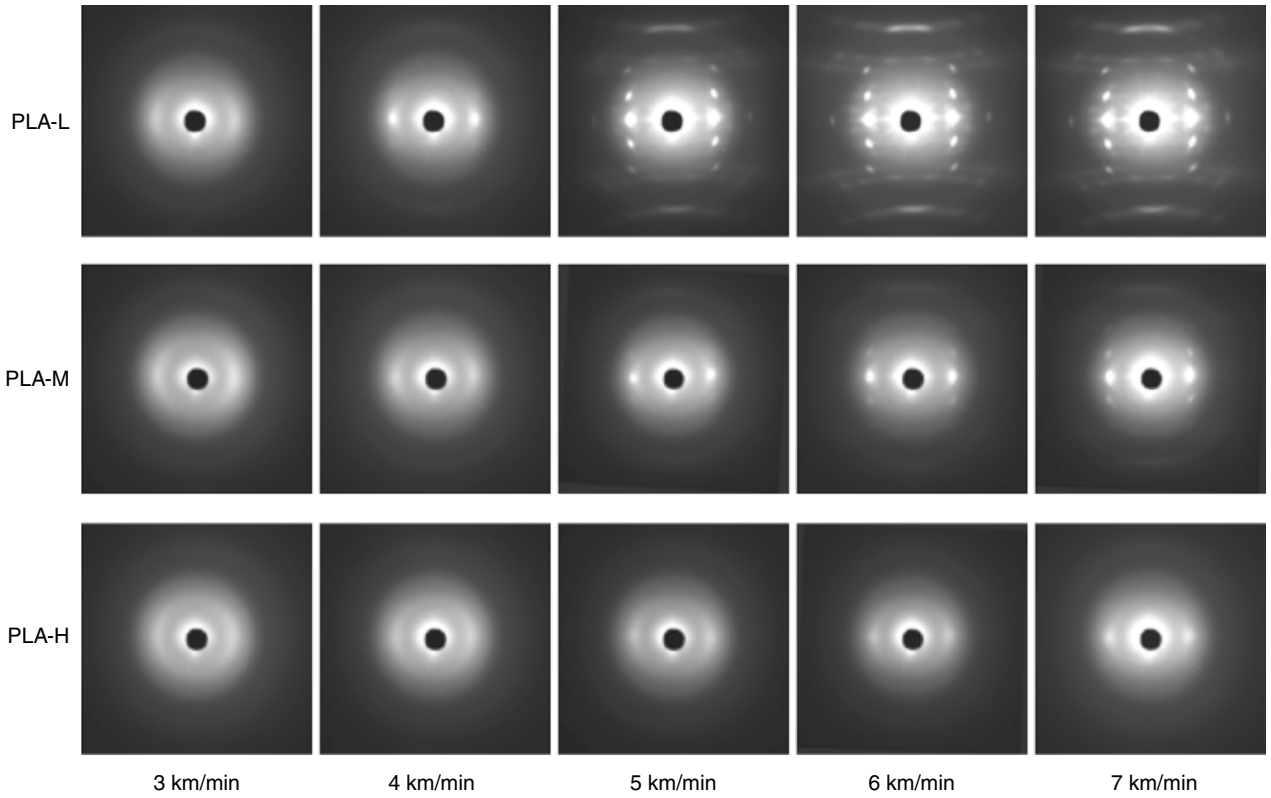


**FIGURE 18.2** Wide-angle x-ray diffraction patterns of as-spun PLA-L, PLA-M, and PLA-H fibers prepared at various take-up velocities. Source: Reproduced from Ref. 10 with permission from Taylor & Francis Group.

sharp reflections on the equator started to appear at 6–7 km/min; however, three-dimensional development of crystalline structure was not confirmed up to the highest take-up velocity of 8 km/min.

From the thinning behavior of the PLA-L and PLA-M spin-lines (Figure 18.1a and b), it was found that the position of solidification, which accompanied the neck-like deformation, shifted toward the spinneret when the take-up velocity was higher than 5 km/min. This result implies that the temperature of orientation-induced crystallization increased with the take-up velocity. Highly developed crystalline structure observed in the WAXD patterns corresponded to the high crystallization temperature in the spin-line. In the case of PLA-H, although clear crystalline reflections did not appear even at high take-up velocities, neck-like deformation was observed. This result implies that the occurrence of neck-like deformation does not directly correlate with crystallization.

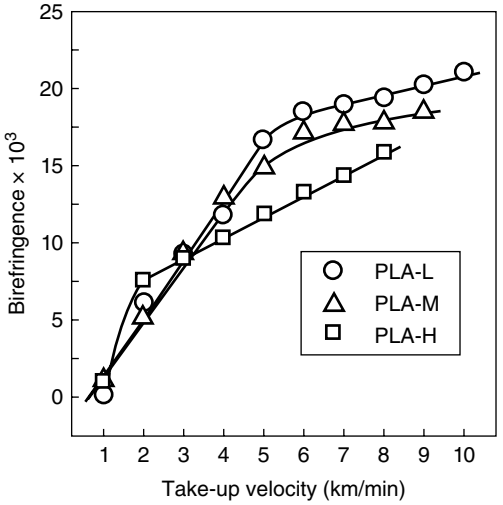


**FIGURE 18.3** Effect of take-up velocity on birefringence of as-spun PLA-L, PLA-M, and PLA-H fibers. Source: Reproduced from Ref. 10 with permission from Taylor & Francis Group.

### 18.2.2 Birefringence

The variations of birefringence of the as-spun fibers as a function of take-up velocity are shown in Figure 18.3. In the low take-up velocity region, birefringence values of the three polymers were comparable; however, when the take-up velocity exceeded 4–5 km/min, when neck-like deformation was observed in the spin-line and the crystalline reflections started to appear in the WAXD pattern, the birefringence values were in the order of PLA-L > PLA-M > PLA-H. The maximum birefringence values for these three polymers were

approximately $21 \times 10^{-3}$, $18 \times 10^{-3}$, and $16 \times 10^{-3}$, respectively. It should be noted that, according to the polymer producer, the viscosity of these three polymers were adjusted to be similar.

For a moderate level of orientation development in polymer melts, birefringence development is expected to follow the stress-optical rule. The stress-optical coefficient of PLLA with 2% D-lactic acid content was reported to be 3.1 $GPa^{-1}$ [16]. Stress-optical coefficients of polymers vary depending on both intrinsic birefringence and rigidity of the molecular chain. Intrinsic birefringence of PLA has been reported to range from $30 \times 10^{-3}$ to $33 \times 10^{-3}$ [17]. The rigidity of PLAs may vary depending on the composition and sequence of L- and D-lactic acid in the molecular chain. It was reported that PLLA chains in solution exhibited higher equilibrium rigidity as compared with poly(D,L-lactic acid) chains [18]; accordingly, variation of the stress-optical coefficient with changing D-lactic acid content of up to 16.4% may provide a certain effect on the development of birefringence in the high-speed melt-spinning process.

On the other hand, when orientation-induced crystallization starts, there can be an effect of the crystallization-induced molecular orientation for the orientation development, i.e., spontaneous orientation development caused by crystallization [1, 11]. In this case, polymers with a high propensity to crystallize are expected to exhibit higher birefringence. More recently, it was reported that high-speed spun fibers of PLLA with D-lactic acid content lower than 0.5% exhibited birefringence of around $23 \times 10^{-3}$ [19], which is higher in comparison with the maximum birefringence values for higher D-lactic acid content polymers shown in Figure 18.3.

It is interesting to note that the intrinsic birefringence of α-form crystals in PLA estimated through the conventional method, i.e., estimation of bond directions from atomic coordinates [20] and summation of bond polarizability [21], is negative with a value of −0.013 [17]. On the other hand, the stress optical coefficient of 3.1 $GPa^{-1}$ [16] is somewhat large in comparison with the value for PET of 4.8–7.8 $GPa^{-1}$ [22] if the intrinsic birefringence for PET crystal of 0.24–0.28 is considered [23]. Further investigation is required to elucidate the orientation behavior of PLA.

### 18.2.3 Differential Scanning Calorimetry

Differential scanning calorimetry (DSC) thermograms of high-speed spun PLA fibers measured at a heating rate of 10 K/min are shown in Figure 18.4. In general, DSC thermograms of PLA-L and PLA-M fibers showed the glass transition, exothermic peak of cold crystallization, and endothermic peak of melting consecutively as temperature increased. On the other hand, the thermograms of PLA-H fibers did not show distinct features besides the glass transition. In the low take-up velocity region, the $T_g$ for PLA-L, PLA-M, and PLA-H was around 60, 52, and 49°C, respectively. The lowering of $T_g$ with an increase in D-lactic acid content may represent the change in molecular rigidity [18].

In PLA-L, the cold crystallization temperature decreased with an increase in the take-up velocity, indicating the molecular orientation effect on the acceleration of crystallization. Similar cold crystallization behavior was

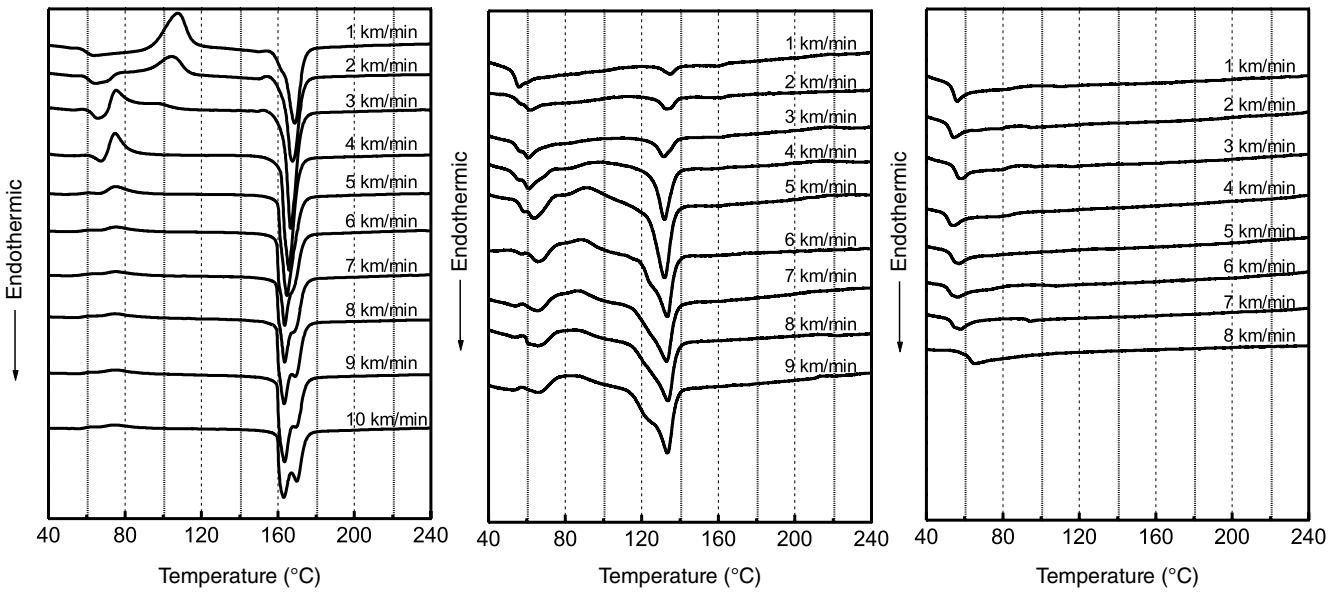


**FIGURE 18.4** Differential scanning calorimetry thermograms of as-spun PLA-L, PLA-M, and PLA-H fibers measured at heating rate 10 K/min. Take-up velocities (km/min) are indicated. Source: Reproduced from Ref. 10 with permission from Taylor & Francis Group.

observed in the DSC thermograms of high-speed spun PET fibers [24]. On the other hand, the melting peak temperature decreased with an increase in the take-up velocity. At 5 km/min, a shoulder started to appear on the higher temperature side of the melting peak and became more distinct with an increase in the take-up velocity. The temperature of the new melting peak was almost identical to the melting temperature of 1 km/min fibers. Mezghani et al. also found a double-melting peak for PLLA fibers produced at 3.1 km/min [6]. The nature of these melting peaks will be discussed in the next section based on the modulated-DSC analysis.

In PLA-M, only a small melting peak was observed at 1 km/min. The melting peak area increased, while the melting peak temperature slightly decreased with increasing take-up velocity. A broad cold crystallization peak appeared from 5 km/min, and its peak temperature decreased with an increase in the take-up velocity. The melting peak temperature was almost constant in this velocity region; however, a shoulder appeared on the low-temperature side of the melting peak. The fact that only the fibers obtained in a high-speed region show a distinct cold crystallization peak indicated that a certain degree of molecular orientation is necessary for PLA-M fibers to crystallize in the DSC measurement at the heating rate of 10 K/min. It should be noted that these fibers are already crystallized through the orientation-induced crystallization in the spin-line. The competition of the heating rate and the crystallization rate during the DSC measurement is the key mechanism for the occurrence of cold crystallization. On the other hand, it was found that the high-speed spun PLA-H fibers did not crystallize during the heating process in the DSC measurement even though increase of crystallization rate induced by orientation was expected. It was reported that even so-called amorphous copolyesters can crystallize under the effect of molecular orientation [25]; however, this is not the case for the PLA-H used in this research.

The crystallinity of the as-spun fibers can be obtained from the heat of fusion estimated by subtracting the heat of cold crystallization from the heat of melting. The heat of fusion of an infinitely large crystal was assumed to be 93.0 J/g [6]. In PLA-L, crystallinity increased steeply from the take-up velocity of 1–3 km/min and reached approximately 45%. In PLA-M, crystallinity increased continuously with the take-up velocity, with a maximum crystallinity of about 15%. Crystallinity of the PLA-H fibers was negligible.

### 18.2.4 Modulated-DSC and Lattice Spacing

It should be noted that the melting behavior of high-speed spun PLA fibers showed an opposite trend as compared with PET; with an increase in the take-up velocity, the melting peak temperature increased and decreased for PET and PLA, respectively [24]. To understand this phenomenon, the melting behavior of high-speed spun PLA fibers was investigated in detail by applying modulated-DSC (m-DSC) analysis, as well as the WAXD measurement to study the temperature-dependent variation of crystalline unit cell size [26, 27].

Analysis of the melting behavior of crystalline polymers using m-DSC generally suggests that the melting and re-crystallization proceed before the complete melting in the heating process. This consideration implies that the melting peak temperature obtained through the measurement with a conventional DSC does not necessarily represent the melting temperature of the originally existing crystals in the test specimen. On the other hand, PLLA is known to have complicated multiple crystalline forms. Regarding the α-form crystals, the disorder-to-order phase transition of α-form crystals, i.e., α′ (or δ)- α transition, has been studied extensively [28, 29].

Results of m-DSC measurement at the heating rate of 2 K/min for the high-speed spun PLA-L fibers prepared at the take-up velocities of 1 and 6 km/min are shown in Figure 18.5. Variations of lattice spacing with increasing temperature at the heating rate of 2 K/min for the (200)/(100) reflection are also shown in the figure. For the 1 km/min fiber, the total heat flow (THF) from the m-DSC measurement showed glass transition, cold crystallization, and melting consecutively with increasing temperature, while there were appearances of an endothermic heat flow in the reversing heat flow (RHF) and an exothermic heat flow in the non-reversing heat flow (NRHF) from around 140°C, indicating that structural change through the melting and recrystallization had started to occur.

In the figures for the variation of lattice spacing, the lines for the ordered α-form crystal and disordered α′(δ)-form crystal are shown for comparison. The slope corresponds to the thermal expansion coefficient of the crystals. The result for the 1 km/min fiber suggested that degree of ordering of the crystals formed in the cold crystallization was in the middle of the α- and α′ (δ)-form crystals, while, during the course of melting and re-crystallization, degree of ordering shifted closer to the α-form crystals rapidly before melting. In other words, the observed melting peak temperature can be attributed to that of the α-form crystal.

On the other hand, for the 6 km/min fiber, the THF, RHF, and NRHF were stable before melting up to around 160°C. The lattice spacing data indicated that the crystals formed in the high-speed melt-spinning process also had an intermediate level of ordering, and there was no improvement of ordering before melting. This result may imply that there is a strong memory effect for the crystalline structure developed in the high-speed melt-spinning process, and therefore structural transition is difficult during the DSC measurement. This is the reason for the lower melting peak temperature observed for the fibers prepared at high take-up velocities.

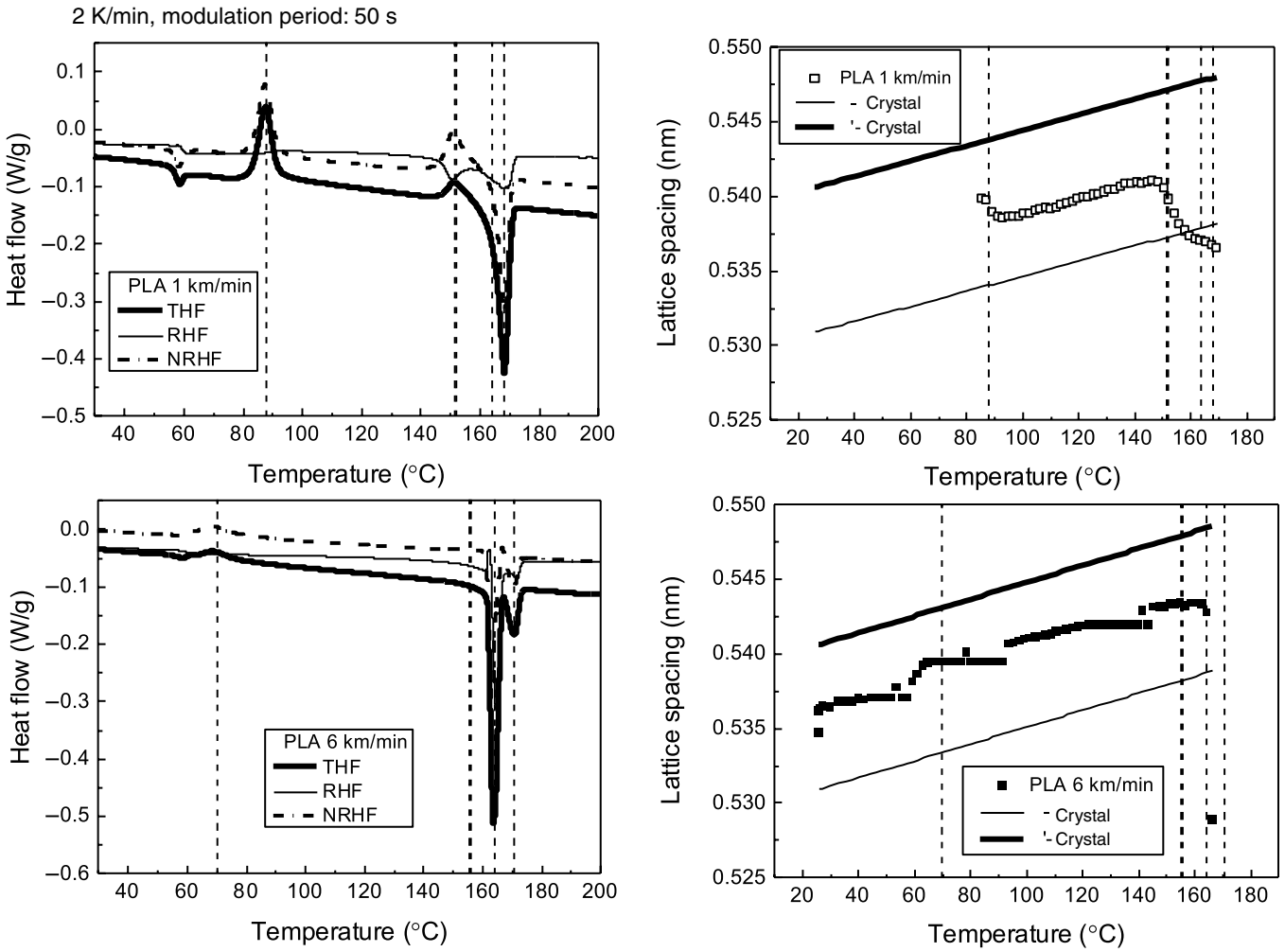


**FIGURE 18.5** Comparison of modulated-DSC thermograms and lattice spacing variations with temperature for PLA-L fibers prepared at take-up velocity 1 and 6 km/min. Source: Reproduced from Ref. 26 with permission from Taylor & Francis Group.

## 18.3 HIGH-SPEED MELT-SPINNING OF RACEMIC MIXTURE OF PLLA AND PDLA

### 18.3.1 Stereocomplex Crystal

It is well known that the mixture of poly(L-lactic acid) (PLLA) and poly(D-lactic acid) (PDLA) chain molecules forms either homocrystals or stereocomplex (SC) crystals [30, 31]. Homocrystals such as α-, β-, γ-, δ-, and ε-forms consist of only PLLA or PDLA molecules, whereas PLLA and PDLA chains with opposite helical hands exist side by side in the SC crystal. The SC crystal exhibits a melting temperature of 220–230°C, which is about 60° higher than those for the homocrystals. The development of SC crystals enhances the thermal resistance of PLA products.

However, the formation of SC crystals from the racemic blend of PLLA and PDLA is not straightforward. From the viewpoint of polymer processing, the SC crystal can bring about difficulty because its melting temperature is close to the thermal degradation temperature of PLA. In addition, to acquire enough improvement in the thermal and mechanical properties of the products, the amount of the SC crystals and their orientation in the products need to be controlled. There exists a competitive crystallization and complicated transition behavior between the homo and SC crystals. Various attempts have been made to promote the formation of SC crystals. For example, researchers have investigated the effect of intensive melt mixing on preferred formation of SC crystals [32], effect of pre-orientation in the amorphous phase on the formation of oriented homo and SC crystals [33], effect of molecular weight on the preferred formation of SC crystals [34], and influence of the melt memory on the formation of homocrystals after the formation of SC crystals [35] and so on.

### 18.3.2 Melt Spinning of PLLA/PDLA Blend

High-speed melt spinning of racemate PLA (r-PLA), i.e., 50 : 50 mixture of PLLA and PDLA molecules, provided by Cargill Dow Polymers LLC (currently Nature Works LLC), was

attempted using a spinneret with a single hole of 0.5 mm diameter at the throughput rate of 3 and 5 g/min [36]. After the spinning experiment at the extrusion temperature of 250°C, extrusion temperature was gradually lowered to 230°C. Surprisingly, extrusion was stable even though the melting temperature of the SC crystal was known to be 220–230°C. The highest take-up velocity of 7.5 km/min was attained for the throughput rate of 5 g/min and the extrusion temperature of 230°C.

Measurement of diameter profiles of the high-speed spinning line for the r-PLA at two extrusion temperatures and two throughput rates revealed the existence of steep diameter attenuation, i.e., neck-like deformation, in the high-speed region of all the extrusion conditions. As in the case of other crystalline polymers, the position of neck-like deformation shifted toward the spinneret with an increase in the take-up velocity, indicating the initiation of crystallization at higher temperatures.

Modeling of the melt-spinning behavior of PET has been reported previously which incorporated the mechanism of orientation development and orientation-induced crystallization into the conventional governing equations, i.e., mass balance, momentum balance, energy balance, and constitutive equations [11]. Kohler et al. improved the modeling through the incorporation of a two-phase model, viscoelastic constitutive equation for amorphous phase, and crystallization kinetic equations for α-form and SC crystals, and applied it to the analysis of the thinning and structure formation behavior of the spin-line of PLLA and racemic mixture of PLLA and PDLA [37].

### 18.3.3 WAXD

WAXD patterns of selected high-speed spun fibers are shown in Figure 18.6. At low take-up velocities, only the amorphous halo was observed. With an increase in the take-up velocity, crystalline reflections started to appear as in the case of the high-speed spinning of PLLAs. In addition to the (110)/(200) reflection of the α-form crystal, the (100) reflection of the SC crystal was clearly observed on the equator for some samples.

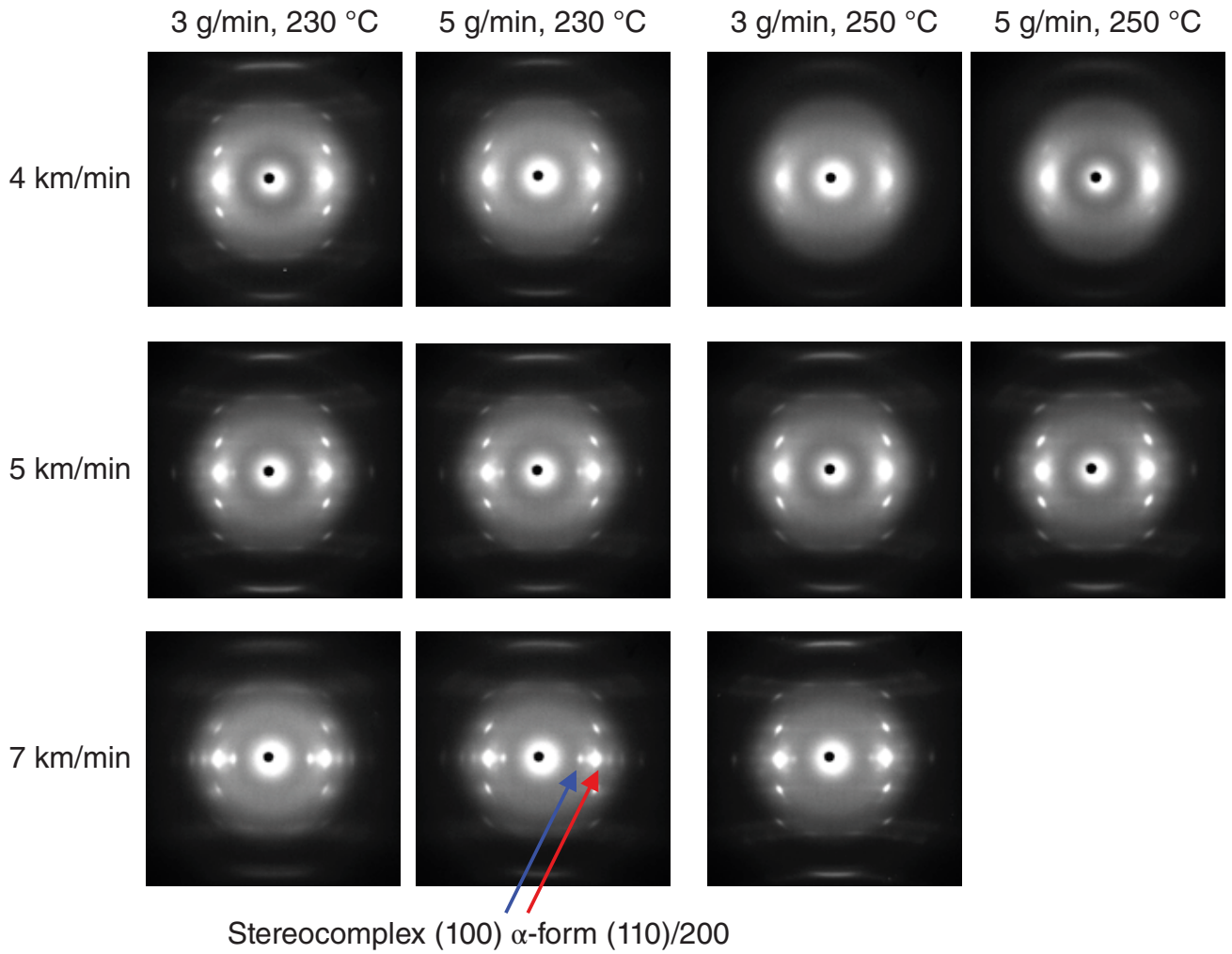


**FIGURE 18.6** Wide-angle X-ray diffraction patterns of as-spun r-PLA fibers prepared at take-up velocities of 4, 5, and 7 km/min under four different extrusion conditions. Source: Reproduced from Ref. 36 with permission from Taylor & Francis Group.

In other words, the structure of the high-speed spun fibers crystallized in the spinning line mainly consisted of the α-form crystal, but coexistence of the SC crystal was also confirmed. It appears that the relative amount of the SC crystal in comparison with the α-form crystal also increased with an increase in the take-up velocity. Comparison of the results for four different extrusion conditions suggested that the decrease of extrusion temperature and throughput rate led to an increase in the formation of SC crystal. It should be noted that the spinning conditions of higher take-up velocity, lower throughput rate, and lower extrusion temperature correspond to the application of higher tensile stress to the spinning line. Accordingly, these conditions generally result in the enhancement of neck-like deformation and orientation-induced crystallization. Crystallization also proceeds at higher temperatures in the spinning line under these conditions. Therefore, it can be concluded that the formation of SC crystal is preferred under high tensile stress and high crystallization temperature.

### 18.3.4 Differential Scanning Calorimetry

DSC thermograms of high-speed spun r-PLA fibers prepared at the extrusion condition of 230°C and 3 g/min are shown in Figure 18.7. A DSC thermogram of amorphous unoriented sample is also shown for comparison. An exothermic peak of cold crystallization was observed in the low-speed region. The peak temperature decreased with an increase in the take-up velocity, indicating the acceleration of crystallization with an increase in the molecular orientation. In the r-PLA fibers obtained at take-up velocities of 1 and 2 km/min, small exothermic and endothermic peaks were detected consecutively at around 160–180°C, and the melting peak of the SC crystal was clearly observed at around 220°C. It should be noted that the melting peaks of both α-form and SC crystals were clearly observed for the unoriented sample. Even though it was confirmed from the WAXD measurement that the fibers prepared in the high-speed region were mainly composed of α-form crystals, no melting peak was observed at the melting temperature of the α-form crystals. These results suggested that complicated phenomena such as melting of α-form crystal and recrystallization of melted molecules into SC crystal were occurring simultaneously at around 160–180°C, although this phenomenon was not detectable in the DSC measurement.

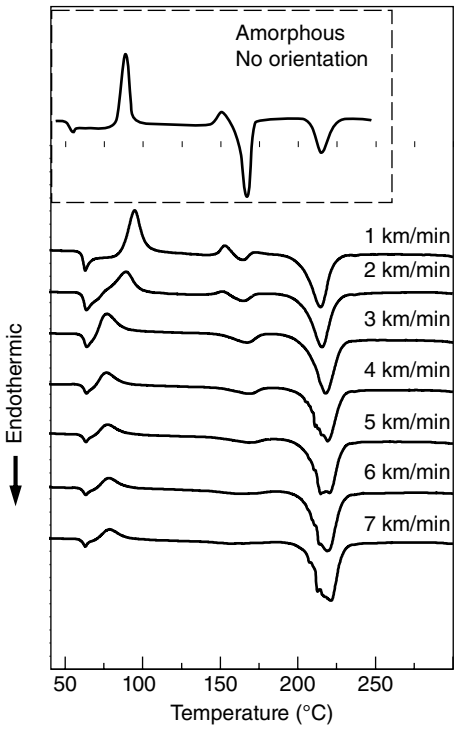


**FIGURE 18.7** Differential scanning calorimetry (DSC) thermograms of as-spun r-PLA fibers prepared under the extrusion condition of 3 g/min and 230°C. Take-up velocity (km/min) are indicated in the figure. Thermogram of amorphous unoriented sample is shown for comparison. Source: Reproduced from Ref. 36 with permission from Taylor & Francis Group.

### 18.3.5 In Situ WAXD upon Heating

To investigate the behavior of crystalline form transition, in situ WAXD measurement with an increase in the temperature was carried out for the high-speed spun r-PLA fibers as shown in Figure 18.8 [38]. The measurement was also carried out for the unoriented amorphous sample for comparison. Variations of integrated intensity on the equator for the α-form and SC crystals were analyzed and plotted as "crystallinity index" in the figure.

For the unoriented sample, there was an evolution of the α-form crystal through the cold crystallization above the glass transition temperature, at around 90°C. The transition from α-form to SC crystal proceeded rapidly near the melting temperature of the α-form crystal, at around 150°C. On the other hand, in the high-speed spun fibers, the amount of SC crystal started to increase and that of α-form crystal started to decrease at a lower temperature. This tendency was more prominent for the fibers prepared at higher take-up velocities. In the 6 km/min fiber, α-form crystal and a small amount of SC crystal originally existed because of the orientation-induced crystallization in the spinning process. The amounts of α-form and SC crystals started to increase steeply from around 90 to 100°C, respectively, while the amount of α-form crystal started to decrease from around 120°C. Obviously, molecular orientation promoted the development of SC crystal. Another interesting feature is the increase in the final melting temperature of α-form crystals. In the 6 km/min fiber, α-form crystal disappeared when temperature was raised to about 200°C. Probably, the existence of SC crystal prevented the melting of α-form crystal to a certain extent, although the reasons are not clear at this moment.

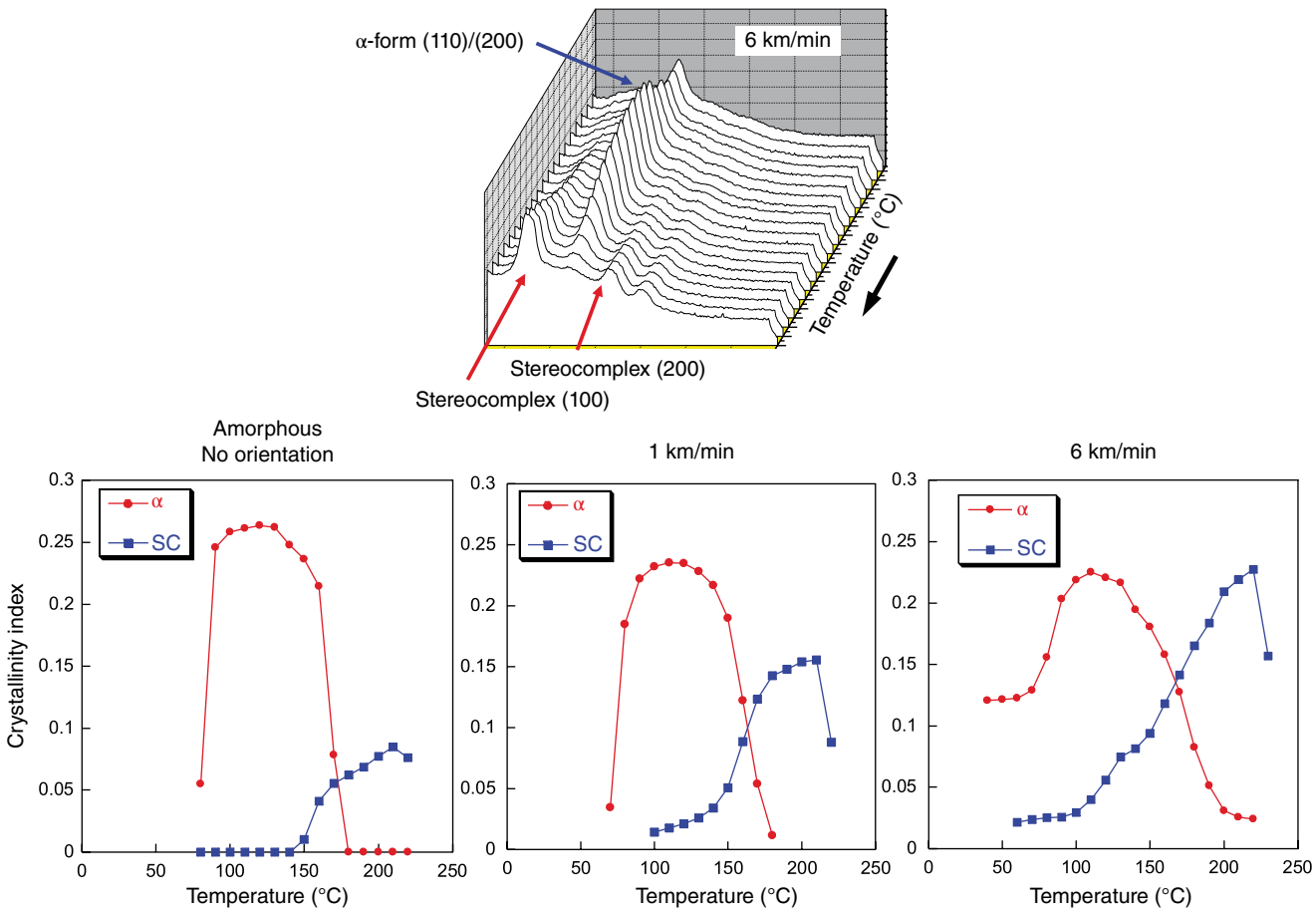


**FIGURE 18.8** Variations of the amount (crystallinity index) of **α**-form and stereocomplex crystals with increasing temperature for amorphous unoriented r-PLA sample, and as-spun r-PLA fibers prepared at take-up velocities of 1 and 6 km/min. Crystallinity index was analyzed from the wide-angle X-ray diffraction intensity distribution curves measured with increasing temperature. As a typical example, original data for the r-PLA fiber prepared at 6 km/min is shown at the top [38].

## 18.4 BICOMPONENT MELT SPINNING OF PLLA AND PDLA

### 18.4.1 Sheath-Core and Islands-in-the-Sea Configurations

Bicomponent spinning is a process in which two polymers of different chemical and/or physical nature are extruded from a common spinneret to form a single fiber [39]. The polymer flows are kept separate up to the spin pack, where they meet and exit together through the spinneret. When the filament leaves the spinneret, it consists of non-mixed components that touch at the interface. Typical cross-sections of bicomponent fibers are core-sheath, side-by-side, segmented pie, and islands-in-the-sea. Bicomponent spinning of PLA with other polymers has been investigated extensively for the improvement of the structure formation behavior, as well as for the incorporation of functionality in the resultant fibers [40–44].

More recently, both PLLA and PDLA with higher optical purities became available in the market. The melt blending of these polymers is anticipated to be more difficult because of a higher tendency for the formation of SC crystals of high melting temperature. An elevated blending temperature for preventing the formation of SC crystal may lead to significant thermal degradation [45]. Therefore, with the aim of avoiding pre-melt blending for the preparation of PLA fibers consisting of highly oriented SC crystal, bicomponent melt spinning of PLLA and PDLA was carried out using the spinning packs for two different cross-sectional configurations, i.e., core-sheath (C/S) and islands-in-the-sea (I/S) fibers, as shown in Fig. 18.9 [46]. In the I/S fibers, 1519 islands were embedded in the cross-section. For the extrusion conditions of 2.5 g/min each for the islands and sea components and the take-up velocity of 6 km/min, diameter of the island component was estimated to be around 500 nm. Two types of optically active poly(lactic acid), PLLA and PDLA with the optical purities

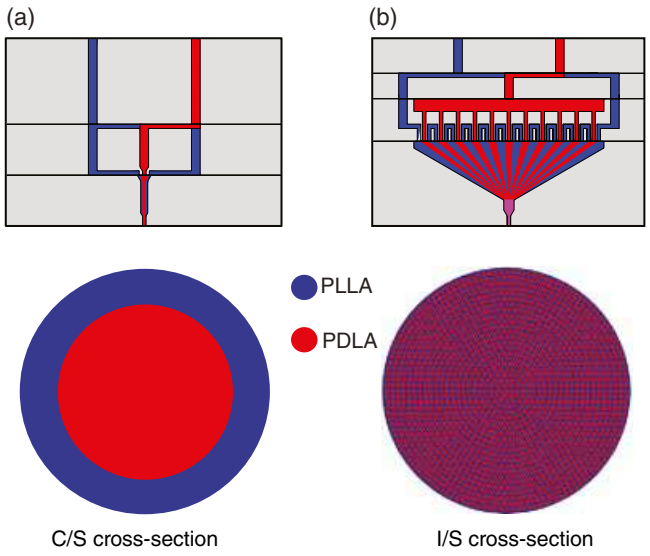


**FIGURE 18.9** Schematic diagrams of the spinning packs for producing (a) C/S (core-sheath) and (b) I/S (islands-in-the-sea) bicomponent fibers. Cross-sectional configurations of the C/S and I/S fibers are also shown. Source: Reproduced from Ref. 46 with permission from The Society of Fiber Science and Technology, Japan.

higher than 99.5% (Total Corbion PLA, Netherlands) were used in this research. Melt flow rates of the PLLA and PDLA were 16 and 25 g/10 min, respectively, implying that PLLA had higher molecular weight than PDLA.

### 18.4.2 Birefringence

Variations of birefringence with the take-up velocity for the C/S and I/S fibers are shown in Figure 18.10. Birefringence increased with the increase of take-up velocity in the low take-up velocity region. For the C/S fibers, birefringence of the sheath part increased suddenly from 4 to 5 km/min and that of the core part reached a maximum at around 5–6 km/min and then decreased. Similar behavior was reported for the high-speed melt spinning of the C/S fibers of low- and high-molecular-weight poly(ethylene terephthalate)s, and the mechanism for the orientation development behavior was explained [47]. In the high-speed spinning process, the component with higher molecular weight (PLLA) starts to crystallize through orientation-induced crystallization. Crystallization causes the solidification of the spin-line, but there can be an orientation relaxation of the PDLA component, which is still in a molten state.

For the I/S fibers, birefringence measurement for individual components was not possible. Mean birefringence of the two components showed steep increases from 4 to 5 km/min. This behavior also corresponded to the starting of orientation-induced crystallization, where the structure development was promoted by lowering the extrusion temperature.

### 18.4.3 DSC

Results of DSC analysis measured at the heating rate of 5 K/min are shown in Figure 18.11. The cold crystallization temperature gradually decreased with the increase of take-up

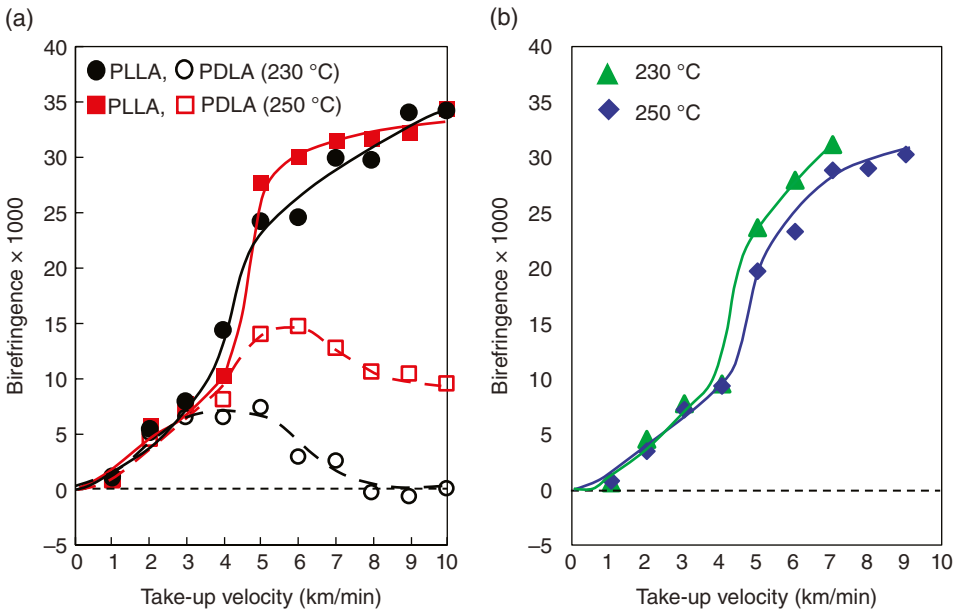


**FIGURE 18.10** Variations of birefringence with take-up velocity for (a) sheath (PLLA) and core (PDLA) components in the C/S (core-sheath) as-spun fibers and (b) I/S (islands-in-the-sea) fibers prepared with extrusion temperatures of 230 and 250°C. Source: Reproduced from Ref. 46 with permission from The Society of Fiber Science and Technology, Japan.

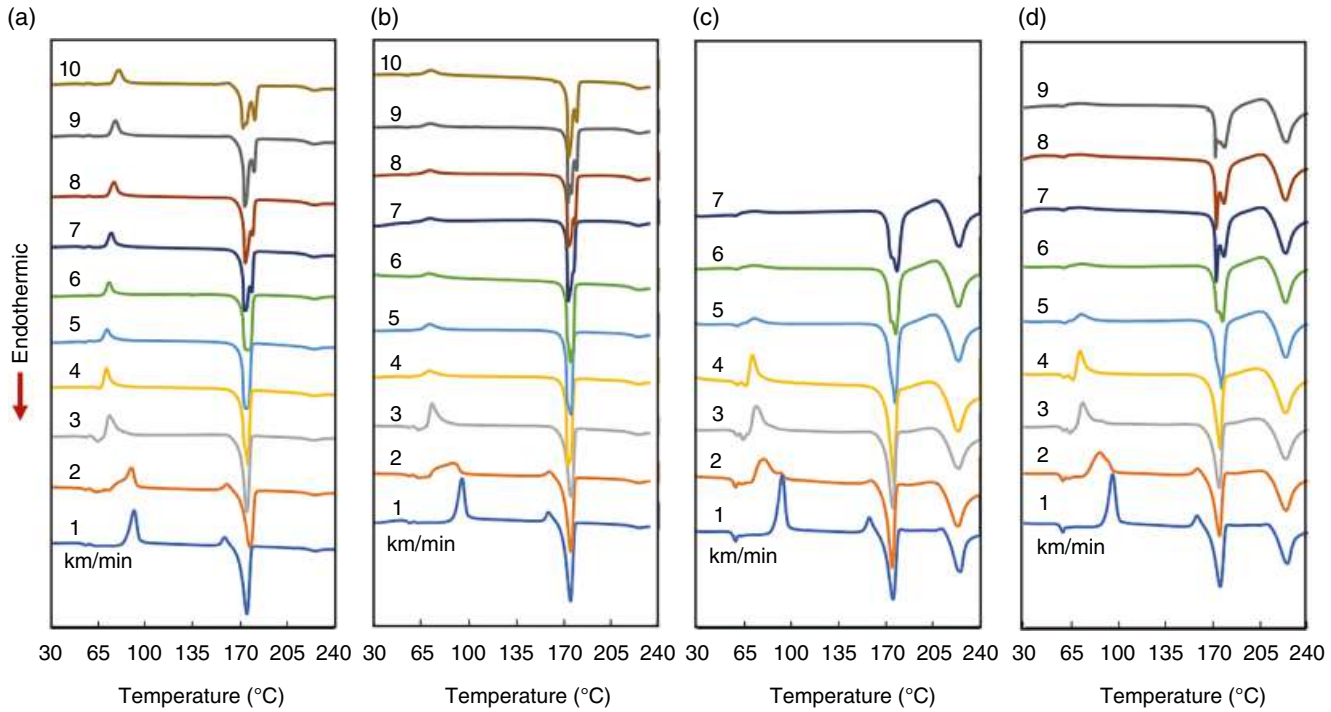


**FIGURE 18.11** Differential scanning calorimetry (DSC) thermograms of as-spun bicomponent fibers with the cross-sectional configuration of C/S (core-sheath) (a) 230°C, (b) 250°C and I/S (islands-in-the-sea) (c) 230°C, (d) 250°C prepared under extrusion temperature of 230 and 250°C. Take-up velocities (km/min) are indicated. Source: Reproduced from Ref. 46 with permission from The Society of Fiber Science and Technology, Japan.

velocity because of the increase in crystallization rate accompanied by the molecular orientation. For the C/S spinning with an extrusion temperature of 230°C, the cold crystallization peak was observed continuously up to the maximum 10 km/min take-up velocity. The peak temperature gradually decreased as the take-up velocity increased from 1 to 4 km/min and then gradually increased with further increase of the take-up velocity. These results are in good accordance with the variations of birefringence of PLLA (sheath) and PDLA (core) components with the take-up velocity shown in Figure 18.10.

For all I/S fibers, it should be noted that a new melting peak was clearly observed at around 225°C, which corresponded to the melting temperature of the SC-crystals. Before the starting of the new melting peak, exothermic heat flow was also observed. The low-speed spun fibers were in an amorphous state, which should crystallize into the α-form crystal through the cold crystallization. The high-speed spun fibers only exhibited crystalline reflections from the α-form crystals in the WAXD pattern, which will be shown in Figure 18.12 in the next section. Therefore, it was suggested that melting of the α-from crystal and recrystallization into the SC crystals occurred during the DSC measurement.

Because α-form crystals are composed of either PLLA or PDLA molecular chains, mutual diffusion of PLLA and PDLA molecular chains is necessary for the formation of the SC crystal, in which PLLA and PDLA chains exist side by side. This means that there was considerable mutual diffusion of PLLA and PDLA molecular chains at the boundary of island and sea components in the I/S fibers. It was speculated that mutual diffusion became viable because of the extremely large interface area in this cross-sectional configuration. By re-examining the DSC data for the C/S fibers carefully, it can be seen that a small melting peak of the SC crystals also existed at around 225°C.

### 18.4.4 Post Annealing

Post annealing of the as-spun fibers was conducted with the fixed-length condition. Considering the melting temperatures for the α-form and SC crystals of 160 and 225°C, annealing temperatures of 120 and 190°C were adopted. Annealing at 190°C was not possible for the C/S fibers because of melting, whereas the I/S fibers kept their shape even at this annealing temperature. After the annealing of the fiber bundle, the low-speed spun fibers stuck together slightly, whereas the high-speed spun fibers were well separated.

WAXD patterns of the as-spun fibers prepared at the extrusion temperature of 230°C and those of corresponding fibers annealed at 120 and 190°C are shown in Figure 18.12. The as-spun fibers with both C/S and I/S cross-sectional configurations exhibited the amorphous halo at 3 km/min, whereas the crystalline reflections from α-form crystals

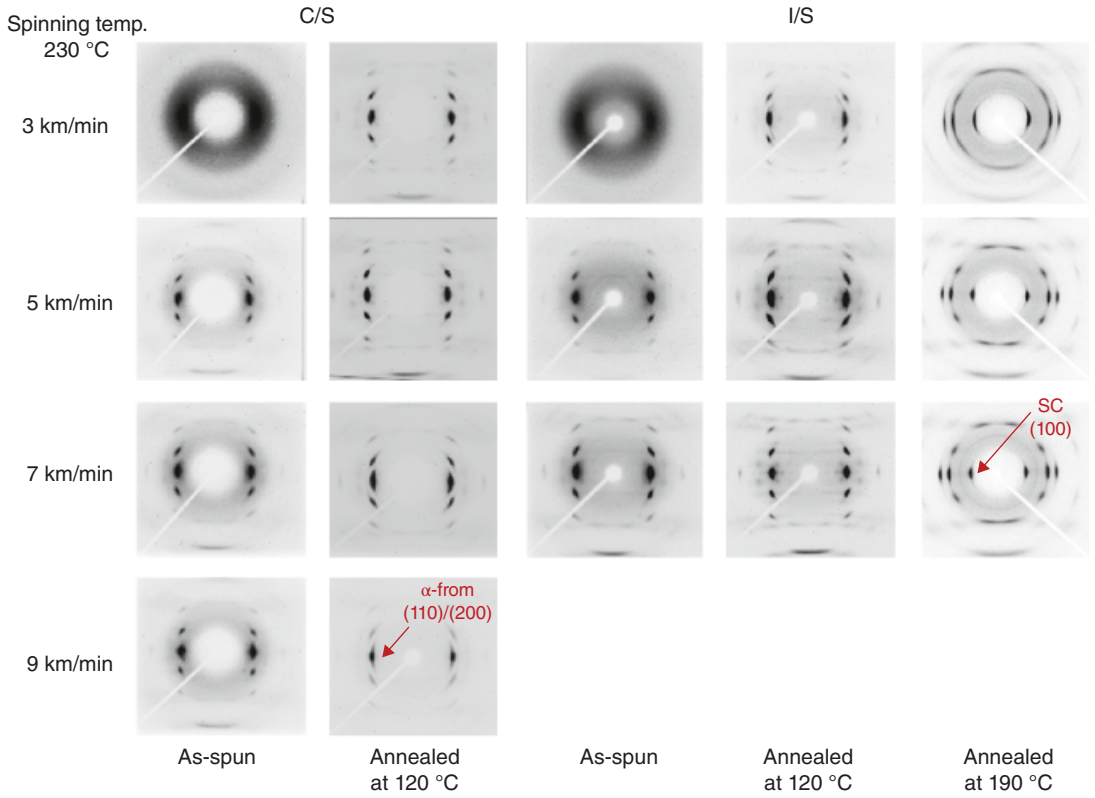


**FIGURE 18.12** Wide-angle X-ray diffraction patterns of as-spun fibers with C/S (core-sheath) and I/S (islands-in the-sea) cross-sectional configurations, and the corresponding fibers annealed at 120 and 190°C. As-spun fibers were prepared at the spinning temperature 230°C. Source: Reproduced from Ref. 46 with permission from The Society of Fiber Science and Technology, Japan.

appeared at 5, 7, and 9 km/min. After the annealing at 120°C, the development of highly oriented α-form crystal was confirmed for all the fibers. For the I/S fibers, the presence of a small amount of oriented SC crystal was confirmed from the appearance of weak reflections from (100) of SC crystal on the equator. When annealing temperature was raised to 190°C, the WAXD patterns for the I/S fibers prepared at 3, 5, and 7 km/min exhibited distinct crystalline reflections due to highly oriented SC crystal where the degree of orientation was slightly lower for the 3 km/min fiber. Even though a weak reflection ring from the α-form crystal of virtually no orientation existed for the 7 km/min, it can be said that the fibers consisting only of highly oriented SC crystals were prepared through the annealing of high-speed spun I/S bicomponent fibers of PLLA and PDLA.

As mentioned previously, the diameter of the islands in the I/S fibers was around 500 nm. In the melt-spinning process, originally PLLA and PDLA molecules were well separated in the fiber cross section. For the development of SC crystal, mutual diffusion of PLLA and PDLA molecular chains is needed over a distance of several hundred nanometers during either the spinning process and/or the annealing process. Assuming that the diffusion occurred only during the annealing process, the diffusion coefficient was estimated. The obtained value of at least $3 \times 10^{-14}$ cm$^2$/s is significantly higher than the reported values for the mutual diffusion at the interface for different polymers [48–51]. There is a possibility of acceleration of diffusion caused by the molecular orientation.

## 18.5 CONCLUDING REMARKS

Because of the presence of asymmetric carbon in the main chain, there is a wide variety of possibilities for the designing of PLA molecules, i.e., random or block copolymerization of L-lactic acid and D-lactic acid, blending of PLA molecules of different degree of copolymerization including pure PLLA and pure PDLA, etc. The formation of SC crystals with extremely high melting temperature in comparison with the homocrystals is another unique feature of PLA. Under the effect of polymer flow during melt processing, structure development behavior can be affected by these unique characteristics of PLA molecules. A strong memory effect presumably originating from the helical conformation of PLA molecular chains was also suggested, whereas there can be a change in the rigidity of molecules depending on the type of copolymerization. In other words, there is a possibility for

the improvement of the characteristics of PLA products through designing PLA molecules by considering the effect of polymer flow on structure development during processing.

## REFERENCES


1. T. Kikutani, Chapter 5, Structure development in synthetic fiber production, in: S. J. Eichhorn, J. W. S. Hearle, M. Jaffe, T. Kikutani (Eds.), *Handbook of Textile Fiber Structure Volume 1: Fundamentals and Manufactured Polymer Fibers*, Woodhead Publishing, Cambridge, 2009, pp. 157–180.
2. K. Saigusa, W. Takarada, T. Kikutani, Improvement of the mechanical properties of poly(glycolic acid) fibers through control of molecular entanglements in the melt spinning process, *J. Macromol. Sci. Part B Phys.* **2020**, *59*(6), 399–414.
3. K. Saigusa, H. Saijo, M. Yamazaki, W. Takarada, T. Kikutani, Influence of carboxylic acid content and polymerization catalyst on hydrolytic degradation behavior of poly(glycolic acid) fibers, *Polym. Degrad. Stab.* **2020**, *172*, 109054.
4. Q. Qin, W. Takarada, T. Kikutani, Fiber structure development of PHBH through stress-induced crystallization in high-speed melt spinning process, *J. Fiber Sci. Technol.* **2017**, *73*(2), 49–60.
5. A. K. Agrawal, Chapter 20, Spinning of poly(lactic acid) fibers, in R. Auras, L.-T. Lim, S. E. M. Selke, H. Tsuji (Eds.), *Poly*(*Lactic Acid*), Wiley, Hoboken, NJ, 2010, pp. 323–341.
6. K. Mezghani, J. E. Spruiell, High speed melt spinning of poly(L-lactic acid) filaments, *J. Polym. Sci. Part B Polym. Phys.* **1998**, *36*(6), 1005–1011.
7. S. Ghosh, N. Vasanthan, Structure development of poly(L-lactic acid) fibers processed at various spinning conditions, *J. Appl. Polym. Sci.* **2006**, *101*(2), 1210–1216.
8. G. Schmack, B. Tändler, R. Vogel, R. Beyreuther, S. Jacoben, H.-G. Fritz, Biodegradable fibers of poly(L-lactide) produced by high-speed melt spinning and spin drawing *J. Appl. Polym. Sci.* **1999**, *73*, 2785–2797.
9. G. Schmack, B. Tändler, G. Optiz, R. Vogel, H. Komber, L. Häußler, D. Voigt, S. Weinmann, M. Heinemann, H.-G. Fritz, High-speed melt spinning of various grades of polylactides, *J. Appl. Polym. Sci.* **2004**, *91*, 800–806.
10. M. Takasaki, H. Ito, T. Kikutani, Structure development of polylactides with various D-lactide contents in the high-speed melt spinning process, *J. Macromol. Sci. Part B Phys.* **2003**, *42*(1), 59–75.
11. J. Shimizu, N. Okui, T. Kikutani, Chapter 7, Simulation of dynamics and structure formation in high-speed melt spinning, in *High-speed Fiber Spinning—Science and Engineering Aspects*, John Wiley and Sons, New York, 1985, pp. 173–201.
12. T. Kikutani, Y. Kawahara, N. Ogawa, N. Okui, Capturing of real image of neck-like deformation from high-speed spinning line, *Sen'i Gakkaishi (J. Soc. Fiber Sci. Technol. Jpn.)* **1994**, *50*(12), 561–566.
13. T. Kikutani, T. Matsui, A. Takaku, J. Shimizu, Diameter measurement in the vicinity of neck-like deformation in high-speed melt spinning process, *Sen'i Gakkaishi (J. Soc. Fiber Sci. Technol. Jpn.)* **1989**, *45*(11), 441–446.
14. T. Kikutani, Y. Kawahara, T. Matsui, A. Takaku, J. Shimizu, Measurement of filament temperature and analysis of orientation-induced crystallization behavior in high-speed melt spinning process, *Seikei-kakou (J. Jpn. Soc. Polym. Process.)* **1989**, *1*(3), 333–339.
15. H. Nishimura, M. Sei, K. Chizuka, M. Masuda, H. Yamazaki, J. Kojima, K. Tamamoto, S. Okamoto, K. Nakamae, M. Kotera, T. Kikutani, S. Sakurai, On-line wide-angle X-ray scattering measurement during high-speed melt-spinning of poly(ethylene terephthalate) fiber, *Zairyo (J. Soc. Mater. Sci. Jpn.)* **2013**, *62*(1), 8–12.
16. J. Mulligan, M. Cakmak, Nonlinear mechanooptical behavior of uniaxially stretched poly(lactic acid): dynamic phase behavior, *Macromolecules* **2005**, *38*, 2333–2344.
17. Y. Ohkoshi, H. Shirai, Y. Gotoh, M. Nagura, Intrinsic birefringence of poly(L-lactic acid), *Sen'i Gakkaishi (J. Soc. Fiber Sci. Technol. Jpn.)* **1999**, *55*, 21–27.
18. G. M. Pavlov, O. A. Dommes, I. V. Aver'yanov, G. F. Kolbina, O. V. Okatova, V. A. Korzhikov, A. V. Dobrodumov, T. B. Tennikova, Conformational differences of poly(L-lactic acid) and poly(D,L-lactic acid) in dilute solutions, *Doklady Chem.* **2015**, *465*(Part 1), 261–264.
19. N. Roungpaisan, W. Takarada, T. Kikutani, High-speed melt spinning of sheath/core bicomponent fibers of poly(L-lactide)s with different molecular weight, *AIP Conf. Proc.* **2019**, *2065*, 030030, 1–4.
20. W. Hoogsteen, A. R. Postema, A. J. Pennings, G. T. Brinke, P. Zugenmaie, Crystal structure, conformation and morphology of solution-spun poly(L-lactide) fibers, *Macromolecules* **1990**, *23*(2), 634–642.
21. C.W. Bunn, *Chemical Crystallography*, Oxford University Press, Oxford, 1961, p. 313.
22. T. Kikutani, K. Nakao, W. Takarada, H. Ito, On-line measurement of orientation development in the high-speed melt spinning process, *Polym. Eng. Sci.* **1999**, *39*(12), 2349–2357.
23. B. Clauss, D. R. Salem, Chapter 13, Density, birefringence and polarized fluorescence, in: D. R. Salem (Ed.), *Structure Formation in Polymeric Fibers*, Hanser, Munich, 2000, pp. 493–520.
24. J. Shimizu, N. Okui, T. Kikutani, Chapter 15, Finer structure and physical properties of fibers melt-spun at high-speeds from various polymers, in *High-speed Fiber Spinning—Science and Engineering Aspects*, John Wiley and Sons, New York, 1985, pp. 429–483.
25. T. Kikutani, K. Morohoshi, H. Y. Yoo, S. Umemoto, N. Okui, Fiber structure development in high-speed melt spinning of copolyesters: poly(ethylene terephthalute-*co*-1,4-cyclohexylene dimethylene terephthalate), *Polym. Eng. Sci.* **1995**, *35*(11), 942–949.
26. M. Takasaki, N. Fukushi, M. Yoshizawa, S. Onosato, M. Hanada, W. Takarada, Y. Kawahara, T. Kikutani, H. Kobayashi, K. Tanaka, Multiple melting behavior of high-speed melt spun polylactide fibers, *J. Macromol. Sci. Part B Phys.* **2017**, *56*(3), 143–160.

27. N. Fukushi, M. Yoshizawa, S. Onosato, M. Hanada, M. Takasaki, W. Takarada, Y. Kawahara, T. Kikutani, H. Kobayashi, K. Tanaka, Analysis of multiple melting of high-speed melt spun polylactide fibers based on kinetic modeling, *J. Macromol. Sci. Part B Phys.* **2018**, *57*(2), 110–128.
28. J. Zhang, K. Tashiro, H. Tsuji, A. J. Domb, Disorder-to-order phase transition and multiple melting behavior of poly(L-lactide) investigated by simultaneous measurements of WAXD and DSC, *Macromolecules* **2008**, *41*, 1352–1357.
29. K. Wasanasuk, K. Tashiro, Crystal structure and disorder in poly(L-lactic acid) δ form (α′ form) and the phase transition mechanism to the ordered α form, *Polymer* **2011**, *52*, 6097–6109.
30. T. Okihara, M. Tsuji, A. Kawaguchi, K. Katayama, Crystal structure of stereocomplex of poly(L-lactide) and poly(D-lactide), *J. Macromol. Sci. Part B Phys.* **1991**, *30*, 119–140.
31. D. Brizzolara, H. J. Cantow, K. Diederichs, E. Keller, A. J. Domb, Mechanism of the stereocomplex formation between enantiomeric poly(lactide)s, *Macromolecules* **1996**, *29*, 191–197.
32. D. Masaki, Y. Fukui, K. Toyohara, M. Ikegame, B. Nagasaka, H. Yamane, Stereocomplex formation in the poly(L-lactic acid)/poly(D-lactic acid) melt blends and the melt spun fibers, *Sen'i Gakkaishi (J. Soc. Fiber Sci. Technol. Jpn.)* **2008**, *64*(8), 212–219.
33. Z. Xiong, G. Liu, X. Zhang, T. Wen, S. Vos, C. Joziasse, D. Wang, Temperature dependence of crystalline transition of highly-oriented poly(L-lactide)/poly(D-lactide) blend: in-situ synchrotron X-ray scattering study, *Polymer* **2013**, *54*(2), 964–971.
34. P. Pan, L. Han, J. Bao, Q. Xie, G. Shan, Y. Bao, Competitive stereocomplexation, homocrystallization, and polymorphic crystalline transition in poly(L-lactic acid)/poly(D-lactic acid) racemic blends: molecular weight effects, *J. Phys. Chem. B.* **2015**, *119*(21), 6462–6470.
35. Y.-F. Huang, Z.-C. Zhang, Y. Li, J.-Z. Xu, L. Xu, Z. Yan, G.-J. Zhong, Z.-M. Li, The role of melt memory and template effect in complete stereocomplex crystallization and phase morphology of polylactides, *Cryst. Growth. Des.* **2018**, *18*(3), 1613–1621.
36. M. Takasaki, H. Ito, T. Kikutani, Development of stereocomplex crystal of polylactide in high-speed melt spinning and subsequent drawing and annealing processes, *J. Macromol. Sci. Part B Phys.* **2003**, *42*(3 & 4), 403–420.
37. W. H. Kohler, P. Shrikhande, A. J. McHugh, Modeling melt spinning of PLA fibers, *J. Macromol. Sci. Part B Phys.* **2005**, *44*, 185–202.
38. T. Kikutani, M. Takasaki, M. Kuroda, H. Ito, Fiber structure development in high-speed melt spinning of poly(L-lactide) with various D-lactide contents and racemate polylactide, *International Conference on Advanced Fibers and Polymer Materials*, Donghua University, Shanghai, 2005, Vol. *1*, pp. 88–91.
39. R. Hufenus, Y. Yan, M. Dauner, D. Yao, T. Kikutani, Chapter 11, Bicomponent fibers, in: J. Hu (Ed.), *Handbook of Fibrous Materials, Vol. 1*, Wiley-VCH Publishing Ltd., Weinheim, 2020, pp. 285–317.
40. S. A. Arvidson, K. C. Wong, R. E. Gorga, S. A. Khan, Structure, molecular orientation, and resultant mechanical properties in core/sheath poly(lactic acid)/polypropylene composites, *Polymer* **2012**, *53*(3), 791–800.
41. C. Prahsarn, W. Klinsukhon, S. Padee, N. Suwannamek, N. Roungpaisan, N. Srisawat, Hollow segmented-pie PLA/PBS and PLA/PP bicomponent fibers: an investigation on fiber properties and splittability, *J. Mater. Sci.* **2016**, *51*(24), 10910–10916.
42. Y. Kawahara, M. Hanada, S. Onosato, W. Takarada, M. Takasaki, K. Takeda, Y. Ikeda, T. Kikutani, High-speed melt spinning of polylactide/poly(butylene terephthalate) bicomponent fibers: mechanism of fiber structure development and dyeing behavior, *J. Macromol. Sci. Part B Phys.* **2019**, *60*(10), 828–846.
43. Y. Kawahara, W. Takarada, M. Yamamoto, Y. Kondo, K. Tashiro, T. Kikutani, Fiber structure, tensile behavior and antibacterial activity of polylactide/poly(butylene terephthalate) bicomponent fibers produced by high-speed melt-spinning, *J. Macromol. Sci. Part B Phys.* **2020**, *59*(7), 440–456.
44. Y. Kawahara, W. Takarada, K. Takeda, Y. Ikeda, K. Onda, T. Kikutani, Dyeing behavior and multi-functionalities of polylactide/poly(ethylene terephthalate) conjugate fibers produced by high-speed melt-spinning, *J. Macromol. Sci. Part B Phys.* **2021**, *60*(1), 63–75.
45. P. E. Le Marec, L. Ferry, J. C. Quantin, J. C. Bénézet, F. Bonfils, S. Guilbert, A. Bergereta, Influence of melt processing conditions on poly(lactic acid) degradation: molar mass distribution and crystallization, *Polym. Degrad. Stab.* **2014**, *110*, 353–363.
46. N. Roungpaisan, W. Takarada, T. Kikutani, Development of polylactide fibers consisting of highly oriented stereocomplex crystals utilizing high-speed bicomponent melt spinning process, *J. Fiber Sci. Technol.* **2019**, *75*(9), 119–131.
47. J. Radhakrishnan, T. Kikutani, N. Okui, High-speed melt spinning of sheath-core type bicomponent fibers of polyesters: high and low molecular weight poly(ethylene terephthalate) systems, *Text. Res. J.* **1997**, *67*, 684–694.
48. S. Yukioka, K. Nagato, T. Inoue, Ellipsometric studies on mutual diffusion and adhesion development at polymer-polymer interfaces, *Polymer* **1992**, *33*, 1171–1176.
49. E. Kim, E. J. Kramer, W.C. Wu, P. D. Garrett, Diffusion in blends of poly(methyl methacrylate) and poly(styrene-*co*-acrylonitrile), *Polymer* **1994**, *35*, 5706–5715
50. H. Qiu, M. Bousmina, Determination of mutual diffusion coefficients at nonsymmetric polymer/polymer interfaces from rheometry, *Macromolecules* **2000**, *33*, 6588–6594.
51. C. Hu, X. Chen, J. Chen, W. Zhang, M. Q. Zhang, Observation of mutual diffusion of macromolecules in PS/PMMA binary films by confocal Raman microscopy, *Soft Matter.* **2012**, *8*, 4780–4787.

# PART IV

# DEGRADATION, ENVIRONMENTAL IMPACT, AND END OF LIFE

# 19

# PHOTODEGRADATION AND RADIATION DEGRADATION

Wataru Sakai and Naoto Tsutsumi

## 19.1 INTRODUCTION

In general, most polymer materials show degradation behavior when exposed to light, resulting in discoloration and/or brittle fracture. This is because chemical bonds in the polymer chain or low-molecular-weight compounds in the matrix absorb light energy, which causes chemical reactions, such as main chain scission, cross-linking, oxidation, or bond cleavage [1, 2]. The photodegradation of polymer materials is particularly accelerated outdoors due to the strong light intensity of the sun, which includes invisible shorter wavelength and higher energy UV radiation. Investigations to prevent photodegradation of polymer materials have been carried out in academic and industrial settings for more than 50 years since the mass production of polymer materials began. Nowadays, it is common that photostabilizers and inhibitors are mixed into the polymer matrix to avoid degradation. However, photo-induced degradation and cross-linking can also be applied actively, such as photoresists in photolithography or surface modifications to develop novel photofunctional polymer materials.

Poly(lactic acid) (PLA) is a photodegradable polymer like most plastics. Therefore, treatment to prevent photodegradation should be considered for PLA products. Because of its relatively short history compared with other more widespread plastics, few reports concerning photodegradation of PLA are found before the 1980s. However, as the development of PLA materials progressed, attention has been increasingly given to the durability of PLA, especially its resistance to heat, light, radiation, and sterilization. On the other hand, when PLA was firstly introduced as a copolyester for sutures in the 1970s, the study of its degradation on exposure to high-energy irradiation began, as this was relevant to sterilization using X-ray, γ-ray, and electron beam (EB). In recent years, the focus on PLA as an environmental material has led to the spread of research on PLA in diverse fields not only as a material but also as a surface modification by light irradiation, improvement of mechanical properties by photo-crosslinking, application as a carrier for photocatalysts, and so on. PLA is also one of the key materials to promote the Sustainable Development Goals (SDGs) as a biomass-derived and biodegradable bioplastic. Thus, the interest in PLA has been increasing [3–5]. This chapter presents the photodegradation and radiolysis of PLA, based on the results of academic research carried out over the past decades.

## 19.2 MECHANISMS OF PHOTODEGRADATION

### 19.2.1 Photon

Light is electromagnetic radiation that has dual properties of both wave and particle. In the field of chemical reactions, it is convenient to treat the light as a quantum particle, called a photon. The energy of a photon at a given wavelength of light is as follows:

$$E = h\nu = \frac{hc}{\lambda} \tag{19.1}$$

where $E$ is the energy of the photon (J/mol), $h$ is the Planck constant ($6.626 \times 10^{-34}$ J s), $\nu$ is the wavenumber ($m^{-1}$), $c$ is the speed of light ($3.000 \times 10^{8}$ m/s), and λ is the wavelength (m). Figure 19.1 shows a series of light ranges and their

*Poly(Lactic Acid): Synthesis, Structures, Properties, Processing, Applications, and End of Life*, Second Edition.
Edited by Rafael A. Auras, Loong-Tak Lim, Susan E. M. Selke, and Hideto Tsuji.

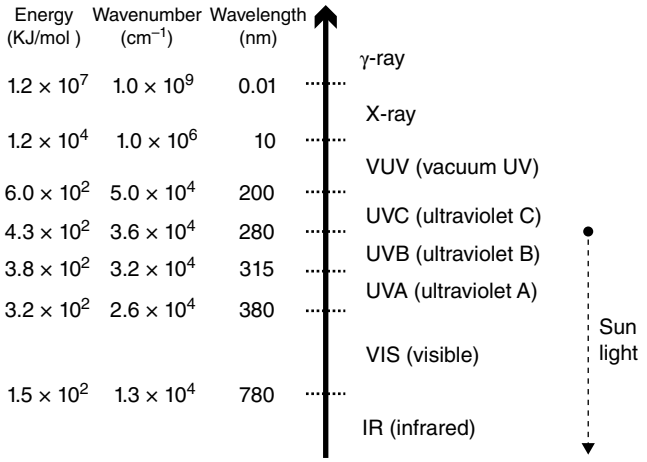


**FIGURE 19.1** Light and high-energy radiations.

energetic properties [2], including IR, UV, and higher energy radiations, X-ray and γ-ray [6]. For example, the wavelength spectrum of sunlight on the ground extends from approximately 280 to 3000 nm. It is usually categorized into three regions: ultraviolet (UV) radiation, visible (Vis) light, and infrared (IR) radiation. UV radiation from the sun can be divided into two regions, UVA and UVB, according to their different effects on biological materials such as human skin. There is a further region of UV radiation with shorter wavelengths, called UVC, which is not included in the sunlight reaching the earth's surface. For sterilization in the medical field, a light of 254 nm in the UVC region is used, which is originally derived from the emission lines of low-pressure mercury lamps of 254 nm. In the future, LED lamps will be widely used as an alternative. The region from 10 to 200 nm, which has wavelengths shorter than UVC, is called vacuum ultraviolet (VUV) in connection with the fact that its wavelength corresponds to the absorption band of oxygen and nitrogen molecules.

Table 19.1 shows bond dissociation energies for some typical bonds in polymers [2, 7] and photon wavelengths that have corresponding energies. The UV radiation from the sun has enough energy to decompose almost all of those bonds. However, although these bond cleavage energies are intrinsically important in the case of thermal processes, not all of the photons that have higher energy than the dissociation energy can initiate photodegradation. This is because photolysis of a molecule essentially depends on whether the photon is absorbed by the molecular bonds and how many photons have been absorbed by the reaction system.

### 19.2.2 Photon Absorption

The photochemical reaction of a material starts with photon absorption. In other words, "only the photons absorbed by the molecule can bring about photochemical reactions." This is the first law of photochemistry, also called the Grotthuss–Draper law. The second law of photochemistry is "one molecule is activated when one photon is absorbed." This is known as the Stark–Einstein photochemical equivalence law. Generally, a particular group in an irradiated molecule absorbs a photon with an appropriate wavelength. When photoabsorption occurs, the molecule in the ground state is electronically excited into a higher energy state. This photoexcitation process is called electron transition where one of the outer electrons is pushed up to a higher energy molecular orbital. These photophysical processes are extensively referred to in the literature; therefore, only basic information related to polymer photodegradation is described here [1, 2, 9].

In an organic molecule, some basic molecular orbitals, such as σ, π, and *n*, are in the ground state, whereas σ* and π* are antibonding orbitals in the excited state. These molecular orbitals are constructed by the linear combination of atomic orbitals. Figure 19.2 summarizes their relative order in energy and the electron transition direction allowed between two molecular orbitals. For example, the C─O bond in an acetone molecule, which is also incorporated in the PLA main chain, is known to have absorption bands at 280 nm due to *n*–π* excitation energy and around 190 nm by *n*–σ* excitation energy. Because radiation intensities in shorter wavelengths below 280 nm are very weak in sunlight, the molecules that have C─O bonds are likely to be photoexcited via the *n*–π* transition. Such active groups that are mainly responsible for photon absorption are often referred to as chromophores.

Photoexcitation does not occur for all molecules with the same probability. This is because photoabsorption depends on the chemical structure of the chromophore group. The Lambert–Beer equation is as follows:

$$\frac{I}{I_0} = 10^{-\varepsilon c l} \tag{19.2}$$

**TABLE 19.1 Bond Dissociation Energy of Some Chemical Bonds and the Corresponding Photon Wavelength [2, 4, 8]**

| Bond | Energy (kJ/mol) | λ (nm) |
|---|---|---|
| C─C | 245–370 | 490–325 |
| C─H | 350–460 | 340–260 |
| C─O | 210–405 | 570–295 |
| C─Cl | 290–315 | 410–380 |
| O─H | 370–470 | 325–255 |
| C─N | 270–300 | 445–400 |
| CO─O | 400–415 | 300–290 |
| C═C | 720 | 165 |
| C═O | 530 | 225 |

Energy and wavelength values are estimated based on the cited references.

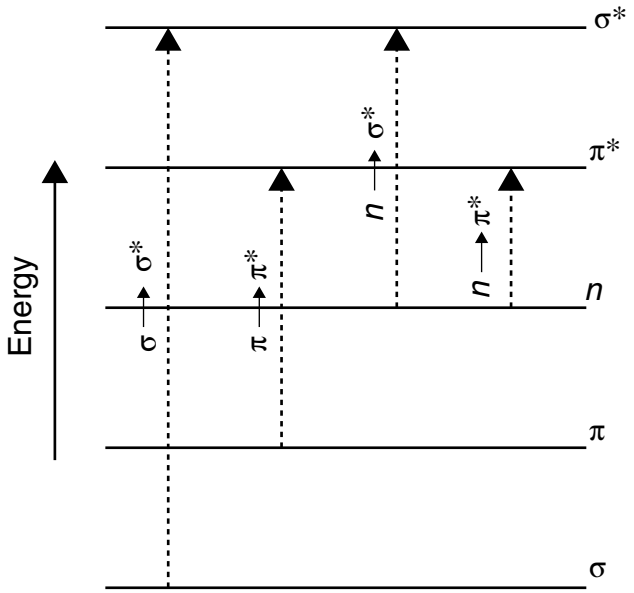


**FIGURE 19.2** Electron transitions between molecular orbitals. *Note*: The distance between orbitals is drawn equally for better comprehensibility.

where $I_0$ and $I$ are the light intensities before and after transmission through the sample; $\varepsilon$ is the molar extinction coefficient (L/(mol cm)), also called molar absorptivity; $c$ is the molar concentration of chromophore in the sample (mol/L); and $l$ is the path length of light in the sample (cm). This equation is often expressed as absorbance $A$:

$$A = \log_{10} \frac{I_0}{I} = \varepsilon c l \tag{19.3}$$

Table 19.2 shows absorption wavelengths and ε for some chemical compounds that have C═C or C═O double bonds. As shown in the table, their absorption range is located at about 180–300 nm and $\varepsilon$ is on the order of $10^0$–$10^2$ in the UVC region, near the short wavelength end of sunlight (~280 nm).

It should be noted that the intensity of the light involved in the reaction is the highest at the surface of the sample and decreases as the light passes into the sample, so that photodegradation is most likely to occur at the surface. Furthermore, during prolonged observation of photodegradation, the concentration of UV-absorbing byproducts may be higher at the surface, thereby reducing the penetration depth of UV light into the sample. This also increases the difference in the distribution of the light intensity in the sample. In addition to the initiators and additives used in the polymerization process, compounds produced during the molding process can become optical impurities that absorb the irradiated light and thus cause photodegradation.

### 19.2.3 Photochemical Reactions of Carbonyl Groups

The PLA chemical structure consists of C─C, C─H, C─O, and C═O bonds. Because the excited state of the C─O group via $n$–π* transition exhibits an antibonding and biradical property (Figure 19.3a), photoexcitation of C═O tends to cause some chemical reactions, such as α and β cleavage (Figure 19.3b), atom abstraction (Figure 19.3c), radical addition, and electron abstraction or electron transfer. On the other hand, single bonds, such as C─C and C─H, absorb at wavelengths shorter than 180 nm. Photo-irradiation in such VUV region is rarely investigated, except under special experimental conditions such as under vacuum, because the absorption by optical glass materials and gas molecules is not small. Therefore, the object of the photodegradability study of PLA is generally to elucidate the reactivity of the C─O chromophore groups under irradiation in the UVB or UVC region depending on whether the effects of sunlight or artificial light are to be investigated, respectively.

## 19.3 MECHANISM OF RADIATION DEGRADATION

### 19.3.1 High-Energy Radiation

The effect of high-energy (ionization) radiation such as X-ray, γ-ray, and electron beam (EB) on polymer materials is as important as photo-irradiation. Some polymer materials

**TABLE 19.2 Absorption Wavelength and Absorption Coefficient for Some Chemical Bonds in Low-Molecular-Weight Compounds and Their Transition Types**

| Bond | Compound | Solvent | $\lambda_{max}$ (nm) | $\varepsilon$ (L/(mol cm)) | Transition |
|---|---|---|---|---|---|
| C─C | Alkane | | <180 | ~1000 | σ–σ* |
| C─C | Benzene | | 200 | 4400 | π–π* |
| | | | 256 | 226 | π–π* |
| C─O | Acetone | Isooctane | 188 | 900 | π–π* |
| | | | 279 | 15 | $n$–π* |
| C─O | Cyclohexanone | Hexane | 285 | 14 | $n$–π* |
| C─O | Ethyl acetate | Ether | 207 | 69 | $n$–π* |

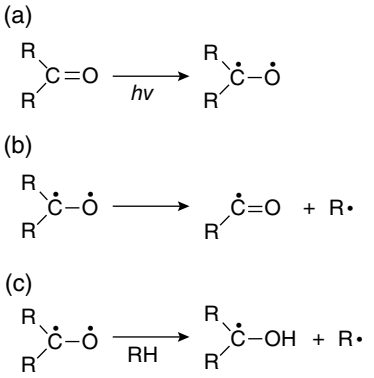


**FIGURE 19.3** (a–c) Various excited states of PLA.

are utilized for medical applications and are sterilized by such radiation or UV irradiation before use. The radiation resistance of these polymeric materials is also important when they are being used in nuclear reactor facilities, radiation equipment, and in space. Moreover, processing by radiation or high-energy ion beam is recently one of the effective methods for modification of surface or bulk properties of polymer materials. As shown in Figure 19.1, X-ray and γ-ray are electromagnetic waves with wavelengths ranging from 10 pm to 10 nm and less than 10 pm, respectively. The energy of the EB is in the order of KeV to MeV, which is close to that of γ-ray. The degradation schemes in organic materials caused by absorption of such high-energy radiation are very different from those produced by UV or Vis photo-irradiation.

### 19.3.2 Basic Mechanism of Radiation Degradation

Since the energies of radiation are more intense than photo-irradiation, they can ionize molecules unselectively through strong interactions with the nuclei or the electron clouds of the molecules (Figure 19.4a) [1, 10–12]. The secondary electrons produced by such interactions have enough kinetic energy to trigger succeeding ionizations and energy excitation of surrounding molecules (Figure 19.4a–c).

These unstable active species further produce many intermediates through side reactions, such as homolytic cleavage, ionic scission, electron transition, and energy transition (Figure 19.4d–j). These intermediates, including the radical species, are then inactivated through neutralization, hydrogen abstraction, or recombination with excess energy loss by chemical reactions and thermal diffusion (Figure 19.4k–n). In this way, the radiation-induced reactions are much different from those produced by photo-irradiation, since ionization and radical reactions can occur simultaneously.

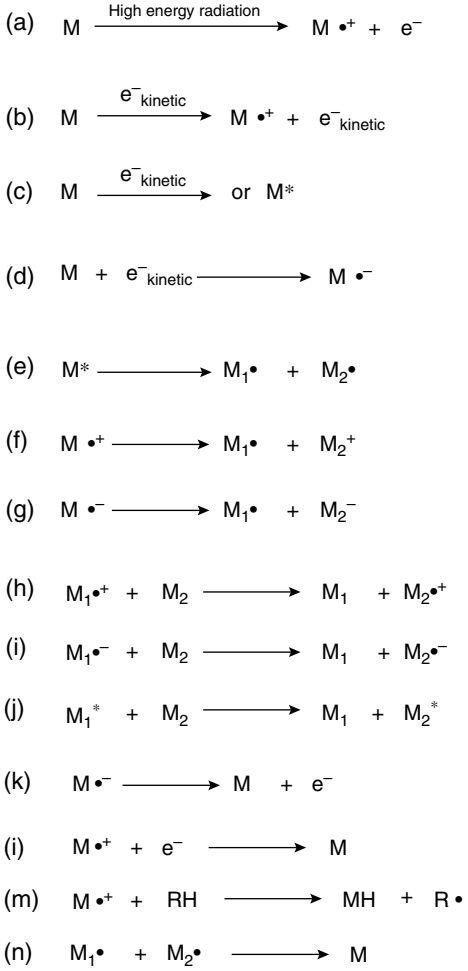


**FIGURE 19.4** (a–n) Ionization of molecules through unselective strong interactions.

## 19.4 PHOTODEGRADATION OF PLA

### 19.4.1 Fundamental Mechanism

As previously mentioned, the most efficient group in PLA for photodegradation is the carbonyl group C═O, which absorbs UV radiation with maximum wavelength at about 280 nm via $n$–$\pi^*$ electron transition. Although the molar extinction coefficient $\varepsilon$ for PLA at 280 nm is very low (less than 100 L/(mol cm)), photodegradation can certainly occur when PLA is exposed to irradiation.

The first published report about photodegradation of PLA may have been the paper by McNeill and Leiper in 1985 [13], although PLA had been utilized as a biocompatible material since the 1970s. McNeill and Leiper examined the photolysis of PLA under vacuum at 30°C for 72 h using a medium-pressure Hg lamp. From the results of volatile products analysis, UV–Vis and IR spectroscopy, and thermal

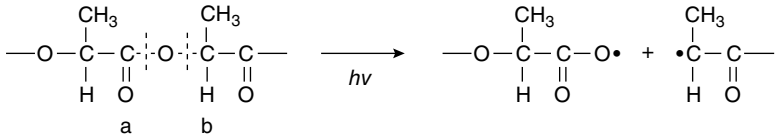


**FIGURE 19.5** PLA decomposition by UV light according to McNeill and Leiper [13].

decomposition, they suggested that PLA decomposition by UV light occurred at the O—C bond in the ester linkage, at the position (b) as shown in Figure 19.5, as in thermal degradation.

The next report on poly(L-lactic acid) (PLLA) photodegradation appeared in 1997 by Ikada [14], who investigated the photodegradation behavior of polycaprolactone (PCL) and PLLA using viscosity measurement, FT-IR and UV–Vis spectroscopy. He showed that the average molecular weight of PLLA rapidly decreased in 1 h of UV irradiation. He also found that the degradation was enhanced by changing the atmosphere from air to $N_2$. This contradictory result is interesting because it is known that polymer degradation in general tends to be accelerated by $O_2$ through an auto-oxidation mechanism [1]. Based on the increased intensity of C═C and OH groups in the IR spectra, Ikada suggested that the main chain scission of PLLA randomly proceeds not through Norrish type I but Norrish type II by UV irradiation (Figure 19.6) [2].

The scheme proposed by Ikada is different from that by McNeill and Leiper [13]. Because the initiation mechanism for photoreaction is triggered selectively by electron transition at C—O, it is acceptable that photodegradation of PLLA is caused by Norrish type II reactions. However, if the —$COO^{\cdot}$ radical abstracts H from a neighboring —$CH_3$ as shown in Figure 19.5, the resulting products —COOH and —CH═$CH_2$ are the same as by the Norrish type II shown in Figure 19.6b.

The degradation behavior of UV-irradiated PLLA was also investigated by Ho and Pometto in 1999, using EB and UV light at 365 nm [15]. While the molecular weight drop due to hydrolytic degradation at 55°C in 10% relative humidity (RH) proceeded slowly for eight weeks, the UV-irradiated PLLA film resulted in large photodegradation rate of weight-average molecular weight ($M_w$) with up to 97% enhancement.

Copinet et al. observed the enhancing effect of UV irradiation on the autocatalysis of hydrolysis in PLLA at different combinations of RH (30, 50, and 100%) and temperature (30, 45, or 60°C) for up to 30 weeks using FT-IR measurements [16, 17]. They observed a faster decrease of crystallinity, glass transition temperature ($T_g$), and $M_w$ due to faster hydrolysis at the ester linkage by increasing RH and temperature, which were accelerated by UV treatment. However, no details about the mechanism of photodegradation or the enhancing effect were suggested.

Tsuji et al. compared the photodegradation behavior of PCL and PLLA comprehensively, under carefully controlled UV irradiation conditions, at 45°C and with 65% RH, using gel permeation chromatography (GPC), differential scanning calorimetry (DSC), tensile testing, and polarized light microscopy [18]. It was found that PCL showed a larger decrease of molecular weight than PLLA after UV irradiation. They suggested that the photodegradation proceeds via Norrish type II reactions as proposed by Ikada in Figure 19.6b [14]. The chemical structure of the two sequential groups adjacent to the ester oxygen is crucial for photodegradability of biodegradable polyesters (Figure 19.7). They also compared the effect of crystallinity on the

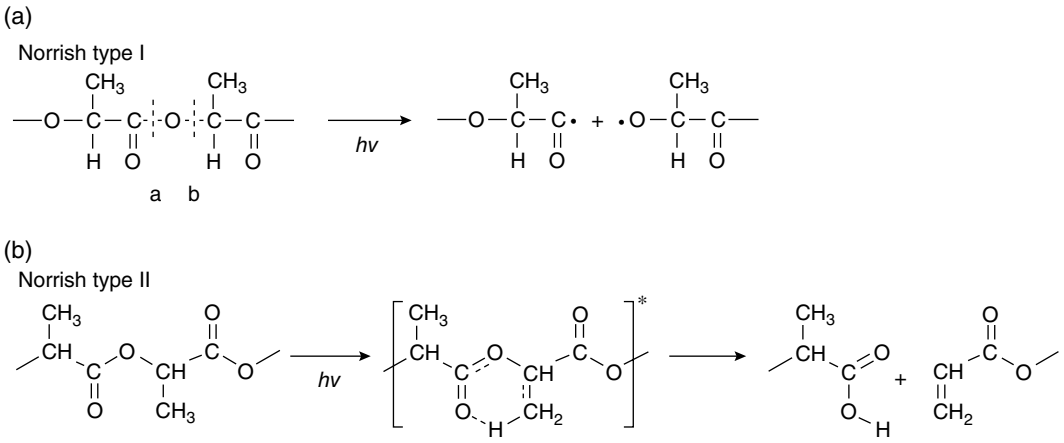


**FIGURE 19.6** (a and b) Main chain scission of PLLA via Norrish type I and II according to Ikada [14].

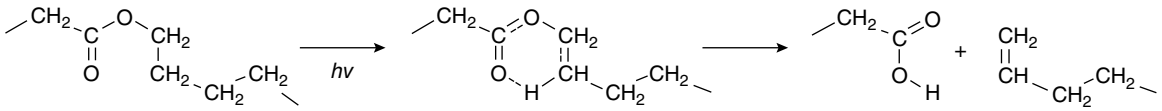


**FIGURE 19.7** Photodegradability of biodegradable polyesters according to Tsuji [18].

photodegradation using PLLA polymers of two different crystallinities: one was less than 2% (PLLA-A) and the other about 35% (PLLA-C). It was found that photodegradation of PLLA chains can occur at random even in the crystalline region of PLLA-C by UV irradiation. This result was remarkably in contrast to the case of hydrolytic degradation of PLLA, where no degradation occurred in the crystalline region. Tsuji et al. presumed that UV light penetration into the specimen was enough for degradation to proceed by the bulk erosion mechanism [18].

As mentioned above, PLA is susceptible to photodegradation through photoexcitation at the C═O group in the ester linkage. Janorkar et al. studied the wavelength effect on PLLA photodegradation using a UV source with a wavelength range of 232–500 nm [19]. It was shown that the degradation of PLLA was minimized when the sample was irradiated through a Pyrex® glass plate. Pyrex glass is not optically transparent at wavelengths below 300 nm in the UV region due to its own absorption. The result implied that the absorption of C═O groups and other efficient groups in PLLA should mainly occur at wavelengths between about 200 and 300 nm. They proposed two mechanisms of PLLA degradation under UV irradiation: one involves a homolytic photolysis at C─O of the backbone leading to hydrogen abstraction (Figure 19.8a) and the other involves photooxidation of PLLA leading to the formation of hydroperoxide derivatives that subsequently degraded into compounds containing a carboxylic acid and unstable diketones (Figure 19.8b). However, these reactions cannot explain the increase of C═C bonds reported by Ikada [14].

Belbachir et al. reported a physically based model for photodegradation effect on elastic–viscoplastic behavior of amorphous PLA films [20]. The simulated results reproduce most of the features of the stress–strain curves (i.e., initial stiffness, nonlinear response, fracture) and showed good agreement with experimental results over a wide range of UV irradiation doses.

### 19.4.2 Photooxidation Degradation

Bocchini et al. carefully observed the FT-IR spectra of PLA photo-irradiated with UV light at wavelength above 300 nm and found growth of a peak at 1845 $cm^{-1}$ [21], which was assigned to an anhydride group, on the basis that by exposing the PLA in an ammonia atmosphere, the peak disappeared, with concomitant increase of peaks ascribed to the formation of carboxylic salt and primary amide groups. They suggested that the anhydride group is formed by the decomposition and β-scission from the hydroperoxide group produced by the photo-oxidative reaction of PLA, as shown in Figure 19.9. Blasco et al. also investigated the UV photodegradation of PLA and observed that the molar mass of specimens followed a second-order law ($1/M = 1/M_0 + kt$). They concluded that the main step involved was random chain scision [22]. They also found that the non-crystallizable groups, such as the anhydride formed during photodegradation, decreased the crystallization rate compared to biodegraded specimens of equivalent molar mass.

As mentioned above, peroxide groups on PLA chains play an important role in photo-oxidized degradation. In such case, chemiluminescense (CL) analysis is a useful method to know the peroxidation state of the sample, which would exhibit a slight emission from the excited carbonyl group (C═O*) and the excited oxygen ($^*O_2$) brought about

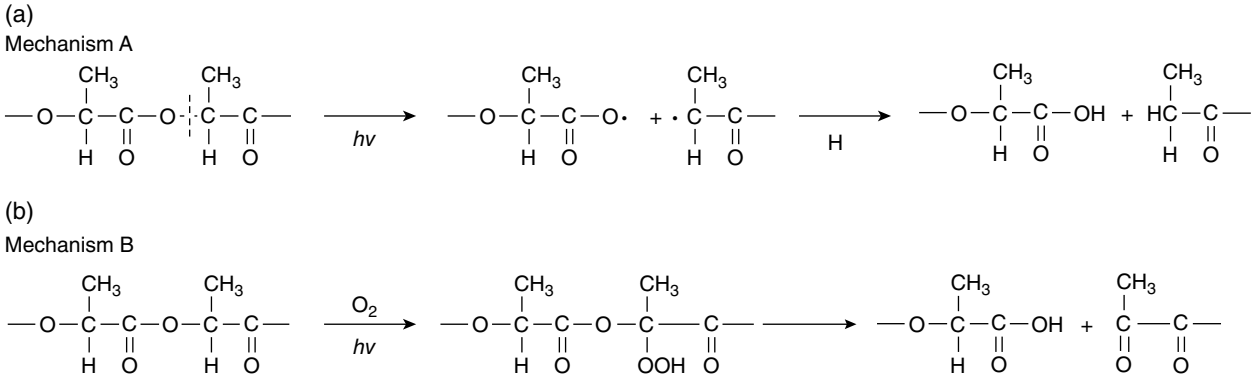


**FIGURE 19.8** (a and b) Mechanism A and B of photodegradation of PLLA under UV irradiation according to Janorkar et al. [19].

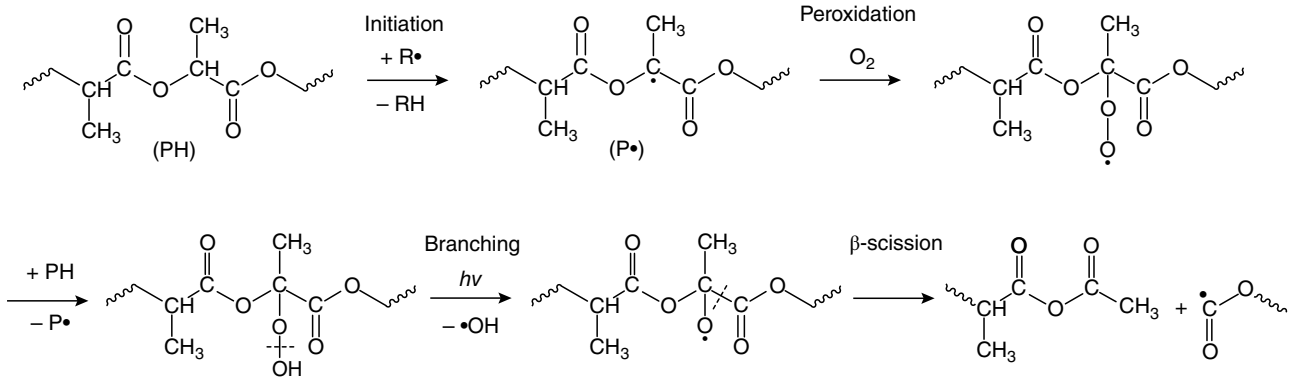


**FIGURE 19.9** Radical oxidation process of irradiated PLA samples, cited with simplification from Ref. 21 reported by Bocchini et al.

by the disproportionation of the two peroxide groups (—O—O·). Rychlý et al. examined UV-irradiated PLA and aromatic–aliphatic polyesters by CL measurement in nitrogen and oxygen atmospheres during the non-isothermal temperature runs. They revealed the existence of two kinds of peroxides in the irradiated samples [23].

### 19.4.3 High-Energy Photo-Irradiation

High-power laser light is often used to fabricate or modify polymers. Hsu et al. used a pulsed KrF excimer laser with a wavelength of 248 nm and pulse width of 25 ns to reduce crystallinity of PLLA films with a surface melting treatment while minimizing chemical modifications [24]. Both short pulse time (ns) and high achievable energy fluence of excimer laser have been used for fabrication of microstructures. Stępak et al. showed some PLLA microstructures made by laser micromachining [25] and investigated the laser-affected zone on PLA surfaces at below or above threshold of laser ablation [26]. When the polymer was exposed to an ultrashort pulse laser with pulse width ~100 fs using a femtosecond laser, ablation occurred through multiphoton excitation, where more than two photons are nonlinearly absorbed by the molecule and the electronic energy state of molecule jumps over the threshold of bonds. Because the excitation time is quite short, the heat damage can be minimized. Yada et al. and Shibata et al. fabricated a laser-induced periodic surface structure (LIPSS) or laser craters on a transparent PLA surface using a femtosecond laser and found the femtosecond laser irradiation at a wavelength of 400 nm accelerates the biodegradation more significantly than using 800 nm laser due to the more decrease in molecular weight induced by the photodegradation [27, 28].

As mentioned above, photo-irradiation in the VUV region needs special conditions and is rare. Li et al. [29] investigated the photodegradation of PLLA using VUV light with a center wavelength of 172 nm generated from an Xe excimer laser, aiming at developing a new PLLA photoresist material. It was revealed that PLLA has a higher degradation rate than poly(methyl methacrylate) (PMMA) under VUV irradiation and the degradation reaction was activated mostly by negatively charged oxygen $O_2^-$. They observed a fast decrease of C═O bonds in 2 min irradiation, the decay of which cannot be explained by the reaction schemes described above where the number of C═O bonds remains stable.

A study of the chirality effect in photolysis of PLA was reported when the ratio of D- to L-isomers differs. It can be said, though, that because photodegradation basically starts at each functional group in the monomers, both isomers should indicate the same chemical decomposition, even though the reaction may proceed enantiomerically. In practice, because the D- and L-isomer ratio greatly changes the polymer crystallinity, the chirality effects must be interchanged with crystalline effects as revealed by Tsuji et al. [18, 30]. Yasuda et al. investigated the characteristic changes in PLA when irradiated with UV-C light ($\lambda$ = 253.7 nm), which is not present in terrestrial sunlight but directly interacts with the carbonyl groups of PLA. It was found that the optical purity of the monomeric units gradually decreased with a marked decrease in molecular weight. This racemization was attributed to the formation of approximately one D-lactate unit at every scission of the PLA chain [31, 32].

### 19.4.4 Photosensitized Degradation of PLA

The wavelength region of photoabsorption for a polymeric material is determined by its chemical structure. If the photosensitivity of the polymer is to be altered, one approach is to change the chemical structure of the polymer to enhance or control the wavelength range of light absorption. The addition of a chromophore with an appropriate light absorption range allows the polymeric material to react indirectly even when irradiated with light in the wavelength range where the matrix polymer has no absorption.

Sakai et al. studied the photosensitized degradation of PLLA using *N*,*N*,*N*′,*N*′-tetramethyl-*p*-phenylenediamine

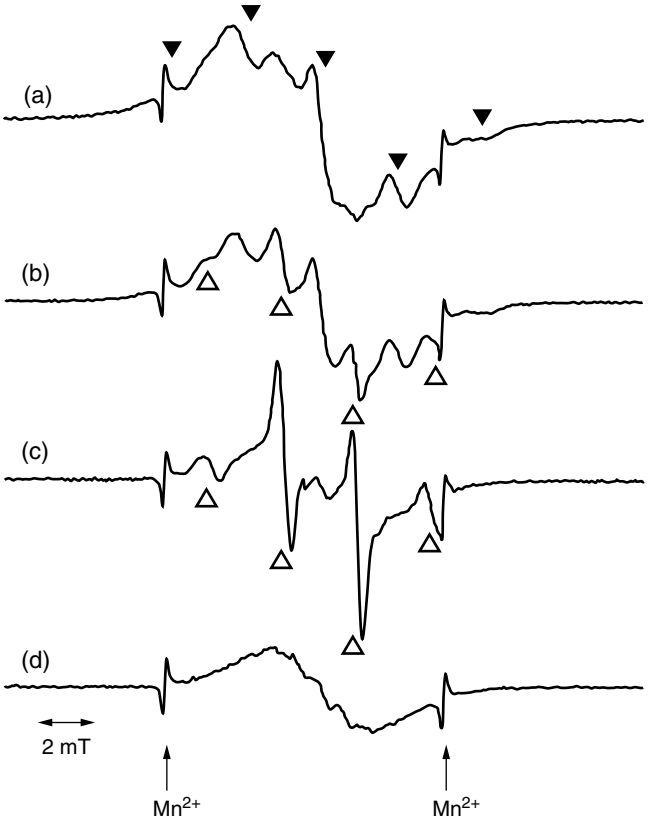


**FIGURE 19.10** ESR spectra of PLA/TMPD at 77 K: (a) after irradiation at 77 K for 1 min, (b) after thermal annealing at 0°C for 1.5 min, (c) after further thermal annealing at 0°C for 20 min, and (d) after further annealing at 20°C for seven days. ▼ and △ indicate the main-chain scission radical of PLA and the main-chain radical, respectively [33].

(TMPD) as a photosensitizer for UV light with $\lambda = 356$ nm, which cannot directly excite the PLLA matrix itself [33]. Electron spin resonance (ESR) spectra were measured under cryogenic light irradiation at 77 K to delay the reaction (Figure 19.10a). The hyperfine structure of ESR spectrum was changed dramatically by stepwise thermal annealing, which revealed the presence of some overlapped radicals, such as $TMPD^{+\cdot}$ radical cations, PLLA main chain scission radicals (Figure 19.11b), and PLLA main chain tertiary radicals (Figure 19.11c). A decrease in molecular weight of PLLA was also observed after irradiation for 5 min. They concluded that an ester radical anion of PLLA ($-COO^{-\cdot}$, Figure 19.11a) produced by capturing the electron ejected from TMPD is the initial species formed in PLLA decomposition. This photosensitized reaction through photoionization of additive was also applied to amorphous PDLLA (poly(D,L-lactic acid)) with ratio of D/L = 25 : 75 and some poly(succinic acid/propanediol) aliphatic polyesters [34, 35]. It was found that not only the chain degradation but also the cross-linking reaction occurred in one of the polyesters, poly[(propane-1,3-diol)-*alt*-(succinic acid)] (3g4).

Tsuji et al. [36] subsequently investigated the photosensitizing effect of TMPD on photodegradation of PLLA-A and PLLA-C for much longer irradiation times than those used by Sakai et al. [35]. They also confirmed that the addition of TMPD effectively enhanced the photodegradation of PLLA films, irrespective of their degree of crystallinity. Moreover, they showed that the UV irradiation affected the thermal properties of PLLA such as $T_g$, cold crystalline temperature ($T_{cc}$), and melting temperature ($T_m$). This implied that the molecular structural changes of chain cleavage, such as C—C formation, and both cross-linking and scission of PLLA occurred.

Recently, it is well known that inorganic catalysts such as $TiO_2$ enhances the degradation of organic materials. There are two types of photoactive $TiO_2$ crystal: anatase and rutile. The anatase type is more likely to exhibit higher catalytic effect upon photoexcitation than rutile due to the narrower band gap. In order to improve the photodegradability of PLA, the photocatalytic degradation of PLA caused by the incorporation of $TiO_2$ nanoparticles into the medium has been studied [37, 38]. $TiO_2$ is electronically excited by UV light with wavelengths of less than 390 nm, producing electron–hole pairs e by electron transfer.

$$TiO_2 + h\nu \leftrightarrow e^- + hole^+$$

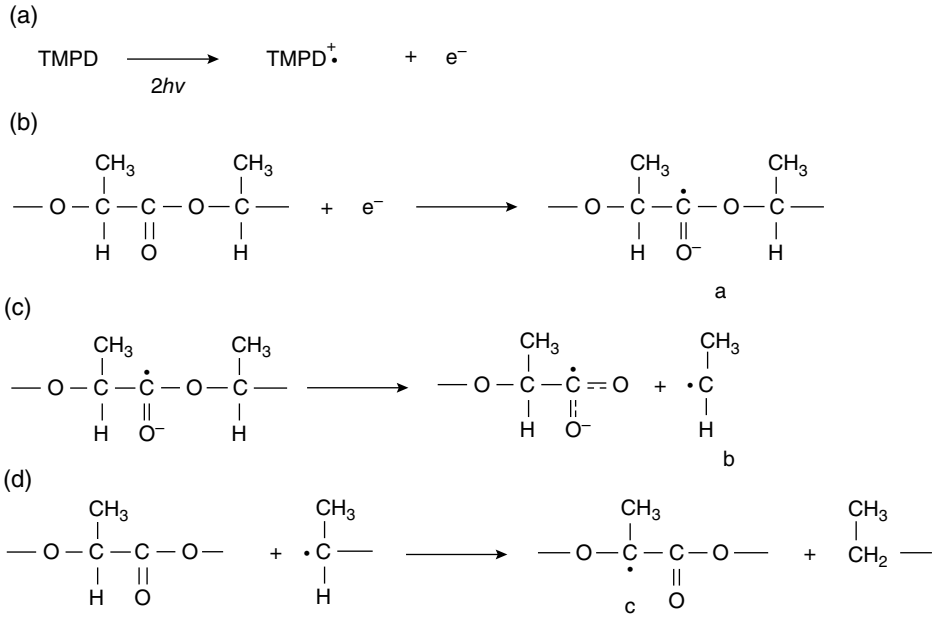


**FIGURE 19.11** (a–d) Production of $TMPD^{+\cdot}$ radical cations (a), main chain scission radicals of PLLA (b), and main chain tertiary radicals of PLLA (c) via photoionization of TMPD, according to Sakai et al. [33].

The excited-state electron–hole pairs move to the nanoparticle surface and react with $H_2O$ or $O_2$ to produce active oxygen species such as $\cdot O_2^-$, $\cdot OOOH$, $\cdot OH$. These active oxygen species are thought to be the key radical species that initiate the degradation of PLA at the boundary of the $TiO_2$ and PLA matrix. This series of radical reactions can also be described as a photosensitized reaction, since $TiO_2$ is activated by relatively long-wavelength UV light, which PLA cannot absorb. $TiO_2$ is originally immiscible with PLA and therefore tends to aggregate in the PLA matrix. Since the photocatalytic effect strongly depends on the dispersion of $TiO_2$ in the sample matrix, some researchers tried surface modification of $TiO_2$ to increase the efficiency of the photocatalytic reaction [39–42]. Luo et al. functionalized the anataze-type $TiO_2$ by grafting lactic acid oligomer onto its surface at about 7 wt% through a solution polycondensation reaction process without using catalyst. They reported a large enhancement of photodegradation of PLA by adding 2 wt% of the modified $TiO_2$ [42].

### 19.4.5 Photodegradation of PLA Blends

The photodegradability of PLA can be modified by blending PLA with other polymers. Kaczmarek et al. found that the photodegradability of PLA was enhanced in blends obtained by photopolymerization of a mixture of PLA and acrylate monomers [43]. Huerta et al. found that PLA-blended PET degraded slightly faster than PET alone in accelerated weathering at 600 h [44]. Malinowski investigated the properties of PLA blends with PCL before and after EB irradiation. It was concluded that the PLA phase is more sensitive to EB than the PCL phase because an increase in the mass flow rate (MFR) with increasing the PLA content and a change in mechanical strength due to the strong effect of PLA degradation on the phase separation structure were observed after EB irradiation. [45]. Salač et al. investigated the additive effects on the photodegradation using orotic acid as a nucleation agent in PLA. The compound decomposed by UV light and slightly accelerated cleavage degradation of PLA chain. The former reaction accelerated the subsequent biodegradation by shortening the lag period [46].

## 19.5 RADIATION DEGRADATION OF PLA

As mentioned above, due to the development of PLA and related biocompatible copolymers, radiation effects on PLA materials due to sterilization have gained more attention since the 1970s. However, basic information about it was rarely reported at that time.

In 1980s, Gupta et al. first investigated the effect of γ-irradiation on viscosity-average molecular weight ($M_v$) of PLA (the ratio of D- and L-isomers was not described) in both air and $N_2$ atmospheres with an exposure below approximately 1 MGy at a dose rate of $2.6 \times 10^{-3}$ MGy/h [47]. They found that both scission and cross-linking reactions compete in the PLA matrix under γ-irradiation; the radiation chemical yield of cross-linking $G(X)$ in air was much lower than in $N_2$ at dose <0.25 MGy, but increased at dose levels >0.25 MGy. It was suggested for the lower dosage that $O_2$ acted as a free radical scavenger resulting in reduced cross-linking, whereas in $N_2$ free radical centers were deactivated by chain

recombination. This $O_2$ effect is contrary to what occurs in photo-irradiation, where the hydroperoxide group on the main chain produced by oxidation is thought to strongly accelerate the photodegradation process in polymers.

Chu compared the radiation effects on two kinds of biodegradable sutures, Dexon® and Vicry®, which were made of poly(glycolic acid) (PGA) homopolymer and poly(glycolide–lactide) (PGL) copolymer, respectively [48]. It was found that PGL fibers were more susceptible to radiation degradation but more resistant to hydrolytic degradation than PGA fibers. They suggested that the methyl group on the lactic acid moiety lowers the probability of radical recombination from radiation chain scission because of steric hindrance and hence increases the probability of degradation.

Birkinshaw et al. examined γ-irradiation effects on compression-molded PLLA [49]. Under 10.0 Mrad and at a 0.156 Mrad/h dose level, which was used in commercial sterilization processes, it was concluded that the degradation in air proceeded through random chain scission without any oxidative reactions. They also calculated the radiochemical yield of scission $G(S) = 2.9$ from the results of GPC. Benyathiar et al. studied the effects of γ-ray and EB irradiation on physical, chemical, mechanical, thermal, and permeability properties of PLA films in detail with different intensity dose levels used in commercial sterilization processes (γ-ray, 1–10 kGy; EB, 1–5 kGy) [50]. No significant color change ($L^*$, $a^*$, and $b^*$), marked decrease of average molecular weight, increase of polydispersity index, decreases of cold crystallization temperature ($T_{cc}$) and melting temperatures ($T_m$), decrease of mechanical strength, and reduction of water vapor permeability were observed. The effects of sterilization by ethylene oxide (55°C, 6.5 h), hydrogen peroxide plasma (28 min), EB radiation (25 kGy), and γ-radiation (25 kGy) on PLA properties were also investigated by Savaris et al. [51]. No significant variations in crystallinity, color, and contact angle were observed. These results indicate that the sterilization process did not cause significant change in the appearance of the PLA material but did cause significant degradation at the molecular level within the sample.

Babanalbandi et al. investigated γ-irradiated PLLA and PDLLA below 10 kGy using ESR measurement at 77 and 300 K [52]. The ESR spectra indicated the formation of some radicals as shown in Figure 19.12, such as (I) main chain radicals produced by dehydrogenation from methine groups; (II) scission radicals resulting from homolytic bond cleavage at the ester groups of the main chain; and (III) acyl radicals. The experimental ESR spectra were well simulated by superimposing each radical spectrum: (I) a quartet with $h_{fcc} = 2.3$ mT; (II) a double quartet with $a_H\alpha = 2.0$ mT and $a_H\beta = 2.3$ mT (apparently like five lines); and (III) a singlet, as shown in Figure 19.13. Although the irradiation mechanisms between γ-irradiation and UV irradiation are different, it is interesting that the radicals I and II in Figure 19.12 are very similar to the results reported by Sakai et al. on photosensitized reaction of PLLA [33]. The $G$ values for radical formation $G(R)$ were obtained from the plots of radical concentration calculated by ESR spectral analysis versus absorbed dose: $G(R) = 2.0$ at 77 K and 1.5 at 300 K for PLLA and 2.4 at 77 K and 1.2 at 300 K for PDLLA [52]. They also determined the $G$ values for cross-linking $G(X)$, as well as scission $G(S)$: $G(S) = 2.4$ and $G(X) = 0.28$ for PLLA and $G(S) = 2.3$ and $G(X) = 0.0$ for PDLLA, indicating that random chain scission is dominant in PLLA under γ-irradiation.

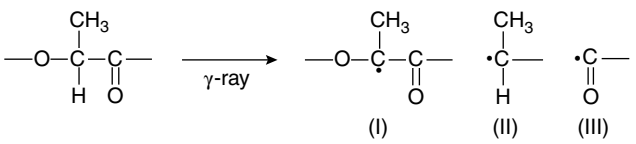


**FIGURE 19.12** Production of (I) main chain radicals, (II) scission radicals, and (III) acyl radicals due to exposure to γ-irradiated of PLLA and PDLLA below 10 kGy, according to Babanalbandi et al. [52].

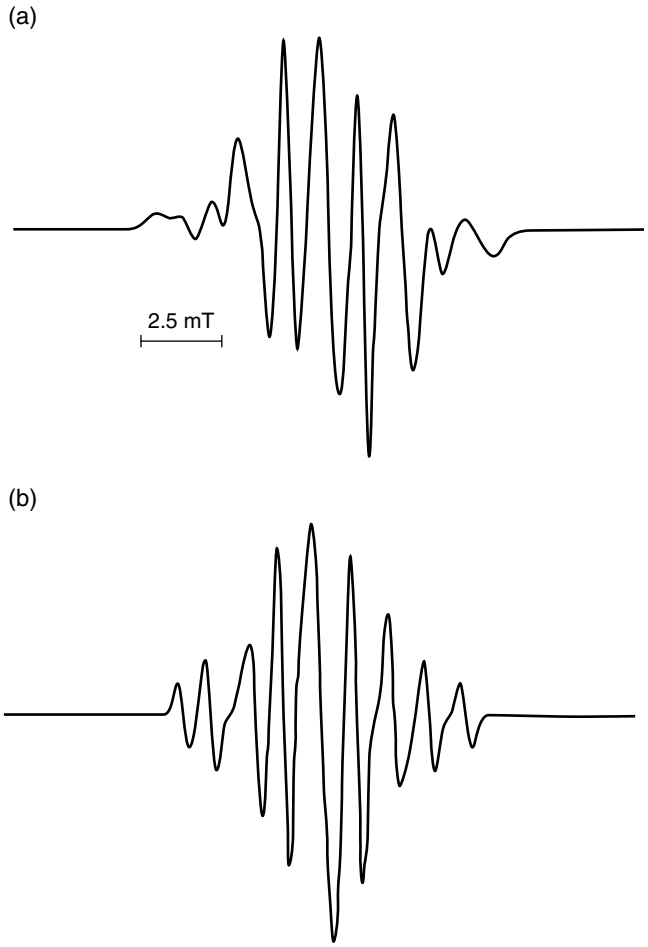


**FIGURE 19.13** Simulation of the ESR spectrum: (a) ESR spectrum of PLA γ-irradiated at 77 K; (b) simulated spectrum of PLA based on the presence of three radicals [52].

Mäder et al. also reported similar distinctive ESR spectra of γ-irradiated PLLA and other biodegradable polymers at 25 kGy by changing the microwave power in ESR measurement in order to observe the saturation effect on the spectrum [53]. Kantoglu et al. observed the radical decay of PLLA, PDLLA, and a random copolymer of poly(L-lactic acid-*co*-glycolic acid) after γ-irradiation in air and vacuum at 25 kGy with a dose rate of 0.59 kGy/h [54]. They observed that the decay curves had to be fitted by applying second-order nonhomogeneous kinetic curves. Kantoglu and Guven also observed the radiation-induced crystallinity damage in PLLA after γ-irradiation in air and vacuum at 80 kGy dose with a rate of 0.59 kGy/h using DSC measurement [55]. Although $T_g$ and $T_m$ of irradiated PLLA were independent of irradiation atmosphere and dose, the crystallinity and the crystalline enthalpy decreased substantially. The radiation yields of a number of damaged units in air and vacuum were calculated to be 0.74 and 0.58 for PLLA, respectively.

## 19.6 IRRADIATION EFFECTS ON BIODEGRADABILITY

The UV irradiation effect on biodegradation was also studied by Tsuji et al. [30] It was shown that the enzymatic weight loss values of irradiated samples were higher for PLLA-A and similar for PLLA-C to that of nonirradiated ones. They suggested that the acceleration effects from decreased molecular weight on enzymatic degradation were higher or balanced with the disturbance effects by the C─C double bond, which was produced during UV irradiation. SEM photographs of PLLA-C taken after irradiation and biodegradation showed fibrous structures remaining (Figure 19.14). These structures may be related to the chains containing or neighboring the C─C double bonds, which were not enzymatically degraded and assembled on the film surface during enzymatic degradation. Jeol and Kim observed an increase in surface hydrophilicity and a decrease in average molecular weight with increasing exposure time when PLA films were exposed to a UV source with wavelengths similar to those of sunlight [56]. The photo-irradiated films were then tested in a modified Sturn test and in compost at 37°C; however, they found that the fastest degradation occurred when the films were exposed to light for 8 h, but that longer exposure resulted in slower biodegradability. In this case, the difference between the apparent biodegradability measured by $CO_2$ and the physical degradation characteristics should be taken into account. EB irradiation was applied by Vargas et al. to improve the biodegradability of PLA plastic waste in compost. It was found that weight loss after six weeks was 9.4% for the 216 kGy dose compared with 1.3% without treatment [57]. The aerobic biodegradation of PLA film

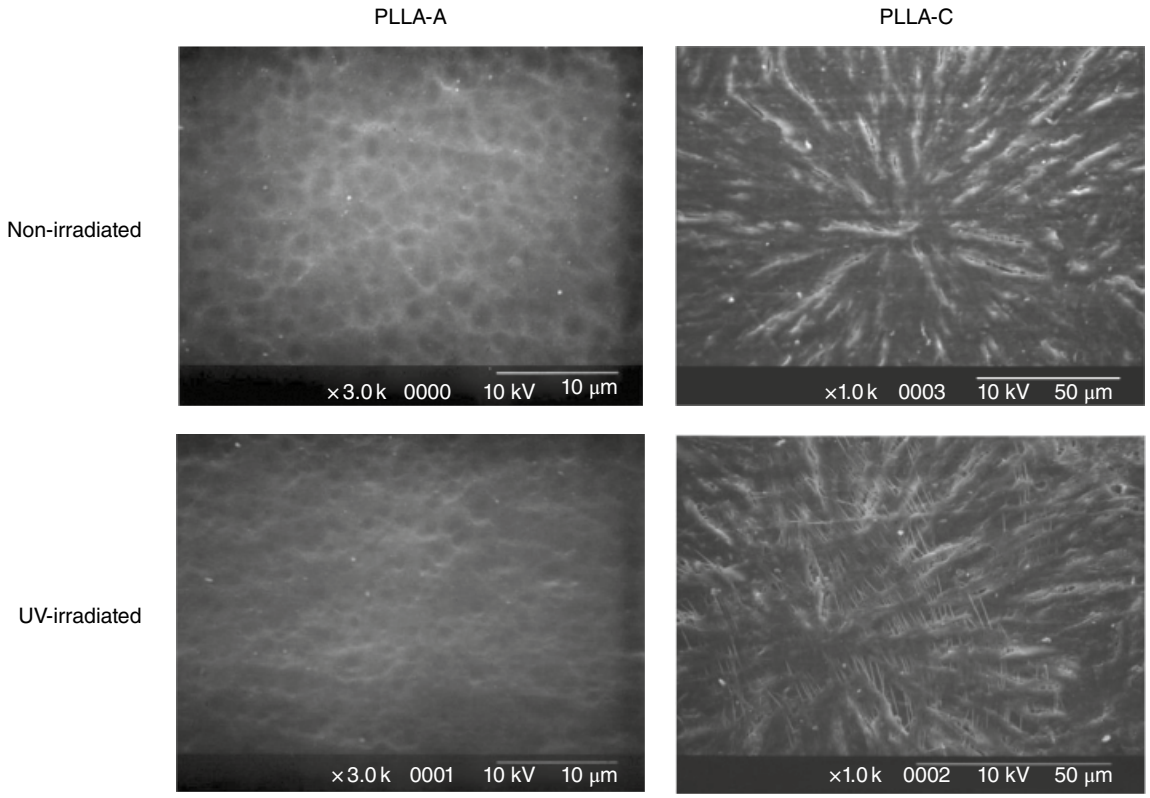


**FIGURE 19.14** SEM photographs of UV-irradiated (60 h) and nonirradiated (0 h) PLLA-A and PLLA-C films after enzymatic degradation for 10 h (PLLA-A films) and 60 h (PLLA-C films). Source: Reproduced from Ref. 30 with permission from Springer Science and Business Media.

irradiated with gamma and electron beam was studied by Benyathiar et al. using a direct measurement respirometric system to investigate the effect of radiation on biodegradation in a simulated aerobic compost environment [58]. Although no different biodegradability was observed between the samples irradiated with the same 30 kGy dose, the irradiated PLA samples stored for three, six, and nine months showed a decrease in averaged molecular weight and a faster biodegradation rate than the control sample significantly.

## 19.7 MODIFICATION AND COMPOSITES OF PLA

The PLA surface has low wettability and poor compatibility to cells due to its low hydrophibicity. Therefore, some attempts have been made to solve this problem by irradiation, such as ionized beam irradiation [59], UV/ozone irradiation [60], or oxygen radio frequency glow discharge [61]. It is also effective to reconstruct the surface of PLA chemically with hydrophilic molecules. UV-induced graft polymerization with hydrophilic monomers and additives can enhance the wettability and cytocompatibility [62–67]. On the other hand, the reduction of rainwater ingress through agricultural nets after hydrophobicity modification of polymer surfaces using photo-initiated chemical vapor deposition (PICVD) has been reported by Knoch et al. [68] Inagaki et al. attempted to modify the surface of PLA film by Ar-plasma, but the surface did not become hydrophilic and bubbles were observed [69]. Chen et al. obtained a long-chain branched (LCB) structure of PLA using a reactive extrusion process with adding multifunctional chemical agent, trimethylolpropane triacrylate (TMPTA), into the PLA matrix during extrusion [70]. The LCV-PLA had a fast crystallization rate, which may expand the use of PLA in some potential applications.

Since polymer composites that contain montmorillonite generally exhibit better physical properties and longer durability, a variety of montmorillonite composites were investigated also in PLA. The results showed that UV irradiation increased crystallinity [71], basic mechanical properties were improved/sustained in accelerated weathering [72], the number of molecular chain breaks in random scission in EB irradiation was reduced [73], and decreased thermal weight loss properties and *G*-value in γ-irradiation [74].

Carbon nanotubes (CNTs) have high electrical conductivity, thermal conductivity, and heat resistance, as well as the effect on nucleating crystallization. PLA nanocomposites containing CNTs showed increased crystallinity, lower tensile strength and strain at failure [75], higher glass transition and melting points, and increase the tortuosity pathway, which reduces the penetration of water molecules deeper into the polymer matrix [76]. The PLA composite with hybrid clay mineral-CNT was also investigated under UV light and it was found that, when 3 wt% of the additive was added to the samples, the 50% weight loss temperature of thermal degradation was reduced by about 10°C, which was further reduced by about 20°C after 300 h of UV irradiation [77].

Composites with nanosilver particles greatly suppressed the photodegradation of PLA due to the effect of light absorption of polyvinylpyrrolidone and scattering of nanoparticles in the nanoparticle coating [78, 79]. The thermal stability was reduced in the system irradiated with gamma-rays by adding zeolite [80], and the photo-oxidative degradation rate was accelerated when $CaSO_4$ was added [81].

PLA has poor thermal resistance above $T_g$. The essential method to improve the thermal durability of PLLA is to strengthen the intermolecular interactions between polymer chains. One of common solutions for this purpose for polymer materials is to induce cross-links in the matrix through photo-irradiation [82]. However, it is not suitable for PLA because of its own photodegradability by photo-irradiation and high-energy radiation. Recently, some successful attempts have been made to induce cross-linking by using EB on samples added with multifunctional molecules such as triallylisocyanurate or blended with other biodegradable polymer, or blended with other biodegradable polymers [83], or to stereocomplex of PLLA and poly(D-lactic acid) (PDLA) [84].

The use of PLA, as a reliable, low-cost and readily available high-dose dosimeter, was attempted by Nuñez and Galindo, and ESR signal response to $^{60}Co$ gamma-ray radiation on PLLA was investigated [85]. Although the irradiated PLA did not show a well-defined narrow-line ESR quartet as was reported by Babanalbandi above [52], the spectrum was well simulated by semi-empirical analysis using a second-order hyperfine coupling equation. As a result of test of signal fading, repeatability, homogeneity, limit, and so on, the accuracy of the PLA-ESR dosimeter was found to be comparable with other systems.

## REFERENCES

1. W. Schnabel, *Polymer Degradation: Principles and Practical Applications*, Hanser International, Munich, 1981, Chapters 4 and 5.
2. J. F. Rabek, *Photodegradation of Polymers: Physical Characteristics and Applications*, Springer, Berlin, 1996.
3. C. Zhang, C. Man, W. Wang, L. Jiang, Y. Dan, *Polym. Plast. Technol. Eng.* **2007**, *160*(2), 1042–1047.
4. E. C. Aguirre, F. I. Franco, H. Samsudin, X. Fang, R. Auras, *Adv. Drug Deliv. Rev.* **2016**, *107*(3), 333–366.
5. S. Teixeira, K. M. Eblagon, F. Miranda, M. F. R. Pereira, J. L. Figueiredo, *J. Carbon Res.* **2021**, *7*(2), 42–86.
6. F. A. Bovey, *The Effects of Ionizing Radiation on Natural and Synthetic High Polymers*, Interscience Publishers, New York, 1958.

7. Bond strengths in polyatomic molecules, in: R. C. Weast, M. J. Astle (Eds.), *CRC Handbook of Chemistry and Physics*, 58th edition, CRC Press, Boca Raton, FL, 1980, pp. F234–F237.
8. L. Yu-Ran, *Handbook of Bond Dissociation Energies in Organic Compounds*, CRC Press, Boca Raton, FL, 2002.
9. N. J. Turro, *Modern Molecular Photochemistry*, Benjamin/ Cummings Publishing, Menlo Park, CA, 1978.
10. R. L. Clough, S. W. Shalaby (Eds.), *Radiation Effects on Polymers, ACS Symposium Series 475*, ACS, Washington, DC, 1991.
11. A. Chapiro, *Radiation Chemistry of Polymeric Systems*, Wiley, New York, 1962.
12. W. Schnabel: *Polymer Degradation, Principles and Practical Applications*, Carl Hanser Verlag, München, 1981.
13. I. C. McNeill, H. A. Leiper, *Polym. Degrad. Stab.* **1985**, *11*(4), 309–326.
14. E. Ikada, *J. Photopolym. Sci. Technol.* **1997**, *10*(2), 265–269.
15. K.-L. G. Ho, A. L. Pometto III, *J. Environ. Polym. Degrad.* **1999**, *7*(2), 93–100.
16. A. Copinet, C. Bertrand, A. Longieras, V. Coma, Y. Couturier, *J. Polym. Environ.* **2003**, *11*(4), 169–179.
17. A. Copinet, C. Bertrand, S. Govindin, V. Coma, Y. Couturier, *Chemosphere* **2004**, *55*(5), 763–773.
18. H. Tsuji, Y. Echizen, Y. Nishimura, *Polym. Degrad. Stab.* **2006**, *91*(5), 1128–1137.
19. A. V. Janorkar, A. T. Metters, D. E. Hirt, *J. Appl. Polym. Sci.* **2007**, *106*(2), 1042–1047.
20. S. Belbachir, F. Zaïri, G. Ayoub, U. Maschke, M. N. Abdelaziz, J. M. Gloaguen, M. Benguediab, J. M. Lefebvre, *J. Mech. Phys. Solids.* **2010**, *58*(2), 241–255.
21. S. Bocchini, K. Fukushima, A. D. Blasio, A. Fina, A. Frache, F. Geobaldo, *Biomacromolecules.* **2010**, *11*(11), 2919–2926.
22. L. S. Blasco, R. Greus, R.G. Alamo, *Polym. Degrad. Stab.* **2013**, *98*(3), 771–784.
23. J. Rychlý, L. Rychlá, P. Stloukal, M. Koutný, S. Pekarová, V. Verney, A. Fiedlerová, *Polym. Degrad. Stab.* **2013**, *98*(12), 2556–2563.
24. S. T. Hsu, H. Tan, Y. L. Yao, *Polym. Degrad. Stab.* **2012**, *97*(1), 88–97.
25. B. D. Stępak, A. J. Antończak, K. Szustakiewicz, P. E. Kozioł, M. R. Wójcik, L. Lazarek, K. M. Proc. *SPIE* **2014**, *9286*, 928611.
26. B. D. Stępak, A. J. Antończak, K. Szustakiewicz, P. E. Kozioł, K. M. Abramski, *Polym. Degrad. Stab.* **2014**, *110*, 156–164.
27. S. Yada, M. Terakawa, *Opt. Express.* **2015**, *23*(5), 5694–5703.
28. A. Shibata, S. Yada, M. Terakawa, *Sci. Rep.* **2016**, *6*(1), 27884–27893.
29. Y. Li, A. Hayashi, M. Saito, M. Vacha, S. Murase, H. Sato, *Polym. J.* **2006**, *38*(4), 395–399.
30. H. Tsuji, Y. Echizen, Y. Nishimura, *J. Polym. Environ.* **2006**, *14*(3), 239–248.
31. N. Yasuda, Y. Wang, T. Tsukegi, Y. Shirai, H. Nishida, *Polym. Degrad. Stab.* **2010**, *95*(7), 1238–1243.
32. N. Yasuda, T. Tsukegi, Y. Shirai, H. Nishida, *Biomacromolecules* **2011**, *12*(9), 3299–3304.
33. W. Sakai, M. Kinoshita, M. Nagata, N. Tsutsumi, *J. Polym. Sci. Part A* **2001**, *39*(5), 706–714.
34. W. Sakai, T. Sadakane, W. Nishimoto, M. Nagata, N. Tsutsumi, *Polymer* **2002**, *43*(23), 6231–6238.
35. W. Sakai, K. Wakabayashi, H. Nishinaka, K. Kawamoto, M. Kinoshita, N. Tsutsumi, *Mater. Res. Soc. Symp. Proc.* **2002**, *708*, 39–44.
36. H. Tsuji, Y. Echizen, S. K. Saha, Y. Nishimura, *Macromol. Mater. Eng.* **2005**, *290*(12), 1192–1203.
37. R. G. F. Costa, G. S. Brichi, C. Ribeiro, L. H. C. Mattoso, *Polym. Bull.* **2016**, *73*(11), 2973–2985.
38. C. Man, C. Zhang, Y. Liu, W. Wang, W. Ren, L. Jiang, F. Reisdorffer, T. P. Nguyen, Y. Dan, *Polym. Degrad. Stab.* **2012**, *97*(6), 856–862.
39. N. Nakayama, T. Hayashi, *Polym. Degrad. Stab.* **2007**, *92*(7), 1255–1264.
40. Y. B. Luo, W. D. Li, X. L. Wang, D. X. Yu, Y. Z. Wang, *Acta. Mater.* **2009**, *57*(11), 3182–3191.
41. Y. B. Luo, X.L. Wang, Y. Z. Wang, *Polym. Degrad. Stab.* **2012**, *97*(5), 721–728.
42. Y. Luo, Y. Cao, G. Guo, *J. Appl. Polym. Sci.* **2018**, *135*(30), 46509.
43. H. Kaczmarek, M. Nowicki, I. V. Kwiatkowska, S. Nowakowska, *J. Polym. Res.* **2013**, *20*(3), 91–103.
44. A.M. T. Huerta, D. P. Ramirez, M.A. D. Crespo, D. D. A. Lopez, D. D. L. Fuente, *Eur. Polym. J.* **2014**, *61*, 285–299.
45. R. Malinowski, *J. Polym. Eng.* **2018**, *38*(7), 635–640.
46. J. Salač, J. Šera, M. Jurča, V. Verney, A. A. Marek, M. Koutný, *Materials* **2019**, *12*(3), 481.
47. M. C. Gupta, V. G. Deshmukh, *Polymer* **1983**, *24*(7), 827–830.
48. C. C. Chu, *Polymer* **1985**, *26*(4), 591–594.
49. C. Birkinshaw, M. Buggy, G. G. Henn, E. Jones, *Polym. Degrad. Stab.* **1992**, *38*(3), 249–253.
50. P. Benyathiar, S. E. Selke, B. R. Harte, D. K. Mishra, *J. Polym. Environ.* **2021**, *B*(2), 460–417.
51. M. Savaris, V. D. Santos, R.N. Brandalise, *Mater. Sci. Eng. C.* **2016**, *69*(1), 661–667.
52. A. Babanalbandi, D. J. T. Hill, J. H. O'Donnell, P. J. Pomery, A. Whittaker, *Polym. Degrad. Stab.* **1995**, *50*(3), 297–304.
53. K. Mäder, A. Domb, H. M. Swartz, *Appl. Radiat. Isot.* **1996**, *47*(11/12) 1669–1674.
54. O. Kantoglu, T. Ozbey, O. Guven, *Radiat. Phys. Chem.* **1995**, *46*(4–6), 837–841.
55. O. Kantoglu, O. Guven, *Nucl. Instrum. Methods Phys. Res. B* **2002**, *197*(3–4), 259–264.
56. H. J. Jeon, M. N. Kim, *Int. Biodeter. Biodegr.* **2013**, *85*, 289–293.
57. L. F. Vargas, B. A. Welt, P. Pullammanappallil, A. A. Teixeira, M. O. Balaban, C. L. Beatty, *Packag. Technol. Sci.* **2009**, *22*(2), 97–106.

58. P. Benyathiar, S. Selke, R. Auras, *J. Polym. Environ.* **2016**, *24*, 230–240.
59. H. Tsuji, H. Sasaki, H. Sato, Y. Gotoh, J. Ishikawa, *Nucl. Instrum. Methods Phys. Res. B* **2002**, *191*, 815–819.
60. G. H. Koo, J. Jang, *Fiber Polym.* **2008**, *9*(6), 674–678.
61. C. M. Alves, Y. Yang, D. Marton, D. L. Carnes, J. L. Ong, V. L. Sylvia, D. D. Dean, R. L. Reis, C. M. Agrawal, *J. Biomed. Mater. Res. B* **2008**, *87B*(1) 59–66.
62. Z. Ma, C. Gao, J. Ji, J. Shen, *Eur. Polym. J.* **2002**, *38*(11), 2279–2284.
63. Z. Ma, C. Gao, J. Shen, *J. Biomater. Sci. Polym. Ed.* **2003**, *14*(1), 13–25.
64. A. V. Janorkar, T. M. Andrew, E. H. Douglas, *Macromolecules* **2004**, *37*(24), 9151–9159.
65. T. Jiang, J. B. Chang, C. Wang, Z. Ding, J. Chen, J. Zhang, E.-T. Kang, *Biomacromolecules* **2007**, *8*(6), 1951–1957.
66. V. Gutierrez, H. Mario, M. G. Ulloa-Hinojosa, J. G. Gaona-Lozano, *J. Appl. Polym. Sci.* **2008**, *110*(1), 163–169.
67. R. M. Rasal, B. G. Bohannon, D. E. Hirt, *J. Biomed. Mater. Res. B* **2008**, *85B*(2), 564–572.
68. S. Knoch, F. Pelletier, M. Larose, G. Chouinard, M. J. Dumontc, J. R. Tavaresa, *Colloids. Surf. A.* **2020**, *598*, 124787.
69. N. Inagaki, K. Narushima, Y. Tsutsui, Y. Ohyama, *J. Adhes. Sci. Technol.* **2002**, *16*(8), 1041–1054.
70. C. Q. Chen, D. M. Ke, T. T. Zheng, G. J. He, X. W. Cao, X. Liao, *Ind. Eng. Chem. Res.* **2016**, *55*(3), 597–605.
71. A. Araújo, G. L. Botelho, M. Silva, A. V. Machado. *Mater. Sci. Eng. B.* **2013**, *3*(2), 75–83.
72. C. Kaynak, B. Sarı, *Appl. Clay. Sci.* **2016**, *121–122*, 86–94.
73. I. Zembouai, M. Kaci, S. Bruzaud, I. Pillin, J. L. Audic, S. Shayanfar, S. D. Pillai, *Polym. Degrad. Stab.* **2016**, *132*(5), 117–126.
74. Y. Yıldırıma, A. Oral, *Radiat. Phys. Chem.* **2014**, *96*, 69–74.
75. G. Gorrasi, A. Sorrentino, *Polym. Degrad. Stab.* **2013**, *98*(5), 963–971.
76. T. Vu, P. Nikaeen, W. Chirdon, A. Khattab, D. Depan, *Biomimetics* **2020**, *5*(4), 61–76.
77. G. Gorrasi, C. Milone, E. Piperopoulos, M. Lanza, A. Sorrentino, *Appl. Clay. Sci.* **2013**, *71*, 49–54.
78. M. Mucha, S. Bialas, H. Kaczmarek, *Res. J. Appl. Sci.* **2014**, *131*(8), 40144.
79. M. Mucha, S. Ksiazek, *J. Chem. Chem. Eng.* **2015**, *9*, 23–30.
80. Y. Yıldırım, A. Oral, *Radiat. Eff. Defect. Solids* **2018**, *173*(5–6) 435–445.
81. M. Gardette, S. Thérias, J. L. Gardette, M. Murariu. P. Dubois, *Polym. Degrad. Stab.* **2011**, *96*(4), 616–623.
82. N. Nagasawa, A. Kaneda, S. Kanazawa, T. Yagi, H. Mitomo, F. Yoshii, M. Tamada, *Nucl. Instrum. Methods Phys. Res. B* **2005**, *236*, 611–616.
83. P. H. S. Kumara, N. Nagasawa, T. Yagi, M. Tamada, *J. Appl. Polym. Sci.* **2008**, *109*(5), 3321–3328.
84. T. M. Quynh, H. Mitomo, L. Zhao, M. Tamada, *J. Appl. Polym. Sci.* **2008**, *110*(4), 2358–2365.
85. F. U. Nuñez and S. Galindo, *Rev. Mex. de Fís.* **2018**, *64*, 472–477.

# 20

# THERMAL DEGRADATION

Haruo Nishida

## 20.1 INTRODUCTION

Poly(L-lactide) (PLLA), prepared by the ring-opening polymerization of L,L-lactide (a cyclic dimer of L-lactic acid), is a well-known crystalline polymer [1–3]. This ring-opening polymerization is an equilibrium reaction, in which the concentration of the cyclic dimer is temperature dependent [4]. Therefore, the lactide is regenerated through the thermal depolymerization of PLLA [5]. Although the thermal degradation of PLLA using catalysts to obtain L,L-lactide is a simple reaction, the actual degradation is complex. For example, the activation energy of degradation, $E$, has been reported to change irregularly in a range of 70–270 kJ/mol as the degradation progresses [6–8]. Moreover, many degradation products have been detected during the pyrolysis of PLLA, especially cyclic oligomers and their diastereoisomers [6, 9]. These issues of complexity were described in a previous review [5]; since then a number of further studies have been carried out, but they have made little scientific progress toward understanding the thermal degradation of PLLA. In some recent papers, the thermal degradation of PLLA is said to be complicated by multiple reactions [10]. However, much of this perceived complexity results from a failure to use appropriate decomposition kinetic models for analyzing complex and multistep reactions. Some of these apparently intractable complications in thermal degradation behavior can be reasonably explained and simplified by analyzing the behavior of each elementary reaction separately and then combining them in a rational way.

In this section, the thermal degradation behavior of PLLA is reviewed and the apparent complexities in its degradation kinetics are discussed, followed by demonstration of how to untangle this complex behavior using the multistep complex reaction analysis method.

## 20.2 THERMAL DEGRADATION BEHAVIOR OF PLLA BASED ON WEIGHT LOSS

### 20.2.1 Diverse Mechanisms

The thermal degradation mechanism of PLLA is more complex than the simple reaction that produces lactides, in that significant amounts of other volatile degradation products are also generated during the thermal degradation process [9, 11, 12]. The thermal degradation mechanisms of PLLA have been reported by several groups (Figure 20.1) [6–9, 11–17].

McNeill and Leiper [9, 11] investigated the degradation of PLLA under both controlled heating and isothermal conditions, reporting that the main products were cyclic oligomers including lactides and other lower boiling point products, such as carbon dioxide, acetaldehyde, ketene, and carbon monoxide. They employed a first-order reaction kinetic equation to calculate the apparent $E$ value, reporting a value of 119 kJ/mol in the range of 240–270°C. Kopinke and co-workers [6, 12] reported a multistep process for PLLA pyrolysis. They found that intramolecular transesterification was a dominant degradation pathway, and that the pyrolysis behavior of pure PLLA differed from Sn-containing

*Poly(Lactic Acid): Synthesis, Structures, Properties, Processing, Applications, and End of Life*, Second Edition.
Edited by Rafael A. Auras, Loong-Tak Lim, Susan E. M. Selke, and Hideto Tsuji.

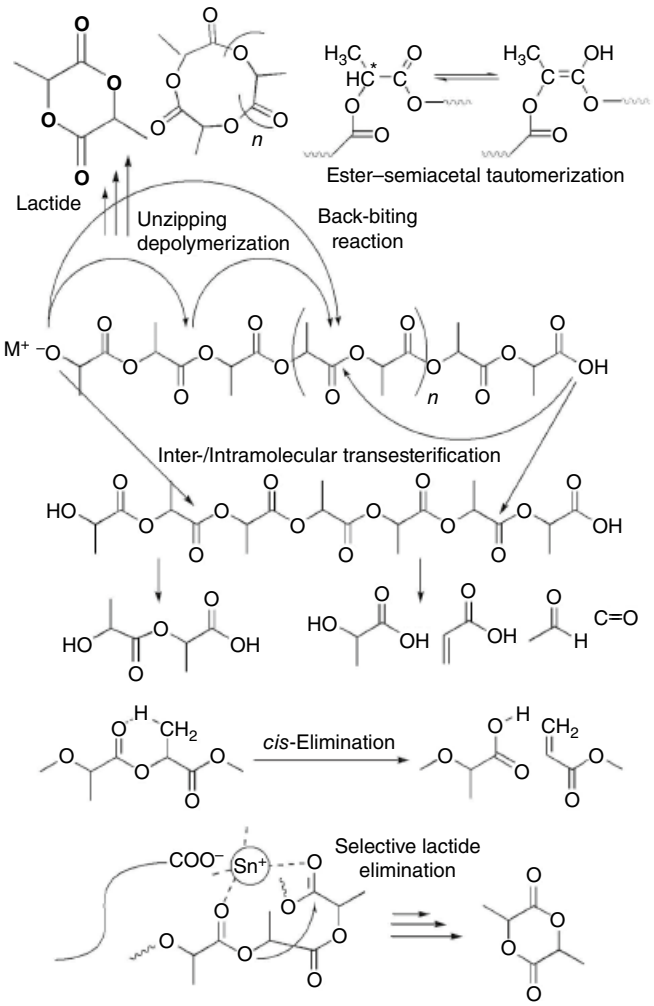


**FIGURE 20.1** Thermal degradation mechanisms of PLLA.

PLLAs. The effect of metal compounds on the pyrolysis behavior of PLLA was also reported by Cam et al. [13]. Babanalbandi et al. [7] reported that the *E* value for PLLA, determined using isothermal methods at 453, 473, 493, 513, 533, and 553 K, decreased from 103 to 72 kJ/mol with an increase in weight loss before increasing to 97 kJ/mol. They postulated that the PLLA degradation process followed complex kinetics, even at low conversion mass. Aoyagi et al. [8] also found that the *E* values changed in the range of 80–160 kJ/mol with weight loss, concluding that the pyrolysis of PLLA involved more than two mechanisms.

Chrissafis [10] reported the thermal degradation of a PLLA nanocomposite with oxidized multi-walled carbon nanotubes (MWCNTs-COOH). He found that as mass conversion progressed, there was a significant variation of *E* value, especially in the case of PLLA alone. He postulated that the decomposition of all the samples took place via a complex reaction involving the participation of at least two different mechanisms. When the experimental data were best fitted against theoretical models for PLLA and composite, an *n*th-order was the closest fit for the first mechanism and *n*th-order with autocatalysis closest fit for the second-mechanism with different *E* values. Unfortunately, the author was unable to support these empirical findings with a rational explanation for the autocatalytic mechanism.

Recently, Ye et al. [18] reported on using Zhuravlev-Lesokhin-Tempelman equation, based on a diffusion mechanism, known as $D_5$ function, to model the thermal decomposition of poly(lactic acid) (PLA) (D-lactate unit: 6%) and its composites with β-zeolite. The equation gave a minimal deviation over almost all the conversion range of pyrolysis of the PLA with β-zeolite composite. Unfortunately, they too were unable to provide a rational explanation linking kinetic analytical conclusions with decomposition products and chemical reaction mechanisms.

### 20.2.2 Factors Affecting the Thermal Degradation Mechanism

***20.2.2.1 Purification*** Thermal degradation behavior of rigorously purified hydroxyl- and carboxyl-end PLLA (PLLA-H) was investigated by means of thermogravimetric analysis (TGA), and pyrolysis-gas chromatography-mass spectrometry (Py-GC-MS) [19]. TGA data revealed that PLLA-H showed a high pyrolysis temperature range of 280–370°C. The apparent activation energy of the degradation reaction, estimated from the TGA curve, was found to be 176 kJ/mol. Kinetic studies indicated that PLLA-H degraded mainly through a random degradation reaction with $A = 2.0 \times 10^{12}\,s^{-1}$, as evidenced by thermal degradation products that included a large number of cyclic oligomers. The main reaction pathway for PLLA-H pyrolysis was regarded as random transesterification (Figure 20.1).

***20.2.2.2 Polymerization Catalyst Residue*** As mentioned in the previous review [5], polymerization catalysts, such as Sn, Zn, and Al compounds, have an extremely important influence on the thermal degradation of PLLA. The application of the Sn catalyst is of special importance because only Sn 2-ethylhexanoate ($Sn(Oct)_2$) is approved by the FDA as a catalyst for food-contact PLLA applications [20]. Reports on the effect of Sn-based catalysts on PLLA thermal degradation have been published by Noda et al. [21], Degée et al. [22], Cam and Marucci [13], Jamshidi et al. [16], Södergård and Näsman [23], Kopinke et al. [6], Zeng et al. [24], and Nishida et al. [25, 26]. However, despite the endeavors of the authors of these studies, many of the papers were unclear as to whether the degradation mechanism was a first-order reaction or a random scission.

To accurately analyze the effect of the Sn atom, our group studied the thermal degradation of PLLA with controlled Sn content in a range of 20–607 ppm [25]. The thermal

degradation of PLLA samples at constant heating rates using TGA indicated that increasing Sn content resulted in a lowering of degradation temperature range and a decrease in *E* value, which converged at about 120 kJ/mol. The kinetic analysis of the dynamic pyrolysis data indicated that the Sn-catalyzed pyrolysis started as random degradation and then shifted to a zero-order weight loss process.

Interestingly, Wachsen et al. [27] and Babanalbandi et al. [7] reported that degradation processes with *E* value of less than 100 kJ/mol were encountered. They suggested that the key to solving this problem lay in the active chain end of the as-polymerized PLLA. Kricheldorf et al. [28] reported that the polymerization of L,L-lactide most likely proceeds via the relatively reactive Sn-alkoxide group. Kricheldorf et al. further pointed out that these Sn-alkoxide groups will be transformed into $-CH(CH_3)-OH$ end-groups via alcoholysis or hydrolysis. Thus, the as-polymerized PLLA (PLLA-ap) and the PLLA precipitated with methanol (PLLA-pr) were prepared from polymerization products leaving an excess amount of Sn compound in the form of catalyst residue. From pyrolyzates and kinetic analyses [26], typical degradation mechanisms of Sn-containing PLLA could be determined, which showed that the thermal degradation reactions of PLLA-ap and PLLA-pr proceeded through a zero-order weight loss process with apparent *E* values of 80–90 and 120–130 kJ/mol, respectively. The possible thermal degradation mechanisms for PLLA-ap and PLLA-pr are the unzipping and intramolecular transesterification reactions caused by Sn-alkoxide chain ends, and the Sn-catalyzed selective lactide elimination caused by Sn-carboxylate chain ends, respectively (Figure 20.1). Both the pyrolysis of PLLA-ap and PLLA-pr produced L,L-lactide selectively. These degradation mechanisms and products are in stark contrast to those of PLLA-H, in which a large number of cyclic oligomers and their diastereoisomers were formed by random degradation.

***20.2.2.3 Thermal Degradation Catalysts*** Although organic tin compounds, especially $Sn(Oct)_2$, are effective catalysts for L,L-lactide production from PLLA [25], there are concerns regarding their toxicity to marine life, resulting in their worldwide ban by the International Maritime Organization. Thus, efforts to discover other catalysts for the depolymerization of PLLA are continuing.

In France, zinc metal has been used for many years as an industrial polymerization catalyst for lactides [29]. Abe et al. [30] who investigated the effects of Zn catalyst residues (diethyl zinc, $ZnEt_2$, and zinc didodecanoxide, $Zn(OD)_2$) reported that residual Zn compounds affected the thermal degradation of PLLA in a similar way to the Sn catalyst, with the outcome dependent on the Zn atom content.

Concerning other metals, it has been reported that when different kinds of metal compounds are blended with PLLA, its pyrolysis behavior can change substantially [13, 31, 32]. Noda et al. [31] and Cam et al. [13] evaluated the activity of various metal compounds as depolymerization catalysts for PLLA. Noda et al. [31] reported the order of activity being Sn > Zn > Zr > Ti > Al. On the other hand, a differing order of Fe > Al > Zn > Sn was reported by Cam et al. [13]. The inconsistency in these results may be attributable to different salts used in their studies.

Interestingly, aluminum hydroxide [$Al(OH)_3$] has been used not only as a polymerization initiator but also as a flame retardant for PLLA. Degée et al. [22] found that the as-polymerized ω-alkoxyaluminum-PLLA with $Al(-O-CH(CH_3)_2)_3$ had a thermal stability comparable to purified PLLA. On the other hand, a large amount (~50 wt%) of $Al(OH)_3$ is required to achieve adequate flame resistance for the PLLA/$Al(OH)_3$ composite [33]. The effects of $Al(OH)_3$ on the thermal degradation of PLLA composites have also been investigated. It was found that at temperatures lower than 250°C, the thermal stability of the composite was improved [34]. This stabilization makes the melt processing of the composite easier than PLLA-ap. Nevertheless, at 250–300°C the depolymerization of PLLA to lactides proceeded selectively by converting PLLA into L,L-lactide with $Al(OH)_3$ acting as a catalyst for the unzipping reaction.

Ideally, the depolymerization catalyst of PLLA should be first of all nontoxic. Secondly, it should be effective in small quantities and capable of selectively converting PLLA to the cyclic dimer L,L-lactide, without causing racemization. One such candidate, discovered after extensive searching, is magnesium oxide (MgO) [19, 35], which appears safe, lowers the degradation temperature range of PLLA, completely suppresses the production of oligomers other than lactides, and avoids the racemization of lactide at temperatures lower than 270°C. When compared to the racemization that occurs with CaO, the anti-racemization effect of MgO is striking, which can be attributed to the lower basicity of Mg than Ca. Furthermore, the catalytic effectiveness of MgO was found to increase with increasing surface area and with the inactivation of the abnormal chemical structures other than the normal $-Mg-O-Mg-O-$ on the solid surface [36, 37].

### 20.2.3 Thermal Stabilization

Södergards et al. [38, 39] reported on the stabilization of Sn-rich PLLA with various types of peroxides. Since the binding energy for electrons in the Sn 3d level increased for PLLA, the stabilization mechanism involves deactivation of the species that catalyze the reversible esterification reaction.

Yuzay et al. [40] reported that PLLA composites including two types of zeolite (5 wt%) showed a complex reaction behavior over lower conversion levels (2.5–10%) and suggested the presence of a complex reaction (multistep reaction) mechanism. Hao and Huang [41] also studied the influence of two different zeolites in PLLA through thermogravimetric

analysis. The thermal degradation features of PLLA/zeolite composites were compared in terms of degradation temperatures and activation energy $E$ value. Calculations indicated that the addition of zeolite-rendered PLLA more thermally stable, requiring higher $E$ values for thermal degradation. On the other hand, Chiang and Wu [42] reported that nanocomposites of PLLA and magnesium/aluminum-layered double hydroxide (MgAl-LDH) reduced the thermal degradation temperature of PLLA. They suggested the presence of complex reaction such as depolymerization and/or inter- and intramolecular transesterification reactions.

Unfortunately, the details of the stabilization mechanism and the kinetic analysis were not clear in these reports.

## 20.3 KINETIC ANALYSIS OF THERMAL DEGRADATION

In order to analyze the complex thermal degradation of polymers kinetically, many kinetic analysis methods have been developed. These methods using different approaches (model-fitting and model-free) have been proposed to determine kinetic parameters. Recently, the model-fitting method using an empirical kinetic model function known as the Sesták-Berggren model [43], which accommodates the physico-chemical and physico-geometrical kinetic models, has been applied to analyze the complex thermal degradation behaviors of PLLA [44–46]. Unfortunately, the kinetic parameters obtained using the Sesták-Berggren equation are often do not have a clear meaning of the degradation mechanism of polymers. Therefore, here, dynamic analysis methods using the kinetic parameters that have clear meanings of the decomposition reaction mechanisms of PLLA is treated.

### 20.3.1 Single-Step Thermal Degradation Process

Thermogravimetry has been used for the analysis of the polymer degradation with remaining weight ratio ($w$), from which the kinetic parameters, such as activation energy ($E$), order of reaction ($n$), and pre-exponential factor ($A$), are determined. Different kinetic models have been developed to analyze the thermogravimetric data with considerable different parameter values [47–58]. The kinetics of thermal degradation have generally been studied using both isothermal and non-isothermal methods. In the earlier literature, isothermal methods were mostly employed for the study of the kinetics of molten-state reactions. During the past four decades, however, non-isothermal methods, for example, the Doyle method [49, 50], Freeman and Carroll method [51], Coats and Redfern method [53], Ozawa method [54], Flynn and Wall method [55, 56], Friedman method [52], Kissinger method [48], and Nishida method [58], have received more attention.

The generalized kinetic expression for the non-isothermal methods is as follows:

$$-\frac{\mathrm{d}w}{\mathrm{d}T}=\left(\frac{A}{\varphi}\right)\exp\left(\frac{-E}{RT}\right)f(w) \tag{20.1}$$

where $\varphi = (\mathrm{d}T/\mathrm{d}t)$ is the heating rate and $f(w)$ is a function representing the reaction model. The specific form of $f(w)$ depends on the type of kinetic process, but usually takes the form $w^n$, where $n$ is the order of reaction. To evaluate the $n$ value for pyrolysis by the differential method, $-\mathrm{d}w/\mathrm{d}T$ is plotted against $(1-w)$ based on Equation 20.1. The plot is then compared with plots for the model reactions, i.e., zero, half, first, and second-order reactions, and random degradation [20]. For random degradation, the least number of repeating units of the residual polymer ($L$) is the variable for the model simulation [47, 58].

The integration value, $-\int \mathrm{d}w/f(w)$, is expressed as follows:

$$-\int\frac{\mathrm{d}w}{f(w)}=\frac{AE}{\varphi Rp(y)}=A\theta \tag{20.2}$$

where $\theta = E/\varphi Rp(y)$ is the "reduced time" [54]. The integral $-\int \mathrm{d}w/f(w)$ has been given by Simha et al. [47] and Ozawa [54], e.g., $-\int \mathrm{d}w/f(w) = 1-w$, $2(1-w^{1/2})$, $-\ln w$, $1/w-1$, and $-\ln\{1-(1-w)^{1/2}\}$ for zero, half, first, second-order reactions, and random degradation ($L=2$), respectively, as model reactions. In the method of integration, the observed remaining weight ratio value $w$ is plotted against $A\theta$ and compared with the model reactions to determine the kinetic parameters.

The methods of differentiation and integration are effective for analyzing the main reactions but are of little use during the early period in the lower range of $(1-w)$. This is because, despite all the model reaction plots being either increasingly or decreasingly curved, they have the same starting point and similar gradients in the early stages with insufficient resolution to distinguish them [5, 59].

For all random reactions, the general relationship between $L$ and $w$ is derived from Equation 20.3 [58].

$$\ln\left\{1-\left(1-w\right)^{1/2}\right\}=-\frac{L}{2}A\theta+\ln\left\{e^{(L/2)A\theta}-\left(e^{LA\theta}-Le^{A\theta}+L-1\right)^{1/2}\right\} \tag{20.3}$$

When $L=2$,

$$\ln\left\{1-\left(1-w\right)^{1/2}\right\}=-A\theta \tag{20.4}$$

$$\ln\left[-\ln\left\{1-\left(1-w\right)^{1/2}\right\}\right]=\ln A\theta=\ln\frac{AE}{\varphi R}-a'-b'\frac{E}{RT}\propto\frac{1}{T} \tag{20.5}$$

where $a'$ and $b'$ are constants. In contrast to Equation 20.2, the plot generated by Equation 20.3 random degradation was distinguishable from the *n*th-order reactions even in the problematic low temperature range. This advantage can be attributed to the fact that with Equation 20.3, all the random degradation models give nearly linear and parallel plots over the whole temperature range with a gradient different from the *n*th-order model reaction curves.

### 20.3.2 Complex Thermal Degradation Process

Equations 20.6 and 20.7 have been proposed by Flynn and Wall [56] for the analysis of complex thermal degradation behavior consisting of two first-order degradation reactions showing weight loss according to the progress of the reaction:

When two first-order reactions compete with each other:

$$w=\exp\left[-\frac{A_1E_1}{\varphi R}p\left(x_1\right)-\frac{A_2E_2}{\varphi R}p\left(x_2\right)\right] \tag{20.6}$$

When two first-order reactions occur independently:

$$w=a\left[\exp\left(-\frac{A_1E_1}{\varphi R}p\left(x_1\right)\right)\right]+\left(1-a\right)\left[\exp\left(-\frac{A_2E_2}{\varphi R}p\left(x_2\right)\right)\right] \tag{20.7}$$

where $A$, $E$, $R$, $\varphi$, $p(x)$, and $a$ are the frequency factor, activation energy, gas constant, heating rate, $\int(e^{-x}/x^2)\,dx(x = E/RT)$, and $w_{1,0}/w_0$, respectively. The complex formulas for the two degradation reactions can be applied only to the reaction combinations involving first-order kinetics. However, in the case of *n*th-order degradation reactions, the more generalized formulas are shown in Equations 20.8 and 20.9 [60, 61]. In these general formulas for two-step complex reactions, the preferential reaction is determined according to the kinetic parameters of each reaction. Therefore, in the case of competitive complex reactions, when the kinetic parameters are significantly different, it is only the preferential reaction that is observable.

When two *n*th-order reactions compete with each other:

$$\begin{aligned}&-\int\frac{dw}{f\left(w\right)}=\frac{A_1E_1}{\varphi R}p\left(x_1\right)+\frac{A_2E_2}{\varphi R}p\left(x_2\right)=A_1\theta_1+A_2\theta_2\\&-\int\frac{dw}{f\left(w\right)}=-\int\frac{dw}{w^n}=-\ln w\quad\left(n=1\right),\frac{1}{n-1}\left(w^{1-n}-1\right)\left(n\neq1\right)\end{aligned} \tag{20.8}$$

When two *n*th-order reactions occur independently:

$$\begin{aligned}&-\int\frac{d\left(w_1/a\right)}{f\left(w_1/a\right)}=\frac{A_1E_1}{\varphi R}p\left(x_1\right)=A_1\theta_{1,a},\\&-\int\frac{d\left(w_2/b\right)}{f\left(w_2/b\right)}=\frac{A_2E_2}{\varphi R}p\left(x_2\right)=A_2\theta_{2,b}\\&a=\frac{w_{1,0}}{w_0},b=1-a\\&-\int\frac{d\left(w\right)}{f\left(w\right)}=-\int\frac{d\left(w_1/a\right)}{f\left(w_1/a\right)}-\int\frac{d\left(w_2/b\right)}{f\left(w_2/b\right)}=A_1\theta_{1,a}+A_2\theta_{2,b}\\&-\int\frac{d\left(w_1/a\right)}{f\left(w_1/a\right)}=-\ln\left(w_1/a\right)\ \left(n=1\right),\frac{1}{n-1}\left[\left(w_1/a\right)^{1-n}-1\right]\\&\qquad\qquad\qquad\qquad\qquad\qquad\qquad\qquad\left(n\neq1\right)\end{aligned} \tag{20.9}$$

Furthermore, the general formulas of the multistep complex reactions are derived as follows [62]:

Multistep competitive complex reactions:

$$\begin{aligned}-\int\frac{dw}{f\left(w\right)}&=\frac{A_1E_1}{\varphi R}p\left(x_1\right)+\frac{A_2E_2}{\varphi R}p\left(x_2\right)+\frac{A_3E_3}{\varphi R}p\left(x_3\right)+\cdots\\&=A_1\theta_1+A_2\theta_2+A_3\theta_3+\cdots\end{aligned} \tag{20.10}$$

Multistep independent complex reactions:

$$\begin{aligned}&-\int\frac{d\left(w\right)}{f\left(w\right)}=-\int\frac{d\left(w_1/a\right)}{f\left(w_1/a\right)}-\int\frac{d\left(w_2/b\right)}{f\left(w_2/b\right)}-\int\frac{d\left(w_3/c\right)}{f\left(w_3/c\right)}+\cdots\\&\qquad=A_1\theta_{1,a}+A_2\theta_{2,b}+A_3\theta_{3,c}+\cdots\\&-\int\frac{d\left(w_1/a\right)}{f\left(w_1/a\right)}=\frac{A_1E_1}{\varphi R}p\left(x_{1,a}\right)=A_1\theta_{1,a}\\&-\int\frac{d\left(w_2/b\right)}{f\left(w_2/b\right)}=\frac{A_2E_2}{\varphi R}p\left(x_{2,b}\right)=A_2\theta_{2,b}\\&-\int\frac{d\left(w_3/c\right)}{f\left(w_3/c\right)}=\frac{A_3E_3}{\varphi R}p\left(x_{3,c}\right)=A_3\theta_{3,c}\\&a=\frac{w_{1,0}}{w_0},\ \ b=\frac{w_{2,0}}{w_0},\ \ c=\frac{w_{3,0}}{w_0},\ \ a+b+c+\cdots=1\end{aligned} \tag{20.11}$$

Yoshikawa et al. [63] introduced the similar formula of the multistep independent complex reaction as follows:

$$\begin{aligned}&\frac{d\alpha}{dt}=\sum_{i=1}^{N}c_iA_i\exp\left(-\frac{E_i}{RT}\right)f_i\left(\alpha_i\right)\quad\text{with}\quad\sum_{i=1}^{N}c_i=1\\&\qquad\text{and}\quad\sum_{i=1}^{N}c_i\alpha_i=\alpha\end{aligned} \tag{20.12}$$

where $c_i$, $A_i$, $E_i$, and $f_i(\alpha_i)$ are the relative contribution, the Arrhenius pre-exponential factor, the apparent activation

energy, and the kinetic model function, respectively, of each reaction stage $i$ for a total of $N$ stages.

In addition, the general formula, in which the competitive and independent reactions are combined, is expressed as follows:

$$-\int \frac{\mathrm{d}(w)}{f(w)} = \left( -\int \frac{\mathrm{d}(w_1/a)}{f(w_1/a)} - \int \frac{\mathrm{d}(w_2/a)}{f(w_2/a)} + \cdots \right) - \int \frac{\mathrm{d}(w_3/b)}{f(w_3/b)} - \int \frac{\mathrm{d}(w_4/c)}{f(w_4/c)} + \cdots = \left(A_1\theta_{1,a} + A_2\theta_{2,a}\right) + A_3\theta_{3,b} + A_4\theta_{4,c} + \cdots \quad (20.13)$$

## 20.4 KINETIC ANALYSIS OF COMPLEX THERMAL DEGRADATION BEHAVIOR

### 20.4.1 Two-Step Complex Reaction Analysis of PLLA in Blends

One common way to improve the properties of PLLA is through the formation of polymer blends and alloys. Many polymers have been used for making these blends and alloys such as polyethylene (PE) [64], polypropylene (PP) [65], polystyrene (PS) [66], poly(methyl methacrylate) [67], bisphenol-A polycarbonate, poly(ε-caprolactone), poly(3-hydroxybutyrate), poly(butylene succinate) (PBS) [68], poly(butylene succinate/adipate) (PBSA), and acrylonitrile-butadiene-styrene (ABS). Despite the fact that some of these PLLA blends/alloys have been commercialized, the thermal degradation behavior of the PLLA component remains elusive.

To achieve selective depolymerization of the PLLA component, polymer blends of PLLA with linear low-density polyethylene (LLDPE) [69, 70], PS [71], PBS [72], and PBSA [72] were prepared and thermally degraded with and without a catalyst. TGA curves of the blends showed two-step weight-loss profiles, in which specific catalysts, such as MgO and $Al(OH)_3$, promoted the PLLA depolymerization selectively, shifting the temperature range for the PLLA component (Figure 20.2) [61].

To clarify the influence of the co-existing polymer, the thermal degradation profiles were analyzed kinetically. From the results, it was found that, even in the presence of MgO and/or $Al(OH)_3$, the presence of LLDPE, PS, and PBS had no effect on the depolymerization behavior of PLLA. Moreover, PLLA was effectively depolymerized into L,L-lactide with a low racemization ratio.

In order to simulate the thermal degradation behavior shown in Figure 20.2 for the PLLA/PS blend, the two-step independent complex reaction given by Equation 20.9 was applied. Analytical results are shown in Figure 20.3 [62]. The measured TGA profile of the PLLA/PS blend was compared with various simulation curves that were produced

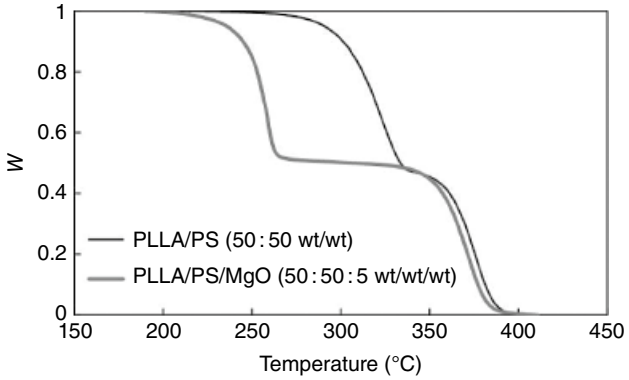


**FIGURE 20.2** Thermogravimetric curves of PLLA/PS (50 : 50 wt/wt) and PLLA/PS/MgO (50 : 50 : 5 wt/wt/wt) at 1 K/min in a constant nitrogen flow (100 mL/min) [61].

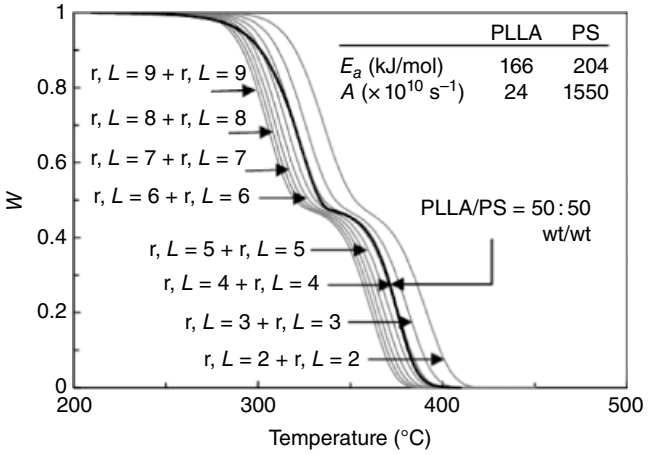


**FIGURE 20.3** TGA profile of PLLA/PS (50 : 50 wt/wt) at 1 K/min in a constant nitrogen flow (100 mL/min) and simulation curves of two-step independent complex reactions [62].

using different kinetic parameters. By comparing a range of simulation curves, the curve (r, $L = 4$ + r, $L = 4$) that combines two random degradation reactions for both components provided a good fit.

In a similar manner, the thermal degradation behavior of a PLLA/PS/MgO blend shown in Figure 20.2 was reproduced by kinetics simulation using Equation 20.9. Analytical results are shown in Figure 20.4 [62]. The simulation curve (1: $n = 0 + 2$: r, $L = 4$) that combines a zero-order degradation reaction of the PLLA component with a random degradation reaction (r, $L = 4$) of the PS component predicted the TGA profile well. Here, the zero-order degradation reaction refers to depolymerization from chain ends by an unzipping reaction.

Comparing the results shown in Figures 20.3 and 20.4, it can be seen that the addition of MgO causes a change in the thermal degradation behavior of the PLLA component by shifting it from the random degradation to the zero-order depolymerization reaction. In other words, it is clear that MgO

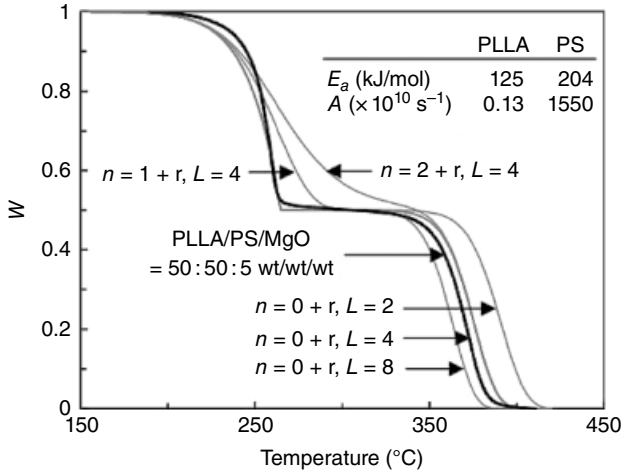


**FIGURE 20.4** TGA profile of PLLA/PS/MgO = 50 : 50 : 5 (wt/wt/wt) at 1 K/min in a constant nitrogen flow (100 mL/min) and simulation curves of two-step independent complex reactions [62].

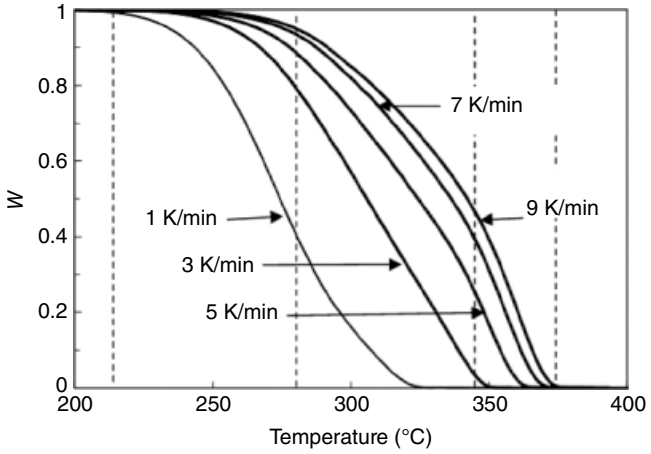


**FIGURE 20.5** TGA profiles of commercially available PLLA measured at various heating rates: 1, 3, 5, 7, and 9 K/min under nitrogen flow of 100 mL/min.

functions as an unzipping depolymerization catalyst that continuously decomposes PLLA into lactide units from the end of molecular chains. On the other hand, MgO has no effect on the thermal degradation of the PS component. From these results, it was found that the presence of MgO had no catalyzing effect on the co-existing polymer PS. Hence, there was no detrimental impact on the effectiveness of the depolymerization of PLLA into L,L-lactide with a low racemization ratio.

### 20.4.2 Multistep Complex Reaction Analysis of Commercially Available PLLA

Commercially available PLLA contains a trace amount of Sn-based polymerization catalyst, which complicates the thermal degradation behavior of PLLA. Figure 20.5 shows TGA profiles measured at different heating rates of 1, 3, 5, 7, and 9 K/min in a nitrogen gas flow [73]. As the heating rate was increased, the TGA profile shifted to the higher temperature side. In addition, the shape of the TGA profile gradually changed with increasing heating rate. The results shown in Figure 20.5 suggest that different modes of thermal degradation proceeded in at least three temperature zones: 215–280, 280–345, and 345–375°C.

Figure 20.6 shows the change in activation energy $E$ value of thermal degradation versus remaining weight $w$ of commercially available PLLA. As the remaining weight $w$ decreased, the $E$ value decreased at first and then started to increase. These changes in $E$ value replicate the results previously reported by Babanalbandi et al. [7]. The specific change in $E$ value suggests that at least three different reactions having different $E$ values proceeded either in combination or successively with the degradation reaction or increase in temperature.

To infer the three degradation reactions that cause changes in the shape of the TGA profile and $E$ value, kinetic analysis was performed by the random decomposition analysis method

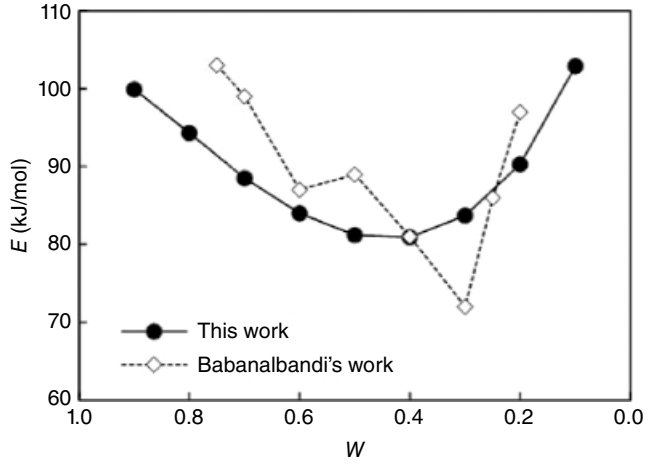


**FIGURE 20.6** Changes in $E$ value on thermal degradation of commercially available PLLA. Results of this work and Babanalbandi's work [7].

using Equation 20.3. The relationships between $\ln[-\ln\{1-(1-w)^{1/2}\}]$ vs $1/T$ for the random degradation and the $n$th-order model reactions (zero-, half-, first-, and second-order reactions) are plotted in Figure 20.7. From the results, it was speculated that commercially available PLLA tended to proceed by random decomposition (r, $L$ = 4) in the early stage of thermal decomposition at a lower temperature range, then shifted to an $n$th-order reaction in the middle stage, and finally returned to random decomposition with other $L$ values at a higher temperature range.

***20.4.2.1 Multistep Independent Complex Reaction Analysis*** The result in Figure 20.7 was reconfirmed by analysis using Equation 20.11 for multistep independent/competitive complex reactions. The analyzed results are shown in Figures 20.8 through 20.11. In Figure 20.8, the

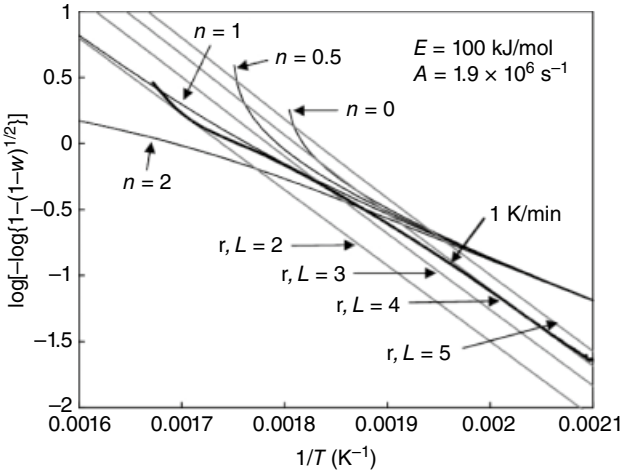


**FIGURE 20.7** Plots of $\log\{-\log[1-(1-w)^{0.5}]\}$ vs 1/T for thermogravimetric data of commercially available PLLA at a heating rate of 1 K/min and for model reactions using the following kinetic parameters: $E = 100$ kJ/mol and $A = 1.9 \times 10^9$ s$^{-1}$. Model reactions: zero order ($n = 0$), first order ($n = 1$), and second order ($n = 2$), and random degradations (r, $L = 2$–4).

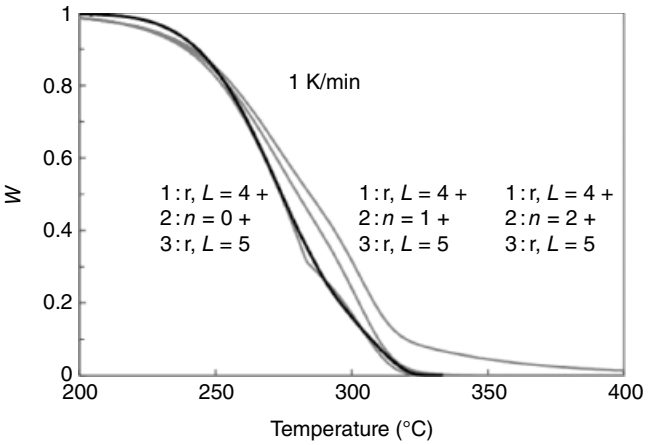


**FIGURE 20.8** TGA profile of commercially available PLLA at a heating rate of 1 K/min and simulation curves of three-step independent complex reactions.

TGA profile measured at a heating rate of 1 K/min was compared with typical simulation curves produced with different kinetic parameters. From this comparison, the simulation curve consisting of three reactions (each weight fractions: 0.3, 0.4, and 0.3), i.e., a random degradation (r, $L = 3$), a zero-order weight loss, and a random degradation (r, $L = 5$), were found to closely match the measured profile. Thus, it was confirmed that the measured profile ($\varphi = 1$ K/min) was reproduced well by the simulation plot of the complex reaction (1; r, $L = 4 + 2$; $n = 0 + 3$; r, $L = 5$).

Next, in Figure 20.9, the profile measured at a heating rate of 5 K/min was also compared with various simulation curves. From these curves, assuming the weight fractions by 0.25, 0.4, and 0.35, the simulation curve consisting of the

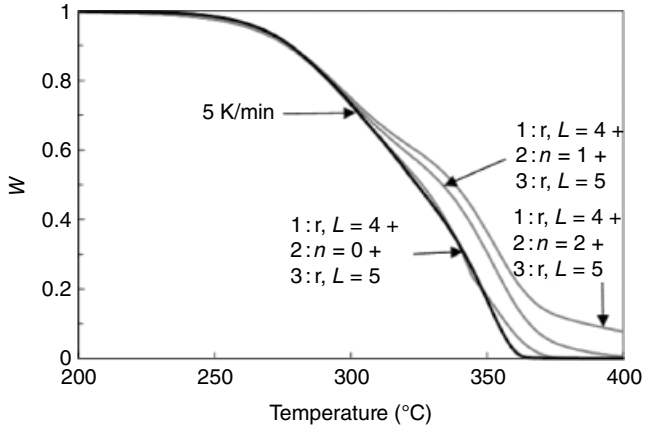


**FIGURE 20.9** TGA profile of commercially available PLLA at a heating rate of 5 K/min and simulation curves of three-step independent complex reactions.

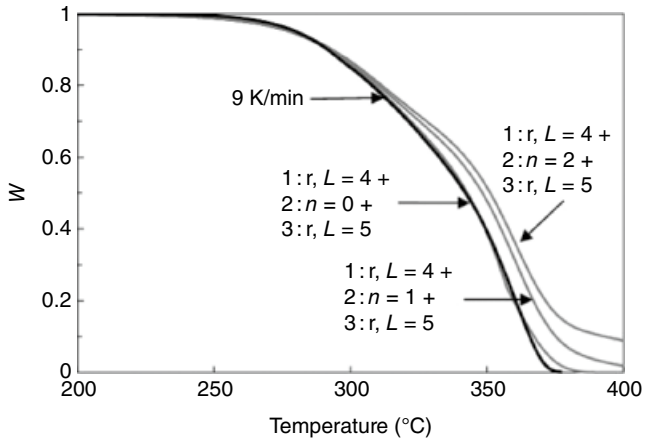


**FIGURE 20.10** TGA profile of commercially available PLLA at a heating rate of 9 K/min and simulation curves of three-step independent complex reactions.

same three reactions (1: r, $L = 4 + 2$: $n = 0 + 3$: r, $L = 5$) was found to closely reproduce the measured profile by using specific kinetic parameter $A$ values. These three reactions gave a simulation curve that matched well with the profile measured at the heating rate of 1 K/min.

Finally, in Figure 20.10, the profile measured at a heating rate of 9 K/min was also compared with various simulation curves in a similar manner. From these curves, assuming the weight fractions of 0.2, 0.35, and 0.45, the simulation curve consisting of the same three reactions (1; r, $L = 4 + 2$; $n = 0 + 3$; r, $L = 5$) with the specific kinetic parameter $A$ values was found to closely reproduced the measured profile.

Table 20.1 lists the kinetic parameters $E$, $A$, $n$, and $L$ values of the best matched simulation curves with the TGA profiles measured at heating rates of 1, 5, and 9 K/min. These quantitative results demonstrate that the thermal degradation behavior of commercially available PLLA consists of at least three different reactions, and that the composition ratio

**TABLE 20.1 List of Kinetic Parameters of Thermal Degradation Simulation Curves of Commercially Available PLLA with a Three-Step Independent Complex Reaction**

| | $\varphi$ (K/min) | First | Second | Third |
|---|---|---|---|---|
| Composition | 1 | 0.3 | 0.4 | 0.3 |
| | 5 | 0.25 | 0.4 | 0.35 |
| | 9 | 0.2 | 0.35 | 0.45 |
| $E$ (kJ/mol) | | 100 | 81 | 175 |
| $n$; random (r), $L$ | | r, $L = 4$ | $n = 0$ | r, $L = 5$ |
| $A$ ($s^{-1}$) | 1 | $1.9 \times 10^6$ | $2.4 \times 10^4$ | $5.5 \times 10^{12}$ |
| | 5 | $3.0 \times 10^6$ | $1.8 \times 10^4$ | $1.2 \times 10^{12}$ |
| | 9 | $3.2 \times 10^6$ | $2.3 \times 10^4$ | $1.4 \times 10^{12}$ |

of each reaction stage changes with the heating rate and the temperature range.

Kameno et al. [44] also studied the thermal degradation behavior of PLLA oligomer (PLAO) involved two partially overlapping mass-loss steps by using Equation 20.12. They reported that the first mass-loss step was the diffusional transfer of lactides from the reaction sites to the top surface of the molten PLAO as the rate-limiting step, and in the second mass-loss step, the overall rate behavior was largely influenced by the bubbling phenomena of degradation products. They analyzed the mass-loss behaviors using the empirical kinetic model function: Sesták-Berggren model SB($m$, $n$, $p$), $f(\alpha) = \alpha^m(1-\alpha)^n[-\ln(1-\alpha)]^p$. As results, they obtained two sets of optimized kinetic parameters ($m$, $n$, and $p$) values: (−0.56, 0.55, −0.32) and (−0.97, 1.21, 1.21) for first and second steps, respectively. They suggested that the physico-geometrical events influenced in the rate behavior of the thermal degradation of PLLA.

***20.4.2.2 Multistep Competitive Complex Reaction Analysis*** The simulations described in above section assume that each elementary reaction proceeds independently. However, it is conceivable that the actual thermal degradation reactions proceed competitively or sequentially. When the reaction proceeds sequentially, it is likely to exhibit a weight loss behavior similar to the independent complex reactions. On the other hand, there is a possibility that the three reactions proceed competitively. Figure 20.11 shows the TGA profile measured at $\varphi = 1$ K/min with typical simulation curves produced by using Equation 20.10 for the multistep competitive complex reactions. It can be seen that the TGA profile measured at $\varphi = 1$ K/min could be reproduced by the competitive complex reactions consisting of random ($L = 4$), first-order ($n = 1$), and random ($L = 5$) reactions. However, it was found that the TGA profiles measured at $\varphi = 5$ and 9 K/min could not easily be reproduced.

Therefore, the seemingly complex thermal degradation behavior of commercially available PLLA was simulated well by using the multistep complex reaction analysis method, and it was postulated that the thermal decomposition behavior

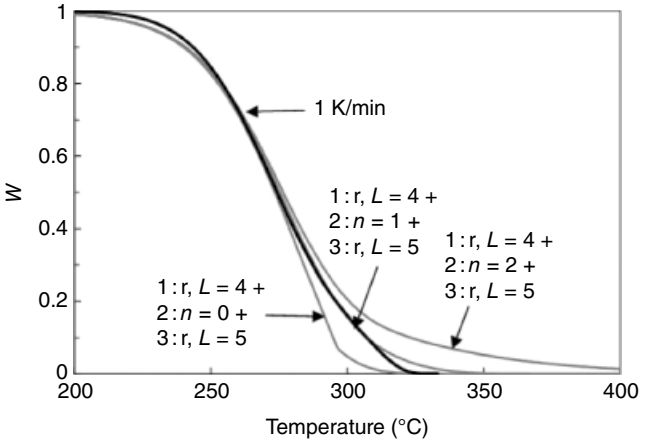


**FIGURE 20.11** TGA profile of commercially available PLLA at a heating rate of 1 K/min and simulation curves of three-step competitive complex reactions.

mainly involved three different decomposition reactions proceeding independently or sequentially. Finally, the multistep complex reaction analysis was found to be effective not only in modeling PLLA degradation but also in the analysis of thermal degradation behaviors of other polymers, blends, alloys, and composites.

## 20.5 THERMAL DEGRADATION BEHAVIOR OF PLA STEREOCOMPLEX: scPLA

An equivalent mixture of optically pure PLLA and PDLA having the same melting point of about 175°C [74] forms a stereocomplex poly(lactic acid) (scPLA), which has a higher melting point (~245°C) than those of pure PLLA and PDLA [75, 76]. It is well known that the scPLA has some properties that are superior to PLA. However, since PLA can easily be hydrolyzed and have poor thermal and photostability, the characteristic degradabilities of such PLA are important in determining how molten scPLA should be processed without causing serious thermal decomposition.

Some reports on the thermal degradation of scPLA have been published [77–83]. Tsuji et al. [77] investigated the thermal degradation of scPLA and found that its enhancement of thermal stability was due to the peculiarly strong interaction between PLLA and PDLA chains even when they are in the melt. The activation energies for thermal degradation were evaluated in a weight loss range of 25–90% on TGA profiles, resulting in 205–297 (scPLA), 77–132 (PLLA), and 155–242 kJ/mol (PDLA). The differences among scPLA, PLLA, and PDLA are considered to be due to differences in both residual Sn contents and numbers of terminal groups acting as starting points of the degradation. Li et al. [83] reported that the molecular weight of PLA displayed significant effects on the thermal performance of scPLA, indicating the improved thermal resistance of high-molecular-weight scPLA. Ajiro

et al. [80] reported that the simultaneous improvement of the melting temperature and the thermal decomposition temperature of poly(lactide)s was achieved by the stereocomplex formation of PLLA and PDLA with aromatic groups at both initiating and terminating chain ends, suggesting that the conjugation of 3,4-diacetoxycinnamic acid at chain ends and the π–π stacking interaction between the aromatic groups contribute to the improvement. Tsuji commented that the balance between terminal aromatic groups and stereocomplexation efficiency is important [82].

On the other hand, Chen and Ren [79] reported that the thermal degradation of scPLA cannot be improved by the stereocomplex structure when including Sn catalyst.

Interestingly, Bao et al. [81] reported that a low-temperature approach to prepare stereocomplex of high-molecular-weight PLLA and PDLA at 160°C achieved the complete stereocomplex crystallites without the formation of homocrystallites, resulting in significant improvements in the crystallinity, melting temperature, and the thermal stability compared with either conventional melt blending or solution casting method.

To clarify the pyrolysis mechanism of scPLA, Fan et al. [78] prepared three scPLA samples with different chain end structures, namely, Sn—O—scPLA, scPLA—$COO^-$ $Sn^+$, and purified metal-free scPLA (scPLA-H). From the analyses of thermal degradation kinetics and pyrolyzates of the scPLA samples, typical degradation mechanisms of these scPLAs have been proposed. The pyrolysis of Sn—O—scPLA proceeds through a main unzipping depolymerization caused by Sn-alkoxide chain ends with apparent $E$ of 80–100 kJ/mol, showing zero-order weight loss behavior. The pyrolysis of scPLA—$COO^-$ $Sn^+$ also proceeds via a zero-order weight loss process consisting of mainly Sn-catalyzed selective lactide elimination with apparent $E$ of 100–120 kJ/mol caused by Sn-carboxylate chain ends. The pyrolyzates from Sn—O—scPLA and scPLA—$COO^-$ $Sn^+$ are predominantly L,L- and D,D-lactides. In the case of scPLA-H, random degradation is the main process, producing a large amount of *meso*-lactide and cyclic oligomers. These degradation mechanisms are nearly the same as those of the corresponding Sn—O—PLLA, PLLA—$COO^-$ $Sn^+$, and PLLA-H, except that the scPLA pyrolysis starts at a higher temperature due to the higher melting point of scPLA.

## 20.6 CONTROL OF RACEMIZATION

Optically pure PLLA is a crystalline polymer with a melting point of about 175°C. However, when the optical purity of PLA is lowered by racemization, its crystallinity decreases, and most of its useful properties are lost [84, 85]. Thus, to be of practical use, PLA must have a high enough optical purity. During the thermal degradation of PLLA, many kinds of diastereoisomers of cyclic oligomers are produced [6, 12, 86, 87]. To control the degradation reaction of PLLA so as to reproduce the optically pure L,L-lactide, it is necessary to clarify its racemization mechanism and discover appropriate catalysts and thermal degradation conditions.

The racemization in the pyrolysis of PLLA has been discussed in some reports [6, 17, 35, 88, 89]. To explain this phenomenon, Kopinke et al. [6] proposed that an ester–semiacetal tautomerization occurred in the lactate unit during the pyrolysis. This speculation was based on the observation of more than two different diastereoisomers of each cyclic oligomer as pyrolyzates. Moreover, it is suggested that possible radical-homolysis pathways cause the racemization through ring-forming processes [6, 17].

Fan et al. [19, 35] found that Ca-ion-catalyzed depolymerization of PLLA with PLLA-Ca caused considerable racemization at temperatures lower than 250°C, forming a large amount of *meso*-lactide as a by-product. They proposed a novel racemization mechanism based on a SN2 reaction at an asymmetrical methine carbon, which occurred as a back-biting reaction from an active chain end structure: R—COO—$Ca^+$ of PLLA [35, 90]. At temperatures over 320°C, side reactions such as the ester–semiacetal tautomerization caused the formation of *meso*-lactide, but not dominantly. At 250–320°C, L,L-lactide is produced exclusively, because unzipping depolymerization proceeds as the main reaction.

The racemization may proceed not only during the depolymerization reaction but also in the state of cyclic monomers obtained after depolymerization. Tsukegi et al. [88] investigated the racemization of the stereoisomer L,L-lactide during heating in the absence of a catalyst, resulting in a high composition of *meso*-lactide, suggesting that the direct racemization of L,L-lactide had occurred. The equilibrium among L,L-, *meso*-, and D,D-lactides was found to converge toward L,L- : *meso*- : D,D-lactides = 1 : 1.22 : 0.99 (wt/wt/wt) after 120 min at 300°C. This composition ratio indicates that in addition to the known racemization reaction of the oligomer chains, direct racemization among the lactides is also important.

Recently, Tsuji and Kondoh [89] reported that *meso*-lactide (MLA) was synthesized by thermal degradation of PLLA at 250 and 300°C. This indicates that the intentional thermal configurational inversion and depolymerization of PLLA and configurational inversion of lactides at the higher temperature as reported by Tsukegi et al. [88] are favorable for the synthesis of MLA in a short period. Interestingly, it was determined that the higher MLA fraction for 250°C compared to that for 300°C at the reaction times when PLLA samples had similar number-average molecular weights can be ascribed to the lower tacticity or higher racemization at chiral carbons in PLA chains. In this report, Tsuji and Kondoh analyzed the changes in molecular weight of residual PLLA. They suggested the random chain scission mechanism of PLLA, despite a serious contradiction between the unzipping depolymerization producing lactides and the random degradation. Fortunately, the report describing a

mechanism to explain this contradiction well has been published by Nishida et al. [25]. They suggested based on the kinetic analysis that the cooperative random transesterification occurred during the unzipping depolymerization of PLLA to show the zero-order weight loss behavior.

## 20.7 CONCLUSIONS

PLLA is well known as a biodegradable and recyclable material that can be converted to the cyclic dimer L,L-lactide. However, the mechanisms of the thermal degradation of PLLA have been regarded as being very complex in behavior. Much of this perceived complexity derives from the lack of technical progress in the kinetic analysis of thermal degradation behavior.

Many efforts have been made to clarify and control the thermal degradation of PLLA. As a result, the effects of some important factors, such as polymerization catalyst residues, chain-end structures, depolymerization catalysts, stereocomplex formation, and racemization, have been clarified. Nevertheless, it has not been possible to clarify the thermal degradation behavior of original PLLA in detail. In order to clearly reproduce the thermal degradation behavior of the original PLLA, the multistep complex reaction analysis method was developed, and its effectiveness demonstrated. That is, the method clarified that the thermal degradation behavior of commercially available PLLA consists of at least three reactions, with the first reaction gradually shifting to the second and third reactions independently or sequentially as the temperature rises. The multistep complex reaction analysis method was able to closely reproduce the thermal degradation behaviors. Moreover, the multistep complex reaction analysis method can be applied not only to PLLA degradation but also to the thermal degradation behaviors of many other polymers, blends, alloys, and composites.

The use of PLLA is expected to become more widespread as one of the solutions to the marine plastic waste problem. However, PLLA is also an excellent recyclable polymer, and this important feature of recyclability is a quality that should be given higher research priority. For this reason, it is vital that efforts continue to be made to understand the thermal degradation behavior of PLLA more accurately, establish the technology to control it, and further improve the accuracy of the simulation.

## REFERENCES


1. C. P. Radano, G. L. Baker, M. R. Smith, *J. Am. Chem. Soc.* **2000**, *122*, 1552–1553.
2. A. Kowalski, A. Duda, S. Penczek, *Macromolecules* **2000**, *33*, 689–695.
3. H. R. Kricheldorf, I. Kreiser-Saunders, A. Stricker, *Macromolecules* **2000**, *33*, 702–709.
4. D. R. Witzke, R. Narayan, J. J. Kolstad, *Macromolecules* **1997**, *30*, 7075–7085.
5. H. Nishida, *Poly(Lactic Acid): Synthesis, Structures, Properties, Processing, and Applications*, John Wiley & Sons, Inc., Hoboken, NJ, 2010, pp. 401–412.
6. F. D. Kopinke, M. Remmler, K. Mackenzie, M. Moder, O. Wachsen, *Polym. Degrad. Stab.* **1996**, *53*, 329–342.
7. A. Babanalbandi, D. J. T. Hill, D. S. Hunter, L. Kettle, *Polym. Int.* **1999**, *48*, 980–984.
8. Y. Aoyagi, K. Yamashita, Y. Doi, *Polym. Degrad. Stab.* **2002**, *76*, 53–59.
9. I. C. McNeill, H. A. Leiper, *Polym. Degrad. Stab.* **1985**, *11*, 309–326.
10. K. Chrissafis, *Thermochim. Acta* **2010**, *511*, 163–167.
11. H. A. Leiper, I. C. McNeill, *Polym. Degrad. Stab.* **1985**, *11*, 267–285.
12. F. D. Kopinke, K. Mackenzie, *J. Anal. Appl. Pyrol.* **1997**, *40*/41, 43–53.
13. D. Cam, M. Marucci, *Polymer* **1997**, *38*, 1879–1884.
14. S. H. Lee, S. H. Kim, Y. K. Han, Y. H. Kim, *J. Polym. Sci. Polym. Chem. Ed.* **2001**, *39*, 973–985.
15. X. Zhang, U. P. Wyss, D. Pichora, M. F. A. Goosen, *Polym. Bull.* **1992**, *27*, 623–629.
16. K. Jamshidi, S. H. Hyon, Y. Ikada, *Polymer* **1988**, *29*, 2229–2234.
17. H. Tsuji, I. Fukui, H. Daimon, K. Fujie, *Polym. Degrad. Stab.* **2003**, *81*, 501–509.
18. Q.-q. Ye, Z. Huang, Y.-h. Hao, J.-w. Wang, X.-y. Yang, X.-y. Fan, *J. Therm. Anal. Calorim.* **2016**, *124*, 1471–1484.
19. Y. Fan, H. Nishida, S. Hoshihara, Y. Shirai, Y. Tokiwa, T. Endo, *Polym. Degrad. Stab.* **2003**, *79*, 547–562.
20. US Food and Drug Administration, Food additives. Resinous and polymeric coatings, *Fed. Regist.* **1975**, *40*(121) C (23 June 1975) (CA 83: 112493h).
21. M. Noda, *Shimadzu Hyoron* **1999**, *56*, 83–86.
22. P. Degée, P. Dubois, R. Jérôme, *Macromol. Chem. Phys.* **1997**, *198*, 1985–1995.
23. A. Södergård, J. H. Näsman, *Polym. Degrad. Stab.* **1994**, *46*, 25–30.
24. C. Zeng, N.-W. Zhang, S.-Q. Feng, J. Ren, *J. Therm. Anal. Calorim.* **2013**, *111*, 633–646.
25. H. Nishida, T. Mori, S. Hoshihara, Y. Fan, Y. Shirai, T. Endo, *Polym. Degrad. Stab.* **2003**, *81*, 515–523.
26. T. Mori, H. Nishida, Y. Shirai, T. Endo, *Polym. Degrad. Stab.* **2004**, *84*, 243–251.
27. O. Wachsen, K. Platkowski, K.-H. Reichert, *Polym. Degrad. Stab.* **1997**, *57*, 87–94.
28. H. R. Kricheldorf, I. Kreiser-Saunders, C. Boettcher, *Polymer* **1995**, *36*, 1253–1259.
29. G. Scchwach, J. Coudane, R. Engel, M. Vert, *Polym. Bull.* **1996**, *37*, 771–776.
30. H. Abe, N. Takahashi, K. J. Kim, M. Mochizuki, Y. Doi, *Biomacromolecules* **2004**, *5*, 1606–1614.


31. M. Noda, H. Okuyama, *Chem. Pharm. Bull.* **1999**, *47*, 467–471.
32. M. Noda, H. Okuyama, *Shimadzu Hyoron* **2000**, *56*, 169–173.
33. H.-J. Sterzel, DE Patent 4,325,849 A1, 1993.
34. H. Nishida, Y. Fan, T. Mori, N. Oyagi, Y. Shirai, T. Endo, *Ind. Eng. Chem. Res.* **2005**, *44*, 1433–1437.
35. Y. Fan, H. Nishida, Y. Shirai, T. Endo, *Polym. Degrad. Stab.* **2003**, *80*, 503–511.
36. T. Motoyama, T. Tsukegi, Y. Shirai, H. Nishida, T. Endo, *Polym. Degrad. Stab.* **2007**, *92*, 1350–1358.
37. H. Nishida, *Encyclopedia of Polymeric Nanomaterials*, Springer-Verlag, Berlin, Heidelberg, 2015, pp. 1640–1650.
38. A. Södergards, M. Niemi, J. F. Selin, J. H. Näsman, *Ind. Eng. Chem. Res.* **1995**, *34*, 1203–1207.
39. A. Södergards, J. H. Näsman, *Ind. Eng. Chem. Res.* **1996**, *35*, 732–735.
40. I. E. Yuzay, R. Auras, H. Soto-Valdez, S. Selke, *Polym. Degrad. Stab.* **2010**, *95*, 1769–1777.
41. Y. Hao, Z. Huang, *Applied Sciences in Graphic Communication and Packaging, Lecture Notes in Electrical Engineering 477*, Springer Nature Singapore Pvt. Ltd., Singapore, 2018, pp. 849–855.
42. M.-F. Chiang, T.-M. Wu, *Compos. Sci. Technol.* **2010**, *70*, 110–115.
43. N. Koga, H. Tanaka, *J. Thermal Anal.* **1994**, *41*, 455–469.
44. N. Kameno, S. Yamada, T. Amimoto, K. Amimoto, H. Ikeda, N. Koga, *Polym. Degrad. Stab.* **2016**, *134*, 284–295.
45. L. A. Pérez-Maqueda, J. M. Criado, P. E. Sánchez-Jiménez, *J. Phys. Chem. A* **2006**, *110*, 12456–12462.
46. F. Carrasco, L. A. Pérez-Maqueda, P. E. Sánchez-Jiménez, A. Perejón, O. O. Santana, M. Ll. Maspoch, *Polym. Test.* **2013**, *32*, 937–945.
47. R. Simha, L. A. Wall, *J. Phys. Chem.* **1952**, *56*, 707–715.
48. H. E. Kissinger, *Anal. Chem.* **1957**, *29*, 1702–1706.
49. C. D. Doyle, *J. Appl. Polym. Sci.* **1961**, *5*, 285–292.
50. C. D. Doyle, *J. Appl. Polym. Sci.* **1962**, *6*, 639–642.
51. E. S. Freeman, B. Carroll, *J. Phys. Chem.* **1958**, *62*, 394–397.
52. H. L. Friedman, *J. Polym. Sci. Part C* **1964**, *6*, 183–195.
53. A. W. Coats, J. P. Redfern, *Nature* **1964**, *201*, 68–69.
54. T. Ozawa, *Bull. Chem. Soc. Jpn.* **1965**, *38*, 1881–1886.
55. J. H. Flynn, L. A. Wall, *Polym. Lett.* **1966**, *4*, 323–328.
56. J. H. Flynn, L. A. Wall, *J. Res. Nat. Bur. Stand.* **1966**, *70A*, 487–523.
57. S. Ichihara, H. Nakagawa, Y. Tsukazawa, *Kobunshi Ronbunshu* **1994**, *51*, 459–465.
58. H. Nishida, M. Yamashita, T. Endo, *Polym. Degrad. Stab.* **2002**, *78*, 129–135.
59. H. Nishida, Y. Tokiwa, M. Yamashita, T. Endo, *Polym. Degrad. Stab.* **2000**, *70*, 485–496.
60. H. Nishida, H. Ariffin, Y. Shirai, M. A. Hassan, *Biopolymers*, Sciyo, Rijeka, Croatia, 2010, pp. 369–386.
61. H. Nishida, *Handbook of Sustainable Polymers: Structure and Chemistry*, Pan Stanford Publishing Pvt. Ltd., Singapore, 2016, pp. 289–329.
62. H. Nishida, *Chem. Eng.* **2014**, *59*, 491–498. in Japanese.
63. M. Yoshikawa, Y. Goshi, S. Yamada, N. Koga, *J. Phys. Chem. B* **2014**, *118*, 11397–11405.
64. K. S. Anderson, S. H. Lim, M. A. Hillmyer, *J. Appl. Polym. Sci.* **2003**, *89*, 3757–3768.
65. H. Nishida, Y. Arazoe, T. Tsukegi, Y. Wang, Y. Shirai, *Int. J. Polym. Sci.* **2009**, 1–9. https://doi.org/10.1155/2009/287547.
66. P. Sarazin, B. D. Favis, *Biomacromolecules* **2003**, *4*, 1669–1679.
67. G. Zhang, J. Zhang, S. Wang, D. Shen, *J. Polym. Sci. Part B Polym. Phys.* **2003**, *41*, 23–30.
68. J. W. Park, S. S. Im, *J. Appl. Polym. Sci.* **2002**, *86*, 647–655.
69. T. Tsukegi, H. Nishida, M. Omura, Y. Shirai, T. Endo, *Kobunshi Ronbunshu* **2006**, *63*, 241–247.
70. M. Omura, T. Tsukegi, Y. Shirai, H. Nishida, T. Endo, *Ind. Eng. Chem. Res.* **2006**, *45*, 2949–2953.
71. M. Omura, T. Tsukegi, Y. Shirai, H. Nishida, *Kobunshi Ronbunshu* **2007**, *64*, 745–750.
72. M. Omura, T. Tsukegi, Y. Shirai, H. Nishida, *Kobunshi Ronbunshu* **2007**, *64*, 751–757.
73. H. Nishida, Y. Shirai, *Proceeding of the 11th Intranational Symposium on Research Association for Feedstock Recycling of Plastics Japan*, 16 September 2008, Kumamoto.
74. C. Migliaresi, D. Cohn, D. E. Lollis, L. Fameri, *J. Appl. Polym. Sci.* **1991**, *43*, 83–95.
75. Y. Ikada, K. Jamshidi, H. Tsuji, S. H. Hyon, *Macromolecules* **1987**, *20*, 904–906.
76. J. R. Murdock, G. L. Loomis, U.S. Patent 4,719,246, 1988; U.S. Patent 4,766,182, 1988; U.S. Patent 4,800,219, 1989.
77. H. Tsuji, I. Fukui, *Polymer* **2003**, *44*, 2891–2896.
78. Y. Fan, H. Nishida, Y. Shirai, Y. Tokiwa, T. Endo, *Polym. Degrad. Stab.* **2004**, *86*, 197–208.
79. D. Chen, J. Li, J. Ren, *J. Polym. Environ.* **2011**, *19*, 574–581.
80. H. Ajiro, Y.-J. Hsiao, T.H. Thi, T. Fujiwara, M. Akashi, *Chem. Commun.* **2012**, 48, 8478–8480 (*2012*).
81. R.-Y. Bao, W. Yang, W.-R. Jiang, Z.-Y. Liu, B.-H. Xie, M.-B. Yang, Q. Fu, *Polymer* **2012**, *53*, 5449–5454.
82. H. Tsuji, *Adv. Drug Deliv. Rev.* **2016**, *107*, 97–135.
83. Y. Li, Q. Li, G. Yang, R. Ming, M. Yu, H. Zhang, H. Shao, *Adv. Polym. Technol.* **2018**, *37*, 1674–1681.
84. S. Brochu, R. E. Prud'homme, I. Barakat, R. Jerome, *Macromolecules* **1885**, *28*, 5230–5239.
85. H. Tsuji, Y. Ikada, *Macromolecules* **1992**, *25*, 5719–5723.
86. F. Khabbaz, S. Karlsson, A. C. Albertsson, *J. Appl. Polym. Sci.* **2000**, *78*, 2369–2378.
87. C. Westphal, C. Perrot, S. Karlsson, *Polym. Degrad. Stab.* **2001**, *73*, 281–287.
88. T. Tsukegi, T. Motoyama, Y. Shirai, H. Nishida, T. Endo, *Polym. Degrad. Stab.* **2007**, *92*, 552–559.
89. H. Tsuji, F. Kondoh, *Polym. Degrad. Stab.* **2017**, *141*, 77–83.
90. Y. Fan, H. Nishida, Y. Shirai, T. Endo, *Green Chem.* **2003**, *5*, 575–579

# 21

# HYDROLYTIC DEGRADATION

HIDETO TSUJI

## 21.1 INTRODUCTION

Polylactide, also known as poly(lactic acid) (PLA), is basically synthesized via the removal of water from lactic acid by condensation polymerization or ring-opening polymerization of lactide (LA), the structure of which is obtained by the removal of two water molecules from two lactic acid molecules. PLA, one of the aliphatic polyesters, is susceptible to hydrolytic degradation, in contrast to aromatic polyesters such as poly(ethylene terephthalate) (PET). The hydrolytic degradation behavior, rate, and mechanism depend on factors such as molecular and higher order structures, as well as medium factors such as temperature, pH, and catalytic species (alkali, enzyme, etc.). Therefore, the hydrolytic degradation behavior, rate, and mechanism are controllable by varying these factors. The hydrolytic degradation rate of PLA should be manipulated when PLA-based materials are used for biomedical, pharmaceutical, and environmental applications. It is known that the in vivo hydrolytic degradation of PLA is comparable to the in vitro hydrolytic degradation rate [1]. Therefore, the in vivo degradation behavior and rate can be predicted from in vitro experimental results to a certain extent. PLA-based biomedical materials should be selected and fabricated to have an appropriate hydrolytic degradation rate in accordance with the healing rate of organs. As pharmaceutical matrices, PLA-based materials should be selected and prepared to have an optimal degradation rate to maintain medicinal concentration in the human body [2, 3]. However, for environmental applications, PLA-based materials should degrade as soon as possible at their end of life. Also, when hydrolytic degradation is utilized for the recycling of PLA to lactic acid, optimum conditions should be selected to attain the highest reaction rate, yield, and optical purity. Optical purity is a crucial factor for the mechanical properties of PLA synthesized from hydrolysis-formed lactic acid, since low optical purity reduces the mechanical properties of PLA. Also, the reaction rate and the yield determine the cost and environmental impact of PLA recycling. On the other hand, for commodity and industrial applications, where PLA-based materials are used as alternatives to petroleum-based polymeric materials, hydrolytic degradation is unfavorable because of reduced mechanical performance. Several articles have included the review of hydrolytic degradation of PLA-based materials [4–14].

## 21.2 DEGRADATION MECHANISM

The molecular structures of linear homopolymers and copolymers of lactic acid, which are often utilized in commodity, industrial, biomedical, and pharmaceutical applications, are summarized in Figure 21.1. Of these polymers, poly(L-lactide) (poly(L-lactic acid) (PLLA)), poly(D-lactide) (poly(D-lactic acid) (PDLA)), and their copolymers having sufficiently long monomer sequences are crystallizable. These PLAs and copolymers belong to the family of aliphatic polyesters, and therefore their ester groups are hydrolytically degraded in the presence of water according to the following reaction:

$$-\mathrm{COO}- + \mathrm{H_2O} \rightarrow -\mathrm{COOH} + \mathrm{HO}-$$

*Poly(Lactic Acid): Synthesis, Structures, Properties, Processing, Applications, and End of Life*, Second Edition.
Edited by Rafael A. Auras, Loong-Tak Lim, Susan E. M. Selke, and Hideto Tsuji.

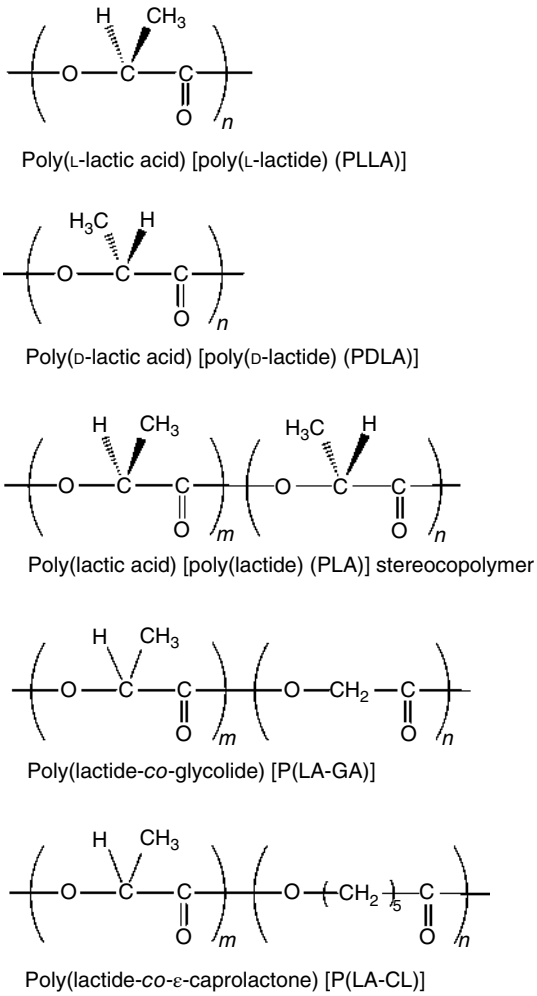


**FIGURE 21.1** Molecular structures of linear homopolymers and copolymers of lactic acid (or lactide).

Table 21.1 summarizes the reported hydrolytic degradation of PLA-based materials. The degradation mechanism, behavior, and rate depend on material and media-related factors, which are summarized in Table 21.2. Also, the indexes (methods) for monitoring the hydrolytic degradation of biodegradable polymers are summarized in Table 21.3.

### 21.2.1 Molecular Degradation Mechanism

In marked contrast to enzymatic degradation, the position of the ester group (chain end or within the chain) does not affect the hydrolytic degradability of PLA-based materials, as long as the polymers are composed of one monomer unit. An exception is the acidic hydrolysis of amorphous poly(DL-lactide) (poly(DL-lactic acid) (PDLLA)) in the solid state reported by Shih [130, 131], where the ester group adjacent to the chain terminal is more susceptible to hydrolytic degradation than that in the middle of the chain. Degradation at the chain ends and in the middle of the chain is, respectively, called exo-chain cleavage and endo-chain cleavage. De Jong et al. [94] reported that the cleavage mechanism of PLA dissolved in solution depends on the media pH. As shown in Figure 21.2, in acidic solution, hydrolytic degradation proceeds via a chain-end scission mechanism in a lactyl monomer unit, forming lactic acid, whereas in an alkaline solution, hydrolytic degradation takes place via backbiting to form a lactyl dimer (lactide) unit, which is further hydrolyzed to give lactoyl lactic acid. Codari et al. investigated the acidic hydrolytic degradation of L- and DL-lactic acid oligomers ($n = 2$–9) and found that oligomers shorter than a critical chain length ($n<7$) exhibited higher degradation rates than longer ones ($n \geq 7$), whereas above this threshold length, the reactivity was independent of chain length [92]. These findings are consistent with the assumption that the ester groups at terminals (α-ester) were hydrolyzed faster than those inside the molecules (β-ester) [92]. The activation energy for hydrolytic degradation was estimated to be 73 and 58 kJ/mol, respectively [92]. Moreover, the hydrolysis kinetics was not affected by chirality [92]. In neutral hydrolytic degradation (NHD), that is, hydrolytic degradation under controlled neutral pH, van Nostrum et al. [93] utilized acetylated and nonacetylated (hydroxy-terminated) L-lactic acid oligomers esterified with *N*-(2-hydroxypropyl) methacrylate and showed that the hydrolytic degradation of hydroxy-terminated L-lactic acid oligomers proceeded via a backbiting cleavage, which resulted in dimer formation, whereas that of acetylated L-lactic acid oligomers took place via random chain cleavage. The results reported by Braud et al. [91] for the hydrolytic degradation of oligomeric L-lactic acid at pH above 6.8 by capillary electrophoresis confirmed the finding by van Nostrum et al. [93]. That is, the concentration of linear dimers was higher than that of the monomer at an early stage and the monomer prevailed at a late stage of degradation. Karlsson and Albertsson [19] investigated the lactide and lactic acid contents in hydrolytically degraded PLLA (not in hydrolysis media) and found that a significant amount of lactic acid was present but a negligibly small amount of lactide was detected. Hakarainen et al. [161] indicated that PLLA was hydrolytically (abiotically) degraded via random cleavage rather than the chain-end cleavage observed for biotic degradation. With respect to the hydrolytic degradation of a monolayer, Kulkarni et al. [112] and Thanki et al. [159] showed that the degradation of PDLLA and poly(DL-lactide-*co*-glycolide) (poly(DL-lactic acid-*co*-glycolic acid) (P(DLLA-*co*-GA))) in an alkaline solution proceeded via chain-end cleavage. Also, the degradation rates of PLLA and PDLLA, as monitored by molecular weight changes, initially increased with degradation time to a maximum value and then decreased [47].

On the other hand, Atkinson and Vyazovkin found that linear one-armed PLLA and P(LLA-*co*-GA) degraded by a random chain scission mechanism while multiarm PLLA and P(LLA-*co*-GA) were degraded by a dual mechanism,

**TABLE 21.1 Reported Articles on Hydrolytic Degradation of PLA-Based Materials [15–354]**

| Type | Polymer | Temp. (°C) | Medium | Specimen State | References |
|---|---|---|---|---|---|
| Nonblended | PLLA | 20 | pH 7.3, 10.5, 10.7 | Solid (monolayers) | [15] |
| | | 21, 37, 45 | Citrate-, phosphate-, carbonate-buffered solution (pH 1.6, 3.0, 5.0, 7.4, 9.6) | Solid (microspheres) | [16–18] |
| | | 23, 50 | pH 7.0, 10.5 ($KH_2PO_4$/KOH solution) | Solid | [19] |
| | | 25 | 0.01 N NaOH solution | Solid | [20] |
| | | 37 | Buffer solution (pH 7) | Solid | [21, 22] |
| | | | Phosphate-buffered solution (pH 6.9, 7.0, 7.4, 7.6) | Solid | [18, 23–42] |
| | | | | Solid (crystalline residues) | [43, 44] |
| | | | | Solid (porous) | [45] |
| | | | | Solid (Nanofiber membrane) | [46] |
| | | | Ringer solution | Solid (including fibers) | [47–49] |
| | | | Simulated body fluid | Solid | [50] |
| | | | NaOH solution (0.01, 0.1, 1, 1.5 N) | Solid (including single crystals) | [39, 51–59] |
| | | | Acetic/orthoboric/orthophosphoric acid buffer solution (pH 2.2, 4.2, 6.0, 7.4, 8.4, 10.1) | Solid (nanospheres) | [60] |
| | | | HCl solution, DL-lactic acid solution (pH 2.0) | Solid | [61] |
| | | | HCl solution (pH –0.9, 0.2), NaOH solution (pH 11.8, 12.8) | Solid (crystalline residues) | [44] |
| | | 37, 60 | Deionized water | Solid | [62] |
| | | 37, 100 | Distilled water | Solid (fibers) | [63–65] |
| | | 40, 50, 60 | NaOH solution (pH 13) | Solid | [66] |
| | | 50 | Water or phosphate-buffered solution | Solid(fiber) | [67] |
| | | 50 | Distilled water (pH 7) | Solid | [68] |
| | | 50, 70, 97 | Phosphate-buffered solution (pH 7.4) | Solid (crystalline residues) | [69] |
| | | 70 | Deionized water | Solid | [70] |
| | | 80 | Phosphate-buffered solution (pH 7) | Solid | [71] |
| | | 80 | Phosphate-buffered solution (pH 7.4), NaOH solution (pH 11) | Solid (fibers) | [72] |
| | | 90 | Phosphate-buffered solution (pH 7.4) | Solid | [73] |
| | | 97 | Phosphate-buffered solution (pH 7.4) | Solid | [74–76] |
| | | 100 | Toluene + montmorillonite K10 | Dissolved | [77] |
| | | 120–350 | Distillated water (liquid state) | Solid or melt | [38, 78–82] |
| | | 160, 180 | Distillated water (liquid state) | Suspensions | [83] |
| | | 5, 25 | Air/water vapor (RH 11–98%) | Solid | [84] |
| | | 100–130 | Air/steam | Solid | [85] |
| | | <170 | Distilled water under microwave irradiation | Solid | [86] |
| | | 130 | Water/ionic liquid | Solid | [87] |

(*Continued*)

**TABLE 21.1** (Continued)

| Type | Polymer | Temp. (°C) | Medium | Specimen State | References |
|---|---|---|---|---|---|
| | | Not specified | NaOH solution (0.1 N, pH 10.7) | Solid (Single crystals) | [88] |
| | | Not specified | NaOH solution (10 g/dL) + citric acid (0.5%) solution | Solid | [89] |
| | Commercial and laboratory-scale synthesized PLLA | 37 | $H_2O$, phosphate-buffered solution (pH 7.4) | Solid | [90] |
| | Oligomers of L-lactic acid | 21 | pH 5.0, 6.8, 7.4, 9.0 | Solid | [91] |
| | ($n$ = 2–9) | 40–120 | pH 2 | Dissolved | [92] |
| | Acetylated L-lactic acid oligomers esterified with *N*-(2-hydroxypropyl)methacrylamide | 37 | Phosphate-buffered solution (pH 7.2) | Solid | [93] |
| | L-Lactic acid oligomers (DP = 7 or 8) | 37 | Acetonitrile + buffer solution | Dissolved | [94] |
| | End-capped PLLA | 60 | Phosphate-buffered solution (pH 7.4) | Solid | [95] |
| | Linear and branched (multiarmed) PLLA | 80 | Ethanol/water = 50 : 50 (v/v) (pH 11) using 3-(cyclohexylamino)-1-propanesulfonic acid (0.1 M) as a buffer solution | Solid | [96, 97] |
| | Branched (multiarmed) PLLA | 37 | Phosphate-buffered solution (pH 7.4) | Solid | [98–100] |
| | | | 1 M NaOH solution (pH 14.0) | Solid | [101] |
| | | 80 | Phosphate-buffered solution (pH 7.4) | Solid | [102] |
| | | | 10% NaOH solution (w/v) | Solid | [103, 104] |
| | Polyesteramide from telechelic oligomers of L-lactide | 37 | Phosphate-buffered solution (pH 6.0, 7.0), Tris–HCl buffered solution (pH 8.0) | Solid | [105] |
| | Peroxide-treated PLLA | 37 | Phosphate-buffered solution (pH 7.4) | Solid | [106] |
| | Electron beam irradiated PLLA | 37 | Phosphate-buffered solution (pH 7.4) | Solid | [107] |
| | UV-irradiated PLLA | 97 | Phosphate-buffered solution (pH 7.4) | Solid | [108] |
| | Cross-linked PLLA | 37 | 0.1M NaOH solution | Solid | [109] |
| | Plasma glow discharged PLLA, Plasma glow discharged PLLA cross-linked with carbodiimide, glutaraldehyde-cross-linked PLLA | 37 | Phosphate-buffered solution (pH 7.4) | Solid | [110] |
| | PDLA | 37 | Phosphate-buffered solution (pH 7.4) | Solid | [33–36] |
| | PDLLA | 20 | pH 3.5, 7.3, 9.95, 10.5, 10.7 | Solid (monolayers) | [15] |
| | | 20,60 | KOH–$C_2H_5OH$ | Solid (microspheres) | [111] |
| | | 21, 37, 45 | Citrate, phosphate, carbonate-buffered solution (pH 1.6, 3.0, 5.0, 7.4, 9.6) | Solid (microspheres) | [16, 17] |
| | | 22 | HCl solution (pH 2.0), phosphate-buffered solution (pH 7.2), NaOH solution (pH 10.5, 10.6) | Solid | [112] |
| | | 23, 37, 45, 70 | Phosphate-buffered solution (pH 7.0) | Solid | [26] |
| | | 25 | 0.01 N NaOH solution | Solid | [20] |
| | | 25, 35 | 0.1 N NaOH solution + acetone/methanol (70/30) | Dissolved | [20] |
| | | 25, 37 | HCl solution (pH 1), phthalate-buffered solution (pH 3), phosphate-buffered solution (pH 7) | Solid | [113] |
| | | Room temperature | 3.75 N NaOH solution | Solid | [114] |

| | | | | |
|---|---|---|---|---|
| | 30 | THF + NaOH and HCl solutions | Dissolved | [115] |
| | 37 | Phosphate-buffered solution (pH 7.4) | Solid | [34, 116–126] |
| | | | Solid (porous under load) | [127] |
| | | Ringer solution | Solid | [47] |
| | | Acidic solution (pH 3.7) | Solid | [122] |
| | | $H_2O$ + Fe(II)/$H_2O_2$, $H_2O$ + Co(II)/$H_2O_2$, $H_2O$ + various metal ions | Solid | [128] |
| | | Acetone + $H_2O$ | Dissolved | [129] |
| | | NaOH solution | Solid | [57] |
| | 60 | Steam (RH 60%) | Solid | [130] |
| | | *p*-Dioxinae-$d_8$ + $D_2O$ + DCl | Dissolved | [131] |
| | 85 | *p*-Dioxinae-$d_8$ + $D_2O$ + 4-*N*,*N*,-dimethylaminopyridine | Dissolved | [130] |
| | Ambient temperature | $H_2O$ + $Na_2HPO_4$ + NaOH (pH 11.4), $H_2O$ + HCl (pH 1.9) | Solid (monolayers) | [132] |
| Oligomers of DL-lactic acid ($n$ = 2–9) | 40, 60 | pH 2 | Dissolved | [92] |
| One- and two-armed PDLLA | 97 | Phosphate-buffered solution (pH 7.4) | Solid | [133] |
| Two- and four-armed PDLLA | | Phosphate-buffered solution (pH 7.4) | Solid | [134] |
| Branched (multiarmed) PDLLA | 37 | 1 M NaOH solution (pH 14.0) | Solid | [101] |
| PDLLA linked with 2,2-bis(2-oxazoline) | 37 | Phosphate-buffered solution (pH 7.4) | Solid | [135] |
| PLA | 25, 40, 55 | Air/water vapor (RH 10%, 50%, 100%) | Solid | [136] |
| | 120–140 | Water/ionic liquid catalyst | Solid | [137] |
| Six-armed PLA (random, heterotactic, isotactic (L/D = 50/50), isotactic (L/D = 100/0)) | 23 | $4.34 \times 10^{-2}$ M 1,5,7-triazabicyclo[4.4.0]dec-5-ene in methanol | Solid | [138] |
| P(LLA-*co*-DLA) | 37 | Phosphate-buffered solution (pH 7.4) | Solid | [39–41, 139–143, 145] |
| | | Alkaline solution (pH 12) | Solid | [145] |
| | | NaOH solution | Solid | [57, 58] |
| | 37, 45, 70 | Buffered solutions (pH 3.0, 7.0, 9.0) | Solid | [26] |
| | 50, 70 | Acetic acid (0.08 M) or sodium bicarbonate (2.4 M)-buffered solutions | Solid | [146] |
| | 90 | Phosphate-buffered solution (pH 7.4) | Solid | [73] |
| Poly(ester-urethane) based on L- and D-lactic acids | 37, 55 | Phosphate-buffered solution (pH 7.0) | Solid | [147] |
| P(LLA-*co*-GA) | 37 | Buffer solution (pH 7) | Solid | [21, 22] |
| | | Phosphate-buffered solution (pH 7.3, 7.4) | Solid | [41, 148–153] |
| | | | Solid (fibers) | [154] |
| | | | Solid (porous) | [155] |
| Electron beam irradiated P(LLA-*co*-GA) | 37 | Phosphate-buffered solution (pH 7.4) | Solid | [156] |
| | | Titrisol (Merk) solution (pH 6.9) | Solid | [157] |
| P(DLLA-*co*-GA) | 20 | pH 10.5 | Solid (monolayers) | [15] |

(*Continued*)

**TABLE 21.1** (Continued)

| Type | Polymer | Temp. (°C) | Medium | Specimen State | References |
|---|---|---|---|---|---|
| | | | NaOH solution, ethylenediamine, or *N*-aminoethyl-1,3-propanediamine solution | Solid | [158] |
| | | 20, 60 | KOH–$C_2H_5OH$ | Solid (microspheres) | [111] |
| | | 22 | HCl solution (pH 2.0), phosphate-buffered solution (pH 7.4), NaOH solution (pH 10.5) | Solid (monolayers) | [112, 159] |
| | | Not specified | 1 N NaOH | Solid | [160] |
| | | 37 | Phosphate-buffered solution (pH 7.3, 7.4) | Solid | [121, 123, 147, 148, 161, 162] |
| | | | Phosphate-buffered solution (pH 7.4) | Solid (porous) | [163–166] |
| | | | Hank's simulated body fluid | Solid (porous) | [167] |
| | | | Phosphate-buffered solution (pH 5.0, 7.4), sodium borate buffer solution (pH 9.2) | Solid | [168] |
| | | | Distilled water, sodium chloride solution, phosphate-buffered solution (pH 7.2, 8.2), $D_2O$ | Solid | [169] |
| | | 60 | Phosphate-buffered solution (pH 7.3) | Solid | [161] |
| | Electron beam irradiated P(DLLA-*co*-GA) | 37 | Phosphate-buffered solution (pH 7.4) | Solid (multilayered) | [170] |
| | P(LA-*co*-GA) | Room temperature | 1 N NaOH solution | Solid (porous) | [171] |
| | | 37 | Deionized water, HPLC grade water | Solid | [172, 173] |
| | | | Phosphate-buffered solution (pH 7.4) | Solid | [172, 174] |
| | | | Phosphate-buffered solution (pH 7.3) | Solid (fibers) | [175] |
| | | | 0.01 M HCl solution (pH 2), phosphate-buffered solution (pH 7.4), 10% NaOH solution (pH > 13) | Solid | [176] |
| | | | HAc/NaAc solution (pH 5.3), phosphate-buffered solution (pH 7.4), $NaHCO_3/Na_2CO_3$ solution (pH 10.1) | Solid (fibers) | [177] |
| | Linear and branched PLLA and P(LLA-*co*-GA) | 37 | Phosphate-buffered solution (pH 7.4) | Solid | [178] |
| | P(L-lactic acid-*co*-L-mandelic acid) | 37 | Tris–HCl-buffered solution (pH 8.6) | Solid | [179] |
| | P(L-lactic acid-*co*-L-hydroxymethyl (or benzyloxymethyl) glycolic acid) | 37 | Phosphate-buffered solution (pH 7.4) | Solid | [180] |
| | P(LLA-*co*-CL) | 23, 37 | Phosphate-buffered solution (pH 7.0, 7.4) | Solid | [181–186] |
| | | 37 | Titrisol solution (pH 7.0) | Solid | [22] |
| | | 37 | HCl/KCl, phosphate-buffered, Tris–HCl-buffered, $Na_2CO_3/NaHCO_3$ solutions | Solid (monofila-ments) | [187, 188] |
| | P(LLA-*co*-CL), PLLA-*b*-PCL | 37 | Phosphate-buffered solution (pH 7.2) | Solid | [189] |
| | Peroxide modified, end-capped, and nontreated P(LLA-*co*-CL) | 25, 43 | Phosphate-buffered solution (pH 7.4) | Solid | [190] |
| | P(DLLA-*co*-CL) | 23, 37 | Phosphate-buffered solution (pH 7.0) | Solid | [182, 183] |
| | | 37 | Phosphate-buffered solution (pH 7.4) | Solid | [181, 191, 192] |
| | P(L-lactic acid-*co*-glycolic acid-*co*-α-L-malic acid) | 37 | Phosphate-buffered solution (pH 7.2) | Solid | [193] |
| | P(LLA-*co*-GA-*co*-CL) | 37 | Phosphate-buffered solution (pH 7.4) | Solid | [151, 194] |

| | | | | |
|---|---|---|---|---|
| P(DLLA-*co*-GA-*co*-CL) | 37 | Phosphate-buffered solution (pH 7) | Solid | [195] |
| P(L-lactic acid-*co*-mandelic acid) | 37 | Phosphate-buffered solution (pH 7.2) | Solid | [196] |
| P(LLA-*co*-β-malic acid) | 37 | Phosphate-buffered solution (pH 7.4) | Solid | [197] |
| P(LLA-*co*-γ-butyrolactone) | 37 | Phosphate-buffered solution (pH 7.0) | Solid | [198, 199] |
| P(LLA-*co*-δ-valerolactone) | 20, 60 | KOH–$C_2H_5OH$ | Solid (microspheres) | [111] |
| | 60 | Distilled water | Solid | [200] |
| P(LLA-*co*-β-methyl-δ-valerolactone) | 70 | Distilled water | Solid | [201] |
| P(DLLA-*co*-adipic anhydride) | 37 | Phosphate-buffered solution (pH 7.4) | Solid | [202] |
| P(LLA-*co*-aspartic acid) | 37 | Phosphate-buffered solution (pH 7.3) | Solid | [203] |
| P(DL-lactic acid-*co*-glycine) | 37 | Phosphate-buffered solution (pH 7.4) | Solid | [204] |
| P(L-lactic acid-*co*-lysine) | 37 | Phosphate-buffered solution (pH 7.1) | Solid | [205] |
| P(DL-lactic acid-*co*-aspartic acid) | 37 | Phosphate-buffered solution (pH 7.4) | Solid | [206] |
| P(LLA-*co*-3-methyl-4-oxa-6-hexanolide) | 37 | Tris, tricine-buffered solution (pH 7.4, 8.0) | Solid | [207] |
| P(LLA-*co*-3,6-dimethyl-2,5-morpholinedione) | 37 | Tricine-buffered solution (pH 8.0) | Solid | [208] |
| P(DLLA-*co*-3,6-dimethyl-2,5-morpholinedione) | 37 | Tricine-buffered solution (pH 8.0) | Solid | [208] |
| P(LLA-*co*-trimethylene carbonate) | 37 | Tris, tricine-buffered solution (pH 7.4, 8.0) | Solid | [209] |
| | | Titrisol solution (pH 7.0) | Solid | [22] |
| P(DLLA-*co*-trimethylene carbonate) | 35, 37 | Phosphate-buffered solution (pH 7.0, 7.4) | Solid | [210–212] |
| P(DLLA-*co*-*rac*-1-methyltrimethylene carbonate) | 35 | Phosphate-buffered solution (pH 7.0) | | [212] |
| P(DLLA-*co*-2,2-dimethyltrimethylene carbonate) | 35, 60 | Phosphate-buffered solution (pH 7.0) | | [212, 213] |
| P(L-lactic acid-*co*-ricinoleic acid) | 37 | Phosphate-buffered solution (pH 7.4) | Solid, liquid | [214] |
| P(L-lactic acid-*co*-bis-2-hydroxyethyl terephthalate) | 45, 60 | Phosphate-buffered solution, phosphate–citrate-buffered solution (pH 7.4) | Solid | [215] |
| PLLA-*b*-PCL | 37, 45, 55 | Phosphate-buffered solution (pH 7.6) | Solid | [216] |
| PLLA-*b*-PCL-*b*-PLLA | 37 | Phosphate-buffered solution (pH 7.4) | Solid | [217] |
| PDLLA-*b*-PCL-*b*-PDLLA | | Phosphate-buffered solution (pH 7.4) | Solid | [218] |
| PLLA–PCL multiblock copolymer | Not specified | Phosphate-buffered solution | Solid | [219] |
| PLLA-*b*-poly(1,5-dioxepan-2-one)-*b*-PLLA and multiblock copolymer | 37 | Phosphate-buffered solution (pH 7.4) | Solid | [220, 221] |
| PLLA-*b*-PEO | 25, 37, 50 | Citrate-, phosphate-, and boric acid–borax-buffered solution (pH 5.0, 7.5, 9.0) | Solid | [222] |
| Linear and branched PLLA-*b*-PEO | 37 | Phosphate-buffered solution (pH 7.2) | Solid | [223] |
| PDLLA-*b*-PEO | 37 | Water | Solid | [224] |
| | | 0.9% NaCl solution | Solid | [225] |
| | | Phosphate-buffered solution (pH 7.4) | Solid | [226] |
| PLA-*b*-PEO | 37 | Aqueous solution (pH 2), phosphate-buffered solution (pH 7.2) | Solid (microspheres) | [227] |
| PLLA-*b*-PEO-*b*-PLLA | 25 | DMSO-$d_6$/$H_2O$ containing small amount of $CF_3COOH$ | Solid | [228] |
| | 37 | Distilled water, deionized water | Solid | [229, 230] |

(*Continued*)

**TABLE 21.1** (Continued)

| Type | Polymer | Temp. (°C) | Medium | Specimen State | References |
|---|---|---|---|---|---|
| | | 37 | Physiological salt solution, phosphate-buffered solution (pH 7.4) | Solid | [231–233] |
| | | 60 | Buffer solution (pH 4, 7, 10) | Solid | [234] |
| | PDLLA-*b*-PEO-*b*-PDLLA | 37 | Deionized water | Solid | [235] |
| | | | Phosphate-buffered solution (pH 7.4) | Solid | [236] |
| | | | NaOH solution | Solid | [237] |
| | PDLLA–PEO block copolymers | 37 | Phosphate-buffered solution (pH 7.4) | Solid | [119] |
| | P(LLA-*co*-GA)-*b*-PEO | 37 | Phosphate-buffered solution (pH 7.2) | Solid | [223] |
| | P(LLA-*co*-GA)-*b*-PEO-*b*-P(LLA-*co*-GA) | 37 | Distilled water | Solid | [229] |
| | P(LA-*co*-GA)-*b*-PEO-*b*-P(LA-*co*-GA) | 37 | Phosphate-buffered solution (pH 7.4) | Solid | [174] |
| | P(DLLA-*co*-CL)-*b*-PEO-*b*-P(DLLA-*co*-CL) | 37 | Phosphate-buffered solution (pH 7.4) | Solid | [238] |
| | P(LA-*co*-GA)–PEO multiblock copolymers | 37 | Phosphate-buffered solution (pH 7.4) | Solid (microspheres) | [239] |
| | Branched PLLA-*b*-PEO | 37 | Phosphate-buffered solution (pH 7.2) | Solid | [223] |
| | Branched P(LLA-*co*-GA)-*b*-PEO | 37 | Phosphate-buffered solution (pH 7.2) | Solid | [223] |
| | P(DLLA-*co*-GA-*co*-ε-CL)-*b*-PEO | 37 | Phosphate-buffered solution (pH 7.4) | Solid | [240] |
| | PLA-*b*-poly(propylene oxide)-*b*-PLLA | 37 | Phosphate-buffered solution (pH 7.2) | Solid | [241] |
| | PLLA-*b*-poly(propylene oxide-*co*-ethylene oxide)-*b*-PLLA | 37 | Phosphate-buffered solution (pH 7.4) | Solid | [242, 243] |
| | PLLA-*b*-poly(succinic anhydride-*co*-ethylene oxide) | 37 | Distilled water | Solid | [244] |
| | PDLLA-poly(tetramethylene ether glycol) | 37 | NaCl solution | Solid | [245] |
| | PDLLA-*b*-poly(ethylphosphate) | 37 | Phosphate-buffered solution (pH 7.4) | Solid | [246] |
| | Poly(orthoester)–*b*-PLA–*b*-poly(orthoester) | 37 | Phosphate-buffered solution (pH 7.4) | Solid | [247] |
| | Poly(1,3-trimethylene carbonate)-*b*-poly(L-lactide-*co*-glycolide) and poly(1,3-trimethylene carbonate-*co*-glycolide)-*b*-poly(L-lactide-*co*-glycolide) | 37 | Phosphate-buffered solution | Solid | [248] |
| | PLA stereo multiblock copolymers | 37 | Phosphate-buffered solution (pH 7.4) | Solid | [249] |
| | PLLA/poly(trimethylene terephthalate) multiblock copolymers | 60 | $Na_2CO_3$/$NaHCO_3$ buffer solution (pH 10) | Solid | [250] |
| | PLLA/polyisobutylene multiblock copolymers | 37 | Phosphate-buffered solution (pH 7.4) | Solid | [251] |
| | PEO/PPO/PLLA multiblock copolymers | 37 | Phosphate-buffered solution (pH 7.4) | Solid | [252] |
| | Pullulan-*g*-PLLA | 37 | Phosphate-buffered solution (pH 7.0) | Solid | [253] |
| | Cellulose-*g*-PLLA | 37 | Phosphate-buffered solution (pH 7.4) | Solid | [254] |
| | Dextran-*g*-oligo PDLLA | 37 | Phosphate-buffered solution (pH 7.3) | Solid, dissolved | [159] |
| | Dextran-*g*-P(LA-*co*-GA) | 37 | Phosphate-buffered solution (pH 7.2) | Solid | [255, 256] |
| | Poly(vinyl alcohol)-*g*-P(LA-*co*-GA) | 37 | Phosphate-buffered solution (pH 7.4) | Solid | [257] |
| | Poly(butadiene)-*g*-poly(L-lactide-*co*- trimethylene carbonate) | 37 | Phosphate-buffered solution (pH 7.4) | Solid | [258] |
| | Poly(PDLLA methacrylate-*co*-*tert*-butyl acrylate) | 20, 37 | Artificial seawater (AFNOR norm) | Solid | [259] |
| | Poly[vinyl-3-(dialkylamino)-alkylcarbamate-*co*-vinyl acetate-*co*-vinyl alcohol]-*graft*-poly(DL-lactide-*co*-glycolide) | 37 | Phosphate-buffered solution (pH 2, 7.4), tris-buffered solution (pH 9) | Solid | [260] |

| | | | | | |
|---|---|---|---|---|---|
| | Poly(2-armed PEO-*b*-PDLLA methacrylate) | 100 | 1 M NaOH solution | Solid | [261] |
| | P(DLLA-*co*-CL) initiated with glycerol and cross-linked with 2,2-bis(ε-caprolactone-4-yl)-propane | 37 | Phosphate-buffered solution (pH 7.4) | Solid | [262] |
| Blend/ composite | High-molecular-weight (HMW) and low-molecular-weight (LMW) PLLA | 37 | Phosphate-buffered solution | Solid | [263] |
| | Self-reinforced PLLA | 37 | Phosphate-buffered solution (pH 6.1) | Solid | [264, 265] |
| | HMW and LMW PDLLA | 37 | Phosphate-buffered solution (pH 7.4) | Solid | [266, 267] |
| | HMW P(DLLA-*co*-GA)/LMW PDLLA | 37 | Phosphate-buffered solution | Solid (microspheres) | [268] |
| | HMW P(LA-*co*-GA)/LMW PDLLA | 37 | Phosphate-buffered solution (pH 7.4) | Solid | [269] |
| | PLLA/PDLA | 20 | pH 10.5 | Solid (monolayers) | [270] |
| | | 37 | Phosphate-buffered solution (pH 7.4) | Solid | [33–36, 271] |
| | | 70, 85, 97 | Phosphate-buffered solution (pH 7.4) | Solid (microspheres) | [272] |
| | Two-armed PDLLA-*b*-PLLA/PDLLA-*b*-PDLA | 80 | Toluene/conc. HCl | Solid | [273] |
| | PDLA/PDLLA | 37 | Phosphate-buffered solution (pH 7.4) | Solid | [120] |
| | PLLA/PGA | 37 | Phosphate-buffered solution (pH 7.3) | Solid | [274] |
| | PLLA/PCL | 20 | pH 10.5 | Solid (monolayers) | [15, 275] |
| | | 37 | Phosphate-buffered solution (pH 7.4) | Solid | [28, 276] |
| | PLLA/P(LLA-*co*-CL) | 50 | Phosphate-buffered solution (pH 7.4) | Solid | [276] |
| | P(LA-*co*-GA)/PCL | 37 | Phosphate-buffered solution (pH 7.4) | Solid | [277] |
| | PLLA/PCL/P(LLA-*co*-CL) or PLLA-*b*-PCL | 50 | Phosphate-buffered solution (pH 7.4) | Solid | [276, 278] |
| | LMW PDLLA/poly(3-hydroxyoctanoate) | 37 | Citrate-, phosphate-, tetraborate-buffered solutions (pH 4, 7, 10) | Solid | [279] |
| | PLLA/poly(butylene succinate) | 37 | NaOH solution (1 N or pH13) | Solid | [280, 281] |
| | PLA/oligomeric poly(hexamethylene succinate) | 37 | Phosphate-buffered solution (pH 7.4) | Solid | [282] |
| | PLLA/poly((butylene adipate-*co*-terephthalate)/chain extender | 60 | 0.1 M NaOH solution | Solid | [283] |
| | PLLA/poly((butylene adipate-*co*-terephthalate)/ silver-loaded kaolinite | 60 | NaOH solution (pH 13) | Solid | [284] |
| | PLLA/PET | 60 | Phosphate-buffered solution (pH 7.2) | Solid (reactively blended) | [285] |
| | PLA/poly(trimethylene terephthalate) | 60 | Phosphate-buffered solution (pH 7.2) | Solid | [286] |
| | PLLA/poly(*p*-dioxanone) | 37 | Phosphate-buffered solution (pH 7.4) | Solid | [287] |
| | PLLA/poly(*p*-dioxanone)/poly(*p*-dioxan-*co*-L-lactide) | 37 | Phosphate-buffered solution (pH 7.5) | Solid | [288] |
| | Linear and branched P(LLA-*co*-DLA-*co*-GA)/ poly(trimethylene carbonate-*co*-ε-caprolactone) | 37 | Phosphate-buffered solution (pH 7.0) | Solid (reactively blended) | [289] |
| | PLLA/poly(aspartic acid-*co*-L-lactide) | 40 | Phosphate-buffered solution (pH 7.3) | Solid | [290] |
| | | 25 | Air (R.H. = 60%) | Solid | [290] |
| | PLLA/PLLA-*b*-poly[2-(perfluorooctyl)ethyl methacrylate] | 39 | Air (R.H. = 88%) | Solid | [291] |

(*Continued*)

**TABLE 21.1** (Continued)

| Type | Polymer | Temp. (°C) | Medium | Specimen State | References |
|---|---|---|---|---|---|
| | PLA/Nylon 6 | 20, 40, 60, 80 | Distilled water | Solid | [292] |
| | PLLA/PEO | 37 | Physiological salt solution | Solid | [232] |
| | PLA/PEO | 37 | Buffered solution (pH 10.6) | Solid | [293] |
| | PLA/chitosan/PCL | Not specified | Phosphate-buffered solution (pH 7.4) or 0.1 M NaOH solution | Solid | [294] |
| | PLA/chitosan/PEO | Not specified | HCl solution (0.1 N, pH 1) | Solid | [295, 296] |
| | PLLA/PVA | 37 | Phosphate-buffered solution (pH 7.4) | Solid | [297] |
| | P(LA-*co*-GA)/PVA | 37 | Water | Solid | [298] |
| | PLLA/poly(methyl methacrylate) | 60 | Phosphate-buffered solution (pH 7.2) | Solid | [299] |
| | | 37 | 1 N NaOH solution (pH 14) | Solid | [300] |
| | PLLA/poly(*p*-vinyl phenol) | 37 | 1 N NaOH solution (pH 14) | Solid | [301] |
| | PLA/poly(ethylene-*co*-glycidyl methacrylate)/ hexagonal boron nitride, electron beam irradiation | 58 | Phosphate-buffered solution (pH 7.1) | Solid | [302] |
| | PDLLA/DL-lactide | 37 | Phosphate-buffered solution (pH 7.4) | Solid | [121] |
| | P(LLA-*co*-GA)/L-lactide | 37 | Phosphate-buffered solution (pH 7.2) | Solid | [303] |
| | PLLA/lauric acid | 37 | Phosphate-buffered solution (pH 7.4) | Solid | [304, 305] |
| | PDLLA/caffeine | 37 | Phosphate-buffered solution (pH 7.4) | Solid | [118] |
| | PLA/citrate esters | 37 | $NaHCO_3$–NaOH solution (pH 10.6) | Solid | [306] |
| | PLLA/sucrose palmitate | 35, 55 | $NaHCO_3$–NaOH solution (pH 10.6) | Solid | [307] |
| | PLLA/Mg powder | 37 | Phosphate-buffered solution (pH 7.4) | Solid | [308] |
| | PLLA/MgO-*g*-PLLA and/or chitin-*g*-PLLA | 37.5 | Phosphate-buffered solution (pH 7.4) | Solid | [309] |
| | PLLA/ZnO nanoparticles | 49 | Distilled water | Solid | [310] |
| | | 58 | NaOH solution (0.25M) | Solid | [311] |
| | | 60, 80 | Phosphate-buffered solution (pH 7.4) | Solid | [312, 313] |
| | PLA/ $Ag_3PO_4$, PLA/ZnO, PLA/$Ag_3PO_4$/ZnO | 70 | Phosphate-buffered solution (pH 7.4) | Solid | [314] |
| | PLLA/$TiO_2$ | 37 | NaOH solution (pH 13) | Solid | [315] |
| | P(DLLA-*co*-GA)/calcium compounds | 37 | Phosphate-buffered solution (pH 7.4) | Solid | [316] |
| | PLLA/TCP (β-tricalcium phosphate) | 37 | Phosphate-buffered solution (pH 7.4, 6.4) | Solid | [317–320] |
| | P(LLA-*co*-DLA) (70/30 or 50/50)/TCP (β-tricalcium phosphate) | 37 | Phosphate-buffered solution (pH 7.4) | Solid | [321] |
| | P(LLA-*co*-ε-caprolactone)TCP(β-tricalcium phosphate) | 37 | Phosphate-buffered solution (pH 7.4) | Solid | [322] |
| | PLLA-*b*-poly(ethylene/hexamethylene–sebacate) TCP (β-tricalcium phosphate) | 37 | Phosphate-buffered solution (pH 7.4) | Solid | [323, 324] |
| | PLLA/hydroxyapatite | 37 | Simulated body fluid, phosphate-buffered solution (pH 7.3, 7.4) | Solid | [325, 326] |
| | PLA/hydroxyapatite | 37 | Phosphate-buffered solution (pH 7.4) | Solid | [327] |
| | PLLA/$SiO_2$ nanoparticles | 37, 55 | NaOH solution (pH 13) | Solid | [328] |
| | PLLA/polyhedral oligomeric silsesquioxanes | 37 | NaOH solution (pH 13) | Solid | [320, 329] |
| | PLLA/organomodified montmorillonite | 35,45 | NaOH solution (pH 13) | Solid | [331, 332] |
| | PLLA/organomodified montmorillonite, organomodified synthetic fluoro mica, sepiolite | 37, 58 | Phosphate-buffered solution (pH 7.0) | Solid | [333] |
| | PLLA/PDLA organomodified montmorillonite | 45 | NaOH solution (pH 13) | Solid | [332] |

| | | | | | |
|---|---|---|---|---|---|
| | PLLA/unmodified or modified vermiculite | 37 | NaOH solution (pH 12.8) | Solid | [334] |
| | PLLA/talc or organomodified talc | 50, 70 | Water | Solid | [335] |
| | P(LLA-*co*-DLA) (85/15)/bioactive glass | 37 | Phosphate-buffered solution (pH 7.4) | Solid | [336] |
| | L-Lactic acid-based poly(ester-urethane)/bioceramics | 37 | Saline solution | Solid | [337] |
| | PDLLA/coral | 37 | Phosphate-buffered solution | Solid | [338] |
| | P(LLA-*co*-DLA) (85/15)/MgO or hydroxyapatite | 37 | Phosphate-buffered solution (pH 7.2) | Solid | [339] |
| | P(DLLA-*co*-GA)/metal salts | 37 | HEPES buffer solution | Solid | [340] |
| | PLLA/nano/micro-diamond | 97 | Phosphate-buffered solution (pH 7.4) | Solid | [341] |
| | PLLA/multiwalled carbon nanotube | 37 | NaOH solution (pH 13) | Solid | [315, 342–344] |
| | PLLA/surface treated multiwalled carbon nanotube | 37 | NaOH solution (pH 13) | Solid | [315] |
| | PLLA/unzipped multiwalled carbon nanotube | 37 | NaOH solution (pH 13) | Solid | [345] |
| | P(DLLA-GA)/single-walled carbon nanotube | 37 | HEPES + NaOH solution (pH 7.0) | Solid | [346] |
| | PLLA/modified and grafted carbon nanofibers | 37 | NaOH solution (pH 13), HEPES + NaOH solution (pH 7.0) | Solid | [346, 347] |
| | PLLA/graphene | 37 | NaOH solution (pH 13) | Solid | [315] |
| | PLLA/graphene and/or PDLA | 30 | NaOH solution (pH 8) | Solid | [348] |
| | PLLA/graphene oxide | 37 | Phosphate-buffered solution (pH 7.4) | Solid | [349] |
| | | 50 | HCl solution (pH 2), distilled water (pH 7), NaOH solution (pH 12) | Solid | [350] |
| | PLA/cellulose nanocrystals | 37 | Phosphate-buffered solution (pH 7.4) | Solid (fiber) | [351] |
| | PLA/cellulose nanocrystals | 37, 60 | HCl solution (pH 2), distilled water (pH 7), NaOH solution (pH 12) | Solid | [352] |
| | PLA/wood flour/bis(2,6-diisopropylphenyl) carbodiimide | 80 | pH 7 | Solid | [353] |
| Coating | PLA | 50 | Phosphate-buffered solution (pH 7.4) | Solid (fiber) | [354] |

**TABLE 21.2 Material and Media-Related Factors That Affect Degradation Behavior and Rate of PLA-Based Materials [3]**

| Material Factors | Media-Related Factors |
|---|---|
| Molecular Structures | Temperature |
| Molecular weight and distribution | pH |
| Tacticity (optical purity) and distribution | Solutes (kinds and concentrations) |
| Comonomer structure, content, and distribution | Enzymes (kinds and concentrations) |
| Terminal groups | Microbes (kinds, number, and culture conditions) |
| Branching | Stress or strain |
| Cross-links | |
| Highly ordered structures | |
| Crystallinity | |
| Crystalline thickness | |
| Spherulitic size and morphology | |
| Orientation | |
| Hybridization (blends and composites) | |
| Material Morphology | |
| Material shape and dimensions | |
| Porosity and pore size | |
| Surface Treatment | |
| Coating | |
| Alkaline treatment | |

**TABLE 21.3 Indexes (Methods) for Monitoring Degradation**

| Material-Based Indexes | Nonmaterial-Based Indexes |
|---|---|
| Weight remaining (gravimetry) molecular weight and distribution (e.g., gel permeation chromatography (GPC)) | Dissolved organic carbon (DOC) or total organic carbon |
| Physical properties (e.g., differential scanning calorimetry (DSC), tensile testing) | Biochemical oxygen demand (BOD) |
| Material morphology (e.g., scanning electron microscopy (SEM), polarized optical microscopy (POM)) | Amount of released carbon dioxide. Amount of released biogas |
| | pH |
| | Absorbance (turbidity) |

i.e., nonrandom chain scission mechanism at or near the branch points followed by random chain scission of the resulting PLLA or P(LLA-*co*-GA) fragments [178]. In NHD of two-armed PDLLA at 97°C, although selective chain cleavage at terminal ester groups or second ester groups from chain terminals, which are induced by two terminal hydroxyl groups, contributed to hydrolytic degradation rout to some extent, the random cleavage of ester groups, irrespective of their position, was the main hydrolytic degradation route for both one- and two-armed linear PDLLAs [133].

With the incorporation of a comonomer or another polymeric block, selective degradation tends to take place. The most representative example is the selective cleavage of ester groups connecting glycolyl units (half of the glycolide (GA) units) in the copolymers of LA and GA and the predominant removal of glycolyl units, resulting in decreasing content of GA units during hydrolytic degradation [111, 148, 149, 157]. As stated below, in regard to the triblock copolymer of PLLA and poly(ethylene oxide) (PEO) (PLLA-*b*-PEO-*b*-PLLA), the ester groups connecting PLLA and PEO, rather than those connecting the lactyl units, were preferentially hydrolytically degraded at an early stage [229, 234]. Chaubal et al. [246] showed that in the NHD of poly(DL-lactide)-*b*-poly(ethylphosphate) (PDLLA-*b*-PEP), the cleavage of the ethylphosphate–lactyl linkage first occurred and then the cleavage of the lactyl–lactyl linkage took place. For this reason, the hydrolytic degradation of PLLA-*b*-PEO-*b*-PLLA and PDLLA-*b*-PEP was faster at an early stage than at a late stage. In contrast, Rashkov et al. [228] and Li et al. [233] reported that the acidic and NHD of PLLA-*b*-PEO-*b*-PLLA was not enhanced due to the phase separation between PLLA and PEO segments and that the hydrolyzability of the ester linkage between PEO and PLA in copolymers is similar to that in PLA segments, and therefore, PEO segments were not released at an early stage of degradation [236]. Further work is required to elucidate the causes for such a mechanism difference.

With respect to graft polymers, the hydrolytic degradation mechanism depends on the solubility of the polymers. For example, oligo(DL-lactide) (DLLA)-grafted dextrans are hydrolytically degraded depending on the solubility of the graft copolymers in water media [159]. Figure 21.3 shows the expected hydrolytic degradation processes for water-soluble and water-insoluble graft copolymers. In both processes, the largest part of the dextran was released in the first two weeks. Also, Li et al. indicated that the ester cleavage mechanism of dextran-*g*-poly(lactide-*co*-glycolide) (P(LA-*co*-GA)) varied depending on the charge type (positive or negative) of the dextran [256]. That is, positively charged diethylaminoethyl dextran chloride-*g*-P(LA-*co*-GA) was randomly cleaved at the ester groups, whereas cleavage at the ester groups in the vicinity of the branching points predominated for negatively charged dextran sulfate sodium-*g*-P(LA-*co*-GA).

When the polymer contains two types of linkages of ester and amide groups, as in the case of polyesteramide synthesized by polycondensation using sebacoyl chloride, 1,6-diaminohexane, and telechelic oligomers of L-lactide (LLA), the ester linkages, not amide linkages, are predominantly cleaved in NHD [105].

During the course of hydrolytic degradation, low-molecular-weight water-soluble oligomers and monomers are formed by the cleavage of chains and are released from the mother materials, resulting in weight loss. The degree of

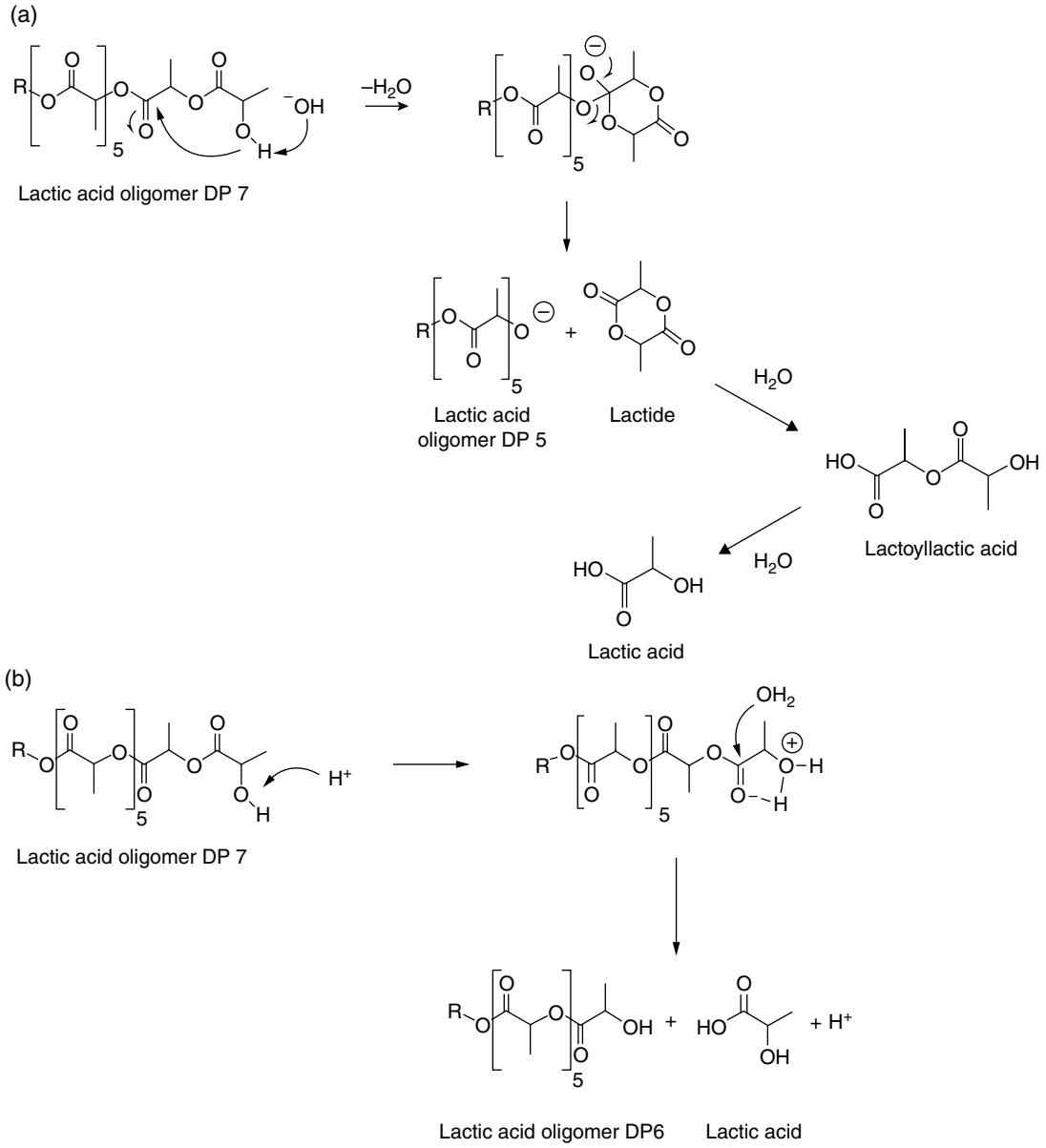


**FIGURE 21.2** Hydrolytic chain cleavage mechanisms of PLLA in alkaline (a) and acidic (b) solutions. *Source*: Adapted from Ref. 94. Copyright 2001, with permission from Elsevier.

polymerization of such water-soluble lactic acid oligomers and monomers formed can be determined by high-performance liquid chromatography (HPLC) or by their chemical shift values from $^1$H NMR spectroscopy [355]. In the case of NHD at 70°C, water-soluble oligomers and monomers were composed of 1–13 lactic acid units, which were not toxic to human umbilical vein endothelial cells [70].

### 21.2.2 Material Degradation Mechanism

A surface erosion mechanism takes place when the hydrolytic degradation rate of the material surface in contact with water (containing catalytic substances such as alkalis and enzymes) is much higher than the diffusion rate of water molecules or catalytic substances within the material. In such a case, the hydrolytic degradation seems to occur solely on the material surface because the hydrolytic degradation rate is much higher on the surface than at the core (Figure 21.4a) [1, 356]. In contrast, a bulk erosion mechanism occurs when the hydrolytic degradation rate of the material surface is lower than the diffusion rate of water, and therefore hydrolytic degradation takes place homogeneously, irrespective of the depth from the material surface (Figure 21.4b). Material thickness is an important factor for determining the hydrolytic degradation mechanism. As can be expected, the hydrolytic degradation mechanism changes from a bulk erosion mechanism to a

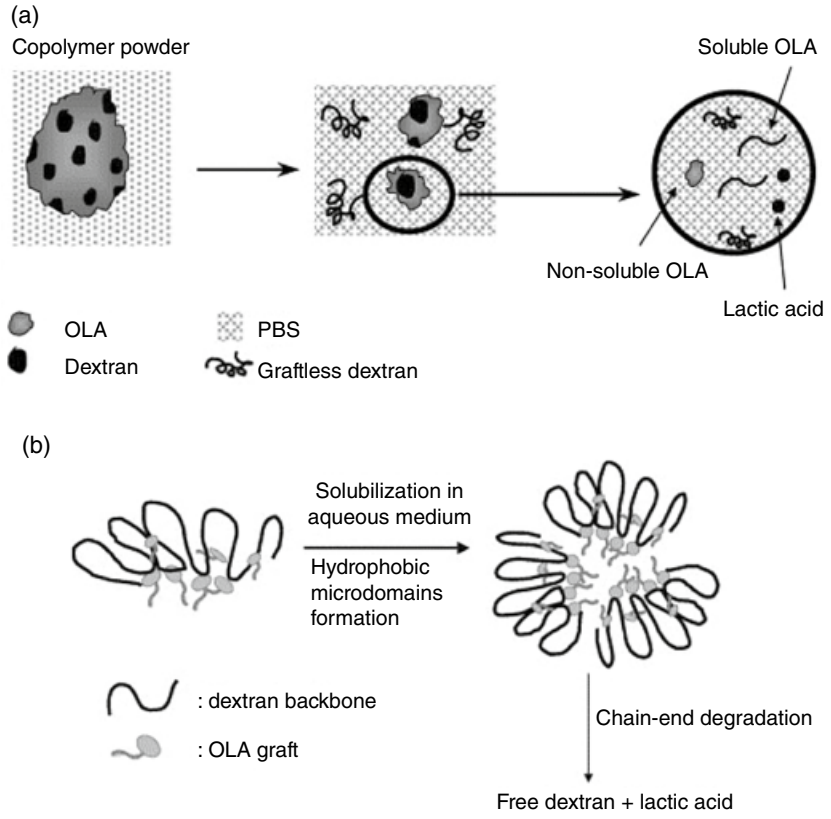


**FIGURE 21.3** Expected processes of hydrolytic degradation of water-insoluble (a) and water-soluble (b) oligo(DL-lactide)-grafted dextrans in a phosphate-buffered solution. *Source*: Reprinted from Ref. 159. Copyright 2005, with permission from Elsevier.

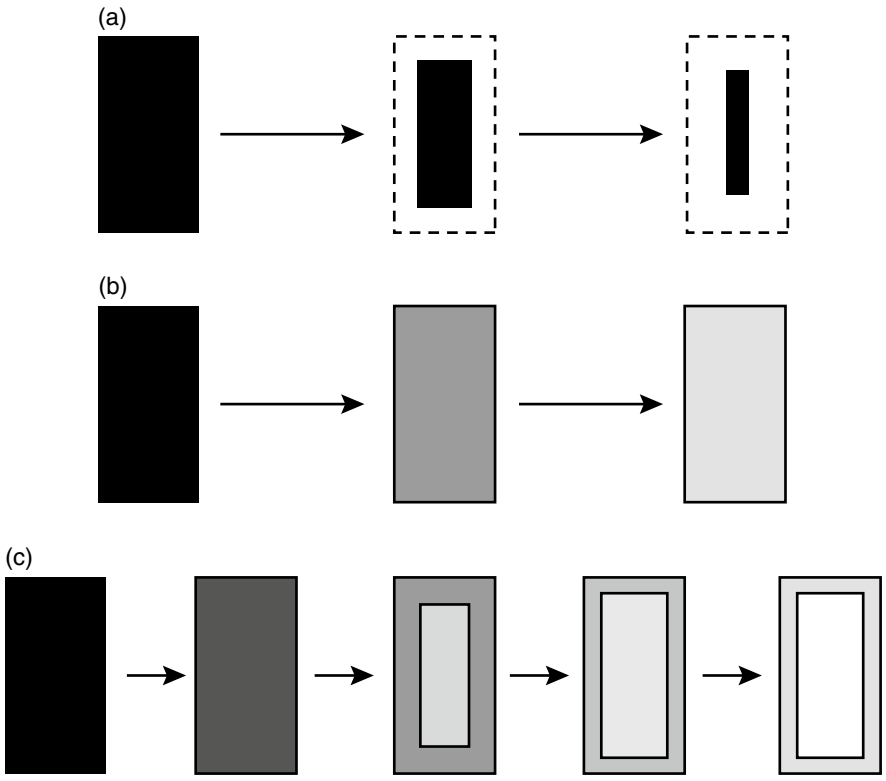


**FIGURE 21.4** Hydrolytic degradation mechanisms of bulky PLA materials: (a) surface erosion, (b) bulk erosion, and (c) core-accelerated bulk erosion [1, 356].

**TABLE 21.4 Critical Thickness ($L_{critical}$) of Biodegradable Polyesters, Above Which Hydrolytic Degradation Mechanism Changes from Bulk Erosion to Surface Erosion [176]**

| Polymer | Molecular Structure/Example | $L_{critical}$ |
|---|---|---|
| Poly(anhydride) | $(-R-CO-O-CO-)_n$ | 75 μm |
| Poly(ketal) | $(-O-CR^1R^2-O-R^3-)_n$ | 0.4 mm |
| Poly(ortho ester) | $(-O-CR^1(OR^2)-O-R^3-)_n$ | 0.6 mm |
| Poly(ε-hydroxycarboxylic acid) | $(-O-(CH_2)_5-CO-)_n$ poly(ε-caprolactone) | 1.3 cm |
| Poly(acetal) | $(-O-CHR^1-O-R^2-)_n$ | 2.4 cm |
| Poly(α-hydroxycarboxylic acid) | $(-O-CH(CH_3)-CO-)_n$, poly(lactic acid), poly(lactide) | 7.4 cm |
| Poly(amide) | $(-NH-R-CO-)_n$ | 13.4 m |

surface erosion mechanism when the material thickness is higher than the critical thickness ($L_{critical}$), as summarized in Table 21.4 [176]. For example, for poly(DLLA-*co*-1,3-trimethylene carbonate (TMC)), cylindrical specimens with diameters of 2.5 mm were hydrolytically degraded in a neutral medium via a surface erosion mechanism [210]. As expected, this means that copolymerization with TMC increased the hydrolytic degradation rate of PDLLA and, therefore, lowered the $L_{critical}$ value.

On the other hand, as reported by Vert and coworkers, in the cases of PDLLA [116], PLLA [24, 29], poly(L-lactide-*co*-glycolide) (poly(L-lactic acid-*co*-glycolic acid) (P(LLA-*co*-GA))) [148], P(DLLA-*co*-GA) [148], PDLLA-*b*-PEO [226], and PLLA-*b*-PEO-*b*-PLLA [233], NHD proceeds via core-accelerated bulk erosion when the materials are thicker than 0.5–2 mm. In such cases, hydrolysis-formed oligomers and monomers with a high catalytic effect are trapped and accumulated in the core part of the materials [357]. This results in accelerated hydrolytic degradation in the core part (core-accelerated bulk erosion), as shown in Figure 21.4c. Therefore, the hydrolytic degradation of PLA proceeds via bulk erosion, core-accelerated erosion, and surface erosion mechanisms for material thicknesses lower than 0.5–2 mm, between 0.5–2 mm and 7.4 cm, and higher than 7.4 cm, respectively.

Two- or more-armed PLLA and PDLLA are different from 1-armed PLLA and PDLLA in that the former has the incorporated coinitiator moiety in the middle of the chains and the chain direction changes (i.e., —CO—O— or —O—CO—) at the coinitiator moiety. Three- or more-armed PLLA and PDLLA are different from two-armed PLLA and PDLLA in that the former has a branching structure. With increasing arm-number or decreasing molecular weight, the density of hydroxy groups that contributes to hydrogen bonding increases, thereby affecting the material degradation mechanism. The degradation mechanism of crystallizable PLLA depends on arm-number, initial crystallinity, and molecular weight [100]. The NHD mechanism of amorphous and crystallized linear two-armed PLLAs (thickness = 100 μm) changed from bulk erosion to surface erosion with decreasing initial $M_n$ [100]. On the other hand, crystallized higher molecular weight branched four-armed PLLAs degraded via bulk erosion, whereas the degradation mechanism of other (low molecular weight and/or amorphous) branched four-armed PLLAs could not be determined [100]. Iñiguez-Franco reported that alkaline hydrolytic degradation of linear one-armed PLLA (thickness = 25 μm) at 80°C proceeded via bulk erosion, whereas branched PLLA (thickness = 21 μm) proceeded via surface erosion [96]. To exclude the effects of crystallizability on hydrolytic degradation, one- and multi-armed PDLLA were used (thickness = 100 μm) [133]. NHD of one-armed PDLLA and two-armed PDLLA at 97°C proceeded via bulk erosion; significant surface erosion occurred in the two-armed PDLLA [133]. The pure effect of branching was investigated using two- and four-armed PDLLA (thickness = 50 μm) [134]. The NHD of two-armed PDLLA and four-armed PDLLA at 97°C proceeded mainly via bulk and surface erosion mechanisms, respectively [134]. However, two-armed PDLLA acquired an additional surface erosion nature with decreasing molecular weight [134]. That is, surface erosion becomes a main degradation mechanism when the density of terminal hydroxy groups that induce hydrogen bonding is high, which probably decreases the diffusion rate of water molecules into the materials.

Li summarized the morphological changes and crystallization during hydrolytic degradation of PLA-based materials as shown in Figure 21.5 [358]. The triangle can be divided into two zones; C zones are composed of intrinsically semicrystalline polymers and A zones of intrinsically amorphous polymers. For A1 polymers, degradation leads to hollow structures that remain amorphous because of the high irregularity of the polymer chain structures. For A2 polymers, degradation leads to hollow structures that will partially crystallize and the crystalline structure of formed crystallites depends on the initial composition. For A3 polymers, no hollow structures can be obtained and both the surface and the interior crystallize [358].

Yoshioka et al. [166] found that the NHD of porous P(LLA-*co*-GA) proceeded via bulk and surface erosion mechanisms for periods shorter and longer than 12 weeks, respectively. That is, the degradation mechanism varied depending on the degradation period.

PLLA, PDLA, and copolymers having sufficiently long monomer sequence length are crystallizable. Upon

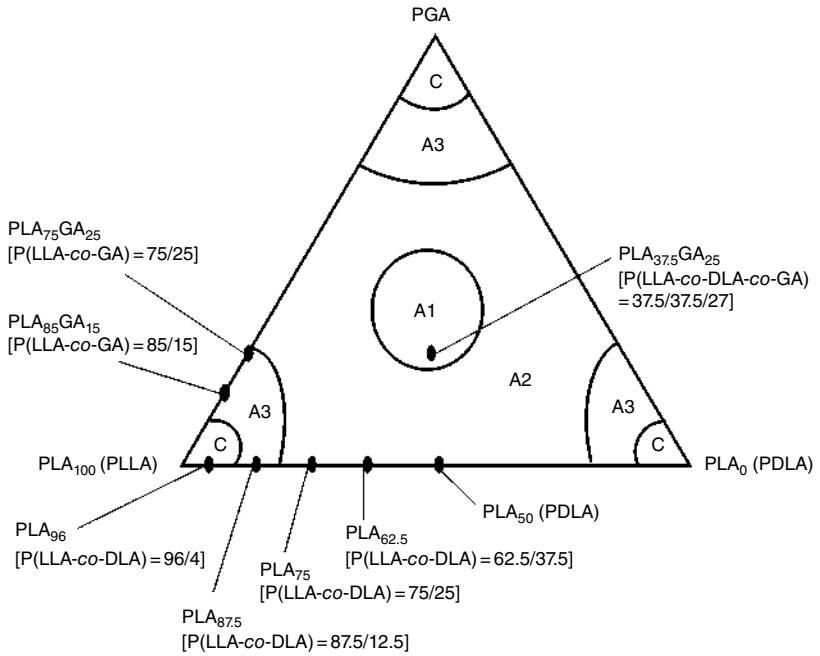


**FIGURE 21.5** Schematic representation of the hydrolytic degradation behavior of P(LA-*co*-GA). *Source*: Adopted from Ref. 358. Copyright 2002, with permission from John Wiley & Sons, Inc.

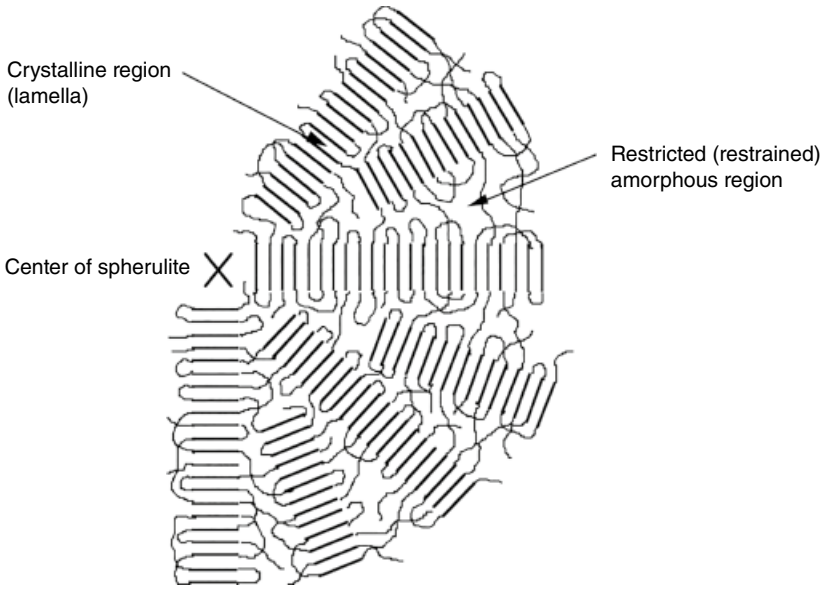


**FIGURE 21.6** Schematic representation of spherulitic structure [356].

crystallization, some amorphous chains are assembled to form crystalline regions, as depicted in Figure 21.6 [356]. Normally, crystallization takes place via the growth of spherulites (i.e., three-dimensional assemblies composed of crystalline and amorphous regions). The chains in the crystalline regions are more hydrolysis resistant compared with those in the amorphous regions because the access of water molecules to the chains inside the rigid crystalline regions is prohibited. This causes selective or predominantly hydrolytic cleavage of chains in the amorphous regions and removal of hydrolysis-formed water-soluble oligomers and monomers. As a result of selective hydrolytic degradation and removal of the chains in the amorphous regions, the crystalline regions remain. Such crystalline regions are called "crystalline residues" (Figure 21.7) [69, 356]. Figure 21.8a shows the gel permeation chromatography (GPC) profiles of crystallized PLLA films hydrolytically degraded in a phosphate-buffered solution (37°C and pH

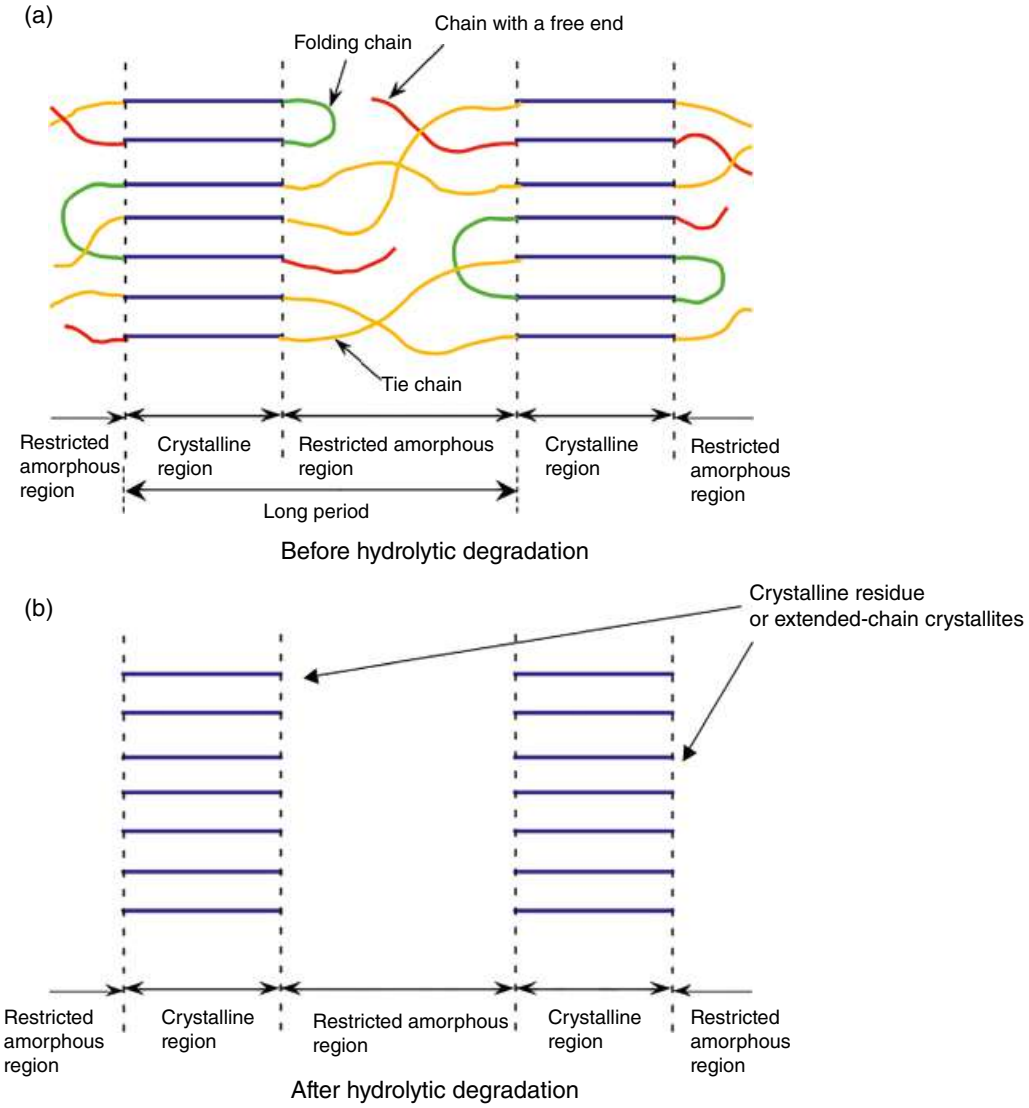


**FIGURE 21.7** Schematic representation of structures of crystallized PLA material (a and b) before and after hydrolytic degradation, or of the formation of crystalline residues (or extended-chain crystallites) [69, 356].

7.4) for different periods [31]. In this case, hydrolytic degradation took place via the bulk erosion mechanism, and therefore the total peak was shifted to a lower molecular weight with degradation time. Specific peaks at $2 \times 10^4$ and $1 \times 10^4$ g/mol were observed for the degradation period of 24 months. The height of the peak at $2 \times 10^4$ g/mol decreased compared to the one at $1 \times 10^4$ g/mol as time increased. These two peaks were attributed to the molecular weight of onefold and twofolds of the chains in the crystalline regions. Therefore, the relative peak height change indicated the hydrolytic scission of folding chains. Similar to this, also in an alkaline medium, the specific peak ascribed to crystalline residues at $1 \times 10^4$ g/mol became higher with degradation time [52] (Figure 21.8b). However, in this case hydrolytic degradation proceeded via a surface erosion mechanism, and therefore the peak appearing at $10^5$–$10^6$ g/mol was ascribed to the core part of the crystallized PLLA that became smaller with an increase in degradation time.

The predominant removal of amorphous chains in Vicryl™ (P(LA–GA) (92/8)) can be understood by the disappearance of amorphous peaks and the enlargement of crystalline peaks observed using infrared spectroscopy with the ATR technique [175]. Wide-angle X-ray diffraction in the [130, 020] directions revealed that crystalline sizes perpendicular to the fiber axis remained unchanged, whereas that in the [002] direction indicated that the crystalline size parallel to the fiber axis significantly decreased [175]. This reflects the fact that hydrolytic degradation proceeds from the folding surface and not from the sides of crystalline regions. Moreover, the decrease of long period, which is defined in Figure 21.7, was traced by small-angle X-ray scattering (SAXS) measurements. Solid-state $^{13}$C NMR spectroscopy revealed that upon

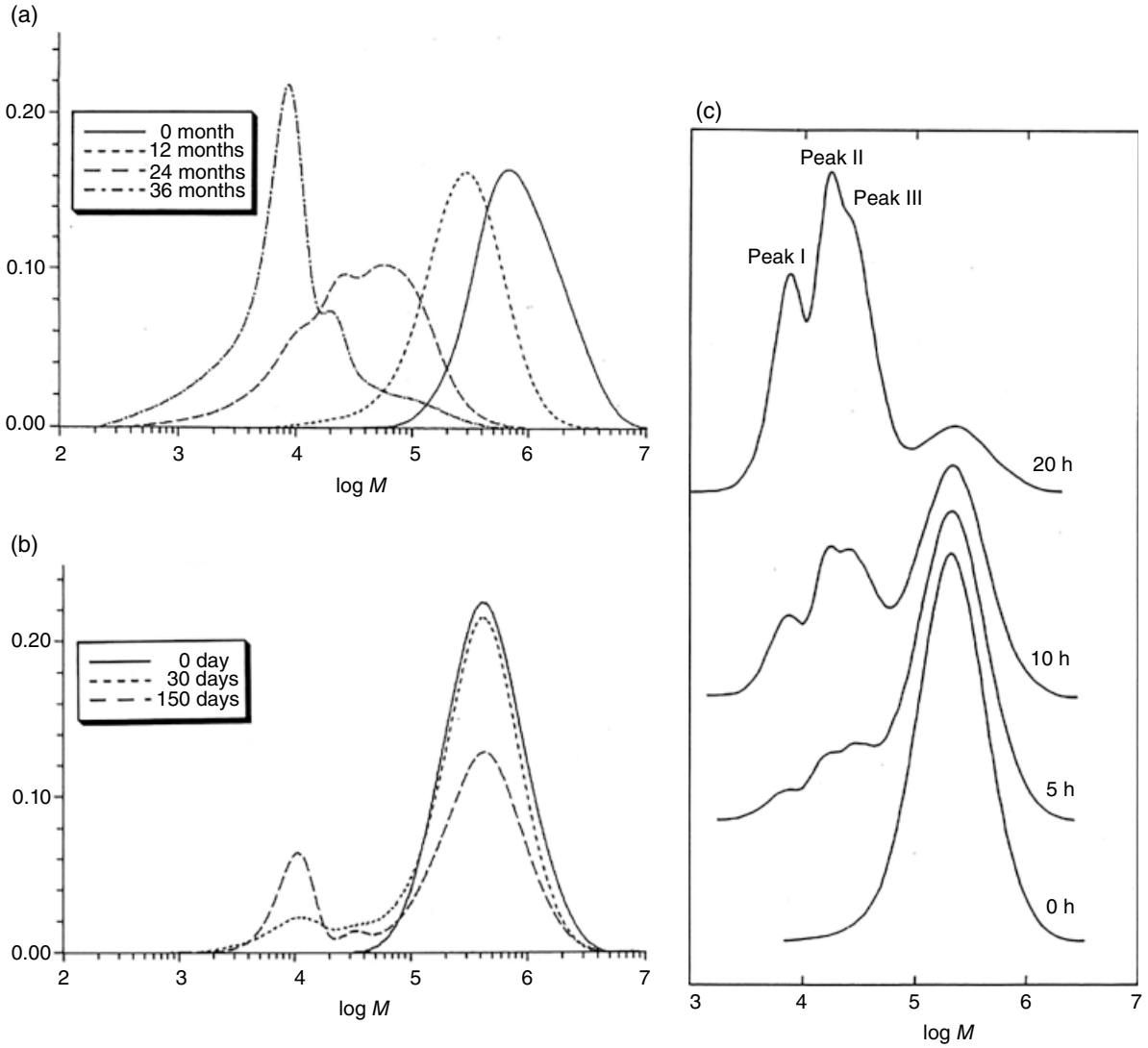


**FIGURE 21.8** GPC profiles of crystallized PLLA films hydrolytically degraded at 37°C in a phosphate-buffered solution (pH 7.4) [31] (a), NaOH solution (pH 12) [49] (b), and proteinase K/Tris–HCl-buffered solution (pH 8.6) [359] (c) for different periods.

hydrolytic degradation, the chain mobility slightly increased in both crystalline and noncrystalline (amorphous) regions by lowering crystalline thickness and shortening noncrystalline (amorphous) chains, respectively [42].

The hydrolyzability of the chains in the amorphous region between crystalline regions is influenced by the types of media. The amorphous region between crystalline regions is called the "restricted amorphous region" or the "restrained amorphous region," while that outside the spherulites or in completely amorphous materials is called the "free amorphous region." The restricted amorphous region contains three types of chains: tie chains, folding chains, and chains with a free end (Figure 21.7a). In acidic, neutral, and alkaline solutions, all three types of chains were cleaved by hydrolytic degradation, but proteinase K catalyzed the cleavage of only the tie chains and the long chains with a free end and not the folding chains and the short chains with a free end. In other words, proteinase K cannot catalyze the hydrolytic degradation of the chains neighboring on the crystalline regions. This is evidenced by the GPC profiles change of crystallized PLLA hydrolyzed in the presence of proteinase K [359] (Figure 21.8c). This is discussed in detail in Chapter 22.

When PLA-based materials are hydrolytically degraded via a bulk erosion mechanism, the degradation can be divided into at least three stages: (i) initial hydration or water absorption of materials; (ii) gradual decrease in molecular weight without weight loss; and (iii) weight loss through the formation and dissolution of water-soluble oligomers and monomers. For P(DLLA-*co*-GA), Huang et al. [167] added a fourth stage wherein the pores diminished or collapsed. In their classification, micropores are formed in the second stage and are enlarged in the third stage. On the other hand,

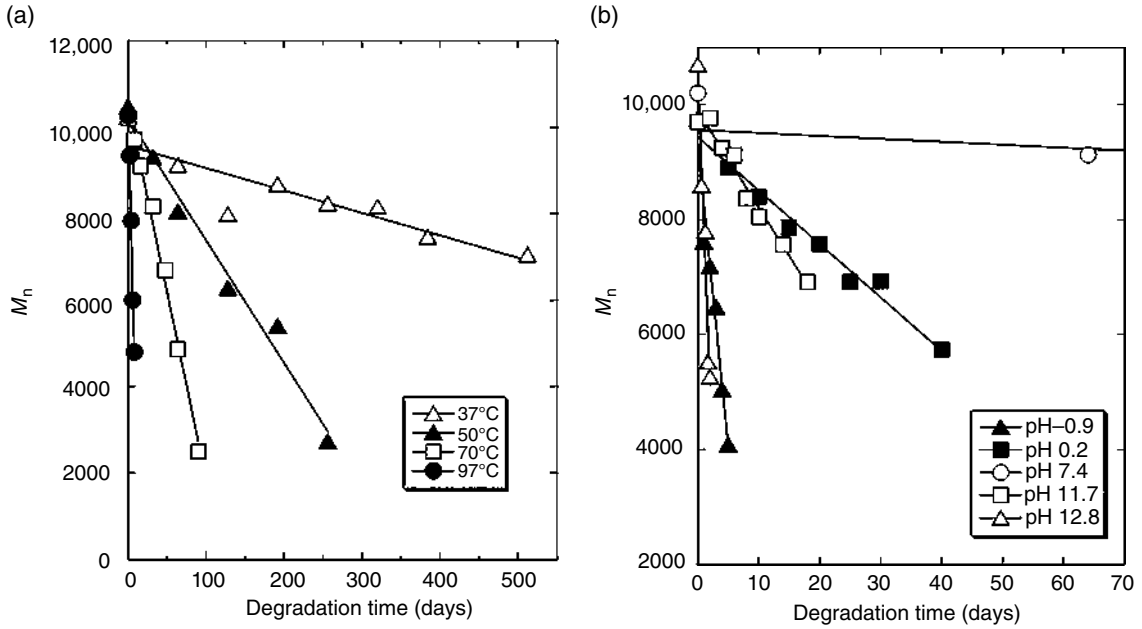


**FIGURE 21.9** $M_n$ change of PLLA crystalline residues during the course of hydrolytic degradation at pH 7.4 and different temperatures (a) [43, 69] and at 37°C and different pH (b) [44].

during the course of NHD of block copolymers of PLLA-*b*-PEO-*b*-PLLA initially having relatively long PLLA units, gels composed of block copolymers having short PLA chains are formed on the material surface and are connected to that surface by PLLA crystallites as a linkage [230].

Iwata and Doi investigated the alkaline hydrolytic degradation mechanism of single crystals of PLLA grown in *p*-xylene solution [53]. Single crystals of PLLA were first degraded at the loose chain-packing region on the crystal edges, and then gradually from both the crystal edges and the tight chain-packing region, accompanied by chain folding on the crystal surface. In contrast, Jo et al. concluded from the low-molecular-weight fractions traced by GPC that the initial stage of alkaline hydrolytic degradation of single crystals of PLLA grown in acetonitrile proceeded in loosely folding chains [88].

### 21.2.3 Degradation of Crystalline Residues

In the first stage of hydrolytic degradation of crystallized PLLA materials, the chains in amorphous regions are predominantly degraded and removed as water-soluble oligomers and monomers (Figure 21.7). As a result, only the crystalline regions remain [28, 31, 32, 52, 75]. Such remaining crystalline regions have extended-chain crystallite structures and are called "crystalline residues." Most of the reported studies on hydrolytic degradation of PLA-based materials are concerned with hydrolytic degradation at an early stage. However, there have been a few studies regarding the late stage of hydrolytic degradation, that is, hydrolytic degradation of "crystalline residues." We have prepared PLLA crystalline residues by accelerated NHD of crystallized PLLA films in a phosphate-buffered solution at pH 7.4. The crystalline residues were hydrolytically degraded at different temperatures and pH 7.4 and at different pH values and 37°C (Figure 21.9) [43, 44, 69]. As seen from Figure 21.9, the number-average molecular weight ($M_n$) of PLLA crystalline residues decreased monotonically with degradation time, and the hydrolytic degradation rate constant ($k$) estimated from the following equation was constant, irrespective of the $M_n$ values:

$$M_n(t_2) = M_n(t_1) - k(t_2 - t_1) \tag{21.1}$$

where $M_n(t_2)$ and $M_n(t_1)$ are the $M_n$ values at the hydrolytic degradation times of $t_2$ and $t_1$, respectively. The obtained $k$ values for PLLA crystalline residues were 5.31, 27.8, 86.5, and 710 g/(mol day) at pH 7.4 for 37, 50, 70, and 97°C, respectively [43, 69]. Utilizing these $k$ values, the overall periods required for crystalline residues having an initial $M_n$ of $1.0 \times 10^4$ g/mol to reach the molecular weight of L-lactic acid, 90 g/mol, were evaluated to be $1.8 \times 10^3$, $3.6 \times 10^2$, $1.2 \times 10^2$, and 14 days for 37, 50, 70, and 97°C, respectively [43, 69]. Joziasse et al. [27] estimated that the resorption times required for as-polymerized or hot-drawn PLLA to be hydrolytically degraded to lactic acid were 40–50 and 50 years, respectively. Also, Suuronen et al. reported that the molecular weight of crystalline residues remained unchanged for three years after their formation in a phosphate-buffered solution at pH 6.1 [265].

The Arrhenius plot of these $k$ values yields the activation energy for the hydrolytic degradation ($\Delta E_h$) of PLLA crystalline residues (which should be α-form considering crystallization temperature of initial PLLA samples). The obtained $\Delta E_h$ of PLLA crystalline residues (α-form) was 75.2 kJ/mol, which was significantly higher than the 50.9 kJ/mol obtained by us for PLLA in the melt in the temperature range of 180–250°C [78], but was slightly lower than the 83.7 and 83.3 kJ/mol reported by Makino et al. [16] for PLLA and PDLLA microspheres, respectively, as solids in a temperature range below the glass transition temperature ($T_g$) (21–45°C). $\Delta E_h$ of PLLA/PDLA stereocomplex crystalline residues was estimated to be 97.3 kJ/mol [58], which was higher than that of PLLA crystalline residues (α-form) (75.2 kJ/mol), as expected.

The melting temperature ($T_m$) of crystalline regions can be expressed as a function of the reciprocal of crystalline thickness ($l_c$), that is, $l_c^{-1}$, according to the Thomson–Gibbs equation given below [361]:

$$T_m(\mathrm{K}) = T_m^0\left[\frac{1-2\sigma_e}{l_c\rho_c\Delta H_m^0}\right] \tag{21.2}$$

where $T_m^0$, $\sigma_e$, $\Delta H_m^0$, and $\rho_c$ are equilibrium $T_m$, specific fold surface free energy, heat of fusion per unit mass, and crystal density, respectively. In the case of PLLA crystalline residues (or extended-chain crystallites), $l_c$ can be estimated from $M_n$ using the following equation:

$$l_c(\mathrm{nm}) = \frac{0.288\times(0.80\times M_n)}{72.1} \tag{21.3}$$

where the chains in the crystalline residues are assumed to take $10_3$ helix with a length of 28.8 nm along the $c$-axis [361, 362] and the amorphous chains on the "fold surface" are negligibly short compared to those of the crystalline chains, while 0.80 is the parameter for PLLA that converts $M_n$ for the polystyrene standard to absolute $M_n$ [75] and 72.1 is the mass per mole of lactyl unit (half of a lactide unit). The $l_c$ value can be calculated using Equation 21.4 from $L$, the enthalpy of melting ($\Delta H_m$), and the $\Delta H_m^0$ values:

$$l_c(\mathrm{nm}) = \frac{L\Delta H_m}{\Delta H_m^0} \tag{21.4}$$

Using Equations 21.3 and 21.4, Equation 21.2 can be written as

$$T_m(\mathrm{K}) = T_m^0\left[\frac{1-626\sigma_e}{\rho_c M_n\Delta H_m^0}\right] \tag{21.5}$$

$$T_m(\mathrm{K}) = T_m^0\left[\frac{1-2\sigma_e}{L\rho_c\Delta H_m}\right] \tag{21.6}$$

To estimate $\sigma_e$, $T_m$ should be plotted as a function of $(M_n)^{-1}$ or $(L\Delta H_m)^{-1}$ (Figure 21.10) [69] according to Equation 21.5 or 21.6. The $\sigma_e$ values were estimated from the slopes and $T_m^0$ using $\rho_c$ of 1.29 g/cm$^3$ [363] and $\Delta H_m^0$ values of 135 [364] or 93 J/g [363]. The obtained $\sigma_e$ values are summarized in Table 21.5 [69, 75, 360, 365–374], together with the reported values [167, 364–366, 371]. As the $\sigma_e$ values estimated using Equation 21.5 depend on $\Delta H_m^0$, we have utilized the representative $\Delta H_m^0$ values of 135 and 93 J/g [363, 364], and the $\sigma_e$ values obtained with these two values are abbreviated as $\sigma_e(135)$ and $\sigma_e(93)$, respectively. The $\sigma_e(135)$ and $\sigma_e(93)$ values estimated for the crystalline residues (extended-chain crystallites) having surfaces composed of very short chains with a free end were 55.6–56.4 and 38.3–38.8 erg/cm$^2$, respectively. The $\sigma_e(135)$ and $\sigma_e(93)$ values estimated from Figure 21.10 using Equation 21.6 are identical (39.9 erg/cm$^2$) because $\Delta H_m^0$ is not explicitly contained in Equation 21.6. In marked contrast with the $T_m^0$ values, the estimated $\sigma_e$ values vary dramatically depending on the procedure and the parameters used for their calculation. The $\sigma_e$ values for PLLA/PDLA stereocomplex have been estimated, using the same procedure for PLLA crystalline residues [272], $T_m^0 = 279$°C [375], $\Delta H_m^0 = 146$ J/g [376]. Thus obtained $\sigma_e(146)$ = 21.1, 32.0, and 26.0 erg/cm$^2$ for hydrolytic degradation at 70, 85, and 97°C, respectively [272].

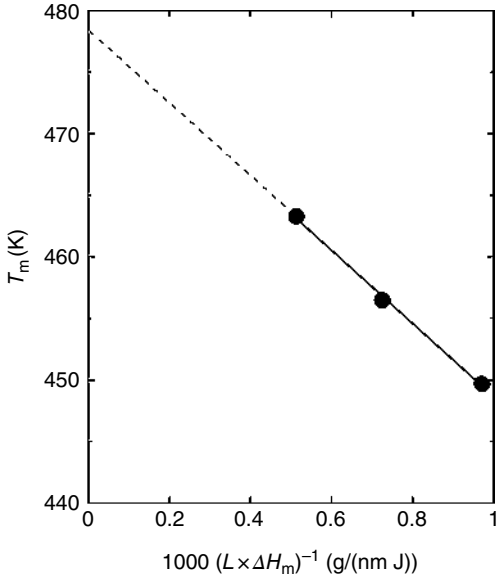


**FIGURE 21.10** $T_m$ of crystallized PLLA films crystallized at different temperatures as functions of $(L\times\Delta H_m)^{-1}$ [69].

A lower $T_m$ appeared in addition to the main $T_m$ when crystallized PLLA films were hydrolytically degraded to a great extent in the presence of proteinase K [359, 377]. In the enzymatic hydrolytic degradation, the tie chains and the chains with a free end in the amorphous regions were predominantly degraded and removed but the folding chains were not degraded, resulting in the formation of surfaces composed of very short chains with a free end and folding chains, which are in contact with the air. The surface

**TABLE 21.5 Equilibrium Melting Temperature ($T_m^0$) and "Folding Surface" Free Energy ($\sigma_e$) for PLLA Having Different "Folding Surface" Structures [69, 75, 360, 365–374]**

| Specimen | Type | Structures of Folding Surface | $T_m^0$ (TG)[a] (K) | $T_m^0$ (HW)[b] (K) | $T_m^0$ (M)[c] (K) | $\sigma_e$(135)[d] (erg/cm$^2$) | $\sigma_e$(93)[e] (erg/cm$^2$) | $\sigma_e$(146)[f] (erg/cm$^2$) |
|---|---|---|---|---|---|---|---|---|
| PLLA | Crystalline residues (extended-chain crystallites) | Very short chains with a free end (neighboring the air) | | | | | | |
| | Hydrolyzed at 50°C [69] | | 464.5 | | | 55.8 | 38.4 | |
| | Hydrolyzed at 70°C [69] | | 464.9 | | | 55.6 | 38.3 | |
| | Hydrolyzed at 97°C [69] | | 464.5 | | | 56.4 | 38.8 | |
| | Crystallized films | Folding chains, tie chains, chains with a free end | | | | | | |
| | Kalb and Pennings [365] | | | 488 | | | | |
| | Vasanthakumari and Pennings [366] | | | 480 | | | 61 | |
| | Tsuji and Ikada [367–369] | | | 478–485 | | | | |
| | Huang et al. [167] | | | | | | 60 | |
| | Miyata and Masuko [364] | | | | | 63–107 | | |
| | Abe et al. [370] | | | | 500.1 | | | |
| | Tsuji et al. [75] | | 478.3[g] | | | 39.9[g] | 39.9[g] | |
| | Single crystals | Folding chains, a trace amount of chains with a free end (neighboring the air) | | | | | | |
| | Hoffman et al. [371] | | | | | | 53 ± 4 | |
| | Kalb and Pennings [365] | | | | | | 75 | |
| PLLA/PDLA stereocomplex | Crystalline residues (extended-chain crystallites) | Very short chains with a free end (neighboring the air) | | | | | | |
| | Hydrolyzed at 70°C [272] | | 279 | | | | | 21.1 |
| | Hydrolyzed at 85°C [272] | | 279 | | | | | 32.0 |
| | Hydrolyzed at 97°C [272] | | 279 | | | | | 26.0 |

[a] The $T_m^0$ value obtained by Thomson–Gibbs equation [360].
[b] The $T_m^0$ value obtained by Hoffman–Weeks procedure [372].
[c] The $T_m^0$ value obtained by Marand et al. procedure [373, 374].
[d] The $\sigma_e$ value for $\Delta H_m$(100%) = 135 J/g for PLLA.
[e] The $\sigma_e$ value for $\Delta H_m$(100%) = 93 J/g for PLLA.
[f] The $\sigma_e$ value for $\Delta H_m$(100%) = 146 J/g for PLLA/PDLA stereocomplex.
[g] The given values have been calculated in the present article based on the data reported in Ref. [75].

structure and environment (neighboring the same type of chains or air) of the crystalline regions after enzymatic hydrolytic degradation are similar to those of the crystalline residues (or extended-chain crystallites), where both surfaces have very short chains with a free end in contact with the air. This observation and Equation 21.2 strongly suggest that the $\sigma_e$ value for a surface composed of very short chains with a free end in the crystalline residues (extended-chain crystallites) is much lower than that for the initial "folding surface" composed of the three types of amorphous chains before hydrolytic degradation. The gradual decrease in $T_m$ at a relatively late stage of hydrolytic degradation of crystallized PLLA materials in vitro in a PBS or the Ringer solution, and in vivo [1], is attributable not only to a decrease in crystalline thickness but also to structural and environmental changes at the "folding surface."

## 21.3 PARAMETERS FOR HYDROLYTIC DEGRADATION

The hydrolytic degradation mechanism, rate, and behavior are affected by the parameters of materials and media, as summarized in Table 21.2. The material parameters include molecular and highly ordered structures, additives including other polymers and fibers, and the material morphology. The medium parameters include the type and concentrations of catalytic species and other solutes, pH, temperature, and the type and density of microbes.

### 21.3.1 Effects of Surrounding Media

Before discussing the effects of material parameters, those of the surrounding media are briefly stated. PLA is utilized as biomedical scaffold material, and therefore in vitro hydrolytic degradation experiments under the conditions of 37°C and pH 7.4, which are very similar to those in vivo degradation experiments in the human body, are frequently utilized [23, 25, 378]. However, for P(LA-*co*-GA) microspheres, enzymatic degradation is reported to be dominant for subcutaneous implantation; its total degradation was faster than NHD [171, 257], and the difference in massive P(LA-*co*-GA) degradation between in vivo and in vitro cases depends on the polymer composition [378]. Furthermore, the degradation rate of PDLLA in the femur was lower than that of NHD in a phosphate-buffered solution [124]. In the human body, hydrolytic degradation of PLA-based materials with normal dimensions (i.e., thickness lower than the critical thickness ($L_{critical}$)) is known to proceed via a bulk erosion mechanism and not a surface erosion mechanism [176].

***21.3.1.1 pH*** Hydrolytic degradation of PLA-based materials involves the cleavage of ester groups, and therefore the reaction is catalyzed by the presence of hydronium and hydroxide ions. The high concentration of hydroxide ions in alkaline media strongly accelerates the hydrolytic degradation of PLA-based materials [16, 17, 51, 52, 54, 145, 177]. Therefore, alkaline media can be used for an acceleration test of hydrolyzable polymeric materials. However, it should be noted that degradation in alkaline media proceeds via a surface erosion mechanism, not a bulk erosion mechanism as in the human body, although the acceleration test is a good method to monitor the hydrolyzability of a polymer (not a material) in a short period. With respect to the hydrolytic degradation of a monolayer, Kulkarni et al. [112] and Thanki et al. [159] indicated that the degradation of PDLLA and P(DLLA–GA) was enhanced at low and high pH and that no significant end cap effect was observed at high pH.

Similar to alkaline media, acidic media accelerate the hydrolytic degradation of PLA-based materials [16, 17, 60]. However, hydronium ions have no significant or a very low catalytic effect on the hydrolytic degradation of PLA-based materials compared with that of alkalis when the molecular weight of PLA is higher than $1 \times 10^5$ g/mol [61, 113, 115]. In contrast, the hydrolytic degradation of poly(L-lactide-*co*-ε-caprolactone) (P(LLA-*co*-CL)) monofilament sutures was not influenced by pH when degradation was monitored by weight loss [188].

***21.3.1.2 Temperature*** The hydrolytic degradation temperature ($T_h$) can be divided into three ranges: $T_h < T_g$, $T_g \le T_h < T_m$, $T_m \le T_h$. Reed and Gilding [21] revealed that the NHD rate traced by mechanical properties dramatically increased when the degradation temperature was elevated over $T_g$. Limsukon et al. reported that in the case of PLA modified with a multifunctional epoxy-based chain extender, short-term hydrolysis behavior at 85°C well predicted the long-term hydrolysis behavior at 40°C in water [97]. The hydrolytic degradation mechanism of crystallizable PLA-based materials varies when the degradation temperature becomes higher than $T_m$. At $T_h$ exceeding $T_m$, crystalline regions melt and disappear, and hydrolytic degradation in the melt takes place homogeneously, as does that in noncrystallizable PDLLA. Figure 21.11 shows the time changes in the GPC profiles of crystallized PLLA films hydrolytically degraded in the solid state at 97°C ($T_h < T_m$) [74] and PLLA hydrolytically degraded in the melt at 200°C ($T_m \le T_h$) [78]. At 97°C (in the solid state), the molecular weight distribution peak shifted as a whole to a lower molecular weight, specific peaks due to the chains in the crystalline residues appeared at 24 h and that at $1 \times 10^4$ g/mol remained (Figure 21.11a), as in hydrolytic degradation at 37°C [31, 32]. In marked contrast, at 200°C (in the melt), the molecular weight distribution peak shifted completely to a lower molecular weight, down to $1 \times 10^3$ g/mol at 21 min without the formation of specific peaks due to the chains in the crystalline residues (Figure 21.11b). Figure 21.12 shows the Arrhenius plot of the hydrolytic degradation rate constant ($k$)

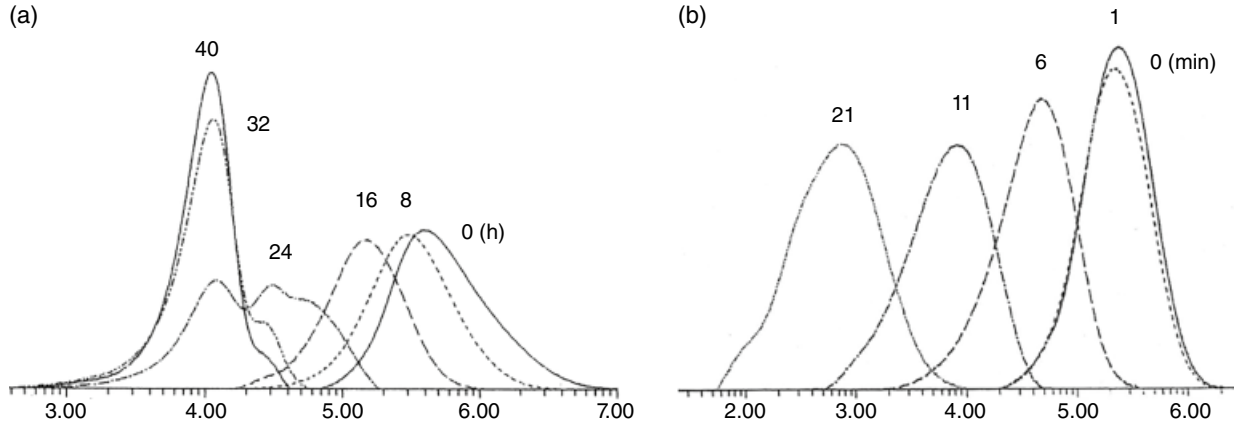


**FIGURE 21.11** GPC profiles of crystallized PLLA films hydrolytically degraded in the solid state at 97°C ($T_h < T_m$) (a) [74] and PLLA hydrolytically degraded in the melt at 200°C ($T_m < T_h$) (b) [78].

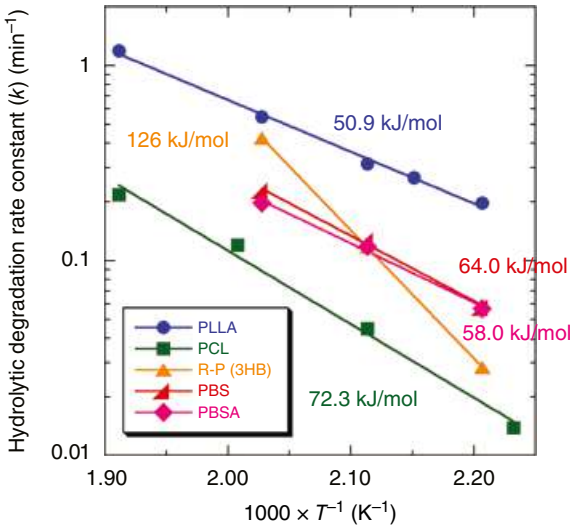


**FIGURE 21.12** Arrhenius plots of PLLA, P(*R*-3HB), PCL, PBS, and PBSA in the melt [78, 380–382].

of PLLA [78] in the melt estimated from the following equation [78, 379], together with those of other biodegradable polyesters derived from hydroxycarboxylic acid or from diol and dicarboxylic acid in the melt [380–382]:

$$\ln M_n(t_2) = \ln M_n(t_1) - k(t_2 - t_1) \qquad (21.7)$$

As seen in Figure 21.12, of the well-known biodegradable aliphatic polyesters, PLLA has the highest $k$ values, at least at 180–220°C ($1000 \times T^{-1} = 2.21$–$2.03\ K^{-1}$). This result indicates that hydrolyzability of PLLA is the highest among the biodegradable polyesters.

The activation energy values hydrolytic degradation ($\Delta E_h$) in the melt were obtained from the plots in Figure 21.12. The $\Delta E_h$ values and equations for $k$ against the degradation temperature are summarized in Table 21.6 [382], together with those for other biodegradable aliphatic polyesters and aromatic PET [383]. The $\Delta E_h$ value (50.9 kJ/mol) for PLLA in the temperature range of 180–250°C [78] is lower than those of aliphatic polyesters, poly(butylene succinate) (PBS), and poly(butylene succinate/adipate) (PBSA) in the temperature range of 180–220°C [382], PCL in the temperature range of 175–250°C [380], poly(*R*)-3-hydroxybutyrate), that is, poly(*R*)-3-hydroxybutyric acid) (P(*R*-3HB)) in the temperature range of 180–220°C [381], and PET in the temperature range of 250–280°C [383]. This again is indicative of PLLA having the highest hydrolyzability among the biodegradable aliphatic polyesters.

On the other hand, the $\Delta E_h$ value (69.6 kJ/mol) for PLLA in the temperature range of 120–160°C (in the solid state above $T_g$) [82] is lower than the 83.7 and 83.3 kJ/mol reported by Makino et al. for PLLA and PDLLA, respectively, in the temperature range of 21–45°C (in the solid state below $T_g$) [16]. This difference is attributable to the enhanced chain mobility above $T_g$ compared to that below $T_g$. Probably, the higher chain mobility enhanced the diffusion of water and resulted in ready hydrolytic degradation and a lower $\Delta E_h$ value. Makino's values [16] are very similar to 87.2 kJ/mol, reported for hydrolytic degradation with high-pressure steam at 100–130°C [85]. For alkaline hydrolytic degradation of PDLLA dissolved in an alkaline solution, Kulkarni et al. [20] reported a $\Delta E_h$ value of 46 kJ/mol.

***21.3.1.3 Effects of Miscellaneous Medium Parameters*** Makino et al. indicated that the alkaline hydrolytic degradation of PDLLA and PLLA increased with an increase in ionic strength [16, 17]. Tsuji and Nakahara [61] found that an aqueous solution containing DL-lactic acid to give pH 2 has no significant catalytic effect on the hydrolytic degradation of PLLA, in marked contrast with the fact that lactic acid and its oligomers formed inside PLA-based materials accelerate hydrolytic degradation [24, 116, 148]. Fan et al. [127] showed that a tensile load and a combination tensile/vertical load enhanced NHD as traced by weight loss

**TABLE 21.6 The Activation Energy of Hydrolytic Degradation ($\Delta E_h$) in the Melt (and in the Solid Only for PLLA) and Temperature Dependence of Hydrolytic Degradation Rate Constant ($k$) Values [78, 82, 380–383]**

| Monomer Type | Polyester | Method | Temperature Range (°C) | $\Delta E_h$ (kJ/mol) | $\Delta E_h$ (kcal/mol) | $k$ (min$^{-1}$) |
|---|---|---|---|---|---|---|
| Aliphatic hydroxycarboxylic acid | PLLA (solid) [82] | $M_n$ | 120–160 | 69.6 | 16.6 | $4.17\times10^{8}\exp(-8.71\times10^{3}T^{-1})$ |
| | PLLA (melted) [78] | $M_n$ | 180–250 | 50.9 | 12.2 | $1.39\times10^{5}\exp(-6.12\times10^{3}T^{-1})$ |
| | P(*R*-3HB) [381] | $M_n$ | 180–220 | 126 | 30.0 | $8.86\times10^{12}\exp(-1.51\times10^{4}T^{-1})$ |
| | PCL [380] | $M_n$ | 175–250 | 72.2 | 17.3 | $3.95\times10^{6}\exp(-8.69\times10^{3}T^{-1})$ |
| Aliphatic dicarboxylic acid/aliphatic diol | PBS [382] | $M_n$ | 180–220 | 62.0 | 15.3 | $1.41\times10^{6}\exp(-7.70\times10^{3}T^{-1})$ |
| | PBSA [382] | $M_n$ | 180–220 | 58.0 | 13.8 | $2.79\times10^{5}\exp(-6.97\times10^{3}T^{-1})$ |
| Aromatic dicarboxylic acid/aliphatic diol | PET [383] | Liquid water concentration | 250–280 | 233 | 55.7 | — |

and molecular weight change. In the case of storage in the air, the hydrolytic degradation rate of PLA increases with relative humidity (RH) and temperature [84, 136].

### 21.3.2 Effects of Material Parameters

By varying the material parameters, the hydrolytic degradation mechanism, behavior, and rate can be controlled. In other words, these parameters are carefully manipulated when PLA-based materials are biomedically and environmentally applied by using the "hydrolyzability" function. In the following section, the NHD conditions are temperature of 37°C and pH of about 7, unless otherwise specified.

#### *21.3.2.1 Molecular Structure*

*21.3.2.1.1 Molecular Weight* Excluding the structure of the monomer unit, molecular weight should be the most crucial factor for determining degradation behavior and rates. Figure 21.13 shows the change in number-average molecular weight ($M_n$) of PLLA with different molecular weights and its copolymers with D-lactide (DLA), glycolide (GA), and ε-caprolactone (CL) (P(LLA-*co*-DLA), P(LLA-*co*-GA), and P(LLA-*co*-CL), respectively) [40, 41, 186]. As can be seen, the effect of copolymerization was dramatic, whereas that of $M_n$ was insignificant or very small, at least in the range of $8\times10^{4}$–$4\times10^{5}$ g/mol [40, 47]. However, at lower molecular weights below $4\times10^{4}$ g/mol, the molecular weight effect was significant for PDLLA [120, 121]. The latter result can be explained by four factors that are caused by a decrease in molecular weight: (i) elevated molecular mobility; (ii) increased density (number per unit mass) of hydrophilic terminal carboxyl and hydroxyl groups; (iii) increased density of catalytic terminal carboxyl groups; and (iv) higher probability of the formation of water-soluble oligomers and monomers upon hydrolytic degradation. Factors (i) and (ii) increase the water diffusion rate and content, enhancing hydrolytic degradation. Factors (i)–(iv) should be dramatic for PLA at a molecular weight lower than $1\times10^{4}$ g/mol. The

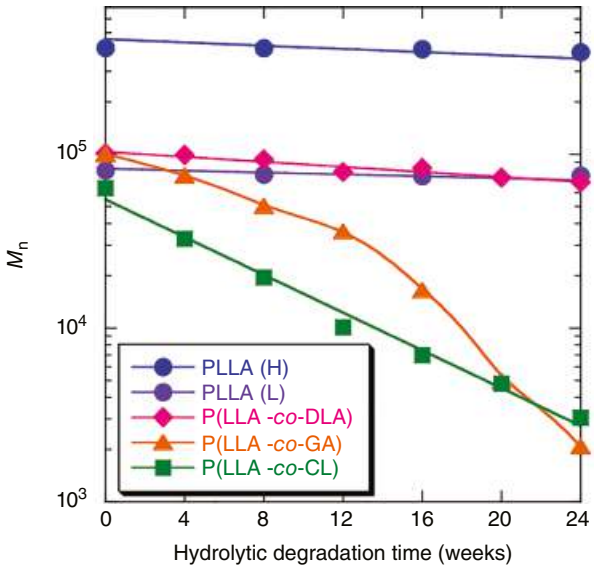


**FIGURE 21.13** $M_n$ change of amorphous PLLA having high and low molecular weights (PLLA(H) and PLLA(L), respectively), P(LLA-*co*-DLA) (77/23), poly(L-lactide-*co*-glycolide) (P(LLA-*co*-GA)) (81/19), and poly(L-lactide-*co*-ε-caprolactone) (P(LLA-*co*-CL)) (82/18) with respect to hydrolytic degradation in a phosphate-buffered solution [40, 41, 186].

NHD of P(DLLA-*co*-GA) with a weight-average molecular weight ($M_w$) of $1.1\times10^{4}$–$1.7\times10^{5}$ g/mol traced by molecular weight decreased with an increase in molecular weight [168]. With respect to branched PLLA coinitiated with glycerol (three-arm) or sorbitol (five-arm), a similar molecular weight dependence is observed for $M_n = 8\times10^{4}$ g/mol in alkaline media when traced by weight loss and total organic carbon (TOC) [103, 104].

*21.3.2.1.2 Tacticity or Optical Purity* As can be seen in Figure 21.13, the effect of tacticity or optical purity of PLA on NHD is much lower than that of an incorporated comonomer other than DLA or D-lactic acid. However, the

lowered optical purity or isotacticity by the incorporation of D-configured lactyl units in L-configured lactyl units and vice versa increased the neutral and alkaline hydrolytic degradation [15, 20, 26, 34, 40, 57, 73, 270]. This can be explained as follows. The low chain regularity of low optical purity PLA causes rather disordered chain packing and, therefore, leads to a high supply rate of water through the polymer matrix in the amorphous regions. It has been reported that even the incorporation of about 1% of the D-lactyl unit enhanced the NHD of PLLA [40]. In some of the reported studies, the crystallinity of PLA during hydrolytic degradation was not controlled or specified, and therefore the effect of crystallinity was not removed. On the other hand, Li et al. [148] found that the NHD rate of P(DLLA-*co*-GA) (75/25) was much higher than that of P(LLA-*co*-GA) (75/25), indicating that the higher tacticity or optical purity of lactyl units disturbs hydrolytic degradation. Similar to this result, P(LLA-*co*-CL) retained a higher molecular weight than P(DLLA-*co*-CL) during NHD [182].

Cameron and Shaver investigated the effects of tacticity on alkaline hydrolytic degradation of PLA and found that the alkaline hydrolytic degradation rate decreased in the following order: random PLA (i.e., P(L-lactic acid-*co*-D-lactic acid))>heterotactic PLA>isotactic PLA (L/D = 50/50, i.e., PLLA/PDLA multiblock copolymer)>isotactic PLA (L/D = 100/0, i.e., PLLA), wherein crystallinity values were not specified [138]. Karst and Yang [384] used molecular modeling to explain the fact that resistance of stereocopolymers poly(L-lactide-*co*-D-lactide) P(LLA–DLA) to hydrolysis is affected by the percentages of L- and D-lactyl units and their arrangement (block or random) in the polymer. It was found that among the stereocopolymers with the longest blocks of L- and D-lactyl units, those containing 50% L-lactyl units had greater hydrolysis resistance and were more stable before hydrolytic degradation compared to stereocopolymers with 26 or 74% L-lactyl units. They explained these results in terms of the amount of stereocomplexes having higher stability formed in the stereocopolymers; that is, the amount of stereocomplexes was higher for block stereocopolymers than for random stereocopolymers and was highest for block stereocopolymers with 50% L-lactyl units.

*21.3.2.1.3 Copolymerization* Of the lactone comonomers, the GA and CL units are frequently utilized to elevate the hydrolytic degradation rate and elongation at break, and to lower Young's modulus of PLA-based polymers. For hydrolytic degradation of P(LA-*co*-GA), Vert and coworkers and other research groups [6, 358, 385, 386] intensively investigated and obtained information that is summarized in several review articles. With respect to the acceleration of alkaline and NHD of LLA-based copolymers, the effect of the incorporation of hydrophilic GA is higher than that of hydrophobic CL [22, 41, 57, 186]. In the case of the NHD of P(LLA-*co*-GA), nonexponential decay was observed for degradation periods exceeding 12 months. In other words, the parameters for exponential decay changed with degradation periods of more than 12 months [41]. The NHD rate of P(LLA-*co*-GA) [21, 155] and the acidic [168], neutral [161–163, 168], and alkaline [168] hydrolytic degradation rates of P(DLLA-*co*-GA) increased with an increase in GA unit content. Schmitt et al. [169] ascribed the high NHD rate of P(DLLA-*co*-GA) with a high GA content to an increase in bound reactive water content, but not of total water content. In the case of the CL unit, the incorporation effect on NHD of PLLA or PDLLA is complicated. That is, the maximum degradation rate traced by molecular weight change was observed at about 60% LA units (40% CL units) [181, 182]. In the case of block copolymers of PDLLA-*b*-PCL, the NHD rate traced by viscosity and weight loss increased with an increase in PDLLA content [216]. Fernández et al. showed that P(LLA-*co*-CL) (74/26) random copolymer had higher NHD rate than that of PLLA-*b*-PCL (74/26) block copolymer [189]. Leng et al. observed a similar trend for NHD of poly(butadiene)-*g*-poly(L-lactide-*co*-trimethylene carbonate) monitored by weight loss and number-average molecular weight [258]. Zhang et al. [194] showed that three monomer-based copolymer P(LLA-*co*-GA-*co*-CL) (63/27/20) nanoparticles had a higher NHD rate compared with that of two monomer-based copolymer P(LLA-*co*-GA) (70/30) nanoparticles, whereas Cai et al. [151] and Sawhney and Hubbell [195] reported that the NHD rate of P(DLLA-*co*-GA-*co*-CL) or P(LLA-*co*-GA-*co*-CL) increased with an increase in GA content or a decrease in CL unit content.

The incorporation of hydrophilic and catalytic β-malic acid units elevated the NHD rate traced by weight loss [197]. Also, Kimura et al. [193] indicated that the incorporation of both glycolic acid and α-l-malic acid in PLLA remarkably enhanced NHD. Nakayama et al. [200] reported that increasing the incorporated content of δ-valerolactone (VL) units in PLLA decreased the NHD rate traced by TOC, whereas the NHD rate of P(LLA-*co*-β-methyl-VL) gave a maximum when β-methyl-VL was 20 mol%. Zhu and Lei [202] reported that the NHD rate of poly(DLLA-*co*-adipic anhydride) increased with an increase in adipic anhydride content. The incorporation of *rac*-1-methyl-TMC at 22 mol% elevated the NHD of PDLLA traced by weight loss, whereas a further increase of *rac*-1-methyl-TMC lowered the degradation rate [212]. Grijpma and Pennings [22], Jie and Zhu [210], and Pêgo et al. [211] showed that the incorporation of TMC up to 50 mol% increased the NHD rate of PLLA and PDLLA monitored by weight loss and molecular weight change. However, Shirahama and Yasuda [207] indicated that incorporation of 3-methyl-4-oxa-6-hexanolide (MOHEL) decreased the NHD of PLLA. Another class of PLA-based copolymers are those with amino acid units. Helder et al. [204] investigated the NHD of P(DLLA-glycine) and found that the degradation rate

monitored by weight loss was the highest at a DLLA content of 80 mol%. Barrera et al. [205] showed that the incorporation of lysine units accelerates the NHD of PLLA traced by weight loss and molecular weight change. Shinoda et al. [203] and Huang and Cui [206], respectively, reported the strong enhancing effects of incorporated aspartic acid units on the NHD of PLLA and PDLLA. Also, Tarvainen et al. [135] reported that PDLLA linked with 2,2-bis(2-oxazoline) had a higher NHD rate than nonlinked PDLLA. Fan et al. performed NHD of poly(1,3-trimethylene carbonate)-*b*-poly(L-lactide-*co*-glycolide) and poly(1,3-trimethylene carbonate-*co*-glycolide)-*b*-poly(L-lactide-*co*-glycolide) with various comonomer ratios and found that the dirandom block structure of the latter had a lower regularity of the chain segments and a higher water permeation rate into amorphous region, causing rapid NHD [248].

The polymerization of LLA, DLLA, LA/GA, and other combinations of LA with comonomers in the presence of hydrophilic poly(ethylene glycol) or PEO segments is frequently used to synthesize block copolymers. These block copolymers can be used as matrices for drug release systems containing hydrophilic drugs. During hydrolytic degradation, the high hydrophilicity of PEO accelerates the diffusion of water into the material and increases its water content, resulting in enhanced cleavage of the ester linkage, while the release of water-soluble PEO causes a rapid increase in weight loss. Therefore, the incorporation of PEO elevates the degradation rate of PLA-based homopolymers and copolymers as traced by molecular weight change and weight loss [119, 174, 222, 224, 229, 231, 235, 239]. Kimura and Lee et al. [241–243] synthesized triblock and multiblock copolymers of PLLA and poly(propylene oxide) (PPO) or poly(ethylene oxide-*co*-propylene oxide), Maeda et al. [244] synthesized diblock copolymers PLLA-*b*-poly(succinic anhydride-*co*-ethylene oxide), and both groups investigated the NHD thereof. The degradation rate increased with an increase in the amount of PPO, poly(ethylene oxide-*co*-propylene oxide), or poly(succinic anhydride-*co*-ethylene oxide). Cho and An [238] investigated the effects of DLLA/CL composition on the NHD of triblock copolymers P(DLLA-*co*-CL)-*b*-PEO-*b*-P(DLLA-*co*-CL) and found that the NHD rate monitored by weight loss increased with an increase in DLLA content. For multiblock copolymers of P(LA-*co*-GA) and PEO, the NHD rate traced by weight loss became higher with an increase in P(LA-*co*-GA) and PEO block lengths, whereas that monitored by molecular weight was similar in both cases when compared at a similar ratio of P(LA-*co*-GA) to PEO. For the NHD of PDLLA-*b*-PEO-*b*-PDLLA or PDLLA–poly(tetramethylene ether glycol) block copolymers under uncontrolled pH in an NaCl solution, the degradation rate traced by viscometry decreased with an increase in the content of relatively hydrophobic polyethers [237, 245]. On the other hand, the effects of incorporation of hydrophobic blocks on the NHD of PLLA-based multiblock copolymers depend on the type of second block. In the case of PLLA-polyisobutylene multiblock copolymers, NHD rate increased with decreasing PLLA block length due to lower crystallinity [251], whereas in the case of PLLA-poly(trimethylene terephthalate) multiblock copolymers, NHD rate increased with an increase in PLLA block fraction [250]. Rahaman and Tsuji synthesized stereo multiblock PLAs having different average block lengths and found that their NHD rate increased with decreasing average block length. Moreover, NHD of the stereo multiblock PLAs with average block lengths higher than 27 and 15 lactyl units was suppressed as compared with that of the PLLA/PDLA blend and the neat PLLA or PDLA, respectively [249].

By graft polymerization, PLA-based materials with a complicated degradation mechanism can be prepared, as depicted in Figure 21.3. Li et al. [255] and Breitenbach et al. [257] synthesized dextran-*g*-P(LA-*co*-GA) and PVA-*g*-P(LA-*co*-GA) and studied the NHD thereof. They showed that graft copolymers had a higher degradation rate as traced by weight loss and molecular weight change than linear P(LA-*co*-GA). Similar results were obtained for PLLA and cellulose-*g*-PLLA [254]. In the case of poly[vinyl-3-(dialkylamino)-alkylcarbamate-*co*-vinyl acetate-*co*-vinyl alcohol]-*graft*-poly(DLLA-*co*-GA), the hydrolytic degradation rate was higher for graft copolymers having shorter poly(DLLA-*co*-GA) side chains [260]. Langlois et al. [259] investigated the NHD of graft copolymers of poly(PDLLA methacrylate-*co*-*tert*-butyl acrylate) in artificial seawater and found that the degradation rate monitored by released lactic acid increased with an increase in the lactic acid content of the polymer. Also, Ohya et al. [253] reported that the NHD rate of pullulan-*g*-PLLA monitored by molecular weight change increased with an increase in the sugar unit content of the polymer.

*21.3.2.1.4 Substituted PLA* PDLLA with methyl side groups, poly(DL-2-hydroxybutanoic acid) (PBA) with ethyl side groups, poly(DL-2-hydroxyhexanoic acid) (PHA) with *n*-butyl side groups, and poly(DL-2-hydroxydecanoic acid) (PDA) with *n*-octyl side groups were synthesized by condensation of each hydroxyalkanoic acid and their NHD rates were estimated by degree of polymerization (DP) [387]. The hydrolytic degradation rate traced by DP and weight loss at 80°C decreased in the following order: PLA > PDA > PHA > PBA and that monitored by DP at 37°C decreased in the following order: PLA > PDA > PBA > PHA [387].

*21.3.2.1.5 Terminal Group* Terminal-group-modified polymers may be classified as copolymers. Terminal groups may be hydrophilic (—OH and —COOH), have a catalytic effect (—COOH), and act as sites where lactide is formed by backbiting (Figure 21.2a). Therefore, hydrolytic degradability can be manipulated by modifying the terminal groups. For example, the incorporation of hydrophobic long

methylene units, such as the dodecyl group ($C_{12}$) in the terminal group, decreased the hydrolytic degradation rate of PLLA [95]. However, the hydrolytic degradation rate of PLLA in which the carboxyl terminal was end capped with dodecanol, while the hydroxy terminal was acylated with the dodecyl group, was very similar to that of PLLA end capped only at the carboxyl terminal. Lee et al. [102] synthesized linear and branched PLLA, and then all their end groups were modified to have ─OH, ─Cl, ─$NH_2$, or ─COOH terminations. Of these modifications, the NHD rate was the highest for PLLA terminated with ─COOH, and those with ─Cl and ─$NH_2$ showed much lower degradation rates. In the case of monolayers, end capping of the hydroxyl group had no significant effect on the alkaline hydrolytic degradation of PDLLA as traced by surface area change [112].

*21.3.2.1.6 Branching* Branching is expected to increase hydrolytic degradation due to the increased number per unit mass of hydrophilic and/or catalytic terminal groups and of terminal groups where LA is formed by backbiting, as shown in Figure 21.2a. Such effects were reported in the literature when the degradation was monitored by weight loss or molecular weight change [99]. Kim et al. [98] studied linear and branched PLA and indicated that branched PLLA had lower and higher hydrolytic degradation rates than those of linear PLA at the early and late stages of degradation, respectively. Hayashi and Tsuji prepared crystallized and amorphous linear two-armed and branched four-armed PLLAs and investigated the effects of branching and crystallinity [100]. The NHD rate at 37°C determined by $M_n$ decrease was higher for crystallized samples than for amorphous samples, whereas that of two-armed PLLA monitored by weight loss was higher for amorphous samples than for crystallized samples [100]. The NHD rate at 97°C monitored by $M_n$ decrease was higher for the two-armed PDLLA (bulk erosion) than for the four-armed PDLLA (surface erosion). Also, the NHD rate of two-armed PDLLA decreased with decreasing $M_n$ [134]. These findings can be explained by the fact that the strength of the surface erosion nature increased with a decrease in $M_n$ [134]. On the other hand, Numata et al. [101] reported that the six branches of *myo*-inositol-coinitiated PDLLA have no effect on alkaline hydrolyzability when compared at a similar total $M_n$ monitored by GPC or the $M_n$ of PDLLA segments traced by $^1$H NMR spectroscopy. In contrast, the 22 branches of polyglycerine coinitiated PDLLA enhanced alkaline hydrolytic degradation [101].

Li and Kissel [223] prepared linear and 4-armed/8-armed branched block copolymers of LLA and GA coinitiated with branched PEO and showed that the branching affected the NHD as traced by weight loss and molecular weight change. On the other hand, Joziasse et al. [289] investigated the NHD of linear and branched P(LLA-*co*-DLA-*co*-GA)/linear poly(TMC-*co*-CL) blends and found that the blends of branched copolymers retained their mechanical properties for longer periods than did the linear copolymers.

*21.3.2.1.7 Cross-linking* Cross-links in PLA-based materials are anticipated to reduce their hydrolyzability because the cross-linked rigid structure is thought to disturb the diffusion of water molecules into the materials, and cross-links in some cases reduce the number of terminal groups. However, cross-linked PLA-based materials are insoluble in normal solvents, and therefore detailed information cannot be derived from hydrolysis experiments that exclude the dry and wet weights of the materials. For example, Younes et al. [262] prepared P(DLLA-*co*-CL) initiated with glycerol and cross-linked with 2,2-bis(CL-4-yl)-propane. The physical properties of cross-linked P(DLLA-*co*-CL) decreased in a logarithmic fashion with degradation time in NHD, indicative of first-order degradation kinetics, and the cross-linked P(DLLA-*co*-CL) degraded relatively slowly, with degradation being incomplete after 12 weeks. Similarly, cross-linked PLLAs showed lower alkaline hydrolysis rates traced by weight loss compared with that of linear one-armed PLLA, and their weight loss and degree of swelling during degradation increased with an increase in average molecular weight between the crosslinks [109].

***21.3.2.2 Highly Ordered Structures*** PLLA crystallizes in α- and δ-(α′-)forms at crystallization temperature ($T_c$) values higher and lower than 120°C, respectively [388]. The thickness of PLLA crystalline region increases with an increase in $T_c$ [32]. Therefore, the crystalline form is controllable by $T_c$, but it should be noted that crystalline thickness simultaneously changes with $T_c$. Crystallinity of PLLA can be controlled by crystallization time at a fixed $T_c$ after melting [31, 367]. Normally, the final crystallinity after the completion of crystallization at a fixed $T_c$ becomes higher with increasing $T_c$ [31].

*21.3.2.2.1 Crystallinity* The chains in crystalline regions are hydrolysis-resistant compared to those in amorphous regions. Therefore, with increasing crystallinity ($X_c$), alkaline and enzymatic hydrolytic degradation rates decrease [51, 52, 359, 377]. However, in the case of NHD of PLLA [30–32, 74, 106], PLLA/PDLA blends [36] and P(LLA-*co*-GA) [152] in neutral media of phosphate-buffered solutions or in the human body at 37°C (except at 97°C [74]), the hydrolytic degradation rate (traced by weight loss, molecular weight change, and mechanical property changes) becomes higher with an increase in $X_c$ (Figure 21.14) [31]. This result was first reported for in vivo degradation of PLLA [389–391] and then also for in vitro degradation. The probable explanation is as follows. Upon the crystallization of PLLA, the hydrophilic terminal groups (─OH and ─COOH) and the

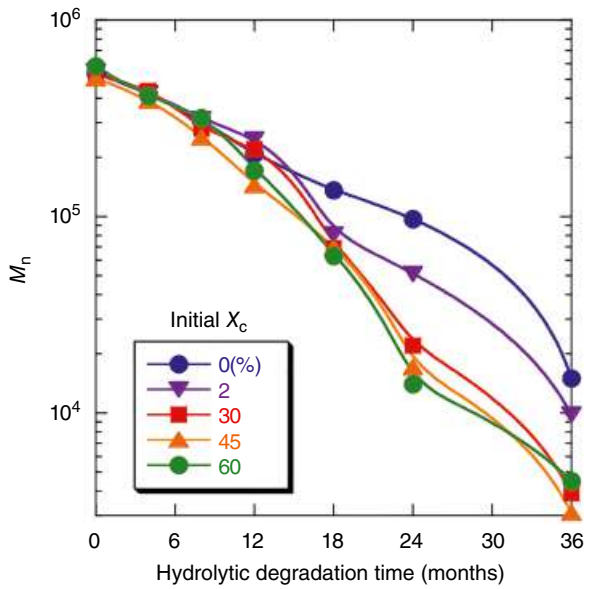


**FIGURE 21.14** $M_n$ change of PLLA films having different initial crystallinity ($X_c$) values during hydrolytic degradation in a phosphate-buffered solution [31].

catalytic terminal group (—COOH) are condensed in the amorphous region between the crystalline regions, as depicted in Figure 21.15 [31, 356]. The empty and solid circles in the figure refer to hydroxyl and carboxyl groups, respectively. The high densities (numbers per unit mass) of the terminal groups will cause loose chain packing in the amorphous region between the crystalline regions compared to the chain packing in completely amorphous film. Such loose chain packing and high densities of hydrophilic terminal groups enhance the diffusion of water molecules and increase the water content. The elevated water supply rate and content and the catalytic effect increased by the high density of the carboxylic group will synergize to remarkably accelerate the hydrolytic degradation of crystallized PLLA films. Moreover, the terminal groups, as sites for the formation of lactoyllactic acid and lactic acid (Figure 21.2), are condensed in the amorphous region between the crystalline regions, and thereby the formed lactoyllactic acid and lactic acid should catalyze the hydrolytic degradation in a restricted area of the amorphous region. This also will further enhance the aforementioned synergy effect. However, according to the report by Li et al. [24], crystallized PLLA had a higher NHD rate than that of amorphous PLLA when degradation was monitored by L-lactic acid release, whereas the relation was reversed when monitored by weight loss and tensile properties. Also, for P(LLA-*co*-GA) (10/90) and PLLA, higher $X_c$ delayed the NHD in phosphate-buffered solution at 37°C traced by weight loss [150] and in distilled water at 50°C monitored by weight loss and viscosity-average molecular weight [68].

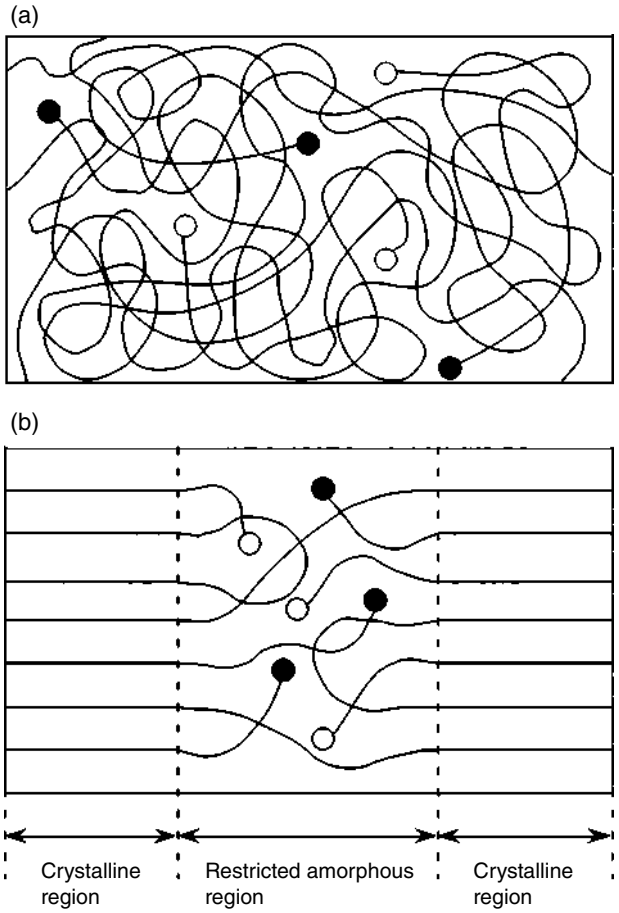


**FIGURE 21.15** Schematic representation of completely amorphous and crystallized PLLA (a) and crystallized PLLA (b) [31, 356].

*21.3.2.2.2 Crystalline Form* As stated above, PLLA crystallizes in α- and δ-(α′-)forms at $T_c$ values higher and lower than 120°C, respectively. The NHD rates of PLLA crystallized at $T_c$ of 100°C (δ-form) and of 120, 140, and 160°C (α-form) in phosphate-buffered solution was mainly determined by crystallinity, not by crystalline form, and increased with an increase in crystallinity. At the late stage of NHD in distilled water at 50°C, PLLA crystallized at 80°C (δ-form) had a higher degradation rate as monitored by weight loss and viscosity-average molecular weight than that of PLLA crystallized at 140°C (α-form), when compared at the similar initial crystallinity values [68].

*21.3.2.2.3 Crystalline Thickness* In the early stage of hydrolytic degradation, wherein mainly amorphous chains are degraded, the crystalline thickness has only an indirect effect on hydrolytic degradation. That is, the crystalline thickness will indirectly alter the crystallinity of materials and, therefore, indirectly affect the hydrolytic degradation rate. In the late stage of hydrolytic degradation, wherein the crystalline residues are degraded, the effect of crystalline thickness is direct and crucial. The molecular weight of crystalline residues

(or extended-chain crystallites) increases with an increase in the initial crystalline thickness before degradation [32, 52, 74, 75]. As expected from Equation 21.1, the hydrolytic degradation time required for the crystalline residues to be completely degraded to lactic acid increases with an increase in their initial molecular weight. In other words, if the crystalline thickness is large, the crystalline residues remain for a long period after the material function is lost.

*21.3.2.2.4 Orientation* In contrast to the enzymatic hydrolytic degradation of PLLA [39, 392], orientation has a relatively small effect on neutral and alkaline hydrolytic degradation. Crystallinity, rather than biaxial orientation, seems to determine the alkaline and NHD rates of PLLA films [39]. On the other hand, Hyon and Jamshidi et al. [37, 63–65] indicated that hydrostatic molecular-oriented PLLA could retain its mechanical performance for a longer period compared with compression molded PLLA. Also, Dias et al. reported that the during NHD, the diameter of electrospun PLLA fibers increased, but their membrane porosity decreased due to the release of internal tensions related to the electrospinning and/or thermal treatment processes [46].

### *21.3.2.3 Polymer Blending, Composites, and Additives*

*21.3.2.3.1 Polymer Blending* Polymer blending is commercially advantageous for preparing PLA-based materials having a wide variety of physical and hydrolytic degradation properties. Five or more factors of a second polymer or an additive are thought to influence the hydrolytic degradation rate, behavior, and mechanism of PLA-based materials in neutral media: (i) miscibility and dispersibility, (ii) hydrophilicity, (iii) acidity or basicity, (iv) molecular weight and distribution, and (v) size and shape of the polymer domain (if the second polymer is immiscible with the first polymer) or additives. For example, the addition of hydrophilic polymers, such as poly(vinyl alcohol) (PVA) [297, 298], PEO [232], poly(glycolide) (i.e., poly(glycolic acid) (PGA)) [274], poly(aspartic acid-*co*-L-lactide) [290], poly(*p*-dioxanone) [287], poly(ethylene-*co*-glycidyl methacrylate) [302], plus hydrophilic and catalytic compounds such as thioridazine [393], hydroxyapatite [325, 327], β-tricalcium phosphate [321], lauric acid [304, 305], oligomeric PDLLA ($M_n = 2.4 \times 10^3$ g/mol) [267], and DL-or L-lactide (in vitro in a phosphate-buffered solution [121, 303] or in vivo [389]), is known to enhance the NHD of PLLA. In the case of PLLA/poly(*p*-dioxanone) blends, the addition of a compatibilizer suppressed the NHD of blends [281]. Normally, the hydrolytic degradation rate constant ($k$) estimated using Equation 21.7 is in the range of $2.2–3.4 \times 10^{-3}$ day$^{-1}$ (0–12 months) [31, 32]. The addition of PVA and lauric acid increased the $k$ value to $9.4 \times 10^{-3}$ [297] and 0.03 day$^{-1}$, respectively [304, 305]. Nijenhuis et al. [232] reported that a PLLA/PEO blend showed different degradation behavior compared to a PLLA-*b*-PEO-PLLA block copolymer. Sheth et al. [293] investigated the alkaline hydrolytic degradation of PLA/PEO blends. Their results suggested that porous PLLA materials were formed upon immersing them in a buffered solution by extraction of PEO from the PLLA/PEO blends, as reported by Tsuji et al. [394], and as a result the blend showed faster degradation compared to PLLA because of increased surface area per unit mass of PLA/PEO blends.

The addition of hydrophobic polymer is expected to decelerate the hydrolytic degradation of PLA. The addition of PCL to poly(lactide-*co*-glycolide) decelerated NHD of poly(lactide-*co*-glycolide), but NHD of PCL was accelerated [277]. Also, phase-separated structure affects surface hydrolytic degradation such as alkaline hydrolytic degradation. For example, Shirahase et al. [300] found that the addition of poly(methyl methacrylate) (PMMA) enhanced the alkaline hydrolytic degradation of PLLA/PMMA blends monitored by weight loss with an increase of PMMA up to 30 wt%, whereas further addition of PMMA lowered the hydrolytic degradation rate. Probably, the hydroxyl ions can diffuse into the interface between phase-separated PLLA and PMMA-rich domains and catalyze the surface hydrolytic degradation of PLLA domains. The hydrolyzable PLLA surface area per unit mass in the blends should be higher than that in pure PLLA, resulting in an elevated degradation rate. However, too much PMMA forms its continuous domain and encapsulates the PLLA domains as particles. This structure disturbed the contact of dispersed PLLA domains with water, resulting in delayed hydrolytic degradation of PLLA domains. In the case of NHD of PLLA/PMMA blends, the degradation rate monitored by overall $M_n$ decreased with an increase in PMMA fraction due to nondegradability of PMMA [299]. The blending of PLLA with PLLA-*b*-poly[2-(perfluorooctyl)ethyl methacrylate] decelerated hydrolytic degradation in air (R.H. = 88%), and crystallization of PLLA widened the difference between neat PLLA and PLLA/PLLA-*b*-poly[2-(perfluorooctyl)ethyl methacrylate] blends [291].

There have been numerous reports with respect to blends of PLA-based polymers with other aliphatic polyesters. Although accelerated NHD of PDLLA was observed upon the addition of oligomeric PDLLA [267], such acceleration was not seen for P(LA-*co*-GA) [269]. The latter result was attributed to the crystallization of P(LA-*co*-GA) induced by oligomeric PDLLA, which lowered the hydrolytic degradation rate, counterbalancing the accelerating effects of oligomeric PDLLA. On the other hand, Mallardé et al. [279] reported that oligomeric PDLLA ($M_n$ = 1100 g/mol) enhanced the alkaline hydrolytic degradation of poly(3-hydroxyoctanoate). Lee et al. [15, 275] found that the dilution effect of slowly degrading PCL on rapidly degrading PLLA increased the alkaline hydrolytic degradation rate of PLLA/PCL blend monolayers with PLLA contents below 50%. Similarly, regarding bulky PLLA-based blends, the

incorporation of PCL or P(LLA-*co*-CL) increased the total NHD rate of the blends as traced by molecular weight, and the enhancing effect was higher for P(LLA-*co*-CL) [28, 276]. Inoue et al. [280] indicated that the incorporation of poly(butylene succinate) lowered the alkaline hydrolytic degradation of PLLA as traced by weight loss, whereas Wang et al. reported the opposite result [281]. Choi et al. [278] compared the difference in the enhancement effect of the addition of relatively random P(LLA-*co*-CL) and PLLA-*b*-PCL on the NHD of PLLA/PCL blends. The incorporation of relatively random P(LLA-*co*-CL) had a higher enhancing effect on the degradation of the blends. Regarding the blends with aromatic polyester, blending PLA with poly(trimethylene terephthalate) [286] and poly(butylene adipate-*co*-terephthalate) [284] was reported to decrease the NHD and alkaline hydrolytic degradation rates determined by weight loss. Compatibilizers (PEO [295, 296] or PCL [294]) of PLA (configuration or OP not specified) [295] or PLLA [294] with chitosan decelerated acidic hydrolysis [295, 296] or NHD and alkaline hydrolysis [294] monitored by weight loss.

A peculiar example is the addition of poly(D-lactide) (i.e., poly(D-lactic acid)) to PLLA. In the blends, the interaction between a PLLA chain and a PDLA chain is much higher than that between PLLA chains or PDLA chains, resulting in a stereocomplex formation [13]. Such strong interaction disturbs the diffusion of water into the material and lowers the hydrolytic degradation rate, whether the stereocomplex is formed in the blends or not [33–36, 271]. For example, as-cast pure PLLA and PDLA films had $k$ values of $1.41 \times 10^{-3}$ and $2.14 \times 10^{-3}\,\text{day}^{-1}$, respectively, whereas the $k$ value of their 1 : 1 blend film was $7.3 \times 10^{-4}\,\text{day}^{-1}$ [33]. That is, the 1 : 1 blend film has a $k$ value one order of magnitude lower than that of nonblended films. A similar result was obtained for the alkaline hydrolytic degradation of PLLA/PDLA blend monolayers [270]. Molecular modeling ascribed the high hydrolysis resistance of PLLA/PDLA blends compared with that of stereocopolymers P(LLA–DLA) with the same L-lactyl unit content to the fact that blends can form more stereocomplexes than stereocopolymers [384]. Similarly to PLLA/PDLA blends, the enantiomeric substituted PLLA/PDLA, i.e., poly(L-2-hydroxybutanoic acid)/poly(D-2-hydroxybutanoic acid) blend, had a lower NHD rate at 80°C compared with unblended poly(L-2-hydroxybutanoic acid) or poly(D-2-hydroxybutanoic acid) [395].

Although in this section, the effects of the incorporated polymers on the hydrolytic degradation of PLA were stated. Hu et al. [292] investigated the effect of incorporated PLA on the hydrolytic degradation of poly(ε-aminocaproic acid) (Nylon 6). They found that hydrolytic degradation-formed lactic acid catalyzed and accelerated the hydrolytic degradation of nylon 6. This can be applied to enhance the hydrolytic degradation of polycondensation-formed polymers catalyzed by hydronium ions.

*21.3.2.3.2 Composites/Additives* Regarding inorganic additives, van der Meer et al. [339], Ara et al. [316], and Imai et al. [323, 324], respectively, reported that the addition of MgO, calcium compounds, tricalcium phosphate, and magnesium neutralized the catalytic carboxyl groups formed by the hydrolytic degradation of P(LLA-*co*-DLA), P(DLLA-*co*-GA), PLLA-*b*-and poly(ethylene/hexamethylene–sebacate) and reduced their NHD rates. In contrast, the addition of magnesium [308] and tricalcium phosphate [320] increased the NHD rate of PLLA traced by weight loss and pH [12] and $M_n$ [320]. Also, Shikinami and Okuno [325] found enhanced hydrolytic degradation of PLLA in the presence of hydroxyapatite. They ascribed the higher hydrolytic degradation rate to the hydrophilic nature of hydroxyapatite and pore formation due to the removal of hydroxyapatite particles. Therefore, the total effect of an additive is determined by the combination of polymer/additive, the additive concentration, morphology and surface properties, and the degradation medium and temperature in each case. Similarly, the addition of ZnO accelerated NHD of PLLA as monitored by pH [312], weight loss [314], $^1$H NMR spin-spin relaxation time, and number-average molecular weight [310] and alkaline hydrolytic degradation of PLLA traced by weight loss [311]. The addition of organomodified montmorillonite or unmodified/modified vermiculites accelerated alkaline hydrolytic degradation of PLLA determined by weight loss [332, 334]. The addition of PDLA to PLLA/organomodified montmorillonite further accelerated alkaline hydrolytic degradation [332]. The addition of organomodified montmorillonite and unmodified sepiolite delayed the NHD of PLA due to their crystallization-inducing effect and/or to their high water uptake reducing the amount of water available for polymer matrix hydrolysis [333]. In contrast, the presence of organomodified synthetic fluoro mica also induced polymer crystallization, but it catalyzed the hydrolysis of PLA [333]. The addition of $Ag_3PO_4$ decelerated NHD at 70°C traced by weight loss [314]. The addition of silver-loaded kaolinite decelerated alkaline hydrolytic degradation of PLA/poly(butylene adipate-*co*-terephthalate)/tetrabutyltitanate (compatibilizer) blend monitored by weight loss, pH, and viscosity [284]. When hydrophilic $SiO_2$ was added to PLLA, the alkaline hydrolytic degradation rate determined by weight loss increased [328]. In contrast, Jo et al. found that the addition of talc or organomodified talc delayed NHD at 50 and 70°C as monitored by $M_w$ [335]. Also, the addition of MgO-*g*-PLLA and/or chitin-*g*-PLLA accelerated NHD of PLLA [309].

Zhang et al. [340] investigated the hydrolytic degradation of P(DLLA-*co*-GA) (50/50) containing various metal salts and discussed the effects of porosity induced by the presence of salt particles, osmotic force caused by the ionic nature of encapsulated salts, neutralization of protons by basic salts

evolved during the hydrolysis of ester linkages, and chemical interaction between ions and functional groups. They indicated that the addition of alkaline metal salts with low water solubility reduced the hydrolytic degradation rate traced by molecular weight because these salts may disrupt the autocatalytic effect caused by the carboxylic group. A similar effect was observed for PDLLA/coral blends, where core acceleration of thick PDLLA specimens was not detected, because of the autocatalytic effect of the formed low-molecular-weight oligomers and monomers was removed by the incorporated coral [338]. In the case of basic additives such as a caffeine base and coral, the overall catalytic effects were determined by base/carboxyl group interaction, crystallization, and matrix-controlled or channeling-controlled diffusion of basic additives [118, 338]. The hydrolytic degradation rate of PDLLA traced by weight loss, molecular weight, and amount of formed lactic acid decreased in the presence of coral. Niemelä et al. [336] investigated P(LLA-*co*-DLA) (85/15) containing bioactive glass and found that the incorporation of bioactive glass lowered the rate of reduction of molecular weight although the decreases in tensile strength and weight remaining were dependent on the amount of added bioactive glass. The addition of sucrose palmitate, a nonionic surfactant, accelerated acidic, neutral, and basic hydrolytic degradation of PLLA traced by weight loss [307].

The addition of nano/micro-diamond decreased the NHD rate of PLLA at 97°C monitored by weight loss and $M_n$ [231]. The addition of single-walled carbon nanotubes has been used to functionalize PLA-based materials [396–398]. Also, the incorporation of nonmodified hydrophobic carbon nanotubes and hydrophilic carbon nanotubes with carboxyl groups on their surfaces, respectively, reduced and enhanced the NHD as traced by weight loss [346]. In contrast, pristine, carboxyl-functionalized, and unzipped multiwalled carbon nanotubes increased the alkaline hydrolytic degradation rate of PLLA as determined by weight loss [315, 342–345], probably due to the increased surface area by the incorporated multiwalled carbon nanotubes. The accelerating effect was higher for carboxyl-functionalized multiwalled carbon nanotube than the pristine one [342]. Further addition of PDLA to PLLA/multiwalled carbon nanotubes increased the alkaline hydrolytic degradation rate [344]. The addition of carbon nanofibers with surfaces modified with carboxy groups promoted alkaline hydrolytic degradation, whereas the addition of PEO-grafted carbon nanofibers suppressed alkaline hydrolytic degradation [347]. The addition of graphene decelerated alkaline degradation of PLLA [350] or PLLA/PDLA (95/5) [348] as monitored by weight loss, intrinsic viscosity, and pH, whereas the opposite result has also been reported [315]. The addition of graphene oxide accelerated acidic, neutral, and alkaline hydrolytic degradation of PLLA traced by weight loss [349, 350]. The addition of cellulose nanocrystals accelerated NHD monitored by molecular weight [351]. The addition of both wood flour and the antihydrolysis agent bis(2,6-diisopropylphenyl)carbodiimide remarkably decelerated NHD at 80°C, although the addition of wood flour or bis(2,6-diisopropylphenyl)carbodiimide alone showed insignificant and very small decelerating effect [353]. The addition of crystalline silk nano-discs decelerated the acidic, neutral, and alkaline hydrolytic degradation of PLA monitored by weight loss and weight-average molecular weight [352].

Even coinitiators remaining after polymerization can be regarded as additives and are reported to have an effect on hydrolytic degradation. For example, zinc metal and derivatives thereof used for polymerization of DL-lactide remained after polymerization and increased water absorption, resulting in a higher degradation rate compared with tin derivative coinitiators [125]. On the other hand, Leenslag et al. [23] showed that the extraction of low-molecular-weight compounds (probably such as unreacted lactide) with ethyl acetate lowered the neutral degradation rate as monitored by molecular weight change and tensile strength.

***21.3.2.4 Material Shapes*** With respect to the material shape, hydrolysis media strongly influence the effect of material shape on the degradation rate. As stated earlier, in neutral media, decreased thickness of materials causes ready removal of formed oligomers and monomers, resulting in a reduced autocatalytic effect and, therefore, a lower degradation rate. Conversely, the core-accelerated erosion mentioned earlier [11, 24, 116, 148, 226, 233] takes place in the case of PLA-based materials with a thickness of over 0.5–2 mm. For these reasons, pore formation decreases the degradation rate of PLA-based materials [155], whereas all degradation rates of PLA-based materials in neutral media are higher for a thick material (85–100 μm) than for a thin material (5–10 μm) [162]. Similar to these results, for P(DLLA-*co*-GA) and PLLA, Wu and Ding [164] and Lee et al. [165], respectively, reported that high wall thickness and low porosity increase the NHD rate because a large wall thickness and small surface area both lead to a slow diffusion rate and high concentration of the degradation products (oligomers and monomers) and thus result in a fast acid-catalyzed degradation.

In contrast, Pegoretti et al. [49] indicated that the NHD of PLLA fibers monitored by molecular weight change was higher for fibers with a smaller diameter (72 μm) than for those with a larger diameter (120 μm). Similar to this result, Chen and Ma [45] showed that nanofibrous foam had a higher NHD rate (traced by molecular weight change and weight loss) than solid-wall foam. Also, Huang et al. [167] indicated that porous P(DLLA-*co*-GA) had a higher NHD rate (monitored by molecular weight) than dense P(DLLA-*co*-GA). Furthermore, for PDLLA monolayers, the degradation rate increased with an increase in surface pressure from

$2\times10^{-3}$ to $1\times10^{-2}$ N/m (corresponding to maximal close packing of all lactyl units), whereas a further increase to $1.45\times10^{-2}$ N/m caused the formation of a three-dimensional structure, resulting in a decreased degradation rate [132]. The reported results in this section indicate that the hydrolytic degradation rate should be determined by the combined effects of the water diffusion rate per unit weight of the material and the concentration of hydrolysis-formed catalytic oligomers and monomers.

On the other hand, pores enhance the alkaline and enzymatic surface hydrolytic degradation of aliphatic polyesters because of the increased surface area per unit mass of porous materials compared with that of nonporous materials [399]. Similar to this, the pores formed by the removal of water-soluble polymers such as poly(*p*-vinyl phenol) from PLLA/water-soluble polymer blends accelerated the alkaline hydrolytic degradation of PLLA as traced by weight loss [301]. Also, pores were reported to accelerate the NHD of PLLA/ZnO nanoparticles monitored by weight loss and pH [313].

***21.3.2.5 Miscellaneous Parameters*** Electron beam irradiation of PLLA and the surrounding gas causes primary radical formation that induces secondary, tertiary, or higher order radical formation and recombination of formed radicals. During the course of these processes, PLLA and copolymers undergo hydrogen abstraction, oxidation, release of carbon dioxide, and so on. Due to these reactions, molecular weight and other molecular changes take place. The higher NHD rates of electron-beam-irradiated PLLA and P(LLA-*co*-GA) are attributable to a lower molecular weight [107, 156]. Such accelerated NHD at 58°C by electron beam irradiation was observed for PLA/poly(ethylene-*co*-glycidyl methacrylate)/hexagonal boron nitride blends [302]. Södergård et al. [106] indicated that peroxide treatment caused faster NHD of PLLA. PLLA showed complicated dependence on UV-irradiation [108]. In an early stage, the degrees of hydrolytic degradation rate determined by weight loss, $M_n$, and $T_m$ were higher for the UV-treated films than those for the UV-nontreated films [108]. In a late stage, the trend traced by $W_{loss}$ was reversed, and the difference in the degrees of hydrolytic degradation between the UV-treated and UV-nontreated films monitored by $M_n$ and $T_m$ became smaller, with the exception of the degrees of hydrolytic degradation of the amorphous films traced by $T_m$ [108]. In contrast, Chandy and Sharma [110] showed that NHD of PLLA was retarded by plasma glow discharge and subsequent cross-linking with carbodiimide or by glutaraldehyde cross-linking. Hirano et al. [86] found that microwave irradiation during hydrolytic degradation induced rapid hydrolytic degradation of PLLA. Also, hydrophobic finishing agent decelerated NHD traced by weight loss and $M_n$ [354].

## 21.4 STRUCTURAL AND PROPERTY CHANGES DURING HYDROLYTIC DEGRADATION

### 21.4.1 Fractions of Components

LA-based copolymers or PLA-based polymer blends contain various types of hydrolyzable linkages between lactides, lactide and comonomer, and comonomers. Normally, the hydrolytic degradation rates of these linkages are different and the monomer components connected with linkages with higher hydrolyzability are predominantly removed. For example, Kamei et al. [111], Li et al. [148], Park [149], and Grijpma et al. [157] investigated the fractional changes of monomers in P(LLA-*co*-GA) and P(DLLA-*co*-GA) during NHD. They found that the GA fraction is reduced during hydrolytic degradation. The relative ratio of L-and D-lactyl units in P(DLLA-*co*-GA) was constant because of the same cleavage rates of ester linkages between D-unit and D-unit, D-unit and L-unit, L-unit and D-unit, and L-unit and L-unit [111]. During NHD, L- or DL-lactyl unit content relative to glycine, ε-caprolactone, or 1,5-dioxepan-2-one content increased in P(DLLA-*co*-glycine) [204], P(LLA--*co*-CL) [184, 185], or PLLA-*b*-P(1,5-dioxepan-2-one)-*b*-PLLA [220], whereas DL-lactyl unit content relative to ε-caprolactone unit content decreased in P(DLLA--*co*-CL) [192]. Cohn and Younes [222] and Youxin et al. [229] indicated that the L-lactyl unit content in PLLA-*b*-PEO and PLLA-*b*-PEO-*b*-PLLA increased with NHD due to the release of water-soluble PEO chains. In contrast, the content of L-lactic acid units decreased in poly(L-lactic acid–bis-2-hydroxyethyl terephthalate) during NHD at 60°C, but such selective removal was not observed at 45°C [215]. In the case of polymer blends, we investigated the hydrolytic degradation of PDLA/PDLLA blends and found that amorphous PDLLA is predominantly degraded and removed from the blends [120].

### 21.4.2 Crystallization

As summarized in Figure 21.5 [358], crystallization of PLA-based materials takes place during hydrolytic degradation [23, 24, 30–32, 40, 47, 51, 62, 74, 75, 146, 148, 152, 184, 186, 338, 358, 400]. Even when amorphous PLLA was used for a hydrolytic degradation test, crystallinity increased with degradation time [23, 24, 31, 40, 62, 146]. Figure 21.16 shows the $X_c$ change of PLLA films having different initial $X_c$ values during hydrolytic degradation in phosphate-buffered solution [31]. Recently, it was suggested by SAXS, differential scanning calorimetry (DSC), and GPC that the crystalline thickness of PLLA increased during NHD [75]. Similarly, L-lactide copolymers of P(LLA-*co*-GA) and P(LLA-*co*-CL) crystallize during the course of hydrolytic degradation [41, 186]. Such crystallization during hydrolytic degradation is faster for rubbery copolymers P(LLA-*co*-CL) [184, 186] and

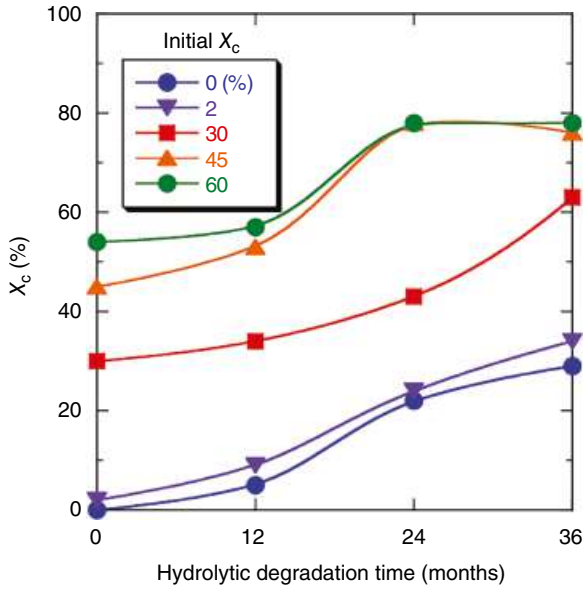


**FIGURE 21.16** Crystallinity ($X_c$) change of PLLA films having different initial $X_c$ values during hydrolytic degradation in a phosphate-buffered solution [31].

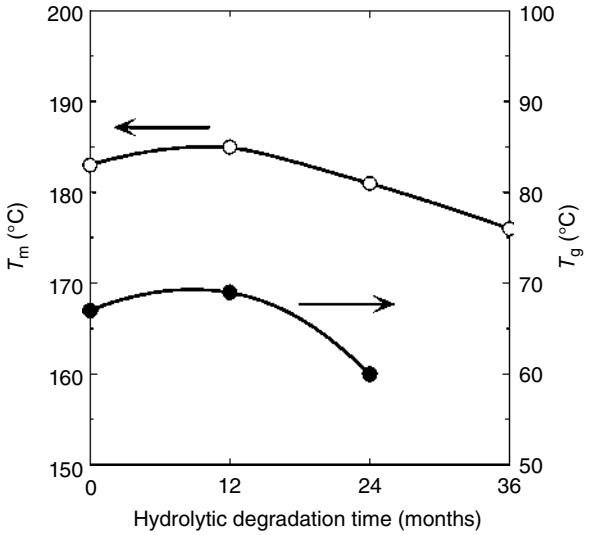


**FIGURE 21.17** Glass transition ($T_g$) and melting temperature ($T_m$) changes of PLLA film having initial $X_c$ value of 56% during hydrolytic degradation in a phosphate-buffered solution [31].

P(LLA-*co*-GA) [41, 152]. Li et al. [184] reported that the selective removal of CL and increased LLA content induced the crystallization of LLA segments in P(LLA-*co*-CL). Shikinami and Okuno [325] found that the crystallization of PLLA during NHD was accelerated by the presence of hydroxyapatite. The incorporation of lauric acid accelerated hydrolytic degradation in a neutral medium and, thereby, enhanced the crystallization of PLLA [305]. For the NHD of P(LLA-*co*-GA) (10/90), new lamellae of GA segments were formed between the old lamellae, resulting in a decreased long period and amorphous region thickness traced by SAXS [150]. Lostocco and Huang [282] showed that in addition to the plasticizing effects of water during NHD, the presence of oligomeric poly(hexamethylene succinate) enhanced the plasticizing effect and accelerated the crystallization of PLA. Regarding the crystallization of block copolymers during NHD, Huang et al. [218] indicated that in PDLLA-*b*-PCL-*b*-PDLLA, the crystallization of rubbery PCL segments was not disturbed by the neighboring glassy PDLLA segments. In addition to crystallization, selective removal of amorphous chains in PLA-based materials increased the crystallinity of PLLA [31, 32, 52, 265]. Regarding the effects of branching, amorphous linear two-armed PLLAs with an $M_n$ below $3.5\times10^4$ g/mol crystallized during hydrolytic degradation, whereas the branching architecture disturbed crystallization of initially amorphous branched four-armed PLLAs during hydrolytic degradation [100]. Stereocomplex crystallization occurred during NHD of stereo multiblock PLAs and PDLLA with average stereoblock lengths higher than seven lactyl units [249].

At a late stage in the acidic and NHD of copolymers containing both L- and D-lactyl units, stereocomplex formation of L-lactyl unit sequences and D-lactyl unit sequences can take place. Reported examples are those for PDLLA [117, 118, 122, 125, 140] and P(DLLA-*co*-CL) [192]. This phenomenon is caused by the selective removal of lactide segments having relatively random L- and D-lactyl unit sequences, leaving the relatively long L- and D-lactyl unit sequences.

### 21.4.3 Mechanical Properties

At a late stage of NHD of PLA-based materials, decrease in mechanical properties takes place, resulting from the decreased molecular weight. However, at an early stage of NHD, some mechanical properties increase due to the stabilized chain packing in the amorphous regions, resulting from low-temperature annealing in the presence of water molecules as a plasticizer [31, 32]. The latter was observed for P(LLA-*co*-CL) (45/55) during NHD at 23 and 37°C [183]. Todo et al. [38] investigated the fracture toughness of PLLA hydrolyzed in a neutral medium for 24 weeks and revealed that the decrease rate of fracture toughness was higher for crystallized PLLA than for amorphous PLLA. This was attributed to deteriorations such as crack formation at the spherulite interface that originated from the chain cleavage.

### 21.4.4 Thermal Properties

Normally, as shown in Figure 21.17 [31] at a late stage in the NHD of high-molecular-weight PLLA, $T_g$ decreases due to enhanced molecular mobility resulting from reduced molecular weight and $T_m$ decreases due to the decreased crystalline thickness and surface structural change of crystalline regions [31, 32, 143]. However, at an early stage of

hydrolytic degradation, the effect of stabilized chain packing in the presence of water under elevated temperature is higher than the reduced molecular weight effect, causing an increase in $T_g$ [31, 32, 143], whereas because of the thickening of crystallites or reduced disorder in the crystalline lattice, a $T_m$ increase can take place. The peak area of melting increases and that of cold crystallization decreases during alkaline and NHD due to crystallization and the selective removal of amorphous chains [24, 30–32, 51, 52, 54, 72].

### 21.4.5 Surface Properties

Hydrolytic degradation causes the cleavage of ester groups, resulting in an increased number of hydrophilic terminal groups (hydroxyl and carboxyl groups). Therefore, the surface hydrophilicity of PLA-based materials increases [55, 56, 123]. Figure 21.18 shows the advancing contact angle ($\theta_a$) change during alkaline hydrolytic degradation and during enzymatic degradation [55]. Alkaline and enzymatic degradation were carried out at 37°C in a 0.01 N NaOH solution (pH 12) and a Tris–HCl-buffered solution (pH 8.6) with proteinase K. As can be seen, the contact angle for water decreased monotonously from 100° to about 85° and 75° with increased degradation time for alkaline and enzymatic treatment, respectively. This indicates in reverse that the surface hydrophilicity of PLLA-based materials is enhanced by alkaline or enzymatic surface treatment. Further hydrophilicity was attained by rising with citric acid solution of alkali-treated PLLA films [89]. At an early stage of hydrolytic degradation, the charge density of PLLA increases due to the formation of hydroxyl and carboxyl groups, whereas at a late stage it decreases due to the release of hydrolysis-formed charged water-soluble oligomers [18]. Also, the surface softness increases due to hydrolysis-formed pores. On the other hand, Saiz-Arroyo et al. [50] showed that the surface mechanical properties of PLLA, such as the creep constant and microhardness, decreased with NHD.

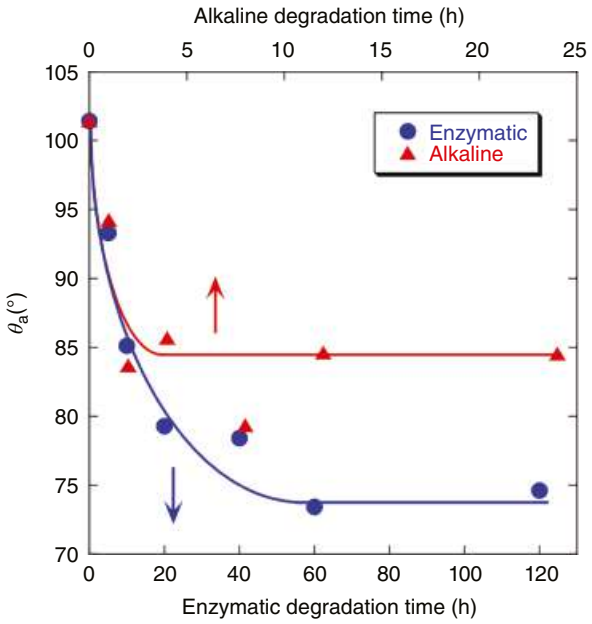


**FIGURE 21.18** Advancing contact angle ($\theta_a$) change during alkaline hydrolytic degradation, together with enzymatic degradation [55].

### 21.4.6 Morphology

As shown in Figures 21.19 and 21.20, the alkaline hydrolytic degradation of partially crystallized PLLA films elucidates the morphology of spherulites by selective removal of amorphous chains, whereas the image contrast of spherulites observed by polarized optical microscopy (POM) decreases after NHD due to disorientation of PLLA lamellae caused by the cleavage of tie chains [31, 52]. Fredericks et al. described the structure of P(LA-*co*-GA) (10/90) (Vicryl™) hydrolytically degraded in a neutral medium as a Swiss cheese formation [175]. During the NHD of PLLA and P(LLA--*co*-CL) fibers, regular patterns of cracks running in the vertical direction to the fiber axis are formed and finally the fibers are fragmented into independent disks [65, 72, 188].

## 21.5 APPLICATIONS OF HYDROLYTIC DEGRADATION

Excluding the specific purposes that utilize the "hydrolyzability" function, such as in biomedical, pharmaceutical, and environmental applications, the method of hydrolytic degradation can be effectively used for the following purposes.

### 21.5.1 Material Preparation

***21.5.1.1 Manipulation of Surface Properties*** PLA-based materials have relatively low hydrophilicity that can reduce the affinity of human body cells for such materials. As stated above, surface treatment involving alkaline or enzymatic surface hydrolytic degradation can enhance hydrophilicity (Figure 21.18) and, thereby, increase human body cell affinity without changing the structure of the core part and the bulk mechanical properties. Alkaline or enzymatic treatment can be utilized for increased surface hydrophilicity by the cleavage of ester groups and the formation of hydrophilic hydroxyl and carboxyl groups on the surface (Figure 21.21). Kimura and Yamaoka [114] revealed that the number of carboxyl groups per unit area increased upon alkaline surface hydrolytic degradation.

Slomkowshi et al. [401] reported that alkaline etching of PLLA microspheres in ethanol containing KOH produced a suspension of aggregated nanoparticles. Also, Nam et al. [160] and Wang and Cai [402] indicated that alkaline hydrolytic degradation of PLLA materials increased surface

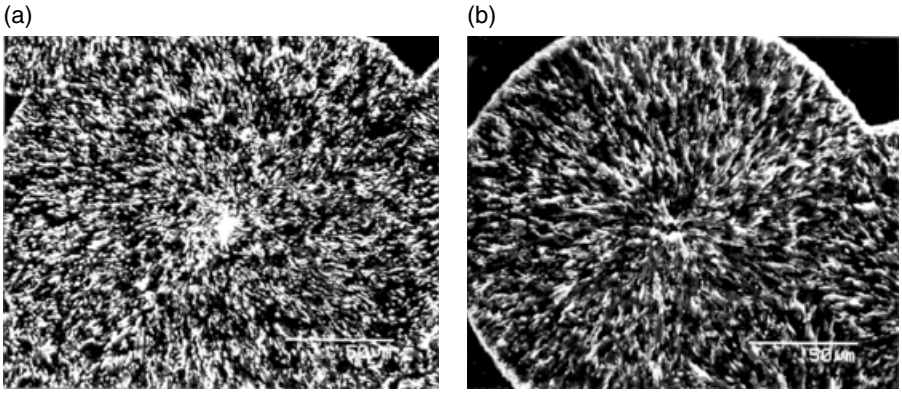


**FIGURE 21.19** Scanning electron photomicrographs of PLLA films containing spherulites after alkaline hydrolytic degradation for 30 days (a) and 150 days (b) [52].

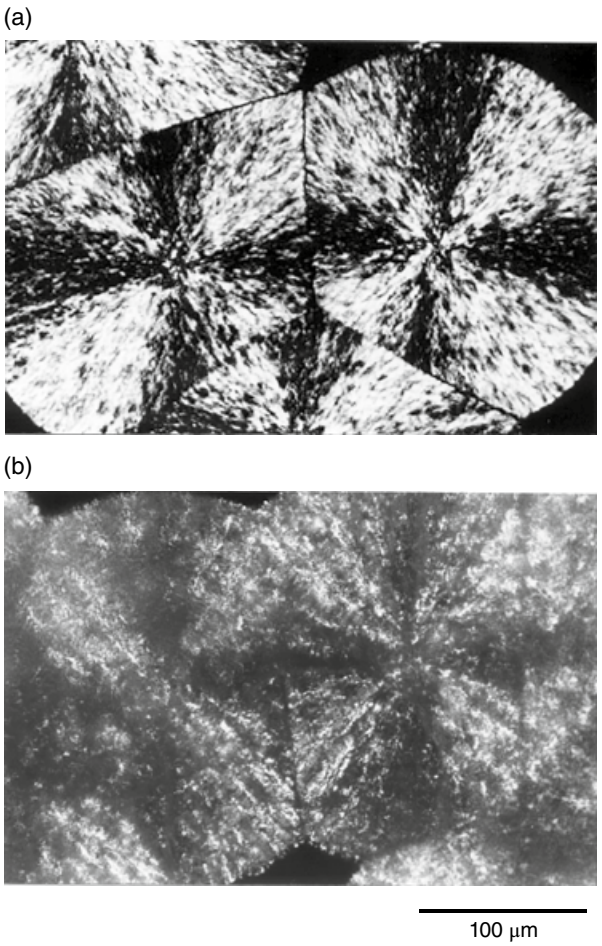


**FIGURE 21.20** Polarized optical photomicrographs of PLLA films containing spherulites before (a) and after (b) NHD [31].

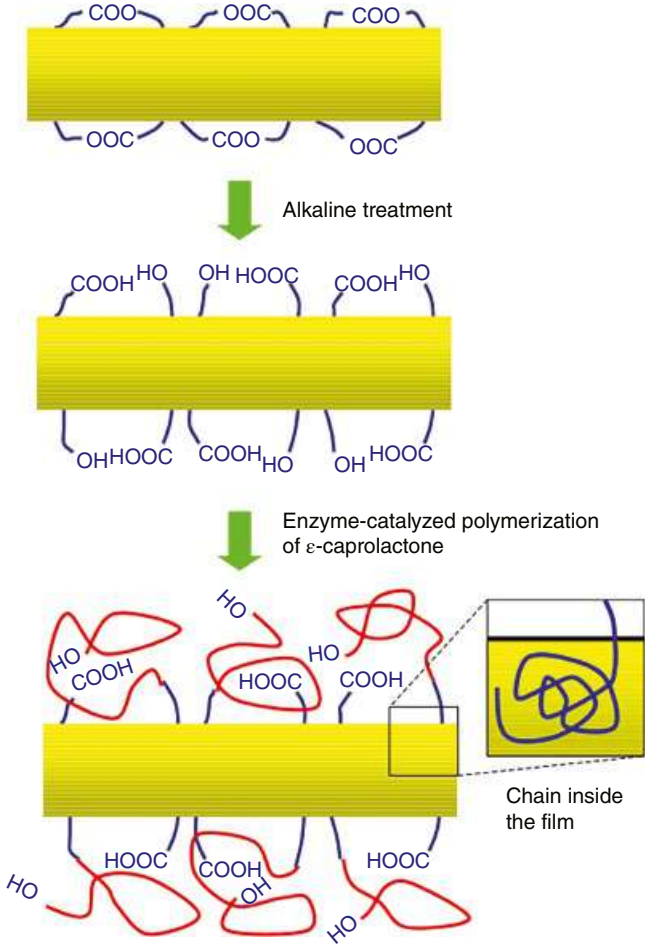


**FIGURE 21.21** Schematic representation of alkaline treatment and graft polymerization of biodegradable polyester film [59].

hydrophilicity and enhanced the cell affinity for the materials. Park et al. [171] found that NaOH surface-treated porous P(LA-*co*-GA) had a higher number of attached chondrocytes, total intracellular protein content, and extracellular matrix components compared with those of nontreated P(LA-*co*-GA). Plasma glow discharge treatment gave PLLA materials higher hydrophilicity compared with that of nontreated materials [110]. However, the difference became insignificant upon immersion in a phosphate-buffered solution for 20 days.

***21.5.1.2 Formation of Reactive Sites on Surface*** Croll et al. [158] utilized surface alkaline hydrolytic degradation of P(DLLA-*co*-GA) using an NaOH solution, ethylenediamine, or an *N*-aminoethyl-1,3-propanediamine solution, and the formed carboxyl or amine groups were used for further grafting of chitosan. Tsuji et al. [59] prepared PLLA films grafted with PCL chains by surface alkaline hydrolytic degradation of PLLA films to have a high number of hydroxyl groups on their surface and subsequent enzymatic graft polymerization of CL coinitiated with surface hydroxyl groups (Figure 21.21).

Also, Tsuji et al. [76] prepared block copolymers by ring-opening polymerization of DLLA coinitiated with PLLA crystalline residues (or extended-chain crystallites) prepared by NHD of crystallized PLLA films. Extended-chain crystallites can act as a macrocoinitiator because they have many hydroxyl groups as terminal groups on their surface. In spite of the activity as the coinitiator, the chains inside the extended-chain crystallites are inert and expected to be protected from intersegmental transesterification between block chains synthesized in the first step (L-lactide chains) and the second step (DL-lactide chains) due to the rigidity of the crystalline lattice.

***21.5.1.3 Preparation of Structured Materials and Nanomaterials*** Rzayev and Hillmyer [403] developed a novel method for preparing nanochannel array plastics with tailored surfaces by self-assembly, alignment of polystyrene (PS)–poly(dimethylacrylamide) (PDMA)–PLA triblock copolymers, subsequent selective hydrolysis and removal of PLA segments from the aligned materials. PDMA blocks appeared on the nanochannel surface after the removal of PLA segments. Also, Ho et al. [406] developed a method for preparing thin film with perpendicularly and cylindrically nanopatterned PS through selective hydrolytic degradation and the removal of PLLA segments from spin coated PLLA-*b*-PS.

Mincheva et al. prepared linear two-armed stereocomplexed PDLLA-*b*-PLLA/PDLLA-*b*-PDLA blends and removal of PDLLA blocks by hydrolytic degradation, resulting in the formation of stereocomplex nanocrystals for reinforcement of conventional PLA-based materials [273].

***21.5.1.4 Preparation of Low-Molecular-Weight PLA*** As stated in the "Molecular Weight" section, it is crucial to control the molecular weight of PLA-based materials for biomedical, pharmaceutical, and environmental applications because the molecular weight determines the hydrolytic degradation rate and drug release profile. Therefore, it is preferred to prepare PLA-based materials having appropriate molecular weights for specific applications and purposes. In conventional methods of ring-opening polymerization of LLA and comonomers or condensation polymerization of L-lactic acid and comonomers, numerous parameters, such as type and concentration of initiator, coinitiator, and catalyst, reaction temperature, time, and pressure, should be accurately controlled for manipulating the molecular weight of the synthesized polymer. The hydrolytic degradation of PLA-based materials in the melt proceeds via homogeneous and random cleavage of chains. Therefore, this could be a simple and effective preparation method for PLA-based materials with different molecular weights because in such a method only the reaction temperature and time need to be controlled, and commercially available high-molecular-weight materials can be utilized as starting materials (Figure 21.22) [78]. As seen in Figure 21.11, when PLLA was hydrolytically degraded in the melt, low-molecular-weight specific peaks ascribed to crystalline residues were not formed.

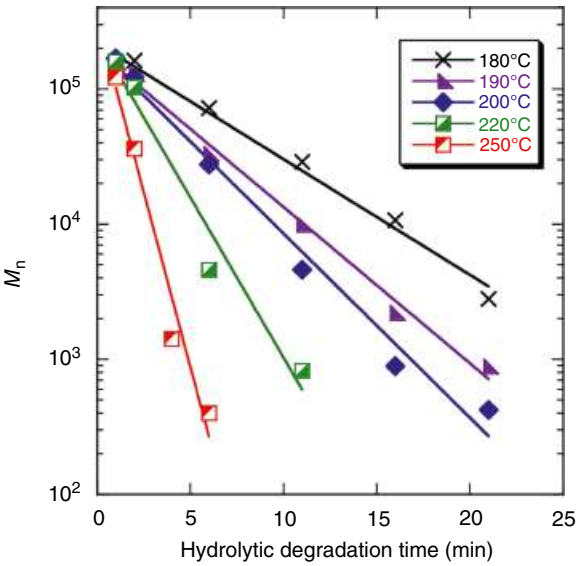


**FIGURE 21.22** $M_n$ of PLLA hydrolytically degraded in the melt as a function of degradation time [78].

## 21.5.2 Recycling of PLA to Its Monomer

As stated above, PLA is susceptible to hydrolytic degradation, and the degradation rate becomes higher with an increase in temperature. Utilizing this trend, the recycling of PLA to lactic acid in high yield is expected to be attained by high-temperature hydrolytic degradation within a short period, such as several tens of minutes. An example is shown in Figure 21.23 [80], where the yield of lactic acid from melted PLLA during hydrolytic degradation in liquid water at temperatures between 160 and 250°C is plotted against degradation time. L-lactic acid was recovered in a yield exceeding 90% at 160–300°C within 180 min and insignificant racemization of formed L-lactic acid took place at degradation temperatures of up to 230°C [78–80, 82]. Here, it should be noted that at the degradation temperature of 160°C, PLLA became a melted material for a period

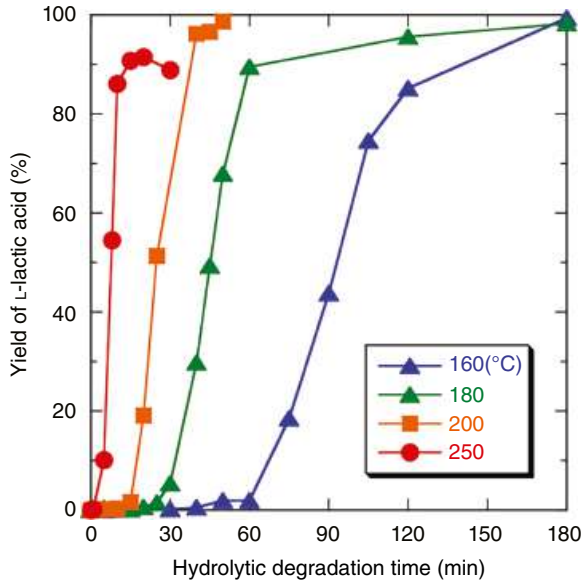


**FIGURE 21.23** Yields of lactic acid from PLLA during hydrolytic degradation at different temperatures between 160 and 250°C are plotted against degradation time [80].

exceeding 50 min because $T_m$ of PLLA (initial $T_m$ = 172°C) was lowered to below 160°C during hydrolysis. However, even at a temperature lower than $T_m$ (120°C), the degradation can form L-lactic acid at around 100% yield when degradation is continued for a long period of 4320 min. Piemonte and Gironi reported that PLLA in aqueous suspension can be hydrolytically degraded to water-soluble monomer and oligomers within 120 min at 160 or 180°C [83]. On the other hand, Okamoto et al. found that hydrolytic degradation of PLLA at 100°C for 6 h in toluene in the presence of montmorillonite K10 gave L-lactic acid oligomers with $M_n$ of ca. 200 g/mol in a yield exceeding 90% and that these oligomers could be readily polymerized to PLLA with $M_w$ over $1 \times 10^5$ g/mol by the use of $SnCl_2$/*p*-toluenesulfonic acid as the catalyst [77]. Hirano et al. reported that microwave irradiation reduced reaction time for recycling of PLLA to lactic acid and optical purity was higher compared with that for the nonirradiated reaction [86]. Song et al. found that the maximum hydrolytic conversion of PLA (93.9%) and the maximum yield of calcium lactate (76.1%) were obtained at 130°C for 2 h using a water/ionic liquid (1-butyl-3-methylimidazolium acetate) mixture [137].

## 21.6 CONCLUSIONS

The rate, behavior, and mechanism of the hydrolytic degradation of PLA-based materials can be manipulated by varying molecular and highly ordered structures, blending, fillers, material shape, and surface structure. Also, hydrolytic degradation can be utilized for the recycling, preparation, and modification of PLA-based materials.

## REFERENCES


1. H. Tsuji, Polylactides, in: Y. Doiand, A. Steinbüchel (Eds.), *Polyesters 3, Biopolymers*, Vol. *4*, Wiley-VCH, Weinheim, 2002, pp. V/129ff.
2. H. Tsuji, Degradation of poly(lactide)-based biodegradable materials, in: L. B. Albertov (Ed.), *Polymer Degradation and Stability Research Developments*, Nova Science Publishers, New York, 2007, pp. 11–59.
3. H. Tsuji, *Degradation of Poly(Lactide)-Based Biodegradable Materials*, Nova Science Publishers, New York, 2007.
4. M. Vert, P. Christel, F. Chabot, J. Leray, Bioresorbable plastic materials for bone surgery, in: G. W. Hasting, P. Ducheyne (Eds.), *Macromolecular Materials*, CRC Press, Boca Raton, FL, 1984, pp. VI/119ff.
5. D. H. Lewis, Controlled release of bioactive agents from lactide/glycolide polymers, in: M. Chasin, R. Langer (Eds.), *Biodegradable Polymers as Drug Delivery System, Drug and The Pharmaceutical Sciences*, Vol. *45*, Marcel Dekker, Inc., New York, 1990, pp. I/1ff.
6. M. Vert, S. M. Li, H. H. Garreau, More about the degradation of LA/GA-derived matrices in aqueous media, *J. Control. Release* **1991**, *16*, 15–26.
7. G. B. Kharas, F. Sanchez-Riera, D. K. Severson, Polymers of lactic acid, in: D. P. Mobley (Ed.), *Plastics from Microbes*, Hanser Publishers, New York, 1994, pp. IV/93ff.
8. D. E. Perrin, J. P. English, Polyglycolide and polylactide, in: A. J. Domb, J. Kost, D. M. Wiseman (Eds.), *Handbook of Biodegradable Polymers*, Harwood Academic Publishers, Amsterdam, 1997, pp. I/3ff.
9. Y. Ikada, H. Tsuji, Biodegradable polyesters for medical and ecological applications, *Macromol. Rapid Commun.* **2000**, *21*, 117–132.
10. S. M. Li, M. Vert, Biodegradation of aliphatic polyesters, in: G. Scott (Ed.), *Biodegradable Polymers: Principles and Applications*, 2nd edition, Kluwer Academic Publishers, Dordrecht, 2002, pp. V/71ff.
11. A. Södergård, M Stolt, Properties of lactic acid based polymers and their correlation with composition, *Prog. Polym. Sci.* **2002**, *27*, 1123–1163.
12. R. Auras, B. Harte, S. Selke, An overview of polylactides as packaging materials, *Macromol. Biosci.* **2004**, *4*, 835–864.
13. H. Tsuji, Poly(lactide) Stereocomplexes: Formation, Structure, Properties, Degradation, and Applications, *Macromol. Biosci.* **2005**, *5*, 569–597.
14. H. Tsuji, Poly(lactide)s and their copolymers: physical properties and hydrolytic degradation, in: P. I. J. M. Wuisman, T. H. Smit (Eds.), *Degradable Polymers for Skeletal Implants*, Nova Science Publishers, New York, 2009, pp. 41–70.
15. W. K. Lee, J. A. Gardella Jr., Hydrolytic kinetics of biodegradable polyester monolayers, *Langmuir* **2000**, *16*, 3401–3406.
16. K. Makino, M. Arakawa, T. Kondo, Preparation and in vitro degradation properties of polylactide microcapsules, *Chem. Pharm. Bull.* **1985**, *33*, 1195–1201.

17. K. Makino, H. Ohshima, T. Kondo, Mechanism of hydrolytic degradation of poly(L-lactide) microcapsules: effects of pH, ionic strength and buffer concentration, *J. Microencapsulation* **1986**, *3*, 203–212.
18. K. Makino, H. Ohshima, Changes in charge density and softness of a poly(L-lactide) microcapsule surface in the hydrolytic degradation process, *Colloid Surf. B* **1996**, *6*, 373–378.
19. S. Karlsson, A.-C. Albertsson, Abiotic and biotic degradation of aliphatic polyesters from "petro" versus "green" resources, *Macromol. Symp.* **1998**, *127*, 219–225.
20. R. K. Kulkarni, E. G. Moore, A. F. Hegyeli, F. Leonard, Biodegradable poly(lactic acid) polymers, *J. Biomed. Mater. Res.* **1971**, *5*, 169–181.
21. A. M. Reed, D. K. Gilding, Biodegradable polymers for use in surgery—poly(glycolic)/poly(lactic acid) homo and copolymers: 2. in vitro degradation, *Polymer* **1981**, *22*, 494–498.
22. D. W. Grijpma, A. J. Pennings, (Co)polymers of L-lactide, 1. Synthesis, thermal properties and hydrolytic degradation, *Macromol. Chem. Phys.* **1994**, *195*, 1633–1647.
23. J. W. Leenslag, A. J. Pennings, R. R. M. Bos, F. R. Rozema, G. Boering, Resorbable materials of poly(L-lactide). VII. in vivo and in vitro degradation, *Biomaterials*, **1987**, *8*, 311–314.
24. S. M. Li, H. Garreau, M. Vert, Structure-property relationships in the case of the degradation of massive poly(α-hydroxy acids) in aqueous media, Part 3: Influence of the morphology of poly(L-lactic acid), *J. Mater. Sci. Mater. Med.* **1990**, *1*, 198–206.
25. Y. Matsusue, T. Yamamuro, M. Oka, Y. Shikinami, S. H. Hyon, Y. Ikada, in vitro and in vivo studies on bioabsorbable ultra-high-strength poly(L-lactide) rods, *J. Biomed. Mater. Res.* **1992**, *26*, 1553–1567.
26. J. V. Seppälä, R. M. H. Malin, Studies of the hydrolytic degradation of some aliphatic polyesters, in: Y. Doi, K. Fukuda (Eds.), *Biodegradable Polymers and Plastics*, Elsevier Science, Amsterdam, 1994, pp. 519–527.
27. C. A. P. Joziasse, D. W. Grijpma, J. E. Bergsma, F. W. Cordewener, R. R. M. Bos, A. J. Pennings, The influence of morphology on the (hydrolytic degradation of as-polymerized and hot-drawn poly(L-lactide)), *Colloid Polym. Sci.* **1998**, *276*, 968–975.
28. H. Tsuji, Y. Ikada, Blends of aliphatic polyesters. II. Hydrolysis of solution-cast blends from poly(L-lactide) and poly(ε-caprolactone) in phosphate-buffered solution, *J. Appl. Polym. Sci.* **1998**, *67*, 405–415.
29. G. Schwach, M. Vert, in vitro and in vivo degradation of lactic acid-based interference screws used in cruciate ligament reconstruction, *Int. J. Biol. Macromol.* **1999**, *25*, 283–291.
30. E. A. R. Duek, C. A. C. Zavaglia, W. D. Belangero, in vitro study of poly(lactic acid) pin degradation, *Polymer* **1999**, *40*, 6465–6473.
31. H. Tsuji, A. Mizuno, Y. Ikada, Properties and morphology of poly(L-lactide). III. Effects of initial crystallinity on long-term in vitro hydrolysis of high molecular weight poly(L-lactide) film in phosphate-buffered solution, *J. Appl. Polym. Sci.* **2000**, *77*, 1452–1464.
32. H. Tsuji, Y. Ikada, Properties and morphology of poly(L-lactide) 4. Effects of structural parameters on long-term hydrolysis of poly(L-lactide) in phosphate-buffered solution, *Polym. Degrad. Stab.* **2000**, *67*, 179–189.
33. H. Tsuji, in vitro hydrolysis of blends from enantiomeric poly(lactide)s Part 1. Well-stereo-complexed blend and non-blended films, *Polymer* **2000**, *41*, 3621–3630.
34. H. Tsuji, Autocatalytic hydrolysis of amorphous-made polylactides: effects of L-lactide content, tacticity, and enantiomeric polymer blending, *Polymer* **2002**, *43*, 1789–1796.
35. H. Tsuji, in vitro hydrolysis of blends from enantiomeric poly(lactide)s. Part 4: well-homo-crystallized blend and non-blended films, *Biomaterials* **2003**, *24*, 537–547.
36. H. Tsuji, C. A. Del Carpio, in vitro hydrolysis of blends from enantiomeric poly(lactide)s. 3. Homocrystallized and amorphous blend films, *Biomacromolecules* **2003**, *4*, 7–11.
37. S. H. Hyon, F. Jin, K. Jamshidi, S. Tsutsumi, T. Kanamoto, Biodegradable ultra high strength poly(L-lactide) rods for bone fixation, *Macromol. Symp.* **2003**, *197*, 355–368.
38. M. Todo, N. Shinohara, K. Arakawa, H. Tsuji, Effect of hydroloysis on fracture behavior of poly(L-lactide), *Kobunshi Ronbunshu* **2003**, *60*, 644–651.
39. H. Tsuji, M. Ogiwara, S. K. Saha, T. Sakaki, Enzymatic, alkaline, and autocatalytic degradation of poly(L-lactic acid): effects of biaxial orientation, *Biomacromolecules* **2006**, *7*, 380–387.
40. S. K. Saha, H. Tsuji, Effects of molecular weight and small amounts of D-lactide units on hydrolytic degradation of poly(L-lactic acid)s, *Polym. Degrad. Stab.* **2006**, *91*, 1665–1673.
41. S. K. Saha, H. Tsuji, Hydrolytic degradation of amorphous films of L-lactide copolymers with glycolide and D-lactide, *Macromol. Mater. Eng.* **2006**, *291*, 357–368.
42. H. Tsuji, S. Kamo, F. Horii, Solid-state $^{13}C$ NMR analyses of the structures of crystallized and quenched poly(lactide)s: effects of crystallinity, water absorption, hydrolytic degradation, and tacticity, *Polymer* **2010**, *51*, 2215–2220.
43. H. Tsuji, K. Ikarashi, in vitro hydrolysis of poly(L-lactide) crystalline residues as extended-chain crystallites. Part I: long-term hydrolysis in phosphate-buffered solution at 37°C, *Biomaterials* **2004**, *25*, 5449–5455.
44. H. Tsuji, K. Ikarashi, in vitro hydrolysis of poly(L-lactide) crystalline residues as extended-chain crystallites: III. Effects of pH and enzyme, *Polym. Degrad. Stab.* **2004**, *85*, 647–656.
45. V. J. Chen, P. X. Ma, The effect of surface area on the degradation rate of nano-fibrous poly(L-lactic acid) foams, *Biomaterials* **2006**, *27*, 3708–3715.
46. J. C. Dias, C. Ribeiro, V. Sencadas, G. Botelho, J. L. G. Ribelles, S. Lanceros-Mendez, Influence of fiber diameter and crystallinity on the stability of electrospun poly(L-lactic acid) membranes to hydrolytic degradation, *Polym. Test.* **2012**, *31*, 770–776.
47. G. Migliaresi, L. Fambri, D. Cohn, A study on the in vitro degradation of poly(lactic acid), *J. Biomater. Sci. Polym. Ed.* **1994**, *5*, 591–606.
48. C. Migliaresi, L. Fambri, Processing and in vitro degradation of poly(L-lactic acid) fibres, *Macromol. Symp.* **1997**, *123*, 155–161.

49. A. Pegoretti, L. Fambri, C. Migliaresi, in vitro degradation of poly(L-lactic acid) fibers produced by melt spinning, *J. Appl. Polym. Sci.* **1997**, *64*, 213–223.
50. C. Saiz-Arroyo, Y. Wang, M. A. Rodriguez-Perez, N. M. Alves, J. F. Mano, in vitro monitoring of surface mechanical properties of poly(L-lactic acid) using microhardness, *J. Appl. Polym. Sci.* **2007**, *105*, 3860–3864.
51. D. Cam, S. H. Hyon, Y. Ikada, Degradation of high molecular weight poly(L-lactide) in alkaline medium, *Biomaterials* **1995**, *16*, 833–843.
52. H. Tsuji, Y. Ikada, Properties and morphology of poly(L-lactide). II. Hydrolysis in alkaline solution, *J. Polym. Sci. Part A* **1998**, *36*, 59–66.
53. T. Iwata, Y. Doi, Alkaline hydrolysis of solution-grown poly(L-lactic acid) single crystals, *Sen'I Gakkaishi* **2001**, *57*, 172–177.
54. X. Yuan, A. F. T. Mak, K. Yao, Surface degradation of poly(L-lactic acid) fibres in a concentrated alkaline solution, *Polym. Degrad. Stab.* **2003**, *79*, 45–52.
55. H. Tsuji, T. Ishida, Poly(l-lactide). X. Enhanced surface hydrophilicity and chain-scission mechanisms of poly(L-lactide) film in enzymatic, alkaline, and phosphate-buffered solutions, *J. Appl. Polym. Sci.* **2003**, *87*, 1628–1633.
56. H. Tsuji, T. Ishida, N. Fukuda, Surface hydrophilicity and enzymatic hydrolyzability of biodegradable polyesters: 1. Effects of alkaline treatment, *Polym. Int.* **2003**, *52*, 843–852.
57. H. Tsuji, Y. Tezuka, Alkaline and enzymatic degradation of L-lactide copolymers, 1. Amorphous-made films of L-lactide copolymers with D-lactide, glycolide, and ε-caprolactone, *Macromol. Biosci.* **2005**, *5*, 135–148.
58. H. Tsuji, Y. Tezuka, K. Yamada, Alkaline and enzymatic degradation of L-lactide copolymers. II. Crystallized films of poly(L-lactide-*co*-D-lactide) and poly(L-lactide) with similar crystallinities, *J. Polym. Sci. Part B* **2005**, *43*, 1064–1075.
59. H. Tsuji, M. Nishikawa, Y. Osanai, S. Matsumura, New strategy for controlling biodegradability of biodegradable polyesters by enzyme-catalyzed surface grafting, *Macromol. Rapid Commun.* **2007**, *28*, 1651–1656.
60. A. Belbella, C. Vauthier, H. Fessi, J.-P. Devissaguet, F. Puisieux, in vitro degradation of nanospheres from poly(D,L-lactides) of different molecular weights and polydispersities, *Int. J. Pharm.* **1996**, *129*, 95–102.
61. H. Tsuji, K. Nakahara, Poly(l-lactide). IX. Hydrolysis in acid media, *J. Appl. Polym. Sci.* **2002**, *86*, 186–194.
62. H. Xu, X. Yang, L. Xie, M. Hakkarainen, Conformational footprint in hydrolysis-induced nanofibrillation and crystallization of poly(lactic acid), *Biomacromolecules* **2016**, *17*, 985–995.
63. S. H. Hyon, K. Jamshidi, Y. Ikada, Melt spinning of poly-L-lactide and hydrolysis of the fiber in vitro, in: S. W. Shalaby, A. S. Hoffman, B. D. Ratner, T. A. Horbett (Eds.), *Polymers as Biomaterials*, Plenum Press, New York, 1984, 51pp.
64. K. Jamshidi, S. H. Hyon, T. Nakamura, Y. Ikada, Y. Shimidu, T. Teramatsu, in vitro and in vivo degradation of poly-L-lactide fibers, in: P. Christel, A. Meunier, A. J. C. Lee (Eds.), *Biological and Biomechanical Performance of Biomaterials*, Elsevier Science, Amsterdam, 1986, pp. 227–232.
65. S. H. Hyon, Surface morphology for poly-L-lactide fibers subjected to hydrolysis, *Sen'i Gakkaishi* **1998**, *54*, 527–531.
66. H.-M. Chen, Y. Shen, J.-H. Yang, T. Huang, N. Zhang, Y. Wang, Z.-W. Zhou, Molecular ordering and α′-form formation of poly(L-lactide) during the hydrolytic degradation, *Polymer* **2013**, *54*, 6644–6653.
67. F. Mai, W. Tu, E. Bilotti, T. Peijs, The influence of solid-state drawing on mechanical properties and hydrolytic degradation of melt-spun poly(lactic acid) (PLA) tapes, *Fibers*, **2015**, *3*, 523–538.
68. N. Zhang, X. Yu, J. Duan, J.-H. Yang, T. Huang, X.-D. Qi, Y. Wang, Comparison study of hydrolytic degradation behaviors between α′- and α-poly(L-lactide), *Polym. Degrad. Stab.* **2018**, *148*, 1–9.
69. H. Tsuji, K. Ikarashi, In Vitro Hydrolysis of Poly(L-lactide) Crystalline Residues as Extended-Chain Crystallites: II. Effects of Hydrolysis Temperature, *Biomacromolecules* **2004**, *5*, 1021–1028.
70. G. Xu, X. Liu, Y. Lin, G. He, W. Wang, W. Xiong, H. Luo, Z. Liu, J. Zhao, Thermal hydrolysis of poly(L-lactic acid) films and cytotoxicity of water-soluble degradation products, *J. Appl. Polym. Sci.* **2015**, *132*, Article number 42064.
71. J. K. Lee, K. H. Lee, B. S. Jin, Structure development and biodegradability of uniaxially stretched poly(L-lactide), *Eur. Polym. J.* **2001**, *37*, 907–914.
72. X. Yuan, A. F. T. Mak, K. Yao, Comparative observation of accelerated degradation of poly(L-lactic acid) fibres in phosphate buffered saline and a dilute alkaline solution, *Polym. Degrad. Stab.* **2002**, *75*, 45–53.
73. J. E. Bergsma, F. R. Rozema, R. R. M. Bos, G. Boering, C. A. P. Joziasse, A. J. Pennings, in vitro predegradation at elevated temperatures of poly(lactide), *J. Mater. Sci. Mater. Med.* **1995**, *6*, 642–646.
74. H. Tsuji, K. Nakahara, K. Ikarashi, Poly(L-lactide), 8. High-temperature hydrolysis of poly(L-lactide) films with different crystallinities and crystalline thicknesses in phosphate-buffered solution, *Macromol. Mater. Eng.* **2001**, *286*, 398–406.
75. H. Tsuji, K. Ikarash, N. Fukuda, Poly(L-lactide): XII. Formation, growth, and morphology of crystalline residues as extended-chain crystallites through hydrolysis of poly(L-lactide) films in phosphate-buffered solution, *Polym. Degrad. Stab.* **2004**, *84*, 515–523.
76. H. Tsuji, M. Nishikawa, Y. Sakamoto, S. Itsuno, Novel preparation method for poly(L-lactide)-based block copolymers: extended chain crystallites as a solid-state macro-coinitiator, *Biomacromolecules* **2007**, *8*, 1730–1738.
77. K. Okamoto, K. Toshima, S. Matsumura, Degradation of poly(lactic acid) into repolymerizable oligomer using montmorillonite K10 for chemical recycling, *Macromol. Biosci.* **2005**, *5*, 813–820.
78. H. Tsuji, H. Daimon, K. Fujie, A new strategy for recycling and preparation of poly(L-lactic acid): hydrolysis in the melt, *Biomacromolecules* **2003**, *4*, 835–840.
79. T. Saeki, T. Tsukegi, H. Tsuji, H. Daimon, K. Fujie, Depolymerization of poly (L-lactic acid) under hydrothermal conditions, *Kobunshi Ronbunshu* **2004**, *61*, 561–566.


80. M. Faisal, T. Saeki, H. Tsuji, H. Daimon, K. Fujie, Depolymerization of poly (L-lactic acid) under hydrothermal conditions, *Asian J. Chem.* **2006**, *19*, 1714–1722.
81. H. Tsuji, R. Okino, H. Daimon, K. Fujie, Water vapor permeability of poly(lactide)s: effects of molecular characteristics and crystallinity, *J. Appl. Polym. Sci.* **2006**, *99*, 2245–2252.
82. H. Tsuji, T. Saeki, T. Tsukegi, H. Daimon, K. Fujie, Comparative study on hydrolytic degradation and monomer recovery of poly(L-lactic acid) in the solid and in the melt, *Polym. Degrad. Stab.* **2008**, *10*, 1956–1963.
83. V. Piemonte, F. Gironi, Lactic acid production by hydrolysis of poly(lactic acid) in aqueous solutions: an experimental and kinetic study, *J. Polym. Environ.* **2012**, *21*, 275–279.
84. V. K. Holm, S. Ndoni, J. Risbo, The stability of poly(lactic acid) packaging films as influenced by humidity and temperature, *J. Food Sci.* **2006**, *71*, E40–E44.
85. A. F. Mohd-Adnan, H. Nishida, Y. Shirai, Evaluation of kinetics parameters for poly(L-lactic acid) hydrolysis under high-pressure steam, *Polym. Degrad. Stab.* **2008**, *93*, 1053–1058.
86. K. Hirao, Y. Shimamoto, Y. Nakatsuchi, H. Ohara, Hydrolysis of poly(L-lactic acid) using microwave irradiation, *Polym. Degrad. Stab.* **2010**, *95*, 86–88.
87. L. Xie, H. Xu, Z.-P. Wang, X.-J. Li, J.-B. Chen, Z.-J. Zhang, H.-M. Yin, G.-J. Zhong, J. Lei, Z.-M. Li, Toward faster degradation for natural fiber reinforced poly(lactic acid) biocomposites by enhancing the hydrolysis-induced surface erosion, *J. Polym. Res.* **2014**, *21*, Article number 357.
88. N.-J. Jo, I. Jung, S. S. Park, W.-K. Lee, C.-H. Lee, Morphological study on mechanical deformation and alkaline hydrolysis of solution-grown poly(L-lactide) crystals, *Mol. Cryst. Liq. Cryst.* **2014**, *599*, 51–54.
89. C. Guo, M. Xiang, Y. Dong, Surface modification of poly (lactic acid) with an improved alkali-acid hydrolysis method, *Mater. Lett.* **2015**, *140*, 144–147.
90. A. Hoüglund, K. Odelius, A.-C. Albertsson, Crucial differences in the hydrolytic degradation between industrial polylactide and laboratory-scale poly(L-lactide), *ACS Appl. Mater. Interfaces* **2012**, *4*, 2788–2793.
91. C. Braud, R. Devarieux, H. Garreau, M. Vert, Capillary electrophoresis to analyze water-soluble oligo(hydroxyacids) issued from degraded or biodegraded aliphatic polyesters, *J. Environ. Polym. Degrad.* **1996**, *4*, 135–148.
92. F. Codari, S. Lazzari, M. Soos, G. Storti, M. Morbidelli, D. Moscatelli, Kinetics of the hydrolytic degradation of poly(lactic acid), *Polym. Degrad. Stab.* **2012**, *97*, 2460–2466.
93. C. F. van Nostrum, T. F. J. Veldhuis, G. W. Bos, W. E. Hennink, Hydrolytic degradation of oligo(lactic acid): a kinetic and mechanistic study, *Polymer* **2004**, *45*, 6779–6787.
94. S. J. de Jong, E. R. Arias, D. T. S. Rijkers, C. F. van Nostrum, J. J. Kettenes-van den Bosch, New insights into the hydrolytic degradation of poly(lactic acid): participation of the alcohol terminus, *Polymer* **2001**, *42*, 2795–2802.
95. K. Kurokawa, K. Yamashita, Y. Doi, H. Abe, Structural effects of terminal groups on nonenzymatic and enzymatic degradations of end-capped poly(L-lactide), *Biomacromolecules* **2008**, *9*, 1071–1078.
96. F. Iñiguez-Franco, R. Auras, J. Ahmed, S. Selke, M. Rubino, K. Dolan, H. Soto-Valdez, Control of hydrolytic degradation of poly(lactic acid) by incorporation of chain extender: from bulk to surface erosion, *Polym. Test.* **2018**, *67*, 190–196.
97. W. Limsukon, R. Auras, S. Selke, Hydrolytic degradation and lifetime prediction of poly(lactic acid) modified with a multifunctional epoxy-based chain extender, *Polym. Test.* **2019**, *80*, Article number 106108.
98. S. H. Kim, Y. H. Kim, Biodegradable star-shaped poly-L-lactide, in: Y. Doi, K. Fukuda (Eds.), *Biodegradable Plastics and Polymers, Studies in Polymer Science*, Vol. *12*, Elsevier Science, Amsterdam, 1994, pp. 464–469.
99. Y. Zhao, X. Shuai, C. Chen, F. Xi, Synthesis and characterization of star-shaped poly(L-lactide)s initiated with hydroxyl-terminated poly(amidoamine) (PAMAM-OH) dendrimers, *Chem. Mater.* **2003**, *15*, 2836–2843.
100. H. Tsuji, T. Hayashi, Hydrolytic degradation and crystallization behavior of linear 2-armed and star-shaped 4-armed poly(L-lactide)s: effects of branching architecture and crystallinity, *J. Appl. Polym. Sci.* **2015**, *132*, Article number 41983.
101. K. Numata, R. K. Srivastava, A. Finne-Wistrand, A.-C. Albertsson, Y. Doi, H. Abe, Branched poly(lactide) synthesized by enzymatic polymerization: effects of molecular branches and stereochemistry on enzymatic degradation and alkaline hydrolysis, *Biomacromolecules* **2007**, *8*, 3115–3125.
102. H. Lee, S. H. Kim, Y. K. Han, Y. H. Kim, Synthesis and degradation of end-group-functionalized polylactide, *J. Polym. Sci. Part A* **2001**, *39*, 973–985.
103. I. Arvanitoyannis, A. Nakayama, E. Psomiadou, N. Kawasaki, N. Yamamoto, Novel star-shaped polylactide with glycerol using stannous octoate or tetraphenyl tin as catalyst: 1. Synthesis, characterization and study of their biodegradability, *Polymer* **1995**, *36*, 2947–2956.
104. I. Arvanitoyannis, A. Nakayama, E. Psomiadou, N. Kawasaki, N. Yamamoto, Synthesis and degradability of a novel aliphatic polyester based on L-lactide and sorbitol: 3, *Polymer* **1996**, *37*, 651–660.
105. V. De Simone, G. Maglio, R. Palumbo, V. Scardi, Synthesis, characterization, and degradation of block polyesteramides containing poly(L-lactide) segments, *J. Appl. Polym. Sci.* **1992**, *46*, 1813–1820.
106. A. Södergård, J. F. Selin, J. H. Näsman, Hydrolytic degradation of peroxide modified poly(L-lactide), *Polym. Degrad. Stab.* **1996**, *51*, 351–359.
107. S. C. J. Loo, H. T. Tan, C. P. Ooi, Y. C. F. Boey, Hydrolytic degradation of electron beam irradiated high molecular weight and non-irradiated moderate molecular weight PLLA, *Acta Biomater.* **2006**, *2*, 287–296.
108. H. Tsuji, K. Shimizu, Y. Sato, Hydrolytic degradation of poly(L-lactic acid): combined effects of UV treatment and crystallization, *J. Appl. Polym. Sci.* **2012**, *125*, 2394–2406.
109. K. A. George, T. V. Chirila, E. Wentrup-Byrne, Effects of crosslink density on hydrolytic degradation of poly(L-lactide)-based networks, *Polym. Degrad. Stab.* **2012**, *97*, 964–971.
110. T. Chandy, C. P. Sharma, Effect of plasma glow, glutaraldehyde and carbodiimide treatments on the enzymic degradation of

poly (L-lactic acid) and poly (gamma-benzyl-L-glutamate) films, *Biomaterials* **1991**, *12*, 677–682.

111. S. Kamei, Y. Inoue, H. Okada, M. Yamada, Y. Ogawa, H. Toguchi, New method for analysis of biodegradable polyesters by high-performance liquid chromatography after alkali hydrolysis, *Biomaterials* **1992**, *13*, 953–958.
112. A. Kulkarni, J. Reiche, A. Lendlein, Hydrolytic degradation of poly(*rac*-lactide) and poly[(*rac*-lactide)-*co*-glycolide] at the air–water interface, *Surf. Interface Anal.* **2007**, *39*, 740–746.
113. N. S. Mason, C. S. Miles, R. E. Sparks, Hydrolytic degradation of poly(DL-lactide), *Polym. Sci. Technol.* **1981**, *14*, 279–291.
114. Y. Kimura, T. Yamaoka, Surface modification and properties of biodegradable polymers based on poly-L-lactides, in: N. Yuiand M. Terano (Eds.), *Surface Science of Crystalline Polymers*, Kodansha Scientific Ltd, Tokyo, 1996, p. XVI/163ff.
115. J. H. Jung, M. Ree, H. Kim, Acid- and base-catalyzed hydrolyses of aliphatic polycarbonates and polyesters, *Catal. Today* **2006**, *115*, 283–287.
116. S. M. Li, H. Garreau, M. Vert, Structure-property relationships in the case of the degradation of massive aliphatic poly-(α-hydroxy acids) in aqueous media, Part 1: Poly(DL-lactic acid), *J. Mater. Sci. Mater. Med.* **1990**, *1*, 123–130.
117. S. M. Li, M. Vert, Crystalline oligomeric stereocomplex as an intermediate compound in racemic poly(DL-lactic acid) degradation, *Polym. Int.* **1994**, *33*, 37–41.
118. S. M. Li, S. Girod-Holland, M. Vert, Hydrolytic degradation of poly(DL-lactic acid) in the presence of caffeine base, *J. Control. Release* **1996**, *40*, 41–53.
119. E. Çellikkaya, E. B. Denkbas, E. Piskin, Poly(DL-lactide)/poly(ethylene glycol) copolymer particles. I. Preparation and characterization, *J. Appl. Polym. Sci.* **1996**, *61*, 1439–1446.
120. H. Tsuji, Y. Ikada, Blends of crystalline and amorphous poly(lactide). III. Hydrolysis of solution-cast blend films, *J. Appl. Polym. Sci.* **1997**, *63*, 855–863.
121. S. H. Hyon, K. Jamshidi, Y. Ikada, Effects of residual monomer on the degradation of DL-lactide polymer, *Polym. Int.* **1998**, *46*, 196–202.
122. S. M. Li, S. McCarthy, Further investigations on the hydrolytic degradation of poly(DL-lactide), *Biomaterials* **1999**, *20*, 35–44.
123. É. Kiss, E. I. Vargha-Butler, Novel method to characterize the hydrolytic decomposition of biopolymer surfaces, *Colloids Surf. B* **1999**, *15*, 181–193.
124. G. G. Henn, C. Birkinshaw, M. Buggy, E. Jones, A comparison of in-vitro and in-vivo degradation of poly(DL-lactide) bioabsorbable intra-medullary plugs, *Macromol. Biosci.* **2001**, *1*, 219–222.
125. G. Schwach, J. Coudane, R. Engel, M. Vert, Influence of polymerization conditions on the hydrolytic degradation of poly(DL-lactide) polymerized in the presence of stannous octoate or zinc-metal, *Biomaterials* **2002**, *23*, 993–1002.
126. J. S. Wiggins, M. K. Hassan, K. A. Mauritz, R. F. Storey, Hydrolytic degradation of poly(D,L-lactide) as a function of end group: carboxylic acid vs. hydroxyl, *Polymer* **2006**, *47*, 1960–1969.
127. Y. B. Fan, P. Li, L. Zeng, X. J. Huang, Effects of mechanical load on the degradation of poly(D,L-lactic acid) foam, *Polym. Degrad. Stab.* **2008**, *93*, 677–683.
128. S. A. M. Ali, P. J. Doherty, D. F. Williams, Mechanisms of polymer degradation in implantable devices. 2. Poly(DL-lactic acid), *J. Biomed. Mater. Res.* **1993**, *27*, 1409–1418.
129. J. A. P. P. Van Dijk, J. A. M. Smit, F. E. Kohn, J. Feijen, Characterization of poly(D,L-lactic acid) by gel permeation chromatography, *J. Polym. Sci. Polym. Chem. Ed.* **1983**, *21*, 197–208.
130. C. Shih, A graphical method for the determination of the mode of hydrolysis of biodegradable polymers, *Pharm. Res.* **1995**, *12*, 2036–2040.
131. C. Shih, Chain-end scission in acid catalyzed hydrolysis of poly (D,L-lactide) in solution, *J. Control. Release* **1995**, *34*, 9–15.
132. Tz. Ivanova, I. Panaiotov, F. Boury, J. E. Proust, J. P. Benoit, R. Verger, Hydrolysis kinetics of poly(D,L-lactide) monolayers spread on basic or acidic aqueous subphases, *Colloids Surf. B* **1997**, *8*, 217–225.
133. H. Tsuji, J. Yamamoto, Hydrolytic degradation and thermal properties of linear 1-arm and 2-arm poly(DL-lactic acid)s: effects of coinitiator-induced molecular structural difference, *Polym. Degrad. Stab.* **2011**, *96*, 2229–2236.
134. H. Tsuji, T. Hayashi, Hydrolytic degradation of linear 2-arm and branched 4-arm poly(DL-lactide)s: effects of branching and terminal hydroxyl groups, *Polym. Degrad. Stab.* **2014**, *102*, 59–66.
135. T. Tarvainen, T. Karjalainen, M. Malin, S. Pohjolainen, J. Tuominen, J. Seppälä, K. Järvinen, Degradation of and drug release from a novel 2,2-bis(2-oxazoline) linked poly(lactic acid) polymer, *J. Control. Release* **2002**, *81*, 251–261.
136. K. L. G. Ho, A. L. Pometto III, P. N. Hinz, Effects of temperature and relative humidity on polylactic acid plastic degradation, *J. Polym. Environ.* **1999**, *7*, 83–92.
137. X. Song, H. Wang, X. Yang, F. Liu, S. Yu, S. Liu, Hydrolysis of poly(lactic acid) into calcium lactate using ionic liquid [Bmim][OAc] for chemical recycling, *Polym. Degrad. Stab.* **2014**, *110*, 65–70.
138. D. J. A. Cameron, M. P. Shaver, Control of thermal properties and hydrolytic degradation in poly(lactic acid) polymer stars through control of isospecificity of polymer arms, *J. Polym. Sci. Part A Polym. Chem.* **2012**, *50*, 1477–1484.
139. K. P. Andriano, T. Pohjonen, P. Törmälä, Processing and characterization of absorbable polylactide polymers for use in surgical implants, *J. Appl. Biomater.* **1994**, *5*, 133–140.
140. S. M. Li, M. Vert, Morphological changes resulting from the hydrolytic degradation of stereocopolymers derived from L- and DL-lactides, *Macromolecules*, **1994**, *27*, 3107–3110.
141. F. W. Cordewener, F. R. Rozema, R. R. M. Bos, G. Boering, Material properties and tissue reaction during degradation of poly (96L/4D-lactide)-a study in vitro and in rats, *J. Mater. Sci. Mater. Med.* **1995**, *6*, 221–217.
142. F. W. Cordewener, F. R. Rozema, C. A. P. Joziasse, Poly (96L/4D-lactide) implants for repair of orbital floor defects: an in vitro study of the material properties in a simulation of the human orbit, *J. Mater. Sci. Mater. Med.* **1995**, *6*, 561–568.

143. M. F. Gonzalez, R. A. Ruseckaite, T. R. Cuadrado, Structural changes of polylactic-acid (PLA) microspheres under hydrolytic degradation, *J. Appl. Polym. Sci.* **1999**, *71*, 1223–1230.

144. J. Kangas, S. Paasimaa, P. Mäkelä, J. Leppilahti, P. Törmälä, T. Waris, N. Ashammakhi, Comparison of strength properties of poly-L/D-lactide (PLDLA) 96/4 and polyglyconate (Maxon®) sutures: in vitro, in the subcutis, and in the achilles tendon of rabbits, *J. Biomed. Mater. Res.* **2001**, *58*, 121–127.

145. P. Taddei, P. Monti, R. Simoni, Vibrational and thermal study on the in vitro and in vivo degradation of a poly(lactic acid)-based bioabsorbable periodontal membrane, *J. Mater. Sci. Mater. Med.* **2002**, *13*, 469–475.

146. X. Zhang, M. Espiritu, A. Bilyk, L. Kurniawan, Morphological behavior of poly(lactic acid) during hydrolytic degradation, *Polym. Degrad. Stab.* **2008**, *93*, 1964–1970.

147. K. Hiltunen, J. Tuominen, J. V. Seppälä, Hydrolysis of lactic acid based poly(ester-urethane)s, *Polym. Int.* **1998**, *47*, 186–192.

148. S. M. Li, H. Garreau, M. Vert, Structure-property relationships in the case of the degradation of massive poly(α-hydroxy acids) in aqueous media, Part 2: Degradation of lactide-glycolide copolymers: PLA37.5GA25 and PLA75GA25, *J. Mater. Sci. Mater. Med.* **1990**, *1*, 131–139.

149. T. G. Park, Degradation of poly(lactic-*co*-glycolic acid) microspheres: effect of copolymer composition, *Biomaterials* **1995**, *16*, 1123–1130.

150. X. H. Zong, Z. G. Wang, B. S. Hsiao, B. Chu, J. J. Zhou, D. D. Jamiolkowski, E. Muse, E. Dormier, Structure and morphology changes in absorbable poly(glycolide) and poly(glycolide-*co*-lactide) during in vitro degradation, *Macromolecules* **1999**, *32*, 8107–8114.

151. Q. Cai, J. Bei, S. Wang, Relationship among drug delivery behavior, degradation behavior and morphology of copolylactones derived from glycolide, L-lactide and ε-caprolactone, *Polym. Adv. Technol.* **2002**, *13*, 105–111.

152. S. C. J. Loo, C. P. Ooi, S. H. E. Wee, Y. C. F. Boey, Effect of isothermal annealing on the hydrolytic degradation rate of poly(lactide-*co*-glycolide) (PLGA), *Biomaterials* **2005**, *26*, 2827–2833.

153. W. S. Pietrzak, M. Kumar, An enhanced strength retention poly(glycolic acid)-poly(L-lactic acid) copolymer for internal fixation: in vitro characterization of hydrolysis, *J. Craniofac. Surg.* **2009**, *20*, 1533–1537.

154. Y. You, B. M. Min, S. J. Lee, T. S. Lee, W. H. Park, in vitro degradation behavior of electrospun polyglycolide, polylactide, and poly(lactide-*co*-glycolide), *J. Appl. Polym. Sci.* **2005**, *95*, 193–200.

155. Q. Cai, G. Shi, J. Bei, S. Wang, Enzymatic degradation behavior and mechanism of poly(lactide-*co*-glycolide) foams by trypsin, *Biomaterials* **2003**, *24*, 629–638.

156. S. C. J. Loo, C. P. Ooi, Y. C. F. Boey, Influence of electron-beam radiation on the hydrolytic degradation behavior of poly(lactide-*co*-glycolide) (PLGA), *Biomaterials* **2005**, *26*, 3809–3817.

157. D. W. Grijpma, A. J. Nijenhuis, A. J. Pennings, Synthesis and hydrolytic degradation behavior of high-molecular-weight L-lactide and glycolide copolymers, *Polymer* **1990**, *31*, 2201–2206.

158. T. I. Croll, A. J. O'connor, G. W. Stevens, J. J. Cooper-White, Controllable surface modification of poly(lactic-*co*-glycolic acid) (PLGA) by hydrolysis or aminolysis I: physical, chemical, and theoretical aspects, *Biomacromolecules* **2004**, *5*, 463–473.

159. P. N. Thanki, E. Dellacherie, J. L. Six, Prevailing mechanisms of the hydrolytic degradation of oligo(D,L-lactide)-grafted dextrans, *Eur. Polym. J.* **2005**, *41*, 1546–1553.

160. Y. S. Nam, J. J. Yoon, J. G. Lee, Adhesion behaviors of hepatocytes cultured onto biodegradable polymer surface modified by alkali hydrolysis process, *J. Biomater. Sci. Polym. Ed.* **1999**, *10*, 1145–1158.

161. M. Hakarainen, S. Karlsson, A.-C. Albertsson, Rapid (bio) degradation of polylactide by mixed culture of compost microorganisms—low molecular weight products and matrix changes, *Polymer* **2000**, *41*, 2331–2338.

162. L. Lu, C. A. Garcia, A. K. Mikos, in vitro degradation of thin poly(DL-lactic-*co*-glycolic acid) films, *J. Biomed. Mater. Res.* **1999**, *46*, 236–244.

163. J. J. Yoon, T. G. Park, Degradation behaviors of biodegradable macroporous scaffolds prepared by gas foaming of effervescent salts, *J. Biomed. Mater. Res.* **2001**, *55*, 401–408.

164. L. Wu, J. Ding, Effects of porosity and pore size on in vitro degradation of three-dimensional porous poly(D,L-lactide-*co*-glycolide) scaffolds for tissue engineering, *J. Biomed Mater. Res.* **2005**, *75A*, 767–777.

165. I. C. Lee, L. P. Cheng, T. H. Young, Role of phase diagram of membrane formation system in controlling the crystallinity and degradation rate of PLLA membranes, *J. Biomed. Mater. Res.* **2006**, *76A*, 842–850.

166. T. Yoshioka, N. Kawazoe, T. Tateishi, G. Chen, in vitro evaluation of biodegradation of poly(lactic-*co*-glycolic acid) sponges, *Biomaterials* **2008**, *29*, 3438–3443.

167. J. Huang, M. S. Lisowski, J. Runt, E. S. Hall, R. T. Kean, N. Buehler, J. S. Lin, Crystallization and microstructure of poly(L-lactide-*co-meso*-lactide) copolymers, *Macromolecules* **1998**, *31*, 2593–2599.

168. X. Wu, N. Wang, Synthesis, characterization, biodegradation, and drug delivery application of biodegradable lactic/glycolic acid polymers. Part II: biodegradation, *J. Biomater. Sci. Polym. Ed.* **2001**, *12*, 21–34.

169. E. A. Schmitt, D. R. Flanagan, R. J. Linhardt, Importance of distinct water environments in the hydrolysis of poly(DL-lactide-*co*-glycolide), *Macromolecules* **1994**, *27*, 743–748.

170. N. K. Chia, S. S. Venkatraman, F. Y. C. Boey, S. Cadart, J. S. C. Loo, Controlled degradation of multilayered poly(lactide--*co*-glycolide) films using electron beam irradiation, *J. Biomed. Mater. Res.* **2008**, *84A*, 980–987.

171. G. E. Park, M. A. Pattison, K. Park, T. J. Webster, Accelerated chondrocyte functions on NaOH-treated PLGA scaffolds, *Biomaterials* **2005**, *26*, 3075–3082.

172. S. S. Shah, Y. Cha, C. G. Pitt, Poly (glycolic acid-*co*-DL-lactic acid): diffusion or degradation controlled drug delivery?, *J. Control. Release* **1992**, *18*, 261–270.

173. M. Sandor, J. Harris, E. Mathiowits, A novel polyethylene depot device for the study of PLGA and P(FASA) microspheres in vitro and in vivo, *Biomaterials* **2002**, *23*, 4413–4423.

174. C. Witt, T. Kissel, Morphological characterization of microspheres, films and implants prepared from poly(lactide-*co*-glycolide) and ABA triblock copolymers: is the erosion controlled by degradation, swelling or diffusion?, *Eur. J. Pharm. Biopharm.* **2001**, *51*, 171–181.

175. R. J. Fredericks, A. J. Melveger, L. J. Dolegiewitz, Morphological and structural changes in a copolymer of glycolide and lactide occurring as a result of hydrolysis, *J. Polym. Sci. Polym. Phys. Ed.* **1984**, *22*, 57–66.

176. F. von Burkersroda, L. Schedl, A. Göpferich, Why degradable polymers undergo surface erosion or bulk erosion, *Biomaterials* **2002**, *23*, 4221–4231.

177. C. C. Chu, A comparison of the effect of pH on the biodegradation of two synthetic absorbable sutures, *Ann. Surg.* **1982**, *195*, 55–59.

178. J. L. Atkinson, S. Vyazovkin, Dynamic mechanical analysis and hydrolytic degradation behavior of linear and branched poly(L-lactide)s and poly(L-lactide-*co*-glycolide)s, *Macromol. Chem. Phys.* **2013**, *214*, 835–843.

179. S. I. Moon, H. Urayama, Y. Kimura, Structural characterization and degradability of poly(L-lactic acid)s incorporating phenyl-substituted α-hydroxy acids as comonomers, *Macromol. Biosci.* **2003**, *3*, 301–309.

180. M. Leemhuis, J. A. W. Kruijtzer, C. F. van Nostrum, W. E. Hennink, in vitro hydrolytic degradation of hydroxyl-functionalized poly(α-hydroxy acid)s, *Biomacromolecules* **2007**, *8*, 2943–2949.

181. T. Nakamura, S. Hitomi, T. Shimamoto, S. H. Hyon, Y. Ikada, S. Watanabe, Y. Shimizu, Surgical application of biodegradable films prepared from lactide and ε-caprolactone, in: A. Pizzoferrato, P. G. Marchetti, A. Ravaglioli, A. J. C. Lee (Eds.), *Biomaterials and Clinical Applications*, Elsevier Science, Amsterdam, 1987, p. 759.

182. M. Malin, M. Hiljanen-Vainio, T. Karjalainen, J. Seppälä, Biodegradable lactone copolymers. II. Hydrolytic study of ε-caprolactone and lactide copolymers, *J. Appl. Polym. Sci.* **1996**, *59*, 1289–1298.

183. T. Karjalainen, M. Hiljanen-Vainio, M. Malin, J. Seppälä, Biodegradable lactone copolymers. III. Mechanical properties of ε-caprolactone and lactide copolymers after hydrolysis in vitro, *J. Appl. Polym. Sci.* **1996**, *59*, 1299–1304.

184. S. M. Li, J. L. Espartero, P. Foch, M. Vert, Structural characterization and hydrolytic degradation of a Zn metal initiated copolymer of L-lactide and ε-caprolactone, *J. Biomater. Sci. Polym. Ed.* **1997**, *8*,165–187.

185. S. I. Jeong, B. S. Kim, Y. M. Lee, K. J. Ihn, S. H. Kim, Y. H. Kim, Morphology of elastic poly(L-lactide-*co*-ε-caprolactone) copolymers and in vitro and in vivo degradation behavior of their scaffolds, *Biomacromolecules* **2004**, *5*, 1303–1309.

186. S. K. Saha, H. Tsuji, Effects of rapid crystallization on hydrolytic degradation and mechanical properties of poly(L-lactide-*co*-ε-caprolactone), *React. Funct. Polym.* **2006**, *66*, 1362–1372.

187. K. Tomihata, M. Suzuki, T. Oka, Y. Ikada, A new resorbable monofilament suture, *Polym. Degrad. Stab.* **1998**, *59*, 13–18.

188. K. Tomihata, M. Suzuki, Y. Ikada, The pH dependence of monofilament sutures on hydrolytic degradation, *J. Biomed. Mater. Res.* **2001**, *58*, 511–518.

189. J. Fernández, A. Larrañaga, A. Etxeberría, J. R. Sarasua, Effects of chain microstructures and derived crystallization capability on hydrolytic degradation of poly(L-lactide/ε-caprolactone) copolymers, *Polym. Degrad. Stab.* **2013**, *98*, 481–489.

190. M. Viljanmaa, A. Södergård, R. Mattila, P. Törmälä, Hydrolytic and environmental degradation of lactic acid based hot melt adhesives, *Polym. Degrad. Stab.* **2002**, *78*, 269–278.

191. M. F. Meek, W. F. A. den Dunnen, I. Stokroos, A. J. Pennings, P. H. Robinso, J. M. Shakenraad, in vitro degradation of poly (DL-lactide-ε-caprolactone) nerve guides, *Cell Mater.* **1996**, *6*, 103–110.

192. G. Kister, G. Cassanans, M. Bergounhon, D. Hoarau, M. Vert, Structural characterization and hydrolytic degradation of solid copolymers of D,L-lactide-*co*-ε-caprolactone by Raman spectroscopy, *Polymer* **2000**, *41*, 925–932.

193. Y. Kimura, K. Shirotani, H. Yamane, T. Kitao, Copolymerization of 3-(S)-[(benzyloxycarbonyl)methyl]-1,4-dioxane-2,5-dione and L-lactide: a facile synthetic method for functionalized bioabsorbable polymer, *Polymer* **1993**, *34*, 1741–1748.

194. H. Zhang, W. Cui, J. Bei, S. Wang, Preparation of poly(lactide-*co*-glycolide-*co*-caprolactone) nanoparticles and their degradation behaviour in aqueous solution, *Polym. Degrad. Stab.* **2006**, *91*, 1929–1936.

195. A. S. Sawhney, J. A. Hubbell, Rapidly degraded terpolymers of DL-lactide, glycolide, and ϵ-caprolactone with increased hydrophilicity by copolymerization with polyethers, *J. Biomed. Mater. Res.* **1990**, *24*, 1397–1411.

196. H. Fukuzaki, Y. Aiba, M. Yoshida, M. Asano, M. Kumakura, Synthesis of biodegradable poly(L-lactic acid-*co*-D,L-mandelic acid) with relatively low molecular weight, *Makromol. Chem.* **1989**, *190*, 2407–2415.

197. B. He, J. Bei, S. Wang, Morphology and degradation of biodegradable poly(L-lactide-*co*-β-malic acid), *Polym. Adv. Technol.* **2003**, *14*, 645–652.

198. A. Nakayama, N. Kawasaki, I. Arvanitoyannis, S. Aiba, N. Yamamoto, Synthesis and biodegradation of poly(γ-butyrolactone-*co*-L-lactide), *J. Environ. Polym. Degrad.* **1996**, *4*, 205–211.

199. A. Nakayama, N. Kasasaki, S. Aiba, Y. Maeda, I. Arvanitoyannis, N. Yamamoto, Synthesis and biodegradability of novel copolyesters containing γ-butyrolactone units, *Polymer* **1998**, *39*, 1213–1222.

200. A. Nakayama, N. Kawasaki, Y. Maeda, I. Arvanitoyannis, S. Aiba, N. Yamamoto, Study of biodegradability of poly(δ-valerolactone-*co*-L-lactide)s, *J. Appl. Polym. Sci.* **1997**, *66*, 741–748.

201. A. Nakayama, N. Kawasaki, I. Arvanitoyannis, J. Iyoda, N. Yamamoto, Synthesis and degradability of a novel aliphatic polyester: poly(β-methyl-δ-valerolactone-*co*-L-lactide), *Polymer* **1995**, *36*, 1295–1301.


202. K. J. Zhu, Y. Lei, Preparation, characterization and biodegradation characteristics of poly(adipic anhydride-*co*-D,L-lactide), *Polym. Int.* **1997**, *43*, 210–216.

203. H. Shinoda, Y. Asou, A. Suetsugu, K. Tanaka, Synthesis and characterization of amphiphilic biodegradable copolymer, poly(aspartic acid-*co*-lactic acid),*Macromol. Biosci.* **2003**, *3*, 34–43.

204. J. Helder, P. J. Dijkstra, J. Feijen, in vitro degradation of glycine/DL-lactic acid copolymers, *J. Biomed. Mater. Res.* **1990**, *24*, 1005–1020.

205. D. A. Barrera, E. Zylstra, P. T. Lansbury, R. Langer, Copolymerization and degradation of poly(lactic acid-*co*-lysine), *Macromolecules* **1995**, *28*, 425–432.

206. Y. S. Huang, F. Z. Cui, Preparation of biodegradable poly(lactic acid-*co*-aspartic acid) by copolymerization processes, *Curr. Appl. Phys.* **2005**, *5*, 546–548.

207. H. Shirahama, H. Yasuda, Synthesis of poly(lactide-*ran*-MOHEL) and its biodegradation with proteinase K, *J. Polym. Sci. Part A* **2001**, *39*, 1374–1381.

208. H. Shirahama, K. Umemoto, H. Yasuda, Synthesis and enzymatic degradation of optically active depsipeptide copolymers, *Kobunshi Ronbunshu* **1998**, *55*, 57–65.

209. C. Tsutsumi, K. Nakagawa, H. Shirahama, H. Yasuda, Synthesis and enzymatic degradation of optically active L-lactide/1-methyltrimethylene carbonate copolymers, *Kobunshi Ronbunshu* **2001**, *58*, 245–253.

210. C. Jie, J. Zhu, Preparation, characterization and biodegradable characteristics of poly(D,L-lactide-*co*-1,3-trimethylene carbonate), *Polym. Int.* **1997**, *42*, 373–379.

211. A. Pêgo, A. A. Poot, D. W. Grijpma, J. Feijen, in vitro degradation of trimethylene carbonate based (co)polymers, *Macromol. Biosci.* **2002**, *2*, 411–419.

212. C. Tsutsumi, K. Nakagawa, H. Shirahama, H. Yasuda, Biodegradations of statistical copolymers composed of D,L-lactide and cyclic carbonates, *Polym. Int.* **2003**, *52*, 439–447.

213. C. Tsutsumi, K. Nakagawa, H. Shirahama, H. Yasuda, Enzymatic degradations of copolymers of L-lactide with cyclic carbonates, *Macromol. Biosci.* **2002**, *2*, 223–232.

214. R. Slivniak, A. Ezra, A. J. Domb, Hydrolytic degradation and drug release of ricinoleic acid–lactic acid copolyesters, *Pharm. Res.* **2006**, *23*, 1306–1312.

215. E. Olewnik, W. Czerwinski, J. Nowaczyk, Hydrolytic degradation of copolymers based on L-lactic acid and bis-2-hydroxyethyl terephthalate, *Polym. Degrad. Stab.* **2007**, *92*, 24–31.

216. W. P. Ye, F. S. Du, W. H. Jin, J. Y. Yang, Y. Xu, in vitro degradation of poly(caprolactone), poly(lactide) and their block copolymers: influence of composition, temperature and morphology, *React. Funct. Polym.* **1997**, *32*, 161–168.

217. H. Qian, J. Bei, S. Wang, Synthesis, characterization and degradation of ABA block copolymer of L-lactide and ε-caprolactone, *Polym. Degrad. Stab.* **2000**, *68*, 423–429.

218. M. H. Huang, S. M. Li, M. Vert, Synthesis and degradation of PLA–PCL–PLA triblock copolymer prepared by successive polymerization of ε-caprolactone and DL-lactide, *Polymer* **2004**, *45*, 8675–8681.

219. C. Teng, H. Xu, K. Yang, M. Yu, The preparation and biodegradable properties of poly(L-lactic acid)-poly(ε-caprolactone) multiblock copolymers, *J. Macromol. Sci. Part A* **2006**, *43*, 1877–1886.

220. K. Stridsberg, A. C. Albertsson, Changes in chemical and thermal properties of the tri-block copolymer poly(L-lactide--*b*-1,5-dioxepan-2-one-*b*-L-lactide) during hydrolytic degradation, *Polymer* **2000**, *41*, 7321–7330.

221. M. Ryner, A. C. Albertsson, Resorbable and highly elastic block copolymers from 1,5-dioxepan-2-one and L-lactide with controlled tensile properties and hydrophilicity, *Biomacromolecules* **2002**, *3*, 601–608.

222. D. Cohn, H. Younes, Compositional and structural analysis of PELA biodegradable block copolymers degrading under in vitro conditions, *Biomaterials* **1989**, *10*, 466–474.

223. Y. Li, T. Kissel, Synthesis, characteristics and in vitro degradation of star-block copolymers consisting of L-lactide, glycolide and branched multi-arm poly(ethylene oxide), *Polymer* **1998**, *39*, 4421–4427.

224. K. J. Zhu, L. Xiangzhou, Y. Shilin, Preparation, characterization, and properties of polylactide (PLA)–poly(ethylene glycol) (PEG) copolymers: a potential drug carrier, *J. Appl. Polym. Sci.* **1990**, *39*, 1–9.

225. X. M. Deng, C. D. Xiong, L. M. Cheng, R. P. Xu, Synthesis and characterization of block copolymers from D,L-lactide and poly(ethylene glycol) with stannous chloride, *J. Polym. Sci. Part C* **1990**, *28*, 411–416.

226. M. Stefani, J. Coudane, M. Vert, Effects of polymerization conditions on the in vitro hydrolytic degradation of plaques of poly(DL-lactic acid-*block*-ethylene glycol) diblock copolymers, *Polym. Degrad. Stab.* **2006**, *91*, 2853–2859.

227. D. Muller, F. Carlsson, M. Malmsten, Adsorption of poly(ethylene oxide)–poly(lactide) copolymers. Effects of composition and degradation, *J. Colloid Interface Sci.* 2001, 116–126.

228. I. Rashkov, N. Manolova, S. M. Li, J. L. Espartero, M. Vert, Synthesis, characterization, and hydrolytic degradation of PLA/PEO/PLA triblock copolymers with short poly(L-lactic acid) chains, *Macromolecules* **1996**, *29*, 50–56.

229. L. Youxin, C. Volland, T. Kissel, In-vitro degradation and bovine serum albumin release of the ABA triblock copolymers consisting of poly (L(+) lactic acid), or poly(L(+) lactic acid-*co*-glycolic acid) A-blocks attached to central polyoxyethylene B-blocks, *J. Control. Release* **1994**, *32*, 121–128.

230. S. M. Li, I. Rashkov, J. L. Espartero, N. Manolova, M. Vert, Synthesis, characterization, and hydrolytic degradation of PLA/PEO/PLA triblock copolymers with long poly(L-lactic acid) blocks, *Macromolecules* **1996**, *29*, 57–62.

231. P. Cerrai, M. Tricoli, L. Lelli, G. D. Guerra, R. Sbarbati Del Guerra, M. G. Cascone, P. Giusti, Block copolymers of L-lactide and poly(ethylene glycol) for biomedical applications, *J. Mater. Sci. Mater. Med.* **1994**, *5*, 308–313.

232. A. J. Nijenhuis, E. Colstee, D. W. Grijpma, A. J. Pennings, High molecular weight poly(L-lactide) and poly(ethylene oxide) blends: thermal characterization and physical properties, *Polymer* **1996**, *37*, 5849–5857.

233. S. M. Li, S. Anjard, I. Rashkov, M. Vert, Hydrolytic degradation of PLA/PEO/PLA triblock copolymers prepared in the presence of Zn metal or $CaH_2$, *Polymer* **1998**, *39*, 5421–5430.
234. D. S. G. Hu, H. J. Liu, Structural analysis and degradation behavior in polyethylene glycol/poly(L-lactide) copolymers, *J. Appl. Polym. Sci.* **1994**, *51*, 473–482.
235. S. S. Shah, K. J. Zhu, C. G. Pitt, Poly-DL-lactic acid: polyethylene glycol block copolymers. The influence of polyethylene glycol on the degradation of poly-DL-lactic acid, *J. Biomater. Sci. Polym. Ed.* **1994**, *5*, 421–431.
236. S. M. Li, I. Molina, M. B. Martinez, M. Vert, Hydrolytic and enzymatic degradations of physically crosslinked hydrogels prepared from PLA/PEO/PLA triblock copolymers, *J. Mater. Sci. Mater. Med.* **2002**, *13*, 81–86.
237. X. M. Deng, C. D. Xiong, L. M. Cheng, H. H. Huang, R. P. Xu, Studies on the block copolymerization of D,L-lactide and poly(ethylene glycol) with aluminium complex catalyst, *J. Appl. Polym. Sci.* **1995**, *55*, 1193–1196.
238. H. Cho, J. An, The effect of ε-caproyl/D,L-lactyl unit composition on the hydrolytic degradation of poly(D,L-lactide-*ran*-ε-caprolactone)-poly(ethylene glycol)-poly(D,L-lactide-*ran*-ε-caprolactone), *Biomaterials* **2006**, *27*, 544–552.
239. M. Penco, S. Marcioni, P. Ferruti, S. D'Antone, R. Deghenghi, Degradation behavior of block copolymers containing poly(lactic-glycolic acid) and poly(ethylene glycol) segments, *Biomaterials* **1995**, *17*, 1583–1590.
240. N. Morakot, J. Threeprom, Y. Baimark, Mechanical properties and hydrolytic degradation of methoxy poly(ethylene glycol)-*b*-poly(DL-lactide-*co*-glycolide-*co*-ε-caprolactone) diblock copolymer films, *E-Polymers* 2008, *1*, Article number 92.
241. Y. Kimura, Y. Matsuzaki, H. Yamane, Y. Kitao, Preparation of block copoly(ester-ether) comprising poly(L-lactide) and poly(oxypropylene) and degradation of its fiber in vitro and in vivo, *Polymer* **1989**, *30*, 1342–1349.
242. C. W. Lee, Y. Kimura, Synthesis and properties of A–B–A block copoly(ester-ethers) comprising poly(L-lactide) (A) and poly(oxypropylene-*co*-oxyethylene) (B) with different molecular weights, *Bull. Chem. Soc. Jpn.* **1996**, *69*, 1787–1795.
243. C. W. Lee, Y. Kimura, in vitro biodegradability and surface properties of block copoly(ester-ether)s consisting of poly(L-lactide)and polyether, *Macromol. Res.* **2003**, *11*, 42–46.
244. Y. Maeda, A. Nakayama, I. Arvanitoyannis, N. Kawasaki, K. Hayashi, N. Yamamoto, Synthesis and characterization of copoly(succinic anhydride-ethylene oxide)-poly(L-lactide) block copolymer, *Polym. J.* **2000**, *32*, 307–315.
245. C. D. Xiong, L. M. Cheng, R. P. Xu, X. M. Deng, Synthesis and characterization of block copolymers from D,L-lactide and poly(tetramethylene ether glycol), *J. Appl. Polym. Sci.* **1995**, *55*, 865–869.
246. M. V. Chaubal, G. Su, E. Spicer, W. Dang, K. E. Branham, J. P. English, Z. Zhao, in vitro and in vivo degradation studies of a novel linear copolymer of lactide and ethylphosphate, *J. Biomater. Sci. Polym. Ed.* **2003**, *14*, 45–61.
247. K. Schwach-Abdellaoui, J. Heller, R. Gurny, Hydrolysis and erosion studies of autocatalyzed poly(ortho esters) containing lactoyl–lactyl acid dimers, *Macromolecules* **1999**, *32*, 301–307.
248. T. Fan, W. Ye, B. Du, Q. Zhang, L. Gong, J. Li, S. Lin, Z. Fan, Q. Liu, Effect of segment structures on the hydrolytic degradation behaviors of totally degradable poly(L-lactic acid)-based copolymers, *J. Appl. Polym. Sci.* **2019**, *136*, Article number 47887.
249. M. H. Rahaman, H. Tsuji, Hydrolytic degradation behavior of stereo multiblock and diblock poly(lactic acid)s: effects of block lengths, *Polym. Degrad. Stab.* **2013**, *98*, 709–719.
250. J. Li, Z.-Q. Jiang, Z.-B. Wang, P. Chen, Y. Li, J. Zhou, J. Liu, Y.-Z. Wang, Q. Gu, Synthesis, crystallization and hydrolysis of aromatic-aliphatic copolyester: poly(trimethylene terephthalate)-*co*-poly(L-lactic acid), *Polym. Degrad. Stab.* **2011**, *96*, 991–999.
251. U. Ojha, P. Kulkarni, D. Cozzens, R. J. Faust, Hydrolytic degradation of polyisobutylene and poly-L-lactide-based multiblock copolymers, *J. Polym. Sci., Part A: Polym. Chem.* **2010**, *48*, 3767–3774.
252. X. J. Loh, Y. X. Tan, Z. Li, L. S. Teo, S. H. Goh, J. Li, Biodegradable thermogelling poly(ester urethane)s consisting of poly(lactic acid)-thermodynamics of micellization and hydrolytic degradation, *Biomaterials* **2008**, *29*, 2164–2172.
253. Y. Ohya, S. Maruhashi, T. Ouchi, Graft polymerization of L-lactide on pullulan through the trimethylsilyl protection method and degradation of the graft copolymers, *Macromolecules* **1998**, *31*, 4662–4665.
254. C. Yan, J. Wu, J. Zhang, J. He, J. Zhang, Hydrolytic degradation of cellulose-graft-poly(L-lactide) copolymers, *Polym. Degrad. Stab.* **2015**, *118*, 130–136.
255. Y. Li, J. Nothnagel, T. Kissel, Biodegradable brush-like graft polymers from poly(D,L-lactide) or poly(D,L-lactide-*co*-glycolide) and charge-modified, hydrophilic dextrans as backbone—synthesis, characterization and in vitro degradation properties, *Polymer* **1997**, *38*, 6197–6206.
256. Y. Li, C. Volland, T. Kissel, Biodegradable brush-like graft polymers from poly(D,L-lactide) or poly(D,L-lactide--*co*-glycolide) and charge-modified, hydrophilic dextrans as backbone—in-vitro degradation and controlled releases of hydrophilic macromolecules, *Polymer* **1998**, *39*, 3087–3097.
257. A. Breitenbach, K. F. Pistel, T. Kissel, Biodegradable comb polyesters. Part II. Erosion and release properties of poly(vinyl alcohol)-*g*-poly(lactic-*co*-glycolic acid), *Polymer* **2000**, *41*, 4781–4792.
258. X. Leng, W. Zhang, Y. Wang, Y. Wang, X. Li, Z. Wei, Y. Li, Hydrolytic degradation of comb-like graft poly (lactide-*co*-trimethylene carbonate): the role of comonomer compositions and sequences, *Polymers* **2019**, *11*, Article number 2024.
259. V. Langlois, K. Vallee-Rehel, J. J. Peron, A. Le Borgne, M. Walls, P. Guerin, Synthesis and hydrolytic degradation of graft copolymers containing poly(lactic acid) side chains: in vitro release studies of bioactive molecules, *Polym. Degrad. Stab.* **2002**, *76*, 411–417.
260. F. Unger, M. Wittmar, F. Morell, T. Kissel, Branched polyesters based on poly[vinyl-3-(dialkylamino)alkylcarbamate-*co*-vinyl acetate-*co*-vinyl alcohol]-graft-poly(D,L-lactide-*co*-glycolide): Effects of polymer structure on in vitro degradation behavior, *Biomaterials* **2008**, *29*, 2007–2014.

261. F. P. W. Melchels, A. H. Velders, J. Feijen, D. W. Grijpma, Photo-cross-linked poly(DL-lactide)-based networks. structural characterization by HR-MAS NMR spectroscopy and hydrolytic degradation behavior, *Macromolecules*, **2010**, *43*, 8570–8579.

262. H. M. Younes, E. Bravo-Grimaldo, B. G. Amsden, Synthesis, characterization and in vitro degradation of a biodegradable elastomer, *Biomaterials* **2004**, *25*, 5261–5269.

263. H. A. von Recum, R. L. Cleek, S. G. Eskin, A. G. Mikos, Degradation of polydispersed poly(L-lactic acid) to modulate lactic acid release, *Biomaterials* **1995**, *16*, 441–447.

264. R. Suuronen, T. Pohjonen, R. Taurio, P. Törmälä, L. Wessma, K. Rönkkö, S. Vainionpää, Strength retention of self-reinforced poly-L-lactide screws and plates: an in vivo and in vitro study, *J. Mater. Sci. Mater. Med.* **1992**, *3*, 426–431.

265. R. Suuronen, T. Pohjonen, J. Hietanen, C. Lindqvist, A 5-year in vitro and in vivo study of the biodegradation of polylactide plates, *J. Oral Maxillofac. Surg.* **1998**, *56*, 604–615.

266. H. Sah, Y. W. Chien, Effects of $H^+$ liberated from hydrolytic cleavage of polyester microcapsules on their permeability and degradability, *J. Pharm. Sci.* **1995**, *84*, 1353–1359.

267. J. Mauduit, E. Pérouse, M. Vert, Hydrolytic degradation of films prepared from blends of high and low molecular weight poly(DL-lactic acid)s, *J. Biomed. Mater. Res.* **1996**, *30*, 201–207.

268. H. Sah, Y. W. Chien, Degradability and antigen-release characteristics of polyester microspheres prepared from polymer blends, *J. Appl. Polym. Sci.* **1995**, *58*, 197–206.

269. G. Schliecker, C. Schmidt, S. Fuchs, R. Wombacher, T. Kissel, Hydrolytic degradation of poly(lactide-*co*-glycolide) films: effect of oligomers on degradation rate and crystallinity, *Int. J. Pharm.* **2003**, *266*, 39–49.

270. W. K. Lee, T. Iwata, J. A. Gardella Jr., Hydrolytic behavior of enantiomeric poly(lactide) mixed monolayer films at the air/water interface: stereocomplexation effects, *Langmuir* **2005**, *21*, 11180–11184.

271. H. Tsuji, M. Suzuki, in vitro hydrolysis of blends from enantiomeric poly(lactide)s, *Sen'i Gakkaishi* **2001**, *57*, 198–202.

272. H. Tsuji, T. Tsuruno, Accelerated hydrolytic degradation of poly(L-lactide)/poly(D-lactide) stereocomplex up to late stage, *Polym. Degrad. Stab.* **2010**, *95*, 477–484.

273. R. Mincheva, Ph. Leclère, Y. Habibi, J.-M. Raquez, P. Dubois, Preparation of narrowly dispersed stereocomplex nanocrystals: a step towards all-poly(lactic acid) nanocomposites, *J. Mater. Chem. A* **2014**, *2*, 7402–7409.

274. Y. You, S. W. Lee, J. H. Youk, B. M. Min, S. J. Lee, W. H. Park, in vitro degradation behavior of non-porous ultra-fine poly(glycolic acid)/poly(L-lactic acid) fibres and porous ultra-fine poly(glycolic acid) fibers, *Polym. Degrad. Stab.* **2005**, *90*, 441–448.

275. W. K. Lee, R. W. Nowak, J. A. Gardella Jr., Hydrolytic degradation of polyester blend monolayers at the air/water interface: effects of a slowly degrading component, *Langmuir* **2002**, *18*, 2309–2312.

276. M. Hiljanen-Vainio, P. Varpomaa, J. Seppälä, P. Törmälä, Modification of poly(L-lactides) by blending: mechanical and hydrolytic behavior, *Macromol. Chem. Phys.* **1996**, *197*, 1503–1523.

277. J. Idaszek, A. Bruinink, W. Święszkowski, Delayed degradation of poly(lactide-*co*-glycolide) accelerates hydrolysis of poly(ε-caprolactone) in ternary composite scaffolds, *Polym. Degrad. Stab.* **2016**, *124* 119–127.

278. N. S. Choi, C. H. Kim, K. Y. Cho, J. K. Park, Morphology and hydrolysis of PCL/PLLA blends compatibilized with P(LLA-*co*-εCL) or P(LLA-*b*-εCL), *J. Appl. Polym. Sci.* **2002**, *86*, 1892–1898.

279. D. Mallardé, M. Vailière, C. David, M. Menet, Ph. Guérin, Hydrolytic degradability of poly(3-hydroxyoctanoate) and of a poly(3-hydroxyoctanoate)/poly(R,S-lactic acid) blend, *Polymer* **1998**, *39*, 3387–3392.

280. K. Inoue, S. O-oya, M. S. Lee, S. Akasaka, S. Asai, M. Sumita, Fractal and degradation process of biodegradable polyester blends, *Sen'i Gakkaishi* **1998**, *54*, 277–284.

281. Y.-P. Wang, Y.-J. Xiao, J. Duan, J.-H. Yang, Y. Wang, C.-L. Zhang, Accelerated hydrolytic degradation of poly(lactic acid) achieved by adding poly(butylene succinate), *Polym. Bull.* **2016**, *73*, 1067–1083.

282. M. R. Lostocco, S. J. Huang, The hydrolysis of poly(lactic acid)/poly(hexamethylene succinate) blends, *Polym. Degrad. Stab.* **1998**, *61*, 225–230.

283. W. Dong, B. Zou, Y. Yan, P. Ma, M. Chen, Effect of chain-extenders on the properties and hydrolytic degradation behavior of the poly(lactide)/poly(butylene adipate-*co*-terephthalate) blends, *Int. J. Mol. Sci.* **2013**, *14*, 20189–20203.

284. S. Girdthep, P. Worajittiphon, T. Leejarkpai, R. Molloy, W. Punyodom, Effect of silver-loaded kaolinite on real ageing, hydrolytic degradation, and biodegradation of composite blown films based on poly(lactic acid) and poly(butylene adipate-*co*-terephthalate), *Eur. Polym. J.* **2016**, *82*, 244–259.

285. I. Acar, A. Kasgöz, S. Özgümüs, M. Orbay, Modification of waste poly(ethylene terephthalate) (PET) by using poly(L-lactic acid) (PLA) and hydrolytic stability, *Polym. Plast. Technol. Eng.* **2006**, *45*, 351–359.

286. H. Zou, C. Yi, L. Wan, W. Xu, Crystallization, hydrolytic degradation, and mechanical properties of poly(trimethylene terephthalate)/poly(lactic acid) blends, *Polym. Bull.* **2010**, *64*, 471–481.

287. X. Xie, W. Bai, D. Chen, C. Xiong, X. Pang, Effect of poly(para-dioxanone) on the hydrolytic degradation of poly(L-lactide), *J. Polym. Environ.* **2015**, *23*, 156–164.

288. X. Xie, W. Bai, C. Tang, D. Chen, C. Xiong, Effects of poly(para-dioxanone-*co*-L-lactide) on the in vitro hydrolytic degradation behaviors of poly(L-lactide)/poly(*para*-dioxanone) blends, *J. Mater. Res.* **2015**, *30*, 860–868.

289. C. A. P. Joziasse, H. Veenstra, M. D. C. Topp, D. W. Grijpma, A. J. Pennings, Rubber toughened linear and star-shaped poly(D,L-lactide-*co*-glycolide): synthesis, properties and in vitro degradation, *Polymer* **1998**, *39*, 467–473.

290. H. T. Oyama, Y. Tanaka, A. Kadosaka, Rapid controlled hydrolytic degradation of poly(L-lactic acid) by blending with poly(aspartic acid-*co*-L-lactide), *Polym. Degrad. Stab.* **2009**, *94*, 1419–1426.

291. Y. Huang, F. Chen, Y. Pan, C. Chen, L. Jiang, Y. Dan, Effect of hydrophobic fluoropolymer and crystallinity on the hydrolytic degradation of poly(lactic acid), *Eur. Polym. J.* **2017**, *97*, 308−318.

292. L. C. Hu, H. Nakata, H. Yamane, T. Kitao, The role of poly(L-lactide) in the degradation of poly(ε-amino caproic acid), *Kobunshi Ronbunshu* **1994**, *51*, 486–492.

293. M. Sheth, R. A. Kumar, V. Dáve, R. A. Gross, S. P. McCarthy, Biodegradable polymer blends of poly(lactic acid) and poly(ethylene glycol), *J. Appl. Polym. Sci.* **1997**, *66*, 1495–1505.

294. N. T. T. Trang, N. T. Chinh, D. T. M. Thanh, T. T. X. Hang, N. V. Giang, T. Hoang, P. M. Quan, L. D. Giang, N. V. Thai, G. Lawrence, Investigating the properties and hydrolysis ability of poly-lactic acid/chitosan nanocomposites using polycaprolactone, *J. Nanosci. Nanotechnol.* **2015**, *15*, 9585−9590.

295. N. T. Chinh, N. T. T. Trang, D. T. M. Thanh, T. T. X. Hang, N. V. Giang, P. M. Quan, N. T. Dung, T. Hoang, Thermal property, morphology, and hydrolysis ability of poly(lactic acid)/chitosan nanocomposites using polyethylene oxide, *J. Appl. Polym. Sci.* **2015**, *132*, Article number 41690.

296. N. T. T. Trang, N. T. Chinh, N. V. Giang, D. T. M. Thanh, T. D. Lam, L. V. Thu, N. D. Quang, T. Hoang, Hydrolysis of green nanocomposites of poly(lactic acid) (PLA), chitosan (CS) and polyethylene glycol (PEG) in acid solution, *Green Process. Synth.* **2016**, *5*, 443−449.

297. H. Tsuji, H. Muramatsu, Blends of aliphatic polyesters: V non-enzymatic and enzymatic hydrolysis of blends from hydrophobic poly(L-lactide) and hydrophilic poly(vinyl alcohol), *Polym. Degrad. Stab.* **2001**, *71*, 403–415.

298. C. G. Pitt, Y. Cha, S. S. Shah, K. J. Zhu, Blends of PVA and PGLA: control of the permeability and degradability of hydrogels by blending, *J. Control. Release* **1992**, *19*, 189–200.

299. N. Boudaoud, S. Benali, R. Mincheva, H. Satha, J.-M. Raquez, P. Dubois, Hydrolytic degradation of poly(L-lactic acid)/poly(methyl methacrylate) blends, *Polym. Int.* **2018**, *67*, 1393–1400.

300. T. Shirahase, Y. Komatsu, Y. Tominaga, S. Asai, M. Sumita, Miscibility and hydrolytic degradation in alkaline solution of poly(L-lactide) and poly(methyl methacrylate) blends, *Polymer* **2006**, *47*, 4839–4844.

301. T. Shirahase, Y. Komatsu, H. Marubayashi, Y. Tominaga, S. Asai, M. Sumita, Miscibility and hydrolytic degradation in alkaline solution of poly(L-lactide) and poly(*p*-vinyl phenol) blends, *Polym. Degrad. Stab.* **2007**, *92*, 1626–1631.

302. A. Kumar, T. Venkatappa Rao, S. Ray Chowdhury, S. V. S. Ramana Reddy, Optimization of mechanical, thermal and hydrolytic degradation properties of poly(lactic acid)/poly(ethylene-*co*-glycidyl methacrylate)/hexagonal boron nitride blend-composites through electron-beam irradiation, *Nucl. Instrum. Methods Phys. Res. B* **2018**, *428*, 38−46.

303. K. Paakinaho, H. Heino, J. Väisänen, P. Törmälä, M. Kellomäki, Effects of lactide monomer on the hydrolytic degradation of poly(lactide-*co*-glycolide) 85L/15G, *J. Mech. Behav. Biomed. Mater.* **2011**, *4*, 1283–1290.

304. A. C. Renouf-Glauser, J. Rose, D. F. Farrar, R. E. Cameron, A degradation study of PLLA containing lauric acid, *Biomaterials* **2005**, *26*, 2415–2422.

305. A. C. Renouf-Glauser, J. Rose, D. F. Farrar, R. E. Cameron, Comparison of the hydrolytic degradation and deformation properties of a PLLA–lauric acid based family of biomaterials, *Biomacromolecules* **2006**, *7*, 612–617.

306. L. V. Labrecque, R. A. Kumar, V. Davé, R. A. Gross, S. P. McCarthy, Citrate esters as plasticizers for poly(lactic acid), *J. Appl. Polym. Sci.* **1997**, *66*, 1507–1513.

307. R. B. Valapa, G. Pugazhenthi, V. Katiyar, Hydrolytic degradation behavior of sucrose palmitate reinforced poly(lactic acid) nanocomposites, *Int. J. Biol. Macromol.* **2016**, *89*, 70−80.

308. C. Shuai, Y. Li, P. Feng, W. Guo, W. Yang, S. Peng, Positive feedback effects of Mg on the hydrolysis of poly-L-lactic acid (PLLA): Promoted degradation of PLLA scaffolds, *Polym. Test.* **2018**, *68*, 27–33.

309. W. Wen, K. Liu, Z. Zou, C. Zhou, B. Luo, Synergistic effect of surface-modified MgO and chitin whiskers on the hydrolytic degradation behavior of injection molding poly(L-lactic acid), *ACS Biomater. Sci. Eng.* **2019**, *5*, 2942–2952.

310. M. Qu, H. Tu, M. Amarante, Y.-Q. Song, S. S. Zhu, Zinc oxide nanoparticles catalyze rapid hydrolysis of poly(lactic acid) at low temperatures, *J. Appl. Polym. Sci.* **2014**, *131*, Article number 40287.

311. L. Pérez-Álvarez, E. Lizundia, L. Ruiz-Rubio, V. Benito, I. Moreno, J. L. Vilas-Vilela, Hydrolysis of poly(L-lactide)/ZnO nanocomposites with antimicrobial activity, *J. Appl. Polym. Sci.* **2019**, *136*, Article number 47786.

312. E. Lizundia, L. Ruiz-Rubio, J. L. Vilas, L. M. León, Towards the development of eco-friendly disposable polymers: ZnO-initiated thermal and hydrolytic degradation in poly(L-lactide)/ZnO nanocomposites, *RSC Adv.* **2016**, *6*, 15660–15669.

313. E. Lizundia, P. Mateos, J. L. Vilas, Tuneable hydrolytic degradation of poly(L-lactide) scaffolds triggered by ZnO nanoparticles, *Mater. Sci. Eng. C* **2017**, *75*, 714–720.

314. H. Rashidi, B. Najaf Oshani, I. Hejazi, J. Seyfi, Tuning crystallization and hydrolytic degradation behaviors of poly(lactic acid) by using silver phosphate, zinc oxide and their nano-hybrids, *Polym. Plast. Technol. Mater.* **2020**, *59*, 72−82.

315. M.-X. Li, S.-H. Kim, S.-W. Choi, K. Goda, W.-I. Lee, Effect of reinforcing particles on hydrolytic degradation behavior of poly (lactic acid) composites, *Compos. B. Eng.* **2016**, *96*, 248−254.

316. M. Ara, M. Watanabe, Y. Imai, Effect of blending calcium compounds on hydrolytic degradation of poly(DL-lactic acid-*co*-glycolic acid), *Biomaterials* **2002**, *23*, 2479–2483.

317. T. Niemelä, Effect of β-tricalcium phosphate addition on the in vitro degradation of self-reinforced poly-L,D-lactide, *Polym. Degrad. Stab.* **2005**, *89*, 492–500.

318. S. Kobayashi, K. Sakamoto, Effect of hydrolysis on mechanical properties of tricalcium phosphate/poly-L-lactide composites, *J. Mater. Sci. Mater. Med.* **2009**, *20*, 379–386.
319. S. Yamaji, S. Kobayashi, Effect of in vitro hydrolysis on the compressive behavior and strain rates dependence of tricalcium phosphate/poly(L-lactic acid) composites, *Adv. Compos. Mater.* **2013**, *22*, 1–11.
320. S. Kobayashi, S. Yamaji, Analytical prediction of hydrolysis behavior of tricalcium phosphate/poly-L-lactic acid composites in simulated body environment, *Adv. Compos. Mater.* **2014**, *23*, 211–223.
321. A. A. Ignatius, P. Augat, L. E. Claes, Degradation behavior of composite pins made of tricalcium phosphate and poly(L, DL-lactide), *J. Biomater. Sci. Polym. Ed.* **2001**, *12*, 185–194.
322. N. Ahola, M. Veiranto, J. Rich, A. Efimov, M. Hannula, J. Seppälä, M. Kellomäki, Hydrolytic degradation of composites of poly(L-lactide-*co*-ε-caprolactone) 70/30 and β-tricalcium phosphate, *J. Biomater. Appl.* **2013**, *28*, 529–543.
323. Y. Imai, M. Nagai, M. Watanabe, Degradation of composite materials composed of tricalcium phosphate and a new type of block polyester containing a poly(L-lactic acid) segment, *J. Biomater. Sci. Polym. Ed.* **1999**, *10*, 421–432.
324. Y. Imai, A. Fukuzawa, M. Watanabe, Degradation of composite materials composed of tricalcium phosphate and a new type of block polyester containing a poly(L-lactic acid) segment, *J. Biomater. Sci. Polym. Ed.* **1999**, *10*, 773–786.
325. Y. Shikinami, M. Okuno, Bioresorbable devices made of forged composites of hydroxyapatite (HA) particles and poly-L-lactide (PLLA): part I. *Basic characteristics, Biomaterials* **1999**, *20*, 859–877.
326. Y. Shikinami, M. Okuno, Bioresorbable devices made of forged composites of hydroxyapatite (HA) particles and poly L-lactide (PLLA). Part II: practical properties of miniscrews and miniplates, *Biomaterials* **2001**, *22*, 3197–3211.
327. M. Kaavessina, A. Chafidz, I. Ali, S. M. Al-Zahrani, Characterization of poly(lactic acid)/hydroxyapatite prepared by a solvent-blending technique: viscoelasticity and in vitro hydrolytic degradation, *J. Elastom. Plast.* **2015**, *47*, 753–768.
328. H.-M. Chen, Y.-P. Wang, J. Chen, J.-H. Yang, N. Zhang, T. Huang, Y. Wang, Hydrolytic degradation behavior of poly(L-lactide)/$SiO_2$ composites, *Polym. Degrad. Stab.* **2013**, *98*, 2672–2679.
329. H. Pan, Z. Qiu, Biodegradable poly(L-lactide)/polyhedral oligomeric silsesquioxanes nanocomposites: enhanced crystallization, mechanical properties, and hydrolytic degradation, *Macromolecules* **2010**, *43*, 1499–1506.
330. Z. Qiu, H. Pan, Preparation, crystallization and hydrolytic degradation of biodegradable poly(L-lactide)/polyhedral oligomeric silsesquioxanes nanocomposite, *Compos. Sci. Technol.* **2010**, *70*, 1089–1094.
331. H. Chen, J. Chen, J. Chen, J. Yang, T. Huang, N. Zhang, Y. Wang, Effect of organic montmorillonite on cold crystallization and hydrolytic degradation of poly(L-lactide), *Polym. Degrad. Stab.* **2012**, *97*, 2273–2283.
332. Y. Li, C. Han, X. Zhang, K. Xu, J. Bian, L. Dong, Poly(L-lactide)/poly(D-lactide)/clay nanocomposites: enhanced dispersion, crystallization, mechanical properties, and hydrolytic degradation, *Polym. Eng. Sci.* **2014**, *54*, 914–924.
333. K. Fukushima, D. Tabuani, M. Dottori, I. Armentano, J. M. Kenny, G. Camino, Effect of temperature and nanoparticle type on hydrolytic degradation of poly(lactic acid) nanocomposites, *Polym. Degrad. Stab.* **2011**, *96*, 2120–2129.
334. M. D. Fernández, M. J. Fernández, Vermiculite/poly(lactic acid) composites: effect of nature of vermiculite on hydrolytic degradation in alkaline medium, *Appl. Clay Sci.* **2017**, *143*, 29–38.
335. M.-Y. Jo, Y. J. Ryu, J. H. Ko, J.-S. Yoon, Hydrolysis and thermal degradation of poly(L-lactide) in the presence of talc and modified talc, *J. Appl. Polym. Sci.* **2013**, *129*, 1019–1025.
336. T. Niemelä, H. Niiranen, M. Kellomäki, Self-reinforced composites of bioabsorbable polymer and bioactive glass with different bioactive glass contents. Part II: in vitro degradation, *Acta Biomater.* **2008**, *4*, 156–164.
337. J. Rich, J. Tuominen, J. Kylmä, J. Seppälä, S. N. Nazhat, K. E. Tanner, Lactic acid based PEU/HA and PEU/BCP composites: dynamic mechanical characterization of hydrolysis, *J. Biomed. Mater. Res.* **2002**, *63*, 346–353.
338. S. M. Li, M. Vert, Hydrolytic degradation of the coral/poly(DL-lactic acid) bioresorbable material, *J. Biomater. Sci. Polym. Ed.* **1996**, *7*, 817–827.
339. S. A. T. van der Meer, J. R. de Wijn, J. G. C. Wolke, The influence of basic filler materials on the degradation of amorphous D- and L-lactide copolymer, *J. Mater. Sci. Mater. Med.* **1996**, *7*, 359–361.
340. Y. Zhang, S. Zale, L. Sawyer, H. Bernstein, Effects of metal salts on poly(DL-lactide-*co*-glycolide) polymer hydrolysis, *J. Biomed. Mater. Res.* **1997**, *34*, 531–538.
341. H. Tsuji, T. Aratani, H. Takikawa, Physical properties, crystallization, and thermal/hydrolytic degradation of poly(L-lactide)/nano/micro-diamond composites, *Macromol. Mater. Eng.* **2013**, *298*, 1149–1159.
342. Y. Zhao, Z. Qiu, W. Yang, Effect of functionalization of multiwalled nanotubes on the crystallization and hydrolytic degradation of biodegradable poly(L-lactide), *J. Phys. Chem. B* **2008**, *112*, 16461–16468.
343. Y. Zhao, Z. Qiu, W. Yang, Effect of multi-walled carbon nanotubes on the crystallization and hydrolytic degradation of biodegradable poly(L-lactide), *Compos. Sci. Technol.* **2009**, *69*, 627–632.
344. Q. Dong, Y. Li, C. Han, X. Zhang, K. Xu, H. Zhang, L. Dong, Poly(L-lactide)/poly(D-lactide)/multiwalled carbon nanotubes nanocomposites: enhanced dispersion, crystallization, mechanical properties, and hydrolytic degradation, *J. Appl. Polym. Sci.* **2013**, *130*, 3919–3929.
345. L. He, J. Sun, X. Wang, X. Fan, Q. Zhao, L. Cai, R. Song, Z. Ma, W. Huang, Unzipped multiwalled carbon nanotubes-incorporated poly(L-lactide) nanocomposites with enhanced interface and hydrolytic degradation, *Mater. Chem. Phys.* **2012**, *134*, 10594–1066.

346. I. Armentano, M Dottori, D. Puglia, J. M. Kenny, Effects of carbon nanotubes (CNTs) on the processing and in-vitro degradation of poly(DL-lactide-*co*-glycolide)/CNT films, *J. Mater. Sci. Mater. Med.* **2008**, *19*, 2377–2387.

347. X.-Z. Jin, X. Yu, C. Qi, X.-D. Yang, Y.-Z. Lei, Y. Wang, Crystallization and hydrolytic degradation behaviors of poly(L-lactide) induced by carbon nanofibers with different surface modifications, *Polym. Degrad. Stab.* **2019**, *170*, Article number 109014.

348. S. Girdthep, W. Sankong, A. Pongmalee, T. Saelee, W. Punyodom, P. Meepowpan, P. Worajittiphon, Enhanced crystallization, thermal properties, and hydrolysis resistance of poly(L-lactic acid) and its stereocomplex by incorporation of graphene nanoplatelets, *Polym. Test.* **2017**, *61*, 229–239.

349. C. Shuai, Y. Li, W. Yang, L. Yu, Y. Yang, S. Peng, P. Feng, Graphene oxide induces ester bonds hydrolysis of poly-L-lactic acid scaffold to accelerate degradation, *Inter. J. Bioprint.* **2020**, *6*, 91–104.

350. J. Duan, Y.-N. Xie, J.-H. Yang, T. Huang, N. Zhang, Y. Wang, J.-H. Zhang, Graphene oxide induced hydrolytic degradation behavior changes of poly(L-lactide) in different mediums, *Polym. Test.* **2016**, *56*, 220–228.

351. C. Xiang, M. W. Frey, Hydrolytic degradation of nanocomposite fibers electrospun from poly(lactic acid)/cellulose nanocrystals, in: J. Hinestroza, A. N. Netravali (Eds.), *Cellulose Based Composites: New Green Nanomaterials*, John Wiley & Sons, Inc., Weinheim, 2014, pp. 117–136.

352. R. Patwa, A. Kumar, V. Katiyar, Crystallization kinetics, morphology, and hydrolytic degradation of novel bio-based poly(lactic acid)/crystalline silk nano-discs nanobiocomposites, *J. Appl. Polym. Sci.* **2018**, *135*, Article number 46590.

353. P. Holcapkova, P. Stloukal, P. Kucharczyk, M. Omastova, A. Kovalcik, Anti-hydrolysis effect of aromatic carbodiimide in poly(lactic acid)/wood flour composites, *Compos. Part A Appl. Sci. Manuf.* **2017**, *103*, 283–291.

354. M. Ma, W. Zhou, Improving the hydrolysis resistance of poly(lactic acid) fiber by hydrophobic finishing, *Ind. Eng. Chem. Res.* **2015**, *54*, 2599–2605.

355. J. L. Espartero, I. Rashkov, S. M. Li, N. Manolova, M. Vert, NMR analysis of low molecular weight poly(lactic acid)s, *Macromolecuels* **1996**, *29*, 3535–3539.

356. H. Tsuji, *Biodegradable Polymers*, Corona Publishing Co. Ltd., Tokyo, 2002 (in Japanese).

357. S. M. Li, M. Vert, Biodegradation of aliphatic polyesters, in: G. Scott, D. Gilead, (Eds.), *Biodegradable Polymers: Principles and Applications*, Chapman & Hall, Cambridge, 1995, pp. 43–87.

358. S. M. Li, Hydrolytic degradation characteristics of aliphatic polyesters derived from lactic and glycolic acids, *J. Biomed. Mater. Res.* **1999**, *48*, 342–353.

359. H. Tsuji, S. Miyauchi, Poly(L-lactide): VI effects of crystallinity on enzymatic hydrolysis of poly(L-lactide) without free amorphous region, *Polym. Degrad. Stab.* **2001**, *71*, 415–424.

360. See, for example, U. W. Gedde, *Polymer Physics*, Chapman & Hall, London, 1995, Chapters 7 and 8.

361. W. Hoogsteen, A. R. Postema, A. J. Pennings, G. ten Brinke, P. Zugenmaier, Crystal structure, conformation, and morphology of solution-spun poly(L-lactide) fibers, *Macromolecules* **1990**, *23*, 634–642.

362. J. Kobayashi, T. Asahi, M. Ichiki, A. Okikawa, H. Suzuki, T. Watanabe, E. Fukada, Y. Shikinami, Structural and optical properties of poly lactic acids, *J. Appl. Phys.* **1995**, *77*, 2957–2973.

363. E. W. Fischer, H. J. Sterzel, G. Wegner, Investigation of the structure of solution grown crystals of lactide copolymers by means of chemical reactions, *Kolloid ZZ Polym.* **1973**, *251*, 980–990.

364. T. Miyata, T. Masuko, Crystallization behavior of poly(L-lactide), *Polymer* **1998**, *39*, 5515–5521.

365. B. Kalb, A. J. Pennings, General crystallization behaviour of poly(L-lactic acid), *Polymer* **1980**, *21*, 607–612.

366. R. Vasanthakumari, A. J. Pennings, Crystallization kinetics of poly(L-lactic acid), *Polymer* **1983**, *24*, 175–178.

367. H. Tsuji, Y. Ikada, Properties and morphologies of poly(L-lactide): 1. Annealing condition effects on properties and morphologies of poly(L-lactide), *Polymer* **1995**, *36*, 2709–2716.

368. H. Tsuji, Y. Ikada, Blends of isotactic and atactic poly(lactide). I. Effects of mixing ratio of isomers on crystallization of blends from melt, *J. Appl. Polym. Sci.* **1995**, *58*, 1793–1802.

369. H. Tsuji, Y. Ikada, Blends of isotactic and atactic poly(lactide)s: 2. Molecular-weight effects of atactic component on crystallization and morphology of equimolar blends from the melt, *Polymer* **1996**, *37*, 595–602.

370. H. Abe, Y. Kikkawa, Y. Inoue, Y. Doi, Morphological and kinetic analyses of regime transition for poly[(S)-lactide] crystal growth, *Biomacromolecules* **2001**, *2*, 1007–1014.

371. J. D. Hoffman, R. L. Miller, H. Marand. D. B. Roitman, Relationship between the lateral surface free energy. sigma. and the chain structure of melt-crystallized polymers, *Macromolecules* **1992**, *25*, 2221–2229.

372. J. D. Hoffman, J. J. Weeks, Melting process and the equilibrium melting temperature of polychlorotrifluoroethylene, *J. Res. Natl. Bur. Stand* **1962**, *66A*, 13–28.

373. H. Marand, J. Xu, S. Srinivas, Determination of the equilibrium melting temperature of polymer crystals: linear and nonlinear Hoffman–Weeks extrapolations, *Macromolecules* **1998**, *31*, 8219–8229.

374. J. Xu, S. Srinivas, H. Marand, Equilibrium melting temperature and undercooling dependence of the spherulitic growth rate of isotactic polypropylene, *Macromolecules* **1998**, *31*, 8230–8242.

375. H. Tsuji, Y. Ikada, Crystallization from the melt of poly(lactide)s with different optical purities and their blends, *Macromol. Chem. Phys.* **1996**, *197*, 3488–3499.

376. H. Tsuji, F. Horii, M. Nakagawa, Y. Ikada, H. Odani, R. Kitamura, Stereocomplex formation between enantiomeric poly(lactic acid)s. 7. Phase structure of the stereocomplex crystallized from a dilute acetonitrile solution as studied by high-resolution solid-state carbon-$^{13}$NMR spectroscopy, *Macromolecules* **1992**, *25*, 4114–4118.

377. H. Tsuji, S. Miyauchi, Poly(L-lactide): 7. Enzymatic hydrolysis of free and restricted amorphous regions in poly(L-lactide) films with different crystallinities and a fixed crystalline thickness, *Polymer* **2001**, *42*, 4463–4467.

378. M. Therin, P. Christel, S. M. Li, H. Garreau, M. Vert, in vivo degradation of massive poly(α-hydroxy acids): validation of in vitro findings, *Biomaterials* **1992**, *13*, 594–600.

379. Y. Cha, C. G. Pitt, The biodegradability of polyester blends, *Biomaterials* **1990**, *11*, 108–112.

380. H. Tsuji, T. Ono, T. Saeki, H. Daimon, K. Fujie, Hydrolytic degradation of poly(ε-caprolactone) in the melt, *Polym. Degrad. Stab.* **2005**, *89*, 336–343.

381. T. Saeki, T. Tsukegi, H. Tsuji, H. Daimon, K. Fujie, Hydrolytic degradation of poly[(R)-3-hydroxybutyric acid] in the melt, *Polymer* **2005**, *46*, 2157–2162.

382. H. Tsuji, Y. Yamamura, T. Ono, T. Saeki, H. Daimon, K. Fujie, Hydrolytic degradation and monomer recovery of poly(butylene succinate) and poly(butylene succinate/adipate) in the melt, *Macromol. React. Eng.* **2008**, *2*, 522–528.

383. J. R. Campanelli, M. R. Kamal, D. G. Cooper, A kinetic study of the hydrolytic degradation of polyethylene terephthalate at high temperatures, *J. Appl. Polym. Sci.* **1993**, *48*, 443–451.

384. D. Karst, Y. Yang, Effect of arrangement of L-lactide and D-lactide in poly[(L-lactide)-*co*-(D-lactide)] on its resistance to hydrolysis studied by molecular modeling, *Macromol. Chem. Phys.* **2008**, *209*, 168–174.

385. M. Vert, S. M. Li, H. Garreau, New insights on the degradation of bioresorbable polymeric devices based on lactic and glycolic acids, *Clin. Mater.* **1992**, *10*, 3–8.

386. M. Vert, J. Mauduit, S. M. Li, Biodegradation of PLA/GA polymers: increasing complexity, *Biomaterials* **1994**, *15*, 1209–1213.

387. H. Tsuji, T. Eto, Y. Sakamoto, Synthesis and hydrolytic degradation of substituted poly(DL-lactic acid)s, *Materials* **2011**, *4*, 1384–1398.

388. H. Tsuji, Quiescent crystallization of poly(lactic acid) and its copolymers-based materials, in: M. L. Di Lorenzo, R. Androsch (Eds.), *Thermal Properties of Bio-based Polymers (Advances in Polymer Science, vol. 283)*, Springer Nature, Cham, 2019, pp. 37–86.

389. T. Nakamura, S. Hitomi, S. Watanabe, Y. Shimizu, K. Jamshidi, S. H. Hyon, Y. Ikada, Bioabsorption of polylactides with different molecular properties, *J. Biomed. Mater. Res.* **1989**, *23*, 1115–1130.

390. H. Pistner, D. R. Bendix, J. Mühling, J. F. Reuther, Poly(L-lactide): a long-term degradation study in vivo: part III. Analytical characterization, *Biomaterials* **1993**, *14*, 291–298.

391. H. Pistner, H. Stallforth, R. Gutwald, J. Mühling, J. Reuther, C. Michel, Poly(L-lactide): a long-term degradation study in vivo: part II: physico-mechanical behavior of implants, *Biomaterials* **1994**, *15*, 439–450.

392. H. Cai, V. Dave, R. A. Gross, S. P. McCarthy, Effects of physical aging, crystallinity, and orientation on the enzymatic degradation of poly(lactic acid), *J. Polym. Sci. Part B* **1996**, *34*, 2701–2708.

393. A. Kishida, S. Yoshioka, Y. Takeda, M. Uchiyama, Formulation-assisted biodegradable polymer matrices, *Chem. Pharm. Bull.* **1989**, *37*, 1954–1956.

394. H. Tsuji, R. Smith, W. Bonfield, Y. Ikada, Porous biodegradable polyesters. I. Preparation of porous poly(L-lactide) films by extraction of poly(ethylene oxide) from their blends, *J. Appl. Polym. Sci.* **2000**, *75*, 629–637.

395. H. Tsuji, A. Okumura, Crystallization and hydrolytic/thermal degradation of a novel stereocomplexationable blend of poly(L-2-hydroxybutyrate) and poly(D-2-hydroxybutyrate), *Polym. J.* **2011**, *43*, 317–324.

396. S. I. Moon, F. Jin, C. Lee, S. Tsutsumi, S.-H. Hyon, Novel carbon nanotube/poly(L-lactic acid) nanocomposites; their modulus, thermal stability, and electrical conductivity, *Macromol. Symp.* **2005**, *224*, 287–296.

397. H. Tsuji, H. Takai, N. Fukuda, H. Takikawa, Non-isothermal crystallization behavior of poly(L-lactic acid) in the presence of various additives, *Macromol. Mater. Eng.* **2006**, *291*, 325–335.

398. H. Tsuji, Y. Kawashima, H. Takikawa, S. Tanaka, Poly(L-lactide)/nano-structured carbon composites: conductivity, thermal properties, crystallization, and biodegradation, *Polymer* **2007**, *48*, 4213–4225.

399. H. Tsuji, T. Ishizaka, Porous biodegradable polyesters. II. Physical properties, morphology, and enzymatic and alkaline hydrolysis of porous poly(ε-caprolactone) films, *J. Appl. Polym. Sci.* **2001**, *80*, 2281–2291.

400. M. Vert, S. M. Li, H. Garreau, Attempts to map the structure and degradation characteristics of aliphatic polyesters derived from lactic and glycolic acids, *J. Biomater. Sci. Polym. Ed.* **1995**, *6*, 639–649.

401. S. Slomkowshi, S. Sosnowski, M. Gadzinowski, C. Pichot, A. Elaisssari, Direct synthesis of polyester microspheres, potential carriers of bioactive compounds, *ACS Symp. Ser.* **1998**, *708*, 143–153.

402. Y. Q. Wang, J. Y Cai, Enhanced cell affinity of poly(L-lactic acid) modified by base hydrolysis: wettability and surface roughness at nanometer scale, *Curr. Appl. Phys.* **2007**, *7S1*, e108–e111.

403. J. Rzayev, M. A. Hillmyer, Nanochannel array plastics with tailored surface chemistry, *J. Am. Chem. Soc.* **2005**, *127*, 13373–13379.

404. R. M. Ho, W. H. Tseng, H. W. Fan, Y. W. Chiang, C. C. Lin, B. T. Ko, B. H. Huang, Solvent-induced microdomain orientation in polystyrene-*b*-poly(L-lactide) diblock copolymer thin films for nanopatterning, *Polymer* **2005**, *46*, 9362–9377.

# 22

# ENZYMATIC DEGRADATION

Ken'ichiro Matsumoto, Hideki Abe, Yoshihiro Kikkawa, and Tadahisa Iwata

## 22.1 INTRODUCTION

### 22.1.1 Definition of Biodegradable Plastics

Ideal biodegradable plastics are defined as materials that are completely degraded to $CO_2$ and $H_2O$ by the action of microorganisms. The precise definitions based on standardized and accepted test methods for "biodegradable plastics" and "degradable" by ISO/TC-61/SC-5/WG-22 (ISO 472/DAM3: Amendment 3: General terms and terms relating to degradable plastics) are as follows [1]:

*Biodegradable Plastics*: A degradable plastic in which the degradation results from the action of naturally occurring microorganisms such as bacteria, fungi, and algae.

*Degradable*: A material is called degradable with respect to specific environmental conditions if it undergoes the degradation to a specific extent within a given time measured by specific standard test methods.

On the other hand, in ASTM D6400-19, "compostable plastic" is defined as follows:

*Compostable Plastic:* A plastic that undergoes degradation by biological processes during composting to yield carbon dioxide, water, inorganic compounds, and biomass at a rate consistent with other known compostable materials and leaves no visually distinguishable or toxic residues.

Biodegradable plastics are expected to be used in the following areas: (i) where plastics can be used in the natural environment, such as agricultural and fishery materials, civil engineering and construction materials, and leisure goods; (ii) where recovery and reuse of plastics are difficult but composting of organic waste is available, such as food packaging, hygienic products, and miscellaneous; and (iii) where specific material properties are required, such as slow release, water retention, medical use, low oxygen permeability, and low melting temperature.

### 22.1.2 Enzymatic Degradation

Biodegradation tests are classified into three groups: (i) environmental degradation, (ii) microbial degradation, and (iii) enzymatic degradation. Environmental degradation is evaluated based on overall biodegradation of materials by measuring the changes in weight loss, tensile strength, surface morphology, molecular weight, and so on under different environmental conditions such as soil, seawater, or river water. Accordingly, this test depends on the characteristics of soil and water, temperature, humidity, precipitation, amount of natural sunlight, and so on. The main evaluation tests for microbial degradation are biochemical oxygen demand (BOD), gas emission ($CO_2$ and methane, primarily), and weight loss measurements. However, this method is also controlled by the load and type of microorganisms, amount and kinds of enzymes secreted by the microorganisms, and so on. Accordingly, the degradation mechanism of polymeric materials at the molecular level is complex.

The main components of biodegradable plastics and polymers are polysaccharides, polyesters, and polyamides, which are hydrolyzed by specific enzymes such as glycosyl hydrolases, ester hydrolases, and peptide hydrolases, respectively. Insoluble biodegradable plastics are degraded into water-soluble materials (e.g., organic acids, oligomers) by the action of enzymes secreted from the microorganisms (enzymatic degradation or primary degradation). These water-soluble materials are metabolized to $CO_2$, $H_2O$, and biomass (complete degradation or microbial metabolism) in microorganisms as shown in Figure 22.1. Many enzymes

*Poly(Lactic Acid): Synthesis, Structures, Properties, Processing, Applications, and End of Life*, Second Edition.
Edited by Rafael A. Auras, Loong-Tak Lim, Susan E. M. Selke, and Hideto Tsuji.

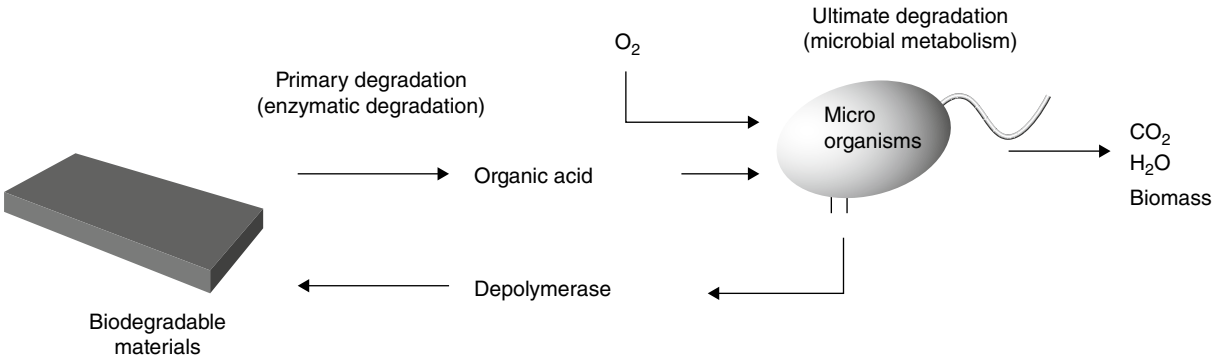


**FIGURE 22.1** Enzymatic degradation and microbial metabolism.

have been isolated and purified for biodegradable polyesters, specifically, for poly(hydroxyalkanoate)s, which are biodegradable polyesters produced from organic acids and glucose by microorganisms [2]. However, until now, no study of the specific enzymes for biodegradation of poly(lactic acid) (PLA) has been reported.

Williams reported the enzymatic hydrolysis of poly(L-lactic acid) (PLLA) in the presence of enzymes such as pronase, proteinase K, and bromelain. However, these enzymes are proteases and not PLLA depolymerases [3]. Regarding PLA stereocopolymers, Fukuzaki et al. reported that the hydrolysis of PLA was accelerated in the presence of specific enzymes, and the most rapid enzymatic degradation of the stereocopolymers was observed on the poly(D,L-lactic acid) (PDLLA) sample containing 50% L-lactic acid (LLA) [4]. Furthermore, Makino et al. showed that the addition of a carboxylic esterase accelerated the decrease in the weight-average molecular weight of PDLLA [5]. Reeve et al. reported the effects of stereochemical composition on enzymatic degradability of PLA films by proteinase K from *Tritirachium album* [6].

Enzymatic degradation is mainly evaluated by means of (i) weight loss of polymeric materials; (ii) optical density of polymer suspensions; (iii) titration of water-soluble materials; (iv) molecular weight measurement; (v) physical property changes; and (vi) surface morphological changes. These methods mainly focus on the polymeric material itself. If specific enzymes were isolated for PLA, the three-dimensional structural analysis of the enzyme molecule would provide very useful information for understanding the enzymatic degradation mechanism at the molecular level.

Biodegradable thermoplastics, such as PLA, have various material shapes, three-dimensional structures, and crystal morphologies. Melt-crystallized and solvent-cast films mainly consist of spherulites including lamellar twisting (Figure 22.2). Fibers have well-organized, oriented lamellar crystals along the fiber axis with high crystallinity, high crystal orientation, and thick lamellar crystals. The fundamental crystal morphology of polymeric material is a lamellar crystal that has chain folding with a period of 5–10 nm. In the chemical or enzymatic hydrolysis of biomaterials, the distribution of crystal regions, lamellar crystal thickness and size, crystal morphology, and structure may play a decisive role in the rate of hydrolysis.

In this chapter, we review the enzymatic degradation mechanisms of PLA prepared from melt-crystallized, solvent-cast, and blend films, mainly by using proteinase K enzyme.

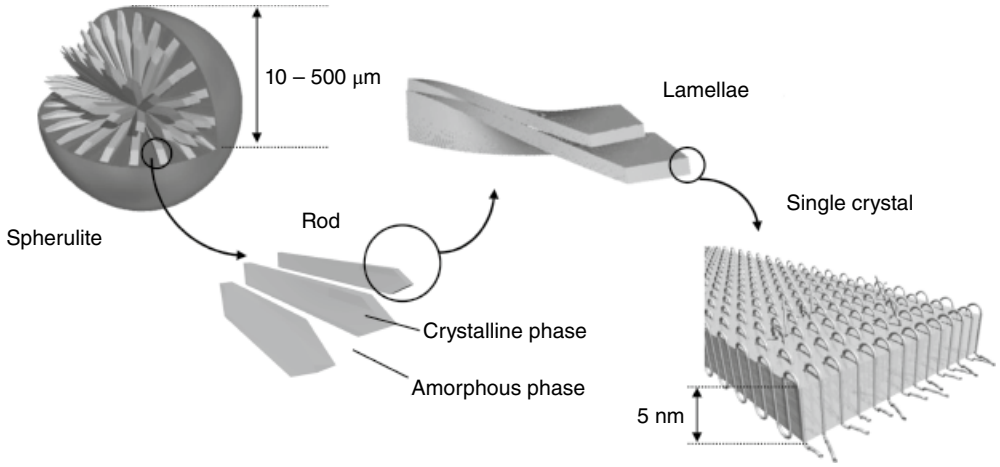


**FIGURE 22.2** Spherulite structure and lamellar crystals in polymeric materials.

The degradation mechanisms of thin films with thickness of about 100 nm and solution-grown lamellar crystals are also discussed. Also, we review the recent advances in characterization of enzymes that degrade PLAs and their copolymers.

## 22.2 ENZYMATIC DEGRADATION OF PLA FILMS

The degradability of PLA materials by various enzymes has been reported [3, 4, 6–19]. In regard to recent reports, see Section 22.5. In particular, the enzymatic degradation of PLLA and its copolymers by proteinase K secreted by the mold *T. album* has been investigated most extensively [3, 6–17].

### 22.2.1 Structure and Substrate Specificity of Proteinase K

Proteinase K is a family of serine proteases with strong activity in hydrolyzing proteins, particularly keratin [20]. It consists of 279 amino acids with a molecular weight of 28,790 Da [21]. The crystal structure of proteinase K molecules has been investigated by X-ray diffraction studies; its shape is a half sphere 4 nm in diameter [22–24]. The catalytic site serine (Ser224) plays a central role in the catalytic reaction and forms a catalytic triad with an aspartate (Asp39) and a histidine (His69). The catalytic residues (Ser224–Asp39–His69) are located on the flat side of the enzyme molecule and participate in a nucleophilic attack on the carbonyl carbon atom of the peptide chain. The enzyme forms a single functional domain structure. From the conformational data of the enzyme complexed with oligopeptides, it is predicted that the catalytic site includes at least 8, and possibly 10, subsites for binding monomer units of polypeptide substrates [25]. It also reveals that the oligopeptide with an extended conformation binds preferentially over the helical conformer [25]. Although the original substrates for the enzyme are peptides, the enzyme can hydrolyze the ester bond of PLLA molecules. Williams first found that proteinase K showed strong effects on PLLA degradation [3].

### 22.2.2 Enzymatic Degradability of PLLA Films

PLLA is a crystallizable polymer with melting temperature at around 175°C. Semicrystalline PLLA films can be prepared by various techniques, such as solution casting with a slow evaporation rate of solvent, isothermal crystallization from the melt, and annealing of amorphous samples. Since PLLA has a glass transition temperature ($T_g$) of 60°C, which is higher than room temperature, a completely amorphous film can be obtained by melt quenching.

Tsuji and Miyauchi prepared amorphous films of PLLA with different number-average molecular weights ($M_n$) ranging from 76,000 to 480,000 Da and performed enzymatic hydrolysis of the films by proteinase K [12]. They found that the rate of enzymatic erosion by proteinase K decreased with an increase in PLLA molecular weight. When the erosion rates were plotted against the inverse of molecular weight ($M_n^{-1}$), the plot revealed a linear relationship, where the intercept of the line at $M_n^{-1} = 0$ gave a positive value (1.75 μg/mm$^2$ h) (Figure 22.3). This result indicates that the hydrolysis of PLLA molecules catalyzed by proteinase K proceeded via *exo*- and *endo*-chain scissions. A similar molecular weight dependence of hydrolysis rate of PLLA materials has been confirmed from the results of enzymatic degradation of branched PLLA samples by proteinase K reported by Numata et al. [26, 27].

Tsuji and Miyauchi prepared a series of semicrystalline PLLA films with different crystallinities by an annealing treatment at 140°C for melt-quenched amorphous samples and investigated the effect of the presence of crystalline regions on the enzymatic degradation rate [13]. Figure 22.4 shows the relationship between the enzymatic erosion rate and crystallinity of PLLA films with annealing treatment at 140°C for 10–45 min. The erosion rate of PLLA films decreased with an increase in crystallinity, indicating that the enzyme predominantly hydrolyzes the PLLA molecules in amorphous regions on the film surface. In addition, the erosion rates of semicrystalline PLLA films revealed a nonlinear relationship with the film crystallinity. To explain the relationship between the erosion rate and the crystallinity, the researchers postulated the presence of two types of amorphous regions, namely, the free amorphous region and the amorphous region that is restricted by the crystalline architecture. It is proposed that the degradation rate of the

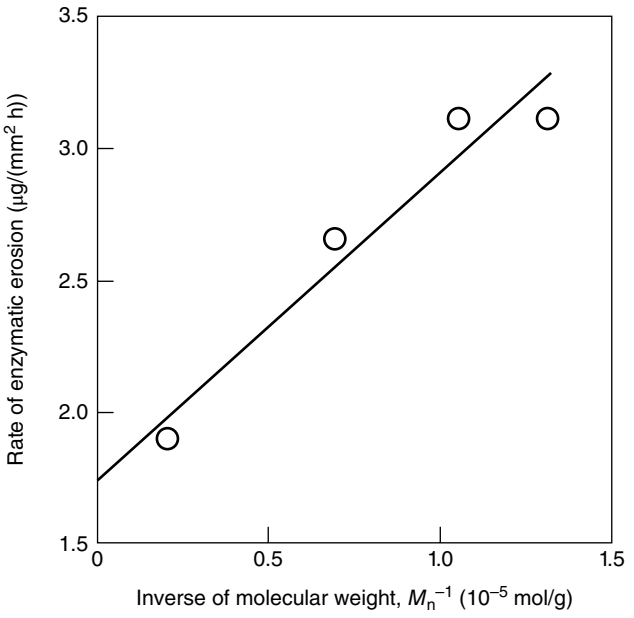


**FIGURE 22.3** Enzymatic hydrolysis rate of PLLA films as a function of the inverse of molecular weight ($M_n^{-1}$). *Source*: Reprinted with permission from Ref. 12. Copyright 2001, American Chemical Society.

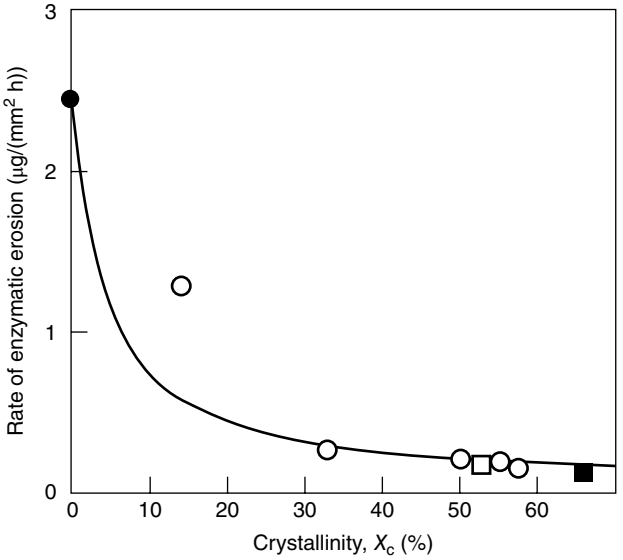


**FIGURE 22.4** Enzymatic hydrolysis rate of PLLA films as a function of the initial crystallinity of semicrystalline PLLA films ($X_c$). PLLA amorphous film (•), PLLA semicrystalline films annealed at 120°C for 600 min (□), 140°C (○) for different time ranging from 10 to 600 min, and 150°C (■) for 600 min [13, 14]. Dotted line represents the simulated profile of degradation rates by assuming successive hydrolysis reaction of amorphous and crystalline regions on the film surface. For the simulation, the enzymatic erosion rate of PLLA film (R) is determined by using the following equation: $1/R = X_c/R_c + (1 - X_c)/R_a$, where $R_c$ and $R_a$ are the erosion rates of crystalline and amorphous regions, respectively, and the values of $R_c = 0.1\,\mu g/(mm^2\,h)$ and $R_a = 2.5\,\mu g/(mm^2\,h)$ are applied.

amorphous regions in the semicrystalline phase (restricted amorphous regions) is lower than that of the completely amorphous regions (free amorphous regions) [13].

On the other hand, the nonlinear relationship for the hydrolysis of semicrystalline PLLA films can be accounted for in terms of successive hydrolysis reactions of amorphous and crystalline regions on the film surface. It is known that the enzymatic degradation of PLLA films by proteinase K progresses on a film surface as a heterogeneous reaction. If the surface of semicrystalline PLLA film is occupied by PLLA crystalline aggregates, such as spherulites, the enzymatic degradation in amorphous and crystalline regions occurs successively from the surface of the film. Therefore, the overall rate of film erosion ($R$) may be expressed by the erosion rates of crystalline ($R_c$) and amorphous ($R_a$) regions with the degree of crystallinity ($x_c$) as follows:

$$\frac{1}{R} = \frac{x_c}{R_c} + \frac{1 - x_c}{R_a} \tag{22.1}$$

Using this equation, the erosion rate of crystalline region ($R_c$) can be estimated from the data in Figure 22.4. The estimated $R_c$ value (0.1–0.2 μg/(mm² h)) is much smaller than the $R_a$ value obtained from a completely amorphous film (2.5 μg/(mm² h)). Thus, the hydrolysis of the crystalline regions is a rate-limiting step in the enzymatic degradation of semicrystalline PLLA film.

Furthermore, it was reported that among semicrystalline PLLA films with similar crystallinity, the films annealed at a higher temperature were more resistant to enzymatic degradation [14]. It has been suggested that the lamellar crystal size of PLLA also plays a decisive role in the enzymatic degradation process. A similar dependence of the enzymatic erosion rate of semicrystalline PLLA on crystal size has been confirmed by Kurokawa et al. [28].

### 22.2.3 Enzymatic Degradability of PLA Stereoisomers and Their Blends

Since the lactyl monomeric unit has a chiral center, various PLA stereoisomers can be obtained by the polymerization of stereoisomers of lactic acids or lactides. Reeve et al. first investigated the stereoselectivity of proteinase K using various PLA stereocopolymers derived from mixtures of L-lactide (LLA) and D-lactide (DLA) [6]. Films of the polymers prepared by solution casting were annealed to crystallize and then exposed to proteinase K. They found that the enzyme preferentially degraded PLLA and not poly(D-lactic acid) (PDLA). A decrease in the L-lactyl repeat unit content ($X_{LLA}$) from 100 to 92 mol% led to a large decrease in crystallinity and corresponding increases in film weight loss rates [6]. However, the experimental results observed here for semicrystalline PLA films are due to the superimposed effects of polymer stereochemistry and material crystallinity on film degradability.

MacDonald et al. [7] prepared melt-quenched amorphous films of PLA stereocopolymers derived from LLA/DLA and LLA/*meso*-lactide (MLA) with 75–95 mol% of $X_{LLA}$. They investigated the effects of stereochemical composition and of repeat unit sequence distribution on enzymatic degradation by proteinase K. They reported that amorphous films of PLA stereocopolymers derived from LLA/DLA with 80–95 mol% of $X_{LLA}$ exhibited almost identical weight loss rates. On the other hand, PLA derived from LLA/MLA showed lower weight loss rates than those of the LLA/DLA series. This finding was tentatively attributed to the inhibiting effect of L-D-L triads present in PLA derived from LLA/MLA [7]. Tsuji and Miyauchi [12] further investigated the effect of stereochemical composition on enzymatic degradability of PLA stereocopolymers derived from LLA/DLA by using amorphous films of PLA with a wide range of $X_{LLA}$ from 0 to 0.99. They reported that the enzymatic erosion rate of the PLA films decreased with decreasing $X_{LLA}$ and finally became zero when $X_{LLA}$ was below 0.3 (Figure 22.5). Furthermore, they considered the average L-lactyl and D-lactyl unit sequential lengths ($l_L$ and $l_D$) of PLA stereocopolymers and concluded that the PLA molecules are enzymatically hydrolyzable when $l_L$ is higher than 3 and $l_D$ is lower than 10. The rate of degradation dramatically decreased as the $l_L$ value decreased from 10 to 3. This result can be easily understood by taking into account the number of

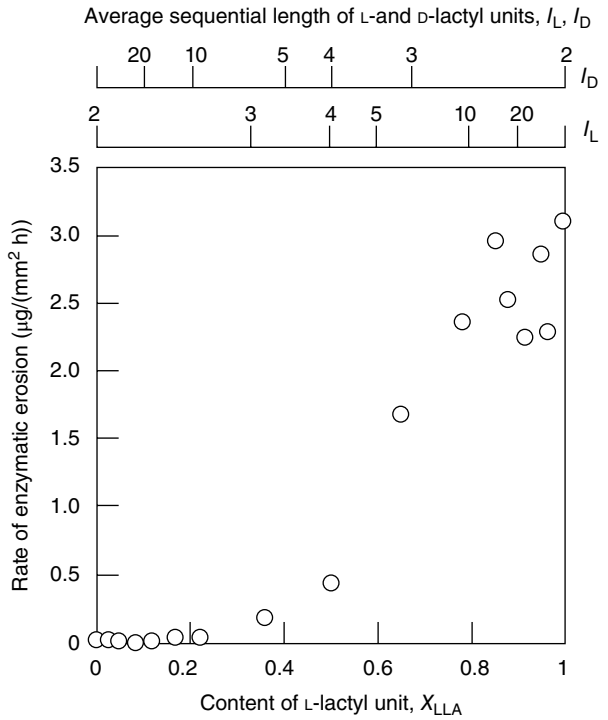


**FIGURE 22.5** Enzymatic hydrolysis rate of PLA stereocopolymer films as functions of L-lactyl unit ($X_{LLA}$) content and of the average sequential length of L-lactyl ($l_L$) or D-lactyl ($l_D$) units. The values of $l_L$ and $l_D$ are calculated by using following equations: $l_L = 2/(1 - X_{LLA})$ and $l_D = 2/X_{LLA}$. *Source*: Reprinted with permission from Ref. 12. Copyright 2001, American Chemical Society.

subsites for the catalytic site of proteinase K. As mentioned above, the catalytic site of proteinase K includes 10 subsites for incorporating monomer units [25]. If the 10 subsites are fully occupied by LLA monomeric units, the ester bond may be quickly hydrolyzed by catalytic amino acid residues. The DLA units cannot bind to the several parts of the 10 subsites owing to their configurational and/or conformational mismatch with the subsites. The rate of ester hydrolysis may decrease as the numbers of subsites occupied by LLA monomeric units is decreased, and ester hydrolysis by proteinase K does not occur when the monomer occupation for the subsites is less than three [12]. When the PLA stereocopolymers between LLA/DLA and LLA/MLA are compared at an identical $X_{LLA}$ value, the $l_L$ value of PLA from LLA/DLA is larger than that from LLA/MLA. As a result, PLA derived from LLA/MLA degrades slower than those from LLA/DLA. Thus, the enzymatic degradation rate of PLA stereocopolymers by proteinase K is strongly dependent on the distribution and sequential length of LLA units in the molecules.

In addition to PLA stereocopolymers, PLA films with different stereochemical compositions can be obtained by blending PLA stereoisomers. The enzymatic degradability of both the enantiomeric blend films from PLLA and PDLA and the diastereoisomeric blend films of PDLLA with either PLLA or PDLA has been investigated by Tsuji and Miyauchi [12]. It is of interest to note that the erosion rates of amorphous films show similar trends with respect to the overall $X_{LLA}$ between enantiomeric and diastereoisomeric blends (Figure 22.6). The enzymatic erosion rate of both blend films decreased with decreasing $X_{LLA}$ and approached zero at $X_{LLA}$ below 0.3, which is very similar to the result for the nonblended PLA films. Since the PLLA and PDLLA components are enzymatically hydrolyzable as opposed to PDLA, the content of hydrolyzable components in the blends with identical $X_{LLA}$ values are apparently different between enantiomeric and diastereoisomeric blends. Therefore, such similarity in trends of the erosion rates with the $X_{LLA}$ value between the enantiomeric and diastereoisomeric blends may be a coincidence. However, these results indicate that the overall enzymatic erosion rate of PLA specimens can be controlled by varying the blending ratio and the types of PLA stereocopolymers.

### 22.2.4 Effects of Surface Properties on Enzymatic Degradability of PLLA Films

Since the enzymatic degradation reaction of PLLA progresses on the surface of materials, it can be predicted that the modification of surface properties will result in a change in enzymatic degradability. Of surface modification techniques, grafting with poly(hydroxyethyl methacrylate) [29], polyacrylamide[29], polymethacrylate [29], and poly(ε-caprolactone) (PCL) [30] and coating with poly(vinyl alcohol) [31] on the PLLA materials have been investigated. It has been found that an alkaline treatment leads to enhancement of hydrophilicity on the surface of PLLA materials [32, 33]. The surface properties of polymeric materials can also be changed by an end-capping technique with various functional groups because chain end groups are segregated on the surface of materials due to free energy considerations. End-capping polymers with functional groups is a good technique to modify the surface properties while limiting change in the bulk properties of the materials. Many types of PLLA samples having various end groups have been synthesized to vary the surface properties of PLLA films [28, 34–39]. For example, it has been reported that the introduction of dodecyl ester ($C_{12}$) at the PLLA chain ends enhances the hydrophobicity on the film surface, while the surface of PLLA film becomes hydrophilic with the introduction of tri(ethylene glycol) monomethyl ether ester (MEEE) (Figure 22.7) [38]. Thus, the surface hydrophilicity or hydrophobicity of PLLA film reflects the hydrophilicity or hydrophobicity of the compounds substituted at the PLLA chain ends.

Kurokawa et al. investigated the enzymatic degradation of amorphous films of PLLA end capped with various alkyl ester chain end groups by proteinase K [39]. They found that the enzymatic degradation of PLLA films with shorter alkyl ester groups (with carbon numbers of 1–11) proceeded homogeneously from the surface of film and that the weight loss of the films increased proportionally with time (Figure 22.8). The film thickness decreased as degradation

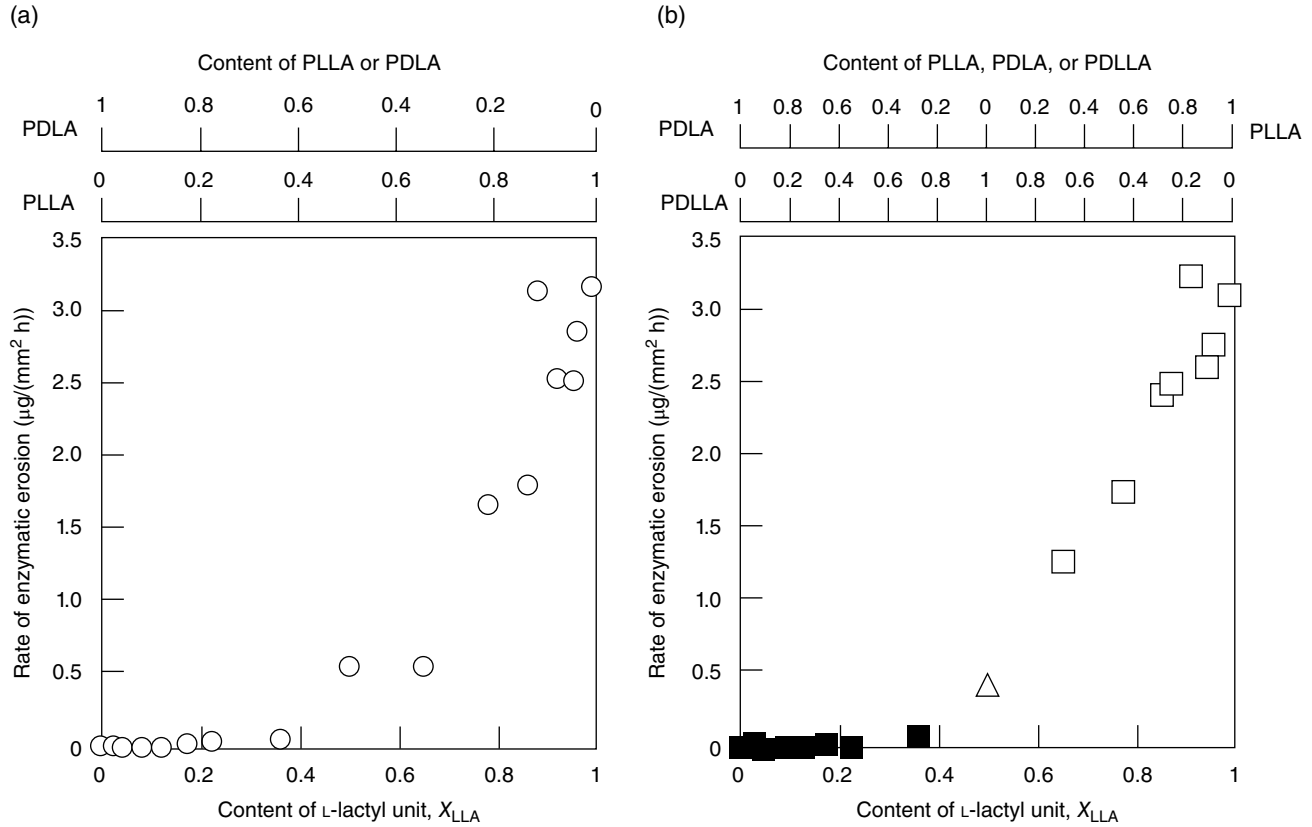


**FIGURE 22.6** Enzymatic hydrolysis rate of (a) enantiomeric blend films from PLLA and PDLA and (b) diastereoisomeric blend films from PDLLA and either PLLA or PDLA as a function of $X_{LLA}$. *Source*: Reprinted with permission from Ref. 12. Copyright 2001, American Chemical Society.

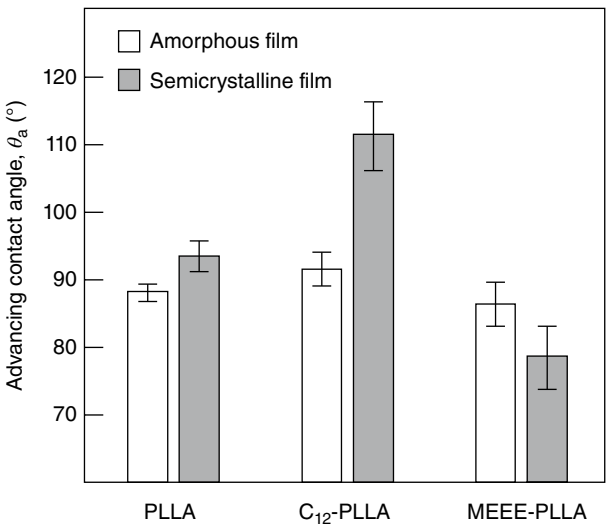


**FIGURE 22.7** Advancing contact angles ($\theta_a$) with water on the surface of end-capped PLLA films. PLLA, non-end-capped PLLA; $C_{12}$-PLLA, PLLA with dodecyl ester chain end; and MEEE-PLLA, PLLA with tri(ethylene glycol) monomethyl ether ester chain end. *Source*: Reprinted with permission from Ref. 38. Copyright 2004, American Chemical Society.

proceeded while the surface remained smooth (Figure 22.9c and e). On the other hand, the introduction of alkyl ester chain ends with carbon numbers of 12–14 induced suppression of the degradation of PLLA film by proteinase K. Substantial erosion took place only at the initial stage of the enzymatic reaction, followed by very small weight loss, as shown in Figure 22.8. The erosion profiles of PLLA films with longer alkyl ester groups ($C_{18}$ and $C_{24}$) were almost identical with the non-end-capped PLLA films. However, the surface of PLLA films with longer alkyl ester groups was blemished, and a sponge-like network structure was formed on the film surface (Figure 22.9i and k), indicating that the enzymatic degradation reaction of PLLA samples with longer alkyl ester groups occurred heterogeneously from the surface to the inside of the film.

Such alkyl ester chain-length-dependent behaviors for the end groups can be explained in terms of the dispersing state of alkyl ester chain ends in the PLLA phase and the solubility of alkyl ester groups in the aqueous phase by reference to the degradation studies on PLLA-based blends as follows. Gajria et al. [40] performed enzymatic degradation of miscible blends of PLLA and poly(vinyl acetate) (PVAc) using proteinase K. The PLLA molecules on the film surface of PLLA/PVAc blends were degraded by the enzyme at the initial

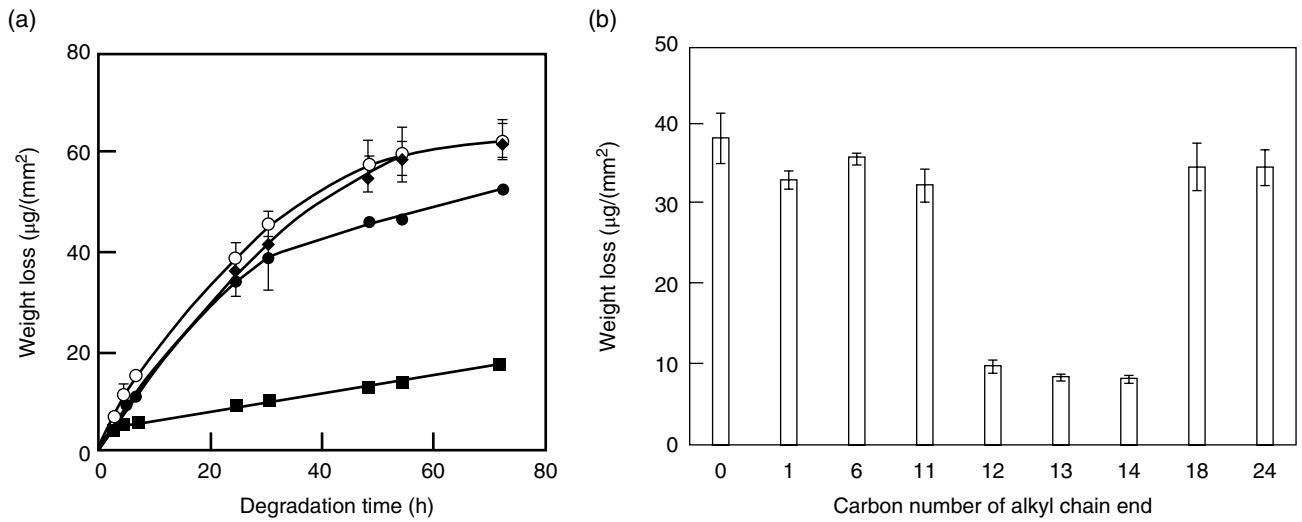


**FIGURE 22.8** Weight loss of amorphous film of PLLA end capped with alkyl ester groups by proteinase K. (a) Time-course changes in weight loss for non-end-capped PLLA (○), PLLA with hexyl ($C_6$-PLLA) (♦), with dodecyl ($C_{12}$-PLLA) (■), and with octadecyl ($C_{18}$-PLLA) (•) ester chain end. (b) Weight loss of PLLA films after enzymatic degradation for 24 h. *Source*: Reprinted with permission from Ref. 39. Copyright 2008, American Chemical Society.

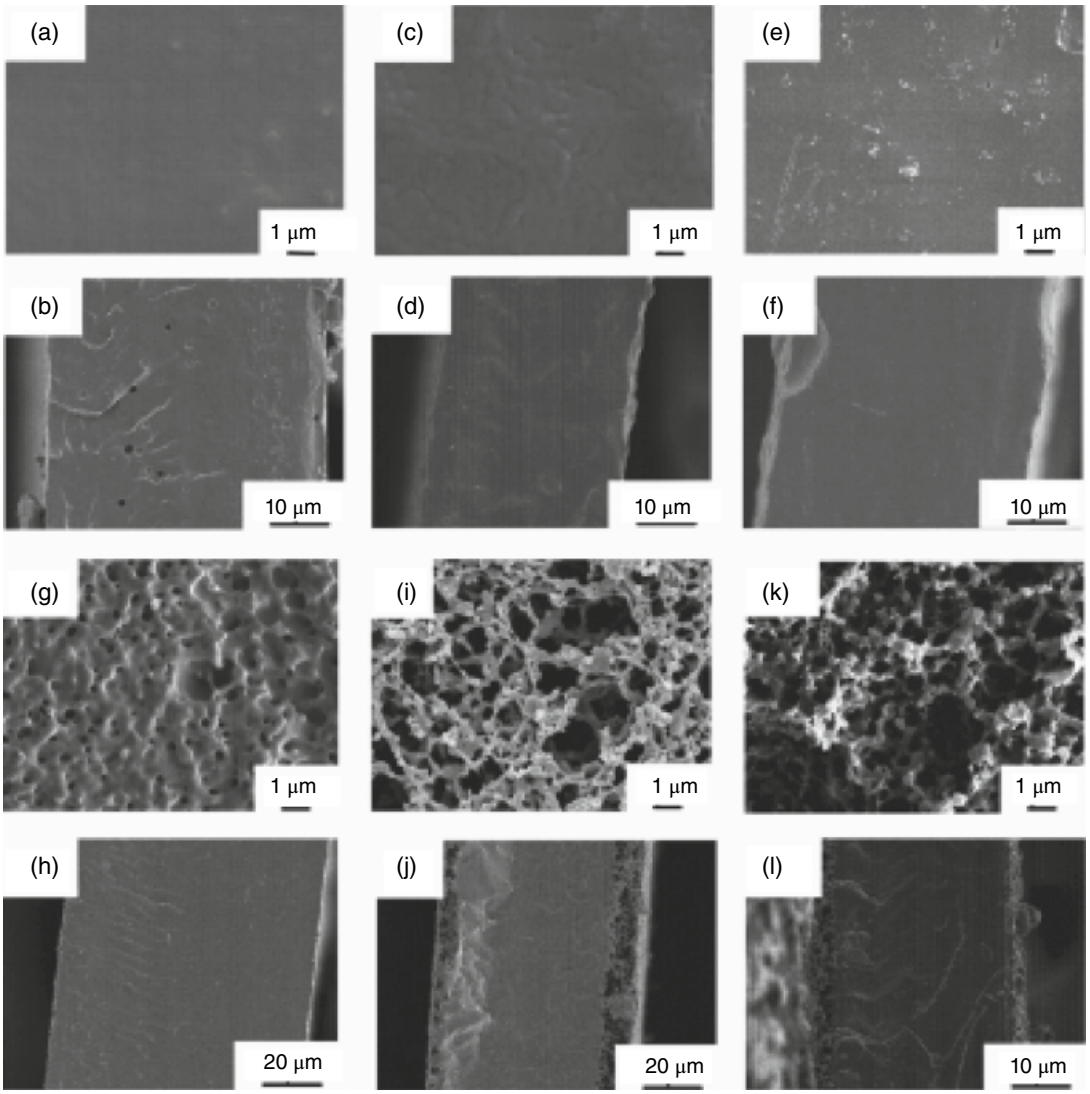


**FIGURE 22.9** Scanning electron micrographs of the surfaces (a, c, e, g, i, k) and cross sections (b, d, f, h, j, l) of end-capped PLLA films after enzymatic degradation for 24 h by proteinase K: (a, b) PLLA, (c, d) $C_1$-PLLA, (e, f) $C_6$-PLLA, (g, h) $C_{12}$-PLLA, (i, j) $C_{18}$-PLLA, (k, l) $C_{24}$-PLLA films. *Source*: Reprinted with permission from Ref. 39. Copyright 2008, American Chemical Society.

stage. After the initial degradation period, enzymatically inactive PVAc molecules covered the film surface and the enzymatic erosion was inhibited. Sheth et al. [41] reported on the enzymatic degradation of PLLA and poly(ethylene oxide) (PEO) miscible blends with proteinase K. Because PEO is a water-soluble component and was released from the blend during the immersion in aqueous solution, the overall erosion rates of the PLLA were accelerated by blending with PEO. In contrast to these miscible blend systems, a heterogeneous degradation profile has been observed for the enzymatic degradation of immiscible PLLA/PCL blends by proteinase K [42–44]. The immiscible blends formed a phase-separated structure and the enzyme hydrolyzed only the PLLA phase, but not the PCL phase. As a result of partial degradation of the PLLA phase, many holes were formed on the surface and inside of the blend films.

In the cases of PLLA samples with alkyl ester chain ends with 12–14 carbons, the PLLA molecules on the film surface are degraded by the enzyme. The alkyl chain end groups are not readily hydrolyzed by proteinase K and remain on the film surface. As a result, during the initial stage of the enzymatic reaction, the alkyl end groups may be concentrated on the film surface and eventually cover it. With an increase in alkyl chain end concentration, the enzymatic erosion on the film surface is retarded at this later stage. On the other hand, alkyl groups with carbon numbers below 11 may be easily released from the film surface into the reaction solution during the hydrolysis of the PLLA molecules. As a result, the PLLA samples with shorter alkyl ester groups have almost the same degradation profiles as non-end-capped PLLA. In the case of PLLA samples with alkyl ester chain ends with carbon numbers over 18, the alkyl chain end groups may assemble with each other owing to the hydrophobic interactions. Such heterogeneous hydrophobic-rich regions are not readily hydrolyzed by proteinase K, while the amorphous regions of the pure PLLA phase can be hydrolyzed easily by the enzyme, resulting in a sponge-like network structure. As a result, at the later degradation stage, the weight loss of the $C_{18}$-PLLA film was smaller than that of the non-end-capped PLLA. This indicates that end capping with functional groups provides a good method of varying the enzymatic degradation rate of PLLA materials with minimal changes to the bulk properties.

In addition, it was found that a PLLA substrate with microporous surface structure can be obtained by enzymatic etching of PLLA with long alkyl ester end groups [39]. Similarly, for immiscible PLLA-based blends, such as PLLA/PCL blend [43, 44], a porous structure can be formed both on the surface and inside of the blend film by selective enzymatic etching. Furthermore, Park et al. [45] demonstrated that films with layered microporous structure were obtained from the films of PLLA/poly[(*R*)-3-hydroxybutyrate] (P(3HB)) blend by cold drawing and selective removal of the PLLA component with alkaline treatment (Figure 22.10). The selective removal of the PLLA component in PLLA/P(3HB) blends may be substituted, of course, by enzymatic treatment. It is expected that these techniques for forming a microporous

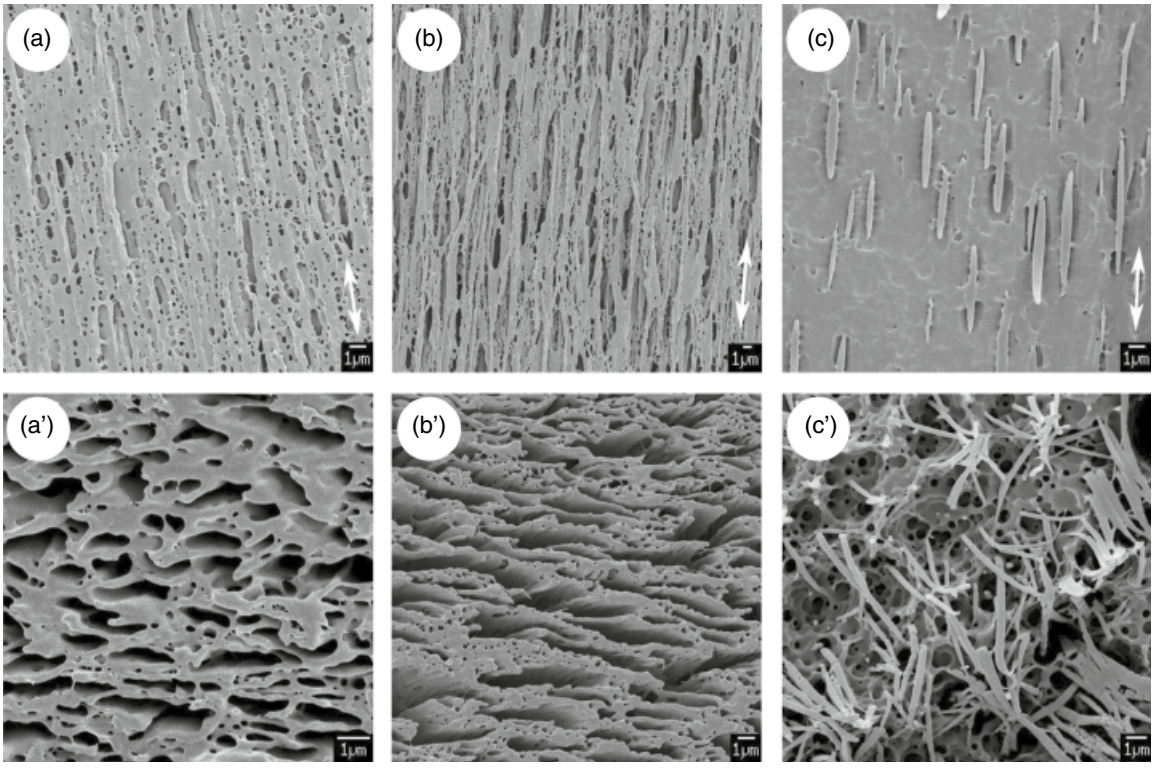


**FIGURE 22.10** Scanning electron micrographs of ultrahigh-molecular-weight PHB/PLLA blends drawn to five times after alkaline treatment at various blend ratios of (a) 7/3, (b) 5/5, and (c) 3/7. Top and bottom columns represent the surface (a–c) and cross section (a′–c′) of each sample, respectively. *Source*: Reprinted with permission from Ref. 45. Copyright 2004, American Chemical Society.

structure can be applied to the fields of bio-based polymeric materials, in particular biomaterials.

## 22.3 ENZYMATIC DEGRADATION OF THIN FILMS

### 22.3.1 Thin Films and Analytical Techniques

Thickness of polymer films can affect the properties of the material such as crystalline morphology [46–48], $T_g$ [49], and crystallization kinetics [50–53], and so on. A polymer film less than 1 μm is generally categorized as thin film and that less than 100 nm can be specially called an ultrathin film [54]. A well-established method to prepare thin films is spin coating of substrate. Important parameters affecting the film thickness are rotation speed, concentration of polymer solution, volatility of the solvent, and so on. A layer-by-layer (LbL) assembly is formed via stepwise deposition through alternate immersion in interactive polymer solutions [55, 56]. The thickness of the LbL film depends on the number of assembly steps. A monolayer of polymers can be obtained by the Langmuir–Blodgett (LB) film balance at the solution/air interface [57]. These thin films have been used to examine the hydrolysis and enzymatic degradation behaviors of PLA materials.

Several analytical methods to determine the crystalline morphology and enzymatic degradation of PLA thin films have been used, such as optical microscopy, scanning electron microscopy (SEM), transmission electron microscopy (TEM), atomic force microscopy (AFM), quartz crystal microbalance (QCM), and so on. These analytical techniques have different resolutions and test environments. Optical microscopy with crossed polarizers can be used to visualize micrometer-scale objects such as spherulites [58, 59]. SEM and TEM are operated in a vacuum and enable the observation of spherulitic to lamellar morphologies in the nanometer scale [58, 59]. AFM is recognized as a powerful tool to characterize polymer surface morphologies at a molecular level [60] and can be used in ambient, vacuum, and solution, as well as at elevated temperatures, which enables the in situ observation of polymer crystallization [61] and enzymatic degradation processes [62]. QCM is known as a sensitive tool to monitor the mass change on a quartz electrode on the nanogram order [63]. In terms of studies of biodegradation, enzymatic adsorption and degradation result in mass increase and decrease, respectively, and they can be monitored as negative and positive frequency changes [64]. By using these analytical techniques, crystalline morphologies and enzymatic degradation in PLA thin films has been investigated.

### 22.3.2 Crystalline Morphologies of Thin Films

Before studying its enzymatic degradation, PLA thin films should be adequately characterized. As stated in Section 22.3.1, crystalline morphologies are affected by the film thickness. A PLLA thin film was obtained by the spin-cast method on a substrate, and the film thickness was controlled by the concentration of the PLA solution. The cast thin film was melted above melting temperature (typically >175°C) and crystallized at elevated temperature. Figure 22.11 shows the effect of film thickness on the crystalline morphologies in PLLA thin films crystallized at 160°C [65]. In film below 30 nm in thickness, dendritic crystals were formed on the basis of diffusion-controlled growth. Thin film of 50–100 nm thickness showed hexagonal crystals, whereas that above 200 nm thickness was composed of highly stacked lamellar aggregates with edge-on and flat-on orientations.

In addition to the film thickness, crystallization temperature affects the resultant crystalline morphologies. In thin films (100 nm in thickness) crystallized at different temperatures, the PLLA crystals exhibited various crystalline morphologies from spherulitic aggregates to hexagonal lamellar stacks [66]. This morphological diversity was explained in

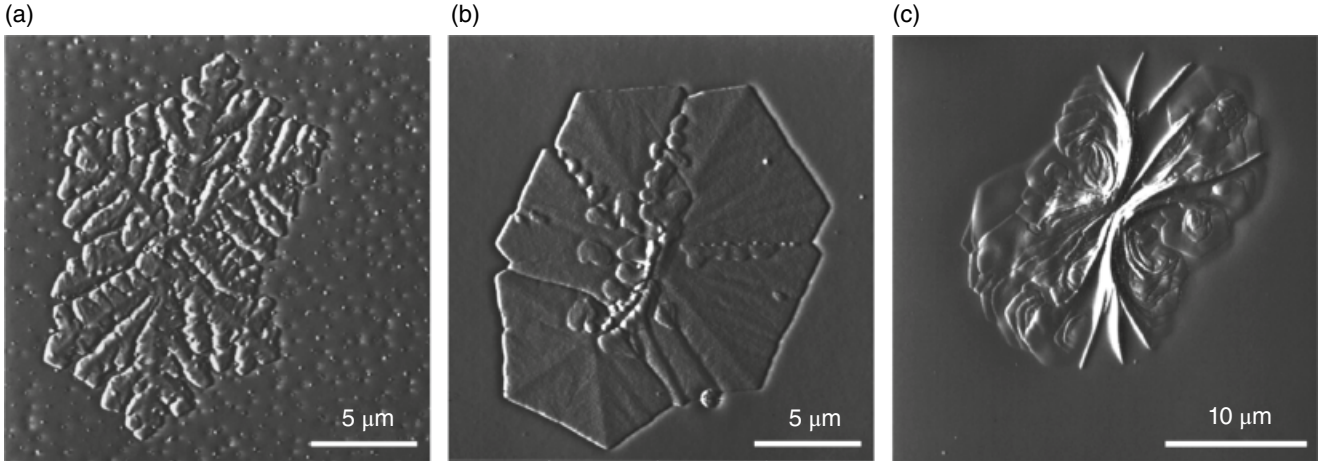


**FIGURE 22.11** AFM amplitude images of PLLA thin films (crystallized at 160°C) prepared from chloroform solutions with the concentrations of 0.25 (a), 0.5 (b), and 2.0% (w/v). The film thicknesses measured by AFM were 20 (a), 50 (b), and 200 nm (c), respectively. (a) Dendritic crystal, (b) hexagonal crystal, and (c) early stage of spherulitic morphology with edge-on and flat-on lamellae. *Source*: Reprinted with permission from Ref. 65. Copyright 2001, American Chemical Society.

terms of regime transition that is governed by both the nucleation rate at the growth front and the lateral spreading rate of the nucleus at the growth face [67]. Maillard and Prud'homme [68, 69] reported that main-chain configurational information of PLA is expressed in lamellar curvature and twisting. Edge-on crystals in PLLA thin film (15 nm in thickness) formed S-shape lamellae, whereas those in PDLA thin film showed Z-shaped morphologies. Since neither pure PLLA nor PDLA forms banded spherulites composed of twisting lamellar crystals, PEO was added to the system to induce the lamellar twisting. The twisting of PLLA lamellae was right-handed, while that of PDLA lamellae was left-handed. In the case of enantiomeric blend thin film (1 : 1) [70], stereocomplexed PLA crystals were formed, exhibiting a triangular shape. The crystal contains alternating packing with threefold symmetry by left- and right-handed $3_1$ helices for PLLA and PDLA chains, respectively [71]. Thus, chirality and stereocomplex formation are also important factors affecting the crystalline morphologies of PLAs.

To achieve a glassy amorphous PLA thin film, the melted thin film should be immediately quenched below $T_g$ (typically <60°C). This procedure provides a quite smooth surface that enables the observation of enzyme molecules of nanometer size (see the next section).

### 22.3.3 Enzymatic Adsorption and Degradation Rate of Thin Films

Partially crystallized PLLA thin film was subjected to enzymatic degradation by proteinase K. In situ AFM observation of PLLA thin film was performed during enzymatic degradation (Figure 22.12) [72]. The amorphous region surrounding the hexagonal crystal was first eroded. Subsequent long-term degradation revealed that the amorphous region under the hexagonal crystal was gradually degraded [73]. This result suggests that the degradability is different even in the amorphous region and is related to the free and restricted amorphous regions as proposed by Tsuji and Miyauchi [13]. The erosion rate of the restricted amorphous region between the hexagonal crystal and the substrate was slower than that of the free amorphous region around the crystal [73]. After enzymatic degradation for 120 min, all the amorphous regions were completely eroded, and only the hexagonal crystals of 25–30 nm in thickness were observed (Figure 22.13), suggesting that proteinase K hydrolyzed the amorphous regions of PLLA much faster than the crystalline regions.

To study the enzymatic degradation of the free amorphous region, completely amorphous PLLA thin film was prepared (see Section 22.3.2), and the erosion rate was directly monitored by using QCM in the nanogram per square centimeter regime [74]. The enzymatic erosion rate was dependent on the concentration of proteinase K, and the thin amorphous film of 100 nm thickness was completely hydrolyzed in 20 min when the concentration of the enzyme was >100 μg/mL. During the course of enzymatic degradation, even if the enzyme solution was replaced with a buffer solution (i.e., no enzyme), there was no retardation of the hydrolysis rate. Actually, weight loss of the thin film continued at the same degradation rate as in the initial condition. Direct AFM observation (Figure 22.14) revealed that the adsorbed proteinase K molecules could not be removed by washing with water, except for 40% ethanol aqueous solution. These results indicate that adsorption of proteinase K onto the PLLA surface is irreversible. The number of adsorbed enzymes on PLLA increased with increasing enzyme concentration. Figure 22.15 shows the relationship between the enzyme concentration and the erosion rate measured by QCM, as well as the number of adsorbed proteinase K measured from AFM images. The concentration dependence of the number of enzymes is in good agreement with that of the erosion rate. From this result, it can be concluded that the erosion rate is determined by the amount of adsorbed proteinase K molecules. Wei and coworkers [75] also reported proteinase K adsorption onto PLA surface, which was revealed by SEM observation, contact angle, and surface tension measurements. In contrast to the adsorption ability onto PLLA surfaces, proteinase K cannot adsorb onto PDLA surfaces. Thus, proteinase K can irreversibly adsorb onto a PLLA surface and catalyze the hydrolysis reaction despite the lack of substrate-binding domains in PHB depolymerases [76].

Since the $T_g$ of PLLA in bulk determined by differential scanning calorimetry (DSC) is generally about 45–60°C, the mobility of the PLLA main chain is negligible at room temperature. Therefore, the hexagonal crystals and the surrounding amorphous regions are hard enough to be observed by AFM at room temperature. Nevertheless, proteinase K can easily hydrolyze such "hard" glassy amorphous PLLA chains. Therefore, AFM in the frictional force mode was used to examine the surface molecular mobility on PDLLA and PLLA thin films under vacuum and aqueous conditions [72]. A lower $T_g$ and a lower cold crystallization temperature of PDLLA and PLLA thin films were detected under aqueous conditions than those in vacuum. The depression in $T_g$ was explained in terms of a plasticizer effect by water molecules that enhanced the molecular mobility at the surface of both thin films. The enhanced molecular mobility of PLLA chains may help the enzymatic attack by proteinase K.

### 22.3.4 Enzymatic Degradation of LB Film

LB films are prepared from the polymer monolayers by compressing until adequate surface pressure is achieved. PLA monolayers are formed on a water surface as a subphase by spreading a dilute PLA solution. When the hydrolyzing enzyme is added to the water subphase, the enzymatic degradation takes place at the interface of the LB film and the aqueous subphase. Therefore, the enzymatic degradation rate can be evaluated on the basis of

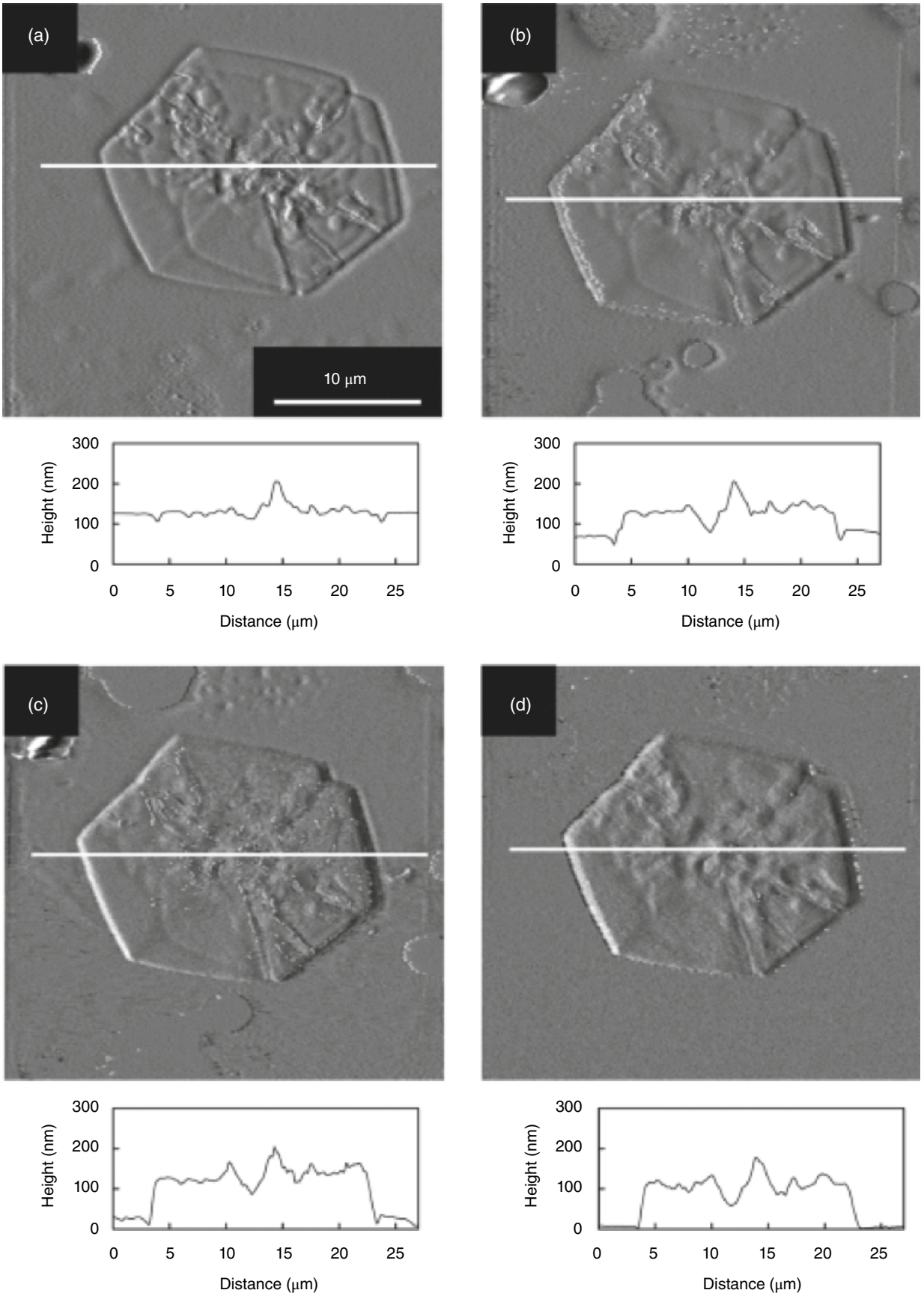


**FIGURE 22.12** AFM amplitude images of PLLA thin film (120 nm in thickness) crystallized at 160°C for 20 min before (a) and during enzymatic degradation by proteinase K (b–d). The first frame (a) was obtained in buffer solution without enzyme. The following frames were recorded in enzyme solution containing 200 μg/mL of proteinase K during enzymatic degradation for 5 (b), 10 (c), and 15 min (d), respectively. The graph under each AFM image is cross-sectional data at the white line region. Before enzymatic degradation, the height of hexagonal crystal was almost identical to that of surrounding amorphous region (a). On starting the enzymatic degradation by proteinase K, height difference between the hexagonal crystal and the surrounding amorphous region increased to 50–60 (b), 90–100 (c), and 110–120 nm (d), respectively. *Source*: Reprinted with permission from Ref. 72. Copyright 2004, American Chemical Society.

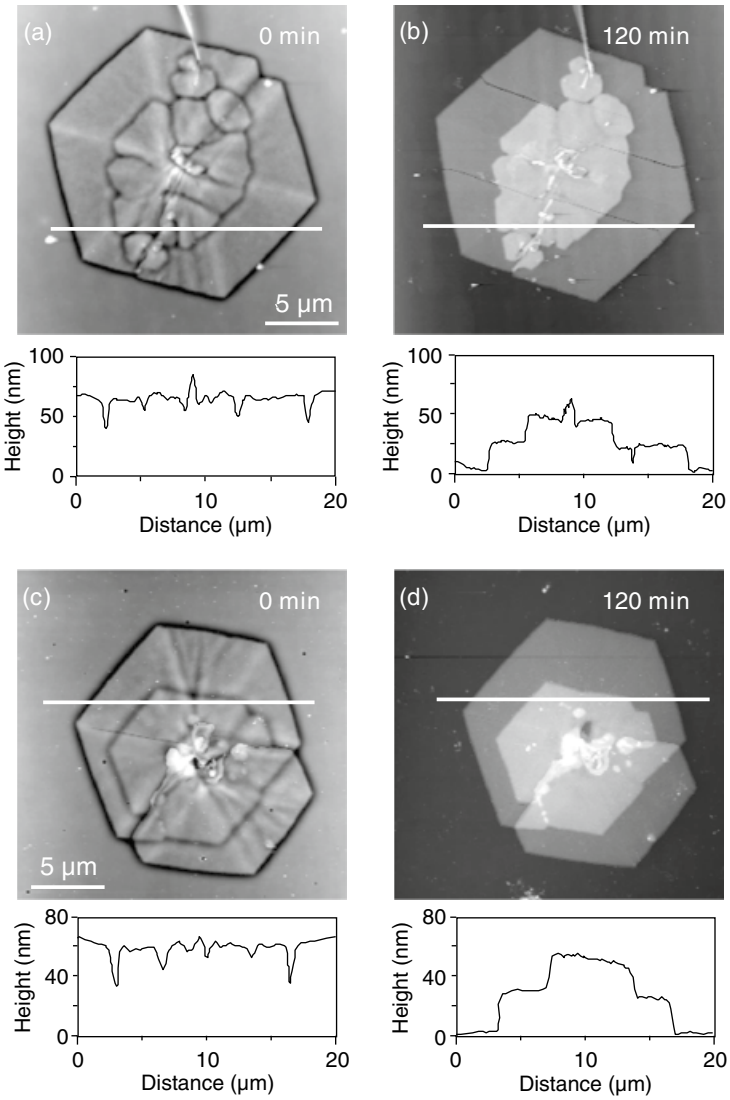


**FIGURE 22.13** AFM height images of PLLA thin films (crystallized at 160°C for 20 min) before (a and c) and after enzymatic degradation by proteinase K (200 μg/mL) for 120 min (b and d). The graph under the height images is line profile data at the white line region in each height image. *Source*: Reprinted with permission from Ref. 73. Copyright 2002, American Chemical Society.

time-dependent measurements of reduction in the area occupied by the LB film maintained at a constant surface pressure [77]. The degradation of a PLLA monolayer was much faster than that of PDLA and PDLA/PLLA monolayers. This means that both PDLA components and stereocomplexed PLA show a strong retardation effect against enzymatic degradation by proteinase K.

For the AFM observation, compressed LB films were deposited on the substrate at a constant surface pressure. The effects of molecular weight, number of branches, and chirality on the enzymatic degradation rate were evaluated by in situ AFM in buffer solution containing proteinase K [27]. The degradation rate was estimated from the time-dependent changes in the occupied surface area of LB film, which was converted to weight loss by taking the density of the PLLA amorphous phase (1.248 g/cm$^3$) into account. Figure 22.16 shows the time-dependent AFM images of PLLA monolayer film during enzymatic degradation. The area of LB film covering the substrate gradually decreased with time, whereas the thickness of the monolayer remained unchanged at 3 nm. Against the six different PLAs with linear, branched, and chirality character, in situ AFM observation was performed and

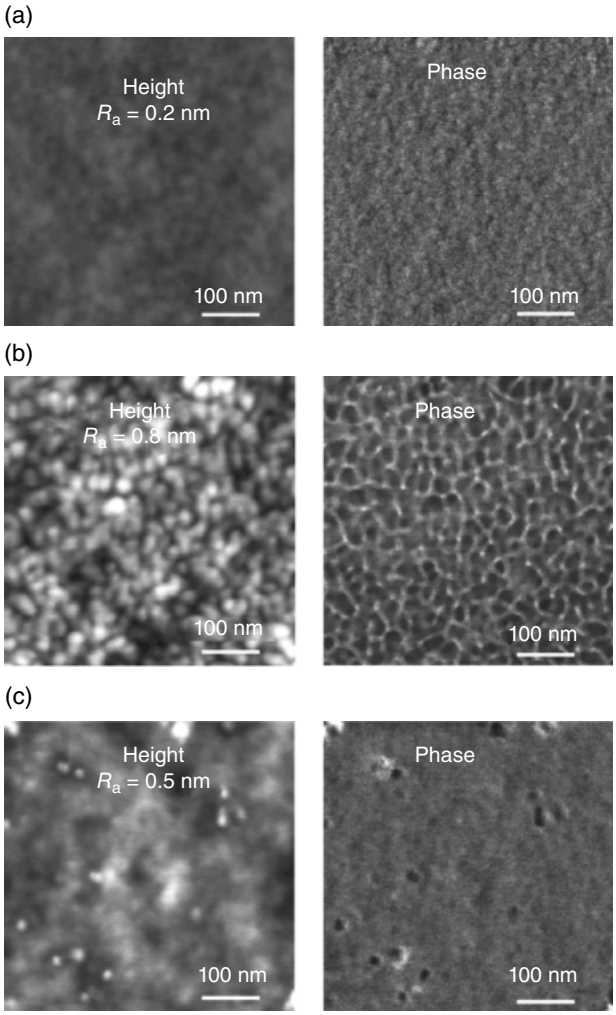


**FIGURE 22.14** AFM height and phase images of (a) PLLA amorphous thin film before enzymatic degradation, (b) proteinase K adsorbed on PLLA surface after enzymatic degradation for 7 min, and (c) PLLA surface washed with 40% aqueous ethanol after enzymatic degradation for 7 min. *Source*: Reprinted with permission from Ref. 74. Copyright 2005, American Chemical Society.

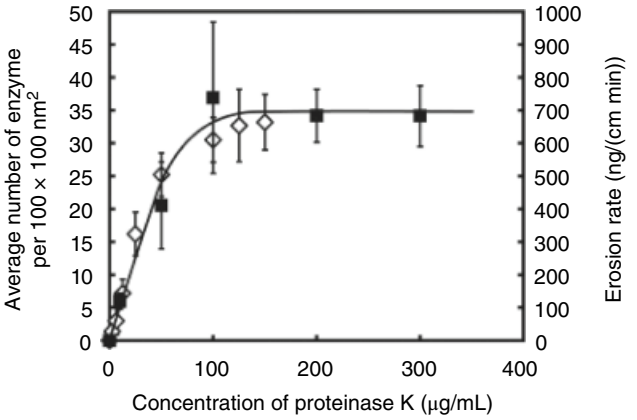


**FIGURE 22.15** Dependence of enzymatic erosion rate (■) and adsorbed enzymes (◊) on the concentration of proteinase K. Erosion rate was measured by QCM, whereas the adsorbed enzymes per $100 \times 100\,nm^2$ PLLA surface after enzymatic treatment for 7 min were measured from AFM images. *Source*: Reprinted with permission from Ref. 74. Copyright 2005, American Chemical Society.

the enzymatic degradation rates were compared. In the linear PLLA case, the erosion rate increased with a decrease in the molecular weight, whereas the branched PLLA exhibited a dependence of the erosion rate on the average molecular weight of the PLLA segment in the branches rather than on the total molecular weight. As stated above, the D-components in the PDLLA hindered the enzymatic attack, resulting in a slower erosion rate as compared with PLLA.

### 22.3.5 Application of Selective Enzymatic Degradation

To highlight the crystalline features inside the polymeric material, etching treatments using acids, bases, and organic solvents have been carried out especially for TEM observation [58, 59, 78]. In these studies, the amorphous region is predominantly removed, but at the same time, the crystalline region is also thought to suffer damage to some extent. In contrast, selective enzymatic degradation of amorphous regions can be used as a mild etching method for PLLA material. Since proteinase K hydrolyzes the PLLA chains in the amorphous regions preferentially to those in the crystalline regions, "enzymatic etching" can be used to study the crystalline lamellae in thin films. The removal of the amorphous region around the crystalline region can be judged from the thickness of the residual crystal. The crystal thickness of PLLA and stereocopolymer thin films after enzymatic degradation measured by AFM was in good agreement with the lamellar thickness measured by small-angle X-ray scattering (SAXS), but not the long period [79]. The linear correlation indicates the complete erosion of the amorphous region, permitting the detailed investigation of "naked" crystalline lamellae in PLLA thin film.

Figure 22.17 shows the PLLA thin film before and after enzymatic degradation by proteinase K for 120 min [80]. Before degradation, lamellar crystals were surrounded by an amorphous region, and the depletion zone at the growth front of the lamellae was clearly visible. After enzymatic degradation, the amorphous region was selectively removed, and only the crystalline lamellae were retained. Flat-on crystals with 25 nm thickness existed perpendicular to the basal edge-on crystal without lamellar twisting and screw dislocation. On the basis of this observation, it was proposed that the change in lamellar orientation from edge-on to flat-on in

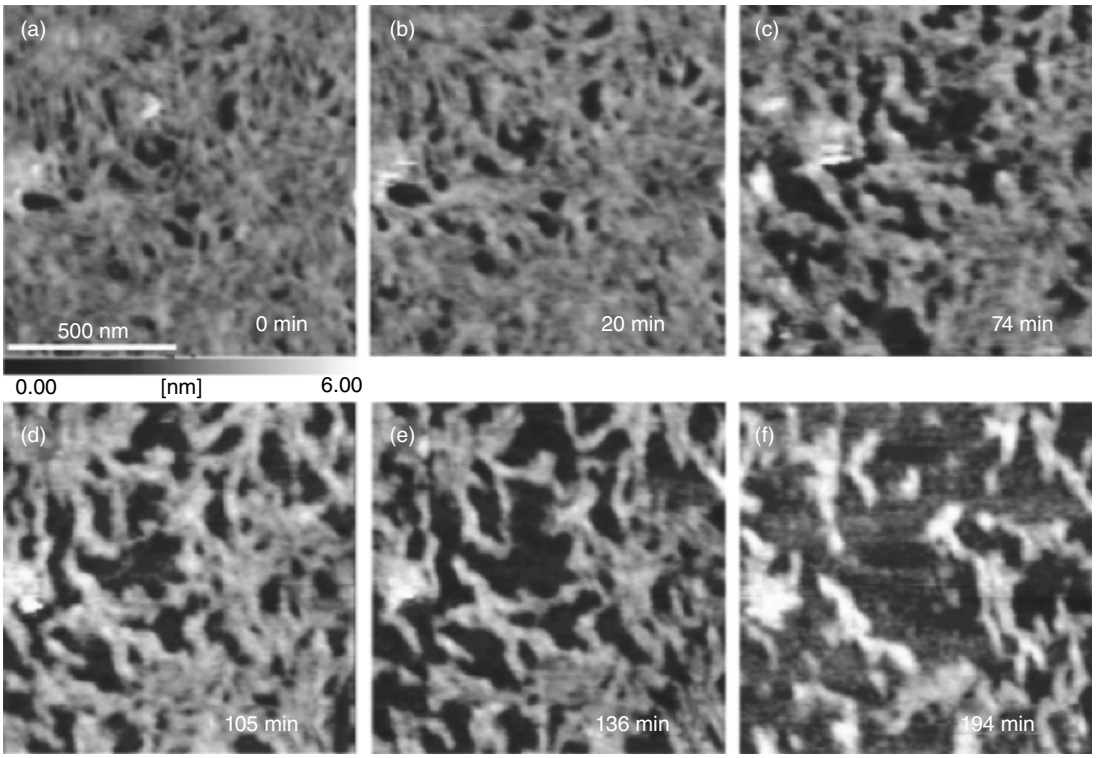


**FIGURE 22.16** Continuous AFM height images of PLLA monolayer ($M_n$ = 84,000 Da) during enzymatic degradation by proteinase K (10 μg/mL). Panel (a) represents the AFM image before degradation, and panels (b–f) are recorded during enzymatic degradation for 20 min (b), 74 min (c), 105 min (d), 136 min (e), and 194 min (f). *Source*: Reprinted with permission from Ref. 27. Copyright 2008, American Chemical Society.

PLLA thin film does not come from twisting, but from derivative growth. This estimation is one of the possible reasons for having no banded spherulites in PLLA films, which are caused by periodical lamellar twisting.

## 22.4 ENZYMATIC DEGRADATION OF LAMELLAR CRYSTALS

To elucidate the mechanism of enzymatic degradation in the crystal region, single crystals are considered a good model substrate. Enzymatic degradation using single crystals has been performed on polysaccharides, for example β(1–4) xylan single crystals with xylanases [81] and lamellar single crystals of nigeran with mycodextranase [82]. These techniques were applied to the enzymatic degradation of P(3HB) [83–85] and its copolymers [86], poly(4-hydroxybutyrate) (P(4HB)) [87], PCL [88], poly(ethylene succinate) (PES) [89], and poly(tetramethylene adipate) (PTMA)[90] single crystals that are biodegradable thermoplastics. In this section, we will describe the morphologies of PLLA crystals grown from dilute solution and the mechanism of enzymatic degradation of lamellar crystals by proteinase K from the mold *T. album* [91, 92]. We will also add some information on the morphologies of PLLA/PDLA stereocomplex single crystals [70, 93].

### 22.4.1 Enzymatic Degradation of PLLA Single Crystals

PLLA solution-grown single crystals were first reported by De Santis and Kovacs [94]. PLLA single crystals have mainly two kinds of morphologies, hexagonal and lozenge shaped with screw dislocation. Figure 22.18 shows electron micrographs of both morphologies with typical electron diffraction diagrams [91]. On the basis of the orthogonal unit cell in PLLA crystals, the lozenge-shaped crystals are considered to occur with {1 1 0} as growth planes, such as flat lamellar polyethylene crystals. Compared to the smooth faces well defined by {1 1 0} of a lozenge-shaped crystal, the growth faces of a hexagonal-shaped crystal, except the {1 1 0} planes, are slightly rough. The thickness of lozenge-shaped crystals at the monolayer parts measured by AFM was 9–10 nm, while that of hexagonal-shaped crystals were 11–12 nm.

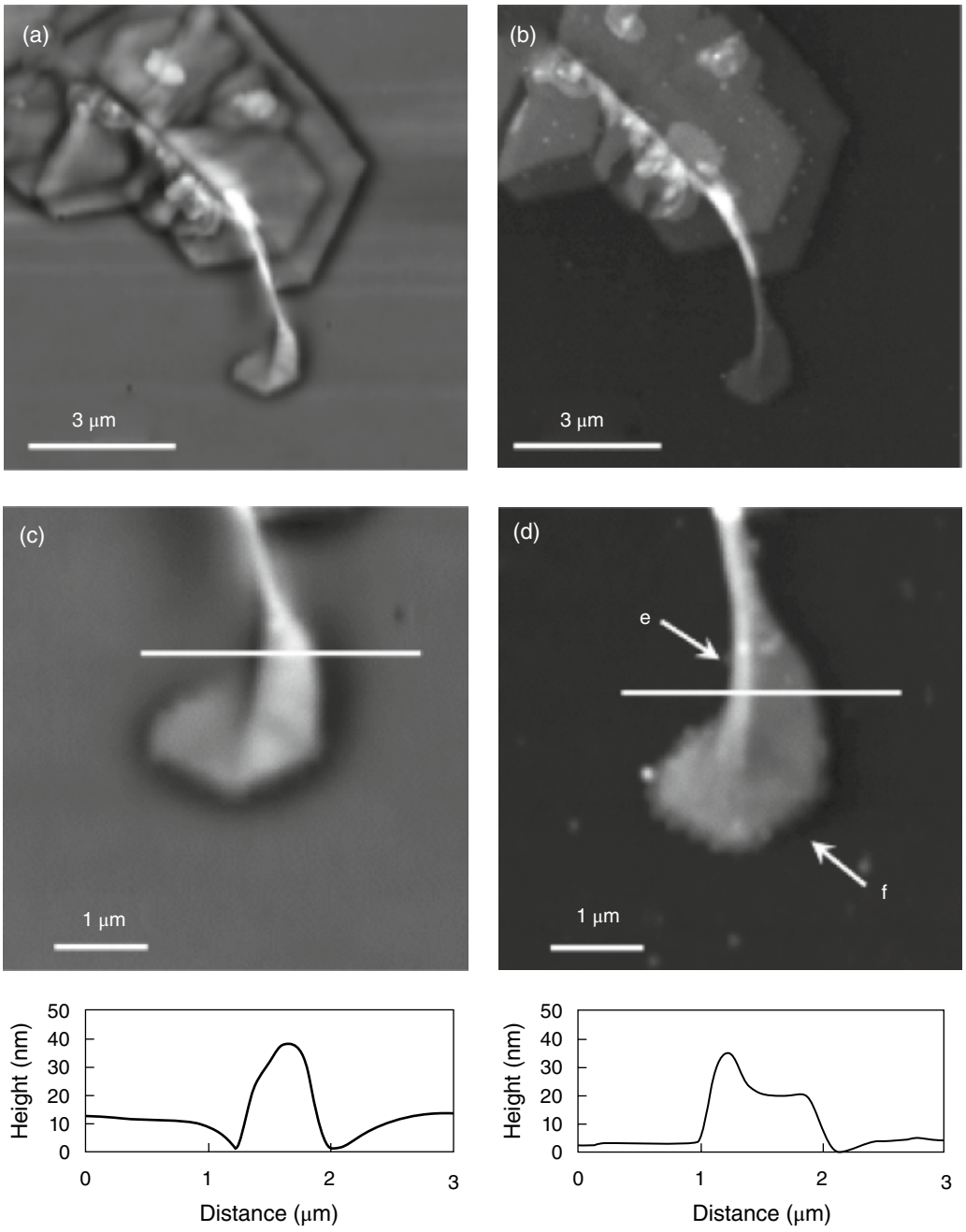


**FIGURE 22.17** AFM height images of PLLA thin films before (a and c) and after enzymatic degradation by proteinase K for 2 h (b and d). Frames (c) and (d) are enlarged images of (a) and (b), respectively. Arrow e denotes the edge-on crystal, whereas arrow f indicates the flat-on crystal. *Source*: Reprinted with permission from Ref. [80]. Copyright 2003, Wiley-VCH Verlag GmbH.

The time-dependent absorbance changes at 210 nm caused by the liberation of lactic acid into the reaction solution from PLLA single crystals in 50 mM Tris–HCl buffer (pH 8.5), with and without 200 μg/mL proteinase K at 37°C, are shown in Figure 22.19. The slight increase of curve B (without enzyme) indicates the hydrolysis of the amorphous region on the crystal surface. However, the rate of this hydrolysis is negligibly small in comparison to that of enzymatic biodegradation by proteinase K (curve A). The electron micrographs of PLLA single crystals after 70 h hydrolysis without enzyme and 50 h enzymatic degradation are shown in Figure 22.20. The morphology and size of the crystals remained unchanged in the absence of proteinase K (Figure 22.20a). On the other hand, PLLA single crystals

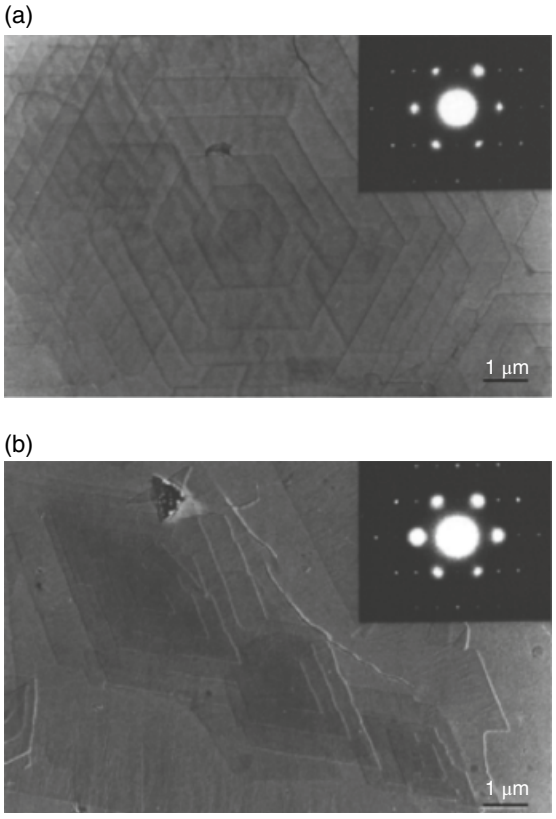


**FIGURE 22.18** Electron micrographs after shadowing with a Pt–Pd alloy of PLLA lamellar crystals grown from a dilute solution of *p*-xylene, and typical electron diffraction diagrams: (a) hexagonal-shaped and (b) lozenge-shaped single crystals. *Source*: Reprinted with permission from Ref. 91. Copyright 1998, American Chemical Society.

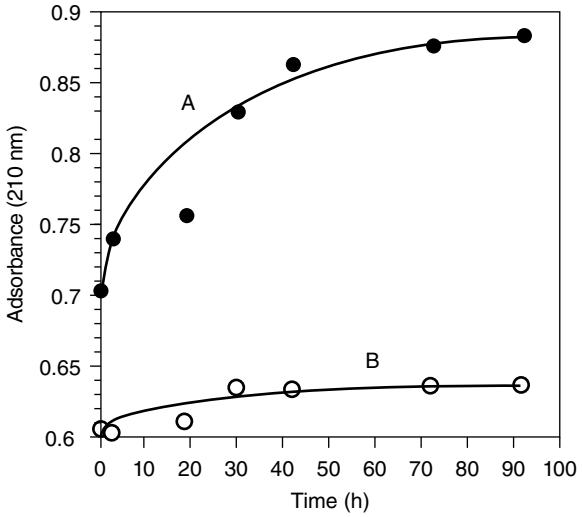


**FIGURE 22.19** Time-dependent changes in the absorbance at 210 nm of the reaction solutions of PLLA single crystals with (curve A: ∘) and without (curve B: •) 200 mg/mL proteinase K at 37°C. *Source*: Reprinted with permission from Ref. [91]. Copyright 1998, American Chemical Society.

degraded from the crystal edges to form a round shape with concomitant reduction in crystal size.

The molecular weights of PLLA single crystals remained unchanged before and after enzymatic degradation as shown in Figure 22.21, indicating that partial enzymatic degradation at the chain-folding surfaces does not take place. In addition, AFM measurements of PLLA single crystals showed that the thickness of monolayer parts also remained unchanged before and after enzymatic degradation, further showing no evidence of enzymatic degradation on the crystal surface. Similar observations have been reported in the enzymatic degradation of P(3HB) [83–85], P(4HB) [87], and PES[89] by some extracellular PHB depolymerases and PCL [88] and PTMA [90] by lipase. Based on these results, the active site of proteinase K also cannot degrade the ester linkage of the chain-folding region due to the steric hindrance of side chains, similar to PHB depolymerases and lipases. Accordingly, proteinase K preferentially attacked the disordered chain-packing region of the crystal edges.

### 22.4.2 Thermal Treatment and Enzymatic Degradation of PLLA Single Crystals

The thermal behavior of PLLA single crystals was first investigated by Miyata and Masuko [95]. They reported that the crystal surface became rough and the lamellar thickness increased by annealing. Because most microscopic studies reported so far were performed ex situ by TEM and AFM, they have not been able to follow the behavior without the influence of sample cooling from the annealing temperature to room temperature on the crystal appearance. Fujita and Doi [96] investigated in situ annealing and melting of PLLA single crystals by temperature-controlled AFM. They reported that thickening of the crystal edges was occasionally observed, indicating that the crystal edges were less perfect than the central, well-ordered region. On the basis of thermal behavior and enzymatic degradation described in the previous section, it can be concluded that the enzymatic degradation and thermal behavior of PLLA single crystals are preferentially initiated at defective sites or phases with higher chain mobility such as crystal edges.

Lee and Iwata reported enzymatic degradation behavior of PLLA single crystals thermally treated below the melting temperature [92]. The lamellar thickness of PLLA lozenge-shaped single crystals increased slightly after thermal treatment without altering their original shapes, which means that the density of the lamellar crystal decreased. This result indicates that less-ordered and loosely chain-folding regions were increased on the crystal surface by thermal treatment. Enzymatic degradation of thermally treated PLLA single crystals progressed from loosely chain-packing regions at both crystal surface and edges, suggesting that

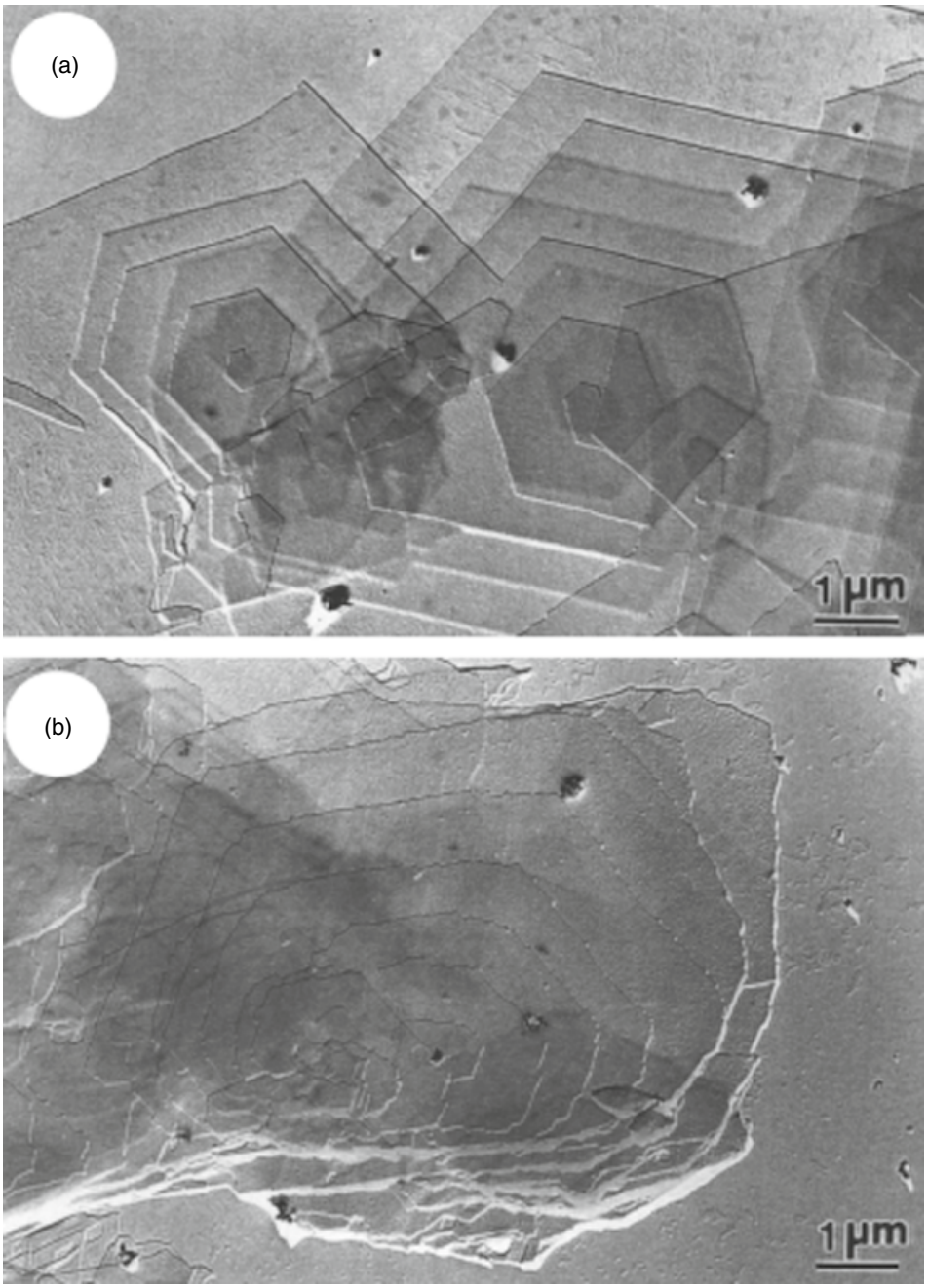


**FIGURE 22.20** (a) Electron micrograph of PLLA single crystals suspended in 50 mM Tris–HCl buffer (pH 8.5) for 70 h at 37°C. (b) Electron micrograph of PLLA single crystals after 50 h of enzymatic degradation by proteinase K at 37°C. *Source*: Reprinted with permission from Ref. [91]. Copyright 1998, American Chemical Society.

enzymatic attack can occur at loosely chain-folding regions on the crystal surface without decreasing the lamellar thickness, as well as those at the crystal edges.

### 22.4.3 Single Crystals of PLA Stereocomplex

PLLA/PDLA stereocomplex has attracted considerable interest because its melting temperature is about 230°C, which is 50°C higher than that of PLLA [97]. Single crystals of stereocomplex were reported by Brizzolara et al. and Cartier et al. [70, 93]. Solution-grown single crystals of PLLA/PDLA stereocomplex, which were prepared from a dilute polymer solution in *p*-xylene, were nearly hexagonal. However, single crystals of stereocomplex formed in thin film at 200°C have a unique crystal morphology with a highly unusual triangular shape as shown in Figure 22.22. Crystal

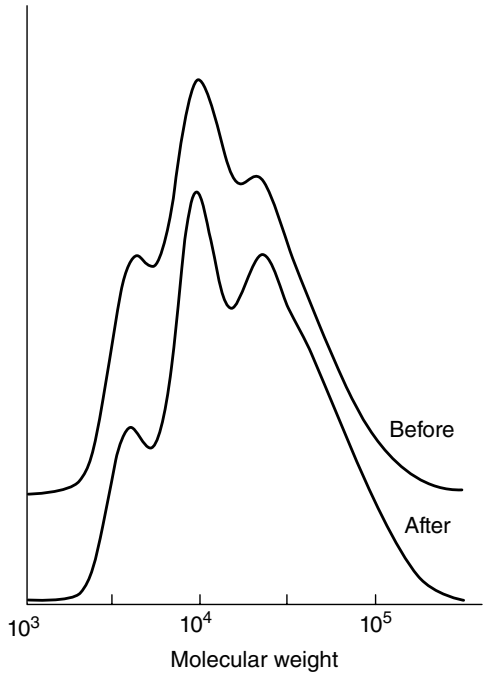


**FIGURE 22.21** Gel permeation chromatograms of PLLA single crystals before and after partial enzymatic degradation by proteinase K at 37°C for 50 h. *Source*: Reprinted with permission from Ref. 91. Copyright 1998, American Chemical Society.

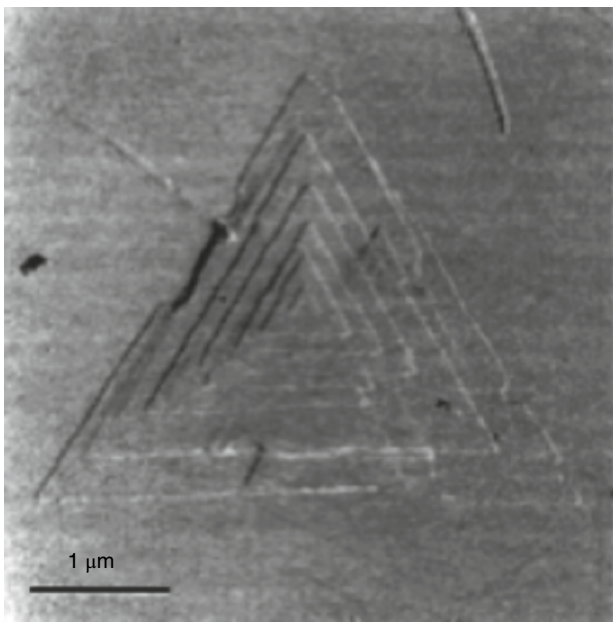


**FIGURE 22.22** Electron micrograph of PLLA/PDLA stereocomplex formed by thin film grown at 200°C. *Source*: Reprinted with permission from Ref. 70. Copyright 1997, American Chemical Society.

structure analysis and enzymatic degradation of PLLA/PDLA stereocomplex single crystal seem to be attractive from the viewpoint of both industrial and scientific aspects in the future.

## 22.5 RECENT ADVANCES IN CHARACTERIZATION OF ENZYMES THAT DEGRADE PLAs INCLUDING PDLA AND RELATED COPOLYMERS

As mentioned above, the stereochemistry of the lactate (LA) unit is a critical factor in enzymatic degradation of PLAs. PLLA is known to be degraded by proteinases, which hydrolyze the proteins composed of L-amino acid residues, and are highly specific to PLLA and have no activity toward PDLA (Figure 22.23). In contrast, little was known about PDLA-degrading enzymes when the first edition of this book was published. Over the last decade, the identification and understanding of PDLA-degrading enzymes, and degrading enzymes of D-LA-containing polymers, have improved. This section summarizes the latest knowledge of PLA-degrading enzymes based on their enantiospecificity. It should be noted that the standard grade chemically synthesized PLAs contain several percent of enantiomer. For instance, PLA 2003D provided by NatureWorks LLC is mainly composed of L-LA and contains 3.5 wt% D-isomer [98]. The $T_m$ of the standard PLA is 150–160°C, while that of PLAs with higher optical purity (>99%) is 170–180°C [99]. In this section, both the standard and high optical purity PLAs, mainly composed of

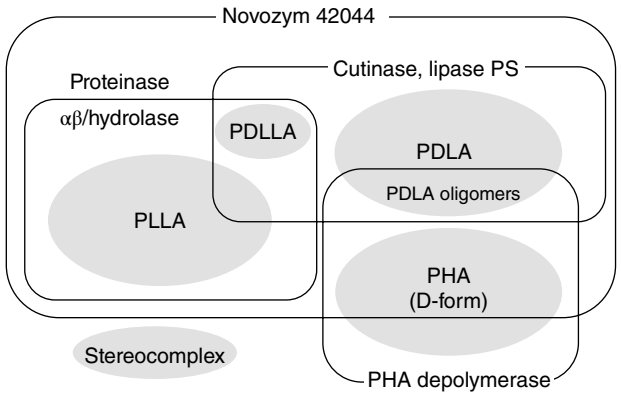


**FIGURE 22.23** Substrate specificity of PLA- and related polyester-degrading enzymes. PDLLA (poly-DL-lactide) is noncrystalline polymer that can be easily degraded by broad range of esterases. Proteinases and αβ/hydrolases are specific to PLLA, while cutinases and several lipases prefer PDLA than PLLA. Lipase Novozym 42044 possesses very broad substrate specificity and degrades also PHB (emulsion). PHA depolymerases have been thought to be highly specific to PHA. Recent studies revealed their degrading activity toward PDLA oligomers.

L- and D-LA, are referred as PLLA and PDLA, respectively. The copolymers with lower enantiopurity are referred as PDLLA.

### 22.5.1 αβ-Hydrolase

αβ-Hydrolase fold enzymes share a similar higher structure composed of α-helixes and β-sheets but possess diverse functions [100]. Several αβ-hydrolases exhibit PLA-degrading activity. The αβ-hydrolases, screened from uncultured microbes, degrade PLLA and/or PDLLA but not PDLA [101]. The αβ-hydrolase ABO2449 from *Alcanivorax borkumensis* and RPA1511 from *Rhodopseudomonas palustris* degrades PDLLA but neither PLLA nor PDLA [102]. From these results, the PLA-degrading αβ-hydrolase unlikely degrades PDLA.

### 22.5.2 Lipases and Cutinase-Like Enzymes

Lipases have various substrate specificities. Lipase PS is presumably specific to PDLA, although the activity of lipase PS is much lower than other PLA-degrading lipases (Figure 22.24) [103]. In contrast, Novozym 42044, which is a lipase from an unknown origin, degrades both PLLA and PDLA [103, 104]. In addition, Novozym 42044 exhibits poly(D-3-hydroxybutyrate) (PHB) emulsion-clarifying activity [104], while other lipases only partly degrade PHB [105, 106]. Novozym 42044 seems to possess exceptionally broad substrate specificity toward aliphatic polyesters.

Cutinase-like enzyme (CLE) has broad substrate specificity toward a variety of polyesters including PDLA. CLE from the yeast *Cryptococcus* sp. Strain S-2 degrades both PLLA and PDLA but preferentially hydrolyzes PDLA at 30°C [103, 107]. The crystallinity of PDLA film incubated with CLE increased once in one to two days, but later decreased. The CLE degrades amorphous region of PDLA faster but also degrades its crystalline region [103]. The enzyme slightly degrades PLLA/PDLA blends, but the amorphous region is likely degraded, and there is no evidence supporting the enzymatic degradation of stereocomplex. A cutinase-type esterase Est119 from *Thermobifida* alba AHK119 formed a clear halo on emulsified plates of Ecoflex, PBSA [poly(butylene succinate-*co*-adipate)], PBS, and PCL [108]. The enzyme formed the halo on PDLA plate although it was less transparent than those of Ecoflex, PBSA, PBS, and PCL. The enzyme formed a halo on PLLA plate but very slowly. No observable halo was formed on PHB plate [109]. These studies demonstrate that CLEs are specific to PDLA compared to PLLA and do not degrade PHB, although PHB is composed of D-3HB units. The measurement of total organic carbon (TOC) from PLLA and PDLA films by CLE from *Cryptococcus flavus* showed a consistent result [110]. A CLE from *Ideonella sakaiensis*

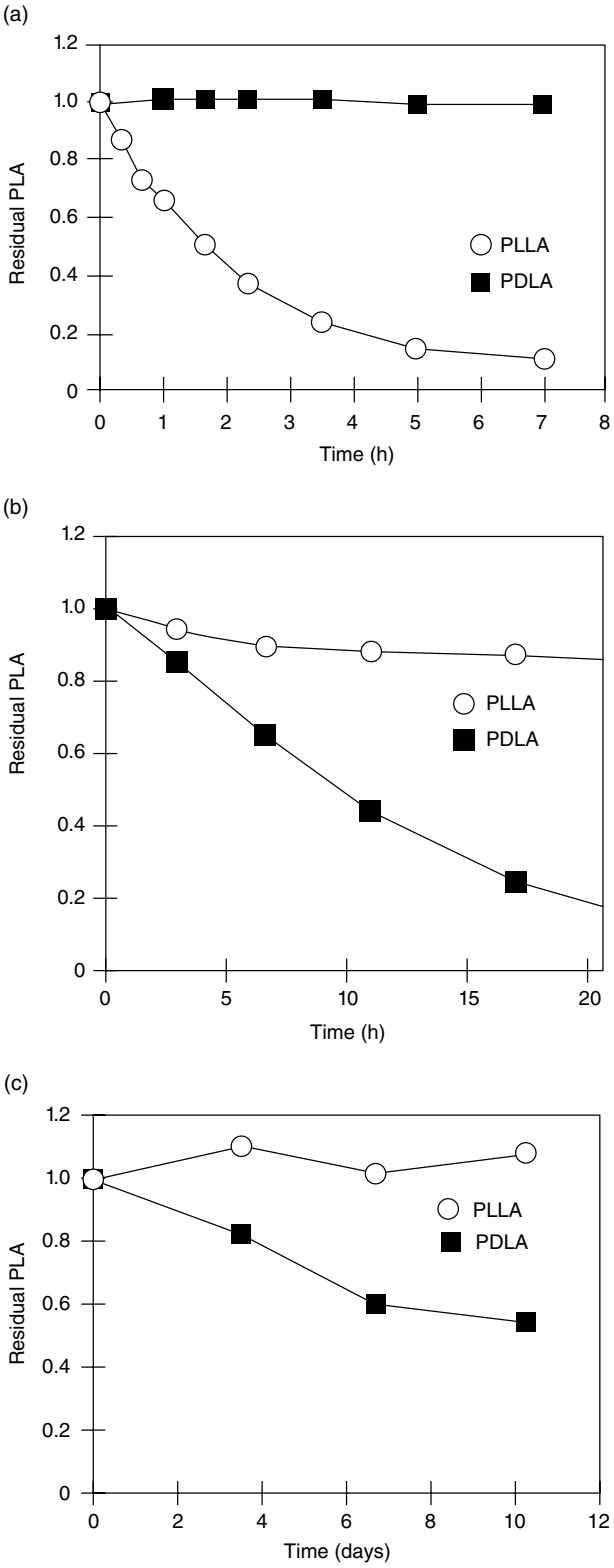


**FIGURE 22.24.** Enzymatic degradation of PLLA and PDLA emulsion. (a) Proteinase K; (b) CLE; (c) lipase PS. Degradation was measured by the decrease of absorbance at 600 nm. *Source*: Reprinted from Ref. 103. Copyright 2011, with permission from Elsevier.

hydrolyzes poly(ethylene terephthalate) (PET) and is known as PETase [111]. Kitadokoro et al. indicated the structural similarity between PDLA-degrading cutinase and PETase [112].

The binding of CLE from *Pseudozyma antarctica* JCM10317 (PaE) to the polyester surface was analyzed using SPR and AFM [113]. PLLA was tested in this study because the PDLA-degrading activity of CLE had not been generally recognized when the study was conducted. As a result, the experiment revealed that the PaE preferably binds to PCL; the binding of CLE to PLLA is very weak. Further studies on the binding of CLE to PDLA are necessary.

The mechanism of enantiomer recognition of proteinases and lipases has been investigated in detail. These enzymes are members of serine hydrolases and have a catalytic triad consisting of serine, histidine, and aspartic acid. These catalytic residues in the enzymes are in mirror-image positions, which probably causes the different affinity toward PLLA and PDLA [103]. The relatively low enantiospecificity of lipases and cutinases as compared with the strict enantiospecificity of proteinases can be explained by the fact that lipids and cutin, which are the natural substrates of lipases and cutinases, have no enantiomers. Proteinases and CLEs degrade PLLA and PDLA, respectively, partly into cyclic oligomers [103].

### 22.5.3 Polyhydroxyalkanoate Depolymerases

Polyhydroxyalkanoate (PHA) depolymerases (PhaZs) [114] are new members of D-LA-containing polymer-degrading enzymes. It has been well known that PhaZs do not degrade PLAs irrespective of the enantiomer of LA. However, PhaZs do degrade PDLA oligomers [115, 116]. The range of degree of polymerization (DP) that can be degraded varies depending on PhaZs. The hidden activity of PhaZs toward PDLA oligomers was found through the studies on biodegradation of poly(D-LA-*co*-D-3HB) random copolymer. The screening of P(67 mol% LA-*co*-3HB)-degrading microbes in soil retrieved many positive samples, and all of them also degrade P(3HB), indicating that P(67 mol% LA-*co*-3HB)-degrading capacity in the soil microbes relates to PHA biodegradation. The isolated P(67 mol% LA-*co*-3HB)-degrading bacteria mainly belong to *Variovorax* or *Acidovorax* species, which possess the *phaZ* genes, the gene products with a *C*atalytic *D*omain type *2* (CD2) [117]. This suggests the role of CD2 in the degradation of D-LA-containing PHA. The PhaZs degrade PDLA oligomers with DP ranging from 10 to 30, but not those ranging from 20 to 40. The DP-dependent degradation of PDLA by PhaZs is related to the conformation of the polymer chain. Molecular dynamics simulation demonstrates that PDLA oligomers with DP of 30 have aggregated forms, while shorter oligomers have more extended forms. The aggregated forms of PDLA oligomer may not be easily loosened by PhaZs [117]. The limitation is dependent on the type of enzyme because certain cutinases can degrade high-molecular-weight PDLA at ambient temperature.

D-LA oligomers are useful not only as a component to be assembled into high-molecular-weight polymers such as polyurethane [118] but also for preparing polymer blends. D-LA oligomers with DP of 30–40 were reported to be effective in forming PLA stereocomplex when they are combined with high-molecular-weight PLLA [119]. However, it should be noted that, to the best of our knowledge, the reported PLLA-, PDLA-, and PDLLA-degrading enzymes do not degrade stereocomplex, although stereocomplex is hydrolytically degradable at a slower rate than PLLA [120–121]. Further studies will be needed on the enzymatic degradability of PLA stereocomplex.

Lee et al. reported that the whole-cell culture of recombinant *Escherihia coli* expressing PHB depolymerase (PhaZ) from *Caldimonas manganoxidans* degraded PLA (presumably standard grade PLLA) at 50°C in 30 days (nearly 100% weight loss) [122]. This result may suggest that PhaZ can degrade PLLA. However, further verification is needed because of the lack of negative control conditions (*E. coli* without PhaZ) and biochemical analysis of the PhaZ.

### 22.5.4 Enhancement of Biodegradability of PLAs

Enzymatic degradation of PLAs has been of interest from the standpoint of the development of biodegradable materials. In order for the materials to be biodegraded by microbes, there are three requirements: (i) the polymers attract the microbes and promote the secretion of degrading enzymes; (ii) the polymer chain is cleaved by the action of enzymes; and (iii) the degradation products are mineralized by microbes. The biodegradation of PLAs is slow in natural environments partly because the enzymes contributing to PLA degradation are unlikely induced by PLAs alone. Therefore, the addition of natural inducers such as proteins, peptides, and amino acids (for PLLA degradation) is needed to promote the secretion of the PLA-degrading enzymes [123]. In fact, biostimulation and bio-augmentation were shown to be effective to enhance the mineralization of PLA in soil [124]. PLA- and other biopolymers-degrading enzymes might be used to accelerate the degradation. These enzymes have been developed for chemical recycling of biopolymers [125]. Another approach to induce the enzymatic degradation of PLAs is by adding the degrading enzyme to the polymer material. PLLA degradation was promoted by embedding immobilized proteinase K [125, 126]. In this approach, thermal stability of the degrading enzyme is a critical factor. The immobilization of enzymes is effective to improve their stability.

The finding of PDLA oligomer degradation by PhaZs expands the potential use of PDLA-related polymers as biodegradable materials because PhaZs are known as ubiquitous enzymes in the environments. Furthermore, the secretion of PhaZs by microbes is induced by the presence of PHA. Thus, D-LA-containing PHA is feasible to meet the aforementioned requirements.

### 22.5.5 Control of Enzymatic Degradation of PLAs

The control of enzymatic degradation of polymeric compounds is a major goal in the development of degradable materials. A strategy to accelerate the enzymatic degradation rate of PLLA by proteinases is blending it with other polymers, such as PBS [127], PBSA [128], and PEG [129]. Such accelerating effect of blends is partly due to the increase in the hydrophilicity [130], as a similar effect was also observed in chitosan grafting with PLA [131]. In addition, blending affects the crystallinity and crystallization of the materials that influences their degradation rate as seen in the blend with PHB [132, 133]. The composite with modified fulvic acid rather decelerated the degradation [134]. PLA composite is also used to control the degradation rate. For instances, PLLA/cellulose composite increased the enzymatic degradation rate by proteinase K [135]. PLA/layered silicate nanocomposites also exhibited enhanced enzymatic degradation [136]. To introduce a switching function of the degradation, the enzymatic degradation of PLLA was controlled by a photo trigger using coating with an azo compound. The PLLA degradation by proteinase was triggered by UV irradiation [137].

As mentioned in this chapter, the specificity of degrading enzymes including enantiospecificity is a critical factor in PLA degradation. The specificity of degrading enzymes toward enzymatically degradable polyesters can be utilized to create porous materials. PLLA and PBS are specifically degraded by proteinase K and cutinase, respectively. Taking advantage of this property, the blend of PLLA and PBS were degraded by these enzymes to form a porous material. This approach improved wettability and hydrophilicity of PLA [138].

Several studies created blends of PLA and nonbiodegradable polymers and investigated their enzymatic degradability. It should be noted that the evaluation of degradability based on weight loss does not indicate the enzymatic degradability (or biodegradability) of the materials. Degradation and eventually mineralization of entire components should be measured to determine the degradability of the material.

## 22.6 FUTURE PERSPECTIVES

Enzymatic degradation of PLA is attracting more research interest partly due to the severe problem of plastic pollution in the environments. In the last decade, it is widely understood that biodegradability of polymeric materials depends on the environment. PLLA is recognized as a compostable plastic and well degraded in the composting conditions, but PLLA does not meet the criteria of ISO and ASTM standards of biodegradability in marine, fresh water, and soil [139]. However, recent studies indicate the potential of PLAs as biodegradable polymers with the combinations of other components. The regulation of biodegradability of PLAs and related polymer will be an important research target.

In the last decade, the understanding of enzymatic degradability of PDLA considerably improved. CLEs are major PDLA-degrading enzymes, and their relation to PETase has been reported. The mechanism of PLLA degradation by proteinases have been extensively studied. The mechanism of CLEs degrading PDLA will be understood at molecular level. For understanding enzymatic degradation mechanisms at the molecular level, in situ experiments during the enzymatic reaction are necessary using in situ AFM and synchrotron radiation.

The enzymatic degradability of the stereocomplex remained unclear. The nonenzymatic hydrolytic degradation rate of streocomplexed PLLA/PDLA blend film is slower than the nonblended film [121], indicating the persistency of the material. Further studies are needed to evaluate the enzymatic degradability and biodegradability of the stereocomplex in the natural environments.

## REFERENCES


1. D. Riggle, *BioCycle* **1998**, *39*, 64.
2. A. Steinbüchel, Y. Doi (Eds.), *Biopolymers*, Vols. 3a (*Polyesters I*) and 3b (*Polyesters II*), Wiley-VCH Verlag GmbH, Weinheim, 2002.
3. D. F. Williams, *Eng. Med.* **1981**, *10*, 5–7.
4. H. Fukuzaki, M. Yoshida, M. Asano, M. Kumakura, *Eur. Polym. J.* **1989**, *25*, 1019–1026.
5. K. Makino, M. Arakawa, T. Kondo, *Chem. Pharm. Bull.* **1985**, *33*, 1195–1201.
6. M. S. Reeve, S. P. McCarthy, M. J. Downey, R. A. Gross, *Macromolecules* **1994**, *27*, 825–831.
7. R. T. MacDonald, S. P. McCarthy, R. A. Gross, *Macromolecules* **1996**, *29*, 7356–7361.
8. H. Cai, V. Dave, R. A. Gross, S. P. McCarthy, *J. Polym. Sci. Part B.* **1996**, *34*, 2701–2708.
9. S. Li, S. P. McCarthy, *Macromolecules* **1999**, *32*, 4454–4456.
10. S. Li, M. Tenon, H. Garreau, C. Braud, M. Vert, *Polym. Degrad. Stab.* **2000**, *67*, 85–90.
11. S. Li, A. Girard, H. Garreau, M. Vert, *Polym. Degrad. Stab.* **2001**, *71*, 61–67.
12. H. Tsuji, S. Miyauchi, *Biomacromolecules* **2001**, *2*, 597–604.
13. H. Tsuji, S. Miyauchi, *Polymer* **2001**, *42*, 4463–4467.
14. H. Tsuji, S. Miyauchi, *Polym. Degrad. Stab.* **2001**, *71*, 415–424.
15. H. Tsuji, Y. Tezuka, *Macromol. Biosci.* **2005**, *5*, 135–148.
16. H. Tsuji, Y. Tezuka, K. Yamada, *J. Polym. Sci. Part B* **2005**, *43* 1064–1075.
17. H. Tsuji, M. Ogiwara, S. K. Saha, T. Sakai, *Biomacromolecules* **2006**, *7*, 380–387.
18. H. Pranamuda, A. Tsuchii, Y. Tokiwa, *Macromol. Biosci.* **2000**, *1*, 25–29.
19. A. Hoshino, Y. Isono, *Biodegradation* **2002**, *13*, 141–147.


20. W. Ebeling, N. M. Hennrich, M. Klockow, H. D. Orth, H. Lang, *Eur. J. Biochem.* **1974**, *47*, 91–97.
21. K. D. Jany, G. Lederer, B. Mayer, *FEBS Lett.* **1986**, *199*, 139–144.
22. C. Betzel, M. Bellemann, G. P. Pal, J. Bajorath, W. Saenger, K. S. Wilson, *Proteins Struct. Funct. Genet.* **1988**, *4*, 157–164.
23. C. Betzel, G. P. Pal, W. Saenger, *Eur. J. Biochem.* **1988**, *178*, 155–171.
24. C. Betzel, S. Gourinath, P. Kumar, P. Kaur, M. Perbandt, S. Eschenburg, T. P. Singh, *Biochemistry* **2001**, *40*, 3080–3088.
25. A. K. Saxena, T. P. Singh, K. Peters, S. Fittkau, C. Betzel, *Proteins Sci.* **1996** *5*, 2453–2458.
26. K. Numata, R. K. Srivastava, A. Finne-Wistrand, A. C. Albertsson, Y. Doi, H Abe, *Biomacromolecules* **2007**, *8*, 3115–3125.
27. K. Numata, A. Finne-Wistrand, A. C. Albertsson, Y. Doi, H. Abe, *Biomacromolecules* **2008**, *9*, 2180–2185.
28. K. Kurokawa, K. Yamashita, Y. Doi, H. Abe, *Polym. Degrad. Stab.* **2006**, *91*, 2333–2341.
29. Z. W. Ma, C. Y. Gao, J. Juan, J. Ji, Y. H. Gong, J. C. Shen, *J. Appl. Polym. Sci.* **2002**, *85*, 2163–2171.
30. H. Tsuji, M. Nishikawa, Y. Osanai, S. Matsumura, *Macromol. Rapid Commun.* **2007**, *28*, 1651–1656.
31. H. Tsuji, T. Ishida, *Macromol. Biosci.* **2003**, *3*, 51–58.
32. H. Tsuji, T. Ishida, N. Fukuda, *Polym. Int.* **2003**, *52*, 843–852.
33. H. Tsuji, T. Ishida, *J. Appl. Polym. Sci.* **2003**, *87*, 1628–1633.
34. S. Stassen, S. Archambeau, P. Dobois, R. Jerome, P. Teyssie, *J. Polym. Sci. Part A* **1994**, *32*, 2443–2455.
35. W. K. Lee, I. Losito, J. A. Gardella, W. L. Hicks, *Macromolecules* **2001**, *34*, 3000–3006.
36. T. Ouchi, T. Uchida, Y. Ohya, *Macromol. Biosci.* **2001**, *1*, 371–375.
37. T. Ouchi, T. Uchida, H. Arimura, Y. Ohya, *Biomacromolecules* **2003**, *4*, 477–480.
38. Y. Kobori, T. Iwata, Y. Doi, H. Abe, *Biomacromolecules* **2004**, *5*, 530–536.
39. K. Kurokawa, K. Yamashita, Y. Doi, H. Abe, *Biomacromolecules* **2008**, *9*, 1071–1078.
40. A. M. Gajria, V. Dav, R. A. Gross, S. P. McCarthy, *Polymer* **1996**, *37*, 437–444.
41. M. Sheth, R. A. Kumar, V. Davé, R. A. Gross, S. P. McCarthy, *J. Appl. Polym. Sci.* **1997**, *66*, 1495–1505.
42. L. J. Liu, S. M. Li, H. Garreau, M. Vert, *Biomacromolecules* **2000**, *1*, 350–359.
43. H. Tsuji, T. Ishizaka, *Macromol. Biosci.* **2001**, *1*, 59–65.
44. H. Tsuji, G. Horikawa, *Polym. Int.* **2007**, *56*, 258–266.
45. J. W. Park, Y. Doi, T. Iwata, *Biomacromolecules* **2004**, *5*, 1557–1566.
46. O. Mellbring, S. K. Øiseth, A. Krozer, J. Lausmaa, T. Hjertberg, *Macromolecules* **2001**, *34*, 7496–7503.
47. K. L. Beers, J. F. Douglas, E. J. Amis, A. Karim, *Langmuir* **2003**, *19*, 3935–3940.
48. C. Qiao, J. Zhao, S. Jiang, X. Ji, L. An, B. Jiang, *J. Polym. Sci. Part B* **2005**, *43*, 1303–1309.
49. J. A. Forrest, K. D. Veress, J. R. Dutcher, *Phys. Rev. E.* **1997**, *56*, 5705–5716.
50. M. M. Despotopoulou, C. W. Frank, R. D. Miller, J. F. Rabolt, *Macromolecules* **1995**, *28*, 6687–6688.
51. S. Sawamura, H. Miyaji, K. Izumi, S. J. Sutton, Y. Miyamoto, *J. Phys. Soc. Jpn.* **1998**, *67*, 3338–3341.
52. H. Schönherr, C. W. Frank, *Macromolecules* **2003**, *36*, 1188–1198.
53. Y. Ma, W. Hu, G. Reiter, *Macromolecules* **2006**, *39*, 5159–5164.
54. C. W. Frank, V. Rao, M. M. Despotopoulou, R. F. W. Pease, W. D. Hinsberg, R. D. Miller, J. F. Rabolt, *Science* **1996**, *273*, 912–915.
55. G. Decher, *Science* **1997**, *277*, 1232–1237.
56. T. Serizawa, Y. Arikawa, K. Hamada, H. Yamashita, T. Fujiwara, Y. Kimura, M. Akashi, *Macromolecules* **2003**, *36*, 1762–1765.
57. A. Ulman, *An Introduction to Ultrathin Organic Films: From Langmuir–Blodgett to Self-Assembly*, Academic Press, London, 1991, 101pp.
58. P. H. Geil, *Polymer Single Crystals*, Krieger Publishing Co., Huntington, NY, 1973.
59. P. J. Barham, Crystallization and morphology of semicrystalline polymers, in: R. W. Cahn, P. Haasen, E. J. Kramer, (Eds.), *Materials Science and Technology*, Vol. *12*, VCH, Weinheim, 1993, pp. 155–208.
60. S. N. Magonov, D. H. Reneker, *Annu. Rev. Mater. Sci.* **1997**, *27*, 175–222.
61. J. K. Hobbs, A. K. Winkel. T. J. McMaster, A. D. L. Humphris, A. A. Baker, S. Blakely, M. Aissaoui, M. J. Miles, *Macromol. Symp.* **2001**, *167*, 1–14.
62. Y. Kikkawa, T. Murase, H. Abe, T. Iwata, Y. Inoue, Y. Doi, *Macromol. Biosci.* **2002**, *2*, 189–194.
63. K. A. Marx, *Biomacromolecules* **2003**, *4*, 1099–1120.
64. K. Yamashita, T. Funato, Y. Suzuki, S. Teramachi, Y. Doi, *Macromol. Biosci.* **2003**, *3*, 694–702.
65. Y. Kikkawa, H. Abe, T. Iwata, Y. Inoue, Y. Doi, *Biomacromolecules* **2001**, *2*, 940–945.
66. H. Abe, Y. Kikkawa, Y. Inoue, Y. Doi, *Biomacromolecules* **2001**, *2*, 1007–1014.
67. D. J. Hoffman, *Polymer* **1983**, *24*, 3–26.
68. D. Maillard, R. E. Prud'homme, *Macromolecules* **2006**, *39*, 4272–4275.
69. D. Maillard, R. E. Prud'homme, *Macromolecules* **2008**, *41*, 1705–1712.
70. L. Cartier, T. Okihara, B. Lotz, *Macromolecules* **1997**, *30*, 6313–6322.
71. T. Okihara, M. Tsuji, A. Kawaguchi, K. Katayama, *J. Macromol. Sci. Phys.* **1991**, *B30*, 119–140.
72. Y. Kikkawa, M. Fujita, H. Abe, Y. Doi, *Biomacromolecules* **2004**, *5*, 1187–1193.

73. Y. Kikkawa, H. Abe, T. Iwata, Y. Inoue, Y. Doi, *Biomacromolecules* **2002**, *3*, 350–356.
74. K. Yamashita, Y. Kikkawa, K. Kurokawa, Y. Doi, *Biomacromolecules* **2005**, *6*, 850–857.
75. Z. X. Zhao, L. Yang, J. J. Hua, J. Wei, S. Gachet, A. El Ghzaoui, S. M. Li, *Macromol. Biosci.* **2008**, *8*, 25–31.
76. D. Jendrossek, Extracellular polyhydroxyalkanoate depolymerases: the key enzymes of PHA degradation, in: Y. Doi, A. Steinbüchel (Eds.), *Biopolymers*, Vol. *3b*, Wiley-VCH Verlag GmbH, Weinheim, 2002, pp. 41–83.
77. W. K. Lee, T. Iwata, J. A. Gardella Jr., *Langmuir* **2005**, *21*, 11180–11184.
78. A. E. Woodward, *Atlas of Polymer Morphology*, Hanser Publishers, Munich, 1988, 13 pp.
79. H. Abe, M. Harigaya, Y. Kikkawa, T. Tsuge, Y. Doi, *Biomacromolecules* **2005**, *6*, 457–467.
80. Y. Kikkawa, H. Abe, M. Fujita, T. Iwata, Y. Inoue, Y. Doi, *Macromol. Chem. Phys.* **2003**, *204*, 1822–1831.
81. H. Chanzy, J. Comtat, M. Dube, R. H. Marchessault, *Biopolymers* **1979**, *18*, 2459–2464.
82. R. H. Marchessault, J. F. Revol, T. F. Bobitt, J. H. Nordin, *Biopolymers* **1980**, *19*, 1069–1080.
83. G. A. R. Nobes, R. H. Marchessault, H. Chanzy, B. H. Briese, D. Jendrossek, *Macromolecules* **1996**, *29*, 8830–8833.
84. T. Iwata, Y. Doi, K. Kasuya, Y. Inoue, *Macromolecules* **1997**, *30*, 833–839.
85. T. Iwata, Y. Doi, T. Tanaka, T. Akehata, M. Shiromo, S. Teramachi, *Macromolecules* **1997**, *30*, 5290–5296.
86. T. Iwata, Y. Doi, M. Shiromo, *Macromol. Chem. Phys.* **2002**, *203*, 1309–1316.
87. F. Su, T. Iwata, F. Tanaka, Y. Doi, *Macromolecules* **2003**, *36*, 6401–6409.
88. T. Iwata, Y. Doi, *Polym. Int.* **2002**, *51*, 852–858.
89. T. Iwata, Y. Doi, K. Isono, Y. Yoshida, *Macromolecules* **2001**, *34*, 7343–7348.
90. T. Iwata, S. Kobayashi, K. Tabata, N. Yonezawa, Y. Doi, *Macromol. Biosci.* **2004**, *4*, 296–307.
91. T. Iwata, Y. Doi, *Macromolecules* **1998**, *31*, 2461–2467.
92. W. K. Lee, T. Iwata, *Ultramicroscopy* **2008**, *108*, 1054–1057.
93. D. Brizzolara, H. J. Cantow, K. Diedericks, E. Keller, A. J. Domb, *Macromolecules* **1996**, *29*, 191–197.
94. P. De Santis, A. J. Kovacs, *Biopolymers* **1968**, *6*, 299–306.
95. T. Miyata, T. Masuko, *Polymer* **1997**, *38*, 4003–4009.
96. M. Fujita, Y. Doi, *Biomacromolecules* **2003**, *4*, 1301–1307.
97. H. Tsuji, S. H. Hyon, Y. Ikada, *Macromolecules* **1991**, *24*, 5657–5662.
98. E. H. Backes, L. D. Pires, L. C. Costa, F. R. Passador, L. A. Pessan, *J. Compos. Sci.* **2019**, *3*, 52.
99. https://www.corbion.com 2022. Access date: 02/02/24
100. A. Rauwerdink, R. J. Kazlauskas, *ACS Catal.* **2015**, *5*, 6153–6176.
101. M. Hajighasemi, A. Tchigvintsev, B. Nocek, R. Flick, A. Popovic, T. Hai, A. N. Khusnutdinova, et al., *Environ. Sci. Technol.* **2018**, *52*, 12388–12401.
102. M. Hajighasemi, B. P. Nocek, A. Tchigvintsev, G. Brown, R. Flick, X. H. Xu, H. Cui, et al., *Biomacromolecules* **2016**, *17*, 2027–2039.
103. F. Kawai, K. Nakadai, E. Nishioka, H. Nakajima, H. Ohara, K. Masaki, H. Iefuji, *Polym. Degrad. Stab.* **2011**, *96*, 1342–1348.
104. K. Matsumoto, S. Terai, A. Ishiyama, J. Sun, T. Kabe, Y. Song, J. M. Nduko, et al., *Biomacromolecules* **2013**, *14*, 1913–1918.
105. R. C. Alejandra, C. M. Margarita, M. C. M. Soledad, *Polym. Degrad. Stab.* **2012**, *97*, 2473–2476.
106. P. Kanmani, K. Kumaresan, J. Aravind, S. Karthikeyan, R. Balan, *Int. J. Environ. Sci. Technol. (Tehran)* **2016**, *13*, 1541–1552.
107. K. Masaki, N. R. Kamini, H. Ikeda, H. Iefuji, *Appl. Environ. Microbiol.* **2005**, *71*, 7548–7550.
108. X. P. Hu, U. Thumarat, X. Zhang, M. Tang, F. Kawai, *Appl. Microbiol. Biotechnol.* **2010**, *87*, 771–779.
109. U. Thumarat, R. Nakamura, T. Kawabata, H. Suzuki, F. Kawai, *Appl. Microbiol. Biotechnol.* **2012**, *95*, 419–430.
110. T. Watanabe, K. Suzuki, Y. Shinozaki, T. Yarimizu, S. Yoshida, Y. Sameshima-Yamashita, M. Koitabashi, et al., *Process Biochem.* **2015**, *50*, 1718–1724.
111. S. Yoshida, K. Hiraga, T. Takehana, I. Taniguchi, H. Yamaji, Y. Maeda, K. Toyohara, et al., *Science* **2016**, *351*, 1196–1199.
112. K. Kitadokoro, U. Thumarat, R. Nakamura, K. Nishimura, H. Karatani, H. Suzuki, F. Kawai, *Polym. Degrad. Stab.* **2012**, *97*, 771–775.
113. Y. Shinozaki, Y. Kikkawa, S. Sato, T. Fukuoka, T. Watanabe, S. Yoshida, T. Nakajima-Kambe, H. K. Kitamoto, *Appl. Microbiol. Biotechnol.* **2013**, *97*, 8591–8598.
114. D. Jendrossek, R. Handrick, *Annu. Rev. Microbiol.* **2002**, *56*, 403–432.
115. J. Sun, K. Matsumoto, J. M. Nduko, T. Ooi, S. Taguchi, *Polym. Degrad. Stab.* **2014**, *110*, 44–49.
116. J. Sun, K. Matsumoto, Y. Tabata, R. Kadoya, T. Ooi, H. Abe, S. Taguchi, *Appl. Microbiol. Biotechnol.* **2015**, *99*, 9555–9563.
117. C. Hori, T. Sugiyama, K. Watanabe, J. Sun, Y. Kamada, T. Ooi, T. Isono, et al., *Polym. Degrad. Stab.* **2020**, *179*, 109231.
118. C. Utsunomia, T. Saito, K. Matsumoto, C. Hori, T. Isono, T. Satoh, S. Taguchi, *J. Polym. Res.* **2017**, *24*, 167.
119. S. Inkinen, M. Stolt, A. Sodergard, *Polym. Adv. Technol.* **2011**, *22*, 1658–1664.
120. E. Wojtczak, T. Biedron, M. Bednarek, *Polym. Bull.* **2019**, *76*, 1135–1149.
121. H. Tsuji, *Polymer* **2000**, *41*, 3621–3630.
122. M. C. Lee, E. J. Liu, C. H. Yang, L. J. Hsiao, T. M. Wu, S. Y. Li, *Biotechnol. J.* **2018**, *13*, 1700560.

123. X. Qi, Y. W. Ren, X. Z. Wang, *Int. Biodeterior. Biodegrad.* **2017**, *117*, 215–223.
124. S. M. Satti, A. A. Shah, T. L. Marsh, R. Auras, *J. Polym. Environ.* **2018**, *26*, 3848–3857.
125. https://carbios.fr/technologies/la-biodegradation/ 2022. Access date (02/24/22)
126. Q. Y. Huang, M. Hiyama, T. Kabe, S. Kimura, T. Iwata, *Biomacromolecules* **2020**, *21*, 3301–3307.
127. K. Shi, Z. Bai, T. Su, Z. Wang, *Int. J. Biol. Macromol.* **2019**, *126*, 436–442.
128. T. Malwela, S. S. Ray, *Int. J. Biol. Macromol.* **2015**, *77*, 131–142.
129. P. Rychter, K. Lewicka, D. Rogacz, *J. Appl. Polym. Sci.* **2019**, *136*, 47856.
130. F. Luzi, E. Fortunati, D. Puglia, R. Petrucci, J. M. Kenny, L. Torre, *Polym. Degrad. Stab.* **2015**, *121*, 105–115.
131. J. Li, M. Kong, X. J. Cheng, J. J. Li, W. F. Liu, X. G. Chen, *Int. J. Biol. Macromol.* **2011**, *49*, 1016–21.
132. F. Luzi, F. Dominici, I. Armentano, E. Fortunati, N. Burgos, S. Fiori, A. Jimenez, et al., *Carbohydr. Polym.* **2019**, *223*, 115131.
133. M. Sednickova, S. Pekarova, P. Kucharczyk, J. Bockaj, I. Janigova, A. Kleinova, D. Jochec-Moskova, et al., *Int. J. Biol. Macromol.* **2018**, *113*, 434–442.
134. H. Zhang, W. Zhen, *Int. J. Biol. Macromol.* **2019**, *139*, 181–190.
135. N. Hegyesi, Y. C. Zhang, A. Kohari, P. Polyak, X. F. Sui, B. Pukanszky, *Ind. Crop Prod.* **2019**, *141*, 111799.
136. N. K. Singh, B. P. Das Purkayastha, M. Panigrahi, R. K. Gautam, R. M. Banik, P. Maiti, *J. Appl. Polym. Sci.* **2013**, *127*, 2465–2474.
137. Y. Kikkawa, S. Tanaka, Y. Norikane, *RSC Adv.* **2017**, *7*, 55720–55724.
138. K. Shi, Q. Ma, T. Su, Z. Wang, *Sci. Rep.* **2020**, *10*, 7031.
139. T. Narancic, S. Verstichel, S. Reddy Chaganti, L. Morales-Gamez, S. T. Kenny, B. De Wilde, R. Babu Padamati, et al., *Environ. Sci. Technol.* **2018**, *52*, 10441–10452.

# 23

# ENVIRONMENTAL FOOTPRINT AND LIFE CYCLE ASSESSMENT OF POLY (LACTIC ACID)

Amy E. Landis, Shakira R. Hobbs, Dennis Newby, Ja'Maya Wilson, and Talia Pincus

## 23.1 INTRODUCTION TO LCA AND ENVIRONMENTAL FOOTPRINTS

Environmental or ecological footprints provide a measure of demands on the earth's resources and originally referred to human demands. Carbon footprinting is a similar measure but only in terms of the amount of greenhouse gases produced. These tools are intended to provide a measure of environmental impact. In essence, footprinting is a subset of life cycle assessment (LCA) that can be applied to human activities, processes, and products such as biopolymers.

### 23.1.1 Life Cycle Assessment

To determine the environmental impacts of a product or a process, an LCA is often conducted. LCA provides a comprehensive and quantitative analysis of the environmental impacts of a product or process throughout its entire life cycle. LCA is a powerful tool widely used for measuring the sustainability of an enterprise or a concept and informing decisions with respect to sustainability and environmental considerations. Guidelines for conducting an LCA are defined by the ISO 14040 series [1]. There are four main stages to an LCA:

1. *Goal and Scope Definition:* Defines the extent of the analysis including the goals and the system boundaries. The functional unit for the LCA is defined within this stage.
2. *Inventory Analysis:* Documents material and energy flows that occur within the system boundaries. It is often called the life cycle inventory (LCI) stage.
3. *Impact Analysis:* Characterizes and assesses the environmental effects using the data obtained from the inventory. It is often called the life cycle impact assessment (LCIA) stage.
4. *Interpretation:* Reviews the results of the LCA, identifies opportunities to reduce the environmental burden throughout the product's life, and provides conclusions and recommendations.

Many organizations have established guidelines for performing detailed LCAs, including the Environmental Protection Agency (EPA), the Society for Environmental Toxicology and Chemistry (SETAC), and the American National Standards Institute (ANSI) [1–4]. All these organizations describe LCA steps similar to those listed above. Numerous methodologies exist to conduct LCAs that differ according to time, information, and monetary constraints. Assessments can range from conceptual models to detailed quantitative analyses. There are a host of LCA software packages and tools available to aid in the construction of an LCA.

LCAs can be comparative or stand-alone (i.e., an analysis of a single product). Through the use of a stand-alone LCA, it is possible to observe which stage (creation, use, or disposal) causes the most impact and may offer suggestions to minimize impacts throughout the product life. Comparative LCAs among possible products help to determine the environmentally preferable alternative.

*Poly(Lactic Acid): Synthesis, Structures, Properties, Processing, Applications, and End of Life*, Second Edition.
Edited by Rafael A. Auras, Loong-Tak Lim, Susan E. M. Selke, and Hideto Tsuji.

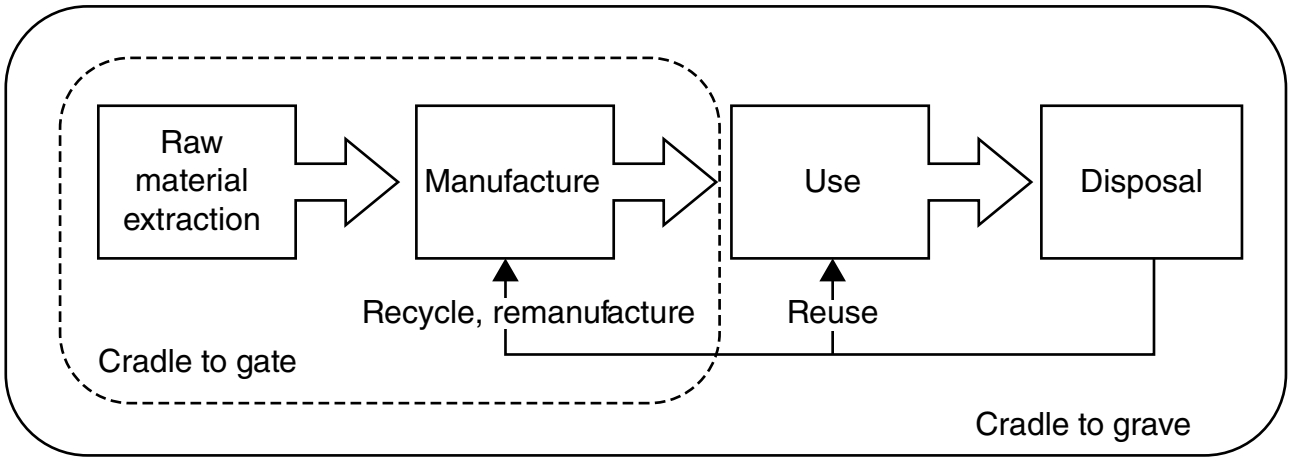


**FIGURE 23.1** Generic life cycle stages.

The system boundaries of an LCA may extend from cradle to gate, cradle to grave, or cradle to cradle. As depicted in Figure 23.1, cradle to gate implies that the LCA covers activities prior to the use phase, while cradle to grave includes the product's use and end of life. Cradle to cradle indicates a product that can be disposed of and returned back to the natural environment; the life cycle of PLA can be considered as such because when PLA degrades, its carbon is recycled back into the environment for uptake as biomass.

### 23.1.2 Uncertainty in LCA

While methods for the incorporation of uncertainty in LCAs have been proposed in the past, the traditional practical applications of LCAs rarely quantify uncertainty or variability. Typically, one number will be used to represent a parameter within the LCI, whereas in many systems one number is insufficient for representing the range, variability, and uncertainty that exist in reality.

Monte Carlo analysis (MCA) can be used in conjunction with LCA to estimate variability and uncertainty. MCA is a tool that simulates a probable range of outcomes from given probability distributions of input variables and can be applied within an LCA framework to capture LCI parameter variability and uncertainty. With the use of MCA, any independent variable with a range of estimates or possible values can be assigned a probability distribution. Output distributions are generated by repeatedly and randomly sampling values from the probability distributions. A simulated outcome distribution can show the most likely scenario, as well as extreme cases that occur infrequently. Monte Carlo analysis within an LCI framework allows the capture of parameter variability and uncertainty. LCIA tools have variability and uncertainty in their factors, as well as uncertainty associated with the model itself (i.e., uncertainty associated with assumptions or boundaries used to construct the model). However, most LCIA tools do not include uncertainty information that can be incorporated into this stage of the LCA.

## 23.2 LIFE CYCLE CONSIDERATIONS FOR PLA

### 23.2.1 The Life Cycle of PLA

LCAs would provide useful environmental information about poly(lactic acid) (PLA). A comparative LCA could evaluate the relative environmental impacts of PLA as opposed to similar petroleum-derived or bio-based polymers such as polyethylene (PE), poly(hydroxyalkanoate) (PHA), or poly(ethylene terephthalate) (PET). A stand-alone LCA could be evaluated to identify areas where environmental improvements can be made during the life cycle and production of PLA.

Once the goal and system boundaries of an LCA have been established, the material and energy flows throughout the system boundaries are tabulated during the LCI. The LCI often begins with the extraction of raw materials and includes transportation of goods, production of materials, use of the product, and disposal of the product, as shown in Figure 23.1. There are many important material flows to be considered in the life cycle of PLA, only a few of which are shown in Figure 23.2.

PLA can be made from a variety of raw materials [5]. The most common feedstock are sugars from sugar cane, beet extracts, whey, and cellulosic materials such as cassava, and corn. When made from corn, PLA is produced via fermentation of corn-derived sugar to lactic acid followed by polymerization. Starch and other valuable coproducts such as feed, oil, and meal are obtained from corn via the wet milling process.

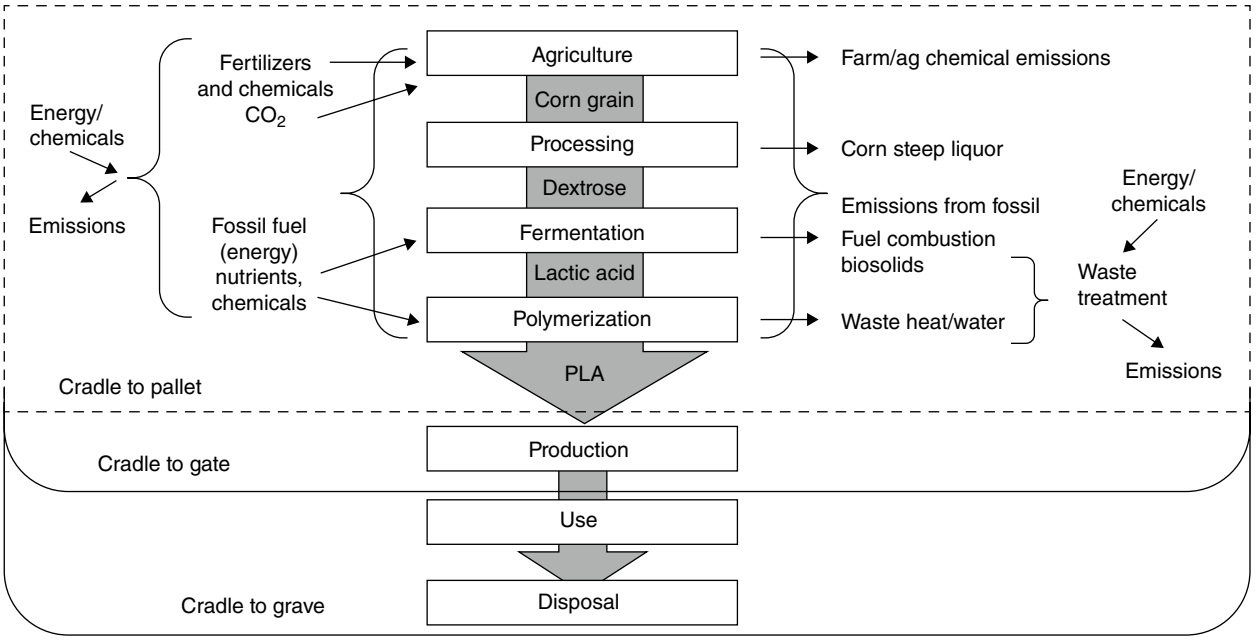


**FIGURE 23.2** Life cycle flows for PLA production from corn.

| Products | Mass(1) | Market(2) |
|---|---|---|
| Starch | 65% | 69% |
| CGF | 22% | 2% |
| CGM | 7% | 8% |
| Oil | 5% | 20% |

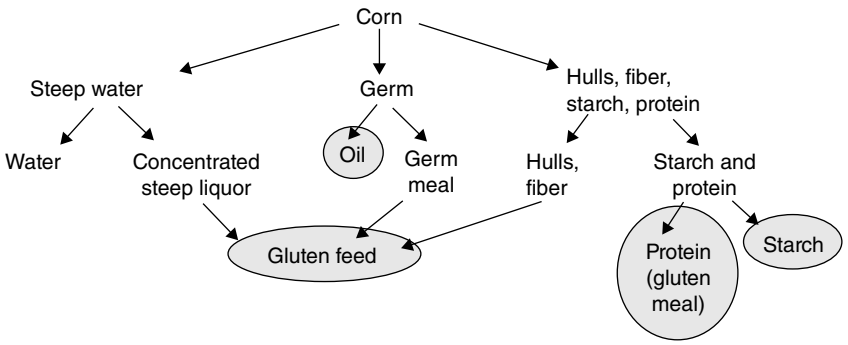


**FIGURE 23.3** Corn wet mill coproducts. *Note*: CGF: corn gluten feed; CGM: corn gluten meal; (1); mass source references: [6–13]; (2): market source references: [14–17].

An important consideration in LCA is the creation of coproducts. The life cycle environmental impacts are shared among the various coproducts; this allocation is called coproduct allocation in LCA. There are numerous methodologies used to allocate environmental impacts to coproducts, and the most common include division of the inventory on a mass basis or on a market basis. Figure 23.3 presents the mass and market allocation schemes for corn-derived products. The product of concern for PLA, starch, has similar allocation percentages regardless of method. The remainder of the products derived from the fermentation and polymerization stages currently produce no additional products of value, and thus no allocation scheme is needed for the flows through these stages.

Lactic acid is created through pure culture fermentation of dextrose. Fermentation requires process and cooling water, microorganisms, growth media (e.g., corn steep liquor from the wet milling process, yeast extract, and minerals), sterilizing agents, pH neutralizers, wastewater treatment, cell and lactic acid separations, and energy reported to be 20 MJ/kg PLA [18–22]. In one method of polymerizing high-molecular-weight PLA, tin catalysts are used to depolymerize the prepolymer to produce a mixture of lactide stereoisomers that, through ring opening polymerization in the melt, are subsequently converted into high-molecular-weight PLA [23]. Other methods of producing PLA are dicussed in Chapters 3 and 4. All the material, chemical, and energy inputs from the production of PLA along with the associated emissions should be included in the LCI.

Industrial food waste can be used to create lactic acid for producing PLA due to its high composition of carbohydrates. Some studies have shown that potato peel waste could produce lactic acid by anaerobic fermentation with

undefined mixed microbial cultures from wastewater treatment plants [24–27]. However, more research is needed to address the impurities present in lactic acid derived from food waste, which ultimately affects the final PLA product. Discovery of practical ways to produce a PLA product from food waste could lead to a cradle-to-cradle system.

The transformation of PLA pellets into commodity goods varies depending on the type of product. PLA is available commercially in many forms, including fibers, films, and extruded and thermoformed containers [28]. Commodity production of PLA can follow many typical petro-polymer routes, including melt spinning, injection molding, and thermoforming [29]. PLA is also commonly used in 3D printing applications [30]. PLA can also be blended with other petropolymers or with natural fibers, including kenaf and flax fibers, which have been used to increase heat resistance and durability of the plastic [31, 32].

### 23.2.2 Energy Use and Global Warming

One of the assumed environmental benefits of biopolymers are their reduction in the amount of fossil fuels and subsequent greenhouse gas emissions compared to their petroleum-derived polymer counterparts [33]. The concept of carbon neutrality or "net zero" emissions of carbon dioxide is an attractive feature of biopolymers with respect to global warming potential (GWP). Within the biopolymer life cycle, the carbon flow is cycled from plant to product, where the plant takes up the amount of carbon utilized for manufacturing the product. The biodegradability of PLA makes it potentially attractive for achieving carbon neutrality or net zero carbon or greenhouse gas emissions resulting from the uptake of $CO_2$ during photosynthesis of PLA's raw materials in an amount equivalent (thus "net zero") to the $CO_2$ emitted during biodegradation. While biopolymers are sometimes said to have net zero carbon emissions, this is true only if the fossil fuel use during farming, fertilizer processing, oil crushing steps, and so on is neglected or offset. When the product life cycle is extended to include these stages, the carbon flows become noncircular. It may be possible to achieve carbon neutrality for the production of biopolymers if all fossil energy is substituted with renewable, carbon neutral energy and/or combined with methods of carbon sequestration [34]. The participation of $CO_2$ in the carbon cycle must be assessed over the entire biopolymer life cycle. Thus, life cycle assessment can aid in quantifying greenhouse gas emissions and fossil fuel usage.

### 23.2.3 Environmental Trade-Offs

While GWP and nonrenewable fuel consumption are important environmental concerns, they are not the only impacts that can be evaluated nor are they the only ones recommended by ISO when reporting environmental impacts. Land use, water use, and water quality are environmental concerns for PLA and other bio-based products since they are derived from agriculture. To address the entirety of environmental implications, it is important to critically examine the materials required, the energy used, and the resultant emissions throughout the entire life of the product from its inception and raw materials extraction to its ultimate disposal, incorporating different media and a broad range of possible conditions.

There are many other environmental impacts that should be evaluated over the life cycle of PLA. For example, nitrate in water bodies is responsible for acidification, eutrophication, and hypoxia, leading to a loss of biodiversity and natural resources. Pesticides in runoff are also hazardous to human and/or ecological health [35]. Air emissions from agricultural systems are also of concern with respect to human health; they typically originate from the combustion of fuels, the application of fertilizers and pesticides, and the particulate matter created during tillage. Air emissions such as $NO_x$, $SO_x$, particulate matter, and volatilized pesticides contribute negatively to human health and ecosystem quality. Intensive farming and erosion can also result in soil degradation.

The environmental trade-offs between PLA and fossil-polymers result from agricultural production of PLA raw materials. Agriculture is one of the major nonpoint source contributors to eutrophication and hypoxia (e.g., within the Gulf of Mexico in the United States) due to the extensive use of fertilizers. Nitrogen and phosphorus are applied as fertilizers to agricultural crops and result in N and P nutrient emissions, which are the primary contributors to hypoxia and eutrophication [36, 37].

Hypoxia is a phenomenon that occurs in aquatic environments as dissolved oxygen becomes reduced in concentration, usually to less than 2 ppm [38]. Hypoxia can be caused by excess nutrients in water. The nutrients of concern are nitrogen or phosphorus; phosphorus is more often the limiting nutrient in freshwater systems, while nitrogen is often the limiting nutrient in marine systems. Despite the fact that less than 5% of phosphorus fertilizers are transported through agricultural runoff, emissions of aqueous phosphorus have proven to be a significant contributor to eutrophication due to the sensitive nature of aquatic autotrophs to phosphorus enrichment [37, 39]. Nutrients causing hypoxia can come from many sources, such as fertilizer runoff from agricultural fields, deposition of nitrogen from the atmosphere, stormwater runoff, and sewage discharges. These nutrients cause enhanced growth and decay of algae and plant matter. As the plant matter degrades, dissolved oxygen is consumed. Lower dissolved oxygen levels result in the death of aquatic plants and animals. The overall effect is called eutrophication. Eutrophication impacts humans as well; it decreases the resource value of water bodies by reducing fish populations

and recreation capacity. Human health impacts can occur when eutrophic waters interfere with drinking water treatment [40]. The most well-known hypoxic area is the "dead zone" in the northern Gulf of Mexico; hypoxic conditions primarily result from nonpoint source nutrient emissions from agriculture within the U.S. Corn Belt. The World Resources Institute and the Millenium Ecosystem Assessment identified over 400 eutrophic and hypoxic systems worldwide [41, 42].

### 23.2.4 Waste Management

The five waste management systems for biopolymers are landfill, composting, incineration, anaerobic digestion, and recycling. In each of these systems, PLA is expected to degrade differently and thus create different environmental effects. Throughout these systems bio-based carbon can be handled in three different ways [43]. The first is considering carbon emissions as carbon neutral because the carbon released by the material is offset by the carbon that was taken up initially. Through this approach, carbon allocation problems are implicitly managed through the carbon content of coproducts [44]. Additionally, carbon can be allocated consistently with the allocation of other environmental burdens while still assuming carbon neutrality. Lastly, some may credit carbon emissions through carbon sequestration as the carbon is stored in the bio-based materials [45]. Knowing what these waste systems are and how PLA behaves in them is essential for understanding why LCA practitioners have found varying results when investigating PLA at its end of life. The waste management systems are outlined below.

Landfilling is the mass burial of wastes, often with a bottom liner separating the wastes from the ground and a covering of soil. This process can occur over decades and throughout this time, the system can undergo many fluctuations in pH, oxygen levels, and temperature [46]. Some advanced landfills and all new US landfills have technology to capture gases that are produced due to the wastes decaying, which help stifle greenhouse gas emissions. However, it should be noted that these systems are not 100% effective.

Many communities are seeking more integrated and sustainable waste management systems. Even though landfilling does not help communities meet their zero waste goals, it is still the backbone of waste management in many countries [47]. This is because it is a relatively inexpensive, well-known technology with lower environmental and economic impacts when compared to uncontrolled dumpsites [47]. Many countries in Latin America, such as Mexico and Brazil, have found success with several open dumpsites being converted into controlled landfills [48].

Incineration is a process where feedstocks such as municipal wastes and biopolymers are converted to steam using a boiler, which is then used to produce energy through a generator [49]. Like petroleum-based polymers, PLA can be incinerated, and the steam can be used in energy production, as well as district heating. Using renewable resources is crucial for the $CO_2$ neutrality of energy recovery [50]. The overall efficiency of these systems can exceed 80%, making incineration a great method of power generation. Despite these benefits, incineration is expensive in terms of operation and maintenance. It also emits greenhouse gases from the burning of petroleum and bio-based feedstocks and has a substantial impact on water depletion due to water needed for the incineration process [51, 52].

Composting is the decomposition of organic matter, such as biopolymers, under controlled aerobic conditions to form a fertilizer or soil amendment [53]. Composting is spurred through a diverse group of microorganisms that use nutrients such as carbon, nitrogen, and phosphorus found in the organic matter to grow. The carbon to nitrogen ratio is critical in the process, as this serves as an indicator of the nutritional balance and the optimum ratio for composting. One of the benefits of compost is the long-term carbon storage to help replenish carbon losses in soil due to agricultural farming [54].

Anaerobic digestion typically involves handling organic solids from municipal wastewater treatment plants [55]. Anaerobic biodegradation usually indicates degradation at mesophilic (37°C) or thermophilic (55°C) biogas plants. In these conditions, a series of metabolic interactions by microorganisms convert organic matter into three main products: methane, carbon dioxide, and biosolids [56]. To ensure the most ideal conditions for the reaction, the carbon–nitrogen ratio must be balanced in addition to the pH being around 7 [57]. Once the process is complete, the digestate residue that remains is rich in nitrogen, phosphorus, and potassium, which are key ingredients in fertilizers. This process produces less heat and biomass compared with aerobic digestion processes such as composting [58].

Recycling is a method of waste treatment where materials that would be discarded are turned into new products. There are two types of recycling, which are mechanical and chemical recycling. Mechanical recycling is the collection, sorting, grinding, and washing of plastics that are then used in the production of new plastic. Chemical recycling changes the molecular structure of the bioplastic, where it is depolymerized into smaller molecules, which are then polymerized to form the recycled plastic [50]. Recycling offers a unique way for products to be incorporated into a "Circular Economy" where a material's value is retained in the economy for an extended period while minimizing or delaying the amount of waste created [59]. Additionally, through the recycling of organic wastes, biodegradable products have an alternative at end of life that effectively sequesters carbon [60].

### 23.2.5 End of Life

In landfill conditions, wastes undergo anaerobic degradation. It has been shown by several studies that PLA will degrade, at least partially, under thermophilic landfill conditions. Kolstad et al. [61] highlighted that amorphous PLA degradation would emit up to 260 mL of methane per gram of biopolymer in landfill conditions. Krause et al. [62] also demonstrated that semi-crystalline PLA could generate significant amounts of methane under thermophilic conditions, while Krause and Townsend [61] found semicrystalline PLA did not biodegrade under accelerated mesophilic optimal landfill conditions.

Biopolymers have high heating values, and since they are renewable, energy recovery technologies such as incineration compete with other forms of waste management that may be viable carbon management strategies [50]. Zhang et al. [52] has shown success in incinerating biopolymers as shown by his experiments. Industrial composting of PLA wastes has been widely studied. Although PLA is bio-based and biodegradable, there have been reports that PLA does not compost as quickly as other materials that are in the compost (e.g., yard trimmings and food waste) [63]. Due to bioplastics' slow degradation rates when compared with other organic material, bioplastics are often screened out of industrial compost facilities and sent to the landfill [63, 64]. Previous research suggests that a pretreatment might enable degradation of bioplastics in compost, but this is not a common practice [65].

The research surrounding the anaerobic digestion of biopolymers is still in its infancy [58]. Despite several tests being conducted, the anaerobic digestion of PLA has been achieved with varying degrees of success. Hamad et al. [66] demonstrated that PLA must be hydrolyzed first to reduce the molecular weight before the biodegradation can start. Through this method, a pretreatment is applied to the biopolymer and then combined with organic fraction of municipal solid waste to form a slurry that can then be anaerobically digested. However, a test from Itävaara et al. [67] showed that PLA could degrade rapidly, up to a rate of 60% during waste disposal in anaerobic treatment facilities without pretreatment. However, it was determined that it could take up to 90 days, which is a lengthy process for industrial anaerobic digestion [61]. Hobbs et al. [68] demonstrated that PLA reached near complete solubilization, 97–99%, when alkaline pretreatment was applied. Beyond that, Yagi et al. [69] showed that PLA was degraded up to 90% in thermophilic temperatures when combined with sludge, without the use of a pretreatment and degraded in mesophilic temperatures although the degradation was much slower.

PLA in recycling scenarios has been found to be a reliable way of managing PLA wastes. However, mass recycling of biopolymers is difficult because there is no large-scale infrastructure to do so [70]. Recycling has seen major reductions in the life cycle impacts of bio-based polymers. The decrease in GWP and fossil fuel depletion is accentuated when using bio-based feedstocks rather than petroleum-based feedstocks [64].

## 23.3 REVIEW OF BIOPOLYMER LCA STUDIES

The environmental performance of PLA has primarily been evaluated from the cradle to gate based on greenhouse gas emissions, nonrenewable energy use, and water use. Previous studies have focused on global warming and fossil fuel usage as the primary metrics for evaluating environmental performance. Nonpoint aqueous emissions are often neglected entirely, while other EPA criteria air pollutants are included in only a few select projects investigating the environmental impacts of bio-based production. Table 23.1 summarizes recent LCA studies on the environmental effects of PLA production. In the past, the research community had shown preference for contaminants that cause greenhouse impacts, as well as for aggregating fossil fuel consumption, with relatively few studies examining other types of environmental degradation.

In summary, the LCA studies show that, assuming current technological and energy use practices, PLA exhibits comparable nonrenewable energy use and greenhouse gas emissions to PE and PET [81, 82]. However, it should be noted that there are still large gaps in bio-based and fossil-based comparative LCAs due to the absence of standardized joint guidelines or product category rules within studies [78, 83].

The life cycle inventory data and environmental impacts of fossil-polymers are often taken from the European Association of Plastics Manufacturers (APME). The APME has an extensive database of LCI data for numerous polymers, including PE, PET, PP, and PS.

### 23.3.1 Cradle-to-Gate and Cradle-to-Grave LCAs

Within early LCA studies, often the life cycle environmental impacts were evaluated only from the cradle to the pellet. The LCA becomes much more complex with the multiple methods of production, products, uses, and disposal. Due to the large amount of uncertainty and variability associated with all these scenarios, LCA practitioners have just recently been able to fully evaluate the entire life cycle of PLA.

The results from Hottle et al. [72] are summarized in Table 23.2; their results show that estimated global warming potential and fossil fuel use during the production process of PLA has similar environmental impacts to other polymers. The production stage of PLA contributes to 50% of the fossil fuels used in the PLA life cycle. The most energy-intensive stage in the cycle is the conversion of sugar cane or starch to

**TABLE 23.1 Overview of PLA LCAs**

| | Environmental Impacts Included | | | | | | |
|---|---|---|---|---|---|---|---|
| Bioproduct | GW | FF | EH | HH | $H_2O$ | eQ | LU |
| PLA production [71] | × | | × | | × | × | × |
| PLA production [72] | × | × | × | × | | | × |
| PLA [73] | × | × | × | | | × | × |
| PLA production [74] | × | × | × | × | | × | × |
| PLA [75] | × | | × | × | | × | |
| PLA [76] | × | × | × | × | × | × | |
| PLA water bottles [77] | × | × | × | × | | | |
| PLA-based food packaging [63] | × | × | | | × | | × |
| PLA [78] | × | | | × | | × | × |
| PLA [79] | × | × | × | × | | × | |

The analyses listed above either included chemicals that typically contribute to the following categories or included a separate impact assessment for the following impact categories: GW: global warming; FF: fossil fuel use; EH; eutrophication; HH; human health (including air quality, carcinogenicity, human toxics, and smog); $H_2O$; water use; EQ; ecosystem quality (including acidification and soil health); LU; land use.

lactic acid. The majority of the energy used in this process is attributed to the electricity used during the fermentation and filtration stages [78, 81, 84]. The PLA GWP presented by various sources differ due to assumptions related to the type of energy use during the fermentation stage, $N_2O$ emissions from agriculture, $CO_2$ credits represented by negative $CO_2$ emissions that can be attributed to carbon soil sequestration with certain types of farming practices, and the embodied carbon within the PLA material also represented by negative $CO_2$ emissions. Agricultural soil and fertilizer $N_2O$ emissions would increase PLA by nearly 0.5 kg $CO_2$ eq./kg PLA in some cases. Other LCAs include the $CO_2$ equivalent carbon contained within the PLA material. The difference that results from this "embodied $CO_2$" would be approximately 1.8 kg $CO_2$ eq./kg PLA. This estimate is based on a PLA molecular weight (MW) of 83,000 g/mol. The MW is reported to have a range of 10,000–300,000 g/mol [62, 63, 85]. However, one must consider whether it is appropriate to attribute a carbon credit to PLA. If PLA biodegrades, the carbon is eventually released to the atmosphere rather than sequestered.

When adding EOL to LCAs, landfilling and composting contribute less to the life cycle of PLA compared to other life cycle stages [72]. Methane production in landfills is a significant factor for global warming impacts associated with biopolymers. Unsurprisingly, recycling provides benefits in the global warming and fossil fuel depletion categories. The results by Hottle et al. [72] show that composting has some environmental advantages, especially when compared to impacts associated with landfilling. But their results show that recycling provides the greatest benefits for PLA at end of life.

The EOL results from Newby et al. [74], Figure 23.4, depict normalized results for incineration and landfilling of PLA for ReCiPe 2016 impact categories. For most of the impact categories, construction of the incineration and landfill attributed less than 15% of total burdens to environmental impacts. The main contributor for most impact categories was the operation for incineration, while some contribution for landfill came from transportation. Incinerating PLA requires more energy when compared with landfilling.

The results from Hobbs et al. [75], Figure 23.5, demonstrates results of two waste management scenarios: anaerobic digestion of treated PLA and composting of treated PLA. The PLA undergoes an alkaline pretreatment to accelerate the degradation of PLA. The pretreatment is accounted for in the end-of life scenarios. Normalized results suggested that co-digestion of food waste and pretreated PLA via anaerobic digestion offers life cycle and environmental net total benefits in several impact categories. Negative emissions or offsets from anaerobic digestion of pretreated bioplastic and food waste are from avoided landfilling of anaerobic digestion sludge, avoided production of synthetic fertilizer and energy.

### 23.3.2 End-of-Life LCAs

LCAs that consider PLA at end-of-life (EoL) differ in how PLA degradation is determined, as well as how electricity production and offsets are allocated. Additionally, the interpretation of the environmental impacts and waste management technology that is considered to be the least harmful is dependent on individual municipalities' waste management goals. This section describes several different EoL methodologies for managing PLA waste and how LCA practitioners include EoL in their modeling approaches.

In many communities, landfilling is an obvious waste management strategy due to its common use to dispose of

**TABLE 23.2 Comparison of Normalized Environmental Impacts for Production vs End-of-life cycle for Landfill and Compost Scenarios**

| | | PLA Amorphous | | | PLA Crystalline | | |
|---|---|---|---|---|---|---|---|
| Impact Category | Unit | Production Inventory Average | Min EOL Only | Max EOL Plus Production | Production Inventory Average | Min EOL Only | Max EOL Plus Production |
| Ozone depletion | kg CFC-11 eq | 0.00E+00 | 3.72E−09 | 5.82E−09 | 0.00E+00 | 3.72E−09 | 5.82E−09 |
| Global warming | kg $CO_2$ eq | 1.15E+00 | 3.08E−01 | 1.95E+00 | 1.15E+00 | 4.54E−02 | 1.46E+00 |
| Smog | kg $O_3$ eq | 2.08E−01 | 9.95E−03 | 2.22E−01 | 2.08E−01 | 7.94E−03 | 2.22E−01 |
| Acidification | kg $SO_2$ eq | 1.64E−02 | 3.36E−04 | 1.76E−02 | 1.64E−02 | 2.78E−04 | 1.76E−02 |
| Eutrophication | kg N eq | 1.30E−03 | 9.68E−05 | 1.31E−02 | 1.30E−03 | 9.68E−05 | 1.31E−02 |
| Carcinogenics | CTUh | 1.75E−11 | 1.33E−09 | 2.48E−09 | 1.75E−11 | 1.33E−09 | 2.48E−09 |
| Non carcinogenics | CTUh | 1.93E−10 | 8.96E−09 | 1.15E−08 | 1.93E−10 | 8.96E−09 | 1.15E−08 |
| Respiratory effects | kg PM 2.5 eq | 5.03E−04 | 2.74E−05 | 5.61E−04 | 5.03E−04 | 2.55E−05 | 5.61E−04 |
| Ecotoxicity | CTUe | 3.40E−04 | 1.61E−01 | 2.10E−01 | 3.40E−04 | 1.61E−01 | 2.10E−01 |
| Fossil fuel depletion | MJ surplus | 3.91E+00 | 6.21E−02 | 4.03E+00 | 3.91E+00 | 6.21E−02 | 4.03E+00 |

Source: Adapted from Hottle et al. [72].

This table presents findings for the production and EOL scenarios of PLA. EOL options include landfilling (amorphous or crystalline) and composting. PLA has high (degradation and no landfill gas capture) and a low (no degradation) emission.

Data taken from Hottle et al. [72]. "Min EOL only" represents LCA results only from the EOL for the lowest EOL scenario. "Max EOL plus production" shows the maximum LCA results from the highest EOL scenario including the production LCA. EOL scenarios included composting and landfilling.

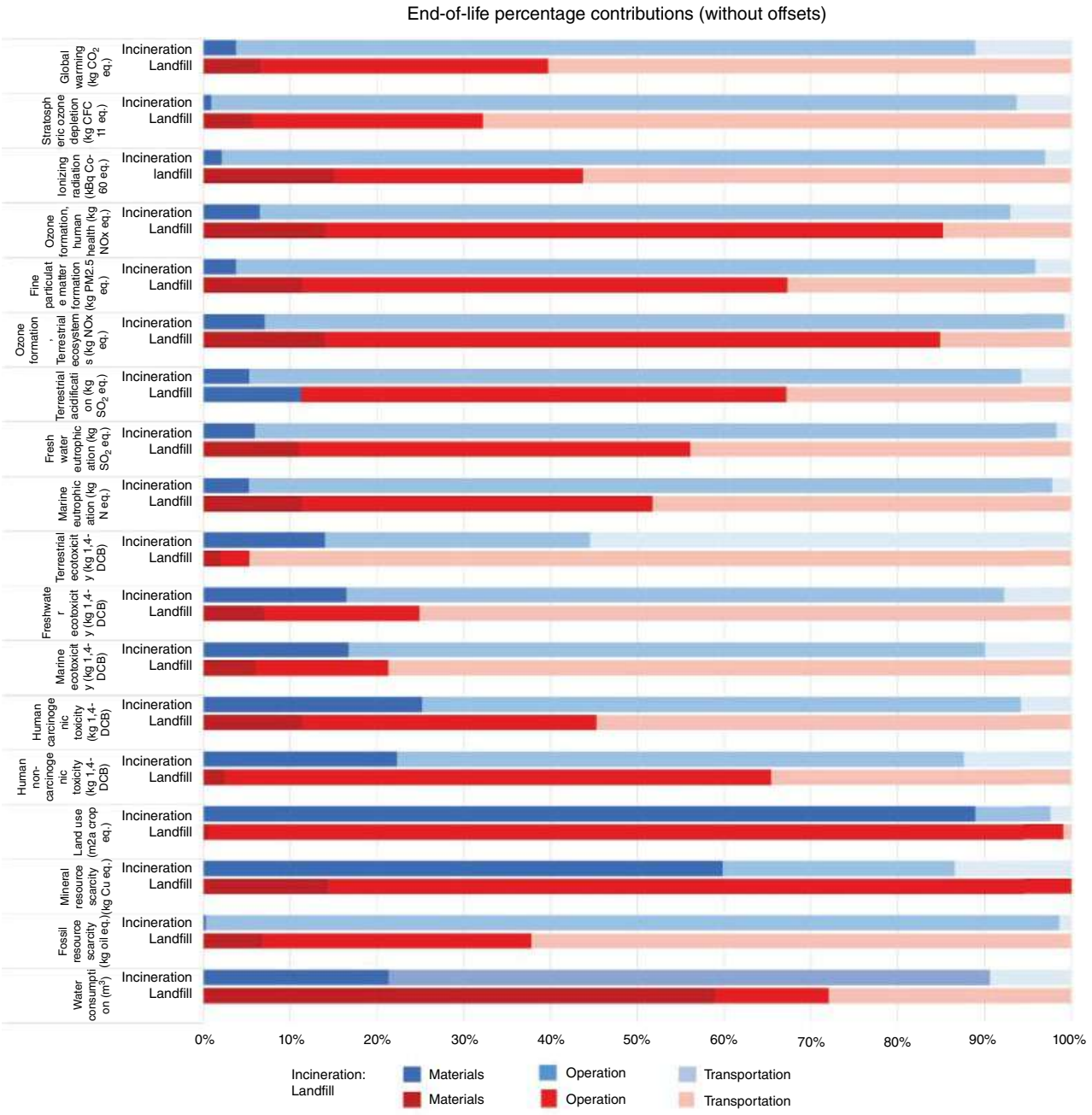


**FIGURE 23.4** End-of-life process contribution for incineration and landfill. Source: Reproduced from Ref. 74.

conventional petroleum-based plastics. Of 14 different EoL LCAs (Table 23.3), 10 of them considered landfilling at the EoL. Only seven of these studies specified the assumptions made when modeling landfills and four of them considered landfill gas capture as an offset [77, 86, 97]. The studies that did not, i.e., those by Kruger et al. [95], Mohee et al. [56] and Lorite et al. [94], assumed that PLA does not degrade, so landfill gas would not need to be captured. Kruger et al. [95] evaluated the best-case scenario in terms of global warming potential for PLA, assuming it did not degrade in the landfill. Throughout the studies that considered landfilling, models differed because of the PLA degradation kinetics, the gas capture efficiency, recovery percentage, electricity production, and thermal recovery. In the studies considered in Table 23.3, 12 of the 14 assessed incineration as a waste management technique. Of these studies, five did not specify if credits for electricity were given [87, 88, 91–93]. Studies by Mohee et al. [56], Gironi and Piemonte [89], and Rossi et al. [90] specified the exact energy values that were provided for a defined amount of PLA. Mohee et al. [56] specified

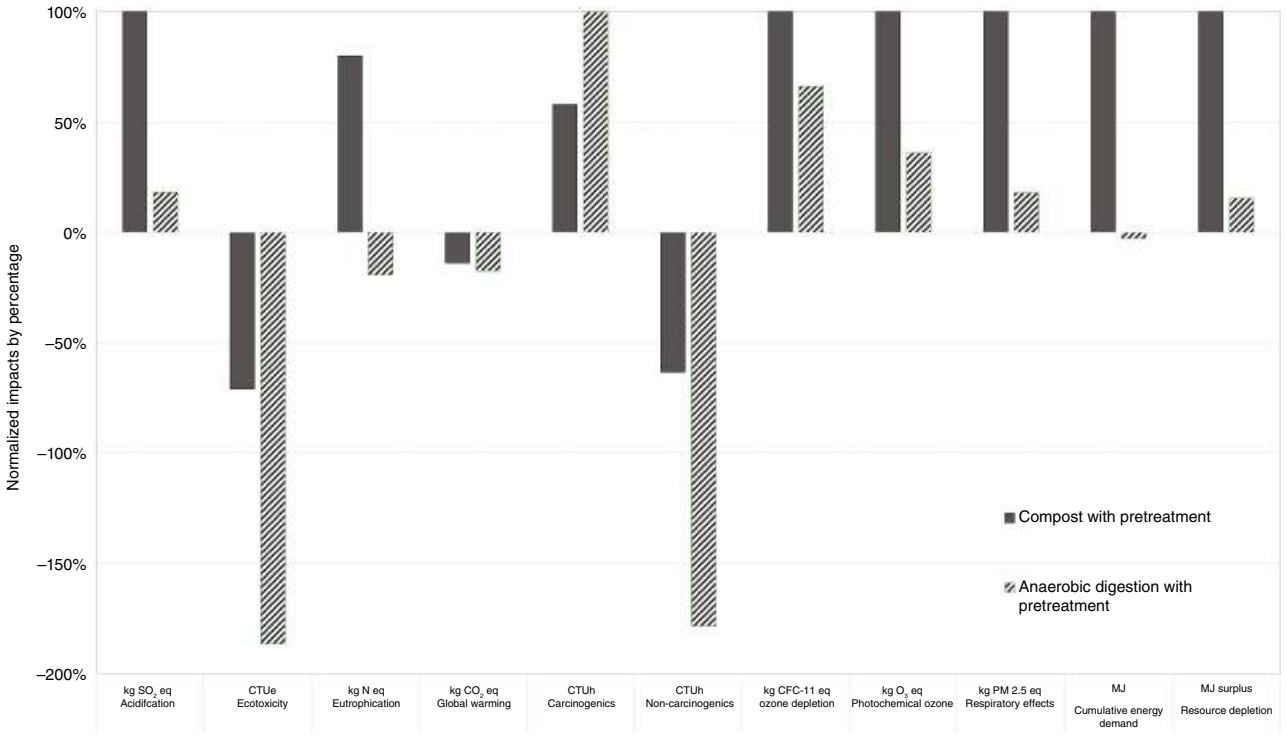


**FIGURE 23.5** Life cycle environmental impacts of PLA. Source: Data obtained from Ref. 75.

3.46 MJ of electricity/kg of PLA, Gironi and Piemonte [89] specified 26 MJ of electricity and 53.3 MJ of thermal energy from 1000 PLA bottles, and Rossi et al. [90] specified 19.5 MJ electricity and 0.78 kWh thermal production/kg of PLA.The LCAs by Kruger et al. [95], Lorite et al. [94], and Hermann et al. [87] specified 11% efficiency for electricity generation, whereas Papong et al. [77] specified 30% efficiency. For thermal energy offsets, Hermann et al. [87], Lorite et al. [94], and Kruger et al. [95] specified 22, 23, and 30% efficiencies, respectively. These values were taken as a proportion of PLA's higher heating value.

Only four studies in Table 23.3 addressed anaerobic digestion. Hermann et al. [87] did not outline any specific information on the methodology that was used. Hermann et al. [87] provided credits for the carbon replacement in digestate that would be used for soil remediation. They estimated 36% electricity generation efficiency and 28% of the electricity being exported after internally powering the digester. Hermann et al. [87] assumed 100% degradation of carbon of PLA with 40% degrading to $CO_2$, 40% to methane, and 20% remaining in the digestate. Piemonte [88] assumed that 85% of PLA would degrade, and 95% of the gas would be recovered. They also specified a 36% efficiency in converting to electricity, which would serve as an offset to the process. Rossi et al. [90] noted an 85.7% carbon degradation with 60% methane and 40% $CO_2$ in the biogas that was credited. Lastly, Rossi et al. [90] assigned credit for substituting peat in digestate and added 10% more emissions from burdens for post-digestion composting with 0.11% methane production.

Industrial composting was considered for handling PLA waste in 12 studies summarized in Table 23.4. For most of these studies, credits were given for the compost replacing either fertilizer or the contents that typically go into fertilizer such as peat and straw. Hermann et al. [87] replaced the peat and straw at a ratio of 1 : 3. Piemonte [88] estimated that 50% of compost displaces about 20% of synthetic fertilizer used during the agriculture stage of PLA production and was credited accordingly. Hermann et al. [87] and Piemonte [88] also predicted 60% degradation of PLA where 95% would degrade to $CO_2$ and 5% into $CH_4$. Hottle et al. [72] and Gironi and Piemonte [89] also used 60% degradation where the 40% that was not degraded would be put into the digestate residue. However, Hottle et al. [72] did not give credit to it as a soil fertilizer, while Gironi and Piemonte [89] and Mohee et al. [56] did. Papong et al. [77] estimated 87% degradation of PLA where the remaning 13% was credited as soil conditioner, and assumed all of the carbon inside was degraded into $CO_2$. Rossi et al. [90] supported that 80% of the PLA carbon would be degraded and went a step further to inspect the compost degradation when it is used and identified that it would emit an additional 301 g of $CO_2$/kg of PLA. [94] Lorite et al. [94] established that 100% of the compost managed would be managed as common biowaste and 100% of the compost would be added as avoided products. Mohee et al. [56] also established that PLA would

**TABLE 23.3 PLA End-of-Life Waste Management. LCA Methodologies Considering Landfill and Incineration as EoL**

| Reference | Landfill | Incineration | AD |
|---|---|---|---|
| Hermann et al. [86] | 0–100% Degradation of PLA, with gas recovery | With energy recovery | Not specified |
| Hermann et al. [87] | NA | Carbon credits for power and heat generation. 11% of high heating value (HHV) power exported, net export of heat 22% of HHV | 40% Carbon stored in soil, carbon credits assigned for soil conditioner replacement. 36% electricity generation efficiency. 28% exported. Carbon credits assigned for soil derived electricity displacement |
| Piemonte [88] | NA | Energy utilized but efficiency not mentioned. | 85% degradation of PLA and MaterBi assumed. 95% gas recovered. 36% efficiency in converting to electricity |
| Gironi [89] | 85% Degradation of PLA 25% recovery of gas. 36% efficiency for electricity generation from gas burning | 26 MJ of electric and 53.3 MJ of thermal energy from 1000 PLA bottles; bottle size not specified | NA |
| Rossi et al. [90] | 1% Degradation of PLA in 100 years, 3.76 g $CH_4$/kg PLA in 100 years, 22% gas recover, 6.1% landfill gas energy into electricity, and 3% into useful heat | LHV 19.5 MJ/kg PLA, substituted electricity by municipal solid waste incineration (MSWI) production, 0.78 kWh/kg PLA, substituted heat by MSWI production 8.25 MJ/kg PLA, 14% net electric efficiency, 41.2% thermal efficiencies | 85.7% Carbon degradation, 60% $CH_4$ and 40% $CO_2$ in biogas, 17.2 MJ/kg PLA recovered, 397 g/kg PLA digestate generated, credits assigned to peat for compost, heat, and energy. 10% emissions for post-digestion composting |
| Papong [77] | 100 Percent degradation, 334 g $CH_4$ /kg PLA, 10% oxidized in the soil; 60% methane recovered and combusted, 30% energy efficiency for methane burned | 30% Electricity efficiency, 20 kWh of electricity are considered for incineration of 1000 PLA bottles; electricity substitutes the grid electricity of Thailand | NA |
| Benetto [91] | NA | Not specified | NA |
| Van der Harst [92] | Not specified, credits given | Not specified, credits given | NA |
| Madival [93] | Not specified, no credits | Not specified, no credits | NA |
| Lorite [94] | No degradation, no landfill gas to be collected or utilized, no credits (Best Case scenario for GWP) | Incineration of waste plastic as the base, avoided products. 11% of the net calorific value is transformed into electric energy and 23% to thermal energy | NA |
| Kruger et al. [95] | No degradation, no gas capture | 11% Recovery as electricity, 30% as thermal energy. Substitutes European grid electricity, and thermal energy serves as process heat replacing heat generated by 50% light fuel oil and 50% natural gas | NA |
| Ingrao [63] | NA | NA | NA |
| Hottle et al. [72] | 37% Degradation over 100 years, and no degradation over 100 years. High emission was modeled as an environmental flow rather than estimating a gas capture efficiency and combustion to make high end bounding scenario | NA | NA |
| EPA [96] | No degradation, no gas capture. Credited for carbon sequestration | Energy value of 0.0176 million British thermal units (MBTUs)/kg of PLA; 17.8% combustion efficiency, avoided products of electricity produced | NA |

NA: Not addressed. Not specified means that the EoL treatment is included in the study but no details were given related to LCA.

**TABLE 23.4 PLA End-of-Life Waste Management. LCA Methodologies Considering Composting and Recycling as EoL**

| Reference | Industrial Composting | Recycling |
|---|---|---|
| Hermann et al. [86] | 55–80% degradation of PLA | NA |
| Hermann et al. [87] | carbon credits for peat and straw replacement, 1 : 3 ratio | NA |
| Piemonte [88] | 50% of compost displaces 20% of synthetic fertilizer used for agricultural stage, 60% degradation, 95% of this degrades to $CO_2$, 5% into $CH_4$ | 90% Used to make a lower grade product which is incinerated after use or same product. |
| Gironi [89] | 60% Degradation. 95% of this degrades to $CO_2$, 5% into $CH_4$ | 100% Closed-loop recycling with same efficiency as PET 1 kg PLA recycled with 90% efficiency |
| Rossi et al. [90] | 1 kg $H_2O$/kg PLA, 80% carbon content degraded fraction in composting 500 g C/kg PLA, 1.03 g $CH_4$/kg PLA, 1464 g $CO_2$/kg PLA, 400 g compost/kg PLA, 62 g $CO_2$/kg PLA, long term $CO_2$ emissions from compost | 0.83 Ratio of primary to secondary PLA. 8% material loss during process, 10% quality loss leading to lower ability of substitution of primary material |
| Papong [77] | 87% degradation of PLA, 13% remaining used as soil conditioner. Assumes 100% of carbon to $CO_2$ which makes it carbon neutral | 90% PLA waste can be converted, 0.6 MJ/kg PLA to convert 0.76 kg PLA/kg PLA (Chemical recycling) |
| Benetto [91] | NA | Not specified, no credits |
| Van der Harst [92] | Not specified, credits given | NA |
| Madival [93] | NA | Not specified, no credits |
| Lorite [94] | 100% Composting managed as composting of common-biowaste and avoided composts via Ecoinvent | NA |
| Kruger et al. [95] | 50% fresh compost in an encapsulated system, 50% treated in an open system. Assumed methane and other volatile organic compounds are emitted | NA |
| Ingrao [63] | Avoided production of chemical fertilizers such as N 0.007 kg/kg of compost and P 0.006 kg/kg, K 0.004 kg/kg. Compost spreading was not considered | NA |
| Hottle et al. [72] | 60% carbon degradation, 95% in $CO_2$, 5% in methane, rest of carbon in compost but credits not mentioned | NA |
| EPA [96] | 100% Composting, avoided fertilizer offset, carbon storage with composting, 52% of compost passive (no further emissions), 0.14 MT $CO_2$ eq./ton PLA | NA |

NA: Not addressed. Not specified means that the EoL treatment is included in the study but no details were given related to LCA.

degrade 100% and used the compost as fertilizer. Ingrao et al. [63] avoided the production of a chemical fertilizer of nitrogen, phosphorus, and potassium per kg of compost.

There are five studies that considered recycling at the EoL (Table 23.4) and four of them specified the methodology used. Piemonte [88] assumed 90% of PLA could be used to make a lower grade product, which would then be incinerated after use. Gironi & Piemonte [89] assumed 100% closed-loop recycling with the same efficiency as PET plastic with 90% efficiency. Rossi et al. [90] assumed a 0.83 ratio of primary to secondary PLA with an 8% loss of material during processing and a 10% quality loss leading to a lower ability of substituting primary material. Papong et al. [77] was the only study that specified a chemical recycling process where 90% of PLA waste could be converted and a 0.76 ratio of new PLA to old PLA could be created. Each of these practitioners used the PLA created from the process as credited to the system.

As discussed in the previous section, the methodologies vary widely on how to manage PLA biopolymers at EoL. The studies investigated mostly used GWP (normalized to kg $CO_2$), as well as single score points, or several midpoint indicators to indicate environmental impact. The values that were explicitly stated, or estimated from figures, have been tabulated in the Table 23.3. However, many of the studies combined the environmental effects from the EoL with the rest of the life cycle, and without separation, EoL impacts, specifically, are impossible to identify. Some studies used functional units such as 1000 PLA bottles in Gironi & Piemonte [89] or 1000 clamshells in Benetto et al. [91], and in these events, values were converted to reflect those of 1 kg of PLA to help aid in comparison. In addition, as with Gironi and Piemonte [89], the GWP gave credit to energy production but did not couple the values with the environmental impacts, which also affected GWP. Lastly, the credits that were given sometimes reflect production processes that varied earlier in the PLA life cycle. Owing to these inconsistencies, it is difficult to come up with a definitive expectation of environmental impact throughout the EoL processes. Besides Hermann et al. [87] considering the sequestration of

the PLA, the lowest reported impacts from the landfill process was from Hottle et al. [72], with the low emission scenario contributing 0.05 kg $CO_2$/kg PLA with the highest reporting from Papong et al. [77] with 5.07 kg $CO_2$/kg PLA (without energy recovery). With incineration, the GWP could range from −0.17 kg $CO_2$/kg PLA as reported from Papong et al. [77] and 1.4 kg $CO_2$/kg PLA as reported from Gironi and Piemonte [89]. Anaerobic digestion based on the studies could range from 0.84 [86] and 0.95 kg $CO_2$/kg PLA [90]. Industrial composing was found to be anywhere between 0.064 kg $CO_2$/kg PLA from Papang et al. [77] and 2.5 kg $CO_2$/kg PLA as reported from Rossi et al. [90]. Recycling values reported from Rossi et al. [90] and Gironi and Piemonte [89] are −0.4 and 0 kg $CO_2$/kg PLA respectively, showing that the environmental GWP impact for recycling methods could likely be less than the others.

Due to discrepancies in values between studies, it can be difficult to see the general trends that correlate with which waste management techniques have the least environmental impact. Much of this is determined by the location where these processes take place and the assumptions that are made. The general trend among these studies is that recycling shows reduced environmental impacts compared to other EoL strategies because of the offsets of reusing the plastic.

The reviewed studies differ widely from each other; most, if not all, assumptions about system boundaries, functional units, and allocations vary greatly (Tables 23.3 and 23.4). It is also important to note that the databases and information used are vital to LCAs and may create inconsistencies when adding EoL data from one database to upstream LCI data from another database [92]. Allocation makes a large difference in terms of overall environmental impact. Some studies assume worst- or best-case scenarios due to the differences of studies in reporting the actual degradation potential of PLA. These can lead to extremely large emission differentials at the EOL. Discrepancies can result between studies based on their choice of electricity source; for example, the study by Hermann and Blok [86] used European energy, whereas Gironi and Piemonte [89] and Piemonte [88] used the US grid electricity mix from ecoinvent. These inconsistencies add variability to the studies, especially when methodologies are not clearly specified, which hinders the reliability and consistency of LCA studies.

In summary, there are many sources of discrepancies in LCA of PLA, not all which can be attributed to a lack of detail. They include true differences in environmental impact in addition to the differences caused by methodological choices. Depending on system boundaries and the waste management system assessed, the EoL stage can represent less than a 5% change in global warming potential when compared with the entire production and transportation processes of PLA [92]. However, EoL processes still play a critical role regionally, where improper and inefficient waste disposal can cause a host of other problems. Additionally, EoL processes can create closed loop systems that can yield a drastic reduction in resource extraction. Systems such as recycling, which have been shown to have the least environmental impact, provide a way to reuse polymers and avoid the need for harvesting virgin resources.

## 23.4 IMPROVING PLA'S ENVIRONMENTAL FOOTPRINT

The final phase of the LCA, interpretation and improvement, is the stage where conclusions are drawn. During this stage, an analysis of major contributions to the environmental impact, sensitivity analysis, and uncertainty analysis are evaluated. Not only are results important to analyze but also it is important to identify what can be learned from the LCA and to identify areas where life cycle environmental improvements can be achieved.

By examining the cradle to gate LCA of PLA in Figures 23.4 and 23.5 and Table 23.2, it is apparent that the majority of environmental impacts from PLA production result from the agricultural and fermentation stages and during EoL. Therefore, improvement of PLA's environmental footprint should first focus on these areas.

### 23.4.1 Agricultural Management

Agriculture contributes significantly to PLA's eutrophication, ecotoxicity, and human health impacts. Agricultural management strategies can be employed to reduce water quality degradation resulting from corn production. Corn farming relies heavily on agricultural chemicals such as fertilizers (which cause eutrophication) and pesticides (which affect human and ecosystem health). Integrating and optimizing farming practices can enable the mitigation of environmental degradation and reduce biopolymers' environmental footprints. There are many agricultural management strategies that can significantly alleviate bioproducts' agricultural environmental impact, such as changes in tillage practices, use of different fertilizer types, and the installation of buffer strips. The possible negative or positive environmental impacts of these agricultural management strategies are summarized in Table 23.5.

Tillage is often practiced as the first step in the preparation for a soil bed to be made suitable for seed germination and seedling development. There are three typical tillage methods: conventional tillage, reduced tillage, and conservation tillage. Conventional tillage involves plowing the soil surface multiple times throughout the harvest season. Conservation tillage includes no-till, where no tilling is done at all aside from planting. Reduced tillage operates equipment at a level between conventional and no-till practices. Compared with conventional tillage, no-tillage often has more environmental advantages including surface runoff

**TABLE 23.5 Agricultural Management Strategies: Potential Life Cycle Impacts**

| Strategy | Eutrophication and Water Quality | Energy and GWP |
|---|---|---|
| Tillage | | |
| Conventional | – | – |
| No-till | ? | + |
| Fertilizer application | | |
| Precision fertilizer application | + | ? |
| Traditional fertilizer application | – | – |
| Fertilizer type | | |
| Synthetic fertilizer | – | – |
| Manure | – | ? |
| Use of buffer strips | | |
| No buffer strips employed | – | NA |
| Buffer strips at farm edge | + | + |

The symbol "–" indicates that the "strategy" may negatively impact the categories listed in the two columns. "+" indicates a positive impact, "?" indicates uncertainty, and "NA" means not applicable.

reduction and soil erosion mitigation. Other possible environmental benefits include reduction of energy consumption required to operate farming equipment and the associated air emissions. One downfall of conservation tillage is that yields are often less than conventionally tilled crops. This difference in yields would be accounted for in an LCA but would affect the energy saved per mass of corn harvested.

The choice of fertilizer type and the amount applied can affect the energy profile, greenhouse gas emissions, and aqueous emissions for corn farming. Both synthetic fertilizers and animal manure are used to enrich soil nutrition. Compared to manure, most commercially synthetic fertilizers contain higher nutrient concentrations by weight and more appropriate nutrient ratios (i.e., N : P : K ratios) and are more readily available to crops when applied to the soil. High gaseous carbon and nitrogen fluxes result from handling and applying manure. Reusing manures, usually originating as waste products of dairy or poultry farms, is often explored as an economical and sustainable alternative to synthetic fertilizers. The manner and timing of agricultural chemical application can also reduce nutrient and pesticide runoff. Approximately 70% of fertilizers applied to fields are immediately lost to the environment. Efficient fertilizer application such as precision knifing could significantly reduce agricultural environmental impacts.

Establishment of buffer strips is used as a farming nutrient management plan. Riparian buffer zones are a recognized agroforestry practice that not only provide phytoremediation for nonpoint source pollutants but also increase biodiversity of terrestrial ecosystems. They can also provide streambank stabilization, moderate flooding damage, control nutrient leaching, sequester carbon, recharge groundwater, and offer recreational opportunities to landowners. The use of buffers at the edges of agricultural lands could reduce nutrient runoff resulting in eutrophication and decrease life cycle greenhouse emissions.

**TABLE 23.6 Sample of Starch Resources**

| Renewable Resource | Region |
|---|---|
| Corn | United States |
| Sugarcane | Brazil |
| Rice | Asia, United States |
| Potatoes | United States, EU |
| Barley, wheat | United States, EU |
| Cassava | EU, Africa, Latin America |
| Others: yam, taro | Africa, Latin America |

### 23.4.2 Feedstock Choice

Agricultural impacts can also be lessened with the use of less intensive agricultural feedstocks that require less fertilizers, chemicals, and energy. Raw materials for PLA production must have certain properties to be competitive on a large scale with petroleum feedstocks. Such desirable characteristics include renewability, cost competitiveness, availability in plentiful supply, amenability to biotechnology or processing technologies, and low energy and chemical production inputs. Such renewable feedstocks must have significant sugar and be suitable for use as feedstocks, thus broadening the range of feedstocks that might be utilized to produce PLA. A comparative LCA will allow the environmental impacts of alternative biomass feedstocks to be quantified. Generally, corn is considered to be a chemical and energy-intensive crop [98]. Potatoes, however, appear to have even higher material and energy demands and would be a worse crop to substitute for corn [99]. Potential feedstocks that have sufficient starch or sugar content to enable fermentation to lactic acid are summarized in Table 23.6.

### 23.4.3 Energy

Improving upon energy consumption throughout the life cycle of PLA can minimize its environmental footprint. First, the utilization of renewable, sustainable energy sources would reduce fossil fuel usage and global warming potential [100]. Second, life cycle stages exhibiting high energy requirements should be identified and their energy needs minimized. For example, one would focus on the fermentation stage, which is the largest consumer of electricity throughout PLA's life cycle.

Currently, electricity is obtained mainly from coal, natural gas, and nuclear resources in the United States. Utilizing renewable energy sources for electricity and less-intensive agricultural practices could yield a net $CO_2$ sequestration for PLA (approximately 2 kg $CO_2$

sequestered/kg of PLA) and significantly less fossil fuel usage (a savings of up to a factor of 11) compared with petro-polymers [71, 81].

As previously mentioned, 53% of the fossil fuel usage during the fermentation stage is actually due to lactic acid distillation and separation steps, while 42% is attributed to electricity used during fermentation and filtration. Fermentation energy can be reduced by employing alternative methods for providing distillation heat such as steam energy from the combustion of corn or corn wet mill byproducts. In addition, renewable energy such as wind power can be used for electricity needs.

PLA has the potential to outperform its petroleum counterparts on a life cycle basis. The opportunity to close the loop on $CO_2$ emissions does exist with extensive use of renewable sources of energy and the use of alternative (i.e., less intensive) crops. However, fossil-based carbon metrics such as global warming and fossil fuel consumption should not be the only metrics for comparing products derived from renewable materials to petroleum ones. The eutrophication impacts arising from intensive agriculture can be mitigated during corn production or by utilizing alternative, less agricultural chemical intensive feedstocks.

### 23.4.4 Design for End of Life

There is an opportunity to better utilize waste management strategies to improve the environmental impacts of PLA, as identified by Hottle et al. [72]. Further improvements to the waste management of PLA could include utilizing the biodegradability of PLA. PLA has been shown to degrade in aerobic and anaerobic environments and optimizing the waste management systems that utilize this degradation (anaerobic digestion and composting) would produce offsets that could decrease the environmental footprint of PLA. Additionally, the establishment of a recycling infrastructure for PLA could be beneficial. LCA studies shows that recycling of PLA could see the greatest benefits realized from the bio-based polymer [72, 77, 97].

## REFERENCES


1. ISO, *Environmental Management—Life Cycle Assessment—Requirements and Guidelines*, International Organization for Standardization, Geneva, 2006.
2. B. W. Vigon, et al., *Life-cycle Assessment: Inventory Guidelines and Principles*, CRC Press, Boca Raton, FL, 2020.
3. J. A. Fava, et al. (Eds.), *A Technical Framework for Life-cycle Assessment*, ed. I. SETAC and SETAC Foundation for Environmental Education, Pensacola, FL 1991.
4. UNEP/SETAC, *Life Cycle Approaches: The Road from Analysis to Practice*, UNEP/SETAC Life Cycle Initiative, Paris, 2005.
5. X. Pan, et al., Polylactic acid (PLA): research, development and industrialization, *Biotechnol. J.* **2010**, *5*(11), 1125–1136.
6. M. S. Graboski, *Fossil Energy Use in the Manufacture of Corn Ethanol*, National Corn Growers Association, Washington, DC, 2002, pp. 1–122.
7. M. Gulati, et al., Assessment of ethanol production options for corn products, *Bioresour. Technol.* **1996**, *58*(3), 253–264.
8. C. E. Wyman,B.J. Goodman, Biotechnology for production of fuels, chemicals, and materials from biomass, *Appl. Biochem. Biotechnol.* **1993**, *39*(1), 41–59.
9. L. R. Lynd, C. E. Wyman, T. U. Gerngross, Biocommodity engineering, *Biotechnol. Prog.* **1999**, *15*(5), 777–793.
10. M. Akiyama, T. Tsuge, Y. Doi, Environmental life cycle comparison of polyhydroxyalkanoates produced from renewable carbon resources by bacterial fermentation, *Polym. Degrad. Stab.* **2003**, *80*(1), 183–194.
11. J. Lunt, Large-scale production, properties and commercial applications of polylactic acid polmers, *Polym. Degrad. Stab.* **1998**, *59*(1–3), 145–152.
12. D.L. Kaplan (Ed.), Introduction to biopolymers from renewable resources, in: *Biopolymers from Renewable Resources*, Springer, Berlin, Heidelberg, 1998, pp. 1–29.
13. H. S. Kheshgi, R. C. Prince, G. Marland, The potential of biomass fuels in the context of global climate change: focus on transportation fuels, *Ann. Rev. Energy Environ.* **2000**, *25*(1), 199–244.
14. M. Patel, et al., Medium and long-term opportunities and risks of the biotechnological production of bulk chemicals from renewable resources, UU CHEM NW&S (Copernicus), 2006.
15. D. Lorenz, D. Morris, *How Much Energy Does It Take to Make a Gallon of Ethanol?*, Institute for Local Self-Reliance, Washington, DC, 1995.
16. M. Crank, et al., Techno-economic feasibility of large-scale production of bio-based polymers in Europe (PRO-BIP), Final report, Department of Science, 2004.
17. USDA, Byproduct credits and net cost calculations, 2006. Available from: https://www.ers.usda.gov › webdocs › DataFiles.
18. T. L. Carlson, E. M. Peters, Jr., Low pH lactic acid fermentation, Google patents, *Appl., P. Int., Editor*, Cargill Incorporated, USA, 1999. Available from: https://patents.google.com/patent/US6475759B1/en.
19. L. Giorno, et al., Study of a cell-recycle membrane fermentor for the production of lactic acid by *Lactobacillus b ulgaricus*, *Ind. Eng. Chem. Res.* **2002**, *41*(3), 433–440.
20. A. M. Eyal, P. R. Gruber, P. McWilliams, D. R. Witzke, A process for the recovery of lactic acid, Google patents, *P. Appl Int*., Cargill Incorporated, USA, 1998. Available from: https://patents.google.com/patent/EP0932594A2/en.
21. B. Dien, N. Nichols, R. Bothast, Fermentation of sugar mixtures using *Escherichia coli* catabolite repression mutants engineered for production of L-lactic acid, *J. Ind. Microbiol. Biotechnol.* **2002**, *29*(5), 221–227.
22. R. Luedeking, E. L. Piret, A kinetic study of the lactic acid fermentation. Batch process at controlled pH, *J. Biochem. Microbiol. Technol. Eng.* **1959**, *1*(4), 393–412.

23. R. Biomass, T. A. Committee, Vision for bioenergy and biobased products in the United States, Washington, DC, 2006. Available from: https://www1.eere.energy.gov/bioenergy/pdfs/final_2006_vision.pdf.
24. S. Liang, A.G. McDonald, E. R. Coats, Lactic acid production from potato peel waste by anaerobic sequencing batch fermentation using undefined mixed culture, *Waste Manage.* **2015**, *45*, 51–56.
25. S. Liang, A. G. McDonald, E. R. Coats, Lactic acid production with undefined mixed culture fermentation of potato peel waste, *Waste Manage.* **2014**, *34*(11), 2022–2027.
26. G. Dreschke, et al., Lactic acid and methane: improved exploitation of biowaste potential, *Bioresour. Technol.* **2015**, *176*, 47–55.
27. E. B. Arikan, H. D. Bilgen, Production of bioplastic from potato peel waste and investigation of its biodegradability, *Int. Adv. Res. Eng. J.* **2019**, *3*(2), 93–97.
28. L. T. Sin, A. R. Rahmat, W. A. W. A. Rahman, *Polylactic Acid: PLA Biopolymer Technology and Applications*, William Andrew, Amsterdam, 2012.
29. P. Gruber, R. Drumright, D. Henton, Polylactic acid technology, *Adv. Mater.* **2000**, *12*(23), 1841–1846.
30. M. Kreiger, J. M. Pearce, Environmental impacts of distributed manufacturing from 3-D printing of polymer components and products, *MRS Proc.* **2013**, *1492*, 85–90.
31. K. Oksman, M. Skrifvars, J.-F. Selin, Natural fibres as reinforcement in polylactic acid (PLA) composites, *Compos. Sci. Technol.* **2003**, *63*(9), 1317–1324.
32. A. K. Mohanty, M. Misra, L. Drzal, Sustainable biocomposites from renewable resources: opportunities and challenges in the green materials world, *J. Polym. Environ.* **2002**, *10*(1), 19–26.
33. U. DOE, B. T. A. Committee, *Vision for Bioenergy and Biobased Products in the United States*, Biomass Research & Development Technical Advisory Committee, Washington, DC, 2002.
34. B. Choi, S. Yoo, S.-I. Park, Carbon footprint of packaging films made from LDPE, PLA, and PLA/PBAT blends in South Korea, *Sustainability* **2018**, *10*(7), 2369.
35. W. E. Pereira, F. D. Hostettler, Nonpoint source contamination of the Mississippi River and its tributaries by herbicides, *Environ. Sci. Technol.* **1993**, *27*(8), 1542–1552.
36. J. N. Galloway, et al., The nitrogen cascade, *Bioscience* **2003**, *53*(4), 341–356.
37. V. Smil, Phosphorus in the environment: natural flows and human interferences, *Ann. Rev. Energy Environ.* **2000**, *25*(1), 53–88.
38. M. C. Scholten, et al., *Eutrophication Management and Ecotoxicology*, Springer Science & Business Media, Berlin, 2005.
39. J. L. Weld, et al., Identifying critical sources of phosphorus export from agricultural watersheds, *Nutr. Cycl. Agroecosyst.* **2001**, *59*(1), 29–38.
40. I. Chorus, M. Welker, *Toxic Cyanobacteria in Water: A Guide to Their Public Health Consequences, Monitoring and Management*, Taylor & Francis, Boca Raton, FL, 2021.
41. M. Selman, et al., Eutrophication and hypoxia in coastal areas: a global assessment of the state of knowledge, *World Resour. Inst.* **2008**, *284*, 1–6.
42. Millennium Ecosystem Assessment, *Ecosystems and Human Well-being: Synthesis*, Island Press, Washington, DC, 2005. Available from: https://www.millenniumassessment.org/documents/document.356.aspx.pdf.
43. M. Weiss, et al., A review of the environmental impacts of biobased materials, *J. Ind. Ecol.* **2012**, *16*(s1), S169–S181.
44. J. Guinée, R. Heijungs, E. Voet, A greenhouse gas indicator for bioenergy: some theoretical issues with practical implications. *Int. J. Life Cycle Assess.* **2009**, *14*, 328–339.
45. M. Brandão, A. Levasseur, Assessing temporary carbon storage in life cycle assessment and carbon footprinting, Report JRC 63225, 2011.
46. P. Kjeldsen, et al., Present and long-term composition of MSW landfill leachate: a review, *Crit. Rev. Environ. Sci. Technol.* **2002**, *32*(4), 297–336.
47. A. Laurent, et al., Review of LCA studies of solid waste management systems—part I: lessons learned and perspectives, *Waste Manage.* **2014**, *34*, 573–588.
48. S. Manfredi, et al., Landfilling of waste: accounting of greenhouse gases and global warming contributions. *Waste Manage. Res.* **2009**, *27*, 825–836.
49. A. Gongora, Sugarcane bagasse cogeneration in Belize: a review, *Renew. Sustain. Energy Rev.* **2018**, *96*, 58–63.
50. K. E. Lorber, G. Kreindl, E. Erdin, H. Sarptas, Waste management options for biobased polymeric composites, In 4th International Polymeric Composites Symposium, 2015, May, pp. 1–9. Available from: https://www.researchgate.net/profile/Hasan-Sarptas/publication/276065476_Waste_Management_Options_for_Biobased_Polymeric_Composites/links/5550921e08ae93634ec94d75/Waste-Management-Options-for-Biobased-Polymeric-Composites.pdf.
51. S. C. Kamate, P. B. Gangavati, Cogeneration in sugar industries: technology options and performance parameters—a review, *Cogener. Distrib. Gener. J.* **2009**, *24*(4), 6–33.
52. D. Zhang, E. A. del Rio-Chanona, N. Shah, Life cycle assessments for biomass derived sustainable biopolymer & energy co-generation, *Sustain. Prod. Consum.* **2018**, *15*, 109–118.
53. L. Ruggieri, et al., Performance of different systems for the composting of the source-selected organic fraction of municipal solid waste, *Biosyst. Eng.* **2008**, *101*, 78–86.
54. Rothamsted, *Rothamsted Long-term Experiments—Guide to the Classical and Other Long-term Experiments*, Rothamsted Research, Harpenden, Herfordshire, 2006.
55. EREF, T.E.R.E.F., Anaerobic digestion of municipal solid waste: report on the state of practice, Internal Research Program, 2015, https://erefdn.org/.
56. R. Mohee, G. D. Unmar, A. Mudhoo, P. Khadoo, Biodegradability of biodegradable/degradable plastic materials under aerobic and anaerobic conditions, *Waste Manage.* **2008**, *28*(9), 1624–1629.
57. V. Massardier-Nageotte, et al., Aerobic and anaerobic biodegradability of polymer films and physico-chemical characterization, *Polym. Degrad. Stab.* **2006**, *91*(3), 620–627.


58. B. Veronika, Anaerobic degradation of bioplastics: a review, *Waste Manage.* **2018**, *80*, 406–413.
59. European Commission, *Closing the loop – An EU action plan for the Circular Economy*, t.C., Communication from the Commission to the European Parliament, the European Economic and Social Committee and the Committee of the Regions, Editor, 2015. Available from: http://eur-lex.europa.eu/legal-content/EN/TXT/?uri=CELEX:52015DC0614.
60. M. Carus, L. Dammer, The circular bioeconomy—concepts, opportunities, and limitations, *Ind. Biotechnol.* **2018**, *14*(2), 83–91.
61. J. J. Kolstad, E. T. Vink, B. De Wilde, L. Debeer, Assessment of anaerobic degradation of Ingeo polylactides under accelerated landfill conditions, *Polym. Degrad. Stab.* **2012**, *97*(7), 1131–1141.
62. M. J. Krause, T. G. Townsend, Life-cycle assumptions of landfilled polylactic acid underpredict methane generation, *Environ. Sci. Technol. Lett.* **2016**, *3*(4), 166–169.
63. C. Ingrao, et al., Polylactic acid trays for fresh-food packaging: a carbon footprint assessment, *Sci. Total Environ.* **2015**, *537*, 385–398.
64. D. Meeks, T. Hottle, M. M. Bilec, A. E. Landis, Compostable biopolymer use in the real world: stakeholder interviews to better understand the motivations and realities of use and disposal in the US, *Resour. Conserv. Recycl.* **2015**, *105*, 134–142.
65. T. A. Hottle, et al., Alkaline amendment for the enhancement of compost degradation for polylactic acid biopolymer products, *Compost Sci. Util.* **2016**, *24*(3), 159–173.
66. K. Hamad, Properties and medical applications of polylactic acid: a review, *eXPRESS Polym. Lett.* **2015**, *9*, 435–455.
67. M. Itävaara, S. Karjomaa, S. Johan-Fredrik, Biodegradation of polylactide in aerobic and anaerobic thermophilic conditions, *Chemosphere* **2002**, *46*, 879–885.
68. S. R. Hobbs, et al., Anaerobic codigestion of food waste and polylactic acid: effect of pretreatment on methane yield and solid reduction, *Adv. Mater. Sci. Eng.* **2019**, *2019*, 1–6.
69. H. Yagi, F. Ninomiya, M. Funabashi, M. Kunioka, Anaerobic biodegradation tests of poly(lactic acid) under mesophilic and thermophilic conditions using a new evaluation system for methane fermentation in anaerobic sludge, *Int. J. Mol. Sci.* **2009**, *10*(9), 3824–3835.
70. A. Soroudi, I. Jakubowicz, Recycling of bioplastics, their blends and biocomposites: a review, *Eur. Polym. J.* **2013**, *49*(10), 2839–2858.
71. E. T. Vink, S. Davies, Life cycle inventory and impact assessment data for 2014 Ingeo™ polylactide production, *Ind. Biotechnol.* **2015**, *11*(3), 167–180.
72. T. A. Hottle, M. M. Bilec, A. E. Landis, Biopolymer production and end of life comparisons using life cycle assessment, *Resour. Conserv. Recycl.* **2017**, *122*, 295–306.
73. W. J. Groot, T. Borén, Life cycle assessment of the manufacture of lactide and PLA biopolymers from sugarcane in Thailand, *Int. J. Life Cycle Assess.* **2010**, *15*(9), 970–984.
74. D. J. Newby, Life cycle assessment of polylactic acid biopolymer industrial waste management techniques in belize, MS thesis, University of Kentucky, 2021.
75. S. R. Hobbs, et al., Life cycle assessment of bioplastics and food waste disposal methods, *Sustainability* **2021**, *13*(12), 6894.
76. C. Moretti, et al., Cradle-to-grave life cycle assessment of single-use cups made from PLA, PP and PET, *Resour.Conserv. Recycl.* **2021**, *169*, 105508.
77. S. Paponge, et al., Comparative assessment of the environmental profile of PLA and PET drinking water bottles from a life cycle perspective, *J. Clean. Prod.* **2014**, *65*, 539–550.
78. S. Walker, R. Rothman, Life cycle assessment of bio-based and fossil-based plastic: a review, *J. Clean. Prod.* **2020**, *261*, 121158.
79. T. A. Hottle, M. M. Bilec, A. E. Landis, Sustainability assessments of bio-based polymers, *Polym. Degrad. Stab.* **2013**, *98*(9), 1898–1907.
80. A. Morão, F. de Bie, Life cycle impact assessment of polylactic acid (PLA) produced from sugarcane in Thailand, *J. Polym. Environ.* **2019**, *27*(11), 2523–2539.
81. E. T. H. Vink, et al., Applications of life cycle assessment to NatureWorks™ polylactide (PLA) production, *Polym. Degrad. Stab.* **2003**, *80*(3), 403–419.
82. T. U. Gerngross, S. C. Slater, How green are green plastics? *Sci. Am.* **2000**, *283*(2), 36–41.
83. S. Spierling, et al., Bio-based plastics—a review of environmental, social and economic impact assessments, *J. Clean. Prod.* **2018**, *185*, 476–491.
84. M. Wang, Updated energy and greenhouse gas emission results of fuel ethanol. Center for Transportation Research, Argonne National Laboratory, 2005. Available from: http://www.transportation.anl.gov/pdfs/TA/375.pdf.
85. P. R. Gruber, et al., Hydroxyl-terminated lactide polymer composition, Google Patents, 1995.
86. B. G. Hermann, K. Blok, M. K. Patel, Twisting biomaterials around your little finger: environmental impacts of bio-based wrappings, *Int. J. Life Cycle Assess.* **2010**, *15*(4), 346–358.
87. B. G. Hermann, et al., To compost or not to compost: carbon and energy footprints of biodegradable materials' waste treatment, *Polym. Degrad. Stab.* **2011**, *96*(6), 1159–1171.
88. V. Piemonte, Bioplastic wastes: the best final disposition for energy saving, *J. Polym. Environ.* **2011**, *19*(4), 988–994.
89. F. Gironi, V. Piemonte, Life cycle assessment of polylactic acid and polyethylene terephthalate bottles for drinking water, *Environ. Prog. Sustain. Energy* **2011**, *30*(3), 459–468.
90. V. Rossie, et al., Life cycle assessment of end-of-life options for two biodegradable packaging materials: sound application of the European waste hierarchy, *J. Clean. Prod.* **2015**, *86*, 132–145.
91. E. Benetto, et al., Using atmospheric plasma to design multilayer film from polylactic acid and thermoplastic starch: a screening life cycle assessment, *J. Clean. Prod.* **2015**, *87*, 953–960.
92. E. Van der Harst, J. Potting, A critical comparison of ten disposable cup LCAs. *Environ. Impact Assess. Rev.* **2013**, *43*, 86–96.
93. S. Madival, et al., Assessment of the environmental profile of PLA, PET and PS clamshell containers using LCA methodology. *J. Clean. Prod.* **2009**, *17*(13), 1183–1194.


94. G. S. Lorite, et al., Evaluation of physicochemical/microbial properties and life cycle assessment (LCA) of PLA-based nanocomposite active packaging, *LWT* **2017**, *75*, 305–315.
95. M. B. K. Kruger, A. Detzel, Life cycle assessment of food packaging made of Ingeo™ biopolymer and (r)PET, 2002.
96. EPA, Waste Reduction Model (WARM), Environmental Protection Agency (EPA), 2020. Available from: https://www.epa.gov/warm/versions-waste-reduction-model-warm#15.
97. F. Gironi, V. Piemonte, Bioplastics and petroleum-based plastics: strengths and weaknesses, *Energy Sour. Part A Recov. Util. Environ. Eff.* **2011**, *33*(21), 1949–1959.
98. R. Frischknecht, et al., The ecoinvent database: overview and methodological framework (7 pp), *Int. J. Life Cycle Assess.* **2005**, *10*(1), 3–9.
99. J. P. Scharlemann, W. F. Laurance, Environmental science: How green are biofuels? *Science* **2008**, *319*, 43–44.
100. I. D. Posen, et al., Greenhouse gas mitigation for US plastics production: energy first, feedstocks later, *Environ. Res. Lett.* **2017**, *12*(3), 034024.

# 24

# END-OF-LIFE SCENARIOS FOR POLY(LACTIC ACID)

Anibal Bher, Edgar Castro-Aguirre, and Rafael Auras

## 24.1 INTRODUCTION

The implementation of bio-based polymers to reduce the dependency on fossil-based resources provides opportunities for advancing global sustainable development goals toward a circular economy [1]. The analysis of the end-of-life (EoL) scenarios of polymers has become a critical issue of the circular economy and for several organizations and countries [2]. Bio-based polymers offer sustainability benefits for the new circular economy, such as renewable resources and lower environmental footprint (EFP) [3].

The optimal EoL scenarios of polymers can differ. So, determining polymers' EoL scenario with the lowest environmental impact depends on several factors such as the nature of the polymer, their end-use purpose, the level of product contamination (e.g., food or chemical residues in packages), as well as the available infrastructure for collection, sorting, and processing. The different EoL scenarios of plastics can be categorized as mechanical recycling, chemical (advanced) recycling, incineration with or without energy recovery, biodegradation in industrial or home composting, anaerobic biodegradation (digestion), and landfilling. The land and aquatic environment should not be considered a disposal environment and should not be designated as an EoL, but as an undesired leakage into the natural system.

Poly(lactic acid) (PLA) is a polymer derived from renewable resources with increasing potential for food and medical packaging, automotive, and agricultural applications [4]. Since PLA is bio-based and compostable, it provides benefits associated with its beginning of life and end of life (Figure 24.1).

Figure 24.2a shows the benefit of PLA being part of the biological carbon cycle in which carbon has the potential to regenerate in a much shorter timeframe when compared with fossil-based polymers. PLA has also been shown to have a lower EFP in some impact assessment categories when compared with conventional polymers, e.g., Figure 24.2b–d show the impacts of two commercially available PLAs, Ingeo™ and Luminy®, on climate change, nonrenewable energy, and water depletion. Morão and de Bie have reported a carbon footprint of around 0.51 kg $CO_2$ eq./kg of PLA resin from cradle-to-gate for PLA resin [6]. A similar value was previously reported for the commercial resin Ingeo™ (around 0.6 kg $CO_2$ eq./kg PLA resin) (Figure 24.2b) [7]. A full discussion of PLA's environmental footprint indicators is provided in Chapter 23.

At its EoL, the environmental benefits of PLA are related to the type of product and application during their service life. This chapter describes the potential EoL scenarios for PLA, and their advantages and disadvantages. Different EoL scenarios would be preferred for various PLA applications and final products. EoL scenarios are discussed in the context of the availability of infrastructure.

## 24.2 TRANSITION FROM A LINEAR TO A CIRCULAR ECONOMY FOR PLASTICS

A circular economy is defined as a system that can restore, retain, and redistribute materials, components, and products back into the system efficiently, for as long as it is environmentally, technically, socially, and economically feasible.

*Poly(Lactic Acid): Synthesis, Structures, Properties, Processing, Applications, and End of Life*, Second Edition.
Edited by Rafael A. Auras, Loong-Tak Lim, Susan E. M. Selke, and Hideto Tsuji.

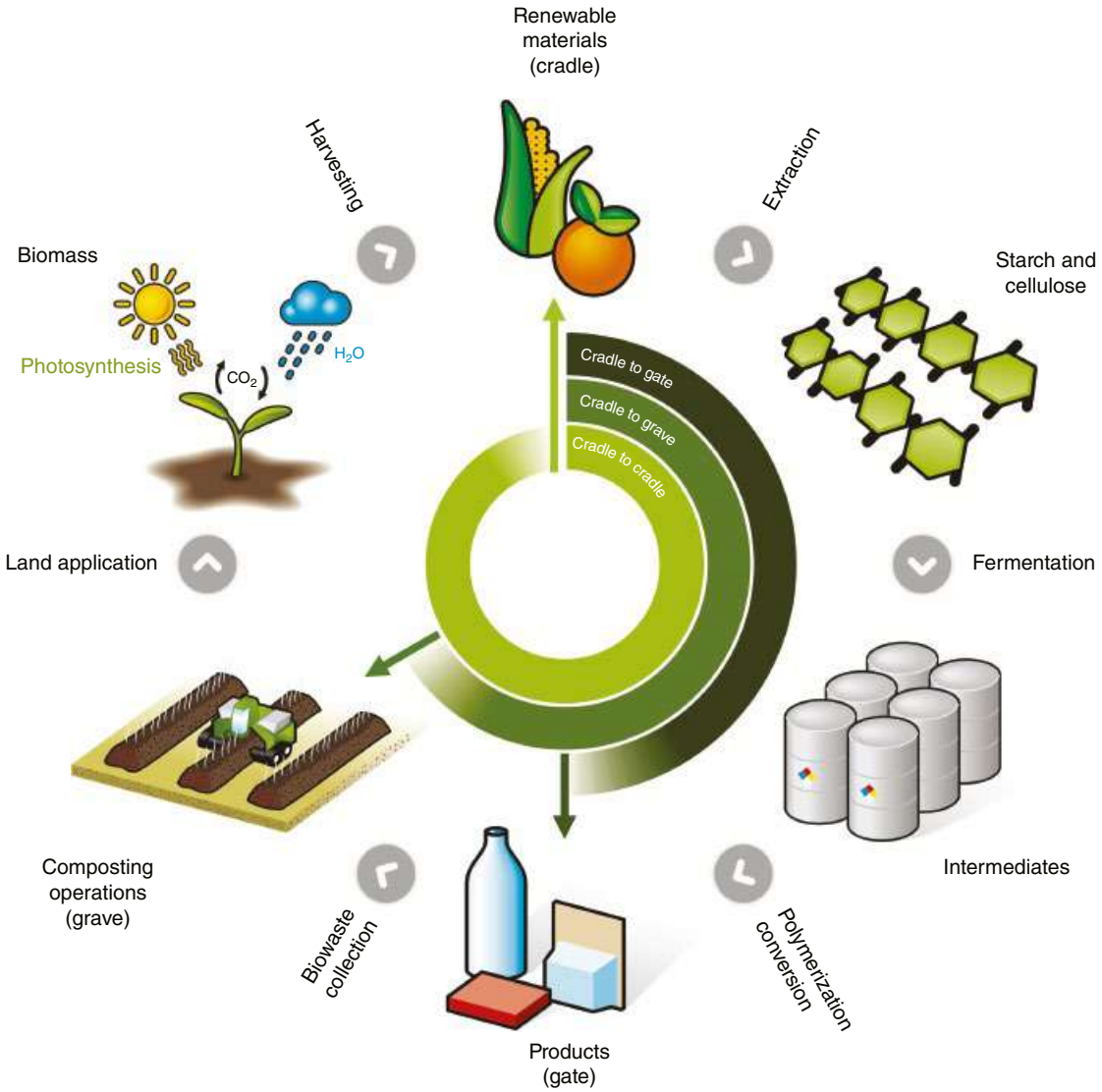


**FIGURE 24.1** Cradle-to-gate, cradle-to-grave, and cradle-to-cradle representing production, consumption, and disposal of bio-based polymers from renewable resources by composting. Source: Reproduced from Ref. [5].

The three main objectives of a circular plastics economy are (i) decouple plastics from fossil feedstocks; (ii) create an effective after-use plastics economy; and (iii) drastically reduce the leakage of plastics into natural systems. So, a waste management system for plastics, per the circular economy concept, intends to minimize materials disposal in landfills while maximizing material reduction and their re-use and recycling (including composting from a biological cycle perspective), avoiding the classical linear flow of production, use, and discard of materials [8]. In the last decade, increasing activities have focused on addressing plastic land and marine pollution and developing policies to prevent waste, mismanagement, and littering, especially for single-use plastics [9, 10]. An important outcome has been that the production of nonbiodegradable single-use plastics is unsustainable in terms of the circular management of plastics [2, 11]. If business continues as usual, projections for the mismanaged global plastic waste per year estimate an increasing trend from 100 million tons in 2020 to ~220 million tons for 2040. However, a potential scenario, considering the improvement of the worldwide waste management system and a shift to a circular plastic economy where use of plastics is highly reduced, and designed for recyclability and/or biodegradability, shows a decreasing trend of plastic pollution by 2040 from 100 to ~25 million tons [12–14].

Thus, turning what is considered waste in a classical linear plastics economy into a valuable resource is a critical element of the circular economy for plastics. If plastics are re-manufactured, re-used, and recycled, this allows for a transition to a circular plastics economy where waste

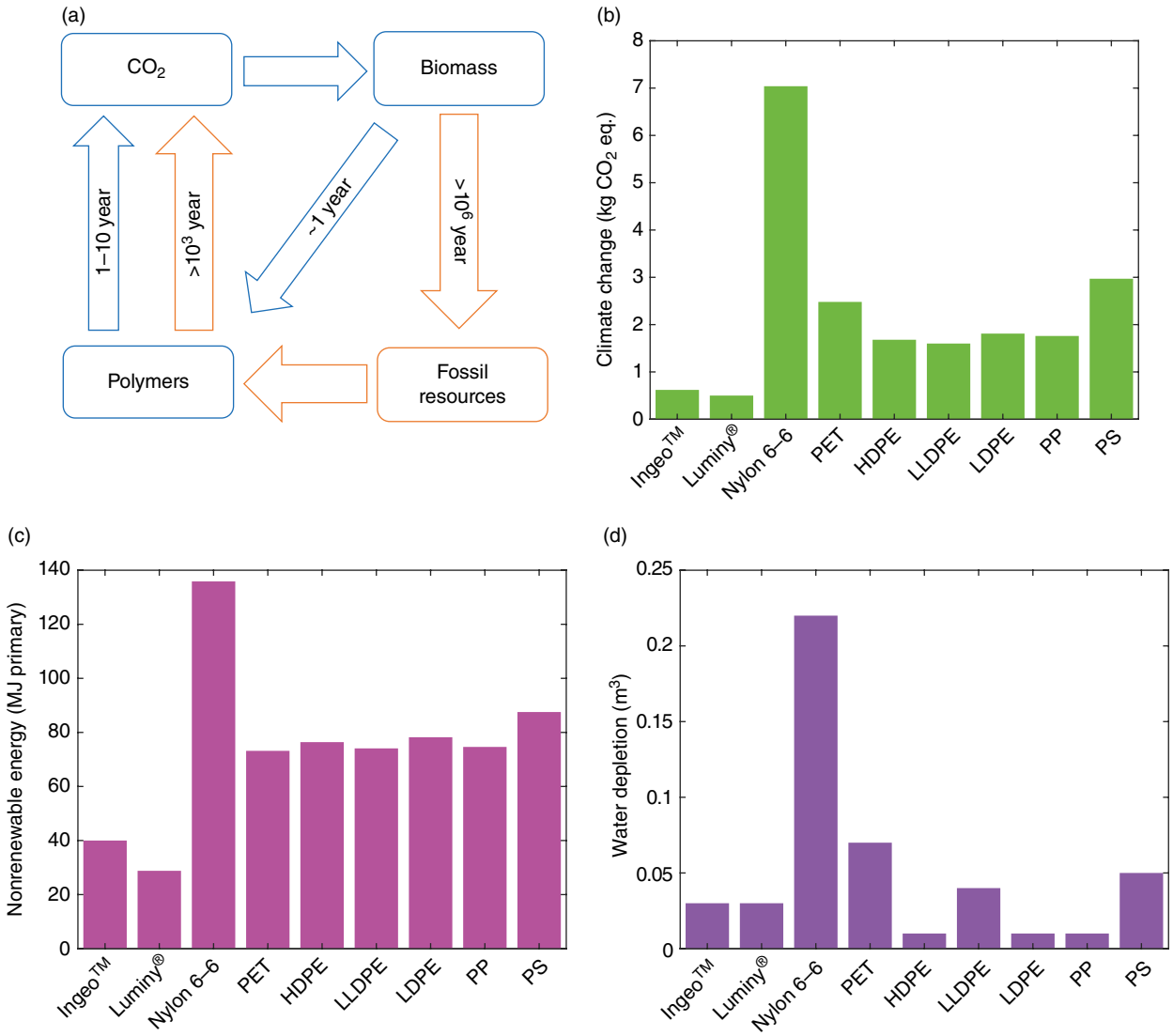


**FIGURE 24.2** Carbon cycle of polymers and environmental footprint (EFP) for PLA and other commercial polymers. (a) Carbon cycle of polymers derived from bio-based and fossil resources; (b) climate change indicator; (c) nonrenewable energy indicator; and (d) water uptake indicator for the production of the current commercial resins PLA Ingeo™, and PLA Corbion Luminy®, and other commercial polymers. Source: Adapted from Ref. [4].

generation is reduced, and resources are used efficiently and sustainably. The waste management system plays an essential role on reducing plastic pollution, along with other initiatives such as encouragement for innovative recycling technologies and incentives for change in consumer behavior [15]. A large portion of plastic waste is generated by packaging. A recent report based on a global assessment of standards, labels, and claims on plastic packaging highlights the importance of providing clear definitions and information to consumers about the reusability or recyclability of plastic packaging [16]. In this context, upstream innovation in packaging targeting the reduction of waste generation in the first place has also been analyzed and encouraged [17].

## 24.3 WASTE MANAGEMENT SYSTEM

The optimal EoL management option for plastics must be assessed to target a lower EFP of the entire system. So, alternative waste management systems are required to meet current and future needs and address land and marine plastics pollution problems [18]. The main objective of the waste management system is to prevent the generation of waste in the first place, recover waste in the second place, and minimize the final disposal of waste. Hence, the first category of the waste management system, waste prevention and reduction, is not strictly considered as an EoL scenario.

Figure 24.3 presents the general waste management system hierarchy showing the most desired and convenient

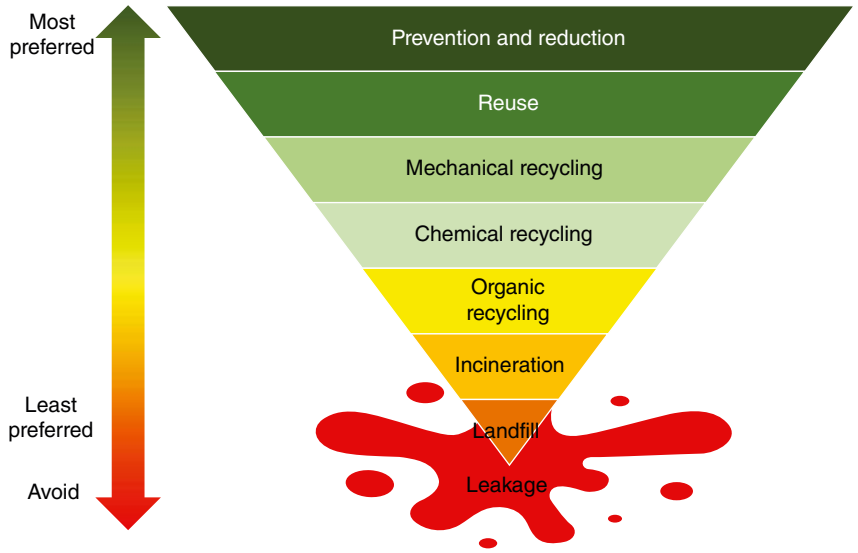


**FIGURE 24.3** Hierarchy of the waste management system showing the most efficient category (prevention and reduction) from an environmental point of view and conservation of resources to the least efficient (landfill). Source: Adapted from Refs. [3, 15, 20].

scenario from a resource conservation perspective. In general terms for plastics, the key to the waste management system is to prevent, reduce, re-use, and recycle the highest amount possible of plastic waste generated, to move from a linear plastics economy to a circular plastics economy, thereby maximizing the conservation of resources and minimizing the amount of plastic leaking to the environment [19].

The waste management system describes, as a hierarchical ranking system, the EoL alternatives based on efficient conservation of resources. The European Commission (EC) and the United States (US) waste management systems are defined in similar ways. The US Environmental Protection Agency (EPA) presents a sustainable materials management system of four levels (i.e., reduction and reuse, recycling/composting, energy recovery, and disposal), and the EC a five-level system (i.e., prevention, reuse, recycling, recovery, and disposal). Despite that, the main goal remains the same: reducing waste to be disposed of to minimize the environmental impacts of the system.

Considering the main four US steps:

1. *Prevention, minimization or source reduction, and reuse*: This level of waste management implies potential waste reduction at the source, which is the most preferred strategy in terms of maximizing the conservation of resources. This strategy has several options and requires manufacturing processes and materials that minimize resource use and maximize the performance of the product by developing clean production and technology, e.g., lightweighting, reuse, remanufacturing, redesigning products, reducing toxicity, buying in bulk, among others. In the packaging area, prevention of potential waste starts at the process level following actions at the marketing, distribution, utilization, and elimination stages. In this context, reducing the amount of fossil-based plastic can be achieved by changing the types of materials used.
2. *Recycling (mechanical, chemical, aerobic organic composting, anaerobic organic digestion)*: The second preferred level of the waste hierarchy is recycling, which includes activities such as collection of used, reused, and unused items. Material recycling systems are complex and consist of interconnected networks, which require seamless transactions between the different stages. To efficiently collect, sort, recycle, and reuse materials, several stakeholders and stages must work together as depicted in Figure 24.4. Recycling and reuse start with consumer engagement. The main factors determining whether a consumer will engage in recycling and material reuse are motivation and convenience. Different approaches vary in the relative importance given to how consumers engage with recycling [21, 22]. The collection stage is mostly defined by the amount of material collected. For packaging, a common collection approach is to allow some or all materials to be mixed in a recycling bin—commingled collection. This often increases participation significantly at the expense of increased separation cost [23, 24]. For recyclable materials to be useful and re-enter the circular economy, they must be separated by the type of material through sortation. Sortation of the commingled materials is done in a material recovery facility (MRF) [25]. Depending on the type of recovered material, the reprocessing steps may be several [26]. Items can be sorted and reprocessed in raw materials that allow the manufacturing of new


**FIGURE 24.4** Steps and stakeholders required for a successful material recycling system.

products via mechanical or chemical recycling. In organic recycling, such as in composting or anaerobic digestion, biological or organic recycling implies returning of biodegradable materials to the ecosystem to fulfill the product's life cycle. The reprocessing facilities are not always close to the communities or MRFs. Hence, the transportation costs between the collection sites, MRFs, and reprocessing facilities should not hinder the recovery and competition with the new or virgin material; situations regularly found for high-density materials such as glass. Finally, end market supply and demand drive the final price of recycled materials [18, 27]. In the case of recycling materials without strong legislation to encourage recycling and incentivize the circular economy, the supply of virgin material competes with post-consumer recycled materials.

Some of the recycling-level benefits are preventing greenhouse gas emissions and water pollutants, saving energy, developing greener technologies, and reducing the need for new combustors and landfills. In packaging, a material is recyclable if it can be collected, sorted, reprocessed, and ultimately reused in manufacturing or making another item. In this context, guidance from organizations and regulatory bodies worldwide, such as the Green Guides from the Federal Trade Commission (FTC) in the United States, helps avoid making environmental claims that mislead consumers [28]. The Sustainable Packaging Coalition (SPC) promotes a standardized labeling system (How2Recycle) to communicate recyclability following the FTC Green Guides in which a product or package is considered widely recyclable only when recycling facilities are available to a substantial majority (at least 60%) of consumers or communities [28, 29]. In this sense, the SPC reported that in 2016 about 73% of US residents had access to curbside recycling programs. Drop-off recycling programs are available to 64% of the US population. For 21% of the population, drop-off programs are the only one available. For 6% of the US residents, no option of recycling program is available [30].

3. *Incineration with and without energy recovery:* For waste that is nonrecyclable from an economical and technical point of view, or if a recycling system is unavailable, incineration with energy recovery is the last option in terms of conservation of energy resources. Several processes, such as combustion, gasification, and pyrolysis, allow the recovery of energy from waste to generate heat, electricity, or fuel. Since both systems, with and without energy recovery, generate a minimal amount of ash to be disposed of, the non-recovery option is the least efficient system of this level.
4. *Disposal in landfills*: Government regulations and standards as they were developed led to modern landfills replacing open dumps. Current landfills are facilities located, designed, operated, and monitored to ensure compliance with laws (including closure requirements). The waste, before its disposal, can be physically, chemically, and/or biologically treated to reduce its volume, toxicity, and hazards. Landfills can generate leachate that can be processed in a leachate treatment system, and methane gas that can be collected and used to generate electricity.

As described, the waste management system considers a hierarchy for waste management to maximize resource conservation and ensure the most environmentally beneficial options. Particular considerations when addressing EoL options for some materials can impact the most convenient EoL scenario. Commercial plastics can be produced using fossil-based or bio-based resources and can be nonbiodegradable or biodegradable. EoL options such as biodegradation (industrial composting, home composting, and anaerobic digestion) are recommended for situations where materials are highly contaminated, e.g., in food packaging. In this situation, a complex contaminated material is not economically viable for mechanical or chemical recycling or recoverable through incineration, and since landfilling should be avoided, which results in compostability as the optimal EoL scenario.

Efforts to shift from a linear economy to a circular economy for plastics by implementing a waste management

system hierarchy must continue to reverse the current global status of polymer flow. In 2016, the plastic economy reported that around 85% of the total plastic waste generated was mismanaged. Approximately 19% was disposed to unmanaged dumps or leaked into the environment, 40% ended in landfills, and 25% was incinerated [31]. Environmental pollution of plastics, microplastics, and nanoplastics leaking to the ocean and everywhere in the biosphere highlights the necessity for a shift to a circular economy. The specific EoL scenarios of PLA will be discussed in the context described above and how it can contribute to a reduction in the amount of plastic leaking to the environment.

## 24.4 END-OF-LIFE SCENARIOS FOR PLA

Consumer habits and preferences toward sustainable materials have changed in the last decades due to an increasing global awareness of sustainability and environmental issues. Thus, as environmental awareness rises, companies and marketers using these materials must be committed to meeting those preferences [32]. So, new sustainable materials are demanded to reduce the environmental impacts associated with conventional materials and its related processes [33]. Among these preferences, there is an increasing demand for bio-based and biodegradable polymers to replace traditional fossil-based polymers [34], which are perceived as materials with higher EFP [7, 35].

PLA is one of the most popular bio-based polymers to address these consumer preferences, and this is reflected by its increasing demand in areas such as food packaging, agricultural mulch films, biomedical devices, fibers for textiles, automotive parts, electronic parts, and filaments for 3D printing, among others [36, 37]. The advantage of PLA is that it can be technically treated in all levels of the waste management hierarchy system previously described, with industrial composting as a potential EoL scenario for single-use contaminated applications such as in food packaging [4, 38, 39]. The optimal EoL scenario is affected by the type of product and its application. When PLA is clean and dry as in automotive parts and filaments, reuse and recycling become viable and convenient EoL alternatives if proper infrastructure exists and enough volume is collected [40]. Biodegradation in composting conditions of PLA has been recommended in situations where the PLA products are highly contaminated as in food packaging products or agricultural films [3].

There are some current limitations to effective recovery of PLA due to its low collection volume, and scarce infrastructure for sorting, recycling, and composting of PLA products at their end-of-life [41]. This is an evolving space, and many efforts are being made to improve the infrastructure and access to recycling and composting for different plastics materials, including PLA. Some organizations such as the Association of Plastic Recyclers (APR), the SPC, Materials Recovery for the Future (MRFF), the Recycling Partnership, Closed Loop Partners, Plastic Recyclers Europe, and Chemical Recycling Europe, among others, are working on initiatives to mitigate current challenges faced by recyclable and compostable materials [42–48].

The actual context of plastic waste at the municipal solid waste (MSW) level in the United States is reflected in the US EPA report, showing that the current situation remains deficient in terms of waste management (Table 24.1) [49]. The 2018 MSW report stated that about 292,360 thousand tons of MSW were generated in the United States in 2018, from which ~23.6% were recycled, ~8.5% were composted, ~11.8% were combusted with energy recovery, and ~50% were discarded in landfills.

Of the total MSW generated in 2018, plastics represented ~12.2% (35,680 thousand tons). From this amount, the total fraction of plastic recycled was ~8.7%, the total fraction of plastics combusted with energy recovery was ~15.8%, and the total fraction of plastics discarded in landfills ~75.6%.

The plastic waste in MSW is divided into durable goods, nondurable goods, and containers and packaging. Plastics in the durable goods section represented around 13,690 thousand tons of plastics generated (38.4%), from which ~6.8% was recycled, ~12.7% combusted with energy recovery, and ~80.5% landfilled. For plastics in the nondurable goods section, around 7460 thousand tons (20.9%) were generated in 2018, from which ~2.4% was recycled, ~19.0% combusted with energy recovery, and ~78.5% landfilled. For plastics in the section of containers and packaging, around 14,530 thousand tons (40.7%) were generated in 2018, from which ~13.6% was recycled, ~16.9% combusted with energy recovery, and ~69.4% landfilled. The amount of composted plastics was not reported for any of these categories, but it is likely to be negligible.

PLA represented around 0.25% of the plastic waste generated (90 thousand tons), with ~78% being nondurable goods (e.g., plastic plates and cups), and ~22% being containers and packaging (e.g., closures, trays, and loose fill). In terms of EoL scenarios, only a negligible value was recycled (less than 5000 tons) and no data was reported for composting, combustion with energy recovery and landfill.

These overall data show a high deficiency in the treatment of plastics waste with a large percentage being landfilled and represent a missing opportunity to collect and recycle more post-consumer plastic and more types of plastic materials, where PLA is still a minor component in terms of volume.

The overall situation in the European Union is different. According to Plastics Europe, 29.1 million tons of plastic waste were generated in 2019. From this total amount, ~32.5% was recycled, almost 43% was combusted with energy recovery, and around 25% was landfilled. However, no specific information on PLA EoL scenarios was provided in the report [50].

**TABLE 24.1 Municipal Solid Waste (MSW), Plastics, and Resins Generated, Recycled, Composted, and Landfilled in 2018 in US (Thousand Tons)**

| | Thousand of Tons[a] | | | | |
|---|---|---|---|---|---|
| Materials | Generated | Recycled | Composted | Incinerated with Energy Recovery | Landfilled |
| MSW | 292,360 | 69,090 | 24,890 | 34,550 | 146,120 |
| Plastics | 35,680 | 3090 | N/A | 5620 | 26,970 |
| *Durable goods* | 13,690 | 930 | N/A | 1740 | 11,020 |
| *Nondurable goods* | 7460 | 180 | N/A | 1420 | 5860 |
| *Containers and packaging* | 14,530 | 1980 | N/A | 2460 | 10,090 |
| Resins | 35,680 | 3090 | N/A | 5620 | 26,970 |
| *PET* | 5290 | 980 | N/A | N/A | N/A |
| *HDPE* | 6300 | 560 | N/A | N/A | N/A |
| *PVC* | 840 | Neg | N/A | N/A | N/A |
| *LDPE/LLDPE* | 8590 | 370 | N/A | N/A | N/A |
| *PP* | 8150 | 50 | N/A | N/A | N/A |
| *PS* | 2260 | 20 | N/A | N/A | N/A |
| *PLA* | 90 | Neg | N/A | N/A | N/A |
| *Other Resins* | 4160 | 1,110 | N/A | N/A | N/A |

Source: Adapted from Ref. [49].
N/A: Not available; Neg: Negligible, less than 5000 tons.
[a] Is not depicted the portion of "Other food management" with 17,710 thousand tons.

### 24.4.1 Prevention and Source Reduction

When considering new applications for PLA to gain market presence, it is relevant to analyze in more detail the preferred EoL scenarios [38]. The waste management hierarchy emphasizes source reduction by designing and redesigning products, especially packaging, to achieve material reduction (lightweighting), longer product life, and reuse [51, 52]. A reduction of the EFP can be achieved when a reduction of weight is implemented during the production stage or a reduction of emissions can be achieved through system optimization.

Material reduction or lightweighting of PLA is a strategy of great interest not only for its economic value but also for waste reduction. However, besides the aim of material reduction, the mechanical, thermal, and barrier properties of PLA must be considered, e.g., in applications like food packaging, maintaining a long shelf life of the product is highly important for both cost and food waste reduction. To avoid performance drawbacks, efforts have been made over the years to produce lightweight PLA materials with good physical and mechanical properties by reinforcing the PLA matrix adding fibers, fillers, composites, and nanocomposites [53–55].

A composite material produced from PLA-sugar beet had lower density compared to neat PLA; however, the mechanical properties were negatively affected due to the added fraction of sugar beet pulp [53]. PLA was also reinforced by using functionalized sepiolite-aminosilane grafted filler and a chemical foaming agent (CFA) to produce lightweight PLA composite with enhanced mechanical properties [54]. Although the addition of CFA significantly reduced the composite density, its mechanical property performance was reduced unless the sepiolite filler was also added. Furthermore, a synergistic effect of the CFA and the functionalized sepiolite filler was reported, where the density was significantly reduced, and the modulus was improved.

The lightweight PLA/cellulose fiber composite was also employed in the automotive industry as a floor-load material [55]. This composite with 50%wt fiber had the highest tensile strength, associated with the ability of the fiber to form hydrogen bonding networks within the PLA matrix. Hence, the composites with 50%wt of fiber fraction and nominal densities of 0.2, 0.3, and 0.4 g/cm$^3$ met the flexural stress and stiffness for the load floor weight of the vehicle specifications [55]. As the market for PLA auto parts increases, it is expected that additional technologies will be developed with the aim of reducing the weight of the PLA-based materials [4].

PLA can be processed using technologies like film extrusion, blown film extrusion, or biaxially oriented film extrusion, which offer the possibility to optimize the amount of resin per unit of area of packaging material needed.

To demonstrate the potential environmental impact of lightweighting PLA, a streamlined Life Cycle Assessment (LCA) was conducted on three hypothetical scenarios from cradle to gate with each scenario reducing the weight of PLA by 1 kg (Table 24.2). The LCA midpoint indicators were reported according to TRACI 2.1 (Tool for the Reduction and Assessment of Chemical and Other Environmental Impacts) per the US EPA specifications, with acidification, eutrophication, particulate matter, and

**TABLE 24.2 Impact Analysis of Each Midpoint Indicator for Scenario 5 (5 kg of PLA) to Scenario 3 (3 kg of PLA)**

| Midpoint Indicators | Scenario 5 | Scenario 4 | Scenario 3 |
|---|---|---|---|
| PLA weight in scenario (kg) | 5 | 4 | 3 |
| Climate change (AR5) (kg $CO_2$ eq.) | 14.81 | 11.85 | 8.89 |
| Climate change, incl. bio. $CO_2$ (AR5) (kg $CO_2$ eq.) | 5.60 | 4.48 | 3.36 |
| PED, nonrenewable (MJ) | 224.64 | 179.71 | 134.78 |
| PED, renewable (MJ) | 138.64 | 110.91 | 83.19 |
| PED, total (MJ) | 363.29 | 290.63 | 217.97 |
| Acidification (TRACI) (kg $SO_2$ eq.) | 0.047 | 0.040 | 0.028 |
| Eutrophication (TRACI) (kg N eq.) | 0.00631 | 0.005 | 0.004 |
| Ozone depletion (TRACI) (kg CFC 11 eq.) | 2.13E−09 | 1.71E−09 | 1.28E−09 |
| Particulate matter (TRACI) (kg PM 2.5 eq.) | 0.003 | 0.002 | 0.002 |
| Smog formation (TRACI) (kg $O_3$ eq.) | 0.803 | 0.642 | 0.482 |
| Water availability (AWARE) ($m^3$ world equiv.) | 6.55 | 5.24 | 3.93 |
| Water consumption (kg) | 191.65 | 153.32 | 114.99 |

smog formation as the midpoint indicators [56]. TRACI 2.1 indicators were not enough to cover all environmental impacts. Therefore, additional indicators were added. The climate change midpoint indicator was based on the characterization factors provided by the IPCC's Fifth Assessment Report (AR5) for a 100-year horizon [57]. The water availability was based on the AWARE (Available Water Remaining) method [58]. The primary energy demand (PED) from renewable and non-renewable resources was also considered for this study [59].

The results from Table 24.2 show that for all midpoint indicators, i.e., climate change, primary energy demand, acidification, eutrophication, ozone depletion, particulate matter, smog formation, water availability, and water consumption, there is a direct reduction of about 20%/kg of PLA lightweighted. These results clearly show a direct environmental benefit provided by implementing a source reduction approach. Other benefits provided by lightweighting include reduction of the EFP during transportation and less material having to be disposed of at the EoL. Water availability and water depletion indicators vary extensively with geographical location, and they are country specific. Crop cultivation locations are important factors to consider when procuring bio-based polymers [6].

### 24.4.2 Reuse

Reuse of materials can maintain the integrity of the material, and in a "reuse at-home" scenario, it has a minimal environmental impact since cleaning is, in general, the only process needed, which tends to have a lower EFP. Products are designed for increased utilization and service life. However, in the area of retail packaging, a wide-scale reuse system has restricted potential, associated with the high costs of returning and managing empty containers to suppliers [60]. In this scenario, the environmental impacts associated with collection and transportation of materials to be reused should also be assessed and taken into consideration as well. In this sense, PLA packaging is not the exception. A smaller-scale reuse system can be considered if PLA products and packaging are reused at the domestic level (for its primary use or other), assuming that the PLA material maintain its desired properties, functionality, and safety [4]. Examples of PLA products that are reusable are dishwasher-proof cups, mugs, plates, and cutlery [61]. Corbion has developed high-heat PLA and stereocomplex PLA technology that allows the product to be reused [3]. A recent development of PLA that is heat resistant and can hold boiling water opens the door for development of PLA products that can be washed and reused [62]. However, extensive research of PLA reuse scenarios is still lacking in the literature.

### 24.4.3 Recycling

Considering the hierarchy of the waste management system, recycling is the next preferable disposal route for PLA. Recycling can be either mechanical, chemical, or biological (composting) [63–65]. Regardless of the advancements in this area, recycling infrastructure is still limited in the waste management system. In this sense, according to the Green Guides, companies cannot make a "recyclable" claim when recycling facilities are not available to at least 60% of the products used by consumers or communities where a product is sold [66]. As reported by the US EPA [49], waste generation of PLA is still considered low in comparison to the traditional resins, making it difficult to recycle in an economically and technically feasible way.

***24.4.3.1 Mechanical Recycling*** Mechanical recycling can be classified as pre-consumer (primary recycling) or post-consumer (secondary recycling). The pre-consumer material is mainly from industrial facilities and is relatively homogeneous in quality and type of polymer; therefore, it can be re-processed relatively quickly. The post-consumer material collected for recycling requires a pretreatment such as washing and sorting due to its heterogeneous material composition with a high content of impurities, before it is shredded and repelletized for reuse. The material obtained by recycling can be used for products similar to those obtained from virgin polymer. However, mechanical and thermal stress during the recycling cycles and the presence of impurities can diminish the properties of the final product [39].

PLA packaging, such as bottles for beverages or clamshells, that has low contamination makes mechanical recycling a viable route for the recovery of PLA [65]. However, the current lack of infrastructure and logistics to recover (collect and recycle) PLA make recycling a problematic route. Furthermore, in existing mechanical recycling facilities, only the polymers that make up a significant portion of the market (i.e., PET, PP, and PE) are sorted and recycled. This situation is not exclusive to PLA, where low volumes of waste generated make the recycling alternative not feasible for sorting and recycling. The economic cost of the recycling process is presently favorable mostly for HDPE, PET, and LDPE [67]; for these three polymers the market demand is higher than for other resins since they have larger established markets to produce new packaging products or other products like fibers, clothes, and textiles [52, 65, 68].

Mechanical recycling would be the easiest and most inexpensive way to recycle clean post-consumer PLA. This route involves recovering, sorting, regrinding, and reprocessing (i.e., melt processing) the PLA waste. However, there is a debate on whether PLA can be successfully recycled in the current plastics recycling infrastructure due to the contamination of the recycling stream [65]. New studies show that, in the worst case scenario, PLA contamination of the plastic recycling stream is not more than the contamination of other traditional plastics [3].

According to Cornell [68], for recycling PLA, this must be either completely fungible with existing recycled resins or be available in sufficient quantity to reach the critical mass needed. There are some initiatives to facilitate the recycling of plastics through the existing infrastructure for recovery and sorting. One important initiative is How2Recycle. This initiative consists of a standardized labeling system intended to communicate recycling instructions to consumers. The initiative wants to counteract the high dispersion of recycling programs, unclear labeling, and inaccurate recyclability claims, mostly in the area of packaging [29]. PLA is still not broadly recycled but addressing critical questions such as correct labeling will help the access of PLA waste to the mainstream of the recycling infrastructure.

Other initiatives are focused on using technologies like near-infrared, black light illumination, or tagging by digital watermarking (e.g., the HolyGrail project) to facilitate the sorting of PLA from the waste stream [69, 70]. In this way, when a sufficient volume of PLA containers is available in the waste stream, recycling stakeholders can explore the means of recovering and cost-effectively recycling PLA. By using near-infrared sorting technologies, purities of around 97% have been obtained for PLA, which is higher than PP (96%), PE (94%), and PET (94%), among others [71]. Organizations such as the Bioplastics Recycling Consortium and Greenplastics, Inc. have developed solutions for post-consumer bioplastic materials [72, 73]. On the other hand, the National Association for PET Container Resources (NAPCOR) and the APR have objected to the initiative of mixing biopolymers like PLA into the existing waste stream of recycled containers. Their concerns are related to the cost of separation and processing, increased contamination, and reduced quality of the recycled material [68, 74]. CreaSolvis®, a solvent purifying technology considered as mechanical recycling, uses physical separation techniques to purify the polymer from contaminants. PLA with around 30% of impurities was successfully purified using this process [40].

Some of the challenges of mechanical recycling are the lack of infrastructure for recycling items and multilayer film structures containing PLA. From the point of view of PLA, studies have shown that reprocessing of plasticized PLA by using thermo-mechanical recycling resulted in a drastic drop of mechanical properties, diminishing the possibility of obtaining high-quality PLA after several cycles of recycling [75]. Mechanical recycling of PLA filled with cellulose fibers and 50% recycled content showed signs of degradation after reprocessing the composite once and for the material exposed to humidity the mechanical recycling reduced mechanical and thermal properties [76, 77]. Chariyachotilert et al. [65] studied the recycling of post-consumer recycled PLA bottles and demonstrated that small reductions of average molecular weight ($M_w$) and number average molecular weight ($M_n$) were observed as the amount of recycled content increased as shown in Figure 24.5. However, in real-life conditions, different grades of PLA (i.e., L- and D-lactide composition) with different types and concentration of additives, optical purity, $M_w$, and $M_w$ distribution, as well as possible thermal, hydrolytic, and UV degradation during and after usage, pose additional challenges for creating a post-consumer recycling market of PLA.

***24.4.3.2 Chemical Recycling*** Even though PLA is not yet sorted out from post-consumer waste due to the small volume generated, MRF separation allows for clean and dry materials to be derived for mechanical recycling. Reprocessed PLA is not approved for use in the production of products for food contact applications. For this reason, an alternative to mechanical recycling is chemical recycling, also known as advanced or tertiary recycling, solvent-based purification or dissolution, depolymerization, feedstock recycling, or resource recovery. Through chemical recycling, plastic waste is broken down using chemical processes and converted into its basic monomeric units that can then be repolymerized into the original plastic [9, 78]. Chemical recycling converts plastics to their basic units by chemolysis using processes such as hydrolysis (water, acids or alkalis), alcoholysis (methanolysis, glycolysis), or aminolysis (amines). The depolymerization by hydrolysis implies the use of water to break the bonds; alcoholysis employs methanol at high temperature and high pressure or glycol in the presence of transesterification catalysts, while during aminolysis a molecule is broken down by reacting with an amine. The enzymatic/catalytic depolymerization where a

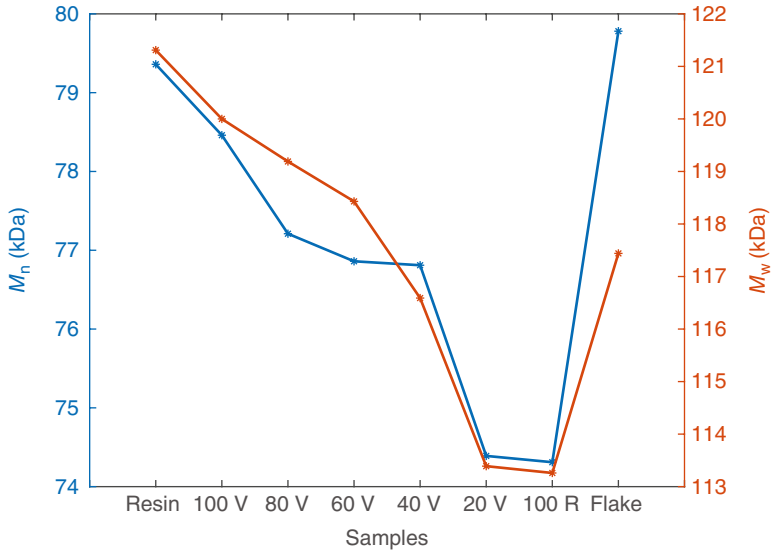


**FIGURE 24.5** Number average molecular weight ($M_n$), and average molecular weight ($M_w$) of PLA resin, 100% virgin PLA and 0% recycled (100 V), 80 V, 60 V, 40 V, 20 V, and 100% recycled (100 R), and flake of PLA sheet samples. Source: Adapted from Ref. [65].

catalyst or enzyme is employed to enable the process is also considered as a viable route of chemical recycling [79–81]. These technologies are not currently widely available in recycling facilities due to their high costs and energy requirements [82, 83]; however, there is a new focus on chemical recycling by governments and organizations as an approach to recovering multilayer polymeric structures [79]. Typical energy recovery routes as pyrolysis and gasification, leading to the production of fuel and gas, are still in development. The main challenges for pyrolysis are associated with better pre-processing, including sorting and separation, reduction of process energy requirements, improving catalyst regeneration, and post-treatment of the resulting pyrolysis oil. Gasification challenges include better pre-processing, identification of potential oxygen sources, and reduction of the associated high capital costs [83].

Two main processes have been used for chemical recycling of PLA, thermal degradation to obtain L-lactide and hydrolysis at high temperature to obtain lactic acid (LA). Depolymerization by thermal degradation (pyrolysis) of PLA can occur at temperatures in the range of 200–300°C. For selective formation of lactide via the unzipping depolymerization mechanism, the addition of metal catalysts such as Sn(II) is necessary [84]. During chemical recycling by hydrolysis, PLA is hydrolyzed at high temperatures to produce LA, which can be readily polymerized to high $M_w$ PLA [63–65]. Besides temperature, hydrolysis is dependent on pH, catalyst concentration, and PLA morphology. The hydrolysis of PLA has been extensively investigated by Tsuji et al. [85] and is lengthily discussed in Chapter 21. The hydrolysis of PLA in the temperature range of 180–350°C was reported with a 5%wt solution of PLA; the optimum temperature for L-lactic acid yield of 90% in 20 min was 250°C. A 95% conversion to LA at temperatures around 170°C during 2 h was reported by Piemonti et al. with concentration of PLA between 5 and 50%wt [86]. Hydrolysis of PLA in water/ethanol solutions (50% ethanol between 40 and 90°C) was reported by Iñiguez-Franco et al.; swelling was observed due to the inclusion of the ethanol, facilitating the sorption of water by hydrolysis. An estimation of 41 h was reported as the time required to achieve 95% conversion to LA at 90°C [87, 88].

PLA can also be depolymerized by alcoholysis. Several alcohol groups can attack the ester bonds via transesterification reactions to generate lactate esters. A catalyst is often required for high depolymerization efficiency when reactions are developed in mild conditions. Some examples are methanol, ethanol, and propanol that yield methyl lactate, ethyl lactate, and propyl lactate. Catalysts as $Zn(Et)_2$, $Zn(Pr)_2$, and $Zn(1)_2$ were effective when depolymerizing PLA via methanolysis [89, 90]. Román-Ramírez et al. investigated the chemical degradation of PLA products (toy, cup, and 3D printing material) into methyl lactate catalyzed by a Zn(II) complex at 70, 90, and 110°C, and a strong correlation for the depolymerization process was found between their model and its experimental data, indicating a higher yield of methyl lactate with higher temperatures and longer reaction times (4 h). On the other hand, lower yields were found in samples with higher amount of additives such as fillers and colorants [91].

A recent development in catalytic chemical recycling is reductive depolymerization. In this process, iridium- and ruthenium-based organometallic complexes, along with an organocatalyst, were used in the presence of hydrogen or a hydrosilane as reagents. Some of the challenges of this novel approach are the development of highly active and recyclable catalysts with high selectivity, low cost, and operability at mild reaction conditions [92].

NatureWorks LLC has successfully recycled off-grade Ingeo™ using chemical recycling [93]. The main disadvantage of chemical recycling is that it is still complex and expensive [65]. On the other hand, the potential of chemical recycling for PLA was demonstrated by an LCA analysis, showing that it is more energetically favorable to produce lactic acid from chemical recycling than from the fermentation of glucose [64].

### 24.4.4 Biodegradation

***24.4.4.1 Aerobic Biodegradation—Industrial and Home Composting*** Single-use PLA is used in flexible packaging. Flexible packaging represents around 50% of the total plastics consumption in packaging, and it is difficult to recover and recycle, leaving biodegradation under composting conditions as an optimal EoL when the plastic is contaminated [94]. Biodegradation is considered as a natural way of recycling [5]. PLA can undergo biodegradation in industrial composting conditions where an initial hydrolytic degradation is the first step, followed by final degradation of PLA by thermophilic microorganisms at around 58°C and 50% relative humidity [5, 95]. Figure 24.6 depicts a typical industrial composting facility where the final products of compostable materials are compost, $CO_2$, $H_2O$, and minerals. For the biodegradation process to take place, three main factors must be considered: the material or substrate (its chemical structure), the environment (temperature, moisture, oxygen, pH), and the microorganism population (metabolic pathways and enzymes) [96, 97].


**FIGURE 24.6** Steps of the composting process in an industrial facility. Source: Reproduced from Ref. [5].

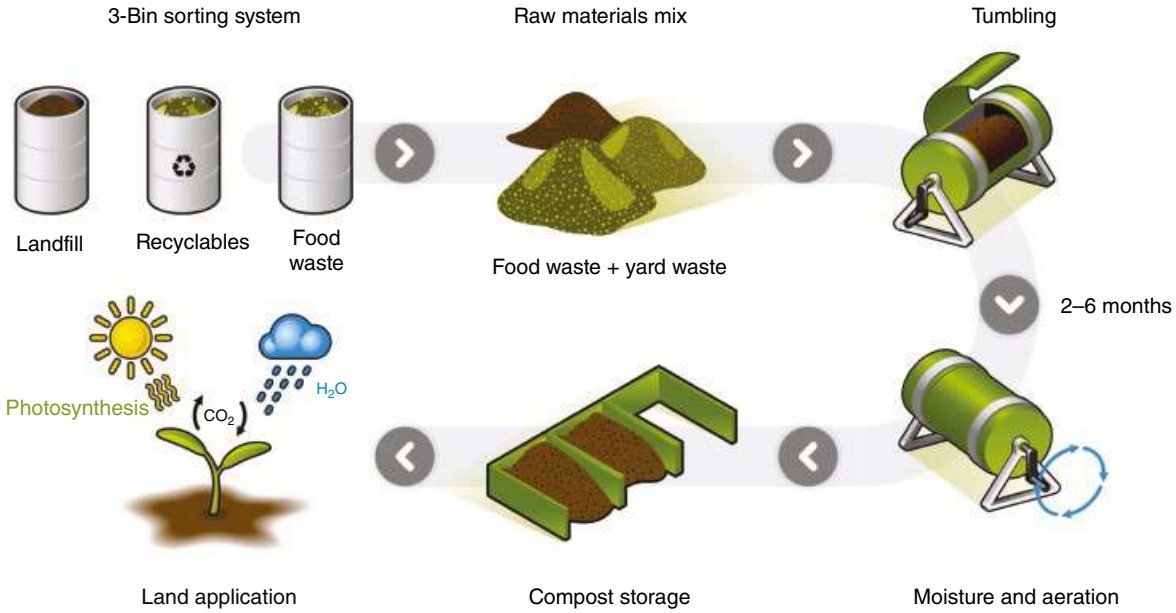


**FIGURE 24.7** Steps of the composting process in a home composting facility. Source: Reproduced from Ref. [5].

Home composting (Figure 24.7) as a EoL option for PLA is still challenging since the rate of biodegradation in mesophilic conditions of PLA is lower than in thermophilic conditions, where the abiotic degradation (i.e., hydrolysis) of PLA tends to be more efficient.

The biodegradation of PLA usually occurs in two main steps. The first is primary or abiotic degradation, where the fragmentation of the polymer chain occurs due to hydrolysis or another mechanism such as oxidative, mechanical, thermal, or radiative. The second and ultimate step is biotic degradation, in which the microorganisms assimilate the low $M_w$ chains formed, giving $CO_2$, biomass, and $H_2O$ (Figure 24.8) [95–98].

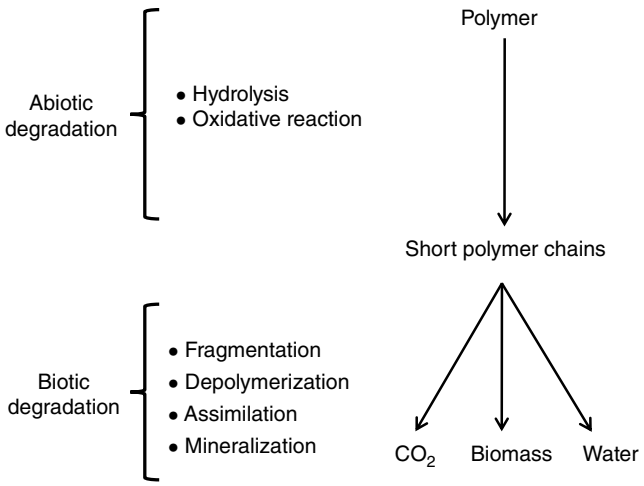


**FIGURE 24.8** Main steps of the polymer biodegradation. Source: Adapted from Ref. [98].

Biodegradation can be evaluated by using various analytical techniques, which can be implemented by using direct or indirect approaches [99]. Respirometric methods are the most preferred when assessing the biodegradation of polymers in laboratory settings or simulated conditions [96]. Respirometric methods use a direct approach by measuring the consumption of $O_2$ or the evolution of $CO_2$ [99]. Several standards have been developed to meet the requirements and the methodologies to assess the biodegradability of plastics under composting conditions. In this sense, ASTM D5338-15 and ISO 14855-1:2005 are the primary standards for measuring the biodegradability of plastics materials under composting conditions by analysis of the evolved $CO_2$ [100–102]. Table 24.3 presents a basic comparison of the requirements between these two standards.

The aerobic biodegradation of PLA films (Ingeo™ 2003D) was evaluated in compost by using an in-house direct measurement respirometer (DMR) following the methodology described elsewhere [104]. Briefly, bioreactors containing PLA and compost, compost only (blank), and compost with cellulose powder (positive reference) were tested at 58°C and 50% RH during a specific period of time. Figure 24.9a shows that the PLA films produced a significantly higher amount of $CO_2$ than the blank, reflecting that the microorganisms could use the carbon from the polymer as a source of energy for their metabolic processes. The amount of $CO_2$ produced for the PLA film is similar to the $CO_2$ evolved for the positive control (cellulose) in the same period. Figure 24.9b depicts the mineralization of PLA and cellulose. The mineralization of PLA films was above 70% after two months of testing. A lag time for PLA can be observed in Figure 24.9b during the first three weeks of the

**TABLE 24.3 General Requirements to Test Biodegradation Under Laboratory Conditions and Comparison Between ASTM D5338-2015 and ISO 14855-1:2005 Standards [100–102]**

| Requirement | | ASTM D5338 | ISO 14855 |
|---|---|---|---|
| Apparatus | Number of bioreactors | At least 12 | At least 9 |
| | Volume of bioreactors | 2–5 L (sufficient headspace) | 2 L or higher (sufficient headspace) |
| | Aeration | Water saturated | Dry or water saturated |
| | | $CO_2$-free | $CO_2$-free |
| | | Accurate flow rate | At pre-set flow rate |
| | Sensor | Specific sensors or appropriate gas chromatographs | Infrared analyzer<br>Gas chromatograph |
| Compost Inoculum | Age | 2–4 months old | 2–4 months old |
| | Homogeneity | Sieved on a screen <10 mm<br>Allows addition of structural material | Sieved on a screen of about 0.5–1 cm<br>Allows addition of structural material |
| | Dry solids | Between 50 and 55% | Between 50 and 55% |
| | Volatile solids | Ash content <70% | No more than 15% of wet or 30% of dry solids |
| | pH | Between 7 and 8.2 | Between 7 and 9 |
| | Production of carbon dioxide | Between 50 and 150 mg of $CO_2$ per gram of volatile solids over the first 10 days | Between 50 and 150 mg of $CO_2$ per gram of volatile solids over the first 10 days |
| | C/N ratio | Between 10 and 40 | Between 10 and 40 |
| Substrate | Shape | Granules, powder, film, simple shapes | Granules, powder, film, simple shapes |
| | Surface area | 2×2 cm max. | 2×2 cm max. |
| | Positive control | Cellulose (particle size <20 μm) | Cellulose (particle size <20 μm) |
| | Negative control | Polyethylene | Not required |
| Other | Temperature | 58 ± 2°C | 58 ± 2°C |
| | Water content | About 50% | About 50% |
| | Ratio of mixture | 6 : 1 sample (dry solids) | 6 : 1 sample (dry solids) |
| | Frequency of measurement | At least daily | At least twice per day |
| | Test period | At least 45 days | Not exceeding six months |
| | Incubation | Dark or diffused light | Dark or diffused light |
| | Oxygen concentration | 6% or higher | 6% or higher |

Source: Adapted from Ref. [103].

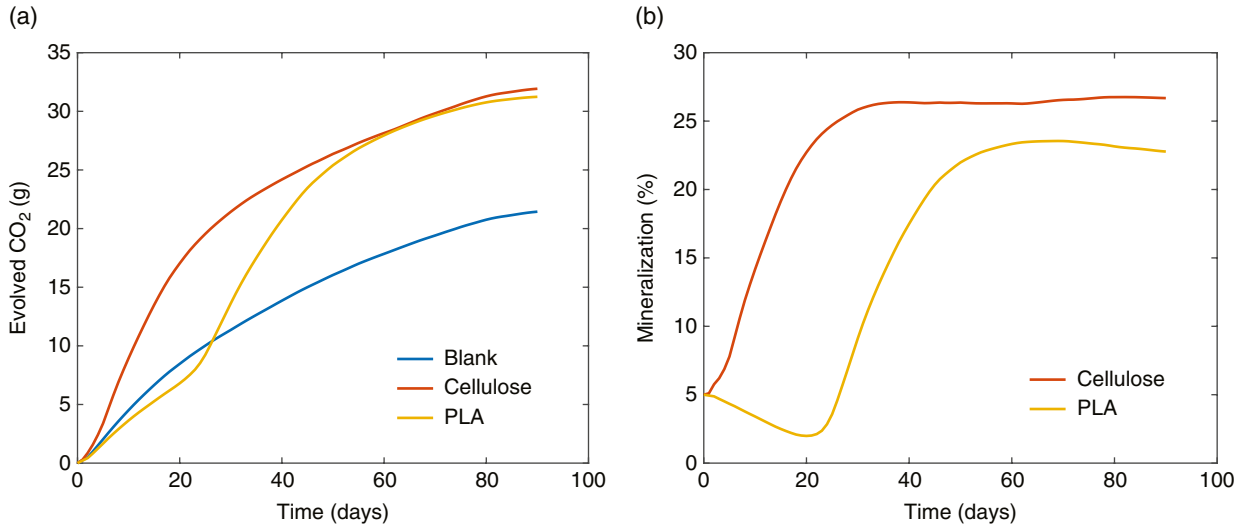


**FIGURE 24.9** (a) $CO_2$ evolution of blank, cellulose, and PLA film; (b) percentage of mineralization of cellulose and PLA films after 90 days of testing. Source: Adapted from Ref. [4].

test, associated with the primary hydrolytic degradation, where the $M_w$ was reduced to values around 9 kDa to be accessible for the microorganisms to start the ultimate degradation step or mineralization.

As previously mentioned, when PLA is highly contaminated, for example, with food in food packaging, composting should be an optimal EoL scenario. However, there are only a few existing industrial composting facilities that allow biodegradable plastics such as PLA to be composted due to a high concern that biodegradable plastics are not easily distinguishable from conventional plastics, hindering quality control and resulting in contamination of the compost stream [38].

Similar to recycling, there is a big challenge in collecting and sorting PLA waste from MSW and sending it to composting facilities for biodegradation. The benefit of PLA by providing an additional option for EoL scenario via composting can only be achieved if the PLA is being disposed of in an appropriate waste management system that allows the biodegradation of PLA [60]. Otherwise, the PLA will behave and accumulate in landfill similarly to other plastics [4]. Initiatives such as the How2Compost label are becoming relevant, providing information about the compostability of products certified by the Biodegradable Products Institute (BPI) [105]. Institutes such as BPI in the United States and Technischer Überwachungsverein (TÜV) Austria in Europe provide certification of compostability for products and packaging. BPI also offers guidelines for labeling and identification of compostable products and packaging [106]. In this direction, proper labeling and identification are vital for successful waste management [16].

Currently, techniques such as bioaugmentation and biostimulation are being investigated to boost the biodegradation of PLA at thermophilic and mesophilic conditions. Bioaugmentation implies a modification of the microbial dynamics by introducing a specific microbial consortium to the environment. Biostimulation implies the introduction of explicit nutritional content to the environment to increase microbial degrading activity [107–109].

***24.4.4.2 Anaerobic Biodegradation—Digestion and Conversion to Biogas*** Anaerobic digestion is also known as bio-gasification and implies the metabolization of biogas methane. The conversion of waste into biogas can be subdivided into four anaerobic steps: hydrolysis, bacterial acidification, acetogenesis, and methanogenesis. The process can be developed at mesophilic or thermophilic conditions, in one or two phases, or as a wet or dry process. In the one-phase process, the complete digestion takes place in one unit. For the two-phase process, hydrolysis and acidification are developed in one tank and methanogenesis in a separate tank. A relative humidity above 85% implies a wet process [110]. Anaerobic digestion also allows for energy recovery.

Studies for over 100 days showed no biodegradation or very low values (around 10%) under anaerobic digestion of PLA in digested sludge [111, 112]. Works based on standard ISO 14853 have examined the anaerobic degradation of PLA, and the authors concluded that no relevant digestion was produced after 28 days of testing at mesophilic conditions [113].

Anaerobic digestion of PLA under solid thermophilic conditions showed relatively higher values in comparison to other biodegradable polymers such as poly(butylene succinate) (PBS) and polyhydroxyoctanoate (PHO) but lower values than poly(ε-caprolactone) (PCL) and polyhydroxybutyrate (PHB) [114].

A comparison anaerobic study of the same PLA type was reported in two tests. A first test, developed for three different humidity and ambient conditions under accelerated landfill conditions, was performed for more than one year; a second test using a high solid (up to 35% of organic waste capability) anaerobic digestion reactor was conducted for more than six months at mesophilic conditions. No significant generation of biogas was reported from the test under accelerated landfill conditions and no significant methane production from the high solid anaerobic digestion reactor [115, 116].

Anaerobic biodegradation of PLA still faces some challenges at the technical scale. Studies comparing anaerobic digestion of PLA at mesophilic and thermophilic conditions showed that thermophilic conditions require the utilization of separate digesters to obtain a meaningful amount of biogas production. However, at mesophilic conditions, no significant biogas was generated at time scales acceptable for an industrial process [117].

### 24.4.5 Incineration with Energy Recovery

Incineration is not only an option for reducing volume but also a technique for waste-to-energy options. Energy is recovered from waste materials and is used for heat or electricity, with final disposal of the fly and bottom ashes [4]. Incineration of waste with energy recovery also offers the possibility of reducing the use of fossil-based resources and other fuel sources. Air pollution is one of the main concerns when addressing waste incineration; however, improvements in gas cleaning technologies have allowed for reduction of pollutants released to the atmosphere due to energy recovery through waste incineration [118, 119].

Recovery processes through thermolysis are technologies producing hydrocarbons that can be used as fuels at higher temperature processes such as pyrolysis, gasification, and hydrogenation. Cracking and gasification are also considered strategies for chemical recovery. Pyrolysis produces liquid and gaseous hydrocarbons at elevated temperatures in the absence of oxygen without a catalyst. Gasification is an aerobic process at high temperatures where the material is

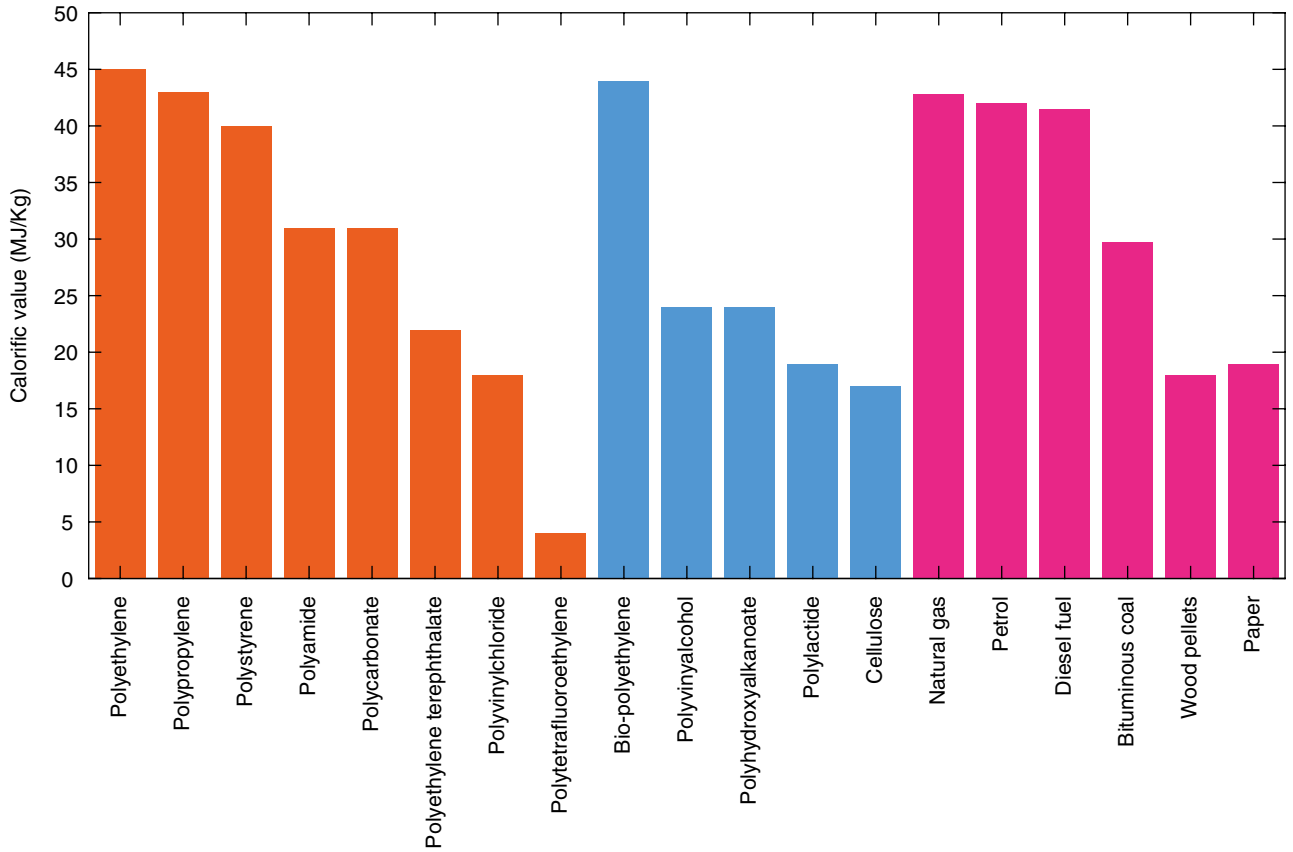


**FIGURE 24.10** Calorific values of several polymers and fuels. Source: Adapted from Refs. [120, 122, 123].

broken down using an oxidizing agent to convert hydrocarbons into syngas. These recovery processes are not considered to be chemical or thermal recycling [78].

Energy is always involved during the manufacturing of plastics. Hence, some of the energy content of the plastics can be recovered when plastics become waste; reasonable energy efficiency can be achieved by using approaches such as co-fueling of kilns [60]. Disposing PLA via incineration is an EoL option that allows the recovery of the energy embedded in PLA [120]. In the context of the circular economy, incineration with energy recovery does not reduce the demand for raw material for plastic production but provides the recovery of the embedded energy [60]. It is also important to consider the composition of the combustion gases and their general impact on the environment [120].

NatureWorks LLC reported that Ingeo™ resin heat content is around 19.5 MJ/kg [121]. This value is in agreement with the calorific values reported by Lauβmann et al. [120] (Figure 24.10), who carried out comparative experiments between biopolymers, fossil-based polymers, and fuels. Their work concludes that PLA and other biopolymers are suitable for energy recovery via incineration since they possess calorific values similar to cellulose-based materials, and they do not generate additional toxic critical substances during combustion [120].

### 24.4.6 Landfill

Landfilling is the less preferable option as an EoL scenario for PLA. The reduction of landfill disposal in the United States from 2005 to 2017 has been just around 2%, from 142,260 to 139,590 thousand tons. Landfill disposal remains the most economical and simple method for handling MSW in the United States [52]. However, landfilling plastics has several negative environmental impacts, such as increasing of waste in the landfill and the generation of gas and leachate, which translate on environmental impacts including health hazards, fires and explosions, vegetation damage, unpleasant odors, landfill settlement, pollution of groundwater, air pollution, and global warming [124]. One of the main drawbacks of disposing plastics in landfills is that most of the plastics do not practically degrade in landfill environments so that they end up accumulating [125] since the landfill environment does not promote degradation and biodegradation. Moreover, landfill conditions can vary considerably by geography [115]. For PLA, moisture and temperature are key factors in promoting biodegradation. These factors affect

the primary hydrolytic degradation and increasing the biodegradation rate of PLA. At mesophilic temperatures, the hydrolytic degradation rate is meager and, as a consequence, the ultimate biodegradation is very low [115].

According to NatureWorks LLC, Ingeo™ is stable in landfill conditions with no statistically significant quantity of methane released [126]. However, studies performed under accelerated landfill conditions at different temperatures and moisture content found that amorphous PLA did generate a small amount of methane when tested at 35°C. Still, no methane was generated in the trial at ambient temperature. For semicrystalline PLA, no significant generation of methane was observed in any of the tests. Kolstad et al. also pointed out that it is highly probable that degradation of PLA in a landfill would require a chemical hydrolysis step before any biodegradation takes place [115].

## 24.5 LCA OF END-OF-LIFE SCENARIO FOR PLA

When having a clean and dry disposed packaging material, it was demonstrated that the optimal EoL scenario for PLA is mechanical recycling. According to Cosate de Andrade et al., mechanical recycling showed the lowest environmental impact compared with other options such as chemical recycling along with composting. From the comparison of both mechanical and chemical recycling, it was observed that energy consumption (electricity) has a large contribution in the impact of chemical recycling [127].

Figure 24.11 shows the midpoint indicators of an LCA for disposed PLA dry packaging where mechanical recycling offers the lower global warming impact of the possible EoL scenarios, followed by anaerobic digestion, incineration, and composting [38]. The study also reports that in the hypothetical case of contaminated PLA packaging with food waste, the recycling option is unattractive from an environmental perspective. Another LCA study conducted by Maga et al. [128] has also showed that recycling (mechanical and chemical) had lower environmental impact than waste incineration for PLA.

As discussed, the incorporation of fillers to reinforce the PLA matrix and obtain lightweight materials is an essential aspect of the prevention and reduction scenario. In this sense, an LCA study of EoL option for PLA/Flax fibers biocomposites showed that mechanical recycling had the lowest environmental impact compared to landfill, incineration, and composting [129]. However, the incorporation of fibers or other fillers may impact the recycling stream due to contamination concerns by the MRFs even if the PLA composites are technically recyclable, i.e., maintaining mechanical and other performance properties after several recycling cycles [76, 77, 130].

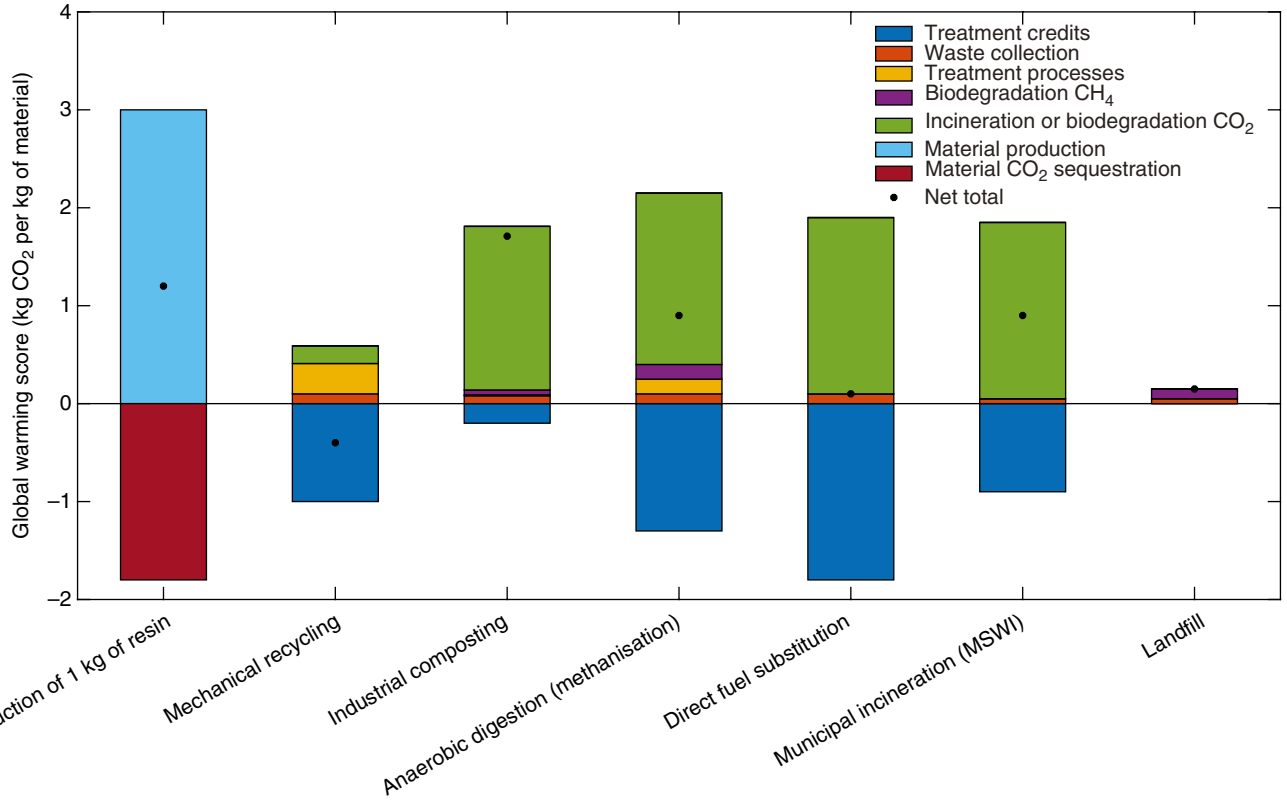


**FIGURE 24.11** Global warming score based on a LCA for EoL scenarios of PLA. Source: Adapted from Ref. [38].

Therefore, mechanical recycling has been shown to be an optimal EoL scenario for PLA, and PLA blends allowed to go through this EoL. Incentives for developing programs for stakeholders and consumers and incorporating resources for collection and infrastructure for sorting and reprocessing are vital issues to address for responsible and sustainable management of PLA.

## 24.6 FINAL REMARKS

In terms of the EoL scenario for PLA, as its use in the global market increases, it will be necessary to reduce its EoL environmental footprint. We have discussed that mechanical recycling offers the lowest environmental impacts for PLA materials that are clean and dry. However, the lack of infrastructure for sorting and reprocessing PLA is still the main drawback of effective mechanical recycling for PLA. Initiatives for proper labeling and new technologies to identify materials can help promote the collection, sorting, and recovery of PLA. Furthermore, PLA material that has been recycled through several cycles presents a reduction of $M_w$ and a loss of properties such as mechanical properties. Therefore, further research is needed for the optimized recyclability of PLA, as well as fully understanding how to recycle PLA produced from different stereoisomer contents.

When low-grade PLA cannot be mechanically recycled, chemical recycling is the next optimal level to recover PLA. Hydrolysis and alcoholysis have lower activation energies than pyrolysis. However, PLA depolymerization via hydrolysis at milder conditions and in the absence of a catalyst is a relatively slow process. Products obtained by chemical recycling can be converted to lactide and polymerized into high $M_w$ PLA. Chemical recycling of PLA is still at the research stage, and mostly done at the industrial (pre-consumer) level rather than at the post-consumer level. Energy consumption seems to be the main drawback to recovering PLA through this route. Chemical recycling offers the possibility of obtaining recycled PLA with similar quality properties to virgin PLA making this process very promising.

Incineration is a viable option for PLA waste when recycling is not an option. According to the study conducted by Rossi et al. [38], incineration showed a lower environmental impact on climate change than composting and similar to anaerobic digestion. Advances in technologies such as pyrolysis and gasification represent potential viable routes to recover PLA while infrastructure for other EoL scenarios is developed and put in place.

Biodegradation, both aerobic and anaerobic, is an acceptable option for PLA materials that cannot be recycled due to high contamination, such as food packaging or agricultural films. Biodegradation in industrial composting conditions is currently the most widely accepted EoL scenario for PLA. Several initiatives by industry coalitions, organizations, communities, and governments are promoting compostable packaging with proper labeling, testing, and certification. Composting facilities should accept additional compostable packaging to bring more food waste into their businesses as the contamination issue is being addressed and improvements in the composting infrastructure are developed.

Landfills are still the most common way for plastic waste disposal in the United States and several parts of the world. So, without an integrated waste management system, waste that can be recycled or recovered for energy ends up in landfills, increasing the volume and environmental hazards associated with landfilling. PLA is still mainly disposed of through this route that misses the benefit that this unique bio-based polymer can bring to the plastic's circular economy.

## REFERENCES


1. United Nations, Transforming our world: the 2030 agenda for sustainable development, 2015.
2. The Pew Charitable Trusts, Systemiq. Breaking the plastic wave: a comprehensive assessment of pathways towards stopping ocean plastic pollution, 2020.
3. Total Corbion PLA, End-of-life options for bioplastics. Clarifying end-of-life options for bioplastics and the role of PLA in the circular economy, 2020.
4. E. Castro-Aguirre, F. Iñiguez-Franco, H. Samsudin, X. Fang, R. Auras, Poly(lactic acid)—mass production, processing, industrial applications, and end of life, *Adv. Drug. Deliv Rev.* **2016**, *107*, 333–366.
5. T. Kijchavengkul, R. Auras, Compostability of polymers, *Polym. Int.* **2008**, *57*, 793–804.
6. A. Morão, F. de Bie, Life cycle impact assessment of polylactic acid (PLA) produced from sugarcane in Thailand, *J. Polym. Environ.* **2019**, *27*, 2523–2539.
7. E. T. H. Vink, S. Davies, Life cycle inventory and impact assessment data for 2014 Ingeo™ polylactide production, *Ind. Biotechnol.* **2015**, *11*, 167–180.
8. Ellen MacArthur Foundation, Rethinking the future of plastics the new plastics economy, 2014.
9. J. N. Hahladakis, E. Iacovidou, S. Gerassimidou, Plastic waste in a circular economy, in: Trevor M. Letcher (Ed.), *Plastic Waste and Recycling*, Elsevier, Academic Press, United Kingdom, 2020, pp. 481–512.
10. J. R. Jambeck, R. Geyer, C. Wilcox, T. R. Siegler, M. Perryman, A. Andrady, et al., Plastic waste inputs from land into the ocean, *Science* **2015**, *347*, 768–771.
11. United Nations Environment Program, *Single-Use Plastics A Roadmap for Sustainanility*, United Nations Environment Programme, 2018.
12. L. Lebreton, A. Andrady, Future scenarios of global plastic waste generation and disposal, *Palgrave Commun.* **2019**, *5*, 6.


13. R. A. Sheldon, Biocatalysis and biomass conversion: enabling a circular economy, *Philos. Trans. R Soc. A Math. Phys. Eng. Sci.* **2020**, *378*.
14. S. B. Borrelle, J. Ringma, K. L. Law, C. C. Monnahan, L. Lebreton, McGivern A, et al., Predicted growth in plastic waste exceeds efforts to mitigate plastic pollution, *Science* **2020**, *369*, 1515–1518.
15. European Commission, Waste prevention and management. Available from: https://ec.europa.eu/environment/waste/index.htm (accessed 17 April 2021).
16. United Nations Environment Programme, *Can I Recycle This? A Global Mapping and Assessment of Standards, Labels and Claims on Plastic Packaging*, United Nations Environment Programme, 2020.
17. Ellen MacArthur Foundation, *Upstream Innovation*, Ellen MacArthur Foundation, 2020.
18. J. Payne, P. McKeown, M. D. Jones, A circular economy approach to plastic waste, *Polym. Degrad. Stab.* **2019**, *165*, 170–181.
19. E. Rudnik, Introduction, in: E. Rudnik (Ed.) *Compostable Polymer Materials*, Elsevier, United Kingdom, 2019, pp. 1–9.
20. U. S. Environmental Protection Agency, Sustainable-materials-management-non-hazardous-materials-and-waste-management-hierarchy. Available from: https://www.epa.gov/smm/sustainable-materials-management-non-hazardous-materials-and-waste-management-hierarchy (accessed 12 January 2021).
21. D. Guerin, J. Crete, J. Mercier, A multilevel analysis of the determinants of recycling behavior in the European countries, *Soc. Sci. Res.* **2001**, *30*, 195–218.
22. F. Lange, C. Brückner, B. Kröger, J. Beller, F. Eggert, Wasting ways: perceived distance to the recycling facilities predicts pro-environmental behavior, *Resour. Conserv. Recycl.* **2014**, *92*, 246–254.
23. J. Hopewell, R. Dvorak, E. Kosior, Plastics recycling: challenges and opportunities, *Philos. Trans. R Soc. B Biol. Sci.* **2009**, *364*, 2115–2126.
24. B. G. Mwanza, C. Mbohwa, A. Telukdarie, The influence of waste collection systems on resource recovery: a review, *Procedia Manuf.* **2018**, *21*, 846–853.
25. M. L. Mastellone, R. Cremiato, L. Zaccariello, R. Lotito, Evaluation of performance indicators applied to a material recovery facility fed by mixed packaging waste, *Waste Manage.* **2017**, *64*, 3–11.
26. D. Kang, R. Auras, J. Singh, Life cycle assessment of non-alcoholic single-serve polyethylene terephthalate beverage bottles in the state of California, *Resour. Conserv. Recycl.* **2017**, *116*, 45–52.
27. Ellen MacArthur Foundation, *The Global Commitment 2020*, Ellen MacArthur Foundation, 2020.
28. Federal Trade Comission, Guides for the use of environmental marketing claims, 2012.
29. How2Recycle. Available at: https://how2recycle.info/ (accessed 8 March 2021).
30. Sustainable Packaging Coalition, 2015–2016 Centralized study on availability of recycling, 2016.
31. McKinsey on Chemicals, No time to waste: what plastics recycling could offer, 2018.
32. United Nations General Assembly, Global sustainable development report, 2015.
33. M. A. Curran, Life cycle assessment: a review of the methodology and its application to sustainability, *Curr. Opin. Chem. Eng.* **2013**, *2*, 273–277.
34. Nova-Institut GmbH, Bio-based building blocks and polymers—global capacities, production and trends 2019–2024, 2020.
35. S. Madival, R. Auras, S. P. Singh, R. Narayan, Assessment of the environmental profile of PLA, PET and PS clamshell containers using LCA methodology, *J. Clean Prod.* **2009**, *17*, 1183–1194.
36. Nova-Institut GmbH, Biobased building blocks and polymers—global capacities, production and trends, 2020–2025, 2021.
37. K. Hamad, M. Kaseem, M. Ayyoob, J. Joo, F. Deri, Polylactic acid blends: the future of green, light and tough, *Prog. Polym. Sci.* **2018**, *85*, 83–127.
38. V. Rossi, N. Cleeve-Edwards, L. Lundquist, U. Schenker, C. Dubois, S. Humbert, et al., Life cycle assessment of end-of-life options for two biodegradable packaging materials: sound application of the European waste hierarchy, *J. Clean Prod.* **2015**, *86*, 132–145.
39. S. Spierling, V. Venkatachalam, M. Mudersbach, N. Becker, C. Herrmann, H.-J. Endres, End-of-life options for bio-based plastics in a circular economy—status quo and potential from a life cycle assessment perspective, *Resources* **2020**, *9*, 90.
40. FNR, PLA in the waste stream, 2017.
41. J. Ren, *Biodegradable Poly(Lactic Acid): Synthesis, Modification, Processing and Applications*, Springer, Berlin, 2010.
42. The Association of Plastic Recyclers, Available from: https://plasticsrecycling.org/ (accessed 25 May 2021).
43. Sustainable Packaging Coalition, Available from: https://sustainablepackaging.org/ (accessed 25 May 2021).
44. Materials Recovery for the Future, Available from: https://www.materialsrecoveryforthefuture.com/ (accessed 25 May 2021).
45. The Recycling Partnership, Available from: https://recyclingpartnership.org/ (accessed 25 May 2021).
46. Closed Loop Partners, Available from: https://www.closedlooppartners.com/ (accessed 25 May 2021).
47. Plastic Recyclers Europe, Available from: https://www.plasticsrecyclers.eu/ (accessed 25 May 2021).
48. Chemical Recycling Europe, Available from: https://www.chemicalrecyclingeurope.eu/ (accessed 25 May 2021).
49. US Environmental Protection Agency, Advancing sustainable materials management: 2018 tables and figures, 2020.
50. Plastic Europe, Plastics—the Facts 2020, 2020.
51. The Waste & Resource Action Programme, Lightweight compostable packaging: literature review, 2006.
52. U. S. Environmental Protection Agency, Advancing sustainable materials management: 2016 and 2017 tables and figures, 2018.

53. L. S. Liu, M. L. Fishman, K. B. Hicks, C.-K. Liu, Biodegradable composites from sugar beet pulp and poly(lactic acid), *J. Agric. Food Chem.* **2005**, *53*, 9017–9022.
54. V. Peinado, L. García, Á. Fernández, P. Castell, Novel lightweight foamed poly(lactic acid) reinforced with different loadings of functionalised Sepiolite, *Compos. Sci. Technol.* **2014**, *101*, 17–23.
55. Y. Du, N. Yan, M. T. Kortschot, Novel lightweight sandwich-structured bio-fiber-reinforced poly(lactic acid) composites, *J. Mater. Sci.* **2014**, *49*, 2018–2026.
56. US Environmental Protection Agency, Tool for the reduction and assessment of chemical and other environmental impacts (TRACI). User's guide, 2012.
57. IPCC, Climate change 2013: the physical science basis, 2013. Available fromt: https://www.ipcc.ch/report/ar5/wg1/ (accessed 23 February 2021).
58. A.-M. Boulay, J. Bare, L. Benini, M. Berger, M. J. Lathuillière, A. Manzardo, et al., The WULCA consensus characterization model for water scarcity footprints: assessing impacts of water consumption based on available water remaining (AWARE), *Int. J. Life Cycle Assess.* **2018**, *23*, 368–378.
59. European Commission, Product environmental footprint category rules guidance, 2018.
60. R. C. Thompson, C. J. Moore, F. S. vom Saal, S. H. Swan, Plastics, the environment and human health: current consensus and future trends, *Philos. Trans. R Soc. B Biol. Sci.* **2009**, *364*, 2153–2166.
61. Eco Concepts. Available from: https://www.ecoconcepts.com.hk/pla-reusable-faq (accessed 28 May 2021).
62. M. Razavi, S.-Q. Wang, Why is crystalline poly(lactic acid) brittle at room temperature?, *Macromolecules* **2019**, *52*, 5429–5441.
63. A. Jarerat, Y. Tokiwa, H. Tanaka, Production of poly(L-lactide)-degrading enzyme by Amycolatopsis orientalis for biological recycling of poly(L-lactide), *Appl. Microbiol. Biotechnol.* **2006**, *72*, 726–731.
64. V. Piemonte, S. Sabatini, F. Gironi, Chemical recycling of PLA: a great opportunity towards the sustainable development?, *J. Polym. Environ.* **2013**, *21*, 640–647.
65. C. Chariyachotilert, S. Joshi, S. E. Selke, R. Auras, Assessment of the properties of poly(L-lactic acid) sheets produced with differing amounts of postconsumer recycled poly(L-lactic acid), *J. Plast. Film Sheeting* **2012**, *28*, 314–335.
66. Environmental claims: Summary of the Green Guides. Available from: https://www.ftc.gov/tips-advice/business-center/guidance/environmental-claims-summary-green-guides (accessed 11 January 2021).
67. How2Recycle, Store Drop-Off. Available from: https://how2recycle.info/sdo (accessed 3 March 2021).
68. D. D. Cornell, Biopolymers in the existing postconsumer plastics recycling stream, *J. Polym. Environ.* **2007**, *15*, 295–299.
69. NatureWorks, Recycling. Available from: https://www.natureworksllc.com/What-is-Ingeo/Where-it-Goes/Recycling (accessed 19 January 2021).
70. Ellen MacArthur Foundation, HolyGrail: tagging packaging for accurate sorting and high-quality recycling, 2019.
71. WRAP, Domestic Mixed Plastics Packaging Waste Management Options, 2008.
72. Packaging Digest, New business buys post-consumer PLA use packaging. Available from: https://www.packagingdigest.com/smart-packaging/new-business-buys-post-consumer-pla-use-packaging (accessed 20 April 2021).
73. Packaging Digest, Sustainable packaging: first new company formed to recycle PLA. Available from: https://www.packagingdigest.com/smart-packaging/sustainable-packaging-first-new-company-formed-recycle-pla (accessed 20 April 2021).
74. Packaging Digest, Napcor refutes claims PLA can be recycled with PET. Available from: https://www.packagingdigest.com/smart-packaging/napcorrefutes-claims-pla-can-be-recycled-pet (accessed 20 April 2021).
75. B. Brüster, F. Addiego, F. Hassouna, D. Ruch, J.-M. Raquez, P. Dubois, Thermo-mechanical degradation of plasticized poly(lactide) after multiple reprocessing to simulate recycling: Multi-scale analysis and underlying mechanisms, *Polym. Degrad. Stab.* **2016**, *131*, 132–144.
76. D. Åkesson, T. Vrignaud, C. Tissot, M. Skrifvars, Mechanical recycling of PLA filled with a high level of cellulose fibres, *J. Polym. Environ.* **2016**, *24*, 185–195.
77. D. Åkesson, S. Fazelinejad, V.-V. Skrifvars, M. Skrifvars, Mechanical recycling of polylactic acid composites reinforced with wood fibres by multiple extrusion and hydrothermal ageing, *J. Reinf. Plast. Compos.* **2016**, *35*, 1248–1259.
78. Zero Waste Europe, Chemical Recycling—7 Steps to Effectively Legislate on Chemical Recycling, 2020.
79. US Department of Energy, Chemical Upcycling of Polymers, 2019.
80. N. Singh, D. Hui, R. Singh, I. P. S. Ahuja, L. Feo, F. Fraternali, Recycling of plastic solid waste: a state of art review and future applications, *Compos. Part B Eng.* **2017**, *115*, 409–422.
81. M. Biron, Recycling, in: Michel Biron (Ed.), *Industrial Applications of Renewable Plastics*, Elsevier. 2017, pp. 67–114.
82. A. Rahimi, J. M. García, Chemical recycling of waste plastics for new materials production, *Nat. Rev. Chem.* **2017**, *1*, 1–11.
83. US Department of Energy, Plastics for a Circular Economy Workshop: Summary Report, 2019.
84. P. McKeown, M. D. Jones, The chemical recycling of PLA: a review, *Sustain. Chem.* **2020**, *1*, 1–22.
85. H. Tsuji, Hydrolytic degradation, in: R. Auras, L.-T. Lim, S. E. M. Selke, and H. Tsuji (Eds.), *Poly(Lactic Acid)*, John Wiley & Sons, Inc., USA, 2010, pp. 343–381.
86. V. Piemonte, F. Gironi, Kinetics of hydrolytic degradation of PLA, *J. Polym. Environ.* **2013**, *21*, 313–318.
87. F. Iñiguez-Franco, R. Auras, G. Burgess, D. Holmes, X. Fang, M. Rubino, et al., Concurrent solvent induced crystallization and hydrolytic degradation of PLA by water-ethanol solutions, *Polymer* **2016**, *99*, 315–323.
88. F. Iñiguez-Franco, R. Auras, K. Dolan, S. Selke, D. Holmes, M. Rubino, et al., Chemical recycling of poly(lactic acid) by water-ethanol solutions, *Polym. Degrad. Stab.* **2018**, *149*, 28–38.

89. F. M. Lamberti, L. A. Román-Ramírez, J. Wood, Recycling of bioplastics: routes and benefits, *J. Polym. Environ.* **2020**, *28*, 2551–2571.
90. L. A. Román-Ramírez, P. Mckeown, M. D. Jones, J. Wood, Poly(lactic acid) degradation into methyl lactate catalyzed by a well-defined Zn(II) complex, *ACS Catal.* **2019**, *9*, 409–416.
91. L. A. Román-Ramírez, P. McKeown, C. Shah, J. Abraham, M. D. Jones, J. Wood, Chemical degradation of end-of-life poly(lactic acid) into methyl lactate by a Zn(II) Complex *Ind. Eng. Chem. Res.* **2020**, *59*, 11149–11156.
92. E. Feghali, L. Tauk, P. Ortiz, K. Vanbroekhoven, W. Eevers, Catalytic chemical recycling of biodegradable polyesters, *Polym. Degrad. Stab.* **2020**, *179*, 109241.
93. NatureWorks, Chemical recycling. Available from: https://www.natureworksllc.com/What-is-Ingeo/Where-it-Goes/Chemical-Recycling (accessed 12 January 2021).
94. BCG, A circular solution to plastic waste, 2019.
95. H. Tsuji, *Degradation of Poly (Lactide)-Based Biodegradable Materials*, Nova Science Publishers, USA, 2008, pp. 1–76.
96. A. A. Shah, F. Hasan, A. Hameed, S. Ahmed, Biological degradation of plastics: a comprehensive review, *Biotechnol. Adv.* **2008**, *26*, 246–265.
97. S. Grima, V. Bellon-Maurel, P. Feuilloley, F. Silvestre, Aerobic biodegradation of polymers in solid-state conditions: a review of environmental and physicochemical parameter settings in laboratory simulations, *J. Polym. Environ.* **2000**, *8*, 183–195.
98. T. Leejarkpai, U. Suwanmanee, Y. Rudeekit, T. Mungcharoen, Biodegradable kinetics of plastics under controlled composting conditions, *Waste Manage.* **2011**, *31*, 1153–1161.
99. V. Mittal, *Characterization Techniques for Polymer Nanocomposites*, Wiley-VCH Verlag & Co., Weinheim, 2012.
100. International Standard, ISO 14855-1 Determination of the ultimate aerobic biodegradability of plastic materials under controlled composting conditions—method by analysis of evolved carbon dioxide, Part 1: general method, 2005, p. 20.
101. International Standard, ISO 14855-2 Determination of the ultimate aerobic biodegradability of plastic materials under controlled composting conditions—method by analysis of evolved carbon dioxide, Part 2: gravimetric measurement of carbon dioxide evolved in a laboratory-scale, 2007, p. 15.
102. ASTM International, Standard test method for determining aerobic biodegradation of plastic materials under controlled composting conditions, incorporating thermophilic Temperatures, 2015, p. 7.
103. E. Castro-Aguirre, Design and construction of a medium-scale automated direct measurement respirometric system to assess aerobic biodegradation of polymers, Master thesis. Michigan State University, 2013.
104. T. Kijchavengkul, R. Auras, M. Rubino, M. Ngouajio, T. R. Fernandez, Development of an automatic laboratory-scale respirometric system to measure polymer biodegradability, *Polym. Test.* **2006**, *25*, 1006–1016.
105. How2Compost. Available from: https://how2recycle.info/how2compost (accessed 15 May 2021).
106. Biodegradable Products Institute, Guidelines for the labeling and identification of compostable products and packaging, 2020.
107. E. E. Raimondo, J. M. Saez, J. D. Aparicio, M. S. Fuentes, C. S. Benimeli, Bioremediation of lindane-contaminated soils by combining of bioaugmentation and biostimulation: effective scaling-up from microcosms to mesocosms, *J. Environ. Manage.* **2020**, *276*, 111309.
108. E. Castro-Aguirre, R. Auras, S. Selke, M. Rubino, T. Marsh, Enhancing the biodegradation rate of poly(lactic acid) films and PLA bio-nanocomposites in simulated composting through bioaugmentation, *Polym. Degrad. Stab.* **2018**, *154*, 46–54.
109. Y. Boonluksiri, B. Prapagdee, N. Sombatsompop, Promotion of polylactic acid biodegradation by a combined addition of PLA-degrading bacterium and nitrogen source under submerged and soil burial conditions, *Polym. Degrad. Stab.* **2021**, *188*, 1–9.
110. H. Endres, A. Siebert-Raths, *Properties and Applications Engineering Biopolymers*, Elsevier, United Kingdom, 2011.
111. P. K. Shin, M. H. Kirn, J. M. Kim, Biodegradability of degradable plastics exposed to anaerobic digested sludge and simulated landfill conditions, *J. Environ. Polym. Degrad.* **1997**, *5*, 33–39.
112. S. Gartiser, M. Wallrabenstein, G. Stiene, Assessment of several test methods for the determination of the anaerobic biodegradability of polymers, *J. Environ. Polym. Degrad.* **1998**, *6*, 159–173.
113. V. Massardier-Nageotte, C. Pestre, T. Cruard-Pradet, R. Bayard, Aerobic and anaerobic biodegradability of polymer films and physico-chemical characterization, *Polym. Degrad. Stab.* **2006**, *91*, 620–627.
114. T. Narancic, S. Verstichel, R. S. Chaganti, L. Morales-Gamez, S. T. Kenny, B. De Wilde, et al., Biodegradable plastic blends create new possibilities for end-of-life management of plastics but they are not a panacea for plastic pollution, *Environ. Sci. Technol.* **2018**, *52*, 10441–10452.
115. J. J. Kolstad, E. T. H. Vink, De B. Wilde, L. Debeer, Assessment of anaerobic degradation of Ingeo™ polylactides under accelerated landfill conditions, *Polym. Degrad. Stab.* **2012**, *97*, 1131–1141.
116. V. Bátori, D. Åkesson, A. Zamani, M. J. Taherzadeh, S. I. Horváth, Anaerobic degradation of bioplastics: a review, *Waste Manage.* **2018**, *80*, 406–413.
117. K. Bernat, D. Kulikowska, I. Wojnowska-Baryła, M. Zaborowska, S. Pasieczna-Patkowska, Thermophilic and mesophilic biogas production from PLA-based materials: possibilities and limitations, *Waste Manage.* **2021**, *119*, 295–305.
118. M. Grosso, A. Motta, L. Rigamonti, Efficiency of energy recovery from waste incineration, in the light of the new waste framework directive, *Waste Manage.* **2010**, *30*, 1238–1243.
119. A. Damgaard, C. Riber, T. Fruergaard, T. Hulgaard, T. H. Christensen. Life-cycle-assessment of the historical development of air pollution control and energy recovery in waste incineration, *Waste Manage.* **2010**, *30*, 1244–1250.

120. C. Laußmann, U. Land, B. Münster, G. H.-J. Endres, F. Hannover, G. U. A.-S. Giese, A. P. Kitzler, Disposal of biopolymers via energy recovery, *Bioplastics Mag.* **2010**, 42–43.
121. NatureWorks, Incineration. Available from: https://www.natureworksllc.com/What-is-Ingeo/Where-it-Goes/Incineration (accessed 20 March 2021).
122. H.-J. Endres, A. Siebert-Raths, H.-J. Endres, A. Siebert-Raths, End-of-life options for biopolymers, in: Hans-Josef Endres, Andrea Siebert-Raths *Engineering Biopolymers*, Germany, 2011, pp. 1–16.
123. Marquard & Bahls. Available from: https://www.marquard-bahls.com/en/news-info/glossary/detail/term/net-calorific-value-gross-calorific-value.html (accessed 4 May 2021).
124. M. El-Fadel, A. N. Findikakis, J. O. Leckie, Environmental impacts of solid waste landfilling, *J. Environ. Manage.* **1997**, *50*, 1–25.
125. S. Selke, Plastics recycling and biodegradable plastics, in: C. Harper (Ed.), *Handbook of Plastics Technologies*, McGraw-Hill, New York, 2006.
126. NatureWorks, Landfill. Available from: https://www.natureworksllc.com/What-is-Ingeo/Where-it-Goes/Landfill (accessed 20 March 2021).
127. M. de Cosate, F. Andrade, P. M. S. Souza, O. Cavalett, A. R. Morales, Life cycle assessment of poly(lactic acid) (PLA): comparison between chemical recycling, mechanical recycling and composting, *J. Polym. Environ.* **2016**, *24*, 372–384.
128. D. Maga, M. Hiebel, N. Thonemann, Life cycle assessment of recycling options for polylactic acid, *Resour. Conserv. Recycl.* **2019**, *149*, 86–96.
129. J. Beigbeder, L. Soccalingame, D. Perrin, J.-C. Bénézet, A. Bergeret, How to manage biocomposites wastes end of life? A life cycle assessment approach (LCA) focused on polypropylene (PP)/wood flour and polylactic acid (PLA)/flax fibres biocomposites, *Waste Manage.* **2019**, *83*, 184–193.
130. J. D. Badia, A. Ribes-Greus, Mechanical recycling of polylactide, upgrading trends and combination of valorization techniques, *Eur. Polym. J.* **2016**, *84*, 22–39.

# PART V

# APPLICATIONS

# 25

# MEDICAL APPLICATIONS

SHUKO SUZUKI AND YOSHITO IKADA

## 25.1 INTRODUCTION

The use of biodegradable materials for medical applications has been studied extensively over the past four decades. The advantages of biodegradable over nondegradable biomaterials are (i) to eliminate the need to remove implants; and (ii) to provide long-term biocompatibility. The most common synthetic biodegradable polymers used in medical applications are poly(α-hydroxyacid)s, including poly(glycolic acid) (PGA), poly(lactic acid) (PLA), and polydioxanone (PDS). Of these polymers, PLA has shown the most promise due to its relatively strong mechanical properties. PLA has been successfully used in many medical implants and is approved by many international regulatory agencies.

The use of PLA in medicine started as early as 1966, when Kulkarni et al. [1] reported the medical application of poly(L-lactic acid) (PLLA). It was observed that the degradation of PLLA powder implanted in guinea pigs and rats gave a nontoxic tissue response. In 1971, Cutright and Hunsuck conducted a follow-up investigation and found applications of PLA as sutures [2] and in orthopedic fixation [3]. Since then, much research has been conducted. However, medical applications of PLA have been limited mainly to bone fixation due to its slow degradation rate. To increase the degradation rate, copolymers with PGA or poly(ε-caprolactone) (PCL) having lower crystallinity were synthesized. This chapter provides an overview of PLA in clinical applications. Although the main focus of this chapter is PLA homopolymers, selected PLA composites and copolymers used for tissue engineering and drug delivery application are also highlighted, since extensive investigations have been performed for these materials over the last few decades. Poly(lactic-*co*-glycolic acid) (PLGA) products are excluded from this section since there are extensive reviews covering these topics.

## 25.2 MINIMAL REQUIREMENTS FOR MEDICAL DEVICES

### 25.2.1 General

All materials intended for use in the human body have to be assessed and approved by the local regulatory agencies prior to market. The minimal requirements of biomaterials intended for medical applications are nontoxicity, effectiveness, sterilizability, and biocompatibility (Table 25.1). Although many currently available biomaterials meet the first three criteria, a lot of them lack biocompatibility.

Biocompatibility is the ability of a biomaterial to perform with desired response(s) in a target application. In other words, biocompatibility cannot be attributed solely to the material properties, but rather, a combination of both material properties and the function it is intended for. Various materials, including polymers, metals, ceramics, and their composites, have been tested as medical devices. These medical devices can be classified into two groups—biodegradable and nondegradable.

At present, there is no nondegradable material that does not trigger any significant foreign body reaction when implanted, as the body fights naturally to defend against the new foreign material, thus evoking immune rejection against or encapsulation of the permanent implant. The fibrous

*Poly(Lactic Acid): Synthesis, Structures, Properties, Processing, Applications, and End of Life*, Second Edition.
Edited by Rafael A. Auras, Loong-Tak Lim, Susan E. M. Selke, and Hideto Tsuji.

**TABLE 25.1 Requirements for Biomaterials [4]**

| Requirement | Properties |
|---|---|
| 1. Nontoxic (biosafe) | Nonpyrogenicity, nonhemolyticity, nonmutagenicity, nonallergicity, nononcogenicity, etc. |
| 2. Effective | Functionality, performance, durability, etc. |
| 3. Sterilizable | Autoclaving, dry heating, ethylene oxide gas, irradiation, etc. |
| 4. Biocompatible | Interfacially, mechanically, and biologically |

encapsulation can cause bacterial infections, which ultimately leads to an unsuccessful implant. Biodegradable polymers have attracted much attention since these materials do not require long-term biocompatibility. Examples of biodegradable polymers in medical applications are listed in Table 25.2. These polymers remain temporarily in the body but disappear via biodegradation over time, thus eliminating the need for a second operation to remove the material after the defect site is healed.

Despite these attractive features, biodegradable polymers are not extensively used in current medical applications for two reasons. First, and most importantly, it is crucial that the degradation rate of the biodegradable polymer match the rate of tissue regeneration [6]. If the polymer degrades faster than tissue regeneration, the patient may experience reoccurrence of the defect. However, if the degradation rate is too slow, the residual polymer may interfere with tissue physiology. The major challenge when designing biodegradable materials is to achieve a perfect tuning of these two parameters, which is further complicated by the fact that the healing process relies on the patient and depends on the extent of tissue damage.

Secondly, degraded substances of the polymer (usually low molecular weight compounds such as unpolymerized monomers, additives, and fragments of polymerization initiators and catalysts) may leach into the patient's body, thus inducing toxicity [4]. These compounds are currently controlled under strict regulatory limits. It is of paramount importance that the safety of degraded substances be meticulously considered since these small molecules are constantly being released in the body.

For hydrolysable polymers, extreme care must be taken during the manufacturing process and storage to prevent material degradation due to moisture. Certain polymers, such as poly(α-hydroxyacid)s, are sensitive to radiation, and therefore the choice of sterilization should also be considered. Often, ethylene oxide, which requires extensive degassing to remove any residual traces of gas, is preferred.

**TABLE 25.2 Medical Applications of Biodegradable Polymers [4, 5]**

| Purpose | Function | Examples |
|---|---|---|
| Operative assist | Bonding, closure, separation | Vascular and intestinal anastomosis, bone fixation, wound cover, hemostasis, vascular embolization |
| Damage healing | Scaffold | Wound healing, tissue growth, organ reconstruction |
| Drug release | Capsulation | Sustained drug release such as antitumor, growth factors to promote healing, antithrombosis, angiogenesis, anti-infection |

### 25.2.2 PLA as Medical Implants

The molecular weight of PLA synthesized from polycondensation of lactic acids is generally too low for medical applications (weight-average molecular weight <20,000 g/mol), and therefore ring-opening polymerization of lactides is often utilized to obtain high molecular weight PLA, unless a rapidly degradable polymer is required for the application. PLLA is a semicrystalline material with a degradation rate of more than two years [7]. In comparison, poly(D, L-lactic acid) (PDLLA), being an amorphous polymer, can easily degrade within 16 months.

The toughness of PLLA can be further enhanced by a drawing process for applications such as bone fixation, which require strength and elasticity similar to those of the native bone tissues. Drawing of PLLA with a weight-average molecular weight over 70,000 g/mol increases the orientation and crystallinity [5]. Another important phenomenon associated with the drawing of PLLA is an increase of piezoelectricity, which will be further discussed in Section 25.3.3.2. Self-reinforcement (SR) is another method used to strengthen PLA for bone fixation applications. This technique bounds polymeric fibers with high modulus and a matrix of the same polymer without any adhesion promoters.

Degradation of PLA by hydrolytic scission of the ester linkages yields lactic acid. Lactic acid is a natural product associated with muscular construction in animals and humans, which can be decomposed by the body's normal metabolic pathways. Lactic acid is converted to pyruvic acid in the body and enters the tricarboxylic acid cycle to yield carbon dioxide and water. Using carbon-labeled PLA, no significant accumulation of degraded products was found in any organ, with minimal amounts found in feces and urine, thus indicating that these products were released through respiration [1]. Since L-lactic acid (LLA) is a naturally occurring stereoisomer of lactic acid, PLLA is more commonly used in medical applications rather than poly(D-lactic acid) (PDLA), which yields D-lactic acid (DLA) when degraded.

PLA and other poly(α-hydroxyacid)s, as well as their copolymers, have been approved by the US Food and Drug Administration (FDA) and by many other international regulatory agencies for implantation in the human body. A number of products are now commercially available and

have successfully been used in the medical field. Despite these successes, there are still disadvantages of PLA such as the degradation products and its hydrophobic nature yet to be overcome.

As mentioned previously, the degradation product, lactic acid (LA), can be decomposed by the body. However, the accumulation of LA, a relatively strong acid, at the implant site, resulting from a "burst" release by bulk degradation of the PLA, will lower the local pH, which then triggers an inflammation response [8, 9]. Such inflammation responses could last for over a year [10, 11]. Another study reported that degradation particles smaller than 2 μm could trigger a foreign body reaction, thus resulting in detrimental effects on the bone tissue [12]. Research aimed at neutralizing the acidic degradation products by adding agents such as calcium carbonate and/or calcium phosphate to the PLLA implants have been studied [13, 14].

Other compounds present in the polymer are trace amounts of initiators, coinitiators, and catalysts. Tin compounds, including tin(II) 2-ethylhexanoate, are examples of the most effective and commonly used initiators for ring-opening polymerization of lactide. Tin(II) 2-ethylhexanoate has been approved by the FDA due to its low toxicity. The residual concentration of tin(II) 2-ethylhexanoate present in the polymer is controlled to a safe level and rigorously monitored. A new range of metal-based initiators and catalysts (e.g., magnesium and calcium) are being studied in the hope to develop more biocompatible materials.

The hydrophobic nature of PLA and other poly(α-hydroxyacid)s results in a low affinity for cells and proteins, thus suppressing tissue formation [15]. This, along with slow degradation of PLA homopolymer, has restricted its use as scaffolds. However extensive investigations have been performed over the past few decades for PLA composite scaffolds, as introduced in Section 25.3.5.

## 25.3 PRECLINICAL AND CLINICAL APPLICATIONS OF PLA DEVICES

### 25.3.1 Fibers

The oldest and broadest medical application of biodegradable polymers is as sutures. The synthetic polymers used for this purpose are mainly PGA or its copolymer with LLA (90 : 10), launched in 1970 and 1974, respectively [16, 17]. PDS sutures were also developed in 1981. Although PLLA is deemed unsuitable for use in sutures due to the slow fiber degradation, it is the preferred material in applications requiring prolonged strength retention. These applications include ligament and tendon reconstruction, as well as stents for vascular and urological surgeries.

PLLA fibers were used clinically to augment ruptured knee ligaments in the early 1990s [18–20]. The most commonly injured ligament during sporting activities or trauma is the anterior cruciate ligament (ACL), which connects the bones of the knee joint. Since a completely torn ACL cannot regenerate by itself, a reconstructive surgery using autografts, such as patellar tendons (part of the tendon in the front of the knee) or hamstring tendons, has to be performed. Polymeric biomaterials, such as polyethylene and polypropylene, are used when autografts are insufficient for the procedure. PLLA fiber, due to its slow degradation rate, is a preferred biodegradable material for this application and has been widely studied. An animal model reported that PLLA had similar improvements in tendon reconstruction when compared to polypropylene [21].

Cooper et al. [22, 23] developed a PLLA 3D construct for ACL reconstruction. It is made of braided fibers with loose braids in the intra-articular region, having pore size of 200–250 μm, and tightly braided at the ends, with pore size of 150 μm, for fixation (Figure 25.1). The rabbit model demonstrated the ability of this construct to allow for bone tissue infiltration and ligamentization, while a large animal (ovine) model revealed complete regeneration of the ACL without PLLA fibers [24, 25]. More recently, a twist-braided PLLA construct made by a custom 3D braiding machine was evaluated in a rabbit ACL reconstruction model, with and without supplementation of bone morphogenetic protein 2 (BMP-2) [26]. The bioengineered ACL matrix demonstrated similar modes of osteointegration as current autografts and allografts. The BMP-2 treatment might enhance osteoblastic activity within the bone tunnels. In the latest development, they added a nondegradable poly(ethylene terephthalate) (PET) fiber to the PLLA matrix to increase strength, with supplementation of the bone marrow aspirate concentrate (BMAC) and growth factors (BMP-2, FGF-2, and FGF-8), which was evaluated in a rabbit model [27]. The results illustrated beneficial effects of bioactive factors and PET incorporation on the ACL regeneration.

Nishimoto et al. investigated a stent-shaped PLLA, fabricated from 0.2-mm diameter fibers, in a medial collateral

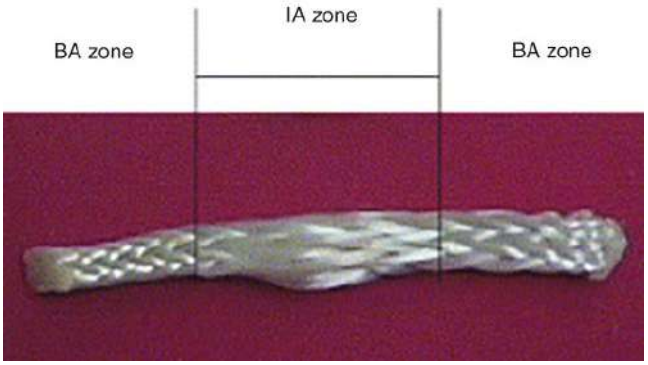


**FIGURE 25.1** 3D PLLA square braid with intraarticular (IA) zone and bone attachment (BA) zones. Source: Reprinted from Ref. 22 with permission from Elsevier.

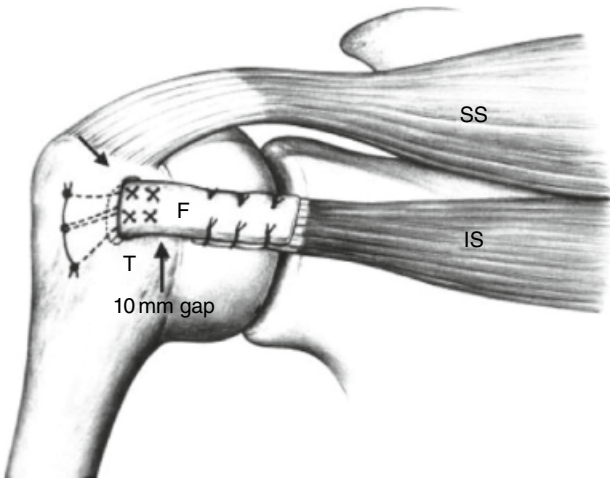


**FIGURE 25.2** Reconstruction of an infraspinatus (IS) tendon by a PLLA felt (F). SS indicates the supraspinatus tendon. Source: Reprinted from Ref. 29 with permission from John Wiley & Sons.

ligament (MCL)-defected rabbit [28]. After 16 weeks post-operation, the PLLA successfully regenerated ligaments with type I collagen expression and fibrocartilage formation, resulting in sufficient mechanical function.

PLLA felts/fabrics have found applications in rotator cuff repairs. Aoki et al. [29] used a PLLA felt as a biodegradable artificial tendon graft for a rotator cuff surgery for the treatment of irreparable rotator cuff tear as shown in Figure 25.2. The felt was obtained by entangling 20 μm diameter fibers, produced by melt spinning of PLLA with a molecular weight of ~215,000 g/mol. Defects created in the infraspinatus (IS) tendons of beagle dogs were reconstructed with the PLLA felt. Histological examinations revealed a three-fold increase in the strength of the felt (due to the infiltration of fibrous tissues) 16 weeks post-operation. Although the degradation rate of the PLLA felt was low, the tensile recovery of the felt graft was excellent. They concluded that the PLLA felt might be a useful material for rotator cuff reconstruction.

Inui and co-workers investigated a double-layered PLLA fabric having smooth exterior surfaces with rough (pile-finished) interior surfaces in a rabbit rotator cuff defect model (Figure 25.3) [30]. This fabric was textured from 23 μm diameter PLLA fibers, with a molecular weight of 86,000 g/mol. Defects created in the IS tendons of rabbits were reconstructed with the PLLA fabric and evaluated histologically and mechanically at 4, 8, and 16 weeks post-operation. Cell migration was observed on the inner, rough surface four weeks post-operation, while the smooth surface prevented cell attachment. After eight weeks, the failure strength of the reconstructed tendon showed no statistical difference with a normal IS tendon, indicating a successful recovery.

X-Repair (Synthasome, San Diego, CA, USA) is a multi-layered woven PLLA felt that is commercially available for rotator cuff repair [31] (Figure 25.4). This product has a tensile strength and stiffness similar to human tendons. A preclinical study using a rotator cuff defect model in dogs demonstrated that the ultimate initial-load directly after implantation was significantly increased when compared with an unaugmented repair, while the stiffness remained unaltered [32]. After 12 weeks, the PLLA felt augmented repairs demonstrated a significant reduction in tendon retraction and were significantly greater in the cross-sectional area, stiffness, and ultimate load than the repairs that were not augmented [32].

PLLA fibers are used as biodegradable stents in cardiovascular and urological surgeries. Metallic stents are traditionally used to treat narrowed or weakened arteries in the body. However, if the stents are covered by the epithelium tissue, an operation is required since they cannot be easily removed by a conventional bronchoscopic procedure [33]. This is an issue for a younger patient who is still growing and requires replacement with a larger stent. Biodegradable

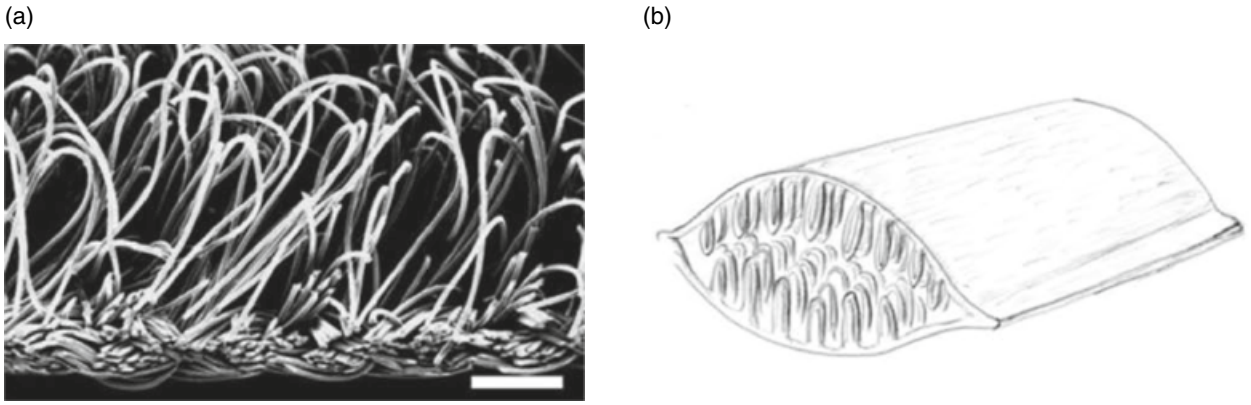


**FIGURE 25.3** (a) SEM image of the rough interior of the pile-finished PLLA fabric. Scale bar represents 50 μm. (b) Schematic representation of a double-layered PLLA fabric [30].

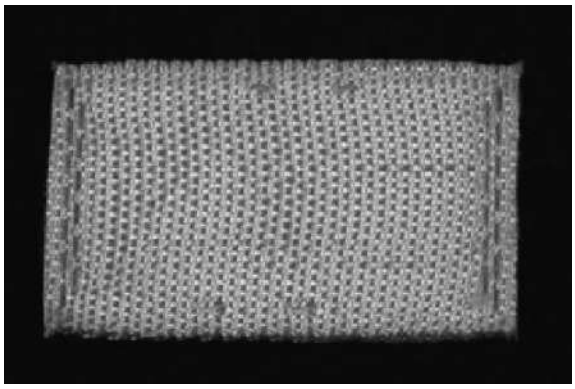

**FIGURE 25.4** Image of X-repair patch. Source: Reprinted from Ref. 31 with permission from Elsevier.

stents have been tested in numerous clinical studies. The degradable polymer is selected based on the duration required for the stent function. For example, PDS and poly(glycolide-*co*-ε-caprolactone) stents can provide temporary support up to five and two weeks, respectively, whereas PLLA fibers are recommended for longer support [34]. PLLA is the most commonly used biodegradable material for coronary stents.

The Igaki-Tamai stent (Kyoto-Medical Planning Co Ltd, Kyoto, Japan) was the first biodegradable stent tested in humans. It is constituted of a zig-zag helical design, made of PLLA monofilament, with a strut thickness of 170 μm and is self-expandable upon heating [35, 36]. The stent struts disappear within three years in vivo. Fifty patients treated with the Igaki-Tamai stent between 1998 and 2000 demonstrated the long-term clinical safety, high survival rate free of cardiac death (98% at 10 years), acceptable major adverse cardiac events, and low scaffold thrombosis rates [36].

Drug-eluting stents have become the current mainstream therapy for coronary artery stenosis due to known extreme low rates of in-stent restenosis [37, 38]. Various manufacturers have introduced PLLA-based, drug-eluting coronary stents commercially, and PLA has also found application in coating materials for drug release. Among them, the most extensively studied stent is the ABSORB BVS (Abbott Vascular, Santa Clara, CA, USA) (Figure 25.5), which is composed of a balloon-expandable PLLA monofilament (thickness 157 μm) with a thin PDLLA coating for controlled release of everolimus [37, 39]. Large-scale clinical trials have been performed since 2010 [38]. However, the ABSORB BVS showed higher rates of thrombosis, target vessel revascularization, and target lesion myocardial infarctions when compared with the cobalt-chromium everolimus-eluting stent group in a recent review [38]. Typically, the struts of PLLA stents should be thicker than those for conventional metal stents in order to provide desirable radial strength. However, this results in poor targeted delivery, platelet deposition, and vessel injury [38].

Despite ABSORB BVS being pulled off the market, second-generation PLLA-based stents have been developed by manufacturers using different strategies, such as thinner struts while maintaining their radial strength, as shown in Table 25.3.

Nondegradable silicone stents are commercially available for use in inoperable, nonmalignant airway disease. Although they are easier to remove than the metallic ones, the larger tube could cause obstruction. Saito et al. [33] compared the biocompatibility and suitability of a tubular biodegradable knitted stent made of PLLA with a conventional silicone stent in normal rabbit airways. Three out of eight rabbits in the silicone stent group died within four weeks of implantation, resulting from airway obstruction by secretions inside the stent lumen, whereas there were none reported in the PLLA stent group. The feasibility of stent delivery and deployment was demonstrated using a balloon expansion technique in a dog model [40].

Another important factor to consider when designing stents is the problems associated with biodegradable stents, such as migration immediately after implantation and rapid disintegration [41, 42]. Isotalo et al. [43] compared the biocompatibility of two different designs of self-reinforced PLLA (SR-PLLA) urethral stents: braided and traditional spiral, as well as stainless steel stents in a rabbit model. They reported a more controlled disintegration of the braided SR-PLLA stent versus the spiral SR-PLLA stent. Although the initial outcomes obtained with PLA based urethal stents in

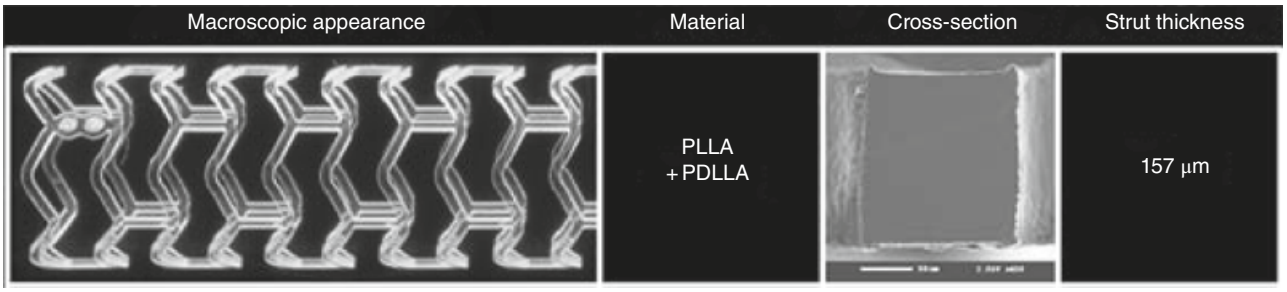


**FIGURE 25.5** Macroscopic and cross-sectional SEM images of ABSORB BVS. Source: Reproduced from Ref. [39] with permission from Elsevier.

**TABLE 25.3 Second-Generation PLLA Stents in Preclinical and Clinical Testing [38]**

| Manufacture | Country | Product Name | Drug | Coating | Strut Size (mm) | Resorption Time (months) | Availability |
|---|---|---|---|---|---|---|---|
| Amaranth | USA | Fortitude | Sirolimus | PDLLA | 150 | 10 | CE mark |
| | | Aptitude | Sirolimus | PDLLA | 115 | >36 | Clinical study |
| | | Magnitude | Sirolimus | PDLLA | 98 | 24–36 | Clinical study |
| Meril | India | MeRes 100 | Everolimus | PDLLA | 100 | 24 | Clinical study |
| ELIXIR | USA | DESolve Cx | Novolimus | PLA based polymer | 120 | 24 | CE mark |
| Shanghai MicroPort Medical | China | Firesorb | Sirolimus | PDLLA | 100–125 | 36 | Clinical study |

animal models were satisfactory, Lumiaho et al. reported degradation of the PLA urethral stent in blocks in a porcine model, resulting in poor ureter drainage [44]. Recent studies for this application tend to focus on using PLGA as a basic material that degrades rapidly and is designed to degrade from the distal to the proximal end to prevent urethral obstruction by fragments [45, 46]. In addition, PLA is often selected as the coating polymer in drug-eluting urethral stents, which have been extensively investigated, in particular for delivery of antitumor drugs [47].

### 25.3.2 Meshes

Barrier membranes are used in guided bone regeneration (GBR) to direct new bone growth in the defects by preventing soft tissue in-growth. It is essential to have a permeable membrane to supply nutrients. Nondegradable membranes such as expanded polytetrafluoroethylene (ePTFE) and ethyl cellulose are often used. However, since a second operation is required to remove nondegradable membranes, commercially available degradable materials are favorably selected for this purpose [48–50]. PLLA meshes have also been extensively investigated for GBR membranes [51–55]. PDLLA and copolymers of PLA are the preferred materials since it is not essential to have a long degradation period. In addition, polymer blends have been explored to provide improved flexibility. Some examples of commercially available PLA products are summarized in Table 25.4.

The high strength of PLLA mesh is favorable when designing 3D structures such as trays and cages. Kinoshita et al. [56, 57] investigated mandibular reconstruction using a PLLA mesh tray and particulate cancellous bone and marrow (PCBM) in 62 patients with tumors, cysts, or alveolar atrophy (Figure 25.6). The PLLA mesh consisted of monofilament with a weight-average molecular weight of 205,000 g/mol, spun, elongated, and woven into mesh. After cutting the PLLA mesh and adjusting it to the shape and size of the bone defect, the tray was filled with PCBM harvested from ilium. The mesh tray was implanted into the jawbone defect and secured using wires. Six months postsurgical clinical evaluations showed excellent results (bone formation range beyond 2/3) in 35 cases (56.5%), good results (bone formation range under 2/3, but reoperation unnecessary) in 17 cases (27.4%), and poor results (cases not falling into either category above) in 10 cases (16.1%).

Composites of PLLA and hydroxyapatite (HA) have been extensively studied for bone application and demonstrated significant improvement of osteointegration compared to pure PLLA [58–60]. Matsuo et al. [61] investigated a PLLA/unsintered HA (u-HA) mesh (Takiron, Osaka, Japan) for mandibular reconstruction in two patients. This composite contained 40% w/w raw particulates of HA for improved osteoconductivity, and gradually degraded in three to five years. A 3D mandible model was created by stereolithography using the computed tomography (CT) images. The PLLA mesh was produced as a customized tray. Mandibular reconstruction was performed using a PLLA/ u-HA mesh tray and PCBM, as well as platelet-rich plasma (PRP). In both cases, no bone resorption was found for over two years with an average CT value of 790 (in Hounsfield units) in the implant sites, which is equivalent to that of the native bone. The group also did a comparative evaluation of a PLLA/u-HA mesh tray with a titanium (Ti) tray for tray fitting and bone quality in a dog mandibular defect model [62]. Bone defects were made bilaterally on the lower borders of the mandible of 14 beagle dogs. The dogs were treated with either a custom-shaped PLLA/ u-HA mesh tray, or a manually adopted Ti tray with PCBM and PRP. It was concluded that the customized PLLA/u-HA mesh tray was adopted more easily and accurately to the mandible, with adequate bone quality achieved at 12 months.

**TABLE 25.4 Commercially available PLA-based GBR membranes**

| Manufacture | Country | Product Name | Material | Resorption Time (Months) |
|---|---|---|---|---|
| Sunstar | Sweden | Guidor | PDLLA and PLLA, with Acetyl tri-*n*-butyl citrate | 13 |
| Curasan Inc | USA | Epi-Guide | PDLLA | 6–12 |
| KLS Martin | Germany | Resorb X | PDLLA | 12–30 |
| Tolmar | USA | Atrisorb | PDLLA dissolved in *N*-methyl-2-pyrrolidone (NMP) | 9–12 |

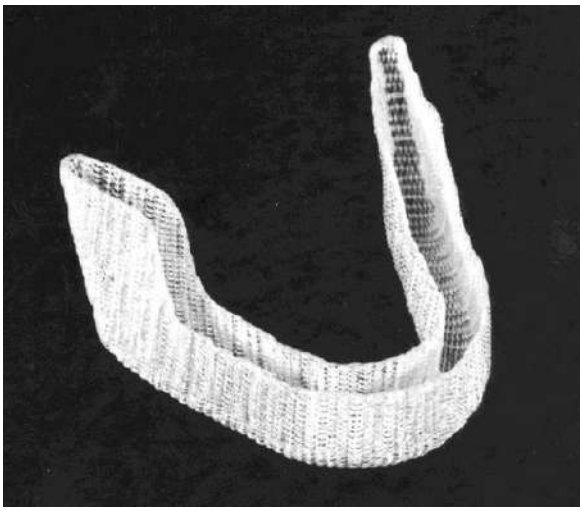

**FIGURE 25.6** PLLA mesh tray (for lower jawbone). The tray may be cut with scissors and is moldable at 70°C [56].

Ochi et al. [63] developed a chondral plug using a PLLA cage with type I collagen sponge, cultured using chondrocytes. This chondral plug can be transplanted using arthroscopy, without the need for arthrotomy—a more invasive surgery. Preliminary results using the osteochondral defect of a rabbit patellar groove revealed a successful transplantation.

### 25.3.3 Bone Fixation Devices

In the past few decades, biodegradable materials are replacing metallic implants for the fixation of fractured bones in the forms of plates, pins, screws, and wires for several reasons: (i) a second surgery is essential to remove metal materials after reunion of the fractured bones. However, removal of the implant may lead to refracturing due to the temporary weakening of the bone; (ii) it is possible that the hard metallic materials can lead to osteoporosis of the bones below the implants due to stress shielding, thus resulting in a fracture near the edge of the material [64, 65]; (iii) there is a risk of toxicity caused by corrosion of the metallic implants [66]; (iv) metallic implants can often interfere or cause distortion in post-operative X-rays, CTs, and MRIs; and (v) the presence of metallic implants may alter local dose distribution (i.e., overdosage in front of and underdosage behind the implants) in patients undergoing postoperative radiotherapy who had tumors removed [67, 68].

The use of degradable materials for this purpose is therefore ideal. Since materials for bone fixation require high strength (similar to that of the bone), PLA has a large potential in this field. Recently, PLA composite-based fixation devices containing bioactive calcium phosphates, such as β-tricalcium phosphate (β-TCP) and HA, have been developed to combat various adverse effects identified in pure polymer devices. Biodegradable orthopedic devices have also been reviewed extensively [7, 69, 70]. Commercially available PLA and its composite bone fixation devices are summarized in Table 25.5. This section introduces the effects of stress shielding and piezoelectricity of PLA, followed by their applications in bone fixation devices.

**TABLE 25.5 Commercially Available PLA Bone Fixatives in the World Market**

| Manufacturer | Country | Product | Material |
|---|---|---|---|
| CONMED (Bionx Implants) | USA | Pin, screw | SR-PLLA |
| | | Meniscus arrow | Drawn PLLA |
| | | Screw, miniplate | SR-P(LLA/DLLA) (70/30) |
| J&J (Codman, DePuy Mitek) | USA | Rivet for skull | PLLA |
| | | Suture anchor | Drawn PLLA |
| Linvatec | USA | Suture anchor | Drawn PLLA |
| | | Interference screw | |
| Phusis | France | Interference screw | P(LLA/DLLA) |
| Centerpulse Orthopedics | USA | Interference screw | PDLLA |
| BIOMET Orthopedics | USA | Miniscrew | Drawn PLLA |
| Gunze | Japan | Pin, screw, miniplate, rod, interference screw | Drawn PLLA |
| Arthrex | USA | Interference screw | Drawn PLLA |
| | | | PDLLA with BCP |
| Takiron | Japan | Pin, screw, miniplate, rod | Drawn PLLA with HA |
| Stryker | USA | Suture anchor | Amorphous PLLA with HA |
| Zimmer Biomet | USA | Suture anchor | PDLLA with β-TCP |
| Anstem Medical | South Africa | Interference screw | PDLLA with β-TCP |
| Inion | Finland | Screw, miniplate | PLLA, PLDLLA, PGA and TMC |

BCP: biphasic calcium phosphate; HA: hydroxyapatite; SR: self-reinforced; β-TCP: β-tricalcium phosphate; TMC: trimethylene carbonate.

***25.3.3.1 Stress Shielding Effect*** The stress shielding effect is a mechanical concept—when two or more components of different elastic moduli make up a mechanical system, redistribution of load, stress and strain will occur toward the stiffer component, such as from bones to metals [71]. In the early healing stage, it is essential that the fixation device is sufficiently stiff in order to stabilize the fracture ends. However, this causes a decrease in stress stimulation, which can lead to osteoporosis, especially during the late healing stage and ultimately can result in fracture and loosening of implants [72–75]. Since biodegradable materials degrade slowly, load transfer to the bone gradually increases, thus reducing the stress shielding effect during the bone healing process [76, 77].

Stress shielding effects of PLLA and stainless steel (SUS304) screws were investigated using rabbit models under a load-bearing condition, as illustrated in Figure 25.7a [78]. While an increase in new bone formation was observed using both screw types, the increase was significantly higher for PLLA screws than for stainless steel screws after 8 and 16 weeks of implantation (Figure 25.7b).

Another study reports the use of PLLA and stainless steel plates (design shown in Figure 25.8a and b) implanted in rabbit femoral shaft osteotomies [79]. The mechanical strength of the united specimens at 8-, 25- and 40-weeks post-implantation is presented in Figure 25.8c. At 25 weeks post-implantation, it was observed that full strength was restored using the PLLA plates, whereas only 30% of the original strength was recovered using the stainless steel plates and was further reduced at 40 weeks. Figure 25.8d showed a decrease in bone thickness for the bone surrounded by the stainless steel plates. The results clearly demonstrate the impact of the stress shielding effect using metal plates on bone loss. The stress shielding effect was eliminated at 25 months when the strength of PLLA plates was reduced to almost zero.

***25.3.3.2 Piezoelectric Effect*** It is well known that bone growth can be enhanced by applying electrical stimulation [80]. Various investigations have revealed that callus formation (which generally occurs at the beginning of bone formation) can be promoted by applying electric fields. Certain materials are capable of generating an electric potential when mechanical stress is applied, known as "piezoelectricity." These materials include crystals and ceramics (including bone). Polymers, such as polyvinylidene fluoride (PVDF), can also exhibit piezoelectricity [81].

It is interesting to note that through increasing the drawing process, PLLA can exhibit a similar degree of piezoelectricity as PVDF. PLLA, a crystalline polymer with an asymmetric carbon present in the repeating unit of the main chain, can exhibit high piezoelectricity when the polymer chains are highly oriented by the drawing process. Unlike PLLA, PDLLA, being an amorphous polymer, does not have any piezoelectric properties regardless of processing conditions. PLLA can therefore aid in promoting pseudo-bone formation via manipulating of the electric potential to change material stress.

The piezoelectric effect of drawn PLLA was investigated using films and rods [82]. As shown in Figure 25.9, the piezoelectric stress ($e_{14}$) and strain ($d_{14}$) constants of the PLLA film increased with increasing draw ratios up to 5, to the maximum values of −20 mC/m$^2$ and −10 pC/N, respectively, which are comparable to PVDF.

This is due to the increased alignment of the PLLA chains caused by drawing. Drawing ratios over 5 resulted in decreased piezoelectric constants, possibly attributed to fibrilization, which rendered disorder and discontinuity of the microscopic crystal arrangement. PLLA rods of different piezoelectric constants were intramedullary implanted in the cut tibiae of cats for internal fixation (Figure 25.10a) [82]. An ultrahigh molecular weight polyethylene (UHMWPE)

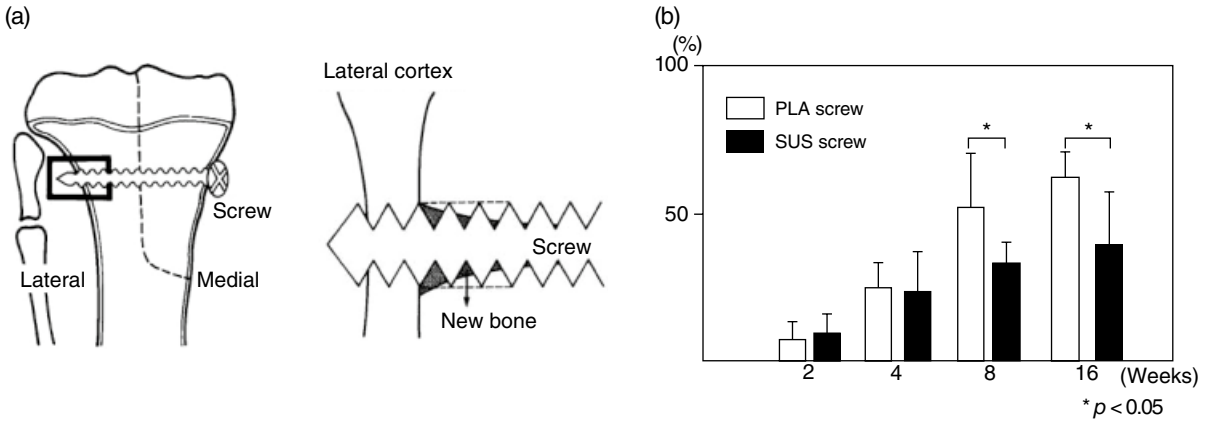


**FIGURE 25.7** (a) Schematic diagram of screw implantation in rabbit tibia proximal osteotomies and new bone formation, (b) new bone formation around PLA and SUS screws expressed as a percentage of the area of the new bone relative to the indentations of screw-threads. Source: Reprinted from Ref. 78 with permission from John Wiley & Sons.

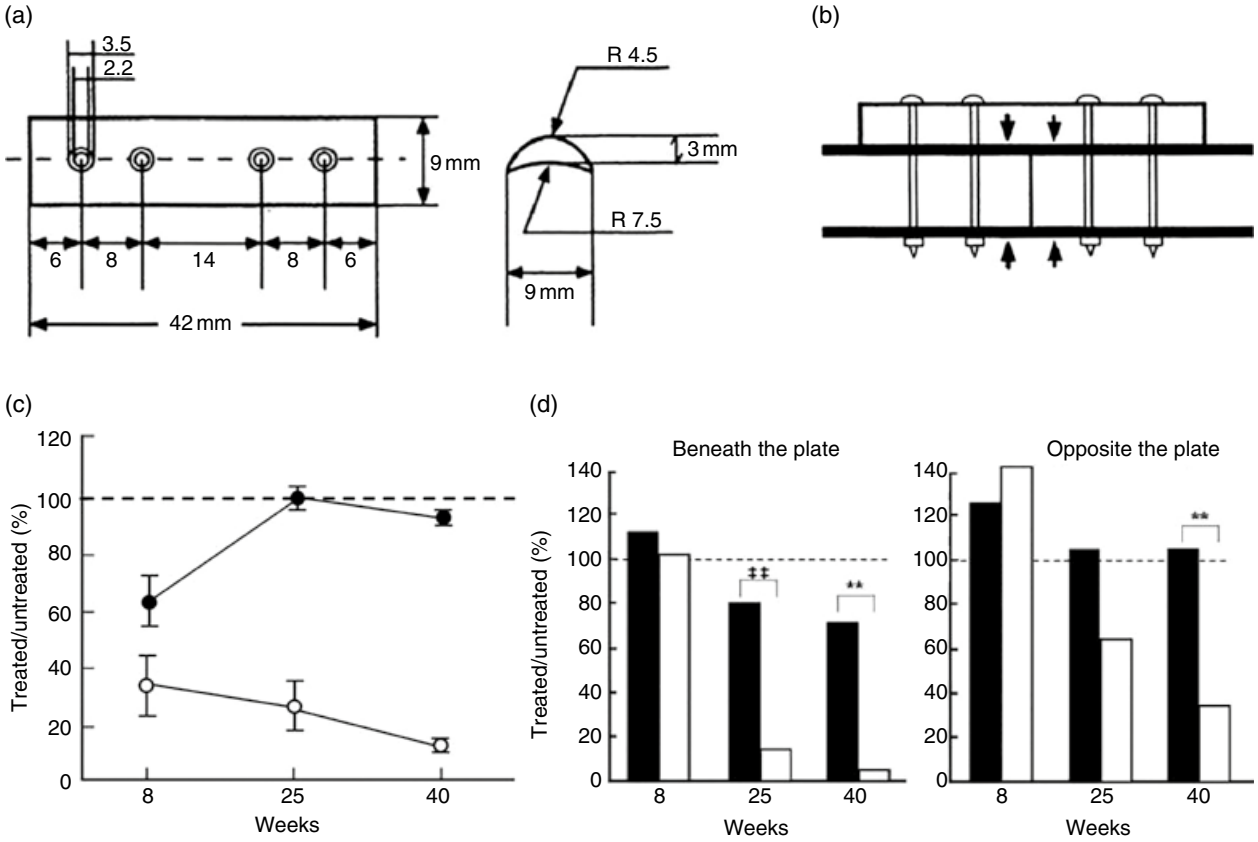


**FIGURE 25.8** (a) Design of the PLLA and stainless steel plates, (b) measured points of cortical thickness beneath (downward arrow) and opposite to (upward arrow) the plates. (c) Changes in the mechanical strength of united specimens using three-point bending. PLLA (●) and stainless steel (○). (d) Cortical thickness below (left) and above (right) the plate. PLLA (■) and stainless steel (□). Ordinate represents percentage of treated/untreated for each femur pair. Source: Reprinted from Ref. [79] with permission from Wolters Kluwer Health.

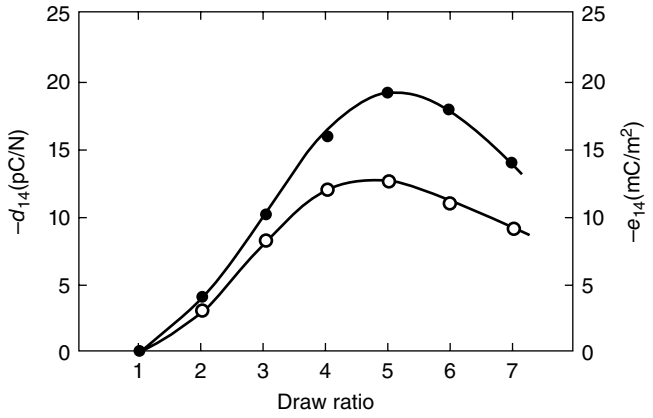


**FIGURE 25.9** The piezoelectric constants (stress: $e_{14}$●, and strain: $d_{14}$○) of PLLA film as a function of the draw ratio at room temperature. Source: Reprinted from Ref. 82 with permission from John Wiley & Sons.

rod (no piezoelectricity) was used as a control. Enhanced fracture healing was clearly observed in the cats implanted with PLLA rods with a high draw ratio after eight weeks (PLLA rods promoted the formation of large callus, unlike undrawn PLLA or PE rods) (Figure 25.10b).

Using the same concept, Tajitsu et al. [83–85] developed electrically controlled PLLA fiber for applications such as tweezers. PLLA fibers having high crystallinity and high orientation of the crystallites were fabricated using high-speed spinning. By applying DC or AC voltage, a pair of

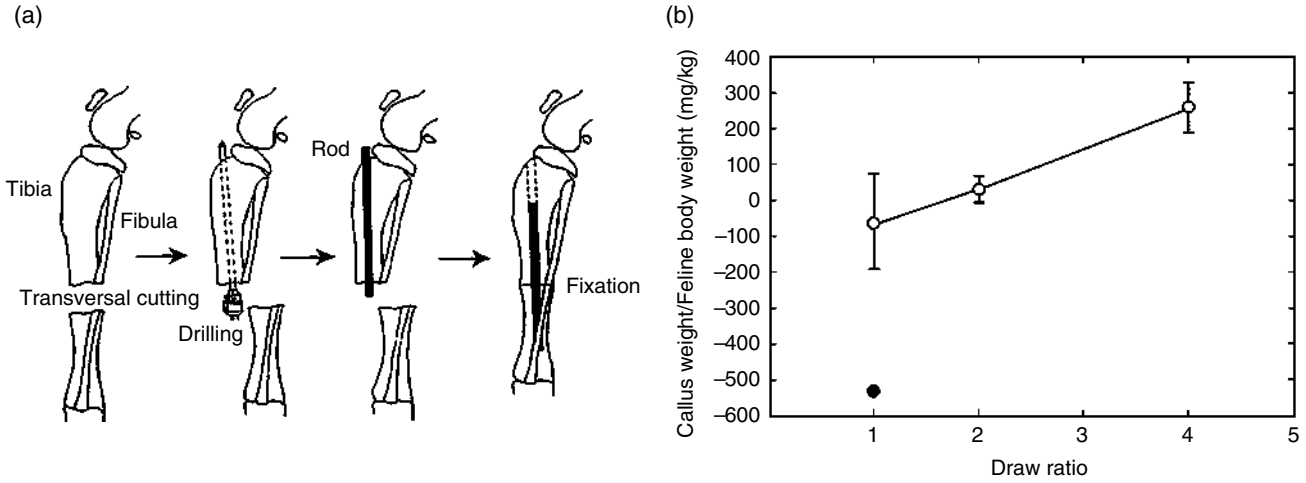


**FIGURE 25.10** (a) Procedure for implantation of the PLLA rods into the intramedullary canal of sectioned cat tibiae. (b) The effect of the drawn ratio of PLLA rod on the weight of callus formation at eight weeks after implantation (n = 4). PLLA (○), UHMWPE (●). Source: Reprinted from Ref. [82] with permission from John Wiley & Sons.

PLLA fibers moved, and were used as tweezers. More recently, they developed a piezoelectric PLLA fabric which was designed to accurately detect twisting, bending and elongation of the fabric. This fabric is used in tailoring smart clothing, being capable of sensing complex human motions [86].

Smith et al. [87] investigated piezoelectric PLLA nanomaterials for applications in mechanobiology. Piezoelectric platforms are attractive when studying the correlation of mechanical and electrical stimuli responses with cellular behaviors. The PLLA nanotubes (diameter of 305 nm and wall thickness 56 nm) were grown using a melt-press template wetting technique [88]. Crystallinity, surface potential, and piezoelectric activity of these nanotubes significantly affected the cellular behavior of human dermal fibroblasts grown on these materials [87].

***25.3.3.3 Screws, Pins, and Rods*** Drawn and SR-PLLA in the form of screws, pins, and rods are widely used for bone fixation. Different sizes and shapes of these materials are currently being marketed (Figure 25.11).

In the past few decades, degradation and biocompatibility of PLA implants were extensively studied. The biocompatibility of PLA implants was adequately demonstrated in many studies [89]. Due to its slower degradation rate when compared with PGA, adverse tissue reaction is often not observed [90, 91], although several adverse effects have been reported and will be discussed later in this section.

Matsusue et al. [92] investigated the degradation of drawn PLLA in vitro and in vivo. Ultrahigh-strength PLLA rods were fabricated using a drawing technique. Rods with a diameter of 3.2 mm and a draw ratio of 2.5 : 1 showed an initial bending strength and a modulus value of 240 MPa and 13 GPa, respectively. The weight of the PLLA rods in the medullary cavity was reduced by 22 and 70% at 52 and 78 weeks, respectively, post-implantation in rabbits. Neither inflammatory nor foreign body reaction was observed histologically in the medullary cavity at 52 weeks. The bending strength, greater than that of human cortical bone, was maintained for eight weeks in the medullary canal.

Hasegawa et al. [93] investigated the long-term degradation effect of drawn PLLA screws using minipig fracture models. Neither granuloma nor fistula formation was observed during the three-year investigation period. PLLA screws substantially degraded between two and three years, with only a small residual degraded product remaining in macrophages at three years. They concluded that the use of PLLA screws for fixation of fractures was not associated with any known side effects and was safe for up to three years.

Ten years of clinical studies on SR-PLLA and SR-PDLLA screws and miniplates used in orthognathic surgery were summarized by Laine et al. [94]. For the 163 patients who underwent a total of 329 orthognathic osteotomies fixed with PLA devices, the outcome was found to be excellent, with very few minor postsurgical complications (8.6%) reported.

The mechanical strength of biodegradable materials used in mandible applications where high forces are generated from constant movement has always been a concern. Maurer et al. [95] tested four clinically used screws (made of PLLA or LLA copolymers) using a finite-element model in the fixation of the bilateral sagittal split osteotomy (SSO), the most common procedure for mandibular advancement (i.e., shifting the lower jaw position forward). All four screws were found to be sufficiently stable at the osteotomy gap as far as the chewing forces were concerned.

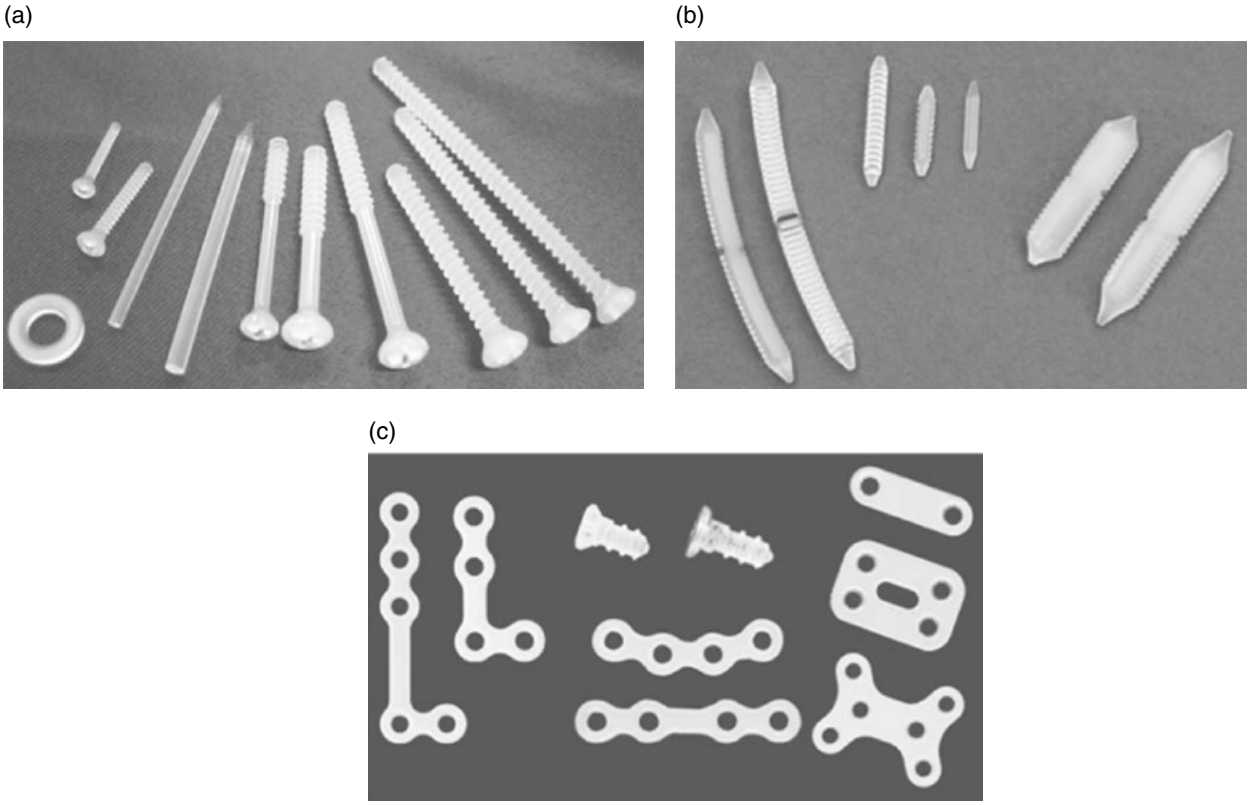


**FIGURE 25.11** PLLA-based (a) screws, (b) rods, and (c) miniplates. Source: Reprinted with permission from Gunze.

Oba et al. [96] compared the stability of drawn PLLA (FIXSORB-MX, Takiron) with titanium screws in the mandible following surgical orthodontic SSO and orthodontic multibracket treatment. No significant differences in the stability of the bony segments were found between 23 patients treated with PLLA screws and 22 patients treated with titanium screws. A slight tendency for clockwise rotation of the distal segment was observed in patients implanted with PLLA screws. It was suggested that fixation of the bony segments with PLLA screws after SSO may be effective in specific cases.

PLLA has been proven to be efficient and safe in the fixation of malleolar fractures [97] and syndesmosis [98]. Böstman reviewed 1223 patients having malleolar fractures treated by internal fixation with biodegradable pins and screws between 1985 and 1994 [97]. The implants used were PGA, PLA, and their copolymers. Only 10 patients (0.8%) experienced side effects, including various local foreign body reactions, synovial irritation, and subsequent degeneration.

While long strength retention time and degradation time of PLLA are not favorable, these parameters can be adjusted by adding PDLLA in the blend. SR-PLLA and SR-P(L/DL)LA (70 : 30) screws were compared for the fixation of ankle fractures [77]. The initial bending and shear strengths of SR-P(L/DL)LA were only slightly lower than those of SR-PLLA. While the ability of SR-P(L/DL)LA to retain its strength was found to be shorter than SR-PLLA (24 vs 36 weeks) in bone, it also degraded at a faster rate [99]. Sixty-two adult patients with ankle fractures were randomized to form two groups. Although syndesmotic ossification was found to be more common in the SR-P(L/DL)LA group during the 1-year follow-up, it was not reported to be statistically significant [77]. Both implant types were found to be suitable for this application. Ito et al. [100] evaluated the use of PLLA screws for fixation in hip surgery for 61 patients with a total of 68 consecutive hip osteotomies. They concluded that while PLLA screws could be used for transfixing an osteotomized acetabulum in a rotational osteotomy, the screw might break when used for a femoral trochanteric osteotomy.

Certain complications associated with PLA materials were reported, despite having many successful applications [101, 102]. Konan and Haddad [103] reviewed the adverse effects of biodegradable interference screws in ACL. Although complications were rare, chondral damage caused by breakage of the screw used in ACL was reported [104–107]. The presence of a broken screw head in the subcutaneous tissue may cause breakage, pain, or foreign body reaction. Therefore, Sugimoto et al. [108] developed a simple procedure to remove the PLLA screw head using a micro-bone-saw.

Dhawan et al. [109] reviewed the complications associated with PLA suture anchors in shoulder surgeries.

Complications such as foreign body reactions, osteolysis, synovitis, chondrolysis, and implant failure were rarely reported. Using biopsy specimens and MRI analysis, McCarty et al. [110] examined complications in 38 patients following PLLA implants for treatment of either labral or rotator cuff repair. Macroscopic intra-articular anchor debris was observed in more than 50% of the patients with complications. High rates of giant cell reaction, papillary synovitis, and significant chondral damage were observed. Crystalline breakdown products of PLLA were found in all cases.

Products made with new PLA composite implants, such as with calcium ceramics (HA and β-TCP), were developed in an attempt to create mechanically stable constructs of improved biocompatibility to minimize complications. Lee et al. [111] compared PLLA and PLLA/HA screws for tibial fixation in ACL reconstruction. The 172 patients who had the arthroscopic ACL reconstruction were evaluated clinically over two years post-surgeries. While no notable clinical differences between the PLLA and PLLA/HA group were identified, the PLLA/HA group did reveal a significant reduction in the extent of tibial tunnel widening and foreign body reactions, as well as a significant increase in screw resorption, when compared with the PLLA group.

***25.3.3.4 Plates*** PLLA plates are mainly used in maxillofacial surgery, as they are not sufficiently strong for load-bearing applications. Suzuki et al. [112] studied a PLLA miniplate system for the treatment of mandibular condylar process fracture in 14 patients (aged $23.1 \pm 5.7$ years). Although two patients experienced mild chronic postoperative tenderness at the implantation site, no wound infection was observed. Satisfactory bone healing was noted in all patients, with no evidence of abnormal resorption during the condylar process.

As PLLA has a lower strength when compared with titanium plate systems, the plate must be of certain thickness in order to provide sufficient strength. However, a thicker plate could trigger complications such as palpability. To overcome this problem, a thinner flat-type PLLA plate system of wider width for strength was constructed (GrandFix-Flat type, Gunze, Kyoto, Japan) (Figure 25.11c). This product was clinically evaluated for the fixation of zygomatic fractures in 12 patients for 6 months and compared with titanium miniplates [113]. Treatment was successful following implantation of the thin PLLA plates, with no complications reported. Hence, it was concluded that the plate was suitable for reducing complications associated with facial palpability.

Copolymers of PLA, blends, and composites have been extensively investigated for plate systems. Among them, as mentioned in Section 25.3.2, the incorporation of unsintered HA (u-HA) was found to provide improved osteointegration and bone healing. SuperFIXORB-MX (also known as OSTEOTRANS MX, TEIJIN Medical Corp., Osaka, Japan) is a PLLA-based plate containing 40% u-HA particles. The plate system was evaluated clinically in 35 patients for fixation of maxillofacial fractures [114]. Although three patients experienced complications (plate exposure in 2 and discomfort in 1), all fracture sites healed, with the plates bonded directly to the bone without interposition of the nonmineralized tissue. Kanno et al. [115] recently published a comprehensive overview of current biodegradable plate systems, including u-HA/PLLA, in oral and maxillofacial surgery. SuperFIXORB-MX was recently used for the fixation of metacarpal fractures in six patients with a total of eight fractures [116]. The patients were followed-up over five years, with positive outcomes in patients treated with the u-HA/PLLA plates. Complete absorption of the plates was achieved in approximately eight years.

Poly(L/D, L-lactic acid) (85/15)(PLDLLA) has also been used clinically for plate systems. Turvey et al. [117] examined the safety and efficacy of poly(L/DL-lactic acid) (70/30) bone plates and screws in craniomaxillofacial surgery for 745 patients who underwent a total of 761 separate operations. The success rate (defined as no breakage or inflammation requiring additional operating treatment) was found to be 94%. There were 14 failed cases due to breakage and 31 cases due to excessive inflammation. All breakages occurred at the mandibular sites with the majority of inflammatory failure occurring either in the maxilla or in the orbit (29 cases) and only two in the mandible. Bone healing was observed at all sites, even when a second surgical intervention for excessive inflammation was required.

PLLA implants have also found applications in spinal surgeries [118]. Metallic spinal instrumentation and implants have been developed to provide immediate structural stability until completion of bone fusion. However, these implants have caused several complications including implant migration and failure, MRI imaging degradation, and stress shielding [118].

A lumbar interbody cage device has also been developed and used effectively for the treatment of patients with various degenerative disorders of the lumbar spine. PLLA cages packed with cancellous bone grafts showed sufficient mechanical strength directly after implantation [119]. In treating patients with lumbar interbody fusion, a high load-bearing condition, the PLLA cage was found to retain its shape, height, and strength, thus allowing fusion to occur [120]. Long-term evaluation in goat lumber interbody fusion demonstrated that the PLLA cage group showed a significantly higher rate of fusion than for titanium cages of the same design after six months of implantation, and complete remodeling after two years [121]. Cages of PLA composites, such as with β-TCP, have also been developed and investigated in vivo, resulting in successful outcomes [122].

Smit et al. [123] evaluated two types of PLA spinal cages, made of either PLLA or poly(L/D,L-lactic acid) (70/30),

packed with bone grafts in a lumbar interbody fusion goat model for two years. While the PLDLLA cage was found to degrade quickly in vivo and failed after three months, the PLLA cage was found to have a much slower degradation profile as compared with the PLDLLA cage, and a higher fusion rate than the titanium cage.

A recent review by Koutserimpas et al. [124] discussed the efficacy and safety of biodegradable implants in spinal fracture intervention in 24 animal and 25 human studies. There was no statistical evidence to support the replacement of traditional instrumentation with biodegradable implants. PLLA was deemed to have more success than PLDLLA. In the lumbar spine animal models, the success rate of PLLA was found to be 75.2% (five studies) as compared with 53.4% for PLDLLA (four studies) ($p$ = 0.003). In clinical trials, PLLA was found to exhibit a 98.7% success rate in the cervical spine (2 studies) as compared with a 90% success rate for PLDLLA (10 studies) ($p$ = 0.015). PLDLLA also had an 84.7% success rate for the lumbar spine in eight studies.

### 25.3.4 Micro- and Nanoparticles, and Thin Coatings

An application of PLLA in the form of injectable microspheres is as temporary fillings in facial reconstructive surgeries. The introduction of highly active antiretroviral therapy in 1996 has significantly decreased the mortality of human immunodeficiency virus (HIV)/AIDS patients. However, this treatment is associated with certain side effects, such as fat loss (lipoatrophy) in the peripheral regions (upper and lower limbs and the face). The US FDA has approved the use of PLLA (Sculptra: Dermik Laboratories, Berwyn, PA) for the restoration and correction of facial fat loss in HIV patients in 2004, following positive results of successful large-scale clinical trials conducted in Europe and the United States [125–127]. The subjects did not experience any acute inflammation, abscess formation, or cytotoxicity either at or remote to the site of implantation.

Although the PLLA implant is not permanent, it can last up to 24 months [128]. The main advantages of this technique are (i) it can be tailored to the changing visage; and (ii) the surgery is not invasive, thus minimizing recovery time [129]. It has also been reported that the degradation and disappearance of PLLA was accompanied by a steady increase of collagen fibers filling the space originally occupied by the implant [129, 130]. However, the mechanism of collagen production via the stimulation of PLLA degradation is not yet fully understood.

PLLA microspheres have also been used as an embolic material in transcatheter arterial embolization—an effective method to manage arteriovenous fistula and malformations, massive hemorrhage, and tumors. Yamamoto et al. [131] evaluated the use of PLLA microspheres (diameters between 100 and 200 μm) as an embolic material in eight patients. The procedure was reportedly successful, with no complications observed. The clinical symptoms were improved immediately following the procedure, and recurrence was not observed during the follow-up period. They concluded that the PLLA particles were suitable for this application and could be easily prepared in any desired size.

Vente et al. [132] evaluated the toxicity of holmium-166 ($^{166}$Ho) loaded PLLA microspheres (diameter of ~30 μm) for transcatheter hepatic arterial embolization in pigs. $^{166}$Ho emits high-energy beta-radiation, as well as gamma-radiation, which facilitates imaging by gamma scintigraphy, SPECT, and MRI. Phase I clinical trial was reported later in 15 patients for radioembolization for the treatment of liver tumors [133]. The results demonstrated the feasibility and safety of the treatment in patients with unresectable and chemorefractory liver metastases, and enabled image-guided treatment.

Microspheres and microcapsules are widely applied in drug delivery systems (DDS) for the prolonged administration of a broad range of medical agents, such as contraceptives, narcotic antagonists, local anesthetics, and vaccines. DDS with peptides and proteins have also attracted much attention, since they are highly effective in comparatively low doses [134]. In recent years, nanospheres and nanoparticles (commonly defined as a size range of 10–1000 nm) have also been extensively studied, as these structures can penetrate through the biological barriers in the tissue system, such as the blood–brain barrier, to facilitate uptake of the drug by the cells [135, 136]. The release of drugs from these DDS systems is based on several mechanisms that include diffusion and polymer degradation (hydrolysis or enzymatic degradation). In many cases, PLGA and a blend of PLA and other faster degrading polymers have been extensively studied since there is a requirement for the material to degrade quickly [137, 138]. The sustained drug delivery systems currently being marketed are mostly based on PLGA [139, 140].

PLLA and PDLLA have also been used for several applications requiring long degradation times [141]. For example, PLA microparticles were explored in ophthalmic applications, such as DDS for glaucoma [142]. A standard treatment for glaucoma is through the administration of a drug, such as eye drops, to reduce the intraocular pressure (IOP). However, patient adherence can be poor, thus reducing the clinical efficacy of this treatment. Several novel delivery systems have been developed to overcome this issue. For example, the use of OTX-TP (Ocular Therapeutix, Bedford, MA, USA), a rod-shaped PEG hydrogel intracanalicular insert containing travoprost encapsulated in PLA microparticles, aids in the slow release (over 90 days) of the drug to the tear film. In a double-blinded Phase IIb clinical trial, 73 patients were randomly allocated to receive either the OTX-TP plug with artificial tear twice daily or a placebo non-eluting plug with

topical timolol 0.5% eye drops [143]. The 90-day results revealed that the IOP was reduced by 4.5–5.7 mmHg and 6.4–7.6 mmHg in the OTX-TP group and the timolol group, respectively. The IOP reduction in the timolol was greater than expected, possibly attributed to the presence of the placebo punctal plug, thus prolonging the contact time of the solution with the ocular surface. A Phase III trial was recently performed with 554 patients to evaluate the efficacy of the OTX-TP plugs without a timolol group. Patients were randomized to receive either the OTX-TP plug or a placebo with a non-eluting plug in both eyes, with follow-up performed fortnightly, from 2 to 20 weeks. The results across all time points showed an IOP reduction of 3.3–5.7 mmHg in the OTX-TP group [144].

The supraciliary delivery of brimonidine-loaded PDLLA microparticles into the eyes of New Zealand white rabbits was investigated by Chiang et al. [145]. This study was aimed at sustained IOP reduction for glaucoma. The first eye received brimonidine-loaded PDLLA microparticles, administrated into the supraciliary space via a shortened 27-gauge hypodermic needle. Two different doses of brimonidine were tested. The other eye received a topical brimonidine and a blank microsphere injection as a control. The results showed a sustained reduction in the IOP (up to 6 mmHg) for the group receiving microcapsules with a high dose formulation (0.9 mg brimonidine) for at least three weeks post injection.

In recent years, there is an increase in research on PLA modifications, such as block copolymers and functionalization, for effective drug delivery [136]. One of the most successful formulations reported in clinical trials is the use of the PLA block copolymer with poly(ethylene glycol) (PEG) system. The PLA block copolymers form micelles with a PLA hydrophobic polymeric core encapsulating hydrophobic drugs, while the hydrophilic PEG corona protects the particles from immune surveillance. An example of such system, Genexol-PM (Samyang Biopharmaceuticals Corporation, Jongno-gu, Seoul, Korea) was approved in 2007 for marketing in Korea. It is based on paclitaxel (PTX)-loaded PDLLA-*b*-PEG micelles (diameters between 20 and 50 nm) for the treatment of breast, ovarian, and lung cancers. Figure 25.12 presents the schematics of the Genexol-PM formulation. Kim et al. [146] investigated the maximum tolerated dosage, dose-limiting toxicities, and the pharmacokinetic profiles of Genexol-PM in a Phase I study consisting of 21 patients with advanced, refractory malignancies. The maximum tolerated dosage of Genexol-PM was found to be 390 mg/m$^2$, which is much higher than that of PTX in the solution form (175 mg/m$^2$). Ongoing Phase II clinical trials are being conducted in the United States and Russia [141]

When administrated by intravenous injection, Genexol-PM requires a higher dose than free PTX to achieve equal tumor accumulation in murine tumor models, due to rapid in vivo drug release. To overcome this problem, Tam et al. [147] developed a prodrug by coupling oligo(lactic acid) onto PTX, which showed an increased drug loading efficiency due to better compatibility with PDLLA-*b*-PEG, and thus slower in vitro release than PTX. It was demonstrated that oligo(lactic acid)$_8$-PTX had higher antitumor efficacy and was less toxic than PTX following an in vivo investigation in rats and mice [148].

BIND-014 (Bind Therapeutics Inc., Cambridge, MA, USA) is another PDLLA-*b*-PEG micelle-based system encapsulating docetaxel evaluated for cancer chemotherapy [149, 150]. BIND-014 was the first clinically tested targeted nanoparticle system and is currently in Phase II studies for patients with advanced breast and non-small-cell lung cancer [141]. It also contains PDLLA-*b*-PEG end-functionalized with small ligands that can selectively bind to a prostate-specific membrane antigen for targeted drug delivery [149]. The micelles (diameter of ~100 nm) are produced using an emulsion process under conditions favoring the presence of the PEG chains at the particle surface. This formulation was demonstrated in multiple animal models to provide up to a 10-fold increase in the effectiveness of

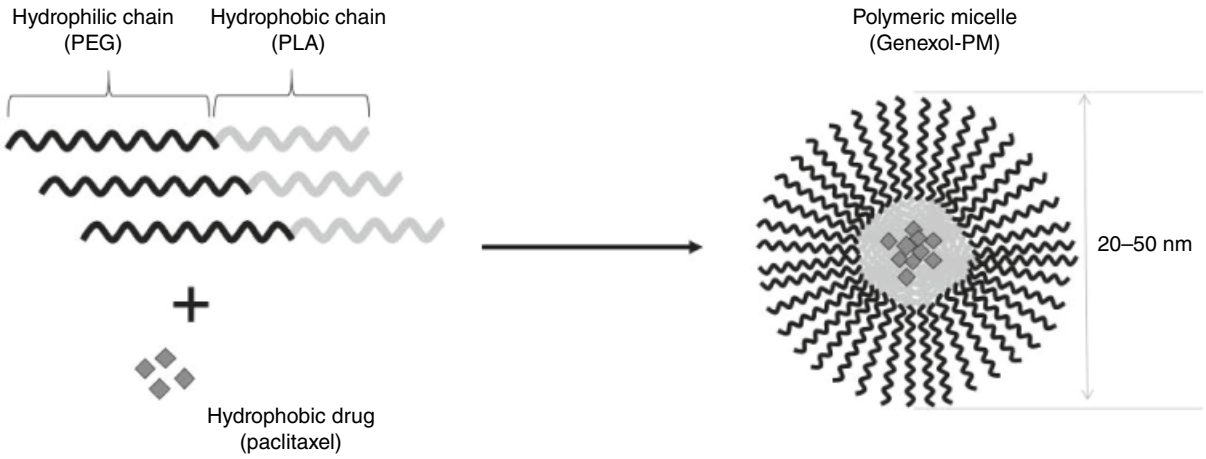


**FIGURE 25.12** Schematic diagram of the paclitaxel-loaded micelle formation. Source: Adapted from Ref. [146].

delivering docetaxel to the tumors as compared with an equivalent dose of free drug, with no increase in toxicity [149].

Niu et al. [151] developed a doxorubicin-loaded stereocomplex micelle drug delivery system using a four-armed PEG-*b*-PDLA and PEG-*b*-PLLA system for cervical cancer chemotherapy. An equimolar mixture of PDLA and PLLA has been reported to form stereocomplexes of distinctive physical and chemical stability, hence improving mechanical and thermal properties, as well as hydrolytic stability [152, 153]. When compared with the PDLA- or PLLA-*b*-PEG-based micelles, the stereocomplex micelles exhibited the slowest doxorubicin release, the most efficient tumor cell uptake, and the best suppression in vitro, as well as increased tumor inhibition rates, in cervical carcinoma mouse models.

PLA has also been extensively investigated as thin DDS coatings on implants. As previously stated, PLA film coatings of micron thickness are often utilized in commercially available drug-eluting coronary stents, using both metallic and biodegradable polymers [154]. Schmidmaier et al. [155] studied a PDLLA coat on metallic implants for the release of growth factors, such as insulin-like growth factor-I (IGF-I) and transforming growth factor-beta 1 (TGF-β1). The growth factors were found to be stable in a thin layer PDLLA coating, with sustained release observed both in vitro and in vivo. Park et al. [156] investigated PLLA films cast on PGA mesh as a carrier for tetracycline in guided tissue regeneration and demonstrated the effectiveness in vivo.

### 25.3.5 Scaffolds

In the recent years, extensive in vitro and in vivo studies have been devoted to PLA-based scaffolds [157–160]. For example, nanofibrous PLA scaffolds, fabricated via electrospinning, have found broad applications ranging from tissue engineering to drug delivery vehicles. Another development is high-resolution 3D desktop printers, in addition to advancements in additive manufacturing, which have allowed fabrication of "ideal" scaffolds with appropriate form and function for targeted tissue engineering applications. Despite the success of this research, clinical translations are still quite limited.

Kurobe et al. [161] evaluated electrospun PLA porous nanofiber conduits with inner diameter of 0.5–0.6 mm for use in small diameter arteries (Figure 25.13). These conduits were surgically implanted in infra-renal aortic interposition in 25 mice. Survival of mice with PLA conduits was excellent (91.6% at 12 months post-implantation), as compared with the control group (83.3% within the same period). Although vessel regeneration was evidenced by 12-month data collected from the cellular infiltration, extracellular matrix deposition, and tissue remodeling, the PLA nanofiber conduits still remained at that time indicating slow degradation for this application. Although the outcomes of small animal studies were promising, PLA nanofiber scaffolds had poor results in large animal models with higher blood pressures, as scaffolds were prone to thrombus formation and graft rupture [162].

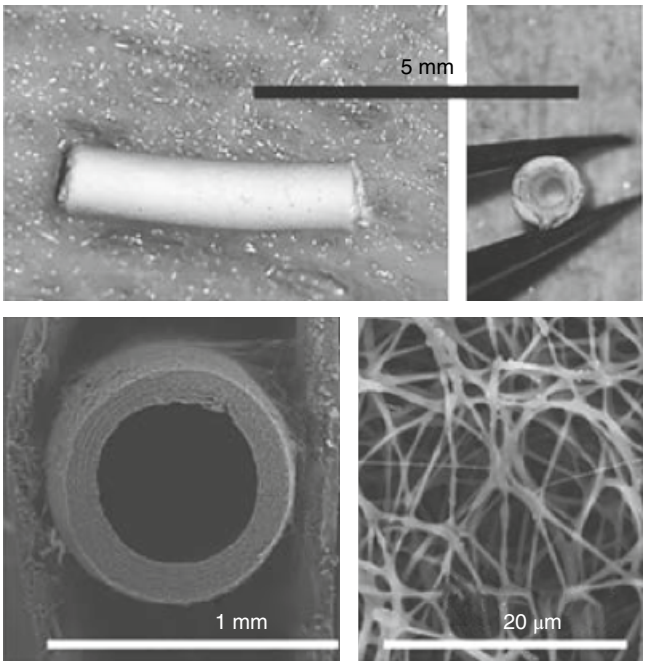


**FIGURE 25.13** Macroscopic and SEM images of electrospun PLA conduits [161].

Mohiti-Asli et al. [163] loaded PLA nanofiber scaffolds with ibuprofen (a nonsteroidal, anti-inflammatory drug) by electrospinning for use in the treatment of acute and chronic wounds. The PLA nanofiber scaffolds containing 20 wt% ibuprofen were evaluated in vivo using a full-thickness wound nude mouse model. The scaffold was found to reduce wound contraction in vivo, and when seeded with skin cells, enhanced new blood vessel formation.

Kobsa et al. [164] synthesized functionalized nanofiber scaffolds made with PLLA, PCL, or PLLA/PCL (50 : 50) blend by electrospinning to allow for controlled delivery of DNA in wound healing applications. Due to the favorable in vitro physical properties and cellular responses exhibited by the PLLA/PCL blend scaffold, it was chosen for further functionalization. Using a layer-by-layer technique, the fibers were coated in alternating layers of polyethyleneimine and plasmids encoding keratinocyte growth factor (pKGF) before application to full-thickness wounds in mice. The pKGF-loaded scaffolds were found to provide significant enhancement in the wound healing process, which was quantified by improvements in the rate of wound re-epithelialization, keratinocyte proliferation, and granulation responses. pKGF delivery was also found to be successful.

Electrospun PLA fibrous scaffolds were also used in bone regeneration applications. Using an electrospinning

technique following a subsequent mechanical expansion process, Shim et al. [165] developed PLLA microfibrous 3D scaffolds. A higher level of osteoblast proliferation was found in 3D scaffolds as opposed to 2D nanofibrous membranes. Cell infiltration and bone formation in the 3D microfibrous scaffolds were demonstrated in vivo using a rabbit calvarial defect model, two- and four-weeks post-implantation.

A 3D cellular construct composed of multilayered cell sheets cultivated on PLLA/gelatin (50 : 50) nanofiber meshes was developed by Ren et al. [166]. The 3D cellular construct was made by stacking four monolayered meshes. Each individual mesh was cultured with bone mesenchymal stromal cells (BMSCs) seven days prior to construction. The resulting 3D cellular construct was incubated for three days before implanting into rat cranial defects. Significant new calcified bone formation was found at 12 weeks post-surgery.

Porous PLA composite scaffolds, fabricated by 3D printers, have been extensively investigated for bone repair applications and hold promise in in vivo studies [167–169]. Zhang et al. [170] evaluated 3D-printed PLA/HA, β-TCP and partially demineralized bone matrix, seeded with BMCs, prior to implantation into a critical-sized rat calvarial defect model. These materials have similar porosity and pore size. The 3D-printed PLA/HA scaffolds were found to have good osteogenic capability and degradation properties with no difference in inflammation reaction when compared with the other two materials.

Surface modification is another approach adopted to improve the biocompatibility and bioactivity of scaffolds. Wang et al. [171] fabricated 3D-printed PLLA scaffolds by creating nanotopographical lamellae patterns with etching in alcohol/alkaline solution, following application of a polydopamine coat via self-assembly of catecholamine. In vitro results revealed a significant enhancement of osteoblast responses through surface modification. A significant improvement in osteogenesis on the scaffold was also observed in vivo using a rat femur defect model for evaluating the nanotopological patterned surface with polydopamine coating.

Liu et al. [172] created a customized porous PLA screw-like scaffold using a desktop 3D printer for fixation in ACL (Figure 25.14). The PLA screw-like scaffolds with/without HA coating and mesenchymal stromal cells (MSCs) loading were used as interference screws for ACL reconstruction in a rabbit model. Significant bone ingrowth and bone-graft interface formation within the bone tunnel were observed at 12 weeks post-surgery using the HA-coated PLA screw loaded with MSCs. The authors concluded that customized fabrication of surgical implants using 3D printers is feasible, effective, and economical since the scaffolds could be easily printed in a clinic.

## 25.4 CONCLUSIONS

Over the past few decades, PLA has found many applications in medicine, in particular, as orthopedic implants. However, these applications are often limited due to a slow degradation rate and high hydrophobicity of PLA implants. Extensive research was carried out to overcome these problems; exemplified by the use of copolymers, blends, and composites. Despite these changes, the function of newer generation implants still does not differ significantly from the original ones that were developed more than 40 years ago. Clinical application as a bone substitute is still restricted to non-load-bearing situations. Despite various preclinical successes, these challenges need to be overcome in order to explore further clinical applications in medical and pharmaceutical fields.

## REFERENCES

1. R. K. Kulkarni, K. C. Pani, C. Neuman, F. Leonard, Polylactic acid for surgical implants, *Arch. Surg.* **1966**, *93*(5), 839–843.
2. D. E. Cutright, E. E. Hunsuck, Tissue reaction to the biodegradable polylactic acid suture, *Oral Surg. Oral Med. Oral Pathol.* **1971**, *31*(1), 134–139.

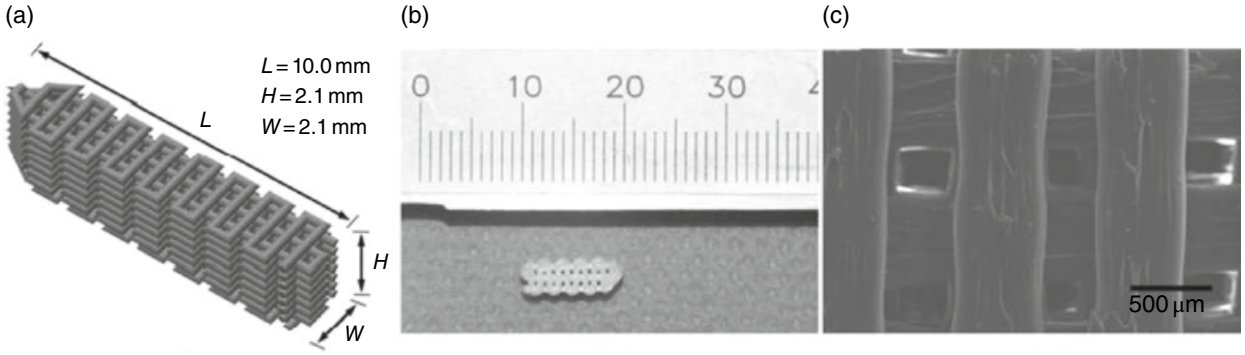


**FIGURE 25.14** PLA screw-like scaffold created using 3D printing. (a) A 3D view of the theoretical design. (b) 3D-printed PLA screw-like scaffold and (c) SEM image of the pure PLA scaffold surface [172].

3. D. E. Cutright, E. E. Hunsuck, J. D. Beasley, Fracture reduction using a biodegradable material, polylactic acid, *J. Oral Surg.* **1971**, *29*(6), 393–397.
4. Y. Ikada, H. Tsuji, Biodegradable polyesters for medical and ecological applications, *Macromol. Rapid Commun.* **2000**, *21*(3), 117–132.
5. H. Ueda, Y. Tabata, Polyhydroxyalkanonate derivatives in current clinical applications and trials, *Adv. Drug Deliv. Rev.* **2003**, *55*(4), 501–518.
6. H. Tsuji, *Poly(Lactic Acid) (Japanese)*, Yoneda Shuppan, Chiba, 2008.
7. J. C. Middleton, A. J. Tipton, Synthetic biodegradable polymers as orthopedic devices, *Biomaterials* **2000**, *21*(23), 2335–2346.
8. M. J. Yaszemski, R. G. Payne, W. C. Hayes, R. Langer, A. G. Mikos, Evolution of bone transplantation: molecular, cellular and tissue strategies to engineer human bone, *Biomaterials* **1996**, *17*(2), 175–185.
9. A. R. Amini, J. S. Wallace, S. P. Nukavarapu, Short-term and long-term effects of orthopedic biodegradable implants, *J. Long Term Eff. Med. Implants* **2011**, *21*(2), 93–122.
10. N. Yoshino, S. Takai, Y. Watanabe, K. Kamata, Y. Hirasawa, Delayed aseptic swelling after fixation of talar neck fracture with a biodegradable poly-L-lactide rod: case reports, *Foot Ankle Int.* **1998**, *19*(9), 634–637.
11. D. Seino, S. Fukunishi, S. Yoshiya, Late foreign-body reaction to PLLA screws used for fixation of acetabular osteotomy, *J. Orthop. Traumatol.* **2007**, *8*(4), 188–191.
12. J. Suganuma, H. Alexander, Biological response of intramedullary bone to poly-L-lactic acid, *J. Appl. Biomater.* **1993**, *4*(1), 13–27.
13. C. Schiller, C. Rasche, M. Wehmöller, F. Beckmann, H. Eufinger, M. Epple, et al., Geometrically structured implants for cranial reconstruction made of biodegradable polyesters and calcium phosphate/calcium carbonate, *Biomaterials* **2004**, *25*(7–8), 1239–1247.
14. H. Eufinger, C. Rasche, J. Lehmbrock, M. Wehmöller, S. Weihe, I. Schmitz, et al. Performance of functionally graded implants of polylactides and calcium phosphate/calcium carbonate in an ovine model for computer assisted craniectomy and cranioplasty. *Biomaterials* **2007**, *28*(3), 475–485.
15. T. I. Croll, A. J. O'Connor, G. W. Stevens, J. J. Cooper-White, Controllable surface modification of poly(lactic-co-glycolic acid) (PLGA) by hydrolysis or aminolysis I: physical, chemical, and theoretical aspects, *Biomacromolecules* **2004**, *5*(2), 463–473.
16. D. K. Gilding, Biodegradable polymers. In: D. F. Williams (Ed.), *Biocompatibility of Clinical Implant Materials*, CRC Press, Boca Raton, FL, 1981, pp. 209–232.
17. J. Kopeček, K. Ulbrich, Biodegradation of biomedical polymers, *Prog. Polym. Sci.* **1983**, *9*(1), 1–58.
18. O. Laitinen, P. Törmälä, R. Taurio, K. Skutnabb, K. Saarelainen, T. Iivonen, et al., Mechanical properties of biodegradable ligament augmentation device of poly(L-lactide) in vitro and in vivo, *Biomaterials* **1992**, *13*(14), 1012–1016.
19. D. Träger, K. Pohle, W. Tschirner, Anterior cruciate ligament suture in comparison with plasty, *Arch. Orthop. Trauma Surg.* **1995**, *114*(5), 278–280.
20. L. Dürselen, G. Hehl, M. Simnacher, L. Kinzl, L. Claes, Augmentation of a ruptured posterior cruciate ligament provides normal knee joint stability during ligament healing, *Clin. Biomech.* **2001**, *16*(3), 222–228.
21. H. Kobayashi, Kawamoto, Y., Hara, S., Tomizawa, N., Gibbons, D. F., VanKampen, C. L., Mendenhall, H. V., Study on bioresorbable poly_L-lactide (PLLA) ligament augmentation device (LAD), *Fourth Japan International SAMPE Symposium*, Tokyo, Japan, 24–28 September 1995.
22. J. A. Cooper, Jr., L. O. Bailey, J. N. Carter, C. E. Castiglioni, M. D. Kofron, F. K. Ko, et al., Evaluation of the anterior cruciate ligament, medial collateral ligament, achilles tendon and patellar tendon as cell sources for tissue-engineered ligament. *Biomaterials* **2006**, *27*(13), 2747–54.
23. J. A. Cooper, J. S. Sahota, W. J. Gorum, J. Carter, S. B. Doty, C. T. Laurencin, Biomimetic tissue-engineered anterior cruciate ligament replacement, *Proc. Natl. Acad. Sci. USA* **2007**, *104*(9), 3049–3054.
24. W. R. Walsh, N. Bertollo, R. A. Arciero, R. A. Stanton, R. A. Poggie, Long-term in-vivo evaluation of a resorbable PLLA scaffold for regeneration of the ACL, *J. Sports Med.* **2015**, *3*(7 suppl 2), 2325967115S00033.
25. P. Y. Mengsteab, L. S. Nair, C. T. Laurencin, The past, present and future of ligament regenerative engineering, *Regen. Med.* **2016**, *11*(8), 871–881.
26. P. Y. Mengsteab, P. Conroy, M. Badon, T. Otsuka, H. M. Kan, A. T. Vella, et al., Evaluation of a bioengineered ACL matrix's osteointegration with BMP-2 supplementation. *PLoS One* **2020**, *15*(1), e0227181.
27. P. Y. Mengsteab, T. Otsuka, McClinton A, N. S. Shemshaki, S. Shah, H. M. Kan, et al., Mechanically superior matrices promote osteointegration and regeneration of anterior cruciate ligament tissue in rabbits, *Proc. Natl. Acad. Sci. USA* **2020**, *117*(46), 28655–28666.
28. H. Nishimoto, T. Kokubu, A. Inui, Y. Mifune, K. Nishida, H. Fujioka, et al., Ligament regeneration using an absorbable stent-shaped poly-L-lactic acid scaffold in a rabbit model, *Int. Orthop.* **2012**, *36*(11), 2379–2386.
29. M. Aoki, S. Miyamoto, K. Okamura, T. Yamashita, Y. Ikada, S. Matsuda, Tensile properties and biological response of poly(L-lactic acid) felt graft: an experimental trial for rotator-cuff reconstruction, *J. Biomed. Mater. Res. Part B Appl. Biomater.* **2004**, *71B*(2), 252–259.
30. A. Inui, T. Kokubu, H. Fujioka, I. Nagura, R. Sakata, H. Nishimoto, et al., Application of layered poly (L-lactic acid) cell free scaffold in a rabbit rotator cuff defect model, *Sports Med. Arthrosc. Rehabil. Ther. Technol.* **2011**, *3*, 29.
31. B. A. Lenart, K. A. Martens, K. A. Kearns, R. J. Gillespie, A. C. Zoga, G. R. Williams, Treatment of massive and recurrent rotator cuff tears augmented with a poly-L-lactide graft, a preliminary study, *J. Shoulder Elb. Surg.* **2015**, *24*(6), 915–921.
32. K. A. Derwin, M. J. Codsi, R. A. Milks, A. R. Baker, J. A. McCarron, J. P. Iannotti, Rotator cuff repair augmentation in a

canine model with use of a woven poly-L-lactide device, *J. Bone Joint Surg. Am.* **2009**, *91*(5), 1159–1171.

33. Y. Saito, K. Minami, M. Kobayashi, Y. Nakao, H. Omiya, H. Imamura, et al., New tubular bioabsorbable knitted airway stent: biocompatibility and mechanical strength, *J. Thorac. Cardiovasc. Surg.* **2002**, *123*(1), 161–167.
34. M. Zilberman, K. D. Nelson, R. C. Eberhart, Mechanical properties and in vitro degradation of bioresorbable fibers and expandable fiber-based stents, *J. Biomed. Mater. Res. B Appl. Biomater.* **2005**, *74*(2), 792–799.
35. H. Tamai, K. Igaki, E. Kyo, K. Kosuga, A. Kawashima, S. Matsui, et al., Initial and 6-month results of biodegradable poly-L-lactic acid coronary stents in humans, *Circulation* **2000**, *102*(4), 399–404.
36. S. Nishio, K. Kosuga, K. Igaki, M. Okada, E. Kyo, T. Tsuji, et al., Long-term (>10 years) clinical outcomes of first-in-human biodegradable poly-L-lactic acid coronary stents: Igaki-Tamai stents, *Circulation* **2012**, *125*(19), 2343–2353.
37. S. Borhani, S. Hassanajili, Ahmadi S., H. Tafti, S. Rabbani, Cardiovascular stents: overview, evolution, and next generation, *Prog. Biomater.* **2018**, *7*(3), 175–205.
38. W. A. Omar, D. J. Kumbhani, The current literature on bioabsorbable stents: a review, *Curr. Atheroscler. Rep.* **2019**, *21*(12), 54.
39. T. Muramatsu, Y. Onuma, H. M. García-García, V. Farooq, C. V. Bourantas, M.-A. Morel, et al., Incidence and short-term clinical outcomes of small side branch occlusion after implantation of an everolimus-eluting bioresorbable vascular scaffold: an interim report of 435 patients in the ABSORB-EXTEND single-arm trial in comparison with an everolimus-eluting metallic stent in the SPIRIT I and II trials, *JACC Cardiovasc. Interv.* **2013**, *6*(3), 247–257.
40. Y. Saito, K. Minami, H. Kaneda, T. Okada, T. Maniwa, Y. Araki, et al., New tubular bioabsorbable knitted airway stent: feasibility assessment for delivery and deployment in a dog model, *Ann. Thorac. Surg.* **2004**, *78*(4), 1438–1440.
41. S. Laaksovirta, T. Isotalo, M. Talja, T. Välimaa, P. Törmälä, T. L. J. Tammela, Interstitial laser coagulation and biodegradable self-expandable, self-reinforced poly-L-lactic and poly-L-glycolic copolymer spiral stent in the treatment of benign prostatic enlargement, *J. Endourol.* **2002**, *16*(5), 311–315.
42. T. Isotalo, M. Talja, P. Hellström, I. Perttilä, T. Välimaa, P. Törmälä, et al., A double-blind, randomized, placebo-controlled pilot study to investigate the effects of finasteride combined with a biodegradable self-reinforced poly L-lactic acid spiral stent in patients with urinary retention caused by bladder outlet obstruction from benign prostatic hyperplasia, *BJU Int.* **2001**, *88*(1), 30–34.
43. T. M. Isotalo, J.-P. Nuutine, A. Vaajanen, P. M. Martikainen, M. Laurila, P. Törmälä, et al., Biocompatibility properties of a new braided biodegradable urethral stent: a comparison with a biodegradable spiral and a braided metallic stent in the rabbit urethra, *BJU Int.* **2006**, *97*(4), 856–859.
44. J. Lumiaho, A. Heino, T. Kauppinen, M. Talja, E. Alhava, T. Välimaa, et al., Drainage and antireflux characteristics of a biodegradable self-reinforced, self-expanding X-ray-positive poly-L,D-lactide spiral partial ureteral stent: an experimental study, *J. Endourol.* **2007**, *21*(12), 1559–1564.
45. A. Kotsar, R. Nieminen, T. Isotalo, J. Mikkonen, I. Uurto, M. Kellomäki, et al., Preclinical evaluation of new indomethacin-eluting biodegradable urethral stent, *J. Endourol.* **2012**, *26*(4), 387–392.
46. A. Kotsar, R. Nieminen, T. Isotalo, J. Mikkonen, I. Uurto, M. Kellomäki, et al., Biocompatibility of new drug-eluting biodegradable urethral stent materials, *Urology* **2010**, *75*(1), 229–234.
47. H. Shan, Z. Cao, C. Chi, J. Wang, X. Wang, J. Tian, et al., Advances in drug delivery via biodegradable ureteral stent for the treatment of upper tract urothelial carcinoma, *Front. Pharmacol.* **2020**, *11*, 224.
48. J. Wang, L. Wang, Z. Zhou, H. Lai, P. Xu, L. Liao, et al., Biodegradable polymer membranes applied in guided bone/tissue regeneration: a review, *Polymers (Basel)* **2016**, *8*(4), 115.
49. S.-W. Lee, S.-G. Kim, Membranes for the guided bone regeneration, *Maxillofac. Plast. Reconstr. Surg.* **2014**, *36*(6), 239–246.
50. I. Elgali, O. Omar, C. Dahlin, P. Thomsen, Guided bone regeneration: materials and biological mechanisms revisited, *Eur. J. Oral Sci.* **2017**, *125*(5), 315–337.
51. Y. Amano, M. Ota, K. Sekiguchi, Y. Shibukawa, S. Yamada, Evaluation of a poly-L-lactic acid membrane and membrane fixing pin for guided tissue regeneration on bone defects in dogs, *Oral Surg. Oral Med. Oral Pathol. Oral Radiol. Endodontol.* **2004**, *97*(2), 155–163.
52. B. Ehmke, S. G. Rüdiger, A. Hommens, H. Karch, T. F. Flemmig, Guided tissue regeneration using a polylactic acid barrier, *J. Clin. Periodontol.* **2003**, *30*(4), 368–374.
53. S. G. Rüdiger, B. Ehmke, A. Hommens, H. Karch, T. F. Flemmig, Guided tissue regeneration using a polylactic acid barrier. Part I: Environmental effects on bacterial colonization, *J. Clin. Periodontol.* **2003**, *30*(1), 19–25.
54. K. Asano, T. Matsuno, Y. Tabata, T. Satoh, Preparation of thermoplastic poly(L-lactic acid) membranes for guided bone regeneration, *Int. J. Oral Maxillofac. Implants* **2013**, *28*(4), 973–981.
55. L. M. Pineda, M. Büsing, R. P. Meinig, S. Gogolewski, Bone regeneration with resorbable polymeric membranes. III. Effect of poly(L-lactide) membrane pore size on the bone healing process in large defects, *J. Biomed. Mater. Res.* **1996**, *31*(3), 385–394.
56. Y. Kinoshita, H. Maeda, Recent developments of functional scaffolds for craniomaxillofacial bone tissue engineering applications, *Sci. World J.* **2013**, *2013*, 863157.
57. K. Yagihara, S. Okabe, J. Ishii, T. Amagasa, M. Yamashiro, S. Yamaguchi, et al., Mandibular reconstruction using a poly(L-lactide) mesh combined with autogenous particulate cancellous bone and marrow: a prospective clinical study, *Int. J. Oral Maxillofac. Surg.* **2013**, *42*(8), 962–969.
58. C. C. P. M. Verheyen, J. R. De Wijn, C. A. Van Blitterswijk, K. De Groot, Evaluation of hydroxylapatite/poly(L-lactide) composites: mechanical behavior, *J. Biomed. Mater. Res.* **1992**, *26*(10), 1277–1296.

59. C. C. P. M. Verheyen, J. R. de Wijn, C. A. van Blitterswijk, K. de Groot, P. M. Rozing, Hydroxylapatite/poly(L-lactide) composites: an animal study on push-out strengths and interface histology, *J. Biomed. Mater. Res.* **1993**, *27*(4), 433–44.
60. T. Furukawa, Y. Matsusue, T. Yasunaga, Y. Nakagawa, Y. Okada, Y. Shikinami, et al., Histomorphometric study on high-strength hydroxyapatite/poly(L-lactide) composite rods for internal fixation of bone fractures, *J. Biomed. Mater. Res.* **2000**, *50*(3), 410–419.
61. A. Matsuo, H. Chiba, H. Takahashi, J. Toyoda, H. Abukawa, Clinical application of a custom-made bioresorbable raw particulate hydroxyapatite/poly-L-lactide mesh tray for mandibular reconstruction, *Odontology* **2010**, *98*(1), 85–88.
62. A. Matsuo, H. Takahashi, H. Abukawa, D. Chikazu, Application of custom-made bioresorbable raw particulate hydroxyapatite/poly-L-lactide mesh tray with particulate cellular bone and marrow and platelet-rich plasma for a mandibular defect: evaluation of tray fit and bone quality in a dog model, *J. Craniomaxillofac. Surg.* **2012**, *40*(8), e453–e460.
63. M. Ochi, N. Adachi, H. Nobuto, S. Yanada, Y. Ito, M. Agung, Articular cartilage repair using tissue engineering technique-novel approach with minimally invasive procedure, *Artif. Organs* **2004**, *28*(1), 28–32.
64. M. C. Kennady, M. R. Tucker, G. E. Lester, M. J. Buckley, Histomorphometric evaluation of stress shielding in mandibular continuity defects treated with rigid fixation plates and bone grafts, *Int. J. Oral Maxillofac. Surg.* **1989**, *18*(3), 170–174.
65. H. K. Uhthoff, M. Finnegan, The effects of metal plates on post-traumatic remodelling and bone mass, *J. Bone Joint Surg. Br.* **1983**, *65*(1), 66–71.
66. H. G. French, S. D. Cook, R. J. Haddad Jr., Correlation of tissue reaction to corrosion in osteosynthetic devices, *J. Biomed. Mater. Res.* **1984**, *18*(7), 817–828.
67. K. R. Postlethwaite, J. G. Philips, S. Booth, J. Shaw, A. Slater, The effects of small plate osteosynthesis on postoperative radiotherapy, *Br. J. Oral Maxillofac. Surg.* **1989**, *27*(5), 375–378.
68. P. Stoll, R. Wächter, N. Hodapp, W. Schilli, Radiation and osteosynthesis. Dosimetry on an irradiation phantom, *J. Craniomaxillofac. Surg.* **1990**, *18*(8), 361–366.
69. W. S. Pietrzak, Principles of development and use of absorbable internal fixation, *Tissue Eng.* **2000**, *6*(4), 425–433.
70. F. A. Barber, Resorbable fixation devices: a product guide, *Orthop. Spec. Ed.* **1998**, *4*, 1111–1117.
71. K. Dai, Rational utilization of the stress shielding effect of implants, in: D. G. Poitout, R. Kotz (Ed.), *Biomechanics and Biomaterials in Orthopedics*, Springer, London, 2004.
72. W. H. Akeson, S. L. Y. Woo, R. D. Coutts, J. V. Matthews, M. Gonsalves, D. Amiel, Quantitative histological evaluation of early fracture healing of cortical bones immobilized by stainless steel and composite plates, *Calcif. Tissue Res.* **1975**, *19*(1), 27–37.
73. L. Claes, The mechanical and morphological properties of bone beneath internal fixation plates of differing rigidity, *J. Orthop. Res.* **1989**, *7*(2), 170–177.
74. H. K. Uhthoff, F. L. Dubuc, Bone structure changes in the dog under rigid internal fixation, *Clin. Orthop. Relat. Res.* **1971**, *81*, 165–70.
75. T. Terjesen, K. Apalset, The influence of different degrees of stiffness of fixation plates on experimental bone healing, *J. Orthop. Res.* **1988**, *6*(2), 293–299.
76. W. J. Ciccone, 2nd, C. Motz, C. Bentley, J. P. Tasto, Bioabsorbable implants in orthopaedics: new developments and clinical applications, *J. Am. Acad. Orthop. Surg.* **2001**, *9*(5), 280–288.
77. A. Joukainen, E. K. Partio, P. Waris, J. Joukainen, H. Kröger, P. Törmälä, et al., Bioabsorbable screw fixation for the treatment of ankle fractures, *J. Orthop. Sci.* **2007**, *12*(1), 28–34.
78. Y. Matsusue, T. Yamamuro, S. Yoshii, M. Oka, Y. Ikada, S.-H. Hyon, et al., Biodegradable screw fixation of rabbit tibia proximal osteotomies, *J. Appl. Biomater.* **1991**, *2*(1), 1–12.
79. S. Hanafusa, Y. Matsusue, T. Yasunaga, T. Yamamuro, M. Oka, Y. Shikinami, et al., Biodegradable plate fixation of rabbit femoral shaft osteotomies. A comparative study, *Clin. Orthop. Relat. Res.* **1995**, (315), 262–271.
80. I. Yasuda, *J. Jpn. Orthop. Assoc.* **1955**, *29*, 351–353.
81. H. Kawai, The piezoelectricity of poly(vinylidene fluoride), *Jpn. J. Appl. Phys.* **1969**, *8*(7), 975–976.
82. Y. Ikada, Y. Shikinami, Y. Hara, M. Tagawa, E. Fukada, Enhancement of bone formation by drawn poly(L-lactide), *J. Biomed. Mater. Res.* **1996**, *30*(4), 553–558.
83. Y. Tajitsu, Piezoelectricity of chiral polymeric fiber and its application in biomedical engineering, *IEEE Trans. Ultrason. Ferroelectr. Freq. Control* **2008**, *55*(5), 1000–1008.
84. Y. Tajitsu, S. Kawai, M. Kanesaki, M. Date, E. Fukada, Microactuators with piezoelectric polylactic acid fibers—toward the realization of tweezers for biological cells, *Ferroelectrics* **2004**, *304*(1), 195–200.
85. Y. Tajitsu, Basic study of controlling piezoelectric motion of chiral polymeric fiber, *Ferroelectrics* **2009**, *389*(1), 83–94.
86. Y. Tajitsu, Smart piezoelectric fabric and its application to control of humanoid robot, *Ferroelectrics* **2016**, *499*(1), 36–46.
87. M. Smith, T. Chalklen, C. Lindackers, Y. Calahorra, C. Howe, A. Tamboli, et al. Poly-L-lactic acid nanotubes as soft piezoelectric interfaces for biology: controlling cell attachment via polymer crystallinity, *ACS Appl. Bio Mater.* **2020**, *3*(4), 2140–2149.
88. M. Smith, C. Lindackers, K. McCarthy, S. Kar-Narayan, Enhanced molecular alignment in poly-L-lactic acid nanotubes induced via melt-press template-wetting, *Macromol. Mater. Eng.* **2019**, *304*(3), 1800607.
89. P. U. Rokkanen, O. Böstman, E. Hirvensalo, E. A. Mäkelä, E. K. Partio, H. Pätiälä, et al., Bioabsorbable fixation in orthopaedic surgery and traumatology, *Biomaterials* **2000**, *21*(24), 2607–2613.
90. O. Böstman, H. Pihlajamäki, Clinical biocompatibility of biodegradable orthopaedic implants for internal fixation: a review, *Biomaterials* **2000**, *21*(24), 2615–2621.

91. P. Nordström, H. Pihlajamäki, T. Toivonen, P. Törmälä, P. Rokkanen, Tissue response to polyglycolide and polylevolactide pins in osteotomized cancellous bone, *Clin. Orthop. Relat. Res.* **2001**, (382), 247–257.
92. Y. Matsusue, T. Yamamuro, M. Oka, Y. Shikinami, S.-H. Hyon, Y. Ikada, in vitro and in vivo studies on bioabsorbable ultra-high-strength poly(L-lactide) rods, *J. Biomed. Mater. Res.* **1992**, *26*(12), 1553–1567.
93. Y. Hasegawa, S. Sakano, T. Iwase, H. Warashina, The long-term behavior of poly-L-lactide screws in a minipig fracture model: preliminary report, *J. Biomed. Mater. Res.* **2002**, *63*(6), 679–685.
94. P. Laine, R. Kontio, C. Lindqvist, R. Suuronen, Are there any complications with bioabsorbable fixation devices?: a 10 year review in orthognathic surgery, *Int. J. Oral Maxillofac. Surg.* **2004**, *33*(3), 240–244.
95. P. Maurer, S. Holweg, W. D. Knoll, J. Schubert, Study by finite element method of the mechanical stress of selected biodegradable osteosynthesis screws in sagittal ramus osteotomy, *Br. J. Oral Maxillofac. Surg.* **2002**, *40*(1), 76–83.
96. Y. Oba, A. Yasue, K. Kaneko, R. Uchida, A. Shioyasono, K. Moriyama, Comparison of stability of mandibular segments following the sagittal split ramus osteotomy with poly-L-lactic acid (PLLA) screws and titanium screws fixation, *Orthod. Waves* **2008**, *67*(1), 1–8.
97. O. M. Böstman, Osteoarthritis of the ankle after foreign-body reaction to absorbable pins and screws: a three- to nine-year follow-up study, *J. Bone Joint Surg. Br.* **1998**, *80*(2), 333–338.
98. W. D. Hovis, B. W. Kaiser, J. T. Watson, R. W. Bucholz, Treatment of syndesmotic disruptions of the ankle with bioabsorbable screw fixation, *J. Bone Joint Surg. Am.* **2002**, *84*(1), 26–31.
99. A. Joukainen, H. Pihlajamäki, E. A. Mäkelä, N. Ashammakhi, J. Viljanen, H. Pätiälä, et al., Strength retention of self-reinforced drawn poly-L/DL-lactide 70/30 (SR-PLA70) rods and fixation properties of distal femoral osteotomies with these rods. An experimental study on rats, *J. Biomater. Sci. Polym. Ed.* **2000**, *11*(12), 1411–1428.
100. H. Ito, A. Minami, H. Tanino, T. Matsuno, Fixation with poly-L-lactic acid screws in hip osteotomy: 68 hips followed for 18–46 months, *Acta Orthop. Scand.* **2002**, *73*(1), 60–64.
101. C. G. Ambrose, T. O. Clanton, Bioabsorbable implants: review of clinical experience in orthopedic surgery, *Ann. Biomed. Eng.* **2004**, *32*(1), 171–177.
102. O. M. Böstman, H. K. Pihlajamäki, Adverse tissue reactions to bioabsorbable fixation devices, *Clin. Orthop. Relat. Res.* **2000**, (371), 216–227.
103. S. Konan, F. S. Haddad, A clinical review of bioabsorbable interference screws and their adverse effects in anterior cruciate ligament reconstruction surgery, *Knee* **2009**, *16*(1), 6–13.
104. B. Lembeck, N. Wülker, Severe cartilage damage by broken poly-L-lactic acid (PLLA) interference screw after ACL reconstruction, *Knee Surg. Sports Traumatol. Arthrosc.* **2005**, *13*(4), 283–286.
105. A. Werner, A. Wild, A. Ilg, R. Krauspe, Secondary intra-articular dislocation of a broken bioabsorbable interference screw after anterior cruciate ligament reconstruction, *Knee Surg. Sports Traumatol. Arthrosc.* **2002**, *10*(1), 30–32.
106. A. Appelt, M. Baier, Recurrent locking of knee joint caused by intraarticular migration of bioabsorbable tibial interference screw after arthroscopic ACL reconstruction, *Knee Surg. Sports Traumatol. Arthrosc.* **2007**, *15*(4), 378–380.
107. T. Takizawa, S. Akizuki, H. Horiuchi, Y. Yasukawa, Foreign body gonitis caused by a broken poly-L-lactic acid screw, *Arthroscopy* **1998**, *14*(3), 329–330.
108. K. Sugimoto, Y. Takakura, Y. Tanaka, K. Kawate, Technique tip: fixation of Mitchell's osteotomy using a PLLA screw, *Foot Ankle Int.* **2003**, *24*(4), 372–373.
109. A. Dhawan, N. Ghodadra, V. Karas, M. J. Salata, B. J. Cole. Complications of bioabsorbable suture anchors in the shoulder, *Am. J. Sports Med.* **2012**, *40*(6), 1424–1430.
110. L. P. McCarty, III, D. D. Buss, M. W. Datta, M. Q. Freehill, M. R. Giveans, Complications observed following labral or rotator cuff repair with use of poly-L-lactic acid implants, *J. Bone Joint Surg.* **2013**, *95*(6).
111. D. W. Lee, J. W. Lee, S. B. Kim, J. H. Park, K. S. Chung, J. K. Ha, et al., Comparison of poly-L-lactic acid and poly-L-lactic acid/hydroxyapatite bioabsorbable screws for tibial fixation in ACL reconstruction: clinical and magnetic resonance imaging results, *Clin. Orthop. Surg.* **2017**, *9*(3), 270–279.
112. T. Suzuki, H. Kawamura, T. Kasahara, H. Nagasaka, Resorbable poly-L-lactide plates and screws for the treatment of mandibular condylar process fractures: a clinical and radiologic follow-up study, *J. Oral Maxillofac. Surg.* **2004**, *62*(8), 919–924.
113. S. Sukegawa, T. Kanno, D. Nagano, A. Shibata, Y. Sukegawa-Takahashi, Y. Furuki, The clinical feasibility of newly developed thin flat-type bioresorbable osteosynthesis devices for the internal fixation of zygomatic fractures: is there a difference in healing between bioresorbable materials and titanium osteosynthesis? *J. Craniofac. Surg.* **2016**, *27*(8), 2124–2129.
114. S. Sukegawa, T. Kanno, N. Katase, A. Shibata, Y. Takahashi, Y. Furuki, Clinical evaluation of an unsintered hydroxyapatite/poly-L-lactide osteoconductive composite device for the internal fixation of maxillofacial fractures, *J. Craniofac. Surg.* **2016**, *27*(6), 1391–1397.
115. T. Kanno, S. Sukegawa, Y. Furuki, Y. Nariai, J. Sekine, Overview of innovative advances in bioresorbable plate systems for oral and maxillofacial surgery, *Jpn. Dent. Sci. Rev.* **2018**, *54*(3), 127–138.
116. K. Kosugi, Y. Zenke, T. Tajima, Y. Yamanaka, K. Menuki, A. Sakai, Long-term outcomes of metacarpal fractures surgically treated using bioabsorbable plates: a retrospective study, *BMC Musculoskelet. Disord.* **2020**, *21*(1), 817.
117. T. A. Turvey, W. P. Proffit, C. Phillips, Biodegradable fixation for craniomaxillofacial surgery: a 10-year experience involving 761 operations and 745 patients, *Int. J. Oral. Maxillofac. Surg.* **2011**, *40*(3), 244–249.


118. A. R. Vaccaro, K. Singh, R. Haid, S. Kitchel, P. Wuisman, W. Taylor, et al., The use of bioabsorbable implants in the spine, *J. Spine* **2003**, *3*(3), 227–237.
119. M. van Dijk, T. H. Smit, S. Sugihara, E. H. Burger, P. I. Wuisman, The effect of cage stiffness on the rate of lumbar interbody fusion: an in vivo model using poly(L-lactic Acid) and titanium cages, *Spine* **2002**, *27*(7), 682–688.
120. M. van Dijk, D. C. Tunc, T. H. Smit, P. Higham, E. H. Burger, P. I. J. M. Wuisman, in vitro and in vivo degradation of bioabsorbable PLLA spinal fusion cages, *J. Biomed. Mater. Res.* **2002**, *63*(6), 752–759.
121. M. van Dijk, T. H. Smit, E. H. Burger, P. I. Wuisman, Bioabsorbable poly-L-lactic acid cages for lumbar interbody fusion: three-year follow-up radiographic, histologic, and histomorphometric analysis in goats, *Spine* **2002**, *27*(23), 2706–2714.
122. L. Cao, Q. Chen, L. B. Jiang, X. F. Yin, C. Bian, H. R. Wang, et al., Bioabsorbable self-retaining PLA/nano-sized β-TCP cervical spine interbody fusion cage in goat models: an in vivo study, *Int. J. Nanomed.* **2017**, *12*, 7197–7205.
123. T. H. Smit, M. R. Krijnen, M. van Dijk, P. I. J. M. Wuisman, Application of polylactides in spinal cages: studies in a goat model, *J. Mater. Sci. Mater. Med.* **2006**, *17*(12), 1237–1244.
124. C. Koutserimpas, K. Alpantaki, M. Chatzinikolaidou, G. Chlouverakis, M. Dohm, A. G. Hadjipavlou, The effectiveness of biodegradable instrumentation in the treatment of spinal fractures, *Injury* **2018**, *49*(12), 2111–2120.
125. A. Redaelli, R. Forte, Cosmetic use of polylactic acid: report of 568 patients, *J. Cosmet. Dermatol.* **2009**, *8*(4), 239–248.
126. G. J. Moyle, L. Lysakova, S. Brown, N. Sibtain, J. Healy, C. Priest, et al., A randomized open-label study of immediate versus delayed polylactic acid injections for the cosmetic management of facial lipoatrophy in persons with HIV infection, *HIV Med.* **2004**, *5*(2), 82–87.
127. M. A. Valantin, C. Aubron-Olivier, J. Ghosn, E. Laglenne, M. Pauchard, H. Schoen, et al., Polylactic acid implants (newfill) to correct facial lipoatrophy in HIV-infected patients: results of the open-label study VEGA, *AIDS* **2003**, *17*(17), 2471–2477.
128. B. Woerle, C. W. Hanke, G. Sattler, Poly-L-lactic acid: a temporary filler for soft tissue augmentation, *J. Drugs Dermatol.* **2004**, *3*(4), 385–389.
129. S. E. Barton, P. Engelhard, M. Conant, Poly-L-lactic acid for treating HIV-associated facial lipoatrophy: a review of the clinical studies, *Int. J. STD AIDS* **2006**, *17*(7), 429–435.
130. D. Vleggaar, U. Bauer, Facial enhancement and the European experience with Sculptra (poly-L-lactic acid), *J. Drugs Dermatol.* **2004**, *3*(5), 542–547.
131. T. Yamamoto, K. Hayakawa, Y. Tabata, Y. Shimizu, Y. Ikada, Transcatheter arterial embolization using poly-L-lactic acid microspheres, *Radiat. Med.* **2003**, *21*(4), 150–4.
132. M. A. D. Vente, J. F. W. Nijsen, T. C. de Wit, J. H. Seppenwoolde, G. C. Krijger, P. R. Seevinck, et al., Clinical effects of transcatheter hepatic arterial embolization with holmium-166 poly(L-lactic acid) microspheres in healthy pigs, *Eur. J. Nucl. Med. Mol. Imaging* **2008**, *35*(7), 1259–71.
133. M. L. J. Smits, J. F. W. Nijsen, M. A. A. J. van den Bosch, M. G. E. H. Lam, M. A. D. Vente, W. P. T. M. Mali, et al., Holmium-166 radioembolisation in patients with unresectable, chemorefractory liver metastases (HEPAR trial): a phase 1, dose-escalation study, *Lancet Oncol.* **2012**, *13*(10), 1025–1034.
134. I. T. Degim, N. Celebi, Controlled delivery of peptides and proteins, *Curr. Pharm. Des.* **2007**, *13*(1), 99–117.
135. J. K. Patra, G. Das, L. F. Fraceto, E. V. R. Campos, M. d. P. Rodriguez-Torres, L. S. Acosta-Torres, et al., Nano based drug delivery systems: recent developments and future prospects, *J. Nanobiotechnol.* **2018**, *16(1):71*.
136. T. Casalini, F. Rossi, A. Castrovinci, G. Perale, A perspective on polylactic acid-based polymers use for nanoparticles synthesis and applications, *Front. Bioeng. Biotechnol.* **2019**, *7*(259):259. doi: 10.3389/fbioe.2019.00259.
137. J. M. Anderson, M. S. Shive, Biodegradation and biocompatibility of PLA and PLGA microspheres, *Adv. Drug Deliv. Rev.* **2012**, *64*, 72–82.
138. D. J. Hines, D. L. Kaplan, Poly(lactic-*co*-glycolic) acid-controlled-release systems: experimental and modeling insights, *Crit, Rev. Ther. Drug Carr. Syst.* **2013**, *30*(3), 257–276.
139. A. Jain, K. R. Kunduru, A. Basu, B. Mizrahi, A. J. Domb, W. Khan, Injectable formulations of poly(lactic acid) and its copolymers in clinical use, *Adv. Drug Deliv. Rev.* **2016**, *107*, 213–227.
140. B. K. Lee, Y. Yun, K. Park, PLA micro- and nano-particles, *Adv. Drug Deliv. Rev.* **2016**, *107*, 176–191.
141. B. Tyler, D. Gullotti, A. Mangraviti, T. Utsuki, H. Brem, Polylactic acid (PLA) controlled delivery carriers for biomedical applications, *Adv. Drug Deliv. Rev.* **2016**, *107*, 163–175.
142. A. A. Aref, Sustained drug delivery for glaucoma: current data and future trends, *Curr. Opin. Ophthalmol.* **2017**, *28*(2), 169–174.
143. C. Wilson, K. N. Sall, S. Bafna, J. P. Gira, McLaurin EB, E. Protzko, et al., Results of a randomized, double-masked, parallel-arm phase 2b study evaluating the safety and efficacy of OTX-TP (travoprost insert) compared to timolol drops for the treatment of patients with open-angle glaucoma or ocular hypertension, *Investig. Ophthalmol. Vis. Sci.* **2017**, *58*(8), 2111.
144. S. Vantipalli, K. N. Sall, E. Stein, H. Schenker, J. Mulaney, R. Smyth-Medina, et al., Evaluation of the safety and efficacy of OTX-TP, an intracanalicular travoprost insert, for the treatment of patients with open-angle glaucoma or ocular hypertension: a phase 3 study, *Investig. Ophthalmol. Vis. Sci.* **2020**, *61*(7), 3488.
145. B. Chiang, Y. C. Kim, A. C. Doty, H. E. Grossniklaus, S. P. Schwendeman, M. R. Prausnitz, Sustained reduction of intraocular pressure by supraciliary delivery of brimonidine-loaded poly(lactic acid) microspheres for the treatment of glaucoma, *J. Control. Release* **2016**, *228*, 48–57.
146. T. Y. Kim, D. W. Kim, J. Y. Chung, S. G. Shin, S. C. Kim, D. S. Heo, et al., Phase I and pharmacokinetic study of Genexol-PM, a cremophor-free, polymeric micelle-formulated paclitaxel, in patients with advanced malignancies, *Clin. Cancer Res.* **2004**, *10*(11), 3708–3716.

147. Y. T. Tam, J. Gao, G. S. Kwon, Oligo(lactic acid)*n*-paclitaxel prodrugs for poly(ethylene glycol)-block-poly(lactic acid) micelles: loading, release, and backbiting conversion for anticancer activity, *J. Am. Chem. Soc.* **2016**, *138*(28), 8674–8677.

148. Y. T. Tam, D. H. Shin, K. E. Chen, G. S. Kwon, Poly(ethylene glycol)-block-poly(D,L-lactic acid) micelles containing oligo(lactic acid)(8)-paclitaxel prodrug: in vivo conversion and antitumor efficacy, *J. Control. Release Offic. J. Control. Release Soc.* **2019**, *298*, 186–193.

149. J. Hrkach, D. Von, Hoff, M. Mukkaram, Ali, E. Andrianova, J. Auer, T. Campbell, et al. Preclinical development and clinical translation of a PSMA-targeted docetaxel nanoparticle with a differentiated pharmacological profile. *Sci Transl Med.* **2012**, *4(128):128ra39*.

150. V. Sanna, N. Pala, M. Sechi, Targeted therapy using nanotechnology: focus on cancer, *Int. J. Nanomed.* **2014**, *9*, 467–483.

151. K. Niu, Y. Yao, M. Xiu, C. Guo, Y. Ge, J. Wang, Controlled drug delivery by polylactide stereocomplex micelle for cervical cancer chemotherapy, *Front. Pharmacol.* **2018**, *9*, 930.

152. Y. Ikada, K. Jamshidi, H. Tsuji, S. H. Hyon, Stereocomplex formation between enantiomeric poly(lactides), *Macromolecules* **1987**, *20*(4), 904–906.

153. K. Fukushima, Y. Kimura, Stereocomplexed polylactides (Neo-PLA) as high-performance bio-based polymers: their formation, properties, and application, *Polym. Int.* **2006**, *55*(6), 626–642.

154. G. G. Stefanini, M. Taniwaki, S. Windecker, Coronary stents: novel developments, *Heart* **2014**, *100*(13), 1051–1061.

155. G. Schmidmaier, B. Wildemann, A. Stemberger, N. P. Haas, M. Raschke, Biodegradable poly(D,L-lactide) coating of implants for continuous release of growth factors, *J. Biomed. Mater. Res.* **2001**, *58*(4), 449–455.

156. Y. J. Park, Y. M. Lee, S. N. Park, J. Y. Lee, Y. Ku, C. P. Chung, et al. Enhanced guided bone regeneration by controlled tetracycline release from poly(L-lactide) barrier membranes, *J. Biomed. Mater. Res.* **2000**, *51*(3), 391–397.

157. P. Saini, M. Arora, M. N. V. Kumar, Poly(lactic acid) blends in biomedical applications, *Adv. Drug Deliv. Rev.* **2016**, *107*, 47–59.

158. G. Narayanan, V. N. Vernekar, E. L. Kuyinu, C. T. Laurencin, Poly (lactic acid)-based biomaterials for orthopaedic regenerative engineering, *Adv. Drug Deliv. Rev.* **2016**, *107*, 247–276.

159. G. Turnbull, J. Clarke, F. Picard, P. Riches, L. Jia, F. Han, et al., 3D bioactive composite scaffolds for bone tissue engineering, *Bioact. Mater.* **2018**, *3*(3), 278–314.

160. S. Liu, S. Qin, M. He, D. Zhou, Q. Qin, H. Wang, Current applications of poly(lactic acid) composites in tissue engineering and drug delivery, *Compos. Part B Eng.* **2020**, *199*, 108238.

161. H. Kurobe, M. W. Maxfield, S. Tara, K. A. Rocco, P. S. Bagi, T. Yi, et al., Development of small diameter nanofiber tissue engineered arterial grafts, *PLoS One* **2015**, *10*(4), e0120328.

162. Y. Matsuzaki, K. John, T. Shoji, T. Shinoka, The evolution of tissue engineered vascular graft technologies: from preclinical trials to advancing patient care, *Appl. Sci.* **2019**, *9*(7), 1274.

163. M. Mohiti-Asli, S. Saha, S. V. Murphy, H. Gracz, B. Pourdeyhimi, A. Atala, et al., Ibuprofen loaded PLA nanofibrous scaffolds increase proliferation of human skin cells in vitro and promote healing of full thickness incision wounds in vivo, *J. Biomed. Mater. Res. B Appl. Biomater.* **2017**, *105*(2), 327–339.

164. S. Kobsa, N. J. Kristofik, A. J. Sawyer, A. L. Bothwell, T. R. Kyriakides, W. M. Saltzman, An electrospun scaffold integrating nucleic acid delivery for treatment of full-thickness wounds, *Biomaterials* **2013**, *34*(15), 3891–3901.

165. I. K. Shim, M. R. Jung, K. H. Kim, Y. J. Seol, Y. J. Park, W. H. Park, et al., Novel three-dimensional scaffolds of poly(L-lactic acid) microfibers using electrospinning and mechanical expansion: fabrication and bone regeneration, *J. Biomed. Mater. Res. B Appl. Biomater.* **2010**, *95*(1), 150–160.

166. Z. Ren, S. Ma, L. Jin, Z. Liu, D. Liu, X. Zhang, et al., Repairing a bone defect with a three-dimensional cellular construct composed of a multi-layered cell sheet on electrospun mesh, *Biofabrication* **2017**, *9*(2), 025036.

167. X. Chen, G. Chen, G. Wang, P. Zhu, C. Gao, Recent progress on 3D-printed polylactic acid and its applications in bone repair, *Adv. Eng. Mater.* **2020**, *22*(4), 1901065.

168. H. Zhang, X. Mao, D. Zhao, W. Jiang, Z. Du, Q. Li, et al., Three dimensional printed polylactic acid-hydroxyapatite composite scaffolds for prefabricating vascularized tissue engineered bone: an in vivo bioreactor model, *Sci. Rep.* **2017**, *7*(1), 15255.

169. X. Li, R. Cui, L. Sun, K. E. Aifantis, Y. Fan, Q. Feng, et al., 3D-printed biopolymers for tissue engineering application, *Int. J. Polym. Sci.* **2014**, *2014*, 829145.

170. H. Zhang, X. Mao, Z. Du, W. Jiang, X. Han, D. Zhao, et al., Three dimensional printed macroporous polylactic acid/hydroxyapatite composite scaffolds for promoting bone formation in a critical-size rat calvarial defect model, *Sci. Technol. Adv. Mater.* **2016**, *17*(1), 136–148.

171. P. Wang, H. M. Yin, X. Li, W. Liu, Y. X. Chu, Y. Wang, et al., Simultaneously constructing nanotopographical and chemical cues in 3D-printed polylactic acid scaffolds to promote bone regeneration, *Mater. Sci. Eng. C Mater. Biol. Appl.* **2021**, *118*, 111457.

172. A. Liu, G. H. Xue, M. Sun, H. F. Shao, C. Y. Ma, Q. Gao, et al., 3D printing surgical implants at the clinic: a experimental study on anterior cruciate ligament reconstruction. *Sci. Rep.* **2016**, *6*, 21704.

# 26

# PACKAGING AND CONSUMER GOODS

Hayati Samsudin and Fabiola Iñiguez-Franco

## 26.1 INTRODUCTION: POLYLACTIC ACID (PLA) IN PACKAGING AND CONSUMER GOODS

Plastics have become pervasive materials due to their unique functional properties and low cost, which contribute considerably to economic development. The production of plastic has increased from 1.5 million tons in 1950 to 359 million tons in 2018 [1, 2]. The global projection of plastic production is 1800 million tons/year by 2050 [3]. Due to the plastic pollution and environmental issues such as global warming, the demand for alternative plastic materials has increased. The worldwide production of bio-based materials was 3.8 million tons in 2019 [2].

The global production of PLA, one of the most commercially successful bio-based polymers, was around 190,000 tons in 2019. The largest PLA producer in the world is NatureWorks LLC in the USA with a total capacity of 150,000 tons. The same plant is installing additional monomer purification technology (~10%) and the installation is expected to complete by the end of 2021 [4]. The second largest plant is operated by Total Corbion's in Thailand with 75,000 tons/annum [5]. Global PLA market is expected to reach around 286.37 kilo metric tons in 2021, and it is valued by revenue at USD 698.27 million of the same year [6]. Recently, Total Corbion has announced its plan to build a new plant in Grandpuits, France. It is expected that this facility will reach a capacity of 100,000 tons annually [7]. By and large, PLA industrial applications can be categorized into consumer durable goods and consumer nondurable goods [8].

PLA properties depend on the polymer architecture and molecular weight, which dictate the final application of the polymer [9]. High-molecular-weight PLA is produced from different combinations of lactic acid (LA) or lactide enantiomers. LA is a chiral molecule having two optically active isomers: L- and D-LAs [10]. Optically active PLAs, poly(L-lactic acid) (PLLA) and poly(D-lactic acid) (PDLA), are comprised of isotactic sequences that are crystallizable. Optically inactive poly(DL-lactic acid) (PDLLA) is composed of isotactic and atactic sequences and therefore is amorphous [11]. A blend of PLLA and PDLA is referred to as stereocomplex or racemic PLA [12]. PLA with L-LA content greater than 93% tends to be semicrystalline, whereas PLA with 50–93% L-LA is amorphous and can be used in applications such as a heat seal layer that requires low sealing temperature [9]. Commercial PLAs are copolymers of L- and D-LAs, where the thermal properties change depending on the ratios. Table 26.1 shows the glass transition temperature ($T_g$) and the melting temperature ($T_m$) of PLA with different copolymer ratios.

Depending on the application, the L/D ratio is adjusted to alter the crystallinity, rheological, and thermal properties. For instance, NatureWorks LLC produces different grades of PLA under the trademark Ingeo™, with properties optimal for various applications as shown in Table 26.2. Figure 26.1 shows the viscosity and D-LA content classification for different Ingeo PLA grades commercialized by NatureWorks LLC. Table 26.3 shows different PLA grades commercialized under the trademark Luminy® from Total Corbion.

*Poly(Lactic Acid): Synthesis, Structures, Properties, Processing, Applications, and End of Life*, Second Edition.
Edited by Rafael A. Auras, Loong-Tak Lim, Susan E. M. Selke, and Hideto Tsuji.

**TABLE 26.1 Transition Temperatures of PLA Copolymers**

| Copolymer Ratio | $T_g$ (°C) | $T_m$ (°C) |
|---|---|---|
| 100 : 0 (L : L,D)-PLA | 63 | 178 |
| 95 : 5 (L : L,D)-PLA | 59 | 164 |
| 90 : 10 (L : L,D)-PLA | 56 | 150 |
| 85 : 15 (L : L,D)-PLA | 56 | 140 |
| 80 : 20 (L : L,D)-PLA | 56 | 125 |

*Source:* Adapted from Ref. 13.

## 26.2 FOOD AND BEVERAGE

### 26.2.1 Evolution of PLA in the Food and Beverage Market

PLA usage in the food and beverage industry has been growing over the past two decades. PLA has been seen as an environmentally friendly alternative to replace fossil plastics. The building block of PLA is derived from renewable crops that sequester $CO_2$ during their growing cycle, thereby removing the need to use fossil resources.

Although PLA has received widespread attention among manufacturers and consumers, its application has been somewhat limited due to its brittleness, moderate barrier properties to moisture and gases that are unsuitable for food contact application. However, since the approval of PLA as a generally recognized as safe (GRAS) material in the 1990s [17–19], many efforts have been made by manufacturers, food industries, and independent researchers to improve its thermal and barrier properties for use as a food packaging material.

In the early 2000s, companies such as Del Monte and Wild Oats Markets used PLA for the packaging of fresh-cut produce and deli food, respectively. In 2003, the first-ever PLA bottles for organic milk were launched by Naturally Iowa Dairy [20]. In the following year, Biota® ("Blame It On The Altitude") marketed PLA bottled water [8]. In 2005, Walmart, the biggest retailer in North America, launched an initiative to encourage suppliers to become more socially responsible through environmentally friendly and sustainable options [18]. By the end of 2005, NatureWorks LLC PLA was used for fresh-cut produce packaging

**TABLE 26.2 Main PLA Grade Commercialized by NatureWorks LLC (Ingeo Portfolio)**

| Category | Grade | Key Features |
|---|---|---|
| Extrusion/thermoforming (series 2000) | 2003D | Used as is or as part of a formulated blend using traditional extrusion equipment |
| | 2500HP | High in viscosity and designed to crystallize during processing |
| Injection molding (series 3000) | 3001D | Unlubricated, medium-flow grade |
| | 3052D | Lubricated, medium-flow grade |
| | 3100HP | Medium viscosity, designed for medium-flow injection molding |
| | 3251D | Lubricated, ultra-high flow rate |
| Films and sheets (series 4000) | 4032D | High heat films |
| | 4043D | General purpose films |
| | 4044D | Reactive extrusion grade |
| | 4060D | Heat seal layer for films |
| Fibers/nonwovens (series 6000) | 6060D | Amorphous-extrusion into mechanically drawn staples fibers, low-melt binder polymer in a sheath-core configuration |
| | 6100D | For lower fiber shrinkage, where higher dimensional stability is required |
| | 6201D | Continues filament/staples for dyed fiber application |
| | 6202D | Staple fibers/spun bond for nonwovens, non-dyed fiber application |
| | 6252D | Melt-blown |
| | 6302D | Amorphous low melt for staple fiber/fiber sheath layer |
| | 6362D | Designed especially for fiber products, where an amorphous structure is desired |
| | 6400D | Monofilaments/BFC/multifilament products |
| | 6752D | Sheath polymer for spunbond applications |
| Foams (series 8000) | 8052D | Expanded foam sheets |
| 3D series for 3D printing (series 3D) | 3D450 | Combining the printability and low warping tendency of Ingeo with optimized adhesion. It provides good adhesion within the support structure, yet allows clean separation from the printed part |
| | 3D850 | This grade exhibits faster crystallization rates and is able to develop improved heat-resistance in 3D-printed parts. This low color resin grade demonstrates the best performance in formulated systems designed to enhance toughness or heat resistance |
| | 3D870 | Engineered to deliver improved heat resistance and high impact strength to 3D-printed parts. This formulated grade achieves thermal and mechanical properties similar to ABS while offering an alternative to styrenic-based materials |

*Source:* Adapted from Ref. 14.

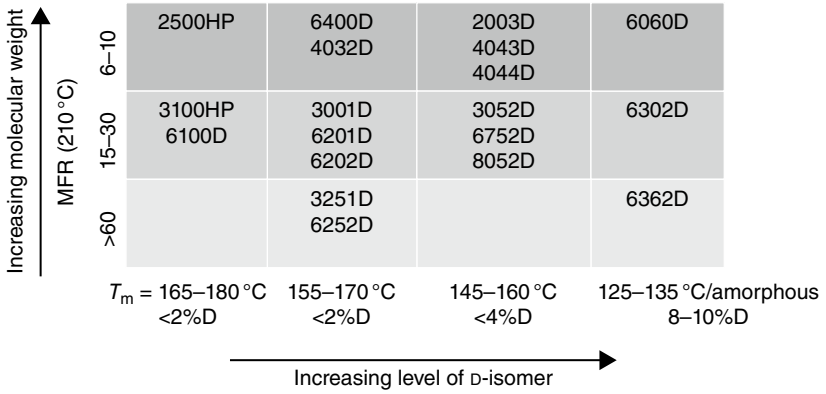


**FIGURE 26.1** Classification of Ingeo PLA grades commercialized by NatureWorks LLC according to their viscosity and D-LA content. *Source:* Adapted from Ref. 15.

**TABLE 26.3 Total Corbion, Luminy Resin Portfolio**

| Grade | Application | Optical Purity | Key features |
|---|---|---|---|
| L105 | Injection molding | >99%L | High-heat, high-flow PLA homopolymer suitable for thin-wall injection molding and fiber spinning. Suitable for the production of semicrystalline parts, which exhibit a higher temperature resistance |
| L130 | Injection molding and fiber spinning | >99%L | High-heat, medium-flow PLA homopolymer. Suitable for the production of semicrystalline parts, which exhibit a higher temperature resistance |
| L175 | Fiber spinning and extrusion/thermoforming | >99%L | High-heat, high-viscosity PLA homopolymer. Suitable for the production of semicrystalline parts, which exhibit a higher temperature resistance |
| LX530 | Fiber spinning | 98%L | Medium-flow, fiber-grade resin suitable for staple fiber or spunbond applications |
| LX575 | Extrusion/thermoforming | 98%L | High-heat, high-viscosity resin that can be used in (film) extrusion processes |
| LX175 | Fiber spinning and extrusion/thermoforming | 96%L | High-viscosity, low-flow, amorphous, transparent PLA resin |
| LX930 | Fiber spinning | 90%L | Medium-viscosity, medium-flow, fiber-grade PLA that can be used as low melting component in sheath-core configurations |
| LX975 | Extrusion/thermoforming | 88%L | High-viscosity resin suitable for use as a heat-seal layer in film applications or as a low-melting component in sheath-core configurations |
| D070 | Nucleating agent | >99%D | When combined with PLA homopolymers will yield a compound that combines good heat resistance with excellent mechanical properties and a reduced processing cycle time |
| D120 | Injection molding, fiber spinning and extrusion/thermoforming | >99%D | High-heat, medium-viscosity, PLA homopolymer suitable for full stereocomplex PLA. The typical ratios are 35–50% Luminy D120 combined with PLLA homopolymers |

*Source:* Adapted from [16].

nationwide [19]. Since then, the market for PLA has grown extensively owing to innovative processing technologies. Many of these technologies are patented by NatureWorks LLC (Cargill, USA), PTT Global Chemical (Thailand), and Total Corbion (Total, France; Corbion, Netherland) [4]. Table 26.4 shows a list of PLA/PLA-based consumer goods in the market.

### 26.2.2 Growing Interest in PLA Serviceware

The use of PLA as the main bio-based polymer has dominated the food and beverage markets all over the globe for a wide range of products since 2005 (Table 26.4). However, its use is still limited to low and moderate thermal exposure applications where moderate mechanical and water barrier properties are required. This has changed since 2013, when additives such as fillers and other biodegradable polymers have been mixed and blended with PLA to achieve enhanced mechanical, barrier, and/or thermal properties for commercial applications. Fillers such as calcium carbonate, clay, and fiberglass have been among the chosen ingredients for improving mechanical properties of PLA, while compounds such as talc and polymers such as poly(methyl methacrylate) and poly(butylene adipate terephthalate) have been used for improving PLA's thermal stability, specifically, the heat distortion temperature. However, novel stereocomplexation of

**TABLE 26.4 Commercially Available PLA/ PLA-Based Consumer Goods**

| Trademark/Commercialized Brand | Year Active | Improved Functions | Applications | Remarks | Refs. |
|---|---|---|---|---|---|
| Tenova, Sweden | 2003–current | None | Shopping bags | Bags composed of 45 wt% PLA and 55 wt% Ecoflex | [8] |
| Biota, USA | 2004–2006 | None | Bottled waters | Advertised as biodegradable bottles<br>No longer on market due to company bankruptcy | [21, 22] |
| Wal-Mart, USA | 2005–current | None | Strawberries, Brussels sprouts | Advertised as biodegradable clamshells<br>Among the first company to use commercialized PLA | [23] |
| Del-Monte, USA | 2005–current | None | Fresh-cut produce | Advertised as biodegradable clamshells | [24] |
| SPAR, Austria | 2005–current | None | Organic pears, apples, tomatoes | Advertised as biodegradable thermoformed with flexible PLA lid | [25] |
| Hypermarket chain Auchan, France | 2005–current* | None | Fresh salads | Advertised as biodegradable containers | [26] |
| Newman's Own, USA | 2005–current* | None | Organic salads | Advertised as biodegradable containers | [27] |
| Pacific Pre-Cut, USA | 2005–current* | None | Freshly prepared salads | Advertised as biodegradable containers | [28] |
| Vitamore®, Ihr Platz (drugstore chain), Germany | 2006–current | None | Bottled beauty, energy and memory drinks | Advertised as 100% bio-based bottles | [29] |
| Huhtamaki, Finland | 2006–current | None | Dessert cups | Advertised as biodegradable containers | [30] |
| Greenware®, Fabri-Kal, USA | 2008–current | None | Cold drink cups, lids and portion containers | 100% biodegradable | [31] |
| Noble Juice, USA | 2008–current | None | Organic and non-organic citrus juice bottles | 100% biodegradable | [32] |
| Apple Inc., USA | 2008–current* | None | iTunes prepaid gift cards | Current status in market unknown | [33] |
| Sant' Anna, Italy | 2008–current | None | Bottled water | 100% biodegradable bottles with PE lids | [34] |
| Fleischmann's®, Blue Bonnet®, Parkay®; ConAgra Foods, USA | 2009–current | Improved shrinkage performance | Tamper evident seals for table spreads | Made of recycled PLA<br>Claimed to reduce 20% of facility's energy consumption | [35] |
| Reddi-Wip®, PAM®; ConAgra Foods, USA | 2009–current | Improved shrinkage performance | Shrink labels for cream whipped topping and cooking spray | Made of recycled PLA<br>Claimed to reduce 20% of facility's energy consumption | [35] |
| Shiseido-Urara, China | 2009–current | None | Bottled shampoo | Favorable reception in Chinese market as an environmentally friendly option<br>Bottles are 50 wt% PLA and 50 wt% HDPE | [36] |
| Wal-Mart; Sams-Club, Mexico | 2010–current* | None | Small white onion | No longer on the market<br>Advertised as biodegradable clamshells | [37] |
| Sunschips®, Frito Lay, USA | 2010–2014 | Thermal resistance | Potato chips bags | Bags withdrawn from the market within a year due to loud crinkling noise<br>Original flavor was retained for a while after incident, but is no longer available<br>Bags composed of 94 wt% PLA, 6 wt% adhesive and ink, 0.2 wt% aluminum liner | [38, 39] |

| | | | | | |
|---|---|---|---|---|---|
| Activia®, Danone, Germany | 2010/2011–current | None | Yogurt | Improved carbon footprint by 25%<br>43% less fossil resource usage than original package | [40] |
| Stonyfield Farm®, USA | 2010/2011–current | None | Organic yogurt multipack cups | Cups composed of 93 wt% PLA, 4 wt% titanium dioxide and 3 wt% compounded additives<br>48% Reduction of greenhouse gas emissions | [41] |
| Polenghi LAS, Italy | 2010–current | None | Bottled lemon juice | Claimed to be first blown extrusion PLA bottle in EU market | [42, 43] |
| Ceramis®, Amcor's Swiss | 2011–current | High barrier toward $O_2$, moisture, aroma compounds | Snacks (pouches)<br>Fruits and vegetables (thermoformed)<br>Breads | Silicon oxide coating provides excellent barrier for PLA | [44] |
| Biopolymer Network | 2017–current | ZealaFoam® EcoBeans | Loose fill for distribution packaging | Expanded PLA foam produced via foaming process with $CO_2$ as the blowing agent | |
| Elk Packaging | 2020–current | None | Numi Overwrap Teabag | Three-layer laminate: Paper/Futamura Natureflex's cellophane/PLA | [45] |

*Source:* Reprinted with a few modifications from Castro-Aguirre et al. [8] and permission from Elsevier.

PLA has been a better and effective approach to tailor the thermal and mechanical properties of PLA [46]. These advancements allow PLA to compete favorably with other commercial fossil polymers such as polyethylene terephthalate (PET), polystyrene (PS), and polypropylene (PP).

The stereocomplexation approach employs the interaction between PLLA and PDLA as previously presented in Chapter 6 (i.e., section 6.5). A strong interaction between L-lactic acid and D-lactic acid segments contributes toward the formation of stereocomplex crystallites [47, 48]. Stereocomplex PLLA or PDLA is capable of crystallizing into α, β or γ form [49]. An equimolar physical mixture of the two enantiomers was reported to produce a new crystallite formation known as the stereocomplex form, contributing to a significant increase in its melting temperature from 180 to 230°C. The mechanism behind the excellent thermal stability of PLA stereocomplex has been widely explained based on the density functional theory. Stereocomplex crystallites were reported to exhibit more thermodynamically stable energy than those of the α, β, or γ form within the range of 0.3–1.3 kcal/mol [49]. However, stereocomplexation alone is not enough to achieve adequate thermomechanical functionality for a wide range of product applications. Thus, additional steps include tackling the molecular architecture of PLA, blending with additives (e.g., impact modifier, filler, nucleating agent), and manipulating crystallization rates through processes such as annealing have been applied for better functionality of PLA. A study by López Rodríguez et al. [50] found through its conducted annealing treatments that the mechanical properties of stereocomplex PLA blend (i.e., tensile strength and elongation at break) were improved significantly due to a higher density of tie chains between crystallites through a mobile amorphous phase, leading to an excellent ductile property of the material. This finding enlightens that improved mechanical properties of stereocomplex crystallites is not a result of the type of crystal polymorphs [47, 50]. On the other hand, from commercial standpoints, PLA resins from NatureWorks LLC have been modified with impact modifiers produced by suppliers such as DuPont, Arkema, Rohm and Haas, and Chemtura for the production of products with improved performance [51]. One example of such an impact modifier is Biomax® Thermal 300 from DuPont that is produced from ethylene copolymer resin with a nucleating agent. This additive provides rapid melt-dispersion for PLA during process, as well as improving PLA's thermal properties and toughness [52]. Arkema produces Biostrength®, an acrylic-based impact modifier that increases PLA impact strength for extruded, thermoformed, calendered, and blow-molded products [53].

In-mold and post-annealing are processing methods to produce PLA cutlery. In-mold annealing is straightforward, wherein in-mold heating of PLA between 100 and 130°C together with lower D-enantiomer content achieves rapid crystallization [54]. On the other hand, post-annealing is a two-step process: (i) molding of PLA cutlery in a cold mold; and (ii) annealing the molded cutlery at the PLA crystallization temperature in a convection oven [54]. There are many variations to the processing of PLA cutlery. WorldCentric®, for instance, produces its line of PLA cutlery with the addition of talc that allows the product to tolerate temperatures up to 93.3°C [55]. Other companies producing PLA-based serviceware products are listed in Table 26.5.

**TABLE 26.5 Selected Examples of Commercially Available PLA Food Serviceware**

| Company | Year | Products | Remarks | Refs. |
|---|---|---|---|---|
| PURALACT®, Netherlands | 2013–current | Single-use hot beverage cups | • Thermoformed containers able to tolerate boiling temperature<br>• Conversion to PLA packaging line is feasible by using an existing PS line | [60] |
| PURALACT, Netherlands | 2013–current | Serviceware | • Comparable impact resistance to ABS<br>• Safe food contact application, and the containers are microwavable | [61] |
| World®Centric, USA | 2019–current | PLA cutlery | • Made from non-GMO sugars (corn, sugarcane)<br>• Products are reusable and dishwasher safe | [55] |
| | | TPLA cutlery | • Addition of talc in the formulation to improve heat resistance (max temp 93.3°C (200°F)<br>• Products are reusable and dishwasher safe | |
| | | ZeroWare™ – Reusable dishware | • PLA is made from corn starch with added talc<br>• Can be reused for at least 100 times | |
| | | PLA cold cup | • Made from non-GMO sugars (corn, sugarcane)<br>• Must be stored under 43°C and from direct light exposure | |

**TABLE 26.5 (Continued)**

| Company | Year | Products | Remarks | Refs. |
|---|---|---|---|---|
| | | PLA hinged clamshell | • Must be stored under 43°C and from direct light exposure<br>• Freezer safe<br>• Not microwaveable<br>• Compost within two to four months in a commercial composting facility | |
| | | PLA deli container | • Must be stored under 43°C and from direct light exposure<br>• Freezer safe<br>• Not microwaveable | |
| good natured® Products Inc., Canada | 2020–current | PLA-based deli & prepared meal container, PLA-based baked goods container, PLA-based fruits and veggies container | • 99% PLA | [62] |
| Biobright, Bright International BV, Belgium | 2020–current | Reusable PLA nonwoven bag, CPLA straws, CPLA tableware, PLA-lined paper cups, lids, container | • Some products are microwave safe | [63] |
| Ecozema®, Italy | 2015–current | Ingeo PLA clamshell box | • Max temperature tolerance: 45–55°C | [64] |
| | | Ingeo PLA cups | | |
| | | Ingeo PLA cups | • Max temperature tolerance: 70°C | |
| | | Ingeo PLA straws | • Max temperature tolerance: 40°C | |
| | | CPLA | • Temperature resistance up to 85°C | |
| 100Bio, USA | 2017–current | PLA foam-based tablewares, fresh food trays | • Heat resistance<br>• Leak resistance and sturdy | [59] |
| | | PLA takeout containers | • *Lid for takeout container are made of rPET | |
| KoreaBiofoam, South Korea | 2019–current | PLA foam-based tray, carriers, bowls, cups | • Food contact safe (FDA compliant)<br>• Pose antibacterial properties | [58] |
| Biodegradable Food Service™, USA | 2007–current | Earth Maize™ | • Made from Ingeo PLA<br>• Temperature resistance up to 43°C<br>• Grease and moisture resistant<br>• Bioflash technology microwavable<br>• Freezer safe (−20°C) | [65] |
| | | Earth Cup™ | • Kraft paper-based cups with PLA coating | |
| | | Earth Bowl™ | • Paperboard bowl lined with PLA<br>• Lid is made from CPLA | |
| | | Earth Cutlery™ | • Temperature resistance up to 85°C | |
| Bonnie Biodegradable (Pty) Ltd, South Africa | 2019–current | PLA cling wrap | • Temperature resistance up to 85°C<br>• Freezer safe | [66] |
| | | PLA straws | • Six-month shelf life | |
| | | PLA cutlery | • Six-month shelf life | |
| | | PLA hot cup lids | • Six-month shelf life | |
| EcoProducts Inc., USA (* there are more products available under this company) | 2007–current | Plantware® cutlery | • CPLA<br>• Temperature resistance up to 93°C | [67] |
| | | GreenStripe® cold cups | — | |
| | | WorldArt™ cold cups | • Temperature resistance up to 40°C | |
| | | GreenStripe hot cups | • Paper cup lined with PLA | |
| | | Ecolid® hot cup lids | • Temperature resistance up to 93°C | |
| SelfEco, LLC, USA | 2016–current | Drinkware | • PLA™ Ingeo | [68] |
| | | Plates | | |
| | | Bowls | | |
| | | Food Cups | | |
| | | Cutlery | | |

(*Continued*)

**TABLE 26.5 (Continued)**

| Company | Year | Products | Remarks | Refs. |
|---|---|---|---|---|
| AMS Compostable, AMS Global Suppliers Group, USA | 2019–current | PLA gloves for food handling<br>PLA cutlery<br>*, ** Paper cups (ripple, double, and single wall) with PLA linings | • *~30 g of PLA was used as a lining<br>• ** PLA lining can withstand up to ~87°C<br>• All products are compostable certified by BPI and OK Home Compost certified by TÜV Austria | [69] |
| Arxxin New Material (Xiamen) Co., Ltd, China | 2003–Current | PLA cutlery<br>PLA clear cups<br>PLA straws | • Products can withstand up to 100°C | [70] |
| Huhtahmaki, USA | 2019–current | Bioware® CPLA cutlery | • Products can withstand up to ~88°C<br>• Resistant to a wide range of temperature from hottest to coldest without warping or melting | [71] |
| Huhtahmaki, UK | 2019–current | Bioware Impresso double-walled hot cup | • 100% PEFC-certified paperboard with PLA coating<br>• Marketed throughout EU | [72] |

*Note*: FDA: U.S Food and Drug Administration; BPI: Biodegradable Products Institute; PEFC: Programme for the Endorsement of Forest Certification.

These companies produce PLA serviceware items that mostly can tolerate temperatures up to a max of 93.3°C.

PLA-based foam has slowly gained momentum. Starting in 2005, the first biodegradable foamed PLA tray was launched by an Italian packaging company, Coopbox Europe S.p.A, under the name Naturalbox, using NatureWorks LLC's Ingeo PLA resin. The foamed sheets were processed using $CO_2$ on a standard tandem extrusion line, where the density was reduced from 1.25 to 0.30 g/cm$^3$. Later, in 2007 Cryovac Inc. (Sealed Air) started to commercialize PLA foams under the tradename of NatureTray [56]. Pactiv in 2010 developed foamed PLA meat trays with Ingeo EarthChoice [57]. Dyne-A-Pak Inc., a Canadian company, produced PLA foam trays for fresh produce with a density of 50–60 kg/m$^3$ [56]. Recently, PLA-based foam serviceware has been produced by companies such as 100Bio™ and KoreaBiofoam that are heat resistant and certified safe for food contact applications [58, 59].

## 26.3 DISTRIBUTION PACKAGING

PLA foams are ideal for short-life applications, such as loose-fill packaging, cushioning, and insulation. Typical polymers used in foam packaging are fossil-based, such as polystyrene and, to a lesser extent, polyethylene and PP [73]. Due to the environmental concern of using these foams for distribution packaging, interest in PLA for these applications has been growing. However, current commercialization of PLA foam is still limited. Since the thermal resistance of low-density PLA foam is limited, the foam tends to deform when in contact with hot foods. Also, chain extenders in PLA that are not approved by FDA mean they cannot be used for direct contact with hot food and beverage products [74].

Foaming of PLA is conducted by dissolving a blowing agent in the polymer matrix and then blowing it in the melt phase. Super-saturation of the blowing agent causes cell nucleation and growth through thermodynamic instability. For PLA foam products, the stabilization of the cell occurs when the temperature reaches below the $T_g$, at around 60°C [75, 76].

In laboratory-scale experiments, both amorphous and semicrystalline PLA polymers have been used. Various technologies are available for large-scale manufacturing of PLA foams. The primary source of packaging foam is extrusion foam. One main requirement for extrusion foaming is melt strength, which is one of PLA's limitations. To modify the rheological behavior, the production of the foam was performed using chain extenders and nanoclays [15]. NatureWorks LLC has a specific PLA grade, Ingeo 8052D, for extrusion foaming of low-density foam sheets. This resin grade is semicrystalline and has 4.7% D-LA [15]. NatureWorks LLC specifies the addition of Joncryl 4368C (BASF) as a branching agent or another masterbatch agent from Clariant. Conventional foaming agents are butane, pentane, and HSFC-15a [77]. Low shear screw technologies have been used for extrusion foaming, such as those developed by Plastic Engineering Associates with Turbo-Screw® [78], licensed in the USA and Europe. This technology is being used to make foam trays.

Particle foam or expandable beads are used to produce molded particle foam products used in packaging of electronics, furniture, and biomedical supplies. The process begins with an expandable polymer bead, which contains a blowing agent, which could be a compressed gas or a volatile liquid. Then, heat is applied to the beads, so they can expand prior to conditioning at a preset temperature and time, and finally they are placed into a mold where heat is applied, forming the solid article [73]. Synbra Technology B.V., a Dutch company, developed an expanded PLA particle foam

material under the tradename BioFoam® [79]. Biopolymer Network offers a commercial expanded PLA foam under the tradename ZealaFoam® EcoBeans, produced via a foaming process with $CO_2$ as the blowing agent, which has excellent impact resistance and insulation properties [80].

## 26.4 OTHER CONSUMER GOODS: AUTOMOTIVE

Plastics have been dominating the automotive industry since they are lightweight, durable, and fuel-efficient. About 33% of the 30,000 car parts are made of plastics such as PP, polyurethane, polyamide, and polyvinylchloride [81]. Although this trend continues, the selection of plastics for car parts has expanded to a green route with PLA as the main option. Modified PLA has been an option for green initiatives in the automotive industry due to its impact resistance, dimensional stability, heat resistance (~140°C), etc. It is an excellent alternative to PET, polyamide, and PP, to name a few [82]. Ford, Toyota, and Mazda are among the first to set targets for replacing petroleum-based plastics with PLA (Table 26.6). In 2006, Mazda became the first automotive company to mass-produce upholstery, floor mats, and other interior parts using PLA [83]. Toyota has been experimenting with several bioplastics such as bio-based polyamide, bio-based polyolefins, and PLA blends [84]. Early experimentation with PLA started in 2003, where PLA/kenaf biocomposites were used to manufacture spare wheel covers and translucent roofs for the Prius and Raum. PLA fiber was used to produce the car floor mats. PLA/PET blends were used for the upholstery part, while PLA/PP blends were used for scuff plates and interior trim [82].

Ford was among the first to initiate the green automotive effort with its soy-based foam seating. They have improved issues associated with bio-based plastics, such as moisture sensitivity and off-odor production during the injection molding process. One of Ford's approaches was introducing nanofillers in the car's bioplastic parts formulation to achieve the needed strength for their application while reducing weight [85]. In a more recent development, in 2018 Noah, the world's first bioplastic car was produced with its body entirely made of PLA and flax. This car was designed by students from Eindhoven University of Technology, Netherlands [86].

## 26.5 OTHER CONSUMER GOODS

Another consumer goods application that has seen increasing PLA use is electronic items. Electronics need a casing for insulation purposes, and the majority of commercial casings are made from petroleum-based plastics such as

**TABLE 26.6 Examples of PLA Uses in Automotive Industries**

| Company | Year | Products | Remarks | Ref. |
|---|---|---|---|---|
| Ford, USA | 2008/2009 | Carpets, mats, interior trims | Issues:<br>• PLA faster decomposition time (~120 days) for a lifetime use<br>• Lengthy molding time (min vs sec) | [87] |
| Toyota, Japan | 2003 | Cover spare wheel translucent roof | Made of PLA/Kenaf biocomposites<br>Used for Toyota model Prius & Raum | [82] |
| | 2003–2015 | Upholstery parts: door, luggage area trims<br>Injection-molded parts: scuff plates, interior trims | PLA/PET blend<br>PLA/PP blend | [82] |
| Mazda, Japan | 2006 | Car seat fabrics<br>Floor mats<br>Pillar cover<br>Door trims<br>Front panels<br>Ceiling material | Made from Biofront™ (the first mass-produced stereocomplexed PLA). The material was co-developed by Mazda and Teijin | [82] |
| | 2015 | Interior parts | Used for MX-5 model<br>88% corn-based | [82] |
| Honda, USA | 2007 | Roof lining<br>Pillar coverings<br>Floor carpets<br>Piece mats<br>Trunk lining | PLA bio-fabric<br>Used for Honda FCX-Clarity | [88] |
| Hyundai, South Korea | 2009 | Interior parts | Blue Will model | [89] |
| Eindhoven University of Technology, Netherland | 2018 | Chassis | High-heat Luminy PLA-grade (Total Corbion) + Flax | [86, 90] |

polycarbonate and acrylonitrile butadiene styrene. PLA naturally does not possess either thermal or impact resistance. Besides, it is not a flame-retardant material for use in electronics. Thus, many companies have attempted to enhance PLA properties to suit electronics applications by introducing plant-based fillers and additives. Kenaf fiber is one of the reinforcement materials used to improve the heat and impact resistance of PLA. Kenaf is native to Africa and Asia. It has long fibers and has been used for many applications requiring thermal insulation, soundproofing, etc., such as in building construction, automotive, and furniture. Toyota, BMW, and Ford have introduced this fiber as part of their material composites, mainly for car interior parts [91]. Similarly, NEC Corporation has employed Terramac® PLA-reinforced Kenaf fiber for its Foma N701iECO cellphone that was launched in 2006. This development was a joint venture between NEC Corporation and Unitika [92]. Kenaf was reported to be able to protect resins from deformation and promote crystallization of PLA that led to improved Young's modulus and heat resistance, with 15% kenaf. A similar material was used to develop La Vie TW and Versa Pro personal computers [93]. Following these developments, NEC enhanced the functionality of the PLA-reinforced kenaf fiber with a charring agent, aluminum hydroxide, and a few other additives (known as NeCycle® bioplastic) [94] to produce eco-friendly flame-retardant components for business/personal computers that were launched in 2010 [93].

However, NEC was not the first to launch such a product. Fujitsu Ltd., Fujitsu Laboratories Ltd., and Toray Industries Inc. became the first successful collaboration to market the FMV-BIBLO NB80K notebook computer in 2005 [95]. This product was developed through experimentation with various flame retardants (i.e., aromatic silicon resin J-052, polydimethylsiloxane DC4-708, and dimethyl siloxane MB50-315 of Dow Corning Toray Silicon Co., Ltd.; methylphenyl system silicon resin X-40-9805 of Shin-Etsu Chemical Co., Ltd.; aluminum hydroxide Pairoraizar HGof Ishizuka glass Co., Ltd.) and resin additives (i.e., PLA H-100J, polyethylene 3000B of Mitsui Chemicals, Inc.; polystyrene 685 of PS Japan Corporation; PP MA-410 of Japanese polyolefin; modified polyphenylene ether 200H, and acrylonitrile butadiene styrene 121 of Asahi Kasei Corporation; polybutylene terephthalate 1401 of Toray Industries Inc., polymethyl methacrylate VH001 of Mitsubishi Rayon Co., Ltd.; polycarbonate/acrylonitrile-butadiene styrene S1100 of Daicel Polmer Ltd.; polycarbonate A1900 of Idemitsu Kosan Co., Ltd.) [96]. They reported that 5 wt%- methylphenyl-silicon resin and 20 wt% aluminum hydroxide were successful in achieving the V-2 rating of the UL94V standard – the Standard for Safety of Flammability of Plastic Materials for Parts in Devices and Appliances Testing. On the other hand, for the development of polymer-alloy technology, PLA with added polycarbonate A1900 was found to have improved Izod impact strength and deflection temperature under load compared to the performance of PLA with the other additives [96].

In another development, the first PLA-based touch screen computer developed by SUPLA Material Technology Co. and Kuender & Co. was showcased at K2013 in Dusseldorf [97]. This technology was based on the third generation PLA from Corbion Purac using lactide building blocks that managed to achieve thermal resistance of up to 120°C with improved impact strength and good scratch resistance. Other projects by Corbion Purac include carpets and furniture designed using PLA-fiber-laminated paneling, toys, and sporting goods (i.e., PLA-based foam surfboard) [98].

Many other PLA-based consumer goods are being developed worldwide, including trash bags, single-use gloves, produce bags, and so on, by becausewecare™, Australia [99], and spunbond nonwoven fabric for shopping bags, mask, garment bags, etc., by Renewable Fibers LLC., USA [100]. In a recent development, a South Korean designer has used PLA combined with 3D printing to create furniture pieces [101]. More development can be expected in this field with major producers like NatureWorks LLC and Total Corbion partnering with many industries. In the future, it will be of no surprise for PLA to become a commodity plastic with a wide range of desirable properties.

## 26.6 CHALLENGES AND FINAL REMARKS

The demand for environmentally friendly plastic options, restricted single-plastic usage, and the advancement of technology have led to a significant expansion of PLA usage worldwide, particularly for consumer goods applications, including food and beverage, packaging distribution, and other consumer goods such as automotive and electronics. With technological advances and collective efforts by bioplastic producers and packaging manufacturers, PLA has emerged as the leading bioplastic material for many applications and has become a great competitor to the existing petroleum-based materials. With PLA plant expansion around the world by dominating producers such as NatureWorks LLC and Total Corbian, more positive outlooks on these developments can perhaps be expected shortly.

Despite all the positive aspects PLA has to offer, the PLA end-of-life scenario remains a challenge mainly due to lack of infrastructure capable of handling this material; specifically, no recycling stream is available, and there is a limited number of organic collection programs around the world. However, the Biodegradable Product Institute of USA (BPI) has recently launched "Guidelines for the Labeling of Compostable Products and Packaging" to assist consumers in identifying and separating compostable plastics such as PLA to avoid cross-contamination with other non-compostable plastics and to facilitate collection through food scrap composting

programs [102, 103]. The guideline highlights the limitations of its recommended approach on the separation of compostable plastics from non-compostable ones based on color, embossing, and print [104]. However, it is unknown how this guideline will help the entire world with different certification schemes. Currently, there are two leading organizations responsible for the issuance of such certifications, which are the BPI in the United States certifying compostable products for the industrial composting environment, and TÜV Austria certifying products for industrial compost, home compost, and marine biodegradation [105]. Despite having some products compostable-certified as indicated on the containers, another question arises: are the compostable containers composted successfully? Early last year, Coop reported that PLA containers used for meat products were not composted as they should; instead, they were burnt by the waste processor, which has prompted Coop to switch from this packaging into recycled options [106].

The emergence of PLA products as part of a strategy to combat environmental issues has provided an option to use compostable polymers to be recovered through composting; however, there are still concerns on the handling and after-use scenarios that need to be looked into.

## REFERENCES


1. L. Neufeld, F. Stassen, R. Sheppard, T. Gilman (Eds.), *The New Plastics Economy: Rethinking the Future of Plastics*, World Economic Forum, Geneva, 2016.
2. P. Skoczinski, R. Chinthapalli, M. Carus, W. Baltus, D. de Guzman, H. Käb, et al., *Biobased Building Blocks and Polymers—Global Capacities, Production and Trends, 2019–2024*, nova-Institut GmbH, Hürth, 2020.
3. D. Qualman, Global plastics production, 1917 to 2050, 2017. Available from: https://www.darrinqualman.com/global-plastics-production/. Accessed November 20, 2020.
4. D. D. Guzman, NatureWorks to expand US PLA production, Green Chemicals Blog, 2020. Available from: https://greenchemicalsblog.com/2020/09/24/natureworks-to-expand-us-pla-production/. Accessed May 31, 2021.
5. K. J. Jem, B. Tan, The development and challenges of poly (lactic acid) and poly (glycolic acid), *Adv. Ind. Eng. Polym. Res.* **2020**, *3*(2), 60–70.
6. Market Watch, Global polylactic acid (PLA) market report 2021 with top countries data and covid-19 analysis to showing impressive growth by industry trends, share, size, top key players analysis and forecast research [press release], Market Watch, 6 April 2021, 2021.
7. Total Corbion, Total Corbion PLA announces the first world-scale PLA plant in Europe [press release], Total Corbion, 2020.
8. E. Castro-Aguirre, F. Iñiguez-Franco, H. Samsudin, X. Fang, R. Auras, Poly (lactic acid)—mass production, processing, industrial applications, and end of life, *Adv. Drug Deliv. Rev.* **2016**, *107*, 333–366.
9. R. Auras, B. Harte, S. Selke, An overview of polylactides as packaging materials, *Macromol. Biosci.* **2004**, *4*(9), 835–864.
10. X. Jiang, Y. Luo, X. Tian, D. Huang, N. Reddy, Y. Yang, Chemical structure of poly(lactic acid), in: R. Auras, L.-T. Lim, S. Selke, H. Tsuji (Eds.), *Poly(lactic acid) Synthesis, Structures, Properties, Processing, and Applications*, John Wiley & Sons, Inc., Hoboken, NJ, 2010, pp. 69–82.
11. H. Tsuji, Autocatalytic hydrolysis of amorphous-made polylactides: effects of L-lactide content, tacticity, and enantiomeric polymer blending, *Polymer* **2002**, *43*(6), 1789–1796.
12. K. J. Jem, J. F. van der Pol, S. de Vos, Microbial lactic acid, its polymer poly (lactic acid), and their industrial applications, in: Chen, G.G-Q. *Plastics from Bacteria*, Springer, Berlin, Heidelberg, 2010, p. 323–346.
13. L.-T. Lim, R. Auras, M. Rubino, Processing technologies for poly (lactic acid), *Prog. Polym. Sci.* 2008, *33*(8), 820–852.
14. NatureWorks LLC. Available from: https://www.natureworksllc.com/What-is-Ingeo. Accessed November 20, 2020.
15. R. Gendron, M. Mihai, Extrusion foaming of polylactide, in: S.-T. Lee (Ed.), *Polymeric Foams: Innovations in Processes, Technologies, and Products*, CRC Press, Taylor & Francis Group, Boca Raton, FL, 2017.
16. Total-Corbion. Available from: https://www.total-corbion.com/luminy-pla-portfolio/. Accessed November 20, 2020.
17. R. Conn, J. Kolstad, J. Borzelleca, D. Dixler, L. Filer, Jr., B. LaDu, Jr., et al., Safety assessment of polylactide (PLA) for use as a food-contact polymer, *Food Chem. Toxicol.* **1995**, *33*(4), 273–283.
18. J. Ahmed, S. K. Varshney, Polylactides—chemistry, properties and green packaging technology: a review, *Int. J. Food Prop.* **2011**, *14*(1), 37–58.
19. Y. Ma, L. Li, Y. Wang, Development of PLA-PHB-based biodegradable active packaging and its application to salmon. *Packag. Technol. Sci.* **2018**, *31*(11), 739–746.
20. A. ElAmin, Wal-Mart signals move to natural packaging, Bakery and Snacks.com, 2005. Available from: https://www.bakeryandsnacks.com/Article/2005/10/27/Wal-Mart-signals-move-to-natural-packaging. Accessed September 25, 2020.
21. PlasticNews, PLA bottle maker biota enters bankruptcy [press release], *PlasticNews*, 2007.
22. R. Lingle, PLA makes splash in bottled water, Packaging World, 2004.
23. NatureWorks LLC, SAM'S CLUB partners with NatureWorks PLA to help the environment [Internet], NatureWorks LLC, 2005 [cited 21 November 2007]. Available from: http://www.natureworksllc.com/news-and-events/press-releases/2005/10-21-05-sams-club-partners-with-natureworks-pla-to-help-the-environment.aspx. Accessed September 10, 2015
24. A. ElAmin, Wal-mart signals move to natural packaging, FoodProductionDaily.com, 2005. Available from: http://www.foodproductiondaily.com/Packaging/Wal-Mart-signals-move-to-natural-packaging. Accessed September 25, 2020
25. SPAR, *Austria Enhances Freshness of Produce with NatureWorks PLA* [press release], NatureWorks, Linz, Austria, 2005.

26. Delhaize expands biodegradable packaging switch, FoodProductionDaily.com, 2006.
27. NatureWorks, *Nature-Based Packaging for Fresh Cut Produce in High Demand* [press release], NatureWorks, Minnetonka, MN, 2005.
28. NatureWorks, *Pacific Pre-Cut Enhance The Freshness of Its Brand with NatureWorks PLA Packaging for Fresh-Packed Salads* [press release], NatureWorks, Minnetonka, MN, 2005.
29. Bioplastics, First PLA bottle in Germany, *Bioplastics* **2006**, 20–21.
30. Bioplastics, Huhtamaki awarded silver: Huhtamaki's PLA dessert cup successful in the annual UK starpack competition, *Bioplastics* **2006**, 7.
31. Fabri-Kal, *Fabri-Kal Announces Addition to Greenware Product Family*, Fabri-Kal, Kalamazoo, MI, 2008. Available from: http://www.fabri-kal.com/fabri-kal-announces-addition-to-greenware-product-family/. Accessed September 10, 2015.
32. NatureWorks, Award, 19 December 2008.
33. R. Thompson, Sustainable is good, 2007, [cited 2015]. Available from: http://www.sustainableisgood.com/blog/natureworks_pla/. Accessed September 10, 2015.
34. Packaging Europe, PLA bottles soon to be released in Italy, Packaging Europe, 2008.
35. ConAgra Foods', *New, Renewable Shrink Film Technology to Reduce Impact on the Environment* [press release], ConAgra Foods, Omaha, NE, 2009.
36. Shiseido, Shiseido to commercialize polylactic acid containers with low environmental load: to be introduced to URARA brand exclusively for the chinese market [press release], Shiseido, 2009.
37. H. Soto-Valdez, PLA clamshells, in: H. Samsudin (Ed.), 2011.
38. D. Sullivan, Chipmaker's all-or-nothing claim sets the bar in big and bold, *BioCycle*, 2010. Available from: http://www.biocycle.net/2010/08/17/chipmakers-all-or-nothing-claim-sets-the-bar-in-big-and-bold/. Accessed September 10, 2015.
39. K. Siranosian, New sunchips bag: 90% plant-based, 100% compostable, TriplePundit, 2010. Available from: http://www.triplepundit.com/2010/02/new-sunchips-bag-compostable/. Accessed September 10, 2015.
40. A. M. Mohan, Danone first to switch to PLA for yogurt cup in Germany, Greener Package, 2011. Available from: http://www.greenerpackage.com/bioplastics/danone_first_switch_pla_yogurt_cup_germany. Accessed September 10, 2015.
41. A. M. Mohan, Stonyfield farm makes studied switch to PLA for yogurt multipacks, Greener Package, 2010. Available from: http://www.greenerpackage.com/regulations/stonyfield_farm_makes_studied_switch_pla_yogurt_multipacks. Accessed September 10, 2015.
42. Polenghi, Bio bottle, Polenghi, 2010. Available from: http://www.polenghigroup.it/en/sostenibilita/. Accessed September 10, 2015.
43. Packaging Strategies, Bio bottle is first in Europe, Packaging Strategies, 21 October 2010.
44. M. Beune, Barrier films: SiOx barrier benefits: paper, film, & foil converter, 2010. Available from: http://www.pffc-online.com/coat-lam/coatings/8832-siox-barrier-benefits-1001. Accessed September 10, 2015.
45. P. Reynolds, Compostable overwrap for tea bags, Packaging World, 2020. Available from: https://www.packworld.com/issues/sustainability/article/21140832/compostable-overwrap-for-tea-bags. Accessed November 20, 2020.
46. W. J. Orts, L. F. Torres, A. Flynn, W. Kelly, inventors, The United State of America, as represented by the Secretary of Agriculture (Wahington, DC, USA), Lapol LLC (Santa Barbara, CA, USA), assignee. High heat deflection temperature polylactic acids with tunable flexibility and toughness USA 2018.
47. H. Tsuji, Poly (lactic acid) stereocomplexes: a decade of progress, *Adv. Drug Deliv. Rev.* **2016**, *107*, 97–135.
48. H. Tsuji, Poly (lactide) stereocomplexes: formation, structure, properties, degradation, and applications, *Macromol. Biosci.* **2005**, *5*(7), 569–597.
49. Z. Li, B. H. Tan, T. Lin, C. He, Recent advances in stereocomplexation of enantiomeric PLA-based copolymers and applications, *Prog. Polym. Sci.* **2016**, *62*, 22–72.
50. N. López-Rodríguez, I. M. De Arenaza, E. Meaurio, J. Sarasua, Improvement of toughness by stereocomplex crystal formation in optically pure polylactides of high molecular weight, *J. Mech. Behav. Biomed. Mater.* **2014**, *37*, 219–225.
51. L. M. Sherman, Enhancing biopolymers: additives are needed for toughness, heat resistance & processability, *Plastics Technol.* **2008**, *54*(7), 58. Available from: https://www.ptonline.com/articles/enhancing-biopolymers-additives-are-needed-for-toughness-heat-resistance-processability. Accessed December 29, 2020.
52. J. Kalkowski, DuPont debuts new modifier for PLA products, Packaging Digest, 2015. Available from: https://www.packagingdigest.com/decorative-materials/dupont-debuts-new-modifier-pla-products. Accessed January 13, 2021.
53. Anonymous, Applications of PLA to grow with new additive developments, Plastemart.com, 2016. Available from: http://www.plastemart.com/plastic-technical-articles/applications-of-pla-to-grow-with-new-additive-developments/1633. Accessed December 29, 2020.
54. S. Manjure, M. Annan, Injection molding of PLA cutlery, *Bioplastics* **2016**, 3, 1–4.
55. World Centric, World Centric, 2019. Available from: https://www.worldcentric.com/. Accessed December 5, 2020.
56. J. H. Schut, Foamed PLA shows promise in biodegradable meat trays, *Plastics Technol.* **2007**, *53*(12), 39–43.
57. M. Thielen, Foam trays in Seattle, *Bioplast. Mag.* 2011, 46.
58. KoreaBiofoam, South Korea, KoreaBiofoam, 2019. Available from: http://www.koreabiofoam.com/en/. Accessed January 13, 2021
59. 100Bio™, 100Bio™, 2017. Available from: http://onehundredbio.com/. Accessed January 13, 2021
60. C. Purac, Bioplastics product profile: PLA thermoformed single-use hot beverage cups, in: C. Purac (Ed.), Total Corbion, 2013. https://www.corbion.com/media/90710/appls-a4-pla-161014-tfcups.pdf. Accessed December 20, 2020.

61. C. Purac, Bioplastics product profile: PLA injection molded serviceware, in: C. Purac (Ed.), Total Corbion, 2013. https://www.total-corbion.com/media/a14b3lrk/total-corbion-pla-product-profiles-190903.pdf. Accessed December 20, 2020.
62. gnP Inc., Canada, good natured Products Inc., 2020. Available from: https://goodnaturedproducts.com/. Accessed December 5, 2020.
63. Biobright, Belgium, Bright International BV, 2020. Available from: https://www.biobright.eu/. Accessed December 20, 2020.
64. Ecozema, Ecozema(R), 2015. Available from: https://ecozema.com/en/. Accessed December 5, 2020
65. BFS™, Biodegradable Food Service™, 2007. Available from: https://earth-to-go.org/. Accessed December 29, 2020
66. BBP Ltd, South Africa, Bonnie Biodegradable (Pty) Ltd, 2019. Available from: https://bonniebio.co.za/ Accessed December 29, 2020.
67. EcoProducts Inc., California, USA, EcoProducts Inc., 2007. Available from: https://www.ecoproducts.com/. Accessed December 9, 2020
68. SelfEco L, New York, USA, SelfEco, LLC, 2016. Available from: https://selfeco.com/. Accessed December 29, 2020
69. Compostable A, Florida, USA, AMS Global Suppliers Group, 2019. Available from: https://amscompostable.com/. Accessed December 29, 2020
70. Arxxin, China, Arxxin New Material (XiaMen) Co. Ltd., 2003. Available from: http://www.ecoarxxin.com/sy.htm. Accessed December 29, 2020
71. Huhtamaki, Cutlery, Huhtamaki USA, 2019. Available from: https://www.huhtamaki.com/en-us/north-america/foodservice/cutlery/. Accessed January 29, 2021.
72. Huhtamaki OYJ, New compostable double walled Impresso hot cup added to the Bioware(R) range [press release], 2019. Accessed January 29, 2021.
73. K. Parker, J. P. Garancher, S. Shah, S. Weal, A. Fernyhough, Polylactic acid (PLA) foams for packaging applications, in: Pilla, S. *Handbook of Bioplastics and Biocomposites Engineering Applications*, John Wiley & Sons, Inc., Hoboken, NJ & Scrivener Publishing LLC, Salem, MA, 2011, pp. 161–175.
74. R. Lee, Know your options for foaming sheet, Plastics Technology, 2015. Available from: https://www.ptonline.com/articles/profile-processor-leverages-people-technology-to-fuel-growth. Accessed December 5, 2020.
75. J. J. Kolstad. Crystallization kinetics of poly(L-lactide-*co*-*meso*-lactide), *J. Appl. Polym. Sci.* 1996, *62*(7), 1079–1091.
76. M. Hartmann, High molecular weight polylactic acid polymers, in: Kaplan, D.L. *Biopolymers from Renewable Resources*, Springer, Berlin, Germany, 1998, pp. 367–411.
77. NatureWorks L, Ingeo™ foam sheet extrusion processing guide. NWPG003_020111, 2012.
78. J. Fogarty, Turbo-Screw™, new screw design for foam extrusion, 2001.
79. Synbra-BioFoam. Available from: https://bewisynbra.com/product/biofoam/. Accessed November 20, 2020.
80. Biopolymer-Network, The revolutionary bioplastic solution. New Zealand, Biopolymer Network, 2017. Available from: http://www.biopolymernetwork.com/content/Zealafoam/76.aspx. Accessed December 2, 2020.
81. P. Khemka, Plastics in the automotive industry—which materials will be the winners and losers?, Nexant, 2019. Available from: https://www.nexant.com/resources/plastics-automotive-industry-which-materials-will-be-winners-and-losers. Accessed March 3, 2021.
82. A. Barrett, History of bioplastics in the automotive industry, *Bioplastic News* **2019**, 1–13.
83. J. Holierhoek, Bio-based plastic is emerging for the automotive industry, Green Light, 2020. Available from: https://greenlight.nl/bio-based-plastic-is-emerging-for-the-automotive-industry/?lang=en. Accessed March 3, 2021.
84. European Bioplastics, Bio-based plastics in the automotive market—clear benefits and strong performance: overview of materials and market development, *Eur Bioplast.* 2020, 1–4.
85. ReliablePlant, Ford researchers aim to create greener, lighter plastics, ReliablePlant, 2021. Available from: https://www.reliableplant.com/Read/20034/ford-researchers-aim-to-create-greener,-lighter-plastics#:~:text=Ford%20researchers%20are%20taking%20a,and%20better%20for%20the%20environment. Accessed March 1, 2021.
86. NOAH, The world's first circular car Material District, 2018. Available from: https://materialdistrict.com/article/noah-worlds-first-circular-car/. Accessed March 1, 2021.
87. R. Miel, Ford explores biodegradable, corn-based plastics MI, USA, *Automotive News*, 2008. Available from: https://www.autonews.com/article/20080616/OEM/306169928/ford-explores-biodegradable-corn-based-plastics. Accessed March 3, 2021.
88. American Honda Motor Co. Inc., Honda FCX clarity—design [press release], American Honda Motor Co. Inc., 2007.
89. SgCarMart, BLUE-WILL—Hyundai charges in with advanced hybrid concept, SgCarMart.com, 2009. Available from: https://www.sgcarmart.com/news/article.php?AID=1996. Accessed March 3, 2021.
90. S. Moore, World's first bio-based, circular car created from PLA, *Plastics Today*, 2018. Available from: https://www.plasticstoday.com/automotive-and-mobility/worlds-first-bio-based-circular-car-created-pla. Accessed March 4, 2021.
91. J. Thomas, Kenaf: Nature's little-known wonder, *The Asean Post*, 2019. Available from: https://theaseanpost.com/article/kenaf-natures-little-known-wonder. Accessed March 12, 2021.
92. Bio-based News, NEC Releases Phone Made With Bioplastic and Kenaf [press release], *Bio-based News*, 2006.
93. NEC, Bioplastics for electronic equipment, NEC Corporation, 2016. Available from: https://www.nec.com/en/global/rd/technologies/bioplastics/bioplastics2.html.Accessed March 3, 2021.
94. NEC, NEC strengthens and expands the use of "NeCycle(R)" bioplastic—bioplastic for use with gas station fueling systems [press release], NEC Corporation, 2014. Accessed March 3, 2021.


95. GreenBiz, Fujitsu develops world's first bioplastic computer cases, GreenBiz, 2005. Available from: https://www.greenbiz.com/article/fujitsu-develops-worlds-first-bioplastic-computer-cases. Accessed March 10, 2021.
96. K. Kimura, Y. Horikoshi, Bio-based polymers, *FUJITSU Sci. Techn. J.* **2005**, *41*, 173–180.
97. Plastics Today, K 2013: PLA bioplastic debuts in touchscreen computer housing, *Plastics Today*, 2013. Available from: https://www.plasticstoday.com/k-2013-pla-bioplastic-debuts-touchscreen-computer-housing. Accessed March 14, 2021.
98. Plastics, Latest generation of PLA, Plastics, 2014. Available from: https://www.plastics.gl/exhibit/latest-generation-of-pla/. Accessed March 10, 2021.
99. becausewecare, becausewecare, 2021. Available from: https://www.becausewecare.com.au/. Accessed March 10, 2021.
100. RenewableFibersLLC, RenewableFibersLLC, 2021. Available from: http://www.renewablefibersllc.com/materials/polylactide-pla/. Accessed March 12, 2021.
101. M. Park, South Korean artist turns to bioplastics for Earth-friendly furniture. Reuters, 2020.
102. Biodegradable Products Institute, Guidelines for the labeling and identification of compostable products and packaging New York, USA, Biodegradable Products Institute, 2020. Available from: https://www.bpiworld.org/Labeling-Guidelines. Accessed December 28, 2020.
103. Businesswire, BPI releases guidelines for labeling and identification of compostable products [press release], New York, USA: Businesswire, 2020.
104. CLSI, *Method for Antifungal Disk Diffusion Susceptibility Testing of Yeasts, Approved Guideline-Second Edition CLSI document M44-A2*, Clinical and Laboratory Standards Institute, Wayne, PA, 2009.
105. UrthPact, Certified compostable products: what to look for and what it means, UrthPact LLC, 2020. Available from: https://www.urthpact.com/certified-compostable-products-what-to-look-for-and-what-it-means/. Accessed December 28, 2020.
106. A. Barrett, Coop stops selling organic meat in PLA compostable containers, *Bioplastics News*, 2020. Available from: https://bioplasticsnews.com/2020/02/12/coop-stops-pla-containers/. Accessed December 28, 2020.

# 27

# TEXTILE APPLICATIONS

MASATSUGU MOCHIZUKI

## 27.1 INTRODUCTION

For the past 50 years, textile materials made from synthetic polymers such as nylon and polyester have been used for industrial applications, as well as for clothing. In some instances, the excellent durability of synthetic polymers has proved to be a major advantage, but in others the great durability of these materials has led to adverse effects.

The current crisis in solid-waste management has led to focused attention on the development of materials that can biodegrade in the natural environment in soil or in compost [1, 2]. Furthermore, in recent years bio-based materials from plants have been utilized as carbon-neutral materials that do not result in the increase of greenhouse gas due to solid waste management, for example, during incineration.

PLA fibers are not only biodegradable but also highly functional due to their intrinsic properties such as bacteriostatic, flame-retardant, and weathering stability [3, 4], when compared with conventional poly(ethylene terephthalate) (PET) fibers. In this chapter, biodegradation mechanism, the key performance features, and potential applications of PLA fiber/nonwoven products are discussed [5–7].

## 27.2 MANUFACTURING, PROPERTIES, AND STRUCTURE OF PLA FIBERS

### 27.2.1 PLA Fiber Manufacture

PLA can be melt-spun into various types of fibers including monofilaments, multifilaments, bulk continuous filaments, staple fibers, short-cut fibers, and spunbond fabrics by conventional melt-spinning machines. The fibers are then drawn and annealed to give good mechanical properties such as high tenacity, good toughness, and dimensional stability [5].

By controlling the ratio of the D- and L-isomers in the polymer chain, it is possible to produce PLA polymers of different melting temperatures. By incorporating polymers with high levels of D-isomer content (~10% D-monomer) into a sheath component, sheath/core-type bicomponent fibers with a sheath melting temperature of 120–130°C can be produced (Figure 27.1). This type of conjugated fiber is utilized as binder fibers in nonwovens for thermal bonding [5].

Furthermore, it is also possible to manufacture side-by-side conjugated PLA fibers in which one component is composed of PLA with lower thermal shrinkage and the other is composed of PLA with higher thermal shrinkage. When exposed to heat treatment, the fibers develop fine spiral micro-crimps due to different thermal shrinkage between the components, as indicated in Figure 27.2. This type of conjugated fiber is utilized as fiber-fill with high bulkiness and good resilience, or as fiber for stretchable nonwovens.

### 27.2.2 Properties of PLA Fibers and Textile

PLA is an aliphatic polyester having no aromatic ring structure, but the yarn properties of PLA are relatively similar to those of PET. However, the density and refractive index of PLA are lower than those of PET, giving it light weight and a deep silky luster without brightness. The moisture regaining and wicking properties of PLA are superior to those of

*Poly(Lactic Acid): Synthesis, Structures, Properties, Processing, Applications, and End of Life*, Second Edition.
Edited by Rafael A. Auras, Loong-Tak Lim, Susan E. M. Selke, and Hideto Tsuji.

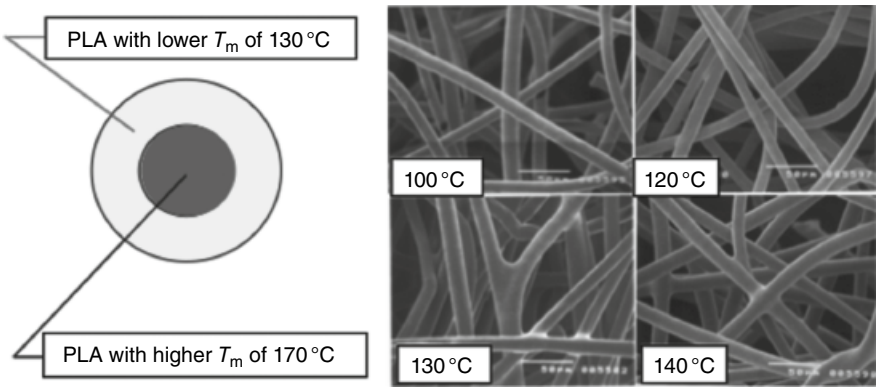


**FIGURE 27.1** Cross-sectional view of sheath/core type of PLA bicomponent fiber and thermal bonding nonwoven made from the sheath/core type of fibers as binder fibers.

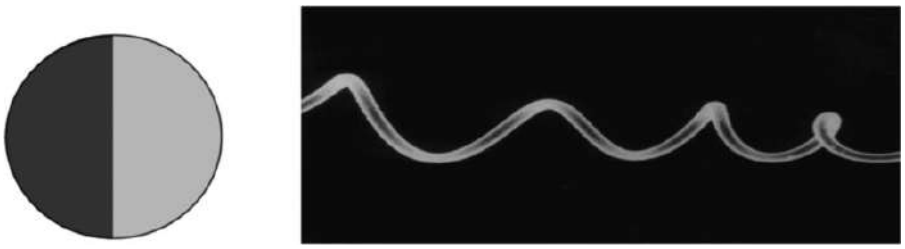

**FIGURE 27.2** Cross-sectional view of side-by-side type of PLA bicomponent fiber and overview of the fiber with fine microcrimps.

PET because PLA is more hydrophilic. Garments made from 100% PLA and its blends with cotton feel more comfortable to the user [4]. In addition, the lower modulus leads to better properties of drape and hand-feel, while the crimp retention property leads to excellent crease resistance. Table 27.1 summarizes the comparisons of the fiber/textile properties of PLA and PET [5–7].

PLA fibers are also dyeable, using dyes dispersion (e.g., Denapla™, Nagase Colors & Chemicals Co., Ltd, Japan) at lower temperature of 100–110°C [8], and it is recommended that the PLA fibers should not be dyed at temperatures higher than 120°C since PLA is more susceptible to hydrolysis at high temperature and humidity, particularly in alkaline conditions, than PET.

### 27.2.3 Effects of Structure on Properties

Crystallinity, crystal structure, morphology, and molecular orientation strongly affect the mechanical, thermal, electrical, and hydrolysis resistance properties of PLA fibers. The crystallization behavior is controlled by molecular characteristics such as molecular weight and the presence of comonomer units in the polymer chain. The crystallization rate decreases and the crystallization half-time lengthens with increasing comonomer (D-lactyl) content in the polymer chain [9].

**TABLE 27.1 Comparison of PLA and PET Fiber/Textile Properties**

| | Properties/ Characteristics | PLA | PET |
|---|---|---|---|
| Resource | Feedstock based | Corn | Petroleum |
| Physical | Specific gravity | 1.25 | 1.34 |
| | Refractive index | 1.40 | 1.58 |
| Drape/hand-feel | Bending modulus ($gf\,cm^2/cm$) | 0.068 | 0.122 |
| | Shear modulus (gf/(cm deg)) | 0.64 | 1.53 |
| Moisture management | cos $\theta$ ($\theta$: contact angle) | 0.254 | 0.135 |
| | Water absorption (wt%) | 0.5 | 0.3 |
| Flame-retardant | Burning time (min) | 2 | 6 |
| | Smoke generation ($m^3$/kg) | 63 | 394 |
| | LOI | 24–30 | 20–21 |
| | Calories of combustion (kcal/kg) | 4500 | 5500 |
| Antibacterial | Bacteriostatic | ≥5.9 | <2.2 |
| | Bactericidal | ≥3.1 | <0 |
| Weathering resistance | Retention of tenacity (%) after 300 h | 95 | 60 |
| Fading resistance | Retention of elongation (%) after 100 h | 100 | 70 |

A high-performance PLA spunbonded fabric with high strength and good dimensional stability has been successfully developed under high air-jet (take-up) velocity of around 5000 m/min. Yarn properties of PLA fibers strongly depend on the take-up speed in high-speed melt spinning. The tensile strength and Young's modulus of PLA fibers increase with increasing take-up speed (Figure 27.3). Figure 27.4 indicates that the thermal shrinkage of PLA fibers reaches the lowest level around 5000 m/min along with high crystallinity induced by higher molecular orientation [3].

### 27.2.4 PLA Stereocomplex Fibers

Ikada et al. [10] found that stereocomplexation or racemic crystallization takes place between PLLA and PDLA units in chloroform solution, forming fibers composed of the stereocomplex by dry/wet spinning. The stereocomplexation is known to occur in solution, as well as in bulk from the melt. Stereocomplex crystallites of PLLA and PDLA have a melting temperature that is 50°C higher than those of homocrystallites of either PLLA or PDLA.

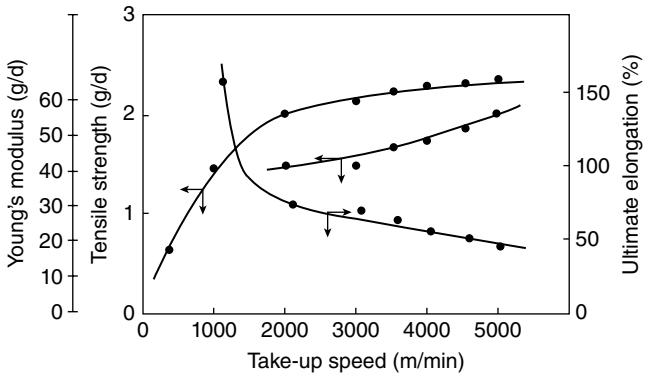


**FIGURE 27.3** Relationship of yarn properties (tensile strength, Young's modulus, and ultimate elongation) and take-up speed for melt spinning of PLA.

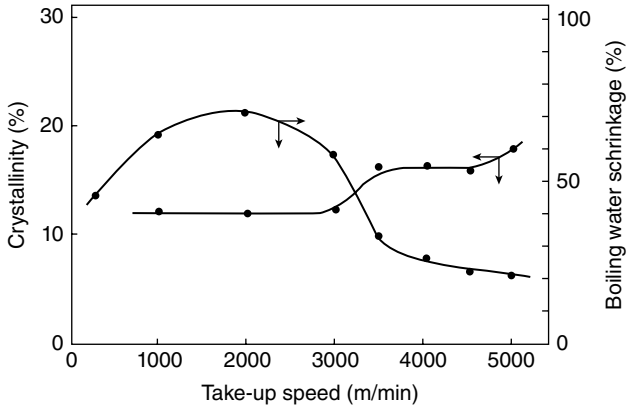


**FIGURE 27.4** Effects of take-up speed during melt spinning on crystallinity and thermal shrinkage of PLA yarn in boiling water.

In high-speed melt spinning followed by drawing and annealing, Kikutani and coworkers [11] found that PLA stereocomplex crystallizes in the blend with 1 : 1 PLLA : PDLA molar ratio, preferably at a take-up speed of more than 4000 m/min. Kimura et al. [12, 13] developed a new process to prepare 100% stereocomplex crystallites having no homocrystallites. These fibers with a melting temperature of 210–220°C are expected to have superior heat resistance for ironing, which typically takes place above 160°C.

PLA stereocomplex has a disadvantage that its melting temperature (220–230°C) is higher than the initial thermal decomposition (>210°C) of PLA, leading to drastic decrease in molecular weight of PLA during the melt-spinning process at 240°C. This is one of the reasons why PLA stereocomplex fibers are not yet commercialized.

## 27.3 KEY PERFORMANCE FEATURES OF PLA FIBERS

### 27.3.1 Biodegradability and the Biodegradation Mechanism

There are discrete differences between enzymatic and chemical hydrolysis, with regards to degradation mechanism, particularly at the first stage of degradation, as shown in Table 27.2 [14].

Enzymatic hydrolysis proceeds only on the surface of the solid substrate characterized by surface erosion and weight loss since the enzymes cannot penetrate the polymeric solid substrate. In this process, the molecular weight does not change during the enzymatic hydrolysis because only the polymer on the surface of the substrate is degraded and the low-molecular-weight degradation products are removed from the substrate by solubilization in the surrounding aqueous medium.

On the contrary, small nonenzymatic catalysts and reagents can diffuse into polymer matrices causing in-depth degradation. Nonenzymatic degradation proceeds initially without weight loss in the first stage of the degradation due to random cleavage of the polymer chain backbone. The

**TABLE 27.2 Differences Between Enzymatic and Chemical Hydrolysis**

| Type | Enzymatic Hydrolysis | Chemical Hydrolysis |
|---|---|---|
| Materials | PHA, PCL | PLA |
| Access point | Outer only | Outer to inner |
| Surface appearance | Rough (eroded) | Smooth (not eroded) |
| Weight loss | Detected | Negligible |
| Molecular weight reduction | Negligible | Detected |
| Degradation mechanism | Surface erosion | Bulk degradation |

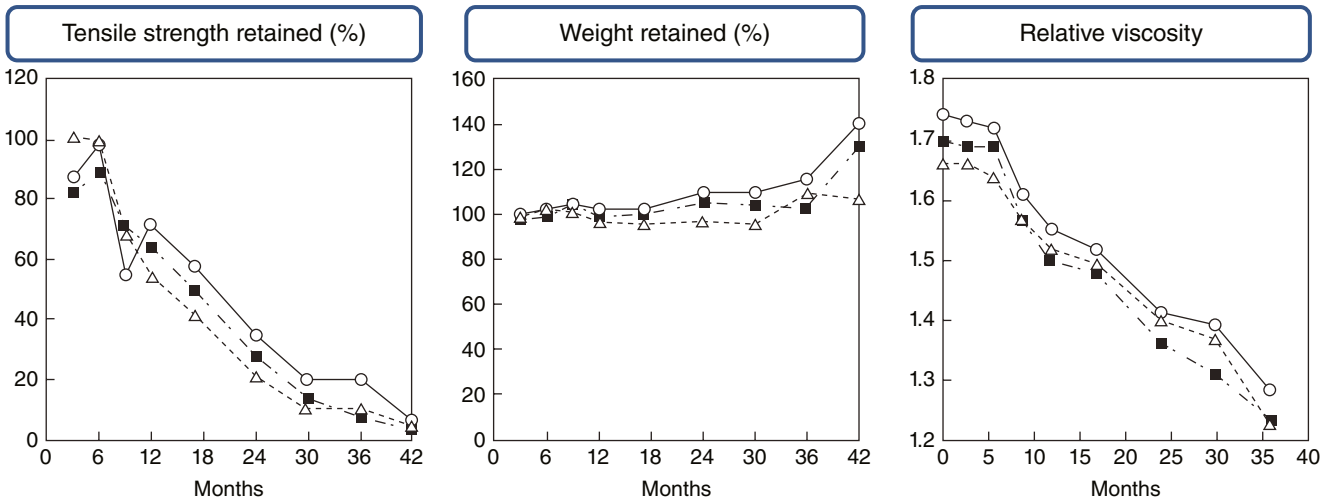


**FIGURE 27.5** Changes in the tensile strength, the weight and the relative viscosity of PLA spunbond (○: 25 g/m², ●: 70 g/m², Δ: 100 g/m²) in the soil burial test for 42 months.

substantial decrease in molecular weight leads to a decrease in mechanical properties such as tensile strength. In the intermediate to final stages of the degradation process, morphological breakdown (i.e., bulk degradation) occurs with fragmentation of the polymer molecules.

PLA is stable in typical end-use and storage conditions at ambient temperature. However, when it is exposed to elevated temperature (>60°C) and relative humidity (>80% RH) conditions, such as in a composting environment, PLA will disintegrate within one week to one month, followed by bacterial attack on the fragmented residues to give carbon dioxide and water. During the primary degradation phase, PLA undergoes hydrolysis that is both temperature- and humidity-dependent but does not involve any microorganisms. As the $M_n$ reaches approximately 10,000–20,000, microorganisms present in the soil begin to digest the lower-molecular-weight oligomers and lactic acid, producing carbon dioxide and water [15]. This two-stage biodegradation mechanism differs distinctly from those of many other biodegradable polymers that degrade by a single-step surface erosion process, involving direct bacterial attack with enzymatic degradation of the polymer.

In natural environments such as in soil or in water, the degradation of PLA proceeds slowly, which is a beneficial feature for agricultural/horticultural, geotextile, and fisheries materials applications. The percentage decrease in the tensile strength and relative viscosity of PLA spunbonded fabrics following soil burial as a function of time, as illustrated in Figure 27.5, indicate that the degradation proceeds slowly but steadily [16]. After three and a half years, the fibers have lost ca. 90% of their initial strength.

On the other hand, Ohkura reported the degradation behavior of biodegradable plastics including poly(3-hydroxybutyrate-*co*-butyl hexanoate) (PHBH), poly(butylene succinate) (PBS), and PLA in sea water, indicating that the percentage retention of bending strength and relative viscosity of PLA after a year had decreased to 87 and 70%, respectively [17]. This information is comparable to the data of the soil burial test as mentioned above, indicating that the percentage retention of tensile strength and relative viscosity of PLA after a year in soil burial test decreased to 87 and 70%, respectively, as shown in Table 27.3 [18]. So, PLA should lose most of its initial strength after approximately four years, both in soil and in sea water.

**TABLE 27.3 Comparisons of PLA Degradation Behavior in Sea Water with That in Soil After a Year**

| Test | Weight Loss (%) | Relative Viscosity Retained (%) | Tensile Strength Retained (%) |
|---|---|---|---|
| **Soil burial** [9] | 0 | 89 | 64 |
| **Sea water immersion** [11] | 0 | 80 | 70 |

On the other hand, when exposed to high-temperature (60–80°C) and high-humidity environments under both aerobic and anaerobic conditions, PLA fibers will degrade rapidly. Figure 27.6 shows the result of aerobic composting at around 60°C for PLA, wool, cotton, and PET fabrics, showing that the PLA degraded more rapidly than natural fibers such as wool and cotton.

The compostability of PLA nonwovens (spunbond fabric, 25 g/m²) was evaluated under simulated composting conditions. The evaluation of the ultimate aerobic biodegradation and disintegration was conducted by measuring the release of biogas and disintegration at 60 ± 2°C after 45 days, according to the ISO 14855 standard procedure. Figure 27.7

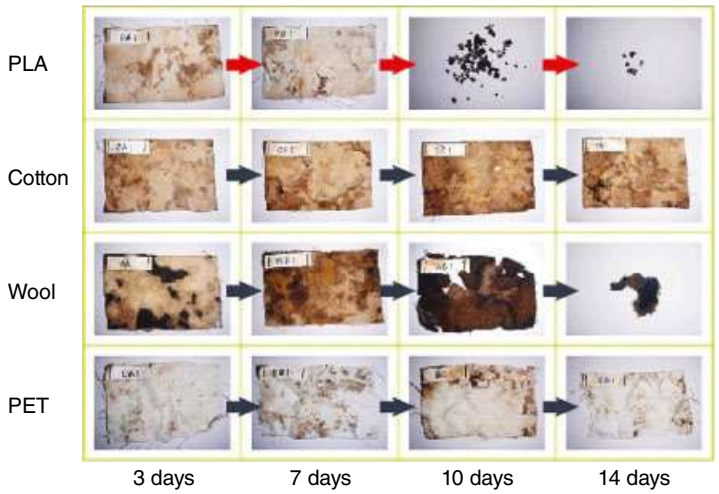


**FIGURE 27.6** Aerobic biodegradation photographs of PLA fabric in compost at 58 ± 2°C in comparison with those of cotton, wool, and PET fabric.

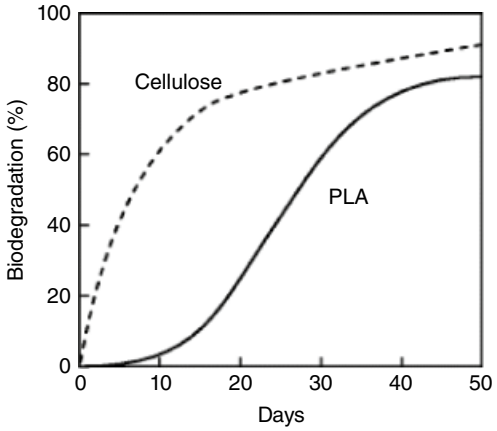


**FIGURE 27.7** Aerobic composting test result of PLA fibers according to ISO 14855.

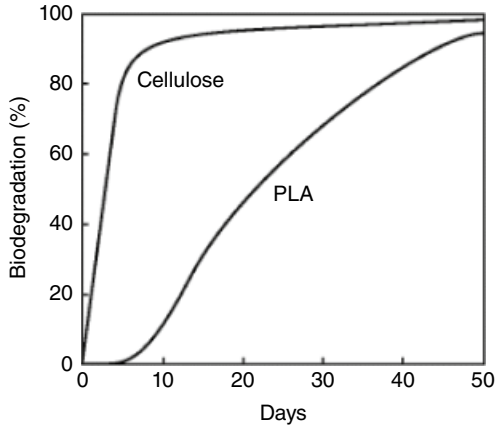


**FIGURE 27.8** Anaerobic digestion test result of PLA fibers according to ISO 15985.

shows the cumulative biodegradation of PLA nonwovens compared with cellulose powder as a positive reference. Here, PLA showed a comparable extent of biodegradability to cellulose after 45 days [3].

In another study, the ultimate anaerobic biodegradability and disintegration under high-solid condition was evaluated based on carbon conversion of the test substance to methane and carbon dioxide after 45 days, according to ISO 15985 [3]. Figure 27.8 shows that anaerobic decomposition of PLA occurs at 52 ± 2°C under static (i.e., non-mixed) conditions.

### 27.3.2 Moisture Management

The moisture regaining and wicking properties of PLA are superior to those of PET (Table 27.1). There has been considerable interest in using PLA either as an inner wicking layer or as an intimate blend with other natural fibers. Garments made from PLA feel more comfortable and can be used for sportswear, as well as shirt. Wearers of PLA fabric will experience improved physiological comfort even under active wear conditions [4].

The wetting and drying behaviors of PLA and PET fabrics have been tested under simulated conditions. Figure 27.9 shows the appearances of PLA and PET fabrics at 1 and 15 min after a drop of water was put on the fabrics. It can be seen that water diffuses faster and dries quicker in the PLA fabric. This excellent moisture transport of PLA fabric leads to a more comfortable feel [5].

### 27.3.3 Antibacterial/Antifungal Properties

The bacteriostatic properties of PLA fibers tested under the standard method using *Staphylococcus aureus* ATCC 6538P as the inoculum, are shown in Table 27.4.

The bacteria cell density after incubation for 18 h at 37°C decreased dramatically from $2.5 \times 10^4$ to $2.0 \times 10^1$ cells/mL

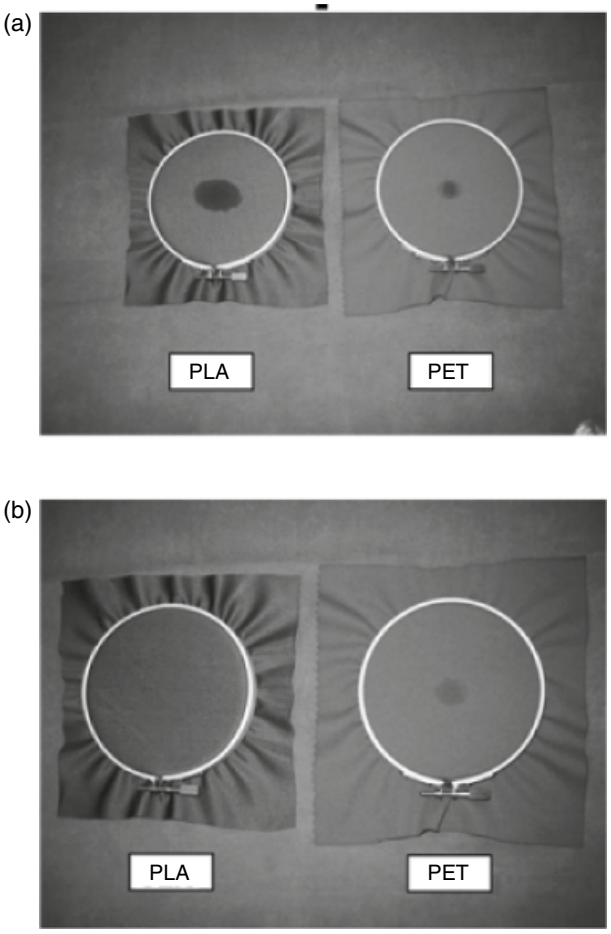


**FIGURE 27.9** Test results for water uptake and transport on PLA and PET fabrics: (a) 1 min and (b) 15 min after placing a drop of water onto the fabric.

for PLA, while for nylon fibers, the cell density increased rapidly to $1.7 \times 10^7$ cells/mL. Similar results were obtained, even when the test was conducted after washing the PLA fibers ten times with nonionic detergent. Furthermore, blending polyester or cotton fibers with PLA fibers did not strongly reduce the bacteriostatic property [3].

It is well known that lactic acid is a strong organic acid, which exhibits antibacterial and antifungal properties. It is hypothesized that small amounts of lactic acid migrating from the PLA fiber matrix may be responsible for the antibacterial/antifungal properties [19]. This unique feature distinguishes PLA from another biodegradable polymers and offers distinct benefits in the areas of food production, sanitation, and agriculture for the prevention of bacterial contamination.

### 27.3.4 Low Flammability

PLA fiber shows improved self-extinguishing characteristics when compared with PET or nylon fibers, although it is not a nonflammable polymer. Gruber and O'Brien [4] reported that PLA fiber burned for only 2 min with low smoke generation (63 $m^2$/kg) after the flame was extinguished, while PET burned for 6 min with higher smoke generation (394 $m^2$/kg). Calories of combustion for PLA fiber (4500 kcal/kg) is comparable to cellulose fiber, but lower than PET fiber (5500 kcal/kg), as shown in Table 27.1. As shown in Table 27.1, the LOI (Limit of Oxygen Index) value of PLA fiber, tested in accordance with JIS K 7201, is larger for PLA fiber (24–30), as compared with PET fibers (20–21) [5, 6]. A larger LOI value for PLA fibers indicates that this material had improved flame-retardant characteristics. The Japan Flame-retardant Fiber Products Association approved PLA conjugated (side-by-side) hollow fiber TERRAMAC™ HP8F (Unitika Fiber Ltd., Japan) without any flame-retardant chemicals as a flame-retardant fiber for fiberfill. In terms of flame-retardant properties under the standard condition of the US Federal Safety Specifications for Vehicles, the FMVSS 302 test demonstrated that PLA fabric performed better than PET fabric, as shown in Figure 27.10. The low flammability and smoke generation of PLA fibers for carpeting, home furnishings, and sheeting fabrics for vehicles lead to improved fire safety.

### 27.3.5 Weathering Stability

The weathering stability of PLA fibers was determined using an accelerated simulated weathering test (Sunshine Weather Meter, Suga Test Instrument Co. Ltd., Japan) and compared with that of PET fibers. Figure 27.11 shows that the weathering stability of PLA fibers is superior to that of PET fibers [5]. These test conditions are considered equivalent to outdoor weathering exposure for three years.

**TABLE 27.4 Antibacterial Activity of PLA Fibers**

| Symbol | Test Specimen | Cell Density $N$ (cells/mL) | log $N$ | Bacteriostatic Activity (log $B$ − log $C$) | Bactericidal Activity (log $A$ − log $C$) |
|---|---|---|---|---|---|
| A | Inoculum | $2.5 \times 10^4$ | 4.4 | — | — |
| B | Control | $1.7 \times 10^7$ | 7.2 | — | — |
| C | PLA fibers | $2.0 \times 10$ | 1.3 | ≥5.9 | ≥3.1 |
| C | After washing | $2.0 \times 10$ | 1.3 | ≥5.9 | ≥3.1 |
| C | PLA/cotton blend | $2.0 \times 10$ | 1.3 | ≥5.9 | ≥3.1 |

Control: nylon fabric for standard; inoculum: *Staphylococcus aureus* ATCC 6538P; detergent: JAFET standard detergent (1.33 mL/L).

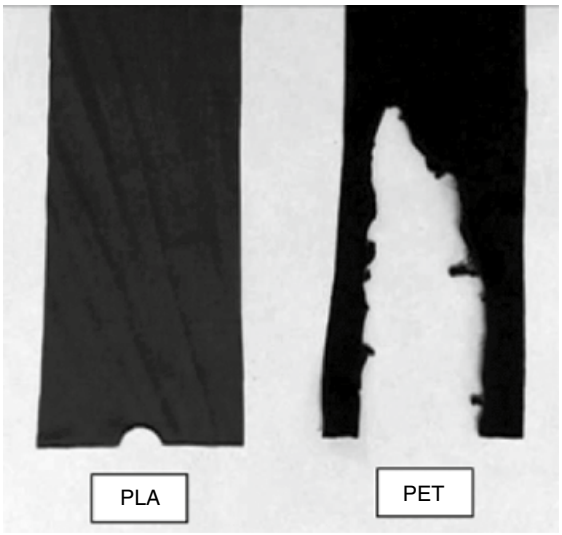


**FIGURE 27.10** Test results for flammability of the fabrics of PLA and PET in accordance with the Federal Safety Standards for Vehicles FMVSS 302.

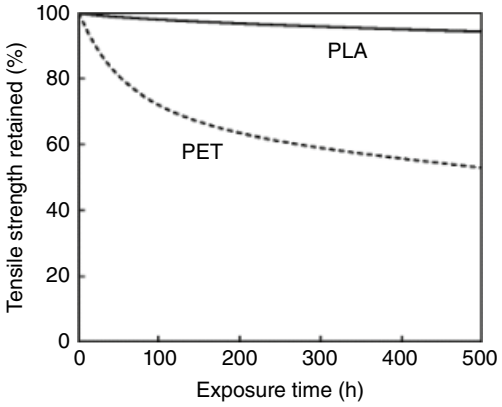


**FIGURE 27.11** Accelerated weathering test result of PLA and PET fibers by Sunshine Weather Meter.

A xenon arc test of fading resistance also demonstrated that PLA fibers perform better than PET fibers, with a 0% loss in elongation at break for the PLA fibers and a 30% loss in elongation at break for the PET fibers, after 100 h of xenon arc exposure [4]. The superior resistance to exposure to daylight with rainfall and UV is an attractive feature that brings promise for potential outdoor applications such as in agricultural, horticultural, geotextile, and industrial areas.

## 27.4 POTENTIAL APPLICATIONS

Many fiber manufacturers, in collaboration with their customers, have been developing commercial applications for PLA fibers. Government efforts will drive further market acceptance, because PLA is viewed as an alternative material to reduce greenhouse gas emissions and wastes after use. The following sections discuss various applications of PLA fibers and the specific properties related to these applications [20–22].

### 27.4.1 Geotextiles

Geotextiles and products for agricultural/horticultural/fisheries applications are used in natural environments, and hence, it is advantageous if they were to disintegrate and degrade completely after their service life is over. Typically, several years of service time is required for applications such as geotextiles for soil erosion control, sandbags, vertical drain sheets, and plant pots. While PLA is fully biodegradable, it is stable in sunshine for several years and degrades only slowly in soil and in sea water [2, 18]. This unique feature offers distinct benefits in the fields of geotextiles and agricultural/horticultural/fisheries applications [16, 20]. For example, Figure 27.12 shows a ground cover sheet made from PLA spunbond fabric with many small holes capable of draining air, water, and roots of plants [20, 22]. Figure 27.13 shows vertical drain sheets made from PLA spunbond fabric for the draining of water and the stabilization of reclaimed land in Tokyo Bay [22].

### 27.4.2 Industrial Fabrics

Both woven and nonwoven fabrics made from PLA fibers are being considered for automobile cabin parts applications, such as floor mats, seat fabric, seat cushions, ceiling fabric, door trim, and partition board. Toyota has already employed a new type of spare-tire box cover using Kenaf/PLA board, which is manufactured by heat-compression molding of a Kenaf/PLA (blend ratio weight-based: 7/3) fiber web [23].

**FIGURE 27.12** PLA ground cover sheet for plants. *Source:* Unitika Ltd.

**FIGURE 27.13** PLA vertical drain sheets. *Source:* Chikami Miltec, Inc.

**FIGURE 27.14** PLA head rest covers. *Source:* East Japan Railway Company.

There are many kinds of fabrics including woven fabrics, mesh fabrics, knitted fabrics, spunbond fabrics, and nonwovens for industrial uses such as signages, awnings, headrest covers, vehicle seat covers, and tarpaulins. Head rest covers made from PLA spunbond fabric are introduced in East Japan Railway Company in Japan (Figure 27.14) [6]. Coating with resin or lamination with film is also used when there is a need for high wet strength and long durability.

### 27.4.3 Filters

One of the potential applications of PLA fibers with good compostability is filters for tea, coffee, and organic wastes. PLA is safe and "generally recognized as safe" for food contact uses [19, 24]. It is approved to FCN (Food Contact Notification) No. 178 (rank: B = H) by FDA. PLA tea bag filters with residual lactide <0.2% are stable such that little hydrolysis and migration occur during typical use of hot water brewing and storage conditions. After use, the structural integrity of PLA fibers decreases as the molecular weight falls under composting conditions with elevated temperature and moisture levels. Eventually the fibers disintegrate and mineralize to carbon dioxide and water along with other organic wastes in the presence of microbes.

**FIGURE 27.15** PLA tea bag filters. *Source:* Yamanaka Industry Co. Ltd.

Yamanaka Industry Co. Ltd. has launched a world-first tea bag filter made from PLA fibers mesh by ultrasonic sealing, Soilon™ (Figure 27.15) [20–22]. It is claimed to offer a pure taste and the finest fragrance without offensive smells, when compared with those from conventional oil-based synthetic fibers such as nylon or polyester. The Soilon tea bag filter is compostable with organic wastes after use and has been certified in accordance with the industrial composting standards, EN13432 and ASTM D6400, by Din Certco and the BPI, in addition to "OK Compost" by Vincotte, for both municipal and industrial composting facilities.

In addition to other liquid filters for juice, liquor, wine, oil, or wastewater, air filters for air conditioning or cleaning are also potential applications of PLA fibers and nonwovens. The use of PLA fiber for air filter applications as an antibacterial/antifungal material will provide benefits for managing sanitary wastes.

### 27.4.4 Towels and Wipes

Towels made from 100% PLA or blends of PLA with cotton feel more comfortable, in addition to fast drying and low shrinkage after drying. Especially, body towels of 100% PLA fibers have a good reputation for not generating bad smells even after long-term use, probably due to the antibacterial/antifungal property of PLA. Figure 27.16 shows body towel made from knitted PLA fabric with a bulky mesh that can


**FIGURE 27.16** PLA body towels. *Source:* Unitika Ltd.

make many fine smooth bubbles on the surface of the PLA fibers, whereas the bubbles disappear soon in the case of silk or cotton [20–22]. The surface of the PLA fibers is moderately acidic, similar to human skin, making it suitable for apparels of baby, child, or allergenic patients having delicate skin because of its nonirritating and comfortable properties.

A potential application of PLA nonwovens is as wipes for baby, industrial, household, and personal care markets. PLA can be directly processed into spunbonded fabrics with good mechanical properties at a high take-up speed, around 5000 m/min. Using binder fibers with a sheath component that has a lower melting temperature of 130°C, nonwovens can be made by conventional thermal bonding lines. Spunlace nonwovens are manufactured through hydroentanglement by high-speed water jets. The superior wicking rate and faster absorbency of PLA lead to wipe applications in nonwovens of 100% PLA or blends of PLA with cotton and rayon. These features enable PLA to be used in a wide spectrum of wipes including baby diapers and wipes, floor and furniture wipes, clean room wipes, food service, and vehicle cleaning.

### 27.4.5 Home Furnishings

PLA fibers meet the requirements of home/office textiles, including desirable sheen, excellent drape and hand, odor and stain resistance, antibacterial/antifungal properties, UV stability, and low flammability. Typical applications of PLA in the home/office furnishing sector are carpet; tile and rugs; draperies including curtains, blinds, and balances; furniture wadding and filling; bedding such as pillows, duvets, sheets, blankets, and wall panel fabrics.

PLA fibers have good crimp retention and elastic recovery leading to excellent shape retention and resilience [4]. These characteristics, together with low flammability, are suitable for fiberfill for pillows, cushions, mattresses, chairs, sofas, and other furniture.

### 27.4.6 Clothing and Personal Belongings

Fabrics of PLA with excellent hand and drape and a silk-like luster are suitable for fashion and formalwear, such as wedding dresses. Better moisture regaining and wicking properties of PLA fibers compared to PET fibers lead to promising applications for various kinds of garments like t-shirts, underwear, intimate wear, casual wear, sportswear, jeans/denim, and jackets. However, the required dyeing technology at lower temperature (105–110°C) with good color fastness and the need to limit ironing to around 120°C have hampered the use of PLA in some apparel applications.

One feature that is inherent to PLA fibers is the ability to hold a crease of fold. This excellent crease retention property facilitates pleats or wrinkles processing of PLA fabrics. For instance, the unique design of the PLA eco-bag (KNA Plus™, Japan) with pleats or wrinkles allows the bags to compactly fold up for storage (Figure 27.17) [25]. These bags have created a sensation in many shops including the Smithsonian Institution.


**FIGURE 27.17** PLA eco-bags. *Source:* kna plus Corporation.

**FIGURE 27.18** 3D-printing PLA filaments and its 3D printings. *Source:* Unitika Ltd.

### 27.4.7 3D-Printing Filament

Acrylonitrile butadiene styrene (ABS) is one of the best-known materials for 3D-printing filament. Despite its desirable properties with superior strength and heat resistance, ABS has inherent disadvantages, such as strong odor emissions and high thermal shrinkage leading to warpage in larger builds, in addition to environmental problems such as high carbon footprint and emission of harmful gases and particles linked. As desktop 3D printing is becoming more widespread, consumers are looking for eco-friendly PLA printing filament. For example, a new type of 3D-printing PLA filament (Terramac, Japan) has been developed recently, which as high transparency, high circularity, and break-resistance (Figure 27.18) [20]. The thermal and flow characteristics allow excellent 3D-printed detail with sharp melting behavior, low emissions, and minimal thermal shrinkage/cracking/warping.

## 27.5 CONCLUSIONS

Since the development of PLA fibers is still in its early stages compared with conventional synthetic fibers, its commercial viability in replacing petroleum-based synthetic fibers has been limited. However, the unique inherent properties of PLA fibers are promising for many applications in the textile industry. Technological improvements in both reducing product/processing costs and widening its material performance are already underway in the industry and academia.

## REFERENCES


1. M. Mochizuki and M. Hirami, Biodegradable fibers made from truly-biodegradable thermoplastics, in: P. N. Prasad. E. Mark and T. J. Fai (Eds.), *Polymers and Other Advanced Materials*, Prenum Press, New York, 1997, pp. 589–596.
2. M. Mochizuki, Properties and application of aliphatic polyester products, in: A. Steinbuchel, Y. Doi (Eds.), *Biopolymers, Vol. 4: Polyesters III*, WILEY-VCH Verlag GmbH, Weinheim, 2002, pp. 1–23.
3. M. Mochizuki, Polylactic acid fibers and nonwovens, in: *Fiber Industry Environmental Manual for the Earth*, SEN-I SHA, Osaka, 1999, pp. 427–440.
4. P. Gruber, M. O'Brien, Polylactide NatureWorks™ PLA, in: A. Steinbuchel, Y. Doi (Eds.), *Biopolymers, Vol. 4: Polyesters III*, WILEY-VCH Verlag GmbH, Weinheim, 2002, pp. 235–250.
5. M. Mochizuki, Polylactic acid as a biodegradable plastic, *Kagaku To Kogyo (Osaka)* **2002**, *76*(6), 278–286.
6. M. Mochizuki, S. Murase, N. Matsunaga, Poly(lactic acid) fiber—environmentally friendly new generation fiber made from plant, *Sen'I Gakkaishi* **2006**, *62*(11), 323–329.
7. M. Mochizuki, Synthesis, properties and structure of polylactic acid fibers, in: J. Hearle, S. Eichhorn, M. Jaffe, T. Kikutani (Eds.), *Handbook of Textile Fiber Structure*, Woodhead Publishing, Cambridge, **2009**, Vol. *275*, pp. 257–275.
8. K. Yamaguchi, Dyeing of polylactic acid fibers, *Text. Process. Technol.* **2001**, *36*, 392–393, 458–464.
9. J. J. Kolstad, Crystallization kinetics of poly(L-lactide-*co*-*meso*-lactide), *J. Appl. Polym. Sci.* **1996**, *62*, 1079–1091.
10. Y. Ikada, K. Jamshidi, H. Tsuji, S.-H. Hyon, Stereocomples formation between enantiomeric poly(lactides), *Macromolecules* **1987**, *20*, 904–906.
11. M. Takasaki, H. Ito, T. Kikutani, Structure development of polylactides with various D-lactide contents in the high-speed melt spinning process, *J. Macromol. Sci. Phys.* **2003**, *B42*, 403–407.
12. H. Yamane, Y. Furuhashi, N. Yoshie, Y. Kimura, Higher-order structures and mechanical properties of stereocomplex-type poly (lactic acid) melt spun fibers, *Polymer* **2006**, *47*(16), 5965–5972.
13. H. Yamane, Y. Furuhashi, Y. Kimura, Higher order structural analysis of stereocomplex-type poly(lactic acid) melt-spun fibers, *J. Polym. Sci. Polym. Phys.* **2007**, *45*, 218–228.
14. M. Mochizuki, M. Hirami, Structural effects on biodegradation of aliphatic polyesters, in: M. Lewin, M. J. W. H. Jaffe, J. H. Wendorfe, and E. Tsuchuda (Eds.), *Polymers for Advanced Technologies*, John Wiley & Sons, New York, **1997**, Vol. *8*, pp. 203–209.
15. J. Lunt, Large-scale production, properties and commercial applications of polylactic acid polymers, *Polym. Degrad. Stab.* **1998**, *59*, 145–153.
16. M. Mochizuki, The roles of biodegradable plastics promoting environmental-friendly agriculture, *WEB J.*, **2001**, *43*, 16–22.
17. T. Ohkura, Biodegradability of microbial-producing polymer Aonilex® in sea water, *BioPla J.* **2016**, *62*, 5–9.
18. M. Mochizuki, Biodegradable plastics to solve the ocean contamination by plastics, *Sen'i Gakkaishi* **2019**, *75*(9), 473–483.
19. M. Mutsuga, Y. Kawamura, K. Tanamoto, Migration of lactic acid, lactide and oligomers from polylactide food-contact materials, *Food Addit. Contam. Part A* **2008** *25*(10), 1283–1290.

20. M. Mochizuki, Material/product designing and market development trends of biodegradable plastics from the view points of plastics wastes management, in: M. Mochizuki *Development of Biodegradable Plastics for Advanced Materials/Technologies—From the View point of Ocean Contamination by Plastics*, NTS, Tokyo, 2019, pp. 219–232.
21. M. Mochizuki, Bio-based man-made fibers for the next generation, *Sen'i Gakkaishi* **2020**, *76*(2), 48–66.
22. M. Mochizuki, *Introduction to Biodegradable Plastics—From Basic to Advanced Technologies along with Applications*, CMC Research, Tokyo, 2020.
23. H. Kawamoto, Mechanical strength of automobile parts made from bio-based plastics, *Mater. Stage* **2006**, *6*(3), 12–19.
24. R. E. Conn, J. J. Kolstad, J. F. Borzelleca, D. S. Dixler, L. J. Filer Jn, B. N. LaDu, M. W. Pariza, Safety assessment of polylactide (PLA) for use as a food-contact polymer, *Food Chem. Toxicol.* **1995**, *33*(4), 273–283.
25. M. Mochizuki, Toxicity and environmental safety of poly(lactic acid) fibers, *Sen'i Gakkaishi* **2009**, *65*(7), 232–236.

# 28

# ENVIRONMENTAL APPLICATIONS

Akira Hiraishi and Takeshi Yamada

## 28.1 INTRODUCTION

Poly(lactic acid) (PLA) and other biodegradable polyesters (BDPs) have gained much interest in environmental applications, including water and wastewater treatment and bioremediation, during the past several decades. One of the major applications in this area involves sorption technology using BDPs for the removal of hydrophobic organic contaminants (HOCs). As marine plastic waste can act as a vector of pollutants in aquatic systems [1], a number of BDPs in their solid state have been found to adsorb aromatics and organohalogen compounds [2]. Much attention has also been paid to the capacity of BDPs for adsorbing oil and its application to oil spill treatment [3]. Another important application to environmental technology is relevant to the supply of BDPs as the substrate for microbial redox processes, in which the target pollutants to be biologically removed are used as terminal electron acceptors. Since BDPs are abiotically hydrolyzed or biologically degraded, they can serve as steady sources of reducing power for the required microbial redox processes. An example of this application is the use of BDPs as a substrate for denitrifying bacteria to remove nitrate from water and wastewater [4, 5], which has been termed "solid-phase denitrification" [4]. Also, BDPs as solid matrices can provide favorable conditions for sustaining the development of microbial films as long as a BDP is added in excess to the system. Once the solid substrate is used up, the biofilm would be washed out. These characteristic features of solid-phase redox processes with BDPs can greatly facilitate process control.

PLA has much longer lifetime in such applications compared with other BDPs in general, because it is more resistant to microbial attack. PLA is chemically hydrolyzed in aqueous solutions, resulting in a slow release of lactic acid. This trait of PLA is disadvantageous for microbial redox processes requiring rapid supplement of the soluble substrate as the electron donor (e.g., the solid-phase denitrification process). This is also the case in anaerobic digestion, if PLA as the solid substrate is applied to enhance methanogenesis with concomitant treatment of plastic waste [6, 7]. On the other hand, the ability of PLA to serve as a long-term source of the organic acid makes its use possible for engineered bioremediation processes in which the microbial redox process involved requires a longer time and constant supply of electron donor to reduce target contaminants. Also, liquid lactic acid oligomers have greater appeal in applications for anaerobic bioremediation of contaminated solid matrices and subsurface environments [8], such as biotreatment of organohalogen-contaminated aquifers and groundwater over extended time periods.

This chapter provides an overview of environmental applications of PLA and other BDPs as the sorbent of HOCs and the substrate for various microbial processes. In particular, it highlights PLA-using solid-phase denitrification processes for water and wastewater treatment, anaerobic digestion, and bioremediation of persistent contaminants.

## 28.2 APPLICATION TO WATER AND WASTEWATER TREATMENT

### 28.2.1 Application as Sorbents

Large numbers of aromatic chemicals and organohalogen compounds released from anthropogenic sources into the environment are recognized as harmful and persistent

*Poly(Lactic Acid): Synthesis, Structures, Properties, Processing, Applications, and End of Life*, Second Edition.
Edited by Rafael A. Auras, Loong-Tak Lim, Susan E. M. Selke, and Hideto Tsuji.

contaminants. The removal of these HOCs from the aquatic phase has been and still is **central to** research in environmental science and technology. It has been shown that plastic debris dispersed as persistent pollutants in marine ecosystems acts as a transporter of HOCs [1, 9, 10]. Aromatic chemicals in foods are adsorbed by polyethylene [11]. Polycyclic aromatic compounds in municipal wastewater treatment plant effluents could be removed by sorption onto polypropylene [12]. The sorption behaviors of HOCs to plastics are complex, affected not only by the properties of both HOCs and plastic but also by the solution chemistry in the environment [13]. In view of the similarity in physicochemical nature between BDPs and conventional petrochemical plastics [14], these polymers may be used as potent sorbents for the removal of HOCs from the aqueous phase.

Matsuzawa et al. [2] studied the removal of different aromatic chemicals as model HOCs from aqueous solutions by sorption onto commercial BDPs, such as PLA, poly(ε-caprolactone) (PCL), poly(butylene succinate) (PBS), poly(butylene adipate/terephthalate) (PBT), poly(3-hydroxybutyrate) (PHB), and poly(3-hydroxybutyrate-*co*-3-hydroxyvalerate) (PHBV). The target HOCs used were biphenyl (BP), bisphenol A (BPA), dibenzofuran (DF), diethylstilbestrol (DES), nonylphenol (NP), phenol, and its chlorinated derivatives, 2-monochlorophenol (2-CP) and 3,5-dichlorophenol (3,5-DCP). They found that all of the BDPs tested, except PLA, adsorbed the aromatic compounds effectively at a removal efficiency of more than 98% at ambient temperature (Table 28.1). When aqueous solutions of phenol and its chlorinated derivatives were treated with BDPs, the removal efficiency increased with increasing numbers of chlorine substituents on the phenol. On the other hand, the chlorophenols were not removed by PLA under the experimental conditions used.

Tubić et al. [15] investigated the sorption of four chlorophenols, 4-chlorophenol (4-CP), 2,4-dichlorophenol (2,4-DCP), 2,4,6-trichlorophenol (2,4,6-TCP), and pentachlorophenol (PCP), onto polyethylene, polypropylene, and PLA. While no significant differences were noted in the sorption behavior of 4-CP among the plastics used, the sorption of 2,4-DCP, 2,4,6-TCP, and PCP varied greatly with polypropylene having the maximum affinity to the chlorophenols.

Although the results of Matsuzawa et al. [2] and Tubić et al. [15] are somewhat different from one another with respect to PLA as the sorbent, the results suggest that the hydrophobic interaction between the polymers and HOCs is one of the important factors affecting the sorption. However, Matsuzawa et al. [2] also found that HOCs adsorbed onto the BDPs were not fully extracted with organic solvents. For example, the total amount of BPA and DF recovered by solvent extraction from the BDPs used as the sorbents accounted for only 19–56% of the initial amount in the respective solutions. One of the possible explanations is that the mechanism of HOC sorption onto the polymers is more than a simple hydrophobic interaction. Otherwise, solvent-induced changes in crystallinity and cristalline structures of PLA [16] may affect the extraction efficiency of adsorbed HOCs.

The adsorptive interaction between BDPs and HOCs is related to the physico-chemical nature of the former compounds, as well as of the latter. A possible determinant of this is glass transition temperature. PCL, PBS, and PHBV have a low glass transition temperature ranging from −60 to 4°C (Table 28.1). These BDPs can adsorb the aromatic compounds effectively at room temperature, and the removal efficiency of the chlorophenols decreases in the following order: PCL (glass transition temperature, −60°C) > PBS (−32°C) > PHBV (4°C). On the other hand, PLA, having a much higher glass transition temperature (60°C), does not adsorb the chemicals effectively at room temperature. Poly(ethylene terephthalate) (PET), with a glass transition temperature of 70°C, shows similar behavior to PLA. Matsuzawa et al. [2] found that PLA can adsorb HOCs in solutions incubated at a temperature greater than its glass

**TABLE 28.1 Sorption of Aromatic Chemicals as Model HOCs by Biodegradable and Conventional Petrochemical Polyesters [2]**

| | Biodegradable | | | | | Nonbiodegradable | |
|---|---|---|---|---|---|---|---|
| Target Aromatic Chemical | PBS (−32°C)[a] | PBT (−30°C) | PCL (−60°C) | PHBV (4°C) | PLLA (60°C) | LDPE (−120°C) | PET (70°C) |
| BP | + | + | + | + | (+) | + | − |
| BPA | + | + | + | + | (+) | − | − |
| DF | + | + | + | + | (+) | + | − |
| DES | + | + | + | + | (+) | (+) | − |
| NP | + | + | + | + | (+) | + | − |
| 2-CP | + | + | + | + | − | − | − |

*Abbreviations and symbols*: BP: biphenyl; BPA: bisphenol A; DF: dibenzofuran; DES: diethylstilbestrol; NP: nonylphenol; 2-CP: 2-monochlorophenol; PBS: poly(butylene succinate); PBT: poly(butylene adipate/terephthalate); PCL: poly(ε-caprolactone); PHBV: poly(3-hydroxybutyrate-*co*-3-hydroxyvalerate); PLLA: poly(L-lactic acid); LDPE: low-density polyethylene; PET: poly(ethylene terephthalate); +: strongly adsorbed; (+): weakly adsorbed; −: not adsorbed.
[a] Figures in parentheses show glass transition temperature.

transition temperature (Table 28.1). The mobility of the amorphous phase of plastics increases above their glass transition temperature, which is possibly critical for increasing the HOC-sorption efficiency. In this context, it is of special interest to further study the relationship between the absorption efficiency and crystallinity of the plastics.

As mentioned above, hydrophobic chemicals are adsorbed onto PLA at >60°C but not at room temperature. This characteristic feature may be exploited for new applications of PLA in which sorption and desorption can be controlled by temperature. We have attempted to adsorb a proton-conducting hydrophobic chemical, such as nitrophenol and chlorophenol, onto PLA at high temperature and then to release it along with hydrolysis of PLA at room temperature (unpublished work). Such a "slow release" of the adsorbed chemical from PLA may be useful for the reduction of excess sludge in the activated sludge system using the chemical uncoupler [17–19].

It has been shown that BDPs are generally superior in HOC removal efficiency to conventional petrochemical plastics such as low-density polyethylene (LDPE) and PET. Although the sorption mechanism for BDPs has not yet been fully understood, it is likely that the physico-chemical characteristics of HOCs, as well as of BDPs, are involved. Possible factors affecting the solubility and sorption of HOCs to biodegradable and nonbiodegradable plastics are hydrogen bonding interaction, π–π interaction, electronic affinity, and van der Waals force [13, 14].

PLA and other BDPs have also been reported to adsorb some metals and oil. For example, Thomas et al. [20] used a PLA/nano chitosan composite to remove cadmium(II) from water. Various bio-based materials with PLA are considered for oil recovery and oil spill treatment [3]. We will refer to this topic briefly in the last section of this article.

### 28.2.2 Application to Nitrogen Removal

***28.2.2.1 Solid-Phase Denitrification*** Biological denitrification is a series of distinct bioenergetic reactions in which nitrate is reduced to nitrogen gas through nitrite, nitric oxide, and nitrous oxide. This biological process is not only a key step in the nitrogen cycle in nature but also is important for nutrient removal in water and wastewater treatment systems. Although wastewater treatment technology including the nitrogen removal system has been basically established, the system confronts a problem that the amount of soluble organic matter as the source of electron donor for microbial activity can become limited at the denitrification step, resulting a decrease in the efficiency of nitrogen removal. Attempts to add liquid substrates such as acetate, methanol, and sludge hydrolysate to the system have been made to overcome this problem. However, it is hard to constantly maintain high activity with such an exogenous liquid substrate and to control a process without secondary organic pollution with the additives.

An alternative strategy to address this problem is the use of polymer solid substrates as carbon and energy sources for microorganisms involved, i.e., the system is known as the solid-phase denitrification process (Figure 28.1) [4, 5]. A number of different solid substrates such as straw, bark, wood, hydrolyzed birch wood, crab-shell chitin, and other biopolymers have been tested for solid-phase denitrification. For this purpose, BDPs that can be used as bioplastic materials are among the most attractive solid substrates because

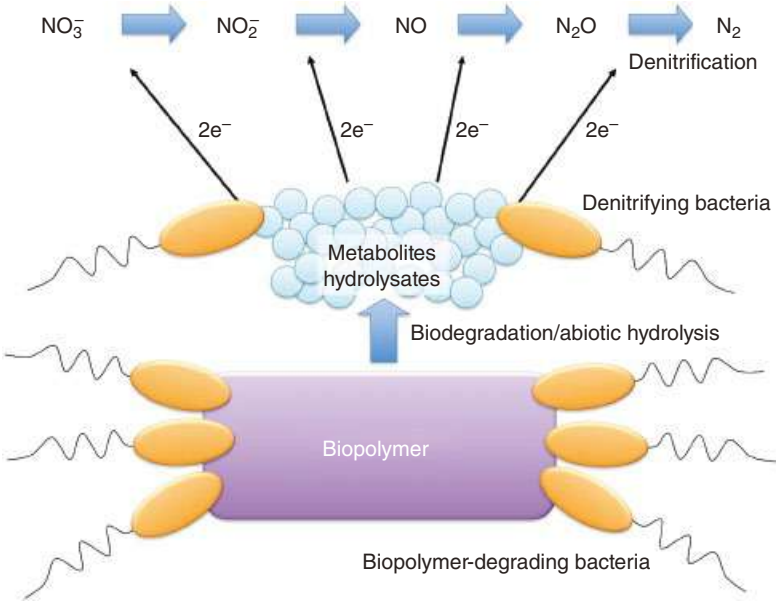


**FIGURE 28.1** Outline of the solid-phase denitrification process using biodegradable polyesters as the solid substrate.

of their excellent biodegradability. The application of BDPs for solid-phase denitrification processes has several advantages over the conventional process, such as a stable long-term supply of reducing power, less risk of secondary organic pollution, and ease of process control.

***28.2.2.2 Degradability of the Solid Substrate*** An important factor to be considered in use of PLA and other BDPs in the solid-phase denitrification process is their degradability, because this factor directly affects in situ denitrifying activity. Information about the biodegradability, biodegradation, and enzymatic degradation of PLA is available in some reviews [21–24]. There is general agreement that PLA is more resistant to microbial attack than BDPs of microbial origin. A possible reason for this is that there are fewer natural products in microbial habitats with structures similar to that of PLA.

While a wide variety of BDP-degrading microorganisms from various environments have been isolated and characterized, the PLA-degrading microorganisms so far described are mostly fungi [25] and actinomycetes asssigned to the genera of the families *Micromonosporaceae*, *Pseudonocardiaceae*, *Streptosporangiaceae*, *Thermoactinomycetaceae*, and *Thermomonosporaceae* [26–28]. Limited members of *Bacteroidetes* and *Proteobacteria* have also been reported to degrade PLA [29–31]. A culture-independent molecular approach has shown that selected members of prokaryotes, such as those of actinomycetes, are likely to play an important role in PLA degradation in compost [32]. The available information has indicated that PLA depolymerases are proteases, lipases, elastases, and cutinase rather than those with high specificity to PLA [21–24]. In a metagenomic approach, genes encoding PLA-degrading enzymes from compost were cloned, and the purified enzymes were esterases that degraded not only PLA but also various aliphatic polyesters [33]. Basically, all these PLA-degrading microorganisms and enzymes are of terrestrial origin, contrasting to the fact that PHB- and PHBV-degrading microorganisms inhabit various environments including aquatic and wastewater treatment systems.

Table 28.2 shows comparative data on the degradability of commercially available PLA and other BDPs in an activated sludge process under denitrifying conditions. PHB, PHBV, and PHBH were degraded faster under these conditions than the other BDPs tested, suggesting that the PHB copolymers are the most suitable as the solid substrates for denitrification processes. High or complete degradability of PHB copolymers has been demonstrated under anaerobic conditions [34–36], as well as in different aerobic environments [37–40]. The commercial PLA products [weight-average molecular weight ($M_w$) $\geq$ 200,000] were hardly degraded under the denitrifying conditions employed. In view of this, together with published data on the natural habitats of PLA-degrading microorganisms, it seems difficult to construct a PLA-dependent solid-phase denitrification process for practical use in which PLA-degrading microorganisms are directly involved. In a PLA-based denitrification process, therefore, nonenzymatic hydrolysis of PLA rather than biodegradation of PLA may be important as the basic reaction to provide reducing power for microbial activity.

**TABLE 28.2 Degradability of Aliphatic Polyester Pellets Under Denitrifying Conditions in Laboratory-Scale-Activated Sludge Reactors Fed with Synthetic Sewage**

| Aliphatic Polyester | Commercial Name as Biodegradable Plastic | Degradability[a] |
|---|---|---|
| PBS | Bionolle | – |
| PBT | Ecoflex | – |
| PCL | Cellgreen PH | + |
| PHB | Biogreen | ++ |
| PHBV | Biopol | ++ |
| PHBH | Green Planet | ++ |
| PLA | Lacea | – |
| PLA | Ingeo | – |

*Source*: Modified from Ref. 4.

[a] Degradability (percent weight loss) within five weeks of incubation at 25°C: ++ indicates >50% degradation; + indicates 10–50% degradation; – indicates <10% degradation.

***28.2.2.3 Denitrification Efficiency*** Among the biopolymers used so far, PHB and its copolymers may be the most suitable solid substrate for denitrification [41], because these polyners themselves are microbial storage materials and thus may be easily metabolized by a broad variety of microorganisms under denitrifying conditions, as well as under aerobic conditions. It has been shown that the PHB- and PHBV-based denitrification processes give higher rates of nitrogen removal than the conventional system in sewage treatment plants. For example, washed PHBV-acclimated sludge [42, 43] and a pure culture system of the denitrifying betaproteobacterium *Diaphorobacter nitroreducens* [44] showed a denitrification rate of approximately 20 mg $NO_3^-$-N/g (dry wt) h with PHBV as the electron donor. The apparent nitrogen removal rate in a PHBV-fed reactor in which organic acids including acetic acid and 3-hydroxybutyrate were produced as the intermediate metabolites reached ca. 60 mg $NO_3^-$-N/g (dry wt) h, possibly because the metabolites could serve directly as electron donors.

PCL as a solid carrier and substrate for denitrification processes is also attractive in light of its biodegradability and production cost [45]. The denitrification rate obtained with PCL is lower than that with PHB copolymers [45, 46]. However, the cost-effectiveness of the PCL-based system estimated on the basis of the total cost of production, quantity required, process control, and so on is comparable to those of the PHB- and PHBV-based process. It is also worth noting

that the HOC removal by sorption and nitrogen removal takes place simultaneously in the PCL-based denitrification process [47].

Despite its low biodegradability, PLA is more economically attractive in practical application because of its wide use as a commercial biodegradable plastic. If PLA waste can be reused as the substrate material, this would greatly reduce cost. So far, few reports have been available on the nitrogen removal system with PLA as the sole solid substrate. Watanabe et al. [48] reported a nitrogen-removal bioreactor that contained gel-immobilized microorganisms and ammonia and PLA plate as an energy source for nitrification and denitrification, respectively. The nitrogen-removal rate in this bioreactor was approximately 3 g-N/day $m^2$-gel surface, and the activity was maintained for over three months without any additional substrate. Rodrigues et al. [49] investigated nitrate removal efficiency using a mixed microbial culture system with PLA, PCL, and starch as the substrate. The nitrate removal rate with starch and PCL was twice as high as with PLA. Fan et al. [50] reported that PLA was inferior to wheat straw when used as the solid substrate for denitrification.

The most important problem in PLA-based applications is to increase the supply of reducing power for denitrification, since commercially available high-molecular-weight PLA is not effective as the source of electron donor required for treatment (see Table 28.2). To overcome this problem, we have attempted to use PLA with different molecular weights for the solid-phase denitrification process [51]. As shown in Table 28.3, good denitrification performance can be achieved in a laboratory-scale reactor when a PLA having an $M_w$ of 9900 is used as the substrate. In this case, the lactic acid released mainly by abiotic hydrolysis of the PLA served as the electron donor for denitrification. We have found that the rate of lactic acid release increased sharply with the low $M_w$ PLA and that no PLA-degrading microorganisms were detected in the reactor (see below).

One of the most important physico-chemical factors affecting the degradability of PLA and other BDPs as the solid substrate is crystallinity. Amorphous BDPs are more degradable than those of crystalline BDPs. In the case of PHB copolymers, the rate of enzymatic erosion of melt-crystallized films decreases with increasing crystallinity [52]. PHB depolymerases predominantly hydrolyze the polymer chains in the amorphous phase and subsequently eroded the crystalline phase. In addition, the enzymatic erosion rate of the crystalline phase in PHA films decreased with increasing lamellar thickness. Therefore, one can assume that the enzymatic hydrolysis of the amorphous regions is a limiting factor for BDP-based solid-phase denitrification. In the case of the PLA-based solid-phase denitrification process, it is important to investigate whether nonenzymatic hydrolysis of the substrate and the resultant denitrification efficiency is related to its crystallinity. Tsuji et al. [53] have shown that the abiotic hydrolysis rate for PLA is enhanced with increasing crystallinity. In fact, the nitrate removal activity of activated sludge using highly crystalline PLA ($X_c$ = 39.4%) was 2.4 times higher than that of nearly amorphous PLA ($X_c$ = 0.9%) [47]. During 57 days of operation, the denitrification reactor with 3% (w/v) highly crystalline PLA removed nitrate completely with a maximum removal rate of 22.8 mg $NO_3^-$-N g/MLSS h [54]. Thus, the apparent denitrification rate in the highly crystalline PLA-added reactor, where its abiotic hydrolysis is accelerated, is comparable to that recorded for the PHBV-added reactor.

**TABLE 28.3 Nitrogen Removal Efficiency in Solid-Phase Denitrification Process with PLA Pellets Having Different Molecular Weights [51]**

| Molecular Weight | Nitrogen Removal Rate (mg $NO_3^-$-N/(g (dry wt) h)) |
|---|---|
| 40,000 | <1 |
| 12,000 | <1 |
| 9900 | 50 |

The formation of microbial colonies and biofilms on solid matrices is important to enhance the total activity in the solid-phase denitrification process. This behavior of bacteria is possibly affected by the surface area and structure of solid substrates. The hydrophobicity and structure of the cell surface and extracellular polymer substance are also connected to the biofilm formation on the solid surface. In the case of PHAs, the hydrophobic adsorption of extracellular PHA depolymerase to the solid substrate triggers an increase in the mobility of molecular chains of single crystals [55]. However, this seems less significant in the PLA-based denitrification process, because PLA-degrading microorganisms and enzymes are unlikely contributors to PLA degradation in this process. Still, the ratio of surface area to molecular weight and crystallinity are the key factors affecting the hydrolysis of PLA and subsequent reducing power supply for microbial activity.

***28.2.2.4 Blend-Supported Nitrogen Removal*** In PLA application for solid-phase denitrification, a number of investigators have used blends of different polyesters and biological materials, such as those of PLA/starch [56–59], PLA/PHBV [60–66], PLA/PBS [67, 68], and PLA/PBS/bamboo [69], as the solid substrate and biofilm carrier. These studies have been conducted by assuming that a blend of PLA with biodegradable polymer of biological origin makes it much more susceptible to microbial attack while maintaining its role as the biofilm support. For example, Xu et al. [60] reported that a PLA/PHBV blend was degraded more rapidly than PLA and PCL. One of the most important subjects in blend-supported solid-phase denitrification is the mixing ratio of materials used. In the case of PLA/starch blends, the nitrate removal efficiency was the highest at a PLA/starch

mass ratio of 5 : 5 [57, 59]. On the other hand, the nitrate removal rate increased with the increasing weight ratio of PHBV/PLA polymers. It is also of particular interest that a fixed-bed system packed with PLA/PHBV blends enhanced nitrification and denitrification simultaneously [66].

Although most of the blend-supported solid-phase denitrification processes studied so far exhibit good performance in nitrogen removal, this may be attributable to the continuous supply of soluble substrates by the preceding biodegradation of the polymer other than PLA. Fourier transform infrared spectroscopy of the effluent in a PLA/PHBV-using denitrification reactor showed that compounds containing hydroxyl groups were produced through hydrolysis [62]. However, information on how PLA is being hydrolyzed to supply denitrifiers with the substrate in such a blend-supported reactor is still fragmentary. Further study should provide more definitive information on the mechanism of hydrolysis in PLA blend-using denitrification processes.

***28.2.2.5 Biodiversity of Microorganisms Involved*** The microbial community analysis of the solid-phase denitrification process is important to understand what kinds of microorganisms are involved and how the community structure is functionally significant in this process. A number of different species of PHB-degrading denitrifying bacteria have been isolated from activated sludge and denitrification processes [42, 70, 71]. Most of these isolates were assigned to genera of the class *Betaproteobacteria*, especially those of the family *Comamonadaceae*. One of the most popular PHB-degrading denitrifiers is *D. nitroreducens* [71]. This bacterium exhibited a high denitrification rate with PHBV comparable to those recorded for PHBV-using solid-phase denitrification processes [44] as noted above. Published reports have suggested the involvement of *D. nitroreducens* and related bacteria in nitrate removal in PHBV- [44] and PLA/PHBV-using [61] solid-phase denitrification processes, although the PHBV-degrading denitrifiers are not always predominant in these processes.

Early microbial community analyses of solid-phase denitrification processes were performed by a combined use of different culture-independent techniques such as polymerase chain reaction (PCR)-aided cloning and sequencing of genes encoding 16S rRNA, BDP-degrading enzymes, and denitrification enzymes, PCR-denaturing gradient gel electrophoresis, rRNA-targeted fluorescence in situ hybridization, and quinone profiling [42–44, 51]. These methods, having different bases of detection, are possibly complementary to each other to correct the technical bias specific to each one. In recent years, next-generation sequencing of 16S rRNA gene amplicons and gene-encoding denitrifying enzymes has been more widely applied for microbial community analysis of solid-phase denitrification processes.

Table 28.4 shows comparative data on the phylogenetic composition of bacteria by culture-independent approaches

**TABLE 28.4 Microbial Community Structure of Solid-Phase Denitrification Processes Using Low $M_w$ PLA and Low $M_w$ [44] and Highly Crystalline PLA [47] as the Substrate**

| Phylum[a]/Class | Low $M_w$ PLA[b] | Low $M_w$ Crytallized PLA[c] | | |
|---|---|---|---|---|
| | | 1%[d] | 3% | 5% |
| *Acidobacteria* | + | – | – | – |
| *Actinobacteria* | – | – | – | – |
| *Bacteroidetes* | ++ | – | (+) | + |
| *Choroflexi* | + | – | – | – |
| *Firmicutes* | ++ | – | – | – |
| *Proteobacteria* | | | | |
| *Alphaproteobacteria* | (+) | – | – | – |
| *Betaproteobacteria* | +++ | ++++ | ++++ | ++++ |
| *Gammaproteobacteria* | + | – | – | – |
| *Delataproteobacteria* | – | – | – | + |
| *Epsilonproteobacteria* | – | – | – | ++ |
| *Planctomycetes* | + | – | – | – |
| *Verrucomicrobia* | (+) | – | – | – |

*Symbols*: ++++; >50% of the total population; +++: 50–>30% present; ++: 30–>10% present; +: 1–10% present; (+): <1% present; –: not detected or negligible.

[a] The new names of phyla with the suffix *–ota* have been proposed [72], but here we use the conventional phylum names.

[b] Information based on the results of 16S rRNA gene lone library analysis.

[c] Information based on the results of next-generation sequencing of 16S rRNA gene amplicons.

[d] Weight/volume (%) in the reactors.

in denitrification reactors using two different PLA carriers, one of which is PLA having an $M_w$ of 9900 [51] and one of which is the low $M_w$ and highly crystallized [54] PLA ($X_c$ = 39.4%). In both systems, the predominant bacteria are members of the *Betaproteobacteria*, especially those of the family *Comamonadaceae* (not shown). Clone library analyses of the transcripts of *nirK* and *nirS* genes, encoding copper- and cytochrome $cd_1$-containing nitrite reductases, respectively, showed that the reactor with the low $M_w$ and highly crystalline PLA harbored active denitrifying bacteria belonging to the families *Comamonadaceae*, *Rhodocyclaceae*, and *Alcaligenaceae* [54]. Bacteria assigned to the *Betaproteobacteria* are also the major constituents of the microbial populations in the denitrification processes with PLA/starch [56], PLA/PHBV [61, 62], and PLA/PBS [67] blends and a PLA/PBS/bamboo composite [69] as the solid substrate.

As mentioned above, members of the *Betaproteobacteria* predominate and played a major role in the PLA-added denitrification process. This fact contrasts sharply with the available information about on PLA-degrading bacterial isolates from the terrestrial environments, most of which have hitherto been identified as being members of actinomycetes [21–24]. Our attempts to isolate PLA-degrading bacteria from PLA-based solid-phase denitrification reactors have been unsuccessful so far. These results provide circumstantial

evidence that abiotic hydrolysis, rather than enzymatic degradation of PLA, is a key step to supply the microorganisms present with lactic acid and their metabolites as carbon and energy sources in the PLA-added denitrification process.

## 28.3 APPLICATION TO METHANOGENESIS

### 28.3.1 Anaerobic Digestion

Organic matter in anaerobic environments is eventually converted to methane and carbon dioxide by collaboration of anaerobes with different metabolic capacities. For methanogenesis from PLA as the substrate in anaerobic digestion, its hydrolysis to L-lactic acid is prerequisite, and the resultant monomer can serve as the carbon and energy source for growth and activity of anaerobic microorganisms. As noted above, PLA hydrolysis in aerobic environments is due to the action of proteases, lipases, and esterases produced mostly by actinomycetes and fungi. However, studies on the biotic PLA hydrolysis in anaerobic environments are limited, and so far, no anaerobic microorganisms capable of hydrolyzing PLA have been reported [73]. Shin et al. [74] reported that PLA was not biologically hydrolyzed in an anaerobic environment during a 100-day long-term investigation. This observation suggests that little biological hydrolysis of PLA can be expected in anaerobic digestion. For good methane production from PLA, a pretreatment that enhances chemical hydrolysis of PLA is required before the anaerobic digestion.

The pretreatments that have been used in this respect include PLA powdering [6, 75], ammonia treatment under high temperature [76–78], high temperature/alkali treatment [79], and adjustment of molecular weight and crystallinity of PLA [80]. In general, the pretreated PLA for enhancing chemical hydrolysis results in good methane production in thermophilic anaerobic digestion at around 55°C. For example, in biological methane potential tests using powder-treated PLA, approximately 80% of PLA was decomposed with concomitant production of biogas with a methane concentration of 55% [75]. In contrast, in mesophilic anaerobic digestion at around 37°C, it is unlikely that methane is produced even from powder-treated PLA [6, 75] or PLA whose molecular weight and crystallinity have been adjusted [80]. In fact, Yagi et al. [6] reported that the powder-treated PLA was degraded by only about 20%, even during 80 days of mesophilic anaerobic digestion. Bernat et al. [81] also showed that mesophilic anaerobic digestion of shredded PLA took four times and more as long as thermophilic anaerobic digestion until the start of methanogenesis. Such a delayed anaerobic digestion period is technically unacceptable in methanogenesis [81]. The reason why methanogenesis proceeds faster in thermophilic anaerobic digestion than in mesophilic anaerobic digestion can be explained by the physical characteristics of PLA. Since the operating temperature range of thermophilic anaerobic digestion overlaps with the glass transition temperature of PLA, the chemical hydrolysis of PLA is enhanced by the easier generation of molecular motion in units of molecular segments, resulting in the achievement of good methane production [80]. On the other hand, because a large number of commercially available anaerobic digestion processes in the world are operated at around 37°C, future development of pretreatments that enable efficient methanogenesis even with mesophilic anaerobic digestion is desired.

### 28.3.2 Methanogenic Microbial Community

Recent 16S rRNA gene-based molecular approaches have provided a deep insight into understanding of methanogenic microbial communities at extremely high resolutions. The phylogenetic information rapidly accumulating has resulted in some interesting findings of microbiota in thermophilic anaerobic digestion that continuously produce methane from PLA [82–84]. However, the prediction of microbial functions based on such phylogenetic data has limitations, and many functional groups of microbes may be still unknown. Here, we focus on L-lactic acid degradation, which is the first microbial reaction process for methane production from PLA. L-Lactic acid in methanogenic environments is degraded to acetic acid and hydrogen by lactate-oxidizing bacteria, and then converted to methane and carbon dioxide by acetoclastic and hydrogenotrophic methanogens.

In themophilic anaerobic digestion in which PLA was continuously treated for 336 days, a core microbiota consisting of three species and completely degrading L-lactic acid to methane was finally formed [82]. This microbiota was composed of lactate-oxidizing bacteria belonging to the class *Thermodesulfovibrionia* and acetoclastic and hydrogenotrophic methanogens. These microorganisms established a low hydrogen partial pressure environment in the thermophilic anaerobic digestion process, thereby enhancing L-lactic acid degradation and methane production. In fact, bacteria of the genus *Thermodesulfovibrio* that degrade L-lactic acid in a syntrophic association with hydrogenotrophic methanogens have been isolated from the thermophilic anaerobic digestion process, and its draft genome sequence has been determined [85].

Members of the genus *Moorella* are another important group of lactate-oxidizing bacteria. A draft genome analysis of a *Moorella* bacterium isolated from a thermophilic anaerobic digestion process for PLA treatment has shown that this microorganism has all the genes encoding enzymes involved in lactate oxidation and those of the methyl and carbonyl branches of the Wood–Ljungdahl pathway, which are responsible for complete conversion of L-lactic acid to acetic acid [86]. Phenotypical and physiological studies have also shown that the *Moorella* isolate is able to completely convert

1 mol of L-lactic acid to 1.5 mol of acetic acid at 55°C, and thus is certainly an acetogen [87]. Large numbers of 16S rRNA gene sequences corresponding to *Moorella* bacteria have been retrieved in several thermophilic anaerobic digestion processes for PLA treatment [82–84], suggesting that these bacteria are ubiquitous in these processes. However, information on the microbiota, in which bacteria belonging to the genera *Thermodesulfovibrio* and *Moorella* coexist, is scanty. More understanding of microbial competition for L-lactic acid during thermophilc anaerobic digestion awaits further study

## 28.4 APPLICATION TO BIOREMEDIATION

### 28.4.1 Significance of PLA Use

Bioremediation technology involves the use of organisms to remove environmental hazards due to chemical contaminants and waste. This technology has gained momentum as a cost-effective and ecologically sound approach for the remediation of various environmental issues, as it can substantially reduce scale of system design, operating costs, and risk of environmental impact, compared to physico-chemical methods. Anaerobic microbial redox processes can work effectively in engineered bioremediation of anaerobically biodegradable contaminants, for which steady and long-term supply of electron donor is generally required for the microbial activity involved. "Slow-release" substrates used for this purpose include biopolymers and food-grade organic compounds such as cellulose, chitin, vegetable oils, and sucrose esters of fatty acids [88]. Also, solid PLA polymers mixed in the aqueous phase can serve as long-term sources of the substrate, because they are expected to slowly release lactic acid upon hydrolysis over extended periods of time. A technique that is increasingly being used to provide the electron donor for anaerobic bioremediation processes involves the application of liquid PLA, especially when target environments to be remediated are soil, groundwater, and subsurface environments.

A commercially available PLA product specifically designed to produce a controlled release of lactic acid is Hydrogen Release Compound (HRC®), which has been developed by Regenesis Bioremediation Products (San Clemente, CA). HRC is a viscous amber-colored liquid containing glycerol tripolylactate. When HRC is applied to in situ environments, hydrolysis or microbial cleavage of its ester bonds slowly releases lactic acid. Then, the organic acid serves as the substrate to stimulate indigenous microorganisms including anaerobic fermentative bacteria, some of which may generate hydrogen as a fermentation product. Thus, the primary advantage of HRC is its ability to serve directly or indirectly as the slow-releasing electron or hydrogen donor for microbial redox processes over an extended length of time.

The production of molecular hydrogen as the result of HRC amendment is very important, because $H_2$ is the electron donor essentially required for anaerobic bioremediation processes in which reductive dehalogenation by strictly dehalorespiring bacteria is involved. Results from various filed applications and laboratory-scale studies have revealed the significance of several factors affecting HRC-using bioremediation processes, such as application types and locations, kinds of contaminants treated, injection/mixing methods, oxygen supply, and system design [89–91].

### 28.4.2 Bioremediation of Organohalogen Pollution

Large numbers of structurally diverse haloorganic compounds are common contaminants in soil, sediment, and groundwater. An example is contamination with aliphatic organohalides including tetrachloroethene (PCE) and trichloroethene (TCE), which have been commonly used as organic solvents and degreasing agents. This contamination is a potential serious threat to drinking water source and human health. Although chlorinated ethenes are among the most recalcitrant contaminants to be treated, biological reductive dehalogenation is gaining acceptance as a feasible approach to engineered remediation of PCE, TCE, and other organohalogen contaminants.

Common electron donor sources considered for bioremediation of organohalogen pollution are lactate, HRC, molasses, vegetable, emulsified vegetable oil, mulch, and compost [92]. Yang et al. [93] reported that the PCE degradation rate in acclimated anaerobic sludge was highest in the presence of lactate as an electron donor. Reductive dechlorination of PCE to ethene occurred with lactate as the best electron donor during anaerobic degradation of toluene in an enrichment culture [94]. A field-scale study showed that TCE was completely converted to ethene during stimulation of in situ microbial activity (i.e., biostimulation) with lactate [95]. Reductive dechlorination of pentachlorophenol (PCP) in paddy soil and column reactors was promoted with lactate, as well as pyruvate, and hydrogen as electron donors [96, 97].

Due to the potential of lactate as the substrate, HRC has been used intensively for bioremediation of organohalogen pollution including PCE contamination in near field-scale simulated aquifers [98, 99] and at dry-cleaning facilities [100]. A microcosm-based study showed that PCE was transformed to TCE and DCE under coupled aerobic/anaerobic conditions where HRC was added as the electron donor and carbon source to promote reductive dechlorination [90]. A system bioaugmented with a competent dehalogenating microbial consortium and supplemented with HRC could enhance PCE dechlorination processes at significantly greater rates than in a system that was biostimulated only [101]. Although several studies have also introduced applications of HRC and other slow-release substrates for

enhanced anaerobic biodegradation of haloaromatic compounds such as PCP, chlorinated benzene, and polychlorinated biphenyls, further study is clearly necessary to evaluate the effectiveness of these applications.

The redox potentials for chloroethenes and other haloorganic compounds are relatively high, ranging from 260 to 570 mV [102]. Therefore, the redox process with the organohalogens as terminal electron acceptors can provide energy sufficient for growth and survival of dehalogenating microorganisms, as this metabolic process is called dehalorespiration. While several strains of dehalorespiring bacteria belonging to different phylogenetic groups have been isolated and characterized, among the best-characterized anaerobic dehalorespiring bacteria related to engineered bioremediation are those of the genus *Dehalococcoides* [92, 102, 103]. Members of *Dehalococcoides* grow slowly with hydrogen as the essential electron donor and chloroethenes and some other haloorganic compounds as the terminal electron acceptor. Therefore, a steady source and readily available supply of molecular hydrogen is prerequisite for stimulating reductive dehalogenation processes with *Dehalococcoides* as the main agent.

Figure 28.2 shows a model process for PLA-amended anaerobic bioremediation of chloroethenes by the *Dehalococcoides*-containing microbial consortium. Utilization of carbon sources by *Dehalococcoides* species has not been fully studied, but acetate is usually used for the cultivation of the organism [104]. Therefore, in the bioremediation process, the added PLA serves not only as the hydrogen donor but also as a carbon source for *Dehalococcoides* through the bioconversion of released lactic acid into acetic acid and hydrogen by co-existing fermenting microbes. This reaction is given by the following formula [105].

$$CH_3CHOHCOO^- + 2H_2O \rightarrow CH_3COO^- + HCO_3^- + H^+ + 2H_2 \quad (\Delta G^{o'} = -4.2 \text{ kJ/mol})$$

It is apparent that the synergistic relationship between the dehalorespiring and fermenting bacteria is indispensable to implement interspecies hydrogen transfer [102]. There are only fragmentary and scattered reports available on how the addition of HRC or solid PLA to contaminated sites affects in situ microbial consortia in terms of quantity, quality, and activity. Further study should provide definitive information about the identity of synergistic microorganisms involved in the PLA-using dehalogenating process.

### 28.4.3 Other Applications

PLA has been used for in situ bioremediation of environments contaminated with non-halogenated aromatics. Mimicking in situ bioremediation of soil contaminated with primarily hexahydro-1,3,5-trinitro-1,3,5-triazine (RDX), but also 2,4-dinitrotoluene (2,4-DNT), and excessive nitrate was performed using bench-scale batch reactors supplemented with HRC, lactate, and corn syrup as hydrogen donors [106]. The reactors were designed to simulate aquifer conditions with site soil and contaminated groundwater. The results of this study indicated that HRC and corn syrup are good electron donors for the remediation of RDX, 2,4-DNT, and nitrate. On the other hand, lactate exhibited less significant effectiveness, in contrast to other observations that lactate serves as one of the most suitable substrates for in situ reductive dehalogenation [93–96].

Environmental applications of PLA have been also made in relation to biological reduction of sulfate and metals.

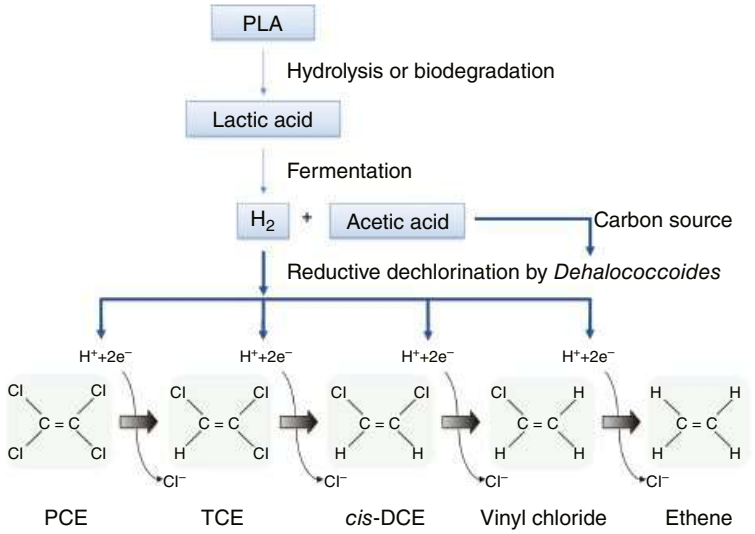


**FIGURE 28.2** Bioremediation model of chlorinated ethenes via reductive dechlorination with PLA added as the long-term source of hydrogen/electron donor.

Edenborn [107] studied the effects of solid PLA and gypsum amendments on bacterial sulfate-reducing activity in zinc smelter tailings. This treatment resulted in promoting sulfate reduction and lowering bioavailable metals including Cd, Cu, Pb, and Zn in the soil with added PLA/gypsum. Geets et al. [108] investigated the effects of HRC and other substrates on the efficiency of in situ precipitation of Zn, Cd, Co, as well as the population dynamics of sulfate-reducing bacteria in contaminated groundwater. They showed that metal precipitation depends on the activity of sulfate reducers, provided that the substrate is continuously added and environmental conditions are strictly controlled. Also, HRC has been successfully used for reduction and immobilization of toxic metals such as hexavalent chromium in laboratory- and large-scale pilot studies [109].

Marconi et al. [110] developed a 3D-printable PLA device to optimize a water bioremediation process. *Chlorella vulgaris* cells were immobilized in an alginate matrix inside the PLA device and tested for nutrient removal from polluted water. During five days of operation, the bioreactor reduced all inorganic nitrogen forms and total phosphorus at least by 90% concomitantly with decreasing aerobic mesophilic bacteria and coliforms.

For bioremediation of oil-contaminated water, Catania et al. [111] investigated biofilms of hydrocarbon-degrading gammaproteobacteria and actinobacteria that developed on biodegradable oil-absorbing carriers, based on PLA and PCL nanofiber membranes. The immobilized biofilms adsorbed 100% of spilled oil immediately and degraded more than 66% over 10 days. Apart from this biotechnological approach, the oil-absorption capacity of PLA has been reported as described above, and their practical application for remedying of oil-contaminated aquatic environments has attracted interest in connection to the development and improvement of PLA-based materials as the biodegradable and renewable sorbent. The PLA-based sorbents studied include electrospun polysulfone/PLA nanoporous fibrous mats [112], ZIF-8@C600/PLA nanofibers [113], PLA/PHB nanofibrous membranes [114], and a foam-like *Calotropis gigantea* fiber/PLA composite [115].

## 28.5 CONCLUDING REMARKS AND PROSPECTS

One of the most characteristic features of PLA and other BDPs is their capacity for absorbing hydrophobic organic compounds. The application of these polymers as the sorbent has great promise to remove HOCs from water and wastewater. In particular, this adsorption technology has in recent years been considered for application to oil recovery from water and oil spill treatment. For the practical use, more development and improvement of bio-based materials including PLA are necessary to enhance the performance of applied devices and achieve cost-effectiveness. A combination of microbial biotechnology and BDP-based adsorption technology is also intriguing, as already seen in biosorbent-biodegrading biofilms on BDP nanofiber membranes for bioremediation of oil-contaminated water [104].

Another promising application of PLA and other BDPs involves the use of these solid substrates in microbial processes in water and wastewater treatment such as nutrient removal and methanogenic processes. The PLA-based system differs from other BDP-based systems in that abiotic hydrolysis is a key reaction to supply the system with soluble substrates. Therefore, a major problem for PLA-dependent denitrification and anaerobic digestion is to control the hydrolysis rate to release the carbon and electron donor sources required for practical treatment. The nitrate removal efficiency of the PLA-dependent denitrification process is as high as that of the PHA-based system provided that low molecular weight and highly crystallized types of PLA are used as the substrate. This is true for anaerobic digestion, in which methane production is enhanced with the modified PLA as the substrate. Since commercially available PLA products are not hydrolyzed at a rate high enough to generate sufficient carbons and electron donors for microbial processes, there is a need to modify the products for practical application.

Cost-effectiveness is another important problem for the PLA-applied microbial processes. Since the PLA-based denitrification process is much more expensive than the traditionally used system with liquid substrates such as acetate and methanol, the feasibility of PLA application depends on its production cost. On one hand, the development of various PLA products suits the need to replace petrochemical plastics with BDPs growing in the market. The reuse of PLA-based plastic waste may help to overcome this problem so that this technology can provide stable and cost-effective treatment of nitrate-containing water and wastewater. This plastic waste may also be a good substrate for methane production in anaerobic digestion.

Although there are rather limited reports on the application of PLA for engineered bioremediation of organohalogen pollution, much has been learned that is helpful in understanding the effectiveness of this technology. In particular, published data indicate the potential usefulness of liquid and low $M_w$ PLA as the substrate in reductive dehalogenation. Nevertheless, there are a number of questions to be clarified in relation to the physiology and ecology of microbial consortia in PLA-amended bioremediation processes. Since organohalogen contaminants may undergo complete degradation by specific combinations of dehalogenating bacteria, fermenting hydrogen-producing bacteria, and some other physiologically different microbes, the community structure of the microbial consortia involved is of great significance to achieve effective bioremediation. Interspecies hydrogen transfer between fermenting bacteria and dehalorespiring bacteria may be an important limiting

factor affecting the total activity of the bioremediation process. Evaluation of PLA-dependent bioremediation processes will require a greater understanding of the synergistic, co-metabolic, and competitive interactions of key microorganisms involved, for which polyphasic approaches by metagenomics, proteomics, and metabolomics as well as culture-independent phylogenetic approaches may be useful.

## ACKNOWLEDGMENTS

We are very grateful to Professor H. Tsuji, Department of Applied Chemistry and Life Science, Toyohashi University of Technology, for critical comments and stimulating discussions. This work was supported in part by grants for Scientific Research from the Ministry of Education, Culture, Sports, Science and Technology, Japan (Nos. 14390028, 17310046, 19651035, and 21510084 for A.H. and 17H03333 for T.Y.). The work (T.Y.) was also carried out as part of a project entrusted to the Research Foundation for the Electrotechnology of Chubu, Yashima Environment Technology Foundation and Nippon Life Insurance Foundation.

## REFERENCES

1. H. Zhang, S. Pap, M. A. Taggart, K. G. Boyd, N. A. James, S. W. Gibb. *Environ. Pollut.* **2020**, *258*, 113698.
2. Y. Matsuzawa, Z. Kimura, T. Nishimura, M. Shibayama, A. Hiraishi, *J. Water Resour. Protect.* **2010**, *2*, 214–221.
3. B. Doshi, M. Sillanpaa, S. Kalliola, *Water Res.* **2018**, *135*, 262–277.
4. A. Hiraishi, S. T. Khan, *Appl. Microbiol. Biotechnol.* **2003**, *61*, 103–109.
5. J. Wang, L. Chu, *Biotechnol. Adv.* **2016**, *34*, 1103–1112.
6. H. Yagi, F. Ninomiya, M. Funabashi, M. Kunioka, *Int. J. Mol. Sci.* **2009**, *10*, 3824–3835.
7. A. Abraham, H. Park, O. Choi, B.-I. Sang, *Bioresour. Technol.* **2021**, *322*, 124537.
8. S. Koenigsberg, A. Willett, M. Sutherland, *Bioremediat. J.* **2006**, *10*, 45–57.
9. S. Endo, R. Takizawa, K. Okuda, H. Takada, K. Chiba, H. Kanehiro, H. Ogi, R. Yamashita, T. Date, *Mar. Pollut. Bull.* **2005**, *50*, 1103–1114.
10. Y. Mato, T. Isobe, H. Takada, H. Kanehiro, C. Ohtake, T. Kaminuma, *Environ. Sci. Technol.* **2001**, *35*, 318–324.
11. P. Simko, *Mol. Nutr. Food Res.* **2005**, *49*, 637–647.
12. V. S. Muhandiki, Y. Shimizu, Y. A. Adou, S. Matsui, *Environ. Technol.* **2007**, *28*, 415–424.
13. F. Wang, M. Zhang, W. Sha, Y. Wang, H. Hao, Y. Dou, Y. Li, *Molecules*, 2020, 25, 1827.
14. R. Auras, B. Harte, S. Selke, *Macromol. Biosci.* **2004**, *4*, 835–864.
15. A. Tubić, M. Lončarski, S. Maletić, J. Molnar Jazić, M. Watson, J. Tričković, J. Agbaba, *Water* **2019**, *11*, 2358.
16. S. Sato, D. Gondo, T. Wada, S. Kanehashi, K. Nagai, *J. Appl. Polym. Sci.* **2013**, *129*, 1607–1617.
17. Y. Liu, *Chemosphere* **2003**, *50*, 1–7.
18. X.-F. Yang, M.-L. Xie, Y. Liu, *Process Biochem.* **2003**, *38*, 1373–1377.
19. Z. Kimura, Y. Hirano, Y. Matsuzawa, A. Hiraishi, *J. Biosci. Bioeng.* **2016**, *122*, 467–474.
20. M. S. Thomas, P. K. S. Pillai, M. Faria, N. Cordeiro, L. Kailas, N. Kalarikkal, S. Thomas, L. A. Pothen, *Appl. Polym.* **2020**, *137*, 48993.
21. Y. Tokiwa, B. P. Calabia, *Appl. Microbiol. Biotechnol.* **2006**, *72*, 244–251.
22. S. M. Satti, A. A. Shah, Polyester-based biodegradable plastics: an approach towards sustainable development. *Lett. Appl. Microbiol.* **2020**, *70*, 413–430.
23. N. F. Zaaba, M. Jaafar, *Polym. Eng. Sci.* **2020**, *60*, 2061–2075.
24. K. Matsumoto, H. Abe, Y. Kikkawa, T. Iwata, Chapter 22, in: R. Auras, L.-T. Lim, S. Selke, H. Tsuji, (Eds.), Poly(lactic acid): Synthesis, Structures, Properties, Processing, Applications, and End of Life, 2nd edition, Wiley.
25. D. Y. Kim and Y. H. Rhee, *Appl. Microbiol. Biotechnol.* **2003**, *61*, 300–308.
26. A. Jarerat, H. Pranamuda, Y. Tokiwa, *Macromol. Biosci.* **2002**, *2*, 420–428.
27. Y. Tokiwa, A. Jarerat, *Biotechnol. Lett.* **2004**, *26*, 771–777.
28. S. Sukkhum, S. Tokuyama, T. Tamura, V. Kitpreechavanich, *J. Gen. Appl. Microbiol.* **2009**, *55*, 459–467.
29. M. Hajighasemi, B. P. Nocek, A. Tchigvintsev, G. Brown, R. Flick, X. H. Xu, H. Cui, T. Hai, et al., *Biomacromolecules* **2016**, *17*, 2027–2039.
30. S. M. Satti, A. A. Shah, R. Auras, T. L. Marsh, *Polym. Degrad. Stab.* **2017**, *144*, 392–400.
31. S. M. Satti, A. A. Shah, T. L. Marsh, R. Auras, *J. Polym. Environ.* **2018**, *26*, 848–3857.
32. P. Sangwan, D. Y. Wu, *Macromol. Biosci.* **2008**, *8*, 304–315.
33. D. Mayumi, Y. Akutsu-Shigeno, H. Uchiyama, N. Nomura, T. Nakajima-Kambe, *Appl. Microbiol. Biotechnol.* **2008**, *79*, 743–750.
34. D. Abou-Zeid, R. Müller, W. J. Deckwer, *J. Biotechnol.* **2001**, *86*, 113–126.
35. K. Budwill, P. M. Fedorak, W. J. Page, *Appl. Environ. Microbiol.* **1992**, *58*, 1398–1401.
36. J. Mergaert, G. Glorieux, L. Hauben, V. Storms, M. Mau, S. Jeans, *Syst. Appl. Microbiol.* **1996**, *19*, 407–413.
37. B. H. Briese, D. Jendrossek, H. G. Schlegel, *FEMS Microbiol. Lett.* **1994**, *117*, 107–111.
38. L. R. Krupp, W. J. Jewell, *Environ. Sci. Technol.* **1992**, *26*, 193–198.
39. J. Mergaert, C. Anderson, A. Wouters, J. Swings, K. Kersters, *FEMS Microbiol. Rev.* **1992**, *9*, 317–321.
40. J. Mergaert, C. Anderson, A. Wouters, S. Jeans, *J. Environ. Polym. Degrad.* **1994**, *2*, 177–183.

41. W. R. Müller, A. Heinemann, C. Schäfer, J. Wurmthaler, T. Reutter, *Water Supply* **1992**, *10*, 79–90.
42. S. T. Khan, Y. Horiba, M. Yamamoto, A. Hiraishi, *Appl. Environ. Microbiol.* **2002**, *68*, 3206–3214.
43. S. T. Khan, Y. Horiba, N. Takahashi, A. Hiraishi, *Microbes Environ.* **2007**, *22*, 20–31.
44. S. T. Khan, Y. Nagao, A. Hiraishi, *AIP Conf. Proc.* **2015**, *1649*, 71–78.
45. A. Boley, W. R. Müller, G. Haider, *Aquacul. Eng.* **2000**, *22*, 75–86.
46. Y. Horiba, S. T. Khan, A. Hiraishi, *Microbes Environ.* **2005**, *20*, 25–33.
47. A. Boley, J. Mergaert, C. Müller, H. Lebrenz, M. C. Cnockaert, W.-R. Müller, J. Swings, *Acta Hydrochim. Hydrobiol.* **2003**, *31*, 1–9.
48. A. Watanabe, H. Uemoto, M. Morisa, S. Saitoh, R. Yoshizaki, *Biol. Sci. Space*, **2004**, *18*, 142–143.
49. A. L. Rodrigues, A. Mosquera-Corral, A. V. Machado, I. Moura, M. I. Matos, A. G. Brito, R. Nogueira, *Water Sci. Technol.* **2012**, *65*, 105–111.
50. Z. Fan, J. Hu, J. Wang, *Environ. Technol.* **2012**, *33*, 2369–2374.
51. M. Takahashi, Y. Tanno, T. Yamada, H. Tsuji, A. Hiraishi, *Microbes Environ.* **2011**, *26*, 212–219.
52. H. Abe, Y. Doi, *Int. J. Biol. Macromol.* **1999**, *25*, 185–192.
53. H. Tsuji, A. Mizuno, Y. Ikada, *J. Appl. Polym. Sci.* **2000**, *77*, 1452–1464.
54. T. Yamada, H. Tsuji, H. Daimon, *Environ. Sci. Pollut. Res.* **2019**, *26*, 36236–36247.
55. T. Iwata, Y. Doi, S. Nakayama, H. Sasatsuki, S. Teramachi, *Int. J. Biol. Macromol.* **1999**, *25*, 169–176.
56. Z. Shen, Y. Zhou, J. Wang, *Bioresour. Technol.* **2013**, *131*, 33–39.
57. C. Wu, D. Tang, Q. Wang, J. Wang, J. Liu, Y. Guo, S. Liu, *Water Sci. Technol.* **2015**, *71*, 1019–1025.
58. Y. Guo, C. Wu, Q. Wang, M. Yang, Q. Huang, M. Magep, T. Zheng, *Front. Environ. Sci. Eng.* **2016**, *10*, 6.
59. M. Yang, X. Wang, S. Liu, C. Wu, Q. Wang, *Biochem. Eng. J.* **2020**, *155*, 107468
60. Y. Xu, T.-L. Qiu, M.-L. Han, J. Li, X.-M. Wang, *Proc. Environ. Sci.* **2011**, *10*, 72–77.
61. T. Qiu, Y. Xu, M. Gao, M. Han, X. Wang, *J. Biosci. Bioeng.* **2017**, *123*, 606–612.
62. Z. Xu, X. Chai, *Int. Biodeterior. Biodegradation*, **2017**, *116*, 175–183.
63. Z. Xu, X. Dai, X. Chai, *Biochem. Eng. J.* **2018**, *131*, 24–30.
64. Z. Xu, X. Dai, X. Chai, *Sci. Total Environ.* **2018**, *634*, 195–204.
65. Z. Xu, X. Dai, X. Chai, *Environ. Sci. Pollut. Res.* **2019**, *26*, 26893–26899.
66. H. Sun, Z. Yang, F. Yang, W. Wu, J. Wang, *Int. Biodeterior. Biodegradation* **2020**, *146*, 104810.
67. R. Zhang, Y. Zhang, F. Lv, H. Wang, S. Tu, *Desalination Water Treat.* **2016**, *57*, 9925–9932.
68. Z. Shen, Y. Yin, J. Wang, *Appl. Microbiol. Biotechnol.* **2016**, *100*, 6047–6053.
69. W. Qi, M. J. Taherzadeh, Y. Ruan, Y. Deng, J.-S. Chen, H.-F. Lu, X.-Y. Xu, *Bioresour. Technol.* **2020**, *305*, 123033.
70. K. Schloe, M. Gillis, B. Hoste, B. Pot, M. Vancanneyt, J. Mergaert, J. Swings, J. Biedermann, R. Süssmuth, *Syst. Appl. Microbiol.* **2000**, *23*, 364–372.
71. S. T. Khan, A. Hiraishi, *J. Gen. Appl. Microbiol.* **2002**, *48*, 299–308.
72. W. B. Whitman, A. Oren, M. Chuvochina, M. S. da Costa, G. M. Garrity, F. A. Rainey, R. Rossello-Mora, B. Schink, et al., *Int. J. Syst. Evol. Microbiol.* **2018**, *68*, 967–969.
73. V. Bátori, D. Åkesson, A. Zamani, M. J. Taherzadeh, I. S. Horváth, *Waste Manage.* **2018**, *80*, 406–413.
74. P. K. Shin, M. H. Kirn, J. M. Kim, *J. Environ. Polym. Degrad.* **1997**, *5*, 33–39.
75. H. Yagi, F. Ninomiya, M. Funabashi, M. Kunioka, *Polym. Degrad. Stab.* **2009**, *95*, 1349–1335.
76. F. Wang, H. Tsuno, T. Hidaka, J. Tsubota, *Bioresour. Technol.* **2011**, *102*, 9933–9941.
77. F. Wang, T. Hidaka, T. Oishi, S. Osumi, J. Tsubota, H. Tsuno, *Water Sci. Technol.* **2011**, *64*, 2135–2142.
78. F. Wang, T. Hidaka, H. Tsuno, J. Tsubota, *Bioresour. Technol.* **2012**, *112*, 67–74.
79. N. Benn, D. Zitomer, *Front. Environ. Sci.* **2018**, *5*, 93.
80. T. Yamada, H. Tsuji, H. Daimon, *J. Environ. Manage.* **2018**, *226*, 476–483.
81. K. Bernat, D. Kulikowska, I. Wojnowska-Baryla, M. Zaborowska, S. Pasieczna-Patkowska, *Waste Manage.* **2021**, *119*, 295–305.
82. H. Yagi, F. Ninomiya, M. Funabashi, M. Kunioka, *Polym. Degrad. Stab.* **2013**, *98*, 1182–1187.
83. H.-C. Tseng, N. Fujimoto, A. Ohnishi, *Bioresour. Technol. Rep.* **2019**, *8*, 100327.
84. T. Yamada, M. Hamada, M. Kurobe, J. Harada, S. Giri, H. Tsuji, H. Daimon, *Microbiol. Resour. Annonc.* **2019**, *8*, e00679–e00719.
85. T. Yamada, J. Harada, M. Kurobe, S. Giri, M.-K. Nobu, T. Narihiro, H. Tsuji, H. Daimon, *Microbiol. Resour. Announc.* **2019**, *8*, e00709–e00719.
86. J. Harada, T. Yamada, S. Giri, M. Hamada, M.-K. Nobu, T. Narihiro, H. Tsuji, H. Daimon, *Genome Announc.* **2018**, *6*, e00517–e00518.
87. S. Giri, M. Hamada, M. Kurobe, T. Hagihara, J. Harada, H. Tsuji, H. Daimon, T. Yamada, AIP Conf. *Proc.* **2019**, *2067*, 020021.
88. R. C. Borden, B. X. Rodriguez, *Bioremediat. J.* **2006**, *10*, 59–69.
89. S. Koenigsberg, A. Willett, M. Sutherland, *Bioremediat. J.* **2006**, *10*, 45–57.
90. D. Lyew, B. Tartakovsky, M.-F. Manuel, S. R. Guiot, *Chemosphere* **2002**, *47*, 695–699.
91. R. C. Wood, J. Huang, M. N. Goltz, *Bioremediat J.* **2006**, *10*, 129–141.

92. B.-E. Jugder, H. Ertan, S. Bohl, M. Lee, C. P. Marquis, M. Manefield, *Front. Microbiol.* **2016**, *7*, 249
93. Q. Yang, H. T. Shang, X. L. Wang, H. D. Li, J. L. Wang. *Biomed. Environ. Sci.* **2006**, *19*, 73–76.
94. H. Shen, G. W. Sewell, *Environ. Sci. Technol.* **2005**, *39*, 9286–9294.
95. B. G. Rahm, S. Chauhan, V. F. Holmes, T. W. Macbeth, K. S. Sorenson Jr., L. Alvarez-Cohen, *Biodegradation* **2006**, *17*, 523–534.
96. N. Yoshida, Y. Yoshida, Y. Handa, H. K. Kim, S. Ichihara, A. Katayama, *Sci. Total Environ.* **2007**, *381*, 233–242.
97. Z. Li, S. Yang, Y. Inoue, N. Yoshida, A. Katayama, *Biotechnol. Bioeng.* **2010**, *107*, 775–785
98. D. T. Adamson, J. M. McDade, J. B. Hughes, *Environ. Sci. Technol.* **2003**, *37*, 2525–2533.
99. M. C. Zanetti, S. Fiore, *Am. J. Environ. Sci.* **2007**, *3*, 151–157.
100. B. W. Vigue, G. Pasrich, S. S. Koenigsberg, *Remediat. J.* **2002**, *12*, 129–140.
101. M. L. Da Silva, R. C. Daprato, D. E. Gomez, J. B. Hughes, C. H. Ward, P. J. Alvarez, *Water Environ. Res.* **2006**, *78*, 2456–2465.
102. A. Hiraishi, *Microbes Environ.* **2008**, *23*, 1–10.
103. H. Smidt and W. M. de Vos, *Annu. Rev. Microbiol.* **2004**, *58*, 43–73.
104. F. E. Löffler, J. Yan, K. M. Ritalahti, L. Adrian, E. A. Edwards, K. T. Konstantinidis, J. A. Müller, H. Fullerton, S. H. Zinder, A. M. Spormann, *Int. J. Syst. Evol. Microbiol.* **2013**, *63*, 625–635
105. R. K. Thauer, K. Jungermann, K. Decker, *Bacteriol. Rev.* **1977**, *41*, 100–180.
106. S. A. Mese, D. W. Lehmpuhl, *Soil Sediment Contam.* **2008**, *17*, 505–515.
107. H. M. Edenborn, *Bioresour. Technol.* **2004**, *92*, 111–119.
108. J. Geets, K. Vanbroekhoven, B. Borremans, J. Vangronsveld, L. Diels, D. van der Lelie, *Environ. Sci. Pollut. Res. Int.* **2006**, *13*, 362–378.
109. B. Faybishenko, T. C. Hazen, P. E. Long, E. L. Brodie, M. E. Conrad, S. S. Hubbard, J. N. Christensen, D. Joyner, et al., *Environ. Sci. Technol.* **2008**, *42*, 8478–8485.
110. P. L. Marconi, A. Trentini, M. Zawoznik, C. Nadra, J. M. Mercadé, J. G. S. Novoa, D. Orozco, M. D. Groppa, *AMB Exp.* **2020**, *10*, 142.
111. V. Catania, F. Lopresti, S. Cappello, R. Scaffaro, P. Quatrini, *New Biotechnol.* **2020**, *58*, 25–31.
112. L. Liu, Z. Lin, J. Niu, D. Tian, J. He, *Adsorp. Sci. Technol.* **2019**, *37*, 438–450.
113. Y. Wang, X. Li, X. Dai, Y. Zhan, X. Ding, M. Wang, X. Wang, *J. Chem. Technol. Biotechnol.* **2020**, *3*, 730–738.
114. J. C. C. Yeo, D. Kai, C. P. Teng, E. M. J. R. Lin, B. H. Tan, Z. Li, C. He, *ACS Appl. Polym. Mater.* **2020**, *2*(11) 4825–4835.
115. W. Xiao, B. Niu, M. Yu, C. Sun, L. Wang, L. Zhou, Y. Zheng, *J. Clean. Prod.* **2021**, *278*, 123507.

# INDEX




*Poly(Lactic Acid): Synthesis, Structures, Properties, Processing, Applications, and End of Life*, Second Edition.
Edited by Rafael A. Auras, Loong-Tak Lim, Susan E. M. Selke, and Hideto Tsuji.